



**ASB2017** AMERICAN SOCIETY  
OF BIOMECHANICS  
UNIVERSITY OF COLORADO **BOULDER**

**ABSTRACTS**

# Table of Contents

Keynote Lectures.....	1
K1_1--X-ray Reconstruction of Moving Morphology (XROMM) Yields New Insights into Musculoskeletal--(Brainerd).....	1
K2_1--Developing useful smart clothing-Where does biomechanics fit--(Steele).....	2
Plenary Award Lectures.....	3
BA_1--and one thing just led to another--(Grabiner).....	3
FA_1--Translational Journeys - From Head Impact Sensors to Wrist Implants to Toy Controllers--(Crisco).....	4
FA_2--Collaborators-A Key to Fun and Exciting Research--(Neptune).....	5
FA_3--Simulated ACL and Menisci Deficiency Predicts Altered Knee Mechanics During Walking--(Smith).....	6
FA_4--Resolving the Debate-Ankle Push-Off During Human Walking Contributes to Accelerating Both--(Zelik).....	8
Wednesday, August 9, 10:30-noon.....	10
S1A--Touch of Grey-The Aging Runner--(Paquette).....	10
P1B_1--Locomotor Adaption to Lateral Center of Mass Movement Amplification Requires Active Stabilization--(Gordon)....	12
P1B_2--Is There a Learning Effect for Balance Assessment Tests--(Orendurff).....	14
P1B_3--Relating Obesity, Cognition and Biomechanics of Fall Recovery in Older Adults- Preliminary Results--(Coon).....	16
P1B_4--Biomechanical Measures of Clinician-Defined Balance Impairments in Persons Post-Arthroscopy for Femo--(Brown).	18
P1B_5--Below-Knee Amputees Make Specific Anticipatory Locomotor Adjustments To Resist Lateral Perturbation--(Major).	20
P1B_6--Altered Sensory Organization during Quiet Stance Following Neurotoxic Chemotherapy--(Monfort).....	22
P1C_1--EMG Assessment of a Shoulder Support Exoskeleton during On-Site Job Tasks--(Gillette).....	24
P1C_2--Spatial Dependency of Shoulder Muscle Demand During Dynamic Unimanual Pushing and Pulling--(McFarland)..	26
P1C_3--Submaximal Normalizing Methods to Evaluate Load Sharing Changes in Repetitive Upper Extremity Work--(McDonald).	28
P1C_4--Shoulder Musculature Activation During Human Brachiation--(MacLean).....	30
P1C_5--MRI vs CT-Based Shape Registration Accuracy for Quantifying Shoulder Motion Using Biplane Fluoroscop--(Akbari-Shandiz).	32
P1C_6--Post-Mastectomy Breast Reconstruction Surgeries Compromise Passive Shoulder Stiffness--(Leonardis).....	34
T1D_1--Human-Exosuit Interfaces Absorb and Return Energy, Reshaping Exosuit to Human Power Flow--(Yandell).....	36
T1D_2--Hopping with a Full-leg Exoskeleton Lowers Metabolic Cost and Muscle Activity--(Allen).....	38
T1D_3--Tuned or Not Ultrasound Measurements of Soleus Fascicle Dynamics During Human Walking with Elastic --(Dick).	40
T1D_4--Effect of Speed on the Mechanics and Energetics of Walking with an Elastic Ankle Exoskeleton--(Nuckols).....	42
T1D_5--Effects of Ankle Exoskeleton Power and Actuation Timing on Movement Variability and Metabolic Cost o--(Antonellis).	44
T1D_6--A Unilateral Ankle Assisting Soft Robotic Exosuit Can Improve Post-Stroke Gait During Overground Wal--(Sloot)..	46
T1E_1--A Mechanical Role for Incompressible Fluid in Stretched Muscle--(Sleboda).....	48
T1E_2--Intramuscular Pressure Variability Differs from Force Variability during Ramped Isometric Contractio--(Davies).....	50
T1E_3--Intraoperative Measurement of Human Muscle Properties--(Evertz).....	52
T1E_4--Reduced Muscle Stem Cell Number Compromises Serial Sarcomere Addition--(Dayanidhi).....	54
T1E_5--Positive Force Feedback Allows For Faster and Safer Recovery in Perturbed Hopping - At A Cost--(Punith).....	56
T1E_6--Stretch-Shortening Cycle Performance in Dancers--(Rice).....	58
Wednesday, August 9, 1:30-3:00.....	60
S2A--ASB-GCMAS Joint Symposium-Technical Challenges in Clinical Motion Analysis-Finding Solutions--(Kaufman).....	60
R2B_1--Effects of Passive and Powered Ankle-foot Prostheses on Level-ground Walking EMG--(Jeffers).....	62

R2B_2--Effects of Different Power of Powered Prosthesis on Gait Asymmetry and Metabolic Cost--(Choi).....	64
R2B_3--Displacements and Strains of the Gel Liner for Below Knee Prosthetic Users--(Lenz).....	66
R2B_4--Temporal Spatial Improvements for Amputees During Rehabilitation--(Kingsbury).....	68
R2B_5--Intact Knee Joint Kinetics During the First Six Months of Prosthetic Use--(Krupenevich).....	70
R2B_6--Longitudinal Changes in Mediolateral Trunk and Pelvic Motion among Persons with Lower Limb Amputatio--(Hendershot).	72
R2B_7--How Do Prosthetic Stiffness, Height, and Running Speed Affect the Biomechanics of Athletes with Bila--(Beck)....	74
R2B_8--Power and Work Generated Throughout the Running-Specific Prosthesis Keel during Running after Amputa--(Baum).	76
R2B_9--Dynamic Balance During Running Using Running-Specific Prostheses--(Sepp).....	78
S2C--ASB-SICB Joint Symposium-Insights from Animal Biomechanics--(Rubenson).....	80
T2D_1--Effects of an Occupational Wearable Assistive Device on Low Back Loads--(Mokhlespour Esfahani).....	83
T2D_2--Workstation Configuration and Packaging Type Influence Grocery Store Cashier Arm Postures--(Lang).....	85
T2D_3--An Investigation of Cervical Spine Kinematics in Various Tablet Reading Postures--(Douglas).....	87
T2D_4--Finger Flexor Tendon and Subsynovial Connective Tissue Motion with External Mechanical Pressure and --(Farias Zuniga).	89
T2D_5--Applied Hand-Rung Forces After a Ladder Perturbation--(Pliner).....	91
T2D_6--Comparison of 50th Percentile Human Headforms to an Adult Male Population Using 3D Modeling and Prin--(Liu).	93
T2E_1--Differences Between In Vivo Tendon Moment Arms Measured Geometrically And From Tendon Excursion--(Baxter).	95
T2E_2--Are Ultrasound-Based Estimates of Achilles Tendon Kinematics Consistent with the Expected Behavior o--(Matijevich).	97
T2E_3--Do Triceps Surae Muscle Dynamics Govern Non-Uniform Achilles Tendon Deformations--(Clark).....	99
T2E_4--How Do Material Transverse Isotropy and Pre-Tension Influence Simulations of Nonuniform Displacement--(Knaus).	101
T2E_5--Assessing Non-Uniform Stiffening of the Achilles Tendon Using Surface Wave Elastography--(Salman).....	103
T2E_6--In Vivo Tendon Stress is Predicted by Non-Invasive Wave Speed Measurement--(Martin).....	105

Wednesday, August 9, 5:30-6:30.....

P3A_1--High-Acceleration Training During Growth Increases Optimal Fiber Lengths in an Avian Bipedal Model--(Salzano).	
P3A_2--In Vivo Determination of Optimal Muscle Fascicle Length and PCSA Using Multi-scale Measurements--(Terrell)....	109
P3A_3--Individuals With Lower Limb Trauma Prioritize Stability Over Maneuverability When Navigating A Virt--(Sheehan).	111
P3A_4--ACL Reconstruction Graft Geometry is Associated With Asymmetric In Vivo Cartilage Contact Patterns--(Vignos).	113
P3B_1--Incremental Lateral Wedging- Effects on Knee Moment in Medial Knee Osteoarthritis--(Mejia).....	115
P3B_2--Effect of the AtlasGäó Knee System on Stress in the Medial Tibial Cartilage--(Hillstrom).....	117
P3B_3--Articular Cartilage Contact during Gait in Obese Individuals with Knee Pain--(Li).....	119
P3B_4--Abnormal Muscle Forces During Gait are Related to Cartilage Health After Hip Arthroscopy in Femoroac--(Samaan).	121
P3C_1--Muscle Contractile Properties in Mice with LGMD2i Muscular Dystrophy--(Rehwaldt).....	123
P3C_2--Towards Subject-Specific Tendon Models- An Experimental and Modelling Framework--(Rankin).....	125
P3C_3--3D X-Ray Motion Analysis Indicates Treadmill Exercise Exacerbates Knee Osteoarthritis in MMT Rats--(Cooper).	127
P3C_4--Putting on the brakes- the effect of drag loading on the maneuverability of bottlenose dolphins--(Shorter).....	129
T3D_1--Rotator Cuff Tendon Forces During Weight-Relief Lift in Tetraplegia--(Peterson).....	131
T3D_2--Upper Extremity Kinematics of Wheelchair Lacrosse Athletes during Overhead Throw--(Riebe).....	133
T3D_3--Handrim Biomechanics of Pediatric Manual Wheelchair Mobility--(Schnorenberg).....	135
T3D_4--The Relationship Between Propulsion Pattern and the Development of Upper-Extremity Pain in Manual Wh--(Walford).	137

T3E_1--The Effect of Lumbar Belts on Psychological and Biomechanical Outcomes--(Shahvarpour).....	139
T3E_2--The Influence of Lumbar Spine Postures on Monitor Location When Using Sit to Stand Workstations--(Fewster)....	141
T3E_3--Time-Varying Contributions to Lumbar Lordosis during and Unstable Sitting Task in People Who Do and --(Viggiani).	143
T3E_4--Landing Mechanics During A Stop Jump In Individuals With Low Back Pain And Low Back Injuries--(Johnson).....	145
<b>Thursday, August 10, 10:30-noon.....</b>	<b>109</b>
R4A_1--Soft Tissue Increases Stability and Propulsion During Human Running--(Masters).....	147
R4A_2--Differential Leg Joint Function During Human Running--(Jindrich).....	149
R4A_3--The Energetics of the Human Foot Across a Range of Running Speeds--(Kelly).....	151
R4A_4--Hip Alignment, Position at Foot Strike and Peak Hip Adduction Angle in Female Runners--(Brindle).....	153
R4A_5--Influence of Stride Frequency on Knee Joint Stiffness and Anterior Tibial Shear Forces in Female Run--(Thakkar).	155
R4A_6--Multiscale Entropy of Center of Mass Acceleration as a Measure for Cumulative Running Fatigue--(Gruber).....	157
R4A_7--Changes in Mechanics Across a Marathon--(Ruder).....	159
R4A_8--Changes In Running Mechanics During The 2016 US Olympic Trials Marathon--(Hunter).....	161
R4A_9--Coasting to a Sub-2-Hour Marathon using an Optimal Drafting Approach--(Arellano).....	163
P4B_1--Gait Effects on Joint Mechanics and Clinical Outcomes in Hip Dysplasia Patients--(Thomas).....	165
P4B_2--Kinematic Variability and Local Dynamic Stability in Individuals with Hip Dysplasia--(Loverro).....	167
P4B_3--Hip Strength and Hip Moments during Gait in Women with and without Stress Urinary Incontinence--(Hartigan).....	169
P4B_4--Hip Lateral Rotator Muscle Force during Variations of the Single Leg Squat--(Khuu).....	171
P4B_5--Deep Hip Muscle Activation Is Altered During Squatting in Symptomatic Femoroacetabular Impingement--(Diamond).	173
P4B_6--Sagittal Plane Hip Impulse During Gait is Greater After Surgical Intervention for Femoroacetabular I--(Malloy).....	175
S4C_1--Enhancing the Biomechanics Classroom with Entrepreneurial Mindset Learning Activities--(Troy).....	177
S4C_2--Active Learning in Biomechanics Using Wearable Sensors--(McGinnis).....	179
S4C_3--Teaching Undergraduate Biomechanics to Students With Diverse Abilities--(Thompson).....	181
S4C_4--The Teaching Repository as a Tool for You--(Bigelow).....	183
S4C_5--Getting Started with the Science of Teaching and Learning (SoTL) in Biomechanics--(Fournier).....	184
T4D_1--Sagittal Plane Control of Trunk Posture after Spinal Cord Injury--(Audu).....	185
T4D_2--What's Your Potential The Influence of Kinematics on a Muscle's Ability to Contribute to the Sit-To--(Schloemer)..	187
T4D_3--Simple and Two-Element Hill-Type Muscle Models Cannot Replicate Realistic Muscle Stiffness--(Marjaninejad)....	189
T4D_4--Modeling Stiffening in the Neck in Specified Directions Through Muscle Coactivation--(Mortensen).....	191
T4D_5--A Mechanistic Damage Model for Ligaments--(Barrett).....	193
T4D_6--Differences in the Active State of a Simulated Ankle Muscle Using Two Foot Models--(Wager).....	195
T4E_1--Effects of Remote Pain on Muscle Fatigue During Repetitive Movements--(Cowley).....	197
T4E_2--Stiffness Perception at the Human Ankle and Knee--(Azocar).....	199
T4E_3--Mechanical and Visual Perturbation of Human Walking to Find General Principles of Locomotion Control--(rafiee).	201
T4E_4--Effect of Mirror Visual Feedback on Motor Adaptation and Learning--(Stone).....	203
T4E_5--Segmental Coordination During Turning In People With Parkinson's Disease--(Curtze).....	205
T4E_6--Specific Manual Tasks Transform EMG into a Probe for Neural Dysfunction in Parkinson's Disease--(Laine).....	207
<b>Thursday, August 10, 1:30-3:00.....</b>	<b>209</b>

S5A--Principles of Energetic Optimization in Healthy and Pathological Movement--(Finley).....	209
P5B_1--Ankle-Foot Orthosis Alignment Affects Center Of Pressure Velocity--(Ruble).....	212
P5B_2--Finite Helical Axis Variation Between Cavus, Neutrally Aligned, And Planus Feet Under Passive Loadin--(Thorhauer).	214
P5B_3--Foot Pressure Analysis to Assess Planovalgus Foot Deformity Correction Using the Calcaneal-Cuboid-Cu--(Karakostas).	216
P5B_4--Concurrent Validity of an Automatic Technique to Calculate Plantar Contact Area at Mid-Stance During--(Lidstone).	218
P5B_5--Running Strike Pattern, Midtarsal Locking, and the Windlass Mechanism--(Bruening).....	220
P5B_6--Net Ankle Pseudo-Stiffness Is Influenced By Walking Speed But Not Age For Older Adult Women--(Collins).....	222
S5C--Non-Academic Career Paths in Biomechanics--(Hass).....	224
T5D_1--Validation of a Model Based Tracking Technique to Measure In Vivo Patellofemoral Kinematics--(Pitcairn).....	226
T5D_2--Intrarater Reliability of a Novel Semi-Automated Approach to Determine Knee Articular Cartilage Morph--(Kwon)....	228
T5D_3--Feasibility of Biplane Fluoroscopy for Quantification of Shoulder Kinematics during Manual Wheelchai--(Mozingo).	230
T5D_4--Comparison of Real-Time MRI Pulse Sequences for Tracking Tissues of the Actively Moving Wrist--(Shaw).....	232
T5D_5--Extended Field-of-View Ultrasound of the Extensor Carpi Ulnaris--(Adkins).....	234
T5D_6--Intra-Op Biomechanical Guidance Improves Articular Fracture Reduction--(Kern).....	236
T5E_1--Explicit Modification of Step Length Asymmetry Transfers to Over-Ground Walking Post-Stroke--(Sanchez).....	238
T5E_2--Plantar Flexor Stimulation Improves Poststroke Gait Kinematics--(Makowski).....	240
T5E_3--A Uni-Lateral Soft Exosuit for the Paretic Ankle Can Reduce Gait Compensations in Patients Post-Stro--(Kudzia).	242
T5E_4--The Influence of Lateral Stabilization on Hemiparetic Walking--(Frame).....	244
T5E_5--Merged Plantarflexor Muscle Excitation Module Predicts Poor Balance in Post-Stroke Hemiparetic Subje--(Brough).	246
T5E_6--Task-Specific Perurbation Training Provides a Viable Rehabilitation Strategy to Reduce Falls in Stro--(Honeycutt).	248
<b>Thursday, August 10, 5:30-6:30.....</b>	<b>250</b>
P6A_1--Residual Limb Skin Strain Within a Socket Prosthesis in Transfemoral Amputees During Walking--(Gale).....	250
P6A_2--Shoulder Posture, Torque Magnitude, and Torque Direction Highlight the Heterogeneous Elasticity of t--(Leonardis).	252
P6A_3--Biaxial Testing of the Passive Properties of Native and Regenerated Muscle Tissue--(Wallace).....	254
P6A_4--Movement Restriction Increases Thoracolumbar Fascia Stiffness in a Porcine Model--(Glinka).....	256
P6B_1--Path-Specific von-Mises Stresses Inflicting the Pre- and Post-THR Femur During Walking--(Bendjaballah).....	258
P6B_2--Evidence of Low Back Injury In The Absence of Radiographic Detection--(Gale).....	260
P6B_3--Bone Microarchitecture and Running Biomechanics in First-Time Marathon Runners--(Sattler).....	262
P6B_4--Finite Element Analysis Prediction Of Glenohumeral Joint Growth Following Neonatal Brachial Plexus I--(Dixit)....	264
P6C_1--Multi-Scale Model in Co-Simulation to Estimate Patellofemoral Contact Stress in Total Knee Replaceme--(Razu)..	266
P6C_2--Biomechanical Gait Variable Estimation Using Wearables after Total Knee Arthroplasty--(Youn).....	268
P6C_3--Concurrent Osteoarthritis of Contralateral Knee Alters Joint Biomechanics of the Knee with a Mobile---(Wang).....	270
P6C_4--Knee Biomechanics of Dissatisfied Total Knee Replacement Patients during Stair Ascent--(Zhang).....	272
T6D_1--Muscle Activity during Postural Stability Tasks- Role of Military Footwear and Workload--(Chander).....	274
T6D_2--Lower Extremity Kinematics in Military Footwear During Slip Events--(Wilson).....	276
T6D_3--The Effects of a Carbon Fiber Shoe Insert on Speed and Power in Collegiate Athletes--(Gregory).....	278
T6D_4--Lower Extremity Stiffness When Running in Minimalist, Neutral, and Ultra-Cushioning Shoes--(Borgia).....	280
T6E_1--Plantar Pressure Changes with Use of a Custom Dynamic Ankle-Foot Orthosis--(Stewart).....	282

T6E_2--Segmental Turning Velocity and Coordination in Adults with mTBI--(Fino).....	284
T6E_3--Individuals With A Prior Traumatic Brain Injury Exhibit Decreased Neuromuscular Complexity During Ga--(Acuna).	286
T6E_4--Plantarflexor Remodeling Following Achilles Tendon Rupture Repair- A Case Study--(Baxter).....	288
<b>Friday, August 11, 1:30-3:00.....</b>	<b>290</b>
R7A_1--Longitudinal Data from Wearable Sensor System Suggests Movement Improves Standing Posture--(McGinnis)....	290
R7A_2--Quantifying the Shoulder Movement of Manual Wheelchair Users in the Real World Using Inertial Measur--(Cain).	292
R7A_3--Joint Moment Estimation Using Inertial Sensor Measurements with Gaussian Process Regression--(Simons).....	294
R7A_4--Accuracy of a Shoe-Worn Device to Measure Running Mechanics--(Hunter).....	296
R7A_5--Using Inertial Sensors for Assessing Performance During Stair Running--(Ojeda).....	298
R7A_6--An Adaptive Filtering Algorithm to Estimate Sprint Velocity Using a Single Inertial Sensor--(Gurchiek).....	300
R7A_7--Energy Expenditure During Exercise Using Novel Piezoelectric Foam Sensors--(Evans).....	302
R7A_8--A Smart Pressure Insole for Gait Retraining Outside of the Laboratory--(He).....	304
R7A_9--Self-report and Performance Measure Outcome Estimation Using Wearables after Total Knee Arthroplasty--(Youn).	306
P7B_1--A New Measure of Trip Risk Integrating Minimum Foot Clearance and Dynamic Stability Across the Swing--(Schulz).	308
P7B_2--Using Detrended Fluctuation Analysis To Assess System Stability During Running--(Agesta).....	310
P7B_3--Do Inverted Pendulum Models of Stability Make Consistent Predictions of Dynamic Balance for Assessin--(Pickle).	312
P7B_4--Does Dynamic Stability Govern Propulsive Force Generation in Human Walking--(Browne).....	314
P7B_5--Aging Effects on Leg Joint Variability during Walking in the Presence Of Optical Flow Perturbations--(Qiao).....	316
P7B_6--How Healthy Older Adults Negotiate Stepping Objects While Walking--(Salinas).....	318
S7C--Jim Hay Memorial Session MTU Mechanics of the Lower Extremity-Lessons Learned from Sport--(McNittGray).....	320
T7D_1--Material Properties of Ankle Plantarflexor and Dorsiflexor Muscles - Effect of Aging--(Lee).....	322
T7D_2--Differences in Hamstring Muscle Quality Between Highly Active and Sedentary Older Adults--(Casto).....	324
T7D_3--Cognitive and Neuropsychological Differences between Elderly Populations with Good and Poor Balance --(Pechtl).	326
T7D_4--The Relationships Between Physical Capacity And Biomechanical Plasticity In Old Adults--(Kuhman).....	328
T7D_5--Age and Falls History Effects on the Modular Control of Walking with Optical Flow Perturbations--(Allen).....	330
T7D_6--Power Training Increased Neuromuscular Activation of the Extensor Muscles During Gait in Old Adults--(Beijersbergen).	332
T7E_1--Does Metabolic Cost Explain Mass-Based Changes in Preferred Reaching Speed--(O'Brien).....	334
T7E_2--Mechanics & Energetics of Walking with a Flat Center of Mass Trajectory--(Johnson).....	336
T7E_3--The Metabolic Cost of Walking on Rough Terrain--(Gast).....	338
T7E_4--Why is the Energy-Speed Curve for Human Walking U-Shaped--(Miller).....	340
T7E_5--A Passive Hip Exoskeleton for Reducing Metabolic Cost of Walking- A Simulation Study--(Saadatzi).....	342
T7E_6--Energy Cost of Walking in a Passive-Elastic Ankle-Metatarsophalangeal Exoskeleton--(Green).....	344
<b>Friday, August 11, 3:30-5:00.....</b>	<b>346</b>
S8A--Osteoarthritis Examined from Full Human to Cellular Perspectives-ASB-OARSI Symposium--(DeVita).....	346
P8B_1--The Effect of Achilles Tendon Moment Arm Length on Stretch-Shortening Cycle Performance in the Verti--(Madden).	349
P8B_2--Biomechanical Differences in Female Athletes with Varying Levels of Leg Stiffness--(Waxman).....	351
P8B_3--Modified Hockey Skate Blade Profiles Affect Skating Biomechanics And Performance--(Vienneau).....	353
P8B_4--Inverse Dynamics of Swinging Baseball Bats of Various Moments of Inertia--(Crisco ).....	355

P8B_5--Energy Generation Strategies Related to Peak Elbow Varus Torque in High School Baseball Pitchers--(McNally)..	357
P8B_6--Arm Slot and its Relation to Shoulder and Elbow Safety and Efficiency in Youth Baseball Pitchers--(Plunkett).....	359
S8C--Unanswered Questions in Biomechanics-Bases of Muscle Force Production--(Herzog).....	361
T8D_1--Power Imbalance Nearly Eliminated in Whole-Body Analysis--(Ebrahimi).....	365
T8D_2--Lower Extremity Joint Kinetics in Young Adults Walking with Varied Step Lengths--(Krupenevich).....	367
T8D_3--The Functional Utilization Of Propulsive Capacity During Human Walking--(Conway).....	369
T8D_4--Joint Power Generation During Gait Across Mood Phases in Bipolar Disorder--(Kang).....	371
T8D_5--Multi-Objective Control of Lateral Stepping While Walking--(Dingwell).....	373
T8D_6--Regulation of Whole-Body Angular Momentum and Muscle Activation During Walking Adaptability Tasks Po--(Vistamehr).	375
T8E_1--Assessing Movement Asymmetry using the Normalized Symmetry Index in ACL Patients--(Queen).....	377
T8E_2--Failure Modalities Induced by a Novel Mechanical Impact Simulator Designed to Induce ACL Failure--(Bates).....	379
T8E_3--Sex Differences in Knee Forces & Moments that Occur with ACL Rupture on Cadaveric Impact Simulations--(Schilaty).	381
T8E_4--The Combination of Tissue Collagen Quantity and Quality Estimated From MR T2 Relaxometry Predicts T--(Beveridge).	383
T8E_5--Effect of Return-to-Sport Training on Gait Mechanics and Knee Loading after ACLR--(Capin).....	385
T8E_6--Knee Force Vector and Tibia Plateau Orientation during The Stance Phase of Gait- A Comparison of ACL--(Zarei).	387
<b>Wednesday Posters: Ergonomics.....</b>	<b>389</b>
001A--Characterization of Force and Impulse for Touchscreen Gestures--(Asakawa).....	389
002B--Gender Differences in Upper Limb Joints Contributions During a Lifting Task--(Martinez).....	391
003A--Hammer Symmetry of Inertia Influences Complexity of Swing Motion--(Ferdous).....	393
004B--Are Psychophysically Determined Safe Lifting Loads Associated with an Underlying Limiting Joint Stre--(Banks).....	395
005A--Force Redistribution for Seated Individuals via Repositioning--(Scott).....	397
006B--Effects of Head-Worn Display Use on Obstacle Crossing Performance in a Simulated Occupational Task--(Kim).....	399
007A--Contact Force Distribution on the Fingers During Spherical Gripping--(Sinsel).....	401
008B--In Vivo Quantification of Muscle Fatigue in Upper Extremity during Pulling and Gripping using Regio--(Zheng).....	403
009A--Changes in Knee Kinetics are Required for Deceleration with Body Borne Load--(Cameron).....	405
010B--The Influence of Hand Location and Exertion Type On Lumbar Twist During Simulated Industrial Tasks--(McKinnon).	407
011A--Tracing on a Touch Screen- Influence of Age, Implement, Hand, and Friction--(Heintz).....	409
012B--Mass Properties Comparison of Dismounted and Ground Mounted Head-Supported Mass Configurations to Ex--(Wurzbach).	411
013A--Effect of Load Carriage Systems on Shooting Performance During a Tactical Engagement--(Higginson).....	413
014B--Muscle Activation & Strength Assessment in Native_Non-Native Sign Language Users--(Roman).....	415
015A--Are Hybrid Sit-Stand Postures a Good Compromise Between Sitting and Standing--(Noguchi).....	417
016B--Postural Evaluation of Dental Care Professionals Using Motion Analysis and Electromyography--(Abnos).....	419
017A--Biomechanical Differences in Lifting Between a Manual Vs. Power Cot--(Capehart).....	421
<b>Wednesday Posters: Exoskeletal Devices.....</b>	<b>391</b>
018B--Biomechanically-Assistive Garment Offloads Low Back During Leaning and Lifting--(Lamers).....	423
019A--Using Elastic Ankle Exoskeletons to Counteract Age-Related Structure-Function Deficits--(Nuckols).....	425
020B--Dynamic Simulation of Elastic Ankle Exoskeleton Effects on Plantarflexor Muscle-Tendon Neuromechanic--(Poppo).	427
021A--An Instrumented Ankle Foot Orthosis for Quantifying the Influence of Plantarflexion Resistance on Jo--(Bolos).....	429

022B--Effect of Powered Exosuit Training on Impulse during Gait--(Bowers).....	431
023A--Assessing Slip and Trip Risks When Wearing an Upper-Extremity Exoskeleton--(Alemi).....	433
024B--Effects of a Leg Kinetic Energy Harvester on Soldiers' Gait--(Batty).....	435
025A--Performance of a Powered Ankle Exoskeleton Using Neuromuscular Model-Based Control Over a Range of W--(McCall).....	437
026B--Ankle Foot Orthosis Stiffness and Margins of Stability During Walking--(Rosenberg).....	439
027A--Comparison of a New Ankle Orthosis to a Standard Brace on Ankle Dynamics During Walking--(Chung).....	441
028B--Emulation- A Quantitative Approach to the AFO Fitting Process--(Totah).....	443
029A--Effects of Personalized Passive-Dynamic Ankle-Foot Orthoses Bending Stiffness on Gait of Individuals--(Koller).....	445
030B--User Biomechanics during Exoskeleton-Assisted Gait- Theoretical Approach and Case Study--(Smith).....	447
031A--Mechanics and Energetics of Walking with a Powered Ankle Exoskeleton Using Neuromuscular Model-Based--(Philius).....	449
032B--Predictive Simulation Framework for Combined Device and Human Mechanics--(Saadatzi).....	451
033A--Design and Control of a Modular Lower-Limb Exoskeleton Emulator for Accelerated Design and Evaluatio--(Heer).....	453
<b>Wednesday Posters: Jumping and Landing.....</b>	<b>425</b>
034B--Mid-Flight Trunk Motion Increased Unilateral Loading During Landing- a Center of Mass Analysis--(Hinshaw).....	455
035A--Performance Constraints do not Alter Landing in Reactive Jumps--(Stephenson).....	457
036B--Kinematic Analysis of Parkour Landings from a Drop Height of 2.7 Meters--(Dai).....	459
037A--Landing Mechanics in Controlled Screening Tasks and Simulated Games in Volleyball--(Beardt).....	461
038B--Implications of Added Body Mass on Lower Limb Joint Kinetics During Vertical Jumping--(James).....	463
039A--Classifying Landing Performance Using Frequency Domain Analyses--(Sha).....	465
040B--Altered Lower Extremity Kinematics and GRFs in Distracted vs. Focused Landing--(Rider).....	467
041A--Differential Effectiveness of Visual Feedback on Drop Landing Performance--(Rutherford).....	469
042B--Gender Differences in Hip Joint Forces during Unilateral Drop Landings--(Irmischer).....	471
043A--Dynamic Postural Stability and Landing Mechanics during a Single-Leg Landing in Individuals with a P--(Winters).....	473
044B--Dynamic Valgus During Drop Landing Results in Decreased Lateral Plantar Pressure--(Ferrigno).....	475
045A--Fatigue-related Changes in Joint Mechanics, Stiffness, and Energy Absorption during Landings--(Fu).....	477
<b>Wednesday Posters: Spine.....</b>	<b>479</b>
046B--Perturbation of Systems Contributing to Control of Posture in Persons with LBP--(Rowley).....	479
047A--In Vivo Human Facet Joint Gapping During Cervical Spine Manipulation--(Anderst).....	481
048B--Impact of External Loading Assumptions on Sagittal L5S1 Moments During Lifting--(Banks).....	483
049A--Estimation of Mechanical Demands of a Lowering and Lifting Task on the Lower Back in Patients with A--(Shojaei).....	485
050B--Effect of Cervical Decompression Surgery on Biomechanics on Neuromuscular Control during Gait in Adu--(Haddas).....	487
051A--Effect of Trunk Position and Angle of Pull on Spinal Loading During a Row Exercise--(Stutzenberger).....	489
052B--The Effect of Twist on the Mechanical Properties of the Intervertebral Disc--(Harvey-Burgess).....	491
053A--Lumbopelvic Postural Control System Organization is Altered in Individuals with Low Back Pain--(Butowicz).....	493
054B--Validating the Use of Ultrasound to Measure Lumbar Vertebral Twist--(Mayberry).....	495
055A--Low Velocity Collision Characteristics Associated with Claimed Low Back Pain--(Fewster).....	497
056B--The Influence Of Walking Breaks While Standing On Gluteus Medius Activity And Low Back Pain--(Daniels).....	499
057A--Validation of Biplane Fluoroscopy for Cervical Spine Kinematics--(Kage).....	501

058B--Flexion Relaxation Response Between People With and Without Standing-Induced Low Back Pain and a Cli--(Baker).	503
059A--A Comparison of Muscle Activity during Spine Extension in People with and Without Standing-Induced B--(Viggiani).	505
060B--Intervertebral Disc Pressure Variation in Cadaveric Thoracic Spines Under Applied Dynamic Moments--(Anderson).	507
061A--Low Back Loading During Sit-to-Stand in People with a Unilateral Transtibial Amputation--(Actis).....	509
062B--The Influence of Walking Breaks on Lumbar Spine Kinematics During Prolonged Standing--(Payne).....	511
063A--The Relationship Between Family History, Biopsychosocial Factors and Seated Posture on LBP Developme--(Barrett).	513
064B--Active End-Range Spine Flexion Changes in Response to Prolonged Sitting--(Snow).....	515
065A--Changes in Trunk Mechanical Properties Following Prolonged Sitting- A Pilot Study--(Park).....	517
067A--Comparison of Lumbar Spine Acceleration Profiles of Every Day Activities and Examination of Their Fr--(Guzman).	519
068B--Differences in Principal Components in Sit-to-Stand in Participants With and Without Lower Back Pain--(Nunez Jr.).	521
069A--The Effects of Breast Size and Body Image on Posture, Muscle Activation and Back Pain During 2 Hours--(Wanninayake).	523
070B--Directional Contact Forces Investigation in the Upper Cervical Spine Under Antero-Posterior Forces A--(Mesfar).....	525
<b>Wednesday Posters: Sport and Exercise.....</b>	<b>527</b>
071A--Effects of Lumbopelvic-Hip Complex Instability on Throwing Mechanics Amongst Female Handball Athlete--(Gilmer).	527
072B--Effect of Hand Position on Scapular Kinematics in a Traditional Push-up--(Arens).....	529
073A--Neural Network Prediction of Joint Torques in Olympic Weightlifting--(Kipp).....	531
074B--Muscle Synergies in Female Athletes with Generalized Joint Hypermobility--(Geiser).....	533
075A--Ice Hockey Skating Mechanics- Transition From Start To Maximum Speed For Elite Athletes--(Budarick).....	535
076B--Ball Contact Initiates Forearm Deceleration in a Volleyball Spike--(Thompson ).....	537
077A--Quantifying Contact Loading During a Volleyball Spike--(Schmitz).....	539
078B--Evaluation of Bicycle Pedaling Ability Using Vertical and Horizontal Components of Pedaling Force Ve--(Kitawaki)..	541
079A--Lower Leg Morphology and Plantarflexion Strength in Dancers--(Rice).....	543
080B--Morphological and Functional Characteristics of 110m Hurdlers- Volume and Isometric Strength of The--(Okutani).	545
081A--Building a Better Gluteal Bridge--(Lehecka).....	547
082B--The Effect of Knee Support on the Lower Body Joint Loads and Motions of Baseball Catchers--(Dooley).....	549
083A--Modifying Stance Alters the Peak Knee Adduction Moment During a Golf Swing--(Hooker).....	551
084B--Leg Muscle Function of Front Row Rugby Union Scrummaging--(Yaghoubi).....	553
086B--Both Anticipation and Dual-Task Alter Lower Limb Biomechanics during a Loaded Single-Leg Cut--(Seymore).....	555
087A--Ball Release Velocity And Pre-Release Range Of Motion For Five Types Of Softball Pitches--(Meyer).....	557
088B--The Influence of Modern Climbing Holds on Finger Forces and Force Dispersion Patterns--(Herman-Dunphy).....	559
089A--Assessing Performance Correlations among Tasks in a Challenging Obstacle Course--(Vitali).....	561
090B--The FIFA11+ and Distribution of Energy Absorbed Across Lower Extremity Joints in Female Soccer Playe--(Marmon).	563
091A--Knee Adduction Moment and Muscle Activation During a Sidecut on a Raised Surface--(Schroeder).....	565
092B--Comparison of Barbell Kinematics in the Hang Clean and Hang Clean High Pull- Implications for Specif--(Light).....	567
093A--Effect of Leg-Drive on Upper Extremity Muscle Activity during a Bench Press--(Chia).....	569
094B--Coordination of the Ankle and toe Joints in Dancers--(Jarvis).....	571
095A--Kinematic Analysis of Trunk Coordination Throughout the Rowing Stroke Sequence--(Minnock).....	573
096B--Effects of Ballistic-intent Training on the Static Force Capacity of the Neck--(Pelland).....	575

097A--Biomechanical Differences Between a Split-Step and Sidestep Cut in Female Tennis Players--(Hamada).....	577
098B--Energy Flow in Youth Baseball Players in Relation to Pitching Performance and Efficiency--(Howenstein).....	579
099A--Effect of Start Technique on Pro-Agility Test Performance in Division I Football Players--(Ficklin).....	581
100B--Kinematic Predictors of Energy Flow in Youth Baseball Pitchers--(Howenstein).....	583
101A--Kinetics Of Steeplechase Hurdling Performance--(Tracy).....	585
102B--Empirical Based Modeling Approach for the Quantification of Dynamic Knee Stability--(Morgan).....	587
103A--Using a Treadmill to Accurately Measure Power Output in Bicycling--(Straw).....	589
104B--Diagnostic Validity of Static and Dynamic Postural Assessments within 24-48 Hours Post-Concussion--(Szekely)....	591
105A--Pelvis Rotational Velocity and Energy During Baseball Batting--(Dowling).....	593
106B--Does the Fibonacci Sequence Predict Segmental Velocities of the Overhand Throw--(Weimar).....	595
107A--Ulnar Collateral Ligament Properties in baseball Pitchers Throughout A Single Collegiate Season--(Curran).....	597
108B--Directional Compression and Muscle Activity in a Retired World Cup Alpine Skier--(Zavala).....	599
109A--Using the Motus Baseball Pitching Sleeve to Compare Pitching and Long Toss Throwing Arm Biomechanics--(O'Loughlin).	601
110B--Comparison of Kinematic and Kinetic Profiles of Lower Limbs during Baseball Pitching in Adolescent P--(Mathews).	603
111A--Evaluation of Static and Sport-Like Postural Tasks 24-48 Hours Post-Concussion--(Szekely).....	605
112B--Biomechanical Differences Between Sexes and Limb Dominance during a Cutting Maneuver--(Craft).....	607
<b>Wednesday Posters: Aging.....</b>	<b>609</b>
113A--Segment Relationships Adapt to Walking Speed Differently in Healthy Young and Elderly Adults--(Craig).....	609
114B--Kinematic Comparison Of Three Postural Limits Of Stability Tests In Community Dwelling Older Adults--(Allison)....	611
115A--Effect of an Older Adult Golf Training Program on Postural Control--(Du Bois).....	613
116B--Effects of Electrical and Mechanical Stimulation on Foot Sensitivity in Healthy Elderly Subjects--(Zippenfennig).....	615
117A--Differences in Coordination Between Young and Old Runners--(Harrison).....	617
118B--Movement Variability During Split-Belt Treadmill Walking In Healthy Older Adults--(Terza).....	619
119A--On How Age, Disease and Biomechanical Capacities Interact to Affect --(Mirshams Shahshahani).....	621
120B--Effects of Golf Training on Gait Parameters in Older Military Veterans--(Marcione).....	623
121A--More Push from your Push-off- Joint-Level Modifications to Modulate Propulsive Forces in Old Age--(Browne).....	625
122B--Let's Face It, I Am Getting Older- A Longitudinal Study of Balance Recovery from Forward Lean Releas--(Carbonneau).	627
123A--The Effect of Attention and Stance on the Rambling and Trembling Components of Postural Sway in Olde--(Hernandez).	629
124B--The Effects of Dual-task Walking and Talking in Different Conditions and Environments on Elderly Gai--(Leeder).....	631
125A--Force Fluctuations During Hybrid Force_Motion Tasks In Young and Older Adults--(Joshi).....	633
126B--High-Density EMG Recordings of Calf Muscle Activity in Older Adults During Walking--(Mani).....	635
127A--Characterizing Hip Motion and Influence of Age During Common Activities--(Fuller).....	637
<b>Wednesday Posters: Clinical Biomechanics.....</b>	<b>639</b>
128B--Individuals with Knee Osteoarthritis show Asymmetry in Pedaling Mechanics--(Buddhadev).....	639
129A--Strength of Arthroscopic Knot Tied with Compromised Suture- Effect of Defect Location--(Grindel).....	641
130B--The Effect of Isolated Weber B Fibular Fracture Displacement on Tibio-Talar Contact Pressures--(Malekzadeh).....	643
131A--Development of a Disposable Point-of-Service Digital Manometry Device to Assess Anorectal Function--(Attari).....	645
132B--Lower Body Kinematics and Joint Reaction Forces with Distal Femoral Endoprotheses Following Limb Sa--(Fritz).	647

133A--Evaluation of Transforaminal Lumbar Interbody Fusion Cage Placement- Minimally Invasive Versus Open--(Cui)...	649
134B--A Biomechanical Comparison of Syndesmotomic Repair Techniques during External Rotation Stress--(Goetz).....	651
135A--An Intra-Operative Biomechanical Guidance System For Reducing Articular Fractures--(Kern).....	653
<b>Wednesday Posters: Gait.....</b>	<b>655</b>
136B--The Anthropometric Model Influences Whole-Body Center of Mass Calculations in Gait--(Catena).....	655
137A--Lower Extremity Kinematics of Cross-Slope Roof Walking--(Brelhoff).....	657
138B--Joint Mechanical Power Compensations While Walking with Ankle Restriction--(Christensen).....	659
139A--Contributions to Increased Walking Speed During Fixed and User-Driven Treadmill Walking--(Ray).....	661
140B--The Examination of Movement Coordination between Barefoot and Minimal Foot Support Boots in Walking--(Wu)...	663
141A--Spatiotemporal Variability of Children's Gait During Walk-to-Run Transitions--(Kung).....	665
142B--Trunk Neuromuscular Control Strategies Among Persons With Lower Limb Amputation While Walking and Pe--(Butowicz).	667
143A--The Impact of Anthropometric Changes and Physical Activity on Dynamic Balance during Pregnancy--(Werner).....	669
144B--Kinematic Gait Characteristics of a Heterogeneous Population--(Thurman).....	671
145A--Mass Affects Kinetic Symmetry In Children's Knees During Gait--(Shultz).....	673
146B--Detection of Gait Pattern Differences Using Fast Fourier Transform Analysis--(Vessicchio).....	675
147A--Do We Minimize Energy When Choosing Between Gait Patterns--(Antos).....	677
148B--Biomechanics of Simulated Weight Gain Compared to an Obese Population during Stair Descent--(Ransom).....	679
149A--The Biomechanical Implications of Simulated Weight Gain on the Lower Extremity during Gait--(Ransom).....	681
150B--Effects of Walking with Increased Step Width on Knee Adduction Moment--(Edd ).....	683
151A--Using Perturbation Experiments to Infer How Humans Control Walking--(Joshi).....	685
152B--Knee Flexion Modifications During Pediatric Gait Using Visual Feedback--(Oliveira).....	687
153A--Lower Extremity Joint Contributions to Frontal Plane Trunk Dynamics in Persons with Lower Extremity --(Yoder)....	689
154B--Asymmetrical Limb Loading Affects Spatial and Temporal Gait Parameter Differently in Comparison to S--(Bowman).	691
155A--The Effects of Gait Speed on Foot Rockers--(Agnew).....	693
156B--To Walk or to Run Metabolic Cost is not the Answer--(Summerside).....	695
157A--Frontal Plane Pelvis-Trunk Coordination During Asymmetric Load Carriage While Walking on an Uneven S--(Wang).	697
158B--Differences in Lower Body Kinetics when Walking and Walking While Holding Weapon Aim--(Neugebauer).....	699
159A--Structural Parameters of the Foot and the Biomechanics of Walking With and Without Wedged Footwear I--(Lewinson).	701
160B--Lower Extremity Joint Stiffness and Work Performed Across Different Walking and Running Speeds--(Jin).....	703
161A--Step Width During Treadmill Walking is Long-Range Persistent--(Oludare).....	705
162B--Application of Harmonic Transfer Functions Method of Analysis to Understand Responses to Mechanical --(Ehtemam).	707
163A--Statistical Evaluation of Walking Velocity and Knee Adduction Moment- Allometric Scaling--(Andrews).....	709
164B--Gait Initiation Mechanisms in Unilateral Transtibial Amputees.--(Roberts).....	711
165A--Do Kinetic Differences Exist During Curb Ascent In Persons With Ertl And Non-Ertl Transtibial Amputa--(Ferris).....	713
166B--Gait Stability in People with Unilateral Transtibial Amputation Across Walking Speeds--(Wedge).....	715
167A--Fourier Analysis of Vertical Ground Reaction Forces in Habitually Unshod Persons--(Trentadue).....	717
168B--Comparisons of the Variability of Accelerations between Left and Right Foot in Human Walking--(Chavanaves).....	719
169A--Preliminary Evidence that Foot Mechanical Energy During Walking is Dissipated as Heat--(Patterson).....	721

170B--Characterizing Ambulatory Tendencies for Lower Limb Amputees--(Kim).....	723
171A--Whole-body and Segmental Angular Momentum During Turning--(Nolasco).....	725
<b>Wednesday Posters: Knee Mechanics.....</b>	<b>727</b>
172B--Effects of Wide Step Width on Stair Ascent Knee Kinetics in Obese Participants--(Yocum).....	727
173A--Central Activation Deficits of the Quadriceps Muscle in Patellar Tendinopathy--(Sprague).....	729
174B--Effect of Fatigue and Real-Time Visual Feedback During Drop Landings on Patellofemoral Joint Stress --(Olbrantz).	731
175A--Differences in Knee Joint Load Distribution with Varying Cartilage Properties--(Kaplan).....	733
176B--Strength Deficits and Knee Biomechanics Symmetry in Young Adult Osteosarcoma Survivors--(Garcia).....	735
177A--Comparison of Knee Kinematics and Kinetics During Stair Descent in Single-Radius and Multi-Radius To--(Sumner).	737
178B--Knee Mechanics and Muscle Activation Timing in Athletes with Complex Knee Injuries--(Hatcher).....	739
179A--Spatial-Temporal Measurements Indicate Knee Loading Asymmetry after Total Knee Arthroplasty--(Ouattas).....	741
180B--Functional Implications of Menstrual Cycle on Knee Laxity, RFD, and EMD--(Hawkins).....	743
181A--FEA of Lateral Meniscus Posterior Root Avulsions on Tibiofemoral Contact Mechanics--(Fojtik).....	745
182B--Surface Stiffness and Knee Joint Load Effects while Running--(Price).....	747
183A--Patellar Forces And Torsions Resulting From Decreased Activation Of The Vastus Medialis Muscle--(Siegel).....	749
184B--Effects of Age, Gender, and BMI on Maximum Knee Flexion in Single and Dual Leg Bodyweight Squats--(Herlihy)..	751
<b>Wednesday Posters: Pathological Gait.....</b>	<b>753</b>
185A--Functional Ballistic Movements in Children with a History of Ponseti Correction for Talipes Equinova--(Berg-Poppe).	753
186B--Postural Control and Activation of Muscles Controlling the Knee in Children with Idiopathic Toe Walk--(Berg-Poppe).	755
187A--Ponseti v. Posteromedial Release- Asymmetry of Foot Pressures in Children with Unilateral Clubfoot--(Wallace)....	757
188B--The Effect of Prolonged Activity and Lower Limb Trauma on Variable Terrain Walking Stability--(Sheehan).....	759
189A--Locomotor Adjustments in Children with and without Down Syndrome while Negotiating Stairs--(Liang).....	761
190B--Coordination Patterns of Muscle Synergies During Gait in Cerebral Palsy--(Steele).....	763
191A--Validity of Using Head Motion to Detect Dual-Task Gait Imbalance in Adolescents with Concussion--(Pitt).....	765
192B--Effects of Surface Irregularity on Hemiplegic Gait after a Novel Robotic 3-D Ankle Training--(Kim).....	767
193A--Combined Pelvic Assistance Force with Visual Feedback to Improve Gait Patterns in Individuals with P--(Hsu).....	769
194B--Real-Time, Autonomous Tracking of Whole-Body Bradykinesia in Parkinson's Disease--(Roy).....	771
195A--Evaluating the Primary Gait Screen as a Measure of Gait Velocity in Persons with Movement Disorders--(Schmitt)..	773
196B--Osteoarthritis Influences Functional Mobility Performance in Patients with Parkinson's Disease--(Roper).....	775
197A--Quantifying Limp Using Temporal Gait Variables--(Hughes-Oliver).....	777
198B--Stabilizing Forces and Energy Cost of Cerebral Palsy Gait with Pediatric Posterior Walker--(Tumperi).....	779
199A--Metabolic and Mechanical Demands of Symmetrical and Asymmetrical Walking on a Split-belt Treadmill--(Stenum).	781
200B--Effect of Frequency on Whole Body Movement Control in Children with and without Down Syndrome During--(Beerse).	783
201A--Biomechanical analysis of Timed Up-and-Go (TUG) test in children with and without Down syndrome--(Beerse).....	785
202B--Parameterizing Joint-level Variability During Walking for Stroke Victims--(Martin).....	787
203A--Torsional Malalignment Syndrome and Maximum Internal Varus Knee Moment During Gait in Individuals wi--(Case).	789
204B--Does Walk-DMC Predict Surgical Outcomes Extension of Synergy Analysis in Cerebral Palsy to a Second--(Shuman).	791
205A--Analysis and Modeling of Gait Biomechanics in Response to Volumetric Muscle Loss Injury--(Dienes).....	793

206B--Application of Temporal Waveforms for Evaluation of Gait Training in Children with Cerebral Palsy--(Hegarty).....	795
207A--The Influence of Locomotor Training on Mediolateral Dynamic Balance in Individuals with Post-Stroke --(Vistamehr).	797
208B--Kinematic Analysis of Sit-to-Walk in Bipolar Disorder--(Kang).....	799
209A--Lower Limb Coordination Difference in a Dynamic Balance Task Following Stroke--(Boehm).....	801
<b>Wednesday Posters: Prosthetics.....</b>	<b>803</b>
210B--Quantifying the Effects of Toe and Ankle Joint Stiffness, and Their Interplay, on Walking Biomechanics--(Honert).....	803
211A--Kinematic Differences in Partial Hand Amputees Using an Externally Powered Hand Prosthesis--(Wanamaker).....	805
212B--Biomechanical Outcomes of Prosthetic Foot Stiffness during Weighted Walking--(Golyski).....	807
213A--Characterization of Prosthetic Feet for Weighted Walking--(Koehler-McNicholas).....	809
214B--Effects of Robotic Prosthesis Controllers and Positive Work on Metabolic Cost--(Handford).....	811
215A--Finite Element Analysis of Socket to Limb Interface Simulating Gel Liner Slip versus No Slip--(Lenz).....	813
216B--A Dart Thrower's Motion Wrist Should Improve Prosthetics--(Davidson).....	815
217A--Preliminary Validation of Transfemoral Prosthetic Gait Simulator--(Henson).....	817
218B--Adaptation to Gradual and Sudden Increases in Prosthetic Ankle Power--(Selgrade).....	819
219A--Is Grasp Performance of a Novel Myoelectric Hand Prosthesis Impacted by Training--(Bhaskaran).....	821
220B--People with Amputation Walking with a Powered Knee Prosthesis Exhibit Varying Asymmetric Behavior--(Brandt).....	823
221A--Increases in ROM and Circumference of the Forearm after 6 Months of Using a 3D Printed Transitional --(Dudley).....	825
222B--Top Sprinting Speed is Influenced By Prosthetic Model, but not Stiffness or Height, for Athletes with--(Taboga).....	827
223A--Kinematic and Kinetic Analysis of a Biarticular Clutched Spring Prosthesis for TT Amputees--(Willson).....	829
224B--The Point Digit- Mechanical Design and Testing of a Ratcheting Prosthetic Finger--(Segil).....	831
225A--Development of Low Cost 3D Printed Transitional Prostheses--(Pierce).....	833
226B--Using Biomimetic Models and Intramuscular EMG for Control of Myoelectric Prostheses--(Mansouri ).....	835
227A--Prosthetic Feet with Biarticular Elements Replicate Gastrocnemius Function in Simulation--(Anderson).....	837
228B--Variable Stiffness Prosthetic Foot--(Glanzer).....	839
229A--Transfemoral Prosthesis Control for Slope Walking with Principal Component Analysis--(Hong).....	841
230B--3D Printed Prostheses- Not Just Plastic Toys--(Than).....	843
231A--Quasi-Passive Two Degree of Freedom Prosthetic Ankle--(Greene).....	845
<b>Wednesday Posters: Rehabilitation.....</b>	<b>847</b>
232B--Automatically Detecting Destabilizing Wheelchair Conditions and Applying Electrical Stimulation to M--(Armstrong).	847
233A--Dynamic Balance is Different Between Fallers and Non-Fallers with Multiple Sclerosis--(Peebles).....	849
234B--Force Distributions on the Fingers when Squeezing a Spherical Rehabilitation Ball--(Wu).....	851
235A--The Effects of a 10-Week Balance, Flexibility, and Resistance Training Intervention on Postural Stability--(Tolbert).....	853
236B--12-Week Exercise Intervention on Joint Kinetics During Curb Negotiation in Cancer Survivors--(Fraijo).....	855
237A--Kinematic and Stability Changes in Women Using a Sacroiliac Belt- A Case-Control Study--(Cigoja).....	857
238B--EMG of Facial Muscles for Subvocal Speech Recognition--(Meltzner).....	859
239A--The Examination of Hip Joint Kinematics with iWalk in Walking Gait--(Champagne).....	861
240B--A Stress Progression Sequence of Exercises During Achilles Tendon Rehabilitation--(Gheidi).....	863
241A--Speed Impacts Maneuver Stability in Individuals With Spinal Cord Injury--(Viramontes).....	865

242B--Effects of Movement Pattern Biofeedback Training After Total Knee Arthroplasty--(Cheuy).....	867
243A--The Effect of Functional Electrical Stimulation Assisted Rowing and Intravenous Zoledronic Acid on T--(Fang).....	869
244B--Sensory Stimulation Can Improve Motor Functions in Individuals with Multiple Sclerosis--(Almuklass).....	871
245A--EMG Responses to Lateral Pelvis Force Perturbation in Humans with Spinal Cord Injury During Walking--(Wu).....	873
246B--Sensor-based Activity Detection and Classification of Manual Wheelchair Users--(Fortune).....	875
247A--Impact of Geared Wheels on Energy Expenditure during Manual Wheelchair Mobility--(Jahanian).....	877
248B--Eccentric Control after Spinal Cord Injury- Translating From an Animal Model--(Worthen-Chaudhari).....	879
249A--Modifications in Wheelchair Propulsion Technique Over Time--(Russell).....	881
250B--A Neuromuscular Control Comparison between Walking Sticks and Walker during Gait in Adult Scoliosis --(Haddas).	883
251A--Biomechanical Evaluation of a Pneumatic Sleeve Orthosis for Lofstrand Crutch-Assisted Gait--(Xiao).....	885
252B--Supervised Walking Exercise Therapy Improves Gait Biomechanics in Patients with Peripheral Artery Di--(Schieber).	887
253A--Design of a Compact and Portable Hand Rehabilitation Device for Stroke-Survivors--(Anil Kumar).....	889
<b>Wednesday Posters: Upper Extremity.....</b>	<b>891</b>
254B--Effects of Push-Up Plus Variants on Upper Extremity Muscle Demands--(Cudlip).....	891
255A--Analysis of Resorative Predictors of Glenohumeral Capsule Plication--(Kraszeswski).....	893
256B--Minimum Detectable Change Values for Upper Limb Kinematics in Healthy Adults--(Engdahl).....	895
257A--Development of a Propulsion-Specific Regression Model to Predict Scapulothoracic Motion--(Cloud).....	897
258B--A Method for Estimating the Load Distribution in the Anterior Bundle of the Ulnar Collateral Ligamen--(Miller).....	899
259A--4DCT For Assessment of Wrist Ligament Injuries--(Zhao).....	901
260B--Synergistic Shoulder Muscle Activation During Arm Elevation in Different Body Positions--(Stapleton).....	903
261A--Movement Toward Predictive Hand Forces--(Drost).....	905
262B--The Effect of Simulated Rotator Cuff Tear Severity on Glenohumeral Joint Force--(Arce).....	907
263A--Biomechanics of Thumb Carpometacarpal Osteoarthritis Progression--(Crisco).....	909
264B--Optimal Placement of Ultrasonic Sensors for Improved Measurement of Scapular Kinematics--(Vicini).....	911
265A--Characterizations of the Electromyography and Vibromyography Signals During Muscular Fatigue in the --(Xu).....	913
266B--The Influence of Resting Pectoralis Minor Muscle Length on Scapular Kinematics--(Pollen).....	915
267A--Assessing Glenohumeral Joint Conformity with a Statistical Shape Model--(Sintini).....	917
268B--A Finite Element Modeling Approach to Studying Instability in Reverse Shoulder Arthroplasty--(Permeswaran).....	919
269A--Wrist Biomechanical Properties via Six Degree-of-Freedom Robotic Testing--(Badida).....	921
270B--Quantifying The Passive Extension Torque Of The Second Metacarpophalangeal Joint--(Mukherjee).....	923
271A--Determining Return of Scapulohumeral Rhythm in Patients After Reverse Shoulder Arthroplasty--(Permeswaran)...	925
272B--Iterative Learning Control of an Elbow Joint Motion Simulator--(Schimoler).....	927
273A--Thumb Carpometacarpal Joint Motion In Asymptomatic Participants--(Cussen).....	929
274B--A Subject-Specific Shoulder Capsule Mesh Model Trained with In-Vitro Data--(Kraszewski).....	931
<b>Thursday Posters: Anterior Cruciate Ligament.....</b>	<b>933</b>
275A--The Influence of Hamstring Stiffness on ACL Loading Characteristics--(Waxman).....	933
276B--Effects of Functional Knee Brace on Symmetry During Landings in ACL-R Patients--(McConnell).....	935
277A--Limb Asymmetries in Post-ACL Reconstruction Patients--(Veltri).....	937

278B--Sex Differences of MCL and ACL Strains with Cadaveric Impact Simulations--(Schilaty).....	939
279A--Short-term Effects of Femoral Nerve Block on Sagittal Plane Gait Mechanics in Individuals Following --(Nagelli).....	941
280B--Inter-joint Compensations During Early Gait in Individuals Following ACL Reconstruction--(Lin).....	943
281A--Simplified Jump Landing Task Does Not Demonstrate Increased ACL Load--(Wilkie).....	945
282B--Male Athletes Who Walk Asymmetrically Report Similar Function to Those Who Walk Symmetrically 1 Year--(Johnson).	947
283A--Effect of Foot Rotation on ACL Injury Risk Variables During Drop Landing--(Peel).....	949
284B--Coordination Variability in the One Leg Hop Test 20 years after ACL Injury--(Srinivasan).....	951
285A--Energy Absorption Strategies and Muscle Strength in Adolescent Males and Females During a Lateral-Ve--(Goto)..	953
286B--Lower Extremity Segment Coordination Following Anterior Cruciate Ligament Reconstruction--(Besand).....	955
287A--Individuals Following Anterior Cruciate Ligament Reconstruction Adjust Center of Pressure Location t--(Chan).....	957
288B--Sex and Leg Differences in ACL Stress During Unilateral Landings--(Weinhandl).....	959
289A--Hamstrings Activity Contributes To Knee Mechanics During Gait Following ACL Reconstruction--(Pamukoff).....	961
290B--Quadriceps Strength And Gait Asymmetry In Individuals With ACL Reconstruction--(Moffit).....	963
291A--Bicomponent Ultrashort Echo Time T2 Comparison of Native vs Reconstructed ACL--(Denning).....	965
292B--Effect of Torque Magnitude and Timing of In Vitro Anterior Cruciate Strain and Joint Kinematics--(Hale).....	967
<b>Thursday Posters: Footwear.....</b>	<b>969</b>
293A--Reliability of a Device to Measure Torsional Stiffness of Running Footwear--(Zifchock).....	969
294B--Influence Of Military Type Footwear And Workload On Co-Contraction Index In Unilateral Static Balanc--(Hill).....	971
295A--Effect of Military Footwear Type on Ankle Stability Following a Simulated Military Workload--(Simpson).....	973
296B--Footwear Differences in Lower Limb Joint Power Generation During Maximal Vertical Jumping--(Smith).....	975
297A--Influence of Minimalist, Neutral, and Ultra-Cushioning Shoes on Joint Coordination During Running--(Borgia).....	977
298B--The Effects Of A Novel Energy Storage And Return Military Boot On Walking Performance--(Ruble).....	979
299A--Influence of Occupational Footwear on Muscle Activity during a Simulated Workload--(Luginsland).....	981
300B--Does Footwear Affect the Rate of Fatigue During Repeated Sprints--(Frank).....	983
301A--Foot Strike Index, Running Cadence, and Loading Rate While Running in a Traditionally Cushioned Zero--(Urrutia).	985
302B--Effect of Differing Running Shoe Midsole Thickness on Gait Kinetics and Kinematics--(Vollmar).....	987
303A--Landing Mechanisms of Grand Jet+- with Soft Shoes and Pointe Shoes in Ballet Dancers--(Lin).....	989
<b>Thursday Posters: Modeling and Simulation.....</b>	<b>991</b>
304B--Ligament Strain Response between Contralateral Pairs of Lower Extremities during In Vivo Landing Sim--(McPherson).	991
305A--The Influence of Femur and Tibia Rotations on Patellar Tendon Stress and Strain- A Sensitivity Analy--(Park).....	993
306B--Anthropometric Scaling of Musculoskeletal Models--(Roos).....	995
307A--Automation of Volumetric Mesh Generation, Mesh Assembly and Model Input from Surface Representations--(Landis).	997
308B--A Three-Dimensional Mesh Wrapping Model of the Gluteus Maximus--(Vigotsky).....	999
309A--Validating Subject-Specific Muscle Architecture Data for Musculoskeletal Models Using Diffusion Tens--(Charles)...	1001
310B--Reducing Passive Muscle Force- a Process for Patient Specific Muscle Model Parameter Calibration in --(Pariser)..	1003
311A--Knee Contact Force Predictions Altered By Objective Functions During Optimization--(Kuska).....	1005
312B--Upper Extremity Model Sensitivity to Ligament Attachment Points--(LeVasseur).....	1007
313A--Simulating the Effects of Squatting on Pelvic Kinematics to Better Understand Implications During Ch--(Hemmerich).	1009

314B--A Database for Musculoskeletal Segment Length and Circumferences for Individualized Anthropometric R--(Owings).	1011
315A--Comparing Subject Specific and Scaled Generic Musculoskeletal Models for Studying Knee Biomechanics--(Charles).	1013
316B--Musculoskeletal Models Scaled with CT Images versus Skin Markers in a Population with Hip Deformity --(Song)....	1015
317A--Assessment of Spasticity By Novel Stretch Reflex Activation Model--(Kang).....	1017
319A--Joint Contact is Sensitive to Geometry Coarseness and Stiffness in OpenSim--(Krach).....	1019
320B--Using Musculoskeletal Models to Estimate the Passive Joint Stiffness--(Zonnino).....	1021
321A--Investigating Uncertainty in Constitutive Modeling of Components of the Human Head--(Brewick).....	1023
322B--Validation of a Musculoskeletal Model Including the Lower Limbs and Lumbar Spine using Intradiscal P--(Actis).....	1025
323A--Development of a Multiscale Model of the Lumbar Spine- Case Study on a Sit-to-Stand Movement--(Honegger).....	1027
324B--Effect of Modeling Approaches on Neck Muscle Moment Arm Calculations--(Suderman).....	1029
325A--Scaling of Subject Muscle Forces for Use in Optimization--(Burnett).....	1031
326B--Modeling Menisci in Finite Element Models of the Knee Joint- Implications on Cartilage Contact Press--(Sadeqi)....	1033
327A--A 3D Model Of The Medial Gastrocnemius Created Based On Ex Vivo Architectural Measurements--(Williams).....	1035
328B--Strain Analysis on the Femoral Neck using Finite Element Model during Stair Navigation--(Deng).....	1037
329A--A Zero-Feedback and Stable Running Model Controlled by a Central Pattern Generator--(Masters).....	1039
330B--Ground Contact Model for Vertical Jumping of Kangaroo Rats--(Javidi).....	1041

**Thursday Posters: Running..... 1043**

331A--Verbal Feedback During A Single Running Retraining Session- Evidence Of A Positive Outcome--(Sharp).....	1043
332B--Influence of Iliotibial Band Syndrome On Pelvis - Thigh Coupling And Coupling Variability During Run--(Foch).....	1045
333A--Changes in Limb Symmetry during a 2 Mile Outdoor Run--(Renner).....	1047
334B--Knees Presenting Varus Thrust do not Increase Knee Adduction when Running with Body Borne Load--(Brown)....	1049
335A--Tibial Shock During Treadmill and Outdoor Running- Are They the Same--(Jamison).....	1051
336B--Does Wasted Impulse Explain Metabolic Power During Downhill Running--(Southern).....	1053
337A--The Effect of Grade on the Biomechanics of Downhill Running in Female Distance Runners--(Wells).....	1055
338B--Footstrike Pattern Effects on Loading in Runners with Transtibial Amputation--(Djafar).....	1057
339A--Step Frequency in Elite Ultramarathoners During a 100-km Road Race--(Burns).....	1059
340B--Knee Joint Stiffness as a Neuromuscular Component of Preferred Speed--(Morgan).....	1061
341A--Effect of Slope and Speed on Kinetics of Jogging with a Backpack--(Malcolm).....	1063
342B--Relationship Between Running Economy and Kinematics of the Upper Extremity and Trunk--(Rhodehouse).....	1065
343A--The Effect of Transitioning from a Rearfoot Strike Pattern to a Non-Rearfoot Strike Pattern on Runni--(Reynolds)....	1067
344B--Coordination and Coordinative Variability of the Lower Limbs in Competitive Male Distance Runners--(Franzese)....	1069
345A--Lower Limb Segmental Variability During a 40-Min Prolonged Run--(Freedman Silvernail).....	1071
346B--Effect of Running Speed on Foot Strike Index, Spatio-Temporal Parameters and Rearfoot Pronation in R--(Fukuchi).	1073
347A--The Coupling Of Footstrike And Stride Length In Running--(Thompson).....	1075
348B--Prediction Equations for Leg Kinematics and Kinetics During Slope Running--(Shkedy Rabani).....	1077
349A--Effect of Transitioning Running Style from a Rearfoot to a Non-Rearfoot Strike Pattern on Impulse pe--(Smith).....	1079
350B--A Biomechanical Investigation of Compensation Strategies Used by Runners in Response to Reduced Core--(Raabe).	1081
351A--Trunk Kinematics Changes With Age and Running Speed--(Kakar).....	1083

352B--Lower Limb Joint Kinematics In Young and Middle-Aged Runners--(Kakar).....	1085
353A--Estimation of Trunk Muscle Activation During Overground Running--(McClellan).....	1087
354B--Effects of Prolonged Running and Training on Tibial Acceleration and Movement Quality--(Paquette).....	1089
355A--Biomechanical Differences between Knee Disarticulation and Transfemoral Amputation while Running- A --(Maun).....	1091
356B--Asymmetric Step Frequencies Increase the Metabolic Cost of Running--(Azua).....	1093
357A--Surface Stiffness Alters Vertical Stiffness without Altering Metabolic Demand--(Goodwin).....	1095
358B--Joint Torque Requirements and Capacities During Running--(Derrick).....	1097
359A--Distance Running Sagittal Plane Hip and Knee Variability During Early and Late Stance and Swing--(Paxton).....	1099
<b>Thursday Posters: Teaching.....</b>	<b>1101</b>
360B--Physical Education as Pedagogical Tool to Enhance Understanding of Biomechanics--(Fournier).....	1101
361A--Motivation, Learning, and Biomechanics--(Fournier).....	1103
362B--High School Biomechanics Course During Summer STEM Program--(Zaferiou).....	1105
363A--A Hands-Off Approach to Student-Centered Learning of Biomechanics and Research Methods--(DiBerardino).....	1107
364B--Putting function back into functional anatomy- Using active learning techniques to emphasize higher--(Feser).....	1109
365A--Simulator Training Leads to Improved Wire Navigation in First Year Orthopaedic Residents--(Long).....	1111
366B--Software-based Training to Enhance Student Learning in Biomechanics--(Takahashi).....	1113
<b>Thursday Posters: Wearable Sensors.....</b>	<b>1115</b>
367A--Asymmetrical Postural Sway as Quantified by the Hurst Exponent Using an Accelerometer--(Heller).....	1115
368B--Validation of Inertial Measurement Units--(Taylor).....	1117
369A--Comparing Inertial Measurement Unit and Optical Infrared Passive Marker-Based Motion Capture Systems--(Valbuena).....	1119
370B--Assessing the Effect of Soldier Equipment on Road March Biomechanics with IMUs--(Hancock).....	1121
371A--Proof-of-Concept- Accelerometer-Based Metrics Predict Injury in NCAA Runners--(Kiernan).....	1123
372B--The Use of a Single Inertial Sensor to Estimate 3-Dimensional Ground Reaction Force during Accelerat--(Gurchiek).....	1125
373A--Use of Inertial Measurement Units (IMUs) in the Analysis of Bounding Rush Performance in Soldiers--(ODonovan).....	1127
374B--Validation of GoPro Camera Motion Capture System with Inertial Magnetic Sensors for Underwater and L--(Yaghoubi).....	1129
375A--Analyzing the Applicability of Wearable Sensors to Measuring Rowing Performance - A Pilot Study--(Schlenker).....	1131
376B--Influence of Accelerometer Range on Accuracy of Foot-mounted IMU Based Running Velocity Estimation--(Potter).....	1133
377A--Quantifications of the Relative Motion between the Body and the Soldier Plate Carrier System--(Leahy).....	1135
378B--Assessing the Validity of the G-Walk BTS on Individuals with Unilateral Transtibial Amputations--(Courtney).....	1137
379A--Evaluation of an Accelerometer to Assess Sagittal Plane Knee Mechanics During a Drop Landing--(Morgan).....	1139
380B--Calibration and Validation of a Novel Force Measurement Glove- Applications in Quantifying Upper Ext--(Hooke).....	1141
381A--Accurate and Robust Gait Event Detection Using Foot-Mounted Inertial Measurement Units--(Cain).....	1143
382B--Evaluation of Ground Reaction Force Asymmetry in Walking and Running Using Force Plates vs. Accelerometers--(Karimpour).....	1145
383A--Validation of An Embedded Inertial Measurement Unit for Trunk Measurements During Simulated Sitting --(Park).....	1147
384B--Accurate Estimation of the Kinematics Using an IMU-Based Motion Capture System--(Hahn).....	1149
<b>Thursday Posters: Balance.....</b>	<b>1151</b>
385A--Age-Related Differences in Postural Control- Effects of Different Visual Manipulations on Dynamic Balance--(Germano).....	1151
386B--Effect of Lower Limb Dominance and Hemiparesis in Postural Control During Quiet Standing--(Cho).....	1153

387A--Influence of Short-Term Visual Deprivation and Reduced Auditory Capability on Quasi-Static Balance P--(Drechsel).	1155
388B--Correlation Between Plantar Vibration Sensitivity and CoP-Parameters During Dynamic Balance--(Wynands).....	1157
389A--Assessing Changes in the Reactive Control of Balance Due to Modifications of Step Length Asymmetry--(Liu).....	1159
390B--Gestational Lumbar Lordosis Interactions with Dynamic Balance Control during Pregnancy--(Wolcott).....	1161
391A--Postural Instability in Patients with Idiopathic Normal Pressure Hydrocephalus- Effect of Shunting--(Hess).....	1163
392B--Effects of a High Intensity Plyometric Training Regimen on Postural Control of Young Adults--(Suresh).....	1165
393A--Time Evolution of Frontal-plane Dynamical Balance During Locomotor Transitions of Altered Anticipati--(Li).....	1167
394B--Velocity-Based Control of Postural Sway in People with a Unilateral Transtibial Amputation--(Kent).....	1169
395A--Standing Balance Responses to Projected Sensory Stimuli in Below-Knee Amputees--(Shell).....	1171
396B--Using Approximate and Sample Entropy to measure Postural Control in Individuals with Ertl and Non-Er--(Murphy).	1173
397A--Unique Balance Domains for BESS (Balance Error Scoring System) and Y-Balance Tests--(Orendurff).....	1175
398B--Postural Stability During Quiet Standing in Persons with Ertl and Non-Ertl Transtibial Amputations--(Rentuma).....	1177
399A--Strength and Skeletal Muscle Troponin in Postural Control--(King).....	1179
400B--Assessment of Single Leg Postural Control Using A Stabilogram Diffusion Analysis after Stabilizing f--(Buchholz)....	1181
401A--Effects of Surface Type on Single-Leg Stance Utilizing Stabilogram Diffusion Analysis--(Robey).....	1183
402B--Impact of Baby Carrying Method on Postural Sway in Prolonged Standing--(Mannen).....	1185
403A--Effects of Mechanical Step Width Manipulation on Dynamic Stability--(Wilson).....	1187
404B--Effects of Local Muscle Fatigue on Dynamic Postural Control- A Pilot Study--(Kurihara).....	1189
405A--Decreased Plantar Sensation Worsens Postural Control--(Ajisafe).....	1191

**Thursday Posters: Bone and Soft Tissue Mechanics..... 1193**

406B--A Database of Soft Tissue Layer Thicknesses in Musculoskeletal Extremities--(Morrill).....	1193
407A--Correlation between Tibial Slope and Ligament Strain during In Vivo Landing Simulation--(Mejia Jaramillo).....	1195
408B--Preliminary Biomechanical Analysis of Superior Capsular Reconstruction Grafts--(Simi).....	1197
409A--Effects of Photobiomodulation Therapy on Achilles Tendon Structure--(Corrigan).....	1199
410B--Effect of Pressure on the Formation of Creases in a Soft Tissue--(Razavi).....	1201
411A--Comparison of Hip Joint Suction Seal in Simulated Labrum Tear--(Choi).....	1203
412B--Effects of Bullet Speed and the Distance Between Shot Position and an Artery on Artery Rupture Proba--(Jo).....	1205
413A--Observation Period Has an Impact on the Outcome of Soft Tissue Material Properties In Vivo--(Sichting).....	1207
414B--Dynamic Response of the Human Penis to Tensile Loading at Various Strain Rates--(Johnson).....	1209
415A--The Correlation of Bone Mineral Density and Cumulative Dynamic Skeletal Loading--(Lowndes).....	1211
416B--Relationship between Metatarsal Bone Mineral Content and Metatarsal Loading During Gait--(Downs).....	1213
417A--The Effect of Inflammation on the Biomechanical Properties of the Intervertebral Disc--(Laird ).....	1215
418B--The Material Properties of Stability Rotator Cuff Tendons Relevant in Reverse Shoulder Arthroplasty--(Permeswaran).	1217
419A--Sport-Related Loading in Athletes Predicts Bone Mineral Content of the Fifth Metatarsal--(Westbrook).....	1219
420B--Assessing Fracture Severity in the TMJ- Can Fracture Energy Be Computed Using CBCT--(Dibbern).....	1221
421A--Relationship Between Tibial Bone Stress and Biomechanical Factors Associated With Stress Fracture--(Meardon)..	1223
422B--Validating the Use of Peripheral Bone pQCT to Predict Femoral Neck Fracture Risk--(Alba).....	1225
423A--A Method for Assessing Mandible Blunt Impact Biomechanics During Anterior-Posterior Blunt Impacts to--(Weisenbach).	1227

424B--Development of a Structural Stochastic Finite Element Model of Trabecular Bone--(Alrafeek).....	1229
425A--Passive Viscoelastic Finger Stiffness Changes Minimally In Individuals With Chronic Hemiparetic Stro--(Binder-Markey).	1231
426B--A Novel Temperature Controlled Wheelchair Cushion for Pressure Ulcer Prevention--(Ersen).....	1233
427A--Finite Element Analysis of the Tibial Tuberosity Osteotomy with Anteromedialization Procedure for Pa--(Bagwell)....	1235
428B--Localized Fracture Risk Under Gait Cycle Loading Correlates Poorly with High Mirels' Scores in Metas--(Permeswaran).	1237
<b>Thursday Posters: Experimental Methods and Tools.....</b>	<b>1239</b>
430B--A Task Progress-Based Performance Measure for Template Tracing Evaluation--(Eakin).....	1239
431A--Simplified Center of Mass Tracking in Ankle Osteoarthritis Patients--(Gladish).....	1241
432B--Are Gait Kinematics Similar Between Ensemble Average and Representative Cycle--(Pimentel).....	1243
433A--Comparison of Patient-Reported Outcomes and Performance-Based Outcome Measures over Multiple Time Po--(Wingate).	1245
434B--Instrumentation for Measurement of Probe Forces and Orientation during Freehand Ultrasound--(Schimmoeller)....	1247
435A--Improved Hip Joint Center Prediction--(Miller).....	1249
436B--Foot Pressure Masking Accuracy and Reliability in Children with Unilateral Clubfoot--(Wallace).....	1251
437A--Accuracy of Simpler and Lower-Cost Technologies to Measure the Initial Lean Angle for Forward Lean R--(Carboneau).	1253
438B--Accuracy of the Milwaukee Foot Model without the Use of X-Ray Offset Measurements--(Kruger).....	1255
439A--Errors in Margins of Stability Associated with the Use of Simplified Body Models during Walking and --(Havens).....	1257
440B--Validating a Novel 3D Scanner Approach for Measuring Swelling During Prolonged Standing--(Driggers).....	1259
441A--Influence of Pelvic Segment Definition Using Landmarks Palpated in a High Flexion Posture on Joint A--(Hemmerich).	1261
442B--Measurement of Interjoint Pressure in the Midfoot using Novel Sensors--(Noginova).....	1263
443A--A Novel Image-Based Non-Invasive Tracking Technique for In-Vivo Surface Kinematics of the Temporoma--(Hu)...	1265
444B--The Reliability of Ultrasound to Identify Cartilage Thickness in Clinical Populations--(Barrow).....	1267
445A--Optimizing a Force Sensitive Resistor System for Wheelchair Instrumentation--(Lopez).....	1269
446B--3D Scanning- An Innovative Method to Personalize Body Segment Parameter Calculations--(Avalos).....	1271
447A--Day-To-Day Reliability of Gait Characteristics and Coordination in Rats--(Raffalt).....	1273
448B--Reliability of Biomechanical Variables Associated with Knee Osteoarthritis During Walking--(Hawkins).....	1275
449A--Reliability Of Retroreflective Markers In Measuring Sagittal Spine Curvature And Pelvic Tilt And Com--(Mousavi)....	1277
450B--Piezo Electric Device For Peripheral Stochastic Subsensory Vibration--(Zunker).....	1279
451A--Stair-specific Calibration Reduces Errors When Using Force-Plate-Mounted Staircases--(Roth).....	1281
453A--Estimating Body Segment Inertial Parameters Using a Kinect V2--(Kudzia).....	1283
454B--Validation of a Data Analysis Method for Use with a Gaze Tracker--(Cullen).....	1285
455A--Feasibility of Optical Motion Capture to Compute Head Impact Kinematics--(Quisenberry).....	1287
456B--Real-Time Feedback To Improve Marker Placement Consistency Among Novice Examiners--(Macaulay).....	1289
457A--Reliability of Ultrasound Elastography Measurements of the Semitendinosus Tendon--(Domire).....	1291
<b>Thursday Posters: Lower Extremity.....</b>	<b>1293</b>
458B--Passive Implanted Mechanism to Improve Foot-Arch Restoration for Adult-Acquired Flatfoot Disorder- V--(Ling).....	1293
459A--Effect of Prophylactic Knee Bracing on Lower Extremity Kinematics in Running and Jumping--(Stephenson).....	1295
460B--Effect of Functional 3D Socks on the Arch of the Foot--(Wakamiya).....	1297
461A--Effect Of Foot Orthotics On Force Distribution In The Ankle And Subtalar Joint- A Cadaveric Study.--(Lechtig).....	1299

462B--Effects of Water Immersion on Plantar Skin Properties and Sensitivity--(Schmidt).....	1301
463A--Thigh-Calf Contact During Six High Knee Flexion Movements- Onset, Range Of Motion, Magnitude, And Co--(Kingston).	1303
464B--Biomechanical Comparison of Warm-up Procedure for Achilles Tendon--(Shen).....	1305
465A--Effects of Kinematics on the Surface Wear Scarring and Wear Debris in Total Ankle Replacement--(Webb).....	1307
466B--A Brief Lower Extremity Grading System (LEGS) to Evaluate Baseline Lower Extremity Analytics in High--(Smith)...	1309
467A--Foot Morphology of School Aged Children in a Developmental Research School--(Williams).....	1311
468B--Activity Related Plantar Temperature Increase in Healthy Subjects--(Yavuz).....	1313
469A--Net Energy Transfer via Biarticular Muscles During Pedaling Flows Distal-To-Proximal Due to Hamstrin--(Gidley)....	1315
470B--Biceps Femoris and Rectus Femoris Activation During Four Postures of High Knee Flexion--(Laudanski).....	1317
471A--Metatarsophalangeal Joint Stiffness at Different Running Speeds--(Day).....	1319
472B--Arch Structure and Loading Pattern Can Predict Running Foot Mechanics--(Henderson).....	1321
473A--Effective Average Ankle Moment Arm at Various Speeds--(Steinbach).....	1323
474B--Planus First Metatarsophalangeal Joint Loading after Cheilectomy and Moberg Osteotomy- A Study of Si--(Morgan).	1325
475A--Hip, Knee, and Ankle Loading Asymmetries Differ--(Ajisafe).....	1327
476B--Decreased Plantar Sensation is Associated with Increased Loading--(Ajisafe).....	1329

**Thursday Posters: Motor Control..... 1331**

477A--Factors Influencing Visuomotor Tracking Performance in Healthy Adults--(Santago).....	1331
478B--Application of a Novel Elastic Force-Field to Influence Lateral Gait Stabilization Strategy--(Bowman).....	1333
479A--Muscle Synergy Extraction from EMG (Electro Myogram) data- A comparison of algorithms (PCA, NNMF, pl--(Singh).	1335
480B--Center of Mass Control and Multi-Segment Coordination in Children During and After Vibration--(Liang).....	1337
481A--Rate Coding and Recruitment of Elbow Flexion Agonists--(Adams).....	1339
482B--Reliability of a Novel Seated Balance Experiment to Assess Trunk Control--(Ramadan).....	1341
483A--Muscular Fatigue Influences Motor Synergies During Push-Ups--(Bell).....	1343
484B--Tales From the Uninvolved Limb- Motor Control in Unilateral Achilles Tendinopathy--(Fietzer).....	1345
485A--Generalization of Split-Belt Locomotor Adaptation- Motorized Treadmill After-effects are Preserved A--(Gregory)....	1347
486B--Motor Unit Activation of Muscle Synergists During Cyclic Upper-Limb Movements--(Kline).....	1349
487A--Stabilization of Leg Length and Orientation Across Different Hopping Frequencies in Children and Adu--(Beerse)....	1351
488B--Movement Variability and Sensorimotor Cortical Activation During Forward and Backward Wakling--(Groff).....	1353
489A--Estimation of Changes in Lumbar Segmental Kinematics Associated with Alterations in Trunk Neuromuscu--(Shojaei).	1355
490B--Exploring Haptic Feedback on Kinesthetic Awareness- A Case Study--(Shattuck).....	1357
491A--Kinematic Measurement and Analysis of Limb Movement during Motor Learning--(Xing).....	1359
492B--Anticipatory Behaviors in Lateral Weight Shifting--(Fox).....	1361
493A--Muscle Recruitment and Coordination During Common Clinical Upper-Extremity Functional Tests--(Peters).....	1363
494B--Reduction in Stability of Manual Behavior in Uncertain Conditions--(Tillman).....	1365
495A--Expectation of Reward Discounts the Cost of Effort in Human Reaching--(Summerside).....	1367
496B--The Effects of Prolonged Standing on Weight-Bearing and Muscle Activation Asymmetries--(Soliday).....	1369
497A--Estimation of Human Ankle Impedance in Late Stance and Implications in Neuromotor Control--(Shorter).....	1371
498B--Identifying Neurophysiological Control Parameters of the Knee--(Popovich).....	1373

499A--Feedback Controller to Adopt Task-Dependent Postures in a Standing Neuroprosthesis--(Odle).....	1375
500B--Neuromechanical Implications of Postural Changes to Motor Learning and Performance--(Cohn).....	1377
501A--Reverse Engineering the Dynamics of Human Pursuit Strategies--(Arumukhom Revi).....	1379
502B--Prediction of Muscle Activations for Reaching Movements using Deep Neural Networks--(Khan).....	1381
503A--Hand-object Kinematics and Gaze Fixation During Bimanual Tasks--(Haji Fathaliyan).....	1383
<b>Thursday Posters: Muscle and Tendon.....</b>	<b>1385</b>
504B--Relationship Between Residual Force Enhancement and Muscle Fatigue--(Fukutani).....	1385
505A--Relationship Between Young's Modulus, Shear Modulus, and Viscosity in Healthy Achilles Tendon--(Zellers).....	1387
506B--Shear Wave Elastography of Exercise-Trained Hamstring Muscles--(Eby).....	1389
507A--Shortening-Induced Force Depression is Modulated in a Time- and Speed-Dependent Manner Following a S--(Fortuna).	1391
508B--Finite Element Analysis of Intramuscular Pressure in the Human Tibialis Anterior--(Wheatley).....	1393
509A--Biomechanical Evaluation of the Suitability of Mouse Models for Human Neuromuscular Disease--(Hu).....	1395
510B--Too Much Work- Revisiting Ultrasound-Based Estimates of Achilles Tendon Energy Storage and Return--(Franz)...	1397
511A--Spatial Tuning of Muscle Elasticity and EMG Activity for the Sternocleidomastoid Muscles--(Luciani).....	1399
512B--HMB Preserves Strength in Contralateral but not in Botox-Injected Musculature in Rabbits--(Fortuna).....	1401
513A--From Hopping on Land to Treading in Water- Understanding Limits on Muscle-Tendon Performance in Chan--(Doering).	1403
514B--Confounding Factors When Analyzing Motor Unit Firing Adaptations During Muscle Fatigue--(Contessa).....	1405
515A--Evidence That Tuning of Muscle Spindles Can Be Decoupled from Muscle Activation--(Jalaleddini).....	1407
516B--Are You Stiff Enough to Respond to Foam Rolling A Dependency on Tissue Properties--(Kram).....	1409
517A--Novel Coupled Framework of In Vitro and In Situ Analysis for Investigating Intramuscular Force Trans--(Meppelink).	1411
518B--Elastic Shape Change and Mechanical Behavior in the Aponeuroses of Jumping and Landing Turkeys--(Arellano)..	1413
519A--Atrophy and Fatty Infiltration of Paretic Elbow Muscles in Individuals with Chronic Hemiparetic Stro--(Garmirian).....	1415
520B--Effect of Short and Typical Resting Pectoralis Minor Length on Muscle Elongation--(Mohring).....	1417
521A--Ultrasound-Based Estimates of Achilles Tendon Moment Arm Depend on the Method of Joint Axis Identifi--(Wade).	1419
522B--Comparison Between Intraoperative Measurement and Biomechanical Modeling to Determine Human Vasti Sa--(Son).	1421
523A--Relation Between Force Steadiness and EMG Amplitude- Effect of Signal Processing--(Peterson).....	1423
524B--Comparing Thoracic Erector Spinae Muscle Thickness and Fibre Angle Between Ultrasound and MRI--(Nairn).....	1425
525A--Similarity of Force Development and Decline in the Stretch-Shorten Cycle--(Fox).....	1427
526B--Interactions between Tendon Stiffness and Spindle Afferent Feedback Determine the Magnitude of Invol--(Nagamori).	1429
527A--Effects of Constrained Force Application on Muscle Work and Efficiency--(Onasch).....	1431
528B--Optimal Fascicle Length Changes Based on Submaximal Force or Activation--(Scalyer).....	1433
<b>Thursday Posters: Slips and Falls.....</b>	<b>1435</b>
529A--Two Cost-Effective Methods for Slip Training Improve Recovery Rate Following Laboratory-Induced Slip--(Allin).....	1435
530B--Static Perturbation Training to Improve Dynamic Stability During Overground Slip in Young Adults--(Saucedo).....	1437
531A--Age and Falls History Effects on Antagonist Leg Muscle Coactivation During Walking With Optical Flow--(Thompson).	1439
532B--Quantifying the Contribution of Counter-rotation Movements during Fall Recovery- A Validation Study--(Rapp).....	1441
533A--Posterior Fall-Recovery Training of Individuals with Chronic Stroke- Preliminary Results--(Pigman).....	1443
534B--Constraining the Arms Reduces Posterior, but Not Anterior, Single-Stepping Thresholds of Fall Recove--(Petersen).	1445

535A--Walking Muscle Synergies Influence Propensity of Severe Slipping--(Nazifi)..... 1447

536B--Translating a Quantified Measure of Fall Risk to Clinical Use- Defining Expected Variability--(Worthen-Chaudhari).. 1449

537A--Assessing Fall Status in Patients with Multiple Sclerosis Using a Wii Balance Board--(Paliwal)..... 1451

538B--Effects of Lower Extremity Muscle Fatigue on Dual-Task Obstacle-Crossing--(Chen)..... 1453

539A--Effects of a Verbal Fluency Task on Stability While Walking and Obstacle Crossing in Aging--(Brinkerhoff)..... 1455

540B--Turn Performance of Individuals with Lower-Limb Loss- Within-Subject Comparisons among Fallers and N--(Akins). 1458

## **X-RAY RECONSTRUCTION OF MOVING MORPHOLOGY (XROMM) YIELDS NEW INSIGHTS INTO MUSCULOSKELETAL FORM AND FUNCTION**

Elizabeth Brainerd, Ph.D.

Professor of Biology and Medical Science

Department of Ecology and Evolutionary Biology

Brown University

Providence, RI USA

Over the past decade at Brown we have developed X-ray Reconstruction of Moving Morphology (XROMM), which combines dual-fluoroscopy with bone models from CT scans to produce highly accurate animations of 3D bones moving in 3D space. In combination with XROMM, radio-opaque markers can be placed in muscles to measure muscle strain (fluoromicrometry). Researchers have used XROMM to study *in vivo* skeletal motion in numerous behaviors and species including: terrestrial locomotion of turtles, alligators, birds, rats, horses, humans and dogs; arboreal locomotion of sloths; jumping in frogs and humans; feeding in ray-finned fishes, geckos, ducks, sharks, stingrays, opossums and pigs; flight in birds and bats; lung ventilation in lizards and alligators; and track formation in dinosaurs. In turtles we found that the pelvis rotates substantially within the shell, thereby increasing stride length during terrestrial walking. In suction-feeding fish we found the use of axial musculature to power rapid expansion of the head for suction feeding. Axial muscles have traditionally been viewed as swimming muscles in fish, but now the structure and physiology of axial muscles should be reevaluated in light of their dual feeding and swimming roles. XROMM combined with fluoromicrometry shows great promise for future insights, due to the combination of 3D skeletal kinematics captured simultaneously with muscle strain from many individual muscles or regions of large muscles.

## **DEVELOPING USEFUL SMART CLOTHING: WHERE DOES BIOMECHANICS FIT?**

Julie Steele, Ph.D. FASMF  
Professor and Director of the Biomechanics Research Laboratory  
School of Medicine  
Faculty of Science, Medicine & Health  
University of Wollongong  
Wollongong NSW 2522 Australia

Wearable sensors make up one of the fastest growing technology markets worldwide, with smart clothing forming a major component of this market. Smart clothing includes items that can sense and monitor human motion and/or specific biophysical signals, as well as items that can respond to these signals. These items have enormous potential to enhance human performance and health. For example, smart clothing can be designed to improve the performance of elite athletes through to simply helping people live healthier and safer lives. However, to be effective it is imperative that wearable devices are designed and developed based on valid and reliable scientific evidence or they risk merely serving as gimmicks. Furthermore, to be comfortable to wear the devices must be designed to suit characteristics of the individuals for which they are designed, taking into account the structure and function of the human body and the forces involved in an activity. For this reason, biomechanics plays a vital role in developing meaningful wearable technologies. This presentation will describe development of the “Bionic Bra”, a unique item of smart clothing, including an overview of the technology underlying the device and how biomechanics has played an integral role in developing this novel concept.

**...and one thing just led to another**

Mark D. Grabiner, PhD  
Professor, Department of Kinesiology and Nutrition  
Professor, Department of Bioengineering  
Director, Clinical Biomechanics and Rehabilitation Laboratory  
Associate Vice Chancellor for Research and Research Integrity Officer  
University of Illinois at Chicago  
Chicago, IL USA

A random encounter in an elevator initiated the pursuit of what initially seemed to be a reasonably simple question: Is it possible to reduce the incidence of falls by older adults? We started with some simple premises that narrowed our focus while at the time defining our experimental approach: avoiding a trip-related fall is a motor skill; the motor skill can be adequately described by some set of key biomechanical variables; intervention that improves the key variables will increase skill level and decrease trip-related falls. Answering this simple question took longer than we expected, but along the way additional questions inspired by seemingly random events created new (and sometimes surprising) opportunities and paths of inquiry.

## **TRANSLATIONAL JOURNEYS – FROM HEAD IMPACT SENSORS TO WRIST IMPLANTS TO TOY CONTROLLERS**

J.J. Trey Crisco, Ph.D.

Henry Frederick Lippitt Professor of Orthopaedic Research

The Warren Alpert Medical School of Brown University and Rhode Island Hospital

Professor of Engineering (Research), School of Engineering, Brown University

Providence, RI USA

We are biomechanists because we are driven by the thrill of applying hard sciences to biological systems. The process of these applications can be referred to as basic science, science that advances a specific field, and this is a lifetime pursuit. Relatively recently, translational science, science that can build upon basic findings and lead to successful products has become the favored science for many academic institutions. For academic biomechanists, embarking on a journey in translational science can be rewarding, humbling, and even a distraction from basic science pursuits. Moreover, financial success, coveted by our academic institutions, may not be the most realistic or rewarding measure of successful translational science. I hope to provide some insights from my perspective into these issues. The talk will focus on my translational works that range from head impact sensing technology, to total wrist implant arthroplasty, to products for therapy and mobility of children with impairments. I will discuss my successes and failures in these translational endeavors with the hope of smoothing some of the bumps and straightening the path for those considering a similar journey.

## **COLLABORATORS: A KEY TO FUN AND EXCITING RESEARCH**

Richard R. Neptune, Ph.D.  
John T. MacGuire Professor  
University of Texas at Austin  
Austin, TX USA

The study of the biomechanics and neuromotor control of human movement is exceedingly complex and involves a wide range of disciplines including engineering mechanics, muscle physiology, neuroscience, control theory, rehabilitation science, modeling and simulation, experimentation, upper extremity, lower extremity, prosthetics, orthotics and so on. It is hard for one to be an expert in each of these fields, and thus collaborations are an effective way to broaden the areas in which one can do research. This talk will highlight my career path and how I've been very fortunate to collaborate with some of the world's leading scientists to do fun and exciting research that would not have been possible without them.

# SIMULATED ACL AND MENISCI DEFICIENCY PREDICTS ALTERED KNEE MECHANICS DURING WALKING

<sup>1</sup>Colin R Smith, <sup>1</sup>Scott CE Brandon, <sup>1</sup>Darryl G Thelen

<sup>1</sup>University of Wisconsin-Madison, Madison, WI, USA  
email: crsmith25@wisc.edu, web: <http://uwnmbl.engr.wisc.edu/>

## INTRODUCTION

Rupture of the anterior cruciate ligament (ACL) leads to an increased risk of early onset osteoarthritis (OA), especially in cases of a concomitant meniscal injury [1]. It has been hypothesized that altered knee mechanics resulting from such injuries contribute to the initiation of OA [2]. However, it is challenging to assess how soft tissue injuries will affect knee mechanics during functional movement. *In vivo* cartilage loading results from the interaction of movement dynamics, neuromuscular coordination, passive ligamentous structures, and cartilage properties and morphology, all of which are known to change following soft tissue injury [3]. We have developed an integrated multibody knee model and movement simulation framework to investigate the influence of these factors on cartilage loading. In this study, we performed virtual resections of the ACL and menisci to study their influence on cartilage loading and functional knee mechanics during walking.

## METHODS

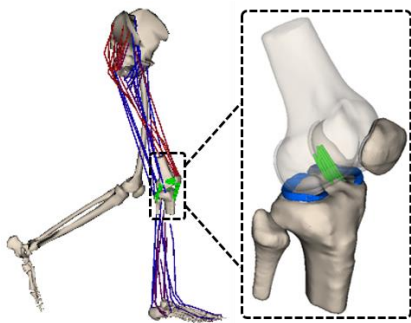


**Figure 1:** Multibody knee model with 6 DOF joints, ligaments, and cartilage and meniscal contact.

A multibody knee model with independent femur, tibia, patella, and medial and lateral menisci bodies was constructed from magnetic resonance images and integrated into a generic musculoskeletal model [2] (Fig. 1). The bodies were connected by six degree of freedom (DOF) joints and constrained by ligaments and articular contact. Fourteen ligaments

and the meniscal horns were represented as bundles of nonlinear springs. An elastic foundation model was used to compute contact pressure for cartilage-cartilage and meniscal-cartilage interactions.

Full body kinematics and ground reaction forces were measured in a motion analysis lab during overground walking (1.2 m/s). A novel simulation routine, Concurrent Optimization of Muscle Activations and Kinematics (COMAK), was used to predict muscle forces, ligament loads, and cartilage and meniscal contact pressures during walking [2]. COMAK simultaneously optimizes muscle activations and secondary knee kinematics (5 tibiofemoral DOF, 6 patellofemoral DOF, and 12 menisci DOF) to satisfy both whole-body and joint-level movement dynamics, while minimizing a weighted squared muscle activation objective function. The simulation was repeated for four cases: intact, ACL deficient (ACLd), menisci deficient and combined ACLd and menisci deficient.

## RESULTS AND DISCUSSION

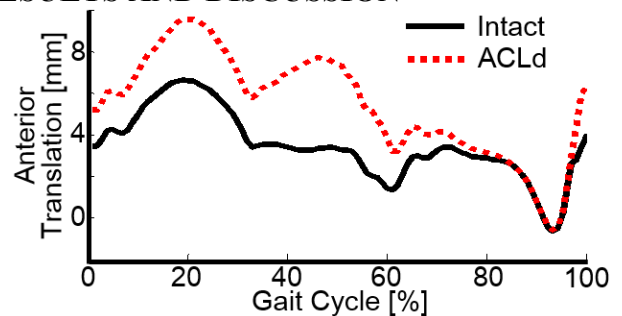


**Figure 2:** Predicted anterior tibial translation in the healthy and ACL deficient knee during walking.

Compared to the intact simulation, the ACLd knee demonstrated increased anterior translation (Fig. 2) and internal rotation throughout stance (max: 4.4 mm, 3°). In early and mid-swing, these kinematics converged towards the intact pattern, but diverged again in terminal swing. A similar trend was predicted for the menisci deficient knee. The

combined ACLd and menisci deficient knee induced substantially larger anterior translation throughout stance, with instances of posterior tibial subluxation in swing.

Both ACL deficiency and menisci deficiency substantially altered cartilage loading on the tibial plateau throughout the gait cycle (Fig 3). At the instant of peak ACL force in the intact simulation, the primary change in the ACLd knee was a posterior shift in the medial (2.4 mm) and lateral (2 mm) center of pressure (COP). In the menisci deficient case, there was an increase in peak pressure (+1.3 MPa) and a posterior shift in the medial COP (1.5 mm). The combined ACLd and menisci deficient knee experienced a dramatic increase in peak contact pressure (+6.2 MPa) and posterior shifts in the medial (9.7 mm) and lateral COP (3.3 mm).

The medial meniscus provided the primary restraint to anterior tibial translation in the ACLd case, along with secondary contributions from the lateral meniscus, MCL, LCL and IT band (Fig. 4). In the menisci deficient knee, the peak loading in the ACL increased by 1.9x to provide anterior restraint. In the combined ACL and meniscus deficient knee, the loading in the MCL increased by 6.6x at the instant of peak ACL loading in the intact knee. In the ACLd and menisci deficient cases, the anterior shift of the tibia oriented the patellar tendon more vertically in the sagittal plane, and thus reduced the anterior restraint required of the passive knee structures. In the combined ACLd and menisci deficient case, the magnitude of the anterior tibial translation resulted in a brief portion of stance where the patellar tendon applied a posterior force to the tibia.

Our simulation predictions corroborate experimental studies of the ACL deficient knee. Using dual fluoroscopy and MRI, Li et al. found a posterior shift

of tibial contact on the medial plateau in ACL deficient knees during lunging [3]. Similar to our simulation predictions, Andriacchi et al found alterations in anterior translation and internal rotation during the terminal portion of swing, which persisted throughout stance [4].

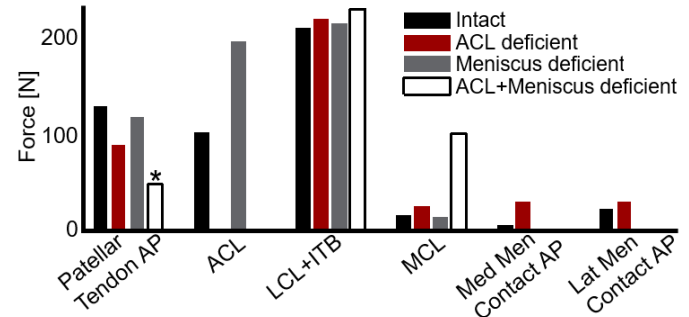


**Figure 4:** Loading in the passive knee structures at the instant of peak ACL force during gait in the intact knee. AP: Anterior force component. (\*) Denotes the patellar tendon applied a posterior force to the tibia.

## CONCLUSIONS

Our simulation predictions suggest that injury to the ACL and/or meniscus leads to altered cartilage contact locations and pressure magnitudes during walking. In the future, we intend to use this simulation framework to investigate muscle coordination and movement strategies that can restore normative cartilage loading patterns in knees with ACL deficiency and/or meniscal damage.

## REFERENCES

- Oiestad BE. *Amer J Sports Med* **37**, 1434, 2009.
- Griffin T. *Exerc Sport Sci Rev* **33**, 195-200, 2005.
- Chaudhari A. *Med Sci Sports Exerc* **40**, 215, 2008.
- Smith CR, et al. *J Knee Surg* **29**, 99-106, 2016.
- Li G, et al. *JBJS* **88**, 1826-34, 2006.
- Andriacchi T, et al. *J Biomech* **38**, 293-98, 2005.

## ACKNOWLEDGMENTS

NIH EB015410, HD084213

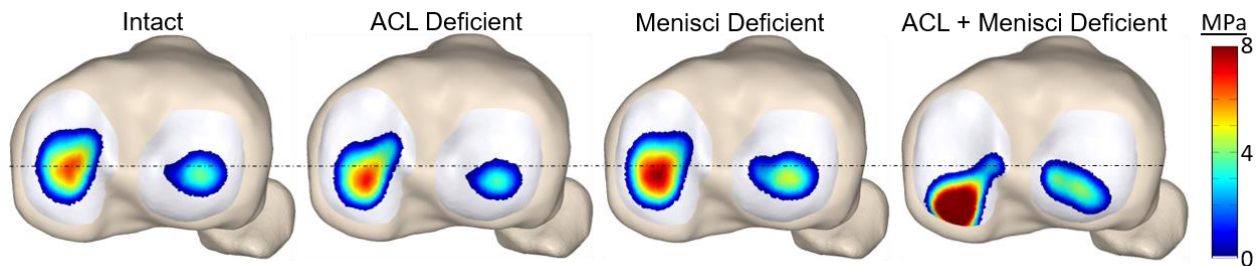


**Figure 3:** Tibial cartilage pressure patterns due to cartilage-cartilage contact at the instant of peak ACL loading in the intact knee for intact, ACL deficient, menisci deficient and combined ACLd and menisci deficient cases.

# RESOLVING THE DEBATE: ANKLE PUSH-OFF DURING HUMAN WALKING CONTRIBUTES TO ACCELERATING BOTH THE SWING LEG AND THE CENTER-OF-MASS

<sup>1</sup>Karl E. Zelik and <sup>2</sup>Peter G. Adamczyk

<sup>1</sup>Vanderbilt University, Nashville, TN, USA

<sup>2</sup>University of Wisconsin – Madison, WI, USA

email1: [karl.zelik@vanderbilt.edu](mailto:karl.zelik@vanderbilt.edu), email2: [peter.adamczyk@wisc.edu](mailto:peter.adamczyk@wisc.edu)

web1: [my.vanderbilt.edu/batlab](http://my.vanderbilt.edu/batlab), web2: <http://uwbadgerlab.engr.wisc.edu>

## INTRODUCTION

Muscle–tendon units about the ankle joint generate a burst of positive power during the step-to-step transition in human walking, termed ankle push-off. However, the functional role of this push-off has been debated for decades, without scientific consensus. One school of thought has emphasized that this push-off power primarily contributes to accelerating the swing leg, while another school of thought has emphasized the effect on accelerating the body’s center-of-mass (COM). There is reasonable empirical evidence to support each perspective, yet these descriptions appear *prima facie* to be in contradiction. The purpose of this work was to unify these seemingly polarized perspectives, and to show that these two possibilities are not mutually exclusive. We demonstrate that both descriptions are valid, and that the principal means by which ankle push-off affects COM mechanics is by a localized action that increases the speed and kinetic energy of the push-off limb. This abstract summarizes findings from our recent JEB Commentary [1].

## METHODS

We reanalyzed level-ground walking data from [2], and computed several energy change and work estimates. First, we partitioned Total (whole-body) mechanical energy change into (a) energy changes due to the motion of the body’s COM (using individual limbs method), plus (b) energy changes due to motion relative to the body’s COM, which we termed Peripheral energy change. Second, we used an alternative way to partition Total mechanical energy change, into contributions from individual body segments and segment groups. For

simplicity, we identified three segment groups: (a) push-off limb (trailing limb thigh, shank, and foot), (b) leading limb and (c) head-arms-trunk. Third, we computed how much of the push-off limb segmental energy change also appears as COM energy change during the push-off phase of gait.

## RESULTS AND DISCUSSION

We found that under normal walking conditions (1.4 m/s), the vast majority (>85%) of push-off limb energy change contributes directly to COM energy change during push-off (Fig. 1). This observation is consistent across gait speed: >80% at 0.9 m/s, and >90% at 2 m/s. Work provided by ankle push-off manifests principally as increased speed of the push-off limb. The push-off limb increases in segmental kinetic energy with little energy transferred to the torso through the hip. But because the limb is included in body COM computations, this localized segmental acceleration also accelerates the COM, and most of the segmental energy change also appears as COM energy change. Thus, ankle push-off primarily contributes to accelerating both the swing leg and the COM during human walking. It is, in fact, the same energy change in both the push-off limb and the COM, with only a small part of limb energy being purely Peripheral (non-COM). Thus, interpretation of ankle mechanics should abandon an either-or contrast of leg swing vs. COM acceleration. Instead, ankle function should be interpreted in light of both mutually consistent effects. This unified perspective informs our fundamental understanding of the role of ankle push-off, and has implications for the design of clinical interventions (e.g. prostheses, orthoses) that restore function to individuals with disabilities.

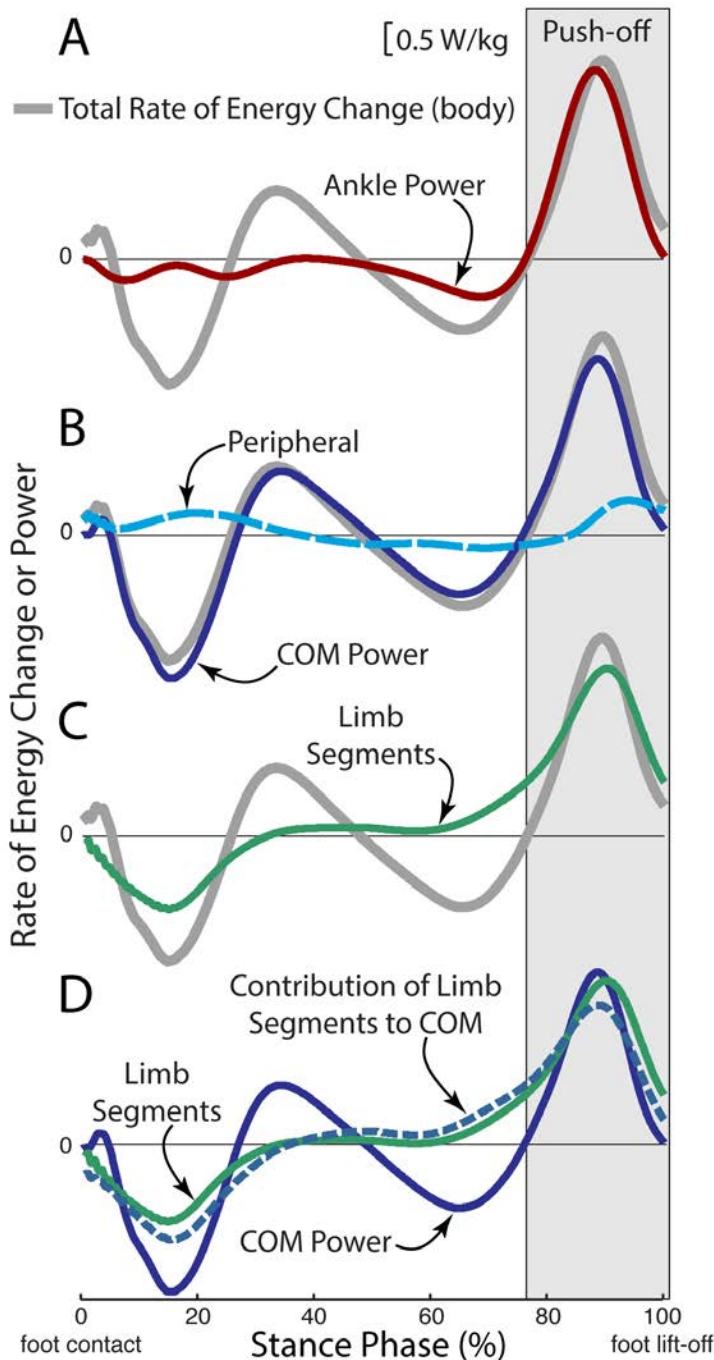


**Figure 1:** Estimates of the rate of energy change ( $\dot{E}$ ) and power (work rate) for an individual limb during human walking. (A) Ankle power (red line) overlaid on Total  $\dot{E}$  (gray line, due to motion of and about the COM). (B) The majority of Total  $\dot{E}$  during Push-off (gray box) is attributable to COM  $\dot{E}$  (blue line), and smaller contributions are from Peripheral  $\dot{E}$  (due to segmental motion relative to the COM, dashed cyan line). (C) The majority of Total  $\dot{E}$  during Push-off is also attributable to segmental  $\dot{E}$  from the push-off limb (green line). (D) The contribution of limb segmental  $\dot{E}$  (green) to overall COM  $\dot{E}$  (solid blue) is shown here in dashed blue. During Push-off, the majority of the limb  $\dot{E}$  goes into this contribution (dashed blue), which in turn accounts for the majority of COM  $\dot{E}$ . Data depicted are inter-subject means at 1.4 m/s ( $N=9$ , [1,2]).

## CONCLUSIONS

The debate whether push-off from ankles powers leg swing or COM rankles.

But a unified view indicates both are true: two effects inextricably tangled.

## REFERENCES

1. Zelik & Adamczyk, *J Expt Biol*, 219(23), 3676-3683, 2016.
2. Zelik, Takahashi & Sawicki, *J Expt Biol*, 218(6), 876-886, 2015.

## ACKNOWLEDGMENTS

The authors would like to thank At Hof, Steven Collins, Philippe Malcolm, Daniel Renjewski, Richard Baker and Kenton Kaufman for their helpful feedback and comments during the preparation of this work. This work was supported in part by the National Institutes of Health [K12HD073945 to K.E.Z.]; and by institutional support from the University of Wisconsin-Madison [to P.G.A.] and from Vanderbilt University [to K.E.Z.].

## TOUCH OF GREY: THE AGING RUNNER

<sup>1</sup>D.S. Blaise Williams III, <sup>2</sup>Julia Freedman Silvernail, <sup>3</sup>Max R. Paquette, <sup>4</sup>Reginaldo K. Fukuchi, <sup>5</sup>Paul DeVita

<sup>1</sup>VCU RUN LAB, Virginia Commonwealth University, Richmond, VA, USA

<sup>2</sup>Department of Kinesiology and Nutrition Sciences, UNLV, Las Vegas, NV, USA

<sup>3</sup>School of Health Studies, University of Memphis, Memphis, TN, USA

<sup>4</sup>Biomedical Engineering, Federal University of ABC, São Paulo, Brazil

<sup>5</sup>Department of Kinesiology, East Carolina University, Greenville, NC, USA

Email: [mrpquette@memphis.edu](mailto:mrpquette@memphis.edu) web: <http://www.memphis.edu/shs/research/mal.php>

### INTRODUCTION

Running has been a popular mode of aerobic exercise in the U.S. for over four decades, and road race participation continues to increase every year. Running is a lifelong activity that can be enjoyed by most, and many runners continue to participate in organized races into their 80s. Unfortunately, more running-related injuries have been reported in older compared to younger runners. Factors that may be related to the greater number of injuries as runners age include changes in tendon composition (i.e., reduced stiffness), reduced muscle strength and joint flexibility and, although controversial, changes in running biomechanics. For this reason, there has recently been a large interest in research focused on age-related changes in running biomechanics, but more work is needed to further understand the mechanisms responsible for age-related declines in performance and higher numbers of injuries in older runners. To this end, many factors need to be studied to bridge the gap between age-related changes in running biomechanics and injury development. This symposium highlights current and new research on the ‘aging’ runner and introduces new research ideas for future work.

#### The symposium will follow this schedule:

Introduction – **Paul DeVita** – 5 mins

Symmetry And Stiffness In The Aging Runner –  
**D.S. Blaise Williams III** – 15 min

Coordination Variability In Older Runners – **Julia  
Freedman Silvernail** – 15 min

Is Running Exposure Protective Against Age-  
Related Biomechanical Changes? – **Max R.  
Paquette** – 15 min

Effects Of Exercise Intervention On Age-Related  
Changes In Running Biomechanics – **Reginaldo  
K. Fukuchi** – 15 min

Discussion – 20 min

### SYMMETRY AND STIFFNESS IN THE AGING RUNNER – Blaise D. S. Williams III

As individuals age, musculoskeletal characteristics such as bone density, joint range of motion, muscle strength and neuromuscular control decrease. These changes likely influence the overall lower extremity mechanics during running. While clear benefits of running exist, the combination of this high stress activity on the aging musculoskeletal system likely results in a different risk of lower extremity injury. In fact, there is an increasing percentage of older runners competing in distance running and a subsequent shift in the overall categories of injuries toward those more common in older runners. If specific differences in lower extremity stiffness and symmetry during running exist in older runners, interventions (i.e., specific training, equipment) targeting these differences in the aging runner should be developed. The availability of these interventions and an understanding of the distinct differences in the aging runner will help to guide decision making and could reduce the risk of running-related injuries and the subsequent deconditioning and disability that may occur with aging. The overall objective of this presentation is to compare the effect of age on dynamic lower extremity stiffnesses (i.e., individual joint and total leg), which contribute to shock attenuation during running and to compare the effect of age on lower extremity symmetry during running, which may be an indicator of declining neuromuscular function.

## **COORDINATION VARIABILITY IN OLDER RUNNERS – Julia Freedman Silvernail**

Running continues to expand in its popularity as a means of physical activity participation. While remaining physically active promotes healthy aging, runners continue to be injured at high rates. This includes an increased risk of some injuries for older runners. Initial biomechanical differences between older and younger runners have been identified when investigating movement characteristics. Yet when recruited to match running volume, these groups tend to look more similar, especially when assessing discrete movement variables. Measures of coordination provide a metric of the underlying organization of movement by quantifying the contributions of individual segments to overall joint motion. Furthermore, how one varies movement coordination upon repetition of a movement provides insight to the flexibility of the system. An injured state leads to a more constrained system where less movement options are available, indicated by a decrease in coordination variability. This presentation will discuss discrete biomechanical comparisons of older and younger runners with similar weekly running volume. Additionally, comparisons of movement coordination and coordination variability between age groups will be presented. This will provide a more robust biomechanical comparison of older and younger runners by utilizing continuous, sensitive measures.

## **CAN RUNNING EXPOSURE PRESERVE AGE-RELATED BIOMECHANICAL CHANGES? – Max R. Paquette**

Aging is associated with loss in functional performance as well as changes in tendon properties and muscle architecture, in particular plantarflexor muscles and Achilles tendon or plantarflexor complex. Mechanical and morphological properties of gastrocnemius can influence their capacity to generate angular power at the ankle joint. Consequently, compared to younger runners, older runners have reduced ability to generate ankle angular power and work during running. This age-related reduction in ankle power generation is paralleled by lower vertical push-off and propulsive ground reaction force in older compared to younger runners. Ultimately, maintenance of ankle joint and plantarflexor power appear to be essential for performing daily activities in addition to more

intense exercise, such as running. It is well accepted that humans are able to adapt and modify their motor task organization using sensory feedback information, especially for repetitive motor task. Repetitive practice enhances motor task organization which maybe a mediator for adaptations to the musculoskeletal system. Endurance running training can have a positive impact on endurance performance, muscle strength, musculotendinous properties, and lower limb joint kinetics in older runners. This author hypothesizes that running training exposure, specifically training intensity, may have preserving effects on lower limb biomechanics of older runners at submaximal running speeds. Further, the author suggests important considerations related to training factors when designing running biomechanics studies in the aging runner.

## **EFFECTS OF EXERCISE INTERVENTION ON AGE-RELATED CHANGES IN RUNNING BIOMECHANICS – Reginaldo K. Fukuchi**

Age-related changes in running biomechanics have been consistently observed in the literature. These changes have been attributed, among other factors, to the loss of strength and flexibility with aging. In fact, few studies, that considered both running biomechanics and the levels of strength and flexibility, have confirmed this association between atypical running biomechanics with general weakness and lack of flexibility. Despite the fact that strengthening and stretching exercises have been recommended to mitigate the effects of aging and to prevent running injuries; and the fact that older age has been considered a risk factor for running injuries, the effects of strengthening or stretching exercises on running biomechanical patterns are poorly understood in older runners. The author will present the findings of a randomized controlled trial study on the effects of exercise intervention on running biomechanics of older runners. Based on these findings, the author will suggest areas to be addressed for future studies. In addition, the author will present a public repository that includes not only running biomechanics data but also data related to running habits, strength, flexibility and foot strike patterns. We suggest that this continually expanding data set would be useful for addressing important biomechanical research questions related to the aging runner.

# Locomotor Adaption to Lateral Center of Mass Movement Amplification Requires Active Stabilization

<sup>1,2</sup>Keith E. Gordon, <sup>1</sup>Mengnan/Mary Wu, <sup>1</sup>Geoffrey Brown, and <sup>3</sup>Jane Woodward

<sup>1</sup> Northwestern University, Chicago, IL, USA

<sup>2</sup> Edward Hines Jr. VA Hospital, Hines, IL, USA

<sup>3</sup> Rehabilitation Institute of Chicago, Chicago, IL, USA

email: [keith-gordon@northwestern.edu](mailto:keith-gordon@northwestern.edu) web: <http://sites.northwestern.edu/agilitylab/>

## INTRODUCTION

Control of frontal-plane stability is critical for community ambulation, but relearning how to control center of mass (COM) dynamics following neurologic injury has proven exceptionally difficult. To effectively enhance locomotor stability we need to develop interventions that target frontal plane COM control. Recent motor learning research suggests that *movement amplification* that increases the intensity and variability of task-specific practice may be an effective strategy for improving control of upper-limb movements [1]. Movement amplification strategies greatly contrast with many existing locomotor training paradigms that employ external *stabilization* techniques to reduce lateral control requirements. Our purpose was to investigate how non-impaired populations respond to a movement amplification paradigm designed specifically to challenge control of frontal-plane COM gait stability. We also compared locomotor adaptations during movement amplification to the effects of frontal-plane COM stabilization.

Specifically, we investigated locomotor adaptation when lateral stability was challenged using a negative viscosity force field that amplified lateral COM velocity, and when lateral stability was assisted using a positive viscosity force field that resisted lateral COM velocity. We hypothesized that participants would *decrease* lateral COM velocity in response to both force fields. We further hypothesized that in the stabilization field, subjects would rely on the external force field allowing a reduction in active control of frontal-plane COM stability. This adaptation would be reflected by a decrease in movement variability and metabolic cost of transport. In contrast, we theorized that in the destabilization field, subjects would increase their

active control of frontal-plane COM stability, as reflected by an increase in movement variability and metabolic cost of transport.

## METHODS

11 young healthy individuals gave informed consent and participated in the study (10 female,  $24 \pm 2.2$  years and  $71 \pm 7.5$  kg). Subjects walked on a wide treadmill that allowed variability in lateral position during three force field conditions that included both laterally stabilizing and destabilizing environments. For all conditions, subjects completed two 5-minute trials of treadmill walking at their preferred speed. Highly controlled lateral forces were applied to a pelvis harness via a set of cables driven by linear motors. The condition order was randomized:

- 1) **Stabilization** – A stabilizing viscous force field applied forces proportional in magnitude and opposite in direction to the subject's lateral COM velocity, reducing the requirements to actively maintain straight-ahead walking.
- 2) **Null** – No forces were applied.
- 3) **Destabilization** – A destabilizing viscous force field applied forces proportional in magnitude and in the same direction as the subject's lateral COM velocity, amplifying the subject's lateral motion. This field increased the requirements to actively maintain straight-ahead walking.

The first trial of each condition allowed the subject to adapt to the novel walking environment. Kinematic and metabolic data were recorded during the last 2 minutes of the second trial of each condition to assess subjects' performance during steady state walking.

## RESULTS AND DISCUSSION

As hypothesized, average peak lateral COM speed per stride during the Stabilization and Destabilization conditions tended to decrease vs. the Null condition (Figure 1). This decrease in COM speed was only significant ( $p < 0.05$ ) for the Stabilization condition. Metabolic cost of transport increased significantly during Destabilization vs. the Null condition ( $p < 0.05$ ) (Figure 1). The lack of change in peak lateral COM velocity when walking in the Destabilizing field (which amplifies movements) suggests that subjects made locomotor adaptations to actively control and reduce their frontal-plane COM dynamics. This control required effort, as evidenced by the significant increase in metabolic cost of transport.

In addition, the variability of peak lateral COM speed between strides increased significantly from Stabilization to Null to Destabilization conditions ( $p < 0.05$ ) (Figure 1). The increase in movement variability when walking in the Destabilization condition may increase movement errors and allow individuals a greater opportunity to practice corrective behaviors required to control lateral COM dynamics.

## CONCLUSIONS

Results from the current study suggest that a movement amplification paradigm can be applied to challenge frontal-plane stability during human locomotion and yields significantly different responses than a stabilization paradigm. Individuals adapted to the destabilizing viscous force field by decreasing lateral COM velocity (similar to the stabilizing field), but increased both metabolic cost of transport and movement variability (in contrast to the stabilizing field). Applying this movement amplification paradigm to gait rehabilitation may be uniquely valuable for training active control of frontal-plane stability.

## REFERENCES

1. Huang, F.C., J.L. Patton, and F.A. Mussa-Ivaldi, *Manual skill generalization enhanced by negative viscosity*. J Neurophysiol, 2010. **104**(4): p. 2008-19.

## ACKNOWLEDGMENTS

Supported by Career Development Award 2 #1 IK2 RX000717 from the U.S. Department of Veterans Affairs. We would like to thank Grace Bellinger for her assistance with data analysis.

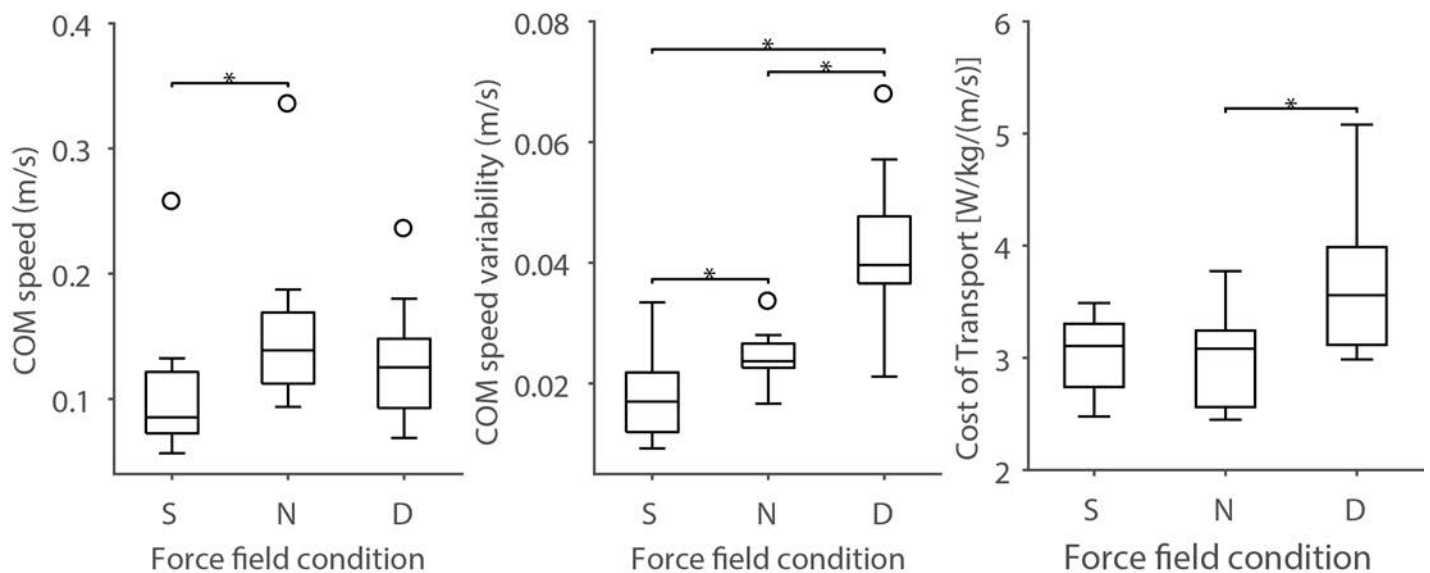


**Figure 1:** Center of mass (COM) speed mean and variability and Cost of Transport for all 11 subjects. S = Stabilization, N = Null, and D = Destabilization condition. \*Significantly different pair at  $p < 0.05$ .

# IS THERE A LEARNING EFFECT FOR BALANCE ASSESSMENT TESTS?

<sup>1</sup> Michael Orendurff, PhD; <sup>2</sup> Christopher Villarosa, BS <sup>3</sup> Joseph Smith, MS, ATC; <sup>3</sup> Charles Chan, MD;  
<sup>1</sup> Carey Hintze, PT, DPT; <sup>1</sup> Kevin Dinglasan, ATC, MS; <sup>1</sup> Kerry Peterson, ATC, MA;

<sup>1</sup> Motion & Sports Performance Laboratory, Stanford Children's Health, Palo Alto, CA, USA

<sup>2</sup> Program in Physical Therapy, University of Washington, Seattle, WA, USA

<sup>3</sup> Stanford Children's Orthopedic & Sports Medicine Center, Palo Alto, CA, USA

Email: [moren@stanford.edu](mailto:moren@stanford.edu), web: <http://www.stanfordchildrens.org>

## INTRODUCTION

Balance is complex construct with many domains. Assessing balance improvements following an intervention requires repeated testing but some question remains as to the learning effect as participants habituate to the balance test [1]. If there is a substantial learning effect from repeatedly undergoing the balance assessment, changes attributable to the intervention would be more difficult to ascertain. Depending on the balance test used, the learning effect may be more substantial.

Observational evidence suggests that individuals become more comfortable with balance tests, performing better on repeated tests.

It was hypothesized that improvements in the performance of the Balance Error Scoring System (BESS) would not be statistically significant with four repeated tests over 10 days, whereas improvements with the Y Balance test would should a statistically significant learning effect over four repeated tests over 10 days.

## METHODS

Sixteen healthy, recreationally active adults gave informed consent to participant in this IRB-approved protocol (9 females, 7 males 29 +/-5 years; low to high intensity exerciser 2-6 x week). Over a 10-day period, each participant completed the BESS and the Y Balance protocol four times following a standardized warm up (Figure 1). The total error score on the BESS test for both firm and foam surfaces was calculated for each day. The total distance achieved in the anterior, posteriolateral and posteromedial directions on the Y Balance test was calculated for each day. Each individual's scores were plotted across days to determine if a statistically significant slope was observed across the days.



**Figure 1.** Balance Error Scoring System (BESS) and Y-Balance tests.

## RESULTS AND DISCUSSION

The relationship between scores on the BESS test across specific days is shown below in Figure 2.

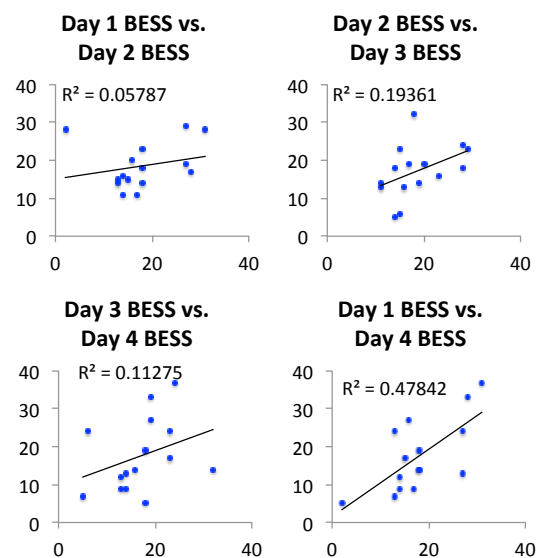


**Figure 2.** BESS scores on Day 1 vs. 2; Day 2 vs. 3; Day 3 vs 4; and Day 1 vs. 4.

The relationship of the scores on the Y Balance test across specific days is shown below in Figure 3.

Contrary to the hypothesis, the slope of the scores on both the BESS and the Y Balance tests did not show a significant slope across the four days ( $P = 0.3-0.9$ ). The score across the four days for each participant are shown in Figure 4.

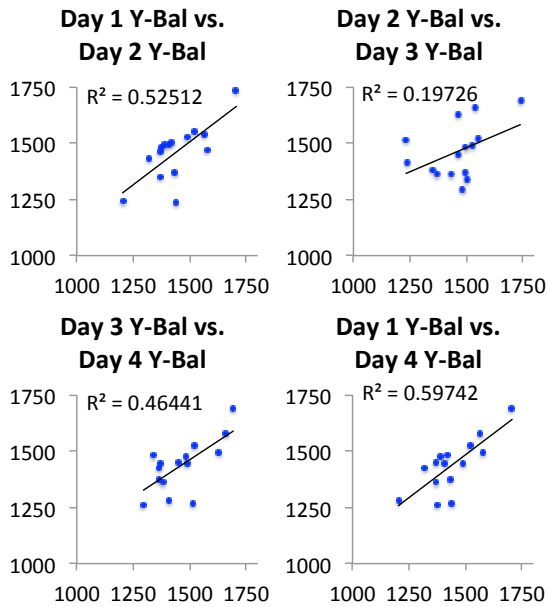


**Figure 3.** Y Balance scores on Day 1 vs. 2; Day 2 vs. 3, Day 3 vs.4; and Day 1 vs. 4.

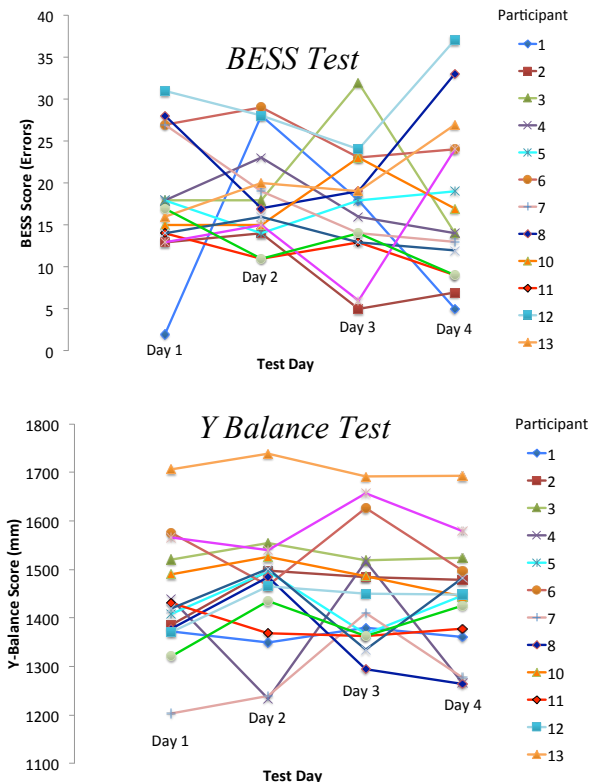


**Figure 4.** Individual scores for each participant across 4 tests performed over a 10-day period.

Only a few participants exhibited an observable trend across the four days, some improving slightly and some worsening slightly. Most participants had high amounts of variance, for example participant 1 on the BESS; despite this the individual had very low variance and almost no trend to their scores on the Y Balance test. These data suggest that there is very little learning effect for either test, even after repeating the tests 4 times in a relatively short period of time. Since many interventions designed to improve balance may last weeks or months it appears unlikely that assessing balance improvements with either the BESS or the Y Balance test would present a confounding learning effect. The BESS is clearly more focused on reducing small errors while in a variety of challenging postures in quiet stance. The Y Balance test is more focused on reaching the limits of stability in three directions, and may be more susceptible to improvements in knee and ankle strength than the BESS. However, neither test specifically mimics the rate of dynamic balance perturbation recovery that likely occurs for individuals to experience a substantial reduction in falls and injuries. Therefore there remains some question as to the most specific and sensitive test battery to determine improvements from injury prevention programs administered to a range of patient populations. Injury prevention programs such as PEP [2] or FIFA 11+ [3] may reduce injuries by improving balance. Either the BESS or the Y Balance tests may be sensitive to these improvements.

## CONCLUSIONS

There does not appear to be any learning affect for the BESS or Y Balance test in active adults over a 10 day test-retest format.

## REFERENCES

1. Plisky PJ, et al. *N Am J Sports Phys Ther* 2009;4,92-9.
2. Manselbaum, BR, et al. *Am J Sports Med* 2005;33,1003-10.
3. Silvers-Granelli H, et al. *Am J Sports Med* 2015;43,2628-37.

## DISCLOSURE

This research was funded by a grant from E2 Technologies who had no influence on the design, conduct, data collection, interpretation or decision to analyze or publish these results.

# RELATING OBESITY, COGNITION AND BIOMECHANICS OF FALL-RECOVERY IN OLDER ADULTS: PRELIMINARY RESULTS

<sup>1</sup> Matthew Coon, <sup>1</sup> Vasanth Subramanian, <sup>1</sup> Jacqueline Ortiz, <sup>1</sup> Noah J. Rosenblatt

<sup>1</sup> Center for Lower Extremity Ambulatory Research, Rosalind Franklin University of Medicine and Science, North Chicago, IL, USA

Email: noah.rosenblatt@rosalindfranklin.edu

## INTRODUCTION

Obesity is a growing epidemic affecting at least 30% of older Americans<sup>1</sup>. Epidemiological studies have shown that obesity increases the risk of falling in older adults<sup>2</sup>, although the mechanisms to explain this are not well established. From a mechanical point of view, following a large change in momentum of the center of mass - as may occur following obstruction of the swing limb during gait (i.e. a trip) - increased inertia due to greater body mass may negatively affect whole-body kinematics and increase the likelihood of a fall. The example of a trip during gait is salient as trips are the leading cause of falls by community-dwelling older adults<sup>3</sup> and the risk of falling in response to a lab-induced trip appears to increase with obesity<sup>4</sup>. However, the effect of body mass on biomechanics of the fall-recovery response following a trip by older adults has not been reported. Given that aspects of the fall-recovery response may involve cortical pathways<sup>5</sup> and that obesity alters brain structure and impairs cognitive function<sup>6</sup>, the latter may partly explain obesity-related falls. However, to our knowledge a relationship between cognitive function in older adults and biomechanics of fall-recovery has not been demonstrated.

The purpose of this on-going study is to provide a modifiable mechanism for obesity-related falls by community-dwelling older adults. Here we use preliminary data collected to date to test the following: H1) obesity negatively impacts biomechanics of fall-recovery following a lab-induced trip; H2) there is a relationship between cognitive function and biomechanics of fall-recovery; H3) the effect of obesity on biomechanics may be partly explained by obesity-related cognitive declines.

## METHODS

To date, 20 participants have been recruited. Inclusion criteria are: 65+ years of age, no neuromuscular conditions that interfere with gait, no joint replacements, ability to walk one mile at any pace without pain or assistive device and body mass in-

dex (BMI) of 18.5-25 kg/m<sup>2</sup> (normal weight) or  $\geq 30$  kg/m<sup>2</sup> (obese). Patients with diabetes had to have their condition controlled and score at least 8/10 on a monofilament test for neuropathy. We analyzed biomechanical data from 13 participants (N=5 normal weight, 74.8 $\pm$ 8.5 yrs, 21.7 $\pm$ 2.0 kg/m<sup>2</sup>, 3 male; N=8 obese, 72.9 $\pm$ 5.0 yrs, 32.9 $\pm$ 1.7 kg/m<sup>2</sup>, 6 males) and measures of cognitive function from 19 participants, including all of those completing the biomechanical data collection (N=8 normal weight, 74.9 $\pm$ 8.7 yrs, 22.4 $\pm$ 2.2 kg/m<sup>2</sup>, 5 male; N=11 obese, 72.2 $\pm$ 5.4 yrs, 33.7 $\pm$ 2.1 kg/m<sup>2</sup>, 8 males). Missing data reflects technical issues, withdrawals or participants not yet completing the study. In addition to using BMI to quantify obesity, participants also received a whole body DEXA scan to quantify percent body fat in the trunk, in the legs and in the whole body. Hip, thigh and waist circumferences were also taken.

Biomechanics of fall-recovery were evaluated using a previously established method<sup>4,7</sup> in which the swing limb was unexpectedly obstructed by a hidden obstacle while the participant wore a safety harness. Motion analysis cameras were used to record the motions of passive reflective markers placed on the body according to the Plug-in-gait model for the normal-weight group and an obesity-specific model<sup>8</sup> for the obese group. From the marker data we calculated: flexion/extension of the trunk and the related angular velocity at the instance that the recovery step made contact with the ground ( $\theta_{\text{trunk}}$ ,  $\omega_{\text{trunk}}$ , respectively), the distance (in the direction of travel) between the trunk center of mass and the toe marker at the same instance ( $\text{COM}_{\text{dist}}$ ), and the total time from the onset of the trip to this instance (recovery time). Similar measures have been shown to affect the likelihood of a successful recovery following a lab-induced trip<sup>7</sup>.

To quantify cognitive function we used four assessments from the NIH toolbox - a validated, tablet-based application to assess cognitive as well as emotional, sensory, and motor function<sup>9</sup>. Assessments included: 1) The Flanker Inhibitory Con-

trol and Attention Test (FIT), to assess executive function; 2) The Picture Sequence Memory Test (PST), to assess episodic memory; 3) the List Sorting Working Memory Test (LST); and 4) The Patten Comparison Processing Speed Test (PCT). Each was scored from 0-100 (mean = 50; standard deviation = 10) after correcting for age based on values from a national database.

To test H1 we used unpaired t-tests to compare kinematics between groups and correlated each kinematic with each anthropometric (BMI, circumferences and fat percentages). To test H2 we repeated the analysis with cognitive scores. To test H3 we planned to analyze only those kinematics that were significantly associated with anthropometrics *and* cognitive scores. We planned to run partial correlations between these kinematics and anthropometrics after covarying for cognitive scores.

## RESULTS AND DISCUSSION

One participant in each group fell (unambiguously relied on the harness to avoid hitting the ground) following the lab-induced trip; both were after-step fallers and included in all analysis.

H1 was not supported. No kinematic differences existed between groups. There were also no significant correlations between any anthropometrics and kinematics and only that between  $\theta_{\text{trunk}}$  and waist circumference “trended” toward significance – e.g.,  $p \leq 0.1$  ( $r=0.64$ ;  $p=0.07$ ). H2 was supported. Specifically,  $\theta_{\text{trunk}}$  was significantly correlated with age-corrected LST score ( $r=.61$ ;  $p=0.04$ ). In addition,  $\text{COM}_{\text{dist}}$  was significantly correlated with age-corrected FIT score ( $r=0.61$ ;  $p=0.03$ ) and with age-corrected PST score ( $r=0.67$ ;  $p=0.01$ ). There was a “trend” toward significance between recovery time and age-corrected PST ( $r=0.48$ ;  $p=0.0097$ ). Given these results, partial correlations were not conducted to test H3. However, to better understand the relationship between obesity and the chosen cognitive assessments in this cohort, correlations were conducted among variables but no significant associations were found.

Given the number of measures to quantify obesity and fall-recovery it is surprising that we observed no significant correlations between the two. However, the sample size may still be too small, particularly given that the variance in anthropometrics is limited by the low number of participants

with Class II and higher obesity ( $\text{BMI} > 35$ ). In addition, a clinically meaningful (albeit non-significant) effect of obesity on fall-risk following a lab-induced fall was previously shown in women only, who may fall at higher rates than men<sup>10</sup>. In contrast, 68% of our participants were male.

The absence of significant associations between obesity and cognitive function is also surprising. However, cognitive function encompasses many domains and the battery of assessments used herein may not directly address previously reported functional changes due obesity<sup>6</sup>. Since beginning this study, the NIH-toolbox has added several cognitive assessments to their battery as well as summative scores of three functional domains based on these assessments. Given our results, it seems reasonable to include these measures and scores moving forward. It is also possible that the strength of the relationship between obesity and cognition was weakened in this cohort given they were fairly active (as per activity data not reported here); physical activity may promote cognitive functioning<sup>6</sup>.

To our knowledge this is the first study to show an association between biomechanics of fall-recovery and cognitive function which seem logical. For example, of the kinematics considered  $\text{COM}_{\text{dist}}$  is the only one that captures coordination of the foot and trunk and it is reasonable that such coordination would rely on attentional resources (FIT score). However, given the time-critical nature the fall-recovery response, we would have also expected PCT to be an important correlate. Regardless, if correlations persist with additional participants, then cognitive training and/or physical activities that improve cognition could help increase efficacy of existing fall-prevention<sup>11</sup> interventions targeting fall-recovery mechanics.

## REFERENCES

1. Flegal KM, et al. *JAMA* **307**, 491-7, 2012.
2. Finkelstein EA, et al. *Am J Health Prom* **21**, 460-8, 2007.
3. Berg WP, et al. *Age Ageing* **26**, 261-8, 1997.
4. Rosenblatt NJ, et al. *APMR* **93**,718-22, 2012.
5. Jacobs JV, et al. *J Neural Trasm* **114**, 1339-48, 2007.
6. Chan JSY, et al. *Front Aging Neurosci* 2013 Dec 20;5:97.
7. Pavol MJ, et al, *J Geron A Biol Sci Med* **56**, 428-37, 2001
8. Lerner ZF, et al. *Med Sci Sports Ex* **46**, 1261-7, 2014
9. Gershorn RC et al, *Neurology* **11**:S2-6, 2013
10. Steven JA, et al, *Inj Prev*, **11**:115-9, 2005
11. Rosenblatt NJ et al, *J Am Geriatr Soc*, **61**:1629-31, 2013.

# BIOMECHANICAL MEASURES OF CLINICIAN-DEFINED BALANCE IMPAIRMENTS IN PERSONS POST-ARTHROSCOPY FOR FEMOROACETABULAR IMPINGEMENT SYNDROME

<sup>1,2,3</sup>Lindsey Brown, <sup>1</sup>Joshua Hoffman, <sup>3</sup>Kathryn Glaws, <sup>4</sup>Cara L. Lewis, <sup>1,2</sup>Michael P McNally, <sup>5</sup>John Ryan, <sup>6</sup>Timothy E Hewett, and <sup>1,3,5</sup>Stephanie Di Stasi

<sup>1</sup> Sports Medicine Research Institute, The Ohio State University Wexner Medical Center, Columbus, OH, USA

<sup>2</sup> School of Health and Rehabilitation Sciences, The Ohio State University, Columbus, OH, USA

<sup>3</sup> Sports Medicine Physical Therapy, The Ohio State University Wexner Medical Center, Columbus, OH, USA

<sup>4</sup> Department of Physical Therapy and Athletic Training, Boston University, Boston, MA, USA

<sup>5</sup> Department of Orthopaedics, The Ohio State University, Columbus, OH, USA

<sup>6</sup> Mayo Biomechanics Laboratories and Sports Medicine Center, Mayo Clinic, Rochester, MN, USA

email: [brown.4119@osu.edu](mailto:brown.4119@osu.edu)

## INTRODUCTION

Persons with femoroacetabular impingement syndrome (FAIS) present with aberrant movement patterns during functional tasks even after surgical intervention.[1] While gait, squatting, and stair climbing are popular tasks for biomechanical evaluation to better assess movement patterns in this population, clinical tests of movement quality have received minimal attention.

The forward step down (FSD) is a clinical tool to evaluate functional quality of movement. Steady balance is one of five clinical criteria evaluated in the FSD task [2] and is commonly impaired in individuals with non-arthritic hip pain.[3] Balance training is one component of post-operative rehabilitation [4] and may significantly contribute to improving quality of movement in this population. Understanding the biomechanical parameters and clinical identification of poor quality of movement in these individuals will better inform targeted intervention strategies.

The purpose of this study was to investigate quality of movement during a FSD in persons after hip arthroscopy for FAIS by identifying biomechanical measures of balance that are associated with clinician-defined balance impairments. We theorized quality of movement is impaired bilaterally, and thus we hypothesized that regardless of limb, persons with clinician-defined unsteady balance during a FSD would demonstrate significantly higher center of pressure displacement area, path length, medial-lateral movement, and peak velocity and

significantly higher lateral trunk, pelvis, hip, and knee excursion compared to persons with steady balance.

## METHODS

Twenty-two participants (15 women) who underwent hip arthroscopy for FAIS consented to participate in this study.

### *Clinician-defined Balance*

For each limb, participants completed five repetitions of a FSD off an 8-inch box. Using 2-dimensional (2D) video of the participant during the FSD, a physical therapist (PT) with a board-certified sports specialty and five years of experience graded quality of movement on predefined criteria.[3] Steady balance was one criterion with participants receiving a dichotomous grade of either steady (0) or unsteady (1) balance.

### *Center of Pressure*

Center of Pressure (CoP) data were collected during the FSD using Bertec force plates. CoP displacement area was measured by calculating the area of an ellipse encompassing 85% of the plotted CoP path during the FSD.[5] CoP path length and medial-lateral movement were calculated by tracking the x and y coordinate positions of the CoP throughout the FSD. CoP peak velocity was defined as the highest change in CoP position over one frame of collected data (0.004sec). All CoP measures were normalized to participant height.

### *Kinematics*

A standard three-dimensional (3D) motion analysis system was used to capture kinematics of the trunk, pelvis, and lower extremity during the FSD. Variables of interest included frontal plane excursion of the trunk, pelvis, hip, and knee.

### Statistical Analysis

Shapiro-Wilk tests confirmed normality for all variables except CoP peak velocity. A multivariate analysis of variance (MANOVA) was performed to assess for interaction of limb (involved or uninvolved) by balance rating (steady or unsteady)( $P < 0.05$ ). If significant interactions were observed, post-hoc t-tests were performed. Main effects were reported if no interactions were found. Related-samples Wilcoxon Signed Rank tests were performed to assess for differences between limbs and balance ratings for CoP peak velocity ( $P < 0.05$ ).

## RESULTS AND DISCUSSION

Thirteen participants (59.1%) were classified as steady on both limbs, three (13.6%) were classified as unsteady on both limbs, two (9.1%) were unsteady on the involved but steady on the uninvolved, one (4.5%) was unsteady on the uninvolved but steady on the involved, three (13.6%) only had the involved limb analyzed due to collection issues (two had unsteady balance and one had steady balance).

**Table 1. Demographics**

Means  $\pm$  standard deviations; Inv. = involved, Un.= uninvolved  
Table excludes participants who only had 1 limb analyzed (n=3)

	Both Steady (n=13)	Both Unsteady (n=3)	Inv. Unsteady (n=2)	Un. Unsteady (n=1)
Age (y)	35 $\pm$ 9	39 $\pm$ 11	42 $\pm$ 4	48
BMI (kg/m <sup>2</sup> )	24.8 $\pm$ 1.7	24.3 $\pm$ 1.37	22.8 $\pm$ 0.6	24.9
Years from Surgery	2.2 $\pm$ 1.1	2.7 $\pm$ 1.0	1.9 $\pm$ 0.1	1.3

There was no significant interaction of limb and balance rating (steady vs unsteady)( $P > 0.10$ ). There was a significant effect of balance rating for trunk, pelvis, and hip excursion and CoP path length medial-lateral movement, and displacement area ( $P < 0.05$ ). Participants with unsteady balance had significantly more trunk, pelvis, and hip excursion, significantly longer CoP path length, significantly

more CoP medial-lateral movement, and significantly higher CoP displacement area (Table 2). There was no significant difference between limbs or balance ratings for CoP peak velocity ( $P > 0.05$ ).

**Table 2. Biomechanical Measures of Balance**

Means  $\pm$  standard deviations; Exc. = excursion; M-L = medial-lateral; CoP values are normalized by height (m)

	Steady	Unsteady	P =
Limbs (N)	30	11	NA
Trunk Exc. (°)	13.4 $\pm$ 5.6	19.5 $\pm$ 7.3	<b>0.02</b>
Pelvis Exc. (°)	10.9 $\pm$ 2.5	15.9 $\pm$ 2.9	<b>0.001</b>
Hip Exc. (°)	18.5 $\pm$ 4.9	25.3 $\pm$ 4.6	<b>0.001</b>
Knee Exc. (°)	12.1 $\pm$ 5.6	12.1 $\pm$ 5.1	0.87
CoP Length (m/m)	0.009 $\pm$ 0.001	0.01 $\pm$ 0.002	<b>0.001</b>
CoP M-L (m/m)	0.004 $\pm$ 0.001	0.005 $\pm$ 0.001	<b>0.001</b>
CoP Area (cm <sup>2</sup> /m)	0.143 $\pm$ 0.047	0.182 $\pm$ 0.067	<b>0.05</b>
CoP Peak velocity [m/(sec*m)]	0.005 $\pm$ 0.002	0.005 $\pm$ 0.002	0.65

These results demonstrate that larger frontal plane trunk, pelvis, and hip excursion and higher CoP variability characterize unsteady balance in individuals who have undergone hip arthroscopy for FAIS.

## CONCLUSIONS

Because abnormal movement patterns persist after surgical intervention for FAIS [1], further investigation is needed to compare quality of movement in this population to movement patterns of healthy controls. Our future work comparing these two populations to better understand contributing factors to steady balance will focus on CoP measurements and kinematic assessment of the trunk, pelvis and lower extremity due to their relationship to clinician-identified balance impairments.

## REFERENCES

1. Rylander J, et al. *J Orthop Res* **31**, 1461-8, 2013.
2. Piva SR, et al. *BMC Musculoskelet Disord.* **7**, 33, 2006.
3. Hatton AL, et al. *Arthritis Care Res (Hoboken)* **66**, 709-16, 2014.
4. Domb BG, et al. *Sports Health* **8**, 347-54, 2016.
5. Saad MC, et al. *J Electromyogr Kinesiol* **21**, 712-8, 2011.

# BELOW-KNEE AMPUTEES MAKE SPECIFIC ANTICIPATORY LOCOMOTOR ADJUSTMENTS TO RESIST LATERAL PERTURBATION

<sup>1,2</sup> Matthew J Major, <sup>1</sup> Xinlin Chen, <sup>1</sup> Chelsi K. Serba, <sup>1</sup> Nicholas Reimold, <sup>1</sup> Franklyn Ndubuisi-Obi, and <sup>1,2</sup> Keith E. Gordon

<sup>1</sup> Northwestern University, Chicago, IL, USA

<sup>2</sup> Department of Veterans Affairs, Chicago, IL, USA

email: matthew-major@northwestern.edu, web: <http://www.nupoc.northwestern.edu/>

## INTRODUCTION

Approximately half of community dwelling persons with lower-limb amputation fall every year [1]. Frontal-plane asymmetries observed during quiet standing [2] suggest that persons with below-knee amputation (BKA) may have limited ability to respond to lateral perturbations during gait. Currently, the mechanisms underlying successful recovery following lateral perturbation are poorly understood. Characterizing the control mechanisms used to maintain locomotor stability may inform interventions to minimize fall risk. This pilot study quantified anticipatory gait adjustments of persons with unilateral BKA when *a priori* information of an impending lateral perturbation is varied. Due to the loss of an active ankle joint and critical forms of proprioception [2, 3], we theorized that persons with BKA will depend on passive stability mechanisms deemphasizing requirements to accurately sense and respond to perturbations. Specifically, we hypothesized that persons with BKA will increase the Margin of Stability (MoS) on their impaired (prosthetic) side during steps prior to a lateral perturbation directed toward their impaired side.

## METHODS

Six subjects with unilateral BKA ( $48 \pm 8$  yrs,  $70 \pm 11$  kg,  $1.7 \pm 0.1$  m) experienced lateral perturbations during a series of treadmill walking trials. *A priori* knowledge of the perturbation direction was randomly varied, but timing of the perturbation was provided through both visual and audio cues. We examined three conditions: 1) Known perturbation direction (toward the impaired or sound limb), 2) Unknown perturbation direction, 3) Baseline - no perturbation. Subjects walked at their self-selected speed for all 30 perturbation trials (6 trials x 3 conditions x 2

perturbation direction). Lateral perturbations of 12% bodyweight were generated by motorized cables attached to a waist harness.

Positions of markers on the fifth metatarsals and pelvis were recorded at 100 Hz (Qualisys, Göteborg, Sweden), and used to define the lateral base-of-support (BoS) and body center-of-mass (CoM), respectively. Matlab (Natick, MA) software estimated MoS of each side as the minimum lateral distance between the extrapolated CoM (XCoM; a velocity-adjusted CoM position [4]) and the BoS during stance. The MoS was averaged for each side across 12 total steps, occurring during the 4 steps prior ( $n-1$  through  $n-4$ ) to perturbation step ( $n$ ).

## RESULTS AND DISCUSSION

Frequency of the side (impaired or sound) of the last heel strike prior to the perturbation step, and MoS for the perturbation conditions during the four steps prior to perturbation compared to baseline are reported in Figures 1 and 2, respectively.

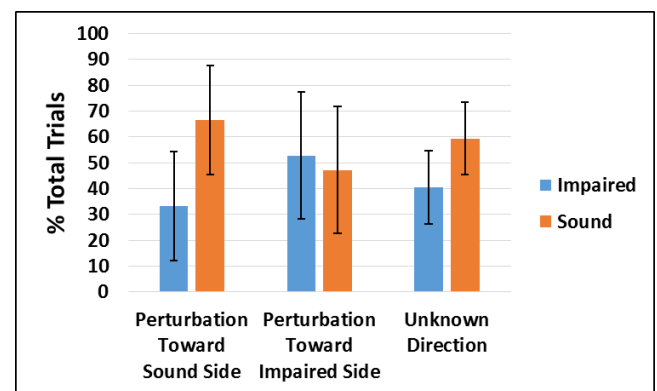


**Figure 1:** Freq. ( $\pm 1$ SD) of heel strike limb at  $n$  step.

Subjects were  $\sim 50\%$  more likely to be on their sound limb when the perturbation was directed toward the sound limb. In contrast subjects were equally likely

to be on their sound or impaired limb when perturbations were directed toward their impaired limb or when the perturbation direction was unknown. These results may suggest a preference to have the sound limb in contact with ground at the time of the perturbation when they are aware that the perturbation will not be toward the impaired side.

The MoS of both limbs did not noticeably change when the perturbation direction was directed toward the sound side. However, when the perturbation direction was unknown or directed toward the impaired side, subjects displayed an increase in the MoS of the impaired limb during the last two steps prior to perturbation ( $n-1$  or  $n-2$ ) when compared to baseline. Across the unknown direction and impaired side perturbation conditions, the average increase in MoS compared to baseline was 12 mm. This increase in MoS may be reflective of using passive mechanisms to reduce the likelihood that the XCoM exceeds the BoS thus requiring a large response to restore balance. Interestingly, when subjects did not expect a perturbation or were aware that a perturbation would be toward their sound side, they walked with relatively symmetric MoS.

These results support the hypothesis that individuals with BKA increase the MoS on the impaired side when the perturbation direction is toward that side. Accordingly, it seems reasonable that when subjects were unaware of the direction of the impending perturbation, they increased impaired side MoS as a precautionary measure for maintaining locomotor balance. This precaution may also be reflected by the generally greater percentage of trials in which subjects were positioned in sound limb stance at the time of perturbation. Overall, given that minimal change to the MoS for either side was displayed

when the perturbation direction was toward the sound side, the results broadly suggest that below-knee prosthesis users may utilize passive mechanisms to enhance stability when they expect to be perturbed toward their impaired side. However, research is needed to better understand the consequences of this strategy when recovering from the type of perturbations imposed in this study.

## CONCLUSION

Persons with BKA seem to emphasize passive mechanisms for maintaining locomotor stability by increasing the MoS on their impaired side when expecting a perturbation toward that limb. Future work will focus on the consequences of such a strategy by exploring the response dynamics following the perturbation for each condition tested.

## REFERENCES

1. Miller WC, et al. *Arch Phys Med Rehabil* **82**, 1031-1037, 2001.
2. Nadollek HS, et al. *Physiother Res Int* **7**, 203-214, 2002.
3. Vrieling AH, et al. *Gait Posture* **28**, 222-228, 2008.
4. Hof A, et al. *Gait Posture* **25**, 250-258, 2007.

## ACKNOWLEDGEMENTS

We thank Geoffrey Brown, and Sean Dwijendra for assistance with device controls and data collection. The work was supported by the Northwestern University Undergraduate Research Assistant Program #999URAP137320, National Institutes of Health's National Center for Advancing Translational Sciences #UL1TR001422 and the Department of Veterans Affairs (#1 IK2 RX001322-01A1, and #1 IK2 RX000717-01).

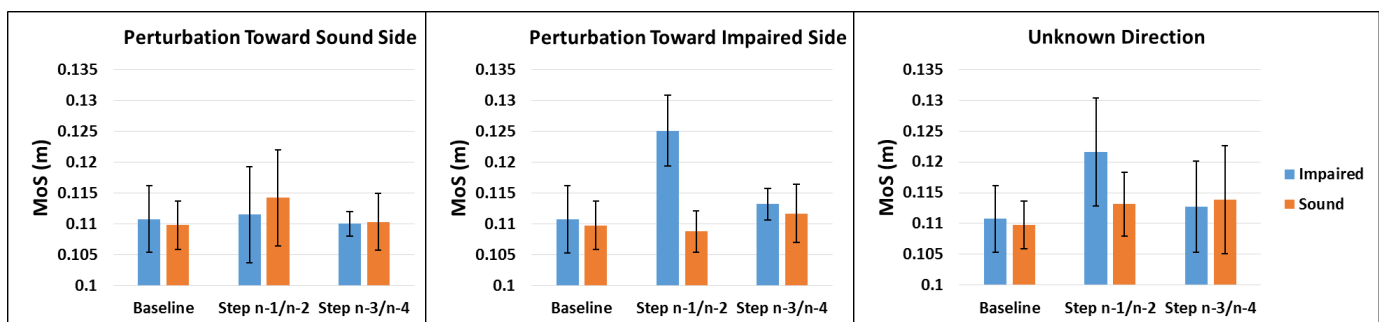


**Figure 2:** Average margin of stability ( $\pm 1SD$ ) of each limb for baseline and for four steps prior to perturbation.

# ALTERED SENSORY ORGANIZATION DURING QUIET STANCE FOLLOWING NEUROTOXIC CHEMOTHERAPY

Scott M. Monfort, Xueliang Pan, Lynette Mesi, Maryam B. Lustberg, and Ajit M.W. Chaudhari

The Ohio State University, Columbus, OH, USA

**email:** monfort.30@osu.edu **web:** <http://u.osu.edu/osusportsbiomechanics/>

## INTRODUCTION

Advances in diagnosing and treating cancer have contributed to improved survival rates and an increasing number of cancer survivors [1]. Many cancer patients receive chemotherapy as a component of an effective anti-cancer treatment, but common chemotherapy agents such as taxanes and oxaliplatin can present patients with adverse effects due to their neurotoxicity [2]. The effects of this neurotoxicity can persist well beyond completion of chemotherapy and are associated with an increased risk of falling [3].

Our previous research has reported the natural history of balance impairments in cancer patients receiving chemotherapy [4]; however, the sensory system mechanisms that may drive this instability are largely unknown. Sensory organization tests have previously been used to systematically interfere with sensory systems to gain insight into postural control strategies and impairments [5]. The purpose of this study was to investigate contributions of sensory system factors to postural instability through a sensory organization approach. Our hypothesis was that cancer survivors who received neurotoxic chemotherapy would rely less on somatosensation during quiet stance.

## METHODS

Seventeen cancer survivors participated in the study after providing IRB-approved informed consent. These participants comprised a group who did not receive chemotherapy (CONTROL; n=6; f/m = 6/0;  $59.3 \pm 9.7$  yrs;  $78.0 \pm 14.1$  kg;  $1.62 \pm 0.05$  m) and a group who recently completed oxaliplatin- or taxane-based chemotherapy (CHEMO; n=11; f/m = 9/2;  $51.7 \pm 12.9$  yrs;  $83.4 \pm 18.8$  kg;  $1.68 \pm 0.05$  m).

Patients completed three 30 second trials of quiet

stance under the following four conditions: Eyes Open (EO)-Rigid surface, EO-Foam surface, Eyes Closed (EC)-Rigid surface, and EO-Rigid with head tilted back at a 45° angle (EO-Tilt). Center of pressure (CoP) data were recorded at 1000 Hz using a balance plate (Bertec Corp.) and low-pass 4<sup>th</sup>-order Butterworth filtered at 20 Hz. The average planar mean velocity (MVEL) over the three trials was used to assess balance for this study. Increased MVEL represents overcorrecting in CoP adjustments [4].

The sensory interference conditions were normalized to EO-Rigid. Increased MVEL during sensory interference conditions were interpreted as a greater reliance on a given sensory system for postural control during natural, unperturbed quiet stance (i.e., 'EC' for vision, 'Foam' for somatosensation, 'Tilt' for vestibular). Additionally, the quotient of EC-Rigid and EO-Foam was used to more directly represent relative reliance on vision versus somatosensation during quiet stance.

Patients also had their vision and somatosensation tested independently of the balance tasks. Visual acuity was assessed using a low-contrast logMAR chart. Passive, ipsilateral joint reposition sense at the ankle was measured to assess proprioception, an aspect of somatosensation. We used a mobile-app (CoreX Therapy) based approach where patients attempted to match an angle of 15° plantarflexion that was previously demonstrated to them. Five trials were collected. The mean absolute error of the three remaining trials after removing the most and least accurate trials was the outcome for this test.

Two-sample independent t-tests were used to test for differences between groups. Additionally, a bootstrapped Pearson correlation analysis between ankle joint reposition error and the ratio of EC to Foam conditions was used to investigate effects of

altered proprioception on postural control strategy in the CHEMO group. Significance was defined at  $\alpha=0.05$  without correcting for multiple comparisons due to the exploratory nature of this study.

## RESULTS AND DISCUSSION

There were no significant differences between groups in age, mass, height, logMAR scores, or ankle joint reposition sense (all  $p>0.05$ ). The CHEMO group demonstrated less of an effect of the somatosensory interference condition (i.e., EO-Foam) compared to the CONTROL group ( $p=0.03$ ) (Table 1). An increased effect of EC relative to Foam in the CHEMO group was also observed ( $p=0.019$ ).

**Table 1.** Effects of sensory interference conditions on MVEL during quiet stance.

	CONTROL	CHEMO	p-value
EO-Rigid (mm/s)	10.3 ± 2.6	15.5 ± 8.3	0.26
EC-Rigid ÷ EO-Rigid	1.4 ± 0.2	1.6 ± 0.3	0.16
EO-Foam ÷ EO-Rigid	2.6 ± 0.5	2.0 ± 0.3	<b>0.03</b>
EO-Tilt ÷ EO-Rigid	1.2 ± 0.2	1.2 ± 0.2	0.90
EC-Rigid ÷ EO-Foam	0.5 ± 0.1	0.8 ± 0.3	<b>0.019</b>

In addition to the group differences, ankle joint reposition sense was significantly associated with the relative effects of the EC and Foam conditions on MVEL ( $r = 0.69$ ,  $p=0.03$ ) in the CHEMO group. This may suggest a shift towards relying more on vision relative to somatosensation in patients with worse ankle joint reposition sense (Figure 1).

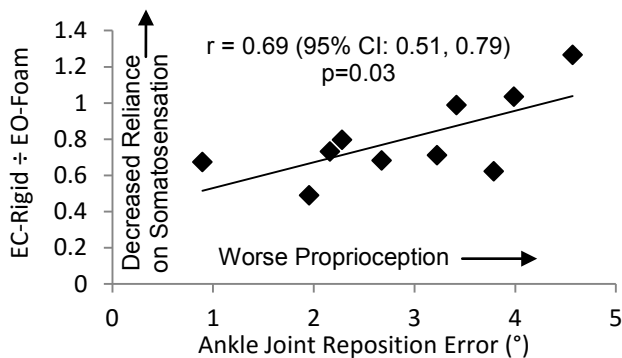


**Figure 1.** Relationship between ankle joint reposition error and relative effect of EC vs. Foam conditions in the CHEMO group. Results of bootstrapped Pearson correlation are shown.

The results of this study support that (1) cancer survivors who complete chemotherapy treatment demonstrate altered balance compared to survivors

who did not receive chemotherapy, and (2) impaired ankle joint reposition sense appears to be associated with these effects. The decreased effect that standing on a foam surface had on the CHEMO group is consistent with these patients compensating for potential diminished somatosensation by increasing reliance on other sensory information (e.g., vision) and less on proprioception that may be impaired during chemotherapy. This interpretation is further supported by worse ankle joint position sense in the CHEMO group being associated with decreased reliance on somatosensation. These findings complement previous findings of exaggerated balance impairments during vision deprived conditions in breast cancer survivors who completed taxane-based chemotherapy [5].

The small sample size is among the limitations of this study. Study enrollment is currently ongoing and the outcomes from additional participants will improve the confidence of our findings and enable a more thorough analysis.

## CONCLUSIONS

Cancer survivors recently completing chemotherapy demonstrated an altered balance control strategy that is consistent with relying less on proprioception during standing balance. These findings support the hypothesized somatosensory-driven mechanism of postural instability in this population and provide guidance for developing interventions that mitigate these detrimental effects of chemotherapy.

## REFERENCES

1. Howlander, *SEER Cancer Stats Review*, 2015.
2. Ocean AJ, Vahdat LT. *Support Care Cancer* 12(9):619-625, 2004.
3. Tofthagen C, et al. *Support Care Cancer* 20:583-589, 2012.
4. Monfort et al., *Gait & Pos*, 48:237-242, 2016.
5. Wampler et al., *Arch Phys Med Rehabil*, 88(8): 1002-1008, 2007.

## ACKNOWLEDGEMENTS

We would like to thank our funding sources:

- NCI R03 CA182165-01
- NSF GRF DGE-13430

# EMG ASSESSMENT OF A SHOULDER SUPPORT EXOSKELETON DURING ON-SITE JOB TASKS

Jason C. Gillette and Mitchell L. Stephenson

Iowa State University, Ames, IA, USA  
email: gillette@iastate.edu

## INTRODUCTION

In 2014, there were 88,980 cases of shoulder injuries that caused individuals to miss work (8.2 cases per 10,000 workers). These shoulder injuries resulted in 26 median days away from work, the longest recovery time of any body part [1]. Common causes of shoulder pain include bursitis, tendinitis, tendon tears, impingement, instability, and arthritis [2]. In order to avoid muscle fatigue and tendinitis, it has been suggested that sustained overhead postures and repeated loads above 40% shoulder strength should be avoided [3].

If worksite modification is limited or not feasible, then an assistive device may be of value to a worker to reduce shoulder loads. For example, a table-mounted arm support was shown to reduce anterior deltoid and upper trapezius muscle activity during pipetting [4]. The purpose of the current study was to assess a passive exoskeleton used by workers during on-site job tasks. This exoskeleton was designed to fit like a backpack frame with cuffs proximal to the elbow that support arm weight during overhead shoulder postures and transfer loads to the pelvis/hip.

## METHODS

Six experienced workers (2 female/4 male, age  $41 \pm 7$  yr; mass  $76 \pm 11$  kg; height  $1.71 \pm 0.08$  m) at two industrial manufacturing sites volunteered for this study. These individuals worked in the following areas: assembly (three workers), painting, parts hanging, and welding. Workers were assessed during a challenging cycle of their job that was repeated during a work shift. The following conditions were compared: 1) consecutive job cycles with and without the exoskeleton, 2) at the beginning and end of the work shift without wearing the exoskeleton that day, and 3) at the beginning and end of the work shift wearing the exoskeleton throughout that day.

Informed consent was obtained from all workers, along with background information, a pre-survey, and a post survey. Data were collected using a Delsys Trigno wireless electromyography (EMG) system at a sampling frequency of 1926 Hz using Delsys EMGworks software. EMG sensors were placed on eight muscles: right and left anterior deltoid, biceps brachii, upper trapezius, and erector spinae. Maximum voluntary isometric contractions (MVIC) were performed in the following postures: shoulder abduction empty can, seated elbow flexion, and prone spinal extension. EMG data were analyzed using custom written code in Matlab.

EMG signals were inspected to remove any non-physiological artifacts. The EMG data were bandpass filtered with a 4<sup>th</sup>-order zero-lag Butterworth filter from 20-450 Hz, and the data were rectified. Next, the EMG data were low-pass filtered at 10 Hz to create a linear envelope. A moving window was used to determine the maximum one second of sustained EMG amplitudes for both the MVICs and job tasks. The maximum one minute of distributed EMG amplitudes measure were determined by dividing the data into consecutive one second intervals and finding the maximum 60 s of muscle activity distributed throughout the job task.

Maximum one second sustained and one minute distributed EMG amplitudes were divided by the maximum one second MVICs to determine a percent of maximum contraction (%MVIC). Next, right and left side muscles were averaged together. The EMG amplitudes presented here are an overall average (consecutive, beginning of shift, end of shift) and the end of shift where fatigue is of most concern. Comparisons were made between job tasks performed without the exoskeleton and with the exoskeleton. Paired t-tests were used for comparisons, with  $p < 0.05$  considered statistically significant (Table 1).

## RESULTS AND DISCUSSION

*Overall.* Maximum one second sustained EMG amplitudes were significantly reduced with the exoskeleton for the biceps brachii ( $p = 0.01$ , 18% reduction) and approached significance for the anterior deltoid ( $p = 0.06$ , 18% reduction). Maximum one minute distributed EMG amplitudes were significantly reduced with the exoskeleton for the biceps brachii ( $p = 0.02$ , 27% reduction) and anterior deltoid ( $p = 0.04$ , 23% reduction), while approaching significance for the erector spinae ( $p = 0.07$ , 19% reduction).

*End of Shift.* Maximum one second sustained EMG amplitudes were significantly reduced with the exoskeleton for the anterior deltoid ( $p = 0.05$ , 31% reduction) and approached significance for the biceps brachii ( $p = 0.08$ , 25% reduction). Maximum one minute distributed EMG amplitudes were significantly reduced with the exoskeleton for the biceps brachii ( $p = 0.03$ , 39% reduction), while approaching significance for the anterior deltoid ( $p = 0.07$ , 28% reduction). Though non-significant, maximum one minute distributed EMG amplitudes with the exoskeleton showed a 28% reduction for the upper trapezius and a 30% reduction for the erector spinae.

Across EMG amplitude measures, the exoskeleton provided the most benefit for the anterior deltoid and biceps brachii. For these two muscles, EMG amplitudes were all significantly reduced or approaching significance with the exoskeleton, along with percent reductions that ranged from 18-39%. The anterior deltoid's primary functions are shoulder flexion and abduction, which were directly assisted by the exoskeleton. While the biceps brachii plays a

secondary role in shoulder movements, the exoskeleton benefits are likely due to increased upper arm stability to indirectly benefit elbow flexion.

One concern with the exoskeleton's design to transfer loads from the shoulder to the pelvis/hip was that muscles of the lower back would have increased muscle activity. However, the EMG amplitudes for the erector spinae with the exoskeleton were reduced 7-30% across measures and even approached a significant reduction for overall maximum one minute distributed EMG amplitude. One potential explanation is that reduced fatigue in the anterior deltoid and biceps brachii helped prevent the worker from using anterior trunk lean as a compensation. Another potential explanation is that the exoskeleton frame promoted a more upright posture.

In summary, the exoskeleton appeared to provide benefits across the muscles tested, although additional participants would allow for further generalization. If we use a 40% strength guideline for repetitive loads, then the anterior deltoid one minute distributed EMG amplitude at the end of shift approaches this value without the exoskeleton (36 %MVIC), while the exoskeleton provides a larger margin of safety (26 %MVIC). Shoulder-supporting exoskeleton usage is most likely to benefit job tasks that involve repetitive overhead movements that challenge the anterior deltoid muscles.

## REFERENCES

1. Bureau of Labor Statistics. *The Economics Daily*, 2015.
2. American Academy of Orthopaedic Surgeons. *OrthoInfo*, 2010.
3. Chaffin DB. *Occupational Biomechanics*, John Wiley & Sons, Inc., 1999.
4. Rempel P, et al. *Work*, **39**, 195-200, 2011.

**Table 1:** EMG amplitudes with and without the exoskeleton at the beginning and end of the work shift.

1 Sec Max (%MVIC)	Overall				End of Shift			
	Deltoid	Biceps	Trap	Spinae	Deltoid	Biceps	Trap	Spinae
Without	63.5±15.8	45.3±17.4	48.1±9.5	52.2±21.6	76.8±29.2	48.9±20.2	51.9±10.5	54.2±35.0
Exoskeleton	52.1±7.5	37.2±15.1*	50.9±5.2	48.4±20.7	52.7±15.0*	36.8±16.2	46.2±11.7	43.7±18.6
1 Min Dist (%MVIC)	Overall				End of Shift			
	Deltoid	Biceps	Trap	Spinae	Deltoid	Biceps	Trap	Spinae
Without	32.0±8.2	19.2±9.1	25.3±6.4	28.7±15.1	36.1±11.4	22.2±12.1	28.1±9.0	30.7±24.9
Exoskeleton	24.8±2.8*	14.0±5.9*	22.2±4.1	23.3±11.1	26.1±8.2	13.5±6.0*	20.3±7.4	21.6±9.8

\*indicates significantly reduced EMG amplitude when wearing the exoskeleton ( $p < 0.05$ )

# SPATIAL DEPENDENCY OF SHOULDER MUSCLE DEMAND DURING DYNAMIC UNIMANUAL PUSHING AND PULLING

Daniel C. McFarland, Michael N. Poppo, Emily M. McCain, and Katherine R. Saul  
North Carolina State University, Raleigh, NC, USA  
email: dcmcfarl@ncsu.edu

## INTRODUCTION

Work-related musculoskeletal disorders (MSD) place a large burden on the economy and workers' health; MSD are the leading cause of work disability and lost productivity [1]. Shoulder MSD worker compensation claims result in the second highest total cost of MSD claims by body region [2], and push-pull tasks, in particular, are significantly related to shoulder complaints [3]. To effectively design workplaces to minimize work-related shoulder MSD, knowledge of the demands placed on shoulder muscles during these tasks is needed; however, little is known regarding shoulder loading during dynamic push-pull tasks [4]. Prior studies on pushing and pulling focused on dynamic full-body tasks (such as cart pushing) and isometric seated tasks [5,6]. Loading under these conditions cannot be directly applied to seated dynamic tasks since EMG and force exertion under dynamic conditions frequently differ from those recorded isometrically [7,8] and foot placement influences pushing force [9]. Therefore, our goal was to quantify how muscle demand, a measure of the overall load placed on the muscular system, varies with task target and task direction.

## METHODS

A series of seated unimanual push and pull tasks were performed by 13 healthy young adults 19 to 32 years old (Fig. 1A).

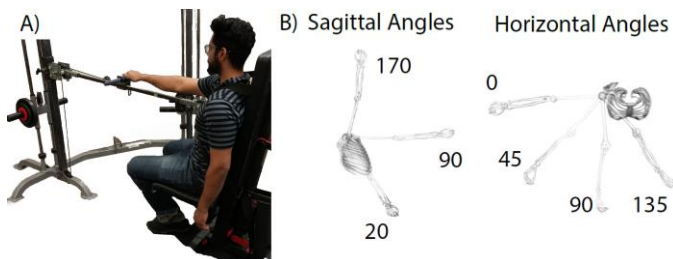


**Figure 1:** A) Subjects pushed/pulled 15% of their isometric max B) Sagittal and horizontal angles

Tasks were performed at a combination of 3 sagittal angles (20°, 90°, 170°) and 4 horizontal angles (0°, 45°, 90°, and 135°) for a total of 12 task targets (Fig. 1B). Electromyographic (EMG) recordings of the anterior, middle, and posterior deltoid, biceps brachii, lateral head of triceps brachii, latissimus dorsi, pectoralis major, and serratus anterior were collected at 2000 Hz. Raw EMG data was post-processed by removing the DC offset, bandpass filtering with cutoff frequencies of 20 and 300 Hz, full-wave rectifying, RMS filtering with a 200 msec window, and normalizing to peak value recorded during the testing protocol.

Muscle demand for each task was calculated as an average of each participant's weighted total of normalized EMG output [10]. Physiological cross-sectional areas (PCSA) from the literature were used to determine weightings for each muscle [11,12,13].

$$\sum_{i=1}^8 Norm\_EMG_i \left[ \frac{PCSA_i}{\sum_{i=1}^8 PCSA_i} \right]$$

Differences in muscle demand were analyzed across sagittal and horizontal task targets using a two-way ANOVA ( $\alpha < 0.05$ ) and Tukey's HSD post-hoc test. Influence of task direction (push or pull) on muscle demand was analyzed with a one-way ANOVA ( $\alpha < 0.05$ ).

## RESULTS AND DISCUSSION

Sagittal target location influenced muscle demand for both pushing ( $p < 0.0001$ ) and pulling ( $p < 0.0001$ ). For pushing, sagittal angle of 170° resulted in a significant increase ( $p < 0.0001$ ) in muscle demand from both angles 20° and 90° (Fig. 2A). For pulling, sagittal angle of 20° resulted in a significant increase ( $p < 0.0001$ ) in muscle demand from both angles 90° and 170° (Fig. 2B). There was no difference in muscle demand among horizontal targets for either task direction.

Dynamic pushing resulted in higher muscle demand than pulling ( $p < 0.0001$ ). Mean muscle demand for pushing was  $0.3144 \pm 0.1072$  whereas mean muscle demand for pulling was  $0.1780 \pm 0.0937$ . Pushing was nearly twice as demanding as pulling, which may make it more likely to cause fatigue and lead to MSD.

Studies of isometric push-pull exertions have reported an increase in total muscle activity – i.e., the summation of EMG levels of the recorded muscles – for more elevated targets for both pushing and pulling [6, 10]. However, in this dynamic study the lowest sagittal target is associated with the largest muscle demand for pulling. One potential reason for this difference is that during a dynamic pull from a low target, subjects must elevate the handle against gravity whereas during a pull from a high target subjects lower the handle. Working against gravity during the pull from the lowest target likely makes this task more demanding. In contrast, subjects in the isometric study maintained the limb posture for the duration of the contraction, and it is well documented that maintaining elevated postures is a risk for fatigue and MSD [6].

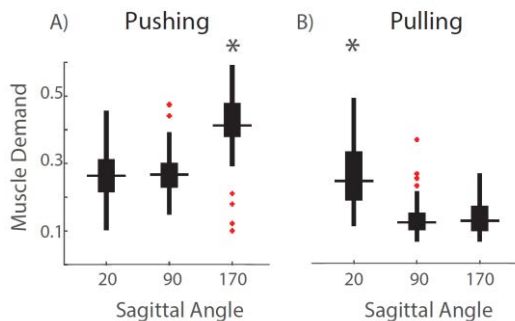


**Figure 2:** Muscle demand during A) pushing and B) pulling to sagittal targets.

Isometric pushing and pulling have been reported to have increased total muscular activity for lateral targets [6], whereas horizontal targets in the dynamic tasks did not influence muscle demand. For the dynamic tasks in this study, pushing/pulling was defined as away from/towards the torso; however, in the prior isometric study, pushing/pulling were always in the anterior and posterior directions. This difference in task definition likely alters limb posture more dramatically among the isometric tasks, and thereby varies muscle demand more markedly across horizontal targets.

Workspaces can be designed based on results from this study to reduce worker fatigue and prevent MSD; however, study limitations should be taken in consideration when interpreting these results. Limitations include potential subject fatigue during testing or asymptomatic injuries. To reduce the effects of fatigue, rest allowances were provided between tasks, and task order was randomized.

## CONCLUSIONS

The primary findings have possible implications for arm function through the workspace:

1. Dynamic pushing and pulling tasks have different muscle demand and workspace location dependence compared to isometric tasks. Thus, care should be used when generalizing from isometric to dynamic tasks for workplace design.
2. Elevating the limb during dynamic pushing and pulling results in increased muscle demand. Thus, workspace design should avoid pushing and pulling tasks that result in motion against gravity. Horizontal target location of the task, however, appears to have reduced influence on muscle demand, and is thus a less important constraint. Priority should be given to locating push tasks at low demand locations since pushing is more demanding than pulling.

## REFERENCES

1. National Academy of Sciences. National Academy Press 2001.
2. Dunning KK. *Am J Ind Med* **53**, 276, 2010.
3. Hoozemans MJM. *J Occup Env Med* **59**,696, 2002.
4. Hoozemans MJM. *Ergonomics* **41(6)**, 757, 1998.
5. Nimbarte AD. *Appl Ergon* **44(5)**, 841, 2013
6. McDonald A. *Appl Ergon* **43(6)**, 971, 2012..
7. Antony NT. *J Electromyogr Kinesiol* **20**,191,2010.
8. Kumar S. *Int J Ind Ergonom* **15**, 427, 1995
9. Rancourt D. *J Mot Behav* **33(4)**, 351, 2001.
10. Nadon AL. *Ergonomics* **59:10**,1294, 2016.
11. Holzbaur KR. *J Biomech* **40(4)**,742,2007.
12. Langenderfer J. *Clin Biomech (Bristol, Avon)* **19(7)**, 664, 2004.
13. Van der Helm FCT. *J Biomech* **27(5)**, 551, 1994.

## ACKNOWLEDGMENT

Funding from CFD Research Corporation

# SUBMAXIMAL NORMALIZING METHODS TO EVALUATE LOAD SHARING CHANGES IN REPETITIVE UPPER EXTREMITY WORK

Alison C. McDonald, Daanish M. Mulla, Peter J. Keir

Department of Kinesiology, McMaster University, Hamilton ON, Canada, L8S 4K1

Email: mcdonaac@mcmaster.ca

## INTRODUCTION

The anatomy of the shoulder allows multiple load distribution strategies between muscles thus load-sharing adaptations to fatigue are expected. The relationship between EMG and muscle force changes with muscle fatigue, making the interpretation of load sharing relationships between muscles challenging when workers are exposed to repetitive demands (McDonald et al, 2015; Tse et al, 2015). Two common methods for normalization include using a maximum voluntary exertion (MVE) or a submaximal reference exertion (RVE); the latter may be better suited to estimate sub-maximal loads (Jonsson, 1982). The purpose of this investigation was to evaluate the efficacy of normalizing EMG data to repeated, static, submaximal exertions to mitigate the fatigue artifact in EMG amplitude, to better reflect load sharing.

## METHODS

Twenty right hand dominant men completed repetitive simulated work tasks, in 60-second work cycles, until exhaustion. Surface EMG (Trigno, Delsys Inc., Natick, MA, USA) was recorded from 11 muscles for a complete work cycle every 3 minutes. Every 12 minutes, participants completed a series of 4 submaximal (30% MVC) and 1 maximal reference exertions. The series of four reference exertions were selected to activate all of the included muscles (Boettcher et al, 2008). Submaximal forces were recorded with a force transducer (Mark-10, Copiague NY) and a manual goniometer confirmed each posture. EMG data were recorded for 3 seconds after achieving the target force. This cycle continued until one of the termination criteria was met: 1) participant declared they could no longer continue, 2) participant was no longer able to complete the work tasks, 3) participant was no longer able to

maintain the 30% MVC force level for any of the 4 reference exertions.

Fatigue was defined as an 8% or greater decrease in median power frequency between reference exertions. Linear envelope EMG was used for the amplitude analysis (2<sup>nd</sup> order, dual-pass BW filter,  $f_c = 4$  Hz). Reference contraction EMG data were used in 6 normalizing methods including a *Standard Normalizing Method (SNM)* (normalized to initial reference exertion) and 5 novel methods (Figure 1).

EMG from one of the work tasks (drill task) was used to evaluate the methods. The novel methods included: (i) *Fatigue Only (FON)*: When myoelectric fatigue was present, the following 12 work cycles were normalized to that reference exertion. All muscles/work cycles not exhibiting signs of fatigue were normalized to the initial reference exertion. (ii) *Linear (LMN)* and (iii) *Cubic (CMN) Models*: A least squares regression model was used to create linear and cubic functions to predict the submaximal EMG amplitude for every third minute. The predicted value was then used to normalize the corresponding work task EMG. (iv) *Points Forward (PFN)*: Each reference exertion was used to normalize the 12 work cycles completed after it. (v) *Points Forward/Backward (PFBN)*: Each reference exertion was used to normalize the 6 work cycles completed before it and the 6 work cycles completed after it.

Random slope, random intercept mixed effects models were used to identify differences between participants and between the normalization methods. All novel methods were compared to the *Standard Normalizing Method*. Pearson product moment correlations assessed how well the predicted points from the linear and cubic normalization models fit the reference exertion data.

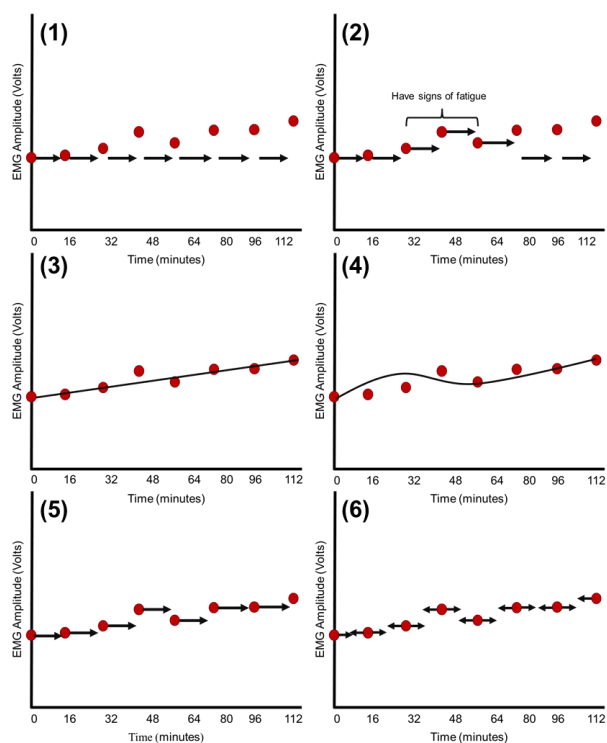


**Figure 1:** Schematic representation of the 6 normalizing methods (1) SN, (2) FON, (3) LMN, (4) CMN, (5) PFN, (6) PRFN. Circles represent mean EMG data during from reference exertions and the black arrows/lines depict which time points are normalized to each reference exertion.

## RESULTS AND DISCUSSION

Participants performed the work cycles for 57-240 minutes, completing between 5-20 sets of reference exertions. The muscles that displayed signs of myoelectric fatigue and the time points where fatigue appeared differed between participants. Shoulder flexion strength decreased from  $108.8 \pm 24.0$  N to  $77.6 \pm 28.6$  N.

The significant differences between the novel methods and the SN method were dependent on the muscle and the number of time points in the analysis. Statistically significant changes were consistent between the FO method and LMN and CMN methods ( $p < 0.05$ ). The amplitude of posterior deltoid muscle was significantly lower when normalized to these 3 methods than when normalized to the standard method (Figure 2). There were more muscles with significant

differences from the SN method with the PFN and PFBN methods.

Correlation analysis showed that the predicted cubic model points correlated better to the actual data points than the linear predicted values.

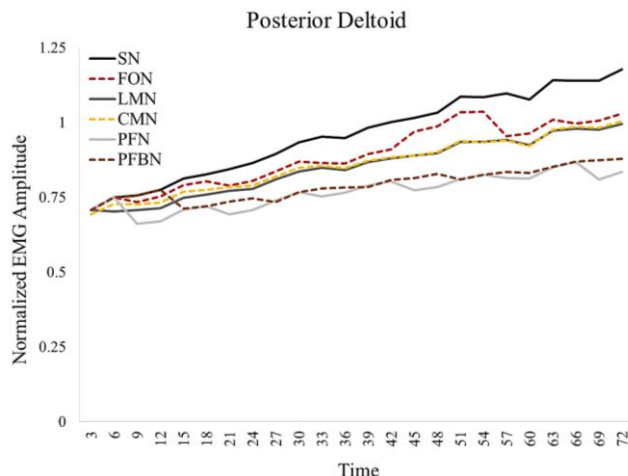


**Figure 2:** Adjusted predictions of the 6 normalization methods with 95% confidence interval for the posterior deltoid muscle.

## CONCLUSIONS

The purpose of this analysis was to develop a method to reduce fatigue artifacts in EMG data, thus results of the PFN, PFBN and FON methods are of interest. These methods are dependent on the local reference data and subject to any variability/fluctuations in these data. The cubic and linear model methods produced results that are consistent with the fatigue only normalizing method, however may be less susceptible to small local fluctuations. Based on the correlation findings, we believe that the Cubic Model Normalizing method has promise as a novel method to mitigate the effects of muscle fatigue on EMG amplitude and improve our understanding of load sharing changes with repetitive work.

## REFERENCES

1. Boettcher, CE et al. *J Orthop Res* **26(12)**, 1591-97, 2008.
2. Jonsson B. *J Hum Ergol* **11**, 73-88, 1982.
3. McDonald, AC et al. *J Electromyogr Kinesiol* **29**, 42-49, 2016.
4. Tse, CTF et al. *J Electromyogr Kinesiol* **29**, 34-41, 2016.

# SHOULDER MUSCULATURE ACTIVATION DURING HUMAN BRACHIATION

<sup>1</sup> Kathleen F.E. MacLean, and <sup>1</sup> Clark R. Dickerson

<sup>1</sup> University of Waterloo, Waterloo, ON, Canada  
email: k4maclea@uwaterloo.ca, web: uwaterloo.ca/diesel

## INTRODUCTION

The human shoulder is highly mobile and is adapted for many different non-locomotor behaviors. Though likely evolving from a weight-bearing locomotor past, the modern human shoulder has reduced power and force capabilities, and is less adapted for overhead postures than its nearest primate relatives [1]. Thus, the modern human shoulder is susceptible to damage in high-load and overhead postures despite an evolutionary history possibly derived from arboreal locomotion [2].

The modern human capacity for and adaptation to climbing behaviors, including brachiation, is unknown. Studying possible ancestral upper extremity behaviors like climbing are of anthropological and biomechanical interest. The purpose of this study was to examine the activation patterns of the shoulder musculature in experienced and inexperienced climbers while performing an overhead brachiation task.

## METHODS

Thirty young adults were recruited, 15 climbers (12M/3F; age 25[3.6] stature 1.71[0.08] m; body weight 66.9[9.0] kg) and 15 non-climbers (12M/3F; 24[2.9]; 1.75[0.07] m; 74.7[12.1] kg). All climbers had > two years of climbing experience and partook in climbing activities at least every two weeks.

Each participant completed a brachiation task across a series of eight horizontally aligned rungs spaced 40cm apart, raised approximately 2.2m off the floor (Figure 1). Six separate brachiation trials were completed. For each trial, right-side EMG (Noraxon, 2 USA Inc., Arizona, USA) was collected for two complete right arm swings, from initial right-arm contact with a rung to subsequent right-arm contact with the next rung, for a total 12

collected brachiation trials. Surface electromyographic (EMG) electrodes were placed over 12 upper extremity muscles: anterior and posterior deltoid, pectoralis major sternal and clavicular head, supraspinatus, infraspinatus, upper and middle trapezius, latissimus dorsi, serratus anterior, biceps brachii and triceps.



**Figure 1:** Experimental climbing setup

EMG was full-wave rectified, high pass filtered at 30Hz, and linear enveloped at 4Hz. EMG was amplitude normalized to muscle specific maximum voluntary exertions (MVE), and time normalized from right arm rung contact (initiating a double arm support phase) to subsequent right arm rung contact (following a right –arm swing phase). Brachiation trials were averaged within participants to obtain a mean representative trial, from which peak and average EMG was extrapolated. Between group comparisons were completed using a one-way ANOVA for each muscle at  $p < 0.05$ .

## RESULTS AND DISCUSSION

No significant differences were found between the climbing and the non-climbing participant group in peak or average EMG for any of 12 muscles measured. Both participant groups had similar

waveform shapes and activation amplitudes in all muscles (Figure 2). No muscle had an average EMG of less than 15% MVE. Four muscles had an average EMG of greater than 30% of MVE: infraspinatus, biceps brachii, serratus anterior and pectoralis major sternal. Peak EMG for all muscles ranged from 30% MVE to over 100% MVE for serratus anterior and pectoralis major sternal.

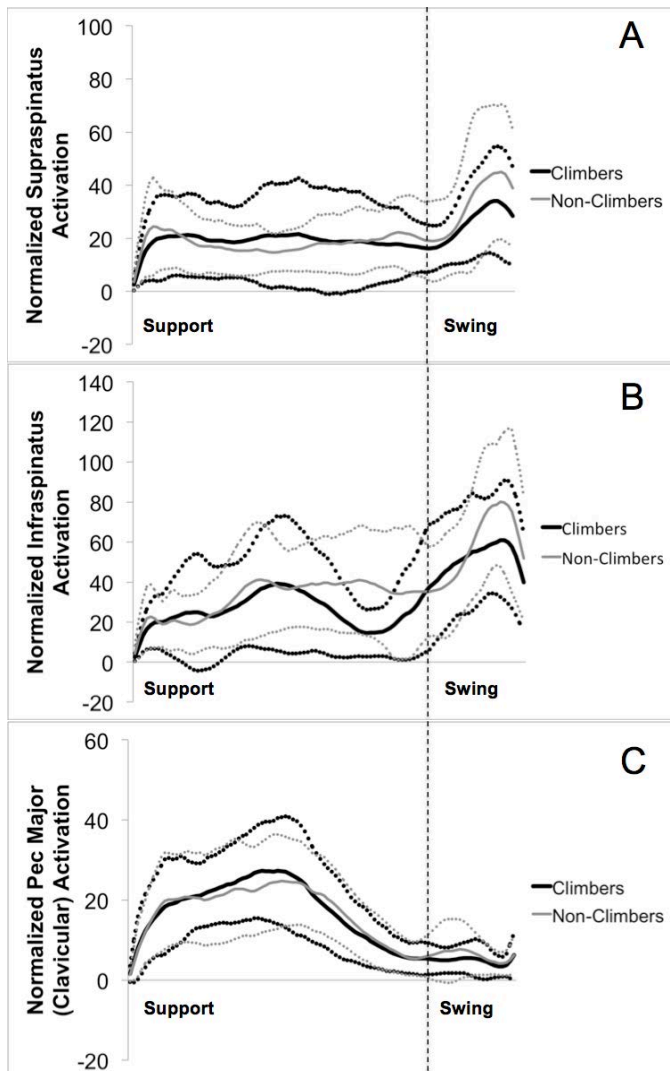


**Figure 2:** Muscle waveforms for right-arm support phase and swing phase of the climb task. Dotted lines represent one standard deviation

The muscle specific waveforms demonstrated the activation pattern of each muscle, giving insight into the role of each of the 12 muscles during the phases of brachiation. Three are shown in Figure 2. Supraspinatus was active throughout, with increased activity in swing to maintain humeral elevation

(Figure 2A). Infraspinatus controlled rotation of the right humerus during the swing phases of both arms, where increases in activation occurred (Figure 2B). Both infraspinatus and supraspinatus also performed the role of stabilizing the position of the humeral head in the glenoid during brachiation [3]. The role of the pectoralis major (clavicular) was isolated to mostly the support phase to stabilize the glenohumeral joint under the high load of full body mass (Figure 2C). It had limited contribution to swing as the unloaded, upward accelerations of the arm likely required the use of other shoulder muscles such as the deltoids.

There was large variability in both participant groups in all muscles, suggesting highly different activation levels and strategies between participants. Most of the shoulder musculature is multifunctional, allowing differences in activation to be compensated for with numerous other synergistic muscles. As no unique muscular activation pattern arose to distinguish participant groups, experience does not appear to be a contributing factor in multifunctional muscular recruitment at the shoulder for a climbing task. Unlike other primates, the non-locomotor, multifunctional evolution of the human upper extremity developed muscular redundancies that may deter the adoption of predictable and efficient biomechanical patterns in brachiation [4].

## CONCLUSIONS

Time normalized muscle waveforms discretized the roles of individual shoulder muscles throughout the support and swing phases of a brachiation task of biomechanical and anthropological significance. Highly variable muscular recruitment strategies were employed in both participant groups, suggesting divergent methods for brachiation independent of climbing experience.

## REFERENCES

1. **Thorpe et al.** (1999), *AmJPhyAnth*, 35, 248-55.
2. **Lewis et al.** (2001), *Physio*, 87, 191-8.
3. **Veeger & van der Helm** (2007), *J Biomech*, 40, 2119-29.
4. **Larson & Stern** (2013). *JHumEvo*, 65, 391-403.

# MRI VS CT-BASED SHAPE REGISTRATION ACCURACY FOR QUANTIFYING SHOULDER MOTION USING BIPLANE FLUOROSCOPY

<sup>1,2</sup> Mohsen Akbari-Shandiz, <sup>2</sup> Rebekah L. Lawrence, <sup>2</sup> Arin M. Ellingson, <sup>1</sup> Kristin D. Zhao, <sup>2</sup> Paula M. Ludewig

<sup>1</sup> Rehabilitation Medicine Research Center, Department of Physical Medicine & Rehabilitation, Mayo Clinic, Rochester, MN, USA

<sup>2</sup> Department of Rehabilitation Medicine, University of Minnesota, MN, USA  
email: shandiz.mohsen@mayo.edu

## INTRODUCTION

Biplane three-dimensional to two-dimensional (3D-2D) registration approaches have been used recently for measuring 3D *in vivo* glenohumeral joint kinematics [1]. In this approach, computed tomography (CT) has become the gold standard for reconstruction of 3D bone models, with high geometric accuracy. One possible alternative, which would not expose subjects to radiation, is magnetic resonance imaging (MRI). However, MRI provides lower bone contrast compared to the CT.

In this study we compared the relative glenohumeral kinematic accuracy of CT-based registration and MRI-based registration with radiostereometric analysis (RSA; gold standard) during dynamic biplanar fluoroscopy to determine if MRI-based registration provides sufficient accuracy for measurements of clinically relevant angular bone and joint parameters.

## METHODS

**Image acquisition.** Two male fresh-frozen cadaveric torsos (age: 72, and 62 yrs.), were imaged with 1.6 mm diameter tantalum beads implanted into the humerus and scapula of the shoulders (three shoulders were analyzed due to technical difficulties with MR imaging of the 4<sup>th</sup> shoulder). The cadaveric torsos were fixed to a custom apparatus that allowed unconstrained motion of the shoulder complex.

A custom biplane fluoroscope was used for all 2D dynamic imaging (consisting of two 65 kW pulsed x-ray generators and two 16 inch image intensifiers, optically coupled to synchronized high-speed video cameras). A custom calibration cube was imaged using the fluoroscopic setup to define the orientation of the x-ray sources and detectors.

Biplane radiographic images of the shoulder were acquired at 60 frames/s (85 kV, 200 mA, 3 ms), while

passively moving the humerus through two simulated motions using a pulley system: frontal-plane elevation and internal/external (IE) rotation.

Prior to the bead implantation, MRI shoulder scans were acquired on a 3T scanner using a VIBE sequence, (Siemens Prisma\_fit; Forchheim, Germany; voxel size: 0.89×0.89×0.9 mm), developed for scanning bones to produce 3D models with high geometric accuracy.

Following tantalum bead implantation in each bone of interest, CT imaging was acquired on a clinical CT scanner (Siemens Somatom Sensation 64; Forchheim, Germany; kVp: 140; voxel size: 0.48×0.48×0.6 mm) to obtain the CT-based 3D bone models and 3D positions of the beads relative to the bone coordinate systems.

**Image analysis.** 3D models of the humerus and scapula were manually segmented from reconstructed CT and MRI images (Mimics; Materialise, Plymouth, Michigan). Coordinate systems were computed for CT-based bone models using ISB anatomical reference frames [2]. To find 3D positions of the beads relative to the MRI-based bone models, the MRI-based surface models were aligned to the CT-based surface models using CloudCompare v2.6.3, retrieved from <http://www.cloudcompare.org/>. First, the 3D models were brought into gross alignment using at least four equivalent landmark pairs. Then, the fine alignment function was applied, which is based on the iterative closest point algorithm (ICP) [3].

To quantify bone rotations and translations, the 3D-2D intensity-based image registration was performed using open-source software (Autoscooper, Brown University, RI, USA) [4]. Using this software, a pair of digitally reconstructed radiographs (DRRs), constructed from the 3D bone models, was manually

matched to each set of two 2D calibrated and undistorted fluoroscopy images (Fig.1). This technique benefits from the bone density information within the bone models rather than using purely external edges. In order to prevent the influence of the implanted beads on image registration, traces of the beads were removed from the CT images manually.

The 3D positions of the beads were tracked from the biplane fluoroscopy images using freely available software (XMA Lab; Brown University) [5]. An independent phantom study, in our lab, has shown this RSA approach to be accurate to within  $\pm 0.2$  mm and  $\pm 0.2^\circ$ .

**Comparison analysis.** We evaluated the accuracy of the 3D-2D registration by computing the root-mean-squared (RMS) error between the 3D-2D registration results and the RSA analysis, for each of six poses of the humerus and scapula across the three shoulders.

## RESULTS AND DISCUSSION

With the CT models, overall RMS errors were 0.6 mm (Max ABS error: 2.3 mm) for all translations, and  $1.1^\circ$  (Max ABS err:  $3.0^\circ$ ) for all rotations for the humerus; and were 0.8 mm (Max ABS error: 2.4 mm) for all translations, and  $0.7^\circ$  (Max ABS err:  $2.0^\circ$ ) for all rotations, for the scapula.

With the MRI models, overall RMS errors for all humerus were 1.6 mm (Max ABS error: 3.9 mm) for all translations, and  $1.8^\circ$  (Max ABS error:  $5.1^\circ$ ) for all rotations; and for scapula, 1.3 mm (Max ABS err: 3.5 mm) for all translations, and  $1.2^\circ$  (Max ABS error:  $3.1^\circ$ ) for all rotations. Detailed results are shown in Table 1.

## CONCLUSIONS

Our results show that, measurement performance with CT-derived bone models was descriptively

superior to measurements performed with MRI-derived models, as we expected. However, our MRI-based registration accuracy indicates that the overall RMS errors were less than 1.6 mm and  $1.8^\circ$  for the humerus and less than 1.3 mm and  $1.2^\circ$  for the scapula, which is an acceptable accuracy for many clinical research questions.

Measuring 3D *in vivo* glenohumeral joint kinematics accurately is important, as it allows for quantification of small changes in clinically relevant parameters.

## REFERENCES

1. Bey MJ, et al. *J Biomech Eng* **128**, 604–9, 2006.
2. Wu G, et al. *J Biomech* **38**, 981–992, 2005.
3. Besl PJ, et al. *IEEE* **14**, 239–256, 1992.
4. Gatesy SM, et al. *J Exp Zool* **313**, 244–261, 2010.
5. Brainerd EL, et al. *J Exp Zool* **313**, 262–279.

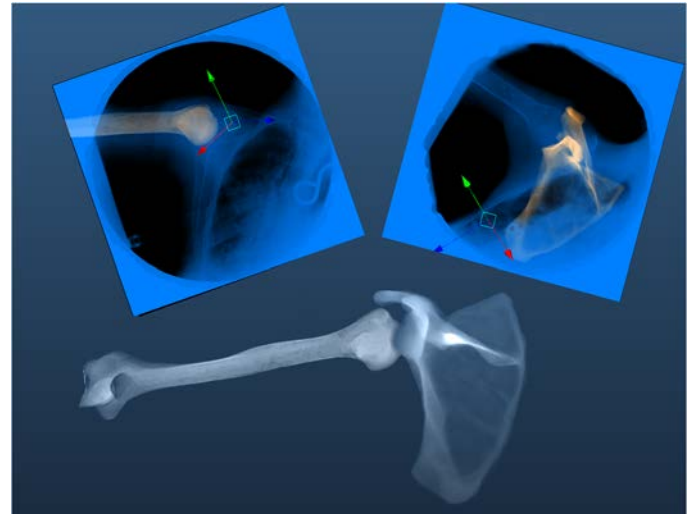


**Figure 1:** Intensity-based image registration.

## ACKNOWLEDGMENTS

This project was supported by Minnesota Partnership for Biotechnology and Medical Genomics (MNP IF #14.02), NIH/NICHD K12HD073945 and F31HD087069.

**Table 1.** RMS error for the CT-based and MRI-based registration relative to RSA across the three shoulders.

Kinematics	RMS error (mm/degree)				RMS error (mm/degree)			
	Humerus				Scapula			
	CT-based		MRI-based		CT-based		MRI-based	
	Elevation	IE	Elevation	IE	Elevation	IE	Elevation	IE
Anterior/posterior translation (mm)	0.4	0.7	1.8	1.9	1.0	0.8	1.7	1.4
Superior/inferior translation (mm)	0.7	0.6	1.1	1.3	0.6	0.4	1.5	1.0
Medial/lateral translation (mm)	0.7	0.5	1.6	1.5	0.9	0.8	1.1	1.2
Flexion/extension rotation ( $^\circ$ )	0.8	1.1	1.5	2.3	0.7	0.5	1.5	1.4
Ab/adduction rotation ( $^\circ$ )	1.0	0.8	1.4	1.8	0.5	0.5	1.0	0.8
Internal/external (IE) rotation ( $^\circ$ )	1.2	1.6	1.7	1.7	0.8	0.8	1.2	1.5

# Post-Mastectomy Breast Reconstruction Surgeries Compromise Passive Shoulder Stiffness

<sup>1</sup> Joshua Leonardis, <sup>1</sup> Brian Diefenbach, <sup>2</sup> Daniel Lyons, <sup>2</sup> Thomas Olinger, <sup>2</sup> Adeyiza Momoh, and <sup>1</sup> David Lipps

<sup>1</sup> School of Kinesiology and <sup>2</sup> Section of Plastic Surgery, University of Michigan, Ann Arbor, MI, USA  
email: jleo@umich.edu, web: <http://www.kines.umich.edu/research/mbil>

## INTRODUCTION

Following a mastectomy, ~70% of breast cancer patients elect to undergo breast reconstruction surgery to replace tissue volume and restore the appearance and feel of natural breast tissue [1]. Implant-based reconstruction has increased in popularity in recent years [2]. The “implant only” technique removes the inferior and medial attachments of the pectoralis major. A tissue expander is placed under the muscle, which is slowly inflated overall several months to stretch the muscle in order to accommodate an implant. In women who undergo radiation therapy, expansion of the pectoralis major is associated with increased reconstruction rates. For these patients, an alternative “lat flap” procedure is performed by removing the medial and inferior attachments of the latissimus dorsi and bringing it from the back into the chest. The implant is then placed between the latissimus dorsi and pectoralis major. Both techniques are associated with functional deficits of the upper extremity, including poorer patient-reported outcomes and reduced strength and range of motion [3]. However, it is unknown how these techniques affect shoulder joint stiffness, a measure that provides insight into a patient’s ability to control her arm during activities of daily living [4]. The present project aims to characterize changes in multidimensional shoulder stiffness following reconstructions utilizing the pectoralis major or latissimus dorsi.

## METHODS

Six “implant-only” and seven “lat flap” female patients at least 18 months post-reconstructive surgery were recruited for this study (Table 1). Four lumpectomy patients whose tumors were surgically removed with the remaining breast intact served as controls. Participants were placed in a removable cast with their elbow flexed 90°, and their shoulder elevated 90° (Figure 1). The cast was attached to the crank arm of a single axis rotary motor with a high-precision encoder and six-degree of freedom load

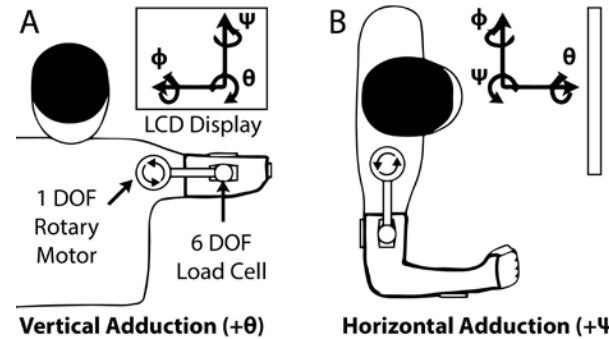


**Figure 1:** A single axis rotary motor perturbed the shoulder in either the vertical (A) or horizontal (B) directions. Visual feedback assisted subjects in matching desired torque.

cell. This motor was centered on the glenohumeral joint and controlled in real time using MATLAB xPC Target (2011a). Strength was measured prior to data collection by performing maximum voluntary contractions (MVC) in vertical add/abduction, horizontal add/abduction, and internal/external rotation.

Subjects were perturbed with small, stochastic perturbations (0.06 rad) for 60 second trials in one of two planes of motion (vertical or horizontal ad/abduction). Lumpectomy controls were only examined in the vertical direction. Resultant shoulder torques were measured as participants were asked to stay relaxed or to maintain a net torque level scaled to  $\pm 10\%$  of their MVC in each perturbation direction. Joint impedance, the dynamic relationship describing the torque response to an imposed change in joint angle, was estimated for each trial using a frequency response function [5]. These estimates were fitted with a 2<sup>nd</sup> order linear model to approximate the inertial, viscous, and stiffness properties of the joint. Two trials were performed in each of the six testing conditions and two perturbation directions, yielding 12 total trials. Between group stiffness comparisons were analyzed with a linear mixed model. T-tests were used to analyze between group strength and within group stiffness data. Bonferroni corrected multiple comparisons were utilized when appropriate. All significances are reported at  $\alpha = 0.05$ .

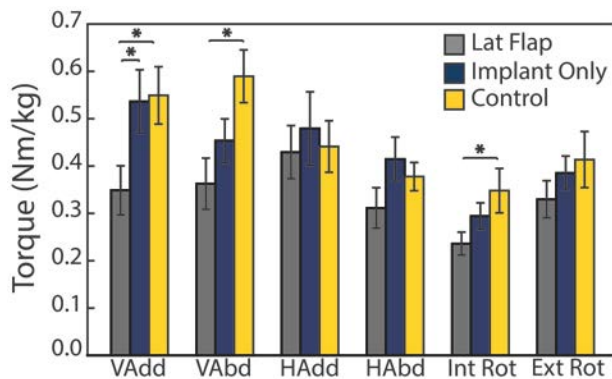


**Figure 2:** Mean maximal shoulder strength in six directions for breast reconstructive surgery patients compared to lumpectomy controls. Error bars represent SE. \* -  $p < 0.05$

## RESULTS AND DISCUSSION

Several significant differences in shoulder strength existed between the experimental groups (Figure 2). The lat flap group exhibited lower maximal vertical adduction torques than both the implant only ( $p = 0.04$ ) and lumpectomy control groups ( $p = 0.04$ ). The lat flap group also exhibited lower vertical abduction ( $p = 0.02$ ) and internal rotation torques ( $p = 0.05$ ) when compared to the control group.

Within the lat flap and implant only groups, passive stiffness was greater in the vertical direction than in the horizontal direction (implant only:  $p = 0.01$ , lat flap:  $p = 0.002$ ). No significant differences were observed within the groups for active stiffnesses, except between vertical adduction and abduction stiffness in the lat flap group ( $p = 0.05$ ).

There was a significant group main effect for passive vertical stiffness ( $p = 0.014$ ). Both lat flap ( $p = 0.041$ ) and implant only groups ( $p = 0.01$ ) exhibited lower passive vertical stiffness when compared to the control group (Figure 3). There were no significant group main effects for active vertical abduction or adduction stiffnesses. In the horizontal direction, there were no significant differences between the implant only and the lat flap group for the passive condition or active horizontal adduction. The lat flap group trended towards a significantly reduced active horizontal abduction stiffness ( $p = 0.064$ ).

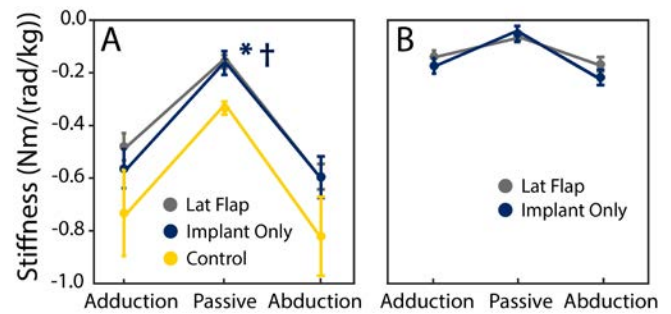


**Figure 3:** Passive and active shoulder stiffness for breast reconstructive surgery patients compared to controls when the shoulder is perturbed in the vertical (A) or horizontal (B) direction. Error bars represent SE. \*, † -  $p < 0.05$ .

Implant-based breast reconstructions significantly affects the passive integrity of the shoulder joint, which may make the joint more prone to future injury. The “lat flap” patients presented additional morbidity relative to the “implant only” patients given their reductions in vertical add/abduction and internal rotation strength. No significant changes in active shoulder stiffness were found when normalized to each patient’s strength. This suggests that other shoulder muscles may compensate for lost function from the pectoralis major or latissimus dorsi. Future studies need to longitudinally examine pre- and post-operative passive and active shoulder stiffness to better appreciate how each reconstruction surgery impacts a given breast cancer patient.

## CONCLUSIONS

Implant-based breast reconstructions negatively reduced the passive integrity of the shoulder joint.

## REFERENCES

- Jagsi et al., *J Clin Onc*, **9**:919-926, 2014
- Cemal et al., *Pl & Rec Surg*, **131**:320-6, 2013
- Koh at al., *J of Surgery*, **79**:42-7, 2009
- Hu et al., *J Neurophysiol*, **105**:1630-41, 2011
- Lipps et al, *IFAC-PapersOnLine*, **48**, 1369-74, 2015

## ACKNOWLEDGEMENTS

Supported by Susan G. Komen grant PDF15329262 and University of Michigan Comprehensive Cancer Center Fund for Discovery.

**Table 1:** Experimental group demographics

	N	Age (yrs)	Ht (m)	Wt (kg)	Days Post Reconstruction
<b>Implant Only</b>	6	49 ± 11	1.64 ± 0.04	73 ± 14	669 ± 99
<b>Lat Flap</b>	7	48 ± 7	1.62 ± 0.06	79 ± 22	754 ± 118
<b>Lumpectomy Control</b>	4	54 ± 7	1.63 ± 0.08	76 ± 8	N/A

# HUMAN-EXOSUIT INTERFACES ABSORB AND RETURN ENERGY, RESHAPING EXOSUIT TO HUMAN POWER FLOW

<sup>1</sup>Matthew B. Yandell, <sup>2</sup>Brendan T. Quinlivan, <sup>2</sup>Dmitry Popov, <sup>2</sup>Conor Walsh, and <sup>1</sup>Karl E. Zelik

<sup>1</sup>Vanderbilt University, Nashville, TN, USA

<sup>2</sup>Harvard University, Cambridge, MA, USA

email: matthew.yandell@vanderbilt.edu, web: my.vanderbilt.edu/batlab

## INTRODUCTION

Soft exosuits and rigid exoskeletons, two types of wearable assistive devices, have demonstrated the potential to improve mobility outcomes for individuals with disabilities, and to augment healthy human performance [1]. However, transmitting power from an assistive device to the human body is challenging because biological tissues and interface materials deform and displace when forces are applied, absorbing power. Inefficient device-to-human power transmission undermines the performance benefits of wearable assistive devices. Experiments on a recent running exoskeleton found that about 50% of the mechanical power provided by the device was lost in transmission to the body [2]. Although the practical difficulties of physically coupling wearable devices to the human body are well-known, only a few studies have published objective data characterizing interface dynamics [3], due partly to the lack of methods to quickly estimate these quantities. The objective of this work is two-fold: first to present a novel methodology for quickly estimating interface power during dynamic tasks using common motion capture and force measurements, and second to apply this method to quantify how a soft robotic exosuit interacts with and transfers power to the human body during locomotion.

## METHODS

We performed a motion analysis study on one healthy male subject (age: 27) wearing a soft robotic ankle exosuit (Fig. 1), similar to [4], while collecting synchronous motion capture, motor encoder, load cell, and ground reaction force data. The subject walked on an instrumented treadmill at 1.5 m/s for 5 minutes while the exosuit generated

plantarflexion assistance about the ankle using a walking controller to apply peak cable force of up to 500 N. We then performed a new biomechanical analysis to quantify exosuit-to-human power transmission using force and motion data, which enabled us to parse augmentation power (powering ankle plantarflexion) vs. interface power (due to deformation and motion of interface materials and underlying soft tissues).

## RESULTS AND DISCUSSION

We found that interface dynamics complicate the transmission of power from wearable assistive devices to the human body, resulting in three key consequences (Fig. 1): (i) During exosuit loading (as applied forces increased), about 55% of exosuit end-effector power was absorbed into the interfaces. (ii) However, during subsequent exosuit unloading (as applied forces decreased) most of the absorbed interface power was returned viscoelastically. Consequently, the majority (about 75%) of exosuit end-effector work over each stride contributed to augmenting ankle plantarflexion. (iii) Ankle augmentation power (and work) was delayed relative to exosuit end-effector power, due to these interface energy absorption and return dynamics.

## CONCLUSIONS

Physical human-device interfaces can absorb and return substantial energy, complicating power transmission. In order to optimize the performance of wearable assistive devices and fully realize their human augmentation benefits, it is important to account for these human-device interface dynamics. Here we present a new method to quantify power transmission and isolate power contributions from human-device interfaces using common force and

motion measurements, which provides insight into how to improve the design and control of wearable assistive devices.

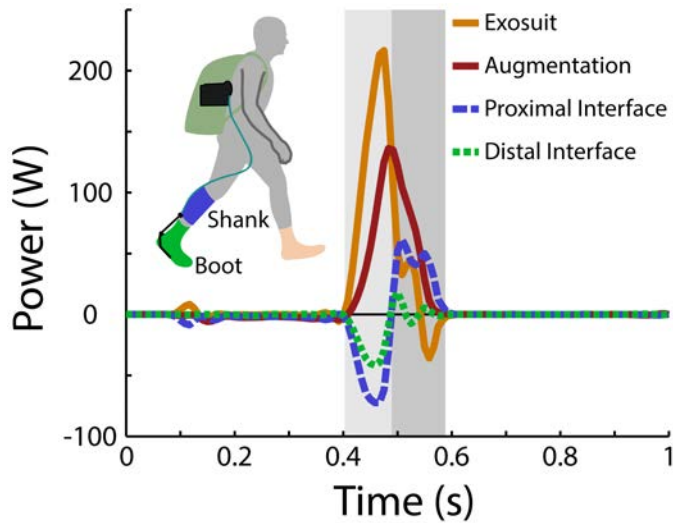


**Figure 1:** Human-exosuit interfaces absorb and return energy, reshaping exosuit to human power flow. Exosuit end-effector power (i.e., device output, orange line) contributes to motion/deformation of the proximal (shank, dashed blue line) and distal (boot, dashed green line) interfaces, and augments ankle plantarflexion (red line). Power is absorbed into interfaces during exosuit loading (as applied forces increase, light gray box), then returned during exosuit unloading (as applied forces decrease, dark gray box), contributing to ankle augmentation. Results are shown for a representative stride.

## REFERENCES

1. Dollar AM, et al. *IEEE Trans. Robot.* **24**, 144–158, 2008.
2. Cherry MS, et al. *J. Appl. Biomech*, 2015.
3. Asbeck AT, et al. *Int. J. Robot. Res.* **34**, 744–762, 2015
4. Lee S, et al. ICRA, Stockholm, Sweden, 2016.

## ACKNOWLEDGMENTS

This research is supported by the Defense Advanced Research Projects Agency (DARPA), Warrior Web Program (W911NF-14-C-0051), the National Science Foundation (CNS-1446464 and DGE1144152) & the National Institutes of Health (K12HD073945). This work was also partially funded by the Wyss Institute, the John A. Paulson School of Engineering and Applied Sciences at Harvard University, & the Vanderbilt University School of Engineering.

# HOPPING WITH A FULL-LEG EXOSKELETON LOWERS METABOLIC COST AND MUSCLE ACTIVITY

<sup>1</sup> Stephen P. Allen, and <sup>1,2</sup> Alena M. Grabowski

<sup>1</sup> University of Colorado Boulder, CO, USA; <sup>2</sup> VA Eastern Colorado Healthcare System, Denver, CO, USA  
email: stephen.allen-1@colorado.edu

## INTRODUCTION

During hopping, leg muscles consume metabolic energy to support bodyweight and modulate leg stiffness [1]. Previous studies have shown that changes in leg stiffness are primarily achieved by adjusting ankle stiffness via the plantar flexor muscles during hopping [2]. Use of an in-parallel, springy, ankle-only exoskeleton reduces metabolic demand 18% and plantar flexor muscle activity 24% when compared to hopping without assistance but equivalent mass of the exoskeleton [3]. Moreover, the use of an exoskeleton acting in parallel to the entire leg with a non-linear stiffness profile, substantially reduces metabolic demand by 24% when compared to normal hopping [4].

The underlying reason for the metabolic reduction when hopping with the full-leg exoskeleton is not fully understood. Therefore, we determined how hopping with springs in parallel to each leg affects the metabolic cost and leg muscle activity during two-legged hopping. We also determined how hopping with weight equivalent to that of the exoskeleton affected metabolic cost and muscle activity. We hypothesized that while using the exoskeleton, subjects would decrease their metabolic demands and leg muscle activity compared to normal hopping and hopping without assistance but with added weight equal to that of the exoskeleton.

## METHODS

9 healthy recreational runners [4M, 5F; Avg(SD): 23(6) yrs; 64.3(6.8) kg] gave written informed consent. Subjects hopped in place on both feet at 2.2, 2.4, 2.6, 2.8, 3.0, and 3.2 Hz to the beat of a metronome during 4 experimental sessions. Each session was performed at the same time of day, and separated by at least 2 days to account for potential fatigue effects. During sessions 1-3, subjects hopped without an exoskeleton (NORM), with the exoskeleton (EXO), and without the exoskeleton but

with weight (WT) equal to that of the exoskeleton (57.9 N). All trials were 5 min, with at least 3 min rest between trials. We measured rates of oxygen consumption and carbon dioxide production (Cosmed K4b<sup>2</sup>, IT) throughout each trial, averaged rates for the last 2 min [4], and calculated net metabolic power (NMP) using a standard equation [5].

During session 4, subjects hopped for 1 min at all frequencies and conditions while we simultaneously collected vertical ground reaction forces (GRFs) (AMTI, Watertown, MA), and surface electromyography (EMG) from the soleus (SO), medial gastrocnemius (MG), lateral gastrocnemius (LG), and rectus femoris (RF) muscles of the right leg (Delsys, Boston, MA) at 1080 Hz.

We used a custom Matlab (Mathworks, Natick, MA) program to determine ground contact events using a 10N vertical GRF threshold and calculate muscle activity. Raw EMG data were bandpass filtered (10-499Hz), rectified, and root-mean-squared with a 50 ms moving window. We analyzed 15 consecutive hops from each trial. For each muscle, we normalized each trial to the maximum of the subject hopping at 2.2 Hz NORM. We calculated whole hop cycle integrals (iEMG) of the normalized EMG for each subject using trapezoidal integration. Onset/offset threshold was established using the average plus 3 standard deviations of clear periods of inactivity as determined by visual inspection [6]. We used a one-way ANOVA to test for significant differences between conditions at each hopping frequency, and performed post-hoc t-tests when applicable. Significance was set to  $p = 0.05$ .

## RESULTS AND DISCUSSION

During EXO trials, average NMP decreased by 16% across all frequencies compared to NORM hopping. Whereas during WT trials average NMP increased

by 15% compared to NORM at 2.4 to 2.8, and 3.2 Hz (Fig 1).

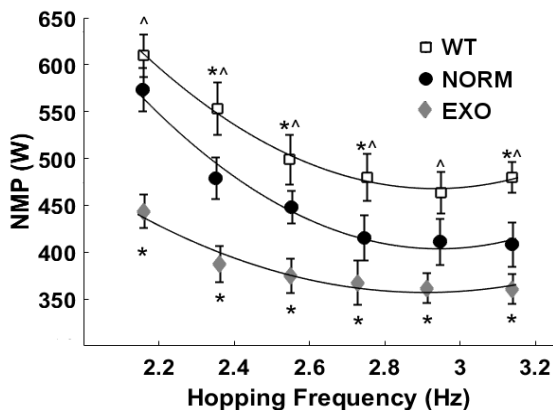


**Figure 1.** Average ( $\pm$  SEM) net metabolic power (NMP) at average hopping frequencies. \*indicates significantly different from NORM ( $p < 0.05$ ). ^indicates significantly different from EXO ( $p < 0.001$ ).

During EXO trials, average MG iEMG decreased by 18% compared to NORM across all frequencies (Fig 2), and average LG iEMG decreased by 20% compared to NORM across 2.6 to 3.2 Hz. In general, MG and LG iEMG during the WT condition were not significantly different than NORM. However, there was one significant difference at 3.2 Hz, where LG iEMG was 11% lower than NORM. There were no significant changes in SO and RF iEMG between conditions.

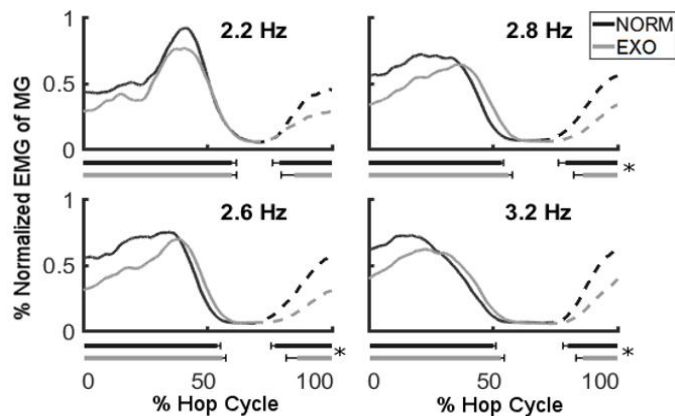


**Figure 2.** Normalized MG EMG group ensemble. Horizontal bars represent average ( $\pm$  SEM) onset/offset timing. \*indicates significantly different onset timing from NORM ( $p < 0.05$ ).

During the EXO conditions, average MG onset timing occurred 9% later in the hop cycle compared to NORM across 2.6 to 3.2 Hz (Fig. 2) and average LG onset timing occurred 7% later in the hop cycle

compared to NORM across 2.8 to 3.2 Hz. Average MG and LG onset timing did not differ in the WT condition compared to NORM, except for 3.2 Hz when LG onset timing occurred 3% later in the gait cycle.

In accordance with previous results [4], we found that use of a full-leg, springy exoskeleton reduces NMP at multiple hopping frequencies compared to NORM, whereas the WT condition increased NMP compared to NORM. However, contrary to our hypothesis, only MG and LG had reduced iEMG during EXO hopping, which could explain the decrease of NMP in the EXO compared to NORM conditions. Previous work found reductions in SO iEMG with an ankle-only exoskeleton [3]; however, the full-leg exoskeleton had no significant effect on SO iEMG. Ensemble plots of the SO EMG depict a visible trend of a reduction within the stance phase of the EXO condition as compared to NORM, but this was not significant.

MG and LG are activated during the aerial phase prior to ground contact during all conditions. However, the EXO condition has a visibly reduced LG and MG EMG during the aerial phase that are not present in NORM or WT. In fact, there were no iEMG or timing differences between WT and NORM. It is likely that subjects may have altered body position, adopted different hopping strategies, or recruited other muscles not analyzed in this study for the WT condition. Further analysis is needed to understand the mechanism responsible for the increase in NMP while hopping with added weight.

## CONCLUSION

Using a full-leg, springy exoskeleton during hopping requires much less metabolic energy than normal hopping, which is likely due to reduced MG and LG muscle activity. In contrast, weighted hopping without an exoskeleton increases metabolic cost, but elicits no change in MG, LG or SO muscle activity.

## REFERENCES

1. Farley C & Morgenroth D. *J Biomech* **32**, 267-273
2. Hobara H, et al. *Neurosci Lett* **418**, 55-59
3. Farris DJ & Sawicki GS. *J Appl Physiol* **113**, 1862-1872
4. Grabowski AM & Herr HM. *J Appl Physiol* **107**, 670-678
5. Brockway JM. *Hum Nutr Clin Nutr* **41**: 463-471
6. DiFabio RP. *Phys Ther* **67**, 43-48

# TUNED OR NOT? ULTRASOUND MEASUREMENTS OF SOLEUS FASCICLE DYNAMICS DURING HUMAN WALKING WITH ELASTIC ANKLE EXOSKELETONS

Taylor J.M. Dick, Richard W. Nuckols, Gregory S. Sawicki

Joint Department of Biomedical Engineering, North Carolina State University and University of North Carolina-Chapel Hill, NC, USA  
email: tjdick@ncsu.edu

## INTRODUCTION

Biologically inspired robotic devices assisting the ankle joint have the potential to augment healthy locomotion [1] and restore impaired neuromuscular deficits as a result of age or disease [2]. Most efficacy studies focus at most on whole body and joint level dynamics, but to date we have a limited understanding of how these devices alter the underlying muscle-tendon behaviour in walking.

Previous work done in our lab has shown that at intermediate stiffnesses, passive ankle exoskeletons reduce the energetic cost of walking by up to 7% [1]. However, at stiffnesses below or above this optimal value metabolic demands are greater than unassisted walking. We theorize that these aforementioned changes in metabolic cost due to stiffness are directly linked to the underlying muscle-tendon dynamics [3]. In this study, we aimed to determine how elastic ankle exoskeletons affect joint mechanics and plantarflexor fascicle dynamics in relation to metabolic cost during human walking. We hypothesized that the stiffest ankle exoskeletons ‘de-tune’ muscle force-length behaviour and offset the benefits of decreased muscle force, leading to suboptimal improvements in metabolic cost. Specifically, we hypothesized that a reduction in the

plantarflexor force requirements would result in a compensatory increase in soleus fascicle lengths due to the decreased stretch of the series elastic element (Achilles tendon).

## METHODS

Eleven subjects (7M, 4F; mean: 27.5y; 74.2kg) completed the IRB approved protocol. We used an exoskeleton emulator to apply a range of ankle exoskeleton rotational stiffnesses ( $k_{\text{exo}}$ ) to the user (0, 50, 100, 150, 250  $\text{Nm rad}^{-1}$ ). The emulator provided torque from benchtop motors to bilateral ankle exoskeletons through a Bowden cable transmission while subjects walked on an instrumented treadmill at  $1.25 \text{ m s}^{-1}$  (Fig. 1A). A torque-angle relationship was imposed to emulate rotational stiffness at the ankle. Following an initial training day, we collected a comprehensive set of kinetic (Bertec), kinematic (Vicon), B-mode ultrasound (Telemed), EMG (Biometrics), and metabolic data (OxyCon Mobile). We performed inverse dynamics analysis (Visual3D) to determine joint moments. Soleus ultrasound images were analyzed [4] to determine time-varying fascicle lengths during walking at the five exoskeleton stiffnesses. We performed an ANOVA to test the effect of  $k_{\text{exo}}$  on soleus fascicle length during walking.

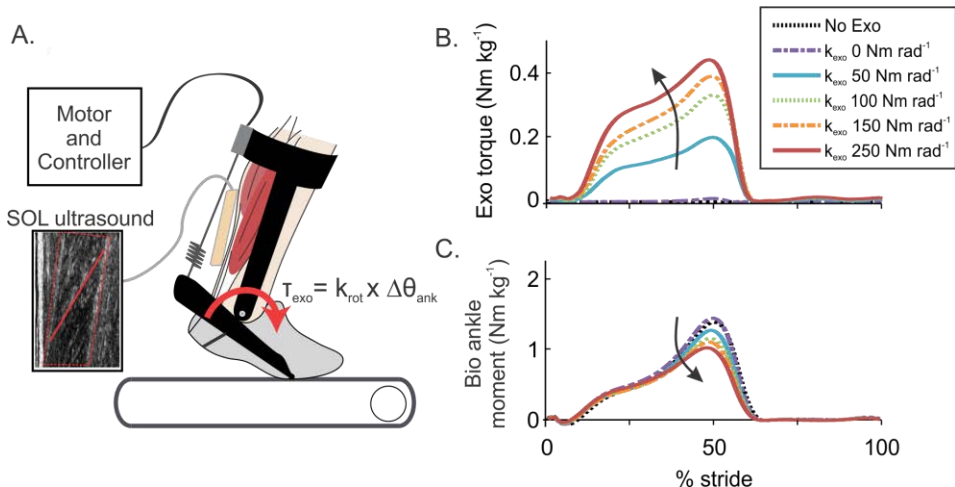


**Figure 1:** (A) Experimental setup. During exoskeleton assisted walking at five stiffnesses, we imaged soleus (SOL) fascicles using B-mode ultrasound. (B) Exoskeleton torque increased with spring stiffness ( $k_{\text{exo}}$ ). (C) Biological contributions to the ankle moment, averaged across the 11 subjects and normalized to body mass, decreased with increased exoskeleton stiffness.

## RESULTS AND DISCUSSION

Exoskeleton torque increased with exoskeleton stiffness ( $k_{exo}$ ) and resulted in a concomitant decrease in the biological ankle moment (Fig. 1 B/C). Compared to the no assistance condition ( $0 \text{ Nm rad}^{-1}$ ), the stiffest exoskeleton condition ( $250 \text{ Nm rad}^{-1}$ ) reduced the peak biological plantarflexion moment by 29%. Increases in  $k_{exo}$  were also accompanied by a reduction in ankle range of motion and therefore total muscle-tendon unit (MTU) length changes. Range of motion decreased from  $-17.7$  to  $15 \text{ deg.}$  at  $0 \text{ Nm rad}^{-1}$  to  $-7.3$  to  $14.3 \text{ deg}$  at  $250 \text{ Nm rad}^{-1}$  which translates to, on average, a 7 mm reduction in MTU length change at the highest stiffness.

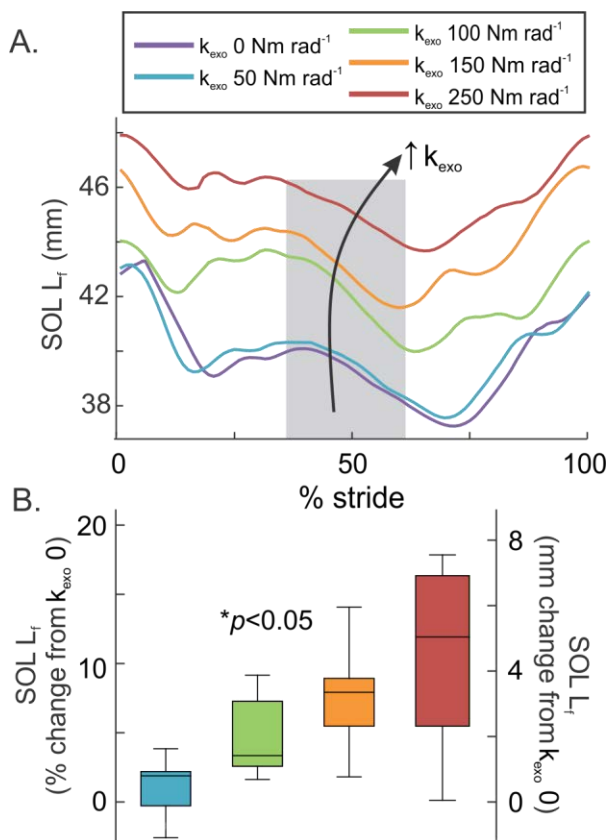


**Figure 2:** Effect of varying  $k_{exo}$  on soleus (SOL) fascicle behaviour during exoskeleton assisted walking. (A) Time-varying fascicle lengths ( $L_f$ ) for 1 subject, averaged over 5 strides and normalized to the stride period, show increases in fascicle operating lengths with increases in exoskeleton stiffness ( $k_{exo}$ ). Shaded region depicts timing of peak MTU length during the gait cycle. (B) SOL fascicle length at peak MTU length in the  $k_{exo} = 0$  condition) are shown as box and whisker plots (median, interquartile range, range) for the 11 subjects.

Despite this reduced MTU length change, and in support of our hypothesis, we found an increase in SOL fascicle length with increasing  $k_{exo}$  (Fig 2A). SOL fascicle length (determined at peak MTU length) increased from 47.5 mm during the no assistance condition ( $0 \text{ Nm rad}^{-1}$ ) to 52 mm at the highest stiffness condition ( $250 \text{ Nm rad}^{-1}$ ) when averaged across 11 subjects (Fig. 2B). This translates to an average SOL fascicle length increase of 11% when the highest exoskeleton stiffness was applied (Fig. 2B).

We found greatest reduction in metabolic cost ( $-4.2\%$  compared to no assistance) at the  $50 \text{ Nm rad}^{-1}$  condition, which coincides with the condition where SOL fascicle lengths were most similar to unassisted walking (Fig 2A). This suggests that, in young healthy adults, small amounts of added stiffness provide some metabolic benefit, but high levels of stiffness likely interfere with the normally efficient and highly tuned plantarflexor muscle-tendon interaction.

## CONCLUSIONS

Our results are consistent with [1] but we now highlight the mechanistic links between disrupted muscle-tendon dynamics and whole body energetic costs during robotically-assisted locomotion. In conclusion, we have shown that exoskeletons which are too stiff shift fascicles towards unfavorable contractile conditions. This effectively ‘de-tunes’ the plantarflexors normal muscle-tendon mechanical behaviour and is a likely contributor to negating metabolic improvements.

## REFERENCES

- Collins SH et al. *Nature* **522**, 212-215, 2015
- Takahashi KZ et al. *J Neuroeng Rehabil* **12**, 23, 2015.
- Sawicki GS & Khan NS. *IEEE Trans Biomed Eng*, **63**(5), 914-923, 2016
- Farris DJ & Lichtwark GA. *Comput Methods Programs Biomed* **128**, 111-118, 2016.

## ACKNOWLEDGMENTS

This project was funded by National Institutes of Health, National Institutes of Nursing Research Award # R01 NR014756 awarded to GSS.

# EFFECT OF SPEED ON THE MECHANICS AND ENERGETICS OF WALKING WITH AN ELASTIC ANKLE EXOSKELETON

Richard W. Nuckols, Gregory S. Sawicki

Joint Dept. of Biomedical Engineering, NCSU and UNC-Chapel Hill, Raleigh, NC, USA  
email: rwnuckol@ncsu.edu

## INTRODUCTION

Our previous research indicates that bilateral elastic ankle exoskeletons with intermediate stiffness springs placed in parallel with the human calf-Achilles' tendon complex reduce the metabolic demand during level walking at 1.25 m/s by 7% [1]. However, whether this same parallel stiffness is optimal at other walking speeds has yet to be determined. Previous work suggests that the quasi-stiffness of the ankle in able-bodied subjects increases with increasing walking speed [2], thus we theorized that optimal stiffness of assistive devices should scale with walking speed.

We hypothesized that 1.) an optimal ankle exoskeleton stiffness exists for each speed, where metabolic demand is reduced relative to no assistance and 2.) as walking speed increases the optimal stiffness should also increase.

## METHODS

We recruited eleven healthy, young adults (7M, 4F; mean:27.5y, 74.2kg) to complete the IRB approved protocol over a four-day testing period. Participants walked at three walking speeds (1.25, 1.5, 1.75 m/s) while we applied five ankle exoskeleton rotational stiffness conditions ( $k_{exo}$ =0, 50, 100, 150, 250 Nm/rad). We delivered mechanical assistance using a custom exoskeleton emulator consisting of bilateral ankle exoskeletons driven by a benchtop motor and transmission, using a control system that imposed a torque-angle relationship to emulate an elastic device providing rotational stiffness.

The order of the four testing days, the purpose, and measurements collected were:

1. Training – 95 minutes (Metabolic Demand)
2. Gait Mechanics (Inverse Dynamics, EMG, B-Mode Ultrasound of Soleus)
3. Steady State Metabolic Demand
4. Stiffness Sweep (Instantaneous Metabolic Demand)

We recorded kinematics using reflective markers (Vicon), muscle activity in the medial and lateral gastrocnemii, soleus, and tibialis anterior using surface EMG (Biometrics), soleus fascicle lengths using B-mode ultrasound (Telemed), and whole body metabolic power with indirect calorimetry (OxyCon Mobile).

We performed a mixed-model ANOVA with a first ( $k_{exo}$ ) and second order term ( $k_{exo}^2$ ) to determine the effect of exoskeleton stiffness on metabolic demand. We then ran a post-hoc pairwise t-tests at each speed to compare the condition that yielded the largest reduction in metabolic cost against the no assistance condition ( $p < 0.05$ ).

## RESULTS AND DISCUSSION

For all walking speeds, exoskeleton torque increased and biological ankle moment decreased with increasing exoskeleton stiffness (Fig 1A). Compared to the no assistance condition (0 Nm/rad), for the stiffest condition (250 Nm/rad) we observed a reduction in average (peak) biological moment of -11% (-29%) at 1.25 m/s, -9% (-22%) at 1.5m/s, and -8% (-22%) at 1.75 m/s. Interestingly, in early stance (0-40%) exoskeleton assistance enhanced total ankle moment while biological moment decreased only slightly. Conversely, in late stance (40-60%) the exoskeleton primarily offset the biological contribution and total ankle moment remained nearly constant or decreased slightly. These changes in ankle joint mechanics were accompanied by systematic decreases in soleus muscle activation across all exoskeleton conditions at all speeds (Fig 1B). At the stiffest condition, we observed on average across speeds a reduction of 17% in integrated soleus EMG during stance phase of walking.

Across speeds, we observed a decrease in relative exoskeleton contribution as walking speed increased. From the slowest to the fastest walking speed, peak

exoskeleton torque decreased by 20% at the highest stiffness despite a 12% increase in peak total ankle torque. This reduction in exoskeleton assistive torque is explained by a decrease in peak ankle dorsiflexion with increased walking speed, suggesting that efficacy of passive devices may be limited by natural ankle joint kinematics especially at fast walking speeds.

Exoskeletons reduced metabolic cost of walking only at the slowest (-4.2% at 1.25 m/s) and fastest (-4.7% at 1.75 m/s) walking speed, and the optimal stiffness did not increase with speed (50 Nm in each case) (Fig 1C). Surprisingly, for walking at 1.5 m/s, exoskeletons increased metabolic cost across all stiffness conditions.

## CONCLUSIONS

Currently we are analyzing ultrasound images of the soleus muscle captured for each stiffness and speed. These data may provide insight into how exoskeletons can disrupt ‘tuned’ ankle dynamics and counteract decreases in biological force and activations offsetting potential metabolic benefits. We are particularly interested in the changes in muscle mechanics at the intermediate speed where we were unable to achieve a reduction in metabolic demand.

The most compliant spring proved effective at both the slowest and fastest, but not the intermediate

walking speed. However, the exoskeleton did not respond to added demands of faster walking in a manner similar to that of biological plantarflexors. Counter to our hypothesis, the optimal elastic ankle exoskeleton spring stiffness did not increase with walking speed.

The metabolic reductions we report here (~5%) still do not approach reductions seen in the most successful active devices (~23%) [3]. Despite this, passive devices remain advantageous given their minimal weight and simplified design in comparison to active systems. In fact, our results suggest that a single compliant exoskeleton spring can achieve metabolic reductions across a range of walking speeds. Furthermore, elastic systems, like the one tested here, may simplify prescription of devices intended to restore structural stiffness to joints in specific populations (*e.g.* older adults).

## REFERENCES

- Collins SH, Wiggin MB, Sawicki GS. *Nature*. 2015
- Shamaei K, Sawicki GS, Dollar AM. *PLoS One*. 2013
- Quinlivan BT et al, *Science Robotics* **2**(2): eaah4416.

## ACKNOWLEDGMENTS

This project was funded by National Institutes of Health, National Institutes of Nursing Research Award # R01 NR017456 awarded to GSS

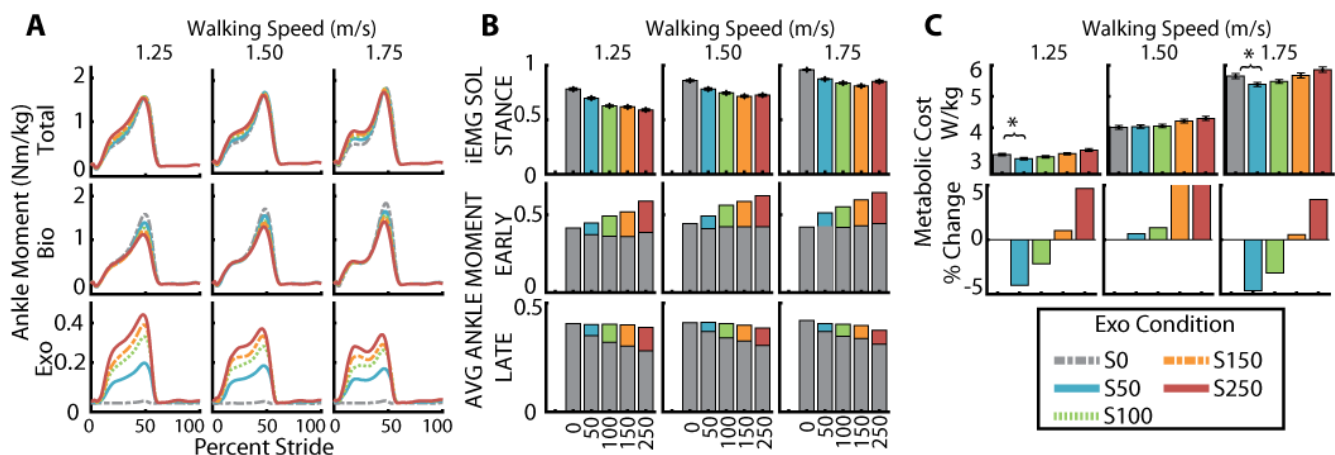


**Figure 1:** Joint dynamics, neuromuscular activation, and whole body metabolic cost changes resulting from applying exoskeleton assistance over a range of walking speeds. **A:** Total, Biological and Exoskeleton Torque **B:** Soleus integrated EMG and average biological moment. Gray bars represent biological contribution and colored bars are exo contribution. **C:** Exoskeleton assistance reduced metabolic demand at the lowest level of assistance for the slowest (1.25 m/s) and fastest (1.75m/s) walking speeds ( $p < 0.05$ ).

# EFFECTS OF ANKLE EXOSKELETON POWER AND ACTUATION TIMING ON MOVEMENT VARIABILITY AND METABOLIC COST OF WALKING

<sup>1</sup> Prokopios Antonellis, <sup>2</sup> Samuel Galle, <sup>2</sup> Jozefien Speeckaert, <sup>2</sup> Dirk De Clercq, and <sup>1</sup> Philippe Malcolm

<sup>1</sup> Department of Biomechanics and Center for Research in Human Movement Variability, University of Nebraska at Omaha, NE, USA

<sup>2</sup> Department of Movement and Sports Sciences, Ghent University, Ghent, Belgium  
email: [pantonellis@unomaha.edu](mailto:pantonellis@unomaha.edu), web: <http://coe.unomaha.edu/brb>

## INTRODUCTION

While humans use many strategies to reduce metabolic energy cost, walking still requires a considerable amount of metabolic energy. Lower extremity exoskeletons have become an established technology designed to reduce metabolic cost. However, it was suggested that they might increase the variability of the locomotor system making the system unstable [1], but optimal assistance settings for gait variability remain unclear. This could be a main concern for people with a mobility disorder.

The purpose of this study was to investigate the effect of ankle exoskeleton power and actuation timing on gait variability and examine if the optimal parameters for gait variability are the same as for metabolic energy cost of walking. We hypothesized that late push-off timing [2,3] and lower push-off work [1] would reduce gait variability.

## METHODS

Ten healthy female subjects participated in this study (age  $23 \pm 1.2$  y; weight  $61.0 \pm 4.5$  kg; height  $168.1 \pm 5.2$  cm). The bilateral exoskeleton consisted of an ankle-foot orthosis at each leg with a hinge at the ankle joint and pneumatic muscles [4].

The experiment consisted of a habituation session and a data collection session. A number of conditions were applied in each session: a Powered-Off condition ( $4.03 \text{ W}\cdot\text{kg}^{-1}$ ), in which subjects walked with the exoskeleton but without assistance from the pneumatic muscles; and 10 powered exoskeleton conditions. The powered conditions were based on a two-dimensional parameter sweep of three actuation timings (36%, 42% and 48%) for which three exoskeleton power levels were applied ( $0.21 \text{ W}\cdot\text{kg}^{-1}$ ,  $0.41 \text{ W}\cdot\text{kg}^{-1}$  and  $0.50 \text{ W}\cdot\text{kg}^{-1}$ ) and a fourth actuation

timing (54%) for which only one power level was applied were used. In the habituation session, subjects learned to walk with the exoskeleton and became accustomed to the experimental set-up. They walked in all powered conditions and the Powered-Off condition on the treadmill at  $1.25 \text{ m}\cdot\text{s}^{-1}$ . Experimental data were collected on a separate day. Each subject performed the same walking protocol as in the habituation session, and all conditions lasted for four minutes.

Subjects wore a face mask connected to a gas analysis system (Cosmed). Exoskeleton sensor data (foot switches, displacement sensors and load cells) was acquired continuously during the entire experiment. Full body 3D kinematics were recorded using 14 infrared cameras (200 Hz; Qualisys).

We quantified the metabolic energy cost of walking based on  $\text{O}_2$  consumption and  $\text{CO}_2$  production during the last two minutes of each condition using a standard equation [5]. Net metabolic cost was calculated by subtracting the metabolic cost of standing at rest from gross metabolic cost during walking and was normalized to body weight.

We quantified the pattern of stride-to-stride fluctuations of the ankle angle kinematics using the largest Lyapunov Exponent [6]. An increase in the largest Lyapunov Exponent indicates higher divergence in the stride pattern (i.e., increased amount of variability), whereas a decrease indicates lower divergence (i.e., reduced amount of variability).

## RESULTS AND DISCUSSION

The Lyapunov Exponent of all powered conditions was lower than that in the Powered-Off condition ( $4.03 \pm 0.74 \text{ W}\cdot\text{kg}^{-1}$ ) (Fig 1). The lowest Lyapunov

Exponent was determined when assistance was achieved at  $48 \pm 1\%$  of the stride and average power of  $0.50 \pm 0.06 \text{ W}\cdot\text{kg}^{-1}$ . These results are different from what was found in a previous study [1] since we found that movement variability was lower during walking with the exoskeleton active.

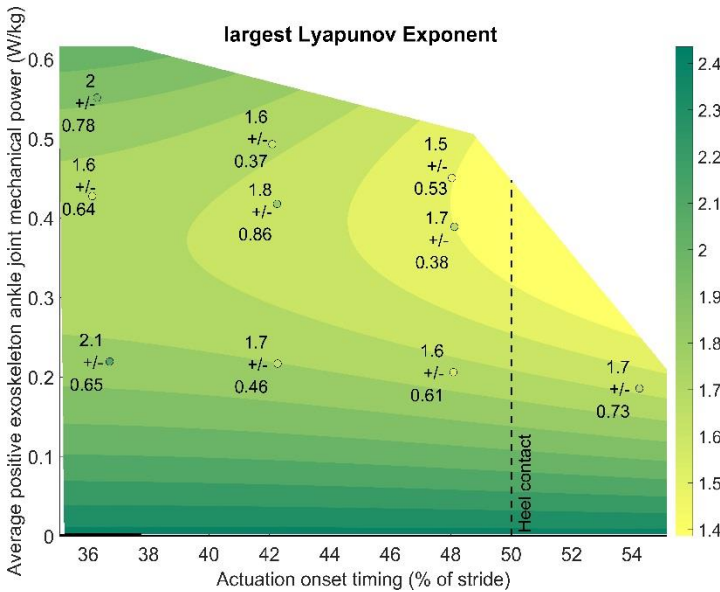


**Figure 1:** largest Lyapunov Exponent for ankle exoskeleton motion across different conditions. largest Lyapunov Exponent is depicted versus actuation timing and average positive exoskeleton power.

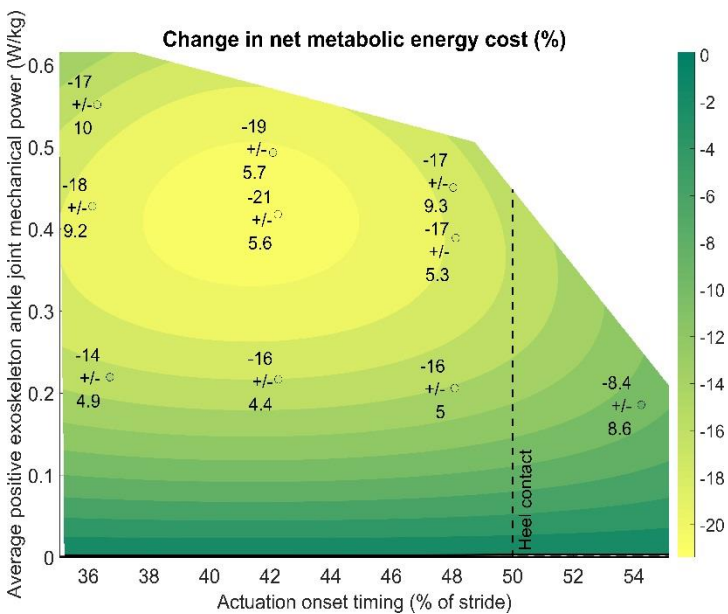


**Figure 2:** Net metabolic energy cost. Net metabolic cost is depicted versus actuation timing and average

positive exoskeleton power. Metabolic cost for the powered exoskeleton conditions is expressed as the reduction versus the Powered-Off condition.

The lowest net metabolic cost was observed when assistance was achieved at  $42 \pm 0.8\%$  of the stride and average power of  $0.4 \pm 0.03 \text{ W}\cdot\text{kg}^{-1}$ , with a reduction of  $21 \pm 5.6\%$  compared to Powered-Off ( $4.03 \pm 0.74 \text{ W}\cdot\text{kg}^{-1}$ ) (Fig. 2). These optimal settings for metabolic cost are different from the optimal settings for reducing variability.

## CONCLUSIONS

We found settings that resulted to a more stable locomotor system and settings that resulted to a 21% reduction in metabolic cost compared to walking with the exoskeleton while inactive. We will apply mixed-model ANOVA to draw clear conclusions about the effects of ankle exoskeleton power and actuation timing on gait variability and metabolic energy cost. Our findings may be broadly applicable to enhance our understanding of the role/ability of lower limb exoskeletons to maintain balance and prevent falls, as well as gaining new insights for optimizing exoskeleton actuation settings to provide a more stable and metabolic efficient human locomotor system.

## REFERENCES

1. Norris JA, et al. *ASME*, 1619-1626, 2007
2. Malcolm P, et al. *J Neuroeng Rehabil* **12**, 2015
3. Bhounsule PA, et al. *Int J Robot Res* **33**, 2014
4. Malcolm P, et al. *PLoS ONE* **8**, 2013
5. Donelan JM, et al. *Proc. R. Soc. London B*, 2001
6. Wurdeman SR, et al. *PLoS ONE* **9**, 2014.

## ACKNOWLEDGMENTS

This study was funded by the Special Research Fund of Ghent University (BOF10/DOC/288). The authors would like to thank Davy Spiessens for the technical support, Ms. Pieter Van den Berghe for his assistance in the data collection, Dr. Brian Knarr for providing the Lyapunov code and feedback on the abstract, and the company Aqtor! (Ghent, Belgium) for their assistance in manufacturing the exoskeleton.

# A UNILATERAL ANKLE ASSISTING SOFT ROBOTIC EXOSUIT CAN IMPROVE POST-STROKE GAIT DURING OVERGROUND WALKING

Lizeth H. Sloom<sup>1,2</sup>, Babak Hejrati<sup>1,2</sup>, Pawel Kudzia<sup>1,2</sup>, Jaehyun Bae<sup>1,2</sup>, Katy Hendron<sup>2,3</sup>, Kathleen O'Donnell<sup>2</sup>, Kenneth G. Holt<sup>3</sup>, Terry Ellis<sup>3</sup>, Louis N. Awad<sup>2,3</sup> and Conor J. Walsh<sup>1,2</sup>

<sup>1</sup> Harvard John A. Paulson School of Engineering and Applied Sciences, Cambridge MA USA

<sup>2</sup> Wyss Institute for Biologically Inspired Engineering, Boston MA USA

<sup>3</sup> Boston University, Boston MA USA

email: walsh@seas.harvard.edu, Web: biodesign.seas.harvard.edu

## INTRODUCTION

Stroke is the leading cause of long-term disability, often resulting in a slow and energetically inefficient gait due to a reduction in push-off power at the end of stance and the inability to lift the foot from the ground during swing (i.e. foot clearance). To improve the quality of life of stroke patients, a soft wearable robot (exosuit) has been developed, which has demonstrated the capacity to improve paretic propulsion, foot clearance and walking efficiency during treadmill walking [1,2].

The long term vision for the exosuit is that it can be used for overground gait training and to improve gait in a community setting. However, it is well known that stroke patients' ambulatory ability on the treadmill and overground are different [3,4]. During overground walking, there is an increase in gait variability due to a lack of an imposed speed, a less restricted walking area and more visual distractions. It is currently unknown if the same benefits observed on the treadmill would be seen during overground walking. Therefore, the objective of this study was to determine if the soft exosuit can improve push-off and foot clearance in patients post stroke during overground walking.

## METHODS

Nine patients with hemiparetic stroke (4 F, 49±13y, time since stroke 4±2y) walked overground at preferred walking speed. They wore a soft robotic ankle-assisting exosuit (Fig. 1) that was designed to transmit assistive forces from a specially designed lightweight body worn actuation system (3.2 kg) to the shank-mounted textile. The soft exosuit provided

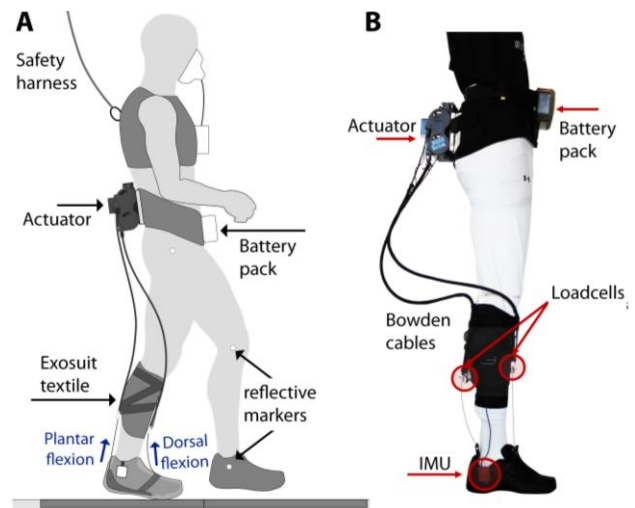


Fig. 1: Experimental setup (A) and exosuit components (B)

ankle plantarflexion assistance during push-off (peak applied force of 25% bodyweight) and ankle dorsiflexion assistance to achieve at least a neutral angle during swing phase [1,2].

Ground reaction forces (ground embedded force plates, AMTI, Watertown, MA) and kinematics (motion capture system, VICON, Oxford, UK) were measured. To understand the effect of exosuit assistance, subjects first walked with it unpowered, followed by a powered exosuit condition. Subjects walked until at least 5 strides were captured per condition with good landing on the force plate.

The propulsion impulse (i.e. the integral over the propulsion force), peak ankle torque during stance, average positive and negative ankle power during second double support, and maximal ankle dorsiflexion during swing and at initial contact were calculated for both the paretic and non-paretic leg. Conditions were compared on a group level using paired t-test (significance set at  $p < 0.05$ ).

## RESULTS AND DISCUSSION

On the paretic side, walking with the powered exosuit improved push-off (Fig. 2). We observed a 14.0% increase in propulsion impulse ( $p=0.03$ ), a 24.5% increase in average positive ankle power ( $p=0.04$ ) and a 41.3% decrease in average negative ankle power ( $p=0.006$ ). The powered exosuit also assisted foot clearance during swing and foot placement on the paretic side in terms of a  $5.2^\circ$  increase in maximal ankle dorsiflexion during swing ( $p=0.002$ ) and a  $4.9^\circ$  increase at initial contact ( $p=0.003$ ). No differences were found for the peak paretic ankle torque or any of the variables from the non-paretic leg (Fig. 3).

These results are similar to our prior work with a tethered soft exosuit that was shown to improve push-off and foot clearance during treadmill walking [1,2]. Taken together, these results suggest that soft wearable exosuit is able to assist post-stroke patients in different walking conditions. Moreover, it provides encouraging evidence that the exosuit technology is able to correctly identify gait events and timely assist paretic ankle deficits during the more variable overground walking.

Overall, the results support the suitability of the exosuit for common overground gait training. Given

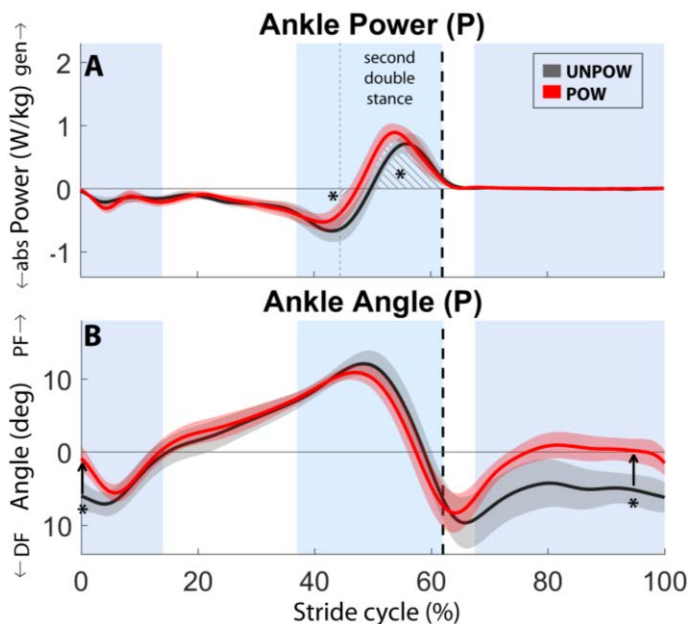


**Fig. 2:** Ankle power (A) and angle (B) for the paretic (P) limb. Mean values, standard error, toe off (dashed vertical line) and timing of support (plantar flexion support: light blue shade; dorsiflexion: blue shade) are indicated.

the known heterogeneity of stroke patients, the wearable exosuit provides exciting opportunities for subject specific gait training, with the potential of tuning the level of assistance to *a patient's* progress.

## CONCLUSIONS

This study demonstrates the capability of a body worn exosuit that targets the paretic ankle to assist push-off and foot clearance in post-stroke patients during overground walking. This builds on past work that demonstrated similar capabilities during treadmill walking. These results are an important step in evaluating and optimizing a wearable soft exosuit for overground gait training in stroke patients and in translating the technology to community-based use. Moreover, we expect that the exosuit can also similarly benefit patients with other gait deficits and neurological disorders.

## REFERENCES

1. Bae J. *IEEE Int. Conf. Rehabil. Robot*, Singapore, Singapore 2015
2. Awad LN, et al. *submitted to Sci Transl Med*, 2016
3. Brouwer B. et al. *Clin Biomech* **24**, 729-734, 2009
4. Harris-Love ML et al. *Neurorehabil Neural Repair* **15**, 105-112, 2001

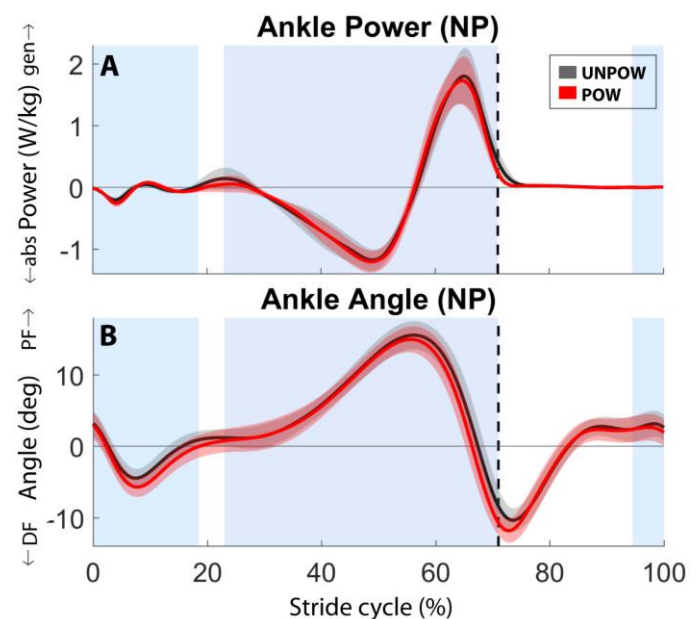


**Fig. 3:** Ankle power (A) and angle (B) for the non-paretic (NP) limb. For explanation see caption of Fig. 2.

# A Mechanical Role for Incompressible Fluid in Stretched Muscle

<sup>1</sup> David A. Sleboda and <sup>1</sup> Thomas J. Roberts

<sup>1</sup> Brown University, Providence, RI, USA  
email: david\_sleboda@brown.edu

## INTRODUCTION

Muscles maintain a constant volume of intracellular fluid. This fluid plays an important role in facilitating normal biochemical function, but its role in determining the biomechanical properties of muscle have been considered in only a few theoretical analyses.

We investigate the mechanical role of fluid within muscle using a combination of physical modelling and experiments on live, isolated skeletal muscle. We test the hypothesis that incompressible muscle fibers can limit reorientation of muscle's extracellular matrix, influencing the passive force produced during stretch.

## METHODS

Passive length-tension profiles for bullfrog semimembranosus muscles were measured before and after increasing intracellular fluid volume. Muscle fluid volume was altered by soaking in dilute, hypotonic physiological Ringer's solution for 1 hour. This allowed movement of fluid from bath to muscle via osmosis. Muscle volume increase was confirmed via separate measurements of muscle weight.

Isolated muscles were clamped at one end to a rigid post and at the other to a force and length-transducing servomotor (Aurora 310 B-LR). Passive tension was recorded at a series of static muscle lengths before and after volume increase. Active length-tension curves were collected prior to measurement of passive tension. All lengths were normalized to the length at maximal force production ( $L_0$ ) and all passive forces were normalized to the passive force produced at 115%  $L_0$  in the isotonic condition.

The mechanical response of muscle to increased internal volume was compared to that of a simple physical model composed of a fluid-filled bladder ensheathed in helical, cross-hatched fibers. The helical sheath represented muscle's collagenous extracellular matrix while the bladder represented a volume of incompressible muscle fibers. Tension produced by the model in response to stretch was measured before and after bladder volume was increased in simulation of the osmotic perturbation applied to muscle.

The effect of volume increase on passive muscle and the physical model were compared. Pre- and post-perturbation length-tension curves were log-transformed so that their shapes could be characterized by slope. The locations of log-transformed curves within the coordinate plane were also compared using the statistical tool SMATR.

## RESULTS AND DISCUSSION

Increasing muscle volume by 40% resulted in 69% increased tension across all muscle lengths studied (fig. 1). The slopes of log-transformed lines for muscle were not significantly different before and after the osmotic perturbation, indicating that increases in tension occurred via a change in the zero-force length, or rest length, of the muscles, rather than by a change in the form of their length-tension curves. Significant differences in the location of the curves within the coordinate plane revealed by the statistical tool SMATR confirmed this interpretation.

The physical model displayed muscle-like length-tension properties which arose from the interaction of the helical sleeve and the fluid-filled bladder. Increasing the internal fluid volume of the fluid

bladder shifted the zero-force length of the model in a manner identical to that described for muscle.

horizontal axis in the untransformed data. Adapted from [1].

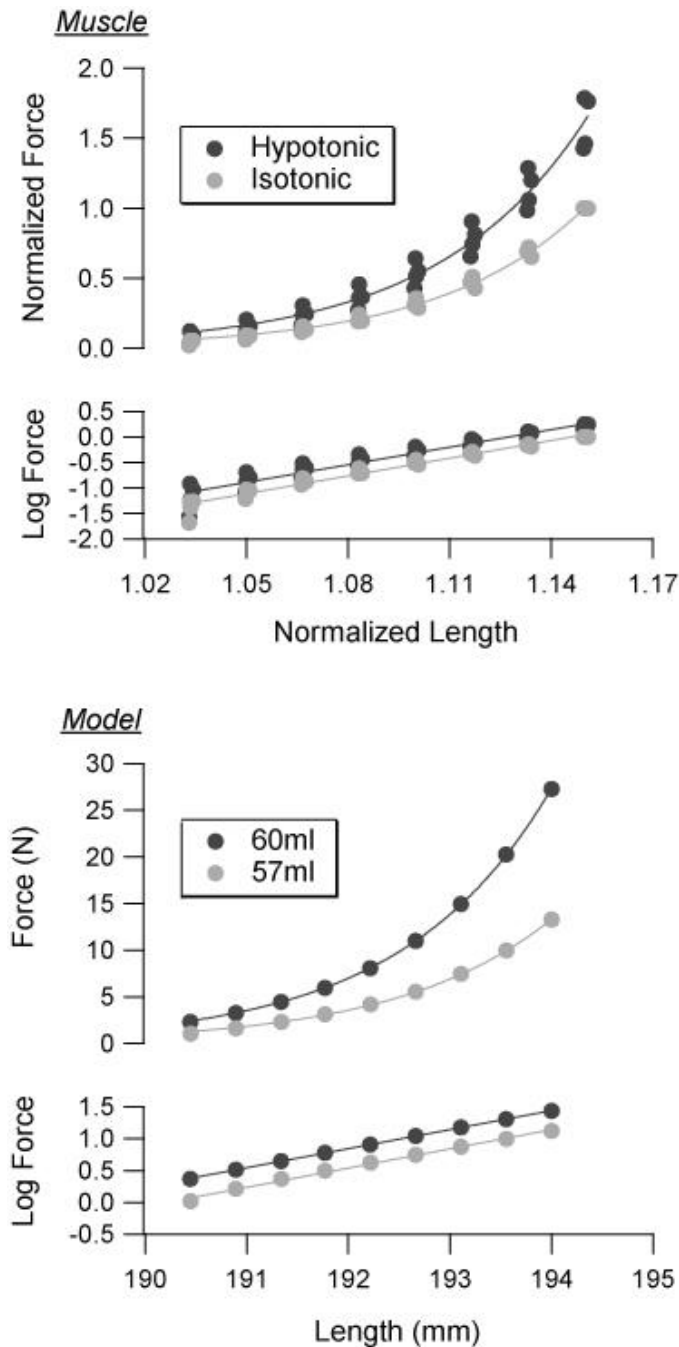


**Figure 1:** Tension produced by passive muscle (n=4) and the physical model before and after fluid volume increase. In both, volume increase caused a vertical shift in the log-transformed length-tension relationship without a significant change in slope. This is the equivalent of a leftward shift along the

Geometric analysis of the model revealed that the volume of space available within the sleeve decreased as a function of length. This occurred as the comprising fibers became aligned with the long axis of the model. Large increases in model tension with stretch occurred only once the internal volume of the helical sleeve approached the constant, incompressible volume of the fluid-filled bladder. At this length, reorientation of the sleeve was inhibited by the incompressible bladder, and further lengthening was made more difficult. We suggest that a similar mechanism contributes to the highly non-linear length tension profile of passively stretched muscle. At short muscle lengths, reorientation of collagen fibers allows the tissue to extend at low stress, but at long lengths this motion is inhibited by the incompressibility of muscle fibers.

## CONCLUSIONS

Our results indicate that fluid acts as a mechanical component of muscle, influencing the passive tension generated in response to stretch. Alterations to muscle fluid volume are shown to alter passive tension, and this same behavior is replicated by a simple physical model of muscle morphology. Our results provide empirical support for existing mathematical models of muscle which incorporate incompressible fluid into their design [2,2], and suggest that activities or pathologies that alter muscle fluid content will influence muscle mechanics.

## REFERENCES

1. Sleboda DA and Roberts TJ. *Biol. Lett.* **13**, 2017.
2. Purslow PP. *J. Biomech.* **22**, 21-31, 1989.
3. Gindre J, et al. *J. Mech. Behav. Biomed. Mater.* **22**, 84-94, 2013.

# Intramuscular Pressure Variability Differs from Force Variability during Ramped Isometric Contractions in Healthy Adults

<sup>1</sup> Brenda L. Davies, <sup>2</sup> Shanette Go, <sup>3</sup> William Litchy, and <sup>1</sup> Kenton R. Kaufman

<sup>1</sup> Department of Orthopedic Surgery, Mayo Clinic, Rochester, MN, USA

<sup>2</sup> Mayo Clinic Medical Scientist Training Program, Mayo Clinic, Rochester, MN, USA

<sup>3</sup> Department of Neurology, Mayo Clinic, Rochester, MN, USA

email: [davies.brenda@mayo.edu](mailto:davies.brenda@mayo.edu)

## INTRODUCTION

Variability is inherent within all biological systems. Human movement appears to have an optimal amount and structure (temporal organization) of variability and disease states tend to cause deviations from this point [1]. It has been suggested that the structure of variability provides insight into system organization and motor control. Previous studies have demonstrated that the structure of force variability is altered in healthy, older adults and individuals with disease, which led investigators to suggest analysis of variability may be applied as a diagnostic biomarker [1-3]. However, the analysis of force variability is currently limited because it only provides a global understanding of skeletal muscle mechanics when measured with conventional clinical tools. Quantification of individual muscle force can refine our understanding of musculoskeletal mechanics and motor control.

Intramuscular pressure (IMP) is the fluid pressure generated within skeletal muscle and is a direct reflection of individual muscle tension [4]. Measurement of IMP has the potential to advance innovative strength assessment techniques. Currently, the variability of IMP is not well characterized. Therefore, the purpose of this investigation was to characterize the structure of the IMP variability during ramped isometric contractions. We hypothesized that the IMP variability would be less than the force variability and that this variability would have a less regular time series structure compared to force variability.

## METHODS

**Subjects:** Sixteen healthy adults (6 females; mean  $\pm$  SD age:  $42 \pm 18.9$  years; BMI:  $25 \pm 4.7$  kg/m<sup>2</sup>) with no history of neurologic or musculoskeletal disease

participated in this study after providing informed consent.

**Experimental set-up:** While subjects were supine, the right ankle was raised until the foot was perpendicular with the shank was parallel to the ground and held in that position with straps placed around the lower leg. A foot strap was secured around the metatarsals and secured to an external load cell (SM-100, Interface Inc., Scottsdale, AZ) in line with the load cell axis and perpendicular to the ankle rotation axis. A fiber optic pressure sensor (FOP-M260, FISO Technologies Inc., Quebec, Canada) was inserted into the tibialis anterior (TA) under ultrasound guidance using a 22-gauge IV catheter. The catheter was oriented toward the distal TA tendon through the skin at a 30° angle until the tip was mid-depth in the TA superficial compartment. The needle was withdrawn and the IMP sensor was advanced through the catheter lumen into the muscle. Force and IMP were simultaneously acquired (2500 Hz) using custom software (LabVIEW, National Instruments, Austin, TX).

**Protocol:** Subjects performed three maximal voluntary contractions (MVC) from which the greatest value was selected. Subjects then performed ramped isometric contractions to 50% MVC at rates of 5, 10, and 15% MVC/second guided by visual feedback. Fifteen trials were performed at each contraction rate, with at least 30 seconds of rest between trials to prevent fatigue.

**Data Analysis:** The unfiltered raw IMP and force time series from the start of force generation to peak force were analyzed using a custom MatLab program (The Mathworks, Inc., Natick, MA). The standard deviation (SD) was used to quantify the amount of

variability present in the force and IMP; a higher SD suggests that the signal has a greater amount of variability. Sample entropy (SampEn) was used to measure the regularity in the IMP and force time series [5]. A more regular time series will have a SampEn closer to zero, while a completely irregular time series will have a SampEn that approaches infinity.

**Statistical Analysis:** Separate repeated measures ANOVAs were performed in JMP software (SAS Institute Inc., Cary, NC) with an alpha value of 0.05. The rate of force development was the independent variable and the force or IMP SD and SampEn were the dependent variables for the respective ANOVA.

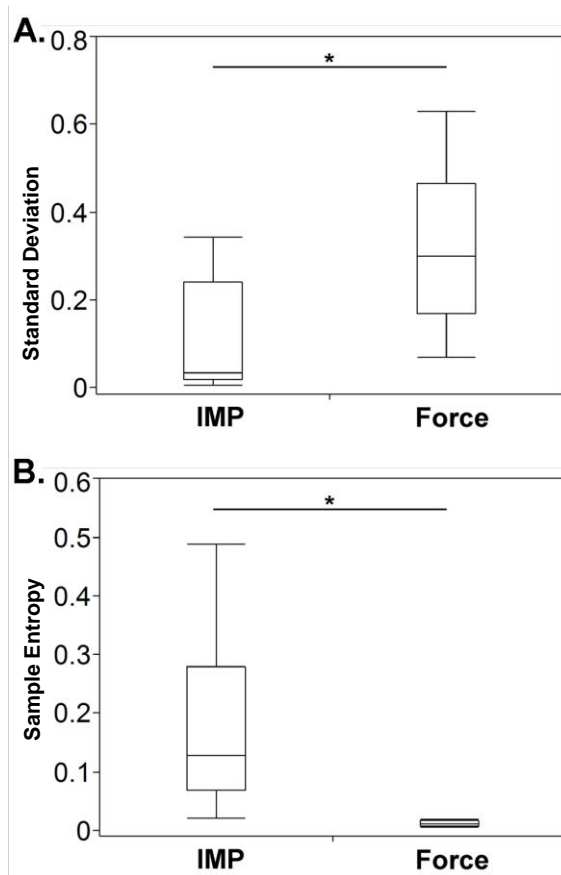


**Figure 1:** **A)** The standard deviation and **B)** sample entropy of the mechanical measure main effects during the ramped isometric contractions (N=14). \* indicates  $p < 0.05$ .

## RESULTS AND DISCUSSION

Fourteen subjects had evaluable data and were included in the final analyses. The mechanical measure main effect revealed that the force SD ( $0.35 \pm 0.13$ ) was higher than the IMP SD ( $0.11 \pm 0.25$ ;  $p < 0.001$ ; Figure 1A), suggesting that there is more variability in the force signal. For the SampEn, there was a mechanical measure main effect displaying that the IMP SampEn ( $0.19 \pm 0.16$ ) was higher than the force SampEn ( $0.01 \pm 0.01$ ;  $p < 0.001$ ). These outcomes suggest that the IMP has a less regular time series than the force. There was not a significant rate of force development main effect or interaction for both the SD and SampEn ANOVA ( $p > 0.05$ ).

These outcomes demonstrate that the IMP of healthy individuals has less variability and a more complex physiological time series signal than force. Moreover, the rate of force development did not appear to influence the SampEn or SD. These outcomes suggest that IMP is highly flexible and can adapt to task demands. Thus, since the structure of variability provides insight into system organization, IMP may be a more accurate reflection of individual muscle motor control than force. Future investigations should seek to quantify the alterations in IMP variability in populations with clinical disorders in order to determine the diagnostic capability of IMP.

## REFERENCES

1. Harbourne RT, et al. *Phys Ther* **89**, 267-82, 2009.
2. Lipsitz LA, et al. *JAMA* **267**, 1806-9, 1992.
3. Arpin DJ, et al. *Res Dev Disabil* **34**, 1134-43, 2013.
4. Winters TM, et al. *Muscle Nerve* **40**, 79-85, 2009.
5. Richman JS, et al. *Am J Physiol Heart Circ Physiol* **278**, H2039-49, 2000.

## ACKNOWLEDGMENTS

Support was provided by NIH grants R01-HD31476 (KRK) and T32-AR056950 (BLD). Any opinions, findings, conclusions, or recommendations expressed in this material are those of the authors and do not reflect the views of NIH.

# INTRAOPERATIVE MEASUREMENT OF HUMAN MUSCLE PROPERTIES

<sup>1</sup> Loribeth Evertz, <sup>1</sup> Christina Webber, <sup>2</sup> Brenda Davies, <sup>3</sup> Richard Lieber, <sup>2</sup> Alexander Shin, and <sup>2,4</sup> Kenton Kaufman

<sup>1</sup> Mayo Clinic Graduate School of Biomedical Sciences, Mayo Clinic, Rochester, MN, USA

<sup>2</sup> Department of Orthopedic Surgery, Mayo Clinic, Rochester, MN, USA

<sup>3</sup> Rehabilitation Institute Chicago, Chicago, IL, USA

<sup>4</sup> Department of Physiology and Biomedical Engineering, Mayo Clinic, Rochester, MN, USA

email: evertz.loribeth@mayo.edu, web: <http://www.mayo.edu/mayo-clinic-graduate-school-of-biomedical-sciences/programs/phd/tracks/biomedical-engineering>

## INTRODUCTION

Tendon and whole muscle transfers are conducted to restore lost motor function. Orthopedic surgeons perform a free functional muscle transfer (FFMT) of the gracilis from the lower limb to the upper limb to regain elbow flexion following an injury to the brachial plexus. The donor muscle often loses one or more grade of muscle strength in the process [1,2]. It is believed that this strength loss may be due to improper tensioning of the muscle during surgery, resulting in sarcomere lengths that are inadequate to achieve the required muscle force production [2].

To increase force production in transferred muscles, a better understanding of in vivo human muscle sarcomere length and other muscle properties are needed. Collection of gracilis muscle properties during surgery, specifically in vivo sarcomere lengths at different joint angles and the associated forces, will provide additional knowledge that may help to improve future computational models and simulations of FFMT surgeries. *We hypothesize that gracilis sarcomere length is on the descending limb of the force-length curve.*

## METHODS

For this study, data were collected during FFMT surgeries. Six subjects (1 female) with an average BMI of  $26.1 \pm 3.3$ , aged  $39 \pm 17$  years consented to participate in the study. Data were collected once the gracilis was isolated under two conditions: tendon attached and tendon transected.

*Tendon attached:* With the gracilis tendon still attached, biopsy clamps were used to collect muscle tissue samples. Joint angles were varied to achieve different muscle fiber lengths (Table 1). After tissue fixation, three fiber bundles were separated from the biopsy samples and placed on glass slides, then three laser diffraction measurements were performed to determine mean sarcomere length for each sample (n=9/sample).

**Table 1:** Joint configurations (JC) for the limb positions used to evaluate changes in sarcomere length.

JC	Hip Rot. (°)	Hip Abd. (°)	Hip Flexion (°)	Knee Flexion (°)
JC1 (n=1)	60	45	45	120
JC2 (n=6)	40	30	45	90
JC3 (n=5)	40	30	45	0

*Tendon transected:* The distal aspect of the gracilis tendon was attached to a custom linear actuator with a clamp used to change muscle length. The same device recorded isometric muscle force production using a load cell (WMC-100, Interface Inc., Scottsdale, AZ), and LabVIEW (National Instruments, Austin, TX). Muscle activation was achieved through stimulation of the obturator nerve and force was recorded during isometric tetanic contractions at three different muscle lengths.

Due to surgical time constraints, data from only two subjects were collected with isometric force measurements recorded at three muscle lengths. To compare the subjects, data were normalized to the maximum force value (Fig. 1(b)).

## RESULTS AND DISCUSSION

*Tendon attached:* Sarcomere length ranged from 2.69-3.88 $\mu\text{m}$  (Fig. 1(a)). Median sarcomere length for JC1 and JC2 was 3.27  $\mu\text{m}$ . Median for JC3 increased to 3.65 $\mu\text{m}$  as illustrated by the grey bars behind sample means (Fig. 1(a)).

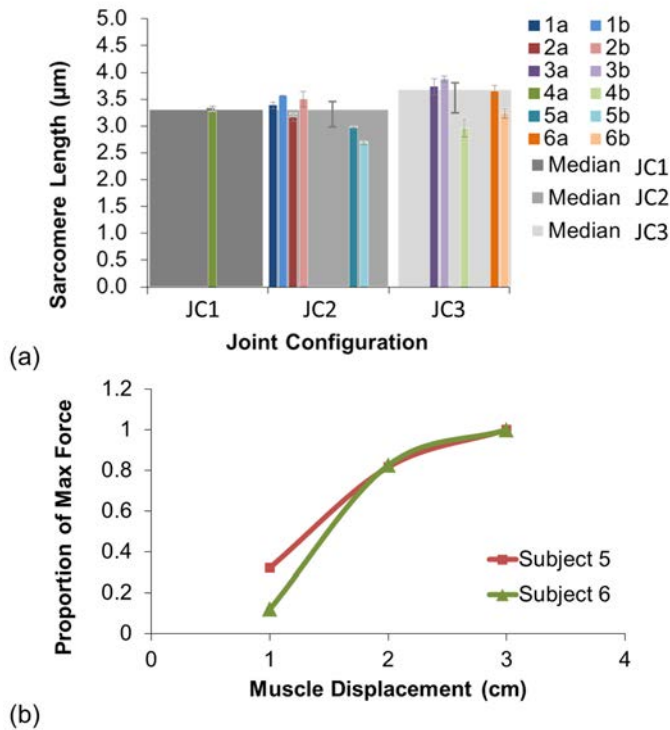


**Figure 1:** (a) *Tendon attached:* Sarcomere length from two biopsies per subject (indicated by 1a and 1b) was measured by laser diffraction. Mean is displayed with colored bars for each sample. Error bars represent standard error of mean. (b) *Tendon transected:* Median sarcomere length evaluated for each joint configuration (JC) is indicated by the grey bars with error bars for the 1<sup>st</sup> and 3<sup>rd</sup> interquartile range.

The measured range of sarcomere lengths (3.27 to 3.65 $\mu\text{m}$ ) at different JC, suggests the gracilis operates, at least in part, on the descending limb of the force-length curve, assuming an optimal sarcomere length of 2.8 $\mu\text{m}$  [3]. This study agrees with data from previous human studies evaluating the upper extremity and the soleus in the lower extremity [4,5].

*Tendon transected:* The isometric tetanic force production followed similar trends for each subject, increasing with each 1cm of muscle displacement

(Figure 1(b)). The increased value seen for Subject 5 at the start value is likely due to additive pretension on the linear actuator. More experiments need to be performed with improved tendon clamping techniques to gain a better understanding of the underlying muscle physiology. It was difficult to ensure the muscle was in its physiological position when starting force measurements.

## CONCLUSIONS

These novel force and sarcomere length data provide insight into the architecture of the gracilis muscle, suggesting it operates on the descending limb of force-length curve. The experimentally obtained patient-specific parameters obtained in this study can be used to reduce the assumptions made in computational simulations of force production. The results can be used to improve musculoskeletal modeling and guide future patient-specific models to advance surgical interventions such as tendon and muscle transfers.

## REFERENCES

1. Barrie KA, et al. *Neurosurgical Focus* **16**, E8, 2004.
2. Lieber RL, et al. *Journal of Hand Surgery* **21**, 612-618, 1996.
3. Walker SM & Schrodt GR. *Anatomical Record* **178**, 63-81 1974.
4. Lieber RL, et al. *The Journal of experimental biology* **200**, 19-25, 1997.
5. Chen X, et al. *Journal of Biomechanics* **49**, 2989-2994, 2016.

## ACKNOWLEDGMENTS

Support was provided by NIH grants R01-HD31476 (KRK) and T32-AR056950 (LQE), NSF Graduate Research Fellowship Grant No. 1255833 (LQE), and the Mayo Clinic Graduate School of Biomedical Sciences. Any opinions, findings, conclusions, or recommendations expressed in this material are those of the authors and do not reflect the views of NIH or NSF.

# REDUCED MUSCLE STEM CELL NUMBER COMPROMISES SERIAL SARCOMERE ADDITION

<sup>1</sup> Sudarshan Dayanidhi, <sup>1</sup> Matthew C. Kinney, <sup>1</sup> Peter B. Dykstra, <sup>2</sup> Charlotte A. Peterson, <sup>2</sup> John J. McCarthy and <sup>1,3</sup> Richard L Lieber

<sup>1</sup> University of California, San Diego, CA, USA

<sup>2</sup> University of Kentucky, Lexington, KY, USA

<sup>3</sup> Rehabilitation Institute of Chicago, Chicago, IL, USA

email: [rlieber@ric.org](mailto:rlieber@ric.org), [sdayanidhi@ric.org](mailto:sdayanidhi@ric.org)

## INTRODUCTION

Children with cerebral palsy (CP), the most common pediatric movement disorder, routinely develop muscle contractures, *i.e.*, muscle excursion limitations that reduce joint range of motion. Unfortunately, their biological basis is poorly understood. Skeletal muscles are composed of myofibers, arranged in parallel and series and made up of basic contractile units: sarcomeres. Serial sarcomere number can increase or decrease under conditions of stretch or slack, respectively. During childhood development, longitudinal growth occurs by sarcomere addition in series. Children with CP have a decreased serial sarcomere number and over-stretched sarcomeres [1, 2], implying reduced ability to add the sarcomeres needed for growth.

Muscle stem cells, *i.e.*, satellite cells, are indispensable for postnatal development, repair and regeneration of skeletal muscles. This stem cell pool is reduced by ~70% in contractures [3]. It is thus possible that, due to reduced muscle stem cell number, inadequate sarcomere addition occurs, leading to muscular contractures. Here we use transgenic mice ( $Pax7^{CreER/+}$ ;  $Rosa26^{DTA/+}$ ), capable of inducible satellite cell ablation, to directly test the hypothesis that adequate satellite cell number is required to add the sarcomeres needed to recover from a contracture.

## METHODS

$Pax7^{CreER/+}$ ;  $Rosa26^{DTA/+}$  ( $Pax7$ -DTA), were used for experiments (N=10, aged 8 weeks) such that treatment with tamoxifen would induce a reduction of satellite cell number by Diphtheria toxin via Cre-Lox recombination but not with a vehicle control.

The right hindlimb was casted in plantarflexion for 2 weeks so that the soleus would lose serial sarcomeres, then treated with tamoxifen or vehicle and allowed to recover for a month after cast removal (Fig. 1A). After a month, maximal dorsiflexion range permissible on the casted side was measured from images and mice were sacrificed and muscles were harvested and used fresh, fixed or frozen.

Flow cytometry was used on fresh quadriceps and gastrocnemius muscles to quantify the number of satellite cells ( $\alpha7$ -integrin<sup>+</sup>/NCAM<sup>+</sup>/CD31<sup>-</sup>/CD45<sup>-</sup>). Serial sarcomere number, myofiber length and sarcomere length were measured in fixed soleus muscles. Collagen content, myofiber areas and muscle area fraction was also calculated from the previously frozen soleii.

## RESULTS AND DISCUSSION

Tamoxifen-treated  $Pax7$ -DTA mice had a significant reduction (~80%) in satellite cell number compared to the vehicle control group ( $p < 0.05$ ), fortuitously similar to that seen in children with CP.

Soleus serial sarcomere number was significantly lower on the tamoxifen-casted side, compared to the contralateral side ( $p < 0.05$ ) while the vehicle control casted side and the contralateral side were similar (Fig. 1B). Soleus sarcomere length was similar in both groups between the casted and uncasted sides. Correspondingly, soleus fiber length was significantly shorter on the tamoxifen casted side compared to the contralateral side, while serial sarcomere number on the vehicle control casted side was similar to the contralateral side.

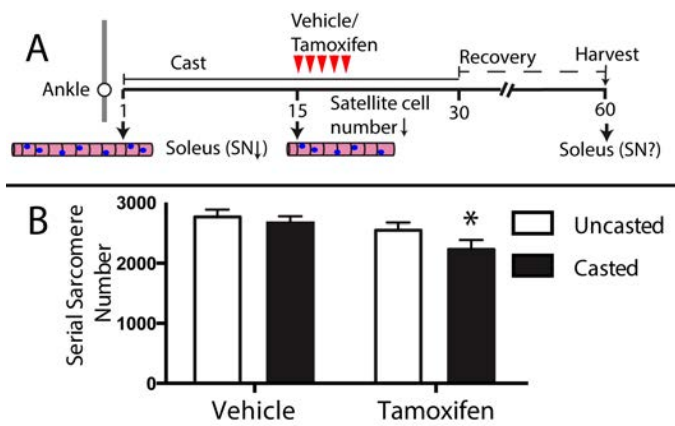


**Figure 1:** Experimental protocol and muscle architecture. A) Mice were in a plantarflexion cast to reduce soleus serial sarcomere number (SN), then treated with either tamoxifen or vehicle-control, cage remobilized for a month and muscles harvested. Serial sarcomere number of the soleus was compared between the groups and sides after the recovery period.

Maximal dorsiflexion angle was similar immediately post-cast. However, at the end of the recovery phase, the tamoxifen-treated casted group was significantly lower compared to the vehicle-treated casted group (Fig. 2A,  $p < 0.05$ ). Importantly, maximal dorsiflexion angles in the tamoxifen-group, *i.e.*, extent of recovery from contracture, was

strongly associated with soleus serial sarcomere number (Fig. 2B,  $p < 0.05$ ,  $r^2 = 0.75$ ). Myofiber areas, muscle area fraction and collagen content were not significantly different between the groups and sides.

## CONCLUSIONS

Here we used a transgenic mouse model to show that recovery from skeletal muscle contracture requires satellite cell-mediated sarcomere addition and that contracture severity is related to serial sarcomere number/fiber length rather than changes in collagen content or in muscle area fraction. These results in a model system test the idea that children with cerebral palsy suffer contractures due to impairment of longitudinal muscle growth because of reduced satellite cell number.

## REFERENCES

1. Smith LR, et al. *J Physiol (Lond)* **589**, 2625-2639, 2011.
2. Mathewson MA, et al. *J Orthop Res* **33**, 33-39, 2015.
3. Dayanidhi S, et al. *J Orthop Res* **33**, 1039-45, 2015.

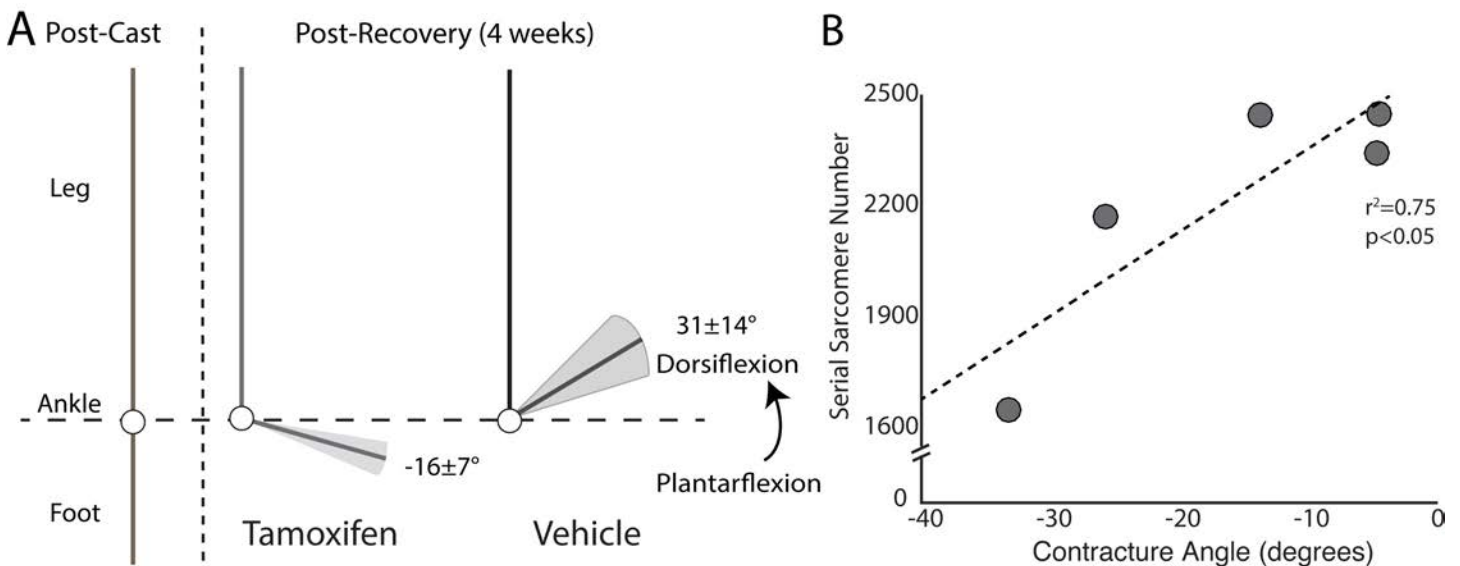


**Figure 2:** Contracture severity one month after remobilization. A) Maximal dorsiflexion angle immediately post-cast and post-recovery in tamoxifen-treated and vehicle control group, B) Association between contracture angle (*i.e.* maximal dorsiflexion angle) and serial soleus sarcomere number in tamoxifen-treated mice.

# POSITIVE FORCE FEEDBACK ALLOWS FOR FASTER AND SAFER RECOVERY IN PERTURBED HOPPING – AT A COST

<sup>1</sup>Laksh Kumar Punith, <sup>2</sup>Michael McKnight, <sup>3</sup>Shreyas Narsipur, and <sup>1</sup>Gregory S. Sawicki

Departments of <sup>1</sup>Biomedical Engineering, <sup>2</sup>Electrical and Computer Engineering and <sup>3</sup>Mechanical and Aerospace Engineering, North Carolina State University, NC, USA  
email: lpunith@ncsu.edu; web: hpl.bme.ncsu.edu

## INTRODUCTION

Legged locomotion research has primarily been interested in the study of steady state behaviors – walking, running and hopping. Several groups have taken a modelling and simulation approach, including some previous work in our lab, to study such behaviors [1]. However, humans – or animals in general – don't locomote in a flat world at constant speed. They need to be able to reject perturbations quickly and safely.

Bipedal birds achieve this by a proximo-distal gradient in their motor control strategy [2]. However, it's less clear what happens at the individual muscle level – especially in humans. Furthermore, the details of the neural control strategy (*i.e.*, reflex feedback vs feedforward contributions) are not well understood.

Modelling is a powerful approach to tackle this problem as the neuromechanics can be explicitly specified. Previous studies of simulated hopping using a model with a muscle *only*, driven by feedback and feedforward neural commands show that positive force feedback leads to improved response to perturbation [3]. However, most animals have tendons that can mechanically buffer unexpected perturbations and potentially limit injurious muscle strains [4]. We hypothesize that reflex feedback in conjunction with tendinous series elasticity can allow a compliant muscle-tendon system to recover from perturbations both rapidly and safely.

## METHODS

We developed a mathematical model of a cyclically stimulated muscle-tendon unit (MTU) (Figure 1). It consists of a massless Hill-type muscle model with a parallel elastic element (PEE) – that together forms the contractile element (CE) – and a nonlinear spring that models the tendinous tissues (series elastic element (SEE)).

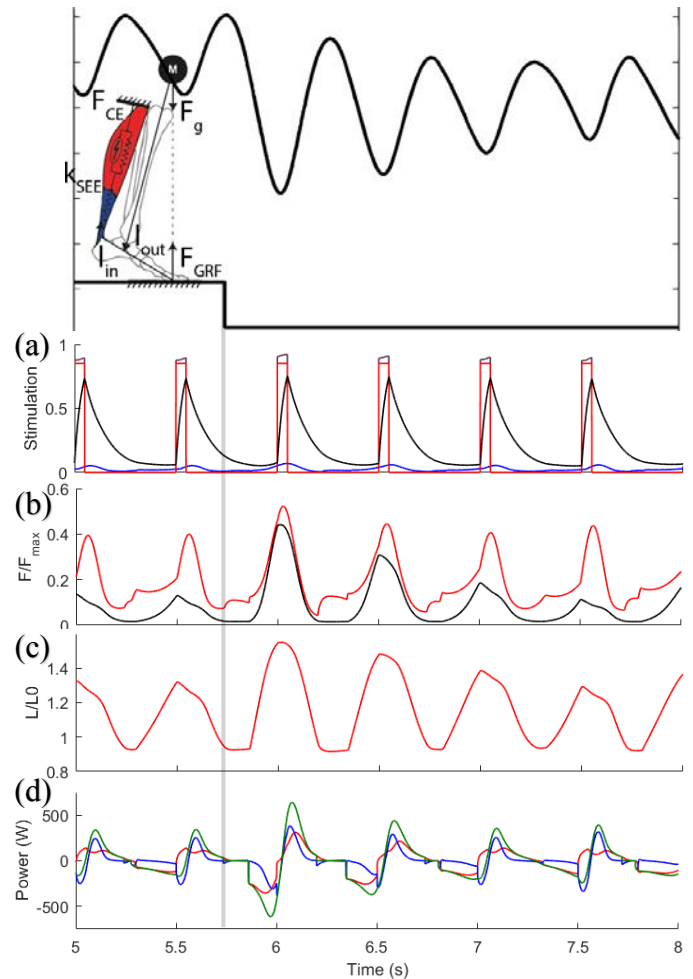


Figure 1: Time series data of (a) **Feedforward, Feedback, Total Stimulation and Activation** (b) **Total and Passive CE Force** (c) **CE Length** and (d) **MTU, CE and SEE Power** for Feedforward Fraction (FF) 0.85 and Positive Force Feedback (PFF) gain  $15 \times 10^{-5} \text{ N}^{-1}$

In the current model, a combination of positive force feedback (PFF) and feedforward (FF) signals stimulate the CE:

$$u(t) = FF(t) + (1 - FF(t)) \cdot \beta \cdot F_{CE}^{\Delta t}$$

where  $FF(t)$  is a square wave with 10% duty cycle and frequency of 2 Hz,  $\beta$  is the feedback gain and  $F_{CE}^{\Delta t}$  is the CE force that is fed back with a physiological time delay of 20 ms.

This stimulation gives rise to an activation  $a(t)$ , which in turn gives rise to active force in the CE in addition to the passive force from the PEE. This total force actuates a point mass in a gravitational field through a mechanical advantage. We apply a perturbation after 10 cycles of hopping to the MTU by virtually moving the ground by  $-5\text{cm}$  ( $\sim 20\%$  MTU slack length). We then allow the model to return to steady hopping. We determine settling time as the time point where the difference in peak total energy levels of the system are within 1% of the energy injected into the system. We calculate metabolic cost based on the velocity of the CE, scale it by activation, integrate it and divide that by body mass and total time to get a mass specific average metabolic rate [5]. To address the hypothesis, we simulated the system at many combinations of feedforward fraction (0-1.0) and positive force feedback gains ( $0-1.8 \times 10^{-6}$ ).

## RESULTS AND DISCUSSION

Increased feedback gain or feedback fraction did not necessarily improve settling time. In fact, whether increasing the feedback percentage or feedback gain, the system first gets slower and then faster at returning to steady hopping (*i.e.*, moving vertically or horizontally across Fig. 2(a)). Interestingly, there are many solutions in the parameter space where settling time is lower (2-5 hops) than the pure feedforward case (6 hops – top left corner of contours in Fig. 2).

Increasing either the feedback fraction or increasing feedback gain, resulted in shorter CE strains during recovery from perturbations (Fig. 2(b)). Compared to the pure feedforward case, CE strains are reduced by up to  $\sim 10\%$  in cases with high feedback. Thus, positive force feedback potentially acts as a safety mechanism that allows the muscle to maintain shorter and thus safer operating lengths in response to sudden perturbation.

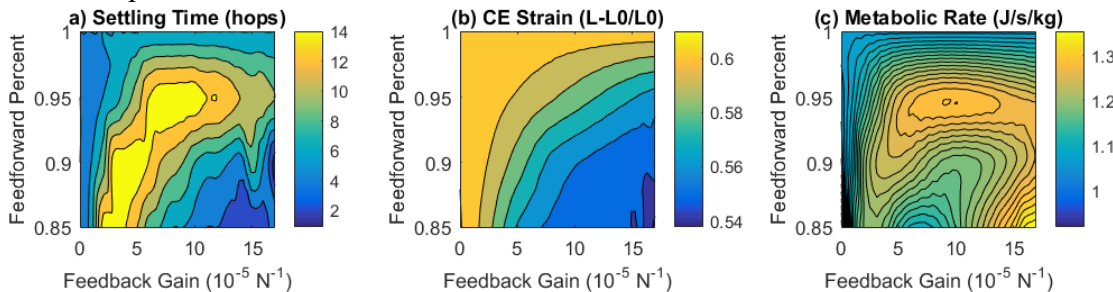


Figure 2: Contours as a function of feedforward (FF) contribution and positive force feedback (PFF) gain for (a) Settling time, (b) Peak strain of CE after perturbation and (c) Mass specific average metabolic rate.

In general, metabolic cost was higher for systems with feedback when compared to purely feedforward control strategies (Fig. 2(c)). For example, the metabolic rate was 20% higher at 0.95 feedforward fraction and  $9 \times 10^{-5} \text{ N}^{-1}$  force feedback gain than the purely feedforward case (1.3 W/kg and 1.1 W/kg). Increased metabolic demand of feedback based neuromuscular control strategies was a result of more reliance on active rather than passive muscle force contributions (Fig 1(b)).

## CONCLUSIONS

Optimally tuned positive force feedback in the context of series compliance within a muscle-tendon unit can facilitate recoveries from unexpected perturbations that are both fast and safe. However, the reduced settling times and safer operating lengths of the contractile element come with a fundamental tradeoff of increased metabolic cost. We have begun to test the predictions of this simple model by examining the behavior of individual muscle-tendon units in both humans (using ultrasound imaging) and on the benchtop (using sonomicrometry) during perturbed cyclic contractions. Insights from these experiments will be used to guide the design of next generation lower-limb robotic devices capable of seamless adjustment to environmental variation.

## REFERENCES

1. Robertson BD and Sawicki GS. J. of Theoretical Biology 353, 121-132, 2014
2. Daley MA and Biewener AA. PNAS 103, 15681-15686, 2006.
3. Haeufle DF, et al. J. R. Soc. Interface 9, 1458-1469, 2012
4. Konow, et al. Proc of the Royal Soc of Lon B: Biol Sci 282.1804 (2015): 20142800.
5. Alexander, R. McN. Journal of Theoretical Biology 184.3 (1997): 253-259.

# STRETCH-SHORTENING CYCLE PERFORMANCE IN DANCERS

Paige E. Rice, Herman van Werkhoven, Edward K. Merritt, Wilton J. Norris,

Jordan P. Rodrigues and Jeffrey M. McBride

Department of Health & Exercise Science, Appalachian State University, Boone, NC, USA

Email: ricepe@appstate.edu

## INTRODUCTION

A minimal amount of research exists in the literature pertaining to quantification of athletic capabilities in the performing arts. Dancers in particular undergo substantial amounts of physically demanding and technical training from a young age. The distinct, aesthetic focus of jumps and leaps in most stylistic choreography results in hyper-plantarflexion and stretch-shortening cycle (SSC) action primarily about the ankle-joint. The SSC is characterized by the active lengthening of the muscle-tendon unit (MTU), which stores elastic strain energy that is subsequently utilized during active shortening of the MTU for enhanced concentric (CONC) performance. Previous findings have suggested that trained athletes who participate in ballistic movements benefit both biomechanically and physiologically from the SSC [1]. Other evidence has shown that dancers possess significantly greater maximal voluntary isometric plantarflexion strength as well as musculo-articular stiffness of the triceps-surae complex than untrained controls [2]. Participation in dance might therefore result in morphology adaptation to the lower leg and contribute to performance. Due to ankle joint dominance in most dance movements, a hopping model might best reflect the SSC capabilities of dancers. Therefore, the purpose of this study was to compare SSC performance during different hopping conditions between dancers and untrained controls. Our hypothesis was that dancers would hop higher and achieve significantly greater relative force and power values when compared to untrained controls.

## METHODS

Twenty healthy, college-aged females participated in the study with no musculoskeletal injury,

neuromuscular disease, or lower limb injury within the past six months. Dancers ( $n = 10$ ; age =  $19.7 \pm 1.3$  yrs; height =  $163.9 \pm 6.6$  cm; body mass =  $62.0 \pm 10.3$  kg; dance training =  $17.0 \pm 1.2$  yrs) were required to currently be training at least three times per week. Untrained controls ( $n = 10$ ; age =  $19.5 \pm 1.1$  yrs; height =  $166.0 \pm 6.8$  cm; body mass =  $69.6 \pm 14.5$  kg) were physically inactive and did not have any background in endurance training, strength training, or dance. Subjects completed four types of hops on a custom-made sled at an inclination of  $20^\circ$  with the knees tethered just proximal of the patella to ensure that the knee joint could not contribute to hopping performance. The sled was equipped with dual force plates at the base, which provided force measurements. A potentiometer was fixed to the top of the sled-carriage, which calculated displacement and thus hopping height measurements. Subjects performed three countermovement hops, and three drop hops at 20cm (DH20), 30cm (DH30) and 40cm (DH40) and were instructed to hop as high as possible during each trial. Two-minute rest intervals were provided between trials. Subjects' greatest hop height was chosen for further analysis and comparison between groups. Forward dynamics were used to obtain a velocity-time curve, allowing for calculation of power from the product of force and velocity. Individual hopping trials were re-sampled to 500 samples using  $\Delta\text{time} = \# \text{ of original samples}/500$ . All force and power measurements were expressed relative to subjects' body mass. Average force- and power-time curves were then generated for each group from each hopping trial and used for further comparison. Displacement-time curves were used in order to define the transition from the eccentric (ECC) phase to the CONC phase.

## RESULTS AND DISCUSSION

Dancers hopped significantly ( $p \leq 0.05$ ) higher than untrained controls during the CMH ( $0.17 \pm 0.03$  m;  $0.13 \pm 0.03$  m), DH20 ( $0.22 \pm 0.04$  m;  $0.17 \pm 0.03$  m), DH30 ( $0.24 \pm 0.05$  m;  $0.17 \pm 0.05$  m) and DH40 ( $0.25 \pm 0.05$  m;  $0.18 \pm 0.05$  m). Dancers had significantly greater relative force during the end of the ECC phase and beginning of the CONC phase than untrained controls during the CMH (Fig. 1). Dancers had significantly greater relative force during DH20, DH30 and DH40 in comparison to untrained controls in the CONC phase (Fig. 1). Dancers also had significantly greater relative power than untrained controls during the CMH, DH20, DH30 and DH40 in the CONC phase (Fig. 2). Relative force and power measurements were significantly related to hop height during all hopping conditions.

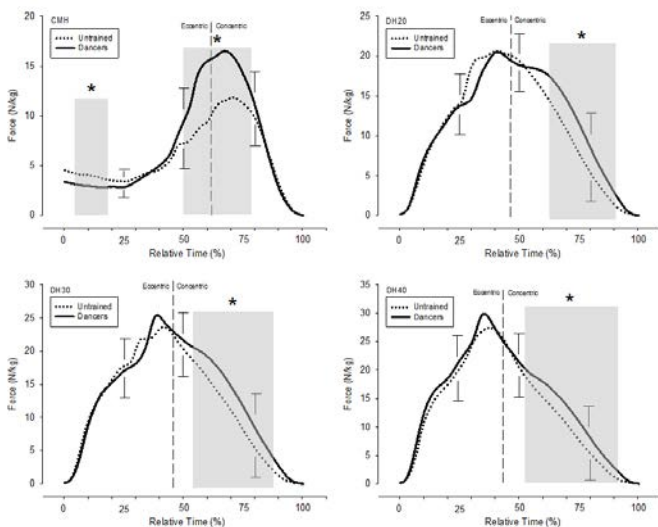


**Figure 1.** Comparison of average force-time curves during all hopping conditions between groups.

The main findings of this investigation provide evidence that participation in dance might result in enhanced SSC performance. Dance involves high volumes of ankle-specific SSC movements during unilateral leaps. Analysis of the gran jeté has shown dancers to perform with small take-off knee angles and large take-off peak power measurements nearing

6,000W [3]. These results are in support of our hypothesis that dancers emphatically use the ankle-joint to transfer power during dance-specific movements.

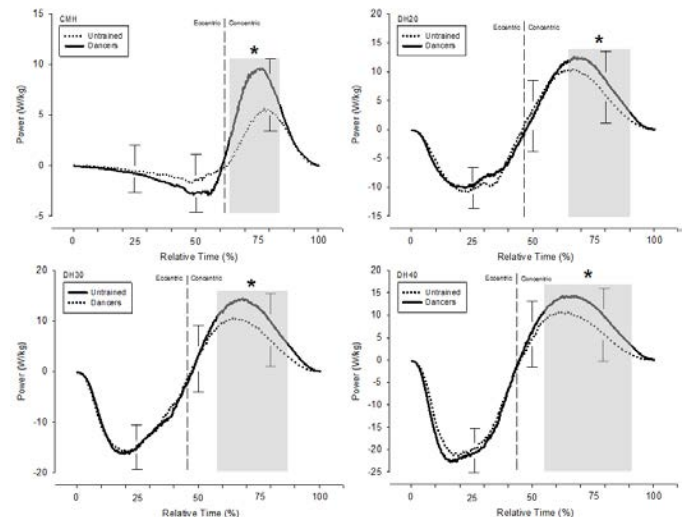


**Figure 2.** Comparison of average power-time curves during all hopping conditions between groups.

## CONCLUSIONS

In conclusion, the current data indicate that biomechanical variables significantly influence dancers' SSC performance, which may be due to muscle-tendon specific adaptations from years of complex movement synchronization. While not the focus of most training for dancers, supplemental plyometric and resistance training might further develop SSC capabilities and ultimately dance performance.

## REFERENCES

1. McBride, JM, et al. *Eur J Appl Physiol* **112**, 3469-77, 2012.
2. Rice, PE, et al. *Journal of Dance Medicine and Science* In Press, 2016.
3. Wyon, M, et al. *Med Probl Perform Art* **28**, 28-32, 2013.

# TECHNICAL CHALLENGES IN CLINICAL MOTION ANALYSIS: FINDING SOLUTIONS

<sup>1</sup> Kenton Kaufman, <sup>2</sup>Sylvia Öunpuu, <sup>3</sup>Kat Steele, <sup>4</sup>Jason Rhodes

<sup>1</sup>Motion Analysis Lab, Mayo Clinic, Rochester, MN, USA

<sup>2</sup>Center for Motion Analysis, Connecticut Children's Medical Center, Farmington, CT, USA

<sup>3</sup>Ability & Innovation Lab: Engineering and Design to Improve Human Performance, University of Washington, WA, USA

<sup>4</sup>Orthopaedics Institute, Children's Hospital Colorado, Aurora, CO, USA

Email: [kaufman.kenton@mayo.edu](mailto:kaufman.kenton@mayo.edu) web: <http://www.mayo.edu/research/labs/motion-analysis>

## INTRODUCTION

Comprehensive motion analysis methodology has been an integral part of the orthopaedic surgical decision-making and outcomes evaluation in the clinical setting for over 50 years. Joint kinematics, kinetics, and electromyographic data have been used to assess and document gait pathomechanics for informed treatment decision-making in the clinical setting. Following treatment, repeat assessments have provided objective documentation of treatment outcomes. This paradigm has facilitated development of new strategies for treatment of gait pathology especially in persons with cerebral palsy. As technology has improved, there is an increased opportunity to determine viable solutions for ongoing issues in clinically based motion analysis. This symposium will combine researchers and clinicians from both the ASB and the GCMAS (Gait and Clinical Movement Analysis Society) to a) delineate ongoing clinical challenges and b) discuss viable solutions to these challenges. We will present clinical issues and their current solutions in some cases and clinical issues that still require creative biomechanical solutions in other cases. In all examples, the symposium will combine a detailed understanding of the clinical question that requires viable implementation options in the clinical setting. It is our goal to develop collaborations between the GCMAS and the ASB so that we can ultimately improve clinical treatment outcomes. The symposium will cover the following topics:

## GAIT AND CLINICAL MOVEMENT ANALYSIS SOCIETY – Kenton Kaufman

The Gait and Clinical Movement Analysis Society (GCMAS) is a multi-disciplinary organization of physicians, allied health professionals, engineers,

biomechanists, and scientists working together to advance scientific knowledge, technical capabilities, and clinical practice in the field of human movement. It was formed in 1995 to improve functional outcomes and quality of life for individuals with any movement disorder at any age. GCMAS members use the latest technology and professional knowledge to measure, evaluate, and understand human movement, provide a forum for professional interaction and exchange of ideas, promote education, stimulate research, and disseminate current knowledge and best practices to enhance human movement and health. Given the cross-disciplinary nature with the ASB, it is hoped that ASB members will consider attending the GCMAS annual meetings. Gait and Posture is the official journal of the GCMAS. More information can be found at <http://www.gcmas.org/>

## UNDERSTANDING THE RELATIONSHIP BETWEEN IMPAIRMENT AND FOOT/ANKLE FUNCTION DURING GAIT IN CHARCOT-MARIE-TOOTH DISEASE – Sylvia Öunpuu

Charcot-Marie-Tooth (CMT) disease is a progressive peripheral neuropathy that impacts gait. The impairments vary depending on phenotype but generally include progressive muscle weakness starting at the foot and ankle muscles. CMT may lead to any one or a combination of deformities such as cavus, claw toes, and limited or excessive passive dorsiflexion range of motion. The impact on gait includes a wide variety of pathology that may include a flail foot, weight bearing on the lateral foot during stance, or toe walking. The complex interaction between cavus deformity, plantar flexor contracture and simultaneous weakness, have implications for surgical correction

of the painful cavus foot. Improved measurement of ankle and foot function during gait is needed to understand the underlying impairments and the possible risks of orthopaedic treatment options. This data will help develop evidenced based treatment indications and ultimately improved outcomes. The typical findings in CMT will be discussed along with our ongoing questions about how to document and understand the relationships that produce foot and ankle function. Other challenges in terms of measuring foot function will be briefly mentioned. We will end with an open discussion with the audience to help clarify the clinical questions and begin to define possible solutions.

### **PATELLAR INSTABILITY: WHAT SHOULD WE MEASURE TO GUIDE TREATMENT? – Jason Rhodes**

Patellar instability is the clinical syndrome due to morphologic abnormalities in the patellofemoral joint where the patella is prone to recurrent lateral dislocation. Most patients with patellar instability are young and active individuals, especially females in the 2nd decade. This presentation will focus how 3D gait analysis is used in pre-operative surgical planning for treatment of patellar instability. Issues with accuracy and repeatability in dynamic coronal and axial kinematic measurements will be presented and discussed. Pre and post-operative cases will be presented to show benefits for this work up to determine needs for different osteotomies and patellar realignment procedures. We will end with an open discussion with the audience to help clarify the clinical questions and begin to define possible solutions.

### **NEUROMUSCULAR CONTROL DURING GAIT IN CEREBRAL PALSY – Kat Steele**

Individuals with cerebral palsy (CP) have impaired movement due to a brain injury near birth. Dynamic electromyography during walking provides insight into when muscle synergists and antagonists are contracting. It is not uncommon in persons with CP to measure muscle activity that is early, prolonged, and out of phase in comparison to typically developing reference data. How does the clinician interpret this information to better understand appropriate surgical intervention?

Understanding how neuromuscular control is altered in CP can provide insight into pathological movement. Electromyographic data from children with CP will be presented, including a discussion of new techniques to quantify patient-specific changes in neuromuscular control to inform treatment planning. Individuals with CP use a simplified control strategy during gait compared with unimpaired individuals. We will explore how these results are similar to synergies during walking among adult stroke survivors, suggesting similar neuromuscular control strategies between these clinical populations

### **TORSIONAL DEFORMITIES AND THE KNEE FLEXION AXIS – Kenton Kaufman**

One of the important roles of clinical motion analysis is documentation of the transverse plane joint motion during gait. A significant part of this procedure is to correctly identify the knee flexion extension axis through identification of the medial and lateral femoral condyles. This is critical as this axis also defines hip rotation and is integral in femoral de-rotation osteotomy decisions. Motion-capture marker misplacement has previously been identified as the largest source of between-laboratory kinematic variability – accounting for up to 75% of the overall variance. Poor identification of the knee axis results in not only error in hip rotation but results in coronal plane knee artifact during maximal knee flexion in swing phase. This is also important in the assessment of maximum knee flexion during landing in the assessment of ACL readiness to return to sport. Examples of motion data for patients with torsional deformities and post ACL reconstruction patients will be presented to illustrate this challenge. This will be followed by a presentation that will outline an efficient algorithm to correct the knee flexion axis post-hoc.

The GCMAS gratefully acknowledges the support ASB for this opportunity.

# EFFECTS OF PASSIVE AND POWERED ANKLE-FOOT PROSTHESES ON MUSCLE ACTIVATION PATTERNS DURING LEVEL-GROUND WALKING

<sup>1</sup> Jana R. Jeffers, <sup>1</sup> Caroline D. Wilson, and <sup>1,2</sup> Alena Grabowski

<sup>1</sup> University of Colorado Boulder, Boulder, CO, USA

<sup>2</sup> Dept of Veterans Affairs Eastern Colorado Healthcare System, Denver, CO, USA  
email: jana.jeffers@colorado.edu

## INTRODUCTION

To accomplish the mechanical tasks required for walking, lower limb muscles are active at different points in the stride [1]. In healthy adults walking at a steady speed over level ground the hip extensors, knee extensors and ankle dorsi-flexors are most active during the beginning of stance and at the end of the leg swing phase [1]. The ankle plantar-flexors are active during mid to late stance when the leg is producing propulsive power to redirect and accelerate the center of mass into the next step [1].

When people with a unilateral transtibial amputation walk on level ground using a passive-elastic (ESAR) prosthesis, they exhibit asymmetric muscle activation magnitudes and durations between their affected leg (AL) and unaffected leg (UL) [2]; the muscles of the AL produce lower peak and average activation, and the muscles of the UL produce higher peak and average muscle activation compared with the same muscles of non-amputees [2]. Powered ankle-foot prostheses have been developed that normalize the metabolic cost and biomechanics of level-ground walking for people with a leg amputation [3]. However, the effects of powered prostheses on muscle activation patterns remain unknown.

Thus, we investigated changes in muscle activation of people with a unilateral transtibial amputation using an ESAR and powered ankle-foot prosthesis during level-ground walking. We hypothesized that integrated electromyography (iEMG) would be lower in all muscles of the UL and higher in all muscles of the AL with use of the powered ankle-foot prosthesis compared to use of an ESAR prosthesis.

## METHODS

Ten otherwise healthy adults (6M, 4F, age 42±11 yrs., height 1.7±0.08 m, biological mass without a prosthesis 77.3±14.8 kg) with a unilateral transtibial amputation gave their written informed consent to participate in this study according to the VA and Colorado Multiple Institutional Review Board.

Subjects walked 1.25 m/s on a dual-belt force-measuring treadmill (Bertec Corp., Columbus, OH) using their own ESAR prosthesis and the BiOM T2 powered prosthesis (BiOM, BionX Medical Technologies Inc., Bedford, MA) for at least 30 seconds while we collected ground reaction force and surface EMG data at 1000 Hz (Noraxon, Scottsdale, AZ). We collected EMG bilaterally from the biceps femoris long head (BF), gluteus maximus ( $G_{MAX}$ ), gluteus medius ( $G_{MED}$ ), vastus lateralis (VL), and rectus femoris (RF), and from the UL lateral gastrocnemius (ULG), soleus (USOL), and tibialis anterior (UTA). We used a 4<sup>th</sup> order recursive butterworth filter with a cutoff frequency of 30 Hz on ground reaction force data and determined heel strike and toe off events with a 20 N vertical ground reaction force threshold. Using a custom Matlab (Mathworks, Natick, MA) script, we band-pass filtered at 10-495 Hz, rectified, and RMS-averaged with a 50ms window the raw EMG data. We then normalized EMG to the maximum signal magnitude for each muscle over a stride while using the ESAR prosthesis. We integrated the smoothed and normalized EMG (*iEMG*) data for each muscle over stance (*iEMG<sub>stance</sub>*) and an entire stride (*iEMG<sub>stride</sub>*). We averaged iEMG for at least 5 strides for each subject. We used dependent t-tests to determine prosthetic device effects on iEMG and set significance at  $p < 0.05$ .

## RESULTS AND DISCUSSION

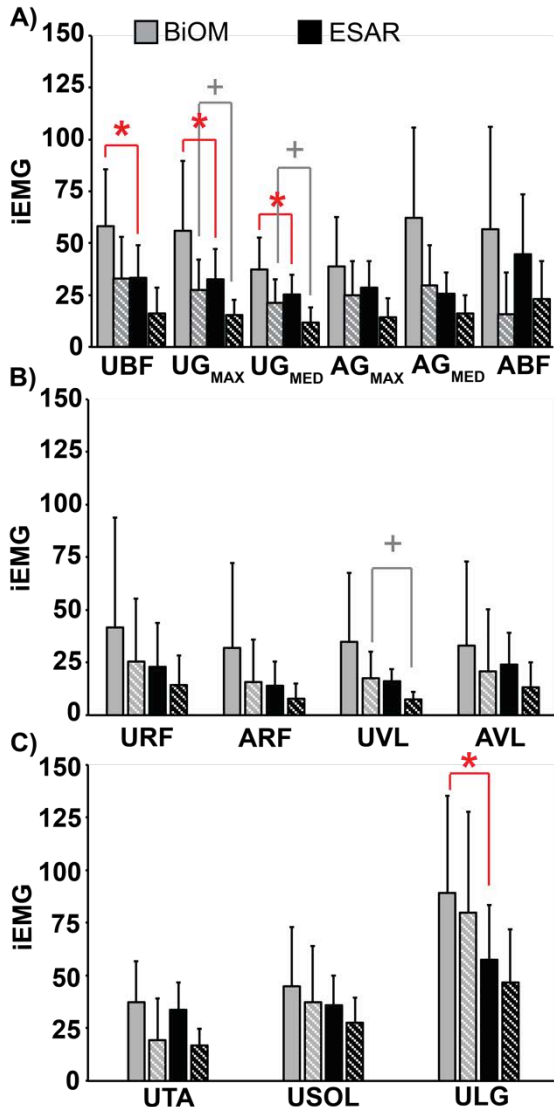


**Figure 1.** Average  $iEMG_{stride}$  (solid) and  $iEMG_{stance}$  (hashed)  $\pm$ S.D. for A) hip extensors, B) knee extensors, and C) ankle flexors/extensors. U is the unaffected leg and A is the affected leg \* indicates significant difference in  $iEMG_{stride}$  and + indicates significant difference in  $iEMG_{stance}$  between prostheses.

$iEMG_{stride}$  (Fig. 1) increased with use of the BiOM compared to the ESAR prosthesis in UBF by 74% ( $p < 0.05$ ),  $UG_{MAX}$  by 71% ( $p < 0.05$ ), ULG by 55% ( $p < 0.05$ ), and  $UG_{MED}$  by 47% ( $p < 0.005$ ). We found no significant effect of foot type on AL  $iEMG_{stride}$  (Fig. 1). Similarly, with use of the BiOM compared to ESAR  $iEMG_{stance}$  (Fig. 1) increased for  $UG_{MAX}$  by 77% ( $p < 0.05$ ),  $UG_{MED}$  by 78% ( $p < 0.005$ ), and UVL by 128% ( $p < 0.05$ ). We found no significant effect of foot type on AL  $iEMG_{stance}$  (Fig. 1).

Contrary to our hypothesis,  $iEMG$  was greater in most UL muscles and not different in AL muscles with use of the BiOM compared to use of the ESAR prosthesis. The greater  $iEMG_{stride}$  and  $iEMG_{stance}$  in the UL could be due to the increased prosthetic mass of the BiOM or an increase in stride length. On average, the BiOM had 1.6 kg greater mass than an ESAR prosthesis. Net metabolic cost (J/s) presumably reflects  $iEMG$  and increased by 7% when 1.7 kg of mass was added to a passive prosthesis during walking in people with a unilateral transtibial amputation [4]. Thus, it is possible that the additional mass of the BiOM compared to the ESAR prosthesis could account for increases in  $iEMG$ . However, because the BiOM provides stance-phase power to the user during the second part of the stance phase [3], it is unclear how added mass and power differentially affect muscle activation patterns. Additionally, subjects increased stride length 5% (0.07m) starting with the AL heel strike and 1% (0.02m) starting with the UL heel strike when walking with the BiOM compared to the ESAR prosthesis, which could increase muscle activation [5].

## CONCLUSIONS

With use of the BiOM powered prosthesis compared to a passive-elastic prosthesis, subjects had greater stride and stance phase muscle activity in their UL biceps femoris, gluteus maximus and medius, lateral gastrocnemius, and vastus lateralis. These differences are likely due to biomechanical changes when walking with the BiOM. Future studies are warranted to examine the relationship between joint kinematics, kinetics and muscle activity when walking with a powered compared to passive ankle-foot prosthesis.

## REFERENCES

1. A.N. Lay, et al. *J Biomech* **40:6** 1276-1285, 2007.
2. E. Isakov, et al. *Prosth Orth Int* **24** 216-220, 2000.
3. H.M. Herr and A.M. Grabowski *Proc Biol Sci* **279:1728** 457-464, 2012.
4. S.J. Mattes et al. *Arch Phys Med Rehabil* **81** 561-568, 2000.
5. P. Högberg *Arbeitsphysiologie* **14:6** 437-441 1952

# EFFECTS OF VARIING POWER OF POWERED PROSTHESIS ON GAIT ASYMMETRY AND METABOLIC COST

Hwan Choi, Emily S. Gardinier, Jeffrey Wensman, C. David Remy, and Deanna H. Gates

University of Michigan, MI, USA

email: gatesd@umich.edu, web: <http://rehab-biomech-lab.kines.umich.edu/>

## INTRODUCTION

People with lower limb amputation have higher energetic costs during walking [1] and walk with increased asymmetry [2] compared to people without amputation. These deficits likely occur because of the functional loss of the plantarflexor muscles, which contribute 80-85% of the total mechanical power generated during the gait cycle [3]. To address this deficit, recent research has focused on the design of devices capable of supplying additional power for push-off. These powered ankle prostheses can increase preferred walking speed, reduce energetic cost and reduce some gait asymmetries in persons with transtibial amputations [4]. It is unclear how much power is required to alleviate the high energetic cost of walking or to minimize asymmetries. While we might attempt to match the work of the intact limb, a prosthetic ankle system experiences losses through the interface (socket) and functions across only one joint, rather than replicating the biarticular nature of the gastrocnemius. Therefore, the purpose of this study was to determine how the amount of power supplied through an ankle prosthesis impacted energetic cost and temporospatial symmetry.

## METHODS

Five individuals with unilateral transtibial amputation (average  $\pm$  SD, height:  $180.0 \pm 0.05$  cm, mass  $96.24 \pm 13.43$  kg, and age:  $46.2 \pm 13.81$  years) were fitted with BiOM T2 powered ankle prosthesis (BIONX Medical Technologies, Inc., Bedford, MA) by a certified prosthetist. Each participant walked on the treadmill with self-selected speed (average  $\pm$  SD,  $1.18 \pm 0.08$  meters/second). Participants were tested the six power conditions of the BiOM controller module (0%, 25%, 50%, 75%, 100%, and prosthetist-chosen).

A 20-camera infrared motion capture system (Motion Analysis, Santa Rosa, CA) was used to acquire three-dimensional marker data at 120Hz. Reflective markers were attached follow by 6 degrees of freedom marker set. Visual 3D (C-Motion, Inc., Germantown, MD) was used to calculate joint kinematics and step length in the sagittal plane from the marker data. We used a portable gas analyzer (K4b<sup>2</sup>, Cosmed, Rome, Italy) to measure the levels of oxygen intake and carbon dioxide output. These respiratory measurements were used to convert the metabolic power using the Brockway equation [5].

Participants were acclimatized for 10 minutes with the prosthetist-chosen power setting conditions on the treadmill. Then, participants walked in each BiOM power condition until respiratory signals reached steady-stated. The condition order was randomized. Step lengths and metabolic power were measured during 3 minutes. Steady-state metabolic powers were normalized by the body weight. The amputated side step lengths were normalized by the intact side step lengths. Gait asymmetry was quantified using an equation (Eqn. 1) proposed by Robinson et al. using amputated step length ( $l_a$ ) and intact step length ( $l_i$ ) [6].

$$Asymmetry = \frac{2(l_a - l_i)}{(l_a + l_i)} \times 100 \quad (1)$$

## RESULTS AND DISCUSSION

As BiOM power increased, metabolic power decreased for participants (Fig. 1). For two of these participants (P3, P4 and P5) metabolic power increased when the prosthesis power was above 75%. Unlike the metabolic power, there were variable changes in gait asymmetry. Participant 5 increased amputated step length and had more symmetric gait

with increased power. However, participant 6 decreased amputated step length and had less symmetric gait. Of the participants who had a symmetric gait in the 0% power condition (P2 and P3), either increased or decreased gait asymmetry. Participant 5 had larger step lengths on amputated side throughout all power conditions and had minimum changes.

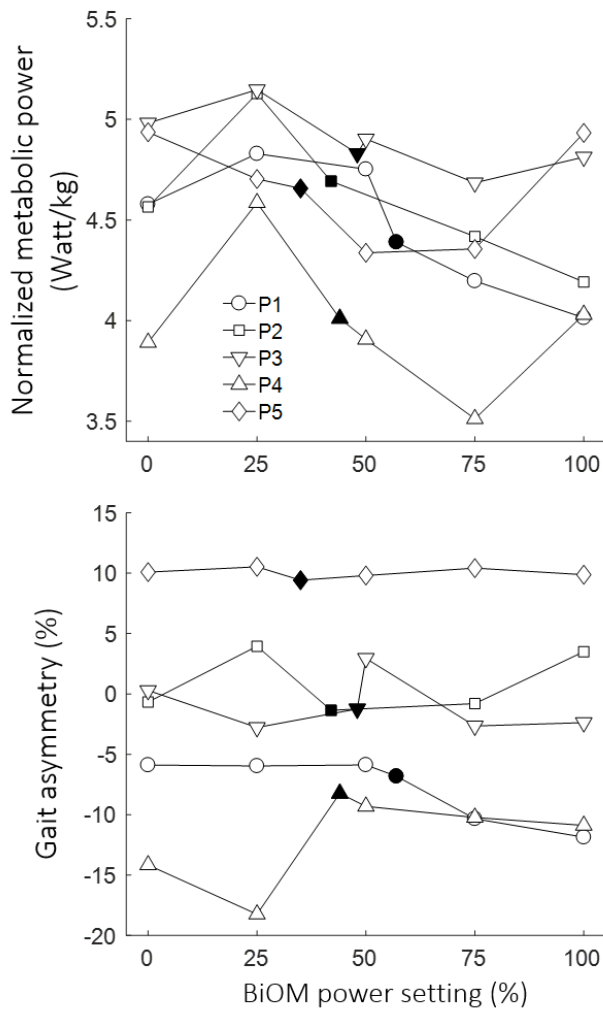


**Figure 1:** Normalized metabolic power (top) and gait asymmetry (bottom). Prosthetist settings were represented with filled symbols. In the gait asymmetry, the value greater than 0 represents amputated side has longer step lengths compared to intact side.

The difference in gait asymmetry with different prosthesis power conditions may be because each individual use different motor adaptive strategies. For example, participants who had decreased step

lengths on the amputated side may have decreased strength or recruitment of residual muscles or had more muscle co-contraction to maintain the balance and this may lead to having more gait asymmetry. Contrarily, a participant who had larger step length on the amputated side with decreased metabolic power (P4) would have benefited from the power of prosthesis.

This suggests that using an optimally tuned powered prosthesis has the potential to decrease metabolic power and improve gait symmetry. Future research will be required to understand the underlying mechanisms by which muscle function changes with the different level of prosthetic power and correlate changes in muscle function with changes in metabolic power and gait asymmetry. In addition to the level of power, different power application during stance phase should also be considered to evaluate how these combinations can produce outcomes.

## CONCLUSIONS

Using a powered ankle prosthesis can reduce the metabolic cost of walking. However, the changes in gait asymmetry were variable between participants. Evaluating metabolic power and gait asymmetry can give guidance to develop an optimally powered prosthesis. This process must consider subject-specific factors to determine the optimal tuning parameters for each individual.

## REFERENCES

1. Torburn L, et al. *J Rehabil Res Dev* **32**, 111-119, 1995.
2. Reft J, et al. *Spinal Cord* **40**, 186-191, 2002.
3. Neptune RR, et al. *J Biomech* **34**, 1387-1398, 2000.
4. Ferris AE, et al. *Arch Phys Med Rehabil* **93**, 1911-1918, 2012.
5. Brockway JM. *Hum Nutr Clin Nutr* **41**, 463-471, 1987.
6. Robinson RO. *J Manipulative Physiol Ther* **10**, 172-176, 1987.

## ACKNOWLEDGMENTS

This study was funded by the NSF 1536188

# DISPLACEMENTS AND STRAINS OF THE GEL LINER FOR BELOW KNEE PROSTHETIC USERS

<sup>1,2</sup> Amy L Lenz, <sup>2</sup> Katie A Johnson, and <sup>1</sup> Tamara Reid Bush

<sup>1</sup> Michigan State University, East Lansing, MI, USA

<sup>2</sup> Mary Free Bed Rehabilitation Hospital, Grand Rapids, MI, USA  
email: lenzamy@msu.edu, web: <http://researchgroups.msu.edu/reidtama>

## INTRODUCTION

In the United States alone, 1.7 million individuals have had a foot or leg amputation [1]. Following transtibial amputation, a gel liner coupled with a prosthetic socket is utilized to maintain ambulation for patients. Pistoning commonly occurs when the prosthetic device translates vertically with respect to the residual limb due to the suspension of the limb [2]. Understanding the limb-to-socket interface is essential for creating a well fit prosthetic device. A few studies have used motion capture to quantify aspects of limb movement within the socket, however a comprehensive assessment of deformation across multiple individuals does not exist [3-4]. To obtain a complete understanding of the limb-device interface, data on how the gel liner deforms and movement of the limb with respect to the prosthesis is a necessity.

The objective of this work was to determine both longitudinal and circumferential displacements of the gel liner and movements of the prosthetic device relative to the gel liner. We hypothesized that larger localized displacements and strains would occur in the distal region of the liner due to pistoning.

## METHODS

Participants included eight transtibial amputees 57.9 +/- 8.2 yrs.; 6 female, 2 male, including one female bilateral amputee. All amputations occurred at least one year prior to the study and were due to traumatic injury, diabetes, or infection. None of the participants needed the use of an assistive device. All participants were seen within six months by a certified prosthetist who deemed their current prosthesis had a proper alignment and fit. All used the equivalent prosthetic

suspensions; a gel liner interface with pin/lock mechanism.

A duplicate socket was manufactured out of a clear thermoplastic material. The duplicates were developed to match the alignment and fit of the participant's prosthetic socket. This allowed reflective thin-disc motion capture markers to be positioned on the gel liner, below the clear prosthetic (Fig 1a). A kinematic assessment compared their gait between the original device and the clear socket to confirm no differences existed. Using motion capture, kinematic data were obtained so residual limb motions within and relative to the socket could be computed.

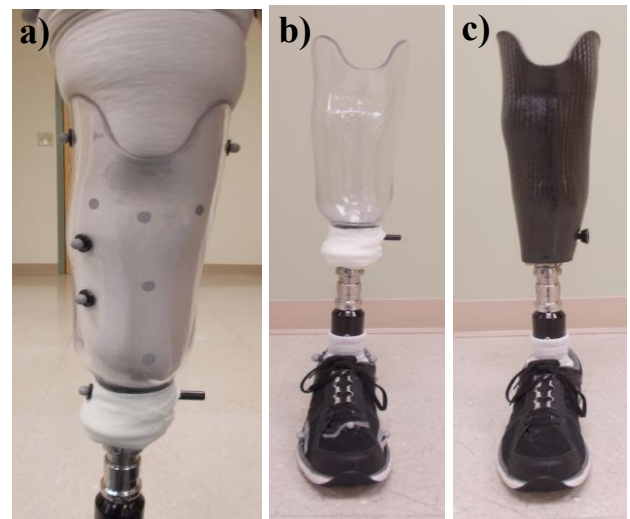


**Figure 1:** a) Clear prosthetic device with markers, b) Clear socket assembly c) Current prosthesis.

Four parameters were quantified: 1) displacement of the gel liner, 2) strain of the gel liner, 3) displacement of the prosthetic socket relative to the limb, and 4) rotation of the prosthetic socket relative to the limb. With these data sets, movements of the gel liner within the socket and relative to the socket were

calculated (Fig 2). Data were analyzed over five gait cycles. Within the four quantified parameters, a one-way ANOVA with Tukey's Post Hoc evaluated statistical differences in anatomical locations with respect to the parameter of interest.

## RESULTS AND DISCUSSION

Highest displacements on the gel liner were observed at the distal fibula (5.93 mm) distal tibia (5.83 mm) and medial side (6.34 mm). When the seven displacements of the liner were compared across each other, the distal measures were statistically different than proximal measures with p values of  $p < 0.05$ . Greatest strains occurred in the proximal tibia (10%), distal tibia (11%) and distal fibular regions (11%). Comparing across all gel liner strain locations the distal measures were significantly different than the proximal data  $p < 0.05$ . Lateral and medial anatomical landmarks had the largest prosthetic socket displacements relative to the limb. When compared across all relative movement measurements the lateral and medial data were larger than all others,  $p < 0.05$ . On average, the greatest relative displacement of  $30.7 \pm 11.4$  mm was observed in the medial proximal soft tissue region, followed by the fibular head with  $27.3 \pm 10.7$  mm. Angular rotation along the anterior, lateral and medial regions of the prosthetic socket relative to the limb showed on average  $5.3 \pm 3.6$ ,  $5.2 \pm 3.5$ , and  $5.4 \pm 3.9$  degrees respectively. The angular rotation data did not yield statistically significant differences in the three anatomical regions.

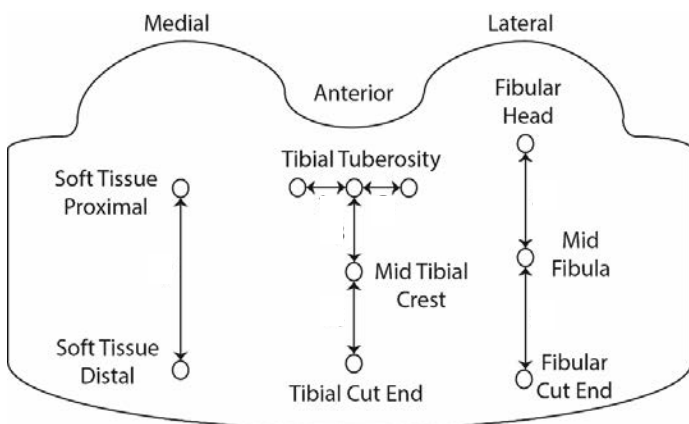


**Figure 2:** Location of anatomically placed markers beneath the clear socket. Displacements and strains were computed between the arrows in the figure.

Results overall confirmed that higher displacements and strains were observed distally as compared to proximally across participants. The reason for this increased distal displacement and strain is related to the suspension method. At the base of the gel liner, a pin system locks to the prosthetic socket, leg and foot. During gait, particularly the swing phase, an elongation of the gel liner occurs due to the suspended weight. Our displacement data are comprehensive in that six regions in the longitudinal direction, two in the transverse direction, three regions of rotation of the prosthetic relative to the leg and relative displacement of the prosthetic to the leg have been determined. Currently, no other data set is available with this number of measures on this large of sample. This mechanics-based information, can inform prosthetists of limb movement within the prosthetic socket and lead to socket or gel liner design changes in the efforts to minimize discomfort, and skin wounds for patients.

## CONCLUSIONS

Our data indicate that the distal interface region is problematic for prosthetic users. To achieve these larger distal displacements either the liner is sliding with respect to the skin or the liner is “sticking” to the skin and shearing tissues below. Either way, a shear force is produced, either at the skin surface or in deeper tissues. Future research will use finite element methods to explore these two scenarios to provide insight into tissue damage common to the distal region of the residual limb.

## REFERENCES

1. Ziegler-Graham K., et al. *Arch Phy Med Reh* **89**, 422-29, 2008.
2. Gholizadeh H., et al. *Clinic Biom* **29**, 87-97, 2014.
3. Childers WL and Siebert S. *Pros Orth Int*, 1-9, 2015.
4. Gholizadeh, H., et al. *Clinic Biom* **27**, 34-39, 2012.

## ACKNOWLEDGMENTS

The authors would like to thank Patrick Logan, CPO.

# TEMPORAL SPATIAL IMPROVEMENTS FOR SERVICE MEMBERS WITH UNILATERAL TRANSTIBIAL AMPUTATION DURING REHABILITATION AT A MILITARY TREATMENT FACILITY

<sup>1</sup>Trevor Kingsbury, <sup>1</sup>Julianne Stewart, <sup>2</sup>Michael Marks, <sup>1</sup>Katherine Sharp, <sup>1</sup>Tatiana Djafar, <sup>3</sup>John David Collins, <sup>1</sup>Jacqueline Moore, and <sup>1</sup>Marilynn Wyatt

<sup>1</sup>Naval Medical Center San Diego, San Diego, CA, USA

<sup>2</sup>Improvement Path Systems, San Diego, CA, USA

<sup>3</sup>BADER Consortium, Newark, DE

email: trevor.d.kingsbury.civ@mail.mil

## INTRODUCTION

Rehabilitation of service members with lower extremity amputation is a critical aspect of returning them to the highest level of function possible. Injured service members were often highly active prior to injury and typically wish to return to activities that demand a high level of performance [1]. Specialized rehabilitation programs at Military Treatment Facilities (MTFs) in conjunction with advanced prosthetic devices allow service members with amputation to pursue their goals. At Naval Medical Center San Diego (NMCS D), the typical rehabilitation course for patients with amputation is broken into four phases: Phases I and II consist of immediate post-op healing and pre-prosthetic training, Phase III introduces prosthetic gait training, and Phase IV initiates higher-level devices and activities as the service member prepares to return to duty or separate from the service [2].

To date, no study has evaluated the improvements in temporal spatial parameters such as velocity, cadence, and step length at specific time points throughout a service member's entire rehabilitation process at an MTF. Temporal spatial parameters are highly related to functional ability and are important when evaluating a patient's ability for activity participation. The purpose of this study is to evaluate the progression of temporal spatial parameters throughout rehabilitation for service members with a unilateral transtibial amputation (TTA). This data can be used to validate the rehabilitation model at an MTF and help give quantitative guidelines and reference data for clinicians in determining course of care for patients with a unilateral transtibial amputation.

## METHODS

A total of 97 patients with a unilateral TTA underwent rehabilitation at NMCS D from 2008-2016 and were studied in the Gait Analysis Laboratory as part of their routine clinical care. Retrospective review excluded patients with contralateral involvement, traumatic brain injury (TBI) affecting gait, and/or less than three gait studies over the course of care. A total of 32 patients fit the inclusion criteria with an average age of  $26.4 \pm 5.0$  years at the time of baseline study. Patients' baseline studies occurred as soon as they were able to ambulate without an assistive device and correlated with early Phase III. Subsequent studies were conducted at six weeks, three months, six months, and one year post baseline. The six week study was performed at approximately the midpoint of Phase III while the three month study was near the conclusion of Phase III. The six month study occurred toward the end of Phase IV, while the one year study was conducted before the patient disengaged from active rehabilitation at the MTF.

Patients were studied in the Gait Analysis Laboratory at NMCS D using a modified Helen Hayes marker set, a 12 camera Eagle Camera system (Motion Analysis Corp., Santa Rosa, CA, USA), and 4 force plates (AMTI, Watertown, MA, USA). Data were processed in Visual 3D (C-Motion Inc., Germantown, MD, USA) and analyzed using R (R Foundation, Vienna, Austria). Temporal spatial variables of interest included velocity (m/s), cadence (steps/min), affected and unaffected step length (m), affected and unaffected stance times (% gait cycle), and step width (m). In addition, Symmetry Index (SI) was calculated for step length

and stance times [3]. Rehabilitation often focuses on minimizing asymmetries, although they are not necessarily functionally detrimental to the patient [4]. Multiple one-way ANOVAs were performed to evaluate a main effect of time with  $p < .05$ , followed by Games-Howell post-hoc tests to determine where significant differences occurred.

## RESULTS AND DISCUSSION

All 32 patients with unilateral TTA were male with an average height of  $1.77 \pm 0.06$  m and an average weight of  $82.1 \pm 17.4$  kg at baseline. Temporal spatial data is reported in Table 1. There were no significant changes in their step width ( $p = .41$ ), affected stance time ( $p = .91$ ) or step length SI ( $p = .58$ ) at any time point. There were significant changes in velocity ( $p < .001$ ), cadence ( $p < .001$ ), affected and unaffected step length ( $p < .001$ ,  $p < .01$ ), unaffected stance time ( $p < .001$ ), and stance time SI ( $p < .01$ ). Velocity and cadence significantly increased at all times compared to baseline (all  $p < .01$ ) and significantly increased at six months and one year compared to the six week time point ( $p < .05$ ). Affected step length significantly increased at all times compared to baseline ( $p < .01$ ) and was also greater at the one year study compared to the six week study ( $p < .01$ ). Unaffected step length increased at three months compared to baseline ( $p < .05$ ). Finally, stance time SI significantly improved at three months compared to baseline and six weeks ( $p < .05$ ) but by 1 year had significantly worsened ( $p < .05$ ).

## CONCLUSIONS

This is the first study to publish rehabilitation outcomes for service members with unilateral TTA

across the duration of rehabilitation at an MTF. Service members had significantly increased velocity, cadence, and step lengths throughout care. Walking velocity matches that of non-injured males by the three month study mark [5]. Compared to baseline, patients are significantly improved both at the end of Phase III of rehabilitation but also have further improvements at the end of Phase IV. This is significant in that they are no longer doing gait specific tasks as part of their rehabilitation course of care, having shifted to high level activities that allow for sport or duty reintegration. Interestingly, stance time SI is the only measure where a significant improvement is seen at the end of Phase III of rehabilitation and regresses over the rest of care. This measure may be acutely sensitive to the part of rehabilitation where active gait retraining is occurring. While all patients progressed through the rehabilitation program, some patients likely had more physical therapy visits than others and thus is a limitation of the study. Future research will look at any physical therapy “dosage” effects to provide additional guidelines for the rehabilitation program.

## REFERENCES

1. Cecere FA. *Military Medicine*, 181, 11/12:1, 2016.
2. Amputation Rehabilitation Protocol. C5 Physical Therapy Division: Naval Medical Center San Diego. Revised December 2010.
3. Blazkiewicz MA. *Acta of Bioengineering and Biomechanics*, 16:1, 29-35, 2014.
4. Hak L. *Physical Therapy*, 94:10, 1480-88, 2014.
5. Oberg T. *JRRD*, 30:2, 210-223, 1993.

**Disclaimer:** The views expressed in this article are those of the author(s) and do not necessarily reflect the official policy or position of the Department of the Navy, Department of Defense, nor the US Government

**Table 1:** Temporal spatial parameters for service members with unilateral TTA throughout rehabilitation. (\* denotes significance from baseline, ^ denotes significance from 6 weeks, “ denotes significance from 3 months, A = affected limb, U = unaffected limb)

Timepoint	Number	Velocity (m/s)	Cadence (steps/min)	A Step Length (m)	U Step Length (m)	A Stance Time (% GC)	U Stance Time (% GC)	Step Width (m)	Step Length SI	Stance Time SI
Baseline	32	1.23 ± 0.14	104 ± 8	0.72 ± 0.05	0.70 ± 0.05	61 ± 2	65 ± 2	0.13 ± 0.03	5.2 ± 4.9	6.0 ± 3.6
6 Weeks	25	1.30 ± 0.13*	106 ± 6*	0.74 ± 0.06*	0.73 ± 0.06	60 ± 2	64 ± 2*	0.12 ± 0.03	3.9 ± 3.4	6.6 ± 4.1
3 Months	27	1.36 ± 0.11*	108 ± 5*	0.77 ± 0.05*	0.74 ± 0.06*	60 ± 2	63 ± 1*	0.12 ± 0.03	4.6 ± 3.6	3.4 ± 2.2*^
6 Months	26	1.41 ± 0.11*^	110 ± 6*^	0.78 ± 0.05*	0.76 ± 0.06*	60 ± 1	63 ± 1*	0.12 ± 0.02	4.8 ± 4.0	4.0 ± 3.2
1 Year	21	1.43 ± 0.12*^	111 ± 6*^	0.80 ± 0.06*^	0.75 ± 0.05*	60 ± 1	62 ± 2*^	0.11 ± 0.02	5.7 ± 3.3	5.6 ± 2.2"

# INTACT KNEE JOINT KINETICS DURING THE FIRST SIX MONTHS OF PROSTHETIC USE

<sup>1</sup> Rebecca L. Krupenevich, <sup>1</sup> Ross H. Miller, <sup>2</sup> Barri L. Schnall, and <sup>2-4</sup> Alison L. Pruziner

<sup>1</sup> University of Maryland, College Park, MD, USA

<sup>2</sup> Walter Reed National Military Medical Center, Bethesda, MD, USA

<sup>3</sup> DoD-VA Extremity Trauma and Amputation Center of Excellence

<sup>4</sup> Uniformed Services University of Health Sciences, Bethesda, MD, USA

email: rlkrup@umd.edu

## INTRODUCTION

Individuals with unilateral lower limb loss are at increased risk for developing knee osteoarthritis (OA) within the intact (contralateral) limb [1]. While the exact mechanism(s) underlying this phenomenon are currently unknown, it is plausible, even likely, that large or unusual loads placed on the intact knee joint may contribute to the “wear and tear” model of OA development and progression [1]. Features of the knee adduction moment (KAM) and the knee flexion moment (KFM) have been previously associated with cartilage degeneration [2,3]. The progression of knee joint mechanics during early prosthesis use is of particular interest because it is important to know when during the rehabilitation process the gait and joint mechanics have “stabilized”. Individuals who have undergone ACL repair, a population with increased risk of OA development similar to limb loss, have been found to exhibit increased contralateral limb loading over time [4]. However, to our knowledge, there have been no longitudinal assessments of biomechanical variables related to OA initiation/progression in individuals with unilateral lower limb loss.

Therefore the purpose of this study was to examine changes in knee joint kinetics of individuals with unilateral lower limb loss as a function of time from independent ambulation. We hypothesized that knee joint moments would increase over time.

## METHODS

Nine male service members with unilateral lower limb loss from traumatic injury (three transfemoral, six transtibial) completed gait analyses at 3 distinct time points: 0, 2, and 6 months after initial ambulation (defined as able to walk 50ft

independently without assistive devices) (Table 1). All participants provided informed consent to procedures approved by the Walter Reed National Military Medical Center Institutional Review Board. Participants walked at a self-selected speed and cadence. Kinematic data were captured using a 23-camera motion capture system (Vicon, Oxford, UK; 120Hz) and kinetic data were captured using six force platforms embedded in a walkway (AMTI, Watertown, MA, USA; 1200Hz). Joint marker placements were completed by one of two trained investigators. Marker position and ground reaction force data were smoothed using a 4<sup>th</sup>-order dual-pass Butterworth filter with cutoff frequencies of 6 Hz and 50 Hz, respectively. Knee joint kinetics were calculated by 6DOF inverse dynamics using Visual3D software (C-Motion, Germantown, MD, USA).

A one-way repeated measures ANOVA ( $\alpha = 0.05$ ) tested for the effect of time on the peak, impulse, and loading rate of the KAM, and peak KFM, with a Bonferonni correction in post-hoc testing. Walking speed and stride length were included to determine if they should be covariates. Effect sizes of 0.01, 0.06, and 0.14 were interpreted as small, medium, and large according to guidelines for  $\eta_p^2$ .

## RESULTS AND DISCUSSION

There was a significant effect of time on stride length ( $p = 0.01$ ,  $\eta_p^2 = 0.42$ ), but not on self-selected walking speed ( $p = 0.13$ ,  $\eta_p^2 = 0.23$ ). After adjusting for multiple comparisons, there were no significant pairwise differences for stride length (all  $p \geq 0.07$ ). Therefore, speed and stride length were not included as covariates in the ANOVA.

Waveforms of the average KAM and KFM at all time points are presented in Fig. 1. There were no

effects of time on peak ( $p = 0.40$ ,  $\eta_p^2 = 0.11$ ), impulse ( $p = 0.80$ ,  $\eta_p^2 = 0.03$ ), or loading rate ( $p = 0.41$ ,  $\eta_p^2 = 0.10$ ) of the KAM, or peak KFM ( $p = 0.11$ ,  $\eta_p^2 = 0.24$ ) (Fig. 2).

The findings reported herein suggest there is not a substantial, acute adaptation of the intact leg to walking with a prosthetic limb. Thus, if an individual walks with large or unusual knee joint loads throughout their rehabilitation, they may continue to walk with large or unusual loads long-term, potentially increasing their risk for developing knee OA in the intact limb.

## CONCLUSIONS

Recently ambulatory individuals with limb loss did not change the major features of the KAM or KFM of their intact knee joint over the first six months of

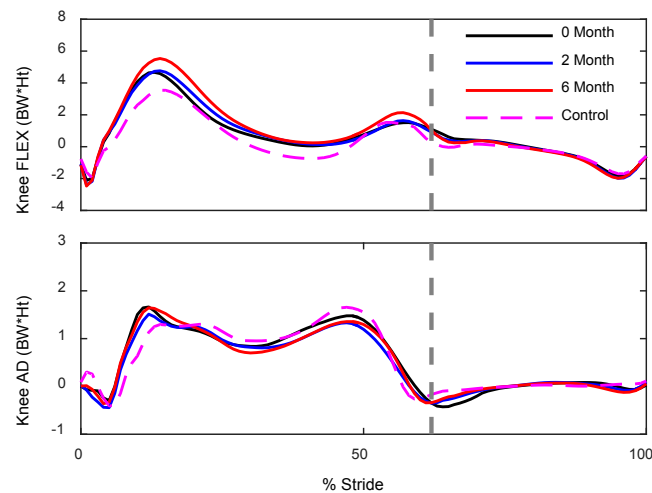


**Figure 1:** Mean knee joint moments in the sagittal (top) and frontal (bottom) plane during walking at self-selected speed. Stride begins and ends at heel strike. Vertical dashed lines indicate toe-off. Data from a non-limb loss group are included for reference (pink dashed).

independently walking with a prosthesis. We speculate that these individuals will maintain this loading behavior until there is a reason to change, such as development of pain in the intact knee joint. Therefore, characteristics of knee joint loading early in the rehabilitation process may be relevant for knee OA risk, and should be considered as targets for therapy prior to the initiation of the disease. Future work should address potential longitudinal adaptations that occur after the first six months of independently walking with a prosthesis and the effects of loading on future joint health.

## REFERENCES

1. Morgenroth DC et al. *PM&R* **4**, S20-S27, 2012.
2. Chehab EF, et al. *Osteoarthr Cartilage* **22**, 1833-1839, 2014.
3. Bennell KL. *Ann Rheum Dis* **70**, 1770-1774, 2011.
4. Webster KE et al. *Gait Posture* **36**, 167-171, 2012.

## ACKNOWLEDGMENTS

This work was supported by the CRSR at USUHS (award #NF90UG) and the DoD-VA EACE. Views expressed are those of the authors and do not reflect the official policy or position of the Army, Navy, or Defense.

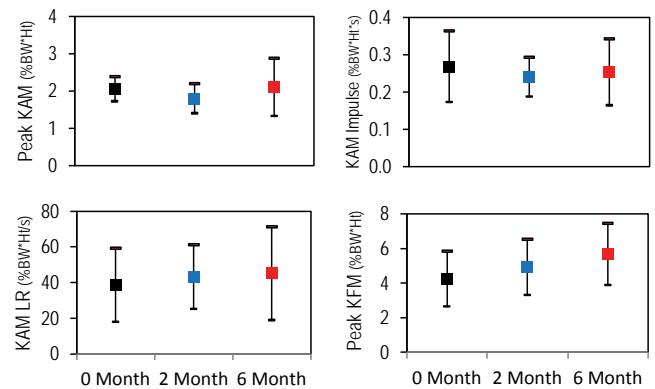


**Figure 2.** Mean and 95% confidence interval for kinetic outcome variables.

**Table 1:** Demographic information at independent ambulation (0 months)

	All (n=9)	Transtibial (n=6)	Transfemoral (n=3)
Age (years)	26±5	25±4	28±6
Height (m)	1.77±0.06	1.79±0.06	1.75±0.07
Mass (kg)	85.0±13.1	82.0±13.5	90.9±12.5
Time from injury (days)	655±1010	217±134	1529±1521
Time from amputation (days)	115±68	130±75	86±47
Time from ambulation (days)	9±1	10±1	8±0

# LONGITUDINAL CHANGES IN MEDIOLATERAL TRUNK AND PELVIC MOTION AMONG PERSONS WITH LOWER LIMB AMPUTATION DURING THE FIRST YEAR OF AMBULATION

<sup>1-3</sup> Brad D. Hendershot, <sup>2</sup> Courtney M. Butowicz, <sup>1,2</sup> Caitlin E. Mahon, <sup>2</sup> Barri L. Schnall, <sup>1-3</sup> Christopher L. Dearth

<sup>1</sup> DOD/VA Extremity Trauma and Amputation Center of Excellence

<sup>2</sup> Walter Reed National Military Medical Center, Bethesda, MD, USA

<sup>3</sup> Uniformed Services University of the Health Sciences, Bethesda, MD, USA

Email: bradford.d.hendershot2.civ@mail.mil

## INTRODUCTION

Persons with lower limb amputation (LLA) often walk with compensational movement strategies involving a prominent reliance on the trunk and pelvis [1]. Resulting increases in trunk and pelvic motions compared to able-bodied individuals have been associated with an elevated risk for low back pain (LBP; [2,3]). In the frontal plane, larger trunk range of motion (ROM) and peak lateral flexion (on the prosthetic side, specifically) among persons with vs. without LLA are often assumed to be a result of an active/learned neuromuscular movement strategy to compensate for weak (or missing) musculature in the residual limb [4]. Identifying the extent to which trunk and pelvic motions change or evolve over time following amputation, particularly beginning at time of initial ambulation, could provide additional insight into contributing factors and, ultimately, guidance for rehabilitation strategies to mitigate deleterious consequences of such motions. Thus, the purpose of this study was to characterize features of trunk and pelvic motion in the frontal plane among persons with LLA as a function of time after amputation. We hypothesized the overall magnitude of mediolateral trunk and pelvic motion would increase with increasing time of ambulation, suggesting a learned proximal movement strategy.

## METHODS

Thirty-two males with unilateral LLA (Table 1) completed gait analyses at 5 distinct time points: 0, 2, 4, 6, and 12 months after initial ambulation (defined as able to walk 50ft independently without assistive devices). Participants walked overground across a 15m level walkway at 3 controlled speeds (completed in a randomized order): Froude2 (mean=0.96 m/s), Froude3 (mean=1.20 m/s), and

Froude4 (mean=1.44 m/s). Full-body kinematics were recorded by tracking (120Hz) reflective markers using a 23-camera motion capture system (Vicon, Oxford, UK). All participants provided informed consent to procedures approved by the Walter Reed National Military Medical Center Institutional Review Board. Note, participants were not required to wear the same prosthetic components throughout, though only 4 of the 32 changed between similar passive energy storage and return feet (all ten with transfemoral amputation wore microprocessor or mechanical knees).

**Table 1.** Mean (SD) participant demographics, obtained at visit t=0, for persons with unilateral transtibial (TT) and transfemoral (TF) amputation. All amputations were the result of traumatic injuries.

	TT (n=22)	TF (n=10)
Age (yr)	27.1 (6.0)	28.5 (6.2)
Stature (cm)	178.5 (4.0)	177.9 (7.8)
Body Mass (kg)	84.2 (11.1)	83.9 (10.8)

Mediolateral trunk and pelvic ROM, and peak trunk lateral flexion in prosthetic limb stance, were computed for each walking speed within Visual3D (C-Motion, Germantown, MD, USA). The trunk was modeled as a single rigid segment, defined proximally by the acromia and C7 vertebrae, and distally at the T10 spinal level. All segmental kinematics were defined in the global coordinate system (relative to vertical). Because not all participants completed all five time points (mean=3, range 2-5), mixed-model repeated measures analyses of variance (ANOVA) were used to compare trunk ROM and peak lateral flexion by group (TT vs. TF) and time, and their first-order interaction. All statistical analyses were performed using SPSS (Version 21, IBM Corp., Armonk, NY, USA), with statistical significance determined when  $p < 0.05$ .

## RESULTS AND DISCUSSION

There were no differences in pelvis ROM by time ( $p>0.09$ ) or between groups ( $p>0.56$ ) at any speed. However, both trunk ROM and peak lateral flexion in prosthetic limb stance decreased (all  $p<0.024$ ) over time (Figure 1), wherein the 0 and 12 month time points were significantly different. At Froude2 and Froude4, these did not differ between groups ( $p>0.28$ ). At Froude3, however, there was a significant interaction between visit and group ( $p=0.014$ ); trunk ROM and peak lateral flexion decreased among persons with TF but not TT amputation, primarily due to the larger values at  $t=0$  among persons with TF amputation.

In contrast to our hypothesis, mediolateral trunk ROM and peak lateral flexion in prosthetic limb stance decreased with increasing time after initial ambulation, regardless of walking speed, most notably within the first 2 months of ambulation among persons with TF amputation. Such a trend suggests mediolateral movements of the trunk and pelvis may be more of a near-term reaction to walking with a prosthesis than a proactive movement strategy learned over time. However, these individuals were also participating in extensive rehabilitation throughout this one-year period and, thus, these changes may also reflect physical therapy and other gait training techniques. Nevertheless, the magnitudes of these motions remain larger than persons without LLA (see gray shaded areas in Figure 1), as well as compared to values reported elsewhere from individuals with LLA who are generally evaluated greater than 12

months post amputation [1,5]; suggesting these motions may continue to change over time. Future work should therefore longitudinally evaluate trunk and pelvic motions for extended durations to capture longer-term changes, particularly when these individuals are no longer receiving frequent rehabilitative care. In summary, data reported here identifies, for the first time, temporal relationships of mediolateral trunk motions within the first year of ambulation among persons with LLA. These data have longer-term implications for the surveillance of LBP onset and recurrence, and may help identify important biomechanical factors in its causation.

## REFERENCES

1. Goujon-Pillet H, et al. *Arch Phys Med Rehab* **89**, 87-94, 2008.
2. Devan H, et al. *Med Hypoth* **82**, 77-85, 2014.
3. Hendershot BD, et al. *Clin Biomech* **29**, 235-42, 2014.
4. Molina RF, et al. *Gait Posture* **37**, 436-9, 2013.
5. Jaegers SMHJ, et al. *Arch Phys Med Rehab* **76**, 736-43, 1995.

## ACKNOWLEDGMENTS

This work was supported, in part, by the Peer Reviewed Orthopaedic Research Program (Award W81XWH-14-2-0144) and the Center for Rehabilitation Sciences Research (HU0001-15-2-003). The views expressed in this abstract are those of the authors, and do not necessarily reflect the official policies of the Departments of the Army, Navy, Defense, nor the United States Government.

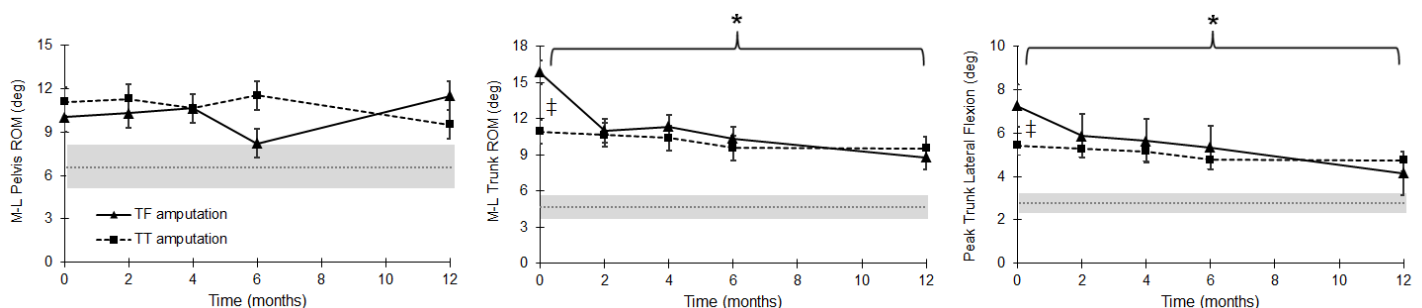


**Figure 1.** Froude3 walking speed. Mean mediolateral (M-L) pelvis range of motion (ROM; left), trunk ROM (middle), and peak trunk lateral flexion in prosthetic limb stance (right) among persons with transtibial (TT) and transfemoral (TF) amputation with increasing time after initial ambulation. Error bars represent standard errors. Grey dotted lines (shaded areas) respectively represent mean (standard deviations) for 6 males without amputation walking at a similar speed. Asterisks indicate significant differences in mean responses between the first (0 month) and last (12 month) time points; group differences within a given time point are also indicated (+).

# How do prosthetic stiffness, height, and running speed affect the biomechanics of athletes with bilateral transtibial amputations?

<sup>1</sup>Owen N. Beck, <sup>2</sup>Paolo Taboga, and <sup>1,3</sup>Alena M. Grabowski

<sup>1</sup>University of Colorado, Boulder, CO, USA

<sup>2</sup>Sacramento State University, Sacramento, CA, USA

<sup>3</sup>Eastern Colorado Healthcare System, Denver, CO, USA

email: owen.beck@colorado.edu

## INTRODUCTION

Athletes with bilateral transtibial amputations compete in events that span a broad range of running speeds. However, to date the biomechanics of only two such athletes have been reported across running speeds [1-3]. Furthermore, it is uncertain if the exhibited biomechanical changes with altered running speed are inherent to athletes with bilateral transtibial amputations, or if they are due to the characteristics of their running-specific prostheses (RSPs) (i.e. stiffness and height). Therefore, the purpose of our study was to quantify how prosthetic stiffness, height, and running speed affect the biomechanics of athletes with bilateral transtibial amputations. We hypothesized that prosthetic stiffness, but not height, would affect biomechanics across running speeds, and that faster running speeds would mitigate the influence of prosthetic stiffness on all tested biomechanical parameters.

## METHODS

Five male athletes with bilateral transtibial amputations gave informed written consent according to the COMIRB and USAMRMC Human Research Protection Office prior to participation. Each athlete performed fifteen sets of running trials lasting 10 strides each on a 3D force measuring treadmill (Treadmetrix, Park City, UT). Each set of trials began at 3 m/s and each successive trial was incremented 1 m/s until the athlete reached top speed. For each set of trials, athletes used a different prosthetic model, stiffness, and height combination. Prosthetic models included the Freedom Innovations Catapult FX6, Össur Cheetah Xtend, and Ottobock 1E90 Sprinter. Prosthetic stiffness conditions were that of the manufacturer recommended and  $\pm 1$  stiffness categories.

Prosthetic height conditions were the International Paralympic Committee's maximum competition height [4] and  $\pm 2$  cm.

We measured ground reaction forces (GRFs) (1000 Hz) throughout each trial and filtered them using a 4<sup>th</sup> order low-pass Butterworth filter (30 Hz). We used the filtered data to calculate the biomechanical variables that influence leg stiffness [2, 5] and running speed [6] from each trial. We determined prosthetic stiffness (kN/m) ( $k_{RSP}$ ) [5], then used it and calculated overall leg stiffness ( $k_{leg}$ ) to compute residual limb stiffness ( $k_{res}$ ) (Equation 1).

$$\frac{1}{k_{leg}} = \frac{1}{k_{res}} + \frac{1}{k_{RSP}} \quad (\text{Eq. 1})$$

We used linear mixed models to assess the influence of prosthetic stiffness, height, and running speed on each biomechanical variable. We set significance at  $p=0.05$ .

## RESULTS AND DISCUSSION

Prosthetic stiffness (kN/m) increased with faster running speeds ( $p<0.001$ ) (Fig. 1). Prosthetic stiffness, height, and running speed all affected biomechanics. Specifically, with stiffer prostheses athletes exhibited greater peak and stance average vertical GRFs ( $p<0.001$ ), increased overall leg stiffness ( $p<0.001$ ), decreased residual limb stiffness ( $p<0.001$ ), decreased ground contact times ( $p<0.001$ ), and increased step frequency ( $p<0.001$ ) (Fig. 2). Increased prosthetic height resulted in lower peak and stance average vertical GRFs ( $p<0.001$ ), as well as longer contact times and step lengths ( $p<0.001$ ). Running speed was inversely associated with overall leg stiffness and residual limb stiffness ( $p<0.001$ ) (Fig. 1).

In contrast to our previous study [5], participants demonstrated an inverse relationship between prosthetic and residual limb stiffness (Fig. 1). Moreover, with increased running speed the influence of prosthetic stiffness was reduced for stance average vertical GRF ( $p < 0.001$ ), residual limb stiffness ( $p = 0.020$ ), contact time ( $p < 0.001$ ), step frequency ( $p = 0.004$ ) (Fig. 2), contact length ( $p = 0.019$ ), the angle swept by the leg spring ( $\theta$ ) ( $p = 0.001$ ), and peak center of mass displacement ( $p < 0.001$ ). No other prosthetic stiffness and running speed interactions achieved significance.

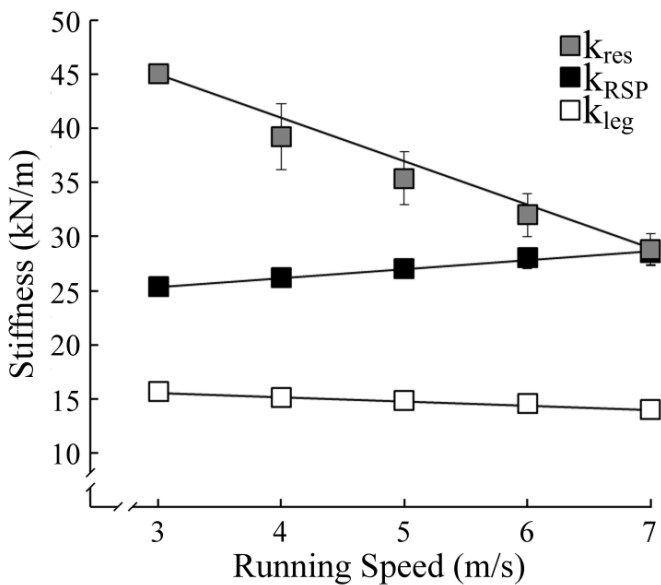


**Figure 1.** Average ( $\pm$ SE) overall leg ( $k_{leg}$ ), prosthetic ( $k_{RSP}$ ), and residual limb ( $k_{res}$ ) stiffness at each running speed and across all prosthetic configurations. Some error bars are hidden behind symbols.

We reject our initial hypothesis because both prosthetic stiffness and height influenced biomechanics across running speeds. We accept our second hypothesis since faster running speeds mitigated the effect of prosthetic stiffness on biomechanics. Furthermore, our participants generally increased both stride length and frequency to achieve faster running speeds. However, for a few trials, some participants improved speed beyond 7 m/s by decreasing stride length and rapidly increasing stride frequency.

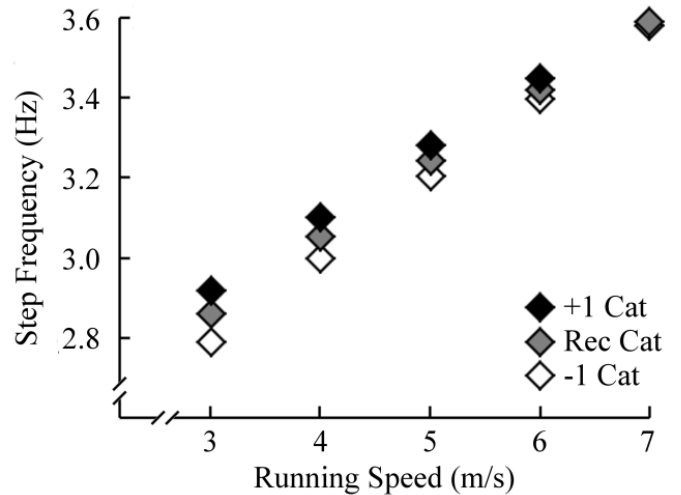


**Figure 2.** Average elicited step frequency across prosthetic models and running speeds while using running-specific prostheses at the recommended and  $\pm 1$  stiffness category (Cat) for a 70 kg subject. Step frequency =  $0.315 \text{ speed} + 0.042 \text{ stiffness (kN/m)} - 0.005 \text{ speed} \cdot \text{stiffness (kN/m)} + 1.258$ .

## CONCLUSIONS

Prosthetic stiffness, height, and running speed affect the biomechanics of athletes with bilateral transtibial amputations. Furthermore, the effect of prosthetic stiffness on biomechanics is reduced at faster running speeds, indicating that prosthetic stiffness has a greater influence on distance running than on sprinting performance for athletes with bilateral transtibial amputations.

## REFERENCES

1. Arellano CJ, et al. *Plos One* **10**, e0115637, 2015.
2. McGowan CP, et al. *J R Soc Interface* **9**, 1975-1982, 2012.
3. Weyand PG, et al. *J Appl Physiol* **107**, 903-911, 2009.
4. IPC Athletics Rules and Regulations, 2014-2015.
5. Beck ON, et al. *J Appl Physiol*, in press, 2017.
6. Weyand PG et al. *J Appl Physiol*, **108**, 950-961, 2010.

## ACKNOWLEDGMENTS

We thank Mike Litavish, Angela Montgomery, Rodger Kram, Freedom Innovations, Össur, Ottobock, and the BADER Consortium, a DoD CDMRP cooperative agreement.

# POWER AND WORK GENERATED THROUGHOUT THE RUNNING-SPECIFIC PROSTHESIS KEEL DURING RUNNING AFTER AMPUTATION

<sup>1</sup> Brian S. Baum, <sup>1</sup> Holly Johnson, <sup>2</sup> Hiroaki Hobara, and <sup>3</sup> Jae Kun Shim

<sup>1</sup> Regis University, Denver, CO, USA

<sup>2</sup> National Institute of Advanced Industrial Science and Technology, Tokyo, Japan

<sup>3</sup> University of Maryland, College Park, MD, USA

email: bbaum@regis.edu

## INTRODUCTION

The ankle joint is the primary power generator for able-bodied runners [1,2]. After amputation this joint is replaced with a mechanical prosthesis that may not fully replace the biological limb's function. Running-specific prostheses (RSPs) are usually modeled as a two-segment rigid body model where the ankle joint is defined by a single point on the keel, which is assumed to be rigid [3]. Consequently, mechanical energy analyses using such a model assume that all of the RSP power and work would be generated at that single point.

However, the RSP most likely does not generate its power and perform work at one point as the keel flexes throughout its length. Oversimplifying a biomechanical model can induce errors in the analysis and any interpretations drawn from such analysis. A multi-segment model can estimate power and work generation at various points throughout the RSP keel, providing a more comprehensive understanding of RSP keel dynamics during running. Identifying how and where the RSP keel generates power and performs work will improve modeling techniques for biomechanical analyses and can inform on prosthesis alignment, training, and RSP designs.

The purpose of this study was to improve our understanding of mechanical energy production in RSPs. We aimed to identify whether RSPs absorb and generate power and perform work throughout the keel at different running speeds. We hypothesized that (1) RSPs absorb and generate power and perform work throughout the keel, (2) RSPs do not absorb and generate power or perform work evenly throughout the keel, and (3) running

speed would not affect keel power and work performance.

## METHODS

Eight males with unilateral transtibial amputation wore their own RSPs to run overground at 2.5, 3.0, and 3.5 m/s.

10 motion capture cameras (Vicon) captured kinematic data at 200 Hz while 10 force platforms (Kistler) captured ground reaction force data at 1000 Hz. A 6-segment RSP model with 5 joints (Fig. 1) was used to estimate mechanical energy throughout the RSP keel. Joint powers and work were calculated at each joint (Fig. 2-3) via inverse dynamics using Visual3D (C-Motion).

A two-factor (Joint x Speed) repeated measures ANOVA determined peak power and total work differences with  $\alpha=0.05$ .

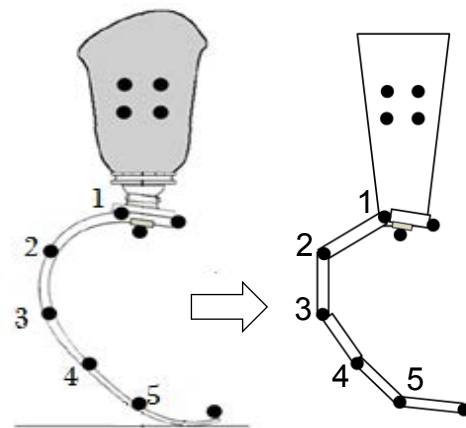


**Figure 1:** Marker placement on RSP keel and resulting 6-segment model. Power and work were calculated at points 1-5.

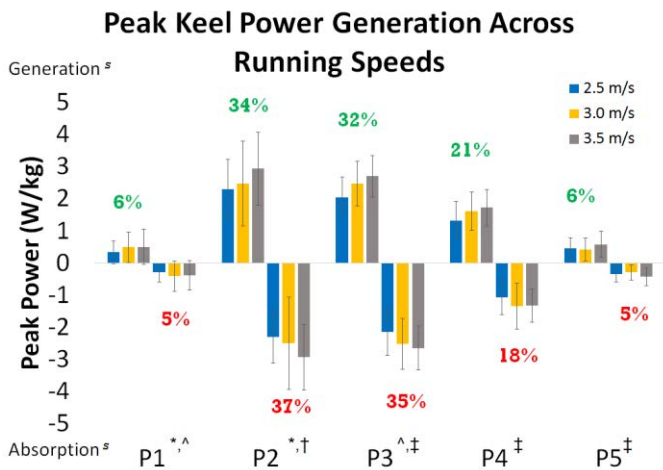


**Figure 2:** Average peak joint powers at each keel point (P1-P5) across speeds. Error bars represent  $\pm 1$ SD. Percentages represent average percent of peak power generated (green) and absorbed (red) by each point across all speeds. Symbols (\*, ^, †, ‡) indicate points that differ from each other ( $P < .05$ ). *s* indicates significant speed effects ( $P < .03$ ).

## RESULTS AND DISCUSSION

*Hypothesis 1 Accepted:* RSPs absorb and generate power throughout the keel, not at one point. Each point on the keel performed work during each running speed condition.

*Hypothesis 2 Accepted:* RSPs do not absorb and generate power or perform work evenly throughout the keel. Points significantly differed from each other in their power absorption and generation (see Fig. 2) and total work performed (see Fig. 3). Points 2, 3, and 4 absorbed and generated 85-90% of the keel power and performed 90% of the total work.

*Hypothesis 3 Accepted:* Total work did not change with speed; No interaction effect (Point x Speed) was observed for either power or work indicating the relative power and work output for each keel point did not change with speed.

*Hypothesis 3 Rejected:* Peak power absorption and generation increased with speed (see Fig. 2).

Past data conflict on whether RSP “ankle” joints produce less or more power and work compared to intact ankle joints [3,4]. Our data indicate that RSPs generate power throughout the keel, and not at one

## Total Work Performed Throughout the Keel

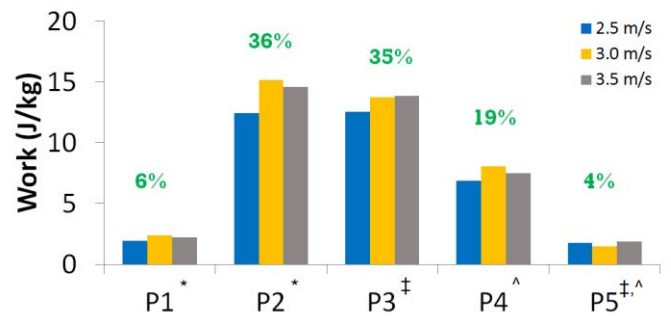


**Figure 3.** Total work performed at each keel point (P1-P5) across speeds. Average percent of work performed by each point across all speeds is shown. \*, ‡, and ^ indicate points that significantly differ from each other ( $P < .05$ ).

point. Modeling RSPs with a single “ankle” joint could induce errors in inverse dynamics analyses and lead to misinterpretations of RSP function.

Altering RSP designs to generate power and work evenly throughout the keel or optimize power generation at one point may lead to greater overall performance. Additionally, different prosthetic alignments may allow runners to optimize RSP power and work generation throughout the keel.

## CONCLUSIONS

Different RSP keel regions absorb and generate different magnitudes of power and perform differing amounts of work. Understanding RSP mechanics requires knowledge of kinematics and kinetics throughout the keel, not at only one point.

## REFERENCES

1. Novacheck TF. *Gait Posture* **7**, 77-95, 1998.
2. Winter DA. *J Biomech* **16**, 91-97, 1983.
3. Buckley JG. *Clin Biomech* **15**, 352-358, 2000.
4. Bruggemann G et al. *Sports Tech* **1**, 220-227, 2009.

## ACKNOWLEDGMENTS

This work was funded by the NIAMS R03 Award #1R03AR062321 and the University of Maryland Department of Kinesiology GRIP awards.

# DYNAMIC BALANCE DURING RUNNING USING RUNNING-SPECIFIC PROSTHESES

<sup>1</sup> Lauren A. Sepp, <sup>2</sup> Brian S. Baum, <sup>2</sup> Erika Nelson-Wong, and <sup>1</sup> Anne K. Silverman

<sup>1</sup> Department of Mechanical Engineering, Colorado School of Mines, Golden, CO, USA

<sup>2</sup> School of Physical Therapy, Regis University, Denver, CO, USA

email: lsepp@mines.edu, web: fbl.mines.edu

## INTRODUCTION

The regulation of angular momentum is important for maintaining balance during gait [1]. For example, individuals who have a history of falling have difficulty controlling angular momentum during fall recovery as compared to those without a history of falling [2]. In addition, the ankle plantarflexors are critical in the regulation of angular momentum [3,4] and fallers have a reduced peak ankle moment during fall recovery [2].

Individuals with a transtibial amputation (ITTA) are characterized by the functional loss of the ankle plantarflexors and have greater ranges of angular momentum during walking [5], which helps explain their greater risk of falling [6] and altered movement strategies. However, whole-body angular momentum has not been examined in ITTA during running.

Understanding movement coordination to provide propulsion, support and balance during running is important in evaluating running performance. Thus, the purpose of this study was to quantify whole-body angular momentum in people with and without transtibial amputations during running. We hypothesized that ITTA using running-specific prostheses (RSPs) would have greater ranges of whole-body angular momentum in all three anatomical planes during running compared to able-bodied individuals.

## METHODS

Five male runners with a unilateral transtibial amputation (mean  $\pm$  SD: height = 1.78  $\pm$  0.09m, mass = 82.9  $\pm$  16.5 kg) and five able-bodied (AB) male runners (mean  $\pm$  SD: height = 1.83  $\pm$  0.06m, mass = 81.3  $\pm$  9.39 kg) participated in the study. Each participant with an amputation ran with their

prescribed RSP. RSP mass and inertial properties were measured for each participant [7]. Participants ran continuously along a 100m track at 3.0 m/s. Speed was monitored using laser sensors during a 25m straightaway. Kinematics were collected at 200Hz using a ten-camera motion capture system and a full-body marker set.

Kinematics were filtered using a fourth-order Butterworth filter with a cutoff frequency of 6 Hz. Whole-body angular momentum ( $\vec{H}$ ) was calculated from body kinematics using a 15-segment model in Visual3D using the following equation:

$$\vec{H} = \sum_{i=1}^n [(\vec{r}_i^{COM} - \vec{r}_{body}^{COM}) \times m_i(\vec{v}_i^{COM} - \vec{v}_{body}^{COM}) + I_i \vec{\omega}_i]$$

where  $\vec{r}_i^{COM}$ ,  $\vec{v}_i^{COM}$ , and  $\vec{\omega}_i$  are the position, velocity, and angular velocity of the  $i$ th segment respectively;  $\vec{r}_{body}^{COM}$  and  $\vec{v}_{body}^{COM}$  are the position and velocity of the center of mass of the whole body respectively; and  $m_i$  and  $I_i$  are the mass and inertia matrix of the  $i$ th segment respectively.  $\vec{H}$  was normalized by participant height, mass, and running speed. Comparisons for overall range of  $\vec{H}$  (peak-to-peak amplitude) between AB and ITTA were calculated using t-tests ( $\alpha=0.05$ ).

## RESULTS AND DISCUSSION

Sagittal and frontal plane  $\vec{H}$  ranges for ITTA were significantly greater ( $p < 0.001$  and  $p = 0.038$ , respectively) compared to AB individuals (Fig. 1), which is consistent with prior studies of walking [5]. Range of  $\vec{H}$  in the transverse plane was not significantly different between groups ( $p = 0.131$ ).

The net external moment equals the time rate of change of  $\vec{H}$ . Thus, greater values of  $\vec{H}$  suggest that ITTA may have difficulty recovering from

unexpected perturbations in the sagittal and frontal planes during running, as a greater external moment is required to restore the  $\vec{H}$  of the body to zero. In addition, ITTA have reduced muscular control at the ankle due to the loss of the plantarflexors, which are critical for balance regulation [3,4]. Thus, ITTA have a reduced capability to quickly modulate the external moment in response to a perturbation.

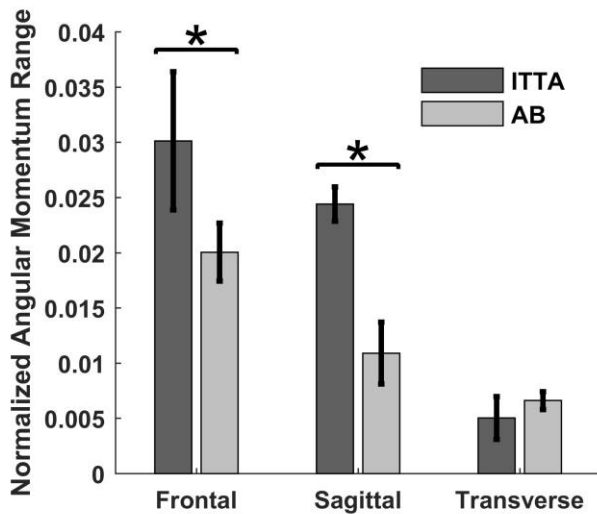


**Figure 1:** Normalized whole-body angular momentum range  $\pm$  one standard deviation in ITTA and AB individuals during running at 3.0 m/s. ‘\*’ indicates a significant difference between groups

Mediolateral ground reaction forces (GRFs) and vertical GRFs factor into frontal plane  $\vec{H}$  through their contributions to the external moment about the body center of mass. A reduction in mediolateral GRFs in the affected limb of ITTA [8] resulted in a reduction in its negative external moment generation toward the affected limb. Thus, the frontal plane  $\vec{H}$  trajectory had a greater positive slope (toward the intact limb) during prosthetic limb stance (~0-33% of the gait cycle, Fig. 2). Larger vertical GRFs during intact limb stance (~50-83% of the gait cycle) [8] contribute to a larger negative external moment (toward the affected limb). These asymmetric GRFs in ITTA result in a greater range of frontal plane  $\vec{H}$  relative to AB participants.

Reduced mediolateral GRFs resulting in an increase in frontal plane  $\vec{H}$  range may provide rationale for prosthetic design considerations. RSPs are typically designed for sagittal plane motion on flat surfaces (like a track). However, restoring mediolateral GRF generation in RSPs could improve their application

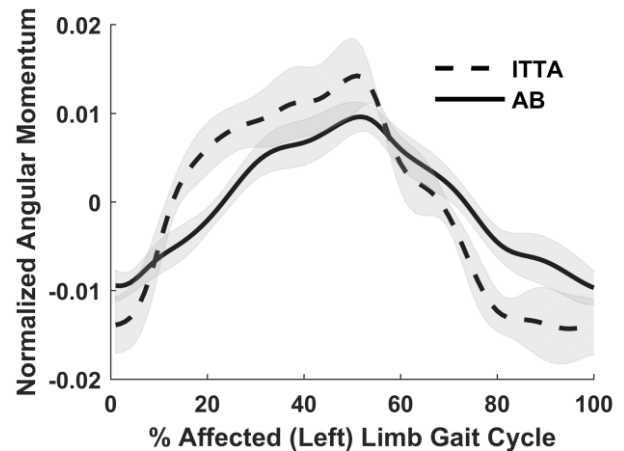


**Figure 2.** Average frontal plane whole-body angular momentum ( $\pm$  1 standard deviation indicated by the shaded area) for the ITTA and AB participant groups running at 3.0 m/s

to uneven surfaces like natural trails, where frontal plane balance is more challenging to maintain.

## CONCLUSIONS

Greater ranges of whole-body  $\vec{H}$  in the frontal and sagittal planes for ITTA during running highlight altered running strategies for ITTA due to the loss of the plantarflexors and subsequent changes in GRFs. Regulating  $\vec{H}$  in the frontal plane by altering prosthesis design to better incorporate mediolateral force control may improve the ability of ITTA to regulate dynamic balance during running.

## REFERENCES

- Herr H, et al. *J Exp Biology* **211**, 467–81, 2008.
- Pijnappels M, et al. *Gait Posture* **21**, 388–94, 2005.
- Neptune RR, et al. *J Biomech* **44**, 6-12, 2011.
- Neptune RR, et al. *J Biomech* **49**, 2975-81, 2016.
- Silverman AK et al. *J Biomech* **44**, 379-85, 2011.
- Miller WC, et al. *Arch Phys Med Rehabil* **82**,1031-7, 2001.
- Baum BS, et al. *Arch Phys Med Rehabil* **94**, 1776-83, 2013.
- Baum BS, et al. *J Appl Biomech* **32**, 287-94, 2016.

## ACKNOWLEDGMENTS

This work was funded by DoD Award #W81XWH-15-1-0518.

## ASB-SICB JOINT SYMPOSIUM: INSIGHTS FROM ANIMAL BIOMECHANICS

<sup>1</sup>Elizabeth L. Brainerd, <sup>2</sup>Suzanne M. Cox, <sup>3</sup>Gregory S. Sawicki, <sup>1</sup>Aaron M. Olsen,  
<sup>4</sup>Brooke E. Flammang, <sup>5</sup>Andrew A. Biewener, <sup>2</sup>Jonas Rubenson

<sup>1</sup>Department of Ecology and Evolutionary Biology, Brown University, Providence, RI, USA

<sup>2</sup>Biomechanics Laboratory, Department of Kinesiology, Penn State University, University Park, PA, USA

<sup>3</sup>Joint Department of Biomedical Engineering, NCSU / UNC Chapel Hill, Raleigh, NC, USA

<sup>4</sup>Department of Biological Sciences, New Jersey Institute of Technology, Newark, NJ, USA

<sup>5</sup>Concord Field Station, Department of Organismal and Evolutionary Biology, Harvard University, Cambridge, MA, USA

Email: [jonas@psu.edu](mailto:jonas@psu.edu) web: <http://sites.psu.edu/biomechanics/>

### INTRODUCTION

The symposium, co-organized by the ASB and the Society for Integrative & Comparative Biology (SICB), aims to foster dialogue between the societies and to stimulate interchange between human-centered and comparative biomechanics fields. The theme of the symposium is the use of the ‘comparative’ approach to uncover biomechanical principles. The symposium will span both terrestrial and aquatic biomechanics. Exchange of technical approaches between fields will also be discussed. Finally, the symposium will showcase examples where the application to humans may not be immediately obvious, but that inspire *unexpected* scientific advances!

Symposium schedule:

Introduction – Jonas Rubenson & Elizabeth (Beth) Brainerd – 10 mins

Avian Model of Exotendons – Suzanne Cox – 15 mins

Mouth Expansion in Catfish Using XROMM – Aaron Olsen – 15 mins

Biomechanics of Strange Fishes (that don’t swim) – Brooke Flammang - 15 mins

Comparative Terrestrial Locomotion: Insights into Human Biomechanics and Biorobotics– Andrew Biewener – 15 mins

Speaker Q & A panel – 20 mins

### ROBOBIRD: AN AVIAN MODEL FOR PASSIVE-ELASTIC EXOTENDONS – Suzanne Cox, Gregory Sawicki & Jonas Rubenson

Limb orthoses, including exoskeletons, are externally worn braces or devices used to improve locomotor deficits, aid rehabilitation or augment human locomotor performance<sup>1</sup>. While robotic and passive exoskeletons have been shown to improve locomotor performance<sup>1</sup>, the limitations of human experimentation have left many important questions unanswered. More specifically, how does exoskeleton design influence muscular-tendon function<sup>2</sup>, and, in turn, locomotor performance?

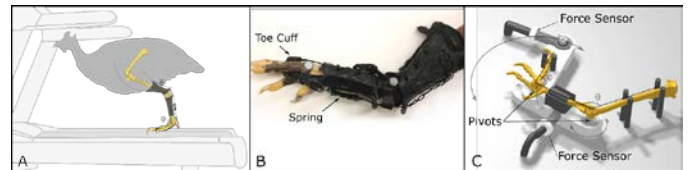


Figure 1: A) Experimental setup B) Exotendon design C) Jig for exotendon moment quantification

Here we present pilot data on a limb orthosis for a bipedal avian model (*Numida meleagris*; Fig 1A-C) that replicates the functionality of current human passive ankle-foot orthoses. In our design, the spring path spans the ankle and metatarsophalangeal (MTP) joints, mirroring the path of several digital flexors and supplementing elastic energy storage during stance phase (Fig 1B). Flexion of the phalanges acts as a natural clutch, disengaging the device during the swing phase. Using intact limb specimens, unaided joint moments at the MTP and ankle (without the exotendon) were subtracted from aided moments to quantify contribution of the exotendon across the span of limb configurations

(Fig. 1C). On combining these data with kinematic analyses of a bird running on a treadmill (n=1; Fig 1A) with and without the exotendon, we observed a 5-10% exo-tendon contribution to the moment at the MTP joint during stance phase (Fig 2). These initial experiments show promise for *in vivo* applications to study neuro-mechanical responses to exotendon augmentation and rehabilitation.

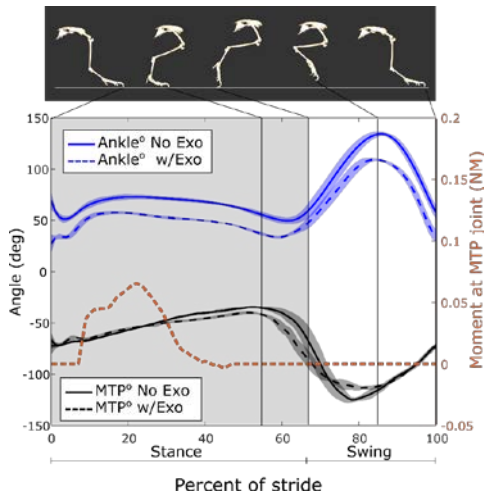


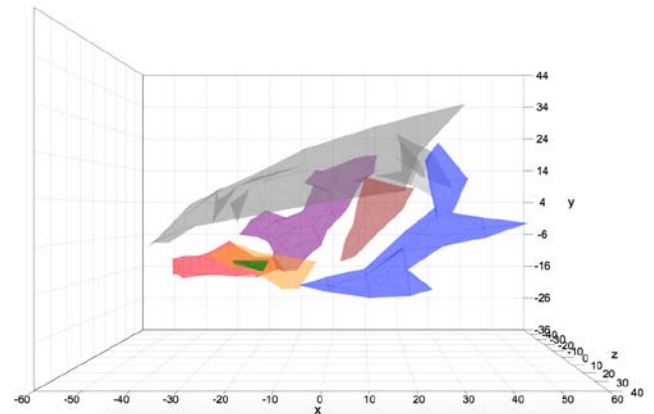
Figure 2: Exotendon moment contribution and its influence on lower limb kinematics

1. Viteckova, S., Kutilek, P. & Jirina, M. Wearable lower limb robotics: A review. *Biocybern. Biomed. Eng.* **33**, 96–105 (2013).
2. Young, A. J. & Ferris, D. P. State-of-the-art and Future Directions for Lower Limb Robotic Exoskeletons. **4320**, 171–182 (2016).

## UNCOVERING MECHANISMS OF MOUTH EXPANSION IN CATFISH USING X-RAY RECONSTRUCTION OF MOVING MORPHOLOGY – Aaron Olsen & Elizabeth Brainerd

The heads of ray-finned fishes contain over 20 mobile skeletal elements, interconnected by a morphologically and functionally varied set of articulations that allow a high degree of mobility. The interconnections among these skeletal elements form a series of coupled mechanisms that can transform input forces at a few elements into rapid expansion of the entire buccal cavity. However, how these mechanisms move and function in three dimensions and how their motion relates to their constituent joints remains unknown. To answer these questions we collected three-dimensional *in vivo* kinematics of seven interconnected cranial bones in channel catfish (*Ictalurus punctatus*)

during suction feeding using X-ray Reconstruction of Moving Morphology (XROMM). We then fit single-joint and multibody models of varying degrees of freedom (DoFs) to the *in vivo* kinematics. As expected, higher DoF models consistently have lower model errors, making it difficult to distinguish between models that have lower error because they better represent the true motion constraints and models that have lower error because they overfit errors. To resolve this, we compare the errors of models fit to the *in vivo* kinematics to the errors of models fit to simulated kinematics. We show how simulated kinematics can be used to establish null expectations for *in vivo* model fitting errors to distinguish between better-fitting and overfitted models. These results contribute to our basic understanding of how articular morphology relates to skeletal motion and demonstrate a model fitting approach applicable to a wide range of musculoskeletal systems.



Funded by NSF 1612230 and 1655756.

## BIOMECHANICS OF STRANGE FISHES THAT DON'T SWIM – Brooke Flammang

There is tremendous morphological and ecological diversity among the approximately 33,000 known species of fishes; this is particularly apparent when looking at their fins. While fishes do use their fins for swimming, fin exaptations for walking or adhering are not uncommon. For example, the blind cave loach, *Cryptotora thamicola*, walks with a salamander-like diagonal-couplet lateral sequence gait. This is accomplished in part by its tetrapod-like pelvis, which unique to other fishes, has an ilium. As a result, *Cryptotora* can support its body

on land for walking and climbing. The functional morphology and biomechanics of this fish may provide insight into the fin-to-limb transition and the origin of tetrapods. Second, remoras are fishes that have evolved a unique adaptive ability: an adhesive disc formed from dorsal fin elements that allows them to attach reversibly to actively deforming wetted bodies of varying roughness and compliance that move at high speed. The adhesive disc is a hierarchical structure, in which the lamellae, spinules, fleshy outer lip, and cranial vessels all contribute to the generation of suction and friction for initial attachment and long-term hold. Continued research on the mechanisms and the material properties of these structures is leading towards a bioinspired adhesive device that will be useful in medicine, ecology, and defense.



### **BIOMECHANICS OF MAMMALIAN AND AVIAN TERRESTRIAL LOCOMOTION: INSIGHTS INTO HUMAN BIOMECHANICS AND BIROBOTIC DESIGN – Andrew Biewener**

Comparative studies of mammalian and avian locomotion provide important insight into the neuromuscular mechanics of movement. The *in vivo* function (fiber strain, force and neural activation) of limb muscles in relation to joint mechanics, recorded across a range of locomotor behaviors, reveals how force and work are modulated in relation to neural activation across movement tasks. Studies of avian bipeds and mammalian quadrupeds suggest the existence of a proximo-distal gradient in muscle function and control. Whereas proximal muscles function to modulate limb work through

feedforward control, distal muscles utilize intrinsic F-L and F-V muscle properties reinforced by reflexive feedback to respond to perturbations for stability during running. Distal muscle-tendon units emphasize economy of muscle force generation and tendon elastic energy recovery, rather than work modulation. Postural changes in limb function dramatically affect musculoskeletal loading patterns, and musculoskeletal features of limb function can be implemented in biorobotic design for legged locomotion. Finally, *in vivo* assessment of muscle function also provides an opportunity to validate Hill-type muscle model predictions, which are frequently used to model and evaluate human movement in normal and pathological conditions. By evaluating the predictive accuracy of Hill-type muscle models, features of the model can be adjusted to improve performance. Improvement in the accuracy of time-varying force produced by muscle models can, in turn, improve their application to studies of human muscle function related to movement performance, rehabilitation and aging.

This work has been supported by NIH AR055648, and DARPA BIOD\_0010\_2003 grants.

### **THE SOCIETY FOR INTEGRATIVE & COMPARATIVE BIOLOGY**

[The Society for Integrative & Comparative Biology \(SICB\)](http://www.sicb.org) fosters research, education, public awareness and understanding of living organisms from molecules and cells to ecology and evolution. SICB encourages interdisciplinary cooperative research that integrates across scales, and new models and methodologies to enhance research and education. SICB has a strong tradition in biomechanics and vertebrate morphology. Discover more about SICB and its vibrant community by attending their annual meeting- the upcoming [2018 meeting](#) is in San Francisco, January 3-7. More information about SICB can be found at their website: <http://www.sicb.org/index.php3> .

The ASB would like to thank SICB and its Officers for supporting this symposium.

# EFFECTS OF AN OCCUPATIONAL WEARABLE ASSISTIVE DEVICE ON LOW BACK LOADS

<sup>1</sup> Mohammad Iman Mokhlespour Esfahani, <sup>1</sup> Mehdi Alemi, <sup>1</sup> Sunwook Kim,  
<sup>2</sup> Ehsan Rashedi, <sup>3</sup> Bochen Jia, and <sup>1</sup> Maury A. Nussbaum

<sup>1</sup> Virginia Tech, Blacksburg, VA, USA

<sup>2</sup> Rochester Institute of Technology, Rochester, NY, USA

<sup>3</sup> University of Michigan – Dearborn, MI, USA

email: nussbaum@vt.edu

## INTRODUCTION

Work involving arm elevation, especially at or above the shoulder level (or, overhead work), is an important risk factor for occupational shoulder musculoskeletal disorders [1]. Overhead work can be unavoidable in some workplaces, yet involves substantial exposure to overexertion, which account for nearly half of shoulder injuries with lost workdays reported in the U.S. [1].

Use of an assistive device can be an effective approach to reduce physical demands involved in overhead work. Earlier, we found that a Wearable Assistive Device (WADE) could substantially reduce upper arm and shoulder loads in overhead work [2]. We recently evaluated a new WADE (EksoBionics Inc., USA), an upper-extremity exoskeletal “Vest” that generates variable forces to support the upper extremities. While this device also reduced shoulder loads, our focus here was to assess potential adverse impacts related to the “loading pathway”, specifically whether use of such a device might increase low-back loading.

## METHODS

Twelve participants (6F & 6M) completed an experiment in which low-back loads were assessed with and without the WADE. Participants completed simulated drilling and light assembly tasks in the experiment. All participants provided informed consent, following procedures approved by Virginia Tech Institutional Review Board.

Training was first provided for the participants to learn the drilling task (see [3] for a task description). In a separate data collection session, three independent variables were experimentally manipulated in a full-factorial design: 1) Vest Intervention (with vs. without); 2) Work Task [drilling (Drilling<sub>LIGHT</sub>), drilling with additional load 2.27 kg (Drilling<sub>HEAVY</sub>), and Wiring]; and, 3) Work

Height [shoulder (SH) vs. overhead height (OH)]. For a given experimental condition, participants completed two trials of each simulated work task. Participants were instructed to complete the trial as quickly and as accurately as possible, and rest periods were provided between conditions.

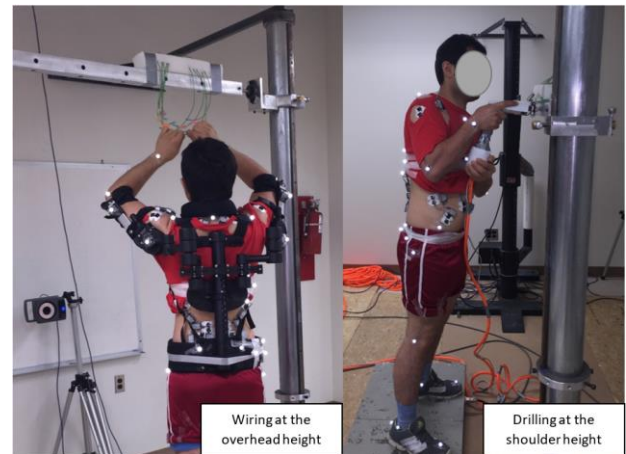


Figure 1. Illustration of drilling and wiring tasks at two work heights.

Muscle activity was monitored using surface EMG (TeleMyo Desktop DTS, Noraxon) over 14 accessible muscles in the lower lumbar region. Initial procedures were completed to calibrate an EMG-based model that estimated spinal loads (see [4] for details). Segmental body kinematics were recorded using surface markers. From the noted model, outcomes measures of peak and mean anteroposterior shear forces ( $F_{AP}$ ) and compressive forces ( $F_{COMP}$ ) were obtained, at the L5/S1 level. Separate mixed-factor ANOVAs were used to evaluate the influences of Gender, Vest, Task, and Height on these measures ( $p < 0.05$ ).

## RESULTS AND DISCUSSION

Peak and mean  $F_{AP}$  were significantly ( $p$ -values  $< 0.01$ ) affected by *Task*, and interaction effects of *Task*  $\times$  *Height* and *Task*  $\times$  *Vest* (Figure 2 Top). Peak

$F_{AP}$  decreased by  $\sim 27\%$  with the vest during shoulder-height work, however it was in general not substantially influenced by vest use.

Peak and mean  $F_{COMP}$  were significantly affected by *Task*, and interaction effects of *Height*  $\times$  *Vest* and *Task*  $\times$  *Vest* ( $p$ -values  $< 0.02$ ; Figure 2 Bottom). Use of the vest reduced peak and mean  $F_{COMP}$  forces respectively by  $\sim 15\text{-}16\%$  and  $\sim 16\text{-}18\%$  during the drilling task at shoulder height. Potential explanations for this decrease are: (1) the mass ( $\sim 6.5\text{kg}$ ) of vest and/or torso flexion created lumbar flexion moments, offsetting extension moments from the drilling task, and (2) participants needed less effort to stabilize their trunk (e.g., reduced co-contraction) because of the rigid and supportive structure of the vest. Further analyses will be needed to investigate these potential mechanisms.

In the current work, some beneficial effects of the vest were demonstrated in terms of low-back loads, though only after a rather short period of task

simulation. Hence, it is unknown whether or to what extent such effects will be maintained (or even increase) over a longer-term period. In addition to reducing shoulder loads, overall the exoskeletal vest led to reduced or comparable low back loads (i.e., both compression and shear lumbosacral reaction forces), especially during the drilling task. Thus, use of such technology may be an effective approach to reduce the physical demands and injury risk involved in overhead occupational tasks.

**Disclaimer:** EksoBionics and The Boeing Co. financially supported this research. While contributing to the study design, they were not involved in data analysis, interpretation, or decision for publication.

## REFERENCES

1. Bureau of Labor Statistics, U.S. Dept. of Labor, 2015.
2. Rashedi, E., et al. *Ergonomics*, 57, 1864-1874, 2014.
3. Alabdulkarim, S., et al. *Ergonomics*, 60, 851-66, 2017.
4. Jia, B., et al. *Int J Ind Erg*, 41(5), 437-446, 2011.

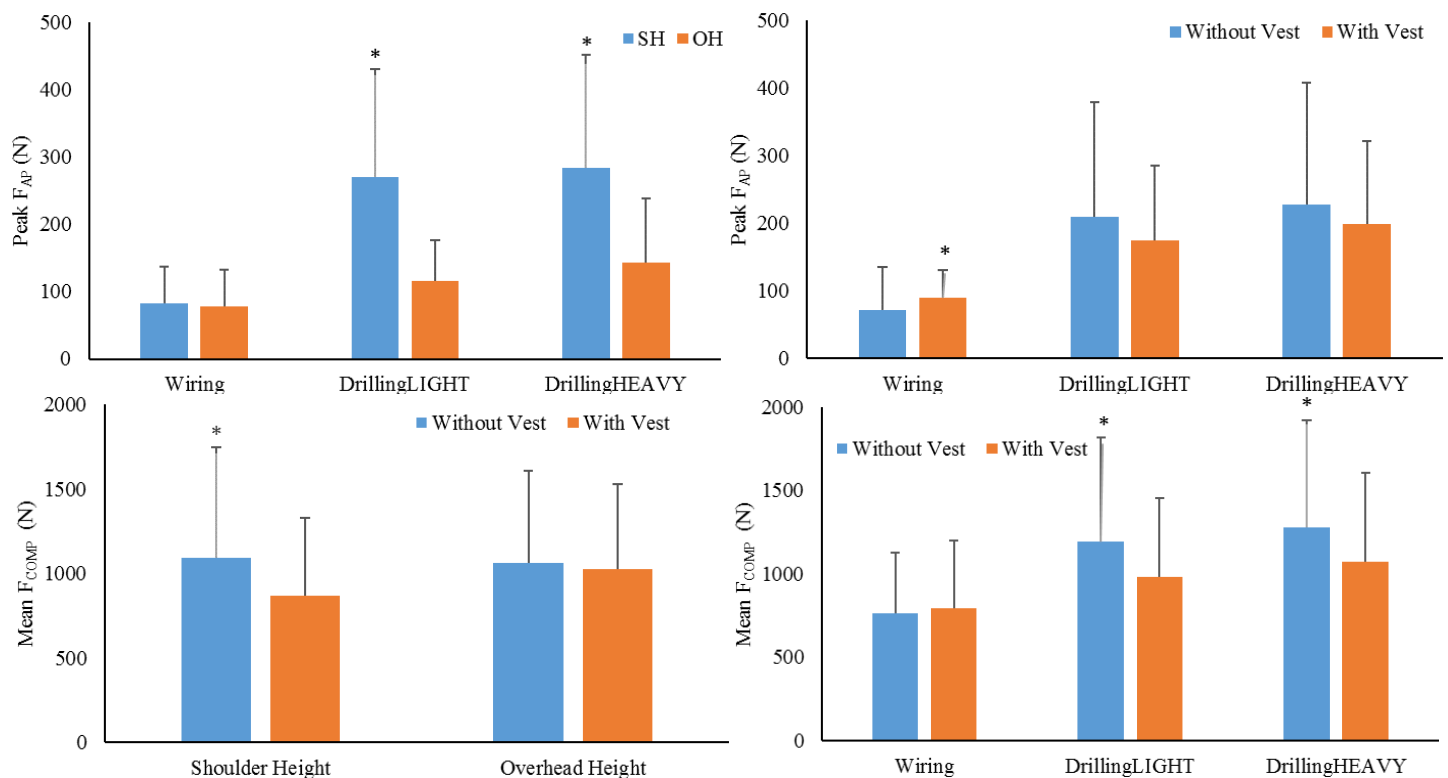


Figure 2. Top: Task  $\times$  Height and Task  $\times$  Vest interaction effects on peak lumbar AP shear forces. Bottom: Height  $\times$  Vest and Task  $\times$  Vest interaction effects on mean lumbar compressive forces. Note that \* indicates significant differences between vest/task conditions, and error bars indicate standard deviations.

# WORKSTATION CONFIGURATION AND PACKAGING TYPE INFLUENCE GROCERY STORE CASHIER ARM POSTURES

<sup>1</sup> Angelica E. Lang, <sup>2</sup> Jacquelyn M. Maciukiewicz, <sup>3</sup> Meghan E. Vidt, <sup>4</sup> Sylvain G. Grenier, and <sup>2</sup> Clark R. Dickerson

<sup>1</sup> University of Saskatchewan, Saskatoon, SK, CA

<sup>2</sup> University of Waterloo, Waterloo, ON, CA

<sup>3</sup> Arizona State University, Phoenix, AZ, USA

<sup>4</sup> Laurentian University, Sudbury, ON, CA

## INTRODUCTION

Upper limb disorders are common in grocery store cashiers, perhaps due to unique exposures. Cashiers have the highest rate of cumulative trauma disorders among all grocery store workers, accounting for up to 35% of all workplace injuries in the retail sector (1). Cashier work tasks involve repetitive movements and prolonged maintenance of awkward postures, such as arm elevation (2). Arm postures are likely influenced by the cashier environment, and certain workstation configurations and packaging containers may alter the physical demands of cashiers (3), increasing their risk for injury.

The purpose of this study was to examine the influence of cashier workstation height, packaging type, workload intensity, and side on arm elevation to delineate postural demands in cashiers.

## METHODS

Fifteen experienced cashiers (7 males, 8 females, age =  $21.5 \pm 1.9$  years) free of self-reported upper-extremity or back injury within the past year participated. The study protocol was approved by the University of Waterloo Research Ethics Board; all participants provided written informed consent.

A simulated cashier station was created for data collection, with dimensions and adjustability matching those of a standard cashier workstation. Participants performed 36 grocery scanning and packing trials. Workstation height (high, medium, low), packaging type (bin, reusable bag, plastic bag), and workload intensity (6 items, 20 items) were systematically tested in a full factorial design.

Motion of the torso and upper limbs was tracked with 8 VICON MX20 (Vicon Motion Systems, Oxford, UK) optoelectronic infrared cameras and reflective markers were placed on the skin near anatomical landmarks per ISB standards. Thoracohumeral angles were calculated for both arms and amplitude probability distribution functions (APDF) created to examine levels of arm elevations for each trial. The amplitudes of the 10<sup>th</sup> percentile, 50<sup>th</sup> percentile, and 90<sup>th</sup> percentile were extracted for each trial and arm.

A mixed effect repeated measures ANOVA with a post-hoc Tukey HSD analysis for gender, intensity, packaging type, and workstation height evaluated the main and interaction effects of each parameters on the different APDF percentiles. Paired t-tests determined bilateral differences (all tests at  $p < 0.05$ ).

## RESULTS AND DISCUSSION

Packing type and workstation height interacted to influence right arm posture at the 90<sup>th</sup> percentile APDF value, considered to be “peak” workload (Figure 1). At the high workstation height, the highest elevation values were for the reusable bags (63.9°), then bins (61.2°) and then plastic bags (55.3°). However, the low height using the bins required the lowest levels of peak arm elevation (48.2°). Moreover, the combinations of reusable bags and low height required similar elevations levels as the combination of plastic bags and medium height, at 50.7° and 50.6°, respectively.

There were also main effects of both packaging type and workstation height for both arms at the 50<sup>th</sup> and 90<sup>th</sup> percentiles. In general, reusable bags required significantly higher arm elevations than both the

bins and plastic bags. Regarding workstation height, the greatest arm elevations occurred while packing at the high heights, followed by the medium height, and then the low height, as expected.

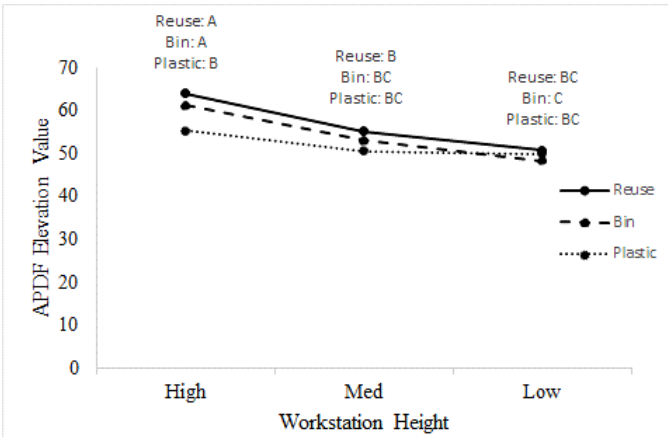


**Figure 1: Interaction of packaging type and workload height for right arm elevation. Levels sharing a letter are not significantly different ( $p < 0.05$ ).**

The differences in arm elevation levels between the different packages are consistent with the geometric profiles of each packaging type. Plastic bags have a low profile, as well as an optional lower bagging area that often cannot be used with the larger reusable options. Bins and reusable bags are taller than plastic bags, with reusable bags being the tallest (1). The main effect of packaging type on arm elevation suggests that reusable bags create the greatest postural demands for the shoulder for cashiers, and the interaction with height, particularly at the highest intensity elevations (90<sup>th</sup> percentile) highlights the need to adjust the workstation to coincide with packaging type to reduce demanding arm postures.

Arm elevation increased with workstation height in the current study, which is a commonly reported phenomena (4). It follows that increasing workstation height would result in greater arm elevations during work. The increased arm elevation

required with workstation height increases and high profile packaging containers, combined with the weighted grocery items, can increase muscular demand (5). This increased muscular demand can initiate muscle fatigue and decreased glenohumeral stability, and instigate shoulder impingement, which is a precursor to many shoulder musculoskeletal disorders (6).

Finally, the right arm had greater arm elevation postures than the left arm. This is likely a consequence of the workstation configuration; groceries were placed to the right of the participant and packaged on the left, resulting in a higher work demand for the right arm. These results indicate that cashiers may benefit from rotation through stations with mirrored layouts.

## CONCLUSIONS

For grocery store cashiers, packaging type and workstation height influence arm postures. The reusable bags and high workstation height required the greatest postural demand, suggesting that when using reusable packaging, workstations should be adjusted to the lowest height, and that lower profile reusable bags should be encouraged.

## REFERENCES

1. Health & Safety Ontario. Retrieved from <http://www.wsps.ca/>
2. Lehman KR, et al. *Ergonomics* **44**, 719-738, 2001.
3. Shinnar A, et al. *Int J Ind Ergon* **34**, 535-541, 2004.
4. Oliveira AB, et al. *Braz J Phys Ther* **15**, 494-502, 2011.
5. Maciukiewicz JM, et al. *Int J Ind Ergon*, in review.
6. Chopp JN, et al. *J Shoulder Elb Surg* **19**, 1137-1144, 2010.

## ACKNOWLEDGMENTS

This project was partially funded by a CRE-MSD seed grant. Equipment used in the grant was funded by the Canada Foundation for Innovation and the Ontario Research Fund.

# AN INVESTIGATION OF CERVICAL SPINE KINEMATICS IN VARIOUS TABLET READING POSTURES

Ethan Douglas and Kaitlin Gallagher

University of Arkansas, Fayetteville, AR, USA  
email: [kmg014@uark.edu](mailto:kmg014@uark.edu)

## INTRODUCTION

In the past five years, tablet ownership in the United States has risen from 4% to almost 50% [1]. Despite recent research associating higher neck flexion angles and muscle activity with handheld computers [2,3], ergonomic standards for these devices do not exist. Previous studies on tablet reading posture have either kept an upright trunk or not assessed different trunk angles when sitting. A survey of high school students reported that seated with a tablet in the lap and a semi-reclined trunk (the hips in front of the shoulders) was the second most common adopted tablet reading position [4]. One recent study examined the effect of a semi-reclined reading position on neck posture and found that increased trunk rotation led to higher neck flexion levels than upright seated positions, but lower neck extensor muscle activity [3]. This study only assessed external measurements of the neck, and so the biomechanical effect of trunk rotation on the cervical spine kinematics is unknown. The purpose of this study was to examine the effect of trunk rotation on cervical spine lordosis and intervertebral joint angles while viewing a tablet computer.

## METHODS

Twenty participants (11 female, weight  $71.1 \pm 11.2$  kg; height  $174.1 \pm 10.2$  cm) aged 18-34 ( $21.3 \pm 1.2$  years) were recruited to participate in this study. The inclusion criteria for participation in this study were no previous neck or spine injury, no chronic headaches, no allergy to rubbing alcohol and have not been exposed to any of the following within the past two years: lumbar spine x-ray, upper GI tract x-ray, barium enema x-ray, or any CT scans. For female participants, an additional inclusion criteria was no chance of pregnancy.

All radiographs were taken by a licensed technician. A lead marker was placed on the right tragus to estimate the head's center of mass. The first image was looking straight ahead (neutral), followed full flexion. Radiographs were then taken with the

participant reading a tablet (iPad2) in their lap in three different postures: 1) Upright seated 2) Semi-reclined ( $20^\circ$  with respect to vertical) 3) Reclined ( $45^\circ$  inclination with respect to vertical) (Figure 1).



Figure 1. Tablet reading positions. (Left to right: Upright, Semi-reclined, Reclined).

All measurements were manually taken by the experimenter using ImageJ and custom MATLAB code. Measurements taken were centroid cervical lordosis (CCL), (represents the lower cervical lordosis angle from C7 to C3 [5]), skull angle with respect to the horizontal, skull-C1, C1-C2, and C2-C3 joint angles, and gravitational moment arm. All measurements were analyzed using one-way repeated measures ANOVAs ( $\alpha=0.05$ ) with a within-factor of position (Neutral/Upright/Semi-reclined/Reclined). Tukey's HSD tests were run to analyze significant main effects.

## RESULTS AND DISCUSSION

There was a main effect of position for CCL ( $p<0.0001$ ), moment arm ( $p<0.0001$ ), C1-C2 ( $p<0.001$ ), C2-C3 ( $p=0.0014$ ), and Skull angle ( $p<0.001$ ). There was no main effect of position for the Skull-C1 angle.

CLL angle became increasingly more flexed when viewing the tablet with an upright trunk compared to the semi-reclined ( $p<0.0001$ ) and reclined trunk ( $p<0.0001$ ) positions. The gravitational moment arm of the head was largest when reading the tablet with an upright trunk compared to the semi-reclined

( $p=0.0248$ ), and reclined ( $p=0.0071$ ) positions (Table 1). The moment arm for the reclined position was not significantly different from neutral. Compared to neutral, the C1-C2 angle was more flexed in the C1-C2 ( $p<0.0001$ ), semi-reclined ( $p=0.0032$ ) and reclined ( $p=0.0010$ ) position. There were no significant differences between C1-C2 for three positions. C2-C3 was also more flexed in the semi-reclined ( $p=0.0008$ ) and reclined ( $p<0.0257$ ) position compared to neutral. The upright position was not different from any of the positions. The skull angle with respect to the horizontal was more flexed than neutral in all positions ( $p<0.001$ ); however, the head experienced the least amount of flexion in the reclined position ( $p=0.0421$ ).

The gravitational moment arm was highest when the person was reading with the upright trunk posture, which agrees with previous findings [2]. Our results also follow previous results demonstrating that the head is more in line with the horizontal in the reclined position versus the semi-reclined and upright sitting positions[4], decreasing the moment arm. Sitting in a reclining position could have some benefits for decreasing the required muscle activation to support the head.

The potential risks of a reclined posture can be seen in the lower cervical spine. While moment arms decreased with trunk rotation, the CCL angle increased. This result is in line with previous work that showed head-to-trunk flexion was greatest in this posture compared to reading a tablet off the lap with an upright posture [3]. Many cervical erector spinae muscles originate inferior to C7 and insert on the upper cervical spine. A larger CCL angle could increase the passive tension applied to the muscles

and ligaments, change where these muscles operate on the force-length curve for active tension development and alter their muscle moment arm.

While the CCL saw increased flexion with the reclined position, there were no subsequent compensations in the upper cervical spine. The intervertebral joints were only slightly more flexed compared to neutral, and the skull-C1 angle was the same for all positions. With the lower cervical spine more flexed with small changes in the upper cervical spine posture, the normal cervical lordosis still will not be maintained. There was also a large variability in the intervertebral joints (Table 1). Participants might adopt different strategies within the cervical vertebrae to achieve similar neck flexion angles. Future work should further investigate this variation in intervertebral joint angles with neck flexion.

## REFERENCES

1. Pew Research Center. <http://www.pewinternet.org/2015/10/29/technology-device-ownership-2015/>
2. Vasavada AN., Nevins DD., Monda, SM., Hughes E., & Lin DC. (2015). *Ergonomics*, **58**(6).
3. Douglas EC & Gallagher KM. (2017). *Applied Ergonomics*, **60**.
4. Shan Z., Deng G., Li J., Li Y., Zhang X., Zhao Q. (2013). *PLoS One*, **8**(10).
5. Ohara. (2006). *Spine*, **31**(22).

## ACKNOWLEDGMENTS

An Arkansas Department of Higher Education Student Undergraduate Research Fund Grant supported this project.

**Table 1:** Mean values and standard deviations of measurements with respect to position. <sup>a</sup>=significant difference between all positions. <sup>bcd</sup>= positions with same letters are not significantly different. - = flexion, + = extension

Measure	Position			
	Neutral	Upright	Semi-Reclined	Reclined
CCL (degrees) <sup>a</sup>	4.8 ± 7.0	-4.4 ± 4.8	-8.2 ± 3.8	-11.0 ± 3.2
Moment Arm (cm)	4.4 ± 0.9 <sup>b</sup>	7.9 ± 1.9 <sup>c</sup>	6.5 ± 1.7 <sup>d</sup>	5.2 ± 2.3 <sup>b</sup>
Skull (degrees)	3.0 ± 5.4 <sup>b</sup>	-21.1 ± 9.1 <sup>c</sup>	-16.2 ± 9.6 <sup>c</sup>	-10.7 ± 12.6 <sup>d</sup>
Skull – C1 (degrees)	-13.2 ± 10.1	-11.4 ± 10.3	-11.9 ± 10.2	-11.4 ± 10.3
C1 – C2 (degrees)	31.2 ± 7.3 <sup>b</sup>	25.5 ± 7.9 <sup>c</sup>	27.5 ± 8.0 <sup>c</sup>	27.2 ± 7.3 <sup>c</sup>
C2 – C3 (degrees)	3.6 ± 5.2 <sup>b</sup>	.47 ± 5.5 <sup>bc</sup>	-1.3 ± 6.7 <sup>c</sup>	.09 ± 5.0 <sup>c</sup>

# FINGER FLEXOR TENDON AND SUBSYNOVIAL CONNECTIVE TISSUE MOTION WITH EXTERNAL MECHANICAL PRESSURE AND PARTIAL OCCLUSION

Amanda Farias Zuniga<sup>1</sup>, Calvin Tse<sup>2</sup>, Peter Keir<sup>1</sup>

<sup>1</sup> Department of Kinesiology, McMaster University, Hamilton, Canada

<sup>2</sup> Rehabilitation Sciences, University of British Columbia, Vancouver, Canada  
email: fariasza@mcmaster.ca

## INTRODUCTION

Carpal tunnel syndrome (CTS) is a highly prevalent neuropathy resulting from median nerve compression, and manifesting into neurological symptoms affecting the hand and wrist. The subsynovial connective tissue (SSCT) is a collagenous network surrounding tendons and the median nerve in the carpal tunnel, and serves to facilitate independent motion between tunnel contents. Cumulative injury to finger flexor tendons and the adjacent SSCT has been postulated as a precursor to CTS development [1]. Moreover, women are more likely to develop CTS [2], suggesting that sex, among other factors, may be a risk factor in CTS development.

Previous investigations have suggested that externally applied pressure to the hand and forearm increase carpal tunnel pressure, subsequently increasing gliding resistance between carpal tunnel contents [3]. Additionally, acute ischemia has been shown to elicit transient CTS symptoms, altering the fluid environment within the tunnel and affecting the viscoelastic properties within [4], ultimately effecting tendon motion.

The current investigation examined the relationship between flexor digitorum superficialis (FDS) tendon–SSCT relative motion with external pressure applied to the hand and forearm, and with local ischemia through brachial (cuff) compression. We hypothesized that each of the compression conditions would increase tendon-SSCT shear strain as measured by their individual tissue displacements

## METHODS

FDS tendon and SSCT motion in 19 healthy subjects (10 men; age= 23 ± 2.2 years) were

measured at baseline and in three experimental conditions: palmar compression (Figure 1A), forearm compression (Figure 1B), and partial ischemia (via brachial arteriovenous occlusion)(Figure 2). Palmar and forearm compression were achieved through custom force applicators using external weights resulting in 5 kg of compression. Participants performed repeated cycles of finger flexion-extension in each experimental condition and at two speeds (0.75 and 1.25 Hz), while tendon-SSCT motion was observed using a Vivid q BT10 sonographic imaging system (GE Healthcare, WI, USA). Colour Doppler imaging was used to measure FDS tendon and SSCT velocities. To compare tendon-SSCT relative displacement, tissue velocities were filtered and integrated to calculate FDS tendon displacement, SSCT displacement, FDS-SSCT relative displacement, and Shear Strain Index (SSI) ( $FDS_{Disp}-SSCT_{Disp}$ ) /  $FDS_{Disp}$ ). This technique using colour Doppler imaging has been validated against cadaveric displacements as an effective method for evaluating tendon-SSCT relative motion [5]. Repeated Measures ANOVAs were performed for each variable and separated by session, and Bonferroni-corrected post-hoc t-tests performed on significant effects.

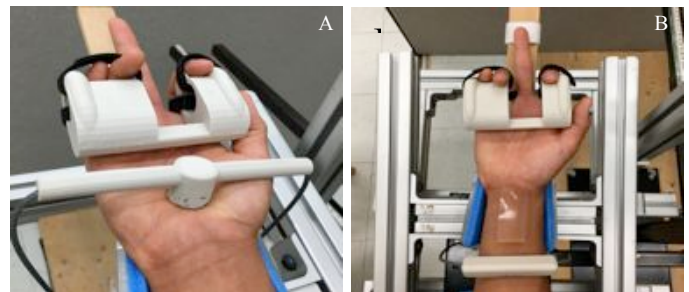


**Figure 1:** Palmar (A) and forearm (B) force applicators with 5kg weight secured via steel cables.



**Figure 2:** Partial ischemia condition with manual blood pressure cuff placed around upper arm and pressure gauge to monitor compression level.

## RESULTS AND DISCUSSION

A significant main effect of compression was found for FDS displacement ( $p < 0.05$ ), with forearm compression resulting in significantly less tendon displacement compared to baseline. Velocity of finger movement during compression significantly affected FDS displacement ( $p < 0.001$ ), SSCT displacement ( $p < 0.001$ ), tendon-SSCT relative displacement ( $p < 0.001$ ) and SSI ( $p < 0.001$ ), whereby fast finger movement decreased tendon and SSCT displacement, and increased tendon-SSCT relative displacement and SSI (Figure 3).

Under partial ischemia, there was a small but significant main effect of ischemia on SSCT displacement ( $p < 0.05$ ) such that ischemia decreased SSCT displacement. Furthermore, fast movement velocity significantly decreased FDS displacement ( $p < 0.001$ ) and SSCT displacement ( $p < 0.001$ ), while tendon-SSCT relative displacement ( $p < 0.01$ ) and SSI ( $p < 0.001$ ) were greater in the fast movement condition (Figure 4). Although not a main objective, further investigation suggests differences in SSCT and FDS displacement under partial ischemia may be explained by sex. A significant Sex  $\times$  Speed interaction effect was observed for both SSCT and FDS displacement under ischemia. For instance, in men, FDS displacement decreased under slow finger movement and increased with fast movement, while FDS displacement in women decreased under both movement speeds. Further post-hoc analysis will aim to explain these sex differences.

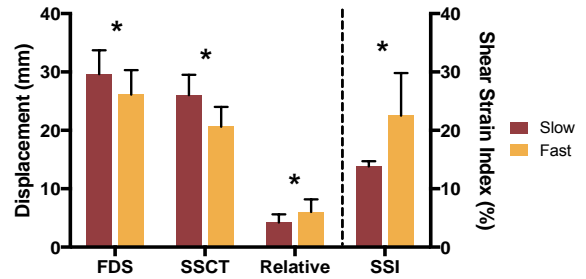


**Figure 3:** Tissue displacement and shear strain index (SSI) for slow and fast movement velocities during the palmar and forearm compression session.

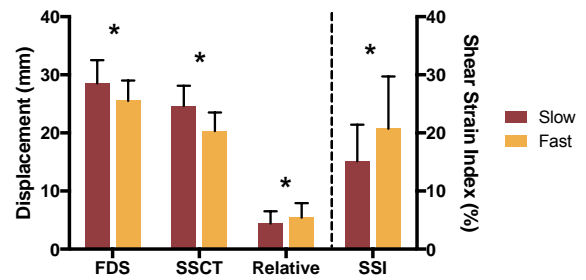


**Figure 4:** Tissue displacement and shear strain index (SSI) for slow and fast movement velocities during the partial ischemia session.

## CONCLUSIONS

Our investigation shows compression and partial ischemia alters FDS tendon and SSCT displacement. Some results suggest greater risk for tendon-SSCT shear injury, particularly under partial ischemia. Faster movement velocities resulted in greater relative tendon-SSCT displacement *in vivo*, an observation previously made in cadaver studies. Preliminary analyses suggest an avenue for sex-related differences in tendon mechanics. This investigation aims to improve the current understanding of mechanisms underlying CTS, specifically related to mechanical compression and ischemia and may be helpful in developing ergonomic interventions.

## REFERENCES

1. Vanhees et al. *J. Orthop. Res.* **11**, 1732-37, 2012.
2. Gruber et al. *J. Med. Ultr.* **43(3)**, 413-20, 2016.
3. Zhao et al. *J. Orthop. Res.* **29(1)**, 62-6, 2011.
4. Faller. *Clin. Exp. Pharma. Physiolo.* **26(1)**, 74-84, 1999.
5. Tat et al. *J Ultrasound Med.* **34(4)**, 679-87, 2015.

## Applied hand-rung forces after a ladder perturbation

Erika Pliner and Kurt Beschoner  
University of Pittsburgh, Pittsburgh, PA, USA  
email: beschorn@pitt.edu

### INTRODUCTION

The majority of fatal falls are to lower levels with ladders accounting for the plurality of these falls [1]. Improved understanding of falling dynamics is critical for developing preventative strategies. For example, previous research on stair fall dynamics have been used to inform handrail design [2]. A significant gap in the ladder fall literature is the magnitude of hand-rung forces applied after a ladder perturbation. The translation of these results will assist in determining whether rung designs enable the force generation required to recover from a ladder perturbation. Furthermore, the interaction between the upper and lower body kinetics during falling are not well understood. This understanding is important since reestablishing the feet back onto the ladder rungs is an important part of recovery process [3]. The purpose of this study is to quantify hand-rung forces during climbing and determine the impact of upper and lower-body responses on these forces.

### METHODS

Thirty-five (13 females) participants climbed a custom-designed, vertically fixed ladder 30 times. Participants experienced a simulated ladder misstep perturbation during six of the climbs (3 per climbing direction) [4]. Onset of perturbation corresponded to the timing of when a person is most likely to experience a slip [3]. Kinetic data was collect from eight unidirectional load cells (2000 Hz) placed on the eighth and ninth rungs (two on the ends of each rung to collect horizontal and vertical forces). Participant safety was ensure with a fall arrest system, and informed consent and IRB approval was obtained prior to testing.

Four hand placement responses from the hand that moved during the perturbation or the hand that was next to move (moving hand) were observed: HP2 – moved two rungs from initial position; HP1 – moved one rung from initial position; HP0 – elevated and returned to initial position; HPN – did not move.

Three foot placement responses were observed after the perturbation: FP2 – both feet reestablished foot placement with the rung(s); FP1 – one foot reestablished foot placement with a rung; FP0 – neither foot reestablished foot placement with a rung. The time window used for all analyses started with the perturbation onset, and the end of the perturbation was defined based on harness forces and downward displacement of the body [4].

The peak horizontal, vertical, and resultant forces applied to rungs 8 and 9 were calculated for the moving hand and the hand that did not move (non-moving hand) during the falling event. The peak forces were only determined if either hand ended or was located on rungs 8 or 9. The separated and combined rungs forces where only assessed if both hands were on these rungs. Peak forces were normalized by body weight. In addition, the angle of the resultant force with respect to the vertical was determined to assist in the characterization of resultant forces applied to a ladder rung.

Repeated-measure ANOVA methods were used with the moving hand, non-moving hand, and combined hands peak resultant force as the dependent variables. The independent variables were subject number (random), gender (confounding), and hand and foot placement response. All analyses were conducted separately for ascent and descent. A Tukey HSD post hoc was run on significant hand and foot placement response effects.

### RESULTS

The non-moving hand peak forces and resultant force angle were greater than those of the moving hand. The combined resultant forces were slightly larger than the subject's body weight for ascent and about 20% larger than their body weight for descent. The combined resultant force angle was about the average resultant force angle from both hands (Table1).

Resultant peak forces were affected by hand and foot placement responses for ascending and descending ladder perturbation recoveries. During ascent, the moving hand had greater peak force for the FP0 compared to the other two foot placement responses. Similarly, the non-moving hand and combined hands had greater peak forces for FP0 than FP2 (Fig.1). In addition, the non-moving hand had greater peak forces for HP0 and HPN compared to HP2 (Fig.2). During descent, applied peak forces were similar across foot responses and varied across hand responses for the moving and non-moving hands. Specifically, the moving hand generated greater force levels for HPN than HP2. The opposite effect occurred with the non-moving hand generating a greater force for HP2 compared to the HPN response.

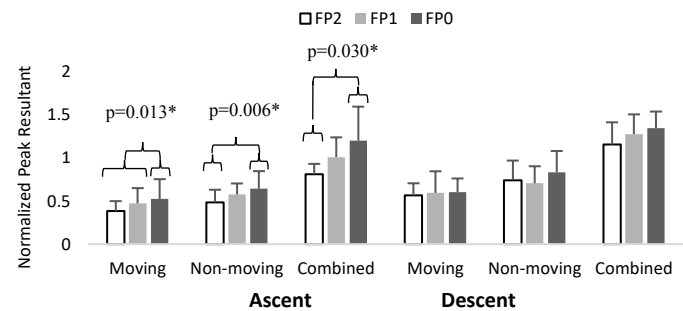


**Figure 1:** Normalized peak resultant forces applied to the rungs across foot placement responses after ascent and descent perturbations.

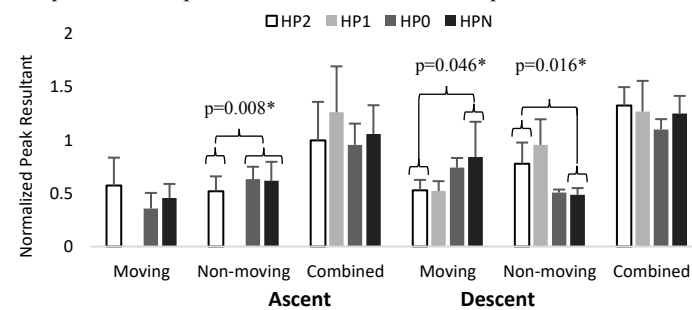


**Figure 2:** Normalized peak resultant forces applied to the rungs across hand placement response after ascent and descent perturbations

## DISCUSSION

Peak resultant forces per hand varied between 47% and 75% of participant body weight (BW). These results add context to previous work that investigated

the peak force persons could generate across different handhold designs. Specifically, we would not anticipate hand forces to be a limiting factor when grasping a horizontal cylindrical rung since the achievable forces on this design are approximately 94%-117% BW [5]. However, hand forces may be a limiting factor when grasping a vertical cylinder (68%-72% BW) or vertical plate (50%-55% BW) [5]. While force distribution varied across the moving and non-moving hand for hand placement responses, the overall combined hand force was similar across hand placement responses. This suggests that the applied forces from the upper body are similar regardless of hand placement response. During ascending ladder perturbations, greater forces were applied to the rungs when neither foot reestablished foot placement with the ladder rung(s). Thus, participants that do not utilize their lower body to recover after a ladder perturbation may need to compensate with a greater upper body response.

## CONCLUSIONS

This study reinforces previous research suggesting that a horizontal cylinder is sufficient to facilitate the generation of hand forces used in response to a ladder perturbation. In addition, this study gives insight on how different hand and foot placement responses facilitate recovery after a ladder perturbation. Overall, these results can be used to support safer ladder handhold designs, and increase the understanding on the interaction between upper and lower body kinetics during falling.

## REFERENCES

1. BLS, *National Census of Fatal Occupational Injuries in 2011*, Washington, D.C., '12
2. Dusenberry et al. *Apl. Ergonomics* 40, 657-69, '09
3. Schnorenberg et al. *J Biomech* 48, 3810-15, '15
4. Pliner et al. *Ergonomics* 57, 1739-49, '14
5. Young et al. *Human Factors*, 51, 705-17, '09

**Table 1:** Average (standard deviation) peak rung forces and resultant force angle for the moving hand, non-moving hand, and combined hands.

	Moving Hand				Non-moving Hand				Combined			
	Horizontal	Vertical	Resultant	Angle	Horizontal	Vertical	Resultant	Angle	Horizontal	Vertical	Resultant	Angle
<b>Ascent</b>	0.18 (0.09)	0.44 (0.19)	0.47 (0.19)	15.8 (25.2)	0.27 (0.05)	0.54 (0.16)	0.58 (0.16)	21.5 (10.8)	0.40 (0.09)	0.98 (0.32)	1.05 (0.32)	18.7 (8.3)
<b>Descent</b>	0.23 (0.13)	0.55 (0.17)	0.59 (0.20)	19.8 (9.8)	0.32 (0.08)	0.69 (0.20)	0.75 (0.22)	21.2 (6.6)	0.48 (0.10)	1.20 (0.21)	1.28 (0.22)	20.9 (3.6)

# COMPARISON OF SURROGATE 50<sup>TH</sup> PERCENTILE HUMAN HEADFORMS TO AN ADULT MALE POPULATION USING 3D MODELING AND PRINCIPAL COMPONENT ANALYSIS

<sup>1</sup> Kristie Liu, <sup>1</sup> David J. Greencorn, <sup>1</sup> Daniel I. Aponte, <sup>2</sup> Shawn M. Robbins, and <sup>1</sup> David J. Pearsall

<sup>1</sup> Department of Kinesiology and Physical Education, McGill University, QC, CAN

<sup>2</sup> School of Physical & Occupational Therapy, McGill University, QC, CAN

email: kristie.liu@mail.mcgill.ca, web: <http://www.mcgill.ca/ihrghome>

## INTRODUCTION

Sport helmets are designed based on surrogate headforms used for impact testing. For ice hockey, the Canadian Standards Association currently requires all testing to be done on the CEN EN 960 standard headform <sup>[1]</sup>, built to the dimensions of a 50<sup>th</sup> percentile male <sup>[2]</sup>. However, head shapes can vary substantially across users of the same head circumference size. This may explain in part why individuals with similar head circumference favour different hockey helmet models and adjustment settings <sup>[3]</sup>. Of greater concern, poor helmet-to-head fit may reduce helmet effectiveness <sup>[4]</sup>.

The objective of this study was to compare the head shapes of two 50<sup>th</sup> percentile male headforms and a subset of the male sample from Greencorn (2017).

## METHODS

3D models of 23 adult male heads and 2 medium sized headforms (CEN EN 960 and NOCSAE) were created using a 3D acquisition protocol. Human subjects in this study were adult Caucasian males (ages 20-32) who exclusively wore medium sized helmets; these subjects will hereafter be referred to as medium heads. 3D acquisition was completed using photogrammetry, a technique that constructs 3D models from overlapping images. A series of digital images were taken of the subjects at multiple angles, and the software AutoDesk ReMake™ was used to render the pictures into 3D models.

Data analysis was completed by comparing three 2D slices taken from the 3D models. First, the 3D models were oriented to have the centre of the Frankfurt Plane (transverse plane passing through the inferior borders of the bony orbit and the upper

margins of the auditory meatus) positioned at the origin. Next, slices were taken at 50mm (Plane 1), 65mm (Plane 2) and 80mm (Plane 3) above the Frankfurt Plane. Principal Component Analysis was performed on Planes 1, 2, and 3 of all subjects to determine the largest components of head shape variability. Z-scores were determined and ranked for each of the three greatest principal components (i.e. PC1, PC2, and PC3) of Planes 1, 2, and 3. Independent samples t-tests were run to compare the average radius of the medium heads to the average radius of the headforms in each of the three planes.

## RESULTS AND DISCUSSION

The ranks of the Z-scores of the CEN EN 960 and NOCSAE headforms demonstrate substantial differences from the median score for most principal components and planes; these ranks are presented in Table 1. PC1 represents difference in scale (or average radius), PC2 represents difference in length to width ratio, and PC3 represents difference in front and back head width. These principal components account for 8-72% of total variability in each plane.

A 50<sup>th</sup> percentile head shape was expected to have Z-score ranks between 8 and 17. For PC1 of all planes, both the CEN EN 960 and NOCSAE headforms ranked within the top 5 scores, thus falling at an end of dataset. This corresponded to the headforms' smaller average radii compared to the medium heads. Across PC2 of all planes, both headforms ranked in the bottom 5 scores, suggesting the headforms are wider and shorter (i.e. more circular) than the rest of the sample. For PC3, CEN EN 960 ranked 18<sup>th</sup>, 15<sup>th</sup>, and 2<sup>nd</sup> for Planes 1, 2, and 3, respectively; Planes 1, 2, and 3 of NOCSAE ranked 13<sup>th</sup>, 12<sup>th</sup>, and 7<sup>th</sup>, respectively.

PC1 indicated that headforms are smaller than the mean of the medium heads: this suggests that headforms may replicate a human cranium without accounting for the thickness of the superficial tissues of the head. The Z-score rankings for PC3 suggest both headforms are near or within the median for the difference in front and back head width at Planes 1 and 2. At Plane 3, both headforms ranked high, indicating a wider front and narrower back; these rankings may reflect incongruency between the medium heads and headforms in this aspect of head shape variability.

Superimposing the average radius of the two headforms with the average radius of the 23 medium heads at Plane 2 in Cartesian and Polar coordinates (Fig 1a and b) revealed significant differences between the average radius of the headforms (n=2) and average radius of medium heads (n=23) at Plane 2 (p=0.019) and Plane 3 (p=0.021), but not at Plane 1 (p=0.065).

## CONCLUSIONS

Despite the small sample size, substantial differences in head shape dimensions from headforms were detected. In particular, significant

differences were found between the mean head radius of two 50<sup>th</sup> percentile adult male headforms and a sample of human subjects. In general, Principal Component Analysis demonstrated neither headform represented a median subject in the three greatest components of head shape variability. The headforms do not represent the median head size of the sample of medium heads. The findings of this study may have implications on future headform design, as sport helmet certification standards require testing on a representative human headform. Further study is in progress to collect a larger sample pool.

## REFERENCES

1. European Standardization Organization. *CEN EN 960:2006*.
2. Pearsall DJ, et al. *ASTM International* **3**, 78-92, 2000.
3. Greencorn DJ. Master's Thesis, 2017.
4. McGuine T, Nass S. *ASTM International*, 1997.

## ACKNOWLEDGEMENTS

I would like to thank Bauer Hockey Corp. and NSERC Canada for funding this study.

**Table 1:** Z-score ranks of CEN EN 960 and NOCSAE headforms in the three largest principal components.

	PC1ISO	PC1NOCSAE	PC2ISO	PC2NOCSAE	PC3ISO	PC3NOCSAE
Plane 1	5	3	23	20	18	13
Plane 2	3	4	23	21	15	12
Plane 3	1	4	22	20	2	7

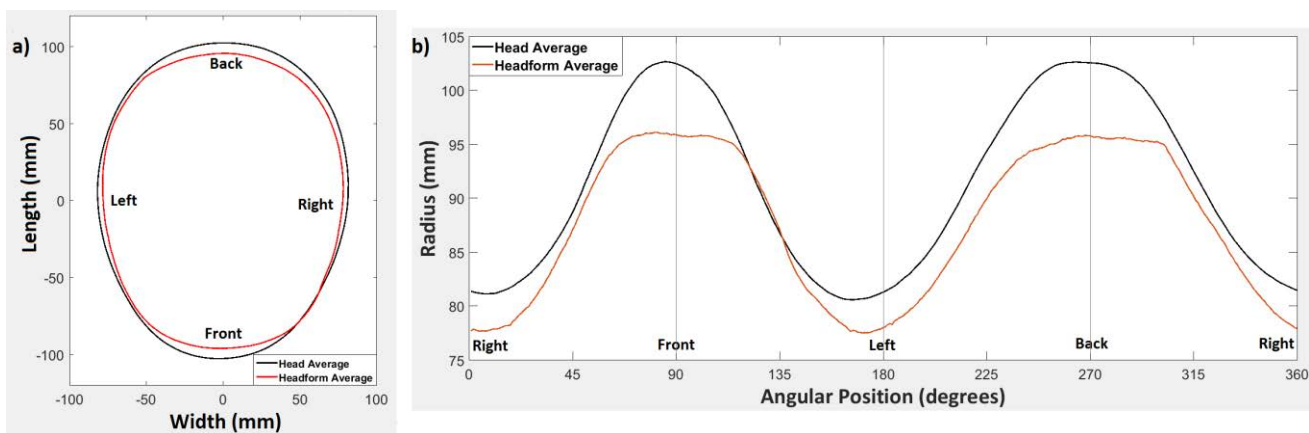


**Figure 1:** a) Average radius of the 2 headforms and the 23 medium heads in Cartesian coordinates; b) Average radius of the 2 headforms and 23 medium heads in Polar coordinates.

# DIFFERENCES BETWEEN *IN VIVO* TENDON MOMENT ARMS MEASURED GEOMETRICALLY AND FROM TENDON EXCURSION

<sup>1</sup> Josh R. Baxter and <sup>2</sup> Stephen J. Piazza

<sup>1</sup> University of Pennsylvania, PA, USA

<sup>2</sup> The Pennsylvania State University, University Park, PA, USA

email: josh.baxter@uphs.upenn.edu, web: <https://www.med.upenn.edu/motionlab/>

## INTRODUCTION

Tendon moment arm is an important musculoskeletal parameter that simultaneously determines muscle mechanical advantage while imposing constraints on muscle function. Despite its relevance to muscle and joint functional capacity [1], variability in moment arm measurements that is attributable to the technique used to measure moment arms limits our understanding of the implications of moment arm for movement capacity.

There are two dominant methodological paradigms for *in vivo* measurement of tendon moment arms: 1) geometric methods that quantify the distance between the tendon line of action and joint center (or axis) of rotation and 2) tendon excursion methods based on the Principle of Virtual Work that take moment arm to be equal to the tendon travel per unit joint rotation. While geometric assessments of moment arm using magnetic resonance (MR) imaging have many advantages [2], tendon excursion measurements that employ ultrasound imaging are attractive alternatives because of their low cost and ease of application. Therefore, the purpose of this study was to compare the moment arms obtained using tendon excursion from ultrasound images to those determined using the geometric technique applied to MR images in the same subjects.

## METHODS

Achilles tendon moment arms were quantified using different techniques in 19 healthy-young males ( $27 \pm 4$  years) in this IRB-approved study. MR images were acquired at neutral ankle position ( $0^\circ$ ),  $10^\circ$  plantarflexion, and  $10^\circ$  dorsiflexion using a 3T scanner (Siemens Trio). Subjects were supine with knees extended and were instructed not to contract their muscles during scanning. The sagittal-plane images acquired in the plantarflexed and dorsiflexed

positions were used to locate the center of tibiotalar rotation, and tendon moment arm was calculated as the shortest distance between tendon line of action and the center of rotation on the neutral-position image [1].

To measure tendon excursion during ankle rotation, the distal muscle-tendon junction of medial gastrocnemius was tracked using B-mode ultrasonography (Aloka 1100; transducer: SSD-625, 7.5 MHz and 39-mm scan width) while the foot was rotated from  $10^\circ$  dorsiflexion to  $10^\circ$  plantarflexion at  $10^\circ\text{s}^{-1}$  in an isokinetic dynamometer (Biodex System 3) [2]. To test the effects of tendon tension on these measurements, subjects performed these plantarflexions while (a) passive, (b) maximally contracting the plantarflexors, and (c) maintaining constant tendon force equal to 30% of the maximum isometric tendon force in neutral position by matching desired torques computed using moment arm versus joint angle relationships previously reported [3].

Moment arms derived from tendon excursion were compared to those determined from the geometric technique using regression analysis.

## RESULTS AND DISCUSSION

All variations of the tendon excursion method yielded smaller moment arms than those determined using the geometric method. Further, there were very weak to moderate correlations across subjects between each tendon excursion moment arm measurement and the moment arm from the geometric method, with  $R^2 = 0.21$ ,  $0.08$ , and  $0.07$  for conditions (a)-(c) as described above. The strongest correlation ( $R^2 = 0.21$ ;  $p = 0.052$ ) with the geometric method was found when tendon excursion was measured during passive ankle movement (Fig. 1).

Geometric method moment arms averaged across subjects ( $53 \pm 6$  mm) agreed with previously reported geometric method values ( $52 \pm 4$  mm) [2]. Moment arms from tendon excursion were about 30% smaller and exhibited twice the variability as geometric method values, also comparing favorably to moment arms measured previously using similar methods [2].

When applied *in vivo*, tendon excursion methods are likely confounded by tendon compliance and an inability to maintain constant tendon tension. When the assumption that the tendon is inextensible [4] is violated and the tendon stretches and relaxes during movement, tendon excursion will underestimate tendon moment arm (Fig. 2). A very stiff tendon or one in which tendon tension is constant will maintain its length and all tendon excursion observed will be attributable to joint rotation. A compliant tendon with varying tension, however, will appear to exhibit less excursion as its length changes, leading to a measurement artifact and an apparently smaller moment arm.

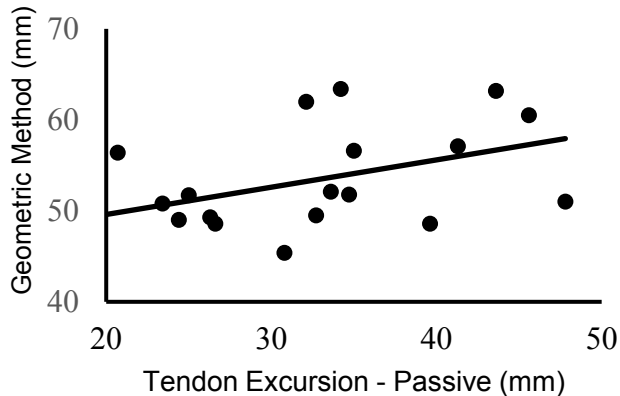


**Fig. 1** Achilles tendon moment arms measured using geometric and tendon excursion methods showed a moderate positive correlation ( $R^2 = 0.21$ ;  $p = 0.052$ ).

The current findings do not agree with a prior report of a strong correlation ( $R^2 = 0.94$ ) between Achilles tendon moment arms in a similar study of the geometric and tendon excursion methods applied in the same subjects [2]. Our sample size was more than twice as large as that of the previous study ( $N = 19$  vs.  $N = 9$ ), which may explain the discrepancy. We performed linear regressions with all combinations

of 9 subjects selected from our sample of 19 subjects ( ${}_{19}C_9 = 92,378$  combinations). These regression models yielded a maximum  $R^2$  value of 0.92, and 11% of the correlations were strong ( $R^2$  greater than 0.50).

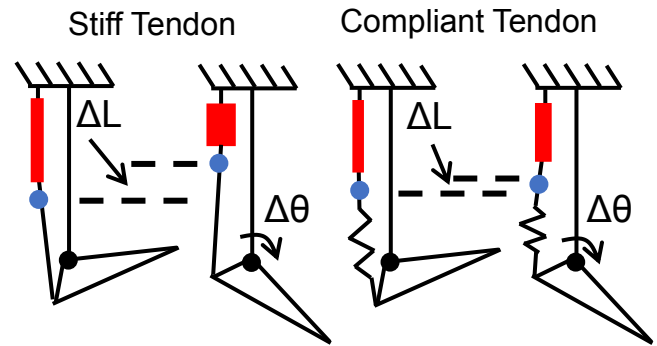


**Fig. 2** Moment arms computed as tendon excursion with respect to joint angle ( $\Delta L / \Delta \theta$ ) will be sensitive to tendon compliance and variation in tendon tension. A very stiff tendon will not produce this artifact, but it will be seen when a compliant tendon stretches and relaxes, resulting in an apparently smaller moment arm.

## CONCLUSION

Achilles tendon moment arms calculated using tendon excursion measured *in vivo* do not appear to be strong surrogate measures for moment arms measured using the geometric method. Moment arms measured using tendon excursion may reflect the mechanical properties of the tendon and an inconsistent application of tendon tension throughout movement. It is important to note, however, that measures of tendon excursion in themselves (due to tendon length changes and joint rotation) may be useful for the insights they provide into muscle fiber length changes during movement.

## REFERENCES

1. Baxter JR, *et al. J Appl Physiol.* **116** (5), 538-544, 2014
2. Fath F, *et al. J Appl Physiol.* **109** (6), 1644-1652, 2010.
3. Maganaris C, *et al. J Physiol.* **510** (3), 977-985, 1998
4. An KN, *et al. J Biomech Eng.* **106** (3), 280-282, 1984

# ARE ULTRASOUND-BASED ESTIMATES OF ACHILLES TENDON KINEMATICS CONSISTENT WITH THE EXPECTED BEHAVIOR OF A PASSIVE ELASTIC TISSUE IN SERIES WITH MUSCLE?

Emily S. Matijevich, Lauren M. Branscombe and Karl E. Zelik

Vanderbilt University, Nashville, TN, USA  
email: emily.matijevich@vanderbilt.edu, web: my.vanderbilt.edu/batlab

## INTRODUCTION

The Achilles tendon (AT) is an important passive elastic structure that facilitates safe and economical human locomotion, and whose behavior informs the development of assistive technologies and rehabilitative interventions. However, quantifying AT kinematics and kinetics *in vivo* is challenging, leading to inconsistent estimates of length change, stiffness and hysteresis in literature [1]. Ultrasound imaging offers one way to non-invasively estimate AT kinematics *in vivo* during human movement, but critical questions remain about which ultrasound methods are most accurate, and if/when each method yields physiologically plausible AT estimates [2]. Two questions motivated this study: (I) Do commonly used ultrasound tracking methods yield similar estimates of AT length change? (II) Are these estimates consistent with the expected behavior of a passive elastic tissue acting in series with a contracting muscle?

## METHODS

Three healthy subjects ( $20 \pm 2$  years,  $75 \pm 10$  kg) performed various movement tasks, during which unilateral lower-limb kinematics (100 Hz, Vicon) and ground reaction forces (1000 Hz, Bertec) were collected synchronously with B-mode ultrasound (~60 Hz, 50 mm depth, Telemed). Subjects provided informed consent prior to participation. To address question (I), we compared AT length change estimates from two commonly used ultrasound methods. For the first method, termed *Indirect*, the ultrasound probe (7 cm linear transducer) was placed on the medial gastrocnemius (MG) muscle belly to track muscle fascicle length changes. Fascicle length was corrected for pennation angle to estimate total muscle length

change. AT length change was then approximated indirectly as the difference between the overall muscle-tendon unit (MTU) length change (estimated from a regression equation using knee and ankle joint angles [3]) and muscle length change. For the second method, termed *Direct Muscle-Tendon Junction (MTJ)*, the ultrasound probe was placed over the MG-AT MTJ. Using optical motion capture and a custom-fixture attached to the probe to track its position, AT length change was more directly estimated as the linear distance between the calcaneus marker (AT insertion) and MTJ. MG muscle length change was also approximated using this method, by subtracting AT from MTU length change (from [3]).

To address question (II), subjects completed three simple tasks in which empirically-estimated AT length changes could be compared to the expected behavior of a passive elastic tendon acting in series with muscle. Tasks were chosen to test combinations of high/low MTU force and large/small MTU length changes. Tasks: (A) Restrained joint calf contractions were performed while seated with a rigid bar affixed above the knees, restricting ankle and knee rotation. Expectation: Small MTU length change and high MTU force would result in substantial AT lengthening, equal and opposite to MG shortening. (B) Heel raises involved contracting the calf muscles while standing to rise onto the toes. Expectation: Large MTU length change and high MTU force would result in AT lengthening. (C) Toe pointing required subjects to hold their foot in the air and plantarflex their ankle. Expectation: Large MTU length change and low MTU force would result in minimal AT length change. Each cycle began/ended with the MG relaxed and the foot in neutral position (i.e., perpendicular to shank).

## RESULTS AND DISCUSSION

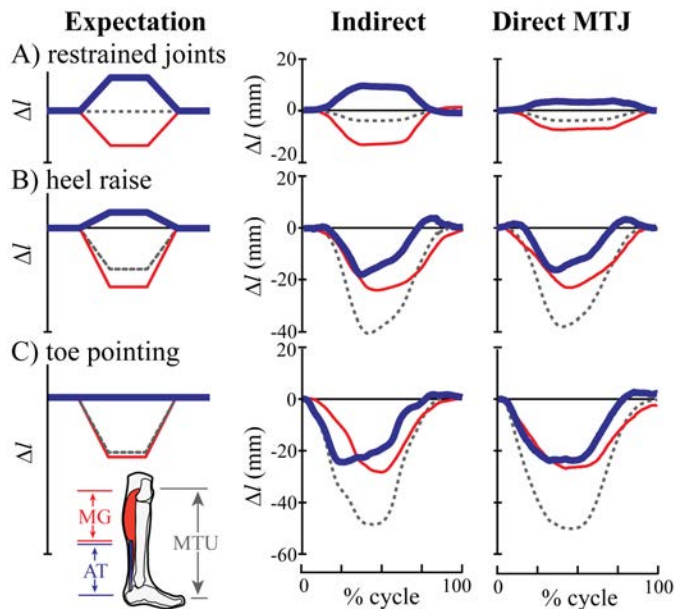


**Figure 1:** AT (thick blue), MG (thin red) and MTU (dashed gray) length changes for one subject during 3 tasks. Data averaged over 5 cycles.  $\Delta l$  = change from relaxed length.

AT length change estimates were strongly correlated between the Indirect and Direct MTJ tracking methods. We found correlation coefficients of  $r = 0.82 \pm 0.06$ ,  $r = 0.89 \pm 0.09$ ,  $r = 0.75 \pm 0.21$  for tasks A, B, and C, respectively (N=3, Figure 1). AT length change estimates were qualitatively consistent with the expected behavior of a series elastic tissue during task A, which involved

minimal changes in MTU length. However, AT length changes were drastically different from expectations for tasks B and C, in which the MTU underwent substantial shortening.

## CONCLUSIONS

Preliminary findings suggest that Indirect and Direct MTJ methods yield similar estimates of AT kinematics for the tasks tested. However, estimated AT kinematics were highly inconsistent with the expected behavior of a passive elastic tissue in series with muscle. In this ongoing study we seek to understand the reasons for and implications of this inconsistency.

## REFERENCES

1. Finni T, et al., *J Appl Physiol.* **114**: 515-517, 2013.
2. Sakuma J, et al., *Eur J Appl Physiol.* **112**: 887-898, 2012.
3. Hawkins D, et al., *J Biomechanics.* **23**: 487-494, 1990.

## ACKNOWLEDGMENTS

This research was supported in part by the National Institutes of Health (K12HD073945).

# DO TRICEPS SURAE MUSCLE DYNAMICS GOVERN NON-UNIFORM ACHILLES TENDON DEFORMATIONS?

William H. Clark and Jason R. Franz

University of North Carolina and North Carolina State University, Chapel Hill, NC, USA  
email: jrfranz@email.unc.edu web: http://abl.bme.unc.edu

## INTRODUCTION

The Achilles tendon (AT) consists of distinct bundles of tendon fascicles arising from the gastrocnemius (GAS) and soleus (SOL) muscles that may act as mechanically independent structures [1]. Indeed, we have shown that these “sub-tendons” exhibit non-uniform displacement patterns during walking, which may reflect sliding between adjacent tendinous structures [2]. While the mechanisms governing these non-uniform displacement patterns have remained allusive, recent computational model predictions implicate differential GAS versus SOL muscle dynamics as a biomechanical candidate [3]. In that study, removing differential GAS versus SOL muscle forces reduced model-predicted tendon non-uniformity by 85%. Thus, here, we implemented a novel dual-imaging approach to investigate triceps surae muscle dynamics as a determinant of non-uniform AT tissue displacements during ramped isometric contractions. We hypothesized that superficial versus deep differences in AT tissue displacements would be accompanied by (and correlate with) anatomically consistent differences in GAS versus SOL muscle shortening.

## METHODS

We have thus far collected data for 8 subjects (age:  $25.4 \pm 5.9$  years, mass:  $71.0 \pm 6.2$  kg, height:  $1.8 \pm 0.1$  m, 3 females and 5 males). Subjects performed three ramped maximum voluntary isometric contractions (MVICs) at each of five ankle joint angles spanning  $10^\circ$  dorsiflexion to  $30^\circ$  plantarflexion in a dynamometer (Biodex System 4 Pro), with the knee flexed to replicate that near the push-off phase of walking. We synchronized two linear array ultrasound transducers to simultaneously record GAS and SOL fascicle kinematics with tissue displacements in their associated tendinous structures (Fig. 1). A 60 mm Teleded Echo Blaster 128 transducer (LV7.5/60/128Z-2) placed over the

medial gastrocnemius and soleus of subjects’ right leg recorded cine B-mode images at 61 frames/s. Simultaneously, a 38-mm transducer (L14-5W/38, Ultrasonix Corporation, Richmond, BC) operating at 70 frames/s recorded ultrasound radiofrequency (RF) data from a longitudinal cross-section of the right free AT, distal to the SOL muscle-tendon junction and secured via a custom orthotic. Subjects’ right foot was barefoot throughout the experiment to facilitate proper placement of the AT transducer. Finally, motion capture tracked right ankle and knee joint kinematics and the positions and orientations of both probes.

Available MATLAB routines based on an affine extension to an optic flow algorithm quantified time series of GAS and SOL fascicle lengths and pennation angles (UltraTrack, [4]), which we combined to compute longitudinal muscle lengths. A custom 2D speckle-tracking algorithm estimated localized displacements of AT tendon tissue, which we averaged in two equally sized tendon depths - superficial and deep - corresponding to tendon tissue

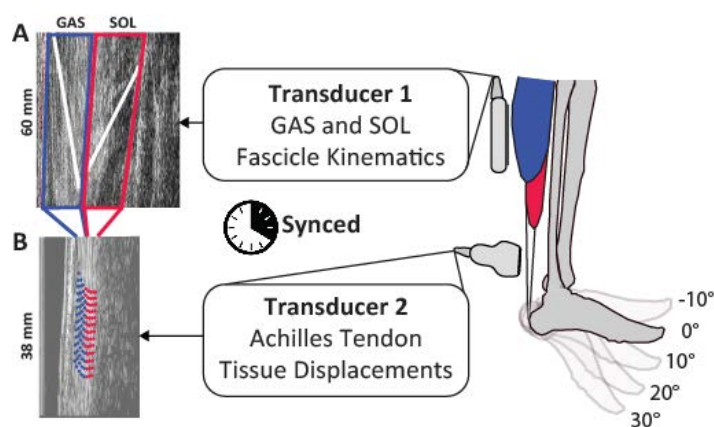


**Figure 1.** Simultaneous ultrasound imaging of the gastrocnemius (GAS), soleus (SOL), and free Achilles tendon. (A) Fascicle lengths and pennation angles derived from cine B-mode images. (B) Custom speckle-tracking of localized Achilles tendon tissue displacements.

thought to arise from GAS and SOL, respectively [2]. A repeated measures ANOVA tested for significant main effects of ankle angle and muscle/tendon (i.e., GAS vs. SOL) on peak muscle shortening and peak tendon lengthening. Finally, we calculated Pearson's correlation coefficients between: (i) GAS and SOL muscle shortening and lengthening in their associated regions of the AT, and (ii) muscle non-uniformity (i.e., GAS versus SOL) and tendon non-uniformity (i.e., superficial versus deep).

## RESULTS AND DISCUSSION

Peak isometric plantarflexor torque decreased progressively from dorsiflexion to plantarflexion across the range of angles tested ( $p < 0.01$ ). For all conditions, SOL shortened by an average of 73% more than GAS during force generation (Fig. 2A). This was accompanied by, on average, 53% more lengthening in the deep versus superficial region of the AT (Fig. 2A). The magnitude of GAS and SOL muscle shortening during force-generation positively

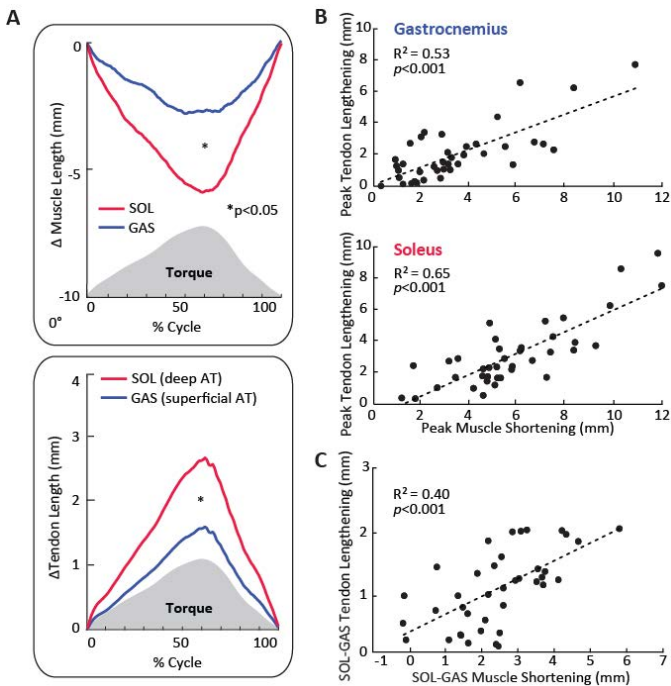


**Figure 2.** (A) Group average muscle shortening and tendon lengthening for the  $0^\circ$  condition. (B) Correlations between peak GAS or SOL muscle shortening and lengthening in their associated regions of the AT. (C) Correlation between superficial versus deep differences in AT lengthening and GAS versus SOL differences in muscle shortening. Both correlations are pooled across all conditions. Asterisks (\*) indicate  $p < 0.05$ .

correlated with lengthening in their associated regions of the AT ( $p < 0.05$ ) (Fig. 2B). Moreover, and consistent with our hypothesis, superficial versus deep differences in AT lengthening positively correlated with anatomically consistent differences in GAS versus SOL muscle shortening ( $p < 0.05$ ) (Fig. 2C). Finally, the strength of these latter correlations exhibited a dependence on plantarflexor torque generation; increased ankle dorsiflexion, conveying an increase in plantarflexor torque generating capacity, elicited stronger correlations between muscle non-uniformity and tendon non-uniformity (e.g., up to  $R^2 = 0.76$  at  $10^\circ$  dorsiflexion,  $p < 0.01$ ).

## CONCLUSIONS

We present *in vivo* evidence that triceps surae muscle dynamics may precipitate non-uniform displacement patterns in the architecturally complex Achilles tendon. Moreover, we present a novel dual-imaging approach to empower simultaneous *in vivo* assessment of muscle and tendon toward an improved mechanistic understanding of triceps surae behavior. Our findings may have important implications for understanding age-associated changes in AT displacement patterns [5], which we suspect alter the muscle contractile behavior of older adults. Specifically, we have proposed that a proliferation of collagen cross-linking and adhesions between adjacent sub-tendons in the AT can unfavorably couple GAS and SOL muscle-tendon dynamics during walking in older adults.

## REFERENCES

1. Szaro P, et al., *Annals of Anatomy*. **191**: 586-593, 2009.
2. Franz JR, et al., *Gait Posture*. **41**: 192-197, 2015.
3. Handsfield GG, et al., *J Biomech*. **51**: 17-25, 2017.
4. Farris DJ, et al., *Comput Methods Programs Biomed*. **128**:111-118, 2016.
5. Franz JR, et al., *J Appl Physiol*. **119**: 242-249, 2016.

## ACKNOWLEDGEMENTS

We thank Ashish Khanchandani, Hannah Mckenney, and Michael Browne for their assistance with data collection. This study was supported by a grant from NIH (R01AG051748).

# HOW DO MATERIAL TRANSVERSE ISOTROPY AND PRE-TENSION INFLUENCE SIMULATIONS OF NONUNIFORM DISPLACEMENTS IN THE ACHILLES TENDON?

<sup>1</sup>Katherine R. Knaus, <sup>2</sup>Geoffrey G. Handsfield, and <sup>1</sup>Silvia S. Blemker

<sup>1</sup>The University of Virginia, Charlottesville, VA, USA

<sup>2</sup>Auckland Bioengineering Institute, Auckland, NZ

email: ker4e@virginia.edu, web: <http://http://bme.virginia.edu/muscle/>

## INTRODUCTION

The Achilles tendon is the largest in the body and plays a critical load-bearing role during walking and running. This tendon has a unique architecture that comprises three subtendons that twist around each other and are each derived from a muscle of the triceps surae. Recent dynamic ultrasound studies have revealed that these subtendons slide past each other during ankle motion, as nonuniform tendon displacements have been observed in both passive and eccentric loading trials [1].

In a recent study, a 3D finite element model (FEM) of the Achilles with its subtendons was developed to explore the mechanisms of this nonuniform displacement [2]. This model showed that inter-subtendon sliding and differential passive muscle force conditions lead to the largest disparity in subtendon displacement. In that study, tendon was modeled as a Neo-Hookean material for simplicity. It is unknown how a more accurate constitutive model containing directional material properties of the collagen fibers in the twisting subtendons would affect simulated displacements. The first goal of this study is to incorporate a transversely isotropic constitutive formulation [3] into the Achilles tendon FEM to elucidate the effect of the material model on displacement nonuniformity.

In addition to *in vivo* displacement measurements, ultrasound can be used to measure local mechanical properties, which can be used to estimate muscle and tendon slack lengths. Recent studies have compared slack lengths of the triceps surae muscles [4] and the medial gastrocnemius and Achilles tendon [5] and found that they occur at different ankle angles. While the individual subtendons were not measured, muscle-tendon and inter-muscle

differences in slack length suggest that these subtendons could also be slack at different ankle angles. Tendon is assumed to be at slack length at the start of finite element simulations, but these differences may be important to consider when modeling Achilles motion. Thus, the second goal is to examine the potential role in displacement nonuniformity of differential subtendon slack lengths by incorporating a pre-tensioning parameter into the material model.

## METHODS

The creation of a free tendon FEM of the Achilles has been previously described in detail [2]. Achilles 3D geometry was constructed from segmented UTE MR images and divided into subtendons based on dissection and MRI of triceps surae locations [Fig. 1A]. Frictionless contact interfaces were assigned between subtendons. To simulate dorsiflexion, a 25° rotation was prescribed to the distal end of the tendon, while the proximal end was constrained to move only proximal-distally. Nodal stiffnesses were applied to the proximal end to simulate passive muscle forces and tuned, in the Neo-Hookean model, to reproduce displacements observed with ultrasound [1].

Simulations were repeated with identical geometry and boundary conditions for tendon modeled as Neo-Hookean and transversely isotropic materials with strain energy density functions:

$$W^{N-H} = C(I_1 - 3) \text{ and } W^{TrIso} = C(I_1 - 3) + W_3(\lambda)$$

Where  $W_3$  defines the relationship between the Cauchy stress ( $\sigma$ ) and the stretch ( $\lambda$ ) along the tendon fiber direction [3]. The stretch is a function of the right Cauchy-Green deformation tensor and vectors defining the fiber directions [Fig 1A], which

were defined using computational fluid dynamics [6]. The stress is in piece-wise exponential form:

$$\lambda \frac{\partial W_3}{\partial \lambda} = \sigma(\lambda) = \begin{cases} L_1 \left( e^{L_2(\lambda - \lambda_{beg})} - 1 \right), & \lambda_{beg} < \lambda < \lambda^* \\ L_3 \lambda + L_4, & \lambda > \lambda^* \end{cases}$$

Where  $\lambda^*$  is the stretch when  $\sigma$  becomes linear, and  $\lambda_{beg}$  is the stretch at the beginning of the simulation. Transversely isotropic simulations were run with  $\lambda_{beg} = 1$  for all subtendons (no pre-tension case). Pre-tension was applied by shifting  $\lambda_{beg}$  (and  $\lambda^*$ ) by a given value, informed by estimated angle of slack length [Fig. 1B]. Differential displacement was compared between Neo-Hookean and transversely isotropic with and without pre-tension by measuring the displacement at the proximal end of each subtendon [Fig. 1C].

## RESULTS AND DISCUSSION

In both the Neo-Hookean and transversely isotropic simulations, the soleus subtendon experienced the largest distal displacement, and the lateral gastrocnemius experienced the least. However, displacements were more nonuniform in the model with transversely isotropic material [Fig. 1C].

Based on muscle and tendon measurements [4,5], the ankle angle at slack length was estimated for the subtendons ( $\angle_{MG} = 42^\circ$ ,  $\angle_{LG} = 37^\circ$ ,  $\angle_{Sol} = 21^\circ$ ). The joint angle at the start of the simulation

occurred at a tendon stretch of 1 ( $\lambda_{beg}$  with no pre-tension), and the tendon stress-strain curves for the subtendons were adjusted accordingly for pre-tension ( $\lambda_{beg, MG} = 0.035$ ,  $\lambda_{beg, LG} = 0.02$ ,  $\lambda_{beg, Sol} = -0.035$ ) [Fig. 1B]. The displacements of the subtendons with pre-tension were different from the no pre-tension case in both the order and the amount of disparity. With pre-tension, the medial gastrocnemius experienced the most displacement, but displacements were more uniform compared to simulations without pre-tension [Fig. 1C].

The directional material model resulted in greater subtendon displacement non-uniformity, so the contribution of differential passive muscle forces may be less than previously estimated and require further tuning [2]. Since inclusion of pre-tension altered the displacement profile of the Achilles, future modeling efforts would benefit from more accurate measurements and incorporation of the angle-specific material properties in the subtendons.

## REFERENCES

1. Slane LC & Thelen DG. *J Biomech*, **47**, 2831-2835, 2014.
2. Handsfield GG, et al. *J Biomech*, **51**, 17-25, 2017.
3. Blemker SS, et al. *J Biomech* **38**, 657-665, 2005.
4. Hirata K, et al. *J Biomech* **48**, 1210-1213, 2015.
5. Hug F, et al. *J Biomech* **46**, 2534-2538, 2013.
6. Inouye J. *Society of Modeling & Simulation Int*, Chicago, IL, USA, 2015.

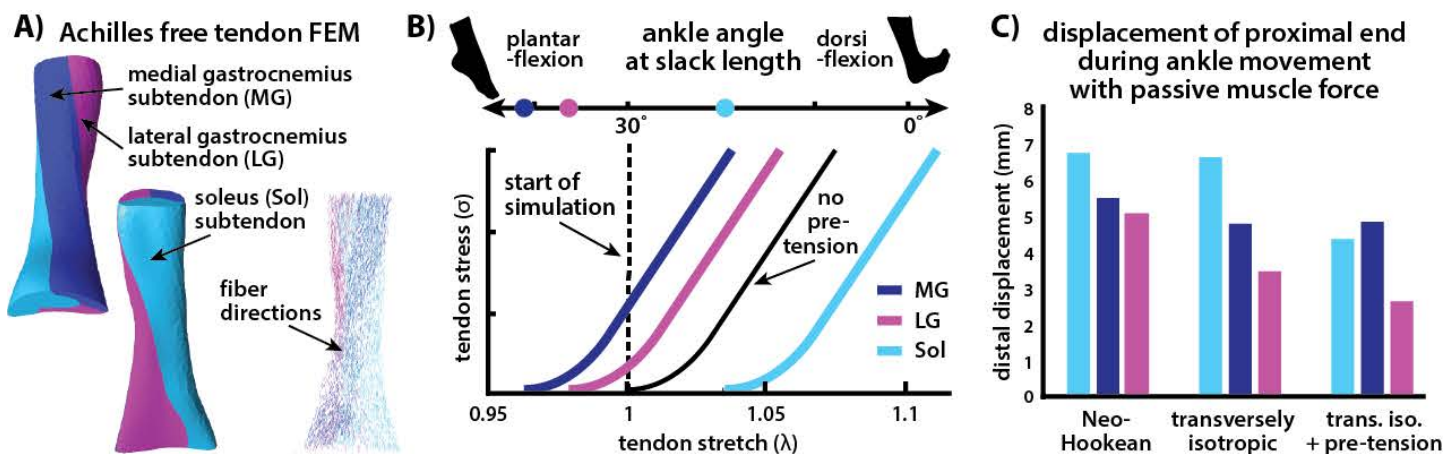


**Figure 1:** A) FEM of the Achilles included unique subtendon structures with defined fiber directions for the medial and lateral gastroc. and soleus. B) The ankle angle at slack length was estimated for the subtendons, and corresponding initial tendon stretch was determined for pre-tension. C) Differential subtendon displacements were determined for simulations with Neo-Hookean and transversely isotropic with and without pre-tension.

# ASSESSING NON-UNIFORM STIFFENING OF THE ACHILLES TENDON USING SURFACE WAVE ELASTOGRAPHY

<sup>1</sup> Muhammad Salman, <sup>2</sup> Karim G Sabra

<sup>1</sup> University of Engineering and Technology, Lahore, Pakistan

<sup>2</sup> Georgia Institute of Technology, Atlanta, GA, USA

<sup>1</sup>email: [msalman3@uet.edu.pk](mailto:msalman3@uet.edu.pk)

<sup>2</sup>email: [karim.sabra@me.gatech.edu](mailto:karim.sabra@me.gatech.edu)

## INTRODUCTION

Currently, noninvasive cost-effective techniques are not available that can quantify in-vivo non-uniform degradation of tendon's mechanical and structural properties associated with localized tendon injuries. This study will demonstrate the applicability of our novel cost-effective surface-wave elastography (SURF-E) method for quantifying spatial variations of tendon mechanical and structural properties in a much broader range of tendon stiffness with various positions and anatomical level than currently available elastography methods do such as Ultrasound (US) and MRI.

## METHODS

Ten healthy men (age:  $22 \pm 5$  years, height:  $175 \pm 9$  cm, body mass:  $72 \pm 8$  kg) were tested with no signs of neuromuscular diseases. The study was approved by the Institutional Review Board (IRB) of the Georgia Institute of Technology. The ankle joint was set to three different values  $70^\circ$ ,  $80^\circ$  and  $90^\circ$  by the help of a goniometer (Fig. 1a). In order to have the data repeatability, leg was restrained in a fixture around calf (Fig. 1b) by the help of a strap and a tong clamp.



Figure 1: a) Ankle angle set by goniometer, b) Fixture around calf, c) Achilles Tendon setup with LDV and shaker rod.

Achilles tendon was marked by five anatomical landmarks each 1cm apart starting from the datum line parallel to the proximal of calcaneus bone (Fig. 1c). Three sections of AT starting from 1 cm above the datum line were quantified for elastic stiffness. The datum line was actuated by an electrodynamic mini-shaker (model 4810, Brüel & Kjær, Nærum, Denmark) to generate band pass filtered frequency (5 Hz-1000 Hz) impulses. Four LDV sensors (PDV 100, Polytec, Irvine, CA, USA) shone along a 5-6 cm long thin retro-reflective adhesive tape (3M). The tape was attached over the tendon from the datum line and 6 cm along the axis of the Achilles tendon. Subjects performed three series of brief contractions for each ankle angle. The measurements were made in a randomized order. The laser elastography measurements were performed on these ten subjects using the similar procedure as described in details in Salman & Sabra [1] and previously validated using soft gel samples [2].

## RESULTS

Fig. 2 consists of four plots obtained from one of the ten subject's data analysis for a  $70^\circ$  ankle angle (dorsiflexion). Fig. 2a is the power spectrum of the four LDV sensors and the shaker excitation. It is clear that the signal ranges from 10 Hz to 500 Hz. The higher the excitation frequency, the lower is the wavelength which gives more localized mechanical properties. Fig. 2b is the application of cross correlation signal processing filter for the four LDV sensors which shine 1 cm apart from each other. The maximum point of these correlation vectors shows that the sensor signal is matched perfectly with the excitation source signal.

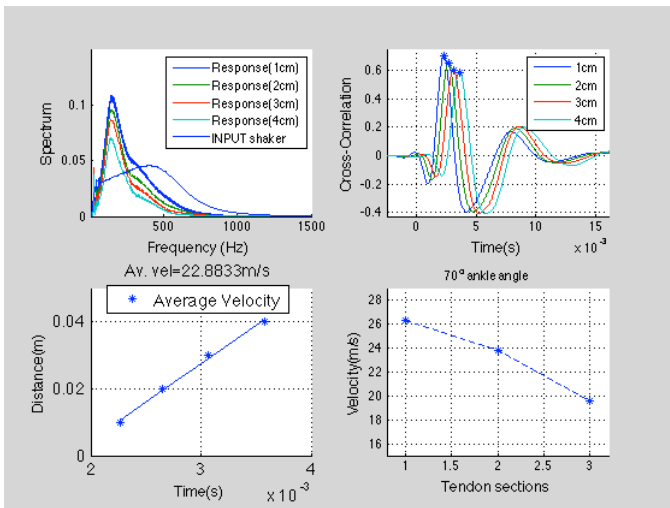


Figure 2(Data analysis of a subject at 70° ankle angle) a)Power spectrum of the sensor and shaker, c) Cross-Correlation signal processing filter, d) Linear fit of four max. peaks in fig. 2c, e) Spatial velocity variation of the AT.

When these peaks are linearly fit they give the slope of an average shear wave velocity as shown in Fig. 2c. When the difference of these peaks is taken we get the velocity slopes which are the spatial velocity variations of the AT as shown in Fig. 2d. Fig. 3 is the the result analysis of ten subjects at three ankle positions. Fig. 3a shows a decreasing trend in the shear wave velocity along the AT. Since wave propagation velocity is the criteria of stiffness of the AT, therefore section I of AT, proximal to calcaneus bone, is at a higher velocity value as compared to the section II and section III which are near the calf muscle. Fig 3b shows the mean of shear wave velocity at three ankle positions.

## DISCUSSION

The measured velocity values in Fig. 3a ranges from (38--10m/s) show that this technique is an objective way to quantify the stiffness of the AT unlike the other techniques such as Ultrasound (US) and MRI techniques which can provide a simple estimate of AT's overall stiffness. High standard deviation in Fig 3a for 70° ankle position as compared to the other two shows the variability of stiffness of AT under high loading. Fig 3b verifies that at low ankle angle, AT becomes stiffer and so does the wave velocity accordingly.

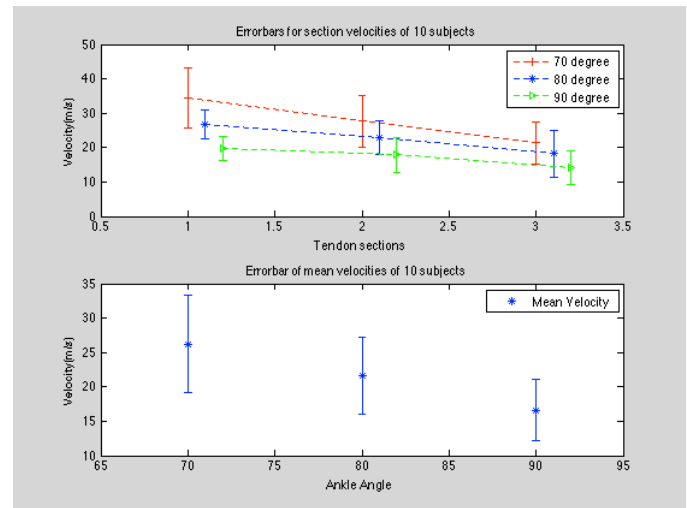


Figure 3 (Data analysis of 10 subjects) a)(Top) Spatial velocity variation of AT at three ankle positions. b)(Bottom) Mean of shear wave velocity along the AT.

## CONCLUSIONS

Developing a low-cost, single LDV-based SURF-E modality as an alternative to using expensive US scanner would broaden the acceptance and clinical usage of transient elastography methods for AT's diagnosis and monitoring the mechanical recovery of injured ATs. SURF-E method would assist the injury risk assessment and patient-specific selection of treatment plans for tendinopathy as well as the monitoring of the efficiency of therapeutic exercise programs which would diminish health care costs associated with the exponentially increasing number of AT injuries. As another advantage, SURF-E method can be performed in near real-time (<3 s) and thus could readily be used to monitor the evolution of the AT.

## REFERENCES

- [1] M. S. K. S. Muhammad Salman, "Assessment of muscle stiffness using a continuously scanning laser-Doppler vibrometer," *Muscle and Nerve*, vol. 50, p. 133–135, 2014.
- [2] S. K. Muhamamd Salman, "Surface wave measurements using a single continuously scanning Laser Doppler Vibrometer: Application to elastography," *Journal of Acoustical Society of America*, vol. 133, p. 1245–1254, 2013.

# IN VIVO TENDON STRESS IS PREDICTED BY NON-INVASIVE WAVE SPEED MEASUREMENT

Jack Martin, Scott Brandon, Emily Keuler, James Hermus, Matthew Allen, and Darryl Thelen

University of Wisconsin-Madison, Madison, WI, USA  
email: jamartin8@wisc.edu, web: <http://uwnmb1.engr.wisc.edu/>

## INTRODUCTION

Understanding tendon tissue loading is crucial to the investigation of musculoskeletal disorders. Unfortunately, assessing *in vivo* loading remains challenging – direct measurements are highly invasive [1], and modeling approaches rely on assumptions of muscle coordination and tissue geometry [2]. We have recently developed a novel non-invasive technique for estimating tendon loads from wave propagation measures. Considering tendon as a tensioned beam, we hypothesized that shear wave speed in tendon should be directly dependent on axial stress [3]. A subsequent *ex vivo* study [3] clearly demonstrated this relationship, showing a strong correlation between tendon stress and squared wave speed (mean  $r^2 = 0.98$ ). We subsequently invented a simple accelerometer-based approach for tracking *in vivo* tendon wave speeds [4]. The purpose of the current study was to investigate the relationship between wave speed and tendon stress for the human Achilles and patellar tendons *in vivo* during isometric contractions.

## METHODS

**Wave tracking.** We constructed a shear wave tensiometer to generate and track transient shear waves in the Achilles and patellar tendons (Fig 1A). Waves were generated using a piezoelectric actuated (Thorlabs PK4JQP1, Newton, NJ, USA), 3D-printed tapper. The tapper was strapped ~7cm superior to the calcaneus for the Achilles tendon and slightly superior to the tibial tuberosity for the patellar tendon. Tendons were tapped in the transverse direction (20 $\mu$ m displacement) at 50Hz, with each tap sending a transverse (shear) wave along the tendon. Two single-axis accelerometers (PCB Piezotronics 352C23/NC, Depew, NY, USA) were positioned over the tendon 10mm and 20mm inferior (Achilles) or superior (patellar) to the

tapper. Transverse acceleration of the tendon was sampled from each accelerometer at 50kHz. Wave speed was calculated using lag in wave arrival time between the two accelerometers (Fig 1B) after each tap, so that wave speed data were collected at 50Hz.

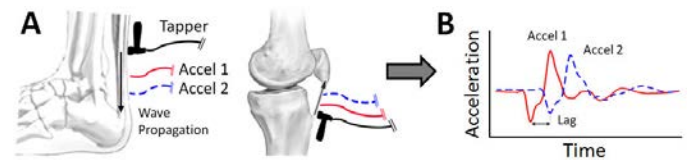


**Figure 1:** A) Schematics of wave speed measurement method for the Achilles and patellar tendons. B) Example shear waves recorded via skin-mounted accelerometers.

**Isometric testing.** Five subjects (3M, 2F) performed isometric contractions cyclically for 8 seconds at 3 rates (0.5, 1.0, 2.0Hz). For Achilles tendon testing, subjects sat in a chair with their ankle dorsiflexed 10 degrees and their knee at 20 degrees flexion. They then pushed against a force plate with a rod positioned under the head of their first metatarsal to control the ankle moment arm. For patellar tendon testing, subjects sat on a bench with their knee at 90 degrees flexion, and pulled against a cable with an in-series load cell. The cable was attached to a brace positioned just above their ankle.

**Analysis.** Tendon stresses were estimated based on measured forces, joint moment arms, tendon moment arms, and tendon cross-sectional areas. Using ultrasound imaging, tendon cross-sectional areas were measured and tendon moment arms were estimated as the perpendicular distance from the trans-epicondylar axis to mid-thickness of the tendon. Wave speed data were low-pass filtered at 20Hz. Correlation between tendon stress and squared wave speed was assessed using the coefficient of determination. A paired t-test ( $\alpha = 0.05$ ) was used to determine whether linear fit slopes were significantly different between the

Achilles and patellar tendons. Inter-subject variability was assessed using the coefficient of variation of fit slopes between subjects. Predicted stresses were calculated using tendon/subject-specific fits of stress versus squared wave speed. Data from all loading rates were pooled for this analysis.

## RESULTS AND DISCUSSION

Tendon wave speeds ranged from ~20-80 m/s in the Achilles tendon and ~10-100 m/s in the patellar tendon through the loading cycles across the 5 subjects. Peak stresses ranged from ~20-100 MPa in the Achilles tendon and ~12-35 MPa in the patellar tendon. There was excellent temporal agreement between squared wave speed and tendon stress (Fig 2A/B). Squared wave speed was highly correlated with tendon stress across all subjects (Achilles:  $r^2 = 0.94 \pm 0.06$ ; patellar:  $r^2 = 0.98 \pm 0.01$ ). Linear fit slopes (Achilles:  $0.013 \pm 0.006 \text{ MPa} \cdot \text{m}^{-2} \cdot \text{s}^2$ ; patellar:  $0.0036 \pm 0.0015 \text{ MPa} \cdot \text{m}^{-2} \cdot \text{s}^2$ ) were significantly different between tendons ( $p < 0.001$ ; e.g., Fig 2C/D), and showed moderate inter-subject variability (Achilles:  $c_v = 0.42$ ; patellar:  $c_v = 0.46$ ).

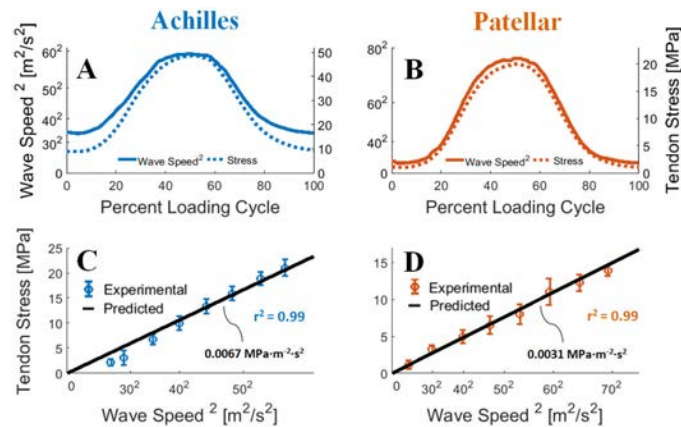


**Figure 2:** A/B) Ensemble mean squared wave speed and tendon stress across all subjects and loading rates. C/D) Predicted tendon stress and binned mean  $\pm$  standard deviation of experimental stress vs. squared wave speed for a representative subject.

These data confirm that the relationship between wave speed and tendon stress observed *ex vivo* holds for the *in vivo* case for both Achilles and patellar tendons. Additionally, this study has established the feasibility of measuring wave speed

at a high rate (50Hz) using skin-mounted accelerometers, making the technique usable for dynamic activities like walking, running, and jumping. Moreover, this study demonstrates the ability to calibrate subject-specific tendon stress-wave speed relationships using simple isometric exertions (e.g., Fig 2C/D). Further experimental and computational study is ongoing to determine the extent to which tendon cross-sectional area, length and architectural features can influence wave speed.

Tendon loading predictions using our shear wave tensiometer have numerous potential applications in biomechanics. First, this technology could be useful in assessing coordination patterns without using cumbersome motion capture and inverse dynamics techniques. Second, direct measurements of tendon stress would be highly useful for validating musculoskeletal models. Finally, and perhaps most impactful, is the potential to use tendon stress measures to diagnose impairments, plan treatments, and track recovery following rehabilitative and surgical interventions.

## CONCLUSIONS

This work has demonstrated the exciting potential for non-invasively tracking tendon wave speeds and using these data to accurately predict tendon stresses *in vivo* during dynamic activity. Future work will aim to better understand the inter-tendon and inter-subject differences observed here, and to apply the technique to important clinical and research applications.

## REFERENCES

1. Fleming BC & Beynonn BD. *Ann Biomed Eng* **32**, 318-328, 2004.
2. Erdemir A, et al. *Clin Biomech* **22**, 131-154, 2007.
3. Martin JA, et al. Proceedings of SB3C'16, National Harbor, MD, USA, 2016.
4. Thelen DG, et al. US Patent App 14/839448, 2015.

## ACKNOWLEDGMENTS

NSF-GRFP (DGE-1256259) and NIH (EB015410). The authors have submitted a patent application [4] on the technology described in this abstract.

# HIGH-ACCELERATION TRAINING DURING GROWTH INCREASES OPTIMAL FIBER LENGTHS IN AN AVIAN BIPEDAL MODEL

<sup>1</sup> Matthew Q. Salzano, <sup>1</sup> Suzanne M. Cox, <sup>1</sup> Stephen J. Piazza, <sup>1</sup> Jonas Rubenson

<sup>1</sup> Biomechanics Laboratory, The Pennsylvania State University, University Park, PA, USA  
email: [salzano@psu.edu](mailto:salzano@psu.edu); web address: <http://www.biomechanics.psu.edu>

## INTRODUCTION

Previous research has shown that fiber lengths of the vastus lateralis and gastrocnemius are longer in human sprinters than in distance runners and untrained controls [1]. Longer fascicle lengths have also been associated with better performance within a group of trained sprinters [2]. In these groups, longer fiber lengths may increase muscle power and work production (independent of PCSA) by reducing fiber strain and relative velocity and thus minimizing force-length-velocity effects.

However, it is unknown if the longer fascicle lengths associated with better sprinting ability are primarily due to genetic variation or if they result from sprint training. Fascicle lengths have been shown to increase in response to stretch [3] but studies examining effects of running training are limited. One study of marathon training showed a decrease rather than an increase in gastrocnemius fiber lengths [4].

The purpose of this study was to determine if optimal muscle fiber lengths are affected by high acceleration running/jumping training during growth, when muscle plasticity may be greatest. We explored this question using a bipedal animal model, guinea fowl, that are fast-growing and amenable to training. We hypothesized that acceleration training during the animals' growth period would result in longer fascicle lengths compared to those measured in a sedentary control group.

## METHODS

Guinea fowl (*Numida meleagris*) were obtained from a regional breeder (Guineafarm, OH). At 4 weeks of age, guinea fowl were split into an Exercise Group (EG; n=15) and Sedentary Group (SG; n=15). The EG were housed in a large, dual-circle pen (each 1.85 m in dia.; ~5.3 m<sup>2</sup>) with ample room for running and perching. The SG were housed in smaller pens (~1

m<sup>2</sup>) to limit movement. Birds were given food and water *ad libitum*.

Along with opportunities for spontaneous movement, the EG were exercised in two ways. An automated boom (Fig. 1) swept through the pen for 10 min h<sup>-1</sup> for 12 h per day to encourage movement. Birds were also manually exercised for 30-40 min per day for 5 days per week in which the animals accelerated in short-duration bouts of running. The SG received no external motivation for movement. The exercise protocol lasted from 4 weeks of age to 14 weeks, when birds were sacrificed. Specimens were imaged using standard x-ray for segment lengths and dual x-ray absorptiometry (DXA) for body composition. Specimens were then dissected to separate the lower limbs. Left limbs were frozen for subsequent measurement of muscle wet mass. Right limbs were fixed in 5% formalin, with joint angles set to approximate the mid-swing phase of running.

The iliotibialis lateralis pars postacetabularis muscle (ILPO; Fig. 1), a large hip and knee extensor was the focus of this study. The ILPO was chosen for initial analysis because it is a major muscle used for locomotion and has been shown to undergo substantial muscle strain during running [5]. The fixed ILPO was dissected free from the limb and photographed for measurement of fascicle pennation angle. Cranial, middle, and caudal portions were sectioned off (Fig. 1), and placed into 30% nitric acid for digestion. Digested muscles were then placed in glycerol for at least one day before small bundles of fibers were transferred to slides. Fiber lengths were measured by digitizing the fiber from high-resolution images. Laser diffraction was used to measure at least 3 different sarcomere lengths across the length of the fibers. Finally, optimal fiber lengths were calculated from the average measured sarcomere lengths per section and the known optimal sarcomere length (2.36 μm) of guinea fowl [5]:

$$L_0 = (2.36/S_L) \cdot FL$$

where  $L_0$  is the optimal fiber length (mm),  $SL$  is the average sarcomere length ( $\mu\text{m}$ ) and  $FL$  is the measured fiber length (mm).

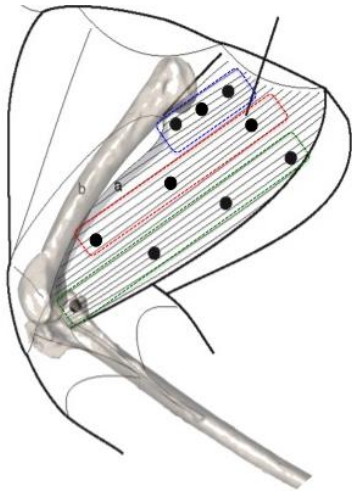


**Figure 1.** Schematic of the ILPO muscle and the cranial (blue), middle (red) and caudal (green) muscle sections and  $SL$  measurements (dots).

## RESULTS AND DISCUSSION

The groups had similar body masses initially (4 weeks-old), but EG body mass was 10% lower than SG by week 6 and throughout the remainder of the experiment ( $p < 0.05$ ). Body composition (percent lean mass) was similar between groups. EG had overall leg lengths 2% shorter than that of SG.

Preliminary tests ( $N = 5$ ) revealed that wet muscle mass, PCSA, pennation angle and  $SL$  were not different between groups. Serial sarcomere number and  $L_0$  were not statistically different between the groups, but showed a trend for increases in the cranial ILPO fibers of the EG ( $p = 0.07$ ).

When normalized to leg length, however, the EG had significantly greater serial sarcomere numbers and longer cranial and caudal  $L_0$  compared to the SG (Fig. 2). These results agree with previous results showing sarcomerogenesis in response to stretch training [3]. However, they contradict findings from a study of endurance training in humans [4] in which shorter

muscle fibers resulted in the gastrocnemius muscle. We interpret this result from differences in the type of training and the functional roles of the muscles studied. Endurance training may lead to adaptations for economical force production favoring short-fibered muscles such as the gastrocnemius. The high-acceleration training in the EG was, on the other hand, hypothesized to lead to longer  $L_0$  that reduces fiber strain and velocity. These activities likely mimicked human sprint-type training as opposed to endurance training.

In conclusion, these findings offer among the first evidence that sprint training during growth may contribute to the observed differences in fiber lengths between sprinters and non-sprinters and between sprinters of varying abilities.

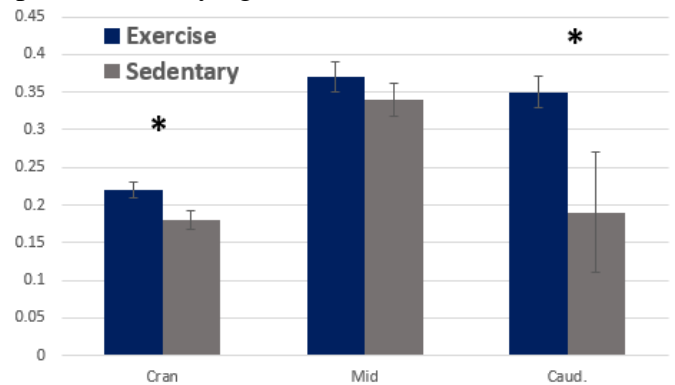


**Figure 2.** Fiber lengths of ILPO normalized to leg length. \* $p < 0.05$  ( $n = 5$  per group)

## REFERENCES

1. Abe T, et al. *Med Sci Sports Exerc* 32(6) 1125-1129, 2000.
2. Kumagai K, et al. *J Appl Physiol* (1985) 88(3), 811-816, 2000.
3. De Jaeger D, et al. *J Appl Physiol* (1985) 118(12), 1467-1473, 2015.
4. Murach K, et al. *Appl Physiol Nutr Metab* 40(1), 99-102, 2015.
5. Carr JA, et al. *J Exp Biol* 214(20), 3405-3413, 2011.

Table 1: Stature and non-normalized muscle parameters.

	Leg Length (mm)	Muscle Mass (g)	PCSA (mm <sup>2</sup> )	Avg. Sarcomere Length ( $\mu\text{m}$ )			Sarcomere Number			Optimal Fiber Length (mm)			Pennation Angle (°)		
				Cran.	Mid.	Cau.	Cran.	Mid.	Cau.	Cran.	Mid.	Cau.	Cran.	Mid.	Cau.
<b>Exercise</b>	264.3	12.6	146.5	2.07	2.17	2.16	24308	41384	39672	57.4	97.7	93.6	14.1	25.2	37.6
<b>Sedentary</b>	272.7	13.2	167.8	2.22	2.27	2.26	21152	39031	37797	49.9	92.1	89.2	14.2	25.2	32.3
<b>p-value</b>	0.11	0.29	0.18	0.13	0.21	0.29	0.07	0.24	0.29	0.07	0.24	0.29	0.47	0.50	0.11

# IN VIVO DETERMINATION OF OPTIMAL MUSCLE FASCICLE LENGTH AND PCSA USING MULTI-SCALE MEASUREMENTS

<sup>1</sup>Evan Terrell, <sup>1</sup>Shawn Russell, <sup>1</sup>Joseph Hart, <sup>1</sup>George Christ, <sup>1</sup>David Weiss, <sup>1</sup>Silvia Blemker

<sup>1</sup>University of Virginia, Charlottesville, VA, USA  
email: et5ee@virginia.edu, web: bme.virginia.edu/muscle/

## INTRODUCTION

It is widely known that the architectural properties of skeletal muscle, including optimal fascicle length ( $l_{fo}$ ) and physiologic cross-sectional area (PCSA), have considerable influence on muscle's ability to generate force and facilitate movement [1]. Because of muscle's hierarchical organization, it is essential to consider architecture across length scales in order to understand these structure-function relationships. While traditional imaging modalities, such as ultrasound and magnetic resonance imaging (MRI), are used extensively to study muscle structure at the fascicle and whole-muscle level, respectively, non-invasive methods of *in vivo* imaging at the length scale of the sarcomere have not been available until recently. Thus, current sarcomere structure data come from cadaveric studies or invasive imaging methods that disrupt muscle tissue and may be limited in their applicability to healthy musculature.

A novel imaging system has been developed that relies on the second harmonic generation (SHG) properties of myosin and a minimally invasive microendoscopic needle to access sarcomeres without the need for incisions or muscle removal [2]. This technology offers an opportunity to image sarcomeres in healthy, living subjects without disrupting muscle structure, and, when combined with traditional imaging methods, provides a comprehensive view of muscle architecture.

The purpose of this study is to use a combination of imaging modalities to provide what we believe are the first *in vivo* measurements of optimal fascicle length in the tibialis anterior (TA) muscle. We have collected image data of TA architecture across length scales using MRI, ultrasound, and *in vivo* SHG microendoscopy to determine  $l_{fo}$  and PCSA of the TA muscle in healthy adults.

## METHODS

Three healthy adult subjects with no history of lower limb injury were recruited for this study (age:  $27.7 \pm 10.8$  years, M/F: 2/1, height:  $172.7 \pm 13.4$  cm, weight:  $66.5 \pm 9.4$  kg). Axial magnetic resonance images of the lower limb were gathered using a 3T Siemens (Munich, Germany) Trio MRI Scanner with a 2D multi-slice sequence and spiral gradient echo. The TA was segmented within the image sequence using an in-house segmentation software created in MATLAB (MathWorks, Natick, MA). TA volume was measured from the 3D surface that was generated by connecting the segmentation contours across image frames.

Muscle fascicle architecture was imaged using a Teleded LS128 ultrasound system with a 60 mm, 7 MHz flat transducer (TELEMED Medical Systems, Milano, Italy). Three panoramic ultrasound image scans were taken of the TA along its path of action from origin to insertion on the dominant leg of each subject. During imaging, the ankle was held at an angle of  $20^\circ$  plantarflexion using a custom brace. Image frames of each panoramic scan were stitched together to produce three complete ultrasound images of the TA in longitudinal cross section for each subject. Muscle pennation angle was measured as the angle between the observed fascicle direction and the internal aponeurosis direction. Muscle fascicle length was measured as the distance along the path of the muscle fascicles between the observed edge of the TA and the internal aponeurosis. Measurements were made in the proximal, middle, and distal third of the muscle length on both the anterior and posterior side of the internal aponeurosis. These measurements were averaged across the three images to determine the pennation angle and fascicle length for each subject [3].

*In vivo* sarcomere length measurements were made using the ‘Zebroscope’ SHG microendoscope system (Zebra Medical Technologies, Mountain View, CA). A high-power laser provided 200 fs pulses of 1030 nm wavelength light, which interacted with the myosin-containing bands of the sarcomere to produce SHG signal. A fiber-optic cable and microendoscopic needle delivered the excitation light into the TA with the ankle joint held at 20° plantarflexion. The needle was oriented within the muscle belly such that the endoscope lens plane was parallel to the TA fascicle direction. The resulting SHG signal was used to produce images of the TA sarcomeres, which allowed for the direct measure of sarcomere length for each subject.

Measured muscle architecture parameters were used to compute  $l_{fo}$  and PCSA.  $l_{fo}$  was computed according to the following equation:

$$l_{fo} = l_f / l_s * 2.7 \mu\text{m}$$

where  $l_f$  is the fascicle length measured from ultrasound imaging, 2.7  $\mu\text{m}$  is the optimal sarcomere length for humans [4], and  $l_s$  is the measured sarcomere length. PCSA was then calculated according to the following equation:

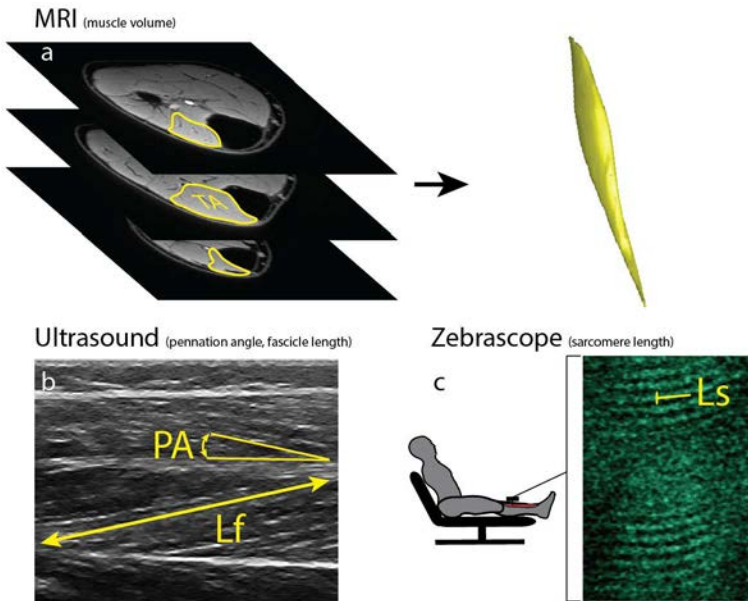


**Figure 1:** (a) Segmentation of the TA in MRI images to produce 3D volume, (b) Measurement of pennation angle (PA) and fascicle length (Lf) in ultrasound images of the TA, (c) Acquisition of *in vivo* SHG images and sarcomere length (Ls) measurement

$$PCSA = V / l_f$$

where  $V$  is the muscle volume measured from MRI.

## RESULTS AND DISCUSSION

At 20° of plantarflexion, pennation angle of the TA was measured at  $8.75 \pm 0.90^\circ$ . The TA fascicle length was measured to be  $6.56 \pm 0.22$  cm and sarcomere length was measured at  $2.83 \pm 0.16 \mu\text{m}$ . The mean TA volume was  $144.8 \pm 30.5 \text{ cm}^3$ . Based on these measurements,  $l_{fo}$  was calculated at  $6.3 \pm 0.5$  cm and PCSA was found to be  $23.0 \pm 5.1 \text{ cm}^2$ .

The values reported here agree well with previously reported architecture measures from cadaveric studies. For the TA, Ward et al. report an optimal fascicle length of  $6.83 \pm 0.79$ . The PCSA reported here is significantly larger than that reported by Ward et al. ( $10.9 \pm 3.0 \text{ cm}^2$ ) due to the larger muscle volume in the healthy subjects compared to the cadaveric specimens [5]. This is consistent with the findings of Handsfield et al [6].

## CONCLUSIONS

This work presents the first reported values of optimal fascicle length computed from *in vivo* muscle architecture measurements of healthy, living subjects and provides important insight regarding the force-length behavior of the TA. Future work will aim to confirm our reported values through the inclusion of additional subjects in our study, consider muscle architecture measurements across ankle joint range of motion, and correlate  $l_{fo}$  and PCSA with measured strength and gait capacities of the TA.

## REFERENCES

1. Lieber, RL, et al. *Muscle Nerve* **23**, 1647-66, 2000.
2. Sanchez GN, et al. *Neuron* **88**, 1109-1120, 2015.
3. Maganaris CN et al. *Eur J Apply Physiol* **79**, 294-297, 1999.
4. Gordon AM, et al. *J Physiol* **184**, 170-192, 1966.
5. Ward SR, et al. *Clinical Orthop Relat Res* **467**, 1074-1082, 2009.
6. Handsfield GG, et al. *J Biomech* **47**, 631-638, 2014.

# INDIVIDUALS WITH LOWER LIMB TRAUMA PRIORITIZE STABILITY OVER MANEUVERABILITY WHEN NAVIGATING A VIRTUAL OBSTACLE COURSE

<sup>1,2</sup>Riley C. Sheehan, <sup>1</sup>Mitchell D. Ruble, <sup>2</sup>Jonathan B. Dingwell, and <sup>1,3</sup>Jason M. Wilken

<sup>1</sup>Center for the Intrepid, Brooke Army Medical Center, JBSA Ft. Sam Houston, TX, USA

<sup>2</sup>University of Texas at Austin, Austin, TX, USA

<sup>3</sup>Extremity Trauma and Amputation Center of Excellence, JBSA Ft. Sam Houston, TX, USA

Email: [riley.c.sheehan.ctr@mail.mil](mailto:riley.c.sheehan.ctr@mail.mil)

## INTRODUCTION

Lower limb trauma (LLT) impairs walking stability [1]. As a result, individuals with LLT often adopt a cautious gait pattern which includes a greater step width. Individuals with LLT also display a greater lateral margin of stability ( $MOS_{ML}$ ) when walking which is related to the force required to move the center of mass outside of the base of support [2]. While this strategy helps maintain the center of mass within the base of support by resisting perturbing forces, the stabilizing effect can also resist intended movements, reducing maneuverability. Thus, we investigated how the cautious gait pattern of individuals with LLT affects their ability to execute lateral walking maneuvers. We hypothesized that individuals with LLT would maintain a wider step width and greater  $MOS_{ML}$  throughout a lateral transition and this would result in poorer transition performance.

## METHODS

Fifteen able-bodied controls and 13 individuals with varying levels of LLT completed 6 trials of a virtual obstacle course at 0.9 m/s (Fig. 1A). The obstacle course consisted of navigating an avatar through a series arches in one of 4 lanes projected on the screen, with the goal of hitting as few arches as possible (Fig. 1B). We tested 2 conditions: “Anticipation” where the transition direction was visible ahead of time and “Reaction” where the transition direction was not visible until exiting the current arch set. We calculated the step width and  $MOS_{ML}$  just prior to and across the transition (Fig. 1C). We also quantified the number of unsuccessful transitions where they collided with one of the arches as a measure of maneuverability. To simplify the analysis and focus on the impact of lower limb trauma, we reduced the dataset by pooling the data from

both directions and only analyzing the more challenging 2-lane transitions. To analyze the effect of LLT on stability and maneuverability we ran a 2-factor (Group x Condition) ANOVA and *post hoc* t-test with Bonferonni-Holm corrections for multiple comparisons with significance defined as  $p < 0.05$ .

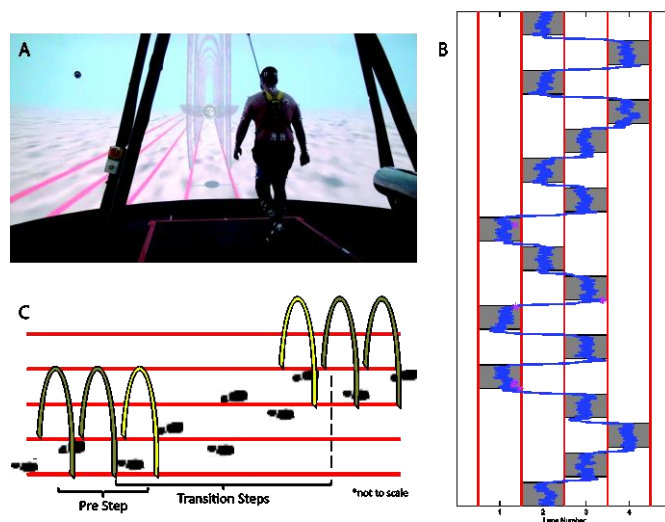


**Figure 1:** A) Patient walking in the VR system, B) Pelvis trajectory during typical obstacle course trial, C) Diagram of the transition task.

## RESULTS AND DISCUSSION

As hypothesized, there was a significant Group effect for both step width ( $p=0.003$ ; Fig. 2A) and  $MOS_{ML}$  ( $p < 0.001$ ; Fig. 2B) during the Pre Step with individuals with LLT maintaining a wider step width and greater  $MOS_{ML}$ . The findings were similar for the values across the transition with a trend towards a significant Group effect for step width ( $p=0.096$ ; Fig. 2C) and a significant Group effect for  $MOS_{ML}$  ( $p=0.001$ ; Fig. 2D) both with the LLT group being greater than controls. This suggests that individuals with LLT prioritize stability and maintain a cautious gait pattern even when preparing for and performing lateral maneuvers.

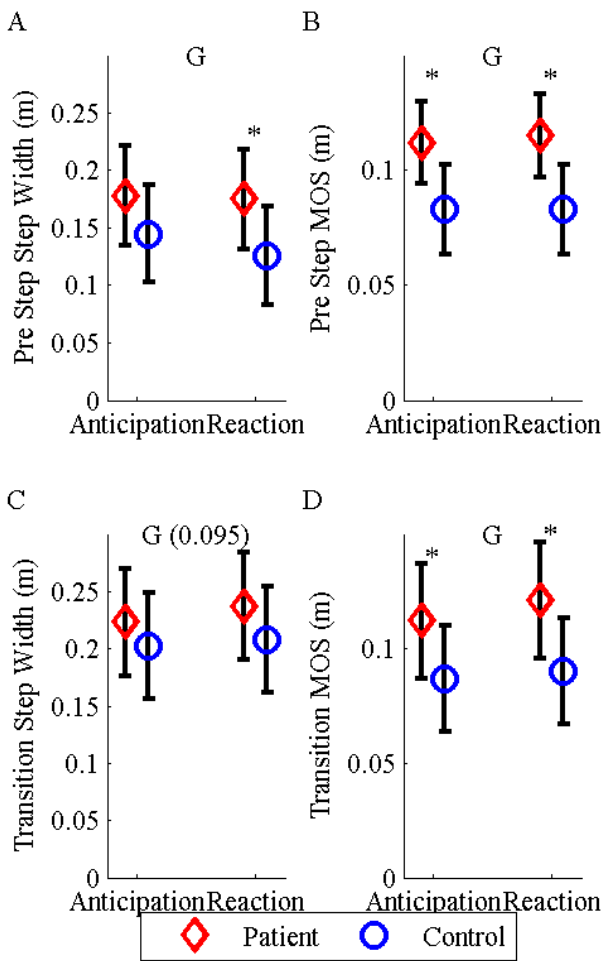


**Figure 2:** Step width and lateral margin of stability (MOS) during the Pre Step (A-B) and across the transition (C-D), respectively.

Further, in support of our hypothesis, there was a significant Group effect for the number of unsuccessful transitions with individuals with LLT performing more poorly than controls ( $p=0.001$ ; Fig. 3). This suggests that the greater priority on stability and reliance on the cautious gait patterns likely impairs transition performance and maneuverability.

## CONCLUSIONS

The individuals with LLT prepared for and transitioned with a wider step width and greater  $MOS_{ML}$ . This suggests that individuals with LLT prioritize stability and retain their cautious gait pattern to the detriment of their maneuverability. By improving individuals' stability and balance confidence through the use of interventions and training, we may be able to reduce patients' reliance on a cau-

tious gait pattern and allow them to develop a more efficient and adaptable gait that can change to meet the specific demands of the environment.

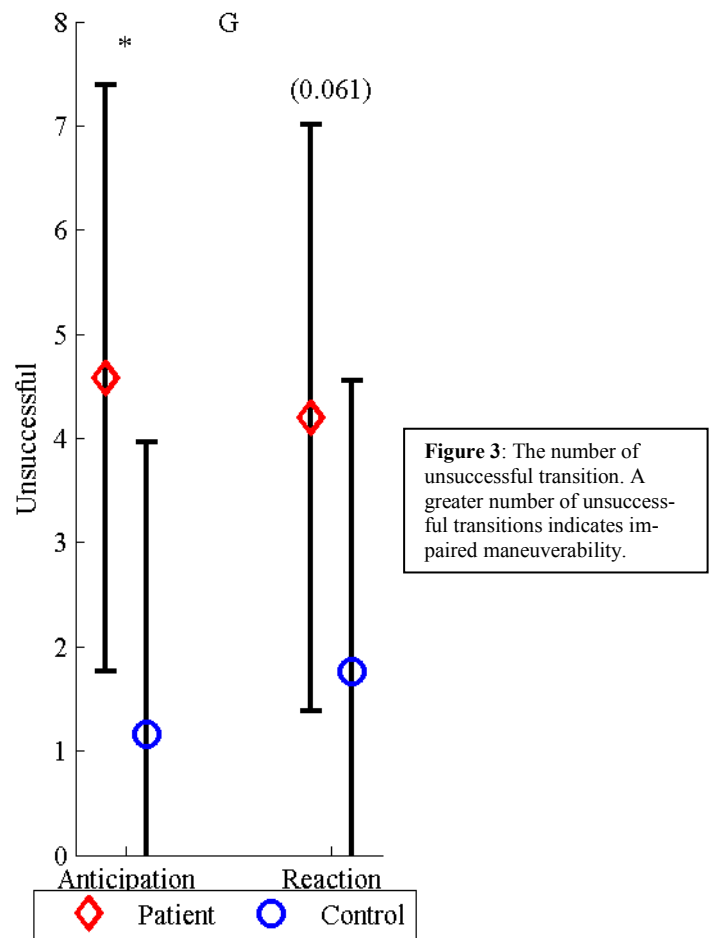


**Figure 3:** The number of unsuccessful transition. A greater number of unsuccessful transitions indicates impaired maneuverability.

## REFERENCES

1. Miller, et al. *Arch Phys Med Rehabil* **82**, 1031-7, 2001.
2. Beltran, et al. *J Biomech* **47**, 1138-43, 2014.

## ACKNOWLEDGEMENTS

DoD/CDMRP/BADER Consortium W81XWH-11-2-0222 (to JBD, JMW, & JPC) and NIH Grant # R01-HD059844 (to JBD & JWM).

## DISCLAIMER

The views expressed herein are those of the authors and do not reflect the official policy or position of Brooke Army Medical Center, U.S. Army Medical Department, U.S. Army Office of the Surgeon General, Department of the Army, Department of Defense or the U.S. Government

# ACL RECONSTRUCTION GRAFT GEOMETRY IS ASSOCIATED WITH ASYMMETRIC *IN VIVO* CARTILAGE CONTACT PATTERNS

<sup>1</sup> Michael F. Vignos, <sup>1,2</sup> Jarred Kaiser, <sup>1</sup> Geoffrey S. Baer, <sup>1</sup> Richard Kijowski, <sup>1</sup> Darryl G. Thelen

<sup>1</sup> University of Wisconsin-Madison, Madison, WI, USA, <sup>2</sup> Boston University, Boston, MA, USA  
email: mvignos@wisc.edu, web: <http://uwnmbl.engr.wisc.edu/>

## INTRODUCTION

Subtle asymmetries in tibiofemoral (TF) kinematics have been detected in ACL reconstructed (ACLR) knees [1,2]. These altered kinematics may produce a shift in cartilage contact regions, which is theorized to initiate osteoarthritis [3]. Additionally, altered TF cartilage contact has been correlated to cartilage damage grade and progression [4,5]. Thus, restoring normal contact patterns with ACLR could prevent early cartilage degradation.

A recent study found that graft tunnel placement impacts TF kinematics during quasi-static lunges, with an antero-proximal femoral tunnel linked to greater anterior translation, medial translation, and internal rotation of the tibia [6]. However, the implications of these altered kinematics on cartilage contact are not well understood. Accordingly, our objective was to investigate the links between TF cartilage contact and ACL graft geometry during a loaded flexion-extension task using dynamic MRI.

## METHODS

The bilateral knees of 18 subjects that underwent a primary unilateral, isolated ACLR were tested (9 M, 24.8±5.7 yrs, 78.9±16.5 kg, 20.2±8.7 months post-op, 9 PT grafts). Bilateral, high-resolution MR images were collected and segmented to create bone, cartilage, and ACL geometries for the ACLR and healthy knees. The location of the ACL femoral and tibial attachments and the orientation of the ACL relative to the tibial plateau were measured bilaterally (Fig. 1A). Non-native ACL graft geometry was characterized by subtracting the healthy from the reconstructed metrics.

During the dynamic MRI protocol, subjects lay supine in the MR scanner with their leg attached to an inertial loading device designed to induce eccentric quadriceps loading at peak knee flexion.

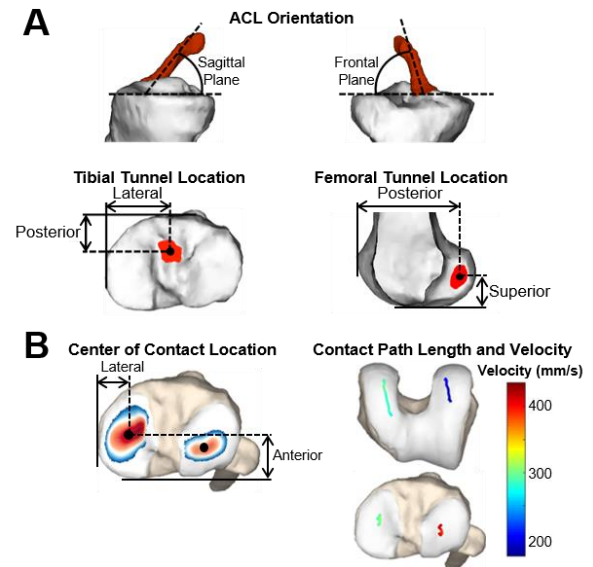


**Figure 1:** A. ACL geometry metrics B. Contact metrics. The sliding length and velocity were computed by subtracting the femur path length and velocity from that of the tibia.

Subjects performed cyclic knee flexion-extension at 0.5 Hz for 5 min while dynamic volumetric images were continuously acquired [7]. Images were retrospectively sorted and reconstructed into 60 frames over the motion cycle. Cartilage contact was characterized by optimally registering the bone and cartilage geometries to the image sets at each frame and computing the overlap of the femur and tibia cartilage. We then extracted the location of the center of contact (COC) on the medial and lateral tibial plateaus at peak flexion (Fig. 1B). Computing the COC location with this method has a maximum error of 0.49mm in the lateral direction and 0.25mm in the anterior direction [8]. We also computed the relative difference (femur subtracted from tibia) in the COC path length and velocity, which have been used as measures of contact sliding length and velocity [4]. Contact asymmetries were determined by subtracting the healthy from the reconstructed metrics. We performed a multiple linear regression analysis to determine the ability of non-native ACL geometry to predict the asymmetry in contact metrics. When a

significant relationship was found ( $p < 0.05$ ), we used the coefficient of the regression model ( $\beta$ ) to determine the sensitivity of each contact metric to non-native graft placement.

## RESULTS AND DISCUSSION

Tibial posterior attachment location and sagittal graft orientation predicted asymmetries in cartilage contact location and sliding length (Fig. 2). A more posterior tibial attachment was linked to a more lateral COC ( $\beta = 0.72$  mm/mm) and greater sliding length ( $\beta = 1.7$  mm/mm) in the medial compartment. A greater sagittal plane angle was linked to a more medial COC on the medial tibia ( $\beta = 0.14$  mm/deg) and decreased sliding length in the lateral compartment ( $\beta = -0.19$  mm/deg).

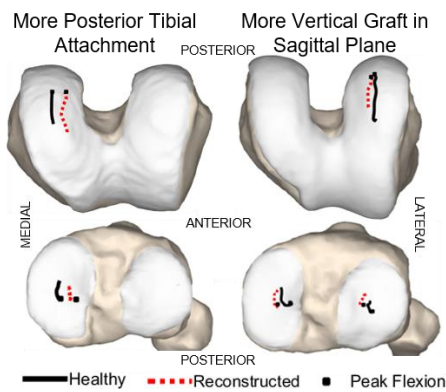


**Figure 2:** Tibia and femur COC paths for representative subjects with only significant differences shown. More posterior tibial attachments predicted more lateral contact and greater sliding length, as seen by the longer reconstructed femur COC path. More vertical grafts corresponded to more medial contact on the medial tibia and decreased lateral compartment sliding length, as seen by the shorter reconstructed femur COC path.

Femoral superior and posterior attachment locations predicted asymmetric sliding velocity magnitudes (Fig. 3). A more anterior femoral attachment was related to greater sliding velocity in the medial compartment ( $\beta = 60$  (mm/s)/mm) and lower sliding velocity in the lateral compartment ( $\beta = -22$  (mm/s)/mm). A more superior femoral attachment was linked to greater sliding velocity in the medial compartment ( $\beta = 22$  (mm/s)/mm).

Our findings suggest that non-native ACL graft placement may contribute to altered cartilage loading in ACLR knees. Recent studies by DeFrate et al. [6] have shown that ACL grafts placed antero-

proximally on the femur, relative to native, tend to be more vertical in the sagittal plane and are linked with greater anterior tibia translation, medial tibia translation, and internal rotation. Similarly, we found links between femoral attachments, sagittal graft angle, and abnormal cartilage contact. The largest contact sensitivity was indicative of substantially greater sliding velocity in the medial compartment in subjects with an abnormally anterior femoral attachment. It was previously found that an increase in sliding velocity of 10 mm/s correlates to approximately a 1 point increase in cartilage damage grade (on a 5 point scale) [4]. Hence, our findings suggest that the early progression of osteoarthritis seen in this population could arise from abnormal contact due to a non-native graft femoral attachment.

## CONCLUSION

This study elucidates links between ACL graft geometry and asymmetric cartilage contact. These findings suggest that altered cartilage loading can potentially be restored through graft placement, which may be important to consider when planning ACLR procedures to restore normative mechanics.

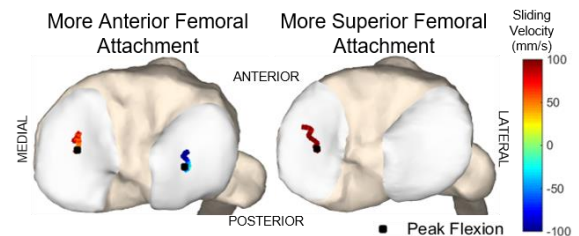


**Figure 3:** Bilateral differences in sliding velocity for representative subjects with only significant differences shown. Anterior femoral attachment was linked to increased medial compartment sliding velocity and decreased lateral compartment sliding velocity. A more superior femoral attachment predicted greater medial compartment sliding velocity.

## REFERENCES

1. Tashman S, et al. *Clin Ortho* **454**, 66-73, 2006.
2. Scanlan SF, et al. *J Biomech*, **43**, 1817-22, 2010.
3. Chaudhari AMW, et al. *MSSE* **40**, 215-222, 2008.
4. Beveridge JE, et al. *J Orthop* **31**, 1745-56, 2013.
5. Anderst WJ, et al. *J Orthop* **27**, 71-77, 2009.
6. DeFrate LE. *J Orthop*, In press, 2017
7. Kaiser J, et al. *MRM* **1316**, 1310-16, 2013.
8. Kasier J, et al. *Med Eng Phy*. **38**, 1131-5, 2016.

## ACKNOWLEDGMENTS

NSF GRFP (MFV): DGE-1256259, NIH EB015410

# INCREMENTAL LATERAL WEDGING: EFFECTS ON KNEE MOMENT IN MEDIAL KNEE OSTEOARTHRITIS

<sup>1</sup> Melvin Mejia, <sup>2,3</sup> Jeffrey L. Cole, <sup>1,2</sup> Peter Barrance

<sup>1</sup> Human Performance and Engineering, Kessler Foundation, West Orange, NJ, USA

<sup>2</sup> Rutgers, The State University of New Jersey, Newark, NJ, USA

<sup>3</sup> Kessler Institute for Rehabilitation, West Orange, NJ, USA

email: [pbarrance@kesslerfoundation.org](mailto:pbarrance@kesslerfoundation.org)

## INTRODUCTION

A 2009 report estimated that osteoarthritis (OA) affected approximately 27 million US adults at that time [1]. In-shoe lateral sole wedging has been proposed as a low cost measure to address varus knee malalignment and associated medial knee OA (MKOA). While one review [2] concluded there was a ‘strong scientific basis for applying wedged insoles in attempts to reduce osteoarthritic pain of biomechanical origin’, another [3] concluded that the use of lateral wedges for MKOA was not supported. Potential benefit derived from lateral wedging has been linked to reduction in the external knee adduction moment (EKAM), with concomitant reduction in medial condylar loading. While some mechanistic study findings have supported this link, others report mixed or contradictory results [4].

Most previous studies of lateral wedging have investigated only one level of wedging - most frequently a 5° lateral wedge. As part of a more comprehensive investigation that incorporates weight bearing MRI of the knee joint, our study explored the effects of incremental increases of lateral wedging on EKAM. In comparison with a non-wedged (neutral) insole, we studied three different levels of wedging at two walking speeds.

## METHODS

We report initial results from all participants recruited to date (n=4, male, 63±6.7 years) in a study that has a target enrollment size of 20. All research procedures were approved by the Institutional Review Board. All participants presented symptomatic, predominantly medial knee osteoarthritis, as confirmed by physical examination and a standing frontal radiograph. Exclusions to

enrollment included: presence of advanced knee OA; history of lower extremity joint replacement or osteotomy; knee surgery in the preceding 6 months; intra-articular viscosupplementation or corticosteroid injection in the preceding 4 months; use of wedged insoles in the preceding 4 months. For each participant, one knee was assigned as the index knee based on the clinical and radiological severity.

All participants were tested in a pair of standardized walking shoes (New Balance MW577), selected according to self-reported shoe size. Four sets of custom insoles were prepared by a professional pedorthist. The base insole was constructed of 5/16” thick neoprene (Spenco®), Spenco Medical Corp., Waco, TX). The neutral (‘N’) insole consisted only of the neoprene layer. Lateral wedging of 3°, 6°, and 9° was added using 1/8” and 1/4” cork layers applied to the full width tapering to zero thickness medially. Lengthwise, wedging was applied from the heel to the metatarsal heads.

Participants were fitted with a custom 42-marker Helen-Hayes kinematic marker set. Marker trajectories were captured using a 12-camera motion analysis system sampling at 120 Hz (Motion Analysis Corp., Santa Rosa, CA). Force data was recorded with two force plates sampling at 2520 Hz (Bertec Corp., Columbus, OH) mounted in the floor.

Initial testing was performed with the neutral insoles. Participants were then asked to walk across the length of the laboratory, first at a “stroll” speed, then at a “brisk” speed. Speeds were self-selected based on verbal cues indicating respectively ‘leisurely walking’ and a faster walk, as if to catch a bus. The average speed of 5 trials for each speed was collected using optical timing gates at the beginning and end of the walk. The subsequent testing order for

footwear condition (N/3°/6°/9°) was randomized. After a brief period of acclimation to each wedge condition, the participant was asked to walk at the ‘stroll’ and ‘brisk’ speeds established during the initial trials, using an audible metronome set to match the cadences to assist in reproducing those baseline speeds. Walking trials were accepted for analysis subject to the following criteria: (1) timing gate speed within  $\pm 5\%$  of targeted speed; (2) kinetic data recorded for the complete stance phase on either or both limbs. Besides the metronome, verbal cueing was provided to facilitate meeting these criteria. At least 3 trials were collected for each limb for each condition.

All kinematic and kinetic post-processing was performed using Cortex (Motion Analysis Corp.) & Matlab (MathWorks, Inc., Natick, MA) software. Marker trajectory data was smoothed using a 6 Hz Butterworth low-pass filter. EKAM profiles were calculated using the Cortex software’s kinetic model and normalized to body weight. The EKAM measure analyzed was the normalized EKAM impulse, calculated as the time integral of the normalized EKAM curve throughout stance.

Data for the index knee were analyzed in this report. Statistical analyses were performed for both speeds, using analysis of variance with lateral wedge level as a repeated factor. Pairwise comparisons were used to test for outcome differences in wedged conditions from the neutral condition. Within wedge conditions, paired t-tests were used to analyze the effect of walking speed. Significance level ( $\alpha$ ) for all statistical testing was set at 0.05.

## RESULTS AND DISCUSSION

In the ‘stroll’ speed, we observed a significant effect ( $p=0.023$ ) of wedge condition, such that EKAM impulse was reduced by the increasing wedge (Fig. 1). At this speed, pairwise testing indicated that EKAM impulse was significantly lower than for the neutral insole for all wedge angles. No significant effect of wedging ( $p=0.383$ ) was found for ‘brisk’ speed, although pairwise testing indicated the EKAM impulse was lower for 3° than N. Mean EKAM impulses were lower for ‘brisk’ than ‘stroll’ speed, significantly at the N and 3° conditions. An

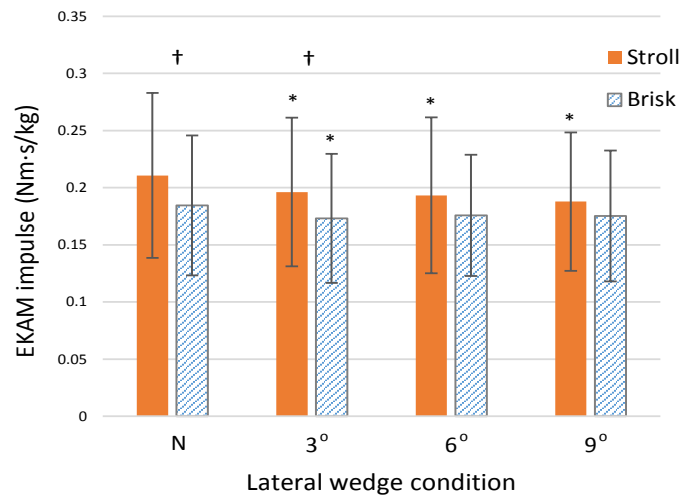


Figure 1: Impulse of normalized knee adduction moment for two walking speeds and 4 wedge conditions. \*: Significant difference of wedge condition from ‘N’, within speed condition; †: significant difference between speeds, within wedge condition.

effect of decreasing EKAM impulse with increasing speed has been reported previously [5].

## CONCLUSIONS

In the ‘stroll’ walking speed, these preliminary results support the hypothesis that incremental lateral wedging monotonically reduces EKAM. At the accelerated speed, the results suggested the presence of a limiting or ceiling effect of lateral wedging on EKAM. Ongoing work will combine these results with a parallel weight bearing MRI investigation of knee joint condylar contact in this cohort, to more clearly describe the biomechanical effects of lateral wedging in MKOA patients.

## REFERENCES

1. Moskowitz, RW. *Am J Manag Care*, 15(8 Suppl):S223-9, 2009
2. Marks, R., et al. *Int J Clin Pract*, 58(1):49-57, 2004
3. Parkes, M. J., et al. *JAMA*, 310(7):722-30, 2013
4. Kakihana, et al. *Am J Phys Med Rehabil*, 86(6):446-54, 2007
5. Robbins, S. M. and Maly, MR. *Gait Posture*, 30(4):543-6, 2009

**ACKNOWLEDGMENTS** - This study was supported by NIDILRR grant 90IF0077 (formerly H133G140183). Additional funding was provided by Kessler Foundation.

# EFFECT OF THE ATLAS™ KNEE SYSTEM ON STRESS IN THE MEDIAL TIBIAL CARTILAGE

<sup>1,3</sup> Rajshree Hillstrom, <sup>1</sup> Oliver Morgan, <sup>2</sup> David Lowe, <sup>3</sup> Anil Ranawat, <sup>3</sup> Austin T. Fragomen, <sup>3</sup> S. Robert Rozbruch, and <sup>3</sup> Howard Hillstrom

<sup>1</sup> Anglia Ruskin University, Chelmsford, Essex, UK

<sup>2</sup> Moximed Inc., CA, USA

<sup>3</sup> Hospital for Special Surgery, NY, USA

email: Rajshree.Hillstrom@anglia.ac.uk, web: <http://anglia.ac.uk/merg>

## INTRODUCTION

Osteoarthritis (OA) is a degenerative joint disease, reported to account for 1% of total deaths worldwide [1]. OA is often caused by increased joint stress and affects the medial knee joint compartment most frequently. The end-stage treatment for OA is total knee replacement (TKR), whereby natural tissues are removed. Although, clinical outcomes are generally satisfactory, a restriction for certain activities, instability, pain, and unmet patient expectations may result.

The Atlas™ implant (Fig. 1), fixed subcutaneously alongside the medial aspect of the joint, is designed to offload the medial compartment of the knee, without violating the natural tissues. This may halt the debilitating symptoms associated with OA progression.

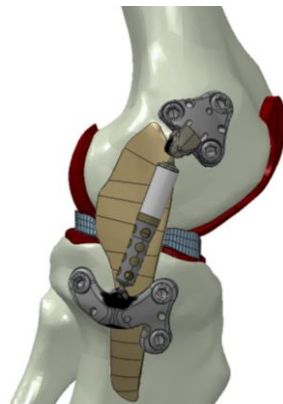


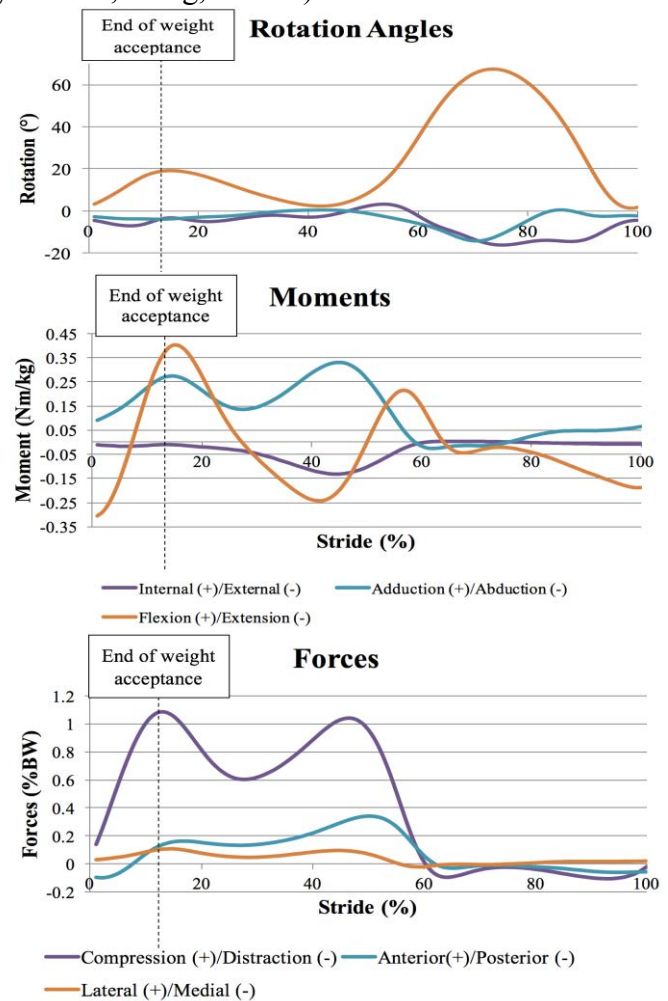
**Figure 1:** The Atlas™ implant fixed to the medial distal femur and proximal tibia.

The aim of this investigation was to study the effect of the Atlas™ knee implant on knee joint contact stress.

## METHODS

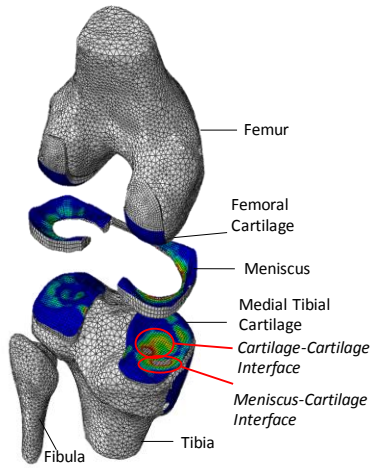
A three-dimensional previously-validated cadaver-specific finite element (FE) knee model [2] was used in this study. Computer aided design models of the Atlas™ components were virtually fixed to the medial aspect of the knee model to simulate

treatment of medial knee OA. To evaluate the knee joint stress distribution within the medial compartment in response to the Atlas™ implant, the model was driven by the loading experienced during the gait cycle (Fig. 2) of a healthy subject with similar anthropometric data as the cadaver (male, 50 years old, 65 kg, 1.65 m).



**Figure 2:** Knee joint angles, forces and moments during the gait cycle of level walking.

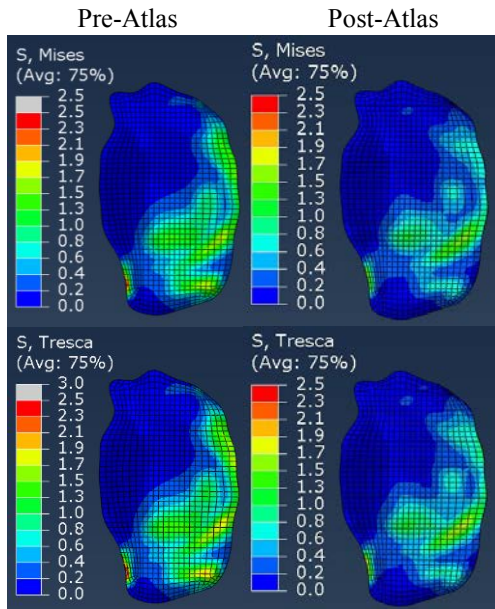
Note that varus thrust is maximum at 20° of knee flexion and 15% of the gait cycle, at the end of weight acceptance (Fig. 2). Peak Tresca and von Mises stress were computed in the medial knee compartment with and without the Atlas™ implant at different points of stance phase.



**Figure 3:** Exploded view of the FE knee model, showing stress distribution on the tibial cartilage and meniscus- cartilage interface were compiled for the quasi-static FE analyses (Fig. 3).

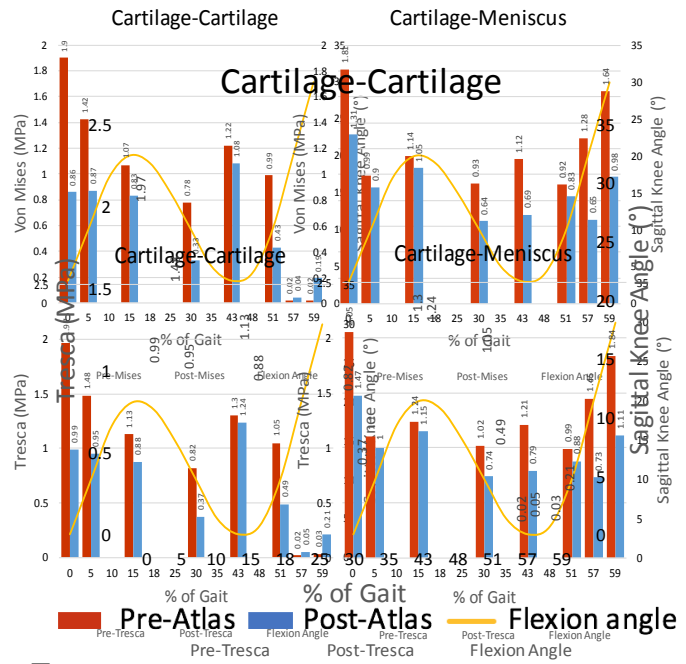
## RESULTS AND DISCUSSION

Figure 4 shows von Mises and Tresca stress values in the medial tibial cartilage, with and without the Atlas™ implant, at end of weight acceptance.



**Figure 4:** (Top) von Mises and (bottom) Tresca stress values on the medial tibial cartilage at the end of weight acceptance.

Peak von Mises and Tresca stress values, with and without the Atlas™ implant, across the stance phase of gait, are compiled in Figure 5.



**Figure 5:** (Top) Peak von Mises and (bottom) Tresca stress values in the medial tibial cartilage at different points of the gait cycle pre- and post- Atlas™. The corresponding knee flexion angle is shown in yellow.

A cadaveric-specific knee FE model was used to compare peak stress values in the medial tibial cartilage with and without the Atlas™ implant at different points during the stance phase of gait. Consistent reductions in peak von Mises stress values, ranging from 11.5% to 56.6% and 9.1% to 49.2%, were noted in the cartilage-cartilage and meniscus-cartilage regions, respectively. Consistent reductions in peak tresca stress values, ranging from 4.6% to 54.9% and 7.3% to 49.7%, were noted in the cartilage-cartilage and meniscus-cartilage regions, respectively.

## CONCLUSIONS

Results of this study show the capability of the Atlas™ implant to offload the medial knee compartment. The clinical significance is that the Atlas™ implant could help delay OA progression, and delay the need for a knee replacement.

## REFERENCES

1. Mathers CD, Loncar D, *Plos Med.* 3(11): e442, 2002
2. Mootanah R. et al., 2014. *CMBBE*, 17(13):1502-1

# ARTICULAR CARTILAGE CONTACT DURING GAIT IN OBESE INDIVIDUALS WITH KNEE PAIN

<sup>1,2</sup>Jing-Sheng Li, <sup>1</sup>Tsung-Yuan Tsai, <sup>1</sup>Guoan Li, <sup>3</sup>David T. Felson, <sup>2,3</sup>Cara L. Lewis

<sup>1</sup>Bioengineering Laboratory, Massachusetts General Hospital and Harvard Medical School, Boston, MA

<sup>2</sup>College of Health and Rehabilitation Sciences: Sargent College, Boston University, Boston, MA

<sup>3</sup>Clinical Epidemiology Research and Training Unit, Boston University School of Medicine, Boston, MA  
email: jsli1@bu.edu

## INTRODUCTION

Obesity is a risk factor for onset of knee osteoarthritis (OA) [1]. Studies using 3D motion capture have reported the gait pattern of individuals with obesity [2]. However, the articular cartilage contact characteristics of the knee joint in obese individuals are still unclear. In this study, we aimed to use a validated dual fluoroscopy imaging system (DFIS) with a subject-specific magnetic resonance (MR) cartilage model to investigate the articular cartilage contact kinematics in obese individuals with knee pain.

## METHODS

Eighteen obese individual with knee pain (age:  $42.4 \pm 9.4$  yrs; body height:  $1.64 \pm 0.09$  m; body mass:  $106.2 \pm 11.9$  kg; body mass index (BMI):  $39.5 \pm 2.5$ ; 15 females, 3 males) with knee pain (visual analog scale:  $63.8 \pm 17.4$  out of 100) were recruited for the fluoroscopic gait analysis. The study protocol was approved by the Institutional Review Board and each subject provided written informed consent. The painful knee of each individual was MR scanned (Philips, Achieva, Eindhoven, The Netherlands) using a Proton Density-Weighted (PDW), Spectral Attenuated Inversion Recovery (SPAIR) sequence. The knee MR images were used to construct the subject-specific bone and cartilage surface models. Each individual was then asked to walk on a treadmill at 1.5 mph (0.67 m/s) and the painful knee was imaged by DFIS (Philips, BV Pulsera, Eindhoven, The Netherlands). Knee positions during the stance phase of the gait cycle were obtained through a 2D to 3D registration procedure. The femoral and tibial cartilage models were mapped to the corresponding bone models at each position. The

cartilage contact was represented by overlapping of the tibial and femoral cartilage surfaces, and the centroid of the overlapped surfaces was defined as the cartilage contact point [3]. The contact points during the stance phase of the gait cycle were described by contact location on the tibial plateau, and the contact and deviation angles on the femoral condyles (Figure 1) [3]. The excursion of contact locations was determined by subtracting the maximum from the minimum during the stance phase of the gait cycle. Paired t-test was used to determine the statistical difference between medial and lateral contact locations. Pearson's correlation analyses were performed to assess the relationship between the excursion of contact locations and BMI/pain status. The alpha level was 0.05.

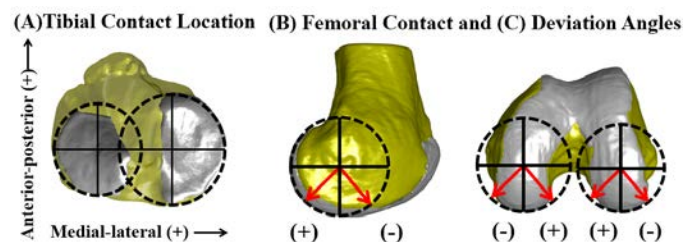


Figure 1. (A) The cartilage contact location on the tibia plateau. The medial-lateral axis is defined first as a line connecting the centroids of the two circles fit to the medial and lateral tibial plateau surfaces. The anterior-posterior axis is created perpendicular to the medial-lateral axis and the long axis of tibia. (B) Femoral contact angle in the sagittal plane is based on the geometric center of each condyle. Positive values indicate the contact point is in the posterior condyle. (C) The deviation angle is in a plane perpendicular to the sagittal plane. Positive values indicate the contact point is in the inner portion of the condyle [3].

## RESULTS

The tibial cartilage contact points in the medial compartment were more anteriorly and medially located compared to the contact points in the lateral compartment during the stance phase of gait (Figure 2A, 2B). The femoral contact angle in both the medial and lateral condyles during the stance phase followed the knee flexion angle, and the medial condyle had a smaller contact angle throughout the stance phase (Figure 2C). The medial condyle had a greater femoral deviation angle than the lateral condyle throughout the stance phase (Figure 2D).

In terms of the excursion of the contact location during the stance phase of gait, the anterior-posterior tibial contact point translated more in the medial compartment than in the lateral compartment (Table 1). Additionally, the femoral contact angle for the medial condyle had a larger excursion compared to the lateral condyle (Table 1). In the correlation analyses, no significant association was found between excursion and BMI or knee pain.

Table 1. Excursion of the tibial and femoral contact locations during stance phase.

	Medial	Lateral	P-value
<b>Tibial anterior-posterior (mm)</b>	7.8 ± 3.2	5.2 ± 1.8	0.003
<b>Tibial medial-lateral (mm)</b>	5.1 ± 2.2	5.9 ± 3.2	0.294
<b>Femoral contact angle (°)</b>	49.6 ± 16.6	36.4 ± 11.1	<.0001
<b>Femoral deviation angle (°)</b>	9.3 ± 3.9	12.0 ± 7.6	0.098

## DISCUSSION

This abstract reported the articular cartilage contact characteristics of eighteen obese individuals with knee pain during the stance phase of the gait cycle. The major tibial contact point translation was in the anterior-posterior direction. The larger anterior-posterior translation in the medial compartment may be helpful to distribute the compressive stress over different areas of the tissue. However, more shear stress may be experienced in the medial plateau during the stance phase of gait when compared to the lateral compartment. This may damage the medial plateau cartilage as shear stress is thought to be a major contributor to the formation of osteoarthritis. In terms of femoral contact angles, the offset implies that the distribution of the contact locations is

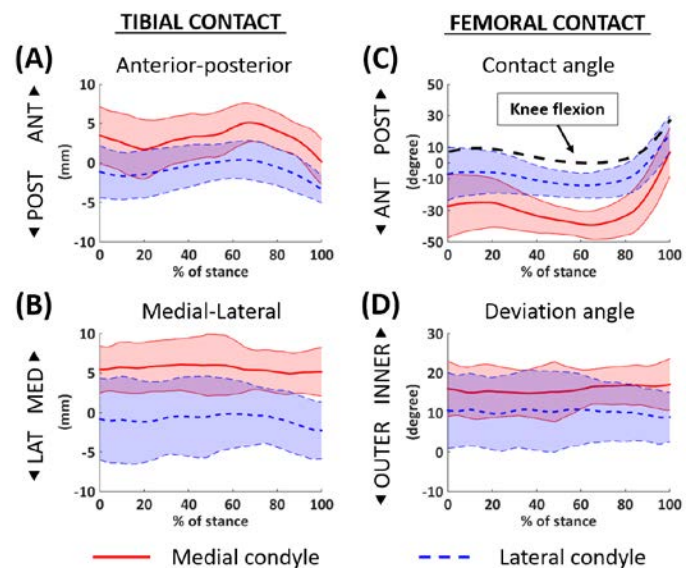


Figure 2. Tibial and femoral articular cartilage contact characteristics. Cartilage contact on tibial plateau along the anterior-posterior direction (A) and medial-lateral direction (B). Cartilage contact angle (C) and deviation angle (D) on femoral condyle.

different between the medial and lateral condyles. The positive femoral deviation angles indicate that both medial and lateral contact points were located in the cartilage on the inner portion of the femoral condyles. Further, the contact characteristics could not be better explained either by BMI or knee pain.

This is the first study, to our knowledge, to investigate the articular cartilage contact mechanism in obese individuals with knee pain. The difference between contact locations in the medial and lateral compartments may provide insights into the pathogenesis of knee osteoarthritis in individuals with obesity.

## REFERENCES

1. Felson DT. *Arthritis Rheum* 41:1343-1355, 1998.
2. Haight DJ. *J Orthop Res* 32, 324-330, 2014.
3. Liu F. *J Biomech* 43:658-665, 2010.

## ACKNOWLEDGEMENTS

This work has been supported by the National Institutes of Health under award numbers P60 AR47785 and K23 AR063235.

# ABNORMAL MUSCLE FORCES DURING GAIT ARE RELATED TO CARTILAGE HEALTH AFTER HIP ARTHROSCOPY IN FEMOROACETABULAR IMPINGEMENT PATIENTS

<sup>1</sup>Michael A. Samaan, <sup>2</sup>Alan L. Zhang, <sup>1</sup>Jan Neumann, <sup>1</sup>Thomas M. Link,  
<sup>1</sup>Sharmila Majumdar, <sup>1,3</sup>Richard B. Souza

<sup>1</sup>Department of Radiology & Biomedical Imaging, University of California, San Francisco, CA, USA

<sup>2</sup>Department of Orthopaedic Surgery, University of California, San Francisco, CA, USA

<sup>3</sup>Department of Physical Therapy & Rehabilitation Science, University of California, San Francisco, CA, USA  
email: [michael.samaan@ucsf.edu](mailto:michael.samaan@ucsf.edu)

## INTRODUCTION

Femoroacetabular impingement (FAI) is a condition in which morphological abnormalities of the hip joint result in mechanical impingement of the joint causing pain and disability during activities of daily living such as gait [1]. Previous studies have shown that when compared to healthy controls, FAI patients exhibit altered hip joint loading patterns during the first half of the stance phase of gait [2] and that hip joint mechanics remain altered after hip arthroscopy [3]. Furthermore, the altered joint mechanics in patients undergoing hip arthroscopy possibly increase the risk of osteoarthritis (OA). Understanding the neuromuscular patterns that occur during gait both before and after hip arthroscopy in FAI patients may provide insight into the possible mechanisms that may potentially lead to hip joint degeneration.

The purposes of this study were to: 1) identify the differences in hip joint muscle force production during gait in subjects with FAI, both before and after hip arthroscopy and 2) determine the relationship between muscle forces and progression of hip joint cartilage abnormalities and composition (assessed with MRI) in FAI patients. We hypothesized that FAI patients would demonstrate abnormal muscle force production during gait both before and after hip arthroscopy and that these abnormal muscle forces would be related to disease severity and its progression.

## METHODS

Thirty-five participants were enrolled in this study. There were 10 FAI patients (40.3±8.7yrs, 7 males, 24.6±3.8kg·m<sup>-2</sup>) and 25 age and BMI matched

controls (CONT, 45.4±12.3yrs, 14 males, 23.7±3.5kg·m<sup>-2</sup>). FAI patients were tested both before and at 7.5±1.3 months after arthroscopic treatment with labral repair and osteochondroplasty. All participants performed 4 successful trials of walking at a self-selected speed, where speeds were controlled to be within 5% of the first successful trial. Static optimization, within OpenSim [4], was used to determine muscle force production, normalized body weight (BW), during the stance phase (initial contact to toe-off) of walking of the gluteus maximus, gluteus medius, gluteus minimus, sartorius, tensor fasciae latae, iliacus, psoas, adductor (magnus/brevis/longus), lateral (LH) and medial (MH) hamstrings, rectus femoris (RF) and the vastii (medius, lateralis and intermedius).

Each FAI patient underwent a hip MRI of the surgical limb using a 3T MR-scanner (GE MR750). Hip joint cartilage abnormalities, in both the acetabular and femoral cartilage regions were assessed before and after hip arthroscopy using a validated MR-based semi-quantitative method called Scoring Hip Osteoarthritis with MRI (SHOMRI) [5] and were summed together to provide a total cartilage score. In addition, T<sub>1ρ</sub> and T<sub>2</sub> mapping [6] of the acetabular and femoral cartilage was performed before and after surgery.

Peak muscle forces in the first and second halves of the stance phase of gait were assessed using one-way ANOVAs and Mann-Whitney U-tests (non-normally distributed data), with a Bonferroni correction of p≤0.004 (0.05/12 muscles). Paired t-tests (p≤0.004) were used to assess differences in muscle force production, T<sub>1ρ</sub> and T<sub>2</sub> mapping (p<0.05) in FAI patients before and after hip arthroscopy. Spearman's (r) and Pearson's (P)

correlations were used to assess for associations between changes in MH, RF and vastii muscle forces with cartilage abnormalities and T<sub>2</sub> mapping in FAI patients, respectively.

## RESULTS AND DISCUSSION

There were no significant differences ( $p > 0.05$ ) in age, BMI or walking speeds between the FAI and CONT groups. Compared to CONT, after hip arthroscopy, the FAI patients exhibited increased MH (FAI:  $1.86 \pm 0.39$  BW; CONT:  $1.41 \pm$  BW;  $P < 0.001$ ), decreased RF (FAI:  $0.29 \pm 0.19$  BW; CONT:  $0.55 \pm 0.25$  BW;  $p = 0.003$ ) and decreased vastii (FAI:  $1.24 \pm 0.36$  BW; CONT:  $2.03 \pm 0.73$  BW;  $p = 0.004$ ) muscle forces during the first half of stance (Fig. 1). Prior to hip arthroscopy, the FAI patients exhibited trends of reduced RF ( $p = 0.02$ ) and vastii ( $p = 0.01$ ) muscle forces during the first half of stance compared to CONT. No differences in muscle forces ( $p > 0.05$ ) were exhibited between the FAI patients and CONT during the second half of stance both before and after hip arthroscopy. In addition, no differences exist in muscle forces during gait or T<sub>1ρ</sub> mapping ( $p > 0.05$ ) within FAI patients after hip arthroscopy. After hip arthroscopy, FAI patients exhibited increased anterior femoral T<sub>2</sub> relaxation times ( $\Delta 2.68 \pm 2.21$  ms,  $p = 0.006$ ). Within FAI patients, a reduction in vastii muscle force was associated with an increased change in the anterior femoral T<sub>2</sub> relaxation time ( $P = -0.70$ ,  $p = 0.03$ ) after hip arthroscopy. No associations between muscle force and cartilage abnormalities were observed.

In the current study, FAI patients demonstrated increased MH, reduced RF and vastii muscle forces during the first half of the stance phase of gait after hip arthroscopy. After hip arthroscopy FAI patients exhibited reduced knee extensor moments during gait compared to controls [4], which may be related to decreased knee extensor force production after hip arthroscopy as shown in the current study. It is

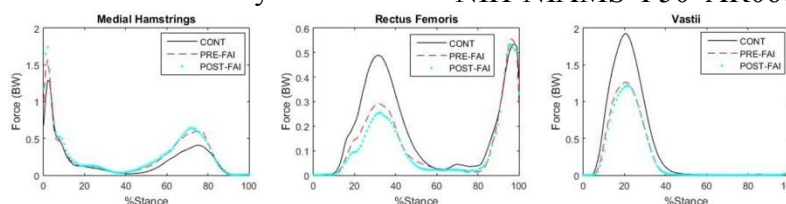


**Figure 1:** Muscle force profiles for the controls and femoroacetabular impingement (FAI) patients during gait.

unclear if these results indicate a role of vastii activation in the pathomechanics of FAI-associated hip OA, or if this represents a simple association as patients reduce vastii activation as an analgesic mechanism to reduce joint compression forces. The increased MH forces exhibited by FAI patients after hip arthroscopy during the first half of stance may cause increased knee flexion and may be a compensatory mechanism of a possible reduced ability to flex the hip joint. Increased vastii muscle force after hip arthroscopy may be a protective mechanism against hip joint degeneration and suggests that quadriceps strengthening may be an important factor in FAI rehabilitation programs. Also, the results of the current study indicate that T<sub>2</sub> mapping may be more sensitive in assessing cartilage degeneration than morphological based cartilage assessments.

## CONCLUSIONS

FAI patients exhibited abnormal muscle forces during the first half of the stance phase of gait. More specifically, vastii strength after hip arthroscopy may affect articular cartilage health. These parameters should be investigated with longer follow-ups and larger cohort sizes.

## REFERENCES

1. Ganz, R, et al. *Clin Orthop Relat Res*, **417**, 112-120, 2003.
2. Samaan, MA, et al. *Am J Sports Med*, **In Press**, 2016.
3. Brisson, N, et al. *Gait Posture*, **37**, 258-263, 2013.
4. Delp, SL, et al. *IEEE Trans Biomed Eng.* **54**, 1940-1950, 2007.
5. Lee, S, et al. *J Mag Res Im*, **41**, 1549-1547, 2015.
6. Li, X, et al. *J Mag Res Im*, **39**, 1287-1293, 2014.

## ACKNOWLEDGEMENTS

NIH-NIAMS P50 AR060752 and F32 AR069458

# MUSCLE CONTRACTILE PROPERTIES IN MICE WITH LGMD2i MUSCULAR DYSTROPHY

<sup>1</sup> Jordan Rehwaldt, <sup>1</sup> B. Dan Rodgers, and <sup>1</sup> David Lin

<sup>1</sup> Washington State University, Pullman, WA, USA  
email: davidlin@wsu.edu

## INTRODUCTION

Muscular dystrophies are particularly debilitating muscle degenerative diseases that compromise myofiber integrity. Interestingly, comprehensive assessments of muscle contractile function in dystrophic animals are surprisingly lacking, and without this essential baseline information, it is extremely difficult to understand how the disease affects motor behavior or to assess whether a novel therapy is effective.

A mouse model for limb girdle muscular dystrophy 2i (LGMD2i) has been developed recently (the P448L mouse) [1], enabling a comprehensive understanding of the disease and the potential development of therapeutics. The objective of our study was to characterize the fundamental contractile properties of the medial gastrocnemius (MG), including force-length (F-L), and force-velocity (F-V) properties. Not only will these data provide a baseline for assessing disease pathogenesis, they will identify novel markers of contractile dysfunction that could prove valuable to drug development efforts. Furthermore, they can elucidate the underlying causes of deficits in motor behavior.

## METHODS

All procedures were pre-approved by the Institutional Animal Care and Use Committee (IACUC) at Washington State University. Experiments were performed on young adult mice (6-7 months old): 5 female wild-type (WT), 5 male WT, 4 female P448L and 6 male P448L mice.

Measurements of *in situ* contractile properties of the MG in a bath at 37°C were made using a whole mouse test system (Aurora Scientific) while operating in either length control mode for isometric contractions or force control mode for isotonic

contractions. F-L properties were estimated from isometric contractions at seven randomized lengths. F-V properties were estimated from contractions with at least 6 isotonic loads (usually 9).

For the F-L data, the analysis included estimates of  $L_o$ , maximal isometric force ( $P_o$ ) and the width of the F-L curve (an indicator of sarcomere inhomogeneity [2], which could occur from structural deficiencies due to the muscular dystrophy). For the F-V data, we estimated maximal shortening velocity ( $V_{max}$ ), normalized maximal power ( $P_{max}$ ), and optimal velocity ( $V_{opt}$ , the velocity at which maximal power occurs). Comparisons were made across all four animal groups using a two-way ANOVA with genotype (P448L and WT) and sex as independent variables and with Tukey's post hoc analysis. Significance was reported at  $P \leq 0.05$ .

## RESULTS AND DISCUSSION

The  $P_o$  was significantly smaller in male P448L mice compared to WT mice in both absolute units (mN; 61% smaller) and when normalized by physiological cross-sectional area (PCSA) (*i.e.*, specific tension; 59% smaller) (Fig. 1). For the female mice, the absolute force was not different between groups, but specific tension was significantly smaller (41%) in P448L mice. These results were a reflection of the larger muscles in female P448L mice relative to WT mice. For both measures, there were no sex differences in either the P448L or WT mice. These results suggest that maximal isometric tetanic contractility is impaired in P448L mice.

Polynomial curves fitted to the normalized F-L data of each animal were used to estimate force-length width, which was found to be similar between all groups (Fig. 1). This result indicated that sarcomere inhomogeneity was not a prevalent feature of LGMD2i mice.

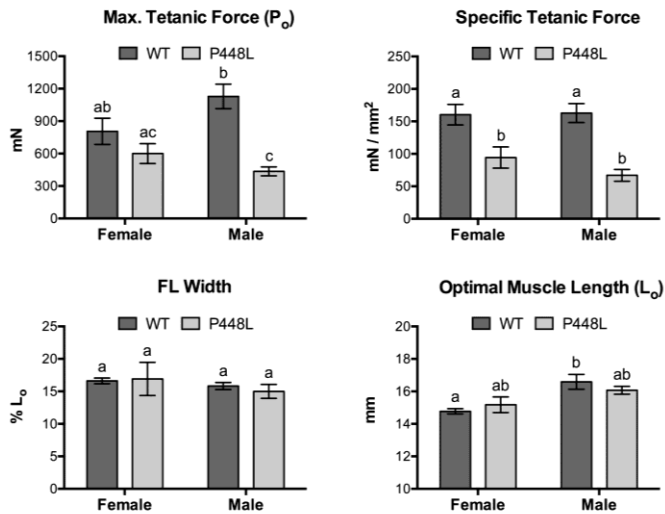


**Figure 1.** Comparison of F-L properties in P448L and WT mice with sex as a factor.

Hill's Equation was fitted to the normalized F-V data and normalized power-velocity (P-V) data of each mouse. From these fits, we could estimate the dynamic contractile properties. Normalized  $V_{max}$  was 36% slower in male P448L mice compared to WT (Fig. 2). Similarly, male-matched comparisons of normalized  $V_{opt}$ , was 35% slower (Fig. 2C). However, no differences were detected in either measures when comparing female groups. These results are again indicative of sexual dimorphism.  $P_{max}$  was lower in P448L males compared to WT mice in both absolute units (75% lower) and when normalized by both fiber length ( $L_f$ ) and PCSA (72% lower) (Fig. 2). Power generation was also lower in P448L female mice (absolute  $P_{max}$  by 34%, normalized  $P_{max}$  48%), though females only differed significantly in normalized  $P_{max}$ . There were no sex differences in normalized  $P_{max}$  in either strain of mice. These results are consistent with the isometric measurements, which were lower in P448L mice, albeit the differences were again greater in P448L males.

## CONCLUSIONS

We quantified the *in situ* contractile properties of the mg in young adult P448L mice, a novel model of LGMD2i. We found that:

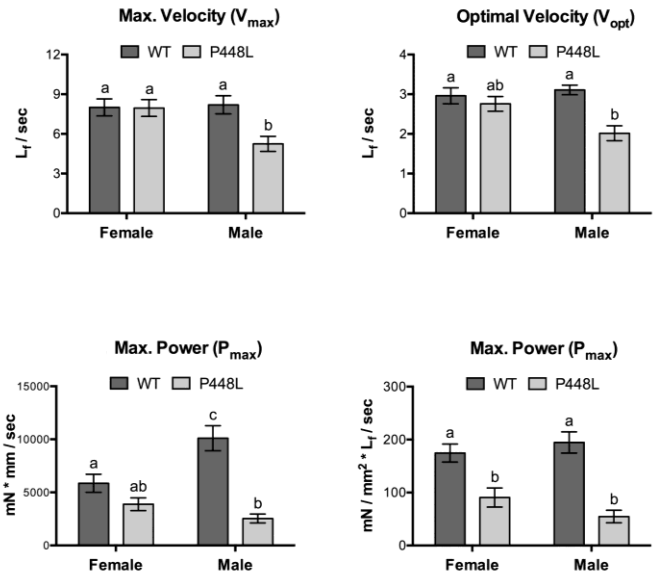


**Figure 2.** Comparison of F-V and P-V properties in P448L and WT mice with sex as a factor.

- Normalized isometric force and power were all significantly smaller in P44L mice compared to sex-matched wild-type mice. These differences were consistent with the replacement of contractile fibers by passive tissue.
- The shape of the active force-length relationships were similar in both groups, regardless of sex, indicating preservation of homogeneous sarcomere structure in P448L mice.
- Sex differences were mostly noted in the F-V curves as maximal and optimal velocities were significantly slower in P448L males, compared to wild-type, but not in P448L females. This suggests that the dystrophic phenotype progresses more quickly in P448L males.

## REFERENCES

1. Qiao C, *et al.* *Mol Ther: J Amer Soc Gene Ther* 22: 1890-1899, 2014
2. Granzier HL, and Pollack GH. *J Physiol* 421: 595-615, 1990

## ACKNOWLEDGMENTS

Support provided by LGMD2i Research Foundation.

# TOWARDS SUBJECT-SPECIFIC TENDON MODELS: AN EXPERIMENTAL AND MODELLING FRAMEWORK

<sup>1</sup> Jeffery W Rankin and <sup>1,2</sup> Craig P McGowan

<sup>1</sup> Department of Biological Sciences and <sup>2</sup> WWAM Medical Education Program,  
The University of Idaho, ID, USA  
email: jwrankin@uidaho.edu

## INTRODUCTION

Forward dynamic simulations of detailed musculoskeletal models are powerful tools for investigating human movement [1]. Combined with experimental data, these tools provide a strong framework for informing clinical practice and improving rehabilitation outcomes. These techniques have broad application and can assist clinicians treating a wide range of populations.

However, existing limitations must be overcome to unlock the unrealized potential of these approaches. To date, generic models are still widely used to study and inform various clinical populations. Advances in rehabilitation methods show that best outcomes are achieved when clinical programs are tailored to a patient's unique needs and pathological condition. Similarly, the use of subject-specific musculoskeletal models is necessary to increase their clinical effectiveness. Researchers have begun to address the limitations inherent in generic models by developing approaches for scaling generic model parameters (e.g., muscle strength, limb masses) [2].

In addition to the aforementioned parameters, the characteristics defining individual muscle-tendon units (MTUs) may need to be tuned to individual patients, especially within populations known to exhibit changes in MTU properties (e.g., aging). In this study, we present a first step in determining the influence that individual MTU properties have on modeling and simulation outcomes, by using an ideal animal model (kangaroo rats) to test the sensitivity of Hill-type muscle parameters on jumping simulation outcomes. Of specific interest is the influence of tendon stiffness, which has been shown previously to greatly influence MTU performance [3].

## METHODS

A detailed musculoskeletal model of the right hind limb of a kangaroo rat (*D. deserti*) was developed from 3D bone scans and muscle dissection (Fig. 1A). A planar model was generated by importing bone scans into SIMM (Musculographics, Inc.) to create five segments that are articulated via seven joints. A total of 21 Hill-type musculotendon actuators were used to represent the major hind limb muscles. Muscle-tendon paths were based on dissection and verified using empirical moment arm data (collected using the tendon-travel method). Tendon parameters were obtained from a generic human model available in OpenSim [2].

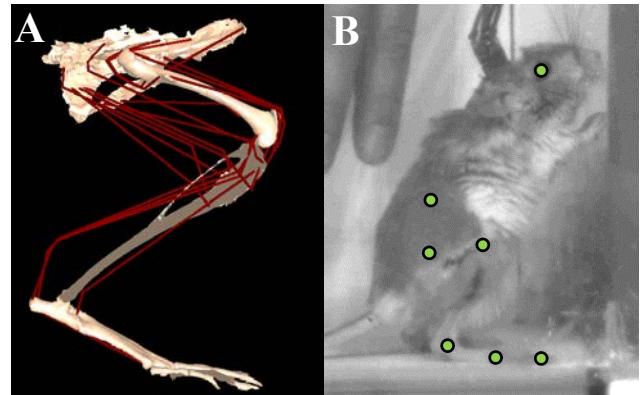


**Figure 1:** A) Kangaroo rat (*D. Deserti*) hind limb musculoskeletal model. MTU are represented by red (grey) lines. B) Experimental jumping setup. Green (grey) circles represent markers used to calculate joint angles.

The model was placed within a dynamic optimization framework where each muscle tendon actuator was excited using a parameterized double-Henning pattern (6 parameters/actuator). An optimal tracking cost function was used to generate forward dynamics simulations that reproduced experimental joint angles during jumping (Fig. 1B).

Five simulations were generated, representing a single representative animal jumping over increasing obstacle heights (20, 25, 30, 35, and 40 cm). MTU and muscle fiber length trajectories of the Gastrocnemius were obtained from each simulation and used for analysis. To evaluate the capabilities of the Hill-type muscle actuators and their sensitivity to tendon parameters, simulated muscle data were compared to experimental MTU and muscle fiber lengths obtained during each jump using sonomicrometry. Muscle excitation timing was also compared to experimentally collected EMG data to verify the feasibility of the optimal simulations.

## RESULTS AND DISCUSSION

In all jump heights, the optimization framework successfully reproduced the major features of the jumping motion with root mean square (RMS) differences between simulated and experimental joint angles averaging <10.5 degrees in all cases. Although total excursion (lengthening + contraction) and contraction only MTU length changes were similar between the simulated and experimental results, the simulations consistently underestimated MTU length changes (Fig. 2A,2C).

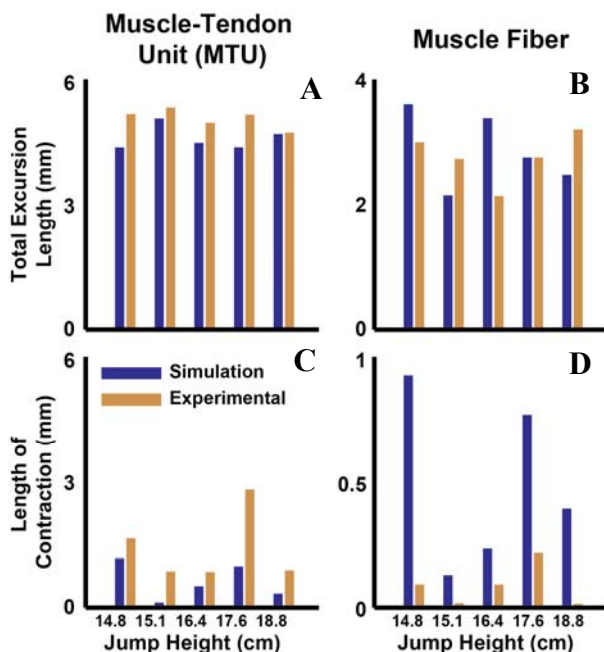


**Figure 2:** Comparisons of total excursion (A,B) and contraction (C,D) lengths for the entire MTU and only muscle fibers.

Total excursions of contractile lengths were variable across simulations (Fig. 2B), likely due to their sensitivity to slight variations in excitation timing during the countermovement phase of the jump. On the other hand, following the countermovement where most of the MTU and fiber contraction occurs, simulated fiber contractions were much greater than those observed experimentally (up to 10% of optimal fiber length, Fig. 2D). The low experimental results are consistent with human jumping studies that suggest ankle extensor muscles act isometrically during the movement [3,4].

## CONCLUSIONS

Relative to human Achilles tendon, kangaroo rat tendons are likely to be stiffer, which would result in relatively higher fiber contractile lengths [5]. Despite this our preliminary data show that, even using a human-based tendon model, simulations may overestimate fiber contractile lengths during jumping. Inaccurate estimations of fiber excursions can limit the utility of detailed musculoskeletal models and simulations in clinical practice and more work is needed to characterize subject-specific variation in tendon properties. Our experimental and simulation framework allows us to test various aspects of muscle-tendon interaction and future simulations specifically detailing the sensitivity of muscle fiber excursion to tendon properties will help determine appropriate parameters for subject-specific human models.

## REFERENCES

1. Neptune, RR, et al. *ESSR* **37** (4), 203-210, 2009
2. Delp, SL, et al. *IEEE TBME* **54** (11), 1940-1950, 2007.
3. Lichtwark, GA, etl al. *JEB* **208**, 4715-4725, 2005
4. Farris, DJ, et al. *JEB* **219**, 528-534, 20016.
5. Biewener, AA, et al. *JEB* **140**, 243-255, 1988.

## ACKNOWLEDGMENTS

We thank Kelsey Blasdell for her assistance in collecting the experimental tendon travel data. Funding for the project was provided by NSF Grant: 1553550 and Army Research Grant: 66554-EG.

# 3D X-RAY MOTION ANALYSIS INDICATES TREADMILL EXERCISE EXACERBATES KNEE OSTEOARTHRITIS IN MMT RATS

<sup>1,3</sup> Elana Cooper, <sup>1</sup> Kevin Hetzendorfer, <sup>2</sup> Liang-Ching Tsai, <sup>1,3</sup> Nick Willett, and <sup>1</sup> Young-Hui Chang

<sup>1</sup> Georgia Institute of Technology, Atlanta, GA, USA

<sup>2</sup> Georgia State University, Atlanta, GA, USA

<sup>3</sup> Emory University, Atlanta, GA, USA

Email: yh.chang@ap.gatech.edu

## INTRODUCTION

Following traumatic knee injury, biomechanical changes in joint loading and chondrocyte metabolism lead to deterioration of articular cartilage and symptomatic presentation of osteoarthritis (OA, [1]). Exercise after traumatic knee injury could alter magnitude and distribution of knee loading necessary to maintain joint health and exacerbate post-traumatic OA. A medial meniscal transection (MMT) rat injury model is often used to evaluate therapeutic interventions on the development of OA following injury [2]. This model allows us to experimentally test OA causes and potential interventions, however, the ability to accurately measure kinematics has been a barrier to relating disease progression to behavioral assays in rats [3]. 3D X-ray Motion Analysis (XMA) using dual-plane, high-speed digital radiography allows accurate measurement of joint kinematics in rats and circumvents skin movement artifact errors common to external marker-based systems [3].

Assessing accurate kinematics with 3D cartilage microstructure and composition allows for a more comprehensive understanding of disease markers and their behavioral presentation in OA pathogenesis. This study tests the effect of an exercise intervention on joint kinematics and cartilage health in a rat knee MMT model of OA. We hypothesized exercise intervention would amplify markers for knee OA disease and cause greater changes in compensatory gait kinematics.

## METHODS

14 male Lewis rats (weight:  $304 \pm 57$  gm) underwent MMT surgery in their left hindlimbs and

were randomly assigned to 1) a non-exercise (NON, N=7) or 2) an exercise (RUN, N=7) group. Rat exercise training consisted of treadmill running 30 minutes per day, 4 days per week at 0.2 m/s. A sham surgery was performed on 6 additional control rats where the MMT was not performed.

Rats were evaluated 8 weeks post-surgery for hind-limb joint kinematics during treadmill locomotion (0.5 m/s) using a high-speed 3D X-ray motion analysis system (100 Hz). Rats were euthanized following testing and 3D bone surface models were generated from whole bone CT scans and aligned with high-speed radiographic images to quantify *in vivo* kinematics (XROMM Autoscooper, Providence RI; Maya, Autodesk). 3D microstructure and composition of the tibial plateau cartilage and subchondral bone were quantified using contrast enhanced microcomputed tomography, EPIC-uCT (50um resolution).

## RESULTS AND DISCUSSION

Hip abduction at midstance is shown to be significantly greater in the RUN rats relative to the sham group ( $p=0.005$ ), whereas NON rats demonstrate increased abduction only at midstance ( $p=0.036$ ) (Fig 1B). RUN rats also demonstrated greater knee varus alignment compared to the sham group at toe-off ( $p=0.036$ ) (Fig 1C). RUN rats showed increased contralateral limb stance support relative to NON and sham groups. Reduced stance time on the injured hindlimb in RUN rats compared to the other groups also revealed a compensatory gait pattern of favoring the injured limb. Increased hip abduction, knee varus alignment, and contralateral limb support time are reflective of gait in persons with mediotibial OA [1], which is also

indicated by an increased exposed bone surface area to the medial tibial plateau in the RUN rats (Fig 2).

Destabilizing the knee joint via meniscal transection alters mechanical stresses to the underlying articular cartilage. Increased degeneration indicated by decreased thickness to the proximal cartilage surface (Fig 2) and higher exposed bone values to medial 1/3 of the mediotibial plateau (Table 1) reflect concentrated force distribution to the area [3] and disrupted joint homeostasis. Attenuation measurements obtained from EPIC-uCT, which are indicators of cartilage health, further support this finding. Increased cartilage attenuation in exercise rats inversely correlates to decreased proteoglycan content and thus an inability to provide sufficient hydrostatic pressurization to resist the mechanical forces that lead to OA progression.

## CONCLUSIONS

The cascading effects of disrupted homeostasis on the cellular level in OA is supported by our measurement of tissue level degradation and changes in gait kinematics. Increased cartilage degeneration, subchondral bone thickening, and

osteophyte formation demonstrated in RUN rats are consistent with end-stage OA. Gait compensations through decreased single limb support time by the injured hindlimb to account for this accelerated OA progression present kinematic gait deviations in RUN rats through varus knee alignment and hip abduction. In contrast, less cartilage degeneration and increased cartilage thickness and volume in NON rats, would suggest a slower progression of OA. Kinematics evaluation at earlier measured time points to assess gait modifications is forthcoming. Quantifying animal behavior with joint structural changes across these time points will be critical for revealing the causal relationship between tissue-level OA markers and changes in gait kinematics. The MMT rat appears to be an effective OA model for evaluating behavioral interventions in combination with cellular therapeutics offering new opportunities to improve current treatment options and disease prevention.

## REFERENCES

1. Favre, et al. *EFORT Open Rev*, **1**:368-374, 2016
2. Willett, et al. *Osteoarthritis and Cartilage* **24**:1604-1612, 2016.
3. Bauman, et al. *J Neurosci Meth*, **186**: 18-24, 2010.

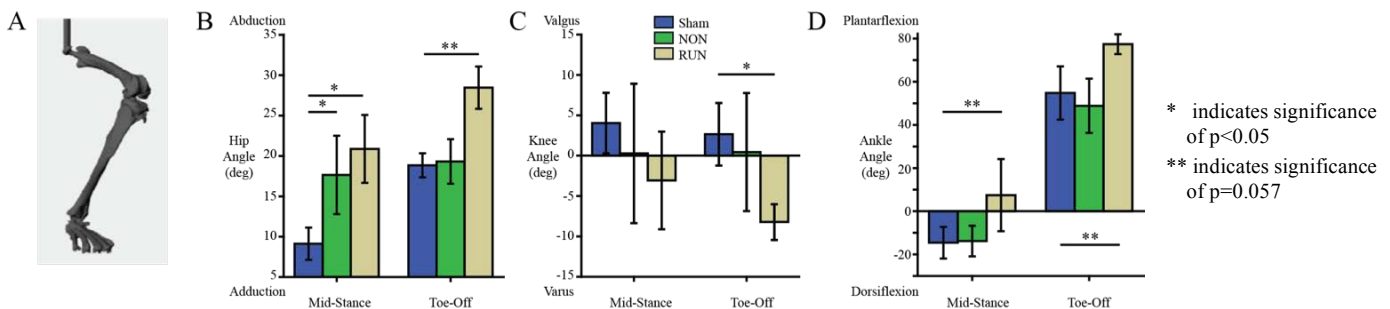
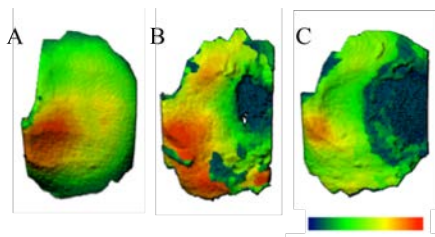


**Figure 1.** A 3D Bone surface model of rat hindlimb used to measure kinematics data (A). Mean  $\pm$  SD Hip abduction (B), knee varus alignment (C), and ankle plantar flexion (D) angles at mid-stance and toe-off.

**Table 1.** Cartilage microstructure and composition (mean  $\pm$  SD)



Cartilage Parameter	Sham	NON	RUN
Total Exposed Bone Area ( $\mu\text{m}^2$ )	0.002 $\pm$ 0.001	0.274 $\pm$ 0.150	0.454 $\pm$ 0.181
Medial 1/3 Exposed Bone Area ( $\mu\text{m}^2$ )	0.004 $\pm$ 0.007	0.398 $\pm$ 0.163	0.554 $\pm$ 0.094
Cartilage Attenuation	1.779 $\pm$ 0.106	1.800 $\pm$ 0.062	1.851 $\pm$ 0.092
Cartilage Thickness (mm)	0.182 $\pm$ 0.425	0.206 $\pm$ 0.027	0.198 $\pm$ 0.037
Cartilage Volume ( $\text{mm}^3$ )	1.169 $\pm$ 0.174	1.280 $\pm$ 0.268	1.060 $\pm$ 0.178

**Figure 2.** Representative proximal views of left medial tibial plateaus showing cartilage thickness maps of sham (A), NON (B), and RUN (C) rats at 8 weeks post-surgery. Accelerated medial cartilage degeneration in rats undergoing elevated exercise treadmill training indicated by areas of thinnest cartilage (dark green).

# Putting on the brakes: the effect of drag loading on the maneuverability of bottlenose dolphins

<sup>1</sup> Annika Stoldt, <sup>1</sup> Makayla Mires, <sup>1</sup> Joaquin Gabaldon, <sup>2</sup> Julie Rocho-Levine, <sup>3</sup> Julie van der Hoop, <sup>4</sup> Michael Moore, and <sup>1</sup> K. Alex Shorter

<sup>1</sup> University of Michigan, Ann Arbor, MI, USA, <sup>2</sup> Dolphin Quest Oahu, Honolulu, HI, USA, <sup>3</sup> Aarhus University, Aarhus, Denmark, <sup>4</sup> Woods Hole Oceanographic Institution, Woods Hole, MA, USA  
email: kshorter@umich.edu

## INTRODUCTION

Maneuverability is vital for animals that must actively hunt highly maneuverable prey. Complex movements are required to out-manuever the prey, which may include rapid changes in velocity and turning radius [1]. There are, however, limitations to maneuverability that are inherent to the animal due to size and dynamic state. For swimming animals, maneuverability is heavily dependent on stability in a fluid environment, which in turn is related to morphological structure [2]. While maneuverability is essential to the success of the animal in the wild, it is difficult to quantify as the marine environment restricts direct observation of these animals during their daily routines. In this study we will investigate the effect of drag loading on the maneuverability of bottlenose dolphins (*Tursiops truncatus*) in a controlled experimental environment. Animal dynamics during a prescribed cornering task were measured and then quantified using a combination of camera-based position measurements, and dynamic information collected from the animal with a bio-logging tag. We expect that additional drag loading will slow the animal down and result in increased maneuverability.

## METHODS

**Experimental set up:** Four dolphins were trained to swim laps around a 750 m<sup>2</sup> (~40 m in diameter) artificial lagoon for ~10 min. During the trials the animals self-selected swimming speeds and four marine mammal specialists stationed around the lagoon used a “point” cue to indicate when the animal should turn and continue swimming to the next turn. The bottom left corner of the lap was selected for the cornering analysis; data 5 m before and after the midpoint of the turn were used to quantify maneuverability. Fig. 1 shows the three drag loading conditions examined: control (C), tag (A), and the tag with added drag loading (A4). In

the A4 condition drag elements increased the tag cross-sectional area by ~800%, resulting in a large increase in drag.

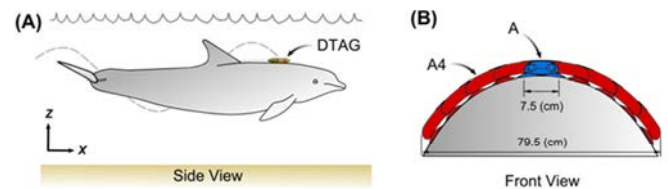


**Figure 1:** Illustration of the dolphin swimming with the tag and the physical elements used to increase drag loading.

**Hardware/Calibration:** Camera data from a GoPro Hero3+ mounted above the lagoon were used to track the animals when visible at the surface. Camera data were calibrated and then hand-tracked to give position, velocity, and acceleration measurements. To supplement camera data, a DTAG3 bio-logging tag was used to measure dynamic information from the animals. Tag sensors include an accelerometer, gyroscope, and magnetometer (all tri-axis), as well as a thermometer, pressure sensor and hydrophones. The tag was attached to the dolphins using four silicone suction cups, mounted ahead of the dorsal fin, oriented with the hydrophone towards the front of the animal. Before the data was used in localization processing, it was calibrated using custom Matlab toolboxes. The study protocol was approved by the University of Michigan Institutional Animal Care and Use Committee and the animal specialists and staff of Dolphin Quest.

**Madgwick Orientation Filtering:** Orientation estimate (pitch, roll, and heading) at the tag was calculated using an algorithm adapted from the method presented in [3]. This method obtains an orientation estimate of the earth frame relative to the sensor frame, through a weighted sum of the gradient-descent optimization of accelerometer, magnetometer and gyrodrometer-based orientation measurements.

**Specific Acceleration Estimate:** Accelerometers measure both specific acceleration created by animal motion and gravitational acceleration. Specific acceleration can be isolated from the measurement by removing the gravitation component using the orientation estimate generated above and the known magnitude and direction of the gravitational acceleration.

**Velocity Filtering:** We employ a modified Kalman filter to improve the horizontal velocity estimate of the animal. Specific acceleration estimated from tag data and external velocity measurements calculated from camera data were combined to provide a more accurate velocity estimate than can be calculated from tag data alone.

**Pose-Graph Localization and GTSAM:** Numerically integrating the filtered velocity yields an initial track of the tagged animal. The track is enhanced through pose-graph localization, implemented with the optimizations on the second generation Incremental Smoothing and Mapping (iSAM2) technique, as part of the GTSAM toolbox [4]. The initial track estimate is decomposed into odometry components, and both track and odometry are inserted into a GTSAM graph, along with video-based position measurements of the animals as ground-truth location measures. Process and measurement noise estimates were defined empirically. The graph is optimized using the GTSAM-based Levenberg-Marquardt optimizer, and yields the final track estimate.

## RESULTS AND DISCUSSION

Data from a representative animal are presented here, with ~30 min of swimming and ~60 cornering events analyzed. Figure 2 presents a representative track estimate along with the camera position measurements (white points) during the A4 condition. The bottom left corner was selected for analysis because the high density of camera based position measurements resulted in the best track estimates. As drag was increased (A and A4), the animal's speed and acceleration around the corner both decreased significantly, Table 1. However, because of the reduced speed the animal was able change heading more rapidly in response to the "point" that initiated the cornering event. This resulted in a decrease in the radius of curvature as drag was increased, Fig 2 and Table 1.

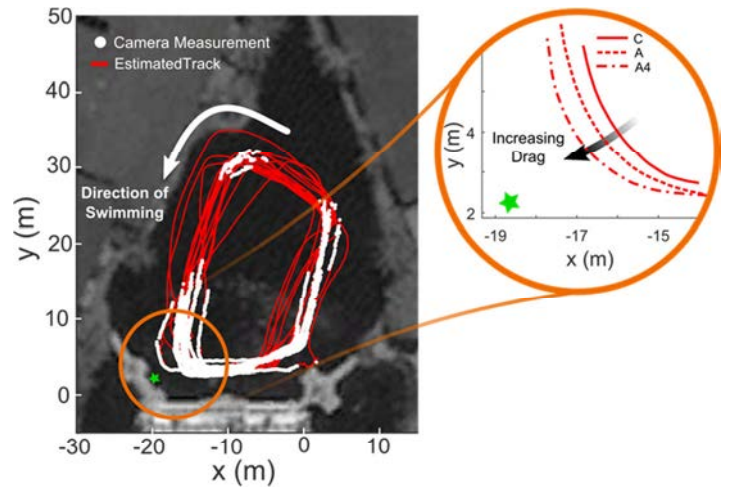


**Figure 2:** Lagoon, camera measurements and estimated track for a representative animals (A4). Detail of the average position for one animal during all conditions.

**Table 1:** Individual animal cornering parameters.

	C	A	A4
Speed - $ \vec{v} $ (m/s)	3.6 (0.7)	3.2 (0.6)	1.8 (0.8)
Acceleration - $ \vec{a} $ (m/s <sup>2</sup> )	2.4 (0.7)	4.1 (1.5)	2.8 (1.4)
Radius - $\rho$ (m)	5.4 (2.3)	4.5 (1.1)	3.6 (0.7)

## CONCLUSIONS

These results demonstrate the potential of this unique experimental environment to examine the swimming biomechanics and maneuverability of dolphins during extended swimming tasks. Similar to terrestrial mammals, dolphins do not perform tight turns at their highest speeds [1]. During the experiment the dolphins decreased overall velocity and acceleration in response to drag loading. But, we observed an increase in maneuverability during the cornering task, with the slower speeds allowing the animal to make sharper turns following the cue. These results support our expectation that maneuverability would increase with added drag loading. Future work will involve processing data from three additional animals, and the development of constraints to control the velocity of the animal in order to further examine the how added drag loading affects the swimming biomechanics of bottlenose dolphins.

## REFERENCES

1. Wilson, AM., et al. *Nature* **489**, 185-189, 2013.
2. Fish, FE. *Integr Comp Biol* **42**, 85-93, 2002.
3. Madgwick, SOH. *IEEE Conf Rehab Rob*, 1-7, 2011.
4. Kaess, M. *Intern Jour Rob Res* **31**, 216-235, 2012.

# ROTATOR CUFF TENDON FORCES DURING WEIGHT-RELIEF LIFT IN TETRAPLEGIA

<sup>1</sup>Carrie L. Peterson, <sup>2</sup>Michael S. Bednar, and <sup>3,4</sup>Wendy M. Murray

<sup>1</sup>Virginia Commonwealth University, Richmond, VA, USA, <sup>2</sup>Loyola University-Chicago, Maywood, IL, USA

<sup>3</sup>Northwestern University, Evanston, IL, USA, <sup>4</sup>Shirley Ryan AbilityLab (formerly RIC), Chicago, IL, USA  
email: clpeterson@vcu.edu

## INTRODUCTION

Pain is prevalent in adults with tetraplegia. The shoulder is the most common location of upper limb pain and is associated with additional losses in function and community mobility. Weight-relief lifting, a movement to lift body weight from the wheelchair seat, must be routinely performed by individuals with spinal cord injury to effectively prevent pressure ulcers, but imparts significant loads on the upper limbs. The triceps play a critical role during weight-relief lift in individuals with paraplegia, who experience lower glenohumeral contact forces relative to individuals with tetraplegia.<sup>1</sup> Individuals with C5 or C6 tetraplegia typically have weak or no residual triceps function. However, active elbow extension can be restored via tendon transfer, a surgical procedure that reassigns the insertion tendon of a non-paralyzed muscle to the insertion site of the paralyzed triceps. The purpose of this study was to compare tendon forces in the rotator cuff during weight-relief lifting in individuals with tetraplegia who have undergone tendon transfer to individuals with tetraplegia without tendon transfer. Rotator cuff tendon forces were compared because rotator cuff disease is the most common cause of shoulder pain in tetraplegia. Tendon forces cannot be directly measured *in vivo* during movement. Thus, musculoskeletal modeling and forward dynamics simulations that replicated the kinematics and kinetics generated by human subjects were analyzed to estimate tendon forces.

## METHODS

Individuals with tetraplegia were recruited for participation (Table 1). The experimental protocol was approved by the Institutional Review Board of Northwestern University. Maximum voluntary joint moments generated by primary upper limb muscle groups were recorded via a load cell interfaced with

a Biodex Multi-Joint System, Pro. For weight-relief trials, subjects were transferred to a chair positioned between two adjustable hand rails. A load cell was interfaced with a custom built handrim to record kinetics during weight-relief lifting trials (Fig. 1). Rigid clusters of non-collinear infrared markers were secured to the thorax, acromion, upper arm, forearm, and hand segments. Kinematics and kinetics were recorded at 74 Hz and 1000 Hz, respectively. Subjects completed six weight-relief lift trials in which they were instructed to lift their body weight using their upper limbs to the best of their ability, to a degree sufficient to relieve pressure under the buttocks, and to hold the lift for five seconds.

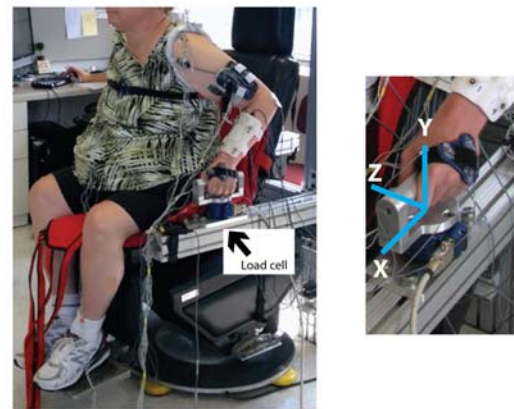


**Figure 1:** Experimental setup during weight-relief lift trials; kinematics and kinetics were recorded.

Two representative individuals with tetraplegia were selected for modeling and simulation based on their injury level and ability to achieve a lift; one with bilateral biceps-to-triceps transfers (Male, 29 years, cf., Table 1, light gray shading) and one with some residual triceps function (Female, 36 years, cf., Table 1, light gray shading). A musculoskeletal model of the nonimpaired upper limb<sup>2</sup> was adapted to model the biceps-to-triceps transfer based on surgical descriptions. Maximum elbow extension strength for the individuals with and without tendon

transfer were 20% and 27% of the maximum isometric elbow extension strength of the nonimpaired model, respectively. The model was driven by 26 Hill-type musculotendon actuators. Maximum force-generating capacity of the upper limb model was scaled to limb strength as measured via maximum joint moments. Forward dynamics simulations that reproduced the kinematics and kinetics recorded from the two participants during the lifting phase were developed using an optimization approach. A simulated annealing algorithm<sup>3</sup> was used to determine muscle excitations that minimized the difference in the simulated and experimental joint angles and handrim forces. Muscle forces were multiplied by the cosine of the pennation angle to estimate tendon forces.

## RESULTS AND DISCUSSION

Rarely an individual with C5 tetraplegia can achieve a weight-relief lift.<sup>4</sup> For the subject in our study, the biceps-to-triceps transfer provided similar elbow extension strength as an individual with C6 tetraplegia with some residual triceps function; in both of these individuals elbow strength was sufficient to lift. Our simulation analysis indicates these two subjects used different muscle coordination patterns to achieve the same task. When normalized to each subject's body mass, peak tendon forces in the individual with residual triceps function were higher relative to the individual with biceps-to-triceps transfer in three of the four muscles of interest: the subscapularis, supraspinatus, and teres minor (Fig. 2). Peak tendon force in the infraspinatus was greater in the individual with biceps-to-triceps transfer (Fig. 2). Overall, relative forces (normalized to maximum isometric force) in the rotator cuff for both subjects were very high, exceeding a previous report in tetraplegia.<sup>1</sup> The relative forces in our study were greater because our model was scaled to represent the strength of the individuals with tetraplegia we

assessed. While van Drongelen et al. did not scale the strength of their model, they found greater relative forces in the rotator cuff in subjects with tetraplegia relative to paraplegia or in nonimpaired subjects.<sup>1</sup> Overall, in our study, peak tendon forces resulting from the weight relief task ranged between 70% and 90% of maximum isometric muscle force, when normalized to subject-specific strength. Peak tendon force in supraspinatus reached 120% for the individual with tendon transfer because passive force was generated.

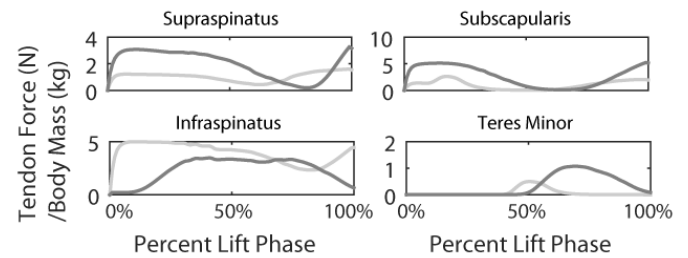


**Figure 2:** Tendon forces in tetraplegia during lift with (light) and without tendon transfer (dark).

## CONCLUSIONS

Tendon transfer can provide weight-relief lifting ability. However, limited elbow extension strength in individuals with tetraplegia, regardless of whether elbow strength is restored via transfer or residual after injury, results in high tendon forces in the rotator cuff.

## REFERENCES

1. van Drongelen S, et al. *Arch Phys Med Rehabil* **86**,1434-40, 2005.
2. Saul KR, et al. *Comput Methods Biomech Biomed Eng*, **18**(13),1445-58, 2015.
3. Goffe WL, et al. *J Econometrics* **60**, 65-99, 1994.
4. Staas WE, et al. *Spinal cord injury and spinal cord medicine*, Lippincot-Raven Publishers, 1998.

## ACKNOWLEDGMENTS

This study was funded by the Craig H. Nielsen Foundation. We thank Jeremy Simon, Florian Billy, and Vikram Darbhe for their help with data collection.

**Table 1:** Characteristics of individuals with tetraplegia who participated in the experimental protocol.

ASIA Motor Level	C7	C6	C5	C6	C5	C5
Gender, Age (years)	F, 53	F, 36	M, 35	M, 31	M, 29	M, 47
Body mass (kg)	91.2	64.9	87.2	143.8	56.6	95.8
Tendon transfer?	No	No	No	No	Biceps-to-Triceps	Deltoid-to-Triceps
Able to lift?	Yes	Yes	No	No	Yes	No

# UPPER EXTREMITY KINEMATICS OF WHEELCHAIR LACROSSE ATHLETES DURING OVERHEAD THROW

<sup>1</sup>Justin M. Riebe, <sup>1</sup>Alyssa J. Schnorenberg, <sup>2</sup>Brian Robertson-Dick, <sup>1</sup>Brooke A. Slavens, and <sup>2</sup>Kenneth Lee

<sup>1</sup>The University of Wisconsin – Milwaukee, WI, USA

<sup>2</sup>The Medical College of Wisconsin, Wauwatosa, WI, USA

email: riebej@uwm.edu

## INTRODUCTION

Since 2001, over 550,000 able-bodied athletes joined organized lacrosse teams in the United States [1]. Similarly, wheelchair lacrosse, founded in 2009, has grown in popularity amongst adaptive athletes. Despite this, there has been no research investigating the biomechanics of the wheelchair lacrosse athletes, particularly about the unique mechanisms for injury the sport may present. Kibler et al. found that a 20% reduction in kinetic energy from the hip and trunk requires a 34% increase in rotational velocity of the shoulder to impart the same force at the hand [2]. Most wheelchair athletes have lower extremity impairments reducing or eliminating their ability to generate forces from the hip and trunk. The resulting increased demands of the shoulder and upper extremity (UE) is highly concerning in a population whom rely on their UEs for mobility and completion of activities of daily living. Investigation of the increased UE demands experienced by manual wheelchair lacrosse players is required to identify additional mechanisms for injury. This will enable the implementation of preventative measures, thereby reducing the risk of injury. This study characterized upper extremity biomechanics during an overhead throw in wheelchair lacrosse athletes.

## METHODS

Five wheelchair lacrosse players with a mean age of 47.4 years ( $\pm 14.9$ ) participated. Subjects used their own sport wheelchair when possible, a 41-inch standard lacrosse stick, and a no-bounce lacrosse ball. Thirty-one passive markers were placed on the subject. Motion data was collected at 240 Hz using a 19 camera Vicon T-Series motion capture system. Subjects were instructed to begin without prior

propulsion of the wheelchair and perform a maximal velocity overhand throw. Three trials from each subject were used for analysis. A custom upper extremity kinematic model [3] was applied, via MATLAB, to determine the three-dimensional glenohumeral (GH), elbow, and wrist joint angles. The start and end of the throw were identified based on definitions used with able-bodied lacrosse players [4] modified for use with wheelchair athletes. Joint angles were time normalized and averaged over the duration of the throw. Group averages were determined for the peak joint angle, and joint range of motion in all three planes for the GH, elbow and wrist joints. Joint angular velocities and accelerations were calculated by taking successive derivatives of the joint angle data; average peak values were obtained.

## RESULTS AND DISCUSSION

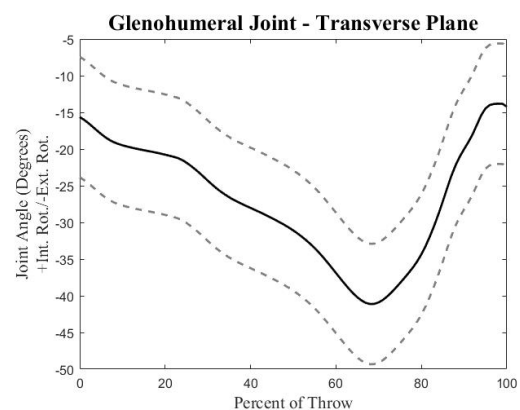


**Figure 1:** Group average (solid) and standard deviations (dotted) of transverse plane glenohumeral joint angle.

The average peak elbow flexion angle ( $115^{\circ} \pm 18.8^{\circ}$ ), and GH external rotation ( $41.1^{\circ} \pm 8.2^{\circ}$ ) are similar to reported values observed in able-bodied lacrosse players of  $100.5^{\circ}$  and  $47.5^{\circ}$ , respectively [5]. Also, the overhead lacrosse throw relies on trunk rotation and extension more than GH external

rotation compared to an overhead baseball throw [5]. This is concerning as many manual wheelchair users may compensate for their inability to produce large degrees of trunk motion with the UEs. Simultaneous high degrees of GH joint abduction and external rotation, as seen here, can lead to tears and recurrent anterior dislocations of the GH joint, with sufficient repetitions [6, 7]. In addition, concurrent high degrees of elbow flexion, also seen here, and biceps activation have been shown to transfers high levels of stress to the glenoid labrum [6]. This is further compounded as the arm reaches its peak external rotation and begins to internally rotate rapidly (Figure 1), while remaining near peak GH abduction. This combined action increases the risk of a labrum tear, which would greatly reduce GH joint function [6].

During the acceleration phase of the throw there are multiple high joint accelerations occurring simultaneously, including 6097 deg/s<sup>2</sup> of wrist flexion, 6888 deg/s<sup>2</sup> of GH joint internal rotation, and 9041 deg/s<sup>2</sup> of elbow joint supination. While these values do not approach those experienced by professional baseball pitchers, they are of still of concern. First, they are occurring simultaneously, stressing multiple structures of the shoulder at the same time. Second, an adult manual wheelchair user likely already has some overuse wear, and is more susceptible to pain and injury development.

## CONCLUSIONS

Overhead throw biomechanics were successfully characterized for 5 wheelchair lacrosse athletes. The

results highlight several potential risk factors. There is already a known high prevalence of pain and pathology development in manual wheelchair users. As many wheelchair athletes are dependent on their upper extremities for mobility it is important to understand these injury mechanisms so steps may be taken to minimize risk of occurrence. Research is underway to compare biomechanics, and muscle activation patterns, of this population to able-bodied lacrosse and wheelchair lacrosse players during overhead and side-arm throws. This information will assist governing bodies in creating rules and regulation necessary to protect wheelchair lacrosse athletes from unnecessary risk of pain and injury.

## REFERENCES

1. www.USlacrosse.org
2. Kibler WB, et al. *Rehabilitation of the Injured Knee*, 1995.
3. Schnorenberg AJ et al. *J Biomech*, **47(1)**, 2014.
4. Mercer JA, et al. *Sport Journal*, **16(1)**, 2013.
5. Plummer HA, et al. *International Biomechanics*, **2(1)**, 2015.
6. Kuhn JE, et al. *J Shoulder Elbow Surg*, 2005.
7. Hara H, et al. *J Shoulder Elbow Surg*, 1996.

## ACKNOWLEDGMENTS

Funded by the Medical College of Wisconsin, Department of Physical Medicine and Rehabilitation, Research Administration Committee Grant Program. Many thanks to Leah Lee, Kristi Lenz, Anna Luterbach, Gretchen Natter, Katherine Reichel, & Noelle Serketich.

**Table 1:** Group average kinematic metrics of the glenohumeral (GH), elbow and wrist joints.

Plane	Joint	Max Angle (deg)	Range of Motion (deg)	Max Angular Velocity (deg/s)	Max Angular Acceleration (deg/s <sup>2</sup> )
Sagittal (flexion + / extension -)	<b>GH</b>	41.0 (±7.7)	28.2 (±7.7)	152 (±74)	2141 (±493)
	<b>Elbow</b>	115 (±18.8)	65.9 (±18.8)	110 (±36)	2022 (±915)
	<b>Wrist</b>	-49.3 (±13.1)	44.9 (±13.1)	340 (±82)	6097 (±3185)
Coronal (adduction + / abduction -)	<b>GH</b>	-48.3 (±8.9)	25.8 (±8.9)	78 (±30)	2943 (±1734)
	<b>Wrist</b>	23.8 (±6.8)	24.5 (±6.8)	210 (±52)	4680 (±2900)
Transverse (internal rotation + / external rot. -)	<b>GH</b>	-41.1 (±8.2)	27.3 (±8.2)	266 (±46)	6888 (±4625)
	<b>Elbow</b>	97.3 (±13.2)	38.3 (±13.2)	224 (±33)	9041 (±6422)

# HANDRIM BIOMECHANICS OF PEDIATRIC MANUAL WHEELCHAIR MOBILITY

<sup>1,3</sup> Alyssa J. Schnorenberg, <sup>2</sup> Lawrence C. Vogel, <sup>2,3</sup> Gerald F. Harris, and <sup>1-3</sup> Brooke A. Slavens

<sup>1</sup> University of Wisconsin-Milwaukee, Milwaukee, WI, USA

<sup>2</sup> Shriners Hospitals for Children, Chicago, IL, USA

<sup>3</sup> Marquette University, Milwaukee, WI, USA

email: paulaj@uwm.edu, web: <http://uwm.edu/mobilitylab>

## INTRODUCTION

There are an estimated 124,000 children under the age of 21 whom use a wheelchair in the United States (U.S.) [1]. Approximately 10,000 individuals sustain a spinal cord injury (SCI) each year in the U.S., with about 20% occurring in those under 20 years of age [2]. SCI often results in physical limitations affecting functional mobility; thereby, making individuals reliant upon wheelchairs.

In adults with SCI, shoulder pain and degenerative changes may develop prematurely due to overuse. A high prevalence of shoulder pain and injury has been observed in adult manual wheelchair users (MWC), with up to 73% of paraplegics reporting upper extremity (UE) pain [3]. However, it should not be assumed that the developing child experiences the same loading demands or is exposed to similar risk factors for injuries as adults. Children are not physically proportionate to adults; therefore, simple scaling of adult dynamics information will not give an accurate representation of the demands of pediatric wheelchair mobility. Due to longer-term wheelchair use in those with pediatric-onset SCI, UE pain and injuries may occur earlier in the lifespan, and severely limit independence, function, and quality of life. Despite this, there is limited research of pediatric wheelchair mobility [4]. Evaluation of pediatric wheelchair mobility is essential to determine differences from adults. This exploratory work aimed to characterize pushrim biomechanics during pediatric manual wheelchair propulsion.

## METHODS

Ten pediatric manual wheelchair users with SCI, and an average age of  $11.5 \pm 4.7$  years (ranging from 6.5 to 19.5 years), participated. Subjects were

diagnosed at least one year prior to the study; average time since injury was  $3.3 \pm 2.1$  years. SCI levels ranged from C3 to T10. The average height and weight was 150.5 cm ( $\pm 28.9$  cm) and 47.7 kg ( $\pm 24.0$  kg), respectively.



**Figure 1:** Representative subject in her personal wheelchair with passive markers on her upper extremity and the wheel axle of the SmartWheel.

Subjects propelled their MWCs along a 15 m level tile walkway using a self-selected speed and propulsion pattern. Markers placed on the subject's third metacarpal joints, and acromions, and on the wheel axle were used for analysis. A 14-camera Vicon MX motion capture system collected bilateral kinematic data at 120 Hz and simultaneously a SmartWheel system collected dominant side 3D force and moment data at the hand-handrim interface at 240 Hz. Up to fifteen stroke cycles per subject were analyzed. To eliminate acceleration and deceleration effects, the first two and last two strokes of any one trial were excluded.

The markers on the acromion process and wheel axle were used to determine the fore-aft (XPOS) and vertical (YPOS) positions of the shoulder relative to the wheelchair axle [4]. The hand and axle markers were used to determine the angle relative to top dead center at which the hand was located on the handrim. The stroke cycle was divided into the contact and recovery phases, with

the contact phase subdivided into the initial contact, propulsion, and release periods [5]. The maximum rate of rise of the resultant force was determined by differentiating the resultant force curve with respect to time, and finding the peak value. Fractional effective force (FEF) was calculated as the percent of the tangential force that contributed to the resultant force.

## RESULTS AND DISCUSSION

### *Temporal-Spatial Parameters*

Subjects propelled at an average speed of 1.17 m/s (+/- 0.28 m/s), covering an average of 1.21 m (+/- 0.19 m) per stroke cycle. Average fore-aft position of the shoulder relative to the wheel axle was aft 59.8 mm (+/- 45.1 mm). Although there is a large variation, this indicates the shoulder is forward of the axle during most of the stroke cycle. The average vertical position of the shoulder relative to the wheel axle was 646 mm (+/- 87 mm). This positively correlated with subject height ( $R^2 = 0.85$ ), as has been found in adults [4]. At initial handrim contact and handrim release, the average angular location of the hand relative to top dead center was 24.6° (+/-15.7°) counter-clockwise, and 52.0° (+/-11.5°) clockwise, respectively. The average transition point between the contact and recovery phases was 36.1% (+/-8.2%) stroke cycle, ranging from 21.0% to 60.8%. While the value falls within the range commonly reported for adult manual wheelchair users of 30 – 50% stroke cycle, there were three subjects with an average stroke cycle transition at 30% of the stroke cycle or less. This may decrease the amount of time available to impart force to the handrim, requiring the child to increase the applied force which adult guidelines discourage.

### *Kinetic Parameters*

As with adults, the pediatric manual wheelchair users experienced braking effects in most, if not all, of their stroke cycles. On average the braking moment about the wheel axle was imparted during 0 - 4.7% (+/- 3.7%) (initial contact period) and 33.7% (+/- 2.5%)–36.1% (release period) of the stroke cycle. Average maximum resultant handrim force over the stroke cycle was 43.5 N (+/- 20.8 N); however, this value ranged widely from 13 N to 116

N. Literature on adult manual wheelchair users, propelling at approximately the same speed, have reported higher average peak resultant forces, between 54.3 N (+/-18.9 N) and 75.5 N (+/-33.2 N), with similar variability [3,5]. The average rate of rise of the resultant force was 1549.3 N/s (+/-939 N/s), again with subjects experiencing values ranging from 337 N/s to 6653 N/s. Adult literature has reported smaller values, with averages and standard deviations between 915 (+/-401) [3] and 1461 (+/-555). The average maximum FEF was 70% (+/- 20%), which is only slightly outside of the adult range of 71% – 80.2% [5].

## CONCLUSIONS

Clinical practice guidelines recommend manual wheelchairs users keep peak forces, rate of rise of force and braking moments to a minimum in order to reduce pain and injury. However, these guidelines were developed for adults, and may not be appropriate for children. Further investigation is required on the impact of the similarities and differences between adult and pediatric MWC discussed here, as well as their correlation to joint biomechanics, stroke patterns, and subject characterizations (time since injury, injury level, etc.). Deeper knowledge of pediatric manual wheelchair biomechanics is essential for understanding the root cause of pain and injury development in order to preserve UE extremity function and joint integrity over their lifespan.

## REFERENCES

1. Brault M. *Curr Popul Rep*, P70-131, 2012.
2. Vogel L, et al. *Orthop Nurs*, **23**, 300-308, 2004.
3. Boninger M, et al. *Arch Phys Med Rehabil* **81**, 608–613, 2000.
4. Kwarciak A, et al. *Arch Phys Med Rehabil* **90**, 20-26, 2009.
5. Finley M, et al. *J Rehabil Res Dev*, **41**, 385-394, 2004.
6. Slavens B, et al. *Front Bioeng Biotechnol*, (**3**), 2015.

## ACKNOWLEDGMENTS

Support provided by the Eunice Kennedy Shriver NICHD of the NIH under Award Number K12HD073945. Research was also supported under a grant from the NIDILRR (grant # 90AR5022-01-00).

# THE RELATIONSHIP BETWEEN PROPULSION PATTERN AND THE DEVELOPMENT OF UPPER-EXTREMITY PAIN IN MANUAL WHEELCHAIR USERS

<sup>1</sup> Shelby L. Walford, <sup>2</sup> Philip S. Requejo, <sup>2</sup> Sara J. Mulroy and <sup>1</sup> Richard R. Neptune

<sup>1</sup> The University of Texas at Austin, Austin, TX, USA

<sup>2</sup> Rancho Los Amigos National Rehabilitation Center, Downey, CA, USA  
email: shelbywalford@utexas.edu, web: <http://www.me.utexas.edu/~neptune/>

## INTRODUCTION

There are currently 3.2 million wheelchair users in the United States, with the vast majority using manual wheelchairs [1]. Of these manual wheelchair users (MWCUs), 253,000 are the result of a spinal cord injury [2]. Because of the consistently high muscle demand on the upper limbs during manual wheelchair propulsion, shoulder pain and injury are prevalent in MWCUs which often leads to a decreased quality of life [3]. Recent studies have analyzed the relationship between a MWCUs' propulsion hand path pattern (Fig. 1) and the upper extremity demand and found that semi-circular (SC) and double-loop patterns (DL) require less muscle power, and therefore are more favorable from an energetics point of view [4,5]. However, it is not known if the less favorable propulsion patterns are more likely to result in shoulder pain over time compared to the more favorable propulsion patterns.

The objective of this study was to determine whether specific propulsion patterns correlate with the development of shoulder pain in MWCUs with paraplegia. We hypothesized that subjects who use the more favorable DL or SC patterns would be less likely to develop shoulder pain over time.

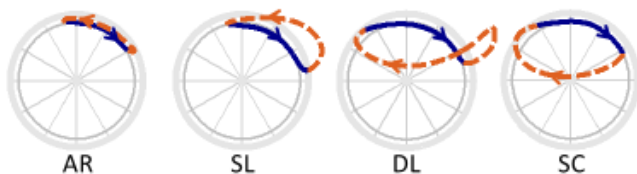


**Figure 1:** The four propulsion patterns are arcing (AR), single loop (SL), double loop (DL), and semi-circular (SC) [4].

## METHODS

Experimental kinematic data from 18 subjects with paraplegia were analyzed at three times: baseline (BL), 18 months after baseline, and 36 months after baseline (17 men; age at BL:  $34.6 \pm 7.0$  yrs; time from injury at BL:  $8.5 \pm 7.0$  yrs). Participants propelled their own wheelchair on a stationary ergometer for a 40-second trial at a comfortable, self-selected speed with data collected during the last 10 seconds. Kinematic data from the wheel, trunk and upper extremities were recorded using a 4-scanner CODA motion analysis system at 100 Hz and were time normalized for each cycle and averaged across cycles. Force data were collected using an instrumented wheel (SmartWheel, 200 Hz) and used to identify the contact and recovery phases of the propulsion cycle using a threshold of 5 N.

Propulsion pattern was identified by the trajectory of the third metacarpophalangeal joint projected onto the handrim plane, and a multiple-rater system was used to subjectively categorize each subject's propulsion pattern (Fig. 1). Additionally, net radial thickness (NRT) and total radial thickness (TRT) were calculated for each trial to quantitatively describe each subject's propulsion pattern [6]. Participants were asymptomatic for shoulder pain at baseline and were classified as having developed shoulder pain if they experienced an increase of  $\geq 10$  points on the Wheelchair User's Shoulder Pain Index at either the 18-month or 36-month follow-up assessment.

To determine whether the development of shoulder pain was related to propulsion pattern, a generalized linear mixed-effects model was used. The fixed effects included propulsion pattern grouping, NRT, and TRT. The random effect was subject with each

having three observations (time points). Fixed effects had a significant influence on the pain score if their coefficients had a p-value less than 0.05.

## RESULTS AND DISCUSSION

Neither NRT, TRT, nor the pattern classification showed a significant relationship between propulsion pattern and pain. Thus, our hypothesis that subjects using a more under-rim propulsion pattern (DL or SC) would be less likely to experience shoulder pain was not supported.

Contrary to what we expected, subjects who did not develop shoulder pain did not use the more favorable patterns (DL and SC) more than the others. Rather, these subjects used the AR and SL patterns more frequently, though not by a significant amount (Fig. 2, Table 1). This result is interesting as the AR and SL patterns tend to require the highest and second highest upper extremity demand over the full cycle, respectively [4]. Additionally, for those who developed pain and did not change patterns over time (Fig. 2), each used a different hand pattern. A potential limitation in this study is that we used muscle power as a surrogate for upper extremity demand which may not be indicative of the biomechanical mechanisms that lead to pain. Also, the lack of statistical significance could be due to too few subjects developing pain relative to the total number of subjects. Future work will be directed at increasing the sample size.

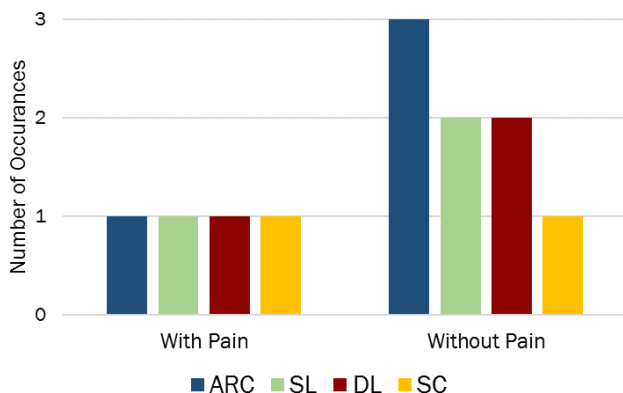


**Figure 2:** Propulsion pattern of subjects who used a stable pattern over time, including those who did and did not develop upper extremity pain.

Subjects who did change their propulsion pattern over time also varied widely in their preferred propulsion pattern (Table 1). Six subjects had at least two different propulsion classifications during the baseline, 18-month, and 36-month data collections. Of these six, only one subject developed pain. However, this subject changed from a SL to DL pattern and ultimately developed shoulder pain.

**Table 1:** Propulsion pattern used by subjects who changed their pattern over the 36-month period.

Subject	Baseline	18	36	Pain (Y/N)
1	ARC	SC	SC	N
2	ARC	SL	SL	N
3	ARC	ARC	SL	N
4	SL	ARC	ARC	N
5	SL	DL	SL	N
6	SL	DL	DL	Y

## CONCLUSIONS

These results suggest that although specific propulsion patterns require less upper-extremity demand than other patterns, the specific pattern used by an individual may not propagate or mitigate shoulder pain. Future work should analyze additional subjects and biomechanical quantities that may be biomarkers for the development of shoulder pain in MWCU.

## REFERENCES

- Centers for Disease Control and Prevention (CDC). *MMWR Morb Mortal Wkly Rep* **58**, 421-426, 2009.
- Centers for Disease Control and Prevention (CDC). *National Center for Injury Prevention and Control; Spinal Cord Injury (SCI): Fact Sheet*. Atlanta, GA, 2006.
- Requejo PS, et al. *Top Spinal Cord Inj Rehabil* **13**, 86-119, 2008.
- Slowik JS, et al. *J Biomech* **49**, 1554-1561, 2016.
- Kwarciak AM, et al. *Disabil Rehabil Assist Technol* **7**, 459-463, 2012.
- Slowik, JS, et al. *Clin Biomech* **30**, 927-932, 2015.

## ACKNOWLEDGMENTS

This study was supported by NIH Grant R01 HD049774.

# The effect of lumbar belts on psychological and biomechanical outcomes

<sup>1,3</sup> Ali Shahvarpour, <sup>2,3</sup> Richard Preuss, <sup>2,3</sup> Michael J.L. Sullivan, <sup>1</sup> Alessia Negrini, <sup>1,3</sup> Christian Larivière,

<sup>1</sup> Institut de recherche Robert-Sauvé en santé et en sécurité du travail (IRSST), Montreal, QC, Canada;

<sup>2</sup> McGill University, Montreal, QC, Canada;

<sup>3</sup> Center for Interdisciplinary Research in Rehabilitation of Greater Montreal (CRIR), Montreal, QC, Canada  
email: ali.shahvarpour@polymtl.ca

## INTRODUCTION

Many patients with low back pain (LBP) may benefit from wearing a lumbar belt (LB) [1], but the mechanisms involved are not fully understood. Two perspectives can be considered, involving pain-related psychological mechanisms and biomechanical mechanisms.

Wearing a LB can produce immediate pain relief which in turn may reduce pain-related fears and catastrophizing, but this has never been formally tested. Biomechanically, a LB can also provide a stiffening effect, leading to a smaller lumbar range of motion (ROM) [2], and decreasing stress on lumbar structures. Our earlier work studied the effect of two flexible LBs (extensible; non-extensible) on lumbar ROM in healthy subjects [2]. These results need to be extended to subjects with LBP.

This study aimed to investigate how wearing an extensible belt (EB) or a non-extensible belt (NEB) affects pain intensity, pain-related psychological variables, and biomechanical (ROM) variables during maximal trunk flexion in subjects with LBP as well as healthy controls (ROM only).

## METHODS

**Subjects.** Non-obese healthy controls (n = 20) and subjects with LBP (n = 40), equally divided by sex, participated. The subjects with LBP had lumbar or lumbosacral pain (with or without radicular pain) for at least 4 weeks.

**Lumbar Belts.** The EB and NEB were chosen based on their functionality at workplace (flexibility and comfort) [2] and had the same dimensions. The tension of the LBs was adjusted at 8.0 kPa, in the

standing upright posture, as measured with a Force Sensing Resistor sensor [2].

**Experimental Conditions.** Starting from the upright posture (knees extended) and following the pace of a metronome, the subjects bent forward maximally (4 s), remained relaxed in that fully-flexed posture (4 s), returned to the upright posture (4 s) and stood quietly (4 s). The task was repeated 5 times, consecutively. The angular kinematics of the trunk was measured with three inertial sensors attached over the sacrum (pelvis), just above the LB (~T9-T10) and at the T1-T2 vertebral level [2]. The ROM of the pelvis ( $ROM_{PE}$ ), lumbar ( $ROM_{LU}$ ) and thoracic spine ( $ROM_{TH}$ ) (Fig. 1) was computed for each quartile (INTERVAL) of the trunk ROM.

**Pain-related variables (subjects with LBP only).** Before performing any flexion trial, pain intensity (0-10 scale) was measured, with and w/o LB. After each flexion trial (with and w/o LB), fear of pain (100 mm visual analog scale) and pain catastrophizing (6-item scale) were also recorded.

**Statistical analyses.** For ROM variables computed for the flexion phase only, 3-way ANOVA for repeated measures (GROUP: healthy vs LBP; CONDITION: no belt (NB) vs with EB vs with NEB; INTERVAL: 0-25 vs 25-50 vs 50-75 vs 75-100% of total trunk ROM) were performed.

## RESULTS AND DISCUSSION

Wearing a LB significantly decreased pain intensity, fear of pain and pain catastrophizing, although the type of the LB did not affect the scores (Fig. 2).

With regard to ROM variables, no GROUP × CONDITION interaction was found, showing the same effect of wearing a LB in both groups. Total

$ROM_{LU}$  for the patient group ( $57.8 \pm 13.1^\circ$ ) was smaller than that for the control group ( $63.6 \pm 12.0^\circ$ ) although the effect was not statistically significant ( $p = 0.072$ ). In contrast,  $ROM_{TH}$  was significantly higher ( $p = 0.027$ ) in the patient group ( $-2.4 \pm 8.2^\circ$ ) compared to the control group ( $-6.6 \pm 6.4^\circ$ ), suggesting compensation between trunk segments.

Total  $ROM_{LU}$  was significantly larger (by  $6-7^\circ$ ) in the NB condition than in both EB and NEB conditions. This was partly compensated for with more  $ROM_{TH}$  (by  $2^\circ$ ) in the EB and NEB conditions.

CONDITION  $\times$  INTERVAL interactions ( $p < 0.001$ ) were seen for  $ROM_{PE}$ ,  $ROM_{LU}$  and  $ROM_{TH}$  (Fig. 3), revealing that wearing either LB had an effect on the movement of the different trunk segments, and that these effects changed over the intervals. The LB reduced the lumbar movement during interval 1 (Fig. 3, middle), which was partly compensated by an increase in  $ROM_{TH}$  (Fig. 3, right). In the final interval (interval 4), however, there was more lumbar movement in the two LB conditions than in the NB condition (Fig. 3, middle), but less pelvic movement (Fig. 3, left).

## CONCLUSIONS

Wearing a LB can produce immediate pain relief as well as reduced pain-related fears and catastrophizing, which may help in initiating a gradual re-exposure to physical work activities (disability prevention perspective), or in helping a worker maintain these activities (secondary prevention perspective), following a LBP episode. Such flexible LBs (EB, NEB) also reduce the lumbar ROM in subjects with LBP in the same way as healthy controls. This effect is compensated for by ROM changes of adjacent trunk segments (pelvis, thorax) during trunk flexion. Whether these compensations are detrimental remains unknown.

## REFERENCES

1. van Duijvenbode IC, et al. *Cochrane Database of Syst Rev* 2, CD001823, 2008.
2. Larivière C, et al. *BMC Musculoskelet Disord* 15, 1-13, 2014.

## ACKNOWLEDGMENTS

The study was funded by IRSST, QC, Canada. We thank Mr. H. Mecheri and Ms. S. Bellfeuille.

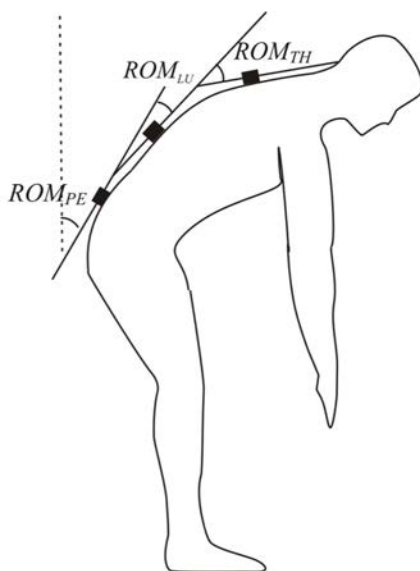


**Figure 1:** Definition of trunk segment angles

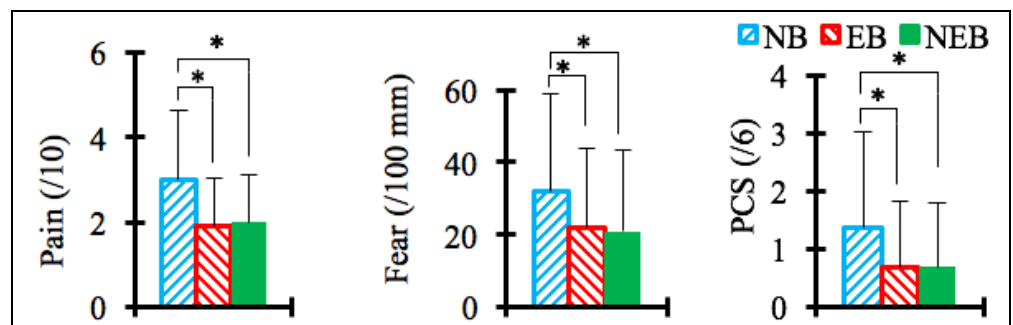


**Figure 2:** Effect of wearing lumbar belts on pain (left), fear of pain (middle) and pain catastrophizing (right) scores. (\*  $p < 0.05$ )

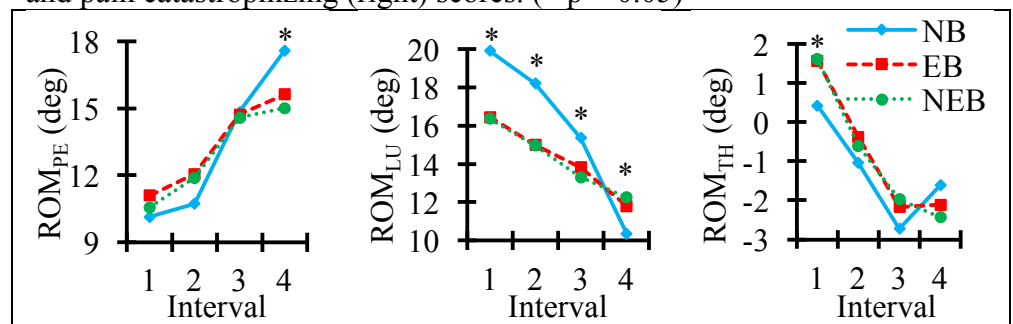


**Figure 3:** CONDITION  $\times$  INTERVAL interaction affected  $ROM_{PE}$ ,  $ROM_{LU}$  and  $ROM_{TH}$ . (\*  $P < 0.05$ )

# THE INFLUENCE OF LUMBAR SPINE POSTURES ON MONITOR LOCATION WHEN USING SIT TO STAND WORKSTATIONS

<sup>1</sup> Kayla M. Fewster, <sup>1,2</sup> Maureen F. Riddell, <sup>1</sup> Jack P. Callaghan

<sup>1</sup> Department of Kinesiology, University of Waterloo, 200 University Avenue West, Waterloo, ON, Canada

<sup>2</sup> Insight + Exploration, Herman Miller, 855 E Main Ave, Zeeland, MI, USA  
email: kfewster@uwaterloo.ca

## INTRODUCTION

A number of research studies have demonstrated the negative health consequences associated with prolonged sitting [1,2]. This has prompted scientists and clinicians to advocate for workers to perform office related tasks while standing, that would be typically done in sitting [4].

In contrast, prolonged standing has been shown to be a risk factor for low back pain (LBP) development [3]. Approximately 50% of asymptomatic individuals are susceptible to acute LBP development during prolonged standing [4,5]. As a result, these findings have led to an emphasis on the importance of movement and varying postures throughout the day with the use of sit to stand workstations. These workstations have shown increased popularity in recent years, demonstrating decreased sedentary behavior, diminished fatigue and greater comfort [6].

The Canadian Standards Association (CSA) Guideline for Office Ergonomics, states that when performing a light office task such as typing, while sitting or standing, the workstation should be set 5 cm below the workers' hand height with elbows bent at 90°, with the monitor placed at or slightly below eye level [7].

Aside from moving the desk when transitioning from sitting to standing, there is a lack of literature regarding the necessary adjustments to other equipment associated with the workstation. A previous analysis has demonstrated that when moving from sitting to standing and following CSA Guidelines, monitor height must be adjusted to keep the monitor at eye level [8]. This suggests that differences in spine posture alignment may exist between sitting and standing. Therefore, the purpose of this study was to evaluate posture in sitting and

standing while adhering to CSA Guidelines. If differences do exist, this study will support changes to office ergonomics guidelines to incorporate monitor adjustments when using sit to stand workstations.

## METHODS

Sixteen participants (8 female and 8 male) were recruited between the ages of 18 and 25 years old. Participants completed 2 different conditions: 1) Sitting Constrained; in which the participants' chair, desk and monitor heights were adjusted according to current CSA seated work guidelines (Figure 1). 2) Standing Constrained; the participants' desk and monitor heights were adjusted according to the current CSA standing work guidelines. In both conditions the participants were constrained to this setup with no freedom to adjust the equipment (Figure 1). Each condition lasted 15 minutes and during each condition participants were randomly assigned the following three standardized computer tasks for five minutes each: 1) Reading short stories on the monitor (READ), 2) Data entry into blank fields on the computer (FORM), and 3) Typing paragraphs as they appear on the screen (MAIL). Each task lasted 5 minutes.

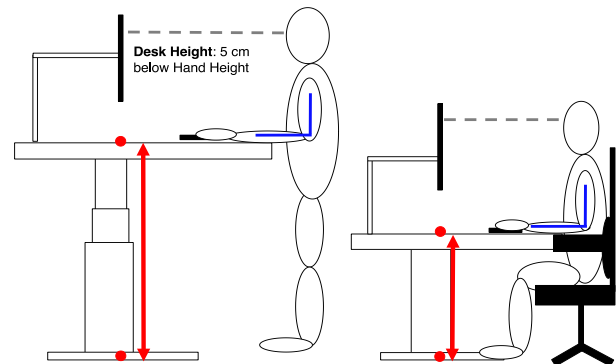


**Figure 1:** Constrained Sitting and Standing workstation setup. Desk height was set to 5 cm below hand height, with the elbows bent to 90°, and the monitor placed at or slightly below eye level

Movement of the head, thoracic, lumbar spine, pelvis and monitor were tracked at 10 Hz using an optoelectronic motion capture system (Optotrak Certus, NDI, Waterloo, Canada). Eye Height relative to Monitor, Lumbar Spine Angle, Trunk Angle relative to vertical and Acromion Process (AC) to Hip distance were calculated as average values across each 5 minute individual task. Lumbar joint angles are expressed relative to individuals' standing postures. A three-way mixed model ANOVA assessed the influence of Condition (Sit vs. Stand), Task (READ, FORM, MAIL), and Gender on posture.

## RESULTS AND DISCUSSION

No significant differences were observed between eye height and monitor height across Condition ( $p = 0.181$ ), or across Task ( $p = 0.056$ ).

There was a significant main effect of Condition ( $p < 0.0001$ ) and Task ( $p = 0.008$ ) for Lumbar Spine Angle. Not surprisingly, there was significantly more lumbar spine flexion in the Sitting condition when compared to Standing. For the main effect of Task, READ resulted in significantly more lumbar flexion in comparison to FORM and MAIL.

A significant main effect of Trunk angle relative to vertical was observed for Condition ( $p < 0.0001$ ). When sitting, participants sat with their Trunk flexed relative to vertical. While standing participants stood with their Trunk extended relative to vertical. (Figure 2).

Significant main effects of Condition ( $p < 0.0001$ ) and Task ( $p = 0.033$ ) were observed for AC to Hip distance. When compared to Standing, the distance between the mid-point of the right and left acromion process to the mid-point of the right and left hip joint center was significantly less (Sitting;  $45.7 \text{ cm} \pm 2.7$ ; Standing  $48.0 \text{ cm} \pm 2.5$ ). For the main effect of Task, Acromion to Hip distance was significantly greater in FORM when compared to READ and MAIL.

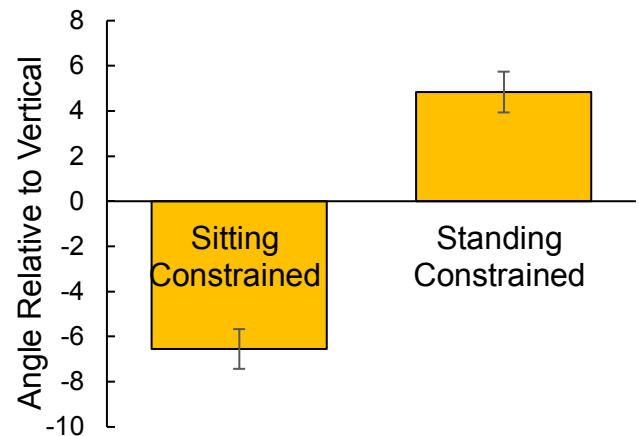


**Figure 2:** Main effect of Condition for Trunk angle relative to vertical. A negative value corresponds to Flexion with respect to vertical while a positive value corresponds to Extension

## CONCLUSIONS

The results from this investigation demonstrate that lumbar spine alignment differences do occur between Sitting and Standing. The observed increased Trunk flexion relative to vertical and decreased distance between AC to hip combined with lumbar spine posture differences explain changes in monitor height when transitioning from sitting to standing and re-adjusting for CSA standards. Results from this investigation support the notion that monitor height adjustments relative to the work surface are necessary when utilizing sit to stand workstations.

## REFERENCES

1. Callaghan JP, et al. *International Journal of Industrial Ergonomics*, 40(2), 165-170, 2009
2. Dunstan DW, et al. *Diabetes Research and Clinical Practice*, 97(3), 368-376, 2012
3. Thorp AA, et al. *Occupational & Enviro Med*, 71(11), 765-771, 2014
4. Marshall et al, *Human Movement Science*, 30(1), 63-73, 2011
5. Nelson-Wong E, et al. *Clinical Biomechanics* 23, 545- 553, 2008
6. Alkhajah TA, et al. *Am J of Prevene Med*, 43(3), 298-303, 2012
7. CSA Group, (CSA Z1004-12). Toronto, Ontario: Author, 2012
8. Riddell MF, et al. 46th Annual ACE Conference, 2015.

# TIME-VARYING CONTRIBUTIONS TO LUMBAR LORDOSIS DURING AN UNSTABLE SITTING TASK IN PEOPLE WHO DO AND DO NOT DEVELOP LOW BACK PAIN DURING STANDING

<sup>1</sup>Daniel Viggiani, <sup>2</sup>Erin M. Mannen, <sup>3</sup>Erika Nelson-Wong, <sup>4</sup>Alexander Wong, <sup>2</sup>Gary Ghiselli, <sup>2</sup>Kevin Shelburne, <sup>1</sup>Jack P. Callaghan and <sup>2</sup>Bradley S. Davidson

Email: [dviggian@uawaterloo.ca](mailto:dviggian@uawaterloo.ca)

<sup>1</sup>Department of Kinesiology, University of Waterloo, Waterloo, ON, Canada; <sup>2</sup>Department of Materials and Mechanical Engineering, University of Denver, Denver, CO, USA; <sup>3</sup>School of Physical Therapy, Regis University, Denver, CO, USA; <sup>4</sup>Systems Design Engineering, University of Waterloo, Waterloo, ON, Canada

## INTRODUCTION

About half of individuals with no clinically-diagnosed low back pain (LBP) will develop LBP when asked to stand continuously for two hours (PDs = pain developers). PDs have shown motor control alterations during standing [1] and are at an increased risk for developing clinical LBP in the future compared to controls (NPDs = not PDs) [2]. Dynamically measured vertebral motion can lend insight into potential mechanisms leading PDs to develop clinical LBP. This study's purpose was to use high-speed radiography to measure intervertebral contributions to lumbar curvature during pelvis-driven lumbar spine motion to determine if PDs and NPDs move their spines differently.

## METHODS

Fourteen participants (8 female) with no history of LBP between 21 and 35 years old performed two testing sessions: 1) standing screening and 2) radiography data collection. The standing session involved participants standing continuously for up to two hours. Prior to and every 15 minutes during the screening, participants reported the intensity of any LBP they experienced on a 100 mm visual analog scale. Any participants reporting pain intensities greater than 10 mm were classified as PDs, with others classified as NPDs [1]. During the radiography data collection, participants sat on an adjustable custom seat with lower limb supports. The seat had a 50 cm diameter hemisphere underneath the seat pan that allowed the seat to tilt freely in all directions and was placed on a rigid table. Participants were instructed to cyclically tilt the seat pan anteriorly (into lumbar extension) and posteriorly (into lumbar flexion) as far as possible while maintaining balance following directed familiarization and practice. Pulsed radiographic images (25 Hz) containing the anterior and posterior

half-cycles were captured of L3 to S1 throughout the entire motions.

Radiographs were undistorted (XMA Lab, Brown University, Providence, RI), and underwent a Matlab-based (ver 2015b, Mathworks, Natick, MA) local contrast enhancement algorithm prior to digitization of four corners of each vertebral body from L3 to S1. Corners were used to compute time-varying sagittal-plane intervertebral joint angles for L3/L4 through L5/S1. Joint angles were expressed as a percentage of the total measurable curve by dividing the raw joint angle by the sum of the magnitudes of all joint angles in order to prevent numerical instability through division by small numbers. The mean contribution across the entire cycle and contributions at the peak total lumbar spine angle (L3-S1) were taken from each joint level for statistical comparisons. Data were stratified by direction of motion (anterior/posterior) and entered into a mixed-model ANOVA using a within factor of joint level (L3/L4 – L5/S1) and a between factor of pain group (NPD/PD). Effect sizes (Cohen's *d*) were calculated for each comparison and bootstrap sampled to produce a 95% confidence interval.

## RESULTS AND DISCUSSION

One male and five females were classified as PDs via the standing screening. Data for the one male PD was excluded as it was incomplete and diverged from the five female PDs. Contributions to lumbar angles were positive in anterior and posterior tilting for NPD and diverged for PD in posterior tilting (Fig. 1).

In the anterior direction (lumbar extension), NPDs and PDs had similar contributions across the entire cycle and also at peak lumbar angle for each joint level ( $p > 0.252$ ; Table 1). However, large effect sizes indicated that PDs may have had greater

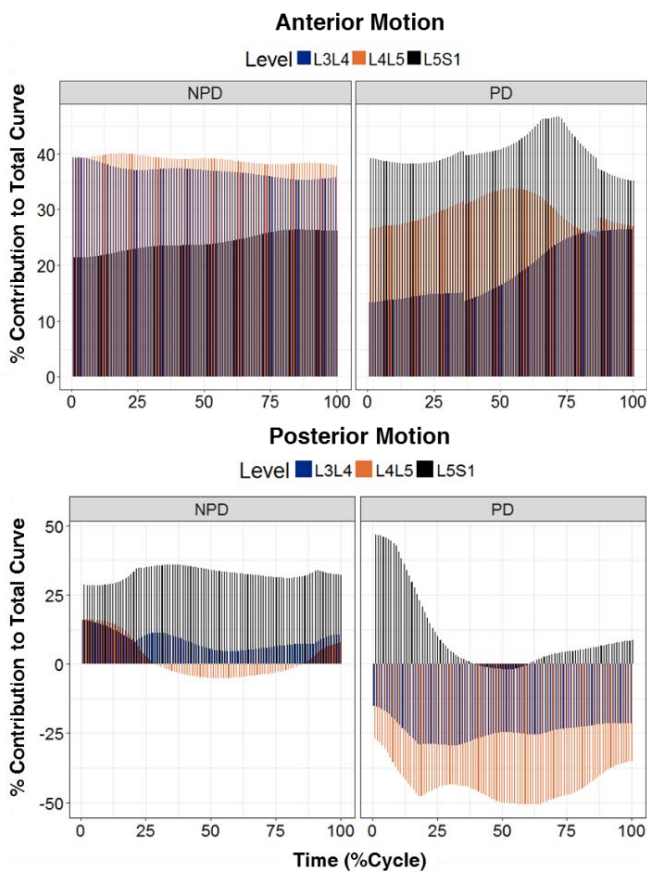


**Figure 1:** Mean contributions to lumbar curvature during anterior and posterior tilting while seated on an unstable seat. Error bars omitted for clarity.

contributions coming from L5/S1 compared to L3/L4 ( $d$  95% CI: 0.91 – 1.10) in this direction (Fig. 1). In the posterior direction (lumbar flexion), PDs appeared to achieve spine flexion mainly through L5/S1, while NPDs appeared to achieve motion primarily through L4/L5 (Fig. 1). There was a main effect of pain group for the mean contributions where PDs had more spine flexion than NPDs in the posterior direction ( $p = 0.016$ ;  $d$  95% CI: 1.01 – 1.71)

**Table 1:** Relative intervertebral joint angle contributions as a percentage of measured lumbar curvature. Data are Mean  $\pm$  SD; positive numbers indicate that the intervertebral joint angle was in extension. Asterisks indicate significant effects of pain group in the posterior direction; different letters indicate main effects of joint level.

		Anterior			Posterior		
		L3/L4	L4/L5	L5/S1	L3/L4 <sup>A</sup>	L4/L5 <sup>A</sup>	L5/S1 <sup>B</sup>
<b>Mean*</b>	NPD	36.9 $\pm$ 13.9%	39.0 $\pm$ 5.5%	24.1 $\pm$ 14.8%	17.0 $\pm$ 29.2%	11.5 $\pm$ 32.9%	35.1 $\pm$ 6.2%
	PD	19.0 $\pm$ 19.7%	29.8 $\pm$ 22.3%	40.6 $\pm$ 22.3%	-24.4 $\pm$ 18.4%	-44.0 $\pm$ 11.8%	10.3 $\pm$ 31.5%
<b>During Peak</b>	NPD	34.6 $\pm$ 11.8%	39.5 $\pm$ 7.7%	25.9 $\pm$ 13.6%	11.0 $\pm$ 30.1%	5.9 $\pm$ 40.7%	36.1 $\pm$ 16.0%
	PD	13.6 $\pm$ 29.8%	27.9 $\pm$ 25.0%	37.6 $\pm$ 16.1%	-17.1 $\pm$ 26.8%	-41.6 $\pm$ 10.5%	14.1 $\pm$ 35.9%

with a similar trend in the contribution at peak lumbar angle ( $p = 0.087$ ;  $d$  95% CI: 0.74 – 1.32; Table 1). L5/S1 was also more extended than L3/L4 and L4/L5 in the posterior direction ( $p < 0.002$ ; Table 1).

## CONCLUSIONS

PDs and NPDs used different regions of their lumbar spines to tilt anteriorly and posteriorly while seated on an unstable chair. These results suggest that PDs adopted an L5/S1-dominant approach to attaining lumbar spine motion while NPDs did not localize motion to a given vertebral level as clearly. The more evenly distributed motion adopted by NPDs may prevent local stress concentrations in the facet joints and surrounding soft tissues and potentially reduce injury risk and pain development [3].

The unstable seat required motion to be driven from the pelvis, contrary to previous studies investigating the development of LBP in PDs, which were performed in standing postures [1]. This study provides evidence of altered spinal kinematics in PDs beyond standing; potentially indicative of generalized, deficient trunk muscle coordination [4]. The transfer of kinematic changes beyond prolonged standing lends further evidence that PDs represent people at an increased risk for developing clinical LBP [2].

## REFERENCES

1. Nelson-Wong E et al. *JEK* **20**(2), 256-63, 2010.
2. Nelson-Wong E et al. *Spine* **39**(6), E379-83, 2014.
3. Cavanaugh JM et al. *J Biomech* **29**(6), 1117-29, 1996.
4. Teyhen DS et al. *Phys Ther* **87**(3), 313-25, 2007.

# LANDING MECHANICS DURING A STOP JUMP IN INDIVIDUALS WITH LOW BACK PAIN AND LOW BACK INJURIES

<sup>1</sup> Alexa K Johnson, <sup>1</sup> Joshua D Winters, <sup>1</sup> Kathleen M Poploski, <sup>1</sup> Nicholas R Heebner, and <sup>1</sup> John P Abt

<sup>1</sup> The University of Kentucky, Lexington, KY, USA

email: johnson.alexa@uky.edu, web: <https://www.uky.edu/chs/research/smri>

## INTRODUCTION

The clinical presentation of low back pain (LBP) is highly variable, therefore it has been recommended that the spine be included with the lower extremities when conducting clinical and movement analyses [1]. LBP is known to increase knee stiffness in runners [2], though information on how joint motion and loading rates may affect each other are unavailable. Likewise, the majority of research on LBP and low back injuries (LBI) has focused on back and trunk biomechanics, independent of the lower extremities. If those with LBP and/or LBI exhibit altered movement in the trunk, additional compensations may exist in the lower extremities, which may lead to the development of an injury in the lower extremity [2].

The purpose of this study is to determine if physically active individuals with a history of LBP or a LBI have altered landing mechanics in a double leg stop jump task, compared to healthy controls. We hypothesize that those with a history of LBP or LBI will have lower loading rates and different lower extremity sagittal plane kinematics at initial contact of a stop jump task, compared to healthy controls, and that such changes are related.

## METHODS

Thirty-five subjects, thirteen with a history of LBP (age  $26.7 \pm 4.1$  yrs; height  $69.5 \pm 1.9$  in; mass  $85.1 \pm 7.3$  kg), nine with a LBI (age  $28.1 \pm 3.6$  yrs; height  $70.8 \pm 2.0$  in; mass  $89.0 \pm 8.1$  kg) and thirteen healthy control subjects (age  $28.2 \pm 5.3$  yrs; height  $70.1 \pm 2.2$  in; mass  $85.8 \pm 9.9$  kg), completed a double limb stop jump. Subjects jumped forward onto two force platforms (Kistler Instrument Corp., Amherst, NY) from 40% of the subject's total body height. They were instructed to jump forward and then vertically as high as possible. Two practice trials were given and variables were averaged across three subsequent trials. Healthy control subjects reported no history of

back or lower extremity injuries, or back pain. The LBP group indicated they suffered from chronic LBP lasting at least 6 months and the first indication of pain reported was an average  $3.0 \pm 2.4$  years ago. The LBI group reported a physician diagnosed herniated disc or bulging disc in the lumbar section of the spine, with injury occurrence ranging from  $2.3 \pm 1.7$  years prior. All subjects reported no pain at the current testing session and were all currently highly physically active.

Raw vertical ground reaction forces (VGRF) were sampled at 1200 Hz and filtered using a fourth order low pass butterworth filter with a cutoff of 50Hz. A custom Matlab code (MathWorks, Natick, MA) was used to calculate loading rates from the VGRF. Peak loading rates were calculated from the onset of force, greater than 20N, to the initial peak VGRF and normalized to body mass. Subjects were outfitted with lower extremity reflective markers and an eight camera three dimensional motion capture system (Vicon Motion Systems Ltd, Centennial, CO) was used to collect bilateral sagittal plane kinematics at the hip, knee and ankle. Kinematic data were sampled at 200 Hz and marker trajectories were filtered using a Woltering filter with a predicted mean square error at 10mm. The plug-in gait model was used to calculate hip flexion at initial contact, knee flexion at initial contact and ankle flexion at initial contact.

Data were summarized using descriptive statistics including means and standard deviations. Analysis of variance was used to compare the mean bilateral peak loading rates, knee flexion at initial contact, hip flexion at initial contact, ankle flexion at initial contact and peak VGRF, between the three groups. A significance level of  $\alpha = 0.05$  was used and post-hoc comparisons were conducted using the Bonferonni adjustment for multiple comparisons. Pearson Correlation Coefficients ( $r$ ) between peak loading rates and lower extremity sagittal plane kinematics at initial contact and vertical ground

reactions forces, in each group were also completed. All data analysis was conducted using SPSS (SPSS 22 IBM Corp, Armonk, NY).

## RESULTS AND DISCUSSION

There were no significant differences in any sagittal plane lower extremity kinematics, VGRF, or peak loading rates between groups (Table 1.;  $p > 0.05$ ). In all groups VGRF were significantly correlated to peak loading rates,  $p < 0.05$ , which was expected as peak loading rates are calculated from the VGRF curve. On the right limb, peak loading rate was significantly correlated to knee flexion at initial contact in the LBP group ( $r = 0.61$ ;  $p = 0.026$ ) and to ankle flexion at initial contact in the LBI group ( $r = 0.75$ ;  $p = 0.019$ ). All other correlations were not significant. Although there are significant correlations between sagittal plane landing at initial contact and peak loading rates, they do not support our initial hypotheses as there were no group differences.

The correlation differences between right and left limbs, or possible limb dominance [3], could play into why we only saw significant correlations on the right side and not the left side. All but one subject, in the LBI group, were right limb dominant. This change in landing strategy between the LBP and LBI groups, from the control group, may be a compensatory strategy adopted due to pain or other mechanisms. If the shock from landing is not adequately distributed it may be an indicator for future injury [2]. Though, in a task in which landing

successfully is not the end goal, landing strategies and shock attenuation may change, as in this case the end goal is to vertically jump as high as possible.

## CONCLUSIONS

It appears that individuals with LBP and/or LBI are not loading different to that of healthy controls during the landing phase, in preparation for an explosive counter movement. The lack of differences may be due to the large between subject variability seen in different landing strategies displayed, and small sample sizes. Analyzing the take-off portion of the stop jump task may provide insight on how LBP and LBI may truly affect performance. Additionally, further research is needed to determine if landing strategies differ when subjects perform more impactful movements with a greater emphasis on shock absorption, like a single limb hop.

## REFERENCES

1. McGregor AH & Hukins DW. *J Back Musculoskelet Rehabil*, **22**, 219-22, 2009.
2. Hamill J, et al. *Res Sports Med*, **17**, 206-73, 2009.
3. Sung et al., *Hum Mov Sci*, **52**, 36-44, 2017.

## ACKNOWLEDGMENTS

This research was supported by the Office of Naval Research N00014-1-15-0069. The content is solely the responsibility of the authors and does not necessarily represent the official views of the Office of Naval Research

**Table 1:** Means and standard deviations of all variables by group. A negative ankle flexion value indicates ankle plantar flexion.

Variable	Group		
	Control Mean $\pm$ SD	LBP Mean $\pm$ SD	LBI Mean $\pm$ SD
Right VGRF (%BW)	228.80 $\pm$ 80.65	239.59 $\pm$ 95.91	206.02 $\pm$ 54.98
Left VGRF (%BW)	250.88 $\pm$ 110.27	237.14 $\pm$ 89.33	211.04 $\pm$ 65.90
Right Peak Load Rate (N/kg/s)	1598.00 $\pm$ 746.58	1617.45 $\pm$ 918.22	1232.84 $\pm$ 474.39
Left Peak Load Rate (N/kg/s)	1685.06 $\pm$ 792.60	1662.53 $\pm$ 979.82	1377.83 $\pm$ 420.61
Right Hip Flexion (deg)	54.57 $\pm$ 11.93	52.67 $\pm$ 14.52	54.58 $\pm$ 13.47
Left Hip Flexion (deg)	54.55 $\pm$ 11.58	52.94 $\pm$ 13.0	56.19 $\pm$ 13.23
Right Knee Flexion (deg)	39.45 $\pm$ 11.37	34.56 $\pm$ 10.02	41.46 $\pm$ 5.96
Left Knee Flexion (deg)	36.81 $\pm$ 11.29	34.59 $\pm$ 10.29	44.12 $\pm$ 8.51
Right Ankle Flexion (deg)	-6.97 $\pm$ 13.09	-9.16 $\pm$ 13.80	-10.19 $\pm$ 10.28
Left Ankle Flexion (deg)	-7.72 $\pm$ 18.22	-6.62 $\pm$ 14.95	-10.43 $\pm$ 17.09

# Soft Tissue Increases Stability and Propulsion During Human Running

Samuel Masters and John Challis

The Pennsylvania State University, University Park, PA, USA  
email: sem361@psu.edu

## INTRODUCTION

Soft tissue moves relative to the skeleton during human locomotion. This motion affect the energetics of human motion [1]. However, the effects of soft tissue motion have not been quantified on the whole-body center-of-mass (COM) control and stability during human running.

A two-body spring-loaded inverted pendulum (SLIP) controlled by a central pattern generator (CPG) can mimic the whole-body COM trajectory and ground reaction force (GRF) during running or hopping [2]. With finely tuned model parameters, this system is asymptotically stable with minimal control feedback. It was hypothesized that adding a soft tissue mass will increase stability and the running velocity of the SLIP model.

## METHODS

The SLIP model contained three masses, a spring connecting the upper body to the lower body, a spring-damper (S-D) connecting the lower body to the ground (Fig. 1), and a S-D connecting the lower body to a soft tissue mass. All S-D values were constant excluding the ground-spring interface. The ground-spring dampening was a function of the dampening coefficient, spring compression and velocity.

The SLIP was powered by an external moment at the spring-ground interface and a propulsive force (PF) that accelerated the whole-system COM. The propulsive phase of the gait cycle started when the SLIP was past vertical and ended when the spring connecting the ground to the lower leg approached its resting length. A tanh function was utilized in order to enforce a zero PF and external moment before and after the propulsive phase.

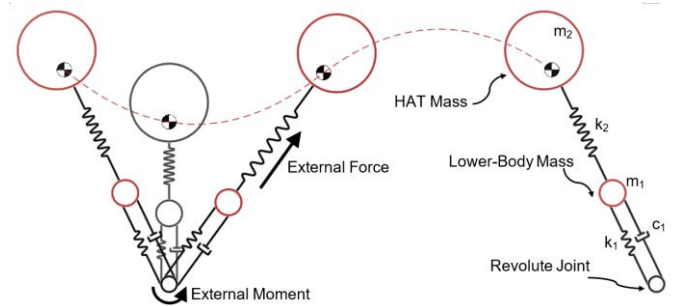


**Figure 1:** Two-mass SLIP model of running with a stance and flight phase. This figure does not include the soft tissue mass.

Vertical stance phase kinematics and GRFs from 10 college-aged male subjects running at  $3.1 \text{ m}\cdot\text{s}^{-1}$  were averaged and used to tune the parameters of the model. The COM vertical position and velocity were fitted with a sine wave to enforce smoothness and cyclical kinematics. All values of force were normalized with respect to body weight (BW). The weight of the lower and upper bodies were 0.165 BWs and 0.835 BWs, respectively. The soft tissue weight was approximately 61% (0.1 BW) of the lower BW.

A particle swarm optimization was utilized to determine the best set of parameters. The S-D parameters were systematically incremented between 100-1000  $\text{BW}\cdot\text{m}^{-1}$  and 0-50  $\text{BW}\cdot\text{s}\cdot\text{m}^{-1}$ , and the SLIP was simulated until its step cycle converged to a period-one gait cycle. These simulations contained minimal control feedback. The angle of the leg increased or decreased proportional to horizontal running velocity.

Stability was measured by two methods. The first method measured the level of noise that induced failure in the SLIP. The magnitude of noise in the spring-ground stiffness was gradually increased until the SLIP fell over. Stability was also measured by increasing the lower spring stiffness value by 100% for a single step and counting the number of steps

until the COM velocity kinematics converged to  $10^{-3}$   $\text{m}\cdot\text{s}^{-1}$  of its period-one gait cycle.

The running speed of the period-one gait cycle for all S-D combinations were used as a measure of efficiency. The propulsion dynamics were the same for all S-D combinations, thus greater running speed was indicative of greater efficiency.

All measurements of performance were compared to a control SLIP. The control SLIP did not have soft tissue.

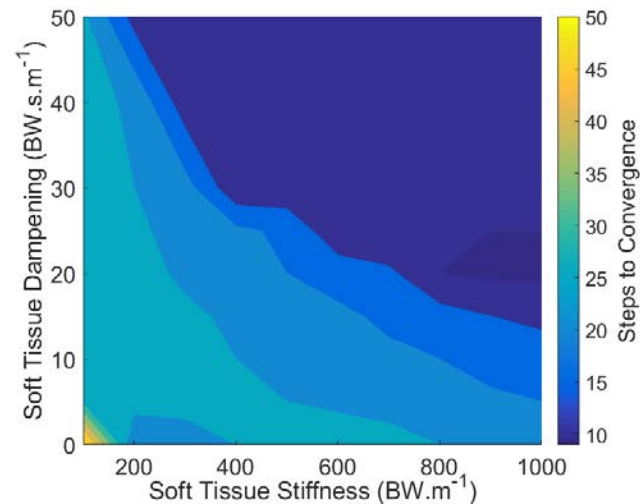
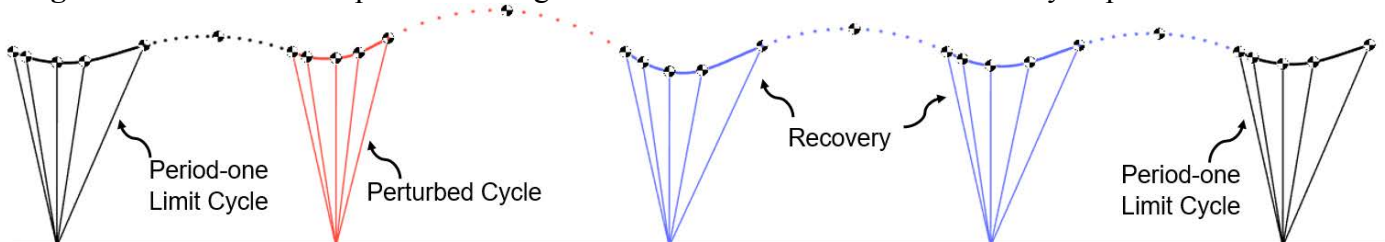


**Figure 2:** A contour plot of the number of steps the SLIP model took for each S-D combination following a perturbation to the spring-ground interface. Dark and light colors indicate greater and lesser stability, respectively.

## RESULTS AND DISCUSSION

The spring stiffness values for the lower and upper springs were  $217.9 \text{ BW}\cdot\text{m}^{-1}$  and  $211.1 \text{ BW}\cdot\text{m}^{-1}$ , respectively. The dampening coefficient for the ground-spring interface was  $23.6 \text{ BW}\cdot\text{s}\cdot\text{m}^{-1}$ . The PF and external moment magnitudes were  $4.15 \text{ BW}$  and  $2.57 \text{ BW}\cdot\text{m}$ .

**Figure 3:** Center of mass position during a simulated trial. Some of the recovery steps have been removed.



The S-D values of the soft tissue had a large effect on the propulsion dynamics of the period-one gait cycle. The SLIP running velocity was proportionally and inversely related to the soft tissue stiffness and dampening, respectively. The horizontal running speed ranged between  $1.9 \text{ m}\cdot\text{s}^{-1}$  and  $3.6 \text{ m}\cdot\text{s}^{-1}$ . The control SLIP ran at a horizontal speed of  $2.2 \text{ m}\cdot\text{s}^{-1}$ . The PF of the control SLIP would have to increase in order to match the running speed of the SLIP with soft tissue for most S-D combinations. This indicated that the SLIP with soft tissue was more efficient than the control SLIP.

Following a perturbation to the leg-ground stiffness, the SLIP with soft tissue performed better than the control SLIP for 94% of the S-D combinations (Fig. 2). The control SLIP took 29 steps before its gait velocity was within  $10^{-3} \text{ m}\cdot\text{s}^{-1}$  of its period-one gait cycle. The number of steps that the SLIP with soft tissue took was between 9 steps and 52 steps (Fig. 3). The bottom of that range occurred at high stiffness and dampening values.

About 98% of the S-D combinations resulted in a SLIP model that could withstand 2x the magnitude of noise relative to that of the control SLIP. The low and high end of the range occurred at zero dampening in the soft tissue. This indicated that a small amount of soft tissue dampening would be sufficient to guarantee greater robustness to noise in the terrain.

The SLIP with soft tissue performed better by all standards measured in this study. It was more stable and ran at greater speeds with the same CPG propulsion dynamics.

## REFERENCES

1. Zelik KE, et al. *J Exp Biol* **218**, 876-886, 2015.
2. Blickhan R. *J Biomech* **22**, 1217-1227, 1989.

# DIFFERENTIAL LEG JOINT FUNCTION DURING HUMAN RUNNING

<sup>1</sup> Devin L. Jindrich, <sup>2</sup> Mu Qiao, and <sup>3</sup> James J. Abbas

<sup>1</sup> California State University, San Marcos, CA, USA

<sup>2</sup> University of North Carolina at Chapel Hill, Chapel Hill, NC, USA

<sup>3</sup> Arizona State University, Tempe, AZ, USA

Email: [djindrich@csusm.edu](mailto:djindrich@csusm.edu), web: <http://faculty.csusm.edu/djindrich/>

## INTRODUCTION

Functional differences among joints may help to coordinate overall leg function during locomotion. The leg may exhibit a proximal-distal gradient in joint mechanical function from power production to spring-like behavior [1]. During walking, human hips produce energy (like motors) and ankles absorb and produce energy (like springs) [2]. The knee exhibits several functions, including motor, energy-absorbing damper, and energy-transferring strut. Distinct joint functions sum together to result in the overall strut-like function of the leg during walking.

When running, legs exhibit overall spring-like function. Spring-like leg function can provide a degree of intrinsic dynamic stability, contributing to locomotion control. However, the contribution of joint functional differences to running leg function and stability is not well understood. We investigated the role of functional differences among leg joints on stability during running maneuvers by testing two hypotheses: (1) that humans exhibit a proximal-distal gradient in joint function during both constant-average-velocity (CAV) running and during sagittal-plane running maneuvers (stepping up and down); and (2) that humans select leg parameters (*e.g.*, stiffness and damping) that optimize intrinsic dynamic stability.

## METHODS

We used a 3-D motion tracking system with 10 cameras (VICON<sup>®</sup> 612, Oxford Metrics Ltd., Oxford, UK) to track whole body kinematics (120Hz, plug-in Gait marker set, 39 markers). We used three stationary force platforms embedded in the ground to record GRFs (3000Hz, 600×400mm, FP4060-NC, Bertec Corp., Columbus, OH, USA). We asked participants to run at a comfortable speed and asked them to perform three tasks (stepping up, CAV running, and stepping down.). Nine males (body mass=74.0±8.2kg, height=1.78±0.06m,

age=27.1±5.7yrs., leg length (greater trochanter to ground)=0.98±0.02m, mean±S.D.) participated.

To categorize leg joint (*i.e.*, hip, knee, and ankle) function, we developed strut, spring, motor, and damper indices (Fig. 1) [2, 3].

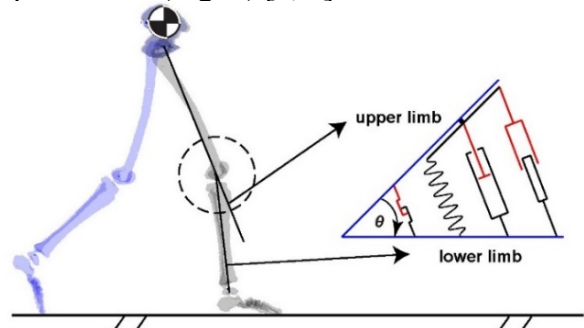


**Figure 1:** Diagram of a leg joint modeled by a strut, motor, spring, and damper in parallel.

The strut index is the dimensionless ratio between the power,  $P_{joint}$ , and moment ( $M_{joint}$ ). A strut index of 100% means a joint has no angular movement while only passing/bearing the moment between two segments; a strut index of 0 means that moments are associated with energy production or absorption. The motor, spring and damper indices characterized the nature of mechanical joint work: energy production, absorption followed by production, and absorption, respectively.

We used experimental data to construct and constrain a dynamic 2D Motor-Damper-Spring model (MDS) with alternate stance and flight phases [3]. The MDS is planar, with three segments: a proximal motor (analogous to the hip), an element with spring and damper in parallel (knee analog), and a distal spring (ankle/foot analog; Fig. 2).

We used forward dynamic simulations to estimate the number of steps achieved by the MDS model before falling on the ground. We quantified stability as the number of steps (# steps) before falling. We performed a sensitivity analysis over a wide

parameter space, and also constrained the model using parameters used by humans.

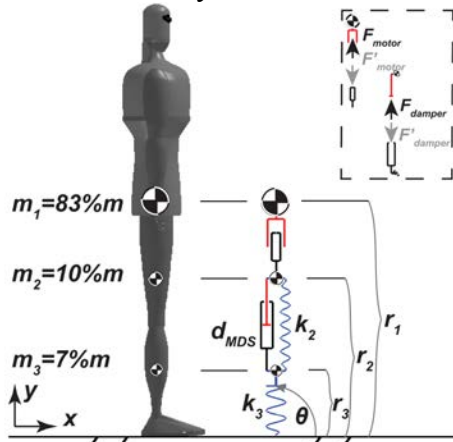


**Figure 2:** Schematic of MDS model.  $k$  is spring constant, and  $d$  is damping constant.

## RESULTS AND DISCUSSION

Consistent with our hypothesis, the hip acted as a “motor,” the knee as a “damper,” and the ankle as a “spring” (Fig. 3) during CAV running and maneuvers.

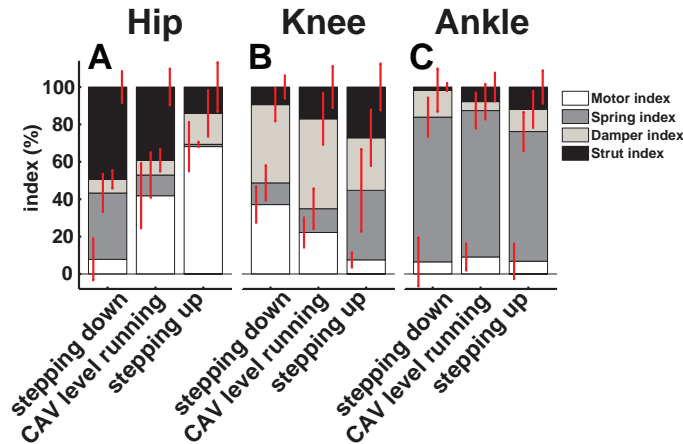


**Figure 3:** Joint functional indices during CAV level running and sagittal-plane maneuvers.

Maneuvers were associated with modest functional changes at the hip and knee joints, with small changes at the ankle joint (Fig. 3). The overall mechanical behavior of leg joints suggests that the MDS model (Fig. 2) is a reasonable representation of leg joint function during running.

The intrinsic dynamics of the MDS model resulted in sustained locomotion on level ground within narrow parameter ranges (Fig. 4; black regions). However, using parameters experimentally derived from humans, the model showed only short-term stability (Fig. 4; symbols). Parameters were

consistent across conditions rather than chosen to maximize stability.

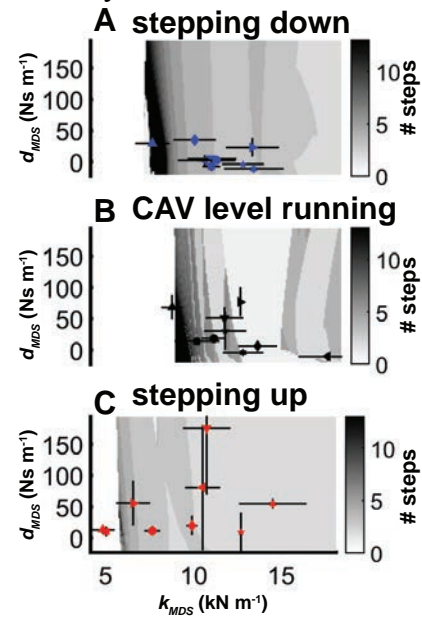


**Figure 4:** Sensitivity analysis of MDS performance relative to stiffness ( $k_{MDS}$ ) and damping ( $d_{MDS}$ ) parameters. Superimposed symbols and STDEV lines represent parameters selected by humans (different symbols represent different participants).

## CONCLUSIONS AND IMPLICATIONS

During constant-average-velocity running and sagittal plane maneuvers, legs showed a proximal-distal gradient in function. The hip, knee and ankle acted as a motor, damper, and spring, respectively. Humans may not optimize intrinsic dynamic stability alone, but may instead choose mechanical and behavioral parameters appropriate for both CAV locomotion and maneuvers. Understanding the contribution of differential joint function to overall leg and body mechanics is an important neuromechanical question with potential implications for athletic training, rehabilitation, prosthetics, and legged robotics.

## REFERENCES

1. Daley, M.A., G. Felix, and A.A. Biewener, *Running stability is enhanced by a proximo-distal gradient in joint neuromechanical control*. Journal of Experimental Biology, 2007. **210**(Pt 3): p. 383-94.
2. Qiao, M. and D.L. Jindrich, *Leg Joint Function during Walking Acceleration and Deceleration*. Journal of Biomechanics, 2016. **49**(1): p. 66-72.
3. Qiao, M., J.J. Abbas, and D.L. Jindrich, *A Model For Differential Leg Joint Function During Human Running*. Bioinspiration & Biomimetics, 2017. **12**(1): p. 016015.

# **The energetics of the human foot across a range of running speeds**

Luke A Kelly, Glen A Lichtwark, Andrew G Cresswell, Dominic J Farris

The University of Queensland, School of Human Movement and Nutrition Sciences,  
Centre for Sensorimotor Performance, Brisbane, Australia, email: l.kelly3@uq.edu.au

## **INTRODUCTION**

The longitudinal arch (LA) of the human foot behaves in a spring-like manner during running. Compression of the LA during early stance allows mechanical energy to be stored in the stretched elastic ligamentous and tendonous tissues that span this structure. In late stance the LA recoils and the elastic structures shorten to return stored mechanical energy to the body. It has been suggested that this mechanism delivers between 8-17% of the mechanical energy required for each stride [1].

In contrast to the LA, the metatarso-phalangeal (MTP) joints are known to absorb mechanical energy during late stance. Thus it is possible that a proportion of the energy returned via LA recoil is actually absorbed at the MTP joints, rather than returned to the body [2].

The notion that positive work is performed about the LA simultaneously with negative work being performed about the MTP joints is somewhat problematic, as the same structures (ie plantar fascia and intrinsic foot muscles) are considered to be the primary source of the mechanical work being performed at both of these joints. Although the same tissue may have a localized effect of performing negative work about a distal joint whilst performing positive work about another proximal joint, it is the net behavior that will contribute to the overall energetics of the system. With this in mind, we suggest it may be more appropriate to consider the energetic function of the LA and MTP joints as part of an entire 'foot' system. Under this scenario the net-work performed by muscles and ligaments acting across both the LA and MTP joints, as well as the contributions of other soft tissues (plantar fat pads etc.) may be adequately captured to reflect the energetics of the foot as an entire system.

Therefore the aim of this study was to quantify the energetic profile of the foot during running and to determine if the foot can indeed be described as spring-like in nature when considering the combined influence of the LA and MTP joints in addition to the other soft tissue structures. We also sought to determine if this energetic profile remained constant across a range of running speeds.

## **METHODS**

Eight healthy participants ran on a force-instrumented treadmill at 2.2, 3.3 and 4.4 m.s<sup>-1</sup> in a counter-balanced order. Three-dimensional motion of fourteen reflective markers attached to the foot, electromyography (EMG) and ground reaction force (GRF) data were captured synchronously during each running trial, with motion data collected at 200 Hz and GRF and EMG data captured at 2000 Hz via a 14-bit analogue to digital converter.

Marker trajectories and GRF data were filtered with a recursive 20 Hz low pass, second order Butterworth filter, while EMG signals were high-pass filtered at 35 Hz using a recursive second order Butterworth filter.

A previously described multi-segment foot model was applied in order to describe rear-, mid- and forefoot motion during running [3]. Foot power was calculated using a unified deformable (UD) segment analysis [2] with the calcaneus applied as the reference segment. Thus foot power reflects the net power contribution of all structures acting distal to the calcaneus segment, including the plantar fascia, intrinsic and extrinsic foot muscles and the plantar fat pads. Negative and positive work performed during stance phase was calculated by applying a trapezoidal integration of joint power curves across the stance phase. In order to describe the spring-like qualities of the foot, a work ratio was calculated at each running speed by dividing the positive work

done by the absolute value of negative work during the stance phase.

Intramuscular EMG was recorded from the two largest intrinsic foot muscles, abductor hallucis (AH) and flexor digitorum brevis (FDB) using previously described techniques [4] to provide further insight into the active muscular contributions to the foot spring function. An EMG root mean square (RMS) signal envelope was calculated using a moving window of 50 ms and each signal was normalized to its peak RMS amplitude found across all conditions. Normalised mean EMG RMS amplitude was calculated during the stance phase for each stride cycle, allowing comparisons in magnitude of stance phase muscle activation between running velocities.

For each individual, the kinetic and EMG data was averaged across a minimum of 10 stride cycles to form individual means for each condition. A one-way repeated measures analysis of variance (ANOVA) was used to describe the influence of running velocity on foot energetics and intrinsic foot muscle activation.

## RESULTS AND DISCUSSION

The foot underwent a phase of negative work from early stance through to mid-stance, followed by positive work in late stance (Figure 1). The magnitude of negative work ( $-0.19 \pm 0.03 \text{ J.Kg}^{-1}$  2.2  $\text{m.s}^{-1}$ ,  $-0.29 \pm 0.04 \text{ J.Kg}^{-1}$  3.3  $\text{m.s}^{-1}$ ,  $-0.42 \pm 0.11 \text{ J.Kg}^{-1}$  4.4  $\text{m.s}^{-1}$ ) and positive work ( $0.18 \pm 0.06 \text{ J.Kg}^{-1}$  2.2  $\text{m.s}^{-1}$ ,  $0.23 \pm 0.10 \text{ J.Kg}^{-1}$  3.3  $\text{m.s}^{-1}$ ,  $0.26 \pm 0.10 \text{ J.Kg}^{-1}$  4.4  $\text{m.s}^{-1}$ ) increased with running velocity ( $P < 0.05$ ). Although a greater amount of negative and positive work was performed about the foot when participants ran faster, work ratio significantly declined with running speed ( $P < 0.05$ ). When running at the slower speed the foot behaved like a spring, returning 98% of the energy stored during early stance (work ratio  $0.98 \pm 0.25$ ). As running speed increased, the foot behaved increasingly like a spring-damper, returning 81% at 3.3  $\text{m.s}^{-1}$  (work ratio of  $0.81 \pm 0.29$ ) and 64% of the energy absorbed during early stance when running at 4.4  $\text{m.s}^{-1}$  (work ratio  $0.64 \pm 0.25$ ).

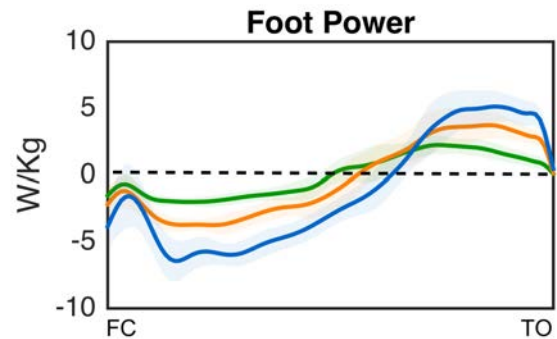


**Figure 1.** Group mean  $\pm$  SD foot power time series data calculated during stance when participants ran at 2.2 (green) 3.3 (red) and 4.4  $\text{m.s}^{-1}$  (blue). Both negative and positive work increased with running speed. Foot contact (FC) and toe off (TO)

Both AH and FDB muscles were active for the entire duration of stance phase, with the FDB muscle displaying a distinct peak in activation during late stance. Mean stance phase activity increased significantly with running speed for both AH ( $21.8 \pm 11.6 \%$ max,  $31.1 \pm 13.7 \%$ max,  $40.0 \pm 17.2 \%$ max) and FDB ( $22.5 \pm 8.4 \%$ max,  $34.8 \pm 12.4 \%$ max,  $46.9 \pm 16.2 \%$ max) indicating that the contribution of these muscles to power absorption and generation increases with running speed.

## CONCLUSIONS

As previously proposed, the foot does behave in a spring-like manner, although it appears that distal structures such as the plantar fat pads and metatarso-phalangeal joints may act to dampen a substantial proportion of the energy that is absorbed within the foot, especially at higher running speeds.

The underlying mechanism for why the foot behaves like a spring-damper at higher running speeds requires further investigation. However, we suggest that damping energy in mid- to late- stance may act to slow centre of pressure velocity and thus possibly improve the gear-ratio of the ankle plantar flexors.

## REFERENCES

1. Stearne ET. al. *SciRep* **19** (6) 19403. 2016
2. Takahashi et. al. *Gait Posture*. **38** 818-23 2013
3. Leardini et al. *Gait Posture* **25** 453-62. 2007
4. Kelly et al. *J R Soc Interface* **12** 20141076 2015

# HIP ALIGNMENT, POSITION AT FOOT STRIKE AND PEAK HIP ADDUCTION ANGLE IN FEMALE RUNNERS

<sup>1</sup>Richard A. Brindle, <sup>1</sup>Clare E. Milner

<sup>1</sup>Drexel University, Philadelphia, PA, USA  
Email: brindle@drexel.edu

## INTRODUCTION

The peak hip adduction angle is a risk factor for the most frequently reported overuse injuries in female runners. Specifically, a large peak hip adduction angle is a risk factor for patellofemoral pain syndrome [1] and iliotibial band syndrome [2] in female runners.

Peak hip adduction angle differences between groups of female runners are often coincident with an offset in angle throughout the stance phase [2]. This offset in hip adduction angle throughout stance may be due to biomechanical differences at foot strike, or anatomical differences between runners. Specifically, a larger pelvis width to femoral length ratio (PW:FL) has been hypothesized to influence the peak hip adduction angle during running [3]. Additionally, the frontal plane position of the pelvis or thigh at foot strike during running may influence the hip adduction angle throughout stance.

Thus, the purpose of this study was to determine if anatomical or biomechanical differences exist between women with large or small peak hip adduction angle during running. We hypothesized that female runners with a large peak hip adduction angle would have a greater PW:FL, and different frontal plane hip, pelvis, and thigh angles at foot strike than those with a small peak hip adduction angle.

## METHODS

As part of an ongoing study, thirty-seven uninjured female runners between 18 and 45 years old participated ( $28 \pm 8$ yr,  $1.66 \pm 0.06$ m,  $62.2 \pm 7.4$ kg,  $23 \pm 10$  miles per week). Participants ran at least 10 miles a week for a year or more. Those with a history

of serious lower extremity injury were excluded. Each participant gave written informed consent.

An eight camera motion capture system and a synchronized force plate recorded marker position at 200 Hz and ground reaction forces at 1000 Hz. Initially, runners were screened for a rearfoot foot strike pattern. Participants changed into shorts and wore laboratory footwear. Retro-reflective markers were attached to both feet and shoes. Running velocity was standardized to 3.7m/s ( $\pm 5\%$ ), and monitored by two photocells connected to a timer. A static trial and five good running trials were collected, and then foot strike pattern was determined using strike index [3]. Of 37 runners screened, 30 were rearfoot strikers and continued in the study. Retro-reflective markers were then attached to the participants' pelvis and right thigh and running gait analysis procedures were repeated.

Hip joint angles and pelvis and thigh segment angles were determined using the joint coordinate system and segment coordinate systems, respectively. Foot strike was the point when vertical ground reaction force surpassed 20N. Anatomical measures were determined from the static trial. Pelvis width (inter-trochanteric distance) was divided by right thigh length (greater trochanter to lateral epicondyle) to calculate each participant's PW:FL.

For analysis, all thirty runners were ranked by their peak hip adduction angle. Dependent variables were averaged for ten runners with the largest peak hip adduction angles (large peak angle group) and ten runners with the smallest peak hip adduction angles (small peak angle group). Between-group differences were interpreted using Cohen's d effect size. Moderate ( $\geq 0.5$ ) or large effects ( $\geq 0.8$ ) which exceeded minimal detectable difference (MDD) were considered meaningful.

## RESULTS AND DISCUSSION

The purpose of this study was to determine if anatomical or biomechanical differences exist between female runners with large or small peak hip adduction angles. We hypothesized that the large peak angle group would have a greater PW:FL and different frontal plane hip, pelvis, and thigh angles at foot strike than the small peak angle group. Our hypotheses were partially supported by the results.

The large peak angle group had a larger peak hip adduction angle and adduction angle at foot strike than the small peak angle group (Table 1). This was expected as comparisons between groups with different peak hip adduction angles found an offset between the frontal plane hip angle ensemble curves throughout the stance phase of running, e.g. [2]. However, frontal plane hip angle at foot strike has not been reported previously in female runners. Thus, reducing hip angle at foot strike may be a way to decrease large peak hip adduction angles in female runners.

The larger hip adduction at foot strike in the large compared to the small peak angle group came from thigh adduction and not contralateral pelvic drop. Pelvis and thigh angle at foot strike have not been reported previously in female runners. These findings suggest that large peak hip adduction angle in female runners is due to thigh rather than pelvis position at foot strike. Thus, reducing thigh angle at foot strike may decrease large peak hip adduction angles in female runners.

The large peak angle group had a moderate effect for greater PW:FL than the small peak angle group. A previous study reported no difference in a similar measure between female runners with different peak hip adduction angles [4]. The large difference in peak hip adduction angle between groups in this study may explain why we found a difference in this ratio. The PW:FL may be useful to clinicians as a simple screening tool for the likely presence of a large peak hip adduction angle in female runners. These results are part of an ongoing study of determinants of the peak hip adduction angle in female runners.

## CONCLUSION

Women with large peak hip adduction angles during running have a more adducted hip and thigh at foot strike, and greater PW:FL than women with small peak hip adduction. Decreasing thigh adduction at foot strike could be a component of treatment for large peak hip adduction angles in female runners. PW:FL may be a useful clinical tool to screen for female runners who may have large peak hip adduction angles.

## REFERENCES

- [1] Noehren, et al. *Clin Biomech* **22**, 951-956, 2007.
- [2] Noehren, et al. *Med Sci Sports Exerc* **45**, 1120-1124, 2013.
- [3] Ferber, et al. *Clin Biomech* **18**, 350-357, 2003.
- [4] Cavanagh and LaFortune. *J Biomech* **13**, 397-406, 1980.
- [5] Willson and Davis. *Clin Biomech* **23**, 203-211, 2008.

**Table 1:** Hip joint and segment angles at foot strike (FS), peak adduction during running, and pelvis width to femoral length ratio during standing in large and small angle groups; mean (SD).

	Small peak angle group	Large peak angle group	Difference	Minimal detectable difference	Effect size
Peak hip adduction angle (°)	12.1 (1.1)	19.3 (2.7)	7.2	3.4	3.9
Hip adduction at FS (°)	8.5 (2.6)	12.9 (2.6)	4.4	2.9	1.7
Contralateral pelvic drop at FS (°)	0.5 (2.4)	1.3 (2.2)	0.8	2.4	0.4
Thigh adduction at FS (°)	4.9 (1.8)	7.4 (1.4)	2.5	1.7	1.6
Pelvis width/Femoral length	0.86 (0.06)	0.92 (0.08)	0.06	0.05	0.7

# **Influence of Stride Frequency on Knee Joint Stiffness and Anterior Tibial Shear Forces in Female Runners.**

Bhushan Thakkar, Kathryn Harrison, Jacqueline Morgan, Gregory Crosswell, Robert Tickes and  
DS Blaise Williams III

VCU RUN LAB, Virginia Commonwealth University, Richmond, VA  
email: thakkarbs2@vcu.edu, web: khs.vcu.edu/about/vcu-run-lab/

## **INTRODUCTION**

The overall incidence of running-related injuries has been found to be 19.4% to 79.3% of recreational or competitive runners who run a minimum of 5 km per training, race, or both. [1] Approximately 50% of all running-related injuries occur at the knee with nearly half of those involving the patellofemoral joint.[1] During running, peak shear stress at the knee occurs around midstance and is tangential to the vertical component of the ground reaction force. Increases in shear forces can potentially alter muscle activation patterns and impact joint stability. [5] High shear has been reported to be detrimental to bone health. [5] During human running, the individual stiffness values of the ligaments, bones, muscles and other musculoskeletal elements are typically integrated together as a simple spring-mass model.[2-3] Running velocity influences vertical stiffness and knee joint stiffness but its relationship with stride frequency (SF) has not been completely understood.[2-4] Luedke et al. in a study on high school runners revealed that runners with  $SF \leq 166$  steps/min were more likely to experience anterior knee pain than those with  $SF \geq 178$  steps/min.[6] The purpose of this study was to compare knee joint torsional stiffness and anterior tibial shear forces in recreational female runners with different stride frequencies.

## **METHODS**

Sixty-four healthy female recreational runners who ran at least 10 miles per week volunteered to participate in the study. Subjects were provided with standard neutral footwear (New Balance, Boston, MA). Gait analysis was conducted on an instrumented treadmill (Treadmetrix, ParkCity, UT). Retroreflective markers were placed on bilateral lower extremities using the modified Cleveland clinic marker set. A 30 second trial was collected using a 5-camera motion analysis system (Qualisys, Goteborg, Sweden) at 120 Hz as

participants ran at a matched pace 2.98m/s. Visual 3D motion analysis software (C-Motion, Germantown, MD) was used to process data. Joint angles were calculated as Cardan angles between adjacent local segments. The knee joint moments were calculated through inverse dynamics and transferred into the segment coordinate system and expressed as internal moments and normalized to body mass and height. Torsional stiffness at the knee (TK) was calculated as the slope of the line through the moment-angle curve from the point of initial contact to maximum knee flexion during the stance phase. Tibial shear (TS) at the knee was defined as the anterior component of the peak forces in the sagittal plane during stance normalized to body mass and height. Three groups of stride frequencies were created: low ( $\leq 164$ ), middle(166-174), high(176-186) steps per minute. Differences in sagittal plane TK and TS were compared utilizing ANOVA and post-hoc Tukey tests were performed for analyzing differences between the three stride frequency groups. SAS®software, Version 9.3 for Windows. Copyright © [2014] SAS Institute Inc., Cary, NC, USA was used for all statistical analysis with an alpha level of 0.05 being considered statistically significant.

## **RESULTS**

Fifty-four subjects were included in the analysis. (Mass:  $61.98 \pm 8.62$ kg, Height:  $1.65 \pm 0.06$ m, BMI:  $22.65 \pm 2.62$ , Age  $35.07 \pm 10.47$  years). Ten subjects were removed from the analysis as their values of either SF, TS or TK were outside of three standard deviations from the mean. There were significant differences between the SF groups when evaluating TS ( $p=0.03$ ) with the low SF group demonstrating the largest shear ( $9.06 \pm 1.41$ N) compared to the middle ( $8.95 \pm 0.95$ N) and high ( $8.06 \pm 1.19$ N) SF groups. Post hoc testing revealed that the low group was significantly different from the high group. A significant difference was also seen with TK

( $p < 0.01$ ) between the three SF groups with the low group exhibiting the highest TK ( $0.08 \pm 0.013 \text{ Nm}^\circ$ ) compared to the middle ( $0.075 \pm 0.01 \text{ Nm}^\circ$ ) and high ( $0.076 \pm 0.01 \text{ Nm}^\circ$ ) SF groups respectively. Further testing showed that the low SF group was different from the middle and high SF groups.

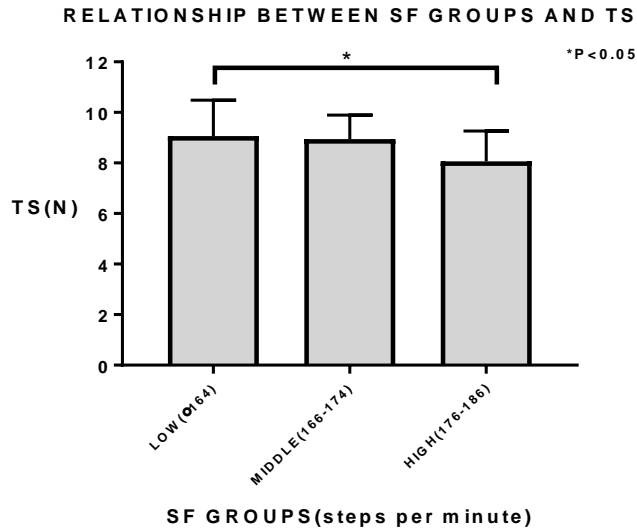


Figure 1: Bar graph demonstrating relationship between the three SF groups and TS.

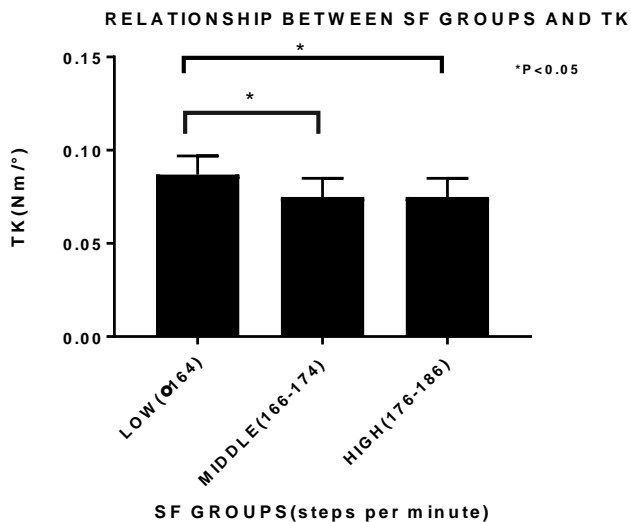


Figure 2: Bar graph demonstrating relationship between the three SF groups and TK.

## DISCUSSION AND CONCLUSIONS

A low stride frequency of less than 166 steps per minute results in an increase in tibial shear forces and concomitant increase in torsional stiffness at the knee joint. This correlates with previous studies which have suggested that low stride frequency leads to increased loading in the knee. Changes in

torsional stiffness could be the result of either increased moment or decreased knee ROM which results in an overall stiffer gait pattern, as the knee is a major contributor to leg stiffness during running.[2,4] Given that the pace was fixed between subjects in the current study, the current study was able to differentiate changes in stiffness and shear based on different stride frequencies. Given the primary role that stiffness plays in the neuromuscular control of movement as well as injury and performance, it is important to note factors that can contribute to its change. Joint stiffness at the knee has been implicated in overuse injuries and degenerative diseases. [3] For example, a more compliant knee joint will attenuate the load placed on the joint to a greater extent than a stiffer joint. Running with a more flexed knee (higher excursion) results in a more compliant knee and increased energy absorption. On further analysis, the current study also showed that the highest stiffness value of the knee joint was due to a relatively greater knee moment in the low SF group ( $1.92 \text{ Nm/kg}$ ) compared to the middle ( $1.67 \text{ Nm/kg}$ ) and high ( $1.65 \text{ Nm/kg}$ ) SF groups. This is likely to place increased compressive forces on the patellofemoral joint as well as on the tibiofemoral joint, thus partially explaining the increases in anterior shear forces. Lack of differences in knee flexion excursion could be attributed to a greater stride length especially in the low SF group which could alter the moment arm, orientation of the ground reaction force and muscle activation. We did not assess the role of muscle contraction and activation, which contributes to the joint moment. Future studies should investigate the role of increasing stride frequency on the ability to alter stiffness and shear in individuals with tibiofemoral joint pathology such as meniscus injuries or knee osteoarthritis.

## REFERENCES

1. Taunton, J.E. *BJSM*, 2002;36(2):95–101.
2. Farley et al, *J Biomech*, 1996;29(2):181-186
3. Hamill et al, *Eur J Spo Sci*, 2014;14(2):130-136
4. Butler et al, *Clin. Biomech*, 2003;18:511-517
5. Shelburne et al, *MSSE*, 2005;37(11):1948-1956
6. Luedke et al, *MSSE*, 2016;48(7):1244-1250

# MULTISCALE ENTROPY OF CENTER OF MASS ACCELERATION AS A MEASURE FOR CUMULATIVE RUNNING FATIGUE

<sup>1</sup>Allison H. Gruber, <sup>2</sup>Max R. Paquette, <sup>2</sup>Kris Camelio, <sup>2</sup>Douglas W. Powell, and <sup>1</sup>Jacob E. Vollmar

<sup>1</sup>Indiana University, Bloomington, IN, USA

<sup>2</sup>University of Memphis, Memphis, TN, USA

email: [ahgruber@indiana.edu](mailto:ahgruber@indiana.edu), web: <http://iubiomechanicslab.weebly.com/>

## INTRODUCTION

The high prevalence of running related overuse injury (RROI) can be attributed largely to rapid increases in training load and inadequate recovery. A healthy runner may not recognize when modifications to a current training program are necessary until after they feel the pain and discomfort associated with “overtraining.” This pain and discomfort may cause a runner to inadvertently alter their running mechanics, causing abnormal loading on the joints and tissues that can eventually lead to injury. Therefore, we suggest that overtraining induces ‘cumulative fatigue’ that results in measurable changes in running gait mechanics prior to the onset of RROI.

Deviations in running mechanics resulting from acute fatiguing bouts have been suggested to cause abnormal loading on the joints and tissues and eventually, lead to injury [1]. To date, changes to running gait patterns resulting from fatigue have only been investigated during or after acute intense runs to exhaustion. Runners in these studies adopted gait characteristics associated with injury development as they reached volitional exhaustion. These characteristics may include increased ground reaction forces, tibial shock, joint stiffness [2, 3], and a decline in center of mass (COM) acceleration complexity [4]. A decline in movement complexity has been suggested to represent an unhealthy system that has a reduced capacity to respond to environmental perturbations [5]. It is unknown if injury-causing gait patterns observed after acute exhaustive runs also occur after more typical submaximal, recreational running bouts or after prolonged training periods of many submaximal running bouts. The purpose of this pilot study was to begin establishing a proof of concept that cumulative fatigue following a submaximal run and following a

prolonged running training period can be identified by a reduction in COM movement complexity. It was hypothesized that COM acceleration complexity would decline after a 30-min submaximal run and after three-weeks of increased running volume.

## METHODS

To date, 12 novice runners who have been running for less than two years, run a minimum average of 10 miles per week, and complete at least three runs per week were included in this study. All participants provided informed consent to participate in the study protocol approved by the IRB. Participants were instructed to reduce their training volume by at least 80% (i.e. training taper) the week prior to the first testing session. During the first testing session, participants completed a 30-min treadmill run at their preferred pace. A 3D accelerometer was secured to the proximal sacrum for which the Z-axis was aligned with the body’s longitudinal axis. The proximal sacrum was used as the estimated location of the participants COM and provided a bony landmark with low soft tissue artifact to mount the accelerometer. Acceleration data were recorded for 30 sec at 200 Hz during the 3<sup>rd</sup> min (pre-run) and 29<sup>th</sup> min (post-run) of the run. Participants rated their lower limb fatigue on a visual analog scale (FVAS; 10 = most fatigued) before and after the baseline treadmill run.

Participants were given a progressive three-week training program scheduled to begin the day after the baseline treadmill run performed in the lab. The program increased weekly mileage by 25% per week for three-weeks and was based on 3–6 runs per week. Participants were encouraged to run at their preferred training pace as long as the prescribed weekly running volume was met. A shoe-worn GPS pod was used to monitor the training adherence by recording

pace and distance per run. Participants returned to the lab the week following the conclusion of the training program to rate their lower-body fatigue and perform a five minute treadmill run at the same speed as the first testing session. COM acceleration was collected during the 5<sup>th</sup> minute of this run (post-train).

The resultant value of the raw COM acceleration data was calculated for each instant then filtered with a Butterworth low-pass filter with a 60Hz cut-off. Complexity of the resultant COM acceleration signal was calculated by multiscale entropy (MSE) [6]. The radius of similarity ( $r=0.001$ ) was determined by calculating 15% of the standard deviation of the original signal. Parameter  $m$  was set to a value of 2 and scale factors 1–8 were examined. The complexity index ( $C_r$ ) was calculated from the area under the MSE curve (sample entropy vs. time scale). Given the small sample size, Cohen’s  $d$  effect sizes were used to determine if the differences in  $C_r$  and FVAS between time points were meaningful.

## RESULTS AND DISCUSSION

Two participants did not complete the training protocol: one due to injury and illness, the other due to noncompliance. Three other participants experienced an injury and two others experienced illness but were able to adhere to the training protocol. The effect of pre-run vs. post-run FVAS was large ( $d=1.41$ ; Table 1) indicating meaningful fatigue perceived by the participants following the 30-min treadmill run. However, mean post-run FVAS was less than 5 on a 1–10 scale which suggests that the treadmill run did not elicit high degrees of lower limb fatigue. Therefore, despite a meaningful change in FVAS, the similarity in pre-run and post-run  $C_r$  was expected ( $d<0.01$ ; Table 1) given that the magnitude of the perceived fatigue was low.

The training protocol was designed to systematically increase the distance of individual sub-fatiguing runs as much as possible without causing injury. This

training program induced a cumulative effect on lower-body fatigue as indicated by greater FVAS post-train than pre-run ( $d=0.79$ ; Table 1). Contrary to the hypothesis, post-train  $C_r$  was moderately greater than that of pre-run and post-run ( $d>0.41$ ). There are two possible explanations for greater COM complexity after the training protocol: (1) running skill of these novice runners improved, increasing the capacity to respond to environmental constraints; or (2) the combination of a novice running pattern and cumulative fatigue following three weeks of intense running training cause COM complexity to increase outside the threshold for optimal health, a continuum that has been proposed by other authors [e.g. 7]. We are currently collecting data on more novice runners, a group of experienced runners, and a control group to provide support for either of these or other explanations. In addition, COM acceleration data is being collected for more than one minute of running to assess complexity over scale factors  $\geq 20$ .

## CONCLUSIONS

The implementation of an intense, three-week running training program increased perceived lower limb fatigue and may also be supported by a change in COM acceleration complexity. Monitoring COM complexity during prolonged running training may help to identify when rest or modifications are needed to avoid RROI development.

## REFERENCES

1. Gerlach KE, et al. *PMed Sci Sports Exerc*, **37**, 657-63, 2005.
2. Dierks TA, et al. *J Biomech*, **43**, 2993-8, 2010.
3. Clansey AC, et al. *Med Sci Sports Exerc*, **44**, 1917-23, 2012.
4. McGregor SJ, et al. *Chaos*, **19**, 26109, 2009.
5. Lipsitz LA. *J Gerontol A Biol Sci Med Sci*, **57**, B115-25, 2002.
6. Costa M, et al. *Phys Rev Lett*, **86**, 068102, 2005.
7. Hamill J, et al. *Clin Biomech*, **14**, 297-308, 1999.

**Table 1:** Lower-body fatigue (FVAS) and complexity index ( $C_r$ ) of the center of mass acceleration pre- and post- the baseline run and after a three-week running training program (post-train) (mean $\pm$ SD).

	Pre-Run	Post-Run	Post-Train	Pre-Run vs Post-Run	Pre-Run vs Post-Train	Post-Run vs Post-Train
FVAS	2.19 $\pm$ 1.69	4.70 $\pm$ 1.87	3.60 $\pm$ 1.86	$d = 1.41$	$d = 0.79$	$d = 0.59$
$C_r$	4.71 $\pm$ 0.99	4.71 $\pm$ 0.96	5.14 $\pm$ 1.10	$d = 0.001$	$d = 0.41$	$d = 0.42$

# CHANGES IN MECHANICS ACROSS A MARATHON

<sup>1,2</sup>Matthew C. Ruder, <sup>1,2</sup>Steve T. Jamison, <sup>1,2</sup>Adam S. Tenforde, <sup>3</sup>Marian T. Hannan and <sup>1,2</sup>Irene S. Davis

<sup>1</sup>Harvard Medical School, Boston, MA, USA

<sup>2</sup>Spaulding National Running Center, Cambridge, MA, USA

<sup>3</sup>TH Chan School of Public Health, Harvard University, Cambridge, MA  
email: matthew.ruder@gmail.com, web: <http://runsnrc.org/>

## INTRODUCTION

Most biomechanics research is conducted within a laboratory setting, either overground or on a treadmill. The recent introduction of wearable devices has allowed biomechanics research to move from the lab to the field. However, since most runners run outside, it is more ecologically valid to measure mechanics in natural environments.

Increased tibial shock (TS) has been associated with running injuries such as stress fractures. [1] It has also been shown that TS increases with fatigue during treadmill running. [2] However, these studies were conducted under tightly controlled conditions in terms of speed, surface, grade, etc. In addition, environmental influences, such as temperature and wind, are also controlled. These factors may contribute to the relationship between fatigue and TS. Fatigue also appears to play a role in strike pattern. Larson has reported that runners who used a midfoot (MFS) and forefoot strike (FFS) early in a race (10 km) changed to a rearfoot strike (RFS) pattern later in the race (32 km). [3]

Therefore, the purpose of this study was to determine if there is an association between footstrike pattern (FSP) changes and TS during a marathon. It was expected that FSP would shift posteriorly over the course of the race and that this shift would be associated with a larger TS increase rather than remaining at a given FSP.

## METHODS

254 runners enrolled in a marathon were recruited. Each subject was provided an inertial measurement unit (IMU) to be worn on their right leg during the marathon. Prior to the race, a mark was placed on the subject's distal, medial tibia, just above the ankle. (Figure 1) The subjects were instructed to place the device over that mark on race day. Additionally, they were taught how to properly affix

and tension the IMU with a strap around the lower leg. A mark placed on the strap was used as a guide. Each subject's device number was written on the outside of their right lower leg in order to identify them on videos taken in the field.



Figure 1: Example of IMU placement

Prior to the race, two areas where the course was level and would allow for optimal camera viewing were identified. Video data (240 Hz) were collected continuously at approximately the 10k and 40k marks in the race. During post-processing, the videos were assessed by study staff to identify subjects' FSP, when possible, at each location.

Acceleration data were sampled in 3 dimensions at 1,000 Hz during the entirety of the race. The resultant acceleration was calculated from the three axes. Tibial shock (TS) was measured as the peak resultant acceleration from each right step during running. TS was averaged for each subject over the 5k period surrounding each video capture point, as 5k split times were made available after the race. Acceleration due to gravity [ $g=9.81\text{m/s}^2$ ] was subtracted from TS resultant accelerations and used to normalize TS to units of gravity [g].

To avoid the confounding effect of pain on mechanics, subjects reporting pain  $>3/10$  on a numeric rating scale prior to the 40th kilometer of the race were excluded ( $n=16$ ). Additionally, runners without complete tibial shock data for the race were excluded ( $n=61$ ). Finally, those who were not identified in the videos at both race points were excluded ( $n=150$ ). This left 37 subjects with complete data which could be analyzed [24 males, 13 females; age= $44.4\pm 12.15$  yr].

Paired t-tests were used to compare TS early (TS\_10k) and late in the course (TS\_40k). As TS has previously been associated with speed ( $5.26 \frac{g}{m/s}$ ), [4] TS\_40k was adjusted for speed differences between the two points (TS\_40k\_ADJ) and compared to early in the race as well. Changes in FSP between the 10k and 40k locations were also tabulated.

## RESULTS AND DISCUSSION

TS\_40k was 13.4% lower than TS\_10k (Figure 2, left;  $p < 0.001$ ). However, speed at the 40k location was 13.7% lower than speed at the 10k location (Figure 2, right;  $p < 0.001$ ). After adjusting for speed, TS\_40k\_ADJ was 5.6% higher than TS\_10k, though this difference did not reach significance (Figure 1, left;  $p = 0.16$ ).

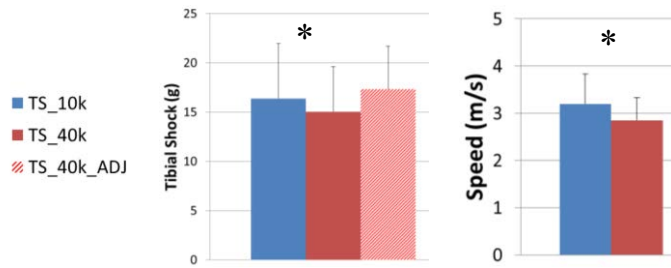


**Figure 2:** Left: Average tibial shock at 10k and 40k race points. Right: Average speed at 10k and 40k race points. Error bars represent standard deviations. \* indicate significant differences ( $p < 0.05$ ).

A summary of FSP and TS changes can be seen in Table 1. 78% of the runners analyzed were RFS, 19% were MFS and 3% were FFS at the 10km race point. Most RFS runners (33/37) retained their FSP throughout the race. These runners experienced a 3.35% increase in speed-adjusted TS.

**Table 1:** Footstrike Pattern at 10k and 40k race points. Total number of observations of each change, if any, recorded. Heavy shading indicates a posterior FSP shift. Light shading indicates an anterior shift. No shading indicates no shift.

10k	40k	n	Average TS_10k[g]	Average TS_40k adj[g]	Percent Diff.
FFS	FFS	1	13.51	12.90	-4.66%
MFS	MFS	2	19.91	19.70	-1.01%
MFS	RFS	5	17.15	18.32	6.59%
RFS	MFS	2	22.66	22.04	-2.75%
RFS	RFS	27	16.22	16.77	3.35%

Only five runners shifted to a more posterior strike pattern as we had hypothesized (all 5 MFS to RFS). This posterior shift in FSP was associated with a 6.59% increase in TS after adjusting for speed, the largest increase observed in our cohort. Two runners changed from a RFS to a MFS. On average these runners demonstrated a decrease in speed-adjusted TS, but only one runner decreased while the other increased. Interestingly, all three runners who maintained a FFS or MFS demonstrated lower speed-adjusted TS later in the race than they did early in the race.

Previous research utilizing a treadmill has shown an increase in TS after a period of exhaustive running, [2] consistent with our results within runners out in the field during an overground marathon race who started with, and maintained, a RFS. Further, the subset of runners that shifted to a more posterior FSP during the race demonstrated an increase in TS. This is also consistent with literature showing that a more posterior strike pattern is related to an increase in loading rates and impacts. Our smallest groups were the most interesting, demonstrating decreases in speed-adjusted TS. More data is needed to understand if this group truly represents what happens under these FSP conditions.

It should be noted that determination of FSP was restricted to one foot contact due to capture volume limitations. It is possible that the captured FSP may not accurately categorize the runner at each point.

## CONCLUSIONS

Tibial shock reduced over the course of the marathon, as did running speed. However, no difference was found when tibial shock was adjusted for speed. In most cases, runners either maintained footstrike angle or shifted posteriorly.

## REFERENCES

1. Milner CE, et al., *MSSE* **38**(2), 323-28, 2006.
2. Verbitsky O, et al., *J Appl Biomech* **14**(3), 300-11, 1998.
3. Larson P, et al., *J Sports Sci* **29**(15), 1665-73, 2011
4. Jamison ST, et al. *ACSM2017*, Denver, CO, 2017.
5. Jamison ST, et al. *ASB2017*, Boulder, CO, 2017.

# CHANGES IN RUNNING MECHANICS DURING THE 2016 US OLYMPIC TRIALS MARATHON

<sup>1</sup>Iain Hunter, <sup>1</sup>Jared Ward, <sup>1</sup>Gill Fellingham, <sup>1</sup>James Tracy, and <sup>1</sup>Andrew Terry

<sup>1</sup>Brigham Young University, Provo, UT, USA  
email: iain\_hunter@byu.edu, web: <http://biomechanics.byu.edu/>

## INTRODUCTION

The 2016 US Olympic Trials Marathon (13 February 2016) resulted in a wide range of finish times perhaps due to the relatively high temperature. There was also a larger field than recent years due to a relaxed qualifying standard. Slower marathoners have greater changes to running mechanics than faster [1]. However, many of these changes are likely due to a slower pace near the end of the race among the slower runners. Other studies found that fatigue cannot be explained by running mechanics [2] and changes in running economy during marathon running cannot be explained by any single kinematic measurement [3].

The 2016 US Olympic Trials Marathon allowed for a unique opportunity for greater detail on the time course of changes in running mechanics comparing slower and faster runners. The course involved a four-lap “P” shaped loop permitting measurements eight times throughout the race. These measurements were approximately every five km.

Realizing that running mechanics do change throughout a marathon, we focused on whether these changes were due to changes in running speed or some other factors. We were also interested in whether the magnitudes of any observed changes in mechanics were correlated with race pace.

## METHODS

Seventy of the 108 finishers of the men’s race were analyzed. They qualified for the race by running under 2:19:00 for a full marathon or under 1:05:00 for a half marathon between 1 August 2013 and 17 January 2016. A Sony a7s ii was placed on each side of Figueiroa Road in between 27<sup>th</sup> and 28<sup>th</sup> Streets ([Course Map](#)). The cameras recorded at 120 Hz with a field of view that could capture at least one full

stride if they ran at least 2 meters from the camera. This allowed measurements of stride rate (SR) and ground time (GT). Stride length was also calculated based upon running paces provided through race results along with the measured SR. All variables were adjusted for running speed through the measurement zone.

We analyzed these data using a repeated measures mixed model in SAS 9.4 (SAS Institute, Cary, NC). As in multiple regression, this method allows estimation of fixed effects (GT/speed and SR/speed). GT/speed was divided multiplied by 100 to make the numbers more readable. The utility of the mixed model also accounts for the covariance structure within subject. Each runner has differences in biomechanics for a variety of reasons. Regressing these data in a traditional sense with multiple observations for each runner would violate assumptions of observation independence, as athletes’ technique measurements throughout the race are likely highly correlated. Adjusting for each athlete’s dependence in this way offers a more accurate estimation of fixed effects of interest along with information on interactions [4].

## RESULTS AND DISCUSSION

Individual GT/speed changes and SR/speed changes were strongly correlated with average race speed. Faster runners had smaller changes in GT/speed and SR/speed even after accounting for differences in running speed through the measurement section (Figure 1). SR and stride length are highly correlated and provided similar findings, so only SR will be discussed here since it was a more accurately determined measurement.

The statistical model used allowed for a collection of other useful information. Early in the race, those with faster finish times had a greater GT/speed, but with

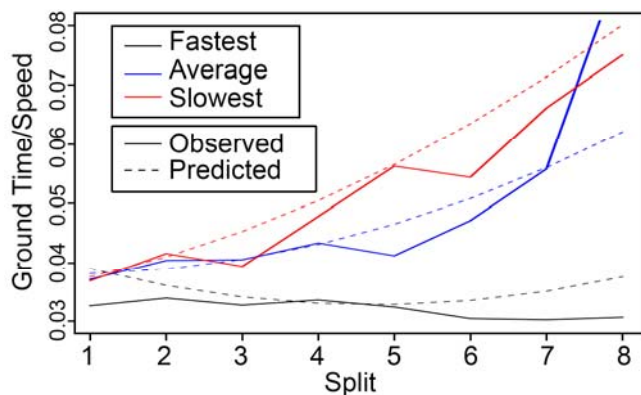


**Figure 1:** Changes in GT/speed for three categories of running ability.

the greater changes the slower finishers exhibited, they spent more time on the ground after adjusting for speed late in the race. Exponential increases in GT/speed and decreases in SR/speed were observed with a major change in both variables around 18-20 miles into the race. This is the stage of a race marathoners often discuss “hitting the wall”. Various physiological, psychological, or nutritional reasons may exist for hitting the wall. Whatever the reason for this event seems to be reflected by changes in some running mechanics.

Differences in training, physiological capacities, pacing, environmental conditions, and nutrition are among potential reasons for changes in the observed running mechanics.

## CONCLUSIONS

Elite male marathoners here exhibit exponential changes in GT/speed and SR/speed, yet the elite runners with faster average race speeds have smaller degrees of change. This was expected. However, it was interesting to note that slower runners spent less time on the ground after adjusting for speed than faster runner early in the race. During the later stages, the slower runners spent more time on the ground after the speed adjustment. The exponential changes in GT/speed and SR/speed coincided with the timing of when “hitting the wall” is often reported.

## REFERENCES

1. Chan-Roper M, et al. *J Sports Sci Med* **11**, 77-82, 2012.
2. Kyröläinen H, et al. *Euro J Appl Phys*, **82**, 297-304, 2000.
3. Hausswirth C, et al. *Int J Sports Med*, **18**, 330-339, 1997.
4. Littell RC, et al. *J Animal Sci*, **76**, 1216-1231, 1998.

## ACKNOWLEDGMENTS

Thank you to USA Track and Field for funding this study.

**Table 1:** Ground Time/Speed regression results

Effect	Estimate	Pr >  t	Interpretation
Mile	0.927	<.001	GT/speed increased as the race progressed
Avg Speed	0.936	0.003	Faster runners had a higher GT/speed than slower
Mile*Avg Speed	-0.201	<.001	Faster runners had more moderate changes in GT/speed as the race progressed
Mile*Mile	0.0049	<.001	Changes in GT/speed were exponential

**Table 2:** Stride Rate/Speed regression results

Effect	Estimate	Pr >  t	Conclusion
Mile	-0.490	<.001	SR/speed decreased as the race progressed
Avg Speed	0.172	0.684	No significant observations comparing faster to slower runners
Mile*Avg Speed	0.0978	<.001	Faster runners had more moderate changes in SR/speed as the race progressed
Mile*Mile	-0.00170	0.010	Changes in SR/speed were exponential

# COASTING TO A SUB-2-HOUR MARATHON USING AN OPTIMAL DRAFTING APPROACH

<sup>1</sup> Christopher J. Arellano and <sup>2</sup> Wouter Hoogkamer

<sup>1</sup> University of Houston, Houston, TX, USA

<sup>2</sup> University of Colorado Boulder, CO, USA

email: [carellano@uh.edu](mailto:carellano@uh.edu), web: <http://uh.edu/class/hhp/people/cjarellano>

## INTRODUCTION

In the Berlin 2014 marathon, Dennis Kimetto established the current world record of 2:02:57 (hr:min:sec), reviving a long-standing controversy as to whether it is possible to break the magical sub-2-hour marathon barrier. Kimetto's overall time translates to an average running velocity of 5.72 m/s, indicating that he needs to increase his velocity to 5.86 m/s, just 2.5% faster to break the sub-2-hour marathon barrier.

Recently, we outlined several biomechanical approaches that could be exploited to improve Kimetto's running economy to a level that would break the 2-hour marathon barrier [1]. The most promising approach would be to reduce the cost of forward propulsion by using a "cooperative drafting" approach, similar to the team trial strategy adopted by cyclists [3], where the runners would take turns in the lead, essentially alternating leading and drafting positions.

Here, we compare improvements in marathon performance time between a "cooperative drafting" and "traditional drafting" approach, where sacrificial runners lead as long as they can while maintaining the target velocity.

## METHODS

To determine how much metabolic energy an athlete needs to save to run 2.5% faster, we use the empirical relation characterizing gross metabolic cost and running velocity originally reported by [2] and adjust the equation to account for the projected frontal area of elite African runners, as described in [1]. Following Kyle and Caiozzo [3], we introduce a shielding factor,  $n$ , with 1 being complete shielding

and 0 being no shielding which yields the following equation:

$$\dot{V}O_2 \text{ (ml O}_2\text{/kg/min)} = 2.209 + 11.39V + 0.02724(1-n)V^3 \text{ (Eq. 1)}$$

Eq. 1 predicts that without any benefits of drafting, a marathon runner with a typical economy requires 72.46 ml O<sub>2</sub>/kg/min to sustain a velocity of 5.72 m/s. According to Daniels and Gilbert [4], an intensity of 84%  $\dot{V}O_2\text{max}$  can be sustained for a 2-hour race (Fig. 1).

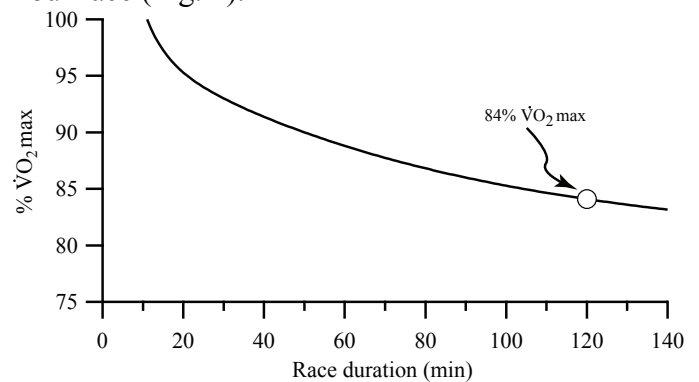


**Figure 1:** Daniels and Gilbert [4] suggest a runner's sustainable % $\dot{V}O_2\text{max}$  exponentially declines as race duration increases.

For both our drafting scenarios, we consider the ideal case that 4 runners work together for a sub-2-hour marathon (e.g., personal best time: Kimetto 2:02:57, Bekele 2:03:03, Kipchoge 2:03:05, and Kipsang 2:03:13). Note that our calculations assume that these 4 runners are all capable of running these times without benefitting from drafting, which is very unlikely.

In the traditional drafting approach, the lead runner maintains a high velocity at a higher %  $\dot{V}O_2\text{max}$  for as long as possible, eventually dropping out when he can no longer sustain the higher %  $\dot{V}O_2\text{max}$ . During this time, the 3 runners behind the lead runner exploit the benefit of drafting and thus can run at the faster velocity while still sustaining 84%  $\dot{V}O_2\text{max}$ . For this "traditional drafting" scenario, we

assume the first runner sustains an intensity of 90%  $\dot{V}O_2\text{max}$  for as long as possible (90% of 84 ml  $O_2/\text{kg}/\text{min}$  [5] = 75.6 ml  $O_2/\text{kg}/\text{min}$ ), then the next runner continues at the same velocity but he can only sustain that for a shorter period of time, since he has already been running at 84%  $\dot{V}O_2\text{max}$ . This process continues until only one runner is left, who then is required to slow down to sustain 84%  $\dot{V}O_2\text{max}$ .

We use the equation by Daniels and Gilbert [4] to predict how long the initial lead runner can sustain 90%  $\dot{V}O_2\text{max}$ ; then use an iterative method (Eq. 2) to solve for how long the next lead runner can sustain that velocity under the constraint that he has been running at 84%  $\dot{V}O_2\text{max}$ .

$$\frac{(T_1 \times 84\%VO_{2max}) + (T_2 \times 90\%VO_{2max})}{(T_1 + T_2)} \leq \frac{DG(T_1 + T_2)}{1} \quad (\text{Eq. 2})$$

In the “cooperative drafting” approach, the only requirement is that on average, the runners consume 72.46 ml  $O_2/\text{kg}/\text{min}$ , the rate needed to run 5.72 m/s without drafting. While leading, a runner would be using metabolic energy faster than this sustainable rate, but while drafting he would be using less metabolic energy, allowing him to recover from the more intense effort. As described in [1], we solve Eq. 1 for the maximum speed, using a shielding factor of 93%.

## RESULTS AND DISCUSSION

As illustrated in Fig. 2, the three lead runners can cover a total distance (before dropping out) of 32.8 km at a velocity of 5.94 m/s. Overall, the 1<sup>st</sup>, 2<sup>nd</sup>,

and 3<sup>rd</sup> runner drop out 50 min, 84 min, and 102 min, respectively. To finish the race, the last runner slows down to 5.72 m/s to sustain 84%  $\dot{V}O_2\text{max}$  as a result of the additional cost of overcoming air resistance. This results in a total marathon time of 1:58:59.

With the cooperative drafting approach, the runners would be able to sustain a velocity of 6.02 m/s throughout the full marathon. This results in a total marathon time of 1:56:49.

## CONCLUSIONS

Our calculations show that “cooperative drafting” is substantially faster than a “traditional drafting” approach where sacrificial runners lead as long as they can to maintain the target velocity. In our ideal scenario, a superfast marathon performance time of 1:56:49 is possible.

## REFERENCES

1. Hoogkamer, Kram, Arellano, *Sports Med*, 2017.
2. Léger and Mercier, *Sports Med*, **1**, 270-277, 1984.
3. Kyle and Caiozzo, *Med Sci Sports Exerc*, **18**, 509-515, 1986
4. Daniels and Gilbert, Tempe, AZ, 1979.
5. Joyner, *J Appl Physiol*, **70**, 683-687, 1991

## ACKNOWLEDGMENTS

We thank our friend Rodger Kram for insightful discussions and for inspiring this collaboration.

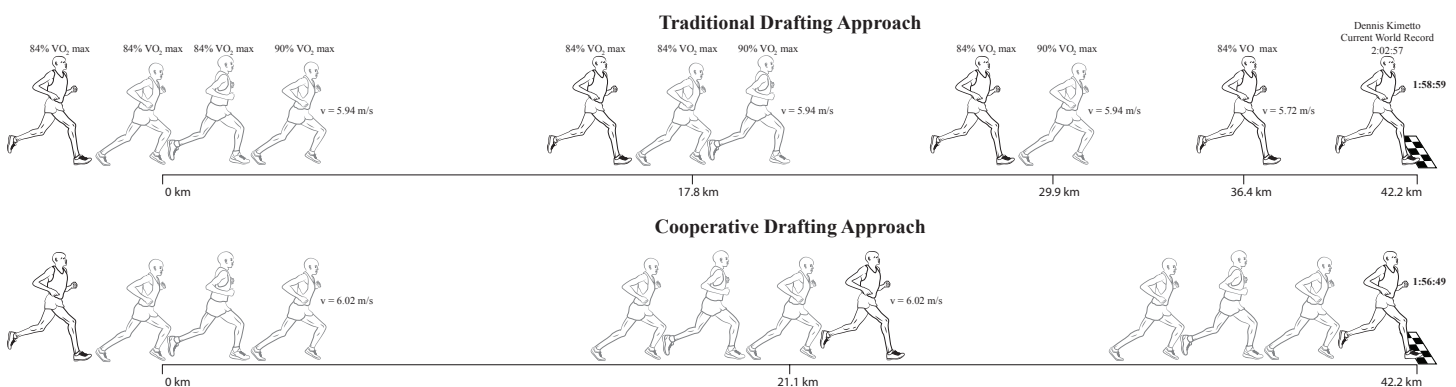


**Figure 2:** Our calculations show that “cooperative drafting” is substantially faster than a “traditional drafting” approach.

# GAIT EFFECTS ON JOINT MECHANICS AND CLINICAL OUTCOMES IN HIP DYSPLASIA PATIENTS

Holly D. Thomas, Kevin N. Dibbern, Michael C. Willey, and Jessica E. Goetz  
University of Iowa, Iowa City, IA  
email: holly-thomas@uiowa.edu, web: <https://uiowa.edu/uiobl/>

## INTRODUCTION

Acetabular dysplasia, a hip deformity that alters joint mechanics, results in pain and hip degeneration at an abnormally young age [1]. One common surgical treatment of acetabular dysplasia is the periacetabular osteotomy (PAO), which permits multiplanar rotational correction of the acetabulum to stabilize the hip joint and reduce contact stress [2]. Orthopaedic surgeons currently utilize 2D radiographic measurements to assess pre- and post-operative lateral coverage and acetabular version [3]. However, it is difficult to quantify the effects of 3D acetabular repositioning with a single 2D radiograph. A realistic computational model of joint mechanics in patients with hip dysplasia would assist surgeons with pre-operative PAO planning.

The use of a rapidly-executing discrete element analysis (DEA) technique allows for analysis of large patient populations in order to establish direct relationships between changes in contact stress and patient outcomes [4]. The accuracy of contact mechanics determined with our custom DEA technique has been validated cadaverically, and we have previously shown that there are significant ( $p < 0.001$ ) differences between a gait cycle specific to hip dysplasia patients [5] and the often utilized Bergmann instrumented total hip gait cycle [6] currently implemented by our algorithm [7]. We have implemented the Bergmann gait cycle due to the increased reliability of gait measurements from instrumented total hip replacements. However, Bergmann gait is not necessarily representative of hip dysplasia patients due to the Bergmann patients' advanced ages and lack of need to prevent hip dislocation. The purpose of this study was to evaluate differences in joint mechanics pre- and post-operatively resulting from the use of the Bergmann-derived gait compared to a dysplastic gait. Furthermore, correlations between pre- and post-operative changes in joint mechanics and

common clinical measures for these patients were evaluated.

## METHODS

Under IRB approval, femoral and pelvic bone geometry from fifteen PAO patients was segmented from pre- and post-operative CT scans using a semi-automated program developed in MATLAB (Mathworks, Natick, MA). The cartilage surfaces were modeled with 1-mm uniform projections normal to the subchondral bone surfaces that were then smoothed toward sphericity using a custom-written algorithm. Each patient model was aligned to the coordinate system defined by Bergmann *et al.* for application of a walking gait cycle. This walking gait was simulated based on forces and rotations measured from patients that received hip implants to treat osteoarthritis [6]. A dysplastic gait cycle was simulated using joint reaction forces and rotations measured using motion capture from hip dysplasia patients [5]. In both cases, the forces applied to each model were scaled based on the patient's body mass. Maximum contact stress and mean contact area were compared for each loading case in both gait cycles. Changes in pre- and post-operative contact measures were then correlated with changes in clinical outcome measures.

## RESULTS AND DISCUSSION

The implementation of the dysplastic gait cycle tended to decrease contact stress post-operatively, whereas use of the Bergmann gait cycle actually increased contact stress (Figure 1). Average maximum contact stress over the entire gait cycle decreased post-operatively by  $0.71 \pm 0.59$  MPa with the dysplastic gait but increased post-operatively by  $1.99 \pm 0.72$  MPa with the Bergmann gait. This is a significant ( $p < 0.05$ ) difference in the change in maximum contact stress between the two gait cycles. Mean contact area decreased after PAO

surgery by  $35.86 \pm 69.23$  MPa with the dysplastic gait and by  $45.56 \pm 60.35$  MPa with the Bergmann gait. There were significant ( $p < 0.05$ ) differences in the change in maximum contact stress in the toe-off phase of gait (Figure 2, left) and significant ( $p < 0.05$ ) differences in the change in mean contact area for midstance and toe-off (Figure 2, middle). Furthermore, the use of the dysplastic gait cycle improved the correlation between change in maximum contact stress and change in VAS pain score (Figure 2, right, dysplastic  $R^2 = 0.2429$  vs. arthritic  $R^2 = 0.0497$ ).

joint. The strongest finding of this work was the tendency for PAO to decrease maximum contact stress when models used dysplastic gait compared to corresponding increases when models used arthritic gait. Additionally, the correlation between change in maximum contact stress and change in VAS pain score improves with the use of a dysplastic gait. These results indicate that inclusion of a dysplastic gait cycle may be extremely important to provide a realistic representation of contact mechanics in hip dysplasia patients and may be necessary to determine correlations between contact mechanics and clinical outcomes.

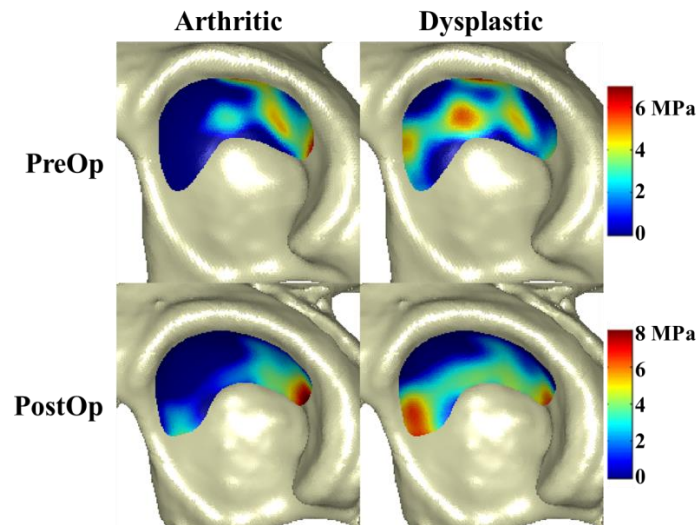


**Figure 1:** DEA analysis of pre- and post-operative acetabular contact stress developed from application of the Bergmann (arthritic) or dysplastic gait cycles.

## SIGNIFICANCE

This work will assist in understanding how pre- and post-operative joint contact mechanics relate to clinical outcomes in hip dysplasia patients, which will enable researchers to provide quantitative assistance to surgeons in order to improve these outcomes.

## REFERENCES

1. Hadley NA, et al. *J Orthop Res* **8**, 504-513, 1990.
2. Siebenrock KA, et al. *Clin Orthop Relat Res* **363**, 9-20, 1999.
3. Gala L, et al. *J Bone Joint Surg Am* **98**, 63-73, 2016.
4. Kern AM and Anderson DD. *J Biomech* **48**, 3427-3432, 2015.
5. Skalshoi O, et al. *Gait & Posture* **42**, 529-533, 2015.
6. Bergmann G, et al. *J Biomech* **34**, 859-871, 2001.
7. Thomas HD, et al. Podium presentation at Midwest ASB Regional Meeting, February 23-24, 2017.

## CONCLUSIONS

Dysplastic gait, in comparison to the gait cycle described by Bergmann (arthritic gait), seeks to minimize risk of dislocation of a less congruent hip

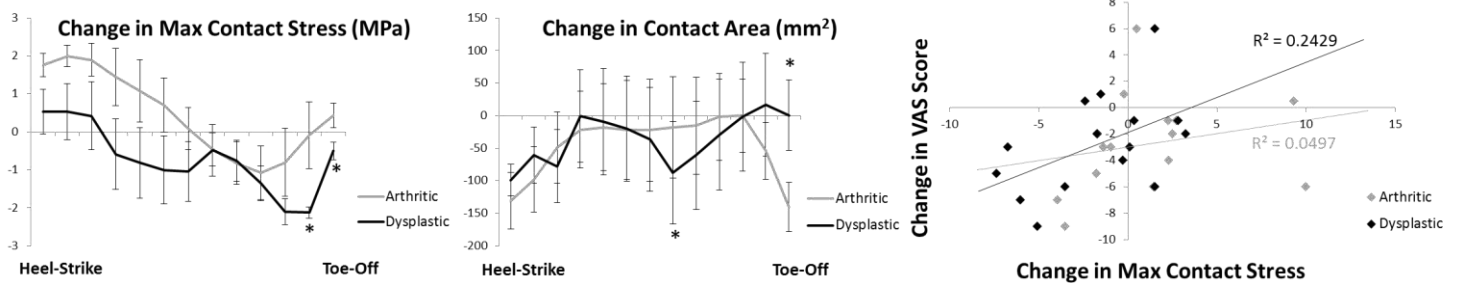


**Figure 2:** Plots of the change in maximum acetabular contact stress (left), change in mean acetabular contact area (middle), and correlation between change in maximum acetabular contact stress and change in VAS pain score (right) due to the implementation of a dysplastic gait compared to the existing Bergmann gait.

# KINEMATIC VARIABILITY AND LOCAL DYNAMIC STABILITY IN INDIVIDUALS WITH HIP DYSPLASIA

Kari L. Loverro, MS, Anne Khuu, and Cara L. Lewis, PT, PhD

College of Health & Rehabilitation Sciences: Sargent College, Boston University, Boston, MA, USA

email: kloverro@bu.edu, web: <http://sites.bu.edu/movement/>

## INTRODUCTION

We previously reported that individuals with hip dysplasia had increased variability in gait kinematics of the hip and pelvis when constrained to a specific walking speed compared to healthy controls [1]. We speculated that the increased variability may indicate a local (hip joint) adaptation to alleviate pain or a lack of neuromotor control. Recently, the use of nonlinear measures to quantify stability of pathological gait has increased due to the ease with which data can be collected [2]. Local dynamic stability measures use nonlinear time series analysis to examine the (in)stability of a system (i.e. a person walking) as it responds to perturbations. Small or large perturbations are recorded as variations in locomotion patterns and can introduce variability into the system [3]. Pain or lack of neuromotor control may produce small perturbations that decrease the dynamic stability of gait.

The purpose of this study was to investigate kinematic variability and local dynamic stability in individuals with hip dysplasia and in healthy controls, and test for differences with walking speed.

## METHODS

Fifteen individuals with either unilateral or bilateral hip pain and dysplasia diagnosed by a physician (14 Female, 1 Male; age  $25.4 \pm 6.0$  yrs; height  $1.64 \pm 0.05$  m; mass  $63.93 \pm 9.82$  kg; UCLA activity score  $7.9 \pm 2.4$ ) participated in the current study. For comparison, 15 healthy individuals also participated in the current research. Healthy participants were one-to-one matched for sex, age, height, mass, and activity score (14 Female, 1 Male; age  $22.3 \pm 3.3$  yrs; height  $1.64 \pm 0.07$  m; mass  $61.94 \pm 7.14$  kg; UCLA activity score  $7.9 \pm 1.9$ ). All participants provided written informed consent.

Participants completed two minutes of walking at three speeds: 1) their preferred (PRF) speed, 2) a prescribed speed (PRSC: 1.25 m/s), and 3) a speed 1.25 times faster (FAST) than PRF. While walking participants were asked to verbally rate their pain on an 11-point (0: no pain-10: extreme pain) numeric rating scale every 30 sec. All healthy controls reported no pain during walking trials, while all individuals with dysplasia reported pain during at least one walking trial.

Kinematic data were collected using a motion capture system (VICON®) while walking on a split-belt instrumented treadmill (Bertec®) to allow for continuous collection of gait. Visual3D (C-Motion, Inc.) was used to measure kinematics of the ankle, knee, and hip joint angles and pelvic and trunk segment angles for every stride of each trial. For each stride, joint and segment angles were time normalized to the gait cycle and exported for the kinematic variability analysis. Filtered velocity data of a marker placed at C7 were exported for the nonlinear analysis.

A custom MATLAB (The MathWorks, Inc.) program was used to determine the minimum number of strides completed across all participants and speeds (95 strides) and calculate peak (min/max) angles for each joint and segment for all 95 strides in the trial. The within-subject mean standard deviation (meanSD) for each dependent variable (angles), for all speed conditions, was extracted for statistical analysis. An additional MATLAB program was used to resample each participant's filtered marker velocity data to ~100 samples per stride and calculate the maximum Lyapunov exponent ( $\lambda_{\max}$ ) of the marker velocity data in all directions of motion.

Kinematic variability was quantified by meanSD where larger values indicate greater variability and local dynamic stability was quantified by the

maximum Lyapunov exponent where smaller values indicate greater stability.

Separate Generalized Linear Models with Generalized Estimating Equation corrections were used to compare the dysplasia group and control group with speed as a within-subject factor and group-by-speed as an interaction factor (SPSS, IBM Inc.). For individuals with unilateral dysplasia, the dysplastic side was used for analysis. For individuals with bilateral dysplasia, the more painful side was analyzed. For controls, the side corresponding to their match was analyzed. Least significant difference post-hoc tests were performed if the factors were significant.

## RESULTS AND DISCUSSION

The results indicate that individuals with hip dysplasia have significantly greater kinematic variability (meanSD) than controls at the hip, pelvis, and trunk (Table 1,  $p \leq 0.035$ ). However, there was no significant difference in local dynamic stability ( $\lambda_{max}$ ) between groups (Table 2,  $p > 0.05$ ). Speed did affect both kinematic variability ( $p \leq 0.004$ ) and local dynamic stability ( $p \leq 0.002$ ). At the ankle and knee, kinematic variability at the PRF speed was significantly greater than at both the PRSC and the FAST speeds. Local dynamic stability in the anterior-posterior and medial-lateral directions was greatest ( $\lambda_{max}$  is the smallest) when participants were

walking at the FAST speed compared to the PRSC and PRF speeds.

## CONCLUSIONS

Increased kinematic variability was detected in individuals with hip dysplasia compared to healthy controls across all speeds, while differences in local dynamic stability were not detected between groups. Both measures detected speed differences. When walking at their PRF speed, participants were significantly more variable at the ankle and knee and significantly less stable at the system level compared to the FAST walking speed. This study indicates that kinematic variability measures and local dynamic stability measures may quantify different parameters depending on the level of analysis and should not be used interchangeably.

## REFERENCES

1. Loverro et al. *Proceedings of ASB* Aug. 2016
2. Dingwell et al. *Chaos* **10**:848-862, 2000
3. Kang et al. *Exp Brain Rsrch* **172**:35-48, 2008

## ACKNOWLEDGMENTS

Research reported was supported by the National Institute of Arthritis and Musculoskeletal and Skin Diseases of the NIH under Award Numbers R21 AR061690 and K23 AR063235.

**Table 1:** Summary of group mean±SD of meanSD for significant kinematic variability variables.

Angle	FAST (meanSD)		PRF (meanSD)		PRSC (meanSD)	
	Control	Dysplasia	Control	Dysplasia	Control	Dysplasia
Hip Extension <sup>a</sup> (°)	0.86±0.20	1.01±0.39	0.94±0.23	1.04±0.30	0.84±0.18	1.14±0.38
Hip Flexion <sup>a</sup> (°)	1.06±0.22	1.20±0.29	1.07±0.25	1.27±0.35	0.98±0.19	1.31±0.31
Posterior Pelvic Tilt <sup>a</sup> (°)	0.81±0.15	0.88±0.17	0.81±0.17	0.91±0.14	0.78±0.09	0.98±0.28
Anterior Pelvic Tilt <sup>a</sup> (°)	0.71±0.21	0.81±0.12	0.74±0.14	0.81±0.18	0.66±0.11	0.88±0.27
Pelvic Hike (°)	0.65±0.18	0.68±0.16	0.60±0.21	0.67±0.16	0.56±0.14	0.73±0.21

Note: a: indicates a significant group effect; b: indicates a significant speed effect

**Table 2:** Summary of mean±SD of local dynamic stability measures.

Direction	FAST ( $\lambda_{max}$ )		PRF ( $\lambda_{max}$ )		PRSC ( $\lambda_{max}$ )	
	Control	Dysplasia	Control	Dysplasia	Control	Dysplasia
Medial-Lateral <sup>b</sup>	0.146±0.022	0.140±0.025	0.154±0.030	0.153±0.020	0.149±0.024	0.160±0.032
Anterior-Posterior <sup>b</sup>	0.401±0.081	0.409±0.050	0.431±0.069	0.432±0.052	0.447±0.065	0.429±0.051

Note: a: indicates a significant group effect; b: indicates a significant speed effect

# Hip Strength and Hip Moments during Gait in Women with and without Stress Urinary Incontinence

<sup>1</sup> Erin H Hartigan, <sup>1</sup> Adrienne McAuley, <sup>1</sup> Mike Lawrence, <sup>1</sup> Willis Brucker,  
<sup>1</sup> Adam King, <sup>1</sup> Brooks Tryon, <sup>1</sup> Mary DeSilva

<sup>1</sup> The University of New England, Portland, ME, USA  
email: [ehartigan@une.edu](mailto:ehartigan@une.edu), web: <http://www.une.edu/wchp/mal>

## INTRODUCTION

Women with stress urinary incontinence (SUI) have reduced isometric hip abduction strength [1]. Strengthening deep hip external and internal rotators in sitting and hip external rotators in side-lying and standing reduces frequency of leaking in women with SUI [2, 3]. Hip muscles play an intricate role in controlling the lower extremity during the stance phase of gait [4], yet gait mechanics in women with SUI are not well understood. Profiles of muscle performance and gait at the hip of women with SUI in comparison to healthy, asymptomatic women will inform clinical practice.

We aimed to describe isometric hip strength and hip angles during gait in women with SUI and to compare values to asymptomatic women. We also explored relationships between hip strength and hip angles and moments, but present here are only preliminary results of the strength and kinematic gait analysis data.

## METHODS

The asymptomatic group (n=16) included women who were over 18 years old, had regular menses, no complaints of pain, no known neurological conditions, and no history of back, pelvic, or lower limb surgeries. The group with SUI (n=7) met the above criteria but reported urine leakage when coughing, sneezing, or exercising.

Testing: Over-ground gait data were collected using 3D cameras (Qualisys) and force plates with 6 degrees of freedom (AMTI). Gait speed was controlled at  $1.3 \text{ m/s} \pm 5\%$ . Data were processed using Visual 3D software (C-Motion). Peak hip angles for all three axes of motion were calculated during three phases of stance: weight acceptance [initial contact (IC) to peak knee flexion (PKF),

mid-stance (PKF to peak knee extension[PKE]), and terminal stance (PKE to toe off)]. Five gait trials were averaged for each limb (i.e. dominant and non-dominant). Maximum voluntary isometric contractions (MVIC) were obtained using a dynamometer (Biodex S4). Hip strength testing via MVICs included hip external rotation and internal rotation in sitting and prone and hip abduction in side-lying. Descriptive statistics [mean (standard deviations)] were calculated for each variable of interest. Limb symmetry indexes (LSI) were calculated as  $100 - (\text{Non-dominant/Dominant} \times 100)$  and defined as clinically different if 15% or greater. Mixed model ANOVAs (limb and group) were used to assess differences. (SPSS, IBM) Significance was set at  $p=.05$ .

## RESULTS

Women in the SUI group were significantly older than those asymptomatic women ( $p<.001$ : 36 (5.5) and 26 (4.2) years old, respectively). Number of pregnancies, BMI, and dominant limb did not differ between groups. Hip strength did not differ between groups, yet hip internal rotation strength in sitting was greater in the dominant limb than non-dominant limb for both group (Table 1). LSI were 18% for SUI and 6% for asymptomatic (i.e., 12.5 and 3.6 Nm/kg, respectively). Limb differences in peak hip internal rotation angles during gait were statistically (Table 2) and clinically different (67%; 5.4 degrees) in the SUI group only.

## DISCUSSION

Although women with SUI do not differ in hip strength, they use asymmetrical hip angles during gait compared to asymptomatic women. Others have reported that asymptomatic women with weak hip strength do not alter peak hip angles

during gait, but instead demonstrated different lower limb coordination patterns in the transverse plane during gait [4]. Gait kinematics in our SUI group present novel findings that hip angles during weight acceptance may be related to pelvic floor muscle dysfunction. Although analyses of hip kinetics and correlations have not been reported and the findings reported here bear further investigation in a larger study, it is possible that closed chain kinetic exercises may benefit women with SUI to restore neuromuscular hip control during the weight acceptance phase of gait.

## CONCLUSIONS

Asymmetrical peak hip internal rotation angles during weight acceptance indicate aberrant

neuromuscular control of the deep hip stabilizers among women with SUI.

## REFERENCES

1. Underwood DB, et al. *J Women's Health Phys Ther.*36(1): 55-61, 2012.
2. Tuttle LJ, et al. *J Women's Health Phys Ther.*40(1): 15-19, 2016.
3. Jorde B and Schweinle W, *J Women's Health Phys Ther.*38(2): 81-89, 2014.
4. Smith JA, et al. *J Orthop Sports Phys Ther.* 44(7): 525-531, 2014.

## ACKNOWLEDGEMENTS

We acknowledge the University of New England's Vice Provost of Research mini grant program, which provided funding for this project.

**Table 1.** Maximal Voluntary Isometric Contractions (Nm/kg), Mean (SD). Abbreviations: SUI = stress urinary incontinence, IR = internal rotation, ER = external rotation

	Asymptomatic Group		SUI group		Differences
	Dominant	Non-dominant	Dominant	Non-dominant	
Hip IR Prone	35.8 (9.0)	37.3 (8.6)	37.8 (5.5)	37.7 (10.1)	
Hip IR Sitting	55.6 (15.7)	52.0 (10.5)	67.7 (13.9)	55.2 (4.5)	Limb p=.022
Hip ER Prone	34.1 (9.1)	33.2 (9.0)	33.6 (8.2)	33.7 (10.2)	
Hip ER Sitting	39.8 (8.0)	39.8 (6.0)	45.7 (10.9)	44.4 (11.8)	
Hip Abduction Side-lying	82.2 (15.8)	81.6 (16.1)	71.8 (15.9)	75.2 (16.5)	

**Table 2:** Peak hip angles (degrees) during three phase of gait, Mean (SD). Abbreviations: SUI = stress urinary incontinence, WA = weight acceptance, MS = mid-stance, TS = terminal stance, IR = internal rotation

	Asymptomatic Group		SUI group		Differences
	Dominant	Non-dominant	Dominant	Non-dominant	
Hip Flexion WA	30.2 (6.6)	27.9 (7.5)	27.4 (6.3)	26.0 (4.7)	Limb p=.017
Hip Extension MS	5.4 (9.1)	4.5 (8.2)	4.9 (8.4)	5.3 (6.5)	
Hip Extension TS	12.6 (8.8)	11.2 (7.5)	13.5 (7.2)	12.6 (6.7)	
Hip Adduction WA	7.7 (2.7)	7.0 (3.2)	9.5 (4.3)	6.9 (4.4)	
Hip Adduction MS	9.1 (2.4)	9.4 (2.8)	11.9 (3.8)	9.2 (3.2)	
Hip Adduction TS	5.8 (3.7)	7.7 (3.6)	8.3 (2.6)	5.6 (4.0)	
Hip IR WA	3.4 (5.3)	4.4 (5.7)	2.6 (6.5)	8.0 (4.6)	Interaction p=.037; Limb SUI only p=.005
Hip IR MS	7.4 (3.3)	8.0 (5.1)	9.2 (6.3)	12.1 (2.2)	
Hip IR TS	7.7 (3.6)	10.9 (5.8)	9.5 (5.5)	12.7 (3.4)	

# HIP LATERAL ROTATOR MUSCLE FORCE DURING VARIATIONS OF THE SINGLE LEG SQUAT

<sup>1</sup> Anne Khuu, <sup>1</sup> Kari L. Loverro, and <sup>1</sup> Cara L. Lewis

<sup>1</sup> College of Health & Rehabilitation Sciences: Sargent College, Boston University, Boston, MA, USA  
email: akhuu@bu.edu, web: <http://sites.bu.edu/movement/>

## INTRODUCTION

The deep lateral rotator muscles of the hip are key stabilizers of the joint [1]. The activity of these rotators, including the quadratus femoris, gemelli, and piriformis, cannot be measured using surface electromyography. Musculoskeletal modeling, however, can give estimations of the force required of these muscle during specific movement tasks.

We have previously demonstrated that the position of the non-stance leg during a single leg squat (SLS) task affects the kinematic and kinetics of the stance leg [2,3]. Variations of the SLS are commonly used in evaluation and treatment for individuals with lower extremity musculoskeletal conditions, but little information is available to direct the selection of the variation.

The purpose of this study was to evaluate hip angles, hip moments, and muscle force of the hip lateral rotators during the SLS with different non-stance leg positions.

## METHODS

Fifteen healthy individuals (8 females, 7 males; age  $22.1 \pm 3.0$  years; height  $1.73 \pm 0.11$  m; mass  $70.4 \pm 11.5$  kg) provided written informed consent and participated in this study. Participants performed 3 SLS tasks, which were differentiated by the position of the non-stance leg. For SLS-Front, the non-stance leg was extended out front during the squat. For SLS-Middle, the non-stance knee was slightly flexed with the non-stance foot adjacent to the stance ankle during the squat. For SLS-Back, the non-stance thigh was vertical and the non-stance knee was flexed  $90^\circ$  during the squat. For each task, participants started standing on both feet with their arms at or out to their sides, positioned their non-stance leg as instructed, squatted as low as possible while maintaining

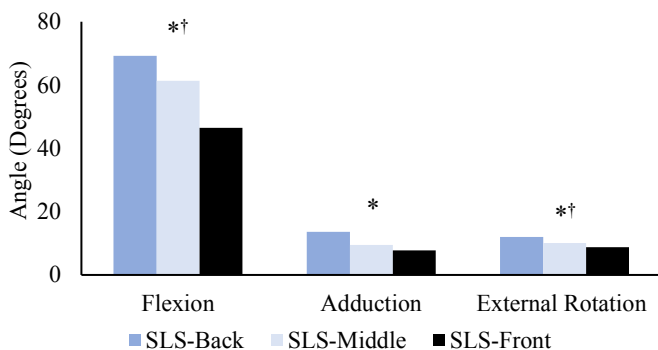
control, and returned to the starting position. Each task was performed 5 times on the right leg. Each performance was recorded as an individual trial. The order of the tasks was randomized. Kinematic data of the trunk, pelvis, and lower extremity were collected using a motion capture system (VICON®). Ground reaction force data were recorded using a split-belt instrumented treadmill (Bertec®). Kinematic and kinetic data were processed in Visual3D (C-Motion) to produce OpenSim compatible motion files. The generic OpenSim gait model (Gait2392) was scaled for each participant according to their height, mass, static calibration data, and segment geometry. In OpenSim, the residual reduction algorithm (RRA) was applied to the simulation. If needed, the RRA was re-run after the model was adjusted to meet the guidelines suggested in the OpenSim software documentation. Next, the computed muscle control algorithm was performed on the simulation to compute the muscle activation levels necessary to track the experimental data. Custom MATLAB code (The MathWorks, Inc.) was used to calculate the average muscle force during the descent phase (start of stance leg flexion to peak knee flexion) and ascent phase (peak knee flexion to returning to standing on both legs) of the gluteus medius (posterior), gluteus minimus (posterior), quadratus femoris, gemelli, and piriformis. In addition, average muscle force was calculated over the 100 ms period surrounding peak knee flexion for each muscle.

The 3D hip angles and moments at peak knee flexion were determined. The muscle force variables of interest were the average muscle force for each of the 5 muscles during the descent phase, the ascent phase, and over the 100 ms period surrounding peak knee flexion. Data were calculated from the first 3 SLS repetitions and averaged per task for analysis. For each variable, a separate one-way repeated measures analysis of variance (ANOVA) was used to test for differences between SLS tasks (SPSS). Least

significant difference post-hoc pairwise comparisons were performed if there was a significant main effect.

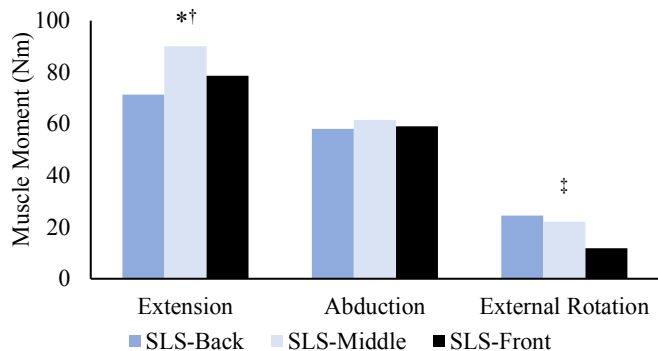
## RESULTS AND DISCUSSION

Performing the SLS with the non-stance leg in different positions affected hip angles and moments, and the force needed from the hip lateral rotator muscles. At peak knee flexion during the SLS-Back, the hip was in more flexion, adduction, and external rotation compared to the other two conditions ( $p \leq 0.04$ ) (Fig. 1). The hip was also in more flexion and external rotation in the SLS-Middle compared to the SLS-Front ( $p < 0.05$ ). In contrast, the hip extension moment at peak knee flexion in the SLS-Middle was larger than in the other two conditions ( $p \leq 0.01$ ), and SLS-Front was larger than SLS-Back ( $p = 0.02$ ) (Fig. 2). The external rotation moment was smaller in the SLS-Front compared to the other two conditions ( $p < 0.01$ ). There were no differences in hip abduction moment between conditions ( $p = 0.45$ ).



\*Significant difference between SLS-Back and other conditions.  
 †Significant difference between SLS-Middle and SLS-Front.

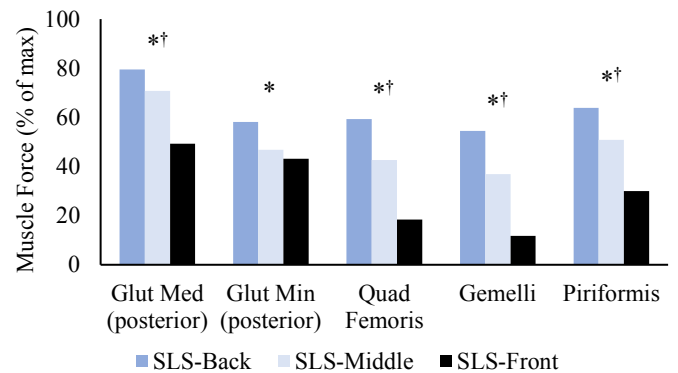
**Figure 1:** Hip angles at peak knee flexion during the single leg squat.



\*Significant difference between SLS-Middle and other conditions.  
 †Significant difference between SLS-Back and SLS-Front.  
 ‡Significant difference between SLS-Front and other conditions.

**Figure 2:** Internal hip muscle moments at peak knee flexion during the single leg squat.

For all muscle force variables for each muscle assessed, the force in the SLS-Back was higher than in the SLS-Front ( $p \leq 0.02$ ) (Fig. 3). Only for the posterior gluteus minimus during the ascent phase was this difference not significant ( $p = 0.23$ ). The SLS-Middle tended to require higher lateral rotator muscle force than the SLS-Front, but this was not significant for the posterior gluteus minimus at peak knee flexion ( $p = 0.49$ ) or during ascent ( $p = 0.84$ ), and for the gemelli during descent ( $p = 0.05$ ).



\*Significant difference between SLS-Back and other conditions.  
 †Significant difference between SLS-Middle and SLS-Front.

**Figure 3:** Estimated muscle force in the epoch surrounding peak knee flexion.

## CONCLUSIONS

SLS-Front requires the least force from the deep hip lateral rotators. As the deep hip lateral rotators are key muscles for hip stability, we would not recommend this variation of the SLS for hip rehabilitation.

## REFERENCES

1. Retchford TH, et al. *J Musculoskelet Neuronal Interact* **13**, 1-12, 2013.
2. Khuu A, et al. *Int J Sports Phys Ther* **11**, 201-211, 2016.
3. Khuu A, et al. *J Orthop Sports Phys Ther* **45**, A130-131, 2015.

## ACKNOWLEDGMENTS

This work was supported by the National Institute of Arthritis and Musculoskeletal and Skin Diseases of the NIH under Award Numbers R21 AR061690 and K23 AR063235.

# DEEP HIP MUSCLE ACTIVATION IS ALTERED DURING SQUATTING IN SYMPTOMATIC FEMOROACETABULAR IMPINGEMENT

<sup>1</sup>Laura Diamond, <sup>2</sup>Kim Bennell, <sup>3</sup>Wolbert Van den Hoorn, <sup>2</sup>Tim Wrigley, <sup>2</sup>Rana Hinman, <sup>4</sup>John O'Donnell, <sup>3</sup>Paul Hodges

<sup>1</sup>Griffith University, Menzies Health Institute Queensland, School of Allied Health Sciences, QLD, Australia

<sup>2</sup>The University of Melbourne, Centre for Health, Exercise and Sports Medicine, VIC, Australia

<sup>3</sup>The University of Queensland, Centre of Clinical Research Excellence in Spinal Pain, QLD, Australia

<sup>4</sup>St Vincent's Hospital, East Melbourne, VIC, Australia

Corresponding author email: [l.diamond@griffith.edu.au](mailto:l.diamond@griffith.edu.au)

## INTRODUCTION

Femoroacetabular impingement (FAI), a structural abnormality of the hip joint, is a significant cause of hip pain and reduced function in younger active adults [1]. Evidence to support FAI as a principal determinant for the future development of hip osteoarthritis is mounting [2]. Yet, current treatments are suboptimal, likely in part due to the absence of experimental data regarding the physical impairments associated with symptomatic FAI. Hip muscle function in this condition has not been well defined. Initial evidence shows altered coordination of deep hip muscle activity in symptomatic FAI during walking [3], despite the generally pain-free nature of this task in FAI, as the hip joint does not move towards the impingement position (deep hip flexion, combined with hip adduction and internal rotation). Hip muscle activity during squatting, a task towards the impingement position, has not been investigated but may provide further insight into the neuromuscular adaptations of this patient population. This exploratory study aimed to investigate activation patterns of the hip muscles during a deep squat in individuals with and without symptomatic FAI.

## METHODS

Fifteen individuals with symptomatic FAI (clinical examination and imaging (alpha angle  $>55^\circ$  (cam FAI), and lateral centre edge angle  $>39^\circ$  and/or positive crossover sign (combined FAI))) and 14 age- and sex-comparable controls without morphological FAI on magnetic resonance imaging underwent testing. Intramuscular fine-wire and

surface electrodes recorded electromyographic (EMG) activity of selected deep and superficial hip muscles during the squatting task. The tri-phase squat included: (i) descent from a standing position to the end of self-chosen available range; (ii) a 3-second hold; and (iii) ascent to the upright standing position. Participants were instructed to use their preferred strategy to squat as deeply as possible at a self-selected controlled pace. Individual muscle EMG patterns were normalized to the mean of the peaks of 5 repetitions, and were statistically compared between groups using a wavelet-based linear mixed effects model based on the technique of wavelet functional ANOVA (wfANOVA) [4]. Demographic and spatiotemporal variables were compared between groups using independent t-tests and Mann-Whitney U tests as required ( $p < 0.05$ ).

## RESULTS AND DISCUSSION

The FAI and control groups were comparable for age, sex, BMI, and dominant leg tested (Table 1). FAI patients reported an average pain score of 2 on an 11-point numerical rating scale after completing the squatting task (range 0-8). There were no between-group differences in leg-length normalized squat depth ( $p=0.12$ ) or ascent speed ( $p=0.11$ ), however, descent speed was significantly slower in the FAI group ( $p=0.05$ ).

During squat descent, FAI patients exhibited greater EMG activity of deep hip external rotator and extensor muscles (gluteus medius (GM), piriformis (PI, Figure 1), obturator internus (OI) and quadratus femoris (QF)) than controls. These muscles have mechanical actions that oppose impingement and

are likely to have an active role in hip joint stabilization. Greater activation may relate to the slower decent speed of FAI patients, and/or be a strategy to stabilize the joint and reduce provocation as the hip approaches deep flexion and impingement.

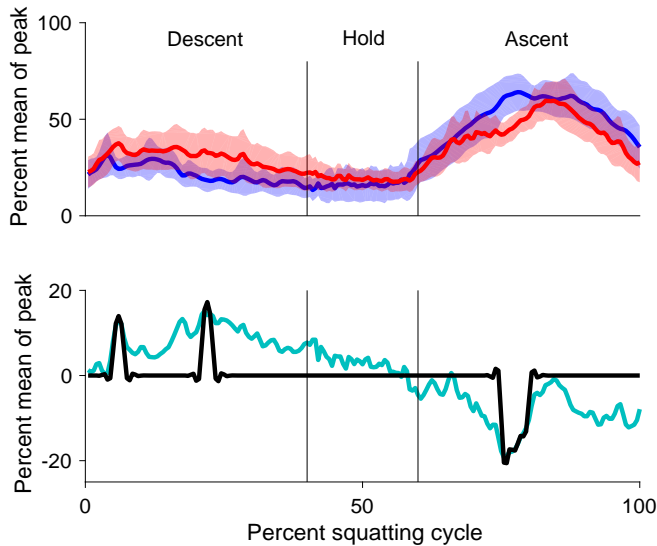


**Figure 1** Ensemble average ( $\pm 1.96 \cdot \text{SEM}$ ) EMG patterns from piriformis for control (blue) and FAI (red) participants over a squatting cycle (top). Average between-group difference (FAI-control; green), significant contrasts (black) (bottom).

During squat ascent, FAI patients exhibited lower EMG activity of deep hip external rotator and extensor muscles (GM, PI and OI) than controls. Gluteus maximus amplitude was also lower than controls during the initial 14% of ascent as FAI

patients moved out of deep hip flexion. Lower activation of these agonists may relate to pain inhibition.

The different squatting strategies exhibited by FAI patients may relate to enhanced protection for the hip, and be favorable for symptoms and function in the short-term. However, there could be long-term consequences if this leads to increased or abnormal joint loading, given that individuals with symptomatic FAI are at risk for further structural damage and early hip osteoarthritis [2].

## CONCLUSIONS

Deep hip muscle activation is altered during squatting in symptomatic FAI. Future studies should examine patients prospectively and post-operatively to establish whether treatments targeted at these features would be potentially beneficial.

## REFERENCES

1. Ganz R, et al. *Clin Orthop Relat Res* **417**:112–20, 2003.
2. Agricola R, et al. *Nat Rev Rheum* **9(10)**, 630-634, 2013.
3. Diamond L, et al. *J Orthop Res* DOI 10.1002/jor.2339, 2016.
4. McKay J, et al. *Neurophysiol* **109**: 591-602, 2013.

**Table 1:** Demographic and clinical characteristics for femoroacetabular impingement and control groups.

Group	Age (yrs)	Males	Height (m)	BMI (kg/m <sup>2</sup> )	FAI type (cam: combined)	Dominant side tested, n (%)	Tegner Activity Level (0-10) <sup>¶</sup>	Pain during squats (0-10) <sup>§</sup>
FAI (n=15)	24.7 (4.9)	11 (73%)	1.76 (0.09)	24.4 (2.5)	11:4	10 (67%)	5.2 (2.1)*	1.9 (2.4)
control (n=14)	27.1 (4.5)	10 (71%)	1.77 (0.08)	23.2 (1.9)	-	9 (64%)	6.6 (1.0)*	-

Values are mean (standard deviation) unless otherwise stated; \*p<0.05; <sup>¶</sup>Tegner scale is 0-10 with zero representing disability and 10 representing competitive sport at the professional level; <sup>§</sup>Numerical Rating Scale ranges between 0-10 with zero representing no pain and 10 representing worst pain possible; FAI, femoroacetabular impingement.

# SAGITTAL PLANE HIP IMPULSE DURING GAIT IS GREATER AFTER SURGICAL INTERVENTION FOR FEMOROACETABULAR IMPINGEMENT SYNDROME

<sup>1</sup>Philip Malloy, <sup>1</sup>Matthew Giordanelli, <sup>2</sup>Antonia Zaferiou, <sup>1</sup>Donald Neumann, and <sup>1</sup>Kristof Kipp

<sup>1</sup>Marquette University, Milwaukee, WI USA  
<sup>2</sup>Rush University Medical Center, Chicago, IL, USA

email: Philip.malloy@marquette.edu

## INTRODUCTION

Femoroacetabular impingement syndrome (FAIS) is a clinical hip disorder that is associated with aberrant hip joint morphology, which results in premature contact between the femur and acetabulum during hip joint motion. FAIS is characterized by anterior hip and groin pain during near end range motion, positive impingement testing, range of motion loss, and imaging findings that point at abnormal structural morphology [1]. FAIS also results in functional limitations while walking, deep squatting, and sitting [2]. Arthroscopic hip surgery for FAIS leads to very good to excellent results in patient reported outcomes; however, information on functional parameters such as gait biomechanics after surgery remains limited [3].

Previous biomechanical studies after hip surgery in people with FAIS show significant improvements in sagittal plane gait kinematics during walking, however, no post-operative improvements in hip joint kinetics were found in these patients [4]. Although arthroscopic hip surgery for FAIS improves patient reported outcomes, it remains unknown if hip joint loading also improves post-operatively. Therefore, the purpose of this study was to determine if sagittal plane joint loading changes after arthroscopic hip surgery for FAIS. It is hypothesized that sagittal plane loading will be greater after hip arthroscopic surgery in persons with FAIS.

## METHODS

Six male and 2 females, who underwent arthroscopic surgical intervention for FAIS, were enrolled in this study. Two patients underwent bilateral surgery for FAIS; therefore, 10 hips were included in the analysis. Hip joint kinetics were measured with 3D

motion analysis and force plates before and greater than one year after arthroscopic hip surgery ( $1.27 \pm .34$  years).

Five gait trials were collected with patients walking at a self-selected speed. Variables of interest were peak sagittal plane hip joint moments and hip joint impulse (Figure 1). Hip joint moments were calculated with inverse dynamics procedures during the stance phase of each walking trial. Joint moments were normalized to body mass ( $\text{N}\cdot\text{m}\cdot\text{kg}^{-1}$ ) and were expressed as external moments. Joint impulse was calculated as the product of the mean external joint moment and change in time during stance phase ( $\text{N}\cdot\text{m}\cdot\text{s}\cdot\text{kg}^{-1}$ ).

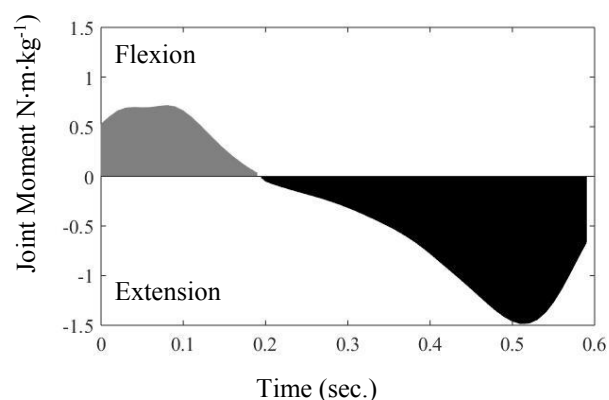


**Figure 1.** Example of hip joint moment during the stance phase of gait. Positive area (grey) indicates hip flexion impulse and negative area (black) indicates hip extension impulse.

An ensemble average of five trials was calculated for each variable of interest and used for analysis. Data are reported as mean  $\pm$  SD. Paired *t*-tests were used to compare pre-operative and post-operative data with an *a priori*  $\alpha$ -level of 0.05.

## RESULTS

The hip flexion and extension impulse during the stance phase of walking were significantly greater after hip arthroscopic surgery (Table 1). Conversely, there were no differences in peak hip flexion and extension moments (Table 1). Moreover, there were no differences in gait speed (Pre:  $1.37 \pm 0.12 \text{ m}\cdot\text{s}^{-1}$ ; Post:  $1.35 \pm 0.06 \text{ m}\cdot\text{s}^{-1}$ ;  $p = 0.641$ ), flexion impulse stance duration (Pre:  $0.18 \pm 0.06 \text{ s}$ ; Post:  $0.17 \pm 0.05 \text{ s}$ ;  $p = 0.585$ ), and extension impulse stance duration (Pre:  $0.49 \pm 0.08 \text{ s}$ ; Post:  $0.50 \pm 0.05 \text{ s}$ ;  $p = 0.389$ ) before and after arthroscopic hip surgery.

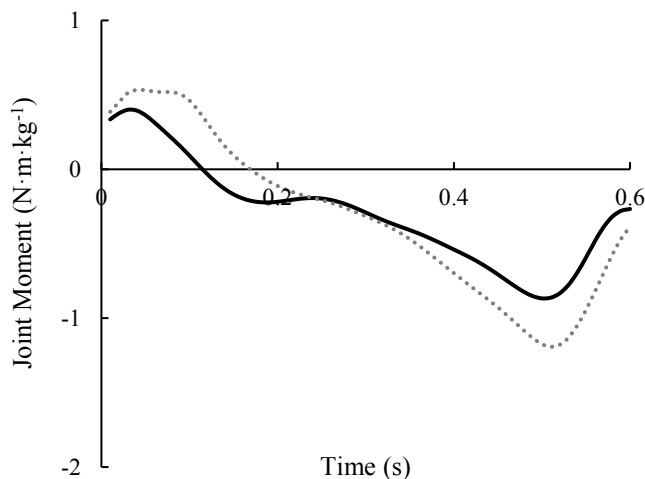


**Figure 2.** Exemplary joint moment curves for a single patient before (black solid line) and after (grey dotted line) hip surgery.

## DISCUSSION

The findings of the current study indicate that patients with FAIS demonstrate greater hip flexion and extension impulse after arthroscopic hip surgery. Since the peak joint moment and stance time did not

differ between pre- and post-operative gait testing, it appears that patients exhibit a higher average joint moment across the stance phase of gait. Perhaps reduced pain or improved muscle function may contribute to this greater sagittal plane joint loading during walking. Future research should investigate whether changes in muscle forces and pain could help explain the increase in joint impulse during gait after hip surgery for FAIS.

## CONCLUSION

Patients who underwent arthroscopic surgery for FAIS demonstrated greater peak flexion and extension joint impulse during the stance phase of gait than compared to before surgery. Patients may exhibit a greater average hip joint moment across the stance phase of gait because of a reduction in pain or improvement in muscle function after hip surgery for FAIS. More research is needed to investigate the exact mechanisms associated with the greater joint impulses after hip surgery.

## REFERENCES

1. Griffin D et al. *Br. J Sports Med* **50**, 1169-1176, 2016.
2. Bedi A, Kelly B. *J Bone Joint Surg* **95**, 82-92, 2013.
3. Clohisy JC et al. *Am J Sports Med* **41**, 1348 – 1356, 2013.
4. Rylander JH et al. *J Orthop Res* **41**, 1461-1468, 2013.

**Table 1.** Peak external hip joint moments ( $\text{N}\cdot\text{m}\cdot\text{kg}^{-1}$ ) and joint impulse ( $\text{N}\cdot\text{m}\cdot\text{s}\cdot\text{kg}^{-1}$ ) in patients with FAIS before and after arthroscopic surgery.

	Before Surgery	After Surgery	P-value
<i>Peak Moment</i>			
Flexion	$.59 \pm .15$	$0.71 \pm 0.23$	.084
Extension	$-.94 \pm .23$	$-1.02 \pm 0.18$	.357
<i>Impulse</i>			
Flexion	$.21 \pm .08$	$.31 \pm .12$	.033*
Extension	$-.35 \pm .10$	$-.50 \pm .08$	.004*

\* indicates statistical significance at  $p < .05$

# ENHANCING THE BIOMECHANICS CLASSROOM WITH ENTREPRENEURIAL-MINDSET LEARNING ACTIVITIES

<sup>1</sup> Karen L. Troy, <sup>2</sup> Laurel Kuxhaus

<sup>1</sup> Worcester Polytechnic Institute, Worcester, MA, USA

<sup>2</sup> Clarkson University, Potsdam, NY, USA

email: ktroy@wpi.edu

## INTRODUCTION

It is well-established that project- and problem-based learning engage students in the classroom. Biomechanics classes offer students the opportunity to build technical proficiency by applying mechanics principles to problems involving living organisms. In addition to this technical proficiency, mindset also matters. [1]

“Entrepreneurial Mindset Learning” (EML), as championed by the Kern Entrepreneurial Engineering Network, offers a framework for faculty to consider outcomes beyond technical proficiency, including stimulating curiosity, making connections, and creating value. These outcomes are synergistic with bioengineering education, which by nature must teach students about biocompatibility, ethical decision making, and other issues unique to working with humans and animals. Using the Entrepreneurial Mindset as a framework when developing course projects offers faculty a structure to enrich content and benefit students.

Here we describe the use of EML as a guide to enrich biomechanics class projects dealing with bone fracture. In each project, specific EML principles were identified with the goal of incorporation into a primarily technical project.

## METHODS

The authors systematically enhanced class projects with EML-inspired tasks. The technical nature of the projects was preserved and strengthened. Specific highlights are described.

**Project 1: Vertebral fracture project, “The Elevator Problem”.** (KLT at WPI, Spring 2017)

An earlier version was implemented by KLT at the University of Illinois at Chicago. This enhanced version emphasizes EML principles.

*Overall Summary of the Project:* Students were given an accident scenario in which an elevator malfunction resulted in injury to an occupant (“Mrs. Albert”). A year later, Mrs. Albert filed a lawsuit against the manufacturer, claiming that her recent

vertebral fracture was caused by the accident. The goal of the assignment was to write an expert opinion, supported with data, summarizing how likely it was that Mrs. Albert’s vertebral fracture was caused by the elevator accident. The EML-enhanced version of the project includes the “twist” in which half the students were “hired” by the elevator company’s attorney, while the other half were “hired” by Mrs. Albert’s attorney. All groups were competing for the attorney’s business, giving an incentive to produce coherent, thorough work.

Student groups are prompted in class to discuss mechanisms of injury, and to identify questions they must answer to determine whether Mrs. Albert had a case. Final reports must provide context, rationale, and citations for assumptions, and students are advised to consider upper and lower limits.

The EML-enhanced version includes additional contextual questions designed to encourage exploration of related material, such as: How much should Mrs. Albert sue for? How could this injury be prevented in the future, given that elevators are necessary? Learning will be evaluated through a structured self-assessment that prompts students to identify and reflect on specific aspects of the project that emphasize various EML principles.

*EML synergies and enhancements:* In addition to traditional engineering project goals of *performing analysis* and *validating* results, this project meets EML goals [2] in the following ways:

- Students must *evaluate the technical plausibility, economic and societal impacts* of both the accident and the lawsuit.
- To determine whether Mrs. Albert had a viable case, they *assess policy and regulatory issues*.
- Students understand vertebral structure and function, and the engineering design of elevator braking systems. This allowed them to *analyze their solutions* in a real-world context.
- By writing an expert opinion, students learn to *communicate their engineering analysis in terms of economic and societal benefits*.

## **Project 2: Cervine cancellous bone as an ex-vivo biomechanical model.** (LK at C.U., Fall 2016)

*Overall Summary of the Project:* Students (26) worked in groups of 3 to analyze the microstructural parameters of cervine vertebral cancellous bone, including trabecular thickness, trabecular number, bone volume fraction, and connectivity density. The overall research question posed was whether cervine vertebral cancellous bone was appropriate for use in biomechanical studies; this question remains unanswered in the literature.

Each group was assigned a unique aspect of the research question, such as age- or sex-differences between specimens. MicroCT scans of cervine lumbar vertebrae and rudimentary instructions for using ImageJ [3] and the BoneJ plugin were provided to students. Each group designed their own analysis and delivered a report, structured similar to a journal paper. These reports were peer reviewed in class. Students could revise their reports for additional credit.

To earn an “A” grade, students had to exceed the minimum requirements by completing additional analysis of their own design and compare to literature beyond that provided. Group report scores were scaled by the individual factor from the CATME peer-evaluation survey. [4]

*EML synergies and enhancements:* This particular project meets EML goals in these ways:

- Students considered the value of an ex-vivo model for laboratory research by *investigating the (research) market*, and *evaluating the societal benefits and sustainability* of ex-vivo animal models for biomechanical studies.
- Students developed curiosity about the use of cadaver specimens in research, and learned about relevant *policy and regulatory issues*.
- Students learned about *intellectual property* surrounding ImageJ.
- Students *communicated the societal benefits* of their conclusion in *economic terms* in reports.

## **RESULTS AND DISCUSSION**

Project #1 was originally implemented in a tissue biomechanics course over a four-week period, and received excellent feedback from students, who enjoyed the context, as well as “being forced to research” and think about their answers. The revised

version presented here includes two classroom periods of worktime, plus one classroom period for discussion of the final product.

Project #2 was implemented in an introductory biomechanics class. Informal observations noted a high degree of student engagement in and outside the classroom. While students initially appeared frustrated by the unconstrained nature of the project and by the gaps in their own knowledge, they displayed confidence in their results by the end, as evidenced by dialogue between groups about choice of methods and realism of results. Several indicated that the experience was meritorious of discussion with prospective employers.

Taken together, these biomechanics class projects provide examples of EML incorporation into otherwise straightforward technical analysis projects. These experiences can inspire students to build *connections* between their classroom experience and the real world, look *creatively* at problems, and *create value* through their work.

## **CONCLUSIONS**

The projects described here required relatively minor edits from previous instantiations to incorporate EML. It is important to note that EML is one framework that can be used to enhance student engagement in the classroom. Many elements of EML are synergistic with fundamental principles behind problem-based learning, flipped classrooms, and other contemporary pedagogical techniques. That is, incorporating elements of EML into existing classroom activities, such as projects, can add value and context to students with only a small effort from the instructor.

## **REFERENCES**

- [1] Osterwelder et al., (2014). *Value Proposition Design*. Wiley.
- [2] <http://engineeringunleashed.com>
- [3] Schneider et al., (2012) *Nature methods*.
- [4] Loughry et al. (2007) *Ed and Psy Meas*.

## **ACKNOWLEDGMENTS**

The authors thank the Kern Family Foundation awards to WPI and Clarkson University for supporting this work.

# ACTIVE LEARNING IN BIOMECHANICS USING WEARABLE SENSORS: A CASE STUDY FROM THE UNIVERSITY OF VERMONT

<sup>1</sup>Ryan S. McGinnis, <sup>1</sup>Ellen W. McGinnis

<sup>1</sup>University of Vermont, Burlington, VT, USA  
email: ryan.mcginis@uvm.edu

## INTRODUCTION

Recent work in engineering education suggests a shift in approach to focus on active engagement of students in the learning process. This approach, so called Active Learning, can include both classroom activities to improve student engagement during lecture, and course-level activities that employ Collaborative (emphasis on student interaction), Cooperative (incentives for student cooperation rather than competition), and/or Problem-Based (student-relevant problems used as motivation) learning approaches. Outcomes have been shown to improve student engagement, academic achievement, and critical thinking, interpersonal, teamwork, and life-long learning skills [1].

Wearable sensors provide a new, and rapid way to directly measure human motion and physiology outside of typical laboratory environments. Because of the ease with which data can be collected, these new devices provide a unique opportunity for developing research methods courses that employ active learning strategies in biomechanics and biomedical signal processing. In so doing students gain valuable experience designing and conducting experiments that use wearable sensors for measuring human motion and physiology, and communicating their findings through written technical reports and oral presentations. This abstract describes our first effort at creating such a course, BME296 – Wearable Sensing in Biomechanics, at the University of Vermont, and details our experience and preliminary outcomes.

## METHODS

To develop this course, we begin with defining goals for student learning. Specifically, we aimed for students to leave the course with experience:

- Reading and discussing primary articles
- Working in groups on biomedical research
- Conducting research with human subjects
- Processing data from wearable sensors to address specific biomechanical hypotheses
- Presenting scientific findings via written and oral communication

The course begins with four units designed to introduce students to typical uses for wearable sensors in research and commercial settings. These include: postural stability assessment [2], fall detection [3] (see Fig. 1), and two units on gait analysis [4, 5].

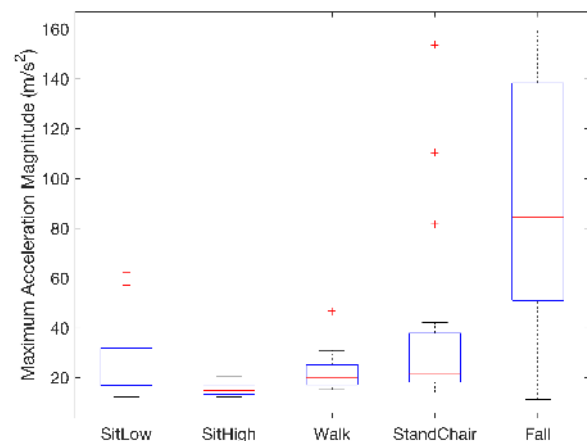


**Figure 1:** Student-designed fall detection experiment performed in BME296. Box plot illustrates quantitative difference between typical Activities of Daily Living and falling.

For each unit, a group of four-six students is responsible for leading discussion on a primary source article, designing and conducting an experiment to replicate the results presented in the article, and facilitating a debrief about the replication experiment including discussion of how the experimental or data analysis methods could be improved in the future.

For each unit, each student is responsible for completing a written summary of the primary source article, developing the method for processing the wearable sensor data described in the article, and using the method to answer a series of data analysis questions. After completing the first two units, students are responsible for writing a formal research report describing the findings from one of the experiments.

The course builds to a final group project that uses data collected from wearable sensors during student-designed experiments to address a hypothesis proposed by each group. For example, one group is currently investigating an old Spanish adage that people with larger feet are more stable. Findings from this project are shared with the instructor and class through written and oral reports.

To enable this course structure, we employ a new wearable sensor system, the BioStampRC (MC10, Inc., Lexington, MA USA – Fig. 2). The BioStampRC system is composed of the skin-worn, conformal BioStamp sensors that provide direct measurement of human motion and biopotentials (e.g., sEMG, ECG), a mobile application for enabling sensor data collection and uploading data from the sensors to cloud storage, and a web application for configuring sensors and downloading data.



**Figure 2:** BioStamp wearable sensor is adhered to the skin, and enables direct sensing of human motion and biopotentials (e.g. sEMG, ECG).

## RESULTS AND DISCUSSION

This elective course is part of a new undergraduate program in Biomedical Engineering at the University of Vermont, and is being offered for the first time during the Spring 2017 semester to 24 upper-level engineering students in Electrical, Biomedical, and Mechanical Engineering. The course is well received by students, with one student noting in midterm evaluations that the course is “showing us better than all of my other classes what a career in BME research might be like.” Moreover, it is providing unique opportunities for student achievement where, one experiment has already resulted in a conference abstract describing the results [6].

However, it is important to note that this teaching approach is not without its challenges. Students accustomed to courses that apply more passive learning approaches often find the transition to active learning difficult. This alternative course structure requires more significant engagement during class, and investigation of problems that do not have clear answers during assignments. The self-directed learning required for successful completion of these assignments can initially be anxiety inducing for some students. However, it can be especially helpful to be transparent and explicit with students about the benefits of this Active Learning approach, and the relevance of the skills that they are learning to their future careers in all areas of engineering.

## REFERENCES

1. Prince, Michael. *J Eng Educ.* 2004;93.3: 223- 231.
2. Mancini M, et al. *J NeuroEng Rehab.* 2012;9:59.
3. Bourke A, et al. *Gait&Posture.* 2007;26:194-199.
4. Aminian K, et al. *J Bio.* 2002;35:689-699.
5. Kang G, et al. *J Bio.* 2016;49:4022-4027.
6. Johnson A, et al. *43<sup>rd</sup> Annu NE BioE Conf*, NJIT, 2017.

# TEACHING UNDERGRADUATE BIOMECHANICS TO STUDENTS WITH DIVERSE ABILITIES

<sup>1</sup>Melissa Thompson

<sup>1</sup>Fort Lewis College, Durango, CO, USA

email: [mathompson@fortlewis.edu](mailto:mathompson@fortlewis.edu) web: [www.fortlewis.edu/exercise-science](http://www.fortlewis.edu/exercise-science)

## INTRODUCTION

Biomechanics courses are taught at both the graduate and undergraduate level and in a variety of schools and programs, including clinical specialties such as physical and occupational therapy, as well as biomedical engineering, biology, kinesiology, exercise science and other programs. Frequently these academic programs present situations in which students have diverse backgrounds in terms of prerequisite knowledge and abilities. Teaching biomechanics to a mixed-ability classroom creates a challenging environment in which the instructor must engage students while maintaining high standards of learning. The ability of an instructor to adapt instruction to meet students' varied learning needs is essential for fostering a positive learning environment in a classroom of varied abilities [1]. Here I describe teaching techniques utilized in undergraduate biomechanics courses in order to enhance learning for students with diverse abilities.

## METHODS

Data was gathered over the course of four years in which multiple undergraduate courses were taught at a small public liberal-arts college. The majority of students were majors from the Exercise Science Department in the degree options of Exercise Physiology and Exercise Specialist. Additionally, each term there were several students from outside the Exercise Science Department, who were primarily majoring in public health, biology and engineering. While the majority of students were exercise sciences majors, there were considerable differences in abilities of students both within and across degree options. For example, the Exercise Physiology option is described as pre-professional training and requires students to take prerequisite math and physics courses. Most students that pursue this major are seeking careers in health care fields,

such as physical and occupational therapy, and graduate school careers. Alternatively, the Exercise Specialist option has no math or physics prerequisites and is aimed at careers in the fitness industry.

Over the four-year period several different teaching techniques were utilized. Data gathered included quantitative scores on specific assignments and exams, as well as overall course grades. Additionally, qualitative student assessments and student feedback were utilized to address the effectiveness of the different teaching modalities.

The selection of different teaching techniques was based on the following questions:

1. How can student ability levels be identified and accommodated?
2. What did students ultimately need to take away from the course?
3. How could content be adapted to engage students of different abilities?

## RESULTS AND DISCUSSION

1. How can student ability levels be identified and accommodated?

An essential first step at being able to teach to a mixed-ability class is to identify student ability levels. Subsequent to this was implementing strategies to address the varied abilities, and in particular offering support for students with deficiencies (Fig 1).

Additionally, the flipped classroom model [2] was utilized as it had a primary benefit of enabling the instructor to identify ability levels and deficiencies in the classroom. Within the flipped classroom model, cooperative learning strategies were employed in which small groups of students with

different ability levels worked together to improve their understanding of specific biomechanics topics or to solve biomechanics problems. These cooperative learning strategies required each member of the team to be responsible for learning all aspects of the topic or problem, as well as being responsible for helping their teammates learn [3].

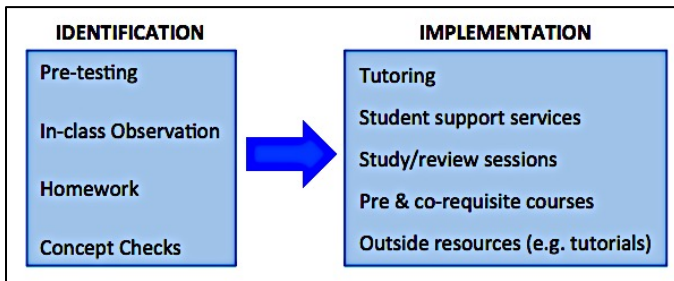


**Figure 1:** Strategies to identify and address student deficiencies.

2. What did students ultimately need to take away from the course?

In the process of determining what students needed to take away from the course I developed what I termed the “barbell framework” in which the majority of the “weight” or focus of the course was content and application, with calculations being an important, but not wholly essential, bridge between these primary concepts (Fig. 2).



**Figure 2:** The barbell framework for undergraduate biomechanics instruction.

Utilizing this approach allowed students to develop an understanding of biomechanical concepts without the risk of losing students who struggled with the computational aspects of the course. With a solid understanding of biomechanical concepts students were better prepared for, and found considerably more meaning in, calculations. The secondary focus of this framework was application

of course concepts, which was essential for demonstrating relevance and significance of the course content.

3. How could content be adapted to engage students of different abilities?

It was determined that a valuable technique for engaging students with varied abilities when covering a variety of different biomechanical topics, was to have students generate ideas for both application and analysis. In this regard, particular emphasis was made to have students apply course content to their career goals and interests. Further, it was also found to be very effective to get to know students and address their particular interests, and to have students share their backgrounds and experiences in an effort to enhance learning.

## CONCLUSIONS

Each student differs in his or her background knowledge, learning style and interests, thereby, presenting a unique opportunity to teach to. Being able to address individual differences and contribute to a student’s intellectual growth is a gratifying experience. When students are involved, explaining, solving, talking, trying, working, and struggling they not only retain information they learn how to ask thoughtful questions, critique information and sharpen their critical thinking skills.

## REFERENCES

1. Tomlinson CA. *How to differentiate instruction in mixed-ability classrooms*. ASCD, 2001.
2. Bishop JL & Verleger MA. *ASEE National Conference Proceedings* **30**, 2013.
3. Dees RL. *J Res Math Educ* **22**, 409-421, 1991.

## ACKNOWLEDGMENTS

A special thanks to Dr. Rodger Kram for instilling my love of teaching biomechanics.

## **The Teaching Repository as a Tool for You**

<sup>1</sup> Kimberly Bigelow and <sup>2</sup>Patrick Rider

<sup>1</sup> University of Dayton, Dayton, OH, USA, <sup>2</sup> East Carolina University, Greenville, NC, USA  
email: Kimberly.bigelow@udayton.edu and Riderp@ecu.edu

### **INTRODUCTION**

The American Society of Biomechanics Teaching Repository was first introduced during the 40<sup>th</sup> Annual Meeting of the American Society of Biomechanics.<sup>1</sup> The Teaching Repository is an on-line resource for individuals interested in biomechanics education at all levels to find – and share – lessons, assignments, labs, resources and more. During this session, we will provide a short tutorial of the Teaching Repository, highlighting how to find information and contribute information. Attendees may wish to follow along on their mobile device or computer. Time will also be provided to get your questions answered and to share your suggestions for an improved repository experience (especially for those experienced users).

### **REFERENCES**

1. Smeesters C & Bigelow K. The New ASB Teaching Repository: Your Go to Place for Biomechanics Teaching Ideas. 40<sup>th</sup> Annual Meeting of the American Society of Biomechanics, 2016.

### **ACKNOWLEDGMENTS**

This session is a contribution of the ASB Education Committee

# GETTING STARTED WITH THE SCIENCE OF TEACHING AND LEARNING IN BIOMECHANICS

<sup>1</sup> Kimberly A. Fournier

<sup>1</sup> University of Rhode Island, Kingston, RI, USA  
email: kimfournier@uri.edu

## INTRODUCTION

*“A paradigm shift is taking hold in American higher education. In its briefest form, the paradigm that has governed our colleges is this: A college is an institution that exists to provide instruction. Subtly but profoundly we are shifting to a new paradigm: A college is an institution that exists to produce learning. This shift changes everything. It is both needed and wanted.”* [1, p. 13]

The scholarship of teaching and learning (SoTL) is a process of applying a scholarly lens to what happens in the classroom [2]. Teaching, learning, and research are synthesized by asking meaningful questions about how students learn and what teaching activities best facilitate their learning [2]. Evidence of thinking and learning is systematically analyzed and the results are used to contribute to a body of knowledge aimed at improving students learning and strengthening teaching practices [2].

In this session, key concepts related to conducting SoTL research will be presented. Topics discussed will include getting started, ethical considerations, design, evidence, best practices, and dissemination of findings. Resources will be made available in the ASB Teaching Repository.

## REFERENCES

1. Barr RB & Tagg J. *Change: The magazine of higher learning*, **27**, 12-26, 1995.
2. Chick N. Retrieved from <https://my.vanderbilt.edu/sotl/understanding-sotl/a-scholarly-approach-to-teaching>. 2017.

## ACKNOWLEDGMENTS

This session is a contribution of the ASB Education Committee

# SAGITTAL PLANE CONTROL OF TRUNK POSTURE AFTER SPINAL CORD INJURY

<sup>1</sup>Musa L. Audu, <sup>2</sup>Lisa M. Lombardo, and <sup>1,2</sup>Ronald J. Triolo

<sup>1</sup>Case Western Reserve University, Cleveland, OH, USA

<sup>2</sup>Cleveland VA Medical Center, Cleveland, OH, USA

email: mxa93@case.edu

## INTRODUCTION

Spinal cord injury (SCI) is a debilitating condition that results in loss of function due to paralysis of muscles of the trunk, legs or upper extremities. Functional Neuromuscular Stimulation (FNS) is a technology that can be used to restore the activity of muscles paralyzed by SCI. This is achieved by applying low-level electric currents to the peripheral motor nerves so as to elicit contractions of the paralyzed muscles and thus restore some or all of the natural movements that were lost. In a survey of individuals with SCI, trunk stability has been ranked third in order of priority by individuals with paraplegia as well as those with quadriplegia [1]. Without trunk control, individuals with SCI have to maintain balance while seated either by holding onto fixed objects with their upper extremities or by using restraints such as belts and straps to keep them constrained to the wheelchair. This greatly limits the workspace that they can explore while seated and reduces their ability to independently perform many activities of daily living (ADLs) and function in typical work environments requiring use of both upper extremities.

The main goal of this study was to use musculoskeletal models to design and test feedback control systems that will stabilize the trunk at erect and non-erect postures so as to expand the seated workspace for individuals with SCI.

## METHODS

A musculoskeletal model of the trunk, pelvis and hips was developed to match the anthropometric characteristics of an individual with SCI (C7 AIS B). The subject had FNS implanted electrodes targeting the core trunk and hip musculature: Erector Spinae, Gluteus Maximus, Hamstrings and Iliopsoas. In simulations with the musculoskeletal model as well as in actual experiments with the subject, it was determined that maximally activating the Erector Spinae muscles

from a forward leaning posture could restore the trunk to an erect posture [2]. To keep the trunk at a forward leaning posture stably for longer periods, a PID feedback controller was designed to modulate the stimulation levels to the hip and back muscles (Figure 1).

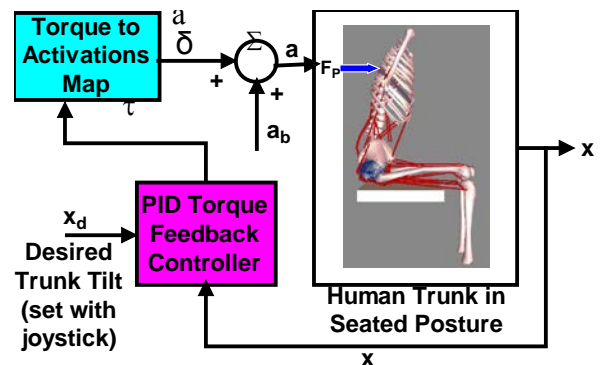


**Figure 1:** Feedback control system for maintaining forward-leaning trunk posture.

In the model, the PID controller was designed on the basis of changes in joint moments at the hips and lumbar back. Changes in trunk tilt  $x$  away from the desired value  $x_d$  caused changes in the feedforward (inverse dynamics) torques at the hips and lumbar joints so as to maintain the trunk at the desired value. The changes in torques were fed to a map that had been developed to convert the torques to corresponding changes in muscle activation levels. These were then fed to the FNS neuroprosthesis control unit to apply to the individual muscles.

To test the controller with a live subject with SCI, the setup depicted in Figure 3(a) and (b) was used. In this setup a wireless sensor consisting of an accelerometer was taped to the chest close to the clavicle and used to measure trunk tilt.

While sitting quietly in her wheelchair with a chest strap attached to the measurement head of a robotic dynamometer, the subject was instructed to use voluntary upper extremity effort to lean forward to an intermediate trunk position, and then release

her arms so that the forward flexed posture was supported completely by the dynamometer. Activation to the back and hip extensor muscles was then increased until the force exerted on the dynamometer head was reduced to zero. This represented the nominal stimulation required to maintain the trunk in the new, non-erect set-point. After returning to upright sitting with voluntary effort, the rope and chest strap were removed and the subject was again instructed to lean forward to the earlier forward flexed position, at which time the feedback controller was activated. When the subject released her arms, stimulation was modulated about the previously determined set-point values to maintain the new posture.

## RESULTS AND DISCUSSION

Typical responses of the model simulations for a movement of the trunk from erect to a forward posture and return are depicted in Figure 2. Figure 3 shows the plot of the trunk tilt as well as changes in muscle activation to keep the trunk at the desired posture.

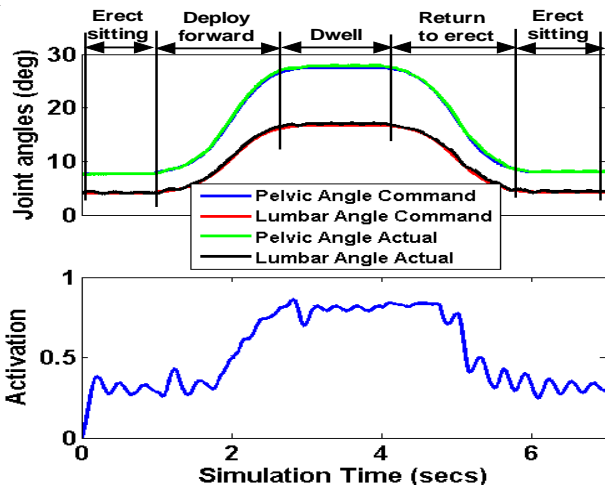


**Figure 2** Simulated Trunk Controller Operation. Top: Pelvic (blue) and lumbar (red) trajectories representing desired trunk movement, and output angles (green, black) achieved by the controller. Bottom: Activation of the *Erector Spinae* specified by the controller.

As shown in Figure 2, muscle activity was primarily required during the dwell phase of the maneuver while the trunk was maintained at the new flexed posture. This confirmed that with suitable choice of stimulus, it is possible to deploy and maintain the trunk at a posture away from erect. From Figure 3(c), as trunk tilt deviated from the

desired value, the controller either increased or decreased stimulation to keep the trunk as close as possible to the original flexed position for upwards of 10 seconds. This would sufficient time for some basic ADLs such as acquiring objects at distances beyond reach while sitting erect.

## CONCLUSIONS

The feasibility of maintaining seated posture in the coronal plane with trunk tilt angles up to  $60^{\circ}$  from erect and for periods up to 10s was established. This exploratory study indicates that the design of FNS systems for maintaining and deploying the trunk at various postures from erect is possible and worth pursuing as an alternative rehabilitation system for individuals with SCI and other paralyzing disorders.

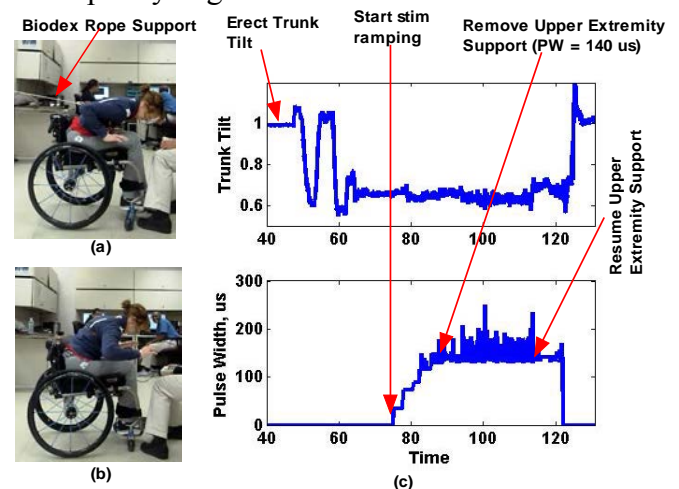


**Figure 3:** Preliminary testing of controller for maintaining trunk at desired forward tilt. (a) SCI subject (C7 AIS B) leaning forward with hands-free while stimulation to the hip and trunk muscles were adjusted to eliminate tension on an instrumented support rope; (b) subject supported at the non-erect set-point by her own stimulated muscles; (c) changes in trunk angle and muscle stimulus for a typical trial.

## REFERENCES

1. Anderson K.D., J.Neurotrauma, 2004; 21 (10) :1371-1383.
2. Murphy et al., Journal of Rehab. Res. and Dev., 2014, (51):747-760.

## ACKNOWLEDGMENTS

This work was supported by DoD (Grant #SC090230) and the VA (Grant #B6406R and Award #A9259-L).

# WHAT'S YOUR POTENTIAL? THE INFLUENCE OF KINEMATICS ON A MUSCLE'S ABILITY TO CONTRIBUTE TO THE SIT-TO-STAND TRANSFER

Sarah A. Schloemer, Laura C. Schmitt, Ajit M.W. Chaudhari, and Robert A. Siston  
 The Ohio State University, Columbus, OH, USA  
 email: schloemer.7@osu.edu

## INTRODUCTION

Induced Acceleration Analysis (IAA) estimates how muscles facilitate movement by supporting the center of mass (COM) against the force of gravity and contributing to the progression of the COM in the direction of movement [1]. Prior IAA studies provide an important baseline of how healthy adults' muscles facilitate motion during activities of daily living (ADLs) [2, 3]. However, the underlying elements of IAA describing the mechanisms by which muscle forces contribute to movement are complex and not fully understood. While muscle force greatly impacts IAA, kinematics influence these forces, as well as muscle moment arms and contributions to movement. This kinematic component of IAA is important, as it has been suggested that for patients to utilize strength gains from rehabilitation, kinematic retraining may be necessary to reprogram the motor pattern [4]. However, existing methods for estimating muscle contributions to movement require extensive time and experimental resources, making patient specific-IAA impractical in a clinical setting. Thus, the purpose of this study was to develop an efficient method for determining how kinematics impact muscle potentials to contribute to ADLs. We present a case-study comparing the effects of kinematics on muscle support potentials in end-stage knee osteoarthritis (KOA) patients and young adults (YA) during the sit-to-stand transfer (STS).

## METHODS

We created a four link sagittal plane (2D; Fig. 1) model with four revolute joints at the origin (contact point between foot and ground), ankle, knee, and hip. Four generalized coordinates ( $\theta_{0-3}$ ) define the models' degrees of freedom. Link masses ( $m_i$ ), lengths ( $L_i$ ), COM positions ( $r_i$ ), and moments of inertia ( $I_i$ ) came from a generic musculoskeletal (MS) model [5]. From Lagrangian dynamics, the equations of motion of the 2D model are given by,

$$[M]\ddot{\theta} = G(\theta) + V(\theta, \dot{\theta}) + S(\theta, \dot{\theta}) + [R]f \quad (\text{Eq. 1}),$$

where  $M$  is the mass matrix,  $\theta$  are the generalized coordinates,  $G$  is the gravitational force,  $V$  is the force due to Coriolis and centrifugal effects,  $S$  accounts for intersegmental forces, and  $f$  contains the muscle forces transformed to a generalized force by  $R$ , containing muscle moment arms. The acceleration solely due to muscle forces can be calculated as

$$\ddot{q}_m = [M]^{-1}[R]f_m \quad (\text{Eq. 2}).$$

A muscle's *potential* to accelerate the body's COM is a muscle's contribution to acceleration per Newton of force ( $\ddot{q}_m [f_m]^{-1}$ ), calculated as

$$\text{Potential} = [M]^{-1}[R] \quad (\text{Eq. 3}).$$

The mass matrix of the 2D model was derived using the linear and angular contributions to the kinetic energy of each of the links in the system [6]:

$$M = \sum_{i=1}^4 (m_i \times J_{vi}^T \times J_{vi}) + (J_{oi}^T \times I_i \times J_{oi}) \quad (\text{Eq. 4}).$$

To obtain muscle moment arms for a given kinematic state, the 2D model's generalized coordinates were transformed to the coordinate definitions of the ankle, knee, hip, and lumbar flexion in the MS model. Pelvic tilt angle was also included in the coordinate transformation as it alters hip and lumbar flexion angles, affecting moment arms and potentials of muscles crossing those joints.

Support potentials of 23 muscles were calculated for 7,824 kinematic states that could be observed in the STS momentum transfer phase [3], when the task of supporting the body is transferred from the seat to the muscles. The muscle potentials predicted by the presented (new) method were verified by potentials estimated using experimental 3D motion capture, modeling, and simulation (traditional) methods [7].

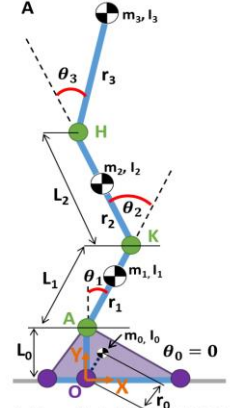


Fig. 1: Four link 2D model. Four revolute joints are at the origin (contact point between foot and ground, O) ankle (A), knee (K), and hip (H). For the STST,  $\theta_0 = 0^\circ$ .

## RESULTS AND DISCUSSION

The new method calculated muscle potentials for a single state in 6-10s using sagittal plane joint angles. The typical frame rate of a video camera commonly used in a clinical setting to capture 2D joint angles is 60 frames (or states) per second and the average STS trial takes 1 second to complete; thus, muscle potentials could be calculated for an entire trial in 10 minutes or less.

Considering a KOA patient with confirmed quadriceps weakness, to maximize the potential of the quadriceps to contribute to support (and decrease the force requirement), the new method predicts that, in a neutral pelvis position, the rectus femoris works with gravity to accelerate the COM downward, but with increasing anterior pelvic tilt the rectus femoris has increasing potential for support (Fig. 2). The new method also predicts the vasti and soleus support potentials would increase slightly with increasing anterior pelvic tilt; however, gluteus maximus potential decreases with increasing anterior pelvic tilt. To maximize the support potential of gluteus maximus, the new method suggests positioning the feet further underneath the COM and increasing lumbar flexion.

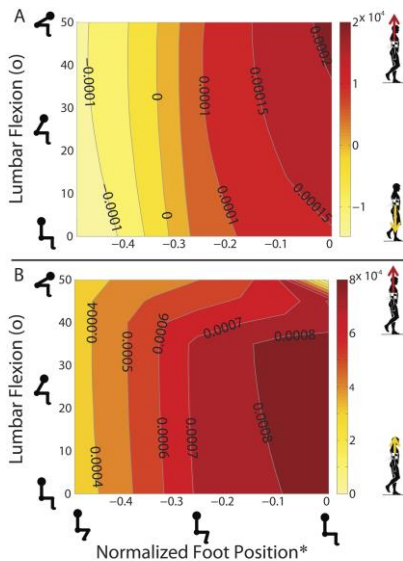


Fig. 2: Rectus femoris support potential at a range of kinematic states for A) 15° and B) 30° anterior pelvic tilt. \*Foot position normalized to leg length.

The new method predicts actual kinematic adaptations used by KOA patients to complete the STS, as confirmed by traditional simulation methods [7], which often require at least 4-6 hours to obtain IAA results for a single trial. During the STS, KOA patients had more rectus femoris support

potential than YA (Fig. 3) with greater anterior pelvic tilt (KOA:  $33.9^\circ \pm 14.0^\circ$  m/Ns<sup>2</sup> YA:  $15.2^\circ \pm 9.5^\circ$  m/Ns<sup>2</sup>) and a slightly more posterior foot position (normalized to leg length; KOA:  $-0.31 \pm 0.15$ ; YA:  $-0.29 \pm 0.11$ ) [7]. However, as

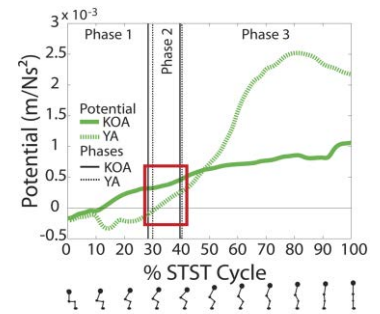


Fig. 3: Rectus femoris support potential produced by KOA patients and YA across one STS cycle [7]. The red box encompasses data from the momentum transfer phase (Phase 2).

predicted by the new method, the increased anterior pelvic tilt angle led to a smaller gluteus maximus support potential in KOA patients ( $0.0006 \pm 0.0003$  m/Ns<sup>2</sup>) than in YA ( $0.0017 \pm 0.0003$  m/Ns<sup>2</sup>). While the new method predicts the compensation strategies observed in the KOA patients, it also suggests additional strategies to further compensate for weakened quadriceps that could be targeted in rehabilitation. The KOA patients could improve overall muscle contributions to support by decreasing their anterior pelvic tilt by 5° and increasing lumbar flexion by 10° to double the gluteus maximus support potential without significantly reducing the rectus femoris potential.

## CONCLUSIONS

This study demonstrates an efficient method to systematically evaluate the effects of kinematic changes on muscle potentials, predict possible sources of pathologic movement, and identify rehabilitation strategies that leverage kinematics and muscle strength to improve mobility.

## REFERENCES

1. Winter D. *The Biomechanics and Motor Control of Human Gait*, University of Waterloo Press, 1987.
2. Neptune, RR, et al. *J Biomech* **41**, 1387-98, 2001.
3. Caruthers, EJ, et al. *J Appl Biomech* **32**, 487-503, 2016.
4. Fisher NM, et al. *Disabil Rehabil* **19**, 47-55, 1997.
5. Delp, SL, et al. *IEEE Trans Biomed Eng* **37**, 757-67, 1990.
6. Craig, JJ. *Introduction to Robotics: Mechanics and Control*, 3<sup>rd</sup> ed. Pearson Education, 2005.
7. Cullen, MK. *Muscle-Driven Simulations of Sit to Stand Transfer in Persons with Severe Osteoarthritis* (Masters' thesis). 2016.

# Simple and Two-Element Hill-Type Muscle Models Cannot Replicate Realistic Muscle Stiffness

<sup>1</sup> Ali Marjaninejad, <sup>1</sup> Babak Taherian, <sup>1</sup> Kian Jalaeddini, and <sup>1</sup> Francisco J Valero-Cuevas

<sup>1</sup> University of Southern California, Los Angeles, CA, USA  
email: marjanin@usc.edu, web: <http://valerolab.org/>

## INTRODUCTION

An important functional property of muscle is to provide stiffness for the limbs [1]. Joint and limb endpoint stiffnesses are critical to control limb posture, movement and interaction with the environment [1,2]. In general, stiffness produces instantaneous resistance to change in muscle length. Stiffness is known to be modulated muscle length (i.e., by joint angles) and muscle activation levels (i.e.  $\alpha$  drive) [3], but the mechanisms that produce them remain unclear.

Hill-type models are a class of normalized lumped-parameter models of muscle of varying complexities that can be scaled to approximate specific muscles. They estimate muscle force as functions of muscle architecture (physiological cross sectional area and pennation angle), kinematic state of muscle (length, and velocity) and the muscle activation level ( $\alpha$  drive) [4,5]. The goal of this project is to assess the ability of Hill-type models to produce muscle stiffness [6].

## METHODS

In this project, we studied versions of two popular Hill-type muscle models. The first model is a simple linear model consisting of series and parallel springs, a viscous element and a contractile element referred herein as the simple Hill-type model without force-length properties (or the Hill-type w/o fl) [4]. The contractile element converts the  $\alpha$  drive to active muscle force. This model, as presented, did not have force-length properties. Thus, we modified it by adding force-length properties to it (i.e., Hill-type w fl). The two-element Hill-type model incorporates two parallel active contractile elements for slow and fast muscle fibers (i.e., Two-Element model) [5]. Note that the active force-length

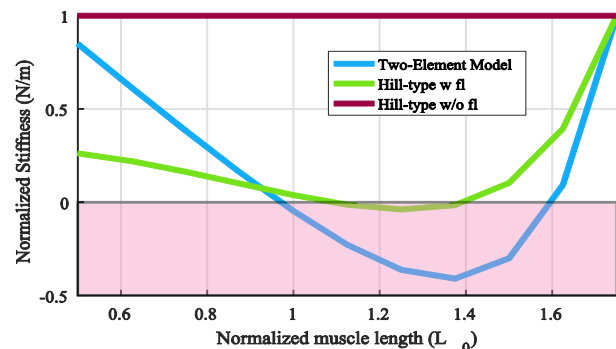


**Figure 1:** Stiffness as a function of muscle length.

properties of muscle (included in the contractile element) are not equivalent to the Hook's law stress-strain relationship. Rather, they represent the active force the muscle can produce at each length for a given activation level [7].

We estimated muscle stiffness in quasi-static condition by applying ten small displacements (of 2.5%  $L_0$ , where  $L_0$  is the optimal muscle length) with the muscle lengths set between 0.5  $L_0$  and 1.8  $L_0$  while the muscle was fully activated. We also calculated values of stiffness at two lengths (0.8 and 1.2  $L_0$ ) for  $\alpha$  drive ranging between 0 to 100 percent in steps of 1%.

## RESULTS AND DISCUSSION

Figure 1 shows stiffness for all models as a function of normalized muscle length. To make figures easier to compare, all figures are normalized to their maximum absolute value. Stiffness for the simple Hill-type model without force-length properties does not depend on muscle length (red). Stiffness varies as a function of muscle length for the other two models (blue and green). However, it becomes negative at some lengths. It is clear that the negative stiffness is not physically possible since it results in instability. Both of the two-Element and modified Hill-type

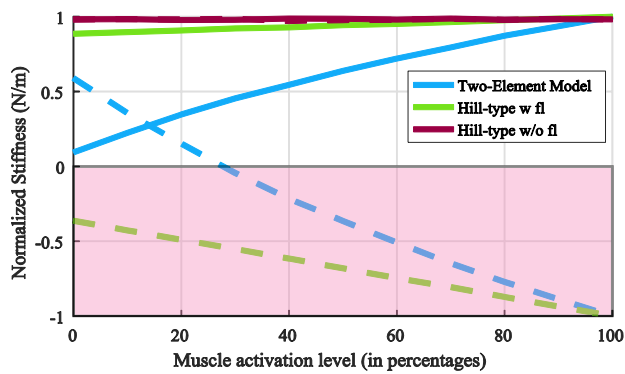


**Figure 2:** Stiffness as a function of muscle lengths equal to  $0.8 L_0$  (solid lines) and  $1.2 L_0$  (dashed lines).

models, however, show patterns similar to that reported in experiments in their non-negative regions [8]. Figure 2 shows the stiffness for all models as a function of muscle activation level at two representative muscle lengths ( $0.8, 1.2 L_0$ ). Once again, stiffness is *not* a function of muscle activation in the absence of force-length properties (red). Stiffness for the two-Element model *does* vary with the muscle activation level for the other two models in a length-dependent manner (blue and green). Interestingly, this change in the stiffness was consistent with the relative proportions of the derivatives of the active and passive parts of the force-length curve. i.e. the more the activation, the larger the weight of the active part. This result is expected considering that activation applies only to the active part of the force-length curve of muscle. As can be seen on the figures, the stiffness can be negative for both length dependent models (blue and green) when the muscle length is longer than  $L_0$ , which demonstrates that the models fail to replicate realistic muscle stiffness.

## CONCLUSIONS

Our results show the simplest Hill-type model fails to reproduce both muscle length and activation dependence of stiffness. The modified and two-element Hill-type muscle models produced stiffness dependence on muscle length and activation, but invariably produce negative stiffness at some muscle lengths, which is not physically realistic. Although force-length properties are very important in explaining stiffness [1,2], Hill-type models cannot

replicate realistic muscle stiffness even when including presence of force-length properties. Future work will explore if dynamic simulations (as opposed to this quasi-static version) and other extensions, such as the inclusion of force-velocity properties, can produce realistic muscle stiffness. If those efforts are unsuccessful, other models such as population-, fiber- and sarcomere-based—although more computationally complex—would need to be preferred.

## REFERENCES

1. Inouye J. M, and Valero-Cuevas F. J. *PLoS Comput Biol*, **12**, p. e1004737, 2016.
2. Babikian S, et al. *J. Nonlinear Sci.*, **26**, 1293–1309, 2016.
3. Mirbagheri M. M. *Exp. Brain Res.* et al. **135**, 423–436, 2000.
4. Shadmehr R, and Wise S. P, MIT press, 2005.
5. Lee S. S. M, et al. *J. Biomech.*, **46**, 2288–2295, 2013.
6. Valero-Cuevas F. J, et al. *IEEE Rev. Biomed. Eng*, **12**, 110-135, 2009
7. Valero-Cuevas F. J. *Fundamentals of neuromechanics*, Springer, 2015
8. Weiss P.L, et al. *J. Biomech.*, **19**, 727-735, 1986.

## ACKNOWLEDGMENTS

This study was supported by NIH-NIAMS under award numbers R01AR050520 and R01AR052345 grants to FVC. This project is also supported by USC graduate school's provost fellowship to A.

# Modeling Stiffening in the Neck in Specified Directions Through Muscle Coactivation

Jonathan Mortensen, Andrew Merryweather

Department of Mechanical Engineering  
University of Utah  
Salt Lake City, UT, USA  
email: Jon.Mortensen@utah.edu

## INTRODUCTION

Neck muscles contract to generate stiffness in preparation for impacts to the head or trunk which alters head kinematics by decreasing maximum accelerations [1, 2]. During unanticipated impacts, or blindsides, the muscle reflex response alone is too slow to develop adequate stiffness. Our current understanding of the role neck stiffness plays in protecting the brain during impacts such as those experienced in popular collision sports is limited. This research aims to develop a musculoskeletal model of the neck to increase our understanding of how muscle contractions initiated with adequate timing prior to an impact affect rotational accelerations of the head.

Previous research modeled coactivation to solve for muscle activations in musculoskeletal models. Three widely used approaches are: maximizing total muscle force, maximizing total muscle activation, and maximizing muscle activation with a constraint of obtaining a certain stiffness level [3-5]. These approaches suggest the need for modeling subject awareness and coactivation. However, the ability to adjust muscle activations based on the direction of an impact is limited. The anatomy of the neck would suggest that it is unlikely that coactivation occurs the same way for all impacts. Our work adds two novel approaches to modeling coactivation that maximizes directional neck stiffness. This exploration of objective functions will allow improved model approximations for experimental data, which will give greater insights to how muscle contraction plays a role in protecting the brain during impacts.

## METHODS

Modifications to an existing model were made to enable the use of dynamic optimization tools in

OpenSim [6]. In order to make the model suitable for dynamic simulations, several modifications were necessary. First, muscles were mirrored across the sagittal plane to produce a more complete muscle set (total number of muscles in the model to 78). Second, values for mass and inertia were added for each solid body represented in the model (i.e. head and vertebrae). Third, joint stiffness caused by ligaments and other passive structures was incorporated. Data from Lee et al. (2006) provided mass and inertia values for each solid body and stiffness properties for each joint.

Muscle properties from the musculoskeletal model were passed into MATLAB, and a function was created to calculate moments generated about various degrees of freedom given muscle activations. Zero net moment was used as a constraint for the optimization problem to calculate muscle coactivation. The MATLAB function is described as:

$$M_k = \sum_{i=1}^{78} a_i f_i r_i$$

where  $M_k$  is the moment about degree of freedom  $k$ ,  $a_i$  is the activation of a single muscle,  $f_i$  is the maximum force a muscle can generate, and  $r_i$  is the moment arm of muscle  $i$  about degree of freedom  $k$ . Coactivation was calculated using objective functions of maximizing activation and maximizing force with the “fmincon” optimizer. This was done to provide a baseline for achieved stiffness with approaches from past research.

Maximizing Stiffness [MS] was achieved in MATLAB by first computing the stiffness each muscle contributes in a specified direction, and then optimizing for the greatest stiffness in that direction. Stiffness was computed by determining the change in muscle force as the head rotates one degree in a

specified direction. This approach allows for the computation of muscle activations that provide maximum stiffness in any direction.

The Push-Pull [PP] approach was performed using OpenSim's static optimization tool. Activations were computed that resist an applied force in a specified direction. Muscle activations were then computed to resist force in the opposite direction which resulted in stable coactivation.

A valid solution was determined when stability requirements satisfied values published in previous research that limit head rotation to 5 degrees or less in 100ms [3].

The computed muscle activations that produced stability were then tested for stiffness (Figure 1). This was done by rotating the model so that gravity acted in the direction of 30 degrees from the sagittal plane and then applying the muscle activations. Both approaches were performed with the specified direction being 30 and 60 degrees from the sagittal plane. Increased stiffness is manifest by decreased deviation of the head from the neutral position.

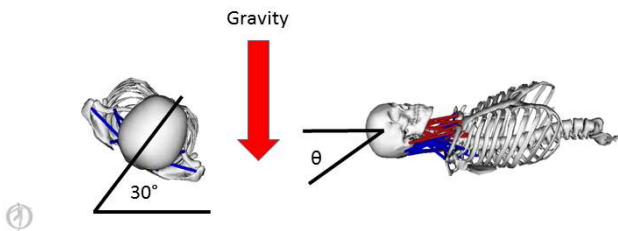


**Figure 1:** Depiction of Stiffness Testing

## RESULTS AND DISCUSSION

The new approaches used in this study were sufficiently stable. Both the MS and PP approaches for 30 and 60 degrees from the sagittal plane obtained higher stiffness levels than maximizing muscle force or muscle activation. The PP approach gave similar results for both the 30 and 60 degree solutions. The MS approaches gave the greatest stiffness of all, with the 30-degree solution being the stiffest.

This work highlights the differences in neck stiffness produced through coactivation to account for forces in off-sagittal-plane directions. This is something that is missing in previous research, but is important to understand the role of muscle contraction during

impacts. This work explored two approaches capable of simulating stiffening response to oblique forces. The MS approach shows particular promise, because it generates the highest stiffness levels achievable through coactivation of muscles alone. Combining this approach with additional constraints on muscle activation levels may be useful to better fit musculoskeletal model parameters to humans preparing for impacts to the head or torso. Future work is needed to confirm the biological significance of this work.

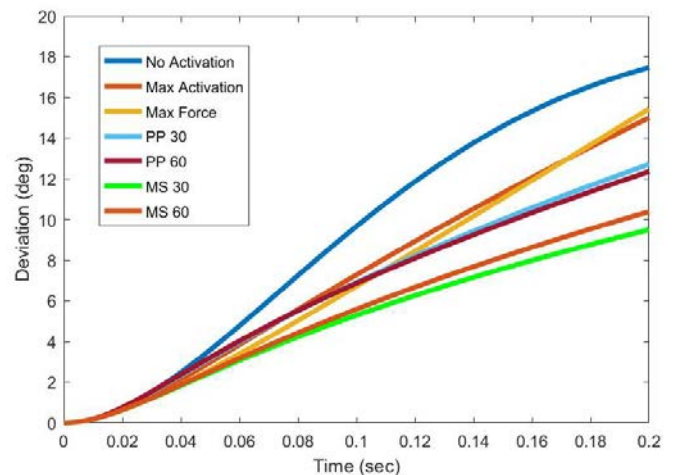


**Figure 2:** Head rotation for each simulation where smaller angles indicate higher stiffness

## REFERENCES

1. Eckner, J.T., et al., *The American journal of sports medicine*, 2014. **42**(3): p. 566-576.
2. Mang, D.W., et al., *The Spine Journal*, 2015. **15**(1): p. 153-161.
3. Chancey, V.C., et al., *Stapp Car Crash Journal*, 2003. **47**: p. 135.
4. Lee, S.-H. and D. Terzopoulos., *ACM Transactions on Graphics (TOG)*. 2006. ACM.
5. Rashedi, E., et al., *Proceedings of the Institution of Mechanical Engineers, Part H: Journal of Engineering in Medicine*, 2010. **224**(3): p. 487-501.
6. Vasavada, A.N., S. Li, and S.L. Delp, *Spine*, 1998. **23**(4): p. 412-422.

## ACKNOWLEDGMENTS

This research was funded in part by grants from the National Science Foundation (#1622741) and NIOSH (NIOSH Education and Research Center training grant T42/CCT810426-10)

# A MECHANISTIC DAMAGE MODEL FOR LIGAMENTS

Jeff M. Barrett<sup>1</sup> & Jack P. Callaghan<sup>1</sup>

<sup>1</sup>Department of Kinesiology, University of Waterloo, Waterloo Ontario, Canada

email: jeffery.barrett@uwaterloo.ca

## INTRODUCTION

The cervical spine is vulnerable to acute injury and the development of chronic pain, often attributed to damage of soft tissues from loading [1]. Computational models of this region may be useful to gain insight into the loads placed on tissues in injurious situations; however, accurate models of tissues are required to ensure that they provide realistic force-deformation predictions.

Unfortunately, most models use phenomenological ligament models that neglect behaviour in the failure region [1]. Therefore, the purpose of this investigation was to test whether a mechanistic model of ligamentous tissue portrays behaviour representative of actual ligament failure and cyclic loading tests.

## METHODS

### *Model Description*

The model tracks the time-evolution of a population of collagen fibres ( $n$ ) in a theoretical ligament, distributed by the length they are stretched ( $x$ ), much like the renowned Huxley muscle model [3] (Equation 1). The initial distribution of collagen fibres is assumed to be normal with a mean  $\mu$  and standard deviation  $\sigma$ . Each collagen fibre is treated as a linear cable with stiffness  $k$  for force calculation (Equation 2). A breaking function describes how quickly collagen fibres will break if they are stretched by a given length, and was assumed to be a step-function.

$$\frac{\partial n}{\partial t} - v \frac{\partial n}{\partial x} = -B_0 \Theta(x - x_0) n(x, t) \quad (1)$$

I.C:

$$n(x, 0) = \frac{1}{\sqrt{2\pi}\sigma} \exp\left(-\frac{(x - \mu)^2}{2\sigma^2}\right)$$
$$F(t) = \int_0^{\infty} kx n(x, t) dx \quad (2)$$

Here:  $n(x, t)$  = Collagen fibres stretched by  $x$  at time  $t$ .

$v$  = The shortening velocity

$\Theta(x)$  = The Heaviside step function

$B_0, x_0$  = Parameters which control how quickly fibres break and at which displacement

$\mu, \sigma$  = The mean and standard deviation of the initial collagen distribution

$k$  = The stiffness of each collagen fibre

### *Experimental Data*

The model was fitted to an experimental average force-elongation curve reported in [2] for the Anterior Longitudinal Ligament (ALL) using scipy's minimize function with five free parameters:  $\mu$ ,  $\sigma$ ,  $k$ ,  $B_0$ , and  $x_0$ . These curves were obtained by loading ligaments from young cadavers ( $n = 21$ ) to failure while measuring elongation and force with strain gauges and linear variable displacement transformers (LVDT) (Omegadyne Inc. Model LC412-500), with averaging across all specimens. The curves themselves are presented in [2].

### *Cyclic Loading*

The fitted model was cyclically loaded to a displacement of 3 mm at 0.5 Hz in order to test if micro-traumas in the ligament model manifest as a plastic deformation.

## RESULTS AND DISCUSSION

### Fitted Model

The model agreed very well with experimental data (Figure 1; parameters in Table 1), with a total RMS error of 14.23 N (1.67 N in the toe-region, and 15.697 N in the failure region), and an  $R^2$  of 0.994.

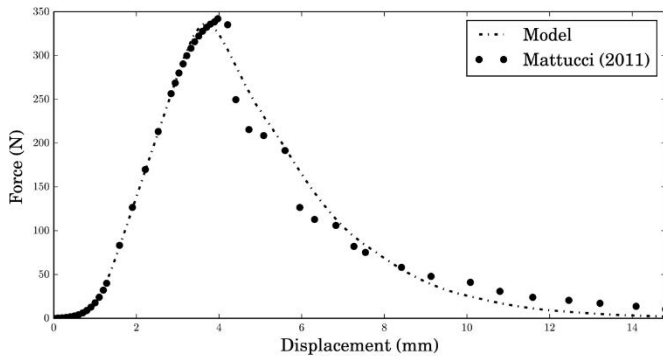


**Figure 1:** The model force-elongation curve versus that obtained from experiment.

### Cyclic Loading

There is a marked decrease in the force production of the ligament with cyclic loading accompanied by a 20% decrease in overall stiffness (Figure 2). Additionally, the ligament returns to a negligible force at a higher degree of strain, indicating plastic deformation of the resting position. With the absence of viscoelastic effects in the model, the observed hysteresis is entirely due to the destruction of collagen fibres.

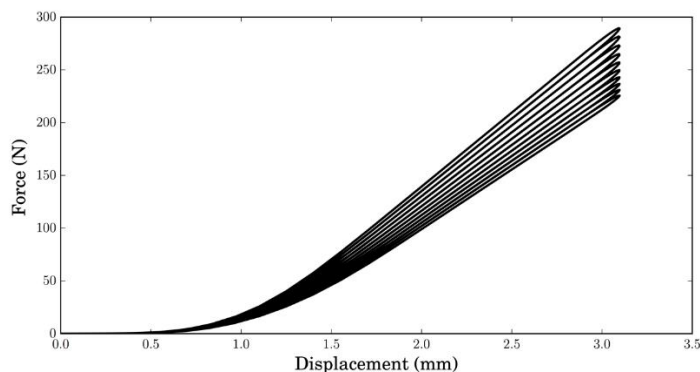


**Figure 2:** Response of the ligament model to cyclic loading.

**Table 1:** Fitted Parameters derived from experimental data for the Anterior Longitudinal Ligament.

$B_0$ ( $s^{-1}$ )	$x_0$ (mm)	$\mu$ (mm)	$\sigma$ (mm)	$k$ (N/mm)
1.39	2.66	-0.985	0.2941	136.7

The presented model opens the doors for future macroscopic models to predict ligament injury, which may have far-reaching applications from ergonomic assessment, to sport, to the analysis of fringe impact scenarios. More theoretically, it amalgamates the study of ligaments and muscles, as it demonstrates that Huxley's equation can be used to model both tissues.

## CONCLUSIONS

This mechanistic model displayed behaviour reminiscent of true ligaments being strained to failure; featuring toe and failure regions that are consistent with the currently accepted mechanisms which govern their shape. Future work could incorporate viscous effects into the model, and validate it by comparing model predictions to other loading conditions.

In cyclic loading the model plastically deforms, a behaviour which is inherently difficult to model. The plastic deformation in the model is governed by the breaking function, which future investigations should attempt to establish more rigorously across different ligaments.

## REFERENCES

1. Yoganandan, N. et al., *Clin Biomech* **16**(1), 1-27, 2001.
2. Mattucci S. *M.A.Sc Thesis University of Waterloo*, 2011.
3. Huxley, AF. et al., *Prog. Biophys Biophys Chem.* **7**, 255-318, 1957.

# DIFFERENCES IN THE ACTIVE STATE OF A SIMULATED ANKLE MUSCLE USING TWO FOOT MODELS

Justin C. Wager and John H. Challis

Biomechanics Laboratory, The Pennsylvania State University, University Park, PA, USA  
e-mail: jcw296@psu.edu

## INTRODUCTION

Muscle-driven simulations of human movement traditionally treat the foot a single rigid segment comprising all the bones proximal to the metatarsophalangeal joint. Recent efforts in kinematic modeling have segmented the foot into three or more links [1, 2] and provided evidence that multisegment and single segment foot models generate different ankle joint kinematics during walking [3]. This difference in ankle joint kinematics could produce a difference in simulated ankle muscle kinematics, thereby leading to changes in the active state required to generate a given joint moment. Though many muscle-driven simulations of human movement utilize a single segment foot, the influence of foot model choices on ankle muscle simulations has not yet been demonstrated. This study aimed to compare the active state of a Hill-type ankle plantarflexor muscle during human running using two different foot models to compute ankle joint kinematics from experimental data.

## METHODS

Marker trajectories and ground reaction forces were collected from seven healthy subjects (3 M, 4 F; age =  $30.7 \pm 10.1$  years; mass =  $66.2 \pm 10.5$  kg) running barefoot at  $3.1 \text{ m}\cdot\text{s}^{-1}$ . The subjects performed three trials using a rearfoot contact pattern. Bony landmarks of the foot and lower leg were tracked using 18 passive retroreflective markers.

Two foot models (single segment and multisegment) were developed within MATLAB 2016a. The single segment foot model was similar to those used in traditional analyses, with one segment to represent the bones between the ankle and metatarsophalangeal joints. In contrast, the multisegment foot model separated the foot into three segments (talus/calcaneus, midfoot, toes) as in [4]. In both models, joint rotation matrices

were decomposed into Cardan angles using a ZXY sequence and angles were normalized to a static trial with the ankle at approximately 90 degrees. The ankle joint angle and ankle resultant joint moment were averaged within subjects and then across subjects to obtain group means. These mean values were used as inputs for a uniarticular ankle plantarflexor muscle model to compare the effect of foot model on ankle muscle active state during running.

The uniarticular ankle plantarflexor muscle was represented as a Hill-type model. The muscle tendon unit length change and muscle moment arm over the stance phase were calculated as in [5, 6]. Force-length, force-velocity, and tendon parameters were taken from [7]. Peak isometric force capacity was set to 6000 N, as in [8] for the combined gastrocnemius and soleus of one leg.

The muscle active state over the stance phase was compared between the two models (single segment foot & multisegment foot) with all parameters held constant except the ankle angles and resultant joint moments computed from the experimental running data.

## RESULTS AND DISCUSSION

The muscle active state differed between the two models during the second half of stance only (Figure 1). Peak active state using the single segment foot model was double that of the multisegment foot model. As no differences were found in the resultant ankle joint moment or muscle force between the two models, the difference in active state was mainly due to the differences in fiber kinematics. Using the multisegment foot model, the fibers operated closer to their optimal length (Figure 2) and shortened at low velocities during late stance (Figure 3), which agrees with experimental ultrasound data for the soleus muscle during running [9].

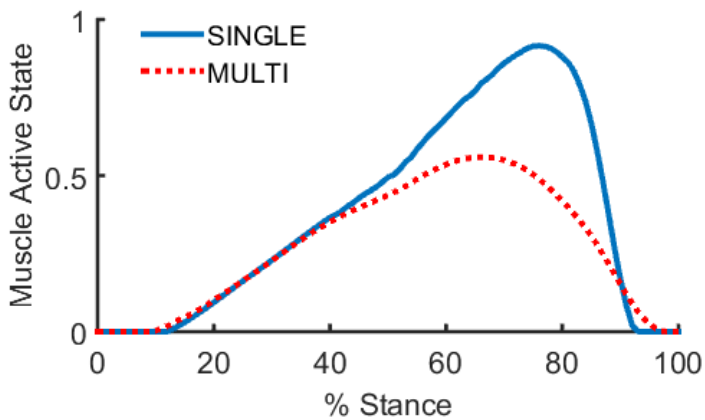


**Figure 1:** Active states of the Hill-type muscle models with a single segment foot or multisegment foot model.

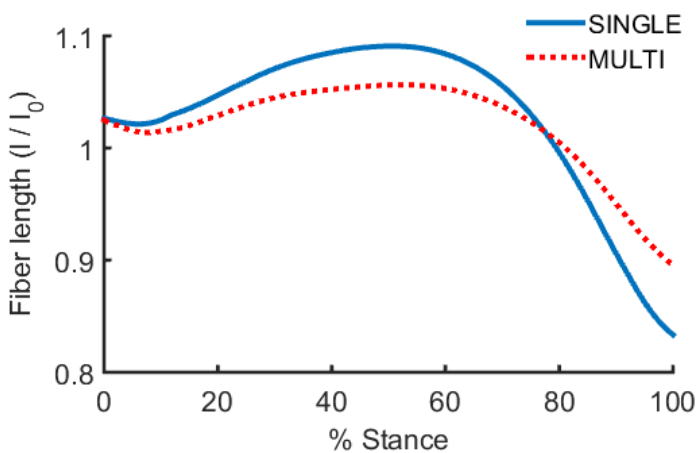


**Figure 2:** Simulated fiber lengths (relative to optimum fiber length,  $l_0$ ) of the Hill-type muscle models with a single segment foot or multisegment foot model.

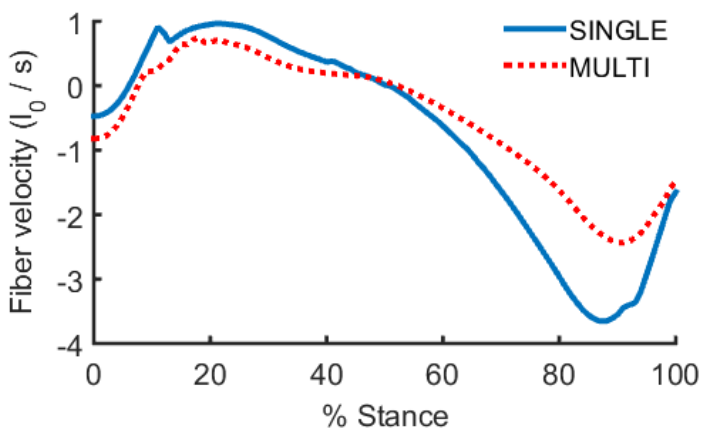


**Figure 3:** Simulated fiber velocities of the Hill-type muscle models with a single segment foot or multisegment foot model. A negative velocity indicates shortening.

## CONCLUSIONS

Muscle-driven simulations of human locomotion have provided significant insights in biomechanics, but most of these simulations have utilized a single segment foot. While this may provide advantages for simulation time and complexity, it may introduce inaccuracies in ankle joint kinematics. These kinematic inaccuracies can propagate to the simulated ankle joint muscles and produce inaccuracies in the active state. Here, a uniarticular plantarflexor muscle driven with ankle kinematics from a multisegment foot model (with the calcaneus tracked separately from the midfoot and forefoot) produced muscle kinematics which were closer to experimental data than an identical muscle model driven with angles from a single segment foot model.

## REFERENCES

1. Carson, M.C., et al. *J Biomech* **34**, 1299–1307, 2001.
2. MacWilliams, B.A., et al. *Gait Posture* **17**, 214–224, 2003.
3. Pothrat, C., et al. *Clin Biomech* **30**, 493–499, 2015.
4. Okita, N., et al. *Gait Posture* **30**, 27–34, 2009.
5. Grieve, D.W., et al. *Biomech VI* **2A**, 405–412, 1978.
6. Bobbert, M.F., et al. *J Biomech* **19**, 887–898, 1986.
7. Challis, J.H. & Domire, Z.J. *Mov Sport Sci/Sci Mot* **90**, 69–78, 2015.
8. van Soest, A. J., et al. *J Biomech* **26**, 1–8, 1993.
9. Lai, A. et al. *J Appl Physiol* **118**, 1266–1275, 2015.

# EFFECTS OF REMOTE PAIN ON MUSCLE FATIGUE DURING REPETITIVE MOVEMENTS

<sup>1</sup>Jeffrey C. Cowley, and <sup>1,2</sup>Deanna H. Gates

<sup>1</sup> School of Kinesiology, University of Michigan, Ann Arbor, MI, USA

<sup>2</sup> Department of Biomedical Engineering, University of Michigan, Ann Arbor, MI, USA  
email: jccowle@umich.edu

## INTRODUCTION

Muscle fatigue is a decrease in force output capacity of muscles. During motor tasks, people can adapt to muscle fatigue by modifying their movement patterns and control strategies. However, this process is cognitively demanding [1]. In complex environments, competing stimuli may affect the way that people are able to adapt during muscle fatigue.

Like muscle fatigue, painful stimuli can cause people to modify their movements [2]. When people experience pain, they direct their attention to the painful area. This can impair motor-cognitive performance [3] and affect the way that people learn motor tasks [4]. In some settings, the cognitive processes related to pain and muscle fatigue may compete for limited mental resources.

This study examined how pain in a remote area of the body affects muscle fatigue during repetitive movements. We hypothesized that pain would reduce the ability to develop successful movement strategies during fatigue, leading to larger errors and faster rate of fatigue.

## METHODS

22 right-handed subjects (11 male) completed the same repetitive task to voluntary exhaustion on two separate days (pain and no pain sessions). They were harnessed to a chair with the right upper arm strapped to a solid brace at  $\sim 90^\circ$  of humeral elevation (Fig. 1A). They grasped a handle attached to a weighted sled (15 % max. elbow flexion strength) and slid the weight back and forth on a low-friction surface in time to a metronome ( $\sim 2.6$  Hz) until they felt they could not continue. In the pain session, ischemic pain was induced in the left arm by applying a blood pressure cuff to the arm (220 mmHg) until subjects

could no longer tolerate the pain or reached a 20 min. safety limit [5]. The fatigue task began when subjects reached a pain threshold ( $\geq 3/10$ ) and continued until voluntary exhaustion. Every 30 seconds, subjective ratings of perceived exertion (RPE) and pain were obtained verbally using numeric scales. Elbow and wrist maximum voluntary contraction strength (MVC) was measured before and after the fatigue task to quantify muscle fatigue. The position of a marker on the handle was tracked at 120 Hz.

Subjects were instructed to maintain movement time so the end of each flexion or extension movement coincided with a metronome beat. Non-dimensional movement distance ( $D$ ) and speed ( $S$ ) were obtained by dividing the length of each movement by forearm length and average speed by forearm length and metronome frequency. A goal equivalent manifold (GEM) was defined as any combination [ $D$ ,  $S$ ] which achieves the correct movement duration (Fig. 1B). Timing errors, and  $D$ , and  $S$  were obtained for all push and pull movements of each fatigue trial. Five equally spaced data bins (160 movements:  $\sim 1$  min.) from each trial were examined, where the first and

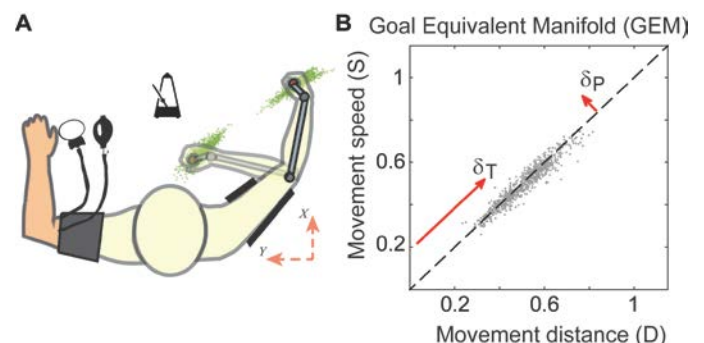


**Figure 1.** Subject setup (A). The task goal was to complete each movement in one metronome beat ( $T$ ). The goal equivalent manifold is shown (B; dashed line). Data points (grey) lying on the dashed line satisfy the timing goal of the task, wherein  $D/S = T$ . Deviations away from the GEM ( $\delta_p$ ) affect performance. Deviations along the GEM ( $\delta_T$ ) do not.

last minutes of fatigue were bins one and five, respectively. Detrended fluctuation analysis was applied to all data series to obtain temporal correlations,  $\alpha$ . The value  $\alpha$  indicates how quickly deviations are corrected in a data series. Lower values indicate that deviations are corrected more rapidly. Dependent measures were analyzed using two-factor within subjects ANOVAs to test for differences due to fatigue state (bin 1-5) and session (pain vs. no pain). Session order was included as a covariate to control for effects of order (pain first vs. no pain first).

## RESULTS AND DISCUSSION

Subjects reported higher pain ratings during the pain session than the no pain session ( $p < 0.001$ ; Fig. 2). They reached an RPE of 8 or greater during all fatigue trials, and MVC strength declined after fatigue in all muscle groups measured ( $p < 0.004$ ).

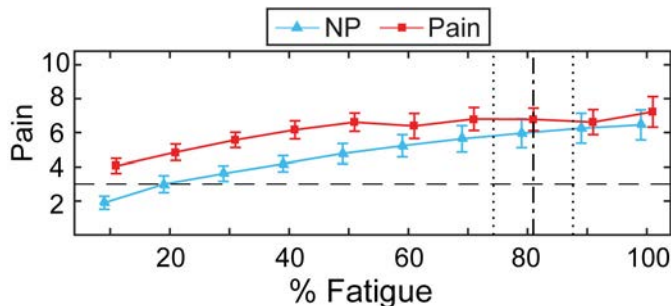


**Figure 2.** Subjective pain ratings during fatigue. Error bars show 95% confidence intervals. Black lines show the pain threshold of 3 (horizontal dashed) and mean cuff deflation time (vertical dash-dot) with 95% confidence interval (dot) during the pain session.

Endurance time increased on the second test day for the subjects who completed the pain session on day one ( $p = 0.014$ ; Fig 3A). Timing errors did not change with pain or fatigue ( $p > 0.13$ ). Deviations perpendicular to the GEM ( $\delta_P$ ) decreased on the second test day, suggesting that subjects improved their ability to maintain the timing goal regardless of session order. Movement distance,  $D$ , speed,  $S$ , and  $\delta_T$  declined during the fatigue task in both sessions ( $p < 0.001$ ; Fig. 3B). Session  $\times$  fatigue interaction effects ( $p < 0.04$ ) indicated that subjects exerted less control (higher  $\alpha$ ) over  $D$ ,  $S$ , and  $\delta_T$  during the first part of the pain session. However, this effect disappeared by the end of the pain session (Fig. 3C).

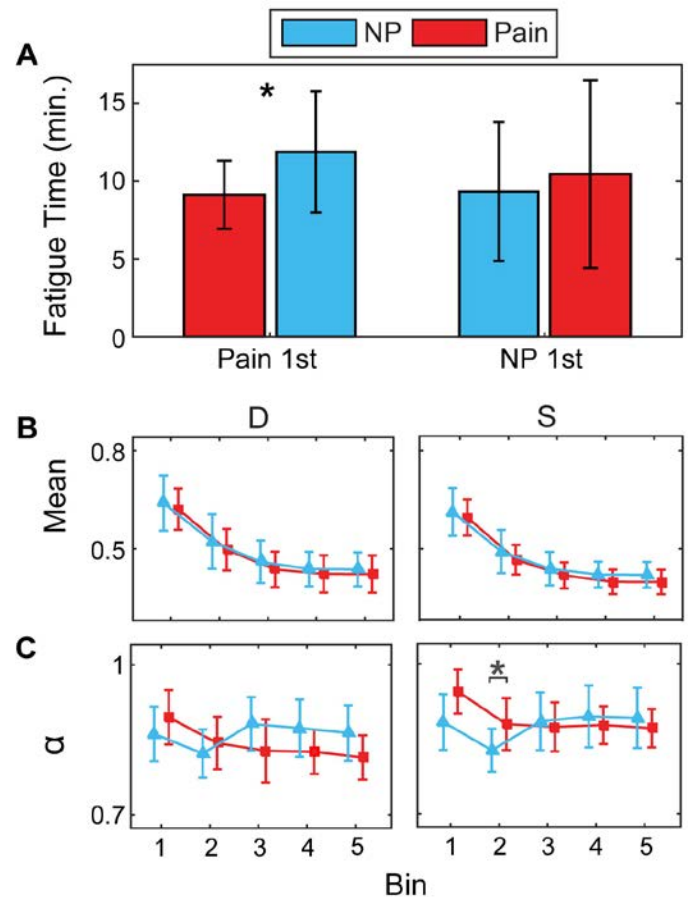


**Figure 3.** Fatigue task duration (A). Mean (B) and temporal correlation,  $\alpha$  (C), of movement distance,  $D$ , and speed,  $S$ . Error bars show 95% confidence intervals. \* indicates a significant difference between sessions.

## CONCLUSIONS

Remote ischemic pain initially caused subjects to reduce movement control, but this effect was reduced quickly as subjects acclimated to the painful stimulus. Previous exposure to the fatigue task and the painful stimulation affected the execution of the task during subsequent sessions. Future work should examine changes in movement control and muscle fatigue in people with chronic pain conditions.

## REFERENCES

1. Terrier R., et al. *J Electromyogr Kinesiol*, 6, e487-93, 2009.
2. Ervilha UF, et al. *Exp Brain Res* **164**, 215-24, 2005.
3. Moseley GL, et al. *Cog Brain Res*, **1**, 188-94, 2005.
4. Dancy E, et al. *Pain*, **8**, 1682-95, 2016.
5. Maixner W, et al. *Clin J Pain*, **9**, 16-25, 1993.

# STIFFNESS PERCEPTION AT THE HUMAN ANKLE AND KNEE

Alejandro F. Azocar and Elliott J. Rouse

Northwestern University, Evanston, IL, USA; Rehabilitation Institute of Chicago, Chicago, IL, USA  
email: erouse@northwestern.edu; web: <http://neurobionics.smpp.northwestern.edu/>

## INTRODUCTION

Regulation of neuromuscular activation during walking causes changes in joint kinetics, kinematics, and mechanical impedance. Joint impedance—the relationship between position and torque—is often parametrized by stiffness, damping, and inertia, and governs energy storage and exchange between joints. Recently, perturbation studies have quantified human joint impedance during gait, providing new insight beyond the traditional biomechanical descriptions of kinetics and kinematics [1]. However, the role of joint impedance in control of locomotion and, consequently, in the development of wearable robotic systems, is not fully understood; in particular, the human ability to sense changes in mechanical impedance properties is unknown.

The purpose of this psychophysical study is to quantify the minimum detectable change in the stiffness component of impedance with the ankle or knee. We sought to determine the just noticeable difference (JND) and corresponding Weber fraction (WF) for stiffness. The JND is the smallest stimulus increment that a subject can detect, and normalizing it results in the WF [2]. We found that subjects can sense a stiffness change of 12% or higher.

## METHODS

Ten healthy, able-bodied subjects (4 female, 6 male; age  $24.9 \pm 3.7$  years; mass  $71.2 \pm 12.4$  kg; mean  $\pm$  s.d.) gave written informed consent to take part in the ankle study, which was approved by the Northwestern University Institutional Review Board; ten healthy, able-bodied subjects (6 female, 4 male; age  $22.2 \pm 2.0$  years; mass  $64.5 \pm 11.0$  kg) gave written informed consent to take part in the knee study. Subjects had neither neurological impairment nor ankle/knee injury.

The Neurobionics Lab Rotary Dynamometer, a frame-mounted motor (Fig. 1, green) with a six-axis

load cell (Fig. 1, pink) used an admittance controller to render the dynamics of a virtual rotational spring-damper system in parallel with the ankle or knee joint. Subjects sat in a Biodex chair and placed their right leg on a plate (Fig. 1, blue) connected to the motor output shaft via a linkage (Fig. 1, yellow); the load cell was attached between the leg plate and the linkage. The ankle or knee joint was aligned with the motor axis and was free to rotate. Subjects were blindfolded and wore noise-reducing headphones to prevent use of visual and auditory cues and to reduce environmental distractions.

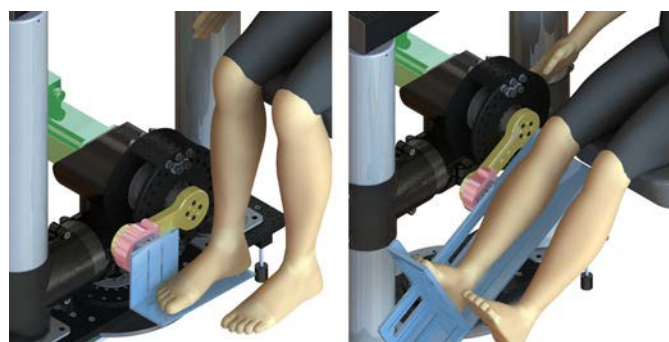


**Figure 1:** Experimental setup for the (left) ankle and (right) knee experiments.

The experiment implemented a two-interval forced-choice (2IFC) paradigm; during each trial, the subjects interacted with the motor while it rendered the spring-damper dynamics. Two sets of dynamics were presented per trial; one with a reference stiffness and the other with a comparison stiffness. Subjects were instructed to interact with the motor by voluntarily extending and flexing the ankle or knee joint. Subjects were exposed to each set of dynamics for eight seconds, then were asked to report which set had a higher stiffness, or resistance to movement. A response of “equal stiffness” was prohibited. Additionally, subjects were not told if their responses were correct or incorrect.

For the ankle experiment, we tested reference stiffness values of 50, 125, and 200 N·m/rad, and for the knee experiment we tested at 125, 200, and

275 N·m/rad. Higher reference stiffness values were too difficult to interact with. The inertia and damping values were 0.3 kg·m<sup>2</sup> and 1 N·m·s/rad, respectively, for all trials.

We implemented Kaernbach's weighted up-down staircase method; this method converges to the JND at the 75% performance point, halfway between guessing (50%) and perfect performance (100%). A base step size,  $\Delta$ , of 5 N·m/rad was used [3]. The better a subject performed, the more challenging the experiment became, and vice versa.

## RESULTS AND DISCUSSION

Stiffness JND increased linearly whereas WF decreased reciprocally for both joints (Fig. 2).

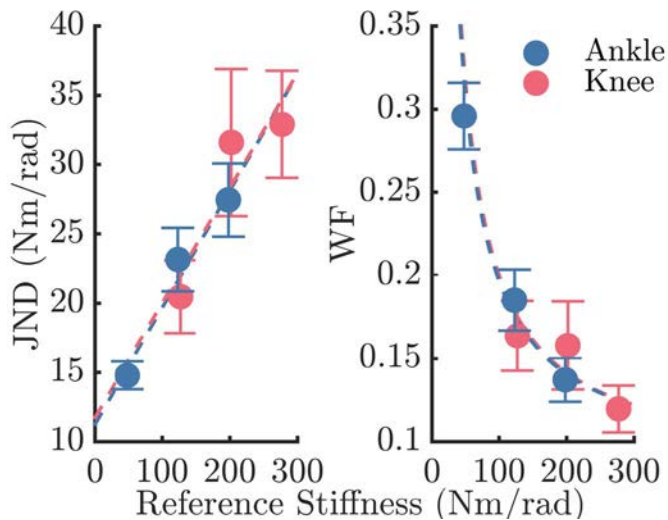


**Figure 2:** JND and WF change with reference stiffness. Error bars denote standard error of the mean. Data are offset for clarity.

At a stiffness level of 275 Nm/rad, the WFs for the ankle and knee were  $0.122 \pm 0.013$  and  $0.120 \pm 0.014$ , respectively (Fig. 3). In other words, stiffness must change by at least 12% at both the ankle and knee for consistent discrimination at a 75% success rate.

Torque perception at the ankle, knee, and elbow, as well as stiffness perception at the elbow, has been studied by other groups [4]–[6]. As Fig. 3 shows, subjects have better stiffness perception at the lower limb than at the elbow; the difference between ankle and elbow perception was significant ( $p = 0.016$ ), in addition to the difference between knee and elbow

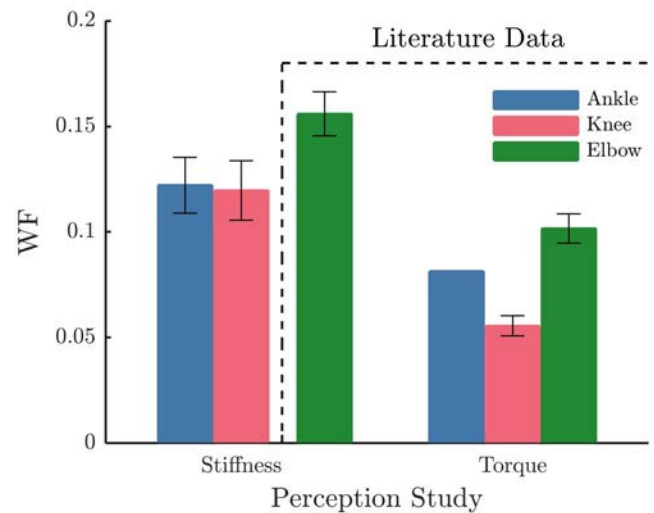


**Figure 3:** Stiffness and torque perception at various joints. Error bars denote standard error of the mean.

perception ( $p = 0.014$ ). Additionally, stiffness perception is worse than torque perception ( $p \leq 0.007$ ). The ability to detect stiffness supports the importance of this impedance parameter in the context of neural control and motor performance, in particular at the ankle and knee joints.

Stiffness perception was also studied to understand the accuracy required by impedance-controlled wearable robotics systems, including exoskeletons. We found that stiffness errors below 12% are permissible; however, it is unclear how errors near the threshold may affect gait dynamics, even if a subject cannot detect the changes. Future research on powered wearable robotic systems will address how continuously-variable impedance affects gait dynamics, and how this relates to perception.

## REFERENCES

1. Rouse EJ, et al. *IEEE Trans. Neural Syst. Rehabil. Eng.* **22**, 2014.
2. Gescheider GA. *Psychophysics: Method, Theory, and Application*, Lawrence Erlbaum Assoc., 1985.
3. Kaernbach C. *Percept. Psychophys.* **49**, 227-229, 1991.
4. Deshpande N, et al. *Arch. Phys. Med. Rehabil.* **84**, 883-889, 2003.
5. Héroux ME, et al. *Arch. Phys. Med. Rehabil.* **86**, 1362-1368, 2005.
6. Jones LA, et al. *Exp. Brain Res.* **94**, 343-351, 1993.

# MECHANICAL & VISUAL PERTURBATION OF HUMAN WALKING TO FIND GENERAL PRINCIPLES OF GAIT CONTROL

<sup>1</sup> Shakiba Rafiee, <sup>1</sup> Tim Kiemel,

<sup>1</sup> Department of Kinesiology, University of Maryland, College Park, USA

Email: [shrafiee@umd.edu](mailto:shrafiee@umd.edu)

## INTRODUCTION

Our research goal is to understand how the nervous system controls locomotion. More specifically, we are interested in identifying general control strategies that the nervous system uses to insure stability in face of different classes of perturbations (both physical and sensory) that naturally occur throughout the gait cycle. To this end, in this study we seek to systematically characterize the properties of neural feedback by examining responses of human walking to small deviations from the desired gait pattern, and to compare the response of the system to different classes of perturbations. Logan et al. [1] previously used simultaneous visual perturbations and upper-body (trunk) mechanical perturbations to investigate the subtasks of controlling orientation relative to vertical (balance) and walking speed. In this study, we take an important next step by studying responses to lower-body perturbations that can potentially affect foot placement.

Foot placement is one of the important strategies that the nervous system can use to stabilize walking. Experimental studies have found that the timing and placement of the foot at heel strike contributes to walking stability (e.g., [2]). Similarly, in simulation studies, controlling the angle of the leg at heel strike ensures stability in simple models of human locomotion (e.g., [3]). In this study we used mechanical and visual perturbations to investigate control strategies that either ensure desired foot-placement or compensate for deviations from it.

## METHODS

We mechanically perturbed walking by applying small continuously-changing forces at the ankles using a spring attached to a motor (Figure 1). We simultaneously applied small continuous sensory perturbations, movement of a virtual visual scene, in order to compare how neural feedback responds to

actual and illusory deviations. The kinematic and muscular responses to the continuous sensory and mechanical perturbations were used to compute phase-dependent impulse response functions ( $\phi$ IRFs) that describe the system responses to small brief perturbations (impulses) applied at any phase of the gait cycle. [4, 1]

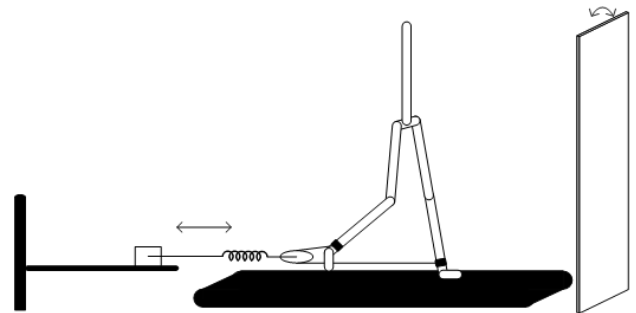


**Figure 1.** Schematic figure of the mechanical and visual perturbation

We collected data from twenty subjects walking on a treadmill for 12 trials each of length 250 seconds. Filtered white noise signals were used to specify the position of the motor (mechanical perturbation) and the velocity of the visual scene (visual perturbation). The kinematic data were collected from right and left sides of the body at external landmarks. The muscular activities were recorded from the right leg and the trunk using surface electromyography (EMG).

## RESULTS AND DISCUSSION

The mechanical perturbation caused zero-latency passive kinematic responses. After some delay, these kinematic deviations were corrected by neural feedback modulating EMG activations at specific phases of gait cycle during which muscles are normally active. We observed similar responses to both forward motion of the visual scene during swing and the mechanical perturbation during swing that caused a forward deviation in foot placement. Both perturbations resulted in increased activation of the

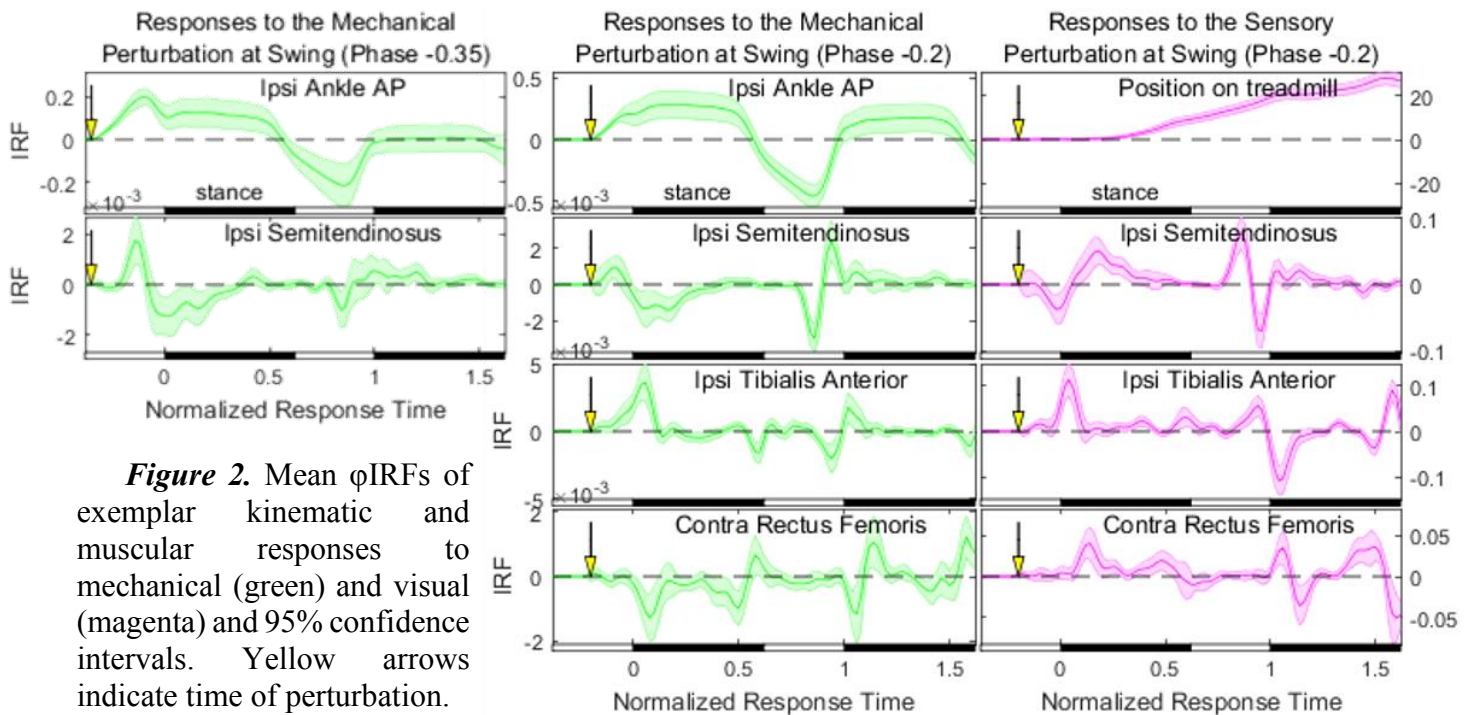


**Figure 2.** Mean  $\phi$ IRFs of exemplar kinematic and muscular responses to mechanical (green) and visual (magenta) and 95% confidence intervals. Yellow arrows indicate time of perturbation.

ipsilateral tibialis anterior (Figure 2) and quadriceps muscles (not shown) in early stance, followed by forward acceleration of the pelvis. These results suggest a general mechanism of early-stance neural control of walking that is used to accelerate the pelvis relative to the foot to correct various kinematic deviations. In the case of the mechanical perturbation, the pelvis is accelerated forward to catch up with foot. In the case of the sensory perturbation, the pelvis is accelerated forward to correct an illusory slowing in walking speed caused by forward visual-scene motion. In contrast to the similar early-stance responses, contralateral rectus femoris activity during the stance-to-swing transition increased in response to the sensory perturbation and decreased in response to the mechanical perturbation (Figure 2). These results are consistent with the presumed role of rectus femoris in controlling cadence, since the sensory perturbation produced a phase advance in the gait cycle, whereas the mechanical perturbation produced a phase delay (not shown). Finally, the ipsilateral hamstring muscle group showed increased activity during swing in response to mechanical perturbations and decreased activity in response to visual perturbations (Figure 2). This discrepancy in behavior is caused by a difference in the strategy used by the nervous system.

In response to mechanical perturbations, a “reactive strategy” partially corrects for the forward displacement of the foot (for perturbations applied in early swing); whereas, in response to visual perturbations, a “compensatory strategy” increases step length to correct for the illusory slowing in speed.

## CONCLUSIONS

In this study, we looked for strategies that the nervous system uses to stabilize walking. We found general control strategies used in the face of both physical and sensory perturbations, e.g., early-stance neural control used to accelerate pelvis through activation of tibialis and other anterior muscles. We also found some characteristic differences in the used control strategies; reactive strategies were used during swing to control foot placement, and compensatory strategies were used during stance to correct for errors in foot placement.

## REFERENCES

1. Logan, D., T. Kiemel, and J.J. Jeka, *Frontiers in Computational Neuroscience*, 2017. **10**(146).
2. Nashner, L.M., *Journal of Neurophysiology*, 1980. **44**(4).
3. Geyer, H., A. Seyfarth, and R. Blickhan, *Proceedings of the Royal Society B: Biological Sciences*, 2006. **273**(1603).
4. Kiemel, T., D. Logan, and J.J. Jeka, *arXiv* 2016.

# EFFECT OF MIRROR VISUAL FEEDBACK ON MOTOR ADAPTATION AND LEARNING

Amanda E. Stone, Matthew J. Terza, Devan R. Ludden, Tiphonie L. Raffegeau, Lisa M. Krehbiel, and Chris J. Hass

University of Florida, Gainesville, FL, USA  
email: stonaman@ufl.edu

## INTRODUCTION

The ability to adapt gait is an important aspect of negotiating a complex and dynamic world. Further, successful rehabilitation is often reliant on an ability to adapt current motor patterns or learn completely new patterns based on task demands. In recent decades asymmetric walking has received attention in gait rehabilitation, particularly post-stroke. In this population, acute split-belt treadmill training has been successfully used to correct asymmetries during both treadmill [1] and overground walking [2] by exaggerating the participants' natural asymmetry. However, it is common that individuals with different injuries or diseases, such as those with cerebellar damage [3], Parkinson's disease [4], or ACL injury [5], may demonstrate difficulty or complete inability to adapt gait on a split-belt treadmill. This highlights the need to develop methods which facilitate adaptation to broaden the split-belt treadmill's utility in clinical use.

Providing visual feedback (FB) has improved rehabilitative outcomes in previous studies. For example, providing task-relevant visual FB accelerated adaptation to a novel task [6,7] while visual distractions impeded it [6]. Many of these FB methods require expensive technical equipment which may not be accessible to all and are often delayed temporally which may impact its effect. One common method for guiding individuals in physical therapy is the use of mirror FB. Frontal plane mirror FB has already been shown to facilitate proper running mechanics and improve motor learning in runners with patellofemoral pain [8]. It is unknown, however, what effect mirror FB may have on individuals' ability to adapt to the split-belt treadmill. The purpose of this study was to evaluate the effects of frontal view mirror FB on adaptation and learning during split-belt treadmill walking.

## METHODS

Thirty-four healthy young adults naïve to the split-belt treadmill volunteered to participate and provided

informed consent. Individuals were divided into a mirror FB group (10 females, 7 males, mean  $\pm$  SD: 21  $\pm$  3 yr, 1.7  $\pm$  0.1 m, 67.2  $\pm$  8.6 kg, 5.0  $\pm$  2.4 hrs/week exercise) or a control group with no FB (10 females, 7 males, 21  $\pm$  3 hr, 1.7  $\pm$  0.1 m, 66.4  $\pm$  15.2 kg, 5.1  $\pm$  1.7 hrs/week exercise).

Three dimensional kinematics were collected while participants walked on the split-belt treadmill. After a five-minute accommodation period, participants walked for five minutes at 0.5 m/s (BASELINE). Gait parameters were averaged over the last five strides of the BASELINE condition. All participants were instructed to look at an X on the wall in front of them. The belts then decoupled and participants walked for 15 minutes at a 3:1 split (1.5 m/s, 0.5 m/s) with their non-dominant leg on the fast belt (ADAPT). Individuals in the visual FB group had a mirror placed two meters in front of them that reflected their lower extremity from the pelvis to the feet. These individuals were instructed to look at their legs in the mirror while walking in the split condition, but no other instruction were given. Gait parameters were analyzed at three different time points during ADAPT: the first five strides (EARLY), the first five strides at the seven-and-a-half-minute mark (MID), and the last five strides (LATE). Following the split condition, participants walked with both belts moving at 0.5 m/s for 10 minutes to washout the effects of the split condition. They then returned to the same 3:1 split condition for 5 minutes (RE-ADAPT) and the first five strides were used to calculate gait parameters.

Asymmetry was defined for step length and double limb support time using the following asymmetry index:

$$\text{Asymmetry} = \frac{(\text{fast leg parameter} - \text{slow leg parameter})}{(\text{fast leg parameter} + \text{slow leg parameter})}$$

Rates of adaptation were quantified as previously described by Malone et al. [2010] with the exception that baseline symmetry was defined as the mean  $\pm$

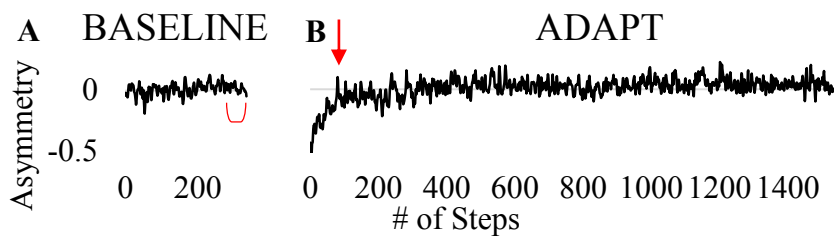


**Figure 1:** Gait parameter asymmetry scores plotted across BASELINE (A) and ADAPT (B). A. Baseline symmetry conditions were determined using the last 30 strides (red bracket). B. Individuals were considered adapted when they had five consecutive strides within the baseline range (red arrow). For example, this participant adapted by stride 109.

SD of the last 30 strides of the baseline trial (not the split condition) (Figure 1).

A  $2 \times 5$  (Group  $\times$  Condition) repeated measures ANOVA was performed to analyze differences in gait parameters. Additionally, a one-way ANOVA was performed to analyze differences in adaptation rate between groups (SPSS,  $p \leq 0.05$ ).

## RESULTS AND DISCUSSION

The mirror FB group showed smaller step length asymmetry ( $p=0.013$ ) and larger double support asymmetry ( $p=0.017$ ) in EARLY compared to the no FB group (Figure 2). The mirror FB group adapted their double limb support time at a significantly slower rate than the no FB group (Mirror FB:  $269 \pm 168$  steps, No FB:  $114 \pm 175$  steps,  $p=0.013$ ). Both groups adapted step length similarly.

Based on previous findings, we initially hypothesized mirror FB would result in motor improvements similar to those present with video camera visual FB [6]. Alternatively, mirror FB could act as a distraction rather than an aid. Individuals who used the mirror for visual FB were initially more perturbed in terms of double support time and able to return to symmetry by LATE adaptation but at a significantly slower rate than those without visual FB. When presented with a mirror, individuals must interpret the viewed image as a mirror interpretation

of themselves, then chose the appropriate course of action, thus leading to a slower rate of adaptation. Additionally, a view of the frontal plane provides little information regarding step length and double support time and therefore individuals in the mirror FB group may have spent more time and resources trying to get useful information out of a potentially useless tool, slowing down the rate of adaptation. Conversely, providing frontal plane mirror FB may distract individuals from the sagittal plane, facilitating a quicker reaction to step length perturbation. This may be beneficial to individuals with step length asymmetries, such as persons who have suffered a stroke.

## CONCLUSIONS

Visual FB via a frontal plane mirror reflection appears to impede double support adaptation, but may improve initial reaction to step length perturbation.

## REFERENCES

1. Reisman, et al., *Brain* **130**, 1861–1872, 2007.
2. Reisman, et al., *Neurorehabil Neural Repair* **23**, 735–744, 2009.
3. Morton, et al., *J Neurosci* **26**, 9107–9116, 2006.
4. Roemmich, et al., *Clin Neurophysiol* **125**, 313–319, 2014.
5. Roper, et al., *Orthop J Sports Med* **4**, 1-9, 2016.
6. Malone, et al., *J Neurophysiol* **103**, 1954–1962, 2010.
7. Roemmich, et al., *Curr Biol* **26**, 2707–2716, 2016.
8. Willy, et al., *Clin Biomech*, **27**, 1045–1051, 2012.

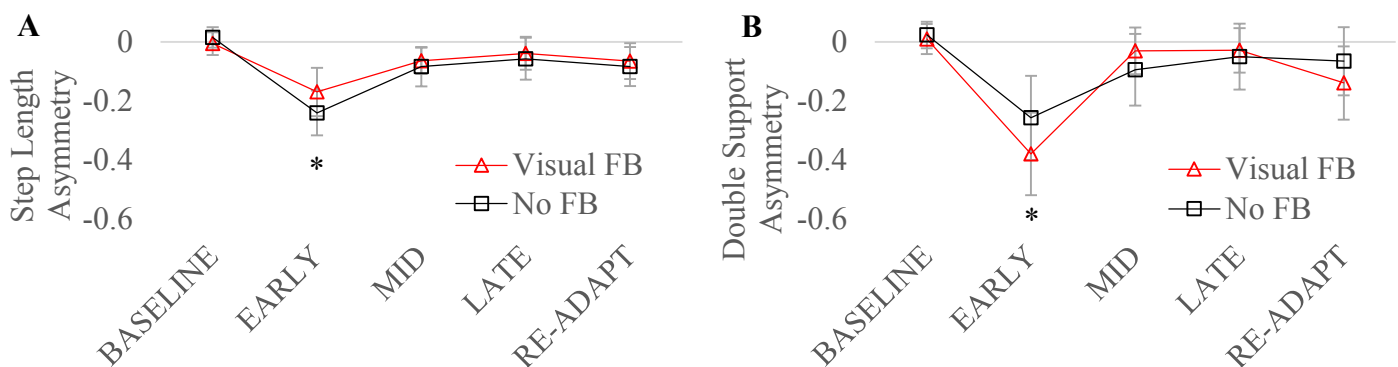


**Figure 2:** Gait parameters (A: step length, B: double support time) across all five conditions.

# SEGMENTAL COORDINATION DURING TURNING IN PEOPLE WITH PARKINSON'S DISEASE

<sup>1</sup> Carolin Curtze, <sup>1</sup> Peter C. Fino, <sup>1</sup> Spencer Smith,  
<sup>1</sup> Patricia Carlson-Kuhta, <sup>1</sup> John G. Nutt, and <sup>1,2</sup> Fay B. Horak

<sup>1</sup> Oregon Health & Science University, Portland, OR, USA  
<sup>2</sup> Veterans Affairs Portland Health Care System, Portland, OR, USA  
email: curtze@ohsu.edu

## INTRODUCTION

The ability to turn safely while walking is crucial for functional mobility. Even early in the disease, people with idiopathic Parkinson's disease (PD) experience difficulties turning. It has been suggested that the segmental coordination of rotation is impaired in people with PD and that they tend to turn 'en-bloc' instead of leading with the head [1].

The goal of this study is to determine the effect of speed, turning angle and antiparkinsonian medication on segmental coordination during turning in people with PD. We hypothesize antiparkinsonian medication will increase turning velocity, but not to alter the segmental coordination.

## METHODS

Seventeen people with idiopathic PD (10 male, 7 female) with a mean age of 71.5 (5.8 SD) years, and a disease severity of Hoehn & Yahr stage 2.

Participants were tested in the practical OFF medication state, after withholding their antiparkinsonian medication for at least 12 hours. Subsequently, they were retested in their ON medication state, 1 hour after taking a supra-threshold dose of levodopa (*i.e.*, 1.25 times of their regular dose).

Participants performed preplanned turns to the left and right, at different turn angles (45, 90, 135, and 180 degrees) while walking at normal and fast speeds. Floor markings similar to a clock face consisting of a turning point in the center and turn

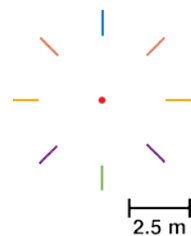


**Figure 1:**  
Experimental setup.

angle marks in the periphery were used as guidance to indicate turn angle (Fig. 1).

Wireless inertial sensors (Opals, APDM Inc.) attached to the lumbar and head were used to capture the sequence and timing of reorientation of body segments at a sampling frequency of 128 Hz (Fig. 2). Outcome measures were peak turn velocity [2] and the lag between head-trunk reorientation when initiating a turn. The onset of segmental reorientation was defined as the time at which the yaw angular velocity exceeded 150% of the range of yaw angular velocity during straight ahead gait.

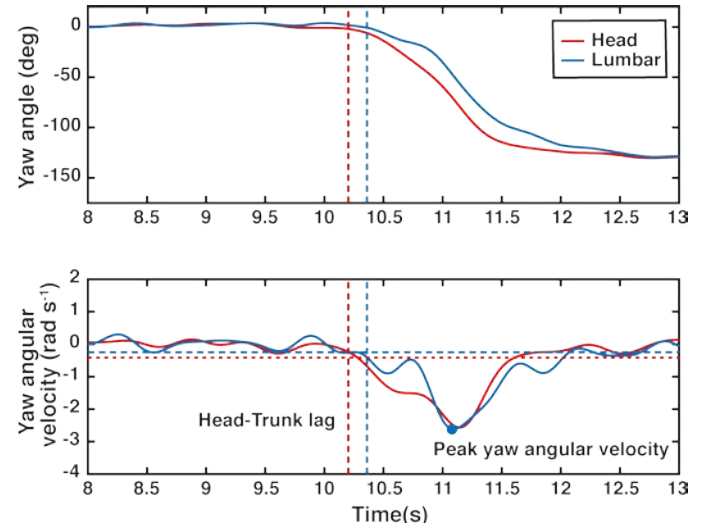


**Figure 2:** Example of a 135-degree turn with cranial to caudal sequence. The head is reorienting into the turn first, followed by the trunk. The onset of segment reorientation (vertical dashed line) the threshold (horizontal dashed line), and the peak yaw angular velocity (circle) are highlighted.

To determine the effect of speed, angle, and medication on turning behavior, linear mixed-effects models were fit for each outcome with random intercepts for each subject to account for within-subject correlations in the data.

## RESULTS AND DISCUSSION

Participants exhibited faster yaw angular velocities at larger turn angles ( $p < 0.001$ , Fig. 3) and when walking faster ( $p = 0.001$ ). Medication state had a significant effect on peak angular velocities; people with PD exhibited significantly lower peak angular velocities during turning in the OFF state compared with the ON medication state ( $p < 0.001$ ).

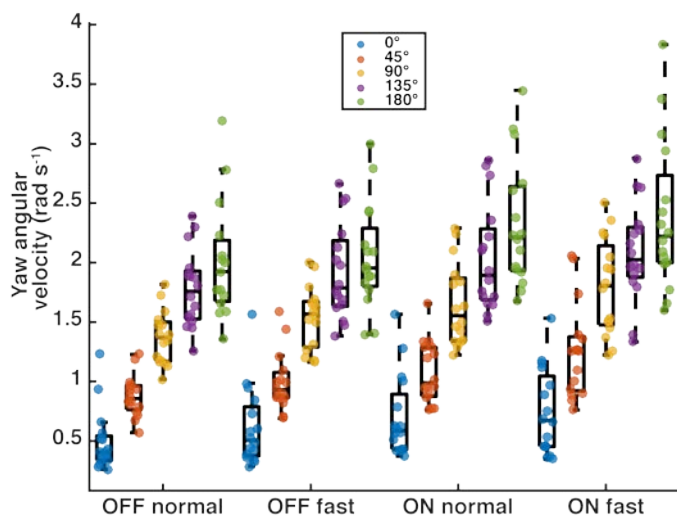


**Figure 3:** Peak yaw angular velocity.

The angle of a turn significantly influenced the delay in initiation of reorientation of the trunk ( $p < 0.001$ ; Fig. 4). At low turning angles, people with PD exhibited a more en-bloc turning strategy, while at larger turning angles, they lead with the head more consistently. Walking at faster speeds reduced the amount of intersegmental reorientation lag between the head and trunk ( $p = 0.03$ ). Medication state did not have a significant effect on the reorientation lag time ( $p = 0.12$ ).

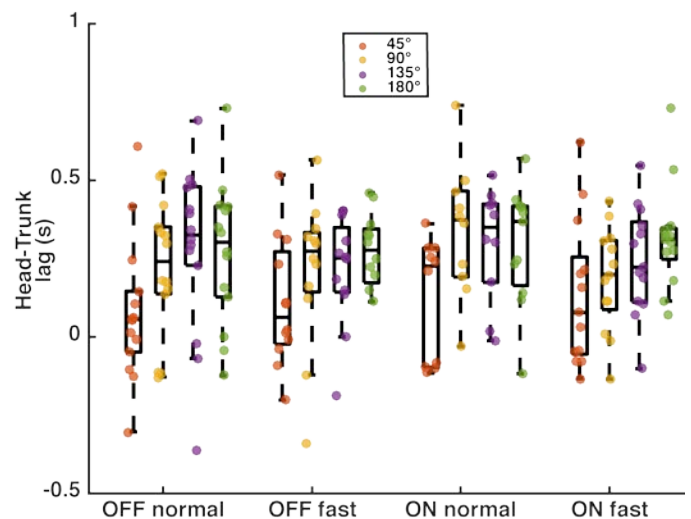


**Figure 4:** Lag of Head-Trunk reorientation.

## CONCLUSIONS

People with PD did not change intersegmental coordination when in ON versus OFF medication state, despite faster turn peak velocities when in the ON medication state. People with PD reoriented their head, with respect to their trunk, later during smaller angle turns compare with large angle turns.

## REFERENCES

1. Akram S, et al. *The Canadian journal of Neurological Sciences* **40**, 520-526, 2013.
2. El-Gohary M, et al. *Sensors* **14**, 356-369, 2014.

## ACKNOWLEDGMENTS

This work was supported by the Medical Research Foundation of Oregon.

## CONFLICT OF INTEREST

Dr. Horak have a significant financial interest in ADPM, a company that has a commercial interest in the results of this research and technology. This potential institutional and individual conflict has been reviewed and managed by OHSU and the VA Portland Health Care System.

# Specific Manual Tasks Transform EMG into a Probe for Neural Dysfunction in Parkinson's Disease

<sup>1</sup>Christopher Laine and <sup>1</sup>Francisco J. Valero-Cuevas

<sup>1</sup> University of Southern California, Los Angeles, CA, USA  
email: [claine@usc.edu](mailto:claine@usc.edu), web: <http://bbdl.usc.edu/>

## INTRODUCTION

Parkinson's disease is the second most common neurodegenerative disease. Without methods for screening and detecting the disease early, diagnosis often occurs only after the nervous system has sustained substantial and irreversible damage [1].

*It may be possible to detect the subtle fingerprints of early disease within patterns of EMG*

Specifically, many of the neural circuits involved in muscle coordination operate at distinct frequencies, and may function to 'bind' multiple muscles together into flexible, task-specific synergies [2]. The oscillatory action of these circuits causes muscles that have been 'bound' together to become synchronized with each other. This can be quantified in the frequency-domain using EMG coherence analysis [2,3].

*Tasks based on muscle coordination could be used to 'probe' the integrity of coordination-related neural circuits*

In this study, we measured EMG-EMG coherence between finger muscles while participants engaged in either a pinch-force modulation task, or a pinch-and-rotate task. One group consisted of healthy adults and a second group consisted of patients with mild-moderate severity Parkinson's disease.

During the rotation task, it was expected that a distinct ~40 Hz drive called the 'Piper Rhythm' would emerge due to the requirement of digit movement [4], but would be notably weak in the patient group, as this drive is reduced by dopamine depletion [5]. The pinch-force modulation task was expected to elicit some 30-50 Hz coherence, but very little at ~20 Hz [6]. Patients were expected to show increased 20 Hz drive, as this may be related to the symptom of bradykinesia [7]. Of course, any

tremor would tend to cause coherence at lower frequencies (<10 Hz).

Our overall hypothesis was that the patient group would show a reduced overall proportion of high (30-50 Hz) frequency coherence in both manual tasks. We also speculate that this reduction could serve as a diagnostic aid if the effects are sufficiently strong.

## METHODS

EMG-EMG coherence was measured between the *abductor pollicis brevis* (APB) of the thumb and *first dorsal interosseous* (FDI) of the index finger of participants as they performed 3-minute manual task trials. The patient group consisted of 11 individuals (ages 42-69, 6 male), all on medication, and our preliminary control group consisted of 10 individuals (ages 24-36, 6 male).

In the first task, participants pinched a small dial as shown in Figure 1 A. They used visual feedback to generate a pinch force that was scaled slowly between 1 and 3 Newtons. The modulation rate was 0.1 Hz for patients and 0.25 Hz for our preliminary control group. In the second task, participants rotated the dial to the left and right  $\pm 22.5^\circ$  at the same frequency. The color of the cursor indicated when forces fell outside of the 1-3 Newton range, to ensure that pinch forces remained similar to the force scaling task.

To evaluate coherence within each task, we calculated a 'gamma ratio' per participant, representing the proportion of total coherence within the 30-50 Hz frequency range. To evaluate differences across groups, we used an unequal variance t-test on ranked data. To evaluate effect size, we calculated Cohen's D. Finally, we evaluated the ability of the 'gamma ratio' to

discriminate patients from controls by determining the area under a Receiver Operating Characteristic curve (ROC\_AUC).

## RESULTS AND DISCUSSION

Figure 1 B and C display the average APB-FDI coherence across all participants in each group, and for each task. The coherence values have been transformed to standard Z-scores prior to averaging. The boxplots in Figure 1 D and E depict the results of calculating the proportion of total coherence in the 30-50 Hz band for each participant, in each group, and for each task. In both the rotation and scaling task, the proportion of coherence in the 30-50 Hz band was low in the patient group relative to the controls.

In fact, during scaling, this ‘gamma ratio’ differed significantly between groups ( $p = 0.0012$ ), showed a large effect size (Cohen’s  $D = 1.08$ ), and good discriminability between patients and controls (ROC\_AUC = 0.81). For dial rotation, this gamma ratio statistically differed across groups ( $p = 8.33e-5$ ), had a very large effect size (Cohen’s  $D = 1.58$ ), and showed excellent discrimination potential (ROC\_AUC = 0.9).

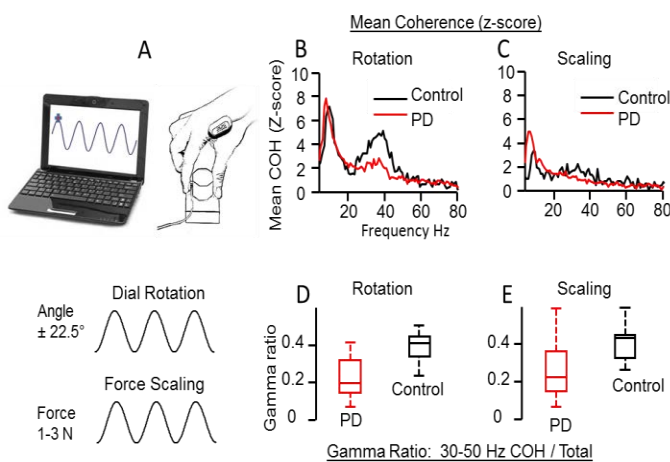


**Figure 1:** EMG-EMG coherence calculated during manual tasks (A) differs between healthy adults and those with Parkinson’s disease (B-E).

It is relevant to note that neural drive to muscles has been studied in Parkinson’s disease before, but the results have not shown diagnostic potential [5]. A major difference between our study and previous work is that we quantify muscle synchronization rather than neural drive to individual muscles. This takes advantage of the interpretation of high frequency EMG coherence as an index of neural ‘binding’ (i.e., an inherently coordination-related phenomenon). Our strategy is also unique in that physical tasks are designed specifically to evoke different frequencies of muscle-synchronizing drive, whose origins are thought to lie within relevant (in this case, disease-affected) neural circuits.

## CONCLUSIONS

Our work demonstrates that simple measures of EMG activity in distinct neuromechanical contexts can be used to probe disrupted neural mechanisms in Parkinson’s disease. This work shows a clear, if preliminary, example of how the specific study of neural drive as subordinate to basic mechanical task demands can be of great benefit in the clinical domain.

## REFERENCES

1. Cheng et al. *Ann Neurol* **67**, 715–25, 2010
2. Nazarpour et al. *J Neurosci* **32**, 12349–12360, 2012
3. Boonstra TW. *Front Hum Neurosci* **7**, 855, 2013
4. Maurer et al. *J Electromyogr Kinesiol* **23**, 673–8, 2013
5. McAuley et al. *J Neurol Neurosurg Psychiatry* **70**, 471–475, 2001
6. Omlor et al., *NeuroImage* **34**, 1191–1198, 2007
7. Little et al. *Exp Neurol* **236**, 383–8, 2012

## ACKNOWLEDGMENTS

This study was supported by NIH-NIAMS under award numbers R01AR050520 and R01AR052345 grants to FVC.

# PRINCIPLES OF ENERGETIC OPTIMIZATION IN HEALTHY AND PATHOLOGICAL MOVEMENT

<sup>1</sup>James Finley, <sup>2</sup>Manoj Srinivasan, <sup>3</sup>Max Donelan, <sup>4</sup>Dinant Kistemaker, <sup>5</sup>Alaa Ahmed,

<sup>1</sup> Biokinesiology and Physical Therapy, Univ. of Southern California, Los Angeles, CA, USA

<sup>2</sup> Mechanical and Aerospace Engineering, The Ohio State University, Columbus, OH, USA

<sup>3</sup> Biomedical Physiology & Kinesiology, Simon Fraser University, Vancouver, BC, Canada

<sup>4</sup> Behavioural and Movement Sciences, VU Amsterdam, Amsterdam, Netherlands

<sup>5</sup> Integrative Physiology, University of Colorado, Boulder, CO, USA

Email: [jmfinley@usc.edu](mailto:jmfinley@usc.edu) Web: [http://pt.usc.edu/Locomotor\\_Control\\_Lab/](http://pt.usc.edu/Locomotor_Control_Lab/)

## INTRODUCTION

The study of human motor control has long been driven by a desire to understand the principles that underlie the selection of motor behaviors. In attempts to identify these principles, a broad class of research has converged on ideas which suggest that motor behaviors may be selected through the optimization of cost functions that include variables such as movement error, reward, and/or effort. Among the broad class of potential cost functions explored in motor control, minimization of energy has often been invoked to explain how we select motor behaviors. However, not all studies provide support for this hypothesis.

In this symposium, we will address the strengths and limitations of the energetic optimization hypothesis in light of current findings from healthy and pathological behavior. We will also ask the more general questions of whether the identification of optimization principles underlying human movement is a worthy quest or whether our efforts should be focused elsewhere. Through an interactive dialogue between the speakers and the audience, we hope to spur a discussion about the evidence for and against the role of energetic optimization in human motor control and highlight potential directions for future research.

## PRESENTATION SCHEDULE

The symposium will proceed according to the following schedule:

Introduction – James Finley – 5 min

Energy Optimality in Unconventional Tasks –

Manoj Srinivasan – 15 min

Energy Optimization and Walking – Max Donelan  
– 15 min

Energetic Consequences of Asymmetry - James  
Finley – 15 min

Kinematic Costs Explain Reaching Movements -  
Dinant Kistemaker – 15 min

Representation of Effort in Decision Making - Alaa  
Ahmed – 15 min

Discussion – 10 min

## ENERGY OPTIMALITY IN UNCONVENTIONAL TASKS IN HUMAN LOCOMOTION AND ITS TRADE-OFF WITH ROBUSTNESS - Manoj Srinivasan

We will begin by explaining how reduced order biomechanical models can be used to predict energetically optimal locomotor behaviors, and will then present evidence from a range of tasks that support the hypothesis that humans optimize energetic cost during walking. In particular, we will present evidence for approximate energy optimality in not just steady straight-line walking, but also in other unconventional situations: unsteady walking

with changing speeds, walking sideways, walking with turns (walking in circles and other complex curves), and recovering from external perturbations during walking. Finally, we will present simple mathematical models of posture (equilibrium) and walking (periodic motion) to examine the trade-offs between energetics on the one hand and stability/robustness on the other. We use numerical optimization to obtain the nominal body motion or state along with feedback controllers that minimize a combination of energy and susceptibility to uncertainty. We find that there is a non-trivial trade-off between these quantities, such that an increase in some kinds of uncertainty also increases the energy cost and also changes the nominal optimal state/motion, for instance, increasing stance width in standing.

### **ENERGY OPTIMIZATION AND THE CONTROL OF WALKING – Max Donelan**

People prefer to move in ways that minimize their energetic cost. Although aspects of this preference may be established over both evolutionary and developmental timescales, we have been interested in the possibility that our nervous systems can optimize energetic cost in real-time. To study this, we use robotic exoskeletons and other mechatronic devices to shift people's energetically optimal gaits to gaits that they don't normally prefer. We find that when subjects are given experience with this new cost landscape, subjects adapt their gaits to converge on the new energetic minimum within minutes and in response to relatively small costs savings. Interestingly, some subjects do not require experience with the cost landscape to initiate energy optimization. This population has naturally high gait variability, suggesting that they are constantly exploring to seek lower cost gaits. However, most subjects do not spontaneously initiate optimization and instead persevere at their originally preferred and now suboptimal gait in the new cost landscape. The experience required to initiate optimization is

experience with a lower cost gait, at which point subjects begin adapting their gait to converge on the new energetic minimum. This behaviour is consistent with a simple reinforcement learning algorithm that selects energetically optimal gaits from a learned prediction of the cost landscape. Our collective findings indicate that energetic cost is not just an outcome of movement, but also plays a central role in continuously shaping it, which is reflected in the algorithms that our nervous system uses to learn new ways of moving through our world.

### **ENERGETIC CONSEQUENCES OF ASYMMETRY IN HEALTHY AND HEMIPARETIC GAIT – James Finley**

Our work focuses on understanding the extent to which asymmetry is actively adjusted during locomotion to reduce energetic cost. We will first present results from studies on healthy individuals adapting to walking on a split-belt treadmill, which can be used to impose a left-right asymmetry in step lengths. In response to this imposed asymmetry, participants gradually adjust their foot placement to adopt steps of equal length. Although this adaptation process is associated with a reduction in metabolic cost, we will show that taking steps of unequal length is often the energetically optimal solution for this task. We will also share recent work exploring the role of energetic optimization in the selection of walking patterns in people post-stroke. Here, we are interested in understanding whether damage to the brain modifies the value placed on different features of walking by, for example, increasing the value placed on stability and being more willing to adopt asymmetric strategies that are energetically costly. We found that spatiotemporal asymmetries were indeed associated with a heightened metabolic cost, and, interestingly, we also observed that people post-stroke do not choose walking speeds that are most economical. The results from these studies highlight the limitations of the energy optimization

hypothesis by demonstrating that both short-term adaptations to imposed asymmetries, and long-term adaptations to brain lesions result in locomotor patterns that are energetically sub-optimal.

### **KINEMATIC COSTS EXPLAIN THE CONTROL OF REACHING MOVEMENTS – Dinant Kistemaker**

It has been widely suggested that central nervous system solves motor behavior redundancy by minimizing a combination of cost variables at the level of kinematics, mechanics and muscle input. To test which variables may underlie the control of arm movements, we had subjects make point-to-point movements while grasping a robotic manipulandum, and we visually perturbed their seen hand position. The robot created a force field (FF) designed to have distinct optimal movements for muscle-input and dynamic costs, yet leaving kinematic cost unchanged. We also used visual perturbations to change kinematic cost, while leaving the dynamical and muscle-input costs unchanged. An optimal control model of the arm, actuated by 6 Hill-type muscle-tendon units, was used to predict movements minimizing various cost variables. The experiments show that after extended exposure to the FF, subjects moved exactly as they did in the absence of the FF, yet were strongly influenced by the small visual perturbations. Experimental results were clearly not consistent with minimization of control and dynamic costs, including mechanical energy. All experimental conditions were adequately predicted by a kinematic cost function comprised of both visually and somatosensory perceived jerk. This study provides evidence that the CNS solves kinematic and mechanical redundancy in separate steps.

### **A REPRESENTATION OF EFFORT IN DECISION MAKING AND MOVEMENT CONTROL - Alaa Ahmed**

Decisions depend on the reward at stake and the effort required. However, these same variables

influence the vigor of the ensuing movement, suggesting that factors that affect evaluation of action also influence performance of the selected action. We describe a mathematical framework that links decision-making with optimality principles in motor control. Each action has a utility, i.e. cost function, which combines the reward at stake with its effort requirements, both discounted as a hyperbolic function of time. The critical assumption of this model is to represent effort via the metabolic energy expended to produce the movement. This energetic representation describes a parameterization of effort as a function of movement duration, mass of the limb, distance, and force, which we confirmed experimentally in reaching movements. Our main result is to show that a single mathematical formulation of action, a utility describing the goodness of the movement via effort, reward, and time, predicts both the decisions that animals make as well as the vigor of the movements that follow. This framework accounts for choices that birds make in walking vs. flying, and the choices that people make in reaching and force production. We suggest that decision-making and movement control share a common utility in which the expected rewards and the energetic costs are discounted as a function of time.

### **AUDIENCE ENGAGEMENT**

Audience participation will be encouraged through real-time feedback using the text message-based audience response system, SMS Poll (<http://www.smspoll.net/>). Specifically, we will administer a pre/post survey to determine the audience's baseline opinions about optimization, and ultimately see if these opinions change in response to evidence presented by the panel. Participants can also pose questions or comment on the topic through the use of the Twitter hashtag #ASB\_Energy. After the conference, the comments, questions, and poll responses will be curated for online storage through Twitter's Moments feature.

# ANKLE-FOOT ORTHOSIS ALIGNMENT AFFECTS CENTER OF PRESSURE VELOCITY

<sup>1</sup>Mitchell D. Ruble, <sup>1,2</sup>Elizabeth Russell Esposito, <sup>1,2</sup>Andrea J. Ikeda, <sup>1,2</sup>Jason M. Wilken

<sup>1</sup>Center for the Intrepid, Department Rehabilitation Medicine, Brooke Army Medical Center, JBSA, Ft. Sam Houston, TX, USA, <sup>2</sup>Extremity Trauma and Amputation Center of Excellence  
E-mail: mitchell.d.ruble.ctr@mail.mil

## INTRODUCTION

Ankle foot orthoses (AFOs) are commonly prescribed to restore function after severe lower extremity injury. Although AFOs can improve pain and the ability to perform daily tasks, they inherently affect gait. For example, a semi-rigid footplate alters how the foot rolls over the ground during gait impacting center of pressure trajectory. The velocity of the center of pressure (vCOP) is a specific measure that has been utilized to help determine different variables such as the dead spot phenomenon in prosthetic gait [1], overall gait efficiency in healthy and injured populations [2], and postural control [3]. Prior research has shown that the vCOP in barefoot walking is characterized by a triple peak pattern at 1) loading response, 2) early-mid stance, and 3) late stance) [2]. The semi-rigid design of AFOs may not allow for biomimetic motion across the three rockers, which may alter both the magnitude and the timing of the vCOP. The specific AFO used in this study was the Intrepid Dynamic Exoskeletal Orthosis (IDEO), a custom, passive-dynamic AFO that has been shown to improve function to a greater extent than other types of AFOs [4]. The purpose of this study was to analyze the effect of IDEO alignment on the peak magnitude and timing of the vCOP.

## METHODS

A total of 12 subjects (11 M, 1 F) with unilateral limb injuries (age  $30 \pm 6$  yrs, height  $1.78 \pm 0.09$  m, mass  $87.3 \pm 9.7$  kg) underwent gait analysis in a motion laboratory (Marker data: 120 Hz, Motion Analysis Corp; Analog data: 1200 Hz, AMTI, Inc.). Three IDEO alignments were tested using a  $3^\circ$  wedge between the footplate and posterior strut (Fig 1): Neutral (Neu) (clinically determined by orthotist),  $3^\circ$  more Dorsiflexed (DF), and  $3^\circ$  more Plantarflexed (PF).



**Figure 1:** The IDEO aligned in dorsiflexion (left) and plantarflexion (right) using a  $3^\circ$  wedge.

Each subject walked at a standardized speed, determined by leg length, until their affected and unaffected limbs made full contact with a force plate 5 times. COP was calculated during a truncated portion of stance phase from ipsilateral heel strike (iHS) to contralateral heel strike (cHS) in Visual 3D. vCOP was calculated as the first derivative of the COP position, and the magnitude and timing of the peak was identified. These dependent measures were compared to data from able-bodied subjects who were group matched for age, height, weight, and leg length.

Data were first tested for normality, and non-normally distributed data were normalized with a logarithmic transformation. A 2-way repeated measures ANOVA (limb x alignment) identified significant main effects and paired t-tests with Bonferroni-Holm corrections identified significant differences between alignments and limbs ( $p < 0.05$ ).

## RESULTS AND DISCUSSION

The  $3^\circ$  modifications in sagittal plane IDEO alignment significantly affected the magnitude and timing of the peak vCOP (Fig 2-3). Significant interaction effects were recorded between limb and alignment for both the magnitude ( $p = 0.002$ ) and timing ( $p = 0.001$ ) of the peak vCOP. The PF alignment of the affected limb had significantly

greater vCOP magnitudes than both the DF ( $p=0.002$ ) and Neu ( $p=0.004$ ) alignments. Additionally, the timings of these peaks were significantly earlier in the PF alignment than the DF ( $p=0.001$ ) and Neu ( $p<0.001$ ) alignments. Patients generally preferred the PF alignment (8/12).

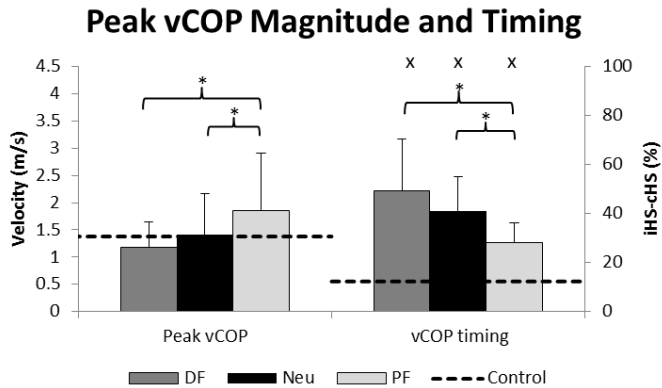


**Figure 2:** Affected limb peak vCOP magnitude and timing with SD bars. \* indicates difference between alignments, X indicates difference from controls.

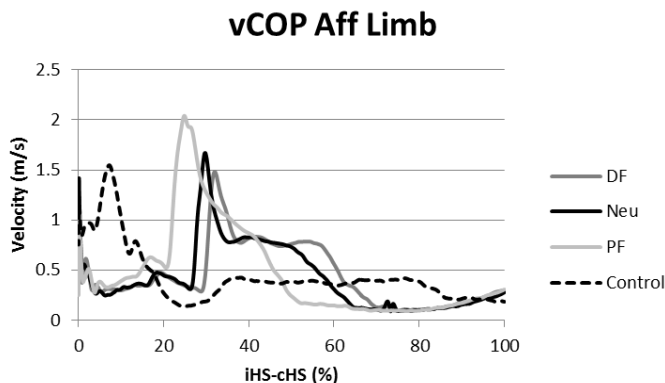


**Figure 3:** Mean vCOP of the affected limb and control data from ipsilateral heel strike (iHS) to contralateral heel strike (cHS) for a representative subject.

Between limb effects were observed for the vCOP magnitudes and timing. The timing of the peak vCOP occurred significantly earlier in the unaffected limb for the DF ( $p<0.001$ ), Neu ( $p<0.001$ ), and PF ( $p<0.001$ ) alignments. However, no significant differences between limbs were found for the vCOP peak magnitudes (DF:  $p=0.115$ , Neu:  $p=0.876$ , PF:  $p=0.193$ ).

Differences between the subject data and the control data were also observed. Peak vCOP timing occurred 25-39% later in the patient data than the control data for the DF ( $p<0.001$ ), Neu ( $p<0.001$ ), and PF ( $p=0.002$ ) alignments. No differences were found between the patient and control data for the peak vCOP magnitudes.

With the earlier and greater peak vCOP magnitudes in the PF alignment, the foot would be expected to transition from heel loading to foot flat faster than the other alignments. However this may not be beneficial for some patients as it may increase the risk of stalling after this rapid peak (Fig 3).

One limitation of this study was that the neutral alignment for each subject was determined by the orthotist's clinical assessment, largely influenced by the subject's pain-free range of motion, and may have differed among subjects.

## CONCLUSIONS

A 6-degree range of changes in the sagittal plane alignment of an AFO significantly influenced the vCOP peak magnitudes and timings. With an increasingly plantarflexed alignment, the peak vCOP magnitudes increased and occurred earlier.

## REFERENCES

1. Klenow TD, et al. *Clin Biomech* **38**, 56-62, 2016.
2. Cornwall MW, et al. *J Am Podiatr Med Assoc* **90**, 334-338, 2000.
3. Palmieri RM, et al. *J Sport Rehabil* **11**(1), 51-66, 2002.
4. Patzkowski JC, et al. *J Bone Joint Surg Am* **94**, 507-515, 2012.

## ACKNOWLEDGEMENTS

Support for this study was provided by the Center for Rehabilitation Sciences Research, Dept. of Physical Medicine and Rehabilitation, Uniformed Services Univ. of Health Sciences, Bethesda, MD.

The views expressed herein are those of the authors and do not reflect the policy or position of Brooke Army Medical Center, the US Army Medical Department, US Army Office of the Surgeon General, Department of the Army, Department of Defense or US Government.

# FINITE HELICAL AXIS VARIATION BETWEEN CAVUS, NEUTRALLY ALIGNED, AND PLANUS FEET UNDER PASSIVE LOADING

<sup>1,3</sup>Eric D. Thorhauer, <sup>3</sup>Matthew W. Kindig, <sup>3</sup>Michael J. Fassbind,  
<sup>2,3</sup>Bruce J. Sangeorzan, and <sup>1,2,3</sup>William R. Ledoux

<sup>1</sup>Department of Mechanical Engineering, University of Washington, Seattle, WA

<sup>2</sup>Department of Orthopaedics and Sports Medicine, University of Washington, Seattle, WA

<sup>3</sup>Center for Limb Loss and Mobility, VA Puget Sound Health Care System, Seattle, WA, USA  
email: ericthor@uw.edu, web: www.amputation.research.va.gov

## INTRODUCTION

Gross anatomical misalignments, such as flatfoot (pes planus) or high-arch foot (pes cavus), affect normal hindfoot and midfoot joint function, increasing risk of injury or degeneration, and reducing overall quality of life. Further, the factors differentiating symptomatic and asymptomatic pes planus subjects are still unclear. Quantification of kinematic variations between foot types is essential to elucidating the complex joint interactions specific to these conditions and aiding surgeons designing procedures and hardware to correct such deformities. Determination of finite helical axes (FHA) of joints in response to passive loading may reveal the “true” joint axes orientations resulting from the guiding articular surfaces and ligaments.

The primary purpose of this study was to quantify hindfoot and midfoot finite helical axes of rotation in four clinical foot type classifications: 1) pes cavus (PC), 2) neutrally aligned (NA), 3) asymptomatic pes planus (APP), and 4) symptomatic pes planus (SPP). The secondary aim was to explore differences between symptomatic and asymptomatic planus feet. We hypothesized that the rotation about, and the orientation of the joint axes in cavus and planus subjects will differ from neutrally aligned feet. Specifically, planus feet would exhibit greater rotation at the midfoot with dorsiflexed, everted, and externally rotated axis orientations, indicative of a flexible foot. SPP differences relative to NA would be exaggerated compared to APP. Additionally, PC subjects would exhibit restricted midtarsal joint motions, and plantarflexed, inverted, and internally rotated axes.

## METHODS

Subjects (17 female/22 male, body mass index (BMI):  $29.1 \pm 6.1$ , age:  $52.4 \pm 8.9$  years) were recruited from the University of Washington and VA Puget Sound Medical Centers with institutional review board approval. Subjects were self-ambulating and classified by an orthopaedic surgeon as: NA: 10, PC: 9, APP: 10, SPP: 10.

Feet were positioned using a custom loading device [1] in eight, equally-spaced, predefined poses inside a magnetic resonance imaging machine (1.5T Phillips Intera Gyroscan, voxel size:  $0.57 \times 0.57 \times 0.70$  mm, SENSE-Flex-M coil). A static imaging volume was acquired at each of the eight poses ranging from maximum plantarflexion, hindfoot inversion, and internal rotation through the neutral position (Path 1), and then from the neutral position to maximum dorsiflexion, hindfoot eversion, and external rotation (Path 2) [1].

Foot and ankle bony anatomy was segmented within subjects, across poses using custom software (Multi-Rigid) [2] that calculates the relative transformation matrices between bone poses. Finite helical axes were calculated directly from the relative homogeneous transforms as outlined by Spoor [3]. The rotation amount and orientation of the FHAs were calculated over Path 1, Path 2, and the overall motion path (Path 1+Path 2) for each subject. FHA orientations were expressed with respect to anatomical coordinate systems based on the inter-malleolar axes [4] and the normal vectors of the loading device platform for each subject.

Differences between foot types were tested using a general linear model (age, sex and BMI included as covariates), and post-hoc comparisons of PC, APP and SPP subjects to the NA group were performed. Linear regressions correlated the rotational contributions of synergistic joint pairs to overall motion (**Figure 1**). Statistical analyses were performed in SPSS (v23, IBM) and significance level was set at  $p < 0.05$ .

## RESULTS AND DISCUSSION

No differences in FHA orientation between both planus and neutral feet were detected. Both planus feet groups had less ankle rotation compared to NA (APP:  $-9.1 \pm 3.5^\circ$ ,  $p = 0.014$ , SPP:  $-12.3 \pm 3.3^\circ$ ,  $p = 0.001$ ) (**Figure 1**). Calcaneal-cuboid joints in SPP subjects had  $4.9 \pm 1.8^\circ$  less rotation than NA ( $p = 0.01$ ). Moderate interactions between BMI and cuboid-fifth metatarsal rotation ( $p = 0.054$ ), medial cuneiform-navicular rotation ( $p < 0.001$ ), and calcaneal-cuboid sagittal plane FHA orientation ( $p = 0.062$ ) were observed. Significant interaction of age and ankle rotation was also observed ( $p = 0.02$ ).

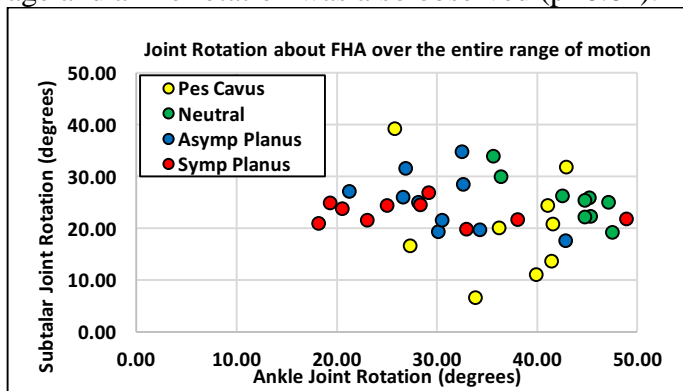


**Figure 1:** Subtalar vs ankle joint rotation for each subject by foot type. SPP exhibited narrow subtalar and wide ankle rotation range. The slope of APP subjects falls between the flat SPP response and negatively correlated NA response ( $R^2 = 0.87$ ).

PC subjects had significantly less rotation through Path 1 at the subtalar ( $7.0 \pm 2.1^\circ$ ,  $p = 0.002$ ), calcaneal-cuboid ( $3.2 \pm 1.3^\circ$ ,  $p = 0.018$ ), and talonavicular ( $10.9 \pm 3.3^\circ$ ,  $p = 0.003$ ) joints compared to NA, suggesting increased midfoot rigidity.

Compared to APP subjects, SPP FHAs were more inverted in the coronal plane for the cuboid-fifth

metatarsal and medial cuneiform-navicular joints. SPP FHAs were more dorsiflexed in the sagittal plane for the calcaneal-cuboid, talonavicular, tibio-calcaneal, and talus-first metatarsal axes, relative to APP.

## CONCLUSIONS

Foot shape deformities disrupt the normal interplay of ankle and subtalar joint axis behavior. Overall, FHA orientations were highly variable for non-neutral groups. The relationships between adult-acquired flatfoot and obesity are highly debated, but increased daily loading may contribute to arch collapse. Future work will investigate relationships between bony morphology, articular surface congruity, and kinematic contributions of foot/ankle motion segments to overall motion.

## REFERENCES

1. Fassbind, MJ, et al. *J. Biomech. Eng.*, **133** (10), 2011.
2. Hu, Y, et al. *J. Biomech. Eng.*, **133** (10), 2011.
3. Spoor, CW. *J. Biomech.* **13** (4): 391-3, 1980.
4. Green, C, et al. *Foot & Ankle Int.* **32** (2): 193-99, 2011.

## ACKNOWLEDGMENTS

Supported, in part, by VA RR&D Service Grant A3030R.

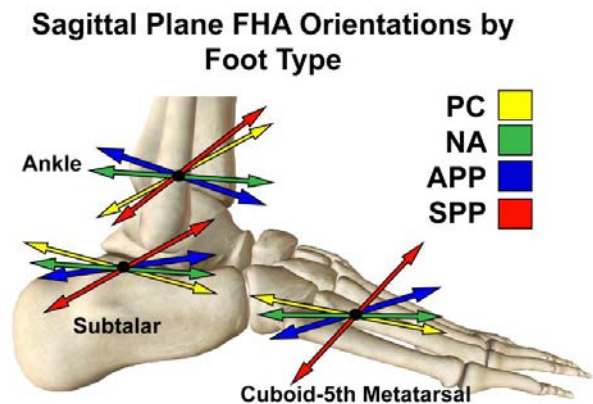


**Figure 2:** Mean sagittal plane FHA orientations by foot type for three selected joints: ankle, subtalar, and cuboid-fifth metatarsal. PC FHAs were plantarflexed for joints distal to the ankle. SPP FHAs were typically dorsiflexed for midfoot joints to a greater degree than APP.

# FOOT PRESSURE ANALYSIS TO ASSESS PLANOVALGUS FOOT DEFORMITY CORRECTION USING THE CALCANEAL-CUBOID-CUNEIFORM OSTEOTOMY

<sup>1,2,3</sup> Karakostas Tasos, <sup>1</sup> Stavropoulos Nicolaos, <sup>2,3</sup> King Erik, <sup>1,2,3</sup> Swaroop Vineeta, <sup>1,2,3</sup> Dias Luciano

<sup>1</sup> Rehabilitation Institute of Chicago, Chicago, IL, USA

<sup>2</sup> Feinberg School of Medicine, Northwestern University, Chicago, IL, USA

<sup>3</sup> Lurie Children's Hospital of Chicago, Chicago, IL, USA

email: tkarakosta@ric.org

## INTRODUCTION

The use of foot pressure distribution analysis in the evaluation of foot deformities has been established [1]. Certain parameters of this analysis, such as the line of progression of the center of force (COF) has been shown to accurately describe lever arm deficiencies that result from foot deformities [2, 3, 4, 5, 6].

One foot deformity, often demonstrated by children with cerebral palsy, which requires careful evaluation and treatment, is the valgus foot. Treatments that have been implemented to address the valgus foot include the triple arthrodesis and the increasingly popular calcaneal-cuboid-cuneiform osteotomy procedure, or triple C (3C) [7]. The 3C procedure combines calcaneal sliding with cuboid and cuneiform wedge osteotomies. Advantages of this procedure include correction of the foot deformity while avoiding long-term complications associated with increased stress on the adjacent joints, which has been found to be related to the triple arthrodesis procedure [7, 8, 9].

However, although to determine the need for the 3C procedure, children often have pre-operative foot pressure distribution analysis, to-date, to the best of our knowledge, there have been no studies that have used pedobarographic analysis to quantify the effects of the 3C procedure. We have assumed that the foot pressure distribution parameters of the COF and peak pressure (PP) would be able to describe the post-operative changes as a function of the procedure. A foot corrected for a valgus deformity should display a more lateral COF trajectory pre-operatively accompanied by a complementary

lateral shift of the PP and, potentially, with a reduction of that pressure in the surgical region. If we can establish foot pressure analysis parameters as a means for assessing planovalgus foot deformity functionally, then we can potentially use it to assess the efficacy of clinical procedures such as the 3C procedure, used to address the deformity. Foot pressure analysis parameters may allow objective assessment of the outcomes of this procedure, which, in turn, will contribute to the effectiveness of the decision making process in addressing valgus foot deformities, as well as monitor progress.

Consequently, the purpose of this study was to determine if selected foot pressure distribution analysis parameters can be used to describe functional changes as a result of the 3C procedure by comparing differences in pre- and post-operative COF trajectory and PP in the surgical region.

## METHODS

This study included twelve subjects (8 males, 4 females, 18 feet) ranging from 6 to 18 years of age. All subjects had a diagnosis of cerebral palsy with valgus foot deformity and had the 3C procedure. Original foot pressure data was collected using the Tekscan HR Mat and related software before and 1 year after surgery. Approximately, three foot pressure distribution trials were selected for each foot for analysis for each pre- and post-operative tests based on the consistency of the COF trajectory and the foot pressure distribution. First, the longitudinal excursion of the COF trajectory was determined and expressed relative to the functional length (the length of the foot in contact with the ground) and estimated actual foot length. Then, we

determined the surgical region and the maximum medial and lateral excursion of the COF trajectory within this region. The excursion was expressed relative to the functional surgical width (the width of the foot in the surgical region in contact with the ground) and estimated actual foot width. The PP within this region was also determined and the distance between the PP location and the functional lateral border of the foot was measured. Pre- and post-operative differences were compared within and across subjects.

## RESULTS

Figure 1 demonstrates the changes in the foot pressure distribution analysis parameters for one of the participants. Sixty nine percent of the feet evaluated demonstrated a longer COF trajectory following surgery. The average percent lengthening relative to the estimated actual foot length was 20% (SD 41). Seventy nine percent of the feet demonstrated a medial to lateral shift of the COF trajectory.

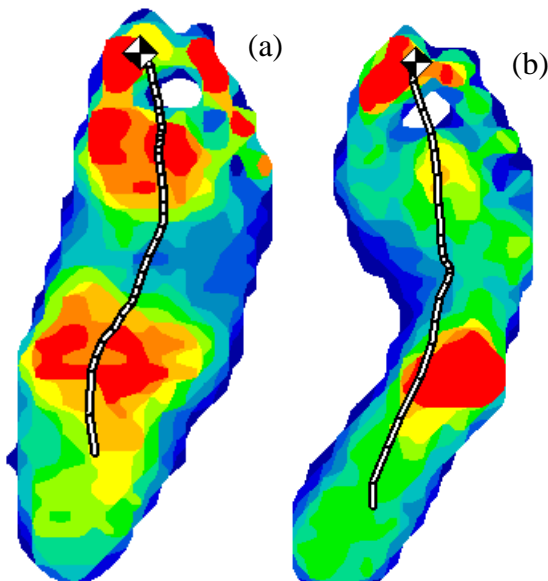


**Figure 1:** Functional changes in foot pressure parameters between pre- (a) and post- (b) surgery using the 3C procedure.

The average percent shift relative to the estimated actual foot width was 7% (SD 11). The PP location demonstrated a medial to lateral shift for eleven of the twelve subjects or 94% of the feet. The average lateral shift of the PP location within the functional surgical width was 22% (SD 22) from the lateral border of the foot. The PP magnitude was reduced for eight of the twelve subjects or 67% of the feet.

## DISCUSSION AND CONCLUSIONS

Following the 3C procedure, most subjects demonstrated a longer COF trajectory, suggesting a greater amount of foot contact with the ground in the longitudinal direction. Furthermore, most subjects showed a lateral shift in the PP location, suggesting that the valgus deformity was reduced. This was complemented by a corresponding lateral shift of the COF trajectory within the functional surgical width.

Consequently, our results suggest that foot pressure distribution analysis is an effective means for assessing the efficacy of the 3C procedure. Pedobarographic analysis can provide information about functional pre- and post-operative differences that can document change.

## REFERENCES

1. Karakostas, T. et al. *Clin Biomech*, **22**, 478-485, 2007.
2. Chang, C.H. et al. *J Ped Orthop*, **22**, 813-818, 2002.
3. Bowen, T. et al. *J Ped Orthop*, **18**, 789-793, 1998.
4. Jameson, E. et al. *J Ped Orthop*, **28**, 254-258, 2008.
5. Davids, J. et al. *Orthop Clin Nor Amer*, **41**, 579-593, 2010.
6. Riad, J. et al. *J Child Orthop*, **1**, 301-312, 2007.
7. Rathjen, K. et al. *J Ped Orthop*, **18**, 775-782, 1998
8. Daglar, B. et al. *J Orthop Sci*, **13**, 41-347, 2008.
9. Stein, H. et al. *Arch Orthop Tr Surg*, 263-269, 1981.

# CONCURRENT VALIDITY OF AN AUTOMATIC TECHNIQUE TO CALCULATE PLANTAR CONTACT AREA AT MID-STANCE DURING GAIT

<sup>1</sup>Daniel E. Lidstone, <sup>3</sup>Louise M. Porcher, <sup>2</sup>Jessica DeBerardinis, <sup>2</sup>Mohamed B. Trabia, and <sup>1</sup>Janet S. Dufek,

<sup>1</sup>Department of Kinesiology and Nutrition Sciences, University of Nevada, Las Vegas, NV, USA,

<sup>2</sup>Department of Mechanical Engineering, University of Nevada, Las Vegas, NV, USA,

<sup>3</sup>ESSO, Saint-Cloud, France

Email: [lidstone@unlv.nevada.edu](mailto:lidstone@unlv.nevada.edu)

## INTRODUCTION

Measuring dynamic footprints during gait can help identify foot deformities and pathology [1] and aid in managing conditions such as diabetic foot pathology [2]. Dynamic footprints are typically produced using electronic pedography [3]. This technique is somewhat limited by the poor resolution of sensor arrays. Also, there exist limited data relative to its reliability and validity. Digital image processing techniques may overcome this limitation through generating high-resolution footprints with adequate frame rates to capture specific events during gait. Image processing has been used to generate static footprints using algorithms that segmented the foot and generated a binary image footprint [3, 4, 5]. This approach requires the foot to be placed on an acrylic sheet and imaged using a digital camera. Previously published techniques used a podoscope in which fluorescent bulbs illuminated the contact area of the foot simplifying image processing [4]. A primary limitation of commercially available podoscopes is their relatively small surface area, which constrains the performance of dynamic movements.

The purpose of this exploratory investigation was to examine the concurrent validity of an automatic digital imaging processing technique to measure plantar contact area during the mid-stance phase of gait with respect to a manual processing method.

## METHODS

*Experimental set-up:* In this institutionally approved study, an elevated acrylic (Plexiglas) walkway (2.54 cm thick, 0.6 m wide, and 1.21 m long) was designed and built to characterize unobstructed gait (Figure 1).

The walkway was extended on both ends of the Plexiglas window (total dimensions: 0.9 m high, 0.6 m wide, 3.6 m long) allowing for unobstructed natural gait. Stairs and guardrails were added for safety and comfort of the participants. LED strips were fitted along the perimeter of the walkway to illuminate the plantar contact area. The light intensity in the testing area was standardized for all data collection sessions, with ambient light also controlled. A high definition camera (Nikon 1 J4, 60 fps, Tokyo, Japan) was placed in a 3D printed camera box directly underneath the center of the walkway to ensure a consistent camera placement for all experiments. The starting position of each participant was marked with tape to help ensure that the right foot of each participant landed near the center of the Plexiglas portion of the walkway without participant targeting.

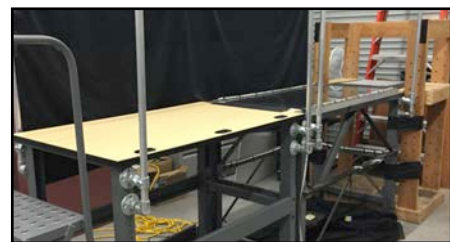


**Figure 1:** Experimental Setup.

All participants (N=42, age=24.3±3.2 years, mass=67.2±16.9 kg, height=1.63±0.08 m) were free from lower extremity injuries and foot deformities. Participants were fitted with tight-fitting black clothing and gloves to reduce noise during image processing.

*Calibration:* A checkerboard (size=20x30 cm, square dimensions=2x2 cm) was placed on the acrylic plate and used to calibrate the images resulting in, 1 pixel-length=0.0016 cm, which was used for calculating contact areas.

*Automated Identification of Plantar Area:* All of the image-processing algorithms were developed in MATLAB, incorporating Image Processing Toolbox functions. A total of 11,564 images were generated from 420 walking trials (N = 42, 10 trials each). The identification process started by cropping each full contact image to a rectangle closely surrounding the foot to simplify image processing. Background noise was filtered. A contour was drawn manually to enclose contact area on a test image during the full contact phase. Red-Green-Blue (RGB) values of pixels within this contour were identified. Average and standard deviation (SD) of the RGB values of all pixels within the contour were calculated. Contact area for all other frames during the full contact phase were identified as those pixels whose RGB values were within the average RGB  $\pm$  twice the SD of the test image. To improve the quality of the identification process, borders were smoothed and gaps were filled.

*Manual Calculation of the Plantar Area:* One hundred frames during the full contact phase of all trials were randomly selected and contact areas were traced by 3 trained researchers using drawing tablets (Wacom, Intuos Pro, Portland, OR). Inter-rater reliability for the manual tracing method was conducted.

*Statistical Analysis:* Statistical tests were performed using SPSS (IBM SPSS Statistics for Windows, Version 23.0, IBM Corp, Armonk, NY). Two analyses were conducted. First, the intra-class correlation coefficient (ICC) was employed to examine the degree of agreement between area measurements of the same image taken by the three researchers. Second, concurrent validity between automated and manual methods were evaluated.

## RESULTS AND DISCUSSION

*Inter-Rater Reliability Results:* The results showed that there existed strong agreement among the 3 researchers (ICC=0.99, 95% CI=0.98-0.99).

*Concurrent Validity Results:* Concurrent validity between the automated and manual methods was acceptable for calculating plantar contact area (ICC = 0.92, 95% CI=0.81-0.96). The average plantar

contact area error between the methods was  $-5.8 \pm 13.1\%$ . This error shows the automatic method underestimated plantar contact area.

*Qualitative Analysis:* An example of images processed using the automatic imaging-processing algorithm and manual tracing method are demonstrated in Figure 2. A common source of error observed in the automatic imaging-processing algorithm was shadow in the mid-arch region. Future studies should aim to reduce these sources of error.

The results from the current study demonstrate a valid approach to produce dynamic footprints for the mid-stance of gait. Future research should examine additional phases during the support phase.

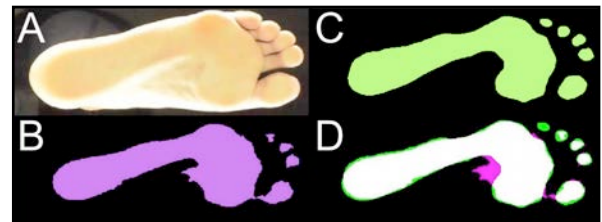


**Figure 2:** Unprocessed image (A), automatic method (B), manual method (C), white shows overlap between the images (D).

## ACKNOWLEDGEMENTS

This publication was made possible by a grant from the National Institute of General Medical Sciences (GM103440) from the National Institutes of Health. This [project's] contents are solely the responsibility of the authors and do not necessarily represent the official views of NIH. The authors would like to appreciate the effort of W. Davis for building the walkway and C. Garcia and A. Trotter for data analysis assistance.

## REFERENCES

1. Fascione J, et al. *J Am Podiatr Med Assoc.*, **104**:125-133, 2014.
2. Shah SR & Patil KM. *IEEE.* 56-59, 2005.
3. Fascione J, et al. *J Am Podiatr Med Assoc.*, **102**(2), 130-138, 2012.
4. Buchelly FJ, et al. *J Phys.*, **705**(1), 2016.
5. Siddiqui HU, et al. *IEEE.* **62**(8),1911-1917, 2015.

# RUNNING STRIKE PATTERN, MIDTARSAL LOCKING, AND THE WINDLASS MECHANISM

<sup>1</sup> Dustin A. Bruening, <sup>2</sup> Michael B. Pohl, <sup>3</sup> Kota Z. Takahashi, <sup>4</sup> Joaquin A. Barrios

<sup>1</sup> Brigham Young University, Provo, UT, USA

<sup>2</sup> Puget Sound University, Tacoma, WA, USA

<sup>3</sup> University of Nebraska at Omaha, Omaha, NE, USA

<sup>4</sup> University of Dayton, Dayton, OH, USA

email: dabruening@byu.edu

## INTRODUCTION

A forefoot strike pattern (FFS) has received considerable attention in running literature due to its theorized benefit in attenuating loading rates, shifting loads distally, and storing/ returning more energy in the foot (compared to rearfoot strike, RFS). While the effects of strike pattern on sagittal plane knee and ankle mechanics have received considerable attention in the literature, less is known about the mechanics of the joints distal to the ankle. Differences in the manner in which the foot is loaded when changing strike pattern [1] may provide an interesting model to test the validity of two traditional clinical models of the foot: midtarsal locking and the windlass mechanism. Research using a multi-segment foot model [2] shows that a FFS is accompanied by a more inverted hindfoot. This could affect midtarsal mechanics via the midtarsal locking mechanism, where hindfoot inversion is purported to reduce flexibility across the joints of the midfoot [3]. In addition, a more anterior center of pressure throughout stance in FFS [1] has the potential to increase the role of the windlass mechanism during push-off, wherein toe extension results in concomitant arch rise [4].

Both the midtarsal locking theory and the windlass mechanism have the potential to alter kinetics across the foot joints. The purpose of this study, therefore, was to explore the effects of running strike pattern on foot kinetics within the context of these clinical theories. We hypothesized that midtarsal locking would result in a less compliant midfoot during loading in FFS, while the windlass mechanism would increase power absorption at the metatarsophalangeal joints and concurrent power generation at the midtarsal joint during push off in FFS.

## METHODS

Eighteen female runners (25±4 yrs., 1.65±0.06 m, 61±7 kg) ran overground at 3.7 m/s using both RFS and FFS patterns. Subjects wore minimalist shoes with cut-outs and reflective markers were placed directly on the skin according to a modified kinetic multi-segment foot model [5]. Marker trajectories and force plate data were collected at 150 and 1,500 Hz respectively.

Midtarsal (MT) and metatarsophalangeal (MP) joints were modeled in Visual 3D software [5]. Joint angles were extracted using a typical Euler sequence. Joint moments and powers were calculated by first partitioning the ground reaction force to each segment sequentially using the center of pressure [6]. Stance was divided into two phases: 1- loading, from initial contact until peak midfoot dorsiflexion, and 2- propulsion, constituting the rest of stance. Metrics differed slightly between the two phases, targeted towards the most dominant foot theory (midtarsal locking in loading and windlass mechanism in propulsion). Range of motion (RoM) and MT joint work (integral of power) were calculated for both phases. MT angular impulse and rotational stiffness (slope of the linear portion of the sagittal plane moment / angle graph) were added to loading, while MP and combined MT/MP joint work were added to propulsion. Strike pattern was compared using paired t-tests ( $\alpha = 0.05$ ).

## RESULTS AND DISCUSSION

LOADING (Table 1): FFS resulted in greater MT dorsiflexion RoM ( $p=0.005$ ), but reduced abduction RoM ( $p=0.003$ ). No differences were observed in frontal plane RoM ( $p=0.122$ ), but the motion

directions were reversed (see [2]), with FFS inverting and RFS everting. MT angular impulse was also greater in FFS ( $p < 0.001$ ), as was MT stiffness ( $p = 0.024$ ). No differences were seen in MT negative work ( $p = 0.912$ ). These results suggest, first, that total MT motion, or deformation, is likely similar between strike patterns, but that MT axes of rotation differ due to changes in postural configuration. The similar deformation occurs despite much greater loading in FFS, suggesting that the altered rotation axes are causing a greater stiffness across the MT joint (i.e. “locking”). This perspective helps explain why energetics conclusions based solely on sagittal plane kinematics [7] differ from tri-planar modeling studies [8, 9] and provides further evidence against any FFS energy storage advantage within the MT joint [8, 9].

**Table 1:** MT joint metrics during loading.

	RFS	FFS	<i>p</i>
ROM (°)			
Dorsiflexion	5.4 ± 1.5	6.4 ± 2.2	0.005
Inversion	(-)3.0 ± 1.3	2.2 ± 1.6	0.122
Abduction	4.5 ± 1.2	3.7 ± 1.2	0.003
Impulse (Nm·s/kg)	.11 ± .02	.16 ± .02	0.000
Stiffness (Nm/°kg)	2.4 ± 0.7	2.8 ± 1.0	0.024
Work (J/kg)	-.11 ± .03	-.11 ± .05	0.912

**PROPULSION (Table 2):** During propulsion, there was greater MT plantarflexion RoM in FFS ( $p < 0.001$ ), but no differences in the other planes ( $p = 0.313, 0.118$ ). By toe off, MT kinematics curves had converged so that there were no distinguishable differences between strike patterns (see [2]). This convergence in MT kinematics suggests that midtarsal locking would affect both strike patterns similarly. However, MP extension RoM was greater in FFS ( $p < 0.001$ ), which appears to engage the windlass mechanism earlier and to a greater extent. This mechanism is evident in the joint work values and illustrated by the power profiles (Figure 1). Although there is greater MT positive work done in FFS ( $p < 0.001$ ), there is also greater concurrent MP negative work ( $p < 0.001$ ), as power is transferred from the MP joint to the MT joint. The integrated manner in which these joints act needs to be considered when evaluating midfoot mechanics (see also [8, 9]). Furthermore, the combined MP and MT work across stance shows no difference between strike patterns ( $p = 0.244$ ), and is a net negative,

suggesting that the foot’s contribution to active propulsion may be limited.

**Table 2:** MT and MP joint metrics during propulsion.

	RFS	FFS	<i>p</i>
MT RoM (°)			
Plantarflexion	7.1 ± 1.7	8.5 ± 2.2	0.000
Inversion	(-) 2.1 ± 1.4	2.5 ± 1.8	0.313
Adduction	4.8 ± 1.5	5.2 ± 1.9	0.118
MP Extension (°)	30.0 ± 3.2	34.8 ± 2.9	0.000
MT Work (J/kg)	.09 ± .04	.15 ± .04	0.000
MP Work (J/kg)	-.16 ± .04	-.23 ± .05	0.000
Combined Work	-.15 ± .04	-.17 ± .06	0.244

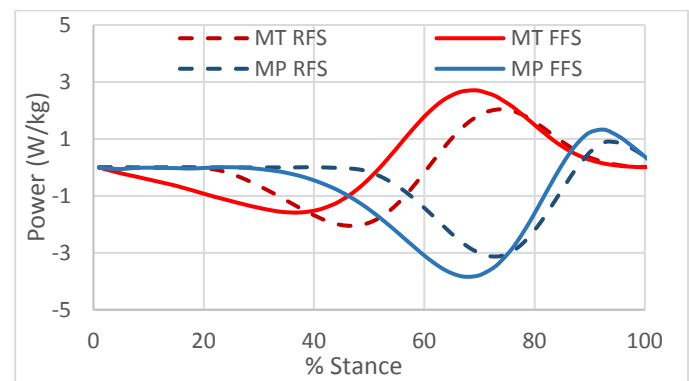


**Figure 1:** MT and MP joint powers across stance

## CONCLUSIONS

The midtarsal locking theory explains why the greater MT joint loading that occurs in a FFS pattern does not result in more negative MT joint work, as altered MT axes stiffen the joint. During propulsion, the windlass mechanism similarly explains why greater MT plantarflexion and positive work do not result in differences in total work done by the integrated MT and MP joints.

## REFERENCES

1. Cavanagh et al. J Biomech, 1980. **13**(5): 397-406.
2. Pohl et al. Clin Biomech, 2008. **23**(3): 334-341.
3. Elftman. Clin Orth, 1960. **16**: 41.
4. Hicks. J Anatomy, 1954. **88**(Pt 1): 25.
5. Bruening et al. Gait Posture, 2012. **35**(4): 529-534.
6. Stefanyshyn et al. J Biomech, 1997. **30**(11): 1081-85.
7. Perl et al. Med Sci Sports Ex, 2012. **44**(7): 1335-43.
8. McDonald et al. PloS one, 2016. **11**(4): e0152602.
9. Wager et al. J Biomech, 2016. **49**(5): 704-709.

# NET ANKLE PSEUDO-STIFFNESS IS INFLUENCED BY WALKING SPEED BUT NOT AGE FOR OLDER ADULT WOMEN

<sup>1,2</sup> John Collins, <sup>1,3</sup> Elisa Arch, <sup>1,3</sup> Jeremy Crenshaw, <sup>4</sup> Kathie Bernhardt, <sup>5</sup> Sundeep Khosla, <sup>6,7</sup> Shreyasee Amin and <sup>4</sup> Kenton Kaufman

<sup>1</sup> Biomechanics and Movement Science Interdisciplinary Program; <sup>2</sup> BADER Consortium; <sup>3</sup> Department of Kinesiology and Applied Physiology, University of Delaware, Newark, DE, USA

<sup>4</sup> Department of Orthopedic Surgery; <sup>5</sup> Division of Endocrinology, Diabetes, Metabolism, and Nutrition, Department of Medicine; <sup>6</sup> Division of Epidemiology, Department of Health Sciences Research; <sup>7</sup> Division of Rheumatology, Department of Medicine, Mayo Clinic, Rochester, MN, USA  
email: jdc@udel.edu

## INTRODUCTION

During stance, the plantar flexors eccentrically control the rate and timing of dorsiflexion [1]. This function controls the shank's rotation and influences the kinetics, energetics, propulsion, support and forward progression of gait [1,2]. Insufficient resistance to dorsiflexion due to plantar flexor weakness results in shorter or asymmetrical step lengths and decreased walking speeds common in patients, such as individuals post-stroke [3].

Resistance to dorsiflexion can be quantified via net ankle pseudo-stiffness (NAS), defined as the slope of the ankle joint moment-angle curve during the second and third rockers [4] of the stance phase of gait. Individuals with plantar flexor weakness are often prescribed Passive-Dynamic ankle-foot orthoses (PD-AFOs) with the intent of using the spring-like bending stiffness of the orthosis to replace a patient's lost dorsiflexion resistance [4]. However, current methods of orthosis fabrication rely on trial-and-error. Beginning with a model-predicted baseline has many benefits, including increased efficiency and rapid, objective fabrication methods. As a first step to developing this baseline model, the purpose of this study was to understand the influence of age and walking speed on NAS beyond the age of 65 years. We hypothesized that NAS would decrease with slower gait and older age.

## METHODS

A total of 113 community-dwelling, ambulatory women between the ages of 65 and 91 (age: 76.3 ± 7.4 yrs; BMI: 27.3 ± 5.0) participated in this IRB-approved study at the Mayo Clinic. Kinematic data

from a 10-camera system (Motion Analysis Corp, Santa Rosa, CA; 120 Hz) and kinetic data from forceplates (2 AMTI, Watertown, MA and 3 Kistler, Amherst, NY 600Hz) embedded in the walkway were processed in Visual3D (C-Motion, Inc, Germantown, MD).

Ankle moments were scaled by body mass, leg length and gravitational constant to create a dimensionless moment [5]. Four to six gait trials were analyzed for each participant. The second and third rockers of stance were defined from the first instance of the plantar flexion moment to the maximum dorsiflexion angle [4]. A Froude-scaled walking speed was also calculated.

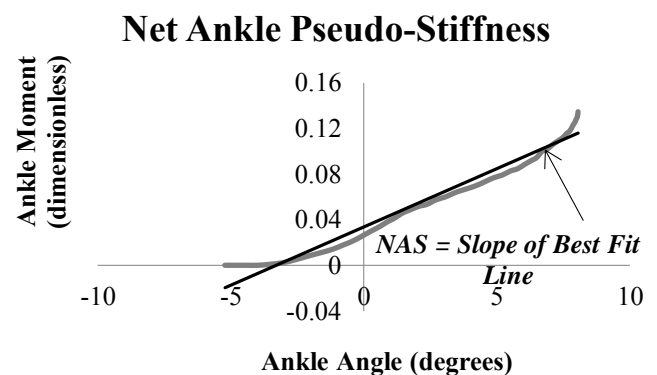


**Figure 1:** The observed ankle angle and moment relationship (gray) for one representative trial. The net ankle pseudo-stiffness (NAS) is calculated from the slope of a best-fit linear regression line (black).

Using custom MATLAB (MathWorks, Inc. Natick, MA) script, NAS was calculated as the slope of a linear regression between sagittal-plane ankle angle and moment for each stance phase (Figure 1). The NAS values were averaged across limbs for each participant. Then, a multivariate linear regression model was used to evaluate the influence of age,

Froude-scaled walking speed, and limb (if necessary) on NAS. Finally, to understand how the components of NAS (change in ankle angle and moment) were influenced by age and walking speed, Pearson correlation analyses were conducted. All statistical analyses were conducted in SPSS (IBM, Armonk, NY).

## RESULTS AND DISCUSSION

Approximately 36% of the variance in NAS was explained by walking speed and age ( $p < 0.001$ ,  $R^2 = 0.355$ ). The NAS increased with walking speed ( $\beta = 0.057 \pm 0.007$ ,  $p < 0.001$ ,  $r = 0.59$ ; Figure 2), but was not influenced by age ( $\beta = 5.0 \times 10^{-5} \pm 4.2 \times 10^{-5}$ ,  $p = 0.23$ ,  $r = -0.11$ ). Further analysis revealed that the change in dorsiflexion angle was negatively correlated with speed, with less dorsiflexion as speed increased ( $r = -0.42$ ,  $p < 0.001$ ). A larger change in the plantar flexion moment was associated with faster walking speeds ( $r = 0.54$ ,  $p < 0.001$ ).

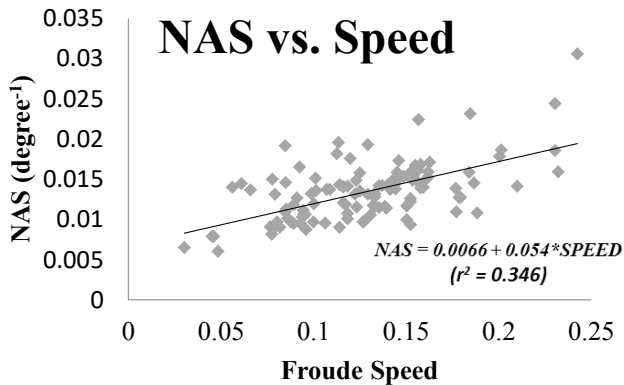


**Figure 2:** The observed relationship between net ankle pseudo-stiffness (NAS) and Froude-scaled walking speed. A linear best-fit line and associated regression equation quantify the positive relationship between NAS and walking speed.

Changes in NAS with speed were influenced by both ankle kinematics and kinetics. With reduced walking speed, the plantar flexion moment decreased and the dorsiflexion angle increased, both of which decreased NAS.

By including a large sample of mobile, elderly women with ages evenly distributed between 65 and 91 years, we were able to treat age as a continuous parameter in the regression analysis. With a patient's weight, leg length and targeted walking speed, a prescribed NAS can be calculated using the regression equation generated in this study (Figure 2). This objectively-determined NAS value could prove critical for effectively personalizing PD-AFO bending stiffness.

## CONCLUSIONS

This study establishes a relationship between gait speed and NAS. PD-AFOs rely on the customized spring-like bending stiffness to replace a patient's lost NAS [4]. Thus, we are providing a foundation for objectively prescribing PD-AFO bending stiffness to achieve a targeted gait speed for older adults with plantar flexor weakness.

## REFERENCES

1. Perry J, Burnfield JM. *Gait Analysis: Normal and Pathological Function*. 2nd ed. Thorofare: SLACK Inc; 2010. doi:10.1001
2. Kepple T, Siegel K, Stanhope SJ. *Gait Posture* **6**, 1-8, 1997.
3. Nadeau S, Gravel D, Arsenault B, Bourbonnais D. *Clin Biomech* **14**, 125-35, 1999.
4. Davis RAB, Deluca PA. *Gait Posture* **4**:224-31. 1996.
5. Hof AL. *Gait and Posture* **4**, 222-23, 1996.

## ACKNOWLEDGMENTS

This work was supported by National Institutes of Health [grant numbers R01AR027065 to SK/SA, T32HD07447 to J. R. Basford, NIH UL1TR000135 to SK], the BADER consortium (DoD/CDMRP award W81XWH-11-2-022) and the Unidel Foundation [to EA].

## NON-ACADEMIC CAREER PATHS IN BIOMECHANICS

Maria Pasquale<sup>1</sup>, Alison Sheets-Singer<sup>2</sup>, Kate Pate<sup>2</sup>, Michael Zabala<sup>4</sup>, Inge Wefes<sup>5</sup>, Chris Hass<sup>6</sup>

<sup>1</sup>Novel Electronics Inc, St. Paul, MN, USA

<sup>2</sup>Nike Sport Research Lab, Portland, OR, USA

<sup>3</sup>Roccor, Engineering and Analysis for Deployable Structure Systems, Longmont, CO, USA

<sup>4</sup>Department of Mechanical Engineering, Auburn University, Auburn, AL, USA

<sup>5</sup>NIH BEST Program for Broadening Experiences In Scientific Training, Biomedical Sciences & Biotechnology Program, Graduate School, University of Colorado Denver|Anschutz Medical Campus, Denver, CO, USA

<sup>6</sup>Department of Applied Physiology and Kinesiology, University of Florida, Gainesville, FL, USA

### INTRODUCTION

According to NIH/NSF reports fewer than half of STEM related PhDs pursue a career in academia, either in research or in teaching, and only 23% of those are in tenure track positions. Importantly, many biomedical-trained scholars enter research roles in industry (18%) and government (6%). Concurrently, the number and diversity of research and development positions for biomechanists in industry has increased. Employers now range from consulting roles (safety/injury), clinical research, health and wellness tracking and preventative care, sports equipment, sports injury and performance consultation, video game and movie animation, and virtual reality development, among others. There are many reasons why individuals with Master's and PhD degrees may pursue opportunities outside of academia; including changing research interests or the appeal of non-academic work, settings, access to more diverse resources for conducting research, job benefits (Sauermaann & Roach, 2012), and the potential to have research outcomes more quickly impact the wider community. Career development training and exposure to opportunities outside of academia is required, but the support and training for this by many institutions is lacking. In this symposium, we will get a glimpse of why several outstanding scientists moved from academia to industry and how their doctoral and postdoctoral training influenced their careers and lives. Panelists will cover "a day in the life," "work life balance," "what skills from your graduate training or research experiences directly translate to a nonacademic position" and "what skills do you wish you would have developed as part of your graduate training that apply to your job today," and will compare and

contrast research endeavors within these two communities. Further, the audience will be able to contrast the career paths and skill sets needed and developed across the variety of companies associated with the panelists. We will also discuss best practices regarding graduate training programs for workforce readiness. Importantly, the panel will discuss the ability to move back and forth between industrial and academic research settings and will highlight the symbiotic nature of this relationship rather than the "either/or" approach that many institutions still promote.

The symposium will follow the proposed schedule:

Introduction- Chris Hass- 2 minutes

Maria Pasquale -12 minutes

Alison Sheets-Singer 12 minutes

Kate Pate-12 minutes

Michael Zabala-12 minutes

Inge Wefes-12 minutes

Panel Discussion / Audience Questions- 28 minutes.

**Maria Pasquale, M.S.**, Director of Application Development for Novel Electronics Inc. For over a decade she has worked building meaningful partners and relationships for novel and maintaining the important relationship between industry and research. Maria studied bioengineering at the University of Pittsburgh where she obtained both her Undergraduate and Master's degree. Maria works closely with the software and hardware development team at Novel to bring new products and customers' wishes to fruition. She continues to

be involved in research projects (design, management, logistics, collection and analysis) with universities, clinical sites, and the military and enjoys this link “back to her research roots.” Maria will discuss important questions to answer before looking for industry positions and the roles that industry sponsors play in the field of biomechanics

**Alison Sheets-Singer, Ph.D.**, Dr. Sheets-Singer is a Senior Researcher in the Nike Sport Research Lab in Portland, OR. The goal of the lab and her research is to enhance athlete performance by creating innovative products and services. Prior to joining Nike, Inc. in 2012, Dr. Sheets-Singer was an Assistant Professor in the Mechanical and Aeronautical Engineering Department at The Ohio State University. Dr. Sheets-Singer will discuss her experiences leading research programs in industry and working with multi-disciplinary teams to create new products, and will compare compare industry and academic research settings.

**Kathryn (Kate) Pate, Ph.D.**, Dr. Pate is currently a Principal Scientist at Roccor (Longmont, Colorado), leading company research efforts in Combat Casualty Care. Dr. Pate has effectively transitioned back and forth between research intensive, teaching, and industry positions. She will describe the skills / experiences from her graduate and postdoctoral training that are similarly valuable among her careers and the skills she wish she would have focused on during her graduate training to prepare her for each of her career roles.

**Michael Zabala, Ph.D.**, Dr. Zabala is an Assistant Professor in the Department of Mechanical Engineering in the Samuel Ginn College of Engineering at Auburn University. Prior to joining the faculty at Auburn in the fall of 2016, Dr. Zabala was a professional consultant at Exponent, Inc. in Atlanta, Georgia, specializing in Injury Biomechanics. He will discuss his academic pathway and will compare and contrast consulting and academic positions. Further, he will provide insights into the process of transitioning back to academia following his consulting career.

**Inge Wefes, Ph.D.**, Dr. Wefes is the Director of the Biomedical Sciences and Biotechnology Program

and Associate Dean of the Graduate School at the University of Colorado Denver|Anschutz Medical Campus. Further, she is the Principal Investigator of a prestigious NIH Best award given to create and implement development opportunities in biomedical science training that will increase the preparedness and employability in the non-academic workforce. Dr. Wefes will discuss best practices and effective programing for career development training for workforce readiness.

# VALIDATION OF A MODEL BASED TRACKING TECHNIQUE TO MEASURE *IN VIVO* PATELLOFEMORAL KINEMATICS

<sup>1</sup> Samuel Pitcairn, <sup>1</sup> Bryson Lesniak and <sup>1</sup> William Anderst

<sup>1</sup> Biodynamics Laboratory, Department of Orthopedic Surgery, University of Pittsburgh PA, USA  
email: swpitcairn@pitt.edu, web: www.bdl.pitt.edu

## INTRODUCTION

The patellofemoral (PF) joint is a common site for non-specific anterior knee pain that occurs in physically active individuals. The pathophysiology of anterior knee pain is not well understood. It is believed that changes in patellar tracking (*i.e.* the changes in anterior-posterior and medial-lateral position, in addition to rotation) may be an underlying cause for PF pain [1].

The movement of the patella within the femoral trochlea is difficult to measure precisely, especially *in vivo*, during dynamic functional activities. Cadaveric studies can provide some insight to PF kinematics, however these studies are unlikely to duplicate the forces or muscle firing patterns of live humans [2]. *In vivo* techniques to measure patella kinematics include intracortical bone pins, externally affixed targets/markers, static and dynamic MRI, and quasi-static radiographs [2-7]. These methodologies provide valuable insight into patella kinematics, however, they are limited by the speed, applied loads, and range of motion that can be analyzed. The aim of the current study was to evaluate the performance of a model-based tracking (MBT) technique for assessing PF motion *in vivo* during dynamic, functional motion.

## METHODS

After obtaining informed consent to participate in this IRB-approved study, nine tantalum beads (1.0 mm dia.; 3 beads per bone) were inserted into the femur, patella, and tibia of two patients undergoing ACL-reconstruction (1 M, 1 F; age 22yrs. and 21yrs, respectively). Both participants completed a standard rehabilitation protocol, and were tested 6 months after surgery. Participants performed three

trials each of over ground walking and stair ascent movements at a self-selected pace within a biplane radiography system (Figure 1).



**Figure 1.** Laboratory setup during stair ascent.

Biplane radiographs were collected at 100 images/s for 1 second during each trial. A high-resolution computed tomography (CT) scan (0.5 x 0.5 x 0.625 mm)(GE LightSpeed Pro 16) was collected after movement testing. The femur, tibia and patella bone tissue was segmented from the CT images (Simpleware software, Exeter, UK). The center of each bead was identified within the CT scans. Voxels containing beads were replaced with voxels containing bone tissue, and the CT slices were reconstructed to create three-dimensional (3D) bone models. Patella motion was tracked using RSA bead tracking as a “gold-standard” and a volumetric MBT process that matches digitally reconstructed radiographs created from the subject-specific bone models to the biplane radiographs [8,9].

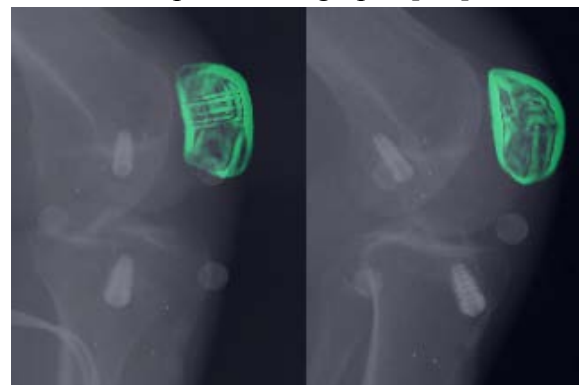


**Figure 2.** Patella bone model (green) tracked onto biplane radiographs.

**Table 1:** Model-based tracking (MBT) patellofemoral joint kinematics. Differences between model-based and bead-based tracking were calculated for each data frame. These differences were used to calculate mean differences (bias) and the standard deviation (precision). Data from level walk and stair ascent trials were averaged separately for each subject and then averaged together to get the values in this table. Standard deviations for each value reflect the inter-trial difference.

	Bias		Precision		RMS error	
	Level Walk	Stair Ascent	Level Walk	Stair Ascent	Level Walk	Stair Ascent
Medial-lateral translation	0.16 mm ± 0.48 mm	0.09 mm ± 0.22 mm	0.45 mm ± 0.22 mm	0.28 mm ± 0.15 mm	0.61 mm ± 0.22 mm	0.39 mm ± 0.16 mm
Anterior-posterior translation	0.28 mm ± 0.02 mm	0.01 mm ± 0.13 mm	0.18 mm ± 0.03 mm	0.08 mm ± 0.05 mm	0.34 mm ± 0.01 mm	0.15 mm ± 0.03 mm
Superior-inferior translation	-0.48 mm ± 0.12 mm	-0.02 mm ± 0.04 mm	0.24 mm ± 0.04 mm	0.14 mm ± 0.03 mm	0.54 mm ± 0.13 mm	0.15 mm ± 0.04 mm
Flexion-extension	0.33° ± 0.82°	0.26° ± 0.57°	1.30° ± 0.19	0.57° ± 0.19°	1.46° ± 0.32°	0.91° ± 0.39°
Tilt	1.19° ± 1.84°	1.36° ± 1.15°	1.17° ± 0.71°	0.87° ± 0.44°	2.25° ± 0.61°	1.85° ± 1.05°
Rotation	3.71° ± 3.80°	-0.23° ± 0.64°	2.38° ± 1.17°	0.79° ± 0.24°	4.56° ± 3.66°	1.09° ± 0.45°

The accuracy of the MBT technique was quantified in terms of bias (the average difference), precision (the standard deviation of the difference) and RMS error. The bead-based and MBT techniques were used to determine the centroid of the three beads implanted in the patella. Six degrees-of-freedom PF joint kinematics were also calculated for each frame of movement (medial-lateral, anterior-posterior and superior-inferior translations relative to the femur, and flexion (*i.e.* rotation about a medial-lateral axis of the femur), tilt (*i.e.* rotation about the patella's long axis), and rotation (*i.e.* rotation about the patella's anterior-posterior axis)) [10].

## RESULTS AND DISCUSSION

Average bead tracking precision (based on the 3D intermarker distances in the patella) was 0.13 mm. Using the bead-based tracking as a gold standard, the precision of the MBT in locating the centroid position of the implanted tantalum beads was  $0.90 \pm 0.2$  mm. In general, kinematic accuracy of the MBT was better in the stair ascent than in over ground walking (Table 1). These kinematic precision values are in line with our previous reports for similar *in vivo* validations for tracking cervical vertebrae (0.33 mm and 1° or less) and tibiofemoral kinematics (0.5 mm and 0.6°) [8,9]. The kinematic RMS error during knee flexion (stair ascent) is similar for translational and slightly higher in rotational measures than previously reported biplane cadaveric knee flexion values (0.395 mm and 0.877°) and cine-MRI knee flexion (0.33 mm and .97°) [2,7]. The ability of this technique to study PF motion during normal weight bearing exercise will help clinicians to better understand the pathology of PF knee pain and the effect of surgical and nonsurgical interventions to treat PF pain. Using cadaver specimens to validate bone tracking does

not provide a realistic representation of all challenges encountered when testing *in vivo*, such as occlusion from the contralateral limb. The patella presents unique challenges when imaging and tracking due to its symmetric shape and small size. These challenges can be overcome through proper placement of the imaging equipment during data collection.

## CONCLUSION

Given appropriate imaging configurations, the volumetric MBT process can track PF kinematics during dynamic functional movements with a precision of 0.45 mm and 2.4° or better.

## REFERENCES

1. Petersen, W, et al. *Knee Surg Sports Traumatol Arthrosc.* **22**(10), 2264–2274, 2010.
2. Bey MJ et al. *J Orthop Surg Res.* **3**, 38, 2008.
3. Fellows RA et al. *J Biomech.* **38**(8), 1643-52, 2005.
4. Koh TJ, et al. *J Biomech.* **25**(6), 637-43, 1992.
5. Suzuki, T et al. *J Biomech.* **45**(14), 2432–2437, 2013.
6. Wilson et al. *J Bone Joint Surg Am.* **91**(3), 558–566, 2009.
7. Behnam et al. *J Biomech.* **44**(1), 193-7, 2011.
8. Anderst et al. *Spine.* **36**(6), 393-400, 2011.
9. Anderst et al. *Med Eng Phys.* **31**(1), 10-6, 2008.
10. Bull AM et al. *Knee Surg Sports Traumatol Arthrosc.* **10**, 184-193, 2002.

## ACKNOWLEDGEMENT

This project was supported by grant R44 AR064620 from the NIH.

# INTRARATER RELIABILITY OF A NOVEL SEMI-AUTOMATED APPROACH TO DETERMINE KNEE ARTICULAR CARTILAGE MORPHOLOGY VIA MRI

Sunku Kwon<sup>1</sup>, Marlee Mason<sup>1</sup>, Alyssa Evans<sup>1</sup>, Merry Taylor<sup>2</sup>, Neal K. Bangerter<sup>2</sup>, J. Ty Hopkins<sup>1</sup>, and Matthew K. Seeley<sup>1</sup>

Department of Exercise Sciences<sup>1</sup>; Department of Electrical and Computer Engineering<sup>2</sup>,  
Brigham Young University, Provo, UT, USA  
Email: [sunkukwon@byu.edu](mailto:sunkukwon@byu.edu)

## INTRODUCTION

Reliable measurement of knee articular cartilage is important for many reasons. Magnetic resonance imaging (MRI) is a direct and noninvasive measurement modality that can be used to detect the morphological (e.g., cartilage thickness and volume) changes in knee articular cartilage. Previously, researchers have used MRI to measure effects of physical exercise on knee articular cartilage morphology, using manual methods of measurement (i.e., each region of interest was manually contoured) [1]. The purpose of this study was to describe our efforts to use a semi-automated approach to reliably measure knee articular cartilage thickness and volume. We hope to establish our ability to do so, so that we can later measure the influence of mechanical load, during physical activity, on knee articular cartilage thickness and volume.

## METHODS

Three recreational runners (1 male and 2 females; Ages: 22, 24, and 26 yrs; Masses: 52, 54, and 72 kg; Heights: 1.75, 1.58, and 1.85 m) received two MRI scans of the right knee, before and after a 60-min run (45 minutes of treadmill running and 15 minutes of overground running). Running speeds ranged from 3.0 to 4.0 m/s. Scans were acquired via a dedicated unilateral knee coil on the 3 Tesla Siemens Trio MRI system (Siemens Healthcare, Erlangen, Germany), using the sagittal 3D double-echo steady-state protocol.

A single rater (one of the coauthors—MM), quantified femoral cartilage thickness and volume for five of the six aforementioned scans, on two occasions that were separated by approximately four weeks. A first pass segmentation for femoral

cartilage thickness and volume was obtained using COLIPE software (Qmetrics, Pittsford, NY, USA) [2]. Next, the aforementioned rater manually adjusted the segmented femoral cartilage that was inaccurately segmented by the software's first pass, for each slice (e.g., see Figure 1). Then, using the COLIPE software and refined segmentations, mean cartilage thickness and volume were recalculated for seven cartilage regions: femur (F), central medial femur (cMF), central lateral femur (cLF), medial trochlear (MFT), lateral trochlear (LFT), posterior medial Femur (pMF) and posterior lateral femur (pLF).

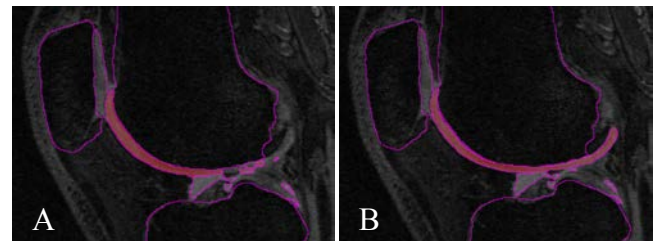


**Figure 1:** Semi-automated segmentation of femoral articular cartilage in the sagittal plane (1 of 160 slices). (A) Initial segmentation via the software; (B) Refined segmentation via the rater.

Intraclass correlation coefficients (ICC) and standard errors of measurement (SEM) were used to assess the intra-rater reliability of the single rater, between the measures of articular cartilage thickness and volume that were quantified four weeks apart. ICC and SEM were calculated using the equations shown at the bottom of Table 1 [3]. The mean square variances for ICC calculation were computed using SPSS (IBM, Armonk, NY, USA).

## RESULTS AND DISCUSSION

Results of the intra-rater reliability analysis are summarized in Table 1. ICC values for all measures of volume were greater than 0.99. ICC values for all measures of thickness, except for one (LFC = 0.76), were greater than 0.91. These high ICC values reflect a high degree of intra-rater reliability between measurement trials, for this specific rater. Differences between the first and second measurements of thickness and volume, for the same rater, are described in more detail in Table 2. Like the ICC values, the data presented in Table 2 also show that our trained examiner was able to consistently (1) adjust the segmentations that were initially established by the software, and (2) derive characteristics of articular cartilage morphology (thickness and volume) via the segmentations.

**Table 2:** Differences between measurements of articular cartilage morphology that were derived from the same MRI scan, four weeks apart.

Region	Thickness (mm)		Volume (mm <sup>3</sup> )	
	Mean Diff (±)	% Diff	Mean Diff (±)	% Diff
F	0.05 (0.03)	2.6	94.9 (67.1)	1.0
cMF	0.08 (0.06)	4.6	19.2 (16.2)	1.2
cLF	0.07 (0.08)	3.3	27.8 (30.1)	1.4
MFT	0.06 (0.11)	3.4	16.5 (8.5)	0.7
LFT	0.02 (0.02)	1.5	4.7 (2.4)	0.4
pMF	0.01 (0.01)	0.5	30.5 (13.8)	1.7
pLF	0.11 (0.23)	4.6	47.7 (32.4)	3.4

The SEM, reported in Table 1, represent an allowed measurement error range, reported in the actual units

**Table 1:** Intra-rater reliability results. Reliability was measured using the intraclass correlation coefficient (ICC), which is a function of between-scans (BMS), trials (TMS), and error (EMS) variances. Standard errors of measurement (SEM) are also reported here.

Region	Cartilage thickness (Mean and SEM unit: mm)						Cartilage volume (Mean and SEM unit: mm <sup>3</sup> )					
	BMS	TMS	EMS	ICC <sub>(2,1)</sub> *	Mean (s)*	SEM*	BMS	TMS	EMS	ICC <sub>(2,1)</sub> *	Mean (s)*	SEM*
F	0.121	0.005	0.001	0.971	1.633 (0.234)	± 0.04	50744895	22025.8	2376.16	0.999	11691.6 (4749.4)	± 74.9
cMF	0.363	0.016	0.002	0.974	1.577 (0.405)	± 0.065	124861.5	236.8	302.79	0.995	1884.8 (758.7)	± 51.6
cLF	0.284	0.011	0.003	0.968	1.646 (0.359)	± 0.064	1500019	1026.69	679.69	0.999	1786.7 (816.8)	± 25.8
MFT	0.141	0.009	0.006	0.911	1.51 (0.257)	± 0.077	1732251	369.15	114.47	0.999	2487.6 (877.5)	± 12.2
LFT	0.041	0.001	0	0.99	1.567 (0.135)	± 0.013	500881.5	0.042	16.39	0.999	1311.7 (471.8)	± 3.4
pMF	0.069	0	0	1	1.708 (0.175)	0	1075844	569.41	533.38	0.998	1972.9 (691.7)	± 21.9
pLF	0.212	0.027	0.029	0.762	1.754 (0.332)	± 0.162	1350560	525.17	5691.38	0.993	1641.2 (775.3)	± 64.3

$$*ICC_{(2,1)} = \frac{BMS - EMS}{BMS + (k-1)EMS + k \left[ \frac{TMS - EMS}{N} \right]}, \text{ where } k=2 \text{ (trials), } N=5 \text{ (number of scans)}$$

$$*SEM = s\sqrt{1 - r}, \text{ where } s = \text{standard deviation of the measurements, } r = ICC_{(2,1)}$$

\*Mean: the mean of the measured values (i.e., cartilage thickness and volume) in 10 scans (5 scans × 2 trials)

[2], which are millimeter (mm) in this case. Note that mean differences shown in Table 2, for both thickness and volume are within SEM range (Table 1). This indicates that the mean differences reported in Table 2 are within an acceptable error range. Although there was generally good intra-rater reliability, the results showed that the rater did have lower reliability for some regions (e.g., pLF thickness). Although we are unsure what the cause of these differences in reliability is, across different femoral regions, we speculate that generally thinner thicknesses may influence segmentation reliability [2]. Finally, it will obviously be important to assess the accuracy of our method. Our values fit well with similar values, from previous literature, describing femoral thickness and volume; however, we still plan to evaluate the accuracy of our measures by comparing our results with results, from the same MRI scans, analyzed by an experienced radiologist.

## CONCLUSIONS

In conclusion, our results show that our trained rater can reliably derive measures of femoral cartilage thickness and volume, from MRI scans, using this semi-automated quantitative analysis method.

## REFERENCES

1. Ho K et al. *Clin Biomech*, **37**, 65-69, 2016.
2. Tamez-Pena J et al. *IEEE Trans Biomed Eng*, **59**(4), 1177-1186, 2012.
3. Denegar C et al. *J Sport Rehabil*, **2**, 35-42, 1993.

# FEASIBILITY OF BIPLANE FLUOROSCOPY FOR QUANTIFICATION OF SHOULDER KINEMATICS DURING MANUAL WHEELCHAIR USE

Joseph D. Mazingo, Mohsen Akbari-Shandiz,  
Cynthia H. McCollough, and Kristin D. Zhao

Mayo Clinic, Rochester, MN, USA  
Email: zhao.kristin@mayo.edu

## INTRODUCTION

The majority of individuals with a spinal cord injury that use a manual wheelchair (MWC) report shoulder pain. Shoulder mechanical impingement, caused by narrowing of the subacromial space during MWC use, is considered a primary extrinsic mechanism associated with shoulder pain and rotator cuff pathology [1]. It has been suggested that a change as small as 1-2 mm in the subacromial space may constitute an overall 10-70% reduction [2]. Thus, marker-based kinematic approaches, which are prone to skin motion artifact, are insufficient for elucidating the biomechanical basis of this problem. 3D-2D model-image registration, using biplane fluoroscopy and computed tomography (CT), has become the gold standard for noninvasive in vivo quantification of bony motion, providing sub-millimeter and sub-degree kinematic accuracy. Investigators have demonstrated the utility of this technique for quantification of shoulder kinematics and changes in the subacromial space, but previous work has mainly been limited to arm elevation tasks in able-bodied individuals. *Thus, the goal of this work was to develop, validate, and demonstrate the feasibility of an approach to quantify shoulder kinematics during MWC use using a clinical biplane fluoroscope.*

## METHODS

A cadaveric validation study was first performed in order to determine the accuracy of this technique. One male fresh frozen cadaver (age 82 yrs.) with the thorax and arms intact was obtained from the Mayo Clinic anatomical bequest program after the protocol was approved by the Mayo Clinic biospecimens subcommittee. 4-6 radiopaque beads were implanted directly into discrete regions of the humerus and scapula of both shoulders in order to conduct radiostereometric analysis (gold standard).

The specimen was CT imaged (Definition Flash, Siemens Healthcare) at 120 kVp, 250 quality reference mAs, 200x200 mm FOV. In order to create 3D models, the scapula and humerus were manually segmented from the image volume by defining regions of voxels that corresponded to each bone (AnalyzePro; Mayo Clinic).

Next, the specimen was secured upright in a custom device that allowed for unconstrained motion of the upper limb, and the glenohumeral joint was centered in the imaging volume of a clinical flat-panel biplane fluoroscope (Artis Zee; Siemens Healthcare). Fluoroscopic images were acquired at 15 frames/second per plane (pulse width= 3.2 ms for each source) during 3 simulated motions, including elevation in the scapular and sagittal planes, and external rotation of the shoulder.

Bone models were registered to fluoroscopic images using freely available model-image registration software (Autoscooper; Brown University). The pose of each model was adjusted such that its DRR was aligned with its fluoroscopic projection in each image plane. RSA was performed using freely available software (XMA Lab; Brown University) in order to track the 3D position of each bead. These positions were used to calculate frame-to-frame motion of bead-based coordinate systems and, therefore, the respective bones to which the beads were rigidly fixed. Global orientation and position data of the bone models and bead clusters were transformed to anatomical coordinate systems for direct comparison using landmarks established by the International Society of Biomechanics [3].

Following IRB approval and informed consent, 1 healthy able-bodied male subject (age 24 yrs.) was enrolled in this pilot study to determine the feasibility of this approach. The subject sat in a rigid low-back manual wheelchair atop a set of stationary manual wheelchair rollers (McLain

Wheelchair Roller; Riverfront Cycle) and the dominant shoulder was centered in the imaging volume of the biplane fluoroscope. Each source and image receptor was positioned to allow unconstrained movement and to provide an imaging volume that captured the shoulder anatomy across its range of motion. After practicing the activity, fluoroscopic images were acquired at 15 frames/second per plane during three cycles of propulsion (Fig. 1). A CT scan of the subject's dominant shoulder will be obtained in order to generate 3D models of the humerus and scapula, conduct 3D-2D registration, and quantify glenohumeral motion.

## RESULTS AND DISCUSSION

We evaluated the accuracy of our approach by computing the absolute difference between 3D-2D model-image registration and RSA for each rotational and translational kinematic parameter (results included in Table 1). For scapula kinematics, the mean absolute difference did not exceed 0.49 mm and 0.27° across all degrees of freedom, with maximum errors of 1.07 mm and 0.77°. For humerus kinematics, the mean absolute difference did not exceed 0.34 mm and 0.44° across all degrees of freedom, with maximum errors of 0.92 mm and 1.09°.

This work defined the accuracy of 3D-2D model-image registration for the quantification of dynamic shoulder motion using a clinical biplane fluoroscope, CT, and open-source DRR-based registration software. Importantly, the observed mean kinematic errors of 0.30 mm and 0.31° were comparable to previous studies (mean kinematic

errors ranging from 0.2 – 0.4 mm, 0.1 – 0.5°). These results supported our decision to proceed with the pilot study on an able-bodied individual, for which preliminary images have been provided (Fig. 1).

Axis	Translation (mm)		Rotation (°)	
	Scapula	Humerus	Scapula	Humerus
<b>X</b>	.36 ± .23	.25 ± .17	.19 ± .13	.42 ± .26
<b>Y</b>	.49 ± .24	.17 ± .14	.15 ± .11	.44 ± .29
<b>Z</b>	.20 ± .16	.34 ± .20	.27 ± .21	.38 ± .24

**Table 1:** Mean absolute difference and standard deviation between 3D-2D registration and RSA.

## CONCLUSIONS

Sub-millimeter and sub-degree kinematic accuracy was obtained using an off-the-shelf clinical biplane fluoroscope, enabling quantification of small changes in subacromial space. Furthermore, our pilot subject study demonstrates the ability to use this approach to obtain biplane fluoroscopy images during manual wheelchair propulsion. Future work will involve application of this technique in individuals with a spinal cord injury in order to determine which MWC-based activities and conditions impose an increased risk of rotator cuff damage.

## REFERENCES

1. Akbar M., et al. *J Bone Joint Surg*, **92**, 23-30, 2010
2. Bey MJ., et al. *J Clin Biomech*, **22**, 767-773, 2007
3. Wu G., et al. *J Biomech*, **38**, 981-992, 2005

## ACKNOWLEDGEMENTS

We thank Mark Hindal for assistance with imaging, Felicia Marquez for contributions to data processing, and NIH/NIAMS T32 AR56950 for supporting this work.

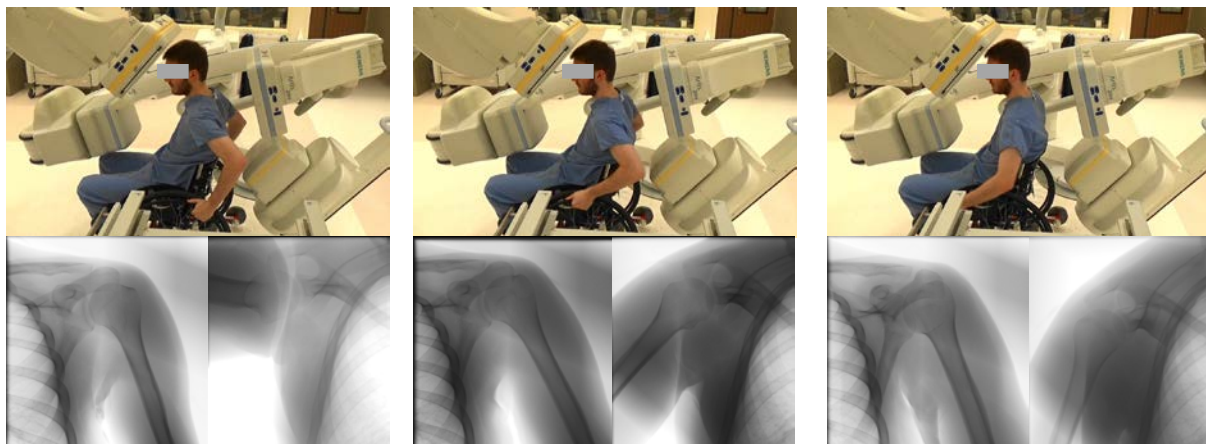


**Figure 1:** Able-bodied subject performing manual wheelchair propulsion. Start of push (left), mid-push (middle), end of push (right). Biplane fluoroscopy images from each image plane at various points during propulsion cycle (bottom row).

# Comparison of Real-Time MRI Pulse Sequences for Tracking Tissues of the Actively Moving Wrist

<sup>1</sup> Calvin B. Shaw, <sup>1</sup> Brent H. Foster, <sup>1</sup> Robert D. Boutin, <sup>2</sup> Robert M. Szabo,

<sup>2</sup> Christopher O. Bayne, <sup>3</sup> Krishna S. Nayak, and <sup>1</sup> Abhijit J. Chaudhari

<sup>1</sup> Department of Radiology, University of California Davis School of Medicine, Sacramento, CA, USA

<sup>2</sup> Department of Orthopedic Surgery, University of California Davis School of Medicine, Sacramento, CA, USA

<sup>3</sup> Ming Hsieh Department of Electrical Engineering, University of Southern California, Los Angeles, CA, USA

email: cshaw@ucdavis.edu, web <http://bme.ucdavis.edu/chaudhari>

## INTRODUCTION

Wrist instability is a major cause of pain, disability, and premature osteoarthritis [1]. In early stages, instability may be difficult to diagnose and pain may only be manifest during joint motion [1]. Clinically, wrist MRI is performed only in the static, neutral position. Therefore, there is no opportunity for assessing early stages of joint instability. Our goal was to implement a quick (<5 min) MRI scan “sequence” as part of our standard clinical wrist MRI exam to assess continuous, active, uninterrupted motion, and extract biomechanical information of relevance to wrist instability.

Two candidate real-time MRI (RT-MRI) pulse sequences were implemented and compared *in vivo*: (1) spoiled gradient echo (fast low angle shot, FLASH) and (2) steady-state free precession (true fast imaging with steady-state free precession, TrueFISP) [2]. We asked (1) can these two RT-MRI sequences provide a direct visualization of the actively moving wrist joints, and (2) which of the two sequences had superior performance with respect to image quality, artifacts and temporal resolution?

## METHODS

Data Acquisition: All protocols were approved by the UC Davis Institutional Review Board. A Skyra 3T System (Siemens Healthcare, Erlangen, Germany) using a 32-channel head radiofrequency coil was used. Preliminary experiments involved phantom scanning and multiple scans of two human participants to optimize scan parameters. The default sum-of-squares based image reconstruction was adopted for all the sequences. RT-MRI datasets were then acquired from three healthy volunteers (age 27±3 years; 2 males). Each sequence acquired 10

different positions of radial ulnar (RU) deviation and clenched fist maneuvers for every subject. Further, each maneuver was repeated thrice to evaluate reproducibility. Finally, the underlying contrast associated with the FLASH sequence was optimized to further improve the visualization of joint spaces by adopting a fat-suppression scheme. The inclusion of fat-suppression marginally increased the temporal resolution by 4%.

Data Analysis: In the first part, the performance of the two sequences was evaluated visually in terms of spatial resolution and degree of artifacts in images. Further, a comparison of the radial and Cartesian (rectilinear) k-space sampling was performed for real-time imaging with the afore mentioned wrist maneuvers. Secondly, fat-suppressed radial-FLASH was evaluated for both spatial and temporal resolution to demonstrate its viability to visualize the moving wrist joints. The scan re-scan reproducibility was quantified by placing regions of interest on the carpal bones and computing the signal-to-noise-ratio (SNR) across all the slices.

## RESULTS AND DISCUSSION

The achievable temporal resolution with the optimized parameters for each sequence is given in Table 1. Note that spatial resolution (determined by the number of radial spokes/Cartesian lines) and temporal resolution are inversely related, therefore there is a trade-off. Radial-FLASH had promising results in terms of spatial and imaging artifacts compared to other sequences (Fig. 1). Although TrueFISP resulted in an appreciably higher image contrast, images were affected by banding artifacts/signal loss (red arrows in Fig. 1) caused by field inhomogeneity that arises due to wrist motion. On the other hand, FLASH provided images

relatively free of banding artifacts, making it a viable scheme for tracking the wrist motion.

The advantage of using radial rather than Cartesian sampling is illustrated in Fig. 1. Radial sampling eliminated wrap around effect (white arrow) since it relied only on frequency-encoding gradients that cover both low- and high-frequency components in every single spoke [2].

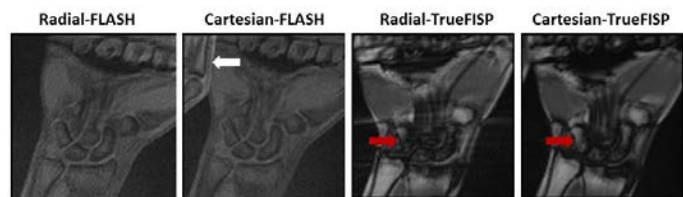


**Figure 1:** Representative coronal slices using radial-FLASH, Cartesian-FLASH, radial-TrueFISP, and Cartesian-TrueFISP from a healthy subject during RU deviation. Red and white arrow(s) point at the banding artifacts and wrap around effect respectively.

The efficacy of the fat-suppressed FLASH in terms of image quality and contrast is illustrated in Fig. 2. The contrast provided by fat-suppressed FLASH was reasonable to distinguish carpal bones and joint spaces of the wrist. Further, Fig. 2 and Table 1 suggests that higher frame rates are possible (up to 7 frames/sec) to assess the wrist kinematics, while maintaining acceptable image quality. Finally, radial-FLASH was also consistent in intersubject and intrasubject reproducibility (Fig. 3).

From our preliminary results, the RT-MRI radial-FLASH sequence demonstrated superiority in its ability to assess the motion of the actively moving wrist. The present study will be extended by increasing the sample size and deriving quantitative measures such as distal radioulnar joint congruity

and changes in the scapholunate interval during wrist motion from the radial-FLASH images.



**Figure 2:** Representative coronal slices (during RU deviation) using fat-suppressed radial-FLASH at 100, 60 and 40 spokes corresponding to 3, 5, and 7 frames/sec.

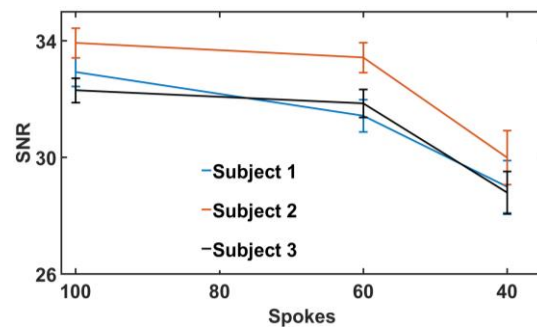


**Figure 3:** SNR versus number of radial spokes (with error bars) for three different subjects (RU deviation) to demonstrate the reproducibility of radial-FLASH.

## CONCLUSIONS

This study designed a feasible RT-MRI protocol and suggests the use of radial-FLASH to achieve adequate spatial and temporal resolution for monitoring active wrist motion.

## REFERENCES

1. Gelberman R, et al. *J. Bone & Surg.* **82**, 577, 2000.
2. Uecker M, et al. *Imaging Med.* **4**, 461-476, 2012.

**Table 1:** Key imaging parameters for FLASH and TrueFISP for the moving wrist in Figs. 1 & 2.

Sequence	R-FLASH	C-FLASH	R-TrueFISP	C-TrueFISP	R-FLASH
Temporal Resolution (ms)	302	351	477	477	134
Voxel Size (mm <sup>3</sup> )	1×1×6	1×1×6	1×1×6	1×1×6	1×1×6
Radial Spokes/ Cartesian Lines	100	112	100	112	40
TR/TE (ms)/Fat-Suppressed	3.02/1.74/No	3.13/1.74/No	4.25/1.75/No	4.77/1.76/No	3.02/1.74/Yes
Bandwidth (Hz/pixel)	990	990	930	930	990
Flip Angle (degrees)	12	12	46	46	12

\*Field of view = 120 mm<sup>2</sup>, number of slices=6, and the imaging plane was coronal for all the five sequences. R-Radial and C-Cartesian

# EXTENDED FIELD-OF-VIEW ULTRASOUND OF THE EXTENSOR CARPI ULNARIS

<sup>1,4,5</sup> Amy N. Adkins, <sup>1</sup> Patrick W. Franks, and <sup>1,2,3,4,5</sup> Wendy M. Murray, PhD

Departments of <sup>1</sup>BME, <sup>2</sup>PM&R, and <sup>3</sup>PTHMS, Northwestern University, Chicago, IL, USA

<sup>4</sup>Shirley Ryan AbilityLab (formerly RIC), Chicago, IL, USA

<sup>5</sup>Edward Hines, Jr. VA Hospital, Hines, IL, USA

email: adkins@u.northwestern.edu

## INTRODUCTION

Fascicle length is an important parameter in defining a muscle's force-generating capacity. Currently, ultrasound is the most common method of measuring fascicle length *in vivo* [1]. However, 24 of 26 forearm muscles have fascicles longer than the field-of-view of common traditional ultrasound (T-US) probes. As such, little work has been done to quantify *in vivo* forearm muscle architecture. The extended field-of-view ultrasound (EFOV-US) algorithm fits together a sequence of T-US images obtained via a continuous ultrasound scan [2], facilitating direct measurement of longer, curved fascicles. Misalignment of the ultrasound probe from the plane of the fascicles has been shown to result in fascicle length error using T-US. Because EFOV-US requires long, dynamic scans, there is concern such misalignment error could aggregate, reducing accuracy and reliability. The objective of this study was to determine the validity and reliability of the EFOV-US method for obtaining fascicle lengths in the extensor carpi ulnaris (ECU).

## METHODS

T-US and EFOV-US images of the ECU were obtained from 8 subjects (4F/4M, ages 23-29, height range 59-73") with no history of musculoskeletal disease or injuries of the upper limb. All subjects provided informed consent; Northwestern University's Institutional Review Board approved this study's procedures.

To evaluate the validity of our measurement protocol, an ultrasound phantom was imaged using EFOV-US. The phantom was constructed to mimic the sonic properties of muscle tissue. Wooden blocks and guitar strings (20-75mm) were measured with a caliper precise to 0.01mm before placement

inside the phantom. Image collection occurred with the ultrasound machine set to EFOV-US mode. Images were exported in DICOM format and object lengths were measured using the segmented line tool in ImageJ (NIH, Bethesda, MD). A Bland-Altman test of agreement was implemented to compare phantom object dimensions measured using the caliper and EFOV-US.

To determine if EFOV-US's long scan yields greater fascicle measurement error than T-US, the right arms of 8 healthy subjects were imaged using both methods. Subjects were seated with their arm rigidly secured in a joint posture that shortened the ECU to the extent that entire fascicle lengths could be captured within a single T-US image (Fig. 1). To enable comparisons between the two methods, the sonographer first obtained an EFOV-US image of the ECU then collected 6 corresponding T-US images that spanned the length of the ECU (Fig. 2). Three corresponding "image sets" (1 EFOV-US and 6 T-US images) were collected per subject. An average of 8 fascicles were measured per method per image set.

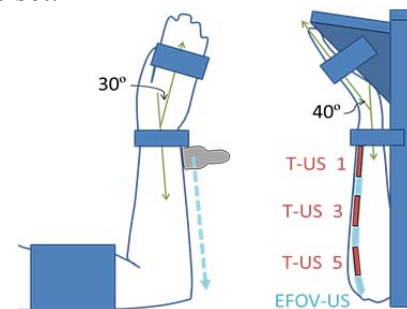


**Figure 1:** Subject's arm position during imaging. Light blue lines indicate the transducer path for a single EFOV-US scan; superimposed red lines illustrate 3 of the 6 corresponding T-US images collected within a given "image set".

A matched-pairs t-test was implemented to compare the average fascicle lengths obtained from the first "image set" collected. A pre-hoc power analysis,

based on uncertainty calculated via the phantom study, indicated that a power greater than 0.80 would be achieved with 6 subjects and an effect size of 1.69. A Bland-Altman plot tested agreement between fascicle measurements obtained using EFOV-US and T-US. The intraclass correlation coefficient (ICC) was calculated from repeated “image sets” to test between trial reliability of EFOV-US.

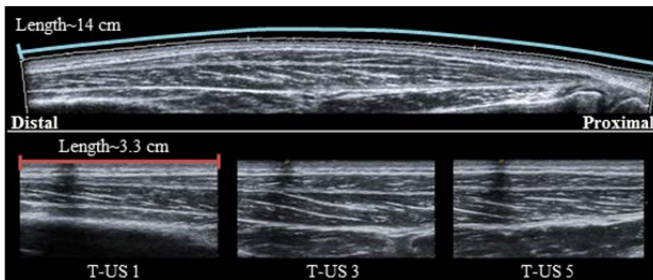


**Figure 2:** EFOV-US image and three example T-US images of the ECU from the same “image set”.

## RESULTS AND DISCUSSION

The measurements from the ultrasound phantom indicate that the EFOV-US imaging and analysis methods produced valid results. We observed an average error of  $2.2 \pm 1.3\text{mm}$  (4.6% average phantom object length). A Bland-Altman plot demonstrated agreement between direct caliper and EFOV-US measurements of the phantom objects (bias =  $-0.67\text{mm}$ , 95% CI:  $-5.57$  to  $4.23\text{mm}$ ).

EFOV-US fascicle measurements are comparable to those obtained from T-US, a well-established method. Average EFOV-US fascicle lengths over the full length of the muscle ( $27.9 \pm 3.7\text{mm}$ ) were not significantly different ( $p = 0.18$ ) than T-US fascicle lengths ( $28.2 \pm 4.0\text{mm}$ ). Bland-Altman analysis also indicates that the two methods agree (bias =  $-0.35\text{mm}$ , 95% CI:  $-1.47$  to  $0.77\text{mm}$ ). Fascicle lengths at the end of the EFOV-US image, where misalignment error associated with the continuous scan would presumably aggregate, were not significantly different ( $p = 0.42$ ) from T-US lengths in the same location within the muscle. Between trial reliability (ICC=0.99 95% CI:0.95-1.00) was excellent [3].

The EFOV-US method is more accurate than an approximation method commonly used when fascicles are longer than the field-of-view of T-US.

Trigonometric estimation was shown to yield an absolute error of  $7.7 \pm 6.2\text{mm}$  in the vastus lateralis, which was approximately 9% of total fascicle length [3]. Our error, determined by the analysis of our phantom images, was 4.6% of object length ( $2.2 \pm 1.3\text{mm}$ ). Notably, differences in fascicle length between the paretic and non-paretic arm of individuals post-stroke are larger than the error observed in our phantom study. For example, a study implementing T-US on the brachialis muscle found fascicles of the paretic arm to be 9-15% shorter (8-21mm) than fascicles of the non-paretic arm [4]. Thus, EFOV-US may be the best available ultrasound imaging approach to study clinically relevant changes in forearm fascicle length.

## CONCLUSIONS

Only one previous study has quantified *in vivo* fascicle lengths in a forearm muscle, despite the ubiquity of ultrasound studies in other muscle groups and the importance of architecture in understanding muscle force generation. The EFOV-US method has the capacity to capture the entire length of the fascicle in one image; this is advantageous in the forearm where over 90% of muscles have optimal fiber lengths longer than the field-of-view of T-US. Utilizing this method in patient populations, such as individuals post-stroke or post-surgery, may enable subject-specific muscle models and improve rehabilitation strategies.

## REFERENCES

1. Kwah, L. et al. *J App Physiol* **114**, 761-69, 2013.
2. Weng, L. et al. *Radiology* **203**, 877-880, 1997.
3. Noorkoiv M, et al. *J App Physiol* **3**, 627-34, 2010.
4. Li L, et al. *ArchPhysMedRehabil* **88**, 243-50, 2007.

## ACKNOWLEDGMENTS

This work is supported by the National Science Foundation Graduate Research Fellowship Program under Grant No. DGE-1324585, as well as NIH R01 D084009 and T32 HD007418. Any opinions, findings, and conclusions or recommendations expressed in this material are those of the authors and do not necessarily reflect the views of the National Science Foundation or NIH.

# INTRA-OP BIOMECHANICAL GUIDANCE IMPROVES ARTICULAR FRACTURE REDUCTION

Andrew M. Kern, Michael C. Willey, J. Lawrence Marsh, Donald D. Anderson  
Department of Orthopedics and Rehabilitation, The University of Iowa, Iowa City, IA  
email: andrew-kern@uiowa.edu, web: <http://www.uiowa.edu/uiobl/>

## INTRODUCTION

Intra-articular fractures (IAFs) often lead to poor outcomes, despite surgeons' best efforts at reconstructing the fractured articular surface. The objective of articular fracture reduction is to lower contact stress within the joint, thereby minimizing risk of post-traumatic osteoarthritis (PTOA). Surgical fracture reductions performed using less invasive approaches (i.e., percutaneously) rely heavily upon C-arm fluoroscopy to judge articular surface congruity. The use of 2D imaging alone for this purpose may prove inadequate<sup>1</sup>.

We explored the value of a biomechanical guidance system for aiding in articular fracture reduction. In five fractured cadaveric ankles, contact stresses, and contact areas were compared in surgeries performed with or without biomechanical guidance.

## METHODS

The biomechanical guidance system uses C-arm fluoroscopic imaging, along with pre-op CT data, to intra-operatively determine fracture fragment poses, (**Fig. 1**). This is done using established 2D-3D registration methods. Optional contact stress analysis provides complementary biomechanical data<sup>2</sup> to inform surgeon decision making.

Five cadaveric ankles obtained from the University

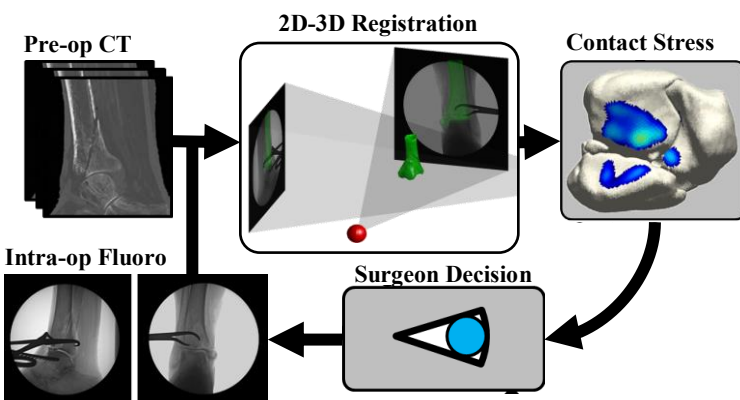


**Figure 1.** Overview of intra-op biomechanical guidance system.

of Iowa Deeded Bodies Program were fractured into clinically relevant patterns using an osteotome and a mallet. Following fracture, the proximal end of the tibia and fibula were potted in bone cement, and a baseline CT image was acquired.

Each fractured ankle was surgically reduced and fixed using percutaneous methods. Surgery was performed twice on each ankle (i.e., 10 surgeries), once in which biomechanical guidance information was shown to the surgeon, and once in which the information was withheld. To mitigate training effects, the order in which surgeries were performed was randomized, three of the ankles were reduced with guidance on their first operation. Repeat surgeries on the same ankle were separated by at least 48 hours, with all fixation hardware removed and incision sites sutured between surgeries.

During surgeries assisted by the biomechanical guidance system, the surgeon was instructed to use the system whenever there was doubt about the state of the reduction. Upon completion of the surgery, the biomechanical guidance system was used once again to determine the final fragment pose and contact stress distribution. A post-op CT scan was obtained to provide gold-standard data.

Following surgical fixation, the post-op result was compared between cases with vs. without information displayed to the surgeon. Contact stress metrics and contact area were compared.

## RESULTS AND DISCUSSION

All surgical reductions were satisfactorily completed. Visual comparisons of contact stress distributions between guided and unguided cases suggest value to using the guidance system (**Fig. 2**). Mean and maximum contact stresses were lower using guidance in four of five cases tested. The average reduction was 0.71 and 1.51 MPa for mean

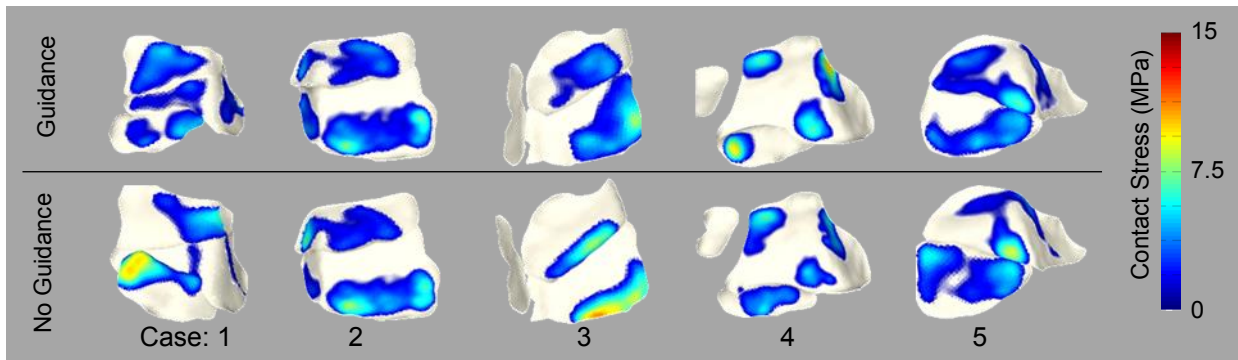


**Figure 2.** Contact stress distributions following definitive reduction with and without biomechanical guidance. Notable improvement (reduction) in contact stress shown in all cases except for case 4.

and maximum contact stress, respectively. Contact area engagement histograms show that unguided cases had greater areas at higher levels of contact stress than did the guidance cases. (Fig. 3)

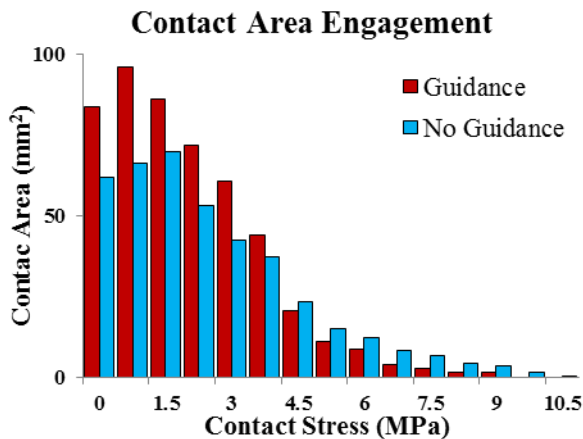


**Figure 3.** Contact stress area engagement histogram. Area reported is mean area across all bins. Note that cases with guidance had less contact area engaged >4.5 MPa.

The single case that did not show a reduction in contact stress with guidance (**Case 4 in Fig. 2**) was unique in that it was the only case with four fracture fragments, and the articular surface was completely separated from the diaphysis of the tibia. The increased complexity of this fracture or the specific fracture pattern may explain the worse outcome using biomechanical guidance.

Due to the prototype nature of this system, it is expected that additional experience with this system will further improve results, as the clinician is able

to better integrate this information. The contact area engagement histogram shows a trend consistent with prior work linking contact stress to PTOA risk, where contact area engaged at contact stresses >4.5 MPa was shown to be particularly deleterious<sup>3</sup>.

## CONCLUSIONS

A biomechanical guidance system was used to aid in the reduction of 5 fractured cadaver ankles. Metrics of contact stress and contact area were improved in four of the five cases tested when the guidance was used. These encouraging results suggest that the provision of intra-op biomechanical information to surgeons has potential to improve long-term outcomes of these difficult fractures. Future work will involve improvement to the core algorithms of the system, additional cadaveric experimentation, and if suitable, eventual translation to the OR.

## REFERENCES

1. Garner, MR et al. *J Orthop Trauma* 29(4): 161-65, 2015
2. Kern, AM, et al. *J Biomech*, 48(12): 3427-32, 2015
3. Anderson, DD et al. *J Orthop Res*. 29(1): 33-39, 2011

## ACKNOWLEDGMENTS

The research reported in this abstract was supported by the National Institute of Arthritis and Musculoskeletal and Skin Diseases of the National Institutes of Health under award number P50 AR055533. Thank you to Steven Long for assistance with surgical preparation and execution

# EXPLICIT MODIFICATION OF STEP LENGTH ASYMMETRY TRANSFERS TO OVER-GROUND WALKING POST-STROKE

<sup>1</sup> Natalia Sanchez and <sup>1</sup> James M. Finley

<sup>1</sup> University of Southern California, Los Angeles, CA, USA  
email: sanc232@usc.edu

## INTRODUCTION

After a stroke, changes in the control of the lower extremities lead to asymmetric step lengths during walking [1,2]. Asymmetries can occur in both directions, with some individuals taking short steps with their paretic leg (and long steps with their non-paretic extremity) or vice versa. However, the degree to which differences in the direction of asymmetry impact the potential for modification of step lengths has not been investigated systematically.

Here, we use visual feedback of foot placement to modify step length asymmetry during treadmill walking in individuals with chronic hemiparetic stroke. We hypothesized that online, visual feedback of actual and desired step lengths could help people post-stroke to improve symmetry. Furthermore, we predicted that this improvement in symmetry would transfer to over-ground walking.

## METHODS

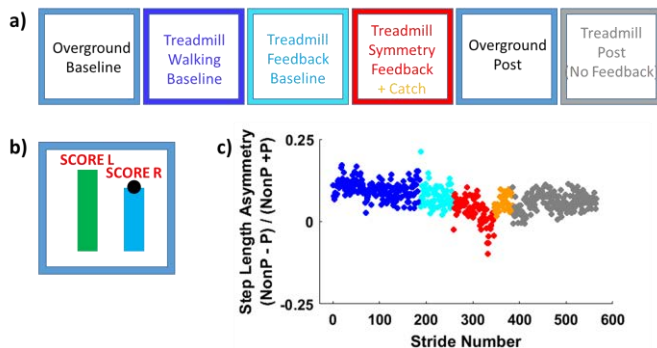


**Figure 1:** a) Experimental protocol b) Visual feedback c) Data from a single participant color-coded to match the corresponding task in (a).

Twelve chronic, hemiparetic stroke survivors participated in this study. Initial walking function was evaluated using the 6-minute walk test. The average speed obtained from this test (or at least 75% of this speed [3]) was used as the target speed for the

treadmill. Motor impairment was quantified using the lower extremity portion of the Fugl-Meyer Assessment.

All participants were tested under the following conditions (sitting breaks of at least five minutes were given between trials): an overground walking trial (OG BASE), a treadmill familiarization trial (FAMILIARIZATION), and a 5-minute treadmill BASELINE trial where we measured their natural step length asymmetry. The visual feedback consisted of two vertical bars corresponding to desired right and left step lengths, and real-time location of their feet was projected onto the bars using markers placed on their ankles (Figure 1b). The length of the bar corresponding to the short step was lengthened to match their long step and generate a symmetric walking pattern (SYMMETRY). Participants then walked across a 4m walkway to determine whether the symmetric walking pattern that was enforced on the treadmill transferred to over-ground walking (OG POST). Finally, participants walked on the treadmill for an additional five minutes to test for retention of the symmetric walking pattern (POST).

Kinematic data for markers placed bilaterally were collected using a ten camera Qualisys Oqus camera system (QTM, Sweden). The fore-aft distance between markers on the lateral malleoli was used to measure step lengths and step length asymmetry (Equation 1).

$$\text{Step Length Asymmetry} = \frac{SL_{NonParetic} - SL_{Paretic}}{SL_{NonParetic} + SL_{Paretic}} \quad (1)$$

Participants were classified as symmetric if the magnitude of their asymmetry was below 0.035. This value corresponds to the mean  $\pm$  two standard deviations of the step length asymmetry measured in healthy participants from a previous study.

## RESULTS AND DISCUSSION

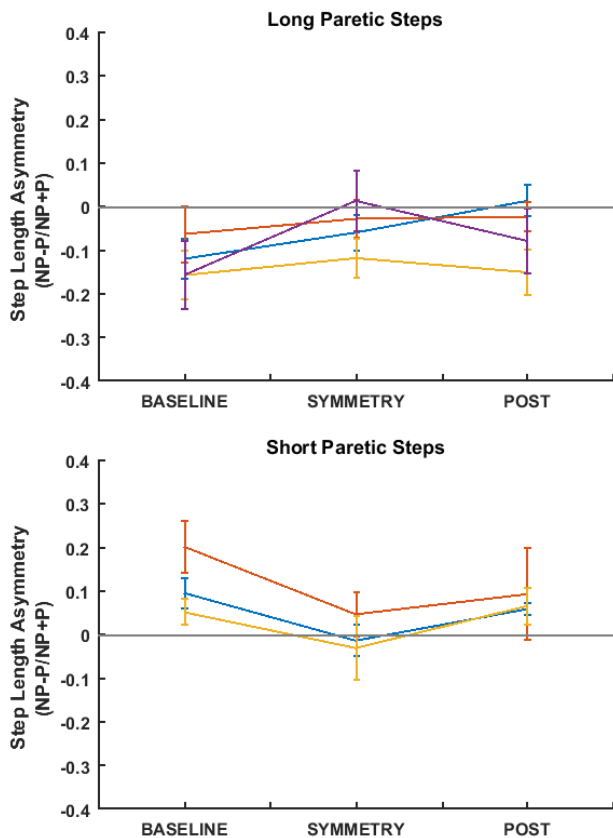


**Figure 2:** Step length asymmetry during treadmill walking for BASELINE, SYMMETRY and POST conditions for each type of asymmetry. Error bars indicate standard deviations.

Of the 12 participants tested, 7 participants were classified as asymmetric. Of these individuals, 3 took short steps with their paretic leg and had step length asymmetries of  $12 \pm 7\%$ , and 4 participants took long steps with their paretic leg and had asymmetries of  $-12 \pm 4\%$ . Aided by visual feedback, participants in the long paretic group reduced their asymmetry by  $60 \pm 35\%$  whereas participants in the short paretic group reduced their asymmetry by  $108 \pm 30\%$  (Figure 2). These preliminary results suggest that participants with short paretic steps may be more capable of using an explicit strategy to improve their symmetry on the treadmill.

After walking on the treadmill, 4/7 participants transferred improvements in symmetry to over-ground walking (Figure 3). The three participants in the long paretic group reduced their over-ground

asymmetry by  $33 \pm 53\%$ , whereas participants in the short paretic group reduced their asymmetry by  $9 \pm 18\%$ . Lastly, some of the improvements in symmetry were retained upon return to the treadmill during the POST trial (Figure 2). Here, we observed a  $58 \pm 44\%$  reduction for the long paretic group relative to BASELINE and a  $25 \pm 37\%$  reduction for the short paretic group.

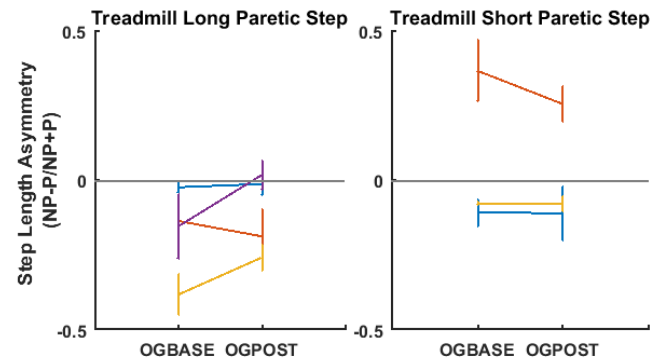


**Figure 3:** Mean (+/-SD) overground step length asymmetry before and after treadmill training.

## CONCLUSIONS

Our results demonstrate that real-time feedback of step length can help to reduce step length asymmetry in chronic post-stroke individuals. Although the observed reductions in asymmetry were acquired on a treadmill using an explicit strategy, practice with a more symmetric pattern generalized to over-ground walking. This result demonstrates that improvements in symmetry were not simply tied to the online, visual feedback, but instead led to a recalibration of participants' walking pattern. Our findings also demonstrate that despite decreased performance of participants with longer paretic steps during on-line feedback, they tended to show greater transfer to over-ground walking and better retention of improvements in symmetry when they returned to the treadmill. These results are preliminary, and it remains to be seen if these patterns hold for a larger sample of participants.

## REFERENCES

- [1] Olney SJ, Richards C. *Gait Posture* 1996;4:136–48.
- [2] Balasubramanian CK, Neptune RR, Kautz SA. *Gait Posture* 2009;29:408–14.
- [3] Savin DN, Morton SM, Whitall J. *Clin Neurophysiol* 2014;125:1012–20.

# PLANTAR FLEXOR STIMULATION IMPROVES POSTSTROKE GAIT KINEMATICS

<sup>1</sup> Nathaniel Makowski, <sup>2</sup> Rudi Kobetic, <sup>2</sup> Kevin Foglyano, <sup>2</sup> Lisa Lombardo, <sup>2</sup> Gilles Pinault, <sup>2,3</sup> Stephen Selkirk, and <sup>2,3</sup> Ronald Triolo

<sup>1</sup> MetroHealth Medical Center, Cleveland, OH, USA

<sup>2</sup> Louis Stokes Cleveland Department of Veterans Affairs, OH, USA

<sup>3</sup> Case Western Reserve University, OH, USA

email: nmakowski@fescenter.org

## INTRODUCTION

Stroke is a leading cause of disability. Resulting hemiparesis limits hip, knee, and ankle movement. Gait impairments increase the likelihood of falls and decrease independence and community involvement. Ankle Foot Orthoses (AFO) and peroneal nerve stimulation assist dorsiflexion to improve toe clearance, reducing fall risk. However, many patients would also benefit from hip and knee assistance. Multi-joint Functional Electrical Stimulation (FES) has been studied as a therapeutic tool; a recent case study demonstrated an implanted multi-joint FES system targeting hip, knee, and ankle muscles improves poststroke gait [1]. Stimulation assistance doubled walking speed. There is further room for improvement as the stimulation pattern did not stimulate plantar flexors, which musculoskeletal models suggest significantly contribute to gait speed [2]. Surface plantar flexion stimulation has modestly improved kinematics [3].

Incorporating plantar flexion stimulation into a gait pattern has been challenging. It requires accurate timing as initiating plantar flexion too early could deter forward progression while stopping stimulation too late could result in toe catching resulting in trips and falls. This study evaluated adding implanted plantar flexion stimulation to a multi-joint FES system and the response to coordinating stimulation with different aspects of gait.

## METHODS

We evaluated plantar flexion stimulation in a single individual. The participant had left sided hemiparesis resulting from a hemorrhagic stroke.

Gait was slow and asymmetric due to lower extremity weakness and hypertonia. He was implanted with a neuroprosthesis 2 years after his stroke [1]. The neuroprosthesis consisted of an 8-channel implanted pulse generator, 8 intramuscular electrodes, and an external control unit. A stimulation pattern was developed to coordinate stimulation with his volitional gait. Stimulating electrodes in the pattern targeted the following muscles: sartorius, tensor fasciae latae, gluteus maximus, quadriceps, and tibialis anterior. A heel switch triggered stimulation transitions between swing and stance phase stimulation.

We compared three walking patterns during a single session. Conditions included 1) no plantar flexor stimulation, 2) gastrocnemius stimulation triggered by -7 degrees stance phase ankle dorsiflexion, and 3) gastrocnemius stimulation triggered by contralateral heel strike. These conditions compare introducing stimulation during the stance phase in anticipation of push off and at the weight transition at the onset of push off. Stimulation parameters were consistently applied to other muscles across trial conditions.

An encoder instrumented on an AFO measured ankle dorsiflexion to trigger stimulation during stance. Stimulation remained on for at least 300ms in this condition and turned off at heel off. A heel switch in the contralateral shoe detected heel strike to trigger stimulation at weight transition. The minimum stimulation duration was 100ms in this condition. Gastrocnemius stimulation durations were chosen to prevent toe catches during early swing.

The participant walked along an 8m walkway while wearing reflective markers on the lower extremities measured by a Vicon motion tracking system. Hip, knee, and ankle angles were calculated using the Vicon software. At least 15 strides per condition were used for analyses.

The primary outcome was joint kinematics. Lower extremity flexion and extension joint angles were time normalized between strides from heel strike to heel strike. Strides were ensemble averaged. Compared kinematic parameters include peak ankle dorsiflexion during push-off, peak ankle dorsiflexion during swing, and peak knee flexion during early swing. Analysis of Variance and post-hoc t-tests evaluated statistical significance.

## RESULTS AND DISCUSSION

Fig. 1 shows the effect of plantar flexor stimulation on stride normalized sagittal plane gait kinematics. Table 1 presents joint angles and statistical comparisons for ankle dorsiflexion during push off and swing as well as knee flexion during early swing. Plantar flexion stimulation reduced dorsiflexion during stance and increased plantar flexion in push-off. Although peak dorsiflexion decreased during swing with plantar flexor stimulation, dorsiflexion stimulation still generated adequate dorsiflexion for toe clearance. Introducing plantar flexor stimulation earlier in the gait cycle was associated with earlier hip flexion.

**Table 1:** Peak joint angles during gait phases.

Peak Angle	Plantar flexion trigger		
	None	Ankle	C. Heel Strike
Push off DF	5.0 (1.6)	-2.1 (3.5)*	-3.7 (2.5)~
Swing DF	10.5 (1.3)	5.6 (1.5)*	8.0 (2.3)†
Knee Flexion	16.9 (1.5)	20.8 (1.8)*	18.9 (1.6)†

\* statistical significance between None and Ankle ( $p < 0.05$ )

~ statistical significance between None and C. Heel Strike ( $p < 0.05$ )

† statistical significance between Ankle and C. Heel Strike ( $p < 0.05$ )

These results suggest the addition of plantar flexion makes plantar flexion push off and swing knee flexion more similar to normal gait. Improved knee flexion contributes to toe clearance as well. Initiating plantar flexor stimulation during mid stance increases the effect on knee flexion. The participant did not have extensive time to practice

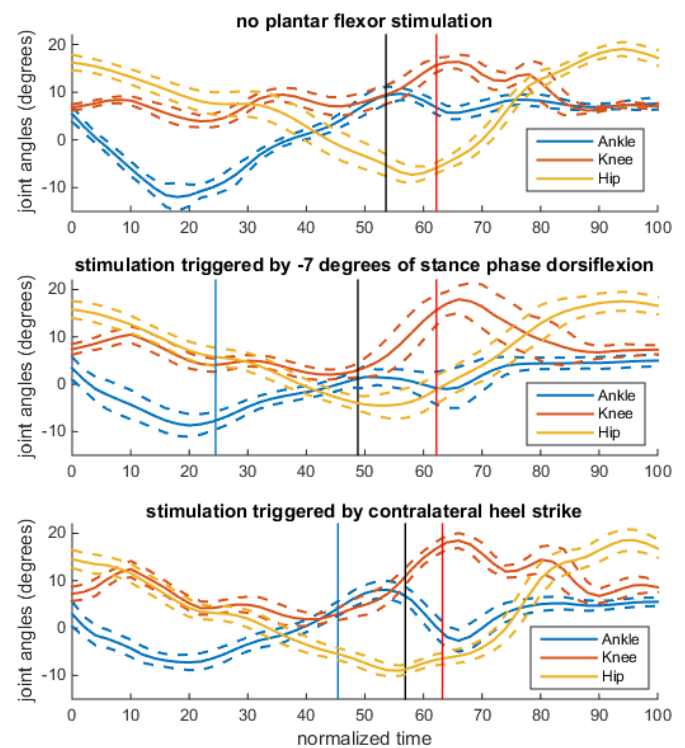


**Figure 1:** Time normalized ensemble averaged strides during stimulation assisted walking with additional plantar flexion stimulation. Red vertical line represents average toe off timing. Blue vertical lines represent the transition to push off while black vertical lines represent the stimulation transition to swing phase.

walking with plantar flexion stimulation incorporated into the stimulation pattern. Further practice walking with plantar flexion stimulation may improve confidence while loading the impaired limb. After additional training, further study should evaluate the effect of plantar flexor stimulation on joint torques, gait speed, and metabolic efficiency. Although this study compared introducing plantar flexor stimulation at two points in the gait cycle, additional optimization of timing would ensure plantar flexor stimulation generates the optimal benefit.

## REFERENCES

1. Makowski NS, et al. *Am J Phys Med Rehabil*, **95**, 880-888, 2016.
2. Neptune RR, et al. *J Biomech*, **34**, 1387-1398, 2001.
3. Kesar KM, et al. *Stroke*, **40**, 3821-3827, 2009.

# A UNI-LATERAL SOFT EXOSUIT FOR THE PARETIC ANKLE CAN REDUCE GAIT COMPENSATIONS IN PATIENTS POST-STROKE

Pawel Kudzia<sup>1,2</sup>, Jaehyun Bae<sup>1,2</sup>, Louis N. Awad<sup>2,3</sup>, Andrew Long<sup>1,2</sup>, Lizeth H. Sloot<sup>1,2</sup>, Katy Hendron<sup>3</sup>, Kenneth G. Holt<sup>3</sup>, Kathleen O'Donnell<sup>2</sup>, Terry Ellis<sup>3</sup>, and Conor J. Walsh<sup>1,2</sup>

<sup>1</sup> Harvard John A. Paulson School of Engineering and Applied Sciences, Cambridge, MA, USA

<sup>2</sup> Wyss Institute for Biologically Inspired Engineering, Boston, MA, USA

<sup>3</sup> Boston University, Boston, MA, USA

Email: walsh@seas.harvard.edu Web: <http://biodesign.seas.harvard.edu>

## INTRODUCTION

Our group has been developing soft wearable robots (exosuits) made from garment-like, functional textiles to augment healthy individuals carrying heavy loads [1] and to assist individuals who have gait impairments due to hemiparesis following a stroke [2]. We have demonstrated that an ankle-joint assisting robot can reduce the metabolic cost of walking in healthy individuals [3]. In patients post-stroke, we have shown that by providing uni-lateral force assistance to the paretic ankle joint during ambulation, we can assist and improve key gait metrics such as foot clearance and paretic propulsion [4].

The goal of this study was to investigate the effects of exosuit provided ankle assistance on common post stroke gait impairments such as reduced step length and compensatory walking strategies resulting from a hemiparetic gait. With this in mind, we sought to evaluate changes in hip hiking, circumduction, and spatiotemporal gait parameters of individuals in the chronic phase of stroke recovery. We hypothesized that walking with the ankle assistance provided while wearing the exosuit will lead to reductions in hip compensations as well as in improvements in spatiotemporal parameters (e.g. longer step length) compared to walking with the exosuit in its unpowered state.

## METHODS

Nine participants with hemiparesis (4F, 49±4y, time since stroke 4.4±1.4y) completed two walking trials on an instrumented treadmill (Bertec Corp., Columbus, OH; 2160Hz) in a motion capture lab (VICON, Oxford Metrics, UK; 120Hz). Each

walking trial was 8 minutes in length with the last two minutes used for analysis. Participants walked on the treadmill at a predetermined overground comfortable walking speed [4]. Patients first walked with the suit unpowered (no assistance) followed by a powered condition. During the exosuit powered condition, assistive forces (approximately 25% body-weight for plantarflexion assistance) from an off-board actuation system were transmitted to the exosuit textile (Fig. 1). The tethered exosuit assisted ankle plantar flexion during the end of stance phase and ankle dorsiflexion during swing phase. Foot mounted IMUs were used to detect the specific gait events with which onset and offset times for the assistive forces were determined [2].

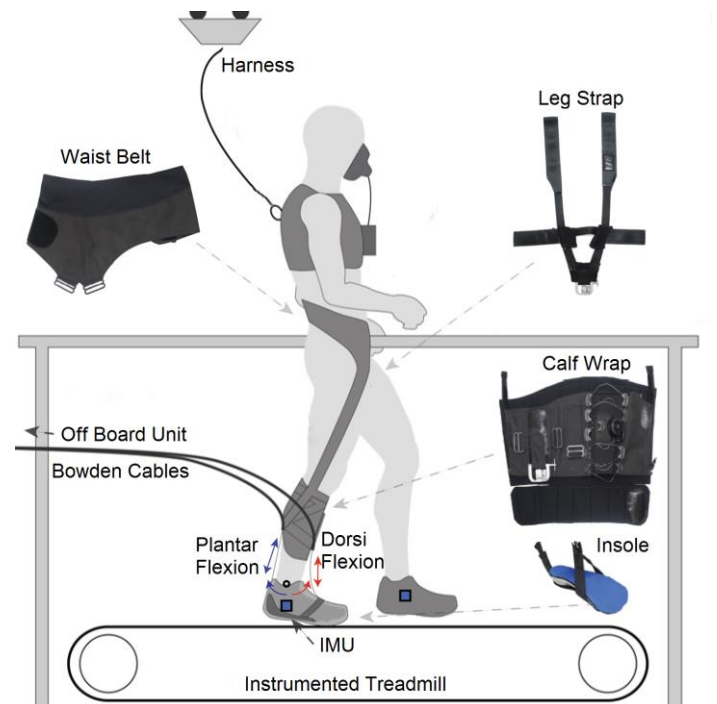


**Figure 1:** Experimental setup and exosuit components

To calculate circumduction, the center of gravity (CoG) of the foot taken from the link-segment model in Visual 3D (C-Motion, Rockville, MD, USA) was used. The difference between the position of the CoG during stance phase and its maximum lateral displacement during swing phase defined the amount of circumduction (Fig.2A) [5]. To calculate the amount of hip hiking, the vertical position of the anterior superior iliac spine (ASIS) markers calculated during quiet standing (static calibration pose taken for kinematic analysis prior to each walking trial) was compared to the maximum vertical position during swing phase (Fig.2B). Lastly, spatiotemporal measures were calculated using heel marker data. Conditions were compared on a group and individual level using a paired t-test ( $p < 0.05$ ).

## RESULTS AND DISCUSSION

Compared to unpowered, walking with the exosuit powered reduced hip hiking by an average of  $27 \pm 6\%$  ( $p = 0.004$ , Fig. 3A) and circumduction by an average of  $20 \pm 5\%$  ( $p = 0.004$ , Fig. 3B) on the paretic side.

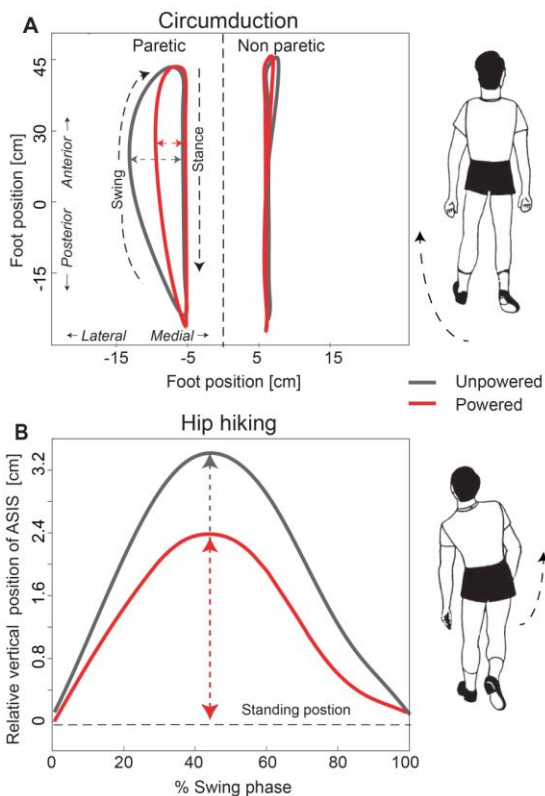


**Figure 2:** Compensatory gait pattern of representative subject showing **A.** Circumduction and **B.** Hip Hiking during exosuit unpowered and powered conditions

At the individual level, each participant presented with a significant decrease in paretic hip hiking and/or circumduction. Step length during the exosuit powered versus unpowered condition increased by  $3 \pm 1\%$  ( $p = 0.002$ ) on the non-paretic side. No significant changes in other spatiotemporal parameters were observed.

These preliminary results suggest that compensatory measures are at least in part secondary deviations resulting from deficits in ankle function. With the known heterogeneity of poststroke walkers, the exosuit provides a platform suitable for subject specific interventions during gait retraining.

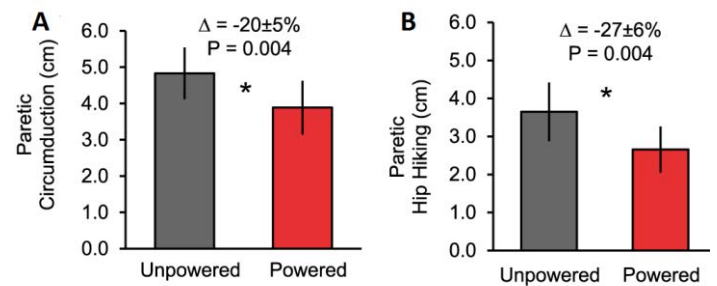


**Figure 3:** Group results showing **A.** Circumduction and **B.** Hip Hiking for the paretic limb comparing exosuit unpowered and powered conditions (mean  $\pm$  SE).

## CONCLUSIONS

This study demonstrated that gait compensations in patients poststroke can be reduced by targeting the paretic ankle with a lightweight, soft wearable robot. This is an important step in evaluating and developing a soft exosuit targeting paretic ankle deficits. Further work will focus on translating these findings to overground studies using a body-worn actuator system. With the ability to control applied forces and timing, such technology can potentially extend to gait impairments related to other neurological conditions.

## REFERENCES

- [1] F. Panizzolo *et al.*, *J. Neuroeng. Rehabil.*, 1, 43, 2016.
- [2] J. Bae *et al.*, *IEEE Int. Conf. Rehabil. Robot.* 2015.
- [3] B. T. Quinlivan *et al.*, *Science Robotics* 4416, 2016.
- [4] Awad LN, *et al.* submitted to *Sci Transl Med*, 2016
- [5] D. Kerrigan *et al.* *Am. J. Phys. Med. Rehabil.*.79, 2000.

# THE INFLUENCE OF LATERAL STABILIZATION ON HEMIPARETIC WALKING

<sup>1</sup> Hannah B. Frame, <sup>2</sup> Christian Finetto, <sup>2</sup> Jesse C. Dean, and <sup>1</sup> Richard R. Neptune

<sup>1</sup> The University of Texas at Austin, Austin, TX, USA

<sup>2</sup> Medical University of South Carolina, Charleston, SC, USA

email: hannah.frame@utexas.edu, web: <http://www.me.utexas.edu/~neptune/>

## INTRODUCTION

Individuals with post-stroke hemiparesis often have reduced mobility and decreased gait symmetry [1]. Since walking is typically a bilaterally symmetric movement, a common goal of stroke rehabilitation is to reduce gait asymmetry caused by stroke-induced hemiparesis. Current rehabilitation strategies often seek to improve gait symmetry by using weight supported treadmill walking or physical therapist directed over-ground walking [2]. Most of these therapies have focused on sagittal plane asymmetry, although frontal plane asymmetry has also been reported [3]. As frontal plane balance is dependent on active stabilization [4], the observed frontal plane asymmetry may be partially attributable to deficits in ensuring balance with the paretic leg.

Whole body angular momentum ( $H$ ) is a promising measure of frontal plane balance, as decreased control of frontal plane  $H$  correlates with lower clinical balance scores in post-stroke individuals [5]. A common response to perceived deficits in frontal plane balance is to use a compensatory gait pattern with increased step widths (as well as reduced cadence and decreased step lengths) [6]. However, while wider steps increase the base of support, they can also increase the peak-to-peak  $H$  in the frontal plane [5]. It is currently not known if removing the need for active control of frontal plane balance would allow stroke patients to reduce their gait asymmetry and range of frontal plane  $H$ .

The purpose of this study was to investigate if external mediolateral stabilization is effective at reducing walking asymmetry in hemiparetic gait. We hypothesized that subjects who were capable of adapting their gait with the addition of mediolateral stabilization (Responders) through a reduction in step width would show improved gait symmetry and decreased range of  $H$  in the frontal plane.

## METHODS

Kinematic data were collected at 120 Hz using a 16-camera motion capture system (PhaseSpace Inc.) from nine hemiparetic post-stroke individuals (4 right hemiparesis, 3 male, age:  $49 \pm 17$  years) during steady state walking on a dual-belt, instrumented treadmill (Bertec Corp.).

Subjects were analyzed during two walking conditions: normal and stabilized. For the normal condition, subjects walked at their self-selected speed on the treadmill for three 30-second trials. The subjects were then fitted with the lateral stabilization apparatus, which applied mediolateral stabilization at the pelvis. Subjects adapted to the added stabilization over a 6-minute period, and once comfortable, completed three 30-second trials at their normal condition self-selected speed. Subjects were classified as a Responder if their step width significantly decreased ( $p < 0.05$ ) between the normal and stabilized conditions as determined by a two-tailed t-test. Step width was defined as the mediolateral distance between heel markers at consecutive heel strikes.

$H$  was calculated using a 13-segment inverse dynamics model, which summed the angular momentum of each segment about the whole-body center of mass ( $CoM$ ).  $H$  was normalized by subject mass, walking speed and height. The range of  $H$  was defined as the peak-to-peak difference in  $H$  over consecutive heel strikes of the paretic leg. Walking symmetry was quantified using a foot placement ratio (the lateral distance between the paretic leg and the center of mass upon heel-strike divided by the sum of the lateral distance of the paretic and non-paretic leg from the  $CoM$ ). A value of 0.5 indicates perfect symmetry while a value larger than 0.5 indicates that the subject placed the paretic leg farther from the  $CoM$  than the non-paretic leg.

A paired t-test was used to test for significant differences between normal and stabilized conditions for the range of  $H$  and symmetry ratio. A change was considered significant if  $p < 0.05$ .

## RESULTS AND DISCUSSION

Of the nine subjects, five were classified as Responders. Despite the decrease in step width, foot placement ratios were not significantly different between conditions ( $0.55 \pm 0.05$  normal vs.  $0.59 \pm 0.06$  stabilized). This result was contrary to our hypothesis and suggests that lateral stabilization does not improve walking symmetry. A study with more subjects and statistical power would be necessary to confirm this finding. It is interesting to note that even though there were no significant differences between the ratios, subjects consistently placed their paretic leg further away from the  $CoM$  even though their overall step width decreased. The strategy of placing the non-paretic leg closer to the  $CoM$  could be the result of no longer needing a non-paretic leg compensatory mechanism to provide balance control.

Also contrary to our hypothesis, the Responders' range of frontal plane  $H$  increased during the stabilized condition ( $p < 0.05$ ) compared to the normal condition (Fig. 1a). This result is surprising, given the observed decrease in step width, and the presumed relationship between narrower steps and lower  $H$ . A possible explanation is that the change in  $H$  was more related to a change in ground reaction force (GRF) rather than foot placement. The time rate of change in frontal plane  $H$  is defined as:

$$\dot{H} = r_{lateral} \times F_{vertical} - r_{vertical} \times F_{lateral}$$

where  $r$  is the moment arm and  $F$  is the GRF acting in the specified direction. A post-hoc analysis showed that the peak vertical GRF only increased  $1\% \pm 0.8$  and  $3\% \pm 1$  for the paretic and non-paretic legs, respectively, thus the increase in  $\dot{H}$  was due to a change in the lateral moment arm or lateral GRF since the vertical moment arm remains largely unchanged. When the step width decreased, the lateral moment arm and lateral GRF also decreased. We assumed that the lateral moment arm decrease would be large enough to reduce  $\dot{H}$ , but that was not the case. The peak lateral GRF decreased by  $34\% \pm 14$  and  $24\% \pm 7$  from the normal to stabilized

condition for the paretic and non-paretic legs, respectively (Fig. 1b), while step width only decreased by  $14\% \pm 10$  between the two conditions, thus resulting in an increase in  $\dot{H}$ .

An alternative explanation for the increased  $H$  range is that the lateral stabilization removed the need for participants to tightly control their frontal plane  $H$ , thus giving participants the freedom to walk with larger ranges of  $H$  without the fear of falling. This possibility requires further investigation.

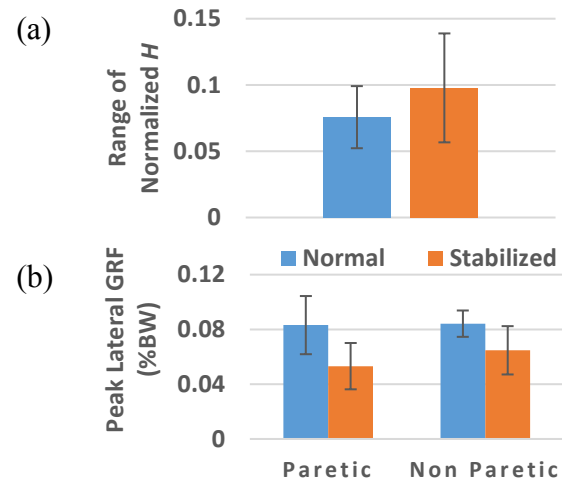


**Figure 1:** a) Peak-to-peak range of  $H$  ( $\pm$ SD) in the frontal plane for normal and stabilized walking, and b) Peak value of lateral GRF ( $\pm$ SD) for normal and stabilized walking.

## CONCLUSIONS

The results suggest that lateral stabilization may not improve walking performance in stroke subjects by decreasing peak-to-peak  $H$  or increasing symmetry. Future studies should examine additional subjects and determine whether increased training with the stabilization influences these results.

## REFERENCES

1. Mozaffarian D, et al. *Circulation* **133**, 447, 2016.
2. Chen G, et al. *Gait and Posture* **22**, 57-62, 2005.
3. Balasubramanian CK, et al. *Gait and Posture* **29**, 408-414, 2009.
4. Bauby CE and Kuo AD. *J Biomech* **33**, 1433-1440, 2000.
5. Nott CR, et al. *Gait & Posture* **39**, 129-134, 2014.
6. Chamberlin ME, et al. *The Journals of Gerontology* **60**, 1163-1167, 2005.

## ACKNOWLEDGMENTS

This study was supported by NIH Grant R21 HD0839.

# MERGED PLANTARFLEXOR MUSCLE EXCITATION MODULE PREDICTS POOR BALANCE IN POST-STROKE HEMIPARETIC SUBJECTS

<sup>1</sup> Lydia G. Brough, <sup>2</sup> Steven A. Kautz and <sup>1</sup> Richard R. Neptune

<sup>1</sup>Department of Mechanical Engineering, The University of Texas, Austin, TX

<sup>2</sup>Department of Health Sciences and Research, Medical University of South Carolina, Charleston, SC  
email: lydia.brough@utexas.edu web: <http://www.me.utexas.edu/~neptune>

## INTRODUCTION

Impaired balance control has a dramatic impact on the lives of individuals post-stroke, with over 70% experiencing one or more falls within 6 months of discharge from the hospital [1]. Falls can lead to injuries with long-term consequences. An increased range of frontal plane whole-body angular momentum ( $H$ ) is often indicative of poor dynamic balance control [e.g., 2]. In healthy walkers, muscle force generation is used to regulate  $H$  during gait [e.g., 3]. Thus, individuals post stroke with impaired muscle coordination patterns may be unable to regulate their  $H$  as effectively.

Prior studies have shown that well-coordinated walking in healthy subjects can be produced by five co-activation modules: 1) hip and knee extensors in early stance, 2) ankle plantarflexors (PFs) in late stance, 3) tibialis anterior and rectus femoris in swing, 4) hamstrings in late swing and early stance, and 5) hip flexors in pre- and early swing [4], and that merged modules in individuals post stroke predict impaired walking performance [5]. Previous research has shown that the PFs are critical to controlling balance in both the frontal and sagittal planes [4, 6]. However, the influence of a merged PF module on balance control is unclear.

The purpose of this study was to determine the influence of a merged PF module on balance control during walking in individuals post stroke by examining the range of  $H$ . Since the PFs are primary contributors to the regulation of frontal and sagittal plane  $H$  [6], we hypothesized that stroke subjects without an independent PF module would have a higher range of  $H$  in both planes than those with an independent PF module.

## METHODS

Kinematic and electromyography (EMG) data were collected from 23 hemiparetic stroke patients (11 left hemiparesis, 10 female; age:  $61 \pm 12$  years) and 15 healthy controls (8 female, age  $55 \pm 8$  years) during 30-second treadmill walking trials at a self-selected speed.

EMG data were processed and analyzed using nonnegative matrix factorization (NNMF) similar to previous work [5]. NNMF determined the minimum number of muscle modules required to account for >90% of the EMG variability and the weighted contribution of each muscle to the module. Subjects were classified as having an independent PF module if NNMF produced a PF module where gastrocnemius and soleus were weighted at 0.4 or greater and all other muscles were weighted at 0.4 or less for at least half of the trials.

A 13-segment inverse dynamics model was used to calculate  $H$  by summing the angular momentum of each segment about the whole-body center of mass in the frontal, transverse and sagittal planes.  $H$  was normalized by subject mass, walking speed and leg length. The range of  $H$  was defined as the peak-to-peak difference in  $H$  in each plane over each stride.

For the range of  $H$  in each plane, an ANOVA with three levels (independent and merged PF module, control PF module) and three two-sample t-tests were used to test for significant differences between each group ( $p < 0.05$ ).

## RESULTS AND DISCUSSION

Seven subjects had an independent PF module (Group A) and 16 did not (Group B). Group B had a

significantly higher frontal, transverse and sagittal range of  $H$  than both Group A and the control group ( $p < 0.05$ ). Group A and the control group were not significantly different from each other in any plane (Fig. 1).

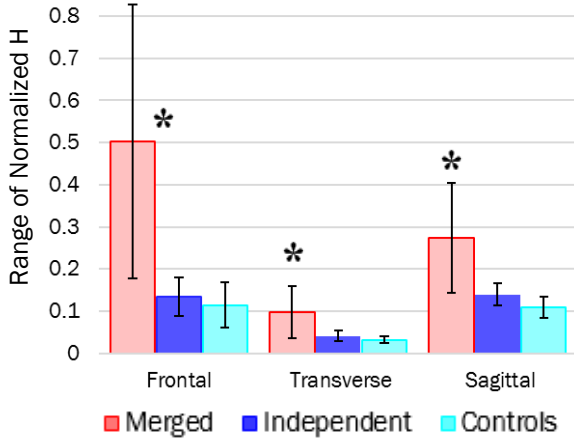


**Figure 1:** Mean ( $\pm$  SD) range of  $H$  in stroke subjects with (Group A) and without (Group B) an independent PF module and in healthy control subjects (\* denotes a significant difference between both of the other groups).

In addition to having a higher range of  $H$ , Group B had more variation in  $H$  between subjects than Group A or the control group (Fig. 2). Thus, having an independent PF module was indicative of a low range of  $H$ , but having a merged PF module yielded a variety of  $H$  patterns.

The higher range of  $H$  in Group B may be the result of the inability to actively regulate  $H$  with the PFs. In the control group, the PFs regulate frontal plane  $H$  by generating vertical and mediolateral ground reaction forces that act to rotate the body towards the contralateral leg [6]. When the PFs are merged with other muscle groups, individuals may not be able to perform this critical biomechanical function. The higher range of  $H$  in Group B may also result from intentional compensation to correct for low paretic propulsion. A number of Group B subjects use a circumduction strategy where they generate angular momentum with the upper body in the frontal and transverse planes to swing the paretic leg forwards. Future work will aim to quantify the contributions of individual body segments to  $H$  to assess which segments contribute to the increased range of  $H$  and

identify rehabilitation strategies for gaining an independent PF module.

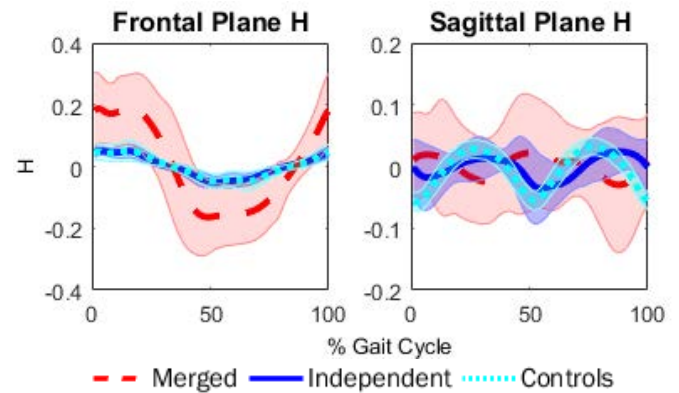


**Figure 2:** Mean ( $\pm$  SD) of frontal and sagittal plane  $H$  during self-selected walking in Group A, Group B and control subjects.

## CONCLUSIONS

These results suggest that an independent PF module is critical for successful balance control. Previous research has shown that stroke subjects can gain independent modules through rehabilitation [7], and thus obtaining an independent PF module should be a crucial aim in stroke rehabilitation.

## REFERENCES

1. Forster, A and Young, J. *BMJ: British Medical Journal* **311**, 83–86, 1995.
2. Nott CR, et al. *Gait Posture* **39**, 129-134, 2014
3. Herr H and Popovic M. *J Experimental Biology* **211**, 467–481, 2008.
4. Neptune RR et al. *J Biomech* **42**, 1282–1287, 2009.
5. Clark DJ, et al. *Journal of Neurophysiology* **103**, 844–857, 2010.
6. Neptune RR and McGowan CP. *J Biomech* **49**, 2975–2981, 2016.
7. Routson RL et al. *Gait Posture* **38**, 511-517, 2013.

## ACKNOWLEDGEMENTS

This work was supported in part by NIH P20HD109040, VA RR&D 1101RX001935 and the Rehabilitation Research & Development Service of the VA.

# TASK-SPECIFIC PERTURBATION TRAINING PROVIDES A VIABLE REHABILITATION STRATEGY TO REDUCE FALLS IN STROKE SURVIVORS: PRELIMINARY RESULTS

<sup>1</sup> Claire F. Honeycutt, <sup>1</sup> Masood Nevisipour, <sup>2</sup> Mark D. Grabiner

<sup>1</sup> Arizona State University, Tempe, AZ, USA

<sup>2</sup> University of Illinois at Chicago, Chicago, IL, USA

email: claire.honeycutt@asu.edu

## INTRODUCTION

Half of the 6.5 million stroke survivors in the United States will fall, making falls the most common and expensive medical complication in stroke survivors. Task-specific training, whose targeted approach allows faster improvements, has become an increasingly credible alternative. Task-specific training is designed to expose subjects to falls in a controlled setting, where injury is not possible, in order to improve their response. Recent results using trip-specific training have revealed a 50% reduction in prospectively measured trip-related falls by middle age and older women [1]. Still, there is very limited information about the effectiveness of task-specific perturbation-based training in stroke survivors. Stroke survivors are afflicted with spasticity, abnormal synergistic patterns of muscle activation, and weakness; therefore it is unclear if the same task-specific training programs that have been implemented in healthy older adults will be effective.

The primary objective of the present study was to determine the impact of a single session of task-specific training on enhancing the compensatory stepping response in stroke survivors. We have previously shown that laboratory induced falls in older adults and stroke survivors are characterized by larger trunk flexion angle, larger trunk flexion velocity, and shorter recovery step length at the first recovery step completion [2,3]. Task-specific perturbation-based training enhances these metrics associated with compensatory stepping as well as reducing number of falls in older adults [2]. Therefore, we hypothesized that trunk kinematics would be significantly modified after training similar to the previously reported results in older women.

## METHODS

Seventeen subjects with unilateral stroke participated in this study. The study was carried out at the University of Illinois at Chicago (UIC) and was approved by Rehabilitation Institute of Chicago, Northwestern and UIC's Institutional Review Boards. Subjects stood on a dual-belt, stepper motor driven and computer controlled treadmill (ActiveStep™, Simbex, Lebanon, NH). Subjects wore a safety harness attached to the ceiling to protect them from falling in the event of an unsuccessful stepping response.

A total number of 27 perturbations were divided into three groups of pre-training test, training, and post-training test. Pre-training and post-training tests consisted of the same 6 perturbations in which 3 posteriorly-directed and 3 anteriorly-directed perturbations were delivered in a randomized fashion. Posteriorly-directed perturbations were designed in three different levels of magnitude (1: small, 2: medium, 3: large). The direction of the perturbation was randomized, but the magnitude was sequenced from small to large for safety. Training consisted of 15 posteriorly-directed perturbations of medium magnitude (displacement: 0.22 m, constant velocity: 0.56 m/s, acceleration/deceleration: 13.89 m/s<sup>2</sup> and -13.89 m/s<sup>2</sup>).

Trials were classified as either a "fall" or "recovery". If the subject became unambiguously supported by the safety harness following a perturbation, that trial was considered as a fall. Twenty-two passive-reflective markers were attached to upper and lower extremities and trunk using a modified Helen Hayes marker set. Dependent variables, including trunk kinematics, step kinematics and center of mass (COM) stability, were calculated for the first recovery step following the perturbation.

## RESULTS AND DISCUSSION

Nine subjects were classified as Fallers (i.e. they fell at least once). Seven of the 9 Fallers fell during both pre- and post-training. Only two Fallers who fell in pre-training could avoid falling in post-training. Still, when all subjects were considered, training led to improvements in the compensatory stepping response. Specifically, Trunk flexion angle and velocity on level 1 and level 2 perturbations (Fig. 1) were diminished indicating enhanced trunk stability. At level 1, Trunk flexion at Step\_Start(SS) and Step\_End(SE) were significantly reduced in post-training trials ( $P=0.016$  and  $P<0.0001$  respectively). At level 2, Trunk flexion velocity at SS and Trunk flexion at SE significantly decreased in post-training trials ( $P=0.006$  and  $P=0.003$  respectively). No significant differences were found in Trunk flexion velocity at SE, Reaction time, Step duration, Step length, Dx and MOS (all  $P>0.05$ ).

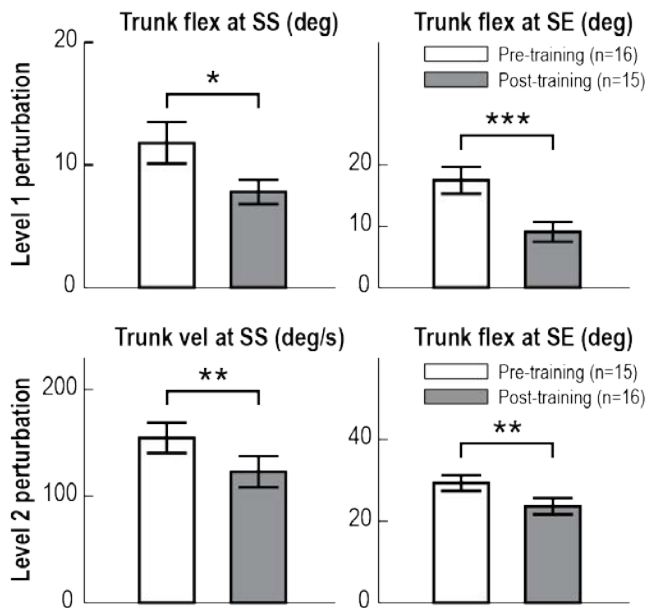


**Figure 1: Pre-training vs. post-training trials comparisons for all subjects.** Figure represents significant differences between pre-training and post-training trials on different levels of perturbation. \* =  $P$ -value  $< 0.05$ , \*\* =  $P$ -value  $< 0.01$ , \*\*\* =  $P$ -value  $< 0.001$ .

Fallers demonstrated changes in a larger number of kinematic and stability variables (8) after training compared to Non-faller group (2) indicating that they were more responsive to training. In addition,

Fallers showed numerous differences from Non-fallers during pre-training but showed enhancements in Trunk movement post-training that made them resemble Non-Fallers. Trunk flexion at SE was significantly different between Fallers and Non-fallers prior to training (at level 1 and 2,  $P=0.028$  and  $P=0.023$  respectively). Further, Trunk flexion velocity at SE was significantly larger for Fallers compared to Non-fallers prior to training (at level 2 and 3,  $P=0.014$  and  $P=0.002$ ). However, Trunk flexion at SE reduced for Fallers after training and was not statistically different from Non-fallers Trunk flexion in pre-training trials (at level 1 and 2,  $P=0.48$  and  $P=0.52$  respectively). Trunk flexion velocity at SE was reduced in Fallers after training and was not statistically different from Non-fallers Trunk flexion velocity before training at level 2 perturbation ( $P=0.22$ ). Training did not adequately decrease these measures at level 3 as Trunk flexion velocity remained significantly different between Fallers and Non-fallers at level 3 ( $P=0.016$ ).

## CONCLUSIONS

These results indicate that despite the unique challenges faced by stroke survivors (e.g. spasticity, abnormal muscle synergies), they are still amenable to task-specific perturbation training. We have previously shown that stroke survivors fall for remarkably similar reasons as other adult populations – most specifically a poor compensatory stepping response including diminished trunk stability and shorter step lengths [3]. While our results here are preliminary in nature and a larger study is needed, the results presented here indicate that task-specific training is a viable rehabilitation strategy to decrease falls in stroke survivors and that it should be pursued as such.

## REFERENCES

1. Grabiner MD, et al. *Medicine & Science in Sports & Exercise*. **44**:2410-2414, 2012.
2. Grabiner MD, et al. *J Electromyography and Kinesiology*. **18**:197-204, 2008.
3. Honeycutt CF, et al. *J Biomechanics*. **49**:3313-3319, 2016.

# RESIDUAL LIMB SKIN STRAIN WITHIN A SOCKET PROSTHESIS IN TRANSFEMORAL AMPUTEES DURING WALKING

<sup>1,2</sup> Tom Gale, <sup>1</sup> Richard McGough, <sup>1</sup> Mark Goodman, <sup>1,2</sup> William Anderst

<sup>1</sup> Department of Orthopedic Surgery, University of Pittsburgh, Pittsburgh, PA, USA

<sup>2</sup> Biodynamics Laboratory, University of Pittsburgh, Pittsburgh, PA, USA

email: thg17@pitt.edu, web: <http://bdl.pitt.edu/>

## INTRODUCTION

For transfemoral amputees, the typical solution to regain mobility is a socket type prosthetic. Due to the various liners and non-anatomical loading the residual limb is subjected to by the socket type prosthetic, discomfort and skin problems are a common occurrence that often lead to reduced activity and quality of life [1]. Although relative motion of the bone to the socket and residual limb motion relative to the socket have been reported [2–4], skin strain occurring within the socket during dynamic functional movement is not well studied. The purpose of this study was to develop a novel method for measuring skin strain within a socket type prosthetic using dynamic biplane radiography.

## METHODS

Two subjects with transfemoral amputations were enrolled in the study. Both participants used a socket type prosthetic with a locking pin liner for anchoring the limb to the prosthetic.

Forty-five to fifty 1.0 mm diameter stainless steel beads were glued on to the residual limb using a grid pattern, with an average distance between beads of 25mm (Figure 1). Based upon bead locations, the residual limb was separated into anterior medial (AM), anterior lateral (AL), posterior medial (PM), and posterior lateral (PL) regions (Figure 1). After the beads were secured to the skin, the participants then put the liner, sock, and prosthetic over the residual limb as they normally would for everyday use.

Participants were imaged standing upright and during walking on an instrumented treadmill (Bertec, OH, USA) at a self-selected speed while

biplane radiographs were collected at 100 images/s (Figure 1). A total of 3 walking trials were collected per subject.

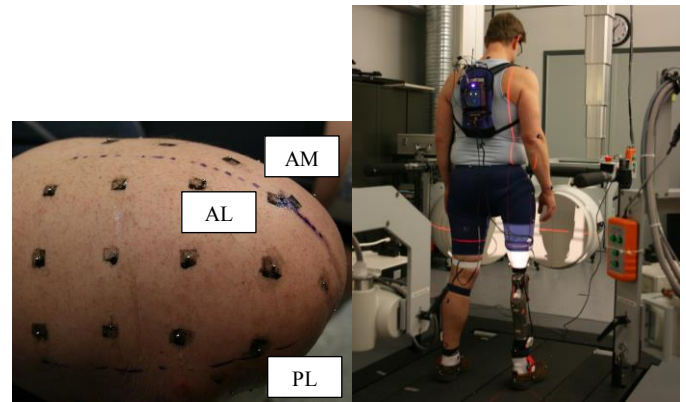


**Figure 1:** Bead grid glued on subject's residual limb with AL, AM, and PL sections visible (left). Subject in upright position within DSX system with prosthetic on over the beads (right).

Dynamic RSA was used to determine bead locations in 3D space during each static and dynamic trial (Figure 2).

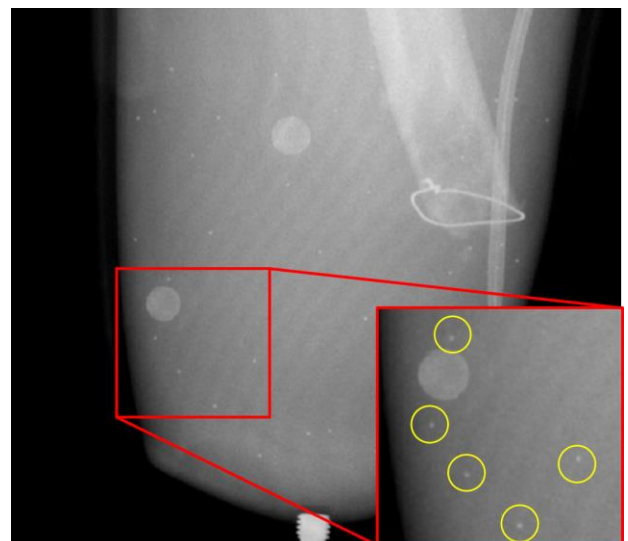


**Figure 2:** A typical frame from one of the biplane radiographic image sequences. Yellow circles highlight the beads glued to the skin.

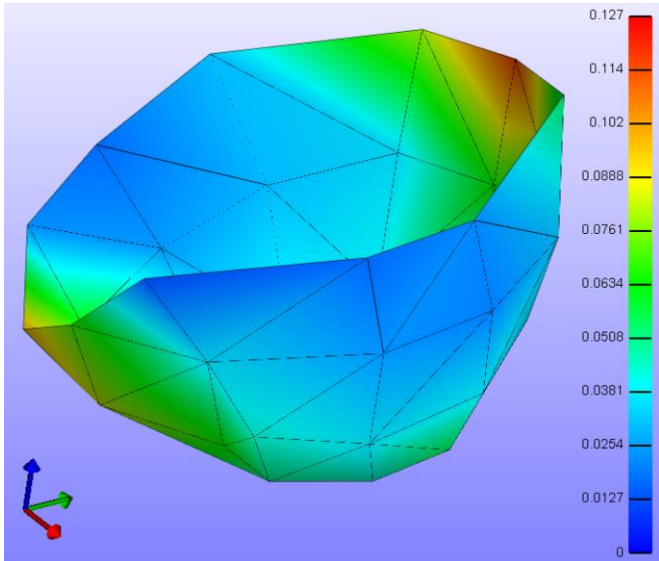


**Figure 3:** The skin surface of the residual limb modeled as shell elements in FEBio. The colormap represents skin strain at one instant of walking.

Bead coordinates in the static standing images were exported as a point cloud and meshed using Geomagic (3D systems, SC, USA). The meshed file was then used in a custom MATLAB (The Mathworks Inc, MA, USA) program in conjunction with the bead coordinates during the dynamic trials to generate a 3D displacement map, formatted for finite element analysis using FEBio (University of Utah, UT, USA). FEBio was used to estimate skin surface strain during walking. Average principal strain  $\left(\frac{\sigma_1 + \sigma_2}{2}\right)$  and maximum shear strains ( $\tau_{max}$ ) were analyzed (Figure 3).

## RESULTS AND DISCUSSION

Dynamic principal strains and shear strains ranged from 4% to 20% depending on participant and anatomic region (Figure 4). The results suggest that skin strain patterns differ greatly from patient to patient and, to a smaller extent, within regions of the residual limb for each individual. This could be due to the location of amputation and the compensatory adjustments to the gait cycle.

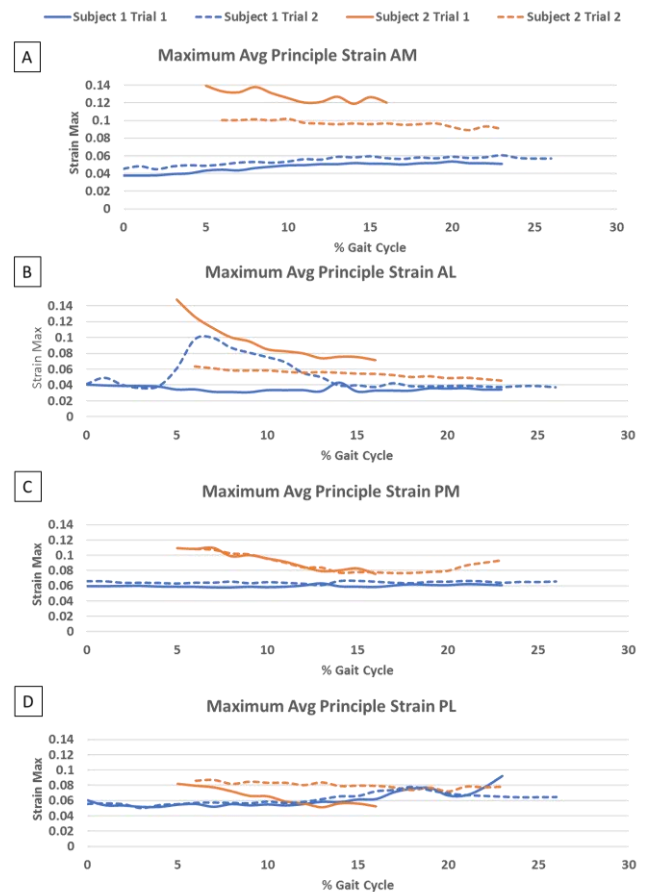


**Figure 4:** Maximum average principal strain over the gait cycle for each anatomic region. Foot strike occurred at 0% gait cycle and mid-stance at approximately 25% of gait cycle.

## CONCLUSIONS

This study demonstrated a novel method for measuring dynamic skin strain in transfemoral amputees wearing a socket type prosthetic. This technique can be used to investigate relationships between skin strain, patient-reported pain and function, and the development of skin-related pathology.

## REFERENCES

1. Meulenbelt HEJ, et al. *J Eur Acad Dermatology Venereol* **21**, 1468-3028, 2007.
2. Papaioannou G, et al. *J Biomech* **43**, 871-878, 2010.
3. Convery P, et al. *Prosthet Orthot Int* **24**, 226-232, 2000.
4. Chong SY, et al. *PLoS One* **11**, p.e0164583, 2016

# Shoulder Posture, Torque Magnitude, and Torque Direction Highlight the Heterogeneous Elasticity of the Pectoralis Major Fiber Regions

<sup>1</sup>Joshua Leonardis, <sup>1</sup>David Desmet, and <sup>1,2</sup>David Lipps

<sup>1</sup> School of Kinesiology, University of Michigan, Ann Arbor, MI, USA

<sup>2</sup> Department of Biomedical Engineering, University of Michigan, Ann Arbor, MI, USA  
email: jleo@umich.edu, web: <http://www.kines.umich.edu/research/mbil>

## INTRODUCTION

The pectoralis major is a wide, flat muscle that consists of two fiber regions with distinctly different architecture. The sternocostal region originates on the sternum and costal cartilage and constitutes roughly two-thirds of the muscles volume. The remaining muscle volume originates on the clavicle and is referred to as the clavicular region. Either region may be harvested individually to provide structural support to the glenohumeral joint when treating irreparable rotator cuff repairs [1]. During clinical decision making, physicians often assume that any function lost due to the disinsertion of either fiber region will be compensated for by the remaining shoulder musculature, giving little consideration to the biomechanical consequences of choosing one region over the other [2]. This lack of consideration is due, in large part, to the limited knowledge regarding each regions elastic properties, characteristics that depict its potential to produce force, and to contribute to shoulder joint function [3]. By characterizing the passive and active elastic properties of each fiber region, one may be better suited to determine the effect their removal has on shoulder function. The present project utilized shear wave elastography to characterize the *in vivo* elastic properties of the individual pectoralis major fiber regions as a function of shoulder position and torques.

## METHODS

The right shoulder of ten male subjects (mean (SD) age: 24 (5) yrs., weight: 81 (14) kg, height: 177 (8) cm) with no history of shoulder injury was placed in a removable plastic cast that was attached to a computer-controlled rotary motor instrumented with a six-degree of freedom load cell. Subjects were positioned in a combination of two shoulder

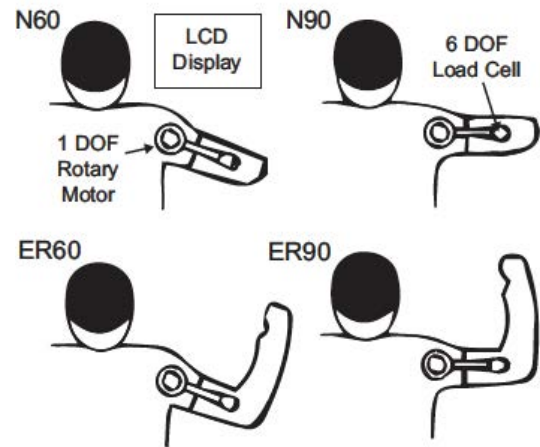


**Figure 1:** Experimental shoulder postures. Subjects were attached to a rotary motor while their shoulder was externally rotated in a neutral (N) or 90° position (ER) and abducted 60° (60) and 90° (90).

abduction angles (60° and 90°) and two external rotation angles (0° and 90°) for a total of four experimental shoulder positions (Figure 1). At each experimental position participants were asked to produce and maintain isometric shoulder torques for approximately five seconds, with the help of visual feedback. These torques were equivalent to 0, 15, and 30% of their maximal voluntary contraction (MVC) in the vertical and horizontal adduction directions. Visual feedback was provided to assist with force accuracy. Surface electromyography data were collected from the pectoralis major, deltoids, trapezius, and latissimus dorsi muscles to further validate task performance.

During each isometric task, a Supersonic Imagine Aixplorer ultrasound elastography machine connected to an SL-15 linear transducer array was used to measure the shear wave velocity (SWV) (Figure 2) of the clavicular and sternocostal regions of the pectoralis major. A greater SWV is associated with a greater shear elastic modulus. Two images were collected from each region for each isometric

force task, resulting in approximately 80 images per subject.

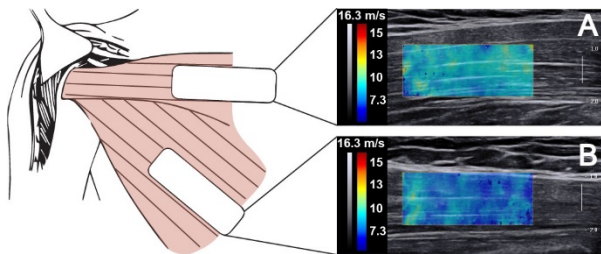


**Figure 2:** Probe locations (left) and representative ultrasound shear wave elastography images of the clavicular (A) and sternocostal (B) fiber regions during 30% MVC horizontal adduction.

One-way ANOVAs were used to assess differences in SWV between fiber regions (clavicular, sternocostal), shoulder positions (N60, N90, ER60, ER90), force directions (horizontal, vertical adduction), and force levels (0, 15, 30% MVC). All significances are reported at  $\alpha = 0.05$ .

## RESULTS AND DISCUSSION

Consistent with the literature, SWVs generally increased with increasing activation for each fiber region in each experimental shoulder position (all  $p < 0.001$ ) [4]. In the clavicular region, SWVs were higher at every experimental shoulder position and force level when force was produced in the horizontal direction (all  $p < 0.001$ ). In the sternocostal region, horizontal adduction torques resulted in higher SWVs at every experimental position except N60 (all  $p < 0.05$ ).

Resting SWVs were higher in the clavicular region for all four experimental shoulder positions (Figure 3) (all  $p < 0.001$ ). For the ER60 and ER90 conditions, there was no difference between the clavicular and sternocostal regions for either force direction at any force level greater than passive. For the N60 and N90 conditions, the clavicular region exhibited significantly higher SWVs at 15% and 30% MVC when force was produced in the horizontal adduction direction (Figure 4). When force was produced in the vertical adduction direction, SWVs were greater in the sternocostal region, but only at 30% MVC (Figure 4).

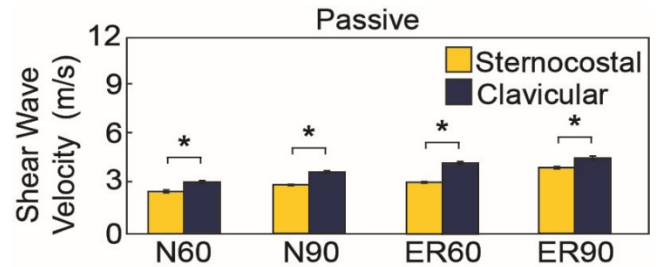


**Figure 3:** Between region passive shear wave velocities for each experimental position.

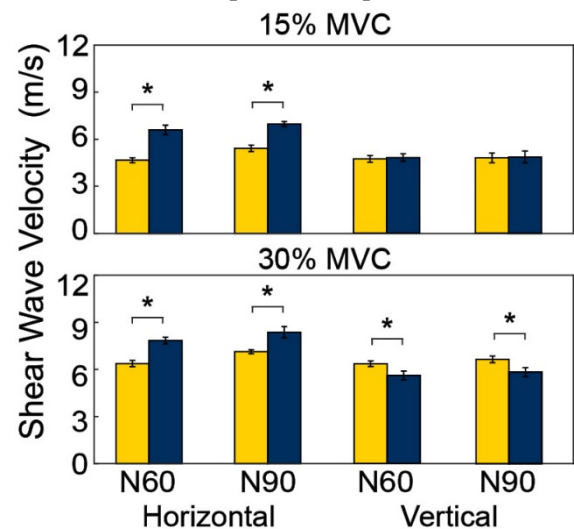


**Figure 4:** Between region 15% (top), and 30% (bottom) shear wave velocities for the N60 and N90 shoulder positions.

Altering shoulder joint position and torque direction underscores the heterogeneous elastic properties of the pectoralis major. The results of this study suggest the clavicular fiber region may contribute more to passive stability and horizontal adduction torques, while the sternocostal fiber region may assist more in vertical adduction torques of greater magnitudes. Additional work is needed to identify the contributions of each fiber region to dynamic movements.

## CONCLUSIONS

The elasticity of the sternocostal and clavicular fiber regions of the pectoralis major are heterogeneous across various postures and contraction levels.

## REFERENCES

1. Valenti et al., *Int Orthopaedics*, **39**:477-483, 2015
2. Carlson et al., *Oral Max Surg*, **15**:565-575, 2003
3. Hu et al., *J Neurophysiol*, **105**:16300-1641, 2011
4. Nordez et al., *J Appl Physiol*, **108**:1389-1394, 2010

# Biaxial Testing of the Passive Properties of Native and Regenerated Skeletal Muscle Tissue

<sup>1</sup> C. Hunter Wallace, <sup>1</sup> Xiao Hu, <sup>1</sup> Juliana Passipieri, <sup>1</sup> J. David Remer, <sup>1</sup> George Christ, and <sup>1</sup> Silvia Blemker

<sup>1</sup> The University of Virginia, Charlottesville, VA, USA  
Email: chw3gr@virginia.edu

## INTRODUCTION

Volumetric muscle loss (VML) refers to a traumatic loss of muscle that has an adverse resultant effect upon function. [1] Currently, there exists no effective clinical treatment for VML that results in a full recovery of muscle function.

Experimental data and computational models show a marked decrease in active force production in muscles with VML injury and a partial recovery of force when repaired. [2] A greater percentage of force recovery is seen when the muscles are repaired with a tissue engineered muscle repair (TEMR) compared to a bladder acellular matrix (BAM) suggesting an advantage to the cell seeding and bioreactor protocols over the use of acellular matrices alone. [2]

In order to fully understand where current methods fall short in regenerating muscle as well as differences between methods, we must first understand the passive properties of both native tissue as well as the regenerated tissue. Once we accomplish this, we can begin to understand how to further improve current methods to bring injured muscle closer to the behavior of native muscle. The goal of this study was to develop a method to use a biaxial testing machine to examine the passive properties of native muscle and then apply this method to measuring the properties of regenerated tissue.

## METHODS

BAM scaffolds were prepared from porcine urinary bladder as previously described. [3] TEMR constructs were then generated from these scaffolds using previously described cell culture, seeding, and bioreactor protocols. [3]

VML injuries were surgically created in 12 week old male Lewis rats as previously described [3]. Briefly, a longitudinal incision was made along the midline of the back, the trapezius muscle was lifted to expose the latissimus dorsi (LD), and an 11x15 mm defect was excised from the medial half. The injured muscle was then treated by either suturing an unseeded BAM scaffold or a TEMR construct to the site of injury.

To obtain the samples for testing, animals were sacrificed at 2 months post-surgery and the LD muscles were isolated from the rats. Samples were excised from within the injured area with care to not include any of the surrounding native muscle tissue. Native samples were taken from the same region in the contralateral LD.

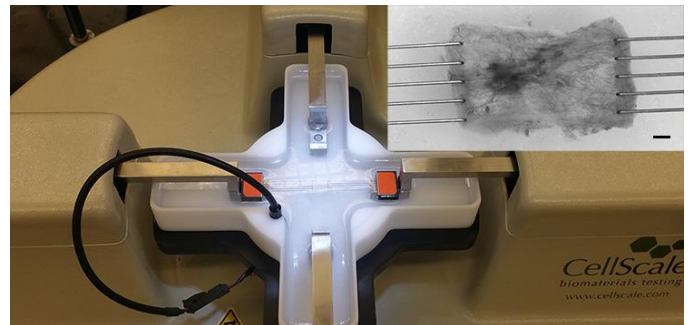


Figure 1: CellScale biotester biaxial testing machine and mounted specimen. Scale bar = 1mm

Immediately after explantation, the samples' unloaded length, width, and thickness measurements were taken. Samples were then mounted on a CellScale BioTester (Fig. 1) and submerged in a room temperature Krebs bath. Samples were stretched at 1% of original mounting length per second until passive resistance began at which point images were taken to be used to measure the mounted length and width in imageJ.

The length at which passive resistance began was defined as optimum fiber length and the new initial length for the tensile testing. Each sample underwent 10 cycles of preconditioning to 10% strain using the

new initial length measurement at 1% strain per second ( $1\%s^{-1}$ ) similar to previous methods. [4] Following preconditioning, the samples were stretched to 10% strain at  $1\% s^{-1}$  for 10 cycles, and finally pulled to failure or a load of 2N at  $1\% s^{-1}$ .

Following testing, the initial size measurements were used to calculate the thickness of the mounted muscle assuming isochoric properties. Using the initial volume and the known displacement rate of the muscle, the cross-sectional area was calculated and subsequently used to calculate stress for each sample. Stress was then normalized using peak isometric stress data obtained from in vitro experiments. [3]

Force, stress and strain data for each sample were resampled and average curves for each treatment group were found. Stress-strain curves were then fit to a previously described model of passive muscle properties. [5]

## RESULTS AND DISCUSSION

The testing protocol was developed in order to obtain repeatable results and we further verified it by comparing native rat LD tissue samples to expected passive muscle behavior in the literature (Fig. 2A). As expected, literature values have a large variance as a result of the differing types of muscles tested as well as the animals tested. Our values fall within this expected range and have a relatively small sample-to-sample variance.

There is not a significant difference in the passive mechanical behavior between tissue regenerated with BAM and tissue regenerated with TEMR (Fig. 2B). Combining this finding with the previous findings of a better active force recovery with the TEMR points toward a recovery of active muscle fibers using this novel treatment given no difference in passive properties but a significant difference in active force production.

## CONCLUSIONS

We have shown here a method that is able to reliably produce stress-strain data from both native tissue as well as regenerated tissue. This method can now be

utilized to investigate the effects of different VML treatments on the passive properties of injured muscle, as well as in other neuromuscular diseases that are known to affect passive muscle properties.

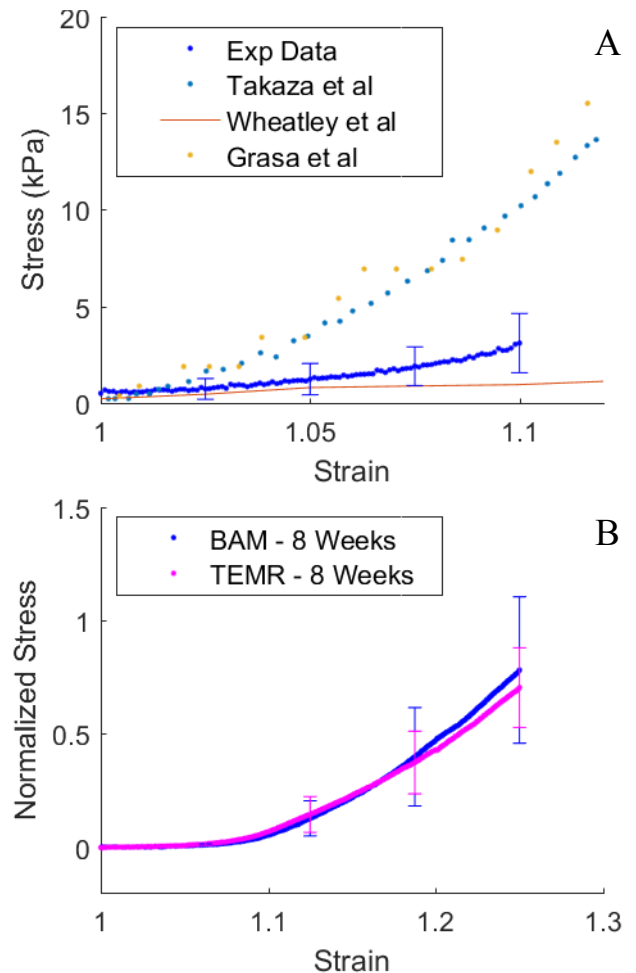


Figure 2: (A) Comparison between native data and literature native muscles and (B) Tissue regenerated with BAM and with TEMR.

## REFERENCES

1. Sawicki Grogan BF and Hsu JR. *J Am Acad Orthop Surg* **19**, S35-7, 2011.
2. Hu X, et al. *Proc. Am. Soc. Biomech*, Raleigh, NC, USA, 2016
3. Corona BT, et al. *Tissue Eng Part A* **18**, 1213-28, 2012
4. Billiar KL and Sacks MS. *J Biomech Eng* **122**, 23-30
5. Blemker S and Delp S. *J Biomech* **38**, 657-65, 2005

# MOVEMENT RESTRICTION INCREASES THORACOLUMBAR FASCIA STIFFNESS IN A PORCINE MODEL

Mike Glinka<sup>1</sup>, Erika Nelson-Wong<sup>2</sup>, Mamiko Noguchi<sup>1</sup>, Helene Langevin<sup>3</sup>, Jack Callaghan<sup>1</sup>

<sup>1</sup>University of Waterloo, Waterloo, ON, Canada

<sup>2</sup>Regis University, Denver, CO, USA

<sup>3</sup>Harvard Medical School, Boston, MA, USA

email: mglinka@uwaterloo.ca

## INTRODUCTION

Historically considered less important than the more specialized organs and muscles it envelopes [1], thoracolumbar fascia (TLF) is now gaining recognition for its potential role in key functions such as stabilizing the lumbar spine, providing attachment for spinal and abdominal musculature, and even sensing body position and pain [1,2]. Thus, its inclusion in pathological models of low back pain (LBP) warrants investigation.

Ultrasound recordings have shown that humans with chronic LBP exhibit increased thickness and decreased mobility in the TLF [2]. Recent work demonstrated similar changes to the TLF in a porcine model subjected to surgical injury combined with movement restriction [3]. To better understand why these functional and morphological changes occur, we sought to investigate if there were associated changes to the porcine TLF stiffness after surgical injury and movement restriction.

## METHODS

Twenty castrated male domestic swine, between 4-6 weeks old, weighing approximately 4-7 kg were acquired from E.M. Parson's Hadley, MA. A stabilization period of 7 days was allowed before subsequent randomization into one of four cohorts: Control (n = 5), Injury (n = 5), Hobble (n = 5), and Injury + Hobble (n = 5) for eight weeks. The injury condition involved a 4x4 cm incision at the L3-4 vertebral level, 2 cm lateral to the midline, between the subcutaneous membranous layer and the perimuscular connective tissue. Hobbled animals were fitted with a harness that constrained the distance between the fore and hind limbs to two-thirds that of unrestrained animals. After 8 weeks,

animals were euthanized and 1x5x3 cm tissue samples were excised. For injured animals, this tissue was extracted contralateral to the injury site. Tissue samples were then immediately frozen in liquid nitrogen.

The TLF samples were transported to the University of Waterloo (Waterloo, ON, Canada) and thawed for dissection. The TLF (perimuscular fascia) was carefully dissected from the underlying muscle and overlying adipose tissue, and cut into 5x5 mm test specimens (Fig. 1).

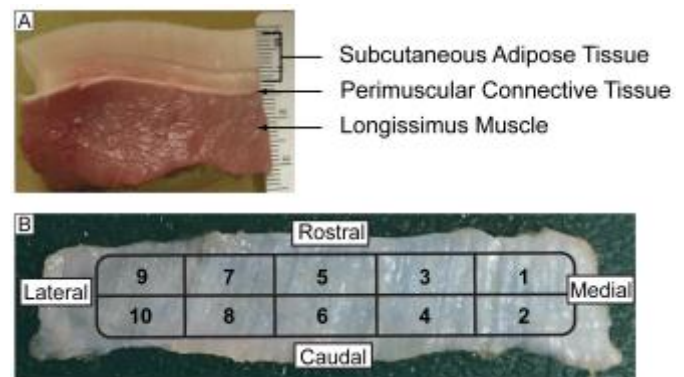


**Figure 1** Perimuscular connective tissue (A) extracted from sample blocks and (B) cut into 5x5 mm specimens.

These 5x5 mm specimens were then mounted onto a displacement-controlled tensile testing apparatus (CellScale, Waterloo, ON). Each specimen was loaded either uniaxially – in the longitudinal or transverse direction, or biaxially – both directions simultaneously. Only the uniaxial longitudinal condition is considered in this submission. The loading protocol was identical for all specimens: preconditioning with 5 cycles of loading/unloading to 10% of initial stretch, followed by 5 cyclic loads to 25%, 35%, and 45% of initial stretch. Initial stretch was defined as the distance between the rakes (which applied the tensile loads) at a preload of 10

mN. All loading and unloading was performed at a 6%/sec stretch rate. Stiffness was calculated from the slope of the linear region of the last two loading curves at each stretch level. A two-factor mixed model analysis of variance was performed to compare stiffness among the four cohorts and three stretch levels. Separate two-factor ANOVAs were then computed at each stretch level with test samples nested within each cohort. An alpha level of 0.05 was used for all tests, with a Bonferroni adjustment for multiple comparisons (SPSS Inc., Chicago, IL).

## RESULTS AND DISCUSSION

Fascia from hobbled animals—whether only hobbled or combined with injury—were significantly stiffer than control fascia, at all three stretch levels ( $F = 9.17$ ,  $p < 0.001$ ; Fig. 2). Specifically, the combo (injury + hobble) and hobble TLF were, on average, 2.4 ( $p < 0.01$ ) and 2.8 ( $p < 0.001$ ) times stiffer than control. Hobble TLF were also stiffer than injured tissue at each stretch level.

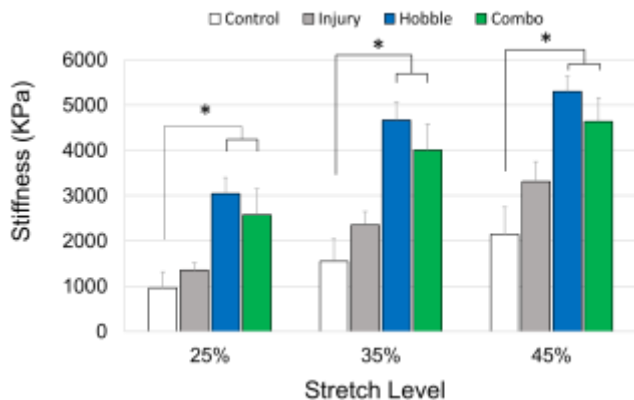


**Figure 2:** Thoracolumbar fascia stiffness at 25%, 35%, and 45% stretch. Significant ( $p < 0.05$ ) differences are denoted by asterisks (\*).

Stretch level significantly affected stiffness ( $F = 105.6$ ,  $p < 0.001$ ) across all cohorts, with tissues becoming progressively stiffer at higher stretch levels.

Individuals with LBP are frequently found to have limited spinal mobility, both gross and segmental. It is unknown if this limited mobility is directly caused by pain, predisposing mechanical factors, or mild trauma such as a muscle strain. Our findings suggest that limiting movement increases local TLF stiffness.

It is well known clinically that restricting joint movement causes adhesions in periarticular connective tissue [4]. Similar pathological processes may have occurred in the dorsal trunk fascia of the hobbled swine in this study, whereby adhesion formation contributed to increased stiffness.

The finding that movement restriction so profoundly increased TLF stiffness beyond that resulting from injury is somewhat surprising. It is possible, however, that the injury was not severe enough to either (1) induce a pathological response on its own or (2) cause animals to voluntarily reduce their mobility. The latter hypothesis is supported by the observation that, before euthanasia, injured animals exhibited no difference in gait speed compared to control animals; only those subjected to mobility restriction walked slower than control animals, even after restraints were removed [3].

## CONCLUSIONS

This study suggests that movement restriction plays a particularly important role in increasing thoracolumbar fascia stiffness. This is a substantial finding highlighting the mechanical contribution of the TLF to the reduced mobility observed in persons with LBP. Future work investigating potential changes to the biochemical composition of the TLF is needed to explain these changes to tissue stiffness. Further, therapeutic interventions aimed at breaking adhesions and reducing tissue stiffness may warrant exploration to determine if mechanical changes associated with LBP can be reversed.

## REFERENCES

1. Willard FH et al. *J Anat*, **221**, 507-36, 2012.
2. Langevin HM et al. *BMC Msk Dis*, **12**, 203, 2011.
3. Bishop JH et al. *PLoS One*, **11**, e0147393, 2016.
4. Tillman LJ. *Biologic mechanisms*, FA Davis, 1992.

## ACKNOWLEDGMENTS

Dr. Callaghan is supported by the Canada Research Chair in Spine Biomechanics and Injury Prevention, Canada. Dr. Langevin is supported by the National Center for Complementary and Integrative Health (NCCHI) ROI AT-004400.

# PATH-SPECIFIC VON-MISES STRESSES INFLICTING THE PRE- AND POST-THR FEMUR DURING WALKING

<sup>1</sup> Mohamed Z. Bendjaballah and <sup>1</sup> Wissal Mesfar

<sup>1</sup> Biomedical Technology Department, College of Applied Medical Sciences, King Saud University  
Riyadh, Saudi Arabia

email: [bendja@ksu.edu.sa](mailto:bendja@ksu.edu.sa), web <http://www.ksu.edu.sa>

## INTRODUCTION

Numerous numerical studies aimed to explore the femoral regions prone to develop stress shielding after a THR. Some researchers adopted the use of a dimensionless factor known as stress shielding rate (SSR). This factor relates the change in the von Mises stress between prosthetic and intact states prorated to that of the intact state [1, 2]. Despite its wide usage in literature, this rate does not capture only the regional stress variation regardless of the stress gradients and intensities. As a consequence, similar rates can occur for two locations with completely different stress gradients rising between the pre- and post-THR cases. Depending on its sign, this rate should be thus used as a dualistic rate that indicates if a site is likely to develop stress shielding or not and must not be used whatsoever in evaluating the stress shielding severity.

The aim of this study is thus to explore the severity of stress shielding by direct investigation of the changes occurring in the von Mises stresses generated under walking activity at specific locations. To achieve this goal, twelve paths were selected in pertinent locations of the intact model and meticulously reproduced in the prosthetic one.

## METHODS

A three-dimensional CAD model of an intact proximal left femur was developed based on series of CT-scan images acquired from a healthy female donor. The prosthetic CAD model was generated by sectioning the femoral head and superimposing the prosthesis' CAD model, which geometry was inspired from a cementless commercial design. Orthotropic and isotropic material properties were

assigned to the cortical and cancellous bone tissues, respectively while 'Ti-6Al-4V' Titanium alloy was chosen for the stem material [3]. A bonded contact was adopted between all interacting components while a fixed boundary condition was set to the bottom surface of the shaft. Loading conditions characteristic of walking activity reported in Ref [4] were implemented in the FE analyses considering our subject's body weight of 700N. The bone tissues and prosthesis were meshed using hexahedral solid elements. Special attention was focused on the meshing operation to reproduce an identical mesh for the bone common to intact and prosthetic models. This procedure helps generate identical paths where the nodal von Mises stresses are explored. Four cardinal locations around the shaft were considered; the lateral, medial, ventral and dorsal. For each of these locations, three distinct paths were further demarcated and represented by sets of nodes located at the inner, middle and outer locations over the cortex thickness (Fig. 1). Direct comparison of the pre- and post-THR von Mises stresses computed along these twelve (12) paths was performed aiming to discern the bony regions prone to develop stress shielding. The static nonlinear FE analyses were performed using Abaqus 6.14.

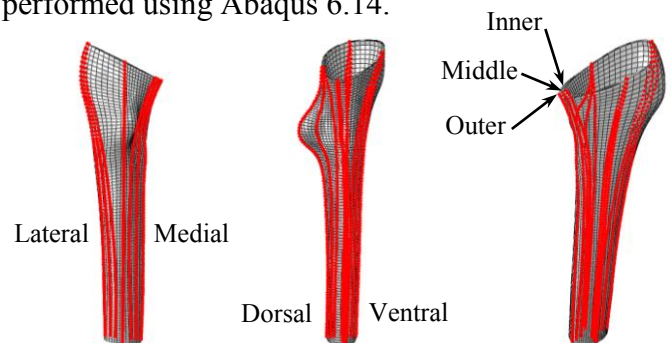


**Figure 1:** Different views of the cortical bone mesh showing node sets composing 12 paths identically demarcated in intact and prosthetic models.

## RESULTS AND DISCUSSION

The von Mises stresses plotted along the normalized distance of the selected paths were found to be in general higher on the outer cortex regardless of the model cases. The highest peak stresses of around 50MPa were computed on the lateral location close to the Vastus Lateralis attachment site (see fig. 2-a) and the dorsal location distally near the model's bottom surface (see fig. 2-d). In the medial region, the stress patterns developed in the intact bone showed that the stresses started at their highest values (~30MPa) proximally to gradually diminish reaching around 12MPa distally. Once the implant is inserted, the stresses dropped drastically to almost vanish at the most proximal region of the shaft. The highest drop (~30MPa) was recorded on the outer cortex of the calcar region (most proximal site of the medial zone, Figure 2-b). Moreover, for this zone, the peri-prosthetic stresses slightly increased in the first quarter of the shaft length and remained almost constant for the rest of the bony shaft (Figure 2-b).

The rest of the bony tissue underwent lesser stress reductions following THR, not exceeding 14MPa computed on the outer cortex of the dorsal region, distal to the lesser trochanter (see Figure 2-d). Along the dorsal and ventral regions, and irrespective of the model condition, pre- or post-THR, the von Mises stress values mainly increased when moving towards the distal direction (see figures 2-c and 2-d).

The highest stress fluctuations were noted in the peri-prosthetic bone close to the implant's tip as well as in bone laying at the muscles' attachments sites. These findings are more tangible at the inner layer for the former case and outer layer for the latter case, respectively. Distal to the implant's tip, the effect of the prosthesis generally disappears, that is, the von Mises stress values computed post-THR literally converged to those obtained in the pre-THR condition.

The use of series of paths generated from node sets identically located in pre- and post-operative models enabled us to make a precise site estimation of the stress change occurring following THR. Our numerical findings were in good agreement with experimental studies nominating the proximal calcar

area, also known as Gruen zone 7, for extensive stress shielding and peri-prosthetic remodeling [5, 6].

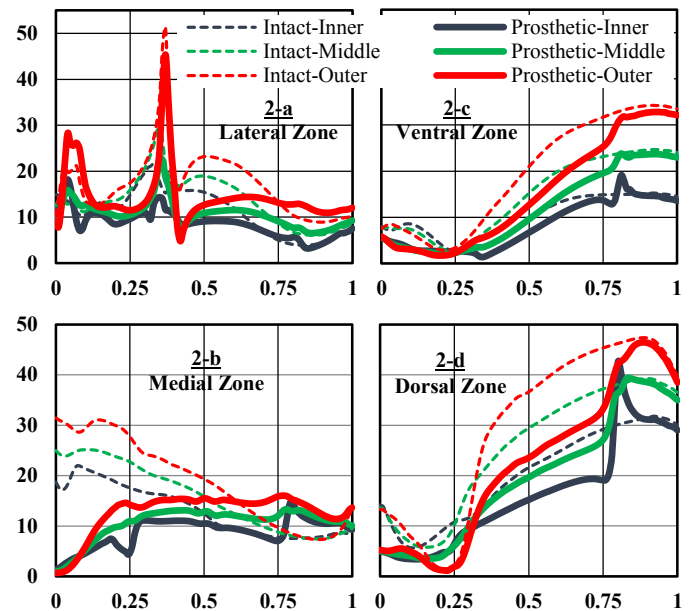


**Figure 2:** von Mises stress distribution in the intact and prosthetic cortical bone computed along the normalized shaft length at the inner (blue), middle (green) and outer (red) paths among the lateral (2-a), medial (2-b), ventral (2-c) and dorsal (2-d) zones.

## CONCLUSIONS

The current study used subject-specific finite element models to accurately predict the sites prone to develop stress shielding and estimate its severity as well. Unlike the SSR which estimates the zonal stress shielding occurrence in a dualistic manner, this study uses the stress decay precisely occurring in a typical site to estimate the severity of stress shielding and the subsequent bone loss expected to occur. Finite element models generated from human cadaveric or patient femora could thus find an extensive use in the pre-planning of THRs through clinical evaluation of new prostheses and/or novel surgical procedures.

## REFERENCES

1. Piao C, et al. *J Orthop Surg Res* **9**, 7, 2014.
2. Li Y, et al. *J Med Biomech* **11**, 140–143, 1996.
3. Caouette C, et al. *Proc IMechE*, **225**, 907-19, 2011.
4. Heller MO, et al. *J Biomech* **38**, 1155-1163, 2005.
5. Taddei F, et al. *Med Eng Phys* **29**, 973–979; 2007.
6. Schileo E, et al. *J. Biomech* **40**, 2982–2989, 2007.

# EVIDENCE OF LOW BACK INJURY IN THE ABSENCE OF RADIOGRAPHIC DETECTION

Nicole C. Gale, Stacey L. Zeigler, Christopher Towler, Kathleen A. Issen, Arthur J. Michalek, and Laurel Kuxhaus

Clarkson University, Potsdam, NY, USA

email: corbienc@clarkson.edu, web: <http://people.clarkson.edu/~lkuxhaus/>

## INTRODUCTION

Low back injuries of varying etiology can occur in bone or soft tissue. Vertebral fractures and soft tissue injuries can occur during the repetitive loading of activities of daily living (ADLs). For example, ring apophysis fractures (RAFs) occur without memorable trauma in healthy young athletes [1-2], and osteoporotic fractures occur without memorable trauma in older adults. We hypothesized that application of high cycle non-traumatic motion to an *ex-vivo* model (absent of bone remodeling) would result in biomechanical symptoms of injury resulting from the combined effects of increased spinal laxity (soft tissue damage) and vertebral fractures. This hypothesis was tested by applying low-load, low-angle cyclic flexion to cervine and cadaver 5-vertebra motion segments. Cervine (white tailed deer, *O. virginianus*) specimens had a similar degree of skeletal maturity and have a similar range of motion [3] to adolescent humans. The cadaver specimens were older with osteoporotic degeneration.

## METHODS

Seven cervine (2 male, 5 female;  $2.4 \pm 0.2$  years) and five human cadaver (1 male, 4 female;  $64.2 \pm 4.8$  years) 5-vertebra motion segments (L1-L5) were prepared [4] and cyclically loaded. X-ray images were obtained before and after cyclic loading on all specimens. Load-displacement, kinematic, and deformation data were collected.

Specimens were loaded (Instron 1331, Norwood, MA) in pin-ended cyclic eccentric axial compression to 20,000 cycles at 0.5Hz, between  $0^\circ$  and  $15^\circ$  of flexion to simulate a low-angle ADL movement. Periodically (after cycles 0, 1,000, 3,000, 6,000, 10,000, 15,000 and 19,995), three-dimensional digital image correlation (3D-DIC) and motion capture imaging occurred during five slower

witness cycles (0.01Hz), the fifth of which were analyzed. Load-displacement data were post-processed (4<sup>th</sup> order Butterworth filter,  $\omega_c=0.01\text{Hz}$ ) using a custom MATLAB code (The MathWorks Inc., Natick, MA). The area, neutral zone length, and slope of each hysteresis loop were computed.

A motion capture system (4 Oqus 500 cameras, Qualisys AB, Sweden) tracked the regional centroid angle ( $\alpha$ ) and the intervertebral angles (IVAs) during the witness cycles. The relative IVAs were computed in QTM (Qualisys Track Manager Version 2.10, Qualisys AB, Sweden). Kinematic data from the analyzed cycles were aligned and then filtered (4<sup>th</sup> order Butterworth filter,  $\omega_c=0.0075\text{Hz}$ , MATLAB). Images for 3D-DIC were captured at 4Hz from two-cameras (Scorpion IEEE-1394, Point Grey Research Inc., Richmond, BC, Canada). During the witness cycles, regions of high localized cortical surface strain were identified using VIC3D 7 (Correlated Solutions Inc., Columbia, SC).

## RESULTS AND DISCUSSION

All tests were completed without obvious evidence of catastrophic fracture and without radiographic evidence of fracture on plain x-rays. The hysteresis loop area trends are similar between the cervine and cadaver specimens (Figure 1), and agree with our previous work [5].

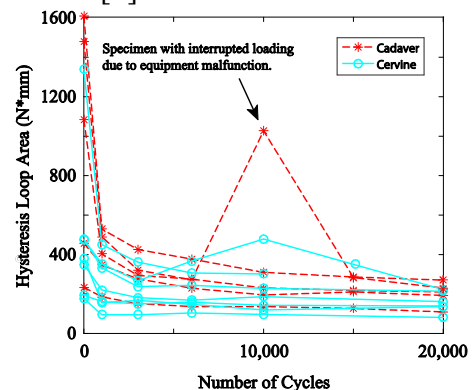
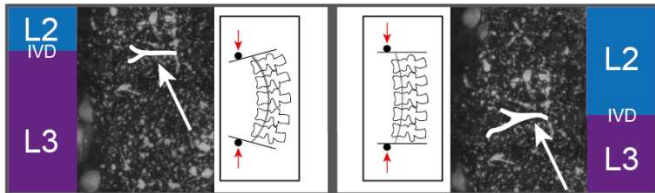


Figure 1: Hysteresis loop area for all specimens.

There is evidence of injury from the surface strain during the witness cycles, despite the absence of radiographic findings. 3D-DIC provides visible evidence of cortical shell cracks opening and closing as early as 6,005 cycles. Comparing images from these specimens (Figure 2) to our previous research [5] that created RAFs under a different loading protocol suggests that the current cervine specimens also have fractures and/or bony injuries.



**Figure 2: Surface strain evidence of fracture in a cervine specimen.**

This evidence is echoed in the observed kinematic changes. The shape of the L2/L3 IVA changes from the beginning of the test to the time of observable crack opening (cycle 10,005), due to the combined effect of injury and disc relaxation (Figure 3). The increase in apparent compliance (increase in angle) near extension from cycle 5 to 10,005 indicates damage and/or disc relaxation, which is consistent with increases in neutral zone length and slope (Figure 4).

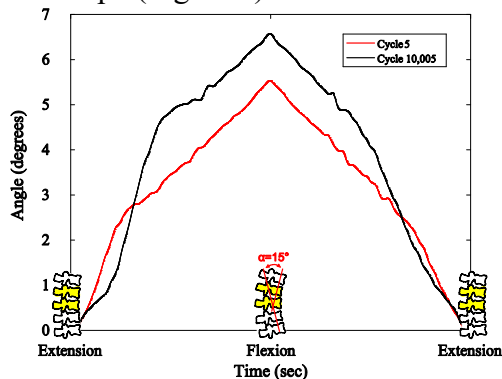


**Figure 3: L2/L3 IVA example.**

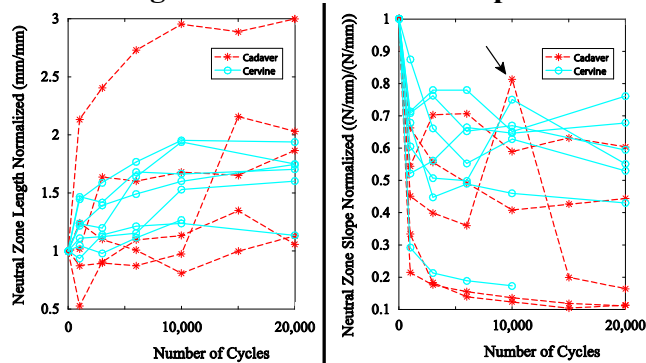


**Figure 4: Neutral zone lengths and slopes.**

The IVAs during each witness cycle show observable change in kinematics throughout the test. When comparing the 5<sup>th</sup> and 10,005<sup>th</sup> cycles there is a clear change in IVA. The angle increases, and the behavior throughout the application of the same displacement condition is markedly different. This change is expected given the increase in neutral zone length, and represents the combined effects of fluid re-distribution in the intervertebral discs and any soft- or hard-tissue damage that occurred during the loading.

## CONCLUSIONS

Both an increase in instability and vertebral injury can occur during low-load, low-angle cyclic loading. An increase in laxity, as evidenced by the increase in neutral zone length and decrease in neutral zone slope, may result in a clinically-significant increase in the risk of hyperflexion injury following prolonged cyclic flexion activities. The bony injuries would likely be symptomatic, but would most likely not be diagnosed as fractures. Our work demonstrates that vertebral injuries can occur in the absence of radiographical findings.

Future clinical work will identify optimal radiographic imaging to detect these injuries. Efforts to prevent and rehabilitate injury in both healthy, physically active adolescents and older adults should consider the role that small movement ADLs may play in injury risk.

## REFERENCES

- [1] Takata K, et al. *JBSJ [AM]*, 70A:589-594, 1988.
- [2] Singhal A, et al. *Ped Neuro*, 49:16-20, 2013.
- [3] Lingle S. *Can J Zoolog*, 71:708-724, 1993.
- [4] Corbiere N, et al. *JBME*, 126:064504-1-4, 2014.
- [5] Corbiere N, et al. *J Biomech*, 49:1477-81, 2016.

## ACKNOWLEDGMENTS

We thank Mark Hedgeland, Mario Ciani, Sandra Thitten, Arlene Roach, Ashley Fish, Glenn Seymour, and Chad Green. The authors have no conflicts of interest.

# Bone Microarchitecture and Running Biomechanics in First-Time Marathon Runners

Hannah E. Sattler<sup>1</sup>, Jessica D. Ventura<sup>3</sup>, Rebecca E. Fellin<sup>4</sup>, Karen L. Troy<sup>2</sup>

<sup>1</sup>Department of Mechanical Engineering, <sup>2</sup>Department of Biomedical Engineering Worcester Polytechnic Institute, Worcester, MA, <sup>3</sup>Department of Kinesiology, Gordon College, Wenham, MA,

<sup>4</sup>Military Performance Division, US Army Research Institute of Environmental Medicine, Natick, MA

email: Jessica.Ventura@gordon.edu, Musculoskeletal Biomechanics Lab: mbl@wpi.edu

## INTRODUCTION

Military recruits commonly sustain stress fractures, an injury common to distance runners, during Basic Combat Training (BCT). Interestingly, the recruits at lowest risk of musculoskeletal injury are those with the fastest 2 mile run time at the start of BCT [1]. It is possible that they participated in more running prior to BCT, which may be protective against injury for the large increase in training volume that occurs during BCT. Studies have shown that bone can adapt its structure to best resist habitual loading, potentially reducing fracture risk. While we have shown that high strain regions in bone experience greater bone apposition than low strain regions [2], the degree to which loading experienced during endurance running changes skeletal microstructure is still not well understood.

Our objective was to quantify changes in running mechanics and bone microstructure in novice marathoners participating in a structured training program. We hypothesized that (1) peak ankle and toe moments would be positively correlated with cortical and trabecular bone microstructure at the distal tibia and first metatarsal, respectively, and (2) change in bone post-marathon training would be positively related to ankle and toe moments.

## METHODS

Fifteen healthy adults training for a first marathon (7 males, age: 36.5±12.9 years, height: 171.4.9±11.9 cm, mass: 77.0±12.9 kg) were recruited. These subjects had never run more than 13.5 miles in a single bout, and had fewer than four weeks of >20 miles/week training over the last five years. Thirteen age and sex-matched physically-active non-runners (6 males, 36.6±12.7 years, 174.2±11.2 cm, 72.8±16.1 kg) were recruited as controls. All subjects provided written informed consent for this ongoing institutionally approved study.

Subjects received high resolution computed tomography (HRpQCT) scans of a 9.02 mm portion

of the right distal tibia (TIB) and first metatarsal (1MT) (Figure 1). Scans were acquired prior to beginning a marathon training regimen for runners and again 5-7 months later, within a month of completing their marathon. Non-runners received scans at a similar time interval.

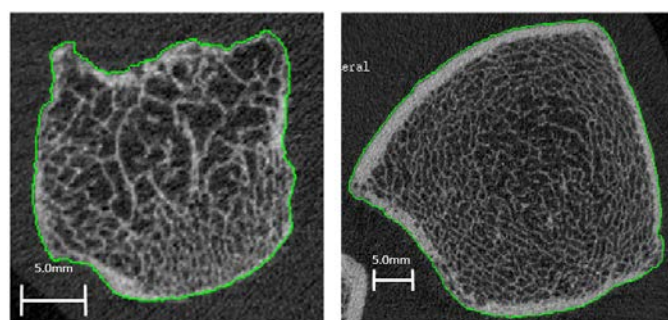


**Figure 1** HRpQCT (XtremeCT, Scanco, Switzerland) image of distal-1M (left) and TIB (right) of a runner. Green line shows segmentation of bone from soft tissue.

Scans were analyzed for a battery of microarchitectural measures including: cortical bone thickness (Ct.Th; mm) and area (Ct.Ar; mm<sup>2</sup>), trabecular number (Tb.N, 1/mm), trabecular spacing (Tb.Sp; mm), volumetric density (BV/TV; mm<sup>3</sup>/mm<sup>3</sup>), trabecular area (Tb.Ar, mm<sup>2</sup>), cortical bone mineral density (Ct.BMD, mg/cm<sup>3</sup>), total area (Tt.Ar, cm<sup>2</sup>), mean slice area (MSA, mm<sup>2</sup>), total bone mineral density (Tt.BMD, mg/cm<sup>3</sup>) and bone mineral content (BMC; g).

Running biomechanics were collected on runners at the beginning of their training and again after their marathon. Three dimensional kinematic and kinetic data were collected while participants jogged around a 50-meter track at their average training speed. Trials were considered valid when the right leg fully hit one of the force plates. For the purpose of this analysis, a simplified two-linkage inverse dynamics model of the right foot and lower leg was used to calculate the forces and moments acting at the ankle and metatarsal joints in the sagittal plane.

Currently, pre- and post- data are available for 7 runners, and complete pre-data are available for 13 runners and 13 non-runners. Baseline bone microstructural data were compared in runners versus non-runners using a t-test. To test whether joint moments were related to bone microstructure, Pearson correlations were calculated for these parameters versus runner pre-data. To examine the dependence of bone adaptation on running biomechanics, percent change in bone microstructure was correlated with baseline running biomechanics parameters.

## RESULTS AND DISCUSSION

At baseline, runners exhibited enhanced cortical and trabecular parameters, indicating increased bone strength compared to nonrunners (Table 1). Although this group was marathon-naïve, these differences suggest that low-volume running in adulthood is beneficial to bone. Self-selection into a marathon training program is likely associated with a life-long commitment to physical activity that may not be as present in the non-runner group. A larger prospective cohort should clarify this point.

**Table 1** Baseline CT measures for TIB in controls vs runners. P-values test for between-group differences. 1MT data were similar.

Measure	Control Mean(SD)	Runner Mean(SD)	P-val
Tb.BMD	172.4(28.1)	211.6(33.7)	0.014
BV/TV	0.144(0.023)	0.176(0.028)	0.013
Tb.Th	0.071(0.011)	0.080(0.010)	0.030
D100	291.8(44.3)	315.0(47.6)	0.012
Ct.Ar	117.5(23.6)	143.3(30.7)	0.035
Ct.Th	1.07(0.24)	1.31(0.26)	0.014

Units: Tb.BMD, mg/cm<sup>3</sup>; BV/TV, mm<sup>3</sup>/mm<sup>3</sup>; Tb.Th, mm; D100 (total bone mineral density), mg/cm<sup>3</sup>; Ct.Ar, mm<sup>2</sup>; Ct.Th, mm.

In runners, bone parameters were closely related to ground reaction forces (GRF) and ankle/toe moments. After normalizing for body mass, several TIB parameters remained correlated with kinetics measures (e.g. Ct.Ar vs. ankle moment  $r=0.58$ ,  $p=0.048$ ; BMC vs. moment  $r=0.64$ ,  $p=0.025$ ). In general, bone mass scales with body mass, but our data suggest that running biomechanics provide an additional important input for bone mass and structure. It is unclear whether this relationship is present in non-runners and whether it is also a reflection of walking moments – a more common daily activity.

Preliminary analysis indicates a trend towards negative relationships between peak GRF and

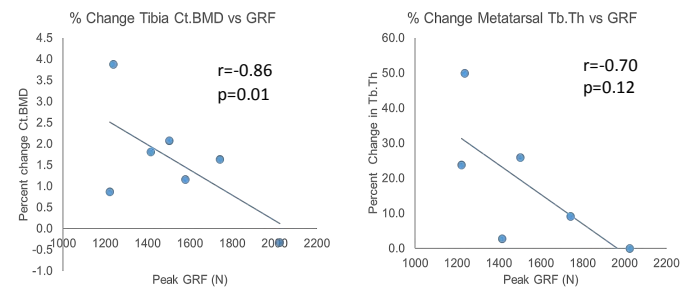


**Figure 2** Change in microstructure was consistently negatively correlated with GRF magnitude. This correlation was weakened by normalizing to body mass. 1MT data were incomplete for one subject.

percent change in both TIB and 1MT bone (Figure 2). Heavier individuals generally generate larger peak GRF and have stronger bone, so it is possible that those with initially weaker bone experience the greatest changes to bone structure. On average TIB bone parameters indicated increased strength (e.g. BMC increased by  $1.2\pm 2.4\%$  from pre to post), and 1MT indicated decreased strength and mineral (BMC decreased by  $2.4\pm 4.5\%$ ), although our sample was small.

The 1MT is loaded primarily in bending in the simplified two-linkage running model. In contrast, the distal tibia is loaded primarily in compression. Whether loading mode, strain rate, or other factors are responsible for the differential effects is yet to be determined. In the future, models will include muscle forces that also contribute to bone loading.

## CONCLUSIONS

Preliminarily, marathon trainees had enhanced bone structure compared to non-runner controls, which may be related to running biomechanics. Improved tibia parameters may indicate a positive effect of marathon training on strength. In the future, an inclusion of musculoskeletal modeling and imaging techniques may better inform stress fracture risk assessment. We expect these trends to be reinforced in the forthcoming full study population.

## REFERENCES

- [1] Jones BH, et al. *MSSE* **25**, 197–203, 1993.
- [2] Bhatia VA, et al. *J Biomech Eng* **137**(1), 2015.

## ACKNOWLEDGEMENTS

The views expressed in this abstract are those of the authors and do not reflect the official policy of the Department of Army, Department of Defense, or the U.S. Government. The investigators have adhered to the policies for protection of human subjects as prescribed in DOD Instruction 3216.02 and the research was conducted in adherence with the provisions of 32 CFR Part 219.

# FINITE ELEMENT ANALYSIS PREDICTION OF GLENOHUMERAL JOINT GROWTH FOLLOWING NEONATAL BRACHIAL PLEXUS INJURY

<sup>1</sup> Nikhil N. Dixit, <sup>1</sup> Daniel McFarland and <sup>1</sup> Katherine R. Saul

<sup>1</sup> NC State University, Raleigh, NC, USA

Email: ndixit2@ncsu.edu, web: <http://www4.ncsu.edu/~ksaul/index.html>

## INTRODUCTION

Neonatal brachial plexus injury (NBPI) occurs in 1.5 per 1000 live births [1]. Children affected with this injury undergo permanent osseous and postural deformities. NBPI presents as either postganglionic injury – resulting in restricted longitudinal growth of paralyzed muscles – or preganglionic injury which causes paralysis without substantial muscle shortening [1]. It is believed that compressive and posterior joint loading subsequent to NBPI increases with shortened muscles, and severe morphological changes are observed in rats with shortened muscles after postganglionic NBPI [3]. Further, the injury imposes a restricted range of motion and reduced limb use, leading to an increase in static loading [2]. Static compressive joint loads are known to significantly inhibit the synthesis of cartilage matrix proteins, while dynamic compression stimulates matrix production in developing bone [2]. It is unknown whether, for NBPI, altered loading due to growth restriction or static loading is the primary driver of joint deformity, and whether the extent of deformity can be predicted. The goal of the study was to evaluate the effect of static vs dynamic joint loading and muscle shortening on the morphology of the developing glenohumeral joint after NBPI.

## METHODS

An iterative finite element modeling approach was used to predict osseous morphological growth in response to biological and mechanical stimuli (Abaqus 6.13.3, Dassault Systemes). We used a thermal expansion analog to capture the biological and mechanical contributions to growth [2]. Biological growth was modeled using a cubic equation which was a function of distance from the growth plate [2]. The mechanical growth was proportional to compressive hydrostatic stress at every node. Stress due to static loads restricted the growth while dynamic hydrostatic stress stimulated growth [2], according to the following equations:

$$\dot{\epsilon}_m = C_d \left( \frac{\sum_{i=1}^N \sigma_{hi}}{N} \right), \text{ for static loads}$$

$$\dot{\epsilon}_m = -C_d \left( \frac{\sum_{i=1}^N \sigma_{hi}}{N} \right), \text{ for dynamic loads}$$

$\dot{\epsilon}_m$  is the mechanical growth rate,  $\sigma_{hi}$  is the compressive hydrostatic stress,  $N$  is the number of movements per step and  $C_d$  is the chondrocyte density. The resultant geometry was the summation of biological and mechanical growth.

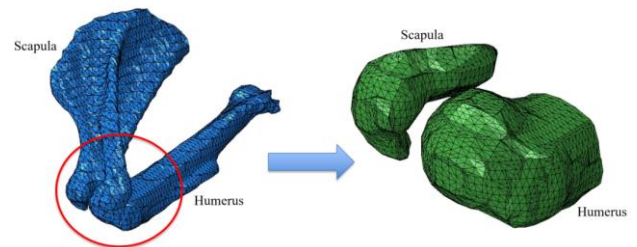


Fig 1: Reduced glenohumeral joint geometry

We created 3 simulations to address our study goals: 1) Dynamic, 2) Static: Preganglionic and 3) Static: Postganglionic. Initial geometry of the glenohumeral joint was the same for all simulations and was derived from micro-CT scans of unimpaired neonatal rats. The geometry was subsequently reduced to the regions near the articulating surfaces to minimize computational time (Fig. 1). For the dynamic simulation, a compressive joint load of 0.1 N was applied under a cyclic motion from 0° to 30° abduction. In the static preganglionic (no muscle restriction) and postganglionic (muscle growth restriction) simulations, the static joint loads were computed with the shoulder in 30° abduction using an upper extremity musculoskeletal model [2] in OpenSim by denervating the NBPI affected muscles and all other unaffected muscles at 30% activation [5]. To evaluate the effect of impaired muscle growth, we performed both simulations with the base musculoskeletal model, and with the affected muscles shortened by 40% relative to the skeletal geometry to represent 8 weeks of the growth period

[3]. The joint loads from OpenSim were incorporated as a displacement boundary condition in Abaqus by considering a joint stiffness of 2kN/mm [6]. The glenoid surfaces for each simulation were measured to assess glenoid inclination angle (GIA), and the glenoid radius of curvature (GRC). GIA is the angle complementary to the angle between the centerline of the spine of the scapula (red) and the tangent line to the rim of the glenoid cavity (Fig. 3).

## RESULTS AND DISCUSSION

Both static conditions (i.e. preganglionic and postganglionic) showed a substantial increase in the GIA and the GRC from the baseline model (Fig. 3, Table 1), confirming that absence or reduction of dynamic loads on the joint following NBPI increases glenoid flatness and declination. In contrast, both GIA and GRC were found to decrease from baseline in the dynamic analysis, retaining the glenoid curvature essential for effective functioning of the glenohumeral joint. Postganglionic simulations exhibited more severe deformity than preganglionic, but changes were less marked than between static and dynamic conditions.

The simulated results compare well with experimental data from a rat study of NBPI in which a postganglionic neurectomy was performed postnatally [3]. An increase in both GIA and GRC in the case of affected rats at 8 weeks postnatal corroborated our simulation predictions that static loads and muscle shortening drive joint deformation due to NBPI. In addition, the magnitude of inclination for postganglionic injury in both experiment and simulation were in close agreement ( $56.1^\circ$  vs  $59^\circ$ , respectively) (Table 1). Limitations in the current simulation should be considered. We modeled a single biological center for the scapula, but there are three growth centers at this stage of development, and each may have different biological growth rates. Differing rates along the glenoid may

contribute to the differences in predicted and experimental GRC.

The computational methodology described here, integrating musculoskeletal joint loading with finite element growth models, provides an important platform to capture the effect of altered musculoskeletal loading following NBPI on the time progression of joint deformation. With this foundation, surgical strategies and effect of intervention timing can be explored.

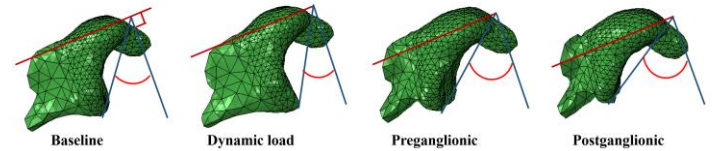


Fig 3: Glenoid deformations in each simulation

## CONCLUSIONS

The study successfully developed a computational framework that captured developmental changes to bone following NBPI, and validated predictions against experimental data. The finite element model predicted that static loading of the joint was primarily responsible for joint deformation due to the neurological injury. The model also captured the effects of altered muscle forces due to preganglionic and postganglionic injuries on a musculoskeletal structure and predicted that postganglionic injuries were responsible for more severe joint deformations, which is consistent with the existing literature [3].

## ACKNOWLEDGEMENTS

This research was funded by NCSRR pilot award.

## REFERENCES

1. Nikolaou S. et al. *J Hand Surg*, 2007-2016, 2015
2. Giorgi M. et al. *J Biomech*, 989-995, 2014
3. Crouch DL. et al. *J Hand Surg*, 303-311, 2014
4. Holzbaur KRS. et al. *BMES*, 829-840, 2005.
5. Cheng W. et al. *J Hand Surg Am.*, 1170-1176, 2015
6. Subic A. et al. *Adv. Material Research*, 3-14, 2013

**Table 1:** GIA and GRC comparison between simulation and experimental results

	FE growth simulation				Experimental data from rat study [3]	
	Baseline	Dynamic load	Preganglionic	Postganglionic	Baseline	Postganglionic neurectomy
Glenoid inclination angle (deg)	38	30	50	59	35.79	56.1
Glenoid radius of curvature (mm)	2.1	1.6	2.6	3.2	2.5	5.6

# MULTI-SCALE MODEL IN CO-SIMULATION TO ESTIMATE PATELLOFEMORAL CONTACT STRESS IN TOTAL KNEE REPLACEMENT

<sup>1</sup> Swithin S. Razu and <sup>1</sup> Trent M. Guess

<sup>1</sup> The University of Missouri, Columbia, MO, USA  
email: swithinr@health.missouri.edu, web: www.mizzoumotioncenter.com

## INTRODUCTION

Total knee arthroplasty (TKA) is a common surgical procedure that attempts to restore the functional mechanics of the normal knee [1]. Recent modifications in design have resulted in substantial decrease in complications such as instability and component loosening. However, complications involving the patellofemoral (PF) joint are the cause of as many as 50% of all total knee revisions [2]. While in-vitro experiments provide an improved understanding of the passive structures of the PF joint, knowledge of in-vivo PF joint stresses during daily activities are limited.

Computational models of the musculoskeletal system provide access to the internal loads at the tibiofemoral (TF) and PF joints based on external measurements. In the past, multibody (MB) dynamics has focused on whole-body dynamic musculoskeletal models while finite element (FE) methods have been used for joint level models. These methods were either isolated or applied at different stages during a simulation. This study introduces a framework for co-simulating MB dynamics and linear FE methods to estimate von Mises stress in the patellar button during smooth, normal and bouncy gait. In this study we also validated the musculoskeletal model by comparing model predictions of TF contact forces to subject specific in-vivo measurements obtained from an instrumented TKA.

## METHODS

The data for this study was collected from an 83-year-old male subject (mass=70 kg and height=172 cm) with an instrumented right TKA that measures the six loading components acting on the tibial tray. The experimental data were provided by the sixth

edition of the Grand Challenge Competition to Predict In-vivo Knee Loads [3].

The subject model (Fig. 2b) was developed in the commercially available multibody dynamic analysis program MSC ADAMS, NASTRAN, and PATRAN (MSC Software Corporation, Santa Ana, CA). The generic musculoskeletal model was comprised of 21 rigid body segments, 53 revolute joints, and 44 right leg muscles [4]. The knee joint (Fig. 2c) consisted of a 12 degrees-of-freedom anatomical right knee that included both the TF and PF joints. The tibial insert was divided into medial and lateral geometries with separate contacts created for each part. The ligaments were modeled as bundles, attached to the bones according to the origin and insertion site footprints based on anatomical studies. Deformable contacts between force plate geometries and shoe geometries were used to model the shoe-ground interface.

This study captures the von Mises stress on the patellar button using rigid-flexible multibody dynamics theory [5]. The patellar button is made flexible using MSC NASTRAN. A FE mesh of the button is generated using MSC PATRAN with tetrahedral elements. The button material is assumed to be linear and isotropic. The material properties were Young's modulus  $5.72E+008$  N/m<sup>2</sup>, Poisson's ratio 0.45, and density 945 kg/m<sup>3</sup>. One attachment node with 6 DOFs is generated at the center of the patella bone. Rigid body spider web elements (RBE2) are used to connect the attachment node to the adjacent surface nodes on the patella button. Thirty fixed boundary mode shapes are exported from MSC NASTRAN.

The experimental motion capture data for smooth, normal and bouncy walking trials provided input to an inverse kinematics step for each model. A feedforward with feedback trim control scheme

(Fig. 1) is used to produce muscle force for muscles with EMG signal. The feedforward muscle scheme incorporates experimental EMG when available with a Hill-type muscle model to produce feedforward muscle force. A feedback scheme is used for remaining muscles.

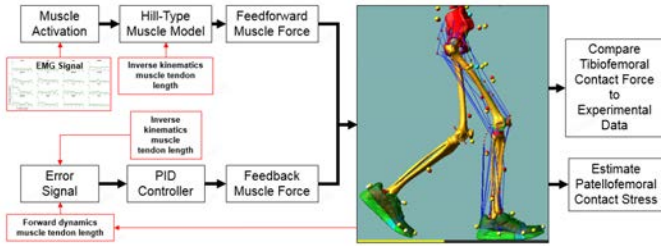


**Figure 1:** Feedforward with feedback control scheme to calculate muscle force and predicting joint contact forces.

## RESULTS AND DISCUSSION

Comparisons of model predictions with measured contact forces showed (Fig. 2a) that the EMG-driven musculoskeletal model using patient-specific input data can estimate tibiofemoral contact forces with root mean square errors (RMSEs) of 0.18-0.29 times body weight (BW) for smooth, 0.15-0.21 BW for normal, and 0.21-0.33 BW for bouncy gait trials. The maximum von Mises stress (Fig. 2b) was computed at the mid-stance (20%, 17%, 22% gait cycle for smooth, normal, and bouncy) when the

average quadriceps muscle force is maximum. The von Mises stresses were 6.4 MPa, 4.7 MPa, and 7.5 MPa for smooth, normal and bouncy gait trials respectively.

## CONCLUSIONS

This study involved co-simulation of a prosthetic patellar button FE model embedded in a validated MB musculoskeletal model of gait. TF contact force RMSEs between model predicted and measured ranged from 0.15-0.33 BW for the three gait types. The von Mises stress in the patellar button increased in smooth and was the greatest in bouncy gait when compared to normal gait due to the increase in flexion angle and quadriceps force.

## REFERENCES

1. Emmerson, KP, et al. *J Bone Joint Surg Br*, **78**(3): p. 441-5, 1996.
2. Rand, JA. *J Knee Surg*, **16**(4): p. 224-8. 2003.
3. Kinney, AL, et al. *J Biomech Eng*, **135**(2): p.021012, 2013.
4. Arnold, EM, et al. *Ann Biomed Eng*, **38**(2): p.269-79, 2010.
5. Bampton, MCC, et al. *AIAA Journal*, **6**(7): p.1313-1319, 1968.

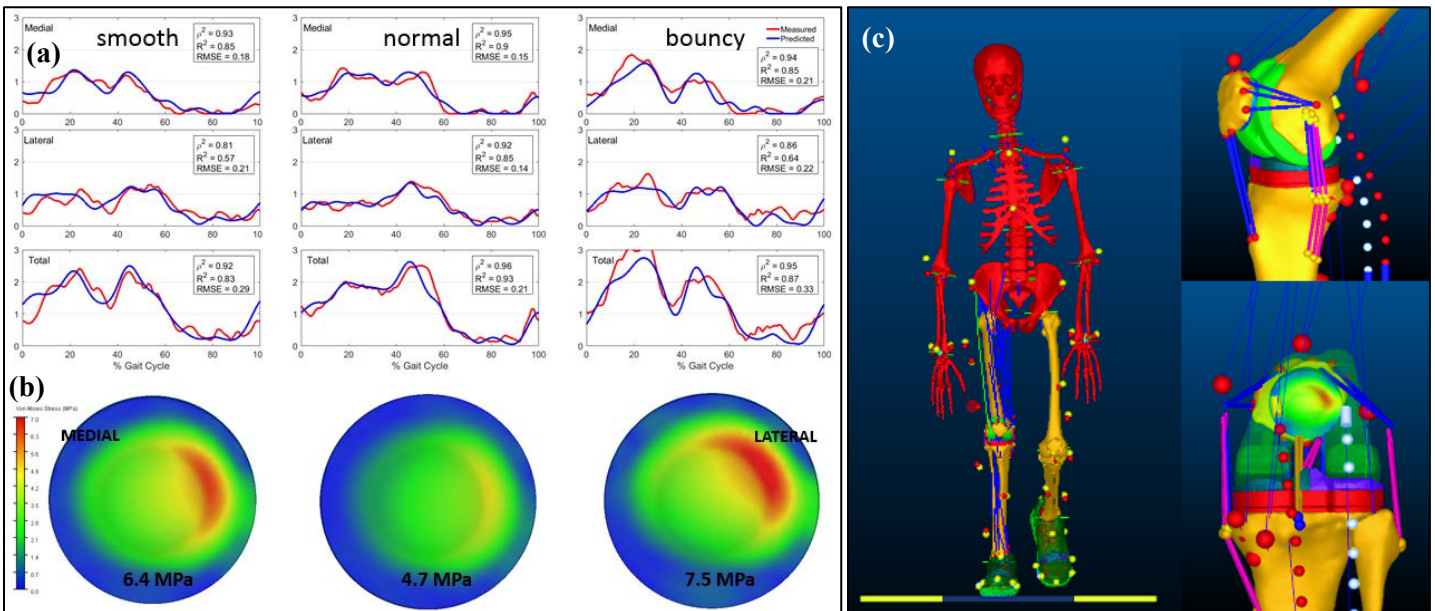


**Figure 2:** (a) Medial, lateral, and total tibiofemoral contact forces compared with in vivo measurements obtained during smooth, normal and bouncy gait; (b) Maximum von Mises stress during mid-stance ; (c) Subject and combined MB-FE knee musculoskeletal model

# Biomechanical Gait Variable Estimation Using Wearables after Total Knee Arthroplasty

Ik-Hyun Youn<sup>1</sup>, Jong-Hoon Youn<sup>1</sup>, Joseph A. Zeni<sup>2</sup>, Brian A. Knarr<sup>1</sup>

<sup>1</sup>University of Nebraska at Omaha, Omaha, NE, USA

<sup>2</sup>University of Delaware, Newark, DE, USA

email: iyoun@unomaha.edu

## INTRODUCTION

Osteoarthritis (OA) of the knee is common disease that impacts functional mobility and quality of life for many individuals [1]. Total Knee Arthroplasty (TKA) is the most common surgical treatment for end-stage OA. While the cause of OA is multifactorial, loading patterns have been correlated with OA progression [2]. Most of the existing data on movement patterns before and after TKA has been assessed using optical motion capture systems and ground reaction forces. However, these measurements are limited to constrained laboratory settings, which may not reflect real-world movement patterns.

Due to the advancement in wearable technologies, wearable sensors have become a viable alternative to assess the initial loading pattern during walking [3]. They are advantageous since they require minimal equipment and can capture kinetic attributes outside of the laboratory setting. Monitoring multiple and sequential kinetic parameters in real-world conditions may lead to a more accurate understanding of the relationship between movement patterns and recovery from TKA. Therefore, the purpose of this study was to estimate kinematic and kinetic gait metrics using two ankle-worn wearable sensors in individuals after unilateral TKA.

## METHODS

15 subjects (1.70±0.1m, 84.5±17.1kg, 67.1±7.5yr, speed=1.13±0.20m/s) after unilateral TKA participated in this study. Data were acquired in the Neuromuscular Biomechanics Laboratory at the University of Delaware. An instrumented split-belt treadmill and an 8 camera motion capture system were used to collect kinetic and kinematic gait variables. Acceleration data were collected using two angle-worn accelerometers. Accelerometers were attached above the lateral malleoli. Each subject

walked at self-selected comfortable walking speed, as determined by a 6 meter walk test, for one minute.

Eleven gait variables were extracted to estimate magnitude, impulse, and angles of initial loading from 3D-acceleration data (Table 1). Then, the wearable sensor-based gait variables were compared to three kinetic and kinematic gait variables averaged across the one-minute trial: maximum knee flexion moment (KFM), maximum knee adduction moment (KAM), and first peak of vertical ground reaction force (vGRF).

**Table 1:** Eleven inertial gait features based on one all-step inclusive and three directional gait feature categories.

Category	Description
Inclusive	Step time
	Step vector magnitude
	Initial loading vector mag.
Lateral	Lateral heel-strike magnitude
	Lateral heel-strike impulse
	Lateral stance phase angle
Vertical	Vertical heel-strike magnitude
	Vertical heel-strike impulse
Anterior	Anterior heel strike magnitude
	Anterior heel-strike impulse
	Anterior stance phase angle

Hierarchical linear regressions were applied to determine contribution of directional gait variables from wearables for each biomechanical gait feature. To analyze directional effect of inertial gait variables, inclusive-, lateral-, vertical-, and anterior-gait inertial variables were sequentially appended as additional dependent variables of regression models.

## RESULTS AND DISCUSSION

Outcomes of the hierarchical linear regression indicated that inertial gait features significantly

estimated all three biomechanical gait features (Table 2). KFM was significantly and solely explained by vertical heel-strike magnitude. The addition of anterior heel-strike magnitude slightly improved the model, but the rest of the nine inertial gait features did not improve prediction of KFM. Lateral heel-strike magnitude and stance phase angle deviation were significant predictors of KAM outcomes after accounting for step time and vector magnitude. For the vGRF prediction model, both lateral and anterior inertial gait features equally contributed to explain 75.4 % of the variance in vGRF measure.

Hierarchical regression models provided evidence that accelerometer-based metrics can be used to predict biomechanical gait variables. With all inertial gait variables, 48.7%, 69.0%, and 75.4% of the variance in KFM, KAM, and vGRF measures were explained, respectively.

Knee flexion moment was primarily explained by vertical inertial gait variables. It is likely that vertical inertial variables are related to limb impact during heel strike. Impact may be partially controlled by knee flexion with an increase in knee flexion during weight acceptance serving to soften impact but subsequently increase peak knee flexion moment. On the other hand, knee adduction moment was primarily explained by lateral inertial gait variables. Gait modifications including increased step width, increased trunk sway and toe-in gait have been shown to be effective at reducing knee adduction moment in healthy population [4]. It is likely that

individuals post-TKA may adapt similar strategies to reduce knee adduction moment as a result of pain or functional compensations. It is reasonable to believe that such gait adaptations may be evidenced through lateral inertial gait variables, given the changes in side to side movement (i.e. swaying, wide steps).

## CONCLUSION

Although generalization to the TKA population as a whole is limited due to the small sample size of this study, the current results provide evidence that inertial measurements can be used to reasonably estimate conventional biomechanical metrics. Future work will examine the relationship between additional kinematic and kinetic variables and inertial variables.

## REFERENCES

1. Ruiz D. et al. *J Bone Joint Surg AM* **16**, 1473-1480, 2013.
2. G.L. Hatfield, et al. *Arthritis Care Res.* **67**. 1004–1014, 2015.
3. Chen, S. et al. *J Biom Heal Inform* **20**, 1521-1537, 2016.
4. Favre, J et al. *J Orthop Res* **34**:1547–1556, 2016

## ACKNOWLEDGMENTS

This work was partially supported by the National Institutes of Health NIH P30-GM103333 and P20GM109090.

**Table 2:** Hierarchical linear regression for three target biomechanical gait variables outcomes.

Model 1 = Inclusive variables

Model 2 = Inclusive + Lateral variables

Model 3 = Inclusive + Lateral + Vertical variables

Model 4 = Inclusive + Lateral + Vertical + Anterior variables

Model	KFM			KAM			vGRF		
	R	Adj. R <sup>2</sup>	ΔR <sup>2</sup>	R	Adj. R <sup>2</sup>	ΔR <sup>2</sup>	R	Adj. R <sup>2</sup>	ΔR <sup>2</sup>
Model 1	0.000	0.000	0.000	0.252	0.128	0.128	0.000	0.000	0.000
Model 2	0.000	0.000	0.000	0.729	0.620	0.492	0.401	0.355	0.355
Model 3	0.511	0.473	0.473	0.753	0.616	-0.005	0.493	0.354	-0.001
Model 4	0.561	0.487	0.014	0.845	0.690	0.074	0.860	0.754	0.400

# Concurrent Osteoarthritis of Contralateral Knee Alters Joint Biomechanics of the Knee with a Mobile-bearing Implant

<sup>1,2</sup> Shangcheng Wang, <sup>3</sup>Zhihong Liu, <sup>1,2</sup> Zheng Xu, <sup>3</sup>Jianming Feng, <sup>3</sup>Lianfu Deng and <sup>1,2</sup> Nigel Zheng

<sup>1</sup> Department of Mechanical Engineering and Science

<sup>2</sup> Center of Biomedical Engineering at UNC Charlotte, NC, USA

<sup>3</sup> Shanghai Institute of Orthopedics and Traumatology, Shanghai Jiao Tong University, Shanghai, China,  
Email: nzheng@uncc.edu, web: <http://coefs.uncc.edu/nzheng/>

## INTRODUCTION

Abnormal knee joint biomechanics during walking have been associated with increased prosthetic wear of a total knee arthroplasty (TKA). Concurrent osteoarthritis of the contralateral knee (CKOA) often requires inter-limb compensation and may have the potential to affect the post-arthroplasty knee biomechanics. While TKA is an effective surgical intervention for knee arthritic pain, CKOA is common among post-TKA patients. When it comes to the management of CKOA, the effect of CKOA on post-arthroplasty knee is often ignored. This study tried to determine if and how CKOA altered knee biomechanics with a mobile-bearing implant.

## METHODS

Patients were selected after a unilateral TKA with mobile-bearing implant (DePuy). The average time past surgery was  $13 \pm 8$  months with a range from 3 to 39 months. At the time of testing, they all could walk without aid, and had no symptoms other than CKOA or any previous injury that would affect gait. A total of 22 patients were recruited. There were 10 CKOA patients (2M/8F, 4L/6R,  $69 \pm 7$  years) and 12 patients (2M/10F, 8L/4R,  $68.8 \pm 5$  years) with asymptomatic contralateral knee. The operated knee of all patients had no or very mild pain at the time of testing.

All subjects signed consent forms after an IRB approved testing protocol was introduced. Each subject walked five times at a self-selected speed in a lab equipped with ten-camera motion capture system (100Hz, MX-F40, VICON, Oxford, UK) and two force plates (1000Hz, AMTI, MA, USA). Marker data was smoothed using a zero-lag 4<sup>th</sup>-order Butterworth filter at a cut-off frequency of 6Hz. A redundant marker set was used to determine the tibiofemoral joint motion which follows our

previously reported study [1]. Intersegment joint loading was obtained through inverse dynamics method. Spatiotemporal parameters, tibiofemoral joint motion and knee joint kinetics were compared between CKOA group and CKNON group using a one-way ANOVA (significance level 0.05). A bivariate correlation analysis was also conducted to investigate the interaction between kinematics and loading.

## RESULTS AND DISCUSSION

**Spatiotemporal:** CKOA group had a bigger stance percentage than CKNON group by 4% gait cycle (GC). CKOA group walked with a 20.5% longer stance phase by 0.17s and 17.5% slower stride speed (Table 1).

**Kinematics:** As knee extended (85%-95% GC), the operated knees in CKOA group were  $5.7^\circ$  less extended than those in CKNON group ( $p < .05$ , Table 1 and Fig. 1). In the transverse plane, a  $3.9^\circ$  more tibia external rotation was observed around heel strike (HS), 95%-20% GC in CKOA group ( $p < .01$ ). Anteroposterior translation was also altered, with about 2mm posterior offset at HS, around mid-stance (25%-35% GC) and around toe-off (60~65% GC).

For range of motion during stance, CKOA group was similar in flexion-extension and anteroposterior translation, but had  $2.5^\circ$  bigger axial rotation range than CKNON group (CKOA,  $9.91^\circ \pm 2.54^\circ$ ; CKNON,  $7.48^\circ \pm 2.55^\circ$ ,  $p < .05$ ).

**Kinetics:** Peak knee axial (vertical) joint force was significantly reduced by 5%BW in CKOA group (Fig. 1 and Table 2,  $p < .01$ ). The peak knee extension moment of CKOA group was also smaller than CKNON group. No difference was found in peak/mean knee adduction/flexion/rotation moment.

**Correlation:** The knee flexion angle at HS was positively correlated with the magnitude of mean

knee flexion moment ( $p < .01$ ,  $r = .77$ ). The tibia external rotation angle at HS was negatively correlated with the magnitude of mean knee adduction moment ( $p < .01$ ,  $r = -0.61$ ) and peak knee rotation moment ( $p < .01$ ,  $r = -0.54$ ). Knee axial rotation range was correlated with rotation angle at HS ( $p < .01$ ,  $r = .63$ ) but not correlated with loading.

**Discussion:** CKOA altered kinematics at HS and increased knee axial rotation range, which might increase the wear rate of the implant [2]. Muscle firing pattern (i.e. a quadriceps overuse pattern) were linked with the extension loss. The internal rotation loss is linked with a reduced mean knee adduction moment which might be a result of front plane

compensation such as trunk leaning in CKOA patients.

## CONCLUSIONS

Concurrent osteoarthritis of the contralateral knee alters the mechanical environment of the knee implant and may affect its function in long-term.

## REFERENCES

1. Wang H., J.E. Fleischli et al. AJSM 41(8):1847-1856, 2013.
2. McEwen, H. M. J. et al. (2005). Journal of Biomechanics 38(2): 357-365.

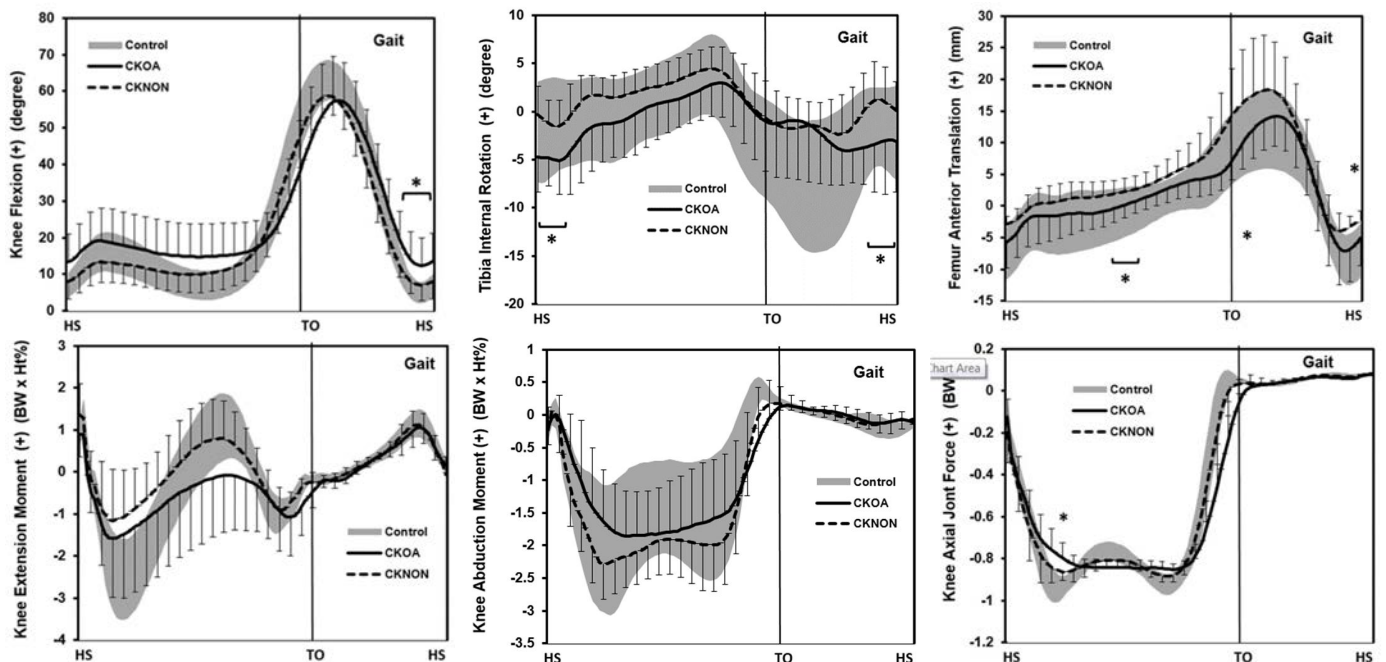


**Figure 1** ensemble average of kinematics and kinetics; HS, TO: heel-strike, toe-off. \* denotes  $p < .05$ .

**Table 1:** Spatiotemporal parameters and kinematic variables at HS. \*\*  $p < .01$ ; \*  $p < .01$ ;

unit	% gait cycle	meter/second	second	degree	degree	millimeter
group	stance phase	stride speed	stance period	Extension	rotation	AP translation
CKOA	64.72 ± 2.61**	0.75 ± 0.15*	0.89 ± 0.17*	11.70 ± 7.09*	-4.67 ± 3.41**	-6.16 ± 3.99*
CKNON	60.32 ± 2.35	0.91 ± 0.14	0.72 ± 0.12	5.82 ± 4.15	-0.71 ± 3.10	-3.18 ± 1.61

**Table 2:** Kinetic variables, force is in body weight (BW)%, moment is in BW x Height (Ht)%.

unit	flexion moment		extension moment	adduction moment		axial joint force
group	peak	mean	peak	peak	mean	peak
CKOA	-1.95 ± 1.15	-0.71 ± 1.08	1.21 ± 0.61*	-2.11 ± 0.79	-1.24 ± 0.64	-0.87 ± 0.03*
CKNON	-1.57 ± 0.90	-0.12 ± 0.65	1.76 ± 0.52	-2.44 ± 0.55	-1.58 ± 0.44	-0.93 ± 0.04

# Knee Biomechanics of Dissatisfied Total Knee Replacement Patients during Stair Ascent

<sup>1</sup>Songning Zhang, <sup>1</sup>Kevin Valenzuela, <sup>2</sup>Harold E. Cates

<sup>1</sup>Biomechanics/Sports Medicine Lab, The University of Tennessee, Knoxville, TN, USA

<sup>2</sup>Tennessee Orthopedic Clinic, Knoxville, TN, USA

email: [szhang@utk.edu](mailto:szhang@utk.edu)

## INTRODUCTION

Total knee arthroplasty (TKA) is a common surgical procedure for treating end-stage knee osteoarthritis (OA). Patients with TKA and knee OA often have difficulty in daily movement tasks such as stair ambulation [2]. Although a majority of TKA patients is satisfied with their surgeries, some TKA patients reported dissatisfaction with decreased capacity of daily living activities [1, 4]. However, it is not entirely clear why the TKA patients are not happy with their TKA procedures.

Previous research on TKA level and stair gait biomechanics has been focused on differences from healthy individuals and between replaced and non-replaced limbs [3, 5]. Research on gait biomechanics of the dissatisfied TKA patients is scarce.

Therefore, the purpose of this study was to compare knee biomechanical characteristics of stair ascent for dissatisfied TKA patients to satisfied TKA patients and healthy controls. It was hypothesized that dissatisfied TKA patients would exhibit decreased knee extension moments and increased knee abduction moments in their replaced limb compared to their non-replaced limb during stair ascent.

## METHODS

Participants were recruited from a local orthopaedic clinic: nine dissatisfied TKA patients (68.0±4.2 years, BMI: 28.4± kg/m<sup>2</sup>, 34.6±14.3 months from surgery) and fifteen satisfied TKA patients (66.6±6.3 years, BMI: 29.1± kg/m<sup>2</sup>, 29.3±12.8 months since surgery). Fifteen healthy controls (60.7±9.2 years, BMI: 25.4± kg/m<sup>2</sup>) were recruited with the same exclusion criteria as the TKA groups. The inclusion criteria for TKA patients were having a unilateral total knee replacement (conducted by a single surgeon) at least 12 months but less than 60 months prior to testing and between the ages of 50 and 75 at the time of testing. Potential participants were

excluded if they had any additional lower extremity joint replacements, any additional diagnosed osteoarthritis of the hip, knee, or ankle, BMI greater than 38, or neurological diseases. TKA patients were then asked, “How satisfied are you with your total knee replacement?” and patients answering “Neutral” were excluded from the study. Any participant who responded “very dissatisfied” or “dissatisfied” was placed into the dissatisfied group and participants who answered “satisfied” or “very satisfied” were placed into the satisfied group.

A 12-camera motion capture system (240Hz, Vicon, UK) and an instrumented staircase (FP-stairs, AMTI, USA) in conjunction with two force platforms (1200Hz, AMTI, USA) were used to collect three-dimensional kinematic and ground reaction force (GRF) data, respectively. Anatomical markers and tracking markers were placed bilaterally on the trunk, pelvis, thighs, shanks, and lab shoes (Noveto, Adidas). Each participant performed five successful stair ascent trials at ±5% of the preferred stair ascent speed. Participants were provided practice trials to become familiar with test settings.

Kinematic and force data were filtered using a low pass fourth-order zero-lag Butterworth filter (8Hz), and processed using Visual3D (5.0, C-Motion, Inc.). Joint moments were computed as internal moments and normalized to mass (Nm/kg).

A 2×3 (limb × group) mixed model analysis of variance (ANOVA,  $p < 0.05$ ) was performed to detect differences between limbs and groups for kinematic and kinetic variables (9.4, SAS). In the presence of a significant interaction or a main effect, *post hoc* comparisons were conducted using paired-sample *t*-tests with Bonferroni adjustments.

## RESULTS AND DISCUSSION

The preferred walking speed for the dissatisfied group (0.53±0.16 m/s) was slower than the satisfied

(0.74±0.10 m/s) and healthy (0.69±0.12 m/s, p<0.0099 for both) group.

Significant interactions were present during stair ascent trials for 2<sup>nd</sup> peak vertical GRF, peak loading-response knee extension moment, knee abduction ROM, and peak loading-response internal rotation moment (Table 1). Post-hoc analysis revealed that the dissatisfied group had lower 2<sup>nd</sup> peak vertical GRFs compared to their non-replaced limb and both the satisfied and healthy groups. The peak loading-response extension moment was lower in the replaced-limb of the dissatisfied group compared to their non-replaced limb and both the satisfied and healthy groups.

For all four variables with significant interactions, the satisfied group was different in their replaced limb compared to their non-replaced limb, experiencing reduced peak vertical GRF, peak loading-response extension moment, and peak loading-response internal rotation moments along with an increased knee abduction ROM. In addition, significant limb main effects were present in the 1<sup>st</sup> peak vertical GRF, peak loading-response abduction moment, and peak push-off abduction moment, with the replaced limbs showing reduced values compared to the non-replaced limbs.

These results showed that the replaced limb of TKR patients had reduced peak vertical GRFs, peak knee extension moment, peak knee abduction moments and peak knee internal rotation moment compared to their non-replaced limbs. More importantly, the dissatisfied TKA patients had slower stair ascent speed, and reduced peak loading-response knee extension moment and peak push-off vertical GRF in their replaced limb compared to their non-replaced limb and satisfied TKA patients and healthy counterparts. Our study has demonstrated that the dissatisfied TKA patients have deficits in not only the speed, but also during loading- response and push-off in stair ascent. Furthermore, it is important to understand associations of other aspects with TKA patient dissatisfactions.

## REFERENCES

1. Boonstra, M. C., et al. (2008). *Knee*, **15**, 390-395.
2. Costigan, P. A., et al. (2002). *Gait & Posture*, **16**, 31-37.
3. Mandeville, D., et al. (2008). *Clinical biomechanics (Bristol, Avon)*, **23**, 1053-1058.
4. Ouellet, D., et al. (2002). *Arthritis Rheum*, **47**, 484-493.
5. Standifird, T. W., et al. (2016). *The Journal of arthroplasty*, **31**, 278-283.

Table 1. Peak GRF and Knee Kinematic and Kinetic Variables during Stair Ascent: Mean ± STD.

Variables	Dissatisfied		Satisfied		Healthy		Int. p value
	Replaced	Non-Replaced	Replaced	Non-Replaced	Dominant	Non-Dominant	
1 <sup>st</sup> Peak VGRF <sup>#</sup>	0.93±0.07	1.01±0.04	0.99±0.04	1.01±0.07	1.02±0.11	1.04±0.08	0.3075
2 <sup>nd</sup> Peak VGRF <sup>**</sup>	1.03±0.09 <sup>ABC</sup>	1.12±0.09 <sup>C</sup>	1.16±0.07 <sup>A</sup>	1.22±0.11 <sup>C</sup>	1.14±0.11	1.14±0.11	<b>0.0338</b>
Extension ROM	53.4±4.9	57.0±5.4	55.3±5.3	56.3±4.5	57.3±4.3	57.1±4.8	0.3572
Loading-response Extension Moment <sup>**</sup>	0.75±0.31 <sup>ABC</sup>	1.11±0.26	1.08±0.26 <sup>A</sup>	1.23±0.23	1.23±0.24	1.19±0.27	<b>0.0003</b>
Abduction ROM <sup>#</sup>	-11.8±7.4	-12.2±6.7	-15.9±4.9 <sup>A</sup>	-9.3±5.3	-13.9±9.1	-12.5±8.0	<b>0.0296</b>
Loading-response Abduction Moment <sup>#</sup>	-0.36±0.16	-0.48±0.14	-0.35±0.15	-0.40±0.17	-0.39±0.20	-0.50±0.15	0.6838
Push-off Abduction Moment <sup>#</sup>	-0.33±0.20	-0.35±0.20	-0.27±0.18	-0.44±0.24	-0.18±0.13	-0.44±0.16	0.1561
Internal Rotation ROM	6.2±5.2	5.4±4.4	2.3±4.2	4.7±3.9	2.0±3.5	3.1±4.8	0.2916
Loading-response Internal Rotation Moment <sup>#</sup>	0.23±0.16	0.30±0.22 <sup>C</sup>	0.24±0.17 <sup>A</sup>	0.38±0.18	0.13±0.10	0.46±0.13	<b>0.0176</b>

<sup>A</sup> Significantly different from contralateral leg of same TKA group, <sup>B</sup> Significantly different from same leg of satisfied TKA group, <sup>C</sup> Significantly different from same leg of healthy group, <sup>#</sup>Limb main effect, \*Group main effect, VGRF – vertical GRF.

# MUSCLE ACTIVITY DURING POSTURAL STABILITY TASKS: ROLE OF MILITARY FOOTWEAR AND WORKLOAD

<sup>1</sup>Harish Chander, <sup>1</sup>Adam C. Knight, <sup>3</sup>John C. Garner, <sup>2</sup>Chip Wade, <sup>1</sup>Hunter DeBusk, <sup>4</sup>Samuel J. Wilson, <sup>4</sup>Jacob Gdovin, <sup>4</sup>Christopher M. Hill & <sup>1</sup>Daniel Carruth

<sup>1</sup>Mississippi State University, Mississippi State, MS, USA; <sup>2</sup>Auburn University, Auburn, AL, USA;

<sup>3</sup>Troy University, Troy, AL, USA; <sup>4</sup>University of Mississippi, University, MS, USA

Email: [hchander@colled.msstate.edu](mailto:hchander@colled.msstate.edu) Web: <http://kinesiology.msstate.edu/>

## INTRODUCTION

Although only a relatively small amount of muscular activity is required to maintain an erect standing posture, the control of it, is complex and involves motor control and neuromuscular systems. When motor or sensory components are altered or defective, body's postural sway generally increases, indicating decreased postural stability. Concurrently, there is an increased demand on the central mechanisms and peripheral muscles to maintain postural equilibrium [1]. An intrinsic human factor, such as a physiological workload leading to muscular fatigue and an extrinsic factor such as, inappropriate footwear that alter lower extremity muscle activity have been shown to contribute to decrements in postural stability and subsequently an increased incidence for falls. Biomechanical analysis of military load carriage has suggested a decrease in postural stability and a greater incidence for injuries [2]. Such physical demands in the military along with inappropriate military footwear might predispose the wearer to inefficient muscular exertion to maintain erect stance and result in postural instability. Therefore the purpose of this study was to analyze the impact of two types of military footwear and a military type workload on muscle activity during postural stability tasks.

## METHODS

The study followed a pre-test-post-test repeated measures design, with a total of sixteen male participants [age:  $26.63 \pm 3.93$  years; height:  $178.04 \pm 6.2$  cm; mass:  $87 \pm 12.4$  kg] tested for muscle activity during postural stability tasks, prior to (PRE) and after a simulated military type 16 kg rucksack carrying workload (POST) [3], in two AR670-1 complaint military footwear on separate days using a counterbalanced footwear assignment. [Boot #1: Belleville TR101 MiniMil ultra-light minimalist tactical military boot (MIN) (mass:  $500.13 \pm 24.1$

gm; sole surface area:  $235.4 \pm 8.2$  cm<sup>2</sup>; flexible boot shaft height: 20 cm; heel-midfoot drop: 2 mm); Boot #2: Belleville 310ST hot weather standard tactical boot (STD) (mass:  $801.13 \pm 40.4$  gm; sole surface area:  $288.6 \pm 24.1$  cm<sup>2</sup>; stiff boot shaft height: 20 cm; heel-midfoot drop: 18 mm)]. Electromyography (EMG) muscle activity from ankle plantar-flexor (PF): medial gastrocnemius and dorsi-flexor (DF): tibialis anterior were assessed using a Noraxon™ TeleMyo EMG system, during sensory organization test (SOT) [eyes open (EO), eyes closed (EC), EO sway referenced vision (EOSRV), EO sway referenced support (EOSRS), EC sway referenced support (ECSRS), EO sway referenced vision and support (EOSRVS)] and motor control test (MCT) [small, medium, large backward (BWS, BWM, BWL) & forward (FWS, FWM, FWL) support translations] on the Neurocom Equitest™ synced with triggered start-stop using a transistor-transistor logic (TTL) pulse. Mean muscle activity during SOT and MCT were calculated after filtering and rectifying the raw data and analyzed using a 2×2 footwear (MIN-STD) × time (PRE-POST) repeated measures ANOVA at an alpha level of 0.05 using SPSS.

## RESULTS AND DISCUSSION

On average, significantly greater muscle activity was required to maintain postural stability in the post workload condition and in STD. Results revealed significant time effect for PF during EO ( $p = 0.006$ ), EC ( $p = 0.016$ ) & EOSRV ( $p = 0.035$ ) conditions. Significant time effect was evident during BWM for DF ( $p = 0.026$ ) and during BWL for PF ( $p = 0.026$ ). Pairwise comparisons revealed significantly greater muscle activity from PF & DF in POST workload compared to PRE workload. Significant footwear × time interaction ( $p = 0.028$ ) was found during BWL for PF with simple effects revealing significantly greater muscle activity in POST workload in STD. The results from the study suggest that a simulated

physiological military type workload with a 16 kg rucksack and wearing the STD boot required greater muscular exertion to maintain postural stability with absent and/or conflicting sensory information in the SOT and during external perturbations in the MCT. Balance results from the SOT and MCT are reported elsewhere, with decreased postural stability in the post-workload condition and superior balance performance in the MIN compared to STD.

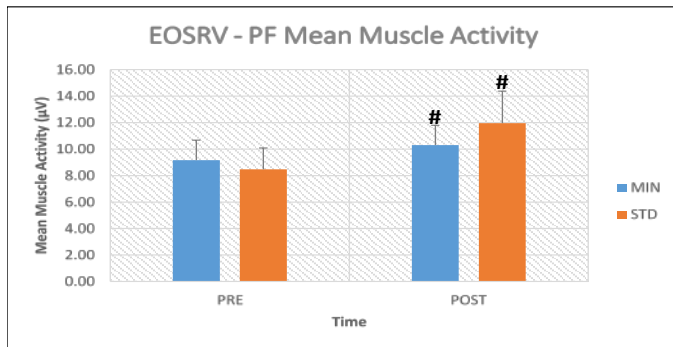


**Figure 1:** Plantar flexor (PF) during eyes open sway referenced vision (EOSRV) condition. # represents significant time difference & § represents significant footwear difference.

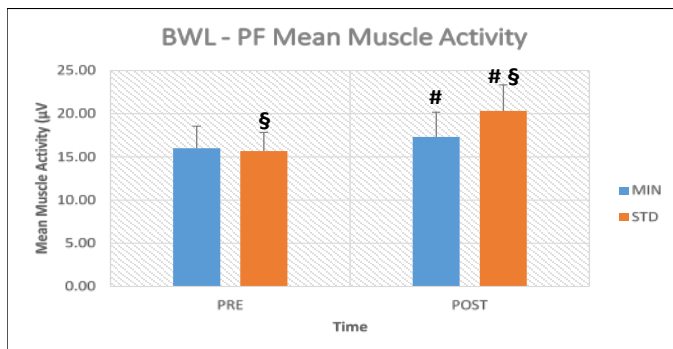


**Figure 2:** Plantar flexor (PF) during backward large perturbations (BWL) condition. # represents significant time difference & § represents significant footwear difference.

Muscular fatigue may impair the proprioceptive and kinesthetic properties of joints by increasing the threshold of muscle spindle discharge, disrupting afferent feedback and ultimately altering conscious joint awareness [4], thereby requiring a greater magnitude of muscle activation to maintain postural control. Results from this study support previous literature, as greater muscle activity was seen in during both SOT and MCT during the post workload conditions, suggesting the need for greater muscular exertion to maintain stability after the workload. Significant differences in EC and EOSRV can be attributed to the reduced activity of the proprioceptive system and the inability of the

postural muscles to produce and sustain a required muscular output [2,4] especially when the postural control system is relying more on proprioceptive system with absent or inaccurate afferent feedback.

Earlier studies have shown that footwear with heavier mass, increases energy expenditure [5] as well an increase in muscular fatigue [6]. The rate of oxygen uptake ( $VO_2$ ) increases by approximately 1% for every 100 gm of mass added to the footwear [5]. Moreover, a lower heel-to-toe drop or minimalist type of foot orientation with an absence of significant heel height, increases postural orientation by minimizing an anterior shift in the body's center of mass and a less severe tipping angle [7], thereby requiring less muscular activity to maintain erect stance. Wearing the STD boot, demonstrated greater muscle activity to maintain postural stability especially in the post workload condition during BWL perturbations. Muscle activity differences between the two military footwear can be attributed to the MIN boot being 300 gm less heavier than STD boot, and incorporating a minimalist sole design with a heel-to-toe drop of 2 mm, with a low heel height compared to the STD's 18 mm, thereby requiring less muscle activation and aiding in a superior performance in the MIN.

## CONCLUSION

Results from the study report a greater requirement of muscular exertion to maintain postural stability after a physiological workload especially in STD military boot. Findings will help offer footwear design suggestions to improve postural stability with minimal muscular exertion and also on work-rest intervals in the military to prevent overexertion induced postural instability.

## REFERENCES

1. Corbeil P et al. *Gait and posture* 18(2), 92-100, 2003.
2. Birrell SA et al. *Gait & posture*, 26(4), 611-614, 2007.
3. DeMaio M et al. *Human Performance Enhancement for NATO Military Operations*, 2009.
4. Gribble P et al. *Arch Phys Med Rehabil*; 85:589-92, 2004.
5. Franz JR et al. *Med Sci Sports Exerc*, 44(8), 1519-1525, 2012.
6. Garner JC et al. *Int. J. Ind. Ergonom*, 43(1), 77-81, 2013.
7. Menant J et al. *Arch Phys Med Rehabil*; 89, 1970-6, 2008.

## ACKNOWLEDGMENTS

This publication was supported by Grant #2T420H008436 from NIOSH. Its contents are solely the responsibility of the authors and do not necessarily represent the official views of NIOSH.

## LOWER EXTREMITY KINEMATICS IN MILITARY FOOTWEAR DURING SLIP EVENTS

<sup>1</sup> Sam Wilson, <sup>2</sup>Harish Chander, <sup>2</sup>Adam Knight, <sup>3</sup>John Garner, <sup>4</sup>Chip Wade, <sup>5</sup>Jacob Gdovin, <sup>1</sup>Christopher Hill,  
<sup>2</sup>Hunter DeBusk, <sup>1</sup>Lauren Luginsland, & <sup>2</sup>Daniel Carruth

<sup>1</sup> University of Mississippi, University, MS, USA; <sup>2</sup>Mississippi State University, Mississippi State, MS, USA;  
<sup>3</sup>Troy University, Troy, AL, USA; <sup>4</sup>Auburn University, Auburn, AL, USA;  
<sup>5</sup>Missouri State University, Springfield, MO, USA  
email: sjwilso2@olemiss.edu, web: hesrm.olemiss.edu

### INTRODUCTION

The term “military personnel” is a large umbrella term for all United States service members regardless of assigned duties. Military personnel jobs vary from infantry, medical personnel, mechanics, flight controllers, pilots and other personnel. Many of the military occupations consist of environments that are further inclusive in extrinsic factors such as diverse terrains, lack of light, increased decibel range, unstable ground surfaces and intrinsic factors such as fatiguing workloads including load carriage. Proper postural control and slip responses are essential in military settings in order to prevent falls. The US Army Annual Injury Epidemiology Report in 2008 found 18.4% of all causes of injuries were attributed to falls/near falls [1]. Slips, trips and falls (STFs) are a consequence of failure of normal locomotion and equilibrium recovery following an induced imbalance [2]. During a slip, there are correctional responses, such as increased knee flexion, and ankle plantar flexion. Footwear characteristics such as the boot shaft height, mass, mid-sole hardness and thickness, elevated heels and type of material of the footwear influence balance and gait and ultimately the slip propensity. Intrinsic factors such as decrements of the postural control systems can contribute to falls. Dysfunction in the visual, vestibular, somatosensory or the musculoskeletal system and any undue muscular fatigue due to excessive workload in the military environment can potentially lead to falls. Thus, the purpose of this study was to examine kinematics of the lower extremity during slip events while wearing military footwear before and after a simulated military workload.

### METHODS

A total of eighteen healthy male adults (Height:  $178.04 \pm 6.2$  cm, Mass:  $87 \pm 12.4$  kg; Age range: 18-35 years) with no history of any musculoskeletal, neurological, cardiovascular or vestibular disorders were recruited for the study. An 8 camera Vicon Nexus (Oxford, UK) 3D motion capture system was used to collect and analyze kinematic gait data. A lower body plug-in gait model from the Helen-Hayes marker system was used for the participant configuration and the kinematic data was sampled at 100 Hz and collected using the Vicon Nexus software. A back-pack type fall arrest system with a movable trolley was used to prevent any undesired falls. Glycerol mixed with water in the ratio of 75% glycerol and 25% water was used as the slippery agent [3]. During the slip trials, glycerol was applied and evenly distributed on a force plate for contact of the leading left leg. Participants were tested using a repeated measures design on two days separated by a minimum of a 72 hours. The footwear used in the study were the Belleville TR101 MiniMil Ultra-Light Minimalist Tactical Military Boot (MIN) and the Belleville 310ST Hot Weather Standard Tactical Boot (STD). Both of these boots comply with the US Army standards for footwear design under regulation AR670-1. Each testing session began with an initial warm up protocol of 10 minutes consisting of body weight squats, high-knees, jogs, gait swings and exaggerated lunges. Participants were strapped to a harness and performed multiple gait trials until normal self-selected pace walking with appropriate foot positioning onto the force plate was achieved. Participants turned away and listened to music on noise cancellation head phones for about 1 minute between each of these normal gait trials. One trial was then chosen to be the unexpected slip (US) and

the contaminant was applied. With the completion of the US and cleaning the floor and footwear, participants performed a similar protocol for the expected slip (ES) with instructions of “will be slippery”. The simulated physiological workload consisting of walking on the treadmill donning the boots and a 16kg weighted back pack. The walking protocol [4] consisted of 3 minute increment periods starting at 3mph at 0% grade, and increasing to 3.5mph and 4mph at 0% grade until minute 9, following which the grade was increased by 5% every three minutes until minute 18. After the load carrying protocol, participants then completed the same set of slip assessments consisting of another set of US and ES as a post-workload measure. A 2 x 2 x 3 (footwear x time x gait trial) repeated measures ANOVA was conducted for ankle, knee, and hip angles at heel strike and 120 ms post heel strike. If main effect significance was observed, post hoc testing was performed using a Bonferroni correction factor. Analyses were performed in SPSS version 24, with an a priori alpha level of 0.05.

## RESULTS AND DISCUSSION

The results revealed footwear main effect significance for the ankle angle at heel strike ( $F(1,17) = 6.546, p = 0.020$ ). Post hoc comparisons suggest an increased dorsiflexion angle at heel strike for the standard boot. A gait main effect was also observed for the ankle angle at heel strike ( $F(2,34) = 19.514, p < 0.0005$ ). For the gait effects, an increased plantarflexion angle was observed between the US, the ES, and the NG trials. For the ankle angle at 120 ms post heel strike, there was a significant gait effect ( $F(2,34) = 3.362, p = 0.047$ ). Comparisons revealed an increased plantarflexion angle in the NG condition compared to the US condition. For the knee angle at heel strike, significant footwear effects ( $F(1,17) = 5.661, p = 0.029$ ) and gait effects ( $F(2,34) = 9.750, p < 0.0005$ ). Footwear comparisons showed increased knee flexion for the standard boot compared to the minimalist. While the gait effect showed greater knee extension angles in the NG condition compared to both the US and ES trials. Slip parameters are reported elsewhere, and revealed increased slip responses in the standard boot compared to the minimalist. The current findings

corroborate those results, and further suggest altered kinematics at the ankle and knee in response to a slip. Specifically, the increased knee flexion in the standard boot could represent a reactionary response to the slip that attempts to lower the base of support, and thus, recover balance [5]. In addition, different gait kinematics could lead to this increased slip propensity, explained by the increased dorsiflexion at heel strike, which may provide a smaller base of support, and decreased dynamic balance.

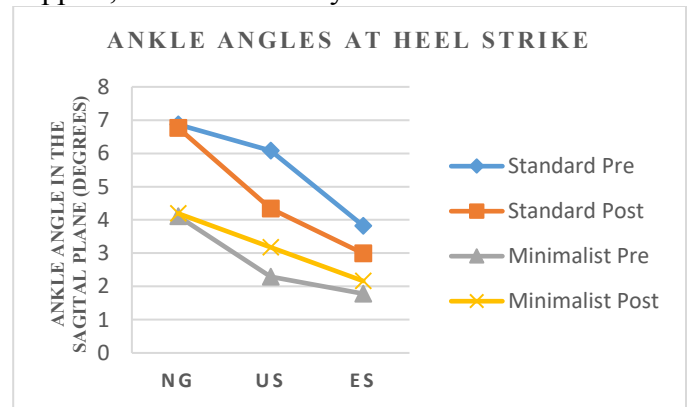


**Figure 1:** Ankle angles at heel strike for the standard and minimalist boot, before and after workload.

## CONCLUSIONS

We observed potential slip response kinematics in the lower extremities dependent on footwear and knowledge of slip. These findings suggest that the minimalist boot may be more appropriate when military personnel could experience unexpected slippery conditions.

## REFERENCES

1. United States Army Medical Department. United States Army Public Health Command. (2008).
2. Gauchard, G., Chau, N., Mur, J. M., & Perrin, P. (2001). Falls and working individuals: role of extrinsic and intrinsic factors. *Ergonomics*, 44(14), 1330-1339.
3. Chander, H., Garner, J. C., & Wade, C. (2015). Heel Contact Dynamics in Alternative Footwear during Slip Events. *International Journal of Industrial Ergonomics*, 48, 158-166.
4. DeMaio, M., Onate, J., Swain, D., Morrison, S., Ringleb, S., & Naiak, D. (2009). Physical performance decrements in military personnel wearing personal protective equipment (PPE). *Human Performance Enhancement for NATO Military Operations*.
5. Lockhart, T. E., & Kim, S. (2006). Relationship between hamstring activation rate and heel contact velocity: factors influencing age-related slip-induced falls. *Gait & posture*, 24(1), 23-34.

## ACKNOWLEDGMENTS

*"This grant report was supported by Grant #2T420H008436 from NIOSH. Its contents are solely the responsibility of the authors and do not necessarily represent the official views of NIOSH"*

# THE EFFECTS OF A CARBON FIBER SHOE INSERT ON SPEED AND POWER IN COLLEGIATE ATHLETES

Robert Gregory, Robert Axtell, Marc Robertson, and William Lunn

Southern Connecticut State University, New Haven, CT, USA

E-mail: [gregoryr3@southernct.edu](mailto:gregoryr3@southernct.edu), Web: <http://www.southernct.edu/running-clinic/>

## INTRODUCTION

Athletes often select equipment, such as running shoes, that is designed to maximize energy storage and return. However, athletic footwear is typically characterized by poor energy storage and return (~1-2%) as a result of current technological limitations in the design of and material properties used in shoe midsole construction [1, 2]. As a result, most of the energy that is stored in a shoe midsole when the foot contacts the ground is lost through heat, friction, and vibrations and, thus, decreases the efficiency of the athlete.

There is limited research to date that has addressed the role of orthotics/shoe insoles on performance improvement. Increasing the stiffness of shoes (via the use of carbon fiber plates inserted into the shoe midsole or under the shoe sock liner) has resulted in a 1.7 cm increase in vertical jump height [3], a 0.7% improvement in sprint performance [4], and a 1% improvement in running economy [5]. While all three of these studies demonstrated improvements in performance when using footwear enhanced with carbon fiber plates, these studies used a flat carbon fiber plate design with a uniform stiffness distribution and limited optimization for the athletes.

The purpose of this study was to examine the effects of a carbon fiber shoe insert on athletic performance. The specific parameters related to athletic performance that were assessed in this study were speed and power. It was hypothesized that the use of a carbon fiber shoe insert will result in improved linear speed (assessed by a 40-yd sprint) and lower-body muscular power (assessed by a vertical jump) through increases in peak ground reaction force (GRF), rate of force development (RFD), and peak power (P).

## METHODS

Twenty-eight male collegiate athletes (NCAA Division II American football skill-position players; age:  $19.4 \pm 1.1$  yr, height:  $178.7 \pm 4.5$  cm, mass  $85.9 \pm 6.9$  kg) participated in this study. Participants provided informed consent according to the policies and procedures of the Institutional Review Board at Southern Connecticut State University.

The participants performed vertical jump and 40-yard sprint tests while using a control shoe insert and carbon fiber shoe inserts (VK Performance Insoles; VKTRY Gear; Milford, CT). The vertical jump was performed on the first day and the 40-yd sprint took place seven days later. Participants used three different stiffness (medium, stiff, and extra stiff) and two different stiffness (medium and extra stiff) carbon fiber shoe inserts during the vertical jump and 40-yd sprint tests, respectively. The shoe insert conditions were presented in random order for both tests; all vertical jump trials (three for each shoe insert) and sprint trials (two for each shoe insert) were separated by a period of 2 min and 5 min, respectively, to minimize the effects of fatigue.

Vertical jump height was determined from takeoff velocity using a force platform (QuattroJump; Kistler Instrument Corp.; Winterthur, SUI), while sprint times (0-10 yd split time and 40-yd total time) were determined using a laser timing system (Power Dash 3x; Zybek Sports; Broomfield, CO). Peak GRF, RFD, and peak P were measured during the vertical jump takeoff via the use of a single force platform and during the sprint start via the use of two force platforms (Type 9260AA; Kistler Instrument Corp.; Winterthur, SUI). A repeated-measures MANOVA was used to compare changes in performance across the shoe insert conditions; the level of significance was set at  $p < 0.10$ .

## RESULTS AND DISCUSSION

The use of a carbon fiber shoe insert resulted in increased vertical jump height. There was no difference in vertical jump height across the four different shoe insert conditions. However, when comparing the control shoe insert versus the optimal stiffness carbon fiber shoe insert for each individual participant, there was a significant ( $p < 0.0005$ ) increase in vertical jump height from  $62.8 \pm 9.4$  cm to  $65.4 \pm 13.0$  cm (a 4.1% increase).

The use of a carbon fiber shoe insert also resulted in improved 0-10 yd split time during a 40-yd sprint. There was no difference in 0-10 yd split time across the three different shoe insert conditions. However, when comparing the control shoe insert versus the optimal stiffness carbon fiber shoe insert for each individual participant, there was a significant ( $p < 0.05$ ) improvement in 0-10 yd split time from  $1.72 \pm 0.07$  s to  $1.69 \pm 0.06$  s (a 1.6% decrease). Even though there was an improvement in 40-yd total time from  $5.06 \pm 0.12$  s to  $5.05 \pm 0.12$  s when comparing the control shoe insert versus the optimal stiffness carbon fiber shoe insert for each individual participant, this difference was not statistically significant ( $p = 0.26$ ).

The increases in performance in both the vertical jump and 40-yd sprint tests were associated with improvements in the movement kinetics of both tasks. The use of the optimal stiffness carbon fiber shoe insert resulted in significant increases in propulsive (vertical) peak GRF ( $p < 0.05$ ), RFD ( $p < 0.005$ ), and peak P ( $p < 0.005$ ) during the vertical jump takeoff (see Table 1). The use of the optimal stiffness carbon fiber shoe insert resulted in significant increases in propulsive (horizontal) peak

GRF for the rear foot ( $p < 0.05$ ), RFD for both the front foot and the rear foot ( $p < 0.05$  and  $p < 0.10$ , respectively), and peak P ( $p < 0.10$ ) during the start of the 40-yd sprint (see Table 1).

The use of a carbon fiber shoe insert did not appear to increase the amount of energy stored and returned during the propulsive phase of the vertical jump takeoff and sprint start. Instead, a carbon fiber shoe insert reduced the amount of energy lost at the metatarsophalangeal joint and resulted in a corresponding improvement in performance in both the vertical jump height and 10-yd sprint time.

## CONCLUSIONS

Increasing footwear bending stiffness through the use of a carbon fiber shoe insert improved both vertical jump and sprint performance. The optimal stiffness was subject-specific. To experience benefits in performance improvement, an athlete must choose the correct stiffness carbon fiber shoe insert that matches his/her body weight and movement biomechanics.

## REFERENCES

1. Nigg BM, et al. *Biomechanics and Biology of Movement*, Human Kinetics, 2000.
2. Nigg BM. *Biomechanics of Sport Shoes*, Benno M. Nigg, 2010.
3. Stefanyshyn DJ, Nigg BM. *Med Sci Sports Exerc* **32**, 471-476, 2000.
4. Stefanyshyn D, Fusco C. *Sports Biomech* **3**, 55-66, 2004.
5. Roy JPR, Stefanyshyn DJ. *Med Sci Sports Exerc* **38**, 562-569 2006.

**Table 1:** A kinetic comparison of the control and optimal stiffness carbon fiber shoe inserts during the vertical jump and 40-yd sprint tests (FF = sprint start/front foot, RF = sprint start/rear foot).

Kinetic Variables	Vertical Jump		40-Yd Sprint	
	Control	Carbon Fiber	Control	Carbon Fiber
Peak GRF (BW)	$3.12 \pm 0.34$	$3.20 \pm 0.40$	$1.03 \pm 0.09$ (FF) $0.76 \pm 0.19$ (RF)	$1.05 \pm 0.13$ (FF) $0.82 \pm 0.15$ (RF)
RFD (BW/s)	$23.6 \pm 4.5$	$25.4 \pm 5.7$	$11.1 \pm 4.2$ (FF) $12.2 \pm 3.6$ (RF)	$12.1 \pm 3.8$ (FF) $13.1 \pm 4.4$ (RF)
Peak P (W/kg)	$85.7 \pm 12.1$	$89.6 \pm 14.8$	$25.1 \pm 10.4$	$27.2 \pm 11.3$

# LOWER EXTREMITY STIFFNESS WHEN RUNNING IN MINIMALIST, NEUTRAL, AND ULTRA-CUSHIONING SHOES

<sup>1</sup> Brianne Borgia, <sup>2</sup> James Becker

<sup>1</sup> California State University, Long Beach, Long Beach, CA USA

<sup>2</sup> Montana State University, Bozeman, MT, USA

email: james.becker4@montana.edu

## INTRODUCTION

The effect of footwear on running mechanics has been a major topic of investigation over the last forty years as changing footwear may impact running performance or alter risk of sustaining a running related injury. Within the last ten years in particular, there has been a substantial amount of research on possible merits and risks associated with using minimalist shoes [1, 2]. At the opposite end of the spectrum, the last five years have seen rising popularity in ultra-cushioning shoes. However, to date there have only been a handful of studies examining these shoes. These studies have reported basic kinematic and kinetic comparisons between minimalist and ultra-cushioning shoes [3], as well as differences in internal loading between the shoe types [4].

One area which has not yet been examined is whether lower extremity stiffness differs when running in minimalist or ultra-cushioning shoes. Stiffness plays a role in both injury and performance, and provides insight into how the neuromuscular system controls movement [5]. As such, understanding how stiffness changes with footwear would provide additional insight into the biomechanical effects of different types of running shoes. Therefore, the purpose of this study was to evaluate changes in lower extremity stiffness when running in minimalist (MIN), traditional (NEUT), and ultra-cushioning (ULTRA) shoes.

## METHODS

Fifteen recreational runners (age:  $23.5 \pm 2.2$  years; height:  $1.68 \pm 0.19$  m.; body mass:  $76.5 \pm 4.5$  kg) participated in this study. All participants were running at least 20 miles per week and were injury

free in the 6 months preceding testing. Participants were provided 3 pairs of laboratory shoes in their self-reported size (MIN shoe: New Balance 1400v3, NEUT shoe: Nike Air Zoom Pegasus 32, ULTRA shoe: Hoka One One Bondi 4, Figure 1).



**Figure 1.** Examples of the three shoes used in the study. Left to right: MIN, NEUT, and ULTRA.

Running kinematics were recorded using a 12-camera motion capture system (Qualisys, Inc., Gothenburg, Sweden) while participants ran on an instrumented treadmill (Bertec Corp, Columbus, OH) at 3.0 m/s. Kinematics and ground reaction forces were sampled at 200 and 1000 Hz, respectively. Participants ran for 10 minutes in each shoe, with data being collected during the last minute. Ten consecutive strides were then extracted for analysis. The order in which participants wore the shoes was randomized.

Raw marker trajectories and ground reaction forces were exported to a custom Matlab (Mathworks, Natick, MA) program where they were filtered using 4<sup>th</sup> order, zero lag, low pass Butterworth filters with cutoff frequencies of 8 Hz and 50 Hz, respectively. Sagittal plane joint angles and moments at the ankle, knee, and hip were then calculated using Cardan angle rotations and standard inverse dynamics techniques. Leg stiffness was calculated using a spring mass model and the methods of McMahon and Cheng [6]. Joint stiffness was calculated by dividing the change in joint moment by the change in joint angle over the absorption portion of stance phase, operationally defined as the time from initial contact until the

ankle reached peak dorsiflexion [5]. To assess whether participants changed their foot strike pattern when changing shoes the strike index was calculated for each step.

One-way repeated measure ANOVAs were used to evaluate differences in strike indices, legs stiffness, and joint stiffness between shoe conditions. When a significant main effect was observed, post hoc comparisons were performed using a Bonferroni correction. A  $p < .05$  was used for all comparisons.

## RESULTS AND DISCUSSION

Strike indices were not different between the MIN ( $24.1 \pm 15.8$ ) and NEUT ( $20.9 \pm 13.6$ ,  $p = .565$ ) shoes. However they were smaller in the ULTRA shoe ( $12.1 \pm 7.5$ ) than in either the MIN or NEUT shoes ( $p = .017$ ,  $p = .033$ , respectively). Though not indicative of a different foot strike pattern, this means that there was a more pronounced heel strike in the ULTRA shoes and that the initial contact point in this condition was closer to the ankle joint center thereby reducing the ankles' ability to absorb energy during the loading phase.

There were no differences in leg stiffness between the three shoe conditions (MIN:  $12.0 \pm 2.0$  kN/m, NEUT:  $12.3 \pm 1.9$  kN/m, ULTRA:  $12.2 \pm 2.3$  kN/m,  $p = .586$ ). Compared to the MIN shoe, the ULTRA shoe resulted in lower joint stiffness at the hip ( $p = .006$ ) and knee ( $p = .047$ ) and higher joint stiffness at the ankle ( $p = .026$ ). There were no differences between the MIN and NEUT shoe at any of the joints (Table 1).

**Table 1.** Mean and standard deviations for hip, knee, and ankle stiffness (N\*m/°) in the minimalist, neutral, and ultra-cushioning shoes. \* indicates significantly different than MIN condition.

	Hip	Knee	Ankle
MIN	$5.1 \pm 2.7$	$6.0 \pm 2.2$	$12.3 \pm 1.2$
NEUT	$4.3 \pm 0.9$	$5.9 \pm 1.7$	$13.0 \pm 1.8$
ULTRA	$3.7 \pm 0.9^*$	$5.3 \pm 1.4^*$	$14.8 \pm 2.4^*$

Our results suggest that while overall leg stiffness remains the same when changing shoe types, the

strategies used by the neuromuscular system to achieve that stiffness varies. The more pronounced heel strike and higher ankle joint stiffness observed in the MIN condition means the ankle is not being used to absorb energy in MIN shoes. This may be one reason why previous studies have reported greater tibial shock [7] and reduced shock attenuation [8] in ULTRA shoes compared to MIN shoes. If the ankle is not helping absorb energy then the other joints must become more compliant, hence the lower joint stiffness in the knee and hip in the ULTRA shoe. However, a more compliant joint will absorb more energy. Whether this is good or bad from an injury perspective remains unknown. But one of the few other studies on maximalist footwear reported higher patellofemoral forces and pressures in ULTRA shoes compared to MIN shoes [4]. Given that the knee is the most common injury site in runners this suggests further studies on injuries associated with ULTRA shoes are needed.

## CONCLUSIONS

These results suggest that compared to MIN and NEUT shoes, running in ULTRA shoes results in re-organization of how the neuromuscular system controls lower extremity stiffness. Implications for this re-organization for injury and performance require further investigation.

## REFERENCES

1. Davis, I. *J. Orthop. Sports. Phys. Ther.* **44**, 775-785, 2014.
2. Perken, K., et al. *Sports Health.* **6**, 475-480, 2014.
3. Sinclair, J., et al. *Footwear Science.* **8**, 33-39, 2016.
4. Sinclair, J. et al. *J. Applied. Biomech.* **32**, 359-364, 2016.
5. Hamill et al., *Europe J. Sport Science,* **14**, 130-136, 2014.
6. McMahon, T., et al. *J. Biomech.* **23**, 65-78, 1990.
7. Ruder, M., et al. *Proceedings of ASB Columbus,* OH, 2015.
8. Sinclair, J., et al. *Movement & Sport. Sci.* **95**, 59-64, 2017.

# PLANTAR PRESSURE CHANGES WITH USE OF A CUSTOM DYNAMIC ANKLE-FOOT ORTHOSIS

Julianne Stewart, Tatiana Djafar, Richard Miltenberger, and Marilyn Wyatt  
Naval Medical Center San Diego, San Diego, CA, USA  
E-mail: julianne.m.stewart.ctr@mail.mil

## INTRODUCTION

Of the combat injuries sustained in the current and recent U.S. military conflicts, injuries involving the extremities comprise the largest category. Limb preservation procedures have become a much more common alternative to amputation after critical limb trauma, but high levels of disability have been reported with both lower limb amputation and lower limb (LL) preservation [1, 2].

The Intrepid Dynamic Exoskeletal Orthosis (IDEO®) is a custom dynamic ankle-foot orthosis developed for use in military service members with critical LL injuries [3]. The IDEO was designed as a high-level functional brace that is thought to transfer loading from the foot to the anterior proximal tibia via deformation of the carbon fiber struts and custom molded tibial cuff that occurs during mid to terminal stance [4]. A proposed mechanism for pain reduction seen with the IDEO is decreased loading or pressure experienced during weight bearing. However, until this study, no actual plantar pressure data had confirmed this unloading during walking gait and this proposed mechanism has not been examined. Additionally, the effects of the brace itself prior to training in use are unknown.

The aim of this study was to evaluate the effect of an IDEO on peak plantar pressure in the total foot as well as in each of eight areas of the foot in a sample with foot and/or ankle injury.

## METHODS

Forty-two participants (40 males) were identified via retrospective review of a clinical registry of patients at Naval Medical Center San Diego. Patients were  $29.7 \pm 8.1$  years old, had unilateral LL injury causing significant deficits to gait and function, were prescribed an IDEO by an orthopedic physician, and were able to walk on level surfaces for at least 15 minutes in each shod and IDEO

conditions. Patients were excluded if they had bilateral LL injury, spine or pelvis injury, or central neurological disorder. For each patient, data collection was performed prior to initiating training in use of the IDEO.

After consenting, each patient was fit with an appropriately-sized pair of novel pedar-x® (novel, Inc., Munich, Germany) pressure-sensitive insoles. For the shod condition, the insoles were placed in the patient's shoes directly underneath his or her feet. For the IDEO condition, the insole on the affected side was placed between the patient's foot and the IDEO footplate. For each condition, the patient walked for two 35-meter trials at a self-selected velocity while plantar pressure data were collected at 50 Hz and transmitted wirelessly to the data collection computer. These trials were performed in a flat, linear hallway without turns or obstacles.

The foot was divided into eight sections for analysis: medial and lateral sections of the hindfoot, midfoot, and forefoot, and greater and lesser toes. A two-way ANOVA with foot (affected and unaffected) and condition (shod and IDEO) as factors was performed for the total foot and for each section. A significance value of  $p < 0.05$  was chosen. Post-hoc t-tests were performed and a Bonferroni correction was applied.

## RESULTS AND DISCUSSION

Peak pressures were significantly decreased in the affected foot with use of the IDEO with up to 64% decreases seen at the forefoot and toes (Fig. 1). Increases in peak pressure of up to 19% were seen in some regions of the unaffected foot as well as the total foot (Table 1).

An interaction effect between foot and condition was found for the total foot and for each of the eight sections of the foot with exception of the medial

midfoot. Additionally, an effect of foot was found for the total foot and all sections of the foot except the lateral midfoot. These findings help provide insight into the mechanism behind the improvement in function and decrease in pain that has been seen with use of the IDEO [5].

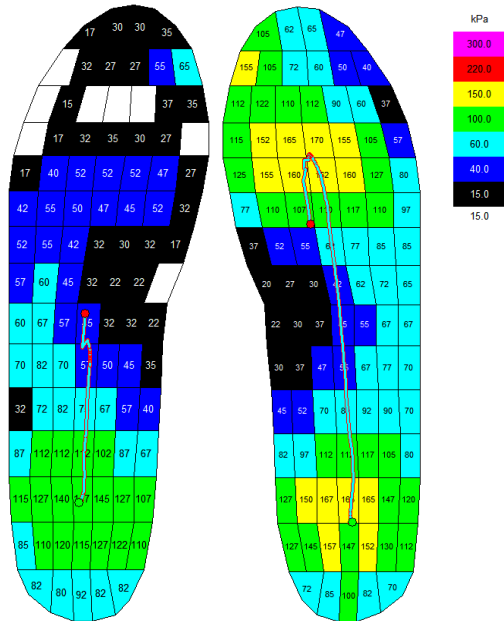


**Figure 1:** Group averaged peak plantar pressures with IDEO affected foot on left and shod unaffected on right.

The slight increases in plantar pressure seen in the unaffected foot with use of the IDEO may be due to increased gait velocity. Velocity during testing was self-selected and was not measured. However, velocity in this patient group during an instrumented gait study performed on the same day was significantly higher ( $p < 0.001$ ) with the IDEO ( $1.19 \pm 0.17$  m/s shod vs.  $1.26 \pm 0.14$  m/s IDEO). Alternately, overloading of the sound limb may be occurring due to unfamiliarity with the IDEO.

## CONCLUSIONS

**Table 1:** Peak pressure mean values  $\pm$  standard deviations in kPa in the total foot and selected foot masks in the affected foot (AF) and unaffected foot (UF) for each shod and IDEO conditions. Cell shading indicates statistically significant difference between shod and IDEO conditions ( $p < 0.0028$ ).

	Total Foot		Med. Hindfoot		Lat. Hindfoot		Med. Forefoot		Lat. Forefoot		Great Toe		Lesser Toes	
	AF	UF	AF	UF	AF	UF	AF	UF	AF	UF	AF	UF	AF	UF
Shod	230.0	258.3	179.2	195.9	175.9	190.0	185.6	226.1	187.1	210.5	165.8	223.0	160.9	202.6
	$\pm$ 47.5	$\pm$ 45.1	$\pm$ 46.6	$\pm$ 40.7	$\pm$ 45.9	$\pm$ 39.7	$\pm$ 58.1	$\pm$ 53.2	$\pm$ 59.2	$\pm$ 51.5	$\pm$ 70.7	$\pm$ 55.5	$\pm$ 69.0	$\pm$ 57.7
	169.3	294.2	157.6	233.5	157.4	235.1	71.1	254.2	67.8	219.4	89.2	245.6	59.3	204.3
IDEO	$\pm$ 36.4	$\pm$ 3.3	$\pm$ 37.9	$\pm$ 60.2	$\pm$ 37.2	$\pm$ 58.4	$\pm$ 40.5	$\pm$ 63.0	$\pm$ 28.5	$\pm$ 50.7	$\pm$ 43.0	$\pm$ 54.8	$\pm$ 21.9	$\pm$ 59.4

Despite a growing body of evidence for functional improvements with use of the IDEO, this is the first study to confirm that this brace can decrease peak plantar pressure, particularly in the forefoot and toes of the affected foot, during walking. This outcome provides insight to clinicians seeking a device to improve painful gait, particularly for conditions of the foot or ankle that produce pain in weight-bearing. Additionally, though the IDEO was designed to enable performance of high-level activities in population with critical limb injury, this study provides support for using the IDEO for walking by those with a diverse collection of injuries.

## REFERENCES

1. MacKenzie EJ, et al. *JAAOS* **14(10)**, S205-S210, 2006.
2. Doukas WC, et al. *J Bone Joint Surg Am* **95(2)**, 138-145, 2013.
3. Owens JG, et al. *J Trauma* **71**, S120-S124, 2011.
4. Patzkowski JC, et al. *J Surg Orthop Adv* **20(1)**, 8-18, 2011.
5. Patzkowski JC, et al. *J Bone Joint Surg Am* **94A(6)**, 507-515, 2012.

## ACKNOWLEDGMENTS

The authors thank Trevor Kingsbury, Katherine Sharp, Jenny Anne Maun, Kimberly Rowe, John David Collins, and Keith Qualls for help with data collection and fabrication of the IDEO. This work was supported with resources provided by EACE.

## DISCLOSURE STATEMENT

The views expressed herein are those of the author(s) and do not necessarily reflect the official policy or position of the Department of the Navy, Department of Defense, or the United States Government.

# SEGMENTAL TURNING VELOCITY AND COORDINATION IN ADULTS WITH MTBI

<sup>1,2</sup> Peter C. Fino, <sup>1</sup> Lucy Parrington, <sup>1,2</sup> Merissa Walls, <sup>1,2</sup> Emily Sippel, and <sup>1,2</sup> Laurie A. King

<sup>1</sup> Oregon Health & Science University, Portland, OR, USA

<sup>2</sup> Veterans Affairs Portland Health Care System, Portland, OR, USA

email: fino@ohsu.edu

## INTRODUCTION

Abnormal standing balance and straight gait have been widely documented in individuals following mild traumatic brain injury (mTBI) [1]. Yet, daily activities require complex movements that involve change of direction and coordinated head and trunk reorientation [2]. Sport-related concussion has been associated with increased intersegmental coordination variability during unplanned turns [2] and decreased center-of-mass speed and curvature when walking around an obstacle [3], but planned turning tasks have not been well explored in populations with mTBI. In particular, it is unclear whether turning performance is associated with self-reported symptoms in individuals with mTBI. As rapid head movements can exacerbate symptoms, individuals reporting mTBI symptoms may limit the velocity of reorientation based on their symptoms. We hypothesized that individuals with mTBI would reduce their reorientation velocity and increase the variability of head-to-trunk coordination during planned turns compared with controls. Further, we hypothesized that the reduction in the velocity and increase in variability would be associated with their self-reported symptom score.

## METHODS

Ten individuals with mTBI {mean (SD) age = 34 (6.7) years, height = 171.8 (8.4) cm, mass = 90.7 (19.9) kg} and 25 healthy controls {age = 28 (8.4) years, height = 169.3 (8.46) cm, mass = 70.3 (13.9) kg} provided informed written consent to participate. All mTBI participants had self-reported complaints of imbalance and a diagnosed mTBI >3 months before the testing session. At the beginning of each session, participants completed the Neurobehavioral Symptom Inventory (NSI). Participants then walked at their comfortable pace around a marked course containing four 45° turns, four 90° turns, and two

135° turns (Figure 1). Each participant completed 12 continuous laps of the course. The first and last laps were excluded from the analysis. Walking speed was determined from the average time to complete each lap. Inertial sensors affixed over the forehead and lumbar region of the spine collected angular velocities of the head and trunk, respectively.

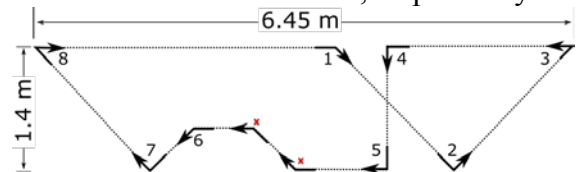


**Figure 1:** Turning course marked with arrows. Eight turns were analyzed, 2 turns (red x) were excluded.

Angular velocities were low-pass filtered at 1.5 Hz. For each turn, the magnitude and time of each peak axial angular velocity was extracted for the head and trunk. Two 45° turns were excluded from the analysis because a clearly defined peak velocity was lacking across all participants. Head-to-trunk coordination was defined as the lag time, calculated as the difference in time between peak velocities of head and trunk for each turn (Figure 2).

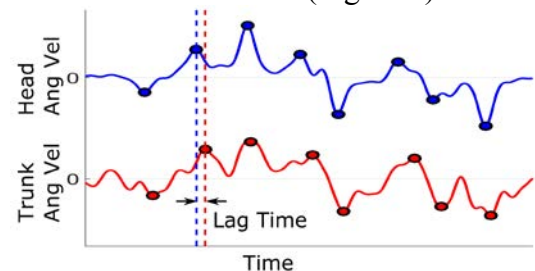


**Figure 2:** Example angular velocity traces showing the peak for each turn (markers) and lag time.

For each participant, the peak angular velocities were averaged across turns of the same angle. Lag time and lag time variability were determined from the mean and standard deviation, respectively, across all turns. Linear mixed models compared the average peak angular velocities between groups after adjusting for covariates of age, height, mass, walking

speed, and turning angle. Independent sample t-tests compared lag time and lag time variability between groups. Pearson correlation coefficients compared the relationship between each outcome and NSI symptom scores within the mTBI group.

## RESULTS AND DISCUSSION

After adjusting for covariates of age, height, weight, walking speed, and turning angle, participants with mTBI had significantly slower peak angular velocities of the head (Figure 3,  $p < 0.01$ ,  $\beta = -0.30$ ,  $SE = 0.11$ ) and trunk ( $p < 0.01$ ,  $\beta = -0.31$ ,  $SE = 0.11$ ) compared with the control group. Lag time did not differ between groups, but lag time variability was significantly higher in the mTBI group compared with the control group ( $p < 0.01$ ,  $g = 0.58$ ).

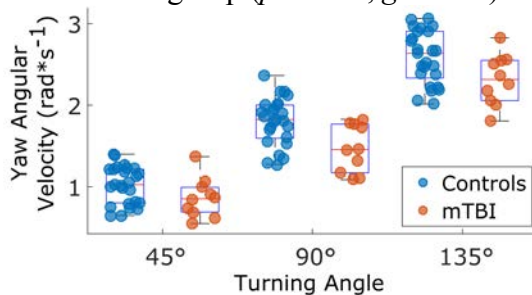


**Figure 3:** Average peak yaw angular velocity of the head for each participant for each turn angle.

Within the mTBI group, NSI total symptom scores were associated with slower average peak angular velocities of the head and trunk during 90° turns ( $r = -0.77$ ,  $p < 0.01$ ;  $r = -0.71$ ,  $p = 0.02$ ). Lag time variability was strongly associated with NSI symptom scores (Figure 4,  $r = 0.87$ ,  $p < 0.01$ ).

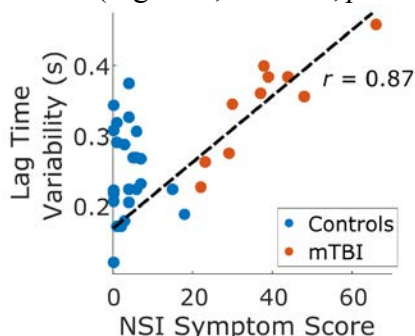


**Figure 4:** Lag time variability was associated with NSI total symptom score in the mTBI group.

The slower peak velocities found in the mTBI group are consistent with previous reports of slower center-of-mass velocities in asymptomatic concussed

athletes during a 90° turn [3]. Notably, the slower angular velocities were significant after adjusting for walking speed, suggesting that the mTBI group may have cut corners to reduce the curvature [3] and angular velocity of each turn. Additionally, our results extend the evidence of increased segmental variability, previously reported during a light-induced turning task [2], to preplanned turns.

Importantly, measures of turning were associated with symptom scores. Standing balance and straight gait deficits are common after mTBI, but they have not been associated with symptom scores [4]. The association between higher symptom scores and measures of turning may be indicative of active avoidance of rapid rotations to prevent exacerbating symptoms. Alternatively, it could suggest symptoms are more apparent during specific dynamic activities such as turning, and such activities may heavily influence the self-reported symptom score given the high prevalence of turning in everyday locomotion. Further study of turning in symptomatic and asymptomatic individuals with mTBI is warranted.

## CONCLUSIONS

Individuals with mTBI adopted slower turning velocities across all turning angles, and exhibited more variable head-to-trunk coordination compared with controls. These results provide knowledge of how self-reported symptoms influence daily locomotor function in adults with mTBI. The association of turning velocity and head-to-trunk coordination variability to self-reported symptoms suggests individuals with mTBI change reorientation patterns to minimize the exacerbation of symptoms.

## REFERENCES

1. Guskiewicz KM, *Clin Sports Med*, **30.1**, 89-102, 2011
2. Powers KC, et al. *Gait Posture*, **39.2**, 728-32, 2014.
3. Fino PC, et al. *J Neuroeng Rehabil*, **13.65**, 1-15.
4. Guskiewicz KM, et al. *J Athl Train*, **36.3**, 263-73, 2001

## ACKNOWLEDGMENTS

Funding was provided by the US Department of Defense (W81XWH-15-1-0620).

# INDIVIDUALS WITH A PRIOR TRAUMATIC BRAIN INJURY EXHIBIT DECREASED NEUROMUSCULAR COMPLEXITY DURING GAIT

<sup>1</sup> Samuel A Acuña, <sup>1</sup> Mitchell E Tyler, <sup>1</sup> Yuri P Danilov, and <sup>1</sup> Darryl G Thelen

<sup>1</sup> The University of Wisconsin–Madison, Madison, WI, USA  
email: saacuna@wisc.edu, web: <http://uwnmbl.engr.wisc.edu>

## INTRODUCTION

Gait and balance disorders are common among individuals who have experienced a traumatic brain injury (TBI). Prior studies have shown that TBI subjects tend to walk slower, take smaller steps, have increased mediolateral sway, and exhibit lower scores on the Dynamic Gait Index [1, 2]. Traditional rehabilitation protocols provide little improvement after the first few months post-injury, leaving many individuals with chronic balance impairments [3]. Interventions that target specific neuromuscular deficits may enhance recovery, but surprisingly little is known about how neuromuscular control of gait is altered following a TBI.

Synergy analyses have gained popularity as an approach for evaluating the complexity of neuromuscular control patterns in neurologically impaired populations. The analysis typically involves the use of matrix factorization algorithms to identify low-dimensional patterns, or synergies, that can describe the variability inherent in an individual's measured muscle activations. A synergy then represents a group of muscles that are generally co-activated, which may represent simplified control. Hence, the variance in muscle activity accounted for by a given number of synergies can provide a measure of the complexity of control used by an individual. Previous studies have shown that neuromuscular complexity, as measured by muscle synergies, is reduced after stroke, Parkinson's disease, spinal cord injury, and cerebral palsy [4, 5]. The goal of this research was to evaluate how the neuromuscular complexity of gait in persons with chronic TBI differs from unimpaired individuals. This synergy analysis provides insight into how leg muscles are controlled after TBI, and may provide a tool to assess changes with rehabilitation.

## METHODS

Twenty healthy young adults (25±3 years, 10 female) and forty-four ambulatory adults with a balance disorder due to a non-penetrative TBI participated in the study (53±9 years, 28 female). Each TBI participant was at least one year post-injury, had previously completed a focused physical rehabilitation program for their TBI, and had reached a plateau in their recovery. All TBI subjects had a dynamic posturography score at least 8 points below normal (Sensory Organization Test, NeuroCom<sup>®</sup>).

Lower extremity electromyographic (EMG) signals were collected bilaterally from six muscles (tibialis anterior, medial gastrocnemius, soleus, vastus lateralis, rectus femoris, semitendinosus) during treadmill walking (60 seconds). Each chronic TBI subject walked at his/her preferred speed (1.0±0.2 m/s). The protocol was repeated on the healthy young adults walking at a speed of 1 m/s. EMG signals were rectified and then low-pass filtered at 10 Hz. Ensemble EMG patterns were created by averaging signals over all gait cycles and normalizing the data to each muscle's root-mean-squared EMG. Non-negative matrix factorization was used to derive the synergies. The walking dynamic motor control index (walk-DMC) was then used to measure the complexity of neuromuscular control during gait [5]. Walk-DMC is a measure of the amount of variance in EMG accounted for in one synergy, relative to that in controls. Higher scores (>100) represent more complexity than the healthy controls, while lower scores (<100) reflect less complexity. For each subject, the walk-DMC score was averaged between left and right legs. A Mann-Whitney test compared the walk-DMC scores between healthy controls and the TBI subjects.

Additionally, a physical therapist evaluated the dynamic gait index (DGI) for each TBI subject. The DGI is an eight task battery (score: 0-24) that scores an individual's ability to walk normally, navigate obstacles, and turn. DGI scores  $\leq 19$  have been associated with fall risk in TBI subjects [2]. DGI was compared to walk-DMC using a Pearson correlation.

## RESULTS AND DISCUSSION

Walk-DMC was significantly ( $p = 0.015$ ) lower in individuals with chronic TBI ( $91 \pm 13$ ), compared to healthy controls ( $100 \pm 10$ ) (Fig. 1). DGI scores for the TBI averaged  $18 \pm 5$ , which is significantly lower than the DGI score of 24 seen in healthy control subjects [2]. As expected, walk-DMC and DGI scores were highly variable in the chronic TBI, with 45% of subjects exhibiting a DGI  $\leq 19$ . For those subjects, who would be classified as at risk for falls [2], walk-DMC was highly correlated with their preferred walking speed ( $R=0.76$ ) (Fig 2).

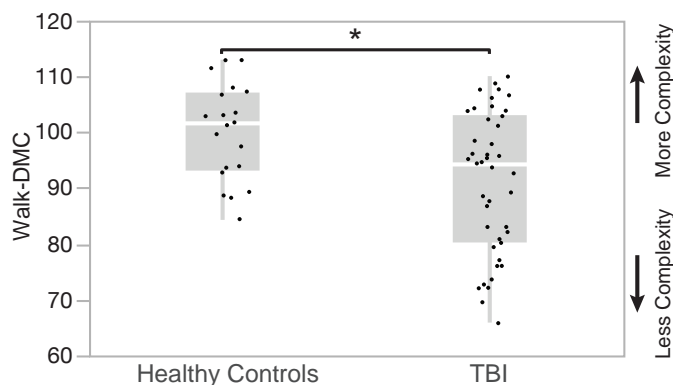


**Figure 1:** Walk-DMC scores for TBI and controls.

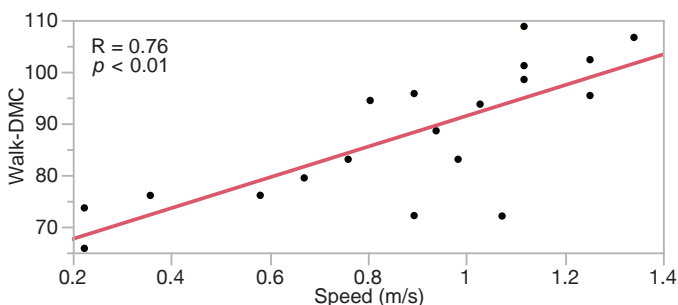


**Figure 2:** Walk-DMC and preferred walking speed were highly correlated for those subjects exhibiting a DGI  $\leq 19$ .

## CONCLUSIONS

This study is the first to show that the complexity of neuromuscular control of gait is permanently altered in many individuals who have previously experienced a TBI. Similar reductions in complexity have been reported in individuals who exhibit gait disorders due to other neurological impairments including stroke, cerebral palsy, and Parkinson's disease. This project is part of a larger neurorehabilitation study investigating the potential to use neuromodulation-enhanced gait retraining to normalize and improve walking in chronic TBI subjects [6]. Beyond simple spatiotemporal gait measures, synergy and walk-DMC metrics could provide greater insight into the underlying changes in coordination that may accompany effective approaches to gait rehabilitation. Further study will involve greater exploration of the synergy patterns and individual muscle weighting to identify the neuromuscular origin of abnormal control in individual subjects, which could be useful for targeting appropriate therapy.

## REFERENCES

1. Vasudevan EVL, et al. *J Neuro Phys Therapy* **38**, 172-182, 2014.
2. Medley A, et al. *Brain Injury* **20**, 1403-8, 2006.
3. Iaccarino MA, et al. *Handb Clinical Neurol* **127**, 411-422, 2015.
4. Ting LH, et al. *Neuron* **86**, 38-54, 2015.
5. Steele KM, et al. *Developmental Medicine & Child Neurology* **57**, 1176-1182, 2015.
6. Danilov Y, et al. *Brain Neurotrauma*, CRC Press, 2015.

## ACKNOWLEDGMENTS

This research was supported by the NIH-NIGMS award #R25GM08325, the TCNL Fund at the UW Foundation, and the Harvey D. Spangler professorship (DT).

# PLANTARFLEXOR REMODELING FOLLOWING ACHILLES TENDON RUPTURE REPAIR: A CASE STUDY

<sup>1</sup> Josh R Baxter, <sup>1</sup> Todd Hullfish, and <sup>1</sup> Wen Chao

<sup>1</sup> University of Pennsylvania, Philadelphia, PA, USA

email: [josh.baxter@uphs.upenn.edu](mailto:josh.baxter@uphs.upenn.edu), web: <https://www.med.upenn.edu/motionlab/>

## INTRODUCTION

Achilles tendon ruptures lead to elongated tendons and reduced patient function. Despite these clinical correlates, the link between muscular shortening constraints imposed by altered tendon properties and muscle remodeling remain poorly understood. Animal studies have shown that muscles rapidly remodel in order to maintain sarcomere shortening dynamics [1,2]. However, the muscular response to extreme changes in shortening demands have not yet been described, which may provide critical information for clinical decision making.

Therefore, the purpose of this study was to establish a framework for linking muscle remodeling and functional deficits in patients recovering from Achilles tendon ruptures. In particular, we aim to identify clinically relevant benchmarks that will guide treatment and better manage expectations. This case study presents a framework that is actively being utilized in a prospective patient registry to confirm a mechanism for muscle remodeling and establish clinical benchmarks for patient success.

## METHODS

A 27-year old male (1.83 m and 84 kg) presented with poor clinical outcomes 2.5 years following an acute Achilles tendon rupture that was surgically repaired by another provider using an open-reduction within 1 week of the initial injury. These poor outcomes were confirmed using a clinical outcome score (ATRS score of 49) [3], evaluation by a fellowship-trained foot and ankle surgeon, and inability to perform a single-leg heel raise. This functional assessment is part of an IRB approved research registry.

Plantarflexor architecture remodeling was quantified under ultrasonography by contrasting the medial gastrocnemius muscles of the affected and unaffected sides. Muscle thickness as well as fascicle

length and pennation were quantified by identifying the superficial and deep aponeuroses and clearly identifiable fascicles.

Plantarflexor function was assessed through a battery of tests including isometric strength testing, single-leg heel raise, and walking. During these activities, the ultrasonography probe acquired images synchronously with motion capture and force plate data. Plantarflexion motion, torque, and power along with fascicle shortening dynamics were calculated to establish the link between muscular and patient function. Fascicle dynamics were tracked using an automated tracking routine that utilizes MATLAB's Computer Vision System Toolbox.

## RESULTS AND DISCUSSION

Muscle remodeling was clearly evident and likely explained the patient's functional limitations observed in this case study. The medial gastrocnemius fascicles of the affected side were 59% shorter, 162% more pennated, and 24% less thick compared to the unaffected side.

Plantarflexor isometric torque was reduced by almost 50% on the affected side, however the percentage of fascicle shortening (41% – 46%) was similar between sides (Table 1). These results suggest that both the affected and unaffected plantarflexor muscles were operating on similar portions of the force-length curves during isometric strength testing.

Despite drastic changes in muscle architecture and isometric strength, walking biomechanics did not differ between the affected and unaffected sides (Table 1). Toe off occurred at 15° plantarflexion with approximately 160 Nm of torque being generated. Gastrocnemius fascicles went through less than 1 cm of excursion, demonstrating how the Achilles tendon can efficiently store and return energy during cyclic tasks – even when constrained by muscular weakness.

**Table 1.** The affected side (surgically repaired tendon) demonstrated large reductions in plantarflexion torque, power, and fascicle shortening during non-cyclic tasks. (~) denotes small difference between sides.

		<b>Affected</b>	<b>Unaffected</b>	<b>% Change</b>
<b>Isometric</b>	Torque	70 Nm	133 Nm	-47%
	Shortening	41% (1.9cm)	46% (5.1 cm)	≈ (-63%)
<b>Walking</b>	Plantarflexion	16°	15°	~
	Torque	160 Nm	156 Nm	~
	Shortening	< 1 cm	< 1 cm	~
<b>Heel Raise</b>	Plantarflexion	12°	40°	-70%
	Torque	140 Nm	140 Nm	~
	Power	100 W	260 W	-62%
	Shortening	1.0 cm	5.4 cm	5 times

Single-leg heel raises are a common clinical exam that demonstrated high sensitivity for muscle structure and function in this case study (Table 1). The affected limb generated one-third as much ankle rotation compared to the unaffected limb. These functional deficits appear to be explained by a 5-fold decrease in fascicle shortening. This decrease in fascicle shortening seems to be compounded by increased shortening pennation (48° compared to 36°), which resulted in a 14% decrease in force transmission along the Achilles tendon line of action.

This case study proposes a framework to rigorously quantify muscle remodeling in response to Achilles tendon injuries – establishing a means to prospectively study the implications of injury and treatments on joint function. Decreases in heel-raise function have been linked to tendon elongation of 3 cm following rupture [4], and our current findings suggest that fascicle remodeling occurs to compensate for tendon elongation at the cost of shortening capacity (Fig. 1). Further, these adaptations appear to be consistent with prior animal work that shows muscle remodeling following acute changes imposed on tendon traveling requirements [1,2].

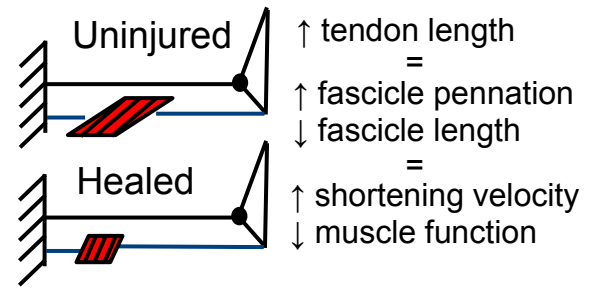


**Fig 1.** Achilles tendon lengthened following surgical repair [4], which appears to elicit muscle remodeling in order to maintain resting tendon tension. This muscle remodeling reduced muscle shortening and function in this study.

Early weight bearing and joint loading following tendon repair improves patient outcomes [5], which may be explained by reduced muscle remodeling and preserved joint function. Utilizing this framework, we have developed an Achilles tendon research registry to prospectively follow patients with tendinopathy and ruptures to develop predictors of success and clinical algorithms for identifying at-risk patients that require additional interventions. As this framework matures, we anticipate that regular patient visits will be completed in under 1 hour and the most descriptive measurements will be translated to clinical tools that can be integrated into the patient care experience.

## CONCLUSIONS

Skeletal muscle responds to tendon injuries in profound and deleterious ways. Utilizing a prospective approach to monitor patient progress may provide clinicians with additional information to tailor rehabilitation and return to activity timelines to optimize healing and long-term outcomes.

## REFERENCES

1. Koh and Herzog. *J Biomech.* **31**, 593-599, 1998.
2. Burkholder and Lieber, *J. Exp. Biology.* **201**, 309-316, 1998.
3. Nilsson-Helander K, et al. *Am. J. Sports. Med.* **35**, 421–426, 2007.
4. Silbernagel KG, et al. *Am. J. Sports Med.* **40**, 1564–1571, 2012.
5. Willits K, et al. *J. Bone Joint Surg. Am.* **92**, 2767-2775, 2010.

# LONGITUDINAL DATA FROM WEARABLE SENSOR SYSTEM SUGGESTS MOVEMENT IMPROVES STANDING POSTURE

<sup>1</sup>Ryan S. McGinnis, <sup>2</sup>Steve DiCristofaro, <sup>2</sup>Nikhil Mahadevan, <sup>2</sup>Ellora Sen-Gupta, <sup>2</sup>Ikaro Silva, <sup>2</sup>Elise Jortberg, <sup>2</sup>John A. Wright, Jr., <sup>2</sup>Roozbeh Ghaffari, <sup>2</sup>AJ Aranyosi, <sup>2</sup>Shyamal Patel

<sup>1</sup>University of Vermont, Burlington, VT, USA

<sup>2</sup>MC10, Inc., Lexington, MA, USA

email: ryan.mcginis@uvm.edu

## INTRODUCTION

Human body posture is an important predictor of human health and as such, is often a target for clinical research, diagnosis, and intervention. For example, upright posture while sitting has been shown to improve stress resilience in asymptomatic patients [1], and to reduce the negative thought bias in depressed patients [2]. Biofeedback has been used to promote improved posture in persons with Parkinson's Diseases [3]. However, effective biofeedback for posture training requires characterization of human body posture outside of the clinic and in the context of specific activities of daily living (ADLs) such as sitting, standing, and lying down. Existing technologies do not provide the contextual activity information needed to interpret posture measurements, and are impractical to wear over multiple days.

To overcome these issues, we present a conformal, wearable sensor system to measure human body posture within the context of activities of daily living and demonstrate its use in the home over 48 hours in healthy subjects. With an eye toward identifying behavioral interventions for improving standing posture, we explore relationships between the time spent completing ADLs and posture, and examine whether particular types of activities could be used to predict improved standing posture.

## METHODS

Data from N=28 subjects (13M/15F; 32+/-12 yrs; 1.72+/-0.11 m; 74.13+/-13.73 kg) over two days (49.34+/-5.42 hrs) were collected for analysis. Each subject was instrumented with BioStamp sensors (Fig. 1a, MC10, Inc. Lexington, MA, USA) affixed

to the skin of the chest and thigh as shown in Fig. 1b. Subjects performed a simple functional calibration (standing in a neutral posture), and then completed their typical daily activities. After 24 hours, subjects met with study staff to remove the BioStamp. This process was repeated on a subsequent day, within 1 week of the initial recording.

The activities completed by each subject are classified according to the machine learning approach described in [4]. Five-second windows of accelerometer data from each sensor are used to compute a set of 62 features which are used as input to a hierarchical tree of binary activity classification models. The output of this tree is an activity classification (Recumbent, Sitting, Standing, or Moving) for each five-second window of data.

Similarly, posture estimates are produced from five-second windows of accelerometer measurements. These measurements are reported in a reference frame ( $F_M$ ) aligned with the measurement axes of the sensor [5] (see Fig. 1b). The orientation of  $F_M$  is arbitrary relative to the anatomical frame of the body ( $F_A$ ). The mapping between  $F_A$  and  $F_M$ , for each subject, follows from the functional calibration activity [5]. Data during each window are averaged to yield the direction of gravity, and transformed into  $F_A$  using this mapping. The projections of gravity onto each axis of  $F_A$  are used to estimate posture angles in the sagittal and coronal planes following standard techniques.

We summarize subject activity patterns by computing the percentage of time spent in each ADL, and define posture quality as the average absolute angular deviation from a neutral standing

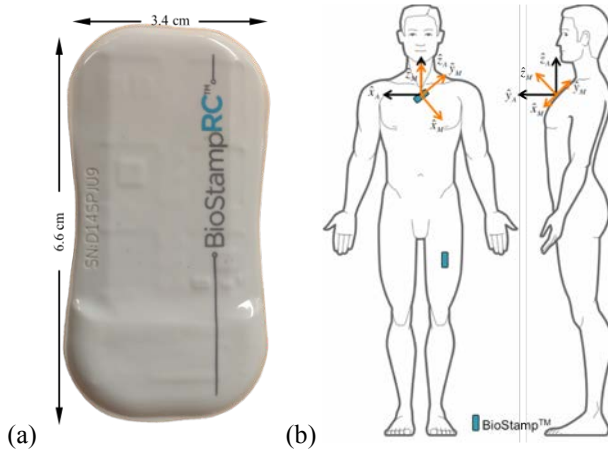


**Figure 1:** BioStamp sensors (a) deployed to the chest and thigh (b) on subjects to characterize posture and ADLs. Posture estimation requires a functional calibration to define the mapping between  $F_A$  (black) and  $F_M$  (orange).

posture in the sagittal plane. Relationships between subject demographics (age, gender, height, weight) and activity patterns are explored using Spearman's rank correlation coefficients. The association between activity patterns and standing posture quality is assessed with linear regression using the isometric log ratio transformation approach [6].

## RESULTS AND DISCUSSION

The correlation coefficients of Table 1 (statistical significance indicated with bolded text) reveal that older subjects spend significantly less time moving and more time sitting than younger subjects. This is especially important as we consider data from a relative young sample (oldest participant was 63 yrs. old), and yet these trends are already apparent.

**Table 1:** Spearman's rank correlation between demographics and percentage of time in each ADL.

	Moving	Sitting	Standing	Recumbent
Age	<b>-0.39</b>	<b>0.44</b>	-0.22	-0.24
Gender	-0.25	-0.07	-0.17	0.18
Height	-0.15	-0.07	-0.16	0.18
Weight	0.04	0.03	-0.13	-0.08

Controlling for age, linear regression reveals an association between standing posture quality and the percentage of time spent moving, sitting, and standing. Model coefficients ( $\beta$ ), standard error (std. err), t-scores ( $t$ ), and p-values ( $p$ ) for the regression are reported in Table 2.

**Table 2:** Regression parameters relating average sagittal standing posture angle and percentage of time spent completing activities.

	$\beta$ (std. err.)	$t$	$p$
Intercept	3.79 (3.94)	0.96	0.35
Age	-4.92 (4.07)	-1.21	0.24
Moving %	-11.75 (3.86)	-3.04	0.01*
Sitting %	8.95 (4.70)	1.90	0.07 <sup>†</sup>
Standing %	7.72 (3.22)	2.40	0.02*
$R^2=0.31$ , * $p < 0.05$ , <sup>†</sup> $p < 0.10$			

Subjects who exhibit better standing posture spend more time moving ( $\beta = -11.75$ ), and less time standing ( $\beta = 8.95$ ) or sitting ( $\beta = 7.72$ ). These results suggest that movement-based intervention programs could provide a means for improving standing posture. Moreover, they demonstrate that interventions that aim to elicit an increase in the percentage of time spent standing (e.g. standing desks), are unlikely to improve standing posture quality. Future studies should further explore these associations with an interventional study to assess the efficacy of behavioral changes (i.e. increased movement, increased standing, etc.) for improving standing posture. In the future, this type of study could further enable investigation of the efficacy of postural and behavioral intervention for improving mental health.

The results presented herein demonstrate that a new conformal, wearable sensor system is able to track activity patterns and posture noninvasively in the home across multiple days. In so doing, we identify relationships between age and activity patterns and between activity patterns and posture quality. These results point toward future interventional studies aimed at improving posture quality and, more generally, the use of this wearable sensor system for studying human behavior outside of typical clinical environments.

## REFERENCES

1. Nair, S et al., *Health Psychol*, **34**, 2015.
2. Michalak, J et al., *Clin Psychol Psychother*, **21**, 2014.
3. Mirelman, A et al., *J NeuroEng Rehab*, **8**, 2011.
4. Patel, S et al., *EMBC*, 2016.
5. McGinnis, RS et al., *IEEE TBME*, **62**, 2015.
6. Hron, K et al., *J of App Stat*, **39**, 2012.

# QUANTIFYING THE SHOULDER MOVEMENT OF MANUAL WHEELCHAIR USERS IN THE REAL WORLD USING INERTIAL MEASUREMENT UNITS

<sup>1</sup> Stephen M. Cain, <sup>2</sup> Emma Fortune, <sup>2</sup> Meegan Van Straaten, and <sup>2</sup> Melissa M. Morrow

<sup>1</sup> The University of Michigan, Ann Arbor, MI, USA

<sup>2</sup> Mayo Clinic, Rochester, MN, USA

email: smcain@umich.edu and Morrow.Melissa@mayo.edu

## INTRODUCTION

The shoulder is the most common site of musculoskeletal pain in people with spinal cord injury (SCI) who use manual wheelchairs (MWCs). Current understanding of shoulder pathology in MWC users points to a “wear and tear” etiology from overuse of an inherently unstable shoulder joint that is poorly designed for weight bearing, mobility, and performing tasks over-head from a seated position [1]. To better understand the mechanisms of shoulder overuse injury, shoulder function in the real world needs to be quantified.

Inertial measurement units (IMUs) provide a relatively inexpensive, robust, simple, and flexible way to measure the acceleration and angular velocity of objects and body segments. Unlike optical-based motion capture, IMUs do not confine data collection to a capture volume defined by camera placement and therefore enable measurement and quantification of human movement in the real world. IMUs can be used to accurately quantify shoulder angles [2]. However, demonstrations of accuracy have been limited to short data collections (< 2 minutes) and require a sequence of properly executed functional movements and/or careful measurement of link lengths to ensure accurate results [2, 3].

The purpose of this study was to develop a methodology to quantify the shoulder movement of MWC users with SCI during day-long data collections in their natural environments. We aimed to meet two criteria: 1) require only functional movements or static calibration postures that can be reliably achieved by all subjects and 2) outcome metrics should not be subject to drift.

## METHODS

In our IRB approved study, subjects ( $n = 5$ ) secured a total of three wireless IMUs (Opal, APDM, Inc.) to their left and right upper arms and thorax utilizing elastic hook and loop straps. For each IMU, we used a custom Kalman filter to estimate its orientation,  $R_{li}(t)$ , relative to an inertial frame defined by the direction of gravity and the initial orientation of the IMU. Because subjects are in a variety of unknown environments with potentially varying magnetic fields throughout the day, we only use accelerometer and angular rate gyro measurements for our orientation estimates. Therefore, we are confident our estimates of orientation relative to gravity are accurate and drift-free, whereas our estimates of the heading or yaw angle of each IMU are drift-polluted.

We instructed subjects to perform the following calibration static postures and dynamic movements after donning the IMUs for the day: 1) static upright posture, neutral shoulders, elbows 90° flexion, arms pressed against torso, 2) static arms straight out in front of body, shoulders 90° flexion, 3) static T-pose, shoulders 90° abduction, hands parallel to ground, 4) dynamic flexion/extension of the torso coordinated with shoulder flexion/extension, and 5) dynamic alternating flexion/extension of the left/right shoulders. All subjects were able to reliably perform calibrations 1 and 4; subjects had difficulty with the other calibrations due to arm movements being restricted by their wheelchairs, torso and abdominal strength, and/or available joint range of motion. Using data from calibrations 1 and 4, we calculated a body segment-to-IMU alignment,  $R_{bi}$ , using an approach similar to [4] for each IMU. The body segment-fixed axes for a given segment were defined as follows: Z-axis aligned with gravity and positive-up when in the calibration 1 posture, X-axis positive-

right and roughly aligned with the rotation axis during calibration 4, and Y-axis defined by the cross-product of the Z and X axes.

We calculated the orientation of each body segment in an inertial frame,  $R_{Ib}(t)$ , as follows:

$$R_{Ib}(t) = R_{Ii}(t)R_{bi}^T \quad (1)$$

Where the subscript  $T$  indicates the transpose of the matrix. The last row of the rotation matrix  $R_{Ib}(t)$  is a unit vector indicating the direction of gravity relative to the body segment,  $\hat{z}_{Ib}(t)$ . Segment elevation angle,  $\theta(t)$ , was calculated as follows:

$$\theta(t) = \cos^{-1}(\hat{z}_{Ib}(t) \cdot [0 \ 0 \ 1]) \quad (2)$$

Segment elevation angles are only dependent on the estimated direction of gravity relative to the body segment, and therefore are a drift-free metric for quantifying body segment motion. An elevation angle equal to zero indicates a body segment is in the same orientation as it was in during calibration 1; non-zero angles indicate deviations from the calibration 1 posture.

## RESULTS AND DISCUSSION

To illustrate the utility of our approach, we present sample results from one subject (male, 22 years, T5-T7 injury level, and 1.7 years post-injury) for a 7 hour long data collection (Fig. 1). The elevation

angle distributions contain several peaks, highlighting that different ranges of elevation angles are required for different tasks throughout the day, including propulsion, body transfer, and reaching tasks. This type of data can be used to determine if certain elevation angle daily distribution profiles are more likely to lead to shoulder pain and dysfunction.

## CONCLUSIONS

Thorax and arm movement can be meaningfully quantified using drift-free estimates of body segment elevation angles, which only require that a subject is able to sit upright and flex/extend the torso and shoulders. Future work will utilize relative orientations of body segments to resolve shoulder plane of elevation and angle of elevation.

## REFERENCES

1. Requejo PS, et al. *Top Spinal Cord Inj Rehabil* **13**, 86-119, 2008.
2. El-Gohary M and J McNames. *IEEE Trans Biomed Eng* **59**, 2635-2641, 2012.
3. Bouvier B, et al. *Sensors* **15**, 18813-18833, 2015.
4. Cain SM, et al. *Gait Posture* **43**, 65-69, 2016.

## ACKNOWLEDGMENTS

This research was supported by the Eunice Kennedy Shriver National Institute of Child Health and Human Development of the National Institutes of Health (R01 HD84423).

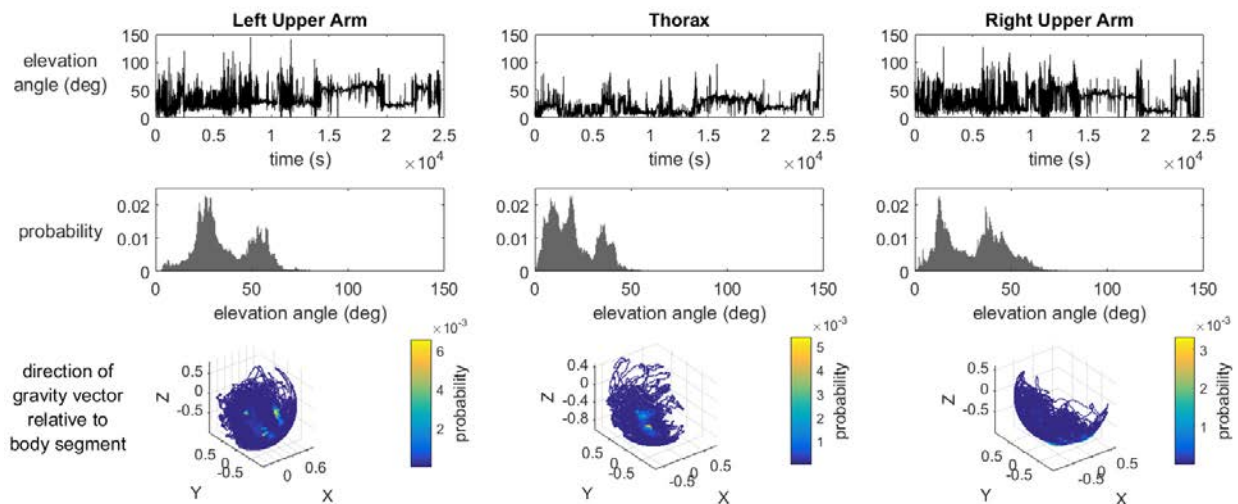


**Figure 1:** Elevation angles versus time (top), elevation angle histograms (middle), and three-dimensional histograms of the gravity vector (bottom) for the left upper arm, thorax, and right upper arm.

# JOINT MOMENT ESTIMATION USING INERTIAL SENSOR MEASUREMENTS WITH GAUSSIAN PROCESS REGRESSION

Craig J. Simons<sup>1</sup>, Cory L. Christiansen<sup>2</sup>, and Bradley S. Davidson<sup>1</sup>

<sup>1</sup>Department of Mechanical & Materials Engineering, University of Denver, Denver, CO, USA

<sup>2</sup>Department of Physical Medicine & Rehabilitation, University of Colorado Denver, Denver, CO, USA

email: [cjsimons@gmail.com](mailto:cjsimons@gmail.com),

web: <http://www.du.edu/rsecs/departments/mme/biomechanics/labs/humandynamics.html>

## INTRODUCTION

Joint moment measurements can provide unique insight into the mechanisms of human movement and thereby offer a powerful metric for clinical evaluation. [1] Traditional methods for determining joint moments require an instrumented gait lab, which limits the range of activities and the population that can be evaluated. Recent developments in the field of wearable inertial measurement units (IMUs) have expanded our ability to quantify human movement outside of traditional movement laboratories.

Because motion data measured with IMUs are typically limited to a subset of segmental kinematics, estimates of joint kinetics are not readily accessible. Conventional inverse dynamics methods provide clear theoretical frameworks enabling equations of motion to be solved for joint moments. However, inverse dynamics methods based exclusively on kinematics information can be insufficient for human motion because both kinematic measurement and parameter uncertainty create outputs that are error prone.

In this investigation, we explored an alternative to inverse dynamics, using IMU data directly with Gaussian Process Regression (GPR), a supervised learning technique, to predict joint moments. To avoid the effects of uncertainties in human data, we made use of a validated kinematic and kinetic dataset from an overdetermined, 7 degree of freedom (DOF) Barrett WAM robotic arm. The goal of the investigation was to establish foundational knowledge for developing a method to estimate joint moments in human movement based only on IMU data.

## METHODS

Gaussian Process Regression (GPR), a supervised learning algorithm, was used to establish a mapping relation from segmental kinematics (measured with IMUs) to the associated joint moments without explicitly modeling the original dynamic process. The GPR mapping relation was learned during a model training phase that uses example data with known kinematic and joint moment values to establish a correlation function between input measurements and target variables (Fig. 1). The training process identifies optimal model parameters for making future joint moment predictions using similar kinematic data.

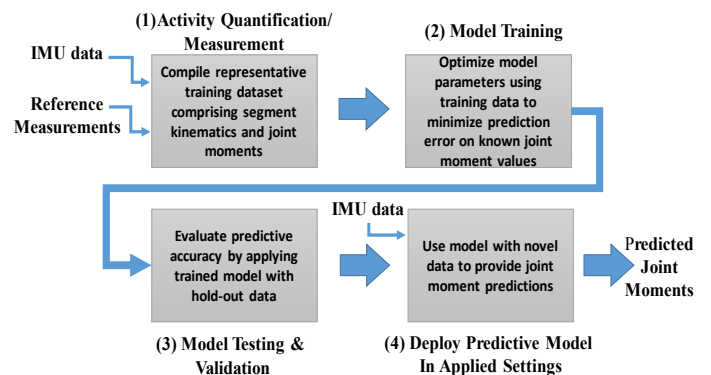


**Figure 1:** Proposed work-flow for enabling joint moment predictions using GPR with IMU data

The 7-DOF robotic arm has two 3-DOF spherical joints (shoulder & wrist) and a 1-DOF elbow. Joints are labeled sequentially from proximal to distal (Fig 2-a). Each joint is individually actuated and the validation data was directly measured at each DOF. Validation kinematics originated as Z-X-Z Euler angles and were transformed into body fixed linear acceleration and angular velocity to simulate IMU data for each of the three arm segments (arm,

forearm, end effector). The simulated IMUs were positioned at the mid-point along the axial length of each segment and initially aligned with the global reference frame.

The validation dataset included 12000 samples (12 sec at 100 Hz) and spanned the range of joint motion using joint-level periodic motion that was phase-shifted at each joint to produce irregular system kinematics. The model was trained using the first 1200 samples and tested on 400 samples at the mid-point of the dataset. Input variables included 3 DOF acceleration and angular velocity from each IMU (18 total). The model predicted 7 joint torques.

## RESULTS AND DISCUSSION

Average moment, standard deviation of the prediction error, and root mean square error are reported for each DOF (Table 1). The ratio of RMS error to joint moment magnitude can be interpreted as prediction accuracy. Prediction results for the primary axes of rotation are displayed in Figure 2.

Within each anatomical joint (shoulder, elbow, wrist) the DOF associated with actuation in the plane of gravity demonstrates greater proportional accuracy than the joints responsible for axial rotation. This may reflect difficulty modeling the subtle dynamics associated with axial rotation.

GPR is well suited to modeling complex dynamic processes (such as human movement) that are difficult to model directly. The GPR model structure easily handles high-dimensional (many DOF) relations and effectively incorporates probabilistic relations embedded within the predictor variables. GPR provides a convenient framework for automating the data processing and results process when deployed for evaluations performed outside of the laboratory.

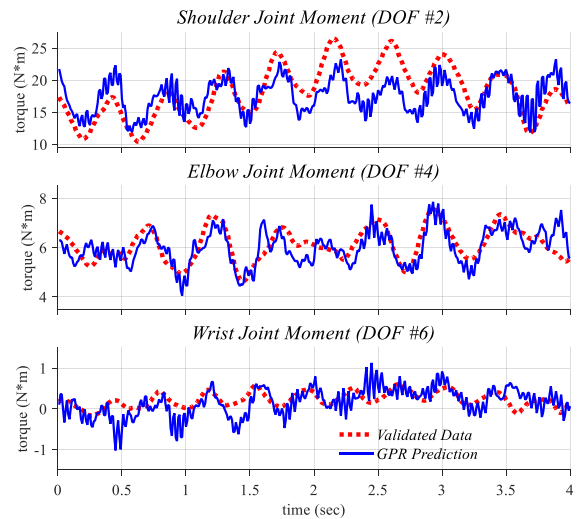
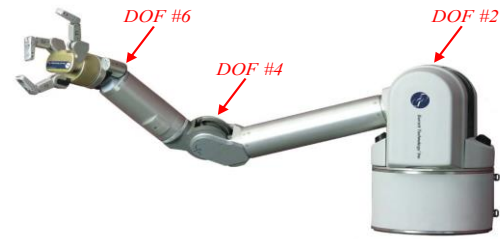


**Figure 2:** Barrett WAM robotic arm with primary rotational joint axes identified (top) and joint moment predictions using GPR with simulated IMU data (bottom)

## CONCLUSIONS

Additional development and refinement of the technique applied to human movement is important to determine the potential for use in achieving research-type kinetic measurements in applied and clinical settings.

Focus of future work will include determining specific training data requirements and establishing the accuracy and capabilities across a range of activities with human subjects.

## REFERENCES

1. Vaughan CL. *Human Movement Science* **15**, 423-443, 1996.
2. Nguyen-Tuong D, et al. *Advanced Robotics* **23**, 2015-2034, 2009.

**Table 1:** Descriptive statistics and error metrics for joint moment prediction at each arm DOF

	Joint Level (DOF)						
	1	2	3	4	5	6	7
<b>Average Moment (N*m)</b>	0.391	18.115	-0.351	6.130	0.070	0.223	-0.007
<b>Std Dev of Error (N*m)</b>	2.671	3.083	1.026	0.500	0.342	0.296	0.319
<b>RMS Error</b>	3.290	2.996	1.039	0.494	0.304	0.201	0.210

# ACCURACY OF A SHOE-WORN DEVICE TO MEASURE RUNNING MECHANICS

<sup>1</sup> Jessica G. Hunter, <sup>1</sup> Ross H. Miller, and <sup>2</sup> Stephen Suydam

<sup>1</sup> University of Maryland, College Park, MD, USA

<sup>2</sup> Milestone Sports, Columbia, MD, USA

email: [jghunter@umd.edu](mailto:jghunter@umd.edu), web: <http://sph.umd.edu/neuromechanics>

## INTRODUCTION

Commercial availability of wearable fitness trackers has grown in recent years, and devices to track variables relating to physical activity have become popular. Some running-specific devices are able to collect sophisticated information relating to running injury and performance variables that have been identified in biomechanics research literature, such as cadence, ground contact time, and vertical oscillation. Additionally, running speed, step length, and loading rates have been associated with running performance, injury, or both [1,2,5]. The general population of runners does not have regular access to instrumented gait analysis, in which cases running-specific devices can provide an affordable and portable alternative for those interested in measuring, tracking, and improving these variables to reduce the high incidence of running-related injuries and improve performance.

Accuracy of measurement is an important factor of a device and may increase its use, in turn improving outcomes for users [3]. The purpose of this study was to compare the accuracy of running metrics from a shoe-worn accelerometer for fitness tracking (the Milestone Pod) to analogous running data from instrumented gait analysis. We specifically tested the accuracy of the Pod for running velocity (VEL), cadence (CAD), ground contact time (GCT), peak knee angle in swing (KA), and vertical average loading rate (VALR).

## METHODS

Institutional approval was obtained and each participant gave written consent. Thirty-nine healthy adults participated in the study (12 males, 27 females, age  $29 \pm 13$  yrs). Subjects were fitted with 33 reflective markers on the pelvis, lower

extremity of the dominant leg and non-dominant foot. The Pod (mass  $\sim 13$  g) was attached to the shoe on the dominant foot by a small rubber carriage. Kinematic data was captured using a 13-camera VICON motion capture system sampling at 200 Hz. Ten embedded force plates recorded ground reaction forces (GRF) at 1000 Hz. Subjects ran around a 50-m indoor track for 3 laps each at 3 speeds: self-selected “normal”, “slow”, and “fast” paces to capture a range of the subject’s typical running mechanics. Running trials were conducted while subjects wore their own running shoes (RS) and standard lab shoes (LS) (New Balance 780v5).

Kinematic and GRF data were processed using Visual3D and MATLAB to determine average VEL, CAD, GCT, KA, and VALR. Data were averaged over all speeds and both shoes to represent intra-subject variance in running training. Raw data were filtered using a Butterworth low-pass filter at 6 Hz for kinematic and 50 Hz for GRF. VALR was calculated as the change in force over the change in time between 20-80% of the time period between initial contact and impact peak and scaled by body weight [4].

A paired-samples *t*-test compared the measurement difference between the Pod and Lab data to zero for all variables ( $\alpha = 0.05$ ). Additionally, a paired-samples two one-sided test (TOST) of equivalence was done between Pod and Lab data ( $\alpha = 0.05$ ). The TOST allows a specified range of difference between variables known as the practical difference (PD). The within trial standard deviation was calculated for both the Pod and Lab system. The average standard deviation of Pod data was used for VEL, CAD, and GCT, and the average standard deviation of Lab data for KA and VALR. Finally, the percent of subjects whose measurement difference fell within the PD was determined.

## RESULTS AND DISCUSSION

Results of the t-test revealed:

- No significant difference between Pod and Lab measurements for GCT ( $p = 0.235$ ,  $ES = 0.12$ ) and KA ( $p = 0.770$ ,  $ES = 0.11$ ).
- Significant differences for VEL ( $p = 0.001$ ,  $ES = 0.41$ ), CAD ( $p = 0.001$ ,  $ES = -0.25$ ), and VALR ( $p < 0.001$ ,  $ES = -0.51$ ).

The TOST between Pod and Lab data showed equivalence for all variables tested:

- VEL, PD = 0.25 m/s ( $p < 0.001$ )
- CAD, PD = 7.83 steps/min ( $p < 0.001$ )
- GCT, PD = 20.0 ms. ( $p < 0.001$ )
- KA, PD = 3.03 deg. ( $p < 0.005$ )
- VALR, PD = 8.51 BW/s ( $p < 0.001$ )

Representative scatterplots of the variables that showed the smallest and greatest differences between Pod and Lab are shown in Fig. 1. The percentage of subjects whose difference between Pod and Lab measurements fell within the practical difference is shown in Figure 1c. The practical difference of KA captured the least number of subjects (17.1%), followed by VEL (52.1%) and VALR (40.6%). CAD and GCT both captured the highest percentage of subjects (both 69.8%).

These results support the general accuracy of the device. The Pod estimates of GCT and KA were most accurate, showing no significant difference from zero. Pod estimates of VEL, CAD, and VALR were equivalent, showing significant differences between Pod and Lab, but the size of the difference was on average smaller than natural within-subject

variance in running mechanics. Although there was no significant difference between the measurement difference and zero for KA, the percentage of subjects whose average KA fell within the practical difference was low. The means of Pod and Lab data were very similar which led to good performance in the  $t$ -test ( $93.7 \pm 9.1$  deg. and  $95.1 \pm 16.0$  deg., respectively). However there was a fairly large (10.3 degree) average within subject difference between Pod and Lab measurements compared to relatively low individual standard deviation within speed and shoe conditions from the Lab data that defined the practical difference (3.03 deg.).

## CONCLUSIONS

The Milestone Pod is effective for measuring kinematic and kinetic running variables. However, refinement of the Pod's capabilities to estimate VEL, CAD and VALR are necessary to improve its versatility and applicability to a greater percentage of users.

## REFERENCES

1. Boyer, E, et al. *Am J of Sports Med*, **43**, 2310-2317, 2015.
2. Clancy, AC, et al. *Med & Sci in Sport & Ex*, **36**, 1917-1923, 2012.
3. Rupp, MA, et al. *Proceedings of Human Factors and Erg Soc*, 1434-1438, 2016.
4. Milner, CE, et al. *Med & Sci in Sport & Ex*, **38**, 323-328, 2006.
5. Tartaruga, MP, et al. *Res Quarterly for Ex and Sport*, **83**, 367-374, 2012.

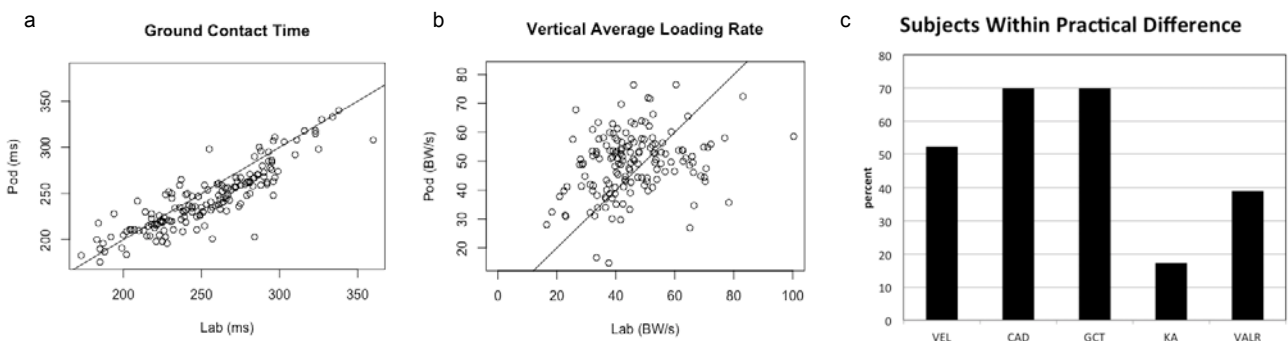


**Figure 1:** a. Pod GCT vs. Lab GCT with a line of perfect fit. b. Pod VALR vs. Lab VALR with a line of perfect fit. c. Percentage of subjects whose difference between Pod and Lab measurements was within the practical difference.

# USING INERTIAL SENSORS FOR ASSESSING PERFORMANCE DURING STAIR RUNNING

<sup>1</sup>Lauro Ojeda, <sup>2</sup>Antonia Zaferiou, <sup>1</sup>Stephen Cain, and <sup>1</sup>Noel Perkins

<sup>1</sup>University of Michigan, Ann Arbor, MI, USA

<sup>2</sup>Rush University Medical Center, Chicago, IL, USA

email: lojeda@umich.edu

## INTRODUCTION

We present a method for using inertial measurement units (IMUs) to estimate stair climbing kinematics during running. Running on stairs can provide important insight into individual's athletic performance and health. In-depth biomechanical analysis of stair running is challenging using traditional optical-based motion capture systems, which are limited to relatively small capture volumes. Most studies that analyze stair climbing focus on functional walking pace [1]. In contrast, we propose using foot-mounted IMUs to capture the foot kinematic motion (acceleration and rotation) during stair running and over large climbing distances. Using this technology, we capture a relatively large number of steps to understand steady state running on stairs. Doing so further provides data essential for within-subject statistical analysis.

IMUs are portable, unobtrusive, and unconstrained (e.g. do not need external references) motion tracking devices. However, IMUs also suffer from several sources of error (e.g. bias instability, scale factor errors, g-sensitivity, temperature sensitivity) that must be accounted for motion tracking applications. When IMUs are mounted on feet, velocity drift error can be estimated using the fact that the foot is essentially stationary during specific times in the stance phase. This velocity error is used to compensate for other system states using a process known as zero velocity update (ZUPT) [2]. We employ this strategy in custom-developed algorithms to accurately reproduce the foot trajectories during stair climbing (see Fig. 1). From these trajectories, we determine important events. Specifically, we estimate stride, swing and stance durations, which reveal climbing speed. In addition, we estimate foot velocity, orientation and position during the entire gait cycle.

The objective of this study is to analyze stair climbing performance while running on stairs. We hypothesize that the stance duration will determine overall

climbing speed since the swing phase duration is largely dictated by the the physical constraints of the stair case (height of risers and width of treads).

## METHODS

We tested 11 healthy volunteer participants (3F, 8M; age: 25.6/3.7 years; mean, SD) The University of Michigan IRB approved the study and all subjects provided informed consent. Subjects were instructed to run up a long stair case at maximum speed, without skipping treads. After pausing for for about 10 seconds, the subjects ran down the same flight of stairs at maximum speed returning to the starting position. The subjects wore two IMU data loggers (Opals, APDM, 128Hz), one mounted on each shoe by attaching it with athletic tape to the top of the laces. Estimated foot trajectories were derived from IMU data according to an algorithm previously validated [2]. The method uses gyroscope and accelerometer data to estimate spatial orientation, and then integrates translational accelerations twice to yield foot velocities and position. Drift (and other inertial sensor errors) were reduced by applying the ZUPT algorithm [2]. Because the riser and tread dimensions of the stairs are known, we added a additional correction to our estimates. In particular, we designed a Kalman filter that uses the riser height as a measurement value that the filter uses to correct the vertical foot position, which is updated by the filter whenever the foot reaches a new tread during the foot fall. After the correction is computed, we used smoothing techniques to provide backward corrections to obtain the complete foot trajectory for each stride. All calculations were performed using custom software developed using MATLAB (MathWorks).

Using the computed foot trajectory and orientation estimations, we determined foot-strike and toe-off times. Foot-strike was defined as the time the foot first contacts a tread. For running on stairs, the toe is more likely to contact the tread first, whereas during normal walk the heel contacts the ground first. Toe-off

time is defined as the time when the foot first loses contact with the tread. Using these foot contact events, the stride duration was estimated as the time between consecutive foot-strike events. The stance time follows from the time between a foot-strike and the subsequent toe-off. Finally, the swing time follows from the time between a toe-off and the subsequent foot-strike (see Fig 1).

## RESULTS AND DISCUSSION

We computed the stance, swing and total stride time for all eleven subjects. We assume left-right symmetry and we combined the results from the left and right feet. During our analysis, we eliminated the first and the last step from each stair run, as we consider them to be transition steps that differ from the steady state stepping that is the focus of our study. In particular, the stair case provided 16 strides total during steady state (eight left and eight right).

Our data analysis shows that in either direction (running up or down the stairs), the stride time was mainly determined by the stance time (see Fig. 2) showing high correlation ( $R^2$  value: up stairs 0.84, down stairs 0.92). During running up stairs, the swing phase time was loosely correlated with the stride time ( $R^2$  value: 0.24), which can be explained by the fact that regardless of the subject speed, the feet must travel approximately the same distance between steps (imposed by the stair design). Subjects make fine adjustments to provide just enough speed to reach the next thread (see Fig. 1). When running down stairs, we found that faster subjects chose to use higher speed during the swing phase at the expense of suffering higher impacts during the foot-strike, as shown by the correlation between the swing phase and stride time ( $R^2$  value: 0.58). Overall, we conclude that stride time is highly correlated with stance time and therefore speed is determined largely by stance time.

In addition to the above conclusion, estimates of foot attitude angles, velocity, and position reveal provide many additional performance metrics that can yield valuable insights into athletic performance such stride variability, ankle flexion and foot clearance.

## REFERENCES

1. Reid SM et al. Gait Posture **31**(2), 197-203, 2010.
2. Ojeda L and Borenstein J, J of Navigation **60**(3), 391-407, 2007.

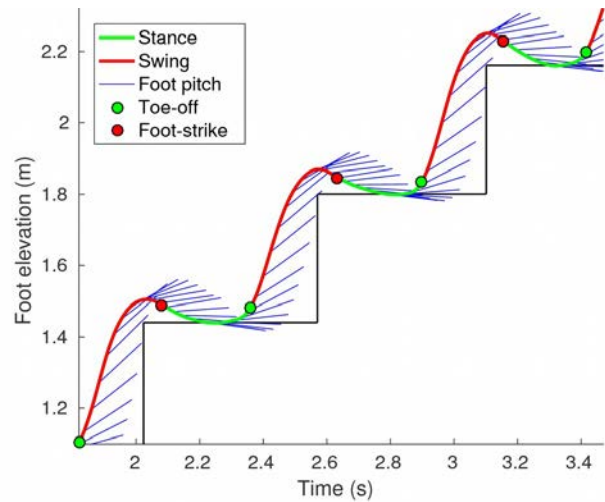


Figure 1: Foot trajectory estimated using IMU sensor data. Close up of a steady state section showing events times, foot orientation, and gait phases.

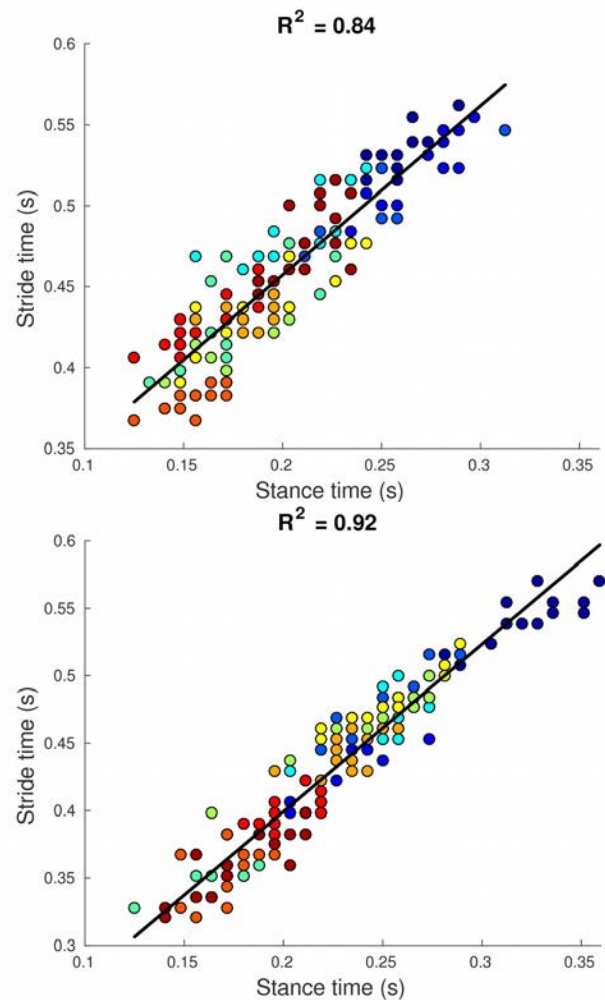


Figure 2: Stance and stride time correlation, each dot represents one stride, and each color represents one subject. Top: Running upstairs. Bottom: Running downstairs.

# AN ADAPTIVE FILTERING ALGORITHM TO ESTIMATE SPRINT VELOCITY USING A SINGLE INERTIAL SENSOR

<sup>1</sup> Reed D. Gurchiek, <sup>2</sup> Ryan S. McGinnis, <sup>1</sup> Alan R. Needle, <sup>1</sup> Jeffrey M. McBride, <sup>1</sup> Herman van Werkhoven

<sup>1</sup> Appalachian State University, Boone, NC, USA

<sup>2</sup> University of Vermont, Burlington, VT, USA

email: [gurchiekrd@appstate.edu](mailto:gurchiekrd@appstate.edu)

## INTRODUCTION

Measuring an athlete's sprint velocity in the field is important for evaluating performance and guiding training interventions [1]. Inertial measurement units (IMUs) are becoming increasingly popular for field-based human movement analyses and may have the means to estimate sprint velocity in the field. Velocity estimates made via integration of the accelerometer signal alone may be subject to error due to a biased signal and/or inaccurate orientation estimates. In this study, we develop and validate a velocity estimation algorithm that uses data from a single sacral worn IMU independent of any external measurement systems.

## METHODS

IMU data may be used to estimate sprint velocity by first expressing the sensor referenced acceleration vector in the world frame and then time integrating the forward component. Error in an estimate obtained this way may originate in the integration of a biased angular rate signal from the gyroscope, integration of a biased acceleration signal from the accelerometer, or an inaccurate estimate of the IMU initial orientation. To compensate for these potential errors, which are expected to increase with time, the algorithm we developed seeks to force constraints on the estimate given the following two assumptions:

(i) the runner's heading during the sprint is expected to be mean zero and

(ii) we expect the following velocity-time relationship as suggested by Furusawa et al. [1]:

$$v(t) = v_m \left(1 - e^{-\frac{t}{\tau}}\right) \quad (1)$$

where  $v$  is the velocity at time  $t$  and  $v_m$  and  $\tau$  describe the sprint running capabilities of the runner.

The quaternion is used to describe the IMU orientation and to express sensor referenced acceleration in the inertial track frame. The initial orientation is estimated during a standing static trial using the on-board accelerometer and magnetometer [2]. The algorithm follows the following steps:

1. Estimate instantaneous IMU orientation via gyroscope integration [3].
2. Decompose the composite quaternion to estimate the sensor's heading and attitude.
3. Linearly detrend the heading estimate to force the mean zero correction of assumption (i).
4. Time integrate the forward acceleration to provide an *a priori* estimate of sprint velocity ( $v^-$ ).
5. Find foot contacts using the forward acceleration signal as described in [4].
6. Fit  $v^-$  data at each foot contact to eq. (1) and determine the associated error ( $E$ ) in the curve-fitting.
7. Beginning with the foot contact where  $E$  was a minimum, determine the correction ( $d_v$ ) provided by the modeled velocity obtained from the curve fitting and the trust factor ( $G$ ) to be given to this correction according to,

$$G = \frac{E_k}{E_k + E_{k-1}} \quad (2)$$

where  $E_k$  and  $E_{k-1}$  are the curve fitting errors associated with  $v^-$  at foot contact  $k$  and  $k-1$  respectively.

8. Correct the *a priori* velocity estimate ( $v^-$ ) according to,

$$v = v^- + G(d_v) \quad (3)$$

9. Time integrate  $v$  to estimate position ( $p$ ) and repeat step 6 and 7 if  $p < 40$  m (sprint distance).

The validity of the velocity estimates from the proposed IMU method was determined by comparison to a previously validated position-time method using photocell data [1]. IMU and photocell data were collected on twenty-eight subjects (male and female sprinters and non-sprinters) for three maximal effort 40 m sprints. Each subject’s best sprint was used for analysis.

The velocity measures used for comparison were average interval velocity (0 – 10 m, 10 – 20 m, 20 – 30 m, and 30 – 40 m), maximal velocity, and instantaneous velocity. Error in the IMU velocity estimates was quantified using relative error (absolute percent difference), root mean square error (RMSE), and Pearson’s product moment correlation coefficient ( $r$ ).

## RESULTS AND DISCUSSION

Comparison of IMU and photocell estimates of average interval and maximal velocity is shown in Table 1. The validity of the IMU estimates may be suggested by significant ( $p < 0.01$ ) correlations with photocell measures, relative error less than 8%, and RMSE between 0.34 m/s and 0.67 m/s. The RMSE of the IMU estimate of instantaneous velocity was  $0.70 \pm 0.26$  m/s and showed strong correlations ( $r = 0.97 \pm 0.01$ ) with photocell estimates.

Fig. 1 shows an example of the result of the filter on the estimated velocity for a single subject. The sinusoidal nature of the true center of mass velocity (due to braking and propulsive impulse at each foot contact) is not expressed in eq. (1) nor in the photocell estimate, which may underlie some of the observed error.

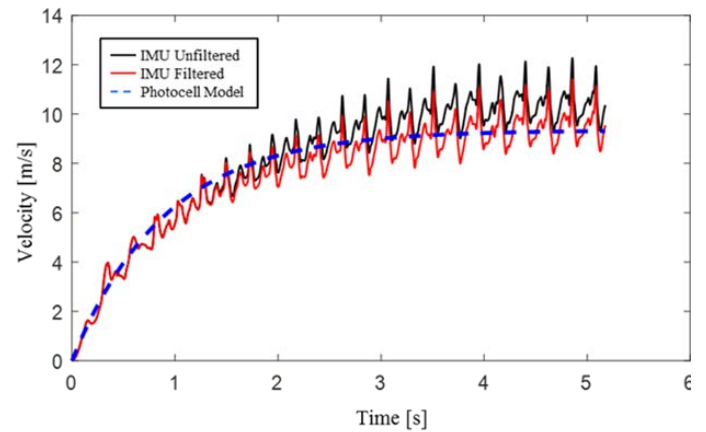


**Figure 1:** Comparison of velocity estimates from reference photocell method (blue dashed line), raw velocity estimate from IMU (solid black line), and velocity estimate from proposed IMU algorithm.

The results of this study suggest IMUs may provide an appropriate means by which to assess sprint velocity. IMUs have been used to measure other variables that may be of interest in evaluating sprint performance (e.g. ground reaction force, joint angles, step frequency, etc.). Future research should investigate the use of IMUs to estimate these other performance variables during sprinting to be used along with sprint velocity in a performance evaluation.

## REFERENCES

1. Samozino, P, et al. *Scand J Med Sci Sports* **26**, 648-658, 2015.
2. Jurman, D, et al. *Sens Actuators A Phys* **138**, 411-420, 2007.
3. Sabatini, AM. *Sensors* **11**, 1489-1525, 2011.
4. Wixted, AJ, et al. *Sports Eng* **12**, 207-212 (2010).

**Table 1:** Comparison of average interval and maximal velocity estimates from IMU and photocell methods. All units m/s except relative error and  $r$ .

		IMU		Photocell		
		Mean $\pm$ SD	Mean $\pm$ SD	Relative Error (%)	RMSE	$r$ ( $p$ value)
Average Interval Velocity:	0m - 10m	4.71 $\pm$ 0.35	4.94 $\pm$ 0.43	5.09 $\pm$ 4.08	0.34	0.81 (< 0.01)
	10m - 20m	7.48 $\pm$ 0.72	7.79 $\pm$ 0.85	5.51 $\pm$ 4.54	0.56	0.83 (< 0.01)
	20m - 30m	8.05 $\pm$ 0.93	8.17 $\pm$ 0.97	6.11 $\pm$ 5.50	0.6	0.80 (< 0.01)
	30m - 40m	8.33 $\pm$ 1.06	8.27 $\pm$ 1.02	7.02 $\pm$ 4.16	0.66	0.79 (< 0.01)
	Max Velocity	8.42 $\pm$ 1.07	8.29 $\pm$ 1.02	7.13 $\pm$ 4.42	0.67	0.80 (< 0.01)

# PREDICTING ENERGY EXPENDITURE DURING WALKING AND RUNNING USING NOVEL PIEZOELECTRIC FOAM SENSORS: A PILOT STUDY

Alyssa Evans<sup>1</sup>, Noelle Tuttle<sup>1</sup>, Steven Morrin<sup>1</sup>, James Tracy<sup>1</sup>, Parker Rosquist<sup>1</sup>, A Jake Merell<sup>3</sup>, Gavin Collins<sup>2</sup>, William Christensen<sup>2</sup>, David Fullwood<sup>3</sup>, Anton Bowden<sup>3</sup>, and Matthew Seeley<sup>1</sup>

Departments of Exercise Sciences<sup>1</sup>, Statistics<sup>2</sup>, and Mechanical Engineering<sup>3</sup>  
Brigham Young University, Provo, UT, USA  
email: alyssa7evans@gmail.com

## INTRODUCTION

By 2030, it is estimated that 1.92 billion people, worldwide, will be overweight or obese [1]. Physical activity can help individuals maintain healthy body mass and decrease risk of certain prevalent diseases (e.g., cancer and diabetes). Wearable devices that can measure activity-based outcomes (e.g., energy expenditure), in real time, can increase exercise motivation, physical activity levels, and weight loss [2]. The ability of commercially-available wearable devices to accurately predict energy expenditure, however, is currently poor enough to have implications for people who desire to use wearables to lose body weight [3].

In our lab, we have developed quasi-piezoelectric, nanocomposite, foam sensors that can be used to sense impact energy in three orthogonal planes. When inserted into the insole of a shoe (Figure 1), data from these sensors strongly correlates to energy expenditure with promising accuracy. These sensors are also robust and relatively inexpensive. The purpose of this study was to test the ability of these sensors, placed in a shoe insole, to predict energy expenditure during walking and running.

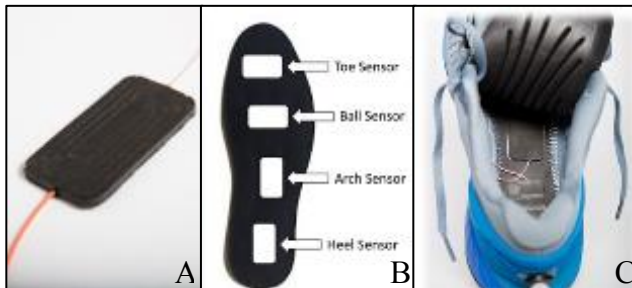


**Figure 1:** (A) the foam sensor; (B) locations of the foams sensors, within the insole; and (C) a photograph of the instrumented athletic shoe.

## METHODS

Six recreational runners (3 males and 3 female,  $24 \pm 1$  years,  $170 \pm 5$  cm, and  $61 \pm 11$  kg) participated in this study. We used a Cosmed K4b<sup>2</sup> portable metabolic analyzer (Cosmed K4b<sup>2</sup>, Cosmed, Rome, Italy) to measure energy expenditure. Subjects first provided informed consent, and then subject demographics were measured. During data collection, participants wore standardized running shoes, and the right shoe was instrumented with our quasi-piezoelectric, nanocomposite foam sensors. Participants completed a 15-min warm-up, at 2.68 m/s, and then completed 5 different trials in a randomized order. Each trial was 4 min of walking or running, at one of the designated speeds: 1.34, 2.23, 2.68, 3.13, or 3.58 m/s. A 1-min walk (1.34 m/s) was completed before and after every trial.

Data from the foam sensors and energy expenditure data were measured throughout the entire collection period (~50 min). Disregarding the transitory periods (first 2 min of each trial), mean energy expenditure was measured for each trial. Using participant weight, height, body mass index, and 8 characteristics of the foam sensor signals (average maximum voltage of the heel, arch, and toe sensor; average minimum voltage of the heel, arch, ball and toe sensor, and absolute integral of voltage curve from the toe sensor), we created a predictive model using a standard linear regression model.

To calculate the out-of-sample root mean square error (RMSE), we performed a cross-validation process where we removed data representing one subject (out-of-sample), fit our model using data from the other five subjects (within-sample), and predicted energy expenditure for the out-of-sample subject. We repeated this process six times, leaving

out each subject in turn, and computed the average RMSE for each walking/running speed, across all subjects.

## RESULTS AND DISCUSSION

Mean RMSE for six within-sample predictions and six out-of-sample predictions are shown in Table 1. Figure 2 shows the distribution of measured and predicted energy expenditure for all six subjects (within-sample subjects and out-of-sample).

Two common wearable devices that are now used to predict energy expenditure during physical activity are the Fitbit Charge HR (Fitbit Inc., San Francisco, USA) and Apple Watch (Apple Inc., California, USA). Our predictive model, based off only 6 subjects, shows somewhat promising results, that are comparable to the two aforementioned devices [3]. On average, the Fitbit Charge HR, which is more accurate than the Apple Watch [3], underestimates energy expenditure by 0.93 Kcal/min. On average, our within-sample RMSE is 0.78 Kcal/min, however, our out-of-sample RMSE is 2.88 Kcal/min. Unlike the Fitbit and Apple

Watch, the accuracies from our model are generally maintained at higher intensity levels. Additionally, we expect RMSE, associated with our model, to decrease, as we increase our sample size and add other independent variables (e.g., gender and accelerometer data, which is also collected from the shoe) to the model.

## CONCLUSIONS

The ability to predict energy expenditure via our novel piezoelectric sensors appears promising; however, more data is needed to create a more accurate model.

## REFERENCES

1. Kelly T, et al. *Int J Obes* **32**, 1431-1437, 2008.
2. Sullivan AN, et al. *Front public Heal.* **4**, 2016.
3. Wallen MP, et al. *PLoS One.* **11**, 2016.

## ACKNOWLEDGMENTS

This work was supported by the National Science Foundation: Grant #'s: CMMI-1235365 & CMMI-1538447.

**Figure 2:** Observed and Predicted EEm measurements for within sample and out-of-sample subjects

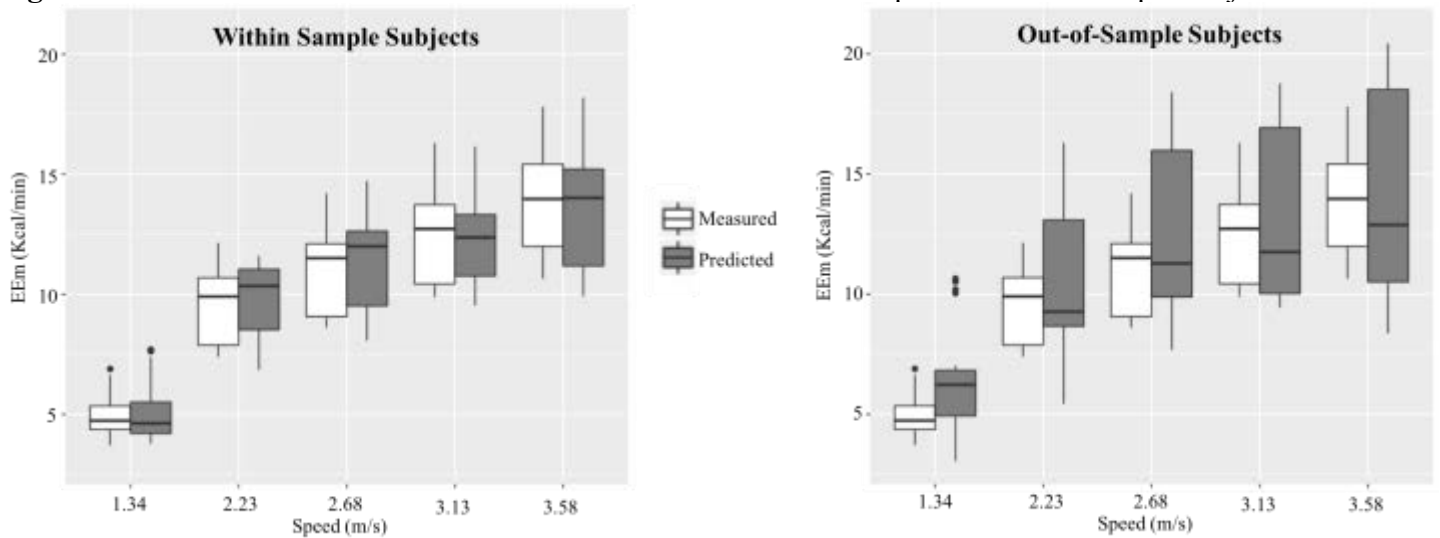


**Table 1:** Average results for six within sample subjects, and one out-of-sample subject.

	1.34 m/s	2.23 m/s	2.68 m/s	3.13 m/s	3.58 m/s
<b>RMSE Within Sample</b> (Kcal/min)	0.61	0.82	0.71	0.71	1.02
<b>RMSE Out-of-Sample</b> (Kcal/min)	1.81	3.05	2.65	2.78	3.36

# A “SMART” PRESSURE INSOLE FOR GAIT RETRAINING OUTSIDE OF THE LABORATORY

<sup>1</sup>Jade He, <sup>2</sup>Kevin Lippmann, <sup>1</sup>Christopher Ferrigno, and <sup>1</sup>Markus A. Wimmer

<sup>1</sup>Rush University, Chicago, IL, USA

<sup>2</sup>Technical University of Munich, Munich, Germany

Email: markus\_a\_wimmer@rush.edu

## INTRODUCTION

Load distribution shifts from the lateral to the medial compartment is related to an increase in knee adduction moment (KAM) [1] and is associated with knee osteoarthritis (OA) [2]. Previously, reductions in KAM occur when barefoot plantar pressure is medialized [3]. This supports the role of altering kinematics of the foot to redistribute loads across the knee joint.

Successfully gait retraining to medialize plantar pressure and lower KAM have been achieved in the laboratory via auditory feedback provided by a high-resolution insole with specifically arranged sensor areas [4]. However, such a plantar pressure-detecting system is comprised of multiple electronics and cables and therefore is unsuitable for gait training in the community. With the ultimate goal of translating pressure-based feedback training into the clinical setting for sufferers of knee OA, the current study employed a pair of fully integrated, slim 13-sensor insoles (OpenGo, Moticon GmbH, Munich, Germany) for measuring and recording real-time plantar pressure distribution (**Figure 1**). A smartphone receives sensor data via ANT wireless technology and provide instant, auditory feedback. Further exploration of using this sensor insole to provide auditory feedback to lower KAM outside of the laboratory is warranted.

In this study, we hypothesize that gait training using auditory feedback from a cable-less, commercially available insole in the in the community will reduce KAM.

## METHODS

This single-day, IRB-approved study tested 11 healthy subjects ( $25.64 \pm 4.67$  yrs; 5M, 6F;  $22.95 \pm 2.83$  kg/m<sup>2</sup>), who self-reported an absence of pain in their lower extremities during the last 48 hours. All subjects wore a pair of standardized, flexible shoes (Dr. Comfort, FlexOA, Mequon, WI, USA) that

contained the insoles. Kinematics, kinetics, and plantar pressure was evaluated for the dominant leg (all right sided).



**Figure 1.** Moticon OpenGo cable-less pressure insoles and their sensor distribution

The testing procedure included a baseline walking assessment, in-lab training and subsequent gait test with feedback, continuation of training outside the lab, and final assessment of memorized gait modification without feedback. For the baseline test, all subjects completed five walking trials at a self-selected speed with their normal gait pattern on a leveled 6-m walkway with their plantar pressure recorded using the insoles. The mean maximum pressure of both sensor S5 and S9 (**Figure 1**) on the lateral side of the foot was calculated. For both sensors, 75% of the mean maximum pressure was set as the training threshold. Each subject received instructions to subtly alter their walking style avoiding the auditory tone from the smartphone. Subjects practiced until they could successfully avoid the feedback tone for several consecutive steps. Then, three walking trials were assessed as the subjects were performing the modification with feedback. Each subject was then instructed to further practice the gait modification while going for a one-mile walk around campus. During this walk, feedback was received through headphones. Upon return to the lab, each subject was asked to walk with the internalized gait modification without

feedback. Five marker-based trials were completed while plantar pressure was recorded as well.

Motion capture was performed using a ground embedded force plate (Bertec, Columbus, OH, USA) to measure ground reaction forces and 12 optoelectric cameras (Qualysis, Gothenburg, Sweden) to capture lower extremity kinematics. A modified Helen Hayes marker set was applied to the lower extremities. Raw kinetics and kinematics were processed in Visual3D (C-Motion, Inc., Germantown, MD, USA) with model templates customized using joint offset for all subjects.

Statistical analyses were performed using IBM SPSS Statistics 22 (SPSS Inc., Chicago, IL). A *p*-value of 0.05 indicated significance. Descriptive statistics were calculated for variables of interest and one-way ANOVA with post hoc Bonferroni were used.

## RESULTS AND DISCUSSION

On average, subjects reduced lateral plantar pressure by 58.96% and 33.58% for S5 and S9, respectively (**Table 1**). Speed, stride, or cadence did not change across three tested conditions (**Table 2**). Compared with normal walking, subjects reduced KAM1 by 15.46 % (0.32%BW\*Ht, *p* = 0.051) and KAM2 by 25.18% (0.71%BW\*Ht, *p* = 0.017) while performing the gait modification cued by feedback. After the additional on-campus training and removing the feedback function on the phone, subjects maintained a 17.87% reduction of KAM1 (0.37%BW\*Ht, *p* = 0.010) and 25.53% of KAM2 (0.72%BW\*Ht, *p* = 0.009). It was encouraging that the KAM reduction was sustained

even without feedback after training. Additionally, knee flexion moment (KFM) did not change while subjects were modifying their gait.

Subject	Reduction of Pressure (%)	
	S5	S9
1	94.12	31.68
2	74.36	32.74
3	-43.03	28.71
4	27.88	20.63
5	47.37	22.73
6	11.97	66.22
7	76.23	29.01
8	92.29	4.51
9	91.82	47.62
10	80.37	61.76
11	95.19	23.72
Mean	58.96	33.58
SD	44.10	18.26

**Table 1.** Reduction of pressure from baseline after on-campus gait training and removal of feedback

## CONCLUSIONS

A commercially available, cable-less insole was capable in training healthy volunteers to medialize plantar pressure and decrease KAM. Further studies have to follow and test the technology on OA patients.

## REFERENCES

1. Kutzner I, et al. PLoS One, **8**(12): e81036, 2013
2. Kumar D, et al. Osteoarthr. Cartil, **21**(2), 298-305, 2013
3. Ferrigno C, et al. Osteoarthr Cartil, **22**(Suppl. 2), S92-93
4. Ferrigno C, et al. J Biomech Eng, **138**(2), 021014, 2016

	Normal Walking		Medialized Pressure with Feedback			Medialized Pressure		
	Mean	SD	Mean	SD	Significance	Mean	SD	Significance
<b>Spatiotemporal Parameters</b>								
Speed (m/s)	1.33	0.17	1.22	0.22	0.336	1.26	0.16	0.745
Stride (m)	1.41	0.11	1.34	0.15	0.367	1.35	0.11	0.630
Cadence (steps/min)	55.84	3.19	54.05	4.47	0.705	55.27	4.11	1.000
<b>Loading Parameters (%BW*Ht)</b>								
KAM1	-2.07	0.41	-1.75	0.32	<b>0.051</b>	-1.70	0.35	<b>0.010</b>
KAM2	-2.82	0.69	-2.11	0.79	<b>0.017</b>	-2.10	0.60	<b>0.008</b>
KFM	2.97	1.09	2.77	0.89	1.000	2.83	1.15	1.000

**Table 2.** Spatiotemporal and kinetics variables of subjects walking in three conditions

# Self-report and Performance Measure Outcome Estimation Using Wearables after Total Knee Arthroplasty

Ik-Hyun Youn<sup>1</sup>, Joseph A. Zeni<sup>2</sup>, Jong-Hoon Youn<sup>1</sup>, Brian A. Knarr<sup>1</sup>

<sup>1</sup> University of Nebraska at Omaha, Omaha, NE, USA

<sup>2</sup> University of Delaware, Newark, DE, USA

email: iyoun@unomaha.edu

## INTRODUCTION

Osteoarthritis (OA) of the knee is a debilitating condition that negatively affects ambulatory function [1]. Although no cure exists, Total Knee Arthroplasty (TKA) is a common procedure to reduce pain for individuals with end-stage OA [2]. Various functional and self-reported measures are used to assess functional ability and impairment before and after TKA. Although questionnaires are cost-effective and easy to administer, these are subjective and may not accurately reflect actual physical impairments or functional deficits. Performance tests can objectively capture mobility capability, but each test only addresses a small aspect of physical function.

Wearable sensor-based ambient gait monitoring is a promising approach that can address some of the limitations of clinical evaluation. This gait monitoring is low cost, portable, and can provide important objective information of mobility characteristics after unilateral TKA in a real-world setting [3]. To implement the wearable approach, effectiveness of the system needs to be carefully evaluated. Therefore, the purpose of this study was to determine if inertial gait features from wearable accelerometers were associated with self-reported and performance-based measures after unilateral TKA.

## METHODS

15 subjects (1.70±0.1m, 84.5±17.1kg, 67.1±7.5yr, speed=1.13±0.20m/s) after unilateral TKA participated in two data collection sessions. In the first session, subjects answered self-reported surveys including knee outcome survey (KOS) and knee injury and osteoarthritis outcomes score (KOOS). Functional testing included the stair climb test (SCT), 6-Minute Walking (6MW), and timed up and go (TUG). In the second session, acceleration data

were collected using two ankle-worn accelerometers. Accelerometers were attached above the lateral malleoli. Each subject walked at self-selected comfortable walking speed, as determined by a 6 meter walk test, for one minute.

**Table 1:** Eleven inertial gait features based on one all-step inclusive and three directional gait feature categories.

Category	Description
Inclusive	Step time
	Step vector magnitude
	Initial loading vector mag.
Lateral	Lateral heel-strike magnitude
	Lateral heel-strike impulse
	Lateral stance phase angle
Vertical	Vertical heel-strike magnitude
	Vertical heel-strike impulse
Anterior	Anterior heel strike magnitude
	Anterior heel-strike impulse
	Anterior stance phase angle

Eleven gait variables were extracted to estimate magnitude, impulse, and angles of initial loading from 3D-acceleration data. Then, the wearable sensor-based gait variables were compared to questionnaires and performance test outcomes. Hierarchical linear regressions were applied to determine contribution of directional gait variables from wearables for each biomechanical gait feature. To analyze directional effect of inertial gait variables, inclusive-, lateral-, vertical-, and anterior-gait inertial variables were sequentially appended to prior regression models.

## RESULTS AND DISCUSSION

Outcomes of the hierarchical linear regression indicated that inertial gait features significantly predicted performance tests (Table 2) and self-

reported measures (Table 3). All three models performed well at predicting performance measures. 70.1 % of TUG score was explained by vertical and anterior inertial variables. 67.6% of 6MW result was explained by anterior variables, and 68.4% of SCT result was explained by inclusive and anterior inertial variables. Self-reported measures were explained well by combinations of inertial gait features. Inclusive and anterior inertial gait features explained 89.0% of variance in KOS Activities of Daily Living Scale (KOS-ADLS). The variance explained for two KOOS subscales (KOOS-Pain and KOOS-Symptom) were 54.7% and 69.0%, respectively. Generally, anterior gait variables improved prediction of clinical measure outcomes. Since the two inertial sensors were attached on ankle, the magnitude of the anteroposterior acceleration is more dominant while walking compared to the other directions. The anterior inertial gait features worked better than inclusive variables including step time and vector magnitude.

## CONCLUSION

Although current results are challenging to generalize due to small sample size, prediction results are promising and may provide additional information about the TKA population. Additional gait characteristics such as symmetry will be analyzed to understand associations between inertial gait features and clinical scores to improve our understanding of the underlying mechanisms behind the observed relationships.

## REFERENCES

1. Ruiz D. et al. *J Bone Joint Surg AM* **16**, 1473-1480, 2013.
2. G.L. Hatfield, et al. *Arthritis Care Res.* **67**. 1004–1014, 2015.
3. Chen, S. et al. *J Biom Heal Inform* **20**, 1521-1537, 2016.

## ACKNOWLEDGMENTS

This work was partially supported by the National Institutes of Health NIH P30-GM103333 and P20GM109090.

**Table 2:** Hierarchical linear regression for three performance tests outcomes.

Model 1 = Inclusive variables

Model 2 = Inclusive + Lateral variables

Model 3 = Inclusive + Lateral + Vertical variables

Model 4 = Inclusive + Lateral + Vertical + Anterior variables

Model	TUG			6MW			SCT		
	R	Adj. R <sup>2</sup>	ΔR <sup>2</sup>	R	Adj. R <sup>2</sup>	ΔR <sup>2</sup>	R	Adj. R <sup>2</sup>	ΔR <sup>2</sup>
Model 1	0.000	0.000	0.000	0.000	0.000	0.000	0.355	0.247	0.247
Model 2	0.000	0.000	0.000	0.211	0.079	0.079	0.404	0.241	-0.006
Model 3	0.439	0.396	0.396	0.211	0.079	0.000	0.534	0.347	0.106
Model 4	0.768	0.705	0.310	0.746	0.676	0.597	0.797	0.684	0.337

**Table 3:** Hierarchical linear regression for three target self-reported survey outcomes.

Model	KOOS-ADLS			KOOS-Pain			KOOS-Symptom		
	R	Adj. R <sup>2</sup>	ΔR <sup>2</sup>	R	Adj. R <sup>2</sup>	ΔR <sup>2</sup>	R	Adj. R <sup>2</sup>	ΔR <sup>2</sup>
Model 1	0.283	0.228	0.228	0.000	0.000	0.000	0.669	0.644	0.644
Model 2	0.431	0.276	0.047	0.384	0.337	0.337	0.669	0.644	0.000
Model 3	0.477	0.268	-0.007	0.384	0.337	0.000	0.697	0.646	0.002
Model 4	0.937	0.890	0.622	0.644	0.547	0.211	0.763	0.698	0.052

# A NEW MEASURE OF TRIP RISK INTEGRATING MINIMUM FOOT CLEARANCE AND DYNAMIC STABILITY ACROSS THE SWING PHASE OF GAIT

<sup>1</sup> Brian Schulz

<sup>1</sup> VA Office of Research and Development, Washington, DC  
email: Brian.Schulz@va.gov

## INTRODUCTION

Minimum toe clearance (MTC), or more generally minimum foot clearance (MFC) when the heel is also considered, is thought to quantify the risk of the toe or foot contacting the ground during the swing phase of gait and initiating a trip [1], but there are methodological issues with this measure and the risk of trip-related falls has been shown to also be associated with gait speed [2].

Proximity of the foot to the ground at midswing would be expected to increase trip risk, but the dynamic stability of the locomotor system would also be expected to relate to trip risk and thus far has not been considered in combination with MTC.

This paper proposes and evaluates a new measure, trip risk integral (TRI), that circumvents many issues with MTC as typically calculated at a single point by considering minimum foot clearance across the entire swing phase and taking into account dynamic stability to estimate risk of falling due to a trip rather than risk of the foot contacting the floor.

## METHODS

Shoes and floor surfaces were digitized and MTC and TRI calculated for unimpaired younger (N=14, age=26±5), unimpaired older (N=14, age=73±7), and older adults who had recently fallen (N=11, age=72±5) walking on surfaces with no obstacles, visible obstacles, and hidden obstacles at slow, preferred, and fast gait speeds.

MTC and MFC were calculated as described previously [3] and TRI was calculated using a version of the margin of stability [4] that was modified to provide a continuous trajectory during the swing phase of gait and negated to indicate the margin of instability (MoI).

To quantify the total trip risk across the swing phase, the integral of MoI/MFC was taken, but spikes in the trip risk trajectory would often occur at

foot liftoff or landing. To exclude these spikes when the foot was intentionally and necessarily in close proximity to the ground, the integral was taken between the time points of peak MFC acceleration to exclude these erroneous spikes and still capture all values between the initial liftoff acceleration of the foot and the terminal deceleration prior to foot contact. The resulting trip risk integral (TRI) is thus calculated as per equation 1:

$$TRI = \int_{FOacc}^{ICacc} \frac{MoI}{MFC} dt \quad (1)$$

A repeated-measures linear mixed model was used to test the effects of the three independent variables of subject group, flooring surface, and actual gait speed on two dependent variables (MTC and TRI) using SAS (SAS Institute Inc., Carey, NC). All interaction effects were also included in the model.

## RESULTS AND DISCUSSION

All subjects walked faster when instructed (F=580, p<0.0001) and slower on surfaces with obstacles (F=8.3, p=0.0006; **Table 1**). Fallers walked slower at all instructed speeds (F=14, p<0.0001).

**Table 1: Mean (SD) of actual gait speeds by instructed gait speeds**

Actual Gait (m/s)	Subject Group	Instructed Gait Speed		
		Slow	Preferred	Fast
Uncorrected	Younger Non-Fallers	0.83 (0.19)	1.19 (0.19)	1.98 (0.40)
	Older Non-Fallers	0.89 (0.25)	1.24 (0.25)	1.85 (0.40)
	Older Fallers*	0.80 (0.18)	0.94 (0.18)	1.18 (0.17)
Normalized (leg lengths/s)	Younger Non-Fallers	0.97 (0.24)	1.40 (0.26)	2.32 (0.52)
	Older Non-Fallers	1.15 (0.35)	1.59 (0.32)	2.38 (0.52)
	Older Fallers*	0.98 (0.23)	1.14 (0.23)	1.43 (0.24)

\* Group effect p<0.0001

MTC and TRI had significant (F≥5, p≤0.005) but differing effects of gait speed and floor surface (**Fig. 1**). As gait speed increased (which increases risk of trip-related falls [2]) MTC indicated less and TRI greater risk, indicating that TRI better quantifies risk of falling due to a trip. While MTC and TRI did

not differ by subject group, strong speed-related effects of TRI ( $F \geq 8$ ,  $p \leq 0.0007$ ) resulted in improved TRI for fallers due to their slower self-selected preferred gait.

### CONCLUSIONS

The proposed trip risk integral (TRI) successfully captures dynamic gait stability and MFC across the swing phase of gait in a single measure that circumvents many of the issues associated with MTC and may better quantify risk of falling due to a trip. These findings demonstrate that slower gait is both an important covariate and potential intervention for trip-related falls.

### REFERENCES

1. Winter DA. *Phys Ther* **72**, 45-6
2. Pavol MJ, et al. *J Gerontol Biol Sci Med Sci.* **56**, M428-37.
3. Schulz BW et al. *J Biomech.* **44**, 1277-84.
4. Hof AL et al. *J Biomech.* **38**, 1-8.

### ACKNOWLEDGMENTS

This work was supported by a VHA RR&D Career Development Award (E4941W). I also thank Wendy Kimmel and Pradeep Ambati for assistance with data collection, Scott Barnett for statistical support, and Stephanie Hart-Hughes and Tatjana Bulat for clinical and editorial support.

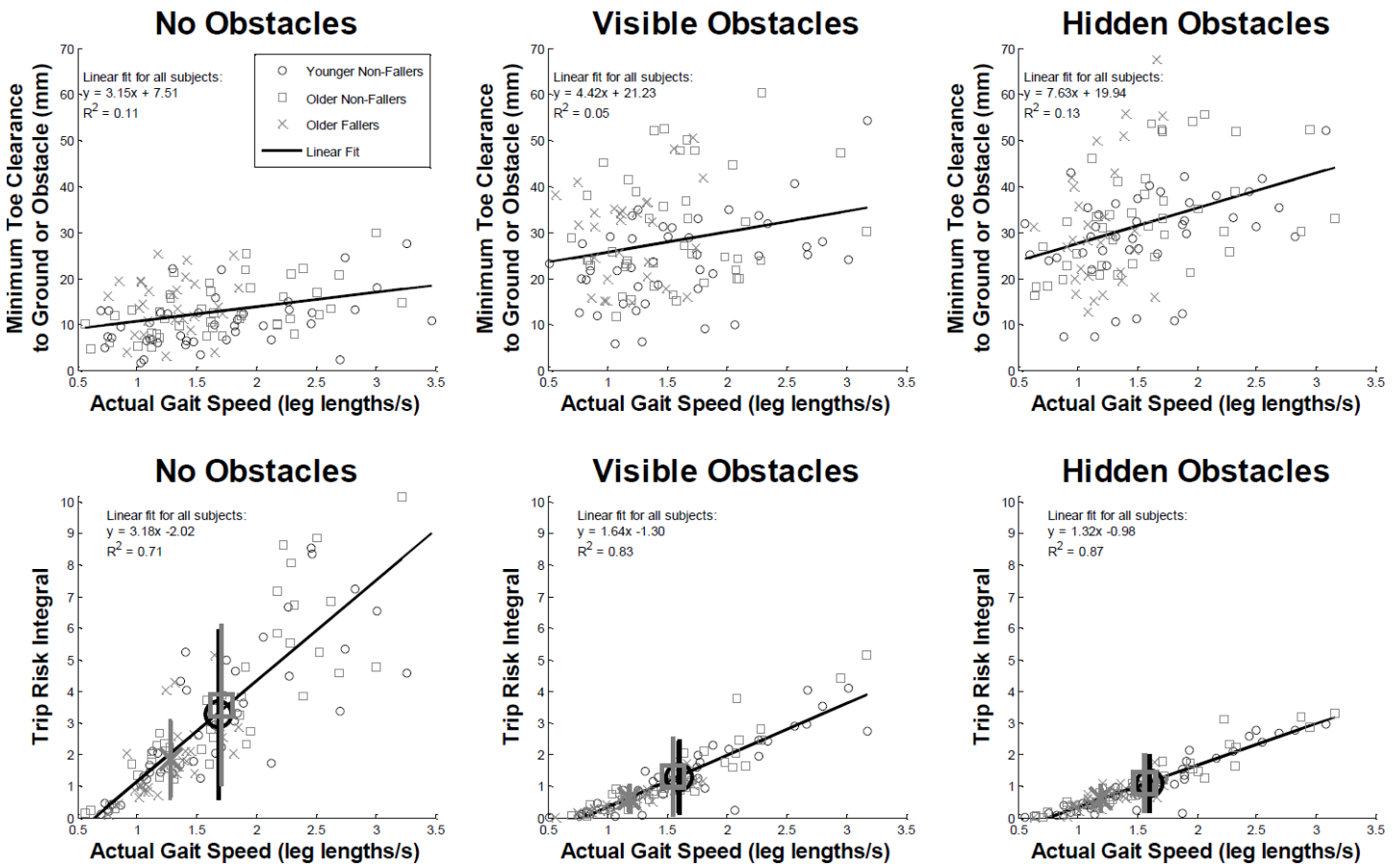


**Figure 1:** Minimum toe clearance (MTC) data (top row) and trip risk integral (TRI) data (bottom row) for younger non-fallers, older non-fallers, and older fallers while walking at three self-selected speeds (slower than preferred, preferred, and as fast as safely possible) on three surfaces: no obstacles (left column), visible obstacles (middle column), and hidden obstacles (right column). Mean  $\pm 1$  standard deviation of TRI values at mean preferred gait speed for each group indicated by large symbols with error bars to illustrate apparent TRI group effect due to slower self-selected gait speeds of fallers.

# USING DETRENDED FLUCTUATION ANALYSIS TO ASSESS SYSTEM STABILITY DURING RUNNING

<sup>1</sup>Cristine Agresta, <sup>1</sup>Jillian Peacock, <sup>1</sup>Jeffrey Housner, <sup>1</sup>Ronald Zernicke, and <sup>1</sup>Jessica Deneweth Zandler

<sup>1</sup>University of Michigan, Ann Arbor, MI, USA

email: cagresta@umich.edu, web: <http://www.mipr.kines.umich.edu>

## INTRODUCTION

Despite extensive research efforts, global risk factors for running-related injury remain largely unidentified. This gap may be due to the traditional linear methods of analysis that comprise the majority of running investigation. These analyses rely on discrete mechanical variables and examination of time-invariant means and variances rather than acknowledging the non-linear dynamics of running in which numerous system components interact to achieve healthy gait. Thus, an alternative dynamical systems approach has been proposed to better elucidate the relation among running mechanics, motor behavior, and injury [1]. This analysis involves studying the adaptability of the motor system during running via concepts related to stability, complexity, and variability.

Stride-to-stride fluctuations in gait patterns have been used to indicate system complexity and adaptability. Detrended fluctuation analysis (DFA) is a common method for examining these deviations in gait and characterizes the statistical persistence (long-range correlation) of a time-series through a single value  $\alpha$ :  $\alpha = 0.5$  indicates no persistence (i.e., white noise);  $\alpha < 0.5$  indicates anti-persistent correlation, in which deviation in one direction is statistically more likely to be followed by deviation in the *opposite* direction, and  $\alpha > 0.5$  indicates persistence, with deviation in one direction statistically more likely to be followed by deviation in the *same* direction. A change in  $\alpha$  in response to a perturbation or a biological stressor may lend insight into motor system flexibility to environmental or task demands. The breakdown of long-range correlations (decreased  $\alpha$ ) in walking gait has typically been viewed as a loss of system complexity and global stability that contributes to functional deterioration often seen with aging and disease. Recently, long-range correlations have been examined in healthy and injured runners in response to changes in running

speed, fatigue, or footwear [2,3,4]. However, unlike walking, there is not a clear direction that delineates healthy versus at-risk (injured) runners. Likewise, interpretation of  $\alpha$  to indicate positive or negative gait adaptation remains unclear.

An important first step in applying these methods to running injury research is to clarify the interpretation of  $\alpha$ . Our primary purpose was to explore changes in long-range correlations in response to an enforced gait perturbation. We sought to determine the extent to which values were predictive of adaptive performance and whether experience (skill mastery) influenced adaptive performance or global system stability.

## METHODS

Forty distance runners (26 M;  $35.6 \pm 10.3$  years old) participated in this study. Runners were free of musculoskeletal injury and had not attempted gait retraining in the last 12 months preceding data collection. Runners were categorized into three groups based on years of distance running experience: 1) novice (0-3 years) 2) intermediate (4 – 10 years) 3) experienced (10+ years).

Participants ran on an instrumented treadmill (h/p/cosmos, Zebris Medical, Germany) at a self-selected speed. Five different step frequencies [150, 160, 170, 180, 190 beats per minute (bpm)] were enforced via an audible metronome and participants were asked to match their footfalls to the beat. Pressure data (120 Hz) were collected from the treadmill using commercial software (Noraxon MyoResearch 3.8) and used to calculate spatiotemporal measures. Metronome onset began after 1 min of free running and lasted for 3 min. The audible beat was washed out with 2 min of white noise and 1 min of silence, for a total trial duration of 7 min. Enforced step frequency order was randomized. Adaptation and de-adaptation were

measured as the time to reach a plateau after onset and cessation of the metronome, respectively.

Generalized linear mixed models were used to determine the extent to which the strength of long-range correlations changed from baseline measures during and following cessation of enforced step frequency perturbations. Additionally, the influence of running experience on  $\alpha$  was examined.

## RESULTS AND DISCUSSION

Baseline  $\alpha$  values did not predict adaptive performance ( $p = 0.30-0.88$ ). However, stride time  $\alpha$  was significantly different between the perturbation and post-perturbation periods ( $p = 0.001$ , Figure 1). All runners had lower  $\alpha$  values during the perturbation period compared to baseline levels. These changes are in line with previous work suggesting the metronome induces a less complex pattern or requires corrective action to maintain stability. Interestingly, values post-perturbation did not return to baseline for any group and were highly variable.

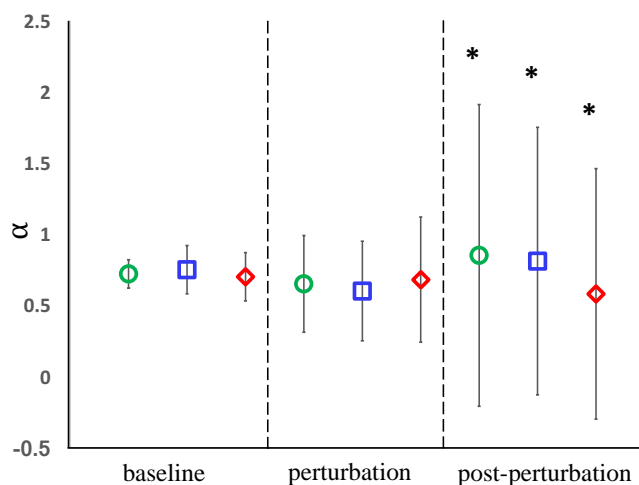


**Figure 1:** Strength of long-range correlations ( $\alpha$ ) for stride time across periods. Green circles: novice; blue squares: intermediate; red diamonds: experienced.

Experience appeared to positively influence adaptability. Baseline  $\alpha$  values were significantly influenced by experience ( $p < 0.05$ ). Likewise, more experienced runners had shorter adaptation times,

were better able to match the desired step frequency, were less perturbed (lower step frequency drift), and were able to successfully match enforced frequencies further away from their preferred step frequency. Experienced runners displayed weaker long-range correlations post-perturbation while correlations in the novice group became stronger.

There is debate about the interpretation of  $\alpha$  in relation to optimal function. Some suggest a higher correlated signal ( $\alpha = 1$ ) is optimal [5] while others suggest an increased correlation represents decreased dynamical degrees of freedom and less flexibility to adapt to perturbations [4]. Given that novice runners have a much higher rate of injury [6] and years of experience usually implies advanced motor skill, it would appear that weaker correlations (lower  $\alpha$ ) are more advantageous for injury resiliency in runners. This is supported by our findings that more running experience corresponded to better adaptive performance. However, the large variability during the post-perturbation period suggests that there is a subject-specific response that warrants further investigation.

## CONCLUSIONS

Nonlinear analysis of long-range correlations during continuous running gait detected changes in response to an external perturbation. This method has the potential to facilitate identification of injury-prone behavior patterns. More research is needed to confirm the appropriate  $\alpha$  interpretation, determine subject-specific responses, and assess sensitivity to specific perturbations.

## REFERENCES

1. Jordan K, et al. *Gait Posture*, **24**, 120-125, 2006.
2. Meardon SA, et al. *Gait Posture*, **33**, 36-40, 2011.
3. Mann R, et al. *Gait Posture*, **42**, 91-95, 2015.
4. van Emmerik REA, et al. *JSHS*, **5**, 3-13, 2016.
5. Hausdorff JM, et al. *J Appl Physiol*, **80**, 1448-1457, 1996.
6. Videbaek S, et al. *Sports Med*, **45**, 1017-1026, 2015.

## ACKNOWLEDGMENTS

This study was funded, in part, by the Michigan Institute for Clinical Health Research, grant UL1TR000433.

# DO INVERTED PENDULUM MODELS OF STABILITY MAKE CONSISTENT PREDICTIONS OF DYNAMIC BALANCE FOR ASSESSING POWERED PROSTHESIS PERFORMANCE ON STAIRS?

<sup>1,2</sup>Nathaniel T. Pickle, <sup>3,4</sup>Jason M. Wilken, <sup>3</sup>Jennifer M.A. Whitehead, <sup>1,5</sup>Nicholas P. Fey and <sup>2</sup>Anne K. Silverman

<sup>1</sup> Depts. of Bioengineering and Mechanical Engineering, University of Texas at Dallas, Richardson, TX, USA

<sup>2</sup>Dept. of Mechanical Engineering, Colorado School of Mines, Golden, CO, USA

<sup>3</sup> Center for the Intrepid, Brooke Army Medical Center, JBSA Ft. Sam Houston, TX, USA

<sup>4</sup>Extremity Trauma and Amputation Center of Excellence, JBSA Ft. Sam Houston, TX, USA

<sup>5</sup>Dept. of Physical Medicine & Rehabilitation, UT Southwestern Medical Center, Dallas, TX, USA

email: nathaniel.pickle@utdallas.edu

## INTRODUCTION

Maintaining dynamic balance while walking on stairs is challenging, particularly for people with a transtibial amputation, who have lost the function of the ankle muscles. A previous study of the range of whole-body angular momentum ( $H$ ) found that powered prostheses do not substantially alter dynamic balance on stairs relative to passive prostheses [1]. Alternative measures of balance based on an inverted pendulum model, such as the extrapolated center of mass [2], foot placement estimate [3,4], and capture point [5,6], may provide new insights. However, muscle power generation/absorption and leg length changes that occur during stair walking may affect some models more than others. Thus, our goals in this study were to 1) compare the three inverted pendulum models and 2) correlate inverted pendulum models and  $H$  in people with a transtibial amputation using powered and passive prostheses on stairs.

## METHODS

Nine able-bodied people (7M/2F, 24.1±5.5 yrs, 92.6±9.2 kg, 1.80±0.10 m) and nine people with transtibial amputation (8M/1F, 30.0±5.6 yrs, 95.6±6.6 kg, 1.81±0.09 m) walked on a 16-step instrumented staircase at a controlled cadence while whole-body kinematics were collected (120 Hz).

We calculated the sagittal-plane extrapolated center of mass (XCOM, Fig. 1a, Eq. 1), with gravitational acceleration  $g$  and constant leg length  $L$  from a static trial.

$$XCOM = x_{COM} + v_x \sqrt{\frac{L}{g}} \quad (1)$$

The foot placement estimate (FPE, Fig. 1b) allows variable leg length (Eq. 2) and incorporates instantaneous  $H$ , expressed as  $J_{COM}\omega_1$ . Conservation of  $H$  about the FPE during foot contact is assumed (Eq. 3), and conservation of energy is applied so the COM comes to rest above the FPE (Eq. 4). Solving numerically for  $\phi$  gives the FPE location.

$$L(\phi) = \frac{h_n}{\cos\phi}, \quad (2)$$

$$mL(\phi)[v_x \cos\phi + v_y \sin\phi] + J_{COM}\omega_1 = [mL(\phi)^2 + J_{COM}]\omega_2 \quad (3)$$

$$\frac{1}{2}[J_{COM} + mL(\phi)^2]\omega_2^2 + mgL(\phi) \cos\phi = mgL(\phi) \quad (4)$$

The capture point (CAP, Fig. 1c) was computed by numerically integrating the system equations of motion (Eqs. 5 and 6) so the center of mass (COM) follows its experimentally measured trajectory  $y_{COM}$  and comes to rest above the CAP location.

$$\ddot{x} = \frac{(x_{COM} - x_{CAP})(g + \frac{d^2 y_{COM}}{dx^2} \dot{x}_{COM}^2)}{(y_{COM} - y_{CAP}) - (x_{COM} - x_{CAP}) \frac{dy_{COM}}{dx}} \quad (5)$$

$$\ddot{y} = \frac{(y_{COM} - y_{CAP}) \frac{d^2 y_{COM}}{dx^2} \dot{x}_{COM}^2 + g(x_{COM} - x_{CAP}) \frac{dy_{COM}}{dx}}{(y_{COM} - y_{CAP}) - (x_{COM} - x_{CAP}) \frac{dy_{COM}}{dx}} \quad (6)$$

Stability metrics were computed as the distance between the XCOM, FPE, and CAP x-locations and the x-location of the leading toe at heel strike ( $u_{max}$ , Fig. 1a), normalized by static leg length.

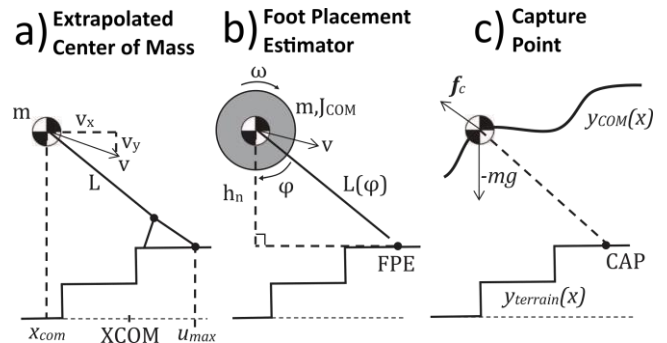


**Figure 1:** Inverted pendulum model diagrams.

Results were compared with a three-factor, repeated measures ANOVA with walking condition, leg type, and metric as fixed effects and subject as a random effect. Pairwise comparisons were adjusted using Tukey's method when significant main or interaction effects were found. We also analyzed the correlation between each stability metric and the range of sagittal-plane  $H$ . All statistical tests had  $\alpha=0.05$ .

## RESULTS AND DISCUSSION

The main effects were all significant ( $p<0.001$ ), as were the interaction effects of condition by leg ( $p<0.001$ ) and condition by metric ( $p<0.001$ ). During stair ascent the effective leg length at heel strike was approximately 20% smaller than in static standing. However, during stair ascent the mean differences were  $0.009\pm 0.005$  (XCOM vs CAP) and  $0.02\pm 0.006$  (XCOM vs FPE), compared to level-ground where the differences were  $0.01\pm 0.006$  (XCOM vs CAP) and  $0.06\pm 0.008$  (XCOM vs FPE). Thus, inverted pendulum models were not highly sensitive to violations of leg length assumptions in stair walking.

There were significant, although small, correlations between the stability metrics and range of sagittal-plane  $H$  in stair descent ( $r\cong -0.19$ ,  $p\leq 0.008$ ), but not in stair ascent. However, a *post hoc* analysis revealed a stronger correlation between the instantaneous value of  $H$  at heel strike and the FPE metric ( $r=-0.50$ ,  $p<0.001$ ). This result indicates that foot placement is important for regulating  $H$  at heel-strike. However, mechanisms like muscle force generation are critical for regulating  $H$  throughout the gait cycle.

Stability metrics were generally more positive in the amputated versus the intact leg, suggesting a conservative prosthetic foot placement strategy. However, when using the powered prosthesis, the

metrics were not significantly different between the amputated and intact legs in stair ascent, suggesting that prosthetic ankle power may help restore bilateral symmetry of dynamic balance during this task.

## CONCLUSIONS

Inverted pendulum models of stability do not appear highly sensitive to leg length assumption violations in stair walking. Foot placement helps regulate  $H$  in early stance, but other mechanisms (e.g., muscle force generation to regulate the net external moment) are also important throughout the gait cycle. People with a transtibial amputation use a conservative prosthetic leg strategy, and powered prosthesis use increases step symmetry in stair ascent.

## ACKNOWLEDGMENTS

The authors thank Kelly Ohm and Audrey Westbrook for assisting with data collection and processing. This work was supported by NIH NICHD Award R03HD075946.

## REFERENCES

1. Pickle NT, et al. *J Biomech* **47**, 3380-9, 2014.
2. Hof AL, et al. *J Biomech* **38**, 1-8, 2005.
3. Wight DL, et al. *J Comput Nonlin Dyn* **3**, 011009-011009-10, 2008.
4. Millard M, et al. *J Biomech Eng-T ASME* **131**, 121001-121001-7, 2009.
5. Pratt J, et al. *Proc 6<sup>th</sup> IEE-RAS Int Conf Hum Rob*, 200-207, 2006.
6. Ramos OE and Hauser K. *Proc 15<sup>th</sup> IEEE-RAS Int Conf Hum Rob*, 851-858, 2015.

The views expressed herein are the authors' and do not reflect the official policy or position of Brooke Army Medical Center, the U.S. Army Medical Dept., the U.S. Army Office of the Surgeon General, the Dept. of the Army, Dept. of Defense, the National Institutes of Health or U.S. Government.

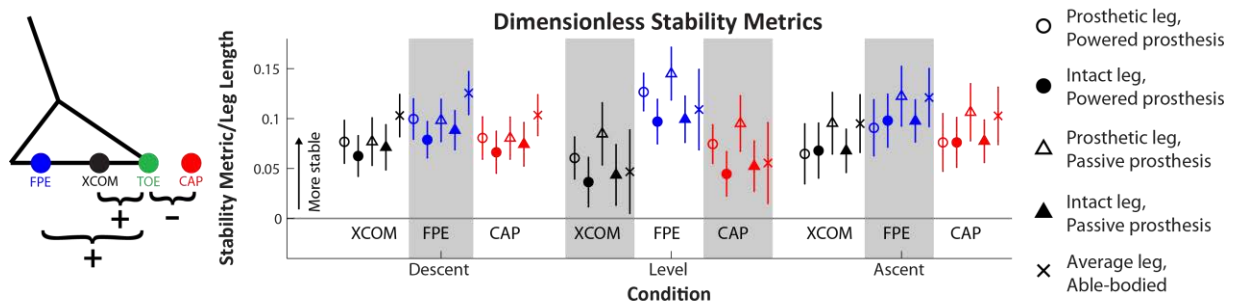


**Figure 2:** Stability metrics for XCOM (black), FPE (blue), and CAP (red).

# DOES DYNAMIC STABILITY GOVERN PROPULSIVE FORCE GENERATION IN HUMAN WALKING?

Michael G. Browne and Jason R. Franz

University of North Carolina at Chapel Hill and North Carolina State University, Chapel Hill, NC, USA  
email: mgbrowne@email.unc.edu, web: http://abl.bme.unc.edu

## INTRODUCTION

Older adults are at an exceptionally high risk of falls, and most of these falls occur during locomotor activities such as walking. Older adults may thus opt to walk slower to improve their resilience to unexpected balance challenges and mitigate their risk of falls. However, prior to eliciting slower preferred speeds, advancing age is accompanied by a precipitous reduction in propulsive forces ( $F_P$ ) exerted during the push-off phase of walking. Winter et al. (1990) originally proposed that many of the hallmark biomechanical features of elderly gait, including reductions in  $F_P$  generation during push-off, reflect the adoption of a safer, more stable pattern of movement [1]. Accordingly, older adults may walk with smaller propulsive forces even prior to walking slower to prioritize stability over mobility. However, direct evidence for tradeoffs between propulsive force generation and walking balance control, independent of changes in walking speed, has remained allusive. As an important first step, the purposes of this study were to investigate: (1) the independent effects of walking speed and  $F_P$  generation on dynamic stability in young adults, and (2) the extent to which young adults prioritize

dynamic stability in selecting their preferred combination of walking speed and  $F_P$  generation. We tested two intuitively sound, but mutually exclusive hypotheses: (i) that walking slower or with smaller  $F_P$  would improve dynamic stability, and (ii) that young adults prefer a combination of walking speed and  $F_P$  generation that maximizes dynamic stability.

## METHODS

Young adult subjects participated in two different but complementary experiments: 12 subjects participated in Experiment 1 (mean  $\pm$  standard deviation, age:  $26.2 \pm 3.1$  years, 6 males/6 females) and 10 subjects participated in Experiment 2 (age:  $24.8 \pm 5.4$  years, 5 males/5 females). Experiment 1 and Experiment 2 both utilized a novel visual biofeedback paradigm based on real-time force measurements from a dual-belt force measuring treadmill (Bertec, Corp., Columbus, OH) (Fig. 1). Specifically, for trials involving this biofeedback paradigm, a custom Matlab (Mathworks, Natick, MA) script continuously computed the average bilateral peak  $F_P$  during push-off from each set of four consecutive steps and projected a visual representation of those values as dots in real-time to

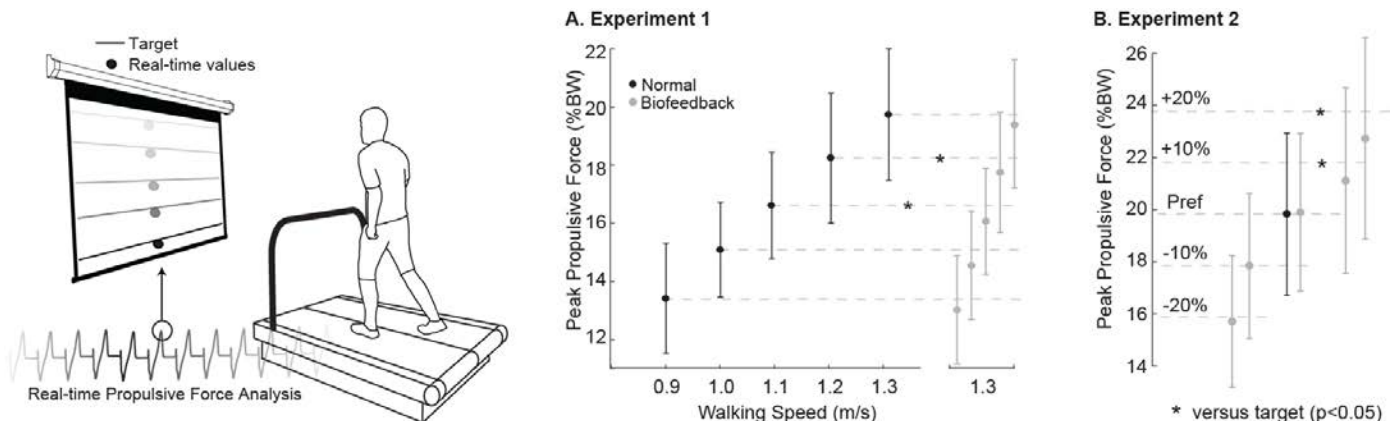


**Figure 1:** Visual biofeedback of  $F_P$  was used in Experiments 1 and 2. Experiment 1 targets were prescribed as  $F_P$  from the slower walking speeds. Experiment 2 prescribed  $\pm 10$  and  $\pm 20\%$  changes in  $F_P$  at preferred speed.

a screen positioned in front of the treadmill (Fig. 1). For Experiment 1, subjects first walked at a range of speeds, from 0.9 to 1.3 m/s in 0.1 m/s increments. Subjects then walked at 1.3 m/s while matching their instantaneous  $F_P$  to target values representing the average extracted from the slower speeds (Fig. 1A). In Experiment 2, subjects first walked at their preferred overground walking speed. Subjects then walked while matching target values representing  $\pm 10$  and  $\pm 20\%$  of preferred  $F_P$  (Fig. 1B). Using motion capture data, we constructed a state vector from the time series of sacrum position and velocity in the anterior-posterior (AP), mediolateral (ML), and vertical directions to calculate short-term maximum divergence (i.e., Lyapunov,  $\lambda_s$ ) exponents [2, 3]. Finally, we analyzed the variability of sacrum kinematics given its complement to dynamic stability within the context of balance control.

## RESULTS AND DISCUSSION

Subjects successfully modulated their  $F_P$  in accordance with all prescribed biofeedback targets (Fig. 1) and biofeedback itself (i.e., normal walking vs. walking with targets representing normal walking) had no discernible effect on dynamic stability. In Experiment 1, walking slower improved dynamic stability despite increasing ML variability. Walking with smaller  $F_P$ , however, increased  $\lambda_s$  by up to 30% (Fig. 2A), with the largest effects in the ML direction. In Experiment 2, increasing or decreasing the  $F_P$  subjects exerted when walking normally at their preferred speed negatively affected metrics of dynamic stability (Fig. 2B). Specifically, walking with 20% larger or smaller than preferred  $F_P$  increased  $\lambda_s$  by 14% and 17%, respectively. In contrast, all components of sacrum variability decreased monotonically with smaller  $F_P$  across the range of biofeedback targets presented (e.g., Fig 2D).

## CONCLUSIONS

Our findings provide the first empirical evidence that that walking slower and walking with smaller  $F_P$  elicit very different effects on local dynamic stability. Consistent with prior studies, walking slower improved dynamic stability despite

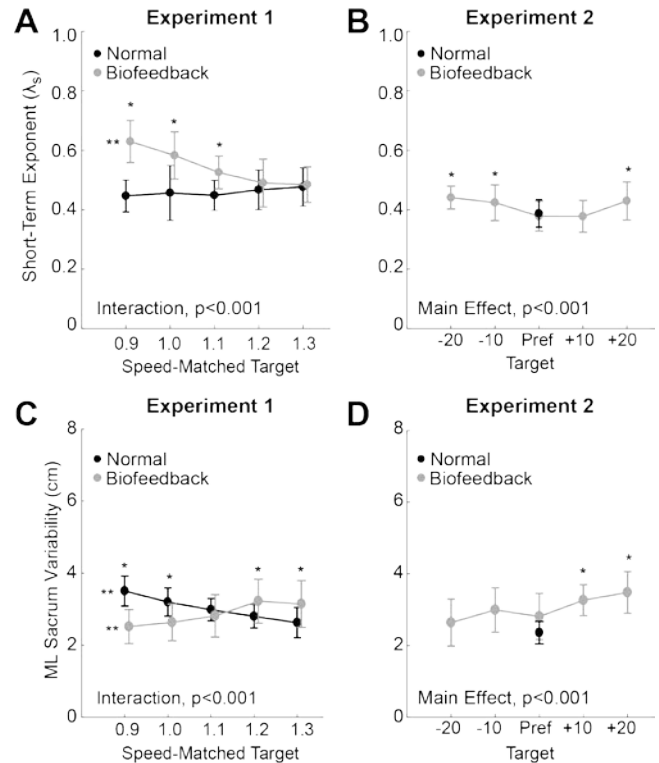


**Figure 2:** Group mean (SE) short-term divergence exponents and ML sacrum variability during walking in Experiment 1 and Experiment 2.

increasing movement variability in young adults. However, contrary to our first hypothesis, walking with smaller  $F_P$  reduced dynamic stability compared to walking normally. Rather, more consistent with our second hypothesis, our findings suggest that young adults adopt an  $F_P$  at their preferred walking speed that maximizes dynamic stability. The age-related reduction in propulsive force generation is likely multifactorial, but precedes the slowing of preferred speed. Winter et al. [1] originally proposed that older adults may reduce  $F_P$  to prioritize stability over mobility. Although an intuitively sound hypothesis, our findings instead allude to unfavorable consequences of reduced propulsive force generation on dynamic stability that may ultimately precipitate walking slower.

## REFERENCES

1. Winter D, et. Al. *Phys Ther.* **70(6)**, 340-7, 1990.
2. Kang H and Dingwell J. *J Biomech*, **27(4)**, 572-7, 2008.
3. Franz J, et. Al. *Hum Mov Sci.* **40**, 381-92, 2015.

# AGING EFFECTS ON LEG JOINT VARIABILITY DURING WALKING IN THE PRESENCE OF OPTICAL FLOW PERTURBATIONS

Mu Qiao, Jody A. Feld, and Jason R. Franz

University of North Carolina at Chapel Hill and North Carolina State University, Chapel Hill, NC, USA

Email: [mu\\_qiao@med.unc.edu](mailto:mu_qiao@med.unc.edu), web: <http://abl.bme.unc.edu/>

## INTRODUCTION

Balance control in older adults is much more susceptible to optical flow perturbations during walking than in young adults, presumably governed by an age-related dependence on visual feedback for motor planning and execution [1, 2]. Balance corrections issued by the central nervous system manifest first at the individual muscle and joint levels before ultimately eliciting adjustments in foot placement from one step to the next. Kinematic variability can provide insight into the magnitude of these step-to-step corrections [3]. However, we currently lack an individual joint-level understanding of how aging affects the neuromechanical strategies used to accommodate optical flow perturbations. Therefore, our purpose was to investigate the effects of aging on leg joint kinematic variability during walking with and without optical flow perturbations of different amplitudes. First, we hypothesized that leg joint variability would: 1) vary across the gait cycle, and 2) increase in the presence of optical flow perturbations. We also hypothesized that, compared to those in young adults, the effects of optical flow perturbations on leg joint variability would be larger and more pervasive in older adults.

## METHODS

11 healthy young (mean±sd, age: 24.8±4.8 years, 5 male, 6 female) and 11 healthy older adults (age: 75.3±5.4 years, 5 male, 6 female) participated. Young subjects walked at 1.25 m·s<sup>-1</sup> and older subjects walked at their preferred overground speed (1.19±0.20 m·s<sup>-1</sup>,  $p=0.15$ ) on an instrumented dual-belt treadmill (Bertec Corp., Columbus, OH). While walking, subjects watched a speed-matched, virtual hallway rear-projected onto a semi-circular screen surrounding the treadmill both with and without continuous mediolateral oscillations of optical flow, applied as the sum of three sine waves (0.125, 0.250, and 0.442 Hz) (Fig. 1). In fully-randomized order, subjects walked for 2 min each with and without

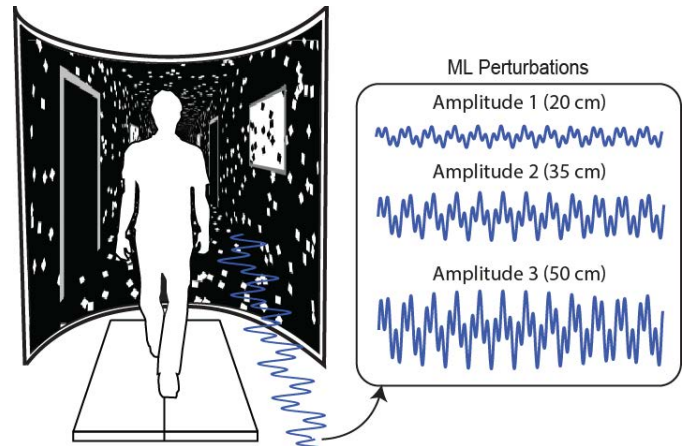


**Figure 1.** Experimental setup and time series of the three optical flow perturbation amplitudes.

optical flow perturbations prescribed by three amplitudes (20, 35, and 50 cm, Fig. 1). A 14-camera, three-dimensional motion capture system (Motion Analysis Corp., Santa Rosa, CA) operating at 100 Hz recorded the trajectories of 33 retroreflective markers placed on the right and left foot, shank, and thigh, and on the pelvis. We calculated hip, knee, and ankle joint kinematics using a global optimization inverse kinematics routine. We calculated time series of sagittal plane hip, knee, and ankle joint angles, and coronal plane hip joint angle. From these, we calculated stride-averaged profiles and the variability of leg joint kinematics using the mean and standard deviation of each outcome measure over the gait cycle. A mixed design 3-way factorial ANOVA determined effects of and interactions between age (young vs. old), perturbation amplitude (0 vs. 20, 35, and 50 cm), and gait cycle (10% bins).

## RESULTS AND DISCUSSION

As hypothesized, during normal walking, hip, knee, and ankle variabilities differed significantly across phases of the gait cycle ( $p$ 's<0.001), and all joints reached their maximum variability immediately following toe-off (*i.e.*, 60-70% cycle) (Fig. 2). Compared to young adults, older adults walked

normally with 33% larger coronal plane hip variability ( $p=0.014$ , Fig. 2D), but no difference in sagittal plane hip ( $p=0.074$ , Fig. 2B), knee ( $p=0.091$ , Fig. 2F), or ankle ( $p=0.091$ , Fig. 2H) joint variabilities.

In young adults, we found a significant effect of perturbation amplitude only on coronal plane hip joint variability ( $p=0.014$ , Fig. 2C), which increased by 39% compared to unperturbed walking. However, in young adults, significant interactions in the sagittal plane revealed that perturbations increased hip joint variability only during midstance and ankle joint variability only at initial contact and terminal stance (hip:  $p=0.020$ , Fig. 2A; ankle  $p<0.001$ , Fig. 2G). As hypothesized, in contrast to their effects in young adults, the effects of optical flow perturbations on leg joint variabilities were larger and much more pervasive in older adults. For example, only in older adults did we find that the increase in coronal plane hip joint variability in the

presence of perturbations ( $p=0.016$ , Fig. 2D) was accompanied by larger sagittal plane hip ( $p=0.045$ , Fig. 2B), knee ( $p=0.048$ , Fig. 2F), and ankle ( $p=0.010$ , Fig. 2H) joint variabilities. These larger effects of perturbations in older adults also manifested over more phases of the gait cycle than in young adults. Moreover, in contrast to young adults who scaled their leg joint variabilities progressively with increasing perturbation amplitude, older adults did not scale their response and were instead disproportionately susceptible to even the smallest amplitude perturbation. Compared to young adults, 20 cm perturbations increased sagittal plane hip, knee, and ankle joint variabilities by an average of 211%, 88%, and 63% more, respectively, and coronal plane hip variability by an average of 68% more in older adults.

## CONCLUSIONS

This study provides joint-level insight into aging effects on the neuromechanical strategies used to regulate walking balance. We first conclude that leg joint variability during walking is phase dependent, with step-to-step adjustments in hip, knee, and ankle joint kinematics occurring predominantly during push-off. Second, young adults accommodated mediolateral optical flow perturbations almost exclusively by increasing variability in coronal plane hip joint angle, likely to orchestrate step-to-step adjustments in lateral foot placement. Finally, in contrast to the localized adjustments in young adults, the same perturbations elicited larger and more pervasive increases in all joint variability outcome measures in older adults. This latter finding suggests that aging not only increases the susceptibility to optical flow perturbations but also negatively affects the joint-level neuromuscular control of walking balance.

## ACKNOWLEDGEMENTS

Jessica Thompson and Heather Stokes for help with data collection. Supported by NIH (UL1TR001111).

## REFERENCES

1. Franz, J.R., et al., IEEE Transactions on Neural Systems and Rehabilitation Engineering, In Press.
2. Franz, J.R., et al., Human Movement Science, 2015. **40**: p. 381-392.
3. Dingwell, J.B., J. John, and J.P. Cusumano, PLoS Computational Biology, 2010. **6**(7): p. 1-15.

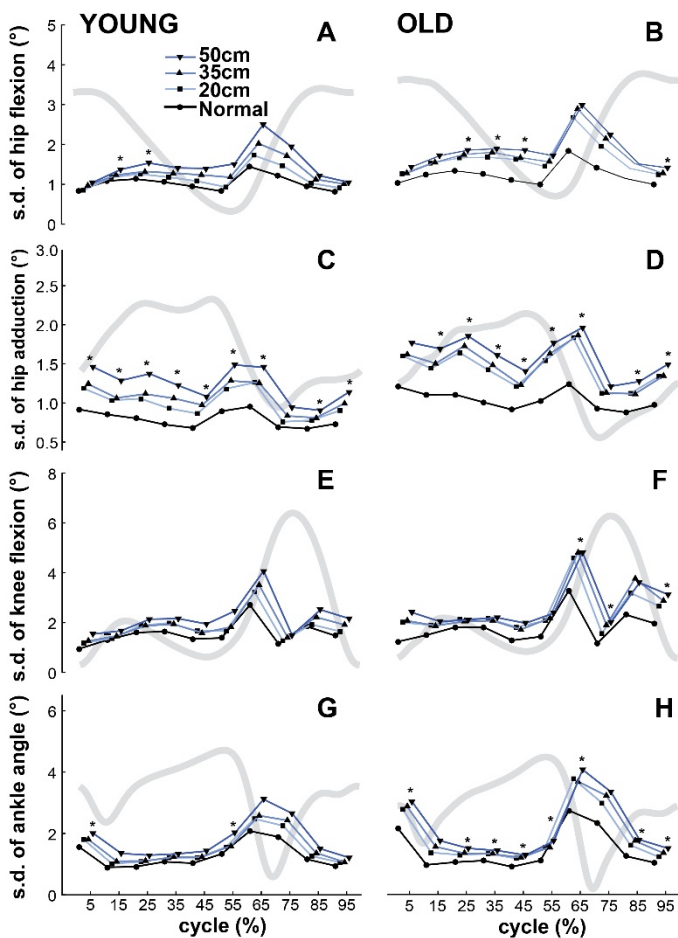


**Figure 2.** Group mean leg joint variabilities (s.d.: standard deviation) in young and older adults. Gray lines show joint angles during normal walking. Asterisks indicate perturbation effects ( $p<0.05$ ).

# HOW HEALTHY OLDER ADULTS NEGOTIATE STEPPING OBJECTS WHILE WALKING

<sup>1</sup>Mandy M. Salinas, <sup>1</sup>Darla M. Castelli, and <sup>1</sup>Jonathan B. Dingwell

<sup>1</sup>The University of Texas at Austin, Austin, TX, USA  
email: flyingcape@austin.utexas.edu

## INTRODUCTION

Executive function (EF) encompasses multiple cognitive processes. A set of skills necessary to formalize goals, plan, strategize, and suppress task-irrelevant information [1]. In everyday life, EF may directly affect walking in contexts that challenge how individuals modify their stepping. Here, we manipulated the cognitive demand of walking by introducing virtual stepping objects (targets and obstacles) designed to disturb the normal walking pattern. We explored how both physical and EF measures affected stepping error performance.

## METHODS

Twenty-one young healthy adults (YH; age 18-29 years) and twenty-one older healthy adults (OH; age 60+ years) walked on a treadmill at  $v_w = 1$  m/s. In the first condition (NWalk), participants were instructed to simply walk. In following two conditions, virtual stepping objects appeared on the treadmill (Fig. 1); and in both conditions, 80% of the stepping objects were colored yellow. Participants were instructed to step on yellow objects (GoYel) while avoiding red objects, and then to step on red objects (GoRed) while avoiding yellow objects. The GoYel Condition accustomed participants to step on yellow objects 80% of the walking trial. The GoRed Condition required participants to *inhibit* this stepping response (i.e. step on yellow) 80% of the trial. Participants completed two 3 minutes trials per condition. Stepping errors partitioned into Go Errors (missed targets) and NoGo Errors (stepped on obstacles).

PHYSICAL AND EF ASSESSMENTS: Each participant also completed a cognitive battery (including MMSE, Go-NoGo Task and Stroop Task; Fig. 2) and several physical (including Timed Up And Go, overground Preferred Walking Speed, and isometric knee extension strength) assessments.

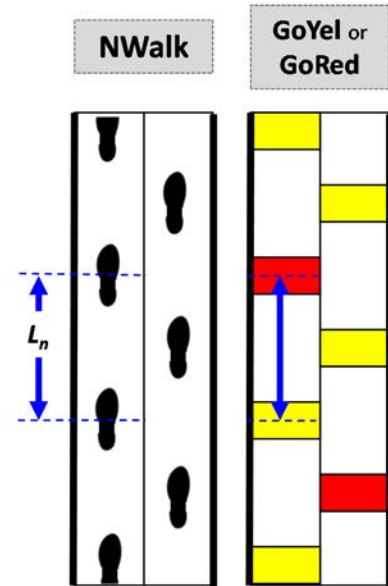


Figure 1: Three Experimental Walking Conditions

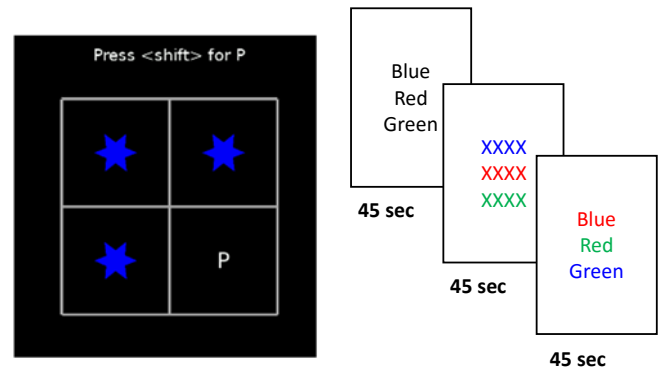
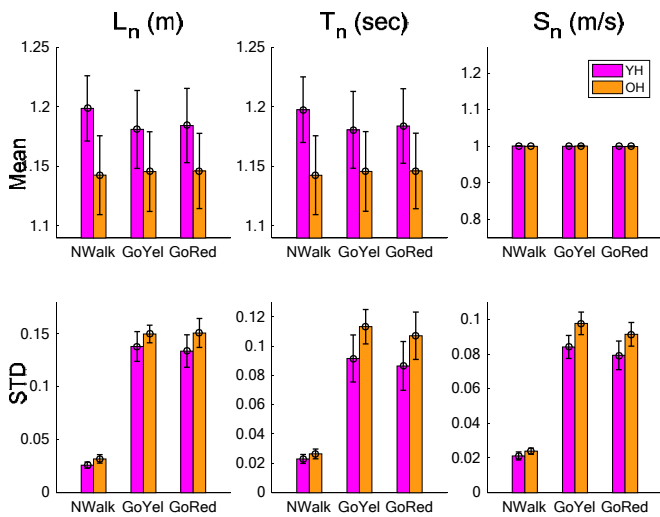


Figure 2: Go-NoGo (GNG) and Stroop Tasks (ST). These cognitive tasks evaluate response inhibition.

## RESULTS AND DISCUSSION

OH adults took shorter and faster strides compared to YH adults (Fig. 3) across all conditions. When virtual stepping objects were introduced (GoYel & GoRed), all participants exhibited increased stepping variability in stride length  $L_n$ , stride time  $T_n$  and stride

speed  $S_n$  (Fig. 3). However, across all conditions, OH adults exhibited greater stepping variability compared to YH adults.



**Figure 3:** Stride Parameter Means and Variability for both YH and OH adults.

STEPPING ERRORS: OH adults made more total stepping errors in both GoYel and GoRed compared to YH adults (top row, Fig. 4).

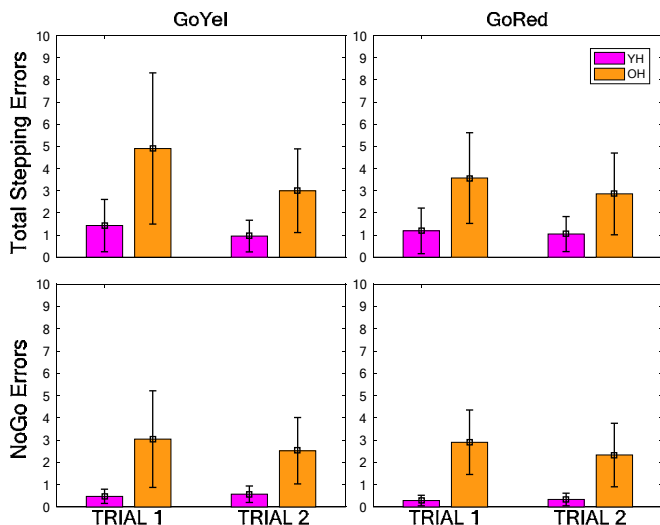


**Figure 4:** Total Stepping Errors and NoGo Errors (stepping on an obstacle) in both object conditions (both Trial 1 and 2 shown).

However, when the total stepping errors were partitioned, OH adults made more NoGo Errors (stepping on an obstacle) compared to YH adults (bottom row, Fig. 4) in both object conditions.

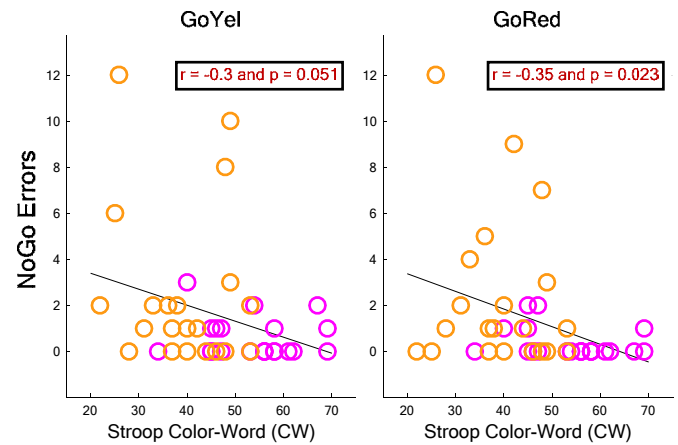


**Figure 5:** Stroop Color-Word (CW) Performance versus stepping NoGo Errors during both object conditions (Trial 2 data shown).

PHYSICAL & EF: OH adults ( $1.48 \pm 0.1$  m/s) preferred slightly faster overground walking speeds compared to YH adults ( $1.33 \pm 0.1$  m/s). For Timed Up and Go (TUG) times, OH adults ( $7.87 \pm 0.4$  sec) were slightly slower than YH adults ( $7.32 \pm 0.5$  sec). OH adults demonstrated slightly less isometric quadriceps strength compared to YH adults. However, no associations were found between any of the physical measures and stepping errors (not shown).

Reduced response inhibition was observed in OH adults compared to YH adults in the Stroop CW condition (not shown). Further, Stroop CW performance was weakly associated with stepping NoGo Errors in the GoRed condition (Fig. 5).

## CONCLUSIONS

Introducing virtual stepping objects within the walking task disrupted the normal walking pattern and did significantly alter walking variability across all participants. OH adults were less successful at negotiating stepping *obstacles* compared to stepping targets. Stepping error performance appeared to be weakly associated to EF (Stroop CW), but was not associated to any of the physical measures

## REFERENCES

1. Rabbitt P. *Methodology of frontal executive function*, 1-38, 1997.

## **JIM HAY MEMORIAL SESSION: MUSCLE-TENDON-UNIT MECHANICS OF THE LOWER EXTREMITY: LESSONS LEARNED FROM SPORT**

<sup>1</sup>Richard L. Lieber, <sup>2</sup>Bing Yu, <sup>3</sup>Darryl G. Thelen, <sup>3</sup> Silvia S. Blemker, <sup>4</sup>Jill L. McNitt-Gray, <sup>5</sup>Walter Herzog

<sup>1</sup> Shirley Ryan AbilityLab, Chicago, IL; <sup>2</sup> University of North Carolina, Chapel Hill, NC;

<sup>3</sup> University of Virginia, Charlottesville, VA; <sup>4</sup> University of Southern California, Los Angeles, CA;

<sup>5</sup> University of Calgary, Calgary, AB

email: mcnitt@usc.edu; walter@kin.ucalgary.ca

This session is dedicated to the memory of Jim Hay, a pioneer in the field of sport and exercise biomechanics and a founding member of ASB. The Jim Hay Memorial Award recognizes the originality, quality, and depth of biomechanics research that addresses fundamental research questions relevant to extraordinary demands imposed in sport and exercise. The Jim Hay Memorial Lecture will be followed by three invited presentations all on the topic of muscle-tendon unit mechanics in the context of sport. The following represents a brief summary of our discussion and the order of presentations for the 2017 meeting.

### **Biomechanical Studies of Muscle Injury**

Richard L. Lieber  
Shirley Ryan AbilityLab

This lecture begins with a brief review of biomechanical and biological studies of eccentric injury in animal models. Basic muscle physiological principles will be illustrated, as well as high-resolution tools to study muscle structure. These basic studies will be used to express a paradigm where high intensity muscle contractions serve as a model to understand normal function. This should set up succeeding talks who will use some of these ideas in more applied settings.

### **Relationship Between Hamstring Flexibility and Strain in Sprinting**

Bing Yu  
University of North Carolina – Chapel Hill

Hamstring muscle injury is one of the most common injuries in sports involving sprinting. Risk factors for hamstring muscle strain injury are still not clear. The literature demonstrates that muscle injury is due to mechanical strain. Our recent studies demonstrated that hamstring muscle-tendon optimal length is correlated with flexibility, and that

hamstring muscle tendon optimal length and flexibility are correlated to the maximal strain of hamstring in sprinting. These results filled gaps in our understanding of risk factors for hamstring muscle strain injury.

### **Modulation of Muscle-Tendon Kinetics with Running Cadence and Speed**

Darryl G. Thelen  
University of Wisconsin

An understanding of muscle-tendon mechanics during running is important for balancing the risk between performance, training and injury avoidance. This talk will review modeling studies we conducted on hamstring demands during high speed running and re-distributions of muscle loading with cadence. We will also introduce a novel shear wave measurement technology which may enable objective assessments of in vivo muscle-tendon kinetics. Such information can be used for biomechanical biofeedback on running form or for tracking recovery following soft tissue injury.

### **The Converging Fiber Hypothesis and Muscle Injury**

Silvia S. Blemker  
University of Virginia

Across the human body, there are several muscles in which fibers converge from a large cross-sectional area in the mid-belly of the muscle to a small cross-sectional area of attachment at the myotendinous junction. However, the classic descriptions of muscle fiber arrangements (e.g., fusiform, pennate, bipennate) do not address the biomechanical implications of this converging fiber phenomenon. Computer models and in vivo dynamic magnetic resonance imaging studies performed by our group have revealed that muscles

with this fiber converging phenomenon have elevated localized tissue strains generally near the myotendinous junction. In this talk, I will present the hypothesis that muscles with fibers that substantially converge to a narrow attachment site have an elevated susceptibility to localized damage during contractions. Further, I will discuss the implications of this concept on (i) strain injury susceptibility in athletes, and (ii) degeneration of muscles due to elevated susceptibility to contraction-induced injury in muscle diseases.

# Material Properties of Ankle Plantarflexor and Dorsiflexor Muscles – Effect of Aging

Sabrina Lee, Amy Xie, Ada Terman, Ricardo Santana, and Kristen Jakubowski

Northwestern University, Chicago, USA

email: [s-lee@northwestern.edu](mailto:s-lee@northwestern.edu), web: <http://www.feinberg.northwestern.edu/sites/pthms>

## INTRODUCTION

Decreased motor performance with increasing age is often associated decreased muscle strength, which in turn, has been attributed to muscle atrophy and changes in muscle architecture. Increased tendon compliance has also been shown to affect muscle mechanics and has been correlated with decreased joint power during push-off. Torque-angle-based estimates of passive muscle stiffness of the ankle are increased in older adults compared in younger adults [1]. However, these methods include contributions from ligaments, joint capsule, multiple muscles and tendons. Elastography is a method that allows quantification of material properties, specifically stiffness, of individual muscles. Shear modulus, as measured using magnetic resonance elastography, showed no significant correlation between age and tissue stiffness [2]. A recent study using shear wave (SW) ultrasound elastography reported increased shear modulus with increasing age in the upper extremity biceps brachii [3]; however, the effects of aging on the lower extremity ankle muscles are unknown.

Thus, the aim of this study was to compare the material properties measured using SW ultrasound elastography, specifically stiffness, of the medial gastrocnemius (MG) and tibialis anterior (TA) between younger and older adults. SW velocity was also compared to measures of joint stiffness, as well as muscle stiffness estimates from torque-angle measures.

## METHODS

Nine young adults (four males, five females,  $21.0 \pm 3.6$  yrs) and five older adults (four males, one female,  $68.8 \pm 5.4$  yrs) participated in the study. Subjects were seated with their knee in maximum extension and their foot secured to a platform of a

dynamometer (System3Pro, Biodex). B-mode and SW elastography ultrasound measurements (Aixplorer, SuperSonic Imagine) of MG and TA muscles were captured, as well as joint angle, torque, and electromyography (Delsys) with the ankle at different angles (0 degrees dorsiflexion (DF), 15 degrees plantarflexion (PF), maximum DF, maximum PF, and two other intermediary angles) while the muscle was passive. SW ultrasound elastography measures the velocity at which shear waves propagate through the tissue [4]. Shear waves will propagate faster in a tissue that has a higher elastic shear modulus. SW velocity was also compared to passive joint stiffness, which was calculated as the change in joint torque as a function of ankle angle. Estimates of MG stiffness from the torque and ankle angle measures were also calculated. The MG moment arm for the ankle range of motion of each subject was obtained from OpenSim using the lower extremity model by Arnold et al. (2010) [5]. The passive force shared by the lateral and medial gastrocnemius was assumed to be proportional to the cross-sectional area such that the passive MG muscle was determined as 61% of the total gastrocnemius force [6]. An Analysis of Covariance was used to compare the SW velocity and joint stiffness between younger and older adults, with ankle angle as the covariate. Correlation coefficient of determination was calculated between SW velocity, joint stiffness, and muscle stiffness estimates.

## RESULTS AND DISCUSSION

Our main findings show that SW velocity in the MG of younger adults was on average 36% greater than older adults ( $p < 0.001$ ) across the ankle range of motion and 54% greater at maximum DF (Fig. 1). There was no difference in SW velocity in the TA between the two groups. Joint stiffness was significantly greater in PF in older adults ( $p = 0.032$ )

and 0.042), but tended to be less in DF compared to younger adults. These results of decreased MG stiffness, as indicated from SW velocity, but increased joint stiffness (similar to the literature) was very surprising. This suggests that MG stiffness does not contribute to the increased joint stiffness of older adults and that other soft tissues and other muscles are the main contributors. This surprising result has substantial implications to our interpretation of joint stiffness and changes in muscle mechanics due to aging. Increased Achilles tendon compliance in older adults has been suggested to affect energy storage during shortening and lengthening cycles. This may also be the case for a more compliant muscle. However, it is unclear if this is an adaptation or a result of changes in muscle composition or structure (i.e. fiber type, collagen content, extracellular matrix).

Our results also indicate that there was a significant correlation between joint stiffness and SW velocity in the MG only in the younger adults ( $r^2=0.46$ ,  $p<0.001$ ); there was no significant correlation between joint stiffness and SW velocity of the TA in both groups. There was no correlation between SW velocity and muscle stiffness estimates from torque-angle measurements. This further suggests that changes in muscle stiffness may be muscle specific and that individual contributions of passive stiffness of muscles and other soft tissues to joint stiffness differ due to aging.

### CONCLUSIONS

These findings indicate that muscle stiffness, as indicated by SW velocity, of the MG is greater in younger adults compared to older adults across the ankle range of motion with the largest difference when the muscle was at the longest. The lack of difference in SW velocity in the TA due to aging suggests that these changes may not be systemic such that all muscles are not affected equally. Tissues other than the primary plantarflexor and dorsiflexors of older adults may contribute differently to joint stiffness than in younger adults. This work has implications for refining and developing training programs focused on muscle properties to prevent mobility loss.

### REFERENCES

1. Gajdosik RL. *Isokinetics Exer* **6**, 163-174, 1997
2. Domire ZJ et al. *J Appl Biomech* **25**, 93-97, 2009.
3. Eby et al. *Clin Biomech*, **30**, 22-27.
4. Bercoff J et al. *Ultra Ferro Freq Contr, IEEE Trans* **51**, 396-409, 2004.
5. Arnold et al. *Ann Biomed Eng* **38**, 269-279, 2010.
6. Gao F et al. *Arch Phys Med Rehabil* **90**, 819-826, 2009.

### ACKNOWLEDGMENTS

We would like to acknowledge our funding source K12HD073945.

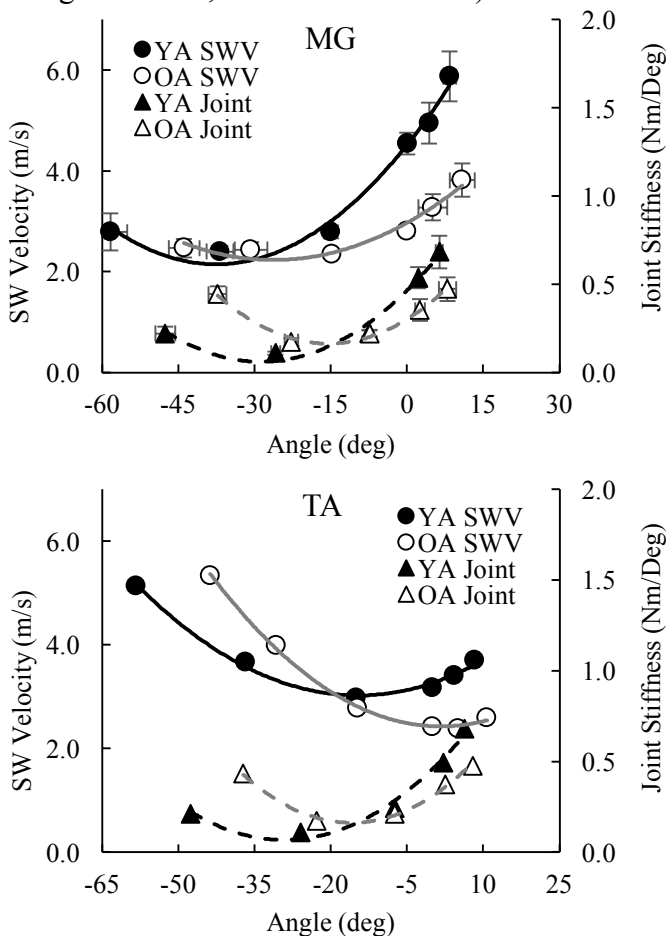


**Figure 1:** Shear wave velocity (SWV) of the medial gastrocnemius (MG, top) and tibialis anterior (TA, bottom) and joint stiffness of younger (filled) and older (unfilled) adults across the ankle range of motion.

# DIFFERENCES IN HAMSTRING MUSCLE QUALITY BETWEEN HIGHLY ACTIVE AND SEDENTARY OLDER ADULTS

Erica Casto, Jocelyn Hafer, and Katherine Boyer

University of Massachusetts Amherst, Amherst, MA, USA  
email: [ecasto@kin.umass.edu](mailto:ecasto@kin.umass.edu)

## INTRODUCTION

Age-related decreases in muscular strength are associated with increased mortality and decreased quality of life (1,2). Knee extensor function is a well-documented determinant of mobility in older adults (1,2). The overall decline in strength with age can occur not only due to loss of muscle mass (sarcopenia), but also a decrease in muscle quality (strength/unit of muscle) (2,3). Few studies account for the potential interaction of age and physical activity on alterations in muscle function with age. While running has been shown to diminish the loss of muscle mass with age (4), the impact of running or high physical activity levels on muscle quality in the aged is not well characterized. A greater understanding of the impact of physical activity on muscle quality may be important as it could have implications for understanding and preventing the onset of age-related musculoskeletal disease.

Poor knee extensor muscle quality has been associated with increased prevalence of knee osteoarthritis in men and women (6). Little work has focused on the changes in hamstrings muscle quality and function with age or disease. Initial work suggests that strengthening of knee flexors may be equally as important as targeting the knee extensors in rehabilitation of knee osteoarthritis (8). A relationship between thigh (knee extensor and knee flexor) muscle strength and increased risk of knee osteoarthritis in women has also been reported (8). There is a need to better understand differences in hamstring function and quality with age as it may be a modifiable factor that influences age-related mobility declines and/or onset of degenerative conditions such as knee osteoarthritis.

The *purpose* of this study was to assess differences in hamstring muscle quality in vigorously active (runners) and sedentary older adults. We hypothesized that runners would have an increased muscle mass, accompanied by an increase in muscle quality.

## METHODS

14 healthy adults, 8 runners (running  $\geq 15$  miles/wk; 4M, 4F,  $62.9 \pm 3.8$  yrs, BMI  $23.2 \pm 2.1$ ) and 6 sedentary (exercising  $\leq 2$  times/wk; 2M, 4F,  $62.6 \pm 4.7$  yrs, BMI  $23.3 \pm 1.3$ ) were recruited to participate in this study. All participants had no history of lower extremity joint injury or surgery, chronic pain, neurological or musculoskeletal diseases. Participants completed two study visits. The first visit was to complete a health-screening questionnaire, assign activity monitors and undergo MRI for hamstring volume assessment. The second visit, 10-14 days later, was to quantify hamstring muscle function. Written informed consent was obtained from all participants as approved by the University of Massachusetts Amherst IRB.

Physical activity was quantitatively assessed using Actigraph GT3X triaxial accelerometers worn at the hip for 7-10 days. Muscle volume was assessed using a 1.5T Siemens MRI. The scan included the length of the thigh from fibular head to greater trochanter with T1 weighted scan sequence (6mm serial axial slice thickness). Hamstring area ( $\text{cm}^2$ ) was measured at 50% of the distance between the femoral condyles and femoral head using custom MATLAB code (Figure 1). Muscle tissue area was distinguished from other tissues based on pixel.

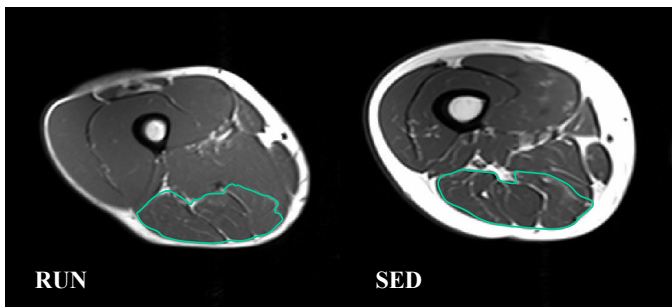


Figure 1: Hamstring muscle area (cm<sup>2</sup>) in RUN vs SED.

Hamstring function was assessed using a Humac Norm isokinetic dynamometer (Cybex, Medway, MA). The protocol included maximal knee flexion isometric contractions and concentric contractions at 90, 180, and 270°/sec throughout a 70° range of motion (20-90°). Two sets of 3 reps were completed at each contraction speed, with 30 seconds rest between sets, and 2 minutes rest between speeds. Peak torque was extracted from the isometric contractions and calculated at the time of peak power for concentric contractions. Muscle quality was then calculated as peak torque divided by the hamstring muscle area for each contraction speed.

A 2-way repeated measures ANOVA was used to compare muscle quality at each contraction speed in RUN vs SED (IBM SPSS software v24, Armonk, NY). An independent samples t-test was used to compare the total hamstring muscle area in the RUN vs. SED groups ( $\alpha=0.05$ ).

## RESULTS AND DISCUSSION

The total hamstring area was 25% greater for the RUN group as compared to the SED group ( $p=0.027$ ). However, despite the increased muscle mass, muscle quality in RUN (mean= 0.289) was lower than in SED (mean= 0.387) at each of the contraction speeds ( $p=0.057$ ), shown in Figure 2. The magnitude of the difference between groups was not different between contraction velocities.

Similar findings were reported for the differences in muscle volume and quality of the knee extensors in this population (9). Similar to the knee flexors, for the knee extensors there was also an inverse

relationship between muscle quality and muscle size. This suggests that although runners are able to mitigate loss of muscle mass with age, they may not maintain muscle quality within the hamstrings.



Figure 2: Muscle Quality: RUN vs SED,  $p=0.057$ .

## CONCLUSIONS

While running appears to be effective for limiting decreases in muscle mass, it may not be effective in maintaining overall muscle quality. Further investigation is needed to assess the mechanism for this unexpected impact of physical activity on muscle function in older adults.

## REFERENCES

1. Newman et al., *J Gerontol*, 61 (1): 72-77, 2006.
2. Lexell, *J Gerontol*, 50:11-6, 1995.
3. Goodpaster et al., *J Gerontol*, 61: 1059-64, 2006.
4. Drey et al., *Clin Physiol Funct imaging*, 2014.
5. Mitchell et al., *Frontiers in physiol*, 260(3), 2012.
6. Conroy et al., *Arthritis Care & Research*, 61(1): 15-21, 2012.
7. Jale et al., *Am J Phys Med & Rehab*, 1995.
8. Culvenor et al., *Arthritis Care & Research*, 2017.
9. Hafer et al., *MSSE*, 48 (5S): 685, 2016.

## ACKNOWLEDGMENTS

ACSM Foundation Doctoral Student Grant, J.F.H.

# COGNITIVE AND NEUROPSYCHOLOGICAL DIFFERENCES BETWEEN ELDERLY POPULATIONS WITH GOOD AND POOR BALANCE AS DETERMINED BY THE FUNCTIONAL GAIT ASSESSMENT

<sup>1</sup> Kenneth Pechtl, <sup>1</sup> April J. Chambers, PhD, <sup>1</sup> J. Richard Jennings, PhD, <sup>1</sup> Mark S. Redfern, PhD

<sup>1</sup> University of Pittsburgh, Pittsburgh, PA, USA  
email: [ajcst49@pitt.edu](mailto:ajcst49@pitt.edu), web: <http://www.engineering.pitt.edu/hmbl/>

## INTRODUCTION

Understanding the cognitive changes that occur in the elderly population that put them at greater risk for poor balance and falls is necessary in order to implement appropriate interventions. Several studies have reported relationships between declining cognitive measures and increases in self-reported falls [1, 2, 3]. However, the falls measure is subject to participant bias that limits the validity of these associations.

Less work has been done on behavioral measures related to balance and falls. The functional gait assessment (FGA) is a measure of walking balance ability. The simple scale has 10 items, each on a 3-point scale with one overall sum. The measure has construct validity and is clinically appropriate for identifying different levels of walking balance [4].

The current study aims to define the neuropsychological and cognitive differences between elderly populations with good and poor balance, as differentiated by the functional gait assessment.

## METHODS

31 healthy elderly adults (18 females, 13 males) with no history of vestibular or neurological disorders were enrolled. Participants with a functional gait assessment score of less than 24 were placed in the Poor Balance group (“ELD-PB”,  $n = 11$ ), and participants with a score of 24 or greater were placed in the Good Balance group (“ELD-GB”,  $n = 20$ ). The ELD-GB group (10 females, 10 males) had an average age of  $75.5 \pm 3.9$ , while the ELD-PB group (8 females, 3 males) had an average age of  $76.9 \pm 4.3$ . Participants were

Caucasian except for 3 African Americans in the ELD-GB group and 2 in the ELD-PB group.

A set of tests ensured that participants were cognitively normal for age (Mini-Mental State Exam, MMSE) and free of major disabilities interfering with their performance (Duke comorbidity scale, Physical Performance Test, preferred gait speed, monofilament test of touch).

The participants then completed a battery of neuropsychological tests. These tests included CNS Vital Signs and the Repeatable Battery for the Assessment of Neuropsychological Status (RBANS). Two tests often used in studies of aging were measured in addition: the digit symbol substitution test and the Trails test. Taken together, these tests assessed short and long term memory, verbal memory, visual memory, psychomotor speed, complex attention, cognitive flexibility, executive function, and simple attention. We also administered the Motor and Perceptual Inhibition Test (MAPIT), a performance measure of choice reaction time and ability to resist perceptual and motor interference, which was previously related to balance [5].

Statistical computations were conducted using Statistica software (Statsoft, Tulsa, OK). Independent samples t-tests were used to compare the cognitive measures between the ELD-GB and ELD-PB groups.

## RESULTS AND DISCUSSION

The ELD-GB and ELD-PB groups were similar in co-morbidities that would confound comparisons and were also similar in overall cognitive function as assessed by the MMSE. Specific

neuropsychological components were also largely similar between groups. This similarity did not extend to all domains, however.

The CNS Vital Signs finger tapping measure was significantly different between the ELD-GB (97.200) and ELD-PB (86.000) groups;  $t(29) = -2.38, p < .05$ , meaning that the ELD-GB group had better fine motor control and motor speed than the ELD-PB group. There is a rather direct relationship between motor control/regulation and balance during gait, which is of clear relevance to falls.

The CNS Vital Signs memory and visual memory domains were significantly different between the ELD-GB (112.150, 112.750) and ELD-PB (102.182, 100.182) groups:  $t(29) = -2.35, p < .05$ ;  $t(29) = -2.25, p < .05$ . Memory and particularly visual memory condition our expectations of the environment that we are moving through. Mild deficits in these domains might hinder anticipation of balance challenges.

The visuospatial constructional index of RBANS was also significantly different between the ELD-GB (100.400) and ELD-PB (88.545) groups;  $t(29) = -2.19, p < .05$ . Good balance relative to poor balance elderly performed better on tasks requiring processing and using visuospatial information.

Finally, susceptibility to perceptual interference as measured by MAPIT was significantly different between groups, where ELD-GB had lower scores (113.806) compared with ELD-PB (162.500);  $t(27) = -2.35, p < .05$ . Relative to the ELD-PB group, the ELD-GB group was slowed less by the perceptual displays, which at first glance would stimulate an incorrect response.

Elderly people with poor balance as determined by a FGA score less than 24 have worse balance because of deficits in basic motor speed combined with some visuospatial deficits appearing in memory, construction, and resistance to interference. This combination of deficits would seem to place them at risk due to slowed reactions to visually confusing challenges in their environment.

## CONCLUSIONS

Taken together, the results suggest a collection of mild deficits that together decrease stability during gait and likely increase risk for falls. When using the FGA as a criterion, a group of factors emerge that overlap only in part with those implicated in falls. Previous studies have found declines in inhibition for single fallers and recurrent fallers [1] as well as lower executive function and attention indices [3]. Similar to these studies, our study found perceptual inhibition differences, but attention and executive function remained similar between groups. This may be due to differences between the groupings using the FGA instead of the self-report falls measure, as well as a difference in the exact measures of attention and executive function.

This study was limited by a small sample size, so replication with larger samples to verify and enhance generalizability is required. Concurrent assessment of functional gait and incidence/prevalence of falls together with neuropsychological testing is needed in the future.

Possible interventions for the elderly population based on these findings include visuospatial training to reduce these deficits.

## REFERENCES

1. Anstey, KJ, et al. *Neuropsychology* **23(4)**, 500-508, 2009.
2. Martin, KL, et al. *Journals of Gerontology* **68(9)**, 1091-1097, 2013.
3. Mirelman, A, et al. *PLoS ONE* **7(6)**, e40297, 2012.
4. Beninato, M & Ludlow, LH. *Physical Therapy* **96**, 456-468, 2016.
5. Jennings, JR, et al. *Experimental Aging Research*, **37**, 179-197, 2001.

## ACKNOWLEDGMENTS

We thank Susan Strelinski and Anita Lieb for their help. This was supported by the NIA (R01AG014116) and Pittsburgh Claude D. Pepper Older Americans Independence Center (P30 AG024827).

# THE RELATIONSHIPS BETWEEN PHYSICAL CAPACITY AND BIOMECHANICAL PLASTICITY IN OLD ADULTS DURING LEVEL AND INCLINE WALKING

<sup>1</sup> Daniel Kuhman, <sup>1</sup> John Willson, <sup>1</sup> J.C. Mizelle, and <sup>1</sup> Paul DeVita

<sup>1</sup> East Carolina University, Greenville, NC, USA

email: kuhmand15@students.ecu.edu, web: <https://www.ecu.edu/cs-hhp/exss/biomechlab.cfm>

## INTRODUCTION

Compared to young adults, old adults exhibit a distal-to-proximal redistribution of joint contributions to support phase mechanics of level walking. This age-associated biomechanical plasticity was quantified by DeVita & Hortobagyi (2000), who reported that hip and ankle joint contributions to total positive work were 16% and 73%, respectively for healthy, young adults and 44% and 51%, respectively for healthy, old adults [1]. Age-associated biomechanical plasticity has also been reported during incline walking. However, while young adults increased both hip and ankle joint torques during incline walking, old adults increased hip but not ankle joint torques [2] suggesting the magnitude of biomechanical plasticity may be task dependent.

Biomechanical plasticity is well established in healthy, old adults. However, not all adults age in a healthy and robust manner; old adults have a wide variation in physical capacity. Understanding the relationship between biomechanical plasticity and physical capacity in old adults may shed a brighter light on age-related declines in neuromuscular function and may lead to improved exercise and rehabilitation strategies for old adults. There is some indication that low- compared to high-capacity old adults exhibit increased magnitudes of biomechanical plasticity [3-5]. Based on these comparisons, we hypothesized that as physical capacity declines, age-associated biomechanical plasticity increases in magnitude. We also hypothesized that the magnitude of biomechanical plasticity would increase during incline compared to level walking; i.e. in the more difficult task.

The purpose of this study was to quantify the relationships between physical capacity and biomechanical plasticity in old adults during level and incline walking.

## METHODS

Data were collected on 32 old (22 female; age = 74.7  $\pm$  4.4 yr.) individuals. Written informed consent approved by the IRB of East Carolina University was obtained from all participants.

Physical capacity was measured using the Short-Form Health Survey Physical Component (SF-36 PC) score. Kinematic and GRF data for the pelvis and right leg were collected using motion capture (120 Hz, Qualisys AB) and force platforms (960 Hz, AMTI). Participants completed 5 successful trials of walking at self-selected speeds over level ground and up a 10° incline ramp.

Kinematic and GRF data were filtered using second-order low pass Butterworth digital filters with cut-off frequencies of 6 & 45 Hz. Joint torques and powers were calculated using an inverse dynamics approach (Visual 3D, C-Motion). To define biomechanical plasticity, we created ratios of support phase hip extensor to ankle plantarflexor peak torques, angular impulses, peak positive powers, and positive work in both level and incline gaits.

Pearson product correlation coefficients were computed between SF-36 PC scores and the four biomechanical plasticity ratios during both walking gaits ( $p < 0.05$ ). In the cases where significant corresponding relationships existed during level and incline walking, 95% C.I.s of regression slopes were computed and compared to determine differences in the magnitude of plasticity in level and incline walking.

## RESULTS AND DISCUSSION

During level walking, significant positive relationships were observed between physical capacity and hip/ankle peak torque, angular impulse, peak positive power, and positive work ratios (Figure

1). During incline walking, significant positive relationships were observed between physical capacity and hip/ankle peak torque, angular impulse, and peak positive power ratios. No significant differences were observed in the magnitude of biomechanical plasticity between level and incline walking (i.e., the beta weights were statistically identical between gaits).

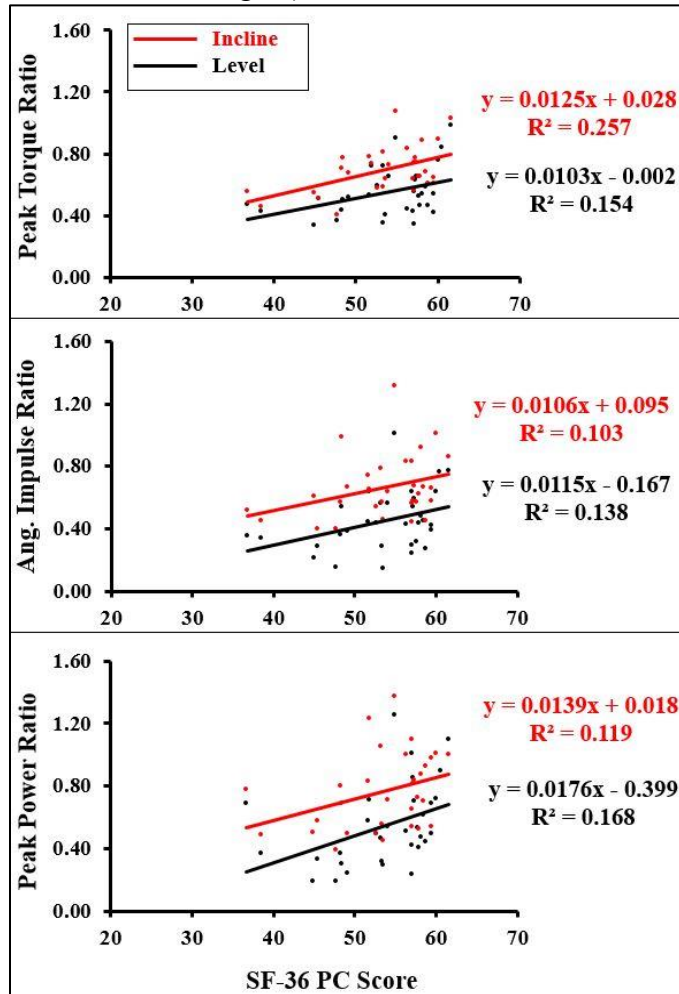


**Figure 1:** Correlations between SF-36 PC scores and biomechanical plasticity ratios and regression equations for each relationship.

**Table 1:** Pearson Correlation Coefficients (r) between biomechanical plasticity ratios and self-selected walking speeds during level and incline walking. Significant r-values are highlighted by **bold** font (p < 0.05).

Pearson Correlation Coefficients				
Plasticity Ratios	Self-Selected Level Walking Speed		Self-Selected Incline Walking Speed	
	r-value	r <sup>2</sup>	r-value	r <sup>2</sup>
Peak Torque	<b>0.518</b>	0.268	<b>0.453</b>	0.205
Angular Impulse	<b>0.353</b>	0.125	0.272	0.074
Peak Power	<b>0.352</b>	0.124	0.293	0.086
Work	0.087	0.008	0.007	0.000

Previous comparisons of high and low-capacity [3], strong and weak [4], and active and sedentary [5] old adults suggested an increased magnitude of biomechanical plasticity in low- compared to high-capacity old adults. Because of this, we hypothesized that an inverse relationship exists between physical capacity and age-associated biomechanical plasticity. Our results do not support this hypothesis. In fact, we report significant positive relationships between physical capacity and biomechanical plasticity during both level and incline walking. Positive relationships between plasticity ratios and self-selected walking speeds during level and incline walking suggest that biomechanical plasticity is an adaptation made by higher-capacity old adults to maintain better walking performance (Table 1). However, it should be noted that the magnitude of the relationships between biomechanical plasticity and physical capacity were moderate at best.

## CONCLUSION

Positive relationships exist between physical capacity and biomechanical plasticity during level and incline walking gait. Incline walking does not appear to increase the per unit magnitude of biomechanical plasticity per unit increase in physical capacity.

## REFERENCES

- DeVita P, et al. *J Appl Physiol* **88**, 1804-1811, 2000.
- Franz J, et al. *Gait Posture* **39** (1), 135-140, 2014.
- Graf A, et al. *Arch Phys Med Rehabil* **86**, 2177-2183, 2005.
- Hortobagyi T, et al. *Eur J Appl Physiol*, 2016.
- Buddhadev H, et al. *Gait Posture* **50**, 131-136, 2016.

## ACKNOWLEDGMENTS

This study was funded by the American Society of Biomechanics Graduate Student Grant-In-Aid

# AGING AND FALLS HISTORY EFFECTS ON THE MODULAR CONTROL OF WALKING WITH OPTICAL FLOW PERTURBATIONS

Jessica L. Allen<sup>1</sup>, Jessica D. Thompson<sup>2</sup>, and Jason R. Franz<sup>2</sup>

<sup>1</sup>Emory University, Atlanta, GA, USA

<sup>2</sup>University of North Carolina at Chapel Hill and North Carolina State University, Chapel Hill, NC, USA  
email: jrfranz@email.unc.edu, web: <http://abl.bme.unc.edu>

## INTRODUCTION

Older adults are at an exceptionally high risk of falls, and most falls occur during locomotor activities such as walking. We recently revealed that gait kinematics in older adults are more susceptible to optical flow perturbations than those in young adults [1], such that balance perturbations during walking could serve as an early identification for falls risk. Altered neuromuscular control of walking balance likely plays an important role in governing an individual's response to balance perturbations. Therefore, the purpose of this study was to investigate aging and falls history effects on the neuromuscular control of leg muscles during walking with and without optical flow perturbations of different amplitudes applied using a custom virtual environment. We used a motor module analysis [2,3] to quantify the complexity and consistency of neuromuscular control underlying walking balance and response to perturbations. We hypothesized that: (i) compared to young adults, aging and falls history would decrease module complexity and consistency, with (ii) larger effects in the presence of balance perturbations.

## METHODS

12 healthy young adults (mean±s.d., age: 24.8±4.8 years, 5M/6F), 11 healthy older adults (75.3±5.4 years, 5M/6F) and 11 older adults with a history of falls (78.0±7.6 years, 4M/7F) walked on an instrumented dual belt treadmill. We defined "falls history" as one or more falls within the last year. Young adults walked at 1.25 m/s while older adults walked at their preferred walking speed (Non-fallers: 1.19±0.20 m/s, Fallers: 1.03±0.22 m/s). Subjects walked while watching a speed-matched, virtual hallway (Fig. 1) with and without continuous mediolateral perturbations of optical flow, applied as the sum of three sinusoids (0.125, 0.250, 0.442 Hz).

In fully randomized order, subjects walked for two minutes with optical flow perturbations of amplitudes 0, 20, 35, and 50 cm.

We collected electromyographic (EMG) at 1000 Hz from seven right leg muscles (Fig. 1) during the second minute. EMG data were high-pass filtered (35 Hz) demeaned, rectified, and low-pass filtered (10 Hz) before being resampled at every 0.5% of the gait cycle. This resulted in an  $m \times t$  matrix for each perturbation condition, where  $m$  is the number of muscles and  $t$  is the time base (i.e.,  $t = \#$  of strides\*201). EMG from each muscle was normalized to the maximum observed across all conditions. We extracted motor modules from each EMG matrix using non-negative matrix factorization, which decomposes EMG such that  $EMG = W * C$  [2,3].  $W$  is an  $m \times n$  matrix and  $C$  an  $n \times t$  matrix of motor module recruitment coefficients, where  $n$  is the number of motor modules and was chosen for each condition such that the 95%

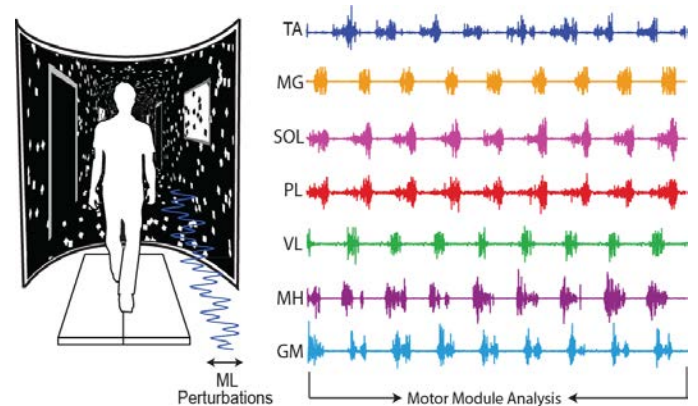


**Figure 1.** EMG was recorded from right leg tibialis anterior (TA), medial gastrocnemius (MG), soleus (SOL), peroneus longus (PL), vastus lateralis (VL), medial hamstring (MH), and gluteus medius (GM) while subjects walked in a custom virtual environment with/without mediolateral optical flow perturbations.

confidence interval of the variability accounted for was > 90% [2]. As a secondary analysis of module complexity we compared the variability accounted for by one motor module [3]. Finally, we examined step-to-step variability of motor module recruitment timing using the average RMSE of the module recruitment coefficients, C [2]. A two-way (group × perturbation) repeated measures ANOVA determined main effects and interactions between factors using alpha=0.05.

## RESULTS AND DISCUSSION

In partial support of our hypothesis, we found that falls history (but not age) was associated with reduced motor module complexity, and that age (but not falls history) was associated with increased step-to-step variability of module recruitment timing. In normal walking, older fallers averaged fewer motor modules ( $2.7 \pm 0.6$ ) than both young adults ( $3.6 \pm 0.5$ ;  $p < 0.001$ ) and older non-fallers ( $3.1 \pm 0.8$ ;  $p < 0.05$ ;

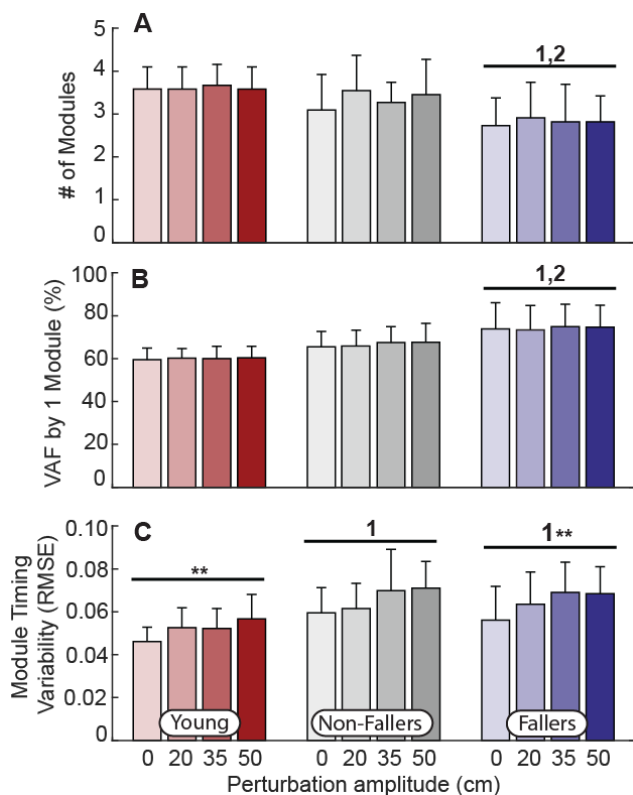


**Figure 2.** Results across all conditions for A: module number, B: variance accounted for by one module, and C: step-to-step module timing variability. Numerical values indicate significant pairwise comparisons between groups (1: vs. young, 2: vs. non-fallers;  $p < 0.05$ ). \*\* indicates significant effects of perturbation amplitude ( $p < 0.05$ ).

Fig. 2A). Similarly, the variance in leg muscle recruitment accounted for by one module was reduced in older fallers compared to young adults ( $p < 0.01$ ) and older non-fallers ( $p < 0.05$ ; Fig. 2B). The step-to-step variability of module recruitment timing in normal walking was on average 25% higher in older compared to younger adults regardless of falls history ( $p < 0.05$ ). This suggests that reduced neuromuscular complexity but not variability is associated with a risk of falling.

Further, we found that step-to-step variability of recruitment timing (and not module complexity) was altered by optical perturbations during walking regardless of age or falls history. Neither measure of module complexity was altered in the presence of optical flow perturbations, which is consistent with prior work suggesting that module complexity is preserved across a variety of walking conditions [4]. In contrast, step-to-step variability of module recruitment timing was increased in the presence of perturbations in both young adults ( $p = 0.02$ ) and older fallers ( $p < 0.01$ ).

## CONCLUSIONS

Here we provide compelling evidence implicating altered neuromuscular control as a mechanism for age-associated falls risk. Moreover, that module complexity was invariant even in the presence of perturbations suggests that the motor repertoire of older adult fallers is a constraint on their ability to appropriately respond to balance challenges during walking. Indeed, only the recruitment timing variability of their available motor modules increased in the presence of balance perturbations.

## REFERENCES

1. Franz JR, et al. *Hum Mov Sci*, **40**, 381-92, 2015.
2. Sawers A, et al. *J Neurophys*, **114**, 3359-73, 2015.
3. Shuman B, et al. *Gait Posture*, **45**, 127-32, 2016.
4. Routson RL, et al. *Physiol Rep*, **2**, e12055, 2014.

## ACKNOWLEDGEMENTS

Supported by NIH grants UL1TR001111 and F32NS087775.

# POWER TRAINING INCREASED NEUROMUSCLAR ACTIVATION OF THE EXTENSOR MUSCLES DURING GAIT IN OLD ADULTS

<sup>1</sup>Chantal Beijersbergen, <sup>2</sup>Urs Granacher, <sup>1,2</sup>Martijn Gäbler, <sup>3</sup>Paul DeVita, and <sup>1</sup>Tibor Hortobágyi

<sup>1</sup>University of Groningen, University Medical Center Groningen, Center for Human Movement Sciences

<sup>2</sup>University of Potsdam, Division of Training and Movement Sciences

<sup>3</sup>East Carolina University, Department of Kinesiology

Corresponding author email: c.m.i.beijersbergen@umcg.nl

## INTRODUCTION

Beyond the visible hallmarks of aged gait, i.e., slowed walking speed, shorter steps, and increased cadence [1], aging also affects the neuromuscular control of gait and old compared with young adults typically walk with greater levels of agonist activation and particularly antagonist coactivation in the lower extremity muscles [2]. Disproportional levels of coactivation are associated with increased metabolic costs and reduced net force [3].

A form of resistance training known as power training incorporates exercises with moderate-to-high loads performed at maximal movement velocities during the concentric phase. It is well-established that power training in old adults results in increased maximal voluntary agonist activation, which contributes to training-induced gains in muscle strength and power [4]. The results on antagonist coactivation after power training are less consistent, as both increased and decreased coactivation were reported when measured during a maximal effort contraction on an isokinetic dynamometer [4]. It is unknown if power training-induced neuromuscular adaptations are also present during walking.

Therefore, for the first time, we examined the effects of 10-weeks of lower extremity power training on neuromuscular activation during walking in community-dwelling old adults. We hypothesized that power training produces correlated improvements in muscle power and gait velocity and increases in agonist activation or decreased antagonist coactivation.

## METHODS

Participants were community-dwelling old adults without mobility limitations who volunteered to participate in the Potsdam Gait Study (POGS). We included data from thirteen participants as a non-exercise control group (age  $69.7 \pm 5.0$  years, Body Mass Index  $25.1 \pm 3.2$  kg/m<sup>2</sup>), and data from twelve participants for the analysis of power training effects (age  $72.1 \pm 5.4$  years, Body Mass Index  $26.2 \pm 4.1$  kg/m<sup>2</sup>). Three participants from the power-training group first had completed the control period.

The power-training program consisted of 30 sessions whereby participants performed leg press, ankle press, knee extension, and knee flexion exercises at 40-60% of their three-repetition maximum (3-RM). Participants were instructed to move the weights rapidly and at high movement velocities during the concentric phase and training progression was based on biweekly measured 3-RM.

Testing was performed before and after the 10-week interventions. We affixed surface electromyographic (EMG) electrodes on five muscles of the right leg, i.e., vastus lateralis (VL), vastus medialis (VM), biceps femoris (BF), gastrocnemius medialis (GM), and soleus (SL).

Participants performed three maximal isometric knee flexor, knee extensor, and plantarflexor contractions while fixed in an isokinetic dynamometer. We recorded torque and EMG activity and took the trial with the highest torque for further analysis. We also recorded EMG activity at a sampling frequency of 1000 Hz during habitual, fast, and standardized walking speeds while participants walked over a 6.5 x 1.5-meter level walkway.

We used the Teager-Kaiser Energy Operator [5] to determine the onset and offset of the main EMG burst for each muscle. We bandpass-filtered the raw-EMG (20-450 Hz) and applied a root-mean-square (RMS) envelope using a 40-ms smoothing window. Next, we performed an amplitude analysis to determine the magnitude of agonist activation and antagonist coactivation. We averaged EMG data from GM and SL to characterize plantarflexor activation and we averaged EMG data from VL and VM to characterize knee extensor activation. We computed gait velocity from kinematic marker data.

Variables were statistically analyzed using a paired t-test comparing pre-post values for power training and control due to the fact that subjects from the control group were included in the intervention group after completion of the control period and subsequent performance of power training. We used simple linear regression analysis to predict changes in isometric torque and gait velocity from changes in neuromuscular activation.

## RESULTS AND DISCUSSION

For all muscle groups, power training increased maximal isometric muscle strength (15-93%,  $p \leq 0.05$ ) and agonist activation (31-53%,  $p \leq 0.05$ ), while antagonist coactivation was unchanged ( $p > 0.05$ ). Changes in agonist activation correlated with changes in muscle strength ( $r = .58$ ,  $p = 0.049$ ), confirming previous findings [4] that mechanisms through which power training improved muscle strength involve increased agonist activation.

Power training non-significantly increased habitual (5%,  $p = .079$ ) and fast (4%,  $p = 0.059$ ) gait velocity. At all speeds, old adults walked with greater knee extensor activation during early stance post-training (16-21%,  $p \leq 0.05$ ). Knee extensor coactivation measured during the main knee flexor burst also increased (19-28%,  $p \leq 0.05$ ). These adaptations did not correlate with changes in habitual or fast gait velocity. We interpret these data to mean that power training increased knee extensor activation and coactivation during heel contact and early stance to stabilize the knee during the loading response.

Power training also increased plantarflexor activation during push-off at all speeds (11-28%,  $p \leq 0.05$ ). At fast speed, changes in plantarflexor activation correlated with changes in gait velocity ( $r = .760$ ,  $p = .004$ , Fig. 1). These data suggest that improved neuromuscular activation of the plantarflexors underlies in part the gains in fast gait velocity.

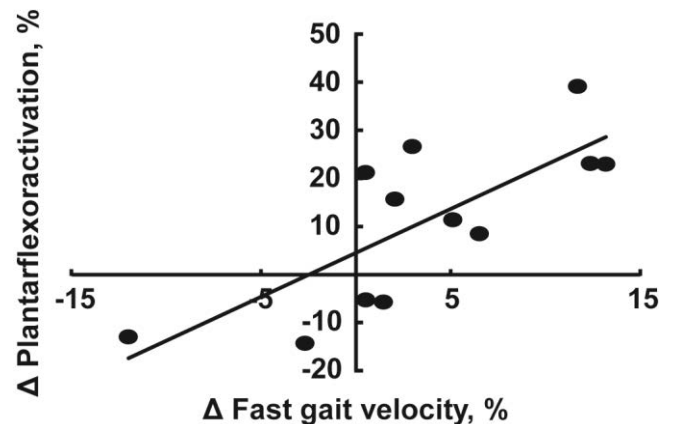


**Figure 1:** Association between power-training induced changes in fast gait velocity and changes in plantarflexor activation during push-off. The association is characterized by  $y = 1.83x + 4.5$ ,  $R^2 = 0.57$  ( $p = 0.004$ ).

## CONCLUSIONS

Power training-induced neuromuscular adaptations included an increase in agonist activation without reductions in antagonist coactivation. Power training may improve healthy old adults' walking performance by increasing neuromuscular activation of the extensor muscles.

## REFERENCES

1. Bohannon RW, et al. *Physiotherapy* **97**, 182-189, 2011
2. Hortobagyi T, et al. *J Gerontol A Biol Sci Med Sci* **66**, 541-547, 2011
3. Mian OS, et al. *Acta Physiol (Oxf)* **186**, 127-139, 2006
4. Arnold P & Bautmans *Exp Gerontol* **58**, 58-68, 2014
5. Solnik S, et al. *Eur J Appl Physiol* **110**, 489-498, 2010

# Does metabolic cost explain mass-based changes in preferred reaching speed?

<sup>1</sup>Megan K. O'Brien, <sup>1</sup>Garrick W. Bruening, <sup>2</sup>Reza Shadmehr, and <sup>1</sup>Alaa A. Ahmed

<sup>1</sup>University of Colorado Boulder, CO, USA

<sup>2</sup>Johns Hopkins University, Baltimore, MD, USA

Email: Garrick.Bruening@colorado.edu

## INTRODUCTION

An open question in motor control is how the brain selects the duration of a movement. We recently proposed a theory capable of explaining both the actions one prefers to take, as well as the speed of the movement that follows [1]. Each movement is assigned a utility consisting of the reward to be acquired minus the effort cost to acquire it, both discounted by time. Critically, the effort cost required to make the movement is represented objectively by its metabolic cost. Previous modeling efforts have assumed that effort costs in reaching scale quadratically with mass [2]. In contrast, empirical measurement of metabolic cost (i.e. objective effort cost) in locomotion suggests a linear scaling [3]. For reaching, the effect of mass on metabolics has not been measured. Here, we quantified metabolic cost of reaching as a function of mass, and then measured how preferred reach speed varied with mass. We asked if changes in speed were consistent with the theoretical predictions of a movement utility where effort of reaching depended on its metabolic cost.

## METHODS

Experiment 1: Metabolic cost of reaching with added mass. We measured the metabolic cost of reaching via expired gas analysis. Eight subjects made horizontal reaching movements while holding the handle of a robotic arm. We computed net metabolic power in four mass conditions: effective mass of robot+human arm of 2.5, 4.5, 6.5, and 10.4 kg. For each condition, subjects performed 5 minutes of reaching at six different movement durations, ranging from 0.4s to 1.3s. A single reach required moving 10cm from a starting circle to a target at the specified duration. Targets were oriented at 45°, 135°, 225°, and 315° in a pseudorandom order. We fit subject data to

determine the relationship between net metabolic power ( $\dot{e}$ ), effective mass of the arm ( $m$ ), reach distance ( $d$ ), and movement duration ( $T$ ) according to the equation:  $\dot{e} = a + bm^i d^j T^{-k}$  Eq. (1).

Experiment 2: Preferred reaching duration with added mass. Twelve additional subjects performed reaches with a similar target set-up but without duration requirements. Subjects were instructed to move at a comfortable speed, and they completed 200 trials in four mass conditions (effective masses of 2.5, 3.8, 4.7, and 6.1kg) in a randomized order. The effect of added mass on preferred movement speed was assessed using a linear mixed model.

## RESULTS

Experiment 1: The metabolic power curves for each mass condition are given in Fig. 1A, with  $i=0.7$  ( $p<10^{-9}$ ),  $b=15.5$  ( $p=0.02$ ),  $a=31.4$  ( $p<10^{-8}$ ),  $k=5$  ( $p<10^{-9}$ );  $j=1.1$  was fit in previous work [1];  $R^2=0.994$ . As expected, increasing mass increased the metabolic cost of reaching, and this effect was more pronounced for faster movements. Importantly, increased mass had a roughly linear effect on the metabolic cost of reaching, consistent with measures in locomotion. We quantified the effect of mass on endpoint variability for fixed movement durations. As expected, variability increased with shorter durations (Fig. 1B,  $p<0.001$ ), but variability did not change with mass ( $p=0.27$ ).

Experiment 2: Added mass increased movement duration (Fig. 2A;  $p<2e-16$ ), decreased peak velocity (Fig. 2B;  $p<2e-16$ ), and did not affect maximum excursion (Fig. 2C;  $p=0.09$ ). To determine if the movement slowing was in response to reduced accuracy with added mass, we turned to the Exp. 1 data (Fig. 1B). In the range of durations that people chose to reach (0.9-1.2sec), there was no discernable effect of mass on variability.

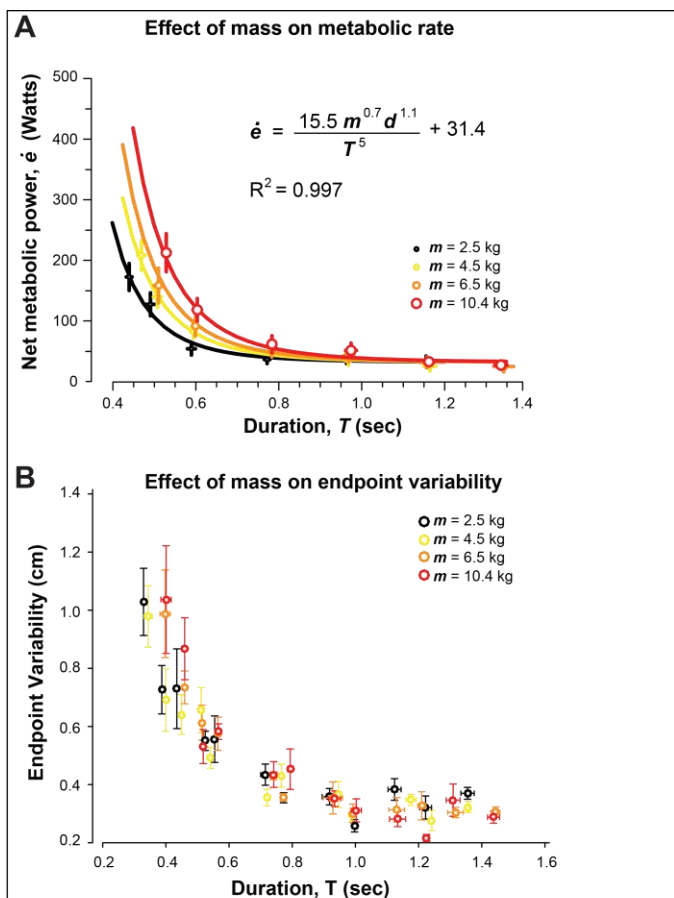


Figure 1. Experiment 1. A: Relationship between net metabolic power and movement duration. Subject data shown by open circles, with standard error. Model fits as curves, resulting in equation. B: Effect of mass on endpoint variability (std). Variability increases with shorter duration ( $p < 0.05$ ), but unaffected by mass ( $p = 0.27$ ).

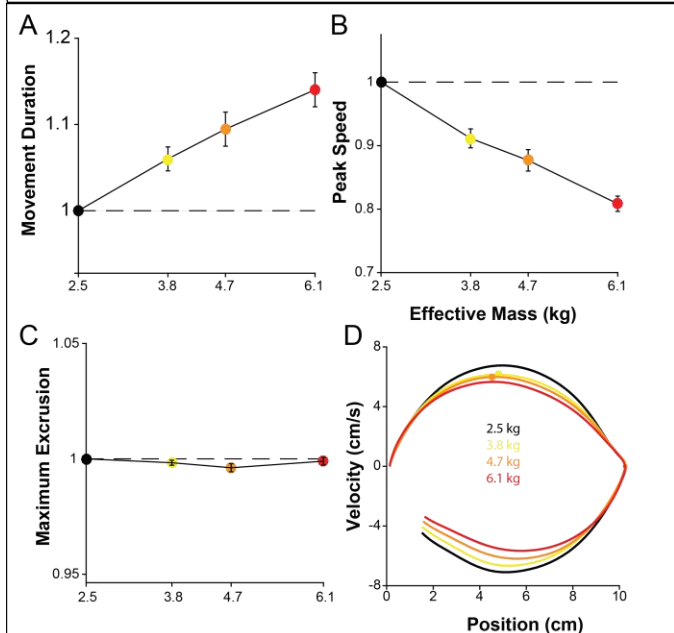


Figure 2. Experiment 2: Effect of mass on preferred duration. Movement duration (A) and Peak Speed (B) decreased with increasing mass at the hand. (C) Maximum Excursion shows no significant effect of mass. All metrics are normalized to the 0 added mass condition, which corresponds to an effective mass of 2.5 kg. (D) Velocity-Position profiles averaged over all subjects for each mass condition. Error bars represent 1 s.e.m..

**Model Predictions.** By integrating Eq. (1) over movement duration ( $T$ ) we have an estimate of effort. We write the utility of that movement as:  $J = (\alpha - aT - bm^i d^j T^{-k})(1 + \gamma T)^{-1}$  Eq. (2), where  $\alpha$  is reward, and  $\gamma$  is the temporal discount factor. To find the models predictions regarding the relationship between movement duration and mass, we set the derivative of Eq. (2) equal to zero and solve for  $T$ . The results are shown in Fig. 3 in both normalized and absolute units (the only free parameter is  $\alpha$ ,  $\gamma$  was set to 1). A model where effort increases linearly with mass ( $i=1$ ) also performs well. In contrast, quadratic scaling ( $i=2$ ) is inconsistent with the data and overestimates the effect of mass on preferred duration.

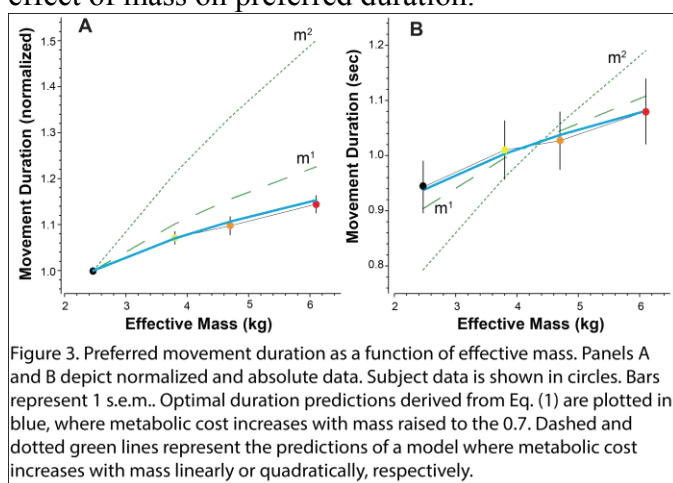


Figure 3. Preferred movement duration as a function of effective mass. Panels A and B depict normalized and absolute data. Subject data is shown in circles. Bars represent 1 s.e.m.. Optimal duration predictions derived from Eq. (1) are plotted in blue, where metabolic cost increases with mass raised to the 0.7. Dashed and dotted green lines represent the predictions of a model where metabolic cost increases with mass linearly or quadratically, respectively.

## CONCLUSIONS

In many models of motor control, effort scales quadratically with mass. Here, we measured metabolics of reaching and found that it increased approximately linearly with mass. Using a model of movement utility where effort was represented objectively as metabolic cost, we found that the speed with which people chose to reach increased at a rate that was consistent with a linear increase in effort as a function of mass.

## References

1. Shadmehr, (2016) A representation of effort in decision-making and motor control. *Curr. Bio.*
2. Torodov, (2002) Optimal feedback control as a theory of motor coordination. *Nat. Neurosci.*
3. Bastien, (2005) Effect of load and speed on the energetic cost of human walking. *Eur. J. Appl. Physiol.*

# MECHANICS & ENERGETICS OF WALKING WITH A FLAT CENTER OF MASS TRAJECTORY

Russell T. Johnson and Brian R. Umberger

University of Massachusetts Amherst, Amherst, MA, USA  
email: [umberger@kin.umass.edu](mailto:umberger@kin.umass.edu), web: <http://umass.edu/locomotion>

## INTRODUCTION

The sinusoidal pathway of the whole-body center of mass (COM) in the sagittal plane during walking has been a topic of study for many years. Early researchers argued that reducing the vertical displacement of the COM should lower the metabolic energy cost of walking [1]. However, recent experimental studies have shown that reducing COM excursion such that it follows a flat trajectory doubles the metabolic cost of transport (COT) [2,3]. These previous studies have shown that humans adopt a flexed limb posture in order to walk with a flat COM trajectory. This flexed posture may explain much of the greater COT, independent of COM motion [4].

One limitation of acute experimental studies is that subjects may not have optimized their gait to novel walking conditions, exaggerating the metabolic penalty. Musculoskeletal modeling and optimal control techniques present a unique way of exploring the influence of walking with a flat COM trajectory without the confounding influence of human adaptation. When viewed together with experimental studies, the modeling approach may provide additional insight on the role of COM motion in locomotor energetics. Thus, our purpose was to investigate the mechanics and energetics of walking with flat and normal COM trajectories using a musculoskeletal modeling approach.

## METHODS

A two-dimensional, 12 degree-of-freedom, 48 muscle model [5] was used within the OpenSim software package. Optimal control simulations of walking (1.3 m/s) with flat and normal trajectories were generated using a direct collocation approach. A weighted multi-objective function was used to minimize the sum of cubed muscle activations plus the deviation from the desired pelvis segment

trajectory, which was used as a surrogate for COM motion as in experimental studies [2,3]. As the pelvis vertical displacement was the only variable that was tracked it allowed the other degrees of freedom, including pelvis segment height and hip, knee, and ankle joint angles, to vary freely within the optimization.

The three specific cases were a normal condition that matched experimental pelvis vertical displacement (Normal), a flat pelvis trajectory matched for final time with the Normal solution (Flat Fixed), and a flat pelvis trajectory where the final time was allowed to vary (Flat) (Fig. 1). The free final time solution allowed the optimization to change stride length and frequency, while the matched final time case had to maintain the stride length and frequency from the Normal condition. The results of the three optimizations were used to compare the COT using a muscle energetics model [6].

## RESULTS AND DISCUSSION

The model was able to produce the desired pelvis displacement trajectories for each of the three conditions (Fig. 1). The joint angles for the Normal condition, despite not being tracked, showed broad

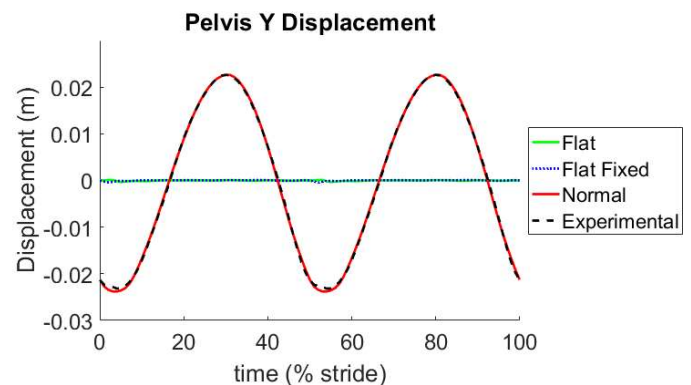


**Fig. 1:** Pelvis vertical displacement. The Normal condition reproduced the experimental mean and Flat conditions kept the pelvis trajectory nearly flat.

agreement with experimental values, with the greatest deviation being relatively less ankle plantar flexion at push off (Fig. 2). The Flat Fixed condition necessarily had the same final time, stride length and frequency as the Normal condition (Table 1). The Flat condition reduced the stride time, resulting in a ~10% shorter stride length.

The Flat Fixed and Flat condition joint angles were similar to each other and represented a more flexed-limb posture around mid-stance than the Normal condition or experimental means (Fig. 2). However, the limb was considerably more extended in the Flat conditions than the postures chosen by humans walking with a flat COM trajectory [2,3]. Thus, the pelvis height was maintained at a relatively high position in these simulations, within a few cm of the mean vertical position of the Normal condition.

The net COT was 11-23% greater in the two Flat trajectory conditions than in the Normal condition (Table 1). This modest increase in COT is considerably less than the ~100% increase reported in experimental studies [2,3]. The model was able to produce a flat pelvis trajectory with a relatively upright posture, avoiding a large increase in energy demands. With feedback or a longer adaptation period, subjects might be able to learn to walk with a flat COM trajectory at relatively low cost by flexing the limbs less. It appears that maintaining a sinusoidal path of the COM in the sagittal plane is energetically beneficial, yet much of the increase in COT reported experimentally may be due to adopting a couched posture rather than the flat COM trajectory, *per se*.

**CONCLUSIONS**

Humans should be able to walk with a flat COM trajectory with only a modest increase in COT. This prediction should be tested experimentally.

**Table 1:** Output variables for the three conditions.

	Flat	Flat Fixed	Normal
Stride Time (s)	0.89	0.99	0.99
Stride Length (m)	1.16	1.28	1.28
Net COT (J/kg/m)	3.11	2.81	2.52

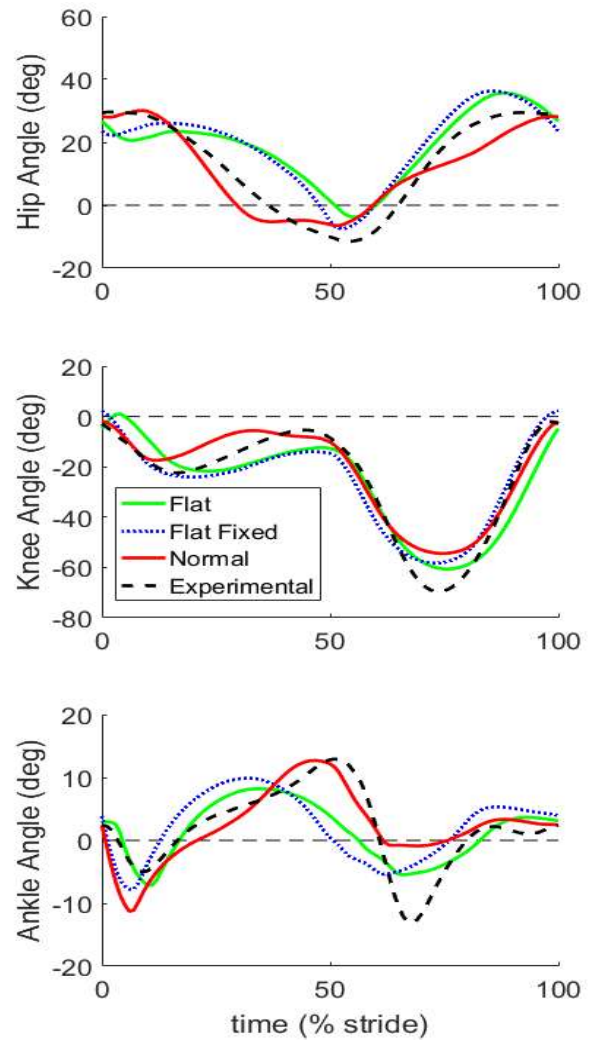


**Figure 2:** Joint angles over a full stride.

**REFERENCES**

1. Saunders JB, et al. *J Bone Joint Surg Am.* **35**, 543-558, 1953
2. Gordon KE, et al. *Arch Phys Med Rehabil.* **90**, 136-144, 2009
3. Ortega JD & Farley CT, *J Appl Physiol.* **99**, 2099-2107, 2005.
4. Carey TS & Crompton RW, *J Hum Evol.* **48**, 25-44, 2005
5. Porsa S, et al. *Ann Biomed Eng.* **44**, 2542-57, 2015
6. Umberger BR, et al. *Comput Methods Biomech Biomed Engin.* **6**, 99-111, 2003.

**ACKNOWLEDGMENTS**

Support: UMass Robinson Fellowship, NCSRR OpenSim Travel Award, NSF (IIS-1526986)

# THE METABOLIC COST OF WALKING ON ROUGH TERRAIN

Koren Gast<sup>1</sup>, Rodger Kram<sup>2</sup>, Raziell Riemer<sup>1</sup>

<sup>1</sup> Ben-Gurion University of the Negev, Beer-Sheva, Israel

<sup>2</sup>Department of Integrative Physiology, University of Colorado, USA

email: rriemer@bgu.ac.il, web: <http://www.bgu.ac.il/~rriemer/>

## INTRODUCTION

Humans have evolved the ability to walk very efficiently [1]. We choose to walk at approximately the speed which minimizes the cost of transport (COT) [e.g. 2], where COT is the metabolic energy expenditure per distance  $\left[\frac{\text{Joules}}{\text{kg}\cdot\text{meter}}\right]$ . The COT for walking on level ground at different speeds can be represented using the following equation form:

$$COT = \frac{b}{v} + mv, \quad (1)$$

Where  $v$  is the speed  $\left[\frac{\text{m}}{\text{sec}}\right]$ , and  $b$  and  $m$  are the equation's constants [2].

However, humans did not evolve to only walk on smooth, level ground, and therefore it is interesting to investigate how different walking surfaces might affect the relations between the energy expenditure and speed. For example, while walking on sand, the relation between COT and speed is linear [3], which means that an optimum COT speed does not exist.

This study investigated the relation between COT and speed for walking on natural outdoor rough terrain to test if there is an optimum speed and if people naturally choose to walk at that speed. Further, we compared our rough terrain results to smooth, level ground walking.

## METHODS

Subjects were 5 males, age 24-29, mass 65-85 kg, height 1.65-1.85 m who gave informed consent to participate. For the rough terrain, subjects walked on a trail 67 m long with small changes in elevation (+/- 1 m). The trail was strewn with rocks and boulders and was relatively straight. The control surface was a 44-meter straight, smooth flat tile floor. The gross energy expenditure rate, was measured with a Cosmed K4b<sup>2</sup> telemetric system.

Two experimental sessions were performed on the rough terrain trail and a third on the level floor. To

allow subjects to adapt to walking on the trail, subjects performed two similar sessions of walking on rough terrain. Here, we report only the results of the second session.

Prior to the first trail session, the subjects were shown the trail and they practiced wearing the metabolic measurement system. The subjects walked out and back on the trail at various speeds. Then, the subjects were asked to walk for 7-9 minutes at their preferred speed. From the time for completion of the trail, average speed was calculated (i.e. the preferred speed). Next, the subjects performed 6-8 trials at different speeds relative to their preferred speed (approximately 50, 75, 100, 125% and 150%), with 5-min rest between trials. Some of the speeds were performed more than once. The order of speeds was randomized for each subject, to avoid adaptation or fatigue effects on metabolic rate. Measurement of the metabolic rate began only after at least 3 min of walking, to capture steady-state energy expenditure. Further, to eliminate the effect of local terrain variation, metabolic rate was averaged over full laps. Only trials with RER (respiratory exchange ratio) < 1 were analyzed. The same procedures were repeated for the floor trials.

*Analysis* We calculated the COT  $\left[\frac{\text{Joules}}{\text{kg}\cdot\text{m}}\right]$  by dividing metabolic rate by the speed and the subject's body mass, we tested several variations of equation (1) and found that the best fit for each of the two-experimental condition was in the form of:

$$COT = a + \frac{b}{v} + mv, \quad (2)$$

To test whether there was a difference in COT between the two surfaces, we used the Chow test using the two equation:

$$COT_{\text{rough terrain}} = \beta_0 + \beta_1 x_1 + \beta_2 x_2 + \varepsilon, \quad (3)$$

$$COT_{\text{floor}} = \alpha_0 + \alpha_1 x_1 + \alpha_2 x_2 + \varepsilon \quad (4)$$

where  $x_1$  is speed<sup>-1</sup> and  $x_2$  is the speed and we fitted 3 parameters for each equation based on 30 valid

observations from the trials on the rough terrain surface and 29 observations from the floor surface.

$$F_{statistic} = \frac{(SSE_a - (SSE_{rt} + SSE_f))/6}{(SSE_{rt} + SSE_f)/(30 + 29 - 2 * 3)}, \quad (5)$$

where  $SSE_a$  is the SSE (sum square of error) calculated on all the observations,  $SSE_{rt}$  is the SSE of the observations from the rough terrain experiments, and  $SSE_f$  is the SSE of the observations from the experiments on the floor surface.

## RESULTS AND DISCUSSION

The COT as a function of speed was 200%-230% greater for the rough terrain surface compared to the smooth, level floor (Table 1) at equivalent relative speeds (Table 1). Further, there was a significant difference in the shape of the COT-speed relations between the two surfaces (Figure 1). While the COT functions were different, both functions have very similar minimum points (1.16 m/sec on rough terrain and 1.18 m/sec on the floor). Further, the subjects' preferred speeds (1.06 m/sec on the rough terrain and 1.17 m/sec on the floor) were very close to the energetic optima (Figure 1).

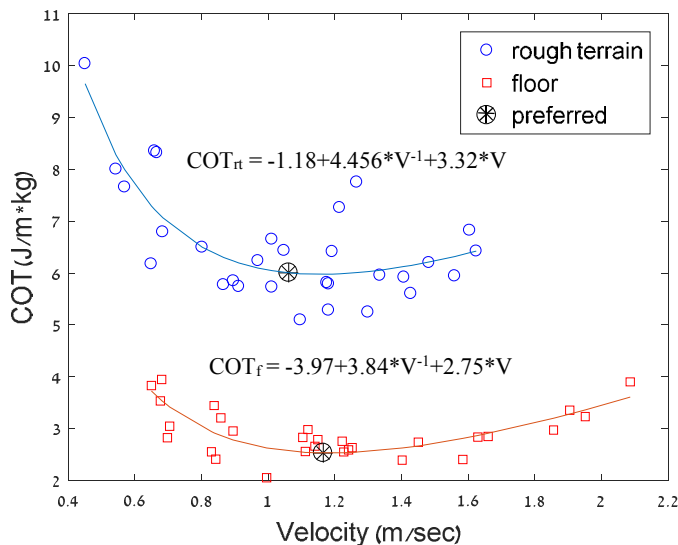


**Figure 1:** COT as a function of velocity. The trend lines were estimated using least squared error minimization.

**Table 1:** Average COT (J/kg•m) for different normalized speed bins and comparing rough terrain to floor.

Normalized speed	50%	75%	Preferred	125%	150%
Average COT rough terrain	7.97(±1.38)*	6.96(±1.15)	5.76(±0.52)	6.20(±0.59)	6.63(±0.63)
Average COT floor	3.44(±0.44)	2.91(±0.39)	2.52(±0.24)	2.65(±0.20)	3.36(±0.34)
Difference (percentage)	231.9%	238.8%	228.2%	234.4%	197.0%

\* Average (±std)

## CONCLUSIONS

The aim of this study was to investigate human walking on rough terrain. When walking on rough terrain, the COT was more than 200% greater than for walking on a smooth floor surface. The preferred walking speed was slower on rough terrain. Interestingly, even on challenging terrain, with considerations such as foot placement, stability, and slipping, there was a speed that minimized the COT and the subjects' preferred speed corresponded to the optimum speed. These findings strengthen the notion that humans sense and prefer speeds that minimize the COT.

*Future work:* Future, experiments should examine different trails, with different terrain roughness. In addition, future research that examines the kinetics and kinematics of the locomotion might explain why the COT is different for walking on different surfaces.

## REFERENCES

- Alexander, R. M. *Principles of Animal Locomotion, Chs 1 and 7* (Princeton Univ. Press, 2003).
- Ralston H. J. *Internationale Zeitschrift Für Angewandte Physiologie Einschliesslich Arbeitsphysiologie*, 17(4), 277–283, 1958.
- Zamparo P. et al. *European Journal of Applied Physiology and Occupational Physiology*, 65(2), 183–187, 1992.

## ACKNOWLEDGMENTS

This study was partially supported by the Helmsley Charitable Trust through the Agricultural, Biomechanical and Cognitive Robotics initiative of Ben-Gurion University of the Negev, and by MAFAT.

# WHY IS THE ENERGY-SPEED CURVE IN HUMAN WALKING U-SHAPED?

<sup>1</sup> Ross H. Miller and <sup>2,3</sup> Elizabeth Russell Esposito

<sup>1</sup> University of Maryland, College Park, MD, USA

<sup>2</sup> Brooke Army Medical Center, San Antonio, TX, USA

<sup>3</sup> Extremity Trauma and Amputation Center of Excellence

email: [rosshm@umd.edu](mailto:rosshm@umd.edu), web: <http://sph.umd.edu/neuromechanics>

## INTRODUCTION

The relationship between the gross energy expended per unit distance traveled (i.e. metabolic cost) and the speed of progression in human walking typically appears U-shaped. In addition, the speed that incurs the lowest metabolic cost is often at or near the individual's preferred walking speed, with faster and slower speeds incurring exponentially greater costs. This result was first reported by Ralston [1] and has been frequently replicated. However, it has not been fully explained why the energy-speed relationship exhibits its characteristic U-shape.

An obvious contributor to the U-shaped curve at slow speeds is the energy cost of basal metabolism, which is an inverse function of walking speed. Thus, basal metabolic cost progressively decreases with increasing speed, suggesting the rise in gross metabolic cost at faster speeds results primarily from muscle energetics. Walking simulations at a range of speeds indicate the iliopsoas and glutei muscle groups are unique compared to other major muscle groups in that they are active primarily during energetically-costly concentric contractions and have little opportunity to store and return elastic strain energy during the stride [2]. The metabolic cost of using iliopsoas and glutei may therefore be expected to increase more dramatically with increasing walking speed than other muscles that can take advantage of energy savings through lengthening contractions and elastic energy return.

Therefore, we hypothesized that the shape of the gross energy-speed curve would be determined primarily by the cost (energy per unit distance) of basal metabolism at speeds slower than preferred, and by the cost of iliopsoas and glutei muscles at speeds faster than preferred.

## METHODS

Optimal control simulations of walking were performed using a 2D musculoskeletal model with 26 Hill muscle models (Fig. 1) [3]. An implicit direct collocation method was used to find the states and controls of the model that minimized the sum of a tracking error plus the gross metabolic cost [3], at five speeds from 0.72-1.67 m/s.

The tracking targets were joint angles and ground reaction forces from 10 healthy young male military service members [4]. Basal metabolic rate was assumed to be 1.0 W/kg. Gross metabolic cost was the sum of the basal and muscle metabolic rates, divided by speed and body mass.

The contribution of each muscle (and of the basal metabolic rate) to the shape of the gross energy-speed curve was determined by calculating the muscle's individual metabolic cost at each speed, then subtracting the cost of the same muscle in the 1.20 m/s simulation, which had the lowest gross metabolic cost.

## RESULTS AND DISCUSSION

The model's metabolic cost and stride duration were within one standard deviation of the human mean at all five speeds, with a U-shaped energy-speed curve (Fig. 2). The model's joint angles and ground reaction forces deviated from the human means by 0.9 standard deviations on average.

No individual muscle had a U-shaped energy-speed curve. Basal metabolism and the energy cost of



**Figure 1:** Model

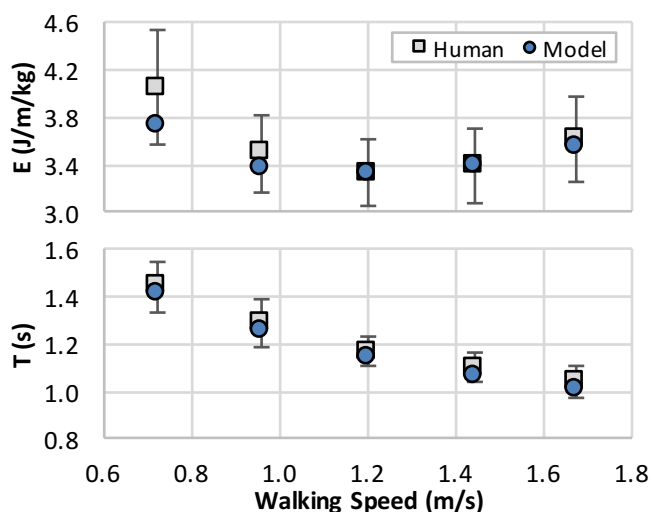


**Figure 2:** Metabolic costs (E) and stride durations (T) at each speed for the model and human data [4].

vasti and hamstrings increased the gross cost at slow speeds, but their contributions were minimal beyond the optimal speed, where the energy cost of iliopsoas and glutei made the greatest contributions (Fig. 3). The other 18 muscles combined made a contribution similar to the iliopsoas (Fig.3).

## CONCLUSIONS

The shape of the gross energy-speed curve in walking is due primarily to basal metabolic rate at slower speeds and to the uniaxial hip muscles at faster speeds. The effect of speed on these muscles is likely due to their architecture (long fibers, short tendon), limiting storage and return of elastic tendon energy, and the fact that they are primarily

used to perform energetically costly shortening contractions. Muscles with similar architecture (e.g. vasti) are activated during less costly lengthening contractions, and other muscles activated during shortening tend to have relatively short fibers and long tendons to take better advantage of tendon elastic energy storage and return (e.g. soleus).

The metabolic costs of individual muscles were not minimized near a common speed (Fig. 3), similar to EMG data from [5], and no muscle had a U-shaped energy-speed curve. Thus, perhaps muscle activity is coordinated to minimize the effect of speed on gross metabolic cost, such that the average cost over the range of typical walking speeds is minimized.

The translational potential of the present results is that individuals who struggle to walk comfortably at moderate speeds or faster may be limited by their uniaxial hip muscles, which are not targeted in strength training as often as other major groups like the quadriceps, hamstrings, and plantarflexors.

## REFERENCES

1. Ralston HJ. *Int Z Ang Physiol* **17**, 277-283, 1958.
2. Neptune RR, et al. *J Biomech* **28**, 135-143, 2008.
3. Miller RH, et al. *J Biomech* **48**, 2858-2864, 2015.
4. Esposito ER, et al. *JRRD* **51**, 1287-1296, 2014.
5. Carrier DR, et al. *PNAS* **108**, 18631-18636, 2011.

The view(s) expressed herein are those of the author(s) and do not reflect the official policy or position of Brooke Army Medical Center, the U.S. Army Medical Department, the U.S. Army Office of the Surgeon General, the Department of the Army and Department of Defense or the U.S. Government.

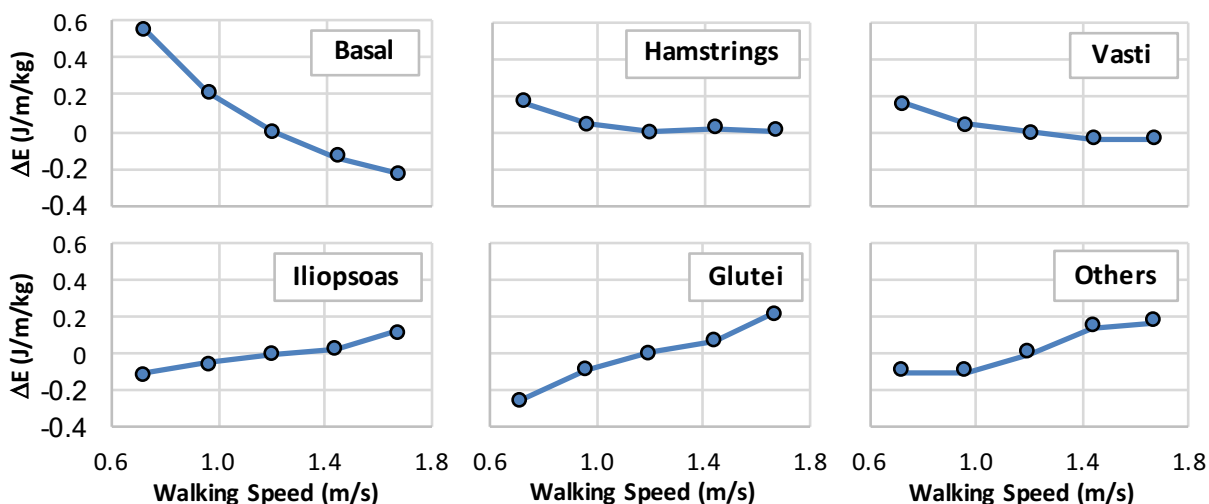


**Figure 3:** Contributions of basal metabolism and selected muscles to the gross metabolic cost (above or below the minimum metabolic cost at the 1.20 m/s walking speed).

# A PASSIVE HIP EXOSKELETON FOR REDUCING METABOLIC COST OF WALKING: A SIMULATION STUDY

Mohammadhossein Saadatzi and Ozkan Celik

Department of Mechanical Engineering, Colorado School of Mines, Golden, CO, USA  
email: msaadatz@mymail.mines.edu, web: brl.mines.edu

## INTRODUCTION

Wearable robots are recently being explored to make walking more efficient, through replacing part of metabolic energy requirement with power provided by exoskeletons. It is shown by Quinlivan et al. [1] that an active exoskeleton with an offboard actuation and power supply system has the capability of reducing metabolic cost of walking up to 23%. However, the weight of such a system that needs to be carried by the wearer in a completely wearable application is a real barrier to net metabolic energy savings during walking. On the other hand, it is shown by Collins et al. [2] that the metabolic cost of human walking can be reduced about 7.5% using an unpowered, clutch-and-spring ankle exoskeleton. This exoskeleton works based on the principle that clutch and spring sustain force passively, unlike muscles and tendons.

In this study, based on the same principle, we have evaluated the feasibility of using a passive hip exoskeleton to reduce the metabolic cost of walking within a predictive simulation framework. Simulations suggest that the proposed hip exoskeleton can reduce the metabolic cost of walking by 10.3% through replacing the power of Iliopsoas muscle group during walking.

## METHODS

In this work, we are using a predictive simulation framework which is created using OpenSim API in C++. In this framework, bipedal walking is generated through optimization of muscle actuation profiles for a musculoskeletal model with 9 sagittal degrees of freedom and 18 muscles.

The actuation profiles for the muscles are determined by minimizing a cost function which

consists of several terms, including target velocity error, metabolic expenditure of muscles, and excessive alternating motion of the upper body. Ten parameters define an actuation profile for each muscle during a gait cycle (90 parameters for all muscles).

Figure 1 shows the results of our predictive simulation framework, and human experimental data (which is taken from [3]) for walking at speed 1.5 m/s. In this figure, the top panel depicts the kinematic trajectory of hip during a stride cycle, the middle panel indicates the Iliopsoas muscle force, and the bottom panel shows Iliopsoas muscle power. According to the depicted experimental data, in the beginning of the gait cycle (from about 15-50% of the gait stride), the Iliopsoas performs negative work (it applies flexion torque while the hip joint is extending). Hence, a torsional spring during this first half of the stride can replace the

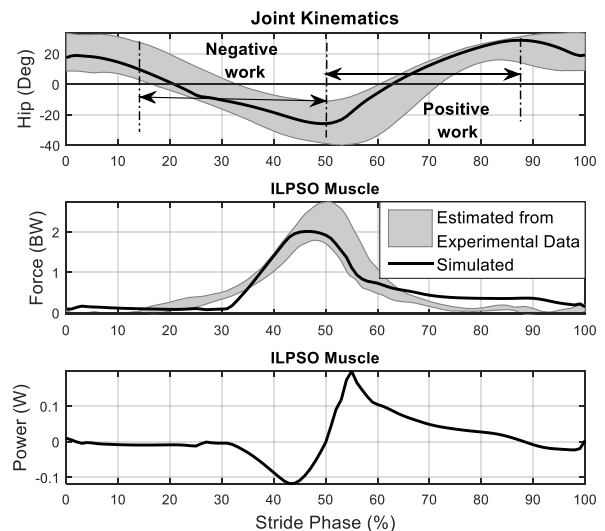


**Figure 1:** Hip angle and Iliopsoas muscle force and power during a gait stride. Experimental data are represented by the shaded region ( $\pm 1$  SD). The solid line represents our predictive simulation results.

negative work done by the Iliopsoas. Also, the energy stored in the spring during the first half of the stride can be used during the rest of the stride to fulfill the positive work normally done by Iliopsoas.

We used our framework to determine the optimal spring parameters around the hip joint to minimize the energetics of walking. Two spring parameters are considered in our optimizations: the optimal stiffness and the equilibrium (free) angle of the torsional spring. The framework optimizes the muscle actuation profiles (90 parameters) and the two exoskeleton parameters simultaneously.

## RESULTS AND DISCUSSION

Based on our framework, an optimal spring (having stiffness of 0.99 (Nm/deg) and equilibrium angle of 10.04 (deg) flexion) is predicted to decrease the metabolic cost of walking by 10.3%. Figure 2 shows the moment generated by Iliopsoas muscle for a stride cycle, during normal gait and during gait with the optimized passive hip exoskeleton. It also shows the moment generated by the proposed exoskeleton if it is worn during walking. It is clear from this figure that the hip exoskeleton has replaced majority of the work done by the Iliopsoas muscle.

Figure 3 shows the metabolic expenditure of walking during normal gait and during gait with the hip exoskeleton. The muscle energetics model proposed by Umberger et al. [4] has been used to compute the metabolic cost of walking (OpenSim API probe class has been used). We note that the

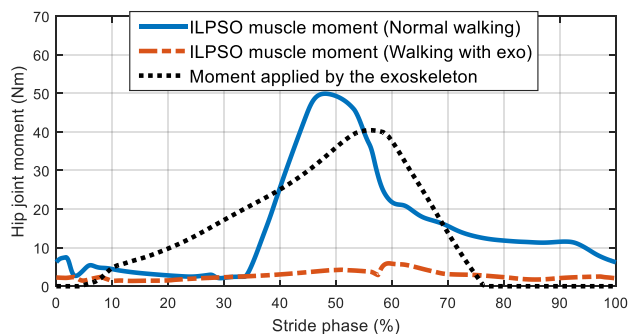


**Figure 2:** Hip joint moment by the Iliopsoas muscle during gait with and without exoskeleton, and the moment generated by the exoskeleton during gait with exoskeleton.

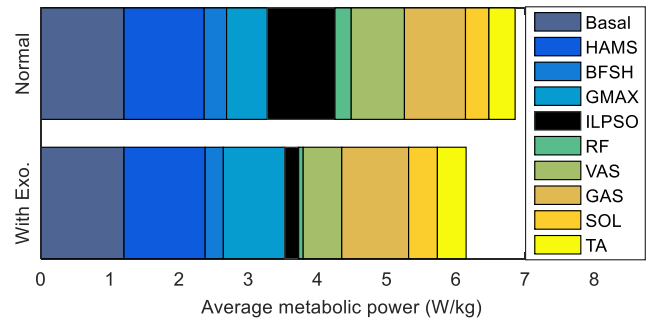


**Figure 3:** Metabolic cost of walking during gait with and without the exoskeleton.

computed metabolic cost of walking is overestimated for either case [4], due to the musculoskeletal parameters and simplifications contained in our model. The hip exoskeleton has changed the metabolic energy expenditure for the muscles, and mainly affected the Iliopsoas. The change in energy expenditure of other muscles originates from the coupled structure of the human musculoskeletal system and multi-articular muscles, which was also noted by Uchida et al. in [5].

## CONCLUSIONS

Our simulation results suggest that it would be feasible to reduce metabolic cost of walking using a passive hip exoskeleton. Verification and tuning of the exoskeleton design through data collection from human subjects constitute our next step.

While current device design efforts have utilized repeated human subjects testing when device parameter values are being explored [6], a predictive simulation framework can be used to explore the device parameter space and to determine the most promising design solutions/parameter values that can be used to inform the human subject experiment design.

## REFERENCES

1. Quinlivan BT, et al. *Science Robotics* **2** (2), 2017.
2. Collins SH, et al. *Nature* **522**, 212-215, 2015.
3. Dorn TW, et al. *PLOS ONE* **10** (4), 1-16, 2015.
4. Umberger BR. *J. R. Soc. Interface* **7** (50), 1329–1340, 2010.
5. Uchida TK, et al. *PLOS ONE* **11** (9), 1-16, 2016.
6. Collins SH. *Proceedings of IEEE-ICM*, VI, Italy 24-27, 2013.

# ENERGY COST OF WALKING IN A PASSIVE-ELASTIC ANKLE-METATARSOPHALANGEAL EXOSKELETON

<sup>1</sup> Brekke A. Green, <sup>2</sup> Gregory S. Sawicki and <sup>1</sup> Jonas Rubenson

<sup>1</sup> Biomechanics Laboratory, The Pennsylvania State University, University Park, PA, USA

<sup>2</sup> Human PoWER Laboratory, Joint Department of Biomedical Engineering, North Carolina State University and the University of North Carolina at Chapel Hill, USA

email: [bag5269@psu.edu](mailto:bag5269@psu.edu); web: [www.locomotionlab.net](http://www.locomotionlab.net), [www.biomechanics.psu.edu](http://www.biomechanics.psu.edu)

## INTRODUCTION

Passive-elastic lower-limb exoskeletons aim to reduce metabolic costs by taking advantage of elastic springs that both provide assistive passive torque and work. While there have been approaches to store and return energy passively across the entire limb [1], the majority of passive-elastic exoskeletons have drawn inspiration from the spring-like mechanics of the human triceps surae. These devices are typically designed with an external spring that parallels the Achilles tendon that stores and returns energy during the stance-phase of walking or hopping.

Emulating the elastic role of the human triceps surae is proving a successful means by which to augment human walking. Indeed, the metabolic energy saving of one such lightweight passive-elastic ankle exoskeleton has recently been shown to lower the metabolic cost of walking below that of normal, instrumented, walking [2]. Here we propose that further advances in passive-elastic assistive exoskeletons may be achieved by drawing inspiration from non-human species that exemplify elastic gait mechanics. Unlike humans that move in a plantigrade posture, the majority of cursorial species walk and run in a digitigrade posture (toe running). This mode of locomotion facilitates elastic energy storage and return in multi-joint muscle-tendon units that cross both the ankle and the metatarsophalangeal (MP) joint. For example, the ostrich has been shown to produce nearly fifty percent of the positive mechanical work of the stance phase of running through elastic recoil at the tarso-metatarsophalangeal joint [3]. This feature of ostrich running is thought to be the main

explanation for how they run with half of the metabolic energy compared to humans [3].

The purpose of the present study was to design and test a biologically-inspired human exoskeleton that emulates the storage and return of elastic energy at both the ankle and MP joints typical of the gait mechanics of efficient non-human cursorial species.

## METHODS

### Exoskeleton Design:

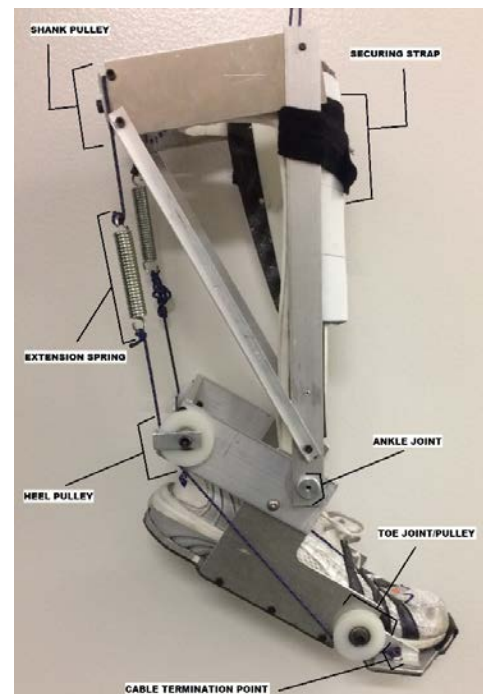


**Figure 1:** Passive-elastic ankle-MP exoskeleton

We designed a passive-elastic exoskeleton (EXO) that was based on a two-joint (ankle and MP)

passive spring design. The EXO consisted of three segments fabricated out of carbon fiber and aluminum: (1) a shank frame; (2) a rear-foot frame mounted directly to a lightweight running shoe that articulated with the shank frame; and (3) a fore-foot plate that was mounted to the sole of the running flat under the toe box (Fig. 1).

The proximal section of the spring cord (Paracord) was aligned in parallel with the triceps surae muscles and ran to a pulley situated on the rear-foot frame behind the ankle. The distal section of the spring continued to a second pulley mounted on the rear-foot frame near the MP joint and terminated on the fore-foot plate. The spring cord looped between the left and right side of the EXO across two pulleys mounted at the top of the shank frame. Two parallel linear steel springs (7 kN/m each) were positioned in the spring cord line behind the calf. This design provided a simultaneous passive-elastic joint moment at the Ankle and MP joints and was capable of transferring energy between the joints.

Metabolic Testing: Pilot experiments measured rates of oxygen consumption (Vista VO2 Lab, Ventura California) in multiple walking trials (1.25 m/s) under three conditions; (1) a control walking condition without the EXO; (2) walking with the EXO but without the passive elastic component engaged; and (3) walking with the EXO fully functional. Standing trials, both under normal and EXO conditions, were collected to determine the net cost of walking (gross metabolic rate minus standing rate). A training period of 20 minutes was used to allow for familiarization with walking in the device both with the spring engaged and when the spring was disengaged.

## RESULTS AND DISCUSSION

The metabolic rates (ml O<sub>2</sub>/kg/min) for walking and standing in the control (no EXO) condition, in the EXO with the spring disengaged, and in the EXO with the spring engaged are presented in Fig. 2

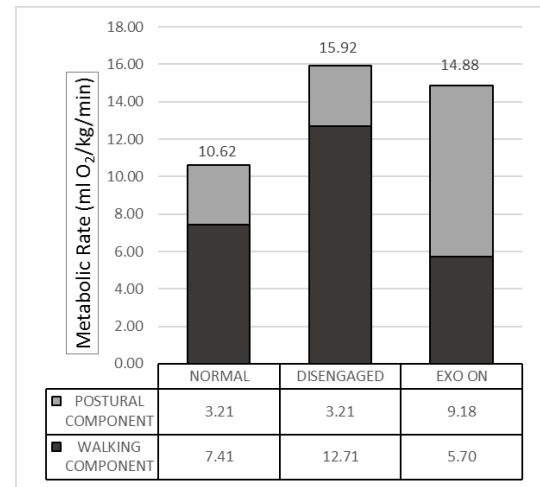


**Figure 2:** The gross oxygen cost measured during walking is represented by the sum of the black and grey bars (standing postural cost). The black bars represent the net oxygen cost of walking.

The gross oxygen cost of walking with the EXO was substantially elevated over the control condition, and is likely explained by the substantial mass of the EXO. Nevertheless, the gross cost of walking in the EXO with the spring engaged was reduced by 6.5%, indicating that the two-joint passive-elastic spring mechanism can reduce walking cost. The net oxygen cost of walking was, surprisingly, 23% lower than the control condition. This value is impressive, but must be viewed cautiously since this arises due to the high cost of standing in the EXO. It is unclear if the same postural cost is present during gait. In summary, pilot data indicate that a biologically-inspired ankle-MP EXO may provide a novel approach for reducing the metabolic cost of human walking.

## REFERENCES

1. Grebowski, AM and Herr, HM. *J Appl. Physiol* 2009, **107**:670-8.
2. Collins SH, Wiggin MB, Sawicki GS. *Nature*. 2015, **522**:212-5.
3. Rubenson, J., Heliam, B.D., Besier, T.F., Lloyd, D.A., and Fournier, P.A. *Journal of the Royal Society, Interface*. 2011 **8**: 740-755.

# OSTEOARTHRITIS EXAMINED FROM FULL HUMAN TO CELLULAR PERSPECTIVES: ASB-OARSI Symposium Sympatico

<sup>1</sup>Cara L. Lewis, <sup>2</sup>Ross Miller, <sup>3</sup>Lou DeFrate, <sup>4</sup>Tim Griffin, <sup>5</sup>Paul DeVita

<sup>1</sup>College of Health & Rehabilitation Sciences, Boston, University, Boston, MA, USA

<sup>2</sup>Department of Kinesiology, University of Maryland, College Park, MD, USA

<sup>3</sup>Department of Orthopaedics, Duke University, Durham, NC, USA

<sup>4</sup>Aging and Metabolism Program, Oklahoma Medical Research Foundation, Oklahoma City, OK, USA

<sup>5</sup>Department of Kinesiology, East Carolina University, Greenville, NC, USA

Email: [devitap@ecu.edu](mailto:devitap@ecu.edu) web: <http://www.ecu.edu/cs-hhp/exss/biomechlab.cfm>

## INTRODUCTION

Osteoarthritis is the most prevalent cause of mobility dependency and disability in the United States and its prevalence is expected to increase over the coming decades. Its etiology and progression involve complex interactions among biomechanical and physiological factors and any cure currently remains elusive. Consequently, OA is an important research focus in both the ASB and the Osteoarthritis Research Society International (OARSI). We now combine researchers from both Societies to identify current practice, experiment, and theory in the scientific investigation and medical treatment of OA. Additionally, our goal is to stimulate increased collaboration between members of ASB and OARSI and between the Societies themselves.

The symposium will follow this schedule:

Introduction – Paul DeVita – 5 mins

Movement Analysis and Gait Retraining – Cara Lewis – 15 mins

Knee Modeling & Cartilage Conditioning – Ross Miller – 15 mins

Overview of OARSI – Tim Griffin - 5 mins

Cartilage Mechanical Environment – Lou DeFrate – 15 mins

Inflammation, Oxidation & Mechanobiology of the knee – Tim Griffin – 15 mins

Discussion – 15 mins

## MOVEMENT ANALYSIS & GAIT RETRAINING – Cara L. Lewis

Evaluating movement kinematics through a visual assessment is an essential part of physical therapy practice. This qualitative assessment of movement, however, does not provide easily quantifiable metrics and is often practitioner-specific. Movement analysis within a three-dimensional motion capture laboratory enhanced with force platform capacity provides a precise quantification of movement as well as the ability to analyze joint forces, moments and powers. These data further combined with electromyography data provide an accurate and sophisticated description of a patient's movement capacity and his or her kinesiological movement solution to the task demands. This added information enables the investigation of the mechanism of injury and potentially successful rehabilitation protocols.

From a clinical standpoint, pain is often used to indicate if the current movement pattern is adaptive or maladaptive. For example, if gait biomechanical changes reduce pain, then those changes are assumed to be favorable and the previous pattern assumed to be detrimental. From a biomechanical standpoint, however, we can investigate why and how those changes may have reduced the pain. This important step allows the physical therapist to not only quantify the alterations for a single individual or group of individuals, but also extrapolate to other groups who may similarly benefit. Thus the combination of the clinical perspective with the biomechanical tools facilitates the development of movement-based physical therapy interventions supported by an understanding of the underlying biomechanical mechanisms.

## **BIOMECHANICAL KNEE MODELING & CARTILAGE CONDITIONING – Ross Miller**

Modeling the loads on the knee during activities of daily living is a growing topic of interest in clinical biomechanics, often motivated by the assumption that relatively high loads prompt the development of knee osteoarthritis under the “wear-and-tear” paradigm. Common approaches include static optimization, reduction models, EMG-driven models, and finite element models. Knee osteoarthritis is notable for the large number of special populations with a relatively high prevalence of the disease, including older adults, obese adults, African Americans, women, individuals with contralateral limb loss, and individuals with prior traumatic knee injuries. This presentation will compare and contrast joint loading in these seemingly disparate populations and will ask how (or if) common features of joint loads may predispose them all to the same chronic disease. The author’s central hypothesis is that if these populations are linked by a primarily-biomechanical factor in their risk for knee osteoarthritis, that factor is likely the conditioning of their cartilage earlier in life affecting their cartilage metabolism and sensitivity to “excessive” or “unusual” joint loads later in life. Thus, predicting the risk for developing OA requires data and models beyond the current loading of the joint.

## **DIVING INTO DIARTHRODIAL JOINTS: IDENTIFYING CARTILAGE MECHANICAL ENVIRONMENT – Lou DeFrate**

Mechanical loading plays an important role in maintaining cartilage health. Altered mechanical loading (potentially due to factors such as joint injury, obesity, and mal-alignment) may contribute to the development of osteoarthritis. However, there are currently limited tools available to quantify the local in vivo mechanical environment of cartilage in humans. While measures of joint alignment on x-ray and gait analysis techniques using markers attached to the skin can provide insights into the amount of force distributed between medial and lateral compartments, it may be difficult to predict the local cartilage tissue response based on these measurements. We now explore how risk factors for

osteoarthritis such as joint injury and obesity influence the local mechanical environment of cartilage during activities of daily living using novel techniques which incorporate MR imaging, biplanar radiography, and 3D modeling tools. Additionally, we will demonstrate the use of imaging biomarkers quantifying changes in cartilage thickness and composition. Together, these measurements can provide new insights into the changes associated with the initiation and progression of OA. Understanding these changes is essential to developing new interventions aimed at the prevention of osteoarthritis.

## **INFLAMMATION, OXIDATION, AND THE MECHANOBIOLOGY OF A RESILIENT JOINT – Tim Griffin**

A central characteristic of OA is the imbalance in the synthesis and degradation of articular cartilage, resulting in the net loss of tissue. This imbalance is attributed in large part to two processes that activate cellular catabolic pathways and impair cell function: inflammation and oxidation. Yet these processes are themselves normally maintained in a balance, for example, by pro- and anti-inflammatory cytokines or endogenous pro-oxidant molecules and anti-oxidant enzymes. Understanding how different types of biomechanical stress sway the balance of joint tissue inflammation and oxidation can provide a more comprehensive understanding of the beneficial and detrimental aspects of biomechanical factors in altering OA risk.

We examined this question in two joint tissues--the infrapatellar fat pad (IFP) and articular cartilage. The IFP is a source of pro-inflammatory cytokines in end-stage OA knees, but it is not known if it is a source of inflammation early in the disease process. We found that the IFP becomes fibrotic without increased inflammation prior to the development of knee OA in obese mice. We hypothesized that the increase in IFP fibrosis was the result of increased joint loading. We tested this hypothesis in non-obese mice following voluntary wheel running. IFP fibrosis and inflammation increased after 3 days of running but resolved by 14 days, indicating that increased loading induces a transient inflammatory response in a healthy knee. In cartilage, we tested

the hypothesis that physiologic levels of cyclic loading improve cellular oxidative balance by enhancing antioxidant capacity. Using *in vitro* compressive loading models with bovine cartilage explants, we found that cyclic loads of 50 and 300 kPa (1 Hz, 12 hrs/day, 2 days) induced a significant increase in total cartilage antioxidant capacity (15% and 115% increase, respectively, over unloaded controls,  $p < 0.05$ ). We are investigating the cellular mechanisms responsible for these load-induced responses that promote oxidative balance.

## **The OSTEOARTHRITIS RESEARCH SOCIETY INTERNATIONAL**

The [Osteoarthritis Research Society International \(OARSI\)](http://www.oarsi.org) is the premier international organization for scientists and health care professionals focused on the prevention and treatment of OA through research, education, advocacy, and the worldwide dissemination of new knowledge. The complexity of OA prevention and treatment requires a multi-disciplinary effort, which includes you! Get involved by participating in OARSI's annual meeting and sponsored workshops. The 2018 and 2019 OARSI World Congresses will be in Liverpool, England and Toronto, Canada in April and May of those years. In fact both Societies hope to have a second combined ASB-OARSI symposium at the 2019 OARSI meeting. Consider the society's journal, [Osteoarthritis and Cartilage](http://www.oarsi.org), for your next publication; it is a highly respected multidisciplinary journal for all OA-related original research articles and reviews. Learn more about OARSI and consider becoming a member by visiting their website at [www.oarsi.org](http://www.oarsi.org).

The ASB gratefully acknowledges the enthusiasm and support of this symposium by OARSI and its Board of Directors.

# THE EFFECT OF ACHILLES TENDON MOMENT ARM LENGTH ON STRETCH-SHORTENING CYCLE PERFORMANCE IN THE VERTICAL JUMP

Thomas Madden, Thanh Tran-Vi, Katherine Knaus, Geoffrey Handsfield, Joseph Hart, and Silvia S. Blemker  
University of Virginia, Charlottesville, VA, USA  
email: tsm3me@virginia.edu

## INTRODUCTION

The enhancement of human movements involving the stretch-shortening cycle (SSC) is evident in motions such as running and jumping. However, the mechanism behind the enhancement is unclear, and less clear are the factors affecting SSC performance. Active force development and elastic energy recoil are thought to be responsible for the increased power output in SSC movements [3]. During the stretch portion, elastic energy is stored in tendons such as the Achilles tendon (AT). Stored energy is potentially reutilized during shortening to augment the power of the motion. For a given joint moment, musculoskeletal modeling illustrates that the amount of energy stored is most sensitive to moment arm (MA) length, and that the two are related inversely [8]. A shorter MA may also aid force and power development by allowing the muscle to shorten at a slower velocity. Observations indicate a shorter AT MA length promotes sprinting ability [2].

The purpose of this study was to determine the effect of MA length on the enhancement of power output in the SSC during vertical jumps. Because a shorter MA may lead to greater elastic energy storage in the tendon [8], we reasoned that AT MA length would correlate inversely with SSC performance in vertical jumping. To test this hypothesis, we used MRI and performance data to determine the relation between MA length and SSC performance in collegiate basketball athletes.

## METHODS

Ten NCAA Division 1 male basketball athletes served as subjects ( $20.1 \pm 1.9$  years,  $198 \pm 7$  cm,  $101 \pm 8$  kg). SSC performance was assessed by comparing peak power output of a jump from a static squat position (squat jump, SJ) to that of a jump with a countermovement (CMJ) [6]. The subjects kept

their hands on their hips during the SJ; in the CMJ, subjects were allowed arm swing in addition to a countermovement. Jump heights were measured using a Just Jump Mat (Probotics, Inc., Huntsville, AL). The best of three jumps were taken as the SJ and CMJ height for each subject. Jump powers (W) were calculated using previously developed equations depending on each subject's jump heights (cm) and body mass (kg) [7]:

$$P_{SJ} = 60.7h_{SJ} + 45.3m - 2055 \quad (1)$$

$$P_{CMJ} = 51.9h_{CMJ} + 48.9m - 2007 \quad (2)$$

SSC performance was quantified as the prestretch augmentation (PA), the increase in jump power from SJ to CMJ relative to SJ [6]:

$$PA = \frac{P_{CMJ} - P_{SJ}}{P_{SJ}} 100\% \quad (3)$$

To produce axial MR images of the lower limbs, subjects were scanned using a 3T Siemens Trio MRI Scanner with a 2D multi-slice spiral gradient echo sequence. AT MA length was approximated as the distance from the center of the ankle joint, defined by the midpoint of a line between the medial and lateral malleoli [5], to the AT (Fig. 1). Measurements were made for the right leg.

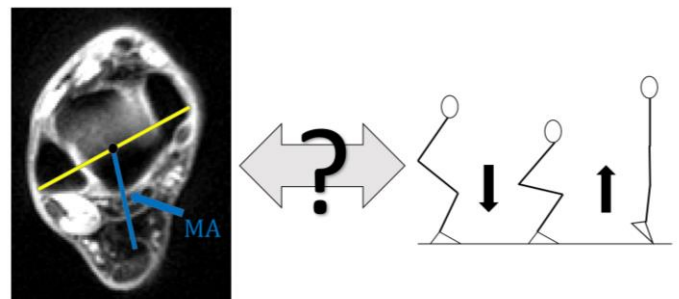


**Figure 1:** (Left) AT MA length was approximated from axial MR images of the ankle joint. (Right) The downward and upward phases of a CMJ is illustrated. The relation between PA and MA length was determined by correlation analysis.

To assess the relationship between MA length and PA, a curve was fit to the data based on an expression for energy stored in a stretched tendon, derived from the tendon force-elongation curve ( $F = ku^n$ ) for a musculoskeletal model [8]. With  $n = 2$  and a given moment,  $M$ , the energy,  $E$ , stored in a stretched tendon depends inversely on MA length,  $r$  [8]:

$$E = \frac{1}{3} k^{-\frac{1}{2}} M^{\frac{3}{2}} r^{-\frac{3}{2}} + C \quad (4)$$

To account for the variation of peak ankle joint moment across subjects, PA was normalized by the product of each subject's mass ( $m$ ) and CMJ height ( $h_{CMJ}$ ), raised to the power of  $3/2$ . This product represents the total work performed during the CMJ, defined as the increase in potential energy of the mass center from take-off to the maximum height of the jump. Because each subject exhibits a similar kinematic pattern, the variation in total work performed accounts for the variation in ankle joint moment. This resulted in the following model equation for relative PA:

$$\frac{PA}{(m \times h_{CMJ})^{\frac{3}{2}}} = Ax^{-\frac{3}{2}} + B \quad (5)$$

## RESULTS AND DISCUSSION

Consistent with our hypothesis, there was an inverse relationship between MA length and relative PA (Fig. 2). Fitting the model curve (Eq. 5) to the data resulted in a significant correlation between MA length and relative PA ( $p < 0.01$ ).

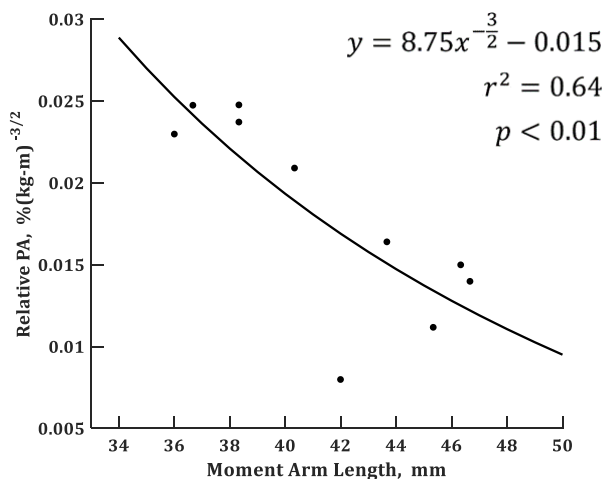


**Figure 2:** A curve, based on Eq. 4, could be used to fit the relative PA vs. AT MA length data.

Vertical jump SSC performance and AT MA length exhibit an inverse relation in the form of the expression for energy stored in a stretched tendon (Eq. 4). This result suggests elastic energy recoil appreciably contributes to SSC performance. Although MA length does not correlate with absolute CMJ height ( $p > 0.10$ ), a shorter MA may allow individuals to perform more efficient movements by reducing the work required of muscle. During the CMJ, subjects were allowed arm swing. While this has been shown to increase CMJ height as compared to no arm swing [4], we reason the difference is not enough to change the outcome of this study because the relative PA still correlated with MA length ( $p < 0.05$ ). Further, the results of this study are consistent with experimental data showing AT MA length to be inversely correlated with running economy [1, 8].

## CONCLUSIONS

Previous research has indicated sprinting ability [2] and running economy [1, 8] to be associated with a shorter AT MA length. In this study, we demonstrated that SSC performance in vertical jumping correlates inversely with AT MA length in collegiate basketball athletes. This relation exhibits the form of the expression for energy stored in a stretched tendon (Eq. 4), suggesting elastic energy is a crucial contributor to SSC performance. Athletic movements involving the SSC appear to favor individuals who have shorter MA lengths.

## REFERENCES

1. Barnes KL, et al. *J Strength Cond Res*, **28**(5), 1289-1297, 2014.
2. Baxter JR, et al. *Proc R Soc Lond [Biol]*, **279**(1735), 2018-2024, 2012.
3. Ingen Schenau, et al. *J Appl Biomech*, **13**(4), 389-415, 1997.
4. Lees A, et al. *J Biomech*, **37**(12), 1929-1940, 2004.
5. Lundberg A, et al. *J Bone Joint Surg*, **71**(1), 94-99, 1989.
6. McGuigan MR, et al. *J Strength Cond Res*, **20**(4), 992-995.
7. Sayers SP, et al. *Med Sci Sports Exerc*, **31**(4), 572-577, 1999.
8. Scholz MN, et al. *J Exp Biol*, **211**(20), 3266-3271, 2008.

# BIOMECHANICAL DIFFERENCES IN FEMALE ATHLETES WITH VARYING LEVELS OF LEG STIFFNESS

<sup>1</sup> Justin P. Waxman, <sup>1</sup> Kevin R. Ford, <sup>2</sup> Anh-Dung Nguyen, and <sup>1</sup> Jeffrey B. Taylor

<sup>1</sup> Department of Physical Therapy, High Point University, High Point, NC, USA

<sup>2</sup> Department of Athletic Training, High Point University, High Point, NC, USA

Email: [jwaxman@highpoint.edu](mailto:jwaxman@highpoint.edu)

## INTRODUCTION

Leg stiffness ( $K_{LEG}$ ) is thought to contribute to an athlete's risk for lower-extremity (LE) injury [1]. However, the potential mechanism(s) by which an athlete's  $K_{LEG}$  contributes to their risk for LE injury is poorly understood. Although several biomechanical characteristics have been identified as prospective risk factors for LE injury [2, 3], the extent to which athletes with varying levels of  $K_{LEG}$  also display differences in biomechanical movement strategies remains unknown. Thus, gaining an understanding of whether differences in  $K_{LEG}$  are accompanied by differences in movement biomechanics is an important first step towards elucidating the potential mechanism(s) by which an athlete's  $K_{LEG}$  may contribute LE injury risk. Therefore, the purpose of this study was to compare differences in sagittal- and frontal-plane biomechanics between adolescent female athletes with varying levels of  $K_{LEG}$ .

## METHODS

Ninety-seven females ( $15.5 \pm 1.3$  years,  $1.7 \pm 0.1$  m,  $60.6 \pm 9.8$  kg) performed a repetitive (i.e. 2.2 Hz), single-leg, vertical hopping task atop a force platform integrated with a 14-camera motion capture system. Three 10-sec trials were recorded on both the dominant and non-dominant leg. Using data from the 6<sup>th</sup> to 10<sup>th</sup> hop of each trial,  $K_{LEG}$  was calculated as the ratio between peak vertical ground reaction force (PvGRF) and maximum center-of-mass (CoM) displacement for each hop [4]. The instants of initial ground contact (IC;  $GRF > 10$  N) and toe-off (TO;  $GRF < 10$  N) for each hop were then used to calculate stance time (from IC to TO), flight time (from TO to IC). Sagittal- and frontal-plane trunk, hip, knee, and ankle biomechanics were also extracted from each

hop. Our biomechanical variables of interest included joint angles at the instant of IC, peak angles and moments throughout stance (from IC to TO), and angular excursions (i.e. peak value – IC value).  $K_{LEG}$ , PvGRF, and moments were normalized to body mass ( $kN \cdot m^{-1} \cdot kg^{-1}$ ), body weight ( $N \cdot N^{-1}$ ), and the product of body height and mass ( $Nm \cdot m^{-1} \cdot kg^{-1}$ ), respectively.

A preliminary repeated-measures ANOVA revealed no significant differences in  $K_{LEG}$ -related variables between dominant and non-dominant legs ( $P > .05$ ). Thus, all variables were averaged across legs for subsequent analyses. Tertiles (i.e. low-, moderate-, and high-stiffness groups) were then established using  $K_{LEG}$  values, and between-group differences in demographics,  $K_{LEG}$ -related variables (i.e. stance and flight times, hopping frequency, CoM displacement, and PvGRF), and hopping biomechanics, were then evaluated using separate one-way ANOVA models.

## RESULTS AND DISCUSSION

Participant demographics, CoM displacement, and hopping frequency, were not statistically different between groups ( $P > .05$ ). However,  $K_{LEG}$ , PvGRF, and flight time significantly increased, and stance time significantly decreased, from the low- to moderate- to high-stiffness group ( $P < .001$ ), indicating that the high-stiffness group experienced higher peak forces and loading rates. Given that performing activities with high GRFs is a risk factor for LE injury, due to higher loading [2], athletes in the high-stiffness group may be producing the very forces in which they should be attempting to avoid. However, we are unaware of any studies that have examined whether healthy athletes with higher  $K_{LEG}$  also display higher peak forces and loading rates during other dynamic tasks. Thus, future work examining such relationships is warranted.

At IC, the high-stiffness group landed with greater lateral trunk-flexion (relative to the stance leg;  $5.3\pm 3.6$  vs  $2.6\pm 3.2^\circ$ ,  $P=.009$ ) and lesser hip-adduction ( $1.4\pm 3.3$  vs  $3.7\pm 2.9^\circ$ ,  $P=.022$ ) angles compared to the low- and moderate-stiffness groups, respectively. Following IC, the high-stiffness group displayed less lateral trunk-flexion excursion compared to the moderate-stiffness group ( $0.8\pm 2.3$  vs  $2.7\pm 3.7^\circ$ ,  $P=.046$ ), greater ankle-dorsiflexion moments compared to the moderate- ( $1.70\pm 0.25$  vs  $1.56\pm 0.17$   $\text{Nm}\cdot\text{m}^{-1}\cdot\text{kg}^{-1}$ ,  $P=.002$ ) and low-stiffness ( $1.70\pm 0.25$  vs  $1.52\pm 0.12$   $\text{Nm}\cdot\text{m}^{-1}\cdot\text{kg}^{-1}$ ,  $P=.022$ ) groups, and greater peak hip-flexion ( $0.59\pm 0.17$  vs  $0.40\pm 0.12$   $\text{Nm}\cdot\text{m}^{-1}\cdot\text{kg}^{-1}$ ,  $P<.001$ ) and ankle-eversion ( $0.48\pm 0.14$  vs  $0.41\pm 0.09$   $\text{Nm}\cdot\text{m}^{-1}\cdot\text{kg}^{-1}$ ,  $P=.038$ ) moments compared to the low-stiffness group. The moderate-stiffness group also displayed greater peak hip-flexion moments compared to the low-stiffness group ( $0.57\pm 0.22$  vs  $0.40\pm 0.12$   $\text{Nm}\cdot\text{m}^{-1}\cdot\text{kg}^{-1}$ ,  $P=.001$ ). Together, these findings suggest that athletes in the high-stiffness group displayed a much more “rigid” hopping strategy compared to athletes in the low-stiffness group, which may help explain why these athletes also displayed greater PvGRF.

While we observed differences in hip and ankle moments, there were no kinematic differences at these joints in their respective planes of motion. As such, the larger hip and ankle moments displayed by the high-stiffness group may be attributed to differences in PvGRF rather than differences in body positioning. In contrast, the larger ankle-eversion moments in the high-stiffness group may be due to the combination of higher PvGRF and greater amounts of lateral trunk flexion. Positioning the trunk lateral to the stance leg can cause the GRF vector to shift laterally, thereby increasing the lever arm relative to the ankle-joint center. Thus, landing with greater lateral trunk flexion at IC, and greater PvGRF, may help explain why the high-stiffness group also displayed greater ankle-eversion moments compared to the low-stiffness group.

The greater lateral trunk flexion observed in the high-stiffness group may be clinically relevant, as this may be a compensatory mechanism for hip-abductor muscle weakness [5]; particularly during single-leg tasks, where adequate neuromuscular control of the hip abductors is essential in positioning the body's

CoM over the base of support to maintain stability. While positioning the trunk lateral to the stance leg can be an effective strategy for reducing hip-abductor demand, the concomitant shift of the GRF vector lateral to the knee-joint center may increase the externally-applied abduction moment, which has been identified prospectively as a risk factor for noncontact ACL injury and patellofemoral pain [2, 3]. While not statistically significant, the high-stiffness group displayed 53% greater peak moments than the low-stiffness group. Our lack of statistically significant findings for frontal-plane knee kinematics and kinetics is likely due to the use of a submaximal hopping task and large variability surrounding group means. Therefore, future studies examining whether  $K_{\text{LEG}}$  is predictive of knee-abduction angles and moments during single-leg tasks with greater frontal-plane demands may clarify how the  $K_{\text{LEG}}$  assessment could identify athletes at increased risk for LE injury. Additionally, because hip-abductor strength was not assessed, it is unknown whether the greater lateral trunk-flexion in the high-stiffness group was due to hip-abductor weakness; thus, future investigations examining this relationship are needed.

## CONCLUSIONS

Healthy, adolescent, female athletes with varying levels of  $K_{\text{LEG}}$  display differences in sagittal- and frontal-plane biomechanics during single-leg hopping. Future studies are needed to determine whether athletes with varying levels of  $K_{\text{LEG}}$  display similar biomechanical differences during more demanding tasks. Because of the large amount of variability in  $K_{\text{LEG}}$  observed in a relatively homogenous sample, future studies examining how  $K_{\text{LEG}}$  contributes to LE injury risk should focus on smaller group subsets that participate in similar activities and have similar training experience.

## REFERENCES

1. Butler RJ, et al. *Clin Biomech*, **18**, 511-517, 2003.
2. Hewett TE, et al. *Am J Sports Med*, **33**, 492-501, 2005.
3. Myer GD, et al. *Clin Biomech*, **25**, 700-707, 2010.
4. Cavagna GA. *J Appl Physiol*, **39**, 174-179, 1975.
5. Dierks TA, et al. *J Orthop Sports Phys Ther*, **38**, 448-456, 2008.

# MODIFIED HOCKEY SKATE BLADE PROFILES AFFECT SKATING BIOMECHANICS AND PERFORMANCE

<sup>1</sup>Jordyn Vienneau, <sup>1</sup>Aimée C. Smith, <sup>1</sup>Sandro R. Nigg, and <sup>1</sup>Benno M. Nigg

<sup>1</sup>University of Calgary, Calgary, Alberta, Canada  
email: javienne@ucalgary.ca

## INTRODUCTION

Biomechanical differences exist between recreational and high caliber ice hockey players [1]. Specifically, high caliber players are able to 1) generate greater total plantar force, 2) extend their hip more at toe-off, and 3) generate a larger hip flexion/extension range of motion during skating maneuvers than their recreational counterparts. These biomechanical differences may help explain the improved skating performance (faster) in high caliber players. However, limited research has been conducted on hockey skates and whether modified skate properties will influence players' performance or biomechanics. One modifiable skate property is the longitudinal radius of the blade, which defines the amount of blade/ ice contact [2]. It has been speculated that a shorter radius allows a player to be more agile in turning movements, while a longer radius enables faster skating due to the increased blade/ ice contact [2].

The purpose of this study was to quantify selected effects of different hockey skate blade profiles on skating performance and skater biomechanics.

## METHODS

Ten male university and collegiate level hockey players participated in this study (Mean  $\pm$  SD: 25.9  $\pm$  6.2 years, 90.2  $\pm$  4.9 kg, 185.2  $\pm$  3.9 cm). All players wore the same CCM Ribcor 44K hockey skate model with three interchanged skate blades. The blade profile conditions were 1) the standard CCM 44K Ribcor profile (Standard), 2) a test profile with a shorter radius than the Standard profile (Agility), and 3) a test profile consisting of two combined radii; a shorter radius for the anterior aspect, and a longer radius for the posterior aspect of the blade (Combo).

Players performed a standardized hockey protocol consisting of forward crossovers, backwards crossovers, and a sprint. Only the data from the backwards crossovers are presented here. Players were instrumented with electro-goniometers to measure hip flexion/extension (Biometrics, AG1500), pressure-sensing insoles to measure in-skate total and regional plantar forces (Pedar-X, novel), and a 3D accelerometer (ADXL 78, Analog Devices USA) on the skate holder for stride detection. Timing lights (TC Timing System, Brower Timing System) were used to measure performance times for each skating maneuver.

## RESULTS AND DISCUSSION

Performance time for backwards crossovers was the best using the Agility blade profile, as the time was 2.3% faster than the standard profile. The combo profile was the slowest with a performance time of 3% slower than the standard profile.

The greatest hip flexion range of motion was observed when skating in the Agility profile (Mean  $\pm$  SE: 25.3°  $\pm$  2.7), followed by the Standard (23.9°  $\pm$  2.0) and the Combo (23.1°  $\pm$  1.9) profiles (Fig. 1). The greatest hip extension at toe-off was observed using the Standard profile (9.3°  $\pm$  1.8), followed by the Agility (10.0°  $\pm$  2.1) and the Combo (11.3°  $\pm$  3.0) profiles.

Players generated greater total plantar force when skating in the Agility and Standard profiles than in the Combo profile (Fig. 2). The increased total force in the Agility profile corresponded to a 2% greater force in the heel region than the Combo profile.

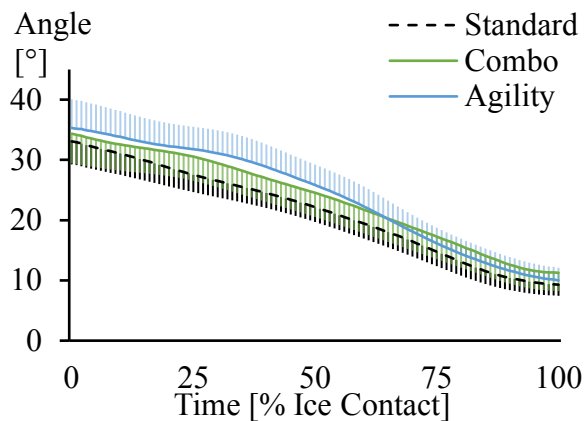


**Figure 1:** Mean  $\pm$  SE hip flexion angle for the inside (left) leg during a backwards crossover.  $0^\circ$  corresponds to full extension.

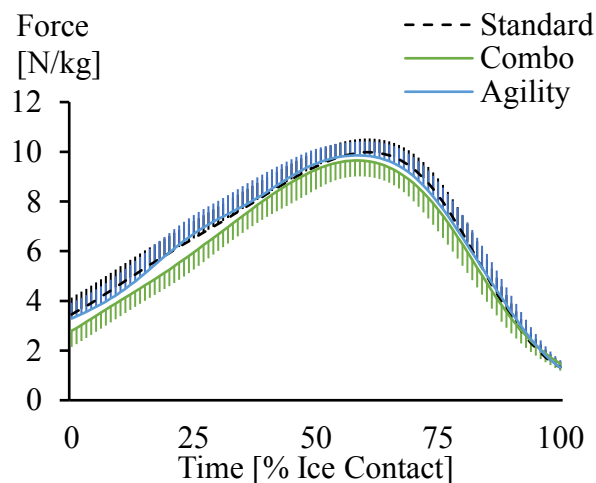


**Figure 2:** Mean  $\pm$  SE total plantar force for the inside (left) leg during a backwards crossover.

It has previously been suggested that a shorter radius would improve a player’s agility [2], which would be beneficial for maneuver such as crossovers. This speculation is supported in this study, where players improved their performance during backward

crossovers in the Agility profile compared to both the Standard profile offered with CCM Ribcor 44k skates, and the Combo profile.

The performance benefits of the Agility profile are supported biomechanically. The Agility blade profile most emulated the elite skating style with an increase in heel force application, and an increase in the hip flexion range of motion [1]. Increased plantar force may allow players to generate more explosive movements, and increasing the hip range of motion maximizes the players blade/ice contact time.

Findings from this study suggest that skate manufacturers should focus on optimizing the skate blade radius, as this parameter appears to positively affect skating performance. Specifically, defenseman perform significantly more backwards skating than offensive players [3], and therefore may benefit most from skates with a shorter radius.

## CONCLUSIONS

In conclusion, changes to hockey skates appear to affect the skating performance of high caliber hockey players, and these enhancements can be supported by biomechanical variables.

## REFERENCES

1. Buckeridge E, et al. *PloS One*, **10**, 1-16, 2015.
2. Lockwood K et al. *J ASTM Int*, **6** (2), 1-8, 2009.
3. Montgomery et al. *Safety in Ice Hockey: Fourth Volume*, ATSM International, 2004.

## ACKNOWLEDGMENTS

The authors would like to thank all participants for their time. This work was supported by Reebok-CCM.

# INVERSE DYNAMICS OF SWINGING BASEBALL BATS OF VARIOUS MOMENTS OF INERTIA

<sup>1</sup> Joseph J. Crisco, <sup>1</sup> Nikolas J. Osvalds, <sup>2</sup> Michael J. Rainbow

<sup>1</sup> Department of Orthopaedics, Alpert Medical School of Brown University and Rhode Island Hospital,  
Providence, RI, USA

<sup>2</sup> Human Mobility Research Centre, Queen's University, Kingston, ON, CA  
email: joseph\_crisco@brown.edu, web: www.brownbiomechanics.org

## INTRODUCTION

Swinging a bat and hitting a ball is a complex task requiring exquisite timing and strength to be successful. In general, at the point of impact, the bat is horizontal and has reached its maximum speed just prior to impact. Increasing a player's maximum bat swing speed is the focus of much instruction and training. The benefit of greater bat swing speed is supported by research studies that have demonstrated that increasing bat swing speed linearly increases batted ball speed, and hence distance. To increase swing speed for a given bat, a player must increase the forces and moments he applies with his hands to the bat during the swing. In a previous study [1], we tracked the full 3-D kinematics of baseball bat swings during a batting cage study of bat performance. We found that bat moment of inertia about the knob (MOI) was the best predictor of the ideal batted ball speed. In this study, we analyze the kinetics of bat swings using those bat kinematics. Specifically, we examined the effects of bat MOI on force impulse and bat speed, and the forces and moments during swings.

## METHODS

Twenty-two ( $n = 22$ ) right-handed male players (mean age: 16, range 13-18) participated in a batting cage study after IRB approval and informed written consent/assent were obtained. Thirteen bat models from six different manufacturers were used in the previous study [1], but only three were selected for this study (Table 1). Five bats of each model were prepared for testing by applying square markers (13mm×13mm) of retro-reflective tape (3M Scotchlite High Gain Reflective Sheeting 7610) along the length of the bat. Four markers were

evenly-spaced circumferentially at approximately 0, 9, 28, 38 and 76 cm from the tip. Baseballs (R100, Rawlings, St. Louis, MO,  $n = 300$ ) were prepared with six uniformly arranged square retro-reflective markers (13mm×13mm).

Testing was held indoors in the Brown University Athletic Center (Providence, RI) over a two-day session. A portable batting cage was assembled (15.2 m×3.0m×4.3m) on the gymnasium floor. The pitching machine (Iron Mike MP5, Master Pitching Machine Kansas City, MO) was positioned within the cage 12.2m from the hitter. Balls were pitched at a speed comfortable to the hitter (range 21.5 – 26 m/s) to maximize the number of hits. Players participated in multiple batting sessions consisting of approximately twenty-five pitches with a single bat. The order of bat models swung by players was selected randomly. Not all bat models were swung by all players.

The pitched ball, batted ball and bat swing were tracked at 300 Hz using an eight-camera Qqus 5-series infrared sensing system (Qualisys, Gothenburg, Sweden). The cameras were mounted on tripods approximately 2.4 m (8 ft) high and positioned behind and to the right side of the batter. Pitched and batted balls were tracked within 3 m (6 ft) of the front of home plate. The system was recalibrated following every 100 pitches, resulting in calibration tolerances less than 0.7 mm. Ball and bat markers were identified within Qualisys Track Manager and exported to Matlab (Mathworks Inc., Natick MA) for subsequent analysis. Ball and bat positions and velocities were calculated using previously developed algorithms [2]. Bat swing speed was computed as the speed of the bat at the tip of the bat.

The forces and moments generated by the hands throughout the duration of the swing were estimated by inputting each bat's physical properties and the 3-D kinematics into Visual3D (C-Motion, Germantown, MD). Linear regression was used to determine if force impulse predicted bat speed. Within each swing, the force and moment time series curves were normalized by their peak value. The normalized curves were then averaged over all players, swings, and bats for qualitative examination. Time of 50% peak values were compared using a paired t-test.

## RESULTS AND DISCUSSION

Force impulse predicted bat speed ( $R^2 = 0.91, 0.84, 0.43$ ) and this linear correlation was constant for each bat model (Fig.1). For the same impulse (e.g. 6.5 Ns) bat speed was significantly ( $P < 0.0001$ ) faster with decreasing MOI.

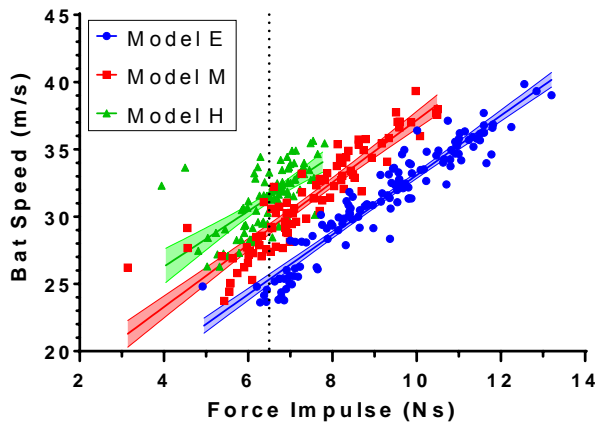


**Figure 1.** Bat speed correlations with force impulse differed (offset, not slope) with bat MOI.

The normalized time series were consistent with a mean standard deviation of 8% and 9% for force and moments, respectively. Additionally, force rose significantly ( $P < 0.001$ ) sooner in the course of the swing than moment, with force reaching 50% of peak at a mean time of 0.045s before ball impact, as

compared to 0.017s for 50% of the peak moment (Fig. 2).

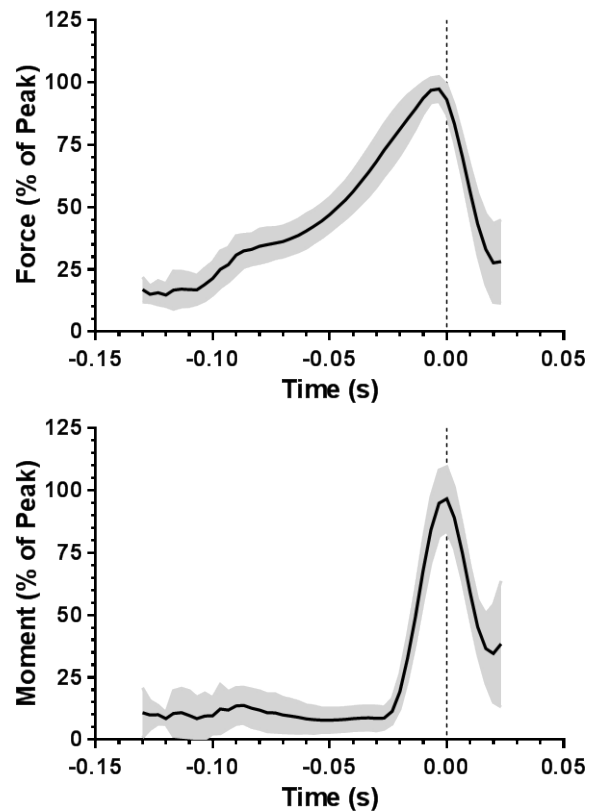


**Figure 2.** Mean (black) and SD (grey) ( $n = 306$ ) of the swing force and moment time series across all bat models, normalized by peak force and peak moment. Time series were synchronized at ball impact (Time = 0.0s).

## REFERENCES

1. Crisco JJ, et al. *J Applied Biomechanics* **30(2)**, 237-243, 2014.
2. Crisco JJ, et al. *Med Sci Sports Exerc* **34(10)**, 1675-84, 2002.

## ACKNOWLEDGMENTS

Funded in part by the National Operating Committee on Standards for Athletic Equipment (NOCSAE) and USA Baseball.

**Table 1:** Physical properties and mean ( $\pm$  SD) bat speed at a specific force impulse value of 6.5 Ns (see Fig. 1).

Bat Model	Hits Analyzed	MOI <sub>knob</sub> (mkg <sup>2</sup> )	Bat Speed (m/s) at Impulse of 6.5 Ns
E (wood)	128	0.231	25.3 $\pm$ 0.2
M (aluminum)	88	0.200	29.1 $\pm$ 0.2
H (composite)	90	0.161	31.4 $\pm$ 0.19

# ENERGY GENERATION STRATEGIES RELATED TO PEAK ELBOW VARUS TORQUE IN HIGH SCHOOL BASEBALL PITCHERS

<sup>1</sup> Michael P. McNally, <sup>1</sup> James A. Oñate, <sup>1</sup> Ajit M.W. Chaudhari

<sup>1</sup> The Ohio State University, Columbus, OH, USA  
email: Michael.mcnally@osumc.edu

## INTRODUCTION

Elbow injuries in high school pitchers are an issue of increasing prevalence, with the number of ulnar collateral ligament injuries increasing nearly 10x in a high school aged population from 2002 to 2011. (Hodgins, 2016). These injuries are often attributed to a combination of overuse, poor conditioning, and/or poor mechanics. While relatively little is known about biomechanical risk factors in high school pitchers, professional pitchers who suffer a serious elbow injury have been shown to have both a greater average pitch velocity (Bushnell, 2010) and greater peak elbow varus torque (Anz, 2010). While there are mixed results on the relationship between ball velocity and elbow varus torque (Hurd, 2012; Post, 2015), theoretically, increasing velocity places more force on the distal end of the kinetic chain, which may result in greater joint torque at the elbow. However, the variance in elbow torque is only partially explained by elbow velocity ( $R^2 = 4.0-37.3\%$ ), and thus is affected by other factors independent of ball velocity.

A common theory among coaches and practitioners is that generating more energy with the lower body, and having sufficient ability to transfer energy through the trunk to the upper body, may aid in reducing load on the arm while improving ball velocity. While plausible, increasing energy transferred from the trunk and legs also results in a greater elbow torque to transfer energy across the elbow (McNally, 2015). Understanding how energy generation strategies during the pitching motion affect elbow load independent of ball velocity are important for practitioners seeking to minimize potential for injury with a neutral or positive effect on performance. Therefore, the purpose of this study was to determine if energy generated by the lower body, trunk, and upper body affects elbow varus torque independent of the effect caused by increased

ball velocity. We hypothesized that energy generated by the legs and trunk would result in reduced elbow varus torque beyond that caused by an increase in hand velocity, while upper body energy generation would result in an increased elbow varus torque.

## METHODS

47 high school baseball pitchers between the ages of 15 and 18 were recruited for participation in this study. After performing a self-selected warm-up, pitchers were recorded using an optical motion capture system (Vicon Inc., Oxford, UK) capturing at 300 Hz while throwing five fastballs at “game like effort” towards a target. Synchronized ground reaction forces were recorded from a custom built pitcher’s mound bolted into four force platforms (Bertec, Co, Columbus, OH, USA), which recorded drive and stride leg ground reaction forces independently at 1500 Hz. The pitch with the highest hand velocity was used for analysis. If full body data were not available due to excessive marker occlusion or markers falling off, the pitch with the next highest velocity was chosen, continuing until the trial with the highest velocity with complete data was determined.

Joint torques and joint powers were calculated using standard inverse dynamics equations using Visual3D software (C-Motion Inc., Germantown, MD, USA). The pitching motion was analyzed from peak knee height to ball release. Peak knee height was determined as the point when the lateral knee joint marker reached its highest vertical position, and ball release was determined as the point 7 ms after the forearm passed a position perpendicular to the ground. Energy generation was calculated for the trunk, and bilaterally for the hip, knee, ankle, shoulder, elbow, and wrist. Energy generation was defined as the amount of positive work – the integral of joint power when joint power is greater than zero

- performed from peak knee height to ball release. Positive joint work was then summed to calculate lower extremity energy generation (hip, knee, and ankle;  $LE_{work}$ ), and upper extremity energy generation (shoulder, elbow, and wrist;  $UE_{work}$ ).

A simple regression was performed to estimate peak elbow varus torque as a function of peak hand velocity. Separate linear regression models were then used to determine the increase in  $R^2$  when including  $LE_{work}$ ,  $Trunk_{work}$ , and  $UE_{work}$ .

## RESULTS AND DISCUSSION

Complete model descriptions including the model input, standard error of estimate,  $R^2$  value, and  $R^2$  increase are shown in Table 1. On average, pitchers generated  $290.6 \pm 72.5$  J of energy with the lower extremity,  $52.7 \pm 24.3$  J with the trunk, and  $104.0 \pm 31.8$  J with the upper extremity. There was a significant association between ball velocity and peak elbow varus torque, with peak hand velocity explaining 56.6% of the variance in elbow varus torque (Table 1, Model A;  $p < 0.0001$ ). Lower extremity work explained an additional 5.4% of the variance in elbow varus torque (Model B;  $p = 0.009$ ), while upper extremity work explained an additional 4.2% (Model D;  $p = 0.020$ ). Trunk work was not associated with an increase in elbow varus torque (Model C). As a secondary analysis, a linear regression was performed to estimate peak elbow torque as a function of peak hand velocity,  $LE_{work}$ , and  $UE_{work}$ . The combined model resulted in an additional 6.45% of variance explained, though neither  $LE_{work}$  or  $UE_{work}$  were independently significant predictors of elbow varus torque.

In contrast to our hypothesis, energy generation by the lower extremity and upper extremity explained only a small amount of the variance in peak elbow varus torque independent of hand velocity. While the inclusion of both lower extremity and upper extremity energy positive work resulted in similar increases in  $R^2$  independently, when considered together, they were not significant predictors of elbow torque independent of ball velocity. Energy generated by the trunk was also not associated with peak elbow torque, which suggests that energy generation strategy may not substantially affect elbow torque above and beyond the effect due to increased hand velocity in high school baseball pitchers. Energetic strategies which emphasize the transfer or control of energy (segment torque power and negative joint torque power, respectively), and energetic transition strategies between fatigued and non-fatigued states, may play more of a role in injury potential, and warrant further investigation.

## REFERENCES

1. Hodgins JL, et al. *Am J Sports Med* **44**, 729-34, 2016
2. Bushnell BD, et al. *Am J Sports Med* **38**, 728-32, 2010.
3. Anz AW, et al. *Am J Sports Med* **38**, 1368-74, 2010.
4. Hurd WJ, et al. *Sports Health* **4**, 415-18, 2012.
5. Post EG, et al. *J Athl Train* **50**, 629-33, 2015.
6. McNally MP, et al. *J Strength Cond Res* **29**, 2708-15, 2015.

**Table 1:** Results from each regression model including model, standard error of estimate,  $R^2$ , and  $R^2$  increase from initial model. Units for  $\tau_{elbow}$  are Nm, for  $v_{hand}$  are m/s, and for work variables are J.

Model	SEE [Nm]	$R^2$	$R^2$ Inc
A: $\tau_{elbow} = -68.03 + 4.93 * v_{hand}$	8.57	0.566	-
B: $\tau_{elbow} = -44.24 + 2.54 * v_{hand} + 0.071 * LE_{work}$	8.02	0.620	0.054
C: $\tau_{elbow} = -67.93 + 4.93 * v_{hand} + 0.001 * Trunk_{work}$	8.67	0.556	-0.010
D: $\tau_{elbow} = -52.96 + 3.69 * v_{hand} + 0.120 * UE_{work}$	8.14	0.609	0.043
E: $\tau_{elbow} = -40.01 + 2.60 * v_{hand} + 0.054 * LE_{work} + 0.080 * UE_{work}$	7.91	0.631	0.065

# Arm Slot and its Relation to Shoulder and Elbow Safety and Efficiency in Youth Baseball Pitchers

<sup>1</sup> Ryan D. Plunkett, <sup>1</sup> Jacob Howenstein, <sup>2</sup> Kristof Kipp, <sup>1</sup> Michelle Sabick

<sup>1</sup> Saint Louis University, MO, USA; <sup>2</sup> Marquette University, WI, USA  
Email: plunkettrd@slu.edu

## INTRODUCTION

Shoulder and elbow injuries are common for baseball pitchers and are becoming more common for youth pitchers as well. Some of the most common injuries are the result of high torques on the elbow and shoulder causing damage to the ulnar collateral ligament (UCL) in the elbow.

Studies have primarily shown pitchers who throw with lesser velocity or have smaller body size encounter less stress [1] and the timing of sequences is important in energy flow especially in reference to pelvic rotation [2].

These findings are important but not always coachable. Arm slot has been defined in a previous study as the combination of trunk tilt, shoulder abduction, and elbow flexion [3]. This same study determined elbow stress increased with elbow flexion and when the arm was more horizontal. While trunk tilt may affect perceived arm slot, we hypothesized that varying degrees of shoulder abduction and elbow angle could impact the UCL. The purpose of this study was to examine arm slot in relation to pitch efficiency and upper extremity moments in the throwing arm.

## METHODS

Fourteen youth baseball pitchers (age: 11.6±1.3 years, height: 1.59±0.12 m, mass: 48.5±13.4 kg, velocity: 56.6±6.9 mph, 11 right-handed/3 left-handed) were recruited for this study. All testing occurred in an indoor research lab equipped with a custom built pitcher's mound with two embedded force plates; one under the rubber and one under the landing area. Reflective markers and marker clusters were attached to each pitcher's upper and lower body. Kinematic data was recorded with a 14-camera motion capture system at 250Hz, kinetic data of the drive (rear) and stride (front) leg were sampled at

1000Hz, and a radar gun was used to record velocity. Each pitcher threw 15 maximal effort fastballs toward a hanging strike zone 46ft from the rubber. The fastest strike thrown for each pitcher was chosen for analysis.

Trunk rotation was positive when rotation passed the point of being square with home plate or being neutral in relation to the pelvis. This is according to the right hand rule about a vertical z-axis.

Correlation was tested using Pearson correlation coefficients. The shoulder, elbow, and trunk orientations were compared to pitch velocity and upper extremity moments normalized for body mass and height. Additionally, upper extremity moments were normalized by velocity to assess the efficiency of the pitch effectively as load/mph [4]. Angles generated from left-handed pitchers were changed in sign to match standard convention used for right-handed pitchers.

The joint angles tested were elbow flexion, shoulder abduction, shoulder elevation, shoulder external rotation, trunk rotation relative to the pelvis, pelvis orientation, and trunk orientation. Additionally, the distance towards home plate between the shoulder and the ball at release was also tested. Outcome variables tested were shoulder abduction moment, shoulder internal rotation moment, and elbow valgus moment. All angle and positioning measurements were collected at ball release.

## RESULTS AND DISCUSSION

The correlations coefficients for all statistically significant relationships are shown in Table 1.

Greater shoulder abduction angle was negatively correlated with increased pitch velocity. Greater external rotation moment significantly correlated with both valgus moment efficiency and shoulder

internal rotation moment efficiency. Values of joint moment efficiency decrease when pitch efficiency increases since the variable is normalized (joint moment per mile per hour pitch velocity). This trend is evident in Figure 2.

Increased transverse plane trunk rotation angle relative to the pelvis correlated with an increased normalized shoulder abduction moment. Increased values of contralateral tilt correlated with increased normalized shoulder abduction moment. Increased trunk rotation relative to the laboratory correlated with less normalized shoulder internal moment.

An interesting correlation is the relationship between greater shoulder abduction and higher velocity. The degree of shoulder abduction is a coachable characteristic and this may suggest arm slot can assist in producing a faster pitch. Also notable is contralateral tilt, which led to increased normalized shoulder abduction moment. This could suggest a more upright trunk during delivery is favorable. The two trunk rotation results had effects on normalized moments of the shoulder. With regards to previous studies' results relating trunk rotation and energy transfer, these may have more to do with the kinematic sequence of the pitch and the degree of trunk opening present at ball release.

Greater external rotation of the shoulder at ball release correlated with improved pitch efficiency for both elbow valgus moment and the shoulder internal rotation moment. This may suggest an earlier release point is favorable, or that greater initial external rotation is a mechanical method for generating more velocity with less stress even without proper kinetic sequencing.

## CONCLUSIONS

The results of this study show the varying factors of arm slot have an effect on the efficiency of a pitch with regards to velocity of the pitch and safety of the pitcher. Because arm slot is a coachable factor and many youth pitchers sustain arm injuries, this topic is deserving of further investigation.

## REFERENCES

1. Sabick, Michelle B., et al. *J Should Elb Surg* **13**, 349-355, 2004.
2. Urbin, M. A., et al. *Am J Sports Med* **41**, 336-342, 2013.
3. Aguinaldo, Arnel L., et al. *J Applied Biomechanics* **23**, 42-51, 2007.
4. Davis, J. T., et al. *Am J Sports Med* **37**, 1484-1491, 2009.

Table 1. Correlation results for key arm slot metrics, (Pearson's r)

Related Variables	Pearson Correlation	Sig. (2-tailed)
Shoulder Abduction and Velocity	-0.676	0.008
Shoulder External Rotation and Shoulder Internal Moment Efficiency	-0.590	0.026
Shoulder External Rotation and Elbow Valgus Moment Efficiency	-0.706	0.005
Trunk Rotation with Respect to the Pelvis (z) and Normalized Shoulder Abduction Moment	0.646	0.013
Contralateral Tilt with Respect to the Lab (z) and Normalized Shoulder Abduction Moment	0.547	0.043
Trunk Rotation with Respect to the Lab (z) and Normalized Shoulder Internal Moment	-0.551	0.041

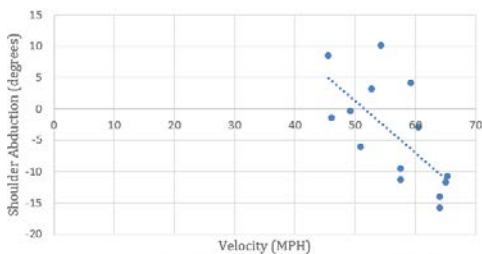


Figure 1. Shoulder Abduction versus Velocity

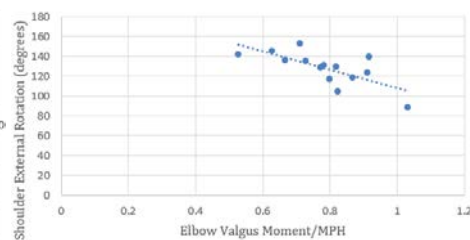


Figure 2. Shoulder External Rotation versus Elbow Valgus Moment/MPH

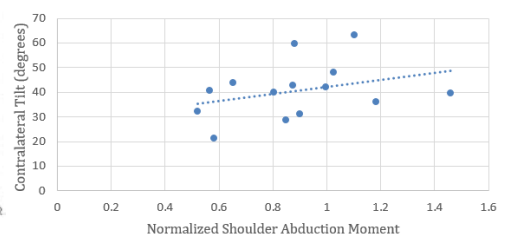


Figure 3. Contralateral Tilt versus Normalized Shoulder Abduction Moment

# UNANSWERED QUESTIONS IN BIOMECHANICS: BASES OF MUSCLE FORCE PRODUCTION

<sup>1</sup> Walter Herzog, <sup>2</sup> Sabrina Lee, <sup>3</sup> Paola Contessa

<sup>1</sup> Human Performance Laboratory, University of Calgary, Calgary, Canada

<sup>2</sup> Neuromuscular Biomechanics Laboratory, Northwestern University Feinberg School of Medicine, Chicago, IL, USA

<sup>3</sup> Delsys and Altec Inc., Natick, MA, USA

Email: [whertzog@ucalgary.ca](mailto:whertzog@ucalgary.ca) web: <https://www.ucalgary.ca/hpl/>

## INTRODUCTION

Despite continual research and development in the field of Biomechanics, several aspects of muscle force production and muscle control remain to be answered or adequately understood. How is force shared among muscles? How do muscle contractile properties and muscle architecture influence the force exerted by muscles? How are motor units controlled to exert muscle force? These are fundamental questions that provide insight into the organization and control of human movement. The symposium will present recent research findings that attempt to resolve current controversies or shed light on these fundamental questions and their impact in sport performance and rehabilitation.

The symposium will follow this schedule:

Introduction – Walter Herzog – 5 mins

The distribution problem in biomechanics – Walter Herzog – 20 mins

Muscle architecture and material properties:  
Influence on muscle function – Sabrina Lee – 20 mins

Neural strategies of muscle force productions:  
controversies and evidences from studies of motor unit behavior – Paola Contessa – 20 mins

Discussion – 25 mins

## THE DISTRIBUTION PROBLEM IN BIOMECHANICS – Walter Herzog

The distribution problem in biomechanics is defined as the determination of the forces of musculo-skeletal structures crossing a joint from the known intersegmental resultant force and moment. The primary musculo-skeletal structures thought to contribute to the intersegmental resultant forces and moments are the muscles, ligaments and bony contact forces. Unfortunately, these forces are hard (not to say impossible) to measure accurately in humans non-invasively, thus only the crudest experimental data are available, typically obtained without proper calibration (in terms of muscle forces), or for non-physiological conditions (contact forces obtained in artificial joints).

However, animal models allow for the accurate measurement of muscle forces and the validation of predicted muscle forces based on musculoskeletal models. This technology has been available for almost forty years now (e.g. (Walmsley et al., 1978)) but has only been used sporadically for validation purposes (e.g. (Herzog et al., 1993; Liu et al., 1999)).

Static optimization algorithms, forward dynamic simulations, and EMG driven musculoskeletal models of muscle force prediction and synergistic force sharing among muscles are used in abundance (for a review see for example (Erdemir et al., 2007; Herzog, 1996)) often with little validation and questionable justification.

Here, I will be showing the wide variety of synergistic force-sharing of the cat triceps surae muscles, and specifically identify surprising results. For example, the result that the smallest muscle of

the group (soleus) contributes the most force for static, and many dynamic movement conditions. Or, that during standing one synergist (soleus) may be highly active and produce great force, while another (medial gastrocnemius) is completely silent, while for a paw shake response, the complete opposite is true, the medial gastrocnemius is highly active while the soleus is silent merely contributing minor passive forces to the movement. It is this complexity of synergistic force sharing that has eluded satisfactory explanation ever since first attempts at muscle force predictions were made (Penrod et al., 1974).

Although I do not have the full solutions to the distribution problem in biomechanics, I sincerely hope that my talk will revive this area of prime importance in biomechanics and movement control research, and might inspire some young scientists to tackle this problem once more with the improved techniques we have available today.

### **MUSCLE ARCHITECTURE AND MATERIAL PROPERTIES: INFLUENCE ON MUSCLE FUNCTION – Sabrina Lee**

Classic research in comparative functional morphology suggests that muscle properties are often optimized to achieve maximal performance for specialized functions. This may include locomotor speed, jump height or distance, and endurance (Hildebrand, 1960; Alexander, 1981; Lieber and Boakes, 1988; Lutz and Rome, 1994). Force modulation, the timing of force generation, and the force-generating capacity of muscle all greatly contribute to the many factors that affect performance. This optimizing of muscle properties for specialized tasks becomes unclear, challenging, and very intriguing in humans as we're not specialized for any movement task, at least not as a species. However, there are examples where groups of individuals may have optimal muscle properties to achieve specialized movements such as in sports (Abe et al., 2001; Kumagai et al., 2000). In particular, the investigation becomes even more intriguing when investigating muscular changes what muscular changes occur in impaired movement.

Muscle plasticity has both its advantages and disadvantages. On one hand, muscle properties can be altered negatively due to injury or pathology. Changes include muscle mass (Malaiya et al., 2007), sarcomere number and length (Lieber et al., 2002), fascicle length (Gao et al., 2008; Barber et al., 2011), pennation angle (Barber et al., 2011; Mohagheghi et al., 2008), stiffness (Sinkjaer et al., 1994; Lee et al., 2015). On the other hand, the muscular system can adapt positively to these disruptive changes, and rehabilitation treatments have great potential to revert these changes or allow muscle properties to adapt in manner such that movement becomes less impaired.

I will discuss how muscle properties such as muscle architecture (e.g. sarcomere length, fascicle length, pennation angle, moment arm) and material properties such as stiffness influence muscle function in healthy and pathologic muscle. With advancement of non-invasive techniques to quantify muscle properties, we are able to glean further insight into the human muscular system. This will help to bridge our knowledge of animal and human muscle mechanics and to decrease assumptions or estimations about muscle properties in humans. This becomes important for aiding clinicians in decision making about diagnosis and treatment-planning.

### **NEURAL STRATEGIES OF MUSCLE FORCE PRODUCTION: CONTROVERSIES AND EVIDENCES FROM STUDIES OF MOTOR UNIT BEHAVIOR – Paola Contessa**

The mechanisms by which the central and peripheral nervous systems control motor units to produce force are still subject to debate. Over the past five decades, the notion that higher-threshold motor units have greater firing rates than lower-threshold ones has been commonly accepted. This notion was derived from electrically stimulated motoneurons in cats (Eccles et al., 1958; Kernell, 1965), and supports the assumption that the firing rates of motoneurons match their mechanical properties to optimize force production. That is, higher-threshold motor units have shorter and bigger force twitches that require higher firing rates to tetanize (Kernell, 2003). Recent empirical data

from voluntary contractions in human subjects (De Luca and Hostage, 2010; among others) have provided abundant evidences in support of a competing theory of motor unit behavior, known as the Onion-Skin scheme (De Luca and Erim, 1996). This construct describes an inverse hierarchical arrangement of motor unit firing rates, where lower-threshold motor units maintain higher firing rates than higher-threshold ones at any time and force during a contraction. This control scheme seems to have evolved not to maximize force, but a combination of force magnitude and duration, thereby proving the capacity to generate muscle force and to sustain it over time.

This symposium will discuss the competing theories of motor unit control, and the empirical data in support of the Onion-Skin scheme. It will also present recent evidences indicating that the Onion-Skin scheme of motor unit firing remains invariant with muscle fatigue.

Conflicting observations on the adaptations of motor unit firing behavior during muscle fatigue have been reported in the literature. This symposium will address some of the discrepant findings, and present several confounding factors in the analysis of motor unit data that can obscure the underlying firing adaptations during muscle fatigue. When these confounding factors are mitigated, empirical data show that motor unit firing rate increases, motor unit recruitment threshold decreases and higher-threshold motor units are recruited during fatiguing contractions. These adaptations can be explained by increasing excitation to the motoneuron pool that compensates for the fatigue-induced decrease in muscle force generation capacity (Contessa et al., 2016), and highlight the influence of mechanical adaptations on motor unit firing behavior during fatigue. Throughout these complementary adaptations, the Onion-Skin scheme that governs motor unit firing behavior appears to be maintained with muscle fatigue.

## REFERENCES

1. Abe, T., Fukashiro, S., Harada, Y. and Kawamoto, K. (2001). Relationship between sprint performance and muscle fascicle length in female sprinters. *J. Physiol. Anthropol. Appl. Human Sci.* 20, 141-147.
2. Alexander, R. M. (1981). Allometry of the leg muscles of mammals. *J. Zool.* 194, 539-552.
3. Barber, L., Hastings, T., Baker, R., Barrett, R., Lichtwark, G. (2011). Medial gastrocnemius muscle volume and fascicle length in children aged 2 to 5 years with cerebral palsy. *Dev. Medicine & Child Neurology* 53(6):543-8.
4. De Luca, C.J., Hostage, E.C., (2010). Relationship between firing rate and recruitment threshold of motoneurons in voluntary isometric contractions. *J. Neurophysiol.* 104, 1034-1046.
5. De Luca, C.J., Erim, Z., (1994). Common drive of motor units in regulation of muscle force. *Trends Neurosci.* 17, 299-305.
6. Contessa, P., De Luca, C.J., Kline, C.J., (2016). The compensatory interaction between motor unit firing behavior and muscle force during fatigue. *J. Neurophysiol.* 116: 1579-1585.
7. Eccles, J.C., Eccles, R.M., Lundberg, A., (1958). The action potentials of the alpha motoneurons supplying fast and slow muscles. *J. Physiol.* 142, 275-291.
8. Erdemir, A., McLean, S., Herzog, W., van den Bogert, A. J., (2007). Model-based estimation of muscle forces exerted during movements. *Clin. Biomech.* 22, 131-154.
9. Gao, F., Grant, T.H., Roth, E.J., Zhang, L.Q. (2009). Changes in passive mechanical properties of the gastrocnemius muscle at the muscle fascicle and joint levels in stroke survivors. *Arch Phys Med Rehabil.* 90(5):819-26.
10. Herzog, W., (1996). Force-sharing among synergistic muscles: theoretical considerations and experimental approaches. *Exercise and Sport Sciences Reviews* 24, 173-202.
11. Herzog, W., Leonard, T. R., Guimaraes, A. C. S., (1993). Forces in gastrocnemius, soleus, and plantaris tendons of the freely moving cat. *Journal of Biomechanics* 26, 945-953.
12. Hildebrand, M. (1960). How animals run. *Sci. Am.* 202, 148-157.

13. Kernell, D., (1965). The limits of firing frequency in cat lumbosacral motoneurons possessing different time course of afterhyperpolarization. *Acta Physiol. Scand.* 65, 87-100.
14. Kernell, D., (2003). Principles of force gradation in skeletal muscles. *Neural Plast.* 1-2, 69–76.
15. Kumagai, K., Abe, T., Brechue, W. F., Ryushi, T., Takano, S. and Mizuno, M. (2000). Sprint performance is related to muscle fascicle length in male 100-m sprinters. *J. Appl. Physiol.* 88, 811-816.
16. Lee, S.M., Spear, S., Rymer, W.Z. (2015) Quantifying Changes In Material Properties Of Stroke-Impaired Muscle. *Clinical Biomechanics* 30, 269-275.
17. Lieber, R. L. and Boakes, J. L. (1988). Muscle force and moment arm contributions to torque production in frog hindlimb. *Am J. Physiol.* 254, C769-C772.
18. Liu, M. M., Herzog, W., Savelberg, H. H. C. M., (1999). Dynamic muscle force predictions from EMG: an artificial neural network approach. *Journal of Electromyography and Kinesiology* 9, 391-400.
19. Lutz, G. J. and Rome, L. C. (1994). Built for jumping: the design of the frog muscular system. *Science* 263, 370-372.
20. Malaiya, R., McNee, A.E., Fry, N.R., Eve, L.C., Gough, M., Shortland, A.P. (2007). The morphology of the medial gastrocnemius in typically developing children and children with spastic hemiplegic cerebral palsy. *Journal of electromyography and Kinesiology* 17(6):657-63.
21. Mohagheghi, A.A., Khan, T., Meadows, T.H., Giannikas, K., Baltzopoulos, V., Maganaris, C.N. (2008). In vivo gastrocnemius muscle fascicle length in children with and without diplegic cerebral palsy. *Dev medicine & child neurology* 50(1):44-50.
22. Penrod, D. D., Davy, D. T., Singh, D. P., (1974). An optimization approach to tendon force analysis. *Journal of Biomechanics* 7, 123-129.
23. Sinkjær, T., Magnussen, I. (1994). Passive, intrinsic and reflex-mediated stiffness in the ankle extensors of hemiparetic patients. *Brain* 117, 355-63.
24. Walmsley, B., Hodgson, J. A., Burke, R. E., (1978). Forces produced by medial gastrocnemius and soleus muscles during locomotion in freely moving cats. *Journal of Neurophysiology* 41, 1203-1215.

# POWER IMBALANCE NEARLY ELIMINATED IN WHOLE-BODY ANALYSIS

<sup>1</sup> Anahid Ebrahimi, <sup>1,2</sup> John Collins, <sup>1</sup> Jill Higginson, and <sup>1</sup> Steven Stanhope

<sup>1</sup> University of Delaware, Newark, DE, USA

<sup>2</sup> Naval Medical Center, San Diego, CA, USA

e-mail: anahide@udel.edu

## INTRODUCTION

A segmental power and energy analysis can be a powerful biomechanical tool for understanding the mechanism driving human movement. Segmental power calculations are traditionally performed using segment endpoint dynamics (traditional kinetic method), but a theoretically equivalent method is to measure changes in the segment's energy state (kinematic method) [1]. Using the change in energy and power relationship, researchers have related work performed by the lower limbs to changes in the energy state of the body [e.g., 2].

However, the traditional kinetic and kinematic methods do not provide experimentally equivalent results for segments proximal to the foot during stance phase of gait [3]. This has been deemed a "power imbalance" and is due to modeling segment endpoints as fixed in the traditional kinetic method. We derived a correction term to account for movement at segment ends to be included in segmental power calculations (corrected kinetic method) [4]. Capturing the magnitude of power imbalance is imperative to effectively interpreting energetic measures in the study of human movement. The purpose of this study was to document the power imbalance between the traditional and corrected kinetic methods to the kinematic method for a whole-body analysis over a gait cycle.

## METHODS

A subset of the data collected by Goldberg and Stanhope was used for data analysis [5]. Eight unimpaired adult subjects (height  $177 \pm 7.5$  cm, mass  $74 \pm 13.1$  kg) walked on a calibrated instrumented split-belt treadmill (Bertec, Columbus, OH) at height-normalized velocities of 0.8 statures/s. Three-dimensional movement data were collected via a six-camera system (Vicon, Los Angeles, CA).

At the segment level, the kinematic method sums the rate of energy change of the segment's gravitational

potential energy, rotational and translational kinetic energy to find segmental rate of energy change. The traditional kinetic method calculates segmental power ( $\vec{P}_m$ ) as the product of net joint moment and joint angular velocity summed with the product of joint intersegmental force and segment endpoint velocity at both distal and proximal segment ends. Distal foot power is calculated as defined previously [6]. The corrected kinetic method includes a derived correction term ( $\Delta\vec{P}c_m$ ) which accounts for movement at segment ends. The correction term is defined in equation 1, where  $\vec{F}_{grf}$  is the ground reaction force,  $\vec{\omega}_m$  is the segment angular velocity of the  $m^{\text{th}}$  segment, and  $\vec{r}_{m/(m-1)}$  is the vector from the distal end of the  $m^{\text{th}}$  segment to the proximal end of the adjoining segment ( $m-1$ ). The corrected kinetic method calculates segmental power as  $\vec{P}_m - \Delta\vec{P}c_m$ .

$$\Delta\vec{P}c_m = \vec{F}_{grf} \cdot (\vec{\omega}_m \times \vec{r}_{m/(m-1)}) \quad (\text{eq. 1})$$

The body was modeled as bilateral feet, shanks, and thighs, with a pelvis and trunk. For each method, body power or rate of energy change was calculated as the sum of the eight segment-level calculations combined. Powers were scaled to body mass.

Power imbalance is defined as the difference between the kinematic method and the traditional (PI<sub>tr</sub>) or corrected (PI<sub>co</sub>) kinetic methods. Two measures were used to capture the magnitude of this difference. First, the root-mean-square error was calculated over the gait cycle using PI<sub>tr</sub> (RMSE<sub>tr</sub>) and PI<sub>co</sub> (RMSE<sub>co</sub>). Second, the percent difference (% Diff) was calculated by taking the portion of absolute PI<sub>tr</sub> or PI<sub>co</sub> work (integration of positive and absolute negative power) divided by the absolute work over the gait cycle using the kinematic method. The % Diff was calculated over the gait cycle (GC) and five intervals of gait: (1) initial double support (DS), (2) first half of single support (SS), (3) second half of SS, (4) terminal DS, and (5) swing (Sw).

## RESULTS AND DISCUSSION

The root-mean-square error reduced from  $0.16 \pm 0.06$  W/kg (RMSE<sub>tr</sub>) (mean  $\pm$  SD) to  $0.03 \pm 0.01$  W/kg (RMSE<sub>co</sub>) with the correction term. In context, the % Diff with PI<sub>tr</sub> can over- or underestimate the work on the body by  $12.3 \pm 4.3\%$  over the gait cycle compared to  $2.8 \pm 0.9\%$  with PI<sub>co</sub>. Figure 1 shows a representative subject's power and rate of energy change for the three methods over a gait cycle. Note that the PI<sub>tr</sub> during swing can be attributed to having the contralateral limb in stance during that phase. The % Diff between absolute work performed during the five intervals of gait are shown in Table 1.

**Table 1:** Percent difference (% Diff) between kinematic and traditional (PI<sub>tr</sub>) or corrected (PI<sub>co</sub>) kinetic methods (mean  $\pm$  SD).

% Diff.	Interval					GC
	1	2	3	4	Sw	
PI <sub>tr</sub>	1.2 $\pm$ 0.8%	2.5 $\pm$ 1.2%	2.0 $\pm$ 1.0%	1.6 $\pm$ 0.3%	5.0 $\pm$ 2.9%	<b>12.3 <math>\pm</math> 4.3%</b>
PI <sub>co</sub>	0.5 $\pm$ 0.3%	0.4 $\pm$ 0.1%	0.5 $\pm$ 0.1%	0.5 $\pm$ 0.2%	0.9 $\pm$ 0.3%	<b>2.8 <math>\pm</math> 0.9%</b>

Researchers have noted two main causes for the lack of equivalence in power and rate of energy change calculations: (1) noise in kinematic data due to a series of differentiations, or (2) accessory motion of skin-mounted markers due to soft tissue movement making segment endpoints inaccurate (violating rigid body assumptions) [1, 3]. While the power correction cannot parse between these two causes, it does account for them to a substantial extent.

Traditional motion capture systems cannot precisely measure real joint translations from surface markers,

which would be necessary to fully interpret the power correction term. However, these results have important implications for the interpretation of power and energy data. Using the power correction term in inverse dynamics calculations can nearly eliminate the power imbalance when tracking power and energy flow through the segments.

## CONCLUSIONS

With the inclusion of a power correction term in the corrected kinetic method, root-mean-square error between the kinetic and kinematic methods decreased by an order of magnitude with the correction term. Power imbalance as a percent difference of absolute kinematic work was reduced from an average of 12% (PI<sub>tr</sub>) to less than 3% (PI<sub>co</sub>) over the gait cycle. The corrected kinetic method facilitates improved accuracy in whole-body energetic analyses.

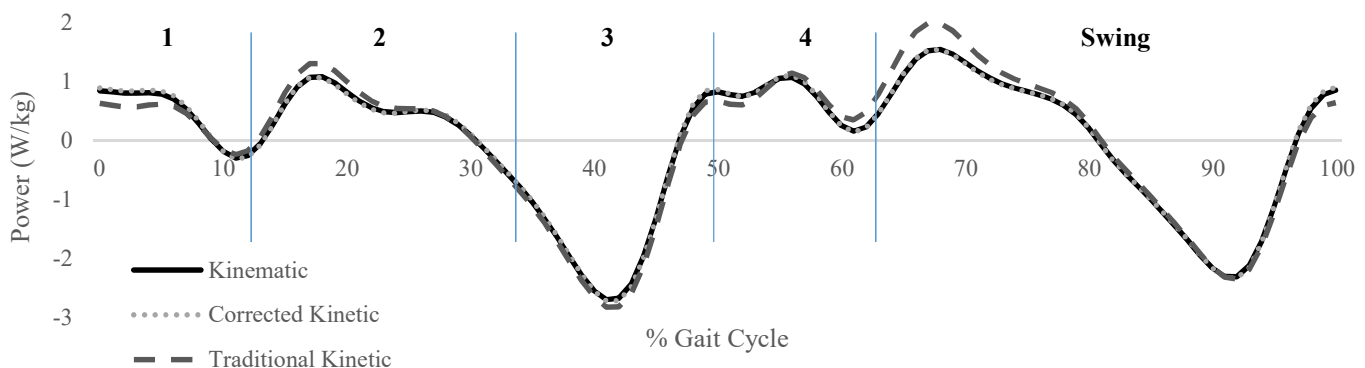
## REFERENCES

1. Zajac FE, et al. *Gait Pos* **16**, 215-32, 2002.
2. Zelik K, et al. *J Exp Bio* **218**, 876-86, 2015.
3. McGibbon C, & Krebs D. *Gait Pos* **7**, 237-42, 1998.
4. Ebrahimi, et al. *Proceedings of ISB '17*, Brisbane, AUS, 2017 (submitted).
5. Goldberg SR, et al. *J Biomech* **46**, 1176-83, 2013.
6. Siegel KL, et al. *J Biomech* **29**, 823-37, 1996.

## ACKNOWLEDGMENTS

Funding provided by the NSF Graduate Research Fellowship (#1247394), the BADER consortium (DoD/CDMRP award W81XWH-11-2-022), and the University of Delaware College of Health Sciences & Mechanical Engineering Department.

**Figure 1:** Representative gait cycle for body power calculated using three methods. Intervals marked with vertical lines: (1) initial double support (DS), (2) 1<sup>st</sup> half of single support (SS), (3) 2<sup>nd</sup> half SS, (4) terminal DS.



# LOWER EXTREMITY JOINT KINETICS IN YOUNG ADULTS WALKING WITH VARIED STEP LENGTHS

Rebecca L. Krupenevich and Ross H. Miller

University of Maryland, College Park, MD, USA  
email: rlkrup@umd.edu

## INTRODUCTION

The ability to walk greatly influences quality of life, particularly in the aging population, but many older adults report difficulty when walking short distances. This difficulty may be reflected by older adult gait mechanics, which differ from the gait of young adults. Specifically, older adults take shorter, more frequent steps when walking at the same speed as young adults, and exhibit greater hip joint torque and power, and less ankle joint torque and power compared to young adults [1]. The cause of this age-related distal to proximal shift in joint kinetics is unknown. Identifying how and why older adults walk differently than young adults may contribute to improving mobility in this population. Previous studies have found that ankle plantarflexor power is a strong predictor of step length [2], and in young adults, walking with longer step lengths results in greater plantarflexor torque [3]. However, the effect of increasing or decreasing step length on joint kinetics in young adults is not clear. Understanding the effect of step length on joint kinetics in young adults is a first step towards identifying factors contributing to the age-related changes in walking mechanics.

Therefore, the purpose of this study was to determine if changes in step length can cause young adults to walk with joint kinetics characteristic of older adults. Previous studies have found reduced ankle joint moments in young adults walking with a shorter step length [3]. Therefore, we hypothesized that ankle plantarflexor moment and power would increase at longer step lengths and decrease at shorter step lengths relative to preferred step length, and hip joint torque and power would decrease at longer step lengths and increase at shorter step lengths, relative to preferred.

## METHODS

Five healthy young adults (4 male, 1 female,  $21 \pm 0.54$  yrs,  $71.6 \pm 15.5$  kg,  $1.73 \pm 0.13$  m) participated in this study after providing written informed consent. Participants performed seven step length conditions: walking with a preferred step length (PSL) and walking with step lengths of  $\pm 5$ , 10, and 15% of step length. Participants adjusted step length by stepping to a metronome beat. Infrared timing gates were used to constrain speed to  $\pm 3\%$  of 1.3 m/s in all conditions. Since walking speed is equal to the product of cadence and step length, holding speed constant and adjusting cadence resulted in changes to step length.

Kinematic data were captured using a 13-camera motion capture system and kinetic data were captured using eight force platforms. Marker position and ground reaction force data were smoothed using a 4<sup>th</sup> order dual-pass Butterworth filter with cutoff frequencies of 6 Hz and 45 Hz, respectively. Knee joint kinetics were calculated by 6DOF inverse dynamics using Visual3D software.

A one-way repeated measures ANOVA ( $\alpha = 0.05$ ) tested for the effect of step length on peak hip and knee flexion and extension moments, and peak ankle plantarflexion moment with a Bonferonni correction in post-hoc testing. Only the PSL and  $\pm 15\%$  conditions were included in the ANOVA due to the small sample size to date.

## RESULTS AND DISCUSSION

Joint moment and power waveforms are presented in Figures 1 and 2. Average stride lengths were 1.26 m, 1.46 m, and 1.63 m for -15% SL, PSL, and +15% SL, respectively. There was a significant effect of step length on peak hip extension ( $p =$

0.003) and flexion moments ( $p = 0.03$ ), peak hip positive power ( $p = 0.03$ ), peak knee flexion moment ( $p = 0.01$ ), and peak knee positive ( $p = 0.49$ ) and negative power ( $p = 0.01$ ). Peak hip extension moment was greater for -15% SL compared to PSL ( $3.83 \pm 0.54$  vs.  $3.24 \pm 0.76$  %BW\*Ht,  $p = 0.03$ ). Peak knee flexion moment was smaller for +15% SL compared to PSL ( $-1.22 \pm 0.19$  vs.  $-1.46 \pm 0.11$  %BW\*Ht,  $p = 0.03$ ), peak negative knee power was smaller for +15% SL compared to preferred and -15% SL ( $-1.17 \pm 0.37$  vs.  $-1.37 \pm 0.15$  and  $-1.71 \pm 0.21$  W/kg, all  $p \leq 0.04$ ). There were no significant pairwise comparisons for peak hip flexion moment (all  $p \geq 0.16$ ) or positive power, or peak knee positive power (all  $p \geq 0.16$ ). There was not a significant effect of step length on peak hip negative power ( $p = 0.82$ ), knee extension moment ( $p = 0.75$ ), peak plantarflexor moment ( $p = 0.39$ ), or peak plantarflexor power ( $p = 0.61$ ).

The kinetic strategies young adults use when walking with different step lengths did not involve adaptations at the ankle. Specifically, peak hip extension moment increased by 18% at shorter step lengths (-15% SL) compared to PSL, and peak knee flexion moment decreased by 16% at longer step lengths (+15% SL) compared to PSL. Similarly, at shorter step lengths, more energy was generated at the hip and absorbed at the knee.

## CONCLUSIONS

Young adults respond to walking with different step lengths by altering hip and knee, but not ankle, joint moments and powers. These findings suggest step length alone does not explain differences in joint kinetics between young and older adults and highlight the need for a similar experiment in older adults to further explain age-related distal to proximal redistribution of joint kinetics. Future work will expand upon these preliminary findings with a larger sample size, more subtle changes in step length, and alternative explanations for the age-related changes in gait mechanics, such as differences in muscle architecture characteristics.

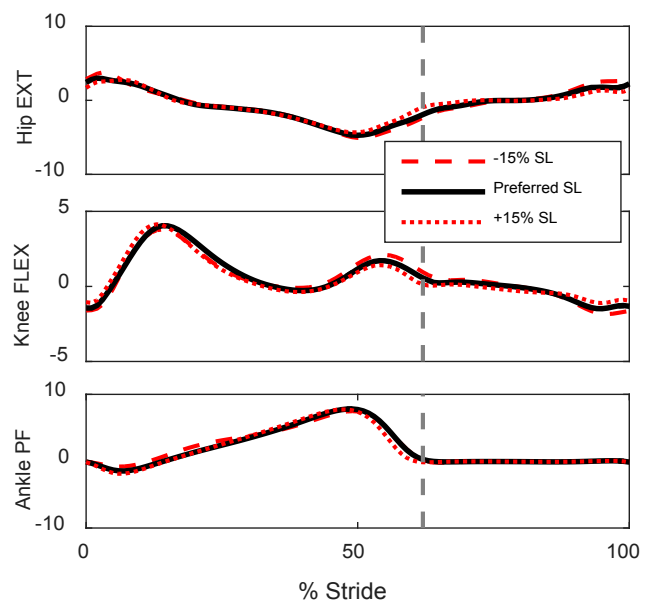


**Figure 1:** Mean hip, knee, and ankle joint moments in the sagittal plane. The stride begins and ends at heel strike. Vertical dashed line indicates toe-off. Units are %BW\*Ht.

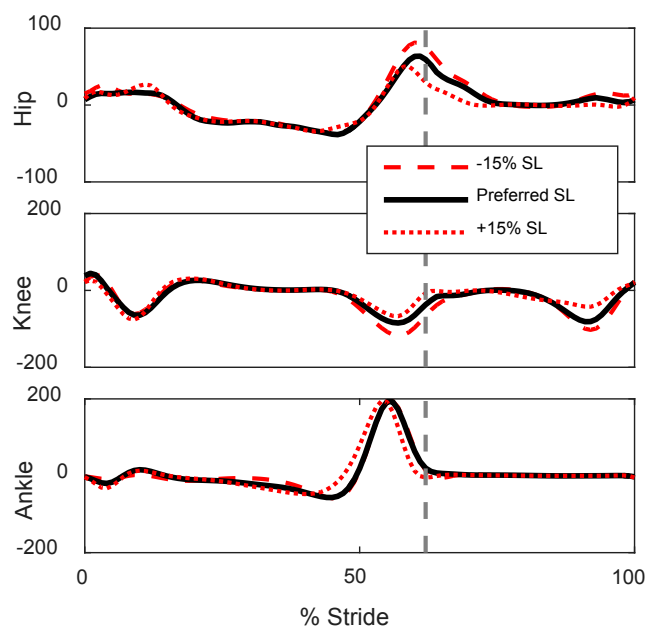


**Figure 2:** Mean hip, knee, and ankle joint powers. The stride begins and ends at heel strike. Vertical dashed line indicates toe-off. Units are W/kg.

## REFERENCES

1. DeVita P, et al. *J Appl Biomech* **17**, 297-311, 2001.
2. Judge JO, et al. *J Gerontol* **51A**, M303-M312, 1996.
3. Umberger BR and Martin PE *J Exp Biol* **210**, 3255-3265, 2007.

# THE FUNCTIONAL UTILIZATION OF PROPULSIVE CAPACITY DURING HUMAN WALKING

Katie A. Conway, Randall Bissette, and Jason R. Franz

University of North Carolina at Chapel Hill and North Carolina State University, Chapel Hill, NC, USA  
email: kaconway@email.unc.edu, web: <http://abl.bme.unc.edu>

## INTRODUCTION

Reduced propulsive forces, arising in part from reduced net ankle joint moment and power generation during the push-off phase of walking, are thought to play an important role in age-related mobility impairment [1]. However, despite their deficits to young adults, older adults retain the capacity to enhance push-off performance, for example during uphill walking [2] and in response to biofeedback [3]. Thus, our ongoing research is based on the working hypothesis that older adults have a considerable but underutilized propulsive reserve available during walking. Conventional methods used to assess neuromuscular reserves (i.e., dynamometry) generally fail to effectively predict age-related changes in plantarflexor performance and/or yield implausible (i.e.,  $\geq 100\%$ ) values of functional capacity utilized (FCU) in walking [4].

As an important first step, the purpose of this study was to gain an improved joint-level understanding of the functional utilization of propulsive capacity during human walking in young subjects, with a special emphasis on the plantarflexor muscles. Ultimately, we intend to test the hypotheses that: (i) young adults' reserve capacity for walking faster

than preferred would correlate with their reserve capacity for increasing propulsion at a preferred walking speed, and (ii) both would yield plantarflexor FCU (%) values less than those obtained using conventional dynamometry.

## METHODS

Seven healthy young adults have thus far participated (age:  $25.6 \pm 7.0$  years, height:  $1.8 \pm 0.1$  m, body mass:  $74.0 \pm 9.7$  kg, 5M/2F). We first recorded subjects' preferred ( $1.3 \pm 0.1$  m/s) and maximum ( $2.6 \pm 0.2$  m/s) overground walking speeds as the time taken to traverse the middle 2 m of a 10 m walkway. Subjects then walked on a dual-belt force measuring treadmill (Bertec, Corp.) for 1 min at their preferred walking speed ("Pref"). Subjects then donned a waist belt that connected to a feedback-controlled, motor-driven system that prescribed horizontal impeding forces according to instantaneous measurements from a load cell (Fig. 1A). Specifically, while subjects walked at their preferred speed on the treadmill, a real-time controller increased the impeding force at a constant rate of 1 %BW per second (Fig. 1B, "Ramp"). Subjects were instructed to maintain their position on the treadmill throughout the ramped protocol while avoiding excessive forward lean. The

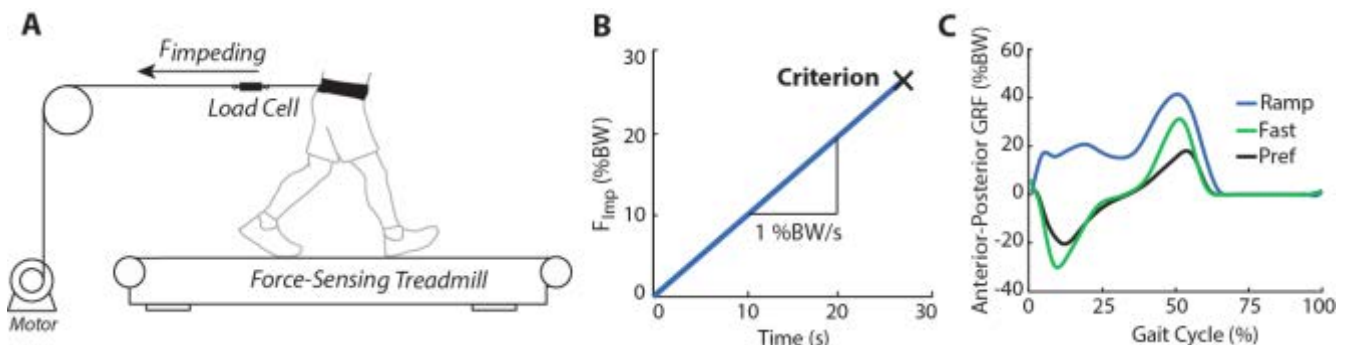


**Figure 1.** (A) Feedback-controlled impeding force system including load cell and motor. (B) Impeding force ( $F_{imp}$ ) ramp condition at 1 %BW/s. (C) Group mean anterior-posterior ground reaction forces (GRF) for preferred (Pref), maximum ramp (Ramp), and maximum walking speed (Fast) trials.

trial was ended following a 0.35 m inexorable posterior translation of the subjects' center of mass, monitored using the motor's encoder. In another trial, subjects walked on the treadmill at their maximum overground walking speed, which they maintained for approximately 10 s ("Fast").

For all treadmill trials, we recorded the 3D trajectories of retroreflective markers on the pelvis and lower limbs (Motion Analysis, Corp.) in synchrony with 3D ground reaction force (GRF) data. Finally, we estimated leg joint moments and powers using inverse dynamics. For the "Ramp" and "Fast" conditions, we extracted all outcome measures from the stride associated with the largest peak anterior (i.e., propulsive) GRF. To compare to more conventional assessments, we also recorded subjects' maximum voluntary isometric ankle moment and maximum isokinetic ankle power at relatively slow (30°/sec) and fast (90°/sec) angular velocities using a dynamometer (Biodex).

## RESULTS AND DISCUSSION

Compared to normal walking, peak propulsive force, ankle moment, and ankle power increased by an average of 68%, 33%, and 115%, respectively, when subjects walked at their maximum speed ( $p$ 's<0.01) (Fig. 1C, Fig. 2). These values also increased by 123%, 35%, and 89%, respectively for the maximum ramp condition ( $p$ 's<0.01). Very surprisingly, peak ankle moment and power generation during the maximum ramp condition were nearly indistinguishable from those during maximum speed walking (Fig. 2) ( $p=0.29$  and  $p=0.21$ , respectively). Finally, isometric plantarflexor testing would have otherwise yielded the incomplete conclusion that subjects utilized, on average, 94% of their maximum available ankle moment when walking at their preferred speed. Rather, true ankle moment utilization resolved in this study averaged only 72-74% of subjects' maximum functional capacity.

## CONCLUSIONS

We present important reference data for the functional utilization of propulsive capacity during

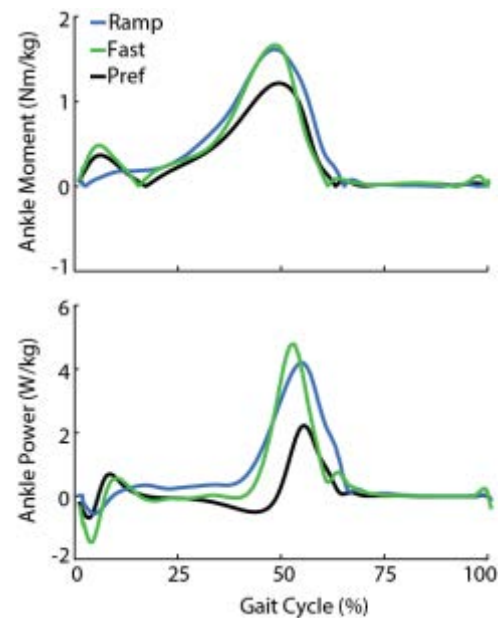


**Figure 2.** Ankle moments and powers over an averaged stride for preferred (Pref), maximum ramp (Ramp), and maximum walking speed (Fast) trials.

walking in young adults. Using a novel ramped impeding force protocol, we discovered that young subjects walking at their preferred speed retain a functional reserve for propulsive forces of 55%, peak ankle moment of 26%, and peak ankle power of 47% during push-off that may not be fully elucidated using conventional dynamometry. Our data also suggest that plantarflexor mechanical performance may be a governing factor in regulating both maximum speed and maximum propulsive force generation during walking. Finally, we introduce a highly functional approach to the assessment of maximum propulsive capacity in walking that may have implications for the tailored prescription of interventions for individuals with propulsive deficits.

## REFERENCES

1. Franz. *Exer Sport Sci Rev*, **44**, 129-35, 2016.
2. Franz, Kram. *J Biomech*, **46(3)**, 535-40, 2013.
3. Franz, Kram. *Clin Biom*, **29(1)**, 68-74, 2014.
4. Anderson, Madigan. *J Biomech*, **47(5)**, 1104-9, 2014.

## ACKNOWLEDGEMENTS

Supported by the UNC University Research Council.

# JOINT POWER GENERATION DURING GAIT ACROSS MOOD PHASES IN BIPOLAR DISORDER

<sup>1</sup> Gu Eon Kang, <sup>1,2</sup> Brian Mickey, <sup>1</sup> Barry Krembs, <sup>1</sup> Melvin McInnis, and <sup>1</sup> Melissa Gross

<sup>1</sup> University of Michigan, Ann Arbor, MI, USA

<sup>2</sup> University of Utah, Salt Lake City, UT, USA

## INTRODUCTION

Bipolar disorder (BD) is characterized by unusual changes in mood, energy and daily tasks [1]. For example, patients with BD experience “high energy” in hypomanic phase and “low energy” in depressed phase [1]. However, these clinical characteristics are described only qualitatively, and have not yet been quantified. Gait is a daily task that requires energy generation for maintaining speed [2], and is altered by emotion in healthy people [3,4]. Since the amount of energy per unit time is power, and power generation in the lower limb is critical for gait [5], investigating joint power generation in gait may fill the gap between qualitative and quantitative descriptions of “energy” that patients with BD experience, which may help to understand more precisely the heterogeneous nature of BD. We aimed to investigate “energy” by quantifying joint power generation in gait across mood phases in BD.

## METHODS

Bipolar patients (n=21) and healthy controls (HC; n=14) recruited from the Prechter Longitudinal Study of Bipolar Disorder at University of Michigan Depression Center were included in this study. All participants had no history of neurological or orthopedic illnesses. HC had no history of personal or familial psychiatric illnesses. The Altman Self-Rating Mania Scale (ASRM) and the Patient Health Questionnaire (PHQ-9) were used to classify bipolar patients by mood phase into hypomanic phase (HM; n=4; ASRM=12.5±5.2; PHQ-9=1.8±1.5), euthymic phase (EU; n=7; ASRM=2.0±1.6; PHQ-9=13.8±7.1) and depressed phase (DP; n=10; ASRM=2.0±1.6; PHQ-9=13.8±7.1).

Marker and ground reaction force (GRF) data were obtained using an optoelectronic motion capture technology with 16 cameras (Motion Analysis, Santa Rosa, CA) at 120 Hz and two force plates (AMTI,

Watertown, MA) at 1200 Hz, respectively. Participants performed level gait for five trials at each of comfortable, slow and fast speeds. Marker and GRF data were low-pass filtered at 6 Hz and 50 Hz, respectively. We used Visual3D (C-Motion, Germantown, MD) to compute kinematic and kinetic variables. One-way ANOVA with Tukey correction was used to compare differences in mean between groups. Then, a linear mixed model with random effects of participants and fixed effects of gait velocity and groups was used to compare differences between groups while accounting for gait velocity.

## RESULTS AND DISCUSSION

Age (39.9±11.7 years) and BMI (25.8±5.3 kg/m<sup>2</sup>) were not different among groups ( $p>.05$ ). Gait velocity was significantly different between groups at comfortable speed (Table 1). Gait velocity was greatest for HM at comfortable speed ( $p<.05$ ), and also tended to be greater than other groups at slow and fast speeds. Gait velocity tended to be least for DP compared to other groups at comfortable speed.

Peak ankle power generation at all speeds, and peak knee power generation at comfortable and fast speeds, were significantly different between groups (Table 1). Peak ankle power generation was greater for HM than for EU, DP and HC at comfortable speed, greater for HM than for EU and HC at slow speed, and greater for HM than for EU at fast speed ( $p<.05$ ). Peak knee power generation was greater for HM than for EU, DP and HC at comfortable speed ( $p<.05$ ), and greater for HM than for HC at slow speed ( $p<.05$ ). Peak knee power generation tended to be the greatest for HM at fast speed. Although peak hip power generation tended to be much greater for HM than all other groups at comfortable and slow speeds, the differences were not significant.

The effects of gait velocity and mood phase on joint powers were separated statistically using a linear

mixed model (Table 2). Peak hip, knee and ankle power generation depended on gait velocity at all speeds ( $p < .05$ ). After accounting for the effects of gait velocity, however, peak ankle power generation was greater for HM than for all other groups at slow and fast speeds, and EU at comfortable speed.

## CONCLUSIONS

Individuals in the HM phase tended to walk faster than other groups at all speeds even though the difference was significant only for comfortable speed trials. Accordingly, peak joint powers also tended to be greatest for HM at the hip, knee and ankle. When the effects of gait velocity were controlled with the linear mixed model, however, group differences in peak joint power generation emerged. Peak ankle power generation was greater for HM than any other group at all speeds. These findings are consistent with qualitative observations of “high energy” for the

HM phase and suggest that biomechanical measures can contribute to the understanding of motor manifestations of BD.

## REFERENCES

1. American Psychiatric Association, DSM-V, 2013.
2. Donlean et al. *J Biomech* 35, 117-124, 2002.
3. Gross et al. *Hum Mov Sci* 31, 202-221, 2012.
4. Kang and Gross. *J Biomech* 49, 4022-4027, 2016.
5. Eng and Winter. *J Biomech* 28, 753-758, 1995.

## ACKNOWLEDGMENTS

This study was funded by American Society of Biomechanics (GIA), Blue Cross Blue Shield of Michigan Foundation, and Rackham School at University of Michigan. We thank Dr. Deanna Gates for help with data collection.

**Table 1:** Mean  $\pm$  standard deviation for gait velocity and peak joint power generation in each group.

	HM	EU	DP	HC
<b>Gait velocity (m/s)</b>				
Comfortable	1.55 $\pm$ 0.15 <sup>HC*,EU*,DP**</sup>	1.21 $\pm$ 0.12 <sup>HM*</sup>	1.15 $\pm$ 0.28 <sup>HM**</sup>	1.21 $\pm$ 0.12 <sup>HM*</sup>
Slow	1.00 $\pm$ 0.21	0.75 $\pm$ 0.19	0.74 $\pm$ 0.27	0.74 $\pm$ 0.17
Fast	2.03 $\pm$ 0.18	1.71 $\pm$ 0.17	1.79 $\pm$ 0.23	1.84 $\pm$ 0.28
<b>Peak hip power generation (W/BW)</b>				
Comfortable	1.34 $\pm$ 0.27	1.18 $\pm$ 0.38	0.96 $\pm$ 0.51	0.88 $\pm$ 0.33
Slow	0.80 $\pm$ 0.31	0.62 $\pm$ 0.32	0.51 $\pm$ 0.28	0.45 $\pm$ 0.24
Fast	2.04 $\pm$ 0.24	2.06 $\pm$ 0.60	1.98 $\pm$ 0.68	1.99 $\pm$ 1.11
<b>Peak knee power generation (W/BW)</b>				
Comfortable	2.07 $\pm$ 1.01 <sup>HC**,EU**,DP**</sup>	0.91 $\pm$ 0.23 <sup>HM**</sup>	0.75 $\pm$ 0.54 <sup>HM**</sup>	0.95 $\pm$ 0.33 <sup>HM**</sup>
Slow	0.67 $\pm$ 0.59 <sup>HC*</sup>	0.29 $\pm$ 0.09	0.30 $\pm$ 0.19	0.26 $\pm$ 0.14 <sup>HM*</sup>
Fast	2.69 $\pm$ 1.20	2.09 $\pm$ 0.75	2.36 $\pm$ 1.13	2.11 $\pm$ 1.15
<b>Peak ankle power generation (W/BW)</b>				
Comfortable	5.29 $\pm$ 0.72 <sup>HC**,EU**,DP**</sup>	3.07 $\pm$ 0.54 <sup>HM**</sup>	3.09 $\pm$ 1.27 <sup>HM**</sup>	3.43 $\pm$ 0.62 <sup>HM**</sup>
Slow	3.09 $\pm$ 1.43 <sup>HC*,EU*</sup>	1.40 $\pm$ 0.68 <sup>HM*</sup>	1.67 $\pm$ 0.91	1.59 $\pm$ 0.72 <sup>HM*</sup>
Fast	7.13 $\pm$ 1.49 <sup>EU*</sup>	4.99 $\pm$ 0.93 <sup>HM*</sup>	5.30 $\pm$ 1.38	5.46 $\pm$ 1.01

Note: Superscript letters are significant differences between groups based on one-way ANOVA: \*  $p < .05$ . \*\*  $p < .01$ .

**Table 2:** Estimates and 95% confidence intervals from linear mixed model for peak ankle power generation.

	Gait velocity	EU	DP	HC
Comfortable	3.62, (2.84, 4.42) <sup>***</sup>	1.01, (0.11, 1.91) <sup>*</sup>	0.75, (-0.10, 1.59)	0.64, (-0.16, 1.44)
Slow	3.71, (3.25, 4.16) <sup>**</sup>	0.83, (0.27, 1.39) <sup>**</sup>	0.57, (0.04, 1.09) <sup>*</sup>	0.52, (0.02, 1.01) <sup>*</sup>
Fast	1.64, (0.67, 2.59) <sup>***</sup>	1.58, (0.08, 3.09) <sup>*</sup>	1.43, (0.06, 2.79) <sup>*</sup>	1.34, (0.04, 2.64) <sup>*</sup>

Note: Asterisks are significant fixed effects of groups (vs. HM) and gait velocity: \*  $p < .05$ . \*\*  $p < .01$ . \*\*\*  $p < .001$ .

# MULTI-OBJECTIVE CONTROL OF LATERAL STEPPING WHILE WALKING

<sup>1</sup> Jonathan B. Dingwell and <sup>2</sup> Joseph P. Cusumano

<sup>1</sup> University of Texas at Austin, Austin, TX, USA; <sup>2</sup> Pennsylvania State University, University Park, PA, USA;  
email: [jd Dingwell@austin.utexas.edu](mailto:jd Dingwell@austin.utexas.edu); web: <http://www.edb.utexas.edu/khe/nbl/>

## INTRODUCTION

Falls are common and perilous events in the lives of the elderly (age  $\geq 65$ ) [1]. Falls to the side are especially dangerous [2] and walking humans are inherently more unstable laterally [3,4]. Most walking environments (sidewalks, store aisles, treadmills, etc.) have finite width. It is unclear how people *regulate* lateral stepping movements in such contexts. Here, we extend a previous framework [5,6] to demonstrate how humans exploit available redundancies to achieve lateral stepping control strategies.

## METHODS

When walking on any defined path (Fig. 1), the only lateral requirement is to not step off the path:

$$-W/2 < [z_L \ z_R] < +W/2$$

where  $W$  is the path width. Due to biomechanical redundancy [6], there are *infinite* choices for each successive step,  $[z_L, z_R]$ . Likewise, our feet are not independent: they are connected to our body. Thus, we presume  $[z_L, z_R]$  act as effectors that enact control over some combination of body position ( $z_B$ ), heading ( $\Delta z_B$ ), or step width ( $w$ ) (Fig. 1). Further:

$$\begin{bmatrix} z_B \\ w \end{bmatrix} = \begin{bmatrix} \frac{1}{2} & \frac{1}{2} \\ -1 & 1 \end{bmatrix} \begin{bmatrix} z_L \\ z_R \end{bmatrix}$$

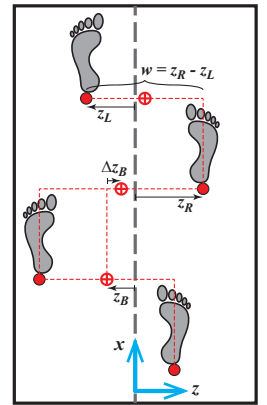
Since this relationship is invertible, specifying either  $[z_B, w]$  or  $[z_L, z_R]$  fully specifies the other. Thus, *position* ( $z_B$ ), *heading* ( $\Delta z_B$ ), and *step width* ( $w$ ) span the set of all possible variables that can be controlled: i.e., all strategies to control lateral stepping when walking on any defined path can be constructed as some combination of *position*, *heading*, and/or *step width* control. We then seek to find the most parsimonious control strategy that captures the variability and step-to-step dynamics we observe in experiment.

Models that control only a single variable ( $z_B$ ,  $\Delta z_B$ , or  $w$ ) do not work (ASB 2016). Likewise, it is impos-

sible to fully control 2 variables simultaneously because each control strategy predicts a *different* foot placement and you cannot put your foot in two places at the same time. Here, we show that multi-objective control models that *balance* control of 2 variables do replicate experimental observation.

**Figure 1:** Candidate variables for lateral stepping control:

- $\{z_L, z_R\} \equiv$  Left & Right lateral foot placements
- $z_B = (z_L + z_R)/2 \equiv$  Absolute lateral deviation of the body
- $\Delta z_B = z_{Bn} + z_{Bn-1} \equiv$  Change in lateral position of the body (a.k.a., “heading”)
- $w = z_R - z_L \equiv$  Step width.



Stochastic control computational models were developed from pre-defined goal functions [5,6]:

$$F = (q_{1n} - q_1^*) + (q_{2n} - q_2^*), \quad q_{1,2} \in \{z_B, \Delta z_B, w\}$$

where each  $q_n$  is a different state variable and the goal was to drive  $F \rightarrow 0$  (i.e., try to satisfy both goals at the same time). The process of regulating step-to-step walking dynamics was modeled as a 2D discrete map, or step-to-step update equation [5]:

$$\begin{bmatrix} q_{1n+1} \\ q_{2n+1} \end{bmatrix} = \begin{bmatrix} q_{1n} \\ q_{2n} \end{bmatrix} + \begin{bmatrix} 1 + \xi_{1m} & 0 \\ 0 & 1 + \xi_{2m} \end{bmatrix} \begin{bmatrix} u_{q1} \\ u_{q2} \end{bmatrix} + \begin{bmatrix} \xi_{1a} \\ \xi_{2a} \end{bmatrix}$$

where the  $\xi$ . were noise terms and the control inputs,  $[u_{q1}, u_{q2}]$  were derived analytically [5] to satisfy:

$$C = \alpha_1 e_1^2 + \alpha_2 e_2^2 + \gamma_1 u_{q1}^2 + \gamma_2 u_{q2}^2$$

where  $e_1$  and  $e_2$  were the errors with respect to each corresponding goal. Thus, these controllers minimized errors in each variable, while also minimizing corrections needed to achieve control. This yielded:

$$\begin{bmatrix} u_{q1} \\ u_{q2} \end{bmatrix} = \begin{bmatrix} -1/(1 + \sigma_{1m}^2 + \gamma_1/\alpha_1) & 0 \\ 0 & -1/(1 + \sigma_{2m}^2 + \gamma_2/\alpha_2) \end{bmatrix} \begin{bmatrix} q_{1n} - q_1^* \\ q_{2n} - q_2^* \end{bmatrix}$$

This control thus takes each new step as a weighted average of the 2 foot placements predicted by each

individual controller. For each possible pair of 2 candidate control variables,  $\{z_B, \Delta z_B, w\}$ , we varied this weighting (from 0% to 100%) and simulated walking for twenty trials of 1000 steps each.

In humans, stepping kinematics were recorded (Vicon) from 13 able bodied participants (age 22-40) who walked in a “CAREN” virtual reality environment [4]. Each participant completed five 3-minute walking trials at a comfortable speed [4].

Stepping parameters analyzed included time series of left ( $z_L$ ) and right ( $z_R$ ) foot placements, lateral position ( $z_B$ ), heading ( $\Delta z_B$ ), and step width ( $w$ ). Means, standard deviations, and Detrended Fluctuation Analysis (DFA)  $\alpha$  exponents [5] were calculated for each time series to compare step-to-step dynamics predicted by each controller to experiment.

## RESULTS AND DISCUSSION

Humans exhibited variability in all stepping variables (Fig. 2; Left). Control models that tried to control either heading & position or heading & step width failed to replicate experimental findings, regardless of the relative proportion of control.

However, the model that traded-off control of absolute position ( $z_B$ ) and step width ( $w$ ) was able to replicate all relevant experimental stepping dynamics when the proportion of control was weighted ~85%-95% towards  $w$ -control, with ~15%-5% towards  $z_B$ -control (Fig. 3).

## CONCLUSIONS

Computational control models yielded directly testable predictions that demonstrate humans adopt *multi-objective* lateral stepping control that prioritizes step width, while trading-off some step width control to maintain lateral position control. Prioritizing step width helps maintain lateral balance [3,4], which is highly relevant for those prone to falling [1,2].

## REFERENCES

1. Robinovich SN, et al. *The Lancet* **381**, 47-54, 2013.
2. Mayhew PM, et al. *The Lancet* **366**, 129-35, 2005.
3. Kuo AD *Int. J Robotics Res* **18**, 917-30, 1999.

4. McAndrew PM, et al. *J Biomech* **44**, 644-49, 2011.
5. Dingwell JB, John J, & Cusumano JP. *PloS Comput Biol* **6**, e1000856, 2010.
6. Dingwell JB & Cusumano JP. *PloS ONE* **10**, e0124879, 2015.

## ACKNOWLEDGEMENTS

DoD/CDMRP/BADER Consortium W81XWH-11-2-0222; NIH Grants R01-HD059844 & R01-AG049735.

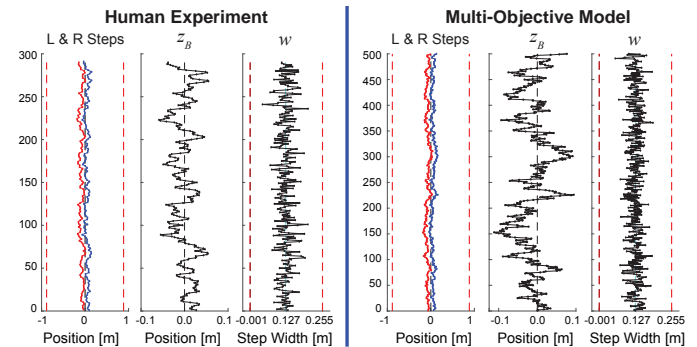


**Figure 2:** Patterns of left ( $z_L$ : red) & right ( $z_R$ : blue) steps, absolute position ( $z_B$ ), and step width ( $w$ ) for a typical human (left) and multi-objective control model (right).

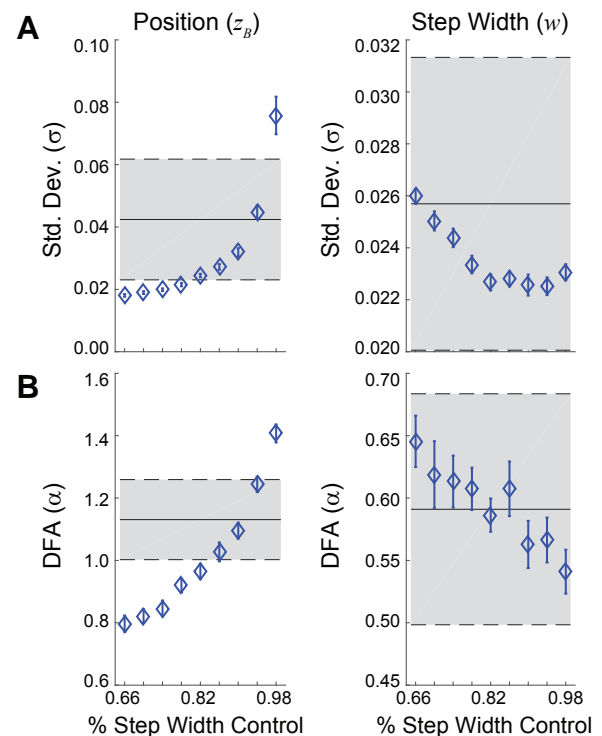


**Figure 3:** Changes in (A) variability and (B) DFA exponents for  $z_B$  and  $w$  for the model (blue diamonds) as the balance of  $w$ -control vs.  $z_B$ -control was varied. Horizontal gray bands indicate mean  $\pm$  SD range for humans.

# REGULATION OF WHOLE-BODY ANGULAR MOMENTUM AND MUSCLE ACTIVATION DURING WALKING ADAPTABILITY TASKS POST-STROKE

Arian Vistamehr<sup>1</sup>, Chitralakshmi K. Balasubramanian<sup>2</sup>, David J. Clark<sup>3,4</sup>, Christy Conroy<sup>1</sup>, Richard R. Neptune<sup>5</sup>, and Emily J. Fox<sup>1,6</sup>

<sup>1</sup> Motion Analysis Center, Brooks Rehabilitation, Jacksonville, FL

<sup>2</sup> Department of Clinical and Applied Movement Sciences, University of North Florida, Jacksonville, FL

<sup>3</sup> Brain Rehabilitation Research Center, Malcom Randall VA Medical Center, Gainesville, FL

<sup>4</sup> Department of Aging and Geriatric Research, University of Florida, Gainesville, FL

<sup>5</sup> Department of Mechanical Engineering, The University of Texas, Austin, TX

<sup>6</sup> Department of Physical Therapy, University of Florida, Gainesville, FL

email: arian.vistamehr@brooksrehab.org

## INTRODUCTION

Although 85% of individuals post-stroke regain some level of steady-state walking function, over one third of these individuals are unable to walk in the community (e.g., [1]). Walking in the community involves performance of adaptability tasks such as obstacle negotiation, stepping up a curb and changing walking direction [2]. Successful performance of these tasks requires the control of dynamic balance, which is a major challenge post-stroke.

Prior studies have shown that the regulation of whole-body angular momentum ( $H$ ) is essential to controlling dynamic balance. For example, older fallers have shown insufficient regulation of angular momentum after a trip [3]. Further, poor regulation of  $H$  during steady-state walking results in a higher peak-to-peak range of  $H$ , which has been associated with lower clinical balance scores in individuals post-stroke [4].

$H$  is primarily regulated by muscle forces through the generation of ground-reaction-forces (GRFs). Simulation analyses of healthy adults during steady-state walking indicate that soleus (SOL), gastrocnemius (GAS), and gluteus medius (GMED) are the primary contributors to the regulation of  $H$  in the frontal plane during late stance [5]. However, plantarflexor weakness is a common impairment post-stroke. Thus, muscle weakness and altered activation may contribute to poor regulation of  $H$  during walking and more challenging adaptability tasks. Further insight into the regulation of  $H$  and the underlying muscle activations post-stroke can contribute to the development of training programs targeted to improve walking adaptability.

Thus, the purpose of this study was to assess the regulation of  $H$  during a variety of walking adaptability tasks in individuals post-stroke and to examine the corresponding changes in the muscle activations relative to steady-state walking.

## METHODS

Three-dimensional kinematics and bilateral surface electromyogram (EMG) data were recorded from 16 individuals with post-stroke hemiparesis (11 left hemiparesis; age:  $60 \pm 12.5$  years; 5 female; self-selected walking speed:  $1.08 \pm 0.29$  m/s). Data was collected during a variety of walking adaptability tasks: self-selected (SS), fastest-comfortable (FC) and backward (BW) walking as well as obstacle negotiation and step up, which were divided into leading and trailing limb phases. These phases included obstacle leading (OBL), obstacle trailing (OBT), step up leading (SUL) and step up trailing (SUT). No orthotics were used. Additionally, data from 10 healthy individuals (age:  $23 \pm 2.9$  years; SS walking speed:  $1.35 \pm 0.13$  m/s) were collected to provide a basis for comparison.

Whole-body  $H$  was calculated in the frontal plane using kinematic data [4]. The regulation of  $H$  was assessed using the peak-to-peak (max-min) range of  $H$  in the frontal plane during single-limb stance (SLS). This phase was selected because  $H$  is regulated by the stance leg through the generation of GRFs, which may be challenging post-stroke. EMG data from SOL, GAS and GMED were high-pass filtered at 30Hz, demeaned, rectified and low-pass filtered at 10Hz using a 4<sup>th</sup>-order Butterworth filter. Muscle activation in each task was quantified by averaging EMG amplitudes of each muscle

during SLS, normalized by the mean amplitude of the same muscle during the SS task.

Significant differences in the regulation of  $H$  between each task versus SS were identified using a paired t-test with Bonferroni adjustment within each condition: paretic SLS, nonparetic SLS, and average of both legs during SLS in healthy controls (HCs). In cases where significant differences were found, comparisons were conducted between the muscle activations during that task relative to the SS task.

## RESULTS AND DISCUSSION

The range of  $H$  in the frontal plane significantly increased during the obstacle and step up tasks relative to the SS task both in individuals post-stroke and in HCs (Fig. 1a). However, note that the baseline range of  $H$  during the SS task is over 65% higher in individuals post-stroke than in the HCs (Fig. 1a'). Thus, overall individuals post-stroke demonstrated higher ranges of whole-body angular momentum during all movement tasks than the HCs. This was particularly evident during the adaptability tasks, which required increased generation of  $H$ .

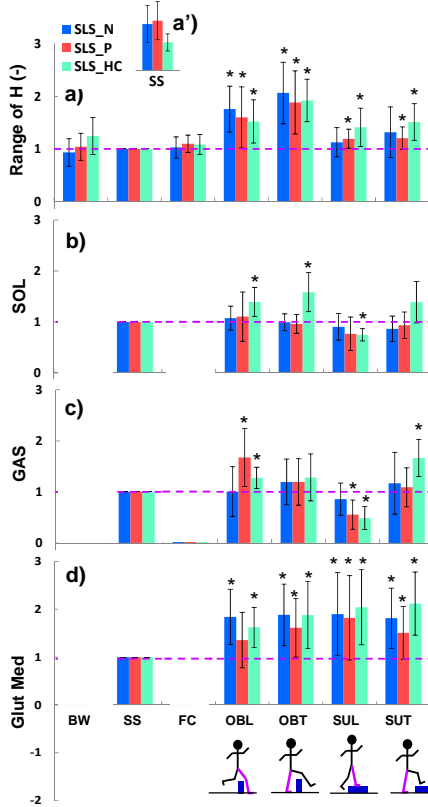


**Figure 1:** Normalized mean ( $\pm$ SD) a) range of  $H$  in the frontal plane, EMG amplitudes of b) soleus, c) medial gastrocnemius, and d) gluteus medius muscles are shown. All figures are normalized with respect to the SS condition and correspond to the single leg stance of the nonparetic leg (blue), paretic leg (red), and average of both legs in healthy controls (green). Significant differences within each group between each task and the SS task are shown with '\*'. Fig. 1a' shows the baseline range of  $H$  in the frontal plane in individuals post-stroke and in healthy controls during the SS task.

For the tasks where the range of  $H$  increased relative to the SS, with the exception of SUL, the

HCs demonstrated a concurrent increase in plantarflexor (SOL, GAS) and hip abductor (GMED) activation (Fig. 1b-d). Interestingly, while individuals post-stroke increased their hip abductor activation, minimal changes in the plantarflexors were evident (Fig. 1b-d). Based on their high range of  $H$  during the SS task (Fig. 1a'), one explanation could be that the individuals post-stroke recruited SOL maximally during the SS task and thus were unable to increase its activation to meet the increased task demands. In the case for GMED, adjustments in muscle activation were more evident across tasks post-stroke. It is possible that this proximal muscle contributed to a lesser extent to the SS task. Further, during the adaptability tasks, the higher pelvic and trunk control requirements along with the commonly used hip strategy post-stroke, may have collectively contributed to the increased GMED activations.

Prior simulation analyses of healthy adults during SS walking have shown the importance of the plantarflexors and the hip abductors in controlling dynamic balance in the frontal plane [5]. Specifically, SOL and GAS act to rotate the body towards the contralateral leg, while GMED acts to rotate the body towards the ipsilateral leg [5]. During these more challenging adaptability tasks, the contributions from these muscles may be even more important for balance control.

In summary, quantifiable deficits in the regulation of  $H$  and muscle activation levels were identified in individuals post-stroke during walking adaptability tasks. Rehabilitation focused on improved muscle activation during such tasks may contribute to recovery of home and community mobility in individuals post-stroke.

## ACKNOWLEDGEMENTS

The authors acknowledge the valuable contributions from Mr. Paul Freeborn in assisting with data collection. This work was supported by Brooks Collaborative Funding, K12 Rehabilitation Research Career Development Program (NIH/NICHHD K12 HDO55929), and the VA R&D Service.

## REFERENCES

1. Lord SE, et al. *Arch Phys Med Rehabil* **85**, 234-9, 2004.
2. Balasubramanian CK, et al. *Stroke Res Treat* 2014.
3. Pijnappels M, et al. *Gait & Posture* **21**, 388-94, 2005.
4. Vistamehr A, et al. *J Biomech* **49**, 396-400, 2016.
5. Neptune RR & McGowan CP, *J Biomech* **49**, 75-81, 2016.

# ASSESSING MOVEMENT ASYMMETRY USING THE NORMALIZED SYMMETRY INDEX IN ACL PATIENTS

<sup>1</sup>Robin Queen, <sup>2</sup>Daniel Schmitt, <sup>3</sup>Shyam Ranganathan

<sup>1</sup>Department of Biomedical Engineering and Mechanics, Kevin Granata Biomechanics Lab,  
Virginia Tech University, Blacksburg, VA, USA

<sup>2</sup>Animal Locomotion Lab, Department of Evolutionary Anthropology, Duke University, Durham, NC, USA  
email: mevan6@vt.edu web: beam.vt.edu/granatalab

## INTRODUCTION

Athletes are at an increased risk of ACL injury during landing tasks, particularly at or immediately following the time of ground contact [1]. Differences in landing mechanics have been reported following ACL-R [2-4]. These movement differences have been proposed as risk factors for subsequent injury to either the ipsilateral or contralateral limb [2]. Asymmetry between limbs is common following ACL-R and has been cited as a potential risk factor for secondary injury [2,3]. Asymmetries in knee flexion angle, and vGRF have been reported in ACL-R populations, and asymmetries in knee extension moment and in frontal plane range of motion have been associated with an increased risk of sustaining a secondary ACL tear following return to sports [2,4].

Symmetry measures such as the Symmetry Index (SI), Ratio Index (RI), Gait Asymmetry (GA) and the Symmetry Angle (SA) have been used in the literature for years to quantify the extent of asymmetry between limbs at different joints. While each of these indices is useful, they all have limitations. For instance, RI tends to very large values as the denominator approaches zero, irrespective of the value of the numerator. The GA uses the natural logarithm and hence is useful only for positive quantities, which may be an issue based on the biomechanical axis system that is defined. The SI is the most generalizable of these indices, but it tends to saturate at its maximum value (max value = 200) when the measured variables are opposite in sign, which is again an issue depending on the variable of interest as well as the type of population being studied.

Another general issue with all these indices (apart from the SI) is that they cannot be used universally across different variables. For the same subject, a

high value of asymmetry in the knee might not be comparable to a high value of asymmetry in the ankle because the symmetry indices in the literature are not standardized, making clinical comparisons more challenging.

Therefore, the purpose of this study was to develop a new symmetry index, based on the SI, which addresses the weaknesses of the other measures in the literature. In addition, this study will demonstrate how this new symmetry measure will allow for comparison across different variables and will demonstrate the advantage of this new symmetry measure when compared to currently available measures.

## METHODS

23 ACL-R athletes (9 males, 14 females, 16.0±1.3 years, 1.69±0.09 m, 72.0±15.7 kg) and 12 control subjects (9 male, 3 female, 22.2±2.2 years, 1.76±0.01 m, 75.6±13.8 kg) participated in the study. All subjects underwent an ACL tibial tunnel-independent reconstruction with a hamstring graft. All subjects signed an approved assent or consent form prior to testing.

46 retro-reflective markers were placed on specific lower extremity landmarks by a single researcher as previously described [4]. An 8-camera motion capture system collected three-dimensional data at 120 Hz (Motion Analysis Corporation, Santa Rosa, CA). Ground reaction forces were measured with two embedded force plates collecting at 2400 Hz (AMTI, Watertown, MA). Each subject performed five vertical stop-jump tasks. The stop-jump task involved a running approach of several steps, a jump off one foot, a two-footed landing, and a subsequent two-footed jump. Subjects were told to approach as quickly as possible and to jump as high as was safely possible. No instruction on landing was given.

Kinematic and kinetic data were collected bilaterally during all trials.

The three-dimensional data was filtered with a 12 Hz low-pass Butterworth digital filter and ground reaction forces (GRF) were filtered at 100 Hz. Time-series curves were generated with Visual 3D software (C-Motion, Bethesda, Maryland, USA) and Matlab (MathWorks, Natick, MA) was used to extract the variables of interest.

Data from the surgical and non-surgical limbs (dominant and non-dominant) of each subject were used to calculate limb symmetry using the previously published SI as well as the newly developed Normalized Symmetry Index (NSI) for each variable using the following formula:

$$NSI = \frac{X_{NSx} - X_{Sx}}{|max(X_{Sx}, X_{NSx})|} * 100\%$$

where  $X_{Sx}$  and  $X_{NSx}$  denote data for the surgical and non-surgical limbs, respectively. An NSI of 0 would represent perfect movement symmetry between limbs. Since repeated measurements were available for each subject, the NSI was calculated using individual measurements and then the mean NSI was calculated. This allowed for the computation of the (intra-class correlation) ICC to evaluate the within and between subject variability in the NSI. A series of independent samples Wilcoxon signed rank tests was performed to compare the NSI in the control and treatment groups for the different variables ( $\alpha=0.05$ ). The non-parametric test is used due to the non-normal nature of the data. Statistical analysis was performed in R.

## RESULTS AND DISCUSSION

To better describe the differences that result from these various measures, we have provided subject specific examples as well as the group comparisons results. The peak valgus angles for the landing trials for a representative ACLR subject (Table 1) demonstrate the between trial variability that exists in this sample. In the calculation of the SI, the large differences between trials has a disproportionate effect resulting in a SI of -200. This difference is reflected when the mean of the SIs and NSIs are computed, yielding a mean SI of -64.17, and a mean NSI of -38.08. If trial 1 is dropped, however, the

mean SI reduces to -37.00, and the mean NSI reduces to -23.2. This illustrates the problem of the robustness of SI as a measure to use in clinical applications.

Table 1: Differences between SI and NSI for a representative subject from the ACLR group

Surgical Peak Valgus	Non-Surgical Peak Valgus	SI	NSI
0.70	-5.57	-200	-112.49
-4.54	-4.45	2.03	2.01
-0.89	-5.54	-144.56	-83.91
-4.73	-3.95	18.07	16.57
-3.50	-3.99	-13.21	-12.39
-3.51	-5.68	-47.33	-38.28
Mean= -2.74	Mean= -4.86	Mean= -64.2	Mean= -38.1

When comparing the two study groups it is clear that the NSI will allow for detection of asymmetries that are not as drastically impacted by between trial variability in joint position.

Table 2: Median Symmetry Measure comparison between the ACL-R and treatment groups using the NSI

	ACLR	Control	p-value
Frontal Plane Knee ROM	17.04	31.25	0.019*
Peak Vertical GRF	17.23	8.96	0.014*
Peak Knee Valgus	42.28	21.60	0.490
Peak Knee Ext Moment	23.87	8.19	0.003*

## CONCLUSIONS

The NSI as a measure of symmetry will allow for the detection of differences between groups as well as allowing for the comparison of the amount of asymmetry across various variables, which is not possible with the previously defined measures of asymmetry due to their measurement limitations.

## REFERENCES

1. Taylor, et al. *JOB*. **44(3)**: 365-71, 2011.
2. Paterno, et al. *AJSM*. **38(10)**: 1968-78, 2010.
3. Butler, et al. *Sports Health*. **6(3)**: 203-9, 2014.
4. Dai, et al. *AJSM*. **40(12)**: 2756-63, 2012.
5. Myer, et al. *JOSPT*. **41(6)**: 377-87, 2011.
6. Manal & Snyder-Mackler. *Oper Tech Orthop*. **6(3)**: 190-6, 1996.
7. Hashemi, et al. *The Knee* **17(3)**: 235-41, 2010.

# FAILURE MODALITIES INDUCED BY A NOVEL MECHANICAL IMPACT SIMULATOR DESIGNED TO INDUCE ACL FAILURE

<sup>1</sup>Nathaniel A. Bates, <sup>1</sup>Nathan D. Schilaty, <sup>1</sup>Christopher V. Nagelli, <sup>1</sup>Aaron J. Krych, and <sup>1</sup>Timothy E. Hewett

<sup>1</sup>Mayo Clinic, Rochester, MN, USA  
email: bates.nathaniel@mayo.edu

## INTRODUCTION

250,000 ACL injuries occur annually and incur over \$2 billion in reconstructive and rehabilitative cost. Hence, it is essential that the orthopedic community better understand the underlying mechanisms that contribute to ACL rupture. A number of impact simulators were developed over the past decade to investigate intra-articular biomechanics at the knee [1]. Most of these platforms were used to investigate the effects of individual elements such as internal tibial torsion, quadriceps force, or hamstrings force on ACL strain during impulse loading. More recently, an impact simulator was designed that was capable of consistently inducing failure on the ACL [2]. However, these failures were mainly tibial avulsions or eminence fractures. Unfortunately, this does not correlate well with the clinical modality of failure observed in surgery. Accordingly, we designed a novel mechanical impact simulator with the intention of addressing this issue. It was hypothesized that our novel impactor design could reproducibly produce ACL failures on cadaveric specimens in modalities that correlate well with clinically observed failures.

## METHODS

35 cadaveric specimens were tested in our novel mechanical impact simulator. Detailed description of the simulator protocol is available in the literature [3]. Briefly, the simulator delivered a series of gravity-driven impulse forces into a ground platform that was aligned with the tibia of lower-extremity cadaveric specimen. Pneumatic actuators simultaneously applied external anterior tibial shear (ATS), knee abduction (KAM), and internal tibial rotation (ITR) forces and torques to the knee joint. All of these applied loads were derived from *in vivo* motion analysis and corresponding biomechanical assessment of athletes performing a drop vertical

jump task off a 31 cm box. A 6-DOF load cell aligned with the long axis of the femur and affixed 20 cm proximal to the joint center point reported loads at the knee. DVRT strain gauges implanted on the ACL and MCL reported ligament strain. A board certified orthopedic surgeon performed clinical and arthroscopic exams pre- and post-testing to assess functional and structural integrity. Injury was attributed to the simulator if exam grades changed between pre- and post-testing. Six specimens were excluded due to unsuitable tissue quality or complications during the testing protocol. 29 specimens remained for analysis (age =  $42.0 \pm 8.5$  years; mass =  $87.6 \pm 21.7$  kg; height =  $175.6 \pm 8.9$  cm; 11 females; 18 males).

## RESULTS AND DISCUSSION

Of the 29 specimens tested, 27 experienced soft tissue failures, of which 25 were ACL failures and 2 were isolated MCL failures (Table 1). The remaining 2 specimens failed via femoral fractures. There was one specimen that received a grade 2 MCL laxity score prior to testing; and thus, was not considered and MCL injury induced by the impact simulator. None of the 29 specimens completed testing without sustaining any injuries. Within the ACL injured specimens, 9 (31%) also expressed concomitant MCL failure induced by the mechanical impact simulator. Twenty of the ACL injuries were complete tears, while 3 were partial tears (Table 2). 17 ACL ruptures were proximal on the femoral side, 6 occurred midsubstance, and 2 were distal on the tibial side (Figure 1). All but one injury reported on the specimens were attributed to the mechanical impact simulations (Table 3).

**Table 1:** Specimen failure modalities.

ACL Rupture	MCL Rupture	Other Soft Tissue	Femur Fracture
86%	38%	3%	7%

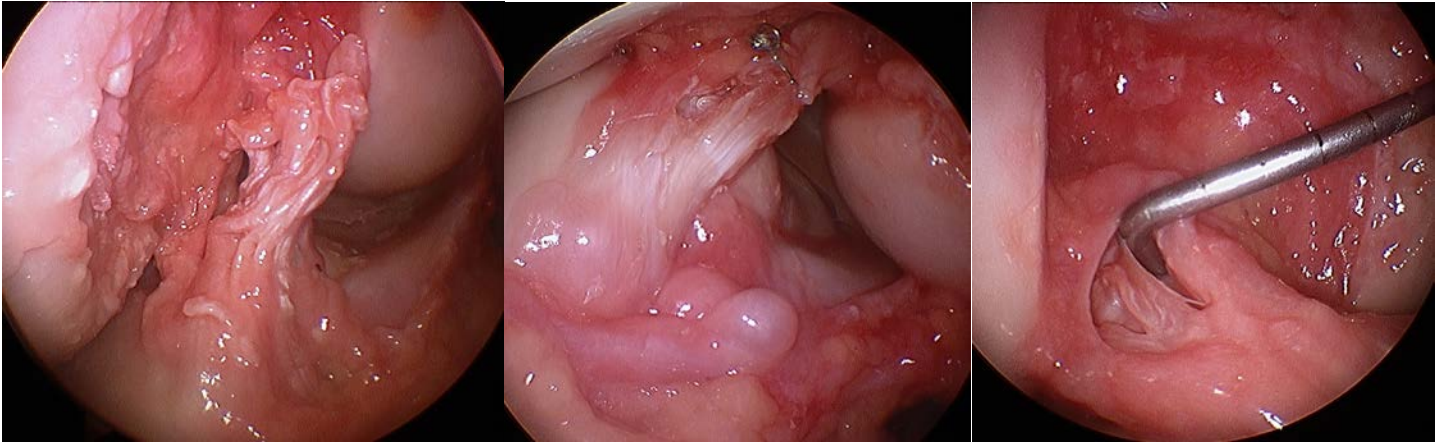


**Figure 1:** Image frames depicting various ACL rupture modalities from the mechanical impact simulator. From left to right, these frames exhibit 1.) a complete femoral avulsion, 2.) a complete midsubstance tear, 3.) a partial midsubstance tear. During a Lachman’s exam, both complete tears were grade 3, while the partial was grade 2.

**Table 2:** ACL rupture locations.

Femoral Avulsion	Mid-Substance	Tibial Avulsion	Complete	Partial
72%	24%	8%	80%	12%

**Table 3:** Number of specimens that recorded positive grades during pre- and post-testing clinical exams. Mean grade for all specimens is in parentheses.

	Lachman	PCL	MCL	LCL
Pre-Test	0 (0.0)	0 (0.0)	1 (0.1)	0 (0.0)
Post-Test	25 (2.5)	0 (0.0)	12 (1.2)	5 (0.4)

The mean peak ACL strain prior to failure in all specimens was  $14.5 \pm 9.0\%$  with a mean peak MCL strain of  $6.8 \pm 8.2\%$ . The mean peak ACL strain prior to failure in the 25 specimens that failed via ACL rupture was  $13.5 \pm 8.2\%$ , with a mean peak MCL strain of  $6.3 \pm 8.7\%$ . The mean peak ACL strain prior to failure in the 10 specimens that sustained MCL injury was  $17.1 \pm 8.6\%$  with a mean peak MCL strain of  $10.5 \pm 9.0\%$ . These values are similar to the peak strain reported in uniaxial ACL failure testing. However, the present ACL strains are smaller than those from a previous injury impactor [2]. This could be a result of the more physiologic loading conditions of our novel device that presented more clinically representative modalities of ACL failure. The increased ACL strain in MCL-injured specimens indicated that the ACL likely compensated for some of the knee restraint lost during MCL injury. Further, the higher strain observed in the ACL vs. MCL is

supportive of literature that indicates the ACL makes greater contributions to knee restraint than the MCL [4, 5].

The injury pattern demonstrated in the 25 specimens that exhibited ACL failure was representative of that which is observed clinically. Femoral side ACL tears are most common, followed by mid-substance tears, followed by tibial avulsions [5].

## CONCLUSIONS

The hypothesis that our novel mechanical impactor would reproducibly create clinically representative modalities of ACL failure was accepted and all results were confirmed by a board certified orthopedic surgeon. The presented simulator is optimized for the study of ACL injury, reconstruction and deficiency in cadaveric models.

## REFERENCES

1. Bates NA, et al. *Clin Bio*, **30**, 1-13, 2015.
2. Levine JW, et al. *Am J Sports Med*, **41**, 385-95, 2013.
3. Bates NA, et al. *Clin Bio*, Accepted: in-press, 2017.
4. Bates NA, et al. *Am J Sports Med*, **43**, 2259-69, 2015.
5. Quatman CE, et al. *Am J Sports Med*, **42**, 177-86, 2014.
6. Kocher MS, et al. *Am J Sports Med*, **30**, 697-703, 2002.

## ACKNOWLEDGMENTS

NIH grant funding R01AR049735, R01AR056259, R01AR055563, T32AR056950, and L30AR070273

# SEX DIFFERENCES IN KNEE FORCES & MOMENTS THAT OCCUR WITH ANTERIOR CRUCIATE LIGAMENT RUPTURE ON CADAVERIC IMPACT SIMULATIONS

<sup>1</sup>Nathan D. Schilaty, <sup>1</sup>Nathaniel A. Bates, <sup>1</sup>Christopher V. Nagelli, <sup>1</sup>Aaron J. Krych, and <sup>1</sup>Timothy E. Hewett

<sup>1</sup>Mayo Clinic Dept. of Orthopedic Surgery, Rochester, MN, USA  
email: schilaty.nathan@mayo.edu

## INTRODUCTION

Females have an increased risk of injury to the anterior cruciate ligament (ACL) compared to their male counterparts [1]. Additionally, 75% of these ACL injuries are non-contact in nature, demonstrating that biomechanical kinetics and kinematics are significant risk factors to this injury. Consequently, it is important to understand the underlying mechanisms of ACL injury to determine the factors that increase ACL injury risk in females. Improved knowledge of the mechanisms of ACL will enhance injury prevention, rehabilitation, and return to sport (RTS) criteria for these athletes.

This current study was designed to specifically determine the mechanisms of loading at the knee that cause ACL failure during a common athletic task – a drop vertical jump (DVJ). It was hypothesized that female limbs would demonstrate differences in knee forces and moments that predispose females to ACL injury compared to males, especially with frontal plane knee abduction.

## METHODS

A custom-designed cadaveric impactor was utilized to simulate athletic DVJs in lower extremities of 35 specimens (22M:13F). Ages of specimens ranged from 24 to 52. Inclusion criteria of the specimens include: no evidence of significant trauma/surgery to lower extremity and no evidence of extended chemotherapy. Specimens were prepared according to specifications outlined in a recent methodology manuscript [2].

*In vivo* kinetics and kinematics of 70 subjects were calculated to determine tertiles of risk (i.e. low, medium, and high) in three degrees of knee forces/moments [i.e. knee abduction moment

(KAM), anterior tibial shear (ATS), and internal tibial rotation (ITR)]. Pneumatic cylinders then applied the designated knee forces/moments to the tibia calculated from the *in vivo* subjects and then a gravity-driven drop sled of 0.5 body weight (34 kg) was released from a height of 31 cm with quadriceps and hamstrings co-contracted with a 1:1 ratio. Single axis and 6-axis load cells recorded vertical ground reaction forces (vGRF) and forces/moments at the knee, respectively. Additionally, two differential variable reluctance transducers (DVRTs) were implanted into the medial collateral ligament (MCL) and the ACL for measurements of ligament strain during loading. Six specimens were excluded for unsuitable tissue quality or complications that arose during the experimental protocol. Four additional specimens were excluded as they did not experience ACL rupture. Twenty-five specimens remained for analysis (16M:9F; **Table 1**).

Statistical analyses were performed with JMP 10 (SAS Institute Inc., Cary, NC) with utilization of one-way ANOVA.

**Table 1:** Specimen Demographics by Sex.

	Males	Females	<i>p</i> -value
<b>Age</b>	42.6 ± 8.1	41.7 ± 8.3	0.7813
<b>Mass (kg)</b>	94.3 ± 17.8	72.5 ± 19.6	0.0094
<b>Height (cm)</b>	180.6 ± 4.9	165.9 ± 3.1	<0.0001

## RESULTS AND DISCUSSION

The cadaveric impactor reliably reproduced clinical ACL ligament ruptures in the 25 specimens included in this analysis (i.e. 17 femoral avulsions, 6 mid-substance ruptures, and 2 tibial avulsions). The vGRF was consistent across all randomized trials. Statistical comparison of vGRF demonstrated no significant difference between males and females with minimum values, maximum values, initial

contact, or 33 msec, 66 msec, or 100 msec post-contact. This is important as significant differences in vGRF would increase forces/moments at the knee. However, consistency of the vGRF across trials demonstrates that biomechanical mechanisms other than vGRF influenced forces and moments at the knee more significantly to induce ACL injury.

With maximum values between sex, females demonstrated a significant increase of maximum knee compression ( $F_{1,24}=6.6497$ ;  $p=0.0168$ ) and a significant difference of maximum knee extension moment ( $F_{1,24}=8.1078$ ;  $p=0.0091$ ). There was a trend towards significance for females to have an increase KAM ( $F_{1,24}=4.0761$ ;  $p=0.0553$ ) compared to males. Normalization of maximum values by body weight and height demonstrated significantly increased KAM ( $F_{1,24}=9.1274$ ;  $p=0.0090$ ) and a significant trend with ITR ( $F_{1,24}=3.4408$ ;  $p=0.0765$ ) of females in comparison to males.

At initial contact compared to males, females exhibited significant more compression of the knee ( $F_{1,24}=12.8497$ ;  $p=0.0016$ ) and significantly greater extension moment ( $F_{1,24}=4.5796$ ;  $p=0.0432$ ). At 33 msec post-impact compared to males, females demonstrated significant trends in lateral translation ( $F_{1,24}=3.2485$ ;  $p=0.0846$ ) and compression ( $F_{1,24}=3.6331$ ;  $p=0.0692$ ). At 66 msec post-impact compared to males, females demonstrated significant trends in lateral translation ( $F_{1,24}=3.5165$ ;  $p=0.0735$ ) and compression ( $F_{1,24}=3.2832$ ;  $p=0.0831$ ). At 100 msec post-impact compared to males, females demonstrated significantly increased knee extension moment ( $F_{1,24}=14.1998$ ;  $p=0.0010$ ) and KAM ( $F_{1,24}=6.6006$ ;  $p=0.0172$ ) (**Table 2**).

These data indicate that with ACL failure trials, females exhibited significantly greater knee

extension moments and compression. When normalized to height and body weight, females exhibited significantly greater KAM compared to males. Relative to load timing characteristics, females exhibited significantly greater knee compression and extension moment at initial contact. At 100 msec post-impact, females demonstrated significantly greater knee extension moment and KAM. Knee extension and KAM are theorized mechanisms that load the ACL and can consequently lead to rupture.

## CONCLUSIONS

Females exhibit greater forces and moments at the knee that predispose them to ACL injury compared to males. Our unique cadaveric simulator reproduced clinical ACL ruptures in both sexes with demonstrations of increased aberrant loading of forces and moments of the knee for females. This evidence indicates that the previous theorized mechanisms of ACL injury [3] (i.e. knee extension, KAM, and ITR) are significant contributors to ACL injury.

## REFERENCES

1. Schilaty ND, et al. *Am J Sports Med*, 2017 (Accepted, in press).
2. Bates NA, et al. *Clin Bio*, 2017 (Accepted, in press).
3. Hewett TE, et al. *Am J Sports Med* **33**, 492-501, 2005.

## ACKNOWLEDGMENTS

NIH funding include: R01AR049735, R01AR055563, R01AR056259 to TEH, and K12HD065987 and L30AR070273 to NDS.

**Table 2:** Forces & Moments at the Knee by Sex at 100 msec Post-Impact.

Force / Moment	Males	Females	p-value
<b>F<sub>x</sub></b> = anterior (+) / posterior (-)	77.3 ± 139.4	-29.8 ± 152.4	0.0875
<b>F<sub>y</sub></b> = lateral (+) / medial (-)	-116.7 ± 87.2	-64.0 ± 80.7	0.1502
<b>F<sub>z</sub></b> = distraction (+) / compression (-)	-88.7 ± 78.6	-25.2 ± 83.4	0.0703
<b>M<sub>z</sub></b> = int. rotation (+) / ext. rotation (-)	54.8 ± 49.6	32.7 ± 53.5	0.3079
<b>M<sub>y</sub></b> = flexion (+) / extension (-)	125.7 ± 45.0	56.4 ± 42.4	0.0010
<b>M<sub>x</sub></b> = abduction (+) / adduction (-)	-27.7 ± 28.6	2.0 ± 26.0	0.0172

# THE COMBINATION OF TISSUE COLLAGEN QUANTITY AND QUALITY ESTIMATED FROM MR T<sub>2</sub>\* RELAXOMETRY PREDICTS TIME-SPECIFIC STRUCTURAL PROPERTIES OF HEALING ACL FOLLOWING ACL REPAIR

<sup>1</sup>Jillian Beveridge, <sup>2</sup>Jason Machan, <sup>3</sup>Edward Walsh, <sup>4</sup>Ata Kiapour, <sup>1</sup>N. Padmini Karamchedu, <sup>1</sup>Kaitlyn Chin, <sup>4</sup>Benedikt Proffen, <sup>4</sup>Jakob Sieker, <sup>4</sup>Martha Murray, <sup>1</sup>Braden Fleming

<sup>1</sup>Warren Alpert Medical School of Brown University, Providence, RI, USA

<sup>2</sup>Rhode Island Hospital Biostatistics Core, Providence, RI, USA

<sup>3</sup>Division of Biology and Medicine at Brown University, Providence, RI, USA

<sup>4</sup>Boston Children's Hospital, Boston, MA, USA

email: braden\_fleming@brown.edu, web: <http://brownbiomechanics.org>

## INTRODUCTION

Magnetic resonance (MR) T<sub>2</sub>\* is an imaging property that reflects collagen organization, with lower T<sub>2</sub>\* relaxation times corresponding to more aligned fibers [1]. The purpose of this study was to develop a T<sub>2</sub>\* relaxometry-based statistical model to predict the structural properties of the healing anterior cruciate ligament (ACL) over a 24-week (w) healing period in a preclinical model of ACL repair. Two hypotheses were tested: (1) that a multiple linear regression model based on both short and long T<sub>2</sub>\* relaxation times would outperform a competing model based on short T<sub>2</sub>\* relaxation times only; and (2) that an optimized prediction model would be capable of predicting ACL structural properties between 6 and 24 weeks post-repair.

## METHODS

Subjects: Twenty-four 15±1 month old (12 castrated males, 12 females; Sinclair Bio Resources, MO) Yucatan minipigs were randomized to receive primary suture repair with (n=12; 6 female) or without (n=12; 6 female) a scaffold to enhance primary healing [2]. All animal procedures were approved by the Institutional Animal Care and Use Committee. In vivo MR imaging: ACLs were imaged (8 per group) at either 6, 12, or 24w after ACL repair using a 512x512 acquisition matrix (voxel size=0.31x0.31x0.8mm) and a 3D gradient 4-echo sequence. Animals were euthanized immediately after imaging, and the hind limbs were harvested and kept frozen until tensile testing. ACL T<sub>2</sub>\* estimation: ACLs were segmented manually by

a single segmenter (Mimics v16, Belgium). T<sub>2</sub>\* relaxation times were calculated on a voxel-wise basis by fitting a monoexponential function to the signal decay across the four echoes. The segmented ACL voxels were then binned into four sub-volumes based on their T<sub>2</sub>\* relaxation times: Vol<sub>1</sub>=0-12.5ms; Vol<sub>2</sub>=12.6ms-25ms; Vol<sub>3</sub>=25.6-37.5ms; Vol<sub>4</sub>=37.6-50ms [3]. Vol<sub>1</sub> is the sub-volume (in mm<sup>3</sup>) of the ACL voxels containing the most organized collagen, whereas Vol<sub>4</sub> is the sub-volume containing the least organized collagen. ACL structural properties: Hind limbs were thawed, dissected leaving only the ACL, and then tensile tested. ACL maximum load, yield load, and linear stiffness were calculated from the load-displacement data determined from the tensile tests [4]. Statistical models: For each structural property, two competing multiple linear regression models were fitted to the data:

1. A 6-parameter model = Vol<sub>1</sub> at 6w, 12w, 24w and (Vol<sub>1</sub> x healing time) interaction

2. A 12-parameter model = the same six parameters as (1), with the addition of Vol<sub>4</sub> at 6w, 12w, 24w; (Vol<sub>1</sub> x Vol<sub>4</sub>) interaction; and three-way (Vol<sub>1</sub> x Vol<sub>4</sub> x healing time) interaction

The Akaike Information Criterion (AIC), which provides an objective measure of the trade-off between goodness of model fit and model complexity, was used to test the first hypothesis by comparing the AIC values of the 6- and 12-parameter models. Lower AIC values indicate superior model performance [5]. To test the second hypothesis, model predictions for each structural property were compared to the measured values in

separate optimized models. The slopes of the optimized models at 6, 12 and 24w were then evaluated to determine whether the slopes contributed significantly to the model predictions at each of the healing time points.

## RESULTS AND DISCUSSION

The AIC values for the multiple linear regression models that were based on both short and long  $T_2^*$  relaxation times were lower than the models based on the shortest relaxation times only (Table 1).

**Table 1.** Regression model AIC values (unitless).

	6-Parameter Model	12-Parameter Model
Failure Load	28.4	23.8
Yield Load	28.6	23.3
Stiffness	29.2	22.0

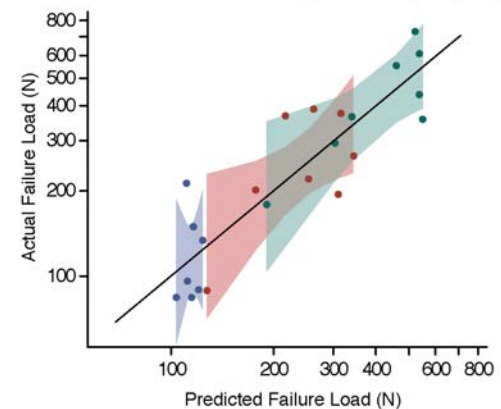
In the optimized 6-parameter ( $Vol_1$ ) only models, the slopes were significant at 12 and 24w, but not at 6w for all structural properties. Conversely, slope was significant at all time points in the 12-parameter ( $Vol_1 + Vol_4$ ) optimized models (Fig 1).

The results supported our hypotheses: the AIC values were lowest in the 12-parameter ( $Vol_1 + Vol_4$ ) models, and the ACL structural properties could be predicted throughout the 24w healing period using this model. Including  $Vol_4$  and its interaction terms had the effect of spreading out the values of the predicted ACL structural properties at 6w, making the slopes significant throughout the 24w healing period. This finding suggests that in addition to the quantity of organized collagen, the amount of disorganized tissue encompassed by the  $Vol_4$  sub-volume is especially important at early time points. We believe that  $Vol_4$  could reflect compositional elements related to the sub-acute healing process that may then modulate collagen organization at later phases of healing following primary ACL repair.

## CONCLUSIONS

Our time-specific,  $T_2^*$ -based prediction model may allow us to estimate the structural properties of ACL repairs in vivo longitudinally.

a. Failure load at 6, 12 and 24w predicted by  $Vol_1$  only



b. Failure load at 6, 12 and 24w predicted by  $Vol_1$  and  $Vol_4$

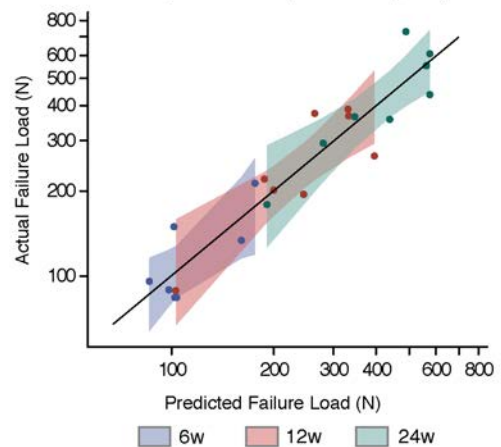


**Figure 1.** Actual versus predicted failure load for (a) the 6-parameter ( $Vol_1$ ) model and (b) 12-parameter ( $Vol_1+Vol_4$ ) model. Shaded regions encompass the 95% confidence intervals of the estimated slopes at each time point. Each circle corresponds to one animal.

## REFERENCES

1. Helms CA, et al. *Musculoskeletal MRI*, Saunders, Philadelphia, 2008.
2. Murray MM, et al. *AJSM* **41**, 1762-1770, 2013.
3. Biercevicz AM, et al. *JOR* **32**, 492-499, 2013.
4. Fleming BC, et al. *AJSM* **37**, 1554-1563.
5. Ramsey FL, et al. *The statistical sleuth: a course in methods of data analysis*, Druxbury, 2002.

## ACKNOWLEDGMENTS

National Institutes of Health (NIAMS 3R01-AR065462-03, NIAMS 1K99AR069004, & NIGMS 5P20-GM104937), and the Lucy Lippitt Endowment.

# THE EFFECT OF RETURN-TO-SPORT TRAINING ON GAIT MECHANICS AND KNEE LOADING IN MEN AND WOMEN AFTER ANTERIOR CRUCIATE LIGAMENT RECONSTRUCTION

Jacob J. Capin, Ashutosh Khandha, P. Michael Eckrich, Ryan Zarzycki, Amelia J. H. Arundale, Kurt Manal, Thomas S. Buchanan, Lynn Snyder-Mackler  
University of Delaware, Newark, DE, USA  
email: capin@udel.edu

## INTRODUCTION

After anterior cruciate ligament (ACL) reconstruction (ACLR), individuals often walk using a “stiff-knee” gait in their involved (ACLR) limb. While gait symmetry (involved vs. uninvolved limb) likely improves over time, gait asymmetries may persist 2 years after ACLR [1]. Moreover, gait asymmetries may be related to poor functional performance [2] and the development of early knee osteoarthritis (OA) after ACLR [3]. Therefore, it is critical to investigate gait mechanics over time after ACLR and the influence of rehabilitation on the presence of gait asymmetries. The purpose of this study was to analyze gait mechanics, including medial compartment tibiofemoral loading, and the presence of gait asymmetries in men and women after ACLR, before and after return-to-sport training. We hypothesized that this training would improve gait symmetry in men and women.

## METHODS

This is a preliminary analysis of an ongoing study that will have 80 participants (40 M, 40 F). Forty-four athletes (age:  $21.1 \pm 7.7$  years, range: 13-54 years; sex: 26 men, 18 women) in jumping, cutting, and pivoting sports participated after primary ACLR when they achieved impairment resolution including quadriceps strength index of  $\geq 80\%$  (post-operative time:  $22.8 \pm 7.4$  weeks, range: 13-40 weeks). All participants underwent motion analysis testing during overground gait with bilateral surface electromyography (EMG). We conducted testing at two post-operative time points: before (pre-training) and after (post-training) a return-to-sport (RTS) training program including strength, plyometric, agility, and secondary prevention exercises.

We used a previously-validated, EMG-informed musculoskeletal model [4,5] to estimate medial tibiofemoral joint contact force. This patient-specific model uses a Hill-type muscle fiber model and establishes optimal muscle parameters (within  $\pm$

20% of normative values) via simulated annealing, in which the squared difference between the internal and external sagittal plane knee moment curves is minimized. Joint contact forces are determined using a frontal plane moment algorithm that balances external knee adduction moment with internal muscle forces. We averaged three predicted walking trials per limb, per subject for analysis. Self-selected gait speed was controlled within subjects to  $\pm 5\%$  across trials and time points. We calculated joint kinematics and kinetics via inverse dynamics using commercial software (Visual3D; C-Motion, Germantown, MD). Knee flexion and adduction moments were normalized by mass\*height ( $\text{kg}\cdot\text{m}$ ) while joint contact forces were normalized by body weight (BW).

We analyzed peak tibiofemoral medial compartment contact force (pMCF), peak knee flexion angle (pKFA) and moment (pKFM), and peak knee adduction moment (pKAM) using 2x2x2 ANOVAs ( $\alpha=0.05$ ): sex (male vs. female), limb (involved vs. uninvolved), and the repeated measure of time (pre-training vs. post-training). We also calculated the proportion of men and women who walked with meaningful gait asymmetries at each time point: we trichotomized participants as overloaders, symmetric, or underloaders by comparing inter-limb differences (involved – uninvolved) to minimal detectable change (MDC) values [6].

## RESULTS AND DISCUSSION

Women walked using larger pMCF ( $p=0.017$ ) compared to men (Table 1). There were main effects of limb for pMCF ( $p=0.003$ ), pKFA ( $p=0.001$ ), and pKFM ( $p<0.001$ ) with smaller values for each variable in the involved versus uninvolved limb. Interestingly, when comparing group mean differences to MDC values [6], both men and women walked with symmetrical joint loading at pre-training. However, at post-training, women as a group underloaded their involved versus uninvolved

medial tibiofemoral compartment while men continued to load symmetrically. This change in loading was due to 9 (of 18) women who had a meaningfully smaller inter-limb loading difference at post-training compared to pre-training. At pre-training, an equal number of women overloaded (N=5) versus underloaded (N=5) their involved knee, while at post-training, all but one women loaded symmetrically or underloaded. In contrast, the proportion of men in each loading classification remained stable over time (Table 2). There were no statistically significant main effects of time, 2-way interactions, or 3-way interactions for any of our variables (kinematic, kinetic, or joint loading).

Our preliminary findings refute our hypothesis and suggest that an RTS training program does not restore gait symmetry. Unexpectedly, while similar proportions of men and women walked symmetrically at pre- and post-training, there was a shift toward underloading among women at post-training. This shift did not occur in men, who remained relatively stable over time: 16/26 (61.5%) men remained in the same loading category, while only 8/18 (44.4%) women were consistent across time. Thus, women and men may respond differently to RTS training.

These differing responses among women and men could influence their subsequent risk for OA. While some studies suggest overloading may place

individuals at risk for OA, other findings indicate underloading 6 months after ACLR may be a risk factor for developing radiographic OA 5 years postoperatively [3]. It is possible that women who initially overload their involved knee may benefit from this type of training while those who underload may benefit from alternative interventions. Further research is warranted.

## CONCLUSIONS

Our preliminary findings suggest RTS training after ACLR does not restore gait symmetry, and men and women respond differently. Surprisingly, women underloaded their involved limb after RTS training, but not before. Further research is needed to fully investigate gait mechanics in men and women after ACLR, and the implications for OA development.

## REFERENCES

1. Capin JJ, et al. *Clin Orthop Relat Res*, 2017, *E-Pub*.
2. Di Stasi S, et al. *Am J Sports Med* **41**, 1310-1318, 2013.
3. Wellsandt E, et al. *Am J Sports Med* **44**, 143-151, 2016.
4. Buchanan TS, et al., *J Appl Biomech* **20**, 367-395, 2004.
5. Manal K, et al. *J Biomed Eng* **135**, 021014, 2013.
6. Gardinier ES, et al. *Gait Posture* **38**, 1051-53, 2013.

## ACKNOWLEDGEMENTS

Funding provided by National Institutes of Health: R01-AR048212, R37 HD037985, R01-HD087459, P30-GM103333, U54-GM104941, and T32-HD00749. Thank you to Georgia Gagianas and Celeste Dix for their data processing.

**Table 1.** There were main effects of sex for pMCF and limb for pMCF, pKFA, and pKFM; values are means (SD) for the involved (INV) and uninvolved (UN) limbs of men and women at pre- and post-training.

Variable	Pre-training				Post-training				p-value			
	Women		Men		Women		Men		Model	Sex	Limb	Time
	INV	UN	INV	UN	INV	UN	INV	UN				
pMCF (BW)	2.93 (0.53)	2.99 (0.59)	2.67 (0.53)	2.87 (0.43)	2.76 (0.39)	3.12 (0.59)	2.63 (0.39)	2.92 (0.42)	0.016	0.017	0.003	0.94
pKFA (°)	21.5 (5.3)	23.0 (4.6)	20.4 (4.8)	23.3 (3.9)	21.0 (5.3)	22.7 (5.1)	19.2 (4.7)	23.1 (4.9)	0.024	0.399	0.001	0.462
pKFM (Nm/Kg*m)	0.42 (0.15)	0.51 (0.14)	0.40 (0.14)	0.51 (0.12)	0.44 (0.16)	0.53 (0.14)	0.41 (0.11)	0.51 (0.13)	0.001	0.360	<0.001	0.594
pKAM (Nm/Kg*m)	-0.27 (0.08)	-0.27 (0.11)	-0.26 (0.07)	-0.27 (0.09)	-0.27 (0.10)	-0.28 (0.11)	-0.25 (0.07)	-0.28 (0.08)	0.98	0.505	0.478	0.91

**Table 2.** There were a similar proportion of men and women who walked with symmetrical pMCF loading at pre- and post-training; however, more women overloaded at pre-training and underloaded post-training.

	Pre-Training			Post-Training		
	Underloading	Symmetric	Overloading	Underloading	Symmetric	Overloading
Women	5	8	5	8	9	1
Men	10	13	3	12	12	2

# KNEE FORCE VECTOR AND TIBIA PLATEAU ORIENTATION DURING THE STANCE PHASE OF GAIT: A COMPARISON OF ACL-RECONSTRUCTED AND CONTRALATERAL KNEES

<sup>1</sup> Milad Zarei, <sup>1,2</sup> Elmar Herbst, <sup>1</sup> James Irrgang, <sup>1,3</sup> Scott Tashman, <sup>1</sup> Freddie Fu, <sup>1</sup> William Anderst

<sup>1</sup> Biodynamics Laboratory, Department of Orthopaedic Surgery, University of Pittsburgh, PA, USA

<sup>2</sup> Department of Orthopaedic Sports Medicine, Technical University Munich, Munich, Germany

<sup>3</sup> University of Texas Health Science Center, Houston, TX

email: milad.z@pitt.edu, web: <http://bdl.pitt.edu/>

## INTRODUCTION

The posterior tibial slope has been discussed as a potential risk factor for anterior cruciate ligament (ACL) injuries [1] due to the anteriorly directed force vector on the knee with axial loading [2]. Video analyses investigating the motion pattern and body position at the time where an ACL injury occurs found that typically subjects land on their heels or the flat foot with the center of gravity being behind the knee joint [3]. In such a position, the effective posterior tibial slope relative to the ground is increased as compared to a static upright standing, where commonly the posterior tibial plateau is measured [3]. Thus, the relationship between the tibial plateau orientation and knee force vector may affect ACL injury. Although computational models to estimate compressive and shear forces at the knee are common (such as inverse dynamics models), no study has investigated the relationship between the knee force vector and subject-specific tibial plateau orientation during dynamic loading. The purpose of this study was to determine the angle between the proximal tibia force vector and the tibial plateau during the early stance phase of walking in ACL-reconstructed and contralateral intact knees. We tested the hypothesis that there are knee (recon vs. intact), compartment (medial vs. lateral) and time related differences in the angle between the knee force vector and the tibial plateau during walking.

## METHODS

Eighteen participants (12 M/6 F, 23.8±9.7 y.o.) who were a part of a larger IRB-approved study of knee kinematics after ACL-reconstruction were included in the present analysis. Six months after

ACL-reconstruction, subjects walked on an instrumented treadmill (Bertec Corporation, Columbus, OH, 1000 Hz) at 1.3 m/s while biplane radiographs of the knee were collected at 100 images per second and overall lower body kinematics were determined using conventional motion analysis (Vicon MX, 100 Hz). Precise kinematics of the tibia and femur were determined using a validated volumetric model-based tracking of the biplane radiographs [4]. Subject-specific inverse dynamics computational models were developed to calculate the forces applied to the tibia from heel-strike through the first twenty percent of the single support phase of the gait cycle. Subject-specific 3D models of the femur and tibia were created from high-resolution CT scans of each knee. Vectors determining the tibial plateau orientation on the medial and lateral compartments of each 3D tibia model were created. The angle between the proximal tibia force (determined through inverse dynamics) and the tibia plateau vector (determined thorough biplane radiographic tracking) was determined.

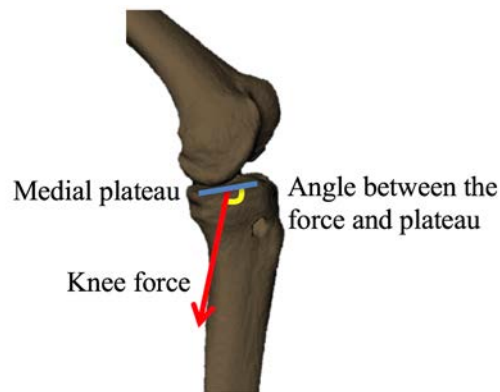


**Figure 1:** The angle between the knee force vector and the tibial plateau.

Statistical analysis was performed every 5% of the gait cycle from foot strike (0%) to midstance (20%). Repeated measures analysis of variance with a post-hoc Sidak test was used to identify differences between legs, compartments, and time instants.

## RESULTS AND DISCUSSION

The results indicate that the angle between the knee force and the tibial plateaus was large during the initial loading phase (0% to 5% of gait cycle) and gradually reduced to approximately 90° at midstance (Figure 2). The angle between the knee force vector and tibial plateau was slightly larger in ACL-R knees, however, this difference was not significant ( $p = 0.179$ ). Likewise, there were no differences between medial and lateral compartments ( $p = 0.21$ ). The angle between the knee force vector and tibial plateaus changed significantly from early stance (0% to 10%) to midstance (15% and 20%) (all  $p < .001$ ). The reconstructed knee tended to be more extended over the first 20% of the gait cycle (Figure 2C).

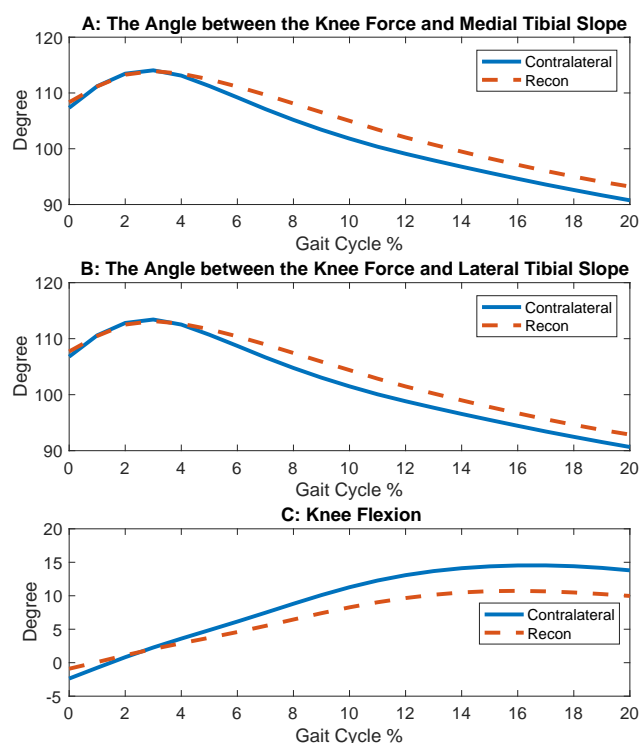


**Figure 2:** A & B: The average angle between the knee force and the medial (A) and lateral (B) tibial plateaus during gait. C: Group average knee flexion.

These results suggest that the proximal tibia force vector has a slightly larger (although non-significant) shear component in ACL-R knees during the initial loading phase of gait. It is possible that walking with more knee extension 6 months after surgery is a coping mechanism to limit the tibial shear force in the ACL-R knee.

## CONCLUSIONS

The most important finding of this study is that the angle of the force vector relative to the tibial plateau surface changes during the initial loading phase of the gait cycle, with a greater portion of the tibial force directed parallel to the tibial plateau during the early loading phase. This result corresponds well to previous research into the common injury mechanism of ACL tears occurring with the knee near full extension [3]. Contrary to our hypotheses, there were no differences between the ACL reconstructed and contralateral healthy knee or between the medial and lateral joint compartments. This novel study, combining surface-based kinematics and kinematics obtained from biplane radiography, is limited by the use of a basic inverse-dynamics model to estimate forces at the knee. More complex musculoskeletal modeling may produce different results. Future analysis will include more complex musculoskeletal modeling and the use of the biplane radiography data (rather than skin-based markers) to estimate joint centers during gait.

## REFERENCES

1. Hashemi J et al., *Am J Sports Med* **62**, 54:62, 2010.
2. Amis AA, *Knee Surg Sports Traumatol Arthrosc*, 197:205, 2013.
3. Boden et al., *J Bone Joint Surg* **18**(9), 520:527, 2010.
4. Anderst et al., *Med Eng Phys* **31**(1), 10:16, 2009.

## ACKNOWLEDGMENTS

This study was funded by NIH/NIAMS, grant number R01 AR 056630.

# CHARACTERIZATION OF FORCE AND IMPULSE FOR TOUCHSCREEN GESTURES

<sup>1</sup>Deanna S. Asakawa, <sup>2</sup>George H. Crocker, <sup>1</sup>Adam Schmaltz, and <sup>1</sup>Devin L. Jindrich

<sup>1</sup>California State University, San Marcos, San Marcos, CA, USA  
<sup>2</sup>California State University, Los Angeles, Los Angeles, CA, USA  
email: [dasakawa@csusm.edu](mailto:dasakawa@csusm.edu)

## INTRODUCTION

Mobile computing and the use of touchscreens has become common for business and personal use [1]. Touchscreen users actuate mobile computing technology by using their fingers. However, the amount of force applied by the fingers during touchscreen gestures is unknown. Exposure to fingertip forces during repetitive touchscreen interaction could potentially increase risk for musculoskeletal injury or disability [2,3]. Also, characterization of fingertip forces and impulses could be used to optimize software design and touchscreen interfaces.

Touchscreen interaction often involves tapping as well as other gestures such as swiping and pinching. The overall goal of this study was to determine the forces and impulses generated by the index finger or index finger and thumb during seven common touchscreen gestures. We hypothesized that compared to tapping, sliding and two-fingered gestures such as pinch and stretch would have smaller resultant forces per finger but larger force impulses. Specifically, based on finger kinematics during touchscreen use [4], we expected tapping to demonstrate the shortest completion time but the highest force.

## METHODS

Thirteen unimpaired participants (6 male, 7 female; age 21-33 years) used a 10.1-inch tablet computer (Galaxy Tab 2, Samsung, Seoul, South Korea) to complete repetitions of touchscreen gestures. All participants provided consent for protocols approved by California State University, San Marcos. Gestures were completed with the dominant hand (11 right-, 2 left-handed). Participants were seated with the touchscreen tablet positioned on a table in front of them. The

participant's sternum was aligned to the center of the tablet computer. The touchscreen computer dimensions were 25.7 x 17.5 x 0.97 cm. A custom software application displayed 6x6 cm square buttons to complete each gesture. The gestures included index finger tap, slide right, slide left, slide up, slide down and index finger and thumb used for pinch (zoom out) and stretch (zoom in). Each of the 7 gestures were presented in randomized order with subjects completing 11 consecutive repetitions. We instructed participants to complete the gestures at a moderate, self-selected pace. The tablet computer was fitted into a rigid plastic case and securely mounted on 6 degree-of-freedom load cell (JR3 Inc., Woodland, CA). calibrated for this study. Calibration and validation of the touchscreen indicated that the measured forces were accurate to within 4% in the range associated with gestures. The 3-dimensional forces and torques applied to the touchscreen were measured at 1000 Hz and were recorded using Labview software (National Instruments, Austin, TX). A manual trigger was used to mark the beginning and end of each gesture during data collection. We calculated forces from the transducer output using the calibration matrix in MATLAB (MathWorks, Natick, MA).

Data were analyzed using Microsoft Excel (Microsoft, Redmond, WA). We computed mean resultant force, impulse for resultant force and coefficient of variation (CoV) for resultant force for each gesture. For pinch and stretch, we calculated force per finger as resultant force divided by two. Gesture completion time was calculated as the duration that a 9-ms moving average of the resultant force was greater than a threshold of 0.2 N. Impulse was computed for resultant forces using the trapezoid rule approximation for the area under the force-time curve. Gestures were compared using repeated measures analysis of variance and Bonferonni's post-hoc comparison.

## RESULTS AND DISCUSSION

Mean( $\pm$ SD) resultant force was greatest for the stretch gesture at 2.05(1.13) N. However, stretch and pinch did not have more average resultant force per finger than single-finger gestures ( $p > 0.05$ ). Contrary to our hypothesis, tap had the lowest mean force of all 7 gestures at 0.50(0.09) N. Resultant force for tap was significantly less ( $p < 0.04$ ) than resultant force for all gestures except slide right. Consistent with our hypothesis, tap had significantly faster completion time than all other gestures studied ( $p < 0.004$ ). Additionally, tap had the lowest CoV for mean resultant force at 18%. CoV for other gestures ranged from slide up at 40% to stretch at 55%.

Each touchscreen gesture had a characteristic impulse profile (Fig. 1). Impulse for the tap gesture 0.07(0.05) Ns was significantly less ( $p < 0.03$ ) than slide up, slide down and pinch (Fig. 2). Stretch had the largest impulse at 2.25(2.11) Ns.

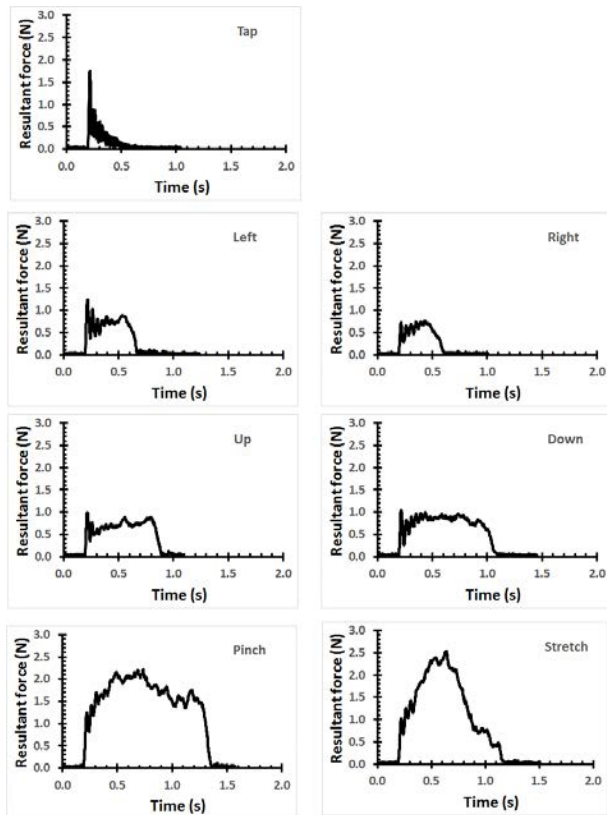


**Figure 1.** Representative force-time profiles for one participant for tap, slide left, right, up, and down with the index finger and pinch and stretch with the index finger and thumb on a touchscreen.

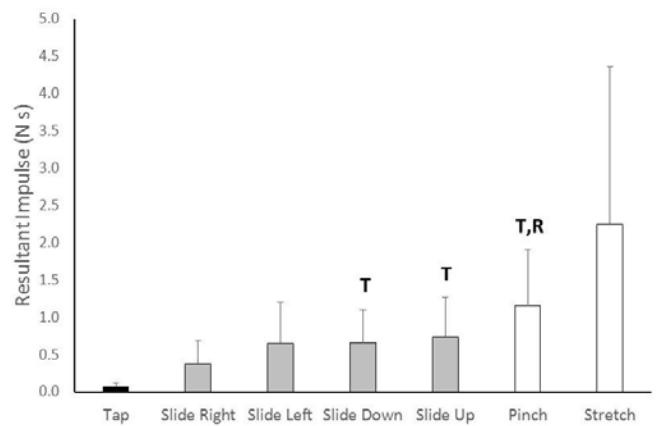


**Figure 2:** Mean resultant impulse for index finger tapping (black bar), index-finger sliding (gray bars), and for two-finger gestures (white bars). Values are mean with error bars for SD for 13 subjects. T and R denote significant difference from tap and slide right, respectively.

The touchscreen gestures studied differed in mean resultant force and impulse measurements. Both the magnitude and duration of force application could potentially influence musculoskeletal exposure during touchscreen use. These findings could be used to optimize design of touchscreen software to minimize the forces and duration of force application. Specifically, these results suggest that to reduce force application to the fingers, index finger tapping could be selected in touchscreen software design over two-finger gestures such as pinch. These data provide a first step toward assessing the potential differences in force and impulse associated with repetitive interaction of the fingers with a touchscreen for tapping, sliding, pinch and stretch gestures.

## REFERENCES

1. Smith, A. *Pew Research Center Report*, 2015.
2. Gerr, F, et al. *Human Factors* **56**, 112-30, 2014.
3. Dennerlein, JT. *Work* **52**, 269-77, 2015.
4. Asakawa, DS, et al. *Appl Ergonomics* **38**, 1861-1868, 20.

## ACKNOWLEDGMENTS

This work was funded by NSF (0964220). We thank Jack Dennerlein and Jong Hwa Lee.

# GENDER DIFFERENCES IN UPPER LIMB JOINTS CONTRIBUTIONS DURING A LIFTING TASK

<sup>1</sup> Romain Martinez, <sup>1</sup> Jason Bouffard, <sup>1</sup> Mickael Begon

<sup>1</sup> Université de Montréal, Département de kinésiologie, Québec, Canada  
email: martinez.staps@gmail.com

## INTRODUCTION

The occurrence of upper limb injuries has been associated with work factors such as overhead work, heavy lifting, repetitive movements and bad postures, but also with individual risk factors including gender. Indeed, even if women are underrepresented in manual handling work, the prevalence of their upper extremity injuries is greater than in men [1].

Differences in motor behavior between women and men have been identified and may contribute to the increased risk of upper limb musculoskeletal disorders among women [2]. Recent studies identified sex differences in trunk and lower limb coordination during manual handling tasks [3]. However, the sex-specific kinematic strategy of the upper limb during a lifting task remains unknown.

This study investigated sex differences in upper limb joints' contribution during a lifting task. Exploring these differences would help us understand the reasons behind the higher prevalence of upper extremity injuries in women.

## METHODS

In total, 25 women (21 ± 2 years; 1.68 ± 0.7 m; 61 ± 8 kg) and 25 men (24 ± 3 years; 1.79 ± 0.8 m; 75 ± 12 kg) took part in this study. The experimental task consisted of moving one box between three adjustable shelves located at hip, shoulder and eye levels. Different box masses were used for men (12 kg) and women (6 kg) to adjust for sex-related differences in maximal force.

Kinematics of the upper arm were recorded with VICON Motion Analysis cameras and the markers set described in [4]. A 25 degree-of-freedom (DoF) kinematic model was constructed using a static trial

(pelvis & trunk [PE/TR; 6 DoF each], sternoclavicular & acromio-clavicular [SC/AC; 3 DoF each], glenohumeral [GH; 3 DoF], elbow & wrist [EL/WR; 2 DoF each]). Centres of rotation was determined using the SCoRE/SARA algorithms (for PE, TR, EL and WR joints) and bony landmarks (for SC, AC and GH joints). Inverse kinematics was performed during lifting trials using an extended Kalman filter algorithm [4].

Then, the contribution of each joint ( $H|_i$ ) to the box elevation was computed by successively resetting joint angles to their reference orientation ( $q_i^{REF}$ ) [5]. Joint contribution refers to the amount of box height achieved by each group of DoF (Algorithm 1).

**Algorithm 1.** Calculation of the joint contributions.  
At time t:

$$\begin{aligned} \text{calculate height}(\mathbf{q}) &= H|_{WR/EL+GH+SC/AC+TR/PE} \quad (1) \\ q_{WR/EL} &= q_{WR/EL}^{REF} \end{aligned}$$

$$\begin{aligned} \text{calculate height}(\mathbf{q}) &= H|_{GH+SC/AC+TR/PE} \quad (2) \\ H|_{WR/EL} &= (1) - (2) \end{aligned}$$

$$\begin{aligned} q_{GH} &= q_{GH}^{REF} \\ \text{calculate height}(\mathbf{q}) &= H|_{SC/AC+TR/PE} \quad (3) \\ H|_{GH} &= (2) - (3) \end{aligned}$$

$$\begin{aligned} q_{SC/AC} &= q_{SC/AC}^{REF} \\ \text{calculate height}(\mathbf{q}) &= H|_{TR/PE} \quad (4) \\ H|_{SC/AC} &= (3) - (4) \end{aligned}$$

$$\begin{aligned} q_{TR/PE} &= q_{TR/PE}^{REF} \\ \text{calculate height}(\mathbf{q}) &= 0 \quad (5) \\ H|_{TR/PE} &= (4) - (5) \end{aligned}$$

Contributions of men's and women's joints were compared using statistical parametric mapping (ANOVA 2-way: sex × height [repeated measures]) for each group of joints.

## RESULTS AND DISCUSSION

A significant main effect (Fig. 1, panel A) of sex on the contribution of the GH joint was found (4-7 and 79-90% of the trial), highlighting a contribution 14% higher for women than for men. Moreover, a significant main effect of sex on the SC/AC joints (11-27% of the trial) and TR/PE (8-32 and 55-100% of the trial) shows those groups of joints contributed 8% and 5% more to box height in men than women.

An interaction between the two factors was found on the SC/AC joints (0-34 and 51-100%) and TR/PE (0-100%). The post-hoc tests (Fig. 1, panel B) revealed that the most significant difference related to the SC/AC joints, with men contributing 18% more than women at the shoulders-eyes condition, followed by the TR/PE at the same height.

Our results support the perspective of a sex-specific kinematic strategy of the upper limb during a lifting task. In particular, we showed that men tend to use a technique which share the motion, and eventually the load, between different groups of joints (GH, SC/AC,

TR/PE) when lifting the box, while women mobilize mainly the glenohumeral joint. We can therefore hypothesize that the force applied to the shoulder is higher in women, thus increasing the risk of injury [6]. The implications of such results argue for a careful consideration of sex during ergonomic interventions, but also during research studies focusing on the upper limb.

## REFERENCES

1. Treaster, D., and Burr, D. *Ergonomics*, **47**, 495–526, 2004.
2. Côté, J. N., et al. *Ergonomics*, **55**, 173–182, 2012.
3. Plamondon, A., et al. *Appl. Ergon.*, **45**, 1558-1569, 2014.
4. Jackson, M., et al., *J. Biomech.*, **45**, 2180–2183, 2012.
5. Robert-Lachaine, X. et al. *Comput. Methods Biomech. Biomed. Engin.*, **18**, 249-258, 2015.
6. Van Rijn, R. M. et al. *Scand. J. Work Environ. Health*, **36**, 189-201, 2010.

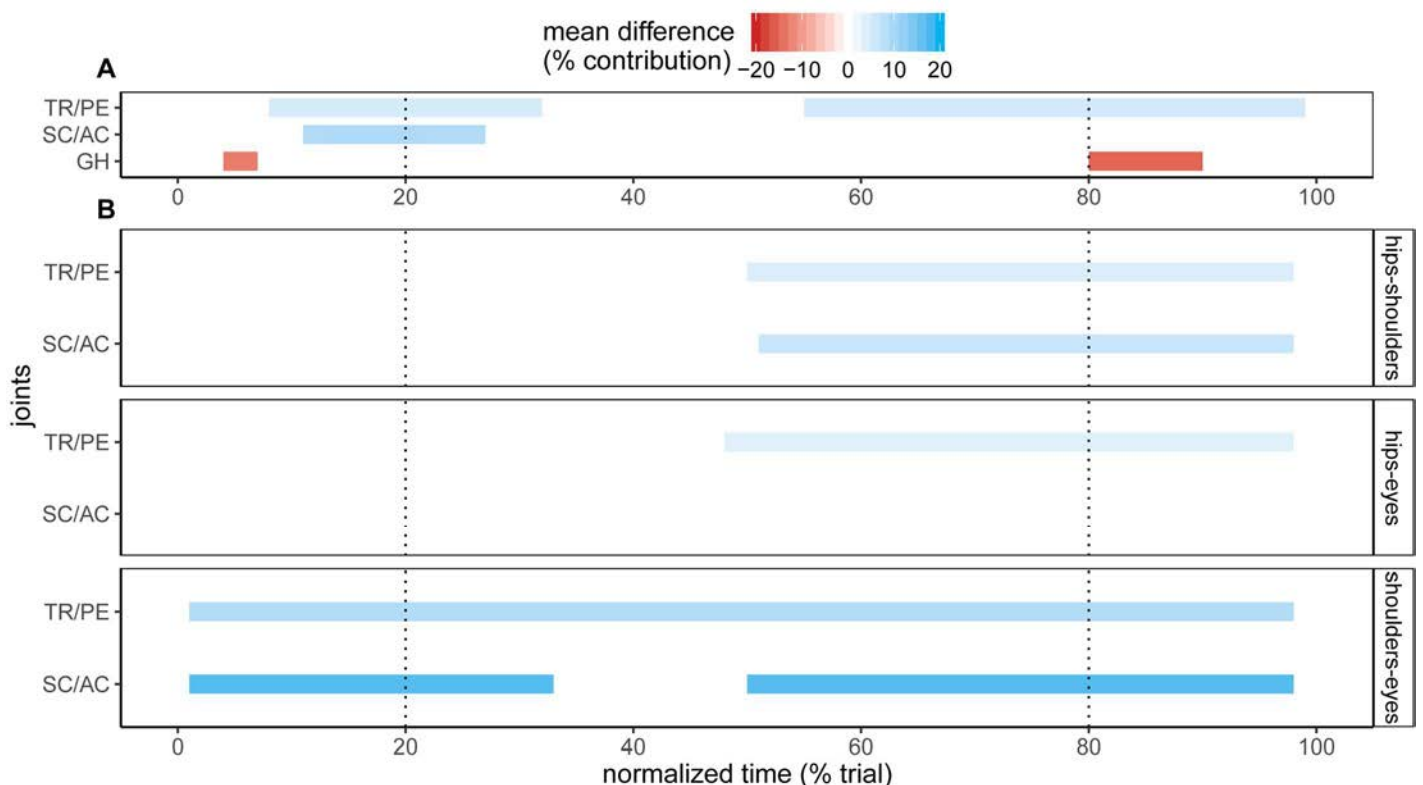


**Figure 1:** Significant group differences found by the statistical parametric mapping on the sex main effect (A) and post-hoc analysis (B) for the three box displacements (hips-shoulders, hips-eyes and shoulders-eyes). Each segment represents a supra-threshold clusters with a color gradient associated with the amplitude of the sex-related difference (blue when men's contribution is higher, red when women's is higher).

# HAMMER SYMMETRY OF INERTIA INFLUENCES COMPLEXITY OF SWING MOTION

<sup>1</sup> Sumaya Ferdous, <sup>2</sup> Nilanthy Balendra, <sup>1</sup> Joseph E. Langenderfer

<sup>1</sup> School of Engineering and Technology, and <sup>2</sup> Doctoral Program in Physical Therapy,  
Central Michigan University, Mt. Pleasant, Michigan, USA  
email: j.langend@cmich.edu

## INTRODUCTION

An object's inertial properties influence the forces and torques required to move the object. The rotational inertia values can be visualized in tensor form as the axes describing an inertia ellipsoid. From the inertia ellipsoid, scalar properties can be calculated which represent the volume (overall object inertia) and symmetry of inertia (Fig. 1). Objects with larger overall inertia require greater torque and muscle forces, while the symmetry of the inertia affects the diversity and patterning of the torque and forces. Previous work in ecological psychology has demonstrated that the relationship between the symmetry and volume of an object's inertia ellipsoid influences effectiveness as a hammering tool [1]. When the magnitude of overall inertia was increased relative to the symmetry of inertia, hammers were more effective. However, these studies did not investigate biomechanics or motor control for functional tasks and did not describe or interpret the entire movement, but only measured outcomes of the task (number of objects hammered in a specific time period) and vertical hammer motion in accomplishing the task.

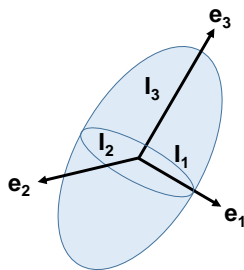


**Figure 1:** Inertia ellipsoid, volume  $V = (4\pi/3)(I_1 I_2 I_3)$  and symmetry  $S = 2I_3/(I_1+I_2)$ .

The purpose of this study was to use principal components analysis (PCA) to characterize upper-extremity kinematics while subjects performed functional hammering with hammers of varying

properties. The goal was to examine the role of hammer symmetry of inertia. The hypothesis was that hammers with greater symmetry of inertia would result in an overall more complex motion as represented by the number of principal components required to explain variance in the motion.

## METHODS

Data were collected with VICON as described previously [2]. Male subjects (N=19) made single strikes of nails using hammers (Fig. 2). Three trials were performed with each hammer. Overall inertia for pairs of hammers (1-2 and 3-4, respectively) were approximately equal. The symmetry of hammers 2 and 4 were 3 and 7 times the symmetry of 1 and 3 (equal symmetry), respectively (Fig 3).



**Figure 2:** Hammers of varying inertial properties.

Coordinates of 16 markers on upper-extremity and hammers were linear-length-normalized from swing initiation to strike/follow-through (trials equal length, 101 points from 0-100% of motion). Data were normalized by the mean marker and norm of the mean in each trial to remove inter-subject anthropometric variation as described in [3]. For each hammer, PCA was performed on the covariance matrix of concatenated data of all trials (19 subjects x 3 trials).

The contribution of each principal component (PC) to the movement of a subject in each trial was

calculated from the normalized variance of the time-series marker data projected onto the principal components. The cumulative normalized variance represents the percentage of variance explained by a given number of PCs for a trial. Differences in cumulative normalized variance for each PC were detected with ANOVA. Additionally, reconstruction of the motion for each PC was performed by projecting marker data onto the principal component and then performing Inverse-Kinematics analysis with OpenSim to calculate joint angles. This analysis allowed for potential qualitative interpretation and visual representation and understanding of how components of the motion variance are partitioned to individual PCs.

## RESULTS AND DISCUSSION

At PC1 and PC2 there were no differences in percent variance explained. For PC3 through PC6 significant differences were found in the percentage of explained variance between the hammers ( $p < 0.001$ ), although significance, differences and effect sizes varied between the different hammers across principal components (Fig. 3). For a given variance level, hammers with greater symmetry of inertia required more principal components to explain the motion.

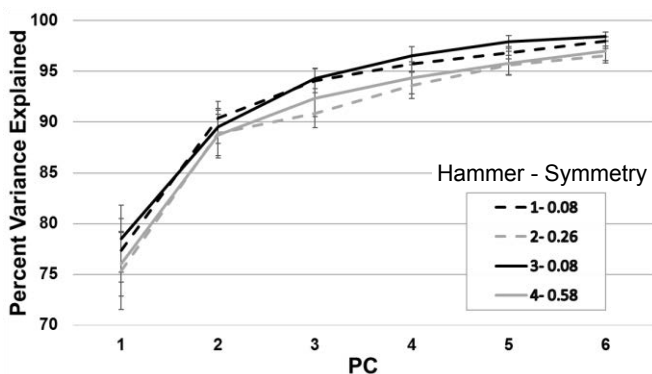


**Figure 3:** Cumulative PC for hammer motion data.

Most of the hammering motion variance is associated with shoulder and elbow flexion and is represented by PC1 (Fig. 4). Other PCs account for less variance indicating subtle differences in secondary degrees of freedom that contributed small but potentially important variations to the motions. For example, PC2 generally corresponded to the reaching involving thorax flexion and elbow extension

required for striking the nail, while PC4 relates to the wrist flexion-extension required for accurate hammer control within the hand.

These results indicate that hammers with greater symmetry of inertia result in a more complex motion as evidenced by the greater number of principal components required to explain variance in motion. These findings confirm results of previous studies [1] which found objects with greater symmetry of inertia were less effective hammers and adds to the understanding of how the symmetry relates to the kinematics of the motion during the entirety of the hammering trial.

These findings have implications for understanding the role of inertial properties of hand held objects in contributing to motion variability as related to difficulty of the task or motion and how control of upper-extremity kinematics, as well as resulting joint and tissue loadings, may be affected.

The model of adding a segment to the upper-extremity with alterable inertial properties presents an intriguing paradigm for understanding not only the role of inertial properties of hand-held objects, but also how inter-subject variability and other situations involving altered segment properties, e.g. obesity, reconstructive surgery/salvage, limb replacement, or prosthesis/exoskeleton, can affect biomechanics and motor control.



**Figure 4:** Interpretation of Principal Components with OpenSim Inverse Kinematics.

## REFERENCES

1. Fitzpatrick, P et al. *Zeitschrift Psycholog* **220**, 23–28, 2012.
2. Balendra, N. and Langenderfer, JE. *App Ergon* **60**, 231-239, 2017.
3. Federolf, P. et al. *J Biomech* **46**, 2626-2633, 2013.

# ARE PSYCHOPHYSICALLY DETERMINED SAFE LIFTING LOADS ASSOCIATED WITH AN UNDERLYING LIMITING JOINT STRENGTH?

<sup>1,2</sup> Jacob J Banks and <sup>2</sup> Graham E Caldwell

<sup>1</sup> Liberty Mutual Research Institute for Safety, Hopkinton, MA, USA

<sup>2</sup> Department of Kinesiology, University of Massachusetts, Amherst, MA, USA  
email: jacob.banks@libertymutual.com

## INTRODUCTION

To combat the high incidence of workplace injuries caused by lifting overexertion [1], ergonomists often rely on tables of maximal acceptable weight limits (MAWL) [2]. Such tables reflect MAWLs for various lifting situations, deemed safe and reasonable by experienced manual materials handling (MMH) workers through an arduous psychophysical research protocol [3]. Application of MAWL tables has demonstrated reductions in workplace injury [4], but their subjective basis provides an intriguing dichotomy between an individual's perception of safe lifting loads and the underlying biomechanical capabilities upon which the perception is based.

Despite advances in motion detection and modeling, there have been a limited number of studies aimed at describing MAWLs in relation to full-body joint demands. Such analysis could identify limiting joints, improve intervention strategies, allow for more personalized MAWLs obtained with less difficulty, and improve our understanding of musculoskeletal safety perception [5, 6].

Therefore, to better understand the psychophysical selection process for safe working loads, a full-body rigid-link joint kinetics model was applied to three different sagittal lifting tasks. Each lifting task was performed at an individually determined MAWL. Our objectives were to examine 1) whether psychophysically determined MAWLs could be characterized by joint kinetics, 2) if individual task MAWLs were linked to the strength of a specific limiting joint, and 3) whether MAWLs across tasks were related by a universal limiting joint strength threshold irrespective of the limiting joint location.

## METHODS

18 healthy, young, fit male participants ( $25 \pm 5$  years;  $178 \pm 6$  cm;  $80 \pm 10$  kg;  $BMI \leq 30$ ) with MMH experience participated in a two-visit protocol designed to minimize the effects of fatigue. During visit 1, following informed consent, an abridged psychophysical protocol consisting of two 20-minute trial-and-error selection periods was used to find individual MAWL loads for three randomly presented lifting tasks: 1) Floor-to-Knuckle (F-K), 2) Knuckle-to-Elbow (K-E), and 3) Knuckle-to-Eye (K-I). For each lift, a custom-built robotic lifting shelf was designed to repeatedly return a 34 x 56 x 16 cm instrumented (AMTI, Watertown, MA) box to the initial position (Fig. 1). Participants were instructed to lift at their own comfortable speed [3], but were paced at 4 lifts/minute with an auditory cue.

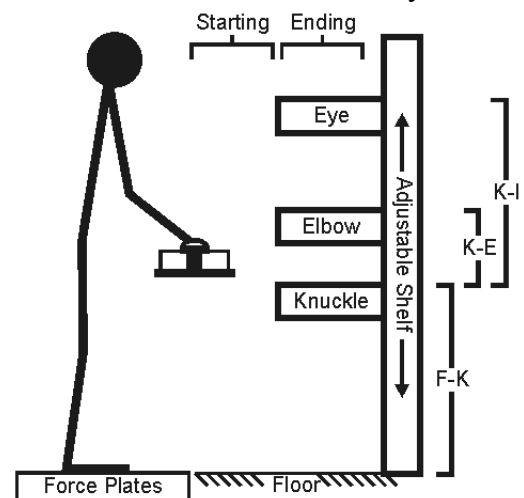


**Figure 1:** Experimental set-up of the starting and ending positions of lifts F-K, K-E, and K-I.

In visit 2, kinematics and kinetics of the three tasks with loads based on the subject-specific MAWLs from visit 1 were recorded. Each lifting motion was recorded at 100Hz using 8 cameras and reflective markers on body segments and the lifting box (Motion Analysis Corporation, Santa Rosa, CA),

along with the ground reaction forces of each foot (Kistler Instruments Corporation, Amherst, NY). Data from three representative lifts for each task are reported. Visit 2 concluded with static maximal voluntary contractions (MVCs) that isolate the shoulder, L5S1, and knee joints, performed at the floor, knuckle and eye lifting positions.

A 3D inverse dynamics model was coded in Matlab (Mathworks, Natick, MA) to determine sagittal joint moments using established body segment characteristics and joint centers [7-9]. Computed external moments were reported relative to their proximal segment's coordinate system. Lift durations were defined by the interval when the measured hand force exceeded 5N. For each participant, shoulder, L5S1, and knee joint moments were normalized to their respective peak MVC values. Peaks for all normalized moments during each lift were extracted. Average MAWLs for the three lifting tasks were calculated and ANOVA tested ( $p < 0.05$ ). A repeated measures ANOVA and Tukey HSD post-hoc test examined differences in normalized peak moments and in the limiting joints for each lift (lift x joint). Limiting joints were identified by the highest normalized peak joint moments for a lift.

## RESULTS AND DISCUSSION

The average MAWLs obtained from the three lifts were:  $19 \pm 5$ ,  $17 \pm 3$ , and  $14 \pm 2$  kg for F-K, K-E, and K-I, respectively (F-K = K-E > K-I). There was a significant joint x lift interaction ( $p < 0.01$ ), with both joint moment patterns and the limiting joint varying by lift (Fig. 2). The lower starting position for F-K challenged the L5S1, whereas the more upright starting postures (K-E & K-I) concluded with a more extended reach that stressed the shoulder. Despite the varied MAWL loads and limiting joints, the normalized peak moments of the limiting joint were similar across the three lifts at ~73% of the joint MVC (F-K = K-E = K-I). These results suggest that a lifter selects a safe MAWL by considering a limiting joint for a particular lifting task. Further, the consistent normalized moment values for the most stressed joints across lifting tasks suggest a universal limiting joint threshold in the MAWL selection process.

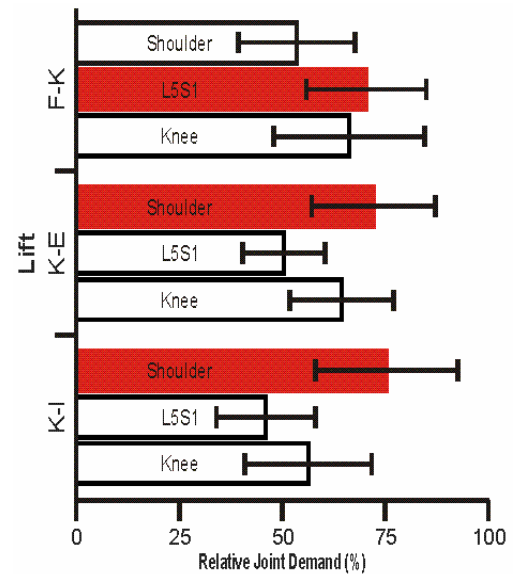


**Figure 2:** Peak normalized shoulder, L5S1, and knee joint moments for each lift. The limiting joint is indicated in red.

The consistent average relative load on the most stressed joint across lifting tasks agrees with a previous study of controlled static postures at a comparable level [5]. This agreement suggests that a universal limiting threshold may hold for both static and dynamic efforts. Future work should examine joint stresses at dynamic loads below and above MAWLs to better understand the MAWL selection process.

Limitations of this study include: 1) participant's interpretation of the psychophysical protocol in MAWL selection, 2) normalizing dynamic joint moments to selected static MVCs, and 3) use of a single nominal lifting frequency.

## REFERENCES

1. Liberty Mutual Workplace Safety Index, 2016
2. Dempsey PG et al. *App. Ergo*, **36**, 489-03, 2005
3. Snook SH & Ciriello VM *Ergo.*, **34**, 1197-13, 1991
4. Snook SH *Ergo.*, **28**, 327-30, 1985
5. Nussbaum MA & Lang A *IJIE*, **35**, 547-57, 2005
6. Fischer SL & Dickerson CR *IJIE*, **44**, 266-74, 2014
7. De Leva P *J Biomech* **29**, 1223-1230, 1996
8. Hanavan EP *AMRL-TR-64-102*, 1964
9. de Looze MP et al. *Clin Bmch*, **7**, 161-9, 1992

# FORCE REDISTRIBUTION FOR SEATED INDIVIDUALS VIA REPOSITIONING

Justin Scott, Tamara Reid Bush

Michigan State University, East Lansing, MI, USA  
email: reidtama@egr.msu.edu

## INTRODUCTION

Most people know someone using a wheelchair, as there are 2.2 million users in the United States [1]. Wheelchair users are at a heightened risk for developing pressure ulcers (PUs) as the tissue in their buttocks is loaded all day with little shifting of this load. PUs are wounds that form when tissue dies, and this death occurs through malnourishment due to lack of blood flow. External pressure on tissue, such as seated loads, diminishes blood flow to the area, putting the area at risk for a PU if the load is not relieved. PUs are costly, painful, and are prone to infection.

Able bodied individuals shift their position or get up if they feel discomfort due to a high pressure on their body. But relief options are limited for wheelchair users. Those with a spinal cord injury (SCI) are not able to feel discomfort [2]. This work investigates loading on the buttocks and back to see what position changes relieve areas of concentrated load, such as the ischial tuberosities (ITs) which is a body region prone to PUs. Our goal is to redistribute the loads occurring on PU prone areas (particularly the ITs) through the development of an articulating chair.

## METHODS

To reach our goal, we developed an articulating chair with independently moving parts to simulate different seated positions [3]. The chair back reclined around the hip joint center. Posture change and leg position were also tested. Rotating the thorax and pelvis supports created 1) kyphotic, 2) neutral and 3) lordotic postures (Figure 1). Two leg positions were tested, a ninety degree knee bend and a straight leg position, each supported by a footrest in front of the chair. A Tekscan mat obtained pressure distributions and center of pressure data on

the seat pan. Pressure measurements were taken at recline angles of 0, 10, 20, and 25 degrees for each leg position and posture.

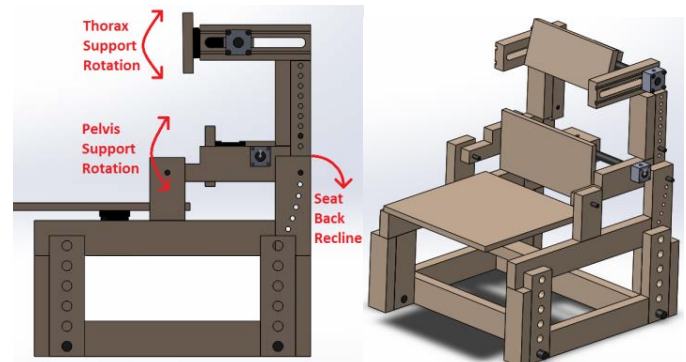


Figure 1. Movement mechanisms of the articulating chair (left) and isometric view (right).

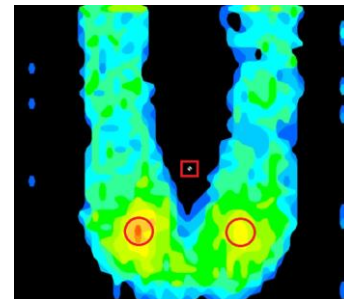


Figure 2. Snapshot from Tekscan mat with Center of Pressure (COP) in the box and ITs circled.

## RESULTS AND DISCUSSION

The pressure data was split on the midline of the participants to consider the left and right sides separately. Values in the y-direction are distances from the back of the buttocks forward, and values in the x-direction are distances from the midline to the left or right. We identified the position of the center of pressure (COP) using the x and y coordinates. On average, a 28 millimeter posterior shift occurred in the COP when reclining from 0 degrees to 25 (Table 1). A 12.7 millimeter posterior shift occurred when changing posture from the lordotic to kyphotic position (Table 2). Both recline and

posture positions show little change in the x direction. When moving the legs from a bent to straight position, a 23.5 millimeter posterior shift in the COP and a 15.6 millimeter shift toward the midline occurred (Table 3).

These COP shifts were measured from the rearmost contact of the buttocks. However, if we look at dynamic movements (Figure 3), we see that in the lordotic posture as compared to the kyphotic posture 1) the full contact area of the buttocks is reduced, 2) the IT pressure is lower, and 3) the IT pressure shifted forward. So, measurement of COP shift from the rearmost position of the buttocks may not truly reflect changes occurring.

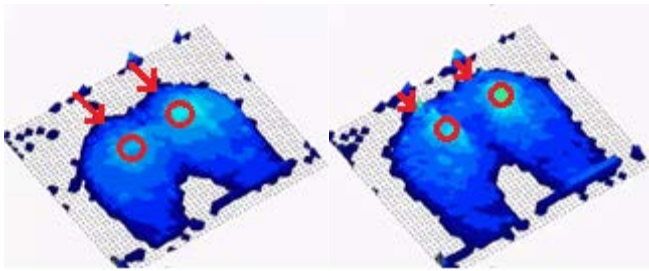


**Figure 3.** Pressure distributions on the seat pan for two postures, lordotic on the left (lower IT pressure peaks shifted forward) and kyphotic (higher pressure peaks shifted rearward) on the right.

Although our numerical data indicate a single motion does not produce a large enough shift in pressure to completely unload the ITs, our measurement approach may not be capturing some of this movement. Additionally a combination of these movements in concert, such as a straightening of the legs while reclining and changing posture,

will create an even larger shift, removing the loading from the ITs. Our long-term goal is to apply these movements to wheelchairs and have them cycle through different postures after a duration of time to automatically shift loads and reduce the risk of PUs.

## CONCLUSIONS

Our initial results have shown a positional shift of the COP when looking at recline, posture change, and foot position while seated. Most movement occurs in the anterior posterior direction. Such movements can be used to load and unload different tissues while in a seated position. A limitation of this study is the small sample size (n=4) and that we have only tested able bodied individuals. Prior to testing people with disabilities, we will incorporate a whole body tilt in addition to articulation and recline to further change loading. Furthermore, we will see if any differences exist between able bodied individuals and those with disabilities.

## REFERENCES

1. NIH Research Plan on Rehabilitation, 2016.
2. National Spinal Cord Injury Statistical Center Data Sheet, 2016.
3. Bush TR, Hubbard RP. *Journal of Biomechanical Engineering.* **129**, 2007.

## ACKNOWLEDGMENTS

Work is supported by NSF CBET, grant 1603646.

**Table 1:** Position of the COP for different recline angles.

Recline Angle (°)	0		10		20		25	
	Left	Right	Left	Right	Left	Right	Left	Right
y position (mm)	115.82±5.59	116.08±8.89	113.03±5.33	115.06±7.87	108.46±4.83	108.46±8.13	107.70±5.33	107.95±7.87
x position (mm)	80.77±4.06	75.44±5.59	83.06±3.56	75.44±5.08	79.76±4.32	75.69±4.06	77.98±3.05	77.22±4.83

**Table 2:** Position of the COP for different postures.

Posture	Kyphotic		Neutral		Lordotic	
	Left	Right	Left	Right	Left	Right
x position (mm)	104.90±14.73	105.66±14.73	106.93±16.00	86.61±22.10	98.55±8.64	94.49±3.05
y position (mm)	74.42±9.91	69.60±12.19	73.91±10.16	71.37±6.86	76.71±9.91	65.79±7.62

**Table 3.** Position of the COP for different leg positions

Leg Position	Left y position (mm)	Right y position (mm)	Left x position (mm)	Right x position (mm)
Knees Bent	128.02±18.29	129.79±23.37	89.66±9.14	85.09±10.92
Straight Legs	97.79±5.84	113.03±8.38	73.66±6.35	69.85±9.14

# EFFECTS OF HEAD-WORN DISPLAY USE ON OBSTACLE CROSSING PERFORMANCE IN A SIMULATED OCCUPATIONAL TASK

Sunwook Kim, Sophia Ulman, and Maury A. Nussbaum

Industrial & Systems Engineering, Virginia Tech, Blacksburg, VA, USA  
Email: sunwook@vt.edu

## INTRODUCTION

Slips, trips, and falls (STFs) continue to be a major cause of occupational injuries and fatalities. For example, STFs accounted for 16.5% of fatal occupational injuries and 27% of lost workday cases in 2015 [1]. The occupational application of smart glasses, or head-worn displays (HWDs), has been explored in diverse applications [2], and may lead to potential benefits since a HWD can project diverse, real-time information in front of one (monocular) or both eyes (binocular) of a user. Though broad evidence supports that an increase in attentional demand and/or cognitive distraction can reduce gait performance [3], there is limited evidence that has been reported regarding the potential impacts of HWD use on gait performance, particularly with respect to obstacle crossing (OC). This study thus assessed the effects of different HWD technologies and information presentation types on OC performance. Two commercially-available HWDs were used, representing binocular (Epson Moverio BT-200) and monocular (Vuzix M100) technologies. Based on earlier work, we hypothesized that the use of a HWD would deteriorate OC performance.

## METHODS

This study involved 12 gender-balanced participants, with self-reported normal or corrected-to-normal vision (contact lenses only), and no recent or current musculoskeletal disorders or injuries. The mean (SD) age, stature, and body mass were 25.3 (6.0) yrs, 177.2 (6.2) cm, and 74.2 (8.3) kg, respectively for males; and 30.2 (14.3) yrs, 164.2 (4.8) cm, and 55.8 (5.4) kg, respectively, for females. Testing was performed with IRB approval, and informed consent was obtained.

A 3×2×2 repeated measures design was used to assess the effects of *Information mode* (paper list, binocular HWD, monocular HWD), *Information type* (text- vs. graphic-based instructions for a simulated assembly task), and *Gender* on OC performance. Participants were provided with consistent shoe types and asked to walk on a linear gait track at a “purposeful” walking speed [4]. After familiarization, participants completed three gait trials to establish a baseline (i.e., no info. mode) and then all the experimental conditions. The order of experimental conditions was counter-balanced.

Triaxial ground reaction forces (GRFs) were collected from two force plates (AMTI, OR-6). Gait kinematics were collected using a 10-camera motion capture system (Vicon, Vero), using passive reflective markers placed on select anatomical landmarks. Eight markers were also placed around the shoe outsole [5], and four markers were placed on each corner of the obstacle (made of dense foam, see Figure 1).

Minimum foot clearance (MFC) and peak required coefficient-of-friction (RCOF) between the shoe and floor surface were used to assess OC performance. RCOF was obtained from each force plate as:  $\sqrt{F_X^2 + F_Y^2}/|F_Z|$  where  $F_X$ ,  $F_Y$ , and  $F_Z$  are the shear and normal GRFs, respectively. Peak RCOF was then extracted [6]. MFC was defined as the lowest location among the reconstructed shoe outsole markers near the mid-swing phase of gait, and was calculated separately for the lead and trail feet over the obstacle [5]. Foot placement location around the obstacle was obtained [7], including the trail horizontal toe and the lead horizontal heel distances (Fig. 1). Obstacle crossing speed (OCS) was estimated as the mean velocity of four pelvis markers during the obstacle crossing step. Mixed-factor analyses of variance were performed on OC

performance measures to assess the effects of gender, *Info. mode*, and *Info. Type*, while including the corresponding baseline measure as a covariate.

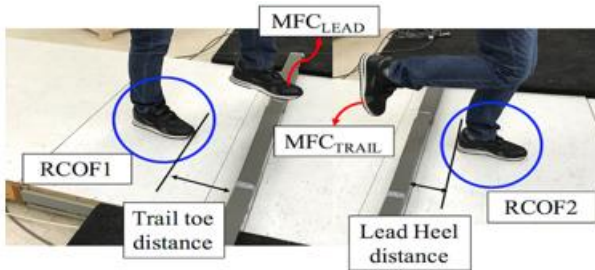


**Figure 1:** OC performance measures obtained.

## RESULTS AND DISCUSSION

Participants exhibited significant changes in some OC performance measures (i.e., RCOF2 or lead heel distance) relative to baseline measures. Additionally,  $MFC_{LEAD}$  was significantly affected by a main effect of *Info. Mode*, and an *Info. Mode*  $\times$  *Info. Type*  $\times$  *gender* interaction effect (Fig. 2).  $MFC_{LEAD}$  was generally comparable between *Info. type* conditions with one exception, and larger for females vs. males.

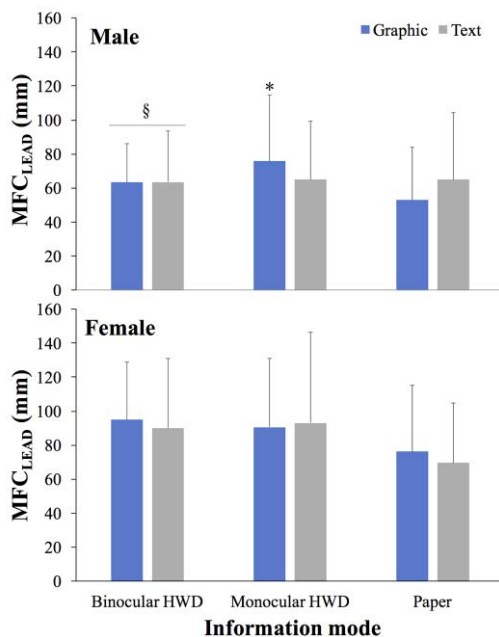


**Figure 2:** Three-way interaction effect of *Info. mode*, *Info. type*, and *gender* on  $MFC_{LEAD}$ . Note: \* and § indicate significant differences between *Info. type* conditions and between genders, respectively.

When attentional demand increases, reducing the OCS may have been a strategy to maintain postural stability (i.e., cautious gait). Use of a HWD resulted

in a slight decrease (~4%) in OCS compared to the baseline, but such a decrease was not apparent for the paper list condition. This may suggest that visuospatial attentional demands were higher with HWD use (vs. the paper list), given that walking/obstacle crossing requires visual and visuospatial information to control limb trajectories [8]. Also, HWD use seemed to cause more conservative obstacle crossing behaviors, which may be gender specific. Common strategies to reduce trip risks include decreasing OCS, increasing  $MFC_{LEAD}$ , and/or increasing the trail toe distance while reducing the lead heel distance [3]. Here, when using the monocular HWD or paper list, males increased the trail toe distance while reducing the lead heel distance. When using a HWD, females exhibited increased  $MFC_{LEAD}$  values.

In summary, we examined the effects of HWD use on OC performance. Our results demonstrate that the use of HWDs may cause the adoption of specific gait strategies. Yet, given potential study limitations (i.e., young participants, rather optimal walking condition), future efforts are needed to understand more completely how HWD use might affect gait performance of diverse working populations, for longer-term use, and under suboptimal or more challenging walking conditions.

## REFERENCES

1. Bureau of Labor Statistics. *bls.gov*, Washington, DC, 2016.
2. Henderson S & Feiner S. *IEEE Trans. Vis. Comput. Graphics*, **17**, 1355-68, 2011.
3. Harley C, et al. *Gait & Posture*, **29**, 428-32, 2009.
4. Beringer DN, et al. *PLoS ONE*, **9**, e96525, 2014.
5. Startzell JK & Cavanagh PR. *Hum Mov Sci*, **18**, 603-11, 1999.
6. Chang WR, et al. *Hum Factors*, **53**, 461-73, 2011.
7. Chen HC, et al. *J Gerontol*, **46**, 196-203, 1991.
8. Patla AE, et al. *J Mot Behav*, **28**, 35-47, 2010.

## ACKNOWLEDGMENTS

This work was sponsored by the Center for Excellence in Logistics and Distribution (CELDi), an NSF Industry/University Cooperative Research Center, under award #0732686.

# CONTACT FORCE DISTRIBUTION ON THE FINGERS DURING SPHERICAL GRIPPING

Erik W. Sinsel, Christopher M. Warren, Daniel E. Welcome, and John Z. Wu

National Institute for Occupational Safety and Health, Morgantown, WV, USA  
email: ESinsel@cdc.gov

## INTRODUCTION

Tool handles are the interfaces between human hands and the tools being operated. The contact conditions in the hand/handle interface may play a role in the comfort and efficiency of the tool operation, as well as in the fatigue of, and injury to, the upper extremity musculoskeletal systems [1]. The size of the handles of power tools has been a major ergonomic consideration for designers wishing to minimize the operating effort and maximize the grip force and torque strength [2]. Previous studies indicate that grip force depends strongly on the handle diameter [3]; the grip effort and injury potential can be reduced by using handles of suitable diameter [4]. However, only cylindrical gripping was considered in the previous studies. The purpose of the current study is to investigate contact force distributions within and across the fingers when gripping a spherical object.

## METHODS

Eight female adults [age 29 (9.1) years, mass 64.6 (7.1) kg, height 163.5 (1.9) cm, hand length 17.2 (0.7) cm] participated in the study, providing informed consent under protocol IRB 11-HELD-02XP approved by the Centers for Disease Control and Prevention. In order to measure contact force, normal force sensors (FingerTPS, Pressure Profile Systems, Los Angeles, USA) were attached to the distal, middle, and proximal phalanges of the four fingers, excluding the thumb (Fig. 1). Each sensor was then individually calibrated at intervals up to 15 N, where an error greater than 2 N prompted a new calibration.

Subjects performed two maximum exertion gripping tasks on a standard tennis ball. A quasi-static portion of each trial was selected and the mean total force across the two trials was used to establish the subject's maximum voluntary exertion (MAX) force value. The subject then performed a random ordering

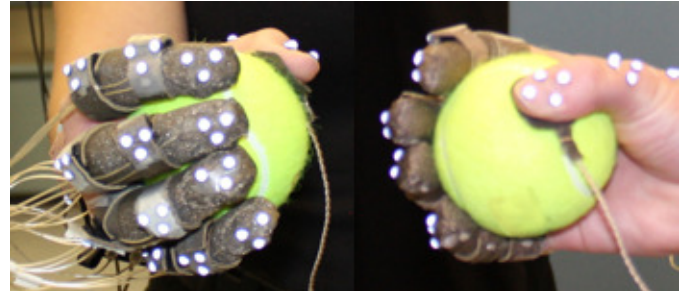


**Figure 1.** Test setup. The subject grips a tennis ball (65 mm diameter); force sensors are located on the palmar aspects of the finger phalanges.

of two trials each at 50% and 25% of MAX. Subjects rested at least 2 minutes between trials. In each trial, an experimenter placed the ball in the subject's instrumented hand; subjects were instructed to not greatly adduct the fingers, avoiding a claw-like posture while gripping.

Sensor data were collected at 40 Hz. During each trial, tare offset data were collected with the sensors not externally loaded; the mean of a one-second range was used to apply a tare to each sensor's data and a zero flooring operation was applied. The mean force for each sensor was calculated over a four-second range with the minimum variance of total finger force.

## RESULTS AND DISCUSSION

The force share among the distal, middle, and proximal phalanges for three grip force levels are shown in Fig. 2. The results show that across all force levels the distal phalanges share approximately 50% of the total force. The proximal phalanges shared approximately 10% of the total force for all grip force levels. Force share for the proximal phalanges was the lowest within the fingers with the exception of the ring finger, where the middle and proximal shares were approximately equal. The grip force level affects the force distributions on the phalanges, however the general trends are not changed.

The force sharing characteristics across fingers are presented in Fig. 3. At all force levels the middle and ring fingers share approximately 50% more force than the other two fingers. The force shares in the middle and index fingers increase with increasing total force level, while the shares in the ring and little fingers decrease.

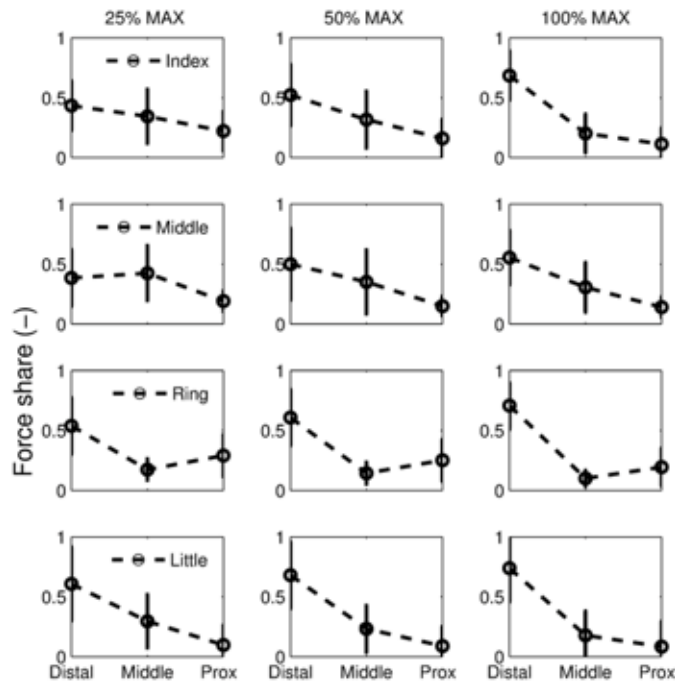


**Figure 2.** Force sharing across the distal, middle, and proximal phalanges for three levels of total finger force (n=8).

In the current study we utilized sensors which were mounted on fingers to evaluate the force on each phalanx when gripping a spherical object. In previous studies [5, 6], contact pressure was measured by using pressure sensor film wrapped on the cylindrical contact surface. It is technically difficult to wrap a pressure sensor film on a spherical surface, while the application of the sensors used in this study is independent of the curvature of the contact surface being gripped.

## CONCLUSIONS

About 60% of the force on the fingers is contributed by the middle and ring fingers and about 40% by the index and little fingers. These characteristics are independent of the total force levels and stiffness of the contact surface (results not shown).

For each of the fingers, the contact force is concentrated mostly on the distal phalanx, independent of the total force. This phenomenon is similar to that observed during cylindrical gripping [5], where the maximal pressure was found on the distal phalanx of the index finger. However, the observed force share pattern in the fingers differs from the previous study: the majority of the finger force is contributed by the middle and ring fingers in spherical gripping, while in cylindrical gripping it is contributed mainly by the index finger [5].

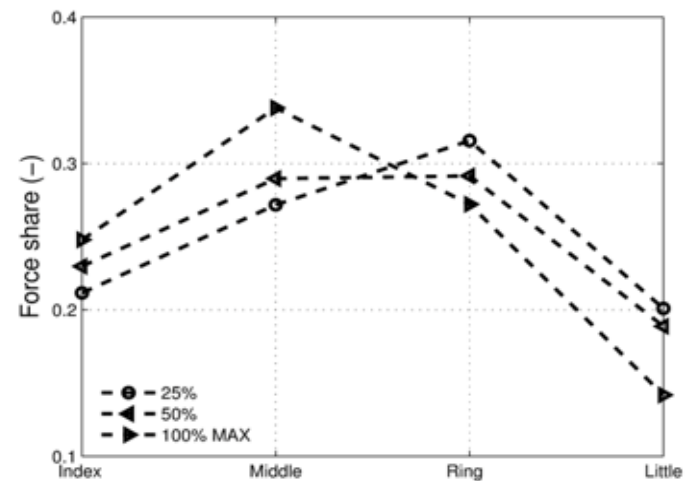


**Figure 3.** Force sharing across the fingers for three levels of total finger force (n=8).

## REFERENCES

1. Fransson C and Winkel J. *Ergon* **34**, 881-92, 1991.
2. Seo NJ, Armstrong TJ, Chaffin DB, and Ashton-Miller JA. *Hum Factors* **50**, 227-36, 2008.
3. Kong YK, Lowe BD, Lee SJ, and Krieg EF. *Appl Ergon* **39**, 191-8, 2008.
4. Freund J, Toivonen R, and Takala EP. *Clin Biomech* **17**, 515-20, 2002.
5. Wu JZ, Dong RG, Warren CM, Welcome DE, and McDowell TW. *Med Eng Phys* **36**, 831-41, 2014.
6. Sinsel EW, Gloekler DS, Wimer BM, Warren CM, Wu JZ, Buczek FL. *Med Eng Phys* **38**, 72-9, 2016.

**DISCLAIMER:** The findings and conclusions in this abstract have not been formally disseminated by the National Institute for Occupational Safety and Health and should not be construed to represent any agency determination or policy.

# IN VIVO QUANTIFICATION OF MUSCLE FATIGUE IN UPPER EXTREMITY DURING PULLING AND GRIPPING USING REGIONAL OXIMETER: A FEASIBILITY STUDY

\*Liyong Zheng, Xueyan S. Xu, Erik W. Sinsel, Daniel E. Welcome, Ren G. Dong, and John Z. Wu

National Institute for Occupational Safety and Health, Morgantown, WV, USA.

\*email: lzheng2@cdc.gov

## INTRODUCTION

Musculoskeletal disorders (MSDs) are responsible for over a third of all sick leaves lasting over nine days in the construction industry [1]. The MSDs in the upper extremity are the second most prevalent type of MSDs [2,3]. It is well accepted that the initiation and development of the MSDs are associated with the muscle fatigue induced by awkward working posture, extended and/or repetitive loading. Ergonomic devices such as wearable robotics or exoskeletons (many specifically focus on the upper extremity) are promising solutions to reduce fatigue and lower risks of the work-related MSDs. To assess effectiveness of those ergonomic products, the first critical step is to quantify fatigue-related changes in the musculoskeletal system *in vivo* and noninvasively and to have a comprehensive understanding of muscle fatigue.

Electromyography (EMG) is commonly used to measure neuromuscular response of muscle fatigue and the median frequency of EMG signals is expected to drop when fatigue occurs. Nevertheless, several studies commented that surface EMG might not be sensitive enough to record low-level muscle activity and the median frequency changes were rather small [4,5]. Recent advances in near infrared spectroscopy (NIRS) technology have provided a noninvasive approach to measure muscle oxygenation and oxidative metabolism, which is believed to investigate a different aspect of the physiological process of fatigue [5]. Previous studies also reported that NIRS results were task- and muscle-dependent [6]. This feasibility study is to test if NIRs is a viable means to quantify fatigue-related oxygenation changes, specifically in upper extremity muscles during pulling and gripping at different postures.

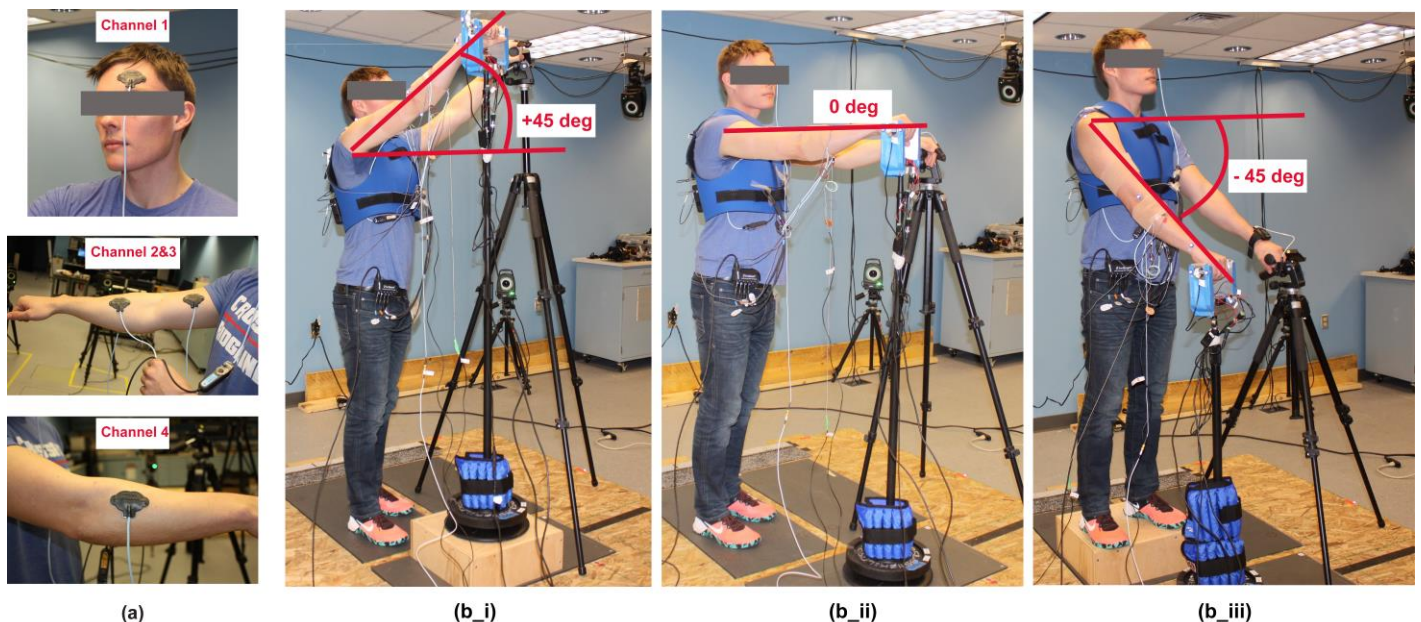


**Figure 1.** (a): Four regional oximetry sensors (channels) were placed on the contralateral forehead (cerebral) and three muscles on the right arm—biceps brachii, flexor carpi radialis, extensor carpi radialis; (b\_i-iii): a subject pulls on an instrumented handle at three different postures (arm angles: +45, 0 and -45 degrees).

## METHODS

A healthy subject (male, 24 years old, 77.6 kg, and 1.75m) was consented to participate in this ongoing NIOSH IRB-approved study. Four regional oximeter sensors (Nonin, SenSmart Model X-100) were placed on the subject's forehead and forearm (Fig. 1a) to measure the oxygenation levels (Oxy). The pulling force was recorded by the force plate (Bertec, 4080-10) and the grip force was measured by the instrumented handle equipped with a pair of force sensors (Interface, SML-100).

Prior to the hold-until-fatigue testing, two types of reference trials—resting and maximum voluntary contraction (MVC)—were recorded at three postures (Fig. 1, b\_i-iii). Three events (Fig. 2) were labeled for the following fatigue tasks in the oximeter: initiate to target two levels of pulling exertions ('a', 30% MVC and 60% MVC), verbally signal the examiner when the subject could not maintain the desired pulling force ('b'), keep the force level as high as possible for about extra 5 seconds, and relax ('c'). The targeted pulling force level was shown on the monitor next to the subject.

## RESULTS

The NIRS measures were found to be markedly responsive to the changes in exertion levels and upper extremity postures (Fig. 2). For the same posture, the muscle oxygenation changes in the 30% MVC trials were noticeably lower than those in the 60% MVC ones; the endurance time was relatively

longer and the force levels remained steadier in the 30% MVC trials as expected [7]. Changes in muscle recruitment were detected when the postures were different: less muscle oxygenation changes were found in the forearm muscles in the overhead posture (Fig. 2, the leftmost column), presumably due to the involvement of the shoulder muscles initiated in the overhead exertions.

## DISCUSSION

These preliminary results demonstrate the promise of NIRS as a feasible approach to quantify muscle fatigue response during functional upper extremity tasks. Further integrative analyses which will also include EMG and vibromyography may provide a complete characterization of onset and progression of muscle fatigue, leading to better assessments and improvement of ergonomic interventions.

## REFERENCES

1. NIOSH. *Worker health chart book*, No. 146, 2004
2. Bureau of Labor Statistics. USDL-22204, 2012.
3. Bureau of Labor Statistics. 2013
4. Knardahl, S. *Work & Stress* **16**,179-189, 2002.
5. Ferguson SA, et al. *Hum Factors* **55** (6),1077-87, 2013
6. McNeil CJ, et al. *Am J Physiol Regul Integr Comp Physiol* **309** (5), R475-81, 2015
7. Mehta RK, et al. *Hum Factors* **56** (4), 645-56, 2014

**DISCLAIMER:** The findings and conclusions in this report are those of the authors and do not necessarily represent the official position of the National Institute for Occupational Safety and Health. The mention of trade names, commercial products, or organizations does not imply endorsement by the US Government.

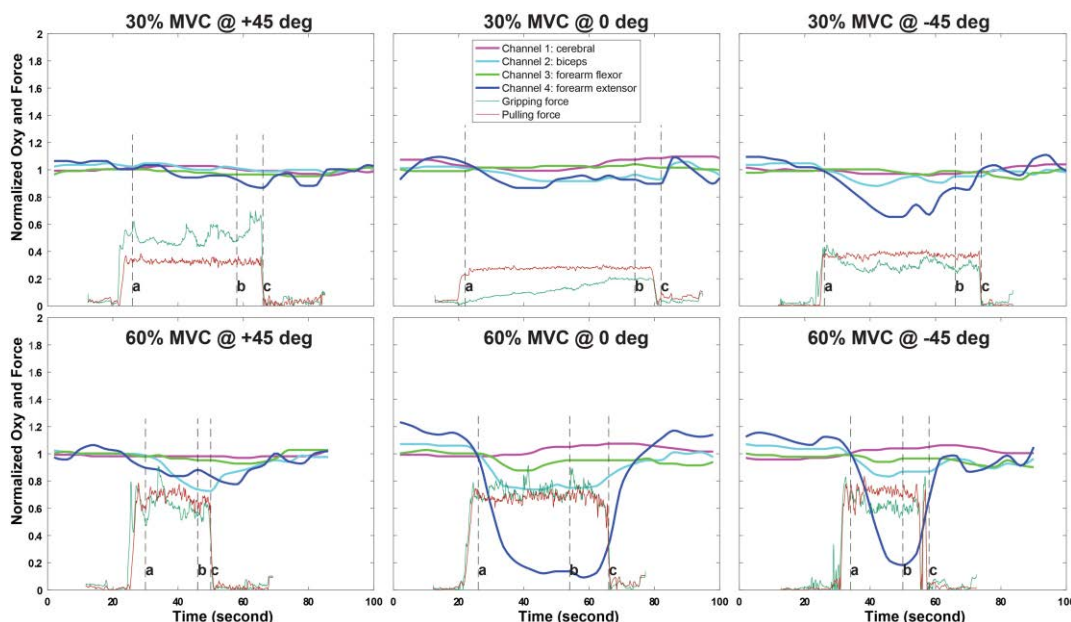


**Figure 2.** Representative normalized cerebral and somatic oxygenation levels (thick lines) along with gripping and pulling force levels (thin lines) during hold-until-fatigue testing at three postures and two levels of exertions (30% and 60% MVC). The oxygenation and force levels were normalized by resting and MVC values. Events labeled: a = start, b = fatigue (signaled by subject), c = relax.

# CHANGES IN KNEE KINETICS ARE REQUIRED FOR DECELERATION WITH BODY BORNE LOAD

<sup>1</sup> Sarah E. Cameron, <sup>1</sup> Jonathan T. Kaplan, <sup>2</sup> Tyler N. Brown, <sup>1</sup> John W. Ramsay

<sup>1</sup> Natick Soldier Research, Development and Engineering Center (NSRDEC) Natick, MA, USA

<sup>2</sup> Dept. of Kinesiology, Boise State University, Boise, ID, USA

email: sarah.e.cameron20.civ@mail.mil

## INTRODUCTION

Transitional periods of dynamic movement, such as transitioning from a run to a walk (RTW) or a walk to a run (WTR) are maneuvers common to military training. In the military, these maneuvers are commonly performed while donning body borne load, sometimes in excess of 45kg. These loads alter lower limb biomechanics causing a significant reduction in performance, as well as increased incidence of musculoskeletal injury. More than 75% of military-related musculoskeletal injuries occur in the lower limb and primarily occur at the knee (1). Donning body borne load, elevates this injury risk and may compromise performance by increasing the mechanical load placed on the joint (2). Load carriers reportedly exhibit increased ground reaction forces and knee joint moments during military activities. But, to date, it is unclear if body borne load increases the frontal and transverse plane knee moments thought to contribute to joint pain, instability and soft-tissue injury (3), particularly during transitional movements common to military training. With that in mind, this study investigated the impact of body borne load on knee joint kinetics and ground reaction force during RTW and WTR transitional movements.

## METHODS

Twenty-one male military personnel (age:  $21.6 \pm 3.1$  yrs, height:  $1.77 \pm 0.56$  m, weight  $79.9.0 \pm 11.6$  kg) participated in this study. For the WTR trials biomechanical data was unavailable for 2 subjects and a reduced sample size of 19 was used. Each participant completed the study maneuvers with three different load configurations: light (LL, ~6kg), medium (ML, 15% of BW) and heavy (HL, 30% of

BW). For the LL, participants wore military equipment (helmet, boots and mock weapon), while for the ML and HL participants added a weighted vest (WeightVest.com Inc. Rexburg, ID, USA) to the LL equipment. The weighted vest was adjusted to have the total load equal either 15% or 30% of participant BW. With each load, participants completed five successful RTW and WTR maneuvers. The RTW consisted of the participant running down a 10m platform at 4 m/s and then transitioning into a 1.5 m/s walk when their dominant leg contacted a force platform (Optima, AMTI, Watertown, MA, USA). Likewise, the WTR required the participant to walk at 1.5 m/s down the platform and transitioning to a 4 m/s run when their dominant limb struck the force platform.

Knee biomechanics were quantified from 3D trajectories of 36 reflective markers. A high-speed stationary recording (240 fps, Opus, Qualysis AB, Gothenburg, Sweden) of each participant was taken to create a kinematic model using Visual 3D (C-Motion, Rockville, MD). The kinematic model consisted of seven skeletal segments (bilateral foot, shank and thigh, and pelvis segments) with 24 DoF. For each trial, synchronous GRF data and marker trajectories were low pass filtered with a fourth-order Butterworth filter (12 Hz). Then, joint rotations were processed using the filtered marker trajectories, while knee joint moments were obtained by processing the filtered kinematic and GRF data.

Peak knee joint moments and GRFs exhibited during stance phase were normalized to BW and submitted to a repeated measures ANOVA to test the effect of load configuration (LL, ML, HL) during the RTW and WTR transitions. Where statistically significant

differences were observed ( $p < 0.05$ ), a modified Bonferroni procedure was used. Where sphericity failed, a Greenhouse- Geisser correction was used.

## RESULTS AND DISCUSSION

Body borne load had a significant effect on peak vertical GRF during the WTR ( $P < 0.001$ ). During the WTR, participants significantly increased vertical GRF from  $1.89 \pm 0.13$  BW with the LL to  $1.92 \pm 0.23$  BW and  $2.04 \pm 0.18$  BW with the ML ( $p = 0.005$ ) and HL ( $p < 0.001$ ) conditions, respectively. However, despite the increased vertical GRF, participants did not exhibit a similar increase in knee joint moments when transitioning from WTR when donning body borne load. Specifically, body borne load had no main effect on peak knee joint flexion ( $p = 0.687$ ), abduction ( $p = 0.92$ ), or internal rotation ( $p = 0.117$ ) moments during the WTR (Table 1). When participants donned body borne load during the WTR, it appears they did not adopt hazardous knee kinetic changes, such as larger knee abduction or internal rotation moments that would increase the injury risk of the acceleration task. Further work, however, is warranted to determine if participants adopted significant kinematic changes that enabled the successful performance, and minimized injury risk, of the WTR.

Body borne load had a significant effect on peak vertical GRF during the RTW tasks ( $P < 0.001$ ). Participants exhibited a peak vertical GRF of  $2.49 \pm 0.25$  BW,  $2.58 \pm 0.25$  BW and  $2.77 \pm 0.25$  BW with the LL, ML and the HL, respectively, during the deceleration of the RTW task. Specifically, during the RTW, the participants exhibited significant increase in peak vertical GRF with the addition of the ML ( $p = 0.025$ ) and HL ( $p < 0.001$ ) compared to the LL configuration.

To maintain lower limb stability and help attenuate the elevated GRFs that resulted with the addition of

load during the RTW, participants increased knee joint moments (Table 1). Participants exhibited a significant increase in peak knee abduction ( $P = 0.006$ ) and internal rotation ( $P = 0.029$ ) moments, but not the peak flexion moment ( $P = 0.415$ ) during the RTW. Specifically, participants increased peak knee abduction moment with the HL ( $p = 0.016$ ) and ML ( $p = 0.008$ ) compared to the LL, and increased the peak internal rotation moment with ML ( $p = 0.050$ ) compared to the LL. These elevated out of plane moments may be indicative of increased risk for injury, as well as instability at the knee. Previous studies have reported a correlation between internal rotation and knee abduction moments and soft tissue injury (4). Further study needs to be done to understand how to minimize these hazardous biomechanical adaptations at the knee during deceleration.

## CONCLUSIONS

Body borne load had a significant effect on knee joint moments when decelerating during the RTW, but not when accelerating during the WTR task. In order to decelerate with body borne load, participants exhibited larger frontal and transverse plane knee moments. These elevated moments may increase injury risk, as well as instability at the knee during the RTW task. Interestingly, participants did not exhibit a similar increase in knee joint moments when performing the WTR with body borne load. Further work is needed to determine if participants can adopt biomechanical patterns that enable successful performance, minimize injury risk, and improve lower limb stability during all military activities.

## REFERENCES

1. Polycyn et al. DTIC document.2002.
2. Andriacchi et al., *Basic orthopedic biomechanics and mechanobiology*.2005.
3. Wang et al., *Research quarterly for exercise and sport*.2013.
4. Quatman, et.al. *British Journal of Sports Medicine*. 2009.

**Table 1:** Mean ( $\pm$  SD) peak knee moments exhibited during the RTW and WTR with each load condition.

Knee Joint Moments (N.m/kg.m)	RTW			WTR		
	LL	ML	HL	LL	ML	HL
<b>Flexion</b>	1.99 $\pm$ 0.28	2.03 $\pm$ 0.29	2.05 $\pm$ 0.3	1.14 $\pm$ 0.05	1.16 $\pm$ 0.18	1.17 $\pm$ 0.19
<b>Abduction</b>	0.07 $\pm$ 0.06 <sup>S*</sup>	0.10 $\pm$ 0.07	0.12 $\pm$ 0.08	0.08 $\pm$ 0.05	0.08 $\pm$ 0.06	0.1 $\pm$ 0.06
<b>Internal Rotation</b>	0.03 $\pm$ 0.03 *	0.05 $\pm$ 0.05	0.05 $\pm$ 0.04	0.06 $\pm$ 0.04	0.05 $\pm$ 0.03	0.07 $\pm$ 0.04

For pairwise comparisons: \*LL-ML, <sup>S</sup>LL-HL, denotes a significant ( $p < 0.05$ ) main effect of body borne load.

# THE INFLUENCE OF HAND LOCATION AND EXERTION TYPE ON LUMBAR TWIST DURING SIMULATED INDUSTRIAL TASKS

<sup>1</sup> Colin D. McKinnon, <sup>1</sup> Clark R. Dickerson, and <sup>1</sup> Jack P. Callaghan

<sup>1</sup> University of Waterloo, Waterloo, ON, Canada  
email: colin.mckinnon@uwaterloo.ca

## INTRODUCTION

Current workstation design guidelines include recommendations for forward and lateral reach distances during occupational tasks based on task frequency and anthropometry. Forward reach guidelines focus on maintaining a neutral shoulder posture since large reaches create large shoulder loads, cause people to fatigue more quickly, and cause more reporting of shoulder pain [1–3]. For lateral reaches, current guidelines are underdeveloped and do not have the same research-based foundation. Rather, lateral reach guidelines generally apply forward reach concepts to the lateral reach envelope determined by worker size and arm length. Low back twisting has been strongly associated with low back pain and injury development [4,5], and the relationship between reaching task hand location and low back twist is currently unknown. The purpose of this study was to investigate low back twist during simulated manual labour tasks across a range of forward and lateral reach distances, task heights, and exertion directions.

## METHODS

Twenty-four (12 male, 12 female) right-handed participants performed single-handed exertions against a load cell (MSA-6, AMTI, USA) attached to the end of a 6-DOF robotic arm (Motoman HP50, Yaskawa, USA). Eleven (11) right-hand target locations (Figure 1) corresponded to Canadian Standards Association forward and lateral reach guidelines for frequent, infrequent and occasional tasks [6]. Exertions were performed at each hand location in all combinations of three directions (forward push, upward exertion, downward exertion), two heights (standing acromion and olecranon heights), and two load magnitudes (40 N, 60% of forward push strength) for a total of 132

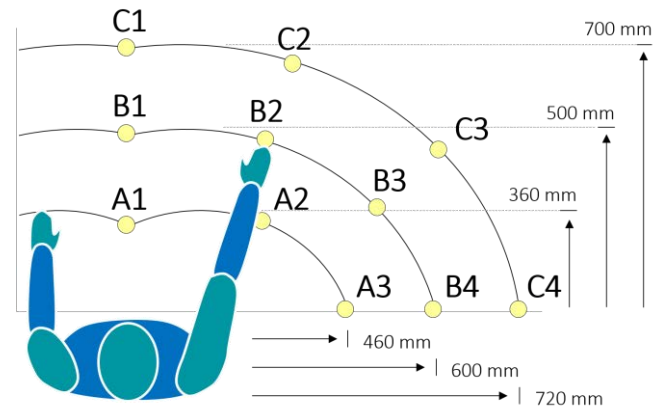


**Figure 1:** Eleven hand target locations used for manual exertions. Targets correspond to current ergonomics reach guidelines (CSA, 2012).

1-second isometric exertion trials. Participant thoracopelvic and right upper limb postures were recorded using 14 reflective markers on bony landmarks and an optical motion capture system (MX20+, Vicon, USA). Thoracopelvic angles (YZX Euler sequence) and right upper arm angles (YXY Euler sequence) were calculated using custom-written Matlab software. Thoracopelvic angles were normalized and expressed relative to a static upright standing trial. Joint angles were compared using a mixed general linear model (RStudio 1.0.136) with sex (M/F), target location (11 levels), height (elbow/shoulder) and direction (up, down, push) as factors ( $\alpha = .05$ ). A Tukey HSD post hoc test tested levels within significant main and interaction effects.

## RESULTS AND DISCUSSION

Significant *target-by-direction* ( $p < .003$ ) and *direction-by-height* ( $p < .03$ ) interactions were observed for all three axes of thoracopelvic motion (axial twist, flexion/extension, lateral bend). These motion axes also showed *target* ( $p < .0003$ ) and

direction ( $p < .007$ ) main effects. Post hoc analyses showed axial twist angle increased with more lateral hand targets, and this increase was generally similar regardless of reach distance (A vs. B vs. C, Fig. 2). Thoracopelvic flexion showed the opposite response, with less flexion at more lateral targets and more flexion with increased reach distance (Fig 2).

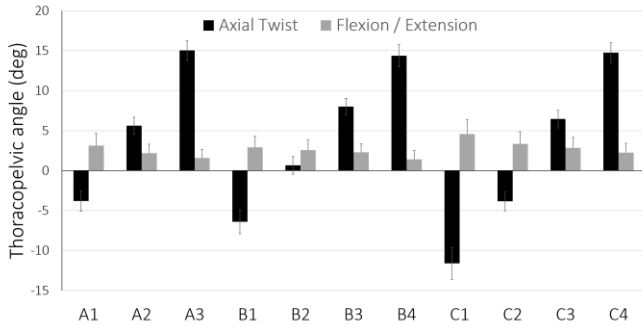


**Figure 2:** Thoracopelvic axial twist angle and flexion angle by hand target location. Positive values show rightward twist and flexion.

These results indicate a trade-off between the twist and flexion motion axes, with opposing postural demands for forward and lateral reaches. It should be noted that mean flexion angle was less than 5 degrees across all hand targets (around 13% of flexion range of motion [7]), whereas axial twist angle was approximately 15 degrees for the most lateral locations, which is nearly 40% of maximum twist range of motion in an upright, neutral posture [8].

Significant *target-by-direction-by-height* ( $p = .01$ ), *direction-by-height* ( $p < .0001$ ), *target-by-height* ( $p < .0001$ ), and *target-by-direction* ( $p < .0001$ ) interactions were observed for glenohumeral elevation angle. Elevation was highest for straight forward targets and decreased laterally (Fig. 3).

Elevation showed similar levels with A and B reached, but increased for C reaches. Plane of elevation showed several significant 2-factor and 3-factor interactions including *direction-by-height* ( $p = .003$ ) and *target-by-direction* ( $p < .0001$ ). Plane of elevation tended to be closer to shoulder abduction for lateral targets and closer to shoulder flexion for forward targets, as expected.

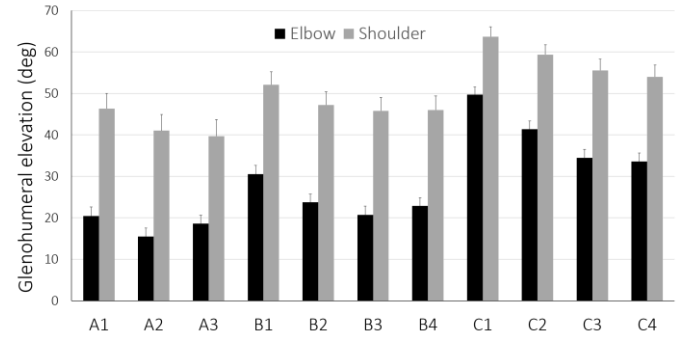


**Figure 3:** Glenohumeral elevation angle by hand target and by target height. Positive values indicate abduction from neutral (arms at sides).

## CONCLUSIONS

The opposing conditions associated with maximum motion for axial twist (lateral, shoulder height, close targets) and glenohumeral elevation (forward, shoulder height, far targets) indicate a complex relationship between thoracopelvic twist and upper limb motion. While close and medium distance targets are reached primarily using lumbar spine motion, farther targets are reached using a combination of lumbar spine motion and increased upper limb elevation. Future work comparing the linear increase of axial twist angles with laterality of hand target and the associated injury risk will assist in definition of safe guidelines for reaching task hand targets.

## REFERENCES

- Anton D, et al. *Ergonomics* **44**(5): 489-501, 2001.
- Brookham RL, Wong JM, Dickerson CR. *IJIE* **40**(3): 337-344, 2010.
- Dickerson CR, Martin BJ, Chaffin DB. *Ergonomics* **49**(11): 1036-1051, 2006.
- Bernard BP. *NIOSH 97B141*, 1997.
- Marras WS. *Ergonomics* **43**(7): 880-902, 2000.
- Canadian Standards Association (CSA). *Z1104-12*, 2012.
- Saur PMM, et al. *Spine* **21**(11): 1332-1338, 1996.
- Drake JDM, Callaghan JP. *Clin Biomech* **23**(5): 510-519, 2008.

# TRACING ON A TOUCH SCREEN: INFLUENCE OF AGE, IMPLEMENT, HAND, AND FRICTION

Brittany D. Heintz and Kevin G. Keenan

University of Wisconsin - Milwaukee, Milwaukee, WI, USA  
email: bheintz@uwm.edu

## INTRODUCTION

Many electronic devices require manipulation of touch screens, a hybrid task requiring both well-directed forces and movements. Hybrid force/motion tasks are challenging motor control tasks [1], especially for older adults [2], which may contribute to decreased use of technology and limit benefits associated with its use (e.g., decreased perceived life-stress and increased social support).

In addition to age-associated differences manipulating touch screens, other factors could influence performance. First, low-friction surfaces, such as those found on many touch screens, lead to impaired motor performance [1, 2]. Second, motor performance is dependent on hand use, and left-hand use by right-handed individuals sometimes leads to decreased dexterity [3]. Third, drawing implement (e.g., finger or stylus) has been shown to both improve and impair performance on touch screens [4]. How these factors interact with age to influence use of touch screens is not clear.

Thus, the purpose of our study was to examine differences between young and older adults tracing an Archimedes spiral on a tablet while swiping against low- and high-friction surfaces using either the finger or stylus with the left or right hand.

## METHODS

26 young (age:  $24.0 \pm 3.8$ ; 15 females) and 24 older (age:  $73.9 \pm 6.4$ ; 14 females) adults volunteered. All participants gave informed consent and were right-handed with no reported neuromuscular problems.

Participants traced an Archimedes spiral displayed on an iPad mini rigidly mounted on a force sensor (Fig. 1A). Spiral tracing was completed using: 1) index finger or a stylus, 2) left or right hand, and 3)

a low- or high-friction touch screen surface [5]. Mean RMS error for each condition was calculated to assess the proximity of the participant's trace to the template [6] (Fig. 1B). Mean downward pressing force and completion time were determined for each condition.

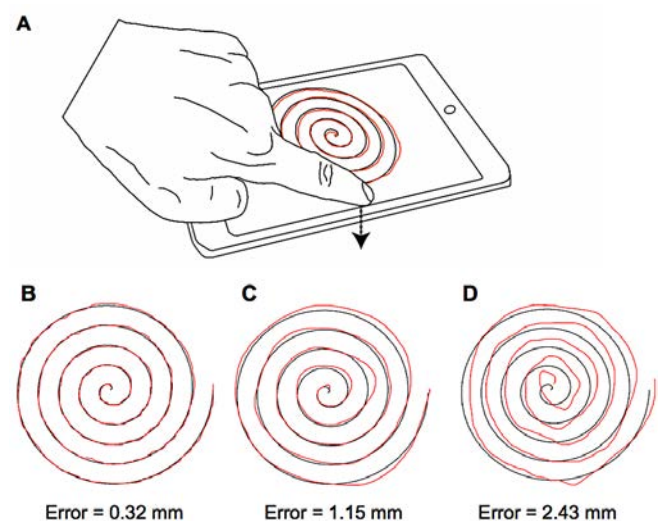


**Figure 1:** (A) Spiral template (black) and subject's trace (red) for the spiral tracing task using the left hand, with normal force aligned with the downward direction (arrow). Representative data for (B) low, (C) medium, and (D) high RMS error.

Additional variables known to change with advancing age were also quantified, as was their relationship to RMS error (e.g., reaction time, fingertip sensory thresholds, and touch screen usage/ownership). Simple reaction time (SRT) and choice reaction time (CRT) tests were completed on a portable laptop. Mean time from stimulus onset to response for 20 trials for each test was determined. Index fingertip sensation was assessed using the standardized von Frey anesthesiometer. A brief survey was given to assess previous touch screen use and ownership.

## RESULTS AND DISCUSSION

Repeated measures ANOVA indicated a significant interaction for RMS error between age and drawing implement (Fig. 2A). In addition, a significant main effect for RMS error was found for hand used and friction condition (Fig. 2B).

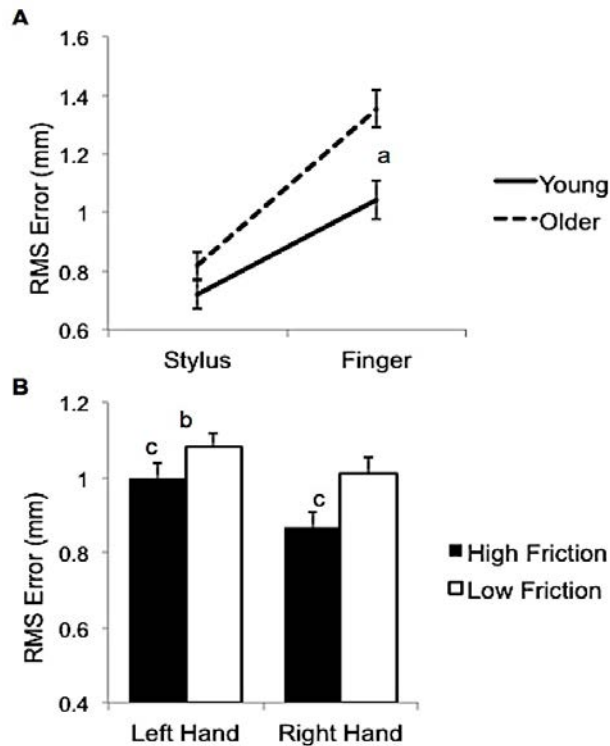


**Figure 2:** RMS error during the spiral tracing task. (A) There was a significant age by implement interaction for the spiral tracing task, with greater RMS error for older vs. younger adults using the finger (<sup>a</sup> $p = .003$ ) and no difference using a stylus ( $p = .165$ ). (B) RMS error decreased using the left vs. right hand (<sup>b</sup> $p < .001$ ), and on the low- vs. high-friction surface (<sup>c</sup> $p < .001$ ).

Sensory thresholds and reaction times were significantly different between young and older adults ( $p < .01$ ), however these and additional variables were not related to increased RMS error in older adults when using their index finger (Table 1).

Though these variables did not correlate with the age-related change in performance when older adults performed the tracing task with their finger (Table 1), one possible explanation for this result may be related to altered visual feedback. The larger size of the fingertip relative to the stylus may occlude a greater area of the display and decrease visual feedback [7], which may be more detrimental for older adults who rely on visual feedback to modify hand trajectories during the task [8].

Results provide evidence for improved touch screen manipulation when using a stylus vs. fingertip by older adults. Moreover, implementing a higher friction touch screen and using the preferred hand improved performance. Further work is necessary to determine whether impaired visual feedback may be responsible for increased RMS error in older adults.

## REFERENCES

- Keenan KG, et al. *J Neurosci* **8**, 8784-89, 2009.
- Keenan KG, et al. *PLoS One* **7**, e48193, 2012.
- Stirling LA, et al. *J Gerontol A Biol Sci Med Sci* **68**, 938-45, 2013.
- Tu H, et al. *Proc. of CHI'12*, 1287-96, 2012.
- Joshi M & Keenan KG. *Exp Brain Res* **234**, 1893-1901, 2016.
- Marmon AR, et al. *Med Sci Sports Exerc* **43**, 560-67, 2011.
- Benko H, et al. *Proc. of CHI'06*, 1263-72, 2006.
- Slavin MJ, et al. *Psych & Aging* **11**, 521-26, 1996.

**Table 1:** Relationship between touch screen performance using the fingertip and completion time, downward force, von Frey index, SRT, and CRT for young and older adults.

	Completion Time	Downward Force	Von Frey Index	SRT	CRT
Young	$r^2 = 0.436$	$r^2 = 0.009$	$r^2 = 0.054$	$r^2 = 0.001$	$r^2 = 0.152$
	$p = 0.002$	$p = 0.643$	$p = 0.255$	$p = 0.909$	$p = 0.049$
Older	$r^2 = 0.090$	$r^2 = 0.005$	$r^2 = 0.025$	$r^2 = 0.024$	$r^2 = 0.057$
	$p = 0.156$	$p = 0.742$	$p = 0.457$	$p = 0.473$	$p = 0.259$

# Mass Properties Comparison of Dismounted and Ground Mounted Head-Supported Mass Configurations to Existing Performance and Acute Injury Risk Guidelines

<sup>1,2</sup> John Wurzbach, <sup>1</sup> SGT Kyle Rybarczyk, <sup>1</sup> B. Joseph McEntire, <sup>1</sup> Dr. Bethany L. Shivers, and <sup>1</sup> Dr. Valeta Carol Chancey

<sup>1</sup> U.S. Army Aeromedical Research Laboratory (USAARL), Fort Rucker, AL

<sup>2</sup> Lailima Government Solutions, LLC, Orlando, FL

email: bethany.l.shivers.civ@mail.mil

## INTRODUCTION

Current U.S. Army head-supported mass (HSM) guidelines, USAARL's Performance Curve (PC) and Acute Injury Risk Curve (AIRC), were developed approximately 20 years ago with a focus on the aviation operating environment. The relationships between mass and vertical and/or longitudinal offset (away from the tragion notch) are critical in assessing risk of performance decrement and acute injury risk. The AIRC was developed with respect to risk of injury during a severe dynamic loading event such as a helicopter crash, and researchers determined change in vertical center of mass (CM) offset to be the best predictor of increased acute injury risk (McEntire, 1998). In comparison, the best predictor of performance decrement was longitudinal CM offset (PC).

The USAARL Curves remain the only established guidelines for U.S. Army HSM, but have limited applicability to individual Soldier movement requirements of the dismounted, ground mounted, and airborne operating environments. Helmet developers and program managers have requested new guidelines be developed for the dismounted, ground mounted, and airborne operating environments that take into consideration currently fielded and proposed HSM configurations. The aim of this project was to measure the mass properties (mass and CM offset) of the currently fielded and proposed HSM configurations and compare them against the existing USAARL Curves.

## METHODS

The mass properties of currently fielded and proposed dismounted and ground mounted helmet systems were measured using the USAARL headform on the Mass Property Instrument (KSR 330-60, Space Electronics). The USAARL headform is representative of the U.S. Army Aviation 50th percentile male. Tested helmets included the Advanced Combat Helmet (ACH), Lightweight ACH, Enhanced Combat Helmet (ECH), Combat Vehicle Crewman helmet (CVC), and a developmental helmet. Helmet attachments included two types of night vision goggles (NVGs), protective masks, spectacles, and one pair of protective goggles. Mass and CM offset were compared against the existing PC (longitudinal offset; X-axis) and AIRC (vertical offset; Y-axis) to assess compliance with the existing guidelines. A total of 50 unique helmet and helmet attachment configurations were assessed.

## RESULTS AND DISCUSSION

Based on the current accepted guidelines, less than 5% (2 of 50) of the measured HSM configurations were acceptable on the AIRC (Figure 1), and 14% (7 of 50) were acceptable on the PC (Figure 2). Twenty-four of the tested configurations exceeded the maximum AIRC and PC recommended mass of 2.5kg, 18 of which had masses greater than 3kg.

Twenty-nine configurations exceeded the maximum vertical offset of 5cm on the AIRC, with ten of those exceeding both maximum mass and maximum vertical offset limits. For example, an extreme HSM configuration (helmet, NVGs, and protective mask) had a mass of 3.4kg with 5.5cm vertical offset and 5.5cm longitudinal offset, exceeding mass and CM offset limits on both curves.

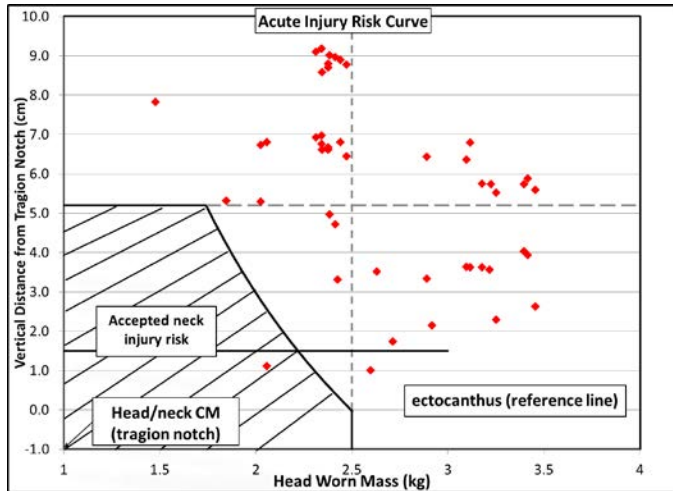


**Figure 1:** Acute Injury Risk Curve with Various Helmet and Helmet Configurations

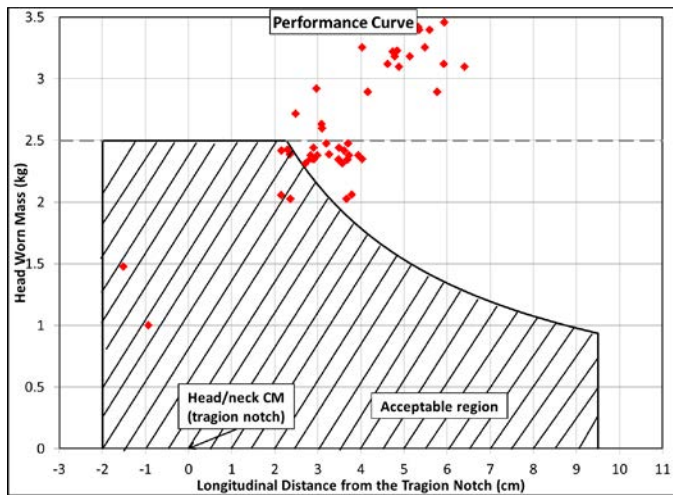


**Figure 2:** Performance Curve with various Helmets and Helmet Configurations

While some individual helmets fell within acceptable limits, the addition of NVGs and protective masks pushed all configurations outside of the recommended guidelines. Frequently used operational configurations, such as the helmet with spectacles and NVGs, exceeded the limits on both AIRC and PC, but were significantly closer to complying with the AIRC and PC curves than less frequently used (worst-case) configurations such as the helmet with NVGs and protective mask.

The current USAARL Curves assess helmets for a small population of the U.S. Army – the Aviator. The ground, dismounted, and airborne Soldier are now exposed to similar helmet loads, but the inertial and moment loading of the cervical spine varies greatly by operating environment.

## CONCLUSIONS

Future curves will need to consider the most likely operating environment, movement techniques, and primary cause of injury. A proposed solution to increased mass and mass offset is to increase or decrease level of protection based on threat. This would allow regulation of the length of time that Soldiers are exposed to extreme HSM configurations. Research should continue to investigate the specific impacts of mass, mass offset, and time of exposure on Soldier health in all operating environments. Guidelines and recommendations developed for the Soldier can be translated to many civilian occupations that use similar, if not identical, HSM configurations such as police SWAT, medical air evacuation pilots and crew, and firefighters.

## REFERENCE

1. McEntire, B.J. (1998). *Mass Requirements for Helicopter Aircrew Helmets*. Ft. Rucker: USAARL

# EFFECTS OF MILITARY LOAD CARRIAGE SYSTEMS ON SHOOTING PERFORMANCE DURING A SIMULATED TACTICAL ENGAGEMENT

<sup>1</sup>Brian K. Higginson and <sup>2</sup>Patrick R. Lindecker

<sup>1</sup>Gonzaga University, Spokane, WA, USA

<sup>2</sup>University of Montana, Missoula, MT, USA

email: [higginson@gonzaga.edu](mailto:higginson@gonzaga.edu)

## INTRODUCTION

Military load carriage systems have recently been found to compromise not only user mobility [1], but also tactical shooting performance [2] and survivability [3] of soldiers. Load carriage systems (such as backpacks) are typically designed to interface with the user directly. In many military applications, duty requirements often dictate that load carriage systems be worn over body armor. This change in load-user interface often results in a subsequent decrease in load stability. In many military career fields, load instability can result in compromised mission-specific task performance and survivability, particularly during tactical engagements. The two most viable solutions to maximize load stability when an external load is worn over body armor is to develop an integrated armor/load carriage system, or modify the existing load carriage systems to provide a more stable load-user interface. While development of integrated armor/load carriage systems are ongoing, the current study aims to determine the effectiveness of an integrated bolster system to stabilize external loads being worn over body armor.

The purpose of this study was to 1) determine the influence of military load carriage systems on tactical shooting performance measures during dynamic target acquisition and engagement tasks, and 2) determine if external load stabilizers can be effectively used to reduce any potential compromises in tactical shooting performance.

## METHODS

Eleven Special Weapons and Tactics (SWAT) team members (Mean  $\pm$  SD: 41.2 $\pm$ 5.7 yrs, 179.3 $\pm$ 6.0 cm, 92.8 $\pm$ 10.1 kg) participated in a simulated tactical

engagement consisting of three separate targets. The first target was located 10 meters directly in front of the shooter and was acquired starting from the rifle ready (contact/close contact) position. The other two targets were located 60° to the right and left of this forward target, at the same linear distance from the shooter. After engaging the first target, the shooter immediately engaged either the right or left target as fast as possible, finishing with the remaining target. Target engagement order was counterbalanced and dictated to the subject in real time using an external auditory cue, coming from the next target to be engaged, immediately prior to engagement of the first target.

The targets were engaged by the shooter using a fully functional weight-matched airsoft M4 Carbine with inertial properties matching those of an actual M4 in use by the U.S. military. An optical targeting system was mounted to the rifle barrel allowing quantification of all shooting performance measures. Shooting performance measures consisted of accuracy, shot placement, time on target, and engagement times (time between shots). Each shooter engaged the three targets under three different conditions: 1) while wearing body armor with no load, 2) while wearing body armor and a 16 kg assault load contained within a standard assault pack, and 3) while wearing body armor and a 16 kg assault load contained within a standard assault pack equipped with a load stabilizer (bolster system). Previous unpublished data from novice shooters indicates that there may be a direction effect, with shooting performance being dependent on whether the right or left target was engaged immediately after the forward target. For this reason, each loaded condition was performed in each direction in replicate (12 shooting bouts total), and averaged (within direction) for analysis.

Shooting outcome measures were compared across conditions using 2 x 3 (direction x load) repeated measures ANOVA ( $\alpha=.05$ ). Sheffé's post-hoc test was performed for any significant main effect of load.

## RESULTS AND DISCUSSION

As seen with previously unpublished data using novice shooters, there was a small, but significant, increase in engagement times of the second target when it was located to the right vs. left of the forward target ( $1.27\pm 0.08$  vs.  $1.16\pm 0.08$  s, respectively;  $p<.001$ ). This was most likely a function of hand/eye dominance of the shooters. Tactical shooting is typically performed using a "both eyes open" strategy. Since all shooters were right handed, this placed the left target closest to their "free" eye, and the right target closest to their "sight" eye. Unlike direction, load had no effect on engagement times while moving from the first to second targets ( $p=.268$ ). Unlike engagement times for the second target, engagement times for the third target were not affected by the direction of acquisition ( $p=.836$ ), but were found to be significantly longer ( $p=.026$ ) for the bolstered condition ( $1.62\pm 0.11$  s) than the unloaded condition ( $1.44\pm 0.09$  s).

Interestingly, after collapsing engagement times across direction and load, it was found that these times did not double from targets 1-2 to 2-3 as expected. Although there was a significant increase in engagement times from targets 1-2 and 2-3 ( $p<.001$ ), the overall magnitude was relatively small ( $1.21\pm 0.08$  vs.  $1.52\pm 0.09$  s, respectively). Given that the angular displacement was twice as great going from target 2-3 as target 1-2 ( $120^\circ$  vs.  $60^\circ$ , respectively), these results indicate that the shooters had an increased angular velocity while engaging the third target when compared to the second.

The time on target prior to engagement was not influenced by direction or load for either the second target ( $p=.310$  and  $p=.402$ , respectively) or third ( $p=.122$  and  $p=.064$ , respectively). This was not unexpected as this target acquisition and engagement task was so dynamic that very little time (0.32 - 0.44 s) was spent on each target, regardless of condition.

Measures of accuracy were not influenced by direction of target engagement or load condition for either the second target ( $p=.251$  and  $p=.591$ , respectively) or third target ( $p=.668$  and  $p=.828$ , respectively) engaged. Similarly, when comparing accuracy between targets 2 and 3, there was no change in accuracy ( $71.5\pm 7.2$  vs.  $68.3\pm 6.4$  mm, respectively;  $p=.400$ ). As with time on target measures, the dynamic nature of this shooting task may have contributed to the lack of differences seen in accuracy measures between conditions and targets. The dynamic nature of this task resulted in relatively large variability between conditions within each subject.

## CONCLUSIONS

The results of this study indicate that engagement times, time on target, and accuracy are minimally affected by load carriage systems during a tactical target acquisition and engagement task. Likewise, from a functional outcomes perspective, the use of a load stabilizer appeared to have little influence on these measures. The lack of significant findings in the current study may be due in part to the highly dynamic nature of this task resulting in relatively large variability between conditions.

This study primarily focused on functional performance outcomes. It may be possible that the use of other more sensitive measures, such as quantifying pack and rifle motion relative to the shooter, may provide more insight into the relationship between load carriage systems and tactical shooting performance. In addition to incorporating more sensitive measures, future research should consider different loads and load distributions, as well as varying engagement strategies and requirements.

## REFERENCES

1. Carlton SD and Orr RM. *Intl J of Occup Safety and Erg* **20**, 33-41, 2014.
2. Palmer JP, et al. *Ergonomics* **56(11)**, 1708-1721, 2013.
3. Billing DC, et al. *J of Str and Cond Research* **29(11S)**, S134-S138, 2015.

# UPPER EXTREMITY MUSCLE ACTIVATION AND STRENGTH ASSESSMENT IN NATIVE AND NON-NATIVE SIGN LANGUAGE USERS

<sup>1,2</sup>Gretchen Roman, <sup>1</sup>Naoaki Ito, and <sup>1</sup>Meghan E. Vidt

<sup>1</sup>Exercise Science and Health Promotion, Arizona State University, Phoenix, AZ, USA

<sup>2</sup>Physical Therapy, Midwestern University, Glendale, AZ, USA

email: garoman@asu.edu

## INTRODUCTION

Over 30% of sign language interpreters are injured on the job [1]. Job demand for interpreters and translators is anticipated to grow 29% by the year 2024 [2]. Because of this projected growth, an even higher number of sign language interpreters are expected to suffer from musculoskeletal (MSK) pain. Most interpreters are non-native American Sign Language (ASL) users – individuals born to non-signing, hearing parents. Native ASL users – Deaf or hearing individuals who have at least one Deaf parent – are an overlooked demographic within sign language interpreting research [3]. Upper extremity (UE) biomechanical considerations unique to the work style of sign language interpreters have long been identified, but only crudely noted. The proposed biomechanical considerations thought to relate with MSK injury include ballistic signing, insufficient micro rest breaks, excessive deviations from neutral wrist, excursions outside the normal interpreting work envelope, and muscle tension [4]. However, little quantitative information is available describing the influence of these biomechanical contributions on the increased MSK injuries reported by non-native ASL users. The focus of this study is to characterize muscle tension and rest in a cohort of native and non-native ASL users while signing. It is hypothesized that non-native users will have worse outcomes, presenting with shorter rest and greater muscle tension, which will be correlated with increased MSK pain and UE weakness.

## METHODS

Five native (4F/1M; 3 Deaf/2 hearing; all right-hand dominant) and 5 non-native (3F/2M; 5 Deaf; 4 right-/1 left-hand dominant) ASL users (age  $41.8 \pm 15.53$  yrs) were studied. Participants interpreted, at a self-selected pace, 3 trials of a 7min source from a video in sign language with audio and closed captioning.

At least 5min rest was given between trials. The third trial was selected for analysis. For all trials, a Noraxon DTS system (Noraxon, Inc., Scottsdale, AZ) was used to measure surface electromyography (EMG). Measures were acquired bilaterally from upper, middle compartments of trapezius, and anterior, middle compartments of deltoid at 1000 Hz. Prior to data collection, maximal voluntary contractions (MVC) were acquired using postures that elicit maximal activity. Surface EMG was processed with a custom Matlab (MathWorks, Inc., Natick, MA) program. Raw EMG signal was band-pass filtered from 10-490Hz with a 4<sup>th</sup> order Butterworth filter, rectified, and enveloped with a 2<sup>nd</sup> order low-pass Butterworth filter with 3Hz cutoff frequency. Signal was normalized by each muscle's corresponding MVC. Micro rest breaks were quantified from processed EMG signal as temporal delay between sequential signs ( $\geq 0.2565$ sec duration with a level of activation  $< 18\%$  of MVC) [5]. Muscle tension was quantified by mean %MVC activation. %rest and %MVC were evaluated across the entire trial duration.

Isometric joint moment was used to assess strength. Measurements were taken at the shoulder for abduction/adduction, flexion/extension, and internal/external rotation with a Humac Norm (CSMI, Stoughton, MA) isokinetic dynamometer. Three 5sec trials were performed for each direction; 1min rest was given between trials and 2min rest was given between tests to offset fatigue [6]. A custom Matlab program was used to identify the maximum joint moment maintained for at least 0.5sec. The maximum value across the 3 trials was evaluated.

MSK pain was measured using a numeric pain rating scale (NPRS) [7]. Participants were asked to rate whether they experience pain from using sign language on a 0-10 scale (0=no pain; 10=worst imaginable pain). A participant with a rating  $> 0$  was

considered to have pain, while a 0 rating was considered without pain.

Group differences between native and non-native ASL users (independent variables) were evaluated using separate Mann Whitney U tests for rest (%rest), muscle tension (%MVC), and strength for self-reported dominant and non-dominant sides (dependent variables). Group differences between those with and without pain (independent variables) were also evaluated using separate Mann Whitney U tests for the same dependent variables. Associations between significant %rest and %MVC findings in the separate muscle compartments were evaluated with corresponding strength measures using Spearman correlation analyses. All analyses were performed using SPSS, (v.23, IBM Corp., Armonk, NY).

## RESULTS AND DISCUSSION

Native ASL users had significantly more %rest compared to non-native in the non-dominant anterior deltoid ( $p=0.009$ ), dominant middle deltoid ( $p=0.047$ ), and non-dominant upper trapezius ( $p=0.047$ ) (Fig. 1). Within the non-native group, there were no differences in the significant %rest measures between those with and without pain (all  $p>0.248$ ). When evaluating the association between significant %rest and corresponding muscle strength, dominant middle deltoid %rest for the non-native group was positively correlated with dominant shoulder abduction ( $r^2=1.0$ ;  $p=0.01$ ).

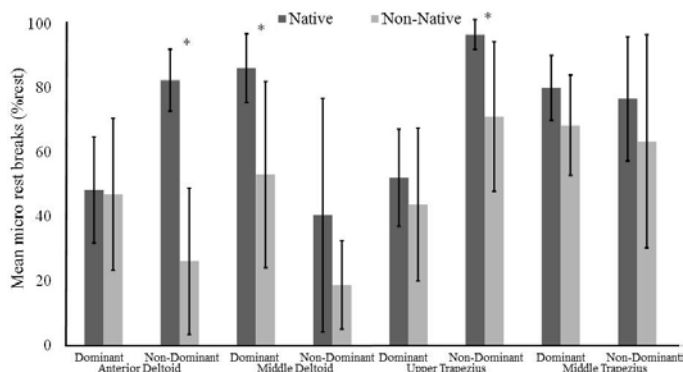


**Figure 1:** Mean (95% confidence interval) micro rest (%rest) for native and non-native ASL users;  $p$ -value $<0.05^*$ .

Non-native ASL users demonstrated greater %MVC activation for non-dominant anterior deltoid ( $p=0.009$ ) and non-dominant upper trapezius ( $p=0.047$ ) (Fig. 2). Within the non-native group, there were no differences in significant %MVC

between those with and without pain (all  $p=0.564$ ). There was no correlation between significant %MVC and corresponding strength for native and non-native groups. UE strength differences were not significant between native and non-native groups (all  $p>0.076$ ), or between those with and without pain (all  $p>0.221$ ).

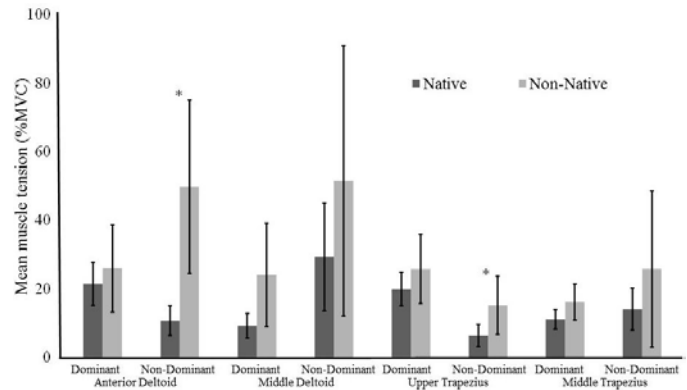


**Figure 2:** Mean (95% confidence interval) muscle tension (%MVC) in native and non-native ASL users;  $p$ -value $<0.05^*$ .

## CONCLUSIONS

Non-native ASL users demonstrated lower %rest, and greater %MVC activation for muscle groups at the shoulder compared to native ASL users. MSK pain was not significantly associated with amount of time spent in rest or muscle tension, which were hypothesized to be indicators of cumulative muscle strain. The association between dominant shoulder abduction weakness and fewer micro rest breaks potentially leads to higher short-term fatigue and greater injury risk long-term. A longer source duration or increased number of trials, and a quantitative measure of fatigue may help to foster a better understanding of the role of muscular fatigue in ASL users. Ongoing work continues to identify primary contributors to increased MSK injury risk in ASL users, including assessments of a larger cohort, and the influence of kinematic and kinetic measures.

## REFERENCES

1. Kroeger, M. *RID Views* **31**, 42-43, 2014.
2. Bureau of Labor and Stats. Occupational Outlook Handbook, 2016.
3. Williamson, A. *MAIS Theses*. Paper 22, 2015.
4. RIT. *Cumulative Trauma Disorder*. Rochester, NY, USA, 2005.
5. Delisle A, et al. *Eur J of Appl Physiol* **95**, 448-460, 2004.
6. Chaffin D. *Am Indus Hygiene Assoc J* **36**, 505-511, 1975.
7. Kahl C, et al. *Phys Ther Rev* **10**, 123-128, 2005.

## ACKNOWLEDGEMENTS

Funding for this project was provided by start-up funds (PI: Vidt) from Arizona State University.

# ARE HYBRID SIT-STAND POSTURES A GOOD COMPROMISE BETWEEN SITTING AND STANDING?

Mamiko Noguchi, Michal Glinka, Maureen F. Riddell, Graham Mayberry, and Jack P. Callaghan

Department of Kinesiology, University of Waterloo, Waterloo, ON, CAN

email: [mnoguchi@uwaterloo.ca](mailto:mnoguchi@uwaterloo.ca)

## INTRODUCTION

Both standing and sitting postures, when maintained statically for a prolonged period of time, are linked to the development of low back pain and discomfort [1]. The range of hybrid sit-stand postures (i.e. perching) offers potential alternatives between sitting and standing. Sit-stand stools allow users to work near their standing height, while offloading some upper body weight onto the stool to relieve lower limb demands. Compared to sitting, perching reduces anterior-posterior shear force at the low back and encourages users to move more frequently [2]; however, it is also associated with increased lower leg swelling, decreased hip comfort [3], and no difference in low back discomfort [2]. Perching also reduces anterior-posterior shear force at the low back when compared to standing [2]; however, lower limb discomfort may be higher or lower depending on the footrest position [2,3,4], and back extensor activity and co-contraction are higher in perching [2]. As these results show, there are some benefits to the use of sit-stand stools; however, questions remain as to whether perched postures are different enough to be a solution for the negative consequences associated with sitting and standing.

Although perching encompasses a range of postures from sitting to standing, there is limited empirical evidence to suggest how a sit-stand stool should be set up. It has been suggested that the lumbar angle closest to neutral with the thigh muscles in passive equilibrium is 135° of trunk-thigh angle in lateral recumbent position [5]. In addition, reclining the chair backrest to 130° reduced the lumbar load by approximately 60% [6]. However, there has yet to be a quantitative study examining whether this angle is in fact optimal and preferred when upright. Therefore, the primary purpose of this study was to identify where lumbar and pelvic angles deviate from sitting and standing and determine three phases: sitting, perching, and standing. The secondary purpose was to examine the differences between phases for trunk and knee extensor muscle activities and ground reaction forces.

## METHODS

Twenty-four participants, 12 males (age  $25.7 \pm 2.3$  years; height  $177.5 \pm 5.6$  cm; mass  $80.2 \pm 15.3$  kg) and 12 females (age  $24.3 \pm 2.2$  years; height  $167.5 \pm 6.1$  cm; mass  $66.0 \pm 8.6$  kg), were recruited. Each participant completed 19 one-minute trials from sitting (90° trunk-thigh angle) to standing (180° trunk-thigh angle) in 5° trunk-thigh angle increments. Three-dimensional kinematic data were collected from trunk, lumbar, pelvis, thighs, and shanks at 50 Hz (Northern Digital Inc., ON), and Cardan angles (sagittal-frontal-transverse) were calculated using Visual 3D (C-Motion, MD). Both lumbar and pelvic angles were expressed as the deviation from the five-second standing trial that was completed before the study began. To assess whether the transition postures significantly deviated from either standing or sitting postures, a statistical approach employing Dunnett's test was performed (R3.3.0 MULTCOMP) for each gender separately.

Electromyography (EMG) data were collected from thoracic erector spinae (TES), lumbar erector spinae (LES), and vastus medialis oblique (VMO) at 2000 Hz (AMT-8; Bortec Biomedical Inc., Calgary, AB). After removing electrical and heart rate artifacts and normalizing the data (%MVC), an average was calculated for each of the one-minute trials. Ground reaction forces were collected at 400 Hz (OR6-7, AMTI Inc., Watertown, MA) and normalized to the participant's body weight (%BW). Similar to EMG, an average of each trial was calculated for each axis of force. Using the classification from each gender, one-way repeated measures ANOVAs were performed to determine the effect of phases ( $p < 0.05$ ).

## RESULTS AND DISCUSSION

Standing lumbar and pelvic angles were different from all other trunk-thigh angles for both males and females ( $p < 0.0001$ ), suggesting that standing is a distinct posture and is difficult to achieve with the current seat interface (e.g. flat, low friction surface) and within the constraints of this study (e.g. feet

position, shank angles). Lumbar angle deviated from sitting at 145° ( $p = 0.0001$ ) and 160° ( $p < 0.0001$ ) trunk-thigh angles for males and females, respectively (Figure 1 top). Pelvic angle was different from sitting at 180° trunk-thigh angle ( $p = 0.004$ ) for males and at 115° and 180° trunk-thigh angles ( $p = 0.025$ ) for females. This gender difference comes from females tending to maintain a more upright posture (less lumbar flexion and more anterior pelvic tilt) compared to males [7], resulting in a wider range of angles that are similar to sitting. Both lumbar and pelvic angles at 135° trunk-thigh angle, as suggested by Keegan [5], were not different from sitting.

The level of muscle activity was low ( $< 10\%$  MVC) in all muscles throughout the trials (Figure 1 bottom). Males exhibited no difference between phases for both trunk extensors (TES  $p = 0.247$ ; LES  $p = 0.319$ ) while a significantly lower VMO activity was seen in standing compared to perching or sitting ( $p = 0.005$ ). Females showed significant differences in all muscles in which TES was higher in sitting compared to perching or standing ( $p < 0.005$ ), LES was higher in standing compared to perching ( $p = 0.015$ ), and VMO was lower in standing compared to perching or sitting ( $p = 0.003$ ). In terms of ground reaction force, all phases were different from each other in the anterior-posterior direction ( $p < 0.001$ ), where perching required approximately 15% BW to maintain postures. Taking both EMG and force data into consideration, the notable differences between phases were in the level of leg effort required to remain upright, which provides insight into considerations for seat designs.

## CONCLUSIONS

Whenever the pelvis is in contact with a low friction supporting surface, changes in lumbar angle do not occur for a wide range of trunk-thigh angles [8]. While the lumbar angle gradually shifted towards neutral from approximately 110° trunk-thigh angle, VMO activity and anterior-posterior shear force at the feet increased, reaching its maximum at 145° trunk-thigh angle. There is no ‘ideal’ seat position that includes all of the benefits from sitting, perching, and standing; however, it is possible to increase the range of perching with fewer lower limb challenges.

Therefore, future chair designs should be focused on reducing discomfort between 115 and 170° trunk-thigh angles with these two key points in mind: 1) the seat interface focusing on pelvis alignment to improve lumbar angles and to offload some of the lower limb demands and 2) the design of the foot support focusing on redirecting force from shear to compression with respect to the lower limb joints [4] while reducing cumbersomeness when it is in use.

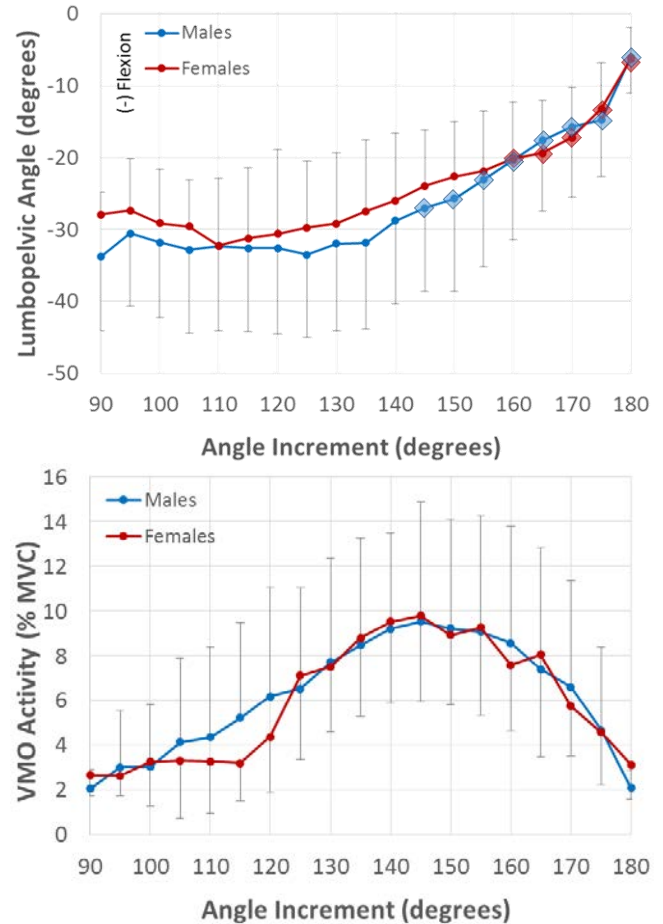


**Figure 1:** Lumbar angle (top) and VMO activity (bottom) from sitting (90° trunk-thigh angle) to standing (180° trunk-thigh angle) postures. The square markers denote significant difference from the sitting posture ( $p < 0.05$ ).

## REFERENCES

- [1] Callaghan JP, et al. *Ergon. Des. Q. Hum. Factors Appl.*, **23**, 20-24, 2015.
- [2] Le P. & Marras WS. *Appl. Ergon.*, **56**, 170-178, 2016.
- [3] Chester M, et al. *Int. J. Ind. Ergon.*, **29**, 289-296, 2002.
- [4] Antle DM, et al. *Int. J. Ind. Ergon.*, **45**, 98-106, 2015.
- [5] Keegan JJ. *J. Bone Joint Surg. Am.*, **35-A**, 589-603, 1953.
- [6] Rohlmann A, et al. *Spine J.*, **11**, 870-875, 2011.
- [7] Dunk KM. & Callaghan JP. *Clin. Biomech.*, **20**, 1101-1110, 2005.
- [8] Dunk KM, et al. *Clin. Biomech.*, **24**, 164-168, 2009.

# POSTURAL EVALUATION OF DENTAL CARE PROFESSIONALS USING MOTION ANALYSIS AND ELECTROMYOGRAPHY

<sup>1</sup>Ricky Abnos, <sup>1</sup>Saefer Siddicky, <sup>1</sup>Maureen Muller, <sup>1</sup>Bonnie Branson, <sup>1</sup>Melanie Simmer-Beck, and <sup>1</sup>Gregory King

<sup>1</sup>University of Missouri- Kansas City, Kansas City, MO, USA  
email: rickyabnos@mail.umkc.edu

## INTRODUCTION

Dental care practitioners frequently encounter neck, back, and shoulder injuries caused by long durations of time in non-neutral positions. Musculoskeletal pain in the upper body appears early in practitioners' careers and often leads to reduced hours or early exit from clinical practice [1-2]. Impairment caused by musculoskeletal disorders (MSDs) on dental operators' clinical activities has a significant impact on the healthcare delivery system and can become a factor in rising costs of healthcare. Several interventions have been suggested to reduce the risks of MSDs among dental operators. Previous studies have used operator awareness [3] and physical fitness [4] to reduce the risk of MSDs in dental practitioners.

Another intervention is the use of magnification loupes to increase visibility of the mouth, thereby improving dental clinicians' posture. Numerous studies have reported the value of loupes for this purpose, but most have used subjective or qualitative data as justification, such as self-reported pain scales and real-time or video evaluations [5-10]. The emergence of motion capture equipment and analysis provides a quantitative method to analyze body kinematics during practice and therefore evaluate whether interventions lead to ergonomic postures [11-15]. Electromyography is another tool which can be used to quantify the effects of intervention through analysis of muscle activity. The purpose of this study was to investigate the feasibility of using motion analysis and electromyography in quantifying dental operator posture. We hypothesized that the use of magnification loupes would exhibit trends toward improved posture, as quantified by upper extremity kinematics and muscle activity.

## METHODS

Two subjects participated in this study, which was approved by the University of Missouri- Kansas City Institutional Review Board. Subjects were selected based on opposing demographics. There was one male subject and one female subject, one of whom was a recent graduate of a periodontal residency program, and the other was a dental hygienist. Both were of similar height. Each operator received a complimentary set of Through-the-Lens (TTL) and Flip-Up lens (FL) loupes (Orascoptic, Middleton, WI, USA). Each subject also used his or her own basic eyewear (BL), including safety lenses worn by the periodontist, and prescription lenses worn by the dental hygienist. Each operator used a light attached to the loupes, and the overhead dental operatory light when using basic eyewear. A standard dental operatory was equipped with 10 OptiTrack Flex 13 motion capture cameras (NaturalPoint, Inc., Corvallis, OR, USA). Each subject was fitted with a motion capture suit to which reflective motion capture sensors were applied. This system measured and recorded 3D positions of the markers during each procedure. Data were collected using Motive software (NaturalPoint), and analyzed using MATLAB (The MathWorks Inc., Natick, MA, USA). Motion data was collected at 120 Hz. Each operator was also fitted with DELSYS Myomonitor IV electromyography (EMG) sensors bilaterally on the upper trapezius and the lumbar erector spinae. Data was collected using the EMGWorks software (DELSYS) at 2 kHz. The operator sat on a stool equipped with a back rest and wheels. Data was collected while the practitioner collected periodontal depths of the patient using a standard probe. The same live patient was used for all procedures, and the type of lenses worn varied for

each of the 3 data collection sessions to minimize practice effects.

Marker position data were used to calculate head angle time series representing forward and lateral angular deviation of the head away from the body midline. Angular range of motion and standard deviations were extracted for 3 different time series: a fixed 40-second duration ( $T_{40}$ ) in which the operator was actively performing the task, the duration in which the operator's chair was between the 9 and 12 o'clock positions ( $T_{9-12}$ ) relative to the patient, and reach-to-reach ( $T_{Reach}$ ), the duration between reaching movements to pick up and set down the probe. To examine muscle activation, raw EMG data was normalized to maximum EMG amplitude within each trial, and root mean square (RMS) values of the EMG data were calculated for  $T_{40}$  time series only.

## RESULTS AND DISCUSSION

Both operators exhibited reduced forward flexion range of motion when using TTL or FL loupes compared to BL conditions. On average, Subject 1 used 50.1% and 48.9% less forward flexion when using TTL and FL lenses respectively, in comparison to the BL lens. Subject 2 on average used 73.9% and 26.6% less forward flexion when using FL and TTL lenses, respectively, in comparison to the BL lens. Table 1 demonstrates the forward flexion range of motion for each of the 3 time series conditions.

**Table 1:** Forward Flexion ROM, in Degrees

	Subject 1			Subject 2		
	$T_{40}$	$T_{9-12}$	$T_{Reach}$	$T_{40}$	$T_{9-12}$	$T_{Reach}$
BL	22.3	19.6	20.2	16.8	18.2	21.7
TTL	12.3	8.5	10.3	12.7	14.3	14.3
FL	10.0	10.8	10.8	0.4	8.7	6.1

No consistent trends were observed in lateral flexion range of motion. This is likely attributable to relatively high variability of head movements in the frontal plane. Additionally, EMG results did not exhibit any consistent trends across testing conditions. This is likely due to the unconstrained time durations across which RMS values were

calculated. In addition to larger sample sizes, future studies using EMG should report muscle activity over smaller and more accurately-defined sub-tasks comprising the overall procedure.

## CONCLUSIONS

In this study, we observed a consistent trend towards improved posture when using magnification loupes during a routine dental procedure. This preliminary analysis provides some basis for the use of motion capture and electromyography in evaluating the effectiveness of ergonomic interventions for medical care providers. This was a pilot study, and further research with a larger sample size is necessary to fully evaluate the utility of motion and EMG analysis of dental operators. Additionally, the clinicians were evaluated in an authentic dental clinical setting not designed for motion capture research, and the suits worn by the practitioners may have interfered with their posture, comfort, and clinical ability. Furthermore this study was conducted without a set period of time or pre-determined order for mouth probing; implementing procedures for these aspects in future studies may improve consistency.

## REFERENCES

1. Morse T, et al. *Work* **35**, 419-429, 2010.
2. Morse T, et al. *J Dent Hyg* **81**, 10, 2007.
3. Kanteshwari K, et al. *Gen Dent* **59**, 476-483, 2011.
4. Valachi, et al. *Dentistry Today* **30**, 144-7, 2011.
5. Dable et. al. *J Indian Prosthodont Soc* **14**, 51-8, 2014
6. Farook et. al. *J Invesitg Clin Dent* **4**, 120-3
7. Hayes et. al. *Work* **53**, 755-62, 2016
8. Hoerler et. al. *J Dent Hyg* **86**, 323-30, 2012
9. Maillet et. al. *J Dent Educ* **72**, 33-44, 2008
10. Perrin et. al. *Swiss Dental Journal* **126**, 222-35, 2016
11. Dalton et. al. *JoVE*, 111, 2016
12. Dowling et. al. *Sports Biomech* **15**, 255-69, 2016
13. Faber et. al. *J Biomech* **49**, 904-12, 2016
14. Paul et. al. *Anatomical Record* 2016
15. Pavan et. al. *Gait & Posture* **38**, 951-5, 2013

# BIOMECHANICAL DIFFERENCES IN LIFTING BETWEEN A MANUAL VS. POWER COT

<sup>1</sup> Steven Capehart, <sup>1</sup>Michael Callihan, <sup>1</sup>Amanda Ransom, and <sup>1</sup>Katherine Worcester

<sup>1</sup>The University of Kentucky, Lexington, KY, USA

Email: steven.capehart@uky.edu

## INTRODUCTION

Musculoskeletal injuries consistently account for about half of all injuries to emergency medical service (EMS) providers (1). These injuries result in lost work time, permanent disability, and high worker compensation costs (2). More than half of all EMS injuries happen when lifting patients and the back is the primary body part affected (3).

National Institute for Occupational Safety and Health (NIOSH) has established safe lifting limits for health care providers of 51 pounds but unfortunately for EMS, many routine lifts, far exceed this recommended compression limit (1). As the prevalence of obesity in the general population increases, the risk for injury to EMS workers who handle and transport patients increases (4).

One such lifting scenario where EMS workers may be at risk of injury occurs when lifting ambulance cots, with patients on them, from the ground to standing height. Implementing mechanical lifting equipment in these situations may reduce the risk of musculoskeletal injury by reducing the force required to lift the patient.

Thus, the purpose of this study was to analyze trunk and lower extremity muscle activity and sagittal plane kinematics and kinetics when lifting a patient between two different cots (mechanically operated cot (Power-cot) and manually operated cot (Manual-cot)).

## METHODS

As of this submission, 10 healthy female nursing students (age  $23.6 \pm 3.2$  weight (kg)  $64.5 \pm 9.8$  height (m)  $142.8 \pm 3.2$ ) and 4 male emergency medical service (EMS) providers age  $34.6 \pm 5.3$  weight (kg)  $80.5 \pm 7.9$  height (m)  $1.78 \pm 0.4$ ) were recruited to take part in a larger study analyzing lifting mechanics during various work-related lifts. The nursing students in this study were untrained as

they have never used the Manual or Power cot before. The EMS providers in this study were considered trained as they have had previous experience using both types of cots regularly.

Stryker EMS provided us with Performance-PRO XT cot (Manual) and Power-PRO XT cot (Power) for comparison in this study (Figure 1A, 1B). The Manual cot features a handle grip that requires two lifters (Figure 1A). For the Manual cot condition, the subjects were at the feet of the cot, while the same trained EMS was lifting from the head of the cot. The mechanically operated Power cot features a battery-powered hydraulic system that raises and lowers the cot with the touch of a button only requiring 1 person. Subjects performed 3 trials lifting the cots from the ground to standing height for each cot. To represent the weight of an average patient, a 75-kg mannequin was secured resting on each cot during collection.



**Figure 1:** A) Manual cot handle vs. B) Power cot handle  
Lower extremity kinematic, kinetic and electromyography were collected during each lift.

Retroreflective markers were placed bilaterally on bony landmarks of the trunk, pelvis and lower extremity and were collected using 10 high speed Motion Analysis Cameras (Motion Analysis Corp, Santa Rosa, CA) at a sampling rate of 200 Hz. Kinetic variables were collected using two Bertec force plates (Bertec Corporation, Columbus, OH) to collect ground reaction forces at 1000 Hz. Joint/segment dynamics were calculated in Visual 3D (C-Motion Inc, Germantown, MD). All kinetic data were normalized to the participants' body mass (kg). Muscle activity (EMG) of the gluteus maximus (GM) rectus femoris (RF), biceps femoris (BF), external oblique (EO), rectus abdominus (RA) and erector spinae (ES) was measured through surface EMG and amplified by a Bagnoli™ 16-channel system (Delsys Inc.)

Statistical comparisons were made via paired t-tests comparing manual vs power cot for both the nursing and EMS groups with  $\alpha = 0.05$  using GraphPad Prism version 7.00 for Windows, GraphPad Software, La Jolla California USA.

## RESULTS AND DISCUSSION

Results of this study found that peak muscle activity of all the trunk and lower extremity muscles were significantly lower ( $p < .001$ ) in the Power Cot condition for both the nurse and EMS groups (Table 1). The most dramatic decrease in peak muscle activity was observed in the RF ( $\downarrow 44.2\%$ ) and BF ( $\downarrow 40.2\%$ ) for the nurse group and RF ( $\downarrow 32.3\%$ ) and GMAX ( $\downarrow 31.9\%$ ) for the EMS group. The Rectus Abdominis had the least amount of change for the nurse ( $\downarrow 1.7\%$ ) and EMS ( $\downarrow 1.8\%$ ).

There was no significant difference between the different lifts for peak trunk or pelvic angle in either

group. Peak hip and knee flexion angle were significantly decreased ( $p < 0.001$ ) during the Power cot condition for both the nurse ( $\downarrow 32^\circ$ , &  $\downarrow 38^\circ$ ) and EMS group ( $\downarrow 25^\circ$ , &  $\downarrow 42^\circ$ ). Peak hip and knee extension moments were significantly decreased ( $p < .001$ ) during the Power cot condition for both the nurse ( $\downarrow 1.1$  Nm/kg, &  $\downarrow 0.23$  Nm/kg) and EMS group ( $\downarrow 0.69$  Nm/kg, &  $\downarrow 0.32$ ).

**Table 1:** Results presented as Peak EMG %MVIC mean and standard deviation. \*  $p < 0.001$  v. Manual

	Nurse		EMS	
	Manual	Power	Manual	Power
<b>ES</b>	37.0 ± 39.7	16.0 ± 23.5*	11.7 ± 2.2	7.1 ± 1.3*
<b>RAB</b>	9.0 ± 3.0	7.3 ± 2.1*	8.4 ± 2.8	6.6 ± 1.5*
<b>RF</b>	70.0 ± 45.3	26.8 ± 28.7*	40.8 ± 38.7	8.5 ± 1.4*
<b>BF</b>	56.8 ± 46.3	16.6 ± 9.9*	37.3 ± 28.2	20.5 ± 11.9*
<b>GMAX</b>	34.0 ± 22.6	12.6 ± 12.3*	51.0 ± 30.0	19.1 ± 11.7*

## CONCLUSIONS

The significantly lower peak muscle activity, and peak joint moments in the Power-cot may indicate that using a Power-cot is much less strenuous and may decrease the risk of musculoskeletal injury when lifting patients.

## ACKNOWLEDGEMENTS

Special thanks to Stryker EMS for allowing the use the Power-PRO XT cot and the Performance-PRO XT cot for our study.

## REFERENCES

1. Lavender. *Applied Ergonomics*, 2007.
2. Walton. *Am. J. Ind. Med.*, 2003.
3. Hogle. *Am J Emerg Med*, 1990
4. CDC.gov

**Table 2:** Results presented as mean and standard deviation. \*  $p < 0.001$  v. Manual

	NURSE		EMS	
	Manual	Power	Manual	Power
Peak Trunk Flexion Angle (°)	62.89 ± 14.67	68.25 ± 15.37	46.65 ± 4.18	56.72 ± 1.30
Peak Anterior Pelvic Tilt Angle (°)	42.45 ± 7.73	42.59 ± 11.11	36.22 ± 16.29	45.38 ± 21.40
Peak Hip Flexion Angle (°)	106.49 ± 19.51	75.84 ± 25.75*	107.00 ± 13.68	81.84 ± 11.98*
Peak Knee Flexion Angle (°)	92.92 ± 29.99	54.48 ± 45.45*	110.45 ± 13.31	67.92 ± 39.06*
Peak Hip Moment (Nm/kg)	1.87 ± 0.45	0.77 ± 0.34*	1.32 ± 0.22	0.63 ± 0.25*
Peak Knee Moment (Nm/kg)	0.46 ± 0.31	0.23 ± 0.44*	0.98 ± 0.28	0.65 ± 0.46*

# BIOMECHANICALLY-ASSISTIVE GARMENT OFFLOADS LOW BACK DURING LEANING AND LIFTING

Erik P. Lamers, Aaron J. Yang and Karl E. Zelik

Vanderbilt University

email: erik.p.lamers@vanderbilt.edu, web: my.vanderbilt.edu/batlab

## INTRODUCTION

Low back pain is the leading cause of limited physical activity, affecting 80-85% of adults in their lifetime [1]. Development of low back pain can result from elevated, prolonged and/or repetitive forces on the spine, which commonly occur during daily activities such as leaning and lifting. Wearable assistive devices (e.g., exoskeletons) are emerging as a potential means of mitigating low back injury risks and associated pain, by offloading the lumbar spine. The majority of these exoskeletal devices have bulky form-factors (designed for use in industrial settings), but are less practical for daily use at home or in other business, social or clinical settings. An appealing, low-profile alternative may be to adapt clothing by embedding structures that assist movement biomechanics. These structures could be entirely passive (springs), quasi-passive (clutchable springs), or active (actuated); where both quasi-passive and active might be controlled via feedback from wearable sensors. The purpose of this initial study was to investigate the degree to which a biomechanically-assistive garment could passively offload lumbar muscles and discs during leaning and lifting.

## METHODS

We developed a biomechanically-assistive garment prototype that passively assists lumbar extension during leaning and lifting, and is sufficiently low-profile to be worn as (or under) clothing. We then tested 8 healthy subjects (7 male, 1 female,  $74 \pm 8.7$  kg,  $1.8 \pm 0.05$ m,  $23 \pm 3$  yrs.) performing leaning and lifting tasks with vs. without the prototype to assess its effect on lumbar muscle activity, which was used as an indicator of biological tissue loading. The prototype consists of an upper-body interface (shirt), a lower-body interface (shorts), and

elastic bands which run along the back, connecting the upper and lower interfaces (Fig. 1A). As the user leans forward, the elastic bands stretch, providing a lumbar extension moment, which reduces moments required by the muscles. Because the elastic bands act with larger moment arms about the spine (than muscles), they provide equivalent extensor moments with smaller force magnitudes, resulting in reduced compressive forces on the spine. Subjects performed 10 trials: (3 leaning angles + 2 lifting weights) x (2 conditions, i.e., with and without the prototype), while we recorded kinematics, force and electromyography (EMG) data. Each subject gave informed consent prior to participation. Subjects leaned forward to a pre-determined angle ( $30^\circ$ ,  $60^\circ$ ,  $90^\circ$ ) for 30 seconds while holding a 4.5 kg weight to their sternum. Subjects then lifted a weight (12.7 or 24 kg) using a squat posture. Mean EMG was used as the main outcome metric for the leaning and lifting trials. Intersubject means and standard deviations were computed. Paired t-tests were performed to assess significance ( $\alpha = 0.05$ ).

## RESULTS AND DISCUSSION

Wearing the prototype during leaning and lifting tasks reduced erector spinae EMG activity (Fig. 1B). Mean EMG was reduced by  $23\% \pm 13\%$  ( $p=0.01$ ),  $27\% \pm 10\%$  ( $p=0.006$ ) and  $43\% \pm 33\%$  ( $p=0.001$ ) for the  $30^\circ$ ,  $60^\circ$  and  $90^\circ$  leaning tasks, respectively (Fig. 1C). Mean EMG was reduced by  $13\% \pm 8\%$  ( $p=0.006$ ) and  $16\% \pm 7\%$  ( $p=0.001$ ) for the 12.7 and 24 kg lifting tasks, respectively.

These EMG reductions suggest that the prototype reduced lumbar muscle forces. Since these muscle forces constitute the majority of compressive force on the lumbar spine [2], these findings suggest that lumbar disc loading may also be reduced. These

results demonstrate the feasibility of biomechanically-assistive garments to reduce lumbar muscle and disc loading, which may help mitigate overuse and/or overloading risks that can lead to low back injury and pain. Future prototypes will integrate quasi-passive structures and wearable sensors in order to control the magnitude and timing of assistance.

## CONCLUSIONS

We found that passive, biomechanically-assistive garments are capable of offloading low back muscles during leaning and lifting, which may reduce force-induced injury risks.

## REFERENCES

1. Hoy D, et al. *Best Prac. & Res. Clin. Rheumatol.* **24**, 155-165, 2010.
2. Potvin JR, et al. *Spine.* **16**, 1099-1107, 1991

## ACKNOWLEDGMENTS

This work was supported by an NSF Graduate Research Fellowship, Vanderbilt Discovery Grant, and NIH K12.

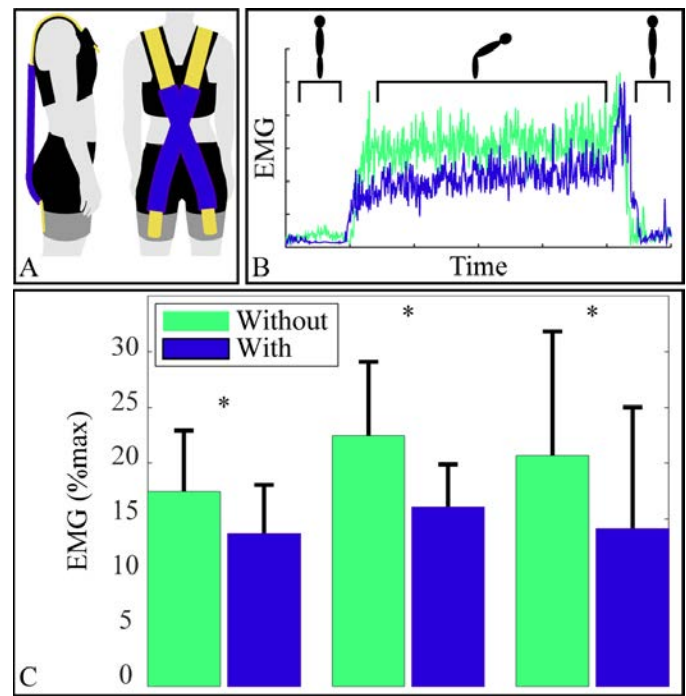


**Figure 1:** (A) Wearable prototype. (B) Representative EMG vs. time plot for leaning. (C) Mean erector spinae EMG was reduced during leaning With (blue) vs. Without (green) the biomechanically-assistive garment prototype.

# USING ELASTIC ANKLE EXOSKELETONS TO COUNTERACT AGE-RELATED STRUCTURE-FUNCTION DEFICITS

Richard W. Nuckols, Taylor J.M. Dick, Jason R. Franz, Gregory S. Sawicki  
 Joint Dept. of Biomedical Engineering, NCSU and UNC-Chapel Hill, Raleigh, NC, USA  
 email: rwnuckol@ncsu.edu

## INTRODUCTION

Elastic exoskeletons have the potential to add structural stiffness about a joint during gait using external springs placed in parallel with biological muscle-tendon units (Fig. 1 A-D). Our previous work has shown that elastic exoskeleton assistance at the ankle leads to decreases in plantarflexor force and activation as well as a decrease in whole body metabolic demand [1]. This is despite evidence for unfavorable changes in fascicle dynamics (*e.g.* longer fascicle lengths) in young adults [2]. Aging on the other hand is associated with a myriad of performance declines. For example, with age comes slower walking speeds and increased metabolic costs [3]. Evidence suggests that the ankle plantarflexors are at the forefront of these performance declines, with age-associated decreases in Achilles tendon (AT) stiffness and muscle force-generating capacity contributing to shorter fascicles and reduced ankle push-off capability in older adults [3,4] (Fig. 1 E-F).

Our aim is to determine whether walking with elastic ankle exoskeletons can augment plantarflexor performance in older adults (Fig. 1). Unlike in young adults, longer fascicle lengths in older adults may lead to improved economy of muscle force production at normal walking speeds [4]. We hypothesized that parallel elastic assistance during walking in older adults would decrease the biological ankle moment, decrease muscle activation, and increase soleus muscle fascicle operating lengths (Fig. 1G).

## METHODS

One elderly subject (female, age: 68) completed the IRB approved protocol. The subject walked for 5 minutes at 1.25 m/s while we applied three exoskeleton assistance levels (stiffness = 0, 100, 150 Nm/rad).

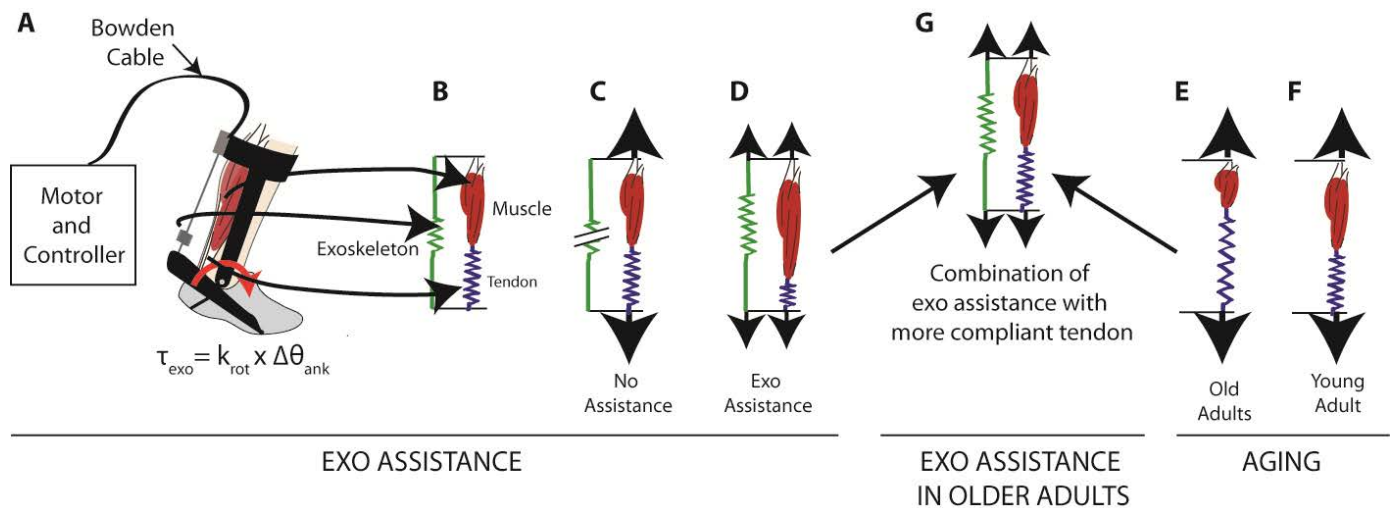


**Figure 1:** Cartoon representation of the expected effect of exoskeleton assistance and aging on the ankle plantarflexors muscle-tendon units (MTU). **A:** Diagram of exoskeleton testbed where plantarflexion assistive torque is applied to the ankle. **B:** Simplified representation of MTU and exoskeleton as parallel force-applying actuators. **C:** Without exoskeleton assistance, the MTU generates the required force for walking. **D:** With exoskeleton assistance, the force is distributed between the parallel elements and force in the MTU decreases leading to a decrease in tendon stretch. **E:** Decrease in tendon stiffness and muscle force-generating capacity associated with aging results in longer tendon length and shorter fascicles compared to **F:** MTU of young adult. **G:** Hypothesized effect of exoskeleton assistance in older individuals. Muscle fascicles return to longer lengths due to decreased tendon stretch as MTU force is offloaded using exoskeleton.

Ankle exoskeleton assistance was delivered to the user through an exoskeleton emulator consisting of bilateral ankle exoskeletons, a benchtop motor and transmission, and a control system (Fig. 1A). A torque-angle relationship was imposed to emulate elastic assistance. We collected a comprehensive kinematic, kinetic, EMG, ultrasound, and metabolic dataset while the subject walked on an instrumented treadmill. Specifically, we recorded kinematics using reflective markers (Vicon), muscle activity in the medial and lateral gastrocnemii and soleus using surface EMG (Biometrics), soleus fascicle lengths using B-mode ultrasound (Telemed), and whole body metabolic power using indirect calorimetry (OxyCon Mobile).

## RESULTS AND DISCUSSION

Compared to the no assistance condition (0 Nm/rad), the stiffest exoskeleton condition (150 Nm/rad) reduced the peak biological plantarflexion moment by 4.8% and the soleus integrated EMG by 12% (Fig. 2A). During stance, average soleus fascicle length increased by 8.5% when high exoskeleton stiffness was applied (Fig. 2C). Assistance also increased the ankle quasi-stiffness (Fig. 2B) and decreased metabolic demand by more than 5%. In this pilot study, the subject obtained the greatest metabolic benefit from the stiffest condition prescribed (150 Nm/rad). Interestingly, this is about twice as stiff as the optimal stiffness in young adults (80 Nm/rad). Due to the structural MTU changes associated with

aging (e.g., reduced AT stiffness), it is unclear whether making the exoskeletons even stiffer could further improve metabolic outcomes.

## CONCLUSIONS

The optimal prescription of elastic ankle exoskeletons has the potential to preserve or restore mobility in our aging population. Ultimately, by personalizing the structural properties of the device to the morphology of an individual user, we may offset unfavorable reductions in tendon stiffness and their metabolic consequences, thereby maximizing independence and quality of life.

## REFERENCES

1. Collins SH, Wiggin MB, Sawicki GS. *Nature*, 2015
2. Sawicki G., et al. *IEEE Trans Biomed Eng.* 2015 Oct 15.
3. Franz, J. R. *Exerc Sport Sci Rev*, 2016 **44**(4): 129-136
4. Stenroth, L., et al. *Med Sci Sports Exerc* 2017 **49**(1): 158-166.

## ACKNOWLEDGMENTS

National Institutes of Health, National Institutes of Nursing Research Award # R01 NR017456 to GSS.

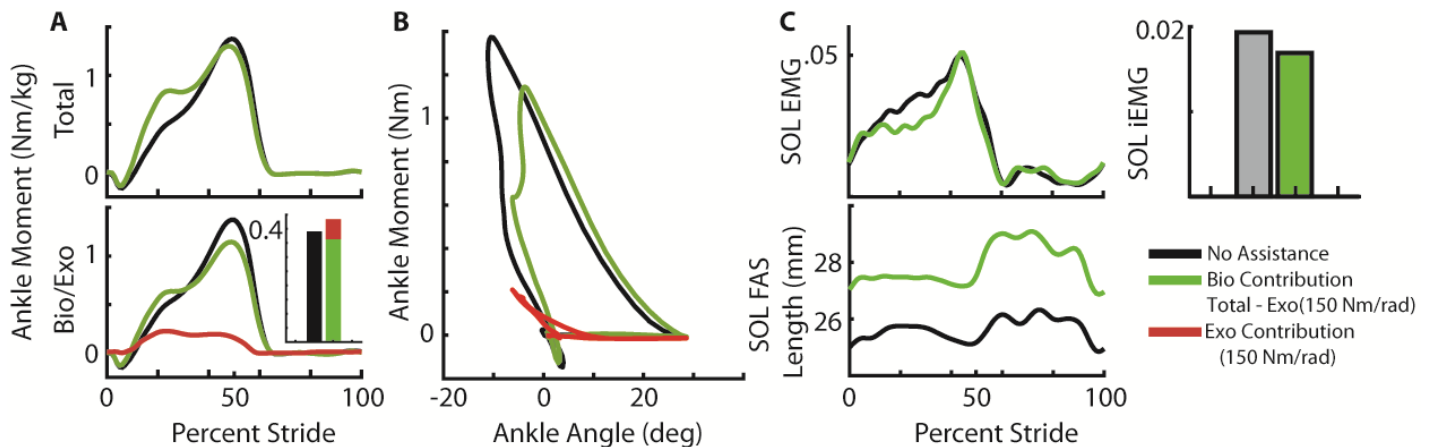


**Figure 2:** Joint and muscle mechanical changes as result of applying exoskeleton assistance. At the ankle joint, exoskeleton assistance results in decrease in biological moment. Soleus activation decreases and length increases with application of rotational stiffness.

# DYNAMIC SIMULATION OF ELASTIC ANKLE EXOSKELETON EFFECTS ON PLANTARFLEXOR MUSCLE-TENDON NEUROMECHANICS DURING WALKING

<sup>1</sup> Michael N. Poppo, <sup>1</sup> Emily M. McCain, <sup>2</sup> Taylor J.M. Dick, <sup>1</sup> Katherine R. Saul and <sup>2</sup> Gregory S. Sawicki

<sup>1</sup> Dept. of Mechanical Engineering, North Carolina State University, Raleigh, NC, USA

<sup>2</sup> Joint Dept. of Biomedical Engineering, University of North Carolina-Chapel Hill and North Carolina State University, Raleigh, NC, USA  
email: mnpoppo@ncsu.edu

## INTRODUCTION

Recent breakthroughs in assistive walking exoskeletons (exos) using a spring-clutch mechanism in parallel with the ankle plantarflexors have been shown to reduce the net metabolic cost of walking by up to 7% [1]. Joint level analysis revealed that this decrease in metabolic cost occurred in a “sweet spot” of stiffness, where walking economy increased and muscle activity decreased. Simple modeling results suggest that plantarflexor muscle mechanics are negatively impacted when working in parallel with an elastic “exo-tendon” [2]. However, the impact of altered ankle kinematics and individual muscle contributions on plantarflexor mechanics and energetics during exo-assisted gait remains unknown. In order to address this knowledge gap, we employed multi-joint models to drive forward simulations with experimental data and investigated the muscle-level impact of exo-assisted walking in the “sweet spot.” We hypothesized that the “sweet spot” occurs when the costs of detuning underlying muscle dynamics to less favorable mechanical conditions and the benefits of reduced muscle force requirements are effectively balanced, resulting in reduced muscle-level metabolic cost.

## METHODS

A subset of data collected from a previous study [1] including four healthy adults (2 F, 2 M;  $21.8 \pm 2.5$  yrs.) walking ( $1.25 \text{ m} \cdot \text{s}^{-1}$ ) at three conditions (no exo, exo with no spring, exo with spring stiffness of  $180 \text{ N} \cdot \text{m} \cdot \text{rad}^{-1}$ ) was analyzed. Kinematic data were collected using a motion capture system (Vicon), ground reaction forces from an instrumented treadmill (Bertec) and muscle activity from a wired electromyography (EMG) system (Biometrics Ltd).

All data were processed using OpenSim and Matlab (MathWorks). A lower limb model [3] was modified by removing all muscles except the medial and lateral gastrocnemii (MG and LG), soleus (SOL), and tibialis anterior (TA) and adding a metabolic probe [4, 5]. This base model was then scaled to each subject’s anthropometry using marker data from static trials. These individualized models were used to create forward dynamic simulations driven by the measured EMG of the muscles crossing the ankle with simultaneously constrained kinematics and ground reaction forces; this method has been previously described for simulating hopping with an exo [6]. Raw EMG data were processed for input to the simulations using custom Matlab scripts that rectified, filtered (4th order band pass filter, 20-300 Hz), and enveloped (rolling root mean square, 100 ms window) the signal. Because EMG from maximum voluntary contraction was unavailable, a subject-specific scale factor was applied to the EMG activation envelope; the value was selected such that the muscle-generated ankle moment during no exo walking minimized errors when compared to the net ankle moment from inverse dynamics [6]. Verification of the models and analyses was done by comparing inverse kinematics, moments and powers from the same subjects previously reported [1]. From these simulations, we analyzed the muscle states including fiber force, activation, fiber length and metabolic power.

## RESULTS AND DISCUSSION

Joint level analyses of kinematics and moments predicted by our simulations are consistent with previously published values [1], and the simulated muscle-generated ankle moments demonstrated similar moment profiles when walking without an

exo and with an exo without a spring. The difference between the biological moment production in the exo no spring and spring conditions was congruent with spring force provided by the exo during stance (0-60% stride); limited differences among all conditions were seen during swing, as expected (Fig. 1).

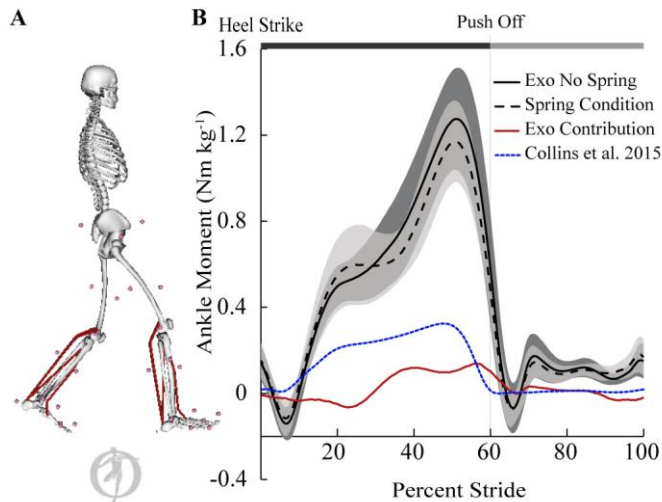


**Figure 1:** **A:** Simulated model **B:** Average summed muscle moment across subjects for exo no spring (solid) and spring (dashed) conditions. Difference in exo no spring and spring conditions yields exo contribution (red), previous findings in blue (dotted).

Muscle-level mechanics of the plantarflexors are dominated by the uniaxial SOL, which accounts for approximately 60% of the summed physiological cross-sectional area. Decreases in the net ankle moment were reflected by a decrease in SOL fiber forces (10.5%) and reduced activations (7.8%) during stance (Fig. 2A,B). SOL force generation ability during stance was not found to be substantially reduced (0.8%) (Fig. 2C). However, in support of our hypothesis, there was an increase in SOL fiber lengths (Fig. 2D). Metabolic power for the

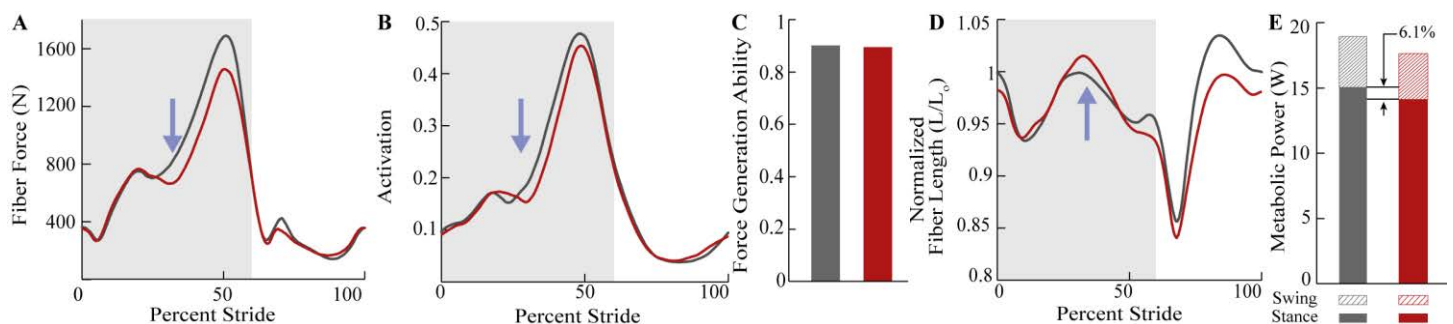


**Figure 2:** Exo no spring (Grey) vs Spring (Red) for SOL **A:** Fiber Force **B:** Activation **C:** Average Force Generation Ability during stance (force per unit activation) **D:** Fiber Length **E:** Average Metabolic Power

SOL was found to decrease (6.1%) in the spring condition compared to no spring (Fig. 2E).

## CONCLUSIONS

Our simulations show reduced biological force production during stance resulting from passive exo assistance. The SOL force-generating ability remained unchanged despite a shift in muscle dynamics. The metabolic cost reduction found in the SOL demonstrates that at the “sweet spot” the trade-off between reduced force requirements and detuned muscle dynamics is managed. Future work will include *in vivo* ultrasound measurements to confirm and expound upon current knowledge of plantarflexor dynamics during assisted walking.

## REFERENCES

- Collins SH, et al. *Nature* **522**, 212-215, 2015.
- Sawicki GS, et al. *IEEE Trans Biomed Eng.* 63(5), 914-923, 2016.
- Arnold EM, et al. *Ann Biomed Eng* **38**(2), 269-279, 2010.
- Umberger BR, et al. *Comput Methods Biomech Biomed Engin* **6**(2), 99-111, 2003.
- Umberger BR, et al. *Exerc Sport Sci Rev* **39**(2), 59-67, 2011.
- Farris DJ, et al. *J Exp Biol* **217**, 4018-4028, 2014.

## ACKNOWLEDGMENTS

We would like to acknowledge Dr. DJ Farris for his assistance in implementing the EMG driven forward simulation framework. National Institutes of Health, National Institutes of Nursing Research Award # R01 NR017456 awarded to GSS.

# AN INSTRUMENTED ANKLE FOOT ORTHOSIS FOR QUANTIFYING THE INFLUENCE OF PLANTARFLEXION RESISTANCE ON JOINT KINEMATICS IN HEALTHY INDIVIDUALS

Nicholas B. Bolus, Caitlin N. Teague, Geza F. Kogler, and Omer T. Inan

Georgia Institute of Technology, Atlanta, GA, 30332, USA  
emails: {nbolus, c.teague, geza, inan}@gatech.edu

## INTRODUCTION

Ankle-foot orthoses (AFOs) are commonly prescribed for individuals with biomechanical deficits of the lower limbs (e.g., foot drop). Traditionally, selection of AFO stiffness has been subjective, based on a practitioner's (e.g., orthotist's) experience and observations to determine a stiffness that maximizes functional mobility during walking. To provide clinicians with quantitative metrics for orthotic prescription, we developed an instrumented ankle foot orthosis (*i*AFO) with embedded sensors that can be used in the clinical setting (Fig. 1). The *i*AFO is capable of measuring orthosis ankle joint kinematics, electromyography, orthosis ankle torque, shank-foot segment orientation, gait state periods, and orthotic interface pressures. These clinically relevant measures are salient for orthotic prescription formulation—particularly for determining the optimal stiffness parameters of an orthosis to maximize each individual's walking performance. We present data from a healthy-subject pilot study using the *i*AFO to investigate the effect of modulating orthotic plantarflexion (PF) resistance on ankle kinematics during level walking. This study will form the foundation for our follow-on work to characterize these kinematics in a larger population of able-bodied subjects and subjects with foot drop.

## METHODS

All studies were approved by the Georgia Tech Institutional Review Board and the Army Human Research Protection Office. Three able-bodied adults (two males, one female) were asked to don the *i*AFO and walk on a level treadmill at a speed of 1 m/s for a set of orthotic stiffness conditions ranging from 0 Nm/° (i.e., unloaded/no springs) to 0.8 Nm/° of PF resistance. Data were recorded continuously for 75 s per trial, and the signals were windowed into individual gait cycles and ensemble-averaged prior to extraction of features as defined below (Fig. 2).

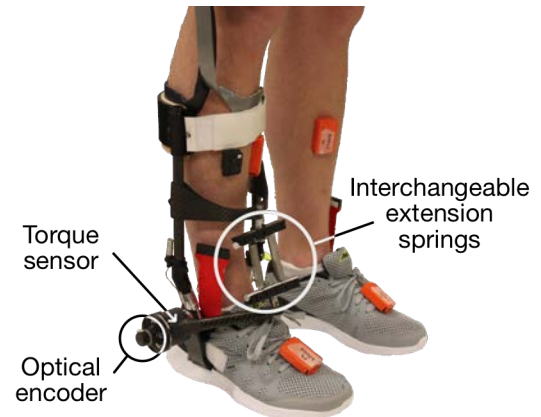


**Figure 1.** The instrumented ankle-foot orthosis (*i*AFO) is a modular, custom-designed, articulated AFO equipped with a variety of sensors to monitor gait parameters in response to varying degrees of orthotic ankle constraint.

## RESULTS AND DISCUSSION

A tendency towards general attenuation of orthosis ankle joint motion in response to increasing PF resistance is evident in the ensemble-averaged waveforms of ankle joint trajectory (Fig. 2). More quantitative trends in specific features of that kinematic data are consistent across all subjects (Fig. 3). For instance, features such as overall range of motion (ROM), excursion of the ankle joint during mid-stance and terminal stance ( $MSt_{\text{excursion}}$  and  $TSt_{\text{excursion}}$ , respectively), and range of motion during swing phase ( $SW_{\text{ROM}}$ ) all decreased in response to increases in PF resistance torque. Interestingly, despite the fact that the device ostensibly *assists* dorsiflexion, the maximum dorsiflexion angle achieved was found to decrease, perhaps suggesting a compensatory mechanism of locomotion in these able-bodied subjects that attempts to counteract any perceived perturbation, assistive or otherwise, in an attempt to restore normal gait mechanics or prioritize stability. We also observed an apparent reorganization in the *timing* of the gait phases, specifically a tradeoff

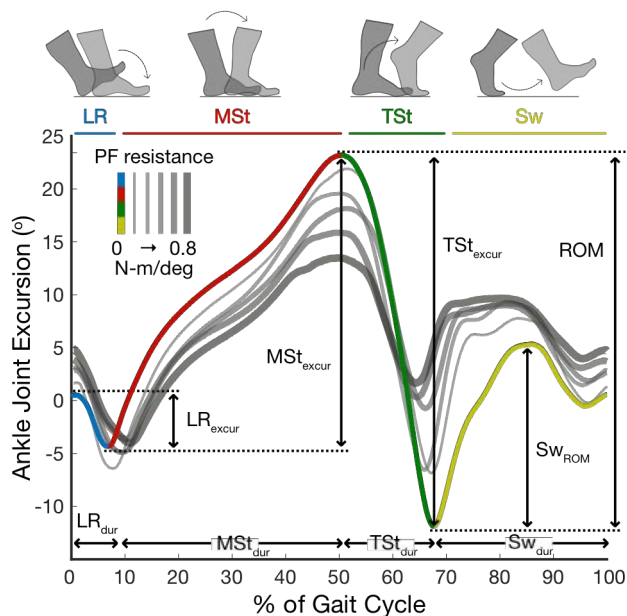


**Figure 2.** Definitions of features of the gait cycle, segmented into four phases—loading response (LR), mid-stance (MSt), terminal stance (TSt), and swing (Sw)—for a representative subject.

between a longer loading response ( $LR_{dur}$ ) and a shorter terminal stance ( $TSt_{dur}$ ). The lengthening of LR is a consequence of the anterior-mounted springs more effectively decelerating the foot after initial contact—an important function of an AFO to prevent “foot slap.” However, as gait velocity was constrained by a constant-speed treadmill, this protraction of LR necessitated a truncation of another phase(s), which we found occurred most prominently in TSt. This siphoning of gait cycle time away from TSt rather than MSt or Sw is likely a matter of walking efficiency: TSt is the phase in which the subject is “fighting against” the imposed orthotic constraint the most, so perhaps the subjects preferentially abbreviated this phase to avoid undue effort, compensating elsewhere along the lower limb, likely at more proximal joints (knee, hip).

## CONCLUSIONS

In this study we found that an increase in orthotic PF resistance led to a general decrease in ankle joint range of motion in healthy individuals, with marked reduction in joint excursion during mid-stance, terminal stance, and swing phase. We also observed a redistribution in the timing of the gait phases: specifically, protraction of loading response and

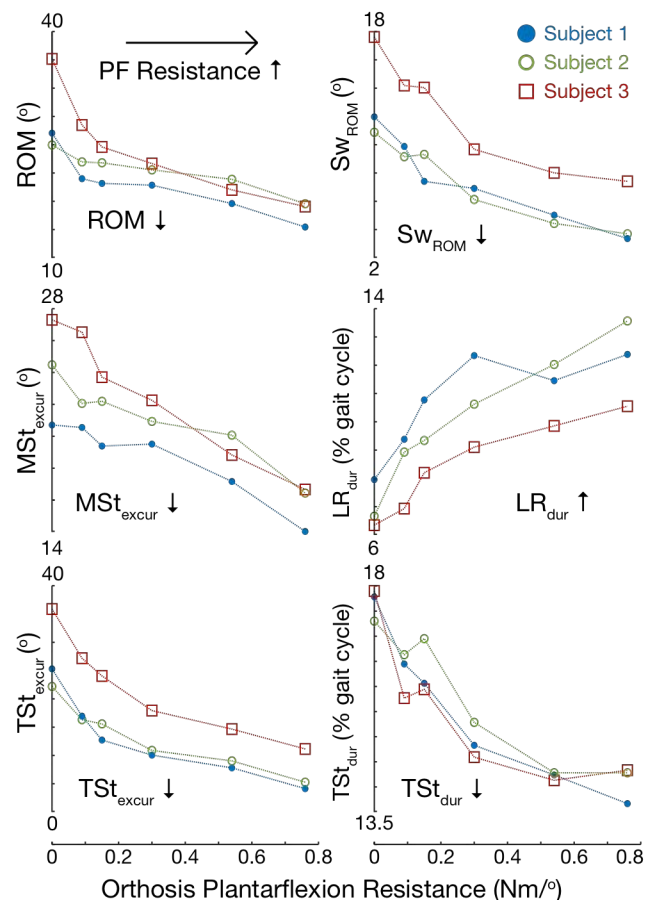


**Figure 3.** Trends in ankle joint kinematic data over a range of PF stiffness conditions ( $n=3$ ).

truncation of terminal stance. We affirmed that our device, the *i*AFO, was capable of decelerating the foot after initial contact and lifting the foot during swing to maintain toe clearance—two key functions of conventional AFOs. Furthermore, this study served to validate the *i*AFO as a clinical tool for monitoring gait parameters during locomotion, preparing us for further investigations on populations with lower limb motor deficits.

## REFERENCES

1. Kobayashi T, et al. (2015) *Clin Biomech* **30**, 775–80.

## ACKNOWLEDGMENTS

This work is based on materials funded in part by the US Army under Grant No. W81XWH-15-1-0479 and expresses the views of the authors only and not necessarily those of the government. NBB is supported by the National Science Foundation Graduate Research Fellowship under Grant No. DGE-16500.

# EFFECT OF POWERED EXOSUIT TRAINING ON IMPULSE DURING GAIT

<sup>1</sup>William Bowers, <sup>2</sup>Fausto Panizzolo, <sup>2</sup>Nikolaos Karavas, <sup>2</sup>Asa Eckert-Erdheim, <sup>2</sup>Christopher Sivi, <sup>2</sup>Andrew Long, <sup>3</sup>Michael LaFiandra, <sup>2</sup>Conor Walsh, and <sup>1,3</sup>Gregory Freisinger

<sup>1</sup>Department of Civil and Mechanical Engineering, United States Military Academy

<sup>2</sup>Wyss Institute for Biologically Inspired Engineering at Harvard

<sup>3</sup>United States Army Research Laboratory, Aberdeen Proving Ground

Email: gregory.freisinger@usma.edu

## INTRODUCTION

As exosuit technology develops, it is important to not only quantify the performance gains that they grant wearers, but also begin to attempt to maximize those gains by implementing training. Although research has been done on creating and refining exosuits themselves, few investigations have measured the effects of training. Developers recommend a varied amount of familiarization, however these recommendations are not always supported by quantitative data. Many studies include at least one initial familiarization session before testing [1,2,4,5], however few focus on the effects of repeated use of exosuit systems [3,6].

The primary purpose of this study was to quantify the effects of training with a powered soft exosuit. This work specifically investigated the braking and propulsive impulse between conditions and over multiple sessions. We hypothesized that braking and propulsive impulses would decrease over the course of a single session and between sessions during powered walking, as the wearer becomes better adapted to the exosuit. We also hypothesized that there would be significantly less braking and propulsive impulse during unpowered walking as compared to powered walking.

## METHODS

Eight male United States Military Academy cadets (age:  $20.6 \pm 1.2$  yr; height:  $1.80 \pm 0.09$  m; weight:  $78.6 \pm 9.2$  kg) participated in this study after providing IRB approved informed consent. The participants completed five sessions over 20 days, utilizing a backpack mounted soft exosuit, which provides assistance in hip extension during stance phase [7]. The exosuit mass was 5.4 kg and the backpack was loaded with an additional 20.4 kg. Each session consisted of 20 minutes of walking

with the exosuit powered on, followed by 5 minutes of walking with the exosuit powered off. Multiple sessions were separated by at least 48 hours to reduce any impact from fatigue. Ground reaction force data was collected using an instrumented treadmill at 1000 Hz from the first two minutes of powered walking (condition A), the last two minutes of powered walking (condition B), and the last two minutes of walking with the exosuit powered off (condition C). Foot strikes from each two minute period were used in follow on calculations ( $94.6 \pm 26.4$  foot strikes per condition).

Braking and propulsive impulse were normalized by body mass and calculated during the right stance phase. Braking and propulsive impulse were found by taking the area under the posterior and anterior ground reaction force curves, respectively. Four different repeated-measure 2-way ANOVAs were used to identify statistical differences within and across sessions. Powered condition A was compared to powered condition B, for both braking and propulsive impulses separately. Powered condition B was compared to unpowered condition C, for braking and propulsive impulses separately. An alpha = 0.05 was chosen to represent a statistically significant difference between conditions and across sessions.

## RESULTS AND DISCUSSION

Mean and standard deviation for braking and propulsive impulses across conditions and sessions are shown in Table 1. For braking, across conditions A and B, main effects were found for subject ( $p < 0.001$ ) and condition ( $p < 0.001$ ), but not for session ( $p = 0.416$ ). For propulsion, across conditions A and B, main effects were found for subject ( $p < 0.001$ ), condition ( $p < 0.001$ ), and session ( $p = 0.001$ ).

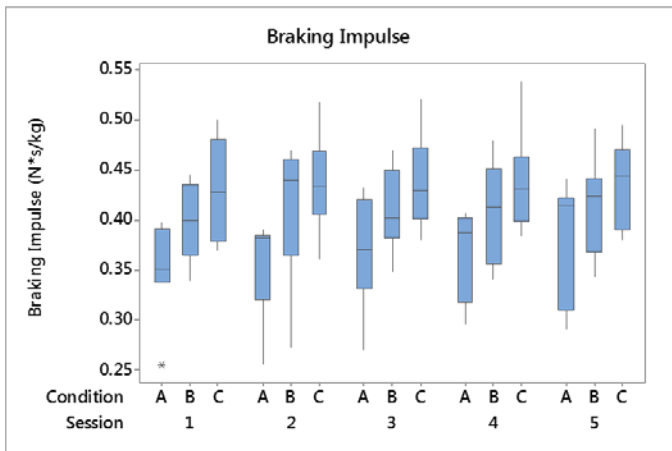


**Figure 1:** Boxplot of braking impulse for five sessions, conditions A, B, and C for each session.

For braking, across conditions B and C, main effects were found for subject ( $p < 0.001$ ), and condition ( $p < 0.001$ ), but not for session ( $p = 0.773$ ). For propulsion, across conditions B and C, main effects were found for subject ( $p < 0.001$ ), session ( $p = 0.001$ ), and condition ( $p < 0.001$ ).

These results indicate that successive training sessions using the exosuit changed how subjects applied propulsive impulse, but do not have significant effects on how they applied braking impulse. Between conditions A and B, from minutes 0-2 of powered walking to minutes 18-20 of powered walking, braking and propulsive impulse increased in magnitude. The highest magnitude of braking and propulsive impulse were recorded during condition C during minutes 23-25 of unpowered walking.

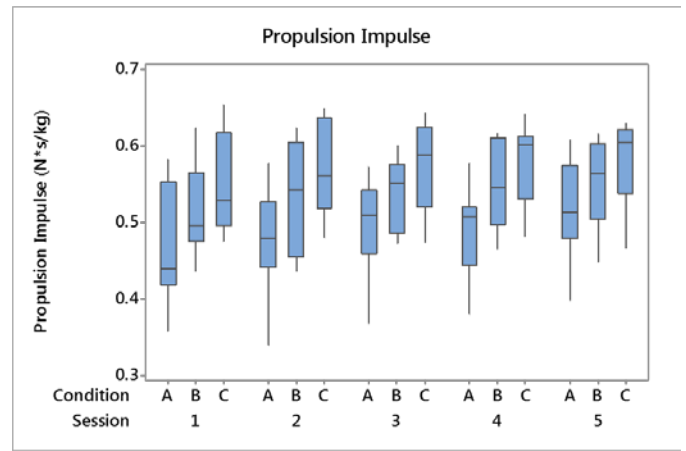


**Figure 2:** Boxplot of propulsive impulse for five sessions, conditions A, B, and C for each session.

## CONCLUSIONS

We identified a significant difference in braking and propulsive impulses between powered and unpowered conditions. Propulsive impulse also changed significantly between multiple training sessions, while no difference was found in braking impulse across sessions. This data supports the notion that individuals may alter ground kinetics over time while using a powered exosuit. More research is required to identify how much training is necessary before steady state kinetics are obtained, and to identify the influence of fatigue and time on impulse.

## REFERENCES

1. Mooney, L.M., et al. *JNER*, **11(80)**, 2014.
2. Collins, S.H., et al. *NATURE*, **522**, 212-215, 2015.
3. Sawicki, G.S., et al. *JEB*, **211**, 1402-1413, 2008.
4. Ding, Y., et al. *JNER*, **13(87)**, 2016.
5. Gordon, K.E., et al. *JBM*, **40**, 2636-2644, 2007.
6. Koller, K.E., et al. *JBM*, **12(97)**, 2015.
7. Karavas, N., et al. *B&B*, **16**, 331-335, 2016

**Table 1:** Braking and propulsive impulses averaged across all eight subjects.

Condition	Braking Impulse (N*s/kg)			Propulsive Impulse (N*s/kg)		
	A	B	C	A	B	C
Session 1	0.35 ± 0.05	0.40 ± 0.04	0.43 ± 0.05	0.47 ± 0.08	0.51 ± 0.06	0.55 ± 0.07
Session 2	0.35 ± 0.05	0.41 ± 0.07	0.43 ± 0.05	0.47 ± 0.07	0.53 ± 0.07	0.57 ± 0.06
Session 3	0.37 ± 0.06	0.41 ± 0.04	0.44 ± 0.05	0.50 ± 0.06	0.54 ± 0.05	0.57 ± 0.06
Session 4	0.36 ± 0.04	0.41 ± 0.05	0.44 ± 0.05	0.49 ± 0.06	0.55 ± 0.06	0.58 ± 0.06
Session 5	0.38 ± 0.06	0.41 ± 0.05	0.44 ± 0.04	0.52 ± 0.07	0.55 ± 0.06	0.58 ± 0.06

Data are shown as mean and standard deviation. Conditions A, B, C are 0-2 minutes powered, 18-20 minutes powered, 23-25 unpowered respectively. Repeated measures 2-way ANOVAs were ran for condition (A vs. B and B vs. C) and session, p-values described in text.

# ASSESSING SLIP AND TRIP RISKS WHEN WEARING AN UPPER-EXTREMITY EXOSKELTON

<sup>1,2</sup> Mehdi Alemi, <sup>1</sup> Mohammad Iman Mokhlespour, <sup>1</sup> Sunwook Kim,  
<sup>3</sup> Ehsan Rashedi, and <sup>1</sup> Maury A. Nussbaum

<sup>1</sup> Occupational Ergonomics and Biomechanics Laboratory, Virginia Tech, Blacksburg, VA, USA

<sup>2</sup> Mechanical Engineering, Virginia Tech, Blacksburg, VA, USA

<sup>3</sup> Rochester Institute of Technology, Rochester, NY, USA

email: nussbaum@vt.edu

## INTRODUCTION

Use of assistive devices is emerging as an effective intervention to reduce physical demands imposed on workers. For example, Rashedi et al. [1] recently demonstrated that using an upper extremity exoskeletal vest with a mechanical arm can reduce physical demands involved in overhead work. Though such devices may effectively control exposure to overexertion, they are generally rigid structures; such rigidity and the added mass may constrain the natural motions of the upper body. This may be a particular concern in terms of occupational slip- and trip-related falls, given that: 1) broad evidence supports that external loads on the body can adversely affect gait performance [2-4]; 2) a change in trunk kinematics can affect gait performance such as step width [5]; 3) post-slip or post-trip trunk kinematics are associated with fall recovery ability [6]; and 4) slips, trips, and falls are a major source of occupational injuries and fatalities [7]. However, little effort has been reported regarding the effects of an assistive device on the risks of slip- and trip-related falls.

This study examined how the use of a newly developed Wearable Assistive Device (WADE) – an upper extremity exoskeletal “Vest” (EksoBionics Inc., USA; Fig. 1) – affects gait performance. The WADE involves shoulder torque generating components and a rigid vertical column along the spine, with mass = 6.5 kg. We hypothesized that wearing the WADE will adversely affect gait performance, due to the rigid structure potentially limiting natural motions of the trunk and the added mass on the trunk.

## METHODS

To assess slip and trip risks, 20 participants (10F & 10M) completed gait trials on a linear walking track (1.5 m × 15.5 m) instrumented with two force platforms (AMTI OR6, Watertown, MA), both with and without the WADE (Fig. 1). All participants provided informed consent, following procedures approved by Virginia Tech IRB.

Participants were provided with standard laboratory shoes, and asked to walk across the track several times with and without the WADE for familiarization. During this familiarization phase, a starting foot position was marked on the walking track, so that participants walked across two force platforms, with each foot and without visible adjustments to gait patterns. Participants completed 10 walking trials at their normal walking speed in each of the Vest Intervention conditions (i.e., with vs. without the WADE on), the order of which was alternated between participants.

During walking trials, triaxial ground reaction forces (GRFs) were sampled at 1 kHz from the two force platforms. Gait kinematics were captured at 100 Hz, using a 7-camera optical motion capture system (Vicon MX-T, Los Angeles, CA), from markers placed over selected anatomical landmarks, and subsequently low-pass filtered (20 Hz, 4<sup>th</sup>-order Butterworth, bidirectional).

For each walking trial, minimum toe clearance (MTC) was calculated for each foot over the force platform to assess trip risks. MTC was defined as the minimum vertical distance between the 2<sup>nd</sup> metatarsal head and the ground during the mid-swing phase of gait. To assess slip risks, the maximum required coefficient of friction (RCOF) was computed as the largest instantaneous ratio of the resultant of transverse and longitudinal shear

GRFs to the normal GRF within 50-200 milliseconds after heel contact [10].

Main and interaction effects of gender and Vest Intervention on each outcome measure were examined using separate repeated measures of analyses of variance (ANOVAs). Statistical significance was determined at  $p < 0.05$ .



Figure 1. Example of a walking trial with the WADE on the linear walking track.

## RESULTS AND DISCUSSION

Our results failed to support the hypothesis, in that neither MTC or RCOF were significantly affected by any main or interaction effects of gender and Vest Intervention (all  $p$  values  $> 0.29$ ). The mean (SD) of MTC and RCOF values were 60.0 (7.7) mm and 0.22 (0.03) with the WADE, respectively; and 60.8 (8.4) mm and 0.22 (0.03) without the WADE, respectively.

The mass of the WADE was 6.5 kg, which was on average close to or less than 10% of participants' body mass. Interestingly, earlier studies have reported that carrying a load less than 10% of body mass does not have substantial effects on trip and/or slip risks, although it can affect spatial-temporal gait characteristics [8,9]. The finding here of no significant effects of WADE on either peak RCOF or MTC confirmed the results of those earlier studies.

In the current study, we found that the upper extremity rigid exoskeletal vest examined imposes no obvious increase in the risk of slips or trips.

However, though not statistically significant, wearing the WADE yielded slightly lower MTC values (by  $\sim 0.8$  mm). Given this, and that a rather simple linear walking task was considered here, further research is needed to set the boundary of working conditions within which gait performance is not compromised with the use of a WADE. For example, the added mass on the body (i.e., from wearing a WADE) may result in a higher postural demand when the wearer needs to walk faster, cross an obstacle, and/or perform different ambulatory activities (e.g., turning, sudden stopping while walking). Moreover, trip and slip recovery were not considered in the current study, and the added weight from the vest might reduce trip and slip recovery capacity of a worker. In addition, kinematics and spatial-temporal characteristics of gait were not considered here, which will be addressed in future study.

**Disclaimer:** EksoBionics and The Boeing Co. financially supported this research. While contributing to the study design, they were not involved in data analysis, interpretation, or decision for publication.

## REFERENCES

1. Rashedi, E., et al., *Ergonomics*, 57(12), 1864-1874, 2014.
2. Qu, X., et al. *Gait & Posture*, 29(1), 23-30, 2009.
3. Rugelj, D., et al. *Applied ergonomics*, 42(6), 860-866, 2011.
4. Schiffman, J. M., et al. *Applied Ergonomics*, 37(5), 607-614, 2006.
5. Arvin, M., et al. *Journal of biomechanics*, 49(13), 3085-3089, 2016.
6. Grabiner, M.D., et al. *J. of Electromyography and Kinesiology*, 18(2), 197-204, 2008.
7. Bureau of Labor Statistics, U.S. Dept. of Labor, 2013.
8. Sukwon, K., et al. *Industrial Health*, 46(1), 32-39, 2008.
9. Rietdyk, S., et al., *Experimental Brain Research*, 165(1), 44-53, 2005.
10. Perkins, P. J., *Walkway Surfaces: Measurement of Slip Resistance*. (pp. 71-71-17), ASTM International, 1978.

# Effects of a Leg Kinetic Energy Harvester on Soldiers' Gait

Jessica Batty, Megan Coyne, Clifford L Hancock, and Karen Gregorczyk  
Natick Soldier Research, Development, and Engineering Center, Natick, MA, USA  
email: jessica.m.batty.civ@mail.mil

## INTRODUCTION

Due to the unique power requirements of soldiers in operational scenarios, the U.S. Army is investigating the use of passive energy harvesting technology. Although energy requirements depend upon the specific mission, on average nine-man squads of infantry soldiers carry a total of 41 kg in batteries during a 72-hour field mission [1]. Wearable energy harvesting systems have the potential to reduce the number of batteries that need to be carried and may enable the development of self-powered wearable devices, such as exoskeletons and prosthetics.

In the present study, a Knee Energy Harvester (KEH) system was evaluated that utilizes the kinetic energy of human movement to produce electrical current. The KEH is composed of two units, one worn on each leg, and the rotation of the thigh and shank segments about the knee joint allows generators within the KEH to convert mechanical work into electrical energy. The electrical energy can then be used to power other devices or to charge batteries. While the KEH allows full range of motion of the knee joint during walking and running, the generators apply a variable resistance torque between 1 and 15 N·m, which could impact gait mechanics. The purpose of this study was to identify the effects of the KEH on gait kinetics and kinematics.

## METHODS

Eight male soldiers (Age, 24±5 yrs; Ht, 176.8±6.5 cm; Wt, 84.1±13.1 kg) performed two 10-min marching trials on a treadmill. The marches were conducted at 1.34 m/s on a 0% treadmill grade, with two different equipment configurations. One configuration included soldier gear and the KEH. The other included the same soldier gear and the KEH was not worn (noKEH). The soldier gear used during all trials weighed 6.34 kg and included combat boots, socks, T-shirt, shorts, a helmet, and a simulated weapon. Additional weight of the KEH

was approximately 0.6 kg. Prior to data collection, subjects familiarized themselves with the KEH during two 2-hr training sessions.

Kinetic and kinematic data were collected using a force plate treadmill (AMTI, Watertown, MA), reflective markers, and an 8-camera (Oqus, Qualysis AB, Gothenburg, Sweden) motion capture system. At 3 min into each trial, force plate and kinematic data were collected over 3-5 right initiated and 3-5 left initiated consecutive strides. Means were evaluated for each leg, and then an overall mean was found for each measure. Ground reaction forces, spatiotemporal measures, and knee joint angles were analyzed. A one-way repeated measures analysis of variance (ANOVA) was used to assess differences between the KEH and the noKEH conditions.

## RESULTS AND DISCUSSION

The ANOVA revealed a significant effect of equipment configuration for impulse ( $p=.014$ ), defined as the integral of the vertical GRF during stance, as well as both average ( $p=.011$ ) and instantaneous peak loading rate ( $p=.016$ ) (Figure 1). The average loading rate was calculated as the slope of the ascending vertical GRF line from heel strike through the first peak vertical GRF, while the instantaneous peak loading rate was the maximum slope achieved along this same line. Compared with the noKEH condition, impulse increased by 2.2%, average loading rate increased by 6.2%, and instantaneous loading rate increased by 14.7% when the KEH was worn.

Analysis of knee joint kinematics indicated that joint movement with the KEH was not the same as movement when the KEH was not used. Knee range of motion (ROM) during the walking task decreased in the KEH condition by 10.5° ( $p=.002$ ). While the maximum knee flexion angle did not statistically differ for the KEH and the noKEH conditions ( $p>.05$ ), wearing the KEH did reduce the maximum

extension angle by  $8.49^\circ$  ( $p=.008$ ). The speed and acceleration of the joint rotation also differed significantly for the KEH and the noKEH conditions. Maximum knee joint angular acceleration decreased by 44.2% ( $p=.003$ ), and maximum knee joint angular extension velocity decreased by 30.0% ( $p=.001$ ) when the KEH was used.

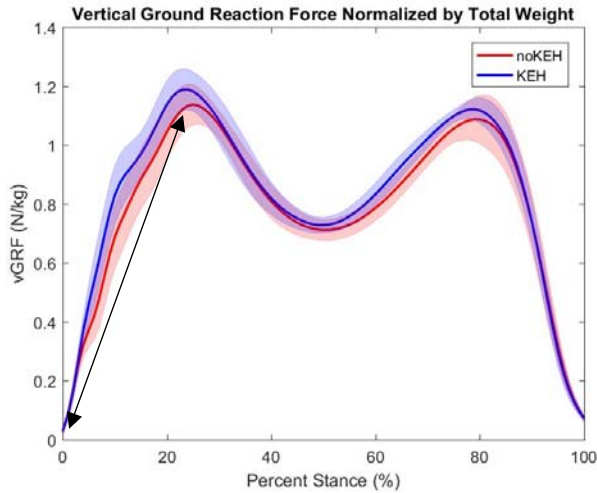


**Figure 1:** Average vertical GRFs for 1.34 m/s walking at 0% grade, normalized by total weight (body weight plus soldier gear and KEH, if applicable). Error bands identify  $\pm 1$  SD. Arrow designates line portion used to calculate loading rates.

Spatiotemporal metrics were also evaluated between the KEH and noKEH conditions (Table 1). Cycle time, step time, and stride length all increased while wearing the KEH ( $p=.001$ , 1.8%;  $p=.001$ , 1.8%; and  $p=.006$ , 1.9%, respectively).

**Table 1:** Example metrics (mean (SD)). All had a significant main effect of equipment configuration ( $p<.05$ ).

Metric	noKEH	KEH
Cycle Time, sec	1.08(.05)	1.10(.04)
Step Time, sec	.54(.02)	.55(.02)
Stride Length, m	2.10(.10)	2.14(.08)
Knee ROM, deg	71.0(4.4)	60.5(2.7)
Max Knee Extension*, deg	5.67(6.3)	-2.82(3.7)

\*Negative extension value indicates flexion, where  $0^\circ$  equals standing calibration knee position.

Considering the overall results of the analyses of the kinetic, kinematic, and spatiotemporal variables, an altered gait pattern emerges that is attributable to use of the KEH. The elevated impulse and loading rates may cause increased strain on the lower extremities, which could increase the likelihood of injury after repeated gait cycles [2].

The reduction of knee joint angular acceleration and velocity was also a key component of the altered gait pattern with the KEH and could be a direct result of the variable resistive torque applied at the knee by the device. Subjects may have compensated for this slower leg motion and limited dynamic ROM by increasing stride length, step time, and cycle time to maintain the overall walking speed of 1.34 m/s.

Given the increased loading rates and impulse demonstrated in the KEH condition as well as the observed kinematic changes at the knee, further analysis of joint kinetics is appropriate to determine if such alterations to normal gait change the manner in which GRFs are transmitted through and absorbed by the body. Additionally, the KEH structure may impact the transfer of GRFs through the connections to the body at the shank and thigh, altering the resultant forces acting on the body. Further characterization of the device’s influence on these forces may mitigate any adverse effects and injury risk indicators.

## CONCLUSIONS

The use of the KEH system resulted in an altered gait pattern for subjects walking at 1.34 m/s on a 0% grade. Altered gait mechanics with the KEH included increased impulse, average and instantaneous peak loading rates, cycle and step times, stride length, as well as decreased knee joint ROM, maximum angular acceleration, and maximum angular extension velocity. While these gait alterations seemingly point to an overall amplified risk of lower-limb injury, further work is required to evaluate the role of the KEH in absorption or transfer of GRFs in order to better understand the cumulative impact of the KEH on gait. Additional investigation to address KEH effects during uphill and downhill walking, as well as jogging conditions is also necessary to evaluate the system as it would be used in the field.

## REFERENCES

1. Draper Laboratory. *OSD Energy Consortium: CONOPS*, 2014.
2. A Hreljac, RN Marshall, PA Hume. *Medicine and science in sports and exercise*, 2000.

# PERFORMANCE OF A POWERED ANKLE EXOSKELETON USING NEUROMUSCULAR MODEL-BASED CONTROL OVER A RANGE OF WALKING SPEEDS

James V. McCall, Sasha A. Philius, Richard W. Nuckols, and Gregory S. Sawicki  
 Joint Dept. of Biomedical Engineering at UNC Chapel Hill and NC State, Raleigh, NC, USA  
 email: jvmccall@ncsu.edu, web: www.bme.ncsu.edu/labs/hpl

## INTRODUCTION

Powered exoskeletons can improve locomotion performance by providing assistive torques to offset biological moments generated by lower-limb joints. So far, the majority of exoskeleton controllers rely on *a priori* tuning of parameters based on a reduced set of locomotor tasks (*e.g.* level walking at preferred speed). This limits their effectiveness to a small subset of functional conditions. To be useful in the real-world, exoskeleton controllers need to be able to automatically adjust to the user and the environment.

The purpose of this study was to explore whether ankle exoskeleton control based on a neuromuscular model could adapt to the increasing mechanical demands associated with increased walking speed (*i.e.*, increased ankle power).

A neuromuscular model (NMM) based controller simulating a Hill-type muscle-tendon with positive force feedback has previously been implemented in an ankle-foot prosthesis [1]. By emulating physiological neuromuscular mechanics, the prosthesis adapted to variable gait speed by way of modulating net work output at each speed. To date, the performance of NMM based controllers has yet to be explored in lower-limb exoskeletons.

We hypothesize that a powered ankle exoskeleton employing a NMM-based controller would automatically adapt to walking speed by 1) increasing net work at increased speeds and 2) maintain reductions in metabolic cost across speeds.

## METHODS

**Exoskeletons:** We provided bilateral plantarflexion assistance via a tethered ankle exoskeleton device. Off-board motors and Bowden cable transmission delivered torque to the custom carbon fiber exoskeletons.

**Controller:** We designed the NMM based controller in Simulink (MathWorks, USA) and implemented it through a dedicated real-time control system which

also handled signal IO (500 Hz, dSPACE, Germany). We calculated applied exoskeleton torque from a load cell (500 Hz, LCM Systems Ltd, UK) placed in series with the applied assistance, and a goniometer (500 Hz, Biometrics, UK) attached to the exoskeleton joint provided real-time ankle angle.

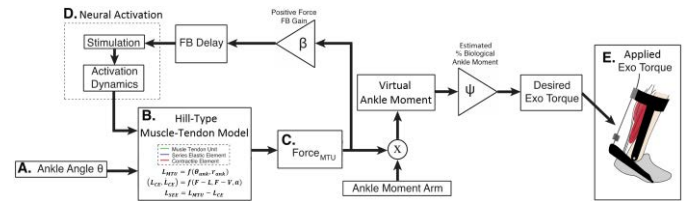


**Figure 1:** Neuromuscular model controller block diagram. Biological force, as computed by the internal muscle-tendon state, is scaled and applied across a moment arm to calculate desired exoskeleton torque.

The NMM based controller implemented in our system was similar to a reflex-based force feedback controller previously demonstrated [1]. A Hill-type muscle-tendon model was the basis for the emulated muscle-tendon unit (MTU) consisting of a contractile element (CE) with both active and passive properties and a series elastic element (SEE) (Fig.1B). We calculated MTU length from ankle angle and musculoskeletal geometry (1.1) and CE dynamics was subject to force-length, force-velocity and activation (1.2). We calculated SEE length as the difference in length of the CE from the MTU (1.3).

$$L_{MTU} = f(\theta_{ank}, r_{ank}) \quad (1.1)$$

$$(L_{CE}, \dot{L}_{CE}) = f(F-L, F-V, a) \quad (1.2)$$

$$L_{SEE} = L_{MTU} - L_{CE} \quad (1.3)$$

MTU force ( $F_{MTU}$ ) was a function of the model's SEE stiffness and strain. In the reflex pathway, we normalized MTU force to  $F_{max}$  and applied a gain (1.2); a 10ms delay was added to emulate a positive force feedback neural reflex signal (Stim) and CE activation dynamics (ACT) were modeled to close the feedback loop (Fig.1D).

We calculated desired exoskeleton torque as a portion of the estimated biological moment.

$$\tau_{exo} = F_{MTU} \times r_{ankle} \times \psi \quad (1.4)$$

where  $\psi$  represented a percentage of the estimated biological torque. We calculated and recorded internal model states ( $F_{MTU}$ ,  $L_{MTU}$ ,  $L_{CE}$ ,  $STIM$ ,  $ACT$ ) in dSpace for 5 second periods for offline analysis.

**Testing Protocol:** Two healthy young adults (M/77.4 kg, and F/75.2 kg) completed the IRB approved protocol. Each subject walked in two conditions (with exoskeleton-No Power and with exoskeleton-Power) and at three speeds for each condition (1.25, 1.50, and 1.75 m/s) for a total of six trials presented in random order. Metabolic power was estimated from indirect calorimetry data collected in minute 5 and 6 of each trial (OxyCon Mobile, Carefusion, USA).

## RESULTS AND DISCUSSION

Mechanical performance of the neuromuscular model (NMM) based controller diminished as walking speed increased. Average exoskeleton torque decreased as speed increased from 1.25 to 1.50 to 1.75 m/s (15.0, 11.6, 8.9 Nm) and peak torque followed a similar trend (Fig. 2a). Net work performed per stride remained nearly constant across speed as the exoskeleton dissipated small amounts of energy in each case.

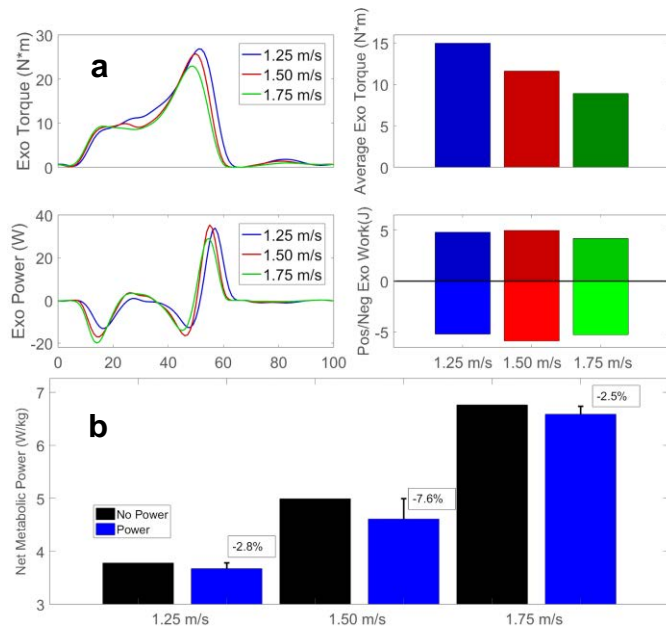


**Figure 2:** Trial results of two subjects walking at different speeds and conditions. **A.** Exoskeleton Torque and Mechanical Power over the stride along with Avg. Torque and Work for each speed. **B.** Net metabolic rate with % reduction displayed for PWR trial compared to NPWR trial at each speed.

Exoskeleton mechanical assistance resulted in reduced metabolic cost across all walking speeds. Compared to the exoskeleton-No Power condition, the reductions in net metabolic rate due to exoskeleton assistance were 2.8%, 7.6%, and 2.5% at 1.25, 1.50 and 1.75 m/s respectively (Fig. 2b).

## CONCLUSIONS

Our initial results indicate that the adaptive properties of NMM-based control seen in prostheses may not generalize to lower-limb exoskeletons. This finding may not be that surprising given that this biologically-inspired control framework is designed to mimic the mechanical performance of biological plantarflexors. In fact, gastrocnemius and soleus muscles exhibit reduced force production at higher walking speeds [2] due to unfavorable force-velocity effects [2,3]. Previous studies on lower-limb prostheses using this control strategy may have avoided this constraint by operating at relatively low walking speeds ( $\leq 1.4$  m/s) [4].

Perhaps an improved class of NMM-based controllers, incorporating a feedforward contribution to neural drive, would lead to improved adaptive performance. For example, adding the user's EMG or some other phase-based signal generator that responds positively to locomotion task demand, on top of reflexive positive force feedback could help counteract the aforementioned performance deficits due to force-velocity effects in the CE component of the NMM.

## REFERENCES

1. Eilenberg MF, *et al.*, *IEEE Trans. Neural Syst. Rehabil. Eng.* 2010;18(2):164-73.
2. Neptune, RR., *et al.*, *Gait Posture*, 2008, 28(1):135-143.
3. Farris DJ, Sawicki GS. *Proc Natl Acad Sci U S A.* 2012; 109(3):977-82.
4. Markowitz, J., *et al. Proc. B. Soc. B.*, vol. 366, no. 1570, 2011, pp. 1621-1631.

## ACKNOWLEDGMENTS

This project was funded by National Institutes of Health, National Institutes of Nursing Research Award # R01 NR017456 awarded to GSS

# ANKLE FOOT ORTHOSIS STIFFNESS AND MARGINS OF STABILITY DURING WALKING

<sup>1</sup> Michael C. Rosenberg, <sup>1</sup> Hwan Choi, <sup>1</sup> Keshia M. Peters, <sup>1</sup> Katherine M. Steele

<sup>1</sup> University of Washington, Seattle, WA, USA

email: mcrosenb@uw.edu, web: <https://depts.washington.edu/uwsteele/>

## INTRODUCTION

Individuals with neurologic impairments often exhibit lower levels of stability during walking than their unimpaired peers. Reduced stability hinders an individual's ability to move safely and autonomously during activities of daily living. Ankle foot orthoses (AFOs) are frequently prescribed to individuals with neurologic impairments to improve gait mechanics and assist walking, but activity-level responses to AFOs are inconsistent. The ankle torques generated by AFOs have been proposed as an efficient way to stabilize the center of mass (COM) during walking [1]. For example, children with cerebral palsy (CP) often have weak ankle plantarflexors, and AFOs may improve stability by enhancing ankle plantarflexor torques. However, studies evaluating AFOs' impacts on gait stability have only compared device types rather than specific AFO mechanical properties [2]. To inform AFO design, a more detailed understanding of how AFO stiffness impacts stability is needed.

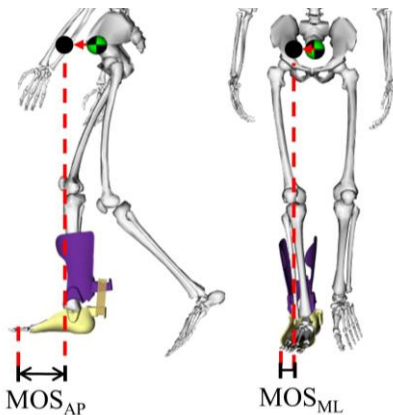


**Figure 1:** Margins of stability (MOS) during AFO-stance. The extrapolated center of mass (black circle) position and velocity are used to compute the anterior-posterior (AP) and mediolateral (ML) margins of stability. Elastic bands (on the back of the AFO) were used to modulate AFO stiffness.

The goal of this study was to evaluate whether AFO stiffness impacts margins of stability (MOS) during level walking. MOS is defined as the minimum distance between the base of support (BOS) of the feet and a vertical projection of a combination of the center of mass (COM) position and velocity (Fig. 1) [3]. A larger minimum MOS has been associated with poorer scores on functional assessments of stability [4]. We hypothesized that mediolateral (ML) MOS would be larger during shoe walking compared to walking with an AFO, and that minimum ML MOS would increase with increasing AFO stiffness.

## METHODS

We collected gait kinematic data from five unimpaired adults, two males, three females: age=24.2 ± 5.4 (avg ± SD), mass=62.9 ± 9.3 kg, height=1.7 ± 0.1 m, during treadmill walking at a fixed slow speed, normalized by leg length. Participants walked with and without a unilateral passive AFO. AFO stiffness was varied from zero to 3.7 Nm/deg using elastic polymer bands (Fig. 1).

We calculated COM trajectories over 25 gait cycles per participant using a 33 degree of freedom model in OpenSim. We then computed the maximum anterior-posterior (AP) and minimum ML extrapolated COM (XCOM, Eqn. 1), which are defined as the sums of the COM position,  $x(t)$ , and the COM velocity,  $\dot{x}(t)$ . The AP and ML BOSs were defined as the positions of the stance limb's toe (AP) and fifth metatarsal (ML) markers. The MOS (Eqn. 2) for each participant and AFO condition can then be computed [3]. To compare between participants, the MOS was normalized by COM height,  $h$ .

$$XCOM(t) = x(t) + \dot{x}(t) \sqrt{\frac{g}{h}} \quad (1)$$

$$MOS(t) = BOS(t) - XCOM(t) \quad (2)$$

To identify differences in maximum AP and minimum ML MOS between shoe walking and walking with AFOs, we performed t-tests with a Bonferroni correction for multiple comparisons (significance level at  $\alpha=0.01$ ). We also performed linear regression to identify relationships between MOS and AFO stiffness.

## RESULTS AND DISCUSSION

The maximum AP MOS was significantly smaller in only the AFO limb for most AFO conditions ( $p<0.001$ ) and there was a trend towards greater minimum ML MOS when walking with an AFO compared to shoe walking (Fig. 2). The minimum ML MOS increased on average by 0.11 in both limbs for the AFO conditions compared to shoes alone. However, there was greater inter-subject variability in minimum ML MOS ( $p<0.001$ ) for the AFO limb compared to the non-AFO limb for all stiffness conditions.

Neither maximum AP nor minimum ML MOS changed with increasing AFO stiffness ( $r^2<0.35$ , slope $<0.004$ ). Conversely, ML MOS increased with step width in the AFO ( $r^2=0.76$ , slope $=0.41 \text{ deg}^{-1}$ ) and non-AFO ( $r^2=0.78$ , slope $=0.29 \text{ deg}^{-1}$ ) limbs. These trends are consistent with studies showing that the modulation of step width may be used to stabilize the COM, and may increase in the presence of new or uncertain environments, such as walking with AFOs [1, 4]. With further adaptation time, step width may decrease as participants become more comfortable with the AFOs.

The small sample size and slow walking speed in this study may have limited our ability to detect changes in MOS when walking with an AFO. Greater walking speed may be required for changes in AFO stiffness to perturb gait enough to impact MOS among unimpaired individuals. Regardless, these findings are consistent with a study that reported slightly larger inter-subject kinematic variability in the AFO limb when walking with an AFO [5], suggesting that changes in minimum MOS of the AFO limb may be harder to predict than those in the non-AFO limb. Understanding the impact of AFOs on stability in CP and other clinical groups is an important area for future investigation.

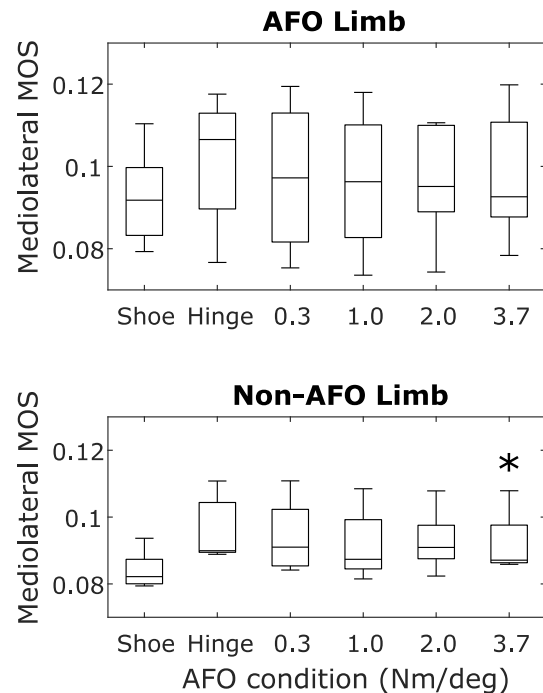


**Figure 2:** Minimum ML MOS for the AFO limb (top) and non-AFO limb (bottom). Asterisks denote significant differences compared to shoe walking ( $p<0.001$ ).

## CONCLUSIONS

These findings are an early step towards quantifying the impacts of AFO mechanical properties on dynamic stability of walking. However, to improve the translational impact of such information to AFO use during daily life, this work should be extended to faster walking speeds and longer adaptation periods in unimpaired adults and individuals with neuromuscular impairments. Using stability to inform device design may improve safety and enhance mobility during daily living.

## REFERENCES

1. Kim M., et al. *Int Conf Rehab Robot*, 1-6, 2013.
2. Lam W., et al. *Gait & Posture*, **22**, 189-197, 2005.
3. Hof A., et al. *J Biomech*, **38**, 1-8, 2005.
4. Vistamehr A., et al. *J Biomech*, **49**, 396-400, 2016.
5. Harper N. G., et al. *Clin Biomech*, **29**, 877-884, 2014.

## ACKNOWLEDGMENTS

This study was supported by the NSF CBET-14526.

# Comparison of a New Ankle Orthosis to a Standard Brace on Ankle Dynamics During Walking

<sup>1</sup>Chloe L. Chung, <sup>1</sup>Denis J. DiAngelo, <sup>2</sup>Douglas W. Powell, <sup>2</sup>Max R. Paquette

<sup>1</sup>Department of Orthopedic Surgery and Biomedical Engineering, University of Tennessee Health Science Center, Memphis, TN, USA; <sup>2</sup>School of Health Studies, University of Memphis, Memphis, TN, USA  
email: [mrpquette@memphis.edu](mailto:mrpquette@memphis.edu), web: <http://memphis.edu/hss/enl/>

## INTRODUCTION

Ankle fractures represent a significant portion of orthopedic trauma injuries that occur in the United States. Patients who sustain irreversible cartilage damage or joint instability from ankle injuries are likely to develop ankle osteoarthritis (OA). Between 70%-80% of ankle OA cases are associated with a previous traumatic injury, a condition known as the Post-Traumatic Ankle Osteoarthritis (PTOA) [1]. PTOA pain and inflammation can be managed noninvasively using orthotics such as the Ankle-Foot Orthosis (AFO) (i.e., brace). A Patellar Tendon Bearing AFO (PTB) applies compression to the lower leg to transfer some weight from the foot and ankle to the lower leg and patellar tendon. This is important since reduced axial ankle loads have been shown to effectively reduce the pain and discomfort of ankle arthritis [2]. However, current AFO designs do not provide a controlled offloading of the ankle joint and tend to limit ankle motion during gait [3].

A new Dynamic Ankle Orthosis (DAO) was designed to provide the coupled benefits of ankle offloading while supporting the range of ankle motion. The DAO applies a distractive force along the axis of lower leg and through the rotational axis of the device, creating an offloading effect. Further, the arrangement of the device's rotational axis with the anatomical axis of the ankle joint allows for a walking range of dorsiflexion ( $\sim 10^\circ$ ), plantar flexion ( $\sim 15^\circ$ ), and some frontal plane motion. The purpose of this preliminary work was to compare ankle joint kinematics and ground reaction force variables between the newly designed DAO and a standard PTB in healthy individuals during level-walking. A non-brace shoe condition (CON) served as the control group. Greater dorsiflexion and eversion excursions while walking were expected in the DAO compared to the PTB.

## METHODS

Three healthy young women ( $22.3 \pm 0.6$  yrs;  $59.8 \pm 9.2$  kg;  $1.62 \pm 0.07$  m) were recruited to participate in this pilot research study. Two braces, DAO and PTB, were fabricated under the supervision of a licensed orthotist (COPI, Memphis, TN) for all participants. Over-ground walking trials were performed wearing shoes with 1) no brace (CON), 2) DAO and, 3) PTB. The DAO distractive force was set to 75N. Participants first completed five over-ground walking trials to measure their preferred walking speed in each condition using photocells and an electronic timer (Lafayette Instruments Inc., IN, USA). Anatomical markers and tracking marker clusters were then placed on both lower extremities and a standing calibration trial was collected. A 9-camera motion capture system (240Hz, Qualisys AB, Sweden) and a force platform (1200Hz, AMTI, Inc., USA) were used to collect kinematic and GRF data, respectively. Participants then completed five over-ground walking trials at a set speed ( $1.4 \text{ m/s} \pm 5\%$ ).

Visual3D biomechanical software (C-Motion, Germantown, USA) was used to process and analyze all data. Joint kinetic variables were calculated using Newtonian inverse dynamics. The mean of each variable during the five walking trials was used for analysis. Due to the preliminary nature of work and small sample sizes ( $n=3$ ), only Cohen's  $d$  effect sizes were reported to assess effect magnitudes with Hopkins' interpretation (i.e., small:  $d < 0.6$ , moderate:  $0.6 \leq d \leq 1.2$ ; large:  $d > 1.2$ ).

## RESULTS AND DISCUSSION

Preferred walking speed was not different between CON and DAO conditions ( $d=0.25$ ) but was faster in CON ( $d=1.20$ ) and DAO ( $d=1.66$ ) compared to PTB walking; both showing large effect sizes (**Table 1**). These findings suggest that DAO does not restrict preferred walking speed unlike the

standard PTB. Step length was longer with DAO ( $d=0.61$ ) and PTB ( $d=0.71$ ) compared to CON. Peak dorsiflexion was greater in DAO ( $13.2^\circ$ ) compared to CON ( $7.7^\circ$ ,  $d=2.92$ ) and PTB ( $7.5^\circ$ ,  $d=3.13$ ) (**Fig. 1**). Dorsiflexion ROM was larger in DAO ( $22.1^\circ$ ,  $d=0.94$ ) but smaller in PTB ( $14.1^\circ$ ,  $d=2.02$ ) compared to the CON ( $18.9^\circ$ ). Only the PTB and CON difference showed a large effect size. Thus, DAO appears to improve dorsiflexion ROM similar to CON compared to PTB. Peak eversion was similar between DAO ( $-3.9^\circ$ ) and CON ( $-3.8^\circ$ ,  $d=0.05$ ), but smaller with PTB ( $-3.3^\circ$ ) compared to CON ( $d=0.21$ ) and DAO ( $d=0.54$ ), but effect magnitudes were all small. Finally, although eversion ROM in CON ( $4.85^\circ$ ) was larger compared to DAO ( $4.05^\circ$ ,  $d=0.52$ ) and PTB ( $0.19^\circ$ ), large effects were only observed between PTB and CON ( $d=6.31$ ) and DAO ( $d=2.87$ ). The DAO allows for greater frontal plane ankle motion than a standard PTB which is more like a non-braced condition.

Bracing conditions had negligible effects ( $d < 0.6$ ) on peak horizontal GRF variables (**Table 1**). However, vertical loading response and push-off peaks were lower in DAO compared to CON ( $d=1.39$  and  $d=0.30$ ) and PTB ( $d=1.42$  and  $d=0.67$ ). PTB increased the vertical loading response ( $d=0.56$ ) and push-off peaks ( $d=0.49$ ) compared to CON. The DAO reduced vertical loading to the body which may promote better tissue recovery during rehabilitation, but more work is needed to fully assess the ankle offloading benefit of the DAO.

## CONCLUSIONS

Findings from this preliminary work support our hypotheses that DAO allows for greater ankle

mobility and reduces vertical loading compared to a standard PTB during walking. We are currently

**Table 1.** Ankle angular kinematics and GRF during walking in the three bracing conditions (mean  $\pm$ SD).

Variables	CON	DAO	PTB
Preferred Speed (m s <sup>-1</sup> )	1.44 $\pm$ 0.08	1.46 $\pm$ 0.07 <sup>b</sup>	1.37 $\pm$ 0.03
Step Length (m)	0.61 $\pm$ 0.03	0.63 $\pm$ 0.03	0.63 $\pm$ 0.03
Horizontal Lateral Peak (BW)	0.02 $\pm$ 0.01	0.02 $\pm$ 0.01	0.03 $\pm$ 0.01
Horizontal Medial Peak (BW)	-0.05 $\pm$ 0.01	-0.06 $\pm$ 0.01	-0.06 $\pm$ 0.01
Horizontal Braking Peak (BW)	-0.14 $\pm$ 0.03	-0.14 $\pm$ 0.03	-0.16 $\pm$ 0.07
Horizontal Propulsive Peak (BW)	0.16 $\pm$ 0.06	0.16 $\pm$ 0.05	0.18 $\pm$ 0.09
Vertical Loading Response Peak (BW)	0.58 $\pm$ 0.14	0.39 $\pm$ 0.14 <sup>a,b</sup>	0.71 $\pm$ 0.28
Vertical Push Off Peak (BW)	0.72 $\pm$ 0.11	0.68 $\pm$ 0.09	0.81 $\pm$ 0.25

Notes: <sup>a</sup>: denotes large effect size vs CON; <sup>b</sup>: denotes large effect size vs PTB. Large  $d > 1.2$ .

expanding the study sample size. Following the completion of this work, we will conduct functional evaluations of the DAO in clinical populations.

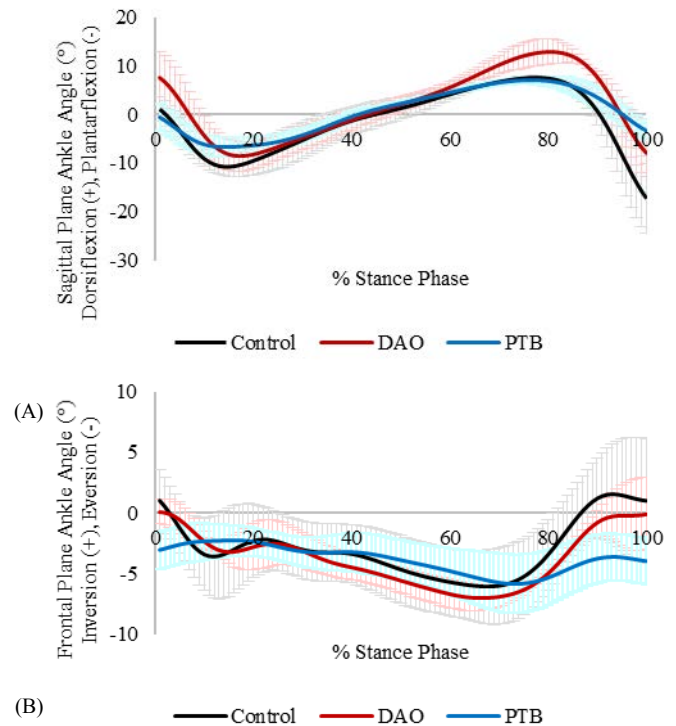


**Fig 1:** Mean Ankle Angles in the Sagittal (A) and Frontal (B) Planes.

## REFERENCES

1. Nguyen, MP et al., *J Bone Joint Surg.* **97**(7):590-596, 2015.
2. DiDomenico, LA et al. *Clin Podiatric Med and Surg.* **29**(3):391-412, 2012.
3. Kitaoka, HB et al. *Arch Phys Med Rehab.* **87**(1):130-5, 2006.

Funding for this study was provided UM Research Investment Foundation and a UT Research Foundation Maturation Grant.

# EMULATION: A QUANTITATIVE APPROACH TO THE AFO FITTING PROCESS

<sup>1</sup>Deema Totah, and <sup>1</sup>Kira Barton

<sup>1</sup>The University of Michigan, Ann Arbor, MI, USA  
email: deema@umich.edu, web: <http://brg.engin.umich.edu/>

## INTRODUCTION

Ankle-foot orthoses (AFOs) are commonly prescribed assistive devices that aid in correcting pathological gait in a wide range of patient populations, from individuals with cerebral palsy to stroke rehabilitation. AFOs come in a variety of designs and sizes, both off-the-shelf and custom-made, to accommodate the diverse population. The AFO fitting process, however, lacks quantitative metrics, and clinicians are left to rely on experience and visual observation of gait to make AFO selection choices.

This work points to the recent interest in emulator technology, which mimics the behavior of active exoskeletons and prosthetic devices with off-board motors [1], as a solution to bridging the gap towards quantitatively determining optimal, personalized AFO designs for patients. A control framework is presented for emulating the torque-angle curve of passive AFOs using an active exoskeleton device. While patients wear the actuated exoskeleton and walk on a treadmill, the off-board controller and motor setup would allow them to ‘try on’ different AFO devices as a sensor suite evaluates their performance. This work includes the exoskeleton design, sensor suite, and simulated control framework, as well as an experimental setup for quantifying the torque-angle curve of passive AFOs.

## METHODS

Taking inspiration from [2], the exoskeleton (Fig. 1) had a single joint at the ankle and consists of a modified surgical shoe, with a rigid foam base, and adjustable metal stirrups. The exoskeleton can be actuated by controlling an off-board motor to pull on a tether attached through a spring to the bottom footplate inside the shoe sole.

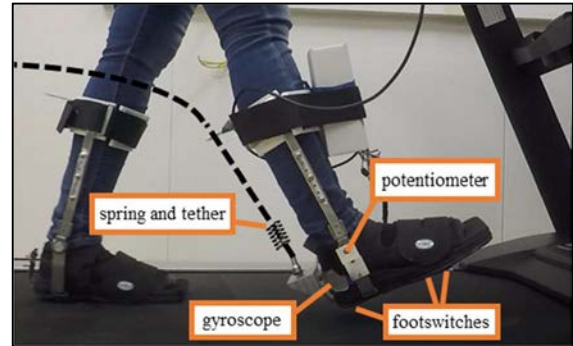


**Figure 1:** The exoskeleton and sensor suite with a diagram of where the spring and tether will connect to deliver torque from an off-board motor.

The exoskeleton was outfitted with a potentiometer to approximate ankle angle and three footswitches (placed underneath the heel (H) and 1<sup>st</sup> and 4<sup>th</sup> metatarsal heads (M1 & M4)) and a gyroscope (posterior to heel) for gait phase detection. An algorithm discussed in [3] is used to identify gait phases. Additionally, the gyroscope is used to identify plantarflexion versus dorsiflexion. The gyro is reset during stance to mitigate drift. The gait phase detection algorithm was tested with a healthy, 26-year old, female subject while walking on a treadmill at 1.5 *mph*.

The control framework was simulated in Simulink and Matlab (Mathworks Inc., Natick, USA). The collected sensor data were stored in Matlab and sampled by the simulation to emulate real-time application. The algorithm first selects an AFO design to emulate. Then, sensor readings are used to determine the gait phase and ankle angle and then command an appropriate exoskeleton torque to the motor driver. Ankle angle and gait phase time histories are collected in a buffer until ten steps are completed. The buffered data is sent to a performance algorithm that calculates a measure of symmetry [4] between the left and right maximum ankle ROM. The process is then repeated for another AFO design selection and a new symmetry metric is

produced. Greater symmetry indicates better patient performance. Once the patient has ‘tried on’ all possible design options, the algorithm chooses the design with the highest symmetry metric as the optimal AFO selection.

The torque-angle curve of a passive AFO was obtained by measuring the displacement of a central rod attached to a wooden pylon fixed inside the AFO (Fig. 2) after a force was applied by tensioning a cable fixed to the rod and to a loadcell. The AFO foot plate was fixed with clamps during the experiment.

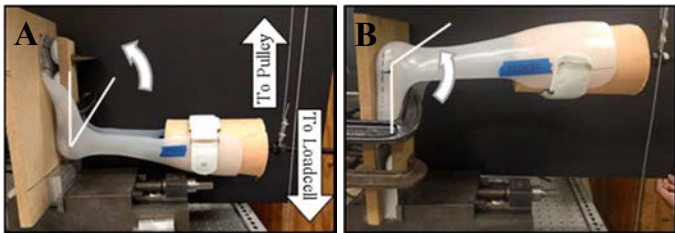


**Figure 2:** Experimental setup to acquire AFO stiffness curves during (A) flexion and (B) extension.

## RESULTS AND DISCUSSION

The gait detection worked well in simulated real-time (Fig. 3) to differentiate steps and gait phases, which were used to prompt the 10-step buffer and calculate the average symmetry metric. The controller used the state and angle to look up the appropriate command torque from the stiffness curves (Fig. 4). In the future, inertial sensing and automation will be added to the stiffness test to capture viscoelastic behaviors.

This framework still needs to be tested on a healthy and pathological patient population. The effectiveness of the emulation will be evaluated by

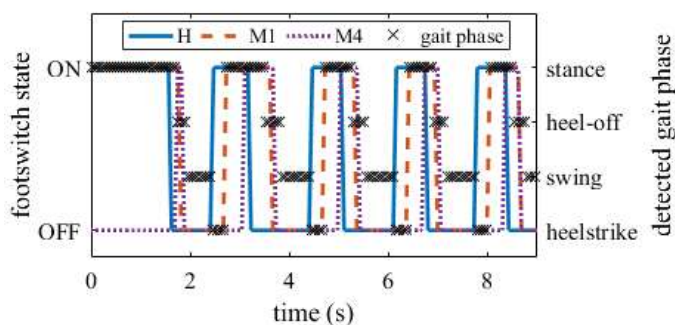


**Figure 3:** Gait detection code identified 4 gait cycle phases (x) based on footswitches (H, M1 & M4) and gyroscope (not shown).

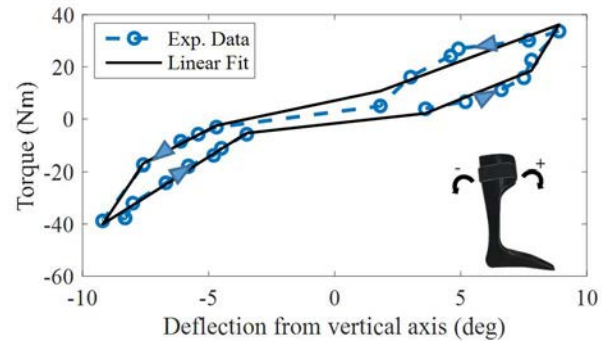


**Figure 4:** The ankle torque-angle curve of a solid-ankle passive, thermoplastic AFO from a static deflection test. Flexion and extension of the AFO was performed. A piece-wise linear fit is applied.

comparing inertial readings and patient feedback between the real, passive and emulated, active AFO versions. The chosen performance metric allows comparison across AFOs and quantifies increased gait symmetry, which is an outcome clinicians look for during their visual evaluation of patients.

Future work will include closing the control loop by utilizing learning control to find the optimal torque-angle curve that maximizes performance and then matching it to available designs. With advances in manufacturing technology, especially additive manufacturing, greater design versatility could allow the creation of unconventional designs to meet customized torque-angle behaviors.

## REFERENCES

- [1] Caputo JM, et al. *2015 IEEE Int. Conf. Robot. Autom.*, 6445–6450.
- [2] Witte KA, et al. *2015 IEEE Int. Con. on Robot. Autom.*, 1223–1228.
- [3] Pappas IP, et al. *IEEE Trans. Neural Syst. Rehabil. Eng.* **9** (2), 2001.
- [4] Chen G, et al. *Gait Posture* **22** (1), 51–56, 2005.

## ACKNOWLEDGMENTS

This work was supported by NSF PFI grant # 1534003 and NIDILRR grant # 90RE5012. The authors thank Devyani Kalvit for aiding in exoskeleton design, and Darren Bolger, CO for providing passive AFOs for testing.

# EFFECTS OF PERSONALIZED PASSIVE-DYNAMIC ANKLE-FOOT ORTHOSES BENDING STIFFNESS ON GAIT OF INDIVIDUALS POST-STROKE

<sup>1</sup> Corey Koller, <sup>2</sup>Cory Cacciola, <sup>3</sup>Darcy Reisman, <sup>1,4,5</sup> Elisa Arch

<sup>1</sup> Biomechanics and Movement Science Interdisciplinary Program, <sup>2</sup> Department of Mechanical Engineering, <sup>3</sup> Department of Physical Therapy, <sup>4</sup> Department of Kinesiology and Applied Physiology and <sup>5</sup> Department of Biomedical Engineering  
University of Delaware, Newark, DE, USA  
email: [ckoller@udel.edu](mailto:ckoller@udel.edu)

## INTRODUCTION

The plantar flexors play a critical role in moving the body forward by eccentrically contracting, during mid- to late- stance, to control shank rotation and forward progression [1]. Insufficient control of the shank's rotation due to plantar flexor weakness [2], an impairment seen in individuals post-stroke [1], may result in gait dysfunctions, such as crouch gait [2] and asymmetric step lengths [3]. Ankle-foot orthoses (AFOs) are rehabilitative devices that can be prescribed to individuals post-stroke who have plantar flexor weakness [2], with the goal of improving gait function [4]. Individuals' post-stroke often experience variable outcomes with currently-prescribed AFOs [5], likely because these AFOs are not properly customized for each individual [6]. We have developed a novel AFO design and prescription process that personalizes the passive-dynamic ankle-foot orthoses (PD-AFO) bending stiffness to each individual to assist their weakened plantar flexors. The bending stiffness can potentially replicate function of the plantar flexors by adding to the resistance needed to control shank rotation [2]. Plantar flexor function can be quantified by the peak plantar flexion moment [7]. Thus, we hypothesize that PD-AFO bending stiffness can be customized to add to an individual post-stroke's peak plantar flexion moment, enabling the net (individual + PD-AFO) moment to reach a typical level. The purpose of this study was to evaluate if personalized PD-AFOs bending stiffness improved the gait of individuals post-stroke.

## METHODS

Three individuals with chronic stroke (> six months post-stroke) consented to participate in this study.

Anthropometric measurements, height, and weight of all subjects were recorded. There were three parts to this study: a baseline visit, PD-AFO manufacturing, and an evaluation visit.

At the beginning of the baseline visit, a 10-meter walk test was performed to measure the subject's self-selected walking speed. The subject then underwent an instrumented gait analysis to collect the data needed to drive personalization of the PD-AFO bending stiffness. For the gait analysis, a seven-camera motion capture system (Motion Analysis Corporation, Santa Rosa, CA) was set up around a split-belt instrumented treadmill (Bertec Corp., Columbus, OH). Retro-reflective markers were attached to specific anatomic lower extremity landmarks. The subject walked on the treadmill at his/her self-selected walking speed while wearing his/her currently-prescribed AFO (Original AFO). Kinematic and kinetic data from 10 gait cycles were captured at 240 Hz and 1200 Hz, respectively. Data were exported into Visual 3D (C-Motion Inc., Germantown, MD) for analysis. Specifically, peak plantar flexion moment during stance was calculated and analyzed.

The PD-AFOs were made out of carbon fiber (CF) composite material. Each PD-AFO was custom fit to the subject's shank and foot by digitally capturing their size and shape using a 3D Fusion FaroArm (FARO Technologies Inc., Lake Mary, FL). The bending stiffness of each PD-AFO was personalized as the difference between the subject's peak plantar flexion moment from the healthy, speed-matched, peak plantar flexion moment obtained from the lab's normative database, divided by a typical dorsiflexion range of motion of 12°.

During the evaluation visit, the subject walked under two conditions: while wearing his/her Original AFO and while wearing the personalized PD-AFO. The same instrumented gait analysis procedures from the baseline visit were used. Peak plantar flexion moment and step length were calculated in Visual 3D and compared across conditions to determine if the individual was able to reach the targeted typical peak plantar flexion moment and if the PD-AFO improved step length symmetry.

## RESULTS AND DISCUSSION

Two females and one male participated in this study (Subject A: male, 61 years, 1.92 m, 81.4 kg; Subject B: female, 37 years, 1.66 m, 74.6 kg; Subject C: female, 62 years, 1.672 m, 76.7 kg). Subjects A, B, and C walked at a scaled velocity of 0.6, 0.4, and 0.3 statures/second, respectively.

Results showed that wearing the PD-AFO increases the peak plantar flexion moment when compared to each subject's Original AFO condition (Fig. 1). While these findings show benefits of the personalized PD-AFO, our hypothesis was not fully supported because the peak plantar flexion moment while wearing the personalized AFO did not return to typical levels (the peak plantar flexion moment of speed-matched typical individuals). Step-length ratio also became more symmetrical with the use of the PD-AFO in comparison to Original AFO for two of the three subjects (Table 1).

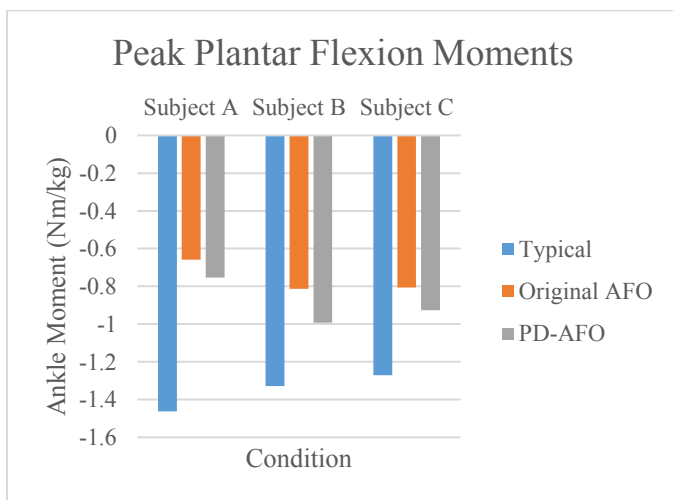


**Figure 1:** Peak plantar flexion moments of the three subjects while wearing the PD-AFO and Original AFO.

**Table 1:** Step-length ratio of the three subjects while wearing the original AFO and PD-AFO.

Step-Length Ratio	Typical	A	B	C
Original AFO	1	1.355	1.111	1.103
PD-AFO	1	1.361	0.978	0.98

## CONCLUSIONS

The goal of this study was to evaluate if the personalized PD-AFO bending stiffness improves the gait of an individual post-stroke. The results indicated that the PD-AFO improved the peak plantar flexion moment and gait symmetry in comparison to each subject's originally-prescribed AFO. However, the personalized PD-AFO did not return the plantar flexion moment and gait symmetry to typical levels. To reap benefits from the PD-AFO bending stiffness, the individual must load the brace into dorsiflexion during mid- to late-stance. The individuals post-stroke, in this study, often did not immediately adjust their gait pattern to properly use the PD-AFO. While this study focused on immediate effects of the personalized PD-AFO, future research should investigate training the individuals how to use the PD-AFOs to determine if even greater benefits can be gained from the personalized bending stiffness.

## REFERENCES

- Perry J. *Gait Analysis: Normal and Pathological Function*, Slack Incorporated, 2010.
- Arch ES, et al. *Ann. Biomed. Eng.*, **43**, 442-450, 2015.
- Esquenazi A, et al. *PM R.*, **1**, 1014-1018, 2009.
- Hesse S, et al. *Stroke.*, **30**, 1855-1861, 1999.
- Harlaar J, et al. *Prosthet. Orthot. Int.*, **34**, 327-335, 2010.
- Condie DN. *Prosthet. Orthot. Int.*, **32**, 313-323, 2008.
- Neptune RR, et al. *J Biomech.*, **34**, 1387-1398, 2001.

# User Biomechanics during Exoskeleton-Assisted Gait: Theoretical Approach and Case Study

Nathaniel I. Smith<sup>1</sup>, Eric Fabara<sup>2</sup>, Jean Francois Daneault<sup>2</sup>, Catherine Adans-Dester<sup>2</sup>, Anne O'Brien<sup>2</sup>,  
Alessandra Scarton<sup>2</sup>, Ugo Della Croce<sup>2</sup>, Paolo Bonato<sup>2</sup>, Karen L. Troy<sup>1</sup>

<sup>1</sup>Department of Biomedical Engineering Worcester Polytechnic Institute, Worcester, MA,

<sup>2</sup>Dept. of Physical Medicine, Spaulding Rehabilitation Hospital, Boston, MA

email:nismith@wpi.edu, ktroy@wpi.edu

## INTRODUCTION

Powered gait-assistive exoskeletons have become increasingly available both in the clinic and in the home. Exoskeletons offer mobility-impaired individuals numerous advantages over wheelchairs, including loading a user's skeleton with external forces. Weight-bearing interventions have been shown to improve bone health in spinal cord injured individuals [1], but little is known regarding the loads imparted by exoskeleton-assisted gait.

Limited data suggests that exoskeleton-assisted gait is relatively slow (0.22 to 0.5 m/s) and that kinematics are affected by walking speed [2]. Joint forces and moments during exoskeleton-assisted gait have yet to be examined extensively. Here we describe a framework for utilizing traditional laboratory motion capture methods to characterize the lower extremity joint forces resulting from and the joint range of motion prescribed by powered exoskeleton-assisted gait. We report data from the first individual who has completed data collection.

## METHODS

*Theoretical Framework:* The underlying theoretical approach to analyzing the biomechanics of exoskeleton-assisted gait described here hinges upon the interaction between the device and the user. Combining these two multi-body systems into a single "lumped" system allows the calculation of lumped net joint moments. Any moments generated by the user's muscles or connective tissues (including any spasticity or contracture) are theoretically represented by the difference between these lumped system joint moments and the torque provided by the device's joint motors, as follows:

$$\text{User-provided moment} = \text{Lumped system moment} - \text{Exoskeleton motor torque}$$

This lumped system approach relies on the assumption that the motor torques reflect all torque provided by the device throughout the gait cycle (i.e. torque is not provided by structural features at end ranges of motion). Additionally, joint angles and reaction forces for the user can be calculated using tracking markers on the user's segments and a measurement or reasonable estimation of the force between the device's footplate and the user's foot. The validity of our estimation of these footplate reaction forces is evaluated and discussed below.

*Case Study:* A 35 year old male ("user") with chronic motor-complete spinal cord injury (ASIA score = A at T4; height: 1.83 m; mass: 65.9 kg) was trained to use the Ekso<sup>TM</sup> powered exoskeleton device (Figure 1) until he was proficient at walking unassisted. The segments of the Ekso were defined with retroreflective markers while the user's segments were defined with marker triads. Anatomical landmarks obscured by the device were located using a marker wand. The user completed four walks across the laboratory while marker positions were collected using a ten camera Vicon system (120 Hz). Ground reaction forces were collected using two force platforms at 1080Hz.

Hip and knee joint angles for the Ekso in the sagittal plane were determined with a six-degree-of-freedom approach, while user joint angles were resolved into joint coordinate systems. User joint reaction forces were calculated using a footplate reaction force estimated from the ground reaction force signal.



**Figure 1.**  
Ekso<sup>TM</sup> powered  
exoskeleton device

Joint moments for the combined user-Ekso system were calculated from the ground reaction force and combined kinematic terms. These combined user-Ekso system joint moments in the sagittal plane were compared to the torque provided by the Ekso joint motors. Strides were defined from Ekso heelstrike to subsequent ipsilateral heelstrike, and left and right stride data averaged together under the assumption of bilateral symmetry.

## RESULTS AND DISCUSSION

The accuracy of our method for estimating footplate reaction forces was deemed acceptable, with RMS differences in acceleration profiles of matched user-Ekso segments of 0.15 - 0.36 m/s<sup>2</sup> throughout the gait cycle. The user achieved an average walking speed of 0.18 m/s. Compared to reported kinematics during assisted gait using a ReWalk exoskeleton [2], the knee and hip ranges of motion, and likely the joint angular velocities, were greater despite a slower walking speed (Table 1).

**Table 1.** User hip and knee ROM and angular velocities.

	Hip	Knee
<b>Range of motion (deg)</b>	38.3	56.1
<b>Max flexion velocity (deg/s)</b>	101.1	121.9
<b>Max extension velocity (deg/s)</b>	49.8	129.3

Knee joint reaction forces, expressed in the tibia anatomical coordinate system, reached a peak value of 0.83 body weight along the longitudinal axis and 0.13 body weight along the anterior-posterior axis, directed inferiorly and anteriorly into the proximal tibia (Figure 2).

Magnitudes of the joint reaction forces experienced by the exoskeleton user never surpassed one body weight. Compared to standing frames, which would be expected to apply a static load of approximately 0.5 body weight per limb, exoskeleton-assisted walking imparts larger and more dynamic forces. These mechanical loading characteristics have been linked to increased bone adaptation [3]. Spasticity or contracture in lower extremity muscles would provide additional bone forces not accounted for in an inverse dynamics solution.

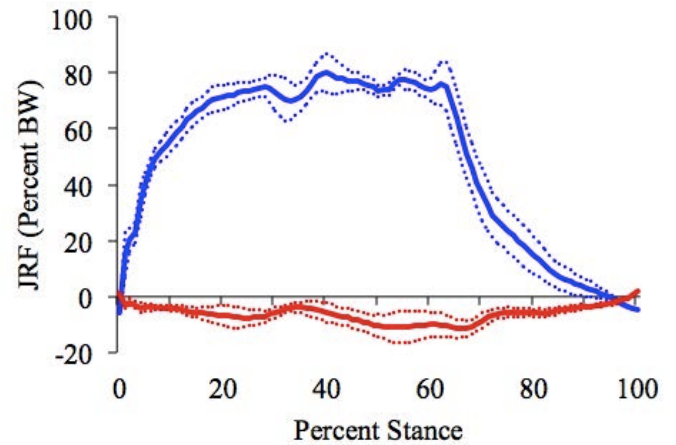


**Figure 2.** Axial (blue) and AP (red) tibia joint reaction forces during stance phase.

Patterns of torque provided by the Ekso joint motors agreed in a general sense with joint moments calculated for the lumped user-Ekso system, but the magnitude and timing of local peaks did not agree well. It was not possible to hardware-synchronize the Ekso and motion capture systems, so visual matching of events was used here but may explain some of the discrepancy. It is also possible that torque is provided passively by joints at terminal ranges of motion (i.e. knees locked), although the measured actuator knee torques do not support this idea. Clarifying these issues would allow future investigations to better quantify the resistive torque between the user and the exoskeleton due to spasticity or contracture, or any assisting torque due to conscious muscle activation in individuals with residual efferent control.

## CONCLUSION

We developed inverse dynamics methods to calculate user joint kinematics and kinetics during exoskeleton-assisted walking. For a case-study individual with SCI, knee ROM was 56.1 degrees, and JRF was 0.83 body weight.

## REFERENCES

- [1] Dolbow DR et al, NeuroRehabil. 2011 p261
- [2] Talaty et al, IEEE Conference on Rehabilitation Robotics, 2013 doi 10.1109/ICORR.2013.6650469
- [3] Turner CH, Bone 1998, p 399

## ACKNOWLEDGEMENTS

Funding provided by Department of Defense under grant #W81XWH-14-1-0611.

# MECHANICS AND ENERGETICS OF WALKING WITH A POWERED ANKLE EXOSKELETON USING NEUROMUSCULAR MODEL-BASED CONTROL - A PARAMETER STUDY

Sasha A. Philius, James V. McCall, Richard W. Nuckols, and Gregory S. Sawicki  
 Joint Dept. of Biomedical Engineering at UNC Chapel Hill and NC State, Raleigh, NC, USA  
 email: sphiliu@ncsu.edu, web: www.bme.ncsu.edu/labs/hpl

## INTRODUCTION

Powered exoskeletons are beginning to break new ground in enhancing locomotion performance for both able-bodied users [1] and individuals with pathologies such as stroke [2]. A major factor in determining exoskeleton performance is the control architecture that is used to generate the commands to motors that apply torques to the lower-limb joints. Approaches to torque control include using preset stiffness and damping values set as a function of joint angle or stride percentage (*i.e.*, impedance control) [1], or using muscle activity of the user (*i.e.*, myoelectric control) [2] to generate a reference signal for the exoskeleton actuators to follow.

Model-based control is another option that may lead to more robust behavior in response to changes in the state of the user or the environment. For example, previous research on a powered ankle-foot prosthesis demonstrated that, with optimized parameter settings, a neuromuscular model (NMM) based on the biological plantarflexors can normalize mechanics and energetics for amputees across a range of walking speeds [3]. It remains to be seen, whether a similar approach can be effective on a powered ankle exoskeleton system.

The purpose of this study was to test the effect of varying the reflex feedback parameters within a NMM-based controller designed to emulate the human ankle plantarflexors on a powered ankle exoskeleton. We hypothesized that increasing reflex feedback gain while minimizing the feedback delay would maximize net exoskeleton work and produce the largest reductions in users' metabolic cost.

## METHODS

**Exoskeletons:** We provided bilateral plantarflexion assistance via a tethered ankle exoskeleton device. Off-board motors and Bowden cable transmission delivered torque to the custom carbon fiber exoskeletons.

**Controller:** We designed the NMM based controller in Simulink (MathWorks, USA) and implemented it

through a dedicated real-time control system which also handled signal IO (500 Hz, dSPACE, Germany). We calculated applied exoskeleton torque from a load cell (500 Hz, LCM Systems Ltd, UK) placed in series with the applied assistance, and a goniometer (500 Hz, Biometrics, UK) attached to the exoskeleton joint provided real-time ankle angle.

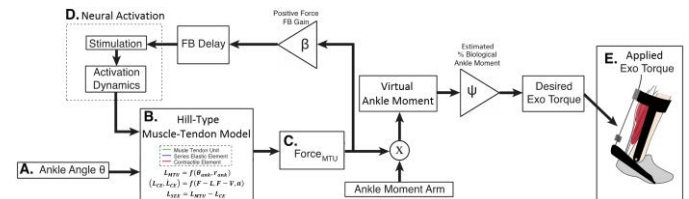


**Figure 1:** Neuromuscular model controller block diagram. Biological force, as computed by the internal muscle-tendon state, is scaled and applied across a moment arm to calculate desired exoskeleton torque.

The NMM based controller implemented in our system was similar to a reflex-based force feedback controller previously demonstrated [3]. A Hill-type muscle-tendon model was the basis for the emulated muscle-tendon unit (MTU) consisting of a contractile element (CE) with both active and passive properties and a series elastic element (SEE) (Fig.1B). We calculated MTU length from ankle angle and musculoskeletal geometry (1.1) and CE dynamics was subject to force-length, force-velocity and activation (1.2). We calculated SEE length as the difference in length of the CE from the MTU (1.3).

$$L_{MTU} = f(\theta_{ank}, r_{ank}) \quad (1.1)$$

$$(L_{CE}, \dot{L}_{CE}) = f(F-L, F-V, a) \quad (1.2)$$

$$L_{SEE} = L_{MTU} - L_{CE} \quad (1.3)$$

MTU force ( $F_{MTU}$ ) was a function of the model's SEE stiffness and strain. In the reflex pathway, we normalized MTU force to  $F_{max}$  and multiplied by a feedback gain. A delay was added to emulate a positive force feedback neural reflex signal (Stim) and CE activation dynamics (ACT) were modeled to close the feedback loop (Fig.1D). We calculated desired exoskeleton torque as a portion of the estimated biological moment.

$$\tau_{exo} = F_{MTU} \times r_{ankle} \times \psi \quad (1.4)$$

where  $\psi$  represented a percentage of the estimated biological torque. We calculated and recorded

internal model states ( $F_{MTU}$ ,  $L_{MTU}$ ,  $L_{CE}$ ,  $STIM$ ,  $ACT$ ) in dSpace for 5 second periods for offline analysis.

**Testing Protocol:** Three healthy-young adults (1 male; average mass  $72.2 \pm 6.1$  kg) completed the IRB approved protocol. Each subject walked at 1.25 m/s with the exoskeletons unpowered, and then powered with four different gains (0.8-2.0 gain sweep) at a set delay (10ms) and four different delays (10-40ms delay sweep) at a set gain (1.2). Metabolic power was estimated from indirect calorimetry data collected in last two minutes of each trial (Carefusion, USA).

## RESULTS

Increases in the NMM controller gain resulted in systematic increases in exoskeleton torque and power output (Fig. 2A, C-D green). The exoskeleton produced net negative work at low gain and net positive work at high gain (Fig.2B, green). In contrast, increasing NMM controller delay generated a decrease in exoskeleton net work (Fig. 2B, blue) and increased torque output to a point of diminishing returns (Fig.2D, blue). Users' metabolic energy consumption was reduced by 4% from the unpowered condition with a 1.2 feedback gain and 10ms delay. All other NMM controller settings increased metabolic demand – 6% in the worst case (Fig. 3).

## DISCUSSION AND CONCLUSIONS

From a mechanical standpoint, the NMM controller functioned as expected with the highest gain and smallest delay providing the most assistance. Surprisingly, this condition did not result in the largest metabolic reduction. Net work delivered by an exoskeleton may not be the only determinant of metabolic benefit to the user. More data and further analysis to examine changes in joint mechanics at the knee and hip, as well as muscle activation patterns may reveal underlying mechanisms driving these observations.

## REFERENCES

- [1] Jackson RW et al., *J. Appl. Physiol.* 2015; 119(5):541-57.
- [2] Takahashi KZ et al., *J. Neuroeng. Rehabil.* 2015; Feb 25; 12:23.
- [3] Herr HM, Grabowski AM. *Proc. Biol. Sci.* 2012; 279(1728):457-64.

## ACKNOWLEDGEMENTS

Funded by National Institutes of Health, National Institutes of Nursing Research Award # R01 NR017456 awarded to GSS.

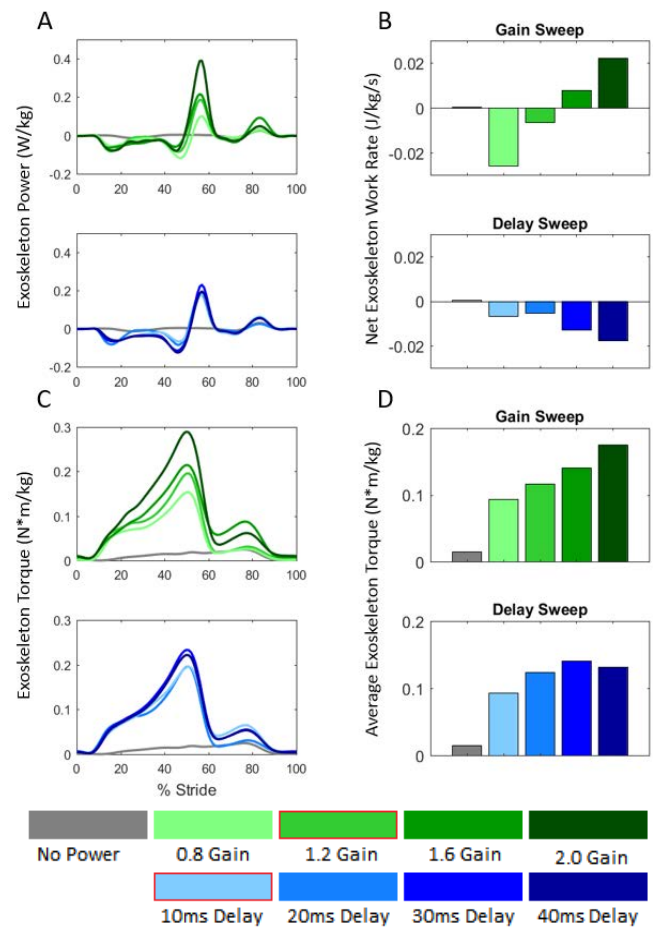


**Figure 2:** In the gain sweep, exoskeleton power (A) and net work rate (B) increased across conditions by increasing the torque profile (C) and average torque (D). In the delay sweep, average torque peaked, before decreasing and net work rate was entirely negative. Darker colors indicate higher values. Red outline indicates base parameters (Gain: 1.2, Delay: 10ms). Curves are study average trajectories.

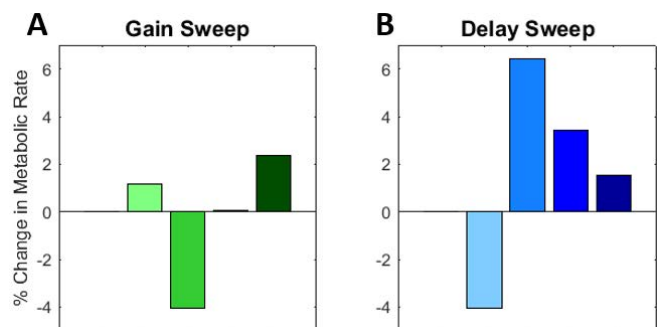


**Figure 3:** Average change in metabolic rate across gain (A) and (B) delay sweeps. Metabolic rate decreased at base (Gain: 1.2, Delay: 10ms) condition, but increased with all other parameter values.

# PREDICTIVE SIMULATION FRAMEWORK FOR COMBINED DEVICE AND HUMAN MECHANICS

Mohammadhossein Saadatzi and Ozkan Celik

Department of Mechanical Engineering, Colorado School of Mines, Golden, CO, USA  
email: msaadatz@mymail.mines.edu, web: brl.mines.edu

## INTRODUCTION

A primary challenge in design of wearable robots and their controllers is the difficulty in device performance prediction due to human adaptation to device dynamics and control. Combined predictive simulations of device and human musculoskeletal mechanics carry the promise to address this challenge and significantly accelerate design, testing and implementation of wearable robots. In this abstract, we present a predictive simulation framework for combined human-robot mechanics of bipedal walking.

## METHODS

The computational framework makes use of OpenSim API in C++ [1]. It employs forward dynamic simulations that are iteratively optimized via Covariance Matrix Adaptation (CMA) [2] to minimize metabolic cost of walking while satisfying a reference walking speed. Employing this single shooting method allows straightforward implementation of a variety of cost functions.

We use a simplified version of the musculoskeletal model “Gait2392-Simbody” available with OpenSim [1], which is commonly used for simulation of bipedal walking. The simplified model has 9 sagittal degrees of freedom and 9 muscle groups on each leg: Soleus, Vasti, Gastrocnemius, Tibialis anterior, Bicep femoris short head, Hamstring, Rectus femoris, Gluteus maximus, and Iliopsoas.

Uniquely, our framework generates bipedal walking through optimization of muscle actuation profiles, eliminating the need for manually-tuned reflex control laws, which were considered in [3,4]. Use of muscle actuation profiles rather than reflex control

laws improves the exploration ability of the optimization and facilitates consideration of different human musculoskeletal models. Additional states can be easily incorporated in our framework to generate bipedal walking for models with different number of muscles.

For the control of locomotion, two controller states are considered, corresponding to support and swing phases, which are detected based on heel strike of the swing leg. Actuations in each state for one leg are mirrored to the other leg. This selection reduces the number of optimization parameters.

Actuation profile of each muscle is defined as a piecewise linear function with 10 parameters (6 parameters for stance phase, and 4 parameters for swing phase). Hence, there are 90 optimization parameters to be determined. To speed up the optimization, routines have been written to terminate the forward dynamic simulation in case of irrelevant solutions.

Complementary to the increased freedom in optimization, we use the computed muscle control (CMC) method to generate favorable initial optimization parameters, which reduce convergence time and probability of getting stuck in local minima. We use Open Science Grid [5], an open source high-throughput computing (HTC) resource, to run multiple simultaneous optimizations so as to identify the solutions that are as close as possible to the global minimum.

A credible simulation of bipedal walking must closely follow experimental human gait data. To validate our simulation, we compare our results with experimental data presented by Dorn et al. in [4].

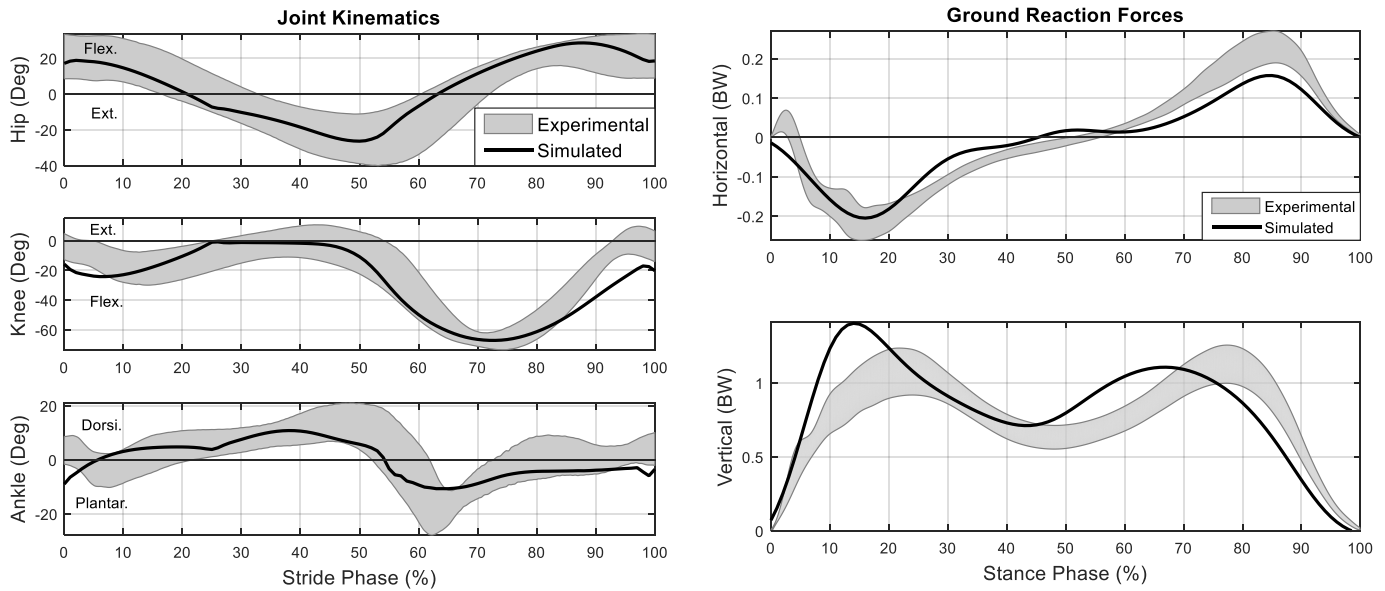


**Figure 1:** Sagittal plane joint kinematics and ground reaction forces for normal (level ground, unloaded) walking at 1.5 m/s. Experimental data for walking are represented by the shaded region ( $\pm 1$  SD) and is from [4]. The solid line represents equivalent simulation results obtained by our predictive simulation framework.

## RESULTS AND DISCUSSION

We successfully used our framework for planar simulation of muscle-driven bipedal walking at 1.5 m/s (Figure 1). Joint angles predicted by our simulations are mostly in agreement with normal human walking. Specifically, joint angles during 88.6 percent of the gait cycle (hip 100%, knee 76.95%, ankle 88.92%) are within 1 standard deviation of experimental data. Also, the ground reaction forces (GRF) of simulated walking reproduce the main features of experimental GRF.

The convergence of the optimization with 90 parameters takes approximately 12 hours on a desktop computer with an eight-core processor. The computational efficiency of our framework and its ability to consider additional parameters for more complex / finer resolution force profiles compatible with human motor control, or external devices, is highly promising.

The framework proposed in this study can be used for design of various types of exoskeletons, including both passive and active, as well as exoskeletons with feedback controllers or optimal actuation profiles. So far, we have used our

framework to perform combined simulation and optimization of passive and active ankle exoskeletons with successful results, which fall beyond the scope of this abstract. Extending our work to simulation of bipedal walking in three-dimensional space and running gait constitutes our future direction.

## CONCLUSIONS

Simultaneous predictive simulation of human and device mechanics has significant potential for facilitating design and control of human augmenting devices. In this work, we presented initial results from the framework we have developed for this purpose.

## REFERENCES

1. Delp SL, et al. *IEEE Trans Biomed Eng* **54** (11), 1940-1950, 2007. 5.
2. Hansen N, et al. *Evol Comput*, **11**(1) 1–18, 2003.
3. Geyer H, Herr H, *IEEE Trans Neural Syst Rehabil Eng* **18**(3), 263-283, 2010.
4. Dorn TW, et al. *PLOS ONE* **10** (4), 1-16, 2015.
5. Pordes, R et al. *J Phys Conf Ser* **78**(1), 012057, 2007.

# DESIGN AND CONTROL OF A MODULAR LOWER-LIMB EXOSKELETON EMULATOR FOR ACCELERATED DESIGN AND EVALUATION OF ASSISTIVE GAIT EXOSKELETON PARAMETERS

Kyle Heer, Jason Lee, Nick Collins, Megan Auger, & Ozkan Celik  
Department of Mechanical Engineering, Colorado School of Mines, Golden, CO USA  
email: kheer@mymail.mines.edu, web: [brl.mines.edu](http://brl.mines.edu)

## INTRODUCTION

Recent advances in robotic technology and control have made robotic exoskeletons and prostheses increasingly viable for a number of applications, including gait assistance [1]. However, difficulty in computational prediction of human adaptation to such devices constrains evaluation of potential device parameters to experimental studies, requiring physical devices that can be worn by a person [2]. For this reason, the use of emulators (testbeds capable of displaying wide ranges of physical parameters to their users) has emerged as an efficient approach to exoskeleton and prosthesis design [2-5]. This abstract describes the implementation of such a device intended for investigation into lower-limb exoskeleton parameters and control strategies.

## METHODS

The emulator (Figure 1) is a modular haptic device capable of closed-loop torque control and real-time angular sensing in up to four simultaneous sagittal-plane lower-limb joints. It comprises five braces to interface with a human user and an actuation cart to house the motors and data acquisition hardware. Table 1 presents a summary of emulator parameters.

Braces for human interface were designed to have sufficient adjustability to accommodate a wide range of user body types and sizes, based on 5<sup>th</sup> and 95<sup>th</sup> percentile values of various anthropometric measurements [6, 7]. In order to minimize mass while maintaining rigidity, all structural components were manufactured from 2024 aluminum. Three human attachment mechanisms are utilized: thin-wall PVC lined with medical foam (leg cuffs), aluminum brackets lined with 1" memory foam (torso brackets), and modified athletic sandals (foot attachment). 10 total functional joint axes provide rotational degrees of freedom (DOF) to the braces.

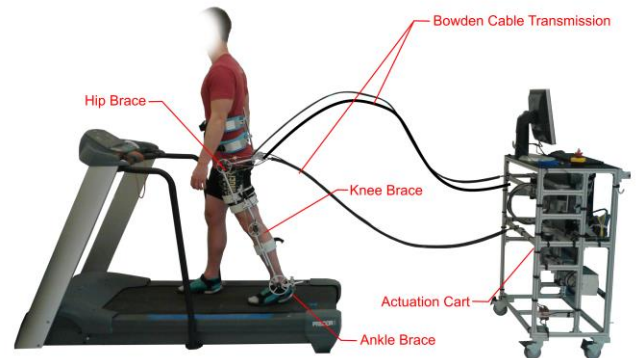


Figure 1: Lower-limb exoskeleton emulator

Four remotely-housed 200 Watt brushless DC motors (Maxon 16-275-EN) are used to independently actuate joints in the exoskeleton braces via Bowden cable transmission – pulleys on the motor output shafts convert torques to tensile forces, which are conducted by a lightweight synthetic fiber (Vectran™) to pulleys at the exoskeleton joint axes. Joint torques and angles are monitored in real time with miniature load cells (FUTEK LSB200) and rotary encoders (US DIGITAL E2-1250) at a frequency of 10 kHz.

Torques applied to the brace joints are controlled with a position feedback controller utilizing a least-squares second order regression model defining the desired motor position as a function of brace joint angle and desired brace torque (Equation 1).

$$\theta_m = A \theta_b + B \tau_{des}^2 + C \tau_{des} + D \quad (1)$$

Where  $\theta_m$  is the desired motor position,  $\theta_b$  is the current brace position, and  $\tau_{des}$  is the desired torque at the brace. Calibration trials conducted over the entire range of continuous torque generation and brace ROM were used to determine coefficients  $A$ ,  $B$ ,  $C$ , and  $D$  in order to account for cable compliance and friction within the Bowden sheath.

**Table 1:** Exoskeleton Emulator Parameters (asterisks denote powered DOF)

	Peak Torque (Nm)	Max Steady-State Torque (Nm)	Mass (kg)	Range of Motion (deg)
Hip	15.6	10.4	2.30	135 F/E*, 70 A/A
Knee	15.6	10.4	0.54	135 F/E*
Ankle	22.8	15.1	1.05	70 D/P*, 35 I/E

To evaluate the performance of the controller, two walking trials were conducted at 1.2 m/s. During the first trial, desired torque was held at zero, so that the motor would let out and take in slack to maintain a constant cable length (transparent mode). In the second trial, desired torque patterns were generated as a function of knee flexion angle to emulate a clutched torsional spring ( $k = 3.18 \text{ Nm/rad}$ ) to resist knee extension during swing. Brace angle, motor position, and resulting tensile forces at the brace were recorded and converted to torque.

## RESULTS AND DISCUSSION

Position controller results for both operation modes are presented in Figures 2 and 3 for three representative gait cycles.

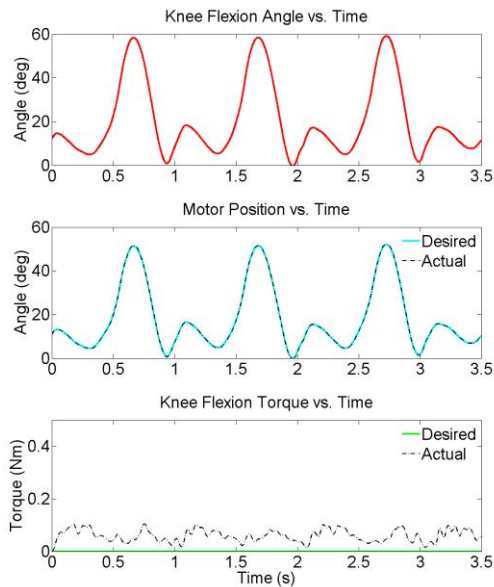


**Figure 2:** Knee flexion angle, desired vs. actual motor position, and desired vs. actual joint torque during treadmill gait with emulator in transparent operation mode

In transparent mode, motor position closely tracked its desired trajectory, and interaction torques remained at or below 0.1 Nm for the entire trial. Motor position tracking was also consistent during spring emulation mode, resulting in torque profiles closely matching their desired trajectories with

minimal delay.

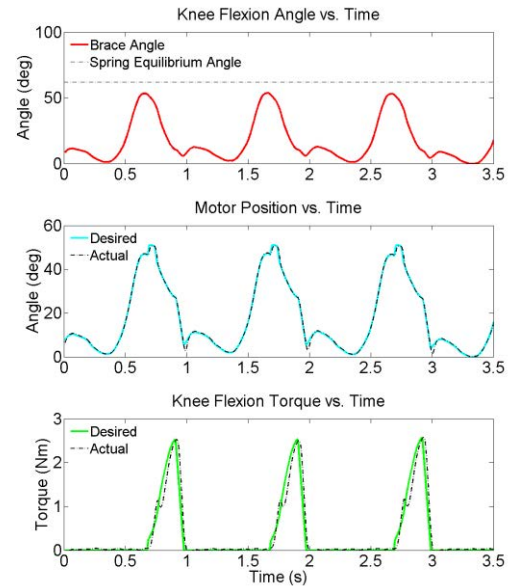


**Figure 3:** Knee flexion angle, desired vs. actual motor position, and desired vs. actual joint torque during treadmill gait with an emulated torsional spring resisting knee extension during swing

## CONCLUSIONS

We have developed, integrated, and characterized a modular lower-limb exoskeleton emulator system with offloaded actuation: an experimental platform to accelerate the identification and testing of exoskeleton design and control parameters. Future work will utilize the emulator to answer research questions related to feasibility of multi-joint spring/clutch driven gait exoskeletons and human joint impedance identification, and to validate results from predictive computational simulations using combined human and device mechanics.

## REFERENCES

1. Viteckova *et al.*, *Biomed Eng*, **33(2)**, 96-105, 2013.
2. Caputo & Collins, *J Bio Eng*, **136(3)** 035002, 2014.
3. Au *et al.*, *Robotics & Automation*, ICRA 2006.
4. Chua *et al.*, *HAPTICS*, 545-549, 2014.
5. Ding *et al.*, *ICRA*, 1327-1334, 2014.
6. Leardini *et al.*, *J. Biomech.* **32(1)**, 99-103, 1999.
7. Fryar *et al.*, *Vital & Health*, **11(252)**, 1-40, 2012.

# MID-FLIGHT TRUNK MOTION INCREASED UNILATERAL LOADING DURING LANDING: A CENTER OF MASS ANALYSIS

Taylor Hinshaw, Daniel Davis, Jacob Layer, and Boyi Dai

University of Wyoming, Laramie, WY, USA  
email: thinshal@uwyo.edu, web: <http://www.uwyo.edu/kandh/>

## INTRODUCTION

Anterior cruciate ligament (ACL) injuries frequently occur in jump-landing tasks. Individuals commonly demonstrate low knee flexion angles, increased knee valgus/varus angles, and increased trunk motion near the time of ACL injury [1]. While the effects of knee biomechanics on ACL loading have been well established, the mechanism between increased trunk motion and ACL injury risk remains unclear. Newton's first law indicates that an individual's total body center of mass (COM) will demonstrate a parabola shaped trajectory while in the air. Because total body COM is composed of multiple segments, movement of specific segments in a particular direction relative to total body COM will result in counter-movements in the opposite direction. Trunk motion in the air is likely to result in motion of the legs simultaneously, and affect landing mechanics.

The purpose of this study was to quantify the effect of mid-flight medial-lateral trunk motion on COM distribution and subsequently landing mechanics. It was hypothesized that medial-lateral trunk motion would cause leg movements in the opposite direction, subsequently resulting in increased impact vertical ground reaction force (VGRF) to the leg that was closer to the total body COM.

## METHODS

Eighteen males and 23 female recreational athletes (age:  $22.0 \pm 3.0$  years; height:  $1.74 \pm 0.10$  m; mass:  $71.0 \pm 13.9$  kg) participated. Forty-four markers were used to establish a full-body model. Kinematic and kinetic data were collected using eight Vicon cameras (160 Hz) and two Bertec force plates (1600 Hz). Participants completed three trials of a jump-landing task in three conditions: reaching left, reaching right, and up. Starting with one foot on each force plate, subjects jumped for maximum height and

land back with one foot on each force plate. In the reaching left condition (Figure 1), participants laterally bended their trunk and reached both hands to the left as far as possible after they reached the maximum height. In the reaching right condition (Figure 2), participants laterally bended their trunk and reached both hands to the right as far as possible after they reached the maximum height. In the up condition (Figure 3), participants reached both hands as high as possible when they reached the maximum height. This task was designed to simulate basketball rebounding and volleyball blocking.

The total body was modeled as four components: the upper body including all segments above the pelvis, the pelvis, the ipsilateral leg of the reaching side, and the contralateral leg of the reaching side [2]. For the up condition, the right side was used as the ipsilateral leg, and the left side was used as the contralateral leg. Time events of initial contact were identified for the ipsilateral and contralateral legs. Time differences were quantified with the initial landing of the ipsilateral leg prior to the contralateral leg defined as positive. At the first foot initial contact, the COM locations of the four body components relative to the total body COM were determined with the direction of the reaching side defined as positive. The peak VGRF during the first 100 ms after initial contact was quantified for each leg.

## RESULTS AND DISCUSSION

The ipsilateral legs landed earlier for the two reaching conditions compared with the up condition (Table 1). At first initial contact, the upper body moved towards the reaching direction while the pelvis and both legs moved in the opposite direction for the two reaching conditions compared with the up condition. The ipsilateral leg experienced the greatest VGRF for the two reaching conditions.

When individuals laterally bend their trunk in mid-flight, the pelvis and two legs moved in the opposite direction. As a consequence, the ipsilateral leg moved closer to the total body COM, and the contralateral leg moved further away from the total body COM, resulting in an asymmetric posture between the left and right leg for landing. First, the ipsilateral leg is likely to land earlier, and the leg landing earlier may experience greater VGRF. Second, utilizing the leg that is closer to the total body COM will result in decreased moment arms from the body weight vector to lower extremity joints, which may decrease joint torques and increase postural stability. These two factors together predispose the ipsilateral leg to experience greater impact VGRF compared with the contralateral leg.

The findings provide insight into understanding increased trunk motion during ACL injuries, and can help explain the prevalence of ACL injury for certain sports. Most jump-landing related ACL injuries in volleyball and badminton are on the knee opposite of the spiking arm or racket arm (dominant arm) [3, 4]. A ball or shuttlecock on a player's dominant side can be reached by extending the dominant shoulder and arm; however, a ball on the non-dominant side may also require lateral trunk bend. The greater mass of the trunk compared with the mass of an arm will induce greater perturbation to the whole body and increase the asymmetries in landing. The increased likelihood of lateral trunk bending towards the non-dominant-arm direction is likely associated with the higher injury rates of the knee opposite to the dominant arm.

While medial-lateral trunk movements may not be avoidable for achieving sports performance, several strategies may be adapted to decrease its impact on landing mechanics. First, after completing the reaching task in the air, participants should try to bend the trunk back to the natural position and establish a symmetric landing posture. Second, individuals may increase the knee and hip flexion in air, which will increase the time for adjusting posture and preparing for a soft landing. Third, when medial-lateral trunk motion is excessive and the contralateral leg is too far away from the total body COM, individuals may land softly on the ipsilateral leg and adopt effective falling strategies.

## CONCLUSIONS

Medial-lateral trunk movements in mid-flight resulted in pelvis and leg movements in the opposite direction, which imposed an asymmetric posture for landing and increased the loading of the ipsilateral leg. The findings provide information for understanding ACL injury mechanism and developing ACL injury prevention strategies.

## REFERENCES

1. Carlson VR, et al. *JBJS Rev* **4**, e5, 2016.
2. De Leva P. *J Biomech* **29**, 1223-1230, 1996.
3. Kimura Y, et al. *Br J Sports Med*, **44**, 1124-1127, 2010.
4. Devetag F, et al. *J Sports Med Phys Fitness*, in press, 2016.



Figure 1. Reaching to the left



Figure 2. Reaching to the right



Figure 3. Up

**Table 1:** Means  $\pm$  Standard Deviations of dependent variables for three jump-landing conditions

	Time Difference in Initial Contact (ms)	Upper Body COM (Body Height %)	Pelvis COM (Body Height %)	Ipsilateral Leg COM (Body Height %)	Contralateral Leg COM (Body Height %)	Ipsilateral Leg Peak VGRF (Body Weight)	Contralateral Leg Peak VGRF (Body Weight)
<b>Left</b>	14.0 $\pm$ 27.0 a	3.8 $\pm$ 1.3 a	-3.3 $\pm$ 1.2 a	3.8 $\pm$ 1.4 b	-10.7 $\pm$ 1.8 a	2.6 $\pm$ 1.0 a	1.7 $\pm$ 0.7 b
<b>Right</b>	16.7 $\pm$ 42.8 a	3.3 $\pm$ 1.5 b	-2.8 $\pm$ 1.2 b	4.1 $\pm$ 1.6 b	-10.1 $\pm$ 1.9 b	2.6 $\pm$ 0.9 a	1.7 $\pm$ 0.6 b
<b>Up</b>	2.6 $\pm$ 5.2 b	-0.2 $\pm$ 0.5 c	0.3 $\pm$ 0.4 c	7.0 $\pm$ 0.9 a	-6.7 $\pm$ 0.81 c	2.3 $\pm$ 0.8 b	2.1 $\pm$ 0.7 a

Note: a>b>c at a significance level of 0.05

# PERFORMANCE CONSTRAINTS DO NOT ALTER LANDING IN REACTIVE JUMPS

Mitchell L Stephenson and Jason C Gillette

Iowa State University, Ames, IA, USA  
email: mitch.stephenson@gmail.com, web: www.kin.hs.iastate.edu

## INTRODUCTION

Non-contact anterior cruciate ligament (ACL) injuries continue to pose a common problem to the athletic community. Recent research [1] has identified the role of reaction time in reactive landing strategies that indicates delayed decision-making for movement direction the instant before lower extremity loading changes movement patterns and decreases performance. It was suggested that a tradeoff between performance and “safe” landing biomechanics may exist, and the previous estimations of lower extremity loading in reactive jump landings may be conservative. An independent investigation partially confirmed this tradeoff in a non-reactive protocol [2].

The current investigation was performed to determine if this tradeoff between performance and loading also exists in a reactive jump landing test. Participants were asked to maintain the movement speed they performed in an anticipated setting during their reactive performances as well. Based on previous results [2], it was expected that the maintenance of the faster movement speed would result in decreased range of motion at the knee and increased vertical ground reaction forces (VGRF).

## METHODS

Nine physically-active, right-foot dominant, uninjured recreational athletes (6 females and 3 males;  $20.8 \pm 1.2$  years;  $1.70 \pm 0.10$  m tall;  $70.7 \pm 11.3$  kg) have volunteered for the ongoing study. Participants provided informed consent, executed a warm-up protocol, and then performed a series of successful practice trials for familiarization.

Participants jumped forward 50% of their height from a 30cm tall block, landed bilaterally on two force platforms (1600 Hz, Advanced Mechanical

Technology Inc., Watertown, MA), and then quickly and fluidly jumped to the left or right  $60^\circ$  from anterior for maximum speed and distance. The jump direction was indicated by one of two lights mounted at eye level in front of the participant. These indicators were lit before the participant began the trial such that the direction was anticipated (AN), or two conditions where the participant had to react to the indicator during the performance: The instant the participant left the 30cm box (RE1), or at the instant they landed on the force platforms (RE2). Participants performed three trials in each direction in each timing condition.

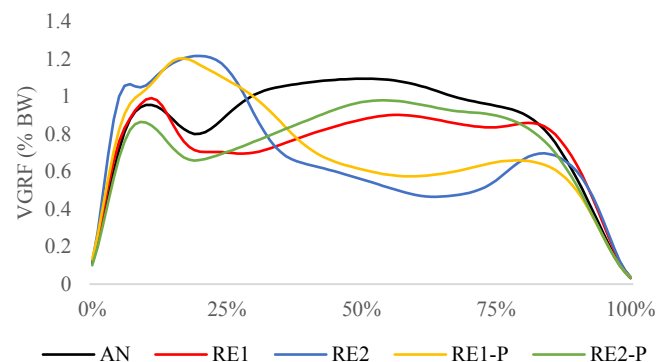


**Figure 1:** Mean VGRF across percentage stance time for each timing condition while jumping right.

The stance time on the force platforms between the two jumps in the AN condition was extracted and averaged. Participants then performed three more trials in each direction for the reactive conditions (RE1-P and RE2-P), but were constrained to maintain the stance time (ST) from the AN conditions. If ST was not fast enough for a trial, it was repeated randomly later until the target ST was reached, or a total of 9 repeats were performed. In the latter situation, the fastest 3 performances were subsequently analyzed.

The jump direction and timing condition were block-randomized and the participant was blinded to these variables. Kinematics of 19 retroreflective markers placed on the right lower extremity, pelvis, and torso were recorded via 8 Vicon cameras at 160Hz through Vicon Nexus 1.8.2 (Vicon Corp, Oxford, UK).

Peak knee valgus and flexion angles as well as the peak unilateral VGRF was extracted during the first 100ms of contact with the force plates. A repeated-measures analysis of variance was performed to compare the effect of the timing condition and performance preservation on knee kinematics and landing VGRF for each jump direction.

## RESULTS AND DISCUSSION

A significant ( $p < 0.001$ ) interaction between the jump direction and timing condition was identified. Significant main effects were identified for knee flexion, VGRF, and ST ( $p < 0.0001$ ). Pairwise comparison results maintaining a false discovery rate (FDR) of 0.05 are presented in Table 1.

As previously reported [1], ST increased from AN to RE1 to RE2. Participants were generally able to reduce ST in the RE-P conditions, but only obtained similarity to the AN condition for RE1-P left jumps; otherwise ST was longer than the AN conditions.

Also similar to previous analyses [1], dependent variables were characteristically unique to jump direction. Knee flexion only changed significantly

for right jumps, remaining shallower in RE2 conditions independent of performance constraints. VGRF changed for both directions, reducing for the left jumps and increasing in the right jumps for the RE2 conditions independent of performance constraints. For right jumps, RE2-P demonstrated slightly less VGRF than the RE2 condition.

Participants were able to consciously reduce their stance times in the constrained conditions, which could have training implications. However, results were otherwise not as expected. Performance constraints did not appear to significantly modify knee kinematics in the first 100ms of landing. Only VGRF for right jumps were affected by the performance constraints in the first 100ms, but this resulted in a *reduction* of VGRF compared to the unconstrained performance.

While it is possible that kinematic and kinetic changes took place beyond the first 100ms of landing (Fig 1), these changes likely do not affect ACL loading [3]. As such, it is likely not necessary to control ST in further reactive jump landing test paradigms. Furthermore it is not likely that previous reactive jump landing investigations underestimated changes in ACL load due to a lack of ST control.

## REFERENCES

1. Stephenson, ML, et al. *Proceedings of ASB'15*, Columbus, OH, USA, 2015.
2. Dai, B, et al. *J Sport Health Sci*, In Press.
3. Koga, H, et al. *Am J Sports Med*, **38**, 2218-2225, 2010

**Table 1:** Peak knee angles, vertical ground reaction force, and stance time (Mean  $\pm$  SE) for each timing condition during the first 100ms of foot contact with the ground. Significance indicated at a 0.05 false discovery rate.

		AN	RE1	RE2	RE1-P	RE2-P
Jump Left	Flexion ( $^{\circ}$ )	63.7 $\pm$ 3.7	63.6 $\pm$ 4.1	67.6 $\pm$ 3.8	64.4 $\pm$ 2.3	65.8 $\pm$ 2.2
	Valgus ( $^{\circ}$ )	8.7 $\pm$ 1.6	9.7 $\pm$ 1.9	8.7 $\pm$ 2.1	9.5 $\pm$ 2.2	8.4 $\pm$ 1.8
	VGRF (%)	2.32 $\pm$ 0.13 <sup>CE</sup>	2.28 $\pm$ 0.13 <sup>CE</sup>	1.84 $\pm$ 0.08 <sup>ABD</sup>	2.45 $\pm$ 0.14 <sup>CE</sup>	1.92 $\pm$ 0.09 <sup>ABD</sup>
	ST (ms)	426 $\pm$ 53 <sup>BCE</sup>	504 $\pm$ 59 <sup>ACD</sup>	688 $\pm$ 37*	438 $\pm$ 51 <sup>BCE</sup>	575 $\pm$ 39 <sup>ACD</sup>
Jump Right	Flexion ( $^{\circ}$ )	78.0 $\pm$ 1.8 <sup>CE</sup>	75.6 $\pm$ 2.3	65.1 $\pm$ 4.8 <sup>AD</sup>	78.3 $\pm$ 1.9 <sup>CE</sup>	64.8 $\pm$ 4.9 <sup>AD</sup>
	Valgus ( $^{\circ}$ )	7.9 $\pm$ 2.3	7.8 $\pm$ 2.1	7.2 $\pm$ 1.1	6.0 $\pm$ 2.5	7.3 $\pm$ 1.5
	VGRF (%)	1.27 $\pm$ 0.07 <sup>CE</sup>	1.24 $\pm$ 0.08 <sup>CE</sup>	1.86 $\pm$ 0.07*	1.07 $\pm$ 0.12 <sup>CE</sup>	1.64 $\pm$ 0.08*
	ST (ms)	432 $\pm$ 54*	513 $\pm$ 57 <sup>ACD</sup>	696 $\pm$ 49*	457 $\pm$ 49 <sup>ABC</sup>	550 $\pm$ 51 <sup>AC</sup>

\*Significantly different than all other timing conditions. <sup>A</sup>Significantly different than AN. <sup>B</sup>Significantly different than RE1. <sup>C</sup>Significantly different than RE2. <sup>D</sup>Significantly different than RE1-P. <sup>E</sup>Significantly different than RE2-P.

# KINEMATIC ANALYSIS OF PARKOUR LANDINGS FROM A DROP HEIGHT OF 2.7 METERS

<sup>1</sup>Boyi Dai, <sup>1</sup>Jacob S. Layer, <sup>1</sup>Taylor J. Hinshaw, <sup>1</sup>Ross F. Cook, and <sup>2</sup>Janet S. Dufek

<sup>1</sup>University of Wyoming, Laramie, WY, USA

<sup>2</sup>University of Nevada, Las Vegas, Las Vegas, NV, USA  
email: bdai@uwyo.edu, web: <http://www.uwyo.edu/kandh/>

## INTRODUCTION

Investigators have examined the effects of landing height and technique on performers' motion, impact forces, and their associated risk of injury [1]. Strategies to decrease injury risk during landing include increasing lower extremity joint range of motion and lengthening landing time [1]. Parkour is a form of acrobatic street gymnastics. One important skill in Parkour is to land safely from a high height. Parkour practitioners use their arms and roll their body during landing [2]. Investigators have quantified landing forces for Parkour landings from a drop height of 0.75 m [2]. How Parkour practitioners effectively execute landings from a high height remains unclear.

The purpose of this study was to compare the center of mass (COM) velocities and accelerations among a traditional squat landing, a Parkour precision landing, and a Parkour roll landing when Parkour practitioners landed from a drop height of 2.7 m.

## METHODS

Seventeen male Parkour practitioners (age:  $23.9 \pm 4.7$  years; height:  $1.78 \pm 0.06$  m; mass:  $67.6 \pm 8.5$  kg; experience in Parkour training:  $7.0 \pm 2.3$  years) participated. All participants were confident and had no anxiety about landing from a drop height of 3 m utilizing each of three landing techniques.

Three video camcorders (60 Hz) were used to record participants' landing motion. The cameras were calibrated for the direct linear transformation procedure using a 32-point calibration frame [3]. Participants performed one trial using each of three landings: squat landing, Parkour precision landing, and Parkour roll landing from a drop height of 2.7 m in a random order. For the squat landing,

participants landed softly with only feet contacting the ground (Figure 1). For the precision landing, participants landed softly with both feet and both hands contacting the ground (Figure 2). For the roll landing, participants landed softly with a rolling motion from both feet to the back (Figure 3).

Twenty-one body landmarks [3] were manually digitized from initial foot contact to the end of the landing, defined as the first frame that the vertical velocity of the COM became positive or one of the feet left the ground, whichever occurred earlier. Three dimensional coordinates of body landmarks were obtained from synchronized two dimensional coordinates and calibration parameters, and filtered at a low-pass frequency of 7.14 Hz [3]. COM of the whole body was calculated [3]. Landing time, COM horizontal and vertical velocities, and accelerations were compared using repeated measures analyses of variance, followed by paired t-tests ( $\alpha=0.05$ ).



**Figure 1. Squat landing**



**Figure 2. Precision landing**

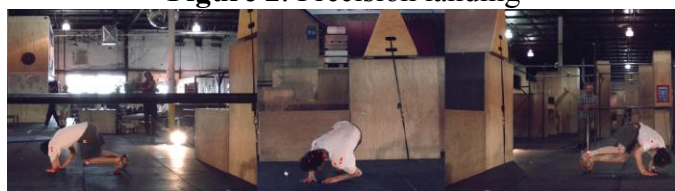


**Figure 3. Roll landing**

## RESULTS AND DISCUSSION

The roll landing resulted in the longest landing time, greatest anterior horizontal velocities at both initial contact and the end of landing, greatest downward vertical velocity at the end of landing, and lowest peak posterior horizontal acceleration during landing compared with the squat and precision landings. The precision landing demonstrated greater anterior horizontal velocities at the end of landing compared with the squat landing (Table 1).

Inappropriate landing techniques can cause excessive impact forces and loading to the lower extremities, resulting in musculoskeletal injuries [1, 3]. In the current study, Parkour practitioners landed from a height of 2.7 m, and no injuries occurred. This evidence suggests that a great initial landing velocity does not necessarily result in injury if appropriate landing techniques are utilized.

Although the roll landing started with the greatest initial anterior horizontal velocity, it also resulted in the lowest peak posterior horizontal acceleration during landing. Most initial horizontal velocity was maintained throughout the landing phase until the downward vertical velocity was largely decreased. The decreased peak posterior acceleration during the roll landing is likely to result in decreased posterior ground reaction forces, which are associated decreased knee extension moments and anterior cruciate ligament loading [3].

A drop landing was studied in the current study, but we speculate that the roll landing will be even more effective when individuals have to jump over a horizontal distance between the drop height and landing height, which will impose a greater

horizontal velocity at initial contact. The rolling motion allows individuals to emphasize decreasing the vertical and horizontal velocities during different time periods. When the vertical velocity is largely attenuated during the landing phase, the horizontal velocity can be subsequently decreased at the end of landing. Dissipating vertical and horizontal velocities separately is likely to decrease the peak loading imposed on the lower extremities.

## CONCLUSIONS

The Parkour roll landing resulted in the least horizontal acceleration during landing and allowed individuals to decrease the vertical and horizontal velocity over a longer period of time, which is likely to decrease the peak loading imposed on the lower extremities. The findings may provide information for developing landing training strategies for decreasing musculoskeletal injuries in high-risk populations such as athletes and military personnel.

## REFERENCES

1. Dai B, et al. *Am J Sports Med* **43**, 466-474, 2015.
2. Puddle DL and Maulder PS. *J Sports Sci Med* **12**, 122-129, 2013.
3. Dai B, et al. *J Sport Health Sci* **4**, 333-340, 2015.

## ACKNOWLEDGMENTS

This study was made possible by a grant from the National Institute of General Medical Sciences (5 U54 GM104944) from the National Institutes of Health. The authors would like to thank Amos Rendao and Ryan Ford at APEX Movement for their help with data collection.

**Table 1:** Mean  $\pm$  standard deviations of dependent variables for three landing conditions

	Landing Time (ms)	Vertical Velocity at Initial Contact (m/s)	Initial Horizontal Velocity at Initial Contact(m/s)	Peak Vertical Acceleration (m/s <sup>2</sup> )	Peak Horizontal Acceleration (m/s <sup>2</sup> )	Vertical Velocity at End of Landing (m/s)	Horizontal Velocity at End of Landing (m/s)
<b>Squat</b>	290 $\pm$ 30 *	-6.3 $\pm$ 0.1	1.4 $\pm$ 0.3 *	46.2 $\pm$ 3.9	-8.6 $\pm$ 2.2 *	0.1 $\pm$ 0.17 *	0.2 $\pm$ 0.2 *
<b>Precision</b>	289 $\pm$ 23 ^	-6.3 $\pm$ 0.1	1.4 $\pm$ 0.2 ^	46.0 $\pm$ 2.5	-7.1 $\pm$ 2.7	0.2 $\pm$ 0.1 ^	0.5 $\pm$ 0.6 *
<b>Roll</b>	320 $\pm$ 37 *^	-6.3 $\pm$ 0.1	2.6 $\pm$ 0.3 *^	45.0 $\pm$ 3.9	-6.0 $\pm$ 2.6 *	-0.3 $\pm$ 0.3 *^	2.8 $\pm$ 0.4 *

Note: significant difference (p<0.05) between two landing conditions with the same symbol

# LANDING MECHANICS IN CONTROLLED SCREENING TASKS AND SIMULATED GAMES IN VOLLEYBALL

Bradley Beardt, Myranda McCollum, Taylor Hinshaw, Jacob Layer, and Boyi Dai

University of Wyoming, Laramie, WY, USA  
email: bbeardt1@uwyo.edu, web: <http://www.uwyo.edu/kandh/>

## INTRODUCTION

Injuries to the anterior cruciate ligament (ACL) are common during jump-landing tasks. Most ACL injuries are non-contact in nature, and ACL injury rates may be decreased through neuromuscular training. Screening and training athletes that are at high risk for ACL injury will increase the efficiency of ACL injury programs.

A controlled jump-landing task has been utilized for screening movement patterns associated with increased ACL loading. Contradicting results have been found for utilizing controlled jump-landing tasks to predict future ACL injuries [1, 2]. One potential reason of a lack of strong predictive value is the discrepancy between the controlled jump-landing task and actual sports environment. It is unknown whether the risky movement patterns identified in a controlled task will remain when athletes compete in game situations. The purpose of this study was to evaluate the differences and correlations in landing mechanics and performance among a controlled jump-landing task, a volleyball-specific jump-landing task, and a jump-landing task performed in a simulated volleyball game.

## METHODS

Thirteen female club volleyball players (age:  $20 \pm 1.7$  years, height:  $167.8 \pm 7.1$  cm, mass:  $66.5 \pm 10.2$  kg) participated. Participants performed five trials each of three jump-landing tasks. The first was a controlled jump-landing task [1] (Figure 1). The second was a jump-landing for spiking a volleyball set to the outside, which only involved a setter and an outside hitter (Figure 2). The third was a jump-landing task for spiking a volleyball set to outside in a simulated game situation, which involved a team on both sides (Figure 3). Jump-landing trials were

recorded simultaneously by three cameras at a sample frequency of 60 Hz. The cameras were calibrated for a direct linear transformation procedure using a 32-point calibration frame [3].

Participants' bilateral shoulders, greater trochanters, knees, and ankles were manually digitized. Three dimensional coordinates of body landmarks were obtained from synchronized two dimensional coordinates and calibration parameters [3]. Participants' stance time, jump height, knee flexion angle at initial contact and peak knee flexion during landing for both left and right legs, and knee-ankle distance ratio at the lowest height were extracted for analysis. Paired t-tests and Spearman's rank correlation tests were performed between two jump-landing conditions for each variable ( $\alpha=0.05$ ).



Figure 1: Controlled jump-landing task

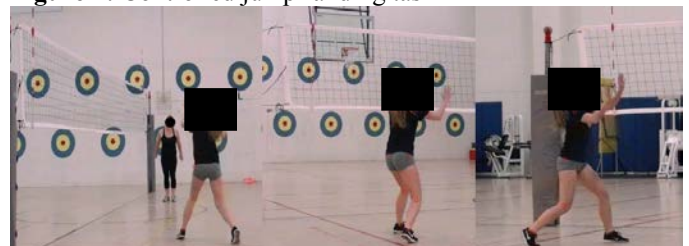


Figure 2: Volleyball specific jump-landing



Figure 3: Jump-landing in a simulate game

## RESULTS AND DISCUSSION

The results of the paired t-tests showed significant differences between the controlled jump-landing and both the volleyball-specific jump-landing and jump-landing in a simulated game for all variables. The Spearman's rank correlation test showed significant correlations for both the volleyball-specific jump-landing and jump-landing in a simulated game for most variables (Table 1).

ACL injuries commonly occur during jump-landing tasks. A controlled drop-jump has been developed to screen movements associated with increased ACL loading to predict ACL injuries with inconsistent findings [1, 2]. The findings of the current study suggest that the landing patterns during a controlled jump-landing task are different and do not correlated well with the landing patterns in a simulated game in female volleyball players. As most ACL injuries occur during actual sports environment, the findings raise concern regarding the testing specificity of utilizing a controlled jump-landing task to screen for risky movement patterns. Screening athletes during actual sports environment is likely to increase the predictive value of using landing biomechanics for future ACL injuries and warrant future investigations.

While screening athletes during sports environment is desirable, requirements of the direct linear transformation procedure such as clear views from cameras, accurate calibration, limited calibration volume, and manual digitizing may compromise its practical application. Other equipment such as inertia sensors and portable goniometers that can be

worn by players without affecting their normal movements may overcome these obstacles.

Meanwhile, the similar and strongly correlated landing patterns between the volleyball-specific landing and landing in a simulated game suggest that a sports-specific task without a simulated game environment could be used as a surrogate when data collection in game situations is not feasible. A volleyball-specific task may be implemented in a lab setting by hanging a ball from a ceiling without involvement of extra players.

## CONCLUSIONS

Landing patterns in a controlled jump-landing task may not represent landing patterns in game situations in female volleyball players. Screening athletes' movement patterns in a sports environment is likely to improve the predictive value of landing biomechanics for ACL injuries. The similarity and correlation between the volleyball-specific landing and landing in a simulated game indicate that it could be possible to utilize a sports-specific landing task in a non-game setting to screen for poor landing mechanics.

## REFERENCES

1. Padua DA, et al. *Journal of Athletic Training*, **50**, 589-595, 2015.
2. Smith HC, et al. *American Journal of Sports Medicine*, **40**, 521-526, 2012.
3. Dai B, et al. *Journal of Sport and Health Science*, **4**, 333-340, 2015.

**Table 1:** Mean  $\pm$  standard deviations of dependent variables for three landing conditions

	Stance Time (ms)	Jump Height (m)	Left Knee Flexion at IC (°)	Right Knee Flexion at IC (°)	Peak Left Knee Flexion (°)	Peak Right Knee Flexion (°)	Knee-Ankle Distance Ratio
Controlled Landing	555 $\pm$ 129 A	0.38 $\pm$ 0.05 B	16.4 $\pm$ 2.6 B	16.3 $\pm$ 4.0 B	86.6 $\pm$ 8.4 A	87.9 $\pm$ 9.0 A	0.79 $\pm$ 0.13 A
Volleyball-Specific Landing	411 $\pm$ 52 C *	0.43 $\pm$ 0.06 A *	39.1 $\pm$ 10.0 A *	23.0 $\pm$ 8.6 A *	48.7 $\pm$ 6.5 B	70.5 $\pm$ 6.4 B *	0.50 $\pm$ 0.09 B *
Landing in a Simulated Game	431 $\pm$ 62 B *	0.44 $\pm$ 0.06 A *	41.5 $\pm$ 9.6 A *	21.2 $\pm$ 6.8 A *	51.1 $\pm$ 6.2 B	69.1 $\pm$ 8.6 B *	0.51 $\pm$ 0.09 B *

Note: significant differences ( $p < 0.05$ ) between two conditions with  $A > B > C$ ; significant correlations ( $p < 0.05$ ) between two conditions with the symbol of \*.

# Implications of Added Body Mass on Lower Limb Joint Kinetics During Vertical Jumping

Hailey N. James, Lindsey E. Allison, Douglas W. Powell, Lawrence W. Weiss, Max R. Paquette  
Musculoskeletal Analysis Laboratory, University of Memphis, Memphis, TN, USA  
email: [mrpquette@memphis.edu](mailto:mrpquette@memphis.edu); web: <http://www.memphis.edu/shs/research/mal.php>

## Introduction

Vertical jump (VJ) ability is considered to be a good predictor of athletic performance and physical capabilities (1). Vertical jump ability is applicable to sports involving high power generation and vertical displacement. For example, basketball players need high power production for rebounds, blocks, and shots. Due to the importance of VJ ability, the maximal vertical jump has been used as a test to monitor improvements in jumping ability following a strength and conditioning program (3). Therefore, it is essential to understand factors that affect lower limb joint powers during jumping. One of these factors is body mass. Following off-season rest periods, athletes may return to training with slightly more body mass due to inactivity or reduced training intensity. In running, added body mass to the trunk (i.e., abdominal area) increases peak knee flexion and extensor moment as a result of increased forward trunk lean (2). Added trunk mass may also alter joint kinetics during vertical jumping which may impact the power contribution of each lower limb joints.

The purpose of this study was to assess the acute effects of added mass equivalent to a 5% increase in body fat on countermovement vertical jump (CVJ) performance and lower limb joint kinetics. We expected a decrease in CVJ performance and a proximal shift in lower limb joint power generation with the added mass.

## Methods

Seventeen recreationally trained young adults (8 women and 9 men) participated in this study (22±2yrs; 70.8±15.2kg; 1.72±0.11m; 15.1±8.1 % body fat). Participants attended one testing session to perform maximal vertical jumping wearing their own footwear. All participants were instructed to refrain from exercise the day before the testing session.

Testing involved measurement of anthropometric variables, a general warm-up on a cycle ergometer, a dynamic warmup including 10 bodyweight squats and 5 jump squats, three maximal unloaded countermovement vertical jumps (**Normal**), and three maximal loaded (**Weighted**) CVJ. During the Weighted CVJ a weight vest with added mass equivalent to a 5% increase in body fat was worn by all participants. Rest periods of at least 75s were provided between maximal jumps. Maximal vertical jump height was standardized to standing reach height. During jumping trials, a 9-camera motion capture system (240Hz, Qualisys AB, Sweden) and a force platform (1200HZ, AMTI, Inc.) were used to collect kinematic and ground reaction force data, respectively.

Visual 3D software (C-Motion, Germantown, MD) was used to process and analyze both kinematic and kinetic data. Newtonian inverse dynamics were used to compute internal joint moments (Nm). Angular joint powers (W) were computed as the product of joint moments and joint angular velocities. The average of all biomechanical variables from each jumping trial during the concentric phase of jumping was used in statistical analyses. Repeated measures ANOVA were used to compare mean from within-subject comparisons (Normal vs Weighted) ( $p<0.05$ ). Cohen's  $d$  effect sizes were also computed to compare the effect magnitude of mean differences.

## Results and Discussion

As hypothesized, vertical jump performance was *greater* during the Normal (41.4±11.1cm) compared to the Weighted condition (39.7±10.6cm;  $p=0.003$ ;  $d=0.16$ ). However, the small effect size suggests that the meaningfulness of this difference is questionable.

Peak plantarflexor, knee extensor and hip extensor moments were greater during the Weighted

compared to Normal jumping condition (**Table 1**). This is not surprising considering the joint moments were not normalized to body mass. The small effect sizes (i.e.,  $d < 0.22$ ) for joint moments suggests that these moment differences have minimal importance. Increased body mass, as simulated by a weighted vest, increases peak knee flexion angle and knee extension moment during running (2). In vertical jumping, the deeper countermovement position would increase ankle and knee ROM, which increases joint lever arms and as a result, increases peak internal moments (**Table 1**). In addition, the deeper countermovement leads to increased forward trunk inclination, and therefore, greater hip flexion. This greater hip flexion with added mass would result in an increased hip extension ROM from the bottom of the countermovement to take-off and a greater lever arm at the hip, which would explain the increased hip extension moment (**Table 1**).

As expected peak lower limb joint powers were redistributed proximally during Weighted compared to Normal jumping (**Figure 1**). However, statistically, condition means were not different at the hip ( $p=0.14$ ;  $d=0.09$ ), knee ( $p=0.30$ ;  $d=0.03$ ), and ankle ( $p=0.15$ ;  $d=0.05$ ) joints. During maximal vertical jumping, the power generated at the knee joint is suggested to be limited due to this forward trunk inclination (4). Although not significant, our findings are similar, such that during the Weighted condition, peak knee power was slightly lower. The observed power redistribution from ankle and knee to the hip during Weighted jumping may be the result of increased angular hip extension velocity. Hip extension velocity may be increased to displace the trunk through the larger angular displacement in an effort to match the timing of joint angular positions at take-off with added trunk mass.

## Conclusions

The findings from this study suggest that added trunk mass to simulate a 5% increase in body fat does not significantly change peak lower limb joint powers during vertical jumping. However, we observed a redistribution in lower limb joint powers from the knee and ankle to the hip joint when mass is added to the trunk. This may suggest that any body mass gained by athletes during the off-season may impact the lower limb joint strategy to produce power during jumping.

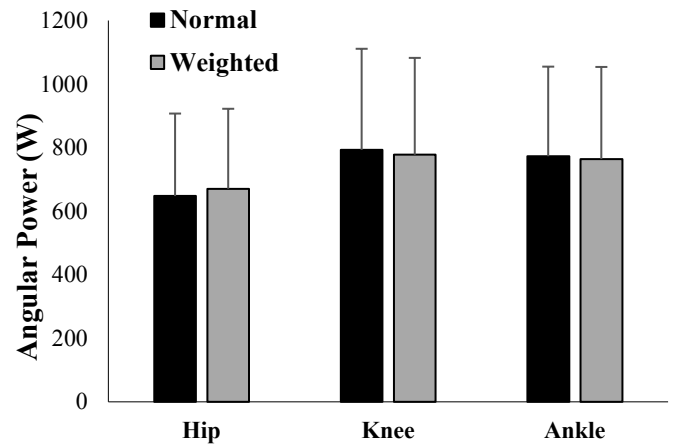


**Fig 1:** Peak hip, knee and ankle angular power generation during the concentric phase of vertical jumping without (Normal) and with added mass (Weighted) (mean  $\pm$  SD).

## References

1. Barker, M. et al. (1993). *Journal of Strength & Conditioning Research*, 7(4), 224-233.
2. Wu, C. H. (2015). University of Jyväskylä: Department of Biology of Physical Activity. Master's Thesis.
3. Umberger, B. R. (1998). *Strength & Conditioning Journal*, 20(5), 70-74.
4. Vanrenterghem, J. et al. (2008). *Journal of Strength & Conditioning Research*, 22(3), 708-714

**Table 1.** Sagittal plane joint ranges of motion (ROM) and peak joint moments during the concentric phase of vertical jumping without (Normal) and with added mass (Weighted) (mean  $\pm$  SD).

Variables	Normal	Weighted	<i>p</i> -values	Effect Size ( <i>d</i> )
Ankle Plantarflexion ROM (°)	58.9 $\pm$ 6.5	59.5 $\pm$ 7.3	0.15	0.08
Knee Extension ROM (°)	90.9 $\pm$ 9.6	91.4 $\pm$ 9.7	0.56	0.05
Hip Extension ROM (°)	91.8 $\pm$ 13.9	92.4 $\pm$ 12.8	0.57	0.05
Plantarflexor Moment (Nm) <sup>a</sup>	117.5 $\pm$ 39.0	121.6 $\pm$ 40.1	0.012	0.11
Knee Extensor Moment (Nm) <sup>a</sup>	126.1 $\pm$ 43.2	132.3 $\pm$ 46.6	0.009	0.14
Hip Extensor Moment (Nm) <sup>a</sup>	173.4 $\pm$ 56.5	186.2 $\pm$ 60.4	0.004	0.22

Notes: <sup>a</sup>: different between conditions. Cohen's  $d < 0.6$  is a small effect size.

# CLASSIFYING LANDING PERFORMANCE USING FREQUENCY DOMAIN ANALYSES

<sup>1</sup> Zhanxin Sha, <sup>1</sup> Zhaoxian Zhou, <sup>2</sup> Boyi Dai, <sup>1</sup> David Dolbow

<sup>1</sup> The University of Southern Mississippi, Hattiesburg, MS, USA

<sup>2</sup> University of Wyoming, WY, USA

email: zhanxin.sha@usm.edu

## INTRODUCTION

Appropriate landing is important for minimizing the risk of injuries during human locomotion such as running, walking, and landing from jump. Incorrect landing techniques may lead to anterior cruciate ligament (ACL) and ankle injuries. There are about 200,000 ACL injuries occurring every year during sport activities. ACL injuries occur during quick deceleration or landing maneuvers in non-contact situations.

A previous study indicated that increased ground reaction forces (GRF) during landing are associated with increased ACL loading [1]. Commonly used GRF variables are calculated from time domain analysis, including peak force, loading rate, and time to peak force. From frequency domain analysis, previous studies identified high and low frequency components during the landing phases from running and walking activities [2-3]. Different frequency content may be related to different landing strategies. However, there is a paucity of study focusing on frequency domain analysis of landing from jumps. Thus, the current study used frequency domain analysis to classify landing performance from counter movement jump (CMJ).

## METHODS

Forty four Division I football players (body mass  $101 \pm 18.96$  kg, age  $21 \pm 2$  years old) participated in the study. All athletes wore training shoes and thirty of them wore the same type of training shoes. The testing included three trials of a countermovement jump. Jumping and landing kinetic variables from dominant and non-dominant legs were measured from two force platforms (AMTI) at a frequency of 1000 Hz. Trials were considered to be valid only when both jump and

landing were on the force platforms. Informed consent was obtained from each athlete in accordance with the protocol approved by the Institutional Review Board.

Jump height (JH) was calculated based on flight time. GRF was normalized to body weight. Direct current component was eliminated from the signal. Frequency components of the vertical force during the landing phase were identified by the Fourier transformation. 99% of the signal power was reconstructed from the inverse Fourier transform of the first several significant components to verify the validity of the Fourier transform.

## RESULTS AND DISCUSSION

The reconstructed signals from components lower than 80 Hz (Figure 1) matched well with the original signals ( $RE < 1\%$ ). Athletes demonstrated different spectra of frequency for left and right legs (Figure 2). Starting from the lowest frequencies, components were added up to a percentage of the total signal power. The result showed that the frequency components of some athletes were below 10 Hz while of some others were always higher than 15 Hz. When athletes were classified into three groups based on spectral ranges at 85 percentage of the total signal power: A: 4-10 Hz, B: 12-27 Hz, and C: 30-44 Hz. There were 11 athletes in group A (JH  $55.9 \pm 5.4$  cm), 29 athletes in group B (JH  $54.7 \pm 10.9$  cm), and 4 athletes in group C (JH  $47.1 \pm 9.0$  cm). Paired T-tests indicated that the JH differences were not statistically significant among these 3 groups ( $p > .05$ ); however, frequency spectra among the 3 groups were significantly different. Therefore, different landing techniques rather than jump height were more likely to affect the frequency components of the landing forces.

Different landings may also relate with different mechanisms of impact attenuation. Previous studies [3,4] demonstrated impact attenuation is a combination of active and passive mechanisms. Active mechanisms involve muscle pre-activation, contraction, and segment configuration. A previous study [1] indicated changing body segments configuration, such as trunk, hip, knee flexion angles and type of foot landing would affect landing time, magnitude and direction of impact force. That may explain the three groups of athletes that had different distributions of frequency components from the current study. Passive mechanisms include bone, articular cartilage, and shoes. Bone and articular cartilage may respond to high and low impact frequencies differently [4]. How this relates with risk of injury still needs to be studied.

## CONCLUSIONS

By applying frequency domain analyses, we have quantified the frequency components of landing forces from CMJ. For athletes with similar jump height, different frequency components distribution were observed. Frequency domain analysis provides another method to classify landing performance. Frequency analysis provides another method to classify landing performance. Future studies may include kinematic information to explore the mechanism of changes in frequency components and whether frequency components are related to potential injury risk factors.

## REFERENCES

1. Dai B, et al. *Am J Sports Med* **43**, 466-474, 2015.
2. Blackmore T, et al. *J Biomech* **49**, 479-483, 2016.
3. Gruber A, et al. *J Sport Health Sci.* **3**, 113-121, 2014.
4. Braggemann G, et al. *Proceedings of ISBS '11*, Porto, Portugal, 2011.

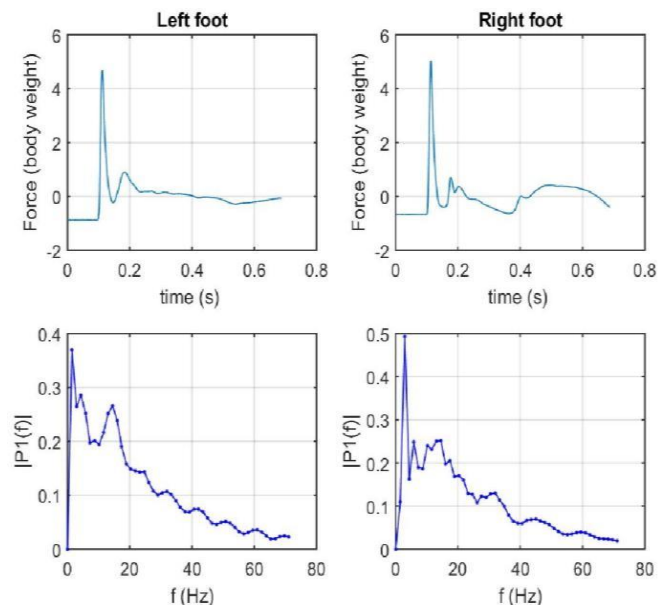


**Figure 1:** Original signals (top) and frequency components (bottom) for the left and right foot.

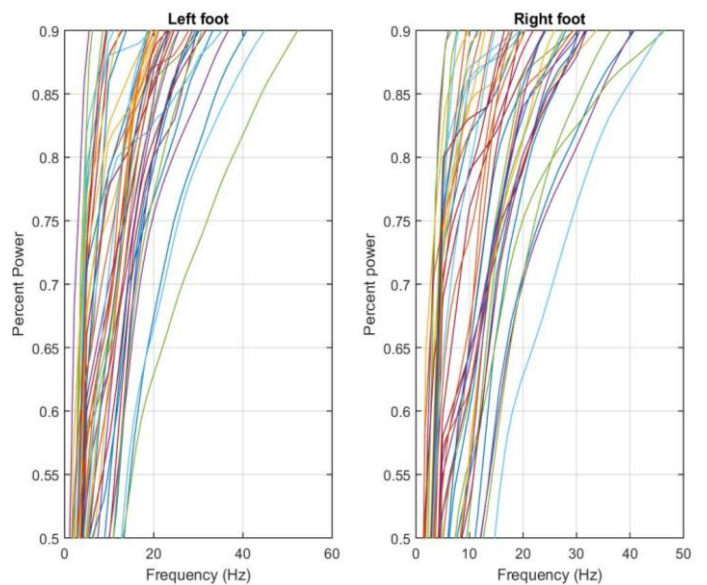


**Figure 2:** Frequency and power distribution for left and right legs from all athletes.

# ALTERED LOWER EXTREMITY KINEMATICS AND GROUND REACTION FORCES IN DISTRACTED VS. FOCUSED LANDING

Patrick Rider, Hannah Ellis, Caroline Yeomans, Alison Ratti, and Nicholas Murray

East Carolina University, Greenville, NC, USA  
email: riderp@ecu.edu

## INTRODUCTION

Soccer is the most popular sport in the world with rapidly growing numbers of female participants. Soccer also has one of the highest injury rates of any sport, especially among female athletes. Most of these injuries occur to the lower extremity. As a result, significant research has been conducted to quantify injury mechanisms in female soccer players and to evaluate training programs that help correct mechanical problems that might place an athlete at a higher risk of injury. For example, athletes who land with more extended knees or with larger vertical ground reaction forces have shown a higher incidence of non-contact ACL tears<sup>1</sup>. Many of these risk factors are modifiable through training and many training protocols have shown promise in reducing injury rates.

The most effective training programs involve incorporating muscle strengthening and plyometric drills, as well as biomechanical feedback from a coach to alter landing kinematics. Athletes are given feedback about body position and are instructed to focus on their landing technique<sup>2</sup>. While this is important for proper instruction and training purposes, it is less clear if these mechanical changes translate to the field where the athlete's focus will be on an external task, such as heading a ball or moving into position to defend in response to an opposing player. The purpose of this study, was to investigate landing mechanics between distracted and focused landing in female collegiate soccer players. We hypothesize that when distracted with an external task, participants will land with more joint extension and greater peak vertical ground reaction forces.

## METHODS

Twelve female Division 1 soccer players completed the study protocol (BMI  $24.7 \pm 2.58$ ). Each participant was cleared by the team athletic training staff prior to protocol implementation. All participants provided university approved informed consent and completed a short questionnaire to obtain information about position (4 defenders, 5 midfielders, and 3 forwards) and weekly training/playing time ( $1050 \pm 228.2$  total minutes per week). Each athlete had on average  $13.5 \pm 2.4$  years of playing experience. Goal keepers were excluded from this study.

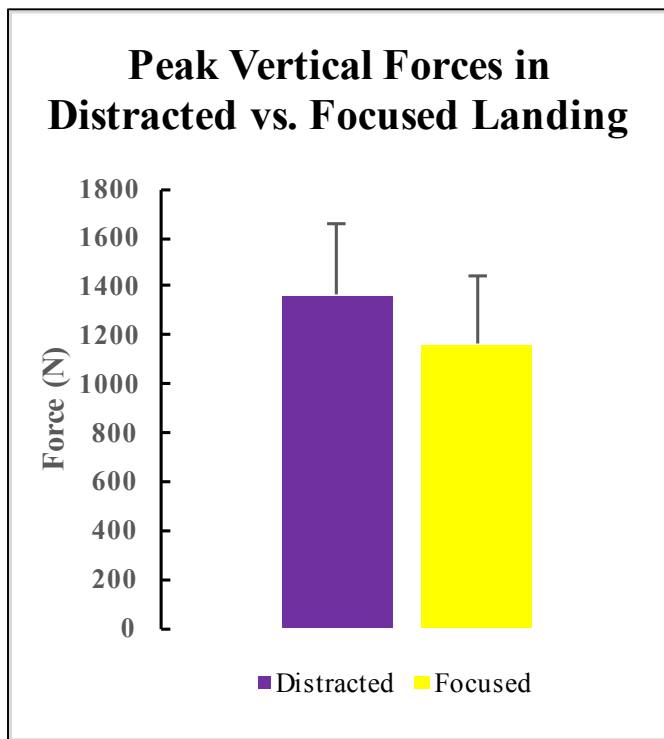
Participants were prepped for trunk and bilateral lower extremity 3D motion capture utilizing two force platforms. They were asked to perform 3 successful trials of 2 separate jump landing tasks. The distracted landing task involved an externally focused task which required the participant to tap their forehead a suspended soccer ball. The ball was suspended on a tether from the ceiling and placed approximately .15 meters anteriorly and .20 meters vertically from the participant's starting position. During the focused landing condition, the participant was instructed to jump and focus their attention on their landing. Peak jump height was not different between the two conditions (Distracted:  $0.27\text{m} \pm 0.6\text{m}$  vs. Focused:  $0.27\text{m} \pm 0.7\text{m}$ ). Condition order was randomized between participants.

## RESULTS AND DISCUSSION

The distracted landing condition showed significant differences in sagittal plane joint kinematics for the hip, knee and ankle at contact compared to the

focused condition (Table 1). Participants in the distracted condition landed significantly more extended at all lower extremity joints.

There was also a large increase in peak vertical ground reaction forces in the distracted landing condition. Results are presented in the following figure.



These results indicate that an athlete’s focus has a significant impact on their mechanical performance of a task and training protocols might benefit from incorporating external focus elements into their design. This finding is supported in the motor control literature as well, in that external focus is

more critical to performance in experienced athletes, while internal focus is more useful when learning a task<sup>3</sup>.

### CONCLUSIONS

The results of this study supported our hypothesis that distracted landing produces more extended joint positions at contact and increases in external ground reaction forces. Additionally, the results support the predictions of the constrained action hypothesis.<sup>4</sup> Jump landing training protocols could potentially be more effective by utilizing externally focused tasks during implementation because this may allow the motor system to more naturally adapt an individual’s landing mechanics. Future studies should investigate whether the incorporation of this type of methodology during jump training provides a better transfer of correct mechanics to in-game situations.

### REFERENCES

- Hewitt, TE. *American Journal of Sports Medicine*, **33**(4), 2005.
- Alentorn-Geli, E. *Knee Surgery, Sports Tramatology, Arthroscopy*, **17**(8), 859-879, 2009.
- Weiss, SM. *J of Sports Sciences*, **26**(10), 1049-1057, 2008.
- Kal, EC. *Human Movement Science*, **32**(4), 527-539, 2013.

**Table 1:** Left and Right Joint Angles at Contact between Distracted and Focused Conditions

Joint Angle at Contact (deg)	Condition			
	Distracted		Focused	
	Right	Left	Right	Left
<b>Hip</b>	-19.0 ± 9.4	-22.1 ± 10.0	-31.2 ± 10.2	-34.4 ± 9.8
<b>Knee</b>	-9.7 ± 4.8	-13.9 ± 5.3	-17.8 ± 7.3	-20.9 ± 6.5
<b>Ankle</b>	-34.4 ± 4.5	-36.9 ± 4.6	-42.2 ± 10.6	-43.3 ± 11.5

# DIFFERENTIAL EFFECTIVENESS OF VISUAL FEEDBACK ON DROP LANDING PERFORMANCE

<sup>1</sup> Drew Rutherford, <sup>1</sup> Abigail Anderson, <sup>1</sup> Alyssa Kompelien, <sup>1</sup> Elizabeth Skaer, <sup>1</sup> Thomas Kernozek, <sup>2</sup> Naghmeh Gheidi

<sup>1</sup> Department of Health Professions – Physical Therapy Program, University of Wisconsin-La Crosse, La Crosse, WI, USA

<sup>2</sup> Department of Exercise and Sport Science, University of Wisconsin-La Crosse, La Crosse, WI, USA  
email: drutherford@uwlax.edu

## INTRODUCTION

Anterior cruciate ligament (ACL) injuries are common in the United States with an annual incidence rate estimated of 250,000 [1]. High vertical ground reaction forces (vGRF) and knee valgus in jump landings are thought to contribute to these injuries. With young females experiencing a risk of ACL injury 2-6 times greater than males [2], they may benefit from focused training interventions on landing strategies.

Performance feedback can be used clinically to assist individuals in developing motor control patterns that decrease vGRF and minimize knee valgus in jump landings [3]. However, there has been disagreement on whether feedback is effective in modifying performance over the long term [4]. It is possible that this effect is mediated by the nature of the deficits displayed in landing performance prior to receiving training.

The aim of this study was to identify whether visual feedback is effective in improving landing kinetics in females presenting initially with high or low vGRF. We also evaluated whether these effects would persist at an immediate post-test and following a 1-week retention.

## METHODS

Forty-nine college-aged females (Age:  $21.2 \pm 1.6$  years, Height:  $169.6 \pm 7.0$  cm, Mass:  $67.7 \pm 9.7$  kg) participated on two days of testing. Each performed a total of 30 drop landings from a hang bar with mid-foot positioned 50 cm above the ground. Kinematic data were collected using a 15 camera motion capture system (Motion Analysis

Corporation, Santa Rosa, CA, USA) sampled at 180 Hz. Bilateral kinetic data of vGRF were collected by two force platforms (Model 4080, Bertec Corporation, Columbus, OH, USA) sampled at 1800 Hz.

Participants performed 6 baseline landing trials (Pre-Test) where they were instructed to land as softly as possible without specific instructions on how to alter their performance. Following a 1-minute rest period, 12 training trials were completed. Post-trial feedback of peak vGRF was given immediately after landing and displayed for 10 seconds. Feedback was provided as a numeric representation in multiples of body weight (BW) on a projector in front of the participant. After the set of training trials, feedback was removed and participants completed 6 Post-Test trials. Participants returned 1 week later for a follow up session of 6 trials without feedback (Retention). They were not provided any instruction on how to lower peak vGRF values to avoid bias.

Means for peak vGRF (BW) were calculated for the Pre-Test, Post-Test, and Retention trial blocks. A hierarchical cluster analysis (HCA) using Ward's method with squared Euclidean distances was performed to yield two different sub-groups based on peak vGRF from the Pre-Test (High Group vs. Low Group). A repeated measures mixed model ANOVA (alpha set to 0.05) was performed on peak vGRF to analyze Group by Time effects. Effect sizes (Cohen's *d*) were calculated between post-hoc comparisons. Statistical tests were completed using SPSS, version 24 (IBM Corporation, Armonk, NY, USA).

## RESULTS AND DISCUSSION

The HCA produced two sub-groups from Pre-Test values: High Group ( $n = 16$ ); Low Group ( $n = 33$ ) (Fig. 1). The ANOVA produced a Group by Time interaction ( $F(2,46) = 13.0, p < 0.001$ ). The High Group with a large initial vGRF ( $4.57 \pm 0.37$  BW) demonstrated a reduction in Post-Test and Retention peak vGRF values from Pre-Test ( $-9.0\%$ ,  $4.16 \pm 0.64$  BW,  $p < 0.001, d = -0.79$ ;  $-12.0\%$ ,  $4.02 \pm 0.43$  BW,  $p < 0.001, d = -1.37$ ). The Low Group with a smaller initial peak vGRF ( $3.31 \pm 0.51$  BW) was not different between Post-Test and Retention values ( $-0.25\%$ ,  $3.30 \pm 0.52$  BW,  $p > 0.05, d = -0.02$ ;  $+4.3\%$ ,  $3.45 \pm 0.53$  BW,  $p > 0.05, d = +0.27$ ) compared to the Pre-Test.

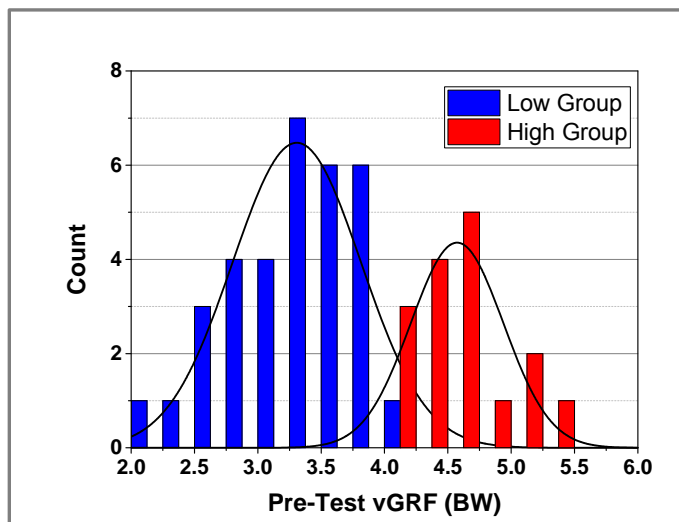


**Figure 1:** Distributions of Pre-Test vGRF values by Group resulting from hierarchical cluster analysis.

The results suggest that participants starting with a high initial vGRF are able to integrate visual feedback of peak vGRF to make meaningful improvements (Cohen's  $d$ : 0.8-1.3) in landing kinetics within-session and at 1-week retention. However, this feedback did not cause a change in vGRF in individuals presenting with a low initial vGRF (Fig. 2). This may represent a floor effect in this performance variable where this group may be already at a reduced risk of ACL injury and the lack of room for improvement would yield negligible gains [3]. Rather than being hindered by an unnecessary form of feedback, these individuals

may instead benefit from feedback of kinematic and other performance variables to lower injury risk factors other than peak vGRF.

## CONCLUSIONS

Visual feedback was shown to be effective for individuals presenting with a high vGRF. This suggests that feedback may need to be matched to an individual's unique needs determined through pre-test screening of landing performance analyzing variables such as peak vGRF. Future efforts will focus on using HCA to classify individuals based on pre-test kinematic performance variables.

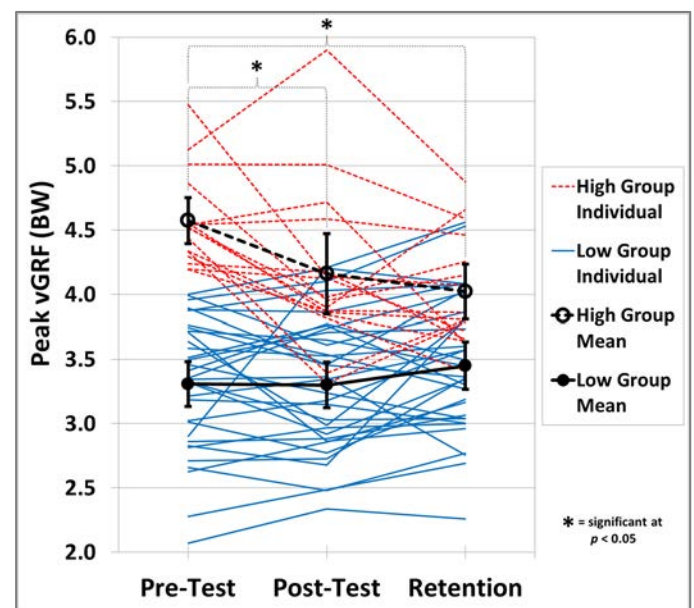


**Figure 2:** Performance curves of peak vGRF by Time condition for all individuals. Group means are shown with  $\pm 95\%$  confidence intervals.

## REFERENCES

1. Griffin LY, et al. *Am J Sports Med* **34(9)**, 1512-1532, 2006.
2. Hewett TE, et al. *Am J Sports Med* **34(2)**, 299-311, 2006.
3. Ericksen HM, et al. *J Orthop Sports Phys Ther* **45(2)**, 112-118, 2015.
4. Etnoyer J, et al. *J Athl Train* **48(2)**, 161-171, 2013.

# GENDER DIFFERENCES IN HIP JOINT FORCE DURING UNILATERAL DROP LANDINGS

<sup>1</sup> Bobbie Irmischer, <sup>1</sup> Hunter Bennett, <sup>1</sup> Zachary Sievert, and <sup>2</sup> Joshua T. Weinhandl

<sup>1</sup> Old Dominion University, Norfolk, VA, USA

<sup>2</sup> University of Tennessee Knoxville, Knoxville, TN, USA

email: birmi001@odu.edu

## INTRODUCTION

Increased forces between the femur and acetabulum are commonly accepted as a mechanism for damage in traditional hip osteoarthritis, and a proposed factor in femoroacetabular impingement [1]. Males have been reported to land with a hip dominant landing strategy that is associated with a reduced risk of knee injury [2]. The resulting hip loading associated with this landing strategy is not fully understood.

Unfortunately, hip joint forces cannot be directly measured via non-invasive methodologies. These forces can, however, be estimated through musculoskeletal modeling using measured kinematics and kinetics [3,4]. A comprehensive understanding of hip joint loading during landing in a healthy population will provide a foundation for comparison to symptomatic pathological hips.

The purpose of this study was to understand if there is an interaction between gender and limb side on hip mechanics during unilateral drop landings. Females have been associated with significantly higher vertical ground reaction forces during landings [5,6]. As such, we hypothesized females would exhibit a concurrent increase in maximum hip joint force (HJF) compared to males.

## METHODS

Forty-two healthy, physically active participants between the ages of 18 and 30 (21 females, 60.37±9.27kg, 1.65±0.07m; 21 males, 80.37±16.26kg, 1.79±0.09m) volunteered to complete single leg drop landings (height = 40cm). Five trials on each landing leg were collected and order was counterbalanced. Ground reaction forces (GRF) and three-dimensional (3D) marker coordinate data were collected synchronously using a Bertec flush mounted force plates (2000Hz) and an

eight-camera Vicon motion capture system (200Hz). Raw 3D marker coordinate and GRF data were low-pass filtered using a 4th-order, Butterworth filter with a cutoff frequency of 10 Hz.

In OpenSim [3], a 19-dof, eight segment generic musculoskeletal model (Gait2392) with doubled strength and activation, was scaled for each subject using individual anthropometric data from a calibration trial. The inverse kinematics problem was solved at each frame to compute model joint angles using a least squares approach while accounting for constraint weights [7]. Inverse dynamics were addressed using calculated joint angles and measured GRF data to identify net joint reaction forces and moments necessary to maintain equilibrium. Muscle forces were estimated using static optimization at each time step with inverse dynamics outputs, external load data, a scaled model and the sum of muscle stress squared as the optimization criteria. The JointReaction analysis algorithm within OpenSim was used to calculate hip joint forces (HJF). Resulting hip torques were verified as null.

The landing phase was defined from initial contact to maximum knee flexion of the landing limb. Resultant HJF and GRF were calculated from force components and normalized by body weight. HJF is expressed as the pelvis on the femur in the femoral reference frame. Timing of peak force represents time from initial contact. Variables of interest were maxHJF, time of maxHJF, maxGRF, 3D hip, knee, and ankle range of motion (ROM), and 3D hip, knee, and ankle angles at initial contact (IC). All variables were evaluated for normality and homogeneity. Separate 2x2 ANOVAs were used to assess differences between each variable with respect to gender and limb side ( $p < 0.05$ ).

## RESULTS AND DISCUSSION

Significant main effects of gender were identified for maxHJF, maxGRF, time of MaxGRF, HipFlexionIC, and HipRotationIC ( $p < 0.05$ ). No other significant main effects were reported for gender. Across all variables examined, there were no significant findings pertaining to main effect for limb nor any interaction effects between gender and limb.

As hypothesized, females performed landings with greater peak resultant GRF and HJF. The HJFs reported in this study are higher than those measured from instrumented prosthesis [4], however, they are comparable to modeling estimates in a young, healthy population [8]. The increased peak forces were present despite a lack of gender differences in lower extremity ROM during the landing phase. PeakGRF occurred earlier in the landing phase in females than males, while MaxHJF timing did not indicate a significant gender effect. This suggests both genders experience MaxHJFs at similar timing between initial contact and maximum knee flexion. Previous research has suggested males absorb more force at the hip during landing while females rely more heavily on the knee [2].

Studies utilizing single leg landings have yielded less consistent findings when compared to those with double leg landings. In the current study, males demonstrated less hip flexion and more internal rotation than females at initial contact. The large standard deviations observed across all variables may indicate that a variety of landing techniques are being employed by participants. Yet, overall, bilateral differences were not identified for any of the kinetic, timing, and angular measures. Similar findings have been reported in studies using healthy populations [5].

## CONCLUSIONS

Bilateral differences were not indicated for unilateral landings with a sample of young, healthy, and recreationally active participants. Females experienced greater GRF and HJF peaks, yet only the GRF timing was different. Examining the muscle kinematics and energetics may help disentangle gender differences in hip loading.

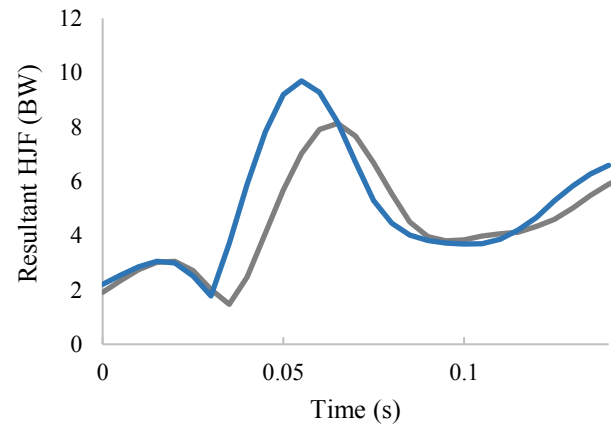


**Figure 1:** Sample male and female HJF for one right leg trial with similar times from initial contact to maximum knee flexion. Grey represents male and blue represents female.

**Table 1:** Pooled limb peak forces, timing, joint angle ROM, and joint angles at initial ground contact (mean  $\pm$  SD).

	Females	Males
<b>Peak Forces (BW) and Timing (ms)</b>		
MaxHJF*	9.32 $\pm$ 1.27	8.09 $\pm$ 1.55
MaxHJF Timing	84.3 $\pm$ 39.1	80.4 $\pm$ 28.3
MaxGRF*	3.84 $\pm$ 0.34	3.51 $\pm$ 0.42
MaxGRF Timing*	65.3 $\pm$ 6.5	69.0 $\pm$ 7.4
<b>ROM (<math>^{\circ}</math>)</b>		
Hip Flexion	18.42 $\pm$ 6.18	17.87 $\pm$ 4.84
Hip Adduction	18.63 $\pm$ 4.03	17.05 $\pm$ 3.91
Hip Internal Rotation	10.88 $\pm$ 4.47	12.12 $\pm$ 4.43
Knee	49.03 $\pm$ 8.73	49.47 $\pm$ 12.23
Ankle	48.70 $\pm$ 6.72	49.37 $\pm$ 9.78
<b>Joint Angles at Initial Contact (<math>^{\circ}</math>)</b>		
Hip Flexion*	7.83 $\pm$ 8.67	1.38 $\pm$ 9.91
Hip Adduction	-20.86 $\pm$ 5.25	-22.62 $\pm$ 4.54
Hip Internal Rotation*	-4.00 $\pm$ 4.76	-8.52 $\pm$ 6.29
Knee	-14.78 $\pm$ 4.42	-14.85 $\pm$ 6.03
Ankle	-27.92 $\pm$ 6.71	-26.56 $\pm$ 10.52

\* Indicates a significant gender difference ( $p < 0.05$ )

## REFERENCES

- Ganz R. et al. *Clin Orthop Relat Res*, **417**:112-20, 2003.
- Weinhandl J. et al. *The Knee*, **22**: 298-303, 2015.
- Delp SL. et al. *IEEE Trans Biomed Eng*, **54**:1940-50, 2007.
- Bergmann G. et al. *J Biomech* **34**:859-71, 2001.
- van der Harst JJ. et al. *Clin Biomech*, **22**: 674-80, 2007.
- Pappas E. et al. *Clin J Sports Med*, **17**: 263-268, 2007.
- Lu TW & O'Connor JJ. *J Biomech*, **32**:129-34, 1999.
- Edwards WB. et al. *Proceedings of the 31<sup>st</sup> Annual ASB Meeting*, Palo Alto, CA, 2007.

# DYNAMIC POSTURAL STABILITY AND LANDING MECHANICS DURING A SINGLE-LEG LANDING IN INDIVIDUALS WITH A PREVIOUS KNEE INJURY

<sup>1</sup> Joshua D Winters, <sup>1</sup> Kathleen M Poploski, <sup>1</sup> Alexa K Johnson, <sup>1</sup> Nicholas R Heebner, and <sup>1</sup> John P Abt,  
<sup>1</sup> The University of Kentucky, Lexington, KY, USA

e-mail: Joshua.winters@uky.edu, web: <https://www.uky.edu/chs/research/smri>

## INTRODUCTION

Altered neuromuscular activation patterns following a musculoskeletal injury may inhibit the control of the lower extremity during dynamic movements. [1] Physically active individuals often perform complex dynamic movements that require both shock absorption and postural stabilization. Postural stability has been linked to ankle and knee injuries [2] and examining factors associated with stabilization may provide insight as to how musculoskeletal injuries may influence stability and joint loading during dynamic movements.

The purpose of this study is to determine if physically active individuals with a self-reported knee injury occurring within the last year have decreased knee extension strength, altered landing mechanics, or altered stabilization strategies during a forward jump single-leg landing task. We hypothesized that those with a history of knee injury will have decreased knee extension strength, land with a stiffened knee strategy, and with less stability compared to controls.

## METHODS

Knee strength and lower extremity kinematics were collected on 31 physically active males, 16 with a previous self-reported knee injury (age  $26.9 \pm 3.9$  yrs; height  $180.48 \pm 6.31$  cm; mass  $83.69 \pm 7.68$  kg), and 15 control subjects without a history of lower extremity injuries (age  $25.2 \pm 2.7$  yrs; height  $179.32 \pm 5.36$  cm; mass  $82.27 \pm 8.02$  kg). All subjects performed a self-reported injury history questionnaire guided by a licensed clinician. Injuries were defined as a musculoskeletal injury event that occurred within the last year from the date of the questionnaire and resulted in altering physical training for at least one day. Healthy control subjects reported no history of lower extremity injuries. Individuals reporting bilateral injuries, neurological conditions, and musculoskeletal injuries affecting other lower

extremity joints were excluded from this analysis. Knee extension strength (KES) was collected using an isokinetic dynamometer (Biodex Medical Systems Inc., Shirley, NY) and normalized to body mass for group comparisons. Lower extremity kinematics, peak vertical ground reaction forces (pkVGRF), and dynamic postural stability index (DPSI), a composite of the anterior-posterior, medial-lateral, and vertical ground reaction forces were collected during a Forward Jump Single-Leg Landing task (FJSL). Subjects were instructed to jump forward, clearing a hurdle approximately 31 cm in height, landing on a single limb, stabilizing rapidly and maintaining postural control following the landing.

Subjects were outfitted with reflective markers and lower extremity kinematics were collected using an 8-camera 3D motion capture system (Vicon Motion Systems Ltd, Centennial, CO) and vertical ground reaction forces were collected by two force plates at 1200 Hz (Kistler Instrument Corp., Amherst, NY). Data were processed with Vicon Nexus software using a Plug-in-Gait model. Marker trajectories were filtered using a Woltering filter with a predicted mean square error at 10mm. Hip, knee and ankle flexion and adduction angles at initial contact (@IC) and peak flexion angles (pkFlex) were recorded from the kinematic analysis.

Independent samples t-tests were used to examine differences in KES, kinematics, and DPSI between those who experienced a knee injury within the last year (INJ) and those with no history of lower extremity injuries (CON). Paired samples t-tests were used to evaluate lower extremity asymmetries between the injured and uninjured limbs within the INJ group using the same measures as the group comparison. Pearson correlation coefficients examined the relationships between KES, landing kinematics, pkVGRF, and DPSI. All data were

analyzed using SPSS (SPSS 22 IBM Corp, Armonk, NY). Significance level was set at  $\alpha = 0.05$ .

## RESULTS AND DISCUSSION

There were no significant differences in KES, pkVGRF, or DSPI between groups ( $p > 0.05$ , respectively). The INJ group had significantly lower KES in the injured limb compared to that of the uninjured limb ( $p = 0.006$ ) and these KES asymmetries were not observed in the CON group ( $p = 0.331$ ), Figure 1). There were no significant differences between the injured and uninjured limb within the INJ group for any of the kinematic measures, pkVGRF or DSPI ( $p > 0.05$ , respectively). Within the INJ group increased KES significantly correlated to a decreased pkVGRF and an improved DSPI (Table 1) but only when landing on the uninjured limb. When landing on the injured limb, KES did not correlate to pkVGRF, DSPI or any kinematic measure ( $p > 0.05$ , respectively). HipFlex@IC correlated to pkVGRF during the FJSL task for both the injured and uninjured limb (Table 1) while AnkleFlex@IC correlated with pkVGRF for the injured limb only (Table 1). Though there were no significant differences between the INJ and CON groups, we found between limb KES asymmetries within the INJ group that were not observed in the CON group. Furthermore, the asymmetrical KES observed in the INJ group may influence pkVGRF and DSPI differently between limbs.

Individuals reporting a knee injury within the last year may experience decreased KES for a significant period of time following the injury. Though asymmetrical KES within the INJ group did not lead to asymmetrical pkVGRF, or DSPI it may have

altered the strategies used between the different limbs to achieve similar shock absorption and stabilization. Based on the lack of correlations between KES and the biomechanical outcomes on the injured side, individuals may attempt to compensate for the decreased KES by relying more on the ankle during landing. Due to the limited sample size, complexity of the task, and the differing severities of the knee injuries further research is needed to determine if specific compensation strategies are utilized for shock absorption and stabilization and examine if these strategies translate to other dynamic movements.

## CONCLUSIONS

Individuals who reported having a knee injury demonstrated KES asymmetries within one year following their injury. Further research is needed to investigate how decreased muscle function, including KES and neuromuscular function following a knee injury influence joint specific loading and dynamic joint stability during both bilateral and unilateral dynamic movements.

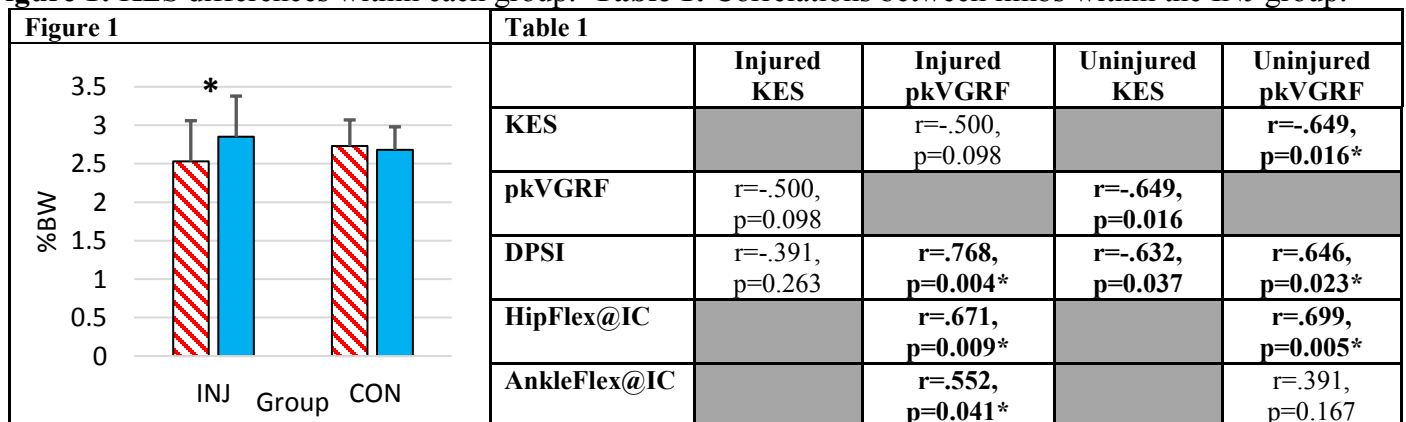
## REFERENCES

1. Swanik et al., *J Athl Train*, **34**, 121-129, 1999.
2. Sell et al., *Physical Therapy in Sport*, **13**, 80-86, 2012

## ACKNOWLEDGMENTS

This research was supported by the Office of Naval Research N00014-1-15-0069. The content is the responsibility of the authors and may not represent the official views of the Office of Naval Research.

**Figure 1:** KES differences within each group. **Table 1:** Correlations between limbs within the INJ group.



# DYNAMIC VALGUS DURING DROP LANDING RESULTS IN DECREASED LATERAL PLANTAR PRESSURE

<sup>1</sup> Christopher Ferrigno, <sup>1</sup> Jade He, <sup>1</sup> Philip Malloy, <sup>1</sup> Markus A. Wimmer

<sup>1</sup> Rush University Medical Center, Chicago, IL, USA  
email: christopher\_ferrigno@rush.edu, web: <http://asb2017.org/>

## INTRODUCTION

Anterior cruciate ligament (ACL) injuries are highly debilitating and commonly occur in sporting activities involving sudden stops and change of direction. Following ACL reconstruction (ACL-R), re-injury rates to the ipsilateral or contralateral knee are as high as 31% [1]. Movement asymmetries such as increased dynamic valgus at the knee during sport-specific tasks such as the box drop vertical jump test (DVJ) are associated with ACL rupture and persist following ACL-R. These aberrant movement patterns place high demands on the ACL, increasing the likelihood of re-injury three-fold [2]. Such patterns are modifiable [3]; therefore, detecting asymmetries during sport-specific tasks is crucial for determining at-risk individuals.

Clinically, identifying lower limb movement anomalies using semi-quantitative two dimensional (2D) video recording or 3D analysis is time consuming and impractical for most settings. Detecting plantar pressure is quick and affordable, making it clinically feasible. Faulty kinematic responses during the DVJ have a large frontal-plane component; therefore, similar medial-lateral pressure shifts likely occur during dynamic valgus.

The purpose of this proof-of-concept pilot study was to explore the plantar pressure response to three different landing strategies during the DVJ. We hypothesized that healthy subjects demonstrate higher lateral plantar pressures during hip abducted landing, while demonstrating lower lateral pressures during hip adducted landing.

## METHODS

Eight healthy participants were enrolled in this institutional review board approved study at Rush University Medical Center (29.9±4.6yrs, 2 women,

BMI=25.3±2.9). All subjects were healthy with a self-reported absence of knee pathology, surgery to the lower extremities, or current pain in their lower extremities.

All subjects wore a standardized shoe (Dr. Comfort, FlexOA, Mequon, WI, USA) containing a pair of fully-integrated pressure-detecting shoe insoles (OpenGo, Moticon GmbH, Munich, Germany) with built-in 13 capacitive sensors (Figure 1).



**Figure 1.** The Moticon OpenGo Insole.

Subjects completed a total of 6 DVJs from a box (31cm high) (Figure 2). For all jumps, subjects were instructed to drop forward off the box and immediately perform a sub-maximum vertical jump. During the first set of 3 jumps, subjects performed their jumps according to previous work [3] with their feet initially positioned 35 cm apart on the box. To increase the dynamic valgus for the final set of 3 jumps, a foam block was placed between the distal thighs. Subjects were instructed to perform the DVJs without releasing the foam block from between their knees.



**Figure 2.** The DVJ. The subject preparing to drop from the box (left) and landing with a self-selected technique (center) or with dynamic valgus (right).

Plantar pressure data was wirelessly downloaded and processed with OpenGo Software (Moticon GmbH, Munich, Germany). The maximum pressure from each of the 26 total sensors was recorded from each during the first half of the initial landing following the drop from the box. The three trials for each DVJ condition were averaged. To examine whether imparting a dynamic valgus resulted in a change in medial or lateral foot pressure, select sensors were grouped to represent the entire lateral foot, medial foot, or different regions of interest during landing (Figure 3). For the medial foot, sensors 0, 2, and 6 were selected since they are likely to contact the floor during the first half of stance (far left). For the lateral foot, sensors 5 and 9 were selected and grouped to capture the plantar loading on the lateral surface for the 5<sup>th</sup> metatarsal heads (sensor 5) and heel (sensor 9) during the first half of stance (far right). Comparisons were made for these specific pressure sensor groupings.

Statistical analyses were performed using SPSS 23 (IBM, Armonk, NY). Paired t-tests were used to compare the plantar pressures of sensor groupings.

## RESULTS AND DISCUSSION

Paired t-tests revealed that jumping with knees directed medially using a foam block resulted in a considerable decrease in plantar pressures in the sensor group representing the entire lateral foot (sensors 5,7,9,11) and select sensors (sensors 5,9) (Table 1). No significant changes were measured in the sensor groupings of the entire medial insole ( $p > 0.152$ ) or selected sensors 0, 2, and 6 ( $p > 0.071$ ).

In this proof-of-concept study, lateral plantar pressure reduced bilaterally during the induced dynamic valgus landings. A larger study to further explore the changes in plantar pressure, as well as the potential for using plantar pressure-based as a feedback training tool, are warranted.

## CONCLUSIONS

This pilot study suggests that plantar pressures decrease in the lateral foot during a landing position which places the athletes at risk for ACL injury or re-injury during sport.

## REFERENCES

1. Leys T, et al. *AmJSportsMed*, **40**, 595-605, 2012.
2. Paterno MV, et al. *AmJSportsMed*, **38**, 1968-1978, 2010.
3. Hewett TE, et al. *AmJSportsMed*, **33**, 592-501, 2005.

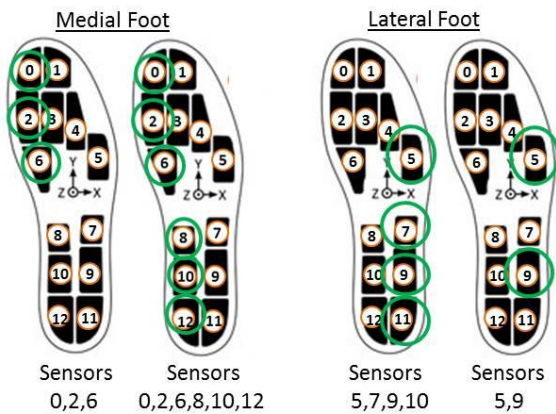


**Figure 3.** Locations of sensor groupings on the OpenGo Insole.

**Table 1:** Plantar pressures in select Moticon OpenGo Insole pressure sensors during undirected (normal) and directed (genu valgum position) initial landings of the drop vertical jump. All pressure values are in N/cm<sup>2</sup>.

	Sum of ALL Lateral Sensors (Sensors 5,7,9,11)			Sum of Sensors Under Lateral Midfoot and 5th Metatarsals (Sensors 5 and 9)		
	Normal Position	Genu Valgum Position (with foam)	p-value	Normal Position	Genu Valgum Position (with foam)	p-value
Right Foot	13.62 (3.63)	6.76 (6.08)	<b>0.014</b>	7.02 (1.27)	3.60 (2.72)	<b>0.008</b>
Left Foot	14.11 (6.14)	7.66 (5.85)	0.067	6.49 (2.74)	4.00 (3.07)	<b>0.021</b>

# FATIGUE-RELATED CHANGES IN JOINT MECHANICS, STIFFNESS, AND ENERGY ABSORPTION DURING LANDINGS

<sup>1,2</sup> Weijie Fu, <sup>1</sup> Xini Zhang

<sup>1</sup> Shanghai University of Sport, Shanghai, China

<sup>2</sup> Spaulding National Running Center, PM & R, Harvard Medical School, Cambridge, MA, USA.

Emails: fuweijie315@163.com; fuweijie@sus.edu.cn

## INTRODUCTION

The lower extremity, especially at ankle and knee joints, is more vulnerable to injuries during movements that involve repetitive landings. Adjustments in landing posture control can be beneficial for mediating the magnitudes of the impact forces, joint loading, and energy absorption [1]. These altered landing strategies, however, will be negatively affected when neuromuscular fatigue has been developed by prolonged exercise [2, 3]. It is noteworthy that a majority of these studies on fatigue effects have demonstrated different responses in both mechanical characteristics and lower extremity control strategies. However, there is limited evidence that indicates whether the biomechanical changes of the lower extremity are related to the type, site, or severity of fatigue.

The aim of this study was to determine the effect of two typical fatigue protocols on sagittal plane joint mechanics, stiffness, and energy absorption during drop landings.

## METHODS

Fifteen collegiate male players (age:  $20.9 \pm 0.8$  yrs; height:  $175.5 \pm 4.2$  cm; weight:  $68.9 \pm 5.5$  kg) with an average of 4.2 years of experience in jumping events were recruited to participate in the study. They were asked to be in the laboratory and to complete landing tasks within one of the two fatigue-induced protocols on two separate days. A period of 1 week rest was required between visits to ensure that fatigue was eliminated and the two protocols would not affect each other.

The participants were asked to complete the bipedal drop landing (DL) tasks from a height of 60 cm.

The DL technique required the participants to step off from a landing platform without losing balance, and as naturally as possible with a toe-heel landing. 5 successful trials were acquired for analysis. The DL tests were performed before and after conducting each of the fatigue-induced protocols.

Constant-speed running fatigue protocol (R-FP) and shuttle sprint + vertical jump fatigue protocol (SV-FP) were used in the study [2, 3]. R-FP required participants to run at 4.0 m/s on a treadmill until they felt fatigue maximally and could not continue running. The participants were considered to have reached a fatigued condition when the HR of the participant reached 90% of his age-based maximum HR. SV-FP consisted of five consecutive vertical jumps followed by a set of 6×10 m shuttle sprints. The participants were required to repeat the above sequence at least five times until they could not reach 70% of the maximal vertical jump height for all five jumps.

During the procedure of either fatigue-induced intervention, the highest HR was recorded. Meanwhile, the rating of perceived exertion (RPE) for each participant was acquired immediately after the intervention was completed. 3D kinematics (Vicon, 240 Hz) and ground reaction force (Kistler, 1200 Hz) were measured simultaneously. The variables included joint moment, stiffness, and energy absorption. The first, second, and third peaks of the hip ( $M_{H1}$ ,  $M_{H2}$ ), knee ( $M_{K1}$ ,  $M_{K2}$ ,  $M_{K3}$ ), and ankle joint movement ( $M_{A1}$ ,  $M_{A2}$ ) were selected [1]. Two-way ANOVAs and paired sample t-tests were used to determine the influence of independent variable (fatigue × protocol) on the dependent variables (kinetics, energy absorption, and stiffness) using SPSS 21.0. The significance level was set at  $\alpha=0.05$ .

## RESULTS AND DISCUSSION

A significant increase in the center of gravity (CoG) displacement (Figure 1) as well as each joint of range of motion was found after fatigue both in R-FP and SV-FP. A significant increase in the  $M_{K1}$  was showed in post-fatigue compared to pre-fatigue using SV-FP, which suggested that knee extensor moment might increase to resist GRF to prevent corruption of lower extremity.

The reduced vertical stiffness in SV-FP might be a protective landing control strategy during the impact phase. The joint stiffness results showed that the contribution in hip and knee were larger than ankle. However, no differences were observed in the stiffness using R-FP which may be explained by the lower-limb biomechanical adaptation for different protocols (Figure 1).

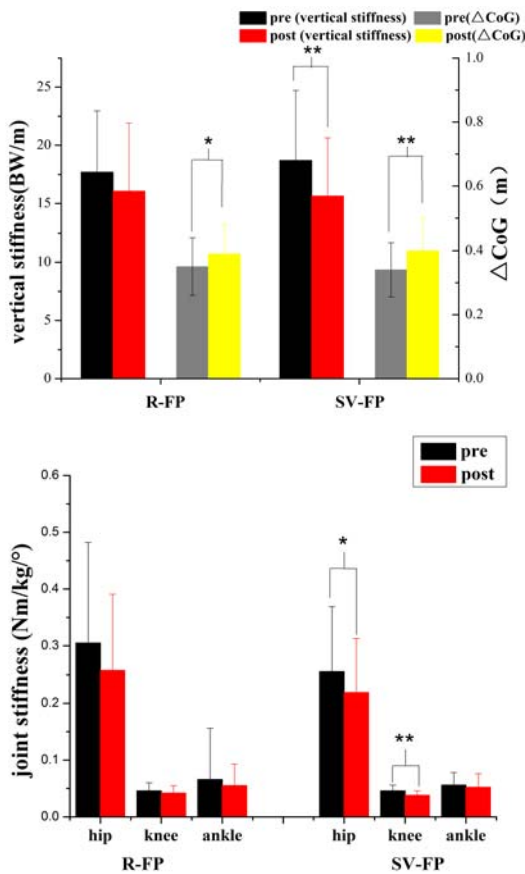


**Figure 1:** Effects of two fatigue protocols on vertical stiffness, center of gravity displacement (CoG, upper), and joint stiffness (lower).

Both fatigue protocols induced similar overall joint energy absorption. Specifically, the knee joint extensors accounting for about 55% of the total energy absorption were the major contributors to energy absorption, then the hip joint extensors group for further absorption during impact. Furthermore, our results revealed that a greater eccentric work was observed at hip joint (+25.1%) in R-FP with a less eccentric work done by ankle muscles (-19.1%). However, no changes were found in joint work for SV-FP which might due to different muscle fatigue induced by different protocols (Figure 2).

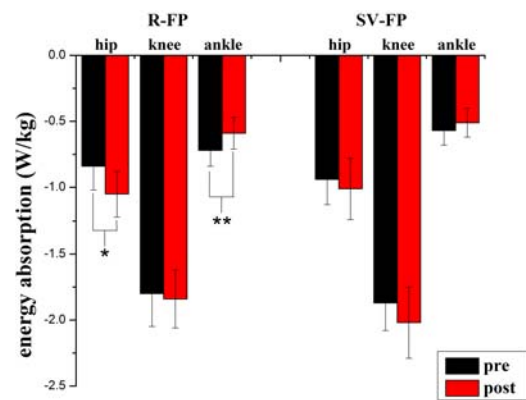


**Figure 2:** Effects of two fatigue protocols on energy absorption of lower extremity during landings.

## CONCLUSION

The control strategies of lower limb in a fatigued condition vs. non-fatigue were varying from different fatigue protocols in terms of kinetics, stiffness, and energy absorption of joints during landings. Specifically, changes in energy absorption were mainly observed in R-FP; while altered joint moments and stiffness were occurred in SV-FP.

## REFERENCES

1. Zhang SN, et al. *Medicine and Science in Sports and Exercise* **32**, 812-819, 2000.
2. Tsai LC, et al. *Science in Sports and Exercise* **41**, 1952-1957, 2009.
3. Quammen D, et al. *Journal of Athletic Training* **47**, 32-41, 2012.

# PERTURBATION OF SYSTEMS CONTRIBUTING TO NEUROMOTOR CONTROL OF POSTURE IN PERSONS WITH RECURRENT LOW BACK PAIN

<sup>1</sup> K. Michael Rowley and <sup>1</sup> Kornelia Kulig

<sup>1</sup> University of Southern California, Los Angeles, CA, USA  
email: krowley@usc.edu, web: pt.usc.edu/krowley

## INTRODUCTION

Non-specific low back pain (LBP) is an incredibly large problem for industrialized nations, with up to 80% of adults experiencing an episode at least once in their lifetime [1] and about a third suffering from recurrent or chronic symptoms [2]. Motor control changes during symptom remission have been identified in patients with recurrent symptoms including delayed and reduced activation of deep trunk muscles [3] and changes in trunk stiffness [4]. Treatment interventions designed from these findings and tested in randomized control trials, however, have not shown greater benefit over usual care [5]. In addition, while many researchers have promoted subgrouping of patients based on psychometrics and movement impairments, little work has been done investigating the interaction between these measures. The purpose of this study was to investigate the effects of dual-task interference on trunk control during a dynamic unstable postural task in participants with and without recurrent LBP. Associations between these effects and psychometric measures were also tested.

## METHODS

Six pain-free control participants (4 Females, 2 Males; Age:  $30 \pm 4$  yrs; Height:  $174 \pm 5$  cm; Weight:  $73 \pm 12$  kg) and four participants with recurrent LBP (3 Females, 1 Male; Age:  $25 \pm 1$  yrs; Height:  $169 \pm 7$  cm; Weight:  $72 \pm 9$  kg) were recruited to participate in the study and signed informed consent per Institutional Review Board guidelines. Control participants had no history of low back pain or any current musculoskeletal or neurological complaints. Participants with non-specific recurrent LBP have had at least two episodes per year for at least one year, but were in symptom remission at the time of testing.

Participants completed three 3 trials of a balance-dexterity task (Fig. 1), adapted from combining a lower-extremity-dexterity test [6] and single-limb balance. They then completed another three trials with a concurrent cognitive dual-task recalling a list of five numbers and performing mental arithmetic on those numbers. Two measures of trunk coordination were calculated: (1) correlation coefficients between motion of the thorax and pelvis in the frontal plane (trunk coupling) and (2) ratio of deep-to-superficial paraspinal muscle activity. Change in trunk coupling was calculated by subtracting trunk coupling R value during the dual-task from trunk coupling R value during the single-task. Participants also completed the validated Movement-Specific Reinvestment Scale (MSRS) [7,8] to provide a quantitative measure of attentional resources they typically devote to their movement. A higher score indicates greater tendency to invest conscious attention in movement. Means were compared between single- and dual-task conditions using dependent t-tests, and correlations were tested using Pearson's test. Statistical significance set at  $\alpha=0.05$ .

## RESULTS AND DISCUSSION

For the six control participants, the change in trunk coupling from single- to dual-task conditions (a positive value indicating an increase in coupling when the dual-task was added) trended toward negative association with MSRS score ( $R= -0.70$ ,  $p= 0.12$ ) (Fig. 2). A subset of three participants underwent EMG instrumentation of the paraspinals. These data indicated that pain-free participants who scored high on the MSRS (and therefore decreased their trunk coupling under dual-task interference) also increased the ratio of deep (multifidus) to superficial (erector spinae) muscle activation ( $R=0.87$ ,  $p=0.33$ ) (Fig. 3). This supports the

hypothesis that a control strategy utilizing increased superficial musculature and decreased deep musculature is not robust to attentional interference as we see the opposite occur in conditions of dual-task interference. The four participants with recurrent LBP showed an association between the change in trunk coupling from single- to dual-task conditions and MSRS score trending in the same direction ( $R = -0.89$ ,  $p = 0.11$ ) (Fig. 2). While the direction was the same as the controls, the data were shifted upward such that all participants increased trunk coupling when the dual-task was added. The deep-to-superficial muscle activation data did not reach significance ( $R = 0.51$ ,  $p = 0.49$ ) (Fig. 3).

These findings indicate that, in pain-free participants, there is no uniform change in trunk coupling during this dynamic task when a cognitive dual-task is added. Importantly, however, the change in dynamic trunk stiffness measured in each individual may be related to his or her score on the MSRS. In persons with recurrent LBP in symptom remission, however, all participants increased trunk coupling when the cognitive task was added, regardless of score on the MSRS. This is quite an

important finding which informs rehabilitation given that dual-tasking is often prescribed during rehab to practice real-life situations. These findings indicate that dual-tasking should be prescribed with caution as it may increase trunk coupling in this patient group. Findings from continued work on this study will help us learn more about interactions between attention, psychometric measures, and motor control measures in patients with recurrent LBP. Understanding these interactions will enhance multi-modal treatments, which up until now have been marginally successful.

## REFERENCES

1. Rubin DI. *Neurol Clin* **35**, 353-371, 2007.
2. Waxman R, et. al. *Spine* **25**, 2085-2090, 2000.
3. MacDonald D, et. al. *Spine* **35**, 818-824, 2010.
4. Hodges P, et. al. *J Biomech* **42**, 61-66, 2009.
5. Macedo LG, et. al. *Phys Ther* **89**, 9-25, 2009.
6. Lyle MA, et. al. *J Biomech* **46**, 998-1002, 2013.
7. Masters R, et. al. *Int Rev Sport Exerc Psych* **1**, 160-183, 2008.
8. Laborde S, et. al. *Pers Individ Differ* **78**, 77-87, 2015.



**Figure 1 (above, left):** Balance-dexterity task.

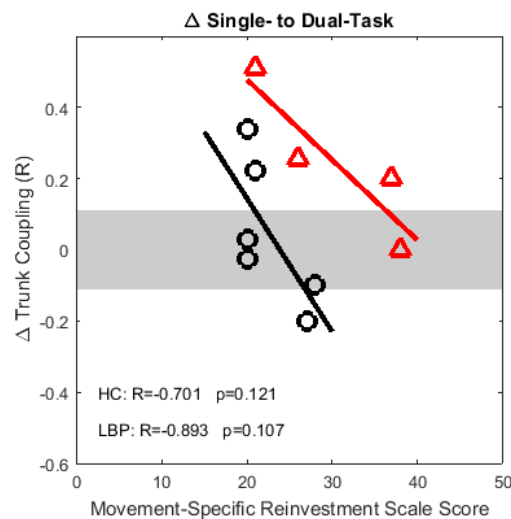
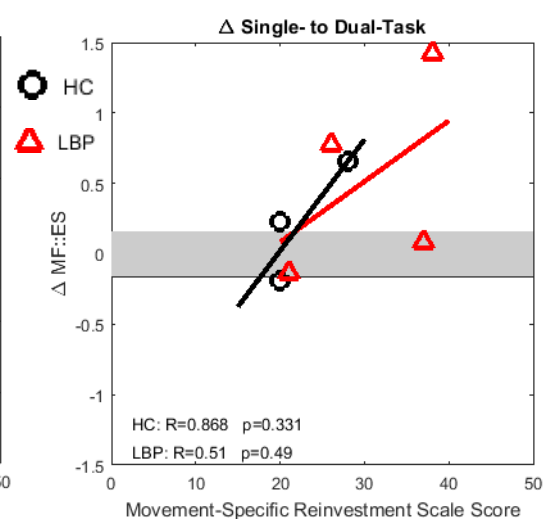


**Figure 2 (above, center):** Change in trunk coupling from single- to dual-task condition (positive indicates trunk coupling increased when dual-task was added) plotted against score on the Movement-Specific Reinvestment Scale (MSRS). Trends toward negative associations between change in trunk coupling and MSRS score can be observed. This association is shifted upward in the LBP group such that all participants increased coupling when adding the dual-task. Gray bar indicates standard error of measure.

**Figure 3 (above, right):** Change in deep-to-superficial muscle activity ratio from single- to dual-task condition (positive indicates multifidus-erector spinae ratio increased when dual-task was added) plotted against score on the Movement-Specific Reinvestment Scale (MSRS). Trends toward positive associations between change in ratio and MSRS score can be observed. Gray bar indicates standard error of measure.



# IN VIVO HUMAN FACET JOINT GAPPING DURING CERVICAL SPINE MANIPULATION

<sup>1</sup> William Anderst, <sup>1</sup> Tom Gale, <sup>1</sup> Kris Gongaware, and <sup>1</sup> Michael Schneider

<sup>1</sup> The University of Pittsburgh, Pittsburgh, PA, USA  
email: anderst@pitt.edu, web: www.bdl.pitt.edu

## INTRODUCTION

Neck pain is one of the most commonly reported symptoms in primary care settings, and a major contributor to increasing healthcare costs[1]. Cervical manipulation is a common and clinically effective intervention for neck pain. However, the biological mechanisms underlying spinal manipulation remain unknown.

Chiropractic spinal manipulations are mechanical events that produce mechanical effects at the treatment site. These mechanical effects may initiate neurologic responses, leading to positive clinical outcome. However, little is known about the biomechanics of spinal manipulation. This lack of knowledge is due, in part, to the inability to accurately measure the intervertebral kinematics of the spine during manipulation.

Considering that previous research has documented pre- to post-manipulation changes in facet gapping[2], and that the cracking sound that is elicited during high-velocity low-amplitude manipulation (HVLA) is believed to be cavitation of the spinal facet joints, it is reasonable to hypothesize that facet kinematics are the (or one of the) primary kinematic mechanisms behind manipulation. Therefore, the purpose of this pilot study was to measure, for the first time, *in vivo* facet joint gapping during cervical spine manipulation.

## METHODS

Ten participants with acute mechanical neck pain were enrolled in this IRB-approved study. Cervical manipulation was performed by a licensed chiropractor within a biplane radiography system (Figure 1). The manipulation was performed using the thumb cervical extension technique. With the patient lying supine, the head rotated 90° away from the clinician, and the target segment on the upside,

the clinician delivered a thrust straight across the articular pillar with the thumb.



**Figure 1:** The biplane imaging system configured to collect dynamic biplane radiographs during HVLA manipulation. The X-ray sources are to the right, and image intensifiers and high-speed cameras to the left, providing sagittal-oblique views of the spine without occlusion from the clinician.

Synchronized, 2.0 ms duration pulsed biplane radiographs were collected at 160 images per second for 0.8 seconds during the manipulation. High resolution CT scans (0.29 x 0.29 x 1.25 mm) of C1-C7 were collected from each participant after the manipulation. A validated volumetric model-based tracking process was used to track bone motion during manipulation with sub-millimeter accuracy[3]. Bone kinematics were filtered using a 4<sup>th</sup>-order Butterworth filter with the filter frequency (10 Hz) determined by residual analysis[4]. Facet joint gapping was calculated as the average distance between adjacent articular facet surfaces.

Outcome parameters included the change in facet joint gap during manipulation (pre-manipulation to peak gap), the rate of facet gapping, and the time to peak facet gap (Figure 2).

## RESULTS AND DISCUSSION

The upper cervical spine was occluded, either by the chiropractor's hands or the patient's mandible, for 3 of the 10 participants. Audible cavitation did not occur for one participant, and the timing between

the manipulation and radiographic imaging was not synchronized for 1 participant, leaving data from 5 participants available for the final analysis (2 M, 3 F; average age: 38±15 yrs.). Motion of 3 to 5 vertebrae from C2 to C6 was tracked during manipulation for each participant.

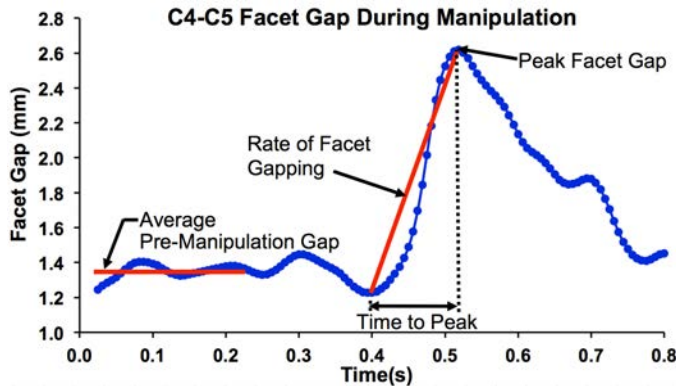


**Figure 2:** Facet gapping during manipulation and measured outcome parameters for one representative subject. Each blue data point represents one frame of tracked motion during the manipulation.

Facet joint gapping consistently occurred across all tracked vertebrae (Figure 3). This result demonstrates that manual manipulation affects the targeted and adjacent motion segments.

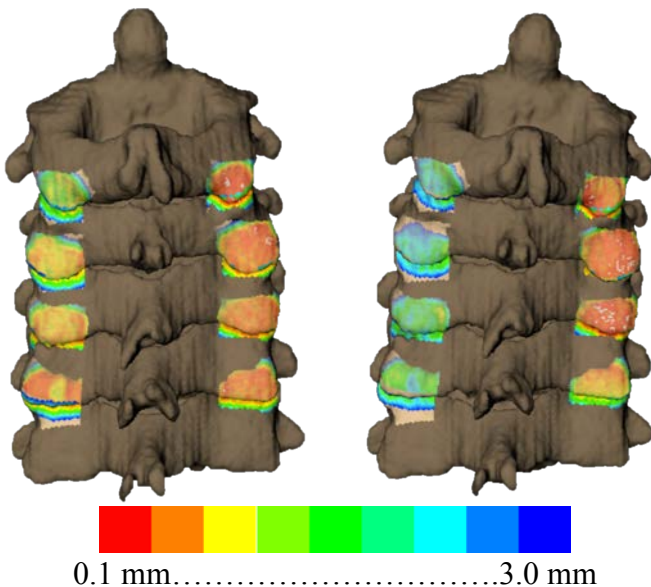


**Figure 3:** A posterior view of the cervical spine pre-manipulation (left) and during manipulation (right). Gapping of the left facet joints is demonstrated by the color-coded facet joint surfaces.

The maximum increase in facet gap from pre-manipulation to peak facet gap averaged 0.98±0.30 mm across the 5 participants, while the average increase in facet gap over all tracked motion segments was 0.78±0.32 mm. This maximum increase in facet gap during manipulation was more than double the peak facet joint distraction that occurs during full ROM flexion/extension in healthy individuals[5]. This finding confirms that manipulation induces facet joint motion beyond the normal physiologic range.

The average time to peak facet gap was 129±55 ms, slightly longer than the previously reported thrust duration during cervical manipulation (90 to 120 ms)[6]. The average rate of facet gapping over all motion segments was 7.4±2.9 mm/s. A strong relationship was observed between the rate of facet gapping and the increase in facet gap during manipulation ( $R^2 = 0.57$ ).

**CONCLUSIONS**

This study is the first to measure facet gapping during cervical manipulation on live humans. These preliminary results improve our understanding of the basic *in vivo* biomechanics of spinal manipulation. Continuing this line of research will allow clinicians and researchers to design better interventions that reliably and sufficiently impact the key mechanisms behind manipulation.

**REFERENCES**

1. Hogg-Johnson, S., et al. *Spine (Phila Pa 1976)*. **33**(4 Suppl) S39-51, 2008.
2. Cramer, G. D., et al. *J Manipulative Physiol Ther.* **36**(4) 203-17, 2013.
3. Anderst, W. J., et al. *Spine (Phila Pa 1976)*. **36**(6) E393-400, 2011.
4. Winter, D. A., *Biomechanics and Motor Control of Human Movement (4th Edition)*. 2009, Hoboken, New Jersey: Wiley.
5. Anderst, W. J., et al. *Spine (Phila Pa 1976)*. **39**(8) E514-20, 2014.
6. Herzog, W., et al. *Spine (Phila Pa 1976)*. **18**(9) 1206-12, 1993.

**ACKNOWLEDGMENTS**

Funding for this project was provided by a grant from the NCMIC Foundation.

# IMPACT OF EXTERNAL LOADING ASSUMPTIONS ON SAGITTAL L5S1 MOMENTS DURING LIFTING

<sup>1,2</sup> Jacob J Banks and <sup>2</sup> Graham E Caldwell

<sup>1</sup> Liberty Mutual Research Institute for Safety, Hopkinton, MA, USA

<sup>2</sup> Department of Kinesiology, University of Massachusetts, Amherst, MA, USA  
email: jacob.banks@libertymutual.com

## INTRODUCTION

Lower back injuries are a major burden on society [1]. To reduce these injuries, potentially harmful tasks need to be identified, assessed, and modified. L5S1 resultant joint moments calculated from inverse dynamic modeling (IDM) are a powerful means of comparing the lower back demands of lifting tasks [2]. The accuracy of IDM moments depends on both the approach used and the veracity of any applied assumptions.

The two fundamental approaches for calculating L5S1 joint moments are characterized as top-down (TD) and bottom-up (BU) [3]. The BU approach requires lower limb segment motion, inertial characteristics and measured foot/ground forces [4]. In contrast, the TD approach uses upper body segments and hand/external load information. Less soft tissue and, thus, greater rigidity of the lower limb segments favors the application of the BU approach when foot/ground forces can be measured. In the absence of measured external forces and moments, or in more natural environments, assumptions of the load must be made. The impact of these assumptions on TD L5S1 resultant joint moments during lifting has not been established.

In this study, we compare the L5S1 resultant joint moment during a sagittal manual materials handling task, calculated from four IDM models: 1) BU with measured foot/ground forces; 2) TD model using a lifting box instrumented with force sensors measuring hand forces (TD\_FS); 3) TD without measured hand forces, but accounting for all known box inertial and kinematic characteristics (TD\_I $\alpha$ ); and 4) TD similar to TD\_I $\alpha$  but simplified by assuming no knowledge of the box's rotational kinematics (TD\_I0).

## METHODS

18 healthy young ( $\leq 35$  years) and fit (BMI $\leq 30$ ) male participants ( $25\pm 5$  years;  $178\pm 6$  cm;  $80\pm 10$  kg) agreed to an institutional informed consent prior to participation in this study.

A custom-built robotic lifting shelf was designed to repeatedly return a box (34 x 56 x 16 cm) to an initial position following each lift. The box handles were instrumented with six-axis force sensors (AMTI, Watertown, MA). The lifting motion was recorded at 100Hz with 8 near infrared cameras and 12.5mm passive reflective markers on the box and participants' body segments (Motion Analysis Corporation, Santa Rosa, CA). Force plates (Kistler Instruments Corporation, Amherst, NY) positioned under each foot recorded ground reaction forces during a 9.1kg lifting task from the floor to a knuckle high shelf (Fig. 1), performed at 4 lifts/minute.

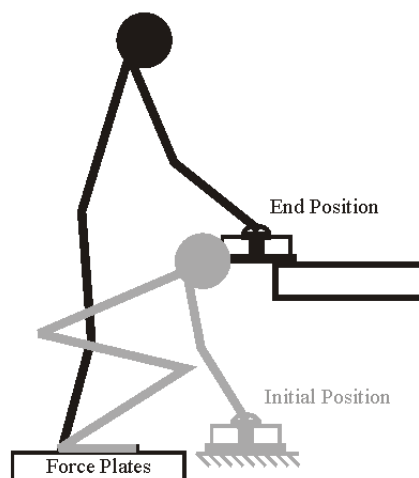


**Figure 1:** Lifting task setup.

A 3D Newtonian-based IDM was coded in Matlab (Mathworks, Natick, MA). Body segment characteristics were defined by de Leva [5] and

Hanavan [6]. The L5S1 joint centers were projected 34% anterior from L5S1 spinous process [7]. Box inertial properties were modeled as a uniform rectangular prism. External sagittal L5S1 moments were reported relative to the pelvis' coordinate system. Lift durations were defined by the interval when the hand force exceeded 5N. For the TD\_I $\alpha$  and TD\_I0 approaches in which the hand force was not directly measured, the period of definable box movement was identified. To minimize effects due solely to modeling upper versus lower body segments, the average difference between the TD moments and a BU L5S1 moment during quiet standing was added to all of the TD moments.

Root mean square (RMS) and peak moments were computed from all L5S1 joint moment curves. Three lifts from each participant were used in repeated measure ANOVAs for both RMS and peak moments to compare the four approaches, with post hoc Tukey testing of model means ( $p < 0.05$ ).

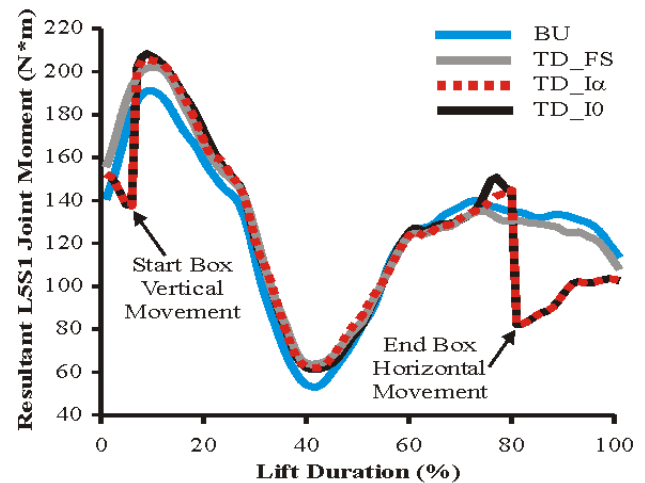
## RESULTS AND DISCUSSION

Table 1 shows that L5S1 moments were influenced by the choice of approach. All TD approaches resulted in significantly greater peaks and RMS than the BU approach. Within the three TD models, peak moments were equivalent (TD\_FS = TD\_I $\alpha$  = TD\_I0), but the RMS moments were higher with the use of the measured hand forces (TD\_FS > TD\_I $\alpha$  = TD\_I0).

As illustrated in Figure 2, load assumptions have the greatest impact on L5S1 moments in the initial and final portions of lifting. This highlights the importance of accurately defining when the load being lifted is in contact with a support surface. Without measured forces, the gradual loading and unloading which occurs as the load transitions from and onto the support surface cannot be assessed accurately.

**Table 1:** Mean  $\pm$  standard deviation peak and RMS values for the four models. Superscripts indicate model significance for peak [ $a \neq b$ ] and RMS [ $x \neq y \neq z$ ] moments ( $p < 0.05$ ). See text for abbreviation definitions.

L5S1 Moment (N*m)	BU	TD_FS	TD_I $\alpha$	TD_I0
Peak	195.2 $\pm$ 22.1 <sup>a</sup>	214.2 $\pm$ 27.4 <sup>b</sup>	219.0 $\pm$ 27.9 <sup>b</sup>	218.9 $\pm$ 28.6 <sup>b</sup>
RMS	144.7 $\pm$ 18.6 <sup>x</sup>	155.7 $\pm$ 23.3 <sup>z</sup>	150.3 $\pm$ 23.2 <sup>y</sup>	150.5 $\pm$ 23.3 <sup>y</sup>



**Figure 2:** Typical resultant L5S1 sagittal joint moment curves.

All TD approaches generated a  $\sim 10\%$  offset in L5S1 moments when compared to the BU approach. This offset is due to varied effects of rigid body segment assumptions, as the massive trunk segment in the TD models is far less rigid and its center of mass less predictable than any lower extremity segment. This discrepancy between average peak L5S1 moment(s) matches previous reports during a similar task [3].

Limitations of this study include: 1) analysis of a single planar task; 2) use of a single lifting speed; and 3) evaluation of only the L5S1 joint moment. It is hypothesized that examination of these limitations would further highlight the differences between the different IDM approaches.

## REFERENCES

1. Liberty Mutual Workplace Safety Index, 2016
2. Occupational Biomechanics, 2006
3. Kingma I, et al. *J Biomech* **29**, 693-704, 1996
4. Desjardins P, et al. *ME&P* **20**, 153-158, 1998
5. De Leva P *J Biomech* **29**, 1223-1230, 1996
6. Hanavan EP *AMRL-TR-64-102*, 1964
7. McNeil T, et al. *Spine* **5**, 529-538, 1980

# ESTIMATION OF MECHANICAL DEMANDS OF A LOWERING AND LIFTING TASK ON THE LOWER BACK IN PATIENTS WITH ACUTE LOW BACK PAIN

Iman Shojaei, Elizabeth G Salt, Quenten Hooker, and Babak Bazrgari  
University of Kentucky, Lexington, KY, USA  
Email: shojaei.iman@uky.edu

## INTRODUCTION

Mechanical loads experienced in the lower back during daily activities have been reported to be different between patients with chronic low back pain (LBP) and asymptomatic individuals. Whether such differences in mechanical loads have a causal role in transition from acute to chronic LBP is unclear. As the first step toward addressing such a research gap, the objective of this study was set to investigate differences in mechanical demands of a lowering and lifting task in the sagittal plane on the lower back between patients with acute LBP and asymptomatic individuals. Under free forward trunk bending and return, we have recently observed that patients with acute LBP adopt larger pelvic rotation and smaller trunk angular acceleration compared to asymptomatic controls [1]. Considering the impact of such kinematics difference on mechanical demands of task on the lower back [2], we hypothesized that the shearing and moment demands of the lowering and lifting task on the lower back to be, respectively, larger and smaller in patients with acute LBP versus controls.

## METHODS

Nineteen females with health-care provider diagnosed acute LBP and nineteen matched asymptomatic controls were included in this study. Prior to data collection, all participants completed an informed consent procedure approved by the University of Kentucky's Medical Institutional Review Board. Participants were instructed to complete one symmetric lowering (a 4.5 kg load) and lifting task at their preferred cadence while standing on the center of a force platform (AMTI, Watertown, MA). Wireless Inertial Measurement Units (Xsens Technologies, Enschede, Netherlands) superficial to the thorax, pelvis, right thigh, and right shank were used to track the motion of these body parts, as rigid bodies. The kinematics and kinetics data were sampled at the respective rates of 50 and 1000 Hz.

A linked-segment model of the lower extremities and pelvis, developed in MATLAB (The MathWork Inc., Natick, MA, USA, version 8.6) [2], was used to estimate the mechanical demands of task on the lower back. The model included rigid bodies of seven segments (bilateral feet, shanks, and thighs as well as the pelvis) that were connected using frictionless point-contact joints (Fig. 1). A “bottom-up” inverse dynamics approach was used to estimate reaction forces and moments at the lower back which was considered to be the superior level of the pelvis. Projections of the lower back reaction forces perpendicular (axial) and parallel (shearing) to the L5-S1 intervertebral discs were calculated to represent the contribution of task demand to the total axial and shearing forces [2] (Fig. 1).

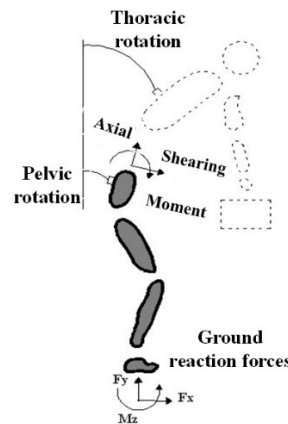


**Figure 1:** The linked-segment model used to estimate the mechanical demands of a lowering and lifting task.

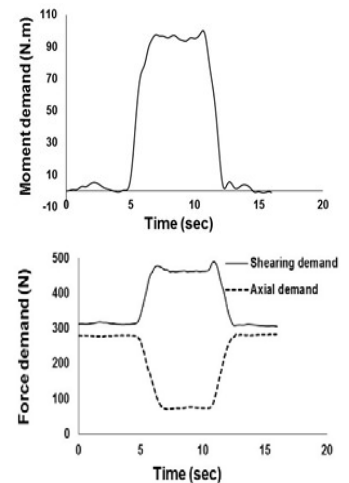


**Figure 2:** A typical example of moment, axial, and shearing components of task demand on the lower back

The axial, shearing, and the moment components of task demand (Fig. 2) at the time of peak moment component (TPMC) as well as the peak pelvic and thoracic rotations along with the corresponding values of lumbar flexion were used as dependent measures for statistical analyses. Univariate analysis

of variance (ANOVA) tests were conducted on the task demand and the kinematics variables.

## RESULTS AND DISCUSSION

The moment component of task demand between patients with acute LBP and asymptomatic controls was not different. However, the shearing and axial components at TPMC were, respectively, larger and smaller in patients (Table 1). Moreover, the patient group completed the task with a smaller thoracic rotation and a smaller lumbar flexion (Table 1).

Our hypothesis on the smaller moment demand of task in patients was driven by our findings of similar peak thorax rotation but smaller peak angular acceleration during free trunk forward bending and return in patients vs. controls [1]. However, the patients adopted a different trunk motion under lowering and lifting task compared to free forward bending and return. Specifically, the thoracic rotation ( $F=0.14$ ,  $p=0.709$ ) and angular acceleration ( $F=0.35$ ,  $p=0.562$ ) at TPMC were not different between patients and controls under lowering and lifting task.

No differences in the moment demand of the task on the lower back between the groups, though an indication of comparable total internal tissue responses to the task demand, doesn't suggest comparable active muscle response. Specifically, the observed smaller lumbar flexion in patients (Table 1) suggests a smaller passive contribution of lower back tissues in offsetting the moment demand of task,

hence an indication of larger active muscle contribution.

Our hypothesis on the larger shearing demand of task in patients with acute LBP versus controls was based on our earlier observation of larger pelvic rotation in patients vs. controls during free forward trunk bending and return [1]. In contrast to free motion, peak pelvic rotation was found to be comparable between the groups (Table 1) during lowering and lifting task. Nevertheless, our hypothesis was approved as pelvic rotation at TPMC, where the statistical analyses for the task demands were performed, was larger ( $F=8.44$ ,  $p=0.006$ ) in patients.

## CONCLUSIONS

In summary, we found patients with acute LBP vs. controls adopt distinct trunk kinematics to perform lowering and lifting task which leads to larger shearing and smaller axial demands of the task on the lower back. Although the potential role of abnormal mechanics of lower back in transition of an acute LBP case to chronic and/or recurrent LBP should be investigated using longitudinal studies, our observation of differences in the lower back mechanics, both kinematics and kinetics aspects, between patients with acute LBP and asymptomatic individuals support such a role.

## REFERENCES

1. Shojaei I, et al. *Clinical Biomech* **41**, 66-71, 2017
2. Shojaei I, et al. *J Biomech* **49**, 896-903, 2016

## ACKNOWLEDGEMENT

This work was supported by an award (UL1TR000117) from NIH.

**Table 1:** Summary of statistics results for the effects of group (patients with acute LBP and controls) on dependent variables. TPMC: Time of peak moment component.

	Task Demands at TPMC						Peak Kinematics					
	Moment		Shearing		Axial		Thoracic Rotation		Pelvic Rotation		Lumbar Flexion	
	F	p	F	p	F	p	F	p	F	p	F	p
Group	0.06	0.806	6.10	<b>0.020</b>	8.10	<b>0.008</b>	7.91	<b>0.009</b>	3.60	0.068	18.06	<b>&lt;0.001</b>
	Mean (SD)		Mean (SD)		Mean (SD)		Mean (SD)		Mean (SD)		Mean (SD)	
Patients	89.5 (19.0)		446.7 (36.0)		74.2 (81.9)		75.2 (10.3)		42.6 (10.2)		32.6 (11.0)	
Controls	89.6 (26.6)		415.5 (47.3)		159.1 (80.8)		85.4 (11.3)		34.0 (11.9)		51.4 (13.4)	

All statistical analyses were performed using SPSS (IBM SMSS Statistics 23, Armonk, NY, USA). A p-value  $\leq 0.05$  (Boldface) was considered as statistically significant.

# Effect of Cervical Decompression Surgery on Biomechanics on Neuromuscular Control during Gait in Adult Cervical Spondylotic Myelopathy Patients

<sup>1</sup>Ram Haddas, PhD, <sup>1</sup>Sujal Patel, MD, <sup>2</sup>Raj Arakal, MD, <sup>3</sup>Theodore Belanger, MD, <sup>3</sup>Kevin L. Ju, MD

<sup>1</sup>Texas Back Institute Research Foundation, Plano, TX, USA

<sup>2</sup>Texas Back Institute, Plano, TX, USA

<sup>3</sup>Texas Back Institute, Rockwall, TX

Email: [rhaddas@texasback.com](mailto:rhaddas@texasback.com)

## INTRODUCTION

Cervical spondylotic myelopathy (CSM) is a neurologic condition resulting from cervical stenosis and spinal cord compression due to degenerative changes within the cervical spine.[1] These changes can include disc herniations, disc osteophyte complexes, ligamentum flavum hypertrophy, spondylolisthesis, or cervical kyphosis.[2] CSM is most common after the age of 50 years, but the age of onset is variable depending on the degree of congenital spinal canal narrowing and other factors.[1] Gait imbalance is a frequent symptom of CSM, and has been reported to be improved by surgical intervention.[3] Clinical studies have determined that individuals with CSM have a slower gait speed, prolonged double support duration, and reduced cadence compared to healthy controls.[4] In fact, difficulty with gait and balance are the most common manifestations of CSM.



**Figure 1.** Preoperative and postoperative MRI of a myelopathic patient

While there may be some debate as to when patients with radiographic cervical stenosis should undergo decompressive surgery, most surgeons will agree on

surgery for patients with moderate or severe myelopathy.[5] The purpose of this study was to evaluate the effect of cervical decompression surgery on the biomechanics and neuromuscular control of the lower extremities and spine during gait in patients with CSM before and after surgical intervention and to compare these parameters to a healthy control group.

## METHODS

Ten subjects with CSM who have been deemed appropriate surgical candidates performed gait analysis one week before (Pre) and 3 months after surgery (Post3). Twenty healthy volunteers served as a control group. Fifty-one reflective markers (9.5 mm diameter) were utilized to collect full body three-dimensional kinematics using 10 cameras (VICON, Denver, CO) at a sampling rate of 100 Hz. Ground reaction forces (GRFs) were measured using three sequential force plates (AMTI, Watertown, MA). Trunk and lower extremity muscle activity was measured using surface EMG electrodes (Delsys, Inc, Natick, MA). For the test, the patient walked barefoot at his/her self-selected speed along a 10 meter walkway. Spine and lower extremity neuromuscular control, spatiotemporal and vertical GRFs were measured and recorded. A 2 factors repeated measures ANOVA was used to determine differences in gait patterns in adult CSM patients before and after their surgery and compared to the healthy controls.

## RESULTS AND DISCUSSION

After cervical decompression surgery, CSM patients had significantly faster walking speed (Pre: 0.82 vs Post3: 1.03 m/s,  $p=0.050$ ), longer step (Pre: 0.48 vs Post3: 0.60 m,  $p=0.013$ ) and stride length (Pre: 0.98 vs Post3: 1.14 m,  $p=0.050$ ). The delay in rectus

femoris onset was significantly improved (Pre: -0.13 vs -0.08 sec,  $p=0.037$ ) after cervical decompression surgery. The duration of semitendinosus and rectus femoris muscle activity decreased (ST: Pre: 53.2 vs 42.9 % of gait cycle,  $p=0.018$ ; RF: 48.8 vs 41.4 % of gait cycle,  $p=0.044$ ) after cervical decompression surgery and approached that of normal controls. The first peak of the vertical GRF was also found to occur earlier (Pre: 21.05 vs Post: 17.90 % of gait cycle,  $p=0.050$ ) after cervical decompression surgery (Figure 2).

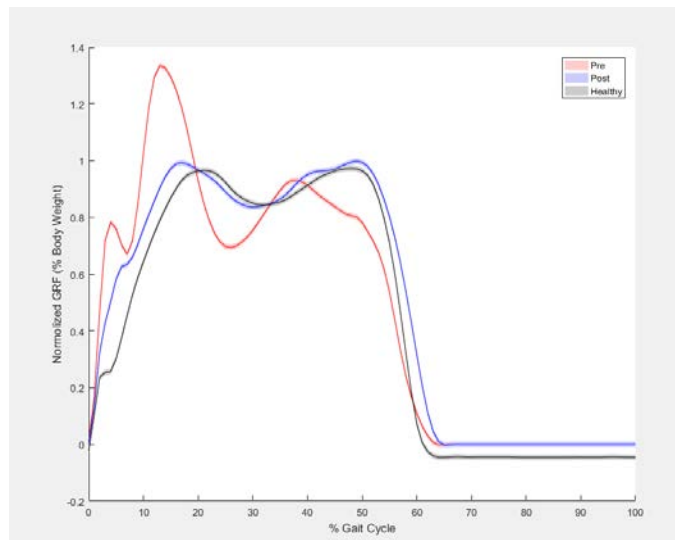


**Figure 2.** Vertical ground reaction forces during gait from a representative patient with cervical myelopathy pre- and post-surgery and healthy adults.

In comparison to the control group, CSM patients preoperatively presented with a significantly slower gait speed (0.24 m/sec;  $p=0.037$ ), decreased step length (0.11 m;  $p=0.014$ ), stride length (0.20 m;  $p=0.019$ ), and increased step width (0.05 m;  $p=0.001$ ). Cadence, stride and stance times, swing-stance ratio, and single support time were not found to be statistically different. Control group muscle onsets were later (Multifidus: 0.69 sec,  $p=0.024$ ; Rectus femoris: 0.51 sec,  $p=0.036$ ; Semitendinosus: 0.38 sec,  $p=0.032$ ; Tibialis Anterior: 0.29 sec,  $p=0.044$ ) in comparison to preoperative CSM patients. Furthermore, control group muscle durations were significantly shorter (Multifidus: 8%

of gait cycle,  $p=0.035$ ; Rectus femoris: 9 % of gait cycle,  $p=0.021$ ; Semitendinosus: 11 % of gait cycle,  $p=0.018$ ; Medial Gastrocnemius: 6 % of gait cycle,  $p=0.049$ ) in comparison to preoperative CSM patients. Moreover, preoperative CSM patients presented with a lower vertical GRF 2nd peak (0.09% of BW;  $p=0.050$ ), later 1st peak (3% of gait cycle;  $p=0.048$ ) and valley (3% of gait cycle;  $p=0.049$ ) in comparison to the healthy group (Figure 2). After surgical decompression, CSM patients had normalization of their gait with only minor differences when compared to the control group.

## CONCLUSIONS

Cervical decompression surgery improved the gait pattern in patients with cervical spondylotic myelopathy. Based on our preliminary results, CSM patients walk slower and with reduced trunk and lower extremity function and efficiency in comparison to a healthy control group. However, surgical decompression resulted in faster walking speeds with longer steps and an increase in spine and lower extremity function and efficiency. These post-operative CSM patients actually had similar walking patterns in comparison to controls. Spine care providers should use gait analysis as part of their clinical evaluation to better understand the effects of the disease and its treatment on their patients' gait, function, and, ultimately, quality of life.

## REFERENCES

1. Rhee JM, et al. *Spine J* **34**(9), 890-5, 2009.
2. Emery SE, et al. *J Am Acad Orthop Surg* **9**(6), 376-88, 2001.
3. Thomas TL, et al. *J Neurosurg* **86**(1), 64-8, 1997.
4. Malone A, et al. *Eur Spine J* **21**(12), 2456-66, 2012.
5. Geck MJ, et al. *Orthop Clin North Am J* **33**(2), 329-48, 2002.

# EFFECT OF TRUNK POSITION AND ANGLE OF PULL ON SPINAL LOADING DURING A ROW EXERCISE

Lyndsay Stutzenberger and Michael Pavol

Oregon State University, Corvallis, OR, USA

email: [stutzenl@oregonstate.edu](mailto:stutzenl@oregonstate.edu)

## INTRODUCTION

Osteoporotic vertebral fractures are common in older age, particularly in women, and can have profound effects on quality of life [1]. Promisingly though, resistance-training programs that include rowing exercises have been shown to improve lumbar bone density [2]. Rowers also have increased lumbar bone density, arguably due to the loads that rows apply to the spine [3]. However, little is known regarding effects of variations in technique on spinal loading during a row exercise. Such knowledge may serve to improve exercise programs against osteoporosis. This study thus determined the effects of trunk position and angle of pull on spinal loading during row exercises.

## METHODS

Five healthy, premenopausal women (mean  $\pm$  SD age:  $43 \pm 3$  years, mass:  $60 \pm 6$  kg, height:  $165 \pm 3$  cm) with recent experience in upper-body strength-training exercises participated in this study after providing informed consent. After a task-specific warm-up, 32 reflective markers were placed on each participant's trunk and lower and upper limbs. Participants performed sets of standing rows against resistance from elastic tubing (Black Mountain Products, Lakemoor, IL). Rows were performed in each of two trunk positions: erect and flexed  $30^\circ$  from vertical, for each of three angles of pull: vertical, angled  $45^\circ$  from horizontal, and horizontal. For vertical and angled rows, the tubing looped through an anchor on the ground ahead of the participant. For horizontal rows, a researcher held the midpoint of the tubing still at the participant's chest height, ahead of her. Tubing used was selected based on calibration equations and measured body dimensions. To perform a row, participants either stood erect or squatted down until one hand reached

a marked position on the thigh at which the trunk would be flexed  $30^\circ$ , as established initially using an inclinometer. Beginning with arms outstretched towards the tubing's anchor point, participants smoothly pulled the tubing's handles to their chest in about 1 s, and with minimal pause, returned to their starting position. Sets of 3-4 repetitions of each row exercise were performed against an aimed-at peak resistance of 111 N. Kinematic data were recorded at 60 Hz with nine motion-capture cameras (Vicon, Los Angeles, CA) and ground reaction forces under the feet were recorded at 360 Hz by side-by-side force plates (Bertec, Columbus, OH). Body dimensions and weight were also measured.

Motion capture and force plate data were filtered at 7 Hz and 14 Hz, respectively. Marker positions relative to body segments and joint centers were then calculated (BodyBuilder, Vicon). Finally, the AnyBody Modeling System (Aalborg, Denmark) was used, with the lumbar spine model from the AnyBody Managed Model Repository (v1.2) and custom models of the lower limbs, to calculate compressive and anteroposterior shear forces at the L5/S1 spinal segment, as well as tubing length, from the collected data. The model was scaled to each participant, and inverse dynamics solutions were found to minimize the sum of the cubed muscle fascicle activations in each frame of data.

Peak spinal forces, normalized to body weight, were averaged across trials for each set, excluding trials with calculated peak tubing forces outside of 89-134 N. Mixed-model multiple linear regression was used to determine the effects of trunk position and angle of pull on peak compressive and anterior shear forces on L5 from S1 and their ratio. Fixed main and interaction effects, as well as random effects of participant, were modeled using dummy-variable or effects coding.  $p < .05$  was used for significance.

## RESULTS AND DISCUSSION

Independent of angle of pull ( $p > .36$  for interaction effect), the peak compressive and anterior shear forces on L5 from S1 during the rows were greater in the trunk-flexed than in the trunk-erect position ( $p < .001$ ; Figure 1, Table 1). This is consistent with the larger moment arms of the head-arms-torso weight and, for vertical and angled rows, of the tubing resistance force with the trunk flexed. The resulting larger external moment would require greater force from the lumbar extensors to offset.

Surprisingly, angle of pull had no effect on the peak compressive and anterior shear forces on L5 from S1 during the rows ( $p > .42$ ; Table 1). Qualitatively, the patterns of loading appeared to differ between angles of pull though, with peak forces typically occurring near the midpoint of vertical rows but near the start or end of horizontal rows (Figure 1). Changes in loading at L5/S1 during the rows reflect changes in both the tubing resistance force and the moment created by the upper limbs' weight. The resistance force is greatest at the row midpoint, but during horizontal rows, the moment created by the limbs' weight is greatest at the start and end. These offsetting influences can explain the present results.

As was true for the peak forces, angle of pull also had no effect on the ratio of peak compression to shear force at L5/S1 in either trunk position (Table 1). This suggests that no angle of pull is optimal for maximizing bone loading while minimizing loading of soft tissue. For peak tubing resistances near 111 N, standing rows at any angle of pull from vertical to horizontal may be equally appropriate for creating a potentially osteogenic stimulus at L5/S1. However, peak resistances larger than 111 N may be needed to produce an osteogenic response [3].

**Table 1:** Mean  $\pm$  SD values of the peak compressive force and peak anterior shear force on L5 from S1, in body weights, and the compression to anterior shear peak force ratio for each row exercise. \*  $p < .001$  vs. Erect.

Trunk Position	Angle of Pull	Compressive	Anterior Shear	Compression:Shear
Erect	Vertical	1.44 $\pm$ 0.19	0.15 $\pm$ 0.02	10.1 $\pm$ 2.0
Erect	Angled	1.85 $\pm$ 0.38	0.27 $\pm$ 0.09	7.2 $\pm$ 1.5
Erect	Horizontal	1.77 $\pm$ 0.32	0.26 $\pm$ 0.11	7.6 $\pm$ 2.4
Flexed	Vertical	2.73 $\pm$ 0.95*	0.45 $\pm$ 0.13*	6.0 $\pm$ 0.6*
Flexed	Angled	2.64 $\pm$ 0.53*	0.53 $\pm$ 0.09*	5.0 $\pm$ 0.4*
Flexed	Horizontal	2.69 $\pm$ 0.67*	0.52 $\pm$ 0.19*	5.4 $\pm$ 0.8*

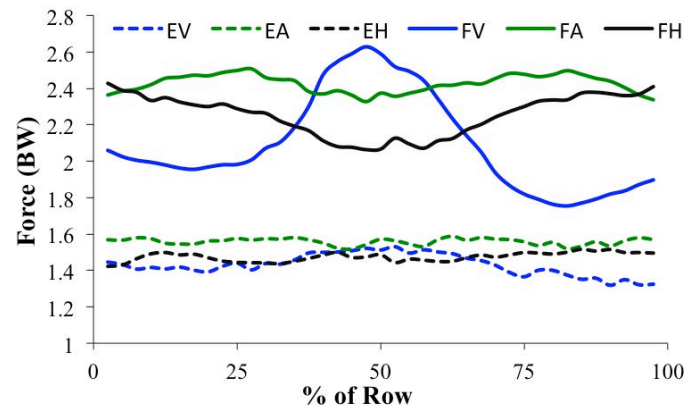


**Figure 1:** Ensemble averages of compressive force at L5/S1 across the row. Timing is in terms of the tubing length, where 50% corresponds to maximal length. Type of row: E=erect, F=flexed, V=vertical, A=angled, H=horizontal. BW=body weight.

## CONCLUSIONS

The present results support the inclusion of row exercises performed in a trunk-flexed position with elastic tubing in exercise programs against spinal osteoporosis, as these produce greater spinal loading than similar rows performed with the trunk erect.

## REFERENCES

1. Briggs AM. *Osteoporosis Int* **18**, 575-584, 2013.
2. Winters-Stone KM, and Snow CM. *Bone* **39**, 1203-1209, 2006.
3. Morris FL, et al. *Int J Sports Med* **21**, 518-523, 2000.

## ACKNOWLEDGMENTS

Partially funded by National Science Foundation Grant DGE 0965820, the NSF IGERT Program in Aging Sciences at Oregon State University.

# THE EFFECT OF TWIST ON THE MECHANICAL PROPERTIES OF THE INTERVERTEBRAL DISC

Maxine Harvey-Burgess, Diane Gregory

Wilfrid Laurier University, ON, CAN

email: [harv8610@mylaurier.ca](mailto:harv8610@mylaurier.ca)

## INTRODUCTION

Herniation is a common injury to the intervertebral disc (IVD) and contributes to low back pain. The IVD contains the nucleus pulposus (NP) surrounded by the multi-layered annulus fibrosus (AF). Within the AF there are two structures which both have important adhesive properties: the interlamellar matrix and the intralamellar matrix. The interlamellar matrix is the area between adjacent AF layers and the intralamellar matrix is the area between collagen fibres of a single layer of the AF. IVD herniation occurs when the NP breaks through the layers of the AF through both the inter- and intralamellar matrices [1].

When combined with flexion, twist has been shown to contribute to low back pain [2]. In vitro, twist combined with flexion has been shown to increase the risk of IVD herniation and damage to the AF [3]. Therefore, it is plausible that twisting of the IVD may damage the inter- and intralamellar matrices due to the tensile and shear forces twist places on the AF. However, it remains unclear how twist affects the mechanical properties of the AF. The purpose of this study was to examine the effect of twist on the mechanical properties of the inter- and intralamellar matrices of bovine IVDs.

## METHODS

This study used 18 bovine IVDs from the caudal region. Dissected functional spine units (FSU) were loaded in a custom twisting jig and a mechanical testing system (MTS, Eden Prairie, MN) (Figure 1). Each FSU was subjected to one of four loading protocols for two hours: (1) 0N of compression and 0° of twist, (2) 1000N of compression and 0° of twist, (3) 0N of compression and 12° of twist, or (4)

1000N of compression and 12° of twist. All FSUs were preloaded with 125N of compression and 0° of twist for 15 minutes prior to the two hour loading protocol.

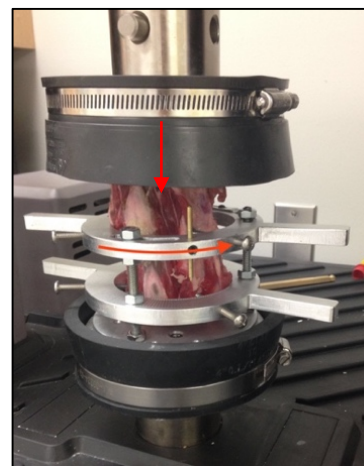


**Figure 1.** An FSU in twist and mounted in the mechanical testing system.

Following mechanical loading, three samples were dissected from each IVD. One sample, containing at least two adjacent layers of the AF, was used for a peel test. During the peel test, the sample was mechanically delaminated to measure interlamellar matrix strength. The variable of interest from the peel test was peel strength.

The other two samples were dissected down to single layers of the AF, which were subsequently mechanically tested in tension until failure. Care was taken to ensure that the collagen fibres of dissected single layers were oriented in the direction of twist. During the single layer tests, tension was applied perpendicular to the orientation of the collagen fibres in order to measure intralamellar matrix strength. The variables of interest from the

single layer testing included toe region stress/strain, stiffness, and yield point.

## RESULTS

Average yield point of the single layer samples exposed to 12° of twist, regardless of the magnitude of compression (0N or 1000N of compression), was 0.42 N/mm<sup>2</sup> (±0.27) while the average yield point of the single layer samples that were not exposed to twist (0N or 1000N of compression) was 0.81 N/mm<sup>2</sup> (±0.48) (p=0.025) (Figure 2).

Additionally, the average yield point of the single layer samples exposed to combination loading (twist and compression) was 0.36 N/mm<sup>2</sup> (±0.13) and the average yield point of the single layer samples exposed to compression-only loading was 0.98 N/mm<sup>2</sup> (±0.45) (p=0.019).

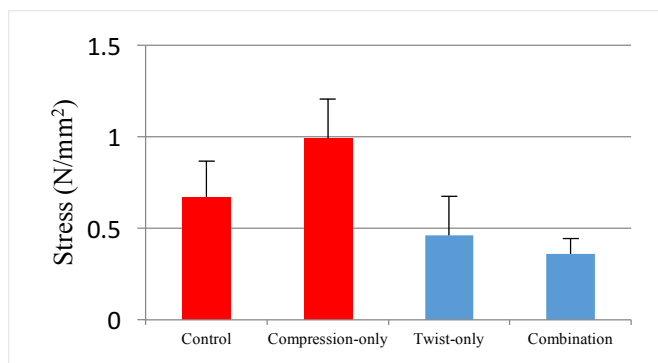


**Figure 2.** Average yield point from the single layer tensile test. The red bars indicate FSUs exposed to 0° twist while the blue bars indicate 12° twist.

Average peel strength of the samples exposed to 12° of twist (0N or 1000N of compression) was 2.10 N/mm (±0.61) and the average peel strength of the samples that were not exposed to twist (0N or 1000N of compression) was 3.46 (±1.83) (p=0.116) (Figure 3).

## DISCUSSION

The single layer samples exposed to twist (0N and 1000N of compression) had significantly lower yield points than the single layer samples that were not exposed to twist (0N and 1000N of compression). This suggests that twist, regardless of compression exposure, negatively affects the strength of the intralamellar matrix. Given that part of herniation progression is migration through clefts in the intralamellar matrix [1], this may explain why risk of herniation is higher when the IVD is twisted.

Though the difference between the peel strength of IVDs exposed to twist compared to those not exposed to twist was not found to be significant (p=0.116), there appears to be a trend of decreasing strength in twisted samples. Therefore, it is possible that twist may be negatively affecting the AF's ability to resist delamination, which would contribute to increased risk of herniation. Further examination is needed to confirm this.

## CONCLUSIONS

The lower yield points observed in the twisted single layer samples compared to those that were not twisted indicated that twist reduced the strength of the intralamellar matrix. Previous research has indicated that twist in combined loading scenarios increases the risk of IVD herniation [3]. According to the results of the current study, this increased risk could be due to twist causing damage to the AF, allowing herniation to occur more easily. Further research should explore the mechanical effects on the AF as a result of combination loading with flexion; a well-established risk factor for herniation.

## REFERENCES

1. Tampier C, et al. *Spine* **32**, 2869-2874, 2007
2. Kelsey JL, et al. *J Orthop Res* **2**, 61-66, 1984
3. Marshall LW, et al. *Clin Biomech* **25**, 6-9, 2010

# LUMBOPELVIC POSTURAL CONTROL SYSTEM ORGANIZATION IS ALTERED IN INDIVIDUALS WITH LOW BACK PAIN

<sup>1</sup>Courtney M. Butowicz, PhD, CSCS and <sup>1</sup>Sheri P. Silfies, PT, PhD

<sup>1</sup>Drexel University, Philadelphia, PA, USA  
email: silfies@drexel.edu

## INTRODUCTION

Movement impairments associated with low back pain (LBP) may result from alterations in the mechanisms by which the central nervous system processes sensory information in the presence of painful and non-painful stimuli. Current evidence proposes that patients with recurrent and chronic LBP exhibit altered sensorimotor integration that is coupled with a reorganization of the somatosensory and motor cortices [1-4]. Biomechanical studies assessing trunk postural control consistently demonstrate degradation in performance (increased center of pressure (COP) movement) in individuals with LBP, but analysis approaches have provided limited insight into the interaction of sensorimotor components of the system [5]. Non-linear analysis of system complexity (sample entropy) may provide information regarding the interaction of components within the neuromuscular control system and allow improved insight into system organizational changes in individuals with LBP.

The purpose of this study was to characterize differences in postural system organization between individuals with and without LBP when lumbopelvic control is challenged during unstable sitting.

## METHODS

Ten individuals with subacute LBP (5 males; age:  $26.1 \pm 12.1$  yrs; stature:  $168.6 \pm 8.7$  cm; mass:  $69.9 \pm 11.0$ kg) and 10 healthy controls [CTR] (5 males; age:  $30.5 \pm 8.5$  yrs; stature:  $169.7 \pm 8.8$  cm; mass:  $75.8 \pm 17.0$  kg) completed a biomechanical test of trunk neuromuscular control. Participants provided written informed consent and all procedures were approved by the local IRB. Trunk neuromuscular control was assessed using a custom apparatus

consisting of an unstable chair situated on an elevated force plate (Kistler, Inc. Fig. 1). Extremity constraints (e.g., arms across chest, feet supported, legs strapped together) required isolated trunk neuromuscular control to maintain upright sitting. Participants performed three-60s trials in an eyes open (EO) and eyes closed (EC) condition with a 60s break between trials [5].



**Figure 1:** Trunk neuromuscular control testing apparatus. Hemisphere under seat creates instability in the sagittal and frontal planes requiring trunk movement to maintain balance.

Force data were collected at 240 Hz (down sampled -120Hz) and COP variables derived to quantify mediolateral (frontal) plane control. Time series data were filtered (2nd-order low pass Butterworth filter at 10 Hz) to eliminate low amplitude measurement noise. A custom Matlab program (Mathworks, Inc.; Natick, MA) was used to calculate sample entropy (SEn; parameters  $r = 0.2$ ,  $m = 3$ ). SEn quantifies the structure of variability over time allowing for continuous assessment of changes in postural organization. SEn examines the logarithmic probability that a time series of data points a set distance apart will demonstrate comparable characteristics on the next comparison segment within the state space [6]. SEn values typically range between 0-2. Lower values represent increased regularity, which was interpreted as a more constrained system with fewer degrees of freedom and less organization of the control system components [7]. Between trial test-retest reliability of SEn was calculated (trial 1 to 3) using an intra-

class correlation coefficient (ICC<sub>2,1</sub>). A two-way ANOVA compared performance differences between groups and conditions (EO, EC) (P<.05) with partial eta squared presented as an index of size of the differences.

## RESULTS AND DISCUSSION

Test-retest reliability was good to excellent (Table). There was a significant main effect of group ( $F_{(1,18)}= 12.87, p= 0.002, \eta_p^2= 0.42$  and a significant interaction effect ( $F_{(1,18)}= 52.97, p< 0.001, \eta_p^2= 0.75$ ). Lumbopelvic system organization within the groups was similar during the EO condition. However, when visual feedback was removed the groups presented a significantly different organizational strategy (Fig. 2). The CTR group's organization became more flexible (higher SEN), while those with LBP became more constrained (lower SEN).

Table. Between Trial Reliability and Standard Error of Measurement

Group	Eyes Open		Eyes Closed	
	ICC	SEM	ICC	SEM
CTR	.77	.05	.88	.10
LBP	.81	.05	.67	.08

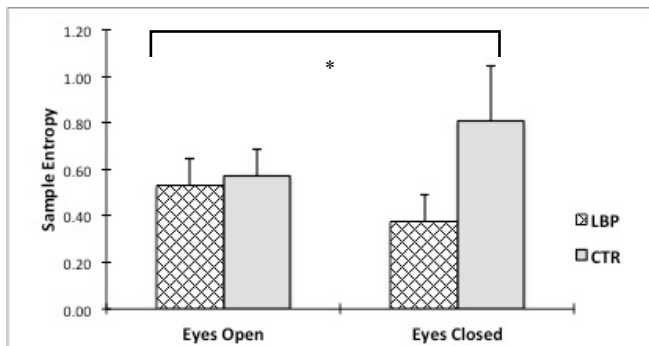


Figure 2: Group means and standard deviations for sample entropy during tests of isolated trunk neuromuscular control in eyes open and eyes closed conditions. CTR- control; LBP - low back pain; \* P<.05

Improved understanding of potential impairments in the interaction of components of underlying control mechanisms (visual, proprioceptive, vestibular, neuromotor) in patients with LBP may assist in therapeutic intervention choices. The significant interaction effect suggests that when a component of the control system (visual input) was removed, the control system's adaption was different between groups. The LBP group became less organized (more constrained), reducing the adaptive capability

of the lumbopelvic postural control system. The CTR group however, became more organized (less constrained), increasing the adaptive capability of the system. As sensory information was removed, the CTR group was better able to reorganize and increase interconnections between proprioceptive, vestibular and neuromotor system components in order to adapt to the challenge of unstable sitting. The response of individuals with LBP to removal of visual input suggests that vision may be a more dominant aspect of their control mechanism. This finding also suggests an inability to adequately reorganize or re-weight system sensory input [8] and may be reflective of impairments within or between the control system components. A similar response was reported following experimental impairment of trunk muscles (fatigue protocol) in which individuals without LBP adapted by increasing organization of the system, while those with LBP demonstrated less system organization during lumbopelvic movements. [9]

## CONCLUSIONS

Individuals with LBP demonstrate altered trunk postural control system organization compared to healthy controls particularly when challenged to adapt or reorganize the system following a perturbation of a system component.

## REFERENCES

- Hotz-Boendermaker S, et al. *Spine* **41**, E667-673, 2016.
- Kregel J, et al. *Semin Arthritis Rheum* **45**, 229-237, 2015.
- Tsao H, et al. *Brain* **131**, 2161-2171, 2008.
- Flor H, et al. *Neurosci Lett* **224**, 5-8, 1997.
- Sung W, et al. *Spine J* **15**, 1772-1782, 2015.
- Pincus SM, et al. *J Clin Monitor* **7**, 335-345, 1991.
- Roerdink M, et al. *Exp Brain Res* **174**, 256-269, 2006.
- Brumagne W, et al. *Neurosci Lett* **366**, 63-66, 2004.
- Bauer CM, et al. *J Electmyo Kines* **33**, 94-102, 2017.

# VALIDATING THE USE OF ULTRASOUND TO MEASURE LUMBAR VERTEBRAL TWIST

<sup>1</sup> Graham Mayberry, <sup>1</sup> Colin McKinnon, <sup>2</sup> Brian Nairn, <sup>2</sup> Janessa Drake, and <sup>1</sup> Jack P. Callaghan

<sup>1</sup> University of Waterloo, Waterloo, ON, Canada

<sup>2</sup> York University, Toronto, ON, Canada

E-mail: graham.mayberry@uwaterloo.ca

## INTRODUCTION

Axial lumbar twist is a significant factor in low back pain development and cause of injuries [1]. The accurate measurement of spinal twisting is important in evaluating its biomechanical properties, yet our ability to measure this movement *in vivo* remains difficult due to skin movement artifacts and technological constraints [2]. Magnetic resonance imaging (MRI), computerized topography, and x-ray instruments have formerly been used as a gold standard for measuring and tracking axial twist of the spine [3,4]. While these results are important, the positions and postures that can be studied are very limited.

The use of ultrasonography (US) to measure tissues below the surface of the skin and lumbosacral motion has been used in previous studies with great success [5,6]. While MRI does represent a gold standard in internal measurements, it is often too costly, inaccessible, or unreasonable for certain postures or environments. The use of US to measure lumbar axial twist of the spine may provide a viable alternative, given its low cost, portability, and availability. The purpose of this study was therefore to validate the use of US to measure axial twist of the lumbar spine by comparing results obtained from MRI technology.

## METHODS

Twenty (10 males, 10 females) healthy participants were recruited for this study with no history of low back pain over the past 12 months who successfully passed the MRI screening process. A Siemens MAGNETOM 3T Trio MRI scanner was used to acquire 3D MRI scans, using a T1-weighted VIBE sequence, while a Sonosite M-Turbo medical

ultrasound imaging system, with a 3-5 MHz linear transducer was used to acquire US images.

Participants were secured to an MRI-safe spine board that had been customized to allow for both US and MR imaging. After manual palpation, a vitamin-E capsule was affixed to the skin so to ensure that the same vertebral levels were being compared. During the imaging session, the participant was imaged using US in either a neutral or an axially twisted (where a 30° padded wedge was locked to the spine board beneath the pelvis) position. The participant was then transferred to the MRI bed by four researchers while the participant remained motionless in order to maintain their position on the spine board. The lumbar spine was then imaged using MRI, followed by the reverse order such that each participant was imaged in both the neutral and twisted positions using both MRI and US.

Intervertebral axial twist was measured using OsiriX (© Pixmeo Sarl, V 5.0.1) and Matlab (9.1, The MathWorks Inc.) for MRI and US data, respectively. External surface markers were adhered to the thorax, pelvis, and US probe in order to determine vertebral body location relative to both the thorax and pelvis. Intervertebral rotation was calculated using spinous processes for all subjects, while a subset of images were used where both spinous process (SP) and transverse process (TP) could be identified. Welch two sample t-tests were used in both the full (measure using spinous process) and subset (spinous and transverse process) of data to compare MRI and US measures, where the motion was calculated relative to the thorax (USThor) and pelvis (USPel). A Bland-Altman plot analyzing agreement between the MRI and both the USThor and USPel measurement techniques was also performed.

## RESULTS AND DISCUSSION

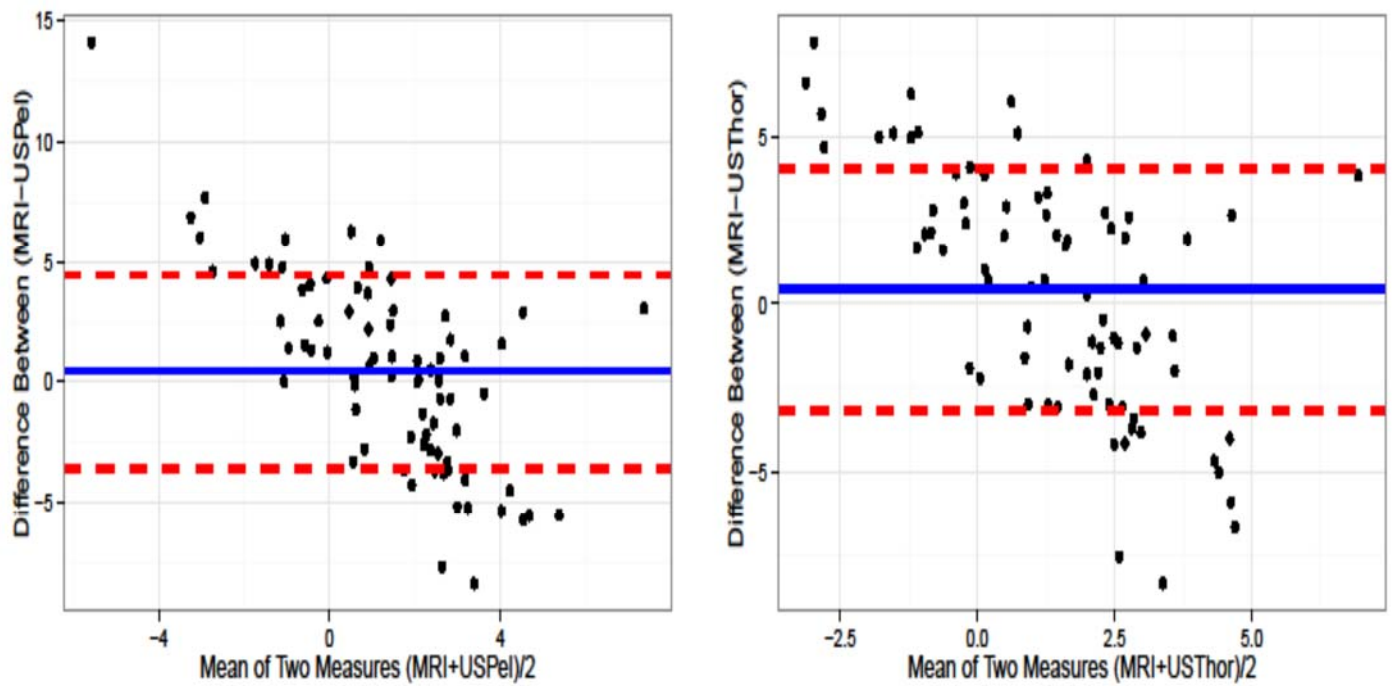


Figure 1: Bland-Altman Plots comparing MRI and US measurements of lumbar axial twist relative to the pelvis (USPel) and thorax (USThor).

T-test results are displayed in Table 1, demonstrating that there were no significant differences between MRI and US measures of axial twist, regardless of landmarks (SP or SP+TP) used. The Bland-Altman plots reveal that lumbar rotation measured using US and MRI are very similar (Figure 1).

The results of this study suggest that US can be a valid tool for measuring axial twist in the lumbar spine. Whether using the SP alone or a combination of SP and TP, it appears that the technique developed to measure rotation using a combination of surface markers and US does not solely depend on the ability to see the entire vertebral structure, leading the authors to believe that imaging of the thoracic spine in this manner would also be valid. Furthermore, we determined that there was no difference in intervertebral angles when calculating angles relative to the pelvis or thorax rigid body surface markers.

## CONCLUSIONS

This validation study has demonstrated that axial twist of the lumbar spine can be measured using the coordinated ultrasound and motion capture approach demonstrated in this study. The ability to use US to accurately measure spinal rotation vastly improves our understanding of how specific tasks and body positions affect the internal structures, thus providing researchers and clinicians an opportunity to better predict spinal motion patterns that result in injury.

## REFERENCES

1. Kelsey, JL et al. *J Orthopaed Res* **2(1)**, 61-6, 1984.
2. Cappozzo, A et al. *Clin Biomech* **10(4)**, 171-8, 1995.
3. Fujii, R et al. *Eur Spine J* **16**, 1867-74, 2007.
4. Ochia, RS et al. *Spine* **31(18)**, 2073-8, 2006.
5. Dupont, AC et al. *J Clin Ultrasound* **29(4)**, 230-6, 2001.
6. van den Hoorn, W et al. *Ultrasound Med Biol* **42(5)**, 1221-9, 2016.

**Table 1:** Results from Welch Two Sample t-test for each MRI comparison of both data sets.

Body Landmark Used in Ultrasound		df	t-value	p-value
Spinous Process	MRI-USThor	109	1.09	0.279
	MRI-USPel	103	1.02	0.308
Spinous and Transverse Process	MRI-USThor	27	0.87	0.389
	MRI-USPel	27	1.12	0.272

# LOW VELOCITY COLLISION CHARACTERISTICS ASSOCIATED WITH CLAIMED LOW BACK PAIN

Kayla M. Fewster<sup>1</sup>, Robert J. Parkinson<sup>1,2</sup>, Jack P. Callaghan<sup>1</sup>

<sup>1</sup>Department of Kinesiology, University of Waterloo, Waterloo, ON

<sup>2</sup>-30- Forensic Engineering., Toronto, ON, Canada

email: kfewster@uwaterloo.ca

## INTRODUCTION

Up to fifty percent of individuals involved in low velocity collisions report low back pain (LBP) [1]. Epidemiological studies suggest there is an association between developing a whiplash neck injury from a motor vehicle collision and reporting low back pain, with the reported incidence of low back pain with a whiplash injury ranging between 40 to 60% of all whiplash cases [2,3].

Despite the statistical relationship, there is a lack of knowledge regarding injury mechanisms associated with LBP reporting. Frequently, lumbar injury (pain) is reported after low velocity collisions, even with little vehicle damage, a lack of objective evidence upon medical examination and negative radiographic evidence. As a result, assessments of injury remain solely reliant on symptom reporting, despite the psychosocial issues known to be present in litigated claims.

To assess causation of low back injuries claimed after collisions, forensic engineering firms are engaged to determine the likelihood that an injury was sustained. As a result, they have unique access to details from the collision to allow for an understanding of the detailed collision characteristics such as vehicle velocity changes and vehicle orientations. In addition, hospital reports and medical records are reviewed to assess the injuries claimed and any associated preexisting medical conditions. This unique source of data provides the rare opportunity to match reported collision circumstances with reported low back injury outcomes, circumventing the need for assessors and researchers to solely rely on occupant recall and reporting in understanding causation.

However, this data is rarely analyzed to understand 'population' trends and relationships. In order to

identify potential low back injury mechanisms resulting from low velocity collisions it is necessary to characterize and identify the physical dynamics of low velocity collisions that result in LBP claims and establish links between collision circumstances and injury outcomes. Therefore, the primary objective of this investigation was to characterize the physical circumstances of low velocity motor vehicle collisions that resulted in claims of low back injury.

## METHODS

This investigation involved the secondary analysis of a data set obtained from a forensic engineering firm based in Toronto, Ontario, Canada. Each analyzed case was obtained from a search of the firm's internal electronic database. The database was searchable by a number of different fields including: start/finish date of the claim, project description and case number.

The searchable database encompassed 15 years of cases (2000-2014), and was searched using specific key words. All cases that were returned based on the search criteria were documented using the case number to keep personal information confidential. Only cases that included a biomechanical evaluation of the injuries sustained in a collision with a collision severity of 25 km/hour or less were included in the analysis. Each identified case was reviewed for specific collision characteristics, injuries claimed and pre-existing medical conditions (Table 1).

Descriptive statistics (mean, SD and ranges) along with proportions across low back injury claims were computed for documented variables. In order to protect the privacy of any involved individuals, all data presented was deidentified and grouped to ensure it was not possible to identify an individual

person or case. This approach was reviewed and approved by the University of Waterloo Office of Research Ethics.

**Table 1:** The documented variables for each case meeting the search criteria

Characteristics Specific to Collision	Occupant Specific Characteristics
Collision Severity	Age
Direction of Collision Forces	Gender
Vehicle Repair Cost	Seating Position
Event Data Present	Claimed Injuries
Tow Away vs. Self Reported	Pre-Existing Medical Complaints
Vehicle Type	Seatbelt Worn
Number of Occupants in Vehicle	Disc Degeneration Present & Level
	Prior Accidents

## RESULTS AND DISCUSSION

In total, 83 cases met the inclusion criteria. The automotive collisions assessed occurred between the years of 2002 and 2014. The mean (SD) age across all claimants was 41.2 (10.6) years, with a range of 15 to 65 years of age. Males and Females were relatively equally distributed across all claims; 45.8 percent of all claimants were male and 54.2 percent of all claimants were female.

Out the 83 cases reviewed, 77% involved a claim of low back injury. Specific to those who claimed low back injury, the mean age was 41.5(10.2), 78% of claimants were the driver of the vehicle and 100% of claimants were wearing their seat belt. The most common pre-existing medical conditions were pre-existing LBP or evidence of lumbar disc degeneration with 63% of claimants either having had a history of LBP or displayed evidence of lumbar disc degeneration, or both (**Figure 1**). Of all low back injury claims, 97% were accompanied by a whiplash and/or whiplash associated disorder claim.

For low back injury claims, a rear-end impact was the most common configuration (70% of all low back injury claims involved a rear-end collision).

The majority of all low back injury claimants experienced a change in velocity of 13 km/hour or less (69%), with 42% of all low back injury claims falling between collision severities of 10 – 12 km/hour. Sedans and minivans were the most common types of vehicles, accounting for 72% and 19% of all vehicles respectively.

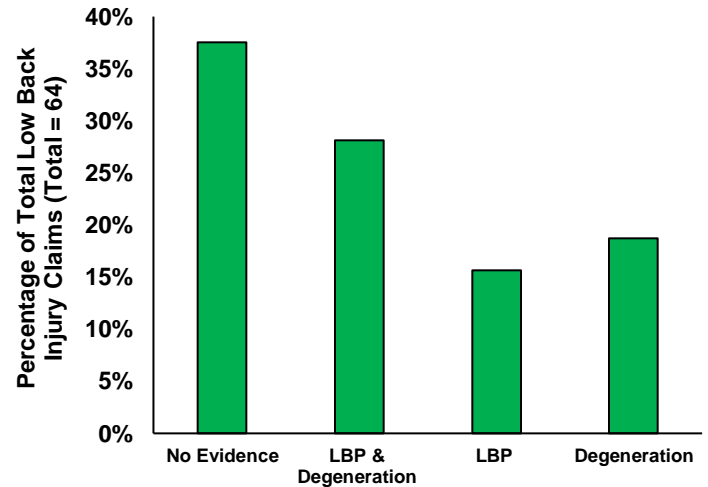


**Figure 1:** Low back injury claims as a function of pre-existing low back medical conditions.

## CONCLUSIONS

Results indicate that rear-end collision severities of 10 – 12 km/hour appear to be particularly common with respect to low back injury reporting; more severe collisions were not associated with greater low back injury reporting. This result contrasts with previously published neck injury risk data which demonstrated the risk of neck injury symptom reporting increases with collision severity [4].

The results of this investigation provide knowledge of collision characteristics that can be employed in future studies on the mechanisms of low back injury in low speed motor vehicle accidents.

## REFERENCES

1. Fast, S. et al. (2002). *Am J Phys Med Rehabil.* 81(9):645-650
2. Beattie, S. et al. (2010). *Injury.* 41(2):144-146
3. Magnússon et al. (1994). *Cepha : Int Journal of Headache*14(3):223–27
4. Krafft et al. (2005). *Folksam Research and Karolinska Inst.* 05-0363

# THE INFLUENCE OF WALKING BREAKS WHILE STANDING ON GLUTEUS MEDIUS ACTIVITY AND LOW BACK PAIN

Bryce Daniels, Marcus Payne, Aaron Caldwell, Matthew Ganio, and Kaitlin Gallagher  
University of Arkansas, Fayetteville, AR, USA  
email: kmg014@uark.edu

## INTRODUCTION

In an attempt to reduce diseases related to sedentary activity, the transition to standing and sit-stand desks in the office workplace has led to more people being exposed to bouts of prolonged standing[1]. Unfortunately, as many as 71% of people will experience low back pain (LBP) during 2-hour bout of prolonged standing[2]. Previously, it has been shown that there is an increased gluteus medius co-contraction in prolonged standing induced LBP developers[2]. Walking could be a practical general back exercise since it increases trunk muscles activation as opposed to standing[3]. To date, there has been no research on how prolonged standing induced LBP developers would be affected by a walking break. The purpose of this study is to compare LBP reports and gluteus medius muscle activity during prolonged standing and prolonged standing with walking breaks. This work can lead to new insight on the potential causes for prolonged standing induced LBP development and the potential for walking breaks as an intervention.

## METHODS

A total of 11 participants, six males ( $22.3 \pm 3.78$  years;  $1.84 \pm 0.08$  m,  $82.9 \pm 8.31$  kg) and five females ( $21.6 \pm 1.82$  years;  $1.62 \pm 0.09$  m;  $56.0 \text{ kg} \pm 7.78$  kg) were recruited for this study. Exclusion criteria included previous low back surgery or injury, an allergy to rubbing alcohol, an implanted pacemaker, or any history of fainting/dizziness. Participants wore running shoes and clothes they would be comfortable standing or walking in for two hours. Participants signed an informed consent prior to beginning the study.

Surface electromyography (EMG) sensors (Delsys, Natick, MA) were used to measure bilateral gluteus medius muscle activity. A disposable razor was used to remove any hair and dead skin cells from the area, then it was cleaned with isopropyl alcohol. Maximum voluntary contractions were measured using bilateral side-lying clamshells. For each muscle, the baseline signal was removed, full-wave

rectified, low pass filtered at 2.5 Hz, and then normalized to its maximum voluntary contraction.

Pain scores for the low back region were collected using a 100 mm Visual Analogue Scale (VAS). Participants were asked to mark their current level of pain on the scale with anchors of “no pain” on the left and “worst pain imaginable” on the right. One scale was filled out immediately upon arrival to the lab to serve as the baseline value. Scales were then filled out at the start of the trial and every 15 minutes for the full two hours. The VAS from the start of the trial was subtracted from all subsequent scores. An increase of 10 mm from baseline categorized a participant as a pain developer (PD)[2].

Participants completed two 2-hour experimental trials separated by at least one week. Participants stood on a treadmill and watched a documentary for either two hours or had a walking break (2 mph) every 25 minutes (100 minutes of standing and 25 minutes of walking). The order of the experimental trials was randomized between participants.

Muscle activation analyzed were taken at three instances (1) for the standing-only trial, (2) the standing portion of the walking break day and (3) walking breaks. An amplitude probability distribution function (APDF) was used to determine the median and range of gluteus medius contraction. Cross-correlation analyses were used to quantify the phase characteristics of the right and left gluteus medius signals[4]. A phase shift of  $\pm 250$  ms was used. The analysis was run on 1-minute blocks of data then averaged over the entire section. A positive cross-correlation coefficient between two muscles indicates that they are acting together, and a negative value indicates they are firing reciprocally.

Due to the lack of non-PDs at this time, the analysis compared variables between conditions. A one-way repeated measures ANOVA with a within factor of condition (standing only, standing on walking break

day, and walking) was run on the median, range, and cross-correlation coefficient. A Tukey HSD post hoc test was run a significant main effect. Significance was set at  $\alpha=0.05$ .

## RESULTS AND DISCUSSION

Out of the 11 participants, eight participants were classified as PDs during the standing visit while only three were classified as PDs during the standing with walking breaks visit. Seven participants reported a lower low back region VAS score on the walking breaks day (Figure 1). None of the participants who were nonPDs in standing were PDs on the walking breaks day.

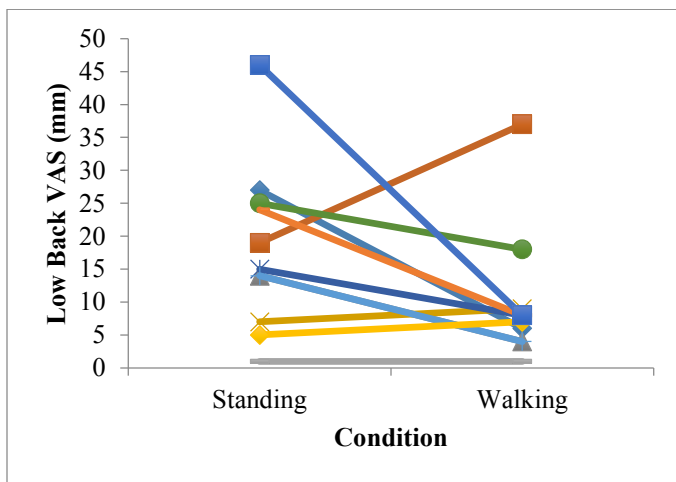


**Figure 1:** Maximum low back region pain scores for the standing-only and standing with walking break trials.

There was a significant main effect of condition for the muscle activation range of the right and left gluteus medius muscles and the cross-correlation coefficient ( $p<0.0001$ ) (Table 1). There was no significant difference for the median %MVC for either muscle. Outcome variables for standing were not significantly different across days. Due to

**Table 1:** APDF median and ranges, and cross correlation coefficients across conditions. Different letters denote significant difference between conditions for that outcome measure.

Measures	Conditions		
	Stand	Stand-Walk	Walking
Median Right Gluteus Medius (%MVC)	4.1 ± 2.2	4.3 ± 4.0	6.2 ± 3.7
Range Right Gluteus Medius (%MVC)	4.7 ± 4.8 <sup>a</sup>	3.3 ± 5.3 <sup>a</sup>	15.9 ± 8.9 <sup>b</sup>
Median Left Gluteus Medius (%MVC)	5.7 ± 5.3	4.5 ± 2.3	6.0 ± 2.2
Range Left Gluteus Medius (%MVC)	5.3 ± 9.4 <sup>a</sup>	4.7 ± 5.3 <sup>a</sup>	19.3 ± 7.3 <sup>b</sup>
Gluteus Medius Cross-correlation Coefficient	0.008 ± 0.18 <sup>a</sup>	0.043 ± 0.18 <sup>a</sup>	-0.571 ± 0.14 <sup>b</sup>

single leg support phase during walking and swing phase of the contralateral leg, it was expected that the range of muscle activity would be higher for walking and demonstrate a more reciprocal firing of the right and left gluteus medius muscles compared to standing.

While we did not assess the difference between PDs and non-PDs as of yet, the increased range of firing and the reciprocal pattern of firing may point to a potential intervention to promote less co-activation of the hip abductor muscles in standing. With more PDs in our current sample, it demonstrates that even those who have been shown to have greater levels of co-activation in prolonged standing have cyclic gluteus medius recruitment in walking.

With the collection of more participants, future work will assess the difference in magnitudes of these correlations to determine if PDs are still co-activating at higher levels than non-PDs during walking. Studies should also assess the impact of walking speed on muscle co-activation.

## REFERENCES

- [1] Davis et al. (2015) *Ergonomics in Design*, **23**(3):9–13.
- [2] Marshall et al. (2011) *Human Movement Science*, **30**(1):63–73.
- [3] Callaghan et al. (1999) *Clinical Biomechanics*, **14**(3), 203–216.
- [4] Nelson Wong et al. (2009) *JOSPT*, **39**(4): 287-295.

## ACKNOWLEDGMENTS

This work was supported by a Southwest Center for Occupational and Environmental Health Pilot Project Training Award (T42 OH008421).

# VALIDATION OF BIPLANE FLUOROSCOPY FOR CERVICAL SPINE KINEMATICS

<sup>1</sup>Craig Kage, <sup>1,2</sup>Mohsen Akbari-Shandiz, <sup>1</sup>Rebekah L. Lawrence, <sup>3</sup>Hana Boudlali, <sup>1</sup>Mary Foltz, and <sup>1,3</sup>Arin M. Ellingson

<sup>1</sup>Department of Rehabilitation Medicine, University of Minnesota, MN, USA

<sup>2</sup>Department of Physical Medicine & Rehabilitation, Mayo Clinic, Rochester, MN, USA

<sup>3</sup>Department of Biomedical Engineering, University of Minnesota, MN, USA

email: ellin224@umn.edu

## INTRODUCTION

Traditional methods of kinematic measurement offer limited ability to determine precise intersegmental motion of the spine. Recently, dynamic biplane fluoroscopic imaging has proven to be an accurate, effective, and non-invasive method of quantifying three-dimensional kinematic motion of the spine and other joints [1-3]. Previous studies have utilized 3D bone models reconstructed from computed tomography (CT) and shaped-matched to biplanar dynamic radiographs to determine underlying kinematics [1]. This approach has been validated previously in the spine by comparison to the standard measure of dynamic radiostereometric analysis (RSA) using implantable tantalum beads [1,2].

The purpose of this study was to validate our dynamic biplane fluoroscopy system's accuracy in the assessment of cervical spine flexion motion through CT-based registration and RSA comparison using a cadaver. Validation is an essential step to complete for each individual fluoroscopy system to ensure accurate and precise results prior to initiating human subject collection. The validation procedure should also closely mirror that of actual human subject collection; for this reason, dynamic activities were simulated using a cadaveric specimen with intact surrounding musculature and soft tissue.

## METHODS

### *Data Acquisition*

Tantalum beads (1.6mm) were inserted into the anterior aspect of the cervical spine vertebral bodies (four in C4; five in C5) of a fresh-frozen cadaveric specimen (male, age 62) to facilitate RSA tracking. CT images were obtained (Siemens Somatom Sensation 64; Forchheim, Germany; kVp: 120;

voxel size: 0.34x0.34x0.6) to generate 3D bone models and establish bead location.

Dynamic radiographic imaging was acquired on a custom biplanar imaging system (Imaging Systems and Services, Inc.; St. Painesville, OH, USA) equipped with 16" image intensifiers and high speed cameras (Xcitex ProCapture). A 55-degree interbeam angle was used with each system parallel to the horizontal and source to detector distance of 152cm (Figure 1). A wedge style radiographic filter (Ferlic Filter Co., LLC, White Bear Lake, MN, USA) was implemented with the following fluoroscopic parameters: 70kv, 250mA, 3.5ms, 60Hz. Cervical flexion was passively simulated from an extended position was obtained with a custom-made apparatus.

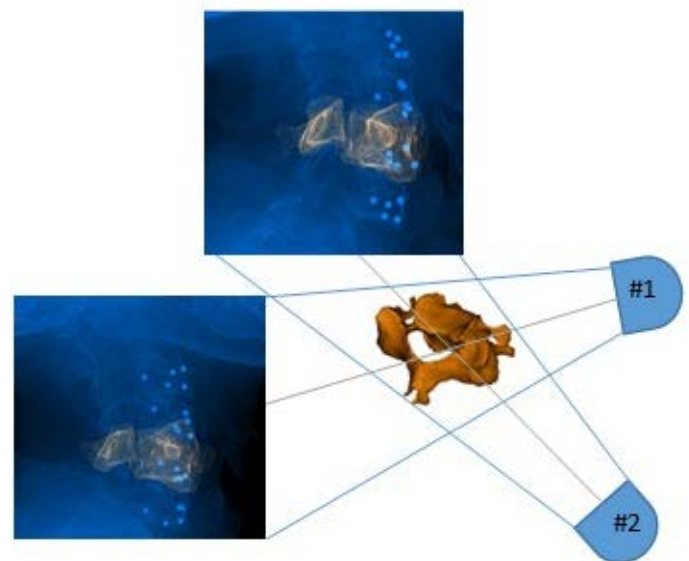


**Figure 1:** Biplanar fluoroscopic set-up with 55° interbeam angle. C5 bone model reconstruction inset.

### *Image Processing*

CT images were reconstructed manually to create 3D bone models of levels C4 and C5 and a local anatomical coordinate system (Figure 2) was assigned (Mimics; Materialise, Plymouth, MI,

USA). Bone model bead positions were masked (ImageJ/Fiji, US NIH, Bethesda, MD, USA) to prevent bead-bias while shape-matching. The masked-models were manually shape-matched utilizing digitally reconstructed radiograph (DRR) projections (Autoscooper, Brown University, RI, USA). Ten equally spaced frames from the dynamic trial (full extension to full flexion) were extracted for analysis. RSA was performed (XMA Lab, Brown University, RI, USA) to determine the 3D location of each bead during flexion. The rotational and translational components were then transformed to a local coordinate system and the values from CT-reconstruction were directly compared to RSA values using a Matlab script (Matlab, R2016B, The Mathworks, Inc., Natick, MD, USA). RMS error, bias, and precision were calculated to examine tracking of individual vertebral segments and relative intersegmental kinematic accuracy.

## RESULTS AND DISCUSSION

Summary statistics are displayed in Table 1.

Tracking of individual vertebral segments resulted in an average RMS error of 1.04° and 0.48mm, average precision of 0.88° and 0.33mm, and average bias ranged from -0.65 to 0.53° and -0.33 to 0.40mm for rotations and translations, respectively.

The relative intersegmental kinematic agreement resulted in an average RMS error of 1.48° and 0.61mm, average precision of 1.31 and 0.61, and average bias ranged from -0.96 to 0.77° and -0.22 to -0.03mm for rotations and translations, respectively.

Flexion/Extension rotations indicated the highest degree of error, despite being nearest to in-plane motion (flexion). However; all error was found to be below two degrees (rotation) and one mm

**Table 1:** Accuracy of dynamic biplane fluoroscopy via CT-based registration vs. RSA for cervical spine flexion. Flexion-Extension (FE), Lateral Bending (LB), Axial Rotation (AR), Anterior-Posterior (AP), Medial-Lateral (ML), Superior-Inferior (SI).

	FE (deg)	LB (deg)	AR (deg)	AP (mm)	ML (mm)	SI (mm)
<b>Individual Segment Registration Accuracy</b>						
RMS Error	1.27	0.88	0.97	0.37	0.54	0.53
Bias	-0.34	0.53	-0.65	0.27	-0.33	0.40
Precision	1.24	0.66	0.74	0.19	0.44	0.36
<b>Relative Intersegmental Kinematic Accuracy</b>						
RMS Error	1.98	1.56	0.91	0.63	0.71	0.50
Bias	0.77	-0.96	0.18	-0.22	-0.03	-0.05
Precision	1.97	1.02	0.95	0.58	0.74	0.51

(translation) for both registration and kinematic comparisons, which is comparable to other validation studies of the spine [1,2].

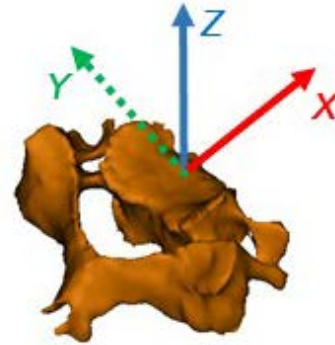


**Figure 2:** Anatomic local coordinate system overlaid on a C5 3D bone model reconstruction (Landmarks: anterior/superior vertebral body, left and right most lateral inferior vertebral notch).

## CONCLUSIONS

The results affirm that our biplane fluoroscopy system is capable of capturing highly accurate bone tracking and kinematic motion of the cervical spine. This validation assessment will serve as the groundwork to proceed on into human subject collection.

## REFERENCES

1. Anderst WJ, et al. *Spine (Phila Pa 1976)* **36**(6), E393-400, 2011.
2. McDonald CP, et al. *Spine J* **10**, 497-504, 2010.
3. Li G, et al. *J Biomech* **41**(7), 1616-1622, 2008.

## ACKNOWLEDGEMENTS

This project was supported by NIH/NICHHD K12HD073945, F31HD087069, and Minnesota Partnership for Biotechnology and Medical Genomics (MNP IF #14.02).

# FLEXION RELAXATION RESPONSE BETWEEN PEOPLE WITH AND WITHOUT STANDING-INDUCED LOW BACK PAIN AND A CLINICAL COMPARISON GROUP

<sup>1</sup>Laura Baker, <sup>1</sup>Connor Longacre, <sup>1</sup>Carol Passarelli, <sup>1</sup>Amy Renslo, <sup>1</sup>Dianne Riggs, <sup>1</sup>Ryan Tollis, <sup>2</sup>Daniel Viggiani, <sup>3</sup>Bradley Davidson, <sup>2</sup>Jack P. Callaghan, and <sup>1</sup>Erika Nelson-Wong

<sup>1</sup>School of Physical Therapy, Regis University, Denver, CO, USA, <sup>2</sup>Faculty of Applied Health Sciences, University of Waterloo, Waterloo, ON, Canada, <sup>3</sup>Department of Materials and Mechanical Engineering, University of Denver, Denver, CO, USA, email: enelsonw@regis.edu

## INTRODUCTION

Low back pain (LBP) is a common and costly condition that is one of the leading causes of disability worldwide, yet contributing factors are currently not well understood. Prolonged standing protocols have been extensively used to investigate predisposing biomechanical factors for LBP development in asymptomatic individuals [1]. One identified factor is an altered flexion relaxation response (FRR) in those developing pain in standing (PD) compared with those who remain painfree (NPD). Healthy individuals are expected to demonstrate a 'typical' FRR with myoelectrical silence of the trunk extensors and increased activity of the hip extensors during standing lumbar flexion [2]. Previous work has shown PDs demonstrate a maladaptive pattern of increased gluteal muscle relaxation during standing trunk flexion compared to NPDs [1].

PDs have been shown to be at increased risk for future clinical LBP compared to NPDs [3]. However, PDs have also demonstrated a favorable response to stabilization exercise approaches commonly used in physical therapy intervention [4]. This has led to the hypothesis that PDs may share similar characteristics to individuals with clinical LBP (CLBP) that respond favorably to similar intervention protocols. Relationships between PDs and patients with CLBP subclassified into a LBP subgroup of Stabilization (ie; expected to respond to stabilization based exercise) have not been investigated previously. The purpose of this study was to investigate FRR differences between individuals categorized as NPD, PD and CLBP, with consideration for potential sex differences. Both PD and CLBP groups were expected to demonstrate decreased gluteal and increased spinal extensor activity during standing flexion, and NPDs

expected to demonstrate the opposite pattern, indicating a typical response for healthy individuals.

## METHODS

Data for this submission are a subset of a larger study. Nineteen individuals (9 male,  $25.4 \pm 5$  yrs old) with no prior history of LBP performed a standing protocol of up to 2 hrs while reporting LBP every 15 min on a 100 mm visual analog scale (VAS). Participants were classified as PD if they reported  $\geq 10$ mm increase in LBP during standing. Eleven individuals (4 male,  $35.8 \pm 11.5$  yrs old) with a recent history (prior 12 months) of CLBP and meeting Treatment Based Classification criteria for Stabilization subgroup [5] were also recruited.

Electromyography data were recorded from 4 bilateral muscle groups (Thoracic Erector Spinae = TES, Lumbar Erector Spinae = LES, Gluteus Maximus = GMx, Biceps Femoris = BF) at 2000 Hz (Bortec, AMT-8, Calgary, AB). Submaximal reference contractions were used for normalization purposes. Participants performed self-paced standing trunk flexion, with a hold in full flexion for approximately 5 seconds. After bias removal, data were full wave rectified and low pass filtered (dual-pass 4<sup>th</sup> order Butterworth,  $f_c=2.5$  Hz). EMG data were plotted for each participant and visually inspected to identify stable windows for upright standing and full flexion. Average activation was calculated across upright and flexion windows for each muscle. FRR was then calculated as the ratio of average upright activation to flexed activation for each muscle [1]. Using this approach, an  $FRR > 1.0$  indicates relaxation during flexion and  $FRR < 1.0$  indicates increased muscle activity during flexion.

To determine if symmetry could be assumed for a data reduction measure, left and right side FRRs for

each muscle were entered into paired t-tests, with non-significant probabilities indicating left/right symmetry. When symmetry could be assumed, left and right sides were averaged to yield a single measure. FRRs were entered into a 3x2 ANOVA (Pain Group x Sex) with alpha = .05.

## RESULTS AND DISCUSSION

Ten of nineteen participants (4 male) were classified as PD with average VAS =  $16 \pm 4.1$  mm (compared with  $2 \pm 2.5$  mm for NPD). No significant differences were found in left/right FRR comparisons, therefore symmetry was assumed for all muscle groups. All muscle groups had a significant main effect of sex, with males having greater relaxation than females of TES, LES and GMx, and females having greater relaxation of BF than males (Figure 1). There was also a significant Pain Group x Sex interaction for TES, with males having higher FRR ( $2.67 \pm 1.44$ ) than females ( $0.72 \pm 0.57$ ) for the NPD group only. There was a main effect of Pain Group on FRR for LES only, with NPD having higher FRR ( $2.97 \pm 2.76$ ) than CLBP ( $1.31 \pm 1.02$ ), neither being significantly different from PD ( $1.79 \pm 1.99$ ).

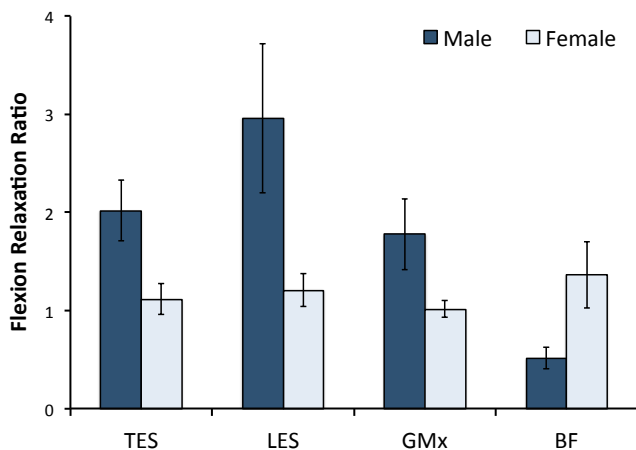


**Figure 1:** Significant ( $p < .05$ ) sex differences were found for muscle relaxation during standing flexion in all muscle groups. Males increased activation of biceps femoris (BF) during flexion, with marked relaxation in the other extensor groups.

Our hypotheses were partially supported, with PD and CLBP groups demonstrating similar patterns of decreased LES relaxation during standing flexion.

Although differences between NPD and PD groups in this measure were not significant, the NPD group did show the expected increased relaxation for healthy individuals, and were significantly different from the CLBP group.

Findings relative to sex differences, independent of pain group were interesting, and consistent across muscle groups. Males in this study appeared to rely on hamstring musculature for standing flexion (increased BF activation at full flexion) with commensurate relaxation of GMx. Females did not show significant relaxation in any of the muscle groups, with average FRRs close to 1.0, indicating relatively equal activation between upright and flexed postures. Compared to males, females utilized a gluteal dominant strategy at the hip.

## CONCLUSIONS

These findings show some differences in flexion relaxation response between individuals who do not experience standing-induced LBP and those with clinical LBP, specifically for the lumbar portion of the erector spinae. It is possible that between group differences were not detected in this study due to small sample sizes. A post hoc power analysis revealed power ranging from 8-49% for detecting between group differences. Males and females showed markedly different responses during the flexion task. Previous work has indicated potential sex differences in hip musculature response to exercise interventions for standing induced LBP [4]. Implications of the current findings related to LBP risk, movement strategy retraining, and therapeutic exercise interventions should be explored further.

## REFERENCES

1. Nelson-Wong E & Callaghan JP. *J Electromyogr Kinesiol*, **20**, 256-263, 2010.
2. Paquet N, et al. *Spine*, **19**, 596-603, 1994.
3. Nelson-Wong E & Callaghan JP. *Spine*, **39**, 1-5, 2014.
4. Nelson-Wong E & Callaghan JP. *J Electromyogr Kinesiol*, **20**, 1125-1133, 2010.
5. Stanton TR, et al. *Phys Ther*, **91**, 496-509, 2011.

# A COMPARISON OF MUSCLE ACTIVITY DURING SPINE EXTENSION IN PEOPLE WITH AND WITHOUT STANDING-INDUCED BACK PAIN, AND THOSE WITH CHRONIC LOW BACK PAIN

<sup>1</sup>Daniel Viggiani, <sup>2</sup>Bradley S. Davidson, <sup>1</sup>Jack P. Callaghan, and <sup>3</sup>Erika Nelson-Wong

<sup>1</sup>Department of Kinesiology, University of Waterloo, Waterloo, ON, Canada; <sup>2</sup>Department of Materials and Mechanical Engineering, University of Denver, Denver, CO, USA; <sup>3</sup>School of Physical Therapy, Regis University, Denver, CO, USA; email: dviggian@uwaterloo.ca

## INTRODUCTION

Transient low back pain (LBP) development during prolonged standing may predict future LBP. People developing LBP from standing (pain developer = PD) are distinguished from non-pain developers (NPD) by increased trunk and hip co-activity [1], and altered vertebral kinematics in lumbar spine extension [2]. However, there have been no direct comparisons of PDs to people with chronic LBP in supported or unsupported spine extension. This study's purpose was to compare muscle co-activity strategies between NPDs, PDs and a chronic LBP group in two lumbar spine extension variants.

## METHODS

Nineteen participants (9 male; 21-40 yrs old) with no history of LBP and 11 participants (4 male; 20-52 yrs old) satisfying the Stabilization subgroup of the Treatment-based Classification [3] (CLBP) were recruited. A previously used standing protocol was used to separate the 19 participants with no prior LBP history into PD (n=10, 4 male; 22-35 yrs old) and NPD (n=9, 5 male; 21-40 yrs old). Participants were classified as PD if they reported  $\geq 10$  mm increase in LBP on a 100 mm visual analog scale during the standing protocol [1,2]. Following instrumentation for EMG and kinematics, participants performed spine extension in two different postures in a randomized order: standing and prone. In standing, participants were instructed to lean backwards (look overhead as far as possible) without translating hips/pelvis, hold in full extension for 3-4 seconds, and return to neutral standing. While prone, participants were instructed to relax on an examination table with their arms supporting their upper body in lumbar extension (pelvis on table) and hold for 30 seconds.

Kinematics of the trunk and pelvis were measured using active marker clusters (Optotrak 3D

Investigator, NDI, Waterloo, ON), and collected at 50 Hz to identify lean, hold and return phases of standing extension based on the trunk-pelvis sagittal angles. Surface electromyography of six muscles bilaterally (T9 Erector Spinae (TES), L3 Erector Spinae (LES), Gluteus Maximus (GMX), Biceps Femoris (BCF), External Oblique (EXO) and Internal Oblique (INO)) were collected at 2000 Hz during both tasks (AMT-8, Bortec, Calgary, ON). Bias-removed EMG signals were rectified, dual-pass filtered (Butterworth, 2.5 Hz cutoff), and expressed as a percent of reference voluntary contractions to represent muscle activations. Muscle co-activity among sets of two to eight muscles (defined in Table 1) were computed based on commonality (the overlap between muscles of a set) and activity level (the mean activity of muscles in a set) [4]. Measures for each set were averaged over phase of standing extension and over the full prone extension period.

**Table 1:** Muscle Set Definitions (BL = Bilateral)

Set Name	Muscles in Set
<i>Trunk8</i>	BL TES, LES, EXO, INO
<i>ATrunk4</i>	BL EXO, INO
<i>PTrunk4</i>	BL TES, LES
<i>LTrunk4</i>	Left TES, LES, EXO, INO
<i>RTrunk4</i>	Right TES, LES, EXO, INO
<i>Hip4</i>	BL GMX, BCF
<i>BL-TES etc.</i>	BL Muscle Pairs

Mixed model ANOVAs with a between factor of Group (NPD/PD/CLBP), and a within factor of Phase (lean/hold/return) or Posture (standing/prone) were used when appropriate. Tukey's test was used for post-hoc investigations of significant findings.

## RESULTS AND DISCUSSION

There was a main effect of Group where PDs had higher commonalities than NPDs in the Hip4 ( $p =$

0.049) and BL-GMX muscle sets ( $p = 0.043$ ), and higher commonalities than CLBPs in the PTrunk4 set ( $p = 0.035$ ) (Fig. 1). There were no Group effects of activity levels ( $p > 0.371$ ), and no Group\*Pain or Group\*Posture interactions on either measure ( $p > 0.076$ ). There were main effects of Posture where holding prone extension produced higher commonalities ( $p < 0.002$  for ATrunk4, PTrunk4, Hip4, and all Bilateral pairs) and lower activity levels ( $p < 0.038$  for Trunk8, ATrunk4, LTrunk4, RTrunk4, BL-LES, BL-EXO and BL-INO) than holding standing extension. The Trunk8, LTrunk4 and RTrunk4 sets had the highest commonalities in the Return phase ( $p < 0.001$ ). Main effects of Phase on activity levels in standing extension were muscle set-dependent. The Hold phase of standing extension had the highest activity levels ( $p < 0.043$ ) within the Trunk8, ATrunk4, LTrunk4, RTrunk4, BL-EXO and BL-INO muscles sets. The Return phase of standing extension had the highest activity levels ( $p < 0.044$ ) in the Hip4, BL-LES, BL-BCF and BL-INO muscle sets.

## CONCLUSIONS

The CLBP group was always similar to the NPD group, with PDs exhibiting higher co-activity in

posterior musculature during standing and prone extension. These findings suggest that PDs activate a greater number of muscles during these extension tasks rather than increasing amplitudes compared to NPD and CLBP counterparts. The current CLBP sample was chosen to reflect a subgroup that was intended to be most similar to PDs in terms of LBP reduction following treatment [1,3]. However, this study demonstrates that people with LBP benefitting from stabilization exercises do not exhibit different amounts of “stabilizing” co-activity than low-risk, asymptomatic controls (NPDs) during standing and prone extension tasks. Co-activity during lumbar spine extension was more dependent on movement phase and posture than pain group status. Further comparisons between PDs and subgroups of people with LBP can further our understanding of how transient LBP develops into chronic LBP.

## REFERENCES

1. Nelson-Wong E. et al. *JEK*, **20**(6), 1125-33.
2. Viggiani D. et al. *Proceedings of CSB*, Hamilton, ON, Canada, 2016.
3. Stanton TR. et al. *Phys Ther*, **91**(4), 496-509.
4. Viggiani D. et al. *CMBBE*, Submitted, 2017.

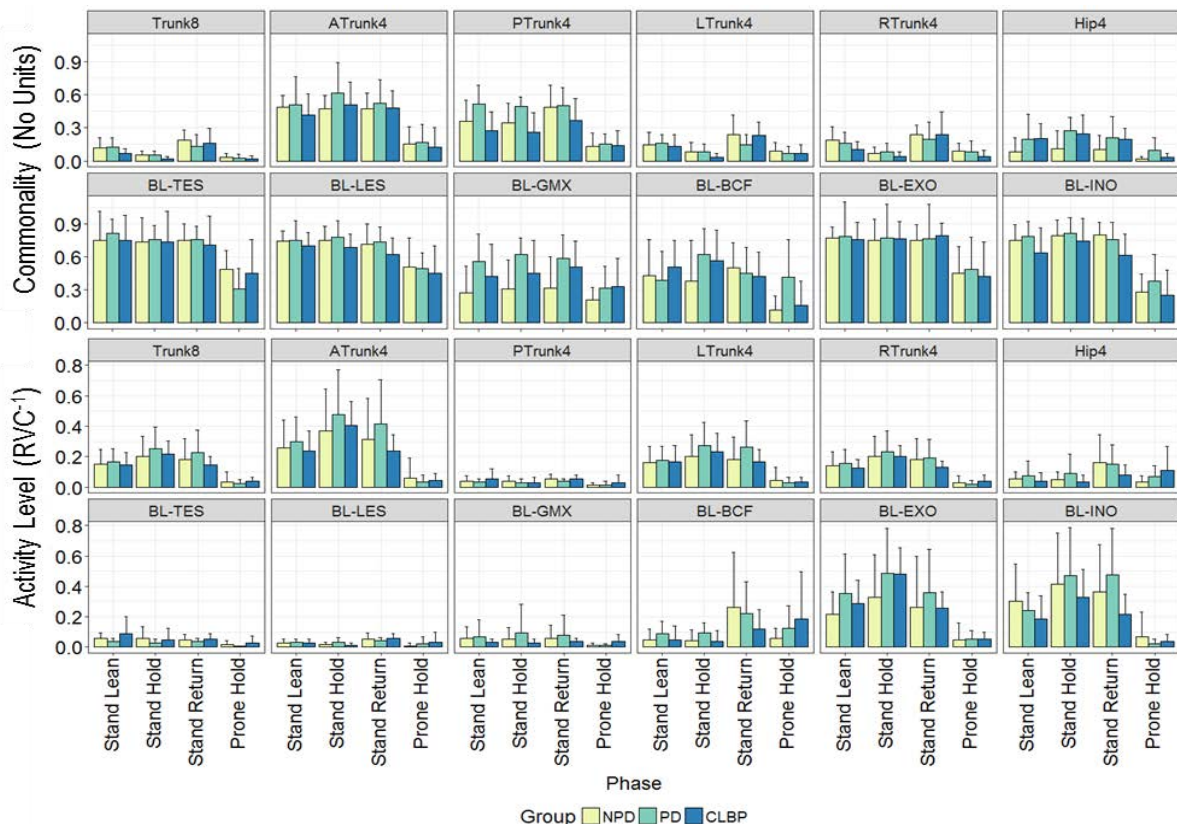


**Figure 1:** Commonalities (Top) and Activity Levels (bottom) during Standing and Prone Extension.

# INTERVERTEBRAL DISC PRESSURE VARIATION IN CADAVERIC THORACIC SPINES UNDER APPLIED DYNAMIC MOMENTS

<sup>1,2</sup>Dennis E. Anderson, <sup>3</sup> Erin M. Mannen, <sup>1</sup> Rebecca Tromp, <sup>3</sup> Benjamin M. Wong, <sup>2</sup> Hadley L. Sis, <sup>2</sup> Eileen S. Cadel, <sup>2</sup> Elizabeth A. Friis, and <sup>1</sup> Mary L. Boussein

<sup>1</sup> Beth Israel Deaconess Medical Center, Boston, MA, USA; <sup>2</sup> Harvard Medical School, Boston, MA, USA

<sup>3</sup> The University of Kansas, Lawrence, KS, USA

email: danders7@bidmc.harvard.edu

## INTRODUCTION

The rib cage is often assumed to add stability or share loads with the thoracic spine. However, the effects of the rib cage on thoracic spine loading are not well studied, in part due to the difficulty in measuring spinal loading within an intact spine-rib cage construct. Intervertebral disc pressures provide a surrogate measure of loading and may be measured in cadaveric spine tests to provide insight into spinal loading. We have previously reported that the rib cage appears to have a limited effect on thoracic intervertebral disc pressures under static compressive follower loads [1]. However, applied pure moments increase intradiscal pressures in lumbar spine specimens [2], but such measurements are lacking in the thoracic region. Thus, our objective was to examine thoracic intradiscal pressures with applied dynamic moments, and to determine the effect of the rib cage on these pressures.

## METHODS

Eight fresh-frozen human cadaveric thoracic spines (T1-T12) with the rib cage intact were obtained (4 female, 4 male, age range 61-71). Specimens were positioned upright in a testing machine (Applied Test Systems, Butler, PA) with a compressive follower load of 400 N applied by means of cables running lateral to the spine, connected to the spine by a rod inserted through each vertebral body with an eye nut at each end. Dynamic pure moments (0 to  $\pm 5$  N·m) were applied in displacement control at 1°/s in three modes of bending: axial rotation (AR), flexion - extension (FE), and lateral bending (LB). Trials were performed first with the rib cage intact, and again after the rib cage was removed by cutting the ribs about 2 cm lateral to the costo-transverse

joints (Figure 1). Disc pressures were measured at T4-T5 and T8-T9 using needle-mounted pressure transducers (Gaeltec, Isle of Skye, Scotland). Pressure measurements were normalized to pressure at 0 N·m, then the slopes of pressure vs. moment magnitude were calculated via linear regressions. The effect of rib cage on pressure-moment slopes were examined with mixed effects models by spinal level and direction of applied moment, adjusting for specimen as a random variable. Analyses were performed with Stata/IC 13.1 (StataCorp LP, College Station, TX).

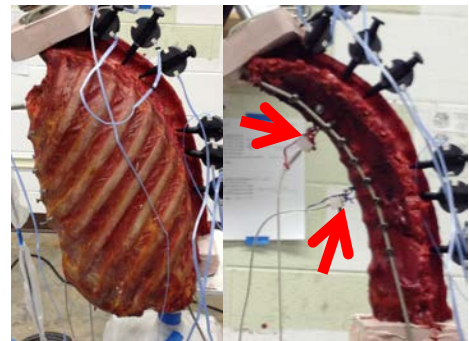


**Figure 1:** Testing was performed with rib cage intact (left) and rib cage removed (right). In both cases, pressure transducers (arrows) were inserted in the in the T4-T5 and T8-T9 intervertebral discs.

## RESULTS AND DISCUSSION

Pressure increased with applied moment (whether positive or negative) in all modes of bending (Figure 2). Flexion (positive) and Extension (negative) pressure-moment slopes differed ( $p < 0.05$ ), so these were analyzed separately; directions were combined for axial rotation and lateral bending analyses. Slopes were significant and positive in AR and LB, in Flexion at T4-T5, and in Flexion at T8-T9 with no rib cage ( $p < 0.05$ , Table 1). The pressure-moment slope was higher with no rib cage

at T4-T5 for all loading directions and at T8-T9 for AR only ( $p < 0.05$ , Table 1).

Removal of the rib cage had the largest impact in AR, increasing the slope about three-fold. Slopes were not significant in Extension, perhaps due to a shift of loading from the disc to the posterior elements as the spine moves into extension [3]. Our previous analysis of the same specimens under static compressive follower loads found unclear and likely minimal effects of the ribcage on disc pressure [1]. Thus, it appears that the rib cage contributes to thoracic spine stability or load sharing more so under applied moments or angular motion more than under compressive loading.

### CONCLUSIONS

Overall, removing the rib cage increased the pressure-moment slope in most conditions, indicating that the rib cage plays an important role in thoracic spine loading. This unique information will be helpful in future studies and modeling efforts to evaluate spinal loading *in vivo*.

### REFERENCES

1. Anderson DE, et al., Journal of Biomechanics, 49(7): 1078-1084, 2016.
2. Rohlmann A, et al., Spine, 26(24): E557-E561, 2001.
3. Adams MA, et al, Clin Biomech (Bristol, Avon), 9(1): 5-14, 1994.

### ACKNOWLEDGMENTS

This study was supported by the National Institute on Aging (K99AG042458) and by a Mentored Career Development Award from the American Society for Bone and Mineral Research.

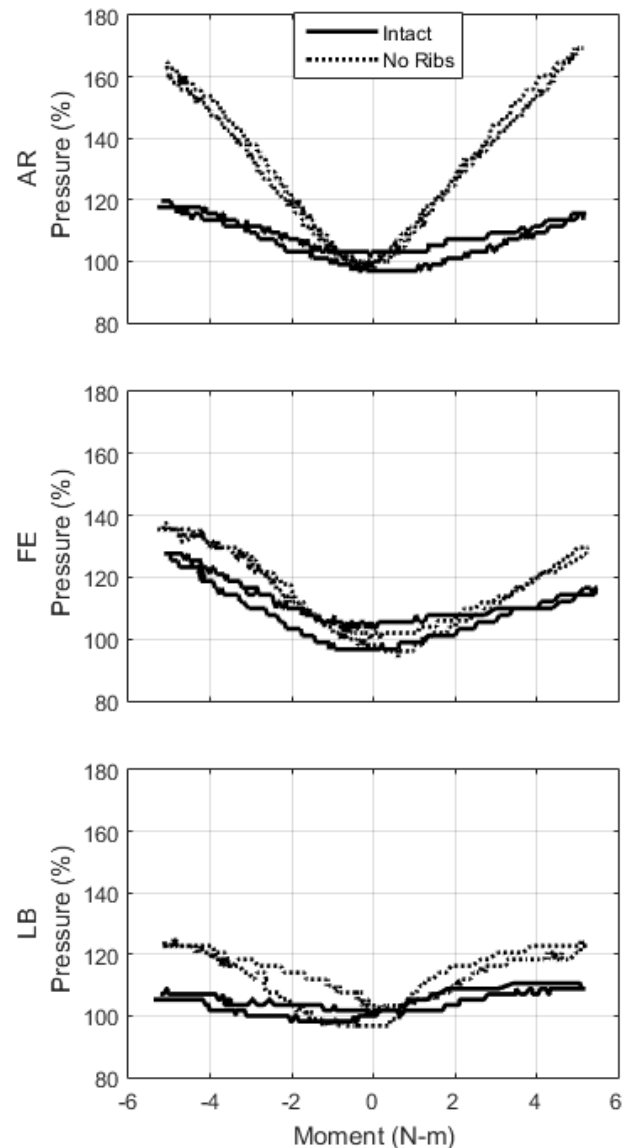


**Figure 2:** Example pressure-moment plots from the T4-T5 disc of one specimen in axial rotation (top), flexion-extension (middle), and lateral bending (bottom). Pressure is normalized to pressure at 0 applied moment.

**Table 1:** Pressure-moment slopes (95% confidence intervals, units of % pressure increase per N·m) with and without the rib cage present. Significant slopes ( $>0$ ) are in bold. \*Different than Intact ( $p < 0.05$ ).

	Rib Cage Intact		Rib Cage Removed	
	T4-T5	T8-T9	T4-T5	T8-T9
Axial Rotation	<b>3.80 (0.60 – 7.00)</b>	<b>3.79 (1.27 – 6.33)</b>	<b>12.83 (9.63 – 16.02) *</b>	<b>9.87 (7.33 – 12.41) *</b>
Flexion	<b>6.34 (2.84 – 9.83)</b>	4.39 (-0.44 – 9.22)	<b>9.44 (5.88 – 13.00) *</b>	<b>6.65 (1.82 – 11.48)</b>
Extension	0.71 (-3.56 – 4.97)	-2.65 (-6.64 – 1.34)	3.60 (-0.72 – 7.92) *	-1.49 (-5.49 – 2.50)
Lateral Bending	<b>2.33 (1.33 – 3.33)</b>	<b>2.30 (0.14 – 4.46)</b>	<b>4.43 (3.37 – 5.50) *</b>	<b>2.50 (0.34 – 4.66)</b>

# LOW BACK LOADING DURING SIT-TO-STAND IN PEOPLE WITH A UNILATERAL TRANSTIBIAL AMPUTATION

<sup>1</sup> Jason A. Actis, <sup>2</sup> Luis A. Nolasco, <sup>2</sup> Deanna H. Gates, <sup>1</sup> Jasmin D. Honegger, and <sup>1</sup> Anne K. Silverman

<sup>1</sup> Department of Mechanical Engineering, Colorado School of Mines, Golden, CO, USA

<sup>2</sup> School of Kinesiology, University of Michigan, Ann Arbor, MI, USA

email: jactis@mymail.mines.edu, web: fbl.mines.edu

## INTRODUCTION

Chronic low back pain (LBP) affects approximately 28% of adults in the U.S. [1], whereas up to 71% of people with a lower limb amputation (LLA) suffer from LBP [2]. Understanding the reasons for this increased prevalence could help to mitigate LBP in people with or without an amputation. People with LLA have altered low back biomechanics during a variety of movements [3,4], and greater low back loading during walking [4], but low back loading in people with a transtibial amputation (TTA) during the sit-to-stand motion (STS) is not well-characterized. Peak L4-L5 loading is greater during STS compared to walking or running [5], and people with a transtibial amputation (TTA) engage in STS approximately 50 times every day [6]. Thus, the purpose of this study was to determine differences in peak L4-L5 compressive loads, and trunk kinematics between people with and without TTA during STS. We hypothesized that, compared to people without an amputation, people with TTA would have greater loading at more extreme trunk angles and a greater range of trunk motion.

## METHODS

Four people without an amputation (Control, 1M/3F, 23.3±2.9 yrs, 1.66±0.06 m, 65.9±9.3 kg) and four people with a unilateral transtibial amputation (TTA, 4M, 45.5±14.8 yrs, 1.84±0.02 m, 99.4±15.3 kg) participated in this study. No participant had more than minimal LBP as indicated by the Modified Oswestry Low Back Pain Questionnaire [7].

All participants performed five self-paced STS trials, beginning seated with hips, knees, and ankles at 90° of flexion and feet hip-width apart on separate force plates recording at 1200 Hz.

Kinematics were collected at 120 Hz with a 20-camera motion capture system and a full-body marker set including markers placed at C7, T8, xyphoid process, and bilaterally at the acromion, PSIS, ASIS, iliac crest, and greater trochanter.

Kinematics and GRFs were low-pass filtered with a 4<sup>th</sup>-order Butterworth filter with cutoff frequencies of 6 Hz and 10 Hz, respectively. An eight-segment model was used to determine the inverse kinematics solution in Visual3D, which was used as input to an OpenSim 3.3 musculoskeletal model of the trunk, lumbar spine, and lower body with 292 Hill-type musculotendon actuators. A static optimization algorithm solved the muscle recruitment problem at each time step by minimizing an objective function of the sum of muscle activations squared. Once muscle forces were estimated, joint contact loads were calculated at L4-L5 throughout the STS motion. Differences between groups in peak load, trunk range of motion (ROM, relative to the lab frame), and trunk angle at the instant of peak load were compared with t-tests ( $\alpha=0.05$ ).

## RESULTS AND DISCUSSION

Compared to control participants, TTA participants had larger peak L4-L5 compressive loads (Table 1), and greater trunk flexion throughout STS (Figure 1). Peak loads occurred shortly after liftoff and prior to peak trunk flexion for all participants. At the instant of peak loading, TTA participants were in postures with significantly greater trunk flexion and lateral bending (Table 1). Previously, the moment of liftoff has been identified as the period of least GRF asymmetry for control participants, and the period of greatest GRF asymmetry for people with TTA [8]. This asymmetry, along with greater ranges of trunk motion, has been suggested as a reason for

greater low back loading in people with an amputation during STS [3].

Both groups had similar ranges of trunk flexion, but TTA participants had larger ranges of motion in lateral bending and axial rotation that approached significance (Table 1,  $p < 0.10$ ). Greater 3D trunk ROM during STS has been seen previously in people with a transfemoral amputation [3], and in people with LBP [9].

**Table 1:** Mean (SD) trunk kinematics (flexion, lateral bending towards the right/intact leg, and axial rotation towards the prosthetic/left leg are positive) and L4-L5 compression (normalized to body weight (BW)) for each group. Significant  $p$ -values for comparisons between groups are in bold.

	Control	TTA	$p$	
Angle at Peak	Flexion	-41.8° (5.1°)	-49.8° (3.2°)	<b>&lt;0.01</b>
	Lateral Bending	-0.5° (1.8°)	3.8° (4.4°)	<b>&lt;0.01</b>
	Axial Rotation	-1.86° (3.3°)	1.5° (4.8°)	<b>0.01</b>
ROM	Flexion	36.1° (18)	38.3° (19°)	0.64
	Lateral Bending	6.6° (3°)	8.1° (2°)	0.09
	Axial Rotation	4.8° (2°)	6.2° (3°)	0.08
Peak L4-L5 Load (BW)	3.46 (0.4)	3.73 (0.4)	0.05	

## CONCLUSIONS

The instant immediately after liftoff has been identified as an important consideration in understanding risks for LBP development. At this instant, people with TTA had greater L4-L5 compressive loading, greater trunk flexion, and greater lateral bending. More extreme trunk postures increase lumbar spine loading [5] and strain on intervertebral discs [10], which suggests a potential pathway to LBP development. Future work will include more participants and identify L4-L5 joint kinematics.

## REFERENCES

- Schiller J, *Vital Heal. Stat.*, **10**, 40–44, 2012.
- Ephraim PL, *et al.*, *Arch. Phys. Med. Rehabil.*, **86**, 1910–1919, 2005.
- Hendershot BD & Wolf EJ, *Gait Posture*, **42**,

204–209, 2015.

- Yoder A, *et al.*, *Gait Posture*, **41**, 757–762, 2015.
- Wilke H, *et al.*, *SPINE*, **24**, 755–762, 1999.
- Bussmann J, *et al.*, *Arch. Phys. Med. Rehabil.*, **89**, 430–434, 2008.
- Fairbank JC & Pynsent PC, *SPINE*, **25**, 2940–52, 2000.
- Agrawal V, *et al.*, *Ergonomics*, **139**, 656–664, 2011.
- Shum G, *et al.*, *SPINE*, **32**, E211–E219, 2007.
- Shah JS, *et al.*, *J. Bone Joint Surg. Br.*, 246–251, 1978.

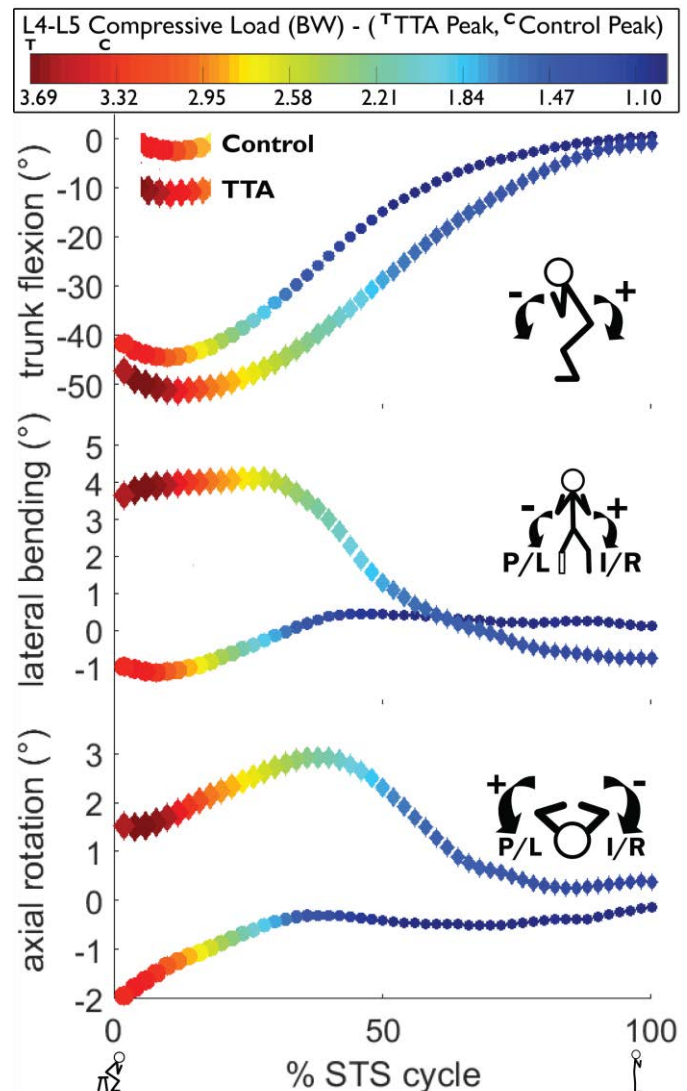


**Figure 1:** Average 3D trunk kinematics and normalized L4-L5 compressive loads from liftoff to the termination of forward trunk velocity (lateral bending positive towards I/R = intact/right side, axial rotation positive towards P/L = prosthetic/left side).

# THE INFLUENCE OF WALKING BREAKS ON LUMBAR SPINE KINEMATICS DURING PROLONGED STANDING

Marcus Payne, Bryce Daniels, Aaron Caldwell, Matthew Ganio, Kaitlin M. Gallagher  
University of Arkansas, Fayetteville, AR, USA  
email: mcpayne@email.uark.edu

## INTRODUCTION

As many as 71% of people experience low back pain (LBP) development during prolonged standing [1]. Both movement and posture based interventions are used to help alleviate low back pain development [2]. Increased lumbar lordosis, or extension, has been found in those who develop pain during prolonged standing [3]. It is possible that movement interventions, such as walking breaks, can alter the posture of the lumbar spine and pelvis, reducing LBP reports; however this has not been assessed. Using indwelling bone pins and motion capture, intersegmental lumbar spine flexion and axial rotation was found to be less than 4 degrees, with the most motion in the frontal plane [4]. The purpose of this study is to investigate how lumbar spine kinematics differ between prolonged standing and walking breaks, and determine the impact on LBP during prolonged standing. We hypothesize that walking will increase lumbar spine movement and LBP reports would be less when walking breaks interrupted standing.

## METHODS

A total of 12 participants (7 males: 18-28 years,  $1.83 \pm 0.08$  m,  $80 \pm 11.4$  kg; 5 females: 19-24 years,  $1.63 \pm 0.05$  m,  $56 \pm 7.7$  kg) have been collected for the study. Exclusion criteria included any previous low back surgery or injury, any allergy to rubbing alcohol, an implanted pacemaker, or any history of dizziness or fainting. Participants were asked to come to the lab on two separate days, separated by at least a week. During one visit, they completed a two hour bout of prolonged standing. During the other visit, they again stood for two hours, but had a 5-minute walking break (2 mph) every 25 minutes (100 minutes standing, 20 minutes walking). The order of the walking and standing trials was randomized. Both trials were completed while standing on a treadmill facing a desk to the side, which facilitated a smooth transition to the walking breaks during the walking trial.

Subjective pain scores for the low back region were collected using a 100mm visual analogue scale (VAS). Participants were asked to mark their current level of pain using a vertical tick on a line anchored with “no pain at all” on the left and “worst pain imaginable” on the right. Scores were collected at the start and every 15 minutes for the duration of the trial. The score at the start of the trial was subtracted from all other scores so each person started with a baseline score of 0. If the participant’s normalized VAS score exceeded 10 mm, they were categorized as a pain developer (PD). Classification into pain groups based on VAS scores has shown to be a repeatable and functional measure [5].

A motion capture system (Qualysis AB, Gotenburg, Sweden) was used to track two rigid bodies throughout the trial. The first rigid body was placed on L1/L2 and the second on the sacrum. Calibration markers were placed bilaterally on the iliac crests and rib cage, and anterior superior and posterior superior iliac spines to create a lumbar region and pelvis segment, respectively. Three-dimensional angles were calculated in Visual3D (C-Motion, Germantown, MD). An amplitude probability function (APDF) was used to calculate the median angle and range between the 10<sup>th</sup> and 90<sup>th</sup> percentiles. The APDF was run on the standing trial, the standing portion of the walking breaks trial, and the walking breaks separately.

Due to lack of non-pain developers at this stage of collection, a one-way repeated measures ANOVA with factor condition (standing only, standing portion of walking trial, and walking breaks). A Tukey post-hoc test was used to test significant main effects. Significance level was set at  $\alpha=0.05$ .

## RESULTS AND DISCUSSION

Seventy five percent of participants were categorized as PDs during the standing-only trial, but only 17% were categorized as PDs during the walking trial (Figure 1). These results demonstrate

that walking breaks during a bout of prolonged standing may be beneficial for reducing prolonged standing induced LBP.

There was a significant main effect for median flexion/extension angle ( $p=0.0021$ ), but not for lateral bend ( $p=0.35$ ) or axial twist ( $p=0.99$ ) (Table 1). The lumbar spine was more flexed during walking compared to the standing trial on the same day, but not across experimental days. While it did not differ from the first day, this is an interesting find as lumbar lordosis angle has been shown to be more flexed in non-PDs compared to PDs [3].

There was a main effect for flexion/extension ( $p=0.0034$ ) and axial twist range ( $p=0.03$ ) (Table 1). Less range of motion was found in walking compared to the standing on the same experimental day. While this may seem counterintuitive, participants were unconstrained in standing, meaning they could move around and did not maintain fixed position. As a result, participants could have had larger excursions in flexion-extension due to voluntary movements in standing, compared to the much more controlled walking condition. The same may be the reason why there was no difference in the lateral bend range of motion, as shifting weight between left and right foot during standing may have resulted in changes in the lateral bend angle. Axial twist range of motion, which increased with walking, is the only movement that could be difficult to perform without voluntary twisting motions.

A limitation to this study is that it is difficult to measure the exact movement at the intervertebral joint level using surface motion capture. As a result, our measurements represent regional differences between the upper lumbar spine and pelvis. This study also did not address different walking speeds and their influence on pain development. Slower

walking speeds may not elicit the same amount of lumbar spine movement, potentially resulting in similar pain scores between slow walking and standing. Future assessments will split participants into pain groups to determine if movement patterns differ between the groups.

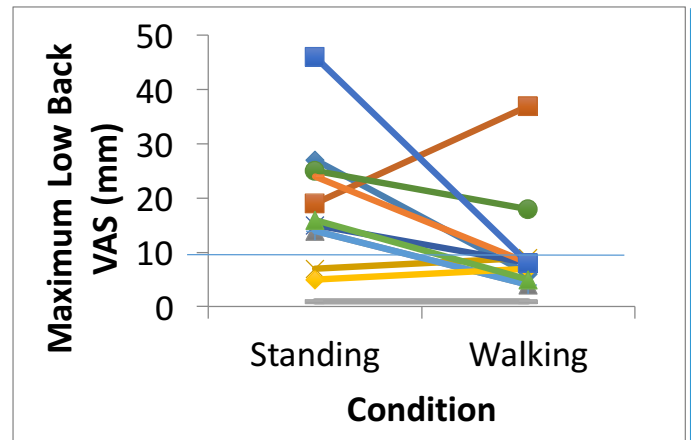


**Figure 1:** Maximum pain scores for the low back region during standing and walking trials.

## REFERENCES

1. Davis KG, Kotowski SE (2011) *Human Movement Science*, 30(1): 63-73.
2. Gallagher KM (2014) *University of Waterloo*, PhD Thesis.
3. Sorensen CJ et al. (2015) *Manual Therapy*, 20(4):553-7.
4. MacWilliams BA et al. (2013) *The Journal of Bone and Joint Surgery*, 95(23):e184-1-8.
5. Nelson-Wong E, Callaghan JP. (2010) *Rehabilitation Research and Practice*, 2010:289278.

## ACKNOWLEDGEMENTS

This work was supported by a Southwest Center for Occupational and Environmental Health Pilot Project Training Award (T42 OH00842

**Table 1.** Mean (standard deviation) of median and range of lumbar angles (degrees) across conditions: standing-only (SO), and the standing part (WS) and walking part (WW) of the walking trial. Negative = flexion; left lateral bend; right axial twist. Superscript letters the same within each angle are not significantly different.

Direction	Flexion/Extension			Lateral Bend			Axial Twist		
	SO	WS	WW	SO	WS	WW	SO	WS	WW
<b>Median</b>	-1.3 (4.1) <sup>a</sup>	-2.6 (6.7) <sup>a</sup>	-8.3 (6.6) <sup>b</sup>	-0.7 (0.8)	0.03 (2.1)	-0.3 (2.1)	-0.2 (2.0)	-0.3 (1.8)	-0.3 (2.5)
<b>Range</b>	8.6 (2.2) <sup>a</sup>	7.6 (2.5) <sup>a,b</sup>	5.8 (1.4) <sup>b</sup>	5.3 (3.0)	3.9 (2.9)	5.8 (2.6)	4.3 (1.2) <sup>ab</sup>	3.6 (1.4) <sup>a</sup>	6.0 (3.9) <sup>b</sup>

# The Relationship Between Family History, Biopsychosocial Factors and Seated Posture on LBP Development in Prolonged Sitting

Matthew Barrett, John Charles Snow, and Diana De Carvalho  
Faculty of Medicine, Memorial University of Newfoundland, St. John's, NL, Canada  
email: [mhb726@mun.ca](mailto:mhb726@mun.ca)

## INTRODUCTION

Low Back Pain (LBP) is one of the major health care issues facing society today<sup>1</sup>. LBP has been linked to occupational postures such as prolonged sitting<sup>2</sup>. However, it appears that some individuals are more likely to develop pain from exposures to sitting than others<sup>3</sup>. Prior work has identified groups of transient pain developers (PD) and non-pain developers (NPD) within study populations<sup>3</sup>. Currently it is not known what factors drive this differential pain response. The purpose of this study is to investigate the relationship between seated spine posture, family history of LBP and biopsychosocial factors between participants that do and do not develop transient pain in response to prolonged sitting.

## METHODS

32 participants (4 females, 28 males, average age 23.5 years  $\pm$  6.9 (SD), height 179.4 cm  $\pm$  7.79 (SD) and mass 77.4 kg  $\pm$  11.1 (SD) were recruited from the local community. Exclusion criteria included a history of tumor, infection, fracture, inflammatory arthropathy and/or previous surgery of the spine. A health screening form including questions on family history of LBP, the Tampa Scale of Kinesiophobia (TSK), and the Back Pain Attitudes Questionnaire (BPAQ) were all completed prior to data collection. Two tri-axial accelerometers (ADXL335, Analog Devices, Norwood, MA, USA) were fixed to the skin in the +y down, +z anterior orientation using double-sided tape overlying the L1 and S2 spinous processes. Accelerometer signals were collected at a rate of 1500 Hz using a 16-bit A/D board (Noraxon DTS, Noraxon Inc, Scottsdale, AZ, USA). Following instrumentation four 5s posture calibration trials were collected: upright standing, maximum extension, maximum flexion (standing) and maximum flexion (seated). Participants were then seated at a computer workstation that consisted of an adjustable height table, desktop computer,

standard keyboard, and the seat pan of a standard office chair. The workstation was individually adjusted to each participant according to ergonomic standards prior to the start of the protocol. Throughout the sitting trial participants completed a standardized typing task that aimed to simulate typical office report writing. Immediately prior to the sitting trial, participants completed a baseline rating of perceived low back pain using a 100 mm visual analog scale (VAS) with anchors of 0 mm (No Pain) and 100 mm (Worst Pain Ever). This rating was then repeated every 7.5 minutes throughout the trial. Accelerometer data were collected continuously throughout the sitting trial in four 15-minute blocks. Accelerometer data were processed using a custom written program (Matlab R2015b The Mathworks Inc., Natick, Massachusetts, USA). This includes calibrating the axes with respect to gravity, converting voltages to accelerations, calculating absolute inclinations from accelerations, smoothing the data using a dual-pass 2<sup>nd</sup> order Butterworth filter with a cut-off frequency of 1Hz and then adjusting the accelerometer inclination according to quadrant (based on the sign combination of the y and z axes). The inclinations of each sensor are then used to calculate the relative lumbar flexion angle and then the normalized lumbar flexion angle, expressed as a percent range of motion. To focus only on changes in perceived pain response, baseline pain ratings were subtracted from each subsequent rating throughout the trial. These baseline-removed ratings of pain were then used to classify participants into three groups based on clinically relevant levels of pain<sup>4</sup>: Pain developers (PD) reported > 20 mm of perceived low back pain, while sub-clinical pain developers (SC) reported > 10 mm but < 20 mm, and non-pain developers (NPD) reported < 10 mm of perceived pain throughout the typing trial. A one-way ANOVA was conducted with a Tukey's post-hoc test to compare the normalized flexion, peak pain rating, and questionnaire scores between pain

groups (SPSS, Version 22.0, IBM, Armonk, NY, USA). Self-reported family history of back pain was correlated to pain group status using Pearson's correlation coefficient. Significance was accepted at the  $p=0.05$  level.

## RESULTS AND DISCUSSION

8/32 (25%) of the study population were identified as PD, 8/32 (25%) as SC, and 16/32 as NPD. Average Peak Pain Ratings for the left and right low back respectively were 2.7(+/-2.83) mm, 2.0(+/-2.62), mm (NPD), 12.7(+/-4.84) mm, 15.2(+/-3.14) mm (SC), and 38.2(+/-19.56) mm, 38.1(+/-20.20) mm (PD). These peak pain ratings were statistically significant between pain groups ( $p=0.0001$ ).

The average normalized lumbar flexion angles adopted by participants throughout the trial were 51.2 (% ROM) +/- 22.57, 60.9 (%ROM) +/- 15.67 and 65.3 (%ROM) +/- 25.29 (Figure 1) for NPD, SC, and PD respectively. Flexion angles were not statistically different between groups ( $p=0.402$ ).

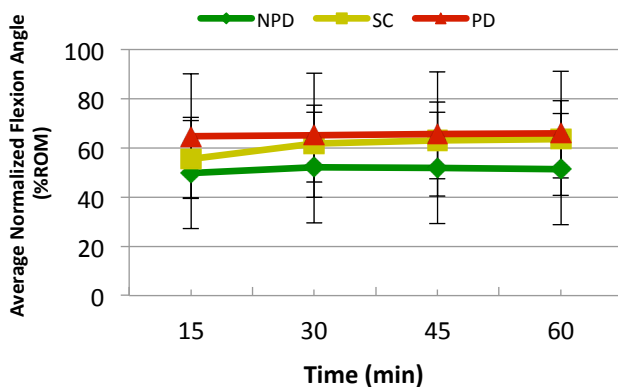


**Figure 1:** Average normalized lumbar flexion angles (%ROM) for all pain groups throughout the typing trial.

With respect to family history of LBP the results suggest no relationship exists with pain group status ( $r^2 = -0.50$ ,  $p=0.799$ ). The TSK and BPAQ show no statistically significant difference between pain groups ( $p=0.303$  and  $p=0.103$  respectively).

Results from this study are similar to previous research by Gallagher et al. (2011) where distinct pain groups emerged in response to prolonged standing. In this investigation a SC group was

identified to be statistically different from both the PD and NPD groups. It is possible that SC individuals did not have enough time to develop into PD since our study only examined a 1-hour exposure, suggesting there are possible differences in response rate between individuals. With respect to seated posture during sitting as indicated by the normalized lumbar flexion angles, it appears that the PD and SC groups adopted more spine flexion for the duration of the hour protocol. This is consistent with previous research where it is hypothesized that flexed postures lead to LBP through mechanisms such as increased disc pressure<sup>5</sup> and/or viscoelastic creep<sup>6</sup>.

## CONCLUSIONS

This investigation found three distinct groups of individuals emerge in respect to perceived pain development during sitting. The identification of the subclinical group suggests that some individuals may develop pain quicker than others. The data from this study showed no relationship between family history, kinesiphobia or negative attitudes towards LBP and pain group. Trends in the data indicate that adopted spine flexion angle may be playing a role. Future work should further investigate the role of spine posture as well as explore the responses in a clinical population.

## REFERENCES

1. Hoy D, et al. *Arthritis & Rheumatism*, **64**: 2028–2037, 2012
2. Lis AM, et al. *Eur Spine J.* **16(2)**:283-298, 2007.
3. Gallagher et al. *Gait & posture.* **34.4**: 490-495, 2011.
4. Sokka. *Clin and Exp Rheum.* **23**: S77-84, 2005
5. Andersson et al. *Clinical Orthopaedics and Related Research* **129** 156-164., 1977
6. McGill & Brown. *Clinical Biomechanics* **7.1**: 43-46, 1992

## ACKNOWLEDGMENTS

This work was funded by a NSERC Discovery Grant. MB is supported by a Dean's Fellowship Award from Memorial University of Newfoundland.

# Active End-Range Spine Flexion Changes in Response to Prolonged Sitting

<sup>1</sup>John Charles Snow, Matthew Barrett and Diana De Carvalho

Faculty of Medicine, Memorial University of Newfoundland, St. John's, NL, Canada

email: jcs505@mun.ca

## INTRODUCTION

Research has identified that most workers are seated for the majority of the workday in developed countries.<sup>3</sup> Sitting often involves non-neutral postures of the spine, at times inducing near end ranges of spinal flexion.<sup>1</sup> Sustaining extreme ranges of flexion for as little as 20 minutes has been shown to alter spine flexibility.<sup>2</sup> However, the effect of near-end ranges, such as those observed in office chairs<sup>1</sup>, has yet to be studied. The purpose of this study was to examine the effect prolonged office chair sitting has on the active maximum spine flexion angle.

## METHODS

26 participants (4 females, 22 males), average age 24.1 years  $\pm$  7.7 (SD), height 179 cm  $\pm$  8.6 (SD) and mass 78.7 kg  $\pm$  10.7 (SD) were recruited from the local population. Exclusion criteria included a history of tumor, infection, fracture, inflammatory arthropathy and/or previous surgery of the spine. Two tri-axial accelerometers (ADXL335, Analog Devices, Norwood, MA, USA) were fixed to the skin in the +y down +x left, +z anterior orientation using double-sided tape overlying the L1 and S2 spinous processes. Accelerometer signals were collected at a sample rate of 1500 Hz using a 16-bit A/D board (Noraxon, Scottsdale, AZ, USA). Following instrumentation, four 10 s posture calibration trials were collected: upright standing, maximum extension, maximum flexion (standing) and maximum flexion (seated). Participants were then seated at a computer workstation that consisted of an adjustable height table, desktop computer, standard keyboard and the seat pan of a standard office chair. The workstation was adjusted to each participant individually prior to the start of the data collection. Throughout the sitting trial participants completed a standardized typing task that involved mimicked report writing. Immediately prior to starting the sitting trial, participants completed a baseline rating of perceived low back pain using a

100 mm visual analog scale (VAS) with the anchors of 0 mm/"No Pain" and 100 mm/"Worst Pain Ever". This rating was then repeated every 7.5 minutes throughout the trial. Accelerometer data were collected continuously throughout the sitting trial in four 15-minute blocks. Following the sitting trial the maximum flexion (standing) trial (10 s) was repeated. Accelerometer data were processed using a custom written program (Matlab R2015b, The Mathworks, Natick, MA, USA) to extract the lumbar angles from the raw accelerometer data as follows: calibrating the sensors with respect to gravity, converting voltages to accelerations, calculating absolute inclinations, smoothing the data using a dual-pass 2<sup>nd</sup> order Butterworth filter (cut-off frequency 1 Hz) and calculating the relative spine angle from the absolute inclinations of the top and bottom sensor. A normalized flexion angle was calculated using the functional range of motion trials and representing the flexion angle as a percentage of maximum flexion range. Normalized flexion angles were averaged over the sitting trial. To represent changes in spine flexibility, a differential lumbar spine angle was calculated by subtracting the pre-sitting trial maximum spine flexion value from the post- maximum flexion value. To focus only on changes in perceived pain ratings in response to sitting, the baseline pain rating was subtracted from each subsequent rating throughout the trial. Baseline-removed ratings of perceived pain were then used to classify participants into three groups according to the peak value rated at any point in the trial: "Pain developers" (PD) > 20 mm of perceived low back pain, "sub-clinical pain developers" (SC) reported >10 mm but < 20 mm, and "non-pain developers" (NPD) reported <10 mm of perceived pain.<sup>3</sup> A one-way ANOVA with a between factor of pain group was conducted for the outcome measures of maximal spinal flexion angle differential, average lumbar spine angle during sitting and peak perceived pain rating (SPSS, Statistics 23, IBM Software, Armonk New York). Tukey's test was

conducted post hoc. For all tests significance was accepted at the  $p=0.05$  level.

## RESULTS AND DISCUSSION

Of the total study population, 23% were identified as PD, 31% as SC and 46% as NPD (Table 1). The average peak pain ratings were  $31.5 \pm 11.4$ ,  $15.2 \pm 3.1$  and  $2.9 \pm 2.8$  for PD, SC and NPD respectively. The peak pain ratings were statistically significant between pain groups ( $p = 0.011$ ). The differential maximum flexion angle increased for all pain groups ( $4.2^\circ \pm 4.2$ ,  $7.3^\circ \pm 5.8$ , and  $0.4^\circ \pm 5.9$  for PD, SC and NPD respectively, Figure 1). These differences were found to be significantly greater in the SC pain group ( $p = 0.023$ ). The average normalized lumbar spine angles adopted by participants throughout the trial were: 64.6 % ROM  $\pm 24.9$  and 53.9 % ROM  $\pm 23.4$ , 51.0 % ROM  $\pm 21.8$ , for PD, SC and NPD respectively. There were no significant differences between pain groups for average normalized lumbar angle adopted throughout the sitting trial ( $p=0.392$ ).

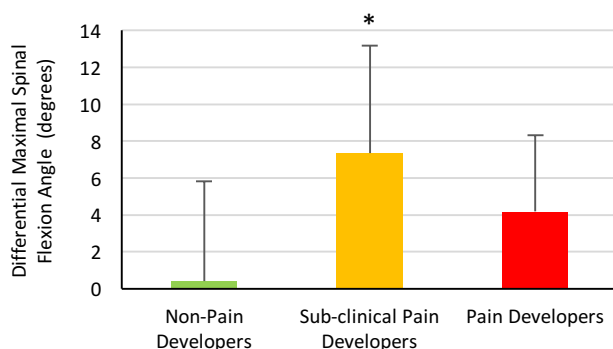


**Figure 1:** The differential angle (representing the difference between pre- and post- sitting trial measures). The SC group exhibited a significant increase in maximum angle (\*).

Similar to the findings of end-range flexion induced flexibility changes<sup>2</sup>, a one-hour exposure to office chair sitting appears to increase the active maximum spine flexion angle. By analyzing this response in the context of perceived pain, our results show that these flexibility changes appear to differ by pain groups. Considering all pain groups sat with similar spine posture throughout the prolonged sitting trial, the mechanism behind this differential pain development remains unknown. It is interesting that significant differences were found in the SC group but not PD group. Perhaps these flexibility changes begin to reverse as pain increases and reactive stiffness sets in. Future work will need to explore this phenomenon in greater detail.

## CONCLUSIONS

This study shows statistically different pain response groups with a 1-hour exposure to sitting. Further, while all groups showed increasing spine flexibility this difference was only significant for the SC group. Such flexibility changes are of clinical importance as they could result in altered spine stability and potential low back injury. Further research needs to be done to determine if this response is dose dependent and/or affects muscle reflex activations.

## REFERENCES

- [1] De Carvalho, D. et al. 2016. *Ergonomics*, **1-37**.
- [2] McGill, S. M., & Brown, S. 1992. *Clinl Biomech*, **7(1)**, 43-46.
- [3] Clemes, SA, et al. 2014. *Occup Med*, **64(3):188-92**.
- [4] Sokka, T. 2005. *Clin rheum* **23(5)**, S77.

## ACKNOWLEDGMENTS

This project was supported by a NSERC Discovery Grant. JCS was supported by the TPMI educational fund.

**Table 1:** Pain Group demographics, average spine posture during sitting and peak pain ratings.

	Average Age	Average Height (cm)	Average Weight (kg)	Average Lumbar Spine Angle (% ROM flexion)	Peak Pain Rating (mm)
Non-Pain Developers	22.1	178.6	76.5	51.0	2.9
Pain Developers	23.2	179.9	79.2	53.9	31.5
Sub-Pain Developers	22.5	177.6	76.0	64.6	15.2

# Changes in trunk mechanical properties following prolonged sitting: A Pilot Study

<sup>1</sup> Jang-Ho Park, <sup>1</sup> Sunwook Kim, and <sup>1</sup> Divya Srinivasan

<sup>1</sup> Virginia Polytechnic Institute and State University, Blacksburg, VA, USA  
email: sdivya1@vt.edu, web: www.oeb.ise.vt.edu

## INTRODUCTION

Low back pain (LBP) is a prevalent (18 %), costly (\$15 to \$50 billion per year in the USA), and often disabling musculoskeletal disorder affecting the general population [1]. Among working-age adults, LBP is quite common among sedentary workers next to workers performing heavy lifting. Sedentary work characteristics may explain such prevalence. No substantial association, however, has been reported between perceived low back discomfort (due to prolonged sitting), and objective measures on postures, muscle activity, and blood oxygenation of the lumbar spine [2]. Hence, the causal relationship between occupational sitting and LBP is still unclear.

While identifying a specific cause of LBP development remains challenging, spinal instability has been considered as an important casual mechanism [1]. Stabilization capacity of the trunk can be quantitatively described using trunk intrinsic stiffness and apparent mass that can be obtained based on a displacement-controlled perturbation paradigm to assess the mechanical behaviors of trunk active and passive tissues. In this study, we test the hypothesis that prolonged sitting to perform a computer-based task would be associated with reductions in trunk intrinsic stiffness and apparent mass, given that performing such task in a sitting position likely involves maintaining the trunk in flexed lumbar postures for a long time, and this would in turn alter mechanical stability of the spine.

## METHODS

Five young adults with no self-reported history of low back pain in the previous 12 months completed the study, after completing informed consent procedures approved by the Virginia Tech Institutional Review Board. Their mean (SD) age, height, and weight were 24.8 (2.6) years, 169.7 (12.9) cm, and 70.8 (10.2) kg, respectively. Each participant

performed a total of 3 hours of computer-based tasks in continuous sitting. Prior to the sitting period, and immediately following the sitting period, participants were asked to rate the pain in the low back region using a visual-analog scale (verbally anchored at 0% for no pain and 100% for worst pain imaginable), and trunk mechanical behaviors were assessed using a sudden perturbation paradigm [3].

For trunk perturbation, participants stood up in a rigid metal frame and wore a shoulder harness that was connected by a rigid rod at the T8 level to a servomotor. Then, a pseudorandom sequence of twelve anterior-posterior perturbations ( $\pm 5\text{mm}$ ) were generated by the servomotor and transferred to the trunk via a rigid rod-harness. During the perturbations, trunk motion was measured using signals from the motor encoder and laser sensor, while applied forces were measured by a load-cell sensor which was placed in-line with the rigid rod (Fig. 1). Participants maintained a constant baseline extensor effort which was set as 10% of maximum voluntary RMS (root-mean-square) EMG in the lumbar erector spinae at the L3 level.

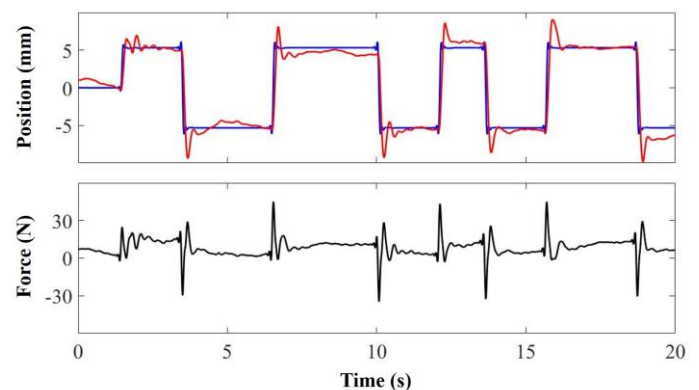


Figure 1: Representative data obtained during a sequence of perturbations [Top: trunk positions measured by the motor encoder (blue line) and measured displacement of T8 level from the laser sensor (red line); Bottom: driving force measured from the load-cell sensor]

Trunk dynamic properties were estimated during a latent period of 60 ms following each perturbation, using a system identification approach relating the measured trunk kinematics to kinetics. A two degree-of-freedom spring–mass–damper system [3] was used to model the trunk (1) and harness-rigid rod assembly (2):

$$F(u, t) = \begin{Bmatrix} F_1 \\ F_2 \end{Bmatrix} = \begin{bmatrix} 2.7 & 0 \\ 0 & m_2 \end{bmatrix} \begin{Bmatrix} \ddot{u}_1 \\ \ddot{u}_2 \end{Bmatrix} + \begin{bmatrix} c_1 & -c_1 \\ -c_1 & c_1 + -c_2 \end{bmatrix} \begin{Bmatrix} \dot{u}_1 \\ \dot{u}_2 \end{Bmatrix} + \begin{bmatrix} k_1 & -k_1 \\ -k_1 & k_1 + -k_2 \end{bmatrix} \begin{Bmatrix} u_1 \\ u_2 \end{Bmatrix}$$

where  $F$  (external force) and  $u$  (displacement) were measured variables,  $m$  (mass),  $c$  (damping), and  $k$  (stiffness) were estimated using a least-squares curve fit procedure. Anteriorly directed perturbations yielding high correlation ( $> 0.99$ ) and low mean square error ( $< 0.005$  N) between measured and model-predicted driving force were selected for further analysis. Intrinsic trunk stiffness and apparent mass for all selected perturbations were averaged to yield one value for each parameter for each subject, prior to sitting and following 3 hours of sitting.

## RESULTS AND DISCUSSION

Table 1 shows the results of the study. Three participants (P2, P4, and P5) showed an average of ~32% increase in low-back discomfort with sitting for 3 hours. This corresponded to ~60% decrease in trunk stiffness and to ~25% decrease in mass. These are in agreement with our hypothesis and aligned with expectations from previous research [3]. However, P1 and P3 presented contrary results: self-reported discomfort was increased by about half as much as the other group (~16%), and trunk stiffness and mass were increased by ~120% and by ~27% after sitting, respectively. These inconsistent results in our limited sub-sample could be due to several

reasons. We speculate that since the reversal in trunk mechanical properties from our expectation was associated with much less discomfort at the end of sitting in 2 participants, there may be some individualized coping strategies associated with prolonged sitting. This may either be that those individuals were not using consistently flexed lumbar postures while sitting or that they may have been sitting in a less “static” manner by employing variable postural/muscle activation strategies. We have recorded the muscle activities from multiple thoracic/lumbar muscles as well as postures during the sitting task. In addition to testing more subjects to improve statistical power, future research will also examine trunk stiffness-related changes of muscle activation and kinematics during the sitting task.

In conclusion, quantifying spinal stability via changes in trunk intrinsic stiffness and apparent mass may be a promising approach to objectively evaluate acute changes in spinal mechanical behaviors as a result of prolonged sitting. This in turn may improve an etiological understanding of why prolonged sitting causes low-back pain, and help inform and set targets for interventions addressing this problem.

## REFERENCES

1. Panjabi, M. M. (2003). Clinical spinal instability and low back pain. *Journal of electromyography and kinesiology*, 13(4), 371-379.
2. De Looze, M. P., et al. (2003). Sitting comfort and discomfort and the relationships with objective measures. *Ergonomics*, 46(10), 985-997.
3. Barzgari, B., et al. (2011). Disturbance and recovery of trunk mechanical and neuromuscular behaviours following prolonged trunk flexion: influences of duration and external load on creep-induced effects. *Ergonomics*, 54(11), 1043-1052.

**Table 1:** Discomfort in low-back and estimated trunk stiffness and mass prior to and following the sitting task

Participant	Low Back Discomfort (%)		Trunk Stiffness (kN/m)		Trunk Mass (kg)	
	Pre	Post	Pre	Post	Pre	Post
P1	19.1	44.1	29.7	96.5	32.6	53.6
P2	3.9	28.9	26.2	5.0	31.3	20.1
P3	0.0	6.4	40.9	50.8	36.4	32.6
P4	2.2	8.7	53.6	34.0	33.2	25.6
P5	0.0	64.7	12.7	5.0	28.3	23.5

# COMPARISON OF LUMBAR SPINE ACCELERATION PROFILES OF EVERY DAY ACTIVITIES AND EXAMINATION OF THEIR FREQUENCY CONTENT

<sup>1</sup> Herb Guzman, <sup>1</sup> Alejandra Barraza, <sup>1</sup> Enrique Bonugli, <sup>1</sup> Lars Reinhart, and <sup>1</sup> Lisa Gwin

<sup>1</sup> Biodynamic Research Corporation, San Antonio, TX, USA

## INTRODUCTION

New miniature accelerometers are based on piezoresistive MEMS (Micro-Electro-Mechanical Systems) elements. These smaller sensors can be easily coupled to the low-back/lower-lumbar spine of a human subject. Studies with larger devices have also been conducted with sensors attached to the low back of human subjects [1]. Based on the literature, no studies have compared every-day activities for lumbar-spine acceleration profiles and their frequency content measured simultaneously with MEMS wireless and wired accelerometers. Research has been conducted on lumbar-spine acceleration profiles and their frequency content during ejection seat tests or other severe lumbar accelerations with live human subjects and/or with Anthropomorphic Test Devices, but not during every-day activities[2],[3].

The purpose of this research was to study the lumbar-spine acceleration profiles and their frequency content of a group of human subjects while they carried out every-day activities. This study also compared the performance of a wireless versus a wired device simultaneously coupled to the lumbar spine of each subject.

## METHODS

Fifteen activities and one roller coaster ride event that humans may experience on any given day were performed by seven healthy subjects (Table 1). The subjects were: three females (21-51 y/o; wt: 61-78 kg; ht: 1.52-1.65 m) and four males (35-50 y/o; wt: 72-88 kg; ht: 1.65-1.86 m). Two types of MEMS accelerometers were fastened to a mount molded to fit the lower lumbar area of each subject. One device was a low-cost, wireless triaxial accelerometer (X16-2, GCDC, Inc.) while the other device was a high-cost triaxial accelerometer wired

to an external data acquisition system (53A, MSI, Inc./TDAS-PRO, DTS, Inc.). The sensors measured three orthogonal translational accelerations near the subjects' L5 [lumbar] vertebrae: Front-to-back acceleration was the x-axis component (forward:+), side-to-side was the y-axis (left:+) and up-down was the z-axis (up:+). The wireless sensor sampling rate was set to its maximum, 400 Hz. The wired system sampling rate was set to its minimum, 500 Hz. Both accelerometers detected steady-state and transient accelerations.

Matlab algorithms compared the lumbar accelerations from both devices as follows: (1) the signals from the wireless sensor were up-sampled to 500Hz to synchronize with those from the wired sensor. (2) The Power Spectral Density (PSD) estimates of each raw signal were computed using Welch's Periodogram to study their frequency content. (3) Based on the PSD estimates, the signals were Low-Pass-Filtered (LPF) at various upper cutoff frequencies. (4) The PSD's were also used to characterize the signal-to-noise-ratios (SNR). (5) The correlation coefficients between the signals from each device were computed for the data from each activity. (6) The root-mean-square-deviations (RMSD) between the signals from each device were also computed. (7) The predominant acceleration components and resultant acceleration magnitudes were determined and their profiles were analyzed.

## RESULTS AND DISCUSSION

The acceleration profiles were examined in terms of their peak accelerations and pulse durations. For a comparison of the pulse *durations*, the accelerations were numerically integrated to obtain *velocities*. Table 1 shows the peak velocities and accelerations for selected subjects in the predominant directions for each every-day activity. The average peak values

are reported for cyclic events such as hopping, walking, etc.

The frequency content of the accelerations in terms of signal power showed three salient frequency ranges: Long-duration events such as vehicle braking had the most significant signal power at approximately 10-Hz or below.

**Table 1:** Summary of Results (BC=Bumper Car).

Activity, LPF Upper Cutoff (Hz)	Peak Velocities, m/s	Peak Accelerations, g's	Correlation Coefficient
Vehicle Braking (10)	(x) 9.1; (z) -1.3	(x) -0.94 ; (z) 1.12	(x) 1.0 ; (z) 0.99
Speed Bumps (50)	(x) -0.4 ; (z) 0.5	(x) 0.47 ; (z) 2.09	(x) 0.98 ; (z) 0.96
Chair Plops (40)	(x) 1.7 ; (z) -1.8	(x) 1.18 ; (z) 3.93	(x) 0.98 ; (z) 0.86
BC Front Impact (100)	(x) -1.9; (z) 0.6	(x) -1.42 ; (z) 1.93	(x) 0.97 ; (z) 0.87
BC Rear Impact (100)	(x) 1.6 ; (z) -1.0	(x) -0.34 ; (z) 2.78	(x) 0.98 ; (z) 0.94
BC Side Impact (100)	(y) 2.1 ; (z) -0.4	(y) 1.76 ; (z) -0.05	(y) 0.91 ; (z) 0.86
Walking (100)	(x) 1.2 ; (z) 0.1	(x) -0.19 ; (z) 1.33	(x) 0.97 ; (z) 0.98
Upstairs Slow (100)	(x) 0.3 ; (z) 0.8	(x) -0.32 ; (z) 1.56	(x) 0.98 ; (z) 1.0
Downstairs Slow (100)	(x) -0.1 ; (z) 0.0	(x) -0.66 ; (z) 1.97	(x) 0.98 ; (z) 0.98
Upstairs Fast (100)	(x) 0.9 ; (z) 1.6	(x) -0.88 ; (z) 2.90	(x) 0.84 ; (z) 0.91
Downstairs Fast (100)	(x) 1.1 ; (z) -0.4	(x) -0.96 ; (z) 3.48	(x) 0.86 ; (z) 0.99
Running (100)	(x) -0.5 ; (z) 1.5	(x) -0.39 ; (z) 4.69	(x) 0.89 ; (z) 0.99
Heel Strikes (100)	(x) 0.1 ; (z) 0.3	(x) 1.23 ; (z) 6.69	(x) 0.93 ; (z) 0.98
Hopping (100)	(x) 0.5 ; (z) 2.2	(x) -4.24 ; (z) 8.15	(x) 0.97 ; (z) 0.96

The signal power of events such as entering/exiting a vehicle, chair plops and traveling over speed bumps extended into frequencies of 40-50 Hz; short-duration events such as heel strikes, running, hopping and climbing stairs tended to have more signal power of up to 100-Hz. Fig. 1 provides an overview of these frequency ranges. Fig. 2 shows examples of acceleration profiles for selected everyday activities and the braking event from a roller coaster ride.

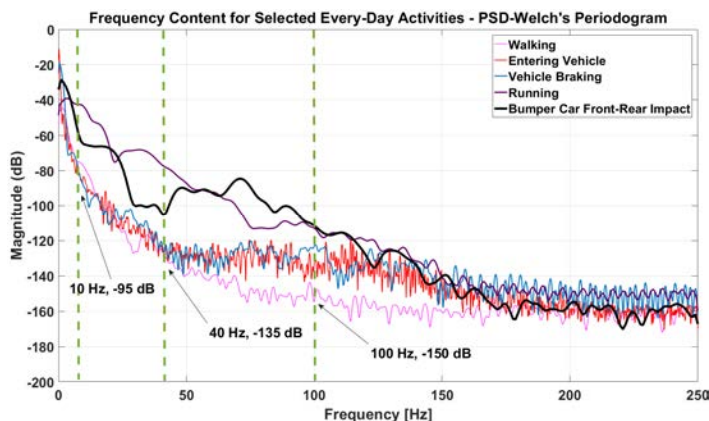


**Fig. 1:** Accelerations frequency content.

The mean percent difference in the calculated peak resultant accelerations differed at most 9.55% between the low cost and the high-end sensor.

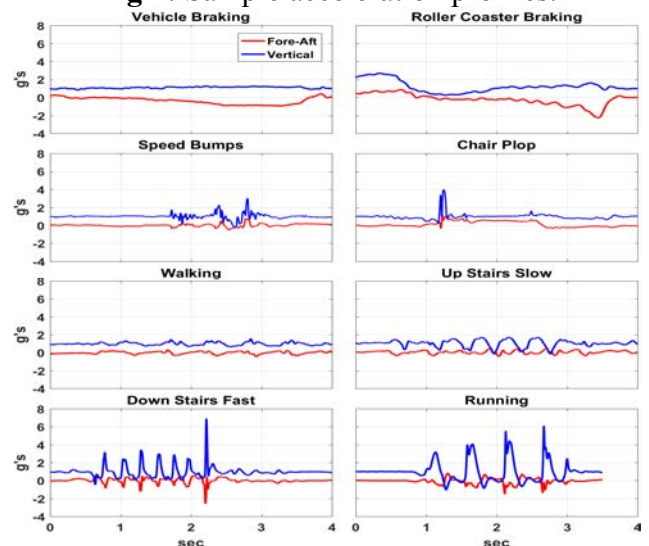
## CONCLUSIONS

The lumbar-spine acceleration profiles and their frequency content were studied for fifteen everyday activities and one roller coaster ride event. Measurements from a wireless (low-cost) and a wired (high-cost) accelerometer were compared. The overall signals of both of these sensors exhibited good correlation (Avg. 95.4%) and low root-mean-square deviations (Avg. 0.103). It was evident that the sampling rates used were limited for some activities. The low-cost device recorded relatively noisier signals than the high-cost device.

## REFERENCES

1. Manoogian SJ; et al. Evaluation of thoracic and lumbar accelerations of volunteers in vertical and horizontal loading scenarios. *Biomechanics, 2010* (SP-2268). SAE #2010-01-0146. 2010.
2. Gallagher, HL, et al. An Analysis of Vertebral Stress and BMD During +Gz Impact Accelerations. *Oak Ridge Institute for Science and Education, TN. 2007.*
3. Jamison D, IV. Mechanical characterization of the human lumbar intervertebral disc subjected to impact loading conditions. Thesis. Drexel University. 2013.

**Fig 2:** Sample acceleration profiles.



# DIFFERENCES IN PRINCIPAL COMPONENTS IN SIT-TO-STAND IN PARTICIPANTS WITH AND WITHOUT LOWER BACK PAIN

Mauricio Nunez Jr, Young-Hoo Kwon  
Biomechanics Laboratory, Texas Woman's University, Denton, TX, USA  
Email: mnunez3@twu.edu

## INTRODUCTION

According to the National Institute of Neurologic Disorders around 80% of adults are affected by lower back pain at some point in their lives. The pain can stem from sprains, strains, herniation, rupture, stenosis, or injury. The etiology of back pain is limitless and ranges from chronic debilitating ailments to acute issues. The problem with back pain is that the symptoms are treated but the root cause is not rectified.

Having imbalances causes some muscle groups to become tightened and others stretched and weakened. The way that these muscle groups are affected can be seen in movement patterns (Nadler et. Al 2000) This study will attempt to identify different movement patterns between self-reported lumbar pain and a control no pain group. The resulting movement strategies, or principle components, will be compared between the two groups.

The purpose of this study was to investigate the kinematic and kinetic differences in non-pain versus self-reported lower back pain and analyze the movement using Principle Component Analysis. The null hypothesis is that there exists no difference in the components of movement between participants with back pain and no back pain.

## METHODS

69 participants ranging from ages 18-35 were selected from the local university student population using emails and flyers. The participants self-reported no lumbar pain versus lumbar pain using a Wong-Baker scale to rate and locate the area of pain. The participants were then divided into a pain and no-pain group; 40 in the control (no-pain) and 29 in the lumbar pain group.

The 10-camera Vicon motion capture system and four AMTI force plates were used for data capture at 100 Hz. The participant was prepped and instructed to stand and sit slowly on a platform 60 cm high and stand back up to complete one stand-sit-stand motion. The task was chosen from normal activities that are repeated various times through a normal day.

Once the data collection for the 3 trials were completed, the 3 trials per participant were averaged. The data was then normalized to only include starting from sitting position to a stand position. The different Principle Components of the marker coordinates were calculated for each participant's average trial. The Eigenvalues, Eigenvectors, and a visual representation of the data was calculated. The results were based on a method previously implemented in a study that analyzed the principle components of alpine skiers (Federolf et. Al 2012). The data used for this study represented the first 10 PCA's that contributed to the overall movement strategy. Each component represented a movement strategy and the results indicated the percent of the strategy used by the participant; if a participant had PC1 of .84, that resulted in the participant using PC 1 as 84% of the overall movement. The resultant components are a method to quantify the different parts of an overall movement. The results were then analyzed using SPSS to evaluate if there were significant differences between participants with lower back pain and the control in the resulting movement strategies.

## RESULTS AND DISCUSSION

Using the results from different components allowed us to analyze the utilization of different movement patterns that muscle groups performed

(Zago et. Al 2016). Since there was 1 dependent variable with 10 levels and 1 independent variable, an independent sample t-test was run and the results demonstrated statistically significant differences in components 4,5,6 and 8 as shown in table 1.

The components that were significant were then analyzed by reconstructing the movement pattern using the PC results to subjectively find a movement strategy for that component. For Example, figures 1 and 2 showed the beginning and end sections of component 8 which was determined to be a knee bending strategy. The video representation demonstrated that the component was an extension and a posterior shift of the knee joint; bringing the knees behind the toes as standing occurred. Component 4 was determined to be a hip strategy in which the hips were posteriorly shifted during the stand. Component 5 was an overall straightening of the body. Component 6 was an adduction of the arms.

## CONCLUSIONS

There were significant differences in certain principle components (4,5,6,8) in a standing test between participants with lower back pain and participants with no lower back pain. We reject the null hypothesis and accept that there is a significant difference between the 2 groups. Further investigation of the timing and velocities of the components will be done in the future to attempt to discover how and why the use of different components is employed by the different groups. Also, kinetic and kinematic data of the involved segments and joints will be further analyzed.

## REFERENCES

1. Federolf, P., Reid, R., Gilgien, M., Haugen, P., & Smith, G. (2014). The application of principal component analysis to quantify technique in sports. *Scandinavian Journal of Medicine & Science in Sports*, *24*(3), 491-499.
2. Nadler SF, Malanga GA, DePrince M et al. The relationship between lower extremity injury, low back pain, and hip muscle strength in male and female collegiate athletes. *Clinical Journal Sport Med* 2000; *10*(2):89-97.
3. Zago, M., Codari, M., Iaia, F. M., & Sforza, C. (2016). Multi-segmental movements as a function of experience in karate. *Journal of Sports Sciences*, 1-8.

	Sig. (2-tailed)	mean Diff.	Std. Error Diff	95% CI of the Difference	
				Lower	Upper
PC1	0.649	0.599	1.309	-2.014	3.212
PC2	0.200	-1.076	0.831	-2.735	0.583
PC3	0.326	-0.554	0.559	-1.669	0.562
PC4	0.000	-0.407	0.091	-0.590	-0.225
PC5	0.000	0.312	0.067	0.177	0.446
PC6	0.000	0.478	0.092	0.295	0.662
PC7	0.248	0.662	0.569	-0.473	1.797
PC8	0.012	-0.089	0.034	-0.158	-0.020
PC9	0.857	0.015	0.084	-0.152	0.182
PC10	0.100	0.059	0.036	-0.012	0.130

**Table 1.** Results of Principle components between the groups differences.

# THE EFFECTS OF BREAST SIZE AND BODY IMAGE ON POSTURE, MUSCLE ACTIVATION AND BACK PAIN DURING 2 HOURS OF PROLONGED STANDING

Susari Wanninayake and Janessa Drake

York University, Toronto, ON, Canada  
email: jdrake@yorku.ca

## INTRODUCTION

Women with large breasts often experience various symptoms such as back pain, neck pain and shoulder grooving from brassier straps [1]. Research has shown that women with large breast sizes can cause greater thoracic kyphosis and lumbar lordosis [1]. These angles improve after women undergo breast reduction surgery [1]. Further, trunk muscle activation has shown to be greater in women with larger breasts compared to women with smaller breasts in some cases [2]. However, it is unclear how women of various breast sizes cope during prolonged exposures. Two hour prolonged standing protocols have been shown to be an effective approach to evaluate spine motion [3].

Additionally, women's breasts can often influence their body image and self-esteem. However, it is unclear whether body image and/or self-esteem influence posture. If other psychological factors such as depression can influence posture, then it is possible that body image and/or self-esteem may also influence posture [4].

The primary objective of this study was to observe how posture in women with various breast sizes respond to prolonged standing. The secondary objective was to determine if there was a possible relationship between body image and posture.

## METHODS

Twenty-one healthy, university aged females (Table 1) were recruited for this study. Each participant measured their two breast circumferences that were used to calculate breast size. The first measurement was taken at the widest point of the breasts (OBCC) and the second measurement was taken under the breast at the mammary fold (UBCC) [5]. Typically,

a 2.54cm (1 in) difference would represent an A cup, 5.08cm (2 in) is a B cup, 7.62cm (3 in) is a C cup, etc. [5]. A ratio of OBCC/UBCC was used to divide participants in breast size groups to factor in different body sizes. Prior to the collection participants completed the Rosenberg Self-esteem Scale (RSES) and the Body Shape Questionnaire (BSQ) to evaluate body image.

**Table 1:** Mean (SD) anthropometrics by comparison groups: small breast size group (SG) and large breast size group (LG).

	SG (n=11)	LG (n=10)
Age (years)	23.36 ±2.58	20.10 ±1.66
Mass (kg)	60.66 ±11.39	61.90 ±7.25
BMI	21.78 ±2.39	22.21 ±2.56
OBCC-UBCC (cm)	7.39 ±2.11	13.97 ±1.80
Avg. Cup Size	~ B-C	~ D-E

Eight muscles bilaterally were recorded by surface electromyography (EMG) electrodes on the abdominal, back and gluteus medius muscles. Maximal voluntary contractions (MVCs) were collected for each muscle group of interest. Using an optoelectronic system, the motion was tracked for: upper thoracic (C7-T4), mid thoracic (T4-T9), lower thoracic (T9-T12) and lumbar (L1-S2) segments.

Participants stood at a table for 2 hours. During this time, they completed 4 quiet tasks (30 min each) in random order. The Visual Analog Scale (VAS) was used to record perceived pain. The participants rated their upper back (C7-T6), mid back (T6-T12), and low back (lumbar) pain every 15 minutes. Maximum change in VAS was calculated. A change equal to or greater than 10mm was considered to be clinically significant [3].

All statistical analyses were performed in SAS 9.4 (SAS Institute Inc., NC, USA). Three way repeated measures mixed model ANOVAs were performed compare sample groups with dependent variables.

## RESULTS AND DISCUSSION

Throughout prolonged standing, segment flexion angular responses over time were similar between breast size groups (Figure 1). But breast size was a significant main effect in upper thoracic and lumbar segments ( $p < 0.032$ ). But, there is a main effect of breast size on segment flexion angles. LG had more flexed upper thoracic and greater extended lumbar angles, but no difference in the mid thoracic angles relative to SG at each time epoch.

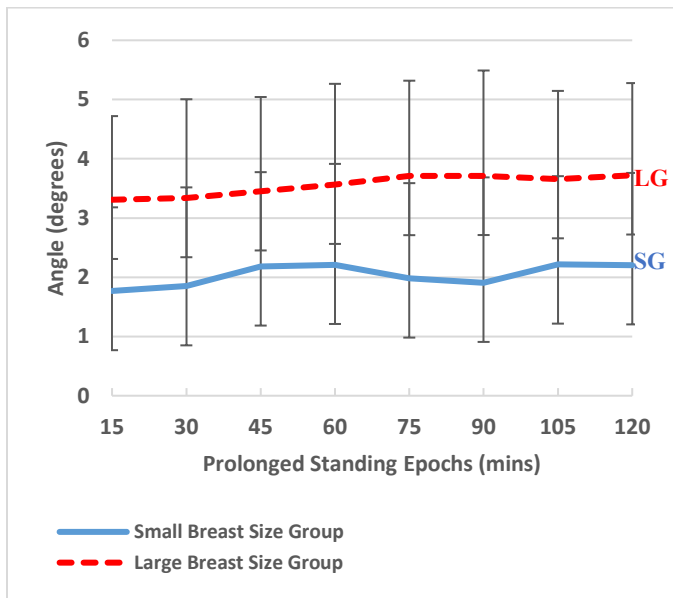


**Figure 1:** Mean upper thoracic segment responses during 2-hr prolonged standing between LG and SG. The initial upright bias was subtracted out.

Four of the 16 muscles showed a significant difference between breast size groups (mean) right rectus abdominis (RRA), left gluteus medius, left external oblique and right thoracic erector spinae at the T4 level, ( $p < 0.031$ ). In general, SG had either greater muscle activation or were no different from LG. This would suggest that the LG group could be relying more on passive tissue. Also, in general SG showed greater variable mean muscle activation than

in LG. It is suspected that this variability in the SG group muscle activation could explain why overall, the LG group had a greater number of pain developers than SG (Table 2).

**Table 2:** Percentage of non-pain developers and pain developers from upper, mid and low VAS scores between SG (n=11) and LG (n=12).

	Upper (%)		Mid (%)		Low (%)	
	NPD	PD	NPD	PD	NPD	PD
SG	45.5	54.5	54.5	45.5	27.3	72.7
LG	10	90	30	70	20	80

There is a possible relationship between self-esteem (RSES) and as well as body image (BSQ) and breast size. The LG group had lower self-esteem and greater body image dissatisfaction than the SG group. These relationships have potential to impact spine angles. However, further research is needed to identify the impact between the psychosocial measures and posture.

## CONCLUSIONS

The more flexed thoracic and more extended lumbar spine angles, differences in EMG and increased pain responses in LG may suggest that women with larger breasts are an important subgroup to be identified in future prolonged standing research. Especially given the potential impact of body image and self-esteem on these responses in LG. Additional participants spanning the A to G+ cup sizes are needed to fully elucidate these relationships.

## REFERENCES

1. Findikcioglu, K, et al. *Aesthetic Plast Surg* **31**, 23-27, 2007.
2. Schinkel-Ivy, A & Drake, J, *J Back Musculoskelt Rehabil* **29**, 741-748, 2016.
3. Nelson-Wong, E & Callaghan, J, *J Electromyogr Kinesiol* **20**, 256-263, 2010.
4. Canales, JZ, et al, *Rev Bras Psiquiatr* **32**, 376-380, 2010.
5. McGhee, D, et al. *Br J Sports Med* **40**, 970-974, 20.

# DIRECTIONAL CONTACT FORCES INVESTIGATION IN THE UPPER CERVICAL SPINE UNDER ANTERO-POSTERIOR FORCES APPLIED TO THE HEAD

<sup>1</sup>Wissal Mesfar, <sup>2</sup>Lucie Pelland, <sup>3</sup>Kodjo Moglo

<sup>1</sup>Biomedical Technology Department, CAMS, King Saud University, Riyadh, KSA

<sup>2</sup>School of Rehabilitation Therapy, Queen's University, Kingston, ON, Canada

<sup>3</sup>Mechanical & Aerospace Engineering, Royal Military College of Canada, Kingston, ON, Canada

email: wmesfar@ksu.edu.sa, web: <http://ksu.edu.sa/en>

## INTRODUCTION

Following external forces applied to the head-and-neck (HN) complex, restraint moments are generated by muscles and the viscoelastic soft tissues of the cervical spine, predominantly ligaments and joint capsules, as well as contact forces at the facet joints and intervertebral discs [1]. Quantification of contact forces in response to applied external forces to the head is necessary to characterize the biomechanical response of the HN in general, and to differentiate injury mechanisms at the craniocervical segment. However, due to the complex osteoligamentous morphology of the craniocervical segment, quantification of the contact force in different directions is difficult to anticipate as they will be dynamically shaped by the active response of soft tissues. In this study, we used finite element modeling to investigate the direction and magnitudes of contact forces at the craniocervical segment under application of external anterior-posterior forces to the head.

## METHODS

Predictions were based on simulations of our validated HN 3D nonlinear complex FE model [2]. For the simulation, neck efforts were assumed to be produced under static conditions to maintain HN stability under an antero-posterior force application. An anterior and posterior forces up to 100N and 350N were applied to the occipital and to the frontal bone of the head, respectively, under the presence of a constant 40N HW applied to its center of mass. The first thoracic vertebra was fixed while the head and cervical vertebrae were free to translate but not to rotate. These boundary conditions reflect the rotation restriction applied by the muscles to each bony

structure of the HN to keep the complex in its neutral posture. The computed reaction moments at the center of mass of each bony structure represent the net muscles moments required to counterbalance the applied force and to maintain static stability of the segment. The contact force between the occipital condyles and the superior articular facets of C1 (C0-C1), the transverse ligament (TL) and the dens at C2 (TL-dens) and at the facet joints between adjacent vertebrae (C1-C3) were also predicted. Finally, the relative translation of the occipital condyles on C1 and between each adjacent vertebra of the cervical spine segment was computed along the three anatomical directions. The static nonlinear FE analyses were performed using Abaqus 6.11.

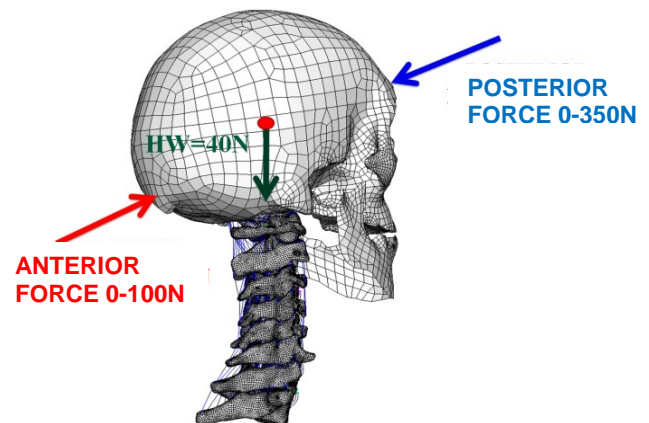


**Figure 1:** Finite Element Model of the head and neck; the location and direction of the externally applied load is shown.

## RESULTS AND DISCUSSION

The CFs at the facets joints of the upper (C0-C3) cervical segments as well as the CF between the transverse ligament (TL) and the Dens of C2 vertebra are shown in Fig 2a-d. The 40N HW produced a total

CF of 29.8N at C0-C1 and 37.1N at C1-C2 oriented mainly to the distal direction (Figs 2b-d). With the application of an antero-posterior load, the contact forces at C0-C1 increased quasi-linearly as a function of the magnitude of the applied force, reaching a maximum of 266N, with a posterior force of 350N, and 84N, with an anterior force of 100N (Figure 2a). At segmental levels below C1, the profile of CFs varied for applied posterior and anterior forces. For anterior forces, the CF on the facet joints and at TL-Dens increased quasi-linearly as a function of increasing magnitude of the applied force (Figures 2a). The predominant CF component of the facets joints segment of C0-C3 was found in the distal direction and pursued by the anterior direction for C0-C1 and C2-C3 and by a posterior force for C1-C2 (Figs 2b, d). In fact, an anterior CF inflects to the HN complex an extra moment applied at the levels of the facets joints requiring an additional net muscles moment to counterbalance the effect of the anterior CFs which is confirmed by a net moment of the whole muscles greater than the maximum moment of the external forces in the HN complex calculated at T1 vertebra. However, for posterior forces, the CF was present mainly at C0-C1 level in the whole directions followed by C1-C2 in the distal direction up to 200N posterior force. The CF at C0-C1 was increased substantially to the right direction after a posterior force of 100N reaching 66N at 350N (Fig. 2c) but remains under 20N in the antero-posterior direction (Fig. 2b) while the force is in the posterior direction.

## CONCLUSIONS

The response of the CFs is mainly related to the shape of the surfaces in contact and the contact response influences directly the muscles response and translations of the vertebra in the joint leading to the development of a coupling phenomenon in which the application of a pure force in the antero-posterior direction, generating external moments in the sagittal plane, leads to a response of the joint in the frontal and transverse planes. This finding may elucidate the understanding of the muscles activities response while a loading is applied in a specific direction and to understand the mechanism of injuries in the cervical spine.

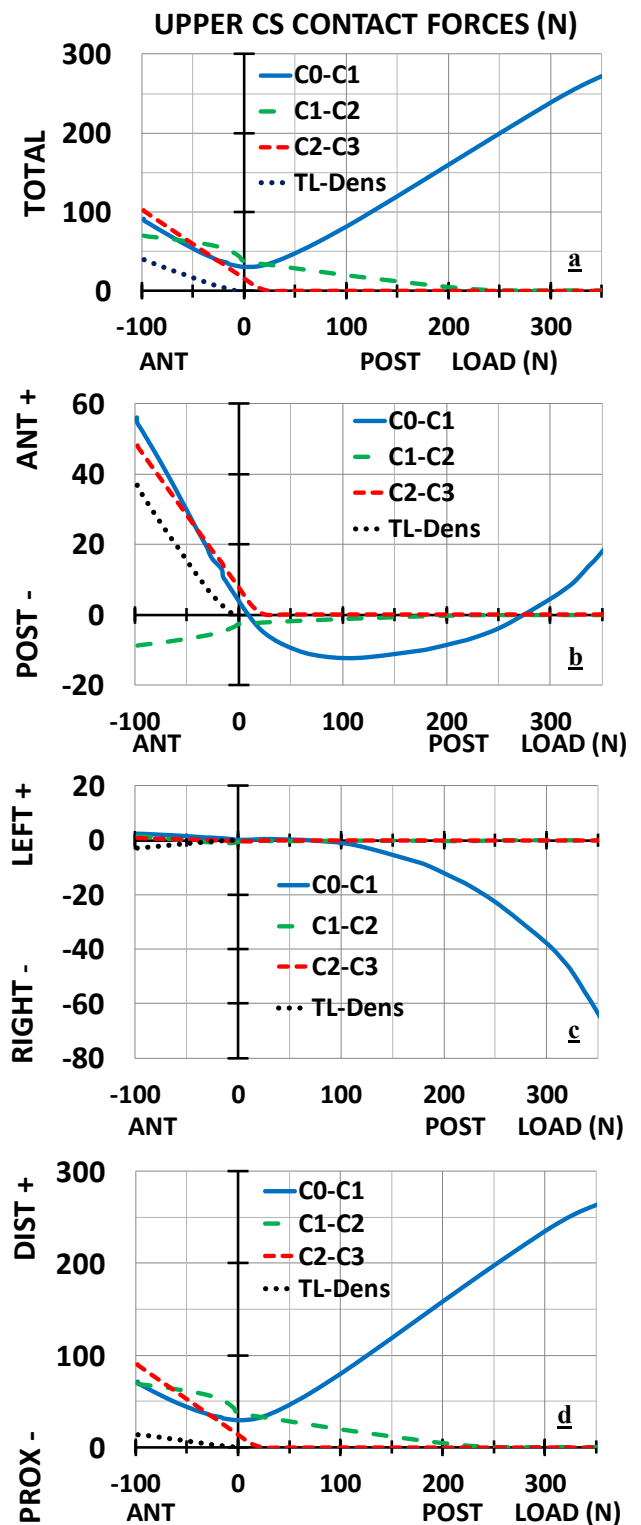


**Figure 2:** Contact forces of the upper cervical joints at the various anatomical directions. The CF are shown over the range of applied anterior and posterior external forces in presence of 40N HW.

## REFERENCES

1. Li-jun et al. *Spinal Cord* **52**, 342-347, 2014.
2. Mesfar and Moglo, *Clin Biomech* **28(8)**, 846-52, 2013.

# EFFECTS OF LUMBOPELVIC-HIP COMPLEX INSTABILITY ON THROWING MECHANICS AMONGST FEMALE HANDBALL ATHLETES

Gabrielle Gilmer, Sarah Gascon, Gretchen Oliver

Auburn University, Auburn, AL, USA

email: ggg0005@tigermail.auburn.edu, web: www.sportsmedicineandmovement.com

## INTRODUCTION

Throwing is a kinetic chain activity that requires coordinated energy transfer from the proximal segments (pelvis and torso) to the most distal segments (arm and hand) [1]. It has been documented that inadequate strength throughout the kinetic chain may contribute to inefficient force production and decrease optimal energy transfer for throwing performance [2]. The sport of team handball (THB) is unique in that it stresses both the lower extremity (LE) in the side-to-side cutting as well as the upper extremity (UE) in the volume of overhand throwing. Additionally, THB requires segmental stability throughout the kinetic chain for efficient dynamic movement. The ability to transfer energy and perform an accurate shot on goal is dependent on the synchronization, stabilization, and strength of the UE and LE.

The lumbopelvic-hip complex (LPHC) is the key component in connecting the UE and LE [2]. Previous research has shown that proper stabilization of the LPHC leads to higher rotational velocities across all segments [3]. Thus, interruptions in this energy transfer may lead to decreased performance and injury susceptibility [2].

Literature has shown injuries of the shoulder and knee in THB account for 44.0% and 26.7% of all injuries, respectively [4]. Even though the injury rates and the importance of energy transfer throughout the kinetic chain are known, there has yet to be a comparison examining LE segments and their contribution to the UE segments in THB athletes. Therefore, the purpose of this study was to examine the relationship between LPHC stability and segmental sequencing during a jump shot. It was hypothesized that LPHC instability would

affect segmental velocity sequencing of the pelvis (PV), torso (TV), humerus (HV), and forearm (FV).

## METHODS

Twenty female THB athletes (26.5±4.7 years; 174.6±4.2 cm; 74.4±6.4 kg) participated. An electromagnetic tracking system was used to collect kinematic data (100Hz) while participants performed three 9-meter jump shots. Data were analyzed across four events: foot contact (FC), maximum shoulder external rotation (MER), ball release (BR), and maximum shoulder internal rotation (MIR).

It is known that dynamic knee valgus indicates LPHC instability, however there are sparse quantitative data indicating what degree of instability is of concern as well as how LPHC instability effects throwing mechanics [5]. The current study utilized FC as the event to classify LPHC instability. This event was chosen because it is early in the throwing motion, and an interruption at this point ultimately cumulates to issues throughout the throw. LPHC instability was classified as 17° or greater knee valgus at FC [6].

## RESULTS AND DISCUSSION

Mann-Whitney U-test was used for analysis. Results revealed statistically significant differences between groups amongst PV at BR ( $p = 0.015$ ). Figure 1 shows the PVs change over the course of the throw. Table 1 shows the TV, HV, and FV medians over the course of the throw. The results from this study reject the hypothesis.

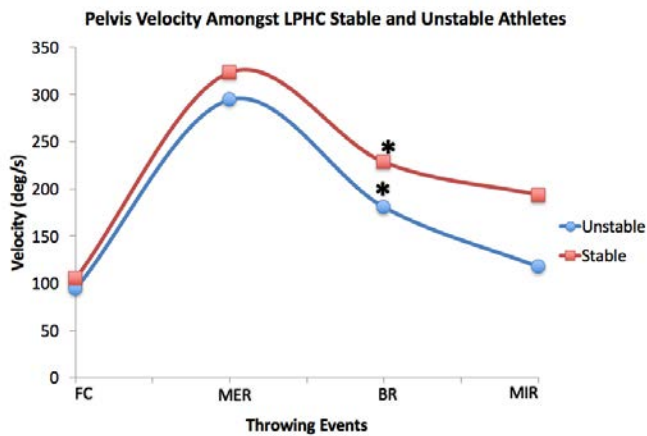


**Figure 1:** Median pelvis velocity values are shown over the course of the throw. Significance was found between groups at BR.

Thus, the authors speculate that LPHC instability could possibly decrease the efficiency of energy transfer through the LPHC and to the upper extremity in these selected athletes. In addition it should be noted that these selected athletes were currently training in the USA Women’s National Team Handball residency program, and it is possible that due to their heavy training regimen, they were still able to stabilize the body even though instability is present.

These finding may also suggest that knee valgus at FC is not a consistent indicator of LPHC instability. It is widely accepted that dynamic valgus is an

indicator for LPHC instability [1], but it remains unclear for what part of the throw and how much valgus deems an individual unstable.

## CONCLUSIONS

The main findings of this study reveal that LPHC instability, as classified at FC, resulted in significant differences between groups in PV at BR. However, it is unknown whether compensations are being made or if FC is a poor indicator of LPHC instability. Therefore, it is recommended that future studies include muscle activation, and further research investigate the best way to classify LPHC instability within a throw among THB athletes.

## REFERENCES

1. Putnam CA. *J Biomech.* **26**, 125-135, 1993.
2. Kibler WB, et al. *Sports Med.* **36**, 189-198, 2006.
3. Saeterbakken A, et al. *Journal of Strength and Conditioning.* **25**, 712-718, 2011.
4. Giroto N, et al. *Scandinavian Journal of Medicine and Science in Sports.* **10**, sms1636, 2015.
5. Alshemimary WK, et al. *Journal of Arthritis.* **4**, 1000210, 2016.
6. Apostolopoulos AP, et al. *Orthopedics & Traumatology.* **96**, 777-783, 2010.

**Table 1:** No significant differences were found amongst the torso, humeral, and forearm velocities. Median values amongst groups are listed.

Segmental Velocities (°s <sup>-1</sup> )	Classification	Throwing Event			
		FC	MER	BR	MIR
<b>Torso</b>	Unstable	201.47	536.43	227.18	160.55
	Stable	213.95	613.14	218.78	180.16
<b>Humerus</b>	Unstable	340.62	818.59	1184.51	724.04
	Stable	295.15	909.70	1233.98	777.92
<b>Forearm</b>	Unstable	444.02	998.22	1684.74	737.04
	Stable	413.61	979.11	1878.06	701.23



## RESULTS AND DISCUSSION

There was no significant interaction between elbow flexion and hand position for upward rotation (UR) ( $p = .938$ ). There was no main effect of elbow flexion for UR ( $p = .232$ ). However there was a main effect of hand position on UR ( $p < .001$ ). Pairwise comparisons indicated that standard and narrow conditions showed greater UR than wide ( $p = .001$  and  $p = .002$ , respectively). However no significant difference was seen between standard and narrow conditions ( $p = .091$ ) (Figure 2).

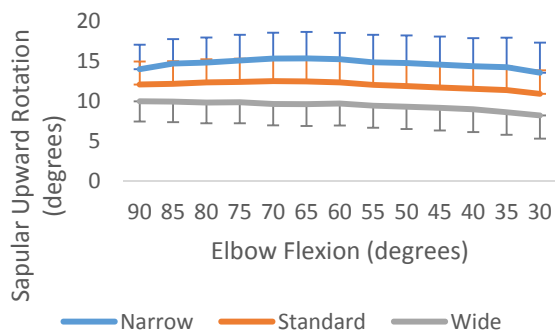


**Figure 2:** Scapular upward rotation (mean  $\pm$  SEM) across elbow flexion angle for each hand position.

There was no significant interaction between elbow flexion and hand position for posterior tilt (PT) ( $p = .821$ ). PT was affected by hand position ( $p = .001$ ), with greater PT in Narrow than in wide conditions ( $p = .004$ ). There was no significant main effect of elbow angle ( $p = .218$ ) (Figure 3).

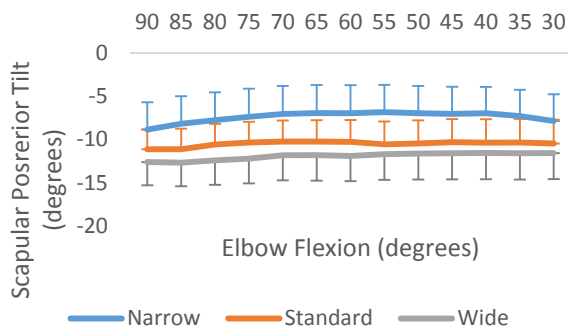


**Figure 3:** Scapular posterior tilt (mean  $\pm$  SEM) across elbow flexion angle for each hand position.

There was no interaction between elbow flexion and hand position on external rotation (ER) ( $p = .073$ ). There were main effects of both hand position ( $p = .021$ ) and elbow flexion ( $p < .001$ ) on ER. ER decreased linearly with elbow extension ( $p < .001$ ) (Figure 4).

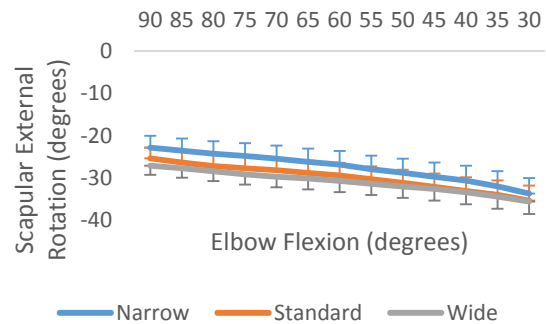


**Figure 4:** Scapular external rotation (mean  $\pm$  SEM) across elbow flexion angle for each hand position.

## CONCLUSIONS

The current data indicates that a narrow hand position shows the greatest amount of UR, ER, and PT during the concentric phase. Furthermore a wide hand position shows the least amount of UR, ER, and PT when compared to standard and narrow. This indicates that a narrow hand position may be more applicable for a rehabilitation setting, as it promotes healthy scapular motion, whereas a wide hand position may put the scapula in a position that is at risk for subacromial impingement.

## REFERENCES

1. Cogley, RM, et al. *J Strength Cond Res* 19, 628- 633, 2005
2. Decker, MJ, et al. *Am J Sports Med* 27, 784-791, 1999.
3. Ludewig, PM, et al. *Am J Sports Med* 32, 484 493,2004.
4. San Juan, JG et al. *BMC Musculoskelet Disord*, 16, 23, 2015
5. Suprak, DN, et al. *J Athl Train.* 48, 826-835, 2011

# NEURAL NETWORK PREDICTION OF JOINT TORQUES IN OLYMPIC WEIGHTLIFTING

Kristof Kipp, Matthew Giordanelli, and Christopher Geiser

Marquette University, Milwaukee, WI, USA  
email: kristof.kipp@marquette.edu

## INTRODUCTION

Biomechanists often analyze joint kinetics because they provide useful information about the neuromuscular and motor control mechanisms during human movement [4]. The problem that sports biomechanists and coaches face is that in order to calculate joint kinetics, they need to collect whole-body kinematic data, ground reaction force data, and anthropometric data.

Neural networks (NN) may provide a viable alternative because they can be used to analyse complex relationships between biomechanical inputs and outputs [1,3]. For example, Liu et al. [3] used a NN to predict lower extremity joint torques during vertical jumps from ground reaction force data (GRF). Further, Hahn and O'Keefe [2] used NN to predict joint torques from kinematic data.

The purpose of this study was to develop and train NN to predict hip, knee, and ankle joint torques from vertical and horizontal motions and mass of a barbell during an Olympic weightlifting exercise.

## METHODS

Seven weightlifters (body-mass:  $106.0 \pm 13.2$  kg; max clean lift-mass:  $126.4 \pm 22.9$  kg) were recruited for this study. After a brief warm-up with several repetitions and sets at lighter loads, each lifter performed two repetitions at 85% of their estimated 1-Repetition Maximum (RM) of the clean exercise.

Sixteen reflective markers were attached to various anatomical landmarks of each lifter's feet, shanks, thighs, and pelvis [2]. In addition, a strip of reflective tape was wrapped around the long axis of the barbell at its mid-point. The three-dimensional position of these markers were recorded with a 6-camera motion capture system at 250 Hz. GRF were collected at

1,250 Hz from two force plates that were built into a 2.4 m x 2.4 m weightlifting platform.

The kinematic and kinetic data were filtered at 6 Hz and 25 Hz, respectively. Lower extremity biomechanics were calculated from a rigid-link model that included a foot, shank, thigh, and pelvis segment. An inverse dynamics procedure, which combined kinematic and GRF data with basic anthropometric data, was used to calculate the net internal joint torques of the hip, knee, and ankle joints [4]. Torques were normalized to each lifter's body-mass and height (i.e.,  $\text{N} \cdot \text{m} \cdot \text{kg}^{-1} \cdot \text{m}^{-1}$ ). Time-series data from the right leg were then extracted and time-normalized to 100% of the pull phase, which was defined as period from when the barbell left the platform to when the GRF fell below 10 Newton's. The horizontal and vertical positions of the barbell were also extracted during the pull phase.

The horizontal and vertical positions as well as the mass of the mass of the barbell served as inputs to a NN to predict the joint torque time-series. The NN consisted of a nonlinear autoregressive network with exogenous inputs, and had a 3-layer input level, a 10-layer hidden level, and a 3-layer output level. The NN was trained with Levenberg-Marquardt back-propagated error correction and had a feedback-delay of 1:2. The NN was developed and trained on data from six of the seven weightlifters, and then tested with data from the one remaining weightlifter (Figure 1) [3]. The performance of the NN was evaluated based on its mean square error (MSE) and inspection of the predicted data output in relation to the actual input data. In addition, the percent difference between actual and predicted peak hip, knee, and ankle joint torques were calculated to provide a pragmatic interpretation of the NN performance [3].

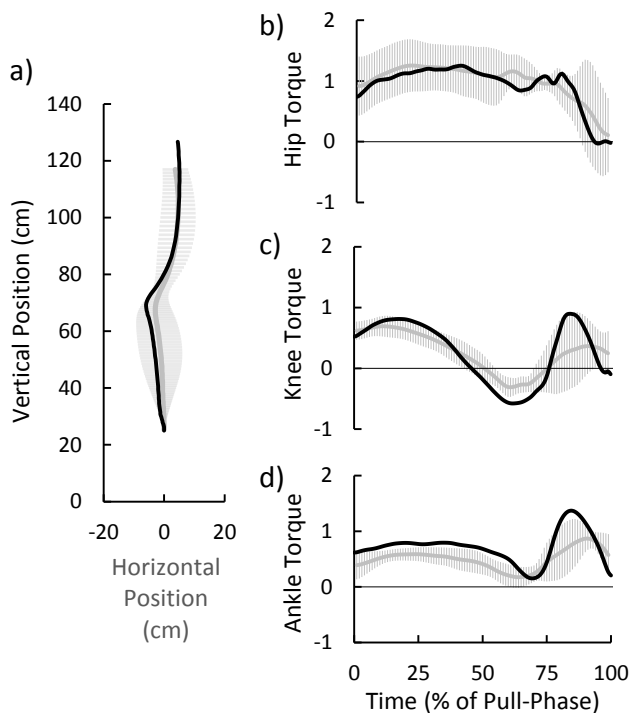


**Figure 1:** Ensemble average (Mean±SD) of training cases (grey line and error bars) and the single test case (black) for a) barbell position and b) hip, c) knee, and d) ankle joint torque data.

## RESULTS AND DISCUSSION

A low MSE ( $4.70e^{-5}$ ) obtained from the training of the NN indicated that the NN effectively captures the relationship between joint kinetic data and barbell mass and kinematic data during the clean.

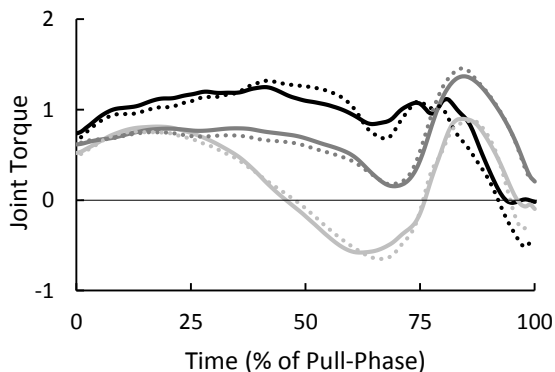


**Figure 2:** Actual (solid line) and predicted (dotted line) hip (black), knee (dark grey), and ankle (light grey) joint torque data.

Further, application of the trained NN to the test case showed that it was possible to predict joint torques from the barbell kinematic data and mass with a low error (MSE = 0.0119) (Figure 2).

**Table 1:** Percent difference (%Diff) between actual and predicted joint torques with NN.

Joint	Actual	Predicted	%Diff
Hip	1.25	1.31	5%
Knee	0.90	0.88	-2%
Ankle	1.36	1.45	6%

The prediction errors (MSE) for the individual joint torques were 0.0266 for the hip, 0.0092 for the knee, and 0.0096 for the Ankle joint. With respect to the peak joint torques, the results of the current study indicate that the vertical and horizontal barbell motions as well as lift mass could predict the joint torques to within 6% (Table 1).

## CONCLUSIONS

This study highlighted the ability of a NN to predict joint kinetic data from barbell mass and kinematic data. Given that the horizontal and vertical motions of the barbell can be easily recorded and processed with low-cost motion analysis solutions, the results of the current study suggest that sports biomechanists and coaches could use NN to readily analyze joint torque data of weightlifters during either practice or competition without expensive equipment or obtrusive instrumentation of athletes.

## REFERENCES

1. Hahn ME & O'Keefe, KB. *J Musculoskel Res* **11**, 117-126, 2008.
2. Kipp K, et al. *J Strength Cond Res* **25**, 1229-1234, 2011.
3. Liu Y, et al. *J Biomech*, **42**, 906-911, 2009.
4. Winter DA. *Biomechanics and motor control of human movement*. John Wiley & Sons, Inc. 2005.

# MUSCLE SYNERGIES IN FEMALE ATHLETES WITH GENERALIZED JOINT HYPERMOBILITY

Christopher F. Geiser, Matthew Giordanelli, Lydia Legler, Courtney Kost, Philip Malloy, and Kristof Kipp

Marquette University, Milwaukee, WI, USA  
email: Christopher.geiser@marquette.edu

## INTRODUCTION

Individuals are characterized as having Generalized Joint Hypermobility (GJH) when they have a greater than normal range-of-motion (ROM) at multiple joints throughout their body, and are often referred to in the common vernacular as “double-jointed”<sup>1</sup>. GJH is more common in females and younger ages<sup>2</sup>. Individuals with GJH who participate in athletic activities are more at-risk for knee injury<sup>3</sup>, injury in general<sup>4</sup>, and they sustain more severe injuries than non-GJH counterparts<sup>4</sup>.

Previous studies have examined whether individuals with GJH attempt to control their joint laxity by altering muscle activation patterns. Subjects with GJH were found to have greater co-activation levels of erector spinae muscle groups and of hamstring and quadriceps muscles, all key joint stabilizing muscle groups, during a balance task<sup>5</sup>. GJH subjects also exhibit greater hamstring and quadriceps co-contraction during gait<sup>6</sup> and during isometric knee flexion<sup>7</sup>, presumably to stabilize their more mobile knee joints. However to date, no analysis of motor control or muscle activation patterns have been done in high level athletes during demanding athletic movement tasks.

Non-negative matrix factorization (NNMF) is becoming a popular tool to evaluate muscle synergies and activation patterns, because it offers unique insight into motor control strategies. NNMF has been used to evaluate clinical differences in motor control strategies between children with cerebral palsy and controls during gait<sup>8</sup>. The goal of the current investigation was to use this technique in the evaluation of control strategies of GJH individuals across multiple stabilizing muscle groups during a complex athletic task, testing the hypothesis that high level female athletes with GJH demonstrate muscle synergies similarly to non-GJH control

subjects from the same team and training background.

## METHODS

Thirty eight athletes from a women’s Lacrosse team were screened for GJH using the Beighton and Horan Joint Mobility Index (BHJMI)<sup>9</sup>. Individuals with a score of 5 or greater were assigned to the GJH group<sup>10</sup>. Individuals with scores of 0 or 1 were used as controls, and those with scores of 2 to 4 were excluded from the study.

Eight wireless surface EMG sensors were placed on each players’ dominant side Gluteus Maximus and Medius, Rectus Femoris, Vastus Lateralis and Medialis, Biceps Femoris, Medial Gastrocnemius and Anterior Tibialis of each subject. Leg dominance was determined by asking which leg they prefer to kick a ball with (right leg in all subjects). The skin was prepared by cleaning with an alcohol wipe and allowed to dry prior to electrode placement, no subjects needed shaving. Sensors were applied with manufacturer adhesives strips and reinforced with flexible adhesive tape.

Subjects performed a single-leg land-and-cut (CUT) task in the lab while EMG and force plate data were collected. The CUT task involved standing on a box, jumping forward and landing on the dominant leg, and cutting immediately 90 degrees away from the land leg. The height of the box was set equal to each subject’s max vertical jump height, as measured from the displacement of a pelvis marker during a maximum countermovement jump. The box was set back from the force plate a distance equal to each participant’s maximum single leg stride distance. This task was chosen because it was a challenging single-leg, athletic-like task that still allowed expedient data collection in a controlled lab setting. To avoid biasing subjects, the same instructions to

“land and quickly cut to the left” were given to each subject. Participants were allowed to practice the task until comfortable, and then performed 3 successful trials. Trials were deemed unsuccessful if the subject could not complete the task, or if they turned and faced the CUT direction instead of facing forward.

EMG and GRF data were collected at 960 Hz. Data were exported for analysis with custom Matlab software. Data were filtered in Matlab using a Bandpass filter with cutoff frequencies of 10Hz to 400Hz. GRF data were used to determine the stance phase of cutting. The stance-phase EMG data for all muscles were time normalized, and ensemble averages were calculated for each of the 8 muscles. The time-normalized ensemble averages for each subject were used as inputs to an NNMF procedure<sup>8,11</sup>. The NNMF algorithms were looped to continue until the variance accounted for (VAF) in the overall muscle activation profiles reached a threshold of 95% using a sum-of-squares approach. The number of activation synergies needed to reach 95% VAF, and the %VAF by the first synergy were used for statistical analysis. The group differences in means for these two variables were analyzed in SPSS with a one-way ANOVA, with significance level set at  $\alpha = 0.05$ . Simple effects sizes were calculated with Cohen’s  $d$ .

## RESULTS AND DISCUSSION

Seven women had a score of 5 or more on the BHJMI (GJH group:  $19.4 \pm 1.0$  years,  $66.0 \pm 6.1$  kg,  $167.3 \pm 3.3$  cm). Eight controls from that same team had a score of 0 or 1 on the BHJMI (CTRL group:  $19.9 \pm 1.2$  years,  $62.1 \pm 7.1$  kg,  $165.3 \pm 7.3$  cm).

The GJH group exhibited fewer muscle synergies than the CTRL group ( $1.67 \pm 0.43$  vs.  $2.25 \pm 0.43$ ;  $p = 0.02$ ,  $d = 1.38$ ), which points to a less complex muscular control strategy during the stance phase in people with GJH.

Although the VAF of the first muscle synergy did not differ significantly between groups (GJH:  $94.4 \pm 1.2\%$ ; CTRL:  $92.0 \pm 2.8\%$ ;  $p = 0.053$ ,  $d = 0.87$ ), the large effect size indicates that there may be clinically meaningful group differences.

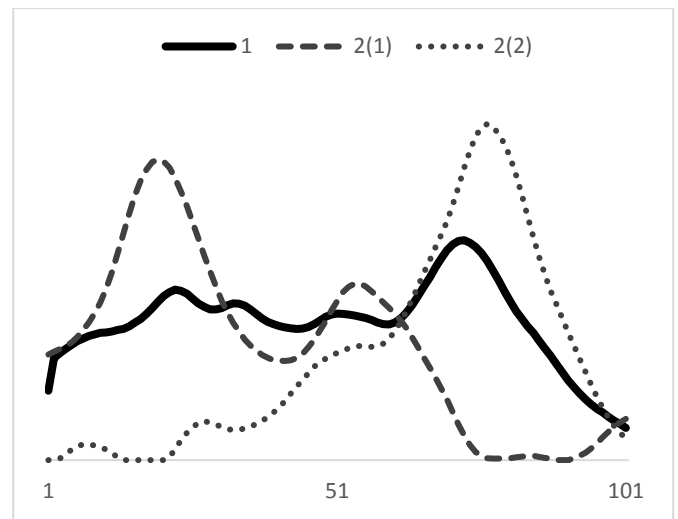


**Figure 1:** Example of synergy activation coefficients for an individual subject with one synergy (1) and a subject with 2 synergies [2(1) and 2(2)] to account for >95% variance in muscle activation patterns.

## CONCLUSIONS

Together, these results provide support for the hypothesis that individuals with GJH use a simpler muscle activation strategy during the execution of an athletic task. The simpler strategy may reflect greater co-contracting of lower extremity muscle groups, which may be a means to better stabilize the lower extremity joints in the face of hypermobility. Given that people with GJH are at greater risk of injury, it would be of interest to further study the association between muscle synergies and risk of injury, as well as the effects of targeted training on muscle synergies in relation to injury risk.

## REFERENCES

1. Grahame, R. *Rheumatology*. 2008;20:106-10.
2. Russek LN. *Phys Ther*. 1999;79(6):591-99.
3. Pacey V. *Am J Sp Med*. 2010;38(7):1487-97.
4. Konopinski. *Am J Sp Med*. 2012;40(4):763-69.
5. Greenwood, NL. *Man Ther*. 2011;16:623-28.
6. Schmid, S. *Clin Biom*. 2013;28:1020-25
7. Jensen, BR. *Mus Nerv*. 2013;48:762-69
8. Steele, KM. *Dev Med Ch Neur*: 2015;57:1177-82
9. Beighton & Horan. *JBJS Br*. 1969;51(3):444-53.
10. Decoster, LC. *JAthTr*. 1999;34(2):99-105
11. Lee & Seung, *Nature*. 1999;401(21):788-91

# ICE HOCKEY SKATING MECHANICS: TRANSITION FROM START TO MAXIMUM SPEED FOR ELITE ATHLETES

<sup>1</sup> Aleksandra Budarick, <sup>1</sup> Jaymee Shell, <sup>2</sup> Shawn Robbins, <sup>3</sup> Philippe Dixon, <sup>4</sup> Tong-Chin Tom Wu, and <sup>1</sup> David Pearsall

<sup>1</sup> Department of Kinesiology and Physical Education, McGill University, Montreal, QC, Canada

<sup>2</sup> School of Physical and Occupational Therapy, McGill University, Montreal, QC, Canada

<sup>3</sup> School of Public Health, Harvard University, Boston, MA, USA

<sup>4</sup> Department of Movement Arts, Bridgewater State University, Bridgewater, MA, USA

Email: [aleksandra.budarick@mail.mcgill.ca](mailto:aleksandra.budarick@mail.mcgill.ca), Web: <http://www.mcgill.ca/ihr/g/>

## INTRODUCTION

Ice hockey is a popular winter sport in North America. Many factors determine strategic gameplay advantage: one fundamental attribute is an athlete's "power skating"; more specifically, one's ability to achieve rapid skating start acceleration up to maximal speed. Coaches emphasize this in training drills based on total time per distance covered; however, discrete trajectory measures of skaters' position over time are required to understand skating technique mechanics to optimize performance. For instance, in sprint running, centre of mass (COM) acceleration profiles can detect key phase transition points that correspond to changes in body segment angles [1]. Similar analyses in ice hockey would allow a comprehensive understanding of the mechanics involved in acceleration to maximal skating speed.

This is the first study to quantify the COM forward velocity-time trajectories of elite ice hockey skaters from start to maximal speed, and to compare the trajectories of male and female athletes.

## METHODS

Nine male (22±1 years) and ten female (21±1 years) elite ice hockey players participated in this study. A single leg jump test evaluated lower limb power. Each participant was instrumented with a full-body marker set, including instrumented skates and a stick. Data was collected on an ice surface at 240 Hz with an 18-camera Motion Capture system (Vicon®, Oxford, UK) (fig 1). The skating acceleration phase (0-15m) and maximal skating phase (19-34m) were

captured independently. For the acceleration phase, the athletes skated between the blue lines, and the first 7 accelerative steps were captured. For the maximal skating trials, the athletes skated from the red goal line to the far blue line, and 4 steps of maximal skating were captured between blue lines.

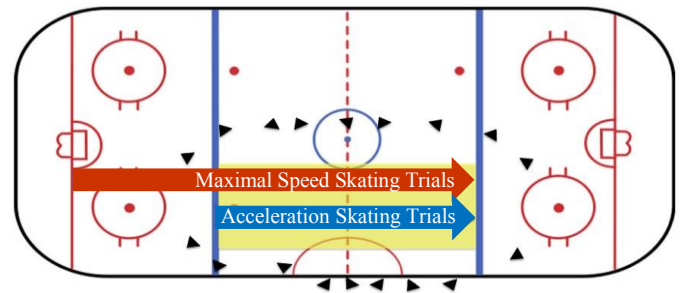


**Figure 1:** On-ice camera set-up (black triangles) and calibrated capture area (yellow shaded area).

The complete skating velocity-time trajectory was generated using logarithmic projection of the accelerative steps' forward velocities. The maximal speed phase steps were plotted on the logarithmic line of best fit according to the respective time (frame) distance between phases for each participant. Data was processed using Vicon Nexus 2.1.1 (Vicon®, Oxford, UK), and Visual 3D software (Ver 5.01.23, C-Motion, Germantown, MD, USA). Data was analyzed using custom MATLAB (Mathworks, Natick, MA, USA) scripts. SPSS Statistic Software (IBM Corporations, Somers, USA, Version 23.0) was used for statistical analysis. Mixed-ANOVAs were used to test for interactions between skater sex and step number on COM measures. A Pearson's  $r$  correlation determined the strength of the relationship between leg power and peak speed. Significance level was set at  $p < 0.05$  for all tests.

## RESULTS AND DISCUSSION

The single leg jump test showed significant differences between females and males on both the right ( $p=0.015$ ) and left ( $p<0.001$ ) sides, with male skaters jumping further in both cases. There was a strong correlation between peak leg power and peak speed ( $R^2=0.81$ ).

Logarithmic COM forward velocity-time profiles from start to maximal speed were similar between male and female skaters, though progressive male velocity gains superseded those of the females, where males were faster ( $p<0.001$ ) at any given distance (fig 2). Males achieved greater peak accelerations in the first 1.25 seconds ( $7.7$  vs  $6.2$   $m/s^2$  for males and females on average over the first four stance phases), but the male vs. female acceleration magnitudes were similar after the first 1.5 seconds of skating. Hence, the leg power output in the first four steps (1.25 seconds) was critical in the skate start performance, so it will be important for coaches to focus on these first four steps, as well as increasing lower body power, to maximize performance.

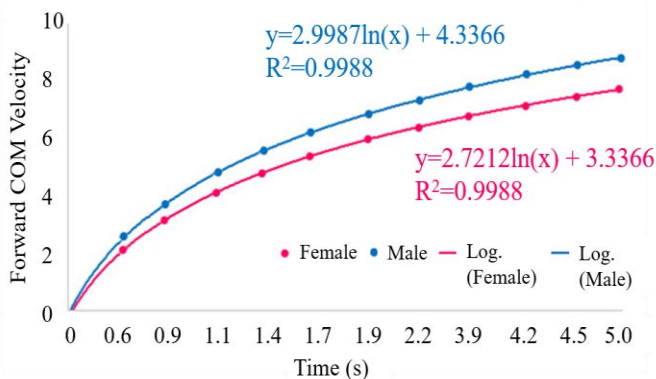


**Figure 2:** The velocity-time progression for males and females from standing start to maximum speed, including logarithmic equations and  $R^2$  values.

After 34 m from the start, body COM forward velocity was still increasing by 0.4 to 0.5 m/s per stride due to the overall positive net forward propulsion. In theory, skaters would reach their ultimate maximal skating velocity once they reach their anaerobic threshold [2]. It is unlikely that an ice hockey athlete would perform an all-out sprint to

exhaustion, especially in a game setting, so these athletes may never actually achieve their ultimate maximal speed. Hence, the maximal speed variables determined in this study are arguably representative of an in-game context.

The maximum acceleration during the first stance phase was  $7.8 \pm 1.6$   $m/s^2$  for females, and  $9.6 \pm 2.0$   $m/s^2$  for males. There was a significant difference of forward acceleration between sexes during the start phase ( $p=0.015$ ), but not during the maximal speed phase. The maximal speed phase within-stride accelerations oscillated between approximately 2 and  $-2$   $m/s^2$ , and the positive acceleration phase exhibited a bimodal pattern. Overall, a transition point between accelerative and maximal skating may be identified at the point at which negative acceleration intervals occur within the trajectory.

## CONCLUSIONS

Using a 3D motion capture system and a whole-body marker set, this study was successful in tracking skater's body COM movement patterns in an open ice surface setting. To the authors' knowledge, this is the first study to quantify the discrete velocity progression of elite ice hockey athletes from start to maximal skating. Overall, elite male and female ice hockey athletes showed similar COM trajectories, though males achieved a faster peak velocity than females, largely due to males' greater acceleration during the initial first four steps after the start. Hence, all things being equal, lower extremity power and starting step techniques are crucial to achieve maximal speed over a 30 m distance.

Future research on ice hockey skating should include kinematic analyses in conjunction with kinetic and/or physiological measures, in order to fully understand the implications of these sex-specific skating patterns on performance.

## REFERENCES

1. Nagahara R, et al. *Biology Open* **3**, 689-699, 2014.
2. Droghetti P, et al. *Eur J Appl Physiol* **53**:299-303, 1985.

# Ball Contact Initiates Forearm Deceleration in a Volleyball Spike

<sup>1</sup> Glen C. Thompson, <sup>1</sup> Dylan G. Schmitz, <sup>1,2</sup> Kayt E. Frisch PhD

<sup>1</sup> Dordt College, Sioux Center, IA, USA

<sup>2</sup> email: [Kayt.Frisch@dordt.edu](mailto:Kayt.Frisch@dordt.edu)

## INTRODUCTION

A previous study has calculated kinetic and kinematic parameters for every arm swing phase prior to ball contact during a volleyball spike [1]. In baseball, a sport with a similar overhand motion, the deceleration phase during pitching has been associated with tensile loads strong enough to peel the biceps and superior labrum complex away from their humeral attachments [2]. Therefore, neglecting to analyze the contact and deceleration phases of the volleyball spike swing may lead to poor estimations of forces in the shoulder.

Minimal research has noted the importance of analyzing the deceleration phase in volleyball. Escamilla et al. presented the idea that contacting the ball produces an equal and opposite direction that acts as the main deceleration of the arm during a spike [3]. This study tests that hypothesis by measuring arm acceleration throughout the course of a volleyball spike to determine when the arm decelerates.

## METHODS

This study evaluated arm motion of five right-handed intercollegiate women's volleyball players. None of the athletes reported current shoulder and/or elbow pain. This study followed a protocol approved by IRB.

Each participant followed standard warm-up procedures prior to data collection. 25 reflective markers were placed on the trunk and upper body and tracked using a 12-camera motion capture system (1280 x 1024 pixels, 240fps, OptiTrack, Beaverton, OR).

Each athlete was asked to spike the volleyball with a live set five times. Small gaps in the marker data were filled using the built-in interpolator, then

exported as .csv files to be analyzed with a previously created MATLAB program (MathWorks, Natick, MA).

Using the marker position data, the angular position, velocity, and acceleration of the forearm with respect to the global coordinate system's x-axis were calculated. These plots were used to assess the rate and temporal location of deceleration of the forearm during a volleyball spike.

## RESULTS AND DISCUSSION

Consistently across multiple trials, for multiple subjects, the deceleration of the arm begins at the point of maximum angular velocity, which corresponds to a point of inflection in the angular acceleration plot. The deceleration phase finishes when the angular velocity reaches its global minimum, which also relates to another point of inflection in the angular acceleration plot. The trends in angular velocity for an experimental spike can be observed in Figure 1:

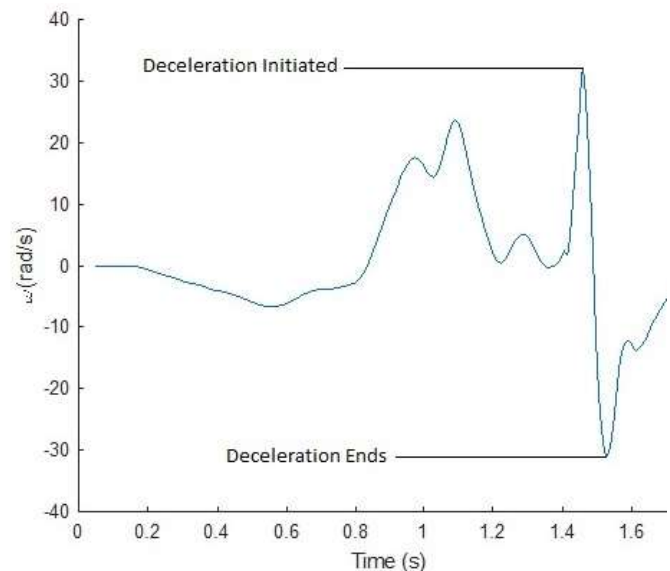


**Figure 1:** Forearm Angular Velocity for a Volleyball Spike

Similarly, the trends in angular acceleration for this spike can be seen in Figure 2:

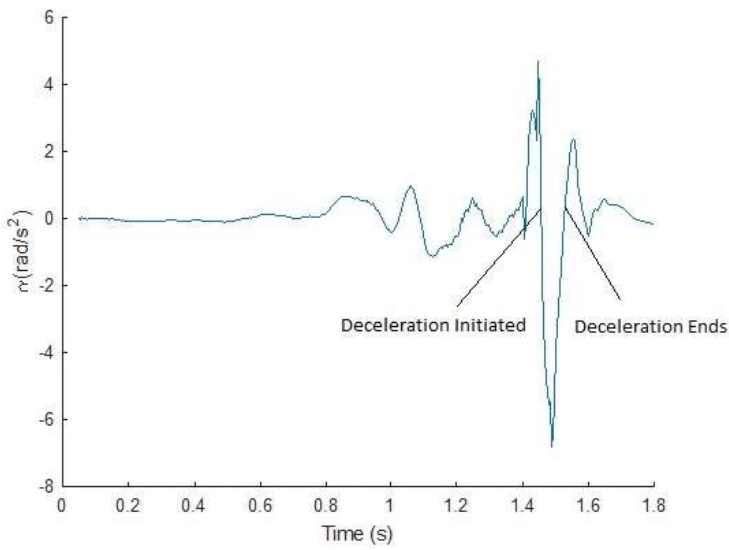


**Figure 2:** Forearm Angular Acceleration for a Volleyball Spike

It was approximated that in this spike, deceleration initiated at 1.45 seconds and finished at 1.55 seconds. This means that the muscles producing the force to spike the volleyball were eccentrically loaded in approximately 0.1 seconds. It is unclear how variation in the rate of eccentric loading affects overall muscle functionality. However, it is possible that variations in loading time affect the muscle's ability to contract repeatedly.

This variance can be caused by many in-game factors. For a volleyball spike, the location of the set can have a large impact on swing mechanics. For example, during a match, the set may be closer to the net than the athlete initially anticipated, causing her to have to adjust her swing. This causes a more rapid

deceleration of the arm after the spike, because the attacker must avoid the net. This rapid deceleration may create a larger load on the rotator cuff, especially the supraspinatus and infraspinatus muscles. Further study is needed to elucidate these possible connections.

## CONCLUSIONS

The results indicate that ball contact initiates a large deceleration during a volleyball spike. This supports the hypothesis that the ball contact initiates deceleration [3]. This emphasizes the need for more information about the contact forces during a volleyball spike. The contact forces during a spike would provide the best estimate for the relatively large deceleration loading on the arm, and help determine if volleyball athletes are subject to the same loading risks that have been associated with shoulder injury in other overhead sports.

## REFERENCES

1. Reeser JC, et al. *Sports Health*, **2**, 368-374, 2010.
2. Burkhart SS, et al. *Arthroscopy: The Journal of Arthroscopic & Related Surgery*, **19**, 404-420, 2003.
3. Escamilla RF, et al. *Sports Med*, **39**, 569-590, 2009.

## ACKNOWLEDGMENTS

The authors would like to thank the Dordt College Engineering Department, the Dordt College Women's Volleyball team, Coach Chad Hanson, the Dordt College Center for Research and Scholarship, and the Carver Foundation.

# QUANTIFYING CONTACT LOADING DURING A VOLLEYBALL SPIKE

<sup>1</sup>Dylan G. Schmitz, <sup>1</sup>Glen C. Thompson, <sup>1</sup>Chad DeGraaf, <sup>1</sup>Boone DeKramer, <sup>1,2</sup>Kayt E. Frisch PhD

<sup>1</sup>Dordt College, Sioux Center, IA, USA

<sup>2</sup>email: Kayt.Frisch@dordt.edu

## INTRODUCTION

The occurrence of shoulder pain and injury in young volleyball players is increasing, and it is likely that this may result from high repetition volume of overhand motions like spiking and serving. Reeser [1] analyzed the pre-contact shoulder kinematics and inferred muscle forces during a spike motion up to the moment of contact. However, the forces between the ball and the hand are thought to be relatively large [2] and should also be considered.

This abstract proposes a method to quantify the forces acting between a volleyball and the hand during a spike or serve. The method requires two distinct parts: (1) Direct measurement of the forces between the ball and the hand via pressure sensors and (2) indirect calculation of the forces in a classical impulse-momentum analysis of motion capture data.

## METHODS

The contact forces were measured using force-sensitive resistors (FSR) (TekScan FlexiForce A201 Sensors), in an inverting op-amp circuit configuration. An ATmega328 microcontroller master-slave system, programmed via the Arduino IDE, read and digitized the analog data outputs.

The slave devices were located on a forearm-mounted apparatus, along with the op-amp chips and resistors. To keep the forearm-mount size to a minimum, the power, input signal, and returning digital data were transmitted to the circuit by shielded wire. Power regulation, signal inversion, and data logging were performed on a larger belt-mounted device.

The digitized sensor output signal was stored to an SD card as a .csv file. Initial calibration of the FSRs generates a linear voltage-to-force conversion

regression, which allows the A/D values to be converted to meaningful force values. Averaging all sensors for each sample time and accounting for the relative areas of the sensor and contact surface gives the contact loading of the volleyball.

Indirect measurement of the contact forces can be achieved by tracking the translation and rotation of a volleyball in 3D space using motion capture. The motion capture software, Motive (OptiTrack, Corvallis, OR), includes spherical rigid-body tracking, so a tetrahedral marker set (4 reflective markers) is used to track the volleyball.

To mitigate marker occlusion, protruding spherical markers were affixed to the surface of the volleyball. Since the protruding markers made serving the volleyball more difficult, some trials used flat sticker reflective markers, but the marker occlusion was so severe that these trials were not considered.

Motive tracked not only the position of each marker, but also the translation and rotation of the spherical rigid body. Using a classical discretized impulse-momentum analysis (Eqn. 1) allowed estimation of the force on the hand:

$$(F)(\Delta t) = m * (v_2 - v_1) \quad (1)$$

The impulse was obtained from the measured velocities immediately before and after hand contact. The impulse is approximated as a constant force over the duration of contact, so the impulse divided by the contact duration gave the average force applied.

## RESULTS AND DISCUSSION

The tetrahedral marker set yielded satisfactory results for tracking the volleyball. The rigid body tracking feature in of Motive indirectly tracked the

geometric center of the ball. The motion capture system successfully logged the volleyball's center of mass (COM) in 3D, as well as the position of each marker (Fig. 1).

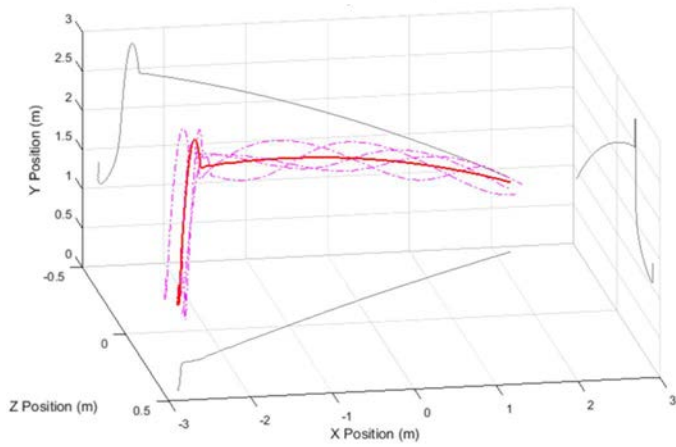


**Figure 1:** Trajectory of the volleyball in 3D. Solid line represents path of COM, dashed lines represent marker paths.

The custom MATLAB (MathWorks, Natick, MA) program used to determine force on the hand calculated the ball's translational velocity components in x, y, and z (Fig. 2). The velocities pre- and post-spike were used as  $v_1$  and  $v_2$ , respectively.

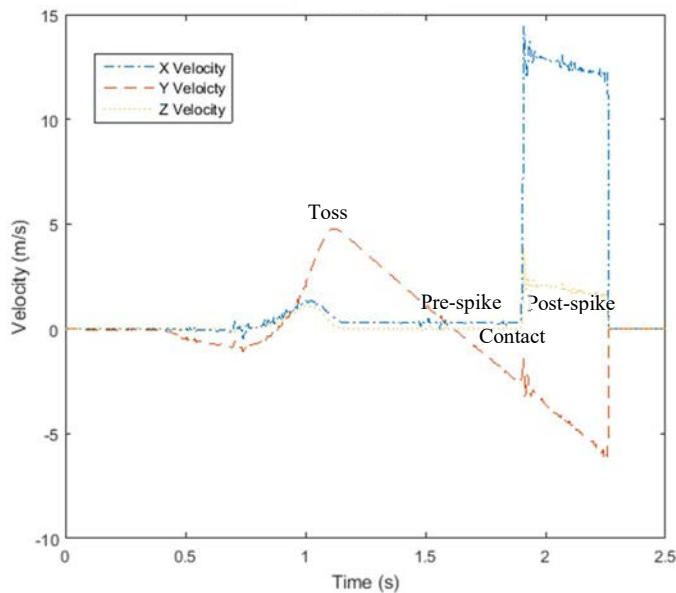


**Figure 2:** Velocity of the COM of the volleyball.

The duration of contact could not be accurately acquired from the motion capture data despite the fact that the frame rate was set to 240 fps. While this frame rate is sufficient for most applications, the duration of the impulse on the volleyball ranged from 10-15 ms, giving at most 3 samples during contact. Preliminary testing with the FSRs gave evidence that the contact duration would average 15 ms, which was used to estimate average loadings up to 400 N based on proof-of-concept tests with collegiate volleyball players.

## CONCLUSIONS

Complementary use of the direct (FSR) method and the indirect (impulse-momentum) analysis allowed estimation of the normal contact forces on the hand for a volleyball spike. Future work will focus on calculating the tangential forces that cause rotation of the volleyball. Additionally, the forces measured will be combined with a kinematics analysis to calculate shoulder loadings during contact.

## REFERENCES

1. Reeser JC, et al. *Sports Health* **2**, 368–374, 2010.
2. Burkhart SS, et. al. *Arthroscopy: The Journal of Arthroscopic & Related Surgery* **19**, 2003

## ACKNOWLEDGMENTS

The authors would like to thank the Dordt College Engineering Department, the Dordt College Women's Volleyball team, the Dordt College Center for Research and Scholarship, and the Carver Foundation.

# EVALUATION OF BICYCLE PEDALING ABILITY USING VERTICAL AND HORIZONTAL COMPONENTS OF PEDALING FORCE VECTOR

<sup>1</sup> Tomoki Kitawaki and <sup>2</sup> Tatsushi Tokuyasu

<sup>1</sup> Kansai Medical University, Hirakata, Osaka, Japan

<sup>2</sup> Fukuoka institute of technology, Fukuoka, Japan

email: kitawaki@hirakata.kmu.ac.jp

## INTRODUCTION

In recent years, a variety of power meters, devices that facilitate measurement of the pedaling force vector, for bicycles has become commercially available [1]. However, few consumer devices exist except for those used experimentally. In this study, the power meter is a pedaling monitoring system (SGY-PM900H90, SGX-CA900: Pioneer Corporation, Kawasaki, Japan) that displays a pedaling force vector to decompose the tangential and normal directions of pedaling force [2].

In order to evaluate bicycle pedaling ability, it is vital to know how riders can effectively exploit their own body weight (BW). However, it is difficult to determine how BW is used via an ability index calculation of the pedaling force vector [3]. Therefore, indices that are more accurate are required.

In this study, we aimed to evaluate the bicycle pedaling ability of amateur cyclists using new indices related to BW. These indices were calculated using the vertical and horizontal components of the averaged pedaling force vector signal obtained via a pedaling monitor system.

## METHODS

The pedaling load for twenty-eight male participants with written consent was increased from approximately 150–300 W in 1 min. intervals via a bicycle trainer (Powerbeam Pro-trainer: CycleOps, Madison, WI). The pedaling force vector output during incremental loading was recorded via a pedaling monitoring system (SGY-PM900H90). Cadence was not specified, i.e., each participant decided on a comfortable cadence. The pedaling

force vector was averaged at each load step, and the vertical and horizontal components, illustrated in Fig. 1, were calculated from the averaged value.

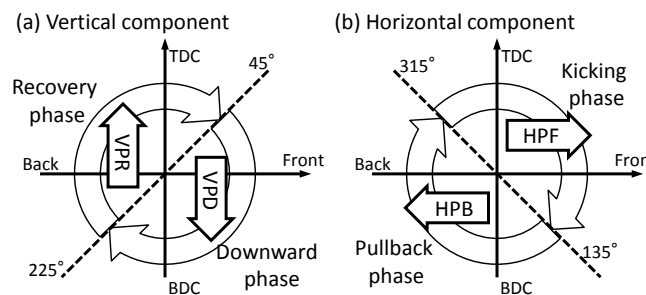


**Figure 1:** Vertical and horizontal components.

The indices calculated from these components of pedaling force are as follows:

- (1) The respective average vertical components in the downward phase (VPD: vertical power downward) and recovery phase (VPR: vertical power recovery).
- (2) The respective average horizontal components in the pullback phase (HPB: horizontal power back) and kicking phase (HPF: horizontal power front).
- (3) Applying a linear regression, standardized to 4.0 W/kg of each index using the corresponding load step value and normalized BW.

We then analyzed the respective correlations between VPD and sumVP (= VPD + VPR), HPB and HPF, and VPD and HPB.

## RESULTS AND DISCUSSION

Participant condition, experimental conditions, and measurement values of indices are listed in Table 1 (mean  $\pm$  SD). Standardization at 4.0 W/kg is practical since the step load of each subject ranged from 2.75 to 5.26 W/kg. To clarify, vertical indices

VPD = 30.9% and VPR = -7.2% mean that 30.9% and 7.2% of BW are on the pedal in the downward and recovery phases, respectively; HPB = 11.9% means that a rearward force equivalent to 11.9% of BW is applied to the pedal in the pullback phase; the value of HPF indicates a small forward pedal force in the kicking phase.

**Table 1:** Participant condition, experimental conditions, and measured values of indices.

<b>Age</b>		39.4 ± 9.4
<b>BW (kg)</b>		63.3 ± 7.6
<b>Height (cm)</b>		170.4 ± 5.5
<b>Step load power (W)</b>	<b>from</b>	171.8 ± 15.4
	<b>to</b>	328.6 ± 39.5
<b>Power weight ratio (W/kg)</b>	<b>from</b>	2.75 ± 0.40
	<b>to</b>	5.26 ± 0.85
<b>Vertical indices (% of BW)</b>	<b>VPD</b>	30.9 ± 4.4
	<b>VPR</b>	-7.2 ± 2.4
<b>Horizontal indices (% of BW)</b>	<b>HPB</b>	11.9 ± 1.6
	<b>HPF</b>	1.0 ± 1.7

Figures 2 and 3 show the relationships of the indices. There is a significant correlation between VPD and sumVP ( $r = 0.832$ ,  $p < 0.001$ ). This means that a participant with a strong downward pedaling force in the downward phase tends to efficiently apply downward force with one leg while raising the other.

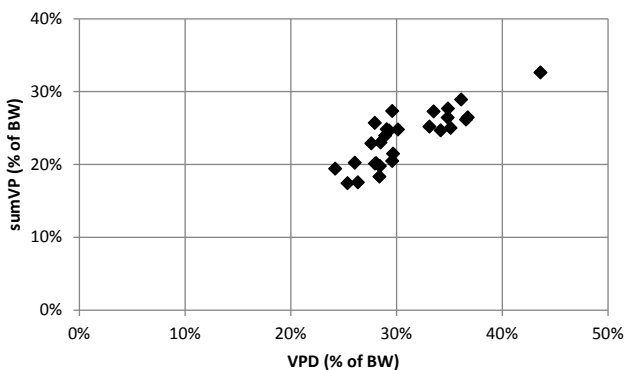


**Figure 2:** Correlation between VPD and sumVP.

In contrast, there is no significant correlation between HPB and HPF ( $r = 0.144$ ) or VPD and HPB ( $r = 0.265$ ). This indicates that most of the participants applied rearward force in the pullback phase and marginal forward force in the kicking phase, and that these forces are independent of each other. In addition, there is no relationship between vertical and horizontal power. From these results, it

is determined that indices are affected by the load applied to the pedal via the force of BW; this reflects the ability to harness one's own BW through pedaling ability. When downward force is large in the downward phase and pulling force is sufficient in the recovery phase, sumVP increases. Thus, the most effective measure of pedaling ability is suggested to be sumVP.

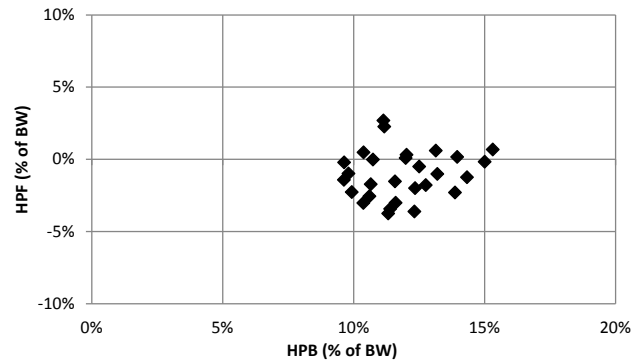


**Figure 3:** Correlation between HPB and HPF.

## CONCLUSIONS

To evaluate bicycle pedaling ability as related to body weight, the indices were calculated using vertical and horizontal components of the averaged pedaling force vector. Conclusions are as follows: (1) the most effective measure of pedaling ability seems to be the difference between downward force in the downward phase and pulling force in the recovery phase, and (2) the horizontal components in the kicking and pullback phases yield marginal influence on pedaling ability.

## REFERENCES

1. Allen & Coggan. *Training and Racing with a Power Meter* (2nd ed.), Velopress, 2010.
2. Pioneer Cyclesports. *Pedaling Monitor Sensor*, Retrieved from <http://pioneer-cyclesports.com/us-en/> on March 1, 2017.
3. Kitawaki et al. *Proceedings of World Congress of Cycling Science '14*, Leeds, UK, **25**, 13-19, 2014.

## ACKNOWLEDGMENTS

This research was supported in part by JSPS KAKENHI Grant-in-Aid for Scientific Research (C), 25350763.

# LOWER LEG MORPHOLOGY AND PLANTARFLEXION STRENGTH IN DANCERS

Paige E. Rice, Herman van Werkhoven, Edward K. Merritt, Wilton J. Norris,

Jordan P. Rodrigues and Jeffrey M. McBride

Department of Health & Exercise Science, Appalachian State University, Boone, NC, USA

Email: ricepe@appstate.edu

## INTRODUCTION

Rigorous training that involves leaping and jumping has been shown to influence skeletal and muscular characteristics. Many common dance movements are associated with high ground reaction forces imposed on the lower leg (LL), which might yield higher levels of bone and muscle strength to sustain such impacts similar to other weight-bearing activities. LL measurements such as bone failure load, similar to ultimate fracture load (UFL), bone stress-strain index (SSI), muscle cross-sectional area (CSA) and muscle power have shown to correlate with one another in a variety of athletes [1, 2]. Past findings have also indicated that muscle CSA is directly proportional to maximal strength levels. Dancers focus a great deal on plantarflexing and generating force about the ankle joint during leaps and jumps that might result in increased maximal voluntary isometric plantarflexion (MVIP) strength. By use of peripheral quantitative computed tomography (pQCT), bone and muscle characteristics can be easily identified without the imposition of overlaying tissues. To our knowledge, no research has reported LL morphology with pQCT and its relationship to strength levels in dancers. The aim of this investigation was to compare relative bone UFL, bone SSI, muscle CSA, fat CSA, and muscle + bone (M+B) CSA of the LL and maximal strength levels between dancers and untrained controls with pQCT.

## METHODS

Twenty healthy, college-aged females participated in the study with no musculoskeletal injury, neuromuscular disease, or LL injury within the past six months. Dancers (D;  $n = 10$ ; age =  $19.7 \pm 1.3$  yrs; height =  $163.9 \pm 6.6$  cm; body mass =  $62.0 \pm 10.3$  kg; dance training =  $17.0 \pm 1.2$  yrs) were required to

currently be training at least three times per week. Untrained controls (C;  $n = 10$ ; age =  $19.5 \pm 1.1$  yrs; height =  $166.0 \pm 6.8$  cm; body mass =  $69.6 \pm 14.5$  kg) were physically inactive and did not have any background in endurance training, strength training, or dance. LL measurements were recorded with pQCT scans at 14%, 38%, and 66% of the tibia length, with 0% representing the base of the tibia. Subjects underwent scanning of both right (R) and left (L) LL. UFL was determined in the x- and y-plane (medial-lateral, anterior-posterior) at the 14% site and normalized to subjects' body mass. SSI was measured at the 14% and 38% sites and again normalized to subjects' body mass. Muscle, fat, and M+B CSA measurements were obtained from the 66% site and normalized to the total area (girth of the leg) provided by the pQCT. Values between groups were then used for comparison. Subjects next completed a MVIP strength test on a custom-made sled at an inclination of  $20^\circ$  (Figure 1).

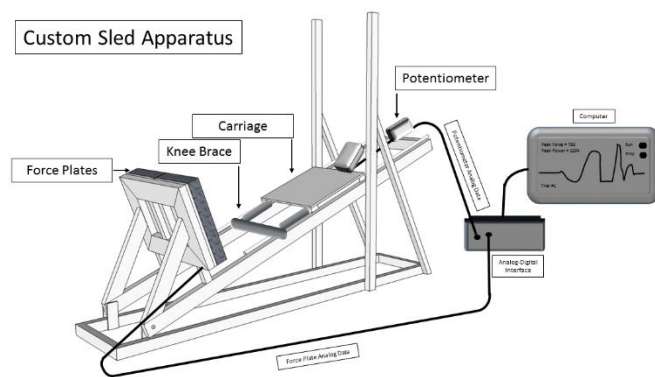


**Figure 1.** Custom Sled Apparatus.

Subjects laid on the sled with a pad behind the knees and a strap fixated proximal of the patella to isolate the ankle joint. Subjects were instructed to perform three, five-second MVIP trials with maximal effort. Two-minute rest intervals were provided in between

each trial. Subjects' trial with the greatest peak force was used for further analysis and normalized to body mass. MVIP data was collected and analyzed in a custom-designed LabVIEW program (National Instruments, Version 8.2, Austin, TX). Statistical significance was set at an *a priori* value of 0.05.

## RESULTS AND DISCUSSION

No significant ( $p \leq 0.05$ ) anthropometric differences existed between D and C. D had significantly greater L x- and R and L y-plane UFL at 14% of the LL (Figure 2), L SSI at 14% and 38% of the LL (Figure 3), and R and L muscle, fat and M+B CSA (Figure 4) than C. D possessed significantly greater MVIP relative peak force than C ( $27.7 \pm 5.7$  N/Kg;  $20.5 \pm 5.1$  N/Kg), which was significantly related to R ( $r = 0.67$ ) and L ( $r = 0.59$ ) LL muscle CSA.

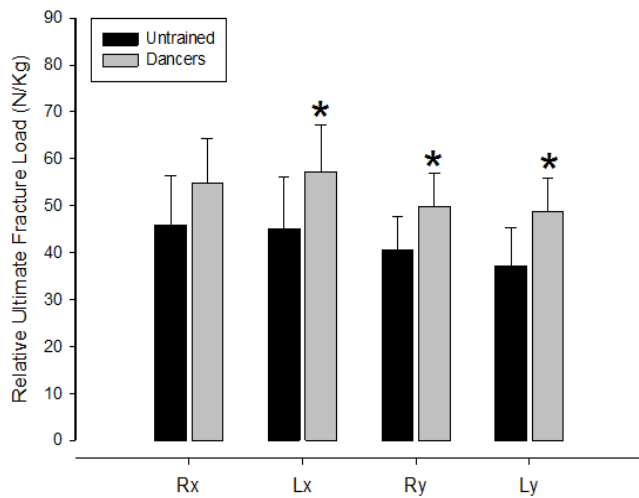


**Figure 2.** Right and left relative ultimate fracture loads at 14% of the lower legs in the x- and y-planes.

The data suggest that involvement in dance might be a stimulus for enhanced lower leg morphology and maximal strength levels. The shear forces that occur during dance leaps have revealed that a high amount of stress is introduced to the lower leg [3]. With improper nutrition, the dance community has been recognized to suffer from lower bone mineral density. However, our data provide evidence that healthily participating in ballistic activity not only fortifies bone strength but also influences muscle

maintenance and fat minimization. The physical demands of dance, therefore, might be contributors to muscle and bone features as well as maximal strength levels.

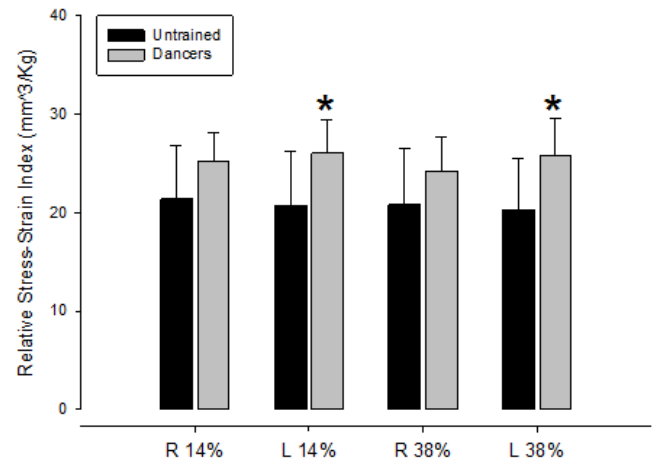


**Figure 3.** Right and left relative stress-strain indexes at 14% and 38% of the lower legs.

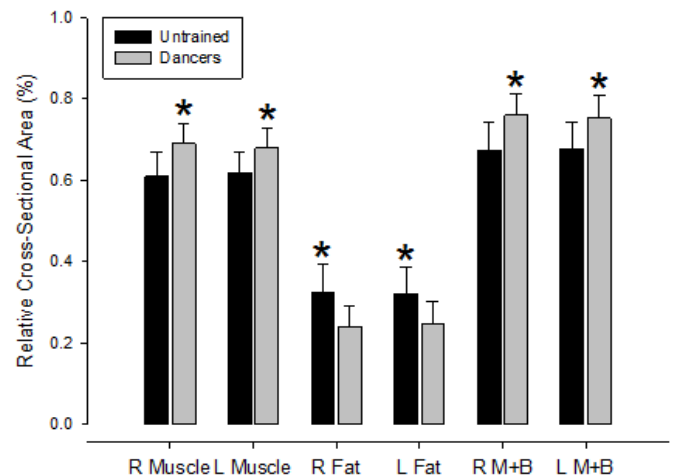


**Figure 4.** Right and left relative muscle, fat and muscle + bone CSA at the 66% of the lower legs.

## REFERENCES

1. Schipilow, JD, et al. *Bone* **56**, 281-9, 2013.
2. Janz, KF, et al. *Med Sci Sports Exerc* **47**, 2201-6, 2015.
3. Simpson, KJ, et al. *Med Sci Sports Exerc* **29**, 928-36, 199

# MORPHOLOGICAL AND FUNCTIONAL CHARACTERISTICS OF 110M HURDLERS: VOLUME AND ISOMETRIC STRENGTH OF THE HIP FLEXOR AND EXTENSOR MUSCLES

Hitoshi Okutani, Tadashi Suga, Tadao Isaka, and Akinori Nagano

Ritsumeikan University, Kusatsu, Shiga, JAPAN  
email: hitokku9pmzi@gmail.com

## INTRODUCTION

Sprint hurdle races, i.e., men's 110m hurdles and women's 100m hurdles, differ from others sprint events in that athletes are required to clear the hurdles. In these sprint hurdle races, hurdlers need to possess two types of techniques, i.e., hurdling technique and sprint technique. Hurdling technique includes take off motion, flight and clearance motion, and landing motion. In the flight and clearance motion, hurdlers swing up and down the leg, clearing the hurdle with flexion and extension of the hip joint. At the same time, hurdlers extend, abduct and supinate the other leg after taking off, in addition to extending and bending the knee joint. The former leg is the lead leg and the latter leg is the trail leg.

Hurdlers have a fixed lead leg and a fixed trail leg to clear the hurdles. The psoas major muscle, which is a hip joint flexor, plays a major role when the hurdlers swing up the lead leg over the hurdles. Therefore, it is assumed that the psoas major muscle of hurdlers have obtained specific morphological characteristics through their training. In addition, hurdlers are likely to show specific functional characteristics together with the morphological characteristics. However, this issue has not been reported in the literature. The purpose of this study was to investigate 110 m hurdlers' morphological and functional characteristics.

## METHODS

Two experiments were conducted in this study. In the first experiment, we determined the volume of the psoas major muscle. Six male collegiate hurdlers (height:  $179.4 \pm 2.5$  cm, body mass:  $65.7 \pm 2.9$  kg) participated in this experiment. The volume of psoas major muscle was determined using

magnetic resonance imaging (Figure 1). The images were taken from the trunk, between the intervertebral disk of the 5th lumbar vertebra to the 3rd lumbar vertebra. The gap between adjacent images was 5mm. We used analysis software (OsiriX Lite) to trace the area of each cross section of psoas major muscle, and calculated the volume using trapezoidal integral. The muscle volume was compared between the lead leg and the trail leg.



Figure 1: MR image of a hurdler

In the second experiment, we determined hip joint flexion/extension torque. Five male collegiate hurdlers (height:  $178.9 \pm 3.25$  cm, body mass:  $65.9 \pm 5.19$  kg) participated in this experiment. Isometric hip joint flexion/extension torque at  $60^\circ$  of hip joint flexion was measured by using Biodex dynamometer. Measurements were repeated for three times, five seconds for each trial, with forty seconds rest intervals. We determined the peak value of the torque from each trial. The average of peak values among the three trials was calculated. The values were compared between the lead leg and the trail leg.

## RESULTS AND DISCUSSION

The purpose of experiment 1 was to investigate if 110 m hurdlers' psoas major muscle has unique

morphological characteristics. The psoas major muscle volume of the lead leg ( $2.22 \pm 0.19 \text{ cm}^3/\text{kg}$ , Figure 2) was significantly greater than that of the trail leg ( $2.08 \pm 0.15 \text{ cm}^3/\text{kg}$ ,  $p < 0.05$ , Figure 2).

The results suggest that the psoas major muscle of the lead leg in hurdlers had hypertrophied through competition-specific training of the motion, i.e., repeated swinging up of the lead leg to clear the hurdles.



Figure 2: Volume of the psoas major muscle

The purpose of experiment 2 was to investigate if 110 m hurdlers' hip joint flexion/extension torque has unique characteristics. In the hip flexion torque, lead leg side ( $1.79 \pm 0.19 \text{ Nm/kg}$ , Figure 3) was significantly greater than that of the trail leg side ( $1.55 \pm 0.09 \text{ Nm/kg}$ ,  $p < 0.05$ , Figure 3). In the hip extension torque, lead leg side ( $3.81 \pm 0.82 \text{ Nm/kg}$ , Figure 4) was significantly greater than that of the trail leg side ( $3.43 \pm 0.76 \text{ Nm/kg}$ ,  $p < 0.05$ , Figure 4).

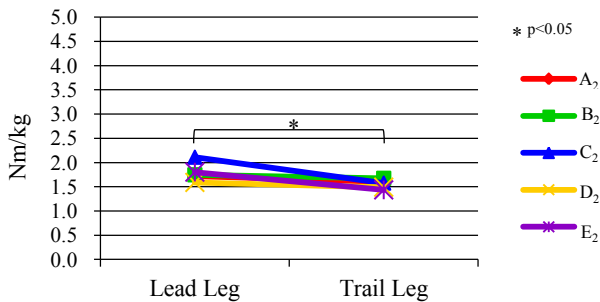


Figure 3: Flexion torque of the hip joint

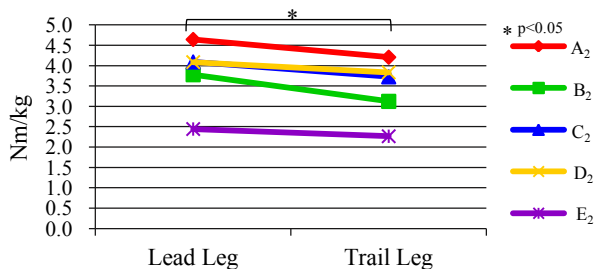


Figure 4: Extension torque of the hip joint

As is well known, muscle strength is related to muscle cross sectional area (Ikai and Fukunaga, 1968). In addition, muscle volume is a major determinant of joint torque (Fukunaga, et al., 2001). As shown in experiment 1, the volume of psoas major muscle of the lead leg was significantly greater than that of the trail leg. The fact that hip flexion torque of the lead leg was significantly greater than that of the trail leg was consistent with these preceding studies.

Similar to hip flexion torque, hip extension torque of the lead leg side was significantly greater than that of the trail leg side. Competition-specific motions of hurdling include rapid swinging down of the lead leg after clearing the hurdle. This may have caused strengthening of hip extensor muscles of the lead leg side compared to the trail leg side.

Okutani et al. (2016) reported that in sprinters, there was no significant difference in the psoas major muscle volume between the right side and the left side. It can be said that the characteristics found in this study are unique to hurdlers.

## CONCLUSIONS

The results suggest that hurdlers had obtained competition-specific morphological and functional characteristics through the training unique to hurdling. The results would be useful in the development of training programs to improve hurdle race performance in the future.

## REFERENCES

- Ikai, M and Fukunaga, T. *Internationale Zeitschrift für Angewandte Physiologie Einschliesslich Arbeitsphysiologie* **26**, 26-32, 1968.
- Fukunaga, T et al. *Acta Physiologica Scandinavica* **172**, 249-255, 2001.
- Okutani, H et al. Proceedings of: BASES Conference 2016, Nottingham, UK, 2016.

# BUILDING A BETTER GLUTEAL BRIDGE: ELECTROMYOGRAPHIC ANALYSIS OF HIP MUSCLE ACTIVITY DURING MODIFIED SINGLE-LEG BRIDGES

<sup>1</sup> BJ Lehecka, <sup>1</sup> Michael Edwards, <sup>1</sup> Ryan Haverkamp, <sup>1</sup> Lani Martin, <sup>1</sup> Kambry Porter, <sup>1</sup> Kailey Thach, <sup>1</sup> Richard Sack, and <sup>1</sup> Nils A Hakansson

<sup>1</sup> Wichita State University, Wichita, KS, USA  
email: bryan.lehecka@wichita.edu

## INTRODUCTION

Gluteal strength plays a role in injury prevention, normal gait patterns, eliminating pain, and enhancing athletic performance. Research shows high gluteal muscle activity during a single-leg bridge compared to other exercises for gluteal strengthening; however, prior studies have only measured muscle activity with the active lower extremity in 90° of knee flexion with an extended contralateral lower extremity [1]. Hamstring cramping has been reported during this standard, which may impede optimal gluteal strengthening [1].

Alterations to the single-leg bridge exercise could result in more efficacious gluteal muscle outcomes. Therefore, the purpose of this study was to determine whether modifications to the dominant leg angles for the single-leg bridge could enhance gluteus maximus and medius activity.

## METHODS

Twenty-eight subjects (16 females, 12 males) were recruited for this cross-sectional study from a population between 18 and 30 years of age who able to perform one hour of low-intensity exercise completed testing in a biomechanics laboratory at the local university. The average age was  $23.4 \pm 2.3$  years, height was  $1.73 \pm 0.11$  m, and weight was  $72.7 \pm 14.0$  kg. The study was approved by the Wichita State University Human Subjects Review Board.

Subjects were familiarized with the testing procedures, electrode placement, stationary bicycle warm-up, maximal voluntary isometric contraction (MVIC) testing, and single-leg bridge variations. Surface electrodes were placed on subjects' dominant leg over the following muscles: ipsilateral

and contralateral quadriceps femoris, ipsilateral biceps femoris, ipsilateral gluteus medius, and ipsilateral gluteus maximus.

Subjects performed a five-minute warm-up on a stationary bicycle prior to performing five variations of the single-leg bridge (Table 1). Bridge variation order was randomized, and the data collector was blind to the position being performed. Subjects were blind to the electromyographic (EMG) activity of their working hip muscles. Subjects performed eight repetitions of each bridge variation to the beat of a metronome set at 60 beats per minute.

EMG data were collected at 3000 Hz (Noraxon, Scottsdale, AZ) as subjects performed maximum voluntary isometric contractions (MVIC) of the muscles of interest and five variations of the single-leg bridge. EMG data were high-pass filtered at 15 Hz and low-pass filtered at 500 Hz using a fourth order Butterworth filter. Filtered data were then smoothed with a 50-millisecond moving average prior to calculating %MVICs for each participant and bridge variation. The mean and standard deviation values of these %MVICs were used in final analysis. Repeated measures analyses of variance (ANOVAs) with Bonferroni corrections were performed for each muscle tested in the five bridge variations. An alpha level of 0.05 was used. SPSS version 23 was used for data analysis.

## RESULTS AND DISCUSSION

Mean EMG measures across subjects expressed as the %MVIC of each analyzed muscle in each of the five single-leg bridge positions are presented in

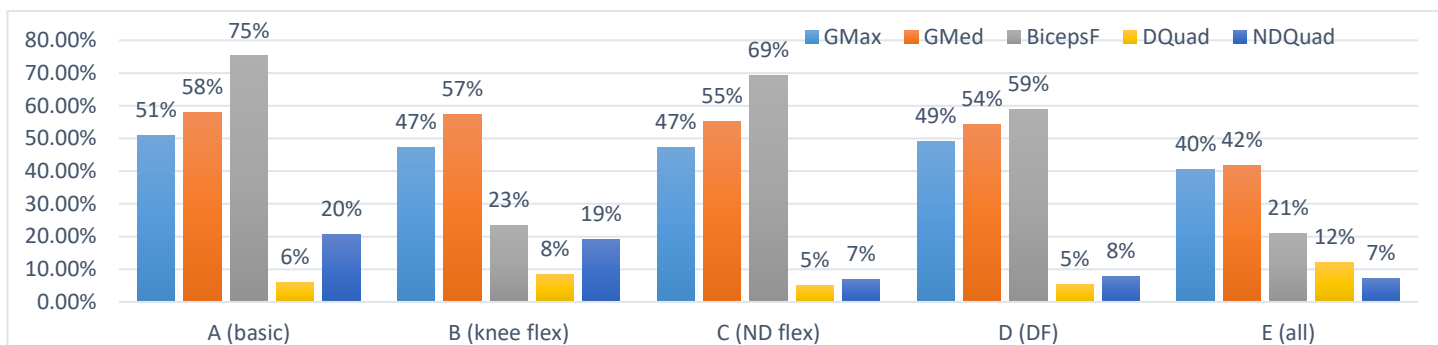


**Figure 1:** Mean EMG activity of five lower extremity muscles during five single-leg bridge variations (GMax = gluteus maximus; GMed = gluteus medius; BicepsF = biceps femoris; DQuad = dominant quadriceps; NDQuad = non-dominant quadriceps)

Figure 1. Gluteus maximus and gluteus medius activation was significantly different between positions A and E only. Biceps femoris activation was significantly different between all positions except A and C; and B and E. Dominant rectus femoris activation was significantly different among all positions except A and B; and C, D, and E.

Hamstring activity was minimized in positions B and E, in which the dominant knee was flexed to 135° instead of 90°. These positions appeared to preferentially activate both gluteal muscles, as gluteus medius and gluteus maximus activation surpassed and essentially doubled biceps femoris activation. However, of the two positions, position B displayed higher %MVIC values than position E for both gluteal muscles (47.35% and 57.23% versus 40.38% and 41.63% for the gluteus maximus and gluteus medius, respectively).

## CONCLUSIONS

The modified single-leg bridge position with 135° of knee flexion (position B) displayed preferential

activation of the gluteus maximus and gluteus medius. This position maintained similarly high gluteal activity while it significantly decreased biceps femoris activity compared to the traditional single-leg bridge position. This modified single-leg bridge position with increased knee flexion on the dominant side may allow more optimal training of the gluteal muscles than the traditional bridge position since the biceps femoris is less likely to be the limiting muscle of the exercise.

## REFERENCES

1. Boren K, Conrey C, Le Coguic J, Paprocki L, Voight M, Robinson TK. Electromyographic analysis of gluteus medius and gluteus maximus during rehabilitation exercises. *Int J Sports Phys Ther.* 2011 Sep; 6(3): 206–223.

## ACKNOWLEDGMENTS

Thanks to Kansas Partners in Progress for helping fund this study.

**Table 1:** Descriptions of the five single-leg bridge variations

Bridge Variation	Description
A (basic)	Subject supine; dominant lower extremity knee at 90 degrees of flexion, and foot flat; non-dominant lower extremity knee extended; arms crossed over chest
B (knee flex)	Identical to position A, except the dominant knee is flexed to 135 degrees
C (ND flex)	Identical to position A, except the non-dominant knee in a resting flexed position and hip in 90 degrees of flexion
D (DF)	Identical to position C, except the dominant ankle is fully dorsiflexed
E (all)	Identical to position D, except the dominant knee is flexed to 135 degrees

# THE EFFECT OF KNEE SUPPORT ON THE LOWER BODY JOINT LOADS AND MOTIONS OF BASEBALL CATCHERS IN DEEP SQUATS

Emily Dooley, James Carr, Eric Carson, and Shawn Russell  
University of Virginia, Charlottesville, VA, USA  
Email: sdr2n@virginia.edu

Website: med.virginia.edu/orthopaedic-surgery/research/the-motion-analysis-and-motor-performance-lab/

## INTRODUCTION

It is estimated that 11.5 million baseball players will take the field this spring in the United States [1]. While not a contact sport, injury prevention and safety are still major areas of concern for amateur baseball players. One example of this is the risk to catchers' knees in both baseball and softball, due to the repeated and prolonged squatting required to play this position, especially for players who begin in little league and progress over the years to college and beyond. It has been determined from a cadaver model that deep knee flexion results in compressive forces across the knee that are 80% higher than normal [2]. This is enough force to reach the damage limits of articular cartilage. "KneeSavers" (Easton, CA) have been developed to try and alleviate some of the knee loads. These are foam wedges worn on the dorsal side of the calf that help support the catchers' weight as they squat (Fig 1). This work develops a method to quantify the kinetics associated with use of knee support.

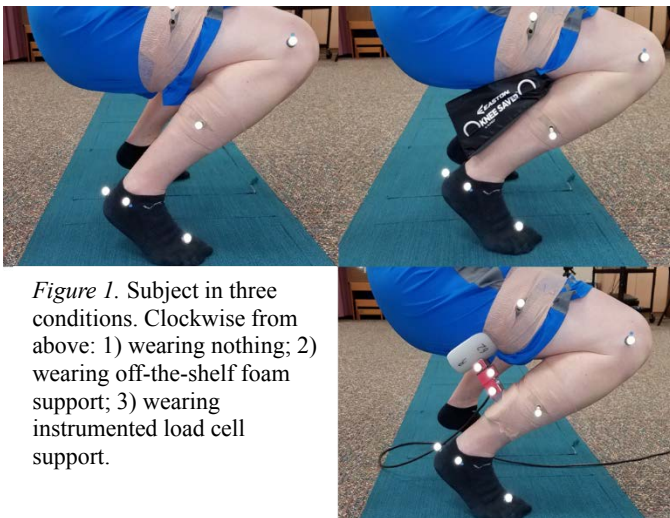


Figure 1. Subject in three conditions. Clockwise from above: 1) wearing nothing; 2) wearing off-the-shelf foam support; 3) wearing instrumented load cell support.

## METHODS

Data was collected for ten subjects, two females and eight males. Subjects were asked to squat into a catcher's stance ( $>130^\circ$  knee flexion) in three conditions: with no device, wearing off-the-shelf foam knee support, and wearing custom built instrumented knee support.

The instrumented knee support consisted of molded support surfaces, single axis load cells, and 3D-printed triad clusters (Fig. 2). The dimensions were set to match those of standard knee supports and were attached at the same location (midcalf).

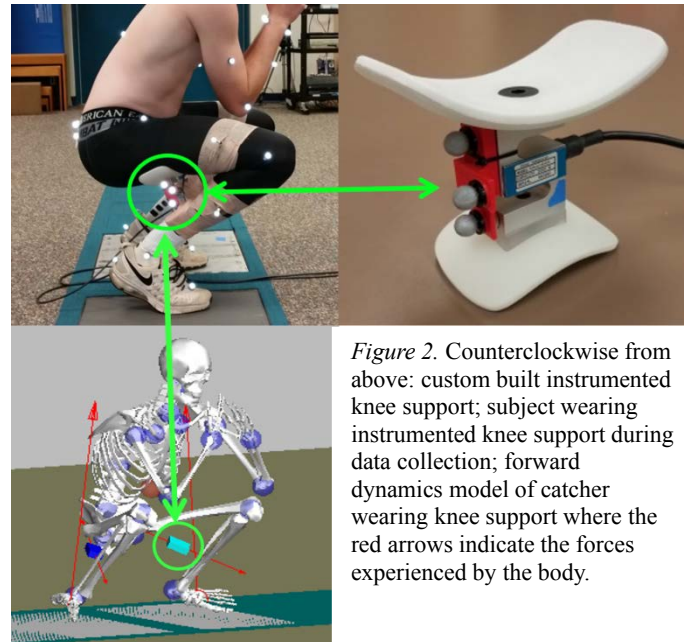


Figure 2. Counterclockwise from above: custom built instrumented knee support; subject wearing instrumented knee support during data collection; forward dynamics model of catcher wearing knee support where the red arrows indicate the forces experienced by the body.

Under each condition the subjects were asked to step onto the force plates, squat and hold to the count of two, rise, and step backwards off of the plates. Subject motion and ground reaction forces were collected via Vicon (PIG marker set) and Bertec force plates. These data were used to populate a custom 43 DoF model (MSC.Adams). The position and direction data from the clusters on the load cell savers combined with the analog force data recorded by the cell allowed the force experience by the knee supports to be incorporated into the model. Specifically, the load cell force was applied along the long axis of the load cell in equal and opposite directions onto the upper leg and lower leg at the point that the force vector from the load cell support crossed each of those bodies (Fig. 2). Sagittal joint kinematics were calculated for each condition. Kinetics were not able to be calculated for condition 2 (off-the-shelf knee support) as the loads they supported were not known. However,

simulations for condition 3 (instrumented knee support) were run twice, once with the measured forces applied and once without the measured forces. This allowed for a comparison of kinetics between knee support and no knee support with kinematics held constant.

## RESULTS

For all three conditions, there were no differences in the sagittal kinematics of the hip, knee, and ankle except in the no support condition where knee flexion was 6.4° greater.

Comparing the same kinematics of wearing the load cell savers, with and without the load cell force applied to the skeleton, there was no difference in hip and ankle sagittal torque, but there was a significant reduction in knee torque with knee support during deep squats. Specifically, a 47% reduction on the dominant side, and a 62% reduction on the non-dominant side (Fig. 3). Similarly, when comparing the condition of not wearing knee support and the instrumented support there was no difference in hip and ankle torque but knee torque differences were reduced with support, 43% and 63% respectively. This is a result of the average force supported through the load cells on each leg being 2.05 +/- .43 N/BM, or approximately 20% of body weight.

## DISCUSSION

The output torque from the no support condition was validated against previously reported knee torque during a squat at 90 degrees [3] results of both models were similar. The reduction in torque at

the knee joint is a critical result. This decrease in torque across the knee decreases the likelihood that the deep knee flexion necessary to squatting in the catching position will reach the damage limit for the cartilage in the knees. In the future this could potentially be modeled by incorporating the force of the quadriceps and patellar tendons about the knee joint center. Since the moment arm of these are approximately one-sixteenth the length of the moment arm to the center of mass, supporting the center of mass with a knee support could dramatically decrease the compressive force experienced in the knee. This compressive force often results in degradation/tears of the meniscus. This could save the catcher's knees from injury and extend the catcher's ability to play baseball.

Regarding the difference in knee angles between subjects wearing nothing and wearing the knee savers, while this angle was statistically significantly different this difference is not functionally different. This means that this difference would not be obvious to the player. It was then concluded that the reduction in torque between the conditions examined would be similar to the reduction in torque between wearing savers and wearing nothing. How knee support effects reaction time becomes a potential reason for not wearing support at higher levels, and should be investigated in the future.

## REFERENCES

1. Futterman, M. (2011) Wall Street Journal.
2. Thambyah, A. et al. (2005) ME&P, 27: 329–335.
3. Han, S. et al. (2013) JHK, 39: 59 – 66.

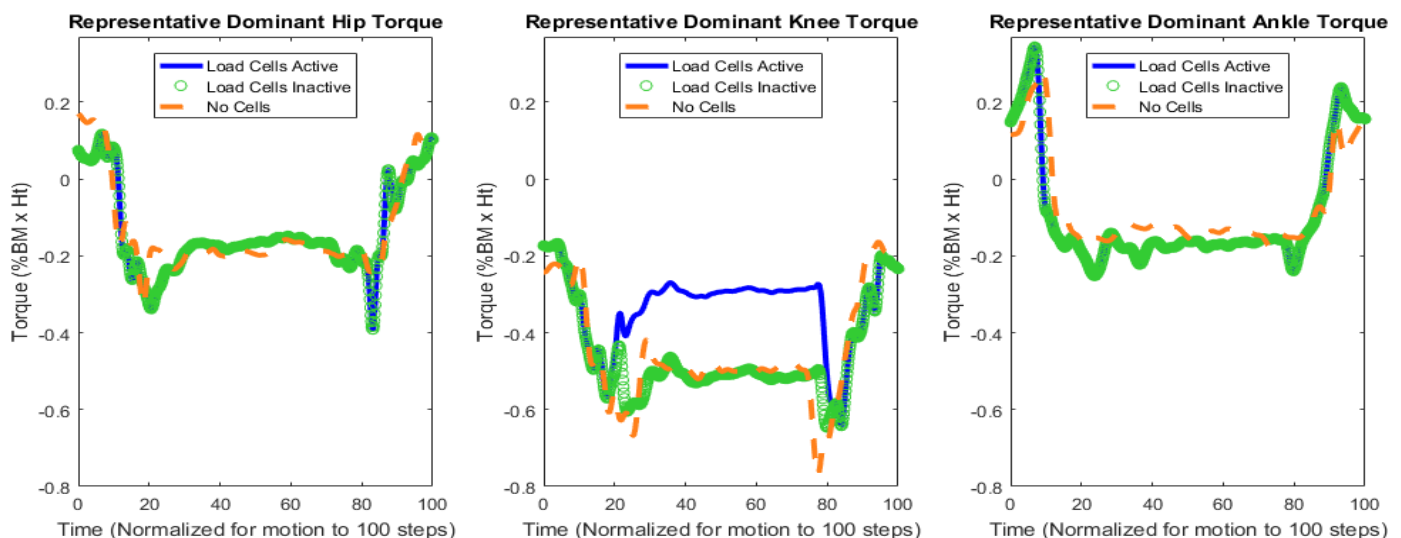


Figure 3. Representative torque plots for dominant sides.

# MODIFYING STANCE ALTERS THE PEAK KNEE ADDUCTION MOMENT DURING A GOLF SWING

<sup>1</sup>Quenten L. Hooker, <sup>1</sup>Robert Shapiro, <sup>1</sup>Terry Malone, <sup>2</sup>Michael B. Pohl

<sup>1</sup>The University of Kentucky, Lexington, KY, USA

<sup>2</sup>University of Puget Sound, Tacoma, WA, USA

Email : [quenten.hooker@uky.edu](mailto:quenten.hooker@uky.edu), [mpohl@pugetsound.edu](mailto:mpohl@pugetsound.edu)

## INTRODUCTION

Although golf is believed to be a low impact activity, previous research suggests up to 72% of golfers have experienced injury [1]. The lead limb knee joint is one of the most frequently injured areas [2]. Although the loads experienced on the knee during the golf swing are not typically large enough to cause acute injury, they might be sufficient to cause damage over time [2]. For instance, the external knee adduction moment, a variable strongly associated with the progression of knee osteoarthritis, is larger in the golf swing ( $0.63 \pm 0.23$  Nm/kg) than gait ( $0.49 \pm 0.19$  Nm/kg) [3]. Since golf is a popular sport, reducing loading and thus injury potential are critical to expand the longevity of one's playing career.

Altering movement patterns is a strategy that can be used to reduce loading on the knee joint. During gait, interventions such as increasing foot angle (angle the feet point outward) and stance width have both been shown to decrease the peak knee adduction moment [4, 5]. It is also possible that the same stance modifications have the potential to reduce loading during the golf swing. For instance, Lynn et al. [3] found a decrease in the knee adduction moment when both feet were externally rotated  $30^\circ$ . However, the aforementioned study did not examine loading in relation to a golfer's self-selected foot angle. Also, to our knowledge no studies have yet explored the effect that stance width has on knee moments during the golf swing.

Although altering stance has been shown to decrease loading at the knee, manipulations to a golfer's stance may have implications on performance. Swing velocity is a relatively simple marker of performance since it is strongly correlated to total driving distance [6]. Therefore, when considering alterations to swing technique, it would be useful to examine whether they have negative implications for swing velocity.

In summary, increasing a golfer's foot angle and stance width may have the potential to alter loading at the knee [3]. Therefore, the purpose of the current study was to examine the effects of various foot angles (i.e. self-selected,  $0^\circ$ ,  $30^\circ$ ) and stance widths (i.e. self-selected, narrow, wide) on the peak knee adduction moment of the lead limb during the golf swing. It was hypothesized that both an externally rotated foot angle and an increased stance width would decrease the peak knee adduction moment during the golf swing. A secondary purpose of the study was to determine what effect the altered stances had on performance (swing velocity).

## METHODS

To date, nine males and one female (age:  $26.0 \pm 5.8$  years, handicap:  $8.7 \pm 6.3$ , height:  $1.8 \pm 0.1$  m, mass:  $81.4 \pm 12.4$  kg) have completed the study protocol. Retroreflective markers were placed on the spine and bilaterally on the pelvis and lower extremity. Participants were then asked to hit three golf drives during each of the following randomly assigned stance conditions: self-selected,  $0^\circ$  (foot angle perpendicular to target line),  $30^\circ$  (foot angle externally rotated from  $0^\circ$ ), 20% narrow (from self-selected stance width), and 20% wider (from self-selected stance width).

3D marker co-ordinate data were collected using ten high speed cameras (Motion Analysis Corp, Santa Rosa, CA) at 200 Hz. An SC100 radar device (Voice Caddie Corp., La Mirada, CA) was used to measure swing velocity. Ground reaction force data were collected using two Bertec force plates (Bertec Corp., Columbus, OH) at 1000 Hz. Joint dynamics were calculated in Visual 3D (C-Motion Inc., Germantown, MD) and normalized to participant body mass. Furthermore, data were time normalized

based on the individual's "top of backswing" and "follow-through" phases (Figure 1).

Repeated measures ANOVA analyses were used to determine if there were differences in the peak knee adduction moment and swing velocity between the stance conditions. When the ANOVA was significant, planned contrasts between the self-selected condition and each of the other stance conditions were conducted.

## RESULTS AND DISCUSSION

Preliminary results show that variations in a golfer's stance have significant effects ( $p < 0.01$ ) on loading at the knee (Table 1). Specifically, the planned contrasts revealed that both the 30° external rotation ( $p < 0.01$ ) and the wide stance width ( $p < 0.01$ ) conditions resulted in a significantly lower peak knee adduction moment compared to the self-selected stance. Therefore, increasing a golfer's foot angle or stance width are both potential mechanisms to reduce the typical external knee adduction moment a player experiences during the golf swing.

Although previous literature has also reported a reduction in the peak knee adduction moment when the feet are placed in greater external rotation, the magnitude of the change differed slightly from our findings. Specifically, Lynn et al. [3] found a 0.09 Nm/kg reduction in the peak knee adduction moment when the feet were externally rotated 30°, while we found a reduction of 0.40 Nm/kg between the 30° and self-selected conditions (Table 1). Considering

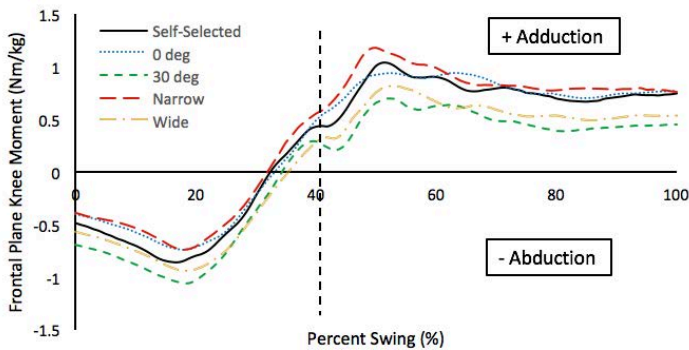


**Figure 1:** Ensemble mean of frontal plane moments for lead limb knee joint. Percent swing is normalized from "top of backswing" to "follow through". Vertical dashed line represents "impact".

participants in the present study used a driver for all golf shots (previous research utilized a 5 iron), we attribute our greater reduction of the knee adduction moment to the typically greater exertion associated with using a driver.

The second purpose of this study was to analyze the effect altering a golfer's stance has on performance. Our data show that altering the golfer's stance resulted in no significant changes ( $p = 0.06$ ) in swing velocity (Table 1). This suggests that the externally rotated foot position and the wider stance were both successful in terms of decreasing the peak knee adduction moment without hindering performance.

**Table 1:** Mean  $\pm$  SD for peak knee adduction moment and swing speed for golf stance conditions

Stance Condition	Peak Knee Adduction Moment (Nm/kg)	Swing Speed (mph)
Self-selected	1.49 $\pm$ 0.58	102.13 $\pm$ 7.59
0 degree	1.43 $\pm$ 0.46	100.37 $\pm$ 7.89
30 degree	*1.09 $\pm$ 0.53	100.57 $\pm$ 8.25
Narrow	1.55 $\pm$ 0.53	99.60 $\pm$ 6.81
Wide	*1.10 $\pm$ 0.51	101.23 $\pm$ 7.57

\* Significantly different from Self-selected ( $p < .01$ )

## CONCLUSION

The preliminary results demonstrate two modifications of the golf stance that can decrease the peak knee adduction moment without altering performance. Considering the prevalence of injury to the lead limb knee joint, modifying a golfer's stance could be used to increase the longevity of their playing career.

## REFERENCES

- 1) Sugaya H, et al. *Human Kinetics*, 83-91, 1998.
- 2) McHardy A, et al. *Sports Med* **36**, 171-87, 2006.
- 3) Lynn SK et al. *J. Sport Sci and Med* **9**, 275-81, 2010.
- 4) Favre et al. *J. Orth Res* **34**, 1547-56, 2016.
- 5) Lynn SK et al. *J. Sci and Med Sport* **11**, 444-51, 2008.
- 6) Hume PA et al. *Sports Med*. **35**, 429-49, 2005.

## ACKNOWLEDGEMENTS

We would like to thank Katherine Worcester and Zachary Lydick for their assistance with data collection

# LEG MUSCLE FUNCTION OF FRONT ROW RUGBY UNION SCRUMMING

<sup>1</sup> Mostafa Yaghoubi, <sup>1</sup> Sally Lark, <sup>1</sup> Philip Fink, and <sup>1</sup> Sarah Shultz

<sup>1</sup> School of Sport and Exercise, Massey University, Wellington, New Zealand  
email: m.yaghoubi@massey.ac.nz

## INTRODUCTION

The purpose of the rugby scrum is to restart play quickly, safely, and fairly after a minor infringement. The scrum is created by eight players from each team, known as front-row pack, who compete for ball possession by binding together in three rows (World Rugby, 2010). The Rugby union scrum comprises of three phases before the ball is introduced: crouch, bind and set. It is important that the front row (comprised of loose head and tight head props, and a hooker) players act in unison, particularly at the bind and set stages. They train for this synchronicity throughout the season, using both live scrimmages and machine-based drills. However, we do not know if the scrum machine simulates live play to the extent that the desired synchronicity is achieved in training. Therefore the purpose of this study was to compare the muscle activation patterns between scrum machine drills and live scrimmages.

## METHODS

Male front row players (N=76; age: 23.6±3.5 years; mass: 104±10.6kg; height: 185±9.5cm) participated in this study. The scrum testing was performed on a scrum sled (Scrum Machines, POWA, New Zealand) and during a live scrum. A 16 channel Noraxon Telemetry DTS EMG telemetry unit, Model 542 DTS EMG (Noraxon US Inc., Scottsdale, AZ) was used to measure bilateral muscle activity of rectus femoris, vastus lateralis and gastrocnemius of tight head and loose head props during scrum (Fig. 1). A digital camera was also synchronized with the EMG system to record the rugby scrum (60Hz) and determine the referee 'set' call while they performed scrum. To normalize the EMG signals during the scrum, participants performed maximal voluntary isometric contractions (MVIC) for each muscle in a randomized order.

All raw EMG signals were rectified and filtered using a 4<sup>th</sup> order Butterworth bandpass filter (frequency band: 5-500Hz). The onset point of muscle contraction was initially identified. The muscle reaction time was calculated as the duration of time from EMG onset to the set call and was normalized to the entire duration of scrum [2]. The rate of muscle recruitment from onset to peak amplitude was calculated using the following equation:

$$V = \frac{\text{Peak amplitude}}{\text{Onset to peak duration}}$$
 To ensure that the data were normally distributed, a log transformation was applied to the rate of muscle recruitment data.

The muscle reaction time, rate of muscle recruitment, and muscle amplitude (as a percentage of MVIC) were analyzed during engagement phase of the scrum. Tests for normality revealed abnormally distributed data for muscle reaction time; thus, comparisons between groups and trials were assessed using Mann-Whitney. Paired t-tests compared muscle recruitment and activity between trials. Statistical significance was set at p<0.05.

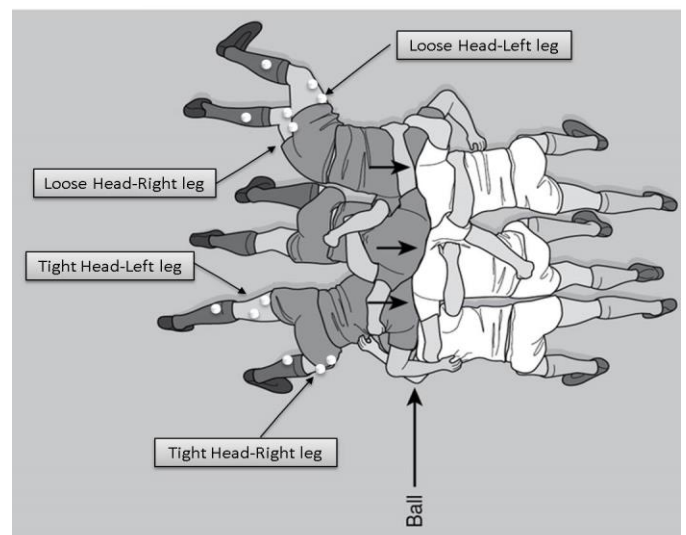


**Figure 1:** Positions of the EMG electrodes on front row of rugby union scrum.

## RESULTS AND DISCUSSION

The muscle reaction time to ‘set’ call was faster when scrummaging live than during the scrum machine drills for all muscles. This quicker reaction time could be due to pre-neuromuscular activation of the musculature. By pre-activating the muscles, they can fire optimally against unpredictable oppositions. Scrumming against the machine operates under an open loop control while a live situation requires close loop control [3], where no adaptations to changing or developing opposing forces are required.

However, the rate of muscle recruitment was significantly higher in the quadriceps muscles when using the scrum machine than in the live situation. Additionally, the muscle amplitude was greater in the vastus lateralis and gastrocnemius during scrum machine drills, compared to live situations. As there is no early push back and no dynamic and opposing front row forces from the scrum machine, the need to pre-activate the musculature becomes irrelevant. Furthermore, the requirement for additional muscle activation for stabilisation purposes is not accounted for when using a scrum machine (Table 1).

## CONCLUSIONS

The scrum machine is ideally suited for functional muscle strengthening during practice. However, scrum training should simulate the live situation as much as possible, to ensure muscle firing patterns can match opposing forces in the most efficient and accurate manner in a game situation.

## REFERENCES

1. Sharp T. *Int J Perform Anal Sport* **14**, 225-237, 2014.
2. Yaghoubi M, et al. *J Applied Biomech* **31**, 79-87, 2015.
3. Shumway-Cook A. *Motor control: theory and practical application*, Lippincott Williams & Wikings, 2007.

## ACKNOWLEDGMENTS

The authors acknowledge P. Silao, for assisting with data collection.

**Table 1:** Mean ( $\pm$ SD) muscle reaction time, recruitment rate, and muscle amplitudes for scrum machine and live scrumming.

	Scrum machine	Live Scrumming	p-value
<b>Reaction Time</b>			
Rectus Femoris	4.65 $\pm$ 4.11	-9.41 $\pm$ 7.37	P<.001
Vastus Lateralis	4.30 $\pm$ 4.10	-11.04 $\pm$ 13.52	P<.001
Gastrocnemius	5.18 $\pm$ 5.91	-5.54 $\pm$ 11.59	P<.001
<b>Recruitment Rate</b>			
Rectus Femoris	3.02 $\pm$ 0.53	2.79 $\pm$ 0.59	0.027*
Vastus Lateralis	3.31 $\pm$ 0.43	2.96 $\pm$ 0.59	P<.001
Gastrocnemius	2.98 $\pm$ 0.58	2.98 $\pm$ 0.57	0.989
<b>Muscle Amplitude</b>			
Rectus Femoris	62.87 $\pm$ 10.50	60.16 $\pm$ 10.02	0.255
Vastus Lateralis	69.18 $\pm$ 9.84	62.89 $\pm$ 10.81	0.034
Gastrocnemius	62.58 $\pm$ 10.81	51.78 $\pm$ 9.01	0.015

# Both Anticipation and Dual-Task Alter Lower Limb Biomechanics during a Loaded Single-Leg Cut

<sup>1</sup> Kayla D. Seymore, <sup>2</sup> Jonathan T. Kaplan, <sup>2</sup> Sarah E. Cameron, <sup>2</sup> John W. Ramsay, and <sup>1</sup> Tyler N. Brown

<sup>1</sup> Boise State University, Boise, ID, USA

<sup>2</sup> U.S. Army Natick Soldier Research Development and Engineering Center, Natick, MA, USA  
email: kaylaseymore@boisestate.edu

## INTRODUCTION

Soldiers simultaneously execute physical and cognitive tasks during military activities. During these activities, soldiers don body borne loads that often exceed 30% of their body weight, altering lower limb biomechanics and decreasing their physical ability. Performing dynamic military activities, such as a single-leg cut, requires a forceful change in direction and produces biomechanical patterns that increase musculoskeletal injury risk [1]. These biomechanical alterations may be further exaggerated with the addition of body borne load or during the performance of a reactive, unanticipated movement. Executing a dual task (combined physical and cognitive) leads to negative performance of either task [2], by producing alterations of lower limb biomechanics [2, 3]. Yet, the impact of a dual cognitive task during dynamic, loaded military activities, such as cutting, is currently unknown. The purpose of this study was to quantify how a dual task impacts the lower limb biomechanics exhibited when performing anticipated and unanticipated single-leg cuts with body borne load.

## METHODS

Twenty-four males ( $20.2 \pm 3$  yrs,  $1.8 \pm 5.2$  m,  $80.3 \pm 11.1$  kg) had hip and knee biomechanics quantified during a series of single-leg cutting tasks. Each participant performed the cuts with three body borne load conditions: no load (NL), medium load (ML, 15% body weight), and heavy load (HL, 30% body weight). During the NL condition, participants wore combat equipment (helmet, boots, and mock weapon) that weighed  $\sim 6$  kg. For ML and HL conditions, participants wore a weighted vest (WeightVest.com Inc. Rexburg, ID, USA) that was adjusted to have the total load (vest plus combat equipment) equal either 15% or 30% of their body weight. With each load, participants performed three anticipated (AN) and unanticipated (UN) cuts with

(DT Cut) and without (Cut) a dual cognitive task. Each cut required participants run at 4.0 m/s down a 10-m walkway and respond to an external light stimulus, by planting their dominant limb on a force plate (Optima, AMTI, Watertown, MA, USA) and cutting at  $45^\circ$  to their non-dominant side. The AN cuts required participants respond to the light stimulus prior to initiating the trial, while UN cuts required participants responded to the light stimulus approximately 500 ms prior to contact with the force platform. The dual task required participants verbally subtract by three from a random number announced at the beginning of each cutting trial.

Hip and knee joint biomechanics of each cut were quantified from 3D trajectories of 36 reflective markers recorded with twelve high-speed (240 fps) optical cameras (Opus, Qualysis AB, Gothenburg, Sweden). A kinematic model with seven skeletal segments (bilateral foot, shank and thigh, and pelvis segments) and 24 DoF was created from a stationary recording. During each cut, synchronous GRF data and marker trajectories were low pass filtered with a fourth-order Butterworth filter (12 Hz). The filtered marker trajectories were processed to solve for the hip and knee joint rotations at each time frame, and filtered kinematic and GRF data were processed to obtain joint moments using Visual 3D (C-Motion, Rockville, MD).

For analysis, subject-based means of hip and knee peak stance (0% - 100%) joint angles and moments were quantified and submitted to a repeated measures linear mixed model. Alpha was set at 0.05.

## RESULTS AND DISCUSSION

The addition of load increased hip and knee joint moments during the single-leg cut. Specifically, the soldiers exhibited greater hip flexion ( $p = 0.001$ ) and internal rotation ( $p = 0.018$ ), and knee flexion ( $p = 0.016$ ) and abduction moments ( $p = 0.001$ ) with the

HL compared to NL, and greater hip flexion moment ( $p = 0.006$ ) compared to ML. Increased knee abduction loads can result in excessive valgus - a risk factor for knee joint injury. To maintain lower limb stability and help attenuate the elevated joint moments that occur with the addition of body borne load, soldiers altered their hip posture during the cut. Soldiers exhibited increased hip flexion ( $p = 0.003$ ) posture with the HL compared to NL, and internal rotation posture ( $p = 0.038$ ) compared to ML. The addition of a body borne load produced no significant adaptation of knee posture. Further research is warranted to determine if adaptations of hip posture are adopted to maintain lower limb stability without compromising the performance of the cut.

Both anticipation and dual task had an impact on lower limb biomechanics during the cut, but did not further exaggerate the lower limb biomechanical adaptations that occur with body borne load. During the UN cuts, soldiers exhibited significantly greater hip ( $p = 0.040$ ) and knee flexion posture ( $p < 0.001$ ), and smaller hip adduction ( $p = 0.001$ ), and knee abduction ( $p = 0.005$ ) and external rotation moments ( $p = 0.026$ ) compared to the AN cut. These findings contradict the existing literature on UN cutting. Reportedly, participants increase frontal plane hip and knee joint motions and loads [4], and potential injury risk, during UN cuts. The current participants, however, adopted hip and knee biomechanical patterns that may decrease injury risk when performing UN cuts with body borne load. Conversely, adding a dual task to the cut may

increase injury risk. Participants significantly decreased hip flexion moment ( $p = 0.027$ ) and knee flexion posture ( $p < 0.001$ ), and increased knee external rotation posture ( $p = 0.034$ ) during DT Cut compared to the Cut (Table 1). The extended knee posture may increase the strain on the musculoskeletal system by reducing the lower limb musculature's ability to absorb and generate energy during the cut [5]. Further work is needed to determine if the knee adaptations evident during the dual task cuts impact soldier performance during such dynamic military activities.

## CONCLUSIONS

The addition of body borne load increased hip and knee joint moments and altered hip posture during the cutting task. But, neither anticipation nor a dual task further exaggerated those biomechanical adaptations. During the UN cuts, participants adopted a biomechanical pattern, including smaller hip and knee frontal plane moments, that are associated with reduced injury risk. However, with the addition of a dual task, soldiers adopted an extended and externally rotated knee that may increase risk of injury.

## REFERENCES

1. Olsen OE, et al. *Am. J. Sports Med* **32**, 1002–1012, 2009.
2. Lin MI, Lin KH. *Front Behav Neurosci* **10**, 1–15, 2016.
3. Al-Yahya E, et al. *Sci. Sports Exerc* **31**, 1176–1182, 2009.
4. Brown TN, et al. *Br. J. Sports Med* **43**, 1049–1056, 2009.
5. Brown TN, et al. *J. Biomech* **47**, 3494–3501, 2014.

**Table 1:** Mean (SEM) peak stance hip and knee joint biomechanics during the single-leg cut.

	Hip Flexion* (°)	Hip Flexion† (N·m/kg·m)	Hip Adduction* (N·m/kg·m)	Knee Flexion*† (°)	Knee Rotation† (°)	Knee Adduction* (N·m/kg·m)	Knee Rotation* (N·m/kg·m)
AN	34.6 (1.7)	-1.29 (0.07)	-0.92 (0.06)	-52.4 (1.7)	-5.9 (0.7)	0.31 (0.03)	0.37 (0.02)
UN	35.9 (1.7)	-1.23 (0.07)	-0.84 (0.06)	-55.7 (1.7)	-6.2 (0.7)	0.27 (0.03)	0.35 (0.02)
Cut	35.5 (1.7)	-1.29 (0.07)	-0.87 (0.05)	-55.0 (1.7)	-5.8 (0.7)	0.29 (0.03)	0.36 (0.02)
DT Cut	35.0 (1.7)	-1.23 (0.07)	-0.89 (0.06)	-53.1 (1.7)	-6.3 (0.7)	0.28 (0.03)	0.36 (0.02)

\*significant difference between anticipation conditions ( $p < 0.05$ )

†significant difference between dual task conditions ( $p < 0.05$ )

# BALL RELEASE VELOCITY AND PRE-RELEASE RANGE OF MOTION FOR FIVE TYPES OF SOFTBALL PITCHES

Ben W. Meyer

Shippensburg University, Shippensburg, PA, USA  
[bwmeyer@ship.edu](mailto:bwmeyer@ship.edu)

## INTRODUCTION

Recent analyses of softball pitching have focused on the fastball, change-up, and screwball pitch types [1,2]. However, in order to succeed at higher levels of play, softball pitchers must also be proficient using other types of pitches such as the curveball and riseball techniques. Figure 1 shows the distinction between a screwball and a curveball for a right-handed pitcher. The focus of several previous investigations has been on pitch counts, injuries, and/or comparisons between novice and expert athletes. This investigation includes the curveball and riseball pitch types, with a focus on the mechanisms of the generation of ball velocity.

Ball velocity is one of the key elements in a pitcher's level of success. One of the factors that may contribute to the generation of a large ball velocity is the pre-release range of motion (ROM). The ROM refers to the distance traveled by the ball from the start of the windmill motion until release.

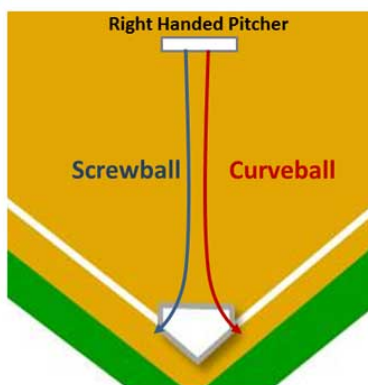


**Figure 1:** Differences between screwball and curveball pitches.

Previous work has assessed the influence of ROM on overhead back (OHB) throw distance [3]. For the

OHB throw, the use of a large ROM did not guarantee a large throw distance in a sample of undergraduate students. The study participants were novices with the OHB technique, and so the present study expands upon this previous work by analyzing a population of subjects who are highly skilled with a variety of softball pitch types.

The purpose of this study was to build upon previous findings for the fastball, change-up, and screwball pitches by adding information about ball release velocity (VR) and pre-release range of motion (ROM) for the curveball and riseball techniques.

## METHODS

Five female NCAA Division II softball pitchers (age =  $20 \pm 1$  yr) participated in the study. Participants performed five pitches for each of the following pitch types: fastball, change-up, screwball, curveball, and riseball. The pitches were performed in a practice session during the spring competitive season. Participants threw for both velocity and accuracy during all trials.

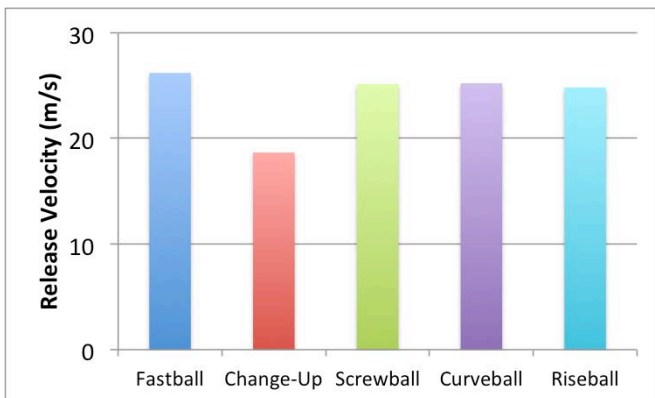
Each trial was recorded with a Casio Exilim EX-F1 camera at a sampling rate of 300 frames per second. Digitizing targets were placed in the plane of motion to calculate reference distances. The center of the ball was digitized in every 3<sup>rd</sup> frame of the video files using Logger Pro software to give data at 0.01 s intervals. The onset of the pitch was determined to be the frame in which the pitcher's hand made its first movement on a continuous trajectory.

The ROM and ball velocities were computed using standard kinematic analysis techniques [2,3]. The three best attempts (for each pitch type) based on

velocity at release (VR) were used in the analysis. Differences between measures were assessed using ANOVA tests with a cut-off for statistical significance set at  $\alpha = 0.05$ .

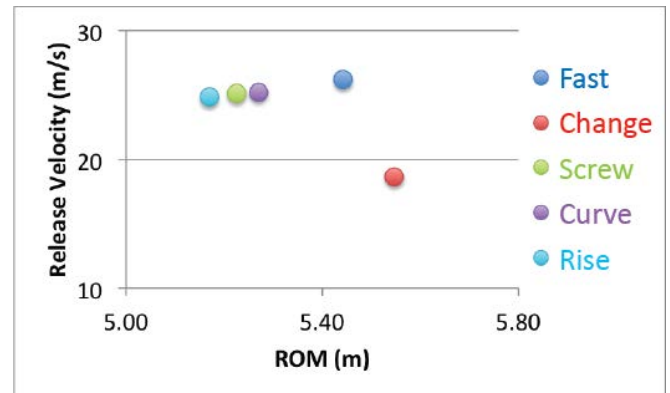
## RESULTS AND DISCUSSION

Figure 2 shows that pitchers achieved the largest VR values using the fastball ( $26.2 \pm 1.4$  m/s) and curveball ( $25.2 \pm 1.3$  m/s), while the smallest VR values were obtained using the change-up ( $18.7 \pm 1.6$  m/s). The fastball, screwball, curveball, and riseball VR values were not significantly different from each other, but VR values for the change-up technique were significantly smaller than all the other techniques. Recent studies [4,5] have shown that female collegiate pitchers throw fastballs in the 22 to 27 m/s range, so the athletes in the present study fall in the higher end of this range.



**Figure 2:** Ball release velocities for the five pitch types analyzed in the study.

Figure 3 shows the relationship between ball release velocity and ROM for all pitch types. Subjects used the largest ROM in the change-up technique ( $5.55 \pm 0.34$  m) and the smallest ROM in the riseball technique ( $5.17 \pm 0.32$  m). Although the fastball technique produced the largest release velocity, the ROM values were not the largest among the pitch types ( $5.44 \pm 0.22$  m). Excluding the change-up technique, results show that an increase in ROM leads to an increase in VR.



**Figure 3:** Relationship between ball release velocity and pre-release range of motion.

## CONCLUSIONS

The results of this project indicate that for a small sample of NCAA Division II softball pitchers, release velocities are very similar (24-26 m/s) for the fastball, screwball, curveball and riseball pitch types. The change-up pitch has distinct VR and ROM characteristics and future studies should investigate other factors that make the change-up such a unique pitching style.

## REFERENCES

1. Meyer, BW. *40<sup>th</sup> Amer Soc Biom*, 2016.
2. Bicko, T. *38<sup>th</sup> MARC-ACSM Meeting*, 2015.
3. Meyer, BW. *37<sup>th</sup> Amer Soc Biom*, 2013.
4. [www.coachup.com](http://www.coachup.com)
5. Ficklin, T. *60<sup>th</sup> ACSM Meeting*, 2013.

## ACKNOWLEDGEMENTS

The author would like to thank the College of Education and Human Services and the softball team at Shippensburg University.

# THE INFLUENCE OF MODERN CLIMBING HOLDS ON FINGER FORCES AND FORCE DISPERSION PATTERNS

Dylan Herman-Dunphy and Deborah L. King

Ithaca College, Ithaca, NY, USA  
email: [dherman2@ithaca.edu](mailto:dherman2@ithaca.edu), web: <http://www.ithaca.edu/hshp/depts/ess/>

## INTRODUCTION

Climbing is one of the fastest growing sports in the world and this growth has evolved with the addition of sport climbing into the 2024 Olympic games. Most research done on the biomechanical effects of climbing holds has focused on the effects of holds on finger forces. How a climber's fingers grab a climbing hold may have a greater effect on finger forces than the depth of the objects being held [1]. However, changing grip position does not affect finger force magnitudes when gripping a simulated climbing hold [2]. Nonetheless, finger forces are unequal across the fingers when using climbing hold grip positions [1,2]. No studies, though, have used modern climbing holds and instead used simulated holds (wood ledges) or outdated style holds.

The purpose of this study was to determine if, when using modern climbing holds, the type of hold affects finger forces as measured by maximum normal and average normal forces. A secondary purpose was to understand the positioning of the fingers on the holds by measuring center of force distance between each finger.

## METHODS

The 19 volunteer subjects were a mix of climbers and non-climbers. Subjects were required to hang onto 7 holds (H1-H7), made by Atomik Climbing Holds, for 1-2s with a 10-minute break between each hang. H1 was a sloper hold at 90 degrees sloping, H2 was a sloper hold at 110 degrees

sloping, H3 was a pinch hold that is 4.5cm wide, H4 was a pinch hold that is 7.0cm wide, H5 was an edge hold that is 60 degree in-cut, H6 was an edge hold that is 70 degrees in-cut, and H7 was an edge hold that is 90 degrees in-cut.

A Tekscan pressure sensor (3000E F-Scan System), designed for insole-shoe pressures, was used to collect data at 63 Hz. After a pilot study to validate the F-Scan system with finger forces, the pressure films were adhered to a thin piece of foam and the climbing holds. Subjects directly held onto the film over the climbing hold for each grip. Average (avg) and maximum (max) normal forces and center of force (COF) distances were collected using the F-Scan analysis software.

Data were analyzed using three, two-way repeated measures ANOVAs and post hoc analysis were done for significant main effects and interactions. Alpha = 0.05.

## RESULTS AND DISCUSSION

There was a significant finger main effect for avg force ( $F_{2,204, 83.738} = 140.132, p = 0.000$ ). The middle finger avg force was 18% greater than index, 29% greater than ring, and 53% greater than pinky. Avg force had a significant hold ( $F_{4,163, 158.189} = 3.394, p = 0.010$ ). For max force there was a significant finger main effect ( $F_{2,166, 80.146} = 131.662, p < 0.001$ ) and a significant hold main effect ( $F_{4,128, 152.750} = 5.562, p = 0.000$ ). H5 was 18% > H4, 16% > H6, and 19% > H7. Similar results were observed for max force for the finger main

effect ( $F_{2,166}$ ,  $80.146 = 131.662$ ,  $p < 0.001$ ) with the middle finger greater than the index, ring, and pinky by the same percentages. For the hold main effect ( $F_{4,128}$ ,  $152.750 = 5.562$ ,  $p < 0.001$ ) though H5 was greater than H1, H4, and H6. .

The limited number of differences in finger forces on the different types of holds supports previous literature [1,2] that grip type or hold type has little effect on finger forces. Surprisingly, though, H5, the 60-degree in-cut edge, repeatedly had greater finger forces for both avg and max force. This indicates there is some effect of climbing hold type on the finger forces. Since H5 had the largest degree of in-cut, it is hypothesized that the angle of the gripping surface may influence finger forces to a significant effect as opposed to grip surface width or depth, for example.

COF analysis showed a COF distance finger main effect ( $F_{1,689}$ ,  $52.372 = 14.781$ ,  $p = 0.000$ ) with COF distance from index to middle finger greater than the distances between the ring and middle fingers or ring and pinky fingers. A COF hold main effect ( $F_{4,024}$ ,  $124.754 = 3.357$ ,  $p = 0.012$ ) suggest that the distances between adjacent fingers vary substantially on the different holds, which was not surprising given the large range in size of each hold. Interestingly, this difference in COF finger distance on the different holds did not affect the pattern of individual finger forces as the middle finger always had the greatest force followed by the index, ring, and pinky.

## CONCLUSION

Regardless of hold type, the distribution of force between the fingers follows the same pattern with the middle having the greatest force and pinky the least. The type of the modern climbing hold, however, has little effect on finger forces; though, the angle of in-cut may affect the finger forces with an inverse relationship between the degree of in-cut

and the magnitude of finger forces. Further research into the biomechanical effects of climbing holds on finger forces should focus on the role that in-cut angle plays in determining finger forces and how that relates to risk of injury.

## REFERENCES

1. Amca A. M., et al. Journal of Sport Science, 2012.
2. Quaine F., et al. Journal of Clinical Biomechanics, 2003.

## ACKNOWLEDGMENTS

Special thanks to Atomik Climbing Holds and Ithaca College for helping sponsor this study.

# ASSESSING PERFORMANCE CORRELATIONS AMONG TASKS IN A CHALLENGING OBSTACLE COURSE

<sup>1</sup>Rachel Vitali, <sup>1</sup>Stephen Cain, <sup>2</sup>Leia Stirling, <sup>1</sup>Noel Perkins

<sup>1</sup>University of Michigan, Ann Arbor, MI, USA

<sup>2</sup>Massachusetts Institute of Technology, Cambridge, MA, USA  
email: vitalir@umich.edu

## INTRODUCTION

Modern warfare requires warfighters to carry increasingly heavy loads that include essentials like body armor, gear, food, and water. Optimizing the load and configuration is critical for maximizing the probability of mission success. The Marine Corps Load Effects Assessment Program (MC-LEAP) was developed to reveal variations in soldier performance due to clothing and individual equipment (CIE) [1]. The program consists of an obstacle course representative of tasks warfighters encounter in combat. Performance for any obstacle is frequently defined by the time required to complete the obstacle. Using this sole measure of performance, we hypothesize that performance on several obstacles are correlated; meaning a decrease (or increase) in performance for one predicts a decrease (or increase) in performance in another. For example, we hypothesize correlated performance in the sprint and agility run since subjects sprint between cones during the agility run. In addition, we expect high correlation in performance between window and wall obstacles since both require upper body strength. If performance on obstacles are highly correlated, one may conclude they do not provide independent measures of performance.

## METHODS

We tested 44 subjects (17 females, 27 males; age =  $20.1 \pm 1.9$  years; body mass =  $74.1 \pm 14.9$  kg; height =  $1.76 \pm 0.12$  m; mean  $\pm$  standard deviation). A subset of 24 subjects (8 females, 16 males) completed the obstacle course a total of four times while carrying 0% (twice), 15%, and 30% of their body weight. All subjects carried a mock-rifle (3.4 kg). The University of Michigan IRB approved the study, and all subjects gave informed consent. The

investigator held an inertial measurement unit (Opal sensors, APDM, Portland OR) with an embedded binary switch that was used to time-stamp the beginning and end of each obstacle, essentially serving as a timing gate. The course (Figure 1) was an abbreviated version of the MC-LEAP containing 10 obstacles. A linear fit and Pearson correlation coefficient was calculated from the data for each possible pair of obstacles. The additional loading conditions produced a wide range of performance, strengthening the validity of these results depicted in Figure 2. If the 95% confidence interval for the slope from the linear fit includes zero, then the correlation between the two obstacles is negligible.

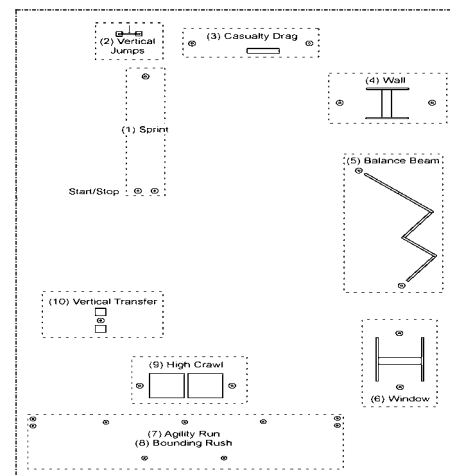


**Figure 1:** Abbreviated MC-LEAP obstacle course.

## RESULTS AND DISCUSSION

The only pair of obstacles that had negligible correlation was the window and casualty drag. If performance in an obstacle was not highly correlated ( $R < 0.7$ ) with any other obstacle, then it could be considered an independent measure of performance. Two obstacles that met this criterion were the vertical jump and balance beam. By contrast, the two

obstacles exhibiting the greatest performance correlation were the vertical transfer and casualty drag ( $R=0.80$ ). These obstacles also had the strongest correlations with subject height ( $R=0.64$  and  $R=0.66$ , respectively), suggesting height could be a confounding variable. As expected, performance in the window and wall obstacles were correlated ( $R=0.79$ ), and variability could derive from differences in subject flexibility or technique since the window obstacle represents a constrained wall [2]. Additionally, performance in the high crawl and bounding rush were highly correlated ( $R=0.76$ ), as both require significant coordination of limbs while in a prone position. Finally, performance in the sprint and agility run were correlated ( $R=0.72$ ) as anticipated from [3] where high performers sprinted in straight lines between cones during the agility run.

## CONCLUSIONS

The overall number of obstacle pairs with highly correlated performance (4) is much less than the total possible number of pairs (54). Thus, this subset of obstacles from the MC-LEAP sufficiently assesses different variables of performance. However, since performance in a few obstacles are significantly correlated (e.g., window and wall), one

obstacle in such a pair might be eliminated without compromising conclusions regarding subject performance. Furthermore, this suggests there is likely a subset of performance variables (i.e., speed, strength, agility, etc.) that contribute to all obstacles to varying degrees depending on the obstacle. It should also be noted that effectively only speed was considered. Other measures of performance would highlight a different skill/technique and generate different correlations. Thus, removal of an obstacle should be considered based on metrics of interest.

## REFERENCES

1. Smith EM and Kelley FL. *Statement before the Tactical Air and Land Forces Subcommittee*, 2013.
2. Cain, et al. *39<sup>th</sup> Annual Meeting of ASB*, Columbus, OH, USA, 2015.
3. Zaferiou AM, et al. *40<sup>th</sup> Annual Meeting of ASB*, Raleigh, NC, USA, 2016.

## ACKNOWLEDGMENTS

This material is based upon work supported by the US Army Contracting Command-APG, Natick Contracting Division, Natick, MA, under contract W911QY-15-C-0053.

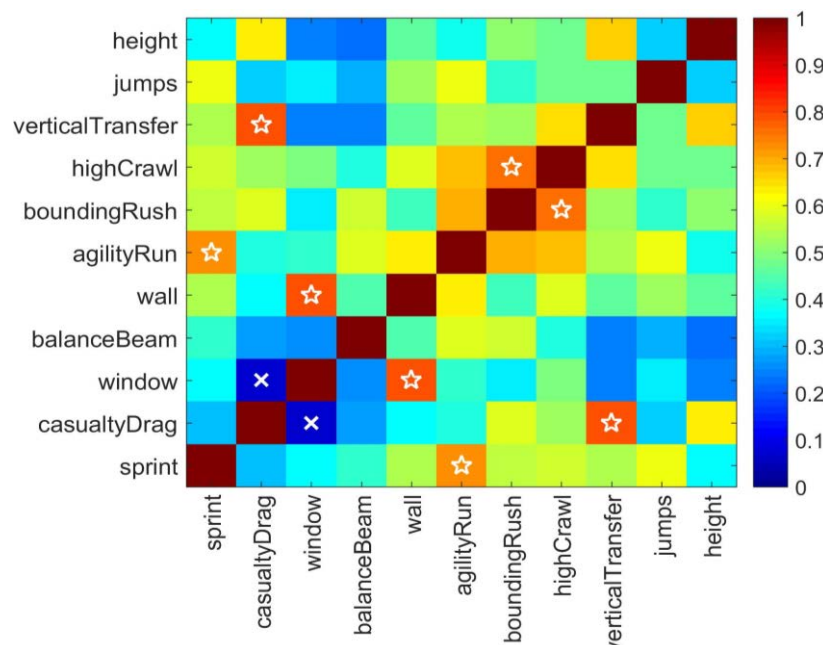


**Figure 2:** Color map of the correlations between the data from the obstacles in the abbreviated MC-LEAP obstacle course. Along the diagonal, the correlations are one (dark red) because they are autocorrelations. The white stars represent obstacle pairs that are highly correlated ( $R>0.7$ ), excluding autocorrelations. The white crosses represent obstacle pairs that have negligible correlation.

# THE FIFA11+ AND DISTRIBUTION OF ENERGY ABSORBED ACROSS LOWER EXTREMITY JOINTS IN FEMALE SOCCER PLAYERS

<sup>1</sup>Adam R. Marmon, <sup>2</sup>Amelia Arundale, <sup>2</sup>Holly Silvers-Granelli,

<sup>2</sup>Ryan Zarzycki, <sup>2</sup>Celeste Dix, <sup>3</sup>Anahid Ebrahimi, <sup>2</sup>Lynn Snyder-Mackler

Departments of <sup>1</sup>Kinesiology and Applied Physiology, <sup>2</sup> Physical Therapy and <sup>3</sup> Mechanical Engineering  
University of Delaware, Newark, DE, USA

[marmon@udel.edu](mailto:marmon@udel.edu)

## INTRODUCTION

The FIFA11+ is an injury prevention program designed as a dynamic warm-up program targeting commonly occurring injuries in soccer, such as anterior cruciate ligament injury [1]. The program is simple to learn, does not require specialized equipment, can be completed in approximately 20 minutes, is progressive so can be used across a range of skill levels, and is very easy to implement. The common goals of injury prevention programs, including the FIFA11+, are to improve core stability, balance and neuromuscular control. The FIFA11+ also incorporates exercises designed to improve the participants' ability to maintain proper joint alignment. Recommendations from the program development team are that the participants should perform the dynamic warm-up at the start of training session at least twice per week. The FIFA11+ has been shown to effectively reduce injury rates [2,3] and increase dynamic balance [4], however, it is unclear if biomechanical changes can be identified that may be contributing to the reduced injury rates. The purposes of this study were 1) to characterize the distribution of energy absorbed by the lower extremity during a deceleration task and 2) to determine if participation in the injury prevention program leads to changes in the distribution of energy absorbed across the joints in the lower extremity. Via the training with the FIFA11+, we hypothesized a reduction in energy absorption at the knee during a deceleration task, which may be compensated for by the more proximal joint (e.g. hip).

## METHODS

Twenty-seven female soccer players (age= 20.3 ± 1.23 yrs; height 1.66 ± .06 m; mass 63.9 ± 5.0 kg) from two Division I Collegiate soccer teams

participated in this study. Participants underwent motion analysis of a deceleration task (Decel) prior to (Pre) and following (Post) a competitive season during which the teams utilized the FIFA 11+ Injury Prevention Program.

The Decel task was completed by having subjects run approximately ten meters, plant their foot on the force plate and decelerate their body, then pushing backward, and running backwards to the initial starting position. Three successful trials were collected from each limb; a trial was deemed successful when the participant cleanly planted the entire foot on the force plate, with no shifting of the foot during the deceleration, and completed the maneuver without any loss of balance.

Motion capture data were acquired via Vicon Nexus software (Vicon Motion Systems, Oxford, United Kingdom) where 22 retro-reflexive markers affixed to anatomical landmarks and 23 markers affixed to rigid, thermoplastic shells were utilized to generate subject specific models. Kinematic and kinetic data were collected at 240 and 1080 Hz, respectively, via 8 cameras and an imbedded forceplate. Kinematic and kinetic data were low-pass filtered using a second-order, zero-phase-lag Butterworth filter with a cutoff frequencies of 6 and 40 Hz, respectively. Visual-3D (C-Motion, Germantown, MD) software was used to calculate kinematic and kinetic variables. The dependent variables for this study include joint power for four constituents of the lower limb (distal foot, ankle, knee and hip) calculated using a 6 degree of freedom method [5]. Negative work was then calculated as the integration of power from initial contact (vertical ground reaction force exceeding 5N) through peak knee flexion angle (PKF). All values were normalized by body mass. Work performed by each constituent was calculated as a

percentage of total (summed distal foot, ankle, knee, and hip) work.

A 2x4 repeated measures ANOVA was completed to assess change in the distribution of negative work performed across the four joints over time. Paired t-tests were used to assess difference in the presence of a significant joint by time interaction. Alpha levels were set at  $p=0.05$ . Huynh-Feldt corrections were applied if the assumption of sphericity was violated.

## RESULTS AND DISCUSSION

There was a significant constituent by time interaction (Figure 1;  $p= 0.011$ ). Paired t-tests indicated significant reduction in the proportion of energy absorbed by the knee (Pre  $47.8 \pm 7.6\%$  and Post  $45.0 \pm 7.1\%$ ;  $p= 0.008$ ) and an increase in the proportion of energy absorbed by the hip (Pre  $34.3 \pm 1.2\%$ , Post  $37.2 \pm 1.5\%$ ;  $p= 0.024$ ). These findings support our hypothesis that after participating in the FIFA11+ program, the hip compensated for the reduce energy absorbed by the the knee. While there were significant differences observed at both the knee and the hip, the effect sizes were large (Cohen's  $D = 0.937$ ). The inherent variability of biomechanical measures, combined with the relatively small sample size available here suggest that a larger data set may be needed before drawing more definitive conclusions.

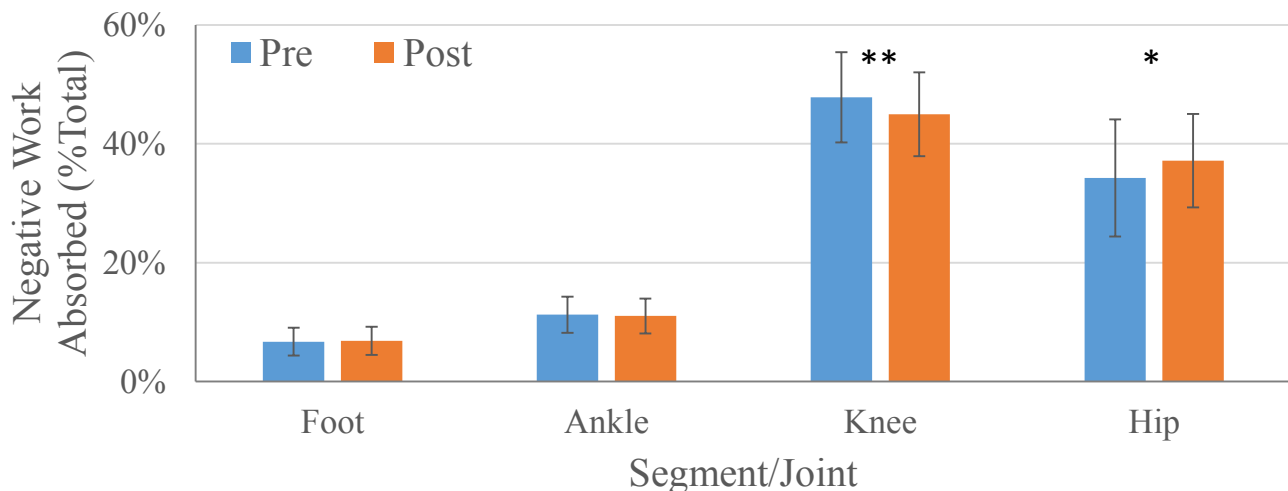


Figure 1. Distribution of negative work for the foot, ankle, knee and hip Pre and Post a season utilizing the FIFA11+ Injury Prevention Program. Significant differences over time  $*p<0.05$ ;  $**p=0.01$ .

## CONCLUSIONS

As a focus of the intervention to improve core stability, balance and neuromuscular control, it is reasonable to expect that participation would lead to reduced energy absorption by the knee, which also led to increased energy absorption by the proximal hip. Participating in the FIFA11+ program has successfully reduced injury, which may be attributed to a shift in energy absorption during deceleration to more proximal muscular. This redistribution of energy absorption at the knee and hip may be a positive result of the FIFA11+ program.

## REFERENCES

- 1-Agel J. *Am J Sports Med*, **33**(4):524-30, 2005.
- 2-Silvers-Granelli H et al. *Am J Sports Med* , **43**(11):2628-37, 2015.
- 3- Bizzini M and Dvorak J. *Br J Sports Med*, **49**(9):577-9, 2015.
- 4- Gomes Neto M et al. *Clin Rehabil*, **1**:1-5, 2016.
- 5- Zelik KE, Takahashi KZ, Sawicki GS. *J Exp Biol* **218**: 876-886, 2015.

## ACKNOWLEDGEMENTS

Thanks to Kelsey O'Donnell and Elise Kraus for their assistance with this project.  
Funding: NIH R01 AR048212 09, NIH P30 GM103333 03, NIH R44 HD068054 05 NSF GRFP 1247394

# KNEE ADDUCTION MOMENT AND MUSCLE ACTIVATION DURING A SIDECUT ON A RAISED SURFACE

Lauren E. Schroeder, Kevin A. Valenzuela, Songning Zhang, John G. Orme, and Joshua T. Weinhandl

The University of Tennessee, Knoxville, TN, USA  
email: Lschroel@vols.utk.edu

## INTRODUCTION

Fast-pitch softball has increased in popularity, with 19,628 NCAA Division I female athletes participating in the 2014-15 season [1]. However, increased participation results in increased chance of injuries. Base running is a major component of the sport, occurring in almost every play of the game. To get from one base to the next, players have to “round the base” by performing a sidecut to the left by planting their right foot on a raised base. Unfortunately, this specific movement has resulted in approximately 187 game-day injuries [2].

This dynamic sidecut movement has been shown to place large loads on the knee ligaments, potentially resulting in anterior cruciate ligament (ACL) injuries [3]. Noncontact ACL injuries account for nearly 31% of all game-day softball knee injuries [2]. Certain biomechanical and neuromuscular abnormalities are common in noncontact ACL injuries. Specifically, increased frontal plane loading [4] and unbalanced quadriceps-to-hamstring co-contraction indices (Q:H CCI) [5] have been identified as primary risk factors for noncontact ACL injuries.

To date, no study has analyzed effects of rounding a base on noncontact ACL injury risk factors in softball players. Therefore, the aim of this study was to determine the effect of a raised surface (i.e. base) during a sidecut on frontal knee loading and muscle activation in recreational softball players.

## METHODS

Nine recreationally active females (age:  $21.8 \pm 2.0$  yrs,  $1.70 \pm 0.03$  m,  $63.7 \pm 5.0$  kg) completed two base running conditions. In the first condition, a sidecut simulating rounding first base was performed with no base (NB) present on the force plate. For the second condition, the same route was performed with a base (WB) present on the force plate. Participants were instructed to stay within a range of  $90^\circ$ - $120^\circ$

during the entrance of the sidecut. Entrance and exit speeds were monitored at  $4.0 \text{ m/s} \pm 0.25 \text{ m/s}$  and  $3.75 \text{ m/s} \pm 0.25 \text{ m/s}$ , respectively. During each trial, right leg 3-D kinematics and kinetics were collected using a 12-camera Vicon motion capture system (200 Hz), ground reaction forces (GRF) were collected with one AMTI force plate (2000 Hz), and muscle activations were measured using the Delsys Trigno wireless electromyography (EMG) system (2000 Hz). Muscles included biceps femoris (BF), semitendinosus (MH), vastus lateralis (VL), and vastus medialis (VM).

Raw EMG data were pre-amplified and band-pass filtered using a 4<sup>th</sup> order Butterworth filter (10 Hz, 350 Hz), full-wave rectified and low-pass filtered (5 Hz) to create a linear envelope. Peak maximum voluntary isometric contraction values for each muscle were used to normalize filtered EMG signals for comparisons (%MVIC). Raw 3D marker coordinate and GRF data were both low-pass filtered using a 4<sup>th</sup> order, Butterworth filter (20 Hz). Q:H CCI was defined as average quadriceps activation divided by average hamstrings activation. A time frame of 50 ms prior to initial contact (pre-contact) and 100 ms after initial contact (post-contact) were used during EMG analysis. Peak internal knee adduction moment was computed in the joint coordinate system and normalized to body mass (Nm/kg).

Paired-samples *t*-tests were used to compare differences between NB and WB initial contact knee abduction angle, peak knee abduction angle, and peak knee adduction moment. A repeated measures 2x2 ANOVA was used to compare Q:H CCI between the conditions (NB and WB) and contact times (pre- and post-contact). The alpha level was set at  $p \leq 0.05$ .

## RESULTS AND DISCUSSION

This study compared frontal knee loading during two base running conditions. It also compared muscle

activations during two base running conditions pre- and post-contact. Our results suggest that performing a sidecut with a raised surface does not significantly alter both peak and initial contact knee abduction angle. Peak knee adduction moment was significantly greater in the NB condition compared to the WB condition (Table 2). A main effect involving contact time was identified for Q:H ratio, indicating a greater Q:H ratio post-contact than pre-contact ( $F_{1,7} = 16.113, p = 0.005$ , Table 1).

It is interesting to note that while participants landed with somewhat larger initial contact and peak knee abduction angles in the WB condition, peak knee adduction moments were significantly larger in the NB condition (Figure 1). These findings contradict what McLean et al. [4] found regarding the causal link between increased initial contact knee abduction angles and the subsequent increased peak knee adduction moments. This suggests contacting a raised surface may provide a more optimal surface to perform and complete the sidecut, causing the GRF to potentially shift more medially compared to cutting on a flat surface.

Q:H CCI#s showed that prior to initial contact, activation between the two muscle groups were somewhat balanced (Table 1). Previous literature has shown that reduced hamstring pre-activation places the ACL at an increased risk of injury due to the inability to properly scale the hamstrings to the same level as the quadriceps [6]. Significantly greater quadriceps activation was seen post-contact. The quadriceps act to prevent the knee from collapsing during any sort of dynamic task, thus explaining the increased activation. Unfortunately, an unbalanced Q:H ratio, with significantly greater quadriceps activation, creates a large anterior shear force, thus increasing the stress on the ACL [5]. Neuromuscular training to improve Q:H CCI could decrease the load applied to the ACL and decrease the risk of injury.

## CONCLUSIONS

These findings suggest that rounding a base, with a controlled foot placement, may reduce ACL injury risk by decreasing the knee adduction moment. Examining movement patterns at the ankle and abnormal foot strikes may provide a better explanation for ACL injuries that occur when rounding a base.

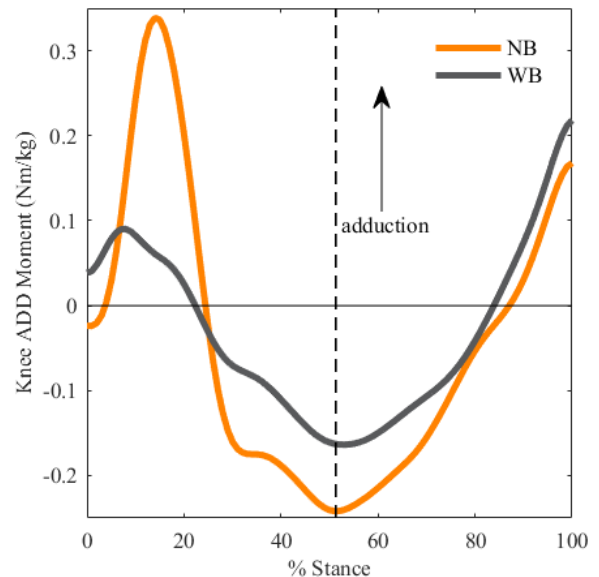


**Figure 1:** Knee adduction moments during NB and WB conditions. Dotted line represents 100 ms after initial contact.

**Table 1:** Mean %MVIC values of Q:H CCI#s between conditions and between contact times.

Q:H CCI#	NB		WB	
	Pre	Post	Pre	Post
	0.92	4.22	1.13	4.17

Pre: 50 ms prior to initial contact, Post: 100 ms after initial contact

Q: VM+VL, H: BF+MH

#: contact time main effect

## REFERENCES

- 1981/82-2014/15 NCAA Sports Sponsorship and Participation Rates Report. NCAA, 2015.
- Marshall, S.W., et al. *J Athl Train* **42**:286-294. 2007.
- Besier, T.F., et al. *MSSE* **33**:1168-1175. 2001.
- McLean, S.G., et al. *Clin Biomech* **20**:863-870. 2005.
- Malinzak, R. A., et al. *Clin Biomech* **16**:438-445. 2001.
- Hanson, A. M., et al. *J Athl Train* **43**:133-143. 2008.

**Table 2:** Knee abduction angles and adduction moments during the two base running conditions (mean±SD).

	NB	WB	p-value	Effect Size (d)
Initial Contact Knee ABD Angle (deg)	-1.01±5.98	-1.72±5.02	0.550	0.14
Peak Knee ABD Angle (deg)	-9.31±4.47	-9.68±3.99	0.632	0.09
Peak Knee Adduction Moment (Nm/kg)	0.54±0.48	0.33±0.32	0.041	0.55

# COMPARISON OF BARBELL KINEMATICS IN THE HANG CLEAN AND HANG CLEAN HIGH PULL: IMPLICATIONS FOR SPECIFICITY OF TRAINING

Scott Light, Stephen Henderson, Melissa Mache

California State University, Chico, CA, USA

email: mmache@csuchico.edu

## INTRODUCTION

The ability to generate power has been previously associated with greater vertical jump heights and faster sprint times [1]. Multi-joint weightlifting exercises, such as the hang clean, that are performed at high speeds and mimic sport specific movements are commonly implemented to help athletes develop power [2, 3]. The hang clean is often broken down into its various components to simplify the movement and help athletes learn and improve specific portions of the lift. For example, the hang clean high pull can be used to help athletes improve technique and triple extension in the hang clean [4]. Independent investigations of the hang clean and hang clean high pull suggest there are similarities in the biomechanics of the two lifts, however, a direct comparison of these lifts is lacking [2, 3]. Furthermore, there are few existing descriptions of Olympic lift performance by women; it remains to be seen if men and women perform these tasks in a similar manner. Thus, the purpose of this study was to compare barbell kinematics of the hang clean and hang clean high pull as a function of sex, with the intent of examining the specificity of the hang clean high pull as a training tool for improving hang clean performance.

## METHODS

Ten men [mean (SD) age: 23 (2) yrs; height 1.76 (0.08) m; mass: 80.9 (10.2) kg] and nine women [mean (SD) age: 23 (1) yrs; height 1.66 (0.06) m; mass: 63.8 (9.5) kg] provided informed consent to participate in this study. All participants were recreationally active individuals with formal training in Olympic lift technique.

Testing took place on two separate occasions, separated by 2 to 10 days. The first testing session

began with a modified version of the Burgener warm-up for Olympic weight lifting. Following the warm-up participants completed a series five repetition hang clean sets to estimate their one repetition maximum (1RM), which was calculated using the Brzycki Formula.

On day two of testing kinematic data were collected during two randomized blocks of trials: five hang cleans and five hang clean high pulls. All lifts were performed at 70% of the participant's 1RM. After the participant completed a modified Burgener warm-up, retroreflective markers were applied to the barbell. Data collection then began with hang clean or hang clean high pull trials. A minimum of 90 seconds of rest was provided between trials and blocks of trials.

Kinematic data were collected at 120 Hz using a 6-camera motion capture system (Motion Analysis). Data were low pass filtered at 8 Hz and used to compute barbell kinematic variables. Vertical bar displacement was analyzed from the instant bar velocity began to increase in the positive direction to maximum barbell height. Maximum vertical velocity, time to maximum vertical velocity, maximum vertical acceleration, and time to maximum vertical acceleration were analyzed from the instant the bar velocity began to increase to the instant of peak vertical velocity of the bar. Values were averaged across trials of the same type. Effects of task and sex on the dependent variables were tested using a 2-way repeated measures ANOVA. Significant interaction effects were explored using t-tests as appropriate. The alpha level was set at 0.05 for the ANOVA and 0.025 for all post-hoc analyses.

## RESULTS AND DISCUSSION

Independent of sex, participants exhibited similar barbell kinematics when performing the hang clean

and hang clean high pull (Table 1). Specifically, there were no differences in the maximum vertical velocity ( $p = 0.513$ ), time to maximum vertical velocity ( $p = 0.151$ ), maximum vertical acceleration ( $p = 0.182$ ), and time to maximum vertical acceleration ( $p = 0.052$ ). The only variable, that differed between the two tasks was the vertical displacement of the bar, which was greater in the hang clean than the hang clean high pull ( $p = 0.007$ ). It is not clear why vertical displacements differed between lifts, however, it is likely that further investigation of the biomechanics of the respective skills could shed light on this difference. That being said, the barbell kinematics indicate that the hang clean high pull is specific to the hang clean and could be an effective tool for improving hang clean performance.

Similarities in barbell kinematics were also present when comparing the performance of men and women during the two lifts (Table 1). Specifically, the vertical displacement ( $p = 0.141$ ), maximum vertical velocity ( $p = 0.090$ ), time to maximum vertical velocity ( $p = 0.0785$ ), and time to maximum vertical acceleration ( $p = 0.792$ ) did not differ between sexes. The only observed difference between sexes was a greater maximum vertical acceleration among men when compared to women ( $p = 0.045$ ). Despite the many similarities between sexes, the difference in acceleration suggests women may benefit from lifting a lighter load to increase vertical acceleration and potentially maximize the development of power.

## CONCLUSIONS

In the current study hang cleans and hang clean high pulls were performed with strikingly similar barbell kinematics. Thus, the present evidence supports the

use of the hang clean high pull as an exercise for improving hang clean performance. Additionally, men and women in the present study performed the two lifts with great similarity. However, researchers should continue to examine the importance of the observed difference in maximum acceleration between sexes. In general, the similarities between tasks and across sexes in the present study suggest that the hang clean high pull is specific to the hang clean and therefore an appropriate training tool for both men and women wishing to improve hang clean performance.

The present results should be interpreted in light of the following cautions: (1) The current study included recreational athletes rather than elite Olympic lifters. Though the present participants had formal training in Olympic lift technique, individuals that are more skilled may perform the lifts differently. (2) We chose to focus on the kinematics of the barbell. The observed similarities in barbell kinematics are telling, however, it is important that future research examine the kinematics and kinetics of the mover to further support the present findings and current strength and conditioning practices.

## REFERENCES

1. Channell, B, et al. *J Strength Cond Res* **22**, 1522-1527, 2008
2. Comfort, P, et al. *J Strength Cond Res* **25**, 3269-3273, 2011.
3. Comfort, P, et al. *J Strength Cond Res*, 1208-1214, 2012.
4. Garhammer, J. *NSCA*, **40**, 61-63, 1984.
5. Haff, G, et al. *J Strength Cond Res* **17**, 95-103, 2003.

**Table 1:** Barbell kinematics during the hang clean and hang clean high pull as a function of sex (Mean + SD).

Variable (Units)	Men		Women	
	Hang Clean	High Pull	Hang Clean	High Pull
<b>Vertical Displacement (m)</b>	0.93 ± 0.06	0.84 ± 0.10*	0.85 ± 0.05	0.82 ± 0.10*
<b>Max Vertical Velocity (m/s)</b>	2.21 ± 0.15	2.22 ± 0.16	2.12 ± 0.14	2.07 ± 0.19
<b>Time to Max Vertical Velocity (s)</b>	0.349 ± 0.071	0.348 ± 0.065	0.361 ± 0.048	0.322 ± 0.059
<b>Max Vertical Acceleration (m/s<sup>2</sup>)</b>	11.9 ± 2.19	11.2 ± 2.49	10.0 ± 2.52†	9.26 ± 1.20†
<b>Time to Max Vertical Acceleration (s)</b>	0.203 ± 0.111	0.227 ± 0.098	0.176 ± 0.077	0.224 ± 0.087

\*  $p < 0.05$  vs. hang clean; †  $p < 0.05$  vs. men

# EFFECT OF LEG-DRIVE ON UPPER EXREMITY MUSCLE ACTIVITY DURING A BENCH PRESS

Justin Chia, Kelsey Miller, and Jacob Gardner

Biola University, La Mirada, CA, USA  
email: jake.gardner@biola.edu

## INTRODUCTION

The bench press is one of the most popular and iconic upper body strength exercises. From competitive to casual, all types of lifters are looking for ways to optimize their bench press. Anecdotal claims from competitive powerlifters suggest that a method known as “leg drive” may allow the bench presser to lift more weight than a standard leg position. One study that examined variability of muscle activity for the bench press in power lifters compared to untrained individuals made an observation that the muscle activity in the vastus lateralis was greater among experienced power lifters compared to untrained lifters [1]. Besides this observation, practically no peer reviewed studies exist regarding how leg activity might affect upper extremity performance in the bench press.

The purpose of this study was to determine if muscle activity of upper extremity muscles differed depending on the involvement of the legs during a bench press exercise. We hypothesized that no differences in upper extremity muscle activity would exist with respect to leg involvement.

## METHODS

Preliminary data from 10 participants (6 male: age  $22.0 \pm 2.1$  yrs, height  $1.71 \pm 0.04$  m, mass  $74.7 \pm 6.4$ , BMI  $25.5 \pm 2.5$  and 4 female: age  $20.5 \pm 1.3$ , height  $1.63 \pm 0.07$ , mass  $60.1 \pm 11.3$ , BMI  $22.4 \pm 2.1$ ) are reported. All participants were recreationally trained and had at least 6 months of regular bench press experience. Additionally, participants were injury free for at least 1 year prior to the start of the study.

Participants attended two testing sessions. The first session served as a test for the participant’s 1-repetition maximum (1RM) for the bench press as well as a familiarization with the leg-drive protocol.

The second session was conducted 1 week later to minimize the potential effects of fatigue or muscle soreness. For this session, surface electromyography electrodes (Noraxon Ag/AgCl Dual EMG, Noraxon USA Inc.) were placed on the right side of the body over the muscle bellies of the sternal fibers of the pectoralis major, the anterior deltoid, and the lateral head of the triceps brachii. A maximal voluntary isometric contraction (MVIC) was performed at mid bench press position (elbows at 90 degrees) for normalization of the three muscles. Participants then performed 3 repetitions in the bench press with a load of 75% of their 1RM in three testing conditions: 1) neutral placement of the feet for stabilization (i.e. standard bench press [2]), 2) feet placed behind the line of the knee on the ground with the instruction to perform leg drive, 3) legs in the air with hips and knees flexed to 90 degrees. For the leg stabilization and leg-drive conditions, vertical and anteroposterior ground reactions forces (GRF) were recorded for the right leg to determine if the subjects were pressing with their legs (AMTI BP600600, 1000 Hz). The three conditions were randomized for each participant.

EMG data were collected through Biopac’s Acknowledge software using BioNomadix wireless transmitters/receivers (Biopac Systems Inc.) collecting at 1000 Hz. The normalized average of the peaks of the three reps for each muscle were analyzed using a repeated-measures ANOVA. A Bonferroni pos-hoc analysis was conducted when applicable to determine where, if any, differences occurred. Because of the low number of participants in this preliminary work, male and female gender groups were combined for statistical analysis. An alpha level of 0.05 was set a priori.

## RESULTS AND DISCUSSION

Graphically, there appears to be a trend for the feet in the air condition to result in greater muscle activations for each of the three muscles analyzed (Figure 1). However, the repeated measures ANOVA revealed no statistically significant differences across conditions for the pectoralis major ( $p = 0.191$ ) or the anterior deltoid ( $p = 0.231$ ). The ANOVA did reveal a statistically significant difference across conditions for the triceps brachii ( $p = 0.046$ ), but the post hoc analysis found no significant pairwise comparisons.

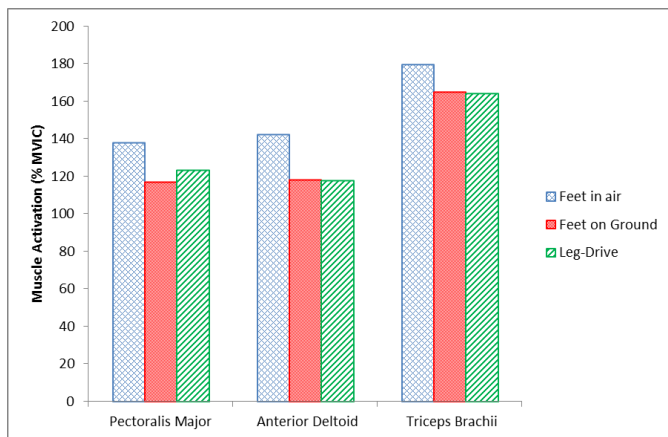


**Figure 1:** Average peak muscle activation of the pectoralis major, anterior deltoid, and triceps brachii muscles across the three leg positions. Mean values are shown in percentage of the peak muscle activation during the 1RM.

When comparing a standard bench press exercise to a bench press performed with leg-drive, our results indicate that a similar amount of motor units are recruited for the task regardless of the leg condition. This begs the question as to what actually lifters are experiencing when they state that it feels easier while using leg-drive. Something to note about the present study is that we required our participants to maintain 5 points of contact with the bench (head, shoulders, buttocks, right and left foot) at all times throughout the lift. In this way, we wanted to eliminate the possibility of an “easier” lift simply by lifting the hips off the bench to effectively change the inclination angle at which the lift is being performed or to shorten the range of motion.

Feasibly, if the lift truly were easier from a muscle activation standpoint, we may actually see less motor unit recruitment during the leg-drive. Less muscle activation would indicate a less demanding task for the central nervous system (CNS) with the same amount of weight being lifted. On a similar note, it is possible that since the weight being lifted was the same across all conditions (75% of 1RM), the CNS only recruited the motor units necessary to perform that task and no more or no less. However, since we did not find a difference in muscle activation between the two conditions, it is clear, at least from a muscle activation standpoint, that leg-drive did not lead to a reduction in motor unit recruitment and thus, the task demand was the same.

While not statistically significant, it is interesting to note a trend appeared for a higher level of motor unit recruitment during the feet in the air condition compared to the other two conditions. Previous research has found that electromyographic activity of trunk stabilizer muscles are increased when performing an unstable compared to a stable bench press [3]. It is possible that the results of the present study may be a similar finding; indicating that not having the feet placed on the ground for stability could result in increased neuromuscular demand by the CNS.

## CONCLUSIONS

Preliminary data from this work indicates that using leg-drive during a bench press does not reduce the demand placed on the central nervous system and thus does not result in decreased muscle activation compared to a standard bench press exercise.

## REFERENCES

1. Kristiansen M, et al. *Scand J Med Sci Sports* **25**, 89-87, 2015.
2. National Strength and Conditioning Association. *Exercise Technique Manual for Resistance Training*, Human Kinetics, 2016.
3. Norwood JT, et al. *J Strength Cond Res* **21**, 343-347, 2007.

# COORDINATION OF THE ANKLE AND TOE JOINTS IN DANCERS

<sup>1</sup> Danielle N. Jarvis and <sup>2</sup> Kornelia Kulig

<sup>1</sup> California State University Northridge, Northridge, CA, USA

<sup>2</sup> University of Southern California, Los Angeles, CA, USA

email: danielle.jarvis@csun.edu

## INTRODUCTION

Dance training emphasizes specialized use of the foot and ankle joints and requires a large range of motion at these joints [1]. Dancers are taught to ‘roll through the foot’ in several types of movements, including jumping. This motion involves allowing the metatarsophalangeal (MTP) joints to stay on the ground as the ankle plantar flexes, then flexing the toes at the end of jump takeoff. Conversely, dancers are taught to land by contacting the ground with the toes first, extending the MTP joints prior to dorsiflexing the ankle.

While dance teachers commonly focus attention on foot and ankle movements, few studies have quantified foot and ankle motion in dancers [2,3], and no study has examined coordination of the ankle and MTP joints during dance movements. Therefore, the purpose of this study was to examine sagittal plane coordination of the ankle and MTP joints during several common dance movements, including relevés, sautés, and saut de chat leap takeoffs.

## METHODS

Ten healthy female dancers (age=27.6±3.2 years; weight=56.3±6.9 kg; height= 1.62±0.06 m) with an average 21.7±4.9 years of dance training were recruited for this study. A three-dimensional motion analysis system was used to collect kinematic data. Participants performed relevés (rising up onto the toes), sautés (vertical bipedal jumps) and saut de chat leaps (split jumps involving both vertical and horizontal movement) (Fig. 1).

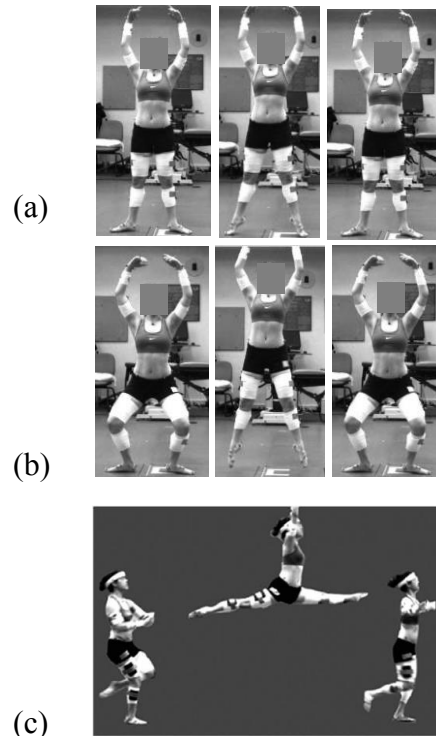


**Figure 1.** Body positioning during dance movements: (a) relevés; (b) sauté jumps; (c) the saut de chat leap, including takeoff, flight, and landing.

The movements were analyzed using a four-segment lower extremity model, which included thigh, shank, foot, and toe segments; the foot was divided at the MTP joints [3]. Sagittal plane kinematics of the ankle and MTP joints were calculated. Angle-angle diagrams of ankle and MTP joint motion were created to examine sagittal plane coordination patterns in the three movements. Based on the angle-angle diagrams, coordination can be described as in-phase, anti-phase, primarily ankle movement, or primarily MTP movement [4].

As the purpose of this study was to examine and describe coordination patterns amongst common dance movements, no statistical analyses were performed at this stage.

## RESULTS AND DISCUSSION

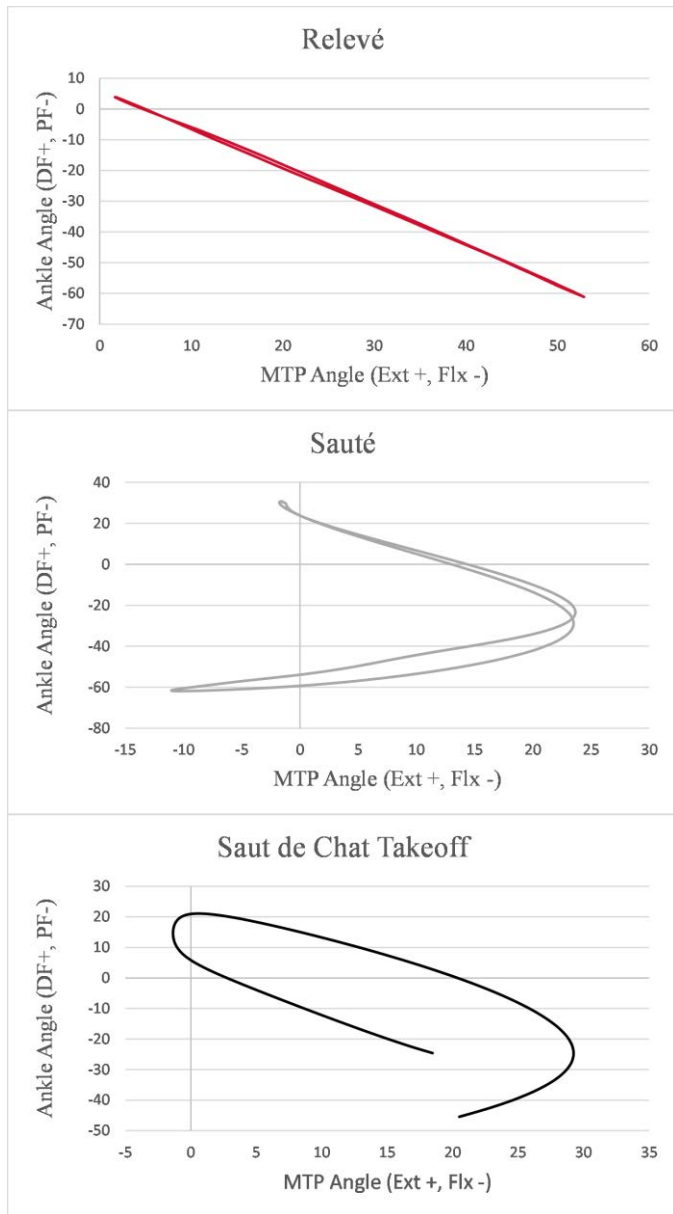


**Figure 2.** Angle-angle plot of mean ankle and MTP displacement for relevé, sauté, and saut de chat.

In the relevé, the movement is anti-phase throughout the entire rising and lowering portions. As the ankle plantar flexes, the MTP joints extend, and as the ankle dorsiflexes, the MTP joints flex (Fig. 2, top).

In the sauté, the movement starts off anti-phase as the ankle plantar flexes and the MTP joints extend. The pattern then shifts to in-phase as the dancer starts to leave the ground, where the ankle continues to

plantar flex while the MTP joints flex to provide additional propulsion off the floor and then achieve the desired aesthetic line while in the air. This pattern is then reversed in landing as the MTP joints first extend as the ankle begins to dorsiflex showing in-phase coordination, then the ankle continues to dorsiflex while the MTP joints flex in an anti-phase coordination pattern (Fig 2, middle).

In the saut de chat leap takeoff, an anti-phase coordination pattern is present as the ankle dorsiflexes and the MTP joints flex while the dancer absorbs weight and prepares to push-off into the air. The anti-phase pattern stays present as the dancer begins to propel off of the ground; the ankle is plantar flexing while the MTP joints extend. Near the end of takeoff, this coordination pattern shifts as the ankle continues to plantar flex and the MTP joints flex to push off of the floor (Fig 2, bottom).

## CONCLUSIONS

This examination of foot and ankle coordination patterns in dancers illustrates the specialized motion of the foot and ankle typically emphasized in dance training. Dancers do in fact move through the foot in both jump takeoffs and landings, demonstrating anti-phase movement of the MTP and ankle joints.

The results of this study provide descriptive evidence of coordination patterns used by trained dancers. Future research could quantify these coordination patterns more specifically using vector coding techniques. The learned coordination patterns at the foot and ankle joints that are seen in trained dancers may be important for successful performance as well as for avoiding injuries. This initial dynamic analysis of sagittal plane MTP and ankle coordination patterns in dancers demonstrates how dancers achieve the aesthetics of foot and ankle motion that are encouraged during training.

## REFERENCES

1. Russell JA, et al. *J Dance Med Sci* **12**, 75-82, 2008.
2. Jarvis DN, et al. *Med Prob Perf Art* **30**,61-65, 2015.
3. Jarvis DN, et al. *J Sports Sci* **34**, 1612-1618, 2016.
4. Chang R, et al. *J Biomech* **41**, 3101-3105, 2008.

# KINEMATIC ANALYSIS OF TRUNK COORDINATION THROUGHOUT THE ROWING STROKE SEQUENCE

McDarragh R. Minnock, Songning Zhang, David R. Bassett, Joshua T. Weinhandl  
The University of Tennessee, Knoxville, TN, USA  
email: mminnock@vols.utk.edu

## INTRODUCTION

Rowing at the elite level requires a high level of physical strength and endurance, as well as technical proficiency. Accurate kinematic sequencing of the rowing stroke (i.e. catch position, drive phase, finish position, and recovery phase) enables the rower to produce powerful and efficient strokes, while also protecting the body from injury [1]. Considering the ‘closed-chain’ and cyclic load-unload nature of rowing, chronic and overuse injuries are the most prevalent of all injuries. Specifically, lower back injuries account for 25% of all rowing related injuries [1, 2].

Previous studies have shown during prolonged sub-maximal ergometer rowing, the total range of lumbar-pelvic motion was markedly increased by about 5° [3]. Similar changes in spinal kinematics were also observed during incremental and maximal effort rowing studies [4-6]. It is important to understand spinal kinematics at different intensities, because the trunk acts as a cantilever and helps in transferring forces throughout the stroke sequence.

There is limited research available on rowing and trunk coordination throughout the rowing stroke sequence. In related coordination studies, angle-angle diagrams were analyzed to assess how two segments move relative to one another at one point in time and determine the variability in movement patterns [7]. Variability in movement is thought to negatively influence the system and potentially lead to injury. However, other studies have shown that variability in movement is essential for the body’s response to complex tasks [7, 8].

The purpose of this study was to observe the influence of rowing stroke intensity on pelvis-lumbar-thoracic coordination. First we hypothesized that the rower would deviate from proper form at 90% split intensity. Secondly, the variability in

pelvis-lumbar-thoracic coordination would increase as the rowing stroke intensity increases.

## METHODS

Ten female rowers from the University of Tennessee, Knoxville Varsity Rowing Team (20.7±2.2yrs, 1.74±0.05m, 69.12±6.2kg) were recruited to participate in this study. They performed an incremental step test on a Concept II model D rowing ergometer (Concept Inc., Morrisville, VT) to measure rowing form at increasing intensities. Intensities were determined from the rower’s average 2,000-meter split time from the previous season. The test began at 70% intensity and increased by 2.5% until reaching 100% intensity. Trials were collected for 30 strokes at the given intensity, followed by 30 seconds rest between trials.

Delsys Trigno wireless inertial measurement unit sensors (IMU) were used to record orientation data throughout the trial (148 Hz). Three sensors were placed on the sacrum, L4, and between shoulder blades. The IMUs recorded the orientation of each segment and XYZ Cardan angles were analyzed.

Data were processed using a customized Matlab code (Mathworks, Inc., Natick, MA) to identify the catch and finish of the 30 strokes. The middle 10 strokes were selected as strokes that best represent rowing form at a given intensity. Data were time normalized to 101 data points to allow for comparison between intensities and participants. A vector coding technique from Needham et al. [7, 8] was used to analyze the coupling angles (CA) and coupling angle variability (CAV) between the pelvis-lumbar and lumbar-thoracic spine at increasing intensities.

Repeated measures ANOVA were used to assess the differences between coupling angle variability at four intensity levels of interest: 70%, 80%, 90%,

and 100%. Follow-up independent t-tests for post hoc comparisons between consecutive intensities were used to identify the point of significant change in rowing form.

## RESULTS AND DISCUSSION

This study measured the coupling angle and coupling angle variability of the pelvis-lumbar and lumbar-thoracic spine at increasing rowing intensities. All participants successfully completed the incremental step-test protocol.

Significant changes in lumbar-thoracic CAV were observed among all participants between the 90%-100% intensities during the second half of the drive phase ( $p < .01$ ). There were changes in the lumbar-thoracic CAV at the other intensity levels (Fig. 1); however, they were found to be not significant. Non-significant changes in lumbar-pelvis coupling angle were observed between 90-100%. There were no significant changes in lumbar-pelvis CAV throughout the incremental step test.

There was significant variability in the lumbar-thoracic spine between 90-100% during drive 2 (Table 1). According to Needham et al. [8] our results suggest that there is more motion in the lumbar spine relative to the thoracic spine. This could indicate earlier extension of the trunk at an earlier point in the drive phase in order to meet performance standards. Although currently there is no research on rowing specific coordination at increasing intensities, we can infer from these results and previous studies that there is more variability in the form of lumbar-thoracic spine when performing at near maximal intensity [4-6]. Increased coordination variability of rowing form may influence the risk of developing lower back injuries.

## CONCLUSIONS

This study addressed movement variability in the rowing stroke sequence at increasing rowing intensities. These results suggest that there is variability in trunk coordination as rowing intensity increases. The repetitive motion of the rowing stroke sequence, in combination with the cyclic loading and unloading of the spine can be harmful to the spinal structure and surrounding tissues. However, further research is warranted to observe the influence of training types, such as prolonged submaximal training or maximal effort tests on trunk coordination

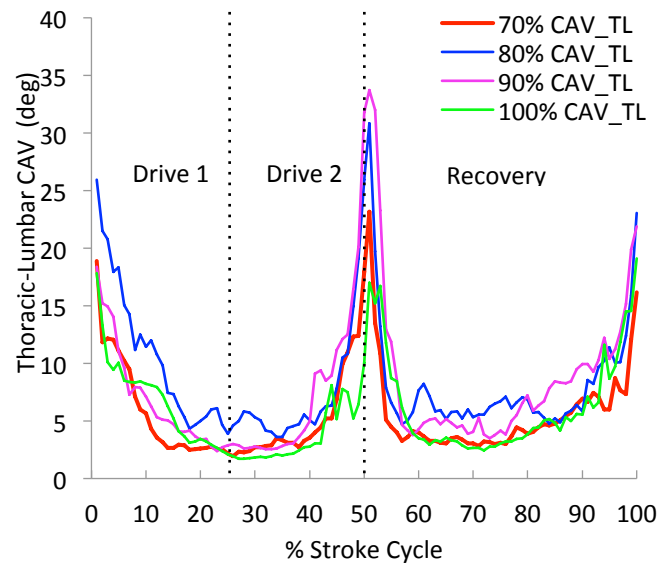


**Figure 1:** Lumbar-thoracic CAV for each of the given intensities across a complete rowing stroke sequence.

## REFERENCES

- [1] Hosea, T. M. et al., " *Sports Health*, **3**, 236-245.
- [2] Rumball, J. S. et al., *Sports medicine*, **6**, 537-555.
- [3] Holt, P. J., et al., *Int J Sports Med*, **8**, 597-602.
- [4] Bull, A. M., et al. *Clin Biomech* **10** 772-776.
- [5] McGregor, A. H., et al., *Med Sci Sports Exerc*, **6**, 1014-1020.
- [6] McGregor, A. H., et al. *J Sports Sci Med*, **1**, 29-35.
- [7] Needham, R. A., et al. *J of biomechanics*, **12**, 3506-3511.
- [8] Needham, R., et al. *J of biomechanics*, **16**, 3911-3912.

**Table 1:** Tables 1 shows the means and standard deviations for CA and CAV for both the lumbar-pelvis and lumbar-thoracic spine during drive 1 (0-25%) and drive 2 (26-50%) at the given intensity. (\* =  $p < .05$ ).

		Drive 1				Drive 2			
		70%	80%	90%	100%	70%	80%	90%	100%
TL	CA	227.4±16.9	237.1±28.5	230.3±24.5	230.0±25.9	225.4±8.3	228.9±20.8	231.4±27.8	233.1±27.7
	CAV	6.2 ±5.1	11.7±12.9	7.6±5.9	7.4±8.34	5.49±2.7	7.8±4.6	8.1±5.4*	3.9±2.6*
LP	CA	216.7±5.7	215.34±9.1	208.5±26.2	199.6±29.8	210.2±10.6	211.1±13.9	200.6±20.7	199.3±23.2
	CAV	5.3±5.5	11.25±13.6	9.0±9.7	8.23±8.6	5.52±3.4	6.7±4.0	8.5±6.2	5.5±2.0

# EFFECTS OF BALLISTIC INTENT TRAINING ON THE STATIC FORCE CAPACITY OF THE NECK

<sup>1</sup> Lucie Pelland, <sup>1</sup> Ian Gilchrist, <sup>2</sup> Wissal Mesfar

<sup>1</sup> School of Rehabilitation Therapy, Queen's University, Kingston, ON, Canada

<sup>2</sup> Biomedical Technology Department, King Saud University, Riyadh, Saudi Arabia

email: Lucie.Pelland@queensu.ca

## INTRODUCTION

Within the context of contact sports, a greater capacity to rapidly increase the stiffness of the neck against an impact may lower the risk for concussion and upper cervical spine injury [1]. In this regard, the contractile rate of force development (RFD) is an important variable, as it determines the potential static strength capacity of the neck that could be developed over the early phase of force application [2]. Static contractions performed with ballistic intent have been shown to facilitate the neural drive necessary to increase contractile RFD [3].

Therefore, our aim was to evaluate the effectiveness of repetitive maximum voluntary static efforts (MVEs) of the neck, performed with ballistic intent, in improving the contractile RFD of the neck and the associated static force capacity available within the first 100 ms of force application.

## METHODS

Twelve physically active males were enrolled, with relevant characteristics as follows: age, 18.6-24.8 years, neck circumference, 36.7-39.5 cm; and neck-to-head ratio, 0.6-0.7

Ballistic intent training and measurement of outcome variables of static force were performed using a Multi-Cervical Unit™. Two blocks of five ballistic intent MVEs were performed along right and left planes of neck flexion, oriented at 45° from the midsagittal plane, with a 3-min rest between blocks and 5-min rest between directions. Visual and auditory feedback of applied force was provided.

Three variables of the moment of static force of the neck were calculated at the level of C3: peak moment of force ( $\vec{M}_{Res}$ , N·m), defined as the largest magnitude

of the moment-time curve developed during each 3-s trial; RFD ( $N \cdot m \cdot s^{-1}$ ), calculated as the rise in the slope of the moment-time curve over the first 100 ms after force onset; and the impulse of static force (ISF,  $N \cdot m \cdot s$ ), defined as the area under the moment-time curve over the first 100 ms after force onset. Facilitation of the neural drive with training was measured from the surface electromyography signal of the sternocleidomastoid (SCM), splenius capitis (SPL) and upper fibers of trapezius (UFT) muscles, bilaterally. Signals were integrated over the 50 ms *prior to* force onset ( $iEMG_{PRE}$ , mV·s).

Outcome variables were measured at baseline, and at 10 min (PT1), 20 min (PT2) and two days (PT3), post-training. Effects of training on the relationship between  $\vec{M}_{Res}$ , RFD and ISF, and the contribution of neural facilitation to RFD, were evaluated using linear regression analyses. The effect size (Cohen's *d*-value) of training on outcomes was calculated.

## RESULTS AND DISCUSSION

Among our twelve participants, peak  $\vec{M}_{Res}$  at baseline ranged between 4.5 and 21.3 N·m, with no between-side difference (paired *t*-test,  $P \geq 0.06$ ). Across all participants and time points of measurement, ballistic-intent training produced a medium-to-large effect on RFD (Cohen's *d*, 0.54 to 0.75; 114-166% increase from baseline) and ISF (Cohen's *d*, 0.51 to 0.66; 133-176% increase from baseline), with a coefficient of variation of the standard error ( $CV_{SE}\%$ ) of 22-24%. The effect size of training on peak  $\vec{M}_{Res}$  was small (Cohen's *d*, 0.20-0.24;  $P \geq 0.07$ ).

Multiple regression plots, relating the effect of training on the three force variables, are shown for all time points of measurements in Figure 1. At baseline, greater magnitudes of RFD and ISF were associated with greater magnitudes of peak  $\vec{M}_{Res}$ .

Training produced a selected increase in RFD and ISF among participants with a lower peak  $\vec{M}_{Res}$  at baseline, with this effect persisting to PT3. A probabilistic sensitivity analysis (PSA), performed using a simulated mean based on the lowest  $\vec{M}_{Res}$  value at baseline (4.5 N·m), indicated that training can be expected to produce an increase in RFD at PT1, that exceeds the upper 95<sup>th</sup> percentile of the proportional increase in RFD for the mean peak  $\vec{M}_{Res}$  of our study group at baseline of 11.2 N·m in 63% of trials.

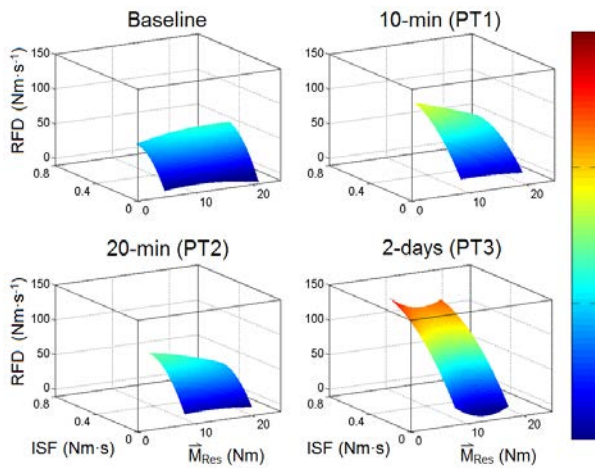


**Figure 1:** Linear regression plots relating the change in RFD and ISF as a function of peak  $\vec{M}_{Res}$ , N·m. The color scale is calibrated to the peak magnitude of RFD across all time-points of measurement.

Training-induced changes in RFD and ISF were associated with a 28.7-71.7% increase in  $iEMG_{PRE}$  of the SCM and SPL at PT1 to PT3 (one-way ANOVA,  $P \leq 0.01$ ), with only a discrete increase for the UFT at PT3 ( $P=0.004$ ). Based on PSA results, participants were classified into low and high baseline peak  $\vec{M}_{Res}$  groups using the mean group value of 11.2 N·m as

the cutoff. Training facilitated an increase in stabilizing  $iEMG_{PRE}$  (Table 1) for the high group (contralateral SCM and ipsilateral SPL;  $P \leq 0.001$ ;  $R^2$ , 0.65), with no effect identified for the low group ( $P=0.59$ ;  $R^2$ , 0.08).

A single bout of ten repetitive ballistic intent MVEs was effective in producing an acute increase in the RFD of the neck, along the direction of training, with an associated increase in ISF capacity at 100 ms. The proportional change in RFD and ISF, across all time points of measurement, was significant at a power of 0.91-0.97 (two-sided). The effects of ballistic intent training were modulated by the underlying coordination of ISF, with a facilitation of the ipsilateral SCM for participants in the low baseline peak  $\vec{M}_{Res}$  group, compared to a facilitation of ipsilateral SPL and contralateral SCM for the high group, this latter pattern of facilitation likely to provide the neck stability necessary for greater magnitudes of ISF and peak  $\vec{M}_{Res}$  to be generated.

## CONCLUSIONS

Ballistic-intent training could provide an easy-to-administer stimulus to enhance the static force capacity of the neck, which could have meaningful application for concussion risk management in contact sports. Learning of effective coordination strategies for individuals with low baseline static force should be considered.

## REFERENCES

1. Gilchrist I, et al. *Journal of Athletic Enhancement*, **4**, 1-19, 2015.
2. Aagaard P, et al. *Journal of Applied Physiology*, **93**, 1318-1326, 2002.
3. Dinn NA, Behm DG. *International Journal of Sports Physiology and Performance*, **2**, 386-399, 2015.

**Table 1.** Predictive contribution of  $iEMG_{PRE}$  to RFD at PT1 for the low and high baseline peak  $\vec{M}_{Res}$  groups

		$R^2$	Model P-value	Significant Normalized Beta Regression Coefficient (P-value)			
				SCM Ipsilateral	SCM Contralateral	SPL Ipsilateral	SPL Contralateral
				PT1	Low	0.08	0.59
	High	0.65	$\leq 0.001$	---	0.37 (0.03)	0.57 (0.003)	---

$R^2$ , coefficient of determination; PT1, 10 min post-training; SCM, sternocleidomastoid; and SPL, splenius capitis.

# BIOMECHANICAL DIFFERENCES BETWEEN A SPLIT-STEP AND SIDESTEP CUT IN FEMALE TENNIS PLAYERS

<sup>1</sup> Adrienne Hamada, <sup>1</sup>Henry Wang, <sup>1</sup>D. Hankemeier and <sup>1</sup>D. Clark Dickin

<sup>1</sup> Biomechanics Laboratory, Ball State University, Muncie, Indiana, USA  
email: amhamada@bsu.edu

## INTRODUCTION

A sidestep cut is a common change of direction movement in sports but is also a common mechanism for anterior cruciate ligament injuries (ACL) [1, 2]. Injuries to the ACL are common in sports such as basketball, soccer and lacrosse but much less common in tennis despite the constant cutting, pivoting and sudden decelerations [3]. The majority of these injuries occur during initial contact with the knee flexed less than 30° and in an abducted (i.e. knocked-kneed) position with the foot rotated outwards [4].

Studies have shown that the use of a split-step could decrease knee loading and injury risk when compared to a sidestep cut [1, 5]. The populations used in these previous studies were not familiar with a split-step. A split-step is a common movement used by tennis players and allows for a quicker reaction time [6]. The landing position of a split-step allows for the body to be more stable as compared to body positioning just before a sidestep cut and allows performers to share forces between feet decreasing peak knee adduction and external rotation [1, 5]. Therefore the purpose of this study was to investigate the differences in joint loading and overall risk factors between a sidestep and split-step cutting maneuver in female tennis players.

## METHODS

Four healthy young females (age: 19.25 ± 1.25 years; mass: 65.6 ± 8.20 kg; height: 1.680 ± 60.69 m) performed two different cuts (sidestep and split-step cuts). Participants were excluded if they had any previous anterior cruciate ligament injuries, other ankle or knee surgeries, current lower extremity injuries, pain, neurological or physiological problems that would prevent them from running and cutting. Participants with a history

of participating in tennis at a USTA 3.0 level or higher with experience playing high school tennis or junior tournaments or adult tournaments or league were included. A sidestep cut in which participants planted one leg and moved in the direction opposite of that leg was performed, along with a split-step cut in which participants performed a bilateral hop with a simultaneous double leg landing then proceeded to perform a sidestep cut. The two cuts were randomized and performed under unanticipated conditions to simulate a game like situation. This was done using a set of timing gates, controlled by a custom program producing images of direction arrows or stop signs. The cutting maneuver was captured using a 12-camera (VICON, Inc., Denver, CO, USA) collecting at 200Hz and two AMTI force Platforms (AMTI, Watertown MA, USA) embedded in the floor sampling at 2000Hz. A modified Plug-in Gait model that included marker clusters on the thigh and shank of each leg was used. Sagittal, frontal and transvers plane joint kinematics were calculated using Visual 3D software (Version 5.0, C-Motion, Germantown, MD, USA). A paired samples t-test was run comparing a sidestep to a split-step with an alpha of p<.05.

## RESULTS AND DISCUSSION

Table 1 shows knee joint angles in all three planes at initial contact for both split-step and sidestep cuts in both directions. Analysis was run on the plant leg comparing the sidestep and split-set cuts in the same direction. During a split-step cut a significant increase in initial contact knee flexion angles were observed compared to the sidestep cut (p<.05). There was also an increase in knee internal rotation at initial contact when performing a split-step as compared to a sidestep cut (p<.05). There were no other significant differences observed between a sidestep cut and split-step cut at the knee joint.

Table 2 shows ground reaction forces during a sidestep and split-step cuts. A significant decrease in peak ground reaction forces were seen during a right split-step cut ( $p < .05$ ). There is was a decrease in breaking forces but was not significant.

The results demonstrate the potential benefits to the use of a split-step cut. The knee flexion angles at initial contact were larger during a split-step cut as compared to a sidestep cut. These angles were observed to be greater than  $30^\circ$  which can decrease the risk of ACL injuries. The decrease in peak ground reaction forces can also decrease the risk of ACL injuries. This decrease in ground reaction forces can be attributed to the ability to share forces between two feet rather than having all of the force being put into one leg. Trewartha et al. (2007) observed that subjects who were better able to share the forces between the two feet show a trend towards decreasing the load placed on the ACL.

## CONCLUSIONS

The preliminary results of this study show that there is the potential of a split-step cut to decrease the risk of ACL injuries by increasing knee flexion angles at

initial contact and decreasing peak ground reaction forces. Since this is a fundamental movement in tennis it is possible that the differences seen are attributed to the experience of the movement. There is the potential for this movement to be translated into other sports but other populations should be trained and tested to see if similar results are achieved.

## REFERENCES

1. Trewartha G, et al. *J Biomech.* **40**, S238, 2007
2. Yu B, et al. *Br J Sport Med.* **41**, i47-i51, 2007
3. Maquirriain J, et al. *Br J Sport Med.* **40**, 451-453, 2007
4. Hewett TE, et al. *NAJSPT.* **5**,434-251, 2010
5. Trewartha G, et al. *Proceedings of ISBS'08*, Korea, 2008
6. Uzu R, et al. *J Sports Sciences.* **27**, 1233-1240, 2009

## ACKNOWLEDGMENTS

Funding source: 2017 Ball State University ASPIRE Grant

Table 1: Knee joint angles at initial contact

Knee Joint Angles at Initial Contact ( $^\circ$ )	Right Sidestep	Right Split-Step	Left Sidestep	Left Split-Step
Flexion(+)/ Extension (-)	19.51 (3.10)*	38.80 (7.31)*	24.09 (4.69)	30.48 (5.48)
Adduction(+)/ Abduction(-)	-.58 (4.60)	-2.93 (5.89)	-5.12 (2.12)	-4.70 (2.23)
Internal(+)/External Rotation (-)	1.37 (5.92)	7.51 (4.42)	6.07 (4.01)*	9.48 (3.16)*

\*Significant differences at  $p < .05$

Table 2: Ground reaction forces

	Right Sidestep	Right Split-Step	Left Sidestep	Left Split-Step
Peak GRF (N/BW)	2.21 (.43)*	1.62 (.29)*	1.99 (.31)	1.70 (.33)
Peak Loading Rate (N/BW)	30.05 (17.34)	52.48 (30.23)	44.83 (28.00)	61.71 (48.15)
Average Loading Rate (N/BW)	21.59 (12.48)	11.85 (5.30)	29.33 (18.68)	13.61 (10.08)
Breaking Force (N/BW)	-.91 (.31)	-.55 (.26)	-.69 (.21)	-.48 (.16)

\*Significant differences at  $p < .05$

# ENERGY FLOW IN YOUTH BASEBALL PLAYERS IN RELATION TO PITCHING PERFORMANCE AND EFFICIENCY

<sup>1</sup> Jacob Howenstein, <sup>2</sup> Kristof Kipp, <sup>1</sup> Michelle Sabick

<sup>1</sup> Saint Louis University, MO, USA

<sup>2</sup> Marquette University, WI, USA

email: jhowens2@slu.edu

## INTRODUCTION

In baseball pitching, shoulder and elbow injuries are prevalent given the ballistic nature of the motion. These injuries, once predominantly seen in older pitchers, have begun to permeate to younger athletes. Because repetitive micro-trauma may lead to acute injuries, understanding how youth pitchers can achieve high performance levels with minimal joint loads could yield important information to help reduce the risk of injury in these athletes [1,2].

Pitchers generate mechanical energy in the lower extremities and transfer it through the trunk and into the upper extremity, ultimately propelling the ball toward home plate. Optimal transfer of energy between segments is critically dependent on the correct muscle activation and timing of sequential steps during the pitching motion [2]. Energy flow (EF) is a measure that quantifies how energy is both generated and transferred among body segments [3]. An optimal, or more efficient, pitching technique would be characterized by larger energy generation and transfer along with smaller joint loads at the shoulder and elbow.

Most pitching studies have focused on the upper extremities and have largely ignored the role of the lower extremities and trunk in relation to pitching performance. Additionally, multiple studies have identified athlete size and pitch velocity as contributors to the magnitude of elbow and shoulder loading [1,4]. Although important, these findings provide limited insight into how to decrease joint loads without a compromise in pitch performance. Therefore, investigation into joint loads with respect to pitch velocity (i.e. joint moment/mph) would likely provide an indicator of pitch efficiency and the trade-off between performance and surrogates for risk of injury [2]. The purpose of this study was

to investigate the relationships between measures of full body energy flow and pitch performance and pitch efficiency.

## METHODS

Fourteen youth baseball pitchers (age:  $11.6 \pm 1.3$  years, height:  $1.59 \pm 0.12$  m, mass:  $48.5 \pm 13.4$  kg, velocity:  $56.6 \pm 6.9$  mph, 11 right-handed/3 left-handed) were recruited for this study. All testing occurred in an indoor research lab equipped with a custom built pitcher's mound with two embedded force plates; one under the rubber and one under the landing area. Reflective markers and marker clusters were attached to each pitcher's upper and lower body. Kinematic data were recorded with a 14-camera motion capture system at 250Hz. Kinetic data of the drive (rear) and stride (front) leg were sampled at 1000Hz, and a radar gun was used to record velocity. Each pitcher threw 15 maximal effort fastballs toward a hanging strike zone 46ft from the rubber. The fastest strike thrown for each pitcher was chosen for analysis.

Elbow valgus and shoulder internal rotation moments were calculated with an inverse dynamics procedure. Energy flow was quantified with a full-body segment power analysis [5]. The rate of work done on each segment by the joint forces (JFP; eqn. 1) and muscle moments (STP; eqn. 2) were summed at the proximal and distal ends of each segment to calculate the total segment power (SP; eqn. 3).

$$\text{JFP} = (\text{joint reaction force}) \cdot (\text{linear joint velocity}) \quad (\text{eqn. 1})$$

$$\text{STP} = (\text{joint moment}) \cdot (\text{segment angular velocity}) \quad (\text{eqn. 2})$$

$$\text{SP} = \text{JFP}_{\text{prox}} + \text{STP}_{\text{prox}} + \text{JFP}_{\text{dist}} + \text{STP}_{\text{dist}} \quad (\text{eqn. 3})$$

When the SP is integrated over a specified interval of time, the result is net energy transfer into or out of the segment. The SP for each segment was thus integrated over the period that it was positive to

calculate the energy it gained and integrated over the period that it was negative to calculate the energy it transferred. EF was normalized to body-mass, whereas upper extremity moments were normalized to body-mass, height, and pitch velocity to calculate pitch efficiency.

Selected EF variables were compared to pitch performance (i.e. ball velocity) and efficiency (i.e. velocity-normalized joint loads) with simple linear regressions.

## RESULTS AND DISCUSSION

A considerable number of the correlations between selected EF variables, pitch velocity, and elbow valgus and shoulder internal moments were significant (Table 1). Pitch velocity was strongly correlated to EF into the drive hip and hand as well as out of the pelvis, shoulder, and humerus. Velocity-normalized elbow valgus and shoulder internal rotation moments were strongly correlated with EF into the drive hip, and out of the pelvis and humerus. Collectively, these correlations point to the importance of energy production and transfer in relation to both velocity and pitch efficiency.

In addition, linear energy toward home plate was strongly related to pitch velocity and efficiency. The four linear energy variables all showed consistent and significant correlations with both pitch velocity and efficiency. In comparison, peak rotational trunk energy had a significant relationship with pitch velocity but not efficiency. No rotational energy

variable had a significant correlation with pitch efficiency. Rotational energy thus appears more important for pitch performance than for pitch efficiency. This study provides evidence that pitch efficiency is not only dependent on an athlete's size and pitch velocity, but also how they generate and transfer energy between body segments.

## CONCLUSIONS

The results of this study highlight the relationships between energy flow and both performance and efficiency measures of baseball pitching. Linear energy from the drive leg and trunk are strongly correlated to pitch velocity and upper extremity loading. Future research should expand the use of energy flow analysis to populations of different ages and larger subject pools. In addition, identifying kinematic predictors of energy flow variables would allow researchers to apply these techniques to athletes in the field without the needing specialized equipment.

## REFERENCES

1. Sabick MB, et al. *J Should Elb Surg* **13**, 349-355, 2004.
2. Davis JT, et al. *Am J Sports Med* **37**, 1484-1491. 2009.
3. Martin C, et al. *Am J Sports Med* **42**, 2751-2760, 2014.
4. Hurd WJ, et al. *Sports Health: Multidisc App* **4**, 415-441, 2012.
5. Gordon DE, et al. *J Biomech* **13**, 845-854, 1980.

Table 1. Correlations between energy flow variables and pitch velocity and efficiency.

	Velocity	Elbow Load Efficiency	Shoulder Load Efficiency
EF into Drive Hip	<b>0.863**</b>	<b>-0.637*</b>	<b>-0.685**</b>
EF out of Pelvis	<b>-0.863**</b>	<b>0.713**</b>	<b>0.742**</b>
EF out of Trunk at Shoulder	<b>-0.845**</b>	0.450	0.524
EF out of Humerus	<b>-0.804**</b>	<b>0.789**</b>	<b>0.758**</b>
EF into Hand	<b>0.750**</b>	<b>-0.592*</b>	<b>-0.634*</b>
Linear Drive Leg Energy	<b>0.908**</b>	<b>-0.718**</b>	<b>-0.756**</b>
Linear Energy, Pelvis to Trunk	<b>0.756**</b>	<b>-0.724**</b>	<b>-0.727**</b>
Peak Linear Trunk Energy	<b>0.746**</b>	<b>-0.803**</b>	<b>-0.774**</b>
Peak Rotational Trunk Energy	<b>0.585*</b>	-0.292	-0.291

**Note:** Significant *p*-values are highlighted in bold font, \*Denotes  $p < 0.05$ , \*\*Denotes  $p < 0.01$   
Efficiency metrics are elbow valgus moment and shoulder internal moments normalized by body mass, height, and velocity (load/mph)

# EFFECT OF START TECHNIQUE ON PRO-AGILITY TEST PERFORMANCE IN DIVISION I FOOTBALL PLAYERS

<sup>1</sup> Travis Ficklin, <sup>2</sup> Panayiotis Papadopoulos, <sup>2</sup> Robin Lund, and <sup>2</sup> Jacob Reed

<sup>1</sup> Dixie State University, Saint George, UT, USA

<sup>2</sup> University of Northern Iowa, Cedar Falls, IA, USA

email: travis.ficklin@dixie.edu

## INTRODUCTION

The Pro-agility test (“20-yard shuttle” or “5-10-5”) is used by football coaches and scouts to assess player acceleration and agility. It is one of the tests administered during the NFL Combine, and draft status is tied to its effective execution.

Athletes begin in a three-point stance with either hand touching the ground. Upon starting, the athlete sprints toward his right (if the right hand was down to start) or left to touch a ground marker five yards away. Then, the athlete turns to sprint ten yards in the opposite direction, touching another marker. Last, he turns again to sprint five yards through the finish line, which is the original start (see Figure 1).

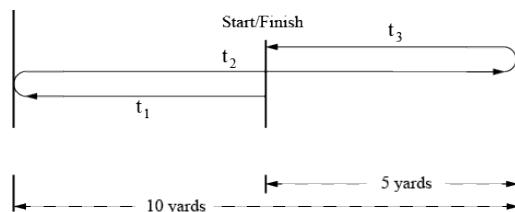


**Figure 1:** The route run during the Pro-agility test. The sequence of moves is labeled  $t_1$ ,  $t_2$ ,  $t_3$ .

Traditionally, players use a crossover step (CS) to start, avoiding a “false” step. However, a “rhythm”, or “drop” step (DS), is natural and has been shown to produce better sprint times for short distances [1,2]. The purpose of this study was to compare a CS start to a DS start in the Pro-agility test to determine which, if either, produces better times.

## METHODS

Study procedures were reviewed and approved by the university IRB, and all subjects provided informed consent. Thirteen Division I football players volunteered to run the test four times in counterbalanced order: twice using a CS start and twice using a DS start. A high-speed video camera

captured each trial at 100 Hz from a position 25 m away from and perpendicular to the line containing the ground markers. Video frames were used to measure the time from start to the first marker touch ( $t_1$ ), from first marker to second marker ( $t_2$ ), and from second marker to finish ( $t_3$ ). Total time ( $t_{TOT}$ ) was the sum of these times. The times from the two DS trials were averaged together, as were the times from CS trials.

Full-body digitization and custom software were used to calculate the center of mass (COM) position, velocity, and acceleration during  $t_1$ . The body’s lean ( $\theta_{LEAN}$ ) with respect to vertical was measured using the vector from the athlete’s trail-foot toe to the top of the trunk. Paired t-tests ( $\alpha = 0.05$ ) were used to find technique differences for times, maximum  $\theta_{LEAN}$ , maximum acceleration ( $a_{COM}$ ), and time to reach both max  $\theta_{LEAN}$  and  $a_{COM}$ .

## RESULTS AND DISCUSSION

Descriptive statistics for all variables are presented in Table 1. Several of the compared variables were shown to be significantly different between trials using a DS start and trials using a CS start.

Specifically,  $t_{TOT}$  was 0.10 s faster, with  $t_1$  taking 0.07 s less time, using a DS start ( $p = 0.02$  and  $p < 0.01$ , respectively). Maximum  $a_{COM}$  in  $t_1$  was the same in both conditions, but subjects reached  $a_{COM}$  0.08 s sooner using the DS start ( $p < 0.01$ ). Even though max  $\theta_{LEAN}$  was similar between techniques, the time to reach it trended significantly less using the DS technique ( $p = 0.06$ ).

A time savings of 0.10 s may seem unimportant, but it can affect an athlete’s ranking in the test heavily. For example, in the 2016 NFL Combine, 51 defensive linemen completed the test, with scores ranging from 4.21 - 5.13 s, and a median of 4.56 s

[3]. If the median player improved his score by 0.10 s, he would have moved up 12 places in rank. This has draft position and related financial implications for the athlete.

The bulk of the time savings occurs during  $t_1$ , and kinematic differences during that portion of the run should be examined. Previous work has indicated that the advantages of the DS stem from two factors. First, a better location of the foot behind the COM allows for bigger horizontal forces. Second, the ballistic placement of the dropped foot leads to an enhanced stretch-shortening cycle (SSC) of propulsive muscles [1,2].

The first of these factors relates to  $\max \theta_{LEAN}$ . Though it was not bigger with the DS start, athletes probably achieved  $\max \theta_{LEAN}$  sooner, meaning that propulsive forces could get bigger sooner. This is supported by their reaching  $\max a_{COM}$  sooner when using the DS start. Though not significantly, athletes continued to gain time during  $t_2$  and  $t_3$ , eventually growing the total advantage to 0.10 s. This may be due to enhanced SSC action at the changes of direction due to carrying slightly more speed at each turn, crating a more ballistic stopping and re-direction (see Figures 2 & 3).

## CONCLUSIONS

When preparing athletes for the Pro-agility test, practitioners seek any potential advantage. The DS start results in a time savings of 0.10 s in this sample, which could help vault players to better rankings and draft positions. Trainers and coaches should try both techniques to see if better times can be achieved using the less-traditional DS start.

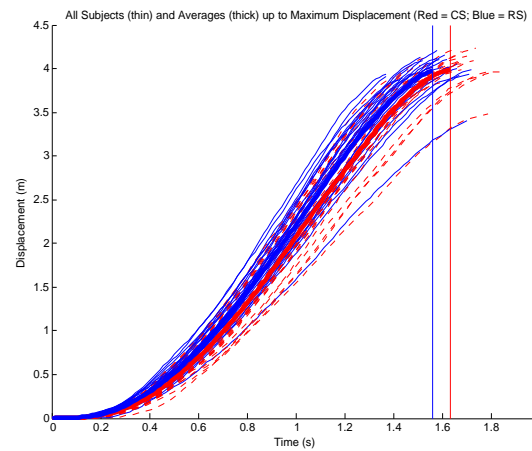


**Figure 2.** COM position during  $t_1$ . Red = CS, blue = DS. Thicker lines represent ensemble averages.

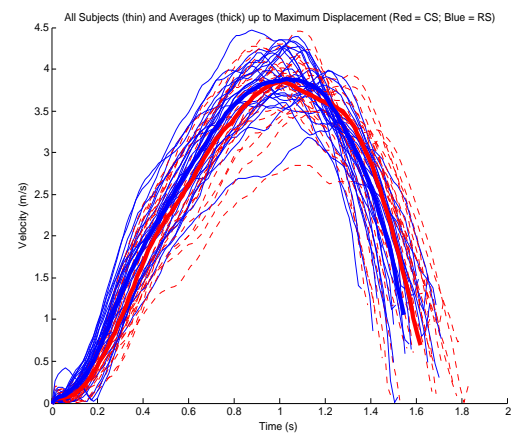


**Figure 3.** COM velocity during  $t_1$ . Red = CS, blue = DS. Thicker lines represent ensemble averages.

## REFERENCES

1. Cusick, JL, et al. *J Strength Cond Res* **28**, 2669–2672, 2014.
2. Frost, DM, et al. *J Strength Cond Res* **22**, 918–922, 2008.
3. 2016 NFL Combine Results - Available from: <http://nflcombineresults.com/nflcombinedata.php>

**Table 1:** Descriptive statistics and results of paired samples t-tests (n=13).

Variable	Crossover Step (CS)		Drop Step (DS)		p
	Mean	SD	Mean	SD	
$a_{max}$ ( $m/s^2$ )	5.42	0.77	5.56	0.65	0.23
$t_{amax}$ (s)	0.46	0.61	0.38*	0.67	.001
$\theta_{lean}$ ( $^\circ$ )	28.4	3.23	28.5	3.18	0.90
$t_{\theta_{lean}}$ (s)	0.54	0.03	0.49	0.09	0.06
$t_1$ (s)	1.62	0.11	1.55*	0.09	.002
$t_2$ (s)	2.23	0.17	2.22	0.18	0.70
$t_3$ (s)	1.23	0.14	1.21	0.11	0.31
$t_{total}$ (s)	5.09	0.35	4.99*	0.35	0.02

# KINEMATIC PREDICTORS OF ENERGY FLOW IN YOUTH BASEBALL PITCHERS

<sup>1</sup> Jacob Howenstein, <sup>2</sup> Kristof Kipp, <sup>1</sup> Michelle Sabick

<sup>1</sup> Saint Louis University, MO, USA

<sup>2</sup> Marquette University, WI, USA

email: jhowens2@slu.edu

## INTRODUCTION

Baseball pitchers generate mechanical energy in the lower extremities and transfer it from proximal to distal segments, through the trunk and upper extremity, to ultimately propel the ball towards home plate [1]. Energy flow (EF) is a measure that refers to how energy is both generated and transferred through the body [2]. The pelvis and trunk link the lower extremities to the arm, thus greater magnitudes of energy flow through the trunk should allow for more energy to be transferred from the lower extremities and core musculature to the throwing arm. Greater magnitudes of EF into the dominant arm from the shoulder have previously been shown to increase serve speeds in tennis players [2]. Little research, however, has applied EF analysis to baseball pitching and no study has applied it to the lower extremities and trunk.

Although information on EF is useful, it is difficult to quantify outside of a research lab. Therefore, the identification of kinematic variables that correlate with greater magnitudes of EF would improve the translation of EF research to the coaching of athletes. The purpose of this paper was to identify kinematic variables that correlate with the magnitude of EF during pitching in youth baseball players.

## METHODS

Fourteen youth baseball pitchers (age: 11.6±1.3 years, height: 1.59±0.12 m, mass: 48.5±13.4 kg, velocity: 56.6±6.9 mph, 11 right/3 left) were recruited for this study. All testing occurred in an indoor research lab equipped with a custom built pitcher's mound with two embedded force plates; one under the rubber and one under the landing area. Reflective markers and marker clusters were attached to each pitcher's upper and lower body.

Kinematic data were recorded with a 14-camera motion capture system at 250Hz. Kinetic data of the drive (rear) and stride (front) leg were sampled at 1000 Hz, and a radar gun was used to record velocity. Each pitcher threw 15 maximal effort fastballs toward a hanging strike zone 46 ft from the rubber. The fastest strike thrown for each pitcher was chosen for analysis.

Energy flow was quantified with a full-body segment power analysis [3]. The rate of work done on each segment by the joint forces (JFP; eqn. 1) and muscle moments (STP; eqn. 2) was summed at the proximal and distal ends of each segment to calculate the total segment power (SP; eqn. 3). The joint between the pelvis and trunk was defined as the midpoint between the two iliac crests.

$$\text{JFP} = (\text{joint reaction force}) \cdot (\text{linear joint velocity}) \quad (\text{eqn. 1})$$

$$\text{STP} = (\text{joint moment}) \cdot (\text{segment angular velocity}) \quad (\text{eqn. 2})$$

$$\text{SP} = \text{JFP}_{\text{prox}} + \text{STP}_{\text{prox}} + \text{JFP}_{\text{distal}} + \text{STP}_{\text{distal}} \quad (\text{eqn. 3})$$

For this paper, we focused on the EF between the pelvis and trunk (Figure 1), as well as the EF out of the trunk through the shoulder joint. The JFP and STP between the pelvis and trunk were analyzed separately while the EF out of the shoulder joint was calculated as the sum of the JFP and STP at the distal end of the trunk. When a component of segment power is integrated over an interval of time, the result is net EF into or out of the segment by that method. The JFP and STP for the pelvis and trunk were integrated over the period each was positive to calculate the energy transferred into them and integrated over the period that they were negative to calculate EF out.

The EF variables of the pelvis and trunk were compared to selected kinematic variables with simple linear regressions. When compared to kinematic parameters, EF was normalized to body mass.

## RESULTS AND DISCUSSION

Multiple kinematic variables had significant relationships with the magnitude of EF through the trunk (Table 1). The maximum linear velocity of the pelvis and trunk and the velocity of both segments at the time of stride contact had significant relationships to the magnitude of JFP between the two segments. These relationships, however, were expected since JFP is the dot product of the force and velocity at a joint. An interesting observation is the stronger relationship between JFP and the peak linear trunk velocity compared to the relationship between JFP and trunk velocity at stride foot contact. The likely explanation for this finding is that the increase in velocity of the trunk, from stride contact to its peak value, is due to the EF from the pelvis via the joint force between the segments.

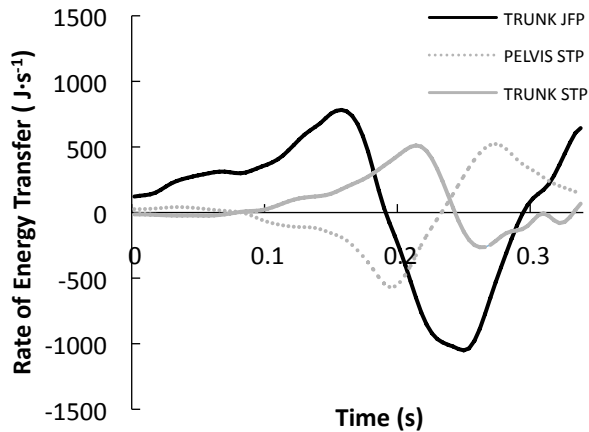


**Figure 1.** Sample energy flow between the pelvis and trunk from stride foot contact to ball release.

Peak trunk flexion angular velocity and the angular velocity of the pelvis relative to the shoulders both had significant relationships to STP out of the pelvis, STP into the trunk, and total EF out of the

trunk at the shoulder joint. Peak trunk angular velocity had a significant relationship with STP out of the pelvis and STP into the trunk. The strong relationship between EF and the angular velocity of the pelvis relative to the trunk underscores the importance of the pelvis leading the rotation of the trunk and creating an angle of separation between the segments. The strong relationship between angular trunk flexion velocity and EF indicates that trunk flexion is an important way to transfer rotational energy up the kinetic chain, even more than axial rotation of the trunk, which had no significant relationship to EF magnitude. Peak angular trunk velocity had the strongest relationship with STP into the trunk, but did not correlate with EF out of the trunk through the shoulder.

## CONCLUSIONS

The best kinematic predictors of energy flow through the pelvis and trunk were peak linear velocities of the pelvis and trunk, angular velocity of the pelvis relative to the trunk, and peak angular trunk flexion velocity. Future research should expand this investigation to larger subject populations and more experienced pitchers with more consistent mechanics.

## REFERENCES

1. Seroyer , Shane T., et al. *Sports Health* **2**, 135-146, 2010.
2. Martin C, et al. *Am J Sports Med* **42**, 2751-2760, 2014.
3. Gordon DE, et al. *J Biomech* **13**, 845-854, 1980

**Table 1:** Correlations between selected kinematic variables and measures of energy flow.

	Pelvis to Trunk JFP	Pelvis STP Out	Trunk STP In	Trunk EF Out at Shoulder
Peak Linear Pelvis Velocity	<b>.694**</b>	.348	.199	.458
Peak Linear Trunk Velocity	<b>.956**</b>	.377	.136	.465
Linear Pelvis Velocity at SC	<b>.776**</b>	.468	.336	.489
Linear Trunk Velocity at SC	<b>.775**</b>	<b>.615*</b>	.509	<b>.538*</b>
Peak Trunk Flexion $\omega$	.043	<b>.797**</b>	<b>.718**</b>	<b>.729**</b>
Peak Trunk Axial $\omega$	.009	.194	.304	.153
Hip/Sho Separation $\omega$	.084	<b>.832**</b>	<b>.817**</b>	<b>.712**</b>
Peak Total Trunk $\omega$	.216	<b>.691**</b>	<b>.847**</b>	.319

**Note:** Significant  $p$ -values are highlighted in **bold** font, \*Denotes  $p < 0.05$ , \*\*Denotes  $p < 0.01$

# KINETICS OF STEEPLECHASE HURDLING PERFORMANCE

<sup>1</sup> James Tracy, <sup>1</sup> Spencer Baker, and <sup>1</sup> Iain Hunter

<sup>1</sup> Brigham Young University, Provo, UT, USA  
email: [iain\\_hunter@byu.edu](mailto:iain_hunter@byu.edu), web: <http://biomechanics.byu.edu/>

## INTRODUCTION

The 3000m steeplechase event requires athletes with a unique combination of endurance, strength, and athleticism. Studies have been completed in recent years focused on kinematics of the steeplechase event, but very little exists on the kinetics.<sup>1,2</sup> Kipp found steeplechase hurdling forces are greater than treadmill running.<sup>3</sup>

This study aimed to determine a kinematic and kinetic analysis of steeplechase hurdling related to horizontal velocity gained or lost upon takeoff and landing.

## METHODS

Eight male collegiate steeplechase athletes were brought to the biomechanics lab. After signing an informed consent approved through the university's institutional review board, they did their typical warmup routine followed by marker placement according to the Vicon Plugin Gait model. A hurdle was placed prior to a 0.6 x 0.9m force platform to measure two hurdle landings, one with the left leg leading and one with the right. Force data were collected at 1000 Hz with motion at 250 Hz. A successful trial was determined when the foot landed completely on the force plate and the designated speed of 4.73 m/s was attained within 5%. This is a little slower than their typical race pace, but constraints of the lab limited us from faster running.

Various characteristics of hurdling technique were measured or calculated using outputs from the Plugin Gait Model. Measurements are illustrated or listed in Figure 1. Change in horizontal velocities were calculated through A/P impulse calculations.

A stepwise linear regression tested for correlations between the loss of velocity during contact with the

ground and the various measures of technique. Correlations were tested between all combinations of predictor variables individually. Some variables were not used in the final regression model based upon them being closely correlated with other potential predictor variables. Separate analyses for takeoffs and landings were completed with alpha set at 0.05. The separation of takeoff and landing trials were needed since the force plates were not in positions that allowed for measurements of both ground contacts in a single jump.



**Figure 1:** Measurements used in analysis are labeled in image. Others included peak vertical force and vertical impulse at takeoff and landing, high point of center of mass, trunk lean at takeoff and landing, and energy during contact with the ground for the hip, knee, and ankle, at takeoff and landing.

## RESULTS AND DISCUSSION

Only takeoff vertical impulse predicted the loss of velocity during takeoff contact. Other measures were non-significant. The horizontal distance between the landing toe and the person's center of mass and the horizontal distance between the landing toe and the hurdle predicted the loss of velocity at landing.

Joint energies during time in contact with the ground were non-significant in the regression analyses.

Graphs of each subject's joint moment profiles for descriptive purposes are included in Figure 2.

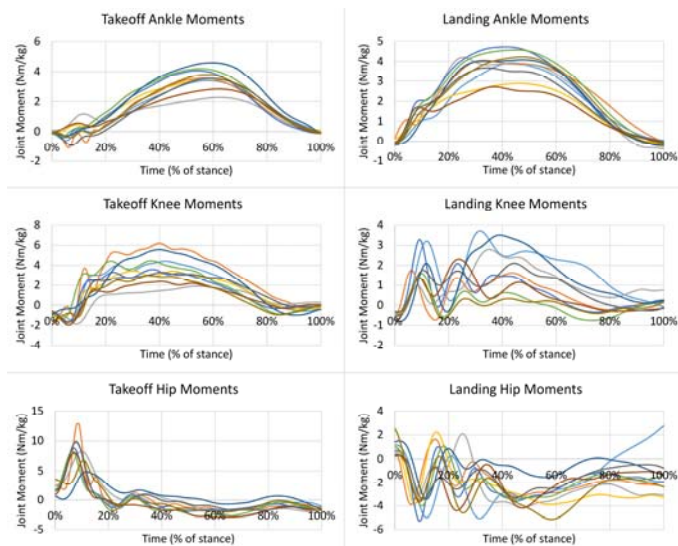


**Figure 2:** Joint moments for takeoff and landing. No significant differences were observed in joint kinetics (specifically joint energy).

Some aspects of steeplechase hurdling technique do not affect the loss or gain of velocity at takeoff and landing. The final model included takeoff vertical impulse, takeoff toe to hurdle distance, knee extension of the lead leg, landing peak vertical force, landing ground time, landing toe to hurdle distance, and landing center of mass to toe distance.

Avoiding large vertical impulses during takeoff allows the athlete to better maintain their horizontal velocity. A forward lean at takeoff was correlated with a smaller peak vertical force at takeoff. This forward lean may be part of the reason vertical impulses were lower. Since both measures were highly correlated with each other, only vertical

impulse was included in the regression. Applying the forces correctly may be more important than body positioning for takeoff, although the one is not independent of the other. A greater vertical impulse was also correlated with a greater high point. Greater takeoff distance was correlated with a center of mass high point farther back from the hurdle. Since the lead leg is farther in front of the center of mass than the trail leg is behind, a high point farther back from the hurdle is desirable.

Correlations of independent variables at landing included: landing closer to the hurdle with longer ground time and a greater forwards lean, a greater forwards lean on landing with a smaller center of mass to toe distance, and a smaller peak force at landing with a smaller toe to hurdle distance. Thus, methods for landing closer to the hurdle and having a smaller center of mass to landing toe distance are connected with more ground time, a greater forwards lean, and a lower peak force.

## CONCLUSIONS

During takeoff, correctly applying forces was more significant than body positioning to successfully maintain horizontal velocity. During landing, the body positioning was more significant than the forces involved to predict obstacle navigation success. However, the kinematics and kinetics are interconnected.

## REFERENCES

1. Hunter I, et al. *J Sports Sci Med* **5**, 318-322, 2006.
2. Hunter I, et. al *J Sports Sci Med* **7**, 218-222, 2008
3. Kipp S, et al. *J Sports Biomech*, 1-14, Sept 2016.

**Table 1:** Descriptive statistics of selected measurements

	Change in Vel (m/s)	Peak Vert Force (BW)	Vert Impulse (BW*s)	Ground Time (s)	CM to Toe (m)	Toe to Hurdle (m)	Ankle Energy (J)	Knee Energy (J)	Hip Energy (J)
<b>Takeoff</b>	-0.71 ± 0.20	4.18 ± 0.66	0.25 ± 0.03	0.18 ± 0.01	0.51 ± 0.04	1.56 ± 0.11	49.3 ± 12.8	11.8 ± 11.8	-10.8 ± 24.1
<b>Landing</b>	0.12 ± 0.18	3.73 ± 0.72	0.14 ± 0.03	0.16 ± 0.01	0.19 ± 0.07	1.07 ± 0.27	-0.25 ± 0.32	-0.28 ± 0.34	-0.69 ± 0.33

# EMPIRICAL BASED MODELING APPROACH FOR THE QUANTIFICATION OF DYNAMIC KNEE STABILITY

<sup>1,3</sup> Kristin D. Morgan, <sup>2</sup> Cyril J. Donnelly, and <sup>3</sup> Jeffrey A. Reinbolt

<sup>1</sup> University of Connecticut, Storrs, CT, USA

<sup>2</sup> The University of Western Australia, Perth, Western Australia, AUS

<sup>3</sup> University of Tennessee, Knoxville, TN, USA

email: kristin.d.morgan@uconn.edu

## INTRODUCTION

Anterior cruciate ligament (ACL) injuries are common sports injuries that impact 1 in every 3,000 individuals [1]. An ACL injury results in the loss of dynamic knee stability, which is critical for the successful execution of movements like single-leg jump landing (SLJL) [2]. Discrete measures are often used to evaluate dynamic knee stability but these measures may not fully capture the altered joint biomechanics. To better capture the changing dynamics, we will implement an empirical based modeling (EBM) approach to quantify dynamic knee stability.

Previous work has assessed dynamic gait stability via methods such as; Lyapunov exponents [3, 4]. This method uses experimental (empirical) gait waveform data to derive models to evaluate gait pattern stability [3, 4]. The EBM approach employed here will use experimental jump landing data to derive a transfer function to evaluate dynamic joint stability via bode stability analysis. A transfer function is the ratio of the models' output response to the input perturbation [5]. Previous studies have used waveform data to develop transfer functions [6, 7]; however, they did not use the transfer function to assess stability.

Thus this study combined multiple techniques to evaluate dynamic knee stability from sagittal plane knee kinematic data in athletes during a SLJL task [3-5, 8]. Surface electromyography (sEMG) data was also analyzed to determine how changes in joint stability relate to changes in muscle coordination. We hypothesize that this technique will be able to differentiate between stable and unstable knee biomechanics and that greater knee flexor-extensor co-contraction will be exhibited during stable jump landings.

## METHODS

Five Australian Football players (age  $20 \pm 1$  yrs;

mass  $87.1 \pm 5.4$ kg; height  $1.90 \pm 0.1$ m) were randomly selected from a larger cohort to perform the six SLJLs each as part of the SLJL protocol (Fig. 1). Sagittal plane knee kinematics were obtained from experimental kinematic marker trajectories. And ground reaction force (GRF) and sEMG data were also synchronously recorded. The sEMG data was collected for six muscles: medial and lateral vasti, hamstrings and gastrocnemii.

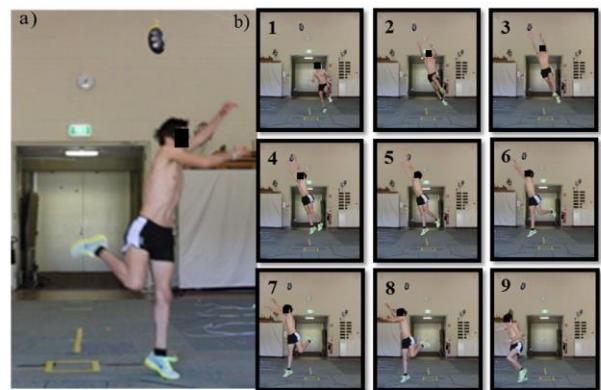


**Figure 1:** Series of images of an individual performing the experimental single-leg jump landing protocol in the laboratory.

The EBM transfer function was developed using the sagittal plane kinematic and GRF waveforms during the weight-acceptance (WA) phase of SLJL. Here the sagittal plane kinematic waveform represented the output response and the GRF waveform represented the input perturbation (Eq. 1).

$$\text{Transfer Function} = \frac{\text{Sagittal plane knee kinematics}}{\text{Ground reaction force waveform}} \text{ Eq. 1}$$

The Laplace transform converted the ratio from the time to frequency domain for the Bode analysis. The gain and phase margins obtained from the Bode stability analysis were used to quantify the individuals' dynamic knee stability. If both the gain margins (GM) and phase margins (PM) were positive, the individual was stable; otherwise they were unstable [5].

The sEMG data was normalized to each muscles peak activation. Directed co-contraction ratios (DCCR) were also calculated for the medial/lateral and flexion/extension muscle groups. The DCCR provides a value between -1 and 1 that indicates the role the agonist (flexor and medial) compared to the antagonist (extensor and lateral) muscles. We computed the integral of the sEMG data during the WA phase for the three muscles and the knee flexors (hamstrings and gastrocnemii) muscle group. A one-way ANOVA and Tukey's post hoc analyses determined if differences between the stable and unstable groups' PMs, sEMG DCCRs and area means were significant ( $\alpha=0.05$ ).

## RESULTS AND DISCUSSION

Twenty-one SLJL trials were classified as stable while nine were classified as unstable and the resulting stable and unstable GM and PM means were significantly different ( $p<0.01$ ;  $p=0.04$ , respectively) (Table 1). The DCCR analysis found that individuals exhibited a more balanced knee flexor-extensor co-contraction during the stable trials than the unstable trials, although the difference was not significant. Overall, all three muscle groups exhibited greater muscle activation during the unstable trials than the stable trials (Table 1). Individually, the gastrocnemii muscles generated significantly greater activation during the unstable trials ( $85.7 \pm 34.1$ ) than the stable ( $57.8 \pm 24.8$ ) ( $p=0.02$ ). Neither the quadriceps nor the hamstrings increase in muscle activation were significant.

The results indicated that the EBM approach successfully assessed and quantified dynamic knee stability during the WA phase of SLJL. And that the stable landings exhibited greater knee flexor-

extensor co-contraction. The gastrocnemii produced a significantly larger increase in activation during the unstable trials, potentially to compensate for the smaller increase in muscle activation by the hamstrings. Previous research has shown that knee flexors and extensors function synergistically to stabilize the knee via joint compression [9]. The disproportionate increase in muscle activation exhibited by the muscle groups during the unstable SLJLs supports this concept. Furthermore, the larger increase in gastrocnemii muscle activation during the unstable landings could represent the muscle activation strategy individuals adopt in attempt to stabilize the knee during unstable SLJLs.

## CONCLUSIONS

This study offers an alternate approach for evaluating dynamic knee stability. The results also provided insight the muscle activation strategies individuals adopt during stable and unstable SLJLs. Future work will investigate how muscle activation timing influences dynamic knee stability.

## REFERENCES

1. Boden BP, et al. *Orthopedics*, **23**(6), 573-578, 2000.
2. Arden CL, et al. *Br J Sport Med* **48**(21), 1543-1552, 2014.
3. Dingwell JB, et al. *J Biomech Eng*, **129**(4), 586-593, 2007.
4. Stergiou N. *Innovative Analyses of Human Movement*, Human Kinetics, 2004.
5. Dorf RC et al. *Modern Control Systems*, Pearson Prentice Hall, 2008.
6. Gruber AH et al. *J Sport and Health Sci Solid*, **3**, 113-121, 2014.
7. LaFortune MA, et al. *J Biomech*, **28**, 113-117, 1995.
8. Morgan KD, et al. *J Biomech* **49**, 1686-1691, 2016.
9. Kvist J, et al. *Med Sci Sport Exerc*, **33**(7), 1063-1072., 2001.

## ACKNOWLEDGMENTS

We thank Caroline Finch, David Lloyd and Bruce Elliot for providing the experimental data (NHMRC grant: 400937).

**Table 1:** Comparison of stability and surface electromyography area and directed co-contraction metrics for stable and unstable single-leg jump landing trials.

Analysis	Variable	Stable	Unstable	P-Value
Stability	Gain Margin (dB)	$138.7 \pm 75.7$	$-36.1 \pm 41.3$	$<0.01^*$
	Phase Margin (deg)	$67.8 \pm 34.5$	$17.4 \pm 96.5$	$0.04^*$
Area	Quadriceps	$74.3 \pm 17.0$	$91.1 \pm 29.5$	0.07
	Hamstrings	$37.3 \pm 18.5$	$56.4 \pm 35.2$	0.07
	Gastrocnemii	$57.8 \pm 24.8$	$85.7 \pm 34.1$	$0.02^*$
	Flexors	$95.1 \pm 42.3$	$142.1 \pm 69.1$	$0.03^*$
DCCR	Hamstrings/Vasti	$-0.42 \pm 0.25$	$-0.49 \pm 0.21$	0.45
	Gastrocnemii/Vasti	$-0.08 \pm 0.21$	$-0.24 \pm 0.19$	0.06
	Flexors/Vasti	$0.28 \pm 0.23$	$0.16 \pm 0.21$	0.17

Using a treadmill to accurately measure power output in bicycling

Asher H. Straw, Jesse Frank, Wouter Hoogkamer, and Rodger Kram

University of Colorado, Boulder, CO, USA

Email: [asher.straw@colorado.edu](mailto:asher.straw@colorado.edu), web: <http://www.colorado.edu/intphys/research/locomotion.html>

## INTRODUCTION

It is easy to accurately measure mechanical power output using a stationary cycle ergometer but stationary cycling is different than actual road cycling. On an ergometer, there is no need for balance and there are no hills. With the advent of inexpensive, on-board, power-measuring hubs, pedals and cranks, it is possible to measure power output in the field on real bicycles. However, some of these devices are of dubious accuracy. Further, outdoor cycling is “noisy” due to variations in road surfaces, incline, velocity and wind. Overcoming air resistance is the major determinant to the power demand in overground cycling yet absent during treadmill cycling but treadmill cycling against resistance eliminates the confound of varying wind experienced during outdoor cycling.

Thus, we explored if a large, inclined motorized treadmill could allow realistic simulation of overground cycling under highly controlled conditions. We were inspired by the great Swedish exercise physiologist, P.O. Åstrand who studied treadmill bicycling in 1953 [1] and humorously noted that his measurements remained particularly consistent “so long as the rider remained on the treadmill”.

Here, we describe our method for using a treadmill to measure mechanical power output and then highlight its utility with three application examples. First, we compared the power required for riding uphill in a seated vs. standing climbing position. Then, we quantified the mechanical power losses due to a novel road bike suspension system. Finally, we used the treadmill to validate a crank-based power measuring device.

## METHODS

On an inclined treadmill, the mechanical power for lifting the mass of the rider and bicycle against gravity,  $P_{\text{vert}}$ , the “vertical power” is calculated as:

$$P_{\text{vert}} = (M + m) g v \sin \vartheta$$

Where  $M$  is the mass of the rider (kg),  $m$  is the mass of the bicycle,  $g$  is  $9.81 \text{ m/s}^2$ ,  $v$  is the treadmill belt velocity (m/s) and  $\vartheta$  is the angle of incline.

The rolling resistance power is calculated as:

$$P_{\text{RR}} = (M + m) g C_{\text{rr}} v \cos \vartheta$$

where  $C_{\text{rr}}$  is the coefficient of rolling resistance. We measure  $C_{\text{rr}}$  by having a subject balance on a bicycle without pedaling while a cord pulls forward on the bike, parallel to the inclined treadmill (Figure 1). The cord passes over a low-friction pulley and we hang weights until the rider remains at one spot on the treadmill in force equilibrium.

$$C_{\text{rr}} = F_{\text{hang}} / F_{\text{N}}$$

where  $F_{\text{N}}$  is the normal component of the weight of the rider + bicycle:  $(M+m) g \cos \vartheta$

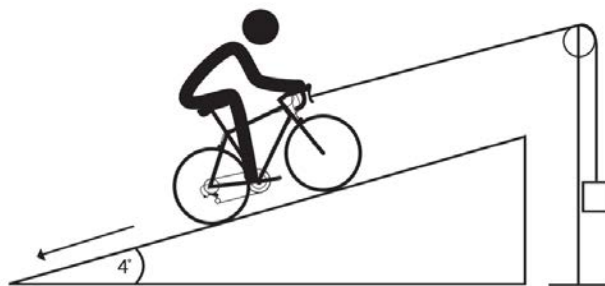


Figure 1. Method for measuring  $C_{\text{rr}}$ .

Finally, we multiply the sum of  $P_{\text{vert}}$  and  $P_{\text{rr}}$  by 1.02 to account for typical drivetrain losses [2].

## RESULTS AND DISCUSSION

We first investigated differences in metabolic and mechanical power output during bouts of seated and standing uphill cycling (n=11). Testing was conducted at 4° at an average power output of 2.85±0.03 W/kg while riding a rigid-framed road bicycle (9.02kg) equipped with a Quarq® crank-based power meter. We averaged rates of oxygen consumption ( $\dot{V}O_2$ ), carbon dioxide production ( $\dot{V}CO_2$ ) for the last 2 minutes of each trial and calculated metabolic power. Metabolic power was ~8 % greater for standing (13.11±0.57 W/kg seated vs. 14.23±0.77 W/kg standing, p <0.001) but there was no significant difference in the mechanical power between the two conditions. (Figure 2).

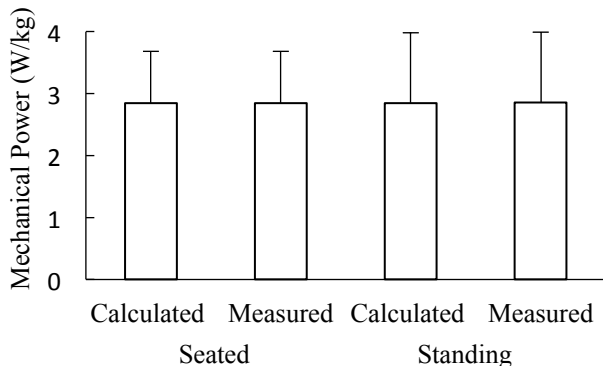


Figure 2. Mechanical power (W/kg) means ± S.D. comparing seated vs. standing.

Next, we investigated differences in metabolic and mechanical power output between a rigid-frame road bicycle without and with a novel front suspension element in the head tube during seated uphill cycling (n=11). The bicycle was designed for rider comfort. However, possible negative effects of the suspension are metabolic and/or mechanical power penalties. Given the extreme repeatability of the treadmill, we were able to discern no differences in either calculated or crank-measured mechanical power (2.85 ±0.05 W/kg) (p = 0.71) between conditions. Metabolic power was not significantly different (13.11 ±0.57W/kg rigid vs. 13.21 ±0.57W/kg compliant, p=0.23). Thus, head tube

suspension system did not require significantly more mechanical or metabolic power compared to riding with the suspension rigidly locked out.

Third, we evaluated the accuracy and precision of six individual units of a newly developed crank-based power meter. We inclined the treadmill to 4.1° degrees and adjusted treadmill speed to achieve 5 power outputs starting at 150W and incrementing 50W every 2 minutes up to 350W. We compared the crank-measured mechanical power to our reference calculated power. We determined an average absolute error of 1.56% (Table 1).

Table 1. Error for crank-power measurements. Difference from Calculated (%)

Meter	% difference
A	+1.16
B	+3.49
C	+0.85
D	-2.06
E	-1.32
F	-0.50

## CONCLUSION

Treadmill bicycling is a realistic and useful simulation of outdoor riding that controls for multiple environmental factors which facilitates collection of accurate and reproducible data.

## REFERENCES

- [1] Åstrand PO. (1953) Study of bicycle modifications using a motor driven treadmill-bicycle ergometer. *Eur J Appl Physiol Occup Physiol* 15(1): 23-32.
- [2] Martin JC, Milliken DL, Cobb JE, McFadden KL, and Coggan AR (1998) Validation of a mathematical model for road cycling power. *J Appl Biomech* 14(3): 276-291.

# DIAGNOSTIC VALIDITY OF STATIC AND DYNAMIC POSTURAL ASSESSMENTS WITHIN 24-48 HOURS POST-CONCUSSION

<sup>1</sup>Brian Szekely, <sup>1</sup>Nicholas G. Murray, <sup>1</sup>Megan E. Mormile, <sup>1</sup>Katelyn E. Grimes, <sup>1</sup>JingJing Yun, <sup>2</sup>Doug W. Powell, and <sup>1</sup>Barry A. Munkasy

<sup>1</sup>Georgia Southern University, Statesboro, GA, USA

<sup>2</sup>University of Memphis, TN, USA

Email: bs07343@georgiasouthern.edu

## INTRODUCTION

An estimated 1.6 - 3.8 million concussions occur annually in the United States [1]. Approximately 30% of sport-related concussions (SRC) experience postural instability immediately post-injury, while 75.6% report dizziness as a debilitating symptom [2,3]. Postural instability post-SRC has been well documented using numerous methods [3]. Kinetic quiet stance measures observed that concussed athletes have elevated postural sway magnitude and greater sway velocity within 24-48 hours post-SRC [4]. In addition, postural instability has been noted within 48-96 hours post-SRC using complex dual-task and dynamic assessments [5]. However, very little is known about the diagnostic validity of these postural assessments post-SRC.

The purpose of this study is to investigate the diagnostic validity of two postural stability methods, quiet upright stance and a sport-like postural task, within 24-48 hours post-SRC.

## METHODS

Twenty-four NCAA Division I athletes with concussions (CON) (12 female, 12 male; age:  $19 \pm 1$  years) and twenty-four matched controls (NON) (12 female, 12 male; age:  $18 \pm 1$  years) participated in this study. All CON were diagnosed with a concussion by the team physician and evaluated within 24 to 48 hours post-SRC. The NON group consisted of NCAA Division I athletes matched to each CON by gender, sport and sport position with no history of concussion or neurological disorder within the past six months. The NON group was measured during preseason participation screening.

All participants completed three trials of eyes open and eyes closed quiet stance for thirty seconds. Additionally, participants completed a sport-like postural task, the Wii Fit Soccer Heading Game (WFS). The WFS uses a Wii Balance Board (WBB) to control an onscreen avatar via an augmented reality environment, and uses internal center of pressure (CoP) measurements to guide the on screen avatar. With the WBB placed on top of the force platform, the athlete swayed their body in an anteroposterior (AP) and mediolateral (ML) direction to move their avatar in a similar fashion to intercept a series of soccer balls while dodging distraction objects.

During both postural tasks, kinetic data was collected from a single force platform (1000 Hz, AMTI, Model OR-6, Watertown, MA.). Raw CoP time-series data in the AP and ML directions were collected using Vicon Motion Capture software (Vicon Motion Ltd., Version 1.8.5, Oxford, England) and further analyzed using custom software (MATLAB 2010, MathWorks, Inc., Natick, MA). Youden's J Statistic, an empirical measure of maximizing the area under the curve, was used to determine performance of the sensitivity (Sn) and specificity (Sp) of Root Mean Square (RMS), Peak Excursion Velocity (PEV), and Sample Entropy (SampEn) in both the AP and ML directions based off the classification of concussion.

## RESULTS AND DISCUSSION

The Youden's J index revealed that during quiet stance, eyes closed PEV in the AP direction ( $y_i = 0.58$ ) had the highest Sn (0.74) and Sp (0.84) in the classification of concussion. During the WFS, RMS in

the ML direction ( $y_i = 0.79$ ) had the highest Sn (0.84) and Sp (0.94), followed closely by RMS in the AP direction ( $y_i = 0.78$ , Sn = 0.89, Sp = 0.89). When quiet stance and WFS were combined, a total Sn of 0.89 and Sp of 0.95 was observed for the above CoP variables (Table 1). No other CoP variables significantly contributed to the diagnosis of concussion. These findings suggest that in a closely matched sample, eyes closed upright stance PEV in the AP direction has good diagnostic validity when attempting to classify concussion. However, the WFS RMS in the AP and ML direction indicated excellent diagnostic validity. This could be due to the sport-like dual-task components of the WFS. This dual-task paradigm may require the athlete to use increased cortical resources to appropriately meet the demands of the postural task more so than quiet upright stance. Therefore, it is recommended that postural stability assessments include both a static quiet stance and sport-like dual-task component in order to maximize the ability to confirm a concussion diagnosis.

## REFERENCES

1. Langlois JA, Rutland-Brown W, Wald MM. The epidemiology and impact of traumatic brain injury. *J Head Trauma Rehabil.* 2006; 21: 375-378.
2. Ciuffreda KJ, Kapoor N, Rutner D, et al. Occurrence of oculomotor dysfunctions in acquired brain injury. *Optometry.* 2007; 78: 155-161.
3. Murray NG, Ambati VNP, Contreras MM, Salvatore AP, Reed-Jones RJ. Assessment of oculomotor control and balance post-concussion: A preliminary study for a novel approach to concussion management. *Brain Injury.* 2014; 28: 496-503.
4. Powers K, Kalmar J, Cinelli M. Recovery of static stability following a concussion. *Gait & Posture.* 2014; 39: 611-614.
5. Cavanaugh J, Guskiewicz K, Giuliani C, Marshall S, Mercer V, Stergiou N. Recovery of Postural control after cerebral concussion: New insights using approximate entropy. *Journal of Athletic Training.* 2006; 41: 305-313.

**Table 1: Specificity, Sensitivity, and Youden Index of Kinetic Posture Metrics**

<b>Posture Metrics</b>	<b>Sp</b>	<b>Sn</b>	<b>Yi</b>
WFS Mean RMS ML	0.95	0.84	0.79
WFS Mean RMS AP	0.89	0.89	0.79
EC Peak Excursion Velocity AP	0.84	0.74	0.58
Combined Model	0.95	0.89	0.84

Note: Sp = specificity, Sn = sensitivity, Yi = Youden index, WFS = Wii fit soccer heading game, EC = eye closed, EO = eyes open, AP = anteroposterior, ML = mediolateral.

# PELVIS ROTATIONAL VELOCITY AND ENERGY DURING BASEBALL BATTING

<sup>1</sup>Brittany Dowling, <sup>1</sup>Walter Laughlin, <sup>1</sup>Caitlin Owen, <sup>1</sup>Ben Hansen, <sup>1,2</sup>Glenn Fleisig

<sup>1</sup>Motus Global, Rockville Centre, NY, USA

<sup>2</sup>American Sports Medicine Institute, Birmingham, AL, USA

email: brittany@motusglobal.com, web: motuslabs.com

## INTRODUCTION

Bat velocity has been identified as a key indicator of batting performance. Increased bat velocity allows for the batter to have increased decision time on whether or not to swing, decreased swing time, and increased batted ball velocity. Coaches and trainers stress the importance of a strong core and the ability to generate rotational velocity during a swing and its relation to faster bat speeds; however, previous research has shown conflicting results. It has been suggested that because youth batters have less body mass or inertia, they are able to move their segments faster compared to adults (1). Conversely, Escamilla et al. (2) reported adult batters had faster pelvis rotational velocities compared to their youth counterparts. Since rotational velocity does not take into account the subject's mass and energy transfer, there may be a more appropriate measure that is related to batted ball velocity. A more useful relationship might be rotational energy – that is, kinetic energy due to rotation. However to date, no batting research has investigated the relationship between pelvis rotational energy and bat velocity. The purpose of this study was to investigate pelvis rotational energy and its potential relationship to bat swing velocity.

## METHODS

A retrospective review identified 200 baseball batters who had previously been tested in the Motus Global lab, including professional, college, high school, and youth batters (Table 1). During testing subjects were instrumented with 45 reflective markers on anatomical land markers. Kinematic data were collected at 480 Hz using an eight-camera 3D motion capture system (Motion Analysis Corp., Santa Rosa, CA, USA). Each participant was allowed unlimited time to warm-up. A standard batting tee was placed in the middle of the capture

volume and the participant was instructed to swing at a baseball placed on the tee. The batting tee was placed 5 cm in front of the lead foot during the stride of the swing and the height of the tee was set at the mid-height of the thigh. The participant was instructed to hit the ball 'up the middle' with a 'game-effort' swing. Testing was completed once the participant successfully hit eight balls. Kinematic data were calculated as previously described (1). Additionally, pelvis rotational energy was computed by modelling the pelvis as a cylinder, and using anthropometric data to calculate inertial properties of the pelvis. The inertia of the pelvis was computed using equation:

$$I_{pelvis} = \frac{mass_{pelvis} * radius\ of\ gyration_{pelvis}^2}{2}$$

The mass of the pelvis was defined as 14.2% of total body mass and the radius of gyration was defined as 34% of the length of the pelvis. The length of the pelvis was defined as 19.1% of the total body height. Rotational energy of the pelvis was computed using the equation:

$$Rot.\ Energy_{pelvis} = \frac{1}{2} I_{pelvis} \omega_{pelvis}^2$$

Per-participant means for the eight swings were computed for each variable and then group mean and standard deviation were computed. Differences between levels of competition (youth, high school, college, and professional) were analyzed using one-way analysis of variance (ANOVA). When the ANOVA indicated significant differences, post hoc paired *t* tests were performed and a Bonferroni correction for multiple comparisons. Additionally, Pearson correlation coefficients were calculated to evaluate the relationship between bat velocity and both pelvis rotational velocity and pelvis rotational energy. The level of significance was set at  $p < 0.05$ .

## RESULTS AND DISCUSSION

Body height, weight, and bat velocity increased significantly with level of play (Table 1). However, there were no differences in pelvis rotational velocity (Table 1) across the competition levels. Even though rotational velocities were not significantly different across levels, there was a trend of decreasing pelvis rotational energy between competition levels with youth batters having the greatest amount. Similar relationships were shown in Escamilla et al.'s (2) study that found no difference in pelvis rotational velocity between adult and youth batters. Conversely, Dowling et al. (1) indicated youth batters had faster pelvis rotational velocity but slower bat velocity.

Pelvis rotational velocity had no correlation to bat velocity within the total group ( $r = 0.12$ ), but was significantly correlated to the professional subgroup ( $r = 0.52$ ) (Table 2). Professional batters were able to transfer more energy to the bat, creating increased bat velocity. The authors of the current investigation believe that the muscle mass about the pelvis, which is involved in the stretch shortening cycle of the lower body during rotation, is essential in transferring energy to the core and upper body during rotation. When comparing batters of different skill level but the same height and weight, researchers established skilled batters had faster bat velocity compared to the unskilled group (3,4). Pure segment rotational velocity may not play as significant a role as initially thought in contributing to bat velocity, although it may still be important once ideal muscle mass is achieved. Therefore, velocity might not be the best measure for bat performance.

Table 1. . Comparison of demographic and kinematic data between competition groups (mean±SD)

	Youth (n=50)	HS (n=50)	College (n=50)	PRO (n=50)	Significance
Age (years)	12±1	16±1	21±1	21±2	*a,b,c,d,e
Body height (cm)	157±12	176±7	180±6	184±5	*a,b,c,d,e,f
Body weight (kg)	48±14	76±20	84±10	91±8	*a,b,c,e,f
Bat velocity (m/s)	25±3	29±3	34±2	36±2	*a,b,c,d,e,f
Pelvis rotational velocity (°/s)	690±88	684±66	673±59	650±71	
Pelvis energy (J)	5±2	10±3	11±2	12±3	*a,b,c,e

Note: HS= high school; PRO= professional. \* Significant differences ( $p < 0.05$ ) among levels. Post-hoc differences between (a) youth and high school, (b) youth and college, (c) youth and professional, (d) high school and college, (e) high school and professional, and (f) college and professional.

When the same breakdown was conducted with pelvis rotational energy, there was a higher correlation to bat velocity ( $r=0.76$ ). Even when batters were separated into competition levels, the correlations are still moderate-strong ( $r = 0.34-0.76$ ). This current study is the first study to investigate the relationship between segmental energy and bat velocity and the authors were able to ascertain a high correlation between the two. Adopting the use of this measurement to further understand how pelvic energy contributes to bat velocity may better describe the differences seen across age groups and different level of play. Further research is needed to understand how this model would apply to other body joints (elbow and knee) and segments (trunk) within the kinetic chain.

## CONCLUSION

Bat velocity had greater correlation to pelvis rotational energy than to pelvis rotational velocity across all batters and within sub-groups. Pelvis rotational energy may be a better measure for understanding a batters ability to generate bat velocity.

## REFERENCES

1. Dowling B, et al. *Sports Biomech* **15**, 255-269, 2016
2. Escamilla RF, et al. *J Appl Biomech*, **25**, 210-218, 2009.
3. Inkster B, et al. *Med Sci Sports Exerc*, **43**, 1050-1054, 2011.
4. Nakata H, et al. *J Phys Fitness Sports Med*, **3**, 457-466. 2014.

Table 2. Calculated Pearson product moment correlation coefficients between pelvis kinematics and bat velocity

	Youth	HS	College	Pro	All
Pelvis rotational velocity	0.1	0.07	0.06	0.52*	.12
Pelvis energy	.76*	.35*	.34*	.62*	.76*

Note: Note: HS= high school; PRO= professional. \* Significant differences ( $p < 0.05$ ) among levels.

# Does the Fibonacci Sequence Predict Segmental Velocities of the Overhand Throw?

Wendi Weimar, Jessica Washington, Brandi Decoux, Sarah Gascon, Gretchen Oliver

Auburn University, Auburn, AL, USA

email: weimawh@auburn.edu, web: <http://www.education.auburn.edu/kinesiology>

## INTRODUCTION

In 1202 Leonardo Pisano published his writing on mathematics in a text entitled *Liber Abaci*. Amongst other topics, he discussed how rabbits multiply in an idealized environment. This sequence, later labeled as the Fibonacci Sequence, is a numerical series in which the resultant sum is a computation of the previous two numbers of the sequence. Specifically, the equation is:

$$X_{n+1} = X_n + X_{n-1}$$

A fundamental representation of this mathematical sequence is 0,1,1,2,3,5,8,13, etc... Further, a mathematical ration of the successive numbers in the aforementioned sequence has often been referred to as the Golden Ration (1.618). While the Golden Ratio has provided aesthetic pleasure in nature and artistic expressions, such as the Golden Spiral seen in spiral galaxies and the quantity of flower pedals, it has also been observed in the human body. Specifically, this ratio has identified the relationship between the lengths of several adjacent anatomical segments, such the upper arm to the forearm, the metacarpals to the phalanges and the upper leg to the lower leg. Additionally, this relationship has also been found in the temporal components of the human gait cycle [1]. However, the identification or correlation of this sequence on various complex movements and the performance outcomes of those motions remain limited. Therefore, the purpose of this project was to determine if the segmental linear velocities during the overhand throw increased in a manner predicted by the Fibonacci Sequence.

## METHODS

The utilized in this project was not collected for the purposes of this project. Instead the data was collected as part of a normative softball study

currently being undertaken in the Sports Medicine and Movement Laboratory at Auburn University in an attempt to identify pathomechanics and improve injury prevention in softball athletes. The throwing data used in this project was from six NCAA Division I collegiate softball players ( $165.3 \pm 6.2$  cm;  $67.1 \pm 5.0$  kg;  $20.8 \pm 1.2$  years). Kinematic data were collected using The MotionMonitor™ motion capture system (Innovative Sports Training, Chicago IL) at a rate of 100Hz. Prior to testing, participants had 15 electromagnetic sensors attached at the following locations: (1) the posterior/medial aspect of the torso at C7, (2) posterior/medial aspect of the pelvis at S1, (3-4) bilateral distal/posterior aspect of the upper arm, (5-6) the bilateral flat, broad portion of the acromion of the scapula, (7-8) bilateral distal/posterior aspect of the forearm, (9-10) bilateral distal/posterior aspect of the lower leg, and (11-12) bilateral distal/posterior aspect of the thigh, (13) superior aspect of the midfoot, (14) superior aspect of the throwing hand at the second metatarsal, (15) and the occipital protuberance. Each participant executed five maximal effort throws to a teammate located at a distance of 60 feet.

To investigate if the summation of speed principle [2] follows a Fibonacci Sequence during the proximal to distal sequencing of the overhand throwing motion, linear velocity of the pelvis, upper arm, lower arm and hand were extracted for analysis. While the trunk was not included in this sequence, due to different computations in segment velocity, it should be noted that the trunk was included as a component of the Fibonacci Sequence. Therefore, the pelvis velocity was chosen as the beginning of the Fibonacci Sequence. The velocity of the pelvis served as the beginning of the series and the sequence was constructed by adding the previous two values together to the next value. In addition to identifying how well the actual velocities compared to the Fibonacci predicted

values, five coaches and one biomechanist who studies throwing, were asked to rank the throwers on the basis of best form, hardest throw and best thrower. This practical knowledge was valuable in evaluating the significance of matching or not matching the Fibonacci Sequence.

## RESULTS AND DISCUSSION

Fitness of the prediction was determined using several methods. The first process was through a regression analysis, which yielded an R2 value of 0.994 (Figure 1). Secondly, Bland Altman plots were constructed and all scores fell within the 95% confidence interval. Moreover, the root mean squared error was also calculated and are presented in Table 1.

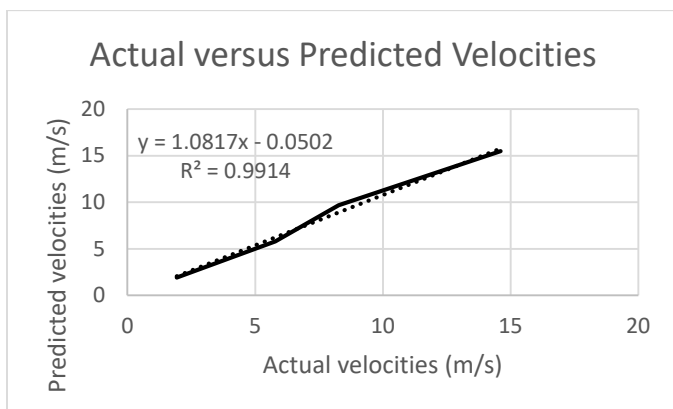


**Figure 1.** The regression of the predicted to actual velocities of the proximal to distal sequence.

	Pelvis	Upper Arm	Forearm	Hand
RMSE	NA	0.703	2.019	2.657

**Table 1.** The root mean squared error measures for each segment. The pelvis values are not available because the pelvis for the actual and predicted were identical.

The results of the analysis indicate that the Fibonacci Sequence can act as a predictor of the actual velocities of the proximal to distal sequence of the overhand throw. While the computations

demonstrated strong numerical similarities, some differences in numerical values did exist and should be addressed. Specifically, a participant, whose velocities varied the most from the predicted velocities, is considered to be a utility player. As such, she is required to adapt her throwing mechanics based on her position on the field. For example, her throwing motion while playing third base, may be different than when playing second base, or even catching. Therefore, future research should consider capturing data from players while on the field, in different playing positions. For a practical opinion, five coaches and one biomechanist who studies throwing were consulted on which participant had the best form, had the hardest throw and was the best thrower. Not surprisingly, each person consulted had a different rubric upon which they based their opinion. However, all but one indicated that they thought that the person whose actual velocities matched the predicted velocities the closest had the hardest throw (this was not proven by the release velocity). Further, when animations of the person that most closely matched the predicted velocities and the person who least matched the predicted velocities were compared in animation form, all coaches/scientist chose the thrower with the velocities that best match the predicted values.

## CONCLUSIONS

This project has indicated that the Fibonacci Sequence can predict the segmental velocities of experienced throwers that follow the proximal to distal sequence. Further research is needed to determine if this sequence can be used to identify level of performance or even predisposition to injuries.

## REFERENCES

- 1) Iosa M, et al. *Biomed Res Int*, 1-7, 2013.
- 2) Bunn, J.W., *Scientific principles of coaching*. Englewood Cliffs, NJ: Prentice-Hall. 1972.

# ULNAR COLLATERAL LIGAMENT PROPERTIES IN BASEBALL PITCHERS THROUGHOUT A SINGLE COLLEGIATE SEASON

<sup>1</sup> Christopher Curran, <sup>1</sup> Patrick Rider, <sup>1</sup> Anthony Kulas, <sup>1</sup> Zachary Domire

<sup>1</sup> East Carolina University, Greenville, NC, USA

email: curran@students.ecu.edu

web: <https://www.ecu.edu/cs-hhp/exss/biomechlab.cfm>

## INTRODUCTION

Approximately 50% of baseball pitchers will have shoulder or elbow pain in the course of a single season [1]. Perhaps the most serious injury for a baseball pitcher is a full tear of the ulnar collateral ligament (UCL) in their throwing arm. The UCL is the primary stabilizer of the medial elbow and is critical to its stability in overhead throwing motions such as baseball pitching [2]. The prevalence of UCL reconstruction, or “Tommy John” surgery, has dramatically increased in the last 20 years in both youth and professional athletes [3].

UCL length and thickness, and the ulnohumeral (U-H) gap have been shown to change in the throwing arms of baseball pitchers compared to their non-throwing arms [4]. Research has shown significant increases in UCL thickness and UCL substance heterogeneity from pre- to post-season in a sample of high school pitchers [5]. However, it has not yet been reported if these changes are consistent in collegiate baseball, which has a much greater work load than high school pitchers.

The primary purpose of this study was to examine changes in UCL structural properties over the course of a collegiate baseball season. A secondary purpose of this study was to examine bilateral differences in UCL structural properties from pre-season to post-season in collegiate baseball pitchers.

## METHODS

UCL structural properties were measured using ultrasound imaging for 10 healthy NCAA Division I collegiate baseball pitchers ( $19.0 \pm 1.3$  yrs). After signing informed consent, bilateral imaging was performed during a pre-season imaging session for both throwing and non-throwing arms. Unilateral imaging was performed bi-weekly throughout the

baseball season to track the structural properties of the UCL in the participants’ throwing arms. At the conclusion of the participants’ regular season, bilateral imaging was again performed to measure post-season structural properties. All imaging data were collected using the Aixplorer ultrasound system (SuperSonic Imagine, Aix-en-Provence, France).

Imaging was performed with participants laying supine, stabilized in  $30^\circ$  of elbow flexion using an adjustable-width arm position splint. Only the upper arm was supported by the splint, allowing for frontal plane movement at the elbow. The joint was loaded by placing a 1-kg weight in the participants’ hand.

UCL length and thickness, and U-H gap space were measured and recorded for each participant (Fig. 1). UCL length was measured from the ligament’s origin on the medial epicondyle of the humerus to its insertion on the ulnar tubercle. UCL thickness was measured as the width of the ligament at 50% of its length. U-H gap space was measured as the distance from the most distal-medial aspect of the trochlea of the humerus to the most proximal-medial aspect of the ulna. U-H gap space was also measured with the forearm supported, and the difference between conditions was termed U-H Gapping.

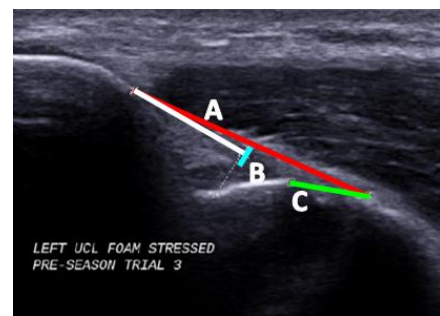


**Figure 1:** B-mode ultrasound image. A) UCL length, B) UCL thickness, C) U-H gap space.

Measurements for each property were taken as the mean value from three trials during each imaging

session. Changes in UCL properties throughout the season were reported as percent change from the initial imaging session. Time by Arm 2x2 ANOVAs were performed to examine differences in the structural properties from pre-season to post-season.

## RESULTS AND DISCUSSION

One participant did not to complete the study following the pre-season imaging. Percent change results for each outcome measure are displayed in Figure 2. Bilateral measurements for Pre- and Post-Season imaging sessions are shown in Table 1.

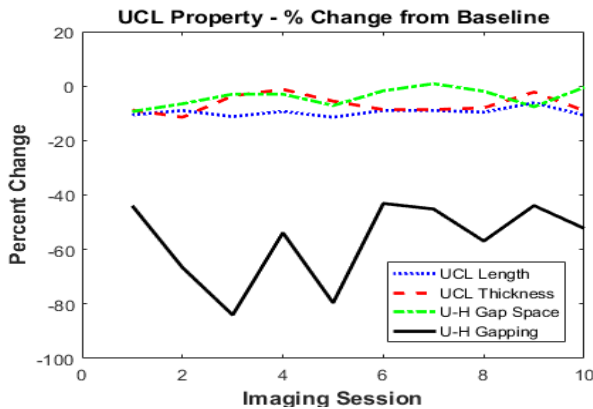


**Figure 2:** Percent change in UCL Structural Measurements of the throwing arm.

There was a main effect for throwing vs non-throwing arm for UCL Thickness, and for Pre- vs Post-Season for UCL Length and UCL Thickness. There were no interaction effects for any of the structural properties. Additionally, there were no trends seen in the structural properties throughout the course of the baseball season.

The decreases in U-H gap space and U-H Gapping in the participants' throwing arms during Post-Season imaging may have been a result of the elevated

throwing load or possible increased joint inflammation, preventing full the medial joint from fully expanding. The large decrease in U-H Gapping shown throughout the season may be indicative of a change in medial joint laxity during periods of elevated loading, and thus may be a useful metric for evaluating injury risk in pitchers. Additionally, fluctuations in these measurements throughout the season may be a result of time from last pitching performance, as we were unable to control for that variable in this study.

## CONCLUSIONS

U-H Gapping may be a good measure for evaluating injury risk, however it showed high variability in the present data. This may be a result of changes in different elbow structures, such as activation in the elbow flexor muscles. This suggests the need for additional methods of measuring UCL properties, including the ligament's material properties (such as modulus) in order to better identify injury risk in pitchers. Additionally, controlling time between an individual's last pitching appearance and the imaging may provide additional insight into the acute effect of pitching on the properties of the UCL.

## REFERENCES

1. Lyman S, et al. *Am J Sports Med.* **30** (4), 463-468, 2002.
2. Callaway GH, et al. *J Bone and Joint Surg.* **79**, 1223-1231, 1997.
3. Fleisig GS. *Sloan Sports Conference*, Boston, MA, USA, 2015.
4. Nazarian LN, et al. *Radiology*, **227**, 149-154, 2003.
5. Marshall NE, et al. *Sports Health.* 7(6): 484-488, 2015.

**Table 1:** Structural Properties of the UCL in mm (mean  $\pm$  SD)

	Throwing Arm		Non-Throwing Arm	
	Pre-Season	Post-Season	Pre-Season	Post-Season
UCL Length <sup>b</sup>	23.01 $\pm$ 1.11	20.52 $\pm$ 1.12	22.02 $\pm$ 1.39	19.67 $\pm$ 1.48
UCL Thickness <sup>a,b</sup>	1.26 $\pm$ 0.13	1.12 $\pm$ 0.06	1.14 $\pm$ 0.05	1.10 $\pm$ 0.09
U-H Gap Space	5.08 $\pm$ 0.91	4.97 $\pm$ 0.80	4.64 $\pm$ 0.87	4.38 $\pm$ 0.74
U-H Gapping <sup>b</sup>	1.14 $\pm$ 0.50	0.69 $\pm$ 0.65	0.35 $\pm$ 0.69	0.17 $\pm$ 0.40

<sup>a</sup>Main effect for Arm (UCL Thickness  $p = 0.008$ )

<sup>b</sup>Main effect for Time (UCL Length  $p < 0.001$ , UCL Thickness  $p = 0.034$ , U-H Gapping  $p = 0.003$ )

# DIRECTIONAL COMPRESSION AND MUSCLE ACTIVITY IN A RETIRED WORLD CUP ALPINE SKIER

Linnea Zavala, Cory Snyder, James Becker, John Seifert

Montana State University, Bozeman, MT, USA  
email: james.becker4@montana.edu

## INTRODUCTION

Directional compression garments are designed to exert a perpendicular force on the underlying tissues to create an increased pressure gradient within the tissue [1]. Two recent studies reported that in competitive alpine skiers, directional compression results in reduced muscle activation, kinematic changes at the hip and knee, and increased fatigue resistance [2, 3]. However, it is not known whether the beneficial effects of directional compression are limited to competitive skiers, or if similar changes in muscle activation would be observed in recreational skiers who are technically proficient in using a carving technique.

The purpose of this study was to examine changes in muscle EMG patterns throughout a day of skiing for a recreational skier technically proficient in using the carving technique when skiing with and without lower body directional compression clothing. In the compression condition, we hypothesized lower EMG intensities (RMS) at the end of the day for vastus lateralis (VL), adductor longus (AL), rectus femoris (RF), gluteus medius (GMed), and gluteus maximus (GMax).

## METHODS

The subject was a 54-year-old, female, retired alpine ski racer who competed on the World Cup circuit from 1979-1990. Additionally, the subject has coached 20 plus years, bringing a unique background and technical proficiency with the carving technique to this study.

The participant skied two days, two weeks apart, first with directional compression tights (Opedix Kinetic Health Gear, Denver, CO, USA) and the second without. Snow and weather conditions were

similar between testing days. Bipolar Ag/AgCl surface EMG electrodes (Trigno, Delsys Inc, MA, USA) were placed on the right leg over the mid belly of the VL, AL, RF, GMed, and GMax muscles. Prior to placing electrodes skin at the placement site was gently abraded and cleaned with rubbing alcohol. Raw EMG signals were amplified at the source and recorded at 1500 Hz (Tringo Personal Activity Monitor, Delsys INC, MA, USA). A gyroscope (Motion Sensor, Electronic Realization, Bozeman, MT, USA) mounted to the back of the boot was used to track ski edge angle at 100 Hz.

Two measurement runs on were taken on each assessment day, one in the morning and one in the afternoon. A course of 12 turns around brush gates, set with 10 m between gates was used for the measurements. Between measurement runs the participant skied their choice of runs throughout the ski area. On the second testing day, this exact sequence of ski area runs was replicated.

Gyroscope data was used to determine turn times by finding the midpoints between maximum and minimum edge angles. For each turn, average root mean squared (RMS) amplitudes from the EMG were found by filtering with a band-pass and then using a 125 ms window with a 62.5 ms overlap. A 2x2 repeated measures ANOVA was used to compare morning and afternoon turn times and RMS for the compression and non-compression conditions (significance level of 0.05).

## RESULTS AND DISCUSSION

No difference in turn times was found for either compression or time of day conditions. RF demonstrated a main effect of condition ( $F = 72.633$ ,  $p < 0.0001$ ) with average RMS values

being lower in the compression condition than the non-compression condition (Table 1). GMed also demonstrated a main effect of condition ( $F = 23.582$ ,  $p < 0.005$ ) with average RMS values being lower in the compression condition than the non-compression condition (Table 1). For all other muscles there were no effects of condition, time of day, or time of day by condition interactions. A ski peak edge angle difference of 4.6% was also observed between the compression (61°) and non-compression (64°) conditions, although these results were not statistically analyzed.

A decrease in muscle activation for skiers in compression garments was previously observed [2,3]. Our findings are consistent with these results for RF and GMed. GMed activity is part of the steering phase of the carving technique and a lower average RMS value in this muscle may be directly related to the decrease in edge angle. In the compression condition we observed a strong decrease in RMS for RF muscle and not for VL. Previous studies have shown a decrease mean frequency in VL and RF as associated with skiing fatigue [4]. Thus, we would expect to see some change in VL activity with fatigue.

A decrease in RMS under a compression condition is not unique to directional compression garments. In 2016, Wang et al. reported a decrease in EMG amplitude in a compression condition for isokinetic measurements of quadriceps muscles under various movement speeds [5]. However, as the purpose of directional compression is to target specific muscles, directional compression in the garment used appears to target RF and GMed, which are

applicable to skiing, although other muscles like VL may be important as well. The effects of decreased RMS on fatigue throughout the day must be considered, but these results provided no detectable differences from morning to afternoon.

## CONCLUSIONS

A retired world cup skier, highly efficient in the carving technique, was observed for two full days of skiing. When wearing directional compression, a decrease in average RMS activity in rectus femoris and gluteus medius was observed. Average peak edge angle also decreased by 4.6% in the compression condition, although this value was not tested for statistical significance. No differences in turn duration or in time of day were observed. Further investigations are necessary to determine the effects that decreased muscle activity due to directional compression garments may have on skier fatigue.

## REFERENCES

1. Fu WJ, et al. *Int. J. of Adv. Robotic Systems* **10**, 6, 2013.
2. Decker M, et al. *Proceedings of ACSM '16*, Boston, MA, USA, 2016.
3. Simons C, et al. *Proceedings of ACSM '16*, Boston, MA, USA, 2016.
4. Kröll J, et al. *J. of Sports Sci. and Med.* **10**, 81-92, 2011.
5. Wang X, et al. *Tech. and Health Care* **24**, S533-S539, 2016.

## ACKNOWLEDGMENTS

This study was funded in by the Rocky Mountain Consortium for Sports Research.

**Table 1:** Mean peak RMS values throughout the turn for each time of day and compression condition.

Factor	Turn Time (s)	Average RMS (V)				
		VL	AL	RF*	GMax	GMed*
AM, Compression	1.203	0.0272	0.0206	0.0204	0.0062	0.0284
	(± 0.162)	(± 0.0052)	(± 0.0066)	(± 0.0028)	(± 0.0020)	(± 0.0095)
AM, No Compression	1.250	0.0271	0.0204	0.0287	0.0094	0.0444
	(± 0.138)	(± 0.0053)	(± 0.0043)	(± 0.0049)	(± 0.0093)	(± 0.0109)
PM, Compression	1.220	0.0248	0.0159	0.0165	0.0057	0.0268
	(± 0.223)	(± 0.0040)	(± 0.0079)	(± 0.0038)	(± 0.00144)	(± 0.0103)
PM, No Compression	1.220	0.0227	0.0181	0.0267	0.0054	0.358
	(± 0.223)	(± 0.0023)	(± 0.0029)	(± 0.0033)	(± 0.0008)	(± 0.0062)

\* Difference observed at  $p < 0.05$

# USING THE MOTUS BASEBALL PITCHING SLEEVE TO COMPARE PITCHING AND LONG-TOSS THROWING ARM BIOMECHANICS

<sup>1</sup> Jaclyn O'Loughlin, <sup>2</sup> Brittany Dowling, <sup>1</sup> Jared Mallard, <sup>1</sup> Christopher Robertson, Ph.D., and <sup>1</sup> Jeffrey Wight, Ph.D.

<sup>1</sup> Jacksonville University, Jacksonville, FL, USA

<sup>2</sup> Motus Global, Rockville Centre, NY, USA

## INTRODUCTION

Routine training for baseball pitchers includes throwing off of the mound as well as high effort flat-ground throws, sometimes greater than 92 m. In theory, increased throwing distance requires the throwing arm to 1) generate and withstand greater loads, 2) generate faster arm speed, and 3) move through a greater range of motion (1). Even though long distance throws are used for conditioning and rehabilitating pitchers, few studies have been conducted examining the effects of long distance throwing and elbow stress. Fleisig et al. (1) used 3D motion analysis to compare pitching and long toss biomechanics and reported maximum distance throws produced greater elbow varus torque than shorter flat-ground and mound throws (1). In contrast, Slenker et al (2) reported no differences in throwing mechanics among all long-toss distances.

Long-toss research is limited likely because it is difficult to complete distance throws in laboratory settings. It is now possible and easier to analyze throwing arm biomechanics using the recently developed pitching sleeve, motusBASEBALL™. This wearable device measures important throwing arm biomechanics and provides researchers the ability to analyze pitchers in field settings.

The purpose of this study was to use the motusBASEBALL to test for differences among baseball pitching and four long-toss distances. Findings from this study may help to better design optimal throwing programs for baseball pitchers.

## METHODS

The participants were college baseball pitchers (n=19; age  $19 \pm 1.3$  years;  $88.3 \pm 8.4$  kg; and  $73.9 \pm 18.6$  cm). During testing, participants were

instrumented with a motusBASEBALL™ sensor and sleeve (Motus Global, Rockville Centre, NY). Participants were allowed to complete their preferred warm-up routine with warm-up throws limited to 16 m. Once the pitcher signaled readiness, five throws were completed at each distance: 27 m, 37 m, 46 m, 55 m. Then, 5 fastballs were thrown from a regulation mound to a catcher (18.3 m away). During long-toss, no instruction or constraints were given for trajectory or crow-hop footwork.

For each throw, the sensor recorded ER (°), elbow varus torque (Nm), and arm speed (°/s). Shoulder ER was measured in reference to the ground. Zero degrees means the forearm is parallel to the ground and pointing anterior. Elbow varus torque was the peak torque measured in Nm. Arm speed was identified represented the maximal rotational velocity of the forearm during the throwing motion.

Data were summarized by computing pooled means and standard deviations for all variables at each throwing distance. For each variable of interest (ER, elbow varus torque, arm speed) a 1-way repeated measures ANOVA was completed with an alpha of 0.05. Post-hoc Tukey analysis were used to determine where significant differences existed among the throws.

## RESULTS AND DISCUSSION

During long toss, pitchers appear to externally rotate their shoulder to an extreme range of motion; the range for the long tosses was approximately 159°-170°. Interestingly, the external rotation achieved appeared to increase slightly as the long toss distance increase. For the two longest throws (46 m & 55 m), the shoulder was externally rotated an additional 5-8° than the shortest throw (27 m). Comparing ER

values from mound pitching to long toss is problematic since the mound has an incline of approximately 8° from the flat ground. The sensor measures ER relative to the ground, not the trunk, and does not account for the incline. Therefore, ER was underestimated (by the slope of the mound). This likely explains why the ER achieved during mound throws was significantly less than all long toss throws. Motus is currently developing a second generation, five device system that will address this issue by comparing the player’s shoulder motion relative to the torso instead of the ground

There were no differences found in elbow varus torque between long toss throw distances as well as mound throws. Interestingly, for all conditions, the means were quite close (53-55 Nm). These findings suggest that all long toss throws generate high magnitude elbow varus torque. Further, the effort of the throw appears to be more related to the magnitude of the varus torque than the distance of the throw. Similarly, for arm speed, the ANOVA revealed no significant findings. Again, for all conditions, the means were quite close (5460-5589°/s). These findings suggest that all long tosses generate arm speed similar to the pitch. These data also suggest

that the effort of the throw determines the magnitude of the arm speed (more so than the distance of the throw).

## CONCLUSIONS

It appears overall that the magnitude of long toss throwing biomechanics are relatively similar to pitching. These findings were consistent with those previously reported by Fleisig and colleagues (1). Coaches and clinicians should be aware that long-toss throws appear to be strenuous on the throwing arm (similar to the baseball pitch). This should be considered when using long-toss programs for practice and rehabilitation.

## REFERENCES

1. Fleisig GS, et al. *J Orthop Sports Phys Ther.* 2011 May. 41:5, 296-303.
2. Slenker NR et al. *Am J Sport Med.* 2014, 42, 1226-1232.
3. Dillman CJ. *J Orthop Sports Phys Ther.* 1993;18(2):402-408.
4. Urbin, M.A, *Amer. J of Sports Med.* 2013. 41:2, 336–342

**Table 1:** Mean and standard deviations of 4 variables in 19 college-level baseball pitchers at 5 different distances.

Throw	Elbow maximum varus torque (Nm)	Shoulder maximum ER (°)	Arm speed (°/s)
<b>Mound pitch 18m</b>	53.7 ± 7.7	156.5 ± 10.5* ♦	5588.7 ± 557.2
<b>Long toss 27m</b>	54.6 ± 7.9	158.9 ± 9.5×	5460.8 ± 713.4
<b>Long toss 37m</b>	55.0 ± 7.4	163.8 ± 8.6	5483.1 ± 657.5
<b>Long toss 46m</b>	55.1 ± 7.9	166.5 ± 8.1 ♦	5489.7 ± 506.3
<b>Long toss 55m</b>	55.3 ± 8.1	170.3 ± 7.6*×	5525.6 ± 468.6

\* - Long toss 55m was significantly greater (p<0.001) than pitch (mound).

♦ - Long toss 46m was significantly greater (p=0.007) than pitch (mound)

× - Long toss 55m was significantly greater (p,0.001) than long toss 27m.

# Comparison of Kinematic and Kinetic Profiles of Lower Limbs during Baseball Pitching in Adolescent Pitchers

<sup>1</sup>Jennifer Mathews,<sup>1</sup> Jacob Howenstein B.S., <sup>2</sup>Kristoff Kipp Ph.D., and <sup>1</sup>Michelle Sabick Ph.D.

<sup>1</sup> Saint Louis University, MO, USA; <sup>2</sup>Marquette University, WI, USA  
email: mathewsjl@slu.edu

## INTRODUCTION

The biomechanics of the lower extremities are a key component in the efficiency of the pitching motion to deliver an effective, yet safe, high-velocity pitch. However, researchers have focused primarily on the kinematics and kinetics of the upper extremity to reduce the risk of injury in throwing athletes. Few studies focus on quantifying lower extremity pitching biomechanics. However, significant shoulder and knee injuries have begun to be diagnosed in younger, adolescent athletes [2]. Kinematic and kinetic variables related to lower extremity movements could provide important information when trying to understand injury mechanisms in the upper extremity in pitchers.

One important skill for high-velocity pitchers is the ability to drive the body over a stabilized stride leg. The landing leg serves as a pivot to transform the forward and downward vertical motions of the trunk into rotational motions of the trunk and arm segments that ultimately generate ball velocity. Studies have shown that greater momentum can be generated by hip extension and abduction and knee extension of the pivot foot, thus improving the quality of the high-velocity pitch [3].

The purpose of this study was to investigate the relationships between the lower limb kinematics and kinetics of adolescent baseball pitchers compared to more skilled pitchers.

## METHODS

Fourteen youth baseball pitchers (age: 11.6±1.3 years, height: 1.59±0.12 m, mass: 48.5±13.4 kg, velocity: 56.6±6.9 mph, 11 right-handed/3 left-handed) were recruited for this study. All testing occurred in an indoor research lab equipped with a custom pitcher's mound with two embedded force

plates; one under the itching rubber and one under the landing area. Reflective markers and marker clusters were attached to each pitcher's upper and lower extremity body segments. Kinematic data were recorded with a 14-camera motion capture system at 250 Hz. Ground reaction forces acting on the drive (rear) and stride (front) leg were sampled at 1000 Hz, and a radar gun was used to record velocity.

Each pitcher threw 15 maximal effort fastballs toward a hanging strike zone 46 ft from the pitching rubber. The fastest strike thrown for each pitcher was chosen for analysis. The variables analyzed were ground reaction forces (GRF) of the stride leg; angular velocity and orientation of the pelvis; and joint kinematics and kinetics of the hip, knee, and ankle joints of the stride leg.

All variables were measured from the instant of stride foot contact (SFC) with the force plate until ball release (BR). The hip, knee, and ankle internal rotation moments were calculated with an inverse dynamics procedure. All joint moments were normalized, and means and standard deviations of these variables were compared to other studies that observed similar kinematics of adolescent and collegiate pitchers [3,4].

## RESULTS AND DISCUSSION

The subject pool for this study was younger than the typical adolescent, high school, or collegiate subject pools of previous studies. Many of the kinematic variables were significantly lower than those described in the literature, likely due to differences in size, development, experience, and muscle strength. However, comparing the ankle plantarflexion (PF) and dorsiflexion (DF) angles and pelvic orientation at SFC and knee flexion/extension angle and moment at BR, the

averages collected in this study fell within the standard deviation of comparable values collected in similar studies (Table 1) [3,4].

The comparisons of the measurements of this study to the literature shed insight into the effects of lower extremity biomechanics on the other aspects of baseball pitching in adolescents. One such correlation is the open foot angle observed at SFC. Open foot placement can cause the pelvis to rotate too soon, which is reflected in the pelvic orientation values. From the current study, the average PF/DF angle of 9.2° was less compared to literature PF/DF value of 17.8° and 13.3°, indicating that these subjects adopted a more open foot placement. Improper foot mechanics and pelvic orientation can produce additional anterior shoulder force and medial elbow force beyond the usual forces applied during the pitching motion [5].

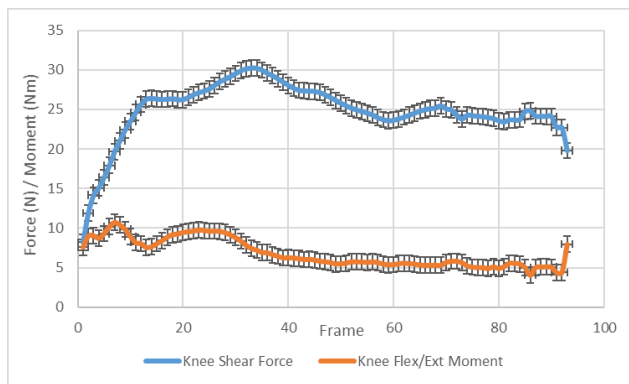


Figure 1. Mean knee shear force and flexion/extension moment on the stride leg during the pitching motion (n=14 subjects).

The moment at the knee and the hip joint angle of the stride leg in collegiate pitchers helps to drive and rotate the knee of the lead leg to accelerate the body forward [3]. The joint kinetics measured in this study were less than those observed in collegiate pitchers, and the assumed conclusion is

that these observed differences are attributed to muscular activities around the hip and knee [3]. While the average moment at the knee is relatively stable due to the moment at the hip, the knee of the lead leg does undergo extensive amounts of shear force. From SFC to BR, the knee shear force reached a maximum value of 30.3 N, which is almost 9% of the average body weight of an 11 y/o boy (Fig. 1) [4]. Forces of this magnitude with high moments and velocity can lead to injury, especially in adolescent knees with little stability. In addition, collegiate pitchers have shown a greater ability than their younger counterparts to generate the momentum of the lower limbs to increase energy of trunk rotation and arm motion [6].

## CONCLUSIONS

In an increasingly competitive environment, implementing current, consistent evidence to identify known risk factors is a key step in decreasing injury risk of adolescent baseball pitchers. Further research should expand upon unsafe or hazardous pitching mechanics and the effectiveness of pitching protocols short- and long-term on safe, effective pitching techniques for adolescent pitchers.

## REFERENCES

1. Seroyer ST, et al. *Sports Health* **2**, 135-146, 2010.
2. Urbin MA, et al. *Am J Sports Med* **41**, 336-341, 2013.
3. Kageyama, M, et al. *J Sports Sci Med* **14**, 246-255, 2015.
4. Kageyama, M, et al. *J Sports Sci Med* **13**, 742-750, 2014
5. Fortenbaugh D, et al. *Sports Health* **1**, 314-320, 2009.
6. Fleisig GS, et al. *Sports Biomech* **8**, 10-21, 2009.

Table 1. Similarities between parameter values measured in this study and other current literature [3,4]

Parameter	Pitching stage	Compared study	Literature Data	Current Study
Knee Flex/Ext Angle (°)	BR	Kageyama, M, et al (2014)	27.5 (37.4)	7.5 (1.6)
Ankle PF/DF Angle (°)	SFC	Kageyama, M, et al (2014)	17.8 (11.2)	9.2 (1.4)
Ankle PF/DF Angle (°)	SFC	Kageyama, M, et al (2015)	13.3 (12.8)	9.2 (1.4)
Pelvic Orientation (°)	SFC	Kageyama, M, et al (2014)	15.7 (8.1)	9.7 (1.7)
Pelvic Orientation (°)	SFC	Kageyama, M, et al (2015)	16.7 (10.4)	9.7 (1.7)
Knee Flex/Ext Moment (Nm)	BR	Kageyama, M, et al (2014)	-0.6 (1.3)	4.4 (3.3)
Knee Flex/Ext Moment (Nm)	BR	Kageyama, M, et al (2015)	-0.5 (1)	4.4 (3.3)

**Note:** Averages are given with standard deviation in parentheses.

# EVALUATION OF STATIC AND SPORT-LIKE POSTURAL TASKS 24-48 HOURS POST-CONCUSSION

<sup>1</sup>Brian Szekely, <sup>1</sup>Nicholas G. Murray, <sup>1</sup>Peter Chrysosferidis<sup>1</sup>, <sup>1</sup>Megan E. Mormile, <sup>1</sup>Katelyn E. Grimes, <sup>2</sup>Doug W. Powell, and <sup>1</sup>Barry A. Munkasy

<sup>1</sup> Georgia Southern University, Statesboro, GA, USA

<sup>2</sup> University of Memphis, TN, USA

email: bs07343@georgiasouthern.edu

## INTRODUCTION

Postural instability is a cardinal sign of a sport-related concussion (SRC) and is commonly assessed by quiet upright static stance [1-4]. However, this type of postural assessment lacks a dual-task component that is found during sport activity. Research involving dual-task postural performance may be more sensitive to deficits in athletic populations [3]. However, additional research is needed to determine if certain types of sport-like postural tasks that include a dual-task are sensitive enough to measure postural instability post-SRC.

The purpose of this study was to examine the effect of a SRC on postural stability using quiet upright static stance and a sport-like dual-task within 24-48 hours post-injury when compared to matched controls.

## METHODS

Twenty-eight NCAA Division I athletes (male: 15, female: 13, age  $19 \pm 1$  years) diagnosed with a sport-related concussion (SRC) and 28 matched controls (NON) (male: 15, female: 13, age  $18 \pm 1$  years) participated in this study. The CONC group was diagnosed with a concussion by the team physician and evaluated within 48 hours post-concussion. The NON group was matched to the

CONC group based on gender and sport, with no prior history (within 6 months) of concussion or neurological issues. All participants completed three eyes open (EO), eyes closed (EC), and sport-like dual-task (SDT) trials. Both the EO and EC tasks consisted of 30 seconds of quiet upright stance, while the SDT was performed over a 62 second interval using the Wii Fit Soccer Heading Game. During the SDT, participants had to control an onscreen avatar while standing on a Wii Balance Board (WBB). The participant shifted their weight to head soccer balls, while avoiding similarly shaped, sized, and colored objects. All participants stood on top of (via the WBB) a single force platform (1000 Hz, AMTI, Model OR-6, Watertown, MA.). Raw kinetic data was exported into MATLAB (MATLAB 2010, MathWorks, Inc., Natick, MA) and further analyzed. Mean Root Mean Square excursions (RMS), Peak Excursion Velocity (PEV) in the anteroposterior (AP) and mediolateral (ML) were calculated per postural condition and exported into SPSS (IBM Inc., version 23, Chicago, IL) for further analysis. Four MANOVAs were run comparing mean differences between groups, with follow up t-tests.

## RESULTS AND DISCUSSION

The results revealed in the EC AP condition, SRC athletes had significantly greater PEV ( $p=0.038$ ) when compared to matched controls (Table 1). In the EC ML condition, athletes had significantly greater RMS ( $p=0.031$ ) than the matched controls. In the SDT AP condition, the results revealed that the CONC athletes had significantly greater PEV ( $p=0.003$ ) and RMS ( $p<0.001$ ) (Table 1). In the SDT ML condition, the CONC athletes had significantly lower PEV ( $p=0.002$ ) and RMS ( $p<0.001$ ) than the NON athletes (Table 1). These findings indicate that postural instability is only present during quiet upright static stance in eyes closed conditions in the current sample. However, during the SDT greater sway magnitude and increased PEV was noted in the AP direction while a reduced sway magnitude and reduced PEV was observed in the ML direction. This could indicate that CONC attempted to adopt a more conservative approach to complete the SDT in the ML direction, while simultaneously being unable to control postural sway in the AP direction. As such, sport-like postural assessments may be more sensitive to postural instability post-SRC due to the increased cognitive load imposed by the SDT. In conclusion, these results suggest that both quiet upright static

stance and SDT can detect postural instability post-SRC.

## REFERENCES

1. Guskiewicz K. Assessment of Postural Stability Following Sport-related Concussion. *Current Sports Medicine Reports*. 2003; 2: 24-30.
2. Cavanaugh J, Guskiewicz K, Giuliani C, Marshall S, Mercer V, Stergiou N. Recovery of Postural control after cerebral concussion: New insights using approximate entropy. *Journal of Athletic Training*. 2006; 41: 305-313.
3. Murray N, Salvatore A, Contreras M, Ambati V, Reed-Jones R. Assessment of oculomotor control and balance post-concussion: A preliminary study for a novel approach to concussion management. *Brain Injury*. 2014; 28:496-503.
4. Powers K, Kalmar J, Cinelli M. Recovery of static stability following a concussion. *Gait & Posture*. 2014; 39:611-614.

**Table 1: Comparisons between groups of quiet upright static stance versus sport-like dual-task in an athletic concussed population and matched control population**

Condition	CONC (Mean $\pm$ SD)	NON (Mean $\pm$ SD)	p-value
EC AP PEV (m/s)	0.11 $\pm$ 0.11	0.06 $\pm$ 0.03	0.038
EC ML RMS (m)	0.006 $\pm$ 0.003	0.005 $\pm$ 0.002	0.031
SDT AP PEV (m/s)	1.69 $\pm$ 1.79	0.61 $\pm$ 0.41	0.003
SDT AP RMS (m)	0.04 $\pm$ 0.03	0.01 $\pm$ 0.01	< 0.001
SDT ML PEV (m/s)	1.14 $\pm$ 1.02	1.96 $\pm$ 0.88	0.002
SDT ML RMS (m)	0.03 $\pm$ 0.03	0.06 $\pm$ 0.02	< 0.001

Note: CON= concussed group, NON= matched control group, SD= standard deviation, EC= eyes closed, SDT= sport like dual task, RMS= root mean square, PEV= peak excursion velocity,

# BIOMECHANICAL DIFFERENCES BETWEEN SEXES AND LIMB DOMINANCE DURING A CUTTING MANEUVER

<sup>1</sup>Amber Craft, <sup>1</sup>H. Wang, <sup>1</sup>L. Judge, <sup>1</sup>D. Clark Dickin

<sup>1</sup>Biomechanics Laboratory, Ball State University, Muncie, IN, USA

Email: [alcraft2@bsu.edu](mailto:alcraft2@bsu.edu)

## INTRODUCTION

Anterior cruciate ligament (ACL) injuries account for 45% of all injuries resulting in 10 or more days of lost participation for athletes, they are also associated with long term health consequences and large financial costs because of surgery [1], [2]. Some risk factors of non-contact ACL injuries include a rapid valgus collapse of the knee joint while near full extension coupled with internal rotation of the tibia, faulty neuromuscular patterns, and anatomical predispositions [3]. The majority of these injuries are seen with dynamic sports movements such as cutting [4].

Limb dominance and sex have also been suggested to play a role in ACL injury risk. The dominant limb is categorized as the limb used for the horizontal movement of the bodies center of mass (i.e., propulsion), whereas the non-dominant limb is used for the vertical movement of the bodies center of mass (i.e., posture and support). Patterns between limb dominance and sex were discovered in an epidemiology study that showed males were more likely to injury their dominant limb ACL (74.1% of the time) while females injured their non-dominant limb ACL more often (68% of the time)[5].

While sex related differences have been reported between the risk of injury more research is needed on the biomechanics of cutting on the dominant and non-dominant limbs to better understand ACL injury risk related to sex and limb differences.

## METHODS

Kinematic and kinetic data was recorded on 9 male and 7 female physically active subjects (age:  $21.06 \pm 2.02$  years; mass:  $75.13 \pm 11.91$  kg; height:  $1.76 \pm .079$  m) with a history of participation in a sport

involving unanticipated cutting. Subjects were excluded if they had any previous ACL injuries, current lower extremity injuries or pain, or neurological or physiological problems that would prevent them from running and cutting. The cutting tasks were captured using a 12 camera Vicon motion capture system (VICON Inc., Denver, CO, USA) collecting at 200 Hz and two AMTI force platforms (AMTI Inc., Watertown, MA, USA) collecting at 2000 Hz with a modified Plug-In Gait marker set. Sidestep cutting was done at a 45 degree angle to the right and left, randomized with trials of running straight or running and stopping in order to make the sidestep cutting maneuvers unanticipated. Frontal, and sagittal initial contact angles at the knee joints, as well as peak vertical ground reaction force normalized to body weight were calculated using Visual 3D software (Version 5.0, C-Motion, Germantown, MD, USA) A repeated measures analysis of variance was performed to test the differences between limb dominance and sex.

## RESULTS AND DISCUSSION

A summary of the kinetic and knee kinematic data is presented in Table 1. As expected, it was found that males had significantly larger ground reaction forces compared to females ( $p < .05$ ). Although no other significant differences were found, it is important to note a few patterns apparent in the means of the different variables. Based on limb dominance, females had smaller initial contact flexion angle on their non-dominant limb compared to their dominant limb, while males showed larger ground reaction forces and a smaller initial contact flexion angle on their dominant limb compared to their non-dominant limb. Between sexes, on the dominant limb males had greater ground reaction forces compared to females, while on the non-dominant limb Females had smaller initial contact knee flexion angles, as

well as a greater abduction angle at initial contact when compared to males.

ACL injuries are known to be multifactorial in nature meaning there is not simply one cause, rather a set of conditions which increase the likelihood of the injury occurring. Many previous researchers have suggested that during cutting when the knee angle of the plant leg is less than 40 degrees there is an increased risk of injury, in the current study subject's initial contact flexion angles put them within that increased risk range, males having an even more extended knee position on their dominant limb and females having more extension on the non-dominant limb [6]. In addition, even small degrees of knee abduction have been shown to increase injury risk, in this study females had greater abduction angles at initial contact compared to males on their non-dominant limb which could indicate females are at a greater risk of injury on that limb when compared to males.

## CONCLUSIONS

The findings of this study show preliminary patterns of differential risk between the dominant and non-dominant limb in both males and females, suggesting males may have an increased risk of ACL injury on their dominant limb while females may have an increased risk on their non-dominant limb. Coaches and athletic trainers should consider limb dominance when creating injury prevention workouts while

working with both male and female athletes because ACL injury risk may be heightened by sex as well as limb dominance. Subjects are continuing to be recruited and additional kinetic and kinematic variables are being examined to expand upon these initial findings to help us further understand the influence of limb dominance and sex on lower extremity movement patterns.

## REFERENCES

1. R. Dick, M. Putuklan, J. Agel, T. Evans, and S. Marshall. *J. Athl. Train* **42**, 2007.
2. L. Griffin *et al.* *J. Am. Acadamy Orthop. Surg* **8**, 2000.
3. D. Daniel, M. Stone, B. Dobson, D. Fithian, D. Rossman, and K. Kenton. *Am. J. Sports Med.* **22**, 1994.
4. J. Hashemi *et al.* *J. Biomech* **44**, 2011.
5. J. Andrews, W. McLeod, T. Ward, and K. Howard. *Am. J. Sports Med* **5**, 1977.
6. M. L. Beaulieu, M. Lamontagne, and L. Xu. *Knee Surg. Sports Traumatol. Arthrosc* **17**, 2009.
7. R. Brophy, H. J. Silvers, T. Gonzales, and B. R. Mandelbaum. *Br. J. Sports Med.* **44**, 2010.
8. B. P. Boden, F. T. Sheehan, J. S. Torg, and T. E. Hewett *J. Am. Acad. Orthop. Surg* **18**, 2010.

## ACKNOWLEDGMENTS

Funding source: 2016 BSU ASPIRE grant

**Table 1.** Averaged kinetic and kinematic variables for males and females on their dominant and non-dominant limbs

Variables	Dominant/Non-dominant	Males	Females
Vertical GRF Peak (BW)	D	3.170	2.450
	ND	2.956	2.474
Knee Flexion at IC (°)	D	23.77	22.14
	ND	24.34	21.5
Knee Abduction at IC (°)	D	-2.63	-5.27
	ND	-2.9	-4.33

# Segment Relationships Adapt to Walking Speed Differently in Healthy Young and Elderly Adults

<sup>1</sup>Jordan J.W. Craig, <sup>1</sup>Adam Bruetsch, and <sup>1</sup>Jessie M. Huisinga

<sup>1</sup>Human Performance Laboratory, The University of Kansas Medical Center, Kansas City, KS, USA  
email: jcraig2@kumc.edu

## INTRODUCTION

Walking at non-preferred gait speed alters variability of foot and trunk motion in healthy young and elderly subjects<sup>1</sup>. While it is known that movement variability of individual segments changes relative to gait speed, it is not clear how relationships between segments are maintained when changing walking speeds, and what role these relationships play in maintaining stability. For example, altered trunk movement could stabilize center of mass motion in order to compensate for altered foot movement, thus maintaining whole body stability even though motion of an individual segment is abnormal. Elderly individuals often have weakness or decreased range of motion, which could alter these segmental relationships and ultimately lead to a higher rate of falls<sup>2</sup>. Therefore, it is important to examine how relationships between trunk and foot movement adapt to challenging gait requirements (i.e. speed) in healthy elderly adults compared to the optimal gait characteristics of healthy young adults.

The aim of the current study was to determine the effects of walking at non-preferred speeds on the relationship between foot and trunk acceleration variability in healthy young and healthy elderly adults in the frontal plane. The frontal plane was examined since gait is laterally unstable, and control of movement in this plane requires active control compared to passive control in the sagittal plane<sup>3</sup>. Since lower body segment motion is mechanically tied to upper body segment motion<sup>4</sup>, we hypothesized that the relationship between trunk and foot acceleration variability will not change significantly with varying gait speed in healthy young or healthy elderly adults.

## METHODS

Twenty healthy young adults (mean 23, range 20-30 yrs.) and twenty healthy elderly adults (mean 73, range 67-85 yrs.) with no history of falls participated in this study. All subjects were free from orthopedic or neurological deficits which may affect their walking or balance. Participants walked

on a treadmill at 80%, 90%, 100%, 110%, and 120% of their self-selected preferred walking speed for 3 minutes at each speed. During all walking trials, participants wore tri-axial accelerometers (Opal, APDM, Portland, OR) on their right ankle and sternum that recorded accelerations at 128 Hz for the duration of each trial. Root mean square (RMS) and sample entropy (SaEn) were calculated for the trunk and foot acceleration time series in the frontal plane using a custom MATLAB script. The segment variability ratio was calculated as the ratio of trunk variability divided by foot variability. A 2 (group) x 5 (speed) ANOVA was performed to examine main effect of group (healthy young, healthy elderly) and walking speed (80%-120%) on the segment variability ratio for RMS and SaEn.

## RESULTS

Preferred walking speed was significantly faster in HY ( $1.25 \pm 0.13$  m/s) compared to HE ( $1.10 \pm 0.27$ ) ( $p=0.02$ ). The segment variability ratio using RMS did not exhibit a main effect of group, but there was a main effect of speed ( $F=9.19$ ,  $p<0.001$ ) where the ratio increased as speed increased (Figure 1). There was a significant speed x group interaction ( $F=5.37$ ,  $p<0.001$ ). One-way ANOVA and post-hoc Tukey's test subsequently determined HE demonstrated no main effect of speed, while HY demonstrated a significant main effect of speed ( $F=5.018$ ,  $p<0.001$ ), where the ratio at 120% preferred walking speed was significantly greater than 80% ( $p=0.002$ ), 90% ( $p=0.005$ ) and 100% ( $p=0.022$ ) of preferred walking speed. The segment variability using SaEn showed a main effect of group ( $F=5.83$ ,  $p=0.02$ ) where the ratio was higher for healthy elderly compared to healthy young adults, and also a main effect of speed ( $F=2.77$ ,  $p=0.029$ ) where the ratio decreased as speed increased.

## DISCUSSION

We hypothesized that a constant relationship between acceleration variability at the trunk and foot segment would be maintained in healthy young and healthy elderly individuals regardless of walking speed. Contrary to our hypothesis, our

results show that healthy young adults adapt to non-preferred walking speeds differently compared to healthy elderly adults, as evidenced by how the segmental ratio changes with respect to walking speed. Specifically, the results showed that healthy young adults adapt their RMS segment variability ratio relative to speed, while healthy elderly adults do not adapt. This may in part be due to the attenuation of accelerations from inferior to superior segments being altered in elderly adults compared to healthy young adults<sup>5</sup>. Previous work has shown that healthy elderly adults prioritize head stability at the cost of adopting an altered trunk coordination strategy compared to healthy younger adults<sup>5</sup>. The altered accelerations at the trunk segment in healthy elderly may lead to a change in the relationship between acceleration variability at the trunk and at the feet which is not adaptable to different gait speeds. The SaEn segment variability ratio results show that there is a main effect of speed across both groups, where the ratio decreases as speed increases. However, the main effect of group for the SaEn segment variability ratio shows that the variability structure at the trunk relative to the feet is different between the two groups. Older adults have shown similar approximate entropy values for trunk accelerations compared to young adults<sup>5</sup>, indicating that our observed differences in segment variability ratio using SaEn may stem from altered acceleration variability at the feet during walking.

RMS segmental ratio is  $<1$  in both groups, indicating that the magnitude of acceleration variability is larger at the foot compared to the trunk for all speeds. The SaEn segmental ratio is  $>1$  in both groups, indicating that accelerations at the trunk are less predictable compared to accelerations at the feet for all speeds. These results indicate that

both groups exhibit less overall motion at the trunk relative to the feet, but more irregular patterns of motion at the trunk relative to the feet across walking speeds. None of the healthy elderly adults in the current study had a history of falls, but it is possible that fall-prone elderly adults exhibit further differences in segment variability ratios compared to healthy young adults, which could be a walking characteristic tied to their instability and fall risk.

## CONCLUSIONS

The relationship between trunk and foot motion likely plays a role in maintaining stability during gait. From our current results, it appears healthy elderly adults with no fall history do not adapt their segmental relationships to task requirements in a way similar to healthy young adults. Future studies should examine the segmental variability ratio in elderly subjects with a history of falls to determine how this measure is related to fall risk.

## REFERENCES

1. Kang HG, et al. *J Biomechanics* **41**, 2008.
2. Kerrigan DC, et al. *Arch Phys Med & Rehab* **82**, 2001.
3. Kuo AD. *Int J of Robotics Research*, **18**, 1991.
4. Adamczyk PG, et al. *J Exp Biology* **212**, 2009.
5. Kavanagh JJ, et al. *Human Mov Sci* **24**, 2005.

## ACKNOWLEDGEMENTS

This work was supported by the American Society of Biomechanics Grant-in-Aid, the NIH Ruth L. Kirschstein National Research Service Award T32 HD057850 from the National Institute of Child Health and Human Development, the National Multiple Sclerosis Society RG 4914A1/2, and the NIH National Center for Advancing Translational Science 1KL2TR00011.

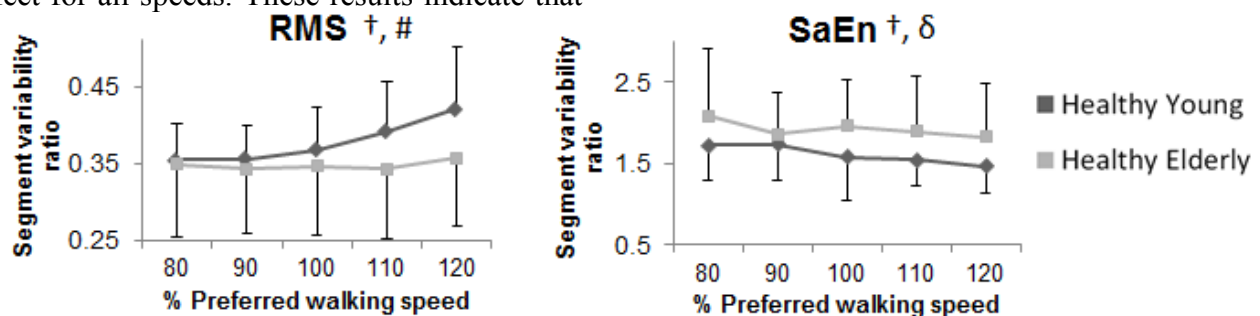


**Figure 1:** Means and standard deviations for segment variability ratio for root mean square (RMS) and sample entropy (SaEn), at 80%-120% preferred walking speed, in healthy young (dark grey) and healthy elderly (light grey) adults. Main effect of speed †; main effect of group δ, significant interaction #.

# KINEMATIC COMPARISON OF THREE POSTURAL LIMITS OF STABILITY TESTS IN COMMUNITY DWELLING OLDER ADULTS

Leslie Allison, Chris Wendt, Alyse Armstrong, Richard Greer, Amanda Akridge, and Samantha Wilson

Winston-Salem State University

Winston-Salem, NC, USA

Email: [wendtc@wssu.edu](mailto:wendtc@wssu.edu)

Web: <http://www.wssu.edu/school-health-sciences/departments/physical-therapy/>

## INTRODUCTION

The Functional Reach Test (FR) is assumed to be a 'low tech' postural limits of stability test that predicts fall risk, despite prior studies demonstrating that it may do neither [1,2]. No prior studies comparing the FRT with both the 'gold standard' computerized Limits of Stability® test (LOS), and the recently developed Sway Sled® test (SS), provided a kinematic analysis of how these tests are actually performed [2,3]. The purpose of this study was to compare the movement strategies used to accomplish these three tests.

## METHODS

Fifteen healthy, community-dwelling older adults (mean age  $71.4 \pm 3.6$  yrs; range 65-80 yrs) were recruited to participate in the study. The majority were female (73%), white (80%), and taking less than four prescription medications (87%). No participant had a history of falls within the last 6 months.

All consented participants performed three tests (FR, LOS, SS) in one visit to the motion analysis lab. For all tests, participants adopted a standardized, height-based foot placement. Passive reflective markers captured motion at the ankle, knee, hip, pelvis, and trunk. For the FR and SS tests, after test familiarization, three trials in each direction (anterior, posterior, left, right) were performed. For the LOS, one practice test and one scored test with targets in eight directions was performed, with only anterior, posterior, left and right directions used for analysis. Five time points were identified in each completed motion, corresponding to 0% (Start), 25%, 50%, 75%, and

100% (Completion) of maximal trunk excursion (Figure 1). For each joint, a 3x5 (Test x Time) RM-MANOVA with planned, post-hoc, Bonferroni-corrected paired samples T-tests analyses were performed.

## RESULTS AND DISCUSSION

All overall multivariate tests were significant for Test, Time, and Interactions, occurring most in the forward (anterior) and backward (posterior) directions, and most at the pelvis and trunk. Post-hoc results for the Forward direction are reported here. Significant differences between tests occurred most often at the pelvis and trunk, and most as the motion progressed (50%, 75% and Completion). Significant differences were found between FR vs SS, FR vs LOS, and SS vs LOS. Differences were greatest between FR and SS, and least between SS and LOS. For example, mean differences in trunk maximal excursion were approximately 22 degrees FR vs SS, and 10 degrees SS vs LOS (see Table 1).

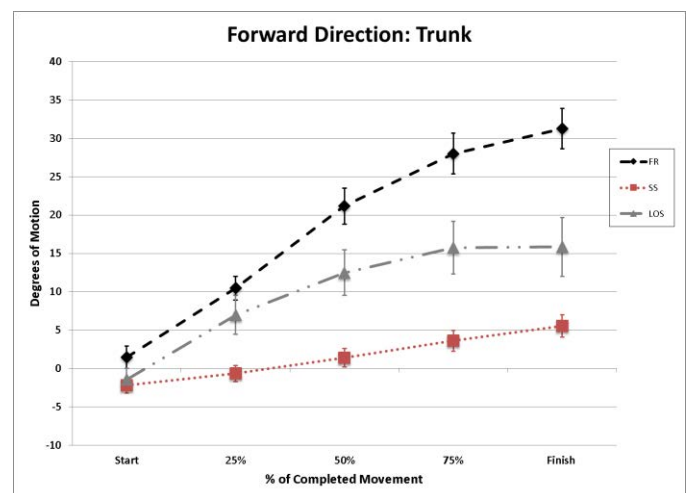


**Figure 1:** Mean Trunk Movement in the Forward Direction between FR, SS and LOS tests.

Restricted postural limits of stability are a risk factor for falls, and accurate measurement is important [4]. These kinematic results extend and support prior research findings indicating that the Functional Reach Test does not measure limits of stability. This may explain the limited predictive validity of the Functional Reach Test for falls.

## CONCLUSIONS

Performance of the Sway Sled® (SS) test most closely resembled the ‘inverted pendulum’ model of postural limits of stability, followed by the computerized Limits of Stability® (LOS), with the Functional Reach Test (FR) least similar. FR performance involves ‘out of phase’ backward

motion at the knee with compensatory forward motion at the trunk, versus the ‘in-phase’ forward motion of the hip, pelvis and trunk in the SS and LOS.

## REFERENCES

1. Wernick-Robinson M, et al. *Arch Phys Med Rehabil.* **80**(3): 262-269, 1999
2. Allison L, et al. Combined Sections Meeting Presentation, APTA. San Diego, Ca, 2013
3. de Warquier-Leroy L, et al. *Ann Phys Rehabil Med.* **57**(6-7): 452-464, 2014
4. Gouglidis V, et al. *Exp Aging Res.* **37**(1): 46-62, 2011

**Table 1:** Mean differences in joint maximal excursion (Completion – Start position) between tests.

	<b>Trunk (deg)</b>	<b>Pelvis (deg)</b>	<b>Hip (deg)</b>	<b>Knee (deg)</b>	<b>Ankle (deg)</b>
<b>FR vs. SS</b>	FR > SS: 22.1	FR > SS: 15.2	FR > SS: 18.7	FR < SS: 4.5	FR < SS: 7.0
<b>FR vs. LOS</b>	FR > LOS: 12.5	FR > LOS: 11.0	FR > LOS: 10.0	FR < LOS: 8.3	FR < LOS: 4.5
<b>SS vs. LOS</b>	SS < LOS: 9.6	SS < LOS: 4.2	SS < LOS: 8.7	SS < LOS: 3.7	SS > LOS: 2.5

# EFFECT OF AN OLDER ADULT GOLF TRAINING PROGRAM ON POSTURAL CONTROL

Andrea M. Du Bois, Nicole Marcione, and George J. Salem, PhD

University of Southern California, Los Angeles, CA, USA  
email: amdubois@usc.edu, web: <http://pt.usc.edu/labs/mbrl/>

## INTRODUCTION

Aging is associated with physiological changes that impair quality of life and increase the risk for falls. A laterally directed fall is more likely to result in a hip fracture, a costly and debilitating injury [1]. Therefore, mediolateral (ML) postural control is of the utmost importance for the aging individual; however, static and dynamic ML postural control decline in older adults [2].

Multimodal exercise programs are effective in improving balance and reducing fall risk [3]. Golf is a popular physical activity that includes intermittent periods of walking equivalent to moderate to vigorous exercise intensity [4], bending over to pick up a golf ball, precise putts that challenge the static postural control of the golfer, and high velocity golf swings. The golf swing requires near maximal activation of the proximal hip musculature including the hip abductors [5], a muscle group that mechanically controls frontal plane balance. The golf swing also requires a bilateral, frontal plane weight shift, challenging dynamic postural control [6]. It is plausible that golf could be used as a therapeutic intervention to improve balance and reduce fall risk in older adults. Therefore, the purpose of this study was to assess the changes in ML postural control following a twelve week therapeutic golf intervention.

## METHODS

Two male older adults (67 y and 70 y) were recruited to participate in the study. The participants completed a 12 week comprehensive golf training program twice weekly for 90 minutes per session. The program was designed to gradually introduce the participants to golf beginning with swing training and gradually progressing to a full round of golf on a 3 par, nine hole golf course.

Before and after the golf training program, participants completed a rapid step test to assess dynamic ML postural control. Participants stood with each foot on separate force platforms (AMTI, Newton, MA; 1500 Hz). They first received a red warning light, followed by either a green or yellow light. If there was a green light, they were instructed to step as quickly as possible onto an elevated force platform (15 cm) with their right foot. If they saw a yellow light, they stepped as quickly as possible with their left foot. A total of five trials per limb were collected in a randomized order.

Temporal measures and center of pressure (COP) dynamics were analyzed for each trial. COP was filtered using a 4<sup>th</sup> order zero-lag Butterworth filter with a 5 Hz cutoff. Temporal measures included weight shift time (WT; time from initiation of movement to lift off of the stepping foot) and step time (ST: lift off to contact with the step). During the weight shift, the net ML COP range (RANGE) and the average ML COP velocity (VEL) were calculated. During the step execution, the mean displacement of the ML COP from the average COP position was calculated (MDISP).

Data was averaged across limbs and trials and presented as means and standard deviations. To represent the magnitude of the change, Cohen's *d* effect sizes were calculated for pre-post values.

## RESULTS AND DISCUSSION

Following the golf training intervention, participants were able to improve their performance on the rapid step test—WT decreased (ES 1.77;  $\Delta = -35.75$  ms). During the weight shift, RANGE (ES 8.34, Figure 1A) and VEL (ES 9.21, Figure 1B) increased. Step initiation requires a bilateral weight shift. First, an individual must shift the COP towards the stepping limb, creating an acceleration

of the center of mass (COM) towards the stance limb. The individual must then rapidly shift the COP towards the stance limb to control the momentum of the COM, allowing for a safe execution of the step [7]. Not only were the participants able to more quickly shift their weight following the golf training program, but they also performed a more dynamic weight shift as demonstrated by the increased RANGE.

2). Thus, the participants not only generated a larger weight shift, but they were better able to control the momentum as demonstrated by the decreased ML COP movements during the step allowing for a more rapid execution of the step.

## CONCLUSIONS

Following participation in a twelve week comprehensive golf training program, the dynamic postural control of the participants improved. Participants were able to execute a rapid step more quickly following golf training. This was accomplished by a larger weight shift that accelerated the COM over the stance leg. The individual was also better able to control the momentum generated during the weight shift, allowing for a more stable and rapid step execution.

Golf is a popular recreational activity that includes multiple components including walking the golf course, bending over to pick up a ball, and dynamic golf swings. Multimodal exercise programs have been shown to be most effective in improving balance and reducing fall risk in older adults. Given this knowledge and the preliminary results of this study, it appears that golf can be utilized as an exercise intervention to improve balance and potentially reduce falls in older adults.

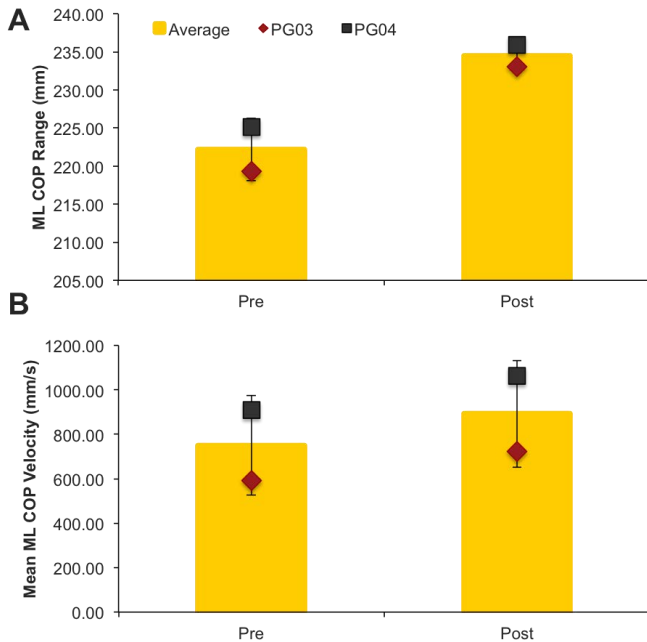


**Figure 1:** COP dynamics during the weight shift before (Pre) and after (Post) the golf training program. A. ML COP range B. Mean ML COP velocity.

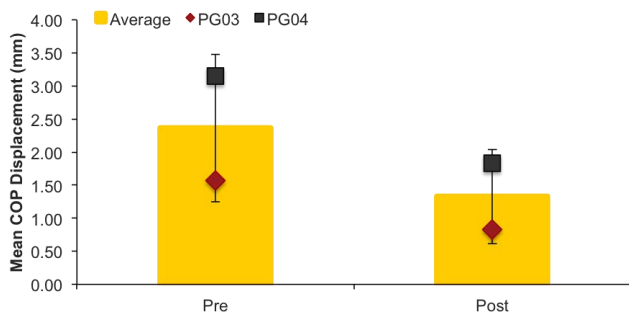


**Figure 2:** Mean ML COP displacement before (Pre) and after (Post) the golf training program.

ST also decreased following the golf training intervention (ES 1.72;  $\Delta = -138.33$  ms). During the step execution, MDISP decreased (ES 2.55, Figure

## REFERENCES

1. Nevitt MC, et al. *J Am Geriatr Soc* **41**, 1226-1234 2008.
2. Jonsson E, et al. *Clin Biomech* **19**, 688-694, 2004.
3. Chodzko-Zajko WJ, et al. *Med Sci Sports Exer* **41**, 1510-1530, 2009.
4. Broman G, et al. *Aging Clin Exp Res* **16**, 375-381, 2004
5. Bechler JR, et al. *Clin J Sport Med* **5**, 162-166, 1995
6. Ball KA & Best RJ. *J Sports Sci* **25**, 757-770, 2007
7. Yiou E & Do MC. *Gait Posture* **32**, 145-147, 2010

# EFFECTS OF ELECTRICAL AND MECHANICAL STIMULATION ON FOOT SENSITIVITY IN HEALTHY ELDERLY SUBJECTS

Claudio Zippenfennig\*, Laura Niklaus, Katrin Karger, Thomas L. Milani

Chemnitz University of Technology, Department of Human Locomotion, Chemnitz, Saxony, Germany

\*email: [claudio.zippenfennig@hsw.tu-chemnitz.de](mailto:claudio.zippenfennig@hsw.tu-chemnitz.de), web: <https://www.tu-chemnitz.de/index.html.en>

## INTRODUCTION

The loss of perception due to reduced plantar sensitivity promotes falling in the elderly [1]. A phenomenon called ‘stochastic resonance’ (SR) attempts to influence sensitive receptors on the footsole with subsensory electrical [2] or mechanical [3] noise stimulation. Positive effects in relation to equilibrium could also be observed with white-noise-like (WNL) electrical stimulation applied to the lateral and medial sides of the knee joint [4]. Furthermore, only one study has investigated the effects of a subsensory noisy vibratory signal after one hour of continuous plantar stimulation [5]. Therefore, the present study investigated the effects of subsensory WNL electrical and mechanical stimulation – applied to the foot sole – on vibration perception thresholds (VPTs) of healthy elderly subjects. Moreover, lasting effects of a short intervention period with these waveforms were examined. We hypothesized that the subsensory electrical as well as mechanical stimulation leads to improvements of foot sensitivity. Lower VPTs were expected.

## METHODS

99 healthy elderly subjects (> 60yrs, 60 ♀ / 39 ♂,  $68.8 \pm 6.0$ yrs,  $165.9 \pm 19.3$ cm,  $75.1 \pm 13.0$ kg) participated in the study. All procedures were executed in accordance with the recommendations of the Declaration of Helsinki and approved by the local ethics committee. Participants were randomly assigned to one of the following groups: vibration (Vi-G), current (Cu-G), control (Co-G), or one of two placebo (PI-Gs). VPTs were measured after a five-minute intervention with either subsensory WNL mechanical (Vi-G) or electrical (Cu-G) stimulation. Co-G had a five-minute rest and both PI-Gs received a five-minute mocked mechanical (PI-Vi) or electrical (PI-Cu)

stimulation. The VPTs were estimated at two randomized anatomical locations (first Metatarsal head (MET I) and heel). All subjects performed the following procedure for each location: baseline measurement, pre measurement as a reliability test, and post measurement after treatment period. VPTs were measured using a TiraVib vibration exciter (TIRA GmbH, Model TV51075, Germany) at 30Hz. The mean of three trials was calculated and used for statistical analyses. The intervention for the Cu-G consists of a WNL electrical stimulation [4]. A two-channel stimulation current unit (Physiomed Elektromedizin AG, Germany) generated a stochastic biphasic current (frequency spectrum 10-100Hz). Electrodes were placed under the hallux and the proximal aspects of the metatarsal heads to stimulate MET I. To stimulate the heel, electrodes were placed at the Achilles tendon above the posterior edge of the calcaneus bone and under the distal area of the plantar calcaneus. Mechanical stimulation in Vi-G took place directly at the two anatomical locations via the vibration exciter. The mechanical signal was adapted to the electrical signal through a self-written Lab-View program. In both intervention groups, stimulation intensity was 90% of the individual perception threshold, which was quantified before measurement. Data was statistically analyzed using parametric and non-parametric tests for dependent samples and Bonferroni correction due to the number of accomplished tests ( $\alpha = 0.05/6 = 0.0083$ ).

## RESULTS AND DISCUSSION

Table 1 shows the results of VPTs after the described five-minute intervention for each group. Vi-G and PI-Vi showed significant increases of their VPTs at MET I or heel (Table 1). While significant changes were also found for Co-G at MET I, all other groups showed no significant differences. The performed Kruskal-Wallis-Test was only statistically significant

for the heel ( $p = 0.005$ ), which was due to the values in Vi-G (Table 1). This leads us to consider whether the five-minute intervention with sub-sensory WNL mechanical stimulation led to a deterioration in foot sensitivity. Considering the PI-Vi, this deterioration seems to have other causes than the intervention. It may be possible that methodological characteristics of the vibration exciter caused these differences. A vibrating probe (diameter 7.8mm) that protrudes 2mm through a hole in a self-constructed wooden footrest was used to measure VPTs. The five-minute intervention as well as mocked mechanical stimulation was realized in a standing position. Therefore, the major pressure on the vibrating probe which prevails in the standing position could have led to skin deformities or to adaptation process resulting in less sensitivity. These changes may influence the way the examined mechanoreceptors function. Considering the other groups, no relevant changes in foot sensitivity were observed after the respective intervention. This is particularly interesting for Cu-G, since other studies consistently demonstrated positive effects of subsensory electrical stimulation [2,4]. A major difference to other studies in the field of SR is the chosen current form. The most commonly used white noise [2,4,5] is a continuous waveform. The waveform in the present study is a frequency modulation caused by random pauses between short triangle pulses (1ms duration). The short pulses of the resulting frequency band of 10-100Hz are possibly too weak to positively stimulate sensory receptors in the foot sole.

## CONCLUSIONS

In conclusion, neither the subsensory mechanical signals nor the electrical signals used in this study had a lasting effect on plantar sensitivity in healthy elderly subjects. In addition to the methodological influences mentioned, the duration of stimulation might be too short. However, studies implementing mechanical stimulation for over an hour also do not show any lasting effects. Further studies should investigate possible lasting effects over a longer period of time (days, weeks, or months) and should use the commonly used white noise.

## REFERENCES

1. Delbaere K, et al. *J Amer Geriatr Soc* **58**, 1679-1685, 2010.
2. Dhruv NT, et al. *Neuroreport* **13**, 597-600, 2002.
3. Khaodhiar L, et al. *Diabetes care* **26**, 3280-3283, 2003.
4. Kimura T & Kouzaki M. *Gait Posture* **37**, 634-636, 2013.
5. Cloutier R, et al. *Annals of neurology* **59**, 4-12, 2009.

## ACKNOWLEDGMENTS

The study was supported by the German Federal Ministry of Education and Research (BMBF, Funding number: 16SV7101).

**Table 1:** Mean±SD of vibration perception thresholds (VPTs) for every condition (baseline, pre, and post intervention), for both anatomical locations (heel and first Metatarsal head, MET I) for each group: vibration (Vi-G), current (Cu-G), control (Co-G), placebo vibration (PI-Vi), and placebo current (PI-Cu). Superscripted symbols represent significant differences: all  $p < 0.0083$

n = 99	Heel [μm]			MET I [μm]		
	Baseline	Pre	Post	Baseline	Pre	Post
VPTs Vi-G [n = 24]	20.1±15.1	18.6±16.5*	40.8±36.4*	30.9±32.4	30.3±23.1	42.5±27.4
VPTs Cu-G [n = 25]	23.4±13.8	22.1±12.1	26.8±21.5	41.8±29.7	43.3±42.4	46.7±31.2
VPTs Co-G [n = 25]	22.3±13.1	22.3±22.2	24.6±21.1	44.2±40.7	42.3±41.2 <sup>#</sup>	50.4±45.6 <sup>#</sup>
VPTs PI-Vi [n = 12]	29.8±28.4	25.1±13.1	44.6±53.6	37.7±23.4	35.2±31.4 <sup>§</sup>	74.0±84.0 <sup>§</sup>
VPTs PI-Cu [n = 13]	16.6±10.8	15.9±11.1	20.6±17.8	30.1±22.4	30.3±23.0	34.5±28.0

# DIFFERENCES IN COORDINATION BETWEEN YOUNG AND OLD RUNNERS

Kathryn Harrison, Jacqueline Morgan, Gregory Crosswell, Yongung Kwon, Bhushan Thakkar, and DS Blaise Williams III

VCU RUN LAB, Virginia Commonwealth University, Richmond, VA  
email: harrisonk3@vcu.edu, web: khs.vcu.edu/about/vcu-run-lab/

## INTRODUCTION

Participation in the sport of running declines sharply after the age of 45 [1]. This may be in part due to increased risk of running-related injury with age [2].

Increase in injury rates amongst older runners may be in part due to altered biomechanics. It has been reported that older runners have decreased range of motion, however the literature is equivocal [3,4]. More consistently, older runners demonstrate reduced power generation at the ankle, which is compensated for by increasing contributions of the hip [5].

The proximal shift in work seen in older runners suggests a change in coordination strategy. It has been hypothesized that disruption in the sequencing of motions associated with loading during running may contribute to injury [6]. Therefore, the purpose of this study was to compare coordination using vector coding between young and older runners.

## METHODS

Twelve young adult males (22(3) yrs, 1.80(.07) m, 78(12) kg) and 12 older males (63(3) yrs, 1.76(.06) m, 73(16) kg) who regularly ran at least 10 miles per week volunteered for this study. Runners were provided with standard neutral footwear (New Balance, Boston, MA). Gait analysis was conducted on an instrumented treadmill (Treadmetrix, Park City, UT). A 20 second trial was collected using a 5-camera motion analysis system (Qualisys, Goteborg, Sweden) at 120 Hz as participants ran at 3.35m/s.

Visual 3D motion analysis software (C-Motion, Germantown, MD) was used to process data. Hip, knee and ankle joint angles were calculated for the stance phase of gait, which was defined using kinetic data from the force plate. Motions associated with

loading response (ie showing a unimodal peak at mid-stance), were selected for analysis. These included rearfoot eversion (EV), tibial internal rotation (TIR), knee flexion (KF) and hip adduction (HAD).

Coordination was assessed using a modified vector coding technique[7]. For each frame, joint position of the distal joint was plotted on the x-axis, and joint position of the proximal joint was plotted on the y-axis. Positive values indicated positions associated with collapse (EV, TIR, KF, HAD). Coordination angle was calculated as

$$\Theta = \tan^{-1}(\Delta p_{\text{proximal}}/\Delta p_{\text{distal}})$$

Where  $\Delta p$  is the change in joint position. Using this scale, positive values indicate in phase motion (eg both joints collapsing) while negative values indicate anti-phase motion (eg. One joint collapsing while the other joint has reversed). Greater magnitude of coordination angle indicates more relative distal motion, while values closer to 0 indicate greater relative proximal motion.

Coordination angles were averaged during four phases of stance previously defined, including impact, loading, propulsion and toe-off. For each couple analyzed (EV-TIR, TIR-KF, KF-HAD, EV-HAD), a MANOVA was used to compare coordination between groups at each phase.

## RESULTS AND DISCUSSION

Coordination through stance phase in younger and older runners is depicted in Figure 1. No significant differences were observed in EV-TIR. Motion was in phase through the first half of stance, with relative TIR increasing until mid-stance. A brief period of anti-phase motion occurred before both motions

occurred in phase, with relative eversion increasing until toe-off.

Similarly, no significant differences were observed in TIR-KF coordination. Knee flexion dominated in early stance, but relative proximal motion declined until mid-stance, at which anti-phase coordination was observed. Following mid-stance relative knee motion increased, dominating propulsion and toe-off.

KF-HAD coordination was significantly different between young and old runners ( $p=.033$ ). Younger runners displayed KF dominated in-phase motion, while older runners had anti-phase motion, as the hip abducted while the knee flexed. Thereafter motion was KF dominated in-phase, until mid-stance when anti-phase motion occurred. During propulsion KF dominated, with relative KF decreasing until toe-off.

There was a trend towards differing EV-HAD between younger and older runners ( $p=.099$ ). Again, the young displayed eversion dominated in-phase motion, while the older demonstrated anti-phase motion. In-phase motion occurred until a period of anti-phase motion at mid-stance. Relative eversion increased during propulsion, and declined through toe-off.

## CONCLUSIONS

Older runners used different coordination strategies between the hip and knee and ankle during the impact phase of running. It appears that older runners do not allow the hip to collapse at impact, possibly to compensate for reduced ability to control the ankle. This is supported by previous work showing a proximal shift in power generation in older runners [5].

This study also found that in both groups, anti-phase motion consistently occurred at mid-stance. It has previously been hypothesized that the collapse motions should peak at mid-stance, and disruption of this synchrony may lead to injury. However younger runners actually appeared to utilize a greater degree of anti-phase motion in the transition from loading to propulsion. Thus this strategy may not be injurious, as previously thought.

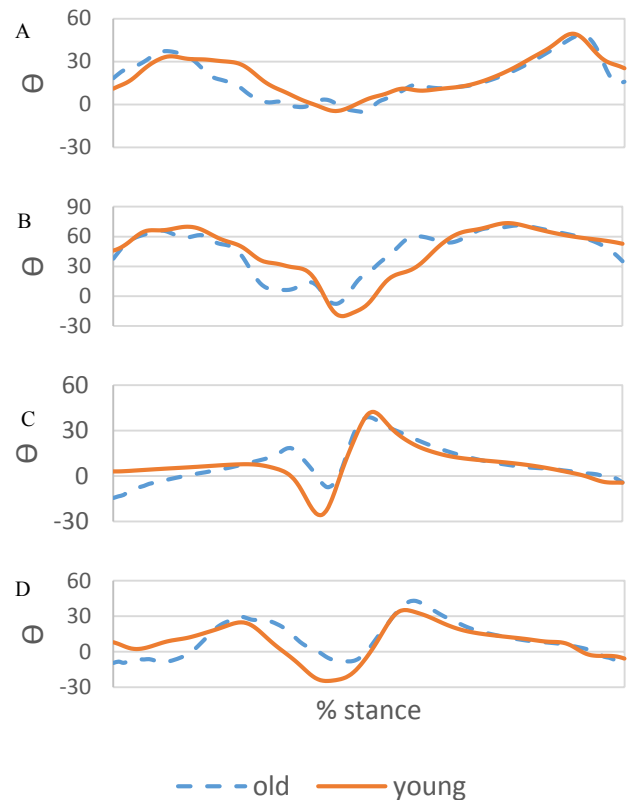


**Figure 1:** Coordination angles of younger and older runners. A) Eversion-tibial internal rotation. B) Tibial internal rotation-knee flexion. C) Knee flexion-hip adduction. D) Eversion-hip adduction.

## REFERENCES

- [1] Running USA. 2016.
- [2] Kluitenberg B, van Middelkoop M, Smits DW, Verhagen E, Hartgens F, Diercks R, van der Worp H. *Scand J Med Sci Sports* 2015;**25**:515-23.
- [3] Fukuchi RK, Stefanyshyn DJ, Stirling L, Duarte M, Ferber R. *Clin Biomech (Bristol, Avon)* 2014;**29**(3):304-10.
- [4] Silvernail JF, Boyer K, Rohr E, Bruggemann GP, Hamill J. *Med Sci Sports Exerc* 2015;**47**(10):2175-80.
- [5] Devita P, Fellin RE, Seay JF, Ip E, Stavro N, Messier SP. *Med Sci Sports Exerc* 2016;**48**(1):98-106.
- [6] James SL, Bates BT, Osternig LR. *Am J Sports Med* 1978;**62**:40-50.
- [7] Ferber R, Davis IM, Williams DS, 3rd. *J Biomech* 2005;**38**(3):477

# MOVEMENT VARIABILITY DURING SPLIT-BELT TREADMILL WALKING IN HEALTHY OLDER ADULTS

<sup>1</sup> Matthew J. Terza, <sup>2,3</sup> Ryan Roemmich, and <sup>1</sup> Chris J. Hass

<sup>1</sup> The University of Florida, Gainesville, FL, USA, <sup>2</sup> The Johns Hopkins University School of Medicine, Baltimore, MD, USA <sup>3</sup> Kennedy Krieger Institute, Baltimore, MD, USA  
email: mjt023@ufl.edu

## INTRODUCTION

The adaptability of movement patterns in the lower extremity joints is essential in achieving optimal foot placement during walking in complex real world environments. Adaptability of movement patterns is evident in the structure of joint variability from stride to stride. Novel physical constraints on the walking system may be used to challenge the walking repertoire of an individual leading to greater exploration of novel and useful dynamics changing the structure of variability.

The split-belt treadmill (SBT) provides one such opportunity to provoke the individual to explore novel movement patterns to improve the adaptability of walking. Although healthy older adults (HOA) appear to demonstrate the same spatiotemporal adaptation to the SBT as healthy young adults (HYA), it is unknown whether potential changes in the variability of movement at the joint level is similar to that of HYAs [1]. Other studies have shown different joint level walking strategies with age, therefore it is possible the HOA versus HYA would exhibit different movement strategies in response to the SBT [2]. Therefore, we sought to compare the structure of the variability of movement during split-belt treadmill walking.

Because previous SBT research has displayed similar spatiotemporal adaptations between HOA and HYA, we hypothesized that HOA would similar changes in joint variability as HYA. We further hypothesized that exposure of the SBT would elicit increased exploration in movement demonstrated by increases in the largest Lyapunov exponent (LyE) of the lower extremity joint angle trajectories over time. Additionally we hypothesized a main effect of age that would reveal the older adults as generally less predictable in their movement variability.

## METHODS

Thirteen healthy older adults (65±8 years old, 7 Males) and fourteen healthy young adults (23±4 years old, 7 Males) volunteered for this study. Individuals were fitted with retroreflective markers in accordance with the Vicon Lower Body Plug-In-Gait model. Motion capture data using an 8 camera Vicon system at 120 Hz were collected as these individuals walked in different conditions on an instrumented SBT.

Individuals walked for five minutes at their self-selected speed to familiarize them with walking on the treadmill. Then individuals walked 2 minutes with the belts tied (moving the same speed) at their fastest comfortable speed and then 2 minutes with the belts coupled at half of their fastest comfortable speed. Participants then walked in the split-belt condition with the belt under their non-dominant leg moving at their self-selected fastest comfortable speed and the belt under their dominant leg moving at half of their self-selected fastest comfortable speed for 10 minutes.

We analyzed the last 30 seconds of both of the baseline conditions and the first 30 seconds of the split-belt condition. We calculated the joint angles at the hip, knee, and ankle of each leg. Because the split-belt treadmill provides a mainly sagittal plane perturbation we analyzed exclusively the sagittal joint angle trajectories. We estimated the largest LyE of these joint angle trajectories during these condition. Higher LyE values indicate less predictable movement and greater movement exploration. To estimate LyE values the data was down-sampled to 60 Hz in accordance with recommendations for accurately estimating Lyapunov exponents in human gait data [3]. The

embedding dimension of the data set was determined to be 5 using the rate of false nearest neighbors algorithm. The time lag for each time series was determined separately using the first minimum of the average mutual information algorithm. LyE was the main outcome measure used to quantify if and to what extent the walking system was being challenged during the split-belt condition.

We exclusively compared the fast leg (the leg on the fast belt in the split-belt condition) and slow leg during split-belt walking to the same leg in the corresponding baseline speed condition (e.g. fast leg in the split-belt condition was compared to the same leg in the tied fast condition). We used a repeated measures multivariate analysis of variance MANOVA (2 x 2 x 6) age group x condition (split versus tied walking) x joint. Post hoc comparisons were made with Benjamini Hochberg corrections for multiple comparisons.

## RESULTS AND DISCUSSION

The statistical tests indicate no interaction between age and condition indicating the split-belt perturbation affects these populations in a similar manner. However, they did reveal significant main effects of age and condition. Post hoc comparisons revealed significant increases in the largest LyE at the hips and knees but not at the ankles during the split-belt condition as compared to the respective tied condition. Meaning regardless of age, this perturbation promotes greater exploration and less predictable motion from stride to stride at these

joints. To this end the SBT may have utility in aging populations as a locomotor training tool by challenging them to explore new patterns of movement in walking. Furthermore, the SBT may also expand the repertoire of adaptive movements in real world situations that involve asymmetric step foot placement. Interestingly, the post hoc pairwise comparison for the main effect of age revealed significant differences at the fast ankle and the fast hip only but in the opposite direction that we hypothesize. HOA were more predictable at these joints. This age effect result may be an indication that there is an interaction between speed and age.

Limitations of these perturbation results may be that they are specific to the speed of the belts during the split condition. Different results may be obtained at slower self-selected speeds.

## CONCLUSIONS

Complex novel walking constraints presented by the SBT may be a viable method for challenging the older adult to explore new walking dynamics, as they respond in a similar manner compared to healthy young adults.

## REFERENCES

1. Roemmich RT, et al. *Clinical Neurophysiology*, **125** 313-319, 2014.
2. DeVita, P, et al. *J Appl Physiology* **88** 1804-1811, 2000.
3. Stergiou, N. *Nonlinear Analysis of Human Movement Variability*, CRC Press Boca Raton, FL, USA ,2016

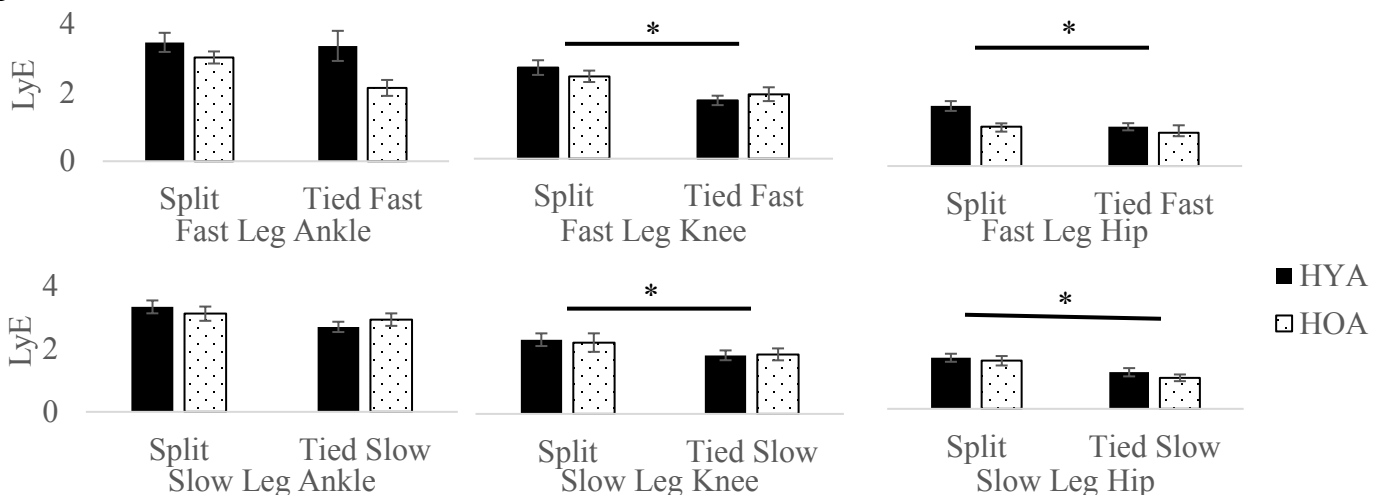


Figure 1: The graphs show significantly decreased predictability of sagittal plane joint movement at the hips and knees during the split condition as compared to the respective tied condition. \*p-value <0.05

# ON HOW AGE, DISEASE AND BIOMECHANICAL CAPACITIES INTERACT TO AFFECT INGRESS/EGRESS FROM A PASSENGER VEHICLE

<sup>1</sup> PM Shahshahani,<sup>1</sup> AS Kapshai,<sup>1</sup> T De Mott,<sup>1</sup> JK Richardson,<sup>2</sup> K Kozak,<sup>2</sup> N Wang,<sup>2</sup> J Wan,<sup>1</sup> JA Ashton-Miller

<sup>1</sup> University of Michigan, Ann Arbor, MI, USA

<sup>2</sup> Ford Motor Company, Dearborn, MI, USA

email: mirshams@umich.edu

## INTRODUCTION

We are not aware of studies of how diseases that commonly affect mobility influence older driver vehicle ingress/egress. Dufour *et. al.* investigated the effect of ingress/egress range of motion requirements on perceived discomfort [1]. Namamoto *et. al.* explored the interaction of age, stature, and vehicle design with the strength requirements for ingress and egress in passenger vehicles [2]. The goal of this study was to quantify how age, osteoarthritis (OA) and diabetic polyneuropathy (PN), muscle strength, measures of functional ability and movement strategy interact to affect vehicle ingress/egress times, because we hypothesized that longer times are associated with greater perceived discomfort ratings. We shall here only report egress times; subject variability is greater in this task [2], and we hypothesized that neither disease nor egress strategy interact with vehicle type in determining egress time.

## METHODS

We recruited elderly subjects aged between 67 and 89 years of age, 23 of whom were healthy, 12 had PN, and 12 had OA. Women comprised 48%, 17%, and 58% of each group, respectively. Subject capacities were measured at the Biomechanics Research Lab on the first visit (**Table 1**). Tests included max isometric hip abduction strength and rate of torque development (RTD), and max isometric knee extension strength. We normalized each strength measurement by subject's weight and height. Functional tests included max one legged balance times (OLB) and timed up and go test (TUG). Cognitive tests included simple reaction time (SRT), recognition reaction time (RRT) [3], Mini-Mental Status Examination (MMSE), and a paper Trails B test. Lower extremity sensory

function was scored using the Michigan Diabetic Neuropathy Score (MDNS).

**Table 1-** Capacities (SD) of participating subjects

Variable	Control (n=23)	Neuropathy (n=12)	OA (n=12)
Age (yrs)	75.6(7.4)	76.8(6.5)	78.6(6.6)
Height (cm)	166.4(9.9)	177.2(7.0)	165.1(9.2)
Weight (Kg)	76.8(13.1)	99.3(15.7)	74.2(15.6)
Norm Knee Ext Torque	0.4(0.2)	0.5(0.2)	0.4(0.1)
Norm Hip ABd Torque	0.5(0.2)	0.4(0.1)	0.4(0.1)
Norm Hip ABd RTD	4.0(2.7)	3.5(2.9)	3.7(1.4)
OLB (sec)	21.6(10.7)	9.1(7.7)	6.7(7.7)
TUG (sec)	10.4(2.3)	12.1(2.1)	13.0(3.2)
MDNS	2.3(2.6)	15.1(3.9)	4.1(2.8)
SRT (msec)	165.8(24.5)	166.2(24.2)	168.2(17.7)
RRT (msec)	250.6(35.0)	239.0(35.8)	254.8(29.6)
MMSE	29.0(1.0)	29.4(0.5)	28.7(1.2)
Trails B (sec)	70.5(33.7)	95.0(49.8)	95.3(33.9)

On their second visit, subjects' ingress/egress was assessed at the Ford Motor Company Human Occupant Package Simulator (HOPS) Laboratory. Standard motion analysis techniques involving surface markers were used along with a reconfigurable setup simulating 7 different passenger vehicle models. Perceived discomfort was rated by a CP-50 scale questionnaire [4] after the subject performed both ingress and egress tasks. Egress strategy was categorized as Left Leg Out (LLO) or Both Legs Out (BLO) strategies [5]. We used linear mixed-effect modeling (LMM) for analyses and a random intercept for each subject to account for the correlation between the repeated measurements. Residuals were considered homoscedastic. R *base* package *ver. 3.3.2* and *nlme ver. 3.1* were used to run the LMM.

## RESULTS AND DISCUSSION

Egress time was not normally distributed so inverse egress time (IET), which was normally distributed, was used as the dependent variable in our analyses.

Disease showed a significant main effect on IET (**Figure 1**). Given no significant difference between the OA and PN groups, these groups were combined in the final statistical model. We also divided our vehicle models into two types based on vehicle package dimensions, with Vehicles 1 and 2 in Type I, and the other five vehicles in Type II.

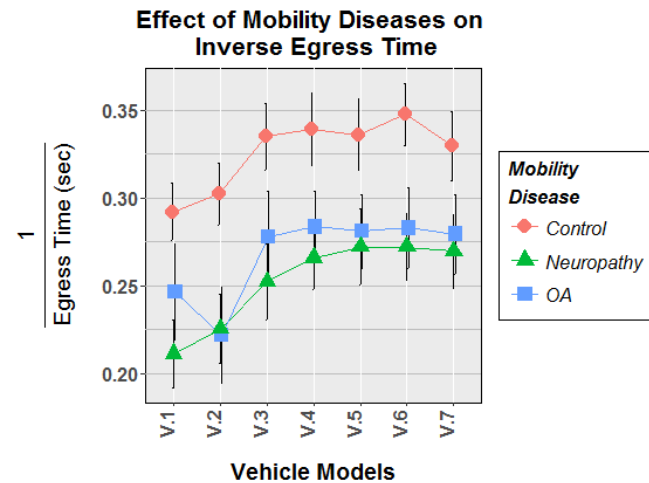


**Figure 1:** The main effect of disease was significant ( $p = 0.01$ ).

The interaction of egress strategy and vehicle model was also significant (**Figure 2**). Both functional capacity measurements showed a significant relationship with IET (**Table 2**). The final statistical model predicting IET on the basis of subject capacities, vehicle type, and egress strategies is shown at right in **Table 2**. The correlation between IET and perceived discomfort was indeed significant and equal to -0.45.

Strengths of the study include the number of subjects and use of LMM to incorporate all the data in the analyses. Limitations included the exclusion of subjects with a BMI exceeding 35 kg/m<sup>2</sup>.

## REFERENCES

1. Dufour F. & Wang X. No. 2005-01-2706. *SAE Technical Paper*, 2005.
2. Namamoto K, et al. *JSAE Review* 24.3 (2003): 335-339.
3. Eckner JT. et al. *Psychol. Assessment* 24.1 (2012): 249.
4. Shen W. and Parsons KC. *International Journal of Industrial Ergonomics* 20.6 (1997): 441-461.

5. Chateauroux E. & Xuguang W. *Applied Ergonomics* 42.1 (2010): 169-177.

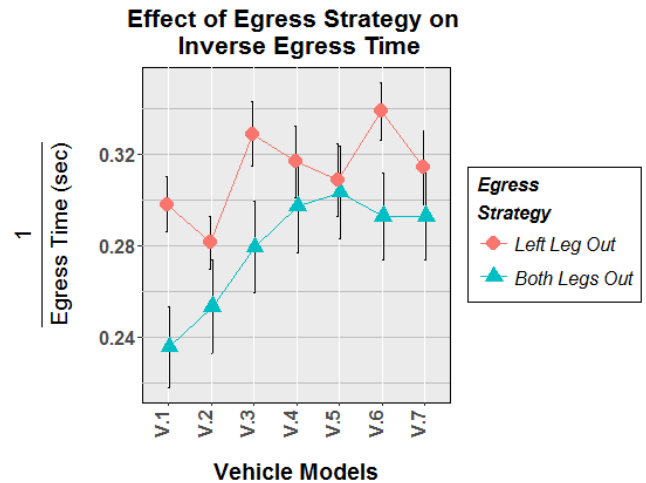


**Figure 2-** The interaction of egress strategy and vehicle model was significant ( $p < 0.0001$ ).

**Table 2-** Summary of the LMMs fitted to IET

	Inverse Egress Time (1/sec)		
	Functional Tests (1)	Subject Capacities (2)	Subject Capacities (3)
OLB (sec)	0.003 (0.001) $t = 3.271^*$		
TUG (sec)		-0.018 (0.004) $t = -4.805^{**}$	
Disease (PN-OA)			-0.045 (0.022) $t = -2.084^*$
Knee Ext Torque ( $\frac{N.m}{Kg.m}$ )			0.096 (0.048) $t = 1.982$
Age (Years)			-0.005 (0.002) $t = -3.290^*$
Weight (Kg)			-0.002 (0.001) $t = -2.874^*$
Type II Vehicle			0.027 (0.009) $t = 2.970^*$
BLO Egress			0.010 (0.014) $t = 0.720$
BLO Egress: Type II Vehicle			0.030 (0.011) $t = 2.653^*$
Intercept	0.247 (0.018) $t = 13.620^{**}$	0.499 (0.044) $t = 11.350^{**}$	0.772 (0.141) $t = 5.478^{**}$
Marginal R <sup>2+</sup>	0.16	0.28	0.35
Conditional R <sup>2+</sup>	0.79	0.79	0.89
Observations	318	318	318
Akaike Inf. Crit.	-952.800	-964.700	-1,017.000

Note: <sup>+</sup>  $p < 0.05$ , \*  $p < 0.01$ , \*\*  $p < 0.001$   
<sup>+</sup>Nakagawa Method

## ACKNOWLEDGMENTS

Funding from the UM - Ford Alliance Grant #N017963. We thank Dr. Andrzej Galecki (UM IOG) for statistical consultation under PHS Pepper Center Grant P30 AG 024824.

# EFFECTS OF GOLF TRAINING ON GAIT PARAMETERS IN OLDER MILITARY VETERANS

<sup>1</sup> Nicole A. Marcione, <sup>1</sup> Andrea M. DuBois, <sup>1</sup> George J. Salem, PhD

<sup>1</sup> University of Southern California, Los Angeles, CA, USA  
email: marcione@usc.edu, web: http://pt.usc.edu/labs/mbrl/

## INTRODUCTION

Maintaining walking ability is critical for seniors in order to stay independent and mobile in the community. With aging, decreased walking speed is associated with reduced stride length (SL) and increased double limb support (DLS) time, and these in turn are associated with poorer health outcomes, disability, hospitalization, increased fall risk and mortality [1,2].

Functional mobility often includes activities where attention is divided. This demand to attend to multiple stimuli in the environment commonly results in detrimental changes to gait speed (GS) and spatio-temporal (ST) gait parameters [2,3]. Moreover, there is strong evidence that poor dual-task (DT) gait performance is a predictor of increased fall risk and impaired cognition [4].

In order address these age-related declines in walking capabilities it is recommended for seniors to get involved with physical activities which include training components of walking, balance, strength, and concentration [5].

Golf is a recreational activity that includes walking over hilly, uneven terrain; and various changes in body position, including high power swings and bending over to pick up a ball. Although there is evidence that golf play is associated with improved balance and walking, golf has received little attention as a *therapeutic intervention* [6]. We hypothesize that golf play is likely to improve walking capabilities and alter ST parameters of gait. The objective of the present study was to examine the influence of a 12-week golf intervention on walking and DT performance in older military veterans.

## METHODS

Fast GS, DT GS and ST gait parameters (stride length: SL and double limb support time: DLS) were measured before and after a 12-week golf intervention (2 x weekly; 90 min per session). Two male participants (74 and 67 years old) completed 5 fast gait and 5 DT gait trials while walking “as fast as possible”. For DT, participants performed a digit subtraction by 3’s task.

A standard lower extremity marker set was used to track lower extremity kinematics with a 10-camera Qualisys (Göteborg, SE) 3D motion capture system. Kinematics were collected at 60 Hz and filtered with a 4th order low-pass Butterworth filter with a 6 Hz cut off. Data was averaged across the 5 trials. Means, standard deviations, change percentage, and effect sizes (ES; Cohens’ d) are presented.

## RESULTS AND DISCUSSION

Participant PG03 attended 20/24 sessions and PG04 attended 22/24 sessions, of the 12-week golf training program. The participants’ fast GS increased by 5.3% and 17.5% (ES 1.26). DT GS increased by 29.2% and 26.1% (ES 3.75) (Fig. 1).

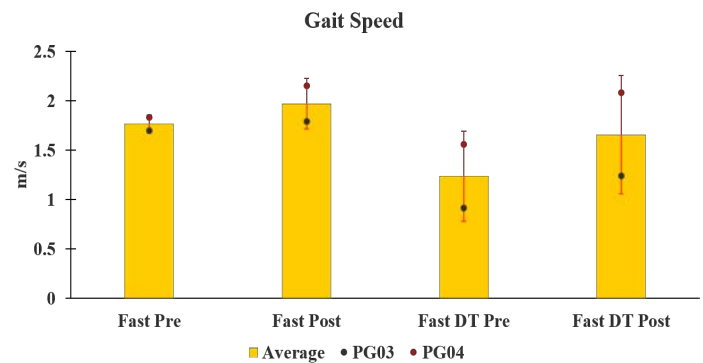


**Figure 1:** Mean fast gait and DT gait speed before (Pre) and after (Post) 12-week golf training intervention.

Fast DT GS was slower than fast GS for both participants at both time points. However, follow-up GS differences between fast and fast DT were not as large as at baseline. PG03 difference decreased by 25.7% and PG04 difference decreased by 34.6%. This decreased difference between pre and post time points suggests that golf training reduced the DT cost of the DT paradigm. Using the measurement of GS under a DT paradigm gives insight into the interlinked relationship between gait and cognition. The higher cognitive demand of the DT digit subtraction task may interfere with shared neural networks and act as a perturbation by disrupting gait control [4]. This study's participants' improved DT GS was accompanied by highly accurate digit subtraction scores, suggesting that the faster gait speeds were not at the cost of reduced cognitive function and that their gait control was not disrupted. Age-associated changes in step parameters include decreased SL and increased DLS time. There is robust evidence that these changes lead to impaired gait and an increase in future fall risk for older adults. Older adults may be using these types of compensatory strategies (modified gait parameters) to increase stability and avoid falls [2]. After completing a 12-week golf training program, during the fast GS, the two participants' SL increased by 44.6% and 8.0% (ES 1.20) and and DLS time decreased by 8.7% and 21.4% (ES 3.54) (Table 1). After completing a 12-week golf training program, during the fast DT GS, the two participants' SL increased by 25.4% and 32.4% (ES 2.95) and DLS time decreased by 21.0% and 43.8% (ES 5.56) (Table 2).

This study's participants had an increase in fast GS, fast DT GS, SL and a decrease in DLS time. These changes are all associated with lower risk for future falls.

## CONCLUSIONS

Both participants had improved gait parameters of fast GS, fast DT GS, SL and DLS following the completion of a 12-week golf training program. They also increased fast DT GS to a greater degree than fast GS alone. These preliminary results suggest that the physical and cognitive demands of golf (navigating the course, walking over hilly, uneven terrain, bending over, swinging, planning and strategizing) may improve gait control and lower future fall risk in older military veterans. Future expansion of this study will inform the development of golf training programs to improve everyday function and quality of life in older adults.

## REFERENCES

1. Studenski S, et al. *JAMA* **305**, 50-58, 2011.
2. Aboutorabi A, et al. *Aging Clin Exp Res* **28**, 393-405, 2016.
3. Smith E, et al. *Gait Post*, **44**, 250-258, 2016.
4. Muir-Hunter SW, et al. *Physiotherapy*, **102**, 29-40, 2016.
5. Chodzko-Zajko WJ, et al. *MSSE*, **41**, 1510-30, 2009.
6. Parkkari J, et al. *Am J Med*, **109**, 102-108, 2000.

**Table 1:** Summary of Fast Gait Parameter Results

Parameter	Participant	Pre	Post	% Change
Stride Length (m)	PG03	1.12(±0.02)	1.62(±0.04)	44.6%
	PG04	1.62(±0.08)	1.75(±0.03)	8.0%
Double Limb Support (s)	PG03	0.23(±0.04)	0.21(±0.04)	-8.7%
	PG04	0.14(±0.04)	0.11(±0.04)	-21.4%

**Table 2:** Summary of Fast Dual-task Gait Parameter Results

Parameter	Participant	Pre	Post	% Change
Stride Length (m)	PG03	1.06(±0.13)	1.33(±0.04)	25.4%
	PG04	1.36(±0.06)	1.8(±0.08)	32.4%
Double Limb Support (s)	PG03	0.43(±0.05)	0.34(±0.03)	-21.0%
	PG04	0.16(±0.05)	0.09(±0.05)	-43.8%

# MORE PUSH FROM YOUR PUSH-OFF: JOINT-LEVEL MODIFICATIONS TO MODULATE PROPULSIVE FORCES IN OLD AGE

Michael G. Browne and Jason R. Franz

University of North Carolina at Chapel Hill and North Carolina State University, Chapel Hill, NC, USA  
email: mgbrowne@email.unc.edu, web: <http://abl.bme.unc.edu>

## INTRODUCTION

Propulsive forces generated during push-off (i.e., the anterior component of the ground reaction force vector;  $F_P$ ) are used to modulate walking speed. Older adults tend to walk slower than young adults. However, even prior to walking slower, older adults walk with a diminished push-off - decreased  $F_P$  accompanied by reduced ankle moment and power generation. These changes may be responsible for unfavorable and metabolically costly increases in mechanical power generated by muscles crossing the hip (i.e., a “distal to proximal redistribution”) [1]. However, despite their apparent deficit to young adults, many older adults retain the capacity to enhance  $F_P$  generation, for example to walk faster, uphill [2], or with appropriate biofeedback [3]. The joint-level modifications used by older adults to augment  $F_P$  generation in walking have yet to be fully elucidated and may be critical to informing the discriminate prescription of strategies to preserve independence in old age.

The purpose of this study was to identify age-related differences in the joint-level modifications used to modulate  $F_P$  generation during walking, an important determinant of push-off performance. We posit that there are two possibilities for older adults to enhance  $F_P$  generation during push-off. First, given the plantarflexors’ role in generating propulsion in young adults, older adults may increase ankle moment and power generation and thereby alleviate compensatory demands at the hip. Alternatively, older adults may opt to rely even more on the hip musculature for power generation, thereby exacerbating their distal to proximal redistribution. Ultimately, we seek an improved understanding of the mechanisms governing diminished push-off in old age and targets for clinical countermeasures.

## METHODS

10 healthy young adults (mean $\pm$ SD; age: 24.8 $\pm$ 5.4 years, 5 males/5 females) and 6 healthy older adults (age: 77.3 $\pm$ 4.2 years, 2 males/4 females) participated in this study. A photo cell timing system first assessed subjects’ preferred overground walking speed (Young: 1.27 $\pm$ 0.14 m/s, Old: 1.26 $\pm$ 0.16 m/s,  $p=0.45$ ). Subjects then walked normally for 60 s on a dual-belt instrumented treadmill at their preferred speed. A custom Matlab script immediately extracted the average  $F_P$  from normal walking for use in the subsequent trials. Subjects then walked at their preferred speed while watching a video monitor displaying their instantaneous  $F_P$ , updating as the average of each 2 bilateral strides (Fig. 1). Then, in 60 s trials, subjects were instructed to modify their instantaneous  $F_P$  to match target values representing normal and  $\pm 10\%$  and  $\pm 20\%$  of normal, shown as horizontal lines. For all trials, a 14-camera Motion Analysis system recorded the trajectories of 33 markers placed on subjects’ pelvis and lower extremities, from which we estimated hip, knee, and ankle joint kinematics and kinetics.

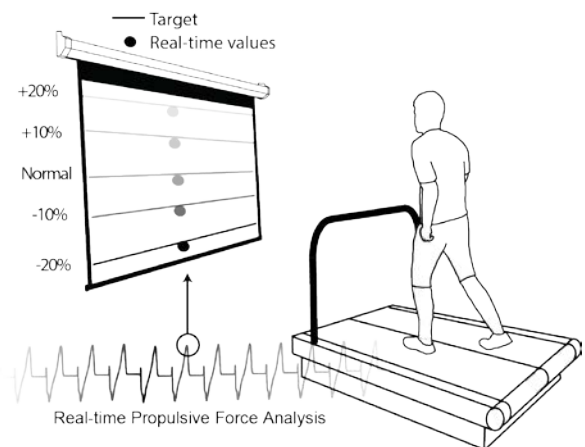


**Figure 1:** Subjects walked with visual biofeedback based on real-time propulsive force measurements.

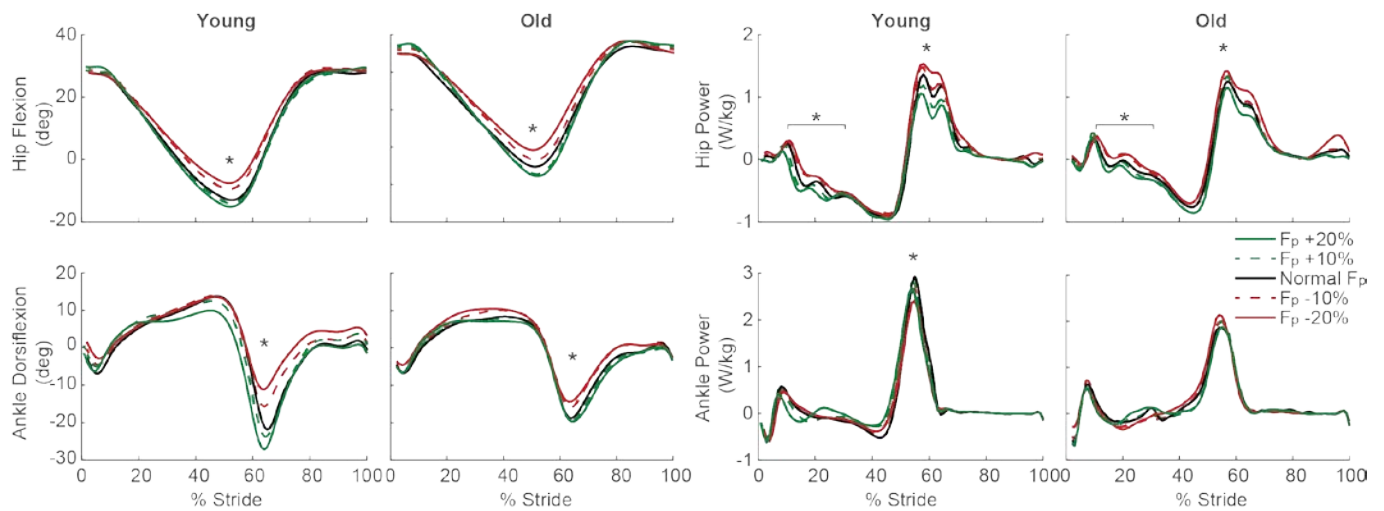


**Figure 2:** Visual biofeedback of propulsive forces ( $F_P$ ) in both young and older adults modified ankle and hip kinematics and hip power generation with minimal change in ankle power generation. (\*Main Effect of  $F_P$ )

## RESULTS AND DISCUSSION

During normal walking, older adults exerted 12% smaller  $F_P$  than young adults and exhibited a characteristic distal to proximal redistribution (i.e., 23% less peak ankle power during push-off and 31% more hip joint positive work during stance). All subjects successfully and systematically modulated their  $F_P$  in accordance with prescribed biofeedback targets. Independent of age, walking with larger (smaller)  $F_P$  increased (decreased) peak hip extension and decreased (increased) the mechanical demands of muscles spanning the hip (Fig. 2). Interestingly, neither young nor older adults enhanced  $F_P$  generation during push-off through increases in ankle power generation. However, this is not to say that subjects could not increase ankle power. Indeed, we recently implemented visual biofeedback based on real-time inverse dynamics and revealed that at least young adults can effectively modulate peak ankle power ( $P_A$ ) through targeted  $P_A$

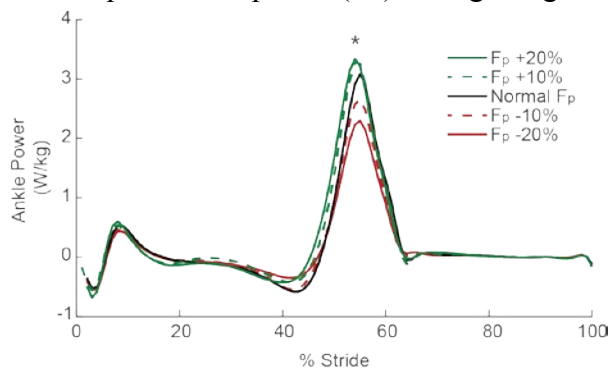


**Figure 3:** Modulation of push-off through direct peak ankle power biofeedback. Young adults ( $n=10$ ).

biofeedback (Fig. 3). We are exploring whether this targeted approach may more directly impact ankle moment and power generation in older adults.

## CONCLUSIONS

Our intuition and prior work led us to anticipate a reversal or an exacerbation of the distal to proximal redistribution in joint power generation when older adults increased  $F_P$  at their preferred speed. Instead, our results reveal an exciting third option: enhancing  $F_P$  via biofeedback improved peak hip extension during push-off and alleviated mechanical power demands at the hip, all without changes in ankle power. Further, older adults walked with increased  $F_P$  without increasing their total positive joint work. Thus, given the same total requisite power generation, older adults got ‘more bang for their ankle power buck’ using biofeedback - larger  $F_P$  with less hip power generation - perhaps in turn yielding faster preferred speeds and/or improved walking economy.

## REFERENCES

1. DeVita P, Hortobagyi T. *J Appl Physiol* **88**(5), 1804-11, 2000.
2. Franz JR, Kram R. *J Biomech* **46**, 535-40, 2013.
3. Franz, Kram. *Clin Biom*, **29**(1), 68-74, 2014.

## ACKNOWLEDGEMENTS

Supported by NIH (R01AG051748) and the UNC-Chapel Hill University Research Council.

# LET'S FACE IT, I AM GETTING OLDER: A LONGITUDINAL STUDY OF BALANCE RECOVERY FROM FORWARD LEAN RELEASES

<sup>1,2</sup> Evelyne Carbonneau and <sup>1,2</sup> Cécile Smeesters

<sup>1</sup> Research Center on Aging, Sherbrooke, QC, Canada

<sup>2</sup> Department of Mechanical Engineering, Université de Sherbrooke, Sherbrooke, QC, Canada  
e-mail: [Cecile.Smeesters@USherbrooke.ca](mailto:Cecile.Smeesters@USherbrooke.ca), web: <http://www.usherbrooke.ca/gmecanique>

## INTRODUCTION

In a cross-sectional study of 52 participants between 19 and 86yrs, Carbonneau and Smeesters [1] showed that the ability to recover balance and avoid a fall using a single step decreased exponentially with age (Figure 1). In particular, we showed that, at the critical age of 51.0yrs, the maximum forward lean angle decreased below one standard deviation of the mean value of 18-year-olds. This decline with age was associated with longer reaction and weight transfer times, slower mean and maximum step velocities and smaller step lengths and heights, but age did not affect step time and step width. Finally, stepping (versus harness) failures increased with age at lean angles larger than maximum. The purpose of this longitudinal study was thus to validate our previous exponential regression curve [1] using a convenience sample of participants whose balance recovery from forward lean releases was repeatedly tested in our laboratory over the past 10 years.

## METHODS

Twelve healthy adults (4 women) had their balance recovery from forward lean releases tested two to six times between the ages of 26.4 and 86.4yrs. At each visit, we determined the maximum forward initial lean angle (starting at ~5deg and increasing in ~2.5deg increments) from which each participant could be suddenly released and still recover balance using a single step.

Using 4 force platforms and 2 load cells at 1000Hz, and 4 optoelectronic position sensors with 24 markers at 100Hz, the following kinematic variables were also obtained: initial lean angle; reaction, weight transfer and step times; mean and maximum step velocities; and step length, height and width at the maximum lean angles.

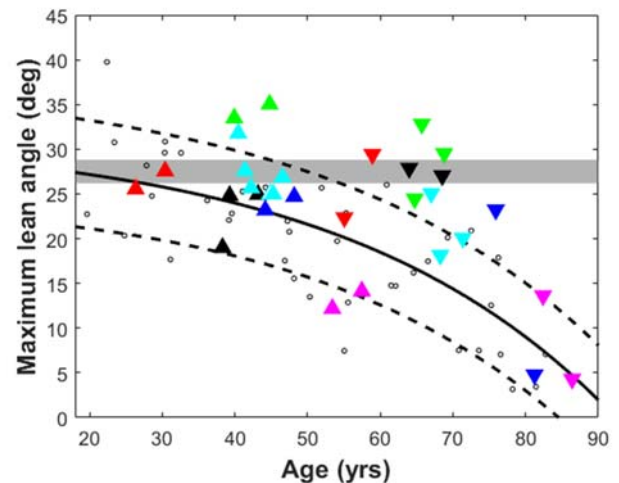


**Figure 1:** Mean±SD exponential regression curve (solid and dashed lines) of the maximum forward lean angle versus age for the 52 participants (black circles) from the cross-sectional study by Carbonneau and Smeesters [1]. The maximum forward lean angle versus age for the 12 participants (colored triangles) from this longitudinal study.

## RESULTS AND DISCUSSION

The maximum forward lean angle versus age points of our 12 participants followed reasonably well our previous exponential regression curve (Figure 1), except in three easily explained cases:

- Participant ▲ (black) did a lot of gardening on the eve of her first point at 38.3yrs, which decreased her maximum lean angle on that day ( $\Delta_{12}=5.8$ deg).
- Participant ▼ (red) started running a year before his second point at 58.9yrs ( $\Delta_{12}=7.1$ deg).
- Participant ▼ (green) started biking the year he retired, right after his first point at 64.7yrs ( $\Delta_{12}=7.1$ deg).

Starting at 40yrs, we started to test systematically the principal investigator of this study (participant ▲, blue) nearly every year. For the previous 10 years,

her maximum lean angle had consistently been at ~27.5deg (Figure 1, gray area), always easily recovering balance at ~25deg, but not at ~30deg and certainly not at ~32.5deg. At 40.5yrs, she obtained an exceptional 31.8deg maximum lean angle (Table 1), after returning from a sabbatical in the Canadian Rockies where she biked to work every day. By 41.4yrs, she was back at 27.6deg. However, let's face it, she is getting older. Indeed, starting at 42yrs, she was no longer able to recover balance at ~27.5deg, especially not during those long winter months. The only exception was her latest test at 46.6yrs, where she just managed 26.9deg late in the summer after biking to work every chance her hectic schedule would permit in an attempt to return to ~27.5deg.

There are not enough data points yet to draw significant trends, but her decline with age appears to be associated with longer weight transfer times and smaller step heights (Table 1). Moreover, as we often see with middle-aged and older adults, the number of protocol infractions her vigilant staff had to ask her to correct has definitely increased:

- Prior to lean release, her eyes were looking at the floor, rather than straight ahead, and her body was not kept in a straight line, her trunk having a smaller initial lean angle than her legs.
- She often attempted to anticipate lean release, obviously starting to react prior to lean release.
- Her heel strikes were definitely less stable at the maximum lean angle.
- At lean angles larger than her maximum, while she used to have only harness failures, stepping failures now often accompanied harness failures. In fact, she knew as soon as the first step was completed that she had failed and, although she could will herself to use only a single step, taking

a second step was more comfortable than falling into the harness. This confirms what we have suspected for several years, as we get older, we are able to respect the single step instruction but are just unwilling to do so [2].

## CONCLUSIONS

This longitudinal study has validated the exponential regression curve obtained in our previous cross-sectional study [1]. Furthermore, it has shown that the ability to recover balance and avoid a fall can be decreased by strenuous work but, more importantly, can also be improved with exercise. Similarly, it has given the principal investigator of this study some interesting insight into why protocol infractions increase with age. Finally, a recent 12-month prospective falls evaluation [3] showed that the maximum forward lean angle significantly predicted a future fall in community-dwelling older adults (65-90yrs). Lean releases could thus be used to screen adults over 50yrs [1] and identify those at risk of falls, or to evaluate the effectiveness of exercise-based fall prevention programs.

## REFERENCES

1. Carbonneau E, Smeesters C. *Gait Posture* **39**, 365-371, 2014.
2. Cyr MA, Smeesters C. *33<sup>rd</sup> Annu Meet Am Soc Biomech*, State College, PA, USA, 2009.
3. Carty CP, et al. *Age Ageing* **44**, 109-115, 2015.

## ACKNOWLEDGMENTS

Marc-André Cyr, Antoine Guillerand, Mathieu Hamel, Kodjo Moglo, Magali Pierre and Alessandro Telonio for technical assistance, as well as NSERC grant 2014-06175 for financial support.

**Table 1:** Effect of age on kinematic variables at the maximum lean angles for participant ▲ (blue)

Age (yrs)	Maximum lean angle (deg)	Reaction time (ms)	Weight transfer time (ms)	Step time (ms)	Mean step velocity (m/s)	Maximum step velocity (m/s)	Step length (mm)	Step height (mm)	Step width (mm)	Failures types (2 trials)
40.5	31.8	83	138	230	4.33	5.56	997	234	-7	SH-SH
41.4	27.6	75	159	218	4.32	6.10	942	215	0	H-H
42.2	25.7	74	149	201	4.24	5.65	853	194	-24	H-H
43	<sup>a</sup>	<sup>a</sup>	<sup>a</sup>	<sup>a</sup>	<sup>a</sup>	<sup>a</sup>	<sup>a</sup>	<sup>a</sup>	<sup>a</sup>	<sup>a</sup>
44.9	~25 <sup>b</sup>	68	171	198	4.16	<sup>a</sup>	824	<sup>a</sup>	<sup>a</sup>	<sup>a</sup>
45.3	25.0	81	157	197	4.93	6.54	972	158	58	H-H
46.6	26.9	49	170	212	4.86	6.81	1030	164	23	H-SH <sup>c</sup>

Failure types: S = Stepping failure, H = Harness failure, SH = Stepping and Harness failure.

<sup>a</sup> Missing data. <sup>b</sup> Estimated data validated by experimental video. <sup>c</sup> Three attempts to anticipate lean release.

# THE EFFECT OF ATTENTION AND STANCE ON THE RAMBLING AND TREMBLING COMPONENTS OF POSTURAL SWAY IN OLDER ADULTS

<sup>1</sup>Manuel Hernandez, <sup>1</sup>Gioella Chaparro, <sup>1</sup>Yaejin Moon, and <sup>1</sup>Jacob Sosnoff

<sup>1</sup>University of Illinois at Urbana-Champaign, Urbana, IL, USA  
email: mhernand@illinois.edu, web: <http://mfp.kch.illinois.edu>

## INTRODUCTION

To maintain balance in an upright stance, humans require a prerequisite amount of cognitive resources that increases with age. Thus, the amount of attention required by an individual to maintain a quiet stance may provide a salient marker of balance dysfunction. To further our understanding of the role of attention in the maintenance of balance, we examine the effect of cognitively demanding tasks and challenging balance conditions, such as a semi-tandem stance, on the rambling (Rm) and trembling (Tr) components of postural sway [1]. Rambling is thought to represent the equilibrium trajectory of the center of mass and is postulated to reflect supraspinal processes [1,2], while trembling represents deviations from equilibrium and may reflect spinal-peripheral processes [1,2]. Given this framework, we hypothesized that rambling would be most affected by divided attention tasks and demonstrate increased relative cerebellar frequency power (0.5-1.5 Hz), particularly in older adults. Secondly, we hypothesized that trembling would be most affected by a challenging balance condition, such as a semi-tandem stance, and demonstrate increased relative reflexive frequency power (1.5-5 Hz), particularly in older adults.

## METHODS

*Subjects.* Healthy young (mean±SD, age 21±2 years, N=20, 10 female) and healthy older adults (age 65±5 years, N=20, 10 female) were recruited from the local community.

*Protocol.* Subjects stood upright, as still as possible, during 60 sec trials in either a comfortable parallel stance with feet side by side (parallel stance), or semi-tandem stance with eyes open. In addition,

subjects were asked to perform a single task or a concurrent cognitive-demanding task in half of the trials, consisting of the backward recitation of alternating letters of the alphabet, using a pseudorandomized starting letter (dual task). Data collection was performed in a single experimental session in a laboratory setting.

*Data Analysis.* Force plate data was collected at 100 Hz using an AMTI Accusway six-degree of freedom force plate. Raw force plate data were processed with a 4th order, zero-lag, low-pass Butterworth filter with a 10 Hz cutoff frequency. The mediolateral (ML) and anteroposterior (AP) components of the center of pressure (COP) were calculated using standard equations. Decomposition of ML and AP COP trajectories into Rm components was achieved by defining instantaneous equilibrium points when the shear force was zero and interpolating between these points using a cubic spline function [1]. Tr components were then calculated by taking the difference between the COP and Rm trajectories, as previously described by Zatsiorsky and Duarte [1]. Rm and Tr trajectories were quantified using the root mean square (RMS) and relative cerebellar and reflexive frequency power (CFP and RFP, respectively). Trials where participants lost balance were eliminated from subsequent statistical analysis. Linear mixed effects models were used to examine the effects of age, stance, and task on outcome measures using R.  $P < 0.05$  was considered statistically significant.

## RESULTS AND DISCUSSION

During split stance conditions, in comparison to parallel stance, all participants swayed with larger amplitudes, as demonstrated by increased ML and AP Rm and Tm RMS ( $p < .001$ ). Older adults, when

successful in maintaining balance, demonstrated decreased AP Rm and ML Tm RMS ( $p < .005$ ) and a significant cohort x stance interaction in AP Rm and ML Tm RMS ( $p < .05$ ), partly consistent with prior results [3]. In addition, during dual task conditions in comparison to single task conditions, increased AP and ML Tm RMS were observed ( $p < .005$ ), suggestive of increased muscle co-contraction.

During dual task conditions in comparison to single task conditions, increased CFP was observed in both AP and ML Rm trajectories ( $p < .005$ ), as observed in **Fig. 1**. However, no significant task x cohort interactions were observed in CFP ( $p > .05$ ). Older adults demonstrated increased AP Rm CFP ( $p < .001$ ). During split stance vs. parallel stance conditions participants demonstrated increased ML and AP Rm CFP ( $p < .001$ ), as well as a significant cohort x stance interaction in both ML and AP Rm CFP ( $p < .001$ ).

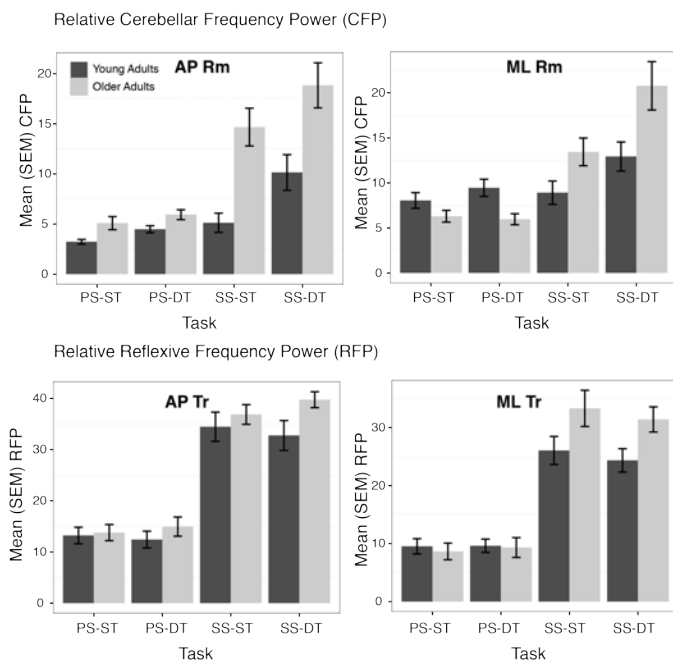


**Figure 1:** Relative cerebellar frequency power (CFP) of AP and ML Rm and relative reflexive frequency power (RFP) of AP and ML Tr during all quiet standing tasks. PS = parallel stance, SS = semi-tandem stance, ST = single task, DT = dual task.

During split stance vs. parallel stance conditions, participants demonstrated increased RFP in both AP and ML Tr trajectories ( $p < .001$ , **Fig. 1**). Furthermore, a significant stance x cohort interaction was observed in ML Tr RFP ( $p < .005$ ), consistent with our hypothesis.

## CONCLUSIONS

We conclude that in balance and cognitively demanding tasks in healthy older adults, stiffening strategies are still employed by older adults to maintain quiet standing, as demonstrated by decreased rambling and trembling RMS. Of novelty, dual tasking led to similar increases in the relative cerebellar frequency power in both AP and ML rambling trajectories across all participants. The similarities across both young and older adults suggests the use of similar mechanisms of postural control during cognitive-demanding tasks in healthy individuals, contrary to our hypothesis that rambling would be most affected by divided attention tasks and demonstrate increased relative cerebellar frequency power (0.5-1.5 Hz), particularly in older adults. Our data is consistent with our hypothesis that trembling would be most affected by a challenging balance condition and demonstrate increased relative reflexive frequency power (1.5-5 Hz), particularly in older adults. Furthermore, it further supports the notion that trembling, in particular, may be useful to quantify changes in reflexive, or peripheral, mechanisms in aging.

## REFERENCES

1. Zatsiorsky VM & Duarte M. *Motor Control*, **3**, 28-38, 1999.
2. Zatsiorsky VM & Duarte M. *Motor Control*, **4**, 185-200, 2000.
3. Sarabon N, et. al. *Gait & Posture*, **38**, 637-642, 2013.

## ACKNOWLEDGMENTS

We would like to thank collaborators in the Motor Control Laboratory for their assistance with data collection.

# THE EFFECTS OF DUAL-TASK WALKING AND TALKING IN DIFFERENT CONDITIONS AND ENVIRONMENTS ON ELDERLY GAIT

<sup>1</sup> Taylor Leeder, <sup>2</sup> Angie Roth, <sup>1</sup> Jennifer Yentes, <sup>2</sup> Julie Blaskewicz Boron

<sup>1</sup> The University of Nebraska Omaha, Department of Biomechanics, NE, USA

<sup>2</sup> The University of Nebraska Omaha, Department of Gerontology, NE, USA  
email: tleeder@unomaha.edu

## INTRODUCTION

Older adults have increased dual-task (DT) costs compared to their younger counterparts, especially when it comes to demanding tasks such as cell phone usage and walking. In an experimental setting using virtual reality (VR), older adults took longer than younger adults to initiate crossing a busy street with traffic; this time difference was compounded during a cell phone conversation, suggesting impairments in the cognitive planning process [1]. When older adults walk and talk at the same time, gait decrements increase. The changes in gait can be measured and used as an indicator of dual-task costs incurred while walking and talking [2]. These costs may help to predict an individual's fall risk, which is important as falls are a common cause of injury among older adults and can lead to morbidity, mortality and an increased possibility of future falls [3].

To our knowledge, no such study has been done comparing walking and talking between a VR and a non-virtual reality (NVR) environment. Thus, the purpose of this study was to compare spatial and temporal gait variables of healthy older adults while walking and talking in different environments and conditions. It was hypothesized that older adults would show significant differences while walking and talking compared to walking only. Additionally, the influence of a VR environment would significantly influence their gait compared to a NVR environment.

## METHODS

Fifteen subjects,  $70.9 \pm 4.7$  years old (40%M/60%F) all right-handed, living independently in the community and free of any disorders that may

interfere with gait or cognition consented to participate in this study. Subjects completed three sessions, all approximately one week apart. During the baseline session, subjects completed three different conversations (in person (IP), on a cell phone (OP), and hands-free (HF)) while seated. Randomization occurred for the subjects to walk on a treadmill in a VR or NVR environment for the other two sessions while talking IP, OP, and in a HF conversation for 10 minutes each. Conversation topics were predetermined and randomized for every subject. A single-task, ten-minute walking only (WK) trial was recorded in each of the last two visits.

In the DT conditions, gait data was collected (100 Hz; Vicon, Oxford, United Kingdom) while subjects walked on a self-paced treadmill (Bertec Corp., Columbus, OH). The self-paced treadmill adjusts to the subject's speed as they walk. Step time, stride time, step length, stride length, step width, stance time, swing time, and double stance time were quantified through custom MATLAB programs (MathWorks Inc, Natick, Mass). Gait variables were compared between environments (VR and NVR) and conditions (IP, OP, HF, WK) using paired samples t-tests. Data was analyzed using IBM SPSS Statistics for Windows (Version 22.0).

## RESULTS AND DISCUSSION

Our hypotheses were partially supported. All conditions were compared but only significant conditions are shown (Table 1). There were no significant differences in any of the gait variables between VR and NVR environments across any DT conditions. However, there were significant differences between WK in VR vs. WK in NVR for

the following gait variables: stance time, swing time, and step width. Furthermore, several other variables came close to significance. Lack of significance could be due to the small sample size, leading to lack of power to detect the differences.

In the VR environment only, significant differences emerged between both OP vs. IP and OP vs. WK. All the gait variables measured, except for step width, were significantly different between the OP and WK conditions. All temporal variables in the OP vs. IP condition were significant (Table 1). No differences were found between any of the other dual-task talking and walking conditions.

Existing literature supports these findings in that older adults change their gait to deal with an additional task like having a cell phone conversation while walking [1,2]. The fact that there were only significant differences found in the OP condition suggests that holding a cell phone is demanding additional resources and not the conversation itself. In addition, the lack of differences present in the HF condition also supports the idea that holding a cell phone is an additional motor task. Furthermore, the idea of visualizing the person you are having a conversation with while OP may impact walking, making it different than a face-to-face conversation. In addition, the optic flow present in VR may affect the sensory system like walking in real-life; stimuli are flowing past the walker with information from the environment affecting how the sensorimotor system responds. This could explain the differences found while using VR.

Overall, the lack of significant differences between conditions and environments could be explained by the nature of our adult population. These older adults were regular exercisers and performed well while walking and talking. Only the addition of holding a cell phone, as opposed to IP and HF, seemed to perturb their gait by increasing stance times and decreasing stride lengths.

## CONCLUSIONS

Significant differences were found in the gait of older adults while walking and talking on a cell phone in a virtual reality environment and a walking only task. Additionally, the presence of VR seemed to impact their gait. This may suggest that using VR could approximate daily life and be used as part of an intervention study to reduce fall risk. In the future, different VR scenes could be used to assess the differences in various real-life situations while talking on a cell phone.

## REFERENCES

1. Neider MB. *Psychol Aging*, **26**, 260-268, 2011.
2. Montero-Odasso M. *J Am Geriatr Soc*, **60**, 2127-2136, 2012.
3. Rubenstein LZ. *Age Ageing*, **35**, Suppl 2:ii37-ii41, 2006.

## ACKNOWLEDGMENTS

Funding by the COBRE Pilot Grant Program NIH Grant P2DGM109090

**Table 1.** P-Values of Selected Gait Variables of Healthy Older Adults Between Different Conditions

	Step Time	Stride Time	Step Length	Stride Length	Step Width	Stance Time	Swing Time	Double Stance Time
<b>Walking Between VR and NVR</b>	0.057	0.056	0.28	0.22	0.047	0.025	0.025	0.21
<b>On the Phone and Walking VR vs. Walking Only VR</b>	0.02	0.028	0.043	0.044	0.13	0.023	0.023	0.042
<b>On the Phone and Walking VR vs. In Person and Walking VR</b>	.006	.007	0.85	0.78	0.14	0.005	.005	0.013

# FORCE FLUCTUATIONS DURING HYBRID FORCE/MOTION TASKS IN YOUNG AND OLDER ADULTS

<sup>1</sup> Mukta Joshi, <sup>1</sup> Brittany Heintz, and <sup>1</sup> Kevin Keenan

<sup>1</sup>Department of Kinesiology and Center for Aging and Translational Research, University of Wisconsin - Milwaukee, Milwaukee, WI

Email: joshi@uwm.edu

## INTRODUCTION

An increase in physiological tremor and a decline in the ability to manipulate objects with the fingers are common consequences of aging. These impairments lead to several limitations in performing activities of daily living (ADLs) such as cooking, feeding, dressing etc. and can lead to dependence and institutionalization<sup>3</sup>. Tremor, both physiological and pathological, manifests itself as an inability to hold a steady force. When individuals are asked to hold a steady force, the force is not constant, but fluctuates about a mean value. These fluctuations in force can be quantified as the standard deviation (or coefficient of variation) of force and reflect the ability of that person to perform a steady contraction.

One critical condition influencing steady force production and dexterous manipulation is the frictional properties of the surface that the fingers contact. For example, force variability was found to be significantly higher when pressing isometrically against a low- vs. high-friction surface<sup>2,5</sup>. Older adults had greater impairments than young adults while pressing down with a steady force on the low-friction surface<sup>2</sup>. This study involved the static task of pressing down with a given force, thus making the normal force the only task-relevant parameter that needed to be controlled tightly. Conversely, when performing a hybrid task of pressing and moving, young healthy participants showed greater normal force variability on a high-vs low-friction surface<sup>1</sup>. In this case producing accurately directed shear forces of sufficient magnitude to enable motion is now a task-relevant parameter and precise control of shear force plays an important role during steady normal force production.

Nonetheless, most studies examining steady force control with advancing age examine static tasks<sup>2,5</sup>. However, these tasks may not best reflect performance on ADLs which involve simultaneous

control of force and motion. Thus, the purpose of this study was to compare force steadiness in healthy young and older adults as they performed static and hybrid tasks on high- and low-friction surfaces.

## METHODS

20 young (18 – 49 years) and 22 older adults (65–89 years) with no reported neuromuscular disorders or upper extremity pathologies were recruited. The iPad without a screen protector served as the high-friction surface (coefficient of friction:  $1.48 \pm 0.46$ ) and the Ionic screen protector placed on the iPad (coefficient of friction:  $0.44 \pm 0.15$ ) was the low-friction surface<sup>1</sup>. A line representing the 2 N target force was given as visual feedback on a 27-inch monitor positioned 1 m in front of the subject. Two targets were displayed as 1.5 cm circles on the iPad touch screen, and they were positioned 8 cm apart from one another. Participants performed two tasks: 1) a force matching task while pressing down statically with their index finger, and 2) a pressing and sliding task moving left/right between the two circles with the index finger pressing against the iPad screen, as previously done in<sup>1</sup>. These tasks were repeated on the low- and high-friction surface. A metronome was set at 60 beats per minute and subjects were instructed to move from one circle to the other at each beat. Each trial was 30s long.

**Data Analysis:** A custom Matlab script was used to calculate the mean and standard deviation (SD) of normal and shear forces for each condition (static/hybrid: left/right) for both low- and high-friction surfaces. SD for force was used as the measure of steadiness.

**Statistical Analysis:** Repeated measures analysis of variance (ANOVA) was performed on SD of normal and shear forces with repeated measures on age, task and friction conditions.

## RESULTS

Normal force variability (SD) was increased on the high- vs low-friction surface during the hybrid task for both the young ( $p < 0.001$ ) and older adults ( $p < 0.001$ ). Figure 1 shows representative data for older adults.

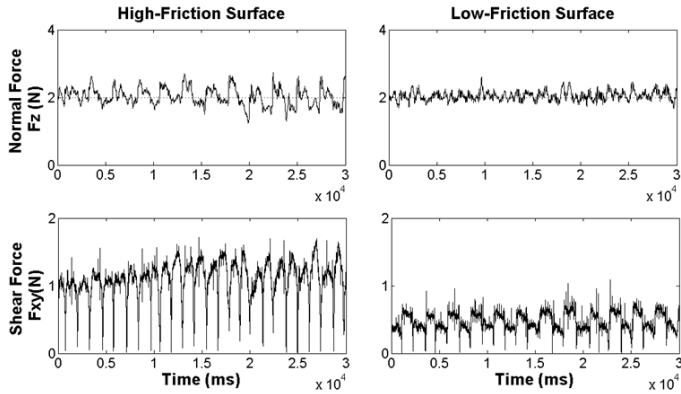


**Figure 1:** Representative data for older adults. *Top row:* Illustrates the visual feedback provided to subjects and that variability in normal force is increased on high- vs. low-friction surfaces. *Bottom row:* As expected, variability in shear force was also greater on high- vs. low-friction surfaces.

While no age effect was observed in variability during the static task ( $p = 0.284$ ), variability on the hybrid task was significantly greater in the older adults than the young adults ( $p = 0.015$ ) (Table 1).

Greater variability in shear force (SD) was observed during the hybrid force/motion tasks than the static task ( $p < 0.001$ ) and on the high-friction surface as compared to the low-friction surface ( $p < 0.001$ ) (Figure 1). The young participants had significantly greater variability in shear force as compared to the older participants during the hybrid task ( $p < 0.001$ ) (Table 1).

## DISCUSSION AND CONCLUSIONS

Older adults showed greater force variability while performing the hybrid force-matching task as compared to the static task where performance was similar between young and older adults (Table 1). This result highlights the importance of examining motor control during hybrid tasks to accentuate potential motor deficits with advancing age.

Greater variability in shear forces in young compared with older adults during the hybrid task may suggest that younger adults were more successful at maintaining a steady downward force ( $F_z$ ) by successfully exploiting variability in out-of-plane directions ( $F_{xy}$ ), consistent with the uncontrolled manifold hypothesis<sup>4</sup>. As shear forces during the hybrid task in older adults were ~34% less than those in young adults, the performance of older adults on the steadiness task may have been impaired by their relative inability to manipulate out-of-plane forces.

It is not clear what neuromuscular mechanisms lead to these changes during hybrid force/motion tasks with advancing age. Future research examining EMG and motor unit activity may allow investigators to determine the neuromuscular mechanisms that vary between young and older participants performing hybrid force-matching tasks.

## REFERENCES

1. Joshi, M.N. and K.G. Keenan, *Exp Brain Res*, 234(7), 1893-901, 2016.
2. Keenan, K.G. and W.V. Massey, *PLoS One*, 7(10), e48193, 2012..
3. Ostwald, S.K., et al., *J Am Geriatr Soc*, 37(10), 963-9, 1989.
4. Scholz, J.P. and G. Schoner, *Exp Brain Res*, 126(3), 289-306, 1999.
5. Seo, N.J., et al., *Hum Factors*, 53(6), 740-8, 2011.

**Table 1:** Variability during the hybrid (left/right) task in normal and shear forces on high- and low-friction surfaces for young and older adults.

	SD of Normal Force (N)	SD of Shear Force (N)	SD of Normal Force (N)	SD of Shear Force (N)
<i>Friction</i>	<i>High Friction Surface</i>		<i>Low Friction Surface</i>	
	Mean $\pm$ SD			
<b>Young Adults</b>	0.254 $\pm$ 0.064	0.723 $\pm$ 0.243	0.213 $\pm$ 0.074	0.323 $\pm$ 0.205
<b>Older Adults</b>	0.335 $\pm$ 0.117	0.436 $\pm$ 0.166	0.276 $\pm$ 0.118	0.234 $\pm$ 0.125

# HIGH-DENSITY EMG RECORDINGS OF CALF MUSCLE ACTIVITY IN OLDER ADULTS DURING WALKING

Diba Mani<sup>1</sup>, Awad M. Almuklass<sup>1</sup>, Landon Hamilton<sup>1</sup>, Taian Vieira<sup>2</sup>, Alberto Botter<sup>2</sup>, Roger M. Enoka<sup>1</sup>

<sup>1</sup>University of Colorado, Boulder, CO

<sup>2</sup>LISiN, Politecnico di Torino, Italy

email: manid@colorado.edu, web: <http://www.colorado.edu/intphys/research/nem.html>

## INTRODUCTION

Advancing age is accompanied by changes in walking performance [1, 2] and a shift in muscle activity away from ankle muscles and up to hip and knee muscles [3, 4]. Most of the information about muscle activity during walking has been obtained from studies in which older adults walked on a treadmill and the activation signals were recorded with sets of bipolar electrodes. Advances in technology, however, now make it possible to quantify activation signals from high-density surface EMG recordings while subjects walk overground.

The purpose of this study was to record the level of activation in the medial gastrocnemius and lateral soleus muscles of older adults as they walked overground at a usual speed. The activation signals were recorded with high-density grid electrodes.

## METHODS

Twenty healthy older adults (12 women,  $72 \pm 4$  yrs) were recruited to participate in up to 4 experimental visits spanning ~10 wks, each separated by at least 3 wks. From these sessions, data from 4 men ( $72 \pm 3$  yrs), acquired over 6 separate sessions, met the inclusion criteria to evaluate activation of the medial gastrocnemius and lateral soleus muscles during overground walking. Subjects were asked to walk at their “comfortable, preferred speed”.

A wearable EMG system was used to acquire high-density recordings. Two 4x8 grid electrodes (1 cm inter-electrode distance) were used: one placed over medial gastrocnemius and the other over lateral soleus. Each grid electrode had 32 detection points spread over 7 rows, and monopolar signals were recorded during the gait cycle. Foot switches were placed beneath the big toe and heel inside the shoe to identify gait events with which to denote EMG onset and offset times.

Decomposition of the high-density EMG recordings yielded 608 steps with a mean of 32 EMG channels per muscle. Those trials with poor recording quality or missing foot switch data, determined via strict Matlab algorithms, were excluded.

Normality tests were performed on the results. The Friedman test for non-parametric data was used to examine EMG amplitude and Wilcoxon Signed Rank test was implemented as a post hoc test with adjusted P-values.

## RESULTS

The mean EMG amplitude and standard deviation for the medial gastrocnemius was  $0.06 \pm 0.00$   $\mu$ V at heel strike,  $0.10 \pm 0.00$   $\mu$ V at mid stance, and  $0.12 \pm 0.00$   $\mu$ V at toe off ( $p < 0.0001$ ). The mean EMG amplitude for the lateral soleus was  $0.07 \pm 0.00$   $\mu$ V at heel strike,  $0.13 \pm 0.00$   $\mu$ V at mid stance, and  $0.14 \pm 0.00$   $\mu$ V at toe off ( $p < 0.0001$ ) (Figure 1). The effect sizes for comparisons between muscles at each time point ranged from -0.510 to -0.602 for medial gastrocnemius and from -0.242 to -0.604 for lateral soleus. Absolute EMG amplitude for lateral soleus was greater than that for medial gastrocnemius at all time points ( $p < 0.0001$ ).

Spatial and temporal information provided by the high-density surface electrodes showed distinct differences in activation between the two muscles, indicating greater muscle activation for lateral soleus.

The amplitude maps show that muscle activation changed during the gait cycle, and that soleus sustained activation levels through to toe off (Figure 2).

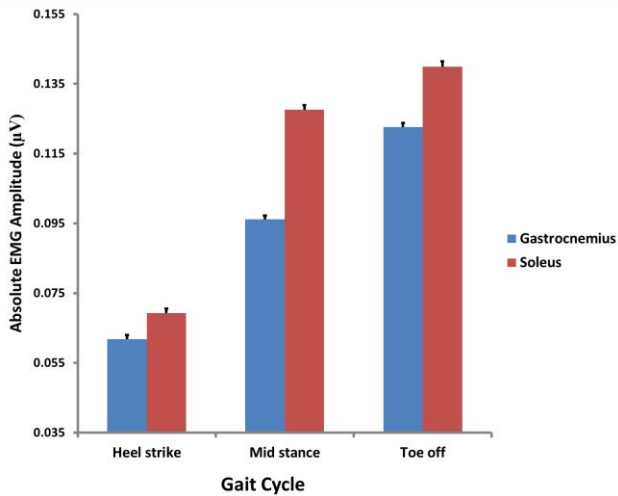


**Figure 1.** Absolute EMG amplitude (mean ± SE) for medial gastrocnemius (MG) and lateral soleus (LS) at heel strike (HS), mid stance (MS), and toe off (TO).

## DISCUSSION

The recordings obtained with high-density grid electrodes provide information about the absolute levels of muscle activation during overground walking. As a result of this technology, it is possible to compare absolute levels of EMG activity across time and muscles. The results show that muscle activation was greater for lateral soleus and was greatest at toe off for both muscles, but was also present during heel strike, likely due to coactivation of the dorsiflexor muscles, as often exhibited by older adults [5].

This technology can provide insight on the distribution of absolute muscle activity within and between leg muscles during overground walking and other mobility tasks. The approach can be used to provide more quantitative information about differences in muscle activation across conditions.

## CONCLUSION

High-density grid electrodes placed on the skin over the triceps surae indicate that the greatest muscle activation occurred at toe off. Compared with medial gastrocnemius, soleus exhibited greater absolute levels of muscle activation during the three phases of the gait cycle.

## REFERENCES

1. Fritz S, et al. *J Geriatr Phys Ther* **32**, 46-49, 2009.
2. Doherty TJ, et al. *Can J Appl Physiol* **18**, 331-358, 1993.
3. Hortobágyi T, et al. *J Appl Physiol* **88**, 1804-1811, 2000.
4. Nashner LM, et al. *Beh Brain Sci* **8**, 135-172, 1985.
5. Kerrigan DC, et al. *Arch Phys Med Rehabil* **79**, 317-322, 1998.

## ACKNOWLEDGEMENTS

Diba Mani was supported by a predoctoral fellowship from an NIH T32 award (AG000279) to Robert S. Schwartz.

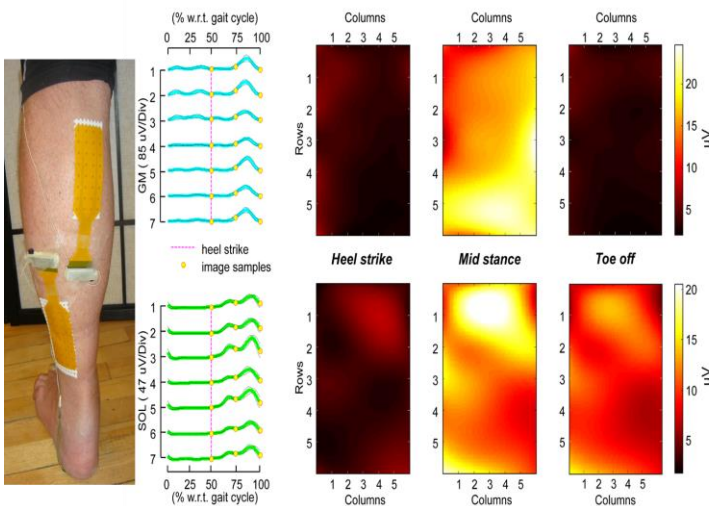


**Figure 2:** A wearable EMG system was placed over the medial gastrocnemius and lateral soleus muscles to record the activation signals during walking. Each row of blue or green traces corresponds to a row in the high-density grid electrode array. The dashed pink line marks heel strike. The yellow circles denote heel strike, mid stance, and toe off. The amplitude maps are associated with these time points.

# CHARACTERIZING HIP MOTION AND INFLUENCE OF AGE DURING COMMON ACTIVITIES

<sup>1</sup> Carley E Fuller, <sup>1</sup>Jenny Tavares, <sup>1</sup>Kevin Bui, <sup>2</sup>Garrison Benton, <sup>1</sup>Jonathan Rylander

<sup>1</sup> Baylor University, Waco, TX, USA

<sup>2</sup> Baylor Scott and White Hillcrest Hospital, Waco, TX, USA

Email: jonathan\_rylander@baylor.edu

## INTRODUCTION

Hip dislocation occurs in between 2% and 11% of total hip arthroplasty patients (THA) [1]. Posterior dislocations occur primarily with internal rotation and flexion of the hip while anterior dislocations occur primarily with external rotation and extension in the hip [2]. Despite the link between hip movement and dislocation, surprisingly little information exists in the literature that details the 3D kinematics of the hip during multiple common activities of daily living. Therefore, doctors are not always able to answer confidently when their patients ask about returning to particular activities following surgery. Additionally, little is known about how these specific hip movement strategies change with age. Therefore, the purpose of this study is to (1) develop normative 3D hip kinematic data for people as they perform common activities of daily living, and (2) determine how hip movement strategies change with age by comparing a group of healthy younger individuals to that of a healthy older group of individuals.

## METHODS

Twenty-three subjects (14 younger aged 19-33 years; 9 older aged 51-68 years; see Table 1 for details) were enrolled in this study.

*Table 1: Subject Demographics*

Group	Avg. Height ± Stdev (cm)	Avg. Weight ± Stdev (kg)	Avg. BMI ± Stdev (kg/m <sup>2</sup> )	Avg. Age ± Stdev (years)	Female:Male
Younger	176.96 (±10.9)	75.16 (±10.0)	24.09 (±3.3)	23.14 (±3.9)	7:7
Older	172.17 (±8.3)	81.97 (±13.5)	27.59 (±3.8)	60.78 (±6.4)	5:4
All	175.08 (±10.0)	77.82 (±11.7)	25.46 (±3.8)	37.87 (±19.4)	12:11

Motion capture was completed with a 14 camera system (Vicon Vantage) using the point cluster marker set developed by Andriacchi et al [3]. A total of 56 activities were performed, 7 of which have been selected for this initial study. The activities of interest for this study include: picking up an object while standing; standing from a chair at a normalized height; standing up from a chair lower than normalized height; standing from a soft and low chair (sofa); tying a shoe on the right foot (on a raised bar) while the left foot is planted on the ground; and ascending and descending stairs.

The analysis was performed using Nexus (Vicon) and custom Matlab scripts to calculate and extract peak 3D hip kinematics. Normalized data tables that displayed the peak angles for each motion were produced for both the younger and older groups. Comparisons between left hip kinematics were made between the younger and older groups using unpaired t-tests ( $\alpha < 0.05$ ) after the data was found to be normally distributed. The left hip was selected because it served as the stance leg while a person tied their elevated right shoe.

## RESULTS

The normative 3D hip kinematic results for each activity for both the younger and older groups of participants are shown below (Table 2). The greatest flexion angles were seen in the ball pick up and shoe tying activities. Abduction was greatest in ball pick up and the stair ascent / descent activities. The greatest internal rotation was seen in the ball pick up, sofa sit to stand, and stair descent activities.

Table 2: Activity Summary

ACTIVITY	Flexion		Abduction		Internal Rot	
	Younger (Stdev)	Older (Stdev)	Younger (Stdev)	Older (Stdev)	Younger (Stdev)	Older (Stdev)
Picking Up: Front to Side	107.4 (±7.3)	108.7 (±8.7)	20.9 (±7.9)	20.4 (±5.9)	20.6 (±6.3)	22.2 (±2.8)
Normalized Chair: Standing Up	89.7 (±9.6)	82.5 (±18.3)	11.0 (±4.1)	7.8 (±3.0)	13.7 (±5.5)	12.4 (±4.7)
Low Chair: Standing Up	94.0 (±13.6)	89.8 (±16.0)	10.3 (±3.8)	9.6 (±2.8)	15.0 (±5.6)	13.2 (±4.6)
Sofa: Standing Up	98.0 (±11.1)	95.0 (±17.7)	13.9 (±4.8)	10.6 (±4.8)	19.6 (±7.4)	15.9 (±6.0)
Stairs: Ascending	68.5 (±3.6)	72.3 (±5.4)	16.7 (±4.2)	17.0 (±3.0)	19.0 (±4.2)	17.9 (±2.1)
Stairs: Descending	46.2 (±5.4)	51.3 (±4.9)	19.2 (±4.1)	18.9 (±1.9)	19.5 (±4.9)	21.9 (±3.9)
Tying Shoe	29.0 (±8.0)	34.2 (±8.1)	8.0 (±3.0)	8.9 (±3.5)	8.1 (±2.6)	11.2 (±3.6)

The effects of age and motion were also analyzed. There was a significant difference in how older and younger subjects performed activities that required a single leg stance position. Older subjects had a significantly greater amount of hip flexion than their younger cohorts for both tying their shoes (+5.2°, p=0.006) and for descending stairs (+5.1°, p=0.02). Although not significant, the older group also had a higher amount of internal rotation while tying their shoes. There was also a significant difference between younger and older subjects for hip flexion when the three sit-to-stand activities were grouped together (-5° in the older group, p=0.009). There were no significant differences at the hip for how young and old subjects performed the picking up activity.

## DISCUSSION

The ball pick up activities employed the greatest range of motion which could put THA patients at risk for dislocation. The pivot and rotation movement is especially risky for patients who have undergone a posterior approach THA since the movement requires a substantial amount of flexion and internal rotation. All of the sit to stand activities also employ a fairly high level of flexion and internal rotation as well, especially when the seat is low to the ground and soft. These activities place the hip at a position near the peak ROM of the hip, close to where the person is at risk of soft and hard tissue impingement. [4]. This able bodied normative hip kinematic data table (and future ones to follow for the additional unreported activities) is necessary to identify

potentially risky activities for patients who have a total hip replacement. Future studies will be performed to identify how these motions are altered in a THA patient population, but this healthy normative data will serve as comparison data and provide doctors and therapists with more information that they can use to instruct post-op care.

Initial comparisons for how age influences hip movement during activities of daily living was also performed using this normative data table and initial differences were identified. For example, the results indicate that older individuals significantly increase their hip flexion while descending stairs. This increased flexion in the older group during stair decent was most likely to ensure that their heel cleared the edge of the step, possibly out of a greater fear of falling. This is speculation, but further analysis will analyze the full body kinematic profiles for both groups during all of the 56 activities to determine how movement profiles change with age. Some of the initial findings, such as the decreased flexion in the older group during sit-to-stand activities might actually indicate a lower risk of hip dislocation in older patients should these trends continue with THA patients. Once the influence of age on hip kinematics is identified, post-surgery instruction and therapy can be more targeted to the individual patient.

The work presented in this study is a critical first step towards a better understanding of how the hip moves during common activities of daily living and how those movements change with age. This data will serve as a foundation for safely collecting similar data with THA patients and for improving the instructions doctors and physical therapists provide their patients post THA.

## REFERENCES

- [1] Ito H, et al. *J. Bone Jt. Surg* **85**, 1725-1732, 2003.
- [2] Fillingham Y, et al. *Am. J. Emerg. Med* **32** 1554e1-1554e3, 2014.
- [3] Andriacchi T, et al. *J Biomech Eng* **120** 743-749, 1998
- [4] Patel A, et al. *J. Arthroplasty* **25** 1275-1281, 2010

# INDIVIDUALS WITH KNEE OSTEOARTHRITIS SHOW ASYMMETRY IN PEDALING MECHANICS

Harsh H. Buddhadev, Daniel L. Crisafulli, David N. Suprak, and Jun G. San Juan

Western Washington University, Bellingham, WA, USA

email: harsh.buddhadev@wwu.edu, web: <http://wp.wwu.edu/biomechanicslab/>

## INTRODUCTION

Cycling is a widely prescribed form of physical activity for individuals with knee osteoarthritis (OA) as it is shown to alleviate knee pain, stiffness, and improve walking speed. Despite the known therapeutic benefits of cycling, no research has examined pedaling mechanics bilaterally in individuals with knee OA.

When pedaling on a stationary ergometer, a person with knee OA can maintain a fixed pedaling intensity, by reducing the power output of the affected leg while simultaneously increasing the power output of the healthy limb because the pedals are connected by a common crank. Such inter-limb compensation of power output may reduce the efficacy and limit the improvements achieved during the rehabilitation process.

Similarly, individuals with anterior cruciate ligament (ACL) deficiency, have also been prescribed with cycling therapeutically, demonstrate significant asymmetry in pedaling mechanics. Under submaximal cycling conditions, the uninjured limb increased its output by 44-50% to compensate for the reduced effort by the ACL deficient leg [1]. However, it is not known whether individuals with knee OA also demonstrate inter-limb asymmetry in pedaling mechanics. Our purpose was to test the hypothesis that individuals with knee OA demonstrate asymmetry in pedaling mechanics.

## METHODS

Twelve individuals with knee OA ( $67.3 \pm 7.6$  years; 6 females and 6 males) and 12 age- and sex-matched healthy controls ( $66.1 \pm 7.3$  years) participated in the study. Local orthopedic surgeons confirmed and diagnosed the grade of radiographic evidence of knee

OA for each side utilizing Kellgren-Lawrence (KS) scale for participants with knee OA. The majority (8/12) of these individuals had bilateral OA, with one side more affected than the other (KS scale grade: More affected side =  $3.0 \pm 0.9$ ; less affected side =  $2.4 \pm 1.1$ ). Limb dominance for participants in the control group was determined by asking which leg they preferred to kick a ball.

Each participant completed a single 1-hour testing session. Following a bicycle set-up procedure that standardized the cycling posture on a Velotron bicycle ergometer, participants completed a 5-minute warm-up ride at 50 W at self-selected cadence. They then completed 2 minutes of pedaling at 100W-60 rpm as crank position, bilateral pedal orientation, and bilateral pedal anterior-posterior and normal pedal reaction forces were sampled synchronously at 250 Hz using a Sensix I-crankset force pedal system. Patients with knee OA confirmed that they were pain free for a week prior to the testing day and the experimental cycling condition was comfortable and did not cause knee pain or discomfort.

The crank position, pedal orientation, and pedal force data were low pass filtered at 4 Hz. The pedal forces were transposed to the crank coordinate system using pedal force, crank position, and pedal orientation data. Effective crank torque on each side was computed as a product of the component of pedal force perpendicular to the crank and length of crank arm. For a given crank cycle, the crank power on each side was computed as a product of average effective crank torque and pedaling cadence. The crank power was then averaged over 60 crank cycles. One-way ANOVA was used to examine the effects of limb-condition (e.g. knee OA- more and less affected leg, control-dominant and non-dominant leg) on average crank power. Significant differences were considered at  $p < 0.05$ .

## RESULTS

Net crank power (i.e. sum of crank power on both sides) and cadence data measured showed that both groups complied with the experimental condition (Knee OA:  $99.3 \pm 3.9$  W and  $60.3 \pm 0.5$  rpm; Control group:  $98.6 \pm 2.4$  W and  $60.2 \pm 0.4$  rpm). As expected, individuals in the control group did not show differences in power generated between their dominant and non-dominant limbs. However, individuals with knee OA demonstrated significant asymmetry in power output between their more and less affected lower extremity. Contrary to our expectations, the more affected leg yielded 11% more power (5.1 W;  $p=0.026$ ) compared to the less affected leg (Figure 1).

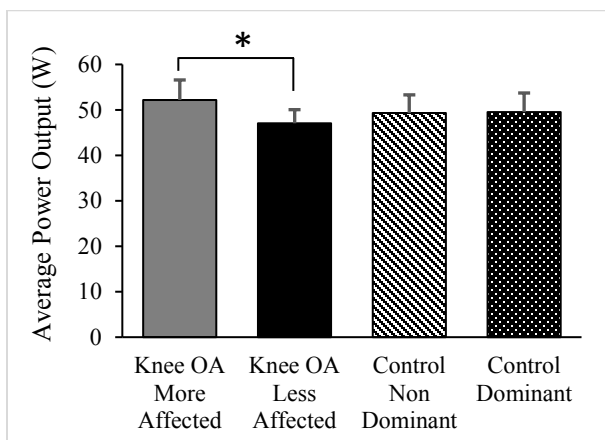


**Figure 1:** Effect of knee OA on average crank power during submaximal cycling at 100 W at 60 rpm. Individuals with knee OA applied more power with their more affected leg compared to their less affected leg ( $*p=0.026$ ). Mean  $\pm$  1 SD

## DISCUSSION

Our data indicates a small but significant asymmetry in crank power output, with the more affected leg yielding more power than the less affected leg. These findings contradict our hypothesis which was based on the logical assumption that grade of knee OA damage is related to function in these individuals. These findings are in agreement with those of Phan et al. [2] and Raynauld et al. [3], who did not find a correlation between function, assessed using Western Ontario and McMaster Universities

Osteoarthritis Index, and KS scores of individuals with knee OA.

Our results suggest that our patients with knee OA favored the more damaged leg rather than avoiding it. During physical therapy, the knee pain of patients with OA is alleviated and they are rehabilitated to gradually increase the use of the more affected leg and overcome compensatory limb avoidance strategies. All our patients had undergone physical therapy for their rehabilitation and they were pain free for at least one week prior to the testing session. Moreover, most of them ( $n=10$ ) were also physically active and engaged in at least 200 minutes of regular moderate intensity physical activity per week. Seven of these individuals also cycled more than 60 minutes on a weekly basis. We speculate that our physically active patients may have become accustomed to favoring the more affected leg during comfortable pain free cycling and thus had greater power output from the more affected compared to the less affected leg.

Excessive asymmetry in power output between the lower extremities can be detrimental to rehabilitation process and joint health of patients with knee OA. Thus, from a therapeutic perspective, our results of asymmetry in power output emphasize the need for monitoring symmetry of effort between legs for individuals with knee OA during cycling. Future studies should examine how inter-limb symmetry in power output during cycling changes through the physical rehabilitation process.

## CONCLUSIONS

Individuals with bilateral knee OA demonstrate asymmetry in crank power output. They apply more power with their more affected compared to their less affected leg.

## REFERENCES

1. Hunt M et al. *Arch Phys Med Rehabil* **85**, 1475-1478, 2004.
2. Phan et al. *Eur Radiol* **16**, 608-618, 2006.
3. Raynauld et al. *Arthritis Rheum* **50**, 608-618, 2004.

# Strength of Arthroscopic Knot Tied with Compromised Suture: Effect of Defect Location

<sup>1</sup>Steven I Grindel, <sup>1</sup>Cameron Best, <sup>1</sup>Jesse Bauwens, <sup>1,2</sup>Linda M McGrady, and <sup>1,2</sup>Mei Wang

<sup>1</sup>Medical College of Wisconsin, Milwaukee, WI, USA

<sup>2</sup>Marquette University, Milwaukee, WI, USA

email: meiwang@mcw.edu

## INTRODUCTION

Suture anchors and sutures are commonly used in arthroscopic orthopaedic procedures. With recent advances in high-strength sutures, the risk of breaking an undamaged suture is relatively low. However, the risk increases substantially if the suture becomes frayed or nicked during arthroscopic procedure, such as being entrapped and pinched by suture-passing instruments. Previously studies have reported the simulation of suture abrasion against its anchor and how it affects its pullout strength in sutures with different materials [1,2]. Similar studies have been conducted with laparoscopic surgeries, where suture damaged by laparoscopic grasping forceps and needle holders [3] or robotic manipulation [4] were shown to have significantly reduced its tensile strength. What is unknown is whether incorporating the instrument-damaged spot of the suture within a suture knot would provide some shielding effect against the weakening strength.

The purpose of this study was to evaluate the effect of defect location on mechanical strength of the suture knot, by incorporating the compromised spot of the suture into the knot, or positioning inside the suture loop, or outside the suture loop.

## METHODS

Three trained orthopaedic surgeons prepared a total of 105 suture knot samples for the study. All knots were tied with No. 2 multi-strand, long chain ultra-high molecular weight polyethylene (UHMWPE) core with a braided jacket of polyester and UHMWPE (FiberWire by Arthrex, Naples, Florida). Stainless steel s-hooks (working load limit: 55lbs) were used to tie the knots. Four study groups were

formed: 1) Control (n=24), where the knots were tied with non-damaged sutures, 2) Knot (n=25), where the damaged spot was incorporated within the knot, 3) Loop (n=29), where the damaged spot was placed inside the suture loop of the knot, and 4) Out (n=27), where the damaged spot was left outside of the suture knot and loop (Fig.1).

To create the damage, suture samples from the three later groups were first placed in a scorpion suture passer (Arthrex, Naples, Florida) along with a spare suture to simulate the entrapment scenario. A controlled abrasion defect was then inflicted in the suture sample by operating the suture passer. Once visual inspection confirmed the defect, a quadruple Duncan sliding knot was tied around the s-hook with the nicked spot placed in its group designated position.

All suture knot samples were tested on a servo hydraulic load frame (Model 809, MTS Systems Corp. Eden Prairie, MN). The s-hook with suture knots tied around it was linked to an I-bolt that was mounted to the crosshead of the MTS system through a hydraulic grip. The two free ends of the suture were wrapped around to a 1-inch diameter steel bar which could rotate freely about its shaft to reduce the friction force on the suture. The suture was then pressed down and secured to the actuator (Fig.2). The fixation point of the suture was marked with permanent ink to verify that no slippage occurred during the test. The exposed suture length was kept at 5 inches for all samples. A 5 N preload was applied to the sample to pretension the specimen and provide a common starting point. The suture sample was loaded to failure at a rate of 1 mm/s. Force and displacement data were collected at 100Hz. Suture failure load was defined as the peak force before its first sudden drop on a force-

displacement plot. Suture breaking point of each sample was noted after the experiment. Comparison of the damaged groups against the non-damaged control was performed using Kruskal-Wallis test and post-hoc nonparametric comparisons with control using Dunn method for joint ranking. All statistical analysis was performed using JMP 12 (SAS, Cary, NC), and with statistical significant level set at 0.05.



**Figure 1:** Illustration of three defect locations: Loop, Knot, and Out.



**Figure 2:** Experimental setup

## RESULTS

Good agreement among the three evaluators were found in mean suture strength of each study group, where deviations of individual mean from group mean was less than  $\pm 5\%$ . The data were then pooled together to evaluate the effect of defect location.

As expected, the non-damaged Control group had the highest tensile strength, with a mean of  $278.1 \pm 32.5$  N. The Knot group, with the defect incorporated within the knot, came second, at  $264.5 \pm 37.9$  N, which was 4.9% lower than Control. The Out group, with defect left outside of the knot

and suture loop, was 11.0% than the control, at  $247.6 \pm 36.0$  N. The weakest group was Loop, with defect located inside the suture loop, at  $236.0 \pm 62.7$  or 15.1% less than the control. Both the Loop group and Out group were significantly weaker than Control ( $p < 0.017$ ,  $p < 0.015$ ). The difference between the Knot and Control was not statistically significant.

All but four of the 24 sutures in Control broke off at the knot, while the four failed inside the suture loop. Majority of the Knot group sutures failed at the knot, while five out of 25 failed inside the suture loop. In Loop and Out groups, approximately half of the sutures broke at the defect spot, while the others failed at the knot.

## DISCUSSION

Results from this study show that incorporating the defect into the knot has the least impact on the strength of the suture knot. The worst choice is to leave the defect inside the suture loop, a 15% reduction in the strength. Limitations of the study include: 1) experiments were conducted without an environmental chamber to mimic in vivo condition these suture knots are applied to. 2) The study design did not include cyclic loading of the samples before load-to-failure test. It is possible that additional dynamic creep may occur in the suture with cyclic loading, and impact the maximum force.

The strength of arthroscopic suture knot plays essential role for the integrity of tissue repairs. Accidental minor damage to the suture does occur during the procedure. Our findings suggest that incorporating the defect within the suture knot is the best option to minimize the effect.

## REFERENCES

1. Wright PB, et al. *Arthroscopy* **22**,1270-1275,2006.
2. Bardana DD, et al. *Arthroscopy* **19**,274-281.2003.
3. Bariol SV, et al. *J Endourology* **19**,1127-1133, 2005.
4. Diks J, et al. *Surg Laparosc Endosc Percutan Tech* **17**,524-527, 2007.

# The Effect of Isolated Weber B Fibular Fracture Displacement on Tibio-Talar Contact Pressures

<sup>1</sup> Stephen Malekzadeh, <sup>2</sup> Jessica Minder, <sup>1</sup> Mark Theiss, and <sup>1</sup> Jihui Li

<sup>1</sup> Inova Fairfax Medical Campus, Falls Church, VA, USA

<sup>2</sup> Columbia St. Mary's Hospitals, Milwaukee, WI, USA

Email: Jihui.Li@inova.org

## INTRODUCTION

The lateral malleolus is important in maintaining a congruent and stable ankle joint. Weber B lateral malleolus fractures, caused by supination and external rotation of the ankle, are the most common type of fracture of the fibula [1]. Controversy still exists regarding surgical necessity of Weber B fractures in cases where the lateral malleolus is fractured and displaced without clinically significant talar shift or medial ankle disruption. Furthermore, the results of current cadaveric biomechanical research reproducing Weber B fractures has yielded conflicting conclusions with regards to its influence upon tibiotalar contact [2-4]. The purpose of this study was to measure the contact areas and peak pressures between the tibial plafond and the talar dome in a cadaveric model with serial displacement of the distal fibula in two isolated Weber B fracture patterns (a transverse fibular fracture and short oblique fibular fracture). Our test hypothesis was that serial displacement of the distal fibula with an intact deltoid ligament complex in this Weber B fracture model would induce no significant changes in contact areas or peak pressures.

## METHODS

12 fresh (6 matched pairs) ankle cadaveric specimens with no prior history of trauma or pre-test laxity were collected from a tissue bank. Skin and subcutaneous tissue were removed from mid-tibia to the hindfoot. The extensor tendons were removed to provide access to the ankle joint. Ankle ligaments, including the deltoid complex, were meticulously maintained. The proximal tibia was potted in a PVC tube using epoxy resin and then mounted onto a Mini Bionix loading machine (MTS Inc. Eden Prairie, MN) and subjected to a 154 lbs

(70kg) axial compressive load (Fig. 1). A Tekscan pressure sensor (model 5033, Tekscan Inc., South Boston, MA) was placed in the ankle joint to monitor the pressure distribution and contact area. Each specimen was first tested at baseline prior to simulated fracture. With a sensor in place, the ankle was subjected to a static, axial load at neutral position, 5 and 10 degrees dorsiflexion, and 5, 10, 15, and 20 degrees plantarflexion using an angled platform. One ankle was randomly selected from each pair to simulate a transverse Weber B fracture with lateral displacement conditions of 2, 4, and 6mm of the distal fibula. A spiral oblique Weber B fracture was simulated on the contralateral ankle with two coupled displacement conditions of the distal fibula (2mm lateral translation and 5 degrees external rotation, then 4mm lateral translation and 10 degrees external rotation). These specimens were then subjected to the same static, axial load and positions as intact specimens for comparative analysis. ANOVA testing was used to compare the peak pressures and contact areas among intact specimens, transverse fracture specimens (TV) and spiral fracture specimens (SR). In statistical analysis a two-sided significance level of 0.05 was selected.

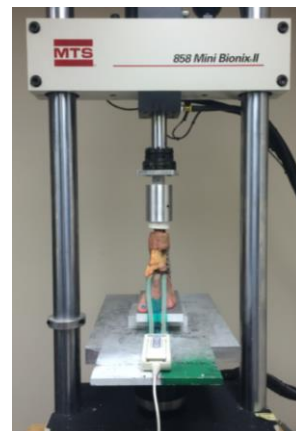


**Figure 1:** Biomechanical testing set-up on Mini Biomix loading machine.

## RESULTS AND DISCUSSION

It was found that at the neutral position (0 degree), intact specimens had similar shape of contact area and pressure distribution with the SR specimens, but not the TV specimens (Fig. 2). The average contact area of the intact specimens (376 mm<sup>2</sup>) was slightly smaller than those of SR specimens (386 mm<sup>2</sup> at 2mm translation and 386 mm<sup>2</sup> at 4mm translation) but not significant (Table 1). TV specimens had larger contact areas (420, 417 and 370 mm<sup>2</sup> at 2, 4, and 6mm translation), but not significant as well. On the contrary, the average peak pressure of the intact specimens (5.7MPa) was slightly higher than SR (5.5 and 5.4MPa at 2, and 4mm translation) and TV specimens (5.3, 5.3 and 5.4MPa at 2, 4, and 6mm translation), but again none of these values were significant. Specimens at other positions (dorsiflexion or plantarflexion) showed a similar trend. In general, more flexion indicated smaller contact areas and higher peak contact pressure, but not significant as well.

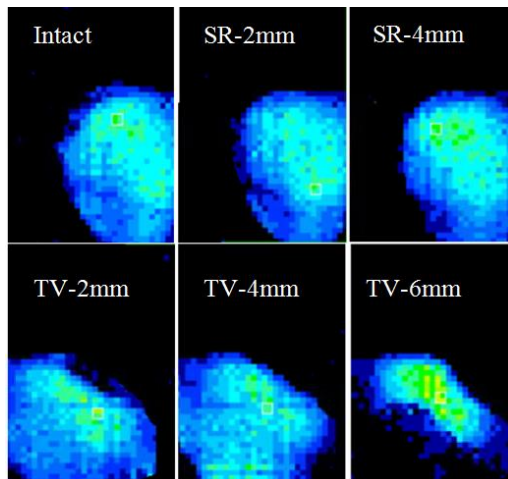


**Figure 2:** Pressure distribution of specimen #3 at neutral position. SR: spiral; TV: transverse.

The results revealed that isolated Weber B fractures (both transverse and spiral oblique models) without clinically significant talar shift or medial ankle disruption does not significantly change the contact area and peak pressures of the tibiotalar articulation. This study supported the conclusions of Clarke et al that isolated Weber B fractures may not require

surgery based on axial load cadaveric observations [3].

**Table 1.** Mean contact areas (cm<sup>2</sup>) and peak pressures. SR: spiral; TV: transverse; Df: dorsiflexion; and Pf: plantarflexion.

Area	Intact	SR-2mm	SR-4mm	TV-2mm	TV-4mm	TV-6mm
10Df	351	400	426	430	422	376
5Df	364	405	417	425	434	386
0	376	386	386	420	417	370
5Pf	357	362	359	410	408	385
10Pf	345	372	364	389	398	359
15Pf	339	342	348	359	392	352
20Pf	306	328	339	336	358	345
Peak Pressure (MPa)						
10Df	5.1	5.1	4.8	4.8	5.0	5.0
5Df	4.8	4.9	5.0	4.8	4.9	5.1
0	5.7	5.5	5.4	5.3	5.3	5.4
5Pf	5.5	5.3	5.5	5.5	5.3	5.3
10Pf	5.9	5.9	5.9	6.0	5.9	5.1
15Pf	6.2	6.0	6.2	6.6	6.0	5.5
20Pf	6.5	6.2	6.2	7.2	6.5	5.6

## CONCLUSIONS

This study suggested that isolated Weber B fractures with the distal fibula displaced laterally up to 6mm or superolaterally up to 4mm lateral translation and 10 degrees external rotation do not cause ankle instability. Interpretation of these results suggested that without significant loss of joint congruence, there is likely no long term pathogenesis of osteoarthritis and pain in this fracture model, therefore mitigating the need for surgery.

## REFERENCES

- [1] Yablon et al., J Bone Joint Surg 1977;
- [2] Curtis et al., Acta Orthop Scand 1992;
- [3] Clarke et al., Foot Ankle Int 1991;
- [4] Harris et al., J Foot Ankle Surg 2004;

## ACKNOWLEDGMENTS

This study was supported by Inova Seed Research Grant.

# DEVELOPMENT OF A DISPOSABLE POINT-OF-SERVICE DIGITAL MANOMETRY DEVICE TO ASSESS ANORECTAL FUNCTION

<sup>1</sup> Ali Attari, <sup>2</sup> William Chey, <sup>2</sup> Jason Baker and <sup>1</sup> James Ashton-Miller

<sup>1</sup> University of Michigan, Department of Mechanical Engineering, Ann Arbor, MI, USA

<sup>2</sup> University of Michigan, Division of Gastroenterology, Ann Arbor, MI, USA

email: attari@umich.edu, web: <http://me.engin.umich.edu/brl>

## INTRODUCTION

Chronic constipation (CC) and fecal incontinence (FI) are common gastrointestinal problems which affect approximately 20% of the North American population [1, 2]. Dyssynergic defecation, which causes CC, is the inability to relax the anal sphincter (AS) and puborectalis (PRM) muscle during defecation. Whereas weakness and injury in AS sometimes result in FI, both problems are typically diagnosed with anorectal manometry (ARM).

In traditional ARM, the AS closure pressure is recorded using a 4 mm diameter catheter with 4 orthogonal pressure sensors. Recently, high resolution systems with many more pressure sensors have become available, but they are expensive, require dedicated space and trained staff at tertiary care medical centers. Many patients go undiagnosed because of limited access to tertiary care centers.

We designed and fabricated a low-cost, disposable, point of service, instrumented glove [3] for community gastroenterologists to assess AS and PRM function during a rectal exam. Termed “Digital Manometry” (DM) it records AS and intrarectal pressures as well as EMG data from the AS and PRM muscles. DM provides similar information to ARM at nearly 3 orders of magnitude lower equipment cost.

## METHODS

The goal of this study was to test anorectal function in 3 healthy young subjects using DM and compare the results with ARM. The DM device consists a disposable instrumented glove (Fig. 1), wrist mounted signal conditioning unit, a data acquisition unit and a laptop.



**Figure 1:** DM disposable instrumented glove

Three MEMs pressure sensors were mounted and wirebonded on a custom designed flexible printed circuit board (FPCB). After encapsulating connections by rigid adhesives, each sensor was covered by a thin layer of silicone rubber to ensure a smooth finish. The FPCB was then wrapped around a glove index digit such that pressure sensors are located on the tip of the distal phalanx, the medial aspect of the middle phalanx and the PIP joint, respectively. The FPCB has two sets of gold plated electrodes on the tip and the shaft of the digit to capture EMG signals from PRM and AS muscles. The entire digit was covered by a latex layer with EMG probes left exposed. Signals from the probe pass through a wrist-mounted signal conditioning unit and a data acquisition device to a laptop computer. Contraction durations in DM was recorded by a digital event marker.

During the study, resting pressures were recorded and then subjects were asked to maximally contract their AS muscle for three 5-10 seconds intervals separated with ~20 seconds rest periods. They were

then asked to simulate defecation by attempting to push out the examiner's finger (Fig. 2) at least three times (Fig. 3).

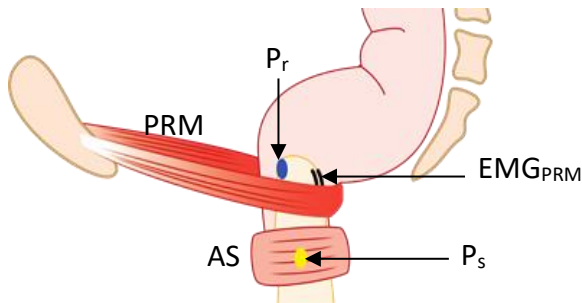


**Figure 2:** Schematic showing of the examiner's finger wearing the DM glove with its pressure transducers for measuring rectal pressure ( $P_r$ ) and AS pressure ( $P_s$ ) and PRM EMG ( $EMG_{PRM}$ )

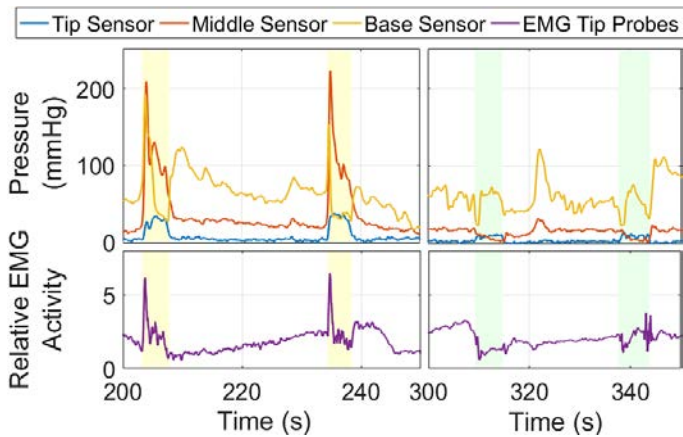


**Figure 3:** Sample AS and rectal pressures (top) and RMS  $PRM_{EMG}$  (bottom) in maximum squeeze (yellow highlights) and simulated defecation (green highlights) from one trial in one subject.

## RESULTS AND DISCUSSION

Sample results may be seen in Fig. 3. When a Bland-Altman [4] analysis was used to study the differences between DM and ARM the mean difference was found to be 9 (mmHg) and limits of agreement  $\pm 44$  mmHg (95%). The slope of the linear regression line between DM and ARM was 0.9. The physical difference between the examiner's finger diameter using DM (i.e., 22 mm) and ARM catheter diameter (i.e., 4 mm) did not lead to a systematic difference in recorded AS pressures as demonstrated by the 9

mmHg difference between ARM and DM results. The one outlier in Fig. 4 could be due to an ARM pressure reading elevated by contact stress or the DM AS pressure sensor being positioned away from the location of maximum AS closure pressure - a change of just one centimeter along the AS can cause a 30% decrease in measured AS pressure [5]. The mean (SD) resting rectal pressure values measured using DM were 29 (13) mmHg.

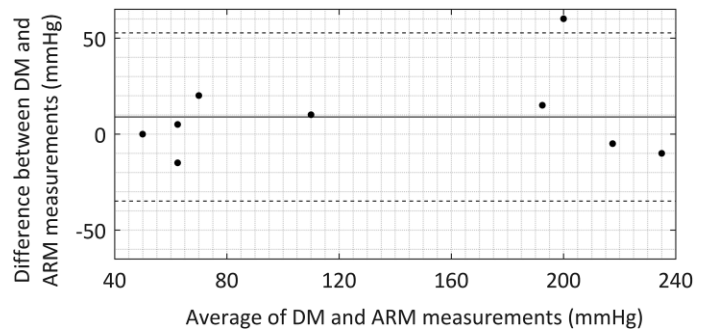


**Figure 4:** Bland-Altman plot showing the limits of agreement (dashed lines) between DM and ARM measurements of AS pressures.

## CONCLUSIONS

DM gave promising measurements of AS pressures at a fraction of the cost of ARM, and via additional pressure and EMG measures an assessment of anorectal functionality not provided by ARM.

## REFERENCES

1. Talley NJ, et al. *J. Gastroenterol.* 102.3, 895-901, 1992.
2. Johanson JF and Lafferty J. *Am. J. Gastroenterol.* 91.1, 33-36, Jan. 1996.
3. Chey WD, et al. US Provisional Patent Appl # 13/714,728.
4. Bland JM and Altman D. *Lancet* 327.8476, 307-310, 1986.
5. Gibbons CP, et al. *Int. J. Colorectal Dis.* 1.4, 231-237, 1986.

## ACKNOWLEDGMENTS

Coulter Foundation and MTrac funding.

# LOWER BODY KINEMATICS AND JOINT REACTION FORCES WITH DISTAL FEMORAL ENDOPROSTHESES FOLLOWING LIMB SALVAGE SURGERY FOR TREATMENT OF OSTEOSARCOMAS

<sup>1,2</sup>Jessica M. Fritz, <sup>1</sup>Christina M.R. Garman, <sup>1</sup>Carolyn I Albert, <sup>2</sup>Jake Bauwens, <sup>2</sup>Donald A Hackbarth, Jr.,  
<sup>2</sup>David M. King, <sup>2</sup>John C. Neilson, and <sup>1,2</sup>Gerald F. Harris

<sup>1</sup>Marquette University, Milwaukee, WI, USA

<sup>2</sup>The Medical College of Wisconsin, Milwaukee, WI, USA  
email: jessica.fritz@marquette.edu

## INTRODUCTION

Bone sarcomas are the fourth most common cancer in individuals under 25 years [1]. Osteosarcoma, the most common subtype of bone sarcomas in this population, is commonly observed in the growing metaphyseal regions of the femur. Limb salvage surgery (LSS) is the standard of care for osteosarcoma in the lower extremities. This complex procedure often involves removal of the tumor and reconstruction of the bone with an implantable metal and polyethylene endoprosthesis. Although LSS has greatly reduced the number of amputations in this population, the procedure is associated with more long-term complications than standard joint arthroplasty. Over time, endoprostheses fail due to aseptic loosening, polyethylene wear, and/or mechanical device fracture. These failure mechanisms indicate that the mechanical loads sustained by the bone-implant construct influence implant survivorship. At present, there is no validated standard method for objective functional outcome measurements following LSS, and only a few studies have reported gait analysis data in this population. These reports have identified two distinct, abnormal sagittal plane knee kinematic patterns during gait: fixed extension (FEx) knee and fixed flexion (FFI) knee. The FEx knee pattern is identified by persistent hyperextension of the affected knee during loading response. The FFI knee pattern consists of a constant knee flexion angle on the affected side during mid-stance (Fig. 1) [2, 3]. Our study aimed to quantify lower body gait kinematics and joint reaction forces (JRFs) of adults who have a distal femoral endoprostheses following LSS. An emphasis was placed on using advanced musculoskeletal modeling techniques to provide the first assessment of internal JRF in this population,

which we theorize can have a significant effect on longevity of the implant, and to examine differences between the FFI and FEx knee pattern groups.

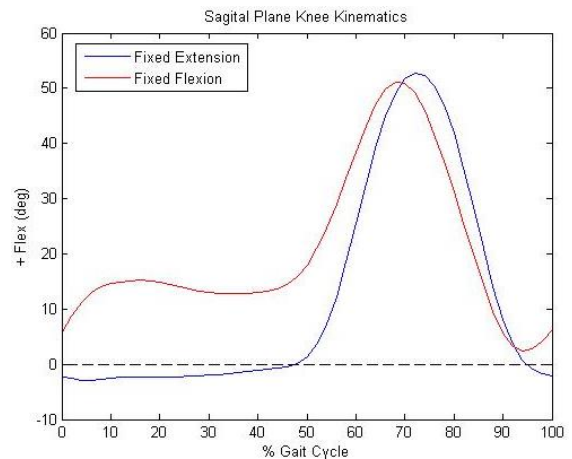


**Figure 1:** Average knee flexion patterns for the fixed extension (blue) and fixed flexion (red) groups

## METHODS

Eight subjects (Age:  $36.3 \pm 18.8$  years; height:  $170.5 \pm 12.3$  cm; weight:  $71.3 \pm 15.7$  kg; 6 F, 2 M) who previously underwent LSS with a distal femoral endoprostheses gave their informed consent to participate in this IRB-approved study. None of the subjects had undergone primary or revision surgery for at least one year prior to this investigation. Three-dimensional gait analysis was performed with a 12-camera motion analysis system (MX model, Vicon Motion Systems Inc., Oxford, UK). An OpenSim gait model, Gait 2392 [4], was used as a basis for creating patient specific models. Each subject's model was altered to exclude musculature removed during the LSS. These models and the subject gait data were input into static optimization and joint reaction analysis algorithms to resolve net joint moments into individual muscle forces and calculate

the axial internal JRF at the knee. The subjects were divided into two groups based on their stance knee flexion patterns (4 FEx, 3 FFI, 1 neutral). A two-way mixed factor analysis of variance (ANOVA) was performed in JMP v12 (SAS, Cary, NC) with significance concluded when  $p < 0.05$ . Post-hoc analyses were completed using a Student's T test. Independent variables included limb, gait pattern, and a limb x gait pattern interaction. Dependent variables included peak knee flexion angle during loading response and peak knee JRF during stance phase. Statistical analyses were performed for the axial JRFs.

## RESULTS AND DISCUSSION

The FEx group exhibited a 37.5% higher axial JRF than the flexed group. While the surgical limb tended towards lower axial JRF, there were no statistically significant differences between surgical and non-surgical limbs. The kinematic analysis of the FEx group revealed a 605% lower peak angle on the surgical side compared to the nonsurgical side. The surgical limb of the FEx group exhibited an 854% lower peak angle than the FFI group's surgical side. Compared to the FFI group, the FEx group showed greater differences between limbs and from normal data in both kinematics and kinetics. The FEx group exhibited more gait dynamics deviations and higher joint reaction forces; putting them at higher risk of pathology or injury in the hip and ankle joints on the surgical limb and/or the contralateral limb (Fig. 2). Push-off power is greatly reduced in the FEx group, although walking speed is not significantly diminished compared to the FFI group (FEx gait speed=0.98 m/s, FFI gait speed=1.06 m/s).

## CONCLUSIONS

Our results indicated that the FEx group was more likely to experience higher axial JRFs compared to the FFI group. This observation suggests the gait pattern adopted by the FEx group may be more damaging to the implant, hence affecting its longevity. Based on the data from this study, we suspect that those patients who exhibit a FEx gait pattern may have instability resulting from weakness or muscle resection. This needs to be further explored. Post-operative quadriceps strengthening and rehabilitation is vital. A post-operative protocol

of gait analysis may be indicated to identify those who are adopting the FEx pattern. Those patients may also benefit from focused gait training as part of their regular rehabilitation protocol.

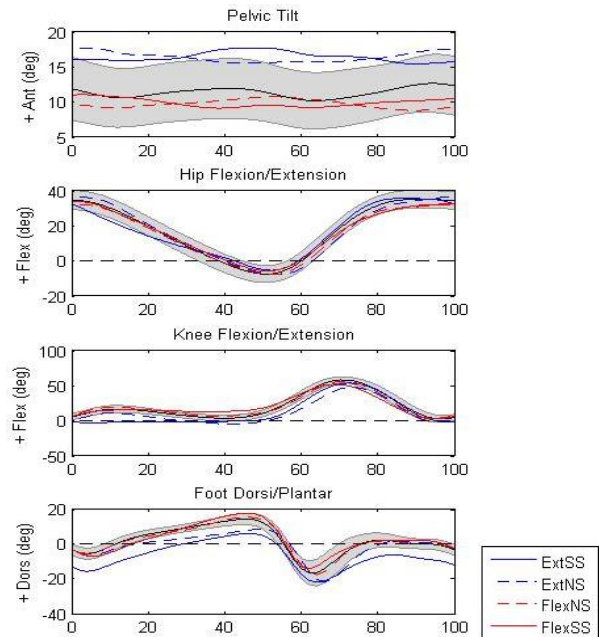


**Figure 2:** Sagittal plane kinematic results throughout the gait cycle. Solid blue line represents the fixed extension surgical limb, dashed blue line represents the fixed extension non-surgical limb, solid red line represents the fixed flexion surgical limb and the dashed red line represents the fixed flexion non-surgical limb. Solid black line and gray band represent the mean and standard deviation of a data set of 48 young adult controls from our motion analysis laboratory.

## REFERENCES

1. Homa, D.M., et al., *Cancer*, 1991. **67**(8): p. 2219-23.
2. Rompen, J.C., et al., *Acta Orthop Scand*, 2002. **73**(4): p. 439-46.
3. Wirganowicz, P.Z., et al., *Clin Orthop Relat Res*, 1999(358): p. 64-74.
4. Delp, S.L., et al., *IEEE Trans Biomed Eng*, 1990. **37**(8): p. 757-67.

## ACKNOWLEDGMENTS

This study was funded by the American Cancer Society through MCW grant number FP8336. Additional support was obtained through NIDILRR grant number 90RE5006-01-00 and grant 90AR5022-01-00. NIDILRR is a Center within the ACL, Department of HHS. The contents of this article do not necessarily represent the policy of NIDILRR, ACL, HHS, and you should not assume endorsement by the Federal Government.

# Evaluation of Transforaminal Lumbar Interbody Fusion Cage Placement: Minimally Invasive Versus Open Surgery

<sup>1</sup>Jingnan Cui, <sup>2</sup>Xinhua Zhan, <sup>2</sup>Liming Cheng, <sup>3</sup>Kerong Dai, <sup>2</sup>Yan Yu, <sup>1,3</sup>Tsung-Yuan Tsai

<sup>1</sup> School of Biomedical Engineering, Shanghai Jiao Tong University, Shanghai, China

<sup>2</sup> Department of Orthopaedic Surgery, Tong Ji Hospital, Shanghai, China

<sup>3</sup> Department of Orthopaedic Surgery, Shanghai 9th People's Hospital, Shanghai, China

email: tytsai@sjtu.edu.cn, web: <http://www.sjtu.edu.cn/>

## INTRODUCTION

Transforaminal lumbar interbody fusion (TLIF)[1] has been a successful treatment to restore disk height and improve the biomechanical stability of the diseased vertebral segments. However, the placement of the fusion cage is based on the surgeon's experiences and could be affected by the surgical approach. Few studies have reported the effects of minimally invasive surgery (MIS)[2] and conventional open surgery on the cage placement. Therefore, the aim of this study was to evaluate and compare the cage positioning of MIS and open surgery. We hypothesized MIS-TLIF could improve the cage placement accuracy with respect to open TLIF.

## METHODS

We retrospectively reviewed all the MIS- and open TLIF cases between Jun, 2013 and Feb, 2015 in our hospital and selected 25 MIS-TLIF and 25 open-TLIF cases for treatment of single-level lumbar degenerative disease. No complications, like cage lipping, sinking or any other untoward effects, have been reported at the time of this study. Anteroposterior and mediolateral radiographs which were taken in routine follow-up at two weeks after surgery were retrieved for data analysis. Three reference markers of the cage were used to determine its position and orientation according to the manufacture design (Fig. 1). Radiographic bony features which have been frequently used in clinical evaluations were digitized for determination of disk dimensions, center of the interbody space, and orientation of the vertebral bodies (Fig. 1&2). The anteroposterior (AP), superoinferior (SI), and mediolateral (ML) distances from the center of the

interbody space to the center of the cage were quantified and normalized according to the vertebral body dimensions in MATLAB (The MathWorks, Natick, USA). The independent t-test was used to compare the cage positioning using MIS- and open TLIF. The significance level was set at 0.05.

## RESULTS

The averages and standard deviations of the normalized distances from the interbody center to the cage center in the MIS-TLIF group were  $-1.9\% \pm 9.4\%$ ,  $2.9\% \pm 9.9\%$ , and  $-0.5\% \pm 6.3\%$  along ML, AP, and SI directions, respectively (Table 1). Corresponding values of the open-TLIF group were  $4.9\% \pm 11.4\%$ ,  $2.6\% \pm 11.7\%$ , and  $-0.6\% \pm 7.0\%$ . Statistically significant difference ( $p = 0.027$ ) was found between MIS- and open-TLIF along ML direction. The spinal cage placement in the MIS-TLIF group is more close to the center of the interbody center along ML direction. No significant differences were reported along the other two directions. Standard deviations of the cage placement were found to be smaller in the MIS-TLIF group (Table 1).

## DISCUSSION

This study successfully quantified the spinal fusion cage position with respect to the interbody space after MIS- and open-TLIF surgery by taking the advantage of the built-in reference points of the fusion cage. The centered cage placement along ML direction is recommended in clinical reports. Our results demonstrated that the MIS-TLIF can produce a more biomechanically favorable cage placement than the open-TLIF. The cage placement precision was also found to be better in the MIS-

TLIF group. Since routine follow-up radiographs were sufficient for the evaluation, no additional radiation exposure is required. This image-based cage placement measurement would be helpful for long-term clinical follow-up for TLIF patients. Additional efforts are guaranteed to determine the accuracy and precision of this measurement.

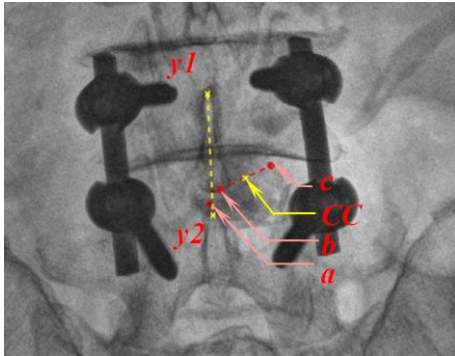


Figure 1. Point CC (Cage Center) was the center of the cage and the line (y<sub>1</sub> y<sub>2</sub>)<sup>-</sup> was the link between spinous processes of vertebrae representing vertical central line of vertebrae. The distance from (y<sub>1</sub> y<sub>2</sub>)<sup>-</sup> to CC was defined as the cage placement along the mediolateral (+/-) direction.

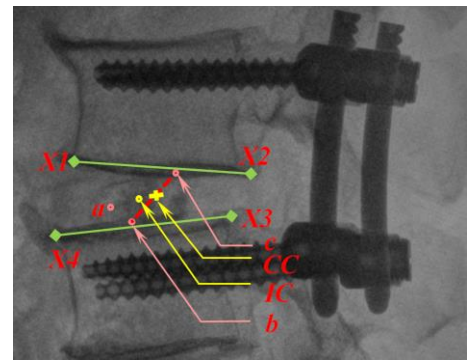


Figure 2. Point CC was the center of the cage. Point IC (Intervertebral Center) was the geometry center of the intervertebral space. The anteroposterior (+/-) and superoinferior (+/-) distances from IC to CC were quantified for evaluation of the cage placement.

## REFERENCES

1. Lowe TG, Tahernia AD, O'Brien MF, Smith DA. Unilateral transforaminal posterior lumbar interbody fusion (TLIF): Indications, technique, and 2-year results. *J Spinal Disord Tech* 2002;15:31-8
2. Foley KT, Holly LT, Schwender JD. Minimally invasive lumbar fusion. *Spine (Phila Pa 1976)* 2003;28:S26-35. doi: 10.1097/01.BRS.0000076895.52418.5E

**Table 1:** Tables may extend across both columns, and those should be included at the bottom of the abstract.

	<b>Mediolateral Distance to the Interbody Space Center (%)</b>	<b>Anteroposterior Distance to the Interbody Space Center (%)</b>	<b>Superoinferior Distance to the Interbody Space Center (%)</b>
<b>MIS Group</b>	-1.9±9.4	2.9±9.9	-0.5±6.3
<b>Open Group</b>	4.9±11.4	2.6±11.7	-0.6±7.0
<b>T-Test P-value</b>	p = 0.027	p = 0.913	p = 0.955

# A BIOMECHANICAL COMPARISON OF SYNDESMOTIC REPAIR TECHNIQUES DURING EXTERNAL ROTATION STRESS

Jessica Goetz, Nathan Davidson, M James Rudert, Andrea Caceres, Matthew Karam, and Phinit Phisitkul

University of Iowa; Iowa City, IA, USA  
email: [jessica-goetz@uiowa.edu](mailto:jessica-goetz@uiowa.edu), web: <https://uiowa.edu/uiobl/>

## INTRODUCTION

The distal tibiofibular syndesmosis is the ligamentous junction between the tibia and fibula at the ankle. During ankle fractures or sprains, individual or all of the syndesmotic ligaments can be torn. Such injuries are often accompanied by disruption of the deltoid ligament complex medially, resulting in a highly unstable joint. It has been reported that 23%-45% of ankle fractures that are treated operatively have syndesmotic disruption that must also be operatively stabilized [1].

Syndesmotic injuries are most often treated surgically by rigidly fixing the fibula to the tibia using screws. However this makes a previously flexible joint completely rigid, which can induce a variety of long-term functional complications. More recently, a flexible tightrope device has begun to see more widespread application for treating these injuries. However the biomechanics of this device are still under investigation [2], often with conflicting results.

The purpose of this work was to compare the mechanical behavior of existing syndesmosis fixation techniques with techniques incorporating various augmentations to improve anatomic realism, and determine which technique would return the rotational ankle mechanics closer to those of an intact ankle.

## METHODS

Ten pairs of fresh frozen through-the-knee cadaveric lower limbs (average age 57.8 years of age, range 37-67; 8 male/2 female) were potted in polymethylmethacrylate bone cement for interfacing with a custom mechanical testing fixture mounted in a Materials Testing Machine (MTS, Eden Prairie, MN). Proximally, the fixture

consisted of a lockable rotary bearing for interfacing with the potted tibial plateau. Distally, the fixture consisted of a lockable xy stage onto which was mounted a plate rigidly immobilizing the potted toes and distal calcaneus (Figure 1). All other joints of the foot were free to move, and the proximal tibiofibular junction was left intact.

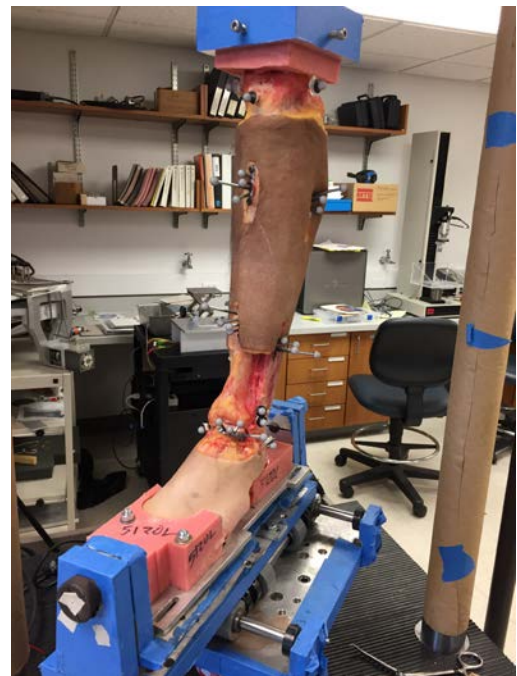


**Figure 1.** Photograph of specimen mounted in MTS for mechanical testing. Blue tape was used to mask reflections during optical marker tracking.

Clusters of reflective markers were mounted on the tibia, fibula, and talus to track bony kinematics. During testing, 750N of compressive axial load was applied to the proximal tibia while the tibia was free to move in rotation and the foot to move in the AP/ML direction. Collars on the xy stage and the rotary bearing were then locked. 100 preconditioning cycles of 5 Nm internal tibial torque (i.e. external foot rotation) were applied. Specimens were allowed to relax for 5 minutes after preconditioning. The definitive torque test

consisted of a single rotation test to 7.5 Nm of torque applied at 1 Nm/sec.

Testing was performed with all ligaments intact and again with the deltoid and syndesmotic ligament complexes completely disrupted. One leg from each pair was then randomly selected to receive “standard” fixation using a standard 4-cortex, 4.5 mm diameter screw, or a tightrope. The fixation was then exchanged and placed through the same hole. The order of fixation placed was also randomized, with 5 specimens having the screw placed before the tightrope and the other 5 having the tightrope placed before the screw. The other ankle from each pair received augmented fixation consisting of a structurally reinforced flexible syndesmosis fixation device, and that device with the addition of suture repairs of the deltoid and anterior inferior tibiofibular ligament. Again, the order of fixation was randomized with n=5 specimens receiving just the structurally reinforced flexible device first and n=5 receiving the additional ligament repair first. The repairs were then exchanged. The rotation angles at 7.5 Nm of applied torque were extracted for comparison of the stability of the different repair strategies (Figure 2).

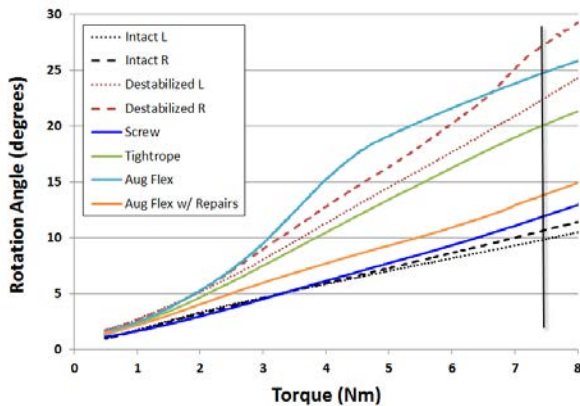


**Figure 2.** Representative torque-angle curves from a single specimen pair. The vertical line indicates 7.5 Nm where the assessment of stability was made.

## RESULTS AND DISCUSSION

Destabilizing the medial and lateral ligaments significantly increased the rotation angle under 7.5 Nm of applied external foot rotation torque. Repair with a screw returned the rotational stability to the joint to near intact levels, whereas the tightrope construct only minimally corrected rotational

instability. The structurally augmented flexible fixation device provided a slight increase in rotational stability over the tightrope device, but did not return the mechanics to intact levels. Addition of ligament repairs to the augmented flexible device successfully returned stability to near intact levels.

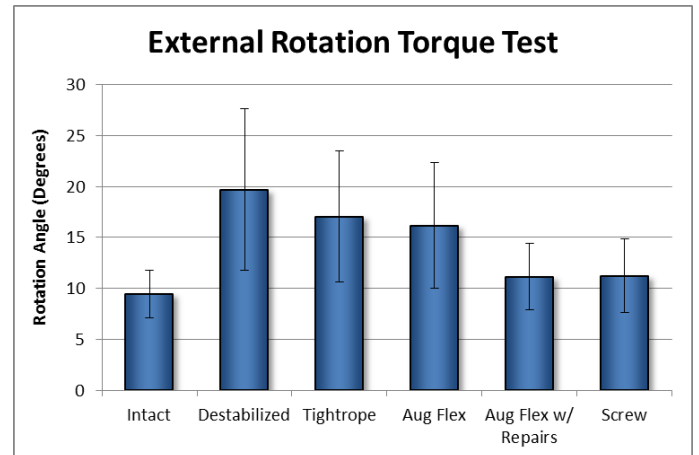


**Figure 3:** Average rotation angle under 7.5 Nm of torque. Error bars indicate standard deviation. n=20 for Intact and the Destabilized conditions, and n=10 for the different repair techniques.

## CONCLUSIONS

Syndesmotic repair has focused on preventing lateral translation of the fibula relative to the tibia using either screws or tightrope repairs. We have found that the tightrope alone is insufficient for restoring rotational stability despite sufficiently preventing coronal plane diastasis. Addition of structural stiffness and/or simulating the anatomic structures disrupted during injury better returned the rotational behavior of a destabilized syndesmosis to normal. This would indicate that there is a need for devices to better recreate the native anatomy.

## REFERENCES

- Schottel PC, et al. *J Orthop Trauma*. 30(2), e36-e40, 2016.
- Clanton TO, et al. *Foot & Ankle Int*. 38(2), 200-207, 2017.

## ACKNOWLEDGMENTS

This work was funded by a research grant from Mortise Medical.

# AN INTRA-OPERATIVE BIOMECHANICAL GUIDANCE SYSTEM FOR REDUCING ARTICULAR FRACTURES

Andrew M. Kern, Michael C. Willey, J. Lawrence Marsh, Donald D. Anderson  
Department of Orthopedics and Rehabilitation, The University of Iowa, Iowa City, IA  
email: andrew-kern@uiowa.edu, web: <http://www.uiowa.edu/uiobl/>

## INTRODUCTION

Patients sustaining intra-articular fractures (IAFs) frequently face poor outcomes. Post-traumatic osteoarthritis (PTOA) is common, partly due to elevated contact stress from residual incongruity following imprecise surgical fracture reduction.

Surgeons already strive to restore an anatomical joint surface, but intra-operative efforts face challenges related to visually judging adequacy of reduction.<sup>1</sup> To address these challenges, we have developed a biomechanical guidance system which uses established 2D-3D pose estimation methods to provide feedback about the positioning of bone fragments. In addition, since a perfectly anatomic reduction can be infeasible, contact stress analysis is used to help the surgeon decide if PTOA-inducing levels<sup>2</sup> are exceeded.

In this study, we present a prototype biomechanical guidance system and report its use in 10 surgeries performed on fractured cadaveric ankles. The accuracy of fragment alignment and contact stress analysis are also evaluated.

## METHODS

The biomechanical guidance system is designed to

provide accurate and useful information to the surgeon relying only upon images from a C-arm fluoroscopy unit. (Fig 1) Before surgery, individual fracture fragments are segmented from a CT scan, and 3D models of the cortical and subchondral bone surfaces are produced. The base fragment, identified as the fragment attached to the tibial diaphysis, is aligned to an anatomical coordinate system for subsequent contact stress analysis.

Intra-operatively, C-arm fluoroscopy (Siemens Cios Fusion) are first acquired, from two different views. Then the orientation of the detector is determined using a custom designed calibration object placed within the field of view. The previously segmented CT data (surfaces, as well as image intensities) are used in a 2D-3D registration algorithm to identify the pose of individual bone fragments. The 3D surface models of the articular bone fragments are displayed to the surgeon in the current state of fracture reduction.

Upon surgeon request, contact stress is computed, (assuming perfect rigid fixation) and overlaid on the 3D model. Contact stress is computed using a previously validated discrete element analysis (DEA) algorithm.<sup>3</sup> The subchondral surface of each bone is offset by 1.7 mm to simulate a uniform cartilage thickness. Contact stresses are computed in

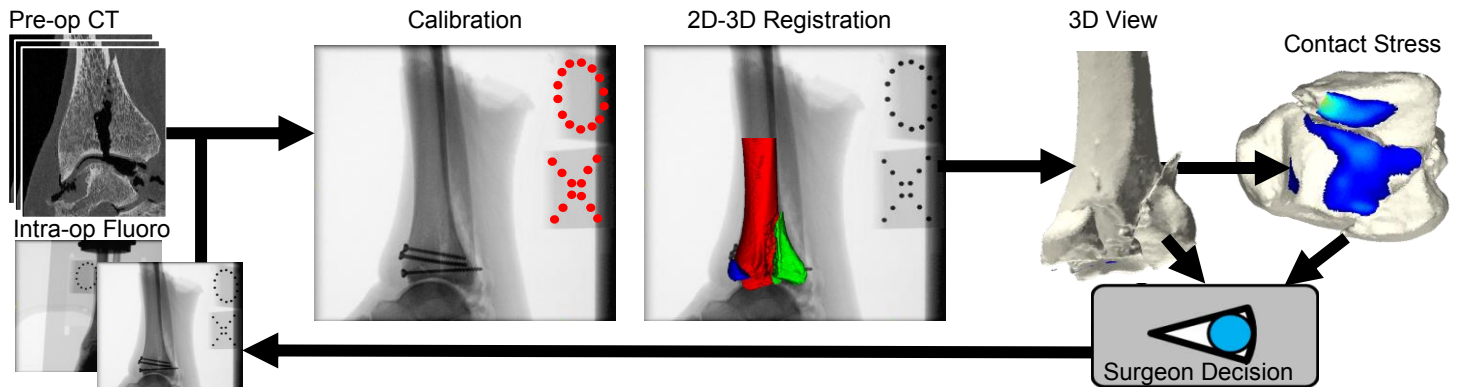


**Figure 1.** Intra-op biomechanical guidance system. Pre-op CT and intra-op fluoro images (calibrated using custom calibration object) enable 2D-3D registration to determine pose of individual fragments. Contact stress results are computed using DEA. Surgeon uses this information to guide their progression through the operation.

a single static pose, with 1000 N axial load applied to the tibia, and 100N applied medially to simulate the stabilizing influence of the fibula.

The system was evaluated in tibial plafond fractures produced in five cadaveric ankles. The fractured ankles were reduced percutaneously, with results recorded by the guidance system. Following final reduction, a post-op CT scan was obtained to provide gold-standard geometric data for evaluation of the registration error of the guidance system. The fixation hardware was removed, and each fractured ankle was reduced a second time (i.e., 10 fracture reductions in total).

Registration accuracy of the intra-op pose data was assessed within Geomagic Studio (3D Systems) by making per-fragment comparisons to surface models of the gold standard data. Accuracy of the intra-op contact stress data was assessed by comparing contact stresses computed using the intra-op pose data to those computed using the gold standard dataset.

## RESULTS AND DISCUSSION

This prototype system was used successfully in 10 simulated surgical procedures. The system was used on average  $4.8 \pm 1.3$  times per procedure. Alignment error in 2D-3D registration is  $0.45 \pm 0.57$  mm in translation and  $2.0 \pm 2.5^\circ$  in rotation. Contact stress distributions and fracture fragment orientations produced by guidance visually compare well to gold standard results (**Fig 2**). The difference in mean and maximum contact stress for intra-op results vs. gold standard are 0.45 (7%) and 1.0 (4%) MPa, respectively.

While there was good alignment accuracy overall, there is substantial variation in alignment error, with alignment errors most commonly present when

small bone fragments are partially occluded by surgical instruments or fixation screws. Continued development of the 2D-3D alignment algorithms and additional experience with the system will likely lead to less frequent alignment failure. Regardless, the contact stress estimates did not vary substantially between intra-operative and gold standard results. This low contact stress error suggests that our guidance system produces results with sufficient accuracy for ongoing study.

## CONCLUSIONS

A system for providing intra-op biomechanical guidance to improve articular fracture reduction has been developed. The system was used successfully in 10 percutaneous cadaveric ankle fracture surgeries. Occasional alignment errors caused by the presence of surgical instruments notwithstanding, this study suggest that the system provides sufficient accuracy to warrant continued evaluation. Future work will involve determining the efficacy of 3D feedback in the OR for improving reduction accuracy and joint biomechanics.

## REFERENCES

1. Garner MR et al. *J Orthop Trauma* 29(4): 161-65, 2015.
2. Anderson DD et al. *J Orthop Res* 29(1):33-9, 2011.
3. Kern, AM, et al. *J Biomech*, 48(12): 3427-32, 2015

## ACKNOWLEDGMENTS

The research reported in this abstract was supported by the National Institute of Arthritis and Musculoskeletal and Skin Diseases of the National Institutes of Health under award number P50 AR055533. Thank you to Tom Bear for help with design and manufacture of calibration hardware.

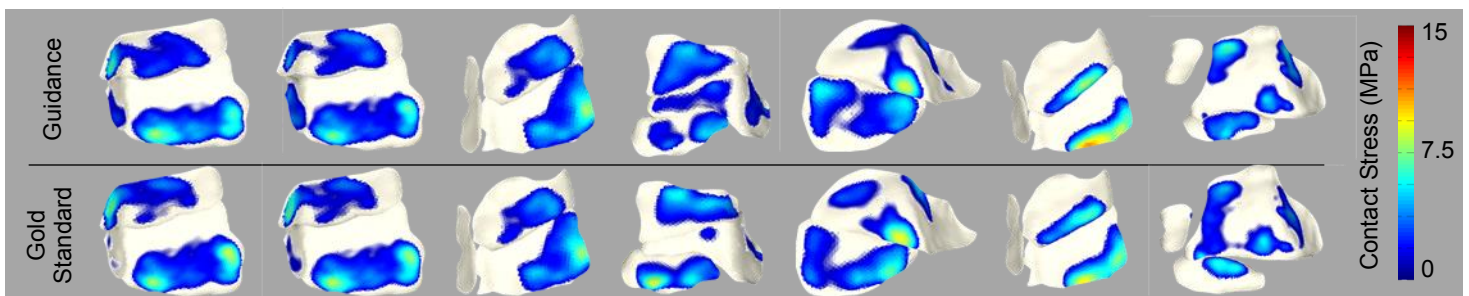


**Figure 2.** Visual comparison between gold standard (CT-based) models and those from the biomechanical guidance system. Cases are ordered left to right by increasing alignment error. Maximum and minimum error cases from the study are represented by the right and left most contact stress plots, respectively.

# THE ANTHROPOMETRIC MODEL INFLUENCES WHOLE-BODY CENTER OF MASS CALCULATIONS IN GAIT

<sup>1</sup> Robert D. Catena, <sup>2</sup> Szu-Hua Chen, and <sup>2</sup> Li-Shan Chou

<sup>1</sup> Washington State University, Pullman, WA, USA

<sup>2</sup> University of Oregon, Eugene, OR, USA

email: [robert.catena@wsu.edu](mailto:robert.catena@wsu.edu), web: <https://labs.wsu.edu/biomechanics/>

## INTRODUCTION

Examining the whole-body center of mass (COM) motion is one of the methods being used to quantify dynamic balance and energy expenditure during gait. One common method for estimating the COM position is to apply an anthropometric model to a marker set and calculate the weighted sum from known segmental COM positions. Several anthropometric models are available to perform such a calculation. However, to date there has been no study of how the anthropometric model affects whole-body COM calculations during gait. This information is pertinent to researchers because the choice of anthropometric model may influence gait findings and currently the trend is for a single model to consistently be used in a study.

## METHODS

We analyzed a single stride of gait data from 103 participants (age 18 to 32, 47 females, average height of 1.75m, average weight of 79.64kg, average BMI of 25.68 kg/m<sup>2</sup>). Fifty-three participants were NCAA athletes or club athletes.

Participants were asked to perform level-walking gait over a 10 m walkway at a self-selected pace. Twenty-nine retroreflective markers were taped to bony landmarks and segments slightly modified from a Helen Hays markers set. A single stride in the middle of the walkway was analyzed. A ten-camera motion capture system captured marker movement at 60 Hz. Marker data were filtered using a 4th order Butterworth filter with a cutoff frequency of 8 Hz.

A 13-segment model of the body was created in Cortex and Biosuite software (Motionanalysis Corp., Santa Rosa, CA). We compared the whole-body

COM motion in each dimension calculated from 4 different anthropometric models [1-4].

We identified the whole body COM location and velocity in each direction at the lead and trailing foot heel strikes and toe-offs. We also identified the total range of motion of the COM in each direction and the maximum velocity of the COM (vCOM) in each direction, as these are commonly used measures of balance control. A within-subject analysis of variance was conducted on each dependent variable to determine the effect of anthropometric model. Follow up pairwise comparisons were conducted using Bonferroni adjustments when appropriate with a significance level (p value) set at 0.01.

## RESULTS AND DISCUSSION

Of all models, Dempster [4] estimates the location of the center of mass highest in the body. The peak medial velocity is also slowest using the Dempster model. The vertical vCOM is highest at specific gait events using Dempster, but peak vertical velocity is only different from the Pavol model.

The Pavol model [2] does not provide much of a different estimate of COM location in the anterior-posterior or medial-lateral directions compared to other models. The vertical COM location estimated by Pavol is in between where other models estimate. The vertical peak velocity is also fastest with the Pavol model.

Plagenhoef [3] consistently estimates the location of the COM in the anterior-posterior direction during heel-strikes about 1 mm off from other anthropometric models. Medial-lateral COM position at heel-strike and total range of motion is

also off from other models. Peak medial-lateral velocity is fastest with the Plagenhoef model.

The de Leva model [1] estimates the COM lowest in the vertical direction of all models. Toe-off anterior velocity and peak anterior velocity is fastest with the de Leva model. Vertical velocity is slowest at heel-strikes using the de Leva model.

The results clearly indicate that COM motion is calculated as statistically different with the use of different anthropometric models. However, while statistically significant, the actual difference between models may not be relevant for level walking gait with respect to anterior-posterior measures of COM motion. Anterior-posterior COM differences were only calculated as being within about a millimeter of each other. COM velocities in the anterior direction were within about two centimeters per second of each model. This amount of difference between models is relatively insignificant compared to the group differences and within-subject variability typically seen in this measure.

Medial-lateral and vertical motions of the COM may be more susceptible to relevant differences between anthropometric models. Medial-lateral COM position between models was within a 1 millimeter difference, however all but the de Leva and Dempster models were statistically different from each other (Table 1). This amount of difference is more important in the medial-lateral direction compared to the anterior-posterior direction. Previous reports have found significant group differences with only a one centimeter difference in COM medial-lateral range of motion [5]. We found a 15 mm/s medial-lateral peak velocity difference between models, representing about a 10% range between models (Table 1). All models were statistically different from each other. Previous reports have found 20 mm/s difference in peak velocity could represent significant group differences [6].

Likewise, consideration should be paid toward choosing the most appropriate anthropometric model when interested in vertical COM motion, as during studies of gait energy expenditure or balance. We found that there was little relevant difference in total vertical range of motion between models, suggesting

that measures of vertical work in gait may not be affected by the anthropometric model. However, we also found that vertical velocity varies widely between anthropometric models, especially at specific events during gait. This may pose a problem for calculations that are velocity based, like kinetic energy. Appropriately identifying the vertical positioning of the COM is also important for some balance measures [6]. The vertical COM position can vary by almost 10% between anthropometric models. The use of the Dempster model may underestimate imbalance in a measure like the inclination angle, while use of the de Leva model may overestimate imbalance [7].

**Table 1.** Average ML COM movement (standard deviation) for each anthropometric model.

<b>Model</b>	<b>[1]</b>	<b>[2]</b>	<b>[3]</b>	<b>[4]</b>
<b>Range (mm)</b>	35.8 (13.7)	36.1 (13.7)	36.6 (13.8)	35.8 (13.7)
<b>Velocity (mm/s)</b>	133.0 (34.0)	130.7 (34.4)	146.0 (34.1)	125.6 (34.4)

## CONCLUSIONS

Our data can provide researchers a priori information on the model determination depending on the particular variable and how conservative they may want to be with COM comparisons between groups. These findings suggest that special consideration should be given the procedural use of an appropriate anthropometric model when medial-lateral or vertical COM motion factors into the dependent variable.

## REFERENCES

1. de Leva P. *J Biomech.* **29**, 1223-1230, 1996.
2. Pavol MJ, et al. *J Biomech.* **35**, 707-712, 2002.
3. Plagenhoef S. et al. *Res Quar Ex Sci.* **54**. 169-178, 1983.
4. Winter DA. *Biomech Motor Cont of Human Mov.* Wiley Interscience, 1990.
5. Catena RD. et al. *Gait Post.* **25**, 406-411, 2007.
6. Catena RD et al. *Neuroeng. Rehab.* **6**. 25
7. Lee HJ and Chou LS. *Arch Phys Med Rehab.* **87**. 569-575.

# LOWER EXTREMITY KINEMATICS OF CROSS-SLOPE ROOF WALKING

<sup>1,2</sup> Scott P. Breloff, and <sup>2</sup> Dwight E. Waddell

<sup>1,2</sup> National Institute for Occupation Safety & Health, Morgantown, WV, USA

<sup>2</sup> University of Mississippi, MS, USA

email: sbreloff@cdc.gov, web: <https://www.cdc.gov/niosh/>

## INTRODUCTION

Since 2011, 173 per 10,000 workers in the construction industry experienced non-fatal falls to a lower level, and 40% of fatal falls in 2015 were falls from height [1]. Considering falls to a lower level accounted for 81% of all fatal falls [1], it is important to determine if occupations that require walking on a sloped surface increase fall risks to the workers.

Sloped gait has been previously studied; up and down slope [2], and cross-slope gait evaluations have been made in low angle conditions (~6 degrees) in a clinical setting [3], or with railroad ballast in an occupational setting [4]. All studies found significant changes versus level walking conditions – ground reaction force, joint moments and sagittal kinematics. While these findings are interesting, they do not replicate the steep surfaces encountered by roofers.

The purpose of this study is to determine how cross-slope walking on a slanted/roof surface alters the lower extremity kinematics of the upper and lower legs compared to level walking. It is hypothesized – in the sagittal plane – the up slope leg will have more flexion in the lower extremity than the level leg while the lower leg will have more extension.

## METHODS

Eleven college-aged male subjects (18.15±15 kg & 180.73±5.89 cm), who were considered inexperienced walking on sloped surfaces, participated in the study. All subjects reviewed and signed an informed consent forms and the study protocol was approved by the University of Mississippi Institutional Review Board.

Subjects completed two separate testing sessions: level surface and sloped surface walking. Due to the complexity and time requirements to install the sloped surface, the testing sessions were not randomized. The level condition consisted of a 10 meter vinyl covered walk-way. The sloped condition was a 4.43m wide x

7.32m long section of 6/12 pitch (~26°) shingled covered roof resting on the laboratory floor (Figure 1).

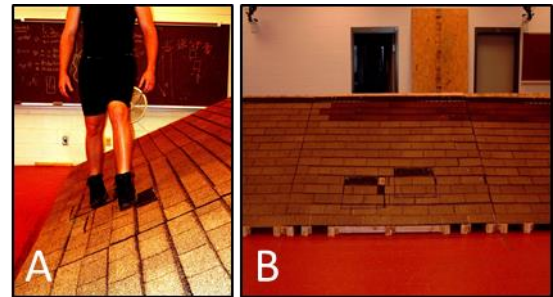


**Figure 1:** A) Frontal view of subject on roof segment. B) Sagittal view of 6-12 pitch roof segment.

Subjects wore spandex clothes and 15 cm high work boots and were outfitted with the plug-in-gait marker set (Vicon, Inc.). The level condition required the subjects to walk across the 10 meter walk way; while the sloped condition had the subjects to traverse the sloped roof section. By traversing the roof section, one foot was higher on the slope (up) and one foot was lower on the slope (down), Figure 1A.

Ten trials from each condition were captured. Lower extremity kinematics (ankle, knee & hip) were calculated using the Plug-in-Gait pipeline in the Nexus software (Vicon). Peak angles (up-slope, down-slope, level) were compared using t-tests. Level data were separated and matched to the corresponding up-slope or down-slope leg. For example, the left leg was down-slope, thus the left down-slope leg peak angles would be compared to the left level leg peak angles. Data analysis was completed using SPSS v22 and *p*-values were set to 0.05.

## RESULTS AND DISCUSSION

All but one (hip extension) of the lower extremity peak angles significantly changed as a result of traversing the sloped roof segment (Table 1). There was no set pattern of the change in kinematics – for

example, the downslope plantarflexion angle decreased compared to level while the upslope foot increased compared to level. Conversely, the knee flexion angle increased from level to slope in the downslope leg and decreased in the upslope leg (Figure 2 & 3; Table 1).

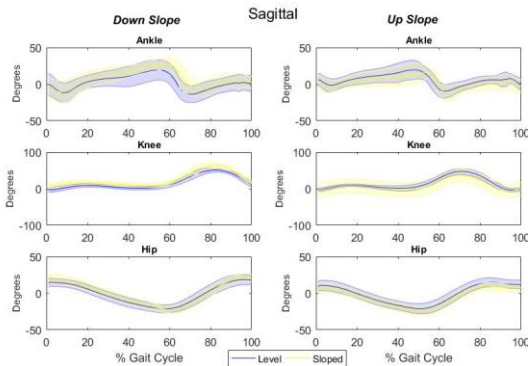


**Figure 2:** Time series histories of lower extremity kinematics comparing level conditions to sloped conditions.

Changes in lower extremity kinematics, posture and gait variability have all been linked to increased risk in falling. Though most of these conclusions are drawn from an elderly population [5], it should not be ignored that the changes in lower extremity kinematics experienced by individuals walking across a sloped surface could lead to the fall risks in the young and healthy.

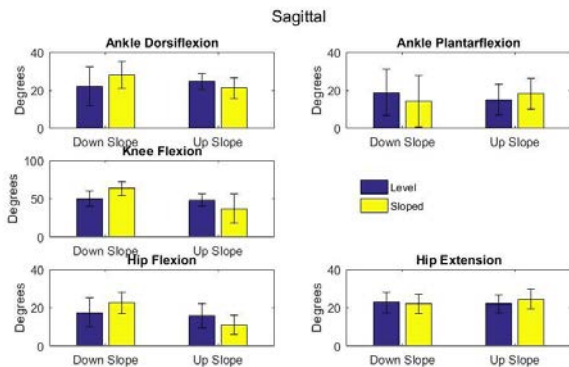


**Figure 3:** Peaks of lower extremity kinematics comparing level conditions to sloped conditions.

**Table 1:** Peak Joint Angles and p-values of the up slope and down slope leg.

Peak Joint Angle (deg)	Down Slope			Up Slope		
	Level	Sloped	p-value	Level	Sloped	p-value
Ankle Plantarflexion	18.9 ± 12.3	13.9 ± 13.5	0.02	15.1 ± 8.0	18.3 ± 8.1	<0.001
Ankle Dorsiflexion	22.1 ± 9.9	28.1 ± 7.2	<0.001	24.5 ± 4.1	21.2 ± 5.5	<0.001
Knee Flexion	50.4 ± 9.7	63.6 ± 9.2	<0.001	48.3 ± 8.0	37.2 ± 18.85	<0.001
Hip Flexion	17.5 ± 7.6	22.6 ± 5.5	<0.001	15.78 ± 6.6	11.1 ± 5.0	<0.001
Hip Extension	22.8 ± 5.4	22.0 ± 4.9	0.28	22.2 ± 4.2	24.5 ± 5.1	<0.001

As an illustration - the increased knee flexion in the downslope leg is similar to what is observed in elderly fallers [5]. Furthermore, the reduced hip flexion in the up slope leg is comparable with a hip flexor muscle contracture.

One limitation of the current study was all subjects walked the same direction on the slope. Therefore, the right leg was always the upslope leg. Furthermore, it was not determined if this was the subjects dominant leg or not. Future studies could compare how dominant vs non-dominant legs respond as upper vs. lower leg.

### CONCLUSIONS

It is apparent that cross-slope walking presents many changes to gait kinematics that associate with increased fall risks. Long term work imposed kinematic changes may make roofers more susceptible to slips, trips and falls, once returning to a level surface. Methods to both combat these changes and educate the workforce are necessary to reduce the injury risk for this worker cohort.

### REFERENCES

1. Bureau of Labor Statistics, Feb 13, 2017.
2. Lay A, et al. *J Biomech* **39**, 1621-1628, 2006.
3. Dixon, et al. *J App Biomech* **26**, 17-25, 2010.
4. Andres RO, et al. *App Erg*, **36**, 529-534, 2005.
5. Kerrigan D, et al. *Arch Phl Med* **82**, 26-30, 2001.

### ACKNOWLEDGMENTS

This research was partially funded by the University of Mississippi's Department of Health, Exercise Science and Recreation Management Graduate Award

**DISCLAIMER:** The findings and conclusions in this report are those of the authors and do not necessarily represent the official position of the National Institute for Occupational Safety and Health. The mention of trade names, commercial products, or organizations does not imply endorsement by the US Government.

# JOINT MECHANICAL POWER COMPENSATIONS WHILE WALKING WITH ANKLE RESTRICTION

Michael Christensen, Anahid Ebrahimi, Teresa Ferrara, Jill Higginson, and Steven Stanhope  
University of Delaware, Newark, DE, USA  
e-mail: mschris@udel.edu

## INTRODUCTION

During gait, individuals with an ankle impairment have restricted ankle function, quantified by reduced ankle mechanical power. These individuals develop compensatory strategies using increased proximal joint (i.e., knee, hip) mechanical power [1]. In order to study the mechanism for this inter-joint mechanical power compensation, researchers have partially restricted ankle function on unimpaired individuals using external ankle foot orthotics (AFOs). While one study reported that unilateral ankle restriction results in an increase in mechanical power at the hip [2], another found bilateral restriction leads to an increase at the knee [3]. However, these studies used AFOs which reduced ankle mechanical power by different amounts. Thus, the primary purpose of this study was to quantify the inter-joint mechanical power compensations when walking with the same amount of ankle restriction unilaterally and bilaterally.

Furthermore, joint mechanical power produced more proximally may lead to an increase in net metabolic expenditure (NME) due to a shift from the highly efficient ankle to the less efficient knee and/or hip [2]. We hypothesized this compensation in joint mechanical power will cause an increase in NME.

## METHODS

Nine healthy subjects (5F/4M,  $1.69 \pm 0.1$  m,  $34 \pm 10$  years,  $75.6 \pm 16.2$  kg) were fitted for AFOs fixed at 90 degrees between the shank and foot to resist dorsiflexion and plantarflexion. Subjects walked on an instrumented split belt treadmill at height-scaled speed of 0.8 statures/s. One 10-minute trial was collected for each of three different conditions while motion (Motion Analysis Corp., Santa Rosa, CA), force (Bertec Corp., Columbus, OH), and metabolic

data (BD, Sydney, Australia) were collected. The subjects walked (1) with standard shoes (Shoes), (2) with an AFO on the dominant (right) limb (RiAFO), and (3) with AFOs on both limbs (BiAFO).

NME (Watts/kg) was calculated by subtracting metabolic expenditure at seated baseline prior to the start of each trial from metabolic expenditure after at least 6 minutes of walking under each condition. Average positive joint mechanical power per stride was calculated at the ankle ( $+\bar{P}_{ankle}$ ), knee ( $+\bar{P}_{knee}$ ), and hip ( $+\bar{P}_{hip}$ ) [4]. Corresponding joint metabolic cost can be estimated for the ankle (MetCost<sub>ankle</sub>), knee (MetCost<sub>knee</sub>), and hip (MetCost<sub>hip</sub>) using efficiency equations [5]. Differences in metrics between conditions were compared using several repeated measures ANOVAs with an overall  $p$  value of 0.05. All post-hoc comparisons reported have been adjusted with the Bonferroni correction using IBM SPSS (IBM Corp., Armonk, NY).

## RESULTS AND DISCUSSION

NME did not significantly change across conditions. Mechanical power and estimated metabolic cost are reported in Table 1.  $+\bar{P}_{ankle}$  and MetCost<sub>ankle</sub> both decreased significantly with unilateral (11% decrease) and bilateral (21% decrease) restriction.  $+\bar{P}_{knee}$ , and MetCost<sub>knee</sub> increased significantly on the impaired limb with unilateral (18% increase) and bilateral restriction (24% increase).  $+\bar{P}_{hip}$  and MetCost<sub>hip</sub> did not significantly change across all conditions.

Interestingly, summed  $+\bar{P}_{knee}$  and  $+\bar{P}_{ankle}$  did not significantly differ across conditions, indicating the knee compensated fully for the decrease in ankle mechanical power (Figure 1).

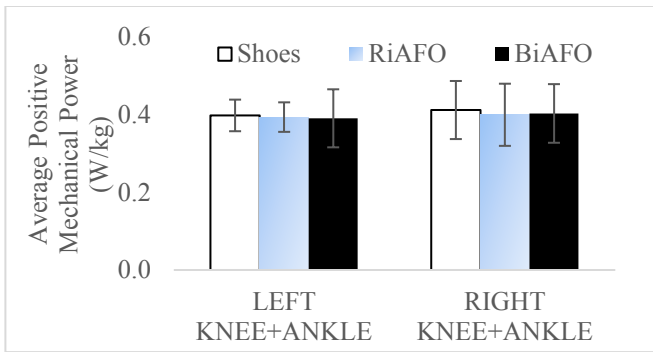


**Figure 1:** Summed knee and ankle average positive mechanical power ( $+\bar{P}_{knee} + +\bar{P}_{knee}$ ) for each limb.

Using the same mechanism to restrict ankle function unilaterally and bilaterally, mechanical power from the ankle was re-distributed to the knee. These findings are similar to data reported on bilateral ankle restriction previously [3]. Wutzke et al. found a primary increase in mechanical power at the hip, but this may be due to differences in the orthotic used to restrict the ankle [2]. A post hoc analysis estimated that Wutzke et al. decreased peak ankle mechanical power by 36% [2], while the present study decreased peak ankle mechanical power by 27%.

Future studies will be necessary to elucidate whether a greater level of ankle restriction will still reveal similar compensatory mechanisms for walking. Although there is a myriad of gait strategies, there appear to be certain requisites which are met. For example, David Winter found the support moment (summed ankle, knee, and hip moment) was similar across walking speeds while individual joint moments varied [6]. It will be important to investigate if total limb mechanical power is one of these requisites of gait such that small inter-joint mechanical power compensations maintain a

constant total limb mechanical power.

## CONCLUSIONS

Compensations for partial ankle restriction occurred at the ipsilateral knee during unilateral ankle restriction and at both knees during bilateral ankle restriction. Interestingly, the increase in mechanical power at the knee compensated for reduced mechanical power at the ankle such that combined ankle-knee mechanical power did not significantly differ across conditions. This re-distribution in mechanical power did not coincide with a significant change in NME.

## REFERENCES

1. Allen JL, et al. *Gait & Posture* **33**, 538-543, 2011.
2. Wutzke CJ, et al. *J Biomech* **45**, 2405–2410, 2012.
3. Huang TP, et al. *J Exp Bio* **218**, 3541–3550, 2015.
4. Buczek FL, et al. *J Biomech* **27**, 1447-1457, 1994.
5. Sawicki GS, et al. *Exerc Sport Sci Rev* **37**, 130-138, 2009.
6. Winter DA. *Hu Mov Sci* **3**, 51-76, 1984.

## Acknowledgements

Funding provided by the NSF Graduate Research Fellowship (#1247394), the Delaware INBRE program (NIGMS 8P20GM103446-16), the University of Delaware College of Health Sciences and Mechanical Engineering Department. The authors thank Independence Prosthetics and Orthotics for assistance with data collections.

**Table 1.** Estimated metabolic cost (MetCost) and average positive mechanical power ( $+\bar{P}_{joint}$ ) for the knee and ankle. <sup>a</sup>Shoes and BiAFO ( $p < 0.05$ ), <sup>b</sup>Shoes and RiAFO ( $p < 0.05$ ), <sup>c</sup>RiAFO and BiAFO ( $p < 0.05$ ).

		Left			Right		
		Shoes	RiAFO	BiAFO	Shoes	RiAFO	BiAFO
MetCost	Knee	0.77 <sup>a</sup> ± 0.067	0.78 <sup>c</sup> ± 0.095	0.95 <sup>a,c</sup> ± 0.149	0.79 <sup>a,b</sup> ± 0.197	0.92 <sup>b</sup> ± 0.189	0.96 <sup>a</sup> ± 0.172
	Ankle	0.35 <sup>a</sup> ± 0.067	0.34 <sup>c</sup> ± 0.047	0.27 <sup>a,c</sup> ± 0.103	0.37 <sup>a,b</sup> ± 0.063	0.29 <sup>b</sup> ± 0.064	0.28 <sup>a</sup> ± 0.078
$+\bar{P}_{joint}$	Knee	0.18 <sup>a</sup> ± 0.016	0.19 <sup>c</sup> ± 0.023	0.23 <sup>a,c</sup> ± 0.036	0.19 <sup>a,b</sup> ± 0.047	0.22 <sup>b</sup> ± 0.045	0.23 <sup>a</sup> ± 0.041
	Ankle	0.21 <sup>a</sup> ± 0.041	0.21 <sup>c</sup> ± 0.029	0.16 <sup>a,c</sup> ± 0.063	0.22 <sup>a,b</sup> ± 0.039	0.18 <sup>b</sup> ± 0.039	0.17 <sup>a</sup> ± 0.047

# Contributions to Increased Walking Speed During Fixed and User-Driven Treadmill Walking

Nicole T. Ray<sup>1</sup>, Brian A. Knarr<sup>2</sup>, Jill S. Higginson<sup>1</sup>

<sup>1</sup>Department of Mechanical Engineering, University of Delaware, Newark, DE, USA

<sup>2</sup>Department of Biomechanics, University of Nebraska at Omaha, Omaha, NE, USA

Contact Email: [nray@udel.edu](mailto:nray@udel.edu)

## INTRODUCTION

Stroke affects nearly 795,000 people annually in the US, making it the leading cause of long-term disability[1]. After stroke, hemiparesis, or unilateral weakness, changes muscle activation and movement patterns and decreases walking speeds[2, 3]. Since decreased walking speeds correspond to diminished quality of life, many poststroke motor rehabilitation programs aim to increase walking speeds[4, 5].

Fast treadmill walking and functional electrical stimulation (FES) of the ankle plantar and dorsiflexor muscles have been added to a 12 week gait training program in an effort to increase walking speed [6]. In these studies, increased anterior ground reaction force (AGRF) and trailing limb angle (TLA) indicated increased walking speeds[7, 8].

To utilize active training principles [9] in gait training, we developed an adaptive, user-driven treadmill controller that adjusts the treadmill's speed to match the user's walking speed in real time. The objective of this study is to determine the relative contribution of AGRF and TLA to increased walking speed during fixed and user-driven treadmill walking. We hypothesize that similar linear relationships exist among walking speed, AGRF, and TLA for both treadmill types.

## METHODS

5 healthy adults (1M 4F, 23.2 ± 5.02 years, 1.67 ± 0.11m, 62.74 ± 10.81kg) with no history of lower limb musculoskeletal injury were recruited for this study. Kinetic and motion capture data were collected using an instrumented split-belt treadmill (Bertec Corp., OH) and an 8 camera motion capture system (Motion Analysis Corp, CA) while participants walked at their self-selected (SS) and fastest comfortable speeds on the fixed and user-driven treadmills for 1 minute each.

Visual3D (C-Motion, Inc., MD) was used to extract walking speed, average peak push-off force (AGRF), and peak TLA (Figure 1). The averages from one randomly selected limb were used for this analysis.

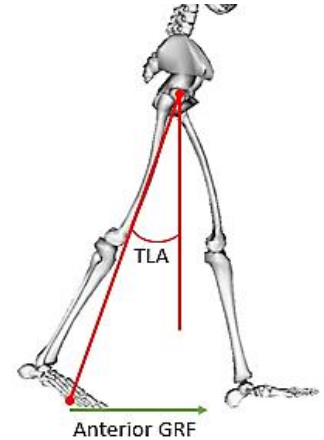


Figure 1: Definition of AGRF and TLA

Linear models were used to describe the relationships between walking speed and AGRF, walking speed and TLA, and AGRF and TLA at both the fast and SS walking speeds to determine the effect of the treadmill mode on gait mechanics.

## RESULTS

Linear models fit to walking speed, AGRF, and TLA are strong and similar at SS speeds, but at fast speeds, the relationships weaken for both treadmill modes (Figure 2, Table 1). AGRF and TLA were highly correlated at both SS and fast speeds (Table 1).

## DISCUSSION

These results show similar linear relationships among walking speed, AGRF, and TLA at the SS speeds for both treadmill types. The highly proportional relationships between SS walking speeds and both AGRF and TLA agree with findings by Hsiao and colleagues [7, 8]. However, at speeds beyond 1.75m/s, these relationships no longer hold. The relationships may change because there are multiple strategies may be used to increase walking speed. For example, one may increase their step length, cadence, or both to increase their walking speed. Despite the user's chosen speed, the relationships among walking speed, AGRF, and TLA do not change in response to the treadmill mode used.

When users walking on a fixed and user-driven treadmill were provided visual flow in a virtual reality environment, there was no significant difference in spatiotemporal parameters, and kinetic and kinematic joint variables [10]. Our results suggest that even without visual flow, our adaptive, user-driven treadmill controller allows users to employ similar strategies to reach their SS and fast walking speeds.

While this study is currently limited in the small sample size (n=5), recruitment is ongoing. The study strengths lie in the homogeneous nature of the population and the control for foot dominance. In addition, these methods control for speed by setting the fixed treadmill to the average speeds from the SS and fast trials on the user-driven treadmill. This additional step isolates the effect of the treadmill controller itself on the user's gait mechanics.

Since active training improves cognitive learning and neuromuscular rehabilitation after stroke, the user-driven treadmill presents the unique opportunity to redefine the standard of care for gait training after stroke. Future work will include spatiotemporal parameters such as cadence as well as kinetic and kinematic measures like knee flexion angle to characterize the gait mechanics used at SS and fast and fast walking speeds on the fixed and user-driven treadmill.

## REFERENCES

1. Benjamin. *Circulation*. pp. 1-485, 2017.
2. Mayo. *Disabil Rehabil*. **21**(5-6) pp. 258-68, 1999.
3. Kesar. *Gait Posture*. **33** (2), pp. 314-7, 2011.
4. Abellan van Kan. *J Nutr Health Aging*. **13** (10), pp. 881-9, 2009.
5. Bohannon. *Int J Rehabil Res*. **14** (3), pp.246-50, 1991.
6. Kesar. *Stroke*. **40** (12), pp. 3821-7, 2009.
7. Hsiao. *J Neuroeng Rehabil*. **12** (1), pp. 40, 2015.
8. Hsiao. *J Neuroeng Rehabil*. **13** (1), pp. 2, 2016.
9. Bulea. *IEEE Annu Conf*. pp. 2111-4, 2014.
10. Sloot. *Gait Posture*. **39** (1), pp. 478-484, 2014.

## ACKNOWLEDGEMENTS

The authors would like to thank NIH P30 103333, NIH P20GM109090, and the UD Helwig Mechanical Engineering Fellowship for their support of this work as well as Kelley Kempinski for her assistance.

Table 1: Summary of linear models fit to walking speed, AGRF, and TLA

Comparison		Slope	Intercept	R <sup>2</sup>
Fixed Mode, SS Speed	AGRF	0.14	0.040	0.96
User-Driven Mode, SS Speed	AGRF	0.14	0.036	0.90
Fixed Mode, Fast Speed	AGRF	0.03	0.213	0.14
User-Driven Mode, Fast Speed	AGRF	0.03	0.206	0.13
Fixed Mode, SS Speed	TLA	7.52	10.561	0.99
User-Driven Mode, SS Speed	TLA	8.32	9.184	0.98
Fixed Mode, Fast Speed	TLA	2.89	17.906	0.19
User-Driven Mode, Fast Speed	TLA	5.17	13.656	0.35

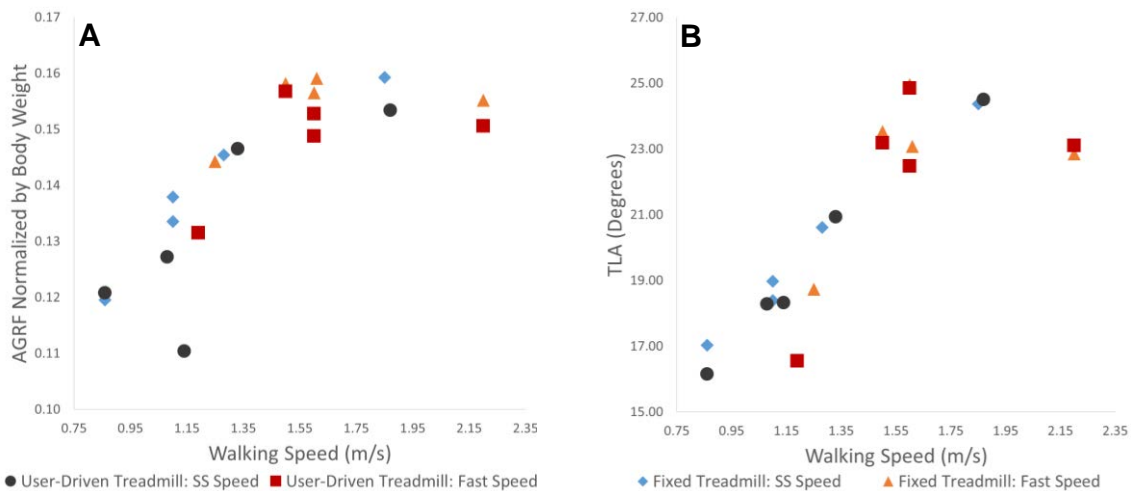


Figure 2: A) Comparison of AGRF normalized by body weight (BW) and walking speed during fixed and user-driven treadmill walking. B) Comparison of TLA in degrees and walking speed during fixed and user-driven treadmill walking.

# THE EXAMINATION OF MOVEMENT COORDINATION BETWEEN BAREFOOT AND MINIMAL FOOT SUPPORT BOOTS IN WALKING

<sup>1</sup>Tom Wu, <sup>1</sup>Seunguk Han, <sup>1</sup>Ariana LaFavre, <sup>2</sup>David J. Pearsall, <sup>2</sup>Pamela J. Russell, and <sup>1</sup>Tyler Champagne  
<sup>1</sup>Bridgewater State University, Bridgewater MA, USA  
<sup>2</sup>McGill University, Montreal, QC, CANADA  
Email: twu@bridgew.edu

## INTRODUCTION

Walking is a fundamental form of human locomotion and is also a basic form of exercise. A typical walking gait consists of both stance and swing phases. During the early portion of the stance phase, the foot pronates after the instant of heel strike. This foot pronation movement helps with shock absorption and ground surface adaptation in walking. The arches under the foot play an important role in assisting with shock absorption, so the selection of proper footwear that can provide proper arch support, particularly for the medial longitudinal arch, is critical [1]. Recently, footwear manufactures have produced boots that have minimal foot support (MFS) for the foot arches. Without proper foot arch support, excessive pronation movements may change the timing and sequencing of the lower extremity joints. This alternation of the joint coordination and sequencing may potentially cause detrimental effect on foot health and lead to lower extremity injury. Therefore, the purpose of this study was to examine the movement coordination between barefoot and minimal foot support boots in walking. The results would help health practitioners to have a better understanding on how minimal foot support footwear could affect walking gait.

## METHODS

Ten college females (age  $21.3 \pm 1.2$  years) were recruited for participation in the study. Approval by the institutional ethics review board was obtained and then prior to the study participants gave written informed consent. All participants warmed up prior to the testing. Five joint reflective markers were placed on the right side of the body at the glenohumeral joint, greater trochanter, lateral epicondyle of the tibia, lateral malleolus, and base

of the fifth metatarsal. During testing, each participant walked for one minute at the speed of 1.3 m/s, a natural walking speed, on a treadmill. Participants walked both barefoot and with the minimal foot support (MFS) boots (UGG classic) with three minutes rest in between. The order of the MFS footwear and barefoot conditions was randomized to reduce the order effect. Data collection concluded in one day with a half hour in duration per participant.

A standard two-dimensional kinematic analysis was conducted with a Casio Camera (Model: EX-FH25) operated at 120 Hz in conjunction with a 650W artificial light to assist in joint marker identification. The Ariel Performance Analysis System (APAS<sup>TM</sup>) motion software was used to obtain angular velocities of the hip, knee and ankle of a gait cycle for each participant. A Butterworth filter function with a cutoff frequency of 10 Hz was applied to the data. The movement coordination pattern was defined as the timing and sequencing of joint movements, and a shared positive contribution (SPC) of proximal to distal joint and a reversed shared positive contribution (RSPC) of a distal to proximal joint based on the angular joint velocity profiles were used to assess movement coordination pattern [2-3]. A SPC or a RSPC of 0% indicates a sequential type of movement, and a SPC or a RSPC of 100% indicates a simultaneous type of movement. Paired sample *t*-tests were conducted at  $\alpha = 0.05$  between barefoot and minimal foot support footwear, and all statistical analyses were conducted with SPSS (v. 23) software.

## RESULTS AND DISCUSSION

Paired sample dependent *t*-tests were conducted on the movement coordination for the hip and knee joint angular velocities and for the knee and ankle

joint angular velocities. There was no statistical significant difference found in the positive contribution of the movement coordination for the hip and knee joint angular velocities ( $p = 0.868$ ) and for the knee and ankle angular velocities ( $p = 0.270$ ) between barefoot and minimal foot support footwear, Table 1.

From the results of this walking gait study, the hip and knee joints showed a slightly more sequential type of coordination whereas the knee and ankle joints showed a more simultaneous type of coordination. When comparing the results to a previous movement coordination study conducted by Wu et al. (2014) on running barefoot and minimalist footwear, similarly, the hip and knee joints were more sequential than the knee and ankle joints that were more simultaneous [4]. Additionally, both positive contributions of the hip and knee joints and the knee and ankle joints were higher in walking than in running. This study supports the notion that when the speed of movement is increased, the movement coordination becomes more sequential [2]. When evaluating the type of sequencing, all ten runners showed a distal to proximal sequencing in the hip and knee joints for both barefoot and minimal foot support footwear and a proximal to distal sequencing in the knee and ankle joints for both barefoot and minimal foot support footwear. These findings are similar as in the previous movement coordination study conducted on running [3]. This study indicates that walking activity, a functional kinetic chain that consists of both open and closed kinetic chains, does not follow the proximal to distal body segmental sequencing as in the open and closed kinetic chains [2,5]. The knee joint initiates the walking motion first and then follows by the ankle and hip joints. The minimal foot support footwear

does not alter the sequencing of the joint coordination pattern, and this may be because these participants already have a low pronation foot profile. Hence, wearing boots with minimal foot support footwear have minimal effect on their walking gait.

## CONCLUSIONS

The purpose of this study was to examine the movement coordination pattern between barefoot and minimal foot support footwear. Ten female participants participated in the study, and each participant walked on a treadmill in barefoot and in minimal foot support (UGG) boots. The results showed no significant change in the timing and sequencing of the walking gait when minimal foot support footwear was worn. This study further reveals the knee joint initiates the lower extremity movement in walking gait, and future studies are warranted to examine the long term effect of wearing minimal foot support footwear and to evaluate movement coordination in other functional kinetic chain activities.

## REFERENCES

1. Genova JM, et al. *J Orthopaedic & Sports Physical Therapy* **30**(11), 664-675, 2000.
2. Hudson, JL *Medicine Science of Sports and Exercise* **18**(2), 242-251, 1986.
3. Wu T, et al. *XVII<sup>th</sup> Canadian Society of Biomechanics*, 2012.
4. Wu T, et al. *7<sup>th</sup> World Congress of Biomechanics*, 2014.
5. McLester J, et al. *Applied Biomechanics: Concepts and Connections*, 2008.

**Table 1:** Movement coordination analysis between barefoot and MFS on the lower extremity

Coordination Pattern	Barefoot	MFS	<i>p</i>
Hip and Knee	44.6 ± 17.6	46.2 ± 20.2	0.868
Knee and Ankle	69.0 ± 28.1	53.8 ± 29.3	0.270

# SPATIOTEMPORAL VARIABILITY OF CHILDREN'S GAIT DURING WALK-TO-RUN TRANSITIONS

<sup>1</sup> Stacey Kung, <sup>1</sup> Philip Fink, <sup>1</sup> Stephen Legg, <sup>1</sup> Ajmol Ali, <sup>1</sup> Sarah Shultz

<sup>1</sup> Massey University, Wellington, New Zealand  
email: s.kung@massey.ac.nz

## INTRODUCTION

Human gait transitions tend to reflect the optimization of gait patterns with changes in task constraints, including the speed of locomotion. As the speed of locomotion changes, adults often choose the more stable and energy efficient gait. Specifically, when walking speeds approach the preferred transition speed (PTS), stride duration variability has previously been shown to increase in adults, which subsequently stabilizes following the walk-to-run transition (WRT) [1]. However, it is unknown whether these self-optimizing tendencies during gait are also present during childhood. Therefore, this study aimed to identify whether children also use the WRT to help stabilize spatiotemporal parameters during gait.

## METHODS

Eleven healthy children (8 females, 3 males; Table 1) completed 2 sessions after written informed assent and parental consent was sought. Participants were first familiarized with the treadmill by walking and running at self-selected speeds for 15 minutes each, followed by three practice transition trials. Session 2 involved a stepped treadmill protocol that started at a self-selected walking pace and the treadmill speed increased by  $0.2 \text{ km}\cdot\text{h}^{-1}$  every 30 seconds until the participant reached a treadmill speed that was  $1.0 \text{ km}\cdot\text{h}^{-1}$  faster than the participants' PTS; the speed was then increased by  $0.5 \text{ km}\cdot\text{h}^{-1}$  until volitional exhaustion. Participants were instructed to start running at the speed that felt most comfortable. The PTS was defined as the speed at which the participant stopped transitioning between walking and running.

Three-dimensional kinematic data were collected at each speed during the stepped treadmill protocol.

Step frequency (Hz) and step length (m) for the left and right legs were calculated for 10 strides at 10 different treadmill speeds, including the participants' self-selected walking speed, five speeds prior to the PTS (i.e. PTS- $1.0 \text{ km}\cdot\text{h}^{-1}$ , PTS- $0.8 \text{ km}\cdot\text{h}^{-1}$ , PTS- $0.6 \text{ km}\cdot\text{h}^{-1}$ , PTS- $0.4 \text{ km}\cdot\text{h}^{-1}$ , PTS- $0.2 \text{ km}\cdot\text{h}^{-1}$ ), the PTS, two speeds following the PTS (i.e. PTS+ $0.2 \text{ km}\cdot\text{h}^{-1}$ , PTS+ $0.4 \text{ km}\cdot\text{h}^{-1}$ ) and a standardized running speed that was  $3.0 \text{ km}\cdot\text{h}^{-1}$  faster than the PTS (i.e. PTS+ $3.0 \text{ km}\cdot\text{h}^{-1}$ ).

**Table 1:** Participants' characteristics and preferred walking (PWS) and transition (PTS) speeds.

	Mean $\pm$ SD	Range
Age (years)	11.55 $\pm$ 0.93	10 – 13
Height (m)	1.55 $\pm$ 0.08	1.45 – 1.69
Weight (kg)	47.12 $\pm$ 10.36	32.00 – 67.86
PWS ( $\text{km}\cdot\text{h}^{-1}$ )	3.8 $\pm$ 0.5	3.0 – 4.8
PTS ( $\text{km}\cdot\text{h}^{-1}$ )	6.6 $\pm$ 0.7	4.9 – 7.7

Standard deviations (SD) of the left and right step frequencies and step lengths were calculated. One-way analyses of variance with repeated measures for speed were used to analyze the effect of speed on the variability of the step frequencies and step lengths. Where significant effects of speed ( $p < 0.05$ ) were found, post-hoc least significant difference (LSD) pairwise comparisons were used to identify the specific relationships ( $p < 0.05$ ).

## RESULTS AND DISCUSSION

There were significant speed effects on the left step frequency ( $F_{(9, 90)}=3.778$ ,  $p < 0.001$ ), right step frequency ( $F_{(9, 90)}=5.534$ ,  $p < 0.001$ ), left step length ( $F_{(9, 90)}=2.459$ ,  $p=0.015$ ) and right step length ( $F_{(9, 90)}=3.952$ ,  $p < 0.001$ ).

When analyzing the walking and running speeds separately, there were generally no significant

differences in the amount of variability of the step frequencies within each mode of gait, irrespective of the speeds, with the exception of walking at PTS-0.8 km·h<sup>-1</sup>. Yet, there is a clear distinction in the variability of step frequencies between the participants' walking and running gaits (Fig. 1). Specifically, the variability of the step frequencies was significantly different between walking and running, suggesting that each mode of gait was associated with different spatiotemporal characteristics during treadmill locomotion.

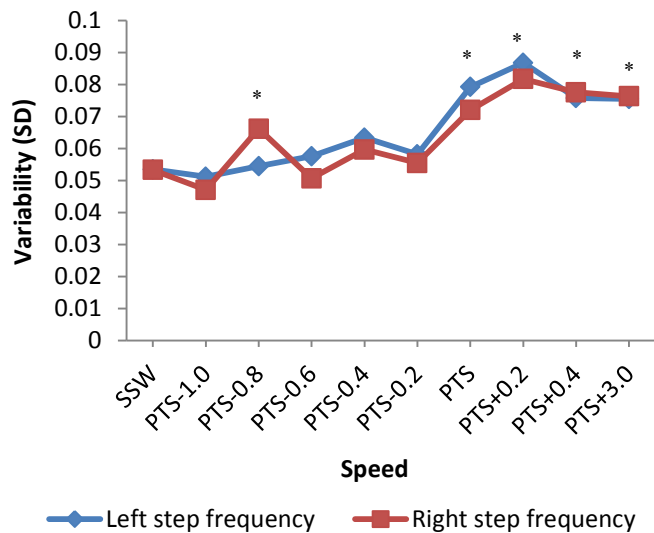


**Figure 1:** Mean variability (standard deviations, SD) of the left and right step frequencies (Hz). Self-selected walking speed, SSW; Preferred transition speed, PTS. \* Significantly different than SSW for step frequency in both limbs.

Interestingly, the participants exhibited a greater amount of spatiotemporal variability following the WRT, which is in contrast to what was observed in adults [1]. Walking may have been the more stable gait pattern in children as it is the more frequently used mode of gait. Additionally, children may have more experience walking at speeds that are faster than preferred if they often walk alongside their parents or other adults, thus contributing to a more stable walking pattern.

Given that there was more spatiotemporal variability during running, the development of a mature, consistent running gait pattern may occur later in children, when compared to walking. Musculoskeletal development during childhood

could be an influencing factor, as limb length is not yet fixed. Therefore, the optimal combination of step length and step frequency may still be subject to change during this period of growth and development, hence the greater variability observed during children's gait transitions compared to adults.

Differences between the inverted pendulum mechanics of walking and the spring-mass mechanics of running may have also contributed to the differences observed between the spatiotemporal variability of walking and running. As the center of mass vaults over a somewhat fixed limb length during walking, step length variability is more limited compared to running where the use of a flight phase could increase variability. To this point, the step length variability was the greatest at the standardized running speed, whereas the self-selected walking speed elicited the least amount of step length variability.

It has been previously observed that slow running is less stable than fast walking [2], which would help explain the initial increase in the step frequency variability following the WRT and the subsequent plateau as the running speed continued to increase towards the preferred running speeds.

## CONCLUSIONS

A lack of stability in 10–13 year old children's spatiotemporal parameters following the walk-to-run transition suggests their running gait patterns may not yet be mature, which could affect their ability to optimize the efficiency and stability of their gait patterns as the speed of locomotion changes.

## REFERENCES

1. Brisswalter J & Mottet D. *Can J Appl Physiol* **21**, 471-480, 1996.
2. Jordan K, et al. *Hum Mov Sci* **28**, 113-128, 2009.

## ACKNOWLEDGMENTS

Anja Fricke for her help with data collection.

# TRUNK NEUROMUSCULAR CONTROL STRATEGIES AMONG PERSONS WITH LOWER LIMB AMPUTATION WHILE WALKING AND PERFORMING CONCURRENT TASKS

<sup>1</sup> Courtney M. Butowicz, <sup>1</sup> Julian Acasio, and <sup>1-3</sup> Brad D. Hendershot

<sup>1</sup> Walter Reed National Military Medical Center, Bethesda, MD, USA

<sup>2</sup> DOD-VA Extremity Trauma and Amputation Center of Excellence

<sup>3</sup> Uniformed Services University of the Health Sciences, Bethesda, MD, USA

email: courtney.m.butowicz.ctr@mail.mil

## INTRODUCTION

Altered trunk-pelvic motions and inter-segmental coordination in persons with unilateral lower limb amputation (ULLA) have been associated with increased risk for secondary health conditions (e.g., low back pain) [1-3]. Kinematic adaptations within these proximal segments may be a result of adopted neuromuscular strategies to account for absent sensory information and/or altered musculoskeletal tissues within the lower extremity due to trauma. In contrast, these adaptations may also indicate impaired trunk neuromuscular control, in that the neuro-musculoskeletal system cannot successfully govern kinematic variability (i.e., mechanical disturbances) and control errors in order to maintain stability. Non-linear analyses quantify the structure of variability over time using stochastic dynamics and may posit how the neuromuscular system controls the trunk in persons with varying levels of limb loss while walking. Thus, the objectives of this study are to: (1) characterize trunk local stability (as an indication of neuromuscular control) in persons with varying levels of ULLA during gait (vs. controls), and (2) evaluate the influences of concurrent cognitive challenges, as the ability to control the trunk during gait requires attentional resources, potentially further influencing trunk stability [4]. We hypothesize that persons with transfemoral ULLA will demonstrate decreased trunk local stability (greater lyapunov exponent) compared to persons with transtibial ULLA and able-bodied controls. Secondarily, persons with transfemoral ULLA will demonstrate larger decreases in local stability with increased cognitive challenge compared to transtibial ULLA and able-bodied controls.

## METHODS

Sixteen males with traumatic ULLA [8 transfemoral (TFA; mean age: 35.4 yrs) and 8 transtibial (TTA; mean age: 33.5 yrs)] and eight controls (CTR; mean age: 27.1 yrs) provided written informed consent, and all study procedures were approved by the local IRB. Participants completed a repeated measures design with three distinct conditions (in random order). For each, participants walked for 8 minutes within the Computer Assisted Rehabilitation Environment (CAREN; Motek Medical BV, Netherlands) at their self-selected speed (mean=1.1±0.2 m/s) while performing a secondary cognitive task (“easy” and “hard”) – each involving distinct attentional demands – or no (“none”) secondary task. For the “easy” task, a single object was displayed on a screen within direct line-of-sight with changing shapes. Participants were asked to press a button whenever a square appeared. For the “hard” task, two objects were displayed simultaneously, with individually changing shapes and colors. Participants were asked to press a button when both objects were either the same shape or same color.

Three-dimensional trunk positions were tracked (120Hz) using a 12-camera motion capture system (Vicon; Oxford, UK). Accelerations were derived using model-based computations in Visual3D (C-motion; Germantown, MD). Local stability of trunk movements was quantified from trunk accelerations using short-term maximum lyapunov exponents ( $\lambda$ ) [5]. Trunk ranges of motion (ROM) were also calculated in each plane as the angular deviation relative to the global coordinate system. A two-way ANOVA compared group (CTR, TTA, TFA) and task (none, easy, hard) for each plane of movement ( $p<0.05$ ). Eta squared for main effects of group are presented as an index of the power of the effect.

## RESULTS AND DISCUSSION

There were no significant interactions between the effects of levels of ULLA and task condition on trunk local stability; however, there were significant main effects of group in the mediolateral,  $F(2,62) = 20.58$ ,  $p < 0.001$ ,  $\eta^2 = 0.39$ , and axial,  $F(2,62) = 28.30$ ,  $p < 0.001$ ,  $\eta^2 = 0.47$  planes. In general, CTR demonstrated less trunk local stability ( $p < 0.001$ ) and smaller trunk ROM ( $p < 0.001$ ) compared to persons with ULLA (Figure 1). However, there were no group differences in anteroposterior plane stability ( $p = 0.34$ ). In the mediolateral and axial planes, TFA demonstrated more trunk local stability, with no differences between cognitive tasks. While the latter is contrary to prior work [6], here we used a different secondary task and a more homogenous sample with respect to age, time since amputation, and walking speed. The concomitant increases in trunk motion and local stability in the TFA group suggest these individuals may employ larger global movements proximally to account for disrupted proprioception and motor function distally. Within these increased global movements, however, this subset of TFA appear to have developed a trunk neuromuscular control strategy that is better able to accommodate increased kinematic variability within the system. This is potentially a compensatory mechanism to prevent balance impairments that can accompany trunk movements outside the base of support. Clinically, rehabilitation goals should aim to increase trunk neuromuscular control via targeted trunk rehabilitation incorporating both anticipatory feed-forward (e.g., active muscle stiffness) and reactive

feed-back (e.g., postural adjustments through proprioceptive mechanisms), resulting in increased local stability and effective control of local mechanical disturbances.

## REFERENCES

1. Hendershot BD, et al. *Clin Biomech* **29**, 235-242, 2014.
2. Russell-Esposito E, et al. *Gait Posture* **40**, 640-646, 2014.
3. Russell-Esposito E, et al. *Clin Biomech* **30**, 1049-1055, 2015.
4. Asai T, et al. *Gait Posture* **38**, 830-836, 2013.
5. Rosenstein MT, et al. *Physica D* **65**, 117-134, 1993.
6. Lamoth JCJ, et al. *Med Engin Phys* **32**, 1009-1114, 2010.

## ACKNOWLEDGEMENTS

This work was supported, in part, by: the Center for Rehabilitation Sciences Research, of the Uniformed Services University of the Health Sciences (DOD Defense Health Program – NF90UG), the DOD-VA Extremity Trauma and Amputation Center of Excellence, and the Peer-Reviewed Orthopaedic Research Program (W81XWH-14-2-0144). The authors wish to thank Alison L. Pruziner, DPT and Vanessa Q. Gatmaitan, MS for their assistance with experimental design and data collection. The views expressed herein are those of the authors and do not necessarily reflect the official policy or position of the Departments of the Army or Defense, nor the United States Government.

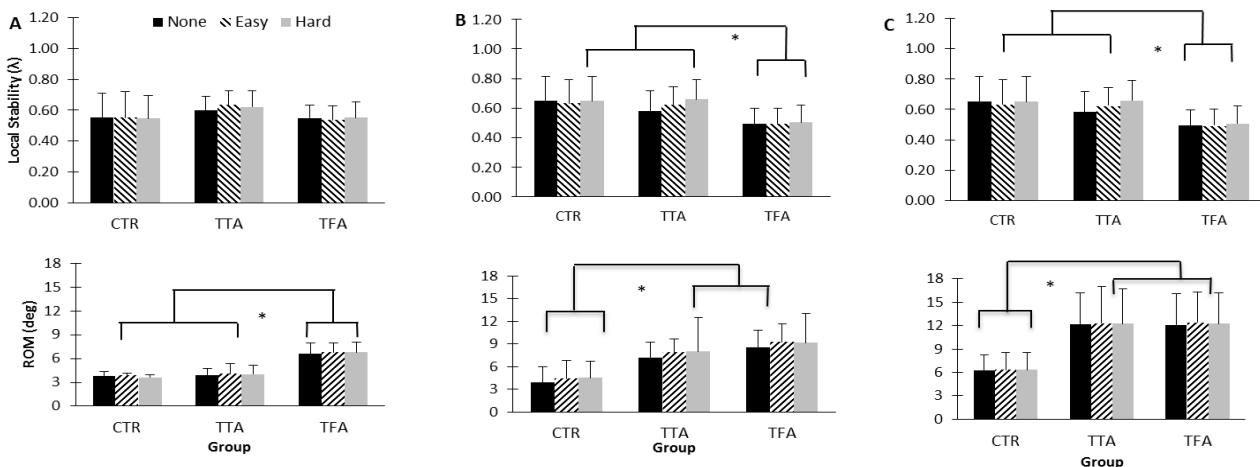


**Figure 1:** Trunk local stability and range of motion (ROM) in the (A) anteroposterior, (B) mediolateral, and (C) axial planes. Asterisks indicate significant ( $p < 0.001$ ) differences between groups.

# THE IMPACT OF ANTHROPOMETRIC CHANGES AND PHYSICAL ACTIVITY ON DYNAMIC BALANCE DURING PREGNANCY

Alexa L. Werner, Kendall M. Iverson, Christopher P. Connolly, Robert D. Catena  
Washington State University, Pullman, WA, USA  
email: [robert.catena@wsu.edu](mailto:robert.catena@wsu.edu), web: <https://labs.wsu.edu/biomechanics/>

## INTRODUCTION

Anthropometric changes and physical activity (PA) participation during pregnancy are potentially two important aspects that may influence balance changes during pregnancy [1, 2]. Understanding balance change among pregnant women is important, as falls are one of the leading mechanisms of injury during pregnancy [2] and result in negative health outcomes for both the mother and fetus. Currently there are few studies that have examined how anthropometric changes impact balance during pregnancy, and so we have a limited understanding of what mechanisms contribute to the increased fall risk of pregnant women. Most studies up to this point have focused on correlating fall risk to gestational age without examining the underlying factors that contribute to dynamic balance. Therefore, the purpose of this study was to compare gestational age, anthropometric changes, and PA during pregnancy as potential correlates to balance changes.

## METHODS

We have currently recruited and tested 33 pregnant participants, but have completed analysis of dynamic balance data for 6 pregnant women (average age of 27.75) from second trimester of pregnancy through birth. Participants were tested once a month.

Participants walked at a self-selected pace on a level treadmill for sixty seconds. Forty-eight retroreflective markers were taped to bony landmarks and segments slightly modified from an established marker set [3]. A ten-camera motion capture system captured marker movement at 100 Hz using Cortex and Biosuite software (Motionanalysis Corp., Santa Rosa, CA) and then low-pass filtered at a 6 Hz cutoff. The entire sixty-second capture was split into individual gait cycles at right heel strikes. The body center of mass (COM) was calculated

using a 13-segment anthropometric model, supported by currently in-review findings. Measures of COM motion with respect to the base of support (BOS), calculated using custom Matlab programs, were used as dependent measures of balance during each gait cycle. Along with gestational age, a range of anthropometric data were collected for all participants at each testing session [4] and used as independent variables. Measures of length were normalized by body height to derive values that could be used for comparison across subjects. Waist circumference and body mass were used to find the changes in weight distribution. To record PA, each participant wore a pedometer (Omron HJ-720ite) during normal daily activities for four days (three weekdays and one weekend day) after balance testing in our lab. We recorded the number of steps and amount of time the pedometer was worn for each day. These data were then averaged into steps/minute to represent PA.

Each independent variable was statistically analyzed using a stepwise multiple regression analysis in SPSS v23 so that the correlation of various independent variables to a balance measure could be compared. Gestational age was included among our other independent variables, as it has been often used in comparison to balance changes during pregnancy.

## RESULTS AND DISCUSSION

Table 1 contains the results of the regression equations for our independent variables.

It appears that waist circumference (as a percentage of body height) and body mass index (BMI) have the greatest correlation to most accepted dynamic balance factors such as step width and minimum distance of the center of gravity (COG) to the BOS. There is a positive correlation between center of mass (COM) medial-lateral (ML) excursion,

maximum COM ML velocity, and step width and waist size. Along with the negative correlation to minimum COG to forefoot boarder, these indicate that balance diminishes as waist circumference and BMI go up. The positive correlation to minimum COG to rear foot border indicates that balance in the posterior direction is not necessarily a concern. While the Pearson coefficient for waist size or BMI alone never exceeds 0.500, when other factors such as gestational age are added into the stepwise regression analysis the R-value can increase to as much as 0.682.

PA had essentially no correlation to balance and interestingly, very little correlation with other independent variables. This suggests that our measure of PA may not have been accurately capturing the physical abilities and/or exercise involvement of these participants. Additionally, gestational age alone had less of a correlation to balance than the correlation of waist size and BMI for the same dynamic balance measures. While the direct correlation does not indicate a strong relationship in the case of either gestational age, waist size, or BMI and dynamic balance, a combination of anthropometric factors correlate well with balance during pregnancy. Also, gestational age is only moderately correlated with anthropometry changes, so anthropometric measures add a unique indication of balance changes not captured by gestational age.

## CONCLUSIONS

Our results combine to show that certain anthropometric changes during pregnancy may be a better indicator than gestational age, or at least different indicator, of balance changes. Physical activity may still correlate with dynamic balance, but our findings from this study do not indicate this to be the case. Future investigations into this relationship will likely require more comprehensive methods of PA assessment. Future research will also examine other potential correlates to balance changes during pregnancy. The observations that COM lateral motions increase in relation to waist size and BMI seem to indicate that these factors may be part of what contributes to the increased fall risk of pregnant women.

## REFERENCES

1. McCrory et al. *JoB*. **43**, 2434-2439. 2010.
2. Weiss H. *AAP*. **40**, 1088-1095. 2008.
3. Catena et al. *Ergonomics*. **58**. 1571-1580. 2015.
4. Pavol et al. *JoB*. **35**. 707-712. 2002.

## ACKNOWLEDGMENTS

This study was funded through a WSU College of Education faculty funding award and a WSU New Faculty award.

**Table 1.** Comparison of Pearson Coefficients for independent variables and stepwise multiple regression model. Subscripts indicate the alphabetical order of the stepwise regression for each dependent variable.

	Pearson Correlation Coefficient									Stepwise Multiple Regression	
	Days to Birth	Waist circumference	Mass (kg)	Mass change	Waist change	Distribution of mass	Distribution change	BMI	Steps per mintue	R-value	P-value
COM ML excursion (mm)	-0.277 <sup>e</sup>	0.312 <sup>d</sup>	0.172	0.012 <sup>f</sup>	0.019	-0.097	0.130 <sup>b</sup>	0.313 <sup>a</sup>	-0.097 <sup>c</sup>	0.371	< 0.001
Max COM ML Velocity (mm/s)	-0.260 <sup>c</sup>	0.338	0.173	0.170	0.000	-0.123 <sup>d</sup>	0.281 <sup>b</sup>	0.366 <sup>a</sup>	0.005	0.483	< 0.001
Min COG to R rear foot border (mm)	-0.430 <sup>d</sup>	0.496	0.167 <sup>c</sup>	0.131 <sup>e</sup>	-0.045	-0.275	0.281 <sup>b</sup>	0.529 <sup>a</sup>	-0.124	0.682	< 0.001
Min COG to R fore foot border (mm)	0.229 <sup>c</sup>	-0.207 <sup>d</sup>	-0.326 <sup>a</sup>	-0.091	-0.096 <sup>g</sup>	-0.183 <sup>e</sup>	0.134 <sup>b</sup>	-0.264 <sup>f</sup>	-0.128	0.434	< 0.001
Step width (mm)	-0.246 <sup>c</sup>	0.342	0.117	0.205	-0.026	-0.188 <sup>d</sup>	0.229 <sup>b</sup>	0.372 <sup>a</sup>	-0.022	0.538	< 0.001

# KINEMATIC GAIT CHARACTERISTICS OF A HETEROGENEOUS POPULATION

<sup>1</sup> Brandon Thurman, <sup>1</sup> Abby M<sup>c</sup>Williams, <sup>1</sup> Lara Pfeiffer, <sup>1</sup> Hanna Slosson, & <sup>1</sup> Michael Bird

<sup>1</sup> Truman State University, Kirksville, MO, USA  
email: mbird@truman.edu; web: hes.truman.edu

## INTRODUCTION

In running gait, the relationship between kinematic characteristics that influence running speed are well researched. Step length (SL) and step rate (SR) are important predictors of run speed [1]. Squadrone & Gallozzi [2] found SL and SR may change when adapting to minimalist running shoes. The relationship between footstrike (FS) pattern and gait kinematics changed when runners changed to minimalist running [3] and has been shown to change during a run [4]. Much of the research performed, however, focused on the homogeneous groups of highly experienced or elite runners. While the relationship between SL, SR, and running speed is not likely to differ for a more heterogeneous population, it is not known how FS pattern may change with running speed within a more general population. Additionally, while much of the previous research classifies FS pattern based on quantitative data, practitioners such as physical therapists often qualitatively classify them. It is important to evaluate the accuracy of these observations in newly trained individuals knowing that self-reported values are not highly accurate [5].

The purpose of this study was to examine the kinematic gait characteristics of a heterogeneous population and to assess the efficacy of qualitative FS pattern assessment.

## METHODS

A heterogeneous group of 258 exercise science students (134 males, 124 females; age: 20.7±1.0 years; height: 1.74±0.11 m; weight: 74.9±8.2 kg) participated. Participants had varying levels of physical fitness and running experience. This study received university IRB approval.

Participants were educated regarding FS pattern

classification prior to data collection. FS pattern was determined by small group consensus and validated using video analysis by well-trained observers (Dartfish Team Pro).

Each participant completed a flying 20 m run at a self-selected slow, medium, fast, and sprint pace. Time was recorded electronically (FarmTek, Polaris) and steps were counted. Running speed (RS), SR, and relative step length (SL/HT) were calculated. A 3x4 ANOVA was run on SPSS to evaluate the three FS patterns and the four paces (alpha=0.05). A Bonferroni correction of alpha level was applied to post hoc tests.

## RESULTS AND DISCUSSION

FS analysis results are displayed in Figure 1. A greater than expected number of midfoot strikers were found at submaximal speeds. The general trend of runners adopting midfoot or forefoot FS patterns as RS increased was expected. Based on video analysis, the newly trained observers were correct for 90-92% of all FS classifications, which is much better than self-reported FS [5]. Most errors appeared to be misclassifications when the runner had FS angles close to a different classification. It is not known how errors in this real-time, subjective classification would improve with experience.

Running speed is the product of step length and step rate [1], yet SL/HT tends to level off at faster speeds. Current results follow the same trends. RS significantly increased across the self-selected paces (p=0.001), with a moderate effect size (ES=0.64), as expected. Forefoot runners were significantly faster than midfoot or heel striking runners at all paces (p=0.001), yet the ES was minute (0.07). There was also an interaction effect between the FS pattern and RS (there were several interaction effects, all with miniscule effect sizes).

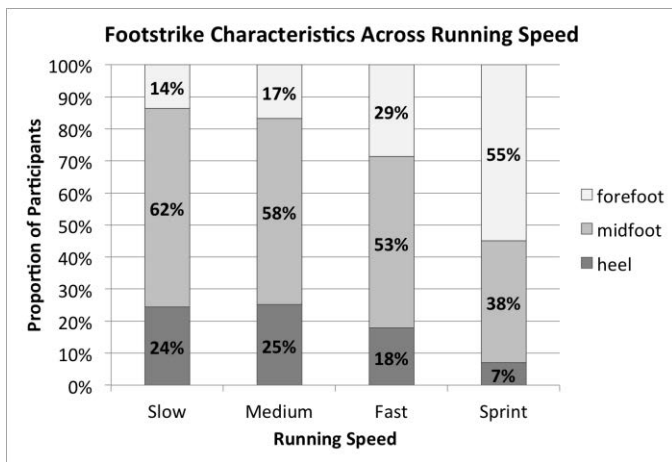


**Figure 1:** FS characteristics across running speeds.

To evaluate the influence of observation accuracy, a subset of 48 subjects was statistically analyzed with the results of video classification of FS pattern. These results were similar to the larger data set. The main effect for running speed was significant (ES=0.64). There was also a significant interaction between FS and RS, but the small difference for forefoot runners no longer remained.

As expected, SL/HT was significantly greater as RS increased (ES=0.43). Forefoot strikers had significantly greater SL/HT than midfoot or heel strikers (p=0.001; ES=0.04). Similar results were found for the subset, where forefoot strikers still had greater SL/HT than midfoot or heel strikers.

Step rate also increased significantly with running speed, as expected (ES=0.51). Forefoot strikers had a significantly greater step rate than midfoot and heel strikers (p=.001, ES=0.02), and there was a significant interaction between RS and FS pattern.

**Table 1:** Footstrike and running pace kinematic characteristics. Running pace data were all significantly different for each variable. \*Significantly different footstrike pattern. †Significant interaction effect between footstrike pattern and pace.

Footstrike Pattern	Running Pace (m/s) <sup>†</sup>				SL/HT				Step Rate (Hz) <sup>†</sup>			
	Slow	Medium	Fast	Sprint	Slow	Medium	Fast	Sprint	Slow	Medium	Fast	Sprint
Heel	3.2 ±0.5	4.1 ±0.5	4.9±0.7	6.2±1.2	0.62±1.0	0.74±0.1	0.83±0.1	0.87±0.1	2.7±0.2	2.9±0.2	3.2±0.3	3.8±0.6
Midfoot	3.2±0.6	4.2±0.6	5.1±0.7	6.4±0.9	0.62±0.1	0.75±0.1	0.86±0.1	0.90±0.1	2.8±0.2	3.0±0.2	3.2±0.3	3.8±0.4
Forefoot*	3.4±0.8	4.5±0.7	5.6±0.7	7.2±0.8	0.65±0.1	0.79±0.1	0.90±0.1	0.96±0.1	2.8±0.3	3.0±0.2	3.3±0.3	4.0±0.4

As with the subset analyzed for RS, the main effect for SR and the interaction between RS and FS pattern remained across speeds, but the greater SR in the forefoot group was not present.

## CONCLUSIONS

This heterogeneous group seemed to run predominantly with heel or midfoot FS pattern at submaximal speeds and increased forefoot FS pattern as speed increased. Perhaps RS and forefoot running are influenced by the same variables; more research is needed to examine this phenomena. A few runners changed FS patterns across pace in less uniform ways, which may be due to classification error or normal variability in FS pattern [4]. We also evaluated the efficacy of qualitative assessments made by newly trained individuals to determine FS pattern. The accuracy rate reflects a degree of potential error in clinical or retail settings where evidence based decisions are determined through observational analysis.

## REFERENCES

1. Hunter, Marshall, & McNair. *Med & Sci in Sports & Exercise* **36**, 261-271, 2004
2. Squadrone & Gallozzi. *J Sports Med & Phys Fitness* **49**, 6-13, 2009.
3. Squadrone, Rodano, Hamill, Preatoni. *J Sports Sciences* **33**, 1196-1204, 2014.
4. Hamill, Russell, Gruber, & Miller. *Footwear Sci*, **3**, 2011.
5. Bade, Aaron, & McPoil. *Int J of Sports Phys Ther* **11**, 2016

# MASS AFFECTS KINETIC SYMMETRY IN CHILDREN'S KNEES DURING GAIT

<sup>1</sup> Sarah P Shultz, <sup>1</sup> Philip W Fink, <sup>1</sup> Stacey M Kung, <sup>2</sup> Mary J Ward, <sup>2</sup> Zolton Antal,  
<sup>3</sup> Sherry Backus, <sup>3</sup> Andrew Kraszewski, and <sup>3</sup> Howard J Hillstrom

<sup>1</sup> Massey University, Wellington, New Zealand

<sup>2</sup> Weill Cornell Medical College, NY, USA

<sup>3</sup> Hospital for Special Surgery, NY, USA

email: s.p.shultz@massey.ac.nz

## INTRODUCTION

Obesity remains a primary risk factor for osteoarthritis (OA) progression, as it can affect all of the tissues within the diarthrodial joint from the biological, mechanical, and structural perspectives. Although OA is often associated with an older cohort, radiographic evidence supports OA development in younger populations. Specifically, obese adolescents displayed cartilage lesions in at least one region of the knee, suggesting early damage to cartilage and increased risk for early progression of OA [1].

Previous research has cited increased sagittal [2, 3] and frontal plane [3, 4] moments in the knees of obese children during walking. With repetitive loading, these increased forces could affect both anterior-posterior and medial-lateral cartilage thickness distribution, respectively. While the increased moments at the knee joint are concerning, there has been no published research that examined whether these increased forces exist bilaterally. Yet, early asymmetries in knee joint loading have been suggested to precede the onset of symptomatic knee OA [5]. Thus, the purpose of this study was to determine the differences in kinetic symmetry between obese and non-obese children.

## METHODS

Twenty-eight adolescents (13-16 years) were classified as non-obese (N=16; age:  $14.7 \pm 1.1$ y; mass:  $54.8 \pm 8.9$ kg; height:  $1.66 \pm 0.10$ m) or obese (N=12;  $14.6 \pm 1.1$ y; mass:  $81.1 \pm 23.4$ kg; height:  $1.64 \pm 0.09$ m), based on international body mass index (BMI) cut-off points [6]. Participants were barefoot and wore tight-fitting clothing; retro-reflective markers were placed according to a previously established protocol [7].

Three-dimensional biomechanics data were collected using a 12 camera motion analysis system and 4 embedded force plates. Participants were asked to walk at their self-selected pace across the 10-m walkway. Five trials were included for processing, based on the following criteria: the presence of bilateral strides, clean footprints on independent force plates, and marker drop-out of less than 20 consecutive frames.

Kinematic and kinetic data were filtered using a bi-directional, low-pass fourth-order Butterworth filter with a cut-off frequency of 6Hz and 40Hz, respectively. Knee joint moments were calculated using inverse dynamics and normalized across stance phase. Bilateral knee joint moments in the sagittal, frontal, and transverse planes were exported for further analysis. Stance phase was subdivided into: loading (1-18%), mid-stance (19-51%), terminal stance (52-84%), and pre-swing (85-101%).

Bilateral kinetic symmetry was represented by an  $R^2$  value, which was calculated between the right and left knee joint moments in the sagittal, frontal, and transverse planes. The total sum of squares (SST) and the error sum of squares (SSE) were calculated:

$$SST = \sum_{j=1}^2 \sum_{i=1}^n (M_{ij} - M_{..})^2$$
$$SSE = \sum_{j=1}^2 \sum_{i=1}^n (M_{ij} - M_{i.})^2$$

where  $M_{ij}$  is the moment at time  $i$ ,  $M_{..}$  is the mean for that moment averaged across both sides of the body and across all time points, and  $M_{i.}$  is the mean across both sides of the body at time  $i$ .  $R^2$  was calculated:

$$R^2 = 1 - \frac{SSE}{SST}$$

$R^2$  values were transformed using Fisher's Z transformation prior to statistical analysis.

Independent t-tests identified group differences in kinetic symmetry for each sub-phase. Statistical significance was set at  $p < 0.05$ .

## RESULTS AND DISCUSSION

Table 1 provides  $R^2$  values for sub-phases that presented significant group differences in kinetic symmetry. Compared to non-obese children, the obese group exhibited significantly greater asymmetry in the sagittal plane knee joint moments during loading and mid-stance sub-phases. Additionally, the obese group presented significantly greater asymmetry in the frontal plane knee joint moments during mid-stance and pre-swing.

**Table 1:** Non-transformed  $R^2$  values for sagittal and frontal plane knee joint symmetry in obese and non-obese children.

	Non-obese (N=16)	Obese (N=12)
<b>Loading</b>		
<i>Sagittal</i>	0.95 ± 0.03*	0.87 ± 0.10
<i>Frontal</i>	0.86 ± 0.18	0.68 ± 0.35
<b>Mid-Stance</b>		
<i>Sagittal</i>	0.88 ± 0.17*	0.71 ± 0.30
<i>Frontal</i>	0.58 ± 0.35*	0.26 ± 0.30
<b>Pre-Swing</b>		
<i>Sagittal</i>	0.74 ± 0.20	0.61 ± 0.29
<i>Frontal</i>	0.82 ± 0.17*	0.61 ± 0.30

\* $p < 0.05$

The majority of group differences occurred in the sub-phases associated with deceleration and weight transfer. Although data were not collected on limb dominance, it would seem that the obese children adapt different strategies when transferring their weight across dominant and non-dominant limbs. The asymmetry in sagittal plane knee joint moments is most consistent during weight acceptance and transfer of the center of mass over the stable foot. Knee flexor moments have a stronger influence early in OA progression and given the timing of the asymmetric over-loading seen in this study, asymmetry in sagittal plane knee joint moments could potentially increase risk of early OA progression in obese adolescents.

The role of altered joint loading in OA progression has been considered in pathological cohorts (i.e. patients with ACL deficiency/injury [8], hip OA [5]), but has not been investigated in otherwise healthy obese individuals. Interestingly, it is suggested that changes in dynamic joint loading at the knee not only precedes onset of symptomatic knee OA, but also appears early in the disease course of hip OA [5]. Because asymmetric joint loading is prevalent at younger ages, the disease course for both knee and hip OA could be established well before an obese individual reaches typically recognized at-risk age ranges. Indeed, radiographic evidence has shown a high incidence of cartilage lesions in the knee joints of obese children with an average age of 14 years [1].

## CONCLUSIONS

Obese children have increased kinetic asymmetry in the sagittal and frontal plane knee joint moments during important sub-phases of stance. The altered joint loading, specifically in the sagittal plane during weight acceptance and transfer, could make obese adolescents highly susceptible to early onset of both hip and knee OA. These risks should be considered when prescribing weight-bearing exercise as part of a weight management program.

## REFERENCES

1. Widhalm HK et al. *Knee Surg Sports Traumatol Arthrosc* **65**, 2615-2622, 2016.
2. Gushue DL et al. *J Pediatr Orthop* **25**, 763-768, 2005.
3. Shultz SP et al. *Arch Phys Med Rehabil* **90**, 2146-2154, 2009.
4. McMillan AG et al. *Gait Posture* **32**, 263-268, 2010.
5. Shakoor N et al. *Arthritis Rheum* **63**, 3853-3858, 2011.
6. Cole TJ et al. *BMJ* **320**, 1240-1243, 2000.
7. Brown AM et al. *Clin Biomech* **39**, 84-90, 2016.
8. Gardinier ES et al. *J Orthop Res* **31**, 458-464, 2013.

## ACKNOWLEDGMENTS

This study was supported by the Weill Cornell Medical College Clinical and Translational Science Center (a Multi-Institutional Consortium).

# DETECTION OF GAIT PATTERN DIFFERENCES USING FAST FOURIER TRANSFORM ANALYSIS

<sup>1</sup> Anthony Vessicchio and <sup>1</sup> Kristin D. Morgan

<sup>1</sup> University of Connecticut, CT, USA  
email: anthony.vessicchio@uconn.edu

## INTRODUCTION

In the United States, an estimated 35 out of 100,000 people suffer an anterior cruciate ligament (ACL) injury each year [1]. Previous studies have analyzed how gait patterns in individuals post ACL reconstruction differ from healthy controls [2-6]. However, these studies have focused on discrete, time domain variables; such as peak knee angle, knee extension moment, and knee excursion. Despite advancements in research and ACL injury prevention programs, ACL injury rates have increased [7]. This indicates that additional information not apparent in the time domain could provide valuable insight into alterations in knee gait patterns in post ACL reconstruction individuals.

Past studies have shown that frequency domain information can be clinically relevant when analyzing gait patterns [8-10]. Both Giakas et al. (1997) and Stergiou et al. (2002) successfully used frequency domain analyses to differentiate between healthy controls and individuals with scoliosis and elderly individuals, respectively, when the time domain variables failed to do so. This study used fast Fourier Transform (FFT) to compare differences in knee gait pattern between healthy and post ACLR individuals. Unlike past studies that focused on the frequency component of FFT alone, and this study focuses on amplitude and phase as well. We hypothesized that the amplitude, frequency, and phase components will be able to detect changes in gait patterns between healthy individuals and individuals post ACLR.

## METHODS

Sixteen control (height  $1.7\pm 0.1\text{m}$ ; mass  $66.7\pm 13.5\text{kg}$ ; age  $20.88\pm 3.9\text{yrs}$ ) and 16 post ACL reconstruction (height  $1.7\pm 0.1\text{m}$ ; mass  $68.83\pm 10.5\text{kg}$ ; age  $19.4\pm 5.1\text{yrs}$ ) participants performed a running protocol and ran at a self-selected speed (control  $2.7\pm 0.4\text{ m/s}$ ; ACLR  $2.7\pm 0.3$

$\text{m/s}$ ) on an instrumented treadmill (Bertec Corp, Columbus, Ohio). Control participants were injury free and ACLR participants were cleared for sports.

Sagittal plane knee kinematics were extracted from processed marker data. The sagittal knee joint time domain data was converted to a frequency domain representation using FFT. The FFT converts a time domain signal into the frequency domain by representing the signal as a series of sinusoids [11]. After being converted to the frequency domain, power and phase spectrums were generated for each signal using a custom MATLAB code (The MathWorks Inc., Natick, MA).

The power spectrum revealed that the majority of the signal energy was contained in the two dominant sinusoids (Fig. 1). Dominant meaning the sinusoids with the largest amplitude excluding the peak at 0 Hz. The amplitude, frequency, and phase components for those two sinusoids for the control left and right limbs and the ACLR individuals injured and non-injured limbs were analyzed. A one-way ANOVA and Bonferroni post hoc analyses were used to determine if between limb amplitude, frequency and phase means were significantly different ( $\alpha=0.05$ ).

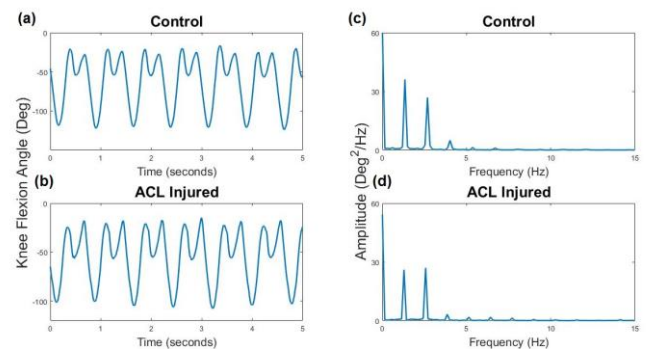


**Figure 1.** Sagittal plane knee kinematics for a (a) control left limb and (b) ACLR injured limb during running. Comparison of power spectrums for the (c) control left and (d) ACLR injured limb.

## RESULTS AND DISCUSSION

The amplitude, frequency, and phase components of the frequency domain all showed significant differences between the control and ACLR limbs. There were significant differences in the frequency and phase components between the ACLR injured and non-injured limbs (Table 1). The second sinusoid of the ACL injured limb group showed a lower amplitude, higher frequency, and lower phase component when compared to the other groups. The first sinusoid of the ACL non-injured limb showed a significantly lower amplitude than the control limbs.

The results presented show that alterations in sagittal plane knee kinematics post ACL reconstruction can be detected from the frequency content of the signal. The amplitude, frequency, and phase components provide a novel way to detect gait pattern abnormalities associated with ACLR. These components may lead to a better understanding of the underlying mechanics involved in gait pattern changes after ACLR. The significant differences between the ACL injured and non-injured limbs support the expected asymmetry between limbs after ACLR [12]. The changes in frequency components may be due to a coping mechanism of the healthy limb present after ACLR.

## CONCLUSIONS

Valuable information can be extracted from sagittal plane knee joint kinematic data by transforming the time domain data into the frequency domain. As hypothesized, variables in the frequency domain such as amplitude, frequency, and phase can be used

to differentiate between healthy controls and subjects who have undergone ACL reconstruction.

Future work will be done to investigate the clinical relevance of these variables. Understanding the underlying mechanics associated with each frequency component may lead to improved ACL injury prevention and rehabilitation programs. Although all of the variables did not present significant differences between groups, the trends in the data lend the need for further investigation. Additional work will be done to analyze these variables in the frontal and transverse planes.

## REFERENCES

1. Donnelly CJ, et al. *Research in Sports Medicine: An International Journal*, **20**, 239-262, 2012
2. Di Stasi S, et al. *Journal of Orthopedic & Sports Physical Therapy*, **45**, 207-214, 2015
3. Hall M, et al. *Gait & Posture*, **36**, 56-60, 2015
4. Gribbin TC, et al. *Clinical Biomechanics*, **32**, 64-71, 2016
5. Devita P, et al. *Medicine & Science in Sports & Exercise*, **30**, 1481-1488, 1998
6. Noehren, B, et al. *Medicine & Science in Sports & Exercise*, **45**, 1340-1347, 2013
7. Mall NA, et al. *The American Journal of Sports Medicine*, **42**, 2363 - 2370
8. Giakas G, Baltzopoulos V, *Gait & Posture*, **5**, 189-197, 1997
9. Gruber AH, et al. *Journal of Sport and Health Science*, **3**, 113-121, 2014
10. Stergiou et al. *Clinical Biomechanics*, **17**, 615-617, 2002
11. Derrick TR. *Research Methods in Biomechanics*. 279-282, 2014
12. White K, et al. *Ortho J Sports Med*. 2013

## ACKNOWLEDGMENTS

We thank Dr. Brian Noehren and his research laboratory for providing the experimental data. And the research was partially funded by NSF IIS 1231545.

**Table 1.** Comparison of the amplitude, frequency, and phase components for the two most dominant peaks between ACLR and control groups

		ACL Injured	ACL Non-Injured	Control Left	Control Right	P-Value
Amplitude (Deg <sup>2</sup> /Hz)	1	28.6 ± 5.9	23.5 ± 3.4 <sup>a</sup>	31.3 ± 6.4 <sup>b</sup>	29.9 ± 6.0 <sup>b</sup>	<0.01*
	2	20.8 ± 3.2 <sup>a</sup>	20.8 ± 3.3 <sup>a</sup>	26.5 ± 5.2 <sup>b</sup>	26.1 ± 4.9 <sup>b</sup>	<0.01*
Frequency (Hz)	1	1.9 ± 1.5	2.6 ± 0.6	1.8 ± 0.7	1.8 ± 0.7	0.07
	2	3.4 ± 3.1 <sup>a</sup>	1.7 ± 0.6 <sup>b</sup>	2.3 ± 0.7	2.3 ± 0.6	0.04*
Phase (Deg)	1	105.0 ± 45.8	88.8 ± 40.1	116.3 ± 34.4	121.5 ± 22.9	0.06
	2	61.9 ± 51.6 <sup>a</sup>	120.3 ± 34.4 <sup>b</sup>	103.7 ± 34.4 <sup>b</sup>	103.7 ± 34.4 <sup>b</sup>	<0.01*

\* denotes significant difference ( $\alpha < 0.05$ )

# DO WE MINIMIZE ENERGY WHEN CHOOSING BETWEEN GAIT PATTERNS?

<sup>1,2</sup> Stephen A. Santos, <sup>1,2</sup> Konrad P. Kording, <sup>1,3</sup> Keith E. Gordon

<sup>1</sup> Northwestern University, Chicago, IL, USA

<sup>2</sup> Rehabilitation Institute of Chicago, Chicago, IL, USA

<sup>3</sup> Edward Hines Jr. VA Hospital, Hines, IL, USA

email: santos@u.northwestern.edu

## INTRODUCTION

Healthy young adults' preferred walking speed, step length, and width minimizes metabolic cost of transport [1, 2]. However, a person's preferred movement may simultaneously satisfy underlying objectives beyond energy efficiency. When forced to, we can choose to walk with many step lengths and widths. Examining the choice between distinct non-preferred stepping patterns, which have different biomechanical (e.g. joint torques) and energetic consequences, can provide insight into the relevant objectives. For example, if a person's only objective is energy efficiency, then equally desirable stepping patterns should have the same metabolic costs.

The goals of this study were to:

- 1) Develop a method to find equally preferable step length-width patterns.
- 2) Test if metabolic cost explains a person's step length-width preferences outside of their normal preferred pattern.

## METHODS

Four healthy young adults (Age:  $27.3 \pm 3.6$ , Gender: 3M) walked on an oversized treadmill at a constant speed (2.7mph), while a projector displayed stepping targets to control step length and step width (Fig. 1A). We defined step length-width patterns as "equally preferred" if there was a 50% chance the participant chose one pattern over another, also known as the point of subjective equality (PSE). To find equally preferred short, long, and wide steps, we used a two-alternative forced-choice paradigm (2AFC). During each trial, participants walked with two different step length-width patterns for 10 seconds: one that remained fixed every trial (fixed choice), and one that was updated based on previous trials (varying choice). The participant chose the step

length-width pattern they preferred most and, as a consequence, walked another 10 seconds with that step length-width pattern. An adaptive staircase algorithm determined the varying step length-width choice for the next trial so the following choice provided more information during later analysis. We chose two fixed "shorter than normal" stepping patterns and then found the equally preferred longer and wider steps by bootstrapping the participant's choices, fitting a logistic function, and calculating the point at which there was a 50% chance of choosing one stepping pattern over another (Fig. 1B). This way we can measure the set of equally preferred movements.

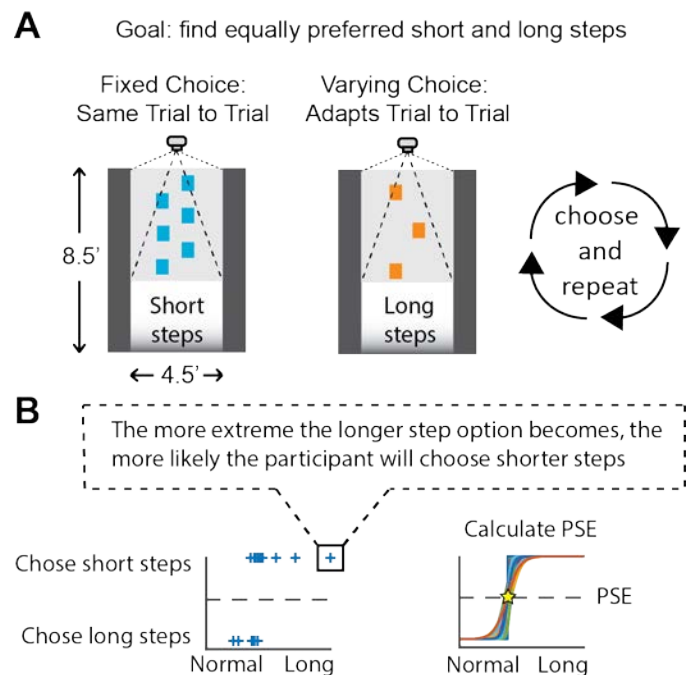


**Figure 1:** A) Example of finding equally preferred shorter and longer steps. B) Calculating equally preferred longer steps, or the point of subjective equality (PSE). A blue cross represents a participant's decision.

Participants then walked for 6 minutes with each equally preferred step length-width pattern to calculate metabolic power using open-circuit respirometry (K4b<sup>2</sup>, COSMED, USA).

## RESULTS AND DISCUSSION

We found equally preferred step length-width preferences using 2AFC. We found that 30 decision trials were sufficient to find step length-width preferences. Ten seconds was a sufficient amount of time to experience each stepping pattern and make a decision, and preferences did not change when participants were given additional time. We also found that step length-width preferences could vary significantly across participants.

Our preliminary results (n = 4) suggest that healthy young adults do not always choose the most energy efficient step length-width pattern (Fig. 2). Three out of the four participants chose longer steps over shorter steps at an increased energetic cost. One participant chose shorter steps over longer steps at an increased energetic cost.

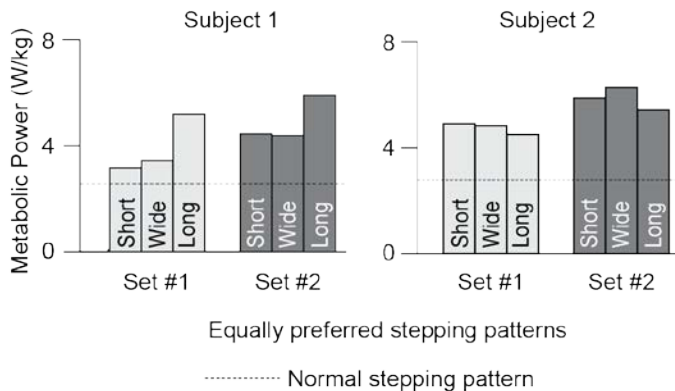


**Figure 2:** Metabolic cost for equally preferred step length-width patterns, outside of a person's normal pattern.

## CONCLUSIONS

We used 2AFC to find equally preferred step length-width patterns. We found that step length-width preferences varied across healthy young adults, and **our preliminary results suggest that energy expenditure cannot fully explain why a person chooses one stepping pattern over another.** In fact, we found a systematic bias towards preferring longer steps to shorter steps. There are likely other factors that influence a person's choice of step length and step width such as stability, joint torques, or comfort. Models and analyses of human locomotion should consider factors in addition to metabolic cost. Future studies can use a similar approach to examine decision making with other parameters of interest (e.g. walking speed).

## REFERENCES

1. Donelan JM, et al. *Proc of the Royal Society B: Biological Sciences*, **268**, 1985-1992, 2001.
2. Zarrugh MY, Radcliffe CW, *European Journal of Applied Physiology* **38**, 215-223, 1978.

## ACKNOWLEDGMENTS

This work was supported by the NIH (T32EB009406)

# SIMULATED WEIGHT GAIN COMPARED TO AN OBESE POPULATION ON LOWER EXTREMITY BIOMECHANICS DURING DESCENDING STAIR WALKING

<sup>1</sup> Amanda L. Ransom, <sup>2</sup> Michelle C. Walaszek, <sup>1</sup> Robert Shapiro, and <sup>1</sup> Lance M. Bollinger

<sup>1</sup> The University of Kentucky, Lexington, KY, USA

<sup>2</sup> Creighton University, Omaha, NE, USA

Email: amanda.ransom@uky.edu, robert.shapiro@uky.edu

## INTRODUCTION

Overweight and obese individuals often use compensatory mechanisms to perform activities of daily living (ADLs), such as descending stair walking [1,2], which may contribute to increased risk of lower extremity injury such as osteoarthritis (OA) [1&3].

Both the amount and location of adipose tissue may be a determinant of certain biomechanical adaptations. An increase in total body and thigh masses has been shown to affect the kinematics and kinetics of the knee in the frontal plane [4 - 6]. Although, the effect of individual segment mass is still relatively unknown [5], we can predict that altering the mass of a segment, such as the thigh, would affect hip and knee kinematic and kinetic variables during descending stair walking.

The exact role of body mass and body mass distribution on obesity-induced biomechanical adaptations are unclear. In an obese population, marker placement becomes difficult due to the excess soft tissue artifact resulting in inaccurate calculations of hip joint centers, which may lead to errors in biomechanical data [7]. Therefore, modeling weight gain may clarify the specific biomechanical adaptations to obesity. The purpose of this study was to compare frontal plane kinematics and kinetics during descending stair walking of an obese population to simulated weight gain (centrally or peripherally) of normal weight individuals.

## METHODS

As of this submission, 15 healthy (5 male; 10 female), normal weight (BMI: 22.3±1.8) participants (age: 23.5 ± 3.7 yrs; height: 1.7±0.1 m; mass: 63.5±11.2 kg) and 5 healthy (1 male; 4 female),

obese weight (OW) (BMI: 33.3±3.2) participants (age: 25.8 ± 5.7 yrs; height: 1.66±0.13 m; mass: 93.4±24.1 kg) have participated in the protocol. Lower extremity kinematic and kinetic, data were collected while descending the stairs. Normal weight participants were loaded with three conditions: unloaded (UL), centrally loaded (CL), and peripherally loaded (PL). For the loaded conditions, participants carried external loads sufficient to increase their BMI by 5 kg/m<sup>2</sup>. For the centrally loaded condition, external load was added to a weight vest. For the peripherally loaded condition, the load was distributed to 50% in the weight vest and 25% to each thigh using specially constructed neoprene sleeves. Normal weight and obese participants descending the stairs at self-selected walking speeds for each condition speed (UL 0.975 ± 0.10 m/s, CL 0.927 ± 0.09 m/s, PL 0.906 ± 0.10 m/s & OW 0.82 ± 0.08 m/s) recorded with Brower Timing Systems, Timing Gates (Power systems LLC, Knoxville, TN). All conditions were randomized and adequate rest was given between conditions.

Retroreflective markers were placed bilaterally on bony landmarks of the trunk, pelvis and lower extremity and 3D data were collected using 10 high speed Motion Analysis Cameras (Motion Analysis Corporation, Santa Rosa, CA, USA) at a sampling rate of 200 Hz. All kinetic data were normalized to the participants' unloaded body weight. The PL condition was corrected for the added mass to the thighs. Force variables were collected using two Bertec force plates (Bertec Corp., Columbus, OH) at 1000 Hz. Joint/segment dynamics were calculated in Visual 3D (C-Motion Inc, Germantown, MD).

The experimental staircase consisted of three steps (step height 16.25 cm, tread length 27.8 cm and step width 95.75 cm) and a platform. No handrail was used but was provided for safety. For each condition

(UL, CL, PL & OW) subjects descended stairs until three valid trials were recorded. A valid trial was defined as walking down the stairs without stumbling and striking the force plate with the dominant leg.

Statistical comparisons were made by a 1-way ANOVA with  $\alpha = 0.05$  and Tukey post-test where appropriate using GraphPad Prism version 7.00 for Windows (GraphPad Software, La Jolla California USA). Data are reported as mean  $\pm$  SD.

## RESULTS AND DISCUSSION

Primary findings in this study, found that the UL was different than the loaded conditions and the obese group during descending stair walking. Specifically, the simulated weight gain and the OW group altered stance phase, step width, peak knee abduction angle, and peak hip abduction angle and abduction moment (Table 1) when compared to the UL condition. Compared to UL, stance duration was higher in CL, PL, and OW ( $p < 0.05$ ). This increase in stance time may help maintain stability and balance when during stair descent [1&2]. Compared to UL, step width was increased in PL and decreased in OW.

OW ( $2.244^\circ \pm 1.22$ ,  $p=0.028$ ) and PL ( $3.351 \pm 4.12$ ) had a significantly lower peak hip adduction angle compared to UL ( $5.336^\circ \pm 3.70$ ). Compared to UL, peak hip abduction moment increased was higher in CL, PL, and OW.

Compared to UL ( $0.055^\circ \pm 2.98$ ), peak knee abduction angle was higher in CL and OW group. No group differences were found when examining knee adduction moment. During level gait, normal weight individuals tend to walk with very little frontal plane knee movement and the knee typically stays adducted throughout stance. The observed change in knee abduction angle could explain the lack of change in knee adduction moment.

Stance phase duration, hip abduction moment, and hip adduction angle are similar between CL, PL and OW suggesting that our model of simulated obesity may mimic some of the biomechanical effects of obesity. It seems that the patterns that are used between all groups (CL, PL & OW) are very similar but there is an increased magnitude in the obese group. However, the magnitude of change in these parameters compared to UL tends to be higher in OW than CL or PL. Therefore, in order to model obesity, we would have to increase the BMI by more than  $5\text{kg/m}^2$ .

Interestingly, simulated obesity and OW elicited different responses in step width and knee abduction angle. Therefore, it is possible that mechanisms other than body mass may influence these parameters in obesity.

## CONCLUSIONS

While these are preliminary results from an ongoing study, they point in the direction suggesting that during descending stair walking weight gain may be able to be modeled. It may be possible to use an acute load to determine the biomechanical effects of weight gain and how this contributes to a chronic condition such as obesity. Further work will consider whether these effects persist in a larger sample.

## REFERENCES

1. Paquette M, et al. *The Knee* **21**, 676-682, 2014.
2. Spanjaard M, et al. *J Exper Bio* **211**, 1368-1375, 2008.
3. Strutzenberger G, et al. *Gait posture* **34**, 119-125, 2011.
4. Kowalk D, et al. *J Biomech* **29**, 383-388, 1996.
5. Westlake CG, et al. *Gait posture* **37**, 359-362, 2013.
6. Segal NA, et al. *AmJ Phys Med Rehab* **88**, 180-191, 2009.
7. McMillan AG, et al. *Gait posture* **32**, 263-268, 2010.

**Table 1:** Results presented as mean and standard deviation. \*  $p < 0.05$  v. Unloaded †  $p < 0.05$  v. OW.

	Unloaded	Central Load	Peripheral Load	Obese Group
Stance phase (% gait cycle)	61.9 $\pm$ 5.3	65.2 $\pm$ 4.5*	66.1 $\pm$ 5.5*	69.0 $\pm$ 3.1*
Step width (m)	0.114 $\pm$ .026	0.114 $\pm$ .037	0.144 $\pm$ .037*†	0.086 $\pm$ .045*
Knee adduction (Nm/kg m)	0.328 $\pm$ .150	0.347 $\pm$ .107	0.345 $\pm$ .095	0.421 $\pm$ .311
Hip abduction (Nm/kg m)	0.777 $\pm$ .016	0.887 $\pm$ .155*	0.887 $\pm$ .120*	0.943 $\pm$ .245*
Knee abduction (°)	0.055 $\pm$ 2.98	0.491 $\pm$ 3.06†	-0.265 $\pm$ 3.16†	0.328 $\pm$ 5.23*
Hip adduction (°)	5.336 $\pm$ 3.70	4.933 $\pm$ 3.75	3.351 $\pm$ 4.12*	2.244 $\pm$ 1.22*

# THE BIOMECHANICAL IMPLICATIONS OF SIMULATED WEIGHT GAIN ON THE LOWER EXTREMITY DURING GAIT

<sup>1</sup> Amanda L. Ransom, <sup>2</sup> Michelle C. Walaszek, <sup>1</sup> Robert Shapiro, and <sup>1</sup> Lance M. Bollinger

<sup>1</sup> The University of Kentucky, Lexington, KY, USA

<sup>2</sup> Creighton University, Omaha, NE, USA

Email: amanda.ransom@uky.edu, robert.shapiro@uky.edu

## INTRODUCTION

Obesity increases risk of lower extremity injury and has been identified as a risk factor for osteoarthritis (OA) [1]. The hip and knee are weight bearing joints, where the combination of an increased load and altered biomechanics, especially in the frontal plane, during walking has been linked to the development and progression of knee OA [1-3]. Overweight and obese individuals use compensatory mechanisms during gait. Compared to their normal weight peers, obese tend to walk with a shorter step length and an increase in step width, which results in a slower self-selected speed [3]. It has been postulated that the slower walking speeds may decrease ground reaction forces and knee moments when walking [1-4].

Obesity is a multifactorial condition comprised of (among others): excess body mass, decreased relative muscle strength and power, decreased agonist recruitment, and premature fatigue. Therefore, the exact role of excess body mass and body mass distribution in obesity-induced biomechanical adaptations are unclear. The purpose of this study was to investigate the independent effects of increasing body mass centrally or peripherally on frontal plane kinematics and kinetics during gait.

## METHODS

As of this submission, 10 healthy (3 male; 7 female), normal weight (BMI:  $23.7 \pm 1.7$ ) participants (age:  $23.7 \pm 4$  years; height:  $1.69 \pm 0.13$  m; mass:  $63.8 \pm 11.6$  kg) have participated in the protocol. Lower extremity kinematic and kinetic data were collected during gait at a self-selected speed. Participants were loaded with three conditions: unloaded (UL), centrally loaded (CL), and peripherally loaded (PL). For the loaded conditions, participants carried external loads sufficient to increase their BMI by 5 kg/m<sup>2</sup>. For the CL condition, external load was

added to a weight vest. For the PL condition, the load was distributed to 50% in the weight vest and 25% to each thigh using specially constructed neoprene sleeves. Participants walked across the walk way at self-selected walking speeds for each condition speed (UL  $1.414 \pm 0.08$  m/s, CL  $1.385 \pm 0.09$  m/s & PL  $1.316 \pm 0.08$  m/s) recorded with Brower Timing Systems, Timing Gates (Power systems LLC, Knoxville, TN). All conditions were randomized and adequate rest was given between conditions. For each condition (UL, CL, PL) all subjects walked until three valid trials were recorded. A valid trial was defined as walking across the force platforms without noticeable changes in gait while striking the force plate with the dominant foot.

Retroreflective markers were placed bilaterally on bony landmarks of the trunk, pelvis and lower extremity and 3D data were collected using 10 high speed Motion Analysis Cameras (Motion Analysis Corporation, Santa Rosa, CA, USA) at a sampling rate of 200 Hz. All kinetic data were normalized to the participants' unloaded body weight. The PL condition was corrected for the added mass to the thighs. Force variables were collected using two Bertec force plates (Bertec Corp., Columbus, OH) at 1000 Hz. Joint/segment dynamics were calculated in Visual 3D (C-Motion Inc, Germantown, MD).

Statistical comparisons were made by repeated measures ANOVA with  $\alpha = 0.05$  and Tukey's post-test where appropriate using GraphPad Prism version 7.00 for Windows (GraphPad Software, La Jolla California USA).

## RESULTS AND DISCUSSION

External loading altered stance phase duration, step width, peak hip adduction angle, peak hip abduction moment, and peak knee adduction moment (Table 1).

Specifically, PL increased the duration of stance phase (~25%;  $p = 0.002$ ) and increased step width (0.029 m;  $p = 0.029$ ) compared to UL. The increase in step width in the PL condition produced a small decrease in peak knee abduction angle ( $p = 0.0505$ ) (Figure 1A,). With the increase in step width, most participants exhibited knee adduction throughout stance.

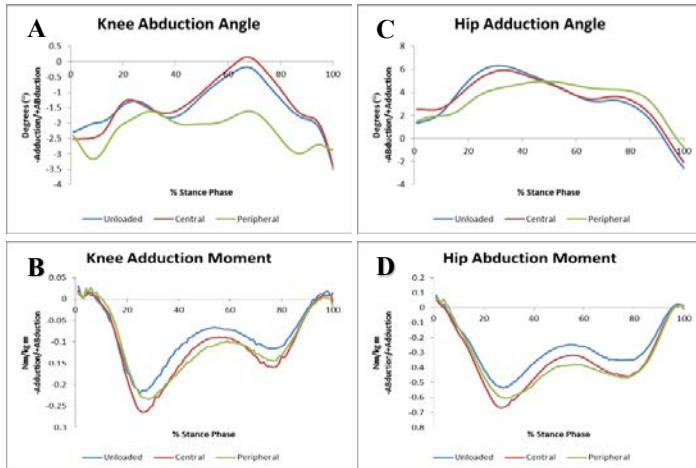


**Figure 1:** Stance phase ensemble curves of the knee abduction angle (A), knee adduction moment (B), hip adduction angle (C) and hip abduction moment (D) during gait N=10.

Peak knee adduction moment was higher in CL ( $0.325 \pm 0.079$  Nm/kg m) than UL ( $0.260 \pm 0.069$  Nm/kg m,  $p=0.002$ ) and PL ( $0.291 \pm 0.076$  Nm/kg m  $p = 0.025$ ). (Figure 1B). Peak knee adduction moment is the only variable that is different between loads.

PL, but not CL, also decreased peak hip adduction angle by approximately  $1.75^\circ$ , compared to UL (Figure 1C  $p=.013$ ). Furthermore, both the CL ( $0.764 \pm 0.108$  Nm/kg m,  $p = 0.005$ ), and PL ( $0.722 \pm 0.096$  Nm/kg m,  $p < 0.001$ ), increased peak hip abduction moment compared to UL ( $0.607 \pm 0.109$  Nm/kg m) (Figure 1B).

In a study comparing normal weight and obese subjects, Browning and Kram [8], found nonnormalized peak knee adduction moments were on average 20 Nm higher in obese subjects. When the joint moments were normalized to body weight McMillan et al. [6], found that during stance the obese subjects had decreased knee adduction moments by 0.04 Nm/kg m. However, these results may be due to differences in normalization methods. Finally, the decrease in moments in McMillan et al. [6], could be a result of decreased gait velocity. Gait velocity was self-selected but the differences between obese and normal weren't reported in their study.

## CONCLUSIONS

These results suggest excess body mass alters frontal plane kinematics and kinetics in a distribution-specific manner during gait. While these are preliminary results from an ongoing study, they point in the direction suggesting that body mass distribution during weight gain may affect biomechanics of the lower extremity during gait. It may be possible to use an acute load to determine the biomechanical effects of weight gain and how this contributes to a chronic condition such as obesity. Further work will consider whether these effects persist in a larger sample.

## REFERENCES

1. Runhaar J, et al. *Obesity reviews* **12**, 1071-1082, 2011.
2. Westlake CG, et al. *Gait posture* **37**, 359-362, 2013.
3. DeVita P, et al. *J Biomech* **36**, 1355-1362, 2003.
4. Naugle KM, et al. *Arch Geron and Ger* **54**, 134-138, 2012.
5. Fregly BJ, et al. *J Ortho Res* **27**, 1016-1021, 2009.
6. McMillan AG, et al. *Gait posture* **32**, 263-268, 2010.
7. Mastaglia SR, et al. *J Clin Densit* **15**, 159-164, 2012.
8. Browning and Kram. *Med Sci Sports Ex* **39**, 1632-1641, 2007.

**Table 1:** Results presented as mean and standard deviation. \*  $p < 0.05$  v. Unloaded †  $p < 0.05$  v. Central.

	Unloaded	Central Load	Peripheral Load
Stance phase (% gait cycle)	$0.649 \pm .005$	$0.662 \pm .006$	$0.675 \pm .009^*$
Step width (m)	$0.102 \pm .006$	$0.104 \pm .003$	$0.131 \pm .004^*$
Knee adduction (Nm/kg m)	$0.260 \pm .069$	$0.325 \pm .079^*$	$0.291 \pm .076^\dagger$
Hip abduction (Nm/kg m)	$0.607 \pm .109$	$0.764 \pm .108^*$	$0.722 \pm .096^*$
Knee abduction ( $^\circ$ )	$0.496 \pm 3.38$	$0.760 \pm 3.48$	$-0.170 \pm 3.08$
Hip abduction ( $^\circ$ )	$8.045 \pm 3.75$	$7.451 \pm 3.41$	$6.277 \pm 3.09^*$

# EFFECTS OF WALKING WITH INCREASED STEP WIDTH ON KNEE ADDUCTION MOMENT

<sup>1</sup> Shannon N Edd, <sup>1,2</sup> Sami Bennour, <sup>1</sup> Baptiste Ulrich, <sup>1,3</sup> Brigitte M Jolles, <sup>1</sup> Julien Favre

<sup>1</sup> Centre hospitalier universitaire vaudois (CHUV), Switzerland

<sup>2</sup> Ecole Nationale d'Ingénieurs de Sousse (ENISo), Tunisia

<sup>3</sup> Ecole Polytechnique Fédérale de Lausanne (EPFL), Switzerland

email: Shannon-Nicole.Edd@chuv.ch

## INTRODUCTION

Knee osteoarthritis (OA) is a leading cause of disability in the elderly, and there is no curative therapy. Disease pathogenesis is not entirely understood; however, gait mechanics have been shown to play a role in medial OA development and progression. The knee adduction moment (KAM) during stance phase, a marker of knee loading, is specifically relevant for this disease. In fact, larger KAM peak during early stance ( $KAM_1$ ) and larger impulse of the KAM during total stance ( $KAM_{impulse}$ ) have been related to OA severity, pain, and loss of cartilage [1].

Therefore, there is a growing interest in gait interventions to decrease these KAM variables [2]. Recently, walking with increased step width has been reported to decrease  $KAM_1$  and  $KAM_{impulse}$ , as well as to decrease the KAM peak during late stance ( $KAM_2$ ) of walking and stair ascent in healthy subjects [3-5]. While these studies, altogether, tested for step width increases in the range of 2-19 cm, a single gait study testing several increases is missing, and the dose-response effect of step width on KAM variables is unknown.

The aim of this study was to characterize the effects of increases in step width from 8 cm to 32 cm on  $KAM_1$ ,  $KAM_2$ , and  $KAM_{impulse}$  in a group of healthy individuals.

## METHODS

Ten healthy subjects (4 female,  $24 \pm 5$  years (mean $\pm$ SD),  $21.4 \pm 1.7$  kg/m<sup>2</sup>) were tested in a gait laboratory after ethics review board approval. Their walking mechanics were monitored following a standard, validated technique using a marker-based motion capture device (Vicon, UK), force plates (Kistler, CH), and the BioMove software (USA) [6].

First, subjects performed five natural walking trials at their preferred walking speed. The normal gait characteristics of each subject, including normal step width (NSW), were calculated based on these trials. Subjects were then asked to walk across the lab while stepping on foot placement targets displayed on the floor. Using the targets, the subjects walked with step width increases of 8, 16, 24 and 32 cm from NSW while preserving their normal foot-progression angle, step length, and speed. Modification trials were recorded in random order.

The percent changes in  $KAM_1$ ,  $KAM_2$ , and  $KAM_{impulse}$  from NSW condition were calculated for each increased step width condition. Student t-tests were used to test these changes versus the null-hypothesis of no change, with  $\alpha=0.05$ . When needed, linear regressions as post-hoc analyses were performed to characterize the associations between step width increase and KAM variables.

## RESULTS AND DISCUSSION

$KAM_1$  was significantly decreased at the 16 cm increase in step width condition ( $p=0.024$ ), but not at the other increased step width conditions (Fig 1A). At all increased step width conditions, both  $KAM_2$  and  $KAM_{impulse}$  were significantly decreased compared with NSW condition (Fig 1B and 1C, respectively,  $p<0.05$ ). Post-hoc regression analyses indicated that six of the ten subjects had significant negative associations between step width increase and changes in  $KAM_1$  and  $KAM_{impulse}$  ( $R^2 > 0.8$ ;  $p<0.05$ ).

The results suggest a sort of threshold response to the decrease in  $KAM_1$  with increased step width. Indeed, while a significant decrease in  $KAM_1$  was found at 16 cm increased step width, this change was not maintained at larger step widths, potentially due to individual compensatory motions at the ankle, hip,

and trunk with such wide steps. This interpretation agrees with the larger inter-subject variations in  $KAM_1$  change at 24 and 32 cm step width increases compared to the inter-subject variations at smaller increases. In fact, while some subjects continued to display decreased  $KAM_1$  at large step width increases, others showed increased  $KAM_1$  from the NSW condition. Thus, care should be taken regarding the amplitude of step width increase in gait retraining programs to reduce  $KAM_1$ .

$KAM_2$  and  $KAM_{impulse}$  were observed to decrease at all increased step widths, and post-hoc regression analyses indicated that there was a linear dose-response for these  $KAM$  variables in 60% of the subjects. There was nonetheless individuality in the  $KAM_2$  and  $KAM_{impulse}$  responses as the regression results showed that  $KAM$  reductions per centimeter of increased step width ranged from 1.0%-1.9% for  $KAM_2$  and 0.9%-2.3% for  $KAM_{impulse}$ . This again supports the need for individual gait retraining programs to reduce medial knee loading ( $KAM$ ).

## CONCLUSIONS

This study highlighted a range of step width increases with consistent  $KAM_1$  reduction for healthy subjects. However, past this range,  $KAM_1$  change became subject-specific. Therefore, while this study confirmed increased step width as a possible gait modification to decrease  $KAM_1$ , this modification may be limited in the amount of  $KAM_1$  reduction it can induce. On the contrary, the decrease in  $KAM_2$  and  $KAM_{impulse}$  was generally continuous with the increase in step width. Even so, large inter-subject variation in  $KAM_2$  and  $KAM_{impulse}$  responses to step width were observed and should be considered in future gait retraining programs. Furthermore, this study was limited to a small group of healthy subjects, and it is of interest to test if these results are also present in medial knee OA patients.

## REFERENCES

1. Bennell K, et al., *Ann Rheum Dis* **70**, 1770-4, 2011.
2. Richards R, et al., *Arch Phys Med Rehabil* **98**, 137-50, 2017.
3. Favre J, et al., *J Orthop Res* **34**, 1547-56, 2016.
4. Fregly BJ, *IEEE Trans Biomed Eng* **55**, 2104-6, 2008.
5. Paquette MR, et al., *J Appl Biomech* **31**, 229-36, 2015.
6. Andriacchi TP, et al., *J Biomech Eng* **120**, 743-9, 1998

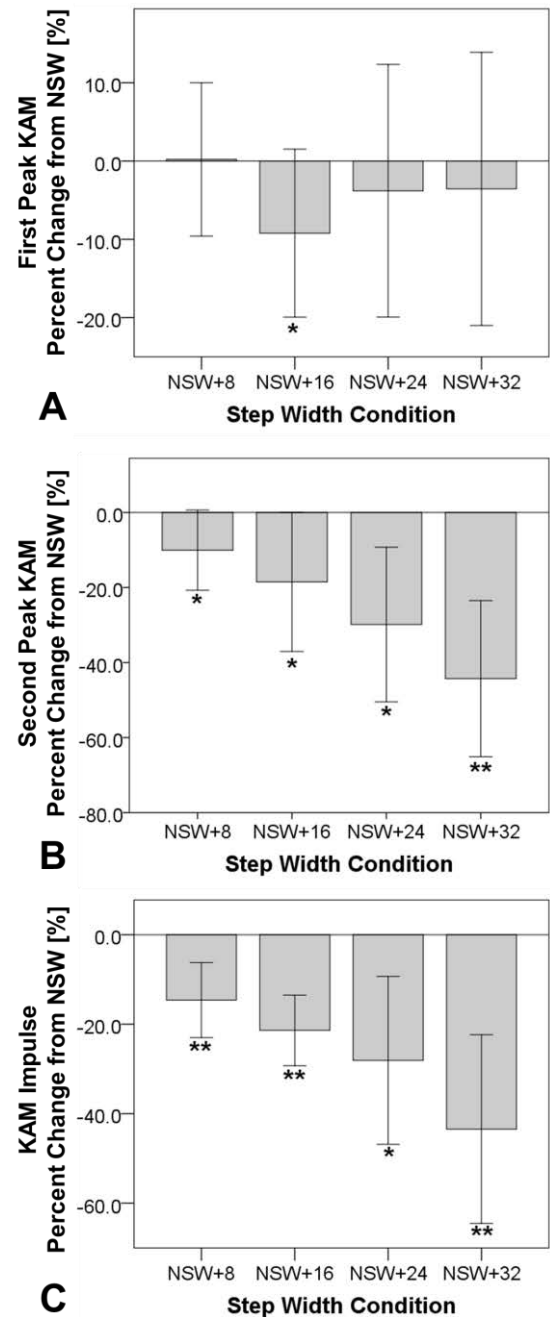


**Figure 1:** Percent changes in  $KAM_1$  (A),  $KAM_2$  (B), and  $KAM_{impulse}$  (C) from NSW condition. Bars indicate standard deviation. T-test for non-zero change: \*  $p < 0.05$ , \*\*  $p < 0.001$

# USING PERTURBATION EXPERIMENTS TO INFER HOW HUMANS CONTROL WALKING

<sup>1</sup> Varun Joshi, and Manoj Srinivasan

Department of Mechanical and Aerospace Engineering  
The Ohio State University, Columbus, OH, USA  
email: [joshi.142@osu.edu](mailto:joshi.142@osu.edu), <http://movement.osu.edu>

## INTRODUCTION

Humans walk stably while also being energy efficient. A better understanding of the human walking controller could help us learn how these potentially opposing objectives are achieved. We perturbed able-bodied human subjects as they walked on a treadmill, and used their kinematic and ground reaction force data to determine how foot-placement and leg-force generation strategies are used to return to steady-state motion [1]. Here, we use data collected from these experiments to derive a controller for two simple models of human walking.

## METHODS

12 subjects (8 male, 4 female) walked for 10 bouts of 4 mins each on an instrumented split-belt treadmill. As they walked kinematic data from 28 markers placed on the torso and lower limbs, along with ground reaction force data from the treadmill were collected. For each individual session, perturbations were either applied in the fore-aft direction (9 subjects) or the medio-lateral direction (7 subjects), with 4 subjects participating in both types of experiments.

Perturbations were applied by humans through inelastic cords, and a load cell in series with the cords measured the magnitude of the perturbation applied. All perturbations were randomly disturbed over the walking bout, with at least 15s and at most 25s of time provided between consecutive perturbations to allow for a return to steady-state. Subjects were made to wear headphones and blinders, to prevent any anticipatory response to the perturbation. All subjects wore a safety harness connected to the ceiling.

We propose two methods for controller derivation, each applicable to a different model of the human walking controller. Both methods measure the deviation of the torso mid-stance state from its nominal value (the mean value during unperturbed walking) and use it as the error term that is being corrected.

1. Consider a biped model that uses the position of the center of pressure (CoP) and the magnitude and direction of the ground reaction force (GRF) as control variables. We can measure the time-varying response of these control variables to a known error in mid-stance torso state. This response can be broken up into many piece-wise linear functions, each mapping the mid-stance torso state into the corresponding control action.
2. Consider a biped model that uses foot-placement and push-off impulse as control variables. First, we use our experimentally collected data to determine a linear function that maps the mid-stance state deviations of human walkers in the  $n^{\text{th}}$  step to the  $n+1^{\text{th}}$  step.

$$\Delta \begin{bmatrix} X_{\text{torso}}(n+1) \\ Z_{\text{torso}}(n+1) \\ \dot{X}_{\text{torso}}(n+1) \\ \dot{Y}_{\text{torso}}(n+1) \\ \dot{Z}_{\text{torso}}(n+1) \end{bmatrix} = J_1 \cdot \Delta \begin{bmatrix} X_{\text{torso}}(n) \\ Z_{\text{torso}}(n) \\ \dot{X}_{\text{torso}}(n) \\ \dot{Y}_{\text{torso}}(n) \\ \dot{Z}_{\text{torso}}(n) \end{bmatrix}$$

For the given biped, we find a corresponding linear function that maps the deviations of torso states and control actions in the  $n^{\text{th}}$  step to the deviations of torso states  $n+1^{\text{th}}$  step.

$$\Delta \begin{bmatrix} X_{\text{torso}}(n+1) \\ Z_{\text{torso}}(n+1) \\ \dot{X}_{\text{torso}}(n+1) \\ \dot{Y}_{\text{torso}}(n+1) \\ \dot{Z}_{\text{torso}}(n+1) \end{bmatrix} = J_2 \cdot \Delta \begin{bmatrix} X_{\text{torso}}(n) \\ Z_{\text{torso}}(n) \\ \dot{X}_{\text{torso}}(n) \\ \dot{Y}_{\text{torso}}(n) \\ \dot{Z}_{\text{torso}}(n) \end{bmatrix} + J_3 \cdot \Delta \begin{bmatrix} I \\ t_{\text{step}} \end{bmatrix}$$

To derive a controller, we relate state-deviations to control-action deviations.

$$\Delta \begin{bmatrix} I \\ t_{\text{step}} \end{bmatrix} = J_4 \cdot \Delta \begin{bmatrix} X_{\text{torso}}(n) \\ Z_{\text{torso}}(n) \\ \dot{X}_{\text{torso}}(n) \\ \dot{Y}_{\text{torso}}(n) \\ \dot{Z}_{\text{torso}}(n) \end{bmatrix}$$

This would give us an effective state transition matrix of the form –

$$\Delta \begin{bmatrix} X_{\text{torso}}(n+1) \\ Z_{\text{torso}}(n+1) \\ \dot{X}_{\text{torso}}(n+1) \\ \dot{Y}_{\text{torso}}(n+1) \\ \dot{Z}_{\text{torso}}(n+1) \end{bmatrix} = J_2 \cdot \Delta \begin{bmatrix} X_{\text{torso}}(n) \\ Z_{\text{torso}}(n) \\ \dot{X}_{\text{torso}}(n) \\ \dot{Y}_{\text{torso}}(n) \\ \dot{Z}_{\text{torso}}(n) \end{bmatrix} + J_3 \cdot J_4 \cdot \Delta \begin{bmatrix} X_{\text{torso}}(n) \\ Z_{\text{torso}}(n) \\ \dot{X}_{\text{torso}}(n) \\ \dot{Y}_{\text{torso}}(n) \\ \dot{Z}_{\text{torso}}(n) \end{bmatrix}$$

We need to solve for  $J_4$ , such that we minimize the error between  $J_1$  for the human and the model

$$J_1^* = J_2 + J_3 \cdot J_4.$$

## RESULTS AND DISCUSSION

Figure 1 shows how we can use piece-wise linear functions to determine the effect of a 0.2 m/s change in mid-stance torso velocity on GRFs over the following stride. We see that a rightward push would lead to a corresponding leftward shift of the time varying GRF. A forward push comparatively leads to a backward shift in GRF during single support but almost no change in GRF while in double support.

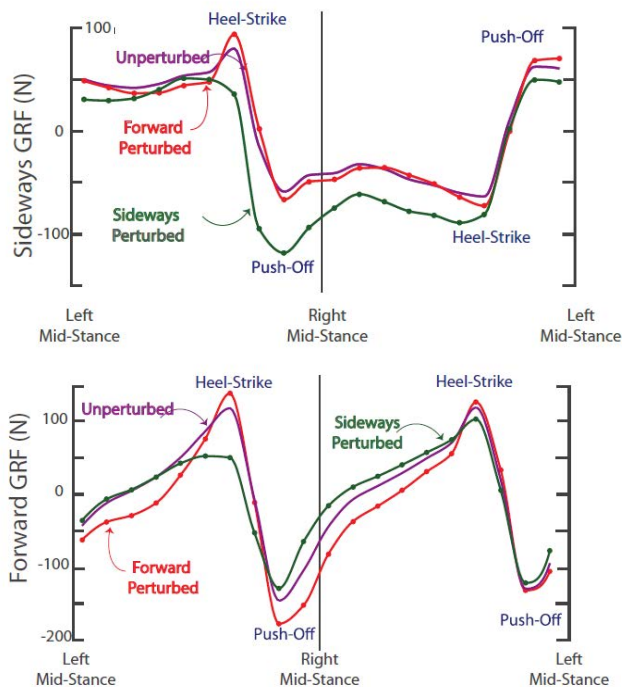


Figure 1. If a perturbation produces a 0.2 m/s deviation in mid-stance velocity in the forward (red curves) or rightward (green curve) direction sideways and forward GRFs are modulated to return to steady-state.

Figure 2 shows how the same change would affect CoP position over the following step. A rightward push causes the CoP to move far rightward and very slightly backward over the next step. An equally large forward push causes the CoP to move very slightly forward during single-stance but does not affect the sideways CoP position at all.

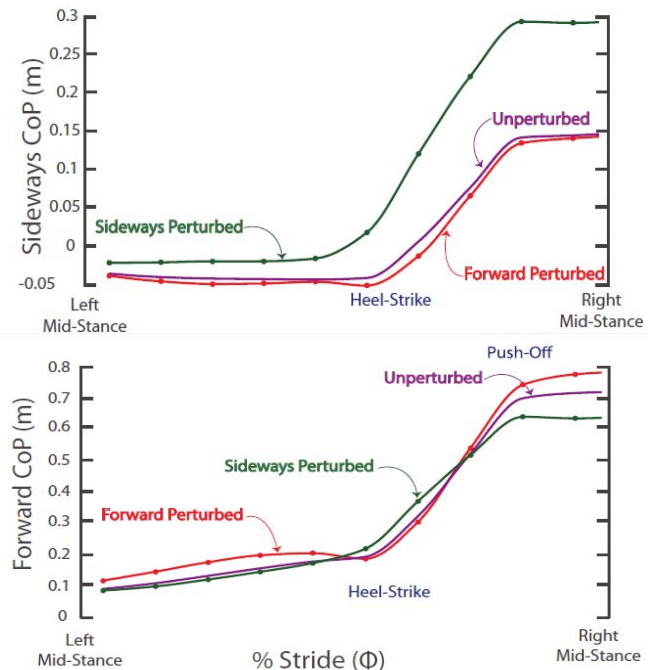


Figure 2. If a perturbation produces a 0.2 m/s deviation in mid-stance velocity in the forward (red curves) or rightward (green curve) direction CoP positions are modulated to return to steady-state.

These models show us how able-bodied humans respond to perturbations, and could be used to quantify how movement disorders impair gait or to measure the effect of rehabilitation techniques. We could also try to use these controllers to design gaits for bipedal robots, to make them more human-like.

## REFERENCES

1. V. Joshi and M. Srinivasan, "Understanding foot placement dynamics and leg-force generation in humans using perturbation experiments", Dynamic Walking 2016

## ACKNOWLEDGMENTS

This work was supported by National Science Foundation grants number 1538342 and 1254842.

# KNEE FLEXION MODIFICATIONS DURING PEDIATRIC GAIT USING VISUAL FEEDBACK

<sup>1,2</sup> Nuno Oliveira, <sup>1,2</sup> Naphtaly Ehrenberg, <sup>2</sup> JenFu Cheng, <sup>2</sup> Sheila Blochlinger, and <sup>1,2</sup> Peter Barrance

<sup>1</sup> Kessler Foundation, West Orange, NJ, USA

<sup>2</sup> Children's Specialized Hospital, New Brunswick, NJ, USA

email: noliveira@kesslerfoundation.org

## INTRODUCTION

Pediatric populations with gait disorders can present temporal and spatial deviations from normative gait that have severe consequences for gait function. Altered sagittal knee motion is one of the most common deviations associated with reduced gait function [1].

Visual biofeedback relies on the sensory integration of real-time visual information to modify specific motor behaviors [2]. While a variety of feedback modalities has been used to modify gait parameters [3], the use of visual feedback to modify knee flexion kinematics during pediatric gait is limited.

The purpose of this study was to investigate how pediatric participants modify their knee flexion patterns during gait using a visual kinematics feedback system (VKFS). Four modifications that increased, and that decreased maximum knee flexion during the gait cycle were tested. The study measured maximum knee flexion angle and full gait cycle error.

## METHODS

Twelve typically developing children and adolescents (6M, 6F; 11.9±2.7 yrs old) participated in the study. All research procedures were approved by the Kessler Foundation Institutional Review Board.

Knee flexion angle data were collected using Inertia Measurement Units (Xsens MTw, Enschede, The Netherlands) with a sampling frequency of 50Hz. Three sensors were fixed to each participant's dominant lower limb. One sensor was placed on the anterior thigh, a second sensor was placed on the posterior shank, and a third sensor was attached to the heel of the participant's shoe. To process and

integrate the data recorded by the sensors into a display for visual feedback, a VFKS was developed in MATLAB (MathWorks Inc., Natick, MA).

After calibrating the flexion angle, participants were asked to walk on the treadmill at a comfortable speed. This speed was used for the duration of each participant's testing. Participants were then asked to walk for 1 min while their natural walking knee flexion pattern was recorded ('gait analysis', GA). A reference gait cycle (RGC) was calculated by averaging 20 time normalized strides. The RGC curve between the two minima before and after maximum knee flexion was amplified and reduced by 20 and 40%, resulting in four different target gait cycles (TGC<sub>+40</sub>, TGC<sub>+20</sub>, TGC<sub>-20</sub>, TGC<sub>-40</sub>). The order of presentation of TGC was randomized, and for each TGC, participants were tested as they walked with real-time visual feedback (FB, 3 min), and with no feedback (NFB, 1 min). During FB trials, participants were asked to experiment with and adopt gait modifications in response to the visual cues displayed by the VKFS. Participants were asked to use the primary full cycle error display to score 'points', and were also provided two assistive cues on peak flexion and timing error (Fig. 1). All feedback was based on the most recent step. In NFB trials, participants were asked to try to maintain the knee flexion pattern previously learned while walking on the treadmill without feedback.

All analyzed cycles were normalized in time (0-100%, interval = 1%). The following measures were calculated for FB and NFB testing conditions by averaging data from the last 10 cycles of the trial. Mean absolute cycle error ('MACE') was calculated as the mean across cycles of the mean absolute difference between the measured angle and the TGC angle. Peak error ('PK') was calculated as the mean across cycles of the absolute error between the measured maximum angle and the maximum angle

of the TGC. Pre-exposure reference values (REF) for each of the above measures at each TGC were calculated by using the 20 RGC cycles as the measured angles.

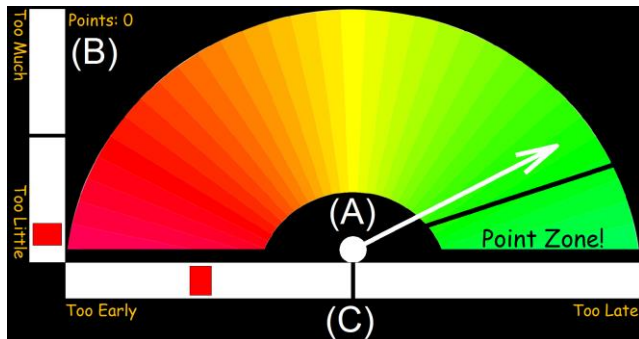


**Figure 1:** (A) The primary feedback needle moved in proportion to the sum of squared angle error across the cycle. A large error was indicated by movement of the needle to the red area, while the green area indicated a small error. A point count was incremented for each gait cycle the needle was in the 'point zone'. Secondary feedback displays indicated signed feedback on (B) magnitude and (C) timing of peak knee flexion.

For both measures and all TGCs, paired sample t-tests with a significance level of 0.05 were used to test for significant differences between REF and FB, NFB conditions.

## RESULTS AND DISCUSSION

For all TGC, PK was significantly smaller for FB than REF (Fig. 2), indicating that participants were able to use the VKFS to change maximum knee flexion in the sense indicated by the target. PK for NFB was significantly smaller than REF for TGC<sub>+40</sub> and TGC<sub>-40</sub>, indicating the ability to maintain aspects of the learned pattern after removal of feedback. However, MACE in FB and NFB was frequently higher than the respective reference measures, and in some cases these increases were significant. Increases in MACE were explained by the results of an examination of the distribution of absolute error across the cycle: decreases in the altered region (peak knee flexion) were offset by increases elsewhere. In some cases these appeared to reflect overall biasing of the gait pattern toward the change intended for peak knee flexion; for example, with TGC<sub>-40</sub>, participants often adopted a pattern with less flexion across the whole cycle. Other changes may have been compensatory motions adopted to facilitate the execution of the targeted patterns.

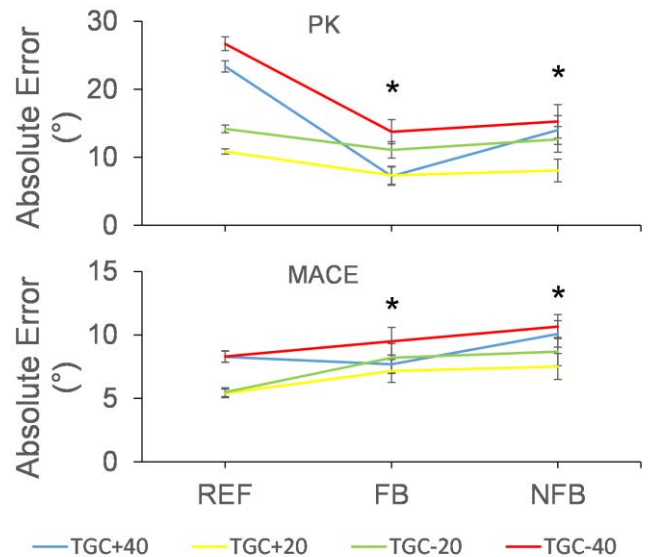


**Figure 2:** Absolute errors for TGCs across testing conditions. Error bars denote group standard errors. \* indicates significant differences between condition and reference for at least one TGC.

## CONCLUSIONS

Maximum knee flexion during typically developing pediatric gait was directed toward specific targets in response to the VKFS. However, overall cycle error was not reduced, indicating that by deviating maximum knee flexion from normal, other parts of the gait cycle were altered. It is possible that reduction in overall error could result from longer FB exposure times. Further work applying the current VKFS in the normalization of pathological gait patterns, rather than deviations from normal gait, might result in reductions of overall error. Additionally, the VKFS error feedback might be weighted to target a specific deviation.

## REFERENCES

1. Sutherland, and Davids, Clinical orthopaedics and related research, 1993. **288**: p. 139-147.
2. Sober, and Sabes, Nature neuroscience, 2005. **8**(4): p. 490-497.
3. Shull, et al., Gait & Posture, 2014. **40**(1): p.11-19.

## ACKNOWLEDGMENTS

Support for this study was provided by Children's Specialized Hospital (New Brunswick, NJ) and Kessler Foundation (West Orange, NJ).

# LOWER EXTREMITY JOINT CONTRIBUTIONS TO FRONTAL PLANE TRUNK DYNAMICS IN PERSONS WITH LOWER EXTREMITY AMPUTATION

<sup>1,2</sup> Adam J. Yoder, <sup>1,2</sup> Shawn Farrokhi, <sup>1,3,4</sup> Christopher L. Dearth, <sup>1,3,4</sup> Brad D. Hendershot

<sup>1</sup> DoD-VA Extremity Trauma & Amputation Center of Excellence

<sup>2</sup> Naval Medical Center San Diego, San Diego, CA

<sup>3</sup> Walter Reed National Military Medical Center, Bethesda, MD

<sup>4</sup> Uniformed Services University of the Health Sciences, Bethesda, MD

Email: adam.j.yoder.civ@mail.mil, web: www.health.mil/eace/

## INTRODUCTION

Persons with unilateral lower extremity amputation (LEA) have altered trunk-pelvis kinematics and joint/muscle forces during walking relative to able-bodied (AB) persons [1,2]. These altered mechanics are believed to be associated with the increased prevalence of and risk for both low back pain (LBP) and falls in persons with LEA. Recent work has demonstrated that in AB walking, all joint moments in the body can contribute to net trunk dynamics, which may include complex inter-planar couplings; for example, the stance limb sagittal ankle moment can induce frontal plane trunk angular accelerations that tend to tilt the trunk ipsilaterally [3,4]. In persons with vs. without LEA, elevated ipsilateral trunk lean during prosthetic limb stance is a commonly reported deviation [1,2]. Therefore, the aim of this exploratory study was to identify the primary contributors to frontal plane angular trunk dynamics during walking of persons with LEA, in comparison to AB walking.

## METHODS

One subject with unilateral transfemoral LEA (TFA), one with unilateral transtibial LEA (TTA), and two AB controls (AB1, AB2), were retrospectively identified from records of the Biomechanics Lab at Walter Reed National Military

Medical Center. Subjects were selected such that self-selected walking velocity (SSWV) fell within +/-5%, and no participants self-reported current LBP at time of data collection (Table 1).

Subjects walked overground along a 15m walkway at SSWV, with full-body kinematics ( $f_s=120\text{Hz}$ ) and ground reaction forces ( $f_s=1200\text{Hz}$ ) respectively measured via a 27-camera motion capture system and six floor-embedded force platforms. One representative prosthetic(right) stance phase was extracted for each subject, kinematic/kinetic data were filtered at 6\25Hz, and an inverse kinematic solution was computed using Visual3D, applying the Gait2392 model definition of the OpenSim software[5]. The Residual Reduction Algorithm was used to compute a set of joint moments that best tracked experimental kinematics while also adjusting trunk center-of-mass location to reduce dynamic inconsistencies. Joint moments and kinematics were input to an induced acceleration analysis, applying a rolling-without-slipping contact constraint at each foot in place of measured forces. For each system force, mean induced angular accelerations were computed using separate positive and negative mean integrals during gait phases of interest [4]. As early stance is generally where elevated lateral lean occurs in persons with LEA, analyzed phases were limited to initial double-limb support (IDS) and early single-limb support (ESS).

**Table 1:** Demographic characteristics and self-selected walking velocity (SSWV) for the able-bodied (AB), transtibial (TTA), and transfemoral (TFA) participants.

	Gender	Age (yr)	Stature (cm)	Mass (kg)	Time Since Amp. (yr)	Prosthetic Componentry	SSWV (m/s, Fr)
TTA	Male	34	177	93	1.29	Renegade <sup>®</sup> (Freedom Innovations)	1.24 (0.17)
TFA	Male	23	174	70	1.25	Ceterus <sup>™</sup> , Power Knee <sup>™</sup> (Ossur)	1.22 (0.17)
AB1	Male	27	176	76	-	-	1.32 (0.20)
AB2	Male	27	172	81	-	-	1.42 (0.23)

## RESULTS AND DISCUSSION

Simulations were successfully generated for each subject, with quality verified against suggested standards [5]. Comparing simulated trunk kinematics (Fig. 1, left) mean trunk lean during ESS was greatest in TTA (5.0°) followed by TFA (3.6°), and AB1\AB2 (0.5° \ 0.1°).

During both IDS and ESS, inter-planar coupling was observed across all subjects. Sagittal ankle and hip moments induced notable contributions to net frontal trunk accelerations throughout stance - in agreement with prior work in AB subjects [3,4]. Contributions from the frontal lumbar moment differed between subjects (Fig 1, right): for TTA a prosthetic(right)-tending acceleration was induced, while for AB1, AB2, and TFA accelerations were intact(left)-tending, although considerably larger in TFA. Comparing AB1 and AB2, AB2 had a larger contribution from stance(right)-side knee Flx\Ext during IDS relative to AB1, while AB1 instead had a larger contribution from trailing(left)-side hip Ab\Ad. This suggests that able-bodied persons may apply notably different underlying mechanics to compose similar net frontal plane trunk accelerations. To facilitate comparison of LEA subjects with AB, the following reasoning was applied; a moment that contributes elevated prosthetic-tending, or reduced intact-tending, acceleration to the cumulative net over IDS (relative to AB1 and AB2), has potential to be associated with subsequent, elevated trunk lateral lean towards

the prosthesis in later stance. For TFA, this highlighted prosthetic-side ankle Flx\Ext and prosthetic-side hip Ab\Ad. In contrast for TTA, this highlighted lumbar frontal moment, followed by prosthetic-side knee Flx\Ext, and prosthetic-side ankle Flx\Ext. The prosthetic ankle contribution was elevated in both TTA and TFA, suggesting adjustment of prosthetic ankle componentry, or distally-targeted gait re-training, may warrant investigation as means to affect elevated lateral trunk lean in LEA patients. However, these simulation-based observations require empirical validation prior to clinical translation.

## CONCLUSIONS

This exploratory study highlights that frontal plane trunk dynamics during level walking in persons with LEA and no LBP are composed of a whole-body balance of system forces, wherein distal prosthetic ankle function may play a role. A larger cross-sectional analysis is needed to ascertain if features observed in these case subjects are characteristic of the broader LEA population, and also if those with versus without LBP differ.

## REFERENCES

1. Yoder, A et al. *Gait & Posture*. **41**:757–62, 2015
2. Hendershot B. *Clin Biomech*. **29**:235–42, 2014
3. Nott C, et al. *J of Biomech*. **43**:2648–52, 2010
4. Klemetti R, et al. *J of Biomech*, **47**:2263–8, 2014
5. Hicks J. *J Biom Eng*. **137**:1-24, 2015

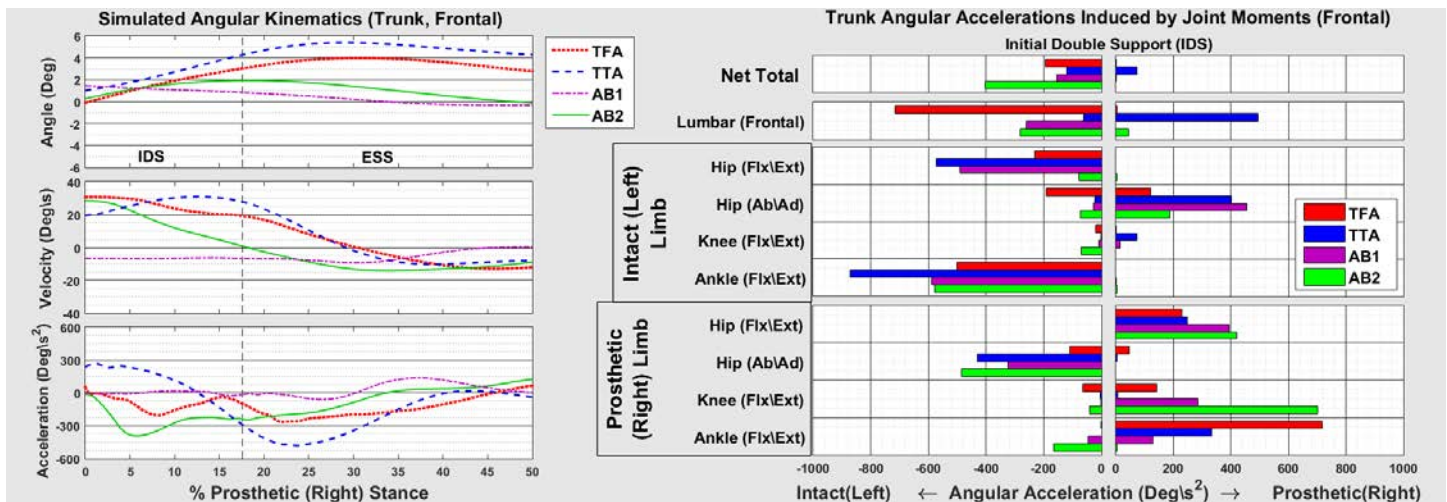


**Figure 1:** Simulated trunk angular kinematics relative to global during initial double support (IDS) and early single support (ESS) (left). Mean, angular accelerations induced on the trunk in the frontal plane by lower-extremity joint moments during prosthetic IDS (right).

# Asymmetrical Limb Loading Affects Spatial and Temporal Gait Parameters Differently in Comparison to Split-belt Adaptation

Lauren Bowman, Troy Rand, M.S., Allison Hoover, Mukul Mukherjee, Ph.D.

The University of Nebraska at Omaha, Omaha, NE, USA

Email: [lbowman@unomaha.edu](mailto:lbowman@unomaha.edu); web: [unonbcf@unomaha.edu](http://unonbcf@unomaha.edu)

## INTRODUCTION

Aging and pathology, such as strokes, can result in asymmetrical walking patterns. Asymmetries may be prominent in the spatial domain (e.g. step length) or the temporal domain (e.g. step time) independently or in conjunction. It is not yet well understood how to target these domains while rehabilitating an asymmetrical walking pattern.

Asymmetrical walking patterns can be induced in healthy individuals through several different tasks including unilateral limb loading and split-belt adaptation. However, these two methods induce asymmetrical walking patterns through different mechanisms. While unilateral limb loading is an external weight added to a limb, it is perceived as one limb being heavier than the other, i.e., an internal perception. In contrast, the split-belt task exhibits an external change to the body because the environment itself is manipulated due to the two belts of the treadmill moving at different speeds. Determining how spatial and temporal components of gait are effected due to limb loading versus split-belt adaptation may give important insight into developing rehabilitation programs for those with asymmetric sensorimotor abnormalities.

Virtual reality (VR) has been shown to effect cadence, temporal walking patterns, and muscle activation during unilateral limb loading<sup>1</sup> while improving adaptability of spatiotemporal characteristics during split-belt adaptation.<sup>2</sup> However, it is not clear how VR effects spatial and temporal symmetry during asymmetrical walking during unilateral limb loading and split-belt adaptation.

The purpose of this study was to determine if spatial and temporal gait symmetries were different between walking with a unilateral limb load versus split-belt adaptation. Additionally, we wanted to determine if

walking in a VR environment had any effect on these differences.

## METHODS

Thirty two young healthy volunteers participated in this study (age  $23 \pm 2.7$  years, mass  $73.6 \pm 13.3$  kg, height  $173.0 \pm 8.6$  cm). All subjects were free of any musculoskeletal or neurological impairments that may have affected their gait or locomotor adaptation. The protocol was approved by the institutional review board of the University of Nebraska Medical Center.

Subjects were exposed to one of two asymmetrical gait patterns: unilateral limb loading or split-belt. Sixteen subjects performed unilateral limb loading and were equipped with an ankle weight weighing approximately 5% of their body weight on their left ankle (Figure 1). They performed four treadmill trials at their preferred walking speed: familiarization, baseline, limb loading, and washout (load removed). Half of these subjects (8) were exposed to VR while half were not (control group).

A second group of sixteen subjects walked on a split-belt treadmill and performed ten treadmill trials at their preferred, fast, or slow walking speed as well as split belt trials with one belt moving at their fast walking speed and the other at their slow walking speed (Figure 1). Half of these subjects were exposed to VR while half were not.

To compare interlimb coordination, the symmetry index (SI) was calculated for step length and step time for all subjects.

$$SI \text{ for Split - belt} = \frac{\text{fast} - \text{slow}}{\text{fast} + \text{slow}}$$

$$SI \text{ for Limb Loading} = \frac{\text{loaded} - \text{unloaded}}{\text{loaded} + \text{unloaded}}$$



Figure 1. The left picture shows unilateral limb loading with the ankle weight fixed to the left ankle. The picture on the right shows a subject doing the split-belt task.

A 3-way mixed model ANOVA was run to compare the task (unilateral limb loading versus split-belt) and vision (virtual reality versus non-virtual reality) for fixed effects and time (baseline, early and late adaptation, early and late washout) for repeated effects.

## RESULTS AND DISCUSSION

*Step length symmetry (Figure 2):* There was a main effect of task [ $F=7.860, p<0.009$ ], and time [ $F=32.142, p<0.0001$ ] but not for vision. There was only a significant interaction for time across task [ $F=19.007, p<0.0001$ ].

*Step time symmetry (Figure 2):* There was a main effect of task [ $F=19.255, p<0.0001$ ], and time [ $F=151.679, p<0.0001$ ] but not for vision. There was a significant interaction for time across task [ $F=76.720, p<0.0001$ ] and time across task across vision [ $F=3.337, p=0.025$ ] and a borderline interaction for time across vision [ $F=2.649, p=0.057$ ].

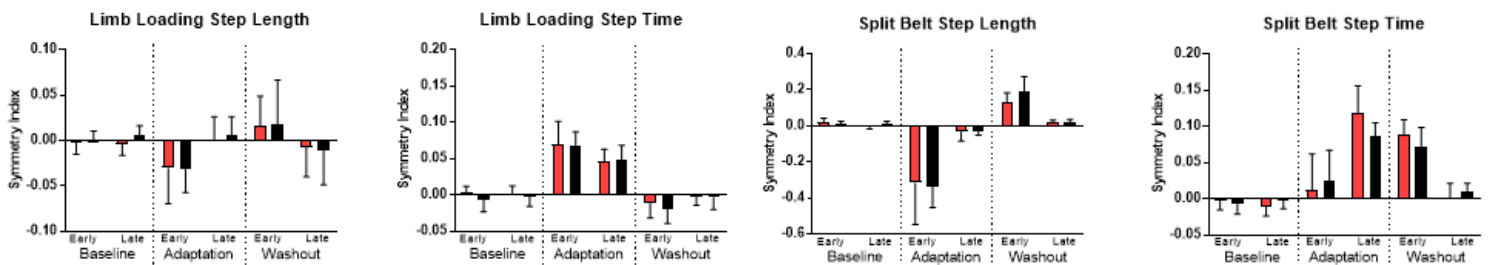


**Figure 2:** Symmetry index for step length and step time for the limb loading task (left side) and split belt task (right side) task. Red bars indicate gait adaptation in VR. The limb loading step length scale is one-fifth the scale of split belt step length for clarity.

## CONCLUSIONS

- 1) Adaptive changes were demonstrated for both limb loading and split-belt adaptation that impacted the temporal gait patterns more than the spatial.<sup>3</sup>
- 2) VR that is known to affect gait patterns also shows differential effects based on type of task and the type of gait variable being studied.
- 3) Asymmetry induced by loading a limb is different from how it is induced by support surface velocity manipulations. This internal versus external induction of asymmetric gait patterns results in different mechanisms of gait coordination.
- 4) Future directions of research would include how internal versus external asymmetry impacts gait variability and how it is impacted by aging.

## REFERENCES

1. Mukherjee M, et al. *J Mot. Beh.* 2011; 43(2):99-109.
2. Eikema DJ, et al. *Exp Brain Res.* 2016; 234(2):511-22.
3. Chien JH, et al. *Exp Brain Res.* 2017.

## ACKNOWLEDGMENTS

This work was funded by the Center for Biomedical Research Excellence grant (1P20GM109090-01) from NIGMS/NIH, NASA Nebraska space grant, and FUSE grant from University of Nebraska at Omaha.

# THE EFFECTS OF GAIT SPEED ON FOOT ROCKERS

Paige Agnew, Francesca Boylan, Kate Emma, Heidi Mickunas, Ayana Phillips, Deborah King

Ithaca College, Ithaca, NY, USA

email: [dking@ithaca.edu](mailto:dking@ithaca.edu), web: <http://www.ithaca.edu/hshp/depts/ess/>

## INTRODUCTION

Locomotion is a foundational component for daily living. Legged locomotion can be broken down into two gait patterns, walking and running [1]. The hip, knee, and ankle joints have different roles depending on the phase of walking & running and must work together to produce and absorb forces to allow efficient movement through the stance phase. In walking, this is accomplished by three rockers: the heel rocker, the ankle rocker, and the forefoot rocker. While the role and movement patterns of ankle and foot have been studied extensively in running, little research has framed foot and ankle motion in running in context of the heel, ankle, and forefoot rockers even though at slow running speeds, 80 to 90% of shod runners' heel strike and exhibit all three rockers [2]. Thus, the purpose of this study is to determine the effect of gait speed on the presence and timing of foot rockers across both walking and running speeds.

## METHODS

Twenty-six healthy college aged students (age (y): 20.4, height (cm): 161.2, mass (kg): 70.1), who give their written informed consent and volunteered to participate. Following a warm-up, subjects completed one-minute walking and running trials at 4 walking speeds and 4 running speeds: 1.16 m/s, 1.46 m/s, 1.65 m/s, 1.92 m/s, 2.24 m/s, 2.68 m/s, 3.13 m/s, 3.58 m/s on a treadmill. One minute of rest at 1.3 m/s was provided between trials.

Nineteen reflective markers placed on key anatomical landmarks were used to create an eight-segment model using a modified Plug-in-Gait marker set (Vicon, Centennial, CO). Motion capture data (Vicon Nexus) was collected at 120 Hz for the last 20 seconds of each trial.

Ten strides of data for each speed were analyzed. Visual 3D was used to calculate the start and stop off the heel, ankle, and forefoot rockers based on guidelines of Bober, et al. [3]. Each rocker was then expressed as a percent of the stance phase. Stride rate and stride length were also calculated. Descriptive statistics were calculated in SPSS for the foot rocker variables. One-way repeated measures ANOVA were used to determine significant differences in the timing of the foot rockers across the treadmill speeds. Post hoc comparison were performed on significant main effects. Alpha = 0.05.

## RESULTS AND DISCUSSION

To date, data has been analyzed for 10 subjects and preliminary statistical analyzes have been performed on these 10 subjects.

Descriptive characteristics of the 5 variables are provide din Table 1. As expected, stride rates (and correspondingly stride lengths) were significantly different across speeds ( $F = 6.86$ ,  $p = .001$ ). Specifically stride rates increased over the first 3 walking speeds (1.16 m/s, 1.46 m/s, 1.65 m/s,  $p < 0.05$  for all). Not all subjects were able to walk at the fastest walking speed, which was near the walk to run transition, introducing large variability in the stride rate and stride length at that speed. None of the running speed stride rates were significantly different from each other.

There was not a main effect for percent of stance in the heel rocker ( $F = 1.051$ ,  $p = .475$ ), ankle rocker ( $F = .51$ ,  $p = .803$ ), or forefoot rocker ( $F = .857$ ,  $p = .605$ ) across speeds. Close examination of the data shows large standard deviations indicating great variability in the time spent in each rocker within each gait speed. Despite this variability, there does appear to be a consistent non-significant drop of time in the heel rocker to decrease across speed.

Once the data from the additional subjects are processed, it will be interesting to see if this drop is statistically significant. There does not appear to be a consistent pattern in the time spent in the ankle or forefoot rockers expressed as a percent of stance.

The data, however, clearly indicate that regardless of speed, there is overlap in the rockers during the gait cycle. Traditionally, the rockers are taught as the heel rocker occurring from heel strike to foot flat, followed by the ankle rocker - representing the tibia rotating forward over the foot - occurring from foot flat to heel off, and then the forefoot rocker - representing motion at the metatarsophalangeal joint - occurring from heel off to toe-off. Our data suggest that the ankle rocker starts prior to foot flat and can continue past heel off. Individual subject analysis also revealed that for some subjects at some running speeds ankle dorsiflexion begins prior to initial contact.

Since the rockers are thought to be pivotal in gait efficiency helping to minimize the motion of the center of mass [4], understanding how they interact at different speeds is valuable for evaluating and planning treatments for gait abnormalities as well as for prosthetic design.

Currently, with only 10 of the 26 subjects analyzed it is premature to conclude that gait speed does not affect the timing of the foot rockers. However, the initial analysis clearly reveals that the foot rockers are not purely sequential at the tested gait speeds. It

is anticipated that data from this study can be used to develop normative values of the timing of the rockers during gait and across speeds and to improve our understanding of the coordinated motion of the foot and ankle towards efficient walking and running.

## CONCLUSIONS

The heel ankle and forefoot rockers do not occur sequential across the gait speeds tested in this study. Speed did not have a statistically significant affect on the time spent in each rocker as a percent of stance.

## REFERENCES

1. Saibene, F., & Minetti, A. E. (2003). *European journal of applied physiology*, 88(4), 297-316.
2. Dugan, S. A., & Bhat, K. P. (2005). *Physical medicine and rehabilitation clinics of North America*, 16(3), 603-621.
3. Bober, T., Dziuba, A., Kobel-Buys, K., & Kulig, K. (2008). *Acta of Bioengineering and Biomechanics*, 10(1), 37.
4. Czerniecki, J. M. (1988). *American journal of physical medicine & rehabilitation*, 67(6), 246-252.

## ACKNOWLEDGMENTS

We acknowledge Rose Paskoff and Eoghan Trihy for their help with data collection and analysis.

**Table 1:** Means and SD of the 5 dependent variables across the 8 gait speeds.

Gait Speed (m s <sup>-1</sup> )	SR (strides/s)	SL (m)	Rockers		
			Heel (%stance)	Ankle (% Stance)	Forefoot (% Stance)
<b>1.16</b>	0.89 ± .03	1.31 ± .05	44.6 ± 13.0	55.5 ± 18.9	42.5 ± 13.7
<b>1.46</b>	1.01 ± .22	1.59 ± .26	32.4 ± 13.9	51.1 ± 19.9	41.1 ± 17.9
<b>1.65</b>	1.07 ± .13	1.61 ± .08	33.8 ± 15.2	41.7 ± 20.5	44.6 ± 15.2
<b>1.92</b>	1.35 ± .44	1.62 ± .42	28.8 ± 12.6	42.5 ± 8.6	56.6 ± 14.4
<b>2.24</b>	1.29 ± .14	1.80 ± .30	23.4 ± 13.6	40.0 ± 20.8	38.4 ± 15.6
<b>2.68</b>	1.37 ± .16	1.92 ± .31	17.5 ± 11.6	34.2 ± 13.8	40.9 ± 15.8
<b>3.13</b>	1.34 ± .12	2.17 ± .29	16.9 ± 10.3	38.1 ± 14.3	44.6 ± 13.7
<b>3.58</b>	1.42 ± .07	2.52 ± .13	27.1 ± 11.2	54.6 ± 15.0	55.5 ± 7.1

# TO WALK OR TO RUN? METABOLIC COST IS NOT THE ANSWER

Erik Summerside, Rodger Kram, & Alaa Ahmed

Department of Integrative Physiology, University of Colorado Boulder, Boulder, CO USA

email: [erik.summerside@colorado.edu](mailto:erik.summerside@colorado.edu)

## INTRODUCTION

Minimization of metabolic cost explains several fundamental observations in locomotion such as preferred step width and length [1,2]. These preferred kinematics during walking seem to minimize the metabolic energy required per unit distance, a metric commonly referred to as cost of transport (COT). Plotting COT as a function of walking speed yields a U-shaped curve (Figure 1A). Interestingly, humans exhibit preferred walking speeds that correspond to the minimum of the COT curve [3]. One difficulty with using COT as a model to explain the preferred walking speed is that it fails to consider two other important movement constraints: time and total distance. According to the COT model, if an individual were given the opportunity to either walk a distance, 'x', or run a distance, 'y,' they should always choose the option to walk. Alternative models based on optimal foraging theory *include* costs for time and distance [4, 5]. For example, when starlings (birds) are given the choice to either walk or fly to food, the preferred mode is best predicted based on minimizing net metabolic rate (net metabolic energy expended divided by time).

We developed a paradigm to probe how metabolic energy, distance, and time explain why humans choose to walk versus run. If decisions were only based on minimizing COT, a participant should always walk (Figure 1A). We hypothesized COT would not predict choice and that there would be situations where running was preferred over walking. Instead of COT, we considered costs that were based solely on total amount of metabolic energy expended, total time spent, and total distance. Figure 1B shows the predictions of each of these three costs (green, red and blue line, respectively). For example, the green line represents the pair of walking and running options that a person would consider equivalent (here on referred to as an indifference point, IP), if he/she only cared

about choosing the option that minimized metabolic energy. In other words, they would consider walking 150m equally preferable as running 100m (asterisk in Figure 1B). For walk distances above this line they would prefer to run, for walk distances below this line, they would prefer to walk.

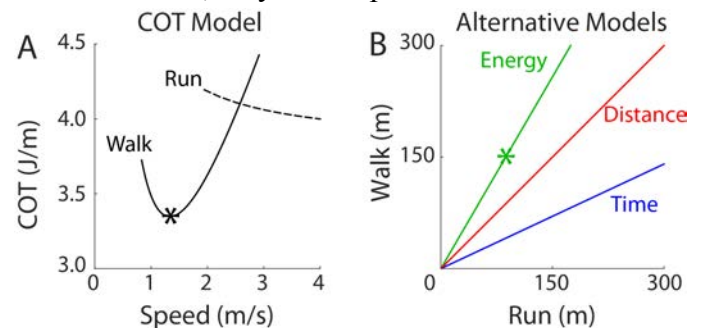


**Figure 1:** A) Metabolic COT for walking (solid line) and running (dashed line) across speeds. Minimization of COT occurs when walking at  $\sim 1.3$  m/s (asterisk). B) Model predictions for indifference points that minimize energy (green), distance (red), and time (blue). An individual that minimizes energy would be indifferent between walking 150m and running 100m (asterisk).

## METHODS

Our experiment took place in a large lighted and climate controlled indoor track facility. Participants (N=20, 12M, 8F) completed a combination of three different types of trials: walk, run, and choice trials. In walk trials, participants walked out to a designated distance and back. In run trials, they ran out to a different designated distance and back. For choice trials, they were given the freedom to repeat either the previous walk or run trial. During all trials, walking and running occurred at self-selected speeds. Participants were informed that the experiment would last two hours and that their decisions during choice trials would not affect the overall duration of the experiment (i.e. always choosing the faster option would not allow them to leave early). All trials ranged in distance between 10-250 meters and took place over 5 blocks. Each block allowed for the measurement of a single IP

which represents the relative walk and run distances where preference for one is equal to the other. Each individual block consisted of four triplets of trials (Walk/Run/Choice). The first triplet of trials in each block consisted of equal walk and run distances. Throughout a block, the run distance did not change. Walk distances were adjusted based on the participant's previous choice. If the choice was run, the walk distance was *shortened* for the next triplet. If the choice was walk, the walk distance was *lengthened*. The walk component of an IP was calculated at the end of each block by averaging the walk distances of the last walk choice and last run choice. IPs from each participant were calculated based on titrated walking distances equal to run distances of 40, 60, 80, 100, and 120m.

We calculated linear models to predict relative walk and run distances that would correspond to equal metabolic energy, distance and time (Figure 1B). Metabolism was not directly measured, but estimated using fitted equations from previously published sources [6,7]. Predictions for metabolic energy and time varied based on an individual's preferred walking and running speeds. To investigate which costs best explained gait preference, we fit a slope through the measured IPs of each participant and compared them to the slopes of each candidate cost.

## RESULTS AND DISCUSSION

All participants made some decisions to run instead of walk, suggesting they were not only minimizing COT. Figure 2A depicts IPs and fitted slope of a single representative participant that minimized time. The average fitted slope of IPs across all participants was 0.73 (0.11) (Figure 2B). This indicates that within the tested distances, running was chosen more often than walking. Average model slopes were 1.72 (0.05) for metabolic cost, 0.47 (0.02) for time, and 1 for distance. The average fitted slope across all participants was different from each of the three proposed models ( $p_{\text{met}} < 0.001$   $p_{\text{dist}} = 0.028$   $p_{\text{time}} = 0.027$ ). Total metabolic energy exclusively explained IPs for only two participants, time explained seven, and distance explained four. Seven participants could not be explained using just one model prediction.

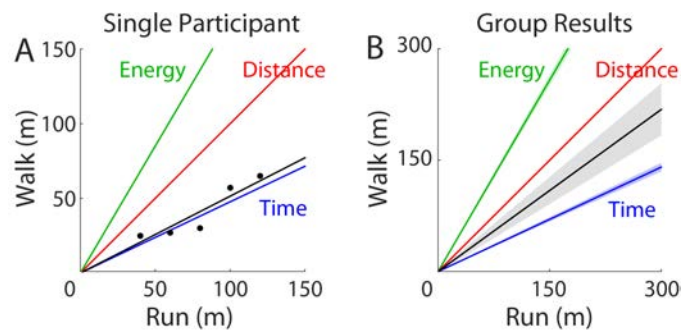


**Figure 2:** A) Indifference points of a single participant with a slope of 0.51 (black) indicating a tendency to minimize time (blue) rather than energy (green) or distance (red). B) Average slope across all participants. Shaded region represents SEM.

We expected individuals who minimized time would move at a faster preferred speed both when walking and running, but found the slope of an individual's IP was not predictive of their preferred walking speed ( $R^2 = 0.075$ ,  $p = 0.245$ ). This suggests participants with faster walking speeds were not making their decisions in order to minimize movement time. Running speed, however, was moderately correlated with an individual's preference for running ( $R^2 = 0.359$ ,  $p = 0.005$ ) that is, faster runners were more likely to choose to run when compared to slower runners.

## CONCLUSIONS

Cost of transport alone was unsuccessful at predicting whether an individual would walk or run. Only two participants exhibited behaviors that minimized the amount of metabolic energy. Instead, most participants minimized time required to complete a trial. These results highlight the importance of considering other costs when explaining locomotion preferences.

## REFERENCES

1. Donelan et al. *Proc. R. Soc. Lond B* 268, 1985-92, 2001
2. Danion et al. *Gait & Posture* **18**, 69-77, 2003
3. Ralston *Int Z Angew Physiol* **17**, 277-283, 1958
4. Shadmehr et al. *Curr Biol* **26**, 1929-1934, 2016
5. Bautista et al. *PNAS* **98**, 1089-94, 2001
6. Zarrugh et al. *J. appl Physiol* **33**, 293-306, 1974
7. Leger & Mercier *Sports Medicine* **1**, 270-77, 1984

# FRONTAL PLANE PELVIS-TRUNK COORDINATION DURING ASYMMETRIC LOAD CARRIAGE WHILE WALKING ON AN UNEVEN SURFACE

Junsig Wang and Jason C. Gillette

Iowa State University, Ames, IA, USA

## INTRODUCTION

Individuals often carry items in one hand instead of both hands during activities of daily living. Asymmetric load carriage is expected to produce a lateral shift of the center of mass and result in increased lateral trunk flexion during walking. Furthermore, carrying asymmetric loads over challenging surfaces such as uneven or irregular terrain may require further postural changes in the upper body.

To our knowledge, no studies exist that investigate pelvis-trunk coordination of asymmetric load carriage while walking on an uneven surface. Describing coordinative patterns of the pelvis-trunk may provide important measures for potential injury risk and development of low back disorders. Therefore, the purpose of this study was to investigate pelvis-trunk coordination in the frontal plane when carrying unilateral versus bilateral loads and when walking on even versus uneven surfaces. We hypothesized that: 1) pelvis-trunk coordination would be more in-phase and less variable during unilateral load carriage as compared to bilateral load carriage and 2) when walking on an uneven surface as compared to an even surface.

## METHODS

Twenty healthy young adults with an age range of 18 to 30 (16 males and 4 females; age  $25.1 \pm 4.0$  years; height  $173.4 \pm 5.2$  cm; mass  $69.9 \pm 7.4$  kg) participated in this study. Three load conditions were tested: no load, 20% body weight (BW) load on one side of the body, and 20% BW load split between both sides of the body. Two hand-held bags were filled with sealed bags of lead shot to match the two loaded conditions. After a warm-up session for one minute, the participants were instructed to walk on both even and uneven surface treadmills at their

preferred pace for 90 seconds under the three load conditions.

An eight-camera Vicon motion analysis system was used to collect three-dimensional kinematic data at a sampling rate of 160 Hz. Twenty retro-reflective markers were placed on bony landmarks. Pelvis and trunk segment angles relative to the laboratory coordinate system were calculated. Gait events were determined by changes in direction of the heel marker anterior-posterior velocity [1]. Fifteen steps were selected and analyzed during the last thirty seconds of each condition.

Kinematic data were low-pass filtered at 6 Hz. Pelvis and trunk ranges of motion (ROM) in the frontal plane were calculated for the stance phase. Segmental angular velocities were calculated from the segment angles utilizing the first central difference method. These data were then used to calculate phase angles from a phase plot, using the arctangent of angular velocity divided by angular displacement at each data point. Continuous relative phase (CRP) was calculated by subtracting the phase angles of the pelvis from the trunk. The CRP was evaluated for pelvis-trunk coordination. A CRP value of  $0^\circ$  indicates completely in-phase coordination, while a CRP value of  $180^\circ$  indicates completely out-of-phase coordination.

Coordination patterns were quantified utilizing mean CRP and CRP variability. Fifteen CRP curves for each participant were used to calculate a mean CRP curve and stride-to-stride variability in CRP. CRP and CRP variability were averaged over the stance phase for statistical analyses. The effect of loading conditions and the effect of different surfaces on pelvis ROM, trunk ROM, mean CRP, and CRP variability were analyzed using repeated measure ANOVA. Holm-Bonferroni post-hoc tests were performed when appropriate. The level of statistical significance for all tests was set at  $p < 0.05$ .

## RESULTS AND DISCUSSION

ANOVA indicated significant main effects of load condition on trunk ROM, mean CRP, and CRP variability (Table 1). Trunk ROM was significantly higher for the 20% BW unilateral load than the 20% BW bilateral load or no load ( $p \leq 0.013$ ). In addition, trunk ROM was significantly increased when comparing the 20% BW bilateral load to no load ( $p < 0.001$ ). Mean CRP and CRP variability were significantly lower for the 20% BW unilateral load than the 20% BW bilateral load or no load ( $p \leq 0.047$ ). CRP variability was significantly decreased when comparing the 20% BW bilateral load to no load ( $p = 0.010$ ).

ANOVA also indicated that CRP variability was significantly higher for the uneven surface than the even surface (Table 1). No interaction effects of the load and surface were found.

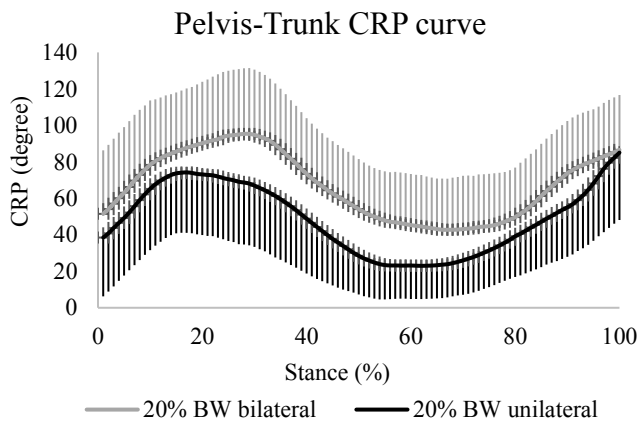


**Figure 1.** Mean CRP curve and CRP variability during 20% BW bilateral and unilateral loads

The present study evaluated frontal plane range of motion and pelvis-trunk coordination when carrying a unilateral versus a bilateral load and when walking on an uneven versus an even surface. Increased trunk ROM was found for the 20% BW unilateral load, while the pelvis ROM was not changed. Therefore, trunk lateral bending motions may be mainly utilized to counterbalance the laterally shifted center of mass when carrying a unilateral load.

The 20% BW unilateral load resulted in greater in-phase and less variable pelvis-trunk CRP, which is consistent with the first hypothesis (Figure 1). Given that there were no changes in pelvis ROM, it appears that changes in coordination may be driven by the trunk. Greater in-phase and less variable pelvis-trunk coordination have been reported in individuals with low back pain [2]. In addition, a lack of coordination variability has been associated with decreased flexibility and increased mechanical stress on the musculoskeletal system [3]. The second hypothesis was not supported as walking on the uneven surface resulted in no change for mean CRP and an increase in CRP variability. The uneven surface may have provided enough of a random perturbation to force the participants into a more variable coordination pattern. In summary, changes in trunk ROM, along with greater in-phase and less variable pelvis-trunk coordination may provide insight into the increased loading and stiffness of the lower back commonly associated with unilateral loads.

## REFERENCES

1. Zeni, JA. et al. *Gait Posture*, **27**(4), 710-714, 2008.
2. Seay, JF. et al. *Clin Biomech*, **26**(6), 572-578, 2011.
3. Hamill, J. et al. *Clin Biomech*, **14**(5), 297-308, 1999.

**Table 1:** Mean and standard deviations for range of motions and coordination parameters under the three load conditions and for the even and uneven surfaces.

	No load	20% BW bilateral	20% BW unilateral	Even	Uneven	Load	Even vs. Uneven	Load ×Surface
Pelvis ROM	7.06 (1.93)	6.82 (1.86)	6.52 (2.15)	6.74 (1.79)	6.85 (1.95)	0.258	0.537	0.693
Trunk ROM	2.49 (0.69)	3.83 <sup>a</sup> (1.22)	<b>4.39<sup>ab</sup></b> <b>(1.90)</b>	3.45 (1.36)	3.69 (1.37)	<b>&lt;0.001</b>	0.099	0.442
Mean CRP <sub>pelvis-trunk</sub>	67.38 (21.18)	67.25 (28.13)	<b>48.77<sup>ab</sup></b> <b>(17.32)</b>	60.14 (25.26)	62.13 (23.81)	<b>&lt;0.001</b>	0.421	0.909
CRP <sub>pelvis-trunk</sub> Variability	35.85 (10.72)	30.69 <sup>a</sup> (10.83)	<b>27.18<sup>ab</sup></b> <b>(8.64)</b>	30.39 (10.15)	<b>32.09*</b> <b>(10.95)</b>	<b>&lt;0.001</b>	<b>0.049</b>	0.806

<sup>a</sup>  $p < 0.05$  vs. no load, <sup>b</sup>  $p < 0.05$  vs. 20% BW bilateral load, \*  $p < 0.05$  even surface vs. uneven surface

# Differences in Lower Body Kinetics when Walking and Walking While Holding Weapon Aim

Jennifer Neugebauer and Maria Talarico

U.S. Army Research Laboratory, Aberdeen Proving Ground, MD, USA  
email: [jennifer.neugebauer.civ@mail.mil](mailto:jennifer.neugebauer.civ@mail.mil), web: <http://www.arl.army.mil>

## INTRODUCTION

Exoskeletons and assistive devices designed for military applications should consider biomechanical differences incurred during operationally relevant movements. To date, exoskeletons have largely been developed for industrial or rehabilitative use and then applied to military applications. For military applications however, user movements may differ from those that a typical person would complete, such as walking with load and walking while shooting (shooting on the move; SM). Previous studies have identified biomechanical differences while walking with load [1] but similar findings have not been reported for a military specific task such as SM, both with and without load. During 'normal' walking, lower limb movement largely exhibits behavior similar to an inverted pendulum [2]. During SM, crouch-like movement patterns are executed to minimize weapon trace motion to improve accuracy. Biomechanical differences may dictate design considerations such as control strategies and/or actuator selection for torque input. There is a need to better understand the biomechanical differences between SM and 'normal' walking in order to account for these differences in exoskeleton design and control. The purpose of this study was to identify lower limb kinetic differences between walking and SM, both with no load and with a 22.7 kg ballistic vest.

## METHODS

Three active duty military ( $37.3 \pm 1.2$  years,  $1.758 \pm 0.092$  m,  $87.1 \pm 16.6$  kg) completed a series of walking and SM trials while carrying either no load (NL) or a 22.7 kg ballistic vest (KIT). Data were collected for 10 seconds every 30 seconds of each 2 minute trial.

Kinematic (240 Hz) and ground reaction force (GRF; 1000 Hz) data were collected simultaneously using a

12 camera motion capture system (Motion Analysis, Santa Rosa, CA) and instrumented force plate treadmill (AMTI Watertown, MA), respectively. Inter-segmental forces, moments, and powers were determined via inverse dynamics methods (Visual3D, C-Motion, Germantown, MD). All strides were averaged for each condition and subject.

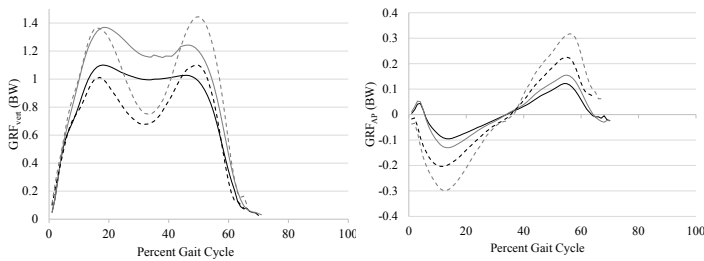
Walking and SM speeds were averaged across all trials and subjects for an overall mean. Peak vertical ( $pGRF_{vert}$ ) and anterior-posterior (AP) GRF ( $pGRF_{brake}$  and  $pGRF_{prop}$ ), vertical and AP impulse ( $Imp_{vert}$ ,  $Imp_{brake}$ ,  $Imp_{prop}$ ), and vertical loading rate ( $LR_{vert}$ ; calculated between 20 and 80% of loading) were calculated for each walk and load. All trials were normalized to a gait cycle and averaged across speed for each load (NL and KIT). Due to the small subject count, cursory statistics (R, R Foundation for Statistical Computing, Vienna, Austria) are presented to guide future studies.

## RESULTS AND DISCUSSION

Biomechanical differences were identified between walking and SM regardless of the load carried. Speed (walking:  $3.0 \pm 0.5$  mph; SM:  $2.8 \pm 0.4$  mph) did not differ between walking and SM ( $p > 0.15$ ). GRFs over the course of the gait cycle differed between SM and walking (Figure 1). For all findings, differences scaled with load (Table 1). Although  $pGRF_{vert}$  did not differ between SM and walking,  $Imp_{vert}$  was greater while  $LR_{vert}$  was lower for SM (Table 1). This relationship suggests that subjects are more slowly loading at heel contact, likely to control body center of mass motion and reduce undesired weapon motion as vertical force increases during stance. Minimizing vertical and AP weapon motion during SM is a primary goal of subjects to maintain target accuracy. This results in a crouch-like gait with increased knee and hip flexion throughout stance phase to minimize and control upper body movement. Continuous knee flexion during SM may contribute to the change in

vertical GRF profile compared to normal gait due to smaller vertical displacement of the body's center of mass. Although due to different causes, children with cerebral palsy exhibit similar hip and knee mechanics during gait as those of SM. Crouched gait reduces the ability to generate similar vertical GRF during normal gait [3], which likely influences the rate of weight acceptance and impulse.

**Figure 1:** GRF<sub>vert</sub> (left) and GRF<sub>AP</sub> (right) for SM (solid) and walking (dashed) with NL (black) and KIT (gray).



Results in the AP direction further support the differences highlighted from the vertical GRFs. Both the braking and propulsive GRFs and impulses were decreased in SM compared with walking (Figure 1).

## CONCLUSIONS

Shooting on the move and walking differ biomechanically and warrant further investigation. Although the results presented are cautionary due to the small subject numbers, the data suggests SM results in greater vertical impulse, lower loading rate, and decreased AP GRFs and impulses. Soldiers and

other tactical operators perform a variety of tasks including fundamental movements (i.e. walking) and more military-relevant movements (i.e. SM). Currently, exoskeletons are developed based on fundamental movements and assume these tasks directly translate to tactical movements. The findings from this study underscore that kinetic differences exist between walking and SM, which suggests that tactical movements may not strictly follow the same patterns as fundamental movements. Understanding biomechanical differences between tasks will provide exoskeleton developers a more comprehensive platform on which to build appropriate control systems and actuation. Future efforts should build on these results, as well as investigate differences in joint moments and powers, the effects of offset loads (larger percentage on back versus front or vice versa) and segmental loads from an exoskeleton.

## REFERENCES

1. Birrell SA, et al. *Gait & Posture* **4**, 611-614, 2007.
2. Cavagna GA, et al. *Am J Physiol* **233(5)**, R243-61, 1977.
3. Hicks JL, et al. *J Biomech* **41(5)**, 960-967, 2008.

## ACKNOWLEDGMENTS

Special thanks to the Warfighters who participated in this study and provided invaluable expertise in order for us to collect operationally relevant data.

**Table 1:** Kinetics ( $\pm$  SD) of SM and NL and with 22.7 kg ballistic vest (KIT). \* indicates trend towards difference ( $p < 0.05$ )

	NL		KIT	
	Shoot on Move	Walking	Shoot on Move	Walking
<b>pGRF<sub>vert</sub> (BW)</b>	1.13 ( $\pm$ 0.04)	1.11 ( $\pm$ 0.09)	1.38 ( $\pm$ 0.07)	1.46 ( $\pm$ 0.12)
<b>pGRF<sub>brake</sub> (BW)</b>	0.19 ( $\pm$ 0.04)	0.23 ( $\pm$ 0.05)*	0.16 ( $\pm$ 0.04)	0.33 ( $\pm$ 0.08)*
<b>pGRF<sub>propulsive</sub> (BW)</b>	0.10 ( $\pm$ 0.04)	0.21 ( $\pm$ 0.04)*	0.13 ( $\pm$ 0.03)	0.30 ( $\pm$ 0.09)*
<b>LR<sub>vert</sub> (BW/s)</b>	7.35 ( $\pm$ 1.1)	6.95 ( $\pm$ 3.3)	9.68 ( $\pm$ 2.0)	8.83 ( $\pm$ 3.2)
<b>Imp<sub>vert</sub> (BWs)</b>	0.57 ( $\pm$ 0.04)	0.52 ( $\pm$ 0.03)*	0.72 ( $\pm$ 0.07)	0.69 ( $\pm$ 0.05)*
<b>Imp<sub>brake</sub> (BWs)</b>	0.02 ( $\pm$ 0.01)	0.04 ( $\pm$ 0.01)*	0.02 ( $\pm$ 0.01)	0.06 ( $\pm$ 0.02)*
<b>Imp<sub>prop</sub> (BWs)</b>	0.02 ( $\pm$ 0.01)	0.04 ( $\pm$ 0.01)*	0.03 ( $\pm$ 0.01)	0.06 ( $\pm$ 0.01)*

# STRUCTURAL PARAMETERS OF THE FOOT AND THE BIOMECHANICS OF WALKING WITH AND WITHOUT WEDGED FOOTWEAR INSOLES

<sup>1</sup> Ryan T. Lewinson, <sup>1</sup> Ryan Madden, <sup>1</sup> Anthony Killick, <sup>1</sup> John W. Wannop, <sup>1</sup> J. Preston Wiley,  
<sup>1</sup> Victor M.Y. Lun, <sup>1</sup> Chirag Patel, <sup>1</sup> Jeremy M. LaMothe, <sup>1</sup> Darren J. Stefanyshyn

<sup>1</sup> The University of Calgary, Calgary, AB, Canada  
email: lewinson@ucalgary.ca

## INTRODUCTION

Wedged footwear is often prescribed to patients with knee osteoarthritis (OA) with the goal of reducing the peak knee adduction moment (KAM) during gait; however, these insoles do not reduce loading for all patients [1]. This has prompted the concept of personalized footwear, whereby footwear is matched to each patient to optimize biomechanical and clinical outcomes. While many researchers have attempted to identify factors that may help predict an individual's biomechanical response to wedged insoles, clinically useful predictors of knee loading and response to wedged insoles remain unknown.

It is often presumed that static foot structure is related to mechanical loads at proximal joints, making some individuals more suited to a particular type of footwear than others. While commonly considered in insole design, limited research exists to support an association between foot structure and knee joint loading or biomechanical response to wedged insoles. In this study, static structural characteristics of the foot were identified in individuals with medial knee OA and the associations between foot structure, knee joint biomechanics and biomechanical response to wedged insoles were assessed.

## METHODS

Thirty patients with medial knee OA participated in this study. The mean (SD) age, mass and height were 60.3 (8.5) years, 83.4 (21.5) kg, and 166.9 (9.5) cm, respectively and 23 were female. All patients were diagnosed clinically by a sport medicine physician and confirmed on x-ray by a radiologist. No patient had a history of joint replacement, or recent history of treatment for their knee OA, including walking aids or braces. Patients with concurrent musculoskeletal pathologies affecting the foot, ankle

or hip were excluded. OA severity of the sample was moderate (Kellgren-Lawrence grade 2.8, SD 1.3).

Patients completed a standing neutral trial as well as 5 gait analysis trials walking at 1.3 m/s in each of 3 footwear conditions: (1) their own footwear, (2) their own footwear with a 6 mm lateral wedge, and (3) their own footwear with a 6 mm medial wedge. Wedged insoles were made by 3D printer from New Balance Inc. (Boston, MA). An eight camera Motion Analysis system recorded 3D trajectories of retroreflective markers placed over each patient's most symptomatic limb at a frequency of 240 Hz, and a Kistler force platform recorded ground reaction forces at a frequency of 2400 Hz during each trial. A standard inverse dynamics approach, as described elsewhere [2], was used to calculate the KAM for each trial. The mean KAM across the 5 trials in each footwear type for each patient was used in subsequent analysis.

Whole-body dual x-ray absorptiometry (DXA) was performed on each patient, and the region distal to the medial and lateral malleoli were identified on the most symptomatic limb to determine foot mass and foot fat content. A 3D foot scanner was used to capture static barefoot foot shape for each patient. A custom Matlab script was written to analyze scans, from which foot length, foot width, arch height and hind foot angle were determined and then verified by an orthopedic surgeon (Figure 1).

Multiple linear regressions ( $\alpha=0.01$ ) were used to assess foot structure characteristics (foot mass, foot fat, foot length, foot width, arch height and hind foot angle) as predictors of KAM during walking, and the change in KAM when wearing a lateral or medial wedge insole.

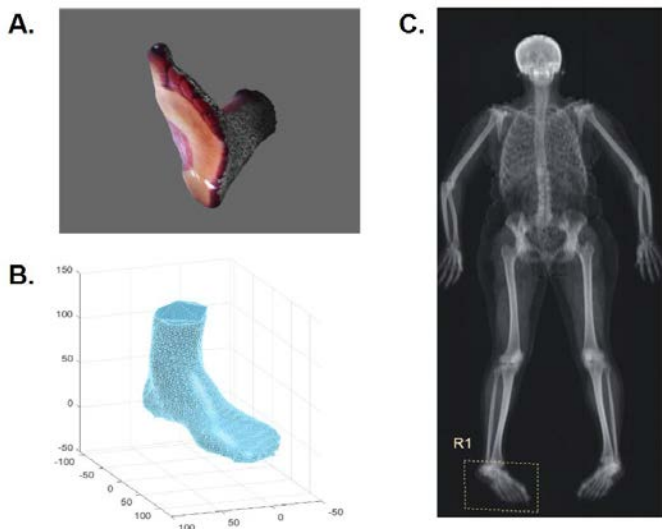


**Figure 1:** (A) a 3D foot scan. (B) Reconstructed mesh used for analysis. (C) DXA used for foot mass and fat measures (designated by region labelled R1).

## RESULTS AND DISCUSSION

Foot mass, foot length and foot width were found to be collinear with other foot structure variables and so were excluded from regression analyses. Using foot fat, arch height and hind foot angle as independent variables representing foot structure, no association was found with KAM magnitude during walking ( $R^2=0.24$ ,  $p=0.060$ ). When evaluating these structural parameters in the context of KAM change in response to wedged insoles, no association was found with KAM change in lateral wedges ( $R^2=0.05$ ,  $p=0.697$ ) or medial wedges ( $R^2=0.02$ ,  $p=0.923$ ). These results were determined using raw magnitude changes in KAM, and remained similar when evaluating changes as percent changes.

Prospective studies evaluating the relationship between static foot structure and clinical disease have not been performed on patients with knee OA; however, in a population of runners, Lun et al. [3] found no relationship between arch height and running injury. The present study adds to this by suggesting that arch height, hind foot angle and foot fat content do not appear to be associated with mechanics at the knee in individuals with knee OA. In addition, while the foot is often discussed as having an influence on dynamic loading at the knee and potentially affecting response to wedged insoles,

these relationships were not identified in the present study. These results question the usefulness of static foot structure measures when prescribing insoles to patients with knee OA.

This study only assessed wedged insoles in patients with knee OA, and thus generalization of the study findings to other insole types or other populations should be done with caution. It is possible that associations between foot structure and baseline knee loading might be observed with larger sample sizes, although this would still not account for the majority of variance in baseline knee joint loading parameters, or change in knee loading with wedged insoles. Thus, other factors remain to be identified that have a larger contribution to knee loading and biomechanical response to insoles. Finally, this study did not assess whether foot structure is associated with clinical response to wedged insoles.

## CONCLUSIONS

Foot structural parameters were not found to be associated with KAM during gait and were not associated with the change in KAM induced by lateral wedge or medial wedge insoles. Taken together, these data suggest that foot structure, as defined in this study, is not associated with gait mechanics at the knee in patients with knee osteoarthritis, and demonstrate that foot structure alone cannot be used to predict biomechanical response to wedged insoles in these patients.

## REFERENCES

1. Lewinson RT, et al. *Ann Biomed Eng* **44**, 3173-3185, 2016.
2. Lewinson RT, et al. *Gait Posture* **50**, 60-68, 2016.
3. Lun VMY, et al. *Br J Sports Med* **38**, 576-580, 2004.

## ACKNOWLEDGMENTS

Alberta Innovates, Canadian Institutes of Health Research, Killam Trusts, Natural Sciences & Engineering Research Council CREATE program, New Balance Athletic Shoe Inc., Vanier program

# LOWER EXTREMITY JOINT STIFFNESS AND WORK PERFORMED ACROSS DIFFERENT WALKING AND RUNNING SPEEDS

<sup>1,2</sup> Li Jin, <sup>1,2</sup> Michael E. Hahn

<sup>1</sup>Neuromechanics Lab, <sup>2</sup>Bowerman Sports Science Clinic, University of Oregon, Eugene, OR, USA  
email: ljin@uoregon.edu, web: <http://bssc.uoregon.edu/>

## INTRODUCTION

Walking and running are primary forms of human locomotion in daily life. Both tasks involve coordination of lower extremity joints, associated with kinematic and kinetic pattern changes. Joint stiffness and stance phase joint work are important for maintaining efficiency when locomotion task or speed changes. Previous studies have separately investigated ankle and knee joint stiffness ( $K_{ankle}$ ,  $K_{knee}$ ) in different movement conditions [1,2], and stance phase joint work ( $W_{joint}$ ) in walking and running [3], respectively. Little is known about the combination of  $K_{ankle}$ ,  $K_{knee}$ , and  $K_{hip}$  patterns, and the relationship between  $K_{joint}$  and  $W_{joint}$ .

For assistive devices, stiffness and work are key features during locomotion. Currently available assistive devices tend to be task-specific, with fixed stiffness and work parameters. The coordination of lower extremity joint stiffness and joint work when locomotion speeds change may be critical to the design of assistive devices suitable for walking and running over different speeds in patient populations. We hypothesized that  $K_{joint}$  and  $W_{joint}$  will increase when locomotion speed increased.

## METHODS

After providing written informed consent for this IRB-approved study, subjects were first instructed to walk on a force-instrumented treadmill (Bertec, Inc., Columbus, OH) across a range of seven speeds from 0.8 to 2.0 m/s (0.2 m/s intervals), for 90 seconds per stage. Then they were asked to run on at six speeds ranging from 1.8 to 3.8 m/s (0.4 m/s intervals), for 75 seconds per stage. Data were extracted from the middle strides of each stage.

Segmental kinematic data were collected at 120 Hz using an 8-camera motion capture system (Motion Analysis Corp., Santa Rosa, CA). Ground reaction force data were collected at 1200 Hz using the force-instrumented treadmill. Kinematic and kinetic data were filtered with a low-pass fourth-order Butterworth filter at 6 Hz and 50 Hz, respectively. Lower extremity joint angles, moments and powers were calculated using the inverse dynamics model in Visual 3D (C-Motion, Inc., Germantown, MD). Joint stiffness ( $K_{joint}$ ) was calculated as a change in joint moment ( $\Delta M_{joint}$ ) divided by joint angular displacement ( $\Delta \theta_{joint}$ ) in the braking phase of ground contact [4]. Stance phase joint positive work ( $W_{joint}^+$ ) and negative work ( $W_{joint}^-$ ) were calculated as the sum of all positive or negative joint power integrated over stance phase time [3], respectively. Statistical analysis was performed using a 2-way ANOVA (joint  $\times$  speed) in SPSS (V22.0, IBM, Armonk, NY). Bonferroni procedure was used for pairwise comparisons.

## RESULTS AND DISCUSSION

To date, six subjects ( $24 \pm 6.7$  years,  $175 \pm 10.9$  cm,  $76 \pm 11.5$  kg) have participated in this ongoing study. Initial analysis indicates that  $K_{knee}$  was

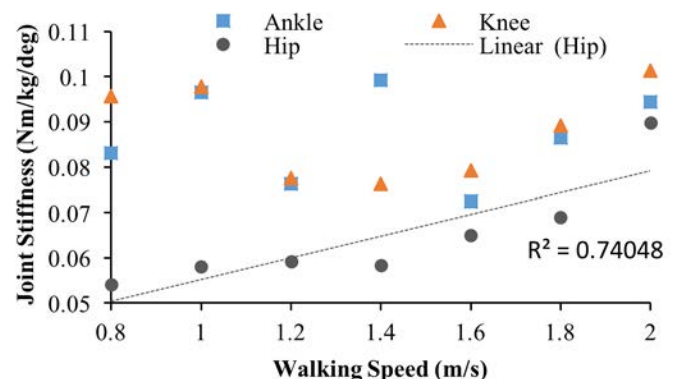


**Figure 1:**  $K_{joint}$  in different walking speeds.

significantly higher than  $K_{hip}$  across different walking speeds ( $p = 0.004$ ) (Fig. 1).  $K_{ankle}$  also tended to be higher than  $K_{hip}$  in walking (Fig. 1). In running conditions,  $K_{ankle}$  was significantly higher than  $K_{knee}$  across speeds ( $p = 0.008$ ) (Fig. 2).  $K_{knee}$  was generally lowest in running (Fig. 2).

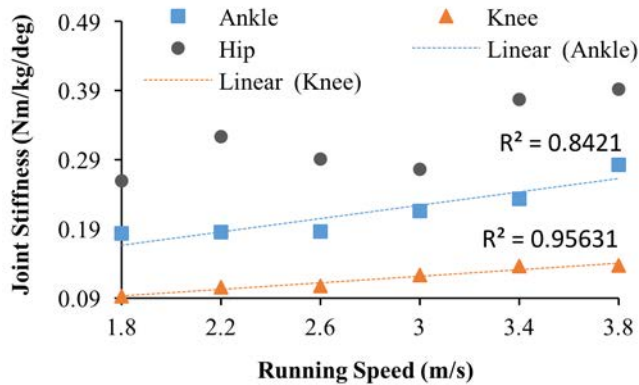


**Figure 2:**  $K_{joint}$  in different running speeds.

In walking conditions,  $W_{ankle}^+$  tended to be higher than  $W_{knee}^+$  and  $W_{hip}^+$  across walking speeds (Table 1).  $W_{ankle}^-$  was significantly lower than  $W_{hip}^-$  ( $p < 0.0001$ ) at 2.0 m/s (Table 1).  $W_{ankle}^-$  at 1.4 m/s was significantly greater than at 2.0 m/s ( $p < 0.0001$ ) (Table 1). In running conditions,  $W_{ankle}^+$  was significantly higher than  $W_{hip}^+$  across different speeds ( $p = 0.012$ ) (Table 2).  $W_{ankle}^+$  tended to be

the highest of three different joints across running speeds (Table 2).

## CONCLUSIONS

The initial hypothesis was partially supported. Variation of  $K_{joint}$  patterns were different between walking and running.  $K_{hip}$  was positively associated with locomotion speed during walking conditions. In running conditions,  $K_{ankle}$  and  $K_{knee}$  were both positively associated with speed. As walking speed increased,  $W_{ankle}^+$  tended to increase, and  $W_{ankle}^-$  decreased.  $W_{knee}^+$  and  $W_{knee}^-$  tended to increase when walking speed increased, indicating that the knee joint is important to absorb and generate energy as speed increases. Lastly, the ankle joint is critical for producing positive work.

## REFERENCES

1. Farley C.T., et al. *J Biomech* **32**(3), 267-273, 1999.
2. Hobara H., et al. *J Biomech* **46**(14), 2483-2489, 2013.
3. Schache A.G., et al. *J Exp Bio* **218**, 2472-2481, 2015.
4. Kuitunen S., et al. *Med. Sci. Sport. Exerc.* **34**(1), 166-173, 2002.

**Table 1:** Joint work in stance phase across different walking speeds. Sample Mean (SD); n = 6.

Joint Work (J/kg)	Walking Speeds (m/s)						
	0.8	1.0	1.2	1.4	1.6	1.8	2.0
$W_{ankle}^+$	0.14 (0.09)	0.18 (0.07)	0.19 (0.09)	0.21 (0.10)	0.23 (0.12)	0.27 (0.17)	0.27 (0.14)
$W_{knee}^+$	0.07 (0.03)	0.05 (0.03)	0.12 (0.05)	0.13 (0.04)	0.17 (0.08)	0.25 (0.14)	0.18 (0.05)
$W_{hip}^+$	0.05 (0.02)	0.09 (0.06)	0.07 (0.04)	0.10 (0.01)	0.09 (0.05)	0.10 (0.07)	0.13 (0.06)
$W_{ankle}^-$	0.22 (0.06)	0.20 (0.10)	0.18 (0.11)	0.19 (0.04)	0.12 (0.06)	0.12 (0.05)	0.08 (0.03)
$W_{knee}^-$	0.04 (0.02)	0.07 (0.08)	0.16 (0.14)	0.15 (0.05)	0.23 (0.26)	0.44 (0.29)	0.22 (0.13)
$W_{hip}^-$	0.07 (0.07)	0.09 (0.13)	0.21 (0.18)	0.13 (0.11)	0.30 (0.36)	0.51 (0.52)	0.21 (0.04)

**Table 2:** Joint work in stance phase across different running speeds. Sample Mean (SD); n = 6.

Joint Work (J/kg)	Running Speeds (m/s)					
	1.8	2.2	2.6	3.0	3.4	3.8
$W_{ankle}^+$	0.44 (0.23)	0.49 (0.31)	0.38 (0.32)	0.46 (0.31)	0.48 (0.34)	0.75 (0.05)
$W_{knee}^+$	0.16 (0.05)	0.22 (0.04)	0.20 (0.06)	0.23 (0.09)	0.22 (0.13)	0.23 (0.10)
$W_{hip}^+$	0.04 (0.02)	0.05 (0.03)	0.17 (0.23)	0.11 (0.10)	0.24 (0.22)	0.14 (0.05)
$W_{ankle}^-$	0.35 (0.12)	0.36 (0.09)	0.31 (0.13)	0.33 (0.14)	0.29 (0.22)	0.47 (0.10)
$W_{knee}^-$	0.34 (0.26)	0.42 (0.13)	0.40 (0.25)	0.57 (0.31)	0.44 (0.17)	0.38 (0.06)
$W_{hip}^-$	0.13 (0.17)	0.09 (0.08)	0.10 (0.11)	0.11 (0.10)	0.09 (0.10)	0.10 (0.05)

# STEP WIDTH DURING TREADMILL WALKING IS LONG-RANGE PERSISTENT

Simisola O. Oludare and Mark D. Grabiner

University of Illinois at Chicago, Chicago, IL USA

Email: soluda2@uic.edu, web: <http://cbr.ahslabs.uic.edu/>

## INTRODUCTION

During treadmill walking, step width has been suggested to have long range (LR) persistence [1,2,3,4] based on detrended fluctuation analysis (DFA). However, DFA does not appear to have the capacity to distinguish between short- and long-range persistence and, in addition, has been reported to falsely detect LR persistence [5,6]. However, during overground walking during eyes opened and eyes closed conditions, step width has been reported to have short range (SR) correlations based on autocorrelation analysis [7] and a modified autocorrelation analysis [8]. These analyses have an advantage of providing a direct assessment of the nature of the persistence evident in a time series.

The purpose of this study was to evaluate step width persistence using the autoregressive moving average/ autoregressive fractional integrated moving average (ARMA/ARFIMA) modeling method [5,6]. The main advantage of this method is the joint estimation of short- and long-range persistence [9]. We hypothesized that step width during locomotion will possess short term correlation structure.

## METHODS

Ten healthy young adults (23.3±1.95 years old, 64.0±16.0 kg, and 165.4±90.3 cm) walked on a microprocessor controlled treadmill for 10 minutes at 2.5 mph.

An eight camera motion capture system operating at 120 Hz tracked the motions of reflective markers placed over the shoe at the heel and 2<sup>nd</sup> metatarsal phalangeal joints (MTPJ), the acromion processes, the anterior superior iliac spines and the level of S2. The markers on the heel and 2<sup>nd</sup> MTPJ were used to construct a single rigid segment from which step width was calculated as the lateral distance between the segment centroids of subsequent foot

placements at the instant of midstance [9].

Midstance was computed as the time at which lateral trunk velocity was zero [9]. The trunk center of mass was modeled as the centroid of the segment defined from the midpoint of the line connecting the acromion processes and the pelvic markers.

Each step width time-series was modeled with 18 ARMA and ARFIMA models (nine of each). Each ARMA model was developed from two inputs, the order of the autoregressive (p) and the order of the moving average (q), which vary from 0 to 2 [5,6]. The ARFIMA models were developed from three inputs, p and q, and the fractional parameter (d). The fractional parameter was quantified from the time series and varies from positive to negative values. A positive d indicates the presence of LR persistence and a d of zero indicates SR persistence.

After the 18 models were developed, the most suitable for the time series was determined using the AIC [5, 6]. The AIC is a goodness of fit statistic that determines the best model as that which accounts for most of the data with the fewest parameters [5, 6]. The AIC values for each model (for each time series) were transformed into a weight that indicated the probability for the i-th model to be the best model given the data and the set of candidate models. These weights were used to determine whether the time series was best described by an ARMA or an ARFIMA model using the following criteria: 1) the best model (i.e. the model with the highest weight) should account for at least 90% of the set of time series (n=10) and if the model is an ARFIMA model, d should be significantly different from 0; and 2) the sum of weights of the nine models should be at least 0.90 for the given time series. If the time series is best described by an ARFIMA model it has LR persistence. To determine if the parameter d was different from 0 we used one-sample t-test against zero (p=0.05).

## RESULTS AND DISCUSSION

Based on the ARMA/ARFIMA modeling, step width time series possess LR persistence. Thus, our hypothesis was rejected. The model which best characterized the step width time series was ARFIMA with higher order autoregressive and moving average parameters,  $p = 1$  or  $2$  and  $q = 1$  or  $2$ , respectively. This indicates that an important aspect of the step width time series can be captured by short term autoregressive and moving average terms [11].

Additionally, a visual examination of a time series generated by ARMA and ARFIMA models also supports this conclusion (Figure 1). Compared to the step width (blue) and the ARFIMA (red) time series, the ARMA (black) time series resembles white noise, a short range persistent process [12].

The maximum weight for each step width time series was for an ARIFMA model and the fractional parameters,  $d$ , were significantly different from 0 ( $p < 0.001$ ) (Table 1). However, only six out of the eleven step width time series had a sum ARIFMA weight greater than 0.90. The average sum of the weights of these six time series was 0.9978, and the average sum of the weights for all ten series was 0.8908.

Table 1. Results from ARMA/ARFIMA and DFA

N	10
ARFIMA as best model	10/10
ARFIMA mean AIC weights	0.89
D (mean±std)	0.25±0.12

Although

this analysis provides evidence that step width demonstrates LR persistence, it does not directly shed any light on possible mechanical or neurological mechanisms underlying LR persistence. However, given that step width has anatomical and physiological constraints, it is possible that during locomotion step width is regulated only when it approaches its limits. This control strategy could result in a LR persistence process which is driven by the superimposition of many SR processes [11,13], thereby providing an explanation for why the autocorrelation analyses

[7,8] and DFA [1,2,3,4] present contradictory results.

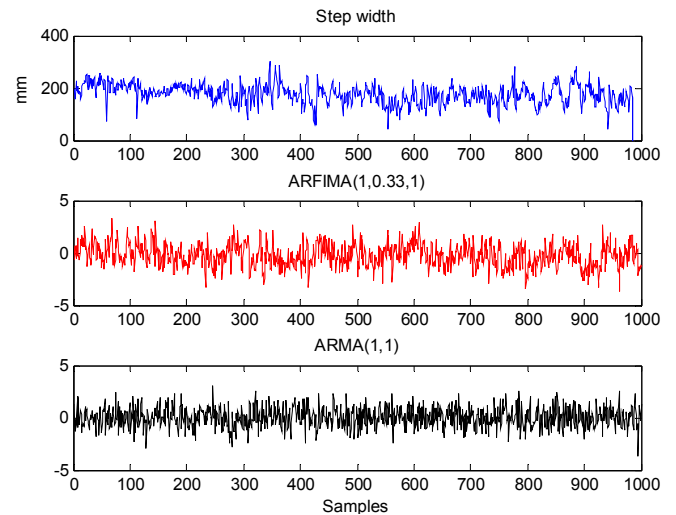


Figure 1. (Blue) Sample Step width time series with average fractional parameter,  $d = 0.33$  (Red) ARFIMA simulation with  $p = 1$ ,  $q = 1$  and  $d = 0.33$  (Black) ARMA simulation with  $p = 1$ ,  $q = 1$

## CONCLUSIONS

The ARMA/ARFIMA analysis indicates that step width during treadmill walking has LR persistence which is consistent with interpretations from DFA. Given the established biomechanical and physiological importance of step width, further study seems warranted to establish how and why persistence is manifested and its potential clinical utility.

## REFERENCES

1. Franz et al. Hum Move Sci. 2016
2. Kaipust et al. Motor Control. 2012
3. Stout et al. Gait Posture. 2016
4. Dingwell et al. 39<sup>th</sup> ASBConference. 2016
5. Delignières and Torre. J Appl Physiol. 2008
6. Wagenmakers et al. Psychon Bull Rev. 2004
7. Collins and Kuo. PLoS One. 2013
8. Grabiner et al. 40<sup>th</sup> ASBConference. 2016
9. Stadnitski. Front Physiol. 2012
10. Hurt et al. Gait Posture. 2010
11. Torre et al. Br. J. Math. Stat. Psychol. 2007
12. Romero and Sancho. Cond. Mat. Stat. Mech. 1999

# APPLICATION OF HARMONIC TRANSFER FUNCTIONS METHOD OF ANALYSIS TO UNDERSTAND RESPONSES TO MECHANICAL PERTURBATIONS IN HUMAN WALKING

<sup>1</sup> Farzad Ehtemam, <sup>2</sup> Sandra K. Hnat, <sup>1</sup> Tim Kiemel, <sup>2</sup> Antonie J. van den Bogert

<sup>1</sup> University of Maryland, College Park, MD, USA

<sup>2</sup> Cleveland State University, Cleveland, OH, USA

email: fehtemam@umd.edu

## INTRODUCTION

Human walking has been studied extensively under approximately steady-state conditions, for example, when subjects walk on a treadmill whose belt moves at a fixed speed. In everyday life, acceleration and deceleration, obstacle negotiation, disturbance rejection, and turning are all examples of behaviors that require modulation of walking speed, which is driven by transient changes in muscle activations [1], [2], [3]. However, even during steady-state walking, the nervous system is continually modulating muscle activations based on sensory information to ensure stability, as evidenced by small continual changes in walking speed and other kinematic variables.

Weak continuous sensory and mechanical perturbations can be used to identify properties of this neural feedback control of steady-state walking [4], [5], based on a local limit-cycle approximation of human gait. Responses to perturbations are characterized in time domain using phase-dependent impulse response functions ( $\phi$ IRFs). A  $\phi$ IRF describes the response to a small brief perturbation (an impulse) applied at any phase of the gait cycle and, by extension, the response to any small perturbation. In this study, we applied this approach to characterize the effects of continually varying treadmill speed on kinematic variables.

## METHODS

The experiment design has been previously described in detail [6]. Twelve subjects walked on an instrumented treadmill (Forcelink, Culemborg, Netherlands) at three different speeds of 0.8, 1.2 and 1.6  $\text{ms}^{-1}$ . Forty seven reflective markers were attached to different anatomical landmarks and the

kinematics were captured using a ten camera motion capture system (Motion Analysis, Santa Rosa, CA, USA). Each trial was ten minutes starting with one minute of normal walking, followed by eight minutes of perturbation, and ending with one minute of normal walking. The perturbation was designed by generating filtered white noise as an acceleration signal in MATLAB (The MathWorks, Inc., Natick, MA, USA) which was then integrated to derive a velocity signal. This signal was commanded to the treadmill using D-Flow software (Motek Medical, Amsterdam, Netherlands).

To approximate walking as a linear time periodic system [7], we replace the time with estimated phase of the gait cycle as the independent variable. Heel-strike times were used to derive a piecewise-linear causal estimate of phase, which was then filtered to obtain a continuous approximation. We then characterized kinematic responses to the perturbation signal (i.e., speed of the belt) in the frequency domain using harmonic transfer functions [4]. An HTF has a “mode” for each integer  $k$  with its own gain and phase functions. The  $k$ -th mode describes the mapping from frequency  $f$  to frequency  $f + kf_0$  where  $f_0$  is the gait frequency. To make it easier to interpret kinematic responses, we converted HTFs to the  $\phi$ IRFs described above. A correction was made for the method used to estimate phase, so that to first order in perturbation size, the resulting  $\phi$ IRFs did not depend on the estimation method [5].

## RESULTS AND DISCUSSION

Figure 1 shows the  $\phi$ IRF between the belt speed and the velocity of right ankle. As we can see in the figure, there is an increase in the velocity immediately after the onset of perturbation (the red

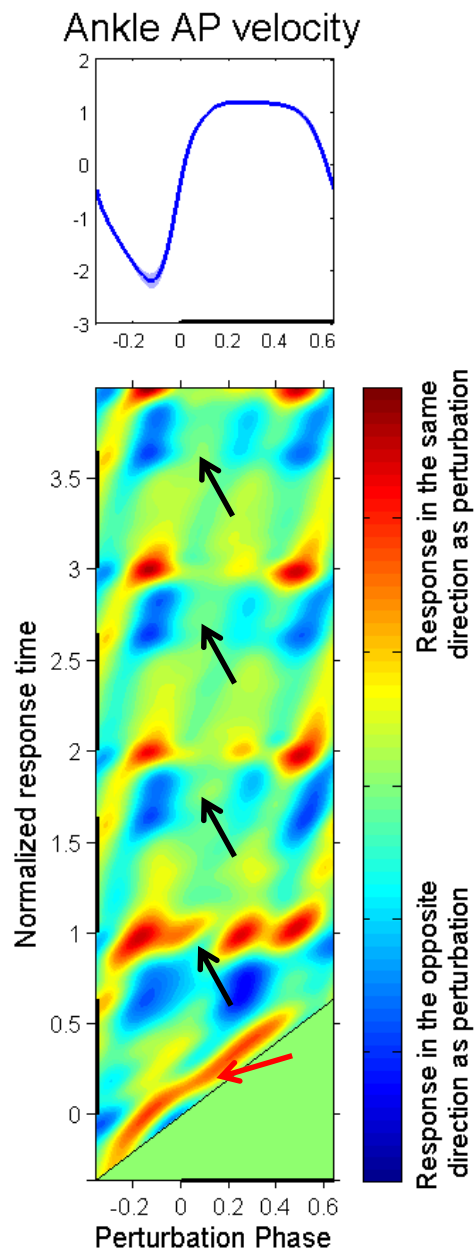


**Figure 1:** *Top:* Mean waveform of the right ankle anteroposterior (AP) velocity across all cycles during the trial. The shaded area shows 95% confidence intervals and the black bar on the horizontal axis marks the stance phase of the cycle. *Bottom:* the  $\phi$ IRF between the belt speed and the ankle velocity for four cycles after perturbation onset calculated from modes  $k$  with  $|k| \leq 3$ . Black bars on each axis mark the stance phase. The color red in the spectrum represents a change in the response in the same direction as the change in perturbation and blue represents changes in the opposite direction. The diagonal line is the onset of perturbation.

area along diagonal marked by the red arrow). Since the input is the speed of the treadmill, we expect to see an impulse in the foot velocity as a response to an impulse in the belt speed. This transient change in velocity is only observed in the first cycle after perturbation and fades away in the following cycles. Another important feature of the observed response is the phase resetting [8], an initial increase in the speed, followed by an immediate decrease, repeated throughout the subsequent cycles (indicated by black arrows in the figure).

The use of  $\phi$ IRFs provides a complete picture of kinematic responses to small perturbations. However, as the size of perturbations increases,  $\phi$ IRFs can be affected by second-order effects, which we are currently investigating by varying perturbation size. We are also measuring electromyographic (EMG) responses, to determine the role of neural feedback in responding to changes in treadmill speed. Longer term, future studies can apply this method to investigate transient responses in geriatric or neurological populations, using kinematic and EMG measures to better understand the neural control mechanisms used to ensure stable walking.

## REFERENCES

- [1] S. A. Chvatal and L. H. Ting, *J. Neurosci.*, **32**, no. 35, pp. 12237–12250, 2012.
- [2] A. J. T. Stevenson, S. S. Geertsen, T. Sinkjær, J. B. Nielsen, and N. Mrachacz-Kersting, *J. Neurophysiol.*, **113**, no. 9, pp. 3151–3158, 2015.
- [3] D. J. Villarreal, D. Quintero, and R. D. Gregg, *IEEE Access Pract. Innov. Open Solut.*, **4**, pp. 893–904, 2016.
- [4] T. Kiemel, D. Logan, and J. J. Jeka, *ArXiv160701746 Q-Bio*, 2016.
- [5] D. Logan, T. Kiemel, and J. J. Jeka, *Front. Comput. Neurosci.*, **10**, 2017.
- [6] J. K. Moore, S. K. Hnat, and A. J. van den Bogert, *PeerJ*, **3**, p. e918, 2015.
- [7] E. Mollerstedt and B. Bernhardsson, *IEEE Control Syst.*, **20**, no. 4, pp. 70–81, 2000.
- [8] T. Yamasaki, T. Nomura, and S. Sato, *Biol. Cybern.*, **88**, no. 6, pp. 468–496, 2003.

# STATISTICAL EVALUATION OF WALKING VELOCITY AND KNEE ADDUCTION MOMENT: ALLOMETRIC SCALING

<sup>1</sup> Samantha Andrews, <sup>1</sup>Elizabeth Parke, <sup>1</sup> Cris Stickley

<sup>1</sup> University of Hawaii, Honolulu, HI, USA  
email: sandrews@hawaii.edu

## INTRODUCTION

Knee adduction moment (KAM) is commonly evaluated in biomechanical research, specifically during the assessment of lower extremity overuse injuries and knee osteoarthritis [1]. However, walking velocity of the pathological group and controls is often different. Previous research has attempted to control for walking velocity differences by implementing a specific walking velocity [2], resulting in one or both groups walking at a non-preferred velocity. This approach, however, is based on the assumption that the relationship between KAM and walking velocity is linear, which has not been previously established. The use of allometric scaling has previously been suggested to control for walking velocity [3] but has not yet been evaluated in young, healthy individuals. Therefore, this study evaluated (1) the relationship between walking velocity and KAM and (2) the effectiveness of allometric scaling of KAM to remove the influence of body mass and walking velocity.

## METHODS

A one time gait assessment was conducted on 63 (Males = 31) healthy, young individuals with a mean height of 170.7 cm (range, 150-186 cm), a mean body mass of 75.7 kg (range, 53-126 kg) and a mean age of 25 years (range, 18-38 years). Patients were asked to walk at a self-selected pace, then at 25% faster and slower than self-selected, while 17 Vicon motion capture cameras (Vicon, Inc., Centennial, CO) collected data from 27 retroreflective markers placed on the lower extremities and trunk. Kinetic data, from one force plate (Advanced Mechanical Technology Incorporated, Boston, MA), were collected at 960

Hz and time synchronized with the kinematic data, collected at 240 Hz.

Log-multilinear regression was used to develop gender specific allometric exponents from only the self-selected velocity data for body mass (BM) and walking velocity (WV) in order to remove the influence of these variables on KAM [4]. Pearson product-moment correlations were performed for raw, ratio and allometrically scaled KAM to evaluate the effectiveness of each scaling procedure.

## RESULTS AND DISCUSSION

The correlation for males between WV and raw KAM (Nm) and between BM and raw KAM were  $r=0.343$  ( $p=0.059$ ) and  $r=0.383$  ( $p=0.033$ ), respectively. For females, the correlation between WV and raw KAM and between BM and raw KAM were  $r=0.255$  ( $p=0.160$ ) and  $r=0.489$  ( $p=0.005$ ), respectively. The correlation for males between WV and ratio-scaled KAM (Nm/kg) and between BM and ratio-scaled KAM were  $r=0.503$  ( $p=0.004$ ) and  $r=-0.124$  ( $p=0.507$ ), respectively. For females, the correlation between WV and ratio-scaled KAM and between BM and ratio-scaled KAM were  $r=0.387$  ( $p=0.029$ ) and  $r=-0.247$  ( $p=0.173$ ), respectively. Raw KAM was allometrically scaled for BM and WV using the following equation:

$$\text{RAW KAM}/((\text{BM}^{\text{exp}})*(\text{WV}^{\text{exp}}))$$

The male exponents for BM and WV were 1.020 and 1.275, respectively. The female exponents for BM and WV were 0.770 and 0.740, respectively. These exponents were used to allometrically scale KAM at each walking velocity condition. The correlations between allometrically scaled KAM and scaling variables at each walking velocity are presented in Table 1.

## CONCLUSIONS

Although ratio scaling for BM was able to remove its effect on KAM, a strong correlation between KAM and WV remained during self-selected walking trials. When allometric scaling was applied, the effect of BM and WV on KAM was completely removed, as indicated by the lack of significant correlation. Successfully removing will allow for better comparison between groups in which WV disparities are present.

When the derived exponents from self-selected velocity were applied to the fast and slow velocity data, allometric scaling was unable to completely remove the effect of WV from KAM. If the relationship between WV and KAM was linear, the application of allometric scaling should have yielded similar results as those produced when applied to self-selected data. However, 10% of the variance in KAM was still attributable to WV, suggesting that walking biomechanics do not change linearly with changes in walking velocity. The lack of linear relationship between KAM and WV is an important distinction, especially when evaluating results from previous research in which walking velocity was prescribed within the methodology.

The results of the current study suggest that the application of allometric scaling is effective in removing the effect of BM and WV from KAM when KAM was evaluated at self-selected walking velocity. However, when applied to fast and slow velocities, allometric scaling by exponents derived from self-selected velocities was unsuccessful. These results indicate the lack of a true linear relationship between walking velocity and KAM, suggesting that the use of prescribed walking velocity could significantly affect biomechanical variables during research. Subjects should complete gait trials at self-selected velocities and allometric scaling should be used to remove the effect of WV, allowing for more accurate comparisons between groups.

## REFERENCES

1. Orishimo KF, et al. *Clin Orthop Relat Res* 470, 1171-1176, 2012.
2. Wilson, JA. *Clin Biomech* 27, 210-212, 2012.
3. Andrews, SN et al. Presented data at ASB, 2016.
4. Vanderburgh, PM, et al. *Med Sci Sports Exerc* 28(5), 626-630, 1996.

Table 1. Correlation between allometrically scaled KAM and scaling variables at each walking velocity

		Males		Females	
		r	p	r	p
Self-Selected	Body Mass	-0.045	0.812	-0.025	0.892
	Velocity	-0.007	0.970	-0.025	0.894
Fast	Body Mass	-0.102	0.585	-0.019	0.916
	Velocity	0.151	0.417	0.027	0.886
Slow	Body Mass	-0.036	0.849	0.122	0.505
	Velocity	-0.216	0.244	-0.209	0.251

r = correlations; p = significant value

# GAIT INITIATION MECHANISMS IN UNILATERAL TRANSTIBIAL AMPUTEES

<sup>1</sup>Mary Roberts and <sup>2</sup>François Prince

<sup>1</sup>Département de kinésiologie, Université de Montréal, Montréal, Québec, Canada

<sup>2</sup>Département de chirurgie, Faculté de médecine, Université de Montréal, Montréal, Québec, Canada  
email: mary.roberts@umontreal.ca

## INTRODUCTION

In the United States, it is estimated that over 1.6 million people are living with an amputation, the most common being the unilateral transtibial amputation and trends indicate that this number is increasing due to dysvascular disease [1].

Walking is the most common form of locomotion and the ability to walk is an indicator of overall health as it dictates autonomy. Of particular interest is the transient process from quiet standing to steady-state walking velocity (SSWV), namely gait initiation.

Although gait initiation in the healthy adult has been well described, few studies have been carried out in the transtibial amputee (TTA) population [2,3]. Moreover, no studies have yet investigated gait initiation in the dysvascular TTA population.

Thus, the purpose of the current study is to compare the biomechanical gait initiation mechanisms of dysvascular TTA to those of healthy controls

## METHODS

Ten participants (7M:3F;  $59.1 \pm 17.3$  years old) with a unilateral dysvascular TTA were recruited via the Institut de Réadaptation Gingras-Lindsay de Montréal. TTA participants were successful prosthetic walkers without aid. Ten healthy controls (8M:2F;  $57.6 \pm 16.4$  years old) were also recruited to participate in this study.

Testing was carried out on a walkway equipped with 3 embedded AMTI (Advanced Medical Technology Inc., MA) force platforms surrounded by an 8 camera OptiTrack motion analysis system (NaturalPoint Inc., OR). From quiet standing, with both feet on side by side force plates, participants

were asked to initiate gait with their right leg and then their left leg. The third force plate was in front of the two others in order to record kinetic data of the first step. A total of 5 trials per side were recorded. Kinetic and kinematic data were both collected at 100 Hz.

Data analysis was carried out using Motive software (NaturalPoint Inc., OR) and a created MatLab program (The MathWorks Inc., MA). Statistics were carried out using SPSS (IBM Corp., NY) with a level of significance set at  $P \leq 0.05$ .

## RESULTS AND DISCUSSION

The mean SSWV attained by controls was  $1.30 \pm 0.23$  m/s and  $1.07 \pm 0.22$  m/s in the TTA group, regardless of the leading limb. This difference was found to be significant. It took an average of 3 steps for controls to reach SSWV and an average of 4 steps for TTA, regardless of leading limb. A large variability (range from 2-7 steps) was observed in the TTA group with regards to the number of steps to reach SSWV. These results corroborate prior findings with regards to a reduced SSWV in a TTA group [4].

The percentage of SSWV reached during the first step was found to be  $74.1 \pm 8.65\%$ , regardless of leading limb in controls and  $72.4 \pm 5.23\%$  of SSWV was achieved during the first step when TTA initiated gait with their intact limb and  $78.6 \pm 6.56\%$  with their prosthetic limb. The difference between the intact and prosthetic limb was found to be significant. The findings as to the percentage of SSWV reached during the first step in controls corroborate prior findings[5]. It is important to note that all TTA participants preferred to initiate gait with their prosthetic limb: in doing so, the intact limb was loaded in order to allow the prosthetic limb to swing forward. TTA are better able to

balance and stabilize on their intact limb, as sensory information is available beneath the foot. Because SSWV was found to be the same regardless of leading limb in the TTA group, the contribution to SSWV produced by each limb is therefore different and it appears as though there is compensation by the intact limb.

The average anterior-posterior ground reaction forces (A/P GRF) recorded beneath the first step are plotted in Figure 1. The reduced SSWV achieved in the TTA group is clearly outlined by the increased braking and reduced propulsion seen below in Fig. 1 with regards to the A/P GRF between both groups. Step time was greater as observed below in Fig. 1 and confirmed by step time when measured from kinematic data (results not shown here).

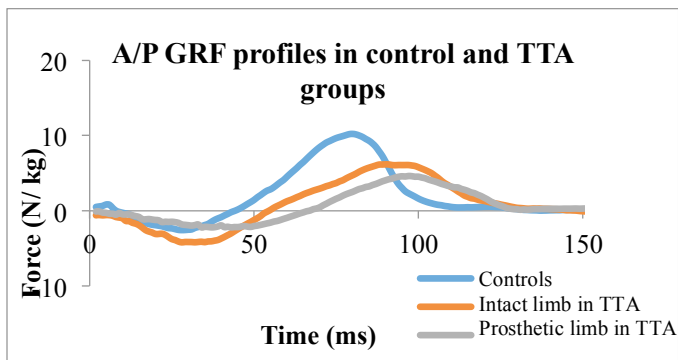


**Figure 1:** A/P GRF profiles of the first step during gait initiation. Force normalized to participant body weight.

As well, the loading rate of the first step vertical GRF were calculated: the loading rate was found to be  $26.1 \pm 5.13$  N/s/kg in controls and  $23.3 \pm 6.69$  N/s/kg and  $17.56 \pm 2.29$  N/s/kg in the intact and prosthetic limb, respectively in TTA. The difference between the intact and prosthetic limb was found to be significant. These results clearly demonstrate a preference for limb loading in the intact limb. This is confirmed by the lower percentage of body weight placed on the prosthetic limb versus the intact limb (results not shown here).

The range of motion (ROM) in the sagittal plane of the hip, knee and ankle, for both limbs, in both conditions are outlined in Table 1. Because the ankle joint is missing in the prosthetic limb, a significant reduction of ROM is observed. Therefore, solely passive energy storage and return is observed within the material of the prosthesis [4].

Because the plantarflexion moment created during push-off is known to be a powerful generator in walking, this reduction of ROM is yet another mechanism leading to reduced SSWV [6]. Also of interest is the reduced ROM at the knee in both the intact and moreover, the prosthetic limb in TTA's. Because of the increased radius of gyration created by a reduced knee flexion during swing phase, the swing time of the limb forward is greater shown by the reduced SSWV (results not shown here). This is further exacerbated in the prosthetic limb.

**Table 1:** ROM of the hip, knee, ankle in sagittal plane.

	Controls	Intact limb	Prosthetic limb
Ankle	$32.2 \pm 6.77^\circ$	$36.5 \pm 14.62^\circ$	$21.8 \pm 12.02^\circ$
Knee	$65.2 \pm 6.33^\circ$	$60.2 \pm 15.78^\circ$	$55.7 \pm 12.99^\circ$
Hip	$50.6 \pm 8.14^\circ$	$46.5 \pm 9.20^\circ$	$47.8 \pm 16.29^\circ$

## CONCLUSIONS

The underlying gait initiation mechanisms employed by dysvascular TTA are different than that of healthy controls, even so in the intact limb. The intact limb contributes a greater extent in achieving SSWV, although the SSWV remains reduced. The implications of understanding daily tasks, such as gait initiation, are paramount to improving rehabilitation, care and quality of life in the growing population of dysvascular TTA individuals. Further studies should aim at understanding the power profiles during gait initiation in such a population.

## REFERENCES

1. Ziegler-Graham K, MacKenzie EJ, Ephraim PL, Trivison TG, Brookmeyer R. *Arch Phys Med Rehabil* **89**:422–9, 2008.
2. Brenière Y, Do MC. *Motor Control* **23**: 235-40, 1991
3. Vrieling AH, Van Keeken HG, Schoppen T, Otten E, Halbertsma JPK, Hof AL, et al. *Gait Posture* **27**:423–30, 2008.
4. Jian Y, Winter DA, Ishac MG, Gilchrist L. *Gait Posture* **1**:9–22, 1993.
5. Prince F, Winter DA, Sjønnensen G. *J Rehabil Res Dev* **35**: 177-185, 1998.
6. Winter DA. *Gait Posture* **3**: 193-214, 1995.

# DO KINETIC DIFFERENCES EXIST DURING CURB ASCENT IN PERSONS WITH ERTL AND NON-ERTL TRANSTIBIAL AMPUTATIONS?

<sup>1</sup>Abbie E. Ferris, <sup>2</sup>Cory L. Christiansen, <sup>1</sup>Gary D. Heise, and <sup>1</sup>Jeremy D. Smith

<sup>1</sup>School of Sport & Exercise Science, University of Northern Colorado, Greeley, CO

<sup>2</sup>Interdisciplinary Movement Science Lab, University of Colorado, Anschutz Medical Campus, Denver, CO

Email: [abbie.ferris@unco.edu](mailto:abbie.ferris@unco.edu); website: <http://www.unco.edu/biomechanics>

## INTRODUCTION

Negotiation of uneven surfaces is especially difficult for those with lower extremity amputations. Relative to age-matched, non-amputees, persons with transtibial amputation (TTA) have an increased risk of falling and fear of falling [1]. Further, persons with TTA report curb negotiation is more challenging than negotiating stairs even though they are encountered with the same frequency [2, 3].

It is also unknown if amputation technique influences an amputee's ability to negotiate a curb. Traditionally, the tibia and fibula are not joined during a TTA (Non-Ertl). However, a transtibial osteomyoplastic amputation (Ertl) uses a "bone bridge" to connect the tibia and fibula sealing the medullary canal. The Ertl technique has been suggested to improve the overall physiology of the residual limb and promote greater distal load-bearing of the residual limb [4, 5].

Therefore, the purpose of this study was to determine if functional ability to negotiate a curb is different between Ertl and Non-Ertl groups. Since it has been suggested the Ertl amputation has an increased capability to bear loads on the distal end of the residual limb, it was hypothesized that those with Ertl amputations would have capacity to store energy at the ankle that can be used in total limb work. Further, the Ertl affected limb would produce greater joint work at the knee, and hip while ascending a curb compared to Non-Ertls.

## METHODS

Two groups of transtibial amputees were recruited: Non-Ertl (n = 7; 88.3 ± 16.0 kg, 1.78 ± 0.08 m; 55 ± 5 years) and Ertl (n = 5; 79.8 ± 15.5 kg, 1.79 ± 0.08 m; 55 ± 8 years). Inclusion criteria included: amputation resulting from trauma, no concomitant musculoskeletal injuries, neurological, or visual

impairments. All participants were physically active at least 3 days per week. Motion data (100Hz) and ground reaction forces (2000 Hz) were collected as participants ascended a 16 cm curb (VICON, UK) (Fig. 1). Participants approached the curb at a walk (~3 m) and ascended the curb at their self-selected walking velocity. **GROUND** and **CURB** steps were analyzed separately.

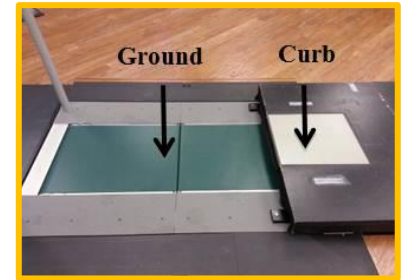


Figure 1. Image of the curb design.

Lower extremity net joint work for the unaffected and affected limbs were calculated. Positive and negative work at each joint were summed to determine the net joint work performed at the hip, knee, and ankle. Total limb joint work was computed as the sum of the net joint work at each joint.

A t-test was used to determine differences in walking speed between groups. A single factor MANOVA ( $\alpha = .05$ ; SAS 9.4, Cary, NC) was used to identify differences in work between groups and limbs.

## RESULTS and DISCUSSION

Both groups walked at similar speeds (1.28 ± 0.20 m/s Ertl vs. 1.28 ± 0.19 m/s Non-Ertl) and all participants were able to perform curb ascent with each limb as the lead limb onto the CURB.

**GROUND Step Results:** Net ankle joint work was significantly larger ( $p < .05$ ) in the unaffected limb of both groups compared with the respective affected limb (Fig. 2). Net work at the knee and hip was not significantly different across limbs. Total limb work was significantly larger ( $p < .05$ ) in both of the unaffected limbs compared to both of the affected limbs (Fig. 2).

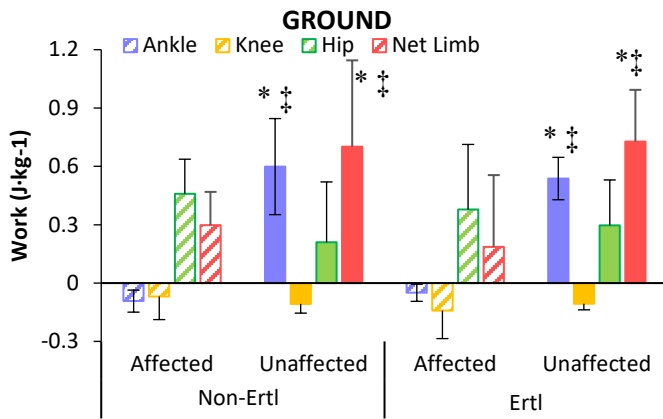


Figure 2. Work for the ankle, knee, hip, and limb for the GROUND step. \*Significantly different from Ertl affected limb; †Significantly different from Non-Ertl affected limb.

**CURB Step Results:** Net work at the ankle was significantly ( $p < .05$ ) smaller for both affected limbs compared to both unaffected limbs (Fig. 3). The Non-Ertl affected limb had significantly greater negative net knee work than both the unaffected limbs ( $p < .05$ ). The Ertl affected limb also produced significantly ( $p = .042$ ) more negative net knee work than the Non-Ertl unaffected limb, but not the Ertl unaffected limb. The Ertl affected limb differed further from the Non-Ertl unaffected limb by producing significantly ( $p = .016$ ) more positive net work at the hip.

Total limb work showed the Non-Ertl affected limb produced significantly ( $p < .05$ ) less work compared to each of the unaffected limbs (Fig. 3). However, no significant differences were found between the Ertl affected limb and each unaffected limb. The contrast of total limb work between the Non-Ertl affected limb and Ertl affected limb approached significance

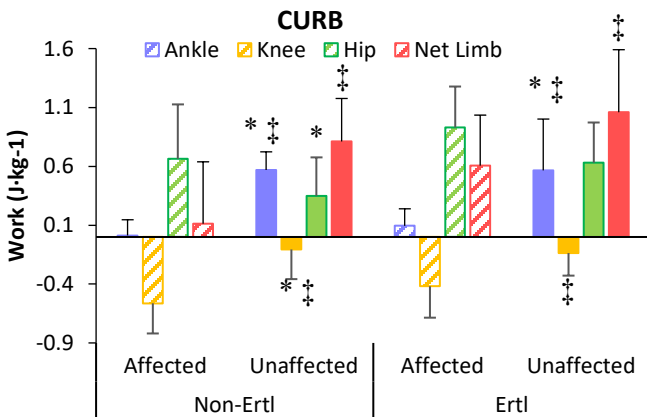


Figure 3. Net joint work for entire limb for the CURB step. \*Significantly different from Ertl affected limb; †Significantly different from Non-Ertl affected limb.

( $p = .0845$ ) suggesting that the Ertl limb overall was performing more net joint work than the Non-Ertl limb.

Results from the CURB step suggest that the unaffected limbs produced a large amount of net work at the ankle. In contrast, the Ertl affected limb produced more net hip work and very little net ankle work. The amount of work produced by the Ertl affected limb at the hip was significantly larger than the Non-Ertl unaffected limb. The inter-limb differences suggest that the affected limbs, regardless of amputation type, adopt more of a hip strategy than a knee strategy (used by the unaffected limb).

Overall, the main finding on the GROUND was that the affected limb of both groups produced significantly less work than the unaffected limb, which was most attributable to the limited amount of ankle work for the affected limb. These results are similar to those reported by Barnett et al. [6] during a similar curb negotiation task in persons with TTA.

Socket type or prosthetic foot type was not controlled which may have affected the way in which the affected limb was used. Importantly, there was no unique socket design in the Ertl group to promote distal residual limb load bearing.

## CONCLUSION

Comparisons between functional outcomes of the Ertl and Non-Ertl groups suggest the Ertl affected limb may behave differently than the Non-Ertl limb by producing more net limb work on the CURB step than the Non-Ertl affected limb, primarily at the hip. This supports our hypothesis that the Ertl limb would produce greater work while negotiating a curb compared to the Non-Ertl affected limb, but this outcome is specific to mechanics on the curb step itself.

## REFERENCES

1. Miller, W., et al. Arch Phys Med Rehabil, 2001. **82**(8): p. 1031-7.
2. Shumway-Cook, A., et al. Phys Ther, 2002. **82**(7): p. 670-81.
3. Larsson, B., et al. Health Qual Life Outcomes, 2009. **7**: p. 44.
4. Dionne, C., et al. J Prosthet Orthotics, 2009. **21**(1): p. 64.
5. Ertl, J., et al. February 15, 2013
6. Barnett, C., et al. Clin Biomech, 2014.

# GAIT STABILITY IN PEOPLE WITH UNILATERAL TRANSTIBIAL AMPUTATION ACROSS WALKING SPEEDS

Ryan D. Wedge, Andrew K. LaPrè, Frank C. Sup, and Brian R. Umberger  
University of Massachusetts, Amherst, MA, USA

email: [umberger@kin.umass.edu](mailto:umberger@kin.umass.edu), web: [www.umass.edu/locomotion](http://www.umass.edu/locomotion), [www.ecs.umass.edu/mie/mrrl](http://www.ecs.umass.edu/mie/mrrl)

## INTRODUCTION

People with lower limb amputation of all levels have an increased incidence of falls [1]. There is considerable interest in how gait stability is regulated in people with lower limb amputation and how this is related to fall risk. People with unilateral transtibial (TT) amputation exhibit many inter-limb asymmetries when walking [2], such as in step length and step time, and these asymmetries may be related to gait stability. It has been shown that step length asymmetry, with a shorter step on the intact side (i.e., a forward step with the intact limb), may enhance gait stability for walking at the preferred speed [3], but the effects across speeds are presently unknown. A better understanding of the inter-relationships among gait stability, asymmetries and walking speed in people with unilateral TT amputation will help inform interventions to reduce the incidence of falls.

The margin of stability [4] is a global (i.e., whole body) measure of gait stability that should be closely related to the risk of falling. Specifically, the backwards MoS (BW MoS) at initial foot contact can reveal the strategies people use to avoid a backwards fall when transitioning onto the lead limb. The BW MoS was previously shown to be greater for the intact limb in people with unilateral TT amputation when walking at preferred speed [3], presumably to compensate for reduced push-off by the prosthetic ankle. Since the mechanisms of maintaining gait stability are of interest across walking speeds, the purpose of this study was to evaluate BW MoS between limbs over a range of speeds in people with unilateral TT amputation.

## METHODS

Data were collected for seven subjects, five with a left-side TT amputation and two with a right-side TT amputation. Four subjects had a shuttle lock

connecting the sleeve and socket, two had a vacuum socket, one was end-bearing, and all seven had a standard pylon and a split toe flex-foot. Subject characteristics are listed in Table 1.

BW MoS at initial foot contact was calculated based on the extrapolated position of the center of mass (CoM) relative to the forward margin of the base of support [3,4]. Kinematic data were captured using a high-speed motion capture system as subject walked overground along a 15 m walkway. CoM horizontal position was determined from markers on the right and left anterior superior iliac spines and posterior superior iliac spines, and then numerically differentiated to determine CoM velocity (vCOM). The forward margin of the base of support was calculated from a marker located on the lateral heel.

BW MoS was determined at initial foot contact for both limbs (prosthetic and intact) for three trials at each of three speeds (preferred and  $\pm 20\%$  of preferred). Dependent variables were tested for differences using 2 (limb)  $\times$  3 (speed) MANOVAs followed by post-hoc tests using the false discovery rate procedure. Due to the preliminary and exploratory nature of the study, significance was evaluated at  $\alpha = 0.10$ .

**Table 1:** Subject demographics: means  $\pm$  SD

Mass (kg)	74.3 $\pm$ 15.0
Height (m)	1.78 $\pm$ 0.09
Slow speed (-20%) (m/s)	1.05 $\pm$ 0.04
Preferred speed (m/s)	1.27 $\pm$ 0.04
Fast speed (+20%) (m/s)	1.55 $\pm$ 0.07

## RESULTS AND DISCUSSION

BW MoS was greater at all speeds for the intact compared to the prosthetic side (Fig. 1A), similar to previous findings at preferred speed [3]. There was a significant effect of speed ( $p < 0.001$ ) and a significant effect of limb ( $p = 0.039$ ) for BW MoS

with no speed-by-limb interaction ( $p = 0.765$ ). Pairwise comparisons showed significant differences in BW MoS between limbs at each speed with moderate to large effect sizes (ES) (slow:  $p=0.092$ ,  $ES=0.44$ ; preferred:  $p=0.022$ ,  $ES=0.90$ ; and fast:  $p=0.052$ ,  $ES=0.78$ ).

There was a significant effect of speed ( $p < 0.001$ ) and a significant effect of limb ( $p = 0.008$ ) for step length with no speed-by-limb interaction ( $p = 0.976$ ). Pairwise comparisons showed significant differences in step length between limbs at the slow speed and large ES for all speeds (slow:  $p=0.030$ ,  $ES=0.91$ ; preferred:  $p=0.103$ ,  $ES=1.09$ ; and fast:  $p=0.126$ ,  $ES=0.84$ ).

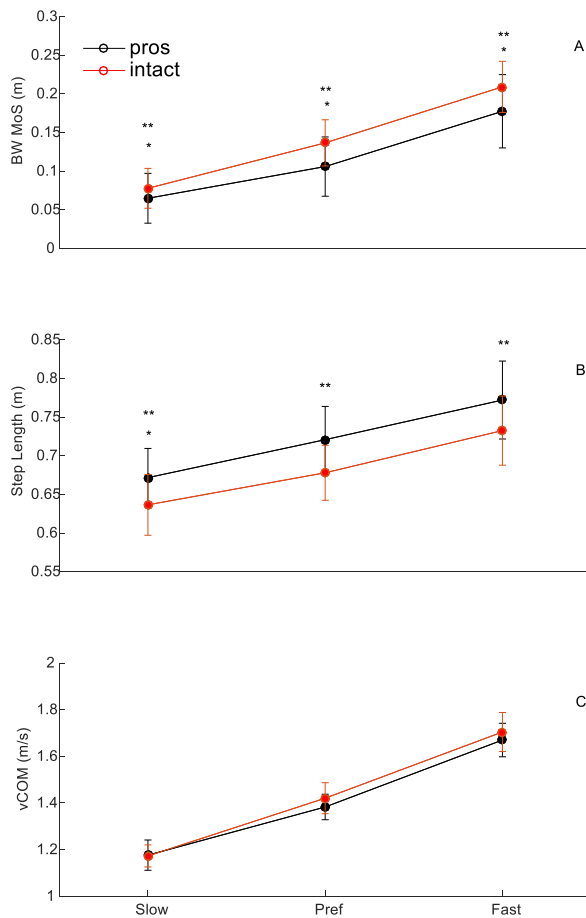


**Figure 1:** BW MoS (A), step length (B), and vCoM (C) for both limbs across speeds. The \* symbol denotes a significant difference between limbs; \*\* denotes a moderate or large effect size.

There was a significant effect of speed ( $p < 0.001$ ) but no significant effect of limb ( $p = 0.302$ ) for

vCoM and no speed-by-limb interaction ( $p = 0.698$ ). All possible pairwise comparisons for speed effects for BW MoS, step length and vCoM were significant (all  $p$ -values  $< 0.01$ ) as was expected given the wide range of speeds (Table 1).

The subjects demonstrated a greater BW MoS on the intact side at initial foot contact across speeds, as had been shown at preferred speed [3]. The greater BW MoS for steps on the intact side was achieved primarily through a shorter step length, rather than a greater vCOM. Due to limitations of a prosthetic limb, subjects may more easily regulate gait stability via step length asymmetry rather than by a greater vCOM, which would require generating more hip work on the prosthetic side and potentially raise metabolic energy expenditure.

This was a preliminary study with a small sample size. Nevertheless, the results were consistent with clear trends and suggest expanding the sample size and testing a greater range of walking conditions.

## CONCLUSIONS

People with unilateral TT amputation achieve greater BW MoS at initial contact on the intact side versus the prosthetic side across walking speeds primarily by utilizing a shorter step length on the intact side, rather than by increasing vCOM. This provides further evidence that gait asymmetries may be functional adaptations that in the case of step length enhance gait stability.

## REFERENCES

1. Miller WC, et al. *Arch Phys Med Rehabil* **82**, 1031-1037, 2001.
2. Sanderson DJ & Martin PE. *Gait Post* **6**, 126-136, 1997.
3. Hak L, et al. *Phys Ther* **94**, 1480-1488, 2014.
4. Hof AL, et al. *J Biomech* **38**, 1-8, 2005.

## ACKNOWLEDGMENTS

Supported by grants from the National Science Foundation (IIS-1526986) and the National Center for Simulation in Rehabilitation Research.

# FOURIER ANALYSIS OF VERTICAL GROUND REACTION FORCES IN HABITUALLY UNSHOD PERSONS

<sup>1,2</sup>Taylor P. Trentadue, <sup>3</sup>Robin M. Queen, <sup>1</sup>Daniel Schmitt

<sup>1</sup>Animal Locomotion Lab, Department of Evolutionary Anthropology, Duke University, Durham, NC, USA

<sup>2</sup>Duke Global Health Institute, Duke University, Durham, NC, USA

<sup>3</sup>Department of Biomedical Engineering and Mechanics, Kevin Granata Biomechanics Lab, Virginia Tech University, Blacksburg, VA, USA  
email: taylor.trentadue@duke.edu

## INTRODUCTION

The spring-loaded inverted pendulum model of human gait represents the limb as a massless strut with the mass concentrated at one end and the joints represented as springs of varying stiffness. [1] This model helps explain the pattern observed during healthy walking where the knee and ankle yield very little. In that context, the spring is relatively stiff and the center of mass (COM) moves upward from heelstrike to midstance, followed by a downward movement from midstance to toe-off. The resulting vertical ground reaction force (VGRF) reflects the acceleration and deceleration of the COM and produces waveforms that include two maxima separated by a local minimum. [2-5] VGRF shape varies with leg spring behaviors and COM acceleration, and it may reflect changes in joint motion, joint function, and health. [6-9]

Musculoskeletal (MSK) health is vital for successful participation in activities of daily life, yet worldwide variation in limb function, especially in the face of changing work roles and dietary patterns globally, remains understudied. Madagascar is experiencing a growing burden of chronic, non-communicable diseases, including MSK conditions. [10] However, no assessments of limb mechanics in a habitually unshod, agrarian sample are available. We used a Fourier analysis of the VGRF to explore limb function in this population.

## METHODS

VGRF data were collected from a sample of habitually unshod persons in the northeastern, rural

SAVA region of Madagascar (n=40; 50% female, mean age  $\pm$  SD = 43.7 $\pm$ 15.8) as well as a sample of habitually shod persons in the U.S. (n=19, 63% female, 53% White, mean age  $\pm$  SD = 31.2 $\pm$ 15.1) using a portable, biaxial force platform (PASCO PS-2142, PASCO Scientific, Roseville, CA). The PASCO force platform measured static forces within 0.1% of known weights (6 kg and 88.5 kg). Participants walked at self-selected speeds across force platforms embedded in the ground or a runway. A total of 400 and 211 valid steps were collected in Madagascar and the U.S., respectively.

To characterize and compare the shape of waveforms within and across populations, normalized VGRF data were filtered using a fourth-order low-pass Butterworth filter with a cutoff frequency of 10 Hz and zero-padded to twice the length of the vector. An eight-term Fourier model with period  $\omega = \pi / \text{contact time (CT)}$  was fitted to the waveforms using MATLAB (MathWorks, Inc., Natick, MA). ANOVA and Tukey's tests were performed to analyze the differences in waveform shape detected by Fourier coefficients within the Malagasy sample and between the Malagasy and U.S. samples.

## RESULTS AND DISCUSSION

In the Malagasy sample, five distinct VGRF waveforms were produced: a characteristic two-peaked waveform ("normal;" n=181), peaks shifted towards the early and late phases of stance in the waveform ("square;" n=74), a flat, plateau-like shape at one maximum and a sinusoidal curve at the other ("trapezoidal;" n=49), a flat curve resembling

that produced during compliant walking (“flat;” n=28), and a curve with  $\geq 3$  distinct peaks oscillating at 100% body weight (“tripeaked;” n=67). Nine coefficients (cosine  $a_{3,4,6,8}$ ; sine  $b_{1,3,5,6,7}$ ) were statistically significantly ( $p < 0.0001$ ) different between the five waveform patterns in the Malagasy sample.

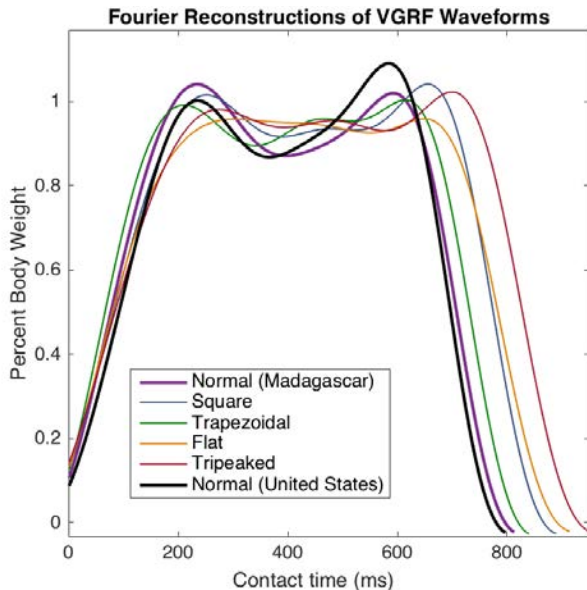


**Figure 1:** Fourier reconstruction of VGRF waveforms. Normal steps in Malagasy and U.S. samples have comparable CT. The other waveforms have significantly longer CT ( $f = 24.09$ ,  $p \ll 0.001$ ).

No statistically significant differences exist in the Fourier coefficients between the normal waveforms in the Malagasy and U.S. at  $\alpha = 0.001$ ; one coefficient ( $a_7$ ) is statistically significant at  $\alpha = 0.05$ .

The gait patterns seen in the Malagasy sample are consistent with those reported as pathological gait patterns in a Western sample and recorded for patients with osteoarthritis. [11, 12] The waveforms in this sample, as seen in Western samples of persons with osteoarthritis, had longer weight receiving phases and CT. [13] Persons in occupations that demand increased physicality often experience MSK pathologies; carrying increased loads or non-standard postures contribute to the burden of MSK disorders, a pattern of labor that may be reflected in these waveforms. [14, 15]

## CONCLUSIONS

Fourier analysis of the VGRF is able to distinguish different gait patterns within a habitually unshod population in rural Madagascar, and it did not detect statistically significant differences in Normal walking VGRFs between agrarian and urban populations. This method identified atypical and potentially pathological patterns that may represent poor lower limb mechanics and joint health. This analysis provides insight into the relationships between cultural and occupational factors and joint mechanics, highlighting the importance of MSK function in a global health context.

## REFERENCES

1. Blickhan R. *J Biomech* **22**, 1217-27, 1989.
2. Alexander RM, et al. *J Zool* **185**, 27-40, 1978.
3. Pandy MG, et al. *Annu Rev Biomed Eng* **12**, 401-433, 2010.
4. Czerniecki JM. *Am J Phys Med Rehabil* **246-252**, 1988.
5. Ayyappa E. *J Prosthet Orthot* **9**, 10-17, 1997.
6. Li Y, et al. *Folia Primatol (Basel)* **66**, 137-59, 1996.
7. Cavagna GA, et al. *J Appl Physiol* **21**, 271-278, 1966.
8. Astephen JL, et al. *J Orthop Res* **26**, 332-41, 2008.
9. Chiu MC, et al. *Gait Posture* **25**, 385-392, 2007.
10. Masquelier B, et al. *Glob Health Action* **7**, 23237, 2014.
11. Jacobs NA, et al. *J Biomech* **5**, 11-34, 1972.
12. Schmitt D, et al. *Gait Posture* **42**, 373-9, 2015.
13. Sims EL, et al. *Aging Clin Exp Res* **21**, 463-469, 2009.
14. Huang TW, et al. *J Exp Biol* **217**, 605-613, 2014.
15. Yasobant S, et al. *Indian J Occup Environ Med* **18**, 75-81, 2014.

## ACKNOWLEDGMENTS

This project was supported by the Duke Deans' Summer Research Fellowship, Duke Undergraduate Research Grants, and Bass Connections. We thank Charles Nunn and Melissa Manus.

# COMPARISONS OF THE VARIABILITY OF ACCELERATIONS BETWEEN LEFT AND RIGHT FOOT IN HUMAN WALKING

Sakdapong Chavanaves, Stephen J. Piazza and Robert B. Eckhardt

The Pennsylvania State University, University Park, PA, USA  
email: pingsakdapong@gmail.com

## INTRODUCTION

Walking, which has been called the most common human activity, features a repetitive sequence of movements with coordination between the left and right limbs to propel the body forward while maintaining stability. The results of several studies have indicated that while there is a considerable degree of symmetry between the left and right limbs in healthy walking gait, there also is evidence of asymmetry in healthy gait [1]. Such asymmetry usually is considered to be a common characteristic of pathological gait such as seen in Parkinson's disease, Huntington's disease, amyotrophic lateral sclerosis and stroke.

While many attempts have been made to research gait symmetry in both healthy and pathological gait, most studies quantified gait symmetry using only spatial-temporal gait variables and joint kinematics and kinetics. Very little is known about symmetry in measures of gait variability, despite indications that gait variability assessment is useful for distinguishing between fall-prone and healthy individuals [2]. The aim of this study was to compare the variability of readings from accelerometers affixed to the left and right feet under various walking conditions.

## METHODS

Seventeen healthy individuals (13 male and 4 female) aged  $26 \pm 6$  years participated in this study. All procedures were approved by the Institutional Review Board of The Pennsylvania State University. Each participant completed two experimental sessions on different days. The participants performed 5-minute walking trials at their preferred walking speed for each of 4 different conditions: treadmill walking (TM), overground

walking on a 2 m x 10 m rectangular path (OG), overground clockwise and counter-clockwise walking along a 1.5 m radius circular path (CW and CCW). In the first session, the participant completed two trials for each condition in random order. In the second session, the participant repeated the same procedure but completed only one trial for each condition in random order.

Participants were provided shoes and a waist belt that were fitted with tri-axial accelerometers (G-Link; LORD Microstrain). The accelerometers measured three-dimensional linear accelerations (not corrected for acceleration due to gravity) at 128 Hz with a maximum lag of  $\pm 100 \mu\text{s}$  between accelerometers.

The first 25 strides of each trial were excluded from analysis to remove transients. Heel strikes were identified as the maximum accelerations (in the axis perpendicular to the plane of the top surface of the shoes) of shoe accelerometers. 150 strides from each trial were used for the analysis.

Each of the acceleration time series along the three orthogonal axes of each accelerometer was separated into time-normalized strides of 101 data points (0%-100% of gait cycle) using a shape-preserving piecewise cubic Hermite interpolation. Variability at each 1% of the gait cycle was determined as the standard deviation of the acceleration from 150 strides. MeanSD-acc was computed as the average standard deviation calculated over the entire gait cycle (the standard deviation at 0% was excluded since it represents the same gait event as at 100%).

We performed two separate 2 x 2 repeated-measures ANOVAs to compare MeanSD-acc between (1) left and right foot x TM and OG and (2) inside and

outside foot x CW and CCW. Bonferroni correction was used to reduce Type 1 error yielding  $\alpha = 0.05/18 = 0.003$  for this study.

## RESULTS AND DISCUSSION

There were significant main effects of (1) TM vs. OG walking condition in all 3 directions, (2) left vs. right foot in the anterior-posterior and the vertical directions (3) inside vs. outside foot in all 3 directions. There were significant interactions between CW vs. CCW walking condition and inside vs. outside foot in all 3 directions.

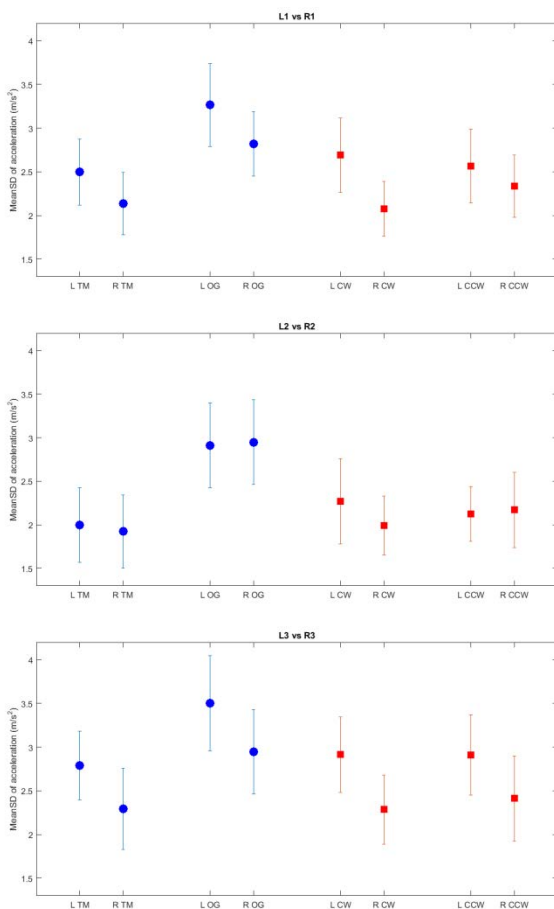


**Figure 1:** MeanSD-acc of L1 vs. R1 (anterior-posterior), L2 vs. R2 (medial-lateral) and L3 vs. R3 (vertical) for four different walking conditions. Each error bar represents  $\pm$  one standard deviation.

Our results showed that MeanSD-acc was larger for the left foot compared to the right foot, except in the medial-lateral direction, in all walking conditions. While results regarding the symmetry of kinematic

and kinetic gait variables are not conclusive [1], we have found that gait asymmetry is apparent in the variability of foot-mounted accelerometer readings. Measurements of upper limb motions have revealed that the dominant-side limb system is specialized for controlling limb trajectory dynamics, while the non-dominant-side limb system is specialized for controlling limb position and stabilization [3]. If similar specialization applies to foot motion, we might expect more consistent foot acceleration trajectories in the dominant foot. Although we did not determine the handedness or the footedness of our participants, previous research indicated that most people are right-limb dominant [4]. If we assume that the majority of our participants are right limb dominant, our results would support the possibility that the smaller MeanSD-acc for the right foot resulted from more consistent control of the right leg dynamics. In addition, it is possible that the lateralization of the foot trajectory control is direction specific, as we observed no difference between left and right foot variability in the medial-lateral direction.

## CONCLUSIONS

The variability of left-foot acceleration is larger compared to that of the right foot, except in the medial-lateral direction, across all the walking conditions tested. This difference may be an indication of both gait asymmetry and motor lateralization. Our results suggest that future studies should not assume the symmetry of gait variability measurements between left and right limbs and that gait variability should be assessed separately for each limb during walking.

## REFERENCES

1. Sadeghi H, et al. *Gait & posture* **12(1)**, 34-45, 2000.
2. Tobes MJ, et al. *Gait & posture* **36(3)**, 527-531, 2012.
3. Sainburg, RL. *Exercise and sport sciences reviews* **33(4)**, 206-213, 2005.
4. Porac C & Coren S. *Lateral preferences and human behavior*. New York, NY: Springer, 1981.

# PRELIMINARY EVIDENCE THAT FOOT MECHANICAL ENERGY DURING WALKING IS DISSIPATED AS HEAT

<sup>1</sup> Jeffrey M. Patterson, <sup>1</sup> Nikolaos Papachatzis, <sup>1</sup> Kota Z. Takahashi

<sup>1</sup> University of Nebraska at Omaha, Omaha, NE, USA  
Email: [jmpatterson@unomaha.edu](mailto:jmpatterson@unomaha.edu), web: [cobre.unomaha.edu](http://cobre.unomaha.edu)

## INTRODUCTION

The human foot contains elastic structures (e.g., plantar fascia) that can store and return mechanical energy [1]. Such structures are thought to play a role in reducing the metabolic energy demands during locomotion [2]. Yet, when accounting for all structures within the foot (e.g., muscles, tendons, and soft tissue deformation), the human foot appears to perform net negative work during walking [3]. It is currently unclear how the body utilizes this net negative work; specifically, whether this energy is used to supplement the body's movement.

There are several possibilities regarding the destination of the foot's net negative work. One possibility is that the foot's energy is transferred proximally through multi-articular muscles (e.g., flexor digitorum or hallucis longus); yet, only a small portion of the foot's energy appears to be transferred through these muscles [4]. Other possibilities may be that the foot's energy dissipates in the form of sound or heat. In fact, walking can induce increases in foot temperature [5], and thus heat transfer may be a plausible outcome for the foot's net negative work.

The purpose of this study was to investigate the link between foot mechanics and temperature regulation. We aimed to increase foot's net negative work by adding mass to the body during walking. We hypothesized that the magnitude of the foot's net negative work would correlate with increased foot temperature during walking with added mass.

## METHODS

One subject (age = 33 yrs, height = 1.74 m, mass = 67.2 kg) completed barefoot walking trials over-ground and on a treadmill, both with and without added body mass. Added mass conditions included 15% body mass and 30% body mass added via a vest

that distributed the mass equally around the core. The order of the three sessions (0, 15%, and 30% added mass) was randomized.

First, baseline temperature recordings were taken at three different sites on the plantar surface of the foot (heel pad, 1<sup>st</sup> and 5<sup>th</sup> metatarsal heads), dorsal surface at the 1<sup>st</sup> metatarsal head, shank (~50% distance between knee and ankle joints), and thigh (~50% distance between hip and knee joints). Then the subject walked over a force plate targeted at 1.25 m/s. After the foot returned to baseline temperature, the subject walked on a treadmill for 10 minutes. Foot, shank, and thigh temperature were recorded after the treadmill trial.

The mechanical power of the foot during the over-ground trials was quantified using a unified deformable segment analysis [6], by modeling all structures distal to the calcaneus as a deforming body [3]. Positive and negative work were quantified by integrating the power with respect to time. The net work was compared with the changes in temperature.

## RESULTS AND DISCUSSION

When the subject walked with added mass, the magnitude of the foot's positive work remained relatively similar. However, the magnitude of negative work increased, and thus the magnitude of net negative work increased; most notably between the 0% and 15% added mass conditions (Figure 1).

After 10 minutes of treadmill walking without added mass, temperatures increased at all sites (Table 1). Temperature increased most notably at the foot, with smaller changes occurring at the shank and thigh. Specifically, the greatest temperature changes occurred at the plantar surface (under the 1<sup>st</sup> and 5<sup>th</sup> metatarsal heads and the heel pad). Walking with added mass magnified this temperature increase,

again most notably at the plantar surface, and most drastically at 30% added mass (Figure 2).

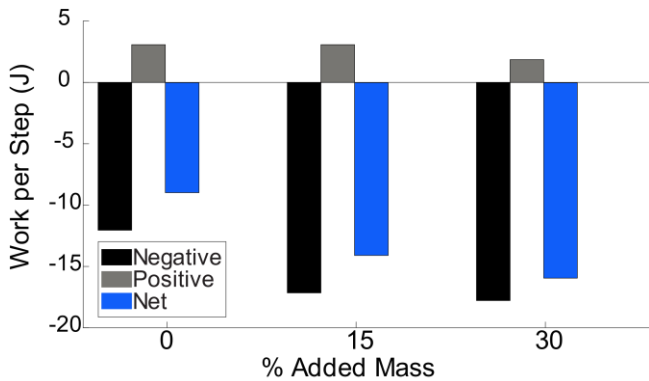


**Figure 1.** With added mass, there was an increase in foot negative work (black), small change in positive work (grey), and an increase in magnitude of net negative work (blue).

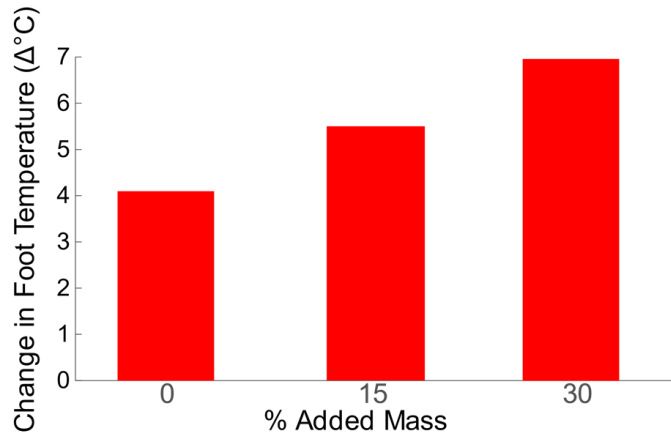


**Figure 2.** During 10 minutes of treadmill walking, the average temperature of the plantar surface increased with added mass.

As the magnitude of foot net negative work increased with added mass, the average temperature of the plantar surface also increased (Figure 3).

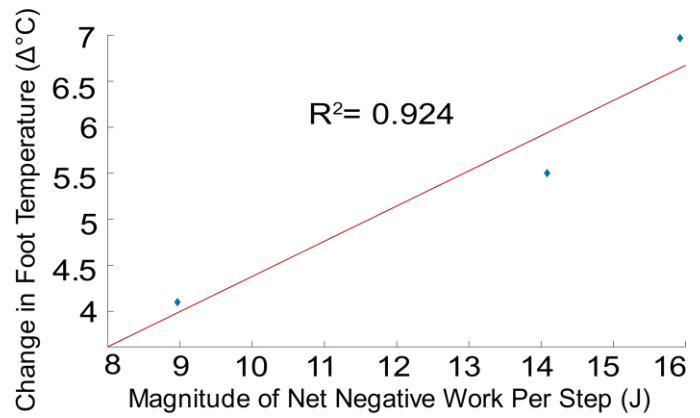


**Figure 3.** The magnitude of net negative worked per step (during over-ground walking) was positively correlated with an increase in average temperature of the plantar surface (during 10 minutes of treadmill walking).

## CONCLUSIONS

These preliminary results support our overall hypothesis that net negative work at the foot may be dissipated as heat. Currently, our analyses cannot parse out the exact source of heat production, such as shear force [5], soft tissue deformation, or muscle force generation. Determining such contributions is expected to give new insights into the mechanism of impaired temperature regulation, such as in patients with diabetes who are prone to ulcer formation in the foot [7].

## REFERENCES

1. Ker RF, et al. *Nature* **325**, 147-149.
2. Stearne SM, et al. *Scientific Reports* **6**, 2016.
3. Worster K, et al. *Proceedings of 40<sup>th</sup> Annual ASB*, Raleigh, NC, USA, 2016.
4. Honert EC, et al. *PLoS One* **11**, e0163169, 2016.
5. Yavuz M, et al. *J Biomech* **47**, 3767-3770, 2014.
6. Takahashi KZ, et al. *J Biomech* **45**, 2662-2667, 2012.
7. Yavuz M, et al. *Diabetes Care* **38**, e178-e179, 2015.

**Table 1:** Temperature measurements after 10 minutes of treadmill walking with added mass.

Temperature (°C)	Plantar Surface of the Foot			1 <sup>st</sup> Met Head (Dorsal)	Shank	Thigh
	Heel Pad	1 <sup>st</sup> Met Head	5 <sup>th</sup> Met Head			
<b>Baseline</b>	21.7	21.0	20.9	21.8	28.6	30.0
<b>0% Added Mass</b>	26.0	25.0	24.9	23.6	29.4	31.0
<b>15% Added Mass</b>	27.1	26.5	26.5	24.0	29.8	31.0
<b>30% Added Mass</b>	29.5	28.0	27.0	24.9	30.8	31.2

# CHARACTERIZING AMBULATORY TENDENCIES FOR LOWER LIMB AMPUTEES

Jay Kim, Audra Davidson, and Deanna H. Gates

University of Michigan, Ann Arbor, MI, USA  
email: jaywoo@umich.edu, web: <http://rehab-biomech-lab.kines.umich.edu/>

## INTRODUCTION

Clinical prescription of prosthetic devices relies heavily on qualitative judgment of a patient's functional ability. The Medicare Functional Classification Level (MFCL) index assigns K-levels based on a patient's mobility and level of community ambulation. Because of its subjective nature, it is unclear if K-levels can accurately describe a patient's mobility across different environments [1,2], or how the potential for ambulation relates to community reintegration. Therefore, it is imperative to move toward a quantitative evaluation scheme.

Many previous studies have used accelerometers to quantify patient walking tendencies, and a few have also utilized Global Positioning System (GPS) devices to measure patient activity in daily life [3]. This study combined the two methods of measurement to provide a quantitative representation of ambulation tendencies with corresponding contextual information i.e., location. The goal of this study was to create a more comprehensive description of a patient's ambulatory profile. These endeavors will develop a better understanding of how best to address the nuanced needs of the diverse amputee population.

## METHODS

Six lower limb amputees ( $49 \pm 18$  years old, 5 male / 1 female) participated in this study (Table 1). Participants wore two accelerometers (ActiGraph, Pensacola, Florida, USA) for seven days. The accelerometers were placed on top of the foot and on the lateral side of the ankle of the affected side. Participants were also given a GPS-enabled smart phone with a location tracking application (Ethica, Saskatoon, Canada).

A modified Theeven cut point [4] was used to detect walking bouts from the accelerometer data. This method accommodates the sedentary nature of the participant demographic. Step counts, average bout durations, and number of bouts per day were derived from accelerometer data.

To quantify community integration, GPS data was used to calculate the amount of time spent at home, near the home, and away from home. Location buffers (Fig 1) of 100 meter and 500 meter radii were created around the home address. Because data was not sampled at a constant rate, data points were linearly interpolated to total 60,480 samples per week (equivalent to 0.1 Hz sampling rate).

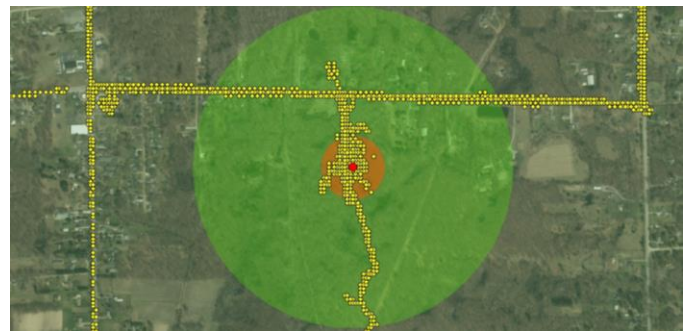


**Figure 1:** GPS points (yellow), participant's home (red), 100m buffer (orange), 500m buffer (green)

## RESULTS AND DISCUSSION

Overall, participants were more active during the week compared to the weekends, which could be attributed to workplace-related activities during the week. While step counts and number of bouts showed higher between-subject variation, average bout duration showed low variability (Fig 2).

Previous studies have used location buffers around the home and pre-determined "community" areas to observe step counts across different areas [4]. Observing the amount of time spent in the buffers of varying radii is a simpler and quicker method that

yields comparable insight into the participant's activity profile and level of engagement in the community. Participants spent the majority of their time at home but also a significant amount of time away from home, which suggests moderate community engagement (Fig 3).

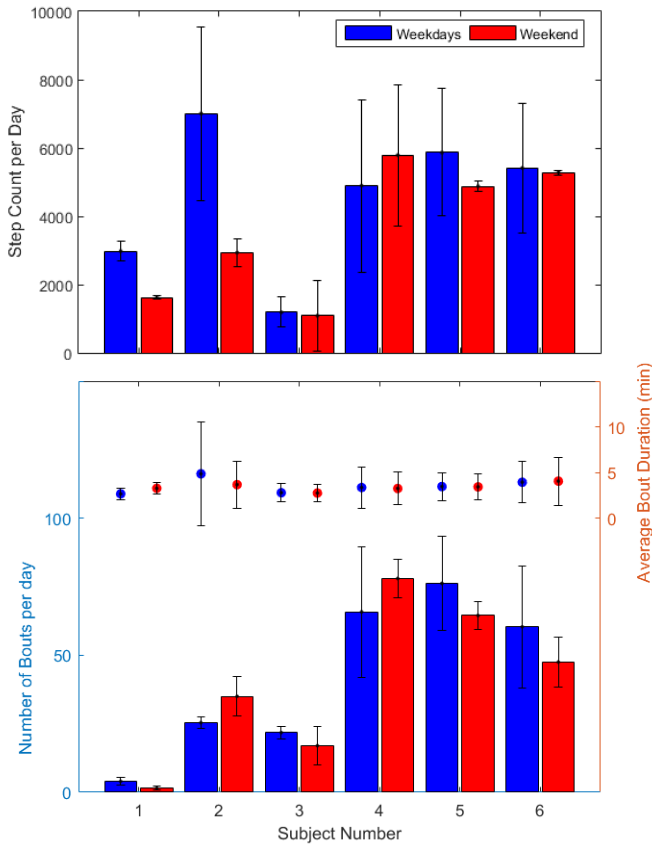


**Figure 2:** Step count per day (top), average bout duration (middle), number of bouts per day (bottom), for all participants

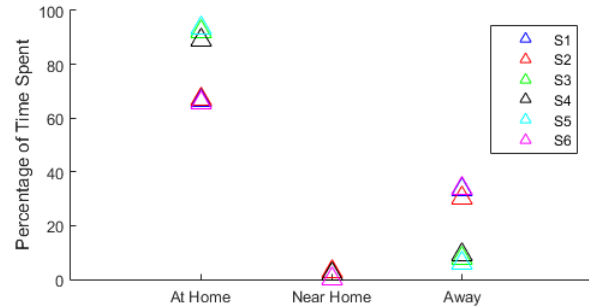


**Figure 3:** Percentage of Time Spent at Home, Near the Home, and Away from Home

Future studies should explore an increased variety of observation parameters to develop a set of characteristics, each uniquely informative. With a more comprehensive participant profile, similarity algorithms could be used to more objectively distinguish participants' ambulatory tendencies.

## REFERENCES

1. Albert, M, et al. *PLoS one*, **8**, e65340. 2013.
2. Corrigan R, et al. *Disability & Rehab*, **30**, 1411-1419, 2008.
3. Hordacre B, et al. *Sensors*, **14**, 5845-5859, 2014.
4. Theeven, PJR, et al. *J Rehab Med*, **44**, 454-461. 2012.

**Table 1:** Participant Demographic

	S1	S2	S3	S4	S5	S6
<b>Age / Gender</b>	43 / F	20 / M	71 / M	39 / M	57 / M	62 / M
<b>Amputation Side / Level</b>	L / Transfemoral R / Transtibial	R / Transfemoral	L / Transtibial	R / Transtibial	L / Transtibial	R / Transtibial
<b>K-level</b>	3	4	3	3	3	3

**Table 2:** Outcome Measures (Mean ± SD)

	Weekdays	Weekend	Total
<b>Step Count per Day</b>	4558.83 ± 1593.07	3598.92 ± 629.68	4284.57 ± 1593.33
<b>Number of Bouts per Day</b>	42.27 ± 11.53	40.58 ± 6.01	41.79 ± 11.18
<b>Average Bout Duration (min)</b>	3.51 ± 2.22	3.40 ± 1.67	3.45 ± 2.07
<b>Percentage of Time at Home (&lt;100m radius)</b>	78.35 ± 12.32	79.58 ± 13.21	78.91 ± 13.86
<b>Percentage of Time Near Home (100m - 500m radius)</b>	1.20 ± 1.30	0.55 ± 0.20	1.02 ± 1.14
<b>Percentage of Time Away from Home (&gt;500m radius)</b>	20.45 ± 12.20	19.87 ± 13.32	20.07 ± 13.66

# WHOLE-BODY AND SEGMENTAL ANGULAR MOMENTUM DURING TURNING

<sup>1</sup> Luis A. Nolasco, <sup>2</sup> Anne K. Silverman, and <sup>1</sup> Deanna H. Gates

<sup>1</sup> School of Kinesiology, University of Michigan, Ann Arbor, MI, USA

<sup>2</sup> Department of Mechanical Engineering, Colorado School of Mines, Golden, CO, USA  
email: lnolasco@umich.edu, web: rehab-biomech-lab.kines.umich.edu

## INTRODUCTION

Whole-body angular momentum is tightly regulated during walking [1] as it is important for maintaining dynamic balance. Decomposition of angular momentum in the three anatomical planes has been used to show differences in task requirements. Upward slope and stair walking require greater frontal range of angular momentum compared to level-ground [2, 3], while the sit-to-stand movement requires greater sagittal angular momentum to successfully complete the task [4]. Turning is another task that presents a greater biomechanical challenge compared to straight-line walking as it requires redirection of the center of mass and asymmetric force generation. Importantly, 34.5% of the steps taken in a given day are turning steps [5]. Therefore, the purpose of this study was to assess whole-body and segmental angular momentum during a 90° right-hand turn compared to straight-line walking.

## METHODS

Six healthy individuals participated in this study. Data in this abstract includes only five of these participants (2F/3M, 25.6±3.4 yrs, 1.73±0.11 m, 76.5±15.4 kg) as they all utilized a similar turning strategy. All participants performed two tasks: straight-line walking and 90° turning at a self-selected speed. Five straight-line walking and five right-hand turns were collected. Turn initiation and termination were defined using pelvic rotation threshold of 5° and 85°. The turn was defined as the heel strike prior to initiation to the heel strike after termination (Fig.1).

55 reflective markers were used to track full body kinematics at 120 Hz using a 20-camera motion capture system (Motion Analysis, Santa Rosa, CA). Kinematics were then low-pass filtered using a 4<sup>th</sup>-order Butterworth filter with a cutoff frequency of 6

Hz. A nine-segment model was created based on segment definitions established by ISB [9].

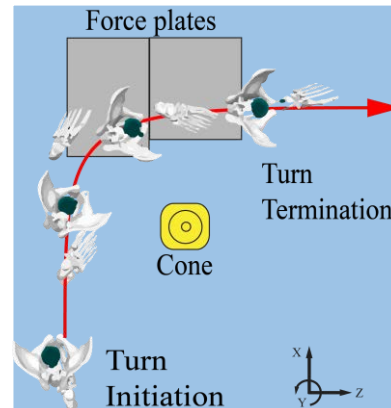


Fig 1. Steps taken during a 90° right-hand turn around a cone.

Segmental angular momenta and whole-body angular momentum were computed about the COM in the three anatomical planes during the middle step of the turn (LHS-LHS) (Fig 1). Whole-body angular momentum was computed as the summation of the segment angular momenta. A rotation matrix was then created based on the center of mass (COM) path trajectory and used to rotate the angular momentum vector from the lab reference frame to the COM reference frame. This calculation ensured that values were interpreted in the body's directions of motion. The peak-peak range of angular momentum in each anatomical plane was then computed for each limb (e.g. sum of thigh, shank and foot segments), torso, and head segments. Paired t-tests were then used to identify differences in whole-body and segmental angular momenta between straight-line walking and turning. Additionally, Cohen's d was used to quantify effect size due to the small sample size.

## RESULTS AND DISCUSSION

The range of whole-body angular momentum did not differ between straight-line walking and turning ( $p = 0.105$ ; Table 1). Differences in segmental ranges of angular momenta were observed in at

least two planes for all four segments analyzed. The right leg angular momentum was greater during turning for the frontal plane ( $p < 0.001$ ,  $d = -3.1$ ), while it was reduced in the sagittal ( $p < 0.001$ ,  $d = 1.31$ ) and transverse planes ( $p < 0.001$ ,  $d = 2.6$ ). The head segment angular momentum was greater in all planes during turning ( $p = 0.012$ ,  $|d| = 0.84$ ). Angular momentum of the left leg was greater during turning in the frontal ( $p < 0.001$ ,  $d > -3.93$ ) and transverse planes ( $p < 0.001$ ,  $d = -1.33$ ) (Fig 2). Throughout the left gait cycle of a turn the right leg generated negative frontal plane angular momentum during the swing phase, counteracting the momentum of the left leg in stance phase. Additionally, the torso range of angular momentum was also greater during turning in the frontal ( $p < 0.001$ ,  $d = -0.81$ ) and transverse planes ( $p = 0.02$ ,  $d = -0.81$ ) most likely used to rotate the body in the direction of turning.

## CONCLUSIONS

Segmental angular momenta can vary dramatically depending on the task. Turning required greater range of angular momentum for all segments compared to straight-line walking, while whole-body angular momentum remained similar during both tasks. Future work will investigate compensation strategies for maintaining dynamic balance during turning in impaired populations.

## REFERENCES

- Herr H, et al. *J Neuroph*, **211**, 467-481, 2008
- Silverman AK, et al. *J Biomech*, **45**, 965-971, 2012
- Silverman AK, et al. *Gait&Pos*, **39**, 1109-14, 2014
- Riley PO, et al. *IEEE Trans Rehab Eng*, **5**, 353-359, 1997
- Glaister BC, et al. *Gait&Pos*, **25**, 289-294, 2007
- Wu G, et al. *J Biomech*, **35**, 543-548, 2002

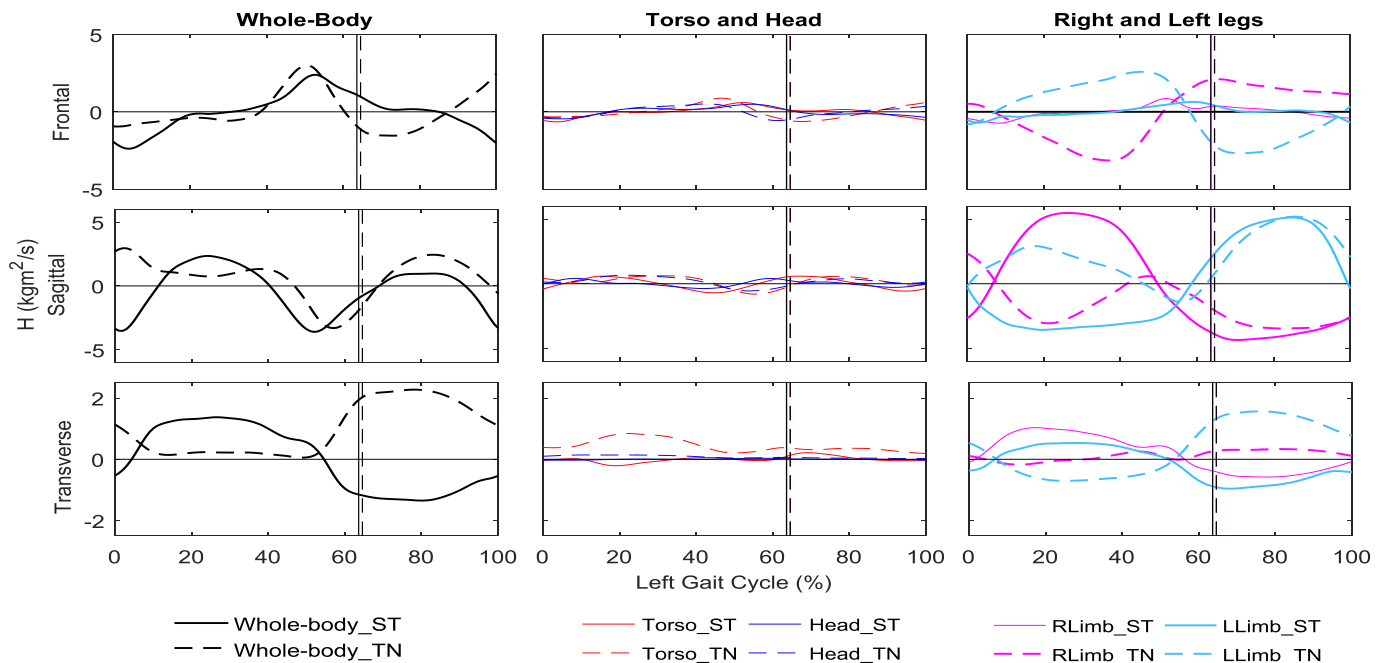


Fig 2. Angular momentum for a gait cycle during turning (TN) and straight-line walking (ST). Segmental contributions to the whole-body angular momentum are presented separately for the torso and head, and lower limbs. Vertical lines display the location of left toe off with the solid line and dashed line corresponding to straight-line walking and turning, respectively.

**Table 1:** Range of whole-body angular momentum for straight-line walking and turning

Plane	Straight-line (kg*m <sup>2</sup> /s) Mean (SD)	Turning (kg*m <sup>2</sup> /s) Mean (SD)	p-value	Cohen's d
Frontal	5.01 (1.91)	5.6 (1.31)	0.258	-0.36
Sagittal	6.51 (2.28)	7.55 (2.64)	0.190	-0.42
Transverse	2.79 (0.51)	2.55 (0.95)	0.343	0.30

# EFFECTS OF WIDE STEP WIDTH ON STAIR ASCENT KNEE KINETICS IN OBESE PARTICIPANTS

<sup>1</sup> Derek Yocum, <sup>1</sup> Joshua T. Weinhandl, <sup>1</sup> Jeffrey T. Fairbrother, <sup>1</sup> Songning Zhang

<sup>1</sup> Department of Kinesiology, Recreation and Sport Studies, University of Tennessee, Knoxville, TN, USA  
email: [dyocum@vols.utk.edu](mailto:dyocum@vols.utk.edu), web: [web.utk.edu/~sals/resources/biomechanics\\_laboratory.html](http://web.utk.edu/~sals/resources/biomechanics_laboratory.html)

## INTRODUCTION

The obese population is 6.8 times more likely to develop knee osteoarthritis (OA) [3]. Medial compartment knee OA is associated with an increased internal knee abduction moment during level walking. Obese participants display an increase in non-normalized peak knee extension moments and knee abduction moments, compared to healthy-weight individuals [2].

Stair ascent studies have found that healthy-weight participants exhibit greater normalized peak knee extension moments and decreased knee abduction moments [6], compared to level walking.

A wider step-width (SW) has been shown to reduce the peak knee extension moment and knee abduction moment during level walking, and stair ascent [1, 4, 7]. However, this has not been studied in an obese population. The purpose of this study was to determine the effects of increased SW on knee biomechanics during stair ascent of obese and healthy-weight participants.

## METHODS

Fourteen healthy-weight (age: 21.6±0.5 years, height: 1.7±0.1 m, mass: 66.3±9.3 kg, BMI 22.5±1.9 kg/m<sup>2</sup>) and ten obese (age: 25.7±5.8 years, height: 1.7±0.1 m, mass: 100.6±12.6 kg, BMI 32.8±2.7 kg/m<sup>2</sup>) participants were recruited to participate in the study. All participants were between 18 and 40 years old. Obese participants had a BMI between 30.0 and 39.9 kg/m<sup>2</sup>, while healthy weight participants were between 18.0 and 24.9 kg/m<sup>2</sup>.

A 12-camera motion analysis system (240 Hz, Vicon Motion Analysis Inc., UK) was used to obtain the three-dimensional kinematics during the test.

Reflective anatomical and tracking markers were placed on both sides of feet, ankles, legs, knees, thighs, and hips. Each participant performed five successful trials of stair ascent in each of two test conditions, preferred and wide SW. SW was defined as the mediolateral distance between the center of masses of both feet during midstance. The wide SW was set as twice the participant's preferred SW, which has been shown to significantly reduce loading-response knee abduction moment [4, 5]. SW was calculated using the second and third steps. A speed range, average speeds ±5%, was used to monitor the speed of movement trials.

A low-pass 4<sup>th</sup> order Butterworth filter at a cutoff of 8 Hz for kinematic and joint moment calculations, and at 50 Hz for GRF calculations. A 2 x 2 (Group x SW) mixed design analysis of variance (ANOVA) was performed to analyze selected variables (22.0 IBM SPSS, Chicago, IL). An *a priori* alpha level was set to 0.05 for all statistical tests.

## RESULTS AND DISCUSSION

A wider SW reduced loading-response peak vertical GRF (p=0.045, Table 1). The obese group demonstrated significantly larger loading-response and push-off peak vertical GRFs (both p<0.001).

Significant Group x SW interactions were observed for both loading-response and push-off peak medial GRFs (all p<0.001, Table 1). This interaction indicated that the obese group increased to greater extents. The post hoc comparisons showed that the obese group had greater mean loading-response peak medial GRF during both preferred (p=0.008) and wide (p=0.001) SW compared to the healthy-weight group. Additionally, the obese group demonstrated greater mean push-off peak GRFs for preferred (p=0.033) and wide (p=0.001) SW (Table 1).

Obese participants had significantly larger loading-response peak knee extension moments ( $p < 0.001$ ). The interaction approached significance for the loading-response peak knee abduction moment ( $p = 0.051$ ) (Table 1). Post-hoc comparisons revealed that only obese participants experienced a decrease in knee abduction moment when SW was increased ( $p=0.020$ ). During push-off, an interaction ( $p=0.022$ ) was seen for peak knee adduction moment, suggesting that the wide SW increased the peak knee adduction moment for both groups, but obese participants showed a greater increase than the healthy-weight group. Post-hoc comparisons revealed that wide SW increased the push-off peak knee adduction moment in both obese ( $p=0.003$ ) and healthy-weight ( $p<0.001$ ) participants. Obese participants had greater push-off peak knee adduction moments during preferred ( $p=0.003$ ) and wide ( $p=0.030$ ) SW conditions.

This study was performed to find differences in knee biomechanics of obese and healthy-weight people during stair ascent at their own preferred and wider SW. We found that obese participants experienced higher medial and vertical GRFs, loading-response peak knee extension moments, and push-off peak knee adduction moments. A significant decrease in the loading-response knee abduction moment in the obese population indicates that a clinical modification to train obese participants to ascend

stairs with a wider SW may lower loading on the medial knee compartment.

## CONCLUSION

Further research should be performed to expose how SW effects biomechanics of the hips and ankles in obese and healthy-weight individuals. Investigation of the effects of increased SW may benefit from investigating muscle activation and joint loading patterns through modeling software such as OpenSim. Lastly, intervention studies on the efficacy of an increased SW gait modification on the obese population are merited to determine the extent in which this modification may help reduce the risk of development of knee osteoarthritis in this population.

## REFERENCES

1. Bennett et al. (2017). *MSSE*, **49**, 563-572.
2. Blazek, K., et al. (2013). *J Orthop Res*, **31**, 1414-1422.
3. Coggon, D., et al. (2001). *Int J Obes Relat Metab Disord*, **25**, 622-627.
4. Paquette, M. R., et al. (2015). *J Appl Biomech*, **31**, 229-236.
5. Paquette, M. R., et al. (2014). *Knee*, **21**, 821-826.
6. Standifird, T. W., et al. *The Journal of Arthroplasty*, **31**, 278-283.
7. Zhao, D., et al. (2007). *Journal of Orthopaedic Research*, **25**, 789-797.

**Table 1:** Peak Mediolateral and Vertical GRFs (N), Knee Extension and Knee Abduction Moments (Nm) for Stair Ascent: mean  $\pm$  STD.

Variable	Healthy		Obese		Int. p	Grp. p	SW p
	Preferred SW	Wide SW	Preferred SW	Wide SW			
LR Peak Vertical GRF	759.6 $\pm$ 96.0 <sup>a,#</sup>	728.6 $\pm$ 85.2 <sup>#</sup>	1079.2 $\pm$ 106.5	1069.0 $\pm$ 150.9	0.296	<b>&lt;0.001</b>	<b>0.045</b>
PO Peak Vertical GRF	823.8 $\pm$ 142.2 <sup>#</sup>	820.3 $\pm$ 118.9 <sup>#</sup>	1136.8 $\pm$ 111.0	1163.0 $\pm$ 114.6	0.349	<b>&lt;0.001</b>	0.472
LR Peak ML GRF	-39.0 $\pm$ 14.1 <sup>a,#</sup>	-91.78 $\pm$ 20.3 <sup>#</sup>	-59.3 $\pm$ 20.4 <sup>a</sup>	-135.5 $\pm$ 35.1	<b>&lt;0.001</b>	<b>0.002</b>	<b>&lt;0.001</b>
PO Peak ML GRF	-29.7 $\pm$ 17.3 <sup>a,#</sup>	-82.2 $\pm$ 24.9 <sup>#</sup>	-48.9 $\pm$ 24.5 <sup>a</sup>	-131.6 $\pm$ 40.1	<b>&lt;0.001</b>	<b>0.004</b>	<b>&lt;0.001</b>
LR Knee Extension Moment	104.1 $\pm$ 22.6 <sup>#</sup>	105.3 $\pm$ 25.2 <sup>#</sup>	153.8 $\pm$ 26.3	159.7 $\pm$ 29.4	0.264	<b>&lt;0.001</b>	0.091
LR Knee Abduction Moment	-21.8 $\pm$ 11.1	-20.7 $\pm$ 7.7	-25.0 $\pm$ 11.3 <sup>a</sup>	-18.5 $\pm$ 14.2	0.051	0.904	<b>0.009</b>
PO Knee Adduction Moment	10.8 $\pm$ 4.2 <sup>a</sup>	15.0 $\pm$ 5.7 <sup>#</sup>	17.7 $\pm$ 15.8 <sup>a</sup>	27.5 $\pm$ 12.6	<b>0.022</b>	<b>0.022</b>	<b>&lt;0.001</b>

a: Significantly different from Wide SW of the same subject group, #: Significantly different from Obese of the same SW, ML: Mediolateral, LR: Loading Response, PO: Push-off Response, GRF: Ground Reaction Force, Int.: Interaction, Grp.: Group Main Effect, SW: Step Width, Bold: p-values indicate significance.

# Central Activation Deficits of the Quadriceps Muscle in Patellar Tendinopathy

<sup>1</sup> Andrew Sprague and <sup>1</sup>Karin Grävare Silbernagel

<sup>1</sup> University of Delaware, Newark, DE, USA

email: [asprague@udel.edu](mailto:asprague@udel.edu), web: <http://www1.udel.edu/dri/tendonteam.html>

## INTRODUCTION

Patellar tendinopathy is a chronic, painful condition of the patellar tendon. It is most prevalent in athletes who participate in jumping sport, such as volleyball and basketball, where high loads are placed on the knee extensor mechanism [1]. Athletes with patellar tendinopathy demonstrate pain, reduced knee extension strength and altered kinetics and kinematics during jumping, compared to healthy controls [2, 3].

Arthrogenic muscle inhibition (AMI) is a reflexive response to joint injury, resulting in the inability to volitionally activate a muscle fully in the absence of muscle or neural tissue damage [4]. AMI of the quadriceps has been observed in patients with knee injuries such as anterior cruciate ligament rupture or reconstruction, knee osteoarthritis, and anterior knee pain [4, 5]. In these conditions, impaired quadriceps activation results in reduced knee extension torque during strength testing. Additionally, it is a contributing factor to decreased neuromuscular control, altered lower extremity kinetics and kinematics, and increased risk of injury [4]. However, AMI has not been investigated in patients with patellar tendinopathy.

The purpose of our study was to determine whether quadriceps AMI, which may contribute to altered biomechanics, is present in patients with unilateral patellar tendinopathy. We hypothesized that the symptomatic limb in patients with patellar tendinopathy would have decreased quadriceps activation compared to the contralateral, asymptomatic limb.

## METHODS

Four subjects (3M:1F) with symptomatic unilateral patellar tendinopathy were recruited. Participants had a mean age ( $\pm$  SD) of 26 ( $\pm$  9) years, height of

72.7 ( $\pm$  6.1) in., weight of 195.2 ( $\pm$  23.1) lbs, and symptom duration of 3.2 ( $\pm$  3.1) months.

Diagnosis of unilateral patellar tendinopathy was confirmed through clinical exam and B-mode ultrasound imaging (LOGIC *e* Ultrasound, GE Healthcare, Chicago, IL). Participants completed the Victorian Institute of Sport – Patellar (VISA-P) Questionnaire to assess symptom severity.

Knee extension peak torque and quadriceps muscle activation was assessed using a Biodex Systems 3 Dynamometer (Biodex Medical System, Shirley, NY) while performing a maximal voluntary isometric contraction (MVIC) with the burst-superimposition method [6]. Participants were seated with the hips at 90° of flexion and the knee at 60° of flexion. Self-adhesive electrodes (6 cm x 8 cm) were placed over the vastus medialis and vastus lateralis muscle bellies. After familiarization with procedures, participants performed a 3-second MVIC. During contraction, a supramaximal, 10-pulse (600  $\mu$ s, 130 V, 100 pulses per second) train of electrical stimulation was delivered to the muscle. Up to 3 trials were completed to ensure the participant had achieved maximal isometric torque prior to burst superimposition. A custom LabView program (National Instruments, Austin, TX) was used to identify the peak MVIC torque and the torque

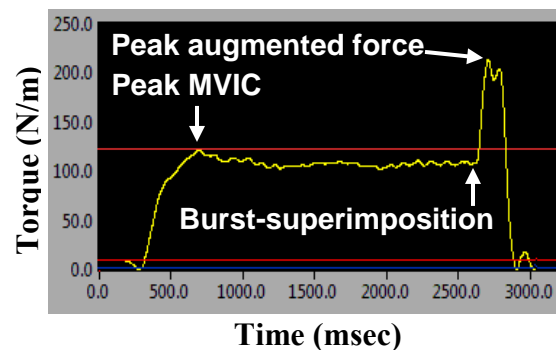


**Figure 1.** Characteristic increase in knee extension torque production with burst-superimposition in a subject with incomplete quadriceps activation.

attributable to the electrical burst (Figure 1.). A central activation ratio (CAR) (MVIC torque/peak torque with burst augmentation) was calculated for comparisons.

Statistical analysis was completed using IBM SPSS Statistics 24. Due to small sample size, the Wilcoxon Signed-Rank test was used to compare limbs. The significance level was set to  $p < 0.05$ .

## RESULTS AND DISCUSSION

Participants had a mean ( $\pm$  SD) tendon thickness of 0.58 ( $\pm$  0.19) cm for the symptomatic limb and 0.47 ( $\pm$  0.21) cm for the asymptomatic limb. Their mean VISA-P score was 57 ( $\pm$  17) points.

All subjects had bilateral deficits in quadriceps activation with a mean CAR of 77.1 ( $\pm$  12.7)% for the symptomatic limb and 75.0 ( $\pm$  16.0)% for the asymptomatic limb (Figure 2). There was no statistically significant difference between CAR in the symptomatic and asymptomatic limbs ( $p > 0.05$ ). Following anterior cruciate ligament reconstruction, a cut-off score of 90% CAR has been established as criteria for return-to-sport [7]. All participants fell below this cut-off, bilaterally, and below normative values for healthy adults ( $94.8 \pm 3.6\%$ ) (Figure 2) [4].

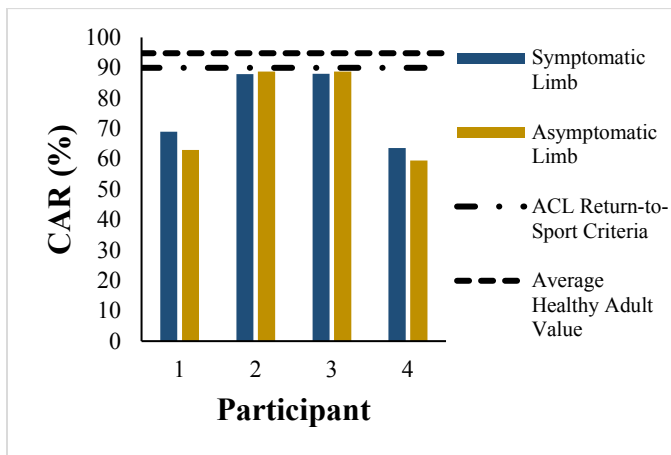


**Figure 2.** Quadriceps central activation ratios (CAR) for the symptomatic limb and asymptomatic limb with cut-off scores for anterior cruciate ligament (ACL) return-to-sport criteria and the normative value for healthy adults.

## CONCLUSIONS

Those affected by unilateral patellar tendinopathy have bilateral reductions in quadriceps activation, which are comparable between the symptomatic and asymptomatic limbs. These values are similar to those observed in the surgical limb of patients 1-month post anterior cruciate ligament reconstruction and well below normative values for healthy adults [8]. This impairment may contribute to alterations in kinetics and kinematics during gait and sport-specific tasks. Clinicians and researchers should be aware of these deficits and how they may impact measures of strength and movement performance. Due to the cross-sectional nature of the study, we are unable to determine whether reduced CAR is a predisposing factor or adaptation to patellar tendinopathy. Prospective studies with larger sample sizes are needed to examine the relationship and how CAR deficits may influence biomechanics and functional performance.

## REFERENCES

1. Ferretti, A. *Sport. Med.* **3**, 289-295, 1986.
2. van der Worp, M, et al. *Br. J. Sports Med.* **45**, 446-452, 2011.
3. De Poel, HJ, et al. *Int J Sport. Med* **35**, 714-722, 2014.
4. Hart, JM, et al. *J. Athl. Train.* **45**, 87-97, 2010.
5. Lewek, MD, et al. *Orthop. Res.* **22**, 110-115, 2004.
6. Snyder-Mackler, L, et al. *J. Bone Joint Surg.* **76**, 555-560, 1994.
7. Adam, D, et al. *J Orthop Sport. Phys Ther* **42**, 601-614, 2012.
8. Drechsler, WI, et al. *Muscle Nerve* **98**, 613-623, 2006.

## ACKNOWLEDGMENTS

This work was supported in part by the National Institute of Arthritis and Musculoskeletal and Skin Diseases of the National Institute of Health under Award Number T32HD007490-13 and by a Florence P. Kendall Doctoral Scholarship from the Foundation for Physical Therapy.

# EFFECT OF FATIGUE AND REAL-TIME VISUAL FEEDBACK DURING DROP LANDINGS ON PATELLOFEMORAL JOINT STRESS IN HEALTHY FEMALE ADULTS

Christina Olbrantz, Jamie Bergelin, Jill Asmus, Thomas Kernozek, Drew Rutherford, Naghmeh Gheidi

University of Wisconsin-La Crosse, La Crosse, WI, USA

email: kernozek.thom@uwlax.edu

## INTRODUCTION

Patellofemoral joint stress (PFJS) may be an important factor in the development of patellofemoral pain (PFP) [1]. Fatigue has been proposed to alter lower extremity mechanics associated with PFP during landing activities [2]. Vertical ground reaction force (GRF) during landing activities may impact PFJS [1].

Our purpose was to determine how healthy females alter their PFJS using visual real-time feedback (RTF) of GRF during drop landings before and after fatigue.

## METHODS

Kinetic and kinematic data respectively, were collected using two force platforms (1800 Hz) and a 15 camera motion analysis system (180 Hz) with forty seven reflective markers. Seventeen healthy females (Age:  $22.5 \pm 1.7$  y; Height:  $188.0 \pm 6.6$  cm; Mass:  $70.8 \pm 5.9$  kg) participated. Each performed a baseline set of five drop landings from a hang bar 60 cm above the ground. After three landing trials for instruction on how the feedback worked, subjects performed an additional five drop landings with visual RTF (RTF condition) displaying their vertical GRF in body weight from a custom program using D-Flow software (Motekforce Link, Amsterdam, Netherlands). RTF displayed a sphere moving on a vertical axis during the landing where a horizontal bar marked the peak vertical GRF. During each drop landing, the numerical value of the vertical GRF from the previous trial was visually displayed for comparison. Subjects were cued to “land softly” before each drop landing to attempt to lower their peak GRF for the next trial. Following the RTF condition, subjects underwent a fatigue protocol

consisting of multiple sets of 15 jump squats. Fatigue was defined as the inability to reach 75% of maximum vertical jump height within two attempts or Borg RPE score  $\geq 17/20$ . After the fatigue protocol, the post-fatigue set of five drop landings with visual RTF was performed (Post-fatigue RTF).

The Human Body Model (HBM) (Motekforce Link, Amsterdam, Netherlands) was used to calculate muscle forces based on an 18 segment, 46 degree of freedom (DOF) musculoskeletal model. Static optimization criteria was used that estimated the muscle forces where the sum of the squared muscle activations were related to the maximum muscle strengths. The total quadriceps force (QF) was determined by summing the rectus femoris, vastus (medialis, lateralis, and intermedius) muscles from HBM. Patellofemoral joint reaction force (PFJRF) was the compressive component of the QF based on knee flexion angle. PFJS was estimated by dividing PFJRF by contact area [3]. A multivariate analysis with repeated measures ( $\alpha = .05$ ) was used to examine differences between conditions (baseline, RTF, Post-fatigue RTF). Follow-up univariate tests were completed to detect differences in each variable between conditions. Statistical calculations were completed in SPSS (IBM, Armonk, NY, USA).

## RESULTS AND DISCUSSION

Multivariate analysis indicated differences across conditions (Wilk's Lambda = .097,  $p = .01$ ). Univariate tests revealed differences for all variables across conditions (baseline, RTF, and Post-fatigue RTF) except peak quadriceps force (Table 1).

Pairwise comparisons were used to examine between testing conditions. Vertical GRF decreased

from baseline to the RTF condition (1.94 BW to 1.78 BW) ( $p = .002$ ) (Figure 1). There was a small increase in GRF to 1.81 BW from the RTF condition to the Post-fatigue RTF condition ( $p = 1.0$ ); overall, there was a 6.4% decrease in vertical GRF from baseline to the Post-fatigue RTF condition ( $p = .118$ ). Peak knee flexion angle increased from 94.0 degrees to 98.4 degrees from baseline to the RTF condition ( $p = .043$ ) and then decreased to 92.3 degrees during the Post-fatigue RTF condition ( $p < .001$ ). Maximum PFJS decreased from baseline to the RTF condition by 3.9% ( $p = .007$ ), then increased from the RTF condition to the Post-fatigue RTF condition by 3.8% ( $p = .034$ ) (Figure 2).

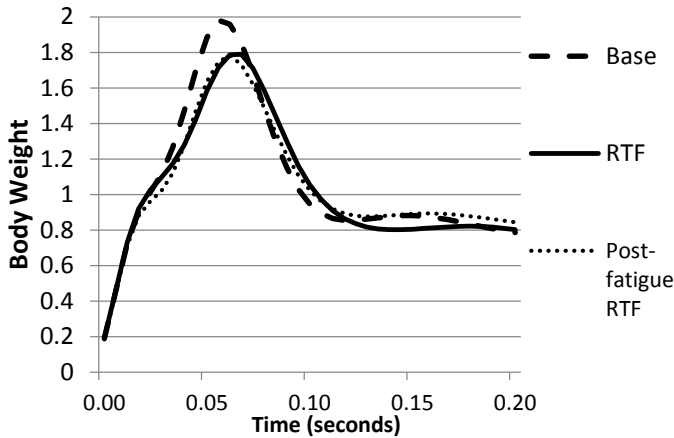


Figure 1. Peak Ground Reaction Force for each landing condition (Baseline, RTF, Post-fatigue RTF)

Patellofemoral joint stress is the interaction between knee flexion, PF contact area, and PF joint reaction

Force [2,3]. The decrease in knee flexion observed in this study during the Post-fatigue RTF condition may be related to the increase in GRF and subsequent increase in PFJS. Therefore, one should consider fatigue state when attempting to use feedback to influence performance.

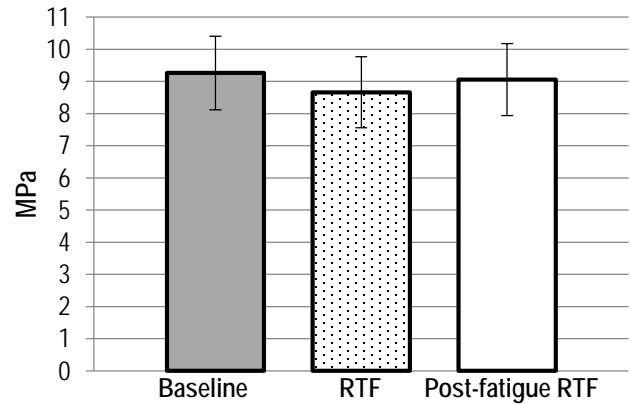


Figure 2. Peak PFJS for each landing condition (Baseline, RFT, Post-fatigue RTF)

## REFERENCES

1. Rothermich MA, et al. *Clin Sports Med* **34**, 313-327, 2015.
2. Brechter, JH, et al. *Med Sci Sports Exerc*, **36**, 1582-1593, 2002.
3. Vannatta CN, et al. *Med Sci Sports Exerc* **47**, 1001-1008, 2015.

## ACKNOWLEDGEMENTS

This study received funding from a UW-La Crosse Graduate Student Research Grant.

**Table 1:** Mean and Standard Deviation Peak GRF, PFJS, PFJRF, QF, joint angles for the three conditions (Baseline, RTF, Post-fatigue RTF). MD is mean difference, ES is effect size and data in parentheses is the standard deviation.

Variable	Conditions			Univariate/Main Effect		Baseline to RTF			RTF to Post-fatigue RTF			Baseline to Post-fatigue RTF		
	Baseline	RTF	Post-Fatigue RTF	F	p-value	MD	p-value	ES	MD	p-value	ES	MD	p-value	ES
Peak vertical GRF (BW)	1.93 (0.40)	1.78 (0.34)	1.81 (0.35)	6.36	0.005	0.154	0.002	0.42	-0.033	1	0.1	0.121	0.118	0.32
Maximum PFJS (MPa)	9.04 (1.48)	8.70 (1.40)	9.04 (1.29)	4.86	0.014	0.34	0.007	0.23	0.34	0.03	0.25	5.00E-04	1	3.61E-03
Knee flexion ROM (degrees)	94.01 (15.04)	98.38 (12.78)	92.30 (12.46)	9.68	0.001	-4.371	0.043	0.31	6.08	0	0.48	1.709	0.857	0.12
Peak quadriceps force (BW)	6.30 (0.65)	6.52 (0.82)	6.62 (0.93)	2.22	0.125	-0.214	0.299	0.29	-0.106	1	0.12	-0.32	0.215	0.4

# DIFFERENCES IN KNEE JOINT LOAD DISTRIBUTION WITH VARYING CARTILAGE PROPERTIES

<sup>1</sup> Jonathan T. Kaplan, <sup>1</sup> John W. Ramsay, <sup>2</sup> Tyler N. Brown, <sup>3</sup> David M. Pierce

<sup>1</sup> Natick Soldier Research, Development, and Engineering Center, Natick, MA, USA

<sup>2</sup> Department of Kinesiology, Boise State University, Boise, ID, USA

<sup>3</sup> Departments of Biomedical and Mechanical Engineering, University of Connecticut, Storrs, CT, USA

Email: Jonathan.T.Kaplan.civ@mail.mil

## INTRODUCTION

Osteoarthritis (OA) of the knee is a detrimental condition for service members and is on the rise [1]. Long-term repetitive loading of the lower extremity during tasks such as walking, running and cutting have been associated with the development of OA. It is known that joint contact forces (JCFs) increase during these tasks when the individual carries additional body-borne loads (BBL). This is a pressing issue for military populations as soldiers carry loads in excess of 30% body weight while completing military relevant training and mission scenarios. How increased JCFs are distributed across the knee joint and within cartilage, and how this may impact the progression of OA, is currently unknown. However, by combining traditional motion capture methods with computational models, it is possible to simulate the cumulative effect of BBL on cartilage.

We investigate two key metrics: interstitial fluid pressure and von Mises solid extra stress. Increased fluid pressure enhances load support, shields the solid matrix, promotes low frictional coefficients and thus reduces tissue and joint wear. von Mises stress in the solid matrix is a scalar measure of distortion energy related to shear stresses. Studies indicate that shear forces play a critical role in the destructive mechanical loading that comprises chondrocyte health and initiates extracellular matrix degradation [2]. We aim to determine how mechanical properties of healthy and diseased cartilage impact the tissue's ability to dissipate forces across the joint associated with varying additional BBL.

## METHODS

Nine male military personnel (participants,  $21.1 \pm 3.8$  yrs,  $72.5 \pm 9.4$  kg,  $1.8 \pm 0.1$ m) completed two test sessions where they donned light or heavy BBL configurations. The light load (LL,  $\sim 6$  kg) was

composed of a helmet, mock weapon, boots, socks and spandex shirt and shorts. The heavy load (HL,  $\sim 40$  kg) consisted of the light load plus body armor with a fabric ammo panel attached on the anterior and a standard issue military backpack. During each test session, individual participants performed three successful run-to-stop maneuvers. These maneuvers required the participant to run down a 10 m walkway at 3.5 m/s and plant their dominant limb on a force platform embedded in the floor, immediately stopping in a low and ready position (i.e. eyes forward, weapon pointed downward at  $\sim 45^\circ$ , legs wide and slightly bent).

We developed OpenSim simulations following methods detailed in Ramsay et al. [3]. While we considered the LL negligible for modeling purposes, for the HL we distributed both a 20-kg body-borne load evenly across the torso and applied at the torso's center-of-mass (CoM) and applied a second 20-kg mass, representing the backpack, 10 cm posteriorly and 5 cm below the torso CoM. We calculated the JCF between the femur and tibia in the longitudinal axis of the tibia for all subjects and averaged them across the two conditions.

Using ABAQUS v6.13 (Simulia, Pawtucket, RI) we created a finite element model including an average femur, tibia, menisci and cartilage using geometries obtained from OpenKnee v1 [4]. We defined the femur and tibia as analytical rigids, menisci as neo-Hookean materials and cartilages as a poroelastic neo-Hookean materials. We completed meshing using the sweep mesh functions in ABAQUS with cartilages defined using C3D4P elements and menisci using C3D4 elements. We simulated varying (two) levels of cartilage health (Healthy and OA) by changing material parameters, cf. Table 1. Simulations were ramped over corresponding time

steps to the maximum JCF calculated from our corresponding OpenSim simulations for both conditions. We applied force to the proximal end of the femur, which was constrained in all degrees-of-freedom except for the axial direction. We constrained the tibia in all axes of rotation.

**Table 1.** Material properties for the FE model [5,6].

Material Properties	Healthy	OA	Menisci
	Cartilages	Cartilages	
$E$ (MPa)	0.5	0.28	28
$k$ ( $10^{-15} \cdot \frac{m^4}{N \cdot s}$ )	1	6	-
$\nu$	0.45	0.45	0.36

## RESULTS AND DISCUSSION

Averaged across 9 participants, the maximum JCFs were 1572.3 N and 2494.5 N for the LL and HL conditions, respectively. We applied these loads to the FE model to obtain distributions of solid von Mises stress and fluid pressure. Peak stresses were primarily distributed where cartilage had direct contact with the menisci, see Fig. 1. Stresses increased in the HL condition compared to the LL condition. The stress appears to be redistributed to the outside boundaries of the condyles in the OA tissue condition.

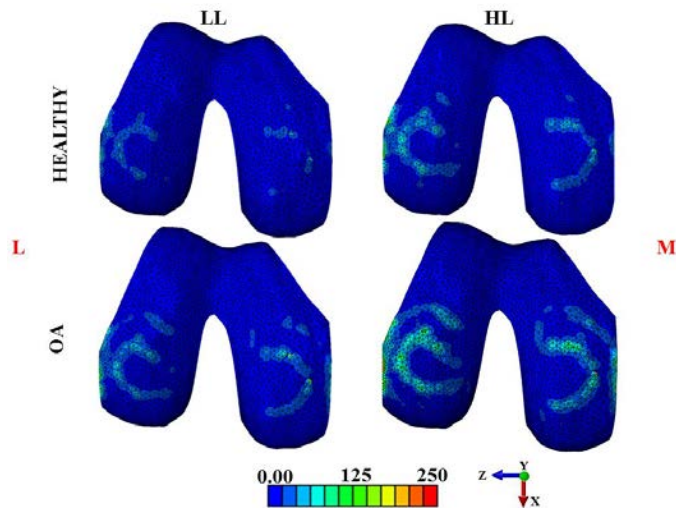


**Figure 1.** von Mises Stress (kPa) distribution for medial (M) and lateral (L) femoral condyles.

The largest fluid pressure (and thus load support) occurs in the healthy tissue during the HL condition, see Fig. 2. Healthy tissue has a lower permeability and thus generates higher interstitial fluid pressure under load to support increasing JCFs without

increasing shear stresses within the tissue. Increased shear forces may expedite the progression of OA.

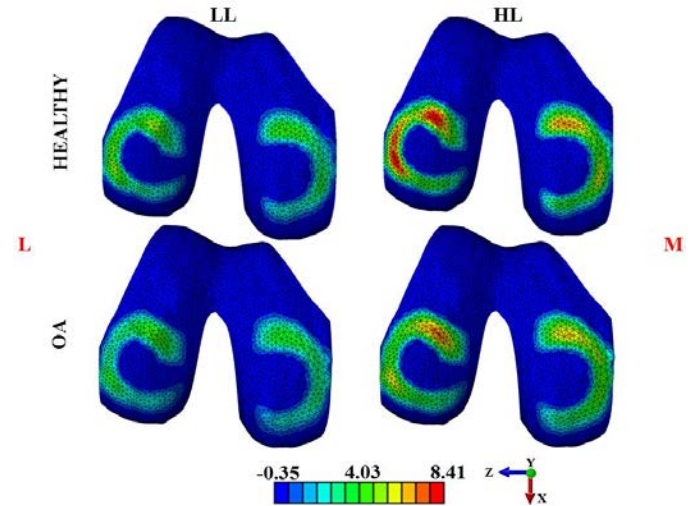


**Figure 2.** Interstitial Pressure (mPa) distribution for medial (M) and lateral (L) femoral condyles.

In our model the primary load bearing surface appears to be the lateral condyle, while higher loads are typically expected in the medial condyle. We attribute this result to the neutral alignment of the femur with respect to the tibia and believe different results could be obtained if we included dynamic rotation of the knee in our simulations.

## CONCLUSIONS

Completing tasks with BBL will increase the amount of force to be distributed across the knee joint. Healthy cartilage provides fluid pressure load support to prevent increased shear stresses that compromise tissue health in the knee. The load carrying capacity of osteoarthritic joints is clearly comprised, resulting in greater intra-tissue stress concentrated particularly at the outside boundaries of the femoral condyles. With models like these, we intend to better understand the long-term impact of load carriage, both in healthy and osteoarthritic populations, in order to maximize the safety and longevity of soldiers, athletes and the general population.

## REFERENCES

- [1] Showery JE, et al. *J. Arthroplasty* **31**, 2108-14, 2016.
- [2] Smith RL, et al. *Biorheology* **37**, 95-107, 2000.
- [3] Ramsay et al, *J. Biomech.* **49**, 3868-3874, 2016.
- [4] Erdemir, A. *J. Med. Devices.* **7**, 040910, 2013.
- [5] Kleeman et al. *Osteo. and Cart.* **13**, 958-963, 2005.
- [6] Mow et al, *J. Biomech.* **17**, 377-394, 1984.

# Symmetry in Strength Deficits and Knee Biomechanics during Loading Response in Young Adult Survivors of Osteosarcoma

<sup>1</sup> Micah Garcia, <sup>1</sup> Joseph Pressey, <sup>1</sup> David Pruitt, <sup>1</sup> Joel Sorger, <sup>1</sup> Erin Kingsley, and <sup>1</sup> Jason T. Long

<sup>1</sup> Cincinnati Children's Hospital Medical Center, Cincinnati, OH, USA  
email: micah.garcia@cchmc.org, web: <http://www.cincinnatichildrens.org/mal>

## INTRODUCTION

With the advent of effective uniform treatment regimens and improved supportive care, the survival rate for pediatric cancers has improved dramatically over the past several decades with 80% of patients now cured of their disease [1]. Osteosarcoma (OST) is the most common malignant bony tumor of children and young adults, typically arising in the metaphyses of long bones during periods of rapid bone growth [2]. OST most commonly develops in the distal femur, proximal tibia, and proximal humerus. Standard treatment consists of chemotherapy. However, surgical resection is the mainstay of local tumor control and is necessary to ultimately achieve a cure. Several approaches to surgical resection are possible, including limb salvage procedures, amputation and rotationplasty. While surgical outcomes are generally associated with acceptable function and patient satisfaction, morbidity may include infection, gait dysfunction, chronic pain, or mechanical failure. This can lead to significant disability with a negative impact on quality of life.

Three-dimensional (3D) motion analysis is a well-established method for quantitative assessment of movement abnormalities in patients with motor impairments. However, there is limited evidence regarding gait abnormalities and associated strength deficits in young adult survivors of OST. The purpose of this study was to assess kinematic and kinetic abnormalities, as well as isokinetic strength deficits in young adult survivors of OST.

## METHODS

Nine young adult survivors of OST were recruited for the study (age:  $24.4 \pm 4.6$  years). Eight of the subjects previously underwent surgical intervention for tumor resection and limb salvage. Study

participation required a single visit to the Motion Analysis Lab (MAL) for testing ( $5.5 \pm 3.3$  years post initial surgery). Subjects were instrumented with 40 reflective markers on the torso and lower extremity, following a modified Helen Hayes marker set. Lower extremity kinematics and kinetics were measured during gait using a 12-camera Raptor4 system (Motion Analysis Corp.; Santa Rosa, CA) with four force plates embedded in the walkway (AMTI; Watertown, MA). Data were captured using MAC Cortex software and post-processed in Visual3D (C-Motion, Inc; Germantown, MD). For this analysis, sagittal plane knee biomechanics were assessed during the first 30% of the gait cycle for both the operative and healthy sides. Symmetry index (SI) was measured as the summed differences in joint angle (or moment) between the operative and healthy limb normalized to total range of motion; higher SI values corresponded to greater asymmetry.

Knee flexion/extension torque was measured via isokinetic strength testing using the Biodex System 4 dynamometer (Biodex Medical Systems, Inc; Shirley NY). Each participant performed a series of flexion/extension cycles at two speeds ( $60^\circ/\text{s}$  and  $180^\circ/\text{sec}$ ). The healthy side was tested first. Verbal encouragement was provided throughout testing, with the participants directed to perform the cycles at full effort and as fast as possible through the full range of motion. During each series of cycles, continuous angle position and torque data were collected from the dynamometer. Each time-series of the cycles were assessed for key angle/torque measures, and peak torque deficits were calculated as the percentage difference between the operative and healthy limbs for the quadriceps and hamstrings. Deficits were calculated as:  $1 - \frac{\text{operative peak torque}}{\text{healthy peak torque}}$

## RESULTS AND DISCUSSION

Blunted knee flexion (Figure 1) and extension demand were observed for patients with higher SI values. Strong correlation was measured between knee angle SI and quadriceps peak torque deficits at both speeds (60 °/s:  $R^2 = 0.93$ ; 180 °/sec:  $R^2 = 0.75$ ). Moderate correlation was measured between knee moment SI and quadriceps peak torque deficits at both speeds (60 °/s:  $R^2 = 0.63$ ; 180 °/sec:  $R^2 = 0.55$ ) (Figure 2).

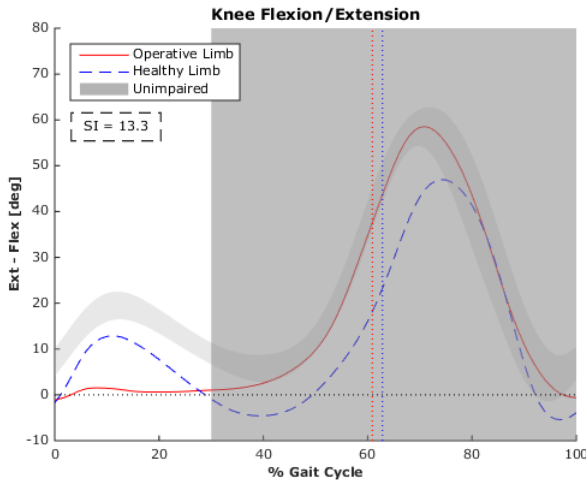


**Figure 1:** Representative sagittal knee kinematics.

Higher SI values and strength deficits were linked to patients with femoral resections. Femoral resection required a prosthetic implant that was designed to allow  $\sim 5^\circ$  of hyperextension to unload the quadriceps during standing and single leg stance. However, some patients regained strength and symmetry

demonstrating that the implant did not automatically lock a patient into a weak leg and hyperextension pattern.

Quadriceps weakness may contribute to the lack of extensor mechanism in the operative limb for patients with greater asymmetry. The limb may have inadequate eccentric strength required to control the flexion response during weight acceptance. Focusing on strength symmetry during rehabilitation may promote improved biomechanical outcomes. A comparison cohort of unimpaired walkers demonstrated knee kinematic and moment SI values of  $5.5 \pm 2.0$  and  $4.1 \pm 2.2$ , respectively. These values corresponded to strength deficits of approximately 20%, which may serve as a quantifiable target during the rehab process.

## CONCLUSIONS

This study demonstrates a link between isokinetic asymmetry and biomechanical asymmetries in the operative and healthy limbs of young adult survivors of OST. Future studies should investigate the biomechanical response to a quadriceps strengthening program in young adult survivors of OST.

## REFERENCES

1. Smith MA, et al. *J Clin Oncol* **28**(15), 2625-34, 2010.
2. Siegel HJ, Pressey, JG, *Expert Rev Anticancer Ther* **8**(8), 1257-69, 2008.

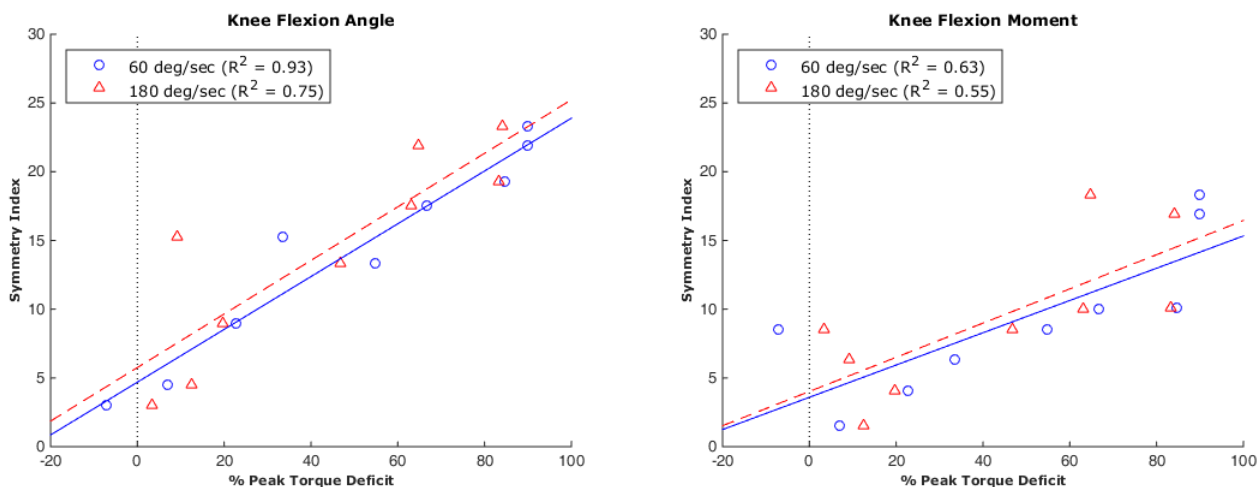


**Figure 2:** Peak quadriceps torque deficits and sagittal plane knee angle and moment symmetric index.

# Comparison of Knee Kinematics and Kinetics During Stair Descent in Single-Radius and Multi-Radius Total Knee Arthroplasty Designs

<sup>1</sup>Bonnie Sumner, <sup>1</sup>John McCamley, <sup>2</sup>David J Jacofsky, <sup>1,2</sup>Marc C Jacofsky

<sup>1</sup>MORE Foundation, Phoenix, AZ, USA

<sup>2</sup>The CORE Institute, Phoenix, AZ, USA

email: bonnie.sumner@more-foundation.org

## INTRODUCTION

Total knee arthroplasty (TKA) is a popular surgical solution to patients suffering from osteoarthritis, with numbers projected to reach 3.48 million by 2030 [1]. Multi-radius (MR) and single-radius (SR) TKAs are two popular design concepts (fig 1). The femoral condyles were first hypothesized to exhibit a single radius of curvature during knee flexion. The last century of research is in agreement that the femoral condyles have a multi-radius curvature with shifting center of rotation during knee flexion [as reviewed in 2]. However, despite greater similarity to the anatomical knee joint, the MR design does not improve walking over SR designs [3].

Previous research in our laboratory found that the SR design TKA more closely replicates normal walking kinematics and kinetics than the MR design. Specifically, knees implanted with MR TKAs had decreased knee flexion and power absorption than SR during level walking [3]. However, during the stance phase of walking knee flexion angle is minimal. Therefore, we aimed to answer whether MR designs more closely replicate normal knee kinematics and kinetics during daily living tasks that require high knee flexion during the loading phase, such as stair descent. We hypothesized that MR knees would more closely replicate the stair descent kinematics and kinetics of healthy age matched controls, than SR knees.

## METHODS

Three groups of subjects participated in accordance with IRB guidelines: TKA subjects with a SR (Stryker Triathlon® Total Knee Replacement System) design (n=8, m=87.4±18.53 kg.), TKA subjects with a MR (Biomet Vanguard Complete Knee System) design (n=8, m=84.3±13.63 kg.), and

age-matched healthy control subjects (n=8, m=76.4±9.22 kg.).

We collected data 1-year post-operatively using ten Eagle-4 digital IR cameras (EVaRT 5.0.4, Motion Analysis Corp., CA) at 120Hz. Subjects wore 28 reflective markers (modified Helen Hayes [4]) while walking at a self-selected pace down a staircase affixed to force platforms (AMTI, MA) sampling at 1,200Hz for at least 5 step cycles.

Orthotrak 6.2.8 (Motion Analysis Corp.) was used to calculate joint kinematic and kinetic parameters. Individual trials for each subject were averaged using the Orthotrak multi-trial processing module. Statistical comparisons of kinetic and kinematic parameters (minimum/maximum of knee angles, moments, and power) were performed with an ANOVA and Tukey's post-hoc analysis using a custom written R programming script (www.r-project.org),  $\alpha = 0.05$ .

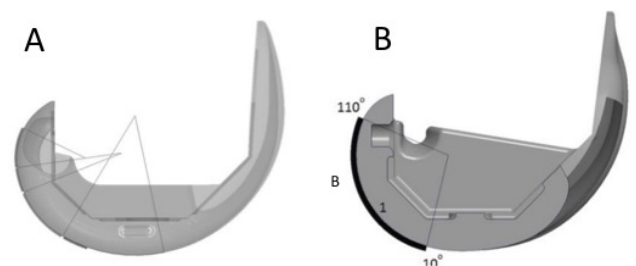


**Figure 1:** Representative multi-radius total knee design (A) and single radius design (B).

## RESULTS

For all three groups knee kinetics and kinematics are comparable to previous research on stair descent [5]. No differences were observed for peak knee abduction angle or frontal moment between the groups ( $p>0.32$ ). The minimum sagittal moment during stance for both the SR and MR knees were both significantly higher than the controls ( $p=0.02$ ,

p=0.05). The peak power absorption was significantly less for SR than MR (p=0.02), but neither was different than the controls (table 1). There were no differences in step width between groups, indicating that the groups may have similar levels of dynamic stability, i.e. neither requires a 'cautious' gait to prevent falling (p=0.62) [6].

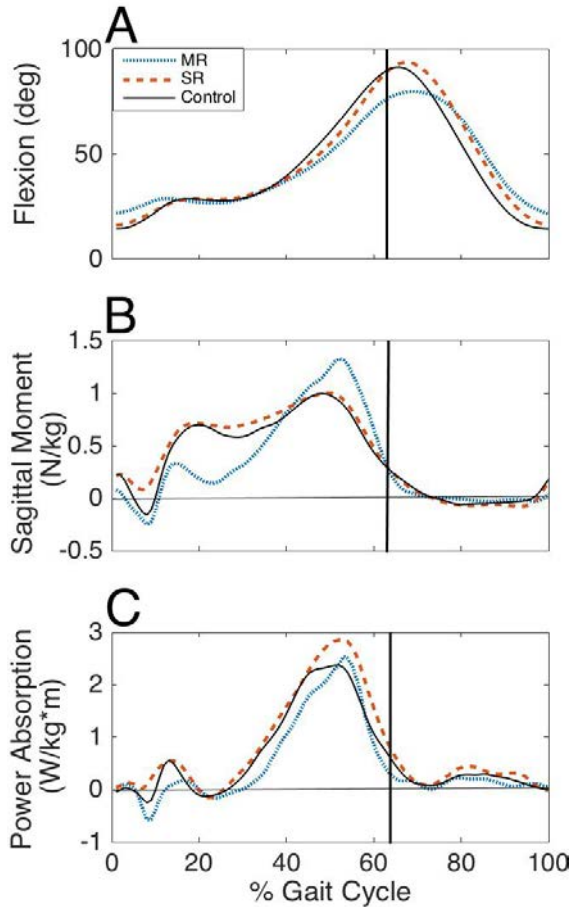


**Figure 2:** Sagittal plane knee flexion (A), moment (B) and power (C) over one gait cycle.

**DISCUSSION**

In contrast to the previous research on level walking, we did not find any significant differences

in knee flexion or peak sagittal moment during stair descent. This may be due to the constraints of the task (i.e. the foot must be placed within the stair dimensions). Although the differences are not enough to establish significance, the MR knees exhibit decreased knee flexion and increased stance moment.

We also found that similar to level walking, peak power absorption during stance is significantly less for the MR compared to SR [3]. This can be attributed to the lower angular velocity for MR patients (fig 2). The MR knee has a reduced radius of curvature at greater knee flexion, reducing the superior-inferior distance of the tibia and femur. This may contribute to laxity of the collateral ligaments, and alter the mechanics of the knee at greater flexion angles [discussed in 3].

**CONCLUSIONS**

Both, MR and SR TKA devices were able to closely replicate normal stair descent kinetics and kinematics. The initial trends suggest that the MR knee performs differently to SR knees especially at higher flexion angles, but statistical power must be improved (via increased sample size) before stronger conclusions can be made.

**REFERENCES**

1. Kurtz S, et al. *J Bone Joint Surg* **89A**, 4, 2007.
2. Wang H, et al. *Clin Orthop Relat Res* **21**, 8, 2006.
3. Larsen B, et al. *J Arthroplasty*, **30**, 6, 2015.
4. Kadaba MC, et al. *J Orthop Res.* **8**, 1990.
5. McFadyen BH and Winter DA. *J Biomech*, **21**, 9, 1988.
6. Young P and Dingwell J. *Gait Posture*, **36**, 12, 2012

Group	Peak Flexion (deg.)	Max Stance Mom (N/kg)	Min Stance Mom (N/kg)	Power (W/kg*m)	Step Width (cm)
MR	92.76±2.51	1.20±0.40	<b>-0.01±0.06</b>	<u>-2.05±0.85</u>	12.78±3.37
SR	95.06±3.48	1.08±0.21	<b>0.03±0.20</b>	<u>-3.03±0.48</u>	13.75±3.20
Control	95.06±3.29	0.92±0.39	-0.21±0.16	-2.64±0.58	12.31±2.22

**Table 1:** Sagittal plane knee flexion, minimum and maximum sagittal moment during stance, knee power, and step width by group. Data is displayed as mean±standard deviation, bolded values indicate significant results from controls, underlined indicate significantly different values from the other knee design.

# KNEE MECHANICS AND MUSCLE ACTIVATION TIMING IN ATHLETES WITH COMPLEX KNEE INJURIES

<sup>1</sup> Courtney Hatcher, <sup>1</sup> Christy Conroy, <sup>1</sup> Fred Baldwin, and <sup>1,2</sup> Emily Fox

<sup>1</sup> Brooks Rehabilitation, Jacksonville, FL, USA

<sup>2</sup> Department of Physical Therapy, University of Florida, Gainesville, FL, USA  
email: courtney.hatcher@brooksrehab.org

## INTRODUCTION

Nearly 50% of all injuries sustained by athletes are to the lower extremities. Approximately 200,000 of these lower extremity injuries occur to the anterior cruciate ligament (ACL) each year, half of which require surgery and/or rehabilitation. Unfortunately, these patients are 15 times more likely to re-injure themselves within the first year of surgery, and only half return to their prior level of activity [1]. Much research has focused on knee mechanics and rehabilitation in patients who have undergone ACL reconstruction (ACL/R) surgery. These studies commonly exclude patients with damage to other structures of the knee. However, at least 50% of ACL-related injuries occur in conjunction with damage to the meniscus, articular cartilage, and/or other ligaments [2].

Since most patients incur injuries involving multiple structures of the knee, it is necessary to expand research and understanding of knee mechanics and muscle activation in these cases. Additionally, there may be key features in patients post ACL/R that apply to patients with complex knee injuries. For instance, it is well-known that ACL/R patients often demonstrate limb asymmetry even after they return to sport, which may be a factor associated with high re-injury rates. Altered muscle activation timing may be an underlying cause to these asymmetries [3]. Prior reports, however, are inconsistent in describing changes in muscle activation timing for patients post ACL/R, and to our knowledge, no studies have compared muscle activation timing in patients with various combinations of knee injuries.

Therefore, the purpose of this case series is to describe knee mechanics and muscle activation timing in athletes with complex knee injuries. These steps are important for guiding research that will

further examine a more diverse knee injury population and contribute to rehabilitation decisions that will help to reduce the risk of re-injury when returning to sport.

## METHODS

Knee mechanics and muscle activation timing in three individuals with different sports-related knee injuries (Age:  $20 \pm 4$  years; 2 males; Time post-surgery:  $20 \pm 6$  weeks) were assessed using three dimensional kinematics, kinetics and surface electromyography (EMG). Individuals performed five repetitions of the single leg land bilaterally from an 8" box, a task commonly used during return to sport rehabilitation testing. Kinematic and kinetic data were used to compare symmetry across subjects, and the symmetry index (SI) was defined:

$$SI = \frac{\text{Uninvolved Limb} - \text{Involved Limb}}{\text{Uninvolved Limb}} \times 100\%$$

where an increase in SI represents greater asymmetry. Data were also collected from a healthy control to provide a basis for comparison (Age: 24 years; Male).

EMG data were collected from the vastus medialis oblique (VMO) during the single leg land. Muscle activation timing during the preparatory phase of landing was evaluated as this phase has previously been identified as a critical time point for knee stabilization. The preparatory phase was defined as 100 ms prior to initial contact, defined as the time point when the foot contacted the force plate [4]. EMG data were demeaned, rectified and smoothed using a fourth order low-pass Butterworth filter with a 10 Hz cutoff frequency. A threshold of 25 times baseline activity was defined as the onset of muscle activation.

## RESULTS AND DISCUSSION

Lower limb asymmetries were evident in patients with knee injuries based on the peak internal knee extensor moment and peak knee power absorption at landing (Table 1). Specifically, the healthy control demonstrated more symmetry for the peak moment and power with an SI of 7.2% and 19.6%, respectively, contrasting from the injured subjects (average peak moment and power SI for injured subjects: 25.2% and 38.5%, respectively). Additionally, delayed muscle activation timing for the VMO was present for subjects 01 and 02 (Table 1, Fig. 1) as compared to the healthy control. More specifically, the onset of muscle activation for the healthy control occurred 40.6 ms into the preparatory phase, differing from subjects 01 and 02 who did not achieve muscle activation until after initial contact.

It has been suggested that patients post ACL/R use imbalanced force absorption strategies, resulting in decreased knee extensor moments on the involved limb [5]. Our findings align with this evidence as all three subjects displayed reduced knee extensor moments on the involved side during landing. Each subject also showed reduced peak knee power absorption at landing on the involved limb which is consistent with previously reported data on the ACL/R population, suggesting that a stiffer landing strategy is possibly being applied.

The results from the EMG data suggest that muscle activation timing is altered in patients with knee injuries. It is well-established that the quadriceps play a major role in stabilizing the ACL during landing [6]. Therefore, delayed activation of the VMO could increase the risk for re-injury, as the quadriceps may not be activating soon enough to provide the appropriate amount of stability.

In summary, the results from this case series provide insight for clinicians that treat athletes with complex knee injuries. These results suggest that

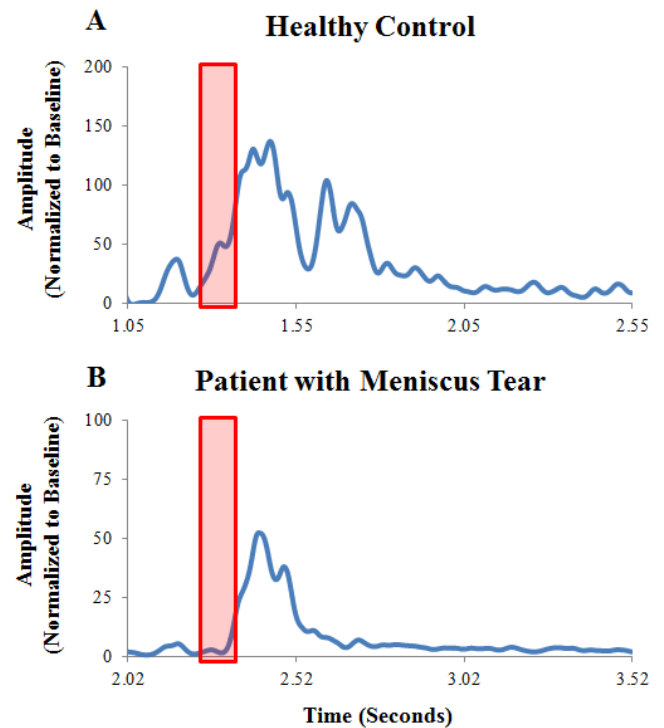


**Figure 1:** Muscle activity of the VMO for the A) left leg of the healthy control and B) involved leg of the patient with a meniscus tear. The shaded box represents the preparatory phase (100 ms) prior to initial contact.

patients who have incurred damage to multiple structures of the knee exhibit altered knee mechanics and muscle activation similar to what has previously been reported on the ACL/R population. By understanding a more diverse knee injury population, targeted rehabilitation programs can be developed to reduce the risk of re-injury in athletes who are returning to sport.

## REFERENCES

1. Paterno MV. *J Athl Train* **50**, 2015.
2. Noyes FR. *Journal of Arthroscopic & Related Surgery* **28**, 123-30, 2012.
3. Hewett TE, et al. *British Journal of Sports Medicine* **39**, 347-50, 2005.
4. Palmieri-Smith, et al. *Journal of Electromyography and Kinesiology* **18**, 973-79, 2008.
5. Paterno MV, et al. *Am J Sports Med* **38**, 1968-78, 2010.
6. Walsh M, et al. *Journal of Athletic Training* **47**, 406-413, 2012.

**Table 1:** Symmetry indices of the peak internal knee extensor moment and peak knee power absorption. Muscle activation timing of the VMO from the beginning of the preparatory phase. \*Indicates onset of muscle activation occurring after the preparatory phase.

Subject	Injury	Peak Knee Extensor Moment SI	Peak Knee Power Absorption SI	Time to Onset for Involved VMO	Time to Onset for Uninvolved VMO
01	ACL + Meniscus Tear	29.7 %	42.8 %	*108 ms	*104 ms
02	Meniscus Tear	14.8 %	31.5 %	*133 ms	*111 ms
03	ACL Tear	31.1 %	41.1 %	32.2 ms	66.6 ms
Healthy Control	None	7.20 %	19.6 %	40.7 ms	

# SPATIAL-TEMPORAL MEASUREMENTS INDICATE KNEE LOADING ASYMMETRY AFTER TOTAL KNEE ARTHROPLASTY

<sup>1</sup>Abderrahman Ouattas, <sup>2</sup>Nicole T. Ray, <sup>2</sup>Joseph A. Zeni, and <sup>1</sup>Brian A. Knarr

<sup>1</sup> Department of Biomechanics, University of Nebraska at Omaha, Omaha, NE 68182

<sup>2</sup> Mechanical Engineering, University of Delaware, Newark, DE 19713

<sup>2</sup> Physical Therapy, University of Delaware, Newark, DE 19713

email: [aouattas@unomaha.edu](mailto:aouattas@unomaha.edu), web: <http://coe.unomaha.edu/brb>

## INTRODUCTION

Total knee arthroplasty (TKA) is the most common surgical procedure to overcome end-stage osteoarthritis (OA) in the knee joint. In the US, more than 700,000 TKA surgeries are performed annually, to which 97% of those due to OA [1]. Within 10 years of the primary TKA, almost 50% of patients undergo a secondary TKA on the contralateral limb due to OA progression [2].

Individuals with end-stage knee OA exhibit asymmetric knee joint loading. This asymmetry is believed to compensate for pain and weakness in the affected limb [3]. While TKA effectively relieves knee joint pain, asymmetric kinematics/kinetics persist post-operation [4]. Post-TKA asymmetric gait patterns use greater joint loading, knee adduction moment and shorter stride length in the non-surgical limb, while showing lower knee flexion angles and shorter stance phase in the surgical limb [5]. It is thought that by shifting more load on the non-surgical limb, the chances of contralateral OA may increase [6]. However, it is difficult to assess loading in clinical settings as the needed equipment can be prohibitively expensive.

Thus, the purpose of this study was to investigate if spatial temporal measurements predict inter-limb loading asymmetry during walking in patients after TKA. We hypothesize that spatial-temporal asymmetry will be positively correlated with loading asymmetry post-TKA.

## METHODS

18 individuals after TKA participated in this study (Table 1). Data were collected using an instrumented split-belt treadmill (Bertec Corp. Columbus, OH) and an 8-camera motion capture system (Motion

Analysis Corp. Santa Rosa, CA). Kinematic data were sampled at 100 Hz and the force data were sampled at 2000 Hz. Subjects performed the 6-meter walk test to determine self-selected (SS) and fast speeds. One-minute walking trials for each speed (SS & fast) were recorded.

Table 1. Subject Information	Mean (SD)
Age	66.1 (5.8)
Mass (kg)	88.4 (19.0)
Height (m)	1.7 (0.1)
Self-Selected Speed (m/s)	1.1 (0.2)
Fast Speed (m/s)	1.4 (0.2)
Time Post-TKA (months)	11.8 (6.7)
Gender	9M/9F
Unilateral/Bilateral	8 Uni / 9 Bi
BMI	29.6 (5.3)

The kinetic and kinematic data were analyzed using Visual 3D (C-Motion Inc. Germantown, MD). Pearson correlation coefficients were calculated using SPSS Statistics (SPSS Inc, IBM Corporation). Inter-limb symmetry ratios were defined as  $S_x/\text{no}S_x$  value. Values above 100% indicate greater loading values on the surgical limb. VGRF values were normalized based on body weight (N/BW). Knee moments values were normalized on body weight multiplied by height (N/BW\*HT).

## RESULTS AND DISCUSSION

Overall, no correlation was found between spatial-temporal (stride length, step length, step time) and loading (1&2 peak VGRF, knee flexion moment, and knee adduction moment) symmetry, with the exception of stride width. Stride width symmetry showed a significant correlation with knee flexion moment symmetry ( $r^2=0.53$ ,  $P<0.001$ ) during fast walking trials (Figure 1). These results not only specify step width as an indicator of knee moment flexion asymmetry, but also suggests that there may exist an optimal range of stride width that is correlated with knee flexion moment symmetry. It

has been previously shown that a wider step width decreases the first knee adduction moment peak in healthy adults [7], but at the cost of increased knee flexion moment while no investigations have been done in post-TKA.

Subjects demonstrated inter-limb loading asymmetry post-TKA, but the direction of asymmetry varied between subjects (Table 2). Patients shifted more load on one limb, which is thought to be the cause of OA progression on the contralateral limb [6]. Within limbs, results showed correlations between stride length and 1st peak VGRF during self-selected (Sx  $r^2=0.49$ , NSx  $r^2=0.48$ ) and fast (Sx  $r^2=0.73$ , NSx  $r^2=0.46$ ) walking, but no significant correlation was recorded between symmetry indices during self-selected and fast walking. This indicates that as stride/step length increases, first peak vertical ground reaction forces increase, but these measurements do not adequately describe VGRF asymmetry post-TKA (Figure 2).

Table 2. Kinetic Symmetry Results			
	Symmetry Index	SS (1.09 m/s)	Fast (1.4 m/s)
Peak Knee Adduction Moment (N.m/BW*HT)	Average	106.64%	110.18%
	Range	48-280%	42-270%
Peak Knee Flexion Moment (N.m/BW*HT)	Average	90.01%	89.70%
	Range	16-151%	36-139%
1st Peak VGRF (N/BW)	Average	97.92%	97.77%
	Range	90-106%	82-109%
2nd Peak VGRF (N/BW)	Average	98.68%	98.05%
	Range	90-106%	87-103%

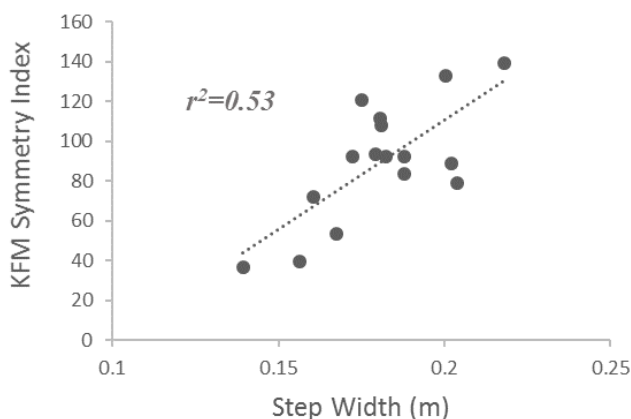


**Figure 1.** Correlation between step width and peak knee flexion moment symmetry at fast walking speed.

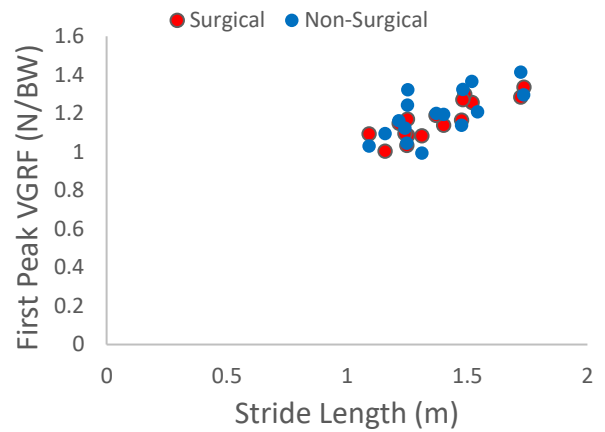


**Figure 2.** Correlation between stride length and 1<sup>st</sup> peak VGRF for surgical and non-surgical limbs at fast walking speed.

## CONCLUSIONS

A significant correlation between stride width and knee flexion moment symmetry index was found, though no other significant correlation between spatiotemporal and loading symmetry indices at either self-selected or fast walking speeds was recorded post-TKA. Future work should examine the mechanisms related to stride width and loading in a TKA population, as well as exploring individual step width in relation to center of mass. Dividing step width into single limb variables will allow exploration into whether asymmetric foot placement is a driving factor in loading asymmetries post-TKA. Overall, however, these findings indicate that clinically accessible methods to assess joint loading are needed to assess interlimb loading asymmetry in post-TKA patients, as simple spatiotemporal measures may not provide proper insight into loading asymmetry.

## REFERENCES

1. Andersson, G. Rosemont, IL: American Academy of Orthopaedic Surgeons **3rd ed.**, 19/45.
2. Shao Y. J. Arthroplasty **28**(10):1842-1845, 2013
3. Zeni J, Higginson J. The knee **18**, 156-159, 2011.
4. Alnahdi AH. J Orthop Res. **29**(5):647-652, 2011.
5. Alnahdi AH, Et al. J Orthop Res **29**,647-652, 2011.
6. Turcot K. Gait Posture **36**(1):68-72, 2012.
7. Favre, J. J Orthop Res **34**(9), 1547-1556, 2016.

## ACKNOWLEDGMENTS

This work was supported by the National Institutes of Health NIH P30-GM103333 and P20GM10909

# FUNCTIONAL IMPLICATIONS OF MENSTRUAL CYCLE ON KNEE LAXITY, RATE OF FORCE DEVELOPMENT AND ELECTROMECHANICAL DELAY

David Hawkins and Amber Sorensen Van Cleave

University of California Davis, CA, USA  
email: dahawkins@ucdavis.edu, web: <http://hpl.ucdavis.edu/>

## INTRODUCTION

Ligament and tendon stiffness affects physical performance and injury risk. Evidence indicates that ligament/tendon stiffness can be affected by fluctuations in hormone levels in women [1], with increased estrogen concentrations associated with decreased collagen synthesis and fibroblast proliferation. Serum estradiol concentrations are typically lowest and highest just before the start of menses and ovulation, respectively [2]. Based on this evidence, it is reasonable to expect that ligament/tendon stiffness would be highest around the start of menses and lowest around ovulation. However, the functional implications of the menstrual cycle on ligament/tendon stiffness are not clear. Several studies have reported no significant effect of estrogen levels throughout the menstrual cycle on knee laxity in women [e.g., 3], while other studies reported significant associations [e.g., 4]. If there are strong functional implications, then there should be differences in functional measures of ligament/tendon stiffness between the start of menses and ovulation.

The purpose of this study was to test the hypothesis that ligament/tendon stiffness is greater at the start of menses compared to ovulation in healthy young women. To achieve this goal, 3 indirect measures of ligament/tendon stiffness; anterior knee laxity (AKL), knee extension rate of force development (RFD), and knee extension electromechanical delay (EMD), were compared between the start of menses and at ovulation over 3 months.

## METHODS

Twenty females, who ranged in age from 18 to 26 years old ( $22 \pm 2$  years, mean  $\pm$  SD) and had a regular menstrual cycle, were recruited. All protocols were approved by the University of California-Davis Institutional Review Board.

AKL, RFD and EMD were quantified using a custom knee arthrometer (CKA) (Fig 1) [5]. Subjects performed a standard 10 minute treadmill walking protocol to warm-up. They were then positioned in the CKA with their right knee secured in a 25-30 degrees flexed position. AKL tests were performed, followed by tests of maximum effort isometric knee extensions.

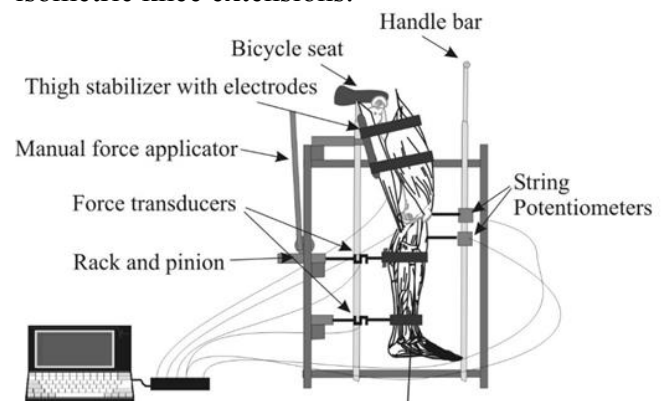


**Figure 1:** Custom knee arthrometer used to quantify AKL, RFD and EMD.

During the AKL test, a  $\sim 2$  second cyclic anterior force (-50 to 250 N) was applied 20 times through a force sensor (LC101-50, Omega Inc, Stamford, CT) positioned on the upper portion of the lower leg while displacement of the tibia relative to the femur was recorded using 2 string potentiometers (SP1-4, Celesco, Chatsworth, CA). Electromyography was used to monitor the activity of the quadriceps and hamstrings. AKL was quantified as the average relative tibial displacement at a 200 N force for the last 10 cycles.

Following the knee laxity test, the strap located approximately 10 cm distal to the knee was removed and the subject performed 4 maximum effort isometric knee extension efforts with each effort separated by approximately 2 seconds. The force developed at the ankle to restrain the leg from moving was recorded along with the muscle activation. The time from the initiation of

quadriceps muscle activation to the time force was detected at the ankle (i.e. EMD), as well as the maximum slope of the force-time response (i.e. RFD) were determined. These tests were repeated for 3 months on the day of the start of menses and on the day of ovulation, determined using ovulation test strips (One Step Ovulation Test Strips, Babi, Beijing, China). A paired T-Test was used to compare the average AKL, RFD, and EMD between start of menses and at ovulation. Significance was set at  $p < 0.05$ .

## RESULTS AND DISCUSSION

Among the 20 subjects who enrolled, 7 chose to discontinue their participation for various reasons. Data from 13 subjects were considered in the analysis.

The group averages for AKL, RFD, and EMD at start of menses and at ovulation were 4.15 mm and 4.39 mm, 1107 N/s and 1093 N/s, and 0.041 s and 0.044 s, respectively. These averages are consistent with the stated hypothesis. If ligament/tendon stiffness is greater at the start of menses compared to ovulation, then AKL should be lower, RFD greater, and EMD lower at the start of menses compared to ovulation. However, AKL, RFD, and EMD responses varied between subjects (Figs 1-3), and there were no significant differences in AKL ( $p=0.23$ ), RFD ( $p=0.86$ ), and EMD ( $p=0.13$ ) between paired averages at the start of menses and at ovulation.

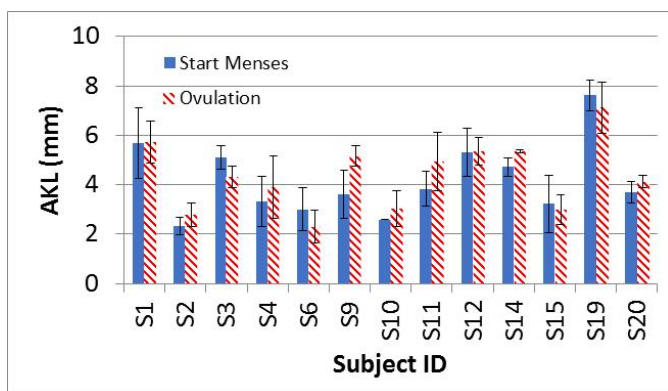


**Figure 1:** Average ( $\pm 1$  std dev) of anterior knee laxity (AKL) for each subject at the start of menses and at ovulation.

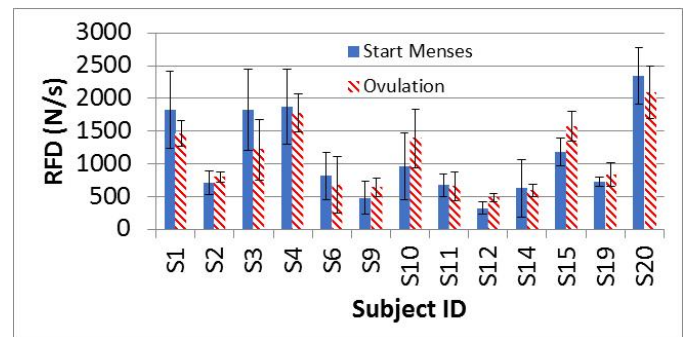


**Figure 2:** Average ( $\pm 1$  std dev) knee extension rate of force development (RFD) for each subject at the start of menses and at ovulation.

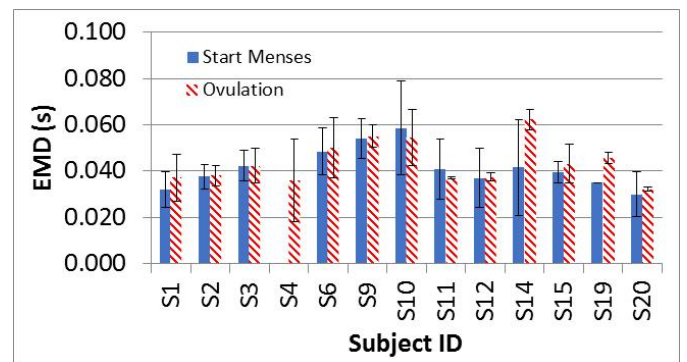


**Figure 3:** Average ( $\pm 1$  std dev) knee extension electromechanical delay (EMD) for each subject at the start of menses and at ovulation. EMD was not successfully recorded at menses for S4.

## CONCLUSIONS

Based on the evidence from this study, there are no generalized functional implications of menstrual cycle on ligament/tendon stiffness.

## REFERENCES

1. Zazulak BT, et al. *Sports Med.* **36(10)**, 847-62, 2006.
2. Stricker R, et al. *Clin Chem Lab Med.* **44(7)**, 883-7, 2006.
3. Van Lunen BL, et al. *J Athl Train.* **38(4)**, 298-303, 2003.
4. Shultz SJ, et al. *J Sports Med Phys Fit.* **45(4)**, 594-603, 2005.
5. Starkel CD, et al. *Austin J Biomed Eng.* **3(1)**, 1034, 2016.

# FEA of Lateral Meniscus Posterior Root Avulsions on Tibiofemoral Contact Mechanics

<sup>1</sup>Erika Fojtik, <sup>2</sup>Andrew Geeslin, <sup>1</sup>Peter Gustafson

<sup>1</sup>Western Michigan University, Kalamazoo, MI, USA

<sup>2</sup>Borgess Orthopedics, Kalamazoo, MI, USA

Email: [erika.g.fojtik@wmich.edu](mailto:erika.g.fojtik@wmich.edu)

## INTRODUCTION

The effects of lateral meniscus posterior root avulsions have been studied in combination with intact meniscofemoral ligaments (MFLs) and deficient MFLs to understand the changes in contact mechanics in the knee and to determine the function of the MFLs. This study was done to validate a patient-specific finite element model (FEM) of a knee against experimental data conducted on cadaveric knees to study the effects of posterior root avulsions of the lateral meniscus.

## METHODS

Magnetic resonance imaging (MRI) was used with 3D Slicer segmentation software to develop the finite element model. Anatomical structures included in the model are the anterior cruciate ligament (ACL), femoral cartilage, femur, fibula, lateral and medial collateral ligaments (LCL/MCL), medial and lateral meniscus, posterior cruciate ligament (PCL), posterior meniscofemoral ligament (pMFL), tibia, and tibial cartilage. The anterior meniscofemoral ligament (aMFL) was omitted from this study due to its lack of presence in the knee. Hypermesh software was used for mesh generation and refinement. Tetrahedral elements were globally used for the model. The model generated from

Hypermesh is shown in Figures 1 and 2 for the anterior and posterior views, respectively. From the model, the following conditions are explored: (1) intact, (2) lateral meniscus posterior root avulsion (LMPRA), and (3) deficient pMFL and LMPRA. The model of each condition maintains a fixed flexion angle of 0° under a 1000 N compressive load. Model outputs include contact pressure and distribution in the tibiofemoral contact region.

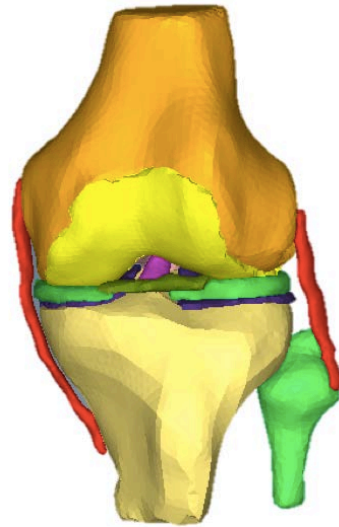


**Figure 1:** Anterior perspective of the knee model in Hypermesh.

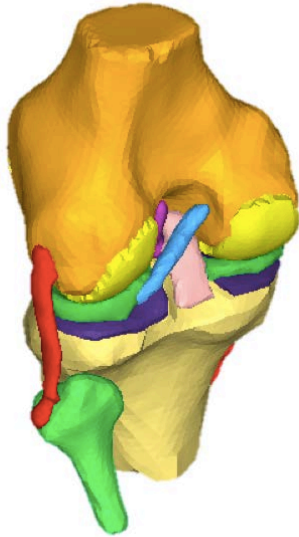


**Figure 2:** Posterior perspective of the knee model in Hypermesh. Posterior meniscofemoral ligament (pMFL) shown in light blue.

## RESULTS AND DISCUSSION

A preliminary set of finite element analyses (FEA) will provide contact pressures and distributions across the tibiofemoral contact region to compare and validate with experimental data. The given experimental data from Geeslin et al. resulted in pressure mapping shown in Figure 3 for the three aforementioned conditions [1]. This work concluded that lateral meniscus posterior root avulsions reduce contact pressure (peak) by 6.1% in the lateral compartment [1]. The absence of the meniscofemoral ligaments, in combination with LMPRA, results in a more severe increase in contact pressure (peak) of 28.2% [1].

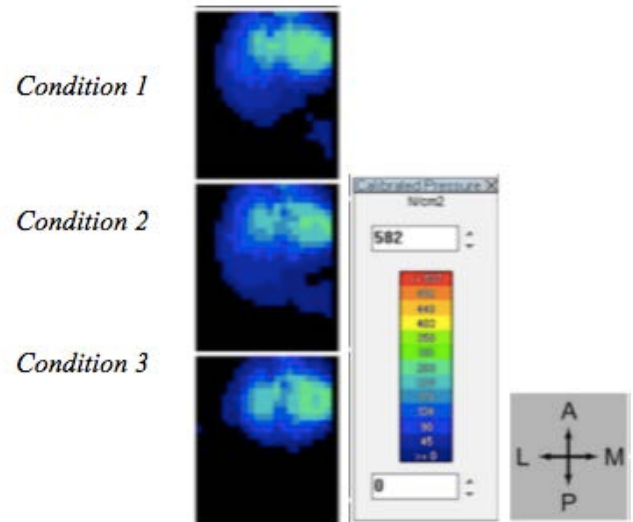


**Figure 3:** Contact pressure maps of the lateral compartment from experimental study done by Geeslin et al. for condition (1) intact knee, (2) LMPRA, and (3) LMPRA and pMFL deficiency. (These graphics were modified with permission from Geeslin [1].)

Development of musculoskeletal finite element models, especially those validated against laboratory experimentation, are critical to describe the biomechanics of dynamic axial loads, rotational loads, and shear stress incident upon the knee. The preliminary results are intended to provide data and insight for future validation of intact and structurally deficient knee joint models. Clinical relevance is based on providing orthopaedic surgeons with an improved knowledge of the biomechanical consequences of the available repair techniques of lateral meniscus posterior root avulsions, and thus improved capability for surgical decision making.

## REFERENCES

1. Geeslin AG, et al. *Knee Surg Sports Traumatol Arthrosc* **24**, 1469-77, 2016.

# **SURFACE STIFFNESS AND KNEE JOINT LOAD EFFECTS WHILE RUNNING**

Victoria A. Price, Daniel J. Kuhman, Stacey Meardon, J. C. Mizelle, Paul DeVita  
Biomechanics Laboratory, Department of Kinesiology, East Carolina University, Greenville NC

## **Introduction:**

Running shoes and surfaces have been developed to help enhance running efficiency and to alter ground impacts by changing the total surface stiffness<sup>3</sup>. Similar to a massed spring, an individual contacts the running surface, flexes their lower limb joints, and stores strain energy through the muscles, tendons, and ligaments. This stored energy is then released back to the limb and the limb joints extend and propel the individual into the next stride<sup>4</sup>. However to maintain global running mechanics, an individual will increase leg stiffness while running across a compliant ground surface and conversely decrease stiffness on harder surfaces. Increasing leg stiffness causes landing impact forces to increase<sup>2</sup> and potentially may counteract beneficial effects of impact load reduction while running on a softer surface. The knee is a determinant for reducing impact forces and changing leg stiffness<sup>2</sup>. Knowing more about knee joint forces while running on surfaces with different stiffnesses has the potential to improve injury prevention strategies.

It was our objective to determine the effect of surface stiffness on knee joint contact forces during running. We expected forces to remain consistent across different surface stiffnesses secondary to leg adjustments. Thus, our hypothesis was that knee joint loads would not be statistically different across varying levels of surface stiffness.

## **Methods:**

We recruited 17 healthy recreational heel strike runners. They provided written informed consent and ran across a 15m track at a consistent pace ( $3.46\text{m/s} \pm 5\%$ ) on 3

ground conditions (hard floor with embedded force plate and 1 and 2 layers of 1.6cm thick Shore00 65 of shock absorbing mat covering the hard surface condition). The study protocol took place over 2 days. On day 1, participants were able to practice running over the various ground conditions at the test speed, on day 2, data were collected. Five successful trials per surface condition were collected using an 8 camera motion capture system (Qualisys Tracking Manager). Kinematic and kinetic data were analyzed through V3D and Quick Basic, and knee joint tibio-femoral (TF) and patella-femoral (PF) forces were estimated through musculoskeletal modeling<sup>1</sup>. Knee joint angular stiffness was also calculated by finding the ratio of the peak torque at the knee joint, simultaneous to the knee joint angular displacement. Data were statistically compared among surface conditions with a one way ANOVA, using three levels and  $\alpha < 0.05$ .

## **Results and Discussion:**

Compressive PF and compressive TF forces were not significantly different between surface conditions supporting our hypothesis. However, knee joint angular stiffness, the rate to the vertical GRF impact peak (vGRF), maximum anteroposterior braking force, and TF shear force for both force magnitude and rate to the maximum force were found to be statistically different and decreased as the surface stiffness decreased (all  $p < 0.03$ ).

Post-hoc testing revealed that knee joint stiffness was less in the softer surface conditions compared to the stiffest condition. Rate to the vGRF impact peak,

maximum anteroposterior breaking force, and the rate to the maximum TF shear force were statistically different between the softest surface stiffness and the stiffer conditions (all  $p < 0.05$ ). Maximum TF shear force post-hoc tests indicated that all stiffness conditions were statistically different from each other (Figure 1).

Our hypothesis was partially supported for knee joint compressive loads but not for the shear loads. As the participants ran across the increasingly dampened surfaces their knee joint angular stiffness decreased. This is contrary to existing literature that suggests an inverse effect between surface stiffness and leg stiffness, which is closely related to knee joint stiffness. In addition, the rate to the vGRF impact peak and the breaking force magnitude decreased with the surface

stiffness. Our data supported the idea that running across differing surface stiffnesses does not statistically alter knee joint compressive forces but can reduce knee joint shear forces. Future research should determine if this strategy is beneficial to a broader range of individuals including those with fore- and mid-foot strike patterns.

**References:**

1. DeVita P, Hortobagyi T. *J Biomech.* 2001;17(4):297-311.
2. DeVita P, Skelly WA. *Med Sci Sports Exerc.* 1992;24(1):108-115.
3. Logan, S., Hunter, I., J. Ty Hopkins, J. T., Feland, J. B., & Parcell, A. C. *J Spts Sci & Med.* 2010, 9(1), 147–153.
4. McMahon TA, Greene PR.. *J Biomech.* 1979;12(12):893-904.

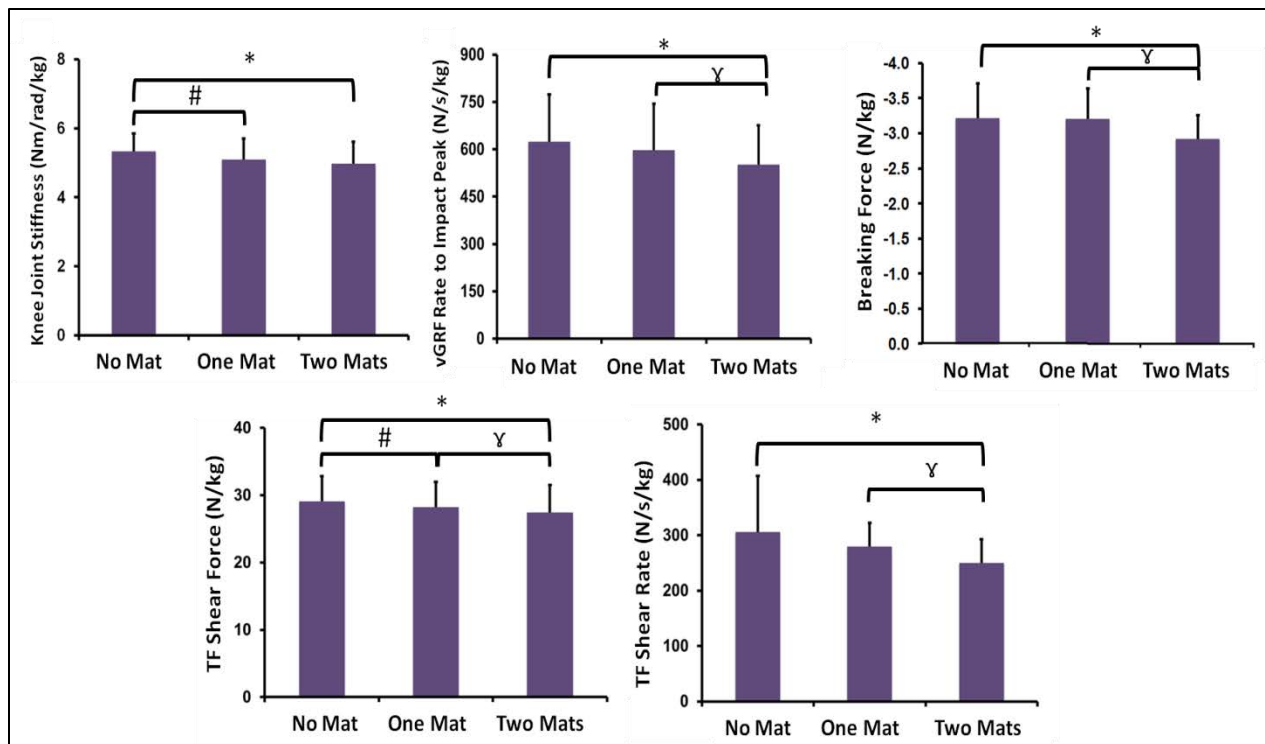


**Figure 1:** Knee joint angular stiffness, vGRF rate to impact peak, breaking force magnitude, TF shear force magnitude and TF shear rate to maximum force. Statistical significance ( $p < 0.05$ ) for No Mat vs One Mat (#), No Mat vs Two Mats (\*), and One Mat vs Two Mats (γ).

# PATELLAR FORCES AND TORSIONS RESULTING FROM DECREASED ACTIVATION OF THE VASTUS MEDIALIS MUSCLE

<sup>1</sup> Sarah E. Siegel, <sup>1</sup> Timothy R. Derrick, <sup>2</sup> Elizabeth R. Boyer

<sup>1</sup> Iowa State University, Ames, IA, USA

<sup>2</sup> Gillette Children's Hospital, St. Paul, MN, USA

email: [sesiegel@iastate.edu](mailto:sesiegel@iastate.edu) : web: [http:// www.kin.hs.iastate.edu/](http://www.kin.hs.iastate.edu/)

## INTRODUCTION

The quadriceps is a powerful muscle group that plays a significant role in many activities of daily living and sports. This group of muscles produces movement at both the hip and knee joint. The knee is a complex joint that must withstand a great deal of stress. The amount of stress placed on the knee puts the joint at risk of injury, dysfunctional movement, and pain.

Patellofemoral pain, also known as anterior knee pain, is one of the most frequent knee conditions seen by sports medicine providers [1]. Dysfunctional tracking of the patella is thought to be a possible cause of such knee pain. There is controversy related to whether or not weakness in the vastus medialis portion of the quadriceps muscle plays a critical role in patellar tracking. It is thought that weakness in the vastus medialis will cause the patella to track laterally.

It has been shown that asymmetric quadriceps loading leads to an alteration in the mediolateral forces [2]. The purpose of this project was to determine if reduced maximal strength of the vastus medialis will cause optimized muscle forces in a musculoskeletal model to increase laterally directed patellar forces or patellar torsion.

## METHODS

Seven young adults (3 males, age: 21.3±2.1 yr; body mass: 68.9±6.7 kg; height: 1.84±0.07 m and 4 females, age: 25.3±5.2 yr; body mass: 56.6±11.3 kg; height: 1.64±0.08 m) with no lower limb injuries and a heel toe running style volunteered to participate.

Running motion data were recorded simultaneously with ground reaction forces Kinematics at 200 Hz using 8 Vicon MX cameras (Vicon, Centennial, CO, USA) and force data at 1000 Hz (AMTI, Watertown, MA). Participants ran at 3.5 m/s with their right foot landing on the force platform.

Two models for each participant were constructed using Matlab. A rigid body model was used to estimate the joint moments using inverse dynamics and a musculoskeletal model was used to estimate length and velocity adjusted maximal dynamic muscle forces and moment arms of 44 muscles in the lower extremity [3]. Muscle forces required to produce the inverse dynamics joint moments were estimated using optimization techniques that minimized the sum of the muscle stress squared and were constrained to equal the moments found using the rigid body model. The moments used as constraints were in the sagittal plane at the ankle, knee and hip, as well as the ankle and hip moments in the frontal plane. The lower and upper bounds of the muscle forces were zero and the maximal muscle forces found using the musculoskeletal model, respectively.

The patellar tendon force was estimated using the quadriceps tendon to ligament force ratio [4]. The muscle and tendon forces acting on the patella were then summed and the medio-lateral directed force and the torsion were selected for analysis. The computer model was then altered to reduce the maximum force producing capabilities of the vastus medialis muscle. The optimization algorithm was applied to the new model and the resultant patellar forces and torsions were recalculated. Reductions of 10%, 20%, 30%, 40% and 50% of the normal vastus medialis force were examined. Peak medio-lateral forces and torsions were identified as a

present of the peak values in the original model. Paired t-tests were utilized to determine the effect of decreased vastus medialis force for each participant, with an alpha criterion of 0.05.

## RESULTS AND DISCUSSION

As expected, the reduced maximum force producing capabilities of the vastus medialis decreased its estimated muscle force. In turn, this increased the vastus lateralis muscle force in order to create enough extensor torque to produce the movement (Figure 1).

Peak patellar mediolateral forces were increased by 2.5% from the 100% condition to the 50% condition while peak patellar torsion was increased by 10.1%. Only the 50% and 60% conditions were statistically significantly different from the 100% condition in these two variables (Table 1).

It should be noted that these results are dependent on the orientation of the muscles relative to the patella. In the Arnold model, the vastus medialis, the vastus lateralis and the patellar ligament tend to pull the patella in a lateral direction. A more

complex model might be necessary to fully understand the loading of the patella. It should also be noted that this technique does not allow for alterations in the kinematics or joint moments that might occur during actual weakening of the vastus medialis muscle.

## CONCLUSIONS

The musculoskeletal model with optimization of muscle forces was able to model the effects of decreased vastus medialis strength. This resulted in small increases in laterally direct patellar forces and somewhat larger patellar torsions.

## REFERENCES

1. Glaviano, N.R. *Inter J Sports Phys Ther*, **10**, 281-290, 2015.
2. Lorenz, A., et al. *The Knee*, **19**, 818-822, 2012.
3. Arnold, E. M., et al. *Annals of Biomedical Engineering*, **38**, 269-279, 2010.
4. Ellis, M. I., et al. *Engineering in Medicine*, **9**, 189-194, 1980.

Table 1. Peak running muscle forces and patellar loading during simulated reduced vastus medialis strength.

Reduction in Vastus Medialis Maximum Force (%)	Peak Vastus Medialis Force (BW)	Peak Vastus Lateralis Force ( BW)	Peak Patellar Lateral Force (%)	Peak Patellar Torsion (%)
100	2.3±1.1	3.0±1.6	100.0±9.0	100.0±5.3
90	2.2±1.2	3.0±1.4	100.6±10.0	103.8±12.9
80	2.1±1.1	3.2±1.6	100.2±10.0	100.0±8.0
70	1.9±.9	3.2±1.6	100.2±10.9	104.1±11.5
60	1.7±.8	3.4±1.7	101.8±9.9	106.2±8.1
50	1.6±.8	3.4±1.7	102.5±8.7	110.1±8.9

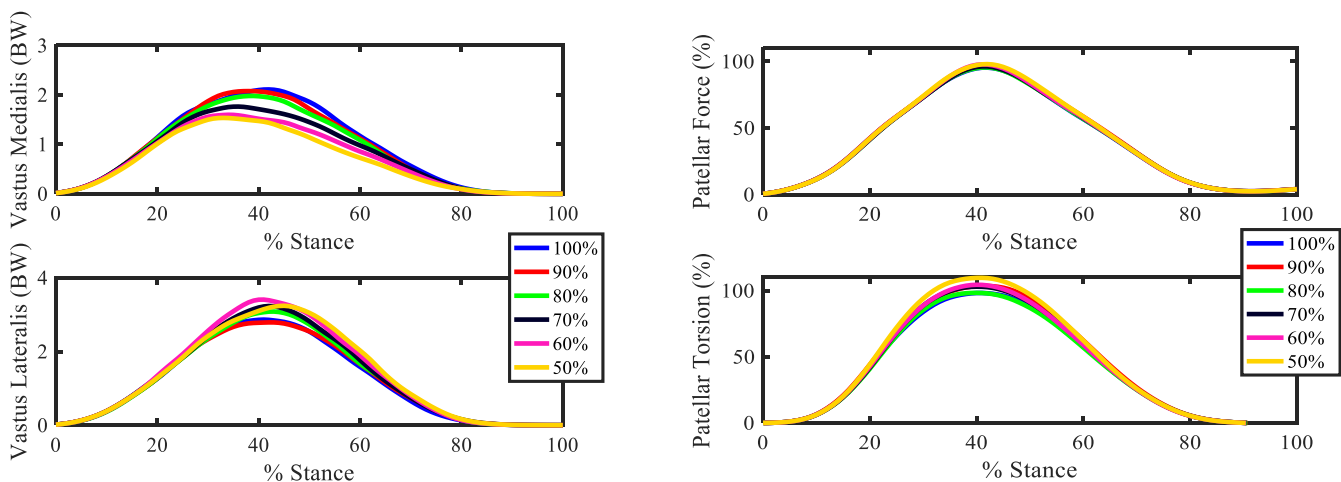


Figure 1. Running muscle forces and patellar loading during simulated reduced vastus medialis strength.

# EFFECTS OF AGE, GENDER, AND BMI ON MAXIMUM KNEE FLEXION IN SINGLE AND DUAL LEG BODYWEIGHT SQUATS

David Herlihy, Kevin O'Brien, and James P. Schmiedeler

Aerospace and Mechanical Engineering, University of Notre Dame, Notre Dame, IN, USA

email: dherlih1@nd.edu, kobrie23@nd.edu, schmiedeler.4@nd.edu

## Introduction

The bodyweight squat is often used for training and biomechanical evaluation, in part because of its similarity to many functional tasks [1]. Squat depth as measured by maximum knee flexion is a common performance metric, so squats may be categorized as partial, half, or deep/full based on that angle [2]. Being overweight, as measured by body mass index (BMI), is known to lead to reduced knee flexion in bodyweight squats [3]. The authors, however, found no literature quantifying differences in bodyweight squat depth associated with age or gender. Expanded use of motion capture systems for biomechanical analysis of large numbers of individuals performing standard motions like the bodyweight squat has enabled a dramatic increase in sample size for quantifying these differences. This work leverages such a data set to determine the effects of age, gender, and BMI on maximum knee flexion in both single and dual leg bodyweight squats.

## Methods

Data were collected from 1068 subjects who participated in biomechanical analysis activities using a markerless motion capture (120 Hz) (Organic Motion, New York, USA) and cloud-based analysis software (DARI, Kansas, USA) system through their employers or educational institutions. All subjects self reported as being healthy and gave their informed consent to have their data, including height, weight, age, and gender, shared without personal identifiers for research and development purposes prior to data collection. This study was approved by the appropriate Institutional Review Board.

The subjects were divided into four groups by age and gender: 133 older males (age range 40-77 years; mean  $\pm$  std dev:  $52 \pm 8.37$  years); 220 older females (40-72:  $51.8 \pm 7.71$  years); 407 younger males (18-24:  $20.3 \pm 1.38$ ); and 308 younger females (18-31:  $21.4 \pm 3.6$ ). Each subject was instructed to perform a dual leg bodyweight squat, a single-leg bodyweight

squat with the left leg, and a single-leg bodyweight squat with the right leg. No instructions about arm placement during the squats were given. The number of other activities each subject performed in his/her data collection session varied. The DARI software computes a large number of kinematic and kinetic quantities for each motion, but this work exclusively analyzed maximum knee flexion angle for each leg.

BMI was computed for each subject as mass in *kg* divided by the square of height in *m*. All data analysis was performed using the software R. An initial multi-factor ANOVA considering all 1068 subjects was used to determine the effects of age, gender, and BMI on maximum knee flexion angle for each of the three types of squats. Since age and gender were both found to be main effects in all three cases, subsequent multi-factor ANOVAs were performed on subject subgroups divided according to age, and single factor ANOVAs were performed on subject subgroups divided according to age and gender to quantify the effect of BMI.

## Results and Discussion

The results of the multifactor ANOVA considering just the younger group of subjects (male and female) determined that BMI was a main effect, but gender was not. As shown in Fig. 1, statistically significant differences were found between the maximum knee flexion angle in the dual leg squat and the single leg squat, but no significant differences were found between the genders for either type of squat. In contrast, the multifactor ANOVA considering just the older group (male and female) found that both gender and BMI were main effects. As shown in Fig. 2, older male subjects exhibited maximum knee flexion angles in both dual leg and single leg squats that were significantly larger than those of older female subjects. The F values from the ANOVAs for the maximum left knee flexion angle in the single-leg squat with the left leg and the dual leg squat are reported in Table 1, and similar values were found for the other angles not reported here.

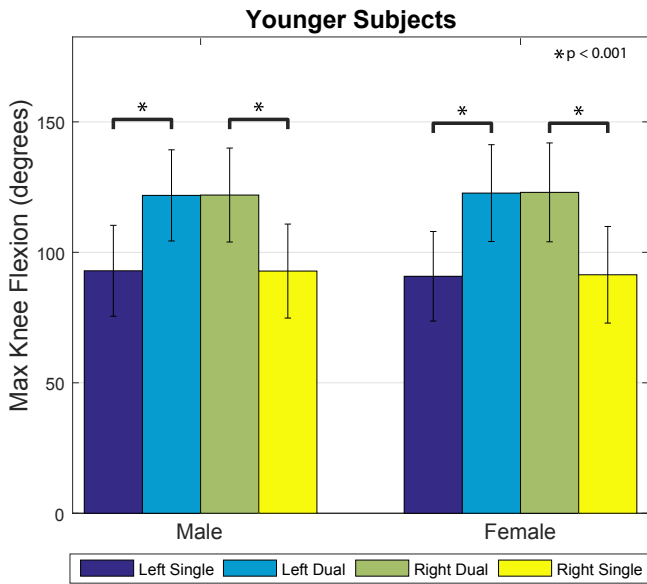


FIGURE 1. Maximum knee flexion in single and dual leg squats for younger subjects.

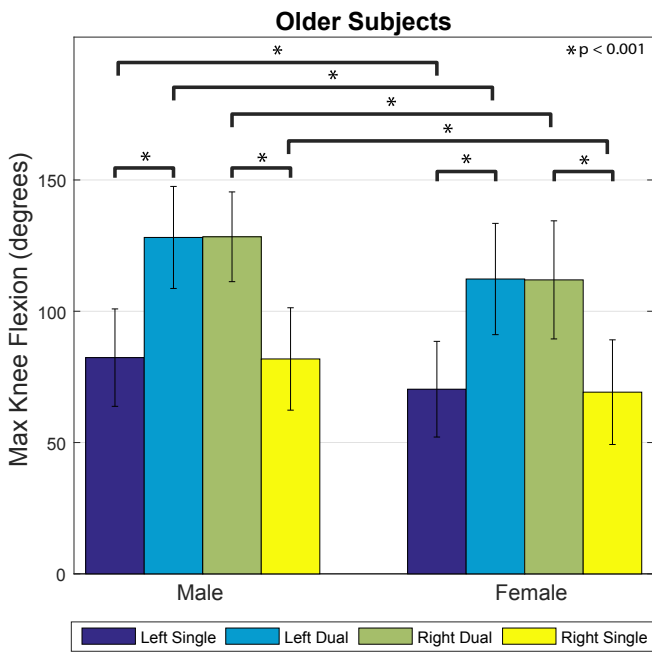


FIGURE 2. Maximum knee flexion in single and dual leg squats for older subjects.

TABLE 1. Effect of gender on maximum left knee flexion in single left leg squats and dual leg squats.

Age Group	F Value (p Value)	
	Single Left	Dual Left
Younger	2.22 (>0.1)	1.99 (>0.1)
Older	49.82 ( $\leq 0.001$ )	81.23 ( $\leq 0.001$ )

The results of the single-factor ANOVAs performed on the older male, older female, younger male, and younger female subgroups indicated that BMI was a main effect on maximum knee flexion for single leg squats in all groups. As BMI increased, the average maximum knee flexion decreased. Table 2 reports the F values for the maximum left knee flexion angle in the single leg squat with the left leg and the dual leg squat. Similar values were found for the angles not reported here. An increase in BMI had a comparatively larger negative effect on maximum knee flexion in both single and dual leg squats for the older female group than the older male group, despite both groups exhibiting a decline. Across all four groups, BMI had a much stronger effect on maximum knee flexion in single leg squats than in dual leg squats. While BMI had a significant effect on the variance of the maximum knee flexion for dual leg squats in both older subject groups, it did not have a significant effect in either younger group in the dual leg squat.

TABLE 2. Effect of BMI on maximum left knee flexion in single left leg squats and dual leg squats.

Grouping	F Value (p Value)	
	Single Left	Dual Left
Older Male	27.64 ( $\leq 0.01$ )	9.68 ( $\leq 0.01$ )
Older Female	64.89 ( $\leq 0.01$ )	18.74 ( $\leq 0.01$ )
Younger Male	61.78 ( $\leq 0.01$ )	1.03 (> .3)
Younger Female	54.43 ( $\leq 0.01$ )	3.99 (> 0.05)

## Conclusions

While younger subjects exhibited no differences in bodyweight squat performance across genders, female subjects exhibited greater degradation of bodyweight squat depth with an increase in age than did male subjects. Furthermore, the effect of BMI was on squat depth was greater for single leg squats than for dual leg squats. These data can inform rehabilitation and athletic training practice.

## References

- [1] M Kritz et al., *Strength Cond J*, 31(1):76-85, 2009.
- [2] B J Schoenfeld, *J Strength Cond Res*, 24(12):3497-3506, 2010.
- [3] A P Glave et al., *J Strength Cond Res*, 26(11):3148-54, 2012.

# FUNCTIONAL BALLISTIC MOVEMENTS IN CHILDREN WITH A HISTORY OF PONSETI CORRECTION FOR TALIPES EQUINOVARUS: PRELIMINARY RESULTS

<sup>1</sup>Patti Berg-Poppe, <sup>1</sup>Renee Burnham, <sup>1</sup>Boni Slagerman, <sup>1</sup>Mark Wilcox, <sup>1</sup>Lana Svien, and <sup>2</sup>Geoffrey Haft

<sup>1</sup>University of South Dakota, Vermillion SD, USA

<sup>2</sup>Sanford Health Systems, Sioux Falls SD, USA

email: Patti.Berg@usd.edu

## INTRODUCTION

Congenital Talipes Equinovarus (CTEV), also referred to as “clubfoot,” is a condition of unknown etiology formed in utero. At birth, an infant presents with inversion, adduction, and equinus of the joints of the foot and ankle to varying degrees.<sup>1</sup> The Ponseti method for correction of clubfoot involves serial manipulations and castings followed by a bracing regimen.<sup>1</sup> While the Ponseti method is the treatment of choice for CTEV, when compared to children born with typical feet, children undergoing the method demonstrate less power and flexibility<sup>2,3</sup> at the foot and ankle, leading to differences in the performance of complex functional activities demanding power and flexibility.

A study of ballistic performance of children post Ponseti correction has not yet been undertaken. Ballistic tasks require complex, rapid, powerful movements to achieve maximal force in a short time.<sup>4</sup> Successful completion of such tasks requires sufficient power<sup>4,5</sup> and flexibility.<sup>5</sup> The purpose of this study was to measure differences in ballistic movements in children with a history of Ponseti correction for CTEV against an age- and gender-matched control group. We hypothesized that children with a history of Ponseti correction would differ from those without CTEV in measures of ballistic movement success due to differences in body structures of the corrected foot/ankle and the elevated demands of ballistic tasks.

## METHODS

Musculoskeletal measures of the lower extremity included strength, passive range of motion (ROM), and closed-chain assessments (Table 1).

A digitized walkway was used to measure ballistic task performance, including standing broad jump, single leg hop, and triple leg hop distances traveled. The standard protocol for the Sargent jump test<sup>6</sup> was used.

## RESULTS AND DISCUSSION

Participants comprised 18 subjects, including 9 children with a history of CTEV following Ponseti correction (CTEV-G) and 9 age- and gender-matched (6 male/group) control group (CG) participants. Matched children did not differ in age (CTEV-G = 8.89±1.27 years; CG = 8.82±1.39 years) or BMI (CTEV-G = 20.2±7.23; CG = 16.25±0.78).

There were no statistically perceived between-group differences in musculoskeletal measures of strength or passive joint range of motion (Table 1). The CTEV-G demonstrated lower degrees of mean passive joint range of motion and greater variability, observed as larger standard deviations. Dorsiflexion strength was greater in CTEV-G and approached significance. A statistically significant difference in closed chain lunge test was observed, with greater degrees of motion identified in CTEV-G (Table 1).

CTEV-G subjects demonstrated poorer ballistic performance than CG subjects; however, the standing broad jump was the only ballistic test to reveal a statistically significant between-group difference (Table 1). No significant correlations were found between ballistic test performance and passive foot or ankle ROM.

## CONCLUSIONS

The CTEV-G showed greater closed kinetic chain dorsiflexion as compared to CG. The greater ROM may be due to mechanical inefficiency during the

stance phase in the gait cycle. The CTEV group may compensate more at the hip, as demonstrated in other studies.<sup>3</sup> Differences in standing broad jump performance may be due to excess DF in the closed kinetic chain of the corrected foot, thereby limiting the full advantage of the stretch reflex used in ballistic tasks. Another possible explanation is a decrease in push-off power, either due to mechanical inefficiency or compensations at the hip joint.

While children with CTEV show poorer jumping distances than matched control subjects for all ballistic tests, these differences did not meet a level of statistical significance, with the exception of the standing broad jump. Ponseti correction alters foot and ankle biomechanics successfully enough that an analysis of ballistic performance does not differentiate children with a history of Ponseti treatment for CTEV from peers unaffected by the congenital condition.

Parents seeking advice about prognosis and outcomes related to their infant's ability to keep up with peers after Ponseti correction for CTEV can be reassured that while deficits in ballistic performance may be present, these deficits are unlikely to significantly impact functional performance in general

## REFERENCES

1. Ponseti IV. The Treatment of Congenital Clubfoot. *Journal of Orthopaedic & Sports Physical Therapy*. 1994;20(1):1-1.
2. Alkjaer T, Pederson EN, Simonson EB. Evaluation of the walking pattern in clubfoot patients who receive early intensive treatment. *Journal of Pediatric Orthopedics*. 2000;20(5):642-647.
3. Karol LA, Jeans K, ElHawary R. Gait analysis after initial nonoperative treatment for clubfeet: intermediate term followup at age 5. *Clinical orthopaedics and related research*. 2009;467(5):1206-1213.
4. Perveen R, Evans AM, Ford-Powell V, et al. The Bangladesh clubfoot project: audit of 2-year outcomes of Ponseti treatment in 400 children. *Journal of pediatric orthopedics*. 2014;34(7):720-725.
5. Wilt F. Plyometrics: What it is and how it works. *Athl J*. 1975;55(5):76, 89-90.
6. Fernandez-Santos JR, Ruiz JR, Cohen DD, Gonzalez-Montesinos JL, Castro-Pinero J. Reliability and Validity of Tests to Assess Lower-Body Muscular Power in Children. *Journal of strength and conditioning research / National Strength & Conditioning Association*. Aug 2015;29(8):2277-2285.

**Table 1. Comparison of Musculoskeletal and Ballistic Task Measures**

	Mean, SD		P
	CTEV	CG	
<b>STRENGTH</b>			
<i>DF Motor Strength (kg)</i>	27.40, 4.40	23.42, 3.64	.053
<b>PASSIVE JOINT RANGE OF MOTION</b>			
<i>Talocrural Dorsiflexion</i>	21.33, 17.47	28.78, 7.01	.262
<i>Ankle Plantarflexion</i>	48.67, 14.30	50.33, 4.52	.746
<i>Midfoot Inversion</i>	41.78, 8.38	46.22, 12.00	.376
<i>Midfoot Eversion</i>	18.44, 4.98	22.89, 8.84	.207
<i>Arc of Passive Ankle Motion</i>	70.00, 27.51	79.11, 8.05	.364
<b>CLOSED KINETIC CHAIN</b>			
<i>Lunge Test<sup>a</sup></i>	41.93, 5.77	34.44, 7.08	.026*
<i>Calcaneal Eversion<sup>a</sup></i>	8.67, 3.39	8.44, 4.36	.905
<i>Heel Rise Test</i>	24.00, 8.73	28.67, 13.75	.403
<b>BALLISTIC TASKS</b>			
<i>Sargent Jump</i>	22.14, 4.00	27.46, 8.03	.101
<i>Single Leg Hop for Distance<sup>a</sup></i>	89.45, 19.51	107.47, 30.74	.157
<i>Standing Broad Jump</i>	113.05, 21.13	136.84, 25.56	.047*
<i>Triple Hop for Distance<sup>a</sup></i>	253.09, 50.91	289.26, 80.35	.271

# POSTURAL CONTROL AND ACTIVATION OF MUSCLES CONTROLLING THE KNEE IN CHILDREN WITH IDIOPATHIC TOE WALKING BEHAVIOR

<sup>1</sup> Patti Berg-Poppe, <sup>2</sup> Lisa Inglis, <sup>3</sup> Jae Yom, <sup>1</sup> Nicole Koskovich, and <sup>1</sup> Nikki Streleck

<sup>1</sup> University of South Dakota, Vermillion SD, USA

<sup>2</sup> Daemen College, Amherst NY, USA

<sup>3</sup> Ohio University, Athens OH, USA

email: Patti.Berg@usd.edu

## INTRODUCTION

Idiopathic toe-walking (ITW) is an atypical toe-toe gait pattern with the absence of heel strike and without a specifically identified etiology.<sup>1,2</sup> Few studies have been published analyzing static postural control and muscle activation patterns in children with ITW.<sup>3,4</sup> This study examined static postural control in children with ITW by measuring loading patterns and activation of muscles controlling the knee using variable sensory conditions.

The purpose of the analysis was to examine knee agonist-antagonist muscle activation to explain center of pressure (CoP) distribution trends under variable postural control conditions.

## METHODS

Surface electromyography (EMG) was applied to rectus femoris (RF) and biceps femoris (BF) to measure the percent of MVIC utilized under a matrix of the firm (Fi) or foam (Fo) surface and eyes open (EO) or eyes closed (EC) conditions for muscles controlling the knee. A ratio was calculated to represent the strength of simultaneous agonist-antagonist contraction. This value was utilized for between-group comparisons and to examine relationships with CoP data.

## RESULTS AND DISCUSSION

Ten children participated in this study. Five children comprised the ITW group (3 male and 2 female; mean age=8.73 years, range 5.92-11.08); 5 age- and gender-matched children comprised the control group (mean age=8.42 years, range 5.67-10.08).

The ITW group demonstrated consistently lower RF and BF activation under all sensory conditions (Table 1). These between-group differences in muscle activation did not meet statistical significance with the exception of BF activation under eyes-closed conditions, showing significantly greater activation of the BF in the control group (Table 1). While activation levels of RF and BF were lower in the ITW group than in the CG under all conditions, RF:BF ratios were much higher in the ITW group.

A comparison of CoP<sub>AP</sub> showed more posterior positioning in the ITW group under all conditions (Table 2); this difference met a level of statistical significance for the FoEC condition alone. As a single group (N=10), there was a negative, high, and significant correlation found between the ratio of RF:BF activation and CoP<sub>AP</sub> positioning under the conditions of FiEO, FoEO, and FoEC; the correlation approached significance under the FiEC condition (Table 3). By group, these correlations were strong for the ITW, but did not meet statistical significance; correlations were much weaker for the CG than for the ITW group (Table 3).

## CONCLUSIONS

A general trend was observed in both groups in which quadriceps activation decreased and hamstring activation increased as sensory conditions become more complex. A trend was also observed in both groups in which CoP position shifted more posteriorly as sensory conditions become more complex. Under all conditions, ITW mean CoP was more posteriorly positioned than CG CoP. The more anteriorly positioned CG showed a more balanced pairing of quadriceps and hamstring muscle activation. In contrast, the ITW group recruited a

greater balance of quadriceps activity in response to a more posteriorly positioned CoP. Because these values capture a 10-second composite timeframe, it is possible that the quadriceps were being called on during the 10-second capture to react to backward sway as the feet were required to maintain a foot-flat position in stance. The reduced levels of activation in comparison to the CG may be explained by compensatory strategies that relied more heavily on control at the ankle or hip for additional postural control.

While these findings are individual rather than group-specific, they suggest insight into the way children utilize musculature at the knee for postural control under a variety of surface and sensory conditions.

## REFERENCES

1. Sala DA, Shulman LH, Kennedy RF, Grant AD, Chu ML. Idiopathic toe-walking: a review. *Dev Med Child Neurol.* 1999;41(12):846-848.
2. Oetgen ME, Peden S. Idiopathic toe walking. *J Am Acad Orthop Surg.* 2012;20(5):292-300.
3. Houx L, Lempereur M, Remy-Neris O, Gross R, Brochard S. Changes in muscle activity in typically developing children walking with unilaterally induced equinus. *Clin Biomech.* 2014;29(10):1116-1124.
4. Horak FB, Nashner LM. Central programming of postural movements: adaptation to altered support-surface configurations. *J Neurophysiol.* 1986;55(6):1369-1381.

**Table 1.** Mean 10-second EMG Activity: Muscles Controlling the Knee

	Rectus Femoris (RF)			Biceps Femoris (BF)			RF:BF Ratio		
	Mean, SD		P	Mean, SD		P	Mean, SD		P
	ITW	CG		ITW	CG		ITW	CG	
<b>FiEO</b>	9.81, 5.20	10.00, 7.40	.777	6.47, 4.03	9.27, 1.32	.177	2.68, 2.56	1.15, .66	.257
<b>FiEC</b>	9.56, 4.69	11.69, 6.82	.582	6.20, 2.58	10.48, 2.38	.026 <sup>a</sup>	2.03, 1.85	1.15, .68	.349
<b>FoEO</b>	9.37, 4.86	11.07, 6.88	.663	5.15, 3.34	9.89, 3.86	.072	2.94, 2.59	1.38, 1.13	.266
<b>FoEC</b>	8.10, 2.28	11.19, 7.10	.380	4.62, 2.44	10.29, 4.38	.043 <sup>a</sup>	2.74, 2.41	1.35, 1.17	.291

<sup>a</sup>P < 0.05

**Table 2.** Mean 10-second Center of Pressure<sup>a</sup> (CoP<sub>AP</sub>) by Surface-Sensory Condition

	CoP <sub>AP</sub> (2-Trial Mean, SD)		P
	ITW	CG	
	<b>Firm Surface x Eyes Open (FiEO)</b>	0.0323, 0.0147	
<b>Firm Surface x Eyes Closed (FiEC)</b>	0.0270, 0.0176	0.0514, 0.0180	.062 <sup>b</sup>
<b>Foam Surface x Eyes Open (FoEO)</b>	0.0083, 0.0294	0.0386, 0.0090	.059 <sup>b</sup>
<b>Foam Surface x Eyes Closed (FoEC)</b>	0.0079, 0.0297	0.0409, 0.0111	.050 <sup>b</sup>

Note:<sup>a</sup>mean position of subject's CoP in the anterior-posterior direction over 10 seconds during quiet stance, higher values represent more anteriorly positioned CoP; <sup>b</sup>approaches significance

**Table 3.** Mean 10-second Center of Pressure<sup>a</sup> (CoP<sub>AP</sub>) vs. Rectus Femoris:Biceps Femoris Activity Ratio

	Full Sample (N = 10)		ITW (n = 5)		CG (n = 5)	
	r	P	r	P	r	P
<b>Firm Surface x Eyes Open (FiEO)</b>	-.684	.029 <sup>b</sup>	-.971	.006 <sup>a</sup>	-.160	.797
<b>Firm Surface x Eyes Closed (FiEC)</b>	-.735	.015 <sup>b</sup>	-.697	.190	.194	.754
<b>Foam Surface x Eyes Open (FoEO)</b>	-.808	.005 <sup>b</sup>	-.708	.181	-.478	.416
<b>Foam Surface x Eyes Closed (FoEC)</b>	-.508	.134	-.708	.181	-.478	.416

Note:<sup>a</sup>mean position of subject's CoP in the anterior-posterior direction over 10 seconds during quiet stance, higher values represent more anteriorly positioned CoP; <sup>b</sup>P < 0.05

# Ponseti v. Posteromedial Release: Asymmetry of Foot Pressures in Children with Unilateral Clubfoot

<sup>1,2</sup>Juanita Wallace, <sup>1,2</sup>Hank White, <sup>1</sup>Sam Augsburger, <sup>1,2</sup>Henry Iwinski, and <sup>1,2</sup>Janet Walker

<sup>1</sup>Shriners Hospitals for Children – Lexington, KY, USA

<sup>2</sup>University of Kentucky, Lexington, KY, USA

email: jjwa234@uky.edu

## INTRODUCTION

Foot loading can be asymmetric between the left and right sides at the onset of independent walking until up to 3-4 years of age [1]. As children mature, symmetry improves due to increased postural stability and motor control [1]. However, previous research has found that for children with unilateral clubfoot, the unaffected side is not normal and displays differences from typically developing feet [2, 3]. In addition, different treatment methods, Ponseti versus comprehensive releases, have been found to produce different outcomes in children with clubfoot (with Ponseti treatment resulting in a more favorable outcome) [4-6]. To date no study has assessed the foot asymmetry between children with unilateral clubfeet that were treated with Ponseti casting versus those treated with posterior medial release (PMR).

## METHODS

Children with unilateral clubfoot treated with Ponseti (N=40) and with PMR (N=40) were retrospectively reviewed for this study. Subjects were age and height matched, but weight was unable to be matched (Table 1). Foot pressure analysis parameters for a 10 area .prc mask [7] was analyzed using the emed® X (Novel Incorporated, Munich, Germany). The areas masks include the total foot, hallux, second toe, third-fifth toes, first metatarsal, second metatarsal, third-fifth metatarsal, medial midfoot, lateral midfoot, medial hindfoot and lateral hindfoot. Parameters analyzed included force time integral (FTI), pressure time integral (PTI), maximum force (MF), mean pressure (MP), contact time (CT), contact area (CA), peak pressure (PP), heel width (HW), forefoot width (FFW), midfoot width (MFW), foot length (FL), medial contact area (MCA) and lateral contact area (LCA).

With the areas and parameters combined there were 82 data points per foot for the final analysis.

The Asymmetry Index (ASI) was used to assess differences between the unaffected and affected side parameters. ASI is defined as

$$ASI = \left| \frac{2(X_U - X_A)}{X_U + X_A} \right| \times 100\%$$

where an ASI of 0 is perfect symmetry [8]. The  $X_U$  and  $X_A$  are the same parameter for the unaffected and the affected sides respectively. Previous research on the ASI has found that an ASI value of  $\leq 10\%$  is acceptable [8].

## RESULTS AND DISCUSSION

The weight of the Ponseti group was significantly larger than that of the PMR group; therefore FTI and MF were calculated as a percent of bodyweight before the ASI was calculated. ASI results show that out of 82 parameters the Ponseti group met  $\leq 10\%$  acceptability in 9/82 (10.9%) parameters and the PMR group met acceptability in 4/82 (4.9%) parameters (Table 2). The remaining parameters had ASI values ranging from 13-87% for the Ponseti group and 11-103% for the PMR group.

There were 20 parameters of the 10 area .prc mask that were significantly different between the Ponseti and PMR treatment groups. For all of these parameters, the Ponseti group demonstrated a lower ASI value (Table 2). Of these variables, 15 were located on the medial side of the foot print. This indicates that there is significantly less asymmetry on the medial side of the foot for the Ponseti group compared to the PMR group ( $p < 0.05$ ).

Both groups demonstrated acceptable symmetry for the total foot print for MF, FFW and FL. When assessing symmetry in masked areas of the foot, only the CT of metatarsals 3-5 reported acceptable symmetry for both groups. The Ponseti group reported acceptable symmetry for CA (total foot,

medial hindfoot, lateral hindfoot), LCA and for MP of the total foot. Previous research has shown that data from the total foot alone does not give a complete picture of the forces affecting the foot when walking [9]. Therefore, for clinicians it is more beneficial to examine pressure under specific regions of the foot instead of the total foot[10]. Results of this study show that if symmetry analysis is only conducted on the total foot print, differences between the Ponseti and PMR treatment groups are not as readily apparent. Therefore, it is recommended that symmetry analysis for children with clubfeet be assessed in specific regions of the foot.

The data in this study reports AIS ranges that exceed those previously found in typically developing children [8] (Table 3). This would indicate that even after surgery, children with unilateral clubfeet do not achieve symmetry that is equal to their able bodied peers. However, these results would support previous assertions that Ponseti treated clubfeet have more favorable outcomes [4-6], due to the Ponseti group reporting double the number of variables with acceptable symmetry and with the ASI values for the 22 variables reported in Table 2 being significantly smaller in the Ponseti group.

## CONCLUSION

The results of this study demonstrate that the Ponseti method was more successful at producing acceptable symmetry of foot pressure variables under specific regions of the foot than clubfeet treated with PMR.

## REFERENCES

1. Bosch, K. Gait and Posture, 2010. **32**: p. 564-571.
2. Cooper, A. Gait and Posture, 2014. **40**: p. 375-380.
3. Favre, P. J Pediatr Orthop, 2007. **27**(1): p. 54-59.
4. Church, C. J Child Orthop, 2012. **6**: p. 51-59.
5. Inam, M. Journal of Surgery Pakistan (International), 2012. **17**(1): p. 109-111.
6. Lykissas, M. World J Orthop, 2013. **4**(3): p. 144-153.
7. Novelgmbh, *Welcome to novel-projects*. 24 ed. 2014, Munich.
8. Bosch, K. Gait and Posture, 2010. **32**: p. 464-458.
9. Hayafune, N. The Foot, 1999. **9**: p. 88-92.
10. Stebbins, J. Gait and Posture, 2005. **22**: p. 372-376.

Table 1. Demographics

	Age (years)	Height (cm)	Weight (kg)*
Ponseti (N=40)	10.84 (0.40)	145.76 (7.39)	51.65 (17.36)
PMR (N=40)	10.90 (0.60)	145.84 (7.48)	43.20 (12.41)

\*Significantly different at p<0.01

Table 2. ASI ≤10% and Significantly Different Parameters (p<0.05)

	PMR	Ponseti	p-value
MF Total	9.98 (7.67)	7.06 (6.23)	0.07
MP Total	10.54 (8.56)	9.88 (7.76)	0.72
CT Metatarsals 3-5	8.83 (14.24)	5.81 (3.50)	0.20
CA Total	13.33 (11.90)	7.43 (6.40)	<b>0.01</b>
CA Medial Hindfoot	13.00 (24.63)	6.87 (7.15)	0.13
CA Lateral Hindfoot	12.82 (20.46)	7.83 (6.81)	0.15
LCA	11.56 (10.57)	9.82 (8.11)	0.41
FFW	9.84 (12.19)	8.31 (6.18)	0.48
FL	8.96 (5.65)	6.24 (4.02)	<b>0.02</b>
PTI Medial Hindfoot	61.25 (44.75)	38.66 (35.34)	<b>0.01</b>
PTI Lateral Hindfoot	55.71 (43.97)	36.05 (31.73)	<b>0.02</b>
PTI Metatarsal 1	81.72 (50.55)	58.56 (45.31)	<b>0.03</b>
PTI Metatarsal 2	57.80 (42.97)	39.98 (27.52)	<b>0.03</b>
PTI Metatarsal 3-5	48.17 (36.46)	33.40 (23.49)	<b>0.03</b>
PTI 2nd Toe	66.39 (49.35)	47.66 (34.56)	<b>0.05</b>
FTI Medial Hindfoot	59.75 (43.99)	38.59 (33.75)	<b>0.02</b>
FTI Metatarsal 2	69.89 (47.23)	41.29 (35.80)	<b>&lt;0.01</b>
FTI Metatarsals 3-5	49.31 (40.52)	33.99 (28.03)	<b>0.05</b>
MF Medial Hindfoot	42.41 (36.55)	27.37 (21.01)	<b>0.03</b>
MF Metatarsal 2	52.56 (37.34)	28.86 (25.59)	<b>&lt;0.01</b>
MP Medial Hindfoot	37.29 (33.11)	28.27 (20.54)	<b>0.05</b>
MP Metatarsal 2	36.50 (29.79)	22.91 (22.26)	<b>0.02</b>
CT 2nd Toe	43.85 (44.84)	28.52 (20.20)	<b>0.05</b>
CA Metatarsal 2	26.44 (20.89)	13.82 (12.68)	<b>&lt;0.01</b>
PP Medial Midfoot	54.05 (46.27)	35.45 (23.70)	<b>0.04</b>
PP Lateral Midfoot	58.98 (44.59)	39.10 (28.54)	<b>0.02</b>
PP Metatarsal 2	48.26 (39.19)	28.72 (27.36)	<b>0.01</b>
PP Metatarsal 3-5	46.42 (36.34)	32.00 (23.63)	<b>0.04</b>
MCA	19.49 (18.85)	10.23 (9.19)	<b>0.01</b>

Bold Variables are p-value < 0.05.

Red Variables are ASI ≤10%

Table 3. Asymmetry Ranges (%) for all parameters and all areas.

	Ponseti	PMR	Typically Developing*
CA	6-74	12-72	<5
PP	28-68	37-65	13-20
FTI	10-100	10-87	5-14
MaxF	7-77	10-86	4-12
CT	7-54	7-47	5-15

\* Bosch & Rosenbaum (2010)

# THE EFFECT OF PROLONGED ACTIVITY AND LOWER LIMB TRAUMA ON VARIABLE TERRAIN WALKING STABILITY

<sup>1</sup>Riley Sheehan, <sup>1,2</sup>Christopher Rábago, <sup>1</sup>Kelly Ohm, and <sup>1,2</sup>Jason Wilken

<sup>1</sup>Center for the Intrepid, Brooke Army Medical Center, JBSA Ft. Sam Houston, TX, USA

<sup>2</sup>Extremity Trauma and Amputation Center of Excellence, JBSA Ft. Sam Houston, TX, USA  
email: riley.c.sheehan.ctr@mail.mil

## INTRODUCTION

Lower limb trauma (LLT) impairs walking stability, especially on variable terrain [1]. Additionally, prolonged activity and load carriage may also impair stability [2]. Military service members are often required to navigate varied terrain for extended periods while carrying loads. In order to maintain military readiness and potentially return to duty, wounded service members must be able to perform these tasks while maintaining stability, avoiding falls which could further injure them. The range of whole-body angular momentum (H) has been used to quantify dynamic stability in various populations and walking conditions with a greater range indicating greater instability [1,3]. We hypothesized that when walking over variable terrain under load carriage, both the frontal and sagittal plane H would: 1) increase with distance walked for both groups, 2) be greater for individuals with LLT than able-bodied controls (AB), and 3) increase with distance at a faster rate for LLT than AB.

## METHODS

Twelve individuals with LLT wearing a custom carbon fiber ankle foot orthosis (1F/11M, 31±5 years, 1.81±0.09 m, 94.8±10.6 kg) and 14 AB (3F/11M, 29±11 years, 1.76±0.10 m, 75.2±12.7 kg) completed a simulated military patrol in a virtual reality environment (Computer Assisted Rehabilitation Environment, Motekforce Link, Amsterdam, NL). Participants wore a Kevlar vest and helmet and carried a mock M4 rifle. The patrol consisted of 8 blocks, each with sections of steady-state platform positions and variable terrain at 1.4 m/s and a graded portion that increased speed and incline with each block. Participants completed as

many blocks as they were able to before quitting or being told to stop due to excessive pain or fatigue.

During the patrol, we collected full body kinematics using a 24-camera motion capture system (Vicon Motion Systems, Oxford, UK). As our measure of stability, we calculated H in the frontal and sagittal planes for each step from a 13-segment model created using Visual 3D (C-Motion Inc, Germantown, MD). The H values were normalized to Height × Body Mass × Walking Speed and averaged for each block for each participant. We focused our analysis on the more challenging variable terrain sections of each block. In order to analyze the influence of prolonged activity and LLT on walking stability, we used a linear mixed-effects model (MATLAB R2015b, The MathWorks Inc, Natick, MA):

$$H = \beta_D \cdot Distance + \beta_G \cdot Group + \beta_I \cdot (Distance \times Group) + (1|Participant)$$

Where H is the range of angular momentum in the frontal or sagittal plane, Distance is the distance walked by the end of each block, Group is coded as 0 for AB and 1 for individuals with LLT, and (1|Participant) represents a random intercept for each participant.  $\beta_D$ ,  $\beta_G$ , and  $\beta_I$  represent the coefficients for Distance, Group, and the interaction between the two, respectively. A coefficient was considered significant if  $p < 0.05$ .

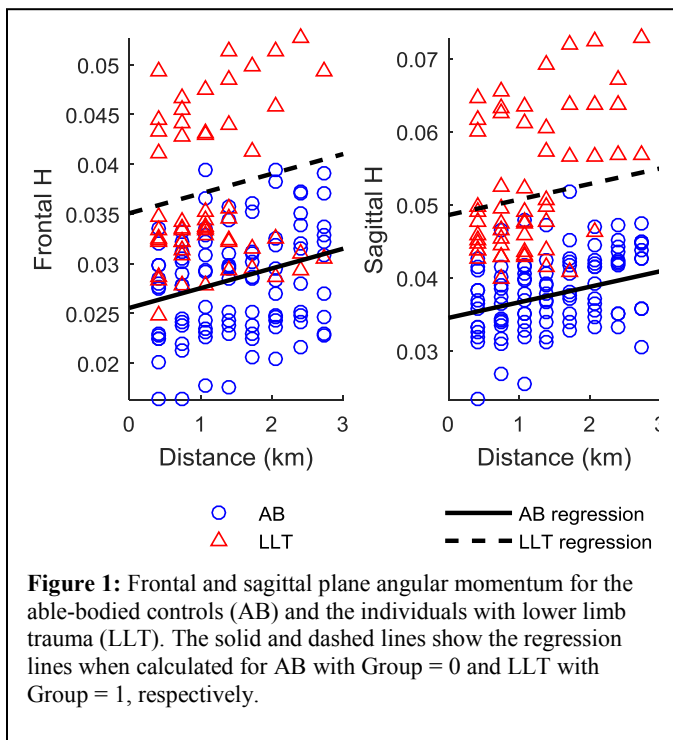
## RESULTS AND DISCUSSION

Overall, the models for both frontal and sagittal plane H had strong fits with adjusted  $R^2$  values over 0.95. Additionally, the coefficients for Distance and Group were significant for both planes, yet the interaction term was not significant (Table 1).

**Table 1:** Values for the linear mixed-effects model coefficients. The Distance coefficient indicates how angular momentum (H) changes with prolonged activity, the Group indicates the baseline difference in H between groups, and the Interaction indicates a difference in the rate at which H changes with distance between the 2 groups. **Bold** coefficients were highly significant with  $p < 0.001$ .

	Distance	Group	Interaction
	$\beta_D$	$\beta_G$	$\beta_{DG}$
Frontal	<b>0.00198</b>	<b>0.00951</b>	-0.00037
Sagittal	<b>0.00213</b>	<b>0.01407</b>	0.00010

In support of our hypothesis, the significant Group effect suggests that individuals with LLT are more unstable than AB when walking over variable terrain. Further, the significant Distance effect indicates that walking stability degrades for both groups following prolonged walking with load carriage. The rate at which walking stability deteriorates appears to be the same for both groups as shown by the lack of a significant interaction effect (Figure 1).



Besides differences in stability, the LLT group also completed fewer blocks on average. As a result, there is a chance that our model is influenced more by the few individuals with LLT that completed all 8 blocks. It is possible that if we had a greater number of participants in the LLT group complete

more blocks, we would have been able to see a difference in the rate of destabilization. Specifically, there may be a point at which stability deteriorates more rapidly in individuals with LLT which may limit task performance. However, task performance by individuals with LLT in this study was primarily limited due to endurance or pain. This means that a stability deficit was likely not the limiting factor for these patients at short distances and that pain and endurance also need to be addressed when returning to occupational tasks.

In a previous study, we found that by exposing an individual with a transfemoral amputation to increasing levels of walking surface pitch and roll oscillations, over time they were able to improve their tolerance, function, and stability [4]. This provides promise that similar interventions may be able to return wounded service members back to comparable levels as their uninjured peers.

## CONCLUSIONS

Although the individuals with LLT started out more unstable, both groups became more unstable at the same rate following prolonged walking over variable terrain. This suggests that if we are able to improve patients' baseline stability, they may be able to achieve the same level of walking stability as uninjured service members, even during long patrols.

## REFERENCES

1. Sheehan RC, et al. *Gait Posture* **41**, 795-800, 2015
2. White SC & Hostler D. *Ergonomics* **22**, 1-9, 2016
3. Herr H & Popovic M. *J Exp Biol* **211**, 467-481, 2008
4. Sheehan RC, et al. *Phys Ther* **96**, 1896-1904, 2016

## ACKNOWLEDGMENTS

Supported by the Center for Rehabilitation Science Research (HU0001-11-1-0004 and HU0001-15-2-0003)

## DISCLAIMER

The view(s) expressed herein are those of the author(s) and do not reflect the official policy or position of Brooke Army Medical Center, the U.S. Army Medical Department, the U.S. Army Office of the Surgeon General, the Department of the Army and Department of Defense or the U.S. Government.

# MOTOR STRATEGY AND LOCOMOTOR ADJUSTMENTS IN CHILDREN WITH AND WITHOUT DOWN SYNDROME WHILE NEGOTIATING STAIRS

Huaqing Liang, Xiang Ke and Jianhua Wu

Georgia State University, Atlanta, Georgia, USA. Email: hliang2@gsu.edu

## INTRODUCTION

Children with Down Syndrome (DS) often show impaired motor control and ability, and walk with a slower speed and a shorter step length compared to typically developing (TD) children [1]. When negotiating an obstacle, children with DS often stop for a longer duration in front of an obstacle before crossing it than their TD peers [2]. When crossing it, children with DS tend to choose a more conservative crawling strategy to reduce the risk of falling [3], and they display a lower toe clearance than TD children [2]. In comparison, stairs negotiation is another setting to study adaptive locomotion in children, but requires moving the center-of-mass up constantly. However, to our knowledge, few studies have been conducted to examine this paradigm in children with and without DS. The purpose of this study was to understand motor strategy and gait adaptation in children with and without DS while transitioning from level surface to stairs.

## METHODS

### *Subjects*

Fourteen children with DS (4M/10F) and fourteen age- and gender-matched TD children (4M/10F) participated in the study. Mean (SD) age of the DS group was 8.6 (1.9) years, height 1.18 (0.11) m, and mass 27.2 (10.4) kg. Mean (SD) age of the TD group was 8.2 (1.9) years, height 1.31 (0.11) m, and mass 29.4 (7.0) kg.

### *Experimental design*

An 8-camera Vicon motion capture system and the Vicon full-body PSIS model was used for data collection. Subjects walked along a 5-meter walkway, and then ascended a three-step staircase. There were three custom wooden staircases with different riser heights: 17cm (LS), 24cm (MS), or 31cm (HS). There were two loading conditions: without ankle load (no load) or with ankle load (ankle load) equaling to 2% of the body weight on each side. There were 6 conditions in total and

subjects completed 5 trials for each condition. The presentation of the conditions was randomized. Subjects were given sufficient rest between conditions.

### *Data analysis*

Motor strategies were categorized as: avoidance, crawling, or walking. If the subject did not ascend the staircase, it was an *avoidance* strategy. When the subject used all four limbs to ascend the staircase, it was a *crawling* strategy. When the subject walked up the staircase, it was a *walking* strategy. The proportion that each strategy was chosen was calculated for each subject under each condition.

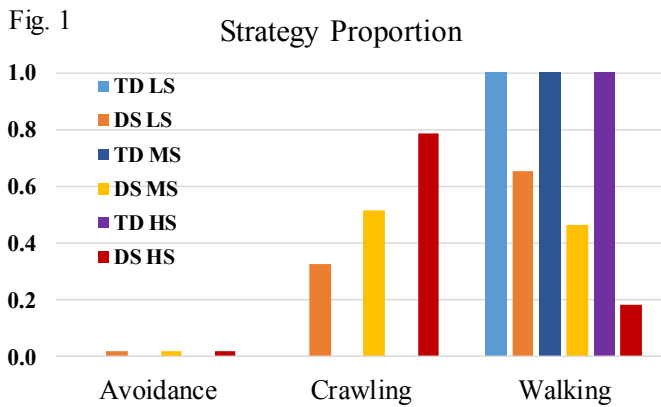
In each trial, the leading foot was defined as the first foot the subject used to ascend the staircase, and the other foot was considered as the trailing foot. The placement of these two feet (i.e., distance between the toe and the staircase) as well as stance time before ascending were calculated for both leading and trailing feet. In addition, vertical toe clearance was calculated as the vertical distance between the toe marker and the height of the stair, and it was only calculated for the trials when subjects used the *walking* strategy. The customized MATLAB program was used for data analysis.

### *Statistical analysis*

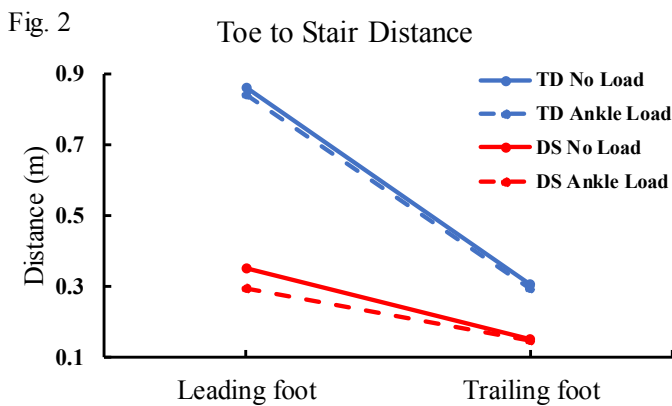
A series of 4-way (group  $\times$  stair  $\times$  load  $\times$  foot) ANOVA with repeated measures were conducted on foot placement, stance time, and toe clearance. Post-hoc pairwise comparisons with Bonforreni adjustments were conducted when appropriate. Statistical significance was set at  $\alpha = 0.05$ .

## RESULTS AND DISCUSSION

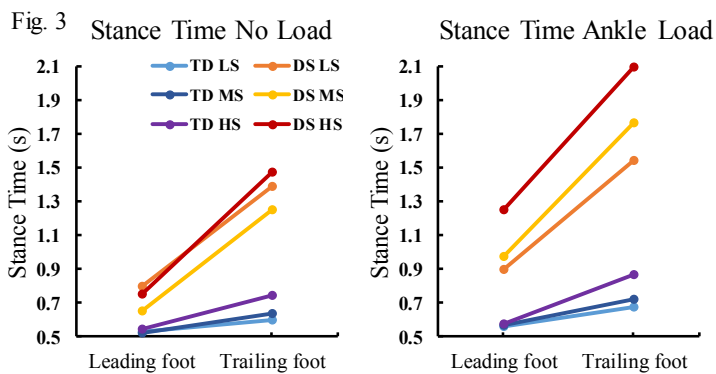
Across the two loading conditions, both groups showed a similar strategy distribution. All the TD subjects walked up the staircase in all conditions (Fig. 1). However, the DS group primarily walked up the stairs in the LS condition but crawled up in the HS condition.



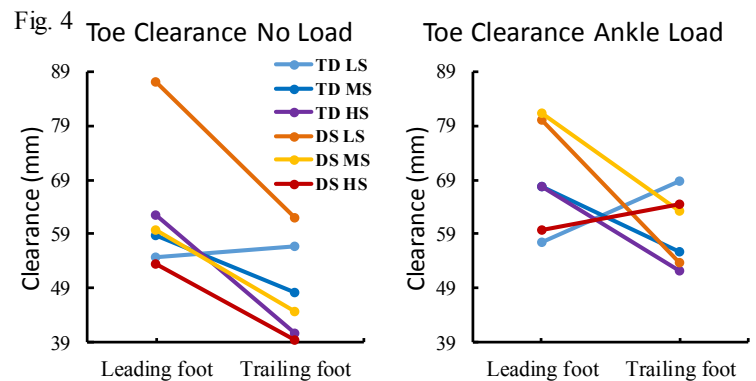
Both groups placed the leading foot further away from the staircase than the trailing foot (Fig. 2). However, the DS group placed both of their feet closer to the stairs than the TD group, and the difference between the placements of the two feet was smaller in the DS group. There was a group by foot interaction and a load by foot interaction (both  $p < 0.05$ ). No effect of stair height was found.



The DS group displayed a longer stance time before negotiating the staircase than the TD group, and both groups showed a longer stance time for the trailing foot than the leading foot (Fig. 3). There was a group



by load, a group by step, and a load by stair interaction (all  $p < 0.05$ ). Post-hoc analysis revealed that stance time was longer in the HS condition than the other two stair-height conditions only with ankle load. Weight appeared to affect only the DS group such that they had longer stance time in MS and HS conditions with ankle load compared to no load.



Both groups generally displayed a higher vertical toe clearance for the leading foot than the trailing foot (Fig. 4). There was a group by load by stair-height interaction, and a group by foot by stair-height interaction (both  $p < 0.05$ ). Without ankle load, the DS group tended to produce a higher toe clearance in the LS condition and a lower toe clearance in the HS condition when compared to the TD group. However, the addition of ankle load resulted in a similar toe clearance between the two groups across three stairs conditions.

## CONCLUSIONS

When ascending stairs, the DS group utilized a conservative *crawling* strategy more often, especially when the stairs were higher. When preparing for the ascent, the DS group placed their feet closer to the stairs, and took longer time in the stance phase than their TD peers. Additionally, the DS group did not show as good adjustments as the TD group in toe clearance when negotiating staircases. All the results suggest that the DS group had limited motor ability when adapting to stairs with different heights.

## REFERENCES

- Galli M, et al. *Gait Posture* **28**, 502-506, 2008.
- Virji-Babul N, et al. *Exp Brain Res* **159**, 487-490, 2004.
- Mulvey G, et al. *Res Q Exerc Sport* **82**, 210-219, 2011

# COORDINATION PATTERNS OF MUSCLE SYNERGIES DURING GAIT IN CEREBRAL PALSY

<sup>1</sup> Katherine M. Steele, <sup>1</sup> Benjamin Shuman, and <sup>2,3</sup> Michael H. Schwartz

<sup>1</sup> University of Washington, Seattle, WA, USA

<sup>2</sup> Gillette Children's Specialty Healthcare, St. Paul, MN, USA

<sup>3</sup> University of Minnesota, Minneapolis, MN, USA

email: kmsteele@uw.edu, web: http://depts.washington.edu/uwsteele

## INTRODUCTION

How individuals with cerebral palsy (CP) and other neurologic injuries recruit and coordinate their muscles to achieve tasks of daily living remains an open question. Muscle synergies provide one method to quantify coordination patterns of multiple muscles during a task [1]. Synergies are calculated from electromyography (EMG) data and identify weighted groups of muscles that are commonly activated together. Among individuals with neurologic injuries, synergies describe greater variance in EMG data compared to unimpaired individuals [2-3], suggesting "simpler" control strategies that may contribute to impaired function.

In CP, synergy complexity is reduced compared to unimpaired individuals during gait and greater reductions are associated with increased functional impairment and worse outcomes after treatment [4]. While synergy complexity provides one measure of impaired motor control, understanding which muscles are activated together in synergies may provide insight into alternative control strategies for locomotion. The aim of this study was to evaluate whether synergy coordination patterns are altered in CP and related to functional ability compared to typically-developing (TD) peers.

## METHODS

We evaluated synergies during gait for 1312 individuals with CP (age: 11.8±7.3 yr, height: 1.3±0.2 m, mass: 36.0±17.3 kg) and 76 TD controls (age: 10.8±3.6 yr, height: 1.4±0.2 m, mass: 40.6±16.4 kg). EMG data was collected over a gait cycle from five muscles: rectus femoris (RF), medial hamstrings (MH), lateral hamstrings (LH), medial gastrocnemius (MG), and anterior tibialis (AT). EMG data was high-pass filtered at 35 Hz,

rectified, low-pass filtered at 10 Hz, and normalized by the maximum value for each muscle [2].

Nonnegative matrix factorization (NNMF) was used to calculate synergies that could explain the greatest variance in EMG data for each individual. Briefly, NNMF identifies the synergy weights ( $W_{m \times n}$ ) and synergy activations ( $C_{n \times t}$ ) for a specified number of synergies ( $n$ ) that minimizes the error:

$$EMG_{m \times t} = W_{m \times n} \cdot C_{n \times t} + \text{error} \quad (1)$$

where  $m$  is the number of muscles and  $t$  is the number of time points. The total variance accounted for (tVAF) by a given number of synergies was calculated as  $1 - \frac{\text{sum of squared error}}{\text{sum of squared EMG data}}$ . K-means cluster analysis was used to identify similar synergies across all individuals. Silhouette analysis was used to identify the number of clusters that best described unique groups of synergies. The silhouette coefficient for a given number of clusters provides a measure of how tightly each cluster is grouped relative to neighboring clusters. For the number of clusters with the maximum silhouette coefficient, we compared the similarity of synergy weights as the average correlation coefficient between the CP and TD groups. Student's t-tests with a Bonferroni correction for multiple comparisons were used to compare tVAF and synergy weights between CP and TD groups.

## RESULTS AND DISCUSSION

Two and three synergies could describe on average 93 and 97% of the variance in EMG data during gait in CP, versus 89 and 96% in TD peers (**Fig. 1**,  $p < 0.001$ ). K-means analysis indicated similar synergy weights between CP and TD groups. For example, in the three-synergy solution ( $n = 3$ ), three clusters provided the most cohesive clusters of synergy

weights, indicating that there were not unique clusters for CP and TD groups.

The average similarity of CP synergy weights and activations to the TD synergies were 0.74 and 0.53, respectively. The gastrocnemius showed the greatest difference in synergy weights, with increased coactivation with other muscles (**Fig. 2**). Individuals with less impairment, as measured by Gross Motor Functional Classification System (GMFCS) Level, had synergies more similar to the TD group. The average similarity of synergy weights and activations were 0.82 and 0.64 for GMFCS Level I and 0.69 and 0.47 for GMFCS Level IV.

## CONCLUSIONS

Individuals with CP did not have distinct patterns of synergy weights during gait compared to TD peers. CP synergies described greater variance in muscle activity and were related to functional impairment in CP, but overall reflect common muscle coordination patterns across diverse gait patterns.

## REFERENCES

1. Tresch MC, et al. *Nature Neuro* **2**, 162-167, 1999.
2. Clark DJ, et al. *J Neurophys* **103**, 844-857, 2010.
3. Cheung VCK, et al. *PNAS* **109**, 14652-6, 2012.

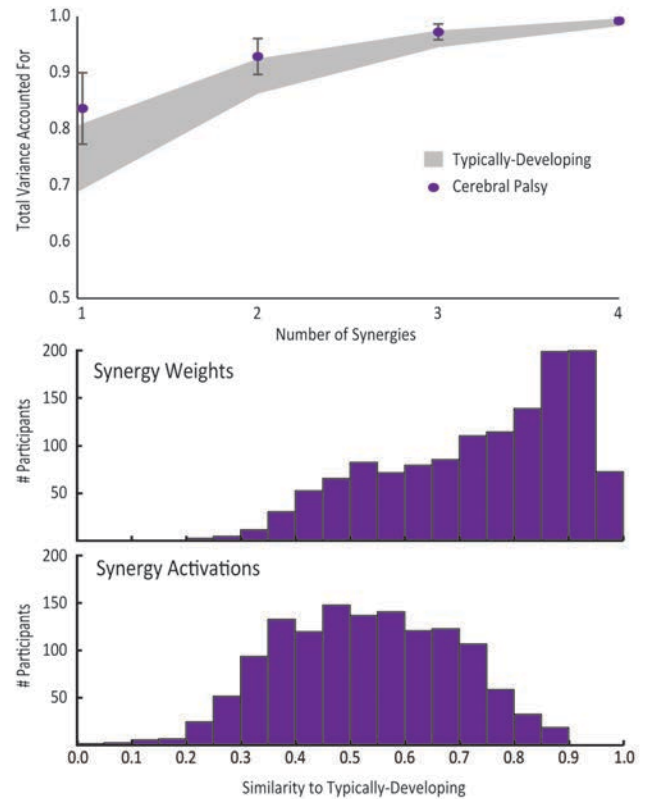


**Figure 1:** Individuals with CP had simplified control (higher tVAF) compared to TD peers. Histograms of similarity of CP synergy weights and activations to TD peers.

## ACKNOWLEDGMENTS

Research supported by NIH NINDS R01NS091056.

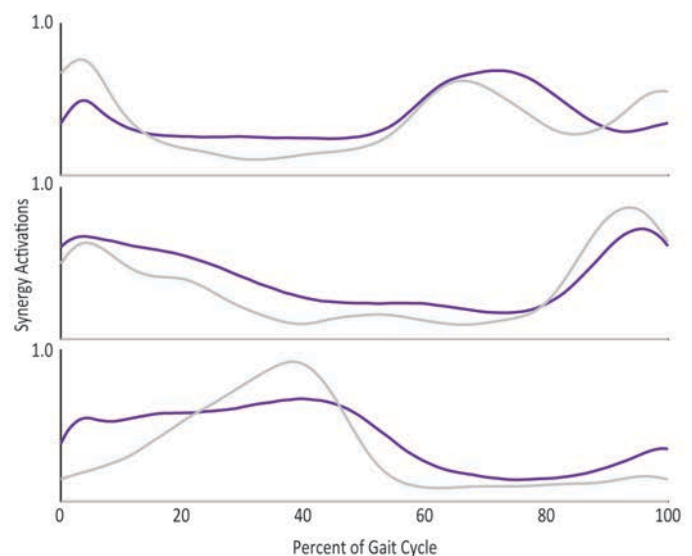
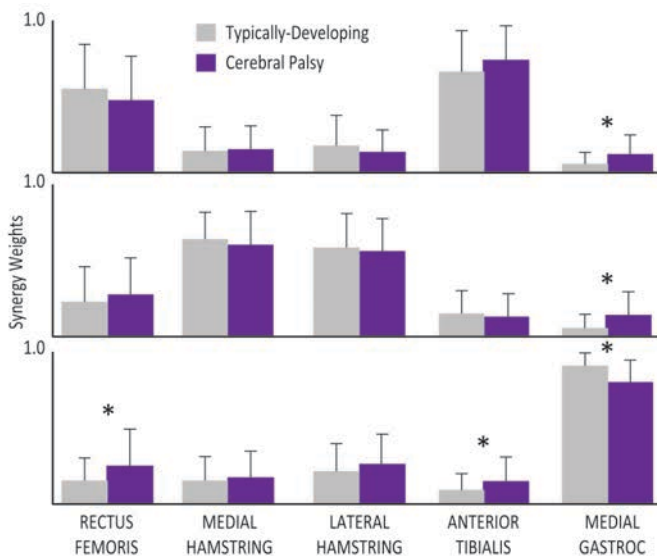


**Figure 2:** Average synergy weights (left) and activations (right) for CP and TD groups. \* indicates a significant difference in synergy weights between CP and TD groups ( $p < 0.003$ ).

# VALIDITY OF USING HEAD MOTION TO DETECT DUAL-TASK GAIT IMBALANCE IN ADOLESCENTS WITH CONCUSSION

Will Pitt and Li-Shan Chou

Department of Human Physiology, University of Oregon, Eugene, OR, USA  
email: [chou@uoregon.edu](mailto:chou@uoregon.edu), web: <http://choulab.uoregon.edu>

## INTRODUCTION

Return to play (RTP) criteria for concussed adolescent athletes vary considerably and are currently based on: time, resolution of subjective symptoms, and normalization of simple balance tasks [1]. Symptom surveys have been shown to normalize within one to two weeks and balance measures can return to baseline in as few as three days. With increasing evidence of long term impairment from repetitive concussive injury, it is essential to institute valid and objective RTP criteria that reliably establish full recovery and reduce risk for successive injury.

Recent investigations of concussion related gait imbalance employ a dual-task paradigm, which combines walking with concurrent cognitive test performance [2]. This line of study has revealed an inability of concussed subjects to control their whole body center of mass (WB COM) as indicated by an excessive medial-lateral (M-L) displacement, faster peak M-L velocity, and slower peak anterior-posterior (A-P) velocity. While these impairments gradually improve over time, they still exist at a significant level as long as two months post injury and, more concerning, worsen when subjects RTP inside of two months [3]. This suggests current RTP criteria may not be sensitive enough to capture lingering deficits in dynamic motor functions, and RTP prior to complete recovery could increase the risk of subsequent injury.

Analysis of the WB COM motion relies on camera-based motion capture technology and requires a whole body retroreflective marker set up. Simplification of the measurement of dual-task gait balance impairment may allow for increased clinical utility and facilitate the application of emerging low cost technologies such as accelerometry. This study

aims to determine if head COM kinematics are able to identifying dual-task gait imbalance previously identified by whole body COM kinematics.

## METHODS

Forty-four high school athletes (8F) were recruited from three local high schools. Twenty-two subjects suffered a concussion in athletics participation were tested within 72 hrs of injury. Concussion diagnosis was made by physicians or athletic trainers [1]. Concussed subjects were matched to healthy controls by sex, height, mass, age, and sport.

Subjects walked at a self-selected pace along a straight walkway under two task conditions: walking only (single-task) and walking while performing a question and answer (dual-task Q&A) battery consisting of spelling a five letter word backwards, or counting backwards by sixes or sevens. Subjects were instructed to look straight ahead at an X placed on the wall during the trial. Data collected from three trials for each condition were used for analysis.

A set of 29 retro-reflective markers were placed on bony landmarks [4]. The head was tracked with five markers: one at the top of each ear, the forehead, back of the head, and on the top of the head such that the plane formed between it and the two ear markers was roughly aligned with the frontal plane. Markers were tracked with a 10-camera motion analysis system, sampling at 60Hz. Marker trajectories were filtered using a low-pass, zero-lag, second-order Butterworth filter with a cutoff frequency of 8Hz. WB COM was calculated as the sum of the weighted masses of 13 body segments. Head COM was defined as the midpoint between the two ear markers.

WB and head COM position data were normalized to one complete gait cycle (heel strike to ipsilateral heel

strike). Total M-L COM displacement was defined as its excursion along the M-L direction. Peak velocities of the COM along the M-L and A-P directions were also identified. Two-way analyses of variance were performed on head COM data for each outcome measure to determine interaction and main effects of group (concussed and control) and condition (single-task and dual-task). Statistical analyses were performed with SPSS version 24 (SPSS Inc., Chicago, IL).

## RESULTS AND DISCUSSION

Concussed subjects were tested at  $2 \pm 0.7$ ,  $8 \pm 1.7$ ,  $17 \pm 3.4$ ,  $31 \pm 4.1$ , and  $59 \pm 3.4$  days after injury. No significant differences were noted between groups for height, mass, or age. Previous statistical analysis of WB COM [2] revealed significant group by task interactions for M-L displacement and peak A-P velocity as well as main effects of group and task for peak M-L velocity.

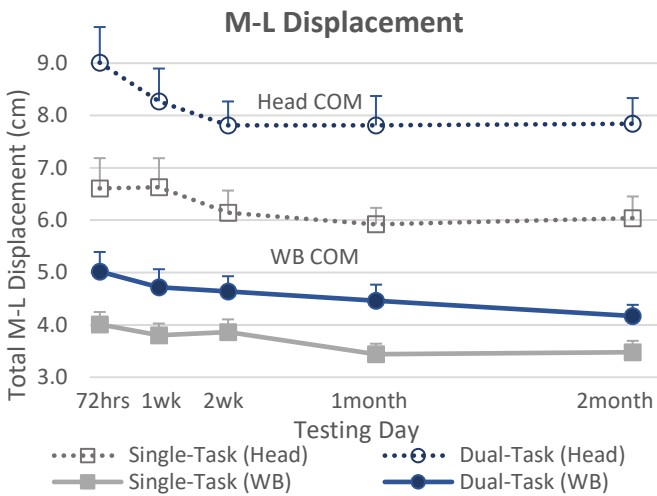


**Figure 1:** Total medial-lateral displacement (mean  $\pm$  SE) of the head and WB COM for concussed subjects during single-task and dual-task conditions

Similar analyses were performed in this study for head COM that did not detect any significant interaction effects for any of the three outcome measures. Further analysis of head peak A-P velocity revealed a significant main effects of group ( $p = .017$ ), however, in repeat analysis with average gait velocity as a covariate, the main effect was reduced to a non-significant level.

Examination of head and WB COM displacements

along the M-L direction revealed similar trajectories through the gait cycle. Head displacement magnitudes were about twice those of the WB, and head trajectory deviations occurred on average 7% sooner than WB deviations (Fig. 2). This suggests the deviation of the head contributes to WB COM M-L displacement rather than being used as a strategy for WB COM stabilization.

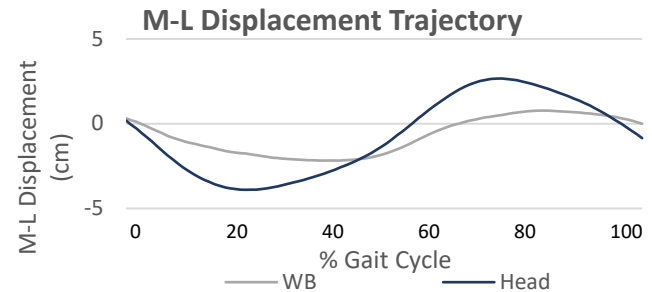


**Figure 2:** Representative plot of the head and WB COM trajectories along the M-L axis.

## CONCLUSIONS

Whole body gait analysis is time consuming and as of now confined to well-equipped gait analysis laboratories. The establishment of head COM kinematics as a sensitive measure of dual-task gait imbalance would facilitate study of this impairment. However, results from this study failed to establish its validity. While the profiles of the head COM data for each of the three outcome measures (Fig. 1) were similar to those of the WB COM, substantial variability in head COM measures likely contributed to the lack of significant effects. The inability to reliably control head orientation without significantly affecting natural movement patterns appears to eliminate the utility of head COM measures in detection of dual-task gait imbalance in concussed individuals.

## REFERENCES

1. McCrory P, et al. *Clin. J. Sport Med.* **19(3)**, 185–200, 2009.
2. Howell DR, et al. *Arch. Phys. Med. Rehabil.* **94(8)**, 1513–1520, 2013
3. Howell DR, et al. *Med. Sci. Sports and Exerc.* **47(4)**, 673–680, 2015.
4. Hahn M and Chou L, *J. of Biomechanics.* **37(6)**, 837–844, 2004.

# EFFECTS OF SURFACE IRREGULARITY ON HEMIPLEGIC GAIT AFTER A NOVEL ROBOTIC 3-D ANKLE TRAINING

<sup>1</sup>Hogene Kim, <sup>1</sup>Ji-Eun Cho, <sup>1</sup>Dohoon Koo, <sup>1</sup>Hwiyoung Lee, <sup>2</sup>Joon-ho Shin, and <sup>1</sup>Sangwoo Cho

<sup>1</sup> National Rehabilitation Center Research Institute, Seoul, South Korea

<sup>2</sup> National Rehabilitation Center Hospital, Seoul, South Korea

email: hogenekim@korea.kr, web: <http://www.nrc.go.kr/nrc/english/>

## INTRODUCTION

Post-stroke hemiparesis is a major source of gait impairments. The kinematic characteristics in such impairments are often described with decreased walking speed and step length, asymmetric joint kinematics, and decreased paretic joint range of motion (ROM) in hip, knee, and ankle joints during gait. Especially the foot drop syndrome, a more ankle extension (plantarflexion) along the talocrural (ankle) axis during mid-swing phase, causes an occasional failure of limb advancements, and increases the trip-related fall risk and fall-related injuries [1].

The reduced ROM at paretic joint in individuals with post-stroke hemiparesis is caused by the increased resistance during passive dorsiflexion. The continuous passive motion for paretic joints helps to increase passive joint ROM by decreasing lower limb joint stiffness, and, in turn, increase gait speed [2].



Figure 1. Ankle Movement Trainer

Ankle Movement Trainer (AMT) was developed to provide 3-D isokinetic ankle movements along talocrural and subtalar axes while seated (Figure1). Ankle joint is defined along 3 orthogonal axes as International Society of Biomechanics recommended for the movement coordinate system [3]. However the subtalar joint is naturally 42 degree tilted on average in sagittal plane [4,5]. The AMT was designed to move along the tilted subtalar joint axis during inversion/eversion.

The objective of this study is that the 3-D isokinetic passive ankle movement training using AMT is effective to improve gait symmetry and walking speed for the individuals with chronic post-stroke hemiparesis. To evaluate the effectiveness of AMT ankle intervention program, we evaluate gait kinematics measured while walking on even and uneven surface, which represents real environment rather than lab environment that provides accurate effects of the developed AMT intervention program.

## METHODS

Total 15 patients with post-stroke hemiparesis (6 females, age:  $64.9 \pm 9.0$  yrs, duration:  $9.5 \pm 5.6$  yrs) were recruited for this study. This study was approved by the NRC Institutional Review Board and all participants signed written informed consent form before the study (NRC2015-03-020).

The AMT exercise program consists of total 12 sessions (four week three sessions per a week) about 30 minutes per a session. A session consists of 20 repetitions of two simple movements (20 dorsi-/plantar flexion; 20 inversion/eversion) and 40 repetitions of two constrained movements (40 Dorsi-flexed Inversion/Eversion; 40 Everted Dorsi-/Plantar flexion).

For gait trials, subjects wore a full-body safety harness. Gait performances were recorded at 100Hz while walking on 10m even and uneven surface total eight times respectively. The even surface was a flat walkway covering with industrial carpet and the uneven surface was fully scattered with wooden triangular pieces with randomized length from 5 cm to 15cm on the flat surface, which was covered with 10m x 1.5m industrial carpet. The kinematic symmetry was evaluated by comparing between paretic and non-paretic kinematics. Walking performances of Pre- and Post- AMT trainings were compared with paired-sample t-test (Significance level:  $p < 0.05$ ).

**Table 1:** Comparison between pre- and post- AMT training in joint kinematics of paretic limbs while walking on even and uneven surfaces (\* is  $p < 0.05$ )

Paretic ROM (deg) (N=15)		Pre-AMT	Post-AMT	P
Even	Hip	29.9 ± 9.7	33.5 ± 8.4	.097
	Knee	40.7 ± 11.3	42.0 ± 12.4	.692
	Ankle	17.0 ± 6.1	18.6 ± 6.1	.316
Uneven	Hip*	23.2 ± 11.4	29.0 ± 9.9	<b>.013</b>
	Knee*	29.7 ± 16.8	35.4 ± 15.3	<b>.034</b>
	Ankle*	12.4 ± 7.1	15.1 ± 7.9	<b>.034</b>

## RESULTS AND DISCUSSION

All subjects successfully participated in 12 AMT training sessions and two pre- and post-AMT training gait evaluations on even and uneven surface.

Table 1 and 2 show the joint and step kinematics while walking on even and uneven surface,

**Table 2:** Comparison between paretic and non-paretic step kinematics while walking on uneven surface and between pre- and post- AMT training (WS: walking speed, SL: step length; SW: step width, ST: step time)

		Paretic Side					Non-paretic Side				
		Pre-AMT		Post-AMT		p	Pre-AMT		Post-AMT		p
		Mean	SD	Mean	SD		Mean	SD	Mean	SD	
Even Surface	WS (cm/s)	39.0	18.9	40.4	17.8	0.440	52.6	24.0	58.1	21.5	0.100
	SL(cm)	29.8	10.8	31.9	9.2	0.059	31.4	11.2	32.9	9.9	0.375
	SW(cm)	16.7	5.2	17.1	5.0	0.390	17.6	5.1	18.0	4.6	0.509
	ST(ms)	840.3	167.5	837.2	143.5	0.866	565.9	274.4	563.3	175.9	0.967
Uneven Surface	WS (cm/s)*	<b>25.7</b>	17.0	<b>32.0</b>	17.8	<b>0.017</b>	35.9	22.6	40.4	24.6	0.101
	SL(cm)*	<b>21.4</b>	10.9	<b>24.3</b>	10.8	<b>0.009</b>	25.0	10.6	26.7	10.8	0.128
	SW (cm)	20.2	6.4	20.9	7.6	0.658	20.4	6.2	20.8	5.4	0.707
	ST(ms)	904.6	181.8	829.6	194.4	0.614	740.8	278.6	678.4	257.3	0.240

compared between Pre- and Post- AMT trainings. There was significant increase in joint ROM in hip, knee and ankle during walking on uneven surface (Table 1), and there were significant increased walking speed and step length in paretic side after the AMT training (Table 2). However, in joint ROM or step kinematics during walking on even surface between Pre- and Post- AMT trainings, there were no significant kinematic changes.

## CONCLUSIONS

Four week 3-D ankle movement training using the developed AMT is effective to increase walking speed, step length and lower limb joint kinematics while walking on uneven surface in the adults with chronic post-stroke hemiparesis.

## REFERENCES

1. Thilman AF, et al. *J Neurol, Neurosur & Psych* **54(2)**, 134-139, 1991
2. Ver C, et al. *Eur Neurol* **76**, 132-142, 2016.
3. Letter to the editor. *J Biomech*, **35**, 543-548, 2002
4. Manter JT, *Ana Rec*, **80(4)**, 397-410, 1941
5. Jastifer JR et al. *Foot*, **24(4)**, 203-209. 2014

## ACKNOWLEDGMENTS

Translational Research Center for Rehabilitation Robots, Korea National Rehabilitation Center, Ministry of Health & Welfare, Korea (#NRCTR-IN16003, #NRCTR-IN17004).

# COMBINED PELVIC ASSISTANCE FORCE WITH VISUAL FEEDBACK TO IMPROVE GAIT PATTERNS IN INDIVIDUALS WITH POST-STROKE HEMIPARESIS

<sup>1</sup>Chao-Jung Hsu, <sup>1</sup>Janis Kim, <sup>1,2</sup>Ming Wu

<sup>1</sup>Sensor Motor Performance Program, Rehabilitation Institute of Chicago, Chicago, IL, USA

<sup>2</sup>Department of Physical Medicine and Rehabilitation, Northwestern University, Chicago, IL, USA  
email: cjhsu@ricres.org

## INTRODUCTION

As individuals with post-stroke hemiparesis typically demonstrate reduced walking velocity and spatiotemporal gait asymmetry, an important goal of rehabilitation is to improve gait pattern. The asymmetrical gait characteristics are associated with reduced weight shifting toward the paretic leg, which may be a consequence of a “learned nonuse” and can be reversed by forced use of the paretic leg. A recent study has applied the concept of constraint induced movement therapy to force use of the paretic leg and promote weight shift towards the paretic leg [1]. Visual feedback is another approach to enhance motor learning for improving weight shift ability in stroke rehabilitation [2]. Potentially, combined constraint induced movement therapy with visual feedback could have a positive impact on gait patterns in individuals with post-stroke hemiparesis.

The purpose of this study was to examine the effects of combined pelvic assistance force with visual feedback during treadmill walking on over-ground spatiotemporal gait characteristics in individuals with post-stroke hemiparesis. We hypothesized that combined pelvic assistance force with visual feedback would improve over-ground spatiotemporal gait characteristics in individuals with post-stroke hemiparesis. The addition of visual feedback would result in greater improvements when compared to pelvic assistance force only.

## METHODS

A total of 15 subjects (age =  $55.4 \pm 7.0$  years) with hemiparesis due to chronic (> 6 months) stroke participated in the study.

Subjects were asked to walk on the treadmill for 2 test sessions: (1) combined pelvic assistance force with visual feedback (COMBINED) and (2) pelvic assistance force only (PELVIC). The order of 2 test sessions was randomized. Each test session was 15 mins with a 10-min sitting break between sessions. Each test session consisted of 5 sections: 1-min baseline, 7-min training, 1-min post-training (no pelvic assistance force/visual feedback), 1-min standing break, and 5-min training. The treadmill speed of each test session was set at subjects' self-selected comfortable speed. In all sessions, subjects wore an overhead harness for safety, and could use the front handrail for safety.

A mediolateral assistance force was applied to the pelvis toward the paretic leg through a customized cable-driven robotic system to facilitate weight shift [3]. The magnitude of assistance force was set at 9% of body weight, and would be adjusted if subjects could not tolerate. The pelvis and ankle positions were recorded using 4 custom designed 3-dimensional position sensors. The recorded ankle position signals were used to trigger the assistance force applied from initial contact to mid-stance of the paretic leg. A custom-written LabVIEW program was used to collect pelvis and ankle position signals at 500 Hz as well as to command assistance force signals to the motors.

Visual feedback was provided through a computer monitor placing in front of the treadmill that displayed vertical bar graphs corresponding to the subjects' weight bearing on the paretic leg. Weight bearing was monitored with a mobile SmartStep device (Andante Medical Devices). When subjects exceeded the target weight bearing, the vertical bar would go above the horizontal line. The target

weight bearing was displayed as a horizontal line graph on the computer monitor and set was at 120% of weight bearing on the paretic leg during baseline.

Spatiotemporal gait variables were evaluated using a 10-m instrumented pressure mat (GAITRite) before and after each test session. Variables of interests included walking velocity, stance time, single leg support time, stride length and step length. Stance time and single leg support time were normalized to the whole gait cycle time (% gait cycle).

Paired-sample t-tests were used to compare: 1) before and after spatiotemporal gait variables within the COMBINED and PELVIC, and 2) change in spatiotemporal gait variables between the COMBINED and PELVIC. Change in spatiotemporal gait variables was computed as  $[(after - before)/before] * 100$ .

## RESULTS AND DISCUSSION

Overground single leg support time ( $p=0.01$ ), stride length ( $p=0.01$ ) and step length ( $p<0.01$ ) significantly improved after the COMBINED (Table 1). Overground walking velocity ( $p=0.02$ ) and step length ( $p=0.01$ ) significantly improved after the PELVIC (Table 1). However, the change in spatiotemporal gait characteristics (velocity,  $p=0.70$ ; stance time,  $p=0.17$ ; single leg support time,  $p=0.47$ ; stride length,  $p=0.30$ ; step length,  $p=0.36$ ) was not significantly different between the COMBINED and PELVIC (Table 1).

Combined pelvic assistance force with visual feedback may facilitate weight shifting toward the paretic leg during stance that might increase paretic leg loading. Increased loading enhanced activation of load-sensitive afferents, which inhibited the initiation of swing and prolonged the duration of single leg support time. Increased loading might also enhance paretic leg hip extension. With the movement of treadmill belt, paretic leg was pulled into more hip extension that resulted in a stretch of hip flexor. The stretch response may induce paretic leg stride forward thus increase the stride and step length.

## CONCLUSIONS

Combined pelvic assistance force with visual feedback improved single leg support time, stride length and step length of the paretic leg in individuals with post-stroke hemiparesis. The addition of visual feedback did not result in greater improvements when compared to pelvic assistance force only. Spatiotemporal gait characteristics after stroke can be improved by applying additional pelvic assistance force and/or visual feedback about weight bearing.

## REFERENCES

1. Aruin AS et al. *Top Stroke Rehabil.* **19**(6),556-63, 2012.
2. Van Vliet PM and Wulf G. *Disabil Rehabil.* **28**(13-14), 831-40, 2006.
3. Wu M, et al. *Gait Posture* 33(2), 256-60, 2011.

**Table 1:** Mean (SD) of spatiotemporal gait variables.

	COMBINED			PELVIC		
	Before	After	Change (%)	Before	After	Change (%)
<b>Walking velocity (m/s)</b>	0.73 ± 0.17	0.76 ± 0.16	5.69±12.90	0.73 ± 0.16	0.77 ± 0.16	6.90 ± 11.08
<b>Stance time (%)</b>	61.34 ± 3.24	61.64 ± 2.81	0.54 ± 2.95	61.42 ± 2.67	60.93 ± 2.89	-0.78 ± 2.67
<b>Single leg support time (%)</b>	26.22 ± 2.87	27.09 ± 3.03	3.40 ± 4.67	25.97 ± 3.10	26.44 ± 3.19	1.98 ± 7.41
<b>Stride length (m)</b>	0.98 ± 0.17	1.03 ± 0.16	5.35 ± 6.98	0.99 ± 0.16	1.02 ± 0.16	3.18 ± 6.12
<b>Step length (m)</b>	0.51 ± 0.08	0.55 ± 0.08	7.46 ± 9.13	0.52 ± 0.08	0.55 ± 0.08	5.42 ± 7.19

# REAL-TIME, AUTONOMOUS TRACKING OF WHOLE-BODY BRADYKINESIA IN PARKINSON'S DISEASE

<sup>1</sup>Roy SH, <sup>2</sup>Shiwani B, <sup>1</sup>Kline JC, <sup>3</sup>Saint-Hilaire MH, <sup>3</sup>Thomas CA, <sup>2</sup>Gennert MA, <sup>1</sup>De Luca G

<sup>1</sup>Delsys, Inc and Altec Inc, Natick, USA

<sup>2</sup>Robotics Engineering Program, Worcester Polytechnic Institute, Worcester, USA

<sup>3</sup>Department of Neurology, Boston University Medical School, Boston, USA

email: [sroy@delsys.com](mailto:sroy@delsys.com), web: <http://www.delsys.com/altec/>

## INTRODUCTION

Sensor-based systems have been used to monitor the motor symptoms of Bradykinesia in Parkinson's disease (PD). But these tool have only been used during scripted activities defined by the Unified Parkinson's Disease Rating Scale (UPDRS), such as repeated finger tapping and opening and closing of the hand [1]. Such approaches lack a complete framework to monitor the full complement of motor symptoms associated with whole-body bradykinesia or track possible fluctuations in severity throughout the day resulting from wearing off [2]. Therefore, we have developed a novel approach to autonomously monitor, in real-time, the symptoms of UPDRS-defined Body Bradykinesia during unconstrained activities of daily living using body-worn sensors and machine learning algorithms.

## METHODS

Patients with mild to moderate Parkinson's disease (n=17, Hoehn & Yahr 1-3) participated in experiments designed to monitor PD motor symptoms during a 3-hour period of unconstrained activities of daily living in a home-like setting. Trigno™ IM wireless sensors (Delsys, Inc. Natick, MA) placed on the distal upper- and lower-limbs of the more symptomatic side of the body were used to record inertial measurement (IMU) and electromyographic (EMG) data. Videos of the subject were recorded and annotated by movement disorder experts to identify activity states and score Body Bradykinesia based on Item 31 of the UPDRS.

We designed a unique algorithm architecture to detect Bradykinetic motor symptoms without a-priori knowledge of movement activities being performed. Because the motor symptoms of Body

Bradykinesia may manifest differently for different activities, we designed a feedforward neural network to autonomously detect walking and non-walking (Figure 1). We tracked Body Bradykinesia separately for these activities by extracting characteristic features of motor symptoms from the recorded IMU-EMG signals. Features of bradykinesia during walking included reduced arm swing, shuffling, reduced cadence, and reduced step length. Features of bradykinesia during non-walking included paucity of movement, reduced amplitude, reduced speed, and hesitancy of movement. Dynamic Neural Network (DNN) algorithms were designed to classify the presence and severity of Body Bradykinesia based on these features. Annotations of the video provided by the clinicians served as the ground truth for assessing accuracy.

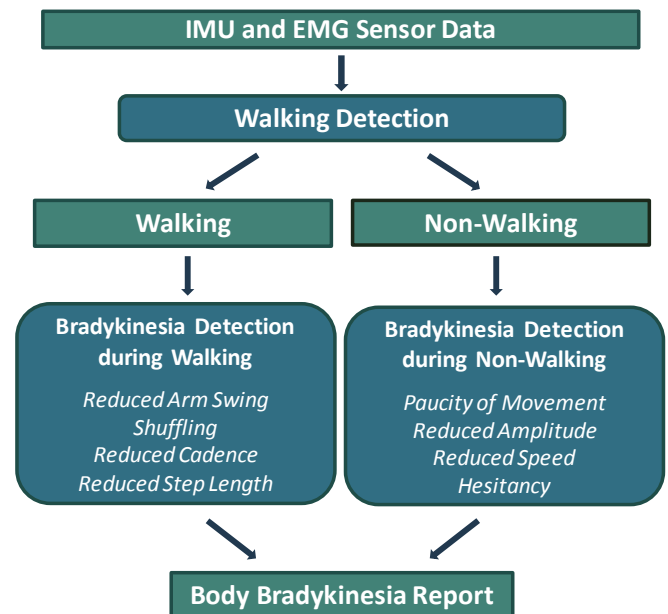


**Figure 1:** Algorithm approach for tracking Body Bradykinesia during unconstrained activities of daily living.

## RESULTS AND DISCUSSION

Our algorithms detected walking and non-walking activities with an accuracy of 99.5% and successfully identified Body Bradykinesia with overall accuracy of 94.6% (Table 1)

Type of activities	Accuracy (%)
Walking	96.7
Non-walking	93.8
Overall	94.6

## CONCLUSIONS

These results demonstrate the first successful sensor-based approach for autonomous monitoring of Body Bradykinesia during activities of daily living. By eliminating the need to perform scripted activities, our approach supports the viability of an ambulatory system that could be used in the home or community to monitor fluctuations of Body Bradykinesia. Similar algorithms are under development for

tracking the full complement of movement disorders associated with PD<sup>3</sup>. When completed, the wearable system will provide comprehensive motor outcome data needed by healthcare providers to better manage medication titration, adjust DBS settings, and establish efficacy for new interventions undergoing clinical trials.

## REFERENCES

1. Kim JW, et al. *Medical & Biological Engineering & Computing*. **49**(3):365-371, 2011.
2. Kubota KJ, et al. *Movement Disorders*. **31**(9):1314-1326, 2016.
3. Roy et al. *Movement Disorders*. **28**(8):1080-1087, 2013.

## ACKNOWLEDGMENTS

Research reported in this abstract was supported in part by the De Luca Foundation and by a grant from the National Institute of Neurological Disorders and Stroke of the National Institutes of Health under award R44NS083098.

# EVALUATING THE PRIMARY GAIT SCREEN AS A MEASURE OF GAIT VELOCITY IN PERSONS WITH MOVEMENT DISORDERS

<sup>1</sup> Abigail C. Schmitt, <sup>2</sup> Chuck E. Jacobson, <sup>2</sup> Michael S. Okun, and <sup>1</sup> Chris J. Hass

<sup>1</sup> University of Florida, Gainesville, FL, USA

<sup>2</sup> University of Florida Center for Movement Disorders and Neurorestoration, Gainesville, FL, USA  
email: a.schmitt@ufl.edu

## INTRODUCTION

Gait performance has received considerable attention in the literature across a variety of clinical populations and age groups. Gait speed is often considered one of the best clinical metrics for assessing movement [1] and is often considered a surrogate for overall morbidity and mortality.

Clinical gait assessments performed overground at a self-selected pace are common, with primary outcomes including gait velocity and spatiotemporal gait characteristics. Typically, several trials of overground gait are collected and outcome metrics are averaged across trials to improve accuracy [1].

In persons with movement disorders there is a need for gait assessments to be more comprehensive as patients often have balance difficulty and trouble with changing direction and initiating and terminating gait. The Primary Gait Screen (PGS) is a new assessment protocol which incorporates gait initiation, turning, and gait termination into the standard overground assessment using the same available space and pressure mat (Fig. 1). To break the assessment into different tasks, the user determines the software processing parameters that work best. The PGS may be a useful assessment to easily capture more comprehensive movement data in clinic in a brief period of time.

However, before the PGS assessment can be accepted we must first test if the gait velocity calculated during PGS is accurate when compared to overground walking. To date, there are no comparisons between simple overground gait assessments at a self-selected pace and the PGS. Thus, the purpose of this study was to determine if the gait velocity calculated during the PGS is an

accurate measure of gait velocity when compared to simple overground walking. Further, we altered processing parameters to determine the most accurate settings to calculate gait velocity.

We hypothesized gait velocity would be faster in the simple self-selected walking trials compared with the PGS trials. Further, we anticipated the most conservative processing of the PGS (i.e., with the greatest cropping) would most closely resemble gait velocity measured during the self-selected walking trials.

## METHODS

Overground gait was assessed in 102 adult patients diagnosed with a movement disorder (47F, 55M; age:  $67 \pm 9$  years). Patients completed a standard protocol on an 8m Zeno Walkway (ProtoKinetics, Havertown, PA) including a single 4x self-selected speed trial (4xSS) and two trials of the Primary Gait Screen, resulting in a total of 4 passes during the PGS. During the 4xSS trial, all patients started 1m before the walkway and turned 1m after the end of the walkway to account for acceleration and deceleration. Further, the first and last 0.6m of the 4xSS trials were excluded to eliminate the first and last steps on the mat for accommodation purposes.

In effort to preserve the clinical applicability of the assessments, the gait velocity data were processed using the Protokinetics PKMAS software. The PGS trials were processed 3 times using 3 different cutoff parameters (1m, 1.5m, 2m). For example, during the 1m cutoff processing, the data from the first meter and last meter of the walkway were ignored in the computation of gait velocity. During the 1.5m cutoff processing, the first and last 1.5m were ignored, resulting in a velocity calculated from the middle 5m

of the walkway. Both trials were processed independently and the resulting gait velocities from the two trials were averaged for each condition.

Paired samples t-tests were used to compare the calculated gait velocities from the PGS cutoffs to the reference group: the 4xSS trial ( $p < .05$ ).

## RESULTS AND DISCUSSION

No significant differences were found in gait velocity between the 4xSS and the computed PGS gait velocities (1m:  $t(101) = 1.157, p = .250$ , Cohen's  $d = 0.037$ ; 1.5m:  $t(101) = -0.951, p = .344$ , Cohen's  $d = -0.029$ ; 2m:  $t(101) = -1.746, p = .084$ , Cohen's  $d = -0.055$ ) (Fig. 2). As evidenced by the very small effect sizes, the mean differences in gait velocity ranged from 0.007 m/s (using 1.5m cutoff) to 0.013 m/s (using 2m cutoff). These differences do not meet the minimally important difference in gait velocity in these populations [2].

These results suggest the PGS may be a useful and accurate clinical assessment of overground walking in persons with movement disorders. To broaden the application of these results, future investigations should expand upon this analysis to look at the gait initiation and gait termination portions of the PGS, in addition to the self-selected gait.

Limitations in this investigation include the diverse sample of patients with varied diagnoses, although

this sample likely represents a realistic cross-section of patients that may be seen in a clinical setting.

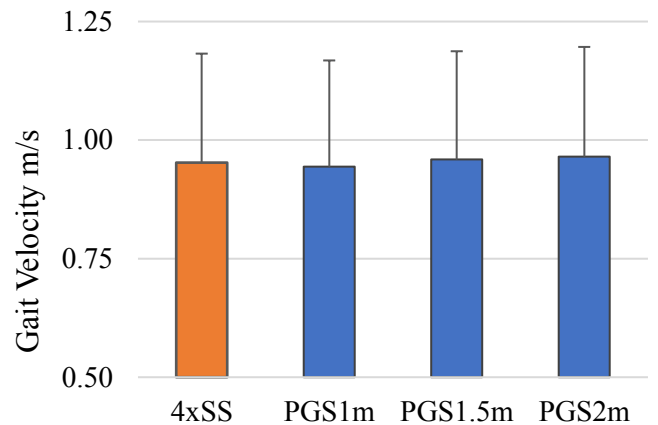


**Figure 2:** Mean and standard deviations of the computed gait velocities for the 4x Self-Selected (4xSS) and Primary Gait Screen (PGS) trials at different cutoff distances.

## CONCLUSIONS

The self-selected walking portion of the Primary Gait Screen does appear to be a good measure of gait velocity in persons with movement disorders.

## REFERENCES

1. Fritz S & Lusardi M. *J Geriatric Phys Ther* **32**, 2, 2009
2. Hass CJ et al. *J Neuro Phys Ther* **38**, 4, 233-238, 2014

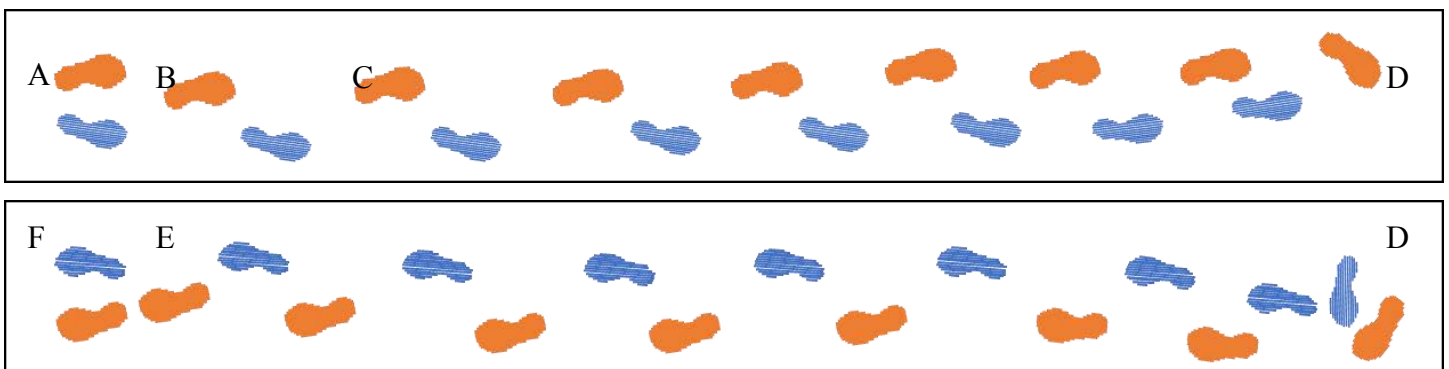


**Figure 1:** Schematic of the Primary Gait Screen (PGS). During the PGS, patients are asked to balance for 10 seconds (A) and initiate gait (B) following an auditory cue (a beep). They are asked to walk at a self-selected pace (C) to the end of the walkway and turn around (D) and walk back to the beginning of the walkway where they should terminate gait (E) and balance for an additional 10 seconds (F).

# OSTEOARTHRITIS INFLUENCES FUNCTIONAL MOBILITY PERFORMANCE IN PATIENTS WITH PARKINSON'S DISEASE

<sup>1</sup> Jaimie A. Roper, <sup>2</sup> Ying He, <sup>1</sup> Samuel Wu, <sup>3</sup> Peter Schmidt, <sup>1,3</sup> Michael S. Okun, <sup>1</sup> Chris J. Hass, and the National Parkinson Foundation Quality Improvement Initiative Investigators

<sup>1</sup> University of Florida, Gainesville, FL, USA

<sup>2</sup> Clarkson University, Potsdam, NY, USA

<sup>3</sup> National Parkinson's Foundation, FL, USA  
email: jaimier@ufl.edu

## INTRODUCTION

Both Parkinson's disease (PD) and osteoarthritis (OA) demonstrate deficits in gait brought about by similar symptoms; stiff joints, slowness, inflexibility, weakness, and a need for assistive devices. Recently, a study by Jones and colleagues [1] reported that arthritis co-occurs in almost 26% of PD patients (n=341). Yet, although similarities in functional impairments exist between the two populations, little is known about the impact of OA on gait impairment in persons with PD. Furthermore, the literature is void of large-scale cohort studies that provide this information.

Understanding the impact of OA on PD is critical to determine the extra burden that OA may contribute to gait impairment in persons with PD and consequently the medical management of these patients. Thus, we sought to understand to what extent OA severity impacts functional mobility performance in patients with PD across time. To investigate this, we evaluated performance times from the Timed Up & Go (TUG) test in patients with PD and OA. Increased OA severity was hypothesized to be predictive of lower functional mobility performance.

## METHODS

We included 4,428 patients with PD from the National Parkinson's Foundation QII database with available timed up and go (TUG) and OA information at baseline and 1-2 years follow-up (9 months to 27 months after baseline) in this analysis. The data were obtained from 16 participating National Parkinson Foundation Centers of

Excellence from within the United States. All participants signed the informed consent.

All evaluations were done in the on medication state. Patients registered in the database between 2009 and 2016 were included. Demographic information of those used in the analysis can be found in table 1.

For the dependent variable, functional mobility, performance was assessed using the TUG test and patients' performance was categorized as either "High" or "Low" functional mobility. High functional mobility performance was defined as performing the TUG in 12 seconds or less [2]. During the TUG test, patients were instructed to stand up from a chair and walk forward at their comfortable speed for 3m, then turn around and walk back to the chair and sit down. The evaluation was timed in seconds from the command, 'go' until the participant made contact sitting in the chair. If the patient could not perform the task without using their hands to push off, they were allowed to perform the test while using their hands or an assistive device to push off the chair. All patients who could not perform the task without using their hands to push off were designated as "Low" functional mobility.

We added sex, age, body mass, and standardized cognition (immediate 5-word recall, verbal fluency, delayed 5-word recall) as covariates to the analysis based on their impact on gait speed and/or their potential to limit mobility [2,3]. To evaluate differences in TUG performance among OA groups we performed a logistic regression while controlling for the pre-specified covariates.

## RESULTS AND DISCUSSION

At baseline 2,538 (57.3%) patients reported no symptoms of OA, 1,047 (23.6%) reported asymptomatic/minimal OA, and 843 (19.1%) reported symptomatic OA (moderate to very severe).

Both the asymptomatic/minimal OA and symptomatic groups had significantly more patients with low functional mobility (TUG>12 seconds), both at baseline (Figure 1). Similar results hold at the 1-2 year follow-up ( $p<0.0001$ ). In addition, there were higher proportion of patients with low functional mobility at follow-up than baseline for all three OA groups, however, the differences among groups in change from baseline to follow-up were not significant ( $p=0.360$ ).

The between group difference remained statistically significant after covariate adjustment with the use of logistic regression. Specifically, at the baseline visit, the odds of having high functional mobility skill for patients with asymptomatic/minimal OA was 1.50 times (95% CI: 1.23-1.84;  $p<0.0001$ ) compared to those with Symptomatic OA; while the odds for patients without OA was 1.71 times (95% CI: 1.43-2.05;  $p<0.0001$ ) compared to those with Symptomatic OA. The between group differences were similar at 1-2 year follow-up, with odds ratio of 1.78 times (95% CI: 1.45-2.19;  $p<0.0001$ ) for those with asymptomatic/minimal OA compared to those with Symptomatic OA; and odds ratio of 1.84 times (95% CI: 1.53-2.04;  $p<0.0001$ ) for those without OA compared to those with Symptomatic OA.

**Table 1:** Sample Demographics

		<b>Total (N=4428)</b>	<b>Absent (N=2538)</b>	<b>Asymptomatic /minimal (N=1047)</b>	<b>Symptomatic (N=843)</b>
<b>Age at first visit (yrs)</b>		66.3±9.6	64.7±10.0	67.9±8.5	68.9±8.8
<b>Age at PD disease onset (yrs)</b>		57.7±11.1	56.3±11.3	59.0±10.5	60.1±10.4
<b>Mass (kg)</b>		79.9±17.9	79.3±17.1	79.7±18.2	82.1±19.7
<b>BMI</b>		27.2±5.7	26.8±5.8	27.2±5.3	28.3±5.8
<b>Male</b>		2881	1763 (69.5%)	632 (60.4%)	486 (57.7%)
<b>Female</b>		1546	775 (30.5%)	414 (39.6%)	357 (42.3%)
<b>Timed Up &amp; Go (seconds)</b>	<i>Baseline</i>	13.2±7.1	11.9±6.3	12.6±6.6	15.1±8.3
	<i>1-2 year follow-up</i>	14.4±7.9	12.9±7.4	13.7±7.4	16.5±9.0

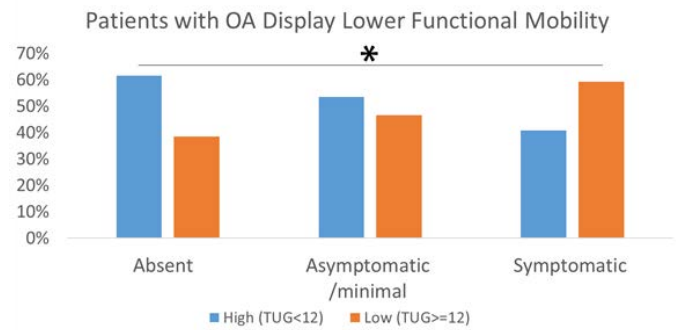


Figure 1. Percentage of patients with high and low functional mobility as measured by the TUG test.

## CONCLUSIONS

This study is one of the first to focus on understanding the influence of osteoarthritis in patients with PD and how this may affect their function and mobility. In summary, functional mobility performance was influenced by OA severity in patients with PD. Specifically, patients with PD who also have a diagnosis of OA have a 1.5-1.8 times increase in risk of displaying low functional mobility. These findings highlight the importance of recognizing the extra burden of OA on functional mobility in patients with PD.

## REFERENCES

1. Jones JD, et al. Parkinsonism Relat Disord **18**, 1073-1078, 2012.
2. Nocera J, et al. *APMR* **94**, 1300-1305, 2013.
3. Yogev-Seligmann G, et al. *Mov Disord*, **23**, 329-342, 2008.

# QUANTIFYING LIMP USING TEMPORAL GAIT VARIABLES

<sup>1</sup>Cherice Hughes-Oliver, <sup>2</sup>Daniel Schmitt, <sup>1</sup>Robin Queen

<sup>1</sup>Department of Biomedical Engineering and Mechanics, Kevin Granata Biomechanics Lab, Virginia Tech, Blacksburg, VA, USA

<sup>2</sup>Department of Evolutionary Anthropology, Duke University, Durham, NC, USA  
email: cnh4ph@vt.edu, web: www.BEAM.vt.edu/granatalab

## INTRODUCTION

Ankle osteoarthritis is a debilitating disease with patients reporting levels of impairment as high as those associated with end-stage kidney diseases, congestive heart failure, and end-stage hip arthritis [1, 2]. There are approximately 50,000 new cases of post-traumatic ankle arthritis reported each year [3]. The ability to quantitatively assess impairment and gait mechanics in clinical settings is challenging. A potential alternative is identifying spatiotemporal variables that are indicative of pathology that can be effectively assessed in the clinic.

The objective of this study was to investigate a clinically-accessible method of identifying gait asymmetries (“limp”) and other changes in patient gait associated with ankle osteoarthritis. We predicted that there would be differences in swing and stance time between affected and unaffected limbs. Sex-specific effects were also investigated to account for sex-based differences, allowing for correction of treatment disparities.

## METHODS

This is a secondary analysis of prospectively collected data on a group of 242 (110 men, 132 women) end-stage ankle OA patients. Only those subjects that have isolated unilateral involvement, no contralateral pain, and no rheumatoid arthritis diagnosis were included (Table 1).

Each subject completed at least four self-selected speed walking trials using an eight-camera motion capture system (Motion Analysis Corporation, Santa Rosa, CA; 120Hz). Heel-strike and toe-off timings were exported from Visual3D after ensuring strike patterns had been correctly identified. Four temporal variables were calculated using a custom Matlab script: stride time, swing time, stance time, and

double support time. Stride, swing, and stance time were defined as heel-strike to heel-strike, toe-off to heel-strike, and heel-strike to toe-off on a single limb, respectively. Left double support time was defined as left heel-strike to right toe-off, and right double support time was defined as right heel-strike to left toe-off. Each temporal variable was averaged across steps for a single trial and then across trials for each subject, and for each limb. Steps per trial and trials per subject both varied between subjects.

An ANCOVA comparing sex and limb (affected and unaffected) while co-varying for average walking speed was run for each variable using JMP Pro 13. All 2-way and 3-way interactions between sex, limb, and walking speed were also examined. An alpha level of 0.05 was used for all analysis.

## RESULTS AND DISCUSSION

No significant 3-way interactions were seen, but several 2-way interactions were significant. (Fig 1). Among the main effect differences, sex-specific effects were seen with men having higher stride, swing, and stance times than women (Fig 1). Limb-specific effects were also seen: swing time was higher on the affected limb and stance time was higher on the unaffected limb. The increase in swing time and decrease in stance time on the affected limb was an expected outcome and may function as a compensatory pattern due to ankle pain on the affected limb.

Effects of walking speed were seen in stride, stance, and double support times but not in swing time. Effects of walking speed on the study variables was sex-dependent for all variables and limb-dependent for all variables except for stride time.

High coefficients of variation, which ranged from 11.6% to 48%, were seen in all study variables and

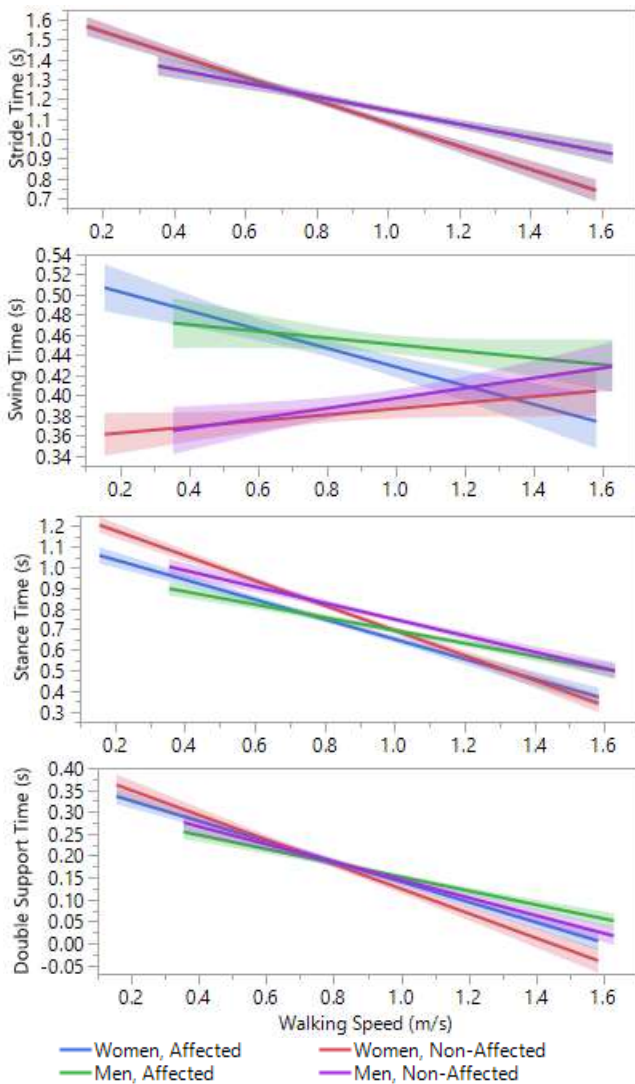


Figure 1: Stride, Swing, Stance, and Double Support Times as a function of walking speed. Results shown by sex and limb differences. \*\*Note: Time scales vary between graphs.

may have restricted significance of results. The highest coefficients of variation were seen in double support time, which also saw the fewest significant effects.

Literature examining sex-specific temporal gait differences in ankle OA patients is limited. It is unclear whether the sex-specific effects observed in this study are present in healthy populations or are a result of sex-specific pain coping compensatory

mechanisms. Similarly to our results, Valderrabano et al found that stride time was not different between limbs in pre-operative ankle osteoarthritis patients [4]. Nuesch, et al. observed no decrease in stance time as a percent of stride time [5], which disagrees with our finding of shorter stance time on the affected limb. Conversely, Shih et al observed decreased stance time and increased swing time on the affected limb, both of which agree with our results [6]. However, Shih et al also saw an increase in double support time on the affected limb, which our results did not reflect.

## CONCLUSIONS

It is possible that temporal variables, which are much easier to collect than 3D motion capture data, can be used to quantify limp and gait compensation; walking speed could play a large role in this quantification, along with limb-specific differences between swing and stance times. These results demonstrate the value of using these simpler variables to evaluate compensation. Results of this study demonstrate the complexity of this patient population and bring up intricacies in studying ankle OA gait. Future studies are needed to better understand variability within the ankle OA patient population and sex-specific differences observed in temporal parameters.

## REFERENCES

1. Saltzman, C.L., et al. J Bone Joint Surg Am, 2006. **88**(11): p. 2366-2372.
2. Glazebrook, M., et al. J Bone Joint Surg Am, 2008. **90**(3): p. 499-505.
3. Saltzman, C.L., et al. Foot Ankle Int, 2009. **30**(7): p. 579-96.
4. Valderrabano, V., et al. Clin Biomech (Bristol, Avon), 2007. **22**(8): p. 894-904.
5. Nuesch, C., et al. Clin Biomech (Bristol, Avon), 2012. **27**(6): p. 613-8.
6. Shih, L.-Y., J.-J. Wu, and W.-H. Lo, Foot & Ankle International, 1993. **14**(2): p. 97-103.

Table 1: Subject Demographics and respective sex-specific p-values

	Height (m)	Weight (N)	Age	Walking Speed (m/s)
<b>Men</b>	1.79±0.08	91.5±15.8	64.2±8.8	0.98±0.25
<b>Women</b>	1.6±0.07	79.5±15.5	62.7±10.2	0.81±0.26
<b>P-value</b>	<0.001*	<0.001*	0.221	<0.001*

# STABILIZING FORCES AND ENERGY COST OF CEREBRAL PALSY GAIT WITH PEDIATRIC POSTERIOR WALKER

Marshall W. Tumperi and Shawn D. Russell

Motion Analysis and Motor Performance Lab  
Department of Aerospace and Mechanical Engineering  
University of Virginia, Charlottesville, VA, USA  
email: sdr2n@virginia.edu,

web: med.virginia.edu/orthopaedic-surgery/research/the-motion-analysis-and-motor-performance-lab/

## INTRODUCTION

United Cerebral Palsy (UCP) reports that an estimated 764,000 individuals in the United States exhibit one or more symptoms of CP, and a recent multisite UCP study of school-age children found that 24.8% of these individuals use walkers [1]. It is estimated that more than 10,000 pediatric walkers are sold each year in the United States [1].

The purpose of a posterior walker is to increase the mobility of the user while maintaining stability and proper posture. Walkers enhance stability by providing both vertical and lateral support at the user's hands. However this increase in stability comes at the cost of having to pull the walker along. Children with CP typically are weaker and fatigue faster than their typically developed peers. Additionally they have been shown to do 59% more work per unit mass on average than TD children [2]. This work develops a method for quantifying the stabilizing forces and the associated increased energetic cost of walking with a pediatric posterior walker for children with CP.

## METHODS

Two children with CP, GMFCS II and IV were instructed to walk in a straight path at their self-selected comfortable walking speed using a custom instrumented posterior pediatric walker (Fig 1). A typical posterior walker was instrumented at the handles with a 6 DoF load cell (ATI) to capture all forces (1080Hz) applied through the handles. Kinematic data was collected at 120 Hz using an 8 camera motion capture system (Vicon) and the full-body Plug-in-Gait marker set in tandem with the 5-point set for the walker located at each handle end (2), load cell locations (2), and center cross bar (1).

Vertical and lateral forces applied to the handles were normalized via body mass to quantify the

stabilizing forces applied by each test subject. The anterior/posterior forces applied at the handle were used in conjunction with the 3D location of the load cells in order to calculate the mechanical work required to move the walker during typical straight walking.



**Figure 1:** Instrumented walker with five markers (left/right grip, left/right sensor, bar) and load cells at connection from handles to walker.

For each time point force, data was subsampled to match kinematic data, and instantaneous work at each handle was calculated as the instant force multiplied by the distance traveled over each time sample. Total work was calculated as the sum of the work done at each handle over the whole trial, these data were normalized by the total linear distance traveled by the walker. Gait events were also identified in order to quantify how the work applied to the walker changed relative to the gait cycle.

## RESULTS AND DISCUSSION

The average total work to move the walker per distance travelled for subject 1 was 9.2(1.9) J/m (GMFCS II) and subject 2 was 15.9(1.9) J/m (GMFCS IV). This compares with the normalized vertical [0.369(0.050) N/kg and 1.9(0.14) N/kg] and lateral [0.0646(0.011) N/kg and 1.41(0.13) N/kg] support forces for each.

Evaluating the instantaneous work relative to gait events shows that a pattern can be seen near foot off (FO) and foot strike (FS) (Fig 2).

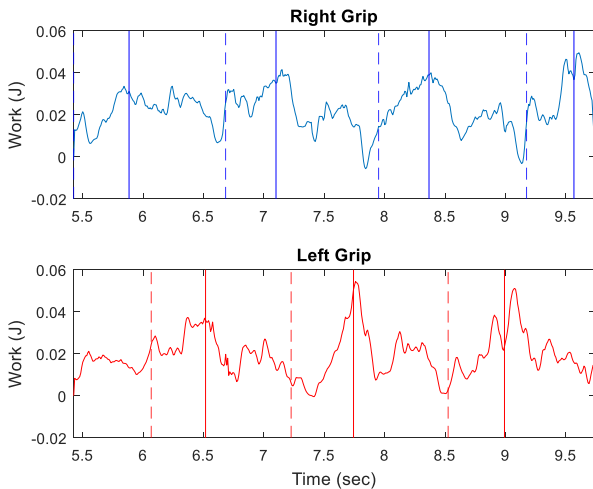


**Figure 2:** Work done on the left and right grips over one trial marked with respective FO events as dashed lines and FS events as solid lines.

Near FO events there is a relative minimum in the amount of work done on the walker, often approaching a negative value. At FS events, we see local maxima reached. These observations reveal how the user has incorporated the walker into their gait. At FO, entering into the swing phase of their gait, the user performs negative or low magnitude work, this coincides with the moment of max power generation needed by the subject during gait to start their next step and move their CoM up and over the stance leg. At FS, entering double support, the user pulled the walker forward with the maximum work observed.

The vertical and lateral forces applied to the walker at the grips reveals how the walker was used for stability and to what extent over the trials (Fig 3). The vertical force shows a similar relationship to the FO and FS events as the total work. During the swing phase between FO and FS, the vertical force increases to a local maxima revealing increasing use

for stability. After FS, the vertical force drops back down as the user is in double support and more independently stable.

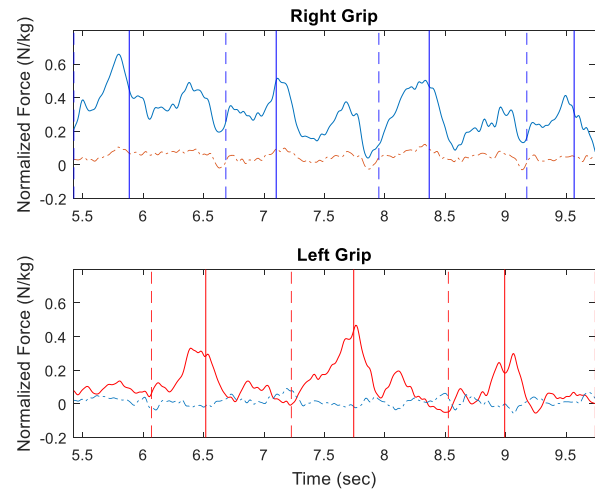


**Figure 3:** Normalized vertical (solid) and lateral (dashed) force where downwards is positive, with FO and FS events marked as dashed and solid lines respectively.

## CONCLUSIONS

The two subjects tested are representative of the extreme walker users, subject one with little reliance on the walker and subject two unable to ambulate without the walker, and were chosen to bracket a typical walker user.

It has been reported that ambulatory children with CP do on average 1.03 J/kg-m of total work while walking without assistive devices [2]. For subject 1, an independent community ambulatory, with a mass of 45kg this equates to approximately 46.4 J/m. So adding the walker their work done would increase by nearly 20%, the increase would be far greater for subject 2.

With the significant increase in work required to use a walker, a child with CP may not be able to use it for long periods of time and thus decrease their overall mobility. The observed patterns in work required and vertical force indicate that a control system for a motorized walker could be designed to decrease the work applied to the walker.

## REFERENCES

1. Koman LA *United Cerebral Palsy*, 1997, 8-1-2005.
2. Russell SD, et al. *J Biomech*, 27, 99-107, 2011.

## ACKNOWLEDGMENTS

This work funded in part by a NIH phase I SBIR

# METABOLIC AND MECHANICAL DEMANDS OF SYMMETRICAL AND ASYMMETRICAL WALKING ON A SPLIT-BELT TREADMILL

Jan Stenum and Julia T. Choi

Department of Kinesiology, University of Massachusetts Amherst, Amherst, MA, USA  
email: jstenum@umass.edu, web: <http://blogs.umass.edu/jtchoi>

## INTRODUCTION

Metabolic and mechanical costs during symmetric walking can be predicted from speed, step length and step rate. How does gait asymmetry affect the energetics of walking? Walking with asymmetric speeds [1] (e.g., on a split-belt treadmill) or asymmetric step durations [2] incurs an added metabolic cost. In split-belt walking, it is not clear if the extra metabolic cost is due to greater mechanical costs, poor efficiency, or a sub-optimal stride rate. We asked whether the mechanical power performed by each leg is dependent only on the ipsilateral leg speed (and independent of contralateral leg speed). We hypothesized that greater mechanical power explains the increase in metabolic power during asymmetrical walking, independent of stride rate.

## METHODS

5 subjects participated (4 male, 1 female; age  $20.4 \pm 1.96$  years; mass  $69.8 \pm 2.7$  kg). First, subjects walked symmetrically at  $1.25 \text{ ms}^{-1}$ ,  $0.75 \text{ ms}^{-1}$  and  $1.75 \text{ ms}^{-1}$  at preferred stride rates. Then, subjects walked symmetrically at  $1.25 \text{ ms}^{-1}$  and, following a 10-minute adaptation period, asymmetrically at belt speeds of  $0.75$  and  $1.75 \text{ ms}^{-1}$  ( $\Delta 1.0 \text{ ms}^{-1}$ ) on a split-belt treadmill at 80, 90, 100, 110 and 120% of their preferred stride rate at  $1.25 \text{ ms}^{-1}$ . Each trial lasted 5 minutes. We calculated net metabolic power from expired air. We calculated the average external positive mechanical power performed on the center of mass by each leg as the dot product of each leg's ground reaction forces and the center of mass velocity (obtained by integrating net ground reaction forces) divided by stride duration. External positive mechanical work is performed during the initial part of single support and during push-off. To characterize the distribution of positive mechanical work during stance, we divided power production during single support by the total amount. Because preferred stride rates at  $0.75 \text{ ms}^{-1}$  and  $1.75 \text{ ms}^{-1}$

approximated 80% and 110% of preferred stride rate at  $1.25 \text{ ms}^{-1}$ , we compared each leg's mechanical variables for symmetrical walking at  $0.75 \text{ ms}^{-1}$  and  $1.75 \text{ ms}^{-1}$  against those of asymmetrical walking at 80% and 110%, respectively (using paired t-tests).

## RESULTS AND DISCUSSION

Preferred stride rates were 44.4, 54.8 and  $62.4 \text{ strides} \cdot \text{min}^{-1}$ , at  $0.75$ ,  $1.25$  and  $1.75 \text{ ms}^{-1}$ . During asymmetrical walking at  $\Delta 1.0 \text{ ms}^{-1}$ , step durations (heel strike to heel strike) from the slow to the fast leg increased (+18 to +23%) while step durations from the fast to slow leg decreased (-19 to -23%) relative to symmetric step durations.

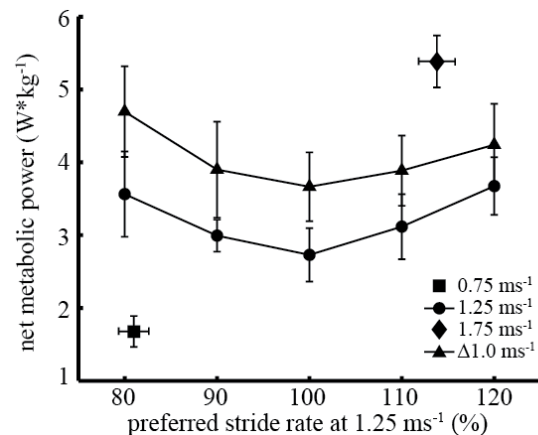


**Figure 1:** Net metabolic power. Error bars are one standard deviation.

Net metabolic power of asymmetrical walking at  $\Delta 1.0 \text{ ms}^{-1}$  was greater than symmetrical walking at the same averaged belt speed, i.e.  $1.25 \text{ ms}^{-1}$ , at all stride rates ( $P \leq 0.018$ ) (figure 1). That is, walking in an asymmetrical environment incurs an added metabolic cost that is independent of stride rate. This is consistent with the added metabolic cost (independent of stride rate) of enforcing asymmetrical step durations with a metronome [2].

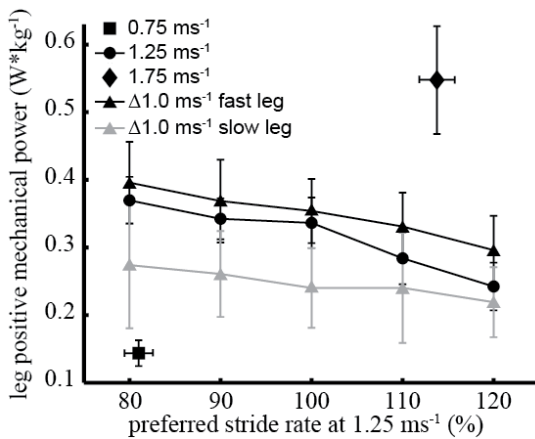


**Figure 2:** External positive mechanical power of each leg. Error bars are one standard deviation.

However, the total external positive mechanical power summed across both legs was not different between asymmetrical walking at  $\Delta 1.0 \text{ ms}^{-1}$  and symmetrical walking at  $1.25 \text{ ms}^{-1}$  (not shown) ( $P \geq 0.291$ ). This is contrary to enforcing step duration asymmetry with a metronome, which resulted in greater external positive mechanical power [2]. During asymmetrical walking at  $\Delta 1.0 \text{ ms}^{-1}$ , positive mechanical power of the fast leg was greater than the slow leg at all stride rates ( $P \leq 0.036$ ) (figure 2). The positive mechanical power of the slow leg during asymmetrical walking was greater than the positive mechanical power performed while walking symmetrically at  $0.75 \text{ ms}^{-1}$  (slow leg's belt speed) ( $P \leq 0.044$ ) even after normalizing to the longer stance duration of the slow leg in asymmetrical walking (1.00 s vs 0.92 s;  $P < 0.001$ ). The positive mechanical power of the fast leg during asymmetrical walking was less than the positive mechanical power performed while walking symmetrically at  $1.75 \text{ ms}^{-1}$  (fast leg's belt speed) ( $P \leq 0.008$ ) even after normalizing to the shorter stance duration of the fast leg in asymmetrical walking (0.54 s vs 0.60 s;  $P < 0.002$ ).

In addition to the greater positive mechanical power performed by the slow leg during asymmetrical walking at  $\Delta 1.0 \text{ ms}^{-1}$  compared to symmetrical walking at  $0.75 \text{ ms}^{-1}$ , a greater proportion of the mechanical work was performed during single support ( $P < 0.016$ ) (figure 3). Because positive external work during single support is performed by work at the hip and knee (and not the ankle), this suggests that positive mechanical work by the slow

leg during asymmetrical walking at  $\Delta 1.0 \text{ ms}^{-1}$  is performed with poor efficiency [3]. The fast leg during asymmetrical walking at  $\Delta 1.0 \text{ ms}^{-1}$  performed a smaller proportion of positive mechanical work during single support than symmetrical walking at  $1.75 \text{ ms}^{-1}$  ( $P < 0.016$ ) (figure 3) which suggests a greater efficiency.

Although joint work is not redistributed by walking speed, efficiency is greatest between 1.25 and 1.75  $\text{ms}^{-1}$  and poorest at  $0.75 \text{ ms}^{-1}$  [4]. The effect of walking speed on efficiency and the redistribution of positive work between single support and push-off during asymmetrical walking likely means that the poor efficiency of the slow leg is not fully balanced by the improvement of efficiency of the fast leg during asymmetrical walking at  $\Delta 1.0 \text{ ms}^{-1}$ .

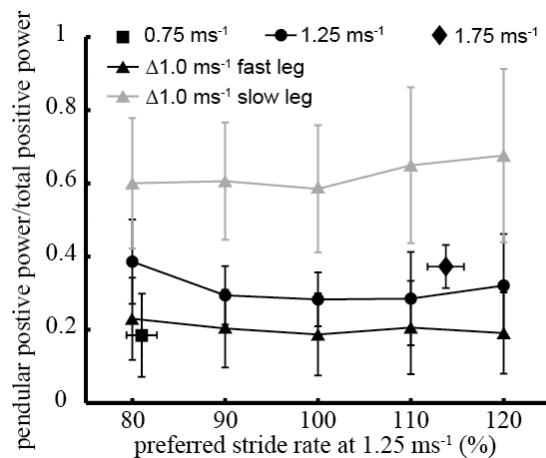


**Figure 3:** Ratio of pendular positive power during single support to the total amount of positive power over stance of each leg. Error bars are one standard deviation.

We have shown that walking in an asymmetrical environment on a split-belt treadmill incurs an added metabolic cost that is independent of stride rate. Contrary to our hypothesis, this is not explained by greater positive mechanical power during asymmetrical walking. Rather, the redistribution of work by the slow leg could explain the increased metabolic cost.

## REFERENCES

1. Finley JM, et al. *J Physiol* 591, 1081-95, 2013.
2. Ellis RG, et al. *Proc R Soc B* 280, 20122784, 2013.
3. Kuo AD, et al. *Exerc Sport Sci Rev* 33, 88-97, 2005.
4. Farris DJ, et al. *J R Soc Interface* 9, 110-8, 2012.

# EFFECT OF FREQUENCY ON WHOLE BODY MOVEMENT CONTROL IN CHILDREN WITH AND WITHOUT DOWN SYNDROME DURING TWO-LEGGED HOPPING IN-PLACE

Matthew Beerse and Jianhua Wu

Georgia State University, Atlanta, GA, USA. Email: [mbeerse1@student.gsu.edu](mailto:mbeerse1@student.gsu.edu)

## INTRODUCTION

Hopping in-place generally follows a spring-mass model for adults and typically developing (TD) children [1]. Increasing hopping frequency demands increased whole-body vertical stiffness and constrained horizontal movement. Children with Down syndrome (DS) often exhibit limited movement ability due to reduced muscle strength, joint coordination, and balance control [2]. It is unknown if children with DS are able to hop outside of their preferred frequency, like their TD peers. This study aimed to assess the whole-body control strategies employed to modulate hopping frequency by children with DS compared to TD children.

## METHODS

*Participants:* Fifteen children with DS and 16 TD children were recruited for this study. Six children with DS were unable to coordinate continuous hopping and were removed from analysis. We age- and sex-matched 9 TD children corresponding to the remaining 9 children with DS. Mean age (SD) was 9.57 (1.53) years, height was 1.22 (0.10) m, body-mass was 30.58 (10.37) kg, and leg length was 0.64 (0.06) m for children with DS (3M/6F) and 9.28 (1.46) years, 1.37 (0.09) m, 32.54 (6.70), and 0.74 (0.07) m for TD children, respectively. Children with DS were shorter in height and leg length, but had similar body mass compared to TD children.

*Experimental design:* Each subject completed three trials of hopping at a self-selected pace to calculate the subject's preferred frequency. We randomly presented four frequency conditions based on their preferred frequency. A metronome led the frequency conditions which consisted of their *preferred* frequency, 20% decrease (*slow*), 20% increase (*moderate*), and 40% increase (*fast*). Two of the DS subjects could complete the *fast* condition so this condition was removed from data analysis.

*Data collection:* Kinematic data was collected using an 8-camera Vicon motion capture system sampling

at 100Hz. We attached a full-body PSIS marker set. Kinetic data was collected using an AMTI force plate sampling at 1000Hz. For each condition, subjects hopped for 20-seconds. Three trials were completed for each frequency condition.

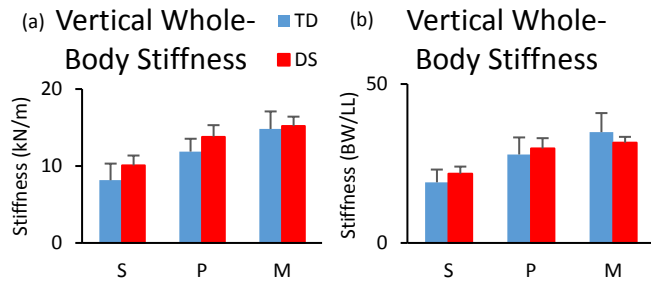
*Data analysis:* We calculated whole-body vertical stiffness as the linear regression slope of vertical ground reaction force (GRF) vs. vertical center of mass (COM) displacement over the stance phase [4]. Vertical COM displacement was calculated by double integration of COM acceleration from the vertical GRF [3]. We also normalized whole-body vertical stiffness by bodyweight (BW) and leg length (LL). For horizontal movement, COM position was estimated from marker data using segmental analysis [2]. We calculated anterior/posterior (AP) and medial/lateral (ML) COM range as the difference between the maximum and minimum positions during stance phase. We calculated AP and ML toe displacement as the difference in position of the toe marker between hops.

*Statistical analysis:* Repeated measures two-way (2 group x 3 condition) ANOVAs were conducted on each raw or log-transformed variable. Bonferroni adjusted post-hoc pairwise comparisons were completed when necessary. A significance level was set at  $\alpha=0.05$ .

## RESULTS AND DISCUSSION

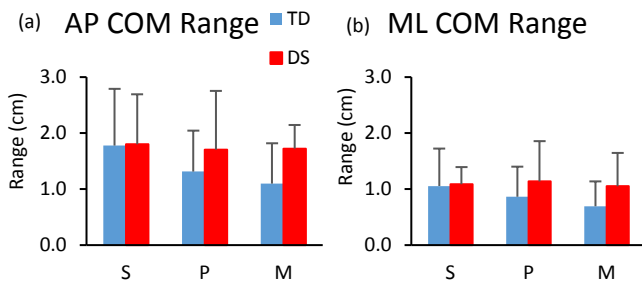
Children with DS hopped at a faster preferred frequency (2.65 Hz) compared to TD children (2.29 Hz). However, children with DS hopped with a similar whole-body vertical stiffness (no group effect for absolute and normalized stiffness). Both children with DS and TD children increased whole-body vertical stiffness when increasing hopping frequency (condition effect for absolute:  $p<0.001$ , normalized:  $p<0.001$ ) (Fig. 1). Both groups increased hopping frequency from *slow* to *preferred* and *slow* to *moderate*, but not *preferred* to *moderate*.

Fig.1



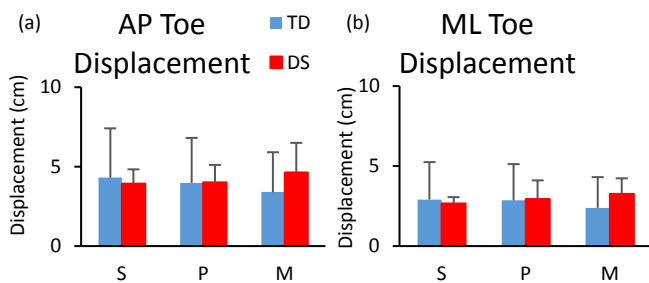
Note: S for *slow*, P for *preferred*, and M for *moderate* frequency condition.

Fig.2



Only TD children decreased AP COM range with increasing frequency (Fig. 2a; group by condition interaction:  $p=0.040$ ). From *slow* to *moderate*, TD children decreased AP COM range ( $p=0.005$ ), resulting in a comparatively greater range in children with DS at the *moderate* condition ( $p=0.012$ ). ML COM range was not different between groups and unaffected by frequency condition (Fig.2b).

Fig. 3



At the *moderate* frequency children with DS increased AP and ML toe displacement, while TD

children decreased (group by condition interaction:  $p<0.001$  for AP and  $p=0.002$  for ML) (Fig. 3a). Both groups decreased stance time with increasing hopping frequency (Table 1). TD children decreased flight time and hopping height with increasing frequency, while children with DS also decreased from *slow* to *preferred*, but increased at *moderate*.

Similar to TD children, children with DS aged 6-11 years are able to modulate their whole-body vertical stiffness and follow a spring-mass model. However, children with DS did not effectively coordinate hopping at the *moderate* frequency condition, demonstrated by hopping height and flight time. This result is similar to previous studies where children with DS, when asked to tap on a pad faster, incorrectly tapped with greater force [4]. Children with DS did not display as much balance control as TD children. TD children reduced AP COM range of motion and AP displacement between hops to increase hopping frequency. Children with DS were unable to modify AP COM range of motion and increased AP displacement between hops at the *moderate* frequency.

## CONCLUSIONS

Children with DS modulate whole-body movement similar to TD children. However, children with DS demonstrate ineffective control strategies and greater horizontal movement when required to hop at a 20% increase (*moderate*).

## REFERENCES

1. Beerse M, & Wu J. *J Biomech* **49**, 3306-3312, 2016.
2. Palisano RJ, et al. *Arch Phys Med Rehabil* **82**, 494-500, 2001.
3. Cavagna GA. *J App Phys* **39**, 174-179, 1958.
4. Frith U, et al. *J Child Psychol Psychiatry* **15**, 293-301, 1974.

Table 1: Mean (SD) of hopping variables	Group	Slow	Preferred	Moderate
Hopping height (cm)	TD	5.38 (2.89)	5.34 (2.34)	4.04 (1.91)
	DS	4.17 (1.27)	3.53 (0.35)	5.11 (0.87)
Stance time (s)	TD	0.31 (0.04)	0.25 (0.02)	0.22 (0.02)
	DS	0.31 (0.05)	0.26 (0.07)	0.24 (0.05)
Flight time (s)	TD	0.19 (0.03)	0.18 (0.02)	0.16 (0.02)
	DS	0.15 (0.07)	0.13 (0.05)	0.15 (0.05)

# BIOMECHANICAL ANALYSIS OF TIMED UP-AND-GO (TUG) TEST IN CHILDREN WITH AND WITHOUT DOWN SYNDROME

Matthew Beerse, Michael Lelko, Jianhua Wu  
Georgia State University, Atlanta, GA, USA. Email: [mbeersel@student.gsu.edu](mailto:mbeersel@student.gsu.edu)

## INTRODUCTION

The Timed Up-and-Go (TUG) test consists of multiple functional tasks of daily living [1]. Specifically, the test requires the participant to stand up from a chair, walk, turn-around, and sit down. The TUG test has been shown to be a valid tool to assess functional mobility in children with DS [1]. While children with DS take a longer time to complete the test compared to typically developing (TD) peers, it is unknown how children with DS perform at each phase of the task. The purpose of this study was to compare the biomechanical pattern of the TUG test between children with and without DS, particularly during the sit-to-stand and walk-out phase.

## METHODS

*Participants:* Fourteen children with DS (4M/10F) and 14 sex- and age-matched TD children were recruited for this study. Mean (SD) age for children with DS was 8.58 (1.91) years, height was 1.18 (0.12) m, body-mass was 27.16 (10.41) kg, and leg length was 0.62 (0.08) m, and for TD children was 8.20 (1.78) years, 1.31 (0.10) m, 29.60 (6.75) kg, 0.71 (0.07) m, respectively.

*Experimental design:* Subjects sat on a chair without side arms, feet in contact with the floor, hip and knee flexed at about 90 degrees and ankle at neutral. Subjects were instructed to stand up from a chair, walk towards a target 3m away, touch the target, turn around, walk back to the chair, and sit down. Subjects completed five trials and were reminded not to run and to walk as fast as possible in each trial.

*Data collection:* We attached a full-body PSIS marker set to the subject and collected kinematic data using an 8-camera Vicon motion capture system sampling at 100Hz.

*Data analysis:* We visually separated the trials into five phases: (1) sit-to-stand, (2) walk-out, (3) turn around, (4) walk-in, and (5) stand-to-sit. We used the criteria below to differentiate the phases across trials

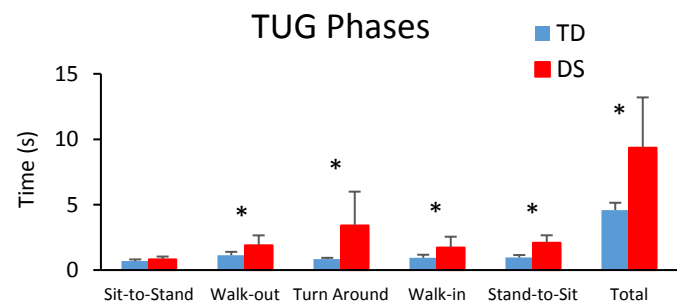
and subjects: sit-to-stand started with the initiation of forward trunk lean and ended with the end of vertical movement of the upper body; turn-around started at the beginning of pelvis rotation and ended when the pelvis orientation returned along the anterior/posterior (AP) axis; and stand-to-sit started at the beginning of pelvis rotation before lowering to the chair and ended with the end of vertical movement of the upper body. The walk-out and walk-in phases were coded as the time between sit-to-stand and turn around, and turn around to stand-to-sit, respectively.

During the sit-to-stand phase we assessed the center-of-mass (COM) excursion and its peak velocity in the AP, medial/lateral, and vertical directions. We also calculated peak extension angle and velocity of the ankle, knee, and hip in the sagittal plane over the entire phase. During the walk-out phase we calculated step length, step width, and walk speed. We normalized step length, step width, and walk speed [2], but statistical results were unaffected.

*Statistical analysis:* Independent t-tests were conducted on the TUG time, each phase duration, and each phase variable to compare the two groups. A significance level was set at  $\alpha=0.05$ .

## RESULTS AND DISCUSSION

Fig. 1

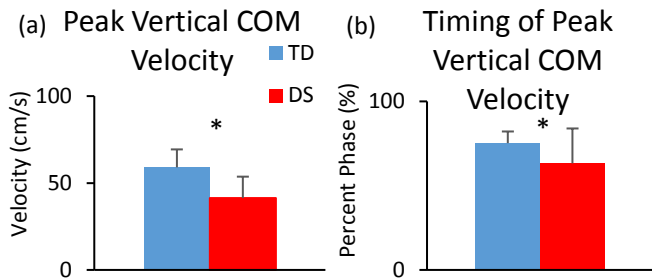


Note: \* indicates statistically significant differences.

Children with DS took longer to complete the TUG task compared to TD children ( $p<0.001$ ) (Fig. 1). On

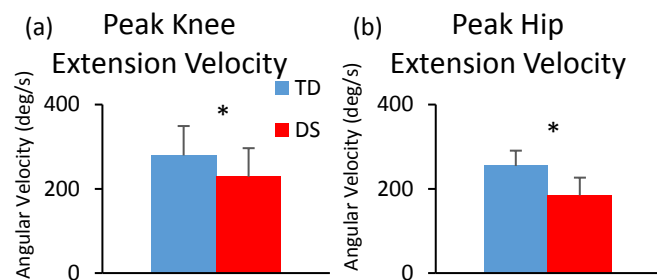
average, children with DS completed the TUG task in 9.35 seconds compared to 4.59 seconds for TD children. Broken down to the five phases, children with DS took longer for each phase except the sit-to-stand phase ( $p=0.054$ ).

Fig. 2



During sit-to-stand, both groups demonstrated similar COM excursion in each direction and peak COM velocity in AP and ML. However, in the vertical direction, the DS group showed a slower peak COM velocity ( $p=0.021$ ) and reached peak velocity earlier in the phase ( $p=0.046$ ) (Fig. 2a-b). Both groups reached similar peak ankle, knee and hip extension angles during the sit-to-stand phase. However, the DS group exhibited slower peak hip and knee extension velocities than the TD group ( $p<0.001$  and  $p=0.046$ , respectively) (Fig. 3a-b).

Fig. 3

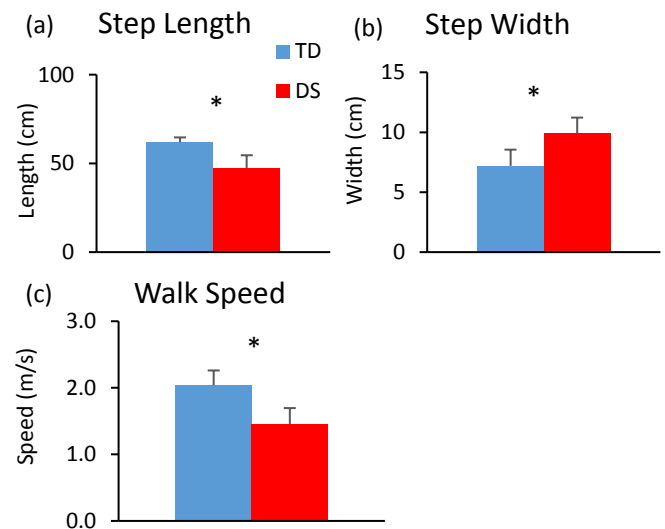


During the walk-out phase, children with DS took shorter but wider steps and walked at a slower speed. There was a group effect for step length ( $p=0.004$ ), step width ( $p=0.013$ ), and walk speed ( $p<0.001$ ) (Fig. 4a-c).

The results of TUG duration are similar to previously published data on children with DS aged 3-13 years [1]. Interestingly, when broken down to each phase, children with DS required more time across each phase, except sit-to-stand (although it approached a

significance). With a similar vertical COM excursion during sit-to-stand, TD children continued to increase vertical COM velocity and reached a greater peak later in the phase. Further, peak extension velocity of the hip and knee joints were lower in children with DS. These results may suggest that TD children may have a better ability than children with DS to transition from sit-to-stand to walking.

Fig. 4



During the walk-out phase, children with DS walked with a spatiotemporal gait pattern typically seen in children with DS at this age range [2]. However, during the TUG test children with DS did walk faster than previously reported preferred walking speeds in this group [2, 3]. Therefore the group difference may suggest a lower capacity for children with DS to modify gait pattern for a specific task, or achieve a fastest walking speed comparable to TD children.

## CONCLUSIONS

The TUG tests consists of separate tasks that assess functional mobility. Children with DS took longer to complete the test and demonstrated slower movement during the sit-to-stand and forward walking phases of the test.

## REFERENCES

1. Nicolini-Panisson RDA, et al. *Dev Med Child Neurol* **56**, 490-497, 2014.
2. Ulrich BD, et al. *Hum Mov Sci* **23**, 133-156, 2004.
3. Smith BA, et al. *Curr Gerontol Geriatr Res*, 1-7, 2012

# PARAMETERIZING JOINT-LEVEL VARIABILITY DURING WALKING FOR STROKE VICTIMS

Anne E. Martin and Mukul C. Talaty

Pennsylvania State University

Email: aem34@psu.edu, mxt103@psu.edu

## INTRODUCTION

Predicting how likely an individual is to fall could improve rehabilitation outcomes, thereby improving the quality of life for millions of individuals. Variability in gait temporal parameters is correlated with fall risk [1] and with clinical measures of gait impairment [2]. Since changes in temporal parameters occur due to changes in joint movements, leg joint variability may provide valuable information about fall risk. Joint variability has been parameterized for young, healthy adults walking at their self-selected speed [3] but not for other populations. Since stroke is a common cause of impaired gait, this abstract presents initial work in parameterizing joint variability for stroke victims. Specifically, it shows that joint variability can be parameterized mathematically using low-order Fourier series for both stroke victims and healthy adults.

## METHODS

Joint angle data from 7 stroke patients (average speed 0.5 m/s), 6 slow, healthy adults (average speed 0.5 m/s), and 7 young, healthy adults (average speed 1.2 m/s) walking overground at their self-selected speed were used. The data from the stroke and slow, healthy subjects were collected using a Coda CX1 (Charnwood Dynamics, Leicestershire, England) active marker motion analysis system system. The data from the young, healthy subjects were collected using a Vicon (camera model: T20S, Oxford, UK) motion capture system. For comparison, artificial joint angle data were created with known variability (filtered zero-mean random noise). A total of 34 strides from each population were used, except for the slow, healthy subject data which had 29 strides. (The young subject data were a subset of the data from [3]). Each stride was divided into stance and swing periods, and the periods were analyzed separately. The affected and contralateral sides were analyzed separately for the stroke subject data, while only the right leg was analyzed for the healthy data.

The per-subject mean motion for each joint was determined and subtracted from the total joint motion for each step (Fig. 1). This gave a time history of the joint variability. To parameterize the variability mathematically, a second-order Fourier series was fit to the stance period variability and a first-order Fourier series was fit to the swing period variability (Fig. 1). The quality of each fit was calculated using the  $R^2$ -value and the normalized root mean square error (RMSE). The normalized RMSE is the RMSE divided by the range of the variability. Pairwise t-

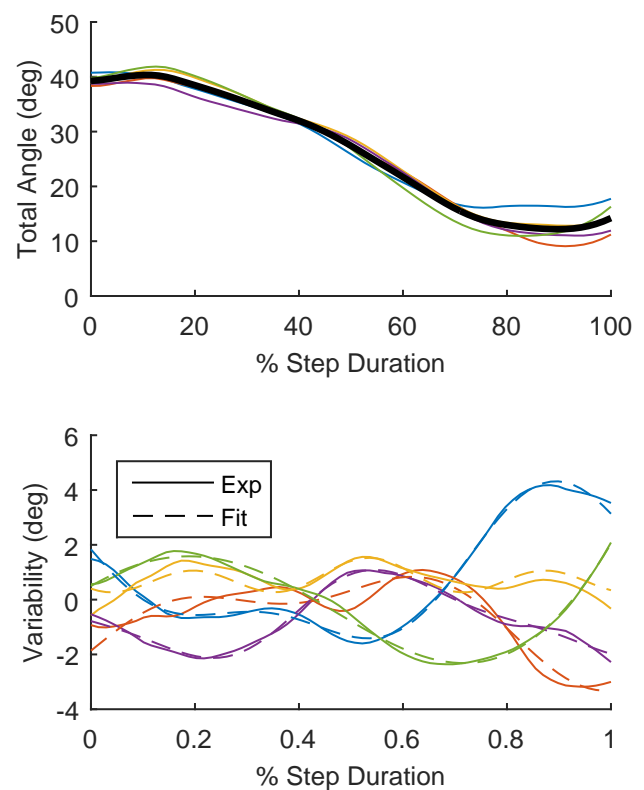


Figure 1: Top: The total (thin lines) and mean (thick line) joint angles. The pointwise difference between the mean and total angle is the variability. Bottom: The experimental variability and the best fit second-order Fourier series. The Fourier series fits the data very well. Both plots show the affected-side stance hip angles for a stroke subject.

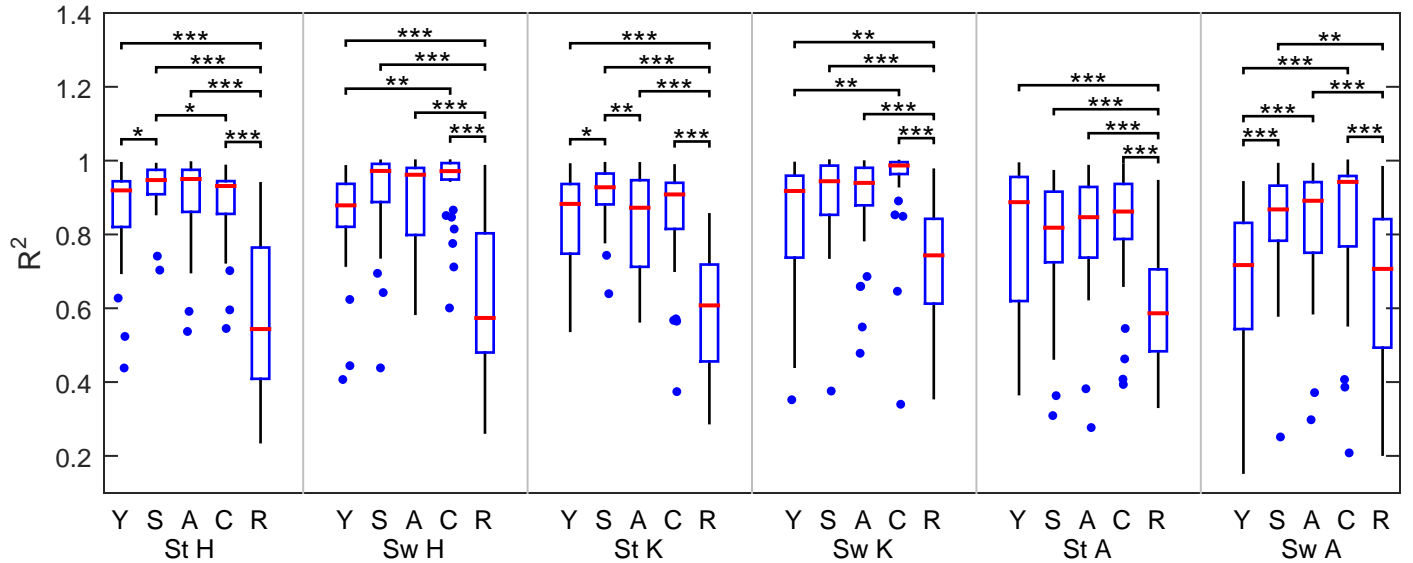


Figure 2: The  $R^2$  values for all groups (Young healthy, Slow healthy, stroke Affected side, stroke Contralateral side, aRtificial), joints (Hip, Knee, Ankle), and periods (Stance, Swing). Larger values indicate better fit. Statistically significant differences are indicated: \* = p-value < 0.05, \*\* = p-value < 0.01, \*\*\* = p-value < 0.001. Statistical significance was similar for the RMSE values. Blue dots indicate outliers.

tests using the  $R^2$ -value and the normalized RMSE were conducted between each of the five groups for each joint and period.

## RESULTS AND DISCUSSION

With the exception of the young swing ankle, low-order Fourier series fit the true experimental data significantly better than the artificial data as expected using both goodness of fit measures (Fig. 2). This provides confidence that the variability is not simply measurement noise and that similarities or differences between populations are true. The fits for the true experimental data were quite good, with  $R^2$ -values consistently above 0.8 and normalized RMSE consistently below 8% of the variability range. For all joints and periods of the stroke subjects, the goodness of fit between the affected and contralateral sides were similar. For the stance joints, the goodness of fit was similar between the young, slow, and stroke subjects. For the swing joints, the goodness of fit was slightly better for the stroke and slow subjects than for the young subjects. This indicates that a second (or first)-order Fourier series well captures the joint variability as a function of step progression in stance (or swing) joints for both healthy adults and stroke victims. This is true despite considerable dif-

ferences in mean walking speed. Further, the systems used to collect the experimental data were different, indicating that joint variability and this parameterization is robust to different data collection methods, at least some gait impairments, and walking speed.

## CONCLUSIONS

The joint variability during walking for both healthy adults and stroke victims has a remarkably similar structure and can be parameterized mathematically using the same method for both populations. Further, the accuracy of the parameterization is similar. The values that define the Fourier series may be different for each population, although this work remains to be done. The full characterization of joint variability will be included in physics-based models of human gait [4] and used to investigate fall risk.

## REFERENCES

- [1] Hausdorff, JM. *Hum Movement Sci* **26**, 555–89, 2007.
- [2] Balasubramanian, CK, et al. *Gait Posture* **29**, 408–414, 2009.
- [3] Martin, AE, et al. *J Biomech* **49**, 3298–305, 2016.
- [4] Martin, AE & Gregg, RD. *IEEE Trans Robot* **32**, 943 – 948, 2016.

# TORSIONAL MALALIGNMENT SYNDROME AND THE MAXIMUM INTERNAL VARUS KNEE MOMENT DURING GAIT IN INDIVIDUALS WITH DISABILITIES

<sup>1</sup> Alexandria Case, <sup>1</sup> K. Mitchell Barr, and <sup>1</sup> Amy Lenz

<sup>1</sup> Mary Free Bed Rehabilitation Hospital Grand Rapids, MI, USA

email: alexandria.case@maryfreebed.com, web: <http://www.maryfreebed.com/>

## INTRODUCTION

Torsional malalignment syndrome (TMS) is defined as the combination of two orthopedic pathologies — femoral anteversion (medial twist in femur) and external tibial torsion (lateral twist in tibia) occurring in the same limb. This creates a “wringing” effect on the knee which may contribute to common knee pathologies such as patellofemoral pain syndrome, cartilage tears, ligament sprains, ligamentous laxity and osteoarthritis [1].

We have observed in our gait analysis laboratory over the years that many patients who present with TMS demonstrate a “valgus thrust” corresponding to an abnormal internal varus knee moment. The purpose of this study is to determine the effects of TMS on maximum internal varus knee moment (MxVKM) in a disabled population. The correlation between the severity of the TMS and the magnitude of the MxVKM will also be analyzed.

We hypothesize that: (a) Patients with TMS will have an increased MxVKM compared to patients without TMS and typically developing peers and (b) For patients with TMS, there will be a moderate positive relationship between the degree of TMS and the magnitude of MxVKM.

## METHODS

This was a retrospective matched comparative correlational design. A comparison of the MxVKM was made among patients with TMS, patients without TMS (nTMS) and typically developing (TD) individuals. The TMS group was made up of 91 limbs from patient ages 4-60 of any diagnosis drawn from the Mary Free Bed Rehabilitation Hospital’s Motion Analysis Center for routine clinical gait analysis between 1994 and 2016.

Limbs were included in the TMS group if they had the following combination of physical exam measurements: a transmalleolar axis >25 degrees external and a difference between hip internal and

external rotation passive range of motion (IR-ER)  $\geq 30$  degrees [2, 3]. In the event that a patient met these criteria on multiple study dates, only the most recent study data was utilized. Any limb which met the criteria was included. (Some patients presented with bilateral, and some with unilateral TMS.) Patients were excluded from the study if the data was collected while the patient was using an assistive device given the interference with the validity of moment data collected. Additionally, patients presenting with an inconsistent gait pattern not definable by a single representative gait cycle were excluded from the study. The non-TMS and normative groups were matched to those patients whose limbs were in the TMS group on the basis of age and gender. The non-TMS group was also matched to the TMS sample based on diagnosis where possible.

The magnitude of counter torsion in patients with TMS was defined using a novel measure we termed the “Torsional Malalignment Syndrome Angle” (TMSA), defined as the sum of the difference between hip internal and external rotation passive range of motion and the degree of external tibial torsion (ETT):  $TMSA = Hip\ IR-ER + TMA$ .

A Lilliefors test was conducted and indicated that the data did not fit a normal distribution. Therefore, a Kruskal-Wallis test and post-hoc Mann-Whitney U-tests were conducted, with an alpha level of  $p < 0.05$  used to establish significance. A Spearman correlation was done to determine the correlation, if any, between the TMSA and the MxVKM of the patients with TMS.

## RESULTS AND DISCUSSION

A Kruskal-Wallis test determined the differences between the MxVKM of the three groups to be statistically significant ( $p = 0.000$ ). Mann-Whitney U-tests between individual groups found statistical significance between all groups; TMS/nTMS, TMS/TD, nTMS/TD ( $p = 0.0013, 0.0000, \text{ and } 0.0000$ ,

respectively). The TMS group median MxVKM was 0.350 Nm ( $\bar{x} = 0.395 \pm 0.31$  Nm, 4.2 times greater than normal; range = 1.524 Nm). The nTMS group median MxVKM was 0.190 Nm ( $\bar{x} = 0.266 \pm 0.26$  Nm; range = 1.763 Nm), 2.3 times greater than normal. The TD group median MxVKM was 0.083 ( $\bar{x} = 0.091 \pm 0.08$  Nm; range = 0.222 Nm). These are represented in (Fig. 1).

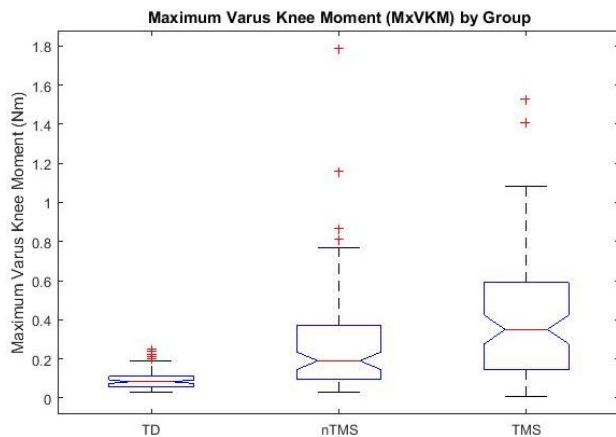


**Figure 1:** Maximum Varus Knee Moment (MxVKM) by Group. The median is indicated by a red horizontal band in each plot, with interquartile ranges annotated with blue bands on each plot. Outliers in each group are noted with red “+” signs.

A Spearman rank correlation coefficient of 0.222 showed a weak correlation between our novel measurement of TMS severity (TMSA) and the magnitude of the maximum varus moment. This highlights the multifactorial nature of an abnormal varus knee moment pattern and the high degree of variability in the sample.

In normal gait, the ground reaction force (GRF) in the frontal plane scarcely ever crosses lateral of the knee joint center, yielding a largely internal valgus knee moment. However, as demonstrated in this study, in disabled patients, the GRF often remains lateral to the knee, leading to an internal varus knee moment. This is believed to occur for a variety of reasons including lower extremity weakness, motor control deficits, excessive lateral trunk sway, midfoot collapse, genu valgus deformity and/or long bone torsion.

Abnormal internal varus knee moments have been found to be associated with ETT in patients with spina bifida (SB) [4]. Surgical correction of ETT in patients with SB via a tibial internal rotation

osteotomy has been found to lead to significant improvement in the varus knee moment postoperatively [5].

In TMS, the tendency for the ground reaction force to pass lateral to the knee joint is believed to be compounded over ETT alone. This is because, in addition to ETT which can cause the weight bearing surface of the foot to be positioned lateral of the weight bearing axis (WBA), femoral anteversion causes the knee joint to be positioned medial of the WBA. This can increase the perpendicular distance of the ground reaction force laterally with respect to the knee joint center and explains, we believe, why the MxVKM was significantly higher in our patients with TMS. The subsequent internal varus knee moment leads to increased compressive forces in the lateral knee compartment and increased distractive forces at the medial knee. In addition, there is a tendency for pathological lateral patellar tracking.

Given the findings of this study, we believe that future research should focus on whether TMS compounds the abnormal effect that ETT alone creates on the varus knee moment. This is clinically significant as it may indicate that treatment of the femur by external rotation osteotomy is necessary in addition to the tibial internal rotation osteotomy to optimize surgical outcomes.

## CONCLUSIONS

Disabled patients have a significantly higher MxVKM than do their non-disabled peers. Those patients with TMS have a significantly higher MxVKM than do matched peers without TMS. Using our novel measure for TMS severity, there is only a weak relationship between the severity of TMS and MxVKM. Further investigation into this relationship may be warranted.

## REFERENCES

1. Leonardi, F. et al. *J Ortho and Traum*, **15**, 131-136, 2014.
2. Swanson, A.B., et al. *Clin Ortho*, **27**, 157-175, 1963.
3. Turner, M.S., et al. *J Bone Joint Surg*, **63**, 396-398, 1981.
4. Lim, R., et al *J Ped Ortho*, **18**, 428, 1998.
5. Dunteman, R.C., et al. *J Ped Ortho*, **20**, 623-628, 2000.

## ACKNOWLEDGMENTS

We thank Rachel Bendewald, Breanna Fink, Jordan Krygsheld, and Alyssa Messner for their assistance in this study.

# DOES WALK-DMC PREDICT SURGICAL OUTCOMES? EXTENSION OF SYNERGY ANALYSIS IN CEREBRAL PALSY TO A SECOND CLINICAL CENTER

<sup>1</sup> Benjamin Shuman <sup>2</sup> Michael H. Schwartz <sup>3</sup> Marije Goudriaan, <sup>3</sup> Kaat Desloovere, <sup>1</sup> Katherine M. Steele

<sup>1</sup> University of Washington, Seattle, WA, USA

<sup>2</sup> Gillette Children's Specialty Healthcare, St. Paul, MN, USA

<sup>2</sup> KU Leuven, Leuven, Belgium

email: brs3@uw.edu, web: <http://depts.washington.edu/uwsteele/>

## INTRODUCTION

The framework of muscle synergies may be useful to evaluate muscle recruitment and coordination in the clinic [1]. In individuals with cerebral palsy (CP), prior research has shown that the dynamic motor control index during walking (walk-DMC) decreases with functional impairment and may be associated with post-treatment outcomes [2, 3]. In evaluating over 400 individuals from one clinical center, prior work demonstrated that individuals with CP with synergies more similar to typically-developing controls were more likely to have positive changes in gait after treatment [3]. The goal of this research was to extend these analyses to another clinical center and evaluate whether synergies may be useful for treatment planning.

## METHODS

Clinical pre-treatment electromyography (EMG) and kinematic data previously collected at the Clinical Motion Analysis Laboratory of the University Hospital Pellenberg, Belgium (CMAL-Pellenberg) from 174 individuals with CP were analyzed. The individuals were distributed between three treatment groups including 62 cases of botulinum toxin type A injection (BTA, M/F: 40/21, age: 6.7±2.9 yr, height: 1.1±0.2 m, mass: 20.7±8.5kg), 46 cases of selective dorsal rhizotomy (SDR, M/F: 23/23, age: 9.2±2.1 yr, height: 1.3±0.1 m, mass: 29.9±6.4kg), and 65 cases of single event multilevel orthopedic surgery (SEMLS, M/F: 38/27, age: 12.2±3.0 yr, height: 1.5±0.2 m, mass: 39.8±14.6 kg). A control group of 13 unimpaired individuals (M/F: 6/7, age: 10.1±3.0 yr, height: 1.4±0.2 m, mass: 39.6±16.4kg) was also analyzed. For each individual, EMG data were analyzed from a random limb from 4 muscles

(medial hamstrings, rectus femoris, gastrocnemius, and tibialis anterior).

EMG data were preprocessed with a 20 to 500 Hz band pass filter, then rectified, and a linear envelope was taken using a 10 Hz low-pass filter. Synergies were calculated using nonnegative matrix factorization. The total variance accounted for by one synergy ( $tVAF_1$ ) was calculated for each individual. Walk-DMC, was calculated as a z-score defined as  $100 + 10 \times [tVAF_{AVG} - tVAF_1] / tVAF_{SD}$  where  $tVAF_{AVG}$  and  $tVAF_{SD}$  are the mean and standard deviation of  $tVAF_1$  from the controls.

Kinematic data for each individual was evaluated pre- and post-treatment using two measures: gait deviation index (GDI) [4] and non-dimensional walking speed. A stepwise regression was used to identify a model that best fit the outcome measures of post-treatment GDI or walking speed. Regressors in the model were pre-treatment GDI or pre-treatment walking speed, walk-DMC, treatment, age, and prior surgeries (yes/no). To minimize the effect of outliers a robust fitting using a bi-square weighting algorithm was used for the output model.

## RESULTS AND DISCUSSION

Walk-DMC distribution was similar across treatment groups (Figure 1, mean 73.4, S.D. 12.6). Overall, we found that there were increases in GDI post-treatment, which were largest for the SEMLS treatment group ( $0.6 \pm 9.2$  BTA,  $1.9 \pm 11.1$  SDR, and  $10.9 \pm 9.1$  SEMLS). We also found an overall decrease in walking speed of  $-0.03 \pm 0.08$  that was similar across all three treatments.

Pre-treatment GDI, and treatment group were significant predictors of post-treatment GDI at

CMAL-Pellenberg (Fig. 2). Walk-DMC was found to be a significant predictor with a positive slope, indicating that higher walk-DMC was associated with higher post-treatment GDI. The effect sizes of pre-treatment GDI, treatment, and walk-DMC were  $43.2 \pm 7.7$ ,  $8.0 \pm 3.6$ , and  $7.4 \pm 7.2$ , respectively. The estimate of pre-treatment GDI slope and intercept by treatment were 0.57 and 24.5 for BTA, 0.99 and -6.60 for SDR, and 0.65 and 25.57 for SEMLS. This illustrates that BTA and SEMLS treatments tended to yield diminishing improvement with increasing pre-GDI. For SDR the model suggests almost no change in GDI post-treatment. The estimate of the pre-treatment walk-DMC slopes was 0.11.

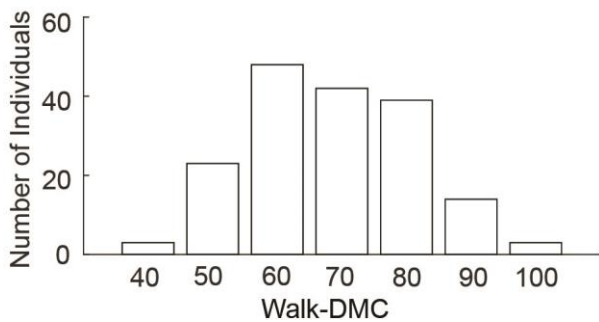


**Figure 1:** Histograms of pre-treatment Walk-DMC

Pre-treatment walking speed and walk-DMC were significant predictors of post-treatment walking speed (Fig. 2). The effect sizes of pre-treatment walking speed and walk-DMC were  $0.42 \pm 0.06$  and  $0.13 \pm 0.07$ . The estimate of the pre-treatment walking speed and walk-DMC slopes were 0.74 and 0.0021 with an intercept of -0.10.

## CONCLUSIONS

Walk-DMC was a significant predictor of post treatment walking speed, but only had a weak prediction of post-treatment GDI for children with CP at this clinical center. These findings confirm prior work finding walk-DMC to be a significant predictor of changes in walking speed after treatment, with higher walk-DMC associated with better treatment outcomes. However, the slope of walk-DMC was smaller with post-treatment GDI at this clinical center, which may be due to differences in the patient populations between centers. Walk-DMC may be most useful in identifying patients with substantial gait deviations (low GDI) but more

typical motor control (high DMC) who may benefit from treatment. Understanding the role of motor control in the evaluation of individuals with CP may help improve treatment outcomes and guide development of new interventions.

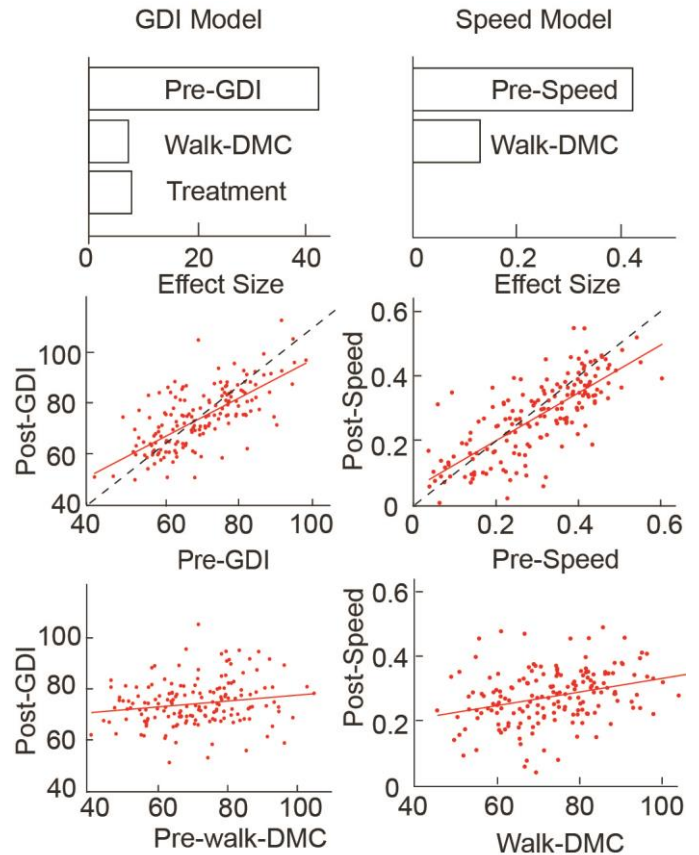


**Figure 2:** The effect sizes and adjusted response plots of the predictors included in the linear models for GDI (left column, treatment not shown) and non-dimensional walking speed (right column). Dashed lines indicate no change from pre-post.

## REFERENCES

1. Ting et al. *NEURON*, 86, 38-54, 2015
2. Steele et al. *DMCN*, 57, 1176-1182, 2015.
3. Schwartz et al. *DMCN*, 58, 1139-1146, 2016.
4. Schwartz et al. *Gait & Posture*, 28, 351-357, 2008.

## ACKNOWLEDGEMENTS

This research was supported by NIH NINDS R01 NS091056 and the University of Washington Institute of Neuroengineering.

# ANALYSIS AND MODELING OF GAIT BIOMECHANICS IN RESPONSE TO VOLUMETRIC MUSCLE LOSS INJURY

Jack Dienes, Xiao Hu, Kevin Janson, Conrad Slater, Robbie Courter, Katie McCormack, George Christ, and Shawn Russell

University of Virginia, Charlottesville, VA, USA

Email: [sdr2n@virginia.edu](mailto:sdr2n@virginia.edu)

## INTRODUCTION

Much research is currently underway to develop novel methods for the regeneration of muscle tissue as treatment of volumetric muscle loss (VML) injury, but few studies have evaluated the relationship between injury and the biomechanics required for normal function. To address this knowledge gap, we have developed a novel method to quantify the changes in gait for rats with tibialis anterior VML injuries that illustrates functional deficit in response to the injury as well as recovery. The ability to measure changes in rat gait parameters will facilitate our ability to quantify relevant functional deficits that result from VML injury, as well as the functional effectiveness of regenerated muscle volume. Data developed from this rat animal model could offer new insight on how to better treat and repair large scale volumetric muscle loss in humans.

## METHODS

Eight (8) twelve (12)-week old female Lewis rats were tested on a Panlab Rat Treadmill at a comfortable walking pace of 40 cm/s with motion capture video recorded at 1, 4, 8, and 12 weeks (W) post-surgery, with baseline testing occurring the week prior to surgery. Before all test runs, each rat was shaved to allow for accurate placement of 3mm and 5mm reflective markers on the bony landmarks of the left anterior superior iliac crest (LASI), right anterior superior iliac crest (RASl), spine, tail, hip, knee, ankle, and toe (Fig. 1). An optimum camera placement setup and calibration frame were developed for the small collection volume necessary to accurately capture the gait of rats. Kinematic data

were collected using a Vicon 7-camera (T40) setup collecting at 120Hz.

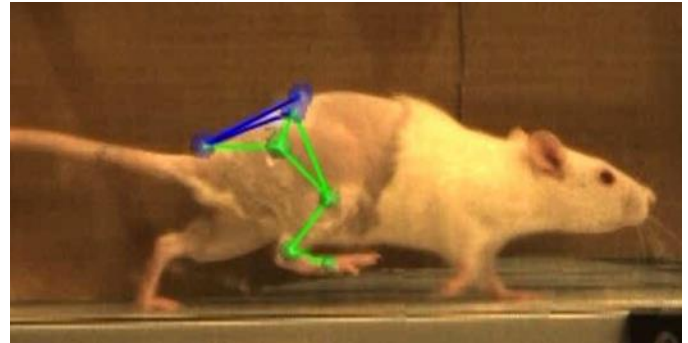


**Figure 1.** Overlay of 3-D markers, LASI, RASI, SPINE, TAIL, HIP, KNEE, and ANKLE on typical rat while walking on the treadmill. Marker locations shown as placed on test animals.

With the cameras calibrated and in place, Vicon Nexus motion capture software was utilized to record each rat walking on the treadmill. Surgery was performed on four of the eight rats and consisted of removal of 20% of the right tibialis anterior muscle in the form of a  $\sim 0.15\text{cm}^3$  rectangular cube with the long axis aligned with the fiber direction. Additionally, the extensor digitorum longus (EDL) and extensor hallucis longus (EHL) synergist muscles were ablated. Motion capture was repeated at 1, 4, 8, and 12 weeks post-surgery on both the injured group and the non-injured control group. All data was normalized to 100% of a complete gait cycle (heel strike to heel strike), with a minimum of three cycles averaged for data at each time point and condition. Cycles were excluded if the rats deviated from a typical walking pattern in any way i.e. sitting, looking up. The 3-D location of the markers on the bony landmarks collected via motion capture was exported for post-hoc kinematic analysis of joints using an OpenSim rat hindlimb model[1] modified

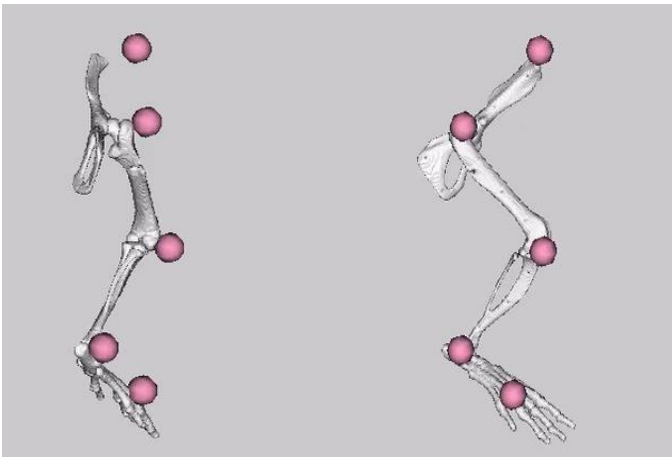


**Figure 2.** Rear (Left) and sagittal (Right) views of modified rat hind limb model developed in OpenSim. Overlay of 3-D marker locations on typical rat while walking on the treadmill. Marker locations shown as placed on model.

for our trials (Fig. 2). Simulations were performed on individually scaled versions of the model to determine gait kinematics. All data was filtered at 30Hz and all post-simulation analyses were performed in Matlab.

## RESULTS AND DISCUSSION

Baseline kinematics were similar to previously reported data on the sagittal kinematics of normal gait in rats[2]. The rats exhibited maximum deviation from normal between week 4-week 8 and slight recovery towards normal by week 12 (Fig. 3). We saw more hip abduction (22.9% W4, 14.8% W12),

more hip external rotation (64.8% W4, 36.9% W12) and more ankle plantarflexion (40.8% W8, 34.9% W12) in the injured animals as compared to their baseline measurements. Data at 1 week post-op was determined to be excessively noisy due to the proximity to surgery, and in the future week 2 will be analyzed instead.

## CONCLUSIONS

These results are indicative of circumduction, a classic compensation for drop foot. The injured rats are increasing the external rotation and abduction of the hip to swing their foot around the body due to their inability to produce sufficient dorsiflexion for foot clearance in swing. The future addition of force plates to analyze dynamics and joint torques for better understanding of musculoskeletal control and joint loads will inform the development of regenerative technologies to aid recovery from VML injuries.

## REFERENCES

1. Johnson et al, 2008, *J Biomech* 41(3) 610-619.
2. Garnier et al, 2007, *Behav Brain Res* 186 57-67.

## ACKNOWLEDGEMENTS

This work was supported in part by the AR<sup>3</sup>T Pilot Funding Program.

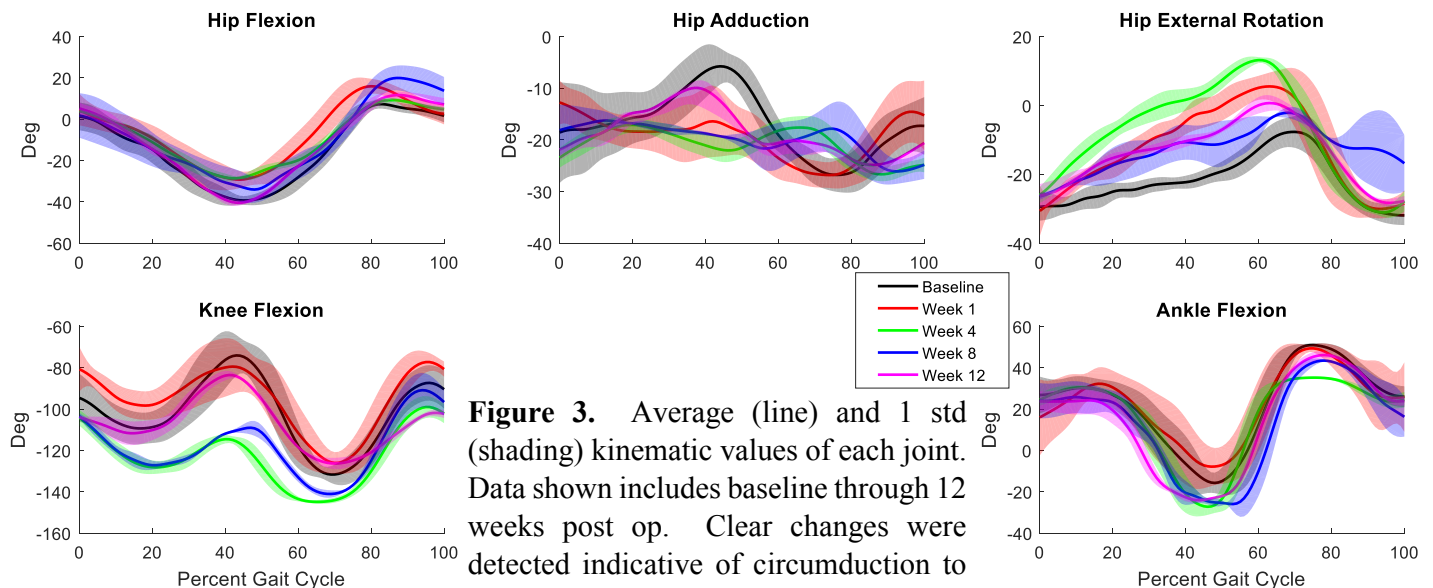


**Figure 3.** Average (line) and 1 std (shading) kinematic values of each joint. Data shown includes baseline through 12 weeks post op. Clear changes were detected indicative of circumduction to compensate for foot drop.

# APPLICATION OF TEMPORAL WAVEFORMS FOR EVALUATION OF GAIT TRAINING IN CHILDREN WITH CEREBRAL PALSY

<sup>1</sup> Amy K. Hegarty, <sup>2</sup> Max J. Kurz, and <sup>1</sup> Anne K. Silverman

<sup>1</sup>Department of Mechanical Engineering, Colorado School of Mines, Golden, CO, USA

<sup>2</sup>Physical Therapy Dept., Munroe-Meyer Institute, University of Nebraska Medical Center, Omaha, NE, USA  
email: ahegarty@mymail.mines.edu, web: fbl.mines.edu

## INTRODUCTION

With advancement and availability of instrumented gait analysis, large amounts of quantitative, interdependent data have become commonplace in the realm of kinematic, kinetic, and musculoskeletal simulation movement studies. However, effective statistical techniques to accurately quantify variance within and between populations or conditions is challenging. Often, hypothesis-driven movement studies target one or multiple time-independent parameters derived from kinematic or kinetic data, such as mean or peak-to-peak values. However, these coarse metrics often mask subtle, yet often clinically relevant, differences in the waveforms.

Waveform analyses derived for use in image processing and pattern recognition have also been effectively used to characterize biomechanical data to evaluate the 3-dimensional (3D) kinematic and force trajectories [1], knee loads during running [2], and muscle activity during balance perturbations [3]. For example, wavelet-based functional ANOVA (wfANOVA) provides a framework to statistically compare time-series curves within the wavelet domain. Wavelet transforms can provide a measure of both frequency content and underlying temporal structure of the data. In wfANOVA, waveform features described in wavelet transformations are statistically compared and can be reassembled in the time domain for interpretation [3].

The purpose of this study was to compare the results of wfANOVA against ANOVA of time-independent metrics (i.e., mean, range of motion) to investigate the effects of gait training on kinematics of children with cerebral palsy (CP). We hypothesized that both statistical approaches would indicate significantly different knee flexion kinematics after gait training. However, we expected that wfANOVA would reveal

additional differences in kinematics that were not apparent from time-independent metrics.

## METHODS

Seven children with spastic CP (6 diplegic, 1 hemiplegic, gross motor function classification system: 6 level II, and 1 level III, age:  $12.4 \pm 2.7$  yrs., height:  $1.48 \pm 0.2$  m, weight:  $43.5 \pm 15.3$  kg) participated in a six-week gait training program. Prior to and following gait training, each child participated in a 3D gait analysis session where lower body kinematics were collected at 120 Hz and filtered at 6 Hz during overground walking. Joint kinematics were calculated using a least-squares optimization algorithm in Visual3D and normalized to the gait cycle (GC) for five walking trials before and after training. Trajectories were generated for each child's more and less affected legs. The less affected leg was defined by higher strength in lower limb isometric joint strength tests.

A linear mixed effects two factor ANOVA model including fixed effects (Training  $\times$  Leg) and a random effect (Subject) was used to model knee flexion time-independent parameters of mean angle and range of motion. The F-test was used to statistically evaluate the effects of the fixed factors within the model ( $\alpha=0.05$ ). Post-hoc two-sample t-test comparisons with Bonferroni corrections ( $\alpha=0.05$ ) were completed where main effects or interaction terms were significant.

Waveform data analysis was completed using wfANOVA. Each knee flexion trajectory (normalized to the gait cycle) was transformed into the wavelet domain using a discrete wavelet transform. The resulting wavelet transform represents a series of coefficients that map to third order coiflet wavelets ordered in time, and grouped

in both low frequency (approximation level) and high frequency (detail level).

A two factor (Training  $\times$  Leg) linear mixed effects ANOVA model with Subject as a random effect was generated for each wavelet coefficient. The F-test was used to evaluate the effects of the fixed factors within the model at each coefficient level. A Bonferroni correction factor was applied to correct field-wide significance level for the F-test ( $\alpha_{\text{fieldwide}}=0.05$ ). For significant main or interaction terms, a post-hoc two sample t-tests were applied with Bonferroni corrections ( $\alpha=0.05$ ).

## RESULTS AND DISCUSSION

The wfANOVA revealed significant differences after gait training whereas the time-independent metric analyses did not. Greater knee flexion was found after training in initial stance (0-25% GC), and terminal swing (90-100% GC) using the wfANOVA (Fig. 1), noted by significant differences in the wavelet domain ( $p<0.006$ ) that were reconstructed in the time domain for interpretation (Fig. 1). Differences in knee flexion between the more and less affected legs were also found primarily during swing (60-90% GC, Fig. 1), noted by significant differences in the wavelet domain ( $p<0.0001$ , Fig. 1).

Significant differences in the knee range of motion were only found between legs, with the less affected leg having a greater range of motion ( $\overline{RoM}_{\text{less aff}} - \overline{RoM}_{\text{more aff}} = 10.8^\circ$ ,  $p<0.0001$ ).

Waveform-based analyses of biomechanical data have the capacity to reveal relevant differences in

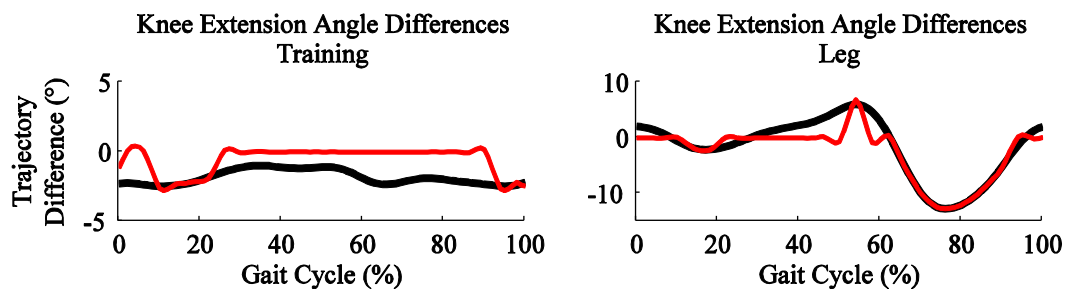


**Figure 1:** Differences in knee flexion angle are shown between pre and post gait training (left) and between the more and less affected legs (right) averaged across the group of children. Mean contrast curves (black) and significant wavelet differences reconstructed within the time domain (red) are shown. When no statistical change in waveform was found, the wavelet reconstructed curve (red) was 0. Positive differences indicate increased knee extension after training (left) or on the less affected leg (right).

gait data that would be otherwise masked by coarse time-independent metrics. These analyses also address several challenges related to biomechanical data analysis, such as temporal dependence and the interdependence of multiple biomechanical measures. Several methods such as wfANOVA [3], statistical parametric mapping [1], and bootstrapping have been effectively used to investigate biomechanical data; however, the utility and clinical relevance of each metric compared to standard techniques should be further investigated.

## CONCLUSIONS

Waveform analyses allow the ability to test generalized hypotheses without requiring *a priori* assumptions of important time phases or specific data features. Gait training resulted in increased knee flexion during initial stance and terminal swing, as indicated by wfANOVA. Differences found using wfANOVA were not apparent when comparing overall mean and range of motion pre/post gait training.

## REFERENCES

1. Pataky T., et al. *J Biomech.* **46**, 2394-401. 2013.
2. Vanrenterghem J. et al. *J Biomech.* **45**, 2444-9. 2012.
3. McKay J. et al. *J Neurophysiol.* **109**, 591-602, 2013.

## ACKNOWLEDGMENTS

This work was partially supported by the NSF GRFP (DGE-1057607).

# THE INFLUENCE OF LOCOMOTOR TRAINING ON MEDIOLATERAL DYNAMIC BALANCE IN INDIVIDUALS WITH POST-STROKE HEMIPARESIS

Arian Vistamehr<sup>1</sup>, Steven A. Kautz<sup>2,3</sup>, Mark G. Bowden<sup>2,3</sup> and Richard R. Neptune<sup>4</sup>

<sup>1</sup> Motion Analysis Center, Brooks Rehabilitation, Jacksonville, FL

<sup>2</sup> Ralph H Johnson VA Medical Center, Charleston, SC

<sup>3</sup> Department of Health Sciences and Research, Medical University of South Carolina, Charleston, SC

<sup>4</sup> Department of Mechanical Engineering, The University of Texas, Austin, TX

email: arian.vistamehr@brooksrehab.org web: <http://www.me.utexas.edu/~neptune>

## INTRODUCTION

Post-stroke hemiparetic gait is associated with a slow walking speed and lack of balance control. Thus, locomotor training, which consists of walking on a treadmill with partial body-weight support and manual assistance from trainers (e.g., [1]), aims to improve the overall mobility. While studies have reported improved walking speed as a result of such training (e.g., [1]), its effect on mediolateral (M/L) balance control is unclear.

One of the conditions for maintaining dynamic balance during walking is to regulate whole-body angular momentum ( $H$ ) through proper foot placement and generation of appropriate ground-reaction-forces (GRFs) (e.g., [2]). That is, the time rate of change of  $H$  is equal to the net external moment determined by foot placement and GRFs from each leg (Fig. 1). Poor regulation of  $H$  during walking results in higher peak-to-peak range of  $H$ , which has shown to be correlated with poor balance scores (Berg and DGI) post-stroke [3]. However, it is not clear if locomotor training improves dynamic balance through improved regulation of  $H$  and how walking speed is related to changes in dynamic balance.

The goal of this study was to assess the influence of locomotor training on M/L balance control during steady-state walking and identify underlying mechanisms associated with the observed changes. Additionally, relationships between the baseline walking speed and the changes in M/L balance control were examined.

## METHODS

Previously collected kinematic and GRF data [1] from 17 post-stroke subjects with hemiparesis pre-

and post-training were analyzed (Table 1). Subjects participated in a 12-week locomotor training program described previously [1]. Three-dimensional kinematics and GRFs were collected within one week of training initiation and completion. Subjects walked on a split-belt instrumented treadmill at their self-selected (SS) walking speed pre-training. During post-training data collection, each subject walked at a speed matched to their pre-training SS speed.

**Table 1:** Participant characteristics: overground SS walking speed and lower extremity Fugl-Meyer (FMA) were assessed pre-training.

	Gender	Age	Side	Months Since Stroke	SS Speed (m/s)	FMA
<b>Group A</b>						
1	M	48	L	59	0.71	25
2	F	45	L	11	0.51	27
3	F	74	R	8	0.79	31
4	M	56	L	12	0.76	24
5	M	54	L	26	0.76	21
6	M	74	R	22	0.48	21
7	M	57	R	32	0.50	20
8	M	68	L	17	0.63	23
9	M	62	L	56	0.60	30
10	M	43	R	11	0.70	23
<b>Mean</b>		<b>58.1</b>		<b>25.4</b>	<b>0.6</b>	<b>24.5</b>
<b>SD</b>		<b>11.3</b>		<b>18.5</b>	<b>0.12</b>	<b>3.8</b>
<b>Group B</b>						
1	M	46	L	9	0.54	21
2	M	64	L	12	0.43	19
3	M	44	L	10	0.50	27
4	F	31	R	10	0.33	18
5	M	57	L	27	0.44	17
6	F	62	L	17	0.43	25
7	M	73	R	7	0.37	21
<b>Mean</b>		<b>53.9</b>		<b>13.1</b>	<b>0.4</b>	<b>21.1</b>
<b>SD</b>		<b>14.3</b>		<b>6.9</b>	<b>0.07</b>	<b>3.7</b>

M/L dynamic balance was assessed using the peak-to-peak range of  $H$  in the frontal plane [3]. Subjects were divided into two groups (Group A: range of  $H$  decreased post-training; Group B: range of  $H$  increased post-training). The range of  $H$  between pre- and post-training during walking was compared

within each group using a paired t-test ( $p < 0.05$ ). A decreased range of  $H$  was associated with improved dynamic balance control. To further understand the underlying mechanisms for any observed changes in  $H$ , GRF peaks and impulses (i.e., time integral of GRFs) were calculated during early (0-50%) and late (51-100%) stance. Also, foot placement was calculated as the vector from the body center-of-mass to the center-of-pressure (Fig. 1). Step width mean and variability were also calculated. Further, Pearson's correlation analyses were performed to examine the relationship between the external moment components and the range of  $H$  in the frontal plane. This study is focused on changes in the vertical GRFs and the M/L foot placement as they are the dominant components of the net external moment in the frontal plane (Fig. 3 in [4]). Lastly, Pearson's correlation analyses were performed to examine the relationship between baseline SS walking speeds and changes in the range of  $H$  from pre- to post-training.

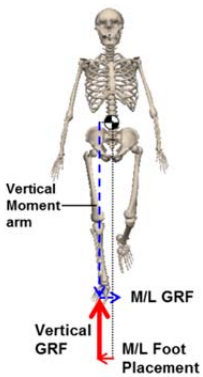


**Figure 1:** The components of net external moment in the frontal plane. Whole-body CoM is shown with  $\bullet$ . The GRF vectors and their corresponding moment arms appear in the same color. The higher magnitude of the vertical GRF compared to other components (after normalizing moment arms and GRFs by body height and weight, respectively) is highlighted by the line thickness.

## RESULTS AND DISCUSSION

Group A decreased their range of  $H$  (-) by 5% ( $p = 0.007$ ) from pre- ( $0.014 \pm 0.004$ ) to post- ( $0.013 \pm 0.003$ ) training. In contrast, Group B increased their range of  $H$  by 9% ( $p = 0.003$ ) from pre- ( $0.014 \pm 0.004$ ) to post- ( $0.015 \pm 0.004$ ) training.

In Group A, the paretic leg M/L foot placement decreased (became narrower) by 8.5% ( $p = 0.002$ ) post-training, which was correlated with a decreased range of  $H$  ( $r = 0.54$ ,  $p = 0.01$ ). Additionally, both step width and step width variability decreased by 5% ( $p = 0.03$ ) and 29% ( $p = 0.001$ ) from pre- to post-training, respectively. There were no significant changes in the peak vertical GRFs. However, the paretic leg vertical GRF impulses increased by 10% ( $p = 0.01$ ) from

pre- to post-training during both early and late stance. Also, the paretic leg vertical GRF impulses were negatively correlated with the range of  $H$  during both early ( $r = -0.41$ ,  $p = 0.07$ , approached significance) and late ( $r = -0.81$ ,  $p < 0.001$ ) stance. These results are consistent with previous work showing that wider paretic foot placement is strongly related to the lower weight bearing of the paretic leg [5].

In Group B, although there were no significant changes in the M/L foot placement, the range of  $H$  was correlated with step width ( $r = 0.74$ ,  $p = 0.002$ ) and the paretic leg M/L foot placement ( $r = 0.77$ ,  $p < 0.001$ ). Additionally, the peak vertical GRFs in the nonparetic leg increased by 4% during early ( $p = 0.02$ ) and late ( $p = 0.01$ ) stance post-training. Also, the range of  $H$  was positively correlated with the nonparetic leg peak vertical GRFs during late stance ( $r = 0.46$ ,  $p = 0.09$ , approached significance) and the nonparetic leg vertical GRF impulses during early stance ( $r = 0.85$ ,  $p < 0.001$ ).

As a whole group, the changes in the range of  $H$  from pre- to post-training were strongly correlated with the baseline SS walking speed ( $r = 0.7$ ,  $p = 0.001$ ). That is, those with a higher (lower) baseline SS walking speed mostly decreased (increased) their range of  $H$  post-training.

In summary, Group A improved their M/L balance control, mainly by narrowing their paretic foot placement and increasing their weight bearing on the paretic side. However, Group B did not improve their M/L balance control, and their nonparetic leg compensations increased post-training. Also, the baseline SS walking speed was a good indicator of those who would improve and those who would not improve their M/L balance control. Future work is needed to expand this investigation to lower level household and higher level community walkers.

## ACKNOWLEDGEMENTS

This work was supported by the Rehabilitation Research and Development Service of the Department of Veteran's Affairs and NIH P20 GM109040.

## REFERENCES

1. Bowden MG, et al. *Arch Phys Med Rehabil* **94**, 856-62, 2013.
2. Pijnappels M, et al. *Gait & Posture* **21**, 388-94, 2005.
3. Vistamehr A, et al. *J Biomech* **49**, 396-400, 2016.
4. Silverman, AK, et al. *J Biomech* **45**, 965-971, 2012.
5. Balasubramanian, C. K., *Clin Biomech* **25**, 483-490, 2010.

# KINEMATIC ANALYSIS OF SIT-TO-WALK IN BIPOLAR DISORDER

<sup>1</sup> Gu Eon Kang, <sup>1,2</sup> Brian Mickey, <sup>1</sup> Barry Krembs, <sup>1</sup> Melvin McInnis, and <sup>1</sup> Melissa Gross

<sup>1</sup> University of Michigan, Ann Arbor, MI, USA

<sup>2</sup> University of Utah, Salt Lake City, UT, USA

## INTRODUCTION

Bipolar disorder (BD) is characterized by periods of mania/hypomania and depression [1]. One clinically important characteristic of BD is unusual changes in performance of daily activities depending on mood [1] but differences in movement characteristics are limited to qualitative and observational descriptors [2]. Sit-to-walk (STW) is a day-to-day activity that requires high level of coordination between two component movements, sit-to-stand and gait initiation [3]. A recent study suggested that STW kinematics change with emotion in healthy individuals [4], suggesting that STW kinematics may change with mood phase in patients with BD. Knowledge of kinematic differences in movement patterns with mood phase in BD may lead to a new quantitative clinical marker for BD. The purpose of this study was to investigate STW kinematics across mood phases in BD.

## METHODS

Twenty bipolar patients and 14 healthy controls (HC) were recruited from the Prechter Longitudinal Study of Bipolar Disorder at University of Michigan Depression Center. Participants had no history of neurological or orthopedic illness that might affect STW. Additionally, HC had no history of personal or familial major psychiatric illnesses. Mood phase of bipolar patients was assessed using the Altman Self-Rating Mania Scale (ASRM) and the Patient Health Questionnaire (PHQ-9). Then, bipolar patients were classified by mood phase into hypomania (HM; n=4; ASRM=12.5±5.2; PHQ-9=1.8±1.5), euthymia (EU; n=7; ASRM=2.0±1.6; PHQ-9=13.8±7.1) and depression (DP; n=9; ASRM=1.9±1.6; PHQ-9=14.6±6.8).

Marker data were collected using an optoelectronic motion capture system with 16 cameras at 120 Hz (Motion Analysis, Santa Rosa, CA). Participants

performed STW from a backless chair (height: 42 cm) for five trials at each of self-selected comfortable, slow and fast speeds. Marker data were low-pass filtered at 6 Hz. Visual3D (C-Motion, Germantown, MD) was used for kinematic analysis. The whole body center-of-mass (COM) was computed from marker data. We identified five events: onset, seat-off, peak vertical (VT) COM velocity, swing leg toe-off and stance leg toe-off [5]. STW duration was defined as the interval between onset and stance leg toe-off, and four relative phase durations were defined as the ratio of intervals between neighboring events to STW duration. Hesitation was defined as the ratio of COM velocity drop in the anteroposterior (AP) direction [6]. COM displacement in the AP and mediolateral (ML) directions, and peak COM velocity in the AP, VT and ML directions were calculated. One-way ANOVA with Tukey correction was used to test significant differences between groups ( $p<.05$ ).

## RESULTS AND DISCUSSION

Age (39.4±11.5 yrs) and BMI (25.8±5.4 kg/m<sup>2</sup>) did not differ between groups. STW duration was not significantly different between groups at any speed (Table 1). Relative phase durations were different between groups only for the last interval between swing leg and stance leg toe-offs (phase 4) at comfortable speed (Table 1). Relative phase 4 duration was 20.3% less for HM than for EU ( $p<.05$ ) at comfortable speed. Hesitation did not differ significantly between groups at any speed but tended to be less for HM than for EU, DP and HC at comfortable and slow speeds. (Table 1).

AP COM displacement was significantly different between groups at comfortable and slow speeds (Table 1). AP COM displacement was greatest for HM compared to all other groups at comfortable speed ( $p<.05$ ). AP COM displacement was also greater for HM than for DP at slow speed ( $p<.05$ ).

ML COM displacement was similar across groups at all speeds ( $6.1 \pm 1.7$  cm).

Similar to AP COM displacement, peak AP COM velocity was significantly different between groups at comfortable speed, and was the greatest for HM ( $p < .05$ ) (Table 1). Peak AP COM velocity also tended to be the greatest for HM at slow and fast speeds. Peak VT COM velocity ( $0.76 \pm 0.18$  m/s) and peak ML COM velocity ( $0.17 \pm 0.04$  m/s) were similar across groups and speeds.

## CONCLUSIONS

Although STW duration was not different among any of the groups, the relative duration of the terminal phase of STW was shorter for HM than for other groups. These results suggest that the time used to execute the STW task does not change with mood phase, but that HM mood phase may impact the coordination of component movements of STW. Further, the HM group maintained momentum in the AP direction more effectively than other groups, as

evidenced by the greater AP COM displacement and AP COM velocity for HM, and suggested by the tendency for hesitation to be less for HM than the other groups. The results also suggest that HM individuals may manage the transition between movement tasks differently than other groups.

## REFERENCES

1. American Psychiatric Association, DSM-V, 2013.
2. Kroenke et al. *J Gen Intern Med* 16, 606-613, 2001.
3. Magnan et al. *Gait Posture* 4, 232-241, 1996.
4. Kang and Gross. *Hum Mov Sci* 40, 341-351, 2015.
5. Kerr et al. *Gait Posture* 26, 11-16, 2007.
6. Kerr et al. *Gait Posture* 37, 598-602, 2013.

## ACKNOWLEDGMENTS

This study was funded by American Society of Biomechanics (GIA), Blue Cross Blue Shield of Michigan Foundation, and University of Michigan Rackham Graduate School. We thank Dr. Deanna Gates for help with data collection.

**Table 1:** Mean  $\pm$  standard deviation for STW variables in each group.

	HM	EU	DP	HC
<b>STW duration (seconds)</b>				
Comfortable	1.77 $\pm$ 0.24	1.85 $\pm$ 0.29	1.87 $\pm$ 0.22	1.87 $\pm$ 0.23
Slow	2.53 $\pm$ 0.55	2.67 $\pm$ 0.34	2.69 $\pm$ 0.52	2.71 $\pm$ 0.40
Fast	1.51 $\pm$ 0.18	1.50 $\pm$ 0.16	1.43 $\pm$ 0.14	1.45 $\pm$ 0.16
<b>Relative phase 4 duration (%)</b>				
Comfortable	22.8 $\pm$ 1.5 <sup>EU*</sup>	28.6 $\pm$ 3.4 <sup>HM*</sup>	24.9 $\pm$ 3.0	25.1 $\pm$ 3.8
Slow	21.7 $\pm$ 1.8	26.1 $\pm$ 3.2	23.5 $\pm$ 3.3	24.3 $\pm$ 3.9
Fast	24.2 $\pm$ 4.4	28.8 $\pm$ 3.4	25.6 $\pm$ 2.3	24.8 $\pm$ 4.0
<b>Hesitation (ratio)</b>				
Comfortable	0.35 $\pm$ 0.11	0.52 $\pm$ 0.20	0.52 $\pm$ .18	0.54 $\pm$ 0.18
Slow	0.67 $\pm$ 0.22	0.82 $\pm$ .11	0.81 $\pm$ 0.20	0.80 $\pm$ 0.19
Fast	0.21 $\pm$ 0.11	0.17 $\pm$ 0.13	0.21 $\pm$ .10	0.26 $\pm$ 0.18
<b>AP COM displacement (m)</b>				
Comfortable	0.97 $\pm$ 0.02 <sup>HC*,EU*,DP*</sup>	0.82 $\pm$ 0.08 <sup>HM*</sup>	0.79 $\pm$ 0.09 <sup>HM*</sup>	0.81 $\pm$ 0.08 <sup>HM*</sup>
Slow	0.35 $\pm$ 0.03 <sup>DP*</sup>	0.35 $\pm$ 0.06	0.32 $\pm$ 0.04 <sup>HM*</sup>	0.34 $\pm$ 0.04
Fast	0.05 $\pm$ 0.01	0.06 $\pm$ 0.00	0.07 $\pm$ 0.01	0.06 $\pm$ 0.01
<b>Peak AP COM velocity (m/s)</b>				
Comfortable	1.48 $\pm$ 0.15 <sup>HC*,EU*,DP*</sup>	1.15 $\pm$ 0.20 <sup>HM*</sup>	1.13 $\pm$ 0.23 <sup>HM*</sup>	1.14 $\pm$ 0.14 <sup>HM*</sup>
Slow	1.12 $\pm$ 0.26	0.80 $\pm$ 0.11	0.83 $\pm$ 0.21	0.82 $\pm$ 0.17
Fast	1.69 $\pm$ 0.11	1.61 $\pm$ 0.12	1.58 $\pm$ 0.22	1.52 $\pm$ 0.17

Note: Superscript letters are significant differences between groups based on one-way ANOVA: \*  $p < .05$ .

# LOWER LIMB COORDINATION DIFFERENCE IN A DYNAMIC BALANCE TASK FOLLOWING STROKE

Wendy Boehm, Kreg Gruben

University of Wisconsin-Madison, WI, USA  
email: wendy.boehm@wisc.edu, web: <https://ncl.labs.wisc.edu/>

## INTRODUCTION

Humans typically accomplish walking despite the dynamic complexity of the task. Following stroke, however, hemiparesis induces additional challenge to that task, often leaving individuals permanently disabled despite therapy. Much evidence indicates that a deficit in lower limb muscle coordination contributes to that challenge, however, precise characterization of the miscoordination and how it disrupts behaviors, as well as therapy to restore walking, have not been attained.

In order to further characterize this impairment, this study analyzed the ground reaction force ( $F$ ) during a bipedal balance task similar to walking in individuals impaired by hemiparesis for comparison with non-impaired individuals. The result was a significant difference in the lower limb muscle coordination pattern between paretic (P) and non-paretic (NP) limbs that predicts walking difficulties, behavioral compensations, and therapy objectives.

Previous study of  $F$  in the sagittal-plane of non-disabled human walking has shown linear relationships between center of pressure (CP) and the tangent of  $F$  direction off vertical ( $\tan(\theta_F)$ ) [1]. During single-leg stance, that CP vs  $\tan(\theta_F)$  relationship is geometrically represented as  $F$  lines-of-action directed through a fixed intersection point above the center of mass (CM) called a divergent point (DP). When the similar relation is extracted using CP with the effect of heel-to-toe foot roll removed, the  $F$  lines-of-action intersect lower ( $xi$ ), near the CM [2].

## METHODS

Nine participants (3 female, age 37-86yrs, 4 right side P) with chronic hemiplegia (>6mo post stroke) and six control (4 female, age 20-53yrs) participants walked on a custom force treadmill

with programmable motion 6-axis foot plates under each foot.<sup>1</sup> All participants walked with a simplified constant-swing-velocity (CSV) foot motion pattern. Control participants additionally walked with a typical swing velocity.  $F$  was recorded at 100Hz for 15s. The principal component of the CP vs  $\tan(\theta_F)$  relationship determined the location of the DP and  $xi$ , which was expressed as fraction of hip height.

## RESULTS AND DISCUSSION

Preliminary results using a simplified calculation of  $xi$  for a subset of subjects show that a line captured most of the CP vs  $\tan(\theta_F)$  variance with DP/ $xi$  (variance accounted for: control walk 99%/95.6%, control CSV walk 99%/97%, stroke CSV walk 93%/97.9%). The DP and  $xi$  locations for typical and CSV walking was above and near the CM (just above the hip), respectively, for the control participants and the NP limb of stroke participants (Fig. 1). In the P limb, DP location was more variable (Fig. 1) and the P  $xi$  was 0.09m anterior of the NP  $xi$  on average.

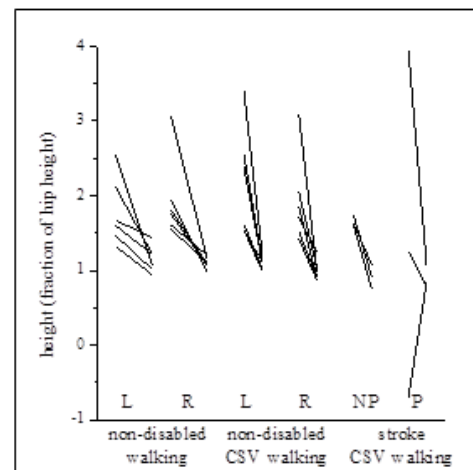


**Figure 1:** Height of intersections points for DP (left end of lines) &  $xi$  (right end of lines) show DP above the CM and  $xi$  near the CM. One line per person per leg.

The tight, anteriorly biased  $xi$  of the P limb captures a specific shift in coordination that is consistent with previously observed anteriorly biased  $F$  in seated tasks [3]. That misdirected  $F$  predicts a range of behaviors to avoid using this control for support, as is commonly observed after stroke [4]. The variable DP shows a change in strategy to accommodate this errant control such that a righting torque is still provided by  $F$  when CP shifts due to body tip.

## REFERENCES

1. Gruben, K. G., & Boehm, W. L. (2012). 31(3), 649-659.
2. Gruben, K. G., & Boehm, W. L. (2014). J Biomechanics, 47(6), 1389-1394.
3. Rogers, L. M., Brown, D. A., & Gruben, K. G. (2004). Gait & Posture, 19(1), 58-68.
4. Boehm, W. L., & Gruben, K. G. (2016). Trans Stroke Res 7(1), 3-11.

# QUANTIFYING THE EFFECTS OF TOE AND ANKLE JOINT STIFFNESS, AND THEIR INTERPLAY, ON WALKING BIOMECHANICS USING AN ADJUSTABLE PROSTHETIC FOOT

Eric C. Honert, Gerasimos Bastas and Karl E. Zelik

Vanderbilt University

email: eric.c.honert@vanderbilt.edu, web: my.vanderbilt.edu/batlab

## INTRODUCTION

The purpose of this ongoing study is to isolate the effects of metatarsophalangeal (MTP) and ankle joint stiffness, and their interplay, on walking biomechanics. The effects of ankle stiffness (in prostheses) and quasi-stiffness (in the biological limb) have been documented in prior literature; however, the effects of MTP joint stiffness – hereafter referred to as toe joint stiffness – are less well characterized. The toe joint undergoes a dorsiflexion range-of-motion in late stance (sometimes referred to as the forefoot rocker phase) comparable to ankle range-of-motion during walking [1]. Walking models also predict that toe joint articulation may improve mechanical cost of transport [2]. However, limited experimental data exist on the effects of toe joint stiffness, or its interaction with ankle stiffness, since toe joint stiffness cannot be easily varied within the biological foot or in commercial prostheses. Here we custom-designed and tested an adjustable prosthetic foot to isolate toe joint, and ankle-toe stiffness effects. This research is expected to provide insight on the functional benefits of toe joint articulation, and may inform optimal toe joint properties to incorporate into prosthetic foot design.

## METHODS

We designed and fabricated a (right and left) pair of adjustable foot prostheses with a sagittal rotational degree-of-freedom to approximate the ankle, and a single rotational degree-of-freedom to approximate the composite toe (MTP) joint axes in the biological foot. This design allows us to independently adjust ankle and toe joint stiffness, and other parameters such as toe length and shape.

Four healthy, non-amputee subjects (2 males, 2 females,  $22\pm 3$  yrs,  $74.8\pm 5.3$  kg,  $1.76\pm 0.07$  m) have thus far participated and provided informed consent for this gait analysis study. Subjects wore the foot prostheses bilaterally below simulator boots (which immobilize the biological ankles). Subjects walked at 1.0 m/s on a split-belt, instrumented treadmill while we recorded ground reaction forces (GRFs) and lower-limb kinematics. Each subject walked with 20 different ankle and toe joint stiffness combinations, which spanned above and below normal ranges [3]. Ankle joint stiffness was varied from 40 to 200 N·mm/deg·kg. Toe joint stiffness was varied from 0 to 10 N·mm/deg·kg, and we also tested an infinitely stiff (locked toe joint) condition. GRFs were used to compute center-of-mass (COM) power through the individual limbs method [4]. COM Push-off work was computed as one key outcome metric, based on prior literature (e.g., [4, 5]).

## RESULTS AND DISCUSSION

Preliminary findings suggest that both toe and ankle joint stiffness affect COM Push-off dynamics, and that the effect of toe joint stiffness is more pronounced with stiffer ankles. We observed that COM Push-off work increased with toe joint stiffness. Given a constant toe joint stiffness, a medium ankle stiffness (100-160 N·mm/deg·kg) resulted in the highest COM Push-off work. Additionally, the effects of toe joint stiffness were larger as ankle stiffness increased, as evidenced by the larger range of COM Push-off work: 4 J at the lowest ankle stiffness vs. 7 J at the highest ankle stiffness (Figure 1).

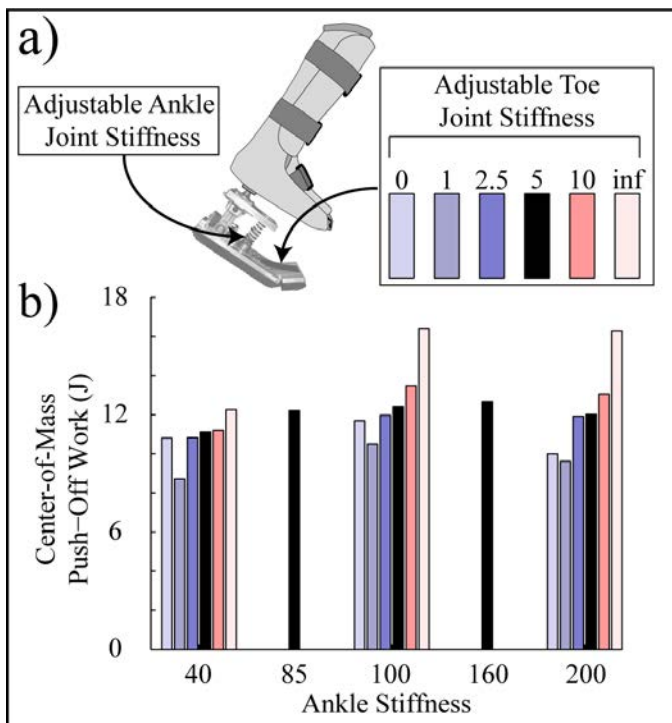


**Figure 1:** a) Adjustable foot prosthesis, and b) center-of-mass (COM) Push-off work during walking at 1.0 m/s for different ankle and toe joint stiffnesses (N=4). All stiffness values are reported in units of N·mm/deg·kg.

In this ongoing study, we also plan to examine GRFs, joint kinematics and kinetics, and metabolic cost. Statistical analysis will be performed after additional subjects are collected. Other foot

parameters such as toe shape, toe length, and foot length will also be varied. Results from this work will be used to inform a follow-up study on individuals with transtibial amputation.

## CONCLUSIONS

Toe joint stiffness affects Push-off dynamics in gait, and the magnitude of this effect increases with ankle stiffness.

## REFERENCES

1. Bruening DA, et al. *Gait & Posture*, **35**:529-534, 2012.
2. Huang Y, et al. *IEEE/ASME ICAIM*, 625-657, 2010.
3. Zhu J, et al. *IEEE Transactions on Industrial Electronics*, **9**: 4797-4807, 2014.
4. Donelan JM, et al. *J. Biomech.*, **35**: 117-124, 2002.
5. Zelik et al., *IEEE TNSRE*, **19**: 411-419, 2011.

## ACKNOWLEDGMENTS

This research was supported by grant funding from NSF (1605200) and NIH (K12HD073945)

# KINEMATIC DIFFERENCES IN PARTIAL HAND AMPUTEES USING AN EXTERNALLY POWERED HAND PROSTHESIS

<sup>1</sup> Andrea B Wanamaker and <sup>1</sup> Ajit MW Chaudhari

<sup>1</sup> The Ohio State University, Columbus, OH, USA

email: wanamaker.178@osu.edu

## INTRODUCTION

Thirty-five percent of the two million amputees in the United States live with loss of an upper limb [1]. Amputation involving the upper limb can result in severe functional deficits, particularly if the thumb or multiple digits are lost; however, the use of an externally powered hand prosthesis can potentially restore user function but it is currently unclear how much of a difference such a prosthesis can make. In addition, it is important to examine how an amputee moves with and without their prosthesis in order to examine potential flow-through conditions due to abnormal upper limb joint motion.

The objective of this research was to identify how partial-hand amputees open a jar with and without their myoelectric hand prosthesis to determine functional differences, specifically in shoulder and elbow kinematics. We hypothesized that using the prosthesis to open the jar would result in reduced joint range of motion (ROM) compared to opening the jar without a terminal device. In addition, we hypothesized that the prosthesis condition would result in biomechanical outcomes similar to healthy cohort outcomes.

## METHODS

Amputee participants were recruited from a local prosthetic clinic. Potential amputee participants had to have a partial-hand amputation (4-digit with intact thumb or 5-digit loss) due to trauma, be over 18 years of age, have a minimum of 10 hours occupational therapy towards learning how to use their prosthesis, have good skin integrity on the residual limb, and have good strength and control of the residual limb: minimum 40° wrist range of flexion/extension, minimum 60° forearm range of supination/pronation, and minimum 10 pounds lateral thumb pinch strength, if applicable.

Healthy two-handed participants were recruited from the local community. Healthy controls had to

be over the age of 18 years and were disqualified if they had previously had surgery on their upper extremities or experienced a severe upper limb injury, such as a torn muscle, ligament or tendon, or a displaced fracture.

The amputee participants performed the testing protocol twice: once with their prosthesis and once without. The two-handed participants also performed the protocol twice: once with their dominant hand as the focus and once with their non-dominant. Condition order was randomized with a fifteen-minute break between to minimize possible learning and fatigue effects. Two trials were collected for each task within each condition for analysis.

Data collection involved collecting 3D motion capture (Vicon) while participants performed various tasks of daily living focusing on upper limb movement. The data and results presented here only encompass a jar opening task. This task was contained within the Southampton Hand Assessment Protocol which requires the participants to complete the task as fast as possible while self-timing [2]. To complete the task, participants start the timer with the hand under assessment, pick up and stabilize the jar with the contralateral hand, twist off the jar lid, set the lid and jar down, and stop the timer. Only the jar opening task is presented here as it was one of the few tasks that all the amputees could successfully complete with and without their prosthesis. In addition, analysis of the SHAP resulted in significant time and functional outcome differences between the prosthesis and non-prosthesis condition for this task.

Upper limb kinematics were calculated using custom Visual3D code. Marker data were filtered using a fourth order low-pass Butterworth filter at 6 Hz. Peak and ROM joint angles for the shoulder, elbow, and wrist were found for each participant for

each condition. The results reflect only the movement that occurred while the participant was in the act of opening the jar. The movement to start and stop the timer and pick up and set down the jar were not included in this analysis. Statistical comparison between conditions was completed using a mixed-effect model with a within-subject (prosthesis vs no prosthesis; dominant vs non-dominant) and between-subjects (amputee vs. two-handed) design with a significance level of 0.05.

## RESULTS AND DISCUSSION

Six male amputees completed the testing protocol (35.7±15.5 yrs, 175.7±7.4 cm, 86.7±20.1 kg). Three were 4-digit (27.7±8.1 yrs, 177.8±9.2 cm, 76.2±6.4 kg) and three were 5-digit partial-hand amputees (43.7±18.6 yrs, 173.5±6.4 cm, 97.2±25.3 kg). Four were amputated on their dominant right side and two on their non-dominant left side. Six male two-handed controls were used for comparison (25.5±3.9 yrs, 182.9±5.8 cm, 83.0±13.3 kg). No differences were found in age or weight between groups, but the controls were taller than the amputee group (p=0.04). Comparison of dominant, non-dominant, prosthesis, and non-prosthesis resulted in multiple significant differences (Table 1).

There were no differences between the prosthesis and either two-handed conditions, indicating that the use of a hand prosthesis does appear to normalize movement. The prosthesis condition had several lower ROMs compared to the non-prosthesis condition, though only one was significant. Shoulder and elbow flexion/extension and adduction/abduction tended towards

significance (p<0.10). Finally, the non-prosthesis condition did result in differences compared to both healthy conditions, indicating a less normative movement pattern

In addition to reducing joint ROM, the use of the prosthesis also reduced the number of attempts made to open the jar. During the non-prosthesis condition, all of the amputees required two or more attempts to twist the lid off as they struggled maintain the appropriate grip. During the prosthesis condition, almost all the amputees made only one twisting motion to open the jar.

## CONCLUSION

The preliminary results presented here indicate that an externally powered hand prosthesis restores function to partial-hand amputees trying to open a jar. Using their hand prosthesis, amputees had similar joint ROMs compared to healthy two-handed controls, while not using the prosthesis resulted in larger joint ROMs, particularly at the shoulder, a possible indicator of potential flow-through conditions.

## REFERENCES

1. Zielger-Graham, et al. *Arch Phys Med Rehabil* **89**, 422-429, 2008/
2. Light CM, et al. *Arch Phys Med Rehabil* **83**, 776-783, 2002.

## ACKNOWLEDGMENTS

We would like to thank Touch Bionics for their financial and in-kind support of this project.

**Table 1.** Ensemble averages (SD) of ROM outcomes for two-handed and amputee groups. Units in degrees. <sup>a</sup> indicates p<0.05 for prosthesis vs non-prosthesis, <sup>h</sup> for dominant vs non-dominant, \* for non-prosthesis vs dominant, ^ for non-prosthesis vs non-dominant.

Outcome		Prosthesis	Non-Prosthesis	Dominant	Non-Dominant
Shoulder ROM	Flex/Ext	17.7±7.3	32.9±18.6 *	9.7±8.1 *	15.9±5.4
	Add/Abd	17.4±9.4	29.3±18.2 ^	17.0±6.0 <sup>h</sup>	12.4±3.2 <sup>h</sup> ^
	Rotation	16.8±8.6 <sup>a</sup>	47.2±22.9 <sup>a</sup> ^*	12.0±4.3 *	21.7±9.3 ^
Elbow ROM	Flex/Ext	19.0±15.9	35.0±20.9 ^	21.9±11.3	14.8±2.5 ^
	Add/Abd	6.8±4.0	16.2±16.7	4.8±2.5	7.5±2.6
	Rotation	32.0±17.3	35.6±16.0	24.5±8.1	19.6±13.6
Wrist ROM	Flex/Ext	20.7±22.3	25.6±44.1	21.3±8.0	29.1±15.1
	Add/Abd	9.9±8.5	17.5±10.5	8.4±2.9 <sup>h</sup>	19.6±8.2 <sup>h</sup>
	Rotation	6.1±6.3	12.1±13.5	8.4±2.6	6.9±2.2

# BIOMECHANICAL OUTCOMES OF PROSTHETIC FOOT STIFFNESS DURING WEIGHTED WALKING

<sup>1</sup>Pawel R. Golyski, <sup>1</sup>Barri L. Schnall, <sup>2,3</sup>Andrew H. Hansen, <sup>2,3</sup>Sara R. Koehler-McNicholas, <sup>1,4,5</sup>Christopher L. Dearth, and <sup>1,4,5</sup>Brad D. Hendershot

<sup>1</sup> Walter Reed National Military Medical Center, Bethesda, MD, USA

<sup>2</sup> Minneapolis Department of Veterans Affairs Health Care System, MN, USA

<sup>3</sup> University of Minnesota, MN, USA

<sup>4</sup> Uniformed Services University of the Health Sciences, Bethesda, MD, USA

<sup>5</sup> DOD/VA Extremity Trauma and Amputation Center of Excellence

email: bradford.d.hendershot2.civ@mail.mil

## INTRODUCTION

Despite the large number of prosthetic feet available to persons with lower limb loss, the mechanical properties best suited to specific ambulatory tasks are largely unknown. In particular, many individuals with lower limb loss wish to engage in activities involving weighted walking - an activity for which some prosthetic feet are marketed. The biological ankle-foot complex exhibits non-linear load-deflection behavior during weighted walking (i.e., there is limited additional deformation at loads exceeding body weight), which maintains roll-over shape with added load. Non-linear stiffness may therefore prevent an effective shortening of a prosthetic foot in response to added load, keeping users from “dropping-off” their prosthesis onto their contralateral limb [1]. Thus, we hypothesized a passive prosthetic foot with non-linear (NL) vs. linear (L) stiffness properties would better accommodate weighted walking, as evidenced by lower contralateral limb loading. Note, two feet tested here were selected based on previous results of mechanical testing of nine prosthetic feet, which identified the single most L and most NL feet (quantified by the difference in maximum instantaneous radius of curvature between loaded and unloaded conditions). As a secondary goal, we also sought to understand the difference in behavior of the prosthetic feet during ambulation, particularly sagittal ankle-foot power, since previous work identified prosthetic ankle-foot power as a determinant of intact limb loading during weight acceptance [2].

## METHODS

A randomized and counterbalanced crossover design was used for eight males with unilateral transtibial amputation (mean [standard deviation] age: 36.9 [7.3] years; time from amputation: 94.2 [45.9] months) who walked along a 15 m walkway in all combinations of the NL and L feet, 2 speeds (1.34 and 1.52 m/s), and with and without added load (i.e., 22kg vest). Full body kinematics and ground reaction forces were respectively collected using an optical motion capture system (Qualisys, Gothenburg, Sweden;  $f=120$  Hz) and force platforms (AMTI, Watertown, MA, USA;  $f=1200$ Hz) embedded in the walkway. All subjects provided informed consent to procedures approved by the Walter Reed National Military Medical Center Institutional Review Board.

With a focus on limb loading and prosthetic foot mechanics, bilateral first peak vertical ground reaction force (vGRF), extrema in prosthetic ankle-foot power [3], and instantaneous roll-over shape radius of curvature of the prosthetic feet [4] were calculated using Visual 3D (C-Motion Inc., Germantown, MD, USA) and Matlab (Mathworks, Natick, MA, USA). Forces and powers were normalized to body weight and added load. For all dependent variables at each speed, two-way repeated measures ANOVAs characterized main effects of prosthetic foot type, load condition, and their first order interaction. The difference in maximum instantaneous radius of curvature between loaded and unloaded conditions was compared at each speed using a paired t-test. Statistical significance was concluded at  $P<0.05$ . All values are reported as mean (standard deviation).

## RESULTS AND DISCUSSION

In contrast to our original hypothesis, the NL vs. L foot was associated with larger intact limb loads during weight acceptance. Specifically, the first peak in intact limb vGRF was significantly larger when participants used the NL vs. L foot at both speeds, though there was no significant difference in the first peak of prosthetic limb vGRF (Table 1). Neither load condition nor the interaction between load and foot type were significant effects for any dependent variables at either speed (all  $P > 0.355$ ). Extrema in prosthetic ankle-foot sagittal power from midstance to toe-off were significantly smaller in the NL vs. L foot, which may partially explain the trends in peak vGRF (Table 1; [2]). There were no significant differences at either speed between the loaded and unloaded maximum instantaneous radii of curvatures of the prosthetic foot roll-over shapes ( $P > 0.745$ ), which were expected to differ with linearity of stiffness. In addition to decreased intact limb loading and increased prosthetic power, the maximum instantaneous radius of curvature was significantly larger in the L vs. NL foot (Table 1), representing greater stability during midstance [4].

While not presented here, the mechanical properties of the two prosthetic feet may explain the deviation from our initial hypothesis. Specifically, overall stiffnesses (%BW/mm) were larger for the NL vs. L foot (NL:  $\sim 0.04$ , L:  $\sim 0.02$  for loads up to body weight; NL:  $\sim 0.09$ , L:  $\sim 0.05$  for loads over body weight). Higher prosthetic foot stiffness has been suggested to result in larger first peak vGRFs on the intact limb [5]. Larger passive prosthetic foot stiffness results in lower energy absorption and proportional return, reducing trailing limb push off power, which is consistent with our results (Table

1). Reduced power has been previously associated with increased intact limb loading and intact external adduction moment at the knee, a biomechanical indicator of the development of intact knee osteoarthritis [2]. Other work has shown clearly that too much compliance can lead to the “drop-off” effect [6]. Together, these results suggest that there may be an optimal prosthetic foot compliance that reduces intact limb loading and provides greater stability, independent of the linearity of stiffness, when walking with added load.

## REFERENCES

1. Hansen, AH, et al. *JRRD* **42**, 381-390, 2005.
2. Morgenroth DC, et al. *Gait & Posture* **34**, 502-507, 2011.
3. Takahashi, KZ, et al. *J. Biomech.* **45**, 2662-2667, 2012.
4. Curtze, C., et al. *J. Biomech* **42**, 1746-1753, 2009.
5. Fey, NP, et al. *Clinical Biomechanics* **26**, 1025-1032, 2011.
6. Klodd, EJ, et al. *JRRD* **47**, 899-910, 2010.

## ACKNOWLEDGMENTS

Support for this project was provided by the BADER Consortium via the Congressionally Designated Medical Research Program (Award # W81XWH-11-2-0222) and the DoD-VA Extremity Trauma & Amputation Center of Excellence (Public Law 110-417, National Defense Authorization Act 2009, Section 723). The views expressed in this abstract are those of the authors and do not necessarily reflect the official policy or position of the Departments of the Army, Navy, Defense, nor the United States Government.

**Table 1:** Mean (standard deviation) biomechanical outcomes between the linear (L) and non-linear (NL) feet, by walking speed. vGRF = vertical ground reaction force, BW= body weight.

	1.34 m/s			1.52 m/s		
	NL Foot	L Foot	P-value	NL Foot	L Foot	P-value
Intact First Peak vGRF (BW+Added Load)	1.22 (0.01)	1.11 (0.01)	0.003	1.27 (0.01)	1.18 (0.01)	0.012
Prosthetic First Peak vGRF (BW+Added Load)	1.08 (0.01)	1.06 (0.01)	0.462	1.11 (0.01)	1.08 (0.01)	0.252
Prosthetic Ankle-Foot Sagittal Power (W/kg)	Max	2.27 (0.15)	<0.001	1.33 (0.11)	2.56 (0.23)	<0.001
	Min	-0.66 (0.02)	<0.001	-0.74 (0.01)	-1.24 (0.03)	<0.001
Maximum Instantaneous Radius of Curvature (mm/foot length)	4.88 (2.09)	6.40 (3.50)	0.018	5.41 (2.08)	7.09 (3.21)	0.009

# CHARACTERIZATION OF PROSTHETIC FEET FOR WEIGHTED WALKING

<sup>1</sup> Sara R. Koehler-McNicholas, <sup>1</sup> Eric A. Nickel, <sup>1</sup> Kyle Barrons, <sup>1</sup> Kathryn E. Blaharski,  
<sup>2</sup> Barri L. Schnall, <sup>2,3,4</sup> Brad D. Hendershot, <sup>1,5</sup> Andrew H. Hansen

<sup>1</sup> Minneapolis VA Health Care System, Minneapolis, MN, USA

<sup>2</sup> Walter Reed National Military Medical Center, Bethesda, MD, USA

<sup>3</sup> DOD-VA Extremity Trauma and Amputation Center of Excellence

<sup>4</sup> Uniformed Services University of the Health Sciences, Bethesda, MD

<sup>5</sup> University of Minnesota, Minneapolis, MN, USA

email: sara.koehler@va.gov

## INTRODUCTION

Following lower-limb amputation, many individuals have the desire to resume physically demanding occupations that require them to carry heavy loads (e.g., military service, firefighters, and farmers). However, it is currently unclear which prosthetic feet are best designed to accommodate heavy load carriage while also providing good overall function and mobility during unweighted activities. In particular, most prosthetic feet deflect proportionally with added loads, thereby resulting in increased prosthetic ankle dorsiflexion [1, 2] and presumably, decreased roll-over shape radii [3]. This tendency suggests that many ankle-foot prostheses may not mimic the physiologic system they are trying to replace during weighted walking.

The goal of this study was to investigate the ability of currently-available prosthetic ankle-foot systems to accommodate weighted walking by examining the mechanical characteristics (i.e., stiffness linearity) and dynamic function (i.e., effective roll-over shape) of prosthetic feet designed for the highest activity users. To evaluate forefoot stiffness linearity, load versus deflection curves were obtained for nine different prosthetic ankle-foot systems. Three research participants then walked with each prosthetic ankle-foot system while quantitative motion analysis was used to obtain effective roll-over shape profiles. We hypothesized that prosthetic ankle-foot systems with a non-linear stiffness profile would better accommodate weighted walking, as evidenced by smaller changes in roll-over shape radii with added load. This study is expected to be useful in guiding the selection of prosthetic feet for high-activity users.

## METHODS

Nine prosthetic feet, all marketed for users in the highest Medicare Functional Classification Level (K4), were investigated in this study (Fig. 1). Load versus deflection profiles were obtained using a servohydraulic universal test frame (MTS 858, MTS, Eden Prairie, MN) with axial/torsional capabilities, a computer-based data acquisition system (Wintest, Bose, Framingham, MA), and a load cell (MTS 661-21A-01, MTS, Eden Prairie, MN). The load frame applied a uniaxial load to the foot. The foot was inserted into a boot (Reebok Hyper Velocity 8'' UltraLight Performance) and mounted in a fixture such that the plantar surface of the boot was set at a 20 degree angle from horizontal, simulating forefoot loading as defined by the ISO 10328 standard. Each foot was loaded to a maximum load of body weight + 22 kg. This represented the peak vertical ground reaction force (GRF) during single-limb support of walking while carrying an additional 22 kg load. Test loads were applied at a rate of 100 N/s, held for 1s, then ramped down at a rate of 100 N/s and held at 0 N for 1s. To compare the mechanical properties of each foot (i.e., linear versus non-linear), load versus deflection profiles were plotted from 50 N of applied load to the maximum load. The best-fit linear slope of the load versus deflection curve was then calculated between 50 N and body weight of each respective subject, corresponding to forefoot stiffness (K1) during unweighted walking. The best-fit linear slope of the load versus deflection curve was also calculated between body weight and maximum load, corresponding to forefoot stiffness (K2) above body weight. Stiffness values were normalized by body weight in order to calculate means across subjects.

Motion analysis data were also collected on three subjects with unilateral, transtibial amputation (age 32-44 years, weight 70-97 kg, height 1.7-1.8 m). A certified prosthetist fit all study feet (tested in random order). Subjects wore the same boot that was used during mechanical testing. Reflective markers were placed on subjects to define an anatomically-relevant socket coordinate system [4]. Subjects then walked at a constant, self-selected speed with and without added weight (22 kg) across two AccuGait force platforms (AMTI, Watertown, MA; sampling rate=1200 Hz) while an 8-camera Oqus 100 motion analysis system (Qualisys Motion Capture Systems, Gothenburg, Sweden; sampling rate=120 Hz) tracked marker trajectories. To calculate roll-over shape, the center of pressure of the GRF was transformed into a socket-based coordinate system with its origin at the knee center [4]. The instantaneous radius of curvature was then calculated for each frame of stance phase [5] and the difference in mean maximum instantaneous radius of curvature was calculated (unweighted-weighted) for each foot across all subjects.

## RESULTS AND DISCUSSION

Mean forefoot stiffness values are shown in Fig 1. Interestingly, K2 forefoot stiffness was higher than K1 for all prosthetic feet tested in this study. These results indicate that to some extent, the stiffness profile of all feet were non-linear, with the Thrive being the most non-linear (i.e., largest difference).

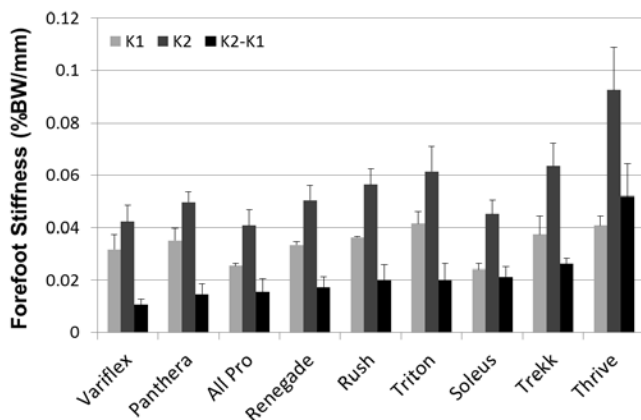


**Fig 1.** Mean forefoot stiffness corresponding to loads up to body weight (K1) and above body weight (K2). Results are sorted by mean difference in K2 and K1, from lowest (left) to highest (right).

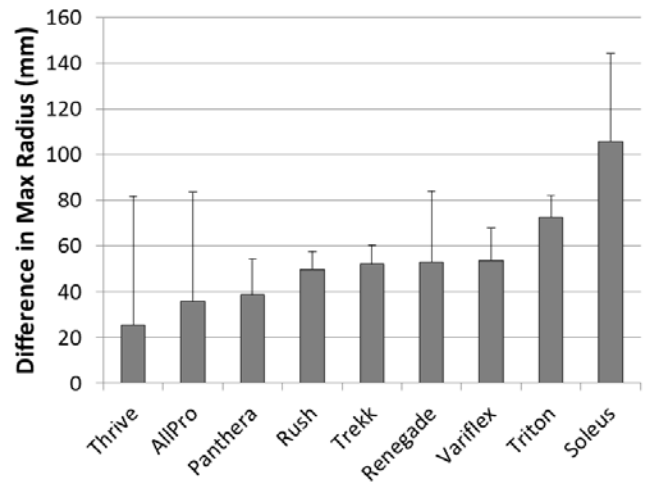


**Fig 2.** Mean difference (unweighted-weighted) in the maximum instantaneous radius of curvature.

Fig 2 shows the mean difference in maximum instantaneous radius of curvature across all subjects. Interestingly, the results of this analysis are consistent with the results of mechanical testing in that the Thrive, with the most non-linear stiffness, exhibited the smallest change in roll-over shape radii with added load. These results suggest that prosthetic ankle-foot systems with non-linear stiffness profiles may better accommodate weighted walking by providing the most biomimetic function for both weighted and unweighted activities. However, further testing is needed to determine the functional implications of these results.

## REFERENCES

1. Doyle SS, et al. *Clin Biomech (Bristol, Avon)* **29**(2), 149-154, 2014.
2. Schnall BL, et al. *J Rehabil Res Dev* **51**(10), 1505-1514, 2014.
3. Hansen AH, et al. *J Rehabil Res Dev* **42**(3), 381-390, 2005.
4. Hansen AH, et al. *Prosthet Orthot Int* **27**(2), 89-99, 2003.
5. Curtze CA, et al. *J Biomech* **42**(11), 1746-1753, 2009.

## ACKNOWLEDGMENTS

Support for this project was provided by the BADER Consortium via the Congressionally Designated Medical Research Program (Award # W81XWH-11-2-0222).

# Effects of robotic prosthesis controllers and positive work on metabolic cost

<sup>1</sup>Matthew Handford and <sup>2</sup>Manoj Srinivasan

<sup>1,2</sup>The Ohio State University, Columbus, OH, USA

email: handford.4@osu.edu, web: http://movement.osu.edu

## INTRODUCTION

The vast majority of lower limb amputees use passive prostheses such as the SACH foot or the Flex foot. These devices have been around since the 1950s and 1980s respectively and have been shown to be detrimental to patients' mobility and metabolic cost. In attempting to create more comfortable prostheses which reduce the metabolic cost of the users, many recent studies sought to develop active prostheses which are capable of providing net positive work to a standard walking gait. Despite the theoretical benefits of active prosthesis, in practice, they only marginally improve amputees' metabolic cost or walking kinematics. In this study, we use a simulation of a person with an ankle-foot prosthesis to observe how increasing the work output of an active prosthesis in 3 different controllers effects the kinematics, and energetics of a walking gait. We also explore how the benefits of each controller change based on gait and environmental changes such as walking speed and ground slope.

## METHODS

Our simulation consists of a sagittal plane model of an amputee with an ankle-foot prosthesis made of seven rigid bodies. Each member is given inertial and dimensional parameters based on previous work [1]. As shown in Fig. 1, all of the biological joints are actuated using 13 uni- and biarticular muscles, whereas the prosthesis is actuated by a single torque motor.

The human-prosthesis model is used to simulate a walking gait by defining a set of contact states, based on heel and toe contact. For each of these contact states we derive ODEs to simulate motion through forward integration [1]. Collisions that occur between these contact states are assumed to be perfectly inelastic. Each of these contact states is

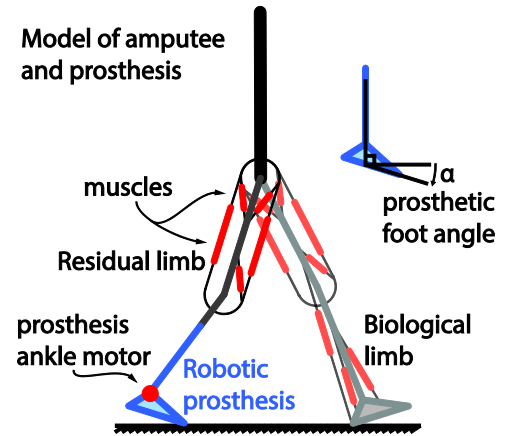


**Figure 1:** Sagittal plane model of human and prosthesis.

then split up into a series of segments to be used in a large scale optimization calculation.

Since people tend to walk in a manner that roughly minimizes metabolic energy [2], we can use energy optimization calculation to predict how a person will move while using a variety of prosthesis controllers. Therefore, we define a cost function based muscle activation, force, and shortening velocity [1], shown below:

$$C_m = \int \sum \left[ 0.05(a + a^2) + a\phi \left( \frac{v}{v_{max}} \right) \right] F_{iso} v_{max} dt$$

We then defined three controllers with which to actuate the ankle-foot prosthesis. The torque-ankle angle relationships are shown in Fig. 2. Each of these controllers was tested with multiple levels of net work to determine their effect on the human metabolic cost and the gait kinematics. Each controller was tested on flat ground at a walking speed 1.3 m/s. After determining that controller 3 produced the smallest metabolic cost, this controller was also tested at other walking speeds and ground slopes.

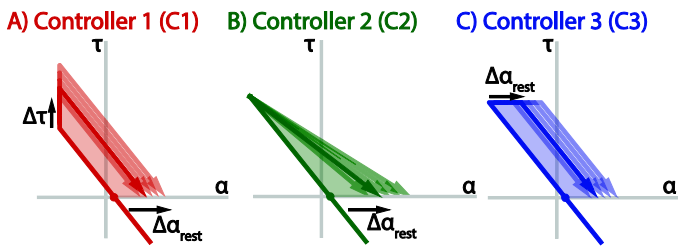


**Figure 2:** Prosthesis controller torque – ankle angle relationship.

## RESULTS AND DISCUSSION

For every controller tested, similar to what has been observed in experimental studies, as the net work of the prosthesis increases, the metabolic cost to the person decreases. However, we also found that at a certain level of work, any additional positive work would produce a higher cost to the person, thus signifying an optimal work. We also found that each controller effected the metabolic cost differently. This shows that not only is work important to metabolic cost, but also the manner in which it is applied needs to be considered. Fig. 3 displays the results for each controller at various levels of work.

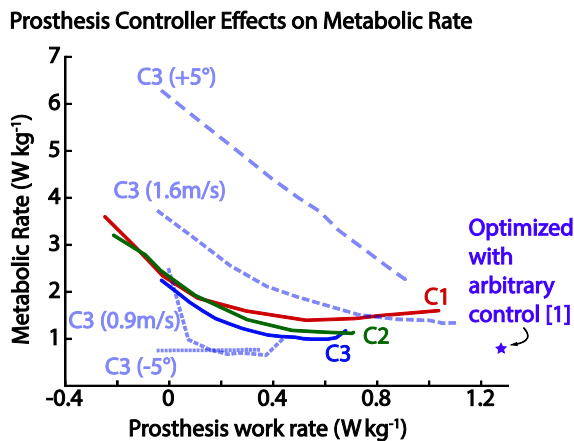


**Figure 3:** Metabolic rate due to various levels of work from all three controllers. Light blue lines show the results from controller 3 at various speeds and ground slopes.

As far as their effect on kinematics, we found that each controller produced an asymmetric gait with % stance time on the prosthesis side increasing along with the addition of work. These results are summarized in Fig. 4. The tendency to spend more time on the prosthesis foot rather than the biological

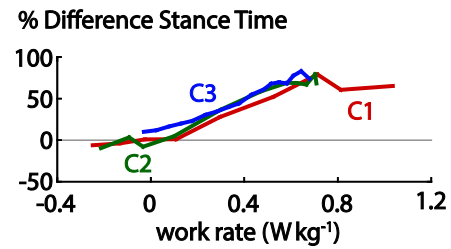


**Figure 4:** The difference in step time between the prosthesis and biological sides.

foot is not seen in experiment. This discrepancy is likely due to the lack of damping in the prosthesis controllers.

After determining which of the three controllers produced the lowest metabolic cost, we tested that controller at walking speeds ranging from 0.9 m/s to 1.6 m/s and with ground slopes ranging from  $-5^\circ$  to  $5^\circ$ . Fig. 3 displays the results from these simulations. For all speeds, we found that the addition of positive work produced smaller metabolic cost. For negative slopes the addition of work to the prosthesis has very little effect on the metabolic cost, while for positive slopes, the metabolic cost is linearly dependent on the work provided. These results lead us to conclude that, in order to get the maximum benefit from an active prosthesis, it may be necessary to build a slope and speed dependency into the controller.

## REFERENCES

1. M. Handford and M. Srinivasan, “Robotic lower limb prosthesis design through simultaneous computer optimizations of human and prosthesis costs,” *Sci. Rep.*, vol. 6, 2016. Gardner JG, et al. *J Biomech* **38**, 1861-1868, 2004.
2. R. H. Miller, “A comparison of muscle energy models for simulating human walking in three dimensions,” *J. Biomech.*, vol. 47, pp. 1373–1381, 2014

## ACKNOWLEDGMENTS

This work was supported by NSF CMMI grant 1300655. We thank Steve Collins and Joshua Caputo for discussions informing this study.

# FINITE ELEMENT ANALYSIS OF SOCKET TO LIMB INTERFACE SIMULATING GEL LINER SLIP VERSUS NO SLIP

<sup>1,2</sup> Amy L Lenz, <sup>1</sup> Sara Roccabianca, and <sup>1</sup> Tamara Reid Bush

<sup>1</sup> Michigan State University, East Lansing, MI, USA

<sup>2</sup> Mary Free Bed Rehabilitation Hospital, Grand Rapids, MI, USA

email: lenzamy@msu.edu, web: <http://researchgroups.msu.edu/reidtama>

## INTRODUCTION

Prosthetic users rely on a well-fitting prosthesis. To accomplish a good fit, the skin on the residual limb is covered by a gel liner, and then the prosthetic device goes over the biological limb and liner. The mechanical interface between the limb and liner results in a complex loading condition at the skin. These loads are contributors to the formation of skin wounds that are highly prone to infection, called ulcers. While extensive linear models have been developed, there is much yet to be understood about key contributors to ulcer formation through the use of non-linear biological tissue modeling. Since this mechanical system consists of a highly non-linear material, i.e. the skin, it is important to use an appropriate material description, otherwise the model results could dramatically overestimate or underestimate the stress magnitude on the skin. Furthermore, a deeper understanding of the interface between the gel liner and residual limb tissue is needed.

Soft tissue modeling research is limited with regard to the use of non-linear neo-Hookean materials implemented in software platforms specifically designed for biological tissues (i.e. FEBio) [1]. Currently, soft tissue models using FEBio study heel ulcers, buttock tissue damage in spinal cord injured individuals, and a single transtibial patient [2-4].

Further, experimental work by the authors [8] showed that during walking, the liner elongated at the distal end of the residual limb. To achieve these larger distal displacements, either the liner is sliding with respect to the skin or the liner is “sticking” to the skin and shearing tissues below.

The purpose of this work was to explore these two scenarios. To accomplish this we developed a soft

tissue model in FEBio and looked at a slip and no slip conditions for three different liners.

## METHODS

A finite element model with a rectangular geometry of 100 mm x 100 mm was developed to represent the body and gel liner interface for a prosthetic user. The model contained four layers: bone, muscle, skin and a gel liner (Fig. 1). Layer thicknesses were 10 mm of bone, 20 mm of muscle, 3 mm of skin, and 9 mm of gel liner [3-7]. Mechanical properties of bone, muscle, skin and a gel liner were adapted from the literature. Specifically, the bone was assumed to be a rigid body ( $E = 7$  GPa;  $\nu = 0.3$ ). The muscle ( $\nu = 0.49$ ;  $\mu = 7.124$  kPa) and skin ( $\nu = 0.495$ ;  $\mu = 31.899$  kPa) were quasi-incompressible and hyperelastic, represented by a neo-Hookean material [3-4]. The gel liner was modeled as an isotropic, linear elastic material. Three liners were modeled and were based on existing liner material: A, B and C with a poisson's ratio of 0.49 and increasing Elastic moduli of 50.05, 55.86 and 56.28 kPa, respectively [5].

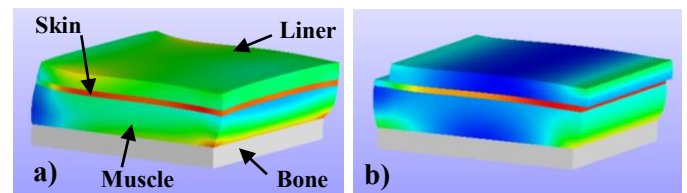


**Figure 1:** a) No slip model and b) Slip model demonstrating effective stress results. Plotted at the same stress color scale, red indicates highest effective stress (Table 1) in the skin layer.

The skin to gel liner interface was modeled in two ways. First, a tied contact was used to computationally represent a no slip condition of the liner with respect to the skin (Figure 1a). Secondly, a sliding contact was defined with a coefficient of friction of 0.3 for all three liner types [5] which

computationally would allow for slip to occur if threshold was exceeded (Figure 1b).

Loading conditions consisted of a 5 kPa distributed pressure at the surface of the gel liner based on experimentally collected force data. Secondly, a prescribed displacement of 6 mm was applied to the liner to represent displacement found in the gel liner for transtibial amputees wearing a gel liner interface with a pin locking suspension design [8].

## RESULTS AND DISCUSSION

In models where slip occurred between the gel liner and the surface of the skin, effective stress was varied throughout the skin layer with the highest stresses occurring in the region identified as element 2 (Figure 2 and 1b); whereas models without slip (Fig. 1a) demonstrated even stresses throughout the interface contact.

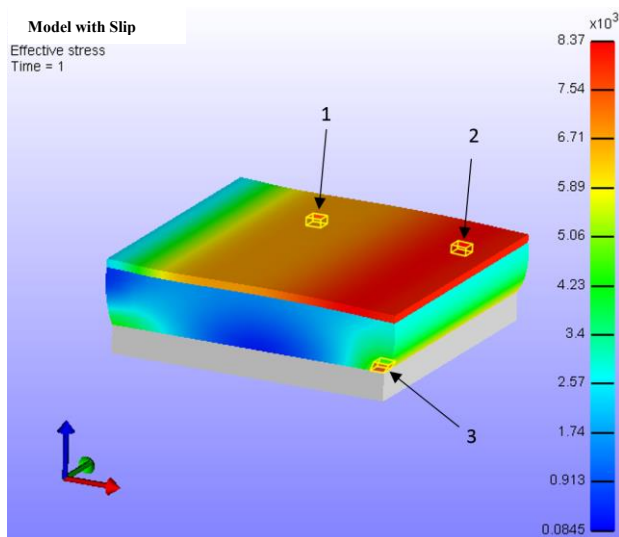


**Figure 2:** Model with slip and gel hidden, demonstrating three locations of effective stress analysis with scale in Pa.

For liner A, with identical loading conditions, the normal compressive stress at the muscle to bone

interface was nearly doubled when compared with the model with slip (Table 1). Additionally, maximum shear stress was increased in all three locations for the model without slip. With increasing prosthetic gel liner stiffness (A to C), models without slip demonstrated slightly decreased compressive stress at the bone to muscle interface. While none of these models exceeded the published ultimate stresses for skin, the deeper tissue stresses and the repeated shear loading which cyclically occurs through the day for prosthetic users is a likely contributor to tissue wounds on the residual limb.

## CONCLUSIONS

Soft-tissue finite element models are needed to improve our understanding of the interface mechanics between prosthetic liners and underlying tissues in prosthetic users. The comparison of slip and no slip conditions present an important clinical question because clinically, slip of the liner with respect the limb is not desired. Additionally, if slip does not occur, the uneven displacements on the liner would produce a shearing of deeper tissue which is also not desirable. Further model studies and experimental data to support these models are warranted. Mechanics based data is a necessity to formulate improved prosthetic fit and design, these additional data are also helpful in guiding prosthetists in the selection of appropriate prosthetic liners for patients.

## REFERENCES

1. Maas SA, et al. *ASME J Biomech Eng* **134**, 2012.
2. Sengeh DM, et al. *J Mech Beh Bio Mat* **59**, 379-392, 2016.
3. Levy A, et al. *J Tissue Viability* **24**, 1-11, 2015.
4. Shoham N, et al. *Adv Skin Wound Care* **28**, 303-316, 2015.
5. Sanders JE, et al. *J Reh Res Dev* **41**, 175-186, 2004.
6. Zollner AM, et al. *J Mech Phys* **28**, 495-509, 2013.
7. Tepole AB, et al. *J Mech Phys* **59**, 2177-2190, 2011.
8. Lenz AL, et al. *ASB'17*, Boulder, CO, USA, In Review

**Table 1:** Liner A comparison for slip versus no slip conditions in three locations. Location 1 and 2 are in the skin layer of the model and location 3 is at the muscle to bone interface (Fig. 2).

	No Slip Model			Slip Model		
	Location 1	Location 2	Location 3	Location 1	Location 2	Location 3
Effective Stress (kPa)	9.12	9.24	9.02	6.71	8.39	5.88
Normal Compressive Stress (kPa)	-4.78	-4.96	-17.69	-5.12	-4.80	-9.40
Max Shear Stress (kPa)	4.98	5.09	5.18	3.88	4.84	3.38

# A DART THROWER'S MOTION WRIST SHOULD IMPROVE PROSTHETICS

Matthew Davidson, Richard Weir  
University of Colorado Denver, Aurora, CO  
email: Matthew.Davidson@ucdenver.edu

## INTRODUCTION

Despite decades of improvement, upper-limb prosthetic devices still do not provide enough functionality for the 41,000 Americans with upper limb amputations. State of the art myoelectric devices work by reading electrical signals from the muscles in the residual limb and translating them into motion of the prosthesis. Non-invasive techniques, such as surface electrodes, are non-specific, picking up data from all extensors or all flexors and providing only two inputs. This means that, although the mechanical challenges of creating a hand and wrist that mimic all 27 degrees of freedom (DOF) of the anatomical limb has been largely solved (see DEKA arm, e.g.), we do not yet have a way to collect enough inputs to effectively control such a complicated device. While many other projects have focused on trying to increase the amount of control inputs, we have attempted to solve this problem by reducing the dimensionality of the device by combining DOF in the wrist into the Dart Thrower's Motion (DTM).

The DTM is a combination of wrist flexion-extension (FE) and radial-ulnar deviation (RU) in a plane rotated along the axis from pure FE. It is particularly useful in performing activities of daily living (ADL) that involve tool use [1]. We previously found this angle to be 26.8 degrees [2]. Our previous work showed that nearly 75% of the functionality of the wrist during grasping can be maintained by reducing the wrist to the single DTM DOF.

We present here the results of testing a new prosthetic device that incorporates the DTM. This device improves functionality while only adding a small amount of complexity. This has the potential to improve the lives of people with upper limb amputations by allowing them to more easily perform ADL and find better jobs.

## METHODS

In a preliminary sample, six adults (age:  $30 \pm 6$  years) with normal physiology performed the Southampton Hand Assessment Procedure (SHAP) while fitted with a splint with a terminal prosthesis simulating an amputation [3]. Participants performed the SHAP with three different wrist configurations: No Wrist, Flexion Wrist, and DTM wrist. Each configuration was tested in a separate session with at least 24 hours of rest in between sessions. At the conclusion of each session, the participants filled out the NASA Task Load Index (TLX), a validated subjective measure of task difficulty.

The SHAP is a validated and standardized measure of hand function that has become standard of care in measuring prosthetics effectiveness. Participants complete 12 movement tasks with abstract objects and 14 ADL objects. The test is based on time-to-completion and produces a score from 0 (no function) to 100 (normal function). The design of the prosthetic hand prevented participants from completing four of the ADL tasks (Buttons, Cut, Tray, and Zip). In order to prevent damage to the equipment, participants simulated pouring water by positioning the cup and counting four seconds before replacing it. Due to large inter-subject variability, we compared data with the intra-subject mean subtracted [3].

The simulated prosthesis consisted of a splint with a commercial quick disconnect attached to the end. We created a custom 1-DOF wrist with rotation and a wedge to create the DTM based on our previous work. The hand was a 1-DOF, 3 finger hand. We used a standard of care state-machine position control system where co-contraction switched between controlling the hand and wrist. The wrist control was disabled for the "no wrist" condition and rotated back to pure FE for the "flexion wrist condition".

EMG signals were recorded from the dorsal and ventral forearm with surface electrodes. The signal was processed in LabView (National Instruments, Austin, TX) and sent to the motors (Faulhaber, Schönaich, Germany) via an Arduino Uno and custom motor controllers (Sigenics, Chicago, IL).

Participants were given up to 15 minutes to practice with the prosthesis before beginning the SHAP. They were given instruction and up to 5 minutes practice time before each task.

This study was approved by the Colorado Multiple Institution Review Board (COMIRB No: 14-0838).

## RESULTS AND DISCUSSION

We found significant differences between SHAP scores of different wrists and that the average SHAP scores for the DTM wrist were higher than those for the FE wrist (ANOVA,  $p < 10^{-7}$ , Tukey confidence interval 95%) [Figure 1]. We also found no difference in TLX (ANOVA,  $p = 0.12$ ) [Figure 2] indicating that controlling the DTM wrist was no more demanding than controlling a FE wrist or a no-wrist system. This supports our hypothesis that including a DTM wrist in a prosthesis will improve functionality without being too difficult to use.

The SHAP score for the no-wrist condition is significantly higher than for the DTM and Fe wrist conditions. This is not surprising since the SHAP is a time-based test and using a second DOF of any kind will add time. Increasing the DOF improves functionality so the increase in time should be offset by a decrease in difficulty. Indeed, most participants commented on how the position of the DTM wrist made many SHAP tasks easier to perform and reduced the need for compensatory motions. In the future, we will analyze shoulder motion to quantify this effect.

Improving the prosthetic wrist can improve the lives of people with amputations by allowing to live independently, engage socially, and find employment. We have shown that the DTM wrist has the potential to be an ideal improvement that balances increased functionality with ease of use. Our next steps are including more able-bodied

participants to improve statistical power, analyzing compensatory shoulder motion, and comparing the results to people with trans-radial amputations.

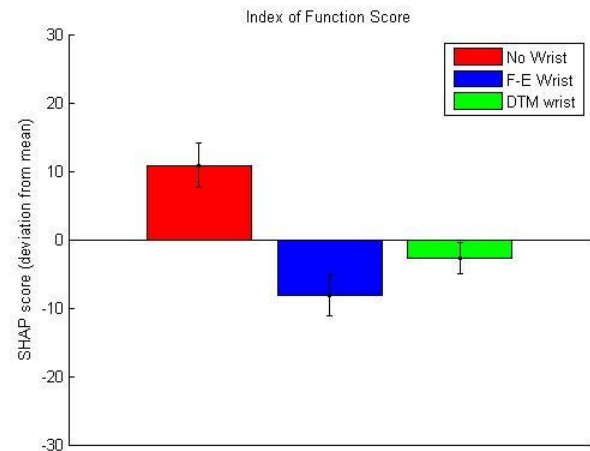


**Figure 1:** Results of SHAP test (intra-subject mean subtracted) indicating that the DTM wrist improves functionality over a FE wrist (ANOVA  $p < 10^{-7}$ , Tukey HSD 95% confidence).

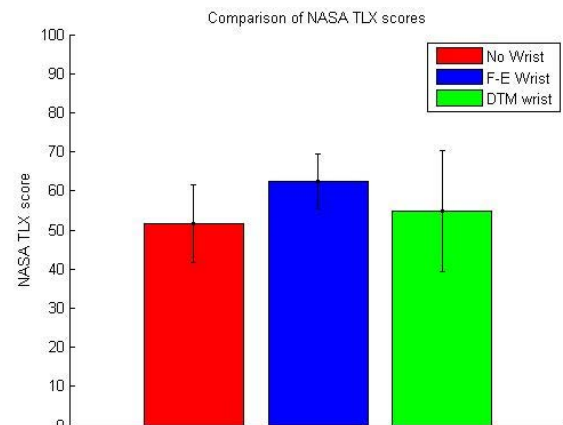


**Figure 2:** NASA Task Load Index for the 3 conditions. Adding FE or DTM wrist to the prosthesis did not significantly increase task load (ANOVA  $p > 0.05$ ).

## REFERENCES

1. Crisco, J, et al. *J Bone and Joint Surgery* **93**, 169-177, 2011
2. Davidson, M. *Rocky Mountain American Society of Biomechanics*, Estes Park, Colorado, USA, 2016
3. Segil, J et al., *IEEE Transactions on Neural Systems and Rehabilitation Engineering* **PP(99)**, 1-1, 2016

# PRELIMINARY VALIDATION OF TRANSFEMORAL PROSTHETIC GAIT SIMULATOR

Dolores Henson, Jessanne Lichtenberg, Raul Saldaña, Sonia Sosa Saenz, Kotaro Sasaki

LeTourneau University, 2100 S Mobberly Ave, Longview, TX, USA  
email: doloreshenson@letu.edu

## INTRODUCTION

When a device to improve the functionality of existing assistive devices is newly designed for patients with mobility impairment, the efficacy of the device needs to be evaluated. During initial prototype evaluations, collecting experimental data from actual patients might be challenging due to limited mobility to access a laboratory and possible secondary conditions prevalent among patients with mobility impairment [1]. Therefore, experiments would be conducted more safely and efficiently if individuals without mobility impairment could perform given simulated motor tasks affected by the impairment. However, the premise is that the tasks accurately represent the characteristic performance of the patients with mobility impairment. For example, unilateral transfemoral prosthetic gait (TPG) is characterized by lower self-selected speeds, shorter prosthetic stance phase, extended knee during stance phase, and increased hip flexor activity [2, 3, 4, 5].

In this study, simulated unilateral TPG performance using an in-house TPG simulator was evaluated. A previous study using a TPG simulator has shown that gait kinematics such as joint angles and stride length parameters are consistent with the data obtained from actual patients [2]. However, up to this date EMG during simulated unilateral TPG has not been analyzed. Therefore, the current study examined hip and knee angles and EMG from four muscles in the simulated prosthetic leg to compare with published data of actual transfemoral amputees.

## METHODS

*Simulator Fabrication:* The TPG simulator was constructed using a set of a mechanical knee, an aluminum pylon, a Niagara foot (Limbs Relief Knee LimbBox, Limbs Int., El Paso, Texas), and a connector (socket) constructed from a sheet of 2-mm thick stainless steel bent into a U-shape to fit around the thigh. A leg brace locked at 110-degree knee

flexion was used to immobilize the subject's lower leg and to securely attach the simulator to the subject's leg. The user wore a knee pad with Velcro to secure the knee in place with the connector (Fig. 1).



**Figure 1.** Fabricated TPG simulator

*Subjects:* Two college students participated in this preliminary study. Both subjects had no prior experience with the simulator and acclimatized themselves to the simulator until they were able to walk down a 30 m track at 60% of their normal gait speed [6]. Subjects wore their own athletic shoes for testing.

*Testing:* 34 reflective markers were attached to anatomical landmarks of the pelvis, legs and feet including the simulator. Using a motion capture system with 7 infrared cameras (T10, VICON, Oxford, UK), kinematic data were captured at 100 Hz during 6-m walk aiming at a target speed of 1.0 m/s, while the subject wore the TPG simulator on his/her dominant leg. The target speed was selected to compare with previous studies using mechanical knees, showing self-selected speeds at or near 1.0 m/s [2, 3, 4]. Five trials were performed for each subject. Wireless surface EMG electrodes (Trigno, Delsys Inc., Natick, MA) were placed on the following muscles in the simulated prosthetic limb: the tensor fasciae latae, gluteus medius, rectus femoris, and semitendinosus [5]. EMG signals were sampled at 1 kHz.

*Data Processing:* Custom-written codes using MATLAB (v8.1, MathWorks Inc., Natick, MA) were used to calculate joint angles and process the EMG data. The kinematic data of all trials of each subject were time-normalized to a full gait cycle and averaged. EMG data were low-pass filtered (10 Hz), rectified, and band-pass filtered (10-400 Hz) to generate EMG linear envelopes, then time-

normalized to a full gait cycle. After taking intra-subject average, the EMG magnitude was normalized to the maximum value over the gait cycle.

## RESULTS AND DISCUSSION

The subjects were able to walk at the speeds near the target speed (1 m/s) after acclimatization (Table 1). The stride length was comparable to a previous study (1.26±0.14 m) with similar gait speed (0.82±0.11 m/s) [2].

**Table 1:** Subject data. Mean gait speed and stride length parameters ± 95% CI interval.

	Subject 1	Subject 2
Gender	Female	Male
Age (yrs)	21	21
Height (cm)	162.6	172.7
Weight (kg)	59.0	87.5
Acclimatization Time (hr)	3.25	1.5
Gait Speed (m/s)	0.85 ± .05	0.97 ± .09
Stride Length (m)	1.19 ± .05	1.13 ± .05

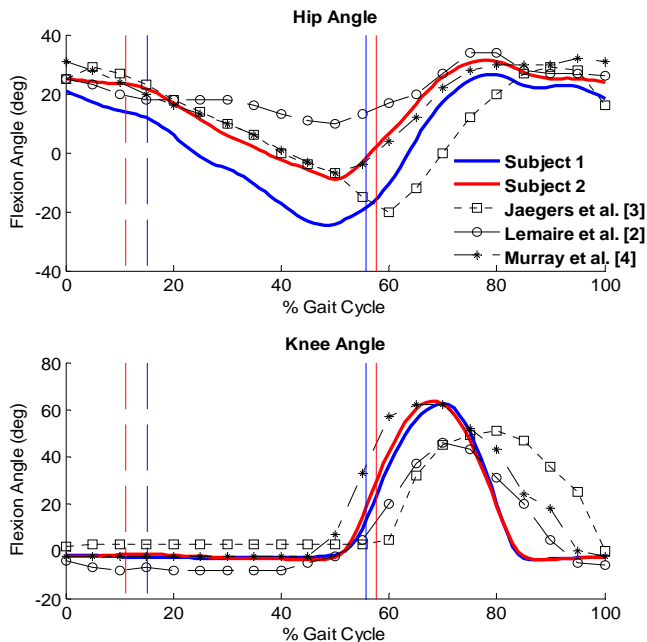


**Figure 2:** Hip and knee angles of simulated prosthetic leg over a gait cycle. Data ensembles the average of all trials. Vertical solid lines indicate the ipsilateral toe-off, and dashed lines indicate the contralateral toe-off.

The joint kinematics of the prosthetic leg (Fig. 2) were in general similar to the literature [2, 3, 4]. Subject 1 showed more extended hip positions during the stance phase, which may be due to the subject attempting to maintain the target speed with shorter single stance duration on the prosthetic side. EMG patterns in Fig. 3 also exhibit similar trends

between subjects and a previous study that exhibited large variability in EMG among three transfemoral amputees [5].

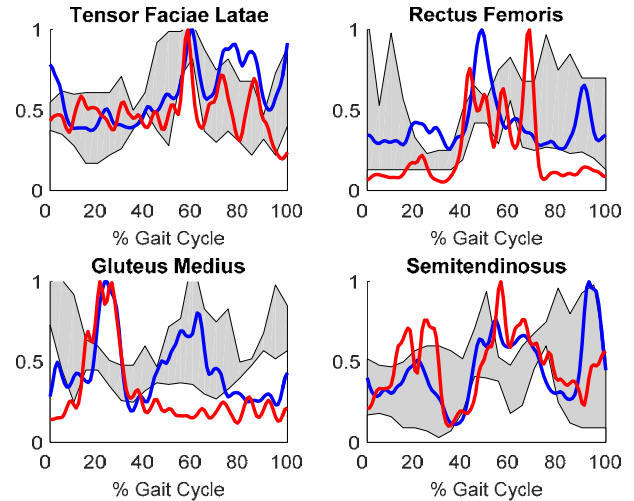


**Figure 3:** EMG linear envelopes over a gait cycle. Blue and red lines represent Subject 1 and Subject 2, respectively. The shaded area represents the range of EMG obtained from three transfemoral amputees in Wentink et al. [5].

## CONCLUSIONS

These preliminary results showed that simulated TPG using the developed simulator may be used to evaluate the efficacy of prototype devices aiming to improve the functionality of existing assistive devices such as prosthetic knees. Collecting data from a larger number of subjects and other biomechanical and physiological data is planned in the future study for further confirmation.

## REFERENCES

1. Gailey R, et al. *J Rehabil Res Dev.* **45**, 15-29, 2008.
2. Lemaire ED, et al. *Arch Phys Med Rehabil.* **81-6**, 840-843, 2000.
3. Jaegers SM, et al. *Arch Phys Med Rehabil.* **76-8**, 736-743, 1995.
4. Murray MP, et al. *Bull Prosthet Res* **10-34**, 35-45, 1980.
5. Wentink EC, et al. *J Neuroeng Rehabil.* **10-1**, 1-11, 2013.
6. Bai TS, et al. *J Med Eng Technol.* **33-2**, 130-135, 2009.

## ACKNOWLEDGMENTS

The authors are grateful to Joseph Wilcox for creating the TPG simulator and to Aaron Panagotopoulos for assistance in data acquisition and processing.

# ADAPTATION TO GRADUAL AND SUDDEN INCREASES IN PROSTHETIC ANKLE POWER

Brian P. Selgrade, Bretta L. Fylstra, and He (Helen) Huang

North Carolina State University/ University of North Carolina – Chapel Hill  
Joint Department of Biomedical Engineering  
email: bpselgra@ncsu.edu, web: <http://nrel.bme.ncsu.edu>

## INTRODUCTION

Previous work demonstrates the benefits of powered ankle prostheses, including reduced metabolic cost, increased gait speed, and reduced intact joint loading [1]. However, few studies explore how amputees adapt to increasing prosthetic joint power, a critical part of powered prosthesis adoption. Sudden perturbations challenge balance more than gradual perturbations [2]. Alternatively, people can adapt to sudden perturbations to minimize energetic cost in only a few steps [3], suggesting sudden perturbations may be preferable to induce an efficient adapted gait.

The purpose of this study was to compare amputee adaptation to sudden and gradual increases in prosthetic ankle power to determine which caused greater changes in compensation from the intact leg. We hypothesized that suddenly increased prosthetic ankle power would induce the wearer to unload the intact limb while gradually increased power would be less perceptible and thus induce less intact limb unloading.

## METHODS

One trans-tibial amputee (male, 114.5kg, 183cm tall) participated in three study sessions – powered prosthesis tuning, powered prosthesis training, and prosthetic power adaptation. In the first two sessions, the power from the BiOM prosthetic ankle (BionX, Bedford, MA, USA) was adjusted to the subject's preferred settings according to the standard BiOM tuning protocol and the subject spent several hours walking with these settings. During the third (adaptation) session, the subject walked on an instrumented treadmill (Bertec, Columbus, OH, USA) at his preferred walking speed (1.2m/s) in two conditions: sudden power increase, and gradual power increase (Fig. 1). In the sudden condition, the subject first walked with power at just below half of

his preferred power level. Next, prosthetic ankle power was increased to the subjects preferred power. After 5 minutes at preferred power, power decreased back to its original, lower level. In the gradual condition, power started at just below half of preferred power and then increased by the smallest possible increment every 15 seconds for 5 minutes, ending at preferred power. After 3 minutes at this constant, preferred power, power decreased back to the lower level.

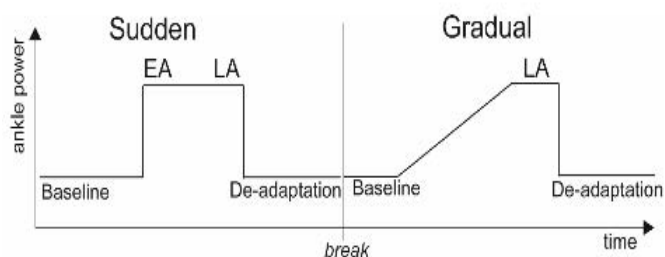


**Figure 1:** Experimental Protocol (EA and LA signify early and late adaptation).

Kinematics and kinetics were collected using an 8-camera system and instrumented treadmill. We used inverse dynamics calculations in Visual 3D (C-Motion, Germantown, MD, USA) and Matlab (Mathworks, Natick, MA, USA) to find joint powers for each stride (Eq 1). We report peak joint powers. We calculated step length symmetry by subtracting left step length from right step length and normalizing by the sum of step lengths [4].

## RESULTS AND DISCUSSION

We found that, as expected, peak prosthetic ankle power increased up to the preferred power level in both the sudden and gradual conditions. However, there were no changes in intact side joint powers or ground reaction force when the prosthetic ankle power increased regardless of condition. Therefore, the hypothesis that suddenly increased prosthetic

ankle power would result in unloading of the intact limb was not supported.

Whereas intact side kinetics were unchanged, peak hip power on the prosthetic side increased when prosthetic ankle power suddenly increased (Fig. 2). This increase in hip power was immediate and disappeared immediately when prosthetic ankle power decreased. This immediate response suggests that the changes in hip power in reaction to increased ankle power are solely due sensory feedback. Rather than slowly updating neural control of his prosthetic side hip, the amputee uses reactive control. Alternatively, in the gradual condition, there was no increase in prosthetic side hip power (Fig. 3), even though prosthetic ankle power was similar in both conditions. This suggests that the increased hip power in the sudden condition results not simply from mechanics but from the underlying motor control.

Despite the changes in prosthetic side joint power, step length symmetry remained constant throughout in both conditions. This apparent mismatch could have occurred because the increase in prosthetic side joint power was too small to have a clear effect on step length or because kinetic asymmetries do not always relate to kinematic asymmetries in amputees [5]. Future research with more subjects is necessary to confirm these results.

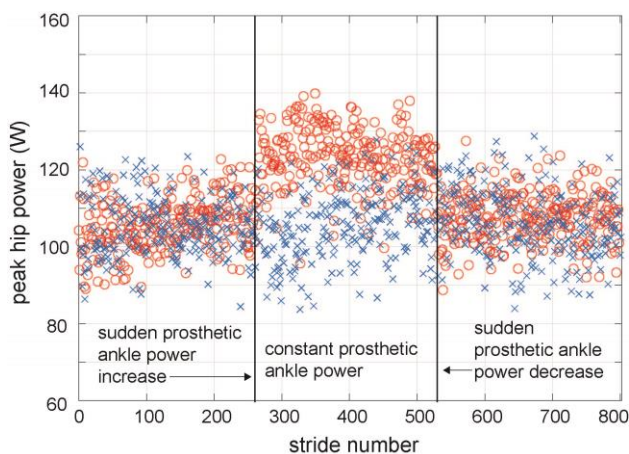


**Figure 2:** Peak hip power for intact (x) and prosthetic (o) sides when prosthetic ankle power was increased suddenly. Hip power increases at the same time as prosthetic ankle power.

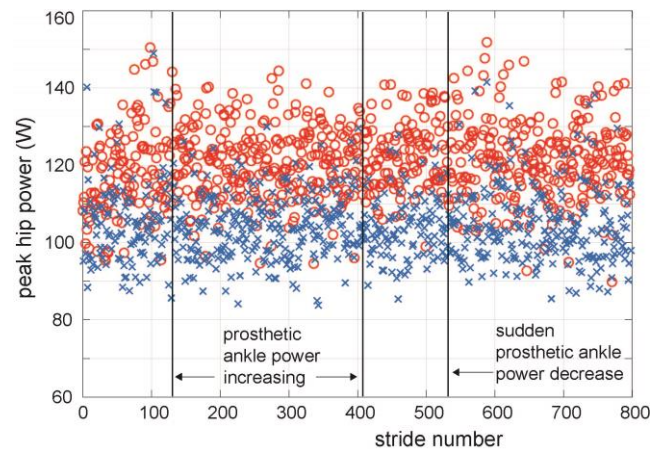


**Figure 3:** Peak hip power for intact (x) and prosthetic (o) sides was unchanged when prosthetic ankle power was increased gradually.

## CONCLUSIONS

While neither sudden nor gradual increases in prosthetic ankle power altered intact leg kinetics, the two conditions did have different effects. Only suddenly increased prosthetic ankle power induced increased prosthetic side hip power, suggesting reactive control of hip power. Additionally, these changes in power did not cause step length symmetry to change. Further research is necessary to confirm these results.

## REFERENCES

1. Caputo JM, Collins SH. *Sci Reports* **4**, 7213, 2014.
2. Sawers A, Kelly VE, Kartin D, Hahn ME. *Gait Post* **38**, 907-911, 2013.
3. Snaterse M, Ton R, Kuo AD, Donelan JM. *J Appl Physiol* **110**, 1682-1690, 2011.
4. Reisman DS, Block HJ, Bastian AJ. *J Neurophysiol* **94**, 2403-2415, 2005.
5. Childers WL, Kogler GF. *J Rehab Res Dev* **51**, 1243-1254. 2014.

## ACKNOWLEDGMENTS

This work was supported by the NSF (Graduate Research Fellowship and NSF 12-580). We thank Zhixiu Han and BionX for their initial help with prosthetic ankle operation and Ming Liu and Alyssa Cox for help with data collection and processing.

# IS GRASP PERFORMANCE OF A NOVEL MYOELECTRIC HAND PROSTHESIS IMPACTED BY TRAINING?

<sup>1</sup>Divya Bhaskaran, <sup>1</sup>Karen Andrews, <sup>1</sup>Ryan Breighner, <sup>2</sup>Sasha Blue Godfrey, <sup>2</sup>Manuel Catalano, <sup>1</sup>Andrew Thoreson, <sup>1</sup>Amanda Theuer, <sup>1</sup>Cesar Lopez, <sup>1</sup>Jonathan Calvert, <sup>2,3</sup>Antonio Bicchi, <sup>4</sup>Marco Santello and <sup>1</sup>Kristin Zhao

<sup>1</sup> Rehabilitation Medicine Research Center, Department of Physical Medicine and Rehabilitation, Mayo Clinic, MN, USA

<sup>2</sup> Advanced Robotic Department, Istituto Italiano di Tecnologia, Genoa, Italy

<sup>3</sup> Centro E. Piaggio, University of Pisa, Pisa, Italy

<sup>4</sup> Arizona State University, AZ, USA

email: Bhaskaran.divya@mayo.edu

## INTRODUCTION

Advances in prosthetic materials and design have provided more upper limb prosthetic options to assist individuals with limb loss to perform their daily tasks. The SoftHand myoelectric prosthesis prototype (SoftHand Pro; SHP) uses robotic technology from the University of Pisa/Istituto Italiano di Tecnologia. The SHP is an anthropomorphic prosthesis that uses standard myoelectric control. This unique, intuitive hand terminal device is light weight, underactuated, and uses a single motor to flexibly control and coordinate finger and thumb motion based on hand synergies.

Preliminary work has determined the feasibility of the SHP in subjects without limb loss during grasping, lifting and releasing objects [1]; these subjects used a 3D-printed harness attached to the forearm in place of a prosthetic socket. However, use of the SHP by subjects with limb loss has not yet been evaluated. This study was conducted to examine functional performance by subjects with transradial limb loss. The study aimed to quantify the ability of subjects with transradial limb loss and age-matched subjects without limb loss to perform a reach-grasp, lift-return (RGLR) task and how task performance may be affected by training with an occupational therapist.

## METHODS

Nine subjects (8 males and 1 female) with transradial limb loss and nine age matched controls (2 males and 7 females) participated in the study.

The protocol was approved by the Institutional Review Board. Subjects with transradial limb loss were fitted with a custom socket prior to testing. The age matched controls used a 3D-printed harness to allow use of the SHP as an extension of their arm. Surface electromyographic (EMG) electrodes were attached on wrist flexors and extensors, to control the closing and opening of the prosthetic hand. Subjects were asked to perform tasks that included reaching, grasping, lifting and then returning (RGLR) an instrumented cylindrical object. The cylinder was instrumented with 6-axis load cells (ATI Industrial Automation) to measure loading applied on the object. Movement of the digits and the object was recorded with an active marker tracking system (PhaseSpace Inc, CA). Red light-emitting diodes were attached to the instrumented object base and the tips of the 1<sup>st</sup> and 2<sup>nd</sup> distal phalanges.

Subjects were seated at a desk with the SHP placed at a standardized resting position and with the instrumented object placed in front of them. After a brief familiarization period with the SHP, subjects performed the task. Subjects were subsequently trained for 6-8 hours by an occupational therapist to use the SHP. At a second data collection session after training, subjects performed the same RGLR task. The task was divided into reaching phase, gripping phase, lifting phase and returning phase. The reaching phase was defined from the point when the hand starts reaching until the hand has reached the object. The gripping phase was defined from the time the hand started to grasp the object until complete grasp was accomplished. The lifting

phase was defined from the time the object was lifted off the desk to the time the object was lifted to the maximum height. The returning phase was defined from the time the object was lowered until the time object reached the desk. Transducer and kinematic data was collected at 96 Hz. Two trials were conducted at each time point.

Data was reduced to several parameters describing key components of the task: (a) normalized arc length of the reach was measured to quantify the trajectory of the reach, (b) duration of each of the phases, (c) velocity of the SHP during each of the phases, (d) maximum loading on the instrumented object during the gripping phase. Variables were examined pre- and post-training and also between subjects with limb loss and age-matched controls with a mixed effects model.

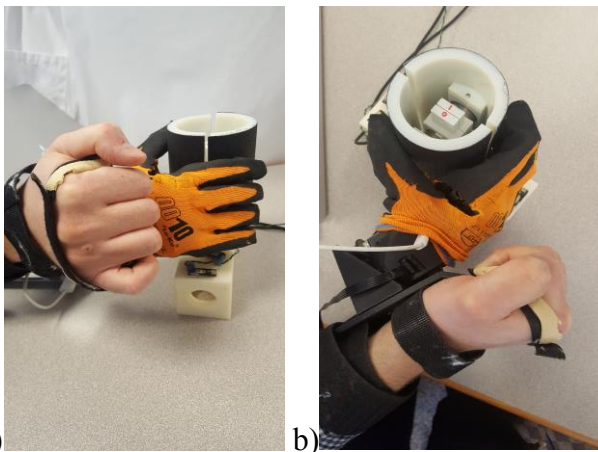


**Figure 1.** Age-matched subject using the SoftHand Pro to grasp the instrumented object, a) sagittal view, b) transverse view.

## RESULTS AND DISCUSSION

The normalized reaching arc length was not significantly different across subjects with limb loss and age-matched controls, pre and post training. This indicates that the subjects with limb loss and controls used a similar trajectory to reach for the cylinder, despite the use of the harness in the control group. The duration of the task phases was also not significantly different across subjects with limb loss and age-matched controls, pre and posttraining for any part of the task. Absence of significant differences in duration parameters

suggests that both the subjects with limb loss and control subjects were able to perform the task in similar times and training did not improve performance within a single training session.

The maximum velocities of the lifting and lowering phases were significantly higher post-training in the subjects with limb loss. However, since, the height of the lift was not standardized, further analysis is required to understand this difference. The maximum force applied on the object was not significantly different across subjects, pre- and post-training. This suggests that irrespective of previous experience with prosthesis, both subjects exerted the same loads on the object. Further analysis is required to understand the time point at which the forces were applied and its relation to the maximum force capability of the SHP.

## CONCLUSIONS

Both transradial limb loss subjects and age-matched controls achieved similar performance during a grasping task. This study implies that the SHP is intuitive and versatile, as even subjects with no exposure to myoelectric control or upper limb prostheses were able to adapt quickly and perform a grasping task successfully and similarly to patients with limb loss.

## REFERENCES

1. Godfrey SB, et al. *Rehabilitation Robotics (ICORR), IEEE International Conference, 2013.*

## ACKNOWLEDGMENTS

This study is supported by the National Institutes of Health (NICHD, R21 HD 081938), The Grainger Foundation, a Mayo Clinic and Arizona State Team Science Award, the European Research Council under the Advanced Grant SoftHands “A Theory of Soft Synergies for a New Generation of Artificial Hands” (no. ERC-291166), and the European Commission projects (Horizon 2020 research program) SOFTPRO (no. 688857).

# PEOPLE WITH AMPUTATION WALKING WITH A POWERED KNEE PROSTHESIS EXHIBIT VARYING ASYMMETRIC BEHAVIOR

Andrea Brandt, Yue Wen, He (Helen) Huang

Joint Department of Biomedical Engineering,  
University of North Carolina at Chapel Hill, Chapel Hill, NC, USA  
and North Carolina State University, Raleigh, NC, USA  
email: [ambrand3@ncsu.edu](mailto:ambrand3@ncsu.edu), web: <http://nrel.bme.ncsu.edu/>

## INTRODUCTION

Modern powered knee prostheses can more closely emulate biological lower limb muscle function than energetically-passive prostheses because they are equipped with a motor and capable of providing greater support and power to the user. Most commonly, the joint mechanics are determined by an impedance controller that modulates knee joint stiffness during predetermined phases based on prescribed impedance control parameters and the user's engagement with the device (i.e. finite state control). As expected using this technology, transfemoral amputees are able to ambulate with more normative (i.e. near able-bodied) mechanics at the prosthetic knee joint [1]. However, no studies to our knowledge report the full-body biomechanics of transfemoral amputees walking with powered knee prostheses. Is there a common gait pattern users adopt when their prosthetic knee moves more naturally?

In the study, we provided transfemoral amputees with near-normative prosthetic knee mechanics with our experimental powered device and evaluated their resulting gait behavior (e.g. center-of-mass motions). Muscle atrophy and remaining physical imbalances may prevent amputees from walking symmetrically, but we hypothesized amputees would not adopt significantly different levels of gait asymmetry with our experimental powered prosthesis. We specifically compared each subject's center of mass forward speed, push-off force impulse, and collision force impulse symmetry.

## METHODS

Three people with transfemoral amputation (20 years male, 61 years male, 27 years female) and functional level K3 (characteristic of typical

community ambulators) provided written, informed consent and participated in our IRB-approved study. A certified prosthetist fit each amputee with our experimental powered knee prosthesis [2], and a trained expert prescribed each amputee with prosthesis impedance control parameters that generated near-normative knee motion. We based this tuning process on the traditional prosthesis control parameter tuning process in a clinic. Each amputee then trained with the device for 3 or more 2-hour sessions, until they reported feeling comfortable walking with the device without assistance.

All subjects walked at 0.6 m/s for three 2-minute trials. We recorded ground reaction forces from a split-belt treadmill (1000 Hz, Bertec Corp.) and full-body motion using an 8-camera motion capture system (42 markers, 100 Hz, VICON). We used standard analysis software (Visual 3D, C-Motion, Inc.) to calculate kinematics, kinetics, and center of mass trajectories. We analyzed the last 10 consecutive strides from each trial to capture steady-state behavior. We filtered the motion and force-plate data using a 4th order Butterworth low-pass filter with a cutoff frequency of 7.5 Hz. To evaluate gait symmetry, we used a standard asymmetry index,  $\frac{(X_{Intact} - X_{Amputated})}{(X_{Intact} + X_{Amputated}) * 0.5} \times 100$ , where X was center-of-mass speed, push-off impulse, and collision impulse. To test for significant differences between subjects, we used one-way ANOVA ( $p < 0.05$ ). If subject was a significant factor, we used Tukey's honest significant difference test to identify how subjects differed.

## RESULTS AND DISCUSSION

All subjects walked with near-normative knee motion at the prosthetic knee joint when using our experimental powered knee prosthesis and subject-specific impedance control parameters (Fig. 1).

Contrary to our hypothesis, all amputee subjects walked with highly varied levels of asymmetric center-of-mass motion (Fig. 2), despite having very similar prosthetic knee motion. Able-bodied people typically walk with the same forward center-of-mass speed during mid-stance, but all amputee subjects walked with varying asymmetric mid-stance speeds (i.e. faster on prosthetic limb) ( $F(2,6)=16.07$ ,  $p=0.004$ ), and subject 2's center-of-mass speed asymmetry ( $M=-31\%$ ,  $SD=3\%$ ) was significantly greater than that of subject 1 ( $M=-21\%$ ,  $SD=2\%$ ) and subject 3 ( $M=-21\%$ ,  $SD=2\%$ ).

Asymmetry in anterior-posterior ground reaction force impulses typically contribute to center-of-mass speed asymmetry. Subjects exhibited varying push-off impulse asymmetry (i.e. push more with intact limb) ( $F(2,6)=32.69$ ,  $p<0.001$ ) and braking impulse asymmetry (i.e. brake more with intact limb) ( $F(2,6)=32.10$ ,  $p<0.001$ ). Interestingly, subject 1's braking impulse asymmetry ( $M=15\%$ ,  $SD=6\%$ ) was significantly lower than subject 2 ( $M=66\%$ ,  $SD=11\%$ ) and subject 3 ( $M=50\%$ ,  $SD=6\%$ ), but his push-off impulse asymmetry

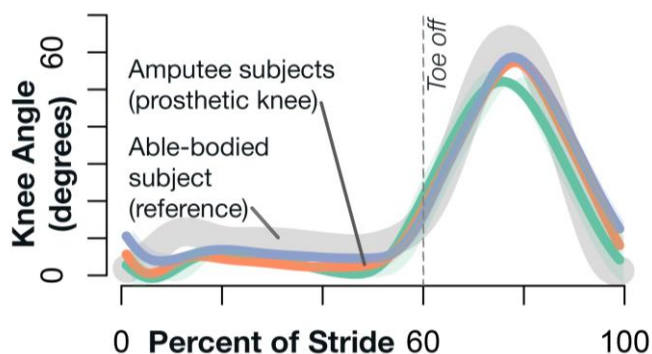


**Figure 1:** With subject-specific prosthetic knee parameters, all amputee subjects walked with a prosthetic knee angle similar to a reference able-bodied subject. All trajectories were normalized to one stride. Vertical dotted line indicates approximate toe off. Line color indicates amputee subjects 1-3 (blue, orange, and green respectively).

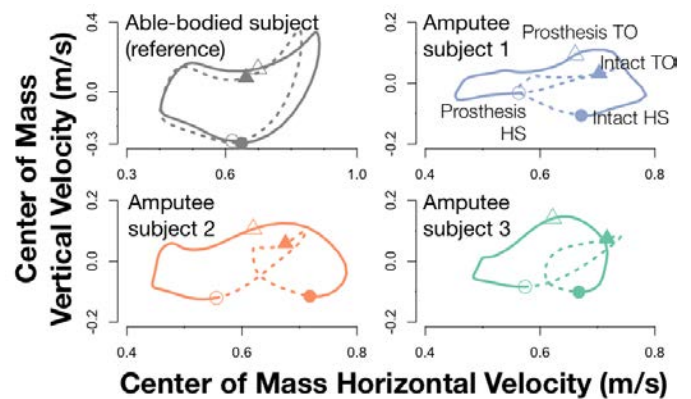


**Figure 2:** Each amputee subject walked with varying levels of asymmetric center-of-mass horizontal and vertical velocity compared to a reference able-bodied subject. All trajectories were normalized to one stride. Line style corresponds to subjects' each limb's initial double support and single support phases (solid for intact limb, dashed for prosthetic limb). Circles represent heel strike, triangles represent toe off, filled point characters represent intact limb gait events, and open point characters represent prosthetic limb gait events.

( $M=93\%$ ,  $SD=7\%$ ) was significantly greater than subject 2 ( $M=57\%$ ,  $SD=11\%$ ) and subject 3 ( $M=43\%$ ,  $SD=5\%$ ).

## CONCLUSIONS

Despite exhibiting similar prosthetic knee motion with our experimental powered knee prosthesis, all amputee users otherwise walked with significantly different levels of gait asymmetry. We will further analyze the force and timing variables that may be contributing to the observed discrepancy in motion to identify possible areas for improvement. With knowledge of the main factors contributing to subject variance and asymmetry, both amputees and engineers may be able make adjustments to allow amputees to reap more benefits from powered prostheses.

## REFERENCES

1. F. Sup, et al. *Int. J. Robot. Res.* **27**, 263-273, 2008.
2. M. Liu, et al. *J. Intell. Robot Syst.* **76**, 461-474, 2013.

## ACKNOWLEDGEMENTS

This work was partly supported by NSF #1406750 & #1361549

# INCREASES IN ROM AND CIRCUMFERENCE OF THE FOREARM AFTER 6 MONTHS OF USING A 3D PRINTED TRANSITIONAL HAND PROSTHESIS

D. Dudley B.S.B.S.E.<sup>1</sup>, J. Peck OTL, CHT<sup>2</sup>, R. Srivastava M.S. CPO<sup>3</sup>, J. Pierce B.S.M.E.<sup>1</sup>, N. Than B.S.<sup>1</sup>, C. Copeland<sup>1</sup> and J. M. Zuniga Ph.D.<sup>1</sup>

<sup>1</sup> Department of Biomechanics, University of Nebraska at Omaha, Omaha 68182, NE, USA

<sup>2</sup> CHI Health Creighton University Medical Center, Omaha 68131, NE, USA

<sup>3</sup> Innovative Prosthetics & Orthotics, Omaha, 68114, NE, USA

email: ddudley@unomaha.edu

## INTRODUCTION

Children's prosthetic needs are complex due to their small size, constant growth, and psychosocial development (Krebs et al., 1991 and Zuniga et al. 2015). Independent of the type of limb deficiency (congenital or traumatic) muscle atrophy, loss of mobility, and asymmetry are typical characteristics of the affected limb (Krebs et al., 1991 and Zuniga et al. 2015). Most upper-limb prostheses for children include a terminal device, with the objective to replace the missing hand or fingers. Electric-powered units (i.e., myoelectric) and mechanical devices (i.e., body-powered) have been improved to accommodate children's needs, but the cost of maintenance and replacement represent an obstacle for many families (Krebs et al., 1991 and Zuniga et al. 2015). The development and use of low-cost transitional prosthetic devices to increase ROM, strength, and other relevant clinical variables would have a significant clinical impact in children with upper-limb differences. Thus, the purpose of the study was to identify anthropometric, active range of motion, and strength changes after 6 months of using a wrist driven 3D-printed transitional prosthetic hand for children with upper limb differences.

## METHODS

*Subjects:* Five children (two girls and three boys, 3 to 10 years of age) with absent digits (one traumatic and four congenital) participated in this study and were fitted with a low-cost 3D-printed prosthetic hand.

*Apparatus:* Anthropometric, active range of motion, and strength measurements were assessed before and

after 6 months of using a low-cost 3D printed prosthetic hand.

*Procedures:* Six variables from the affected and non-affected hand including circumferences, skin folds, and active ROM for flexion, extension, radial deviation, and ulnar deviation were measured on each research participant by a trained occupational therapist.

*Data Analysis:* Seven separate two-way repeated measures ANOVAs [2 x 2; hand (affected versus non-affected) x Time (before and after)] were performed to analyze the data. A p-value of  $\leq 0.05$  was considered statistically significant for all comparisons.

## RESULTS AND DISCUSSION

There were significant hand  $\times$  time interactions for the forearm circumference [F(1,4) = 16.90;  $p = 0.02$ ], active ROM flexion (Fig. 1) [F(1,4) = 12.70;  $p = 0.02$ ], and active ROM extension values [F(1,4) = 8.80;  $p = 0.04$ ]. There were no significant hand x time interaction, however, for wrist flexion strength [F(1,4) = 1.48;  $p = 0.29$ ], wrist extension strength [F(1,4) = 0.05;  $p = 0.84$ ], active ROM UD [F(1,4) = 0.65;  $p = 0.5$ ], active ROM RD [F(1,4) = 1.77;  $p = 0.25$ ], and forearm skinfold values [F(1,4) = 4.24;  $p = 0.11$ ].

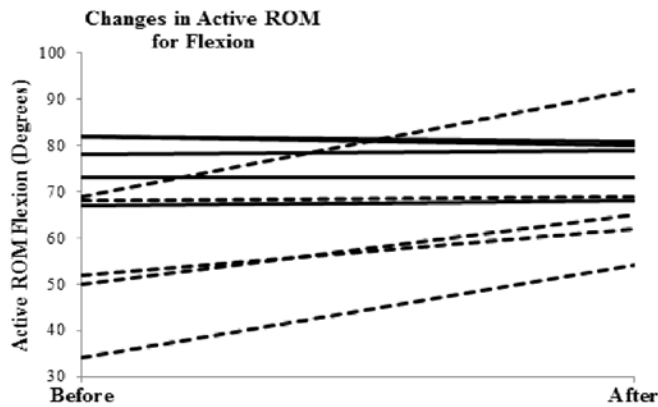


**Figure 1.** Shows individual changes for active range of motion (ROM) for wrist flexion before and after a 6 month period of using the low-cost 3D printed transitional prosthetic device.

The main finding of the present investigation was that the usage of a low-cost 3D printed transitional prosthetic hand significantly increased forearm circumference (Before= $16.70 \pm 1.86$  cm and After= $17.80 \pm 1.48$  cm), wrist active ROM flexion (Before= $54.60 \pm 14.48^\circ$  and After= $68.40 \pm 14.29^\circ$ ), and active ROM extension (Before= $40.40 \pm 37.75^\circ$  and After= $47.00 \pm 36.42^\circ$  cm) on a small sample of children with upper-limb differences. Thus, the Cyborg Beast transitional prosthetic hand represents low-cost prosthetic solution for those in need of a transitional device to increase ROM.

## CONCLUSIONS

Although, durability and environment are factors to consider when using 3D printed prostheses, the practicality and cost effectiveness represents a promising new option for clinicians and their patients.

## CLINICAL APPLICATIONS

Six months of using this 3D printed transitional prosthesis increased forearm circumference, wrist active ROM flexion, and active ROM extension in children with upper-limb differences

## REFERENCES

1. Krebs, D. E., Edlestein, J. E. & Thornby, M. A. 1991. Prosthetic management of children with limb deficiencies. *Phys Ther*, 71, 920-34.
2. Zuniga, J., Katsavelis, D., Peck, J., Stollberg, J., Petrykowski, M., Carson, A. & Fernandez, C. 2015. Cyborg beast: a low-cost 3d-printed prosthetic hand for children with upper-limb differences. *BMC Res Notes*, 8, 10.

# Top sprinting speed is influenced by prosthetic model, but not stiffness or height, for athletes with bilateral transtibial amputations

<sup>1</sup>Paolo Taboga, <sup>2</sup>Owen N Beck, & <sup>2,3</sup>Alena M Grabowski

<sup>1</sup>Kinesiology and Health Science Department, California State University, Sacramento, CA, USA

<sup>2</sup>Integrative Physiology Department, University of Colorado Boulder, CO, USA

<sup>2</sup>Eastern Colorado Healthcare System, Department of Veterans Affairs, Denver, CO, USA

email: [paolo.taboga@csus.edu](mailto:paolo.taboga@csus.edu)

## INTRODUCTION

Running specific prostheses (RSPs) used by athletes with leg amputations are made of carbon-fiber and intended to replicate the spring-like sagittal plane actions of a biological ankle. However, the passive nature and hysteresis [1] of RSPs impairs the rapid application of vertical [2] and horizontal [3] forces on the ground. Previous research has shown that use of RSPs that provide greater elastic energy return ( $\dot{E}_{RSP}$ ) improves running economy at speeds  $\leq 3$  m/s [4], but it is unclear how  $\dot{E}_{RSP}$  affects top speed sprinting. At speeds greater than  $\sim 6$  m/s, non-amputee runners progressively increase their dimensionless leg stiffness ( $K_{leg}$ ) with speed, while sprinters with unilateral and bilateral leg amputations maintain the same  $K_{leg}$  in their unaffected leg and decrease  $K_{leg}$  in their affected legs, respectively [5]. The increase in  $K_{leg}$  for non-amputee runners at faster speeds results from increased peak vertical ground reaction forces ( $vGRF_{peak}$ ), and constant leg compression ( $\Delta L$ ); leading to greater elastic energy storage and return at progressively faster speeds. We hypothesized that stiffer RSPs would allow faster top sprinting speed compared to softer RSPs due to potential increases in  $K_{leg}$ . Since  $K_{leg}$  is influenced by total leg length, we also hypothesized that increasing RSP height would permit faster top sprinting speed. Lastly, we hypothesized that RSPs with greater energy return would allow faster top sprinting speeds, compared to RSPs with lower  $\dot{E}_{RSP}$ .

## METHODS

Five male sprinters with bilateral transtibial amputations gave written informed consent prior to participation according to the COMIRB and USAMRMC Human Research Protection Office. A certified prosthetist fit each athlete with three

different models of RSPs: Freedom Catapult FX6, Össur Cheetah Xtend and Ottobock 1E90 Sprinter. The recommended stiffness category was selected based on each manufacturer's suggestion and the recommended height was set at the maximum allowable height ( $H_{t0}$ ) for each runner according to IPC rules [6]. If  $H_{t0}$  could not be set due to RSP design and residual limb anatomy, the baseline height was set as close to  $H_{t0}$  as possible.

Each sprinter performed three sets of trials at the recommended, +1, and -1 stiffness categories for each RSP model in a randomized order, while maintaining  $H_{t0}$ . Then, the category that allowed the top running speed for each model was selected and height was changed ( $\pm 2$  cm with respect to  $H_{t0}$ ).

Each set of sprint trials started at 3 m/s with speed incremented by 1 m/s until subjects approached their top speed. Then, smaller speed increments were employed until subjects reached top speed, defined when subjects could not maintain their position on the treadmill for 10 consecutive strides.

All trials were performed on a 3D force-measuring treadmill (Treadmetrix, USA) sampling at 1000 Hz. We used a custom Matlab program (MathWorks, USA) to condition signals (30 Hz low-pass 4<sup>th</sup> order Butterworth filter) and determine contact time ( $t_c$ ), aerial time,  $vGRF_{peak}$  and stance average vertical ground reaction force. We identified when the horizontal force crossed 0 N to determine braking (brake) and propulsive (prop) portions of the stance phase and calculated peak horizontal forces ( $hGRF_{brake}$ ,  $hGRF_{prop}$ ) and impulses ( $hIMP_{brake}$ ,  $hIMP_{prop}$ ). We then normalized all forces and impulses to the body weight of each subject including their running gear (both sockets and prostheses).

For each trial we calculated  $\dot{E}_{RSP}$  as:

$$\dot{E}_{RSP} (J/kg \cdot m) = \frac{k_{RSP}(\Delta d)^2(1-Hst_{RSP}/100)}{2L_{step}m} \quad (1)$$

where  $k_{RSP}$  is RSP stiffness,  $\Delta d$  is RSP compression,  $Hst_{RSP}$  is percent RSP hysteresis,  $L_{step}$  is step length and  $m$  is the mass of the subject [4]. We used a linear mixed model to determine the effects of RSP model, stiffness, and height on top speed. We used a second linear mixed model to determine the effects of  $\dot{E}_{RSP}$  on top speed. We then used a third linear mixed model to predict top speed based on all the measured biomechanical parameters.

## RESULTS AND DISCUSSION

We found a significant effect of RSP model on top speed. Use of the Cheetah Xtend and 1E90 Sprinter RSPs allowed 8.0% ( $p < 0.001$ ) and 8.3% ( $p < 0.001$ ) faster top speeds, respectively, compared to use of the Catapult RSPs. We found no significant effect of stiffness category or height ( $p = 0.84$  and  $p = 0.76$ , respectively) on top speed. Elastic energy return ( $\dot{E}_{RSP}$ ) had an effect on top speed ( $p = 0.046$ ), such that a higher  $\dot{E}_{RSP}$  resulted in faster speed (Fig. 1):

$$TopSpeed = 0.514 \times \dot{E}_{RSP} + 7.712 \quad (2)$$

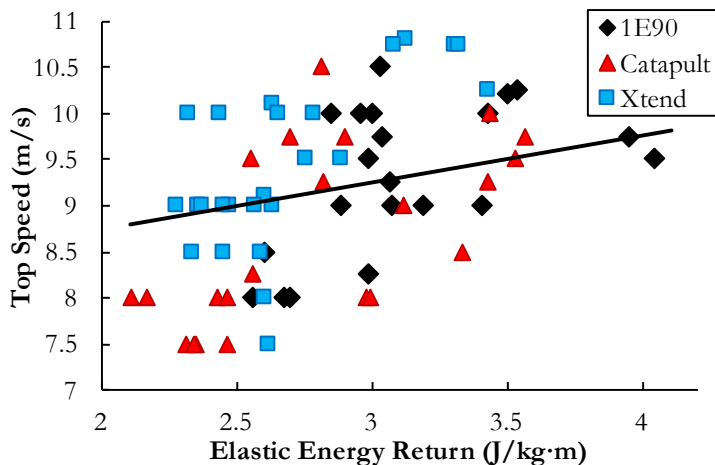


**Figure 1:** Top speed vs. elastic energy return. The black line is the regression line obtained from the second linear mixed model (Eq. 2).  $R^2 = 0.397$ .

We found that among all biomechanical variables,  $t_c$ ,  $vGRF_{peak}$  and  $K_{leg}$  affected top speed ( $p < 0.001$  for all 3 variables), where shorter  $t_c$ , greater  $vGRF_{peak}$ , and lower  $K_{leg}$  resulted in faster speed:

$$TopSpeed (m/s) = -65.33 \times t_c + 1.35 \times vGRF_{peak} - 0.1476 \times K_{leg} \quad (3)$$

( $R^2 = 0.924$ ) where  $t_c$  is measured in seconds,  $vGRF_{peak}$  in BW and  $K_{leg}$  is dimensionless stiffness.

## CONCLUSIONS

We found that top sprinting speed is influenced by prosthetic model but not prosthetic stiffness or height, and greater prosthetic elastic energy return allows faster top speeds in sprinters with bilateral transtibial amputations.

Across different RSPs, sprinters with bilateral leg amputations achieved faster sprinting speeds by shortening contact time, increasing peak vertical ground reaction force and reducing normalized leg stiffness.

## REFERENCES

1. Beck, O.N., et al., PLoS One, 2016. **11**(12): p. e0168298.
2. Grabowski, A.M., et al., Biol Lett, 2010. **6**(2): p. 201-4.
3. Brüggemann, G.P., et al., Sports Technology, 2008. **1**(4-5): p. 220-227.
4. Beck, O.N., et al., J Appl Physiol, 2017: jap-00587
5. McGowan, C.P., et al., s. J R Soc Interface, 2012. **9**(73): p. 1975-82
6. <http://www.paralympic.org/athletics/rules-and-regulations/rule>

## ACKNOWLEDGMENTS

We thank Valerie Daniels, Mike Litavish, Angela Montgomery, Rodger Kram, Freedom Innovations, Össur, Ottobock, and the BADER Consortium, a DoD CDMRP cooperative agreement.

# KINEMATIC AND KINETIC ANALYSIS OF A BIARTICULAR CLUTCHED SPRING PROSTHESIS FOR TRANSTIBIAL AMPUTEES

<sup>1,2</sup>Andrea Willson, <sup>2</sup>Chris Richburg, <sup>1,2</sup>Anthony Anderson,  
<sup>2,3</sup>Joseph Czerniecki, <sup>1</sup>Katherine Steele, <sup>1,2</sup>Patrick Aubin

<sup>1</sup>Department of Mechanical Engineering, University of Washington, Seattle, WA, USA  
<sup>2</sup>VA Puget Sound RR&D Center for Limb Loss and Mobility (CLIMB), Seattle, WA USA  
<sup>3</sup>Department of Rehabilitation Medicine, University of Washington, Seattle, WA USA  
email: amw13@uw.edu, web: <http://faculty.washington.edu/paubin/wordpress/>

## INTRODUCTION

There are a number of biomechanical differences between amputee gait and healthy gait. In healthy gait, the ankle plantar flexor muscles have distinct important roles; the biarticular gastrocnemius (GAS) spans both the ankle and knee joints, and helps to propel the leg into swing phase, while the uniarticular soleus (SOL) acts just at the ankle to propel the body forward [1]. The lack of the GAS muscle is associated with elevated activation of knee and hip flexors as well as decreased ankle push-off power. These differences can lead to secondary conditions such as back pain and knee pain.

Current prosthetic devices are able to recreate SOL function to some extent, but no devices have a biarticular component to replicate the functional role of GAS. To help improve amputee gait we have developed a foot-ankle prosthesis with a clutched spring that spans both the knee and ankle joints. We hypothesize that this spring element can emulate GAS function and reduce gait compensations to improve amputee walking and quality of life.

## METHODS

The biarticular prosthesis (BP) consists of the subject's prescribed socket, a pylon in series with an iPecs 6-DOF load cell, and a single axis College Park Venture foot (Fig. 1). Uprights extend from the pylon, hinge at the knee joint, and continue to mid-thigh where a thigh cuff supports the clutched spring. The tension spring is attached posteriorly, and spans both the knee and ankle joints, and a recoil spring ensures that the string remains slackless. The instrumented pylon detects

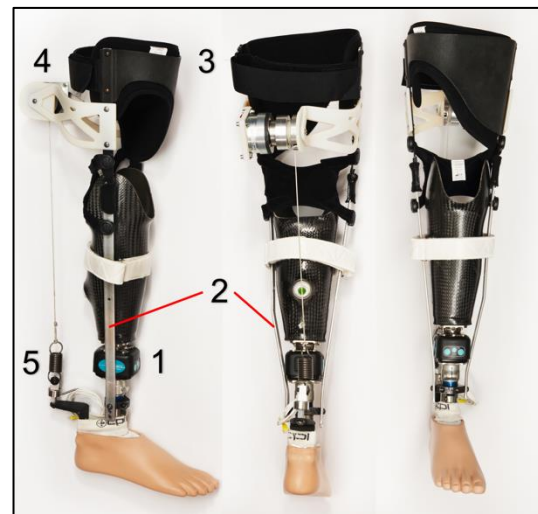


**Figure 1.** Biarticular Prosthesis. 1: iPecs 6-DoF Load Cell, 2: uprights, 3: thigh cuff, 4: ratcheted clutch, 5: spring (medium stiffness configuration).

heel strike to engage the ratcheted clutch. The ratchet coils in the string until the distance between the proximal and distal attachment points reach a minimum (at 15-20% of the gait cycle), the spring is then stretched as stance phase continues contributing to a knee flexion and ankle plantarflexion torque. Once the spring tension and pylon axial force drop below a threshold during toe-off, the clutch disengages the spring in preparation for swing phase.

With IRB approval, data was collected and analyzed for one amputee subject (to-date), female age 54, wearing the BP. Vicon motion capture tracked a marker set of 77 markers (placed on anatomical landmarks as well as in segment clusters). Ground reaction forces, BP spring force, and pylon data (from iPecs) were also recorded during bouts of treadmill walking. EMG signals were also collected for major gait muscles of the lower limb. The subject first walked on their prescribed prosthesis,

then the BP with various force conditions: off mode (spring disconnected), recoil spring only, then 1.8 N/mm, 3.7 N/mm, and 10.5 N/mm springs attached respectively. Finally, we collected data using the subject's preferred spring configuration, while providing them with feedback via a real-time plot of the BP spring force. Subjects were instructed to try to maximize the spring force peak as they walked. The one subject presented here chose the stiffest (10.5 N/mm) spring for the feedback condition.

OpenSim [2] was used to analyze the kinematics and kinetics of the collected data. We developed an amputee musculoskeletal model based on the full body model from Rajagopal et al. [3]. Mass and inertial properties of the residual limb/prosthesis were modified to match typical amputees [4,5], and the residual limb was scaled based on the socket to pylon length ratio. The model was scaled to the specific subject, then inverse kinematics and inverse dynamics were performed. The spring force measured experimentally was applied to the model as an external force, such that the joint torque contributions from the BP spring could be delineated from the internal muscle torques.

## RESULTS AND DISCUSSION

The inverse kinematics results show a difference in knee angle between the different conditions during late stance (Fig. 2). As the BP spring stiffness increased, knee extension in late stance decreased. Additionally, the BP has a substantial effect on the knee moment of the affected limb (Fig. 3). The BP pulls the knee toward flexion, particularly in mid and late stance (40-60% of gait cycle), and this flexion moment increases in magnitude as the BP spring stiffness increases. However, the net knee flexion moment is smaller in magnitude at the higher spring stiffness, which is likely due to kinematic deviations (Fig. 2). As the BP spring stiffness increased the BP contribution to ankle moment increased, but the gains were minimal.

The stiffest spring, under the feedback condition provided the largest contribution to net ankle torque, 14.64% at the peak plantar flexion moment. This same spring condition also shows the largest spring torque contribution at the knee, 147% of the total. This indicates that knee extensor muscles are

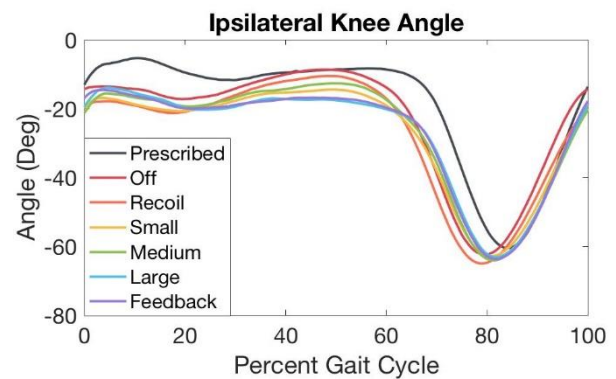


**Figure 2.** Average ipsilateral knee angle with prescribed and different BP spring configurations.

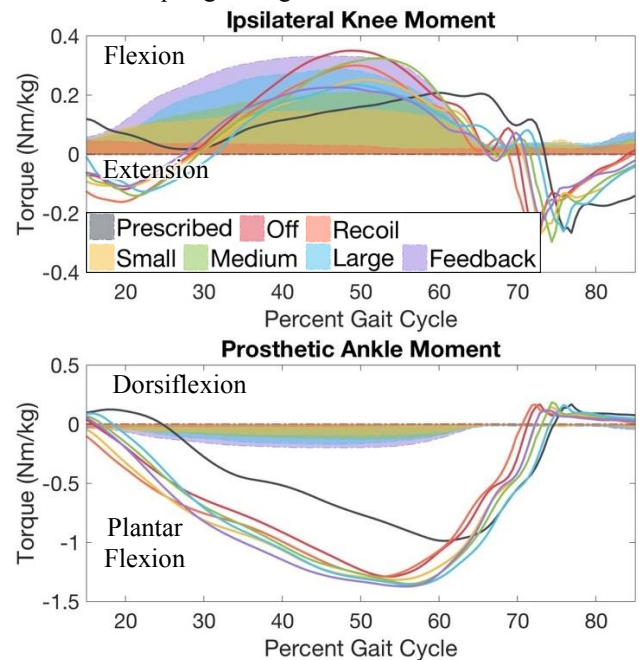


**Figure 3.** Average ankle and knee moments of the affected limb in prescribed and different BP spring conditions. Solid lines show the total joint moment, and shaded regions are the BP spring torque contribution.

over-active to counteract this large flexion torque. Data for 5 additional subjects is currently being collected to further understand the effects of a BP on amputee gait and the impacts of feedback training. Understanding whether mimicking the biarticular action of the GAS can enhance prosthetic function will inform future device design.

## REFERENCES

1. Neptune RR, et al. *J Biomech*, **34**, 2001.
2. Delp SL, et al. *IEEE Biomed Eng*, **53**, 2007.
3. Rajagopal A, et al. *IEEE Biomed Eng*, 2015.
4. Silverman AK, Neptune RR. *J Biomech*, **45**, 2271-2278, 2012.
5. Smith JD, et al. *J Vis Exp*, **87**, 2014.

# The Point Digit: Mechanical Design and Testing of a Ratcheting Prosthetic Finger

<sup>1</sup> Jacob L. Segil, <sup>2</sup> Stephen Huddle, <sup>2</sup> Levin Sliker, <sup>2</sup> Richard F. ff. Weir

<sup>1</sup> University of Colorado Boulder, CO, USA

<sup>2</sup> University of Colorado Denver, CO, USA

email: jacob.segil@colorado.edu

## INTRODUCTION

The largest population of upper-limb amputees is those with partial-hand amputations (including digit, multiple-digit, or partial-digit loss). This population outnumbers all other levels of upper-limb amputees by a ratio of 10:1 [1]. With 500,000 people in the U.S. currently living with minor upper-limb loss [1], a product effectively serving this population would have a significant clinical impact. However, current commercial products for partial-hand amputees do not satisfy all of the needs of these patients; passive fingers are seen as being difficult to fit and operate. While electric-powered fingers and their ancillary components are expensive, fragile, and cumbersome. We developed a passive, ratcheting prosthetic finger that is manufactured using metal laser sintering rapid manufacturing technology, namely the *Point Digit* (Figure 1). Here we present the mechanical design and testing of the *Point Digit* in order to validate its efficacy for use in a clinical setting.

The *Point Digit* is a purely mechanical prosthetic finger (i.e., no actuation, electronics, etc.). A ratchet positions the finger into one of ten distinct levels of flexion. The ratchet ensures that the finger is non-backdrivable. An EOS M270 direct metal laser sintering 3D printer manufactures most components of the *Point Digit* using maraging steel powder (EOS MaragingSteel MS1). This material has a yield strength of 152 ksi and modulus of elasticity of 23 Msi. An internal honeycomb structure maintains strength and reduces weight of the individual components. The length of the *Point Digit* can be scaled between 80 mm to 105 mm in length, which nearly encompasses the ranges of finger lengths for 25 – 75th percentile males and 50-100th percentile females. The average finger mass of all lengths of the *Point Digit* is 50 g fully assembled.

The extension of the *Point Digit* can occur in two ways: 1) a self-locking button releases the ratchet and

extends the finger or 2) the full flexion of the finger causes the finger to spring-back to full extension. By allowing external features to position the finger in both flexion and extension, the contralateral limb is not required for use of the *Point Digit* (i.e. – one-handed operation).

A kinematic linkage system couples all three joints of the *Point Digit*. This linkage system flexes all three joints at an anatomically appropriate rate. The linkage system ensures a finger that behaves similar to the intact limb while maintaining mechanical strength.

Finally, the *Point Digit* provides an anatomically appropriate center of rotation of the metacarpophalangeal joint. This feature ensures a clinically sound system that easily integrates into a prosthetic socket. A mounting bracket provides a method for prosthetists to install the *Point Digit* into the prosthetic socket and ensure appropriate positioning of the finger with respect to the physiological limb.

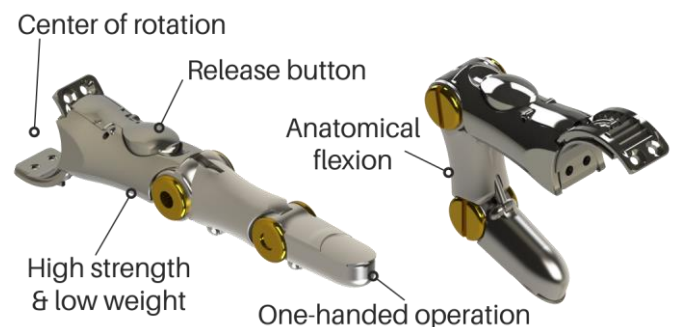


**Figure 1:** Features of the *Point Digit* include anatomically appropriate center of rotation, high strength-low weight, one-handed operation, and others.

## METHODS

Static and dynamic testing procedures were performed to determine the mechanical properties of the *Point Digit*. An Instron 5869 universal tensile testing machine performed the static testing procedure. The chucks in the Instron machine secured the finger in a partially flexed position. Then, a tensile test was performed by loading the finger in 10 lb. increments in tension until catastrophic failure. The load was released after each cycle to produce a hysteresis curve at each loading increment until failure. This loading method simulated the application of pinch forces to the distal phalange of the *Point Digit*. Two *Point Digits* were tested to failure.

The dynamic testing was performed using a custom built finger cycler (Figure 2). The finger cycle consisted of a custom LabView program which commanded a DC motor while measuring the current and position of the finger. The finger cycler drove the finger between full extension and full flexion to ensure that the finger would ratchet, spring-back, and reset appropriately over many cycles. Five *Point Digits* were tested to 10,000 cycles.

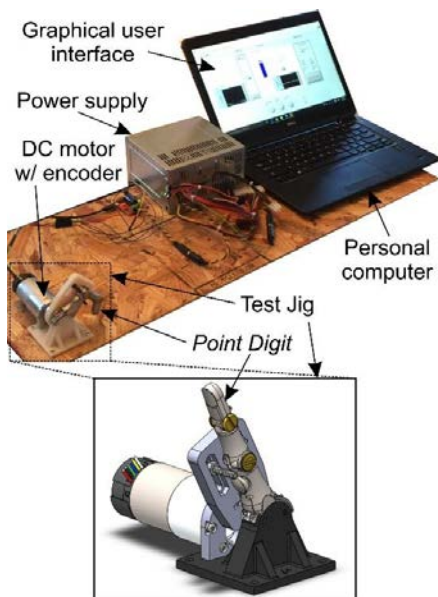


**Figure 2:** Finger cycler for dynamic testing consisting of a computer, custom control software, power supply, DC motor with encoder, and custom mounting hardware. Finger position and current consumption were recorded.

## RESULTS AND DISCUSSION

Two *Point Digits* were tested to static failure. In both cases the digits withstood over 250lbs of pinch force before failure. The failure mechanism consisted of a direct shear failure of the proximal link bar pin. This failure mechanism proved to be an advantageous design feature where the pin can easily be replaced and thereby repair the finger. Figure 3 depicts the applied pinch force compared to the displacement of the finger over the final loading cycle before failure of the finger.

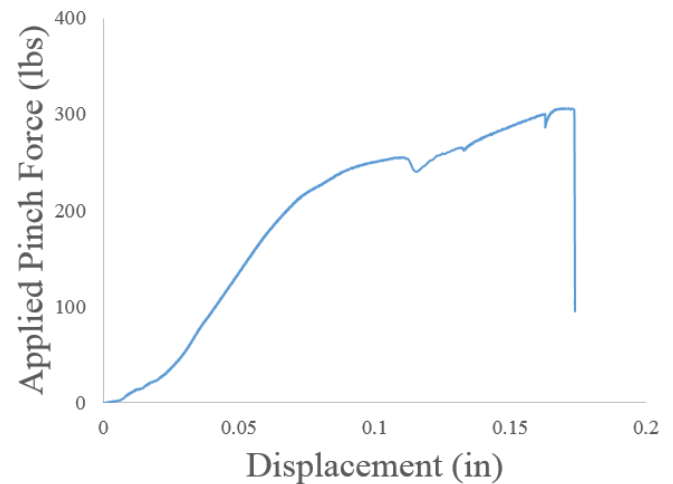


**Figure 3:** The force-displacement curve for a static failure of the *Point Digit*.

The dynamic testing of multiple *Point Digits* confirmed that the mechanism could withstand 10,000 cycles of flexion/extension. Some tests were interrupted due to replacement of linkage pins, tightening of threaded fasteners, etc. However, all fingers successfully achieved 10,000 cycles without fatigue failure or impaired performance.

The mechanical testing of the *Point Digit* confirmed that the mechanical design of the finger can withstand typical loading scenarios in a clinical setting. Future work will entail case studies with partial hand amputees and tests of activities of daily living with the *Point Digit*.

## REFERENCES

1. K. Ziegler-Graham et al., "Estimating the prevalence of limb loss..."Arch. of physical medicine and rehabilitation, vol. 89, no. 3, pp. 422-429, 2008

# DEVELOPMENT OF LOW COST 3D PRINTED TRANSITIONAL PROSTHESES

James Pierce B.S.M.E., Nicholas Than B.S., Drew Dudley B.S., Jorge Zuniga Ph.D.

Department of Biomechanics, University of Omaha 68182, NE, USA  
email: jepierce@unomaha.edu, web: cobre.unomaha.edu

## INTRODUCTION

There are increasing numbers of children with traumatic and congenital amputations or reductions. The Centers for Disease Control and Prevention estimates that about 1,500 babies are born with upper limb reductions every year, and of these only 1 in 9,400 children is considered for prosthetic fitting. This disparity between instances of amputation/reduction and prosthesis prescription is a result of high cost and complex needs, due to children's small size, constant growth, and psychosocial development [1, 2].

Families' financial resources play a crucial role in the prescription of prosthetics for their children, especially when private insurance and public funding are insufficient. Electric-powered (i.e., myoelectric) and body-powered (i.e., mechanical) devices have been developed to accommodate children's needs, but the cost of maintenance and replacement represent an obstacle for many families. Due to the complexity and high cost of these prostheses, they are not accessible to children from low income, uninsured families, or to children from developing countries [1, 2].

Advancements in computer-aided design (CAD) programs and additive manufacturing offer the possibility of designing and manufacturing prostheses at a very low cost [2]. The purpose of the present investigation was to demonstrate the manufacturing methodology of 3D printed transitional prostheses, examine improvement in perceived changes in quality of life, daily usage, and activities performed with these types of devices.

## METHODS

Nine children (two girls and seven boys, 3 to 16 years of age) with upper-limb reductions (one traumatic and eight congenital) were fitted with our 3D printed

transitional prostheses and were asked to complete a survey.

Inclusion criteria included boys and girls from 3 to 17 years of age with unilateral upper-limb reductions.

Exclusion criteria included upper extremity injury within the past month and any medical conditions that would be contraindicated with the use of our 3D printed prostheses prototypes, such as skin abrasions and musculoskeletal injuries.

The study was approved by the Creighton University Institutional Review Board and all the subjects completed a medical history questionnaire. All parents and children were informed about the study and parents signed a parental permission. For children 6 to 17, an assent was explained by the principal investigator and signed by the children and their parents.

The survey was developed to estimate the impact of our prosthetic device including items related to quality of life, daily usage, and type of activities performed.

## RESULTS AND DISCUSSION

After approximately 1 to 3 months of using our 3D printed prostheses, 11 children and their parents reported some increases in quality of life (4 indicated that was significant and 7 indicated a small increase), while 1 indicated no change.

Nine children reported using the device 1 to 2 hours a day, 3 reported using it longer than 2 hours and 1 reported using it only when needed.

Furthermore, children reported using our 3D printed prostheses for activities at home (9), just for fun (10),

to play (6), for school activities (4), and to perform sports (2).

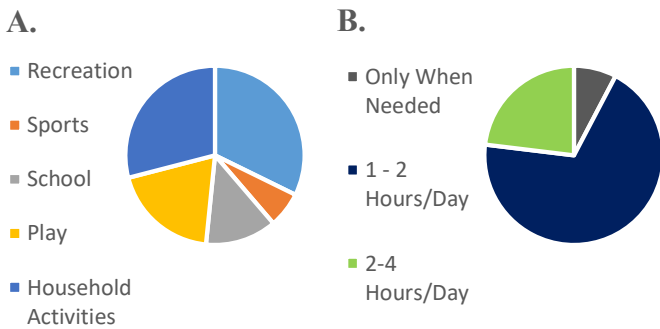


**Figure 1:** Qualitative usage metrics for 3D printed prostheses. A: Activity Type; B: Daily Hours Used

Four children reported malfunctioning and/or breaking of the 3D printed prosthetic device.

The main finding of our survey was that our 3D printed transitional prostheses have a great potential to positively impact quality of life, daily usage, and can be incorporated in several activities at home and in school. However, 36% of our research participants reported durability issues and/or malfunctioning of these devices. There is a need to develop more durable, medical grade 3D printed prosthetic devices to solve these durability constraints.

The proposed solution to this issue is a stepwise improvement of the prosthesis design through user feedback. The relative speed at which modifications can be performed through the use of CAD and 3D printing allows for many iterations of a design to be produced, fitted and evaluated over the course of weeks, rather than months, or years, as with traditional prostheses. [1]

Unfortunately, some observed inaccuracies with collected survey results have been noted in related studies, and a more quantitative method for determining usage is desired. This would allow for more informed future design modifications and more downstream functionality.

A prototype of an appropriate quantitative test apparatus for usage has been constructed, and will be validated in future studies.

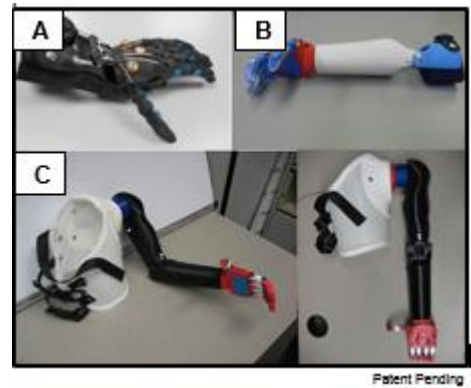


**Figure 2:** Shows some of the 3D printed transitional prostheses prototypes developed by our research team. A: Hand prosthesis (Cyborg Beast); B: Below Elbow Device; C: Prosthetic Shoulder.

## CONCLUSION

Although durability and environment are factors to consider when using 3D printed prostheses, the practicality and cost effectiveness represents a promising new option for clinicians and their patients. The technology opens up the possibility to help clinicians working in rehabilitation to establish guidelines for prosthesis prescription, establish effective rehabilitation programs, and create new prosthetic designs with the ultimate goal of improving self-esteem and quality of life for children with upper-limb reductions.

3D printing technology for the development of prosthetic devices is at a very early stage. The supervision of a certified prosthetist is crucial for the proper development and use of 3D printed prostheses.

3D printed transitional prostheses have a great potential to positively impact quality of life, daily usage, and can be incorporated in several activities at home and in school.

## REFERENCES

1. Krebs DE, Edelstein JE & Thornby MA, *Phys Ther*, **71**, 920-934, 1991.
2. Zuniga JM et al., *BMC Res Notes*, **8**, 10, 2015.

# USING BIOMIMETIC MODELS AND INTRAMUSCULAR EMG FOR CONTROL OF MYOELECTRIC PROSTHESES

<sup>1</sup>Misagh Mansouri, <sup>2</sup>Sergiy Yakovenko, <sup>2</sup>Valeriya Gritsenko, <sup>2</sup>Matthew Boots, <sup>2</sup>Anton Sobinov, <sup>1</sup>Carl Beringer, <sup>1</sup>Michael L Boninger, <sup>1</sup>Lee E Fisher, <sup>1</sup>Jennifer L Collinger, <sup>1</sup>Robert A Gaunt

<sup>1</sup>University of Pittsburgh, Pittsburgh, PA, USA

<sup>2</sup>West Virginia University, Morgantown, WV, USA

email: m.mansouri@pitt.edu, web: <http://rnel.pitt.edu/>

## INTRODUCTION

Commercial myoelectric prostheses have limited capabilities to simultaneously control multiple degrees of freedom. Although challenges exist in the mechatronics of the prostheses themselves, controlling these devices through myoelectric signals remains a significant challenge. These prostheses typically rely on signals recorded from surface EMGs placed on the residual limb, which are not the full set of extrinsic hand muscles required to actuate individual fingers. Also, standard control approaches often use pattern recognition or map the activity of a muscle (or group of muscles) to specific prosthesis movements while largely ignoring the underlying biomechanics. Here, we use a detailed musculoskeletal model that leverages anatomical and physiological knowledge of muscle function and hand biomechanics to interpret the activity of EMG signals. In addition, we use data-driven approaches to investigate the relationships between coordinated hand muscle activity, recorded using intramuscular EMG, and individual joint movements in able-bodied subjects and an amputee. The results from these analyses can be used to inform controller design for our biomimetic model.

## METHODS

All procedures were approved by the University of Pittsburgh Institutional Review Board and the US Army Human Research Protection Office. Nine able-bodied subjects and one transradial amputee were recruited for this study. We recorded intramuscular EMG (iEMG) from 16 extrinsic hand muscles targeted using ultrasound. The open-loop data collection experiments included 45 movement trials that included individual finger and wrist movements

in different wrist postures (flexed, extended, pronated, supinated and neutral). iEMG signals were recorded at 30 kHz, high-pass filtered at 20 Hz, rectified, and then low-pass filtered at 4 Hz. Kinematic data from the arm and hand were collected using 15 electromagnetic sensors (Ascension trakSTAR) and recorded at 100 Hz. We used an OpenSim upper extremity model [1] and modified it by including additional degrees of freedom (DoF) for the wrist and fingers (18 DoFs and 28 musculotendon actuators). The real-time myoelectric prosthetic simulation and control pipeline is shown in Figure 1. The real-time forward dynamic simulations were implemented in MuJoCo physics engine [2]. To speed up simulations, the moment arms matrices and muscle lengths was calculated through pre-compiled functions in MATLAB based on the OpenSim model's musculoskeletal geometry.

Principal component analysis (PCA) and hierarchical clustering analysis (HCA) were applied to the movement trials to compare EMG activity variance across all the different movements in able-bodied subjects and the amputee participant.

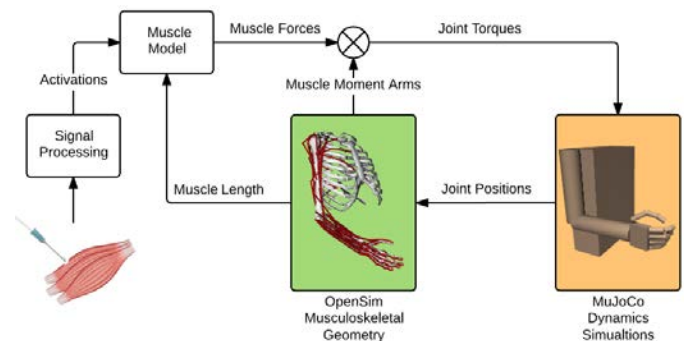


**Figure 1:** Real-time muscle-actuated prosthetic control pipeline using a biomimetic model.

## RESULTS AND DISCUSSION

Our forward dynamic simulations in MuJoCo were achieved in less than 1 ms using our biomimetic model. Simultaneous control of 3-4 DOFs (wrist, thumb, index finger and coupled middle-ring-pinky fingers' flexion/extension) was achieved in able-bodied subjects and an amputee, although maintaining static postures currently remains a challenge. Simulations are stable, although noise in input EMG signals can result in large changes in output joint torque. Furthermore, we typically do not have complete coverage of all finger flexors and extensors, which can lead to imbalances in joint torques across the wrist and may limit current model performance.

We found a major difference in the number of principal components (PCs) required to explain 90% of the variance in the EMG data between the amputee (5 PCs) and able-bodied subjects (10-11 PCs) (Figure 2). The differences in the number of PCs between able-bodied subjects and the amputee could potentially be explained by the reduced muscle set in amputees, challenges related to muscle targeting, or more interestingly, changes in the ability to voluntarily make certain movements as a result of the chronic limb loss. HCA clustered the movement trials from all subjects into four major subgroups consisting of wrist flexion/extension, wrist pronation/supination, wrist adduction /abduction, and all fingers based on all 10 subjects' EMG activity patterns. The HCA results from the amputee subject performing 7 different finger flexion/extension movements is shown in Figure 3.

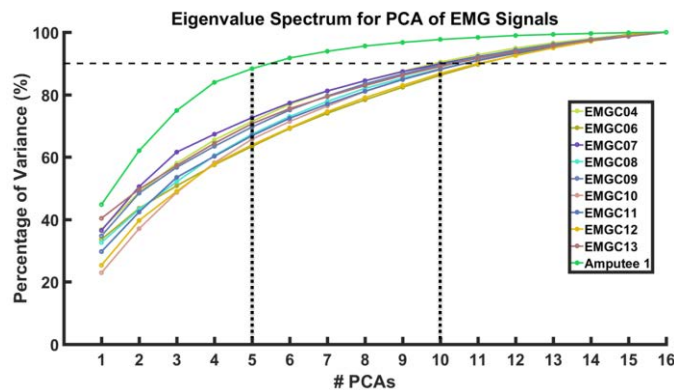


**Figure 2:** Number of PCAs representing the variance of EMG data in able-bodied subjects and an amputee.

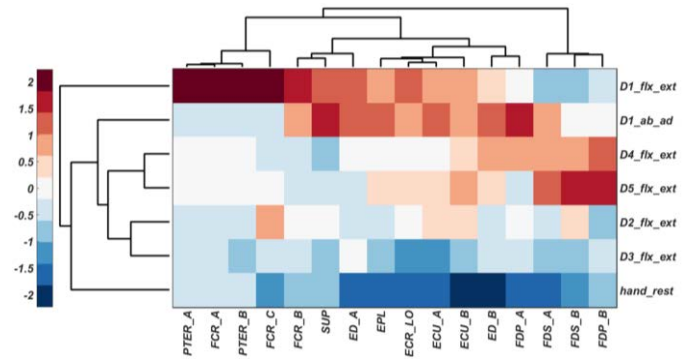


**Figure 3:** Hierarchical clustering shows a subset of finger movements for the amputee subject using dendrogram and heat map. Each EMG channel was standardized across all movements using the z-score.

Analogous movement trials and muscle groups were clustered together. The HCA results can be used to help visualize and understand the underlying neural and biomechanical patterns of EMG activity and as a way replace the missing muscles in amputees. The results of PCA and HCA in this study will be used to improve the design of bio-inspired controllers that generate prosthesis control signals from the biomechanical function of the muscles and the resulting movement dynamics.

## CONCLUSIONS

We have created a model that enables real-time simulation of the complete wrist and hand dynamics and that can be driven by EMG signals. We believe that this biomimetic approach to controlling myoelectric prostheses has the potential to improve prosthetic performance, but can also be used to improve our understanding of the basic biomechanical functions of hand muscles and the resulting movement dynamics.

## REFERENCES

1. Saul KR, et al. *J CMBBE* **18(13)**, 1445-58, 2015.
2. Todorov E, et al. *Proceeding of IROS '12*, 2012.

## ACKNOWLEDGMENTS

This work is sponsored by U.S. Army Research Office and the Defense Advanced Research Projects Agency (DARPA) under Cooperative Agreement NumberW911NF-15-2-0016.

# PROSTHETIC FEET WITH BIARTICULAR ELEMENTS REPLICATE GASTROCNEMIUS FUNCTION IN SIMULATION

<sup>1,2</sup> Anthony Anderson, <sup>1,2</sup> Andrea Willson, <sup>2</sup> Chris Richburg, <sup>3</sup> Joe M. Czerniecki, <sup>1,2</sup> Patrick M. Aubin

<sup>1</sup> Department of Mechanical Engineering, University of Washington, WA, USA

<sup>2</sup> Center for Limb Loss and Mobility, VA Puget Sound Health Care System, WA, USA

<sup>3</sup> Department of Rehabilitation Medicine, University of Washington, WA USA

email: paubin@uw.edu, web: <http://www.amputation.research.va.gov/>

## INTRODUCTION

Transtibial amputees compensate for absent leg musculature with numerous unwanted gait adaptations. Prosthetic users generally walk with a slower self-selected walking speed, gait asymmetries, over-active hip flexors, and deficient prosthetic ankle joint power generation [1].

Prosthetic energy storage and return (ESR) feet passively approximate ankle function, but they lack a biarticular coupling between the knee and ankle. In the intact limb, this coupling is provided by the gastrocnemius muscle. Previous gait simulation studies have shown that while ESR feet can replicate soleus function, they fail to deliver the benefits of biarticular gastrocnemius function [2].

For this study, two spring-damper models of uniarticular and biarticular prosthetic ESR feet were developed to determine the importance of biarticular function in prosthetic design. These models passively generate joint moments in response to prescribed motions. We use these generalized models to determine performance bounds on the entire class of uniarticular and biarticular prosthetic ESR feet. We hypothesize that the model with both uni- and biarticular elements will generate moments more representative of healthy gait than the model with a uniarticular element only.

## METHODS

A previously developed Opensim [3] model was used to simulate healthy gait over the course of one stance period. Data collection procedures are described in [4]. The 10 degree of freedom model

was actuated by 18 Thelen muscle models, and was scaled to the 72 kg participant.

Inverse kinematics, the residual reduction algorithm, and static optimization were performed to determine sagittal plane knee ( $\theta_k$ ) and ankle angles ( $\theta_a$ ) as well as knee ( $\tau_{k,healthy}$ ) and ankle ( $\tau_{a,healthy}$ ) moments for the healthy individual. The gastrocnemius' contribution to the knee moment was calculated and defined as  $\tau_{k,healthy}^{GAS}$ . The soleus' and gastrocnemius' contribution to ankle moments were also determined.

A uniarticular prosthetic foot model (UNI) was developed with the following mathematical form:

$$\tau_a^{UNI} = a_1\theta_a + a_2\theta_a^2 + a_3\dot{\theta}_a \quad (\text{eq 1})$$

Where  $\tau_a$  is prosthetic ankle moment, and  $\theta_a$  is the ankle angle as defined above. Constant parameters  $a_1$  and  $a_2$  are linear and nonlinear contributions to rotational stiffness,  $a_3$  is damping. The rest angle of the uniarticular spring was defined to be zero degrees. By definition, this model produced no knee moments.

The biarticular prosthetic foot model (BI) was defined as:

$$\theta_{a,k} = \theta_a + \theta_k + b_1 \quad (\text{eq 2})$$

$$\tau_k^{BI} = c_1\theta_{a,k} + c_2\theta_{a,k}^2 + c_3\dot{\theta}_{a,k} \quad (\text{eq 3})$$

$$\tau_a^{BI} = c_4\theta_a + c_5\theta_a^2 + c_6\dot{\theta}_a + \tau_k^{BI} \quad (\text{eq 4})$$

For the BI model,  $\theta_{a,k}$  was defined as the rotational equivalent of the gastrocnemius musculotendon length. Ankle dorsiflexion ( $+\theta_a$ ) and knee extension ( $+\theta_k$ ) increase  $\theta_{a,k}$ ; the parameter  $b_1$  was the spring's rest angle. The BI model has one uniarticular

nonlinear torsion spring and one biarticular nonlinear torsion spring with constant stiffness and damping parameters  $c_1$  through  $c_6$ .

For both prosthetic foot models, the constant parameters were computed by solving a constrained least squares optimization problem in MATLAB. Ankle and knee angles from healthy walking were input into equations 1 through 4. The optimizer then chose stiffness and damping parameter values that minimized the difference between the models' ankle ( $\tau_a$ ) and knee ( $\tau_k$ ) moments and the target biological moments. The target ankle moment was defined as the total healthy experimental ankle moment ( $\tau_{a,healthy}$ ), while the target knee moment was only the gastrocnemius contribution to the biological knee moment ( $\tau_{k,healthy}^{GAS}$ ).

## RESULTS AND DISCUSSION

The optimizer was able to find stiffness, rest length and damping parameters (Table 1) such that both the uniarticular and biarticular models closely matched the target biological ankle moment (Fig 1).

The ability of the uniarticular model to produce appropriate ankle moments implies that ESR feet can theoretically be designed to generate both soleus and gastrocnemius contribution to ankle moment through a single uniarticular passive mechanical element.

At the knee joint, the biarticular model was able to closely match the gastrocnemius' contribution to the knee moment. As predicted, the biarticular model more closely mimics healthy human gait kinetics.

Interestingly, the optimal uniarticular ankle spring with an added biarticular component was less stiff than a uniarticular ankle spring alone. As current ESR feet are optimized to work without biarticular elements, adding these elements to existing feet may be an ineffective approach, rather, foot stiffness and

biarticular element stiffness may need to be designed in parallel for optimal performance.

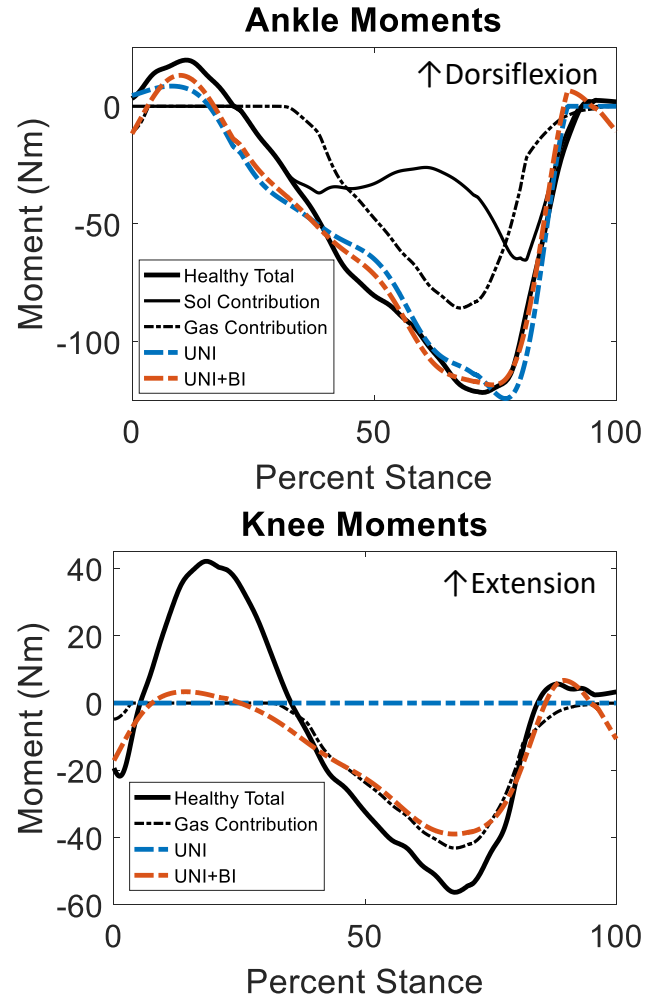


**Figure 1:** Biological and passively generated ankle (top) and knee (bottom) moments

## REFERENCES

1. Winter, D.A., et al. *J. Biomech*, 1988
2. Zmitrewicz, RJ, et al. *J. Biomech*, 2006
3. Delp SL, et al. *IEEE Biomed Eng*, 53, 2007.
4. Chand, et al. *Comput Methods Biomech Biomed Engin*, 2012

**Table 1:** Optimized parameters.

	Linear Ankle Stiffness	Nonlinear Ankle Stiffness	Linear Knee-Ankle Stiffness	Nonlinear Knee-Ankle Stiffness	BI Spring Rest Angle	Damping
UNI	-4.40	-0.44	-	-	-	0
BI	-4.74	-0.16	-0.78	-0.02	16.90	0

# VARIABLE STIFFNESS PROSTHETIC FOOT

Evan M. Glanzer, Peter G. Adamczyk

University of Wisconsin-Madison, Madison, WI, USA  
email: eglanzer@wisc.edu

## INTRODUCTION

Energy storage and return (ESAR) prostheses passively store and return energy to the user through deflection of compliant leaf spring keels. The driving mechanical property in this process is the stiffness of the foot, which must be chosen to achieve an optimum in overall function across all the user's activities. Since these devices are passive, they cannot adapt to changes in activity. In contrast, the natural lower limb continuously adapts its behavior for different activities, including simple changes such as walking faster or slower, or larger changes such as negotiating ramps and stairs. For example, push-off work and peak push-off power increase with increasing walking speed in a healthy human ankle [1], whereas the prosthetic-side leg of an ESAR prosthesis user provides a constant amount of push-off work across all speeds [1].

We propose to address this shortcoming in adaptability through a new prosthesis concept, the Variable Stiffness Foot (VSF), which directly varies the forefoot stiffness of an ESAR-type foot through a low-power internal mechanism. Prior results show that a more compliant forefoot returns more energy to the user [1]; therefore, we plan to continually modulate forefoot stiffness in the VSF to achieve optimal energy return for each walking speed. We hypothesize that a softer forefoot will be better for faster walking because more energy will be returned to the user [2], which is more similar to healthy ankle function. In this study, we investigated the range of stiffness achievable in the latest VSF prototype and its effects on energy return in walking.

## METHODS

### Design

The VSF design (Figure 1) varies the forefoot

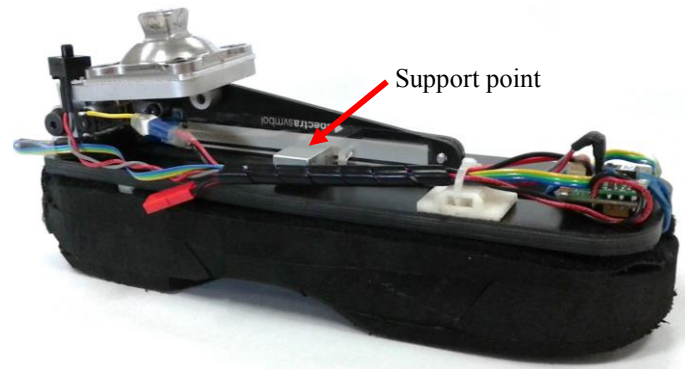


**Figure 1:** Variable stiffness foot prototype

stiffness of an ESAR-type foot by changing the position of a support point behind the flexible keel during swing phases. As this support moves, the length of the freely deflecting forefoot section is altered, which in turn changes the effective forefoot stiffness. Using linear compression testing, we estimated forefoot stiffnesses from 10 to 46 N/mm (Figure 2). In order to achieve quick adjustments, the foot was designed to complete a full-range adjustment in roughly two seconds, which represents about four swing phases of walking.

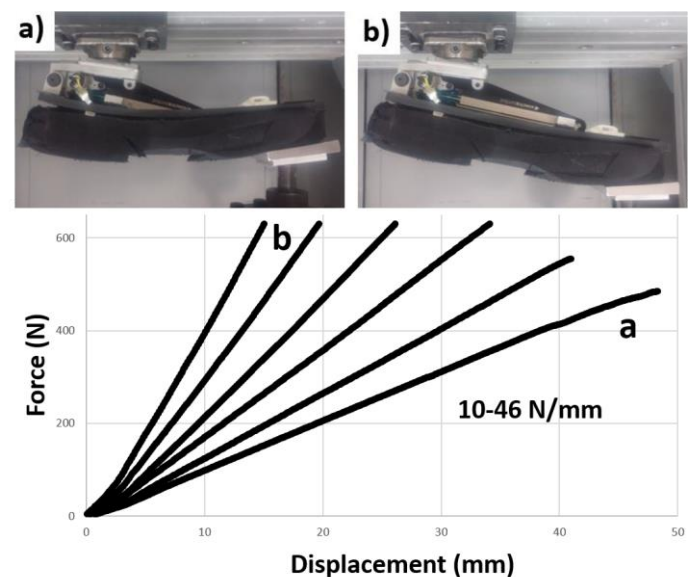


**Figure 2:** Compression testing: a) Softest b) Stiffest

## Validation

We performed a pilot study to validate the effects of the VSF mechanism on energy storage and return. Three non-amputees walked overground on the prosthesis using an ankle-immobilizing boot, with the VSF set to five stiffness levels. We estimated the power flow into and out of the prosthesis using a deformable-body model [3].

## RESULTS AND DISCUSSION

Our analysis focused on device performance rather than how the prosthesis characteristics translated to the joint mechanics of the user. Peak push-off power increased as expected with a more compliant forefoot (Figure 3). Energy returned to the user in push-off showed a similar trend (Figure 4).

However, both peak power and energy return at the softest setting are lower than in the next stiffer setting. This is caused by the softest setting being too compliant for the subject's body mass. The forefoot has a displacement limit that is being reached causing the "bottom-out" effect. A correlation between the minimum useable stiffness and body mass could be studied in the future. This correlation could then be programmed into our controller to avoid the "bottom-out" zone.

## CONCLUSIONS AND FUTURE WORK

Our device demonstrates similar characteristics in

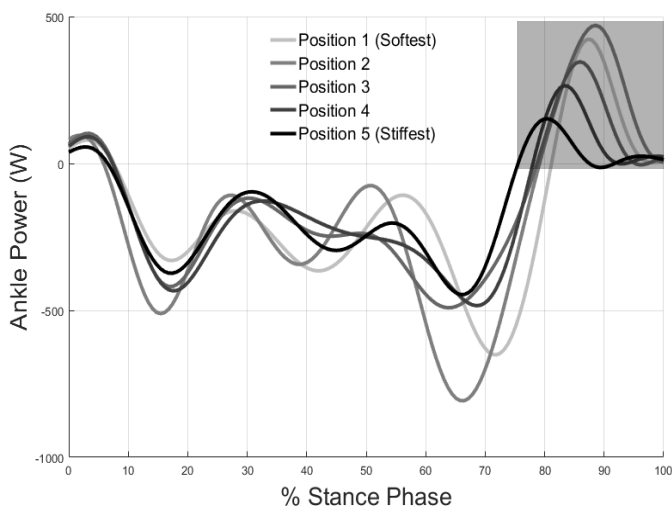


**Figure 3:** Peak ankle push-off power decreases with increasing foot stiffness. Push-off work is highlighted in the gray area. Data is from a single participant.

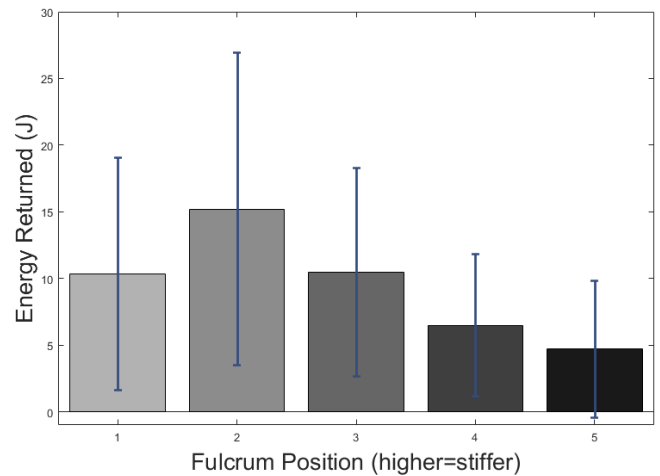


**Figure 4:** Energy returned generally decreased with increasing foot stiffness, with the exception of the first fulcrum position due to a "bottom-out" effect.

power and energy return with changing stiffness as previous studies [2]. In upcoming testing, we will use an onboard controller to adjust the stiffness of the foot in real time to match different activities in persons with amputation. First, we will investigate stiffness changes based on walking speed. This adjustment is expected to influence subjective user preference as well as biomechanical data in ways that have not been tested before. We will also use onboard sensors (Figure 1) to adapt to other foot motions, including up and down slopes and stairs, based on real-time estimates of foot trajectory [4]. Data from these trials will further inform the potential benefits of using a variable stiffness prosthesis, and provide insight into potential design improvements for future devices.

Stiffness has important consequences for proximal joints as well, such as knee moment [2]. We attempted to measure changes in knee flexion moment with changing stiffness but due to the use of the ankle-immobilizing boot, we did not observe significant correlations. Future work will investigate these effects in persons with amputation.

## REFERENCES

1. Adamczyk *et al*, *IEEE TNSRE*, **23**, 776-785, 2015.
2. Adamczyk *et al*, *Hum. Mov. Sci.*, In Review.
3. Takahashi *et al*, *J. Biomech*, 45:15, 2662-7, 2012.
4. Rebula *et al*, *Gait & Post.*, 38:4, 974-80, 2013.

# TRANSFEMORAL PROSTHESIS CONTROL FOR SLOPE WALKING WITH PRINCIPAL COMPONENT ANALYSIS

<sup>1</sup> Woolim Hong and <sup>1</sup> Pilwon Hur

<sup>1</sup> Texas A&M University, College Station, TX, USA  
email: ulim8819@tamu.edu, pilwonhur@tamu.edu, web: [http:// hurgroup.net/](http://hurgroup.net/)

## INTRODUCTION

A powered transfemoral prosthesis is an assistive device for the amputees who lost their lower limb including the knee that supports their daily locomotion [1]. For the amputee patients, walking on various sloped surfaces are one of the most challenging tasks in their daily lives. However, the existing (both passive and active) prostheses cannot fully accommodate the functions.

Trajectory generation for the powered prosthesis is an important procedure to design an appropriate controller that mimics human walking. Trajectory has to be generated for each gait cycle in real time to produce stable, robust and human-like walking. However, real-time trajectory generation is not a simple task and requires high computational loads, which is usually not tractable for the low profile single board computers. Recently, an algorithm for online trajectory generation for the powered transfemoral prosthesis was proposed using spline-based real time optimization. However, this method is applicable only for the upslope walking [1].

In this study, we generate the desired trajectories for various sloped surfaces with a small set of data using Principal Component Analysis (PCA). PCA lets us reduce a complex data set to a lower dimension [2] to perform the slope walking in different inclination with the prosthesis in real-time. Through PCA, we extract two principal components and their coefficients from the ankle and the knee, respectively. By curve fitting the coefficients of the principal components, we estimate the appropriate coefficients corresponding to the slope angle. In other words, we generate the adequate trajectories from the linear combination of the dominant principal components and their coefficients using only the inclination information. We also utilize a

low gain PD controller and the spline generation [1] to adapt the unexpected slope and smoothly blend into the appropriate trajectories corresponding to the new slope.

## METHODS

To collect the data for the PCA analysis, we collected human walking data and joint trajectories for the ankle and knee with a motion capture system (Oqus 210c, Qualisys North America, Inc., Highland Park, Illinois, USA). We put 13 reflective markers on the body of the healthy young adult to capture the subject's joint trajectories while walking on a treadmill. The inclination of the treadmill was varied with 7 different inclination angles:  $-15^\circ$ ,  $-10^\circ$ ,  $-5^\circ$ ,  $0^\circ$ ,  $5^\circ$ ,  $10^\circ$ , and  $15^\circ$ . We set the limit of the slope angle at  $\pm 15^\circ$  since the angles exceeding  $\pm 15^\circ$  are rarely encountered in the daily living.

PCA was performed on the joint trajectories to extract the principal components required to reconstruct the various sloped surface trajectories. PCA provided us the most significant principal components that are the most highly correlated to human joint trajectories with a minimum amount of information [2].

It should be noted that the first gait cycle with the heel strike does not have the defined trajectories, which causes discontinuity in trajectory. To resolve this issue, a cubic spline based optimization is used to have smooth transition between each slope [1]. Also, for the slope adaptation during the heel contact, we used a low gain PD controller to avoid the discrete motion due to the new slope [1].

## RESULTS AND DISCUSSION

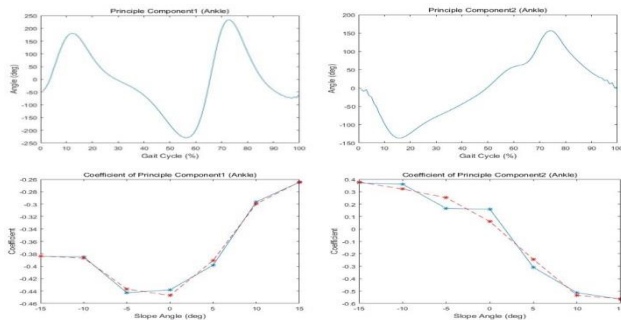


**Figure 1.** Results of PCA. The principal components (PC) of the knee joint angle (left top: 1<sup>st</sup> PC, right top: 2<sup>nd</sup> PC). The coefficients of the principal components (left bottom: 1<sup>st</sup> PC, right bottom: 2<sup>nd</sup> PC).

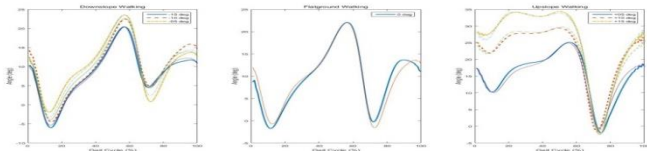


**Figure 2.** Regenerated Ankle Joint Trajectories with Optimized Coefficients and Corresponding Principal Components. Downslope walking trajectories from  $-15^{\circ}$  to  $-5^{\circ}$  (left). Flat ground walking (mid). Upslope walking from  $5^{\circ}$  to  $15^{\circ}$  (right).

It was found that the walking pattern for the downslope was different from that of upslope walking. When the subject walked on the downslope surfaces, the ankle joint angle seemed to remain the same as the level walking regardless of the inclination angles. For the knee joint, as the inclination angle increases, the deviation of the joint trajectory became significant. On the other hand, when the subject walked on the upslope surfaces, both the ankle joint and the knee joint angle increase as the inclination angle increases for the range of 0%-40% and 80%-100% of the gait cycle; interestingly, in the mid-range of the gait cycle, they merged to the flat ground walking trajectory [1].

Figure 1, 3 shows the results of PCA from the ankle joint and the knee joint, respectively. We chose two of the most dominant principal components and their coefficients to generate the joint angle pattern. We solved an optimization problem to curve the coefficient plots for calculating the appropriate coefficients corresponding to the slope angle. As Figure 2 shows, with these 2 principal components and the optimized coefficients, we could generate the ankle joint trajectories for 7 slopes with 0.9815 correlations. From Figure 4, the correlation result of the regenerated trajectories with the results of PCA was 0.9959.

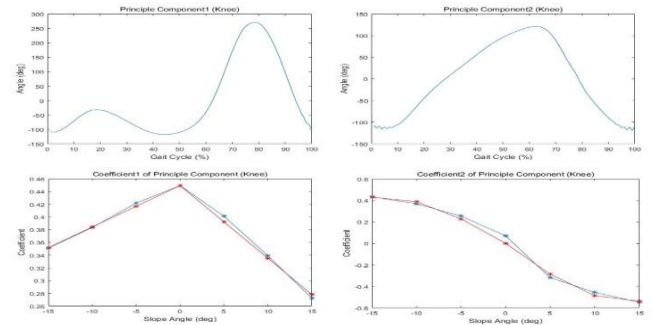


**Figure 3.** Results of PCA. The principal components (PC) of the knee joint angle (left top: 1<sup>st</sup> PC, right top: 2<sup>nd</sup> PC). The coefficients of the principal components (left bottom: 1<sup>st</sup> PC, right bottom: 2<sup>nd</sup> PC).

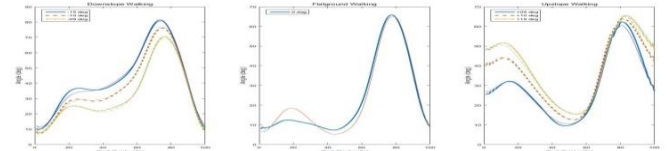


**Figure 4.** Regenerated Knee Joint Trajectories with Optimized Coefficients and Corresponding Principal Components. Downslope walking trajectories from  $-15^{\circ}$  to  $-5^{\circ}$  (left). Flat ground walking (mid). Upslope walking from  $5^{\circ}$  to  $15^{\circ}$  (right)

In general, to generate the trajectories for each slope with the increment of  $1^{\circ}$ , we need 31 trajectories for the ankle and the knee, respectively. Yet, using PCA, we need 4 trajectories (two principal components for each joint) and the corresponding coefficients with high correlation. It was shown that all sloped trajectories within  $\pm 15^{\circ}$  with the linear combination of these components and coefficients could be reconstructed.

## CONCLUSIONS

This research showed that PCA can be used to generate joint trajectories for various slopes from the linear combination of a small number of the components and their coefficients. A low gain PD control and the spline generation along with the PCA-based trajectory generation could adapt the control of transfemoral prosthesis to various slopes without any conflicts [1]. For the future work, we expect to extend this idea to the different situations for the prosthesis control with the unified controller.

## REFERENCES

1. Victor P, et al., IEEE/RSJ International Conference on Intelligent Robots and Systems, 2016
2. Jonathon S. *CoRR*, **abs/1404.1100**, 2014

# 3D Printed Prostheses: Not Just Plastic Toys

Nicholas Than, James Pierce, Drew Dudley, Jorge Zuniga

University of Nebraska at Omaha, Omaha, NE, USA  
email: [nthan@unomaha.edu](mailto:nthan@unomaha.edu), web: <https://cobre.unomaha.edu>

## INTRODUCTION

For children with upper-limb amputations, it is not easy to obtain prostheses. Because of their constant growth and frequent need for larger prostheses, insurance companies refuse to pay, citing cost as a prohibitive factor, and committing to payments only once children are grown. There is ample evidence, however, that early prescription and use of an upper-limb prosthesis is beneficial to amputees [1]. To better care for children and adults with upper-limb amputations, it is necessary that cheaper, more accessible prostheses are developed.

Within the last decade, consumer-grade 3D printers have experienced an explosion in popularity, due to decreasing costs, technological advances, and larger media exposure. Use of 3D printers allows cheap, rapid prototyping, and enables laypeople to quickly and easily create objects that would otherwise require prohibitive resources or expertise.

The cheap, accessible nature of 3D printing has led to the formation of large communities of enthusiasts. Subsets of these communities have, in fact, begun development of prostheses and other assistive devices – with several communities being dedicated solely to designing, printing, and donating upper-limb prostheses. In addition, many academic institutions have begun lines of research with 3D printed prostheses – but because of the field's relative infancy, there is much skepticism in regards to the use of these devices [2].

Several articles – both peer-reviewed and not [2] – suggest that 3D printed prostheses are not functional, and that these devices are little more than novelties. Negative reviews on 3D printed prostheses are frequently given, citing a dearth of evidence supporting prosthesis acceptance and durability. It is also frequently noted that few papers exist, if any, that show improvement of function

with 3D printed prostheses. Therefore, the purpose of this study was to determine whether or not upper-limb amputees improved in function with use of 3D printed prostheses.

## METHODS

This study recruited 11 upper-limb amputees with no neurological deficits. All subjects were children (ages 3-15) with no physical abnormalities, aside from their amputated limb. Prostheses were designed in Autodesk Fusion 360 (Autodesk Inc., San Rafael, California, US), and were printed on Ultimaker 2 Extended+ 3D printers (Ultimaker, Geldermalsen, The Netherlands).

To properly fit prostheses, anthropometric measures are required of a subject's affected limb. Usually, these measurements are taken in-person by a certified prosthetist – however, in this study, limbs were measured at a distance in a manner previously described and validated by Zuniga et al. [3]. Subjects sent pictures of their affected limbs with measuring tapes or rulers nearby to reference for scale, and an open-source program called Tracker (Open Source Physics, Boston, MA, US) was used to determine residual limb size and range of motion. A board-certified occupational therapist and hand therapist performed final fitting procedures of each 3D printed prosthesis.

Upon receiving their 3D printed prosthesis, subjects performed the box and blocks test (BBT, Fig. 1) – a quick (1 min), simple test to assess hand function, whereby a subject uses one arm to move 2.5 cm wooden blocks over a partition, from the ipsilateral to the contralateral side. The test was completed with both the prosthetic and biological hands, and subjects revisited the lab to complete the same test 6 months later. Data was analyzed using a two-way repeated measures ANOVA, comparing prosthetic versus biological hands and BBT scores before and

after 6 months of use. Significance for this study was set at  $p \leq .05$ .

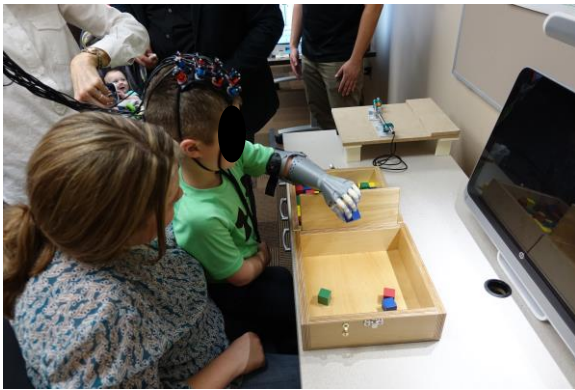


**Figure 1:** Subject completing BBT with prosthesis.

## RESULTS AND DISCUSSION

The ANOVA revealed significant differences between baseline and 6-month scores with subjects' prosthetic hands, but not with their biological hands (Table 1). Finding a change in the prosthetic hand but not the biological hand is important, as the study population consisted entirely of children. Because of their constant growth and maturation, it was necessary to rule out motor development as a reason for increased BBT scores. As there was a lack of difference in biological hand performance before and after 6 months, it can be inferred that the subjects' aging and consequent motor development did not significantly alter BBT performance.

It is important to note that no therapies or interventions were present in this study; the increases in score were due to the subjects' normal use of their prostheses, without any significant training. This lends great credence to the thought that 3D printed prostheses can, in fact, be used as functional prostheses. Furthermore, it is frequently seen that conducting therapies and teaching subjects how to use traditional prostheses (and indeed most tools) can improve function greatly. Considering the already-apparent learning that is occurring with this

3D printed prosthesis, it is logical to assume similar learning principles hold true.

Concerns over 3D printed prosthesis durability are valid, as some subjects did report breaking of prosthetic fingers – however, this study's prosthesis was designed with replacement of parts in mind, and thus it was quite easy to 3D print new fingers and replace them.

Despite the fact that the results of this study were quite expected, it is important not to ignore these findings. Several reviewers have claimed that 3D printed prostheses are not backed by research, and are not able to be used functionally; this study has shown otherwise, and has addressed concerns of function. Durability may be an issue with 3D printed prostheses, but given the ease with which broken parts can be re-printed and replaced, smart prosthetic design may allow users to overcome this. The use of 3D printers has enabled quick and cheap creation of prostheses. Several models of 3D printable prostheses have been made – and several may be flawed – however, this study has found that amputees can improve function with 3D printed prostheses, and that while prosthesis durability may be a problem, replacement of parts is not.

## CONCLUSIONS

For many, high costs prohibit purchase of an upper-limb prosthesis. Recent development in 3D printing technology has allowed cheap and rapid distribution and development of these prostheses. Many authors have suggested lack of function in 3D printed devices, but this study has found otherwise.

## REFERENCES

1. Resnik L, et al. *Arch Phys Med Rehabil.* **93** 710-717, 2012.
2. ten Kate J, et al. *Disabil. Rehabil. Assist. Technol.* **12(3)**, 300-314, 2017.
3. Zuniga JM, et al. *BMC Research Notes* **8:10**, 2015

**Table 1:** Table shows the mean and standard deviation of blocks moved at baseline and 6-month collections

	Baseline (blocks moved)	6 months (blocks moved)
Prosthetic Hand (Significant)	6 ± 12	13 ± 12
Biological Hand (Non-significant)	46 ± 19	48 ± 13

# Quasi-Passive Two Degree of Freedom Prosthetic Ankle

<sup>1</sup>Michael J. Greene, <sup>2</sup>Peter G. Adamczyk

<sup>1</sup>Department of Mechanical Engineering, University of Wisconsin- Madison, WI, USA

email: [greenes@wisc.edu](mailto:greenes@wisc.edu),

## INTRODUCTION

Humans are known to have less stability in the lateral direction during gait. This is especially the case for amputees. Missing one or more limbs reduces the ability to control the body's motion, making overall balance a challenge. With current technology, amputees have trouble walking on slopes and uneven ground. This is largely due to the inability to control the prosthetic ankle. Some active and semi-active prostheses have the ability to adapt their dorsiflexion/plantarflexion (DP) angle to match up- and down-slopes. However, studies have shown that lateral balance is subject to more active control compared to fore-aft balance [1]. Prosthesis users remain disadvantaged in this lateral direction, as they lack the ability to control ankle inversion/eversion (IE) in the prosthetic limb as the natural ankle does. We are developing a semi-active smart prosthetic ankle that can adapt its angle in both DP and IE directions. The prosthesis will actively adjust through angles of  $\pm 10^\circ$  from neutral, in any combination of DP and IE. For the present pilot study, we sought to verify this range of motion and perform a preliminary investigation of its effects on ankle moments in the sagittal and frontal planes during walking. We hypothesized that a plantarflexed alignment would lead to earlier increases in the measured plantarflexor moment; that dorsiflexed alignment would have the opposite effect, a delayed increase in moment; and that inversion and eversion alignment would vary the magnitude of the frontal plane ankle moment.

## METHODS

### Ankle Design

The angle of the prosthetic ankle can be controlled  $\pm 10^\circ$  about any arbitrary axis orthogonal to the longitudinal axis of the ankle module. This effectively makes a 2-axis foot that can be manipulated in both the plantarflexion/ dorsiflexion and inversion/eversion directions. The ankle mechanism is made up of two short cylindrical spacers with their mating ends cut at complementary angles of  $5^\circ$  to form two wedge-shaped inclined planes. These inclined planes rotate independently

about the longitudinal axes of the upper and lower halves of the ankle module (effectively the axis of the tibial pylon and the foot prosthesis' top surface normal). If the two planes are aligned in complementary positions, ankle alignment is neutral (Figure 2). If one plane is rotated relative to the other, the mating faces push against each other and force a change in ankle alignment. Using all combinations of upper and lower rotation angles, the ankle angle can be up to twice the face angle of the wedge ( $\pm 10^\circ$ ), in arbitrary directions including DP, IE or combinations of the two.

The inclined surface between the two plates creates a twist-out moment on each plate due to the contact force resulting from the ankle moment, which is held in balance by friction on both the angled face and the opposite flat face. Analysis of these balancing moments reveals that a friction coefficient as low as 0.05 is sufficient to ensure locking at a face inclination angle up to  $5.7^\circ$ , even in the worst configuration (Neutral). The actual friction coefficient is closer to 0.1, ensuring that the current face angle of  $5.0^\circ$  is well within the safe range. Tensile loads and internal/external rotation moments are supported by a 2-axis universal joint running axially through the center of the module.



Figure 1: Prosthetic Ankle Parts (left to right): shims, u-joint, two inclined planes with friction pads, top flat plate, and male pyramid



Figure 2: Prosthetic Ankle fully assembled

### Ankle Validation

Three able-bodied subjects wearing ankle-immobilization boots tested the ankle module in five target configurations: neutral alignment, and 10° dorsiflexion, plantarflexion, inversion, and eversion. Subjects completed 3 walking trials in each configuration, while standard motion capture and force plate data were recorded. The subjects' gait patterns were analyzed using custom MATLAB code implementing standard inverse dynamics techniques. We measured outcomes of observed ankle angle and ankle joint moment in the sagittal and frontal planes for each condition.

### RESULTS AND DISCUSSION

Stance phase data are presented in this study (0-60% of gait cycle), as the mechanics of ankle alignment primarily affect this phase of gait. Ankle angles were observed to vary in increments of roughly 10° in both sagittal and frontal plane angles, as expected from the 10° setting increments (Figure 3). Despite variance in the Neutral angle across subjects (due to variations in attachment to the ankle immobilization boot), all the different configurations followed the expected relationships among the different angle settings.

Preliminary observations suggest that plantarflexed posture leads to earlier increases in the ankle plantarflexion moment (Figure 4). The dorsiflexed posture appeared to delay the increase of ankle moment a little later in the gait cycle. Thus our hypothesis appears supported. However, later ankle moment relationships did not show a systematic trend, indicating a need for further study of the dynamic interaction between alignment and ankle mechanics.

Inversion and Eversion postures did not appear to shift the ankle moment higher or lower. This could be a result of kinematic compensation (e.g. changes in step width or leaning to the sides to cancel the effect). Further investigation will determine the adaptations the subjects used in these cases.

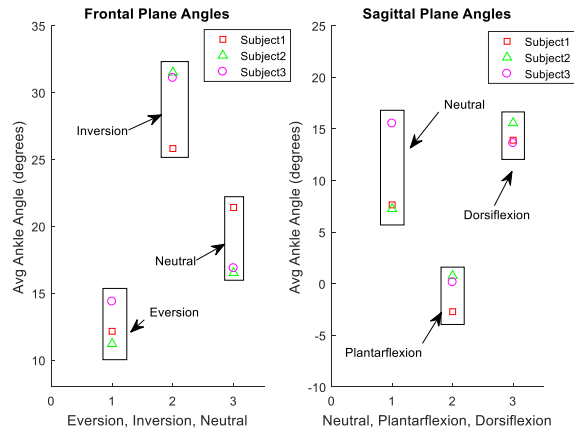


Figure 3: Average ankle angle for each subject

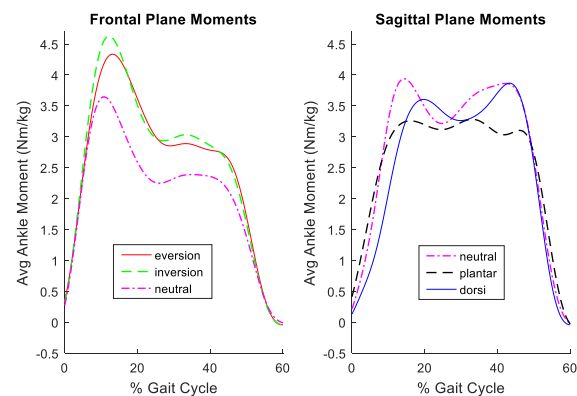


Figure 4: Example Frontal and Sagittal Ankle Moments

### ONGOING AND FUTURE WORK

Ongoing work is focused on continuing this characterization of mechanical behavior of the prosthesis and automating the ankle movement to accommodate different slopes. Automation will also ensure accuracy when changing ankle angle.

Additional work in the immediate future will focus on testing ankle, knee and hip mechanics across variations in alignment in persons with unilateral lower limb amputation.

### REFERENCES

[1] Bauby *et al. J. Biomech.*, 33:11, 1433-440, 2000.

### ACKNOWLEDGEMENTS

This work was supported by institutional funds from the University of Wisconsin – Madison and the Wisconsin Alumni Research Foundation.

# **AUTOMATICALLY DETECTING DESTABILIZING WHEELCHAIR CONDITIONS AND APPLYING ELECTRICAL STIMULATION TO MAINTAIN SEATED POSTURE**

Kiley Armstrong<sup>1,2</sup>, Musa Audu<sup>1,2</sup>, and Ronald Triolo<sup>1,2,3</sup>

<sup>1</sup> Case Western Reserve University, Department of Biomedical Engineering, Cleveland, OH

<sup>2</sup> Louis Stokes Cleveland VA Medical Center, Research Department, Cleveland OH

<sup>3</sup> Case Western Reserve University, Department of Orthopedics, Cleveland OH

Email: kla34@case.edu

## **INTRODUCTION**

Injuries that occur within the thoracic and lumbar regions of the spinal cord typically results in paralysis of the lower extremities and trunk. According to a study surveying 681 people with paraplegia, trunk stability is among the top functions people want restored<sup>1</sup>. For people with the inability to control their trunk, perturbations can cause destabilization and a loss of erect posture, limiting their mobility and independence. Common perturbations experienced by manual wheelchair users that contribute to destabilization are collisions and sharp turns.

Functional electrical stimulation (FES) is used to maintain trunk stability, as well as providing a method to regain an erect posture following a perturbation<sup>2</sup>. Applying FES at the onset a destabilizing event, such as a collision or sharp turn, is expected to increase trunk stability, maintain erect posture, and boost users' confidence in their wheelchair during daily activities.

The goal of this study is to automatically detect potentially destabilizing conditions faced by manual wheelchair users with spinal cord injuries and activate the appropriate muscles to prevent falls and stabilize the seated operator.

## **METHODS**

Wireless inertial measurement units with tri-axial acceleration and gyroscopic sensors were mounted on the wheelchair frames and backs of two individuals with low cervical and thoracic level injuries, see table 1. Kinetic data was collected using Vicon motion capture system, which tracked the position of the wheelchair and subject throughout each trial. Subjects sat passively in a manual wheelchair attached to a guidance track as it descended a ramp to ensure consistent velocity through a sharp 90 degree turn and sudden stop

simulating a collision. An algorithm using the accelerometer and gyroscopic data was created to detect the turns and collisions, and trigger appropriate stimulus patterns. Acceleration in the anterior and posterior (A/P) and angular velocity in the superior and inferior (S/I) direction provided distinct features to discriminate between destabilizing collisions and turns, respectively. During calibration, collision thresholds were determined by taking the mean of the maximum A/P acceleration peak from 20 trials and subtracting two standard deviations. The turn thresholds were determined in the same way using the S/I angular velocity. During testing, the algorithms were applied in real time to activate a pre-programmed pattern to oppose lateral bending or prevent forward leaning and maintain erect posture throughout the events. Subjects rated their perceptions of safety with and without stimulation via the Usability Rating Scale (URS)<sup>3</sup>. Post-processing of the kinetic data allowed calculation of the maximum lateral and forward trunk angle during turns and collisions, respectively, as well as the time to return to erect posture during collision. Erect posture was achieved when the subjects returned to less than 6 degrees of flexion.

## **RESULTS AND DISCUSSION**

Analysis of the kinetic data revealed a difference between maximum trunk angle with and without stimulation applied, as well as a difference in return time to erect posture. Table 2 summarizes the kinetic results of the collisions for both subjects. According to the URS data, subjects reported a significantly increased feeling of safety and stability during collisions ( $Z = -2.539$ ,  $p = 0.011$ ) with a median URS score of 1.5 with and -1.5 without triggered stimulation to the appropriate muscles to resist the destabilizing event. Similarly, during

turns, subjects felt a significant increase in safety and stability ( $Z = -3.100$ ,  $p = 0.002$ ) with a median URS score of 0 with and -1 without triggered stimulation.

**REFERENCES**

1. Anderson, KD. *Journal of Neurotrauma* **21**(10).
2. Murphey, JO, et al. *Journal of Rehabilitation Research and Development* **51**(5).
3. Steinfeld E, Danford G, editors. “Enabling environments: measuring the impact of environment on disability and rehabilitation.” *New York: Kluwer/Plenum*; 1999.

The authors would like to thank Lisa Lombardo, PT, for her expertise and assistance in preparing and conducting the experiments.

This work was supported by Merit Review #RX-001204 (R. Triolo, Principal Investigator) from the Rehabilitation R&D Service of the US Department of Veterans Affairs and utilized the facilities and resources of the Louis Stokes Cleveland VA Medical Center. The contents do not represent the views of the US Department of Veterans Affairs or the United States Government. Human studies approval by LSCVAMC IRB protocol number 07101-H36, ‘A Neuroprosthesis for Seated Posture and Balance.’

**ACKNOWLEDGMENTS**

**Table 1:** A summary of clinical characteristics of participants in this study. Labels: QL = Quadratus Lumborum, ES = Erector Spinae, GM = Gluteus Maximus, IL = Iliopsoas, PA = Posterior Adductor.

Subject	Age	Gender	Injury Level	AIS Grade	Date of Injury	Date of Implant	Muscles Stimulated during Coll	Muscles Stimulated During R Turns	Muscles Stimulated During L Turns
IST-04	44	F	C7	C	3/13/98	8/26/10	ES, QL, GM, PA	R ES, R/L GM, R QL, R/L PA	L ES, R/L GM, L QL, R/L PA
STR-03	41	F	C6	B	9/02/07	3/06/12	PA, GM ES, QL, IL	R ES, R/L GM, R QL, R/L PA, R/L IL	L ES, R/L GM, R/L PA, R/L IL

**Table 2:** A summary of the kinetic results, including maximum trunk angle and return time, for collisions and turns with and without stimulation.

		IST-04		STR-03	
		With Stim	Without Stim	With Stim	Without Stim
<i>Collisions</i>	<b>Mean Max Forward Trunk Angle (deg)</b>	33.23 ± 9.76	33.60 ± 7.01	13.94 ± 2.12	14.47 ± 2.20
	<b>Return Time to &lt; 6 degrees (seconds)</b>	0.77 ± 0.26	2.00 ± 1.96	0.30 ± 0.06	0.34 ± 0.10
<i>Right Turns</i>	<b>Mean Left Trunk Tilt (deg)</b>	2.15 ± 1.65	5.11 ± 1.49	3.72 ± 0.97	3.11 ± 0.45
<i>Left Turns</i>	<b>Mean Right Trunk Tilt (deg)</b>	3.80 ± 1.51	6.51 ± 0.58	3.63 ± 0.46	1.84 ± 1.01

# Dynamic balance is different between fallers and non-fallers with multiple sclerosis

<sup>1</sup>Alex Peebles, <sup>1</sup>Adam Bruetsch, <sup>2</sup>Sharon Lynch, and <sup>1</sup>Jessie Huisinga

<sup>1</sup>Human Performance Laboratory, University of Kansas Medical Center, Kansas City, KS, USA

<sup>2</sup>Department of Neurology, University of Kansas Medical Center, Kansas City, KS, USA

email: apeebles@ku.edu

## INTRODUCTION

Multiple sclerosis (MS) is a progressive autoimmune disease which negatively effects gait and balance. Around 60% of persons with MS (PwMS) experience falls, which often results in injuries, fear of falling, and activity curtailment [1]. Falls most commonly occur during functional mobility, and are most commonly attributed to loss of balance [2]. While fall occurrence is high, not all PwMS experience falls, potentially due to differences in motor control impairments or gait adaptations. Compared to healthy controls, PwMS have altered footfall and trunk motions during gait, however it is unclear if these alterations are specific features seen in PwMS who fall and therefore likely contribute to fall risk [3, 4]. The purpose of this study is to identify specific biomechanical features of gait which are different between fallers and non-fallers with MS by examining both foot and trunk motion. We hypothesize that fallers will 1) have increased gait variability and 2) walk more cautiously compared to non-fallers. With a better understanding of gait features which are different in fallers, we can highlight the gait features that should be monitored early in PwMS to specifically diagnose dynamic imbalance and fall risk.

## METHODS

Fifty-five PwMS (27 non-fallers and 26 fallers; EDSS<5.5) who were able to walk 25 feet unassisted were enrolled in the present study. The fallers group had 2 or more falls in the previous six months and non-fallers had no previous falls.

	NF (n=28)	FA (n=27)	P-value
Age	45.9 (9.5)	46.6 (10.1)	1.000
Gender (F/M)	20/8	19/8	-
BMI	28.0 (6.5)	28.6 (8.4)	1.000
EDSS	1.80 (0.93)	2.87 (1.22)	<b>0.001</b>
PWS (m/s)	0.73 (0.23)	0.51 (0.30)	<b>0.012</b>

Subjects walked at their preferred pace on a treadmill for three minutes. Kinematic data was collected using retroreflective markers placed bilaterally over lower limb anatomical landmarks (60 Hz, 8-camera motion capture system, Motion

Analysis, Santa Rosa, CA, USA). Step length and step width were defined as the anterior-posterior (AP) and mediolateral (ML) distance between contralateral heel markers at each heel strike. Variability of both step length and step width was assessed using coefficient of variation. Margin of stability (MoS) was calculated as the distance between the extrapolated (velocity-adjusted) center of mass and the base of support, in the AP and ML direction at each heel strike. Variability of MoS was assessed using coefficient of variation.

Wireless inertial sensors (Opal, APDM, Portland, OR, USA) measured trunk accelerations (128 HZ, midline of the sternum) concurrently during the treadmill walking. Linear accelerations were measured in the AP and ML axis and analyzed independently. Root mean square transforms were used to describe the dispersion of each signal. Raw acceleration time series were then down-sampled to 60 Hz and truncated to the middle 60 strides to evaluate their temporal structure using Lyapunov exponents. Delay-embedded state spaces were reconstructed using an embedded dimension of 7 for each axis and a time delay of 6 and 8 for the AP and ML direction, respectively.

Independent t-tests were used to identify differences between fallers and non-fallers for each outcome variable. The left and right legs were treated independently for foot motion and MoS.

## RESULTS

In the ML direction, fallers had an increased ML MoS variability compared to non-fallers, with no other differences between groups identified. In the AP direction, the fallers group walked with a decreased step length, decreased AP MoS, increased variability of step length, and increased variability of AP MoS.

## DISCUSSION

Frontal plane stability requires active control where sensory feedback during mid swing is integrated

and lateral step placement is adjusted to appropriately decelerate and redirect the center of mass [5]. There were no differences between groups for step width variability or ML trunk acceleration variability but ML MoS variability, which describes the interaction between the center of mass and base of support, was increased in the fallers group. This shows that fallers were less able to appropriately control their step placement to maintain a consistent ML MoS. Similar results were obtained in the sagittal plane with an increased AP MoS variability and step length variability in the fallers group. This supports the idea that step placement in fallers likely contributed to their fall risk.

The second part of the hypothesis was that fallers would walk more cautiously than non-fallers, which was partially supported since fallers walked with slower and shorter steps than non-fallers but with a decreased AP MoS. A cautious gait would be characterized by increased MoS. Slow and short steps are also indicative of cautious gait as they minimize the forward excursion of the center of mass beyond the stance foot and allow for more response time to perturbations [6]. Previous work in PwMS who were not separated based on falls history actually showed that slower walking leads to an increased AP MoS relative to healthy controls [7]. Here, lower AP MoS in fallers compared to non-fallers is likely another indicator of their fall risk since a smaller MoS indicates the center of mass is closer to leaving the AP base of support.

The gait impairments observed could be attributed to many physiological impairments of MS including slowed neural conduction speed, sensory loss, and spasticity which could all hinder inter-stride adaptability. While these impairments are generally found in all PwMS, it's likely that fallers have more severe physiological impairment leading to worse dynamic balance.

## CONCLUSIONS

The present work provides evidence that within a group of PwMS, there are gait differences between those with a falls history and those with no fall history, specifically that foot placement in the frontal plane and AP MoS are different in the fallers. These findings are novel and significant, as the two groups studied had the same disease, were both mild-moderately disabled and ambulatory, yet they had distinct biomechanical differences in their gait. This suggests that future studies investigating gait in PwMS should include fall history as a covariate.

## REFERENCES

1. Peterson et al. *Arch of phys med and rehab*, **89**, 2008.
2. Peterson et al. *Arch of phys med and rehab*, **94**, 2013.
3. Sosnoff et al. *Gait & posture*, **36**, 2012.
4. Huisinga et al. *Annals of biomed engineering*, **41**, 2013.
5. Rankin et al. *J neurophysiology*, **112**, 2014.
6. Maki, BE. *J American geriatric society*, **45**, 1997.
7. Peebles et al. *J biomechanics*, **49**, 2016.

## Acknowledgements

This work was supported by the National Multiple Sclerosis Society RG 4914A1/2 and the NIH National Center for Advancing Translational Science 1KL2TR00011

Table 1: Comparison of foot and trunk motion between fallers and non-fallers with MS. RMS – root mean square; LyE – Lyapunov exponents; CV – coefficient of variation.

	Anterior-Posterior			Mediolateral			
	NF	FA	Paired t-test	NF	FA	Paired t-test	
Step Length (cm)	44.84 (10.43)	35.02 (14.27)	<0.001*	Step Width (cm)	10.06 (3.77)	10.23 (4.95)	0.991
Trunk AP RMS	0.80 (0.25)	0.77 (0.27)	0.672	Trunk ML RMS	0.83 (0.25)	0.71 (0.30)	0.094
AP MoS (cm)	37.45 (7.34)	29.24 (11.82)	<0.001*	ML MoS (cm)	16.31 (3.13)	16.04 (3.37)	0.650
Step Length CV (%)	5.41 (2.77)	10.47 (7.24)	<0.001*	Step Width CV (%)	23.90 (10.05)	20.88 (11.73)	0.170
Trunk AP LyE	0.0265 (0.0095)	0.00262 (0.0075)	0.898	Trunk ML LyE	0.0216 (0.0121)	0.0283 (0.0149)	0.070
AP MoS CV (%)	4.86 (2.90)	10.32 (8.27)	<0.001*	ML MoS CV (%)	8.19 (2.29)	10.24 (3.36)	0.001*

# FORCE DISTRIBUTIONS ON THE FINGERS WHEN SQUEEZING A SPHERICAL REHABILITATION BALL

\* John Z. Wu, Erik W. Sinsel, Christopher M. Warren, and Daniel E. Welcome  
National Institute for Occupational Safety and Health, Morgantown, WV, USA.

\*Email: [jwu@cdc.gov](mailto:jwu@cdc.gov)

## INTRODUCTION

Musculoskeletal disorders (MSDs) of the hand and fingers are found to be related to occupational activities in multiple industrial sectors [1]. One of the effective intervention methods for the work-related MSDs of the hand is hand excises and rehabilitations [2,3]. The hand rehabilitation or therapy ball is one of the most popular commercially available types of hand exercise and rehabilitation equipment. The distributions of the contact pressure at the interface between the therapy ball and hand/fingers affects the joint moment of each finger, thereby affecting the distributions of the forces among the muscles of the fingers. A better understanding of the biomechanics of the therapies would help to improve the hand rehabilitation strategy and to achieve more effective outcomes. The goal of the current study is to quantify the distributions of the dynamic contact forces between the hand/fingers and therapy ball.

## METHODS

Eight female adults [age 29 (9.1) years, mass 64.6 (7.1) kg, height 163.5 (1.9) cm, hand length 17.2 (0.7) CM] participated in the study. The contact force sensors (or PPS sensor) (FingerTPS, Pressure Profile Systems, Los Angeles, USA) were attached to the distal, middle, and proximal phalanges of the four fingers excluding the thumb (Fig. 1). Each pressure sensor was individually calibrated before being used for the data collection. Subjects were instructed to perform two maximum voluntary exertion gripping tasks on a typical spherical rehabilitation ball. A quasi-static portion of each exertion was selected and the mean total force across the two trials was used to establish a maximum total grip force value, or the maximum grip (MAX). The subjects were then requested to perform a random ordering of two exertions at 25% and 50% of MAX. Subjects rested at least two minutes between trials. Before and after each trial, subjects were instructed to adopt a “handshake” posture, with the wrist neutral and fingers extended. After collection of baseline tare data at the start of the trial, an experimenter placed the ball in the subject’s instrumented hand. Subjects were instructed to not greatly adduct the fingers,



**Figure 1.** Test set-up. **Left:** A subject holds a hand rehabilitation ball, with all force sensors being attached. **Right:** The subject applied the maximal grip force to squeeze the ball.

avoiding a claw-like posture, while gripping. The force sensor data were collected at 40 Hz. The mean force values were calculated from a four-second range with the minimum total force variance during the exertion.

## RESULTS

The force share among the distal, middle, and proximal finger segments of the four fingers for grip force levels of 25%, 50%, and 100% of MAX are shown in Fig. 2. Our results show that the force sharing on the finger segments for the index finger is nearly independent of the grip force levels, whereas the grip force levels affect the force sharing on the fingers segments for the other three fingers. The force share on the distal segment increases with increasing grip force; the force share on the middle segment decreases with increasing grip force; and the force share on the proximal segment is nearly constant for all grip force levels. The results show that the distal fingers segments share approximately 50% of the total force of the finger, whereas the proximal segments took the least force share (approximately 10%). The grip force level affects the force distributions on the finger segments, however, the general trends are not changed.

The effects of the grip force on the force sharing on the four fingers are analyzed in Fig. 3. The middle and ring fingers share approximately 50% more force than the other two fingers. The force share on the ring finger decreases with increasing grip force level, while those in the middle and index fingers increase with increasing grip force level.

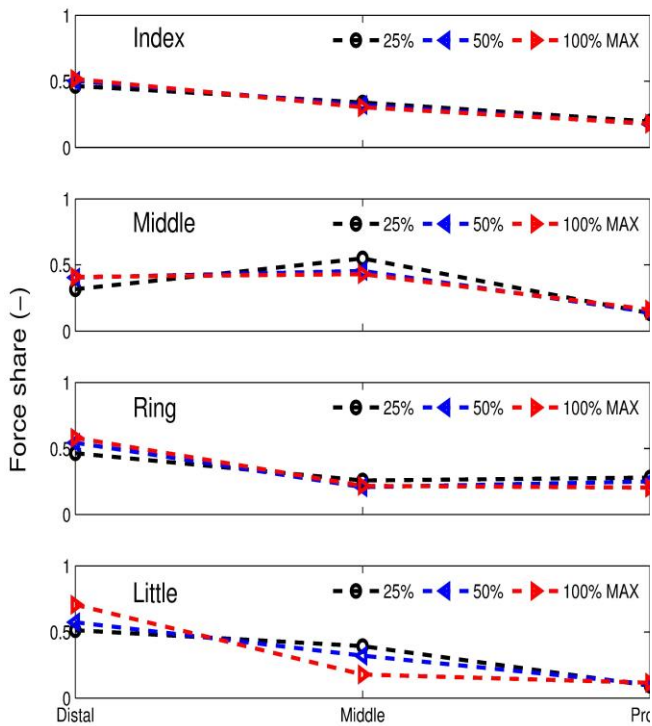


**Figure 2.** Force sharing in finger segments for three grip force levels.

## DISCUSSION AND CONCLUSIONS

Our results indicated consistently that the hand grip force is contributed about 60% and 40% by the middle/ring fingers and by the index/little fingers, respectively, independent of the grip force levels and stiffness of the contact surface (results not shown).

For index, ring, and little fingers, the contact force is concentrated most on the distal segment during squeeze, independent of the grip force levels. However, for the middle finger, the maximal force sharing can be on the distal or middle segment, depending on the grip force level (Fig. 2). This phenomenon is different from those observed in the cylindrical grip tests, where the maximal pressure was always on the distal segment of the index finger [4]. The force share pattern in the fingers observed in

the current study is quite different from the previous study: the majority of the hand grip force is contributed by the middle and ring fingers in the spherical grip, while it is mainly contributed by the index finger in the cylindrical grip [4].

One advantage for the current study over the previous studies is that we measured the contact forces on the fingers using individual PPS sensors. In the previous studies [5], the contact pressure was measured by using pressure sensor film that was wrapped on the contact surface of the object. For the rehabilitation ball, it deforms so much during squeeze (Fig. 1, Right), that it is impossible to wrap a pressure sensor film on the contact surface. In comparison, the application of the PPS sensors is independent of the curvature of the contact surface.

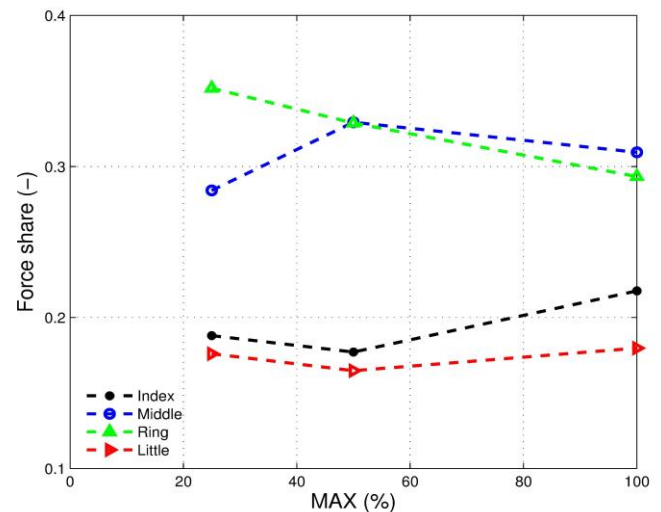


**Figure 3.** Force sharing in fingers for three grip force levels.

## REFERENCES

- [1] Marras WS, Cutlip RG, Burt SE, Waters TR. *Appl Ergon.* 2009. 40(1):15-22.
- [2] Melvin JL. *Am J Occup Ther.* 1985. 39(12):795-8.
- [3] Seu M, Pasqualetto M. *Hand Clin.* 2012. 28(1):87-100.
- [4] Wu JZ, Dong RG, Warren CM, Welcome DE, and McDowell TW. *Med Eng Phys.* 2014. 36(7):831-41.
- [5] Sinel EW, Gloekler DS, Wimer BM, Warren CM, Wu JZ, Buczek FL. *Med Eng Phys.* 2016. 38(2):72-9.

**DISCLAIMER:** The findings and conclusions in this report are those of the authors and do not necessarily represent the official position of the National Institute for Occupational Safety and Health. The mention of trade names, commercial products, or organizations does not imply endorsement by the US Government.

# The Effects of a 10-Week Balance, Flexibility, and Resistance Training Intervention on Postural Stability in Persons with Multiple Sclerosis

<sup>1</sup> Derek Tolbert, <sup>1</sup> Faizan Akram, and <sup>1</sup> Bradley Bowser

<sup>1</sup> South Dakota State University, Brookings, SD, USA

email: derek.tolbert@sdstate.edu, web: <http://www.sdstate.edu/health-and-nutritional-sciences>

## INTRODUCTION

Multiple Sclerosis (MS) is a chronic neurodegenerative disease that currently affects over 2.3 million people worldwide. Common symptoms include postural imbalance, postural asymmetry, and muscular weakness [1, 2, 3, 4].

Research has shown that progressive resistance training (PRT) is beneficial for improving muscular strength and functional performance in persons with MS (PwMS) [2]. However, there is contradicting evidence on the benefits of PRT for improving balance in PwMS.

The purpose of this study is to determine if a 10-week exercise training program combining balance, flexibility, and PRT will improve balance in PwMS. We hypothesized that the intervention would reduce sway velocities, ranges, and loading asymmetry (LA) during sit-to-stand movements and a hand-washing simulation (HW).

## METHODS

Twelve participants (54±8 yrs; 1.68±0.1m; 80.5±22.2kg; EDSS 4.3±1.9) diagnosed with relapsing-remitting MS participated in this study. Participants experiencing a flare-up or change in medication within the last 3 months, receiving steroid injections within the past 60 days, or having other musculoskeletal or neurological conditions were excluded from this study. Postural and strength data were collected pre- and post-intervention.

*Dynamic Posturography:* A non-functional sink was set at a standard height in front of the participant (Figure 1B). Participants were instructed not to lean or rest on the sink during the collection. Participants

simulated rinsing the hands, lathering the hands with soap (simulated by a ball of putty), rinsing the hands once again, and shutting off the faucet. Five trials were performed with one minute of rest between trials. Participants also completed 5 trials of a sit-to-stand movement at preferred (pSTS) and fast (fSTS) speeds (Figure 1A). Ground reaction forces (1000Hz) were collected for 5s during the washing portion of the HW trials and for 8s after the start of the STS movements. Center of Pressure data were calculated and used for all postural variables as described in Chung et al. [4].

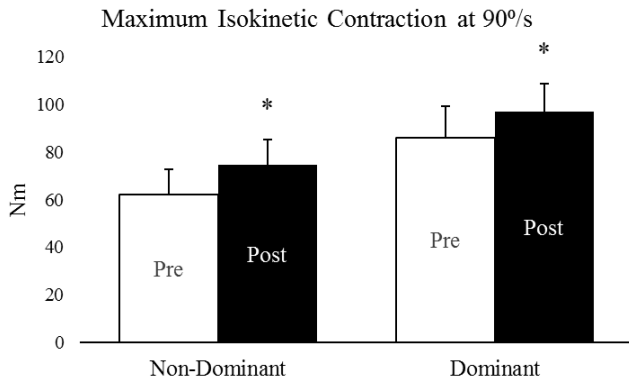
*Strength Assessment:* Participants completed three isokinetic knee extensions of each leg at an angular velocity of 90 °/s. The highest of the 3 trials was used to determine leg extension strength for each leg.



**Figure 1A-B:** 1A: Participant preparing to complete a STS movement. 1B: Participant completing a HW simulation assessment.

*Intervention:* Participants completed 10-weeks of supervised exercise training that included PRT, static stretching, and balance training. Sessions

occurred twice/week, began with a 5-minute warm-up, followed by light static stretching, balance training, and PRT. Static stretches were held for 2-sets of 30s on all major muscle groups. Balance training involved resisting perturbations to an outstretched fitness ball while standing on a foam pad. Two sets of 10-repetitions were completed for all PRT exercises targeting all major muscle groups. Resistance was increased once participants successfully completed all repetitions for a particular exercise over 2 sessions.



\* p-value <0.05 from pre to post

**Figure 2:** Strength during isokinetic knee extension in PwMS.

## RESULTS AND DISCUSSION

Results are summarized in Table 1. Significant changes were seen in isokinetic strength measures for both dominant and non-dominant legs (Figure 2). For postural measures, LA during HW decreased significantly, but no other changes were observed. The principle of specificity may help explain why improvements were only seen in the HW task as our balance training most closely resembled the HW task. It is also important to note that LA values were higher for HW compared to STS. This may be due to the dual-task nature of HW.

**Table 1:** Balance during HW, pSTS, and fSTS movements.

Variables	HW		pSTS		fSTS	
	Pre	Post	Pre	Post	Pre	Post
AP Absolute Length (mm)	251±50	255±55	371±87	379±113	376±376	364±103
ML Absolute Length (mm)	269±64	292±75	340±84	333±95	346±105	325±83
AP Max Velocity (mm/s)	239±46	232±45	357±93	330±95	406±88	378±82
ML Max Velocity (mm/s)	242±56	252±58	364±87	357±70	470±248	442±215
Loading Asymmetry	.159±.091	.125±.081*	.108±.062	.112±.069	.114±.059	.105±.074

**Legend:** HW = Hand Washing, pSTS = Preferred-speed Sit-to-Stand, fSTS = Fast-speed Sit-to-Stand, \* p-value <0.01 from pre to post

During HW, participants had to focus on operating the faucet, reaching for the soap, lathering, washing, and rinsing their hands all while trying to maintain balance. It is interesting to note however, that no changes for anterior-posterior and medial-lateral (AP/ML) stability were found during the HW tasks after the intervention.

Previous research has shown a significant relationship between LA and AP/ML stability [4]. However, our results indicate that improvements in strength and LA do not always result in changes to AP/ML stability.

## CONCLUSIONS

Muscular weakness is a commonly reported symptom of MS. Our data indicate that 10-weeks of balance, flexibility, and PRT is sufficient to elicit significant improvements in muscular strength and to reduce LA during HW.

As our sample size is small, future studies with larger sample sizes are needed to confirm our findings. Future interventions may also want to incorporate greater exercise variety. Current recommendations often include video game based programs, dual-task training, or the use of supplementary tactile feedback [3].

## REFERENCES

1. Bowser B, et al. *Clin Biomech*, **30**, 788-794, 2008.
2. Kjolhede T, et al. *Mult Scler* **18**, 1215-28, 2012.
3. Cameron MH, et al. *Curr Neurol Neurosci Rep* **10**, 2010.
4. Chung LH, et al. *Med Sci Sports Exerc* **40**, 1717-24, 2008.

# EFFECTS OF A 12-WEEK EXERCISE INTERVENTION ON JOINT KINETICS DURING CURB NEGOTIATION IN CANCER SURVIVORS

<sup>1</sup>Anastacia Y. Fraijo, <sup>1</sup>Grace Rhodehouse, <sup>2</sup>Trista L. Olson,  
<sup>1</sup>Reid Hayward, and <sup>1</sup>Jeremy D. Smith

<sup>1</sup>University of Northern Colorado, Greeley, CO, USA, School of Sport & Exercise Science

<sup>2</sup>St. Cloud State University, St. Cloud, Minnesota, USA, Department of Kinesiology  
email: Anastacia.Fraijo@unco.edu, web: <http://www.unco.edu/biomechanics/>

## INTRODUCTION

In 2016, an estimated 1.6 million people were newly diagnosed with cancer in the United States and many of them will be 65 years of age or older [1]. A common side effect of many cancer treatments is chemotherapy-induced neuropathy, which can lead to a loss of balance and an increased risk of falling [2]. Risk of falling is even greater when people have to negotiate obstacles such as curbs, stairs, or other changes in elevation. Exercise has been shown to reduce other side effects of cancer treatments, such as cardiotoxicity [3], but it is unclear whether exercise benefits gait mechanics in a way that might reduce the risk of falling and aid in obstacle negotiation for cancer survivors. Thus, the purpose of this study was to investigate the effects of a 12-week exercise intervention on joint kinetics during curb negotiation in cancer survivors.

## METHODS

Fourteen cancer survivors (8 females, 6 males, age = 64±9 yrs, height = 1.72±0.08 m, mass = 80±26 kg) participated in this study. All participants were recruited from the University of Northern Colorado Cancer Rehabilitation Institute. Each participant completed a pre-assessment session in which medical histories, aerobic fitness, and strength capabilities were assessed. These data were then used to design a specific 12-week exercise intervention for each participant. The 12-week exercise intervention included aerobic, strength/resistance, balance and flexibility training 2 – 3 times per week.

Prior to (pre) and immediately following (post) the 12-week training intervention, each participant's gait was assessed while negotiating a curb. Motion (100 Hz, VICON) and ground reaction forces (2000 Hz,

AMTI) were measured for three trials while participants walked up the curb at a freely chosen speed. Marker coordinates ( $F_c = 6$  Hz) and ground reaction forces ( $F_c = 50$  Hz) were filtered in Visual 3D (C-Motion) using a recursive Butterworth digital filter.

To recreate a curb in the laboratory, two force plates embedded in tandem in the floor and a third force plate mounted on a steel frame was placed in line with the other two force plates. The third force plate was 16 cm higher than the ground plate which modeled the sidewalk curb outside our lab. By using this set up we were able to collect a step on the ground (GROUND) prior to the curb and a step up to the curb (CURB). Sagittal plane kinematics and kinetics were analyzed for the CURB and GROUND leg during three successful trials. A successful trial occurred when complete contact was made with the force plate for the GROUND plate and the CURB plate. Peak joint angular velocities, moments, powers, as well as minimum toe clearance, center of mass velocities, and work were identified from each trial and then averaged for inclusion in statistical analyses. A series of ANOVAs were used to identify differences between pre- and post-test measures ( $\alpha = .05$ ) for the ground and curb leg.

## RESULTS AND DISCUSSION

Joint angular velocities and walking speed were not significantly different between pre- and post-test sessions. However, during late swing phase, the knee flexor moment increased significantly from pre- to post-test conditions ( $p = .006$ ) in the CURB leg. Significantly more power was absorbed at the ankle at about 50% of the gait cycle ( $p = .012$ ) and generated at about 60% of the gait cycle ( $p = .025$ ) for the CURB leg after training. Significantly more power was also generated at the hip at approximately

20% of the gait cycle for the GROUND leg. Overall, the total work performed at the ankle on the CURB increased significantly after training ( $p = .037$ ). Toe clearance over the CURB decreased significantly after training ( $p = .005$ )

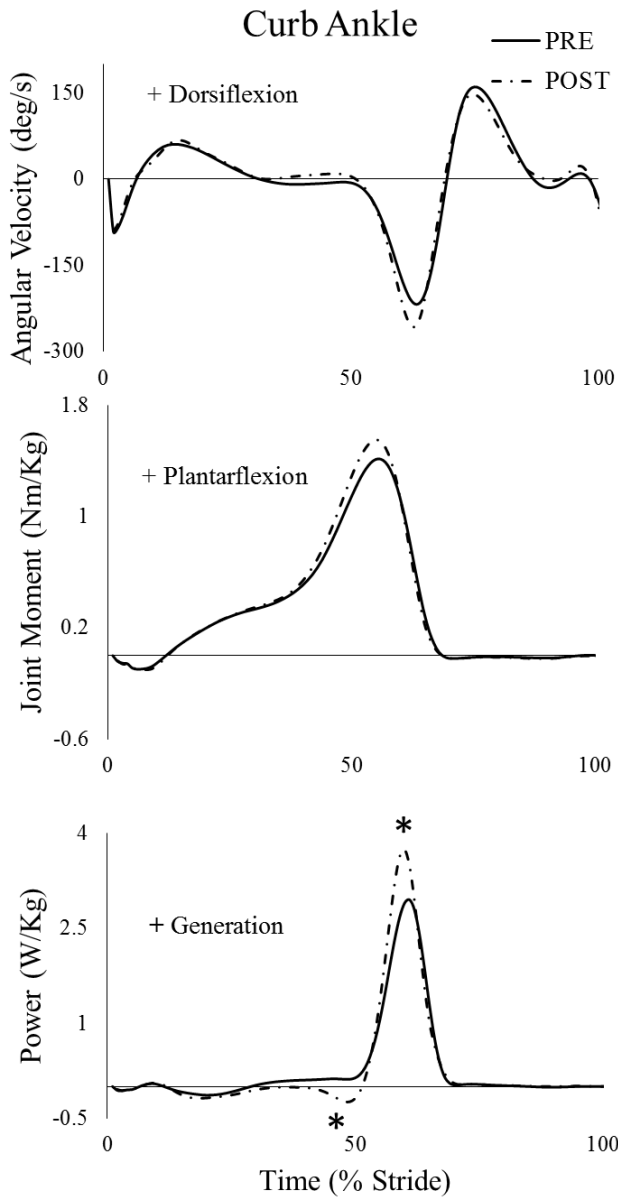


**Figure 1:** Mean joint power at the ankle of the CURB leg. \* indicates significant difference between pre- and post-test sessions.

Previous studies have reported that fallers tend to generate less power at the ankle during push-off when compared to non-fallers [4]. The decrease in ankle power that has been found in previous studies is thought to be caused by a decrease in plantarflexor strength. Thus, cancer survivors in the current study likely lowered their risk of falling after the 12-weeks of training due to the increased power output at the ankle.

Recently, it was also reported that young adults transitioning from level walking to climbing stairs have a minimum toe clearance over the first stair of approximately 7 cm [5]. Given that the minimum toe clearance for study participants decreased after training, this might indicate a more confident gait for these cancer survivors after training.

## CONCLUSIONS

Ankle joint power output during curb negotiation increased following 12-weeks of exercise in cancer survivors. These observed changes in ankle power are consistent with reduced risk of falling among older adults.

## REFERENCES

1. Society AC. Cancer Facts & Figures. In: Society AC, ed. Atlanta 2015.
2. Winters-Stone et al., *Arch Phys Med Rehabil* 92, 646-652, 2011.
3. Lien CY, et al.. *J Physiol Biochem* 71, 668-79, 2015.
4. Kerrigan et al. *Arch Phys Med Rehabil* 81, 730-702, 2000.
5. Ajisafe, T., et al. *Appl Ergon* 59, 203-208, 2017.

**Table 1:** Mean and standard deviations for resultant distance of the toe, center of mass (COM) velocity and total work at the ankle joint.

	Pre	Post
<b>Resultant toe cross (cm)</b>	13.15 ± 1.28	12.21 ± 0.98
<b>COM velocity (m/s)</b>	1.28 ± 0.15	1.34 ± 0.17
<b>Ankle Total Work (J)</b>	0.43 ± 0.11	0.50 ± 0.14

# KINEMATIC AND STABILITY CHANGES IN WOMEN USING A SACROILIAC BELT: A CASE-CONTROL STUDY

<sup>1</sup> Sasa Cigoja, <sup>1</sup> Marc LeVangie, <sup>1</sup> Louise-Helene Gagnon, <sup>1</sup> Magali Robert, and <sup>1</sup> Benno M. Nigg

<sup>1</sup> Human Performance Laboratory, University of Calgary, Calgary, AB, CA  
email: sasa.cigoja1@ucalgary.ca

## INTRODUCTION

Pelvic girdle pain (PGP) is defined as pain from the posterior iliac crest to the gluteal fold in the area of the sacroiliac (SI) joint [1]. It is estimated that PGP can be seen in approximately 20% of women [1, 2]. PGP is generated due to failure to adequately transfer load through the lumbo-pelvic region, which affects lumbo-pelvic stability [1]. Lumbo-pelvic stability, however, is influenced by the SI joint's anatomy (form closure), compressive forces acting across the SI joint (force closure) and neuro-motor control [1, 3, 4]. Compression of the pelvis often provides symptomatic relief to those suffering from PGP [5] and it has been suggested to improve lumbo-pelvic stability [4]. Thus, one of the management options for patients with PGP is the use of an SI belt [1]. Furthermore, studies have shown that the application of the belt alters recruitment of muscles during walking. Therefore, the purpose of this study was to further investigate if the application of the SI belt influences other biomechanical factors, such as stability and lower limb kinematics in women with and without PGP during standing and walking tasks.

## METHODS

This is a case-control study that enrolled five female subjects with PGP (age:  $33.8 \pm 0.8$ , parity: 1 [range: 0, 4], BMI:  $23.8 \pm 2.9$ ) and five matched control subjects (age:  $33.8 \pm 3.6$ , parity: 1 [range: 0, 3], BMI:  $24.2 \pm 3.4$ ). Women were considered cases if they presented PGP and lumbo-pelvic instability. Lumbo-pelvic instability was assessed performing four clinical tests which included the posterior pelvic pain provocative test, Fabers test, Gaenslen's test and palpation of the dorsal ligament. A subject was identified having PGP when two or more tests were positive. Additionally, the active straight leg

raise test had to be positive on at least one side. Subjects had to perform three different tasks with the belt on and off, respectively. The tasks included quiet stance on a force plate, walking over a force plate at controlled speed, and walking at self-selected speed. Pressure distribution and lower limb kinematics were collected while standing using a force plate, pressure insoles and motion capture system. Three-dimensional ground reaction forces and lower limb kinematics were collected while walking at controlled speed, and pressure distribution was collected while walking at self-selected speed.

## RESULTS AND DISCUSSION

All subjects showed a significant decrease ( $T_{1,9} = 5.564$ ,  $p < 0.001$ ) in the 95% confidence ellipse area of the center of pressure (CoP) data during standing when the SI belt was applied, regardless if they were subjects with PGP or healthy controls (Table 1). On average, the 95% confidence ellipse area of subjects with PGP ( $33.27\% \pm 4.73$ ) decreased more when the SI belt was applied compared to the group of healthy controls ( $26.35\% \pm 13.09$ ). The decrease in 95% confidence ellipse area was not statistically significant between the group with PGP and healthy controls. Four out of five patients with PGP showed a greater increase in stability than the matched control subjects. It is hypothesized that with an increase in sample size the effect of the belt between the two groups would become statistically significant.

**Table 1:** The 95% confidence ellipse area of the CoP data for subjects with PGP (S1-S5) and healthy controls (C1-C5) with and without wearing the SI belt while performing the standing task.

Subject	Belt Off [mm <sup>2</sup> ] (SD)	Belt On [mm <sup>2</sup> ] (SD)	Decrease of area [% of Belt Off condition]
S1	51.78 (1.40)	32.10 (16.43)	38.01
S2	60.01 (34.12)	44.54 (26.23)	25.78
S3	16.37 (6.74)	10.79 (7.71)	34.09
S4	26.34 (9.25)	17.86 (7.65)	32.19
S5	22.45 (2.19)	14.31 (1.61)	36.26
C1	26.54 (1.59)	21.35 (2.17)	19.56
C2	25.33 (9.52)	20.03 (0.17)	20.92
C3	31.64 (0.45)	27.63 (14.95)	12.67
C4	14.47 (0.40)	7.83 (1.82)	45.89
C5	40.16 (21.27)	27.02 (3.08)	32.72

Eight out of ten subjects showed significantly higher hip internal rotation ( $T_{1,9} = 2.680$ ,  $p = 0.025$ ) and knee external rotation ( $T_{1,9} = -3.122$ ,  $p = 0.012$ )

during the standing task while wearing the SI belt. Furthermore, all ten subjects showed a significant increase in hip abduction ( $T_{1,9} = -10.146$ ,  $p < 0.001$ ) and knee adduction ( $T_{1,9} = 5.167$ ,  $p < 0.001$ ) at heel strike while walking at controlled speed when the SI belt was applied.

## CONCLUSIONS

This study was able to provide evidence that wearing an SI belt leads to a significant increase in stability in patients with PGP and in healthy control subjects. The results showed a trend that wearing an SI belt affects patients with PGP more than healthy subjects. Furthermore, the results showed that wearing an SI belt leads to a significant change in lower limb kinematics in women who are suffering from PGP and in healthy control subjects during standing and walking.

## REFERENCES

1. Vleeming, A. et al., *Eur Spine J.* **17**: 794-819, 2008.
2. Simopoulos, TT. et al., *Pain Physician.* **15**: E305-344, 2012.
3. Pardehshenas, H. et al., *Journal of Bodywork and Movement Therapies.* **18**: 633-642, 2014.
4. Arumugam, A. et al., *Manual Therapy.* **17**: 275-284, 2012.
5. Beales, D. et al., *Manual Therapy.* **15**: 190-199, 2010.

# EMG OF FACIAL MUSCLES FOR SUBVOCAL SPEECH RECOGNITION

<sup>1,2</sup>Meltzner GS, <sup>3</sup>Heaton JT, <sup>4</sup>Deng Y, <sup>1</sup>Roy SH, <sup>1</sup>Kline JC, <sup>1</sup>De Luca G

<sup>1</sup> Delsys, Inc. and Altec, Inc, Natick, USA

<sup>2</sup>Vocal ID, Inc, Belmont, USA

<sup>3</sup>Harvard Medical School Department of Surgery, MGH Voice Center, Boston, USA

<sup>4</sup>BAE Systems Inc, Burlington, USA

email: [sroy@delsys.com](mailto:sroy@delsys.com), web: <http://www.delsys.com/altec/>

## INTRODUCTION

Each year thousands of individuals require surgical removal of their larynx due to trauma or disease, impairing their ability to vocalize speech. Studies of alternative forms of communication have reported that synergistic activation of muscles involved in speech – which largely remain intact after laryngectomy – produce unique combinations of surface electromyographic (sEMG) signals when articulating different phonemes [1]. This is true even when speech is mouthed or spoken in a silent (unvoiced) manner, indicating that the use sEMG signals for speech recognition has the potential to be a powerful platform to help individuals communicate subvocally. Therefore, we developed a system to record sEMG signals from muscles of the face and neck during silently mouthed speech in patients with laryngectomy and translated patterns of sEMG signals into words using phoneme-based silent speech recognition.

## METHODS

Experiments were conducted with n=7 participants with laryngectomy (mean 64 years). Custom-designed Trigno™ mini sEMG sensors (Delsys, Inc. Natick, MA) were strategically placed on 8 muscles of the face and neck previously identified as those most involved in the articulation of speech (Fig. 1) [1]. A vocabulary of 1000 commonly used English words primarily from the TIMIT data corpus were used to test different combinations of phonemes. Words were presented in token sentences on a computer screen for subjects to silently recite by mouthing the words. A two-stage speech recognition algorithm was designed to process the sEMG signals recorded during silent speech. First, signal segments containing speech data were

identified by a finite state Speech Activity Detection (SAD) algorithm and processed with speaker-dependent window lengths and frame rates to compute Mel-frequency cepstral coefficients (MFCC) [2]. Hidden Markov Models were used to develop a multi-stage phoneme-based speech recognition model specific to each subject. The models were trained on 550 sentences and tested on 430 sentences. All words presented in the testing data were unique and did not appear in the training data.

## RESULTS AND DISCUSSION

We found that the synergistic activation of speech muscles while mouthing different words produced discriminable combinations of sEMG signals that could be used for speech recognition. From the full 8-sensor set, word error rates were on average 11.1% for all subjects tested. When we tested the best 4-sensor combination from each subject (Table 1 and Figure 1), we found average word-errors rates only moderately increased to 14.1%, indicating the potential to simplify the system for in-home use.

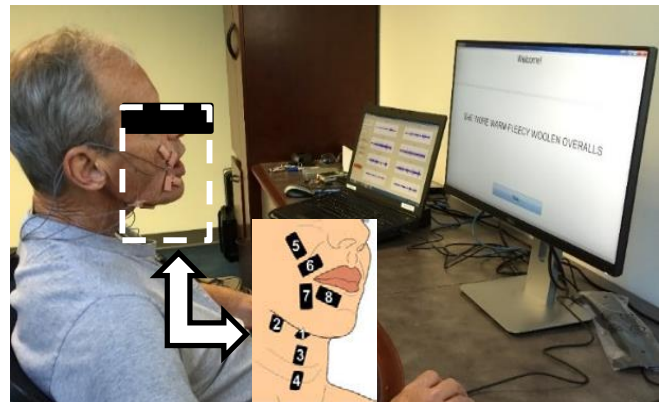


**Figure 1.** Subject operating data acquisition system. The callout shows the sensor location and numbering scheme.

**Table 1. Word Error Rates (WERs - %) per subject**

Sensor#	S1	S2	S3	S4	S5	S6	S7
{1,5,7,8}	14.8	18.7	20.8	27.1	11.6	18.8	18.7
{2,4,5,7}	23.3	20.5	<b>13.8</b>	24.1	14.3	20	15.6
{2,5,6,7}	<b>10.6</b>	<b>19.2</b>	15	<b>17.5</b>	14.4	15.8	<b>14.4</b>
{3,5,6,7}	15	30.8	19.7	19.2	<b>10</b>	<b>13.1</b>	18.1
<b>8 Sensors</b>	10	13.6	13.3	12.8	8.7	8.9	10.2
<b>Mean</b>	15.9	22.3	17.3	22.0	12.6	16.9	16.7
<b>BEST</b>	10.6	19.2	13.8	17.5	10	13.1	14.4

## CONCLUSIONS

These results provide first-of-its-kind demonstration that unique combinations of sEMG signals obtained from synergistic activation of muscles involved in speech articulation can be used for recognition of silently mouthed words in patients with laryngectomy. While there is room to improve the accuracy possibly through increased training data, inclusion of further speaker-dependent parameters or alternative algorithm approaches, the ability to recognize words using phoneme-based patterns of

sEMG provides an impactful first-step towards developing a practical body-worn system for alternative communication for persons with laryngectomy.

## REFERENCES

1. Colby G, et al. *34th Annual IEEE ICASSP*, Taipei, Taiwan, 473-476, 2009.
2. Deng Y, et al. *Proc. 15th Annual Interspeech Conf.* Singapore, 1164-1168, 2014.

## ACKNOWLEDGMENTS

Research reported in this abstract was supported in part by the De Luca Foundation and by a grant from the National Institute on Deafness and Other Communication Disorders of the National Institutes of Health under award R44DC014870.

# THE EXAMINATION OF HIP JOINT KINEMATICS WITH iWALK IN WALKING GAIT

Tyler Champagne<sup>1</sup>, Tom Wu<sup>1</sup>, David J Pearsall<sup>2</sup>, Pamela J. Russell<sup>1</sup>, and Ariana LaFavre<sup>1</sup>

<sup>1</sup>Bridgewater State University, Bridgewater MA, USA

<sup>2</sup>McGill University, Montreal, Canada

Email: t1champagne@student.bridgew.edu

## INTRODUCTION

Standard underarm crutches have long been used as a method to re-enable an individual to perform normal walking. An average of 6.5 million people use an assistive device such as crutches to assist with mobility in the US alone [1]. Crutches have been found to compress the radial nerve which can cause pain, tenderness, and motor weakness as well as the ulnar nerve which can lead to nerve damage and neuropathy [2-3]. The iWalk has been introduced to the market as a new type of hands free crutch in an attempt to eradicate the stress applied to the underarms with traditional crutches, however the effects of the device on walking gait have yet to be researched. Symmetrical walking gait is essential to maintain upright positioning and forward propulsion. When walking gait is rendered asymmetrical, it opens an individual up to problems such as lower back pain, osteoarthritis, and a higher potential of falling [4]. Therefore, the purpose of this study was to examine the symmetry of walking gait with an assistive device

## METHODS

Ten healthy, injury-free University female students with an average age of  $20.2 \pm 1.6$  years old were recruited to participate in the study. Prior to the study, approval by the institutional ethics review board was obtained. After obtaining approval, written informed consent from each participant was received. Each participant was allowed to become acquainted with the iWalk before beginning the walking sequence. Ten joint reflective markers were placed on both sides of the body at the shoulder (gleno-humeral joint), hip (greater trochanter of the femur), knee (lateral epicondyle of the tibia), ankle (lateral malleolus) and toe (base of the fifth metatarsal). The participant walked barefoot on a

treadmill (Model: Milestone 4200) at a speed of 1.03 m/s for thirty seconds to obtain normal lower extremity walking data. Next, the participant was introduced to the iWalk and fitted on the right leg side only for the device. Once adjustments were made to the device, straps were fitted accordingly, and balance was obtained by the participant, they began walking on the treadmill at. Three cycles of heel strike, mid-foot support, and toe off were recorded for analysis.

Two high speed Casio cameras (Model EX-FH25) were positioned to capture the sagittal views of both right and left sides at 120 Hz. Two 650W spot lights were used in conjunction with each camera to assist in joint marker identification. All video trials were transferred onto a computer in the Biomechanics Lab for gait analysis. Three successful walking gait cycles were used for analysis. To determine a successful walking gait selection, a heel strike, mid-foot support, and toe off phase needed to be present and identifiable. The instant of these three phases of walking gait were measured at the hip joint in both normal walking and iWalk conditions. A 2D kinematic walking gait analysis was conducted with Aerial Performance Analysis System (APAS<sup>TM</sup>) motion software. Dependent sample t-tests were conducted with Bonferroni adjustment and all statistical analyses were conducted with SPSS software.

## RESULTS AND DISCUSSION

Dependent sample t-tests were conducted with Bonferroni adjustment for multiple comparisons ( $\alpha = 0.05 / \# \text{ of comparisons} = 0.05 / 4 = 0.0125$ ; IBM SPSS) between right and left sides of iWalk and barefoot walking on the treadmill for each participant during heel strike, mid-foot support, and toe off phases (Table 1).

Hip kinematic alterations between the iWalk and normal walking gait were identified; specifically, the ipsilateral side iWalk vs barefoot hip angle at heel strike, mid-foot support, toe off. The iWalk decreased ipsilateral hip extension angles by 18 degrees, with minimal effect on the contralateral hip, except for mid-foot support.

Hip range of motion typically varies from 30 degrees flexion at heel strike to 10 degrees extension at push off during walking over ground [5]. The decreased ipsilateral hip flexion during swing may be due to the additional weight of the iWalk device on the lower limb as well as the subject's attempt to minimize ground impact force i.e. given the lack of dampening provided by normal knee-ankle-foot at heel strike, stride length on the ipsilateral side was foreshortened.

## CONCLUSIONS

This study used ten healthy female students to examine effects of using the hands-free crutch on the lower limb kinematics at heel strike, mid-foot support, and toe off phases of walking gait. The iWalk device permitted functional bilateral walking, though ipsi-contra-lateral gait symmetries were evident. The results showed that the iWalk does

result in a significant change to the individual's hip angle when compared to normal barefoot walking. This could result in an asymmetrical walking gait with extended use. Therefore, this study concludes the iWalk hands free crutch will indeed alter walking gait. Future studies are warranted to examine lower limb kinematics with both genders over a longer time period to address long term issues.

## REFERENCES

1. The Centers for Disease Control and Prevention. *How many people use assistive devices?*, 2012.
2. Choi, et al. *Ultrasonography*, **34** (4), 275–291, 2015.
3. Jacobson J., et al. *Semin Musculoskelet Radiol Seminars in Musculoskeletal Radiology*, **14** (05), 473-486, 2010.
4. Gouwanda, D. *Journal Of Mechanics In Medicine & Biology*, **14** (1), 2014.
5. Perry, J. *Clin Orthop* 102:18, 1974.

## ACKNOWLEDGMENTS

This study was supported by the 2016 ATP Summer Grant from the Office of Undergraduate Research, Bridgewater State University.

**Table 1:** Hip joint angle at Heel Strike, Mid-Foot Support, and Toe Off. Data are means (SD). \*  $p < 0.0125$

	Heel Strike	Mid-Foot Support	Toe Off
<b>Right Barefoot</b>	159.6° (5.7°)	171.7° (5.6°)	174.1° (3.9°)
<b>Right fitted with iWalk (ipsilateral)</b>	145.1° (6.6°)	149.2° (8.5°)	155.8° (10.7°)
<i>p</i>	0.00*	0.00*	0.00*
<b>Left Barefoot</b>	156.4° (6.2°)	169.7° (6.8°)	172.6° (4.6°)
<b>Left not fitted with iWalk (contralateral)</b>	155.6° (7.8°)	164.9° (8.3°)	172.5° (5.9°)
<i>p</i>	0.45	0.008*	0.96

# A STRESS PROGRESSION SEQUENCE OF EXERCISES DURING ACHILLES TENDON REHABILITATION

<sup>1</sup>Naghmeh Gheidi, Thomas Kernozek, Andrew Revak, Keith Diers, <sup>2</sup>John Willson

<sup>1</sup>University of Wisconsin La Crosse, La Crosse, WI, USA

<sup>2</sup>East Carolina University, Greenville, NC, USA

e-mail: ngheidi@uwlax.edu

## INTRODUCTION

Achilles rupture and tendinopathy both are common tendon injuries in the lower leg [1]. Therapeutic exercise is thought to be beneficial to rehabilitation efforts for Achilles tendinopathy or for the post-surgical management of tendon repair. Progressive prescription of therapeutic exercises to expose patient to an appropriate load is a key factor for successful recovery from Achilles tendon (AT) injuries. The current standard rehabilitation regimens use different exercises including heel raising, squats, lunges, hopping, walking and running within different stages of rehabilitation [2-3]. The rehabilitation exercises that are used to load the AT in both a safe and progressive manner providing for a rapid return to sport remain somewhat unclear. The knowledge of AT loads during a variety of common activities is required to design a safe and effective rehabilitation regimen. Our aim was to compare the estimated AT loading during a several exercises to inform exercise progression for AT rehabilitation.

## METHODS

Eighteen healthy and physically active males were examined (Age:22.1±1.8years, height:177.7±8.4cm, weight=74.29±11.3kg). Kinematic and kinetic data were recorded respectively with 15 Motion Analysis cameras (180Hz) and force platforms (1800Hz). The kinematic and kinetic data, and muscle forces were calculated from a 44 degree of freedom (DOF) musculoskeletal model with 18 rigid segments using the Human Body Model (HBM, Motek Medical, Amsterdam, Netherlands) via inverse dynamic based static optimization routine. The muscle forces were used to quantify total AT force by summing the muscle forces of the medial and lateral gastrocnemius and soleus for each exercise. The AT stress was calculated by dividing the AT force by the participant specific AT cross-sectional area which was measured by ultrasonography. Peak stress rate was determined from the instantaneous slope of the

stress versus the time curve. Subjects performed five repetitions for all 11 exercises including tandem, Romberg, and unilateral standing (U-standing), Unilateral (U) and bilateral (B) heel raising (HR), bilateral (B) and unilateral (U) jump landing (Jump-Land), squat, forward lunge (FL), walking, and running in a random order.

A multivariate analysis of variance (MANOVA) with repeated measures ( $\alpha=0.05$ ) was used to compare the AT stress, stress rate, and force across the 11 exercises. Post hoc comparisons were performed with the Bonferoni procedure. All statistical procedures were performed using SPSS (Version 23, IBM, Armonk, NY, USA).

## RESULTS AND DISCUSSION

The MANOVA revealed differences between tasks (Wilk's lambda=0.006, P-value<0.001). Follow-up univariates depicted differences in peak AT stress, force, and stress rate during 11 exercises. Table 1 shows the mean and standard deviation for peak AT stress, force, and stress rate for each exercise.

Figure 1 depicts the AT stress time series throughout the performance of each exercise. It is observable that the timing of peak AT stress was somewhat unique for each exercise. However, some exercises showed similar AT loading patterns but with different magnitudes like the bilateral and unilateral Jump-Land (at 0-30% for landing, ≈80-100% for jumping) and during stance of walking and running. The peak AT stress for the bilateral and unilateral jump-land occurred during the jumping portion of the exercise. Similarly, during running and walking, the peak AT stress occurred during push off phase of the performance. AT stress during the Romberg, unilateral standing and tandem exercises were quite uniform loading patterns since these exercises were less dynamic with muscle force requirements needed for postural control in a set position. During both heel raise exercises (B-HR and U-HR), the peak AT stress occurred during raising portion rather than lowering

while the forward lunge showed a rather unique pattern where the peak AT stress occurred during raising ( $\approx 70\%$ ). Figure 2 depicts the AT stress in order of magnitude for all 11 exercises. Categories were determined from AT stress based on statistical differences between exercises. In general, AT rate of loading follows largely a similar pattern of loading as AT stress. In general, our AT force values are well below the reported AT failure load 5579N [4].

AT peak stress, force and stress rate were lowest during the Romberg and tandem exercise while standing on both legs. Changing from bilateral to unilateral exercise increased the force and stress. More dynamic exercises (squat and lunge) increased the stress rate. The bilateral and more static exercises with less stress and stress rate may be more desirable earlier in the rehabilitation process. Unilateral and more active exercises may be more useful in later exercise progressions. Understanding loading for each of these exercises may aid in planning the timing and sequencing of exercise progression in a AT rehabilitation program.

**Table 1:** Mean and standard deviation (Mean $\pm$ sd) for AT loading during each exercise.

	AT Stress(MPa)	AT Force (BW)	AT Stress Rate (MPa/s)
Squat	18.23 $\pm$ 8.10	0.77 $\pm$ 0.35	35.30 $\pm$ 18.20
Romberg	21.43 $\pm$ 6.98	0.91 $\pm$ 0.3	17.61 $\pm$ 6.00
Forward Lunge (FL)	40.96 $\pm$ 18.89	1.72 $\pm$ 0.74	128.18 $\pm$ 65.48
Bilateral Heel Raise (B-HR)	44.60 $\pm$ 11.89	1.89 $\pm$ 0.41	220.46 $\pm$ 111.47
Tandem	46.05 $\pm$ 18.88	1.93 $\pm$ 0.74	16.77 $\pm$ 8.62
Unilateral Standing (U-Standing)	52.17 $\pm$ 12.93	2.18 $\pm$ 0.38	18.29 $\pm$ 8.58
Walk	86.17 $\pm$ 28.32	3.71 $\pm$ 1.29	403.42 $\pm$ 163.20
Bilateral Jump-Land (B-jump-land)	91.90 $\pm$ 35.98	3.88 $\pm$ 1.43	1173.67 $\pm$ 618.30
Unilateral Heel Raise (U-HR)	95.07 $\pm$ 33.73	3.98 $\pm$ 1.06	296.03 $\pm$ 185.56
Run	97.80 $\pm$ 50.83	4.15 $\pm$ 2.03	1200.11 $\pm$ 561.11
Unilateral Jump Land (U-Jump-Land)	158.55 $\pm$ 71.60	6.68 $\pm$ 2.66	1985.73 $\pm$ 1036.60

## REFERENCES

- Hess, GW. Foot & Ankle Specialist. **3**, 29–32, 2010.
- Kountouris A, et al. Best Pract Res Clin Rheumatol. **21**, 295-316, 2007.
- Kangas, N, et al. J Trauma. **54**:1171-1181. 2003.
- Wren T.A.L. Clinical Biomechanics. **16**, 245-251, 2001.

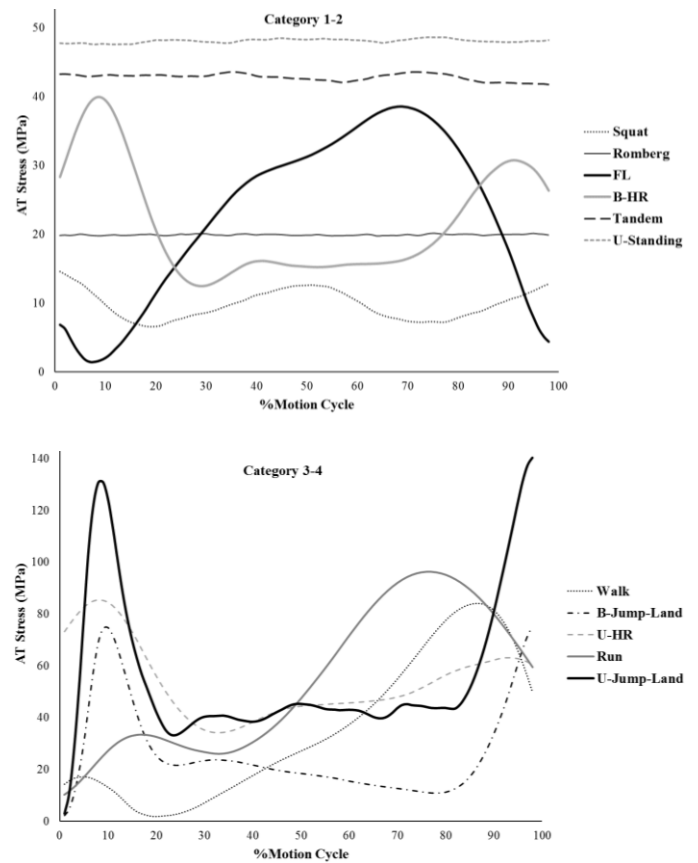


**Figure 1:** Ensemble average AT stress (MPa) for each exercise in category 1-2 and category 3-4 (below).

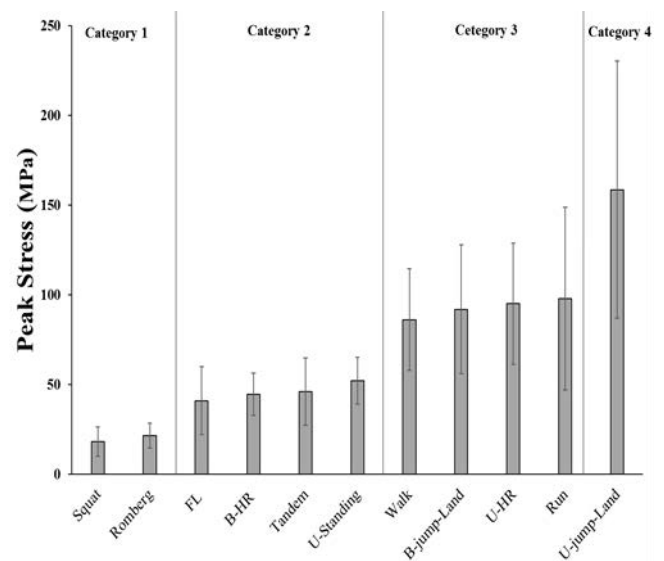


**Figure 2:** Peak AT stress categories based on the univariate differences between exercises.

# SPEED IMPACTS MANEUVER STABILITY IN INDIVIDUALS WITH INCOMPLETE SPINAL CORD INJURY

<sup>1</sup>Carolina Viramontes, <sup>1</sup>Mengnan/Mary Wu, <sup>1</sup>Julian Acasio, <sup>2</sup>Janis Kim, and <sup>1,3</sup>Keith E. Gordon

<sup>1</sup>Northwestern University, Chicago, IL, USA

<sup>2</sup>University of Illinois Chicago, Chicago, IL, USA

<sup>3</sup>Edward Hines Jr. VA Hospital, Hines, IL, USA

email: keith-gordon@northwestern.edu web: <http://sites.northwestern.edu/agilitylab/>

## INTRODUCTION

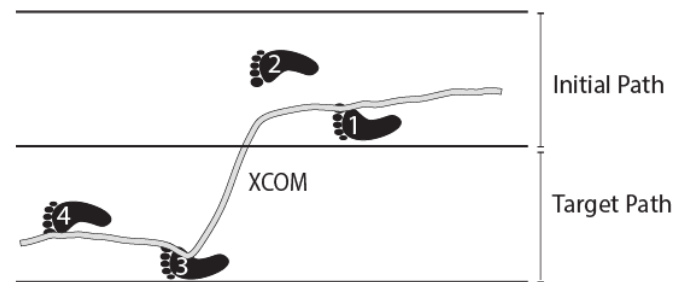
Avoiding obstacles and turning corners are essential for community ambulation but can be challenging for individuals with incomplete spinal cord injury (iSCI). To remain stable during maneuvers, people with sensory-motor deficits rely heavily on passive mechanisms (e.g. large margin of stability) that indiscriminately resist both external perturbations and volitional impulses intended to change trajectory. The proportional relationship between effort to maneuver and passive mechanisms of stability creates a speed-stability trade-off [1]. For a given volitional impulse, the speed of the maneuver will decrease as passive stability increases. As individuals with iSCI have both balance and strength deficits, situations requiring rapid maneuvers may result in a compromise between maneuver speed and stability.

In the current experiment, we examined speed-stability trade-offs as individuals with iSCI performed a simple overground walking maneuver at preferred and fast speeds. Previous studies found that non-impaired individuals reduced their lateral margin of stability (MOS) to facilitate rapid walking maneuvers [2]. Based on this finding, we hypothesized that when challenged to perform rapid walking maneuvers, individuals with iSCI would choose gait patterns that sacrifice passive stability.

## METHODS

Eleven ambulatory individuals with iSCI gave informed written consent and participated in the study. Participants performed straight-ahead walking and maneuvers at comfortable and fast speeds. For straight-ahead walking trials, participants walked

within a straight 7.5 x 0.5m path. During each maneuver trial, participants initially walked straight for 4.5m followed by a lateral maneuver to a parallel path (Figure 1). Once in the new path, participants continued walking forward. During “fast” trials, participants were instructed to walk and maneuver as quickly as possible while maintaining safety. At each speed, participants performed five straight-walking trials and 10 maneuver trials (five maneuvers to the left and right).



- 1) Setup step
- 2) Pushoff step
- 3) Landing step
- 4) Recovery step

**Figure 1:** Experimental Setup and representative locations of extrapolated center of mass (XCOM) and individual foot placements during a comfortable speed maneuver to the left.

Motion capture cameras recorded whole-body kinematics. For each trial, maneuver performance was quantified by time to complete the maneuver and center of mass (COM) path length during the maneuver. To examine lateral stability, we calculated the minimum lateral margin of stability (MOS) [3] during four maneuver steps (Fig. 1). The Setup step was initiated by the last heel strike before the maneuver began. This was followed sequentially by a Pushoff step, Landing step, and Recovery step. A decrease in MOS during a step indicates a decrease

in passive lateral stability and an increase in susceptibility to external perturbations.

Student t-tests or Wilcoxon Sign-Rank tests (when t-test assumptions were violated) were used to compare the effect of speed on performance metrics of Maneuver Time and COM Path Length. Repeated Measures ANOVAs were used to compare the effects of step (the four maneuver steps and a baseline straight-ahead walking step) and walking speed (fast and comfortable) on MOS.

## RESULTS AND DISCUSSION

### Maneuver Performance

Maneuver Time and COM Path Length (Wilcoxon:  $p = 0.003$  and  $p = 0.041$ , respectively) were significantly decreased for fast vs. comfortable walking speeds.

### Lateral Margin of Stability

The repeated measures ANOVA found a significant main effect of step ( $p < 0.0005$ ) and significant interaction between step and speed ( $p = 0.004$ ) on Lateral MoS (Figure 2).

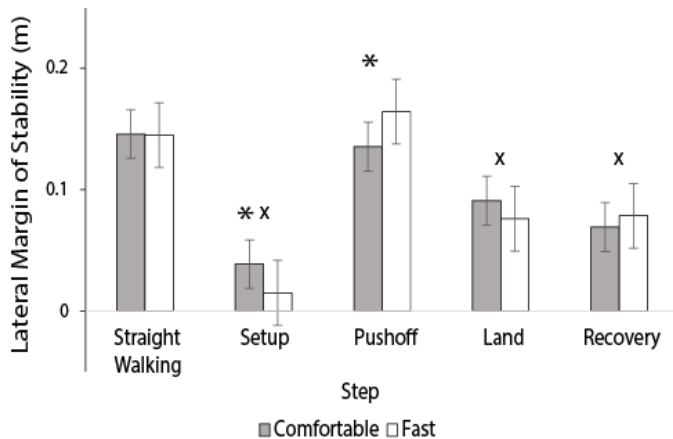


**Figure 2:** Minimum Lateral Margin of Stability for each step and condition. \*Significant difference between speeds. <sup>x</sup>Significant difference from Straight Walking step.

The Setup step had a significantly smaller minimum lateral MOS than every other step (Bonferroni-corrected pairwise comparisons of the Setup step vs.

Straight Walking, Pushoff, Landing, and Recovery steps all  $p \leq 0.002$ ). The minimum lateral MOS of the Setup Step decreased at the fast vs. comfortable walking speed ( $p = 0.026$ ). The minimum lateral MOS of the Pushoff step increased at fast vs. comfortable speed ( $p = 0.007$ ).

Our results show that individuals with iSCI reduce their passive lateral stability in anticipation of performing a lateral maneuver. This strategy reduces an individual's passive resistance to impulses directed in the intended maneuver direction. This reduction in lateral MOS should allow individuals to increase the rate at which they can initiate a maneuver for a given volitional impulse. However, this strategy also reduces passive stability in the maneuver direction, increasing susceptibility to external perturbations.

## CONCLUSIONS

These results suggest that individuals with iSCI choose to sacrifice stability for speed when asked to perform rapid maneuvers. This trade-off might translate to an interaction between community ambulation ability, walking speed, and fall risk. This finding also highlights how speed can be manipulated in a training environment to increase the challenge of maintaining stability during maneuvers.

## REFERENCES

1. Acasio, J., et al. *Gait Posture*, 2016. **52**: p. 171-177.
2. Wu, M., et al. *Plos One*, 2015. **10**(7).
3. Hof, A.L., et al. *J Biomech*, 2005. **38**(1): p. 1-8.

## ACKNOWLEDGMENTS

This work was supported by Merit Review Award #I01RX001979 from the United States Department of Veterans Affairs Rehabilitation Research and Development Service and the Northwestern University Undergraduate Research Assistant Program.

# EFFECTS OF MOVEMENT PATTERN BIOFEEDBACK TRAINING AFTER TOTAL KNEE ARTHROPLASTY

<sup>1</sup>Victor Cheuy, <sup>1</sup>Brian Loyd, <sup>1</sup>Michael Bade, <sup>1,2</sup>Cory Christiansen, <sup>1,2</sup>Jennifer Stevens-Lapsley

<sup>1</sup>Physical Therapy Program, University of Colorado, Aurora, CO;

<sup>2</sup>Geriatric Research Education and Clinical Center, VA Eastern Colorado Health Care System, Denver, CO  
email: [victor.cheuy@ucdenver.edu](mailto:victor.cheuy@ucdenver.edu)

## INTRODUCTION

Quadriceps muscle weakness has profound functional consequences after unilateral total knee arthroplasty (TKA). Compared to healthy controls, patients take twice as long to ascend and descend a flight of stairs, and report moderate to extreme difficulty [1]. A direct mechanism related to functional performance may be asymmetrical compensatory movement patterns. Characterized by low knee extension moments (KEM) and chronic quadriceps disuse in the surgical limb, these patterns promote quadriceps weakness and chronic functional limitations. The existence of these patterns pre-TKA suggest they are learned as compensation for chronic unilateral knee osteoarthritis pain. However, resolution of pain post-TKA has no effect on movement pattern resolution. Instead, innovative biofeedback training may remediate these atypical movement patterns. A strength of this study is that the tools and strategies are commercially available and simple to apply in real-world settings, including the clinic, patient home, and community. The purposes of this study were 1) to assess asymmetry in KEM during step ascent/descent, and 5-time sit-to-stand; 2) to determine if asymmetry was associated with impairment and function; and 3) to compare long-term quadriceps strength outcomes to controls without biofeedback after TKA.

## METHODS

7 older adults (63±7yrs; 5M/2F) received biofeedback during rehab from Pedoped instrumented insoles (Novel) for 8 weeks. Pedopeds give patients weight-bearing feedback in dynamic tasks such as level ground walking and stair climbing. Movement pattern training was integrated into a progressive rehab program, involving ROM, strengthening, and stretching exercises. Intervention acceptance was

measured with the IMI interest and enjoyment subscale, with a mean score of  $\geq 5/7$  considered positive. All patients were tested within 2 weeks prior to TKA, and 2 and 6 months after TKA. 3D kinematic and kinetic data were collected from an 8 camera motion analysis system (100Hz) and force plates (2000Hz). A 15 segment, subject specific model was used, and joint moments calculated using inverse dynamics. 5 sit-to-stand transitions assessing movement quality were performed to a metronome to control speed (1.5Hz). 3 trials were performed bilaterally for step ascent and descent. The ascent leading limb and descent trailing limb were used for analysis. KEM symmetry was calculated as surgical divided by non-surgical limb values. Knee pain was rated by self-report (NPRS). Knee total active range of motion (AROM) was quantified by goniometer. Quadriceps strength (QSR) was calculated using max isometric knee extension torque recorded from an electromechanical dynamometer (CSMI). AROM and strength were converted to a symmetry ratio. The stair climb test (SCT) assessed the ability to ascend/descent a 10-step flight of stairs. A separate 5-time sit-to-stand test (FTSST) measured the time needed to perform 5 transitions as fast as possible. A control group (n=11; 67±8yrs; 5M/6F) with TKA provided QSR data. They received identical rehab but no biofeedback. Differences in KEM symmetry between pre-op and 6-months post-op were calculated using a paired samples t-test. Pearson's  $r$  were calculated between KEM and outcomes measures. Difference in 6 month post-op QSR between groups was calculated using an independent samples t-test.

## RESULTS AND DISCUSSION

The intervention was acceptable to patients, with a mean IMI score of 6.2 (1.1). In the treatment group, sit-to-stand and ascent KEM symmetry returned to pre-op levels at 6 months ( $p=.87$  &  $.89$ , respectively);

descent KEM symmetry was trending towards improvement compared to pre-op ( $p<.1$ ) [Fig. 1]. KEM symmetry during ascent/descent were positively correlated with QSR at 2 and 6 months [Table 1]. Descent KEM was negatively correlated with SCT time at 2 months post-op. Compared to controls, the treatment group was trending ( $p<.1$ ) towards better QSR at 6 months [Fig. 1].

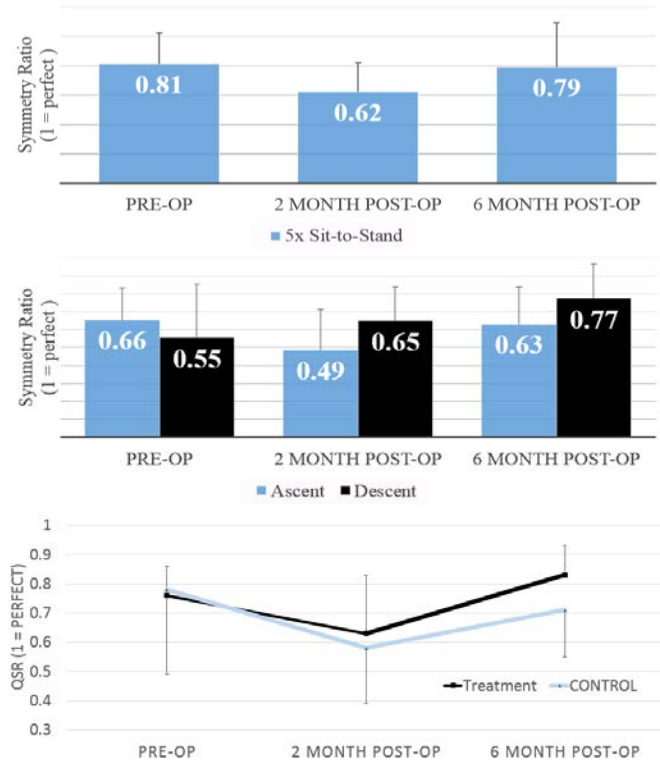


**Figure 1.** KEM symmetry with sit-to-stand (top) and ascent/descent (middle). QSR over time (bottom). Mean (SD) bars shown.

While motor learning through feedback and practice schedules is not a novel rehab tool in neurological populations, use of the methods for retraining movement patterns is innovative for rehab after TKA. Initial data presented elsewhere suggest that this approach also improves patient engagement in rehab post-TKA [2]. The ability for patients to

receive biofeedback during routine daily activity adds significant breadth to the number of home- and clinic-based functional tasks used in the movement pattern training. These results support associations previously found between quadriceps strength and loading asymmetry during functional tasks in patients with TKA [1, 3]. While TKA improves in pain and ROM, these do not correlate with improved movement symmetry. Based on these preliminary results, movement asymmetry may be a modifiable target during rehab, and the remediation of asymmetry through motor learning feedback may reduce deficits in quadriceps strength and function.

## CONCLUSIONS

The results provide preliminary support for the hypotheses that adding rehab with novel movement pattern training may improve KEM symmetry, which may be linked to recovery of QSR. It is reasonable to consider KEM symmetry as an important component to early rehab after TKA, and further study through a large RCT is warranted, investigating whether targeting asymmetry early may attenuate prolonged strength and function deficits. Normalizing movement patterns may also reduce contralateral joint disease and the need for a future TKA.

## REFERENCES

- Christiansen C, et al., *Arch Phys Med Rehabil.* **92**, 1624-9, 2011.
- Bade M, et al., *APTA CSM.* Abstract 2013.
- Alnahdi A, et al., *Knee Surg Sports Traumatol Arthrosc.* **24**, 2587-94, 2016.

## ACKNOWLEDGEMENTS

Funding: NIH R56 AG04894

**Table 1.** Pearson's  $r$  [95% CI] between KEM symmetry and outcome measures over time. \* $p<0.05$ , † $p<0.01$ .

Variable	2 months, $r$			6 months, $r$		
	Ascent	Descent	STS	Ascent	Descent	STS
NPRS	.12 [-.98,.91]	.20 [-.85,.97]	-.29 [-1,.71]	.33 [-.95,.88]	.22 [-.81,.90]	.16 [-.88,.91]
AROM	.05 [-.92,.99]	.33 [-.96,.95]	-.10 [-.93,.96]	-.41 [-.59,-.98]	-.25 [-.98,.99]	-.30 [-1,.94]
QSR	.86* [.46,1]	.90* [.67,1]	.26 [-.73,1]	.83* [-.29,.99]	.95† [.15,1]	.74 [-.1,1]
SCT	-.56 [-.99,.10]	-.92* [-1,-.37]	N/A	-.46 [-1,.16]	-.42 [-1,.29]	N/A
FTSST	N/A	N/A	-.40 [-.96,.86]	N/A	N/A	-.39 [-.99,.27]

# The Effect of Functional Electrical Stimulation Assisted Rowing and Intravenous Zoledronic Acid on Tibial Stiffness in Spinal Cord Injury

<sup>1</sup>Ying Fang, <sup>2,3</sup>Leslie L. Morse, <sup>2</sup>Nguyen Nguyen, and <sup>1</sup>Karen L. Troy

<sup>1</sup> Worcester Polytechnic Institute, Worcester, MA, USA

<sup>2</sup> Craig Rehabilitation Hospital, Englewood, CO, USA

<sup>3</sup>University of Colorado School of Medicine, Aurora, CO, USA

email: yfang3@wpi.edu

## INTRODUCTION

People with spinal cord injury (SCI) experience rapid and severe bone loss in their lower extremities. Decreased bone mineral density and associated deteriorations to bone structure significantly reduce proximal tibia and distal femur strength. As a consequence, individuals with SCI have a high risk of fracture at these regions [1].

Reducing the rate of fractures in this population through interventions that strengthen bone remains an important clinical goal. In this context, therapies that prevent bone loss or that stimulate an anabolic response in bone have been proposed. Zoledronic acid (ZA) is a potent and long-acting bisphosphonate that inhibits osteoclastic resorption and is commonly prescribed for osteoporosis. It has been shown to decrease hip bone loss in acute SCI [2]. Functional electrical stimulation (FES) assisted rowing is an exercise that includes mechanical stimulation to the lower extremities, which is potentially osteogenic. The degree to which FES-rowing, ZA, or a combination is effective in improving distal femur or proximal tibia mechanical behavior in SCI is not known. Our **purpose** was to measure changes to torsional and compressive stiffness at the proximal tibia among people with SCI who underwent FES-rowing training with or without ZA treatment.

## METHODS

### Subjects

Seventeen subjects were selected from a cohort of adults with SCI (**Table 1**) who participated in a one-year clinical trial that included interventions for FES-rowing and ZA. Subjects were excluded if they did not row, or if they received treatments other than rowing and ZA that could affect bone turnover (ie. statin use).

### Finite element (FE) predicted stiffness

Each subject received two CT scans of their knee region before and after the intervention. Each scan included a calibration phantom (MindWays, Austin, TX) to convert CT Hounsfield units (HU) to bone equivalent density ( $\rho_{ha}$ , g/cm<sup>3</sup>). A 0.15 g/cm<sup>3</sup> threshold was used to identify the periosteal surface. Segmented integral bones were resampled to isotropic voxels with 1.5 mm edge length and directly converted to voxel based FE models with linear hexahedral elements using established methods [3]. Elements were assigned material properties based on density-elasticity relationship of  $E_3 = 6570 \rho_{app}^{1.37}$ , where  $E_3$  is axial elastic modulus (MPa) and  $\rho_{app}$  is apparent density ( $\rho_{app} = \rho_{ha}/0.626$ , g/cm<sup>3</sup>) [4, 5]. Anisotropy was assumed to be the same throughout with  $E_1 = 0.574 \cdot E_3$ ,  $E_2 = 0.577 \cdot E_3$ ,  $G_{12} = 0.195 \cdot E_3$ ,  $G_{23} = 0.265 \cdot E_3$ ,  $G_{31} = 0.216 \cdot E_3$ ,  $\nu_{12} = 0.427$ ,  $\nu_{23} = 0.234$ , and  $\nu_{31} = 0.405$ , where subscripts 1 and 2 denote the medial and anterior directions, respectively [6].

Epiphyseal and metaphyseal regions were defined as 0 – 10% and 10 – 20% tibia length, as measured from proximal end. The FE model of each region was subjected to either a fixed axial (compression) or torsional displacement. Surface nodes at distal end of tibial models were fully constrained. The reaction force, or torque, was used to calculate compressive (K; kN/mm) and torsional (T; Nm/deg) stiffness [3].

### Statistical analyses

Repeated measures analysis of variance (RMANOVA) was performed with factors of time (baseline versus follow up), intervention (rowing vs. rowing+ZA), and site (epiphysis vs. metaphysis). Student's t-tests were used to compare total and monthly change between the acute (injured 0-3 years) and chronic group (injured >3 years).

## RESULTS AND DISCUSSION

We observed an interaction between site and time in T ( $p = 0.039$ ), and a main effect for time and site on all variables. Overall, bone stiffness decreased over the intervention period, and the change was significant in both K ( $p = 0.013$ ) and T ( $p = 0.013$ ) for epiphysis, but not metaphysis (**Figure 1**). Although the interventions did not result in increased bone stiffness, previous studies have shown dramatic bone loss in individuals with recent SCI (injured <6 months) [3]. In our cohort, we observed monthly losses in K and T that were greater in acute vs. chronic groups, but that were overall much smaller than those previously reported with recent SCI (**Figure 2**). The present cohort showed similar patterns of stiffness loss as reported in those with recent SCI, with the epiphysis most affected.

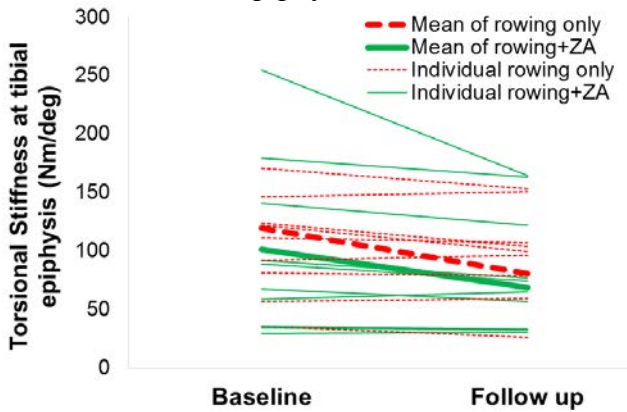


**Figure 1.** Torsional stiffness at epiphysis of rowing and rowing+ZA groups at baseline and follow up.

Both rowing only and rowing+ZA groups showed decreases in bone stiffness. However, some individuals had increases (**Figure 1**). Based on their training record, rowing dose was not related to K or T, indicating that additional factors are contributing to an individual's overall response.

Interestingly, we found that baseline tibial stiffness is a good predictor of its monthly changes at the epiphysis region ( $R^2 = 0.766$  and  $0.634$  for K and T, respectively; **Figure 3**). In other words, people with

stronger bones tend to lose strength faster, which may suggest an asymptotic approach towards a “physiologic endpoint” for bone loss after SCI.

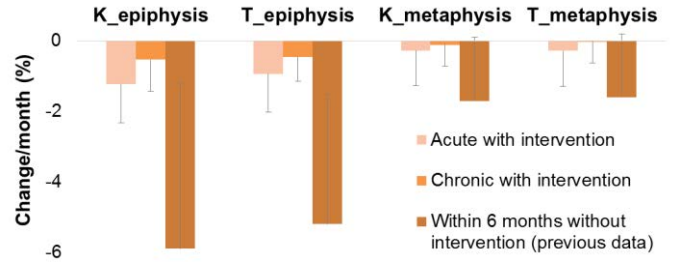


**Figure 2.** Monthly change in compressive (K) and torsional (T) stiffness between baseline and follow up.

## CONCLUSIONS

FES-rowing with and without ZA appears to attenuate loss in bone strength in individuals with SCI. Further investigation is needed to elucidate the factors that causes different individual responses.

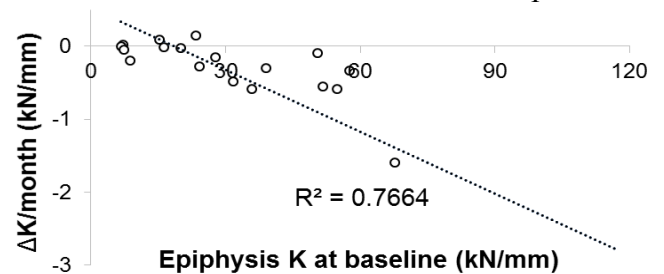


**Figure 3** Relationship between baseline compressive stiffness (K) and monthly change post injury.

## REFERENCES

- [1] Morse LR, et al. *Osteoporos Int* **20**, 385-392, 2009.
- [2] Bubbear JS, et al. *Osteoporos Int* **22**, 271-279, 2011.
- [3] Edwards WE, et al. *Osteoporos Int* **25**, 1005-1015, 2014.
- [4] Rho JY, et al. *Med Eng Phys* **17**, 347-355, 1995.
- [5] Dalstra M, et al. *J Biomech* **26**, 523-535, 1993.
- [6] Rho JY. *Ultrasonics* **34**, 777-783, 1996.

## ACKNOWLEDGMENTS

This study received support from the Department of Defense (W81XWH-10-1-1043). The code to generate FE models from CT data was developed by W. Brent Edwards.

**Table 1:** Subject characteristics: mean (standard deviation). ZA: zoledronic acid

	Acute (< 3 years since injury)			Chronic ( $\geq 3$ years since injury)		
	ZA (N=5)	No ZA (N=3)	All (N=8)	ZA (N=5)	No ZA (N=6)	All (N=11)
Age (yr)	32.5 (12.9)	26.8 (3.8)	30.4 (10.4)	36.0 (10.0)	42.3 (11.4)	39.4 (10.7)
BMI (kg/m <sup>2</sup> )	25.7 (4.8)	23.5 (1.8)	24.9 (3.9)	23.7 (3.8)	24.1 (6.0)	23.9 (4.9)
Year post injury (yr)	1.1 (0.8)	2.0 (0.5)	1.5 (0.8)	14.3 (13.5)	17.9 (14.2)	16.3 (13.3)
Rowing (months)	11.2 (3.0)	7.3 (3.2)	9.8 (3.5)	10.7 (4.5)	11.4 (3.0)	11.0 (3.7)

# SENSORY STIMULATION CAN IMPROVE MOTOR FUNCTIONS IN INDIVIDUALS WITH MULTIPLE SCLEROSIS

<sup>1,3</sup> Awad M. Almklass, <sup>1</sup> Daniel F. Feeney, <sup>1</sup> Robyn A. Capobianco, and <sup>1,2</sup> Roger M. Enoka

<sup>1</sup>Department of Integrative Physiology, University of Colorado, Boulder, CO, USA

<sup>2</sup>Department of Mathematics, University of Colorado, Boulder, CO, USA

<sup>3</sup>College of Medicine, King Saud bin Abdulaziz University for Health Sciences, Riyadh, KSA  
email: awad.almklass@colorado.edu, web: <http://www.colorado.edu/intphys/research/ncm.html>

## INTRODUCTION

Multiple sclerosis (MS) is a neurological disorder that affects approximately 400,000 people in the US. The primary cause of MS is a loss of myelin that reduces signal transmission and processing within the nervous system. Common symptoms reported in the first year of the disease include sensory impairment, fatigue, reduced mobility, and declines in hand function [1]. Sensory symptoms, such as numbness, tingling, or the sensation of pins-and-needles, are observed in ~69% of individuals with MS [2]. The onset of these symptoms varies, but 39% of individuals with MS exhibit these symptoms in the early stages of the disease [3]. There is a strong association between loss of sensation in the limbs and declines in both walking performance and manual dexterity. Interventions that target sensory systems can elicit significant symptom relief and gains in clinical measures of physical function.

The purpose of the current study was to assess the influence of sensory stimulation using augmented transcutaneous electrical nerve stimulation (aTENS) applied to leg and hand muscles on clinical tests of motor function in individuals whose mobility had been compromised by MS. The tests assessed walking endurance, walking speed, sit-to-stand ability, and manual dexterity. We hypothesized that aTENS would acutely improve performance on the clinical tests of motor function and reduce self-reported levels of walking disability (MS Walking Scale-12).

## METHODS

The ongoing study has enrolled 10 of the planned 15 participants. The age (mean  $\pm$  SD) of these individuals was  $55 \pm 5$  yrs and their Patient-Determined Disease Steps (PDDS) scores were  $2.6 \pm 1.4$  (0 = no disability, 8 = bedridden) and the MSWS-12 scores were  $35.5 \pm 12.2$  (12 = no walking disability, 60 = extreme disability).

Participants visited the lab on two occasions with one week between visits. Each visit involved the participant performing four tests of motor function and completing two health-related questionnaires (PDDS and MSWS-12). The four clinical tests were the chair-rise test, assessment of maximal walking speed (25-ft walk test), measurement of walking endurance (6-min walk test), and a test of manual dexterity (grooved pegboard test). The pads through which aTENS was delivered were attached to the limbs during both visits and were placed over the hip flexors and dorsiflexors for the affected leg, and over the median nerve and the thenar eminence of the dominant hand. However, current was only delivered to the pads during the second visit while participants performed the four tests of motor function. The stimulation comprised asymmetrical rectangular, biphasic pulses (0.2 ms) at a rate of 50 Hz.

## RESULTS AND DISCUSSION

The participants experienced statistically significant improvements (Table 1) in the chair-rise test (30-s count), walking endurance (distance walked in 6 min), and pegboard time, but not the time to walk 25 ft (maximal walking speed). Also, they reported a statistically significant reduction in walking disability (MSWS-12 score), but not the PDDS score.

The average improvement after acute exposure to aTENS was (mean  $\pm$  SD) 3.3  $\pm$  4.1% for the 6-min distance, 21.2  $\pm$  14.2% for the chair-rise test, 10.3  $\pm$  10.9% for the pegboard test, and 20  $\pm$  13% for the MSWS-12 score. The magnitude of the benefit that can be obtained with more prolonged treatment remains to be determined.

## CONCLUSIONS

Stimulation of sensory fibers with augmented TENS evoked clinically significant improvements in three of the four tests of motor function and the self-reported level of walking disability in persons who were moderately disabled by MS. Moreover, the improvements in function were immediate.

**Table 1.** The mean  $\pm$  SD for the tests without stimulation (control) and with stimulation (aTENS).

	<b>Control</b>	<b>aTENS</b>	<b>Effect size</b>
<b>Chair-rise test (30-s count)</b>	11.4 $\pm$ 3.9	13.8 $\pm$ 4.9*	-0.63
<b>6-min walk test (m)</b>	399 $\pm$ 167	410 $\pm$ 170*	-0.48
<b>25-ft walk test (s)</b>	6.5 $\pm$ 2.9	6.2 $\pm$ 2.8	-0.38
<b>Pegboard test (s)</b>	110 $\pm$ 44	98 $\pm$ 39*	-0.54
<b>MSWS-12 (score)</b>	36 $\pm$ 12	29 $\pm$ 13*	-0.58
<b>PDDS</b>	2.6 $\pm$ 1.4	2.0 $\pm$ 1.4	-0.37

\*P < 0.05 relative to control. Normality tests were performed and related samples Wilcoxon signed rank test was performed.

## REFERENCES

1. Kister I, et al. *Int J MS Care*. **15**: 146- 158, 2013.
2. Rae-Grant AD, et al. *Mult Scler* **5**: 179–183, 1999.
3. Paty DW. *Demos Medical Publishing*, New York, 2000.

## ACKNOWLEDGMENTS

Presented results do not include a control group, but such a group will be added subsequently. Awad M. Almuksas was supported by King Saud bin Abdulaziz University for Health Sciences Riyadh, KSA.

# EMG RESPONSES TO LATERAL PELVIS FORCE PERTURBATION IN HUMANS WITH SPINAL CORD INJURY DURING WALKING

<sup>1,2</sup> Ming Wu, <sup>1,2</sup> Chao-Jung Hsu, <sup>1,2</sup> Zev Rymer, <sup>1</sup> Weena Dee

<sup>1</sup> The Rehabilitation Institute of Chicago, Chicago, IL, USA

<sup>2</sup> Northwestern University, Chicago, IL, USA

email: [w-ming@northwestern.edu](mailto:w-ming@northwestern.edu)

## INTRODUCTION

Balance control plays a crucial role during locomotion in humans with SCI. Recent studies indicate that there is a strong relationship between balance and walking capacity in patients with SCI [1]. Improved balance control allows a patient to walk with fewer assistive devices and therefore walk faster and more efficiently for both short and long distances. Therefore, it seems that balance is one of the most important factors affecting walking in chronic SCI patients. Thus, we postulate that improved balance control, particularly lateral balance, which needs active control to stabilize lateral motion in humans walking, may facilitate locomotion in humans with SCI. However, current balance training paradigms in patients with SCI primarily focus on standing or sitting balance, which may have limited transfer to walking [2], suggesting a need for developing new dynamic balance training paradigms.

The goal of this study was to examine the neuromuscular responses of humans with SCI when a perturbation force was applied during walking. We hypothesized that a pelvis perturbation force in the mediolateral direction during walking would provide additional challenges to the balance system of humans with SCI and evoke postural reactions to counteract the external perturbation force.

## METHODS

Ten individuals with chronic (> 12 months) motor incomplete SCI (i.e., AIS, C or D) were recruited to participate in this study. All research on human subjects were conducted with authorization of the Northwestern University Medical School Institutional Review Board. Written informed

consents were obtained from all subjects before their participation.

A custom designed cable-driven robotic system was used to apply controlled pelvis perturbation force. The cable-driven system consists of 2 nylon-coated stainless-steel cables (1.6mm), driven by 2 motors (AKM43H, Kollmorgen, Drive amplifier, Servostar 30661) and cable spools, and affixed to a custom waist belt that is strapped to the pelvis.

A controlled lateral force with the magnitude was set at ~9% of body weight, which was adjusted based on the tolerance of each subject, was applied bilaterally to the pelvis while subjects walked on a treadmill. The perturbation force was applied at 3 different phases (i.e., early stance, late stance, early swing phase) with the order of test session was randomized across subjects with 1 minute standing break was inserted between two test sessions. Electromyograms (EMG) from 8 muscles on the weaker leg were recorded using surface electrodes with a sampling frequency at 500 Hz.

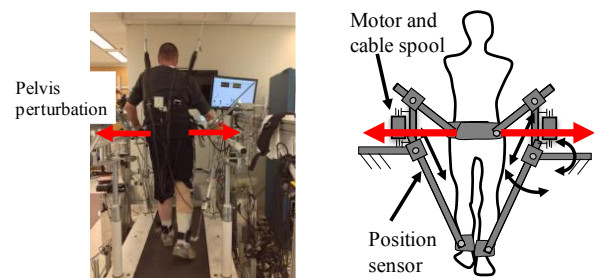


**Figure 1:** This figure illustrates the cable-driven robotic system. A PC was used to control coordinate movement of two motors.

All EMG data were filtered, rectified and smoothed using a second order Butterworth filter with a low-pass cutoff frequency at 20 Hz. The smoothed EMG

signals were averaged over the middle consecutive 10 strides for each condition, and normalized to the peak EMG signal obtained from the maximum walking speed trial. EMG activity was further integrated during stance and swing phase of gait. A repeated measures ANOVA was used to compare the difference with significance was set at  $\alpha < 0.05$ .

## RESULTS AND DISCUSSION

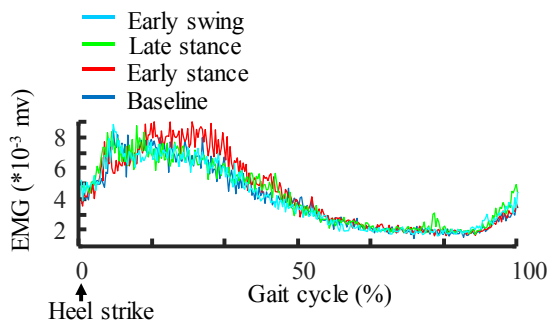


**Figure 2:** The ensemble average traces of the rectified EMG of the hip abductors (ABD) during baseline, with early stance, late stance, and early swing phase pelvis force perturbation. Data shown were average across 10 subjects.

Applying lateral pelvis perturbation force induced enhanced muscle activities of the hip abductors (ABD) and rectus femoris (RF) of the ipsilateral leg during stance phase. Specifically, the integrated muscle activities of ABD significantly increased when lateral pelvis perturbation force was applied ( $p = 0.002$ , ANOVA). Post-doc test indicated that the integrated EMG of ABD significantly increased from  $51.1 \pm 33.1$  at baseline to  $60.0 \pm 36.9$  (normalized) when perturbation force was applied during early stance phase ( $p = 0.002$ ), and increased to  $56.0 \pm 36.1$  when the force was applied during late stance phase, although this was not significant ( $p = 0.11$ ), and slightly increased to  $53.5 \pm 33.0$  when the force was applied during swing ( $p = 0.65$ ). In addition, the integrated muscle activity of RF significantly increased when the perturbation force was applied ( $p = 0.003$ ). Post-doc test indicated that the integrated EMG of RF significantly increased from  $48.0 \pm 30.1$  at baseline to  $57.8 \pm 37.7$  when perturbation force was applied during early stance phase ( $p = 0.06$ ), and increased to  $63.2 \pm 40.7$  when the force was applied during late stance phase ( $p = 0.002$ ), and slightly increased to  $53.9 \pm 37.1$  when the force was applied during swing phase ( $p = 0.41$ ).

Applying lateral pelvis perturbation force during walking may induce enhanced muscle activities of ABD and RF, suggesting subjects may increase muscle activation of hip ABD and RF to counteract the pelvis perturbation force and stabilize the standing leg during walking. Further, we observed a greater increase in muscle activities of hip ABD during early stance phase than that during late stance phase. A possible reason may be because the direction of perturbation force is consistent with the lateral movement of the pelvis when the force was applied during early stance phase. Thus, the perturbation force may facilitate pelvis movement to the lateral direction, which may force subject to generate additional torque to counteract the perturbation force. In contrast, when the perturbation force was applied during late stance phase, the direction of perturbation force is opposite to the movement of the pelvis. Thus, the effect of perturbation force on the hip ABD was damped. In addition, we observed no significant changes in muscle activity of hip ABD when the perturbation force was applied during early swing phase of the ipsilateral leg, probably due to subjects were primarily relying on the contralateral leg (i.e., the standing leg) to stabilize the pelvis for this case.

## CONCLUSIONS

Applying a lateral pelvis perturbation force may provide additional challenges to the mediolateral balance control in humans with SCI during walking. Repeated exposure to pelvis perturbation training may improve motor control of hip abductors, which may facilitate improvements in lateral balance of humans with SCI during locomotion.

## REFERENCES

1. Forrest, GF, et al. *Arch Phys Med Rehabil* **93**, 1553-64, 2012.
2. Winstein, CJ, et al. *Arch Phys Med Rehabil*, **70**, 755-762, 1989.

## ACKNOWLEDGMENTS

We thank Ms. Janis Kim for her assistance in subject recruitment and data collection. This study was supported by NIH/NICHD R01HD083314.

# SENSOR-BASED ACTIVITY DETECTION AND CLASSIFICATION OF MANUAL WHEELCHAIR USERS

<sup>1,2</sup>Emma Fortune, <sup>2</sup>Beth Cloud, <sup>1</sup>Dennis Murphree, <sup>2</sup>Kristin Zhao, and <sup>1,2</sup>Melissa Morrow

<sup>1</sup>Robert D. and Patricia E. Kern Center for the Science of Health Care Delivery, Mayo Clinic, Rochester, MN

<sup>2</sup>Rehabilitation Medicine Research Center, Mayo Clinic, Rochester, MN

email: Fortune.Emma@mayo.edu

## INTRODUCTION

People with traumatic and non-traumatic spinal cord injuries (SCIs) make up 20% of the 1.5 million manual wheelchair (MWC) users in the U.S., with 12,000 traumatic SCIs occurring every year [1]. Shoulder pain is the most common musculoskeletal pain site in MWC users [2] and can significantly limit function and quality of life, with an incidence ranging from 31 to 73% [3]. It is often caused by rotator cuff tears and tendinopathies resulting from shoulder impingement [4]. Overuse, particularly during overhead and weight bearing movements, is thought to be a major causal factor [5]. However, little is known regarding MWC users' cumulative exposure of the shoulder joints to activities of daily living (ADLs) which pose impingement risk.

To better understand the link between MWC use and shoulder impingement, it is important to objectively classify the type and quantify the frequency of ADLs performed in MWC users' everyday life. Previous studies have used multiple accelerometers or a single body-worn accelerometer in combination with a gyroscope-based wheel rotation monitor to identify wheelchair propulsion from other activities mostly unrelated to shoulder overuse [6]. An ADL classification method using fewer monitors would be less cumbersome and including more ADLs related to shoulder overuse could provide additional information in regards to estimating shoulder impingement risk.

This study's aim is to develop and validate an algorithm in a semi-controlled laboratory setting with the potential to accurately detect and classify shoulder overuse activity and identify wheelchair propulsion from non-propulsion activity in MWC users in their natural environment.

## METHODS

Two 25 year old male MWC users with SCIs have been recruited for this study to date. Inclusion criteria include use of a MWC as the primary mobility mode for at least one year, C6 and below traumatic or non-traumatic SCI, and active shoulder range of motion within limits needed for the tasks performed during the study. The study protocol was approved by the Mayo Clinic IRB and written informed consent was obtained before participation.

The subjects performed multiple trials of MWC-related activities of daily living including (1) reaching for an object with 90° of shoulder elevation, (2) reaching for an object overhead, (3) cross-body lifting of backpack between the ground and a table, (4) wheelchair transfers, (5) wheelchair propulsion on a ramp (15 propulsion cycles), and (6) wheelchair propulsion on level ground for a two minute duration (Fig. 1).

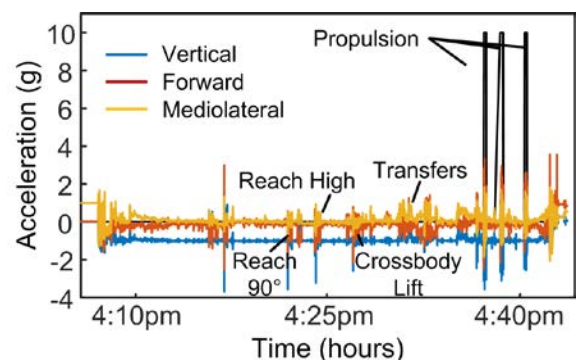


**Figure 1:** Raw tri-axial upper arm acceleration data for one subject during the lab-based protocol.

Continuous tri-axial acceleration data were collected at 128 Hz from one Opal IMU (APDM Inc, Portland, OR, USA) secured to the left upper arm with a strap. Continuous video data were

simultaneously acquired at 60 Hz.

Activity was detected from the acceleration data and peak detection was performed on all identified activity segments using our activity and adaptive threshold peak detection algorithms previously developed for activity and step detection in able-bodied subjects [7] in MATLAB (Mathworks, USA). Active time in seconds and propulsion peaks were validated by comparison to video recordings. Activity cycles were then identified as the acceleration time series data between consecutively detected peaks within identified activity segments. For each activity cycle, six features were extracted for use as predictors (Fig. 2). These resulting six predictors were then fed into a neural network designed using the single layer perceptron architecture. After splitting the data into class-stratified training and test sets, a grid search was conducted over tunable network parameters and model performance was evaluated via five-fold cross validation. The top performing model had a weight decay of 0.1 and 19 nodes in the hidden layer.

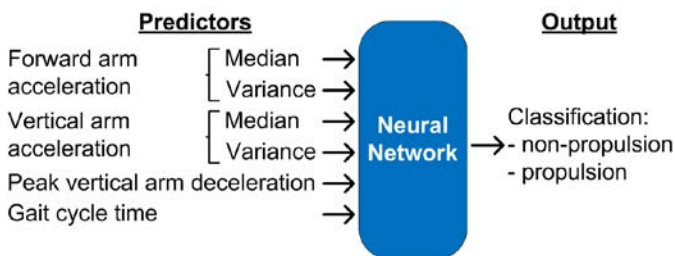


**Figure 2:** Pattern classification algorithm.

## RESULTS AND DISCUSSION

The accuracy of detected active seconds during propulsion and non-propulsion activities was 100% and 93% for subject 1 and 100% and 86% for subject 2, respectively. Propulsion peaks were detected with 100% accuracy with no false positives or negatives detected. The out-of-sample cross validation performance yielded an area under the receiver operator curve (AUC) of 0.97 for differentiating between propulsion and non-propulsion activity (Fig. 3), while its holdout set AUC was 0.95. The model's sensitivity, specificity and accuracy, when using a classification threshold

of 50%, were 0.96, 0.95 and 0.95, respectively, similar to or greater than previous studies [6].

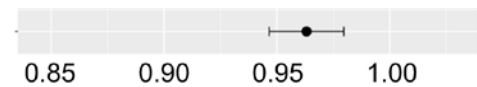


**Figure 3:** Area under the curve estimation for differentiating between propulsion and non-propulsion activity using five-fold cross-validation.

The algorithm is being further developed and validated to discriminate between the other investigated activities based on their distinct acceleration patterns and in combination with IMU-derived shoulder kinematics. Future work will determine the frequency with which MWC users perform the specific ADLs in their free-living environments and combine this exposure data with the relative impingement risk of ADLs to determine a measure of cumulative impingement risk of MWC-associated ADLs.

## CONCLUSIONS

The high AUC obtained with cross-validation suggests that our feature extracting algorithm may be able to accurately identify and differentiate between propulsion and non-propulsion activity of MWC users in their free-living environments using one IMU worn on the upper arm, which remains to be confirmed with additional subjects currently being recruited.

## REFERENCES

1. National Spinal Cord Injury Statistical Center. *J Spinal Cord Med*, **31**, 357-8, 2008.
2. Cooper R et al. *Team Rehab Rep*, **9**, 35-8, 1998.
3. Sie I et al. *Arch Phys Med Rehab*, **73**, 44-8, 1992.
4. Ludewig P et al. *Man Ther*, **16**, 33-39, 2011.
5. Soslowsky L et al. *Ann Biomed Eng*, **30**, 1057-63, 2002.
6. Nooijen C et al. *J NeuroEng Rehab*, **12**, 11, 2015.
7. Fortune E et al. *Physiol Meas*, **36**, 2519, 2016.

## ACKNOWLEDGMENTS

Funding is provided by the Craig H. Nielsen Foundation and the NIH (R01 HD84423).

# IMPACT OF GEARED WHEELS ON ENERGY EXPENDITURE DURING MANUAL WHEELCHAIR MOBILITY

<sup>1</sup> Omid Jahanian, <sup>1</sup> Taylor W Rowley, <sup>1</sup> Scott J Strath, <sup>2,3</sup> Barbara Silver-Thorn, and <sup>1</sup> Brooke A Slavens

<sup>1</sup> The University of Wisconsin–Milwaukee, Milwaukee, WI, USA

<sup>2</sup> Marquette University, Milwaukee, WI, USA

<sup>3</sup> Medical College of Wisconsin, WI, USA

email: jahanian@uwm.edu, Web: www.uwm.edu/mobilitylab/

## INTRODUCTION

Manual wheelchair users often participate less in physical activities (PAs) than able-bodied individuals [1], which increases cardiovascular disease risk and incidence of secondary medical conditions. New wheelchair designs and enhanced self-awareness of activity level could help manual wheelchair users increase their PA levels and to have a healthier life style. Previous research has indicated that using geared wheels, a novel technology for manual wheelchair users, may enhance individuals' function and participation due to significant reductions in biomechanical demands [2,3] and shoulder pain [4]. However, the impact of geared wheels on metabolic demands during manual wheelchair mobility has yet to be investigated.

The objectives of this study are to compare metabolic demands during standard and geared manual wheelchair mobility and to identify the contributing factors impacting energy expenditure during manual wheelchair propulsion. Using a repeated measures design, the following hypotheses were tested:

- Manual wheelchair mobility energy expenditure increases with the use of geared wheels in comparison to standard wheels
- Wrist acceleration and heart rate during manual wheelchair propulsion are significant factors contributing to the variability of energy expenditure

## METHODS

Three able-bodied individuals (males, age: 21 years, height:  $180 \pm 6$  cm, weight:  $89 \pm 15$  kg) were recruited for this study. This study was approved by the University of Wisconsin-Milwaukee (UWM)

Institutional Review Board (IRB). On the first day, anthropometric and demographic information were collected at the UWM Physical Activity and Health Research Lab and resting metabolic rate (RMR) was measured following an overnight fast. Respiratory exchange measurements were determined by an indirect calorimeter (ParvoMedics 2400 TrueOne, Sandy UT) using a flow-through canopy hood [5].

PA assessment was completed at the UWM Mobility Lab on the second day. Participants were asked to propel both standard (direct drive) and geared (gear ratio 1:1.5) manual wheelchairs on a passive wheelchair ergometer instrumented with a speedometer for seven minutes at two different speeds (1.5 and 2 mph). Participants used a Breezy manual wheelchair (Sunrise Medical LLC.) equipped with geared wheels (IntelliWheels, Inc., Champaign, IL). Seven minutes of rest separated each activity. Oxygen consumption was measured using the COSMED *K4b<sup>2</sup>* portable gas analysis system (COSMED, Rome, Italy) during manual wheelchair propulsion. The COSMED *K4b<sup>2</sup>* software was used to establish summary estimates of energy expenditure, including oxygen uptake [ml/min], and energy expenditure [kcal/min]. PA energy expenditure (PAEE) was calculated as the difference between the energy expenditure measured during PA testing and the resting energy expenditure (calculated from RMR). Participants wore accelerometers (ActiGraph GT3x, ActiGraph LLC, Fort Walton Beach, FL) over the posterior dorsal aspect of their wrists. Heart rate was also recorded throughout testing using a heart rate monitor (Polar, Polar Electro Inc., Lake Success, NY, USA) secured around the chest. Stroke cycle frequency during the tasks was calculated based on the sagittal plane kinematics of the third metacarpal marker, using a

3D Vicon T-series motion capture system (Vicon Motion Systems, Oxford, UK).

Steady-state or near-steady-state (<15% coefficient of variation) energy expenditure data were obtained by averaging breath-by-breath measures across 30-second periods [6] to derive oxygen consumption values for 3-7 mins. Oxygen consumption measured from each participant was divided by their measured RMR value to compute subject specific metabolic equivalent tasks (METs) [5]. Statistical analyses were conducted using IBM SPSS software; analysis included paired samples t-test ( $p = 0.05$  significance level) and multiple linear regression analysis.

## RESULTS AND DISCUSSION

The results indicated that METs increased during geared wheel compared to the standard wheel (direct drive) condition, see Table 1. METs increased by 15% ( $p = 0.001$ ) during the geared wheel condition and 1.5 mph speed. Dominant wrist acceleration and relative heart rate (recorded heart rate minus resting heart rate) were significantly correlated with PAEE by Spearman ranks of 0.74 and 0.66, respectively (Figure 1). Using dominant wrist acceleration (Acc) and relative heart rate (HR) as predictors in a multi-regression model explained 78% of the variability in PAEE ( $PAEE = 0.012 \text{ Acc} + 0.23 \text{ HR} - 0.66$ ). The addition of relative heart rate to a wrist acceleration only model significantly improved model performance ( $p < 0.01$ ). The notable increase in the stroke frequency during geared wheel condition (Table 1) could be the main reason for the observed increase in METs and energy expenditure.

## CONCLUSIONS

Using the proposed method, the difference in energy expenditure during use of geared wheels and direct

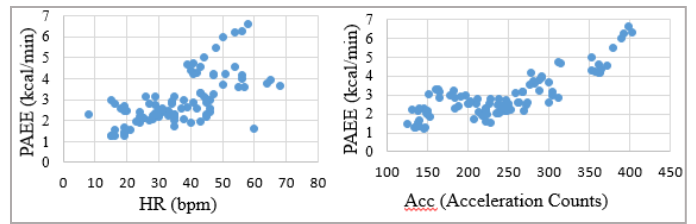


**Figure 1:** Relative Heart rate with PAEE (left) and wrist acceleration with PAEE (right) scatter plots.

drive wheels was detected successfully. Further investigation is underway with a larger population of manual wheelchair users with spinal cord injury. Development of activity specific models for predicting energy expenditure with acceleration and heart rate as primary predictors and wheel type as a covariate at various speeds is warranted. Mixed models with random intercept or slopes will be investigated. The outcomes from this study may ultimately improve manual wheelchair prescription and long-term transitional care for individuals with spinal cord injury.

## REFERENCES

1. Conger S, The *University of Tennessee*, 2011.
2. Howarth SJ, et al. *Clin Biomech* **25**: 21–28, 2010.
3. Jahanian O, et al. *Proceedings of IEEE EMBC*, Orlando, FL, USA, 2016.
4. Finley M, et al. *Arch Phys Med Rehabil* **88**: 1622–1627, 2007.
5. Strath S, et al. *Physiological Measurement* **36(11)**: 2335, 2015.
6. Hiramath S, et al. *The Journal of Spinal Cord Medicine* **34(1)**: 110-117, 2011.

## ACKNOWLEDGMENTS

The content of this work was developed under a National Institutes of Health (NIH) SBIR Phase II grant number 2R44HD071653- 02 and a student research grant from UW-Milwaukee College of Health Sciences.

**Table 1:** Mean stroke frequency, METs and total energy expenditure for different conditions.

Wheel Condition	Speed (mph)	Stroke Frequency (1/min)	METs	Tot. EE (kcal)
Direct Drive	1.5	49 ± 7	2.17 ± 0.25	12.01 ± 1.78
	2	55 ± 7	2.70 ± 0.31	15.07 ± 1.23
Geared	1.5	57 ± 5	2.52 ± 0.25	14.26 ± 1.96
	2	75 ± 15	3.75 ± 0.27	21.48 ± 3.92

## ECCENTRIC CONTROL AFTER SPINAL CORD INJURY: TRANSLATING FROM AN ANIMAL MODEL

Lise Worthen-Chaudhari<sup>1</sup>, Kevin O'Brien<sup>2</sup>, Albert Olszewski<sup>2</sup>, Timothy Faw<sup>3</sup>, Michael McNally<sup>4</sup>, James P. Schmiedeler<sup>2</sup>, and D. Michele Basso<sup>4</sup>

<sup>1</sup>The Ohio State University, Department of Physical Medicine and Rehabilitation, Columbus, OH, USA

<sup>2</sup>The University of Notre Dame, Department of Aerospace and Mechanical Engineering, South Bend, IN, USA

<sup>3</sup>The Ohio State University, Neuroscience Graduate Program, Columbus, OH, USA

<sup>4</sup>The Ohio State University, School of Health and Rehabilitation Sciences, Columbus, OH, USA

email: lise.worthen-chaudhari@osumc.edu

### INTRODUCTION

Despite the importance of lower extremity power absorption during gait [1,2], deficits in power absorption and associated eccentric motor control after incomplete spinal cord injury (iSCI) have yet to be characterized in humans. An animal model of iSCI, found that aberrant, prolonged semitendinosus (ST) burst activity occurred predominantly during eccentric phase of gait known as weight acceptance (WA) [3]. Specifically, the length of eccentric contraction in ST during WA correlated to recovery level, as measured in open field walking, with shorter ST bursts in WA correlating to better open field walking function ( $r^2=0.9697$ ;  $p<0.05$ ). The purpose of the current study was to provide the first translation of these animal model results to human health and provide a preliminary evaluation of ST eccentric activity in WA among individuals with iSCI. We hypothesized that individuals with incomplete spinal cord injury (iSCI) would show more eccentric ST activity in WA than healthy controls walking at speed-matched or self-selected pace.

### METHODS

Research was reviewed and approved by The Ohio State University's Institutional Review Board for Biomedical Human Subjects Research. Data from three individuals with iSCI who used a walker as an assistive aid and three individuals with no neurologic impairment are presented (see Table 1 for matching characteristics). Individuals with iSCI had previously participated in locomotor training within a physical therapy clinic, but had been discharged from that training at least 6 month prior to participation in the current study.

Individuals with iSCI were asked to walk at their comfortable walking speed using the assistive aids each individual typically used in their community. Healthy controls were asked to walk at their self-selected, or freely chosen, pace (SS) and at their slowest possible pace (SLOW). Bilateral joint power and muscle activity data were collected during walking and reduced using Visual 3D software as follows. Kinematic data were collected (Vicon) at 200Hz using a point cluster technique (PCT) marker set of 47 lower extremity markers tracked during dynamic trials plus 8 markers placed on anatomic landmarks during an initial static trial then filtered (Butterworth, low pass 8 Hz). Ground reaction forces (GRFs) were acquired at 2000 Hz from a series of 6 force platforms (Bertec) mounted flush with the surrounding floor and filtered (critically damped low pass filter, 10Hz). Muscle activity was recorded at 2000 Hz from the semitendinosus bilaterally then reduced in custom software written in Matlab (Butterworth low pass 6 Hz). We defined a muscle as "on" within dynamics trials if activity exceeded the resting activity mean plus 2 standard deviations. All data were interpolated to 1000 points per stride. Interpolated EMG data were converted to root-mean-square (RMS) of the signal (50 sample window; 10 sample overlap) and normalized to the max RMS value per trial.

We defined the weight acceptance phase as starting at foot contact with the force platform and ending at the first peak in the vertical GRF. Hip and knee joint power information was used to determine if ST was acting concentrically, eccentrically, or isometrically while on. To characterize the amount of ST eccentric activity during the WA phase we

calculated the negative “work” done by the ST by integrating the area under the muscle activity curve [4] while the muscle was acting eccentrically and refer to this as ST eccentric contribution to WA. To characterize the duration of eccentric activity in WA we calculated how long ST was acting eccentrically as a percent of the phase duration.

When comparing motor control between pathologic and non-pathologic there is precedent for matching self-selected walking conditions [4] as well as for speed-matching [5,6]. Because there is a compelling argument for each approach, matching by comfort vs matching by speed, we compared iSCI free walking, which was typically slow ( $0.291 \pm 0.133$  m/s), to healthy controls walking at two different speeds: their slowest possible speed ( $0.258 \pm 0.133$  m/s; no metronome used) and their SS speed ( $1.410 \pm 0.137$ ). To evaluate differences in ST behavior between these conditions, Student’s t-tests (2 tailed; heterogeneity assumed; performed in Microsoft Excel) were used to compare variables of interest between each healthy control walking speed condition and SCI free walking.

**RESULTS AND DISCUSSION**

Individuals with iSCI demonstrated more ST eccentric contribution during WA (mean  $-0.251 \pm 0.145$ ) than did healthy controls walking at slow ( $-0.069 \pm -0.020$ ;  $p = 0.0263$ ) or SS pace ( $0.0 \pm 0.0$ ;  $p = 0.008$ ). In addition, eccentric activation lasted longer among iSCI participants ( $29 \pm 13\%$  of WA) than among healthy controls walking at slow ( $9 \pm$

$2\%$  of WA;  $p = 0.011$ ) or SS pace ( $0 \pm 0\%$  of WA;  $p = 0.026$ ).

**CONCLUSIONS**

ST eccentric activity is aberrant (prolonged) during WA among individuals with iSCI. Because ST activity in WA has been found to play a role in central pattern generator signaling [see 3 for review], refinement of ST eccentric activity during WA might represent a promising clinical target. Future work will evaluate the effectiveness of interventions targeted to improve ST eccentric activity during WA.

**REFERENCES**

1. Winter DA. *J Biomech* **13(11)**, 923-7, 1980.
2. Liu MQ et al. *J Biomech* **39(14)**, 2623-2630, 2006.
3. Hansen et al. *Brain & Behavior* **2 (5)**, 541-552, 2012.
4. Hayes et al. *Clinical Neurophysiology* **125(10)**, 2024-2035, 2014.
5. Worthen-Chaudhari et al. *Gait & posture* **39(1)**, 588-592, 2014.
6. Worthen-Chaudhari et al. *Gait & posture*, **41(2)**, 597-602, 2015.

**ACKNOWLEDGMENTS**

This work was funded by the NIH (R21 HD082808, F31 NS096921), the Craig H. Nielson Foundation (316282), and the Ohio Chapter of the Fraternal Order of Eagles. We thank Daniel Melcher and Phillip McHenry for assistance with participant scheduling and data collection.

**Table 1:** Matching characteristics of participants with and without iSCI and mean variables of interest per group (mean  $\pm$  SD; \* $p < 0.05$  & \*\* $p < 0.01$  when data are compared to iSCI).

	Matching Characteristics		
	BMI	Age (years)	Gender (female/male)
SCI (n=3)	$29.9 \pm 6.6$	$37.0 \pm 3.5$	2/1
Healthy Control (n=3)	$28.3 \pm 4.5$	$35.3 \pm 10.6$	2/1
	Variables of Interest		
	Gait speed (meters/sec)	ST duration (%phase)	ST ecc contribution
SCI	$0.291 \pm 0.133$	$29 \pm 13$	$-0.251 \pm -0.145$
Healthy Control SLOW	$0.258 \pm 0.133$	$9 \pm 2$ *	$-0.069 \pm -0.020$ *
Healthy Control SS	$1.410 \pm 0.137$ **	$0 \pm 0$ **	$-0.000 \pm -0.000$ **

# MODIFICATIONS IN WHEELCHAIR PROPULSION TECHNIQUE OVER TIME

<sup>1</sup> Ian M. Russell, <sup>1</sup> Edward V. Wagner, <sup>2</sup> Philip S. Requejo, <sup>2</sup> Sara Mulroy, <sup>3</sup> Mary M. Rodgers, and <sup>1</sup> Jill L. McNitt-Gray

<sup>1</sup> University of Southern California, Los Angeles, CA, USA

<sup>2</sup> Rancho Los Amigos National Rehabilitation Center, Downey, CA, USA

<sup>3</sup> University of Maryland School of Medicine, Baltimore, MD, USA

email: irussell@usc.edu

## INTRODUCTION

Preservation of shoulder function is important for manual wheelchair (WC) users with spinal cord injury (SCI). Manual WC propulsion is an effective form of low-cost wheeled mobility as it preserves upper body strength, cardiovascular conditioning, and community participation. Clinicians and researchers have suggested that the repetitive mechanical loading of the shoulder during propulsion may be a factor contributing to the high prevalence of shoulder pain among the SCI population. Current experimental research and clinical guidelines promote improved interaction between the individual and the WC as a means to mitigate detrimental mechanical loading of the shoulders[1]. The mechanical demand imposed on the shoulder (net joint moment (NJM)) is affected by orientation of the resultant reaction force (RF) relative to the forearm[2,3]. Model simulation results indicate a 2-fold increase in RF magnitude can result in minimal changes in shoulder NJM magnitude without decrements in performance if the orientation of the RF relative to the upper extremity segments is modified[2]. The aim of this study was to determine if individuals using manual WCs use the same propulsion technique over time, and if not, what aspects of their technique were regulated and were there observed differences in technique between individuals that did and did not develop shoulder pain over 18 months.

## METHODS

One hundred sixteen experienced manual WC users with paraplegia ( $9 \pm 6$  yrs post SCI, 103 Males, 13 Females) from the Rancho Los Amigos National Rehabilitation Center outpatient clinics volunteered in accordance with the Institutional Review Board. Individuals were excluded from participation if they

reported a history of shoulder pain at entry into the study. Participants were classified as having developed shoulder pain over the longitudinal study if their score on the Wheelchair User's Shoulder Pain Index increased by  $\geq 10$  in the three year follow-up period (48 developed shoulder pain, 68 remained pain-free). Upper extremity kinematics (VICON, 100Hz) and pushrim RF (SmartWheel, 200Hz) were collected during manual WC propulsion on a stationary ergometer at self-selected fast condition at entry into the study (Baseline) and 18 months later (Follow Up). Upper extremity joint kinetics were calculated using custom MATLAB code. Within-subject comparisons were done using a modified step-down Fisher-type method to test for statistical significance.

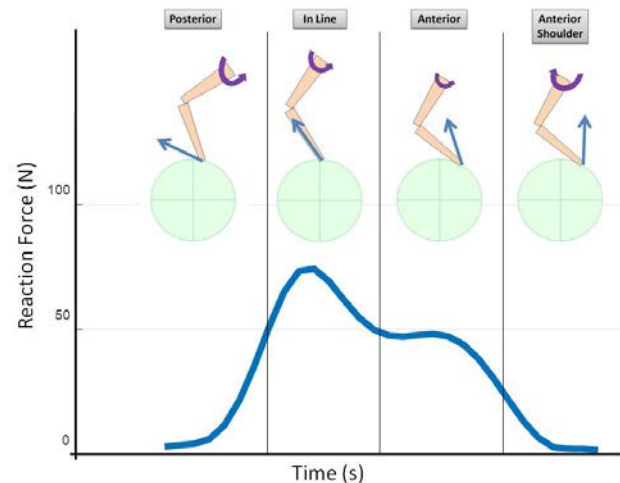


**Figure 1:** RF impulse ( $RF_{imp}$ ) is parsed into intervals based on RF orientation relative to forearm: RF orientated posterior to forearm ( $RF_{post}$ ), inline ( $\pm 5$  deg) with forearm ( $RF_{inline}$ ), anterior to forearm but posterior to shoulder ( $RF_{ant}$ ), and anterior to shoulder ( $RF_{antSh}$ )

Mechanical demand on the shoulder was quantified as the integral of the shoulder NJM ( $NJM_{imp}$ ) during

contact with the handrim. Factors influencing the shoulder  $NJM_{imp}$  also analyzed included  $RF_{imp}$ ,  $RF_{imp}$  parsed by intervals based on RF orientation relative to the forearm (Fig. 1) and contact duration. The shoulder NJM depends on the proximal distal moments created by the Net Joint Forces about the center of mass (CM) of the forearm and upper arm segments as well as the adjacent joint NJM at the elbow. When the RF is oriented anterior to the forearm CM but posterior to the shoulder joint, an elbow extensor NJM is needed to achieve the observed motion and contributes to a smaller required shoulder NJM because the elbow NJM is in the same direction as the shoulder NJM. In contrast, when the RF is oriented posterior to the forearm CM or anterior to the shoulder, a larger shoulder NJM is required to achieve the observed motion because elbow NJM is opposite the direction of shoulder NJM. When the RF is inline with the forearm CM, the affects of the elbow NJM on shoulder NJM are minimized because elbow NJM is at its smallest magnitudes. Modifying more  $RF_{imp}$  to be generated during  $RF_{inline}$  and  $RF_{ant}$ , while keeping total  $RF_{imp}$  the same would reduce shoulder  $NJM_{imp}$ .

## RESULTS AND DISCUSSION

The results indicate manual WC users modify their propulsion technique over time. Specifically, 46/48 of the individuals developing pain and 60/68 individuals remaining pain-free altered some aspect of shoulder  $NJM_{imp}$ ,  $RF_{imp}$ , RF orientation relative to the forearm, or contact duration. Nineteen subjects among the pain-free group showed reductions in shoulder  $NJM_{imp}$  and on average reductions were 40% ( $\pm 20\%$ ) of their  $NJM_{imp}$  during the Baseline collection. Eight subjects among the pain group showed reductions in shoulder  $NJM_{imp}$  and similarly reductions were 43% ( $\pm 13\%$ ) of their  $NJM_{imp}$  during the Baseline collection. RF orientation,  $RF_{imp}$ , and contact

duration were manipulated in both directions by subjects in both pain-free and pain groups( Table 1). Only 27 subjects out of the total population of 116 made technique modifications contributing to reductions in  $NJM_{imp}$ . Strategies chosen to reduce  $NJM_{imp}$  among those 27 subjects were varied and involved combinations of one or more modifications in the features analyzed. The most common technique adjustment to accomplish the reduction in  $NJM_{imp}$  among the population was to reduce  $RF_{imp}$  (19/27). Ten subjects decreased contact duration and five re-oriented RF. These results indicate modifications in RF orientation relative to the forearm,  $RF_{imp}$ , and contact duration were technique modifications implemented by individuals that remained pain-free or developed pain over 18 months. These results indicate that individuals with and without pain can modulate these attributes known to contribute to the mechanical demand imposed on the shoulder during manual WC propulsion at self-selected fast speeds.

## CONCLUSIONS

Knowledge of how experienced manual WC users adapt their propulsion technique over time provides an important step in identifying effective and feasible propulsion strategies for mitigating mechanical demand imposed on the shoulder and preserving shoulder function.

## REFERENCES

1. Consortium for Spinal Cord Medicine *Paralyzed Veterans of America*, 2013
2. Munaretto et al. *Clin Biomech* (Bristol, Avon).2012;27(3):255-262.
3. Raina et al. *J Spinal Cord Med*.2012;35(3):148-155.

## ACKNOWLEDGMENTS

This study was supported by the ARCS Foundation scholarship

**Table 1:** Number of subjects with significant shifts of  $\geq 10\%$  compared to Baseline propulsion cycles.

	Increased $NJM_{imp}$	Decreased $NJM_{imp}$	Increased $RF_{imp}$	Decreased $RF_{imp}$	Increased Contact Duration	Decreased Contact Duration	RF Re-orientation (towards $RF_{ant}$ , $RF_{inline}$ )
Pain (48)	17	8	15	7	16	14	19
Pain-Free (68)	13	19	11	18	22	16	20

# A Neuromuscular Control Comparison between Walking Sticks and Walker during Gait in Adult Scoliosis Patients

R. Haddas, PhD<sup>1</sup>, I. Lieberman, MD<sup>3</sup> and Rumi Singh Kakar, PT, PhD<sup>2</sup>

<sup>1</sup>Texas Back Institute Research Foundation, Plano, TX

<sup>2</sup>Ithaca College, Ithaca, NY

<sup>3</sup>Texas Back Institute, Plano, TX

Email: [rhaddas@texasback.com](mailto:rhaddas@texasback.com)

## INTRODUCTION

Adult degenerative scoliosis (ADS) is associated with progressive and asymmetric degeneration of the disc and facet joints, which typically lead to stenosis.[1] By virtue of the narrowed spinal canal associated with the degeneration these patients frequently develop back pain, as well as leg pain, weakness, and numbness.[2] Patients with degenerative adult scoliosis demonstrate an altered gait pattern.[3] For many patients with ADS a walking aid is beneficial to offset the increased energy expenditure, reduce muscle effort and assist with balance. Walkers are frequently prescribed in an effort to improve balance, mobility, and reduce lower back pain, but a review of the literature reveals conflicting evidence regarding their effectiveness.[4] Clinical experience has shown the use of walking sticks rather than a walker promotes a more upright posture. The walking sticks are beneficial pre-operatively not only in terms of deformity progression and line of sight, but also for patients postoperatively to help maintain surgical correction of their kyphotic deformities. The purpose of this study was to evaluate the impact of different assistive devices on the neuromuscular control of the trunk and lower extremities during gait in preoperative ADS patients.

## METHODS

Eighteen subjects (Age:  $67.3 \pm 7.2$ , H:  $1.65 \pm 0.07$  m, W:  $78.8 \pm 21.7$  kg, 10 females) with symptomatic degenerative scoliosis (VAS low back:  $6.09 \pm 2.36$ , VAS leg:  $5.62 \pm 3.29$ ) who have been deemed appropriate surgical candidates performed gait analysis under 3 testing conditions; 1. with walking sticks, 2. with walker, and 3. without any walking device a week before the surgery. Ag/AgCl surface EMG electrodes were bilaterally placed on the following muscles: external oblique (EO), Multifidi (MF) at level of L5, Erector Spinae (ES) at level of L1, Rectus Femoris (RF), Semitendinosus (ST), Gluteus Maximus (GM), Tibialis Anterior (TA), and Medial Gastrocnemius (MG). EMG data were

recorded using a Delsys® system (2000 Hz) along with locations of 51 markers using 10 camera Vicon® (100 Hz) as the patient walked barefoot at his/her self-selected speed along a 10m walkway for 5 acceptable trials. RMS EMG was scaled to the peak value of the BASE RMS EMG. A repeated measurement ANOVA ( $p < 0.05$ ) design for peak RMS, onset times, Time to Peak and onset durations was used to compare the walking conditions. Post hoc pairwise t-tests with Bonferroni corrections were used if group main effects were found.



Figure 1. Gait with walking sticks and with walker in adult degenerative scoliosis patients

## RESULTS AND DISCUSSION

Only significant main effect for groups for peak RMS activation was observed for left MH but pairwise comparisons displayed no differences. (Table 1). Significant group effects for onset times were observed for left and right EO, MF, ES, left MH (no pairwise differences) and left and right GA and TA with earliest activation in walking sticks, followed by walkers and then unassisted gait (Table 1). Walking sticks group had the smallest onset time (earliest activation in the gait cycle) compared to walkers or no device. This suggests early core muscles activation need with walking sticks to potentially help in stabilizing the pelvis as the lower limbs advance during the gait cycle. Significant group effects for time to peak were observed for right EO and MF, right and left RF and left MH, and right GA and TA (Table

1). Time to peak was highest for walking sticks compared to gait unassisted or with walkers. Pairwise differences were mainly observed between walking sticks and unassisted but not with other comparisons except for left RF and MH. Lastly, significant group effects for onset durations were only observed for right RF and, left GA and right TA (Table 1). Pairwise comparisons for all three of the above comparisons showed shortest onset durations with walking sticks followed by unassisted and then walkers.

Overall, minimal to no differences in peak RMS magnitudes were observed between the three test conditions during the gait cycles but some differences were observed for the temporal variables of activation. Classifying these muscle groups based on their location and actions, explains their purpose during the gait cycle and how it changes with different gait conditions. Based on early onset of activation and greater time to peak for trunk muscles, it is suggested that during locomotion with walking sticks, core muscles are working to stabilize the pelvic motion early in the gait cycle potentially for postural control and limiting non essential trunk movements but this activation is not sustained. Walkers provide a longer and sustained core muscle activation, which could possibly be caused by the forward trunk lean posture assumed with walkers. At the hip and knee joints, quadriceps were active early in the gait cycle with both walkers and walking sticks very similar to unassisted walking. The group differences observed were of relatively very small magnitudes. At the ankle joint, both GA and TA were active for similar durations and peaked about the same time in walking sticks, with largest differences observed between

walking sticks and walkers. This suggests individuals co-activated these muscles throughout the gait cycle but no differences in peak magnitudes were observed between assistive devices.

## CONCLUSIONS

Results suggest that walking sticks can potentially promote trunk and lower extremity gait mechanics and thus neuromuscular control comparable to that of gait without any assistive device. With preoperative walking stick training, surgical correction of deformity, and postoperative use of walking sticks, improvement in both sagittal parameters and kinematics as compared to a walker can be expected. Although the differences in magnitudes between comparisons was small and should be cautiously interpreted on a case-by-case basis, we anecdotally recommend the use of walking sticks to assist with ambulation in symptomatic adult degenerative scoliosis patients. Further studies are in progress to fully understand the effect of assistive devices in facilitating and promoting normal neuromuscular control during ambulation in ADS patients.

## REFERENCES

1. Kotwal S, et al. *HSS J* 7(3), 257-264, 2011.
2. Kotwicki. T, et al. *Adolesc Health Med Ther* 4, 59–73, 2013.
3. Yang. JH, et al. *Eur Spine J* 22(11), 2407–2413, 2013.
4. Bryant MS, et al. *Disabil Rehabil Assist Technol* 7(2), 149–152, 2012

Table 1: Onset times, Time to Peak and Onset Durations of the comparisons with significant main effect differences between groups for 100% of gait cycle.

Onset Times	p-values	Time to Peak	p-values	Onset Duration	p-values
R_EO	0.0307	R_EO	0.034	R_RF <sup>b,c</sup>	0.006
R_MF <sup>a</sup>	0.0150	R_MF <sup>a</sup>	0.028	L_GA <sup>a,b</sup>	0.066
R_ES <sup>a</sup>	0.0147	R_RF <sup>a</sup>	0.008	R_TA <sup>b</sup>	0.047
L_EO	0.0245	L_RF <sup>a,b</sup>	0.000		
L_MF <sup>a</sup>	0.0118	L_MH <sup>a,b</sup>	0.004		
L_ES	0.0264	R_GA <sup>a</sup>	0.013		
L_MH	0.0302	R_TA <sup>a</sup>	0.005		
R_GA <sup>a</sup>	0.0310				
L_GA <sup>a</sup>	0.0333				
R_TA <sup>a</sup>	0.0241				
L_TA <sup>a</sup>	0.0254				

<sup>a</sup>: Significant difference between Walking sticks and No device; <sup>b</sup>: Significant difference between Walking sticks and Walkers; <sup>c</sup>: Significant difference between Walkers and No device

# BIOMECHANICAL EVALUATION OF A PNEUMATIC SLEEVE ORTHOSIS FOR LOFSTRAND CRUTCH-ASSISTED GAIT

<sup>1</sup>Chenzhang Xiao, <sup>2</sup>Omid Jahanian, <sup>2</sup>Brooke A. Slavens, and <sup>1</sup>Elizabeth T. Hsiao-Wecksler

<sup>1</sup>Mechanical Science and Engineering, University of Illinois at Urbana-Champaign, Urbana, IL, USA

<sup>2</sup>Occupational Science and Technology, University of Wisconsin-Milwaukee, Milwaukee, WI, USA  
email: [cxiao3@illinois.edu](mailto:cxiao3@illinois.edu)

## INTRODUCTION

The palm and hand of Lofstrand crutch users can experience up to 50% body weight along with hyperextension of the wrist during swing-through gait [1]. Such repetitive, large loads and extreme wrist posture may lead to wrist strain and the development of carpal tunnel syndrome [2]. To address these issues, we previously developed a passive orthosis that attached to the crutch and reduces wrist extension and redistributed palmar loads away from the carpal tunnel region to the adductor pollicis area (Fig. 1a) [3]. However, all loading still passed through the palm.

Thus, we designed a second version with an active pneumatic sleeve orthosis attached to the crutch cuff that was made to transfer loads from the palm to the forearm (Fig. 1b) [4]. The sleeve orthosis is composed of a coiled soft pneumatic Fiber Reinforced Elastomeric Enclosure (FREE) actuator [5] constrained at both ends by hinged splints attached to the crutch cuff. Once pressurized with air to 206.84 kPa (30 psig), the FREE contracts in the longitudinal direction and expands in the radial direction, providing a constriction pressure supporting the forearm while holding the wrist in a more neutral position. As a consequence of the constriction pressure on the forearm, movement of the forearm tendons and ligaments are restricted and has the added benefit of potentially reducing wrist extension.

This paper describes biomechanical testing to evaluate the effectiveness of the pneumatic sleeve orthosis on healthy adults performing swing-through gait. We hypothesize that the pneumatic sleeve orthosis transfers load from the handle to the crutch cuff, reduces and redistributes palm pressure, and reduces wrist extension.

## METHODS

### Subjects

Eleven able-bodied subjects (5M; 18-32 yrs; average height 171.6 cm; average weight 67.4 kg) were evaluated. The study was approved by the Institutional Review Boards at the University of Wisconsin – Milwaukee (UWM) conducted at the Mobility Lab at UWM and consent was obtained from all participants.

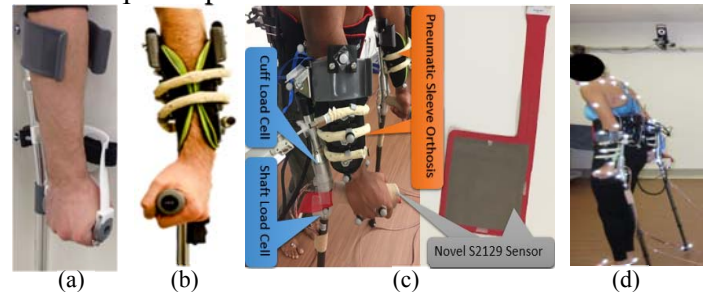


**Figure 1:** (a) Passive Orthosis, (b) Pneumatic Sleeve Orthosis, (c) Testing equipment, (d) A subject in the test

### Data Collection

Kinematics, crutch forces, palmar and forearm pressure data were collected during the tests. Kinematic data were collected at 120 Hz using a 15-camera motion capture system (T-series, Vicon, Oxford, UK) and custom upper extremity marker set (Fig. 1d) [6]. A pair of custom instrumented Lofstrand crutches with three-axis embedded load cells located below the cuff and handle bilaterally were used to collect crutch forces at 960 Hz (Fig. 1c) [7]. Palmar pressure on the dominant side was measured at 60 Hz with a 16 × 16 flexible matrix array (S2129, 1cm × 1cm unit cell, Novel Inc., Germany) wrapped around the grip using established method (Fig. 1c) [3]. Four low-pressure sensors (S2011, 1 cm diameter, Novel Inc.) were spaced around the inside of the sleeve to collect sleeve constriction pressure.

### Experimental Protocol

Each participant was given 15-30 minutes to acclimate to the swing-through gait pattern. Participants were asked to perform swing-through gait over a 6m-long walkway at a self-selected

speed for two testing conditions: with and without the pneumatic orthosis (randomized order). Five trials were collected for each condition with at least one minute of rest time between trials.

#### Data processing

Kinematic data were post-processed using Vicon Nexus and MATLAB software. Wrist flexion/extension angle was computed and averaged over five gait cycles with and without the orthosis for each subject. Mean peak wrist extension and wrist flexion/extension range of motion (ROM) were reported for each subject. Peak crutch cuff and shaft forces (normalized by body weight) on the dominant side were calculated in MATLAB. Palmar and sleeve pressure data were analyzed using Novel Pliance and MATLAB. Due to presentation of asymmetric swing through gait, the data for two subjects were not included in this analysis. Parameters analyzed were peak wrist extension angle, flexion/extension ROM, peak palmar pressure, and peak cuff and shaft forces. A repeated measures MANOVA was run to assess the effect of orthosis use (SPSS v23). Follow-up univariate ANOVAs were examined for significant parameters. Significance level was set at  $\alpha = 0.05$ .

### RESULTS AND DISCUSSION

The MANOVA test ( $p=0.004$ ) and follow-up univariate ANOVAs identified significant effects of the pneumatic orthosis use during swing-through gait of healthy participants (Table 1). Kinematic results indicated a significant reduction in peak wrist extension angle (-7.84%,  $p=0.005$ ) and wrist flexion/extension ROM (-35.50%,  $p=0.001$ ) when using the orthosis. The mean wrist extension angle was lower during the body swing phase of the gait cycle (Fig. 2). Normalized peak cuff force was significantly higher with orthosis use ( $p<0.001$ ), while there was no significant difference in forces recorded in the shaft ( $p=0.7$ ). These results indicated a transfer of forces to the crutch cuff of 10.3% instead of the majority of the load going through the handle. The normalized peak palm pressure was also reduced significantly with

orthosis use by 7.5% ( $p=0.023$ ). Mean pressures in the sleeve remained under 3.79 kPa (28.46 mm Hg) while using the orthosis. (Sustained constriction pressures above 4.67 kPa (35 mm Hg) can cause blood flow restriction [8])

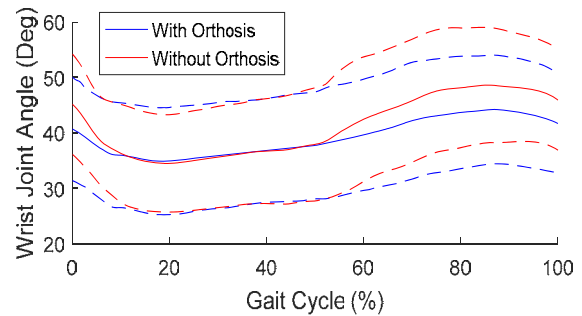


**Figure 2:** Mean wrist joint angles in the sagittal plane (extension (+)). Group mean profile (solid line) and  $\pm 1SD$ (dotted line), 0% and 100% gait cycle is defined as heel strike.

### CONCLUSIONS

We have shown the effectiveness of the pneumatic sleeve orthosis in transferring loads from the Lofstrand crutch handle to the crutch cuff, significantly reducing wrist extension angle and decreasing peak palmar pressure. This promising device may ultimately decrease the risk of wrist strain and carpal tunnel syndrome for long-term Lofstrand crutch users.

### REFERENCES

1. Slavens BA, et al. *Gait Posture* **30**, 511–517, 2009
2. Scanion A, et al. *J Neuroscience Nursing* **41**, 140-147, 2009
3. Farooq D, et al. *EMBC*, Dallas, TX, USA, 2016
4. Xiao C, et al. *J Med. Devices* **10(2)**, 020959, 2016
5. Krishnan G, et al. *ASME-IDETC/CIE*, Chicago, IL, 2012
6. Schnorenberg AJ, et al. *J. Biomech* **47**, 269-276, 2014
7. Slavens BA, et al. *J. Biomech* **44**, 2162-2167, 2014
8. Daly CH, et al. *J Tissue* **16**, 17-21, 2006

### ACKNOWLEDGMENTS

This work was supported by the NSF Engineering Research Center for Compact and Efficient Fluid Power #0540834. Special thanks to Dr. Girish Krishnan, Gaurav Singh, Alyssa Schnorenberg, Justin Riebe, and Novel Inc. for their generous help in this project.

**Table 1:** Mean cuff and shaft forces, palmar and sleeve pressures, wrist extension and ROM (\*:  $p<0.05$ )

Orthosis use	Peak cuff (N/kg)*	Peak shaft (N/kg)	Peak palm pressure (kPa/kg)*	Peak Ext. (deg)*	Flexion/Extension ROM (deg)*
With	0.42 $\pm$ 0.10	4.13 $\pm$ 0.20	1.72 $\pm$ 0.55	46.10 $\pm$ 9.70	11.41 $\pm$ 4.86
Without	0.14 $\pm$ 0.07	4.10 $\pm$ 0.35	1.86 $\pm$ 0.58	50.02 $\pm$ 9.84	17.69 $\pm$ 5.12

# Supervised Walking Exercise Therapy Improves Gait Biomechanics in Patients with Peripheral Artery Disease

<sup>1</sup>Molly Schieber, <sup>2,3</sup>Iraklis I. Pipinos, <sup>2,3</sup>Jason M. Johanning, <sup>2</sup>Holly K. DeSpiegelaere, <sup>1</sup>Benjamin Senderling, <sup>2</sup>Cassidy Berlin, <sup>1</sup>Sara A. Myers

<sup>1</sup>Department of Biomechanics, University of Nebraska at Omaha, Omaha, NE, USA

<sup>2</sup>Omaha Veterans' Affairs Medical Center, Omaha, NE, USA

<sup>3</sup>University of Nebraska Medical Center, Omaha, NE, USA

email: samyers@unomaha.edu, web: cobre.unomaha.edu

## INTRODUCTION

Peripheral artery disease (PAD) is a common manifestation of atherosclerosis affecting the blood flow to the legs. The most common presentation of PAD is intermittent claudication; a condition in which when the patient walks the metabolic demands of the lower limbs exceed the limited supply of blood, causing ischemia, and exercise-induced discomfort and decreased walking ability [1]. Walking exercise is the first line of treatment in patients with claudication with the best results achieved in patients undergoing supervised exercise therapy for at least three months. Supervised walking exercise results in increased maximum walking distances comparable to those seen following surgical revascularization, despite the fact that blockages remain [2]. With this study we tested the hypothesis that supervised exercise training of PAD patients with claudication improves walking distances in association with improved gait biomechanics.

## METHODS

Forty-seven patients (age:  $69.2 \pm 7.0$ ; height (m):  $1.75 \pm 0.7$ ; mass (kg):  $89.4 \pm 18.7$ ) were seen at the Omaha Veteran Affairs Medical Center vascular clinic and evaluated by one of two vascular surgeons. Patients had no history of previous revascularization and were absent of all musculoskeletal and neurological symptoms that could limit gait in addition to PAD. Informed consent was obtained from all subjects prior to starting the twenty-four week (three sessions per week), supervised walking exercise therapy. Therapy protocol was designed following recommendations by the American College of

Sports Medicine and in concordance with previous studies that best produced increases in walking distances [3]. Each session included a 5 minute warm-up, 50 minutes of intermittent exercise on a treadmill, and 5 minutes of cool down activities.

All patients underwent gait analysis before and immediately following exercise therapy. First patients performed the Gardner Max Walk Test [4]; a progressive, graded treadmill protocol at 0.89 m/s that begins at 0% grade, and increases by 2% every two minutes. Initial claudication distance was recorded as the first indication of claudication pain from the patient. The total distance patients were able to walk before stopping because of pain was recorded as maximum claudication distance.

After sufficient rest, each participant was instructed to walk over a 10-meter pathway at a self-selected pace to commence the overground trials where marker trajectories (Motion Analysis Corp, Santa Rosa, CA) and ground reaction forces (kinetics; 600 Hz; AMTI force platforms) were recorded. Each patient was tested before (pain free) and after (pain) the onset of claudication pain. After completing the pain free condition, symptomatic claudication pain was induced by completing the six minute walk test [3]. All patients at baseline experienced a "moderate to severe level of pain" in the leg used for analysis. Immediately after, patients returned to the walkway to perform the walking trials for the pain condition. Five walking trials were collected from each leg of the participants in both conditions.

Joint kinetics and kinematics were calculated for the sagittal plane during the stance phase of walking. Ground reaction forces and joint angles, torques, and powers for the ankle, knee and hip were

analyzed using MATLAB (Mathworks, Inc., Natick, MA) and Visual 3D (Germantown, MD, USA). A paired t-test evaluated walking distances and a two-factor, intervention (pre/post) and condition (pain free/pain), repeated measures ANOVA evaluated gait dependent variables ( $p < 0.05$ ).

## RESULTS AND DISCUSSION

Our hypothesis was partially supported. Both walking distances (Figure 1) and several, but not all, gait biomechanics variables significantly improved following supervised walking exercise therapy.

Gait, Intervention Factor. In the weight acceptance phase of stance, a main effect was found for hip extensor torque and peak lateral ground reaction force. In the single-limb support phase of stance, a main effect was found for ankle power absorption. In the propulsion phase of stance, main effects were found for ankle and hip power generation (Table 1), and peak propulsive ground reaction force. The mean values improved from pre to post intervention, becoming more similar to normative data for healthy controls, for all main effects [4].

Gait, Condition Factor. In the weight acceptance phase of stance, a main effect was found for ankle, knee, and hip joint angles as well as ankle torque, braking impulse, and the peak lateral ground reaction force. In single-limb support phase of stance, a main effect was found for ankle power absorption. In the propulsion phase of stance, main effects were found for ankle angle, torque, and power generation, knee power absorption, peak ground reaction propulsive force and push-off vertical force. In all main effects, mean values worsened in the pain condition compared to pain free in both sessions.

Weakness in the posterior compartment muscles of the calf is a consistent and key factor underlying the gait adaptations patients with PAD experience at

baseline [4]. Improvements in ankle power during single support and the propulsion phase of gait before and after the onset of claudication pain reflect improvements in this area.

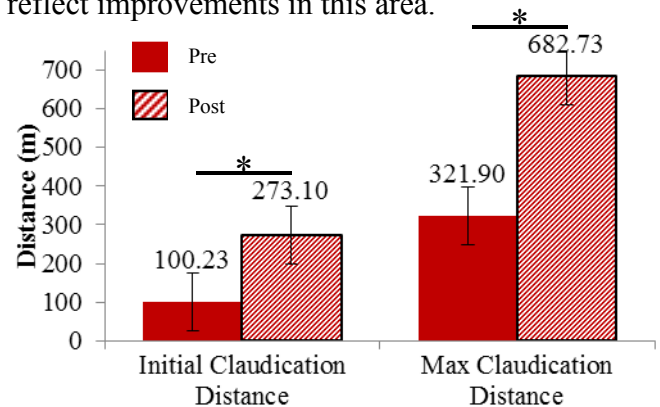


**Figure 1.** Walking distances before (pre) and after (post) the exercise intervention therapy.

## CONCLUSIONS

Six months (72 sessions) of supervised exercise therapy produces significant increases in the treadmill walking distances of patients with claudication. These increases are associated with concurrent improvements in gait biomechanics at the level of the ankle and the hip. Exercise therapy produces strengthening of the gluteus and the foot flexor muscles and this strengthening appears to be the main mechanism producing the improvements of the walking ability of patients with claudication.

## REFERENCES

1. American Heart Association. *About PAD*; 2014.
2. Murphy TP, et al. *J A Col of Card* **65**, 2015.
3. Regensteiner JG. *ACSM's Guide*, 732, 2001.
4. Koutakis P, et al. *J Vasc Surg*. **52**, 340-347, 2010.

## ACKNOWLEDGMENTS

Funding by NIH (R01AG034995; P20GM109090), VA RR&D (1I01RX000604) and NASA Nebraska Space Grant.

**Table 1.** Means and standard deviations (W/kg) for ankle and hip powers during the propulsion phase of stance

Dependent Variable	Before Exercise		After Exercise		$P_{\text{Intervention}}$
	Pain-free	Pain	Pain-free	Pain	
<b>Hip Power Generation</b>	$0.71 \pm 0.2$	$0.83 \pm 0.2$	$0.69 \pm 0.4$	$0.77 \pm 0.4$	<b>0.003</b>
<b>Ankle Power Generation</b>	$2.15 \pm 0.5$	$2.43 \pm 0.6$	$1.86 \pm 0.7$	$2.16 \pm 0.7$	<b>0.003</b>

# DESIGN OF A COMPACT AND PORTABLE HAND REHABILITATION DEVICE FOR STROKE-SURVIVORS

<sup>1</sup> Namita Anil Kumar and <sup>1</sup> Pilwon Hur

<sup>1</sup> Texas A&M University, College Station, TX, USA  
email: namita.anilkumar@tamu.edu, pilwonhur@tamu.edu

## INTRODUCTION

About 795,000 people experience strokes in the US, annually [1], with many suffering from the hand disabilities post stroke. The effects of such disabilities include weakened grip strength, lack of muscle coordination, and hand spasticity [2]. Although commercially available products like Saeboglove, Musicglove and Exo-Glove enable in-home hand rehabilitation, they have limitations that considerably prevent their broader usage: (i) they focus on specific hand functions, (ii) they require a considerable active range of motion to operate, and (iii) they are inapt for patients with hand spasticity [2]. Hence, a new compact and portable Hand Rehabilitation Device (HRD) is proposed that would rehabilitate the hand in a holistic manner. The HRD (US Patent Application: 62/413,130) is a fully actuated rotor-gimbal assembly, which when actuated imposes a gyroscopic torque on the user's hand. Unlike the current products, the developed gyroscopic torque does not demand the user's input.

## METHODS

Based on a customer needs analysis and a competitive benchmarking, it was gathered that a device that imposes a torque on the hand would aid in rehabilitation. There are two kinds of therapies that can be implemented with such a device: one involving synchronization of the hand movement with the generated torque and another requiring the user to resist the torque. While the former relaxes the hand muscles and combats hand spasticity [2], the latter increases hand muscle strength and coordination [4]. It was decided that the HRD should produce a minimum 0.7Nm gyroscopic torque (the amount required to open a jar's lid – an activity performed during physical therapy) [5]. The mass of the device was limited to approximately 550g (mass of a commonly carried half-liter water bottle) so that

the device does not strain the user's hand. Portability is another desired feature so that users can undergo rehabilitation anywhere and at any time.

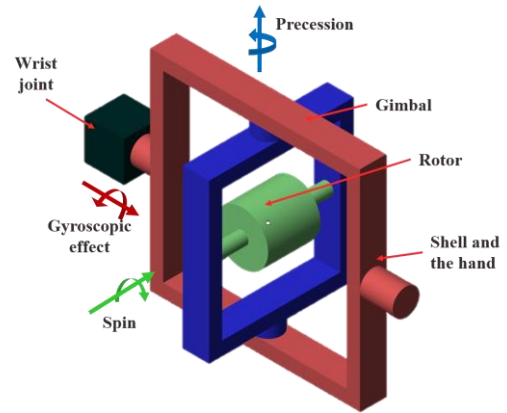


**Figure 1:** A schematic of the device

Consider Fig. 1 where red, blue and green components represent the user's hand, gimbal and the rotor, respectively. When the rotor spins about its axis and the rotor-gimbal assembly precess about the gimbal's axis, a gyroscopic torque is generated and acts on the user's hand. To understand the working principle, a proof-of-concept (POC) model and mathematical simulations were created.

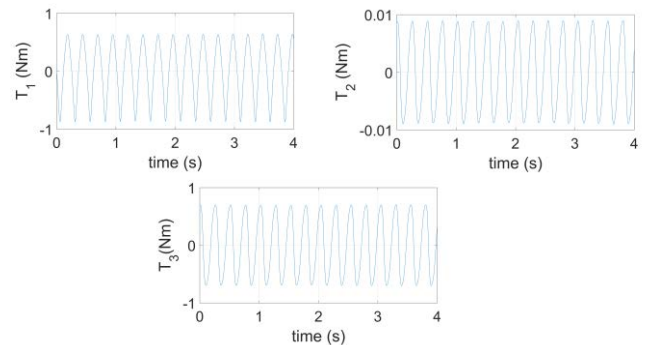


**Figure 2:** Theoretical torques achievable by the device for the specifications provided in Table 1.  $T_1$  is the torque about wrist flexion and extension,  $T_2$  is the torque about radial and ulnar deviations, and  $T_3$

is the torque about pronation and supination of the wrist.

The POC consisted of a fully actuated rotor-gimbal assembly was constructed. It was observed that the hand was forced to move about the wrist in a circular manner when no restriction was posed against the torque. Additionally, imposed hand motion can be manipulated by varying the motion of the rotor-gimbal assembly. Further the mathematical simulations revealed that for given parameters of the device, such as inertia and mass, a torque of magnitude 0.8Nm was attainable. These simulations were used to select the design parameters of the device.

## RESULTS AND CONCLUSION

The greatest challenge of the design process involved lessening the weight and size of the device. Owing to the size requirements of the embedded subsystems, the desired spherical shape could not be acquired and thus an oblong shape had to be adopted. The final product was designed to resemble an American football, so that it would appeal to the user and prospectively add a fun element to the rehab process. To make the device portable, the electronics were initially conceived to be embedded in the device. Since this idea conflicted with the need for compactness and lightness, the electrical systems are placed external to the device in a satchel that the users can wear. While the wires to the gimbal's motor are easily drawn through a hole in the bottom end cap, the wires for the rotor assembly are mechanically coupled to the motor's leads via a slip ring assembly. This enables the free precession of the rotor assembly without any entanglement of wires. To ensure symmetry in the design and to avoid rotary imbalances, the rotor and the gimbal housings were directly integrated with the permanent magnet rotor of the chosen brushless DC motors.

Currently, a dynamic analysis of the design is being carried out to determine the output torques, which will be followed by a biomechanical analysis to i) attest the safety of the device and ii) examine muscle activation patterns due to the output torque. Upon fabrication, the device's performance will be evaluated by investigating the relation between the muscle activation patterns and the hand functional

recovery of stroke survivors. Fugl-Meyer hand function will be evaluated.

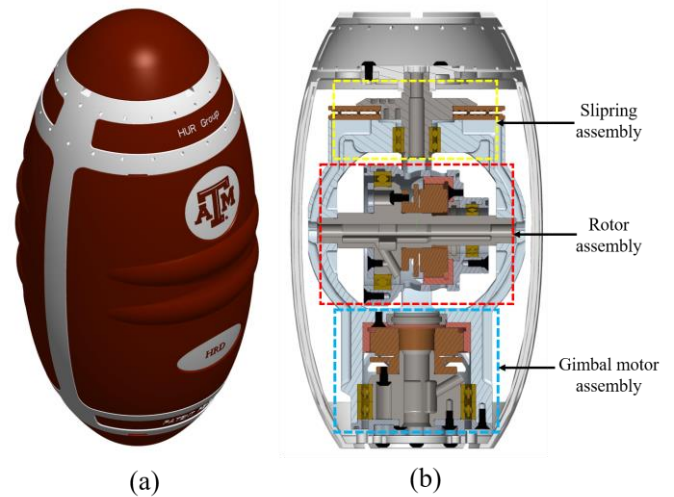


**Figure 3:** (a) Isometric view of the device (b) Cross-sectional view of the device with major subsystems highlighted.

Given the novelty of the device, more efficient and affordable hand rehabilitation for stroke patients is expected. In addition, the application of the device can be extended to other patients with hand function problems including patients with arthritis, Carpal Tunnel Syndrome, and those recovering from hand injuries/surgeries.

## REFERENCES

1. Stroke center  
<http://www.strokecenter.org/patients/about-stroke/stroke-statistics/>
2. Smania, N et al. European Journal of Phy. and Rehab. Med. 2010
3. Kuchinke, LM, and Bender, B, IEEE RAS and EMBS International Conference on Biomed. Rob. and Biomech. 2016
4. Sequeira, G., et al., Arch. Of Phy. Med. and Rehab. 2012
5. Lamercy, O. et al., IEEE Trans. on Neural Sys. and Rehab. Engg. 2007

## ACKNOWLEDGEMENTS

We thank Trifolium Engineering Pvt. Ltd. India for assistance with the design of the rotor-gimbal assembly.

# EFFECTS OF PUSH-UP PLUS VARIANTS ON UPPER EXTREMITY MUSCLE DEMANDS

<sup>1</sup>Alan C. Cudlip, <sup>1</sup>Andrew J. Ho, and <sup>1</sup>Clark R. Dickerson

<sup>1</sup>Department of Kinesiology, University of Waterloo, Waterloo, ON, Canada  
email: accudlip@gmail.com, web: <http://ahs.uwaterloo.ca/kin/research/diesel/index.html>

## INTRODUCTION

The push-up plus requires virtually no equipment and be performed almost anywhere, making it a staple exercise in fitness and rehabilitation programs. The push-up plus (PUP) variation adds active scapular protraction to the end range of a regular pushup to emphasize serratus anterior activation, a muscle active in preventing scapular “winging” [1]. Alterations to the PUP technique can help to meet specific exercise goals, but is used to increase serratus activation in rehabilitation studies. Other alterations of the standard pushup include changes in hand location or internal/external hand rotation, but little is known on how modifications affect upper extremity activation levels. Effective quantification of the effect of altering hand and arm setups during push-up plus on muscle activation levels (particularly in the serratus) would provide clinicians with insight for exercise prescription, particularly in cases of scapular dyskinesis. The purpose of this study was to examine the upper extremity when manipulating hand position, arm position and contact area during the PUP exercise.

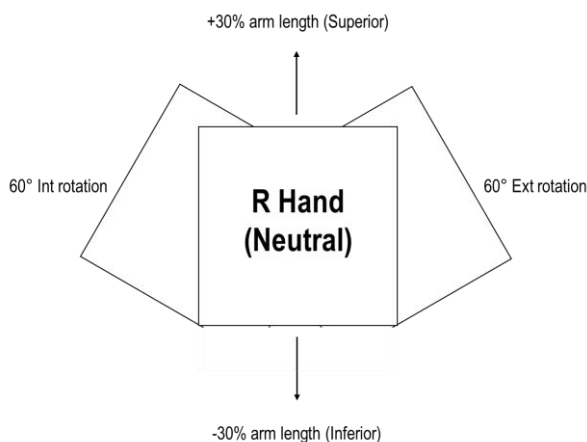


**Figure 1.** Participants completed PUP exertions in combinations of hand contact area (knuckles or palms), arm rotation (neutral, internal or external rotation) and arm location (shoulder height, superior or inferior).

## METHODS

Twenty university-aged males ( $23.1 \pm 2.4$  years,  $1.75 \pm 0.09$  m,  $77.7 \pm 13.1$  kg) completed 18 PUP trials with 3 factors: contact area (knuckles/palms), arm rotation (neutral/ $60^\circ$  internal rotation/ $60^\circ$  external rotation) and hand location (shoulder height/ $\pm 30\%$  arm length superior/inferior) (Figure 1).

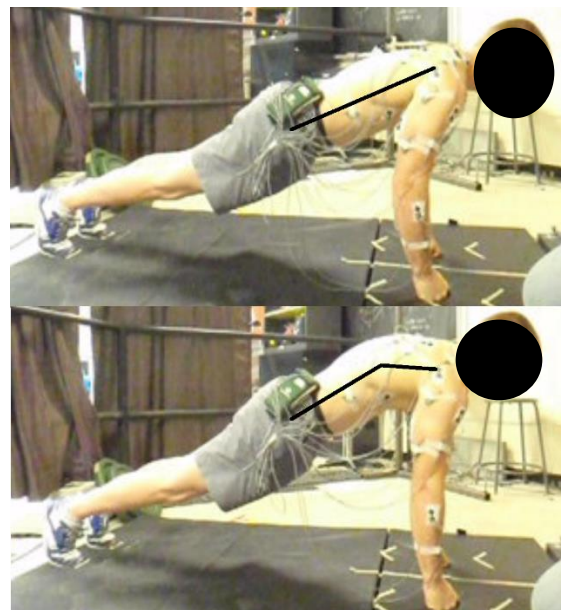


**Figure 2.** Participants completed a standard pushup (top), then moved into the PUP extension (bottom), designed to elicit serratus activity. The black line indicates changes in body posture from increased scapular protraction during the PUP.

All trials were completed on a gym mat, and used a fixed cadence for two repetitions per trial, totaling 18 trials (Figure 2). Surface electromyography was collected from 14 sites overlying muscles of the right arm and shoulder at 1500Hz (Noraxon Telemetry 2400 T G2), linear enveloped and normalized to muscle specific maximal outputs. Cadence was fixed for each trial, with 4s per rep: 1s eccentric loading, 1s concentric pushing up, 1s to push upward to the PUP extension, 1s to return to neutral. Mean and peak values were extracted for each muscle, and a 3-

way ANOVA (2 contact areas \* 3 arm rotations \* 3 hand locations) including interactions was used to determine effects of PUP variants on normalized EMG.

## RESULTS AND DISCUSSION

Hand\*Location interactions occurred in mean activity for 6 of 14 muscles ( $p=0.0001-0.0228$ ), with inferior arm positions and palms contact generally eliciting greater activation. This interaction resulted in increases of up to 20 %MVC in mean infraspinatus activity (from 23% to 43%MVC) and a 33%MVC in peak triceps activation from 37% to 70%MVC. Hand\*Rotation interactions were present in the biceps, triceps, and forearm muscles ( $p=0.0001-0.0449$ ), with knuckles increasing mean and peak activation, and external rotation increasing biceps activation, while the opposite increased triceps activation. A main effect of hand location existed in 85% of mean or peak EMG tests ( $p=0.0001-0.0155$ ), with inferior hand positions increasing activation and superior positions decreasing activations compared neutral, with some exceptions. These changes were as high as 18 %MVC increased from superior to

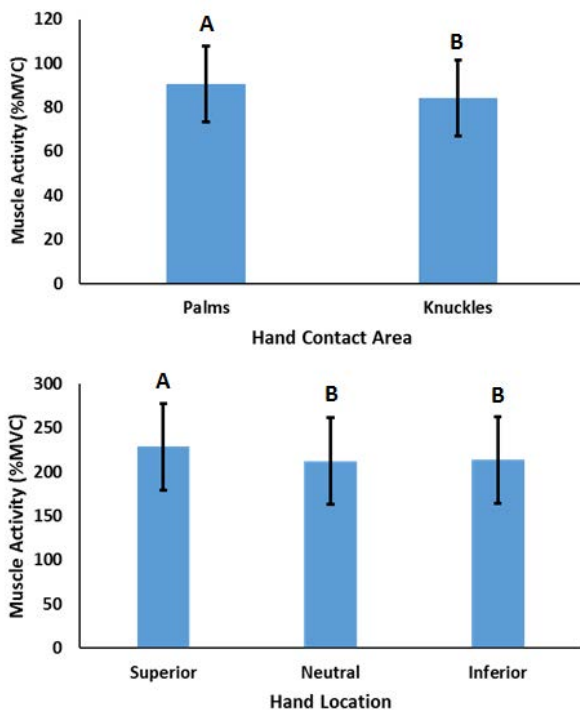


**Figure 3.** Few statistical significant effects existed for serratus, with main effects of hand contact area ( $p=0.0033$ ) and hand location ( $p<0.0001$ ) altering mean and peak activation, respectively; significant differences denoted by letters.

inferior hand positions in infraspinatus, and 34 %MVC increases in lower trapezius.

Serratus activation did vary across most scenarios, with only main effects of hand contact area in mean activity ( $p=0.0033$ ) and arm location in peak activity ( $p<0.0001$ ) (Figure 3). Serratus mean activity increased using palm contact surfaces, and peak activity increased in superior hand positions, but both of these increases were less than 10% increases in activation compared to standard postures. Hand rotation did not increase serratus activation, contrary to previous findings [2]. If the goal is to increase serratus activation in the PUP, altering location or contact surface beyond the standard position appears to provide only marginal benefits.

Altering hand location was the most common and largest influence on mean or peak muscular activity, modulating activity in every muscle except the wrist extensors. Moving the hand to an inferior position increased activation. Smaller elevation angles in the flexion plane decrease available moment arms for some muscles of the upper extremity [3], including the middle deltoid and pectoralis major, prime movers during the push-up. While significant differences exist between these positions for most muscles, some differences in activation may be unobserved using our current methods. Examining only mean and peak muscle activation across all phases of the lift may have washed out some phasic differences. Our future work will examine potential phasic differences on muscular activation, as well as examination of activation ratios between synergistic muscle pairs.

## CONCLUSIONS

Clinicians commonly prescribe the PUP to increase serratus activation, but little evidence exists to support potential benefits from moving beyond the standard pushup position to modify this activation. However, there were many activation increases in other muscles, warranting consideration for rehabilitation of other muscles beyond serratus.

## REFERENCES

1. Decker et al, *Am J Sports Medicine*, 1999.
2. Yoon et al, *Phys Ther Korea*, 2010.
3. Kuechle et al, *J Shoul Elb Surg*, 1997.

# ANALYSIS OF RESORATIVE PREDICTORS OF GLENOHUMERAL CAPSULE PPLICATION

<sup>1</sup>Andrew Kraszewski, <sup>1</sup>Andreas Kontaxis, <sup>2</sup>Stephanie Mayer, <sup>1</sup>Russell Warren

Hospital for Special Surgery, New York, NY; Children's Hospital Colorado, Aurora, CO  
email: kraszewskia@hss.edu, web: [https://www.hss.edu/research-staff\\_kraszewski-andrew.asp](https://www.hss.edu/research-staff_kraszewski-andrew.asp)

## INTRODUCTION

Glenohumeral capsule plication aims to restore the mechanical properties of the tissue to a pre-pathologic state. There is a lack of biomechanical data to guide surgical technique. Clinicians assess shoulder laxity and diagnose pathology using manual load-response (laxity) testing. The predictive accuracy of laxity tests is not well understood.

**Objectives were to: 1) estimate the magnitude of restorative plication, and 2) find laxity predictors of restoration in terms of direction and elevation.**

## METHODS

*Specimen Preparation & Testing.* Fourteen fresh frozen cadavers were CT-scanned, and then dissected down to the capsule. Marker clusters were rigidly attached and anatomic landmarks calibrated with 3D motion capture (0.2mm average residual). Each specimen was potted in rigid fixtures then attached to a glenohumeral laxity device (Figure 1).

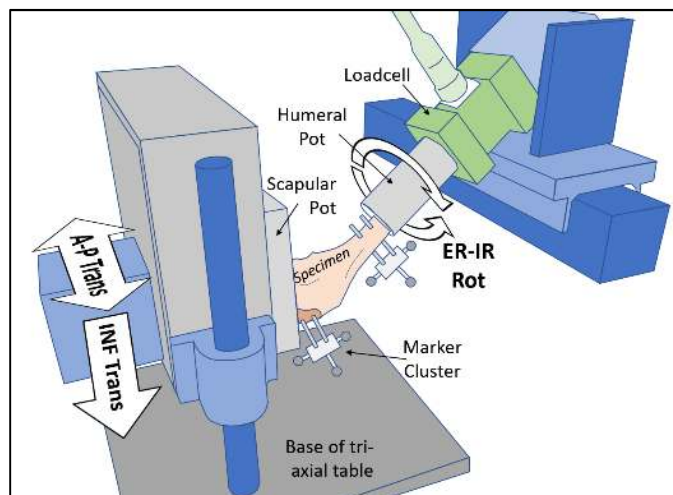


**Figure 1:** Illustration of capsular laxity testing device. The specimen (center) was inverted.

Translational laxity in anterior, posterior and inferior directions was measured at 10lbs applied force. Rotational laxity in external and internal axial

directions was measured at 2.0Nm applied moment. Laxity was tested across five physical levels (baseline, lax, and 5mm, 10mm, 15mm plication) and four positions (0°, 20°, 40°, 60° scaption).

*Data Analysis & Prediction.* Laxity values were offset to the baseline. The Lax level was set equal 0mm. Simple linear regressions (SLRs) were run with the x-intercept calculated as  $-\beta_0/\beta_1$ , to represent restorative plication magnitude (Figure 2).

The scalar plication independent variables were converted to ordinal categorical dependent variables. An ordinal multinomial logistic regression was run for every unique combination of physical and position level, totaling  $\sum_{i=1}^{20} \binom{20}{i} = 1,048,575$  models. Model performance criteria were AIC, classification (C1%), and a custom criterion  $C_p = -AIC + C1\%$ , where AIC is the Akaike Information Criterion and C1% is the classification percentage of the nearest physical level (Lax, 5mm, 10mm, or 15mm) to the average restorative magnitude.

## RESULTS AND DISCUSSION

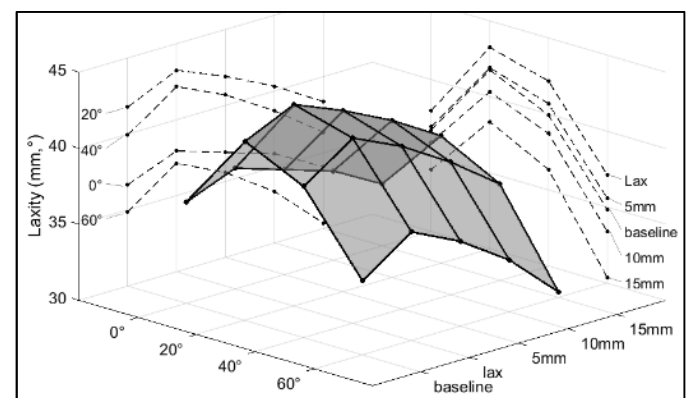


**Figure 2:** Glenohumeral laxity (vertical = direction-averaged laxity) across physical level and position.

The laxity response was complex and varied with physical level and position (Figure 2). Based on these values SLR x-intercepts were calculated for 20 tests (Figure 3, Table 1). Of them, 15 had significant slope

parameters – none were anterior tests. 10 had significant y-intercepts and slopes, the majority being rotational laxity tests. For these the average restorative plication magnitude was  $6.2 \pm 2.5$ mm.

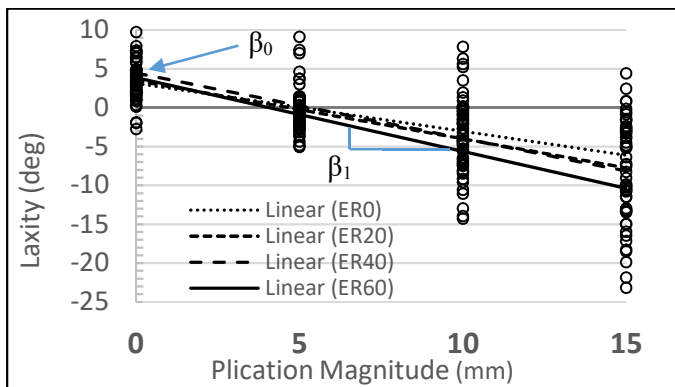


**Figure 3:** External rotation SLR per position. The horizontal axis is plication magnitude (Lax = 0mm).

**Table 1:** SLR results: All laxity tests with significant  $\beta_1$  (2nd). X-intercepts for significant  $\beta_1$  (4<sup>th</sup> col) and significant  $\beta_0$  and  $\beta_1$  (5<sup>th</sup> col).

Laxity Test	$\beta_0$ p-value	$\beta_1$ p-value	x-inter. $\beta_1$	x-inter. $\beta_0$ & $\beta_1$
POST <sub>0</sub>	.104	.003	5.0	
POST <sub>20</sub>	.253	<.001	2.6	
POST <sub>40</sub>	.296	.001	2.8	
POST <sub>60</sub>	.044	<.001	3.8	3.8
INF <sub>20</sub>	.068	.001	4.7	
INF <sub>40</sub>	.021	<.001	4.3	4.3
INF <sub>60</sub>	.085	<.001	3.4	
ER <sub>0</sub>	.044	<.001	5.1	5.1
ER <sub>20</sub>	.002	<.001	4.7	4.7
ER <sub>40</sub>	<.001	<.001	5.3	5.3
ER <sub>60</sub>	.006	<.001	4.1	4.1
IR <sub>0</sub>	.015	<.001	6.4	6.4
IR <sub>20</sub>	<.001	<.001	8.1	8.1
IR <sub>40</sub>	<.001	<.001	9.4	9.4
IR <sub>60</sub>	<.001	<.001	11.0	11.0
<b>AVG (SD)</b>			<b>5.4 (2.4)</b>	<b>6.2 (2.5)</b>

The average restorative magnitude was closest to the 5mm level, and this classification percentage (CI%) was calculated with the other performance metrics (Figure 4). The best Cp model had 10 predictors where the best AIC model had 5 predictors, and the best CI% model had 7 predictors.

The best model per criterion are shown in Table 2. Common tests among models were ANT<sub>20</sub> and IR<sub>40</sub>. Best Cp had similar classification to AIC but double

the predictor count. A 7-predictor model achieved 100% classification of the 5mm category.

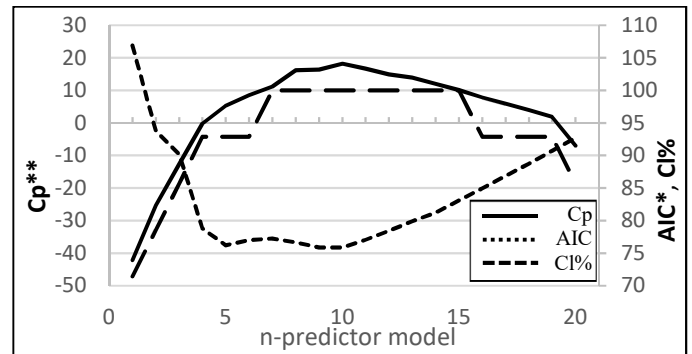


**Figure 4:** Criterion performance metrics. \*Smaller AIC is better. \*\*AIC, CI% lines do not sum to Cp.

**Table 2:** Best model per criterion, showing # of predictors, 5mm classification and laxity predictors.

Model	# Pred	5mm %	Laxity Model Predictors
Cp	10	<b>75.9</b>	ANT <sub>20</sub> , INF <sub>40</sub> , INF <sub>60</sub> , ER <sub>0</sub> , ER <sub>20</sub> , ER <sub>60</sub> , IR <sub>0</sub> , IR <sub>20</sub> , IR <sub>40</sub> , IR <sub>60</sub>
AIC	5	<b>78.6</b>	ANT <sub>20</sub> , POST <sub>40</sub> , INF <sub>60</sub> , ER <sub>20</sub> , IR <sub>40</sub>
CI%	7	<b>100.0</b>	ANT <sub>20</sub> , ANT <sub>40</sub> , INF <sub>20</sub> , ER <sub>40</sub> , IR <sub>0</sub> , IR <sub>40</sub> , IR <sub>60</sub>

## CONCLUSIONS

We have presented experimental shoulder laxity data and an analysis to estimate restorative capsule plication magnitude. The 5-predictor AIC model was parsimonious, but costly in classification compared to the accurate 7-test model. Clinical metrics, e.g. Grade, were not collected, but recent work suggests a moderate relationship between objective laxity and Grade.[1]

A customizable framework was offered to assess accuracy of clinical shoulder tests. Our work stresses the importance of combining translational and rotational tests to refine prediction. Future work will validate with more clinical metrics and outcomes.

## REFERENCES

1. Staker JL et al. *Proceedings of the International Shoulder Group*, Winterthur, Switzerland, 2016.

## ACKNOWLEDGMENTS

HSS Soft Tissue Fund

# MINIMUM DETECTABLE CHANGE VALUES FOR UPPER LIMB KINEMATICS IN HEALTHY ADULTS

Susannah M. Engdahl and Deanna H. Gates

University of Michigan, Ann Arbor, MI, USA

email: sengdahl@umich.edu web: <http://rehab-biomech-lab.kines.umich.edu/>

## INTRODUCTION

When evaluating upper limb performance, it is important to choose tasks that challenge the limits of a patient's ability [1]. For example, the tasks should require use of the distal joints if distal joint deficits are expected. However, it can be difficult to decide which tasks are most relevant for an evaluation since the kinematic redundancy of the upper limb makes it possible to accomplish any task using a variety of movement patterns. In order to select appropriate tasks, it is helpful to understand which joints are most important for accomplishing the task and how reliably movements made with those joints can be measured.

A useful metric for quantifying expected variation in a movement is the minimum detectable change (MDC), or the smallest change in a measurement that is above the level of error [2]. Large MDCs may indicate high levels of natural variability in a movement (or high levels of measurement error), suggesting that task might be inappropriate for use in an evaluation. Therefore, the purpose of this work was to quantify MDCs for upper limb kinematic measurements during activities of daily living (ADLs). The ADLs used in this study were specifically selected for their suggested relevance to functionality in individuals with stroke and upper limb loss.

## METHODS

Nineteen healthy, right-handed adults (mean age = 22 +/- 4 yrs; 9 male) participated in this study. Participants completed two identical experimental sessions, at least one day apart. During each session, participants performed six ADLs with the right arm: 1) apply deodorant to the contralateral axilla (DEO), 2) turn a doorknob (DOOR), 3) answer a desk telephone (PHONE), 4) place a pushpin in a bulletin

board (PIN), 5) wipe a plate with a towel (PLATE), and 6) pour a glass of water from a pitcher (WATER). Each ADL was repeated ten times at a comfortable pace.

Twenty-four reflective markers were placed on the arms and trunk to track the movements of seven body segments using a 19 camera motion capture system. Marker position data were filtered using a fourth-order low-pass Butterworth filter with a 6-Hz cutoff frequency. Joint angles for the trunk, shoulders, elbows, and wrists were computed using rotations defined by ISB [3] and time-normalized to 100% of task completion.

For each joint, the specific peak angles necessary to perform each ADL were determined. Within- and between-session MDCs for the peak angles were calculated according to  $MDC_{95} = SEM * 1.96 * \sqrt{2}$ , where 1.96 corresponds to a 95% confidence interval and SEM (standard error of measurement) is the square root of the mean square error term from the two-way ANOVA [4]. Within-session MDCs were calculated using the 10 individual repetitions from the first session. Between-session MDCs were calculated using averages of the 10 repetitions from each session.

## RESULTS AND DISCUSSION

There was considerable variability in the MDCs (range: 0.7° - 24.6°) depending on the ADL and joint angle (**Fig. 1**). The average within-session MDC was 7.4° (trunk: 3.6°, shoulder: 8.0°, elbow: 8.7°, wrist: 9.6°). In general, between-session MDCs were slightly higher than within-session MDCs. The average between-session MDC was 10.6° (trunk: 3.4°, shoulder: 13.0°, elbow: 12.9°, wrist: 13.3°). This trend is likely due to the fact that there are more potential sources of variation when measurements are made during multiple sessions compared to a

single session. Specifically, small differences in the experimental set-up and marker placement between sessions may lead to higher between-session MDCs.

There is no universally accepted standard for interpreting MDC magnitude. Instead, MDCs should be considered in context of the specific joint and ADL for which they were quantified. This is especially true given the smaller magnitude of trunk and wrist angles compared to shoulder and elbow angles. Consequently, the trunk and wrist MDCs tended to represent a larger percentage of the average peak angles than the shoulder and elbow angles. For example, the within-session MDCs for the wrist and trunk respectively represented 55% and 64% of the average peak angles, while the shoulder and elbow MDCs represented only 14% and 21%.

These results demonstrate the importance of selecting ADLs for assessing upper limb

performance based on which joint angles are important to the assessment. For example, PHONE had low MDCs for elbow flexion but high MDCs for wrist extension. PHONE might be a good choice if elbow flexion is important, but not if wrist extension is important. Another ADL (such as DOOR) would be more appropriate for assessing wrist extension.

Although this work focused on healthy adults, the results will eventually be used to help choose tasks for evaluating patient performance. Future work will also quantify MDCs for a broader range of ADLs.

## REFERENCES

1. Kontaxis, A, et al. *Clin Biomech* **24**, 246-53, 2009.
2. Wilken, JM, et al. *Gait Posture* **35**, 301-07, 2012.
3. Gates, DH, et al. *Am J Occup Ther* **70**, 2016.
4. Weir, JP. *J Strength Cond Res* **19**, 231-40, 2005.

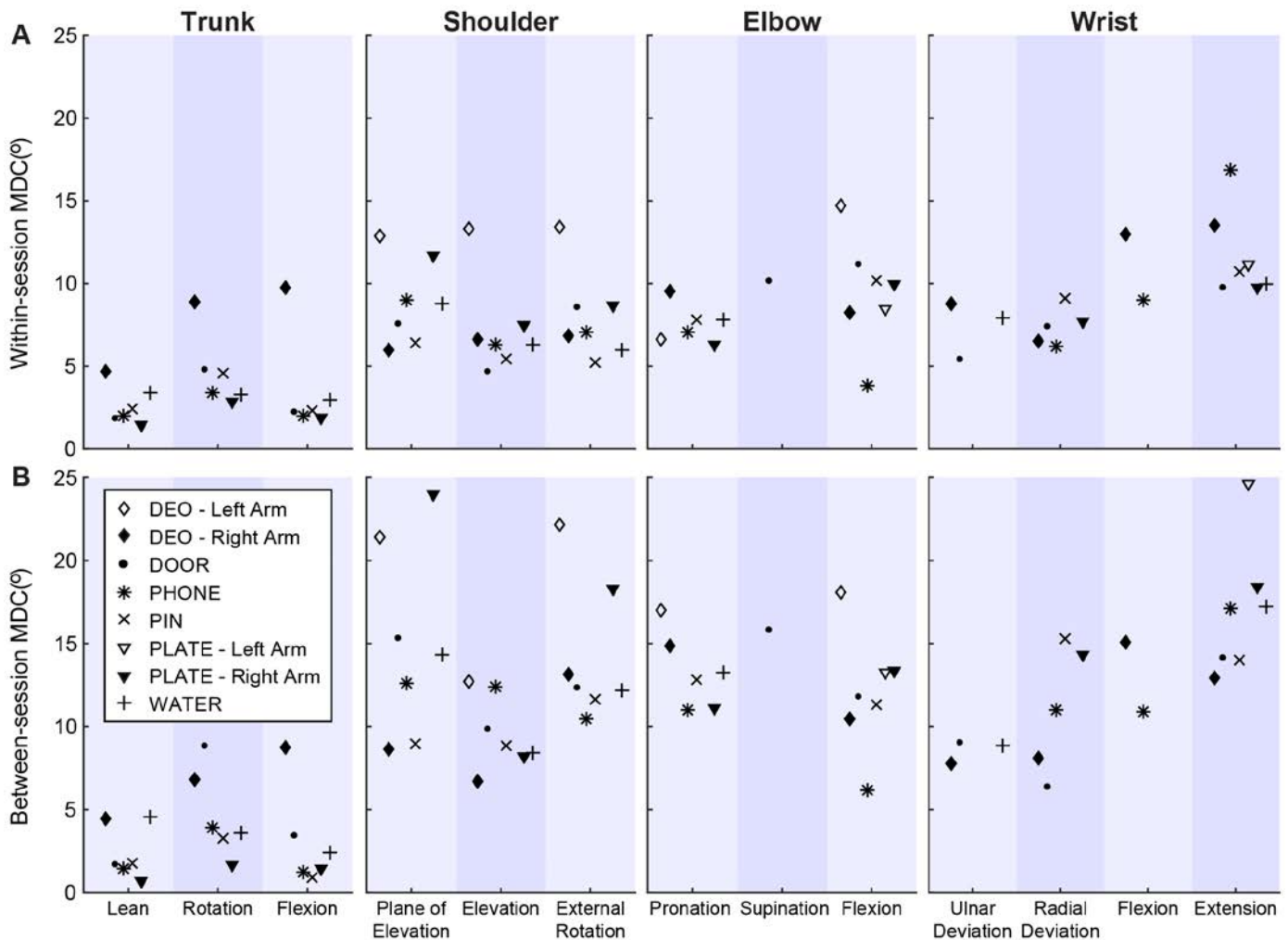


**Fig. 1:** Within-session (A) and between-session (B) MDCs for all activities of daily living.

# DEVELOPMENT OF A PROPULSION-SPECIFIC REGRESSION MODEL TO PREDICT SCAPULOTHORACIC MOTION

<sup>1,2</sup>Beth A. Cloud, <sup>3</sup>Ryan J. Lennon, <sup>1</sup>Felicia M. Marquez, and <sup>1</sup>Kristin D. Zhao

<sup>1</sup>Rehabilitation Medicine Research Center, Department of Physical Medicine and Rehabilitation

<sup>2</sup>Program in Physical Therapy, Mayo Clinic School of Health Sciences, Mayo Clinic College of Medicine and Science

<sup>3</sup>Division of Biomedical Statistics and Informatics

Mayo Clinic, Rochester, MN, USA

email: zhao.kristin@mayo.edu

## INTRODUCTION

Musculoskeletal models are commonly used in biomechanics research and allow for the evaluation of physical phenomena that cannot be measured or are difficult to measure directly, such as muscle forces. The utility of these models relies on the accuracy with which they were developed.

In musculoskeletal shoulder models, kinematics of the scapula relative to the thorax are commonly described using regression models. Regression models have defined equations that can predict the orientation of the scapula based on humerothoracic motion [1-3] and have been built into commonly used musculoskeletal models [4].

The existing scapular regression models were developed using the movement of non-pathological individuals during elevation in multiple planes with or without varying degrees of axial rotation [1-3]. These have been subsequently applied to model a wide range of activities including manual wheelchair (MWC) propulsion [5-6]. It is possible that different types of activities, such as propulsion, and/or individuals with neuromuscular impairments will utilize different rhythms between the scapula and humerus. Therefore, a regression model based on elevation data in able-bodied individuals may not be the best option for modeling MWC propulsion. *The purpose of this study was to develop a propulsion-specific shoulder regression model that predicts scapulothoracic motion from humerothoracic motion in individuals with spinal cord injury and to compare the accuracy of the output to a previously published regression model.*

## METHODS

Data from two IRB-approved studies that included a kinematic evaluation of MWC propulsion were compiled to create the data set for developing the

regression models. All participants had spinal cord injury (SCI) or spinal cord disease that led to at least one year of MWC use. Additional information about the primary studies has been published elsewhere [7-8].

Participants propelled in their personal MWC on a custom set of stationary rollers at a self-selected speed. Data were captured at either 120 or 240 Hz with electromagnetic sensors (Liberty, Polhemus) placed on the thorax at the sternum, scapula at the acromion, and humerus via thermoplastic cuff. The thorax, scapula, and humerus segment coordinate systems were defined according to ISB standards [9]. Motion was quantified with Euler sequences: humerothoracic (HT, YX'Y'') and scapulothoracic (ST, YX'Z''). Data captured at 240 Hz were down-sampled to 120 Hz.

The three HT rotations (plane of elevation [Y], elevation [X'], axial rotation [Y'']) were used as input variables for predicting ST motion via multivariable regression. A regression model was developed for each ST rotation (internal/external rotation [Y], upward/downward rotation [X'], anterior/posterior tilt [Z'']) during both the push and recovery phases of propulsion (6 regression models total). All frames of data during each phase of propulsion were utilized. Due to strong correlations between the HT input variables, these predictors were transformed using principal components analysis. Five parameters were estimated for each regression analysis (3 linear terms, 1 quadratic, and an interaction.) After estimating the regression parameters, the coefficients for the principal components were transformed to coefficients for the original predictors to define the regression model equations. Lastly, previously published shoulder regression models [3] were applied to the data set.

## RESULTS AND DISCUSSION

A total of 31 individuals (25 male, 42±11 years old, 16.0±9.6 years of MWC use) were included in the data analysis. SCI levels ranged from C6/7 to L2.

Individual regression models were defined for each of the ST rotations in both push and recovery utilizing individual HT variables, squared factors, and interaction factors. (Table 1). Each participant contributed an average of 520 data points (range 353 to 700).

The root mean square error (RMSE) of the six regression models ranged from 7.3 to 10.0° (Table 2). The mean square errors (MSE) of the regression models developed in this study were found to be roughly equivalent to, if not smaller than, the errors produced by an established shoulder regression model [3] when predicting ST motion (Table 2).

## CONCLUSIONS

The regression models presented here demonstrate similar levels of accuracy in predicting ST motion during propulsion as other regression models have demonstrated for elevation-based tasks [1-3]; though both the established regression models and this one leave room for improvement. Propulsion-specific regression models may better predict

certain ST motions during propulsion (namely upward/downward rotation and anterior/posterior tilt during the push phase and anterior/posterior tilt during the recovery phase) than a model developed from elevation-based motion. Investigation is ongoing to determine if including participant factors in the regression improves the prediction accuracy.

## REFERENCES

1. deGroot JH & Brand R. *Clin Biomech* **16**, 725-43, 2001.
2. Grewal TJ & Dickerson CR. *J Biomech* **46**, 608-11, 2013.
3. Xu X, et al. *J Biomech* **47**, 1206-10, 2014.
4. Holzbaur KS et al. *Ann Biomed Eng* **33**, 829-40, 2005.
5. Rankin JW, et al. *J Biomech* **44**, 1246-52, 2010.
6. Slowik JS, et al. *J Biomech* **49**, 1554-61, 2016.
7. Zhao KD, et al (2015). *Front Bioeng Biotechnol*
8. Cloud BA, et al. *Arch Phys Med Rehabil* (accepted).
9. Wu G, et al. *J Biomech* **38**, 981-92, 2005.

## ACKNOWLEDGMENTS

Funding for the studies contributing to this data set was provided by the Paralyzed Veterans of America, NIH (NIH/NCATS: TL1 TR000137), and the Foundation for Physical Therapy (PODS II).

**Table 1:** Regression Model Equations

Predictor Variable	ST Y		ST X'		ST Z''	
	Push	Recovery	Push	Recovery	Push	Recovery
Intercept	21.6	29.3	5.00	6.22	-5.60	-5.21
HT X'	-0.12	0.03	0.15	0.14	0.13	0.24
HT Y	0.40	0.25	0.15	-0.01	-0.05	-0.07
HT Y''	0.25	0.16	-0.20	-0.07	-0.13	0.07
(HT X') <sup>2</sup>	2.2 x10 <sup>-06</sup>	-2.1 x10 <sup>-05</sup>	1.4 x10 <sup>-04</sup>	3.5 x10 <sup>-05</sup>	-7.8 x10 <sup>-05</sup>	-8.8 x10 <sup>-05</sup>
(HT Y) <sup>2</sup>	-2.4 x10 <sup>-05</sup>	-7.6 x10 <sup>-04</sup>	9.7 x10 <sup>-04</sup>	-1.0 x10 <sup>-04</sup>	-1.4 x10 <sup>-03</sup>	-3.0 x10 <sup>-04</sup>
(HT Y'') <sup>2</sup>	6.8 x10 <sup>-05</sup>	4.8 x10 <sup>-04</sup>	1.4 x10 <sup>-03</sup>	7.7 x10 <sup>-04</sup>	1.9 x10 <sup>-04</sup>	-1.3 x10 <sup>-03</sup>
HT X'* HT Y	-9.0 x10 <sup>-07</sup>	-3.1 x10 <sup>-04</sup>	7.4 x10 <sup>-04</sup>	7.7 x10 <sup>-05</sup>	-7.0 x10 <sup>-04</sup>	-3.7 x10 <sup>-04</sup>
HT X'* HT Y''	-3.1 x10 <sup>-05</sup>	-1.2 x10 <sup>-04</sup>	-8.9 x10 <sup>-04</sup>	-3.8 x10 <sup>-04</sup>	1.4 x10 <sup>-04</sup>	7.1 x10 <sup>-04</sup>
HT Y* HT Y''	-5.7 x10 <sup>-05</sup>	1.1 x10 <sup>-04</sup>	-2.5 x10 <sup>-03</sup>	-7.9 x10 <sup>-04</sup>	1.0 x10 <sup>-03</sup>	1.7 x10 <sup>-03</sup>

ST Y: scapulothoracic internal/external rotation; ST X': ST upward/downward rotation; ST Z'': ST anterior/posterior tilt; HT X': humerothoracic elevation; HT Y: HT plane of elevation; HT Y'': HT axial rotation

**Table 2:** Performance of the Regression Models

Response	ST Y		ST X'		ST Z''	
	Push	Recovery	Push	Recovery	Push	Recovery
RMSE, ° (this study)	10.0	9.1	9.2	7.5	7.9	7.3
MSE, °-squared (this study)	99.6	82.9	85.5	55.9	61.9	53.0
MSE, °-squared (prior study [3])	92.4	79.1	83.0	88.6	90.1	66.4

ST Y: scapulothoracic internal/external rotation; ST X': ST upward/downward rotation; ST Z'': ST anterior/posterior tilt; RMSE: root mean square error; MSE: mean square error

# A Method for Estimating the Load Distribution in the Anterior Bundle of the Ulnar Collateral Ligament (UCL)

DB Jordan<sup>1</sup>, PJ Schimoler<sup>1,2</sup>, A Kharlamov<sup>2</sup>, MC Miller<sup>1,2</sup>  
<sup>1</sup>University of Pittsburgh, Pgh, PA; <sup>2</sup>Allegheny General Hospital, Pgh, PA  
email: mcmiller@wpahs.org

## INTRODUCTION

Ruptures of the medial ulnar collateral ligament (mUCL) of the elbow are a frequent occurrence for athletes who engage in repeated overhand pitching motions. The mUCL experiences distraction as the joint opens with a valgus load, leading to damage that ultimately can lead to complete failure. While the general mechanical behavior of the mUCL is known [1], a greater understanding of the load distribution between the anterior, middle, and posterior bands of the mUCL can help the development of improved repair options. In order to load the UCL in a manner analogous to the opening of the joint with a valgus load, a special fixture and experimental protocol were developed to adapt a biaxial load frame to elbow testing. The fixture had to grip the ulna and humerus with an intact mUCL while a series of displacement-controlled loads were imposed on the specimen at different flexion angles. Repetition of the test protocol after sequential transection of the anterior band then could provide the necessary data to determine the loads borne by each band of the ligament, using the principle of superposition. The working protocol hypothesis was that the anterior band would support more of the overall imposed load than the posterior band at lower flexion angles.

## METHODS

The method for estimating the load carried by the anterior band of the mUCL is made possible by a customized fixture which allows application of load at multiple flexion angles. There are three main aspects of the fixture. The first is the inclusion of elbow flexion angle as an independent variable in the experiment. The fixture allows the flexion of the mounted specimen through a range of angles that vary in increments of fifteen degrees up to a maximum flexion angle of 105°. The second feature of the fixture allows for the displacement-

controlled distraction of the mounted specimen along the long axis of the ulna at different speeds. This action subjects the specimen to loading scenarios that mimic the valgus opening of the joint. The loads needed to achieve the imposed displacements are monitored in the output. The third feature utilizes the loadframe's rotational degree of freedom. This feature enables the carry angle of the mounted specimen to be adjusted as needed in order to maintain proper joint capsule contact and alignment. In that the ulna is aligned along the distraction axis of the loadframe, rotation of the humerus by means of the loadframe's axial rotation accommodates the differences in alignment caused by the carry angle.

An initial experiment to test each of these features was performed on a single cadaveric specimen. The experiment began with the dissection of the specimen and exposure of the mUCL. Tracking markers of 0.8 mm diameter were fixed with small amounts of cyanoacrylic adhesive to the anterior and posterior bands of the anterior bundle of the mUCL. The ulna and humerus of the specimen were then each mounted into aluminum cylinders filled with polyester resin and stabilized with hardener (Fig. 1). The specimen was then positioned into the loadframe (MTS 858 Bionix) to undergo distraction at 0-105° of flexion with 15° flexion angle increments. The anterior band of the mUCL was then transected from the ligament and the test was repeated. Data processing included the construction of force-strain plots fitted to the standard piecewise model for biological tissues [2]. The strain in the posterior band was quantified in both displacement-based ulnar distractions and this posterior band strain was used to align the force-strain plots of the intact and partial ligament. Through the use of the superposition principle, an estimated force-strain profile was constructed for the transected anterior band. The loads in the

anterior and posterior bands were collated for chosen strain values: 0.5%, 1%, 1.5%, and 2%.

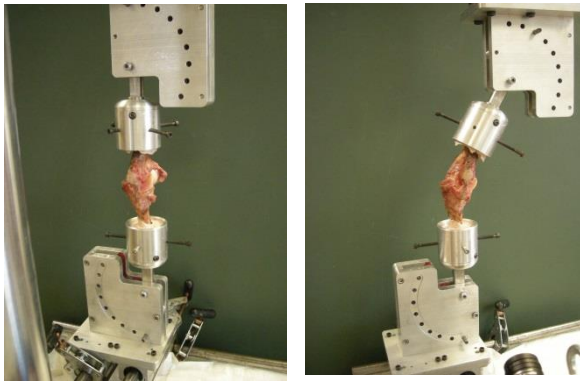


**Figure 1:** Specimen in the Test Fixture

## RESULTS AND DISCUSSION

The load borne by the posterior band increased with flexion angle as evidenced by increases seen between the case of 15° of flexion (Fig. 2) and 75° (Fig. 3) of flexion. The total load in the ligament and the load in the posterior band are the measured values and the anterior band load estimation is the difference. The load in the anterior band remained approximately the same at each level of strain.

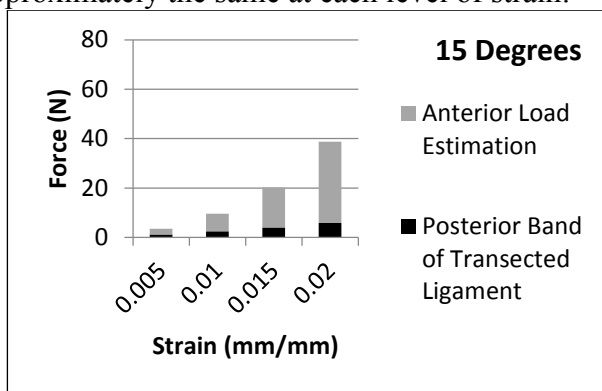


**Figure 2:** Anterior Load Estimation for 15 Degrees of Elbow Flexion

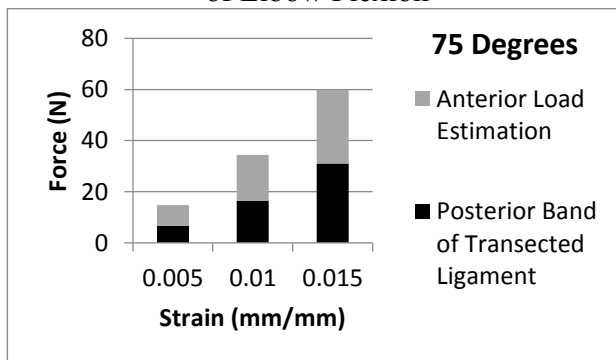


**Figure 3:** Anterior Load Estimation for 75 Degrees of Elbow Flexion

The anterior band supported most of the load in the mUCL at 15° of elbow flexion. Similar results were observed for angles up to 60° of flexion. This result agrees with the previous observations by Regan et al. that the anterior band of the mUCL remains taught at angles lower than 85° during valgus loading [1]. It was also noted that as the flexion angle increased, the load for the posterior band of the transected ligament increased in percentage of the total load imposed, consistent with the findings of Lee et al. who showed a positive correlation between posterior band strain and flexion angle, concluding that its contributions toward valgus stability increased with increasing flexion angle [3].

## CONCLUSIONS

The initial results demonstrate that the proposed method for estimating the load carried in the anterior band of the mUCL was effective. The features of the fixture permitted load consistent with ulnar distraction, permitted complete elbow flexion and accommodated difference in elbow orientation caused by the carry angle. Confidence in the method is derived from the initial results which follow a consistent trend and display behavior that is in agreement with the accepted literature.

Future iterations of the experiment will exploit the method more fully in order to investigate the consistency of these results across a larger sample size. The addition of a marker set for the middle band and an added experimental set with removal of this middle band will allow a better estimation of load distribution.

## REFERENCES

- 1.) Regan W.D., Korinek S.L., Morrey B.F. *Biomechanical Study of Ligaments around the Elbow Joint*, 1991.
- 2.) Fung Y.C., *Biomechanics: Mechanical Properties of Living Tissues*, 1993.
- 3.) Lee T.Q., Jackson T.J., Jarrell S.E., Adamson G.J., Chung K.C., *Biomechanical Differences of the Anterior and Posterior Bands of the Ulnar Collateral Ligament of the Elbow*, 2014.

## 4DCT FOR ASSESSMENT OF WRIST LIGAMENT INJURIES

<sup>1</sup> Kristin Zhao, <sup>1</sup> Ryan Breighner, <sup>1</sup> Sanjeev Kakar, <sup>1</sup> David Holmes, III, <sup>1</sup> Cynthia McCollough, <sup>1</sup> Shuai Leng, and <sup>1</sup> Steven Moran

<sup>1</sup> Mayo Clinic, Rochester, MN, USA  
email: zhao.kristin@mayo.edu

### INTRODUCTION

The wrist joint permits complex motion of the upper extremity that is crucial for both precision and power movements during daily activities; therefore, wrist injuries which result in osteoarthritis (OA) come at a significant socioeconomic cost due to time off work, surgical fees and associated morbidity. Injury to the scapholunate interosseus ligament (SLIL), which connects the scaphoid and lunate bones in the proximal carpal row, is one of the most important and common upper extremity injuries. Accurate diagnosis of the location of SLIL injuries is crucial for providing the most effective treatments so that the location of the tear can be considered in a tailored treatment plan.

Current diagnostic approaches for SLIL injury include magnetic resonance imaging, which lacks the specificity to assess injury location, and wrist arthroscopy, which is invasive and results in an injury grade that is subjective and prone to interobserver variability. We believe that our high spatial and temporal resolution 4D (3D + time) CT technique (4DCT) has the potential to enable accurate quantification of key metrics during wrist motion in patients with SLIL injury, leading to improved clinical practice by replacing invasive and inaccurate diagnostic tests.

### METHODS

Six patients (2 females, 4 males) were recruited as part of an IRB-approved pilot study, demonstrating the novel information obtained from 4DCT. All ten patients had clinical suspicion of unilateral SLIL injury, including tenderness over the scapholunate joint, negative radiographs, equivocal MRI, and no history of wrist injury. They underwent 4DCT imaging on each wrist separately during flexion-

extension, radial-ulnar deviation, and dart thrower's motions. Each wrist was scanned for 2 seconds as the patients moved their wrists using an established non-gated 4DCT technique [1]. Dynamic scans during each of the motions resulted in 18 image volumes across the 2 second trials. Two patients, 53 year old female (Case 1) and 44 year old male (Case 2), underwent diagnostic wrist arthroscopy and the presence of scapholunate instability was confirmed. The first patient (Case 1) had Geissler 3 instability; the second (Case 2) had Geissler 4 [2] findings [3].

4DCT image sequences obtained from the individual cases were further analyzed to map the distance between the scaphoid and lunate during the wrist motions using established image processing techniques [1, 4]. Distance maps are color representations of the distances calculated between the two bone surfaces. These maps provided insight into the magnitude and location of diastasis at the scapholunate joint.

### RESULTS AND DISCUSSION

The distance maps for the radial-ulnar deviation motion in two cases are shown in Figure 1, indicating dorsal diastasis (suggesting dorsal ligament injury alone) (Fig. 1: Case 1) and subtle uniform diastasis (suggesting complete dorsal through volar ligament injury) (Fig. 1: Case 2). Distance maps for four more subjects (who did not have confirmation of injury with arthroscopy) are shown in Figure 2.

The abnormal motion between the scaphoid and lunate can be accurately quantified using the described technology to potentially allow surgeons to more accurately diagnose the location of SLIL injury.

**REFERENCES**

1. Leng, S., K. Zhao, M. Qu, K.N. An, R. Berger, and C.H. McCollough, Dynamic CT technique for assessment of wrist joint instabilities. *Med Phys*, 2011. 38 Suppl 1: p. S50.
2. Geissler, W.B., [Arthroscopic management of scapholunate instability]. *Chir Main*, 2006. 25 Suppl 1: p. S187-96.
3. Kakar, S., R.E. Breighner, S. Leng, C.H. McCollough, S.L. Moran, R.A. Berger, and K.D. Zhao, The Role of Dynamic (4D) CT in the Detection of Scapholunate Ligament Injury. *Journal of Wrist Surgery*, 2016. (epub ahead of print)

4. Zhao, K., R. Breighner, D. Holmes, 3rd, S. Leng, C. McCollough, and K.N. An, A technique for quantifying wrist motion using four-dimensional computed tomography: approach and validation. *Journal of Biomechanical Engineering*, 2015. 137(7).

**ACKNOWLEDGMENTS**

This project was supported by the National Institutes of Health (NIAMS AR057902) and the Mayo Clinic Center for Individualized Medicine.

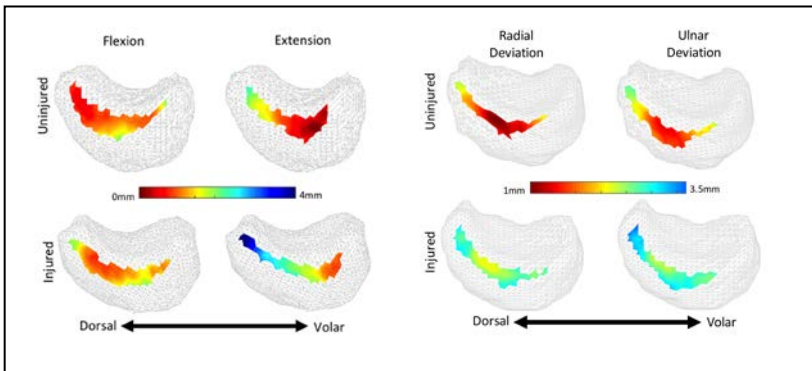


**Figure 1.** (Case 1, LEFT) Sagittal view of the articular surface of the lunate. Color corresponds to interosseous distances at flexion/extension extrema during 4DCT imaging. The injured side (bottom row) exhibits considerable dorsal diastasis during extension, suggesting dorsal ligament disruption. (Case 2, RIGHT) The injured side (bottom row) exhibits uniform, though moderate diastasis. Red indicates the scaphoid and lunate are closer together (ligaments are intact) and blue demonstrates the carpal bones are separated after a ligament injury Note: patient right-side lunate mirrored for comparison purposes.

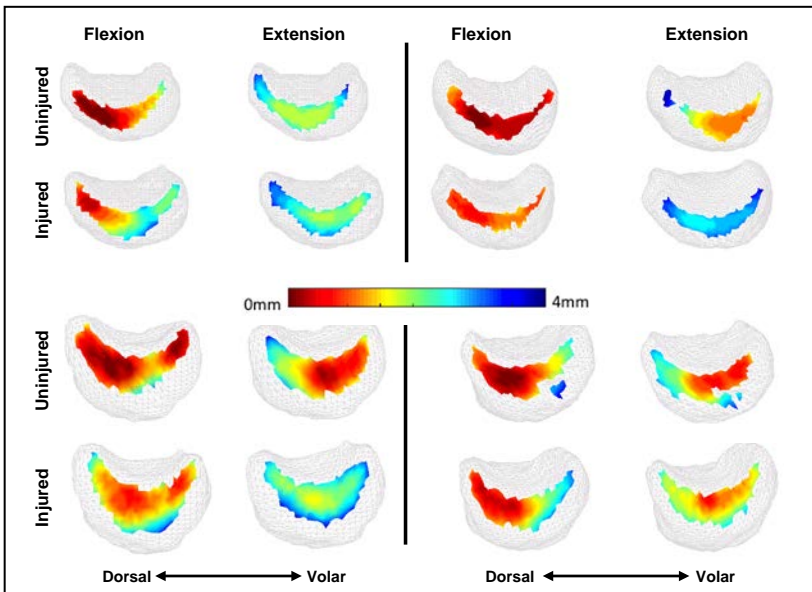


**Figure 2.** Sagittal view of the articular surface of the lunate for four additional patients. Color corresponds to interosseous distances at flexion/extension extrema during 4DCT imaging. The injured side (bottom row) exhibits variable amounts of gapping across subjects, likely indicating different ligament injury locations.

# SYNERGISTIC SHOULDER MUSCLE ACTIVATION DURING ARM ELEVATION IN DIFFERENT BODY POSITIONS

<sup>1</sup>David Stapleton, <sup>2</sup>Samuel DeBoer, <sup>2</sup>Traci Bush, <sup>1,2</sup>Vassilios Vardaxis

<sup>1</sup>Human Performance Laboratory; <sup>2</sup>Department of Physical Therapy, Des Moines University, IA, USA  
email: David.Stapleton@dmu.edu

## INTRODUCTION

In non-pathological shoulder complex function, the humerus and scapula move in a predictable pattern identified as “normal scapulohumeral rhythm”, viewed on the scapular plane as the relative motion between the scapulothoracic and glenohumeral joints [1]. This rhythm is largely dependent on the activation pattern of the muscles that move and stabilize the shoulder complex. The activation of these muscles seems to increase with increased humeral elevation [2] and was shown to operate in synergistic activation patterns which are affected by pathology and level of impairment [3].

Gravitational compensation affects the amplitude of the shoulder kinematics and muscle activity during reaching tasks [4]. The direction of external force and gravity relative to the shoulder complex was also found to affect the normal glenohumeral joint mechanics [5] and was shown to predict scapular motion [6]. In this study we attempt to quantify the synergistic activation between each of the three parts of the deltoid (anterior, middle and posterior; AD, MD and PD, respectively) and the upper trapezius (UT) during elevation of the arm in flexion and abduction. Analysis of these elevation tasks was completed in four body positions commonly used in evaluation and intervention protocols which affect the gravitational load direction relative to the shoulder complex.

## METHODS

Eighteen (18) right-handed male adults aged 24.0 ( $\pm 1.68$ ) years with no history of shoulder pathology participated in the study. Subjects were asked to perform abduction and flexion of the right arm (without additional load) in seated, sidelying, prone, and supine positions from a resting arm position (at the side of the body) to 120°. Motion capture (10-

camera Motion Analysis Corp.) was used to track the elevation of the arm (using planar projection of the torso and the upper arm on the movement plane). Surface electromyography (EMG) data for the AD, MD, PD, and UT was recorded using the MA-300 system (Motion Lab Systems, Inc.). EMG signals were differentially amplified and sampled at 1200 Hz per channel using a 16 bit A/D convertor.

Data analysis was performed using MATLAB. Activation patterns were demeaned, band-pass filtered (10-450 Hz), and enveloped via RMS. Manually resisted muscle specific maximum voluntary isometric contractions were used to normalize the data. The activation level was assessed on three 30° elevation segments (between 0-90°) measured by motion capture. The synergistic activations for each of the deltoids paired with the UT (AD-UT, MD-UT, and PD-UT) averaged over the elevation segment were evaluated using an activity-scaled co-activation (AsCA) algorithm.

$$AsCA = \left( \frac{EMG_1}{EMG_2} \right) * (EMG_1 + EMG_2) * 100$$

where,  $EMG_1 < EMG_2$ . Three-way RM-ANOVA (task by position by elevation segment) was used to analyze the paired synergistic activations (AsCAs).

## RESULTS AND DISCUSSION

There was a 3-way interaction effect only for the PD-UT ( $p < 0.05$ ). Position by elevation and task by elevation, 2-way interaction effects were found for all muscle pairs ( $p < 0.01$ ), and position by task 2-way interaction effects were found for PD-UT ( $p < 0.01$ ) and MD-UT ( $p < 0.05$ ) muscle pairs only.

The synergistic activation between UT and each of the deltoids showed significant arm elevation main effects ( $p < 0.001$ ) (Figure 1). These observed arm elevation effects reflect increased co-activation and

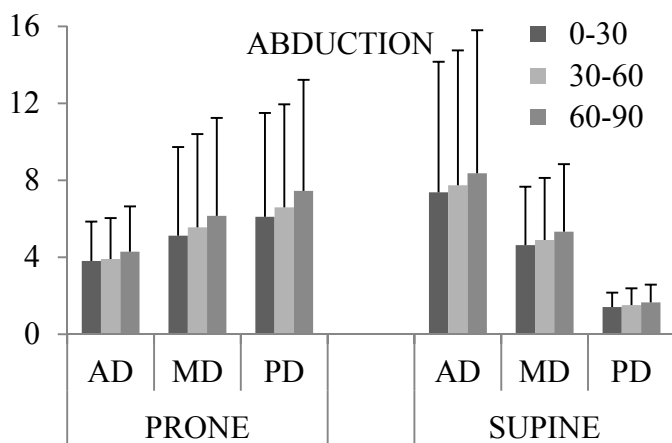


**Figure 1:** AsCAs (mean  $\pm$  SD) for the abduction task in prone and supine positions. Arm elevation and position effect on co-activation between the UT and each of the 3 parts of the deltoid are shown.

suggest higher demands for scapular stability with arm elevation regardless of task and position. Significant ( $p < 0.001$ ) position main effects were also observed for all AsCAs. There was higher co-activation for seated and sidelying as compared to prone and supine positions for the abduction task. During flexion the seated co-activation was the highest for the AD-UT and the lowest for MD-UT and PD-UT, highlighting the anterior deltoid role. Interestingly, the co-activation of the MD-UT and PD-UT were highest in the sidelying position during flexion, underscoring the demand on these muscles to counter gravity in this position. Task main effects were only found for MD-UT and PD-UT ( $p < 0.001$ ).

There was a synergistic co-activation arm elevation trend for all muscle pairs and highest co-activation

values were observed for the AD-UT in the seated and supine positions ( $p < 0.05$ ) (Table 1). The PD-UT showed highest co-activation in the prone position for both tasks ( $p < 0.05$ ). Relatively high MD-UT co-activation was observed, only during abduction, for seated and sidelying positions (Table 1). Co-activations (while relatively high) in sidelying position were not significantly different amongst muscle pairs. The low co-activation values observed were due to the nature of the tasks evaluated. The role of the serratus anterior and lower trapezius was not assessed.

## CONCLUSIONS

The observed modulation of the expected co-activations between the upper trapezius and the deltoids by arm elevation, body position, and task should be accounted for during clinical protocols. Further investigation of additional synergies under more demanding tasks will refine and enhance rehabilitation protocols and improve biomechanical models of the shoulder.

## REFERENCES

1. Freedman L, Munro RR. *JBJS* **48A**, 1503-10, 1966.
2. Ludewig PM, et al. *JOSPT* **24**, 57-65, 1996.
3. Roh J, et al. *Front Hum Neurosci* **9**:6, 2015.
4. Prange GB, et al. *J Electromyogr Kines* **19**, e40-9, 2009.
5. Howell SM, et al. *JBJS* **70A**, 227-32, 1988.
6. De Groot JH, et al. *Clin Biomech* **16**, 735-43, 2001.

**Table 1:** Muscle pair scaled co-activation (AsCA) values (mean  $\pm$  SD).

Muscle Pair Co-activation	Abduction Task					
	Sidelying Position			Seated Position		
	0-30	30-60	60-90	0-30	30-60	60-90
AD-UT	12.3 $\pm$ 14.9	13.0 $\pm$ 15.9	14.0 $\pm$ 17.6	13.2 $\pm$ 8.9	14.4 $\pm$ 8.9	16.5 $\pm$ 9.2
MD-UT	10.7 $\pm$ 10.0	11.1 $\pm$ 10.2	11.7 $\pm$ 10.9	10.2 $\pm$ 5.0	11.1 $\pm$ 5.5	12.3 $\pm$ 5.8
PD-UT	7.7 $\pm$ 4.8	08.0 $\pm$ 4.9	8.4 $\pm$ 5.3	6.8 $\pm$ 5.1	7.4 $\pm$ 5.7	8.2 $\pm$ 6.2
Flexion Task						
AD-UT	7.9 $\pm$ 7.6	8.0 $\pm$ 7.9	8.1 $\pm$ 7.8	12.1 $\pm$ 9.8	12.9 $\pm$ 10.3	14.6 $\pm$ 11.5
MD-UT	7.7 $\pm$ 6.7	7.6 $\pm$ 6.5	7.8 $\pm$ 6.5	2.1 $\pm$ 1.4	2.3 $\pm$ 1.3	2.6 $\pm$ 1.4
PD-UT	6.4 $\pm$ 5.1	6.5 $\pm$ 4.8	6.7 $\pm$ 4.6	1.2 $\pm$ 1.1	1.2 $\pm$ 1.0	1.2 $\pm$ 0.8

## MOVEMENT TOWARD PREDICTIVE HAND FORCES

Joshua P. Drost, Tamara Reid Bush  
Michigan State University, East Lansing, MI, USA  
email: drostjos@msu.edu, reidtama@msu.edu

### INTRODUCTION

Almost everything people do in their daily lives uses their hands. Therefore, when the hand is impaired, it is critical that we understand how much function was lost and where, so that the best possible treatment can be provided. Currently, loss in hand function is determined using surveys, pain scales and radiological exams, all of which are subjective; objective methods to quantify changes in hand function are needed [1, 2]. A hand model that includes the total *force and motion* abilities of a patient will allow health care experts to easily compare changes in hand function, leading to improved rehabilitation and treatment strategies.

Previously, we modeled changes in the motion abilities of the hand caused by arthritis [3]. This model included the full range of motions of the hand; however, force data for each finger were not incorporated into that model. Both motion and forces are necessary to generate a comprehensive hand model for clinical use. To facilitate translation into a clinical environment, it would be optimal to take only a few force measures and be able to predict the forces occurring in the range of movement.

Thus, the goal of this work was to develop a model that could predict the forces over the kinematic workspace of participants with and without reduced hand functionality.

### METHODS

Sixteen participants (7 female and 9 male, average age 25.6 years, SD 6.1 years) without any reported injury or arthritis, termed “Healthy”, and fifteen participants (13 female and 2 male, average age 73.5, SD 4.8 years) with doctor diagnosed osteoarthritis, termed “Arthritic”, were included in this study.

Forces due to changes in flexion/extension of the index finger were measured using a “U-shaped” metal bracket placed in seven positions along a line, each 15mm apart. The participant was asked to push on the bracket, and then pull with maximum force using the pad of the index finger (Figure 1 A&B).

Maximum abduction/adduction forces were also measured in six positions. Three of the positions were at maximum extension (called “Adduction/Abduction Push”—Figure 1C) and the other three were at a mid-range flexion of the interphalangeal joints (called “Adduction/Abduction Pull”—Figure 1D).

After collection, the data were analyzed in terms of the 1) fingertip posture ( $x,y,z$  coordinate) 2) the direction of the force applied as an angle in the sagittal plane ( $\theta$ ), and 3) force magnitude. A linear mixed effect model was then created for each health and gender population. The model included the covariates of normalized distal and palmar displacement ( $x, y$ ), angle ( $\theta$ ) and angle squared ( $\theta^2$ ) along with their interactions. Subject number was used as a random variable to remove variance between subjects.

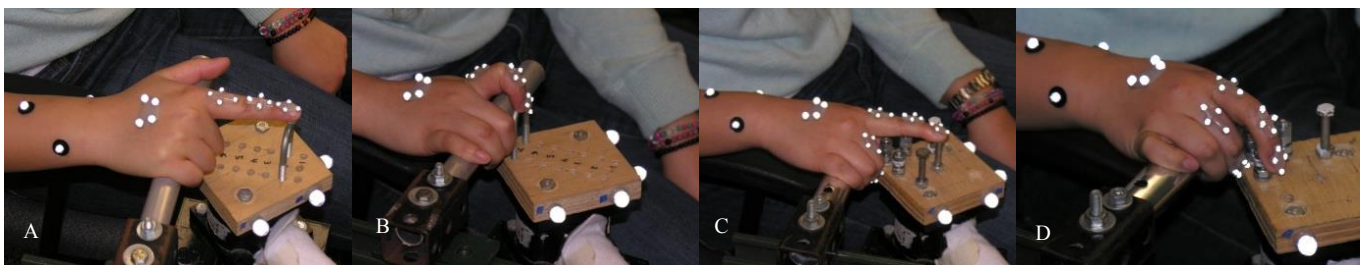


**Figure 1: Experimental setup and force data for (A) flexion/extension push, (B) flexion/extension pull, (C) adduction/abduction push and (D) adduction/abduction pull trials**

## RESULTS AND DISCUSSION

Sagittal plane views of force data from the arthritic female population are presented in Figure 2 (Left). Forces were plotted based on the finger posture in 3D space and normalized for finger length. The origin for all data was at the MCP (metacarpal phalange) joint of the index finger. The plots are oriented so that a fully extended index finger sits along the horizontal axis with the pad of the index finger pointing in the positive vertical direction.

The population forces as predicted by the model are also shown (Fig. 2, Center). The covariates (fingertip position and force direction) are the same as the observed data, but the forces have been predicted using the model. As can be seen, our model can closely predict the forces over the range of motion tested. The model was also used to estimate forces over the entire range of motion for the index finger for the both the healthy and arthritic populations.

Figure 2 (Right) shows the predicted force for the entire kinematic space. The multi directional arrows, show the range of force directions the positions of application, and the colors indicate magnitudes of force. The subject variance has been removed, so this represents the average abilities of an arthritic female.

This prediction model is the first step in being able to use limited clinical measures to create a complete mapping of the forces of the hand. Such a model will

give clinicians an additional tool for diagnosing disorders, tracking therapy, and identifying treatment to help patients gain back function.

Currently the model has been developed for the index finger. Future work will include forces and associated models for all fingers. Also, measures of motion and force will be gathered prior to intervention; mid-way through rehabilitation and after rehabilitation is complete to test its usefulness in a clinical situation.

There is a need for an objective method for diagnosing loss in hand function. This model is highly innovative and useful: comparisons between and individual's abilities and the population models will allow clinicians to determine what function was lost and how much was restored due to treatment.

## ACKNOWLEDGEMENTS

The authors would like to thank the Pearl J. Aldrich Endowment for funding as well as Sam Lietkam, Wu Pan, and Jessica Buschman for their assistance.

## REFERENCES

- [1] Chung K C., et al The Journal of Hand Surgery, 575-587. 1998.
- [2] Katz S, et al. Journal of the American Medical Association, 914-919. 1963.
- [3] Leitkam S, Bush TR. ASME Journal of Biomechanical Engineering. 2015.

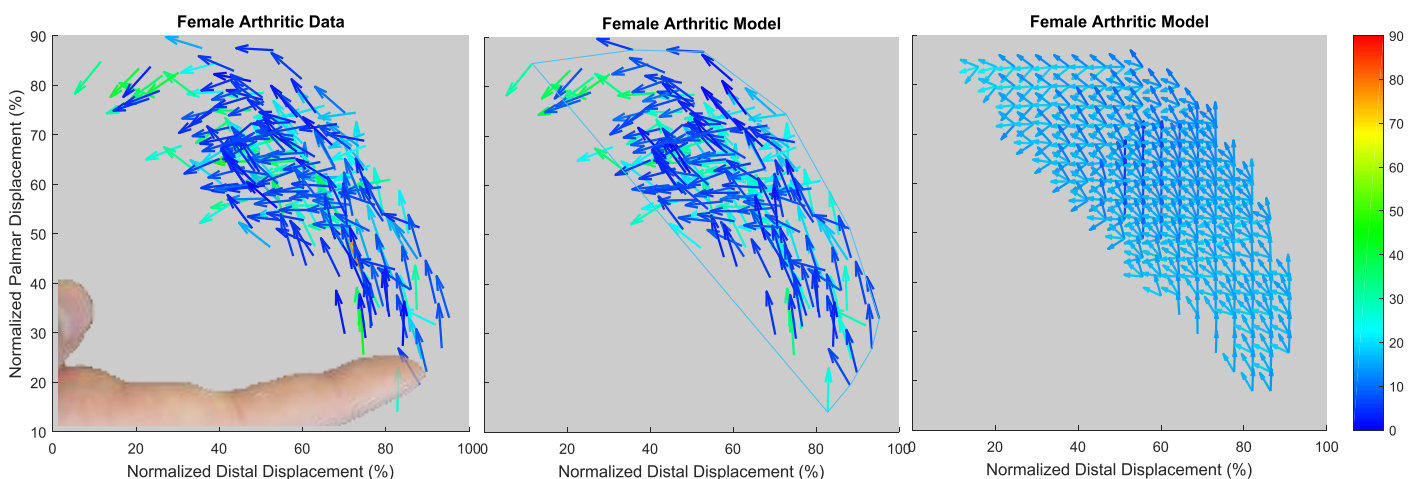


**Figure 2: Sagittal projection of force data for the arthritic female population. A finger has been superimposed over the image to help represent position and direction of forces. Left: measured forces for the population. Center: model prediction of forces. Right: prediction of forces over *entire range of motion*, not just the measured locations.**

# THE EFFECT OF SIMULATED ROTATOR CUFF TEAR SEVERITY ON GLENOHUMERAL JOINT FORCE

<sup>1</sup>Rich Arce, <sup>1</sup>Meghan E. Vidt

<sup>1</sup>Exercise Science and Health Promotion, Arizona State University, Phoenix, AZ, USA  
email: mvidt@asu.edu

## INTRODUCTION

Increased age is associated with rotator cuff (RC) tears [1], which can affect the integrity of tendons and muscle force distribution across the glenohumeral joint [2]. A change in force distribution across the glenohumeral joint can affect resultant joint contact force (JCF), potentially affecting stabilization, and increasing risk of joint damage or injury progression. The RC musculature is critical for stabilizing the humeral head in the glenoid fossa. However, it is unknown how alterations to these muscle forces affect loading at the glenohumeral joint. While JCF cannot be feasibly measured *in vivo*, computational musculoskeletal models enable prediction of these forces under different scenarios of muscle force contribution to gain insight into resulting joint forces, and to make inferences about possible implications for the RC tear population. The purpose of this study is to use a simulation-based approach to evaluate the effect of systematic variations of muscle force distribution on glenohumeral joint force.

## METHODS

A computational musculoskeletal model of the upper limb [3] representing the muscle force characteristics of a healthy older adult male [4] was implemented in OpenSim [5]. Peak isometric muscle force of each RC muscle path in the model was systematically reduced to a percentage of maximum force to simulate increased RC tear size (Table 1). Modulations were made to supraspinatus (S), infraspinatus (IS), subscapularis (SS), and teres minor (TM). A baseline configuration, in which all muscle forces were maintained at nominal older adult values (i.e. 100%), and 7 tear sizes, in which RC muscle forces were reduced incrementally, were evaluated. The influence of static posture on

glenohumeral joint contact force was evaluated. Static postures included 30°, 45°, 60°, and 90° thoracohumeral elevation in the frontal plane. In all assessments, shoulder rotation was set to 0°, elbow flexion was 90°, and forearm rotation was 0°. Dynamic simulations of movement were performed for each static posture and tear size, for a total of 32 simulations. Simulations were conducted using the computed muscle control (CMC) tool [6] in OpenSim, with static postures for model degrees of freedom used as an input. Muscle excitation time histories calculated by CMC were used to calculate glenohumeral JCF with OpenSim's joint analysis tool. Output from 0.25-0.5sec of each 2sec static trial was evaluated to ensure consistency across output for each posture and tear scenario.

**Table 1:** Increased tear size was simulated by decreasing peak isometric force for model muscle paths. Percentages represent the proportion of the model's nominal peak isometric force. S=supraspinatus; IS=infraspinatus; SS=subscapularis; TM=teres minor.

Tear Scenario	S	IS	SS	TM
Baseline	100%	100%	100%	100%
S50	50%	100%	100%	100%
S0	0%	100%	100%	100%
IS75	0%	75%	100%	100%
IS50	0%	50%	100%	100%
IS25/SS75	0%	25%	75%	100%
IS25/SS50	0%	25%	50%	100%
IS25/SS25	0%	25%	25%	100%

Results of the joint force analysis were evaluated using a custom Matlab (The MathWorks Inc, Natick, MA) program. Data was filtered using a dual pass windowing filter. Force components were transformed into the scapula's reference frame, which is aligned with the scapular plane, by applying a 30° anterior rotation about the superior-inferior axis. The resultant JCF was calculated and the peak resultant force identified. Magnitude of peak

resultant force and its compressive component were compared to baseline for each RC tear scenario at each elevation angle. Resultant force components were projected onto the glenoid fossa to assess changes to peak resultant joint force location with each tear scenario and for each elevation angle.

## RESULTS AND DISCUSSION

Increased simulated tear severity resulted in a decrease in overall force production for most trials (Fig. 1). The 30° posture maintained a peak JCF of at least 82% for all scenarios until both IS and SS were at 25% of nominal force. The 45° posture declined to <50% of nominal peak resultant joint force when SS was at 75% of nominal force. Postures at 60° and 90° showed a JCF reduction with increased RC tear severity. It is likely that a smaller moment contribution from upper limb mass contributed to the smaller changes in JCF observed for 30° and 45° postures compared to 60° and 90° postures. Both the 60° and 90° postures experienced a decrease of 60% and 64%, respectively, from baseline to the most severe RC tear.

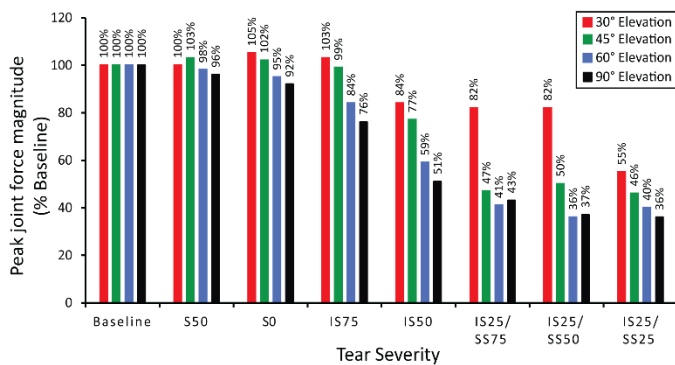


**Figure 1:** % change from baseline in peak JCF magnitude with increased RC tear severity and elevation angle.

There was an overall trend of decreased compressive force with increased RC tear severity, which supports the effect of decreased compressive contributions from markedly reduced muscle force generating capacity from a RC tear. For all elevation postures examined, compression was lowest and remained consistent once SS tear was introduced. While some increases in compression were observed for 30° and 45° postures for smaller simulated RC tears (Fig.2), the corresponding magnitude of the resultant JCF (Fig.1) was not markedly increased, suggesting that

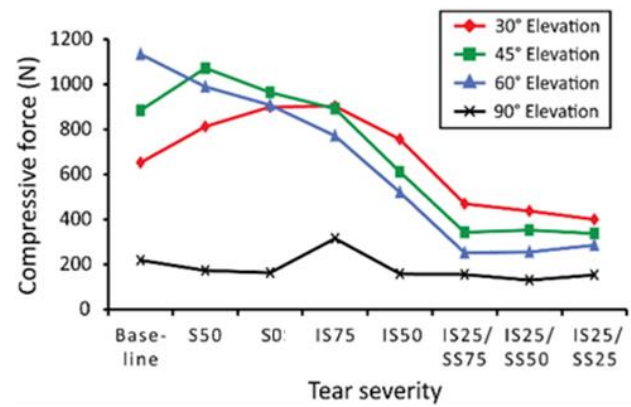


**Figure 2:** A: Regression of compression force as tear severity rises.

remaining musculature in small RC tears may prioritize compression to maintain joint stability. In all simulations, peak resultant force was maintained within the glenoid boundary. Forces were localized at the inferior-posterior aspect for 30°, 45°, and 60° postures, with a more anterior-inferior location observed for 90° postures.

## CONCLUSIONS

We conclude that both posture and increased RC tear size influence the magnitude and compressive component of JCF. Despite the increased risk associated with decreased compressive components of joint force, all peak forces were localized within the glenoid for these static simulations, suggesting that these postures pose less of a risk than those in which forces are not localized within the glenoid boundary. Additional work is currently underway to examine the influence of postures in other planes (e.g. scapular plane), and apply these methods to detailed analysis of dynamic functional tasks, which are most relevant to patients with RC tears.

## REFERENCES

1. Yamamoto A, et al. *J Shoulder Elbow Surg* **19**, 116-120, 2010.
2. Hughes VA, et al. *J Gerontol A Biol Sci Med Sci* **56**, B209-B217, 2001.
3. Saul K, et al. *Comput Methods Biomech Engin* **18**, 1445-1458, 2015.
4. Vidt, ME, et al. *J Biomech* **45**, 334-341, 2012.
5. Delp SL, et al. *IEEE Trans Biomed Eng* **54**, 1940-1950, 2007.
6. Thelen DG, et al. *J Biomech* **36**, 321-328, 2003.

# BIOMECHANICS OF THUMB CARPOMETACARPAL OSTEOARTHRITIS PROGRESSION

<sup>1</sup>Joseph J. Crisco, <sup>1</sup>Douglas C. Moore, <sup>1</sup>Amy M. Morton, <sup>2</sup>Amy L. Ladd, <sup>1</sup>Arnold-Peter C. Weiss

<sup>1</sup>Department of Orthopaedics, Alpert Medical School of Brown University and Rhode Island Hospital, Providence, RI, USA

<sup>2</sup>Chase Hand Center, Department of Orthopaedics, Stanford University School of Medicine, Stanford, CA, USA

email: joseph\_crisco@brown.edu, web: www.brownbiomechanics.org

## INTRODUCTION

Degenerative changes in both cartilage and bone typify thumb carpometacarpal (CMC) osteoarthritis (OA). Despite the prevalence of thumb CMC OA, which affects 20-25% of adults over the age of 50 – and up to 80% of those aged 71-80 – the natural history of the disease is not well characterized. Physical examination and plain radiographs are used for staging OA disease, with progressive joint narrowing associated with more advanced disease. However, limited data exists on typical rates of this disease progression in the thumb. Therefore, the two aims of this study were to estimate the rate of cartilage thinning in early thumb CMC OA, and to determine whether the rate differs between men and women.

## METHODS

OA progression and cartilage thinning were assessed using a large database of clinical, image, and biomechanical data collected as part of a longitudinal study of thumb CMC biomechanics and OA progression. This specific study focuses on the rates of clinically-staged disease progression and cartilage thinning.

Study subjects included 92 patients with nascent thumb CMC OA at enrollment, defined as pain and positive clinical signs with at most minor radiographic changes (49F and 43M between the ages of 45 and 75 yrs); as well as 46 healthy subjects (Controls) recruited to meet specific age and sex criteria (12 young females (YF) and 10 young males (YM) between the ages of 18 and 25 yrs, and 13 older females (OF) and 11 older males (OM) between the ages of 45 and 75 yrs). IRB

approval was obtained before enrollment. Assessments were performed on all subjects at enrollment (Yr 0 or baseline), and at 1.5 and 3 years post-enrollment for the OA patients.

Clinical stage was assigned using a modified version of the Eaton-Glickel radiographic classification system (Stage 0: Pain, but normal radiographs. Stage 1: Mild joint widening or narrowing. Stage 2: Narrowing, debris < 2mm, sclerosis, contour changes. Stage 3: Marked narrowing, debris > 2mm, contour changes. Stage 4: Stage 3 + additional joints). Cartilage thinning was assessed using high-resolution CT volume images (voxel size 0.4x0.4x0.625mm<sup>3</sup>) of the thumb in a splinted neutral position (HiSpeed Advantage 16 slice scanner, GE Medical, Milwaukee, WI). Bone surface models were generated via semi-automated thresholding/manual editing, and the trapezial and MC1 subchondral articular facets were modeled as NURBS surfaces (Geomagic 12, 3D Systems, Rock Hill, SC. USA). Interbone distances, calculated as the shortest distances between vertices on the overlapping regions of the NURBS surfaces, were used to estimate total cartilage thickness (trapezium + MC1). The interbone distances were averaged to yield a single mean joint space width for each joint analyzed.

Linear regressions of OA Grade and mean joint space as functions of time were used to estimate the rate of disease progression and cartilage thinning. A one-way ANOVA (with Tukey's post-hoc multiple comparisons) was used to compare the mean joint space width of the Controls (grouped by age and sex) to those of the patients (at baseline, year 0 and year 3).

## RESULTS AND DISCUSSION

In our study population, thumb CMC OA progressed at a rate of 0.3 OA staging points per year over the evaluation period ( $P < 0.001$ ), resulting in an average increase of one OA stage by the 3-year follow-up (Fig. 1). There were no significant differences in the rate of disease progression in men and women.

The mean ( $\pm 1$  SD) joint space of the younger Controls was 1.4 mm ( $\pm 0.2$  mm), which was not significantly different than that of the older Controls ( $1.3 \pm 0.2$  mm) (Fig. 2). However, the mean joint space at enrollment in patients with early thumb CMC OA was 0.35 mm narrower than the average joint space of the healthy Controls ( $P < 0.001$ ) (Fig. 2). Over the 3 year course of follow-up there was significant ( $P < 0.03$ ) joint space narrowing in the OA patients, at a rate of approximately 0.07 mm/yr. This rate of narrowing amounted to an average loss of joint space width of 0.22 mm (or 20%) over the 3 year period. There was no difference in the loss of joint space between males and females.

In this study we quantified rates of disease progression and cartilage thinning using data from a longitudinal study of thumb CMC biomechanics and OA progression. Our primary assumptions were that our study populations were representative of the general population, and that interbone distance is a reasonable surrogate for cartilage thickness. We found steadily decreasing cartilage thickness with disease progression between enrollment and our 3 year follow-up. Our disease progression data suggests a 10-12 year horizon to end-stage (Stage III/IV) disease; our estimated 0.07 mm/yr. rate of cartilage loss predicts ~50% cartilage thinning by 7 years, and complete erosion by 14 years. Interestingly, our OA patients presented at baseline with significantly thinner cartilage (narrower interbone distance) than our normals (1.0 mm vs. 1.3 mm). This may reflect pre-symptomatic disease-related thinning or, possibly, congenitally thin cartilage. We are currently unable to differentiate between the two. Future follow-ups will allow us to refine the rate of OA progression, and the timing of surgical intervention, which we anticipate will be

influenced by symptom severity (i.e. pain, function) rather than solely anatomy-related.

## CONCLUSIONS

Early thumb CMC osteoarthritis was demonstrated to progress in the first three years after diagnosis. Despite sex-related differences in prevalence, sex was not a factor in progression in our cohort.

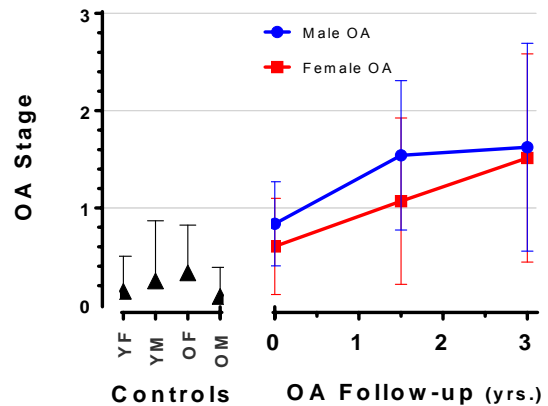


**Figure 1.** Radiographic OA stage for Controls (younger females (YF), younger males (YM), older females (OF), and older males (OM)) at their single assessment and for patients with early stage OA at baseline, 1.5 and 3 yrs. follow-up.

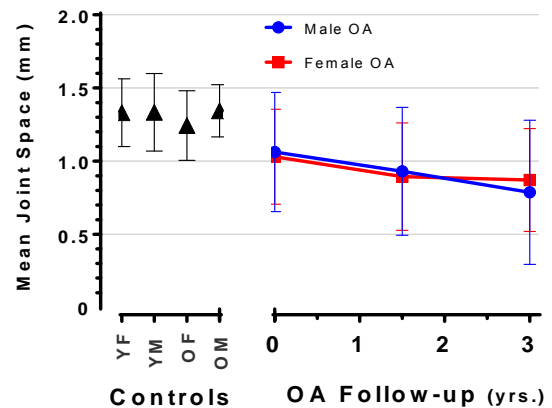


**Figure 2.** Mean (SD) joint space width, a surrogate for cartilage thickness, of the Controls and the patients over the 3 years of the study.

## ACKNOWLEDGMENTS

Supported in part by NIH/NIAMS R01AR059185

# OPTIMAL PLACEMENT OF ULTRASONIC SENSORS FOR IMPROVED MEASUREMENT OF SCAPULAR KINEMATICS

Anthony Vicini and Michelle Sabick

St. Louis University, St. Louis, MO USA

Email: [avicini@slu.edu](mailto:avicini@slu.edu)

## INTRODUCTION

Historically, x-ray imaging has been used to quantify scapular position, but it suffers from inaccuracies due to its 2D nature and involves ionizing radiation. The gold standard for tracking scapular motion is to use bone pins; however this method is invasive and not suitable for clinical situations [1]. Skin mounted optical sensors are an attractive method of quantifying scapula kinematics, but they are not accurate for overhead arm motions [1].

The major issue in tracking scapular kinematics with optical sensors is relative motion between the skin and scapula. Marker placements have been optimized into locations where the skin lies in close proximity to the bone in order to minimize such error. However, ultrasound coupled sensors have the ability to resolve the position of bone relative to skin, making this constraint unnecessary. Following work presented at ASB 2016 in which the quantity of ultrasound coupled sensors required for scapular tracking was optimized, the purpose of this study was to identify appropriate sensor locations to maximize the accuracy of scapular measurement using a reasonable number of sensors [2].

## METHODS

In this study, we built upon previous work, where the quantity of sensors was optimized [2]. Based on these results, a simulated annealing procedure was used to identify optimal locations to place sets of 3,

4, or 5 ultrasound sensors over the scapula to track its position and orientation.

Scapular models used in this experiment were extracted from CT images from the Laboratory of Human Anatomy and Embryology, University of Brussels (ULB), Belgium. CT images were created using a pitch of 0.7, increment of 1.0 mm, voltage of 120 kV, and amperage of 266 mA. Images were thresholded at 266 HU before manual adjustment to yield only the underlying bone. The files were then processed using Python 3.6.

Points on the scapula were randomly selected from a subset of locations visible to ultrasound sensors mounted on the skin to simulate a sensor pointed at each coordinate. Noise was added to points to correspond with error seen in ultrasound imaging of bone [3]. Each point was then rotated and translated by values meant to simulate realistic scapular displacement relative to the skin in overhead arm movements [4]. Displaced points were matched back to their most likely initial positions on the scapula using an iterative closest points algorithm.

After measuring the target registration error (TRE), new points adjacent to the previous ones were selected. The procedure was repeated with these points, and a subsequent trial was repeated using points based off of either the first or second trial. Which set was used to continue was based on the TRE and the current “temperature” of the simulation, which decreased over the course of the run to converge upon a specific point. By allowing worse performing points to be accepted in this

algorithm, the simulated annealing protocol is able to better converge upon complex data like the optimum sensor position [5].

The simulated annealing procedure was conducted on the Kepler supercomputing system at St. Louis University. Fifty simulations were repeated for each quantity of sensors (3, 4, or 5), each of which took approximately 9 hours to run. The data was analyzed using K-means clustering, which had cophenet values of approximately 0.86, representing a moderately high quality solution.

## RESULTS AND DISCUSSION

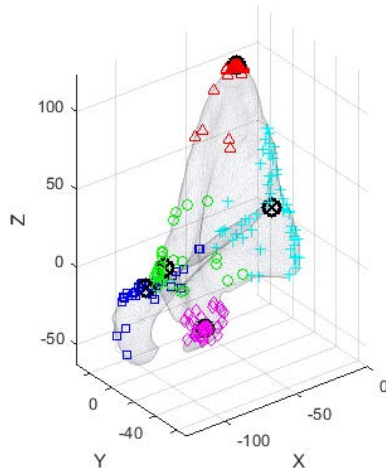


**Figure 1:** Predicted locations of ideal sensor placements using a set of five sensors.

The result of each run was a set of points that corresponded to the ideal placement location of ultrasonic probes to measure scapular location. The final positions of these sensors were overlaid in 3D on the scapula model (Fig 1). Predicted sensor locations tended to be in areas of sharp geometry changes on the bone.

K-means allowed determination of the relative accuracy of each pattern of sensor placements, where low values represent a greater likelihood of the number of unique sensor clusters (Fig 2). Similarly valued numbers at lower quantities than the number of sensors used would imply that one of

the clusters is not needed, whereas higher quantities would imply that there is more than one distinct pattern.

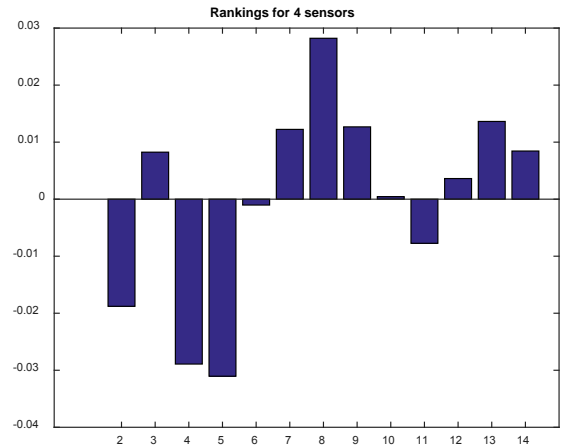


**Figure 2:** Rankings using 4 sensors show that there are 5 distinct clusters and multiple ideal arrangements are possible.

## CONCLUSION

This data represents the initial analysis of ideal ultrasonic sensor placement for tracking of scapular position in simulations representing overhead arm positions. Higher precision trials are currently running on the Kepler supercomputer to refine sensor placement, which minimized the error from over 80 mm of RMS error to sub-millimeter levels in simulations. Subsequent clinical testing is in planning.

## REFERENCES

1. Karduna AR, et al. *J Biomech Eng* **123** 184-190, 2001.
2. Vicini A, et al. *Amercian Society of Biomechanics Summer Conference*, 2016. Awaiting Publication.
3. Jain AK, et al. *Proceedings of SPIE'04*, San Diego, CA, 2004.
4. Matsui K, et al. *J Orthop Sci* **11**, 180-184, 2006.
5. Kirkpatrick SC, et al. *Science* **220.4598** 671-680, 1983.

# CHARACTERIZATIONS OF THE ELECTROMYOGRAPHY AND VIBROMYOGRAPHY SIGNALS DURING MUSCULAR FATIGUE IN THE UPPER EXTREMITY – A PILOT STUDY

\*Xueyan S. Xu, Liying Zheng, Erik W. Sinsel, Daniel E. Welcome, Ren G. Dong, and John Z. Wu  
National Institute for Occupational Safety and Health, Morgantown, WV, USA.  
\*Email: fze2@cdc.gov

## INTRODUCTION

Muscle fatigue is a complex, multifaceted phenomenon and is most commonly defined as an inability to maintain a required force level after prolonged use of the muscle [1]. It is generally accepted that muscle fatigue is associated with the initiation and development of musculoskeletal disorders (MSDs). In order to reduce work-related MSDs, ergonomic solutions, such as various wearable robotics, have been proposed and developed. Since the initial goal of the engineering intervention is to reduce the muscular fatigue of the workers, the assessment of the muscle fatigue becomes a critical step to evaluate the efficiency and effectiveness of an ergonomic product. The purpose of the current study was to evaluate the characteristics of the electromyography (EMG) and vibromyography (VMG) signals of the upper extremity during a fatigue protocol. We were especially interested in the frequency domain of these signals, since they were less noisy and were found to be associated with the muscle fatigue of the rectus femoris (RF) and vastus lateralis (VL) in the literature [2].

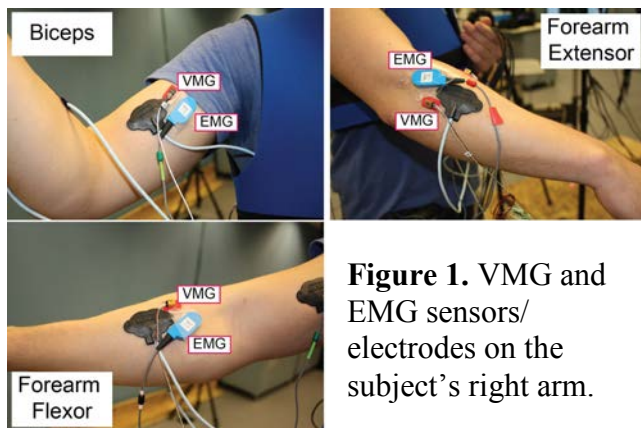


**Figure 1.** VMG and EMG sensors/ electrodes on the subject's right arm.

## METHODS

A healthy male subject (24 years old, 77.6kg, and 1.75m) consented to participate in this ongoing NIOSH IRB-approved study. The EMG and VMG signals were measured during controlled pulling tasks from three muscles of the subject's dominant right arm (biceps brachii, flexor carpi radialis, and

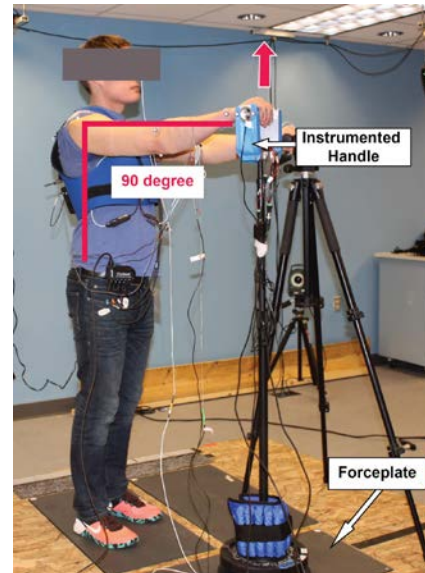


**Figure 2.** Side view of one selected test setup: a subject grips and pulls the instrumented handle with the shoulder flexion/extension at a 90-degree angle.

extensor carpi radialis, Fig 1). The loading system consisted of an instrumented handle and a pole (Fig 2). The height of the pole was adjustable to fit each subject and to assure predetermined posture. Grip force was measured by a pair of force sensors (Interface SML-100) within the instrumented handle, and the lift force was measured by the force plate (Bertec, 4080-10). The subject was instructed to pull the handle vertically while keeping the shoulder flexion/extension angle at 45, 90, or 135 degrees, and the elbow flexion/extension angle always at 0 degrees. Posture-specific pulling maximum voluntary contraction (MVC) was determined first. Then, during each test trial, after approximately 10-seconds in position resting, the subject was required to exert 60% pulling MVC and report fatigue onset. After self-reported fatigue, the subject was advised to try keeping the loading level for up to 10 seconds. There were three-minute rest breaks between trials.

A multi-channel EMG system (Motion Lab Systems Inc., MA-300) with pre-amplified electrodes (MA411) were used to acquire surface EMG signals. The EMG electrodes were placed on the skin surface approximately along the muscle fiber directions. The VMG signals were measured using tri-axial accelerometers (Endevco, M35B, mass = 0.55g). The

accelerometers were glued onto 3D-printed flat adapters, which were attached to the skin surface using double-sided adhesive tape (Fig 1). The sensors and electrodes were then wrapped with elastic cloth wrap to secure their placement. Both EMG and VMG signals were recorded in a motion capture software (Vicon Motion System Ltd., Nexus 2.3) at 1000 Hz, and analyzed in Matlab (Mathworks, Inc.). Root mean square (RMS) value of the raw EMG and VMG (total tri-axial acceleration) and the spectra characteristics (median and peak frequency) of filtered EMG and VMG were calculated for one-second non-overlapped sliding windows.

## RESULTS

Representative results from a specific trial with 90-degree arm posture are displayed in Figure 3. The top two plots show the magnitude (RMS) of VMG and EMG during the entire hold-until-fatigue test trial, which clearly demonstrated the onset of the muscle activities associated with fatigue. The EMG magnitude of the biceps and forearm extensors seem marginally increased during the stage when the subject reported fatigue. The most commonly identified trend of decreasing median frequency (MDF) during fatigue process was only found in EMG. However, the magnitude of the VMG spectra were obviously lower in the fatigue stage compared to that in the earlier part of 60% MVC. As expected, magnitude and spectra at resting were small.

## DISCUSSION AND CONCLUSIONS

Combining VMG and EMG might be a potential tool to evaluate muscle fatigue. In addition to observing the MDF change to assess muscle fatigue as suggested in the previous study [2], we suggest also considering the frequency and magnitude of the major peaks in the VMG spectra. In general, we want to draw attention to magnitude analysis of the signals besides the conventional frequency domain investigation. When tracking the entire resting-hold-until-fatigue process, the MDF might not be appropriate to detect the muscular fatigue status. Since the VMG at resting contains only background noise and is negligible, MDF calculated from these noise signals are meaningless. Further analysis of EMG and VMG data is needed to confirm the findings in this pilot study.

## REFERENCES

- [1] Latash ML, et al. *Brain Research* 961, 229-242, 2003.
- [2] Herzog W, Zhang YT, Vaz MA, Guimaraes AC, Janssen C. *Muscle Nerve*. 17(10):1156-61. 1994

**DISCLAIMER:** The findings and conclusions in this report are those of the authors and do not necessarily represent the official position of the National Institute for Occupational Safety and Health. The mention of trade names, commercial products, or organizations does not imply endorsement by the US Government.

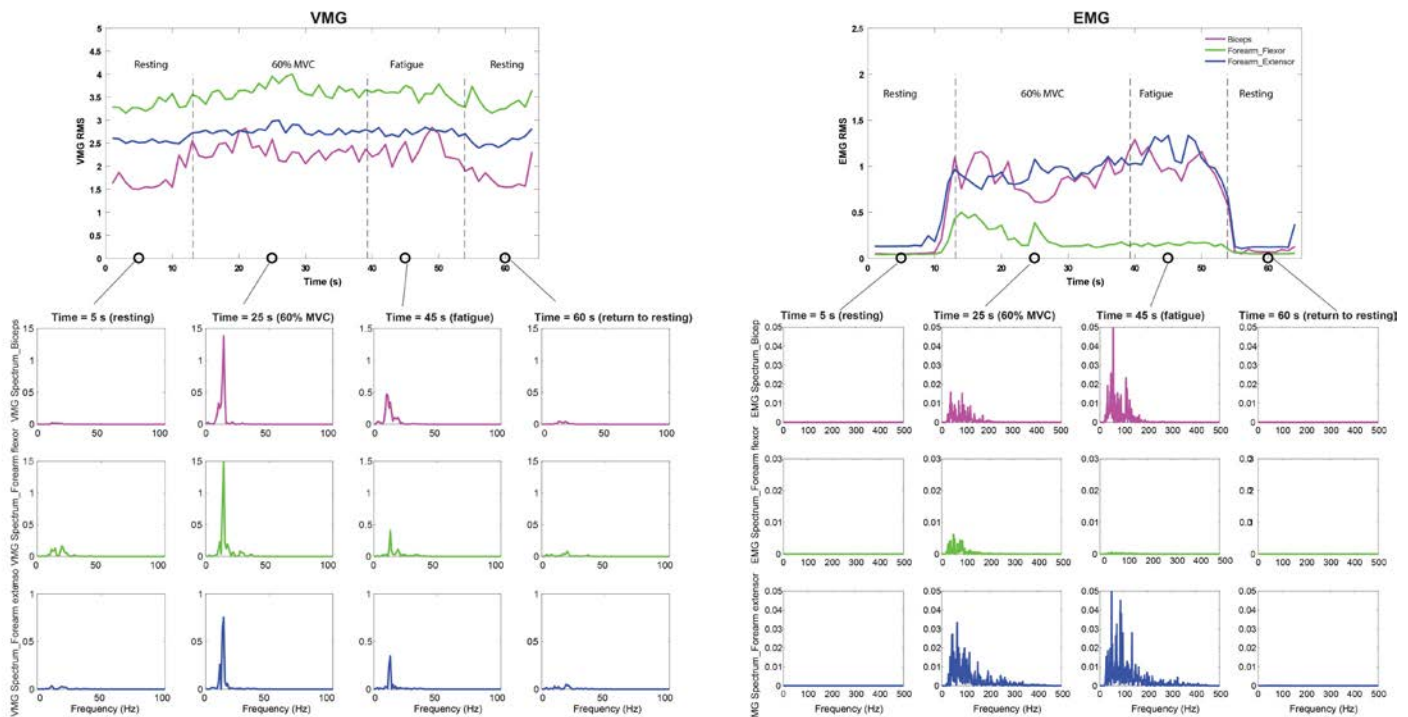


**Figure 3.** RMS of the VMG and EMG, and the representative spectrum analysis results—sampled (1-second) at different muscle status [(1) resting, (2) pulling at 60% MVC, (3) self-reported fatigue but keep pulling and trying to maintain 60% MVC, and (4) return to resting].

# THE INFLUENCE OF RESTING PECTORALIS MINOR MUSCLE LENGTH ON SCAPULAR KINEMATICS

Travis Pollen, Jason Mohring, Kelly Gerrity, Noel Goodstadt, Margaret Finley, and David Ebaugh

ReHAB Group, Drexel University, Philadelphia, PA, USA

email: [trpollen@drexel.edu](mailto:trpollen@drexel.edu), web: <http://drexel.edu/cnhp/academics/departments/Physical-Therapy/>

## INTRODUCTION

Based on the Alignment-Impairment model resting length of the pectoralis minor muscle (PMm) is believed to have a significant effect on scapular alignment and movement [1]. It has been shown that individuals with short resting PMm length have increased scapular internal rotation (SIR) and reduced scapular posterior rotation (SPR) during constrained humeral elevation tasks compared to individuals with long resting PMm length [2]. Moreover, these altered scapular rotations have been linked to subacromial impingement, rotator cuff disease, and glenohumeral instability [3,4]. Based on this information, clinicians often attempt to stretch the PMm of their patients with shoulder pain.

It is currently unknown, however, whether scapular rotations differ between individuals with short and typical resting PMm length. From a clinical perspective, this comparison is generally more pertinent than the comparison between groups with short and long resting PMm length. Additionally, typical human movement is rarely restricted to any one plane of motion, and scapular kinematics have been shown to differ between constrained and unconstrained tasks [5]. Therefore, the purpose of this study was to determine whether scapular rotations during constrained and unconstrained overhead reaching differ between individuals with short and typical resting PMm length.

## METHODS

Twenty-six individuals (sex = 17 females, age =  $26 \pm 4$  years, height =  $1.69 \pm 0.08$  m, mass =  $66.3 \pm 10.4$  kg) volunteered to participate in the study. Participants provided informed consent as per the research protocol approved by Drexel University's Institutional Review Board. To determine resting

PMm length, the coracoid process and fourth rib were palpated and marked. The distance between these marks was measured with the Palpation Meter (Performance Attainment Associates, St. Paul, MN). Resting PMm length was normalized to height to calculate the pectoralis minor index (PMi) [2]. Groups were assigned as follows: short ( $PMi < 8.9$ ) and typical ( $8.9 \leq PMi < 10.5$ ).

Flock of Bird sensors (Ascension Technology Corporation, Burlington, VT) were affixed to the participants' sternum, upper arm, and acromion on their dominant side and their trunk, humerus, and scapula were digitized using The Motion Monitor™ software (Innsport Inc., Chicago, IL). Three-dimensional kinematics were collected for three repetitions each of four arm elevation tasks: constrained = flexion, abduction, and scaption; unconstrained = overhead reach to a shelf. The shelf was set to a height above the participant's shoulder equal to 50% of their arm length [5]. Task order was randomized. For constrained tasks, participants were instructed to raise their arm over three seconds and lower over three seconds. For the unconstrained task, participants were instructed to imagine they were picking up an object from the shelf with their palm facing down.

Data were processed in Matlab (MathWorks, Natick, MA) using a custom-written program. For each task, SIR, SPR, and scapular upward rotation (SUR) (Fig. 1) were extracted at four points of humeral elevation ( $30^\circ$ ,  $60^\circ$ ,  $90^\circ$ , and  $120^\circ$ ) and averaged across repetitions. Twelve mixed model ANOVAs were conducted (one for each scapular rotation and overhead reaching task) with humeral elevation as the within-subjects factor and PMi group as the between-subjects factor. Main effects and interactions were deemed significant for  $p < 0.05$ .

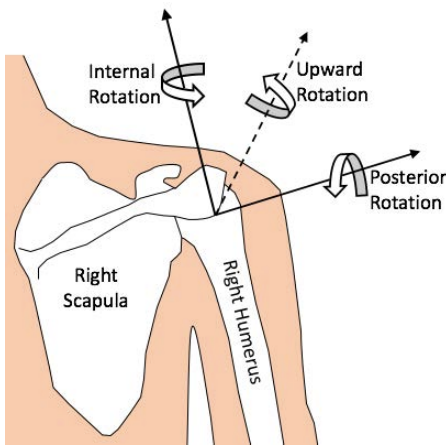


**Figure 1:** Posterior view of the right scapula and coordinate axes about which scapular internal/external, upward/downward, and posterior/anterior rotations occur.

## RESULTS AND DISCUSSION

No significant interactions occurred between humeral elevation and group for any of the four tasks. Significant main effects of group were noted for SUR in scaption ( $F(1,24) = 4.447, p = 0.046, \eta_p^2 = .156$ ), abduction ( $F(1,23) = 4.408, p = 0.047, \eta_p^2 = .161$ ), and the shelf ( $F(1,24) = 4.628, p = 0.042, \eta_p^2 = .162$ ). On average, individuals in the short group had  $6.3^\circ$ ,  $7.2^\circ$ , and  $5.8^\circ$  more SUR than individuals in the typical group for scaption, abduction, and the shelf task, respectively. No other significant main effects of group were noted. Significant main effects of humeral elevation were observed for 9 out of the 12 scapula rotations. However, these main effects were not of interest to our research question.

Our results differ from those reported by Borstad and Ludewig [2], who found increased SIR and reduced SPR in individuals with short resting PMm length compared to those with long resting PMm length. We found no differences in those scapular rotations. However, we found more SUR for the short group on three of the four tasks tested. The discrepancies between our results and Borstad and Ludewig's may be attributable to the differences in the groups compared within each study. In our study, we compared individuals with short and typical resting PMm length, while Borstad and Ludewig compared individuals with short and long resting PMm length.

The comparison of short and typical resting PMm length may be more relevant to clinicians, who generally wish to know how their patients compare to a typical population.

A previous study found differences in scapular kinematics between constrained and unconstrained tasks [5]. Thus, the fact that the short group in this study exhibited increased SUR for the unconstrained shelf task in addition to the constrained scaption and abduction tasks lends further support to our findings. However, the cause of this increased SUR is unclear at this time. Our next step will be to determine whether the observed differences fall within the limits of normal movement variability. Regardless, the majority of previous studies of individuals with shoulder pathology identified decreased (not increased) SUR as a potential risk factor [3]. Thus, from a clinical perspective, a greater amount of SUR in a patient may not be cause for concern.

## CONCLUSIONS

In this study, individuals with short resting PMm length exhibited more SUR during both constrained and unconstrained overhead reaching tasks than individuals with typical resting PMm length. Because there is little evidence correlating increased SUR with shoulder pathology [3], the common clinical practice of stretching the PMm in individuals with a short resting PMm length may not be appropriate.

## REFERENCES

1. Borstad JD. *Phys Ther* **86**, 549-557, 2006.
2. Borstad JD, Ludewig PM. *J Orthop Sports Phys Ther* **35**, 227-238, 2005.
3. Ludewig PM, Cook TM. *Phys Ther* **80**, 276-291, 2000.
4. Ludewig PM, Reynolds JE. *J Orthop Sports Phys Ther* **39**, 90-104, 2009.
5. Amasay T & Karduna AR. *J Orthop Sports Phys Ther* **39**, 618-627, 2009.

## ACKNOWLEDGMENTS

Thank you to Dr. Joseph Sarver for lending his expertise with the data processing software.

# ASSESSING GLENOHUMERAL JOINT CONFORMITY WITH A STATISTICAL SHAPE MODEL

Irene Sintini<sup>1</sup>, William Burton<sup>1</sup>, James Brownhill<sup>2</sup>, Peter Laz<sup>1</sup>

<sup>1</sup>Center for Orthopaedic Biomechanics, University of Denver, Denver, CO, <sup>2</sup>DePuy Synthes, Warsaw, IN  
email: Irene.Sintini@du.edu, Peter.Laz@du.edu

## INTRODUCTION

The mechanics of the shoulder are dependent on the underlying anatomy. Specifically, glenohumeral conformity, defined as the ratio between the humeral and glenoid radii of curvature, influences the contact mechanics and kinematics (translations) of the joint. The glenohumeral joint presents different curvatures in the coronal and transverse planes and, in both planes, has minimal geometrical constraint, deriving most of its stability from the surrounding soft tissue [1]. Further, when considering total shoulder arthroplasty (TSA), a major cause of revision is loosening of the glenoid component [2], which is influenced by implant conformity [3]. Noting tradeoffs between load transfer and constraint, recommendations on implant conformity remain unclear [3]. A systematic quantification of natural joint conformity can support implant design. Prior studies have assessed variation in glenohumeral anatomy with 2D [4] and 3D [2] measurements, relying on manual processing of the geometries. Statistical shape models (SSM) describe the full 3D shape of a bone and enable consistent, automatic anatomical measurements on populations. Prior studies have assessed morphological variation in the shoulder [5,6], but have not investigated joint conformity. The objective of this study was to develop a joint-level SSM of the humerus and scapula to investigate variation in 3D shape, with a focus on conformity.

## METHODS

The training set consisted of 37 left humeri and scapulae from healthy subjects and cadavers (age:  $73 \pm 14$ , 17 females and 20 males, 10 Caucasians and 27 Asians). Bones were segmented from CT scans and the reconstructed geometries were meshed with triangular elements (Fig. 1). A median geometry was chosen as the template; all subjects were registered to the template to establish nodal correspondence. The SSM was created by applying

principal component analysis to the nodal data representing each subject. Only geometry, and not joint alignment, was considered. Modes of variation described the anatomic variation present in the population, and each instance was represented as a series of principal component (PC) scores. Anatomical measurements were automatically performed, including humeral head and glenoid radii of curvature from best-fitting circles in the coronal and transverse planes, and from the best-fitting sphere (Fig. 1) [2]. Glenohumeral conformity and radial mismatch were computed as the ratio and difference, respectively, between the radius of the humeral head and the radius of the glenoid [2,3]. Anterior-posterior (AP) width and superior-inferior (SI) height were computed for the glenoid. Anatomical measurements and PC scores were assessed with Pearson's correlation coefficients (R).

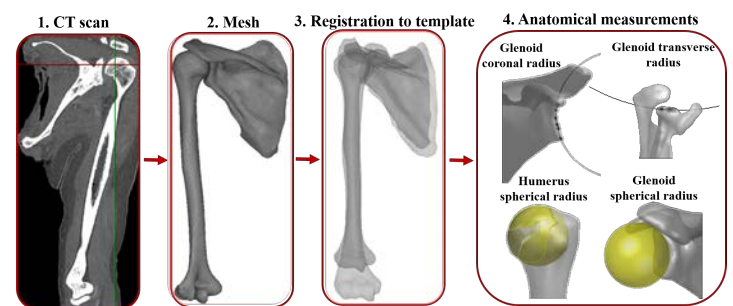


**Figure 1:** Workflow to create a statistical shape model of the shoulder.

## RESULTS AND DISCUSSION

Variation in the humeral anatomy was described as a series of modes of variation (Fig. 2); mode 1 described scaling of the bones (56% of variation explained), while mode 2 (12%) and mode 3 (6%) captured morphological changes in the distal humerus, including the epicondyles, and shoulder blade. Mode 1 was correlated with the head radius ( $R=0.71$ ), glenoid dimensions ( $R=0.66$  for SI height,  $R=0.61$  for AP width), conformity in the transverse plane ( $R=0.48$ ) and the glenoid spherical

radius of curvature ( $R=0.44$ ). Mode 4 (5% of variation explained) was correlated with spherical glenohumeral conformity ( $R=0.41$ ) and radial mismatch ( $R=-0.42$ ) (Fig. 2).

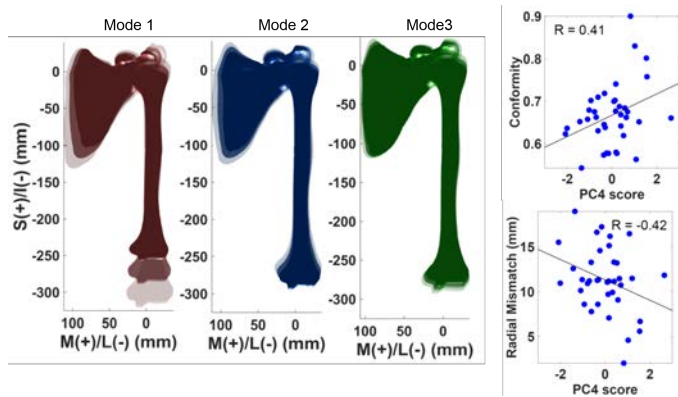


**Figure 2:** Shape modes for the first three principal components shown at mean  $\pm$  2 standard deviations (left). Correlation between the fourth PC and spherical conformity and radial mismatch (right).

Measurements of humeral and glenoid radii of curvature (Table 1) for the training set were consistent with values in the literature [2,4]. A large range of variation was observed in conformity, as evidenced by the standard deviations (Table 1) and scatter in radii data (Fig. 3). The radius of the humeral head was highly correlated ( $R=0.83$  for both AP and SI) with the size of the glenoid (Fig. 3); however, only a moderate correlation was found between the humeral head and the glenoid radius of curvature in the transverse plane ( $R=-0.44$ ), and no correlation in the coronal plane.

The current analysis was based on bone; studies have reported that the glenoid cartilage surface has a smaller radius of curvature than the subchondral bone [1]. Accuracy of the measurements was limited by the resolution of the CT scan (1 mm slice thickness) and the segmentation process. With the ability to characterize 3D variation in anatomy, the joint-level SSM developed in this study is well

suiting to investigate natural glenohumeral conformity, and to inform the design and sizing of TSA implants to restore normal biomechanics.

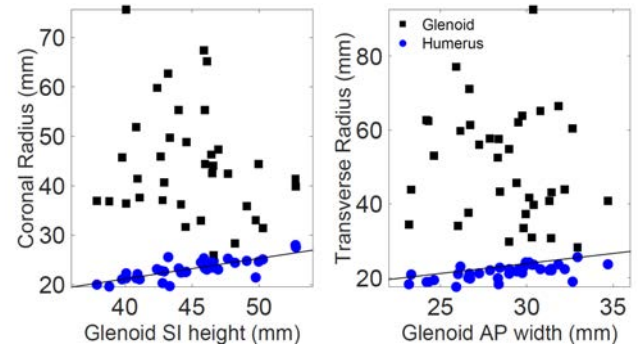


**Figure 3:** Relationship between glenoid and humeral head radii of curvatures with glenoid size. Note: an outlier with a flat glenoid was excluded.

## CONCLUSIONS

A joint-level SSM quantified the shape variation of the glenohumeral joint, which is important to understand natural shoulder constraint and support the design of shoulder implants. A large range of variation was observed in glenohumeral conformity. The humeral radius was strongly correlated with glenoid size, but not with glenoid radii of curvature.

## REFERENCES

1. Kelkar R, et al. *J Should El Surg* **10**, 73-84, 2001.
2. Walch G, et al. *Bone Joint J* **95**, 1377-1382, 2013.
3. Terrier A, et al. *J Should El Surg* **15**, 515-520, 2006.
4. McPherson EJ, et al. *J Should El Surg* **6**, 105-112, 1997.
5. Mutsvangwa T, et al. *IEEE Trans Biomed Eng* **62**, 1098-1107, 2015.
6. Yang YM, et al. *Comp Meth Bio Biomed Eng* **11**, 19-30, 2008.

## ACKNOWLEDGMENT

This study was supported in part by DePuy Synthes.

**Table 1:** Mean  $\pm$  std. deviation for humeral and glenoid radii of curvature, radial mismatch, and conformity.

	Coronal Radius	Transverse Radius	Spherical Radius
<b>Humeral Head (mm)</b>	$23.1 \pm 2.0$	$21.4 \pm 2.1$	$21.9 \pm 1.7$
<b>Glenoid (mm)</b>	$44.4 \pm 11.2$	$53.9 \pm 25.3$	$33.2 \pm 4.5$
<b>Radial Mismatch (mm)</b>	$22.9 \pm 11.3$	$32.4 \pm 26.3$	$11.3 \pm 3.6$
<b>Conformity</b>	$0.55 \pm 0.14$	$0.46 \pm 0.17$	$0.67 \pm 0.07$

# A FINITE ELEMENT MODELING APPROACH TO STUDYING INSTABILITY IN REVERSE SHOULDER ARTHROPLASTY

Vijay Permeswaran, Jessica E. Goetz, Donald D. Anderson

The University of Iowa, Iowa city, IA, USA  
email: vijay-permeswaran@uiowa.edu, web: <https://uiowa.edu/uiobl/>

## INTRODUCTION

Reverse shoulder arthroplasty (RSA) is an effective treatment for relieving pain and restoring function to individuals suffering from glenohumeral arthritis secondary to rotator cuff deficiency[1]. However, RSA has suffered from high early to mid-term rates of complication, with instability one of the most common complications. To study instability following RSA, we modified a previously reported finite element approach [2, 3] to include continuum elements representing the stabilizing influence of the subscapularis and infraspinatus tendons.

## METHODS

Axial PD Cube sequence MRI images were obtained of an intact cadaveric shoulder on a 3T GE Discovery 750W MRI Scanner (GE Healthcare, Chicago). The MRI images were segmented using Seg3D (CIBC, Salt Lake City, UT) to produce bone and tendon surfaces, as well as tendon insertion site data. The bone surfaces were smoothed using Geomagic Studio (3DS, Rock Hill, SC).

RSA implant hardware was placed within the bony geometry of the shoulder following manufacturer guidelines. This involved adjusting the humerus surface from an anatomic position into an RSA position (medial and inferior to anatomic) using Geomagic. Fully hexahedral meshes were generated in TrueGrid (XYZ Scientific Applications, Livermore CA). All resulting FE analyses were run in Abaqus/Explicit (Dassault Systemes, Vélizy-Villacoublay, France). The tendon surfaces were meshed in an undeformed state, and then displaced within the model along with the humerus (Figure 1).

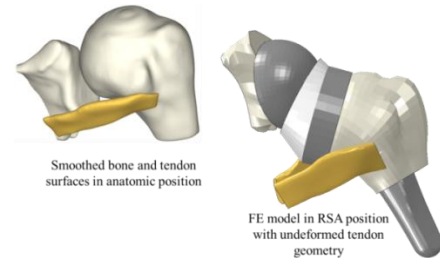


**Figure 1:** Original anatomic position of bone and tendon surfaces (left), with the RSA position of the meshed humerus and tendon in the undeformed state (right).

All tendons were assigned hyperelastic material properties using the *data point input* option in Abaqus. Source stress and strain data were from previously performed physical testing of the rotator cuff tendons.

The FE analyses consisted of three separate steps, the first two of which were used to tension the tendons while the position and rotation of the humerus was fixed. In the first step, the proximal free ends of the tendons were displaced toward their anatomic origins and 5 mm outward from the joint, to avoid any contact with bone or implant surfaces. In the second step, the proximal ends of the tendons were displaced 5 mm towards the joint, with contact now enforced between all surfaces, effectively wrapping the tendons around the glenosphere, polyethylene liner, and humeral tray.

During the third step, the humerus was prescribed to externally rotate about its long axis from neutral to 45° of external rotation. The translations of the humerus were free to displace, such that the tension and wrapping of the soft tissue dictated the position of the humerus during rotation. Three different combinations of proximal-end-tendon boundary

conditions (BCs) were evaluated during the external rotation step to represent the antagonistic eccentric contraction of the subscapularis during external rotation: (BC1) holding the proximal end of the tendon fixed in all translations, (BC2) fixing only the AP and superior/inferior (SI) translations while applying a 1000 N medially-directed load, and (BC3) applying a 1000 N load along the line of action of the tendon while allowing free translation. The subluxation of the humerus was measured for all three BCs, where subluxation was measured as the distance between the centers of rotation of the polyethylene liner and glenosphere.

## RESULTS AND DISCUSSION

For each of the three BCs, impingement was computed between the polyethylene liner and inferior glenoid bone. The primary impingement occurred at the same amount of external rotation for all cases. However, different behavior of the subscapularis tendon was observed for each, as well as different amounts of humeral subluxation. The least subluxation was computed for BC1 (2.99 mm), followed by for BC2 (3.67 mm), and the humerus subluxed the most for BC3 (4.93 mm).

The BC1 case created stable behavior of the tendon, and the tendon orientations stayed relatively fixed during the external rotation. However, excessive force (3123 N) was generated in the tendon, with associated high contact stresses (560 MPa) at the impingement site. In the BC2 case, the proximal end of the tendon translated only 8.8 mm laterally, with significantly less force developing in the AP (400 N) and SI (594 N) directions. Finally, the BC3 case displayed the most interesting result, as the tendon slid inferiorly under the humeral tray during external rotation (Figure 2).

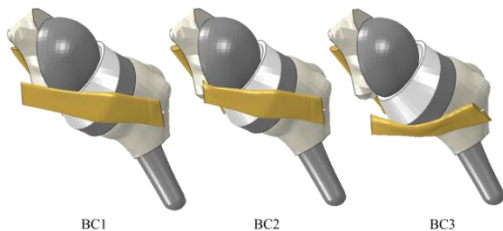


**Figure 2:** All cases are shown at the end of external rotation movement. The sliding inferior translation of the tendon is shown on the right model.

The benefit of this approach over those previously used is the inclusion of continuum tendon elements. Previously, rotator cuff soft tissues were represented as spring elements with no contact modeling to apply a buttressing, distributed load over the polyethylene liner (as would be seen *in vivo*). This new continuum element approach also provides the ability to study edge loading that develops in the polyethylene liner during impingement (Figure 3).

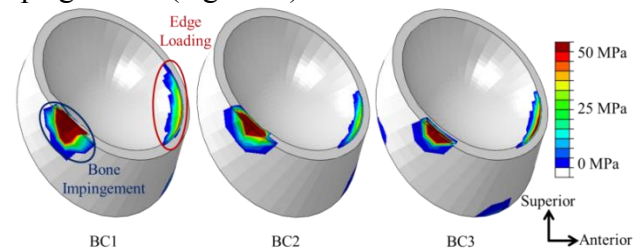


**Figure 3:** Contact stress plots of the BC1, BC2, and BC3 cases. The large contact patch located posteriorly is the impingement site with the bone, while edge loading can be seen anteriorly and inferiorly in all models

## CONCLUSIONS

We developed a finite element modeling approach to study stability in RSA using continuum element representation of soft tissue constraints, including the subscapularis and infraspinatus tendons. The boundary conditions explored at the proximal ends of these tendons influence the mechanics of the joint and need to be validated. The modeling approach allows computation of complex tendon wrapping and instability of an *in vivo* joint.

## REFERENCES

1. Boileau et al. *JSES*, 2006. **15**(5): 527-40
2. Hettrich et al. *JSES*, 2015. **24**(11): 1774-81
3. Permeswaran et al. *J Biomech*, 2016. **49**(13): 3069-73

## ACKNOWLEDGEMENTS

This research was generously funded by the University of Iowa Graduate College as well as the University of Iowa Carver College of Medicine.

# WRIST BIOMECHANICAL PROPERTIES VIA SIX DEGREE-OF-FREEDOM ROBOTIC TESTING

<sup>1</sup> Rohit Badida, <sup>1</sup> Joseph Crisco, <sup>1</sup> Douglas Moore

<sup>1</sup> Department of Orthopaedics, Warren Alpert Medical School of Brown University and Rhode Island Hospital, Providence, Rhode Island, USA

## INTRODUCTION

Clinically, mobility of the wrist is described in terms of the four anatomical directions of motion: flexion, extension, radial deviation, and ulnar deviation. However, the normal activities of daily living involve coupled motions that are combination of these directions. For example, the path from radial extension to ulnar flexion, commonly termed the “dart thrower’s motion”, is crucial for many of the activities of daily living, as well as for occupational and recreational hand use [1].

Determining the biomechanical properties of the wrist in all directions of physiological motion is required to characterize the mechanical properties of the wrist joint. Fully characterizing the mechanical properties of the wrist will advance our understanding of this complex joint. In doing so it will aid in improving orthotic and wrist implant designs, and provide a benchmark for the evaluation of treatments. Characterizing the wrist’s six degree-of-freedom (DOF) flexibility requires a sophisticated six DOF testing strategy.

Accordingly, the objective of this study was to develop a protocol for determining the complete mechanical properties of the wrist using a six degree-of-freedom (DOF) robot musculoskeletal simulator.

## METHODS

Our approach to six DOF robotic wrist simulation was based upon previous experimental protocol that used a two DOF standard material tester [2]. A six axis industrial robot (KUKA KR 6 R700, Augsburg, DE) was integrated with simVITRO labview-based control software (Cleveland Clinic, Ohio, US). The robot is equipped with a multi-axis load cell (ATI, Apex, NC) at the end effector for the measurement of forces and torques in all three Cartesian directions. This interface provides a flexible

musculoskeletal simulator to control and report joint kinetics and kinematics.

To evaluate the protocol a single forearm/hand specimen was prepared by 1) K-wire pinning to fix neutral pronosupination, 2) resection of the digits (at the metacarpophalangeal joints) and proximal 1/3 of the radius and ulna, and 3) potting in fast-setting urethane resin (Smooth-On, Easton, Pennsylvania). The distally-potted metacarpals were mounted to the robot end effector and the proximally-potted forearm was fixed to a mounting pedestal rigidly affixed to the robot base.

After mounting, the spatial relationships between the robot, load cell and the specimen were established using a 6-DOF digitizing probe (Optotrak, NDI, CA). Radius- and 3<sup>rd</sup> metacarpal-based coordinate systems were generated via the digitization of bone-based anatomic landmarks determined within a specimen-specific CT scan.

The Radial coordinate system construction:

$O_r$  – An origin at the midpoint of a line passing from the radial styloid to the ulnar styloid ( $Z_R$  axis)  
 $R_y$  - Pointing proximally, through the centroid of four points digitized around radial and ulnar shaft  
 $R_x$  - Pointing volarly, generated by crossing  $R_y$  and the  $Z_R$  axis  
 $R_z$  – Pointing radially, generated by crossing  $R_x$  and  $R_y$ .

The 3<sup>rd</sup> Metacarpal coordinate system construction:

$O_m$  – An origin at midpoint of ulnar and radial margins of the base of MC3 ( $Z_M$  axis)  
 $M_y$  - Pointing proximally, from the centroid of four points around the distal end of MC3 to  $O_m$ .  
 $M_x$  - Pointing volarly, generated by crossing  $M_y$  and the  $Z_M$  axis  
 $M_z$  – Pointing radially, generated by crossing  $M_x$  and  $M_y$ .

The wrist was tested using pure and combined wrist rotations produced using defined rotational trajectories in each of the four anatomic directions, as well twenty coupled directions (e.g. radial flexion or radial extension). End effector motion was controlled using a hybrid protocol. Rotations were controlled using position control and translations were controlled using force control. Supination/pronation rotation was set to zero. Joint forces were set to 0N and the joint translations were recorded. For each trajectory, the wrist was ramped to 150° in the specified direction and was terminated on reaching a resultant torque of 2 Nm. Data was acquired digitally at a rate of 50 Hz. Torque-rotation curves for each trajectory were reduced to yield ROM and average stiffness. The ROM and stiffness envelopes were constructed by compiling the respective values for each testing trajectory and plotting them on polar plots.

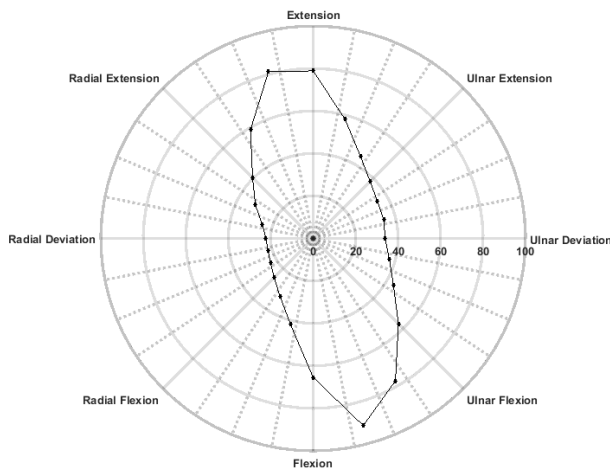


Figure 1 – Wrist ROM envelope (Degrees)

## RESULTS AND DISCUSSION

The principal direction of the wrist ROM envelope was oriented obliquely to the anatomical directions, from radial extension to ulnar flexion (Fig. 1). The largest wrist range of motion was 91.2° in the direction of ulnar flexion, 15° oblique from pure flexion. The values in the orthogonal directions of flexion and extension were 65.4° and 75.9° respectively. The largest range in the extension component was in radial extension, 15° from extension with a value of 81.3°. The ROMs in pure ulnar and radial deviation were 33.8° and 22.3°, respectively. Thus, the largest range of motion for

the wrist was oriented obliquely from radial extension to ulnar flexion.

The smallest stiffness value of 0.02 Nm/Deg was in the ulnar flexion direction and the largest stiffness value of approximately 0.1 Nm/Deg in the radial flexion direction. The principal axis of the stiffness envelope was oriented orthogonal to the principal axis of the ROM envelope.

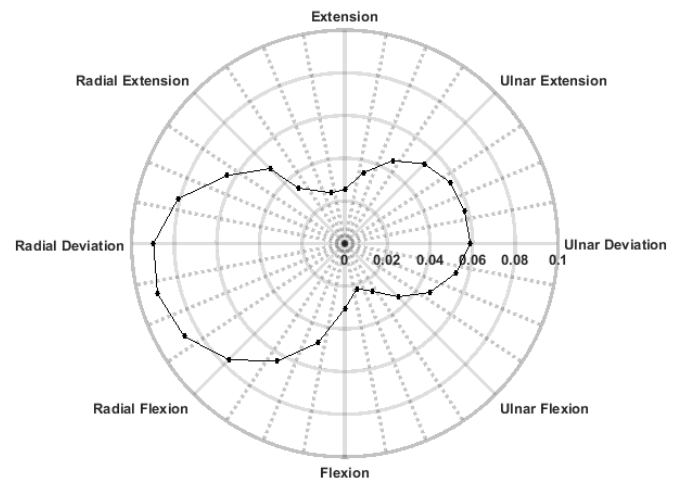


Figure 2 – Wrist stiffness envelope (Nm/Degree)

Musculoskeletal simulation using robotic testing provides an innovative and powerful technique to understand wrist biomechanics because of its multi-dimensional characteristics. A previous robotic wrist study employed a Gough-Stewart testing platform [3], but it had limited ROM (<20°). Our robotic test interface allows us to produce pure and coupled motions about wrist circumduction at 1° interval with range of motion up to 150°.

## REFERENCES

1. Palmer et al., *J Hand Surg (A)*, 1985
2. Crisco et al. *J Bone Joint Surg Am*, 2011
3. Fraysse et al. *Journal of biomechanics*, 2014

## ACKNOWLEDGEMENTS

We thank Tara Bonner, Callan Gillespie and Robb Colbrunn for their consultation regarding data acquisition using the KUKA robot and simVITRO.

# QUANTIFYING THE PASSIVE EXTENSION TORQUE OF THE SECOND METACARPOPHALANGEAL JOINT

<sup>1</sup> Gaurav Mukherjee, <sup>1,2</sup> Patrick M. Aubin and <sup>1</sup> Katherine M. Steele

<sup>1</sup> Department of Mechanical Engineering, University of Washington, Seattle, WA, USA

<sup>2</sup> Center for Limb Loss and Mobility (CLIMB), VA Puget Sound Health Care System, Seattle, WA, USA  
email: kmsteele@uw.edu

## INTRODUCTION

Impairments of the hand drastically impact an individual's ability to live independently. Neuromuscular injuries such as cerebral palsy, stroke, and spinal cord injury, in addition to arthritis and traumatic injury cause hand impairments for 15.2 million people in the United States alone. Joint stiffness is a key characteristic of many hand impairments. Comorbidities such as fixed contractures, hypertonia, atrophy due to disuse, and spasticity affect joint stiffness. Quantifying the finger joint stiffness of healthy individuals is an important first step to subsequent analyses of individuals with impairment. Careful quantitative measurement of joint stiffness has the potential to improve the diagnosis and treatment of diseases that affect the hand.

This paper presents results from a study quantifying the passive torque required to extend the index finger about the metacarpophalangeal (MCP) joint, in a quasi-static manner, from flexion to extension among unimpaired individuals.

## METHODS

In a study approved by the Institutional Review Board at the University of Washington, the extension torques for the second MCP joint were measured on both hands for 22 healthy subjects without hand impairments recruited from the University of Washington. Two subjects had incomplete datasets and were excluded. The subjects were equally distributed between males and females; all were right hand dominant. Detailed anthropometric measures, both summary body measures such as age, height, weight (Table 1), and hand specific measures such as lengths and volumetric data of the hand, and index finger were collected.

**Table 1:** Average anthropometric data, 20 subjects.

	Age (Years)	Height (m)	Weight (N)
Males (10)	26.4 ± 4.8	1.78 ± 0.07	701 ± 94
Females (10)	23.9 ± 4.0	1.65 ± 0.06	613 ± 70

Passive joint torque about the second MCP joint was measured at different angles during the extension of the second digit using a novel device that applies an external torque to the digit, while constraining the wrist at 0 degrees of extension (Fig. 1). We measured the passive internal joint extension torque in two conditions randomized on each index finger: a splinted condition (S), with extended and locked proximal interphalangeal (PIP) and distal interphalangeal (DIP) joints, and the second, the non-splinted (NS) with a neutral and unlocked PIP and DIP joint.

Angular information was collected with a video camera, in synchrony with force information ( $F_{LC}$ ) collected using a load cell (25 lbs). The video data was used to compute the angle of the MCP joint,  $\theta_{mcp}$ . These data ( $30 \pm 8$  trials) for each hand were used to compute the net passive extension torque over the range of motion for each subject computed as the difference between the torque applied by the taut string and the torque due to gravity. Dynamics were ignored because of the quasi-static nature of the test. The finger was slowly moved from 50 degrees of flexion to 0 degrees, corresponding to the long axis of the proximal phalanx aligned with the long axis of the metacarpal.

We used a two-sample t-test for independent means and unequal variance, to test our hypothesis that the mean passive extension torque about the MCP joint at 0, 10, 20, 30, 40 and 50 degrees of flexion are the same for males and females, and for dominant and

non-dominant hands. For testing the hypothesis that the mean passive extension torque about the MCP joint at 0, 10, 20, 30, 40 and 50 degrees of flexion are the same for the splinted and non-splinted conditions for each subject, we used a two-sample paired t-test. We tested our hypothesis that S and NS conditions would not affect the torque significantly with a two-sample paired t-test.

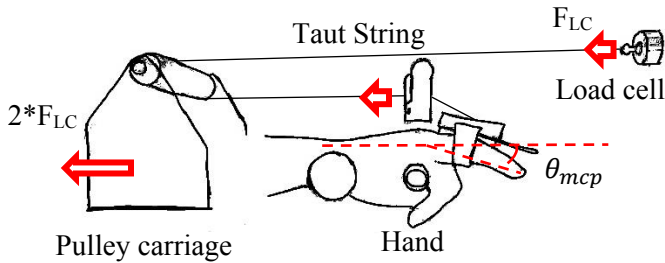


**Figure 1:** Extension torque about the MCP is measured as the difference between the torque due to the string and the torque due to gravity.

## RESULTS AND DISCUSSION

The extension torque, when the finger was in full extension (0 degrees, splinted, dominant hand), was  $10.95 \pm 2.38$  N-cm for males, and  $5.03 \pm 1.60$  N-cm for females (Fig. 2). Males had significantly higher torques for 0, 10, 20, and 30 degrees of finger flexion ( $p < 0.0029$ ). The extension torques about the MCP joint of the dominant hand were not found to be significantly different from the non-dominant hand for males ( $p > 0.6300$ ) or for females ( $p > 0.2200$ ). In the non-splinted condition, the extension torques were found to be significantly higher than the splinted condition among females, for 0, 10 and 20 degrees of flexion ( $p < 0.0120$ ). No significant difference was observed in the extension torques for males between the splinted and non-splinted conditions ( $p > 0.0930$ ), however.

We also found that torques at full extension, (0 degrees, splinted, right hand) are significantly higher than previously reported values [1], both among males ( $p < 0.0485$ ) and among females ( $p < 0.00018$ ). Interestingly, we also observed that the males have higher variance in both the splinted and non-splinted

case, which increases as the finger is extended further.

Normalizing the splinted torque by body weight times height (BWH), hand weight times hand length (HWHL) and finger weight times finger length (FWFL) decreased inter-subject variability by 9%, 18% and 21% respectively, demonstrating that finger specific measures are a better normalizing parameter for hand torques.

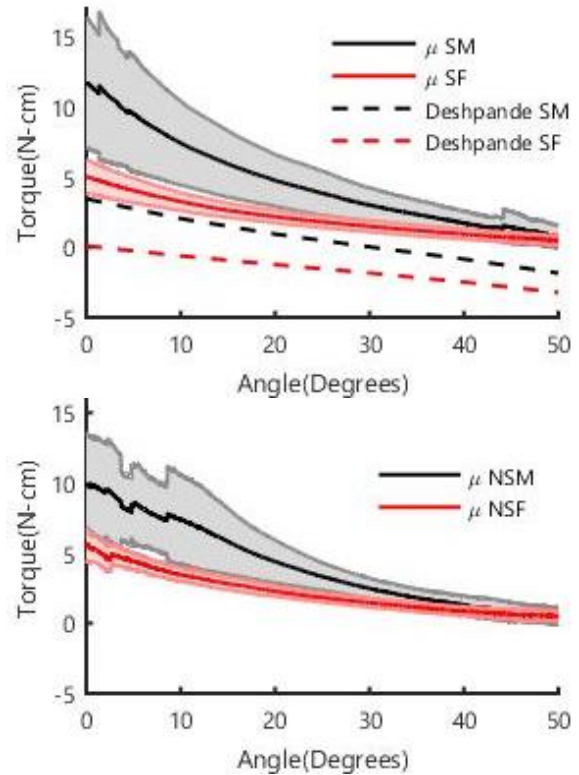


**Figure 2:** Top: torque vs angle curves for splinted males (SM) and females (SF) compared to results reported by [1], bottom: torque vs angle curves for non-splinted males (NSM) and females (NSF)

## REFERENCES

1. Deshpande et al., IEEE Trans. Biomed. Eng., 2012.

## ACKNOWLEDGEMENTS

The authors would like to acknowledge Keshia Peters, Eamon McQuaide, William Kuykendall and Srinivasan Iyer for their assistance

# DETERMINING RETURN OF SCAPULOHUMERAL RHYTHM IN PATIENTS AFTER REVERSE SHOULDER ARTHROPLASTY

Vijay N. Permeswaran, James R. Hall, Andrea P. Caceres, Donald D. Anderson, Jessica E. Goetz, and Carolyn M. Hettrich

The University of Iowa, Iowa City, IA, USA  
email: andrea-caceres@uiowa.edu, web: <https://uiowa.edu/UIOBL>

## INTRODUCTION

Reverse shoulder arthroplasty (RSA) is used for restoring pain-free function and range of motion to patients with glenohumeral arthritis and rotator cuff deficiency [3]. By reversing the ball-and-socket anatomy of the shoulder, the deltoid can compensate for rotator cuff weakness that limits arm elevation. Despite high success rates in terms of restoring pain-free mobility, patients with RSA suffer from high midterm (6-12 month) complication rates [2]. The most common complication, scapular notching, occurs when undesired contact between the humeral cup and inferior glenoid damages the implant and/or scapular bone.

Scapulohumeral rhythm (SHR) is the ratio of glenohumeral (GH) to scapulothoracic (ST) motion (Figure 1). Studies of scapular notching have presumed an immediate return to normal SHR post-RSA, which omits the recovery time and any residual abnormalities in ST motion that may influence the risk or severity of scapular notching. This study used an EOS radiographic system to image the scapula and humerus at 3 poses 6 months and 12 months post-RSA implantation to determine if a healthy SHR had returned.

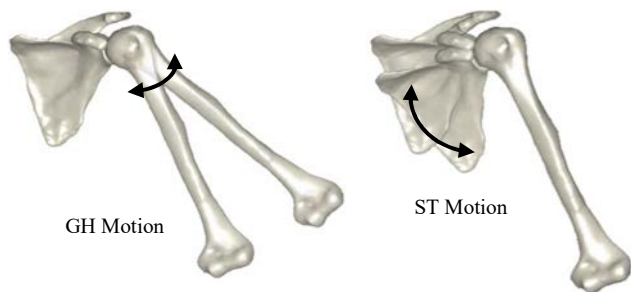


**Figure 1:** Scapulohumeral rhythm (SHR) is the ratio of glenohumeral motion (left) to scapulothoracic motion (right).

## METHODS

EOS radiographic images of the shoulder were captured for 9 patients 6 and 12 months after RSA with a Tornier Aequalis Ascend Flex (Wright Medical, Memphis, TN). EOS uses low dose x-rays to acquire simultaneous orthogonal radiographs. Images of the scapular plane and a plane orthogonal to it were acquired with the patient holding their arm at 60°, 90°, and 120° of abduction (Figure 2).

The RSA implant geometries (provided by Tornier Inc.) were imported into MATLAB (MathWorks, Natick, MA). A 3D-to-2D model image registration method previously reported by our group [1] was used to obtain the 3D pose of the glenosphere and humeral stem.

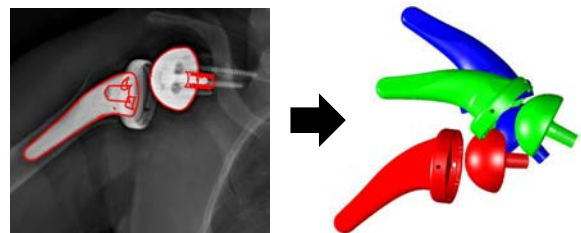


**Figure 2:** EOS images were aligned in 3D and then used to find the exact angle of the glenoid and humeral component.

From the 3D coordinates, humeral and scapular angles were calculated for the three arm abduction positions. Using Geomagic software, cylinders were fit to the distal aspect of the stem and glenosphere post to represent functional axes of the humerus and scapula, respectively.

The known axes of the cylinders of the humeral stem and glenosphere post were transformed from Cartesian coordinates to Euler coordinates using the values calculated from the alignment algorithm. This determined the angle between each component to a

neutral arm position for each angle of abduction (Figure 2). The SHR was then calculated between 60° and 90° and again between 90° and 120° using the formula ( $SHR = (\Delta H - \Delta S) / \Delta S$ ), where  $\Delta H$  and  $\Delta S$  represent the change in rotation of the humerus and scapula respectively [5]. The SHR was then divided into glenohumeral and scapulothoracic components for subjects at 6 and 12 months.

## RESULTS AND DISCUSSION

Patients 6 months post-RSA had an average SHR rhythm from 60° to 90° of 0.97:1 while 90° to 120° was 0.86:1. The average SHR of 0.91:1 calculated in this study for patients 6 months post-RSA differs from previously reported 37 month post-RSA value 1.3:1 [5] and the normal SHR of 2:1 [4] (Figure 3).

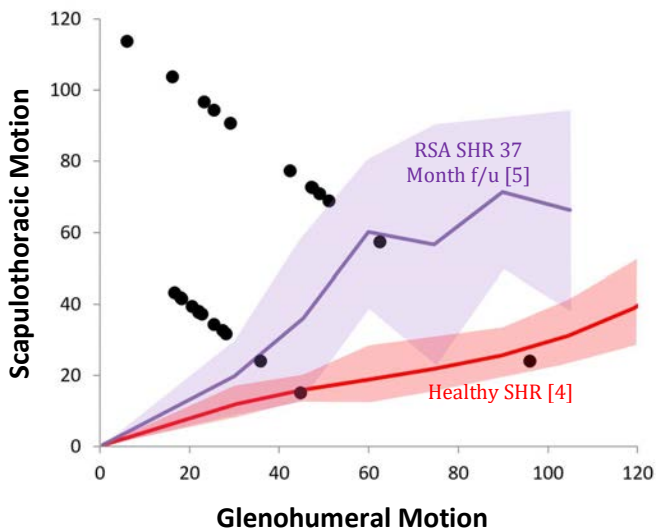


**Figure 3:** SHR values plotted as contributions of glenohumeral and scapulothoracic motion to total abduction value for all subjects at 6 and 12 months.

Preliminary data suggests high variability between each patient's 6 month and 12 month scans (Figure 4). Whereas two patients experienced lower SHRs at 12 months, one had a higher SHR.

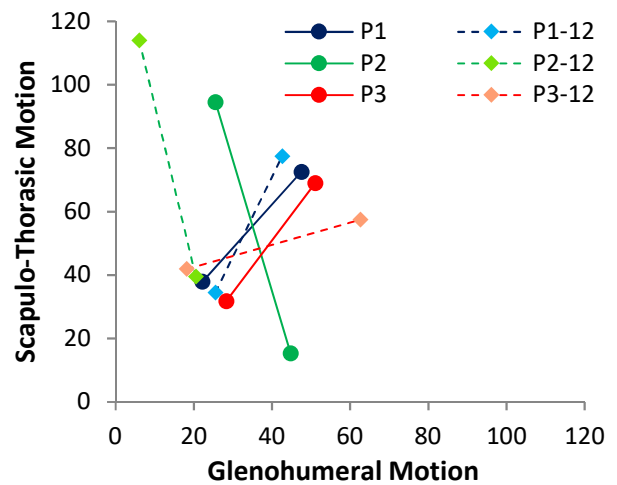


**Figure 4:** Comparison of GH and ST data for patients 6 months and 12 months post-RSA.

## CONCLUSIONS

The return of scapulohumeral rhythm may be important in understanding complications such as scapular notching in patients with RSA. Patients in this study are likely still regaining strength and function at 12 months post-RSA. Variations in recovery regimen and preexisting conditions may have influenced 6 and 12 month scapulohumeral rhythm data. These results indicate abduction ability is regained post-RSA implantation, but with increased ST motion producing a greater likelihood of impingement, which may partly explain why scapular notching is so common after RSA.

## REFERENCES

- [1] Anderson DD, et al. *Comput Math Methods Med.* **67**(8): 1112-8, 2015
- [2] Bosali KI, et al. *J Bone Joint Surg Am.* **88**:2279-92, 2006
- [3] Frankle M et al. *J Bone Joint Surg Am.* **87**(8):1697-1705,2005.
- [4] Inman V et al. *Clin Orthop Relat Res* (330): 3-12, 1996
- [5] Walker D et al. *J Shoulder Elbow Surg* **24**(15): 1129–1134, 2015

## ACKNOWLEDGEMENTS

Funding was generously provided by Tornier, Inc.

# ITERATIVE LEARNING CONTROL OF AN ELBOW JOINT MOTION SIMULATOR

<sup>1,2</sup> Patrick J. Schimoler, <sup>2</sup> Jeffrey S. Vipperman, <sup>1,2</sup> Mark Carl Miller

<sup>1</sup> Allegheny General Hospital, Pittsburgh, PA, USA

<sup>2</sup> University of Pittsburgh, Pittsburgh, PA, USA

email: pjs50@pitt.edu

## INTRODUCTION

Joint motion simulators (JMSs) are cadaveric testbeds for joint related orthopaedic research. Typically, a JMS rigidly fixes one side of a joint while actuating the free side with cables attached to its tendinous insertions with the goal of generating motion and joint loading that is as physiologic as possible. State of the art JMS control systems mix feedforward and feedback methodologies to control joint position and tendon tension [1].

Numerous factors complicate JMS control. Moment arms are a nonlinear function of joint position. Cable slack prevention, an added stability condition, arises from the uni-directional nature of cable actuation and is further complicated if small tendon tensions are desirable. Some muscles affect multiple degrees of freedom (DOFs) demanding more complicated multivariable control methods. Specimens vary in size and degrade quickly making modeling and / or identification difficult.

This study validates a combination of three control methods applied to an existing elbow JMS [2]: decoupled feedback control, antagonist tension switching, and iterative learning control (ILC). These methods combat the aforementioned control complications. Mixtures of decoupled feedback control and switching control have already been successfully applied in anthropomorphic robotics [3]. Here, the additions of ILC and a different kind of switching control, the tension measurement that closes the tension control loop is switched instead of the actuator that receives the tension controller's output signal, make this approach unique.

## METHODS

The AGH elbow JMS simulated four muscles (brachialis, biceps, pronator teres, and triceps) to actuate both kinematic DOFs: flexion / extension (FE) and pronation / supination (PS). A proportional controller generated control signals from comparisons of references and measurements for both joint position and antagonist tension. A linear map formed from identified stiffnesses and moment arms decoupled these control signals into individual muscle commands. A switching algorithm closed the antagonist tension control loops with the smaller of the brachialis and triceps tensions for FE and the smaller of the biceps and pronator teres tensions for PS preventing slack while allowing low tendon tensions. After each trial, an ILC generated new references for the next trial as a function of the previous trial's references and tracking errors.

Two fresh-frozen cadaveric elbows were chosen to bound typical cadaveric elbow sizes. The specimens were transected mid humerus and the hands were removed. The four simulated muscles were dissected down to their forearm insertions.

The JMS was commanded to track three motion types: PS while maintaining constant FE, FE while maintaining constant PS, and simultaneous FE and PS. Motions were smooth curves from 30° to 120° to 30° in 5s; 15° to 105° to 15° was used for the large arm's PS ROM because of a lack of pronation. Fixed angles were set at 30°, 90°, and 120°; 15°, 90°, and 105° were used for the large arm's pronation angles. Antagonist tension references were 0.75 LBS. The elbow was oriented with either a horizontal or vertical flexion plane. Forty iterations of the ILC were performed. RMS and max errors were calculated in both DOFs for joint position and antagonist tension.

## RESULTS AND DISCUSSION

After 40 trials (Table 1), RMS (max) joint position errors were between 0.1° and 1.4° (0.1° and 3.2°). RMS (max) antagonist tension errors were between 0.1 LBS and 0.2 LBS (0.1 LBS and 0.7 LBS) after 40 trials.

**Table 1:** RMS (and max) joint position errors. The left-hand column describes first the motion DOF and second the constant DOF's reference.

	Large Arm		Small Arm	
	Hor.	Vert.	Hor.	Vert.
<b>FE Position (°)</b>				
<b>FE Low</b>	0.6 (1.3)	0.4 (1.0)	0.5 (1.6)	0.5 (1.2)
<b>FE 90</b>	0.6 (1.1)	0.5 (1.1)	0.5 (1.4)	0.4 (1.1)
<b>FE High</b>	0.5 (1.1)	0.5 (0.9)	0.5 (1.6)	0.5 (1.2)
<b>PS 30</b>	0.1 (0.2)	0.2 (0.8)	0.1 (0.2)	0.2 (0.4)
<b>PS 90</b>	0.1 (0.2)	0.1 (0.2)	0.1 (0.1)	0.1 (0.1)
<b>PS 120</b>	0.1 (0.1)	0.1 (0.3)	0.2 (0.4)	0.1 (0.1)
<b>Sim.</b>	0.7 (2.5)	0.8 (2.2)	0.5 (1.3)	0.4 (0.9)
<b>PS Position (°)</b>				
<b>FE Low</b>	0.1 (0.4)	0.1 (0.1)	0.1 (0.1)	1.2 (3.2)
<b>FE 90</b>	1.4 (2.3)	0.9 (2.1)	0.5 (1.2)	0.1 (0.1)
<b>FE High</b>	0.1 (0.2)	0.7 (1.4)	0.2 (0.2)	0.1 (0.1)
<b>PS 30</b>	0.4 (0.8)	0.5 (1.3)	0.3 (0.8)	0.4 (1.3)
<b>PS 90</b>	0.2 (0.4)	0.2 (0.5)	0.2 (0.5)	0.1 (0.3)
<b>PS 120</b>	0.2 (0.7)	0.2 (0.8)	0.2 (0.4)	0.1 (0.3)
<b>Sim.</b>	0.5 (1.4)	0.5 (1.6)	0.3 (0.8)	0.3 (0.8)

Over 40 trials, RMS joint position errors in the DOF with motion were reduced nearly monotonically (Figure 1). By the 40<sup>th</sup> trial, joint position tracking in the DOF with motion was similar regardless of specimen or flexion plane orientation (Figure 2). Joint position in the constant DOF and antagonist tension typically showed less dramatic error reductions because they started with smaller errors prior to the ILC application. The large arm suffered from oscillations at the FE natural frequency which increased errors in joint position and antagonist tension. An elbow JMS [1] designed to actuate an elbow in any orientation was tested in the horizontal and vertical configurations (and two others) tested here and produced RMS FE joint position errors of 2.2° and 1.7°, respectively.

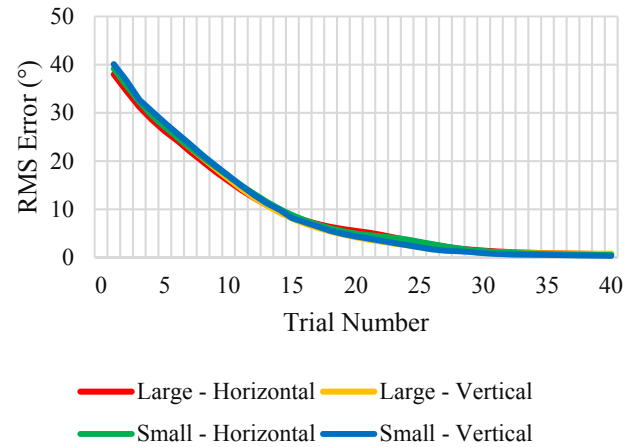


**Figure 1:** RMS FE joint position error during simultaneous FE and PS.

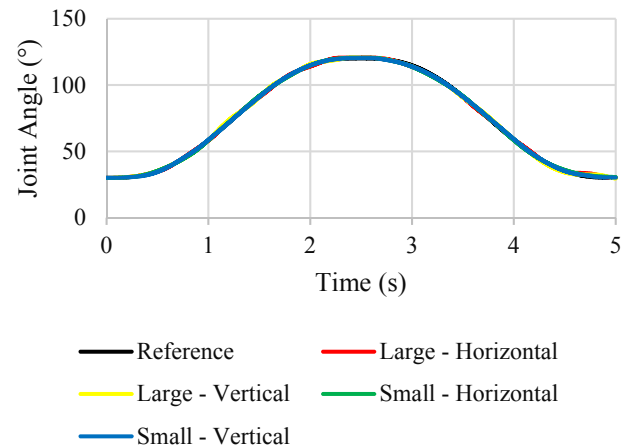


**Figure 2:** FE joint position tracking during simultaneous FE and PS during the 40<sup>th</sup> trial.

## CONCLUSIONS

JMS control is complicated by nonlinear moment arms, uni-directional actuation, muscles that interact with multiple DOFs, and specimens that vary in size and degrade quickly. Despite these difficulties, this abstract shows a combination of decoupled feedback control, antagonist tension switching, and ILC allows for accurate joint position control in both FE and PS with small antagonist tensions.

## REFERENCES

1. Ferreira. PhD, U Western Ontario, 2011.
2. Kuxhaus et al. *J Med Dev* **3**, 1-7, 2009.
3. Potkonjak et al. *Int J Adv Rob Sys* **8**, 143-155, 2011.

# THUMB CARPOMETACARPAL JOINT MOTION IN ASYMPTOMATIC PARTICIPANTS

<sup>1,2</sup> Amber R. Cussen, <sup>3</sup> Gail A. Shafer, and <sup>1</sup> Tamara R. Bush

<sup>1</sup> Department of Mechanical Engineering

<sup>2</sup> College of Osteopathic Medicine, <sup>3</sup> Mid-Michigan Center for Orthopedic Rehabilitation

<sup>1</sup> Michigan State University, East Lansing, MI, USA

email: cussenam@msu.edu

## INTRODUCTION

The thumb carpometacarpal (CMC) joint produces complex movements and is responsible for nearly 50% of upper arm function [1]. In half of aging adults, osteoarthritis develops in the thumb CMC joint impairing thumb range of motion (ROM). In this population, attenuated thumb function is presents with difficulty completing activities of daily living, buttoning clothing and opening tasks [2]. In severe cases, thumb CMC joint OA is debilitating and patients lose their functional independence.

Although many studies have evaluated thumb CMC joint motion, few have looked at motion outside of anatomical planes. In a clinical setting, goniometry is used to measure ROM, but it can only measure motion in a single anatomical plane at a time and has poor interrater reliability with differences of 7-9° between providers [3]. Current methods to measure thumb motion solely within anatomical planes has little relevance in functional hand use. For example, when reaching to grasp an object, we generally have our thumb partially radially abducted and partially palmarly abducted, resulting in motion in both the radial abduction-adduction and palmar abduction-extension planes. We hypothesize that motion capture analysis of thumb motion can be used to improve upon our knowledge of functional thumb motion, providing new measures to evaluate the differences between thumb motion in healthy and disease states.

## METHODS

Standard ROM (Figure 1) and maximal spread between index and thumb finger (functional abduction) were measured in three asymptomatic participants (ages 22-29, 1 male and 2 females).

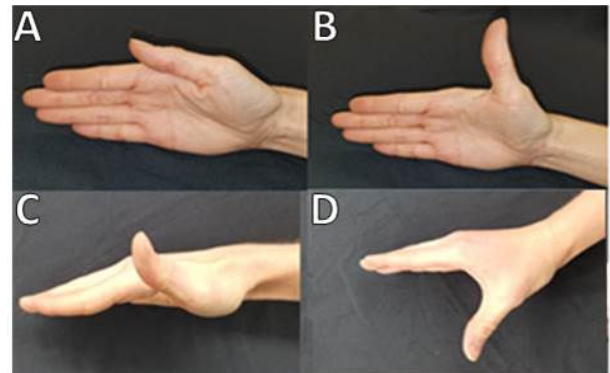


**Figure 1:** Range of motion series. a) adduction, b) radial abduction, c) extension, and d) palmar abduction.



**Figure 2:** Placement of motion capture targets on hand to capture 3D functional movements.

Repetitive thumb circumduction was evaluated in two asymptomatic participants (ages 19-22, female) and 1 osteoarthritic participant (age 66, female). Motion data were collected using a motion capture system. A total of 15 reflective targets (8 markers and 7 pods shown in Figure 1) were used to identify thumb motion and interactions with the index finger.

## RESULTS AND DISCUSSION

Each participant completed a series of motions (Figure 1) to obtain the standard clinical measures. Additionally, 3D functional measurement were captured. Functional movements consisted of

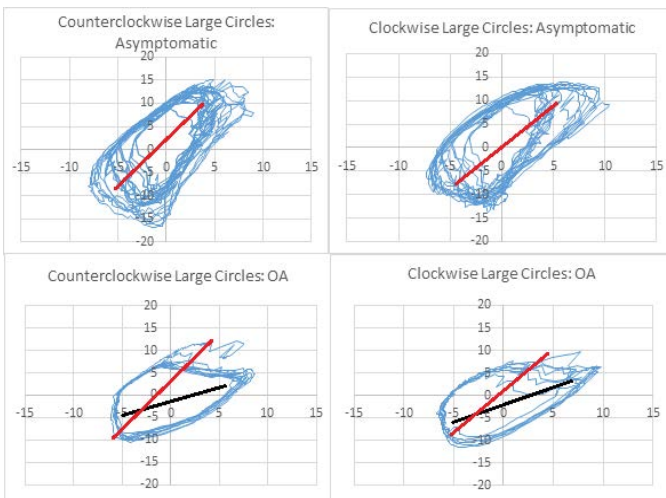


**Figure 3:** Repetitive thumb circumduction (top) asymptomatic participant and (bottom) OA participant. Line overlays show the orientation of the circular movement is shifted between the two participants. The largest radii (red line depicts asymptomatic) is shifted in the OA participant (black line).

maximal thumb and index finger spread and thumb circumduction tasks. Functional abduction was the sum of motion found in radial and palmar abduction directions but allowed for greater spread between the thumb and index finger than isolated palmar or radial abduction alone (Table 1). The larger distances translate to larger motions.

On average, our OA participant took longer to complete thumb revolutions than the asymptomatic participants in the circumduction task. The axis of CMC joint motion was altered in our OA participant and had limited motions compared to asymptomatic controls (Figure 3 and Table 2). Based on our initial findings, OA participants may demonstrate a shift in their axis of motion during circumduction tasks,

**Table 1:** Maximum distance between distal pods during range of motion, a larger distance indicates a larger angle. For abduction tasks, distance was measured between distal thumb and index phalanges markers. For opposition, distance was measured between the distal thumb marker and the marker at the base of the 5<sup>th</sup> metacarpal.

	Asymptomatic #1	Asymptomatic #2	Asymptomatic #3
Radial abduction	154.4 mm	133.4 mm	139.9 mm
Palmar abduction	150.6 mm	140.8 mm	141.5 mm
Functional abduction	168.4 mm	145.1 mm	152.9 mm

**Table 2:** Average time for a revolution (seconds/revolution) in clockwise (CW) and counterclockwise (CCW) circumduction tasks.

Task	Asymptomatic #1	Asymptomatic #2	OA
CW	1.89 ± 0.1	2.12 ± 0.2	2.47 ± 0.3
CCW	2.1 ± 0.2	1.9 ± 0.2	2.01 ± 0.3

however additional data are necessary to confirm this trend. These initial results also suggest that functional measures indicate a larger motion, and by gathering both dynamic data sets and movements that relate to functional measures, we may be able to improve our understanding of kinematics in OA participants. In particular, if we can identify measures that are more sensitive to changes, early onset of functional loss could be identified and interventions prescribed earlier.

Functional measures differ from the planar measures that are typically gathered in a clinical setting and may provide additional insight with regard to joint laxity issues or changes that occur during therapies. A limitation of this work is that our sample is small and results are initial data sets. Additional data collection is ongoing and will be compared in depth to standard clinical measures.

## REFERENCES

1. Luker KR, et al. *Clin Orthop Relat Res* **472**, 1123-1129, 2014.
2. Arden N. *Best Pract. Res. Clin. Rheumatol* **20(1)**, 3-25, 2006.
3. Lewis E, et al. *Am J Occ Ther* **64**, 555-561, 2010.

## ACKNOWLEDGMENTS

We thank our participants and lab members, in particular Josh Drost and Megan Luzenski, for their help with data collection. Funding for this project was provided by MSUCOM Research & Advanced Studies Program/DO-PhD program.

# A SUBJECT-SPECIFIC SHOULDER CAPSULE MESH MDOEL TRAINED WITH IN-VITRO DATA

Andrew Kraszewski, Andreas Kontaxis

Hospital for Special Surgery, New York, NY, USA

email: kraszewskia@hss.edu, web: [https://www.hss.edu/research-staff\\_kraszewski-andrew.asp](https://www.hss.edu/research-staff_kraszewski-andrew.asp)

## INTRODUCTION

The contribution of the glenohumeral shoulder capsule to glenoid loading is only generally understood. Upper extremity musculoskeletal models do not typically include this soft tissue. Better understanding of its function through computer simulations is necessary.

**The objective of this work was to: 1) describe a mesh wrapping model of the glenohumeral capsule, and 2) train the mesh with an in-vitro laxity dataset and report its accuracy.**

## METHODS

*Specimen Preparation & Testing.* Fourteen fresh frozen cadavers were CT-scanned, and then dissected down to the capsule. Marker clusters were rigidly attached and anatomic landmarks calibrated with 3D motion capture (0.2mm average residual). Each specimen was potted in rigid fixtures then attached to a glenohumeral laxity device (Figure 1).

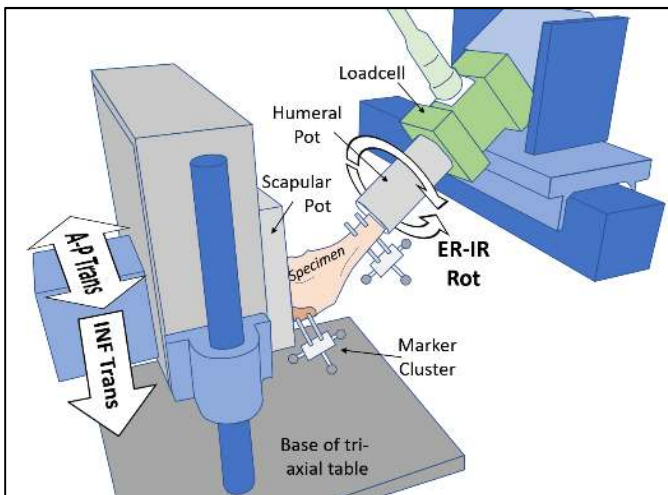


**Figure 1:** Illustration of capsular laxity testing device. Each specimen (center) was inverted.

Rotational laxity in external and internal axial directions was measured at 30fps at  $5.0^{\circ}\text{s}^{-1}$  of applied rotation, up to 2,000 N-mm. Laxity was tested across

five physical levels (baseline, lax, and 5mm, 10mm, 15mm plication) and four positions ( $0^{\circ}$ ,  $20^{\circ}$ ,  $40^{\circ}$ ,  $60^{\circ}$  scaption).

*Data Processing & Modeling.* The training data subset was internal and external axial rotation trials recorded in the baseline condition in all four scaption positions. Six degree-of-freedom glenohumeral position and axial torque were normalized to integer frame increments of axial rotation from zero to maximum torque. Four points on the glenoid capsule insertion and five on the humeral insertion were taken from 3D CT reconstruction. They were interpolated using a cubic spline to 24 origin to insertion points. Five transverse (circumferential) lines were used between origin and insertion (Figure 2). The articular humeral surface was a 23.0mm radius sphere modeled after the CT.

Per frame, mesh nodes were solved for with nonlinear optimization by minimizing a cost function summing the weighted squared inter-node lengths. Origin to insertion line lengths were weighted per published data.[1,2] Slack length was set to zero and the nodes were constrained not to penetrate the sphere.

Then, the mesh stiffnesses (weights) and slack lengths were trained (optimized), keeping the mesh coordinates constant, by minimizing the sum squared error between the mesh-estimated torque and in-vitro torque. Torque RMSE was calculated between the in-vitro data and the model for each direction-position combination. All mesh calculations were performed in MATLAB.

## RESULTS AND DISCUSSION

A single specimen's data was used to train the subject-specific mesh model. The torque-angle profiles (Figure 3) show good agreement with the mesh model and experimental values for external rotation, averaging 82.2 N-mm error. Internal

rotation agreement was worse, averaging 287.7 N-mm (Table 1). For internal rotation, as scaption increased so did RMSE error; furthermore, errors at the beginning and end of the trials were higher than external rotation.

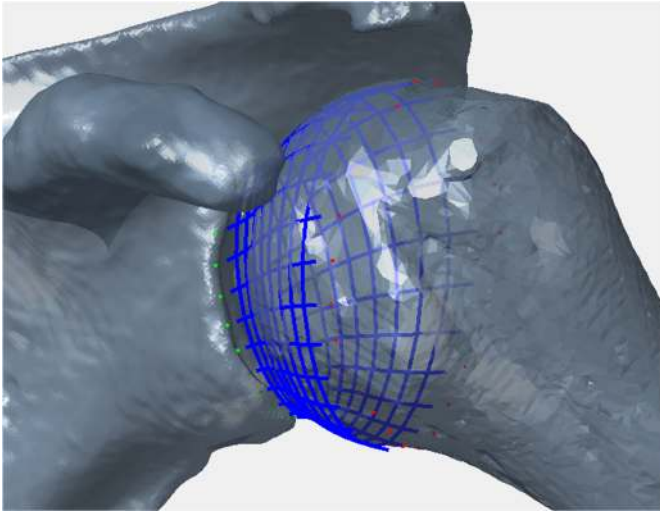


**Figure 2:** Example 3D rendering of the capsule mesh model.

## CONCLUSIONS

The capsule mesh model torque prediction was better in external rotation than in internal rotation. Mesh models are more computational efficient than finite element models, and can be more easily combined with musculoskeletal models. Therefore, they can be viewed as an intermediate solution between current independent muscle lines and more sophisticated approaches.

Future work will refine the model using a broader approach that includes simultaneous optimization of element properties and mesh coordinates. Mesh models are expected to have important applications in both orthopaedic and sports performance arenas.

## REFERENCES

1. Bigliani LU et al. *J Ortho Res*, 1992.
2. Ticker JB et al. *J Shoulder Elbow Surg*, 1996.

## ACKNOWLEDGMENTS

HSS Soft Tissue Fund

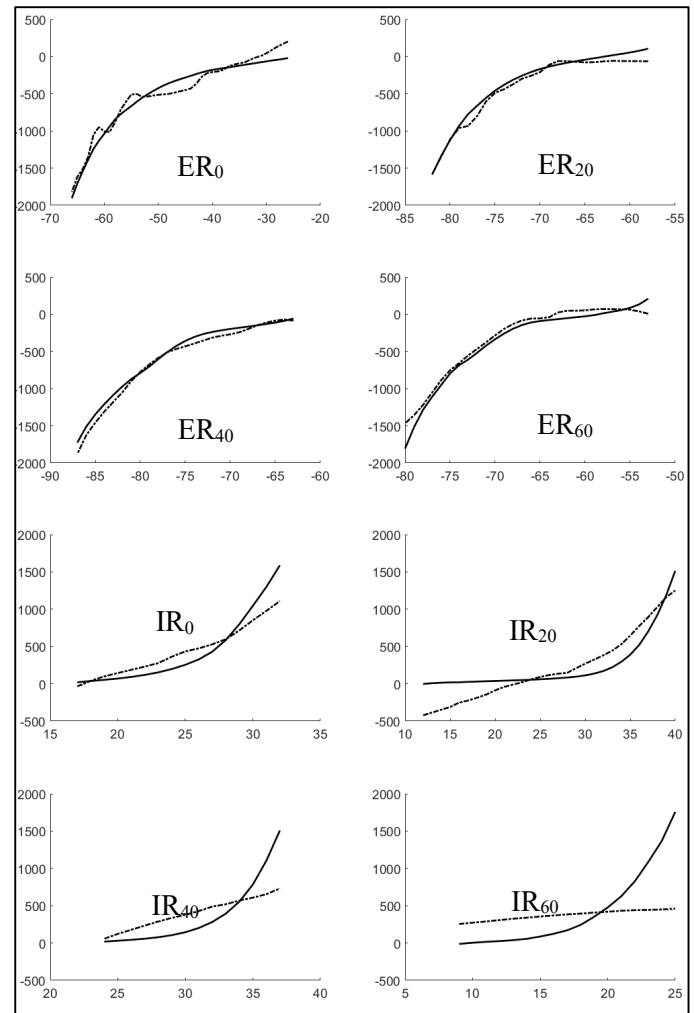


**Figure 3:** Torque-angle profiles. The vertical axis is torque (N-mm) and horizontal axial rotation ( $^{\circ}$ ). The solid line represents in-vitro torque and dotted line is mesh estimated torque.

**Table 1:** RMSE between mesh-estimated torque and experimental in-vitro torque for eight test motions.

Test Motion	RMSE (N-mm)
ER <sub>0</sub>	110.4
ER <sub>20</sub>	77.5
ER <sub>40</sub>	69.7
ER <sub>60</sub>	99.3
IR <sub>0</sub>	179.7
IR <sub>20</sub>	211.4
IR <sub>40</sub>	287.8
IR <sub>60</sub>	472.0

# THE INFLUENCE OF HAMSTRING STIFFNESS ON ACL LOADING CHARACTERISTICS

<sup>1</sup> Justin P. Waxman, <sup>2</sup> J. Troy Blackburn, <sup>1</sup> Christopher K. Rhea, <sup>1</sup> Randy J. Schmitz,  
<sup>1</sup> Robert A. Henson, & <sup>1</sup> Sandra J. Shultz

<sup>1</sup> Department of Kinesiology, University of North Carolina at Greensboro, Greensboro, NC, USA

<sup>2</sup> Department of Exercise and Sport Science, University of North Carolina at Chapel Hill, Chapel Hill, NC, USA

Email: [jpwaxman@uncg.edu](mailto:jpwaxman@uncg.edu), Web: <https://kin.uncg.edu/research/labs/anrl-lab/>

## INTRODUCTION

Hamstring musculo-articular stiffness ( $K_{HAM}$ ) is a modifiable neuromechanical property that may contribute to anterior cruciate ligament (ACL) loading and noncontact ACL injury risk by helping control sagittal-plane tibiofemoral forces and motions. Individuals with higher  $K_{HAM}$  display biomechanical characteristics associated with lesser ACL loading during controlled non-weight bearing perturbations [1] and double-leg jump landings [2] compared to individuals with lower  $K_{HAM}$ . However, these associations have been made with males and females combined in the same analyses, and without equal sex-stratification. Because females display lesser  $K_{HAM}$  [3], and biomechanical characteristics indicative of greater ACL loading [4], compared to males, it is difficult to tease out the unique contribution of  $K_{HAM}$  to ACL loading characteristics versus other sex-dependent factors. Additionally, noncontact ACL injuries more frequently occur during single-leg rather than double-leg jump landings [5]; however, the extent to which  $K_{HAM}$  contributes to ACL loading characteristics when landing on a single leg is unknown. Therefore, the purpose of this study was to determine, within each sex, the extent to which  $K_{HAM}$  predicts biomechanical characteristics of ACL loading during a single-leg stop-jump (SLSJ) task, after controlling for body positioning at initial ground contact (IC).

## METHODS

$K_{HAM}$  and SLSJ landing biomechanics were assessed in 36 males ( $21.5 \pm 2.0$  yrs,  $1.8 \pm 0.1$  m,  $81.4 \pm 11.0$  kg) and 33 females ( $21.1 \pm 2.0$  yrs,  $1.7 \pm 0.1$  m,  $63.0 \pm 9.1$  kg) following a 5-minute warm-up.  $K_{HAM}$  was assessed via free-oscillation, using a standardized assessment load equal to 10% body mass [1, 3]. SLSJ

landing biomechanics were assessed via a force platform integrated with an 8-camera motion tracking system. The SLSJ consisted of the following: 1) a single-leg forward broad jump to the force platform from a starting distance equal to 40% body height, 2) a single-leg landing on the force platform followed by an immediate single-leg jump for maximum vertical height, and 3) a second single-leg landing back on the force platform. Data from 5  $K_{HAM}$  trials and 5 SLSJ trials were averaged.  $K_{HAM}$  data were normalized to body mass whereas force-related data were normalized to body weight.

Sex differences were confirmed via separate one-way analyses of variance. The extent to which  $K_{HAM}$  predicted ACL loading characteristics, after controlling for body positioning at IC (i.e. trunk center-of-mass position relative to the center-of-pressure, hip-flexion angle =  $HF_{IC}$ , and knee-flexion angle =  $KF_{IC}$ ), was determined via separate, sex-specific, hierarchical multiple linear regression analyses. A single ACL loading characteristic (i.e. anterior tibial translation = ATT, anterior tibial acceleration = ATA, or proximal tibia anterior shear force = PTASF) was used as the criterion variable in each model. Body positioning variables were collectively entered into the first block as suppressor variables, and  $K_{HAM}$  was entered into the second block to determine its independent contribution.

## RESULTS AND DISCUSSION

Females were significantly shorter ( $p < .001$ ), had less body mass ( $p < .001$ ), displayed greater  $K_{HAM}$  ( $13.4 \pm 2.6$  vs  $15.1 \pm 2.3$   $N \cdot m^{-1} \cdot kg^{-1}$ ,  $p = .005$ ), and performed the SLSJ with less  $KF_{IC}$  ( $2.9 \pm 6.9$  vs  $-0.9 \pm 8.1^\circ$ ,  $p = .041$ ) than males. Our finding that females displayed lesser  $KF_{IC}$  than males is consistent with previous work [6]. However, this is the first study to

our knowledge to observe higher normalized  $K_{HAM}$  in females compared to males, as previous work has found females to display lesser  $K_{HAM}$  using identical assessment methodology [1]. Nonetheless, these between-sex differences indicate that our decision to use sex-specific regression models was justified.

When examining the extent to which  $K_{HAM}$  predicted ACL loading characteristics, after controlling for body positioning at IC, only the full prediction models for ATA (females) and PTASF (males and females) were significant. When predicting ATA, the linear combination of body positioning and  $K_{HAM}$  predicted 28.0% ( $p = .049$ ) of the variance in ATA. Once differences in body positioning were controlled for ( $R^2 = .277, p = .023$ ), the  $K_{HAM}$   $R^2$  change was not significant ( $R^2\Delta = .003, p = .720$ ). Additionally, only the parameter estimate for  $HF_{IC}$  was significant ( $0.074, p = .014$ ); and the relationship was such that, after holding all other predictors constant, greater  $HF_{IC}$  predicted greater ATA. Similarly, the combination of body positioning and  $K_{HAM}$  predicted 36.9% ( $p = .005$ ) and 33.7% ( $p = .018$ ) of the variance in PTASF for males and females, respectively. Once differences in body positioning were controlled for (males:  $R^2 = .295, p = .010$ ; females:  $R^2 = .319, p = .010$ ), the  $K_{HAM}$   $R^2$  change was not significant for either sex (males:  $R^2\Delta = .074, p = .065$ ; females:  $R^2\Delta = .018, p = .393$ ). Only the parameter estimate for  $KF_{IC}$  was significant (males:  $p < .001$ ; females:  $p = .005$ ); and the relationship was such that, after holding all other predictors constant, greater  $KF_{IC}$  predicted greater PTASF. These findings collectively indicate that  $K_{HAM}$  was not a unique predictor of ACL-loading characteristics in either sex when landing on a single leg.

While higher  $K_{HAM}$  values have been shown to be associated with lesser ATT and PTASF, these relationships were established using non-weight bearing perturbations [1] and double-leg jump landings [2], respectively, whereas we used a SLSJ as our model for injury. This distinction between tasks is important because between-task differences have the ability to influence initial body positioning, which can in turn influence the functional role of the hamstring and quadriceps muscles on knee-joint biomechanics, and ultimately ACL loading

characteristics. In this regard, it is likely that the SLSJ used in this study elicited a more upright landing style (more posterior trunk center-of-mass position and lesser  $HF_{IC}$  and  $KF_{IC}$ ) compared to the double-leg jump landing used previously [2], which may have reduced the hamstrings ability to effectively resist ACL loading characteristics. Thus, between-task differences may have contributed to our contradictory findings, and caution should be taken when attempting to compare our findings to prior work.

## CONCLUSIONS

After controlling for initial body positioning,  $K_{HAM}$  was not a significant predictor of ACL loading characteristics during the SLSJ in either sex. These findings differ from previous work examining other tasks and suggest that  $K_{HAM}$  may not be as effective at resisting biomechanical characteristics of sagittal-plane ACL loading during a single-leg landing, which is performed in a more upright/erect landing style. While additional studies are needed to better understand the functional role of the hamstrings during dynamic single-leg movements, current injury prevention strategies are encouraged to equally focus on improving  $K_{HAM}$  and promote safer (more flexed) landing positions.

## REFERENCES

1. Blackburn JT, et al. *Clin Biomech*, **26**, 278-283, 2011.
2. Blackburn JT, et al. *J Athl Train*, **48**, 764-772, 2013.
3. Blackburn JT, et al. *Clin Biomech*, **24**, 65-70, 2009.
4. Chappell JD, et al. *Am J Sports Med*, **30**, 261-267, 2002.
5. Olsen OE, et al. *Am J Sports Med*, **32**, 1002-1012, 2004.
6. Chappell JD, et al. *Am J Sports Med*, **35**, 235-241, 2007.

## ACKNOWLEDGMENTS

Funding for this study was provided by the American Society of Biomechanics' Graduate Student Grant-In-Aid program.

# THE EFFECTS OF AN EXTENSION CONSTRAINT FUNCTIONAL KNEE BRACE ON LIMB SYMMETRY IN SINGLE- AND DOUBLE-LEG LANDINGS IN ACL-RECONSTRUCTED PATIENTS

<sup>1</sup>Evan McConnell, <sup>2</sup>Thomas K. Miller, <sup>1</sup>Jonathan Gladish, <sup>1,2</sup>Robin M. Queen

<sup>1</sup>Department of Biomedical Engineering and Mechanics, Kevin Granata Biomechanics Lab, Virginia Tech, Blacksburg VA, USA

<sup>2</sup>Department of Orthopaedic Surgery, Virginia Tech Carilion School of Medicine, Roanoke, VA  
email: rmqueen@vt.edu web: beam.vt.edu/granatalab

## INTRODUCTION

Approximately 100,000 ACL reconstructions (ACL-R) are performed in the United States each year.<sup>1</sup> Physicians commonly prescribe the use of a functional knee brace for ACL-R patients as they resume activity to protect the knee and reduce re-injury risk. The effects of these braces on movement and loading patterns have been previously analyzed, specifically to assess the brace's effect on side-to-side symmetry in movement and loading patterns.<sup>2</sup>

Previous work has examined the utility of different movement tasks in assessing return-to-sport (RTS) readiness. Assessing side-to-side symmetry in hop distance during a series of single-leg hopping tests has been the primary method of determining RTS readiness, but these tests have not been previously characterized by measures of movement quality.<sup>4</sup> Therefore, the purpose of this study was to examine loading patterns during a variety of single leg and bilateral jumping tasks in ACL-R patients in order to quantify the effects of time since surgery and functional knee bracing on loading symmetry using a novel, single sensor insole. Based on previous work, we hypothesized that brace wear and time since surgery would affect side-to-side symmetry in loading patterns.

## METHODS

Thirty ACL-R patients (9 males, 21 females; 19.4±4.2 years old; 1.73±0.07m; 72.36±13.50kg; 6.8±1.2 months after ACL-R) participated in the study. Subjects were tested at the time of physician clearance to return to sport-specific activities, and 17 of the subjects repeated the testing again three months later. All subjects received a custom fit, extension constraint functional knee brace (DonJoy Orthopaedics, Vista, CA) prior to participation. Subjects were instructed to wear the brace during all

activities more dynamic than walking throughout the course of the study. All subjects signed either an IRB approved consent or assent form prior to testing.

The testing protocol consisted of a battery of tests done in a braced and a non-braced condition, with testing order being randomized between conditions for each subject. The test battery included three countermovement jumps and a series of single-leg hops. The single-leg hop tasks included two trials each of a single (SH), triple (TH) and crossover (CH) hop for maximum distance and a 6-meter speed hop (6m).<sup>5</sup> These tasks were completed first on the nonsurgical limb followed by the surgical limb. A set of single-sensor force-sensing insoles (pedoped, Novel Electronics, St. Paul, MN) was used to record the normal force between the foot and the shoe during all tasks (100Hz). Data was collected and stored on an iPad via Bluetooth. Physical performance metrics were also recorded and included countermovement jump height, hop distance and hop speed.

A custom written Matlab (MathWorks, Natick, MA) program was used to analyze each limb's peak load during all tasks. In addition, loading rate (LR) was determined for the single hop and countermovement tasks. Values were averaged across trials for each subject, for each limb for every movement task. A limb symmetry index (LSI) was calculated for each variable based on the following equation:

$$LSI = \frac{|X_{Sx} - X_{NSx}|}{0.5 * (X_{Sx} + X_{NSx})} * 100\%$$

where  $X_{Sx}$  and  $X_{NSx}$  denote data for the surgical and contralateral limbs, respectively. This created a set of LSI values for each variable at each time point and in each bracing condition. A Shapiro-Wilk test for normality revealed that many of the variables were

not normally distributed. As a result, a series of Kruskal-Wallis ANOVAs were performed to detect differences in the LSI values with regards to testing timepoint and bracing condition ( $\alpha=0.05$ ). All statistical analysis was performed in JMP Pro 12 (SAS, Cary, NC).

## RESULTS AND DISCUSSION

Side-to-side symmetry in the single hop peak load was significantly improved at the second testing time point (Table 1). No other significant differences were observed for the other variables of interested when examining changes based on brace condition or time.

The LSI values for peak load during the single leg hopping tasks fell mostly below the 10% symmetry benchmark that is used to determine RTS readiness. However, the LSI values for peak load during the countermovement jump were above this benchmark, meaning that considerable loading asymmetry between limbs existed during this task. This agrees with previous work that has shown significant side-to-side differences in peak vGRF during bilateral landing.<sup>2,3</sup> These data show that ACL-R athletes may utilize different landing strategies between single leg and bilateral tasks. Additionally, the LSI values given for loading rates during the single hop and countermovement jump tasks were also well above the clinical asymmetry benchmark. This is in agreement with other work that has reported significant side-to-side asymmetry in loading rates during a bilateral landing task.<sup>6</sup> These results indicate that loading rate may be an important metric to consider when assessing an ACL-R athlete's readiness to return to sport.

The data show that the presence of the brace did not significantly change side-to-side symmetry in

loading parameters or in performance metrics (Figure 1). These results differ from previous work that reported increases in peak vGRF values in both

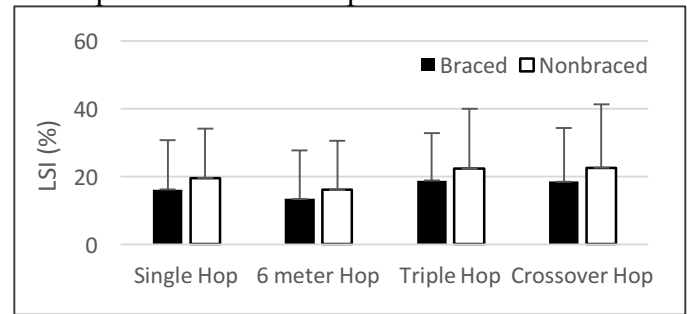


**Figure 1:** LSI Values for Hop Distances Between Bracing Conditions

limbs while wearing a brace during a bilateral landing task.<sup>2</sup> The lack of differences between the braced and non-braced conditions could have been altered based on subjects' compliance to the brace wear instructions. Future work is needed to assess brace wear compliance as well as assessing potential sex-specific response to brace wear.

## REFERENCES

1. Benedetto, PD. *Knee Surg Relat Res* 28, 319-324, 2016.
2. Butler, RJ. *Sports Health* 6, 203-209, 2014.
3. Dai, B. *AJSM* 40, 2756-63, 2012.
4. Gustavsson A. *Knee Surg Sports Traumatol Arthrosc* 14, 778-788, 2006.
5. Noyes, FR. *AJSM* 19, 513-518, 1991.
6. Paterno, MV. *Clin J Sport Med* 17, 258-262, 2007.

## ACKNOWLEDGMENTS

This work was funded in part by a grant from DonJoy Orthopaedics.

**Table 1:** LSI Values for Loading Between Days and Bracing Conditions.

		SH vGRF	SH LR	6m vGRF	TH vGRF	CH vGRF	VJ vGRF	VJ LR
Day 1	Braced	13.9±9.1	98.4±44.1	10.2±8.9	8.8±6.4	7.1±4.6	51.7±30.7	59.5±35.1
	Nonbraced	15.3±10.8	106.0±51.3	8.7±6.8	9.7±7.6	13.0±18.5	52.4±32.2	64.8±43.7
Day 2	Braced	8.6±6.5	85.9±55.8	7.6±5.0	8.7±6.9	6.6±2.9	38.7±20.3	52.9±35.1
	Nonbraced	9.1±7.1	83.4±47.5	8.3±5.4	13.9±21.2	6.6±4.0	41.3±26.2	49.6±34.6
Testing Time p-value		0.002	0.085	0.555	0.906	0.186	0.090	0.255
Bracing Condition p-value		0.754	0.829	0.731	0.589	0.130	0.812	0.901

# LIMB ASYMMETRIES IN POST-ACL RECONSTRUCTION PATIENTS

<sup>1</sup>Nicole Veltri, <sup>2</sup>Mark Vorensky, <sup>1</sup>Patrick McKeon, <sup>1</sup>Rumit Singh Kakar

<sup>1</sup>Ithaca College, Ithaca, NY, USA

<sup>2</sup>University of Rochester Medical Center, Rochester, NY, USA

email: nveltri@ithaca.edu

## INTRODUCTION

Anterior Cruciate Ligament Reconstruction (ACLR) after a complete tear is intended to restore stability and functionality of the limb. At the conclusion of an athlete's rehabilitation, it is common practice to undergo return to sport (RTS) testing focused on assessing strength and function. Tests involving unilateral hops, isokinetic strength and postural stability are conducted to ensure a safe RTS. RTS testing has become common practice, as young athletes have a high secondary reinjury rate of 23%<sup>1</sup>. Reinjury often leads to removal from sport, diminished quality of life, and greater potential for long-term degeneration<sup>1,2</sup>. Limb asymmetries could potentially lead to re-tear of the affected limb (AL) or a new tear of the contralateral unaffected limb (UAL). Therefore, the objective of this study was to compare the performance of the AL and UAL >12months post-ACLR during RTS testing and to interlimb differences observed in healthy controls. Secondary objective was to correlate isokinetic movement tests and functional RTS testing procedures.

## METHODS

11 ACLR subjects (9 females, 2 males,  $22.4 \pm 3.7$  years old,  $5.4 \pm 4.2$  years post-op) participated in this study. The RTS protocol for this study included the following: Y-excursion tests, single hop for distance (SLH), triple hop for distance (TH), triple cross-over hop for distance (TCH), and timed 6m hop (**Figure 1**). Y-excursion was performed anteriorly (Y-A), posteriolaterally (Y-PL) and posteriomediaally (Y-PM). All RTS tests were performed and recorded over 3 acceptable trials per limb. Additionally, participants performed a Weight-Bearing Lunge (WBL) recorded over 6 acceptable trials per limb. Lastly, isokinetic testing of concentric peak torque of quadriceps and hamstrings at 60°/sec, 120°/sec, and 300°/sec using Biodex System 4 Dynamometer MVP™. The AL ACLR was compared to the dominant limb (DL) and the UAL was compared to the non-dominant

limb (NDL) of controls. DL was determined by which leg subjects choose to kick a ball<sup>3</sup>. The LSI was calculated using the formula  $LSI = 100*(AL/UAL)$  or  $100*(DL/NDL)$  to determine the percentage of ability between limbs. An  $LSI < 85\%$  or  $LSI > 115\%$  is considered a clinically important difference. Correlation statistics were collected to identify potential relationships between isokinetic and functional testing performed.

## RESULTS

For all RTS measures, no clinically important differences were found when comparing LSIs for subjects post-ACLR. When comparing those subjects to healthy controls, no clinically important differences were found as well. Full LSI data can be seen in **Table 1**. Correlation statistics between RTS tests and isokinetic tests of subject's post-ACLR are shown in **Table 2**. For the affected limb, isokinetic testing for knee flexion at 300°/sec showed a moderate correlation to all Y excursion tests and isokinetic testing for knee extension at 300°/sec showed a moderate correlation to all hop tests. Small correlations were found between all isokinetic testing <300°/sec and functional tests.

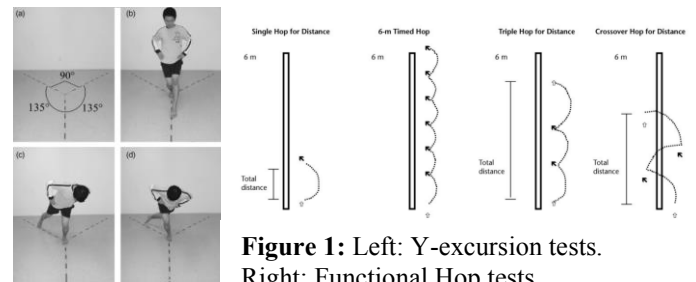


**Figure 1:** Left: Y-excursion tests. Right: Functional Hop tests

## DISCUSSION

For athletes >1 year post-ACLR, no clinically important differences in LSI were found between the affected and unaffected limbs for RTS testing. Additionally, no clinically important difference in LSI was found when compared to healthy controls. However, the high rate of a second ACL tear on the affected or unaffected side continues to be a common concern reported in the literature<sup>1</sup>.

This is likely due to the complex anatomical and pathomechanical nature of the injury. Although the results show minimal differences in LSI, RTS testing may need to be qualitative as well as quantitative, including evaluations of proper landing mechanics and patient reported outcomes. Evaluating kinematics during RTS testing may improve the sensitivity of this assessment.

High speed knee extension isokinetic testing at 300°/sec moderately correlates to SLH ( $r = 0.67$ ), TH ( $r=0.66$ ), and TCH ( $r=0.63$ ). High speed knee flexion isokinetic testing at 300°/sec moderately correlates to Y-A ( $r=0.56$ ), Y-PM ( $r=0.53$ ), and Y-

## CONCLUSION

RTS tests did not produce any clinical differences between the limbs or groups. This protocol, commonly used by clinicians, evaluates an individual's ability to safely return to high-level athletics post-ACLR. Given the high prevalence of reinjury, all objective data should be utilized from functional and isokinetic testing. Future study should include kinematic and kinetic assessment during functional testing along with their relationship to isokinetic testing to test for an athlete's readiness for return to sports.

PL ( $r=0.55$ ). It is important to note the small correlation between both isokinetic tests at  $<300^\circ/\text{sec}$  and functional tests ( $r=0.01-0.44$ ). Isokinetic testing can provide detailed objective data, such as quadriceps:hamstring ratio, peak torque, and peak torque/body weight. Functional testing can provide information regarding landing mechanics and gross power produced by the limb. Isokinetic and functional testing each provide specific information to fully assess an athlete's readiness for return to sport.

## REFERENCES

1. Wiggins AJ, et al. *Am J Sport Med.* 44(7):1861-1876, 2016.
2. Filbay SR, et al. *Am J Sport Med.* 2014;42(5):1247-1255, 2013.
3. Wilk KE, et al. *J. Orthop. Sports Phys. Ther.* 20(2):60-73, 1994.
4. Basnett CR, et al. *Int J Sports Phys Ther.* 8:121, 2013.
5. Barber, S. D. S. *Clin. Orthop. Relat. Res.* 255(255):204-214, 1990.
6. Zwolski C, et al. *Am J Sport Med.* 44(8):2030-2038, 2016.
7. Lund-Hanssen H, et al. *Scand J Med Sci Spor.* 6(3):172-175, 2007.
8. Hoch MC, et al. *Man Ther.* 16(5):516-519, 2011.
9. Wyatt MP, et al. *J. Orthop. Sports Phys. Ther.* 3(2):48-56, 1981.
10. Li RC, et al. *Br J Sports Med.* 30(2):156-160, 1996.

Variables	ACLR (%)	Controls <sup>4-10</sup> (%)
SLH (cm)	97.0 ± 12.5	99.5
TH (cm)	98.9 ± 7.6	99.5
TCH (cm)	98.6 ± 8.7	99.5
6m Hop (sec)	98.8 ± 8.0	101.3
Y-A (cm)	100.2 ± 5.3	100.0
Y-PM (cm)	97.0 ± 11.5	101.0
Y-PL (cm)	98.0 ± 4.9	101.1
WBL (cm)	110.3 ± 35.8	100.8
60°/sec Ext	101.5 ± 18.1	98.0
60°/sec Flex	105.7 ± 16.3	104.0
120°/sec ext	106.2 ± 26.6	98.9
120°/sec flex	107.2 ± 17.6	97.3
300°/sec ext	104.9 ± 16.9	97.9
300°/sec flex	97.6 ± 29.2	97.8

**Table 1:** LSI (%) between AL and UAL during RTS tests compared to controls from literature. LSI (limb symmetry index); ACLR (ACL reconstruction) Control data extrapolated from literature<sup>4-10</sup>.

RTS Tests	Isokinetic Testing (°/sec)											
	60		120				300					
	Flexion	Extension	Flexion	Extension	Flexion	Extension	Flexion	Extension	Flexion	Extension		
SLH	0.12	0.15	0.11	0.16	0.18	0.05	0.31	0.08	0.44	0.24	0.67 <sup>†</sup>	0.01
TH	0.31	0.31	0.23	0.31	0.36	0.19	0.38	0.29	0.63 <sup>†</sup>	0.40	0.66 <sup>†</sup>	0.18
TCH	0.24	0.27	0.23	0.40	0.22	0.12	0.34	0.30	0.40	0.31	0.63 <sup>†</sup>	0.33
Y-A	0.23	0.29	0.08	0.30	0.31	0.20	0.15	0.36	0.56 <sup>†</sup>	0.45 <sup>†</sup>	0.43	0.19
Y-PM	0.30	0.22	0.08	0.14	0.32	0.39	0.05	0.27	0.53 <sup>†</sup>	0.29	0.49 <sup>†</sup>	0.39
Y-PL	0.28	0.04	0.05	0.05	0.37	0.20	0.09	0.02	0.55 <sup>†</sup>	0.06	0.31	0.24

**Table 2:** Correlation statistics between return to sport (RTS tests and peak isokinetic torques for ACLR.

AL (affected limb); UAL (unaffected limb); RTS (return to sport); SLH (single-leg hop); TH (triple hop); TCH (triple cross-over hop); Y-A (anterior Y-excision); Y-PM (posteromedial Y-excision); Y-PL (Y-posteriolateral);

† moderate correlation:  $0.45 < r < 0.70$

# SEX DIFFERENCES OF MEDIAL COLLATERAL AND ANTERIOR CRUCIATE LIGAMENT STRAINS WITH CADAVERIC IMPACT SIMULATIONS

<sup>1</sup>Nathan D. Schilaty, <sup>1</sup>Nathaniel A. Bates, <sup>1</sup>Christopher V. Nagelli, <sup>1</sup>Aaron J. Krych, and <sup>1</sup>Timothy E. Hewett

<sup>1</sup>Mayo Clinic, Dept. of Orthopedic Surgery, Rochester, MN, USA  
email: schilaty.nathan@mayo.edu

## INTRODUCTION

Females have an increased risk of injury to the anterior cruciate ligament (ACL) compared to their male counterparts [1]. Additionally, 75% of these ACL injuries are non-contact in nature, which indicates that neuromuscular and biomechanical kinetics and kinematics are significant risk factors for this injury. Consequently, it is important to understand the underlying mechanisms of ACL injury to determine the factors that increase ACL injury risk in females. Improved knowledge of the mechanisms of ACL will enhance injury prevention, rehabilitation, and return to sport (RTS) criteria for these athletes.

This current study was designed to investigate the sex differences of loading at the knee that cause ACL and MCL strain during a common athletic task – a drop vertical jump (DVJ). It was hypothesized that female limbs would demonstrate increased ACL strain compared to males and that MCL strain would not vary between sexes.

## METHODS

A custom-designed cadaveric impactor was utilized to simulate athletic DVJs in lower extremities of 35 specimens (22M:13F). Ages of specimens ranged from 24 to 52. Inclusion criteria for the specimens were: no evidence of significant trauma/surgery to lower extremity and no evidence of extended chemotherapy. All specimens were CT and MRI imaged prior to dissection. Specimens were prepared according to specifications outlined in a recent methodology manuscript [2].

*In vivo* kinetics and kinematics of 70 healthy athletic subjects were calculated to determine tertiles of risk (i.e. low, medium, and high) in three degrees of knee forces/moments [i.e. knee

abduction moment (KAM), anterior tibial shear (ATS), and internal tibial rotation (ITR)]. Pneumatic cylinders then applied the designated knee forces/moments calculated from the *in vivo* subjects at the tibia and then a gravity-driven drop sled of 0.5 body weight (34 kg) was released from a height of 31 cm with quadriceps and hamstrings co-contracted with a 1:1 ratio. Single axis and 6-axis load cells recorded vertical ground reaction forces (vGRF) and forces and moments at the knee, respectively. In addition, two differential variable reluctance transducers (DVRTs) were implanted into the medial collateral ligament (MCL) and the ACL, respectively, for measurements of ligament strain during simulation. Six specimens were excluded for unsuitable tissue quality or complications that arose during the experimental protocol. 29 specimens remained for analysis (18M:11F; **Table 1**).

**Table 1:** Specimen Demographics by Sex.

	<b>Males</b>	<b>Females</b>	<b>p-value</b>
<b>Age (yrs)</b>	42.7 ± 7.8	40.9 ± 9.7	0.5843
<b>Mass (kg)</b>	96.3 ± 19.5	73.4 ± 17.7	0.0037
<b>Height (cm)</b>	181.5 ± 5.5	166.0 ± 3.3	<0.0001

Statistical analyses were performed with JMP 10 (SAS Institute Inc., Cary, NC) with utilization of one-way ANOVA.

## RESULTS AND DISCUSSION

The cadaveric impactor reliably reproduced clinical ACL ligament ruptures (i.e. 17 femoral avulsions, 6 mid-substance ruptures, and 2 tibial avulsions) in 25 of 29 specimens included in this analysis (86.2%). With males and females combined, the average maximum ACL and MCL strain was  $14.5 \pm 9.0\%$  and  $6.8 \pm 8.2\%$ , respectively. These data indicate that even with high levels of knee abduction

loading, the ACL bears more load than the MCL during functional movement of the DVJ [3].

Comparison of maximum, minimum, initial contact, and post-impact (33, 66, and 100 msec) ACL strain of males vs females did not demonstrate any significant differences. However, there are trends indicative of increased ACL strain in females and the average strain of females with each analysis was a higher value than that of males, although not significantly different (**Figure 1**).

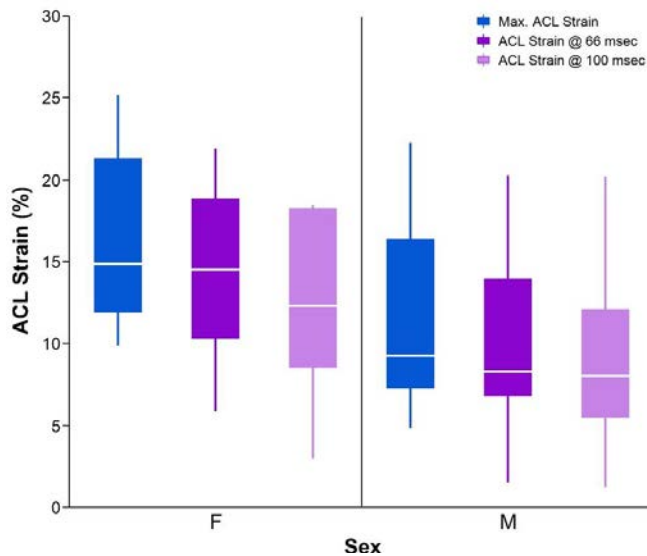


**Figure 1: ACL Strain by Sex.** Females demonstrate higher values of ACL strain at maximum, and 66 and 100 msec post-impact than males.

As ligament failure strength can be dependent upon the cross-sectional area of the ligament, we normalized ACL strain by ACL cross-sectional area. After normalization, significant trends became apparent with females exhibiting greater ACL strain at maximum ( $F_{1,28}=4.1350$ ;  $p=0.0519$ ), and at 66 msec ( $F_{1,28}=4.1660$ ;  $p=0.0511$ ) and 100 msec ( $F_{1,28}=3.0014$ ;  $p=0.0946$ ) post-impact.

Comparison of maximum, minimum, initial contact, and post-impact (33, 66, and 100 msec) MCL strain of males vs females did not demonstrate any significant differences between sexes. After normalization by cross-sectional area of the MCL, no additional significance between sexes was observed with all previous comparisons.

For additional comparisons of ACL and MCL strain values, we compared 25 specimens (17M:8F) that all had successfully acquired data for the randomized loading trial of 67% KAM, 67% ATS, and 67% ITR. Analysis demonstrated that there were no significant differences between sexes with or without normalization to cross-sectional surface area. However, females demonstrated higher ACL strain values as reported earlier (**Figure 1**).

The current state of this study (with fewer female specimens tested than males and with 9 additional female specimens to be tested) may significantly under power the statistics reported in this abstract. We anticipate that the outcomes of ACL strain will demonstrate improved significance with females with further testing that will equal power between sexes. Another limitation of the study is the large variability that DVRTs are known to exhibit when implanted in soft tissue structures. However, even with the high variability of DVRTs, we have maintained consistency with sensor placement and calibrations.

## CONCLUSIONS

Females exhibit greater values of ACL strain than males during similar loading trials and greater ACL strain values at maximum strain, and at 66 and 100 msec post-impact, although these findings are not currently significant.

## REFERENCES

- Schilaty ND, et al. *Am J Sports Med*, 2017 (Accepted, in press).
- Bates NA, et al. *Clin Bio*, 2017 (Accepted, in press).
- Bates NA, et al. *Am J Sports Med* **43**, 2259-2269, 2015.

## ACKNOWLEDGMENTS

NIH funding include: R01AR049735, R01AR055563, R01AR056259 to TEH, and K12HD065987 and L30AR070273 to NDS.

# SHORT-TERM EFFECTS OF FEMORAL NERVE BLOCK ON SAGITTAL PLANE GAIT MECHANICS IN INDIVIDUALS FOLLOWING ACL RECONSTRUCTION

<sup>1</sup> Christopher Nagelli, Stephanie Di Stasi<sup>2</sup>, Albert Chen<sup>2</sup>, Timothy E. Hewett<sup>1</sup>

<sup>1</sup>Orthopedic Biomechanics Laboratories and Sports Medicine Center, Mayo Clinic, Rochester, MN, USA

<sup>2</sup>Sports Medicine Research Institute, The Ohio State University Wexner Medical Center, Columbus, OH, USA  
email: nagelli.christopher@mayo.edu

## INTRODUCTION

Anterior cruciate ligament reconstruction (ACLR) is a common outpatient knee surgery. Femoral nerve blocks are often, though somewhat randomly used to manage postoperative pain and improve patient satisfaction and function. A systematic review of pain management after ACLR observed that a single-shot femoral nerve block provides superior analgesia compared to placebo for up to 24 hours. However, the use of nerve block in these patients has also led to apparent quadriceps motor deficits. This is evident in recent studies that have reported that patients who were treated with a femoral nerve block during ACLR demonstrated significantly greater deficits in isokinetic knee extension and flexion strength 6 months after ACLR.<sup>1</sup> These same patients who received a nerve block were also 4 times less likely to meet return-to-sport criteria 6 months after ACLR.<sup>1</sup>

Residual movement deficits are commonly observed in patients following ACLR. Changes in ambulatory kinematic and kinetic measures persist for several years following ACLR and are directly implicated in the development of post-traumatic osteoarthritis.<sup>2</sup> To date, no study has described the short-term effects of temporary blockade of sensorimotor pathways for ACLR on gait biomechanics. Therefore, the purpose of this study was to determine the impact of femoral nerve block on ambulatory biomechanics 6 and 12 weeks after ACLR. We hypothesized that patients who received femoral nerve block would demonstrate significantly greater sagittal plane asymmetries at the hip and knee joints during ambulation.

## METHODS

With IRB approval, 16 patients scheduled to undergo ACLR were randomized into a group that received a femoral nerve block (ACLR-NB; n=7) or

a control group (ACLR; n=9) (Table 1). All patients received a hamstrings autograft during a standardized ACLR surgical procedure. The patients randomized into the nerve block group received a standard-of-care single-injection bupivacaine femoral nerve block for ACLR. Post-operative physical therapy was implemented per the institution's clinical practice guidelines following ACLR.

Patients were assessed 6 weeks after ACLR. Gait analysis was performed using a 12 infrared camera, 3-dimensional motion analysis system (Cortex, Motion Analysis Corporation, Santa Rosa, CA). Patients were fitted with 55 retroreflective markers in a modified Helen Hayes configuration and completed 5 successful trials during which they walked over ground-embedded force plates at a consistent, self-selected speed (Bertec, Columbus, OH). Sagittal plane hip and knee joint angles at initial contact and peak extension and flexion moments were reduced using custom software (Matlab and Visual 3D). A 2x2 analysis of variance was performed to assess the interaction and main effects of group and limb. *Post-hoc* t-tests will be used to test for significant differences between limbs ( $\alpha=0.05$ ).

**Table 1: Study Cohort Demographics**

Group	Subjects (M/F)	Age (yrs±SD)	Height (m±SD)	Weight (kg±SD)
Nerve Block	7(6/1)	28.4±11.9	1.75±0.1	81.6±14.5
Control	9(7/2)	19.8±8.5	1.73±0.1	76.2±13.1

## RESULTS AND DISCUSSION

No significant interactions were observed for any of the sagittal plane hip and knee angles and moments. However, a significant main effect ( $p=0.001$ ) of

limb was observed for knee flexion angle at initial contact (**Figure 1**). Also, a significant main effect ( $p=0.041$ ) of limb was observed for peak knee flexion moment (**Figure 2**). The ACLR limbs demonstrated lower knee flexion angles at initial contact and peak knee flexion moments than the uninjured limbs.

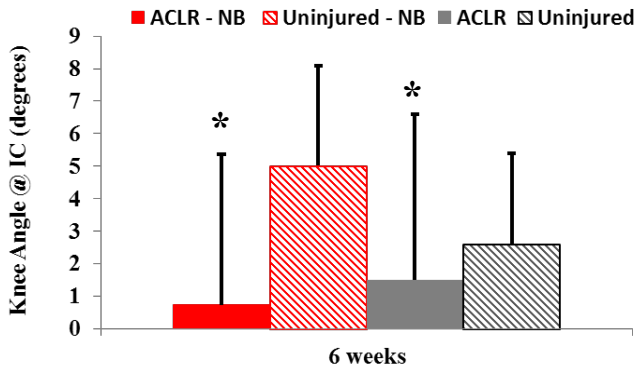


**Figure 1:** Knee Flexion Angle at Initial Contact for the Nerve Block and Control Groups 6 weeks after ACLR. \*ACLR limbs significantly different from uninjured limbs.

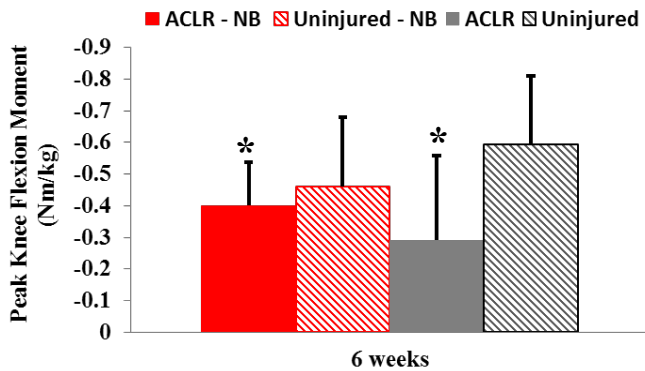


**Figure 2:** Peak Knee Flexion Moment for the Nerve Block and Control Groups 6 weeks after ACLR. \*ACLR limbs significantly different from uninjured limbs.

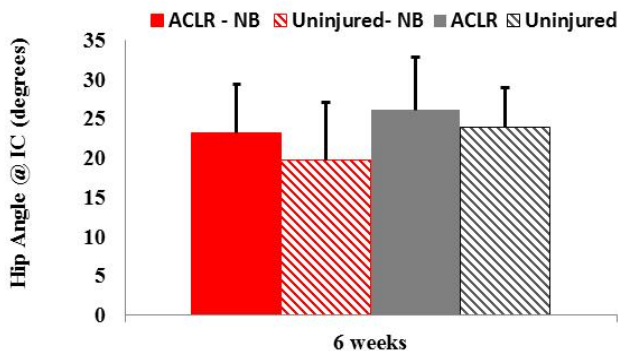


**Figure 3:** Hip Flexion Angle at Initial Contact for the Nerve Block and Control Groups 6 weeks after ACLR

We anticipated that the femoral nerve block group would demonstrate more pronounced sagittal plane

deficits than the control group. Recently published work from this cohort showed that participants who received a single shot femoral nerve block demonstrated larger deficits in isometric quadriceps strength 6 weeks after ACLR compared to those who did not receive a nerve block.<sup>3</sup> However, this preliminary study is limited by the minimal number of patients in each group. Interestingly, the nerve block group's involved limb did demonstrate lower hip and knee flexion angles (**Figure 2 and 3**) than the control group, which indicates the potential for additive, detrimental biomechanical effects induced by a temporary cessation of sensorimotor activity. Significant side to side differences found in this study are consistent with the literature that has reported altered hip and knee mechanics during gait in patients assessed early after acute ACL injury.<sup>4</sup>

The present findings indicate that continued evaluation of gait abnormalities in a larger sample of patients is important for determination of the potentially harmful effects of femoral nerve blocks on knee function following ACLR. Differentiation of the effects based on the type and duration of nerve block is critical for finding safe and effective means for analgesia for outpatient ACLR.

### CONCLUSIONS

To the investigators' knowledge, this is the first study to investigate the effects of femoral nerve block on early post-operative gait mechanics in patients undergoing ACLR. The results of the study indicate that the use of femoral nerve block for ACLR may be associated with adverse effects on hip and knee function during gait. Restoration of normal biomechanics during gait is important for mitigation of the risks for the long-term sequelae such as osteoarthritis. Further investigation of the effects of nerve block on function in a larger sample is required as these findings may have important clinical relevance.

### REFERENCES

1. Luo et al., Am J Sports Med, 2015
2. Andriacchi et al., Clin Ortho Relat Res, 2006.
3. Magnussen et al., J Knee Surg, 2016
4. Rudolph et al., J Electromyogr Kinesiol, 1998.

### ACKNOWLEDGMENTS

The authors would like to acknowledge the graduate students and staff that have helped with data collection in the Sports Medicine Research Institute at Ohio State and the Biomechanics Laboratories at Mayo Clinic. DJO.

# INTER-JOINT COMPENSATIONS DURING EARLY GAIT IN INDIVIDUALS FOLLOWING ACL RECONSTRUCTION

<sup>1</sup> Paige E. Lin, <sup>1</sup> Ming-Sheng Chan, and <sup>1</sup> Susan M. Sigward

<sup>1</sup> University of Southern California, Human Performance Laboratory, Los Angeles, CA, USA  
email: paigeeli@usc.edu, web: <http://pt.usc.edu/labs/hpl/>

## INTRODUCTION

Restoration of normal gait mechanics is observed clinically by 3 months post-anterior cruciate ligament reconstruction (ACLR) [1]. However, biomechanical studies have reported reductions in knee flexion range of motion across stance throughout rehabilitation [2-4]. The presence of altered knee kinematics in the absence of observable gait deficits suggests individuals are compensating for such deficits to normalize gait.

While biomechanical studies suggest a persistence of altered knee kinematics during gait, no differences between limbs in peak or average hip or ankle kinematics have been reported in the literature [3,4]. The absence of kinematic differences at adjacent joints may suggest that individuals do not alter kinematics at adjacent joints to compensate for limited knee flexion. It is also possible that these alterations are not reflected in peak or average angles. Thus, these analyses may not be sensitive enough to identify intralimb compensations, as they are limited to angles identified at discrete time points and peaks for each joint. Further, the timing of these peaks do not necessarily correspond across joints, limiting our understanding of how joints coordinate their actions to compensate for altered knee mechanics.

The purpose of this study is to quantify lower extremity joint coordination and identify compensatory strategies by comparing inter-joint coordination in sagittal plane kinematics during gait between individuals 3 months post-ACLR and controls.

## METHODS

Thirteen individuals (9F,  $23 \pm 7.0$  yrs)  $91 \pm 18$  days post-ACLR without observable gait deficits and thirteen healthy controls (4F,  $24 \pm 5.7$  yrs) walked at a standardized velocity of 1.4m/s ( $\pm 5\%$ ). Five

successful stance phase trials were collected for each limb: ACLr and non-surgical (NS) for the ACLr group and the control (CTRL) limb. Control limbs were averaged for analyses.

Three-dimensional kinematics were collected using an 11-camera motion capture system (250 Hz; Qualisys, Inc. Sweden) or a 14-camera motion capture system (340 Hz; BTS Bioengineering Corp., Italy). Sagittal plane ankle, knee and hip angles were calculated and stance phase was normalized to 101 data points for further analysis.

Inter-joint coordination was quantified from joint angle-angle plots by calculating coupling angles ( $\gamma$ ) between the joints at corresponding time points. Coupling angles were determined using vector coding techniques by connecting two consecutive time points on an angle-angle plot and determining the counterclockwise angle of this line relative to the right horizontal (Figure 1a). A custom MATLAB script was used to calculate coupling angles between two sagittal plane joint coordination couplings: hip-knee and knee-ankle using the following question:

$$\gamma_{j,i} = \tan^{-1}((y_{j,i+1} - y_{j,i}) / (x_{j,i+1} - x_{j,i}))$$
where  $0^\circ \leq \gamma \leq 360^\circ$ , and  $i$  is a percent of stance of the  $j$ th trial.

Coupling angles of hip-knee and knee-ankle angle-angle plots were calculated between all adjacent time points in the ACLr, NS, and CTRL limbs during loading response (LR; 0-25% of stance). Coupling angles were categorized into one of four coordination patterns: in-phase, anti-phase, knee phase, and ankle or hip phase (Figure 1b). The frequency of phase angles that fell into each coordination pattern was determined for each trial during LR and expressed as a percentage of coordination pattern frequency.

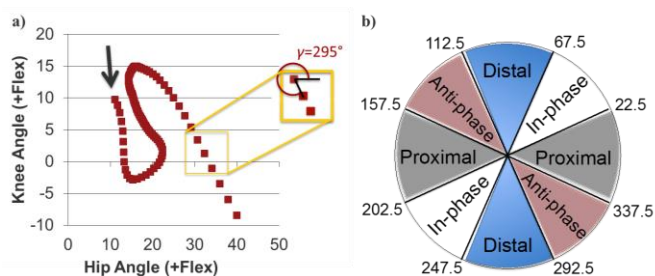


**Figure 1:** a) Determination of coupling angle with arrow denoting heel strike of stance; b) Categorization of coupling angles into coordination patterns.

The dependent variable, coordination pattern frequency, is a discrete variable; therefore, non-parametric Kruskal Wallis tests were used to compare mean rank differences in coordination pattern frequency (anti-phase, in-phase, proximal phase, or distal phase) between limbs. Mann-Whitney U tests were used for post hoc analyses;  $\alpha=0.05$ .

## RESULTS AND DISCUSSION

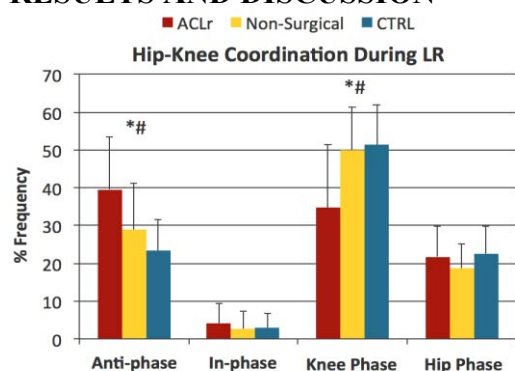


**Figure 2:** Hip-knee coordination during loading response in the ACLr, NS, and CTRL limbs (\* $p<0.05$  ACLr-NS; # $p<0.05$  ACLr-CTRL).

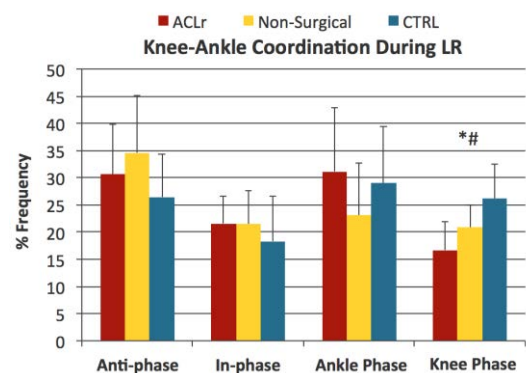


**Figure 3:** Knee-ankle coordination during loading response in the ACLr, NS, and CTRL limbs (\* $p<0.05$  ACLr-NS; # $p<0.05$  ACLr-CTRL).

During LR, the frequency of knee phase motion was reduced in the ACLr limb compared to the NS and CTRL limbs for hip-knee (35% vs. 50% and 51%, respectively;  $p=0.017$ , Figure 2) and knee-ankle (17% vs. 21% and 26%;  $p=0.001$ , Figure 3) couplings. Anti-phase hip-knee coordination was greater in the ACLr limb (40% vs. 29% and 23%;  $p=0.001$ , Figure 2). No differences in inter-joint coordination between the NS and CTRL limbs were observed.

## CONCLUSIONS

Decreased knee phase motion in both couplings is consistent with limited knee motion previously reported. Differences in inter-joint coordination indicate intralimb hip and ankle compensations in the ACLr limb that occur at a time when gait is normalized clinically. Specifically, the decrease in knee phase motion and concurrent increase in anti-phase motion seen in hip-knee coordination was driven by increased hip extension in the surgical limb during early LR. In knee-ankle coordination, a decrease in knee phase motion was driven by increased plantarflexion motion in the surgical limb. The lack of differences between the non-surgical and control limbs suggests that inter-joint coordination is not altered in both limbs following ACLr.

The intralimb compensations in the surgical limb may aid in restoring the appearance of unimpaired gait following ACLr. This is of concern as altered gait mechanics have been attributed to the development and progression of knee osteoarthritis in this population. Future work is needed to investigate how alterations in inter-joint coordination relate to changes in knee loading.

## REFERENCES

1. van Grinsven S, et al. *Knee Surg Sports Traumatol Arthrosc* **18**(8), 1128-1144, 2010.
2. Sigward SM, Lin PE, Pratt KA. *Clin Biomech* **32**, 249-254, 2016.
3. Di Stasi SL, et al. *Am J Sports Med* **41**(6), 1310-1318, 2013.
4. Devita P, et al. *Med Sci Sports Exerc* **30**(10), 1481-1488, 1998.

# SIMPLIFIED JUMP LANDING TASK DOES NOT DEMONSTRATE INCREASED ACL LOAD

Kaitlyn M Wilkie, Mitchell L Stephenson, and Jason C Gillette

Iowa State University, Ames, IA, USA  
email: k.wilkie.21@live.com, web: www.kin.hs.iastate.edu

## INTRODUCTION

Prevention of anterior cruciate ligament (ACL) injuries continues to allude researchers and practitioners. More recent literature has tested lower extremity and ACL loading mechanisms in a reactive test in an attempt to better reflect athletic on-field experiences [1]. This has led to an inflation in methodological complexity [2] that may reduce duplicability and ecological validity, and complicate subsequent implementation by researchers in slightly different settings.

As such, the current project was performed in order to improve upon previous methods [2] by simplifying the task in order to increase ecological validity and decrease independent variable space while producing similar responses.

## METHODS

Ten recreationally-active, uninjured students were recruited as participants (5 females and 5 males;  $21.6 \pm 1.7$  years;  $1.75 \pm 0.04$  m tall;  $71.5 \pm 13.6$  kg). They individually completed an informed consent process, performed a warm-up, and then practiced the following movement before data collection.

Similar to previous research [2], participants started on a 30cm tall block placed 50% of their height away from a landing zone. They jumped forward from this block and landed bilaterally with each foot on a force platform (1600 Hz, Advanced Mechanical Technology Inc., Watertown, MA). Participants then quickly jumped to the left or right  $60^\circ$  from their initial forward direction as far as possible. This angle was chosen instead of  $90^\circ$  after feedback from a focus group indicated it was more natural of a performance.

The direction of the jump was indicated to the participants by one of two LED lights placed at eye

level in front of the jumping area. Controlled by an Arduino Mega microcontroller, the lights were illuminated either before the participant began the trial so they could pre-plan their movement or only after the participant landed on the force platforms, so participants had to react to the direction. Simplifying from four reactive timing conditions to only providing the directional signal at landing eliminated the need to instrument the 30cm tall block and provided more of a worst-case difference between the timing condition implementations.

Participants performed five trials in each timing condition and in each jump direction, for a total of 20 recorded jumps. Order of testing was double-blind randomized by the Arduino microcontroller via a seeded Durstenfeld technique. The microcontroller also randomly injected three “catch” trials into the order of testing; in this condition no directional signal was illuminated. This allowed for verification that the participant was not attempting to predict the jump direction, and inflated the number of potential responses in order to maintain a similar requisite response time [3] to previous investigations [2].

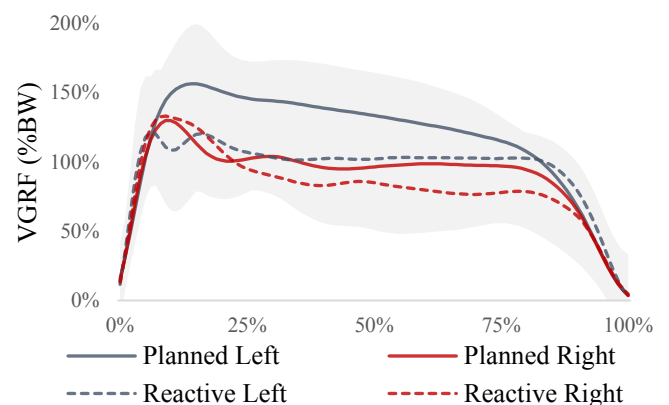


**Figure 1:** Mean unilateral VGRF across percentage stance time for each timing condition while jumping right. Shaded area is  $\pm$  standard deviation range.

A total of 19 retroreflective markers placed on the right foot, leg, pelvis, and torso were recorded by 8 Vicon cameras through Nexus 1.8.2 (160Hz, Vicon Corp, Oxford, UK). Right knee flexion and valgus angles were calculated for the performance; initial values at the first instant of force platform contact and peak values from the first 100ms of contact [4] were extracted. Similarly, peak unilateral vertical ground reaction forces during the same time window were identified and scaled to participant bodyweight. A repeated-measures ANOVA was calculated to determine the differences between jump direction and timing of the directional signal on dependent variables.

## RESULTS AND DISCUSSION

A significant main effect for timing condition was identified for each VGRF ( $p = 0.042$ ) and ST ( $p=0.001$ ), but no other variables ( $p > 0.15$ ). False discovery rate-corrected (*a priori* 0.05) pairwise t-tests did not identify any significant differences for the VGRF between the timing conditions. Significant differences were identified for ST relative to timing condition, and are presented in Table 1.

Similar to previous reports, ST increased in a reactive performance compared to a planned [2]. The grand mean change in ST of 175ms between these conditions is slightly less than theorized by the implications of Hick's Law [3], but similar to previous research [5].

In contrast to previous research [1,2,5], no significant kinematic or kinetic changes were identified between the timing conditions or jump directions. Given that the largest changes in similar variables were previously identified between these two timing conditions, these results are surprising. It is possible that the change in jump direction was not dramatic enough to alter landing techniques during initial contact with the force platform or during the first 100ms of landing. This is not entirely consistent with previous findings, however.

## CONCLUSION

Due to the lack of significant differences in kinematics and kinetics during landing between the timing conditions, caution is suggested if implementing a similarly simplified task. It is possible that the currently presented task does not exacerbate variables associated with ACL load adequately to be a valuable testing paradigm. It is also possible that the unchanged ACL load variables are related to an inflated ST. The potential relationships between ST and ACL load variables are being further studied by the current researchers.

## REFERENCES

1. Almonroeder, TG, et al. *Int J Sports Phys Ther*, **10**, 918-928, 2015.
2. Stephenson, ML, et al. *Proceedings of ASB'15*, Columbus, OH, USA, 2015.
3. Hick WE. *Q J Exp Psychol*, **4**, 11-26, 1952.
4. Koga, H, et al. *Am J Sports Med*, **38**, 2218-2225, 2010.
5. Stephenson, ML, et al. *Proceedings of ASB'16*, Raleigh, NC, USA, 2016.

**Table 1:** Initial and peak knee angles, vertical ground reaction force, and stance time (Mean  $\pm$  SE) in planned and reactive jump directions.

	Planned		Reactive	
	Jump Left	Jump Right	Jump Left	Jump Right
Initial Flexion (°)	25.1 $\pm$ 3.2	27.5 $\pm$ 3.0	26.5 $\pm$ 2.6	26.5 $\pm$ 2.8
Peak Flexion (°)	69.0 $\pm$ 4.7	71.8 $\pm$ 4.0	71.5 $\pm$ 2.4	73.9 $\pm$ 2.8
Initial Valgus (°)	1.9 $\pm$ 1.3	-0.2 $\pm$ 2.2	1.2 $\pm$ 1.3	0.6 $\pm$ 1.3
Peak Valgus (°)	8.6 $\pm$ 1.9	7.5 $\pm$ 3.0	7.6 $\pm$ 2.0	6.6 $\pm$ 2.3
Peak VGRF (%)	1.88 $\pm$ 0.09	1.55 $\pm$ 0.09	1.73 $\pm$ 0.10	1.68 $\pm$ 0.08
ST (ms)	381 $\pm$ 36 <sup>A</sup>	449 $\pm$ 39 <sup>A</sup>	572 $\pm$ 85 <sup>B</sup>	608 $\pm$ 47 <sup>B</sup>

<sup>A</sup>Significantly different than Reactive. <sup>B</sup>Significantly different than Planned.

# MALE ATHLETES WHO WALK WITH GAIT ASYMMETRIES REPORT SIMILAR FUNCTION TO THOSE WHO WALK SYMMETRICALLY 1 YEAR AFTER ACL RECONSTRUCTION

<sup>1</sup>Jessica L Johnson, Jacob J. Capin, and Lynn Snyder-Mackler

<sup>1</sup>The University of Delaware, Newark, DE, USA  
Email: jljohn@udel.edu

## INTRODUCTION

Anterior cruciate ligament (ACL) injuries often cause significant limitations in both activities of daily living and sports. Patients demonstrate altered gait patterns up to 2 years after ACLR, with knee excursion asymmetries in both weight acceptance and mid-stance during gait. Additionally, altered kinetics and kinematics may contribute to the development of joint degeneration and premature osteoarthritis due to the change in load-bearing position[1].

Previous research has investigated the relationship between gait asymmetries and functional exams[2], and self-report outcomes and return to sport[3]. However, there is currently no evidence that investigates the difference between gait asymmetries and self-report outcomes at 1 year after ACLR. We hypothesized that male athletes with asymmetrical knee excursion patterns during gait would have lower self-reported outcomes scores.

## METHODS

Thirty-eight male athletes (age  $24.4 \pm 7.5$  years) completed biomechanical gait assessment 1 year after ACL reconstruction. Inclusion criteria included: age 13-55, >80% quadriceps strength index (QI), and participation in jumping, cutting, and pivoting sports >50 hours per year. All participated in a secondary prevention program[4]. We analyzed participants' walking patterns using an eight-camera motion capture (VICON, Oxford, UK) at 120 Hz and an embedded force platform (Bertec Corp., Columbus, OH) at 1080 Hz. We used 39 retroreflective markers on the bilateral lower extremities and pelvis for motion analysis testing. Participants walked over-ground at a self-selected gait speed maintained to  $\pm 5\%$  across trials. Data were processed using commercial software (Visual3D; C-Motion, Germantown, MD).

We dichotomized asymmetric (Asym) and symmetric (Sym) as a difference in sagittal plane knee excursion between the surgical limb and non-surgical limb that met or exceeded the minimal clinically important difference (MCID) of 3 degrees[5]. We did this at both weight acceptance (WA) and mid-stance (MS) and compared each excursion group separately.

Participants also completed self-report outcome measures: International Knee Documentation Committee Subjective Knee Evaluation Form (IKDC) and Knee Injury and Osteoarthritis Outcome Score (KOOS).

We used independent t-tests to compare outcome measures between groups. Alpha was set to 0.05 a priori.

## RESULTS

The mean difference between limbs (involved – uninvolved) for knee excursion was  $-3.6 \pm 3.5^\circ$  at WA and  $-4.6 \pm 4.5^\circ$  at MS.

There were no statistically significant differences between self-reported outcomes in men who walked symmetrically versus asymmetrically (Table 1). The mean differences between the groups were smaller than the MDC for the self-reported outcomes scores.

## DISCUSSION

The purpose of this study was to compare self-reported outcomes in male athletes who walked symmetrically vs asymmetrically 1 year after ACLR. We found no statistically significant or clinically meaningful difference among men who walked with knee excursion symmetry vs asymmetry on any self-reported outcomes measure.

A lack of difference between groups may be in part due to the stringent criteria all participants passed prior to enrollment. With these standards for

inclusion, we are not able to compare participants with lower baseline function and possible asymmetry during gait.

As part of a larger study, these men also completed an additional secondary prevention program and were required to meet stringent criteria prior to returning to sport. Most participants had full participation in activities of daily living (KOOS ADL score 99.0±2.8) and higher level activities (KOOS Sport/Rec 93.7±9.5) with little pain (KOOS Pain 96.3±4.5). This additional rehab and high functional level may have reduced the impact of gait asymmetries on self-reported outcomes.

We are the first to assess differences in self-reported outcomes in male athletes with and without gait asymmetries 1 year after ACLR. A study in total knee arthroplasty (TKA) patients found that 1 year after TKA, participants had improved self-reported outcomes from prior to surgery to one year after surgery, but these self-reported outcomes did not differentiate between those with and without gait asymmetries[6]. Additionally, Boonstra et al[7] found that post-TKA, patient-based scales were largely influenced by pain. This may suggest that once post-surgical pain is resolved, participants overestimate function[6]. Most participants in our study reported very little pain and high ADL participation regardless of detectable gait asymmetries. This may suggest similar influences of pain on perceived function in the ACLR population.

Additionally, our participants were men who participated in high level activities prior to injury and

completed an additional secondary prevention program after ACLR. High functional level and additional rehab may diminish the impact of gait asymmetries on self-reported outcomes, although further research is necessary.

## CONCLUSION

We found no statistically significant or clinically meaningful difference between male athletes who walked with knee excursion asymmetry and those who did not on any self-reported outcomes measure 1 year after ACLR.

## REFERENCES

1. Erhart-Hledik et al. *J Orthop Res.* 2016.
2. Di Stasi SL, et al. *Am J of Sports Med.* **41**, 1310-1318, 2013.
3. Logerstedt et al. *J Orthop Sports Phys Ther.* **44**, 914-923, 2014.
4. Capin JJ, et al. *J Orthop Res.* 2016.
5. Di Stasi SL, Snyder-Mackler L. et al. *Clin Biomech (Bristol, Avon).* **27**, 360-365, 2012.
6. Naili JE, et al. *Knee Surg Sports Traumatol Arthrosc.* 1-9, 2016.
7. Boonstra MC, et al. *The Knee.* **15**, 390-395, 2008.

## ACKNOWLEDGEMENTS

Funding provided by the National Institutes of Health: R01-AR048212, R37 HD037985, P30-GM103333, U54-GM104941, and T32-HD00749. Thank you to Amelia Arundale, Kathleen Cumber, Ryan Zarzycki, Celeste Dix, Angela H. Smith, and Martha Callahan for their invaluable assistance.

**Table 1 Means and Standard Deviations of Scores on Selected Outcome Measures (t-tests)**

		IKDC	KOOS S/R	KOOS QOL	KOOS Pain	KOOS Symptoms	KOOS ADL
WA	Sym (N=15)	96.9 ±4.7	94.7 ±10.4	85.8 ±18.7	97.8 ±3.0	93.6 ±8.7	99.4 ±1.6
	Asym (N=23)	91.5 ±12.1	93.0 ±9.0	81.8 ±14.0	95.4 ±5.1	86.0 ±15.2	98.9 ±3.5
		p=0.06	p=0.61	p=0.46	p=0.15	p=0.09	p=0.56
MS	Sym (N=13)	92.9 ±10.9	93.0 ±9.5	86.1 ±16.8	95.9 ±4.4	89.3 ±11.8	98.5 ±4.5
	Asym (N=25)	93.9 ±9.9	94.0 ±9.7	82.0 ±15.7	96.6 ±4.7	88.9 ±14.4	99.4 ±1.5
		p=0.77	p=0.78	p=0.47	p=0.70	p=0.93	p=0.41

# Effect of Foot Rotation on ACL Injury Risk Variables During Drop Landing

<sup>1</sup>Shelby A. Peel, <sup>1</sup>Brian M. Matthews, <sup>1</sup>Tanner A. Thorsen, <sup>1</sup>Joshua T. Weinhandl

<sup>1</sup>University of Tennessee, Knoxville, TN, USA

email: speel@vols.utk.edu

## INTRODUCTION

Landing is considered one of the “high-risk” sporting movements that can lead to ACL injury [1]. Because of this, much attention has been placed on kinematic and kinetic variables associated with landing and how they relate to ACL injury risk. One such variable is foot progression angle (FPA).

Previous research has found landing with a “toe-in” position of 30° increases peak hip adduction, knee internal rotation angles and moments, as well as peak knee abduction angles, and decreases peak hip flexion angles [2]. Landing with a “toe-out” position has been shown to decrease these ACL injury variables [2]. However, participant FPA in the previous study was assessed using three different conditions: 1) neutral FPA of 0°, 2) toe-in FPA of 30°, and 3) toe-out FPA of 30°. No study thus far has assessed changes in FPA relative to a person’s natural FPA (self-selected) and the influences this would have on ACL injury risk variables. Currently, it is also unknown if smaller changes of FPA (i.e. 15° of toe-in or toe-out) also influence ACL injury risk variables the same as a more aggressive FPA (i.e. 30° of toe-in or toe-out).

Therefore, the purpose of this study was to assess the effects of changes in FPA from self-selected in 15° intervals on ACL injury risk variables during drop landings in healthy, recreationally active, males and females.

## METHODS

Ten healthy, active participants (five females, five males) volunteered for the current study and provided written informed consent. Participants also completed the Lower Extremity Functional Scale to ensure they qualified to participate.

At the start of their testing session, participants were fitted with a standardized lab shoe (Adidas Noveto)

and asked to complete a five-minute warm-up. After completing the warm-up, anatomical markers and tracking marker clusters were placed on the right leg of the participants (despite leg dominance). A three-second static calibration trial was collected, and data collection began.

An overhead hang bar was adjusted so that participants’ feet were 40cm above the force plate. Five drop landing trials from the hang bar were collected at the participant’s self-selected FPA. An average self-selected FPA was taken from the five self-selected trials and used to determine the 15° toe-in, 30° toe-in, 15° toe-out, and 30° toe-out FPAs. Drop landing tasks after the self-selected condition were counterbalanced and five trials of each condition were collected. A customized MATLAB code (MathWorks, Natick, MA) was used to provide real-time feedback of drop landing FPA during the toe-in and toe-out conditions to eliminate a targeting effect.

A 12-camera motion capture system (200Hz, Vicon, Centennial, CO, USA) and a force platform (2000Hz, AMTI, Inc., Watertown, MA) were used to collect marker coordinate and GRF data, respectively. Visual3D biomechanical software (C-Motion, Germantown, MD, USA) was used to process and analyze all data. Marker coordinate and GRF data were filtered using fourth-order Butterworth low-pass filters with cut-off frequency of 10Hz. 3D joint kinematics were calculated using a joint coordinate system approach. 3D internal joint moments were calculated using standard inverse dynamics techniques and expressed in the joint coordinate system. Joint moments were normalized to body mass.

A 2x5 (gender x task) repeated measures ANOVA was used to compare dependent kinematic and kinetic variables (v23.0, SPSS Inc., Chicago, IL). Significant interactions and main effects were examined with *post hoc* pairwise comparisons with

Bonferroni adjustments. Significance was set at  $p < 0.05$ .

## RESULTS AND DISCUSSION

Initial contact hip internal rotation, knee abduction, and knee external rotation angles as well as peak knee internal rotation moment were all significant between drop landing tasks ( $p < 0.05$ ). Initial contact knee flexion angle, as well as peak hip external rotation, knee extensor, and knee adduction moments were not significant for any task or gender difference ( $p > 0.05$ ). Peak knee adduction moment displayed a trend toward significance ( $p = 0.057$ ).

Our data supports previous studies that suggest landing with a “toe-in” FPA increases ACL injury risk kinematic variables [2]. Specifically, hip internal rotation, and knee abduction angles at initial contact increased as toe-in FPA increased, indicating greater medial knee collapse. Females experienced greater peak knee extensor, adduction, and internal rotation moments compared to males regardless of FPA. However, our kinematic and kinetic magnitudes are not consistent with that of previous research [2]. This is most likely due to the changes in FPA based on the participants self-selected FPA and not a neutral or 0° position. On average, self-selected FPA for the current study’s participants was 20° of toe-out.

Therefore, our 30° toe-in from self-selected condition would only result in approximately 10° of toe-in. Differences in landing task (i.e. drop landing vs. jump landing) may also play a role in magnitude differences.

## CONCLUSIONS

Our results suggest that landing with a toe-in FPA will increase the magnitude of ACL injury risk variables of the hip and knee. Females demonstrate a greater magnitude of these variables with toe-in FPA of 15° and 30° compared to males. However, while hip and knee ACL injury risk variable magnitudes increase, they may not reach a high enough magnitude that would put athletes at a “high-risk” of an ACL injury as seen in previous ACL injury risk studies [3].

## REFERENCES

1. Shimokochi Y et al. *J Athl Train.* **43**, 396-408, 2008.
2. Tran A et al. *J Exp Orthop.* **3**, 2016.
3. Seering W et al. *J Biomech.* **13**, 785-794, 1980.

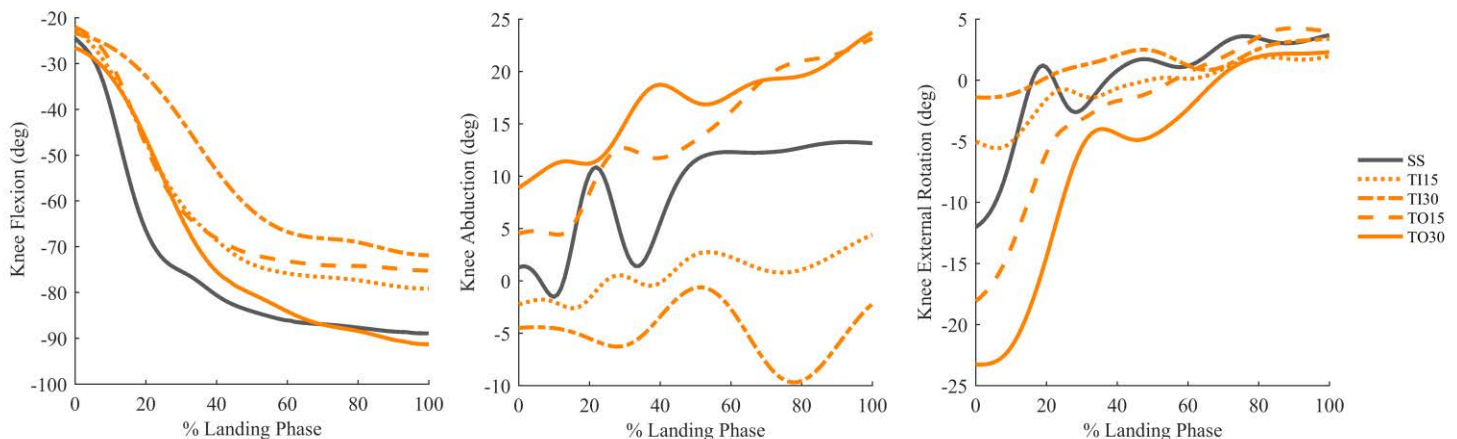


**Figure 1.** Mean ensemble curves for 3D knee joint angles during five drop landing conditions: 1) self-selected FPA (SS; grey solid line) 2) toe-in 15° FPA (TI15; orange dotted line), 3) toe-in 30° FPA (TI30; orange dot-dash line) 4) toe-out 15° FPA (TO15; orange dash line), and 5) toe-out 30° FPA (TO30; orange solid line).

# COORDINATION VARIABILITY IN THE ONE LEG HOP TEST 20 YEARS AFTER ACL INJURY

<sup>1</sup> Divya Srinivasan, <sup>2</sup> Eva Tengman, <sup>2</sup> Charlotte Häger

<sup>1</sup> Virginia Polytechnic Institute and State University, Blacksburg, VA, USA

<sup>2</sup> Umeå University, Sweden

email: sdivyal@vt.edu

## INTRODUCTION

One of the most common tests used in rehabilitation for clinical assessments of functional performance following ACL injury is the one-leg hop forward where the jump distance is measured<sup>1</sup>. The standard way to evaluate the performance in this test is by using the limb symmetry index (LSI), which is the ratio of the jump distance for each of the two legs<sup>1</sup>. However, LSIs of similar magnitude could be achieved by very different limb kinematics, and merely reporting the LSI for jump length does not provide any information about the movement quality and the associated kinematic alterations that may prevail post-injury.

In this context, movement variability has now been accepted in both sports and clinical biomechanics to play a functional role in neuromuscular adaptations. This role includes facilitating adaptations of the individual motor system to processes such as learning, aging, and changing constraints such as pain, fatigue and injury e.g. 2-3. There are reports of different movement variability patterns in the short-term after ACL injury, but to the best of our knowledge, no study has assessed whether the intra-individual variability of joint kinematic patterns is still altered in ACL injured patients in the very long term. The aim of this study was to determine whether coordination variability of the hip-knee joint couplings during the one-leg hop was altered about 20 years after ACL injury compared to healthy knee controls.

## METHODS

This study is part of a large cross-sectional study of >100 individuals. Specifically in this study, 33 individuals who had undergone ACL injury and subsequent treatment using reconstruction surgery were compared with 33 age and gender matched

healthy controls. After warm-up and practice, all participants performed one-leg hops for maximal distance starting on one leg in an upright position from a force-plate, jumping forward as far as possible and landing on the same leg while maintaining balance on the ground. Hops were performed until 3 successful hops could be performed on each leg.

A 3-D motion capture system (Qualisys) was used to movement kinematics, from which knee and hip angles were computed. Force plate and marker data were used to compute take-off and landing instants for each jump, and a 100ms duration prior to take-off and 100ms duration following landing were defined as take-off and landing phases respectively. All the hip and knee joint angles were extracted during the take-off and landing phases for each of the three jump for further analysis. The following intra-limb couplings were investigated: knee abduction-adduction/hip abduction-adduction, knee abduction-adduction/hip rotation and knee abduction-adduction/hip flexion-extension. Angle-angle plots were created for each coupling, and joint coordination was quantified using a vector coding technique<sup>4</sup>. Briefly, coupling angles were calculated using the orientation of the resultant vector of each angle-angle plot to the right horizontal between every two successive data points of each trial. The standard deviation of the coupling angles across the three trials was then calculated for each time point, and then pooled across the whole trial by computing the overall root mean square. Thus this yielded a measure of between-trial, within-subject variability. This procedure was repeated separately for the take-off phase and the landing phase and for each lower extremity coupling using the 3 successful hops. Data from the injured legs of the ACL group were compared with the dominant leg of the non-injured controls.

## RESULTS AND DISCUSSION

Figure 1 shows the coordination variability of the injured side of the ACL group in comparison with the coordination variability exhibited by healthy controls during the take-off and landing phases.

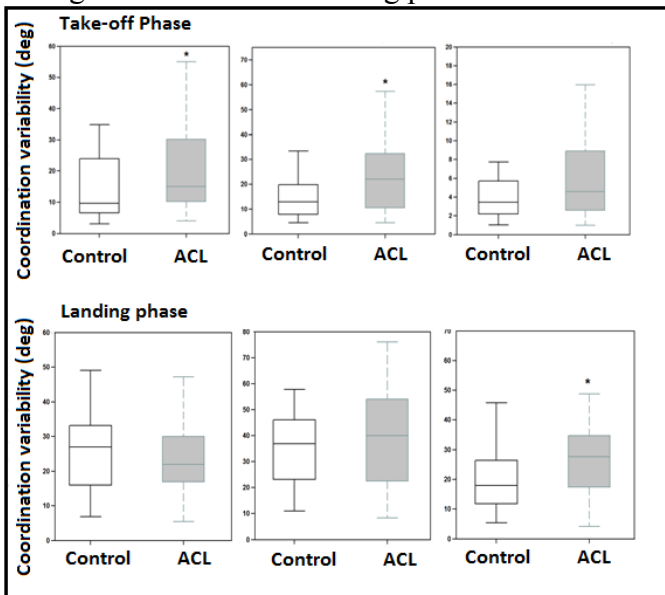


Fig. 1: Coordination variability (SD of vector coupling in degrees) of knee abduction/adduction coupled with hip abduction/adduction (left), hip rotation (center) and hip flexion/extension (right) during the take-off and landing phases of one-leg hops. Box plots show median values, 25th and 75th percentiles, and minimum and maximum values of each variable across all subjects in the group. Asterisk indicates a significant difference ( $p < 0.05$ ) in Mann Whitney U test between the control and ACL groups.

On average, the ACL group exhibited ~50% more variability in knee-hip abduction/adduction than the control group and nearly 60% more variability in knee abduction/adduction-hip rotation than the control group during the take-off phase. The ACL group exhibited ~ 50% more variability in knee abduction/adduction-hip flexion/extension coupling than the control group during the landing phase.

Our results of greater variability in hip-knee coordination in ACL group compared to healthy controls is in agreement with earlier studies <sup>e.g.,5</sup> who have investigated these couplings in the short-term after injury. Such increased variability has been suggested to be due to the absence of proper neural feedback mechanisms due to altered proprioception, despite the regaining of mechanical stability in individuals undergoing ACL reconstruction. For the first time, we have shown that such an effect is present even 20 or so years after injury. Furthermore, in our study, the injured and control groups were not significantly different in terms of hop length as

normalized to body length during the one-leg hop test. However, the injured groups showed significantly lower knee function (worse Lysholm knee scores and Knee injury and Osteoarthritis Outcome Scores). There were also significantly higher limb asymmetries (i.e. worse LSI scores) reported in the injured group than the control group, although the LSI of both groups were above 90% and hence classified as normal. Thus, although both groups showed similar performance in the one-leg hop test and had sufficiently “normal” limb symmetry, the injured group showed different joint coordination variability than the control group. This greater variability correlated with worse scores on tests of self-reported knee function.

## CONCLUSIONS

Improving our understanding of coordination variability and applying methods assessing intra-individual movement variability may provide more insight into mechanisms governing adaptations of neuromuscular control following injury, also in the very long term.

## REFERENCES

1. Augustsson, J., et al. (2004). "Ability of a new hop test to determine functional deficits after anterior cruciate ligament reconstruction." *Knee Surg Sports Traumatol Arthrosc* 12(5): 350-356.
2. Heiderscheit, B. C. (2000). "Movement variability as a clinical measure for locomotion." *Journal of Applied Biomechanics* 16(4): 419-427.
3. Stergiou, N., et al. (2006). "Optimal movement variability: a new theoretical perspective for neurologic physical therapy." *J Neurol Phys Ther* 30(3): 120-129
4. Heiderscheit, B. C., et al. (2002). "Variability of stride characteristics and joint coordination among individuals with unilateral patellofemoral pain." *Journal of Applied Biomechanics* 18(2): 110-121.
5. Pollard, C. D., et al. (2015). "Altered lower extremity movement variability in female soccer players during side-step cutting after anterior cruciate ligament reconstruction." *Am J Sports Med* 43(2): 460-465

# ENERGY ABSORPTION STRATEGIES AND MUSCLE STRENGTH IN ADOLESCENT MALES AND FEMALES DURING A LATERAL-VERTICAL JUMP AT RETURN TO SPORT FOLLOWING ANTERIOR CRUCIATE LIGAMENT RECONSTRUCTION

<sup>1</sup>Shiho Goto, <sup>1</sup>J Craig Garrison, <sup>1</sup>Joseph Hannon, <sup>1</sup>James Bothwell, <sup>2</sup>Kelci Besand, <sup>1</sup>Angellyn Grondin

<sup>1</sup>Texas Health Ben Hogan Sports Medicine, Fort Worth, TX, USA

<sup>2</sup>Texas Christian University, Fort Worth, USA

Email: [ShihoGoto@texashealth.org](mailto:ShihoGoto@texashealth.org);

Website: <https://www.texashealth.org/sports-medicine/Pages/Research-and-Clinical-Trials.aspx>

## INTRODUCTION

Asymmetries of the lower extremity functions have been identified in individuals following anterior cruciate ligament reconstruction (ACL-R) [1-3] which could contribute to recurrent anterior cruciate ligament (ACL) injury. Deficits in the ability to absorb forces through the lower extremity increases strain in the ACL, which could potentially lead to ACL re-injury. There are no studies examining energy absorption (EA) strategy between the ACL-R and contralateral (CON) limbs in adolescent males and females at a time of return to sports (RTS) following ACL-R. The purpose of this study was to examine the differences of EA pattern in the lower extremity in the ACL-R limb and contralateral limbs in adolescent males and females

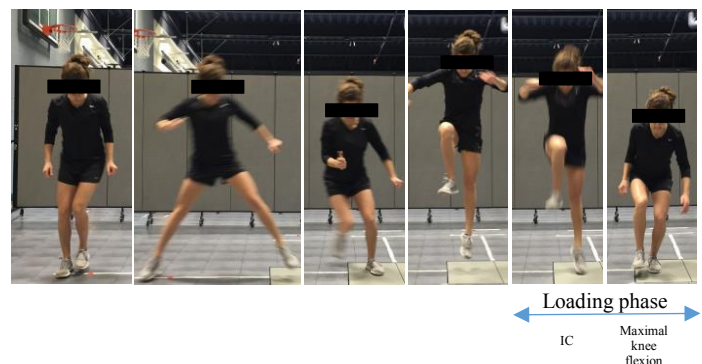
## METHODS

Cross-sectional descriptive study design was used. A total of fifty-three participants with ipsilateral ACL-R who were at a time of RTS following ACL-R volunteered (Male = 21: Age =  $15.67 \pm 1.20$  years, Ht =  $176.80 \pm 7.85$ cm, Mass =  $75.97 \pm 16.0$ Kg; Female = 32: Ht =  $164.35 \pm 6.89$ cm, Mass =  $66.41 \pm 6.89$ Kg).

Joint net power (J) was assessed using an eight-camera motion capture system and two forceplates while participants performed three separate lateral-vertical jump (LVJ) tasks (Figure 1). They stood lateral to the forceplate, located at 50% of their height. Participants then pushed off the ground with their non-testing limb, hopped onto the forceplate with their testing-limb followed by immediate

maximal vertical jump, and landed on the forceplate with their testing-limb. Immediately after landing back onto the forceplate, they were required to balance for approximately 2 seconds. Isokinetic strength of the quadriceps (QUADS) and hamstrings (HAMS) at 60 deg/sec was collected using an isokinetic dynamometer. Maximal voluntary isometric strength of the hip abductor (HAB), hip external rotators (HER), and hip extensors (HEXT) were assessed using a handheld dynamometer. All data were assessed bilaterally in order of uninvolved limb, followed by involved limb. Energy absorption of the hip, knee, and ankle joints were calculated by integrating the negative part of the power curve during the loading phase of the second landing of the LVJ and normalized to the product of height and weight (Ht\*BW) and averaged across three trials. Total EA was calculated as a sum of EA of each joint. Isokinetic strength of the QUADS and HAMS was normalized to body weight (BW) and averaged across 5 trials. Peak MVICs of the HAB, HER, and HEXT was normalized to the BW and averaged across 2 trials. Separate paired t-test were performed to examine the difference between the ACL-R and contralateral limbs in each group (male and female).

**Figure 1. Lateral-hop vertical jump (LVJ)**



## RESULTS AND DISCUSSION

During the loading phase of the LVJ, total EA was significantly decreased in both males ( $p=0.006$ ) and females ( $p=0.047$ ) in the ACL-R limb compared to the CON limb. Adolescent males demonstrated decreased EA at the knee ( $p<0.001$ ) and ankle ( $p<0.001$ ) joints in the ACL-R limb while adolescent females demonstrated increased hip EA ( $p=0.009$ ), and decreased knee ( $p<0.001$ ) and ankle ( $p=0.008$ ) EAs compared to the CON limbs (Table1).

For muscle strength, both groups had significantly decreased QUADS (Male:  $p<0.001$ ; Female:  $p<0.001$ ) and HAMS (Male:  $p=0.038$ ; Female:  $p=0.029$ ) strength, compared to the CON limbs. No significant differences were observed in the gluteal muscle strength (Table 2).

Following ACL-R, adolescent males and females demonstrated altered EA strategies in the ACL-R limb compared to the CON limb during the LVJ. In the ACL-R limb, adolescent males avoided the usage of knee and ankle joints to absorb forces while adolescent females relied more on the hip joint and avoided use of the knee and ankle joints,

in relation to the CON limb. These results suggest that adolescent males and female adopted different strategies to absorb forces during the LVJ. Since both groups displayed decreased QUADS and HAMS strength, these muscles may play an important role in absorbing forces through the lower extremity.

## CONCLUSIONS

Both male and female adolescents displayed different EA absorption strategies during the LVJ at a time of RTS following ACL-R. Increasing QUADS and HAMS strength may improve the EA pattern in the ACL-R limb, which could help develop a more symmetrical landing pattern.

## REFERENCES

1. Abourezk MN. *The American journal of sports medicine*. 2017 Jan;45(1):97-105..
2. Palmieri-Smith RM. *The American journal of sports medicine*. 2015;43 (7):1662-1669.
3. Schmitt LC. *Medicine and science in sports and exercise*. 2015;47(7):1426-1434.

**Table 1:** Energy absorption (Ht\*BW) side to side difference (\*indicates significant difference.  $p < 0.05$ ).

<i>Male</i>	Hip	Knee	Ankle	Total
<b>Involved</b>	-0.088 ± 0.042	-0.066 ± 0.030*	-0.065 ± 0.013*	-0.220 ± 0.070*
<b>Uninvolved</b>	-0.082 ± 0.031	-0.091 ± 0.033	-0.072 ± 0.011	-0.246 ± 0.055
<i>Female</i>				
<b>Involved</b>	-0.091 ± 0.035*	-0.055 ± 0.021*	-0.060 ± 0.013*	-0.206 ± 0.054*
<b>Uninvolved</b>	-0.078 ± 0.031	-0.074 ± 0.027	-0.066 ± 0.015	-0.218 ± 0.053

**Table 2:** Muscle strength (BW) side to side difference. (\*indicates significant difference.  $p < 0.05$ ).

<i>Male</i>	QUADS	HAMS	HER	HEXT	HAB
<b>Involved</b>	1.77 ± 0.43*	1.07 ± 0.25*	0.20 ± 0.07	0.24 ± 0.08	0.24 ± 0.07
<b>Uninvolved</b>	2.42 ± 0.54	1.14 ± 0.23	0.20 ± 0.07	0.24 ± 0.08	0.24 ± 0.07
<i>Female</i>					
<b>Involved</b>	1.26 ± 0.26*	0.87 ± 0.18*	0.16 ± 0.03	0.22 ± 0.06	0.22 ± 0.04
<b>Uninvolved</b>	1.75 ± 0.38	0.91 ± 0.15	0.16 ± 0.03	0.22 ± 0.06	0.22 ± 0.05

# LOWER EXTREMITY SEGMENT COORDINATION FOLLOWING ANTERIOR CRUCIATE LIGAMENT RECONSTRUCTION

<sup>1,2</sup>Kelci B. Besand, <sup>2</sup>James M. Bothwell, <sup>2</sup>J. Craig Garrison, <sup>2</sup>Shiho Goto, <sup>2</sup>Joseph P. Hannon, <sup>2</sup>Angellyn Grondin, and <sup>1</sup>Adam C. King

<sup>1</sup>Texas Christian University, Fort Worth, TX, USA

<sup>2</sup>Ben Hogan Sports Medicine, Fort Worth, TX, USA  
email: k.besand@tcu.edu

## INTRODUCTION

The anterior cruciate ligament (ACL), along with preventing anterior translation of the tibia, provides important sensory information regarding the knee joint. ACL injury disrupts this information, leading to altered neuromuscular control of the lower extremity. Following ACL reconstruction (ACLR) it has been suggested that, if not addressed properly, neuromuscular deficits may occur [1]. Segment coordination is a measure of neuromuscular control that provides information about how adjacent segments move in relation to each other and should be relearned during rehabilitation. Using segment coordination variability as an indicator of poor neuromuscular control may lead to a better understanding of ACL injury risk and missing components of rehabilitation. Some authors suggest that there is an optimal level of variability for motor tasks with anything above or below this level leading to injury [2]. This range has yet to be identified but may prove to be an important factor in ACL injury and rehabilitation.

The current study aims to contribute to the existing literature by investigating lower extremity coordination differences between ACLR patients and control subjects during a jump-landing task. It was hypothesized that ACLR patients would exhibit altered lower extremity segment coordination patterns when compared to the control group.

## METHODS

Thirty-five young females participated in the current study. Ten (age =  $15.7 \pm 0.95$  yrs, mass =  $65.81 \pm 13.37$  kg, height =  $163.83 \pm 8.84$  cm) were released from physical therapy for return-to-sport following ACLR of the right leg. Twenty-five (age

=  $15.24 \pm 1.2$  yrs, mass =  $58.05 \pm 8.83$  kg, height =  $164.57 \pm 5.66$  cm) had no previous lower extremity injury. All subjects were right-leg dominant. Subjects completed three trials of a jump-landing task from a 30 in box placed 50% of the subject's height behind two ATMI force plates (Advanced Mechanical Technology, Inc., Watertown, MA). Subjects jumped from the box, landed on the force plates, and immediately completed a maximal vertical jump. Kinematic data were collected using a 10-camera Qualisys Motion Capture System (Qualisys AB, Göteborg, Sweden) and were filtered using a fourth-order Butterworth filter and 12 Hz cut-off frequency. Joint couplings were created from the kinematic data and then used to create relative motion (angle-angle) plots as a function of anatomical plane. Statistical calculations from relative motion plots were adopted from a modified vector-coding technique [3] and included two measures: (1) relative motion area and (2) vector-coding that calculated an angle, with respect to the right horizontal, of the vector formed between two consecutive data points on the relative motion plot. Statistical analyses included separate repeated-measures ANOVAs conducted on dependent variables with leg, joint coupling, and anatomical plane as the repeated, within subject factors, and injury group as the between subject factor. An alpha value of 0.05 was used to define statistical significance.

## RESULTS AND DISCUSSION

The results of the vector coding analysis revealed significant main effects of coupling ( $p < 0.0001$ ) and plane ( $p < 0.0001$ ). The main effect of leg was found to be non-significant ( $p = 0.847$ ), but a significant triple interaction was found between leg, plane, and

test group. Specifically, in the frontal plane the coordination pattern of the right leg differed for the ACLR subjects compared to the control group ( $p = 0.008$ ). Additionally, a trend toward significance was found between groups for the coordination pattern of the left leg in the transverse plane ( $p = 0.076$ ). The mean vector coding angle was higher for the ACLR group for the right leg in the frontal plane, but was lower for the left leg in the transverse plane compared to the mean coordination of the control group (Fig. 1).

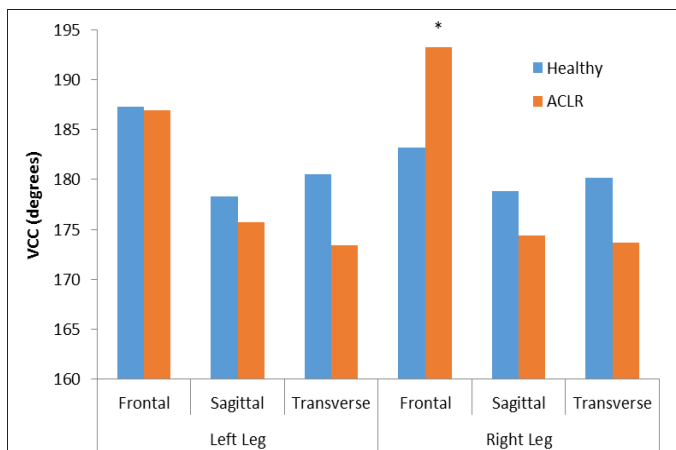


**Figure 1:** A comparison of mean coordination in the control group and ACLR group across all planes for each leg. \*indicates a statistically significant difference in coordination pattern between injury groups in the frontal plane ( $p = 0.008$ ).

The significant main effect of coupling shows that the lower extremity segments use varying coordination patterns during the dynamic task of drop landing to vertical jump performance. Additionally, the plane effect further illustrates the multi-dimensional aspect of the drop landing movement that is not typically addressed in most injury risk models.

The finding of an altered coordination pattern for the injured limb following ACLR compared to healthy controls suggests that athletes may be returning to competition while using movement patterns that place them at risk for further injury. The coordination differences suggest that a neuromuscular control component to ACL recovery may need additional attention during the rehabilitation process.

The findings also suggest that a compensatory strategy may be used in the uninjured limb of ACLR individuals. This result was highlighted by the trend toward significance of the coordination pattern, primarily in the transverse plane. As patients return-to-sport, it is likely that they will exhibit a disinclination to use their injured leg, leading to improper movement patterns. This may also lead to altered coordination patterns of the uninvolved leg as they attempt to correct for movement of the involved leg, potentially increasing the risk of injury. Lastly, many rehabilitation exercises focus on actions in the frontal and sagittal planes, such as controlling medial displacement of the knee and absorbing force during landing by increasing knee flexion, but observing motion in the transverse plane is a greater challenge. This may lead to a lack of feedback regarding transverse plane motion and a decreased ability to correct for movement pattern alterations when completing a dynamic task outside of a controlled setting.

## CONCLUSIONS

The significant triple interaction of leg, group, and plane confirmed the hypothesis that ACLR patients would exhibit altered coordination patterns when compared to control subjects. Additionally, coordination patterns of the injured leg may affect the uninjured leg and contribute to re-injury rates on the contralateral, as well as ipsilateral, side. Coordination changes can reveal how underlying tissues are deformed during motor tasks, and a better understanding of lower extremity coordination deficits following ACLR is needed to establish effective rehabilitation protocols to prevent secondary ACL injury. Overall, further investigation is needed to fully understand the implications of altered coordination patterns following ACLR.

## REFERENCES

- Blache Y, et al. *Int J Sports Med* **38**, 159-167, 2017.
- Pollard CD, et al. *American Journal of Sports Medicine* **43**, 460-465, 2015.
- Sparrow WA, et al. *Journal of Motor Behavior* **19**, 115-129, 1987.

# INDIVIDUALS FOLLOWING ANTERIOR CRUCIATE LIGAMENT RECONSTRUCTION ADJUST CENTER OF PRESSURE LOCATION TO REDISTRIBUTE EXTENSOR LOADING

<sup>1</sup>Ming-Sheng M. Chan, <sup>1</sup>Paige E. Lin, <sup>1</sup>Susan M. Sigward

<sup>1</sup>Human Performance Laboratory, University of Southern California, Los Angeles, CA, USA  
email: mingshec@usc.edu, web: <http://pt.usc.edu/mingshec/>

## INTRODUCTION

Individuals following anterior cruciate ligament reconstruction (ACLR) adopt loading strategies that shift the mechanical demands away from the surgical knee during bilateral tasks [1]. A strategy that shifts demands within the limb away from the knee and toward the hip extensors has been described during squatting [1]. Individuals 7 months post-ACLR exhibited a 25.5% lower knee extensor moment along with a 49.1% higher hip extensor moment, resulting in almost a two-times greater hip to knee extensor moment ratio in the surgical limb compared to the non-surgical limb (surgical: 163% vs. non-surgical: 87.5%) [1]. These data highlight between-limb differences in the distribution of extensor moments during squatting.

Distribution of extensor demands within the limb can be accomplished by altering joint kinematics, adjusting the position of center of pressure (CoP), or a combination of the two [2]. Theoretically, an anterior position of the CoP shifts the vertical ground reaction force vector closer to the knee joint and further from the hip joint, decreasing the demand on the knee extensors and increasing the demand on the hip extensors (Figure 1). However, it is not known if the distribution of sagittal plane extensor demands during squatting is accomplished by altering CoP position in individuals following ACLR.

The purpose of this study was to determine the relationships between CoP position and sagittal plane moments distributions both within- and between-limbs.

## METHODS

Eleven individuals (7 females,  $25.3 \pm 10.7$  yrs) 5 months ( $148.8 \pm 9.2$  days) following ACLR were enrolled in this study. They performed 2 sets of 5

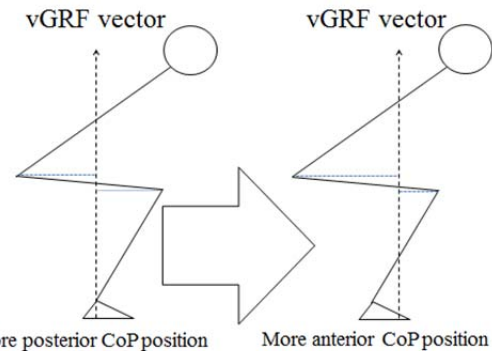


**Figure 1:** Conceptual diagram of the relationship between CoP position and joint moment distributions in the sagittal plane.

consecutive bilateral squats with bodyweight resistance.

Kinematics (250 Hz) were collected using a 11-camera motion capture system (Qualisys, Göteborg, Sweden). Ground reaction forces (1500Hz) were quantified using AMTI force platforms (AMTI, MA, USA). Three dimensional joint kinematics, ground reactions forces and anthropometrics were used to calculate net joint moments using standard inverse dynamics equations (Visual3D, C-Motion Inc., MD, USA). Kinetic data were normalized to body mass. Peak knee extensor moment (kEXT), peak hip extensor moment (hEXT), and CoP position were identified during the deceleration phase ( $0^\circ$  to maximum knee flexion angle).

Foot length was defined as the distance between markers placed on the second toe and the heel (Figure 2). CoP position ( $CoP_{pos}$ ) was calculated as distance from the heel and

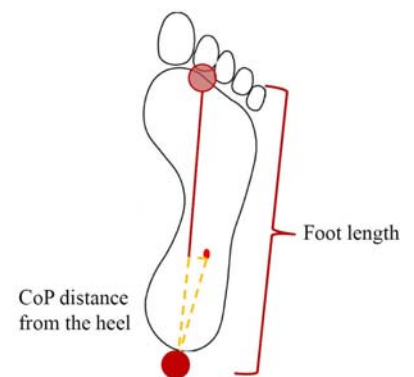


**Figure 2:**  $CoP_{pos}$  (the yellow dash line). 2<sup>nd</sup> toe and the heel markers

normalized to the individual's foot length (Figure 2).  $CoP_{pos}$  at kEXT was identified. A greater number indicates a more anterior  $CoP_{pos}$ .

To reflect the relative extensor moment distribution between the hip and the knee within the limb, a hip to knee ratio (hEXT/kEXT) was calculated for each limb. A hEXT/kEXT > 1 indicates a more hip dominant strategy with a greater extensor moment in the hip relative to the knee.

Between-limb ratios (surgical limb / non-surgical limb) were calculated for  $CoP_{pos}$  and (hEXT/kEXT) to reflect the relative differences between limbs in extensor moment distribution and COP position. Between-limb ratios > 1 indicate that the surgical limb has a more anterior  $CoP_{pos}$  and a greater relative hip extensor moment contribution in the surgical limb. A total of 6 squats (the middle 3 squats of each trial) were chosen for data analysis.

Separate univariate linear regressions were used to determine if the  $CoP_{pos}$  was predictive of the extensor moment distribution for each limb and if the relative difference between limbs in  $CoP_{pos}$  predicted of the relative difference between limbs in extensor moment distribution ( $\alpha = .05$ ).

## RESULTS AND DISCUSSION

When considering each limb,  $CoP_{pos}$  was a significant predictor of the hEXT/kEXT (surgical:  $R^2 = .62$ ,  $p = .004$ ; non-surgical:  $R^2 = .38$ ,  $p = .042$ ; Figure 3, a and b). A greater hEXT/kEXT ratio was related to a more anterior  $CoP_{pos}$ .

When considering differences between limbs in extensor moment distribution and COP position, the between-limb  $CoP_{pos}$  ratio was a significant predictor of the between-limb hEXT/kEXT ratio ( $R^2 = .49$ ,  $p = .017$ ; figure 3, c). A larger between-limb hEXT/kEXT ratio was related to a larger  $CoP_{pos}$  ratio.

## CONCLUSIONS

At 5 months post-surgery,  $CoP_{pos}$  explained 62% and 38% of the variance in the hEXT/kEXT in the surgical and non-surgical limbs, respectively. A more anterior  $CoP_{pos}$  was related to a more hip dominant strategy. As the  $CoP_{pos}$  was positioned more anteriorly, the extensor demand at the knee decreased while the demand at the hip increased.

When considering between-limb differences, those who exhibited a more hip dominant strategy in their surgical limb compared to their non-surgical limb also positioned their COP more anteriorly in the surgical limb. This suggests that individuals following ACLr may adopt a strategy that positions the CoP more anteriorly to reduce the demands on the knee extensors in the surgical limb.

## REFERENCES

1. Salem GJ, et al. *Arch Phys Med Rehabil* **84**(8), 1211-1216, 2003.
2. Gruben KG, et al. *J Biomech* **45**, 1661-1665, 2012.

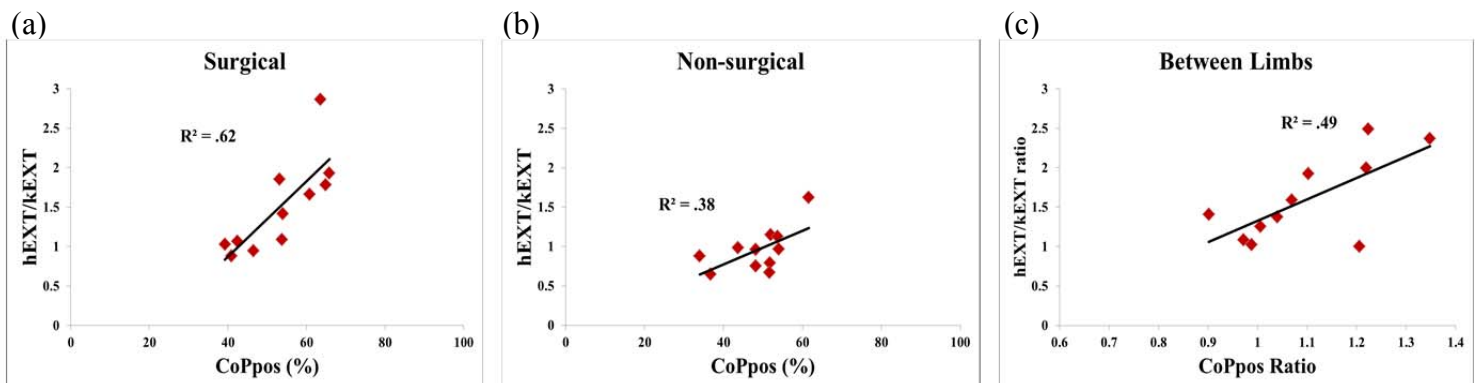


**Figure 3:** The relationships between  $CoP_{pos}$  and hEXT/kEXT (a: surgical, b: non-surgical), and the relationship between  $CoP_{pos}$  ratio and hEXT/kEXT ratio (c).

# SEX AND LEG DIFFERENCES IN ACL STRESS DURING DROP LANDING

Joshua T. Weinhandl, Ashley N. Grillo, and Onyebuchi N. Okereke

University of Tennessee, Knoxville  
email: jweinhan@utk.edu

## INTRODUCTION

The prevalence of anterior cruciate ligament (ACL) injuries in athletic populations is well documented [1], and a majority of these injuries are caused by noncontact mechanisms [2]. Furthermore, recent epidemiological evidence indicates that females are more than twice as likely to have a first-time noncontact ACL injury compared to males [3].

Epidemiological evidence also suggests leg dominance may serve as an etiological factor with regard to ACL injuries [4,5]. Negrete et al. [4] reported a possible association between leg dominance and ACL injury in females but not in males. Likewise, females appear more likely to injure the ACL in their supporting leg, whereas males tend to injure their kicking leg ACL [5].

Therefore, the purpose of this study was to determine if there is an interaction between gender and leg side on ACL stress during unilateral landings. We hypothesized that females would experience increased ACL stress compared to males, and a concurrent increase in related ACL injury risk variables. We also hypothesized that ACL stress and related ACL injury risk variables would be greater in the non-dominant leg compared to the dominant leg (preferred kicking leg).

## METHODS

Twenty-one recreationally active women (60.3±9.3 kg, 1.65±0.07 m) and twenty-two recreationally active men (82.3±18.3 kg, 1.79±0.09 m) volunteered to perform unilateral landings from 40 cm on their dominant and non-dominant legs. Dominant leg was defined as the preferred kicking leg. Prior to data collection, participants were informed of study procedures and provided written informed consent in accordance with institutional guidelines. Marker coordinate data (200 Hz, Vicon) and ground reaction force data (2000 Hz, Bertec) were collected simultaneously for all trials.

OpenSim (v3.3 <http://simtk.org>) was used to simulate all right and left leg landing trials [6]. An 8 segment, 23 degrees-of-freedom (*dof*) musculoskeletal model, with 92 Hill-type muscle actuators (modified from Gait2392), was scaled to match each participant's anthropometry based on experimentally measured anatomical landmarks. The knees were modified to be 3-*dof* joints (i.e., flexion-extension, adduction-abduction, internal-external rotation). Knee adduction-abduction and internal-external rotation *dof* were modeled as universal joints, with the same center of rotation as the flexion-extension *dof*, which was modeled as a planar joint, allowing the tibia to translate relative to the femur as a function of knee flexion angle. Static optimization was used to calculate the muscle forces required to reproduce the joint moments of each trial. The optimization minimized the sum of muscle activations to distribute muscle forces. Simulated knee joint reaction forces and moments, along with hamstrings, quadriceps and gastrocnemius muscle force estimates were input into a three-dimensional knee model to estimate ACL loading [7]. ACL stress was then estimated using average, gender specific measurements of ACL mid-substance area (females: 58.29 mm<sup>2</sup>; males: 83.54 mm<sup>2</sup>) [8].

A 2×2 repeated measures ANOVA was used to assess sex and landing leg differences in peak ACL stress. Other variables of interest included initial contact knee angles, maximum knee angles, and maximum knee moments of the landing leg. Landing phase was defined as initial contact to maximum knee flexion of the landing leg. ACL stress and knee moments were normalized to body mass. Significance for all tests was set at  $p < 0.05$ .

## RESULTS AND DISCUSSION

There were no significant sex×leg interactions for any of the variables examined. However, the interaction for peak ACL stress approached significance ( $p=0.077$ ). A significant main effect of

sex was identified for only peak ACL stress ( $p < 0.001$ ). The main effect of leg was significant for maximum knee internal rotation angle ( $p = 0.009$ ), maximum knee adduction moment ( $p < 0.001$ ), and maximum knee internal rotation moment ( $p < 0.001$ ).

Our first hypothesis that females would experience increased ACL stress compared to males, and a concurrent increase in related ACL injury risk variables was partially supported. Females experienced a peak ACL stress of  $0.15 \pm 0.03$  MPa·kg<sup>-1</sup>, compared to the  $0.12 \pm 0.03$  MPa·kg<sup>-1</sup> peak ACL stress experienced by males, regardless of landing leg. This finding is consistent with the increased rates of noncontact ACL ruptures in females [1]. However, there were no other sex differences observed, suggesting that factors contributed to the increased ACL stress in females besides knee mechanics. Examining hip and ankle mechanics may help explain the sex differences in peak ACL stress observed in the current study.

Our second hypothesis that ACL stress and related ACL injury risk variables would be greater in the non-dominant leg was also partially supported. While the sex×leg interactions for peak ACL stress was not significant ( $p = 0.077$ ), females seemed to show increased stress in the non-dominant ACL. Furthermore, there were alterations in knee mechanics. Specifically, non-dominant leg landings were characterized by a 2.2° increase in maximum knee internal rotation angle, as well as 67% and 125% increases increase in maximum knee adduction and maximum knee internal rotation moments, respectively. These variables are commonly associated with ACL injury risk [2], but their relationship to ACL stress remains unclear.

## CONCLUSIONS

Females experienced greater ACL stress during unilateral landings even though there were no other sex differences observed. This finding suggests females may be more susceptible to ACL injury when presented with unexpected perturbations that increase the load applied to the ACL. Our results also indicate that frontal and transverse plane knee loading is increased during non-dominant leg landings, even though ACL stress is unchanged.

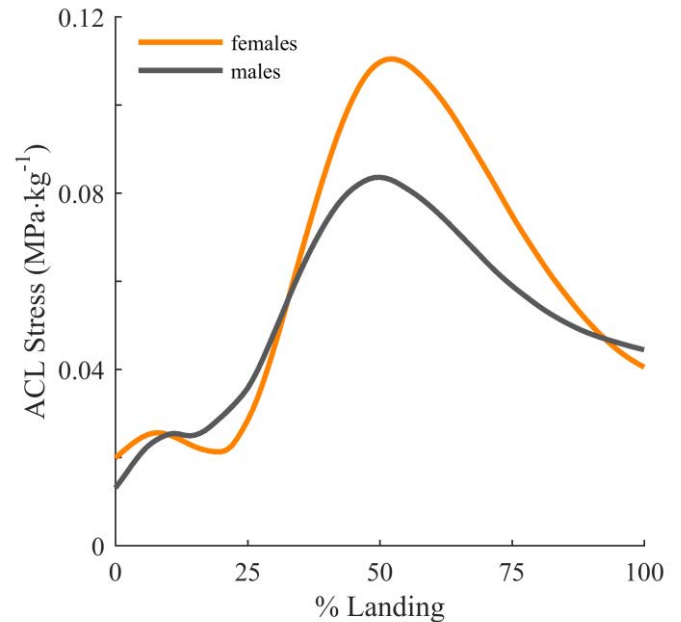


**Figure 1.** ACL stress (MPa·kg<sup>-1</sup>) during unilateral landings for females (orange) and males (gray).

## REFERENCES

1. Agel J, et al., *AJSM*. **33**:542-31, 2005.
2. Hewett TE, et al., *AJSM*. **34**:299-311, 2006.
3. Beynon BD, et al., *AJSM*. **42**:1806-12, 2014.
4. Negrete RJ, et al. *JSCR*. **21**:270-3, 2007.
5. Brophy R, et al. *BJSM*. **44**:694-7, 2010.
6. Delp SL, et al., *IEEE TBE*. **54**:1940-50, 2007.
7. Weinhandl JT, et al., *Clin Biomech*. **28**:655-63, 2013.
8. Chandrashekar N, et al. *AJSM*. **33**:1492-8, 2005.

Table 1. Variables exhibiting significant main effects for sex or leg during unilateral landings (mean ± stdv).

	Dominant		Non-dominant	
	Women	Men	Women	Men
Peak ACL stress (MPa/kg) §	0.16 ± 0.03	0.12 ± 0.03	0.15 ± 0.03	0.12 ± 0.03
Maximum knee internal rotation (deg) *	9.8 ± 3.3	9.2 ± 5.3	12.9 ± 4.6	10.5 ± 5.1
Maximum knee adduction moment (Nm/kg) *	0.11 ± 0.11	0.13 ± 0.10	0.21 ± 0.25	0.18 ± 0.11
Maximum knee internal rotation moment (Nm/kg) *	0.04 ± 0.04	0.04 ± 0.02	0.09 ± 0.05	0.09 ± 0.04

§ Significant main effect for sex

\* Significant main effect for leg

# HAMSTRINGS ACTIVITY CONTRIBUTES TO KNEE MECHANICS DURING GAIT FOLLOWING ACL RECONSTRUCTION

<sup>1</sup>Derek N. Pamukoff, <sup>1</sup>Tyler J. Moffit, <sup>1</sup>Michael N. Vakula, <sup>1</sup>Skylar Holmes, and <sup>1</sup>Melissa M. Montgomery

<sup>1</sup>California State University, Fullerton, Fullerton CA  
email: dpamukoff@fullerton.edu

## INTRODUCTION

Individuals with anterior cruciate ligament reconstruction (ACLR) are at greater risk for knee osteoarthritis due to alterations in walking biomechanics [1]. For instance, individuals with ACLR have lesser knee flexion angles (KFA) and external moments (KFM) [1], partially due to quadriceps dysfunction [2]. However, hamstrings co-activation is also elevated in individuals with ACLR [2, 3], which may influence sagittal plane knee mechanics during gait, and confound the interpretation of reduced KFA and KFM. Therefore, the purpose of this study was (1) to compare knee mechanics (KFA and KFM), and quadriceps and hamstring activation between the injured and uninjured limbs of individuals with unilateral ACLR during gait, and (2) to examine the association between KFA and KFM, and quadriceps and hamstrings activation in the injured limb. We hypothesized that the injured limbs would have lesser KFA and KFM, lesser quadriceps activity, and greater hamstrings activity compared to the uninjured limb. We also hypothesized that greater quadriceps activity would be associated with greater KFA and KFM, and that greater hamstrings activity would be associated with lesser KFA and KFM.

## METHODS

Twenty-three individuals with primary unilateral ACLR volunteered to participate in this study (83% Female; Age =  $22.1 \pm 2.5$  years; Height =  $1.67 \pm 0.07$  m; Mass =  $69.2 \pm 13.5$  kg; Time Since ACLR =  $50.3 \pm 22.6$  months; International Knee Documentation Committee Score =  $85.3 \pm 10.3$ ; Graft Type: Patellar Tendon Autograft = 14, Hamstrings Autograft = 4, Allograft = 5).

Static markers were placed bilaterally on the iliac crest, greater trochanter, medial and lateral femoral

epicondyles, medial and lateral malleoli, and the first and fifth metatarsal heads. Rigid clusters of 4 markers were affixed to the pelvis, and bilaterally to the foot, shank, and thigh. Static markers were removed after a standing calibration trial. Surface EMG sensors were placed bilaterally on the vastus lateralis, vastus medialis, biceps femoris, and medial hamstrings. Ground reaction force, marker position, and EMG data were sampled while participants walked in laboratory standard neutral cushion footwear at a self-selected speed that was maintained within  $\pm 5\%$  across 5 trials. Participants walked across a 10m runway and made contact with consecutive force plates in the center of the runway.

Data were exported to Visual 3D for model construction, and further processed using a custom LabVIEW program. Kinematic and kinetic variables included the peak KFA and KFM during the first 50% of the stance phase. Raw EMG data were band-pass filtered from 20-350Hz, full-wave rectified, and low-pass filtered at 20Hz to create a linear envelope [2]. The processed signals were normalized to the EMG signal from maximal voluntary isometric contractions that were obtained prior to the gait trials, and the integral from 100ms prior to heel contact to peak knee flexion during the first 50% of stance phase was extracted [2]. Integrals for the vastus lateralis and vastus medialis, and biceps femoris and medial hamstrings, were averaged to create composite values of quadriceps and hamstrings EMG activity, respectively.

KFA, KFM, quadriceps activity, and hamstrings activity were compared between limbs using paired samples-tests. Pearson correlations were used to evaluate associations between the KFA and KFM, and quadriceps and hamstrings activity. Exploratory multiple linear regression analyses were used to predict KFA and KFM using quadriceps and hamstring activity as predictors.

## RESULTS AND DISCUSSION

Gait speed was not associated with KFA ( $r = 0.14$ ,  $p = 0.31$ ), KFM ( $r = 0.23$ ,  $p = 0.28$ ), quadriceps activity ( $r = 0.20$ ,  $p = 0.35$ ), or hamstrings activity ( $r = 0.25$ ,  $p = 0.17$ ) in this sample; and therefore, was not accounted for in statistical analyses.

Hamstrings activity ( $53.7 \pm 25.1$  vs.  $35.8 \pm 20.4$ ,  $p < 0.01$ ) and peak KFM ( $0.06 \pm 0.02$  vs.  $0.04 \pm 0.02$  Nm/BW\*ht,  $p = 0.02$ ) were greater in the injured compared to uninjured limb. No difference was found between the injured and uninjured limbs in quadriceps activity ( $44.4 \pm 30.3$  vs.  $51.6 \pm 30.7$ ,  $p = 0.13$ ) or KFA ( $25.7 \pm 6.2$  vs.  $26.1 \pm 7.8^\circ$ ,  $p = 0.31$ ). Greater quadriceps activity was associated with a larger KFA (Fig. 1,  $r = 0.42$ ,  $p = 0.02$ ), and greater hamstrings activity was associated with a smaller KFM (Fig. 1,  $r = -0.35$ ,  $p = 0.05$ ). The association between quadriceps activity and KFM (Fig. 1,  $r = 0.29$ ,  $p = 0.09$ ), and hamstrings activity and KFA (Fig. 1  $r = -0.13$ ,  $p = 0.29$ ) were not significant.

Multiple linear regression indicated that hamstrings and quadriceps activity explained 24% of the variance in KFM and approached significance ( $F_{2,20} = 3.2$ ,  $p = 0.06$ ). Hamstrings activity ( $\beta = -0.41$ ,  $p = 0.05$ ), but not quadriceps activity ( $\beta = 0.37$ ,  $p = 0.07$ ) predicted KFM. Secondly, hamstrings and quadriceps activity explained 18% of the variance in peak knee flexion angle, but this model was not significant ( $F_{2,20} = 2.2$ ,  $p = 0.14$ ). The variable inflation factor due to any correlation between hamstrings and quadriceps activity was 1.04, confirming the absence of multicollinearity.

Previous studies indicate that individuals with ACLR have lower KFA and KFM in their injured compared to uninjured limb [1, 2]. These gait alterations are often attributed to a reduction in quadriceps function (i.e. quadriceps avoidance gait) that is common following ACLR [2, 4, 5]. However, many of these studies [1, 6] have failed to account for the contribution of increased hamstring activity, which is also common following ACLR [2, 3]. Hamstrings activity influences net knee joint moments, and future studies should account for hamstrings activity during gait analyses in individuals with knee pathology.

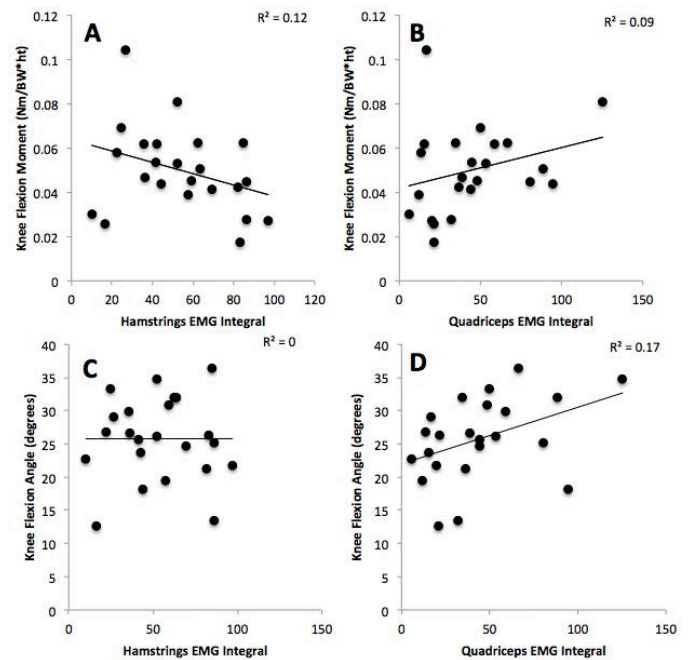


**Figure 1:** Associations between (A) KFM and hamstrings activity; (B) KFM and quadriceps activity; (C) KFA and hamstrings activity; (D) KFA and quadriceps activity

## CONCLUSIONS

These findings suggest that both hamstrings and quadriceps activity contribute to sagittal plane knee mechanics during the stance phase of gait in individuals with ACLR. Future longitudinal studies should examine the influence of elevated hamstrings activity on long-term knee joint health.

## REFERENCES

1. Hart, H.F., et al., *Br J Sports Med*, 2016. **50**(10): p. 597-612.
2. Lewek, M., et al., *Clin Biomech (Bristol, Avon)*, 2002. **17**(1): p. 56-63.
3. Pamukoff, D.N., et al., *Journal of Athletic Training*, 2017. In press.
4. Blackburn, J.T., et al., *Medicine & Science in Sports & Exercise*, 2016. **48**(9): p. 1664-70.
5. Kuenze, C., et al., *Med Sci Sports Exerc*, 2014. **46**(6): p. 1067-76.
6. Asaeda, M., et al., *Knee*, 2017. In press.

## ACKNOWLEDGMENTS

Supported by: CSU Program for Education and Research in Biotechnology New Investigator Grant

# QUADRICEPS STRENGTH AND GAIT ASYMMETRY IN INDIVIDUALS WITH ACL RECONSTRUCTION

Tyler J. Moffit, Michael N. Vakula, Skylar Holmes, Melissa M. Montgomery, Derek N. Pamukoff

California State University, Fullerton, USA  
email: tmoffit@fullerton.edu

## INTRODUCTION

Quadriceps dysfunction is common following anterior cruciate ligament reconstruction (ACLR), and contributes to post-traumatic knee osteoarthritis (KOA) (4). Achieving >90% symmetry has been established as adequate for return to physical activity following rehabilitation (3, 4). Despite rehabilitation, quadriceps strength in the injured limb commonly fails to reach the strength of the uninjured limb (1). During walking, the quadriceps attenuate ground reaction force (GRF). In individuals with ACLR, decreased quadriceps function contributes to aberrant walking mechanics that may contribute to KOA (2). Moreover, quadriceps asymmetry predicts self-reported physical function (5). However, it is unclear if strength asymmetry is associated with asymmetry in functional tasks, such as gait.

The purpose of this study was to (1) examine the association between quadriceps strength asymmetry and gait asymmetry in individuals with ACLR, and (2) to compare gait biomechanics between individuals with high and low quadriceps strength symmetry between limbs. Dependent variables included the peak ground reaction force (GRF), peak knee flexion angle (KFA), and peak knee flexion moment (KFM). We hypothesized that strength symmetry would be associated with symmetry in KFA, KFM, and GRF during gait. We also hypothesized that individuals with high asymmetry would have greater GRF, and lesser KFA and KFM in their injured compared to uninjured limbs during gait.

## METHODS

Quadriceps function and gait biomechanics were assessed in 20 individuals with primary unilateral ACLR (Table 1).

**Table 1:** Participant Demographics

Demographics	
Sex (% female)	85%
Age (years)	21.9 ± 2.5
Height (m)	1.67 ± .07
Mass (kg)	68.8 ± 13.5
Time since ACLR (months)	49.5 ± 22.6
IKDC score	84.5 ± 10.3
<i>Graft type</i>	
Patellar tendon (n)	13
Hamstring tendon (n)	2
Allograft (n)	5

Peak torque (PT) was assessed using maximal voluntary isometric contractions (MVIC) at 45° of knee flexion. Each subject performed 3 MVICs on the injured and uninjured limb in a random order. The highest trials were normalized to body mass for analysis, and used to establish the symmetry index (SI). SI was derived by dividing the PT of the injured limb by the uninjured limb (3).

$$SI\% = \left( \frac{\text{Injured limb}}{\text{Uninjured limb}} \right) * 100$$

The SI was used to determine the percent asymmetry between limbs. A mean split of 84% SI was used to dichotomize the group into high SI (>84% symmetry; n=7, mean SI=94%) group (HIS), and low SI (<84% symmetry; n=8, mean SI=76%) group (LSI). The mean SI was near the range of previously established values (90%) (3), and deemed adequate to divide the sample.

Marker position and force plate data were sampled during 5 walking trials in neutral cushion footwear, at a self-selected speed that was maintained within ±5% across 5 trials. Participants walked over 2 consecutive force plates, striking the first plate with their right foot and the second with their left. Position and force data were exported to Visual 3D

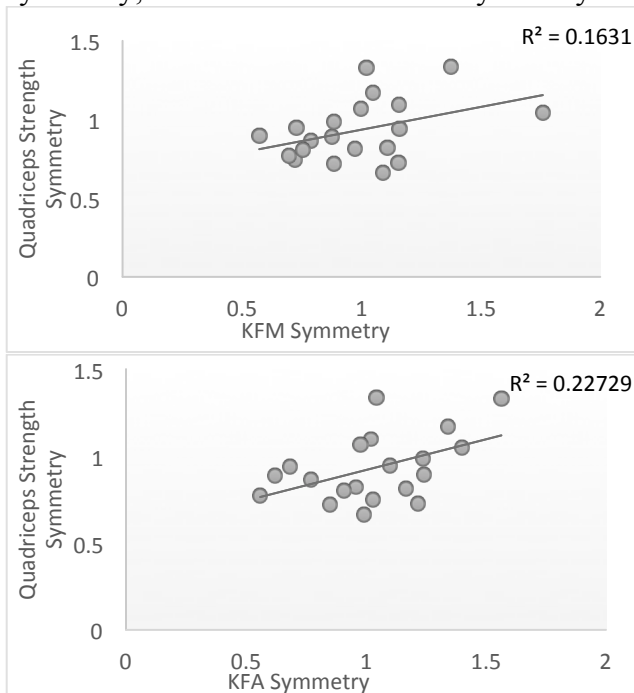
for model construction, and further analyzed using a custom LabVIEW program. Peak KFA and external KFM was calculated during the first 50% of the stance phase for each trial, and the average of all trials was used for analysis. The SI equation was also used to calculate GRF, KFA, and KFM symmetry.

Independent samples t-tests were used to compare GRF, KFA, and KFM between the HSI and LSI groups in the injured limb. Pearson correlations were used to examine the association between quadriceps strength SI and gait SI (KFA, KFM, and GRF) among all participants.

## RESULTS AND DISCUSSION

A trend was observed ( $P = 0.12$ ,  $d = 0.63$ ,  $LSI = 1.15 \pm 0.10$ ,  $HSI = 1.08 \pm 0.18$ ), indicating a higher peak GRF in the injured limb in the LSI compared to the HSI group. No differences were found in KFA ( $P = 0.27$ ,  $LSI = -26.55 \pm 6.02$ ,  $HSI = -29.05 \pm 9.13$ ) or KFM ( $P = 0.23$ ,  $LSI = 0.067 \pm 0.03$ ,  $HSI = 0.06 \pm 0.02$ ) between groups. Quadriceps Strength symmetry was associated with KFA symmetry ( $R = 0.48$ ,  $P = 0.02$ , Fig 1) and KFM symmetry ( $R = 0.40$ ,  $P = 0.04$ , Fig 1).

**Fig 1:** Associations between: Top – KFM PT symmetry; Bottom – KFA sand PT symmetry



Asymmetrical quadriceps strength is associated with asymmetrical gait characteristics (KFA and KFM) in individuals with ACLR. As such, strength asymmetries may contribute to asymmetry in movement patterns that may preferentially load the injured or uninjured limb. Furthermore, greater GRF in the injured limb of the LQI group may contribute to post-traumatic KOA. Therefore, rehabilitation protocols should consider restoring quadriceps strength symmetry, rather than bilateral quadriceps strengthening.

## CONCLUSIONS

Individuals with ACLR have quadriceps strength asymmetry that influences walking asymmetry (KFA and KFM). We observed some evidence that those with low quadriceps strength symmetry (i.e. a weaker injured compared to uninjured limb) experience greater GRF during walking compared to those with high quadriceps strength symmetry. Rehabilitation strategies should consider restoring strength symmetry between limbs to assist in improving long term joint health.

## ACKNOWLEDGMENTS

Supported by: CSU Program for Education and Research in Biotechnology New Investigator Grant

## REFERENCES

1. Ardern CL et al. *Am J Sports Med* 39: 538-543, 2011.
2. Blackburn et al. *Med Sci Sports Exerc* 48: 1664-1670, 2016
3. Ithurburn MP et al. *Am J Sports Med* 43: 2727-2737, 2015.
4. Palmieri-Smith RM and Lepley LK. *Am J Sports Med* 43: 1662-1669, 2015.
5. Pietrosimone B, et al. *Med Sci Sports Exerc* 48: 1671-1677, 2016.

# BICOMPONENT ULTRASHORT ECHO TIME $T_2^*$ COMPARISON OF NATIVE VS RECONSTRUCTED ACL

<sup>1</sup> Sarah C. Denning, <sup>1</sup> Michael F. Vignos, <sup>1</sup> Fang Liu, <sup>1</sup> Richard Kijowski, <sup>1</sup> Darryl G. Thelen

<sup>1</sup> University of Wisconsin-Madison, Madison, WI, USA  
email: scdenning@wisc.edu, web: <http://uwnmb1.engr.wisc.edu>

## INTRODUCTION

Rates of graft rupture following anterior cruciate ligament reconstruction (ACLR) have been reported at 6% [1]. Post-surgical vascularization and graft remodeling are critical to maintain long-term health and strength of the tissue. Prior studies have explored the potential of using magnetic resonance (MR) imaging to track ACL graft remodeling. Indeed, these studies have found that grayscale values of contrast-enhanced [2] and  $T_2^*$  weighted [3] MR images correlate to mechanical strength. However, tendons and ligaments are generally difficult to visualize with MRI, appearing dark due to rapid signal decay.

Recently developed technologies have allowed for implementation of faster echo times, better to image these tissues with higher contrast. Ultrashort echo time (UTE) sequences allow for collection of multiple echoes that can then be used to calculate  $T_2^*$  relaxation parameters with an exponential fit [4]. More recent studies have explored the use of a bicomponent exponential fit of  $T_2^*$  signal decay, which is believed to provide a quantitative measure of the tightly bound and free water in the tissue [5]. The ratio of bound and free water has been linked to localized tissue damage in tendon [6]. In this pilot study, we explore the potential for bicomponent UTE imaging as an *in vivo*, non-invasive diagnostic assessment of ACL graft health.

## METHODS

Four subjects with a primary unilateral, isolated ACLR were tested (2 hamstring and 2 patellar tendon grafts). Both knees were scanned in a 3T MR scanner (Discovery MR750, GE Healthcare, Waukesha, WI) with a padded knee extremity coil (InVivo, Orlando, FL). High resolution sagittal plane images at 16 different TEs from 0.032 to 30 ms

were collected. We segmented the ACL in the UTE images, and then co-registered the UTE images to locally align the ACL in each image set. Bicomponent exponential fitting of the signal intensity through time was conducted on each voxel in the segmented ACLs to get measures of the short and long  $T_2^*$  relaxation times [5]. We also computed the percentage of the signal due to the short  $T_2^*$  relaxation component (i.e.  $T_2^*$  fraction) as a measure of the fraction of bound water in the tissue (Fig. 1).

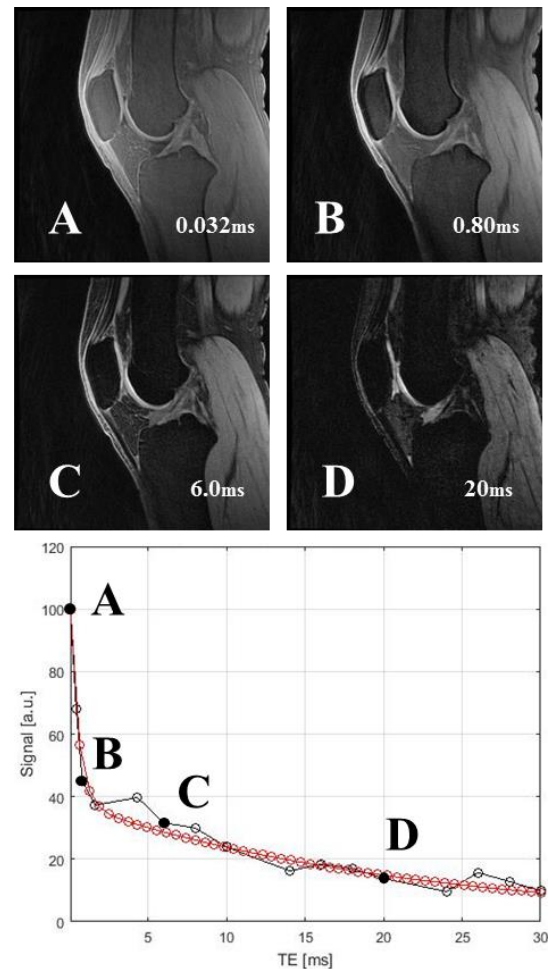


**Figure 1:** A-D) Sample image data collected with different echo times. Lower plot shows the bicomponent exponential fit of the signal intensity over the full range of the sampled echo times.

## RESULTS AND DISCUSSION

Short and long  $T_2^*$  measures averaged 4.3 and 36.6 ms, respectively, in the native ACLs (Table 1). The average  $T_2^*$  fraction was 50%, which is low relative to typical ligaments and tendons [6]. For each of the subjects, the short and long  $T_2^*$  measures were longer in the ACL graft than the native, contralateral ACL (Fig 2). The fraction of bound water was also increased in the reconstructed knee, averaging 57% across the four subjects (Table 1). Some subjects exhibited a substantial amount of heterogeneity of the quantitative MR metrics over the native and

reconstructed ACL, such that further tuning of the UTE sequence may be needed to enhance consistency and quality of the quantitative maps.

**Table 1.** Average  $T_2^*$  relaxation times in a slice of segmented ACL or graft.

	Native	Reconstructed
<b>Short <math>T_2^*</math> (ms)</b>	4.31±0.38	4.95±0.67
<b>Long <math>T_2^*</math> (ms)</b>	36.6±3.8	40.3±4.4
<b><math>T_2^*</math> Fraction</b>	0.503±0.057	0.567±0.047

## CONCLUSION

This study shows that it is feasible to perform ultrashort TE imaging of reconstructed ACLs and provides some evidence that quantitative MR metrics are not normalized in reconstructed ligaments. Further study is needed to assess whether the metrics reflect the health and strength of the tissue, which would support the use of UTE imaging to track tissue recovery following reconstructive surgery.

## REFERENCES

1. Salmon, L., et al., *Arthroscopy* **21**, 948-957, 2005.
2. Weiler, A., et al. *The American Journal of Sports Medicine* **29**, 751-761, 2001.
3. Biercevicz, A.M., *The American Journal of Sports Medicine* **41**, 560-566, 2013.
4. Chang, E., et al. *Journal of Magnetic Resonance Imaging* **41**, 870-883, 2015.
5. Liu, F., Kijowski, R. *Muscles, Ligaments and Tendons Journal*, in-press.
6. Kijowski, R., et al. *Journal of Magnetic Resonance Imaging*, in-press.

## ACKNOWLEDGMENTS

NSF GRFP (MFV) – DGE-1256259, NIH AG051748, EB015410.

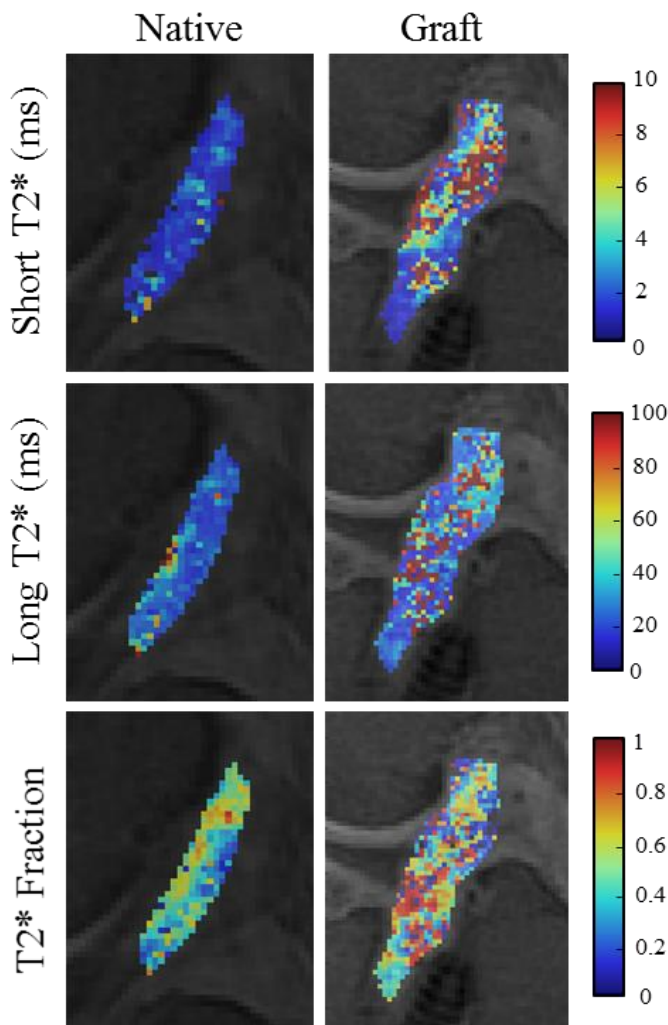


**Figure 2:** ACL color maps for short and long  $T_2^*$  measures along with the short fraction for a both knees of a representative subject showing large bilateral differences.

# EFFECT OF TORQUE MAGNITUDE AND TIMING OF IN VITRO ANTERIOR CRUCIATE STRAIN AND JOINT KINEMATICS

<sup>1</sup> Rena Hale, <sup>1</sup>Nathan D. Schilaty, <sup>1</sup>Nathaniel A. Bates, <sup>1</sup>Christopher V. Nagelli, <sup>1</sup>Aaron J. Krych, and <sup>1</sup>Timothy E. Hewett

<sup>1</sup> Mayo Clinic, Dept. of Orthopedic Surgery, Rochester, MN, USA  
email: hale.rena@mayo.edu

## INTRODUCTION

Approximately 75% of anterior cruciate ligament (ACL) ruptures occur in non-contact scenarios [1]. Often, this is the result of an impulse force within the first 50 ms of initial ground contact created from a rapid deceleration or change of direction [2]. Subsequently, it is important to understand the underlying mechanisms of ACL injury to determine the factors that increase risk of ACL injury. Improved knowledge of knee mechanics will enhance injury prevention, rehabilitation, and return to sport (RTS) criteria.

This current study was designed to mimic the mechanisms of a drop vertical jump (DVJ) *in vitro*. The DVJ is a motion used to determine athletes with a higher risk of ACL failure [3]. The goal of this study was to determine if magnitude of external moments and timing post-impact effected ACL strain and joint kinematics. We hypothesized that higher torque would generate greater anterior tibial translation, internal rotation, and ligament strain at 33 and 66 ms post-impact.

## METHODS

A novel cadaveric impactor was utilized to simulate a DVJ in lower extremities of 12 specimens (7 right, 5 left). Specimens ranged from 24 to 52 years of age. Specimens had no evidence of significant trauma/surgery to lower extremity and no evidence of extended chemotherapy. Specimens were dissected and prepared according to specifications outlined in Bates et al, 2017.

*In vitro* kinetics and kinematics were calculated from DVJ's of 70 subjects. Data was used to determine the mechanisms of risk in three degrees of knee forces/moments [i.e. knee abduction

moment (KAM), anterior tibial shear (ATS), and internal tibial rotation (ITR)]. Pneumatic cylinders applied the designated knee forces/moments (Table 1) to the tibia calculated from the *in vivo* subjects. A gravity-driven drop sled of 333 N was released from a height of 31 cm with quadriceps and hamstrings co-contracted with a 1:1 ratio. 3D markers were placed on the tibia and femur to determine joint kinematics (Northern Digital, Ontario, Canada). A differential variable reluctance transducers (DVRT) was implemented into the ACL to measure change in ligament strain during loading. Kinematic data is presented as the mean change in tibial position with respect to the femur. Knee abduction was not reported due to unresolved marker error.

**Table 1** *In vitro* Knee Forces and Moments Applied during Impact

Population Percentage	KAM (Nm)	ITR (Nm)	ATS (N)
0%	1.7	1	47
67%	26.8	18.6	80
120%	68.8	64.4	235

Statistical analyses was performed with JMP 10 (SAS Institute Inc., Cary, NC) with utilization of matched pairs and one-way ANOVAs with an alpha level < 0.05.

## RESULTS AND DISCUSSION

Results from this study indicate that magnitude of external forces and timing post-impact affects joint kinematics and ACL strain. Internal rotation and anterior tibial translation were significantly greater in the 120% condition then at the 67% at initial

contact (IC), 33 ms, 66 ms, and 100 ms after impact (Table 2). At 33ms after contact, internal rotation was  $14.94 \pm 17.14$  mm in the 120% condition and  $-1.42 \pm 15.03$  mm in the 67% ( $p < 0.05$ ). 120% condition generated  $3.99 \pm 5.09$  mm of medial translation and 67% applied  $-2.67 \pm 2.71$  mm at IC ( $p < 0.05$ ). Though kinematics changed with higher impact, the mean ACL strain did not. Lack of statistical significance in ACL strain is due to the physiological variations of ligament laxity between specimens.

Results from the timing test indicate that kinematics and strain significantly change post-impact under lower torque. In the 67% condition, 33ms post-impact, the knee experienced significantly high compression ( $0.62 \pm 1.15$  mm) flexion ( $-2.79 \pm 1.30$  mm), and lateral translation ( $-5.45 \pm 7.82$  mm). Knee anterior tibial translation ( $8.85 \pm 5.15$ ) also significantly increased at 33ms. At 66ms after impact, the knee experienced maximum ACL strain ( $6.93 \pm 7.71\%$ ) and increased internal rotation ( $4.51 \pm 9.96$  mm). The knee also returned to neutral flexion/extension and medial/lateral alignment. The higher torque load test did not result in significantly different joint kinematics or ACL strain at IC, 33 ms, 66 ms, or 100 ms post-impact.

Limitations in this test included physiological differences in ligament laxity and bone geometry, as well as innate error in the DVRT's.

## CONCLUSIONS

We hypothesized that higher external joint force would generate greater anterior tibial translation, internal rotation, and ligament strain at 33 and 66 ms post-impact. Results verify that increased torque during a simulated DVJ effects change in tibiofemoral kinematics but not ACL strain. Externally applied loads change a knee's kinematic response. At lower loads the 33 ms and 66 ms time points following impact generated the larger tibial translations, rotations, and ligament strain. Thus, these should be a time point of focus for ACL injury prevention. Future studies should focus on applying *in vitro* combinations external torque i.e. KAM, ATS, and ITR magnitudes during impact to further understand mechanisms of ACL injury.

## REFERENCES

- Schilaty ND, et al. *Am J Sports Med*, 2017 (Accepted, in press).
- Bates NA, et al. *Clin Bio*, 2017 (Accepted, in press).
- Hewett TE, et al. *Am J Sports Med* **33**, 492-501, 2005.

## ACKNOWLEDGMENTS

NIH funding include: R01AR049735, R01AR055563, R01AR056259 to TEH, and K12HD065987 and L30AR070273 to NDS.

**Table 2:** Anterior cruciate ligament strain and knee joint kinematics with 67% and 120% external forces

	67% External Forces			
	Initial Contact	33ms	66ms	100ms
ACL Strain [% (SD)]	2.83 (4.28) <sup>+</sup>	2.50 (3.09)	6.93 (7.71) <sup>+</sup>	4.82 (4.71) <sup>+</sup>
Flexion [° (SD)]	-1.03 (1.33)	-2.79 (1.30) <sup>+</sup>	-1.09 (1.86)	0.20 (1.52)
Internal Rotation [° (SD)]	1.97 (10.96)	-1.42 (15.03)	4.51 (9.96) <sup>+</sup>	7.06 (14.09)
Anterior Translation [mm (SD)]	3.46 (5.35)	8.85 (5.15) <sup>+</sup>	3.22 (5.52)	2.89 (4.90)
Lateral Translation [mm (SD)]	-2.67 (2.71)	-5.45 (7.82) <sup>+</sup>	-2.75 (4.14)	-1.51 (3.58)
Compression [mm (SD)]	-0.28 (0.62)	0.62 (1.15) <sup>+</sup>	0.29 (0.83)	-0.20 (1.02)
	120% External Forces			
	Initial Contact	33ms	66ms	100ms
ACL Strain [% (SD)]	5.68 (8.02)	6.29 (9.30)	7.59 (12.63)	7.99 (12.91)
Flexion [° (SD)]	1.88 (2.33)	1.97 (2.55)	1.42 (1.65)	1.31 (1.59)
Internal Rotation [° (SD)]	11.62 (13.41) <sup>*</sup>	14.94 (17.14) <sup>*</sup>	13.22 (15.36) <sup>*</sup>	9.33 (11.18)
Anterior Translation [mm (SD)]	5.83 (6.96) <sup>*</sup>	5.82 (6.83)	6.31 (8.49) <sup>*</sup>	3.91 (4.80) <sup>*</sup>
Lateral Translation [mm (SD)]	3.99 (5.09) <sup>*</sup>	4.15 (4.86)	4.08 (4.97)	5.06 (5.88)
Compression [mm (SD)]	1.92 (2.94)	2.66 (3.52)	2.47 (3.21)	2.31 (2.83)

<sup>+</sup> denotes significance between time points. <sup>\*</sup> denotes significance between magnitude.

# RELIABILITY OF A DEVICE TO MEASURE TORSIONAL STIFFNESS OF RUNNING FOOTWEAR

Rebecca Zifchock, Michaela Sulley, Gary Helton, Gregory Freisinger,  
Frank Blackmon, Roderick Wilson, and Donald Goss

United States Military Academy, West Point, NY, USA  
email: rebecca.zifchock@usma.edu

## INTRODUCTION

Load-bearing exercises such as running and marching account for up to 78% of injuries during Army basic training [1]. Previous literature suggests that there are intrinsic risk factors associated with running, such as high tibial shock values and extreme foot pronation/supination [2, 3]. However, there is also evidence to show that extrinsic factors, such as footwear, may influence injury risk. Butler et al. [4] showed that a cushioning shoe is particularly effective for attenuating shock, while a motion control shoe can reduce rearfoot motion. Therefore, it is important to understand footwear structure, so that its relationship injury susceptibility in runners may be studied more closely.

Torsional shoe stiffness has been previously quantified to assess the shoe's cushioning and support in a single metric [5]. It measures the resistance of the shoe to twisting about its long axis between the heel and the toe box. Assessment of shoe torsional stiffness has previously been conducted using expensive devices that cannot be easily transported for use in most laboratories and clinics. Therefore, the purpose of this study was to present and validate the reliability of a novel device designed to quantify torsional shoe stiffness, as well as heel thickness. This device was intended to be portable, lightweight, and inexpensive, without sacrificing accuracy and validity.

## METHODS

The Shoe Stiffness in Torsion Measurement (SySTM) device was designed specifically to be portable, inexpensive, and reliable for rapid measurement of torsional stiffness, as well as heel

thickness, for running footwear. Torsional stiffness was calculated by the following equation:

$$(L * T) / \phi$$

Where **L** is the length of the shoe, **T** is the torque, and  $\phi$  is the angle of displacement between the toe box and the heel counter of the shoe. An additional measure of heel thickness was also of importance for shoe structure characterization.

The SySTM device is shown in Figure 1. The entire device is 44 x 23 x 18cm (approximately 0.02 m<sup>3</sup>), and has a mass of 6kg. The *rotational platform* is attached to the *torque watch insert* and allowed to swivel with low friction through a stationary block, against which the front toe of the shoe is meant to rest. A “hook and loop” strap is threaded through the *rotational platform* to secure the toe box. The *rear platform* can slide with low friction along the *base* to accommodate a shoe ranging from women's size 4 to men's size 16. The *heel stop* can be rotated along the *threaded rod* to make contact with the insole of the shoe, as far against the posterior heel counter as possible. Not shown in this illustration are the four commercial items that provide the required measurements and standardization: (1) Powered hand drill which imparts approximately 1 N-m of torque to rotate the *heel stop* down into the heel counter until the clutch slips. (2) Set of calipers is used to measure the heel thickness by measuring the length of *threaded rod* remaining above the cross bar of the *rear platform* once the *heel stop* is engaged. (3) Metric scale used to measure the total length, **L**, of the shoe. (4) Torque watch used to record the peak torque, **T**, at the standardized rotation,  $\phi$ , of 30 degrees from horizontal.

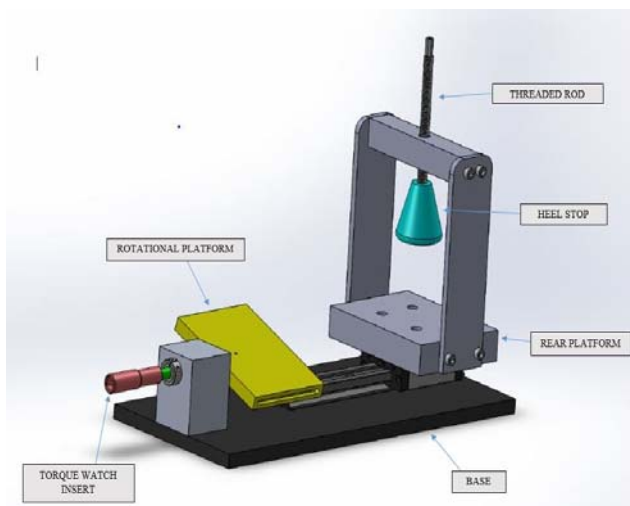


**Figure 1:** The SySTM device as designed

Six individuals were trained on how to use the SySTM device. They each measured six different types and sizes of shoes (right side only). Each rater measured each shoe, in a randomized order, three times, the first was removed and considered a familiarization trial. For each independent measurement, heel thickness, length of the shoe, and torque required to achieve 30 degrees of rotational displacement in the medial and lateral directions were recorded in order to calculate the torsional stiffness in both directions.

The inter-rater and intra-rater reliability of the heel thickness, medial torsional stiffness, and lateral torsional stiffness were assessed through the calculation of interclass correlation coefficients (ICCs). A (2,1) model was reported upon such that these results could be generalized to any group of raters who would take a single measurement to characterize a shoe. In order to assess inter-rater reliability, only the second trial was entered into the model to calculate the reliability between testers. In order to assess intra-rater reliability, the data from the first and second trials were assessed against each other for each of the raters.

## RESULTS AND DISCUSSION

Table 1 shows the ICC values for inter-rater and intra-rater reliability of the device for quantifying medial and lateral torsional stiffness, as well as heel thickness, all of which fell into an excellent range of clinical reliability [6]. The mean medial torsional

stiffness deviation was 1.64 N-m<sup>2</sup>, which is 15% of the mean of that variable for all devices. The mean lateral torsional stiffness deviation was 1.33 N-m<sup>2</sup>, which is 13% of the mean of that variable for all devices. The mean heel thickness deviation was 0.65 mm, which is 1% of the mean of that variable for all devices.

**Table 1:** ICC Values

	<b>Medial Torsional Stiffness</b>	<b>Lateral Torsional Stiffness</b>	<b>Heel Thickness</b>
Inter-Rater ICC (2,1)	0.90	0.86	0.96
Intra-Rater ICC (2,1)	0.91	0.92	0.99

Heel thickness was a particularly reliable measure, as it is derived from a single measure of the threaded rod after it is lowered. Conversely, torsional stiffness is derived from measures of shoe length and torque (at a standardized angle). The combination of any small errors in these three measures likely contribute the variability.

## CONCLUSIONS

The results of this study suggest that the SySTM device is a reliable device for the measurement of shoe torsional stiffness and heel thickness. It is also significantly more portable and less expensive than the industry standards which typically use custom jig in an Instron testing machine (Instron; Norwood, MA). This makes it a feasible option for laboratories and clinics that may require a table-top device that can be stored when not in use.

## REFERENCES

1. Hauret KG, et al. *Am J Prev Med*, 38(1 Suppl), S61-70, 2010.
2. Milner CE, et al. *Med Sci Sports Exerc*, 38(2), 323-328, 2006.
3. Pohl MB, et al. *J Biomech*, 41, 1160-1165, 2008.
4. Butler RJ, et al. *Gait Posture*, 26, 219-225, 2007.
5. Hillstrom HJ, et al. *J Am Podiatr Med Assoc*, 103(4), 297-305, 2013.
6. Cicchetti DV. *Psych Assess*, 6(4), 284-290, 1994.

# INFLUENCE OF MILITARY TYPE FOOTWEAR AND WORKLOAD ON CO-CONTRACTION INDEX IN UNILATEARAL STATIC BALANCE

<sup>1</sup>Christopher M. Hill, <sup>2</sup>Hunter DeBusk, <sup>1</sup>Sam J. Wilson, <sup>3</sup>Jacob R. Gdovin, <sup>1</sup>Caleb C. Williams, <sup>1</sup>Lauren A. Luginsland, <sup>2</sup>Adam C. Knight and <sup>2</sup>Harish Chander

<sup>1</sup>University of Mississippi, University, MS, USA; <sup>2</sup>Mississippi State University, Mississippi State, MS, USA

<sup>3</sup>Missouri State University, Springfield, MO, USA

Email: [cmhill1@go.olemiss.edu](mailto:cmhill1@go.olemiss.edu) web: [hesrm.olemiss.edu](http://hesrm.olemiss.edu)

## INTRODUCTION

Military personnel are consistently exposed to occupation related workloads, which have demonstrated an increased risk of musculoskeletal injuries [1]. Falls account for 18.4% of all cause injuries among military service personal [2]. Intrinsic human factors such as muscular fatigue, especially of the lower extremity and extrinsic environmental factors such as footwear, impact the ability to maintain balance. In order to react to balance perturbations, co-contraction of agonist-antagonist pairs of the lower extremity muscles increases to create stability around a joint, by generating stiffness in the agonist and antagonistic muscles pairs [3]. Moreover both footwear characteristics and lower extremity muscular fatigue have been shown to alter co-contraction [4,5]. Human-environment physical interaction is primarily mediated through footwear, thus usage and access to occupationally appropriate footwear is critical in balance performance. Although, there is considerable amount of literature discussing balance performance in various types of footwear, there remains a dearth in the literature concerning how a minimalist style military boot affects balance characteristics in a trained population. The purpose of the study is to assess the level of lower extremity agonist-antagonist muscular co-contraction during unilateral balance tasks before and after a military style physiological workload, in two different military approved footwear, Belleville 310ST hot weather standard tactical boot (STD) and Belleville TR101 MiniMil ultra-light minimalist style military boot (MIN).

## METHODS

The study was conducted in a repeated measures pre-test-post-test design with twenty-two healthy

male adults (age:  $22.2 \pm 2.7$  years; height:  $177 \pm 6.8$  cm; mass:  $79.8 \pm 9.7$  kg) with no history of musculoskeletal, orthopedic, neurological, cardiovascular, and vestibular abnormalities. Data collection procedures included an initial familiarization of the balance and workload protocols. The experimental testing involved participants tested on two separate days separated by at least 48 hours on two of the military footwear (STD, MIN) with a counter balanced footwear assignment. Participants performed dominant leg unilateral static balance trails (1L), prior (PRE) to and after (POST) a military type workload. The workload included an increasing speed and grade on a treadmill while donning a 16 kg backpack. Muscle activity was collected on medial gastrocnemius (Plantar Flexor-PF), tibialis anterior (Dorsi Flexor-DF), peroneus longus (Evertor- EV), and tibialis posterior (Invertor-IN) using BIOPAC EMG system. Balance was assessed in three sensory conditions: eyes-open (EO), eyes-closed (EC), and eyes-open foam (EOF). Co-contraction between the muscle pairs were calculated using the Co-Contraction Index (CCI) for the agonist-antagonist pairs of DF & PF and IN & EV using mean muscle activity the following equation [6]:

$$(EMG_{Least} + EMG_{Most}) \times EMG_{Least} / EMG_{Most}$$

A 2 (Footwear - STD x MIN) x 2 (Workload - PRE x POST) repeated measures ANOVA was used to analyze CCI at an alpha level of 0.05 using SPSS21.

## RESULTS AND DISCUSSION

Significant interaction was found for PF-DF CCI [F (1, 21) = 5.899,  $p = 0.024$ ,  $\eta^2 = 0.219$ ] in EC sensory condition (Fig. 1). Pairwise comparisons for simple main effects for interaction revealed significant differences for PRE with higher in CCI MIN

compared to STD and for STD with higher CCI in POST compared to PRE significant at  $p = 0.019$  and  $p = 0.031$  respectively. No significant footwear x time interaction or significant differences for main effect footwear or time was found in IN-EV muscle pairs across sensory condions.

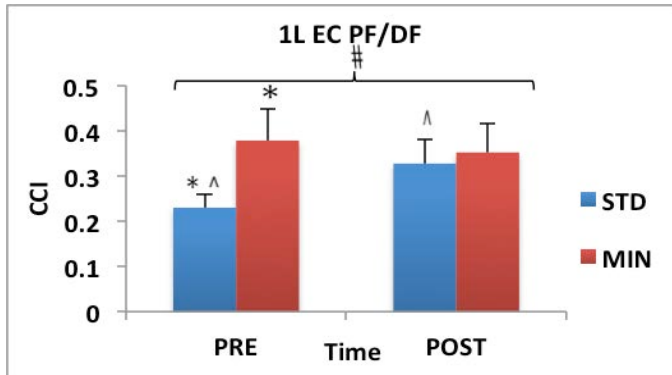


**Figure 1:** Muscle co-contraction index for eyes-closed unilateral balance medial gastrocnemius (PF) and tibialis anterior (DF). # denotes significant interaction; \* denotes significant differences for footwear across time and ^ denotes significant differences for time across footwear.

MIN demonstrated a higher CCI in the PF-DF pair before the military workload. The minimalist boot features a thin insubstantial shaft in comparison to the standard footwear, which features a stiff thick boot shaft suggesting that in acute conditions the thick boot shaft decreases muscular exersion of the muscles around the ankle. Moreover, thin, less stiff boot-shafts may allow for greater range of motion (ROM) at the ankle in dorsiflexion and plantarflexion [5]. However, after workload in order to compentsate for fatigue an increase in CCI was needed to stabilize the ankle joint while donning STD. Thus after workload, the surrounding ankle musculature is similarly effected by the boot shafts. Additionally, CCI increased in the post workload condition while donning STD. Previous literature has displayed increase in the rate of energy expindature and muscular fatigue when a greater mass is placed on a footwear [7,8]. STD is 300 g heavier than MIN footwear, suggesting that the increase in CCI after the occupational workload, may be result of the increased STD mass, while the lighter MIN maintained a similar CCI to its PRE workload condtion.

Our results displayed greater co-contraction in the eyes-closed condition which supports previous literature that reported greater co-contraciton in altered visual information [9]. Once visual feedback was altered, increased co-contraction of PF-DF pair was needed to maintain balance. Greater co-contraction of this agonist-antagonist muscle pairs was exhibited in MIN pre workload in eyes closed condition. However post workload, a similar CCI is found between footwear suggesting that while wearing STD an increase reliance is placed on proprioceptive infomration from the muscles around the ankle joint in order to compensate for the lack of visual information and muscular fatgiue.

## CONCLUSION

In conclusion, CCI for plantarflexor and dorsiflexor pairs was significantly higher in the acute testing condition for the minilmist footwear, suggesting the specific design characteristic of an insubstantial boot shaft increased co-contraction of agonist-antagonist muscle pairs. However, both types of footwear did not differ in CCI after workload suggesting that other footwear design characteristics such as footwear mass, influence muscular cocontraction after an occupational related workload.

## REFERENCES

- Leggat et al. *J Muscoskel Pain*, **15**, 2007.
- Gribble, P., & Hertel, J. *Archi Phys Med Rehab*, **85**, 589–592, 2004.
- Winter et al. *J Neurophy*, **80**, 1211-122, 1998.
- Böhm & Hösl *J of Biomech*, **43**, 2467-2472, 2010.
- Hautier et al., *Med Sci Sports Exerc*, **32**, 2000.
- Rudolph et al. *Knee Surgery, Sports Traum, Arthroscopy*, **8**, 262-269, 2000.
- Franz JR et al. *Med Sci Sports Exerc*, **44**, 1519-1525, 2012.
- Garner JC et al. *Int. J. Ind. Ergonom*, **43**, 77-81, 2013
- Benjuya et al. *J Gerontol A Biol Sci Med Sci*, **59**, 2004.

# EFFECT OF MILITARY FOOTWEAR TYPE ON ANKLE STABILITY FOLLOWING A SIMULATED MILITARY WORKLOAD

<sup>1</sup>Jeffrey Simpson, <sup>1</sup>Hunter DeBusk, <sup>2</sup>Christopher Hill, <sup>1</sup>Brandon Miller, <sup>1</sup>Adam Knight<sup>1</sup>, and <sup>1</sup>Harish Chander

<sup>1</sup>Mississippi State University, Mississippi State, MS, USA

<sup>2</sup>University of Mississippi, University, MS, USA

email: [jds1313@msstate.edu](mailto:jds1313@msstate.edu)

## INTRODUCTION

The United States Army Annual Injury Report identified that acute sprains/strains accounted for 9.3% and 51.0% of military hospitalizations and outpatient visits [1]. Of these injuries, lateral ankle sprains (LAS) resulted in 36% of days limited on duty due to injury. Military personnel are frequently exposed to environmental hazards such as irregular and/or uneven terrain, which may increase the susceptibility for lower extremity injuries. Although the specific mechanism of LAS injuries in military occupations is unknown, high incidence rates in athletics have been reported when landing on uneven surfaces, resulting in excessive inversion of the foot/ankle complex [2].

Augmented ground reaction forces (GRF) upon landing can increase the risk of injury, especially when the ankle is forced into inversion. [3]. Contradicting evidence regarding high and low-shaft athletic footwear suggests other mechanical design characteristics such as shaft stiffness, which reduces inversion range of motion (ROM), and mass of the footwear may influence the rate and amount of inversion when the foot/ankle is forced into inversion [4-5]. Therefore, selection of improper footwear, specifically in military populations that perform daily, occupational, and training tasks on uneven terrain, could increase the risk of LAS injuries.

Service members are provided with standard issue military footwear they are required to wear during active duty. Recently, minimalist footwear designs have been incorporated into military footwear, which feature a lighter mass, more flexible shaft, and a thin midsole in comparison to the standard issue footwear. Providing alternative footwear selections for service members may reduce the risk

of injury. However, the effectiveness of a minimalist boot design on ankle stability in military populations is unknown. Thus, this study examined the influence of a standard and minimalist military boot on GRFs during an inversion perturbation following a simulated military workload.

## METHODS

Twelve healthy adult males (age:  $22.0 \pm 2.0$  y; height:  $178.0 \pm 7.1$  cm; mass:  $81.1 \pm 10.6$  kg) who were moderately active with no self-reported history of musculoskeletal injuries completed the study. Participants completed two testing sessions, separated by at least 72 hours, with a crossover counterbalanced footwear assignment. Footwear used in the study was a standard boot (Belleville 310T hot weather standard tactical boot (STN); mass:  $801.13 \pm 40.4$  g) and a minimalist boot (Belleville TR101 MiniMil ultra-light minimalist tactical boot (MIN); mass:  $500.13 \pm 24.1$  g). Ankle stability was assessed before and after a simulated military workload using an outer sole with fulcrum, which created an inversion perturbation of 25 degrees upon landing [6]. A fulcrum (FUL) or a flat (FLT) outer sole was attached to the bottom of the participants' footwear without the participant having knowledge of the type of outer sole. After the outer sole was attached, participants stepped down from a 27 cm box onto an AMTI (Watertown, MA, USA) AccuGait force platform. A total of 10 successful trials, 5 with FUL and 5 with FLT were completed. Following completion of the ankle stability protocol, participants completed a simulated military workload on a treadmill wearing a 16-kg rucksack that has previously been utilized by DeMaio et al. [7]. After completion of the simulated workload, a post-workload ankle stability protocol was completed.

Data from the force platform was acquired and values of the maximum vertical ( $F_z$ ), anterior/posterior ( $F_y$ ), and medial/lateral ( $F_x$ ) GRFs were obtained and normalized to multiples of body weight for each footwear condition. Time to peak  $F_z$  was also obtained. Separate 2 (footwear) x 2 (time) RM-ANOVAs were computed for FUL and FLT conditions ( $p \leq 0.05$ ).

## RESULTS AND DISCUSSION

Cumulative means  $\pm$  SD are reported in Table 1. For the FUL condition, a significant footwear main effect for the  $F_x$  variable ( $p = 0.010$ ) was identified. In the FLT condition, analyses showed a significant footwear main effect for the  $F_y$  variable ( $p = 0.024$ ). For both footwear main effects, the MIN boot resulted in significantly less max force than the STN footwear. No other significant interactions or main effects were identified.

The primary purpose of this study was to examine ground reaction forces during a dynamic inversion perturbation following a simulated workload in two types of military footwear. In the current study, the main findings were that MIN demonstrated a significantly less peak  $F_x$  during the FUL condition and a significantly less peak  $F_y$  during the FLT condition (Table 1). These findings may be attributed to the differences in mechanical design characteristics of the boots. Although increased  $F_x$  during the FUL condition could be due to the greater STN boot mass, greater shaft stiffness in the STN boot could potentially limit ROM that might influence  $F_x$  during an inversion perturbation.

Moreover, increased shaft flexibility featured in the MIN boot might allow for greater ROM that could also impact the GRF during an inversion perturbation. Although this interpretation is difficult without ankle kinematics, allowing for greater inversion ROM in the MIN boot may have negative implications for risk of injury when the foot/ankle complex is unexpectedly forced into inversion.

Inadequate military footwear may help explain the high incidence of lower extremity injuries. Although results showed reduced  $F_x$  during FUL in MIN boots, mechanical design characteristics such as mass and shaft stiffness may potentially influence other parameters of ankle stability during an inversion perturbation. Future research should examine kinematic parameters of ankle stability to determine the impact of various mechanical design characteristics of military boots on ankle stability.

## REFERENCES

1. Dada-Laseinde E, et al. *US Army Annual Injury Epidemiology Report*, 2009.
2. Suda EY, et al. *J Electromyography and Kinesiology* **19**, 84-93, 2009.
3. Hertel J. *J Athletic Training* **37**, 364-375, 2002.
4. Fu W, et al. *J Foot and Ankle Res* **7**, 7-14, 2014.
5. Ricard MD, et al. *J Athletic Training* **35**, 38-43, 2000.
6. Knight AC & Weimar WH. *Sports Biomech* **11**, 402-413, 2012.
7. DeMaio M, et al. *Human Performance Enhancement for NATO Mil Ops*, 2009.

**Table 1.** Ground reaction force data normalized to multiples of body weight.

	Fulcrum		Flat	
	Pre-Workload	Post-Workload	Pre-Workload	Post-Workload
<b>STN</b>				
$F_z$	1.97 $\pm$ 0.40	1.98 $\pm$ 0.40	2.52 $\pm$ 0.54	2.54 $\pm$ 0.50
$F_y$	0.06 $\pm$ 0.04	0.05 $\pm$ 0.04	0.14 $\pm$ 0.07	0.13 $\pm$ 0.10
$F_x$	0.17 $\pm$ 0.05	0.15 $\pm$ 0.03	0.12 $\pm$ 0.04	0.13 $\pm$ 0.04
<b>MIN</b>				
$F_z$	2.01 $\pm$ 0.32	2.00 $\pm$ 0.33	2.58 $\pm$ 0.51	2.54 $\pm$ 0.58
$F_y$	0.05 $\pm$ 0.05	0.05 $\pm$ 0.03	0.11 $\pm$ 0.08 <sup>†</sup>	0.09 $\pm$ 0.07 <sup>†</sup>
$F_x$	0.12 $\pm$ 0.02 <sup>†</sup>	0.13 $\pm$ 0.03 <sup>†</sup>	0.12 $\pm$ 0.03	0.13 $\pm$ 0.03

<sup>†</sup> indicates significantly less than STN ( $p \leq 0.05$ ).

# Footwear Differences in Lower Limb Joint Power Generation During Maximal Vertical Jumping

<sup>1</sup>Ross E. Smith, <sup>1</sup>Douglas W. Powell, <sup>2</sup>John Harry, <sup>1</sup>Lawrence W. Weiss, <sup>1</sup>Max R. Paquette

<sup>1</sup>School of Health Studies, University of Memphis, Memphis, TN, USA

<sup>2</sup>Department of Kinesiology & Nutrition Sciences, University of Nevada, Las Vegas, Las Vegas, NV, USA

Email: [mrpquette@memphis.edu](mailto:mrpquette@memphis.edu), Web: <http://www.memphis.edu/shs/research/mal.php>

## INTRODUCTION

The field of exercise science is rampant with research on minimal footwear in runners. Minimal footwear, in attempts to mimic barefoot conditions, prioritizes lighter and more flexible shoe materials and a smaller heel-to-toe drop than standard sport footwear [1]. Studies focused on comparing performance variables among footwear types during non-running sport tasks are scarce, however. Greater soleus muscle activity while wearing standard training footwear compared to minimal footwear has been observed during maximal vertical jumping [2]. However no changes in maximal vertical jump performance were observed between footwear [2]. Although muscle activity measures provide important insight into muscular control during vertical jumps, joint power contributions indicate the net muscular contributions of involved musculature during jumping. Joint power contributions during jumping between different types of footwear have not yet been studied.

The purpose of this study was to compare lower limb joint power contributions and maximal jump height in athletes while wearing standard training shoes and minimal shoes. We hypothesized that minimal footwear would yield higher peak ankle joint power contributions but lower peak knee or hip power than standard footwear. Consequently, we also expected no differences in maximal vertical jump height between footwear conditions.

## METHODS

To date, six athletes (2 women; 22±1 years; 1.59±0.0 m; 57.8±10.0 kg, 4 men; 25±4 years; 1.78±0.10 m; 77.1±8.9 kg) who played in jumping sports or performed squats or weightlifting movements three or more times each week participated in the study. Before testing, participants completed a five-minute stationary bike warm-up followed by three 12-touch dot drills. Reflective

markers were placed on the pelvis, thighs, shanks and feet. A 9-camera motion capture system (240Hz, Qualisys AB) and a force platform (1200Hz, AMTI, Inc.) were used to collect kinematic and GRF data, respectively. Each athlete performed three practice jumps at less than maximal effort and three maximal countermovement vertical jumps (CMVJ) in both minimal and standard shoes from a self-selected stance width. Participants were instructed to jump maximally using a Vertec™ apparatus for external motivation. Participants were allowed to jump with their preferred technique (i.e., unrestricted). Standing reach height was measured at the start of jumping trial in both shoes to standardize jumping height. Unilateral limb (self-reported dominant) data from the maximal CMVJ were recorded.

Visual3D biomechanical software (C-Motion, USA) was used to process and analyze all data. Sagittal plane joint kinetics were calculated using Newtonian inverse dynamics equations and joint powers were calculated as the product of joint moments and angular velocities. Peak joint angular powers, joint moments and ranges of motion (ROM) during the concentric phase of the jump were analyzed. The average of each variable during the three CMVJ per footwear condition was used for analysis. A repeated-measures ANOVA with footwear condition as the within-subject factor was used to evaluate all variables ( $p < 0.05$ ). Cohen's  $d$  effect sizes were calculated to assess effect magnitudes.

## RESULTS AND DISCUSSION

As expected, vertical jump height was not different between footwear (**Table 1**). This finding is congruent with reports of no differences in vertical jump height between minimal and standard footwear [2]. Contrary to our hypothesis, ankle joint plantarflexor power was not larger for minimal

compared to standard footwear. Although ankle ( $p=.43$ ;  $d=.32$ ) and hip power ( $p=.78$ ;  $d=.11$ ) were not different between footwear, peak knee extensor power was smaller in the minimal compared to the standard shoe ( $p=0.05$ ;  $d=.18$ ). (Figure 1). There were no differences in sagittal peak joint moments, or joint ROM between footwear conditions ( $p>0.05$ ; Table 1). Although it has been shown that jumping in minimal footwear increases propulsive activation of the soleus [2], this could be a result of an increased proprioceptive load. Minimal footwear have much thinner soles than traditional, which has previously been associated with greater sensory input [3], and could have manifested as increased soleus activity [2]. This increased soleus activity could be a natural strategy that occurs in minimal footwear to account for the lack of stabilizing structures within the shoe when compared to standard shoes. While we expected greater ankle joint powers to manifest similar to what is observed in minimal footwear with runners [4], the vertical jump movement does not necessitate the same stretch-shortening cycle demand at the ankle that running does.

Considering that vertical jump heights were unchanged between footwear but that peak knee power was slightly greater in minimal footwear, our participants may have adopted a different jumping strategy in the novel footwear condition (i.e., participants had no jumping experience in minimal footwear). Since sagittal plane joint ROMs were unchanged between footwear conditions (Table 1), participants may have adopted a kinematic trunk or arm strategy to achieve similar jump heights in minimal footwear. Although we observed a small difference in knee joint power production in minimal compared to standard footwear, the small

effect size suggests that this difference is not meaningful.

## CONCLUSIONS

Our preliminary findings with a small sample size suggest that there are no meaningful differences in ankle, knee and hip power production during vertical jumping between minimal and standard footwear conditions. We are in the process of collecting more data from more male and female participants to better understand these footwear differences and, to assess any sex differences in joint power contributions during CMVJ.

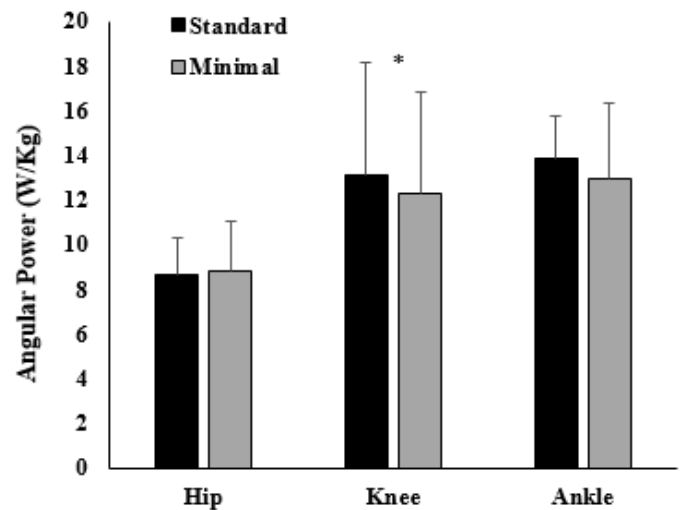


Fig 1: Peak lower limb joint powers during the concentric phase of the vertical jump in standard and minimal footwear (mean + SD).

## REFERENCES

1. Esculier, et al. *J of Foot and Ankle Res*, 8(1):1-9, 2015
2. Harry, et al. *JSCR*, 29(6):1657-1665, 2015
3. Rose, et al. *Proceedings of the ASB Meeting*, 2011
4. Paquette, et al. *Footwear Science*, 5(1):9-18, 2013

Table 1. Lower limb peak sagittal moments and ranges of motion (ROM) for standard and minimal footwear conditions (mean ± SD) with  $p$ -values and Cohen's  $d$  effect sizes.

Variables	Minimal	Standard	$p$ -values	$d$
Ankle Plantarflexor Moment (Nm/kg)	-1.87 ± 0.33	-1.90 ± 0.20	0.74	0.12
Knee Extensor Moment (Nm/kg)	1.98 ± 0.43	2.03 ± 0.44	0.14	0.13
Hip Extensor Moment (Nm/kg)	-2.26 ± 0.45	-2.24 ± 0.46	0.74	0.05
Ankle Dorsiflexion ROM (°)	-55.5 ± 9.0	-57.4 ± 6.4	0.41	0.23
Knee Flexion ROM (°)	84.3 ± 7.3	83.8 ± 6.9	0.64	0.08
Hip Extension ROM (°)	84.2 ± 10.7	-85.5 ± 9.1	0.54	0.14
Jump Height (Meters)	0.44 ± 0.11	0.45 ± 0.12	0.47	0.05

# INFLUENCE OF MINIMALIST, NEUTRAL, AND ULTRA-CUSHIONING SHOES ON JOINT COORDINATION DURING RUNNING

Brianne Borgia<sup>1</sup> and James Becker<sup>2</sup>

<sup>1</sup>California State University, Long Beach, CA, USA

<sup>2</sup>Montana State University, Bozeman, MT, USA

email: james.becker4@montana.edu

## INTRODUCTION

Due to the synchronous movements of the lower extremity during the stance phase of gait, abnormal or excess motion of the foot can cause a disruption in joint actions [1]. Joints such as the knee may be especially sensitive to disruptions in timing [2] which may explain why knee injuries account for up to 25% of all running injuries [3]. Changing the footwear a runner uses is one mechanism which might potentially influence both foot function and the relative timing of joint movements. Changing footwear might also effect coordination and coordination variability between adjacent segments or joints, and thereby impact stresses placed on the joint [4].

In regards to the influence of footwear on joint coordination, it been previously shown that during the stance phase of running, peak eversion occurs significantly earlier when running in a shoe with a softer midsole compared to a harder midsole [3]. Additionally, when running barefoot verse shod appears to change both the amount and relative timing of knee joint flexion and extension [5].

Maximalist, ultra-cushioning shoes are rapidly growing in popularity. However, currently there is no data in the literature regarding how these shoes impact joint coordination. Therefore, the purpose of the study was to examine differences in inter-joint coordination and coordination variability when running in minimalist (MIN), neutral cushioning (NEUT) and ultra-cushioning (ULTRA) shoes.

## METHODS

Sixteen recreational runners (age:  $23.5 \pm 2.2$  years; height:  $1.68 \pm 0.19$  m.; body mass:  $76.5 \pm 4.5$  kg) participated in this study. All subjects were injury

free 6-months prior to and at the time of testing. Subjects were provided 3 pairs of shoes in their self-reported size. (Min shoe: New Balance 1400v3, Neut shoe: Nike Air Zoom Pegasus 32, Ultra shoe: Hoka OneOne Bondi 4).

Running kinematics were recorded using a 12-camera motion capture system (Qualisys, Inc., Gothenburg, Sweden) sampling at 200 Hz while participant ran on an instrumented treadmill (Bertec Corp., Columbus OH) at 3.0 m/s. Participants ran for 10 minutes in each shoe condition, with the first 9 minutes allowing familiarization to the footwear and data collected during the last minute. Marker trajectories were recorded for thirty seconds during the last minute of the 10-minute trial, from which ten consecutive steps were selected for analysis.

Raw marker trajectories were exported to Visual 3D (C-Motion, Inc., Rockville MD) where they were filtered using a 4<sup>th</sup> order, zero lag, low-pass Butterworth filter with a cutoff frequency of 6 Hz. Joint angles for the knee and segment angles describing the orientation of the rearfoot and tibia segments relative to the laboratory coordinate system were calculated. Angles were normalized to 100% of stance phase and exported to a custom LabView Program (National Instruments, Austin TX) where the following dependent variables were calculated: the position at initial contact, peak position during stance phase, and range of motion.

A modified vector coding approach [6] was used to determine the segment couplings between rearfoot and tibia, tibia and knee, and rearfoot and knee. Coupling angles were calculated at each point during stance phase and categorized into one of four patterns: proximal phase, in-phase, distal phase, or anti-phase. The frequency of each pattern were specifically quantified during early (ES: 0-33%),

mid (MS: 34-66%), and late stance phase (LS: 67 – 100%).

Differences in segment and joint kinematics were evaluated using a one way repeated measures ANOVA. Differences in average coordination patterns were evaluated using a two way (period of stance x shoe condition) repeated measures ANOVA. All statistical analyses were performed with an alpha of  $p < .05$ .

## RESULTS AND DISCUSSION

There was a significant period of stance by shoe interaction for average tibia-knee coupling angles ( $F_{4,60} = 3.507$ ,  $p = 0.012$ , Figure 1). Pairwise comparison revealed that during MS average coupling angles were larger in the MIN shoe ( $146.9 \pm 94.9$ ) compared to the ULTRA shoe ( $96.6 \pm 78.35$ ) condition ( $p = .029$ ). During MS in ULTRA conditions tibia-knee coordination was primarily in the distal phase, dominated by tibia motion. However, in the MIN condition tibia-knee coordination during MS was dominated by antiphase motion. No differences in coupling angles were observed for rearfoot-tibia or rearfoot-knee coordination at any of the three phases of stance. There were no statistically significant difference between shoe conditions for any of the segment or joint angle variables (Table 1).

The main finding from this study was higher amount of antiphase motion during MS in the MIN shoe condition. This coordination pattern means the tibia was internally rotating while the knee was extending. Previous research has suggested that this

type of motion may increase torsional stress on the knee joint [7]. While the results of this study provide insight into the role of footwear on joint coordination, additional studies are necessary to determine if these coordination patterns relate to injury incidence when using ultra-cushioning shoes.

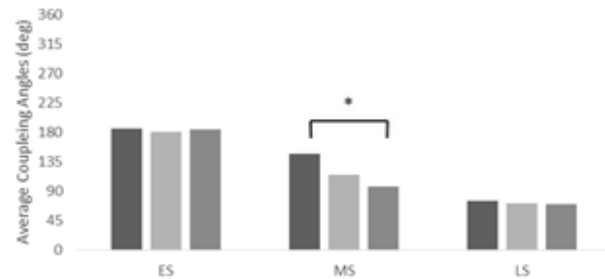


**Figure 1.** Average period of stance x shoe interaction coupling angles of tibia I/R –knee F/E during early stance (ES), mid stance (MS) and late stance (LS) \* indicates significant difference at  $p < 0.05$  level.

## REFERENCES

- DeLeo A.T., et al. *Clinical Biomechanics* **19**(10), 983-991.
- Hamill J., et al. *Med Sci Sports Exerc* **24**(7), 807-813, 1992.
- van Gent R.N., et al. *British Journal of Sports Medicine* **41**(8), 469-480, 2007.
- Silvernail J.F., et al. *Med Sci Sports Exer* **47**(10), 2175-2180, 2015
- De Wit B., et al. *Journal of Applied Biomechanics* **16**, 169-179, 2000
- Chang R., et al. *Journal of Biomechanics* **41**(14), 3101-3105, 2008.
- Pohl, M.B., et al. *Gait and Posture* **25**, 295-302, 2007.

**Table 1:** Mean Values ( $\pm$ standard deviations) for rearfoot frontal plane, tibia transverse plane, and knee sagittal plane kinematics during the stance phase for Min, Neut, and Ultra shoe conditions. IC: initial contact, Peak: peak motion, ROM: range of motion.

		Minimalist	Neutral	Ultra	
Rearfoot	IC	0.88 $\pm$ 4.00	1.94 $\pm$ 4.54	0.67 $\pm$ 5.42	F =.523, p =.604
	Peak	-10.00 $\pm$ 3.45	-9.29 $\pm$ 4.13	-9.11 $\pm$ 5.74	F =.247, p =.785
	ROM	10.88 $\pm$ 2.49	11.22 $\pm$ 2.83	9.78 $\pm$ 3.01	F = 1.001, p = .392
Tibia	IC	5.38 $\pm$ 4.27	4.0 $\pm$ 7.03	2.09 $\pm$ 8.32	F = 1.371, p = .286
	Peak	0.638 $\pm$ 4.64	-2.40 $\pm$ 6.00	-4.29 $\pm$ 8.34	F =3.009, p =.082
	ROM	4.74 $\pm$ 4.12	6.40 $\pm$ 2.81	6.38 $\pm$ 2.65	F =.982, p =.399
Knee	IC	13.92 $\pm$ 5.22	13.30 $\pm$ 5.71	10.73 $\pm$ 5.15	F =2.737, p =.099
	Peak	36.15 $\pm$ 5.41	36.04 $\pm$ 6.47	33.55 $\pm$ 5.57	F =3.325, p =.066
	ROM	22.23 $\pm$ 4.01	22.74 $\pm$ 3.74	22.82 $\pm$ 3.22	F =.248, p =.784

# THE EFFECTS OF A NOVEL ENERGY STORAGE AND RETURN MILITARY BOOT ON WALKING PERFORMANCE

<sup>1</sup>Mitchell D. Ruble, <sup>1</sup>Starr E. Brown, <sup>1,2</sup>Elizabeth Russell Esposito, <sup>1,2</sup>Jason M. Wilken

<sup>1</sup>Center for the Intrepid, Department Rehabilitation Medicine, Brooke Army Medical Center, JBSA, Ft. Sam

<sup>2</sup>Extremity Trauma and Amputation Center of Excellence, JBSA Ft. Sam Houston, TX, USA

E-mail: mitchell.d.ruble.ctr@mail.mil

## INTRODUCTION

Footwear science aims to advance comfort, safety, and economy of motion. Prior research has studied the effects of footwear design on impact loading, energy return, comfort, and movement control [1]. However, biomechanical studies examining the effects of military boot design on performance and injury prevention are limited [2].

Injury prevention is a priority within the military health system. Musculoskeletal injuries are prevalent and largely occur due to overuse and joint disorders [3]. In-shoe interventions may be beneficial, and using prescription orthotics as a preventative measure has been shown to reduce injury development in military recruits [4]. An energy storage and return orthosis (ESRO) was developed for this study to improve the biomechanical performance of Service Members. The purpose of this study was to determine how the ESRO integrated within military boots impacts performance in Service Members.

## METHODS

13 active duty Service Members (age:  $30 \pm 10$  yrs, height:  $1.77 \pm 0.06$  m, mass:  $86.12 \pm 10.35$  kg, 12 male 1 female) with no recent injuries underwent two sessions of gait analysis in a motion laboratory. Kinematic (120 Hz, Motion Analysis Corp), force plate (1200 Hz, AMTI, Inc.), EMG (1200 Hz, Motion Laboratory Systems, Inc.), and metabolic (Parvo Medics) data were recorded as subjects walked at a set speed (4mph). EMG and metabolic data were collected on a treadmill and joint kinematic and ground reaction force data were collected overground. A standard issue military boot and a boot with an integrated ESRO orthotic were tested in a randomized order (Figure 1). The

ESRO boots were, on average, 234g (0.52lbs) lighter than the standard boots.



**Figure 1:** Top: Image of the standard boot (left) and test ESRO boot (right). Bottom: Image of the ESRO (left) and full assembly (right).

Five strides of kinematic/kinetic data and 10 strides of EMG data were analyzed. Lower extremity joint angle, moment, and power data were calculated and peak values during key points of stance and swing were identified. Integrated EMG activity from the gluteus maximus, gluteus medius, rectus femoris, vastus medialis, biceps femoris, lateral gastrocnemius, medial gastrocnemius, soleus, and tibialis anterior was analyzed during 6 phases: 0-10%, 10-30%, 30-50%, 50-60%, 60-80%, and 80-100% of the gait cycle. Metabolic rate was calculated as the average rate during 2 minutes of steady state walking.

A 2-way repeated measures ANOVA (boot x phase of gait) and post-hoc paired t-tests with Bonferroni-Holm corrections identified significant differences in the EMG data. Paired t-tests with Bonferroni-Holm corrections identified significant differences

between boots for the kinematic, kinetic and metabolic data ( $\alpha = 0.05$ ).

## RESULTS AND DISCUSSION

The ESRO boot produced a small (2.8%) but significant and consistent reduction in metabolic rate ( $p < 0.001$ ) (Fig 2). The reduction in mass of the ESRO boots likely contributed to part of the improved metabolic performance. The ESRO may have also contributed. Prior literature indicates that for every 100g added to the ankle, the metabolic rate increases by 0.8% at 4mph [5]. Therefore a 234g decrease in footwear mass would equate to an expected 1.9% decrease in metabolic rate. The ESRO may have contributed to the remaining reduction in metabolic rate but its independent effects cannot be conclusively determined.

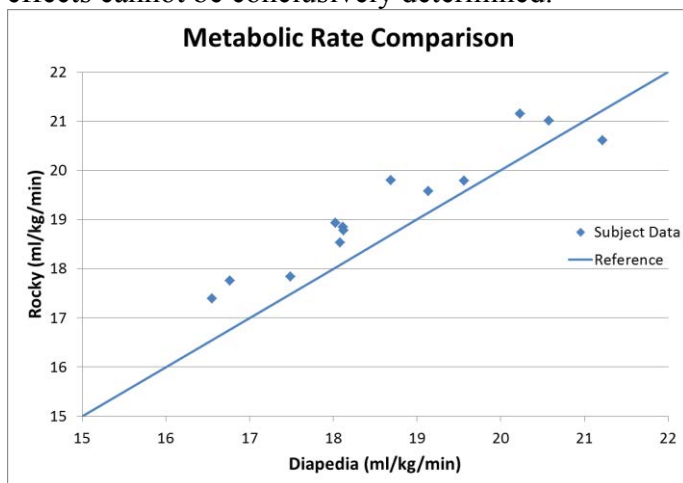


**Figure 2:** Metabolic rate comparison between the standard boot and ESRO boot.

The internal knee extensor moment and knee power absorption in late stance both significantly decreased in the ESRO boot ( $p < 0.014$ ). The difference was 0.05 Nm/kg for the extensor moment and 0.37 for power absorption. The lack of other significant biomechanical changes suggests the ESRO boot may not increase the risk of musculoskeletal injuries.

EMG remained largely unchanged between conditions. However, there was a significant interaction effect between the boot type and phase of gait for the tibialis anterior ( $p = 0.047$ ) and the biceps femoris ( $p = 0.001$ ). The tibialis anterior had a significant 6% reduction in activity in the ESRO

boot during late stance ( $p < 0.001$ ) and a 17% reduction in early swing ( $p = 0.006$ ). It is possible that these reductions may have played a small role in reducing the metabolic rate of walking, but the tibialis anterior is not a large muscle and accounts for only a minor portion of the overall energy expenditure.

There were several limitations. First, the 4mph speed may not highlight the aspects of the boots at different speeds (running). In addition, there was no accommodation time for the boots, which often require a “break-in” period for comfortable use. Finally this abstract does not report all the variables that may be associated with overuse injuries.

## CONCLUSIONS

The novel boot with the ESRO demonstrated reduced metabolic cost with few altered biomechanics. The reduced mass of the ESRO boot likely drove the significant decrease in metabolic activity, and the ESRO integrated within the boot may have also contributed. The reduction was small, but may have important performance implications over time. Overall, the reductions in cost occurred without largely impacting overall gait mechanics and muscle activity.

## REFERENCES

1. Nigg B, et al. *Keynote Lecture of 7<sup>th</sup> Symposium on footwear biomechanics*, 2005.
2. Trone, D.W. et al. *National Technical Information Service*, 1997.
3. Hauret KG, et al. *Am J Prev Med*, **38**(1 Suppl), S61-70, 2010.
4. Baxter ML, et al. *Mil Med*, **176**(3), 291-96, 2011.
5. Miller JF, et al. *J Appl Physiol*, **62**(4), 1497-1501, 1987.

## ACKNOWLEDGEMENTS

This study was funded through an Army Phase II SBIR grant W81XWH-12-C-0041.

The views expressed herein are those of the authors and do not reflect the policy or position of Brooke Army Medical Center, the US Army Medical Department, US Army Office of the Surgeon General, Department of the Army, Department of Defense or US Government.

# INFLUENCE OF OCCUPATIONAL FOOTWEAR ON MUSCLE ACTIVITY DURING A SIMULATED WORKLOAD

<sup>1</sup> Lauren A. Luginsland, <sup>2</sup> Harish Chander, <sup>3</sup> Chip Wade, <sup>4</sup> John C. Garner, <sup>1</sup> J. Derek Eason, <sup>1</sup> Samuel J. Wilson, <sup>5</sup> Jacob R. Gdovin, <sup>1</sup> Christopher M. Hill, <sup>2</sup> Adam C. Knight, and <sup>2</sup> Daniel Carruth

<sup>1</sup> The University of Mississippi, Oxford, MS, USA; <sup>2</sup> Mississippi State University, Starkville, MS, USA  
<sup>3</sup> Auburn University, Auburn, AL, USA; <sup>4</sup> Troy University, Troy, AL, USA  
<sup>5</sup> Missouri State University, Springfield, MO, USA

Email: lluginsl@go.olemiss.edu Web: hesrm.olemiss.edu

## INTRODUCTION

Falls in the work place are a major economic burden. The Bureau of Labor Statistics reported a total of 4,679 workplace fatalities, and a total of 316,650 non-fatal workplace injuries that were due to falls in 2014. Moreover, the leading event or exposure for occupational injuries and illness were workload overexertion [1]. Previous literature has suggested that occupational footwear can cause balance decrements [2,3,4], as can occupational workloads [3,4]. Occupational footwear, while designed primarily for safety, may not provide proper ankle and foot support and predispose the body to postural control decrements, particularly when exposed to extended durations of an occupational workload. Thus, the purpose of this study was to examine differences in muscle activation levels of the lower extremities while wearing different types of occupational footwear during a simulated extended duration occupational workload. The current footwear are standard footwear of the construction and manufacturing industry, and include the Work Boot (WB) (mass:  $0.39 \pm 0.06$  kg; boot shaft height: 18.5 cm), Tactical Boot (TB) (mass  $0.53 \pm 0.08$  kg; boot shaft height: 16.5 cm) and Low Top Shoes (LT) (mass:  $0.89 \pm 0.05$  kg; boot shaft height: 9.5 cm).

## METHODS

Fifteen healthy male adults (aged  $23.6 \pm 1.2$  years; height of  $181 \pm 5.3$  cm; weight of  $89.2 \pm 14.6$  kg), with no history of orthopedic, musculoskeletal, cardiovascular, neurological, or vestibular

abnormalities participated in this study. For the purposes of this abstract, 8 subjects are considered. Participants were tested on three separate days while wearing a randomly assigned occupational footwear, separated by a minimum of 72 hours. The experimental session included an extended duration of a simulated occupational workload which included walking for 4 hours with muscle activation measured every 30 minutes (Pre, 30, 60, 90, 120, 150, 180, 210 & 240 min). Participants were instructed to walk at a self-selected pace and a self-selected path on a hard firm surface until every 30 minute interval to complete muscle activity testing. Muscle activation testing was performed using maximal voluntary contractions (MVCs) of six lower extremity muscles, the quadriceps, hamstrings, plantarflexors, dorsiflexors, ankle inverters, and everters. Surface electromyography signals were recorded from the right leg musculature: tibialis anterior (TA), medial gastrocnemius (MG), semitendinosus (H) and vastus medialis (Q), soleus (IN) and peroneus longus (EV). The EMG signals were recorded using silver/silver chloride monopolar surface electrodes. The ground electrode was placed on the tibial tuberosity. The EMG was recorded using Noraxon® MyoResearch software (Noraxon U.S.A. Inc. Scottsdale, AZ.). Raw EMG data were collected at 1,500 Hz, band-pass filtered (20-250Hz) and rectified prior to analysis. Three maximal voluntary contractions, five seconds in duration were performed for each muscle. Quadriceps and hamstring MVCs were performed while seated on a weight bench, plantarflexion, and dorsiflexion MVCs were performed in the standing position. The mean muscle activity for each MVC were obtained

and averaged together across the three trials for analysis. Mean muscle activity during the MVCs were analyzed using a 3 x 9 (Footwear [WB, TB, LT] x time [Pre, 30, 60, 90, 120, 150, 180, 210, 240]) repeated measures ANOVA. If main effects or interaction differences were observed, simple effects were calculated while applying a Bonferroni correction factor for multiple comparisons. All statistical analyses were performed in SPSS version 22 with an a priori alpha level of 0.05

## RESULTS AND DISCUSSION

A significant main effect for time was found for IN MVC ( $F(8,56) = 2.819, p=0.011$ ). Pairwise comparisons for main effects revealed significant differences with higher MVC at minute 30 than minute 120 and a higher MVC at minute 60 than minute 120 at  $p=0.042$  and  $p=0.028$  respectively. A significant main effect for time was found for Q MVC ( $F(8,56) = 4.909, p > .001$ ). Pairwise comparisons for main effects revealed significant differences with higher MVC at minute 30 than minute 240 at  $p=0.024$ . No significant differences were observed between the footwear conditions.

The significant main effects for time in the IN and Q MVCs may suggest that fatigue affected the most distal part of the lower extremity (IN) after 120 minutes, earlier than the more proximal and larger muscle (Q) at the 240 minute time point. The results agree with the literature, which shows that MVC's should decrease due to the lack of motor unit recruitment with the increase in strenuous workloads [2,4,5].

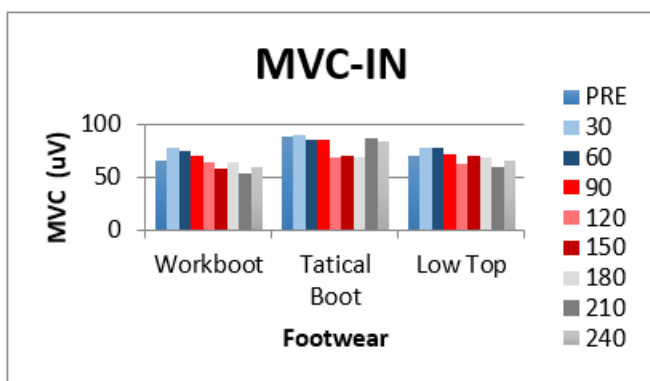


**Figure 1:** Mean MVC's of the inverter muscle (IN) at nine time points.

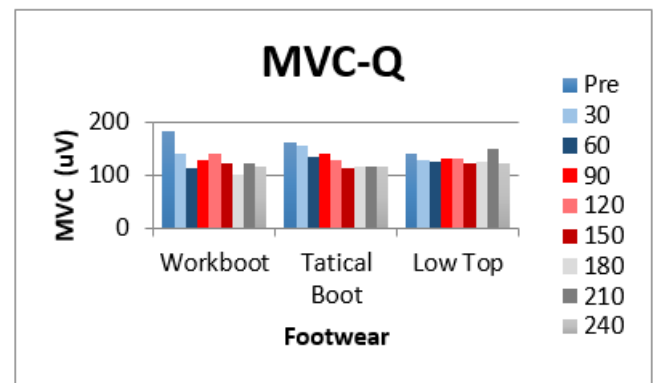


**Figure 2:** Mean MVC's of the vastus medialis muscle (Q) at nine time points.

A decline in the capacity to recruit muscle fibers may indicate tiredness, discomfort, and injuries associated with long duration walking and standing, [6,7]. This may become dangerous, especially in occupational settings, due to the elevated stress placed on the postural control system by hazardous environmental factors [8].

## CONCLUSIONS

Although the footwear analyzed in the current study may not significantly influence on MVC's, we cannot dismiss the possibility that footwear with different physical characteristics may alter the MVC's. It is also possible that footwear specially designed for the occupational work environment may influence muscle activity during a period longer than 4 hours. Therefore, future research should utilize a similar protocol over a longer duration.

## REFERENCES

1. Bureau of Labor Statistics: US Department of Labor, (2014).
2. Chander, H., Garner, J. C., & Wade, C. (2014). Impact on balance while walking in occupational footwear. *Footwear Science*, 6(1), 59-66.
3. Chander, H., Wade, C., & Garner, J. C. (2015). Impact of Occupational Footwear on Dynamic Balance Perturbations. *Footwear Science*, 7: 2, 115-126.
4. Garner, J. C., Wade, C., Garten, R., Chander, H., & Acevedo, E. (2013). The influence of firefighter boot type on balance. *International Journal of Industrial Ergonomics*, 43(1), 77-81.
5. Chander, Morris, Wilson, Garner, and Wade. (2016). Impact of alternative footwear on human balance. *Footwear Science*, 8(3).
6. Davidson, B.S., Madigan, M.L., Nussbaum, M.A., 2004. Effects of lumbar extensor fatigue and fatigue rate on the postural sway. *European journal of applied physiology*; 93(1-2), 183-189.
7. Pline, K. M., Madigan, M. L., & Nussbaum, M. A. (2006). Influence of fatigue time and level on increases in postural sway. *Ergonomics*, 49(15), 1639-1648.
8. Kincl, L. D., Bhattacharya, A., Succop, P. a, & Clark, C. S. (2002). Postural sway measurements: a potential safety monitoring technique for workers wearing personal protective equipment. *Applied Occupational and Environmental Hygiene*, 17(4), 256-66.

# DOES FOOTWEAR AFFECT THE RATE OF FATIGUE DURING REPEATED SPRINTS?

<sup>1</sup>Nicholas S. Frank, <sup>1</sup>Bryan R. Picco, <sup>1</sup>Bryan P. Conrad

<sup>1</sup>Nike Sports Research Lab, Beaverton, OR, USA  
email: nick.frank@nike.com

## INTRODUCTION

Basketball is a game of multiple, high intensity sprints covering an average of 15m [1]. Sustaining sprint performance over the course of a game is challenging: speed and distance traveled significantly decrease in the second half of games.

Recent work has shown the negative effect of footwear with increased longitudinal bending stiffness on the ability to accelerate, demonstrating that greater stiffness is related to slower acceleration over short distances [2]. It remains unknown if flexible footwear helps with sprinting performance over time as is the case in basketball. Therefore, the purpose of this work was to determine if shoes with different bending stiffness influence initial sprint performance and the overall performance decrement throughout a repeated sprint test.

## METHODS

Nine male basketball players (30.2± 4.2 yrs., 1.88 ± 0.04 m, 93.9 ± 7.6 kg) participated in this study. Three different shoes were compared which differed only in their bending stiffness. During three separate visits to the laboratory, athletes performed the repeated sprint ability test (RSA) once per visit and wore a different shoe each time. The RSA is a fatiguing performance drill that tests an athlete's anaerobic capacity [3]. The test consists of ten repeated shuttle sprints that are 30 meters in length (15m + 15m) with thirty seconds of rest between each sprint. If the athlete exerts maximal effort on each sprint, their speed will decrease with each repetition as the effects of fatigue increase. From this decay in performance, the rate of fatigue can be calculated [3]. Previous work has identified that initial performance and the rate of fatigue are positively correlated and have been shown to differentiate endurance athletes from athletes who participate in team sports. [4].

Faster initial sprint times are associated with greater decay in performance over the course of the drill [5]. Conversely, slower initial times are associated with smaller decay rates. Performance was assessed by using wireless timing gates placed ten meters apart. One set of gates was placed at the start/finish line, while the second timing gate allowed for the change of direction speed to be measured (Fig. 1).

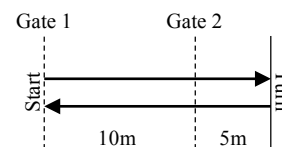


**Figure 1:** Placement of timing gates with respect to the 15m shuttle course allowed for linear sprint and change of direction performance to be measured.

Dependent variables included performance decrement ( $S_{dec}$ ), best lap time, fastest turn, total test time and average lap time. Performance decrement was calculated as:

$$S_{dec}(\%) = \left\{ 1 - \frac{(S_{avg})}{S_{best}} \right\} \times 100$$

A one-way repeated measures ANOVA was used to test for the effect of visit order followed by a separate analysis comparing footwear conditions if an order effect didn't exist.

## RESULTS AND DISCUSSION

In general, sprint times were slower throughout the progression of RSA for all athletes on all visits. A significant order effect was found for performance decrement ( $P < 0.01$ ) and best lap time ( $P < 0.01$ ). Initial sprint times were fastest in the first visit of the study. Additionally, performance decrement was the greatest in the first visit of the study and decreased on each subsequent visit (Fig. 2). There was no order

effect for the total test time and average lap time (Table 1).

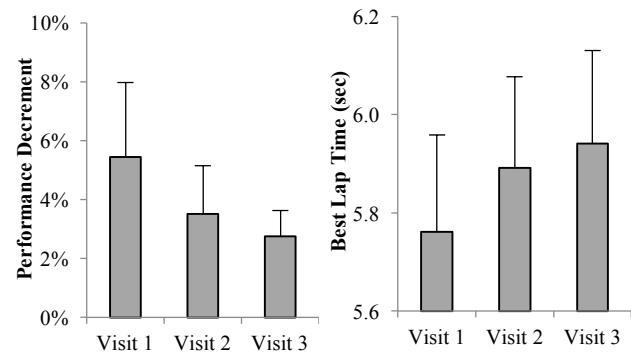


**Figure 2:** Performance decrement (left) decreased from visit to visit, while best lap time increased (right).

Total time to complete the drill was similar across all three shoe conditions. Specifically, the total times for the flexible, medium and stiff conditions were  $58.37 \pm 3.76$ ,  $57.96 \pm 3.25$  and  $58.12 \pm 2.89$  seconds, respectively ( $P = 0.76$ ). Additionally, the average lap time was the same across all three shoe conditions which were  $6.11 \pm 0.23$ ,  $6.06 \pm 0.14$  and  $6.08 \pm 0.20$ , for the flexible, medium and stiff shoes ( $P = 0.70$ ).

The original purpose of the study was to determine the effect of bending stiffness over the course of repeated sprints. As there were no differences in total time to complete the test across shoes, it appears that the range of stiffness tested in this experiment are not great enough to cause a change in performance.

Interestingly, a systematic strategy across study visit was observed in the results. It appears that athletes may have elected to run slower on the initial sprints in visits two and three. This order effect may have been to reduce the discomfort/fatigue associated with the test, based on the experience from the first visit. Additionally, using a different strategy from visit to

visit caused a lot of variability across shoe conditions, potentially overshadowing any footwear effects.

## CONCLUSIONS

Increasing bending stiffness did not affect the total time of the RSA. The range of stiffness tested in this study may be different from previous work.

It was found that athletes self-optimize their performance of the RSA test to produce the same average work load yet with slower initial sprint times. This strategy may have been employed as a way to reduce the discomfort associated with high intensity exercise. The strong order effect observed prevents confirmation of the original purpose to see if initial sprint performance is improved in flexible footwear.

These findings suggest that future work should consider how to measure maximal effort exercise across multiple sessions. One way to mitigate these findings may be through real-time motivational feedback to the athlete.

## REFERENCES

1. Ben Abdelkrim N, et al. *J. Strength Cond. Res.* 24.9, 2330–2342, 2010.
2. Willwacher S, et al. *Ftwr Sci* 8, 99-108, 2016.
3. Castagna C, et al. *J Strength & Cond.* 21.4, 1172-1176, 2007.
4. Bishop D, et al. *J Sci Med Sport* 4, 19-29, 2001.
5. Hamilton A, et al. *J Sports Sci* 9, 371-382, 1991.

**Table 1:** Mean performance measures across each visit of the experiment.

	Visit 1	Visit 2	Visit 3	<i>p</i>
Performance Decrement	5.4% ± 2.5%	3.5% ± 1.6%	2.4% ± 0.7%	< 0.01
Best Lap Time (s)	5.76 ± 0.20	5.89 ± 0.19	5.94 ± 0.18	< 0.01
Fastest Turn (s)	2.35 ± 0.15	2.41 ± 0.1	2.43 ± 0.09	0.06
Total Test Time (s)	58.03 ± 3.61	58.25 ± 2.73	58.16 ± 3.55	0.92
Average Lap Time (s)	6.08 ± 0.26	6.1 ± 0.17	6.08 ± 0.15	0.93

# FOOT STRIKE INDEX, RUNNING CADENCE, AND LOADING RATE WHILE RUNNING IN A TRADITIONALLY CUSHIONED ZERO-DROP SHOE

<sup>1</sup> Macy Urrutia, <sup>1</sup> Travis Ficklin, <sup>2</sup> Robin Lund, and <sup>1</sup> April Ficklin

<sup>1</sup> Dixie State University, Saint George, UT, USA

<sup>2</sup> University of Northern Iowa, Cedar Falls, IA, USA  
email: travis.ficklin@dixie.edu

## INTRODUCTION

Lower extremity injuries are common to runners, including - but not limited to - stress fractures from repeated impact and loading. Though there are many contributors to such injuries, loading rate (LR), which is the rate of vertical ground reaction force development, has been implicated in particular [1].

Some kinematic parameters of foot strike may be tied to helping reduce LR. Among these are potentially foot strike index (SI) and running cadence (RC). SI is a measure of how far forward on the sole of the foot initial impact with the ground occurs (measured as a percentage of foot length). Running cadence is measured in steps (foot strikes) per minute. It is possible that further forward SI and increased RC may help reduce LR [2,3].

Zero-drop (ZD) shoes (Altra Running, Logan, UT) have no difference between forefoot and rearfoot midsole stack heights. The makers of the shoe suggest that this encourages less overstriding, leading to increased RC and a more forward SI. However, the effect of this footwear on these variables is not fully understood.

The purpose of this study was to compare SI, RC, and LR for runners when running in the ZD shoe to running in three other shoes: traditional (TR), stability (ST), and maximalist (MX).

## METHODS

All study procedures were reviewed and approved by the University IRB, and all subjects provided informed consent. Thirty runners (15 M, 15 F) ran for three-minute bouts at a time on a treadmill at their preferred, self-selected pace. They ran in each of the four shoes in counterbalanced order. After the

three-minute bout on the treadmill, subjects ran across a force platform at the same pace.

The right lower extremity was marked with retro-reflective markers and the last 30 seconds of treadmill running, as well as the force plate run, were recorded using a multi-camera 3D system. High speed video (300 Hz) and digitization were used to measure SI [4]. Custom software was used to make subsequent calculations for SI, RC, and LR during initial impact. Paired t-tests ( $\alpha = 0.05$ ) were made to identify any differences between shoes among these variables.

## RESULTS AND DISCUSSION

Descriptive statistics for all variables are presented in Table 1. Several differences are noted in response to the study purpose.

First, SI was further forward for the ZD shoe than for TR shoes ( $p=0.002$ ), ST shoes ( $p<0.001$ ), and MX shoes ( $p=0.004$ ). Next, RC was increased in the ZD shoe over the TR ( $p<0.001$ ) and MX shoes ( $p=0.012$ ), but not the ST shoe. Last, LR was reduced in the ZD shoe compared to the TR shoe ( $p=0.009$ ) and MX shoe ( $p=0.019$ ), but not the ST shoe. A secondary analysis did not reveal direct correlations between SI and LR, or between RC and LR.

Taken together, these findings underscore the complexity of the leg spring, and the importance of considering it as a complete mechanism., rather than focusing on any one characteristic of impact mechanics. In this sample, LR was reduced in the ZD shoe compared to two others. However, even though this was seen concurrently with an increased cadence and a more forward foot strike overall, the variability in LR was not directly explained by either of these variables. This suggests that it is a combination of factors that predicts LR (rather than

any single one), and that different runners experienced different combinations of factors.

However, the current results suggest that the ZD design does have an effect on running mechanics somehow, and that some of these effects occur immediately. For example, there was an overall more-forward SI in the ZD shoe. The majority of this result came from a large effect for a handful of subjects who dramatically changed their SI in the ZD shoe but not in the other shoes (see Figure 1). In previous studies, such a big change typically resulted from instruction and/or the removal of shoes altogether [5]. The current subjects received no instructions other than to run at their preferred pace on the treadmill for three minutes.

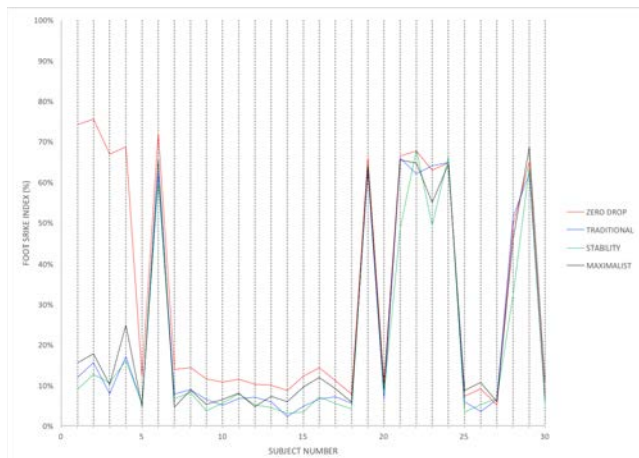


Figure 1: Foot strike index for each subject by shoe. 100% is toe, 0% is heel.

Additionally, increased cadence naturally occurred overall in the ZD shoe. Because speed was held constant, this is tied to reduced stride length, implying a probable overstride reduction. This was likely a contributor to reduced LR as well. Further analysis revealed an attendant increase in knee flexion excursion during weight acceptance in the ZD shoes compared to the TR shoe ( $p = 0.002$ ).

It is evident that runners experienced mechanical changes during impact that taken together likely contributed to the reduced LR, which they would experience as a softer landing. While no one factor may have done this directly, the combination of factors possibly related to the ZD design seems to have changed the leg spring for many of the runners.

## CONCLUSIONS

Overall, there was a reduced loading rate in runners who tried the zero-drop shoe design when compared to loading rates in traditional and maximalist shoes. A combination of factors probably led to this result, but among them may be increased cadence and a more forward foot strike, as well as an associated increase in knee flexion during landing. More research is needed on the long-term effects that adapting to these changes may have for the runners over time, but those who wish to increase cadence and/or land more forward on the foot when running should consider the zero-drop design.

## REFERENCES

- Zadpoor, A., Nikooyan, A. *Clin Biomech* **26**, 23-8, 2011.
- Hamill, J., et. al. *Footwear Sci* **3**, 33-40, 2011.
- Lenhart, R., et. al. *Med Sci Sport Exc* **46(3)**, 557-64, 2014.
- Larson, P. *J Appl Biomech* **19**, 153-68, 2003.
- Squadrone, R., et. al. *J Sports Sci* **33**, 1196-1204, 2015.

## ACKNOWLEDGMENTS

Funding and shoes for this study were generously provided by the Altra Running shoe company.

Table 1: Descriptive statistics and results of paired samples t-tests (n=30).

	Zero-drop (ZD)		Traditional (TR)		Stability (ST)		Maximalist (MX)	
	Mean	SD	Mean	SD	Mean	SD	Mean	SD
Loading Rate (BW/s)	53.9 <sup>1</sup>	+/- 18.6	63.1	+/- 23.1	57.2	+/- 21.0	60.1	+/- 19.5
Stride frequency (steps/min)	168.9 <sup>2</sup>	+/- 10.3	166.2	+/- 10.0	168.0	+/- 8.8	167.2	+/- 9.2
Strike Index (% of foot)	32.9 <sup>3</sup>	+/- 28.4	21.9	+/- 24.8	20.0	+/- 23.3	23.3	+/- 24.2
Knee flexion excursion (degrees)	29.0 <sup>4</sup>	+/- 6.9	26.2	+/- 5.9	28.4	+/- 4.8	28.8	+/- 3.9

KEY: 1 = Less than TR & MX; 2 = Greater than TR & MX; 3 = Further forward than all others; 4 = Greater than TR

# EFFECT OF DIFFERING RUNNING SHOE MIDSOLE THICKNESS ON GAIT KINETICS AND KINEMATICS

<sup>1</sup> Jacob E. Vollmar, <sup>2</sup> Ryan Chang, <sup>2</sup> Jason Leach, <sup>2</sup> Bethany Wilcox, and <sup>1</sup> Allison H. Gruber

<sup>1</sup> Indiana University, Bloomington, IN, USA

<sup>2</sup> Reebok International Ltd., Canton, MA, USA

email: [ahgruber@indiana.edu](mailto:ahgruber@indiana.edu), web: <http://iubiomechanicslab.weebly.com/>

## INTRODUCTION

Running shoes design and construction is ever changing and has resulted in a wide variety of shoes available for commercial purchase including the Hoka One One to Vibram FiveFingers. Arguments both for and against the benefits of cushioning in running shoes have been made; in particular, whether cushioning has a protective or detrimental effect on running related overuse injuries. Recently, a new paradigm has been proposed which argues that the cushioning of the shoe is not as important as the perceived comfort of the shoe and ease of preferred movement path the shoe allows [1]. This hypothesis is possible given that runners tend to normalize joint stiffness and impact force characteristics and tibial shock in response to varying shoe and surface conditions [e.g. 2]. The result that impact forces increase as cushioning increases is counterintuitive. It would be expected that greater midsole cushioning would create a softer landing, similar to the effect of bending the knees when landing from a jump. It has yet to be investigated whether the timing between peak vertical impact force and peak tibial acceleration are changed with varying midsole thicknesses. Although impact forces increase with greater cushioning, a delay in the timing between peak impact force and peak tibial acceleration may indicate that more shock is attenuated by the shoe rather than the tissues of the foot and leg.

The purpose of this study was to examine the effects of an increase of 3 mm and 6 mm in shoe midsole thickness on the timing and magnitude of peak vertical impact force and peak tibial acceleration. It was hypothesized that the delay between the timing peak impact and peak tibial acceleration would increase as midsole thickness increases.

## METHODS

To date, seven healthy, male rearfoot runners between the ages of 18 and 40 volunteered to participate in this study. All participants read and agreed to IRB documents before participating. Participants were outfitted with retroreflective markers secured to anatomical points on their right foot, right leg, and pelvis. The three models of shoes were tested which were identical in all aspects except their midsole thickness (18 mm, 21 mm, and 24 mm). Participants ran in all three shrouded shoe models at  $3.5 \text{ m/s} \pm 5\%$  across a force platform (1200 Hz) imbedded in an 18m runway. Nine infrared Qualisys motion capture cameras recorded the position of the retroreflective markers (240 Hz). A triaxial accelerometer secured to the anteromedial aspect of the distal right tibia was used to measure tibial shock during the stance phase (1200 Hz). Camera, force platform, and accelerometer data were time synchronized. Impact-related variables were assessed from the vertical ground reaction force (vGRF) using previously established methods [3]. A repeated measures ANOVA ( $\alpha=0.05$ ) with Tukey's post hoc comparisons was used to compare the kinetic and kinematic variables between the three midsole thickness conditions. Given the small sample size, Cohen's  $d$  was also used to determine if the none statistically significant differences displayed meaningful trends.

## RESULTS AND DISCUSSION

There was a significant decrease in average vertical loading rate, a significant decrease in instantaneous vertical loading rate, and a significant decrease in peak tibial acceleration as midsole thickness increased (Table 1). Time to peak vGRF impact increased as midsole thickness increased but was not statistically significant ( $p>0.05$ , Table 1). Time to

peak tibial acceleration increased with increased thickness for 18 mm to 21 mm ( $d = 0.37$ ), did not differ between 18 mm thickness and 24 mm ( $d = 0.09$ ), and decreased with increased thickness from 21 mm to 24 mm ( $d = 0.78$ ). No change in the magnitude of the vGRF impact peak was detected between midsole conditions ( $p > 0.05$ , Table 1). No differences in joint kinematics were observed ( $p > 0.05$ ).

The decreases in the average and instantaneous vertical loading rates of the vGRF were consistent with previous studies and may be attributed to an increase in the time to peak impact rather than a significant decrease in the impact peak magnitude [4, 5]. The lack of difference in the kinematic variables might be explained by the identical heel-toe drop between the three shoe thickness models tested [6]. Previous research that showed kinematic differences with differing shoe thicknesses had differences in heel-toe drop between shoe conditions [7]. The lack of kinematic difference could also be explained by the preferred movement path paradigm [1].

The 24 mm thickness condition resulted in the longest delay between the vGRF impact peak and peak tibial acceleration. The smallest difference in timing between peaks occurred with the 21 mm thickness condition (Table 1). The 21 mm condition also resulted in the greatest vGRF impact peak magnitude and longest time to peak tibial acceleration.

## CONCLUSIONS

Increasing the midsole thickness of running shoes from 18 mm to 21 mm to 24 mm reduced ground impact characteristics without changing gait kinematics. The increased delay between peak vGRF impact and peak tibial acceleration may suggest a greater role of the shoe in modulating the tibial shock as midsole thickness increases from 18 mm to 24 mm. Further analysis and more subjects may be needed to explain the inconsistent results with the intermediate, 21 mm thickness condition. The data may indicate an “optimal” midsole thickness for creating less injurious impact conditions.

## REFERENCES

1. Nigg B.M., et al. *Br J Sports Med*, **49**, 1290-1294, 2015.
2. Ferris D.P. & Farley CT, *J Appl Physiol*, **82**, 15-22, 1997.
3. Milner C. E., et al. *Med Sci Sports Exerc*, **38**(2), 323-328, 2006.
4. Addison, B.J., et al. *Journal of Biomechanics*, **48**, 1318–1324, 2015.
5. Hamill, J., et al. *Footwear Science*, **3**, 33–40, 2011.
6. Chambon, N., et al. *Gait & Posture*, **40**(1), 58–63, 2014.
7. Nigg, B.M., et al. *Journal of Biomechanics*, **20**(10), 951–959, 1987.

**Table 1:** Mean±1SD vertical ground reaction force and tibial acceleration characteristics for three differing midsole thickness conditions. Statistical difference between conditions is denoted by  $\alpha$  (18 mm vs. 21 mm),  $\dagger$  (18 mm vs. 24 mm), and  $*$  (21 mm vs. 24 mm) ( $p < 0.05$ ).

	18 mm	21 mm	24 mm	p-value
Active Peak (BW)	2.5791 ± 0.1082	2.5800 ± 0.1416	2.6061 ± 0.1612	> 0.05
Impact Peak (BW)	1.7090 ± 0.1459	1.7340 ± 0.1650	1.7166 ± 0.1967	> 0.05
Vertical Loading Rate (BW/s)	63.8525 ± 9.2255 $\alpha\dagger$	57.9069 ± 10.0463 $\alpha$	55.8325 ± 7.2916 $\dagger$	0.0086
Instantaneous Vertical Loading Rate (BW/s)	98.2785 ± 13.1000 $\alpha\dagger$	88.9592 ± 14.9163 $\alpha*$	78.7651 ± 11.6935 $\dagger*$	0.0001
Tibial Shock (g)	6.0909 ± 0.7533 $\alpha\dagger$	5.1878 ± 0.9745 $\alpha*$	4.3109 ± 0.7156 $\dagger*$	0.0002
Time to Peak vGRF Impact (s)	0.0360 ± 0.0037	0.0396 ± 0.0057	0.0400 ± 0.0019	> 0.05
Time to Peak Tibial Acceleration	0.0241 ± 0.0593	0.0392 ± 0.0215	0.0271 ± 0.0093	> 0.05
Time between peaks	0.0119 ± 0.0556	0.0004 ± 0.0158	0.0129 ± 0.0074	> 0.05

# Landing Mechanisms of Grand Jeté with Soft Shoes and Pointe Shoes in Ballet Dancers

<sup>1</sup> Hsiu-Chen Lin, <sup>2</sup> Tzu-Han Lee, <sup>3</sup> Hsiu-Chen Yeh, <sup>4</sup> Hao-Ling Chen, and <sup>5</sup> Wei-Chun Hsu

<sup>1</sup> Department of Physical Therapy, China Medical University, Taichung, Taiwan

<sup>2</sup> Department of Physical Therapy and Assistive Technology, National Yang-Ming University, Taipei, Taiwan

<sup>3</sup> Division of Physical Medicine and Rehabilitation, Taoyuan Armed Forces General Hospital, Taoyuan, Taiwan

<sup>4</sup> Department of Occupational Therapy, National Taiwan University, Taipei, Taiwan

<sup>5</sup> Graduate Institute of Biomedical Engineering, National Taiwan University of Science and Technology, Taipei, Taiwan

email: hclin@mail.cmu.edu.tw, web: <http://cmupt.cmu.edu.tw/english/index.html>

## INTRODUCTION

Ballet requires a unique balance of athleticism and artistry. Several jumping and landing skills, such as ballonné and grand jeté, will be performed frequently. Grand jeté is a big leap in the form of splits, and the lower extremity would bear substantial impacts during the landing. Two potential contributing factors of ballet dancer's injuries are excessive ground reaction forces and shoe type [1]. The jumping/landing tasks usually have large impacts on the lower extremities, but neither the flat shoes nor pointe shoes could provide significant shock absorption for dancers. Landing on extreme plantar-flexed postures after a grand leap are the frequent circumstances that cause injuries in ballet dancers. The most common injury is ankle inversion sprains, which also have high rate of recurrence and subsequent disability and residual symptoms [2]. These observations lead to a result that impacts at landing have to attenuate by good rolling-down mechanism at the ankle-foot region and also coordinated movements in the lower extremities. However, previous literature seldom reported the descriptions of joint mechanics in lower extremities during the jumping/landing tasks. Therefore, the aim of this study is to investigate the joint mechanics in lower limbs during the landing of grand jeté with flexible ballet (or soft) shoes and pointe shoes in young female ballet dancers.

## METHODS

Nineteen healthy collegiate ballet female dancers were recruited for detailed biomechanical analysis.

Each participant was asked to warm-up first, and then perform grand jeté at least for five times wearing first with soft shoes and then pointe shoes in our motion analysis laboratory equipped with six infrared camera (Vicon MX, Oxford Metrics, UK) and three mounted force platforms (AMTI Inc., Watertown, MA, USA) to collect the kinematic and kinetic simultaneously. Several events during a grand jeté were determined by the currencies of the maximal knee flexion angle, highest body center of mass, foot touch-down on the ground, foot rolling-down to maximal ankle dorsi-flexion angle, and the lift-off from the ground (Fig. 1). The joint angles, moments in the lower extremity starting from the landing to the rolling-down phase in a grand jeté on the force platform were concentrated and the peak values were obtained and used for further analysis. All the dependent variables will be analyzed using SPSS statistical software to determine the differences between shoe types.

## RESULTS AND DISCUSSION

The results showed the significant differences between shoe types occurred mainly in hip and ankle-foot region (Table 1). In the sagittal plane, significant larger hip flexion angle, more forefoot plantar-flexion angle and smaller hip flexor moment at the touch-down were found in the pointe shoe condition. Then, the larger hip flexed angles and ankle plantar-flexion angle were also found in the rolling-down phase. In the frontal plane, smaller midfoot eversion at the touch-down but larger ankle eversion angle during the rolling-down phase were demonstrated in the pointe shoe condition. In the

transverse plane, the larger forefoot internal rotation angle and larger external rotator moment at the knee joint but smaller at the ankle joint were found.

Different landing mechanism would affect the magnitude of the ground reaction force [3]. When wearing different shoe types, the ballet dancers learned to adapt themselves with different landing mechanisms. With the restriction at the toe-box of the pointe shoes, the dancers would land with less forefoot dorsi-flexion but with more flexed hip joint. While wearing the soft shoes, the mid-foot could land with a more everted position, which indicated a flexible foot structure that benefits the shock absorption. Therefore, another strategy occurred during the rolling-down phase with larger knee internal rotator moment.

## CONCLUSIONS

This study aimed to investigate the different landing mechanisms when performing a grand jeté with soft and pointe shoes in young ballet dancers. It has

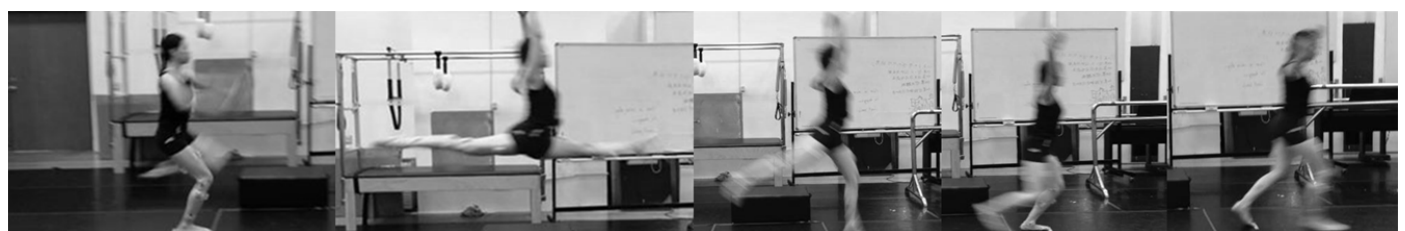


**Figure 1:** Events during a grand jeté.

**Table 1:** Selected joint angles and moments at touch-down and peak values during the rolling-down phase in the landing of grand jeté wearing flat or pointe shoes in the healthy young female ballet dances.

Event Variables \ Shoe type	At touch-down		Rolling-down (minimal)		Rolling-down (maximal)	
	Soft	Pointe	Soft	Pointe	Soft	Pointe
<b>Joint angles</b>						
Hip flexion/extension	22.5±7.7	24.5±7.7*	20.3±6.6	22.5±7.7*	34.6±7.3	37.3±6.7*
Ankle dorsi/plantar-flexion	-26.3±3.8	-24.8±4.9	-26.3±3.8	-24.8±4.9	30.3±4.8	34.0±5.9*
Forefoot dorsi/plantar-flexion	0.39±0.7	-0.02±0.7*	-0.49±0.7	-0.72±0.7	1.02±0.7	0.68±0.7
Ankle inversion/eversion	-0.65±5.7	0.13±6.0	-11.5±4.3	-13.7±4.7*	-0.18±5.5	-0.32±5.9
Midfoot inversion/eversion	-4.4±4.4	-0.82±5.2*	-5.0±4.3	-2.9±4.6	1.69±3.9	2.05±4.4
Forefoot Int./Ext. Rotation	1.92±1.9	2.95±2.7	-0.84±1.9	1.27±2.4*	2.81±2.2	4.42±2.8
<b>Joint moments</b>						
Hip Extensor/Flexor	-9.27±3.7	-7.91±3.5*	-12.9±3.4	-11.7±3.6	13.5±4.7	13.8±7.0
Knee Int./Ext. Rotator	0.03±0.14	-0.03±0.22	-1.71±1.15	-1.53±1.18	2.47±1.37	3.16±1.80*
Ankle Int./Ext. Rotator	-0.31±0.30	-0.38±0.46	-10.1±2.24	-8.95±2.4*	-0.27±0.31	-0.29±0.57

\* indicated statistical significance

accumulated 3-D biomechanical information from the joints of the lower extremities in the landing of grand jeté. This information can be the references for proper landing mechanism and would be helpful in future training strategies in young ballet dancers and rehabilitation of the injured dancers.

## REFERENCES

1. Nunes NM, et al. *Pediatr Phys Ther* **14**, 100-106, 2002.
2. Campoy FA, et al. *Clin J Sport Med* **21**, 493-498, 2011.
3. Chockley C. *J Dance Med Sci* **12**, 5-8, 2008.

## ACKNOWLEDGMENTS

We wanted to express our gratitude to all the participants and also the financial supports the Ministry of Science and Technology of Taiwan (MOST 103 - 2410 - H - 039 - 007 -).

# LIGAMENT STRAIN RESPONSE BETWEEN CONTRALATERAL PAIRS OF LOWER EXTREMITIES DURING *IN VIVO* LANDING SIMULATION

<sup>1</sup>April L. McPherson, <sup>1</sup>Nathaniel A. Bates, <sup>1</sup>Nathan D. Schilaty, <sup>1</sup>Christopher V. Nagelli, <sup>1</sup>Aaron J. Krych, and <sup>1</sup>Timothy E. Hewett

<sup>1</sup>Mayo Clinic, Rochester, MN, USA  
email: [mcperson.april@mayo.edu](mailto:mcperson.april@mayo.edu)

## INTRODUCTION

Biomechanical measures of limb asymmetries during *in vivo* investigations have been identified as a risk factor for primary and secondary anterior cruciate ligament (ACL) injury.[1,2] Recent methodological developments have applied *in vivo* knee kinetics to exert physiologically relevant landing forces on cadaveric lower extremities to mimic ACL injury risk.[3] It is unknown whether contralateral ACLs respond and subsequently fail in a consistent manner during simulator testing. Thus, the objective of the study was to determine if contralateral pairs exhibit different ligament strain responses during simulated *in vitro* landing. It was hypothesized that contralateral lower extremities would exhibit similar ligament strain responses.

## METHODS

A novel mechanical impact simulator was used to simulate the impulse ground reaction force generated during an *in vivo* landing task.[3] External knee abduction moment (KAM), anterior shear (ATS), and internal tibial rotation (ITR) were applied to the specimen in a randomized order of pre-determined magnitudes. External load magnitudes were determined from a previous *in vivo* study of a healthy athlete cohort who performed a drop vertical jump (DVJ) task. Ligament strains were recorded by differential variable reluctance transducers (DVRT) implanted on the ACL and medial collateral ligament (MCL). Eleven pairs of cadaveric lower extremities were obtained from an anatomical donations program (n = 5 female, n = 6 male; age = 42.4 ± 8.6 years; mass = 87.7 ± 21.6 kg; BMI = 29.1 ± 6.6). Analyses of ligament strains were performed between dominant and non-dominant sides. Paired *t*-tests were used to

analyze the data for significant differences ( $p < 0.05$ ) between contralateral pairs.

## RESULTS AND DISCUSSION

Prior to failure, contralateral pairs exhibited no significant differences in maximum ACL strain ( $p = 0.07$ ) or maximum MCL strain ( $p = 0.38$ ) during a simulated DVJ landing (**Table 1**). These findings are consistent with a previous investigation of contralateral differences using *in vivo* kinematics to drive a robotic simulation, which similarly reported no differences in peak ligament strain between contralateral limbs.[4] Whereas previous ligament strain testing studies isolated ligaments by removing the surrounding tissues and used a uniaxial testing device, the current study is a novel way to investigate ligament strain response with all surrounding structures intact in a physiologically relevant manner.

**Table 1:** Maximum ligament linear strain percentage values recorded prior to specimen failure

	Dominant	Non-dominant
ACL	12.05 ± 3.84%	19.18 ± 12.19%
MCL	4.21 ± 7.60%	8.04 ± 9.85%

\*No statistically significant difference between sides ( $p < 0.05$ )

Contralateral pairs tended to fail at similar externally applied loads and with similar pathologies (**Table 2**). Fourteen of the 22 specimens survived to the complete high-risk loading condition (i.e. 100\_100\_100). Interestingly, 12 of these 14 specimens represent 6 contralateral pairs that both reached the complete high-risk trial. For those specimens that survived the complete high-risk trial, the impulse force was adjusted to half the body weight and KAM, ATS, ITR were each increased 20% until the specimen failed.[3]

Findings from this study indicate that limb dominance does not affect the failure threshold of the ligament, since no differences in ligament strain were observed between dominant and non-dominant sides. This may indicate that limb asymmetry is not solely determined by the structure of the ligament, but rather by the product of multiple extrinsic factors and loading mechanisms that influence ACL response. Previous research has demonstrated limb asymmetries observed *in vivo* that increase ACL injury risk can be corrected with neuromuscular training.

The current study is not without limitations. DVRTs are known to have large variability when implanted in soft tissue structures. It also should be noted that failure of three specimens was not due to ACL rupture, but rather femoral fracture or MCL rupture. These three specimens exhibited intact ACL structures in post-testing orthopedic examinations. The remaining nineteen specimens exhibited clinically representative ACL failures, most commonly femoral avulsions. The three non-ACL failure specimens were included in the data analysis in order to represent ligament strain response between contralateral pairs for the comprehensive set of failure mechanisms observed during the landing simulation test. Ligament strains from the trial that induced the failure for each specimen were included in the analysis.

## CONCLUSIONS

There were no significant differences in ACL or MCL strain values between limb sides during *in vitro* simulation testing. This finding indicates that limb dominance does not influence the failure threshold of the ACL, since there was no significant difference in failure strains. As such, it is likely that the mechanical and structural properties of the ACL are comparable between contralateral pairs from the same, healthy specimen. In addition, this study clarifies that observed limb asymmetries *in vivo* are likely more attributable to factors external to the ACL such as neuromuscular control, loading pattern, intra-articular geometry, and lower extremity kinematics.

## REFERENCES

1. Hewett TE, et al. *Am J Sports Med.* **33**, 492-501. 2005.
2. Paterno MV, et al. *Clin J Sport Med.* **17**, 258-62. 2007.
3. Bates NA, et al. *Submitted for Publication.* 2017.
4. Bates NA, et al. *J Biomech.* 2016.

## ACKNOWLEDGMENTS

NIH grant funding R01AR049735, R01AR056259, R01AR055563, T32AR056950, and L30AR070273

**Table 2:** External loads of the trial that caused failure and pathology of specimen failure

Specimen #	Dominant Side		Non-dominant Side	
	Load	Location	Load	Location
<b>1 (F)</b>	100_100_100	Femoral avulsion	100_067_067	Partial tear: PL bundle
<b>2 (F)</b>	033_067_000	Femoral fracture	067_033_000	Partial tear: PL bundle
<b>3 (M)</b>	120_120_120	Femoral avulsion	160_160_160	Mid-substance
<b>4 (M)</b>	220_220_220	Femoral avulsion	120_120_120	MCL failure
<b>5 (F)</b>	100_100_100	Femoral fracture	180_180_180	AM femoral avulsion; PL mid-substance
<b>6 (M)</b>	180_180_180	Partial tear	200_200_200	Femoral avulsion
<b>7 (F)</b>	067_000_033	Femoral avulsion	067_033_000	Femoral avulsion
<b>8 (M)</b>	120_120_120	Femoral avulsion	100_067_067	Femoral avulsion
<b>9 (M)</b>	140_140_140	Femoral avulsion	220_220_220	Femoral avulsion
<b>10 (M)</b>	120_120_120	Femoral avulsion	200_200_200	Femoral avulsion
<b>11 (F)</b>	033_100_067	Femoral avulsion	100_100_067	PL tibial avulsion, AM blowout

Load is indicated as KAM\_ATS\_ITR with varied magnitudes (0%/33%/67%/100%)[3]

# THE INFLUENCE OF FEMUR AND TIBIA ROTATIONS ON PATELLAR TENDON STRESS AND STRAIN: A SENSITIVITY ANALYSIS

Kyung-Mi Park<sup>1</sup>, Tzu-Chieh Liao<sup>1</sup>, Christopher M. Powers<sup>1</sup>, and Joyce H. Keyak<sup>2</sup>

<sup>1</sup>University of Southern California, Los Angeles, CA, USA

<sup>2</sup>University of California, Irvine, CA, USA

Email: powers@usc.edu, web: <http://pt.usc.edu/labs/mbrl/>

## INTRODUCTION

Patellar tendinopathy is a common condition in athletes who perform repetitive jumping and landing movements. The incidence rate of patellar tendinopathy has been reported to be as high as 45% and 30% among elite volleyball and basketball players, respectively [1].

Excessive patellar tendon loading is considered to be the primary cause of patellar tendinopathy [2-3]. It has been proposed that abnormal lower extremity kinematics can contribute to increased patellar tendon loading. In particular, a previous study has reported greater knee internal rotation and hip abduction in persons with patellar tendon abnormality compared to controls [2]. Although altered lower extremity kinematics in the frontal and transverse planes may be a risk factor for patellar tendinopathy, a comprehensive analysis in the context of patellar tendon loading has not been performed.

The purpose of this study was to determine the influence of femur and tibia rotations in the frontal and transverse planes on peak patellar tendon stress and strain using three-dimensional (3D) subject-specific finite element (FE) modeling. We hypothesized that increased rotations of the femur and tibia in the frontal and transverse planes would result in increased peak patellar tendon stress and strain.

## METHODS

A 3D FE model of the knee joint was developed from a healthy female participant (28 years of age). Subject-specific input parameters included 1) patellofemoral joint (PFJ) geometry, 2) weight bearing PFJ kinematics, and 3) quadriceps muscle forces (Fig. 1). Subject-specific PFJ geometry and morphology, weight-bearing PFJ alignment, and

quadriceps muscle morphology were obtained from magnetic resonance (MR) imaging. Lower extremity biomechanics data (kinematics, kinetics, and EMG) were collected during a squatting task (45° of knee flexion).

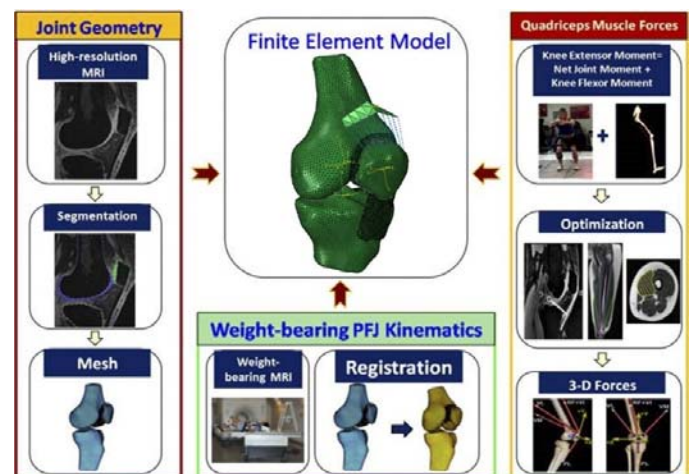


**Figure 1:** 3D subject-specific finite element model framework.

Detailed descriptions of subject-specific inputs for the FE model have been described in previous publications [4-5]. The patellar tendon was modeled as homogeneous elastic and transversely isotropic using tetrahedral continuum elements. Elastic constants for patellar tendon were determined based on the data obtained by Rawson et al [6].

To examine the influence of femur and tibia orientation on patellar tendon stress and strain, the femur and tibia were rotated about their respective axes from the natural weight-bearing position to 10° (2° increments). The process was repeated for the transverse plane (internal and external rotation) and frontal plane (abduction and adduction) (Fig. 2). Quasi-static loading simulations were performed using a nonlinear FE solver in ABAQUS.

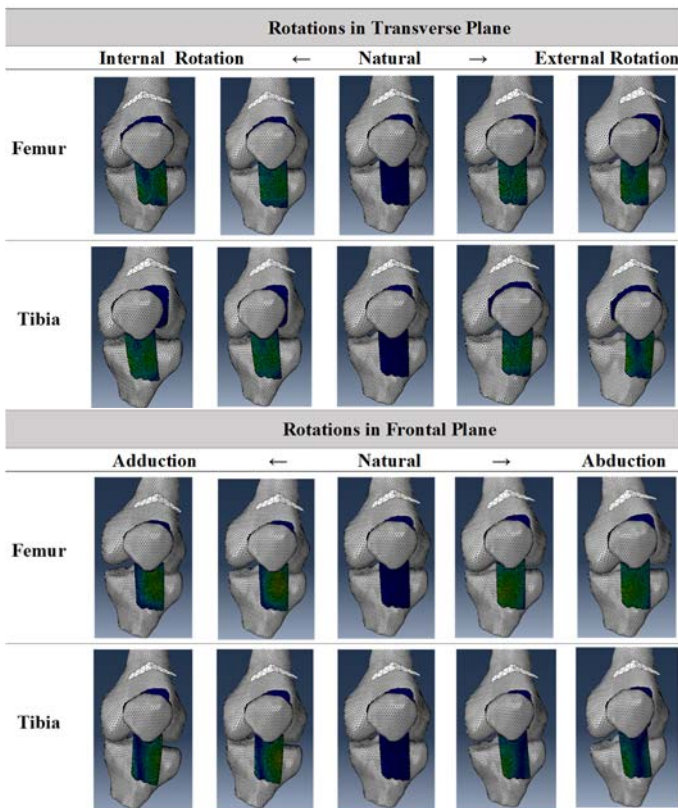


**Figure 2:** Finite element model simulation for femur and tibia rotations in transverse and frontal

Patellar tendon stress and strain were quantified in terms of maximum principal stress and strain, respectively. The peak values of patellar tendon stress and strain were calculated as the mean of the top 5% of elemental stress and strain values, and was used for statistical analysis.

## RESULTS AND DISCUSSION

Both femur and tibia motions demonstrated a linear increase in patellar tendon stress and strain values during both frontal and transverse rotations in either direction (Fig. 3 & 4). In general, transverse plane motions had a greater influence on patellar tendon stress and strain than frontal plane motions. In the frontal plane, tibia rotations had a greater influence on peak patellar tendon stress (Fig. 3a) and strain (Fig. 4a) compared to femur rotations. In the transverse plane, femur and tibia rotations influenced patellar tendon stress (Fig. 3b) and strain similarly (Fig. 4b).

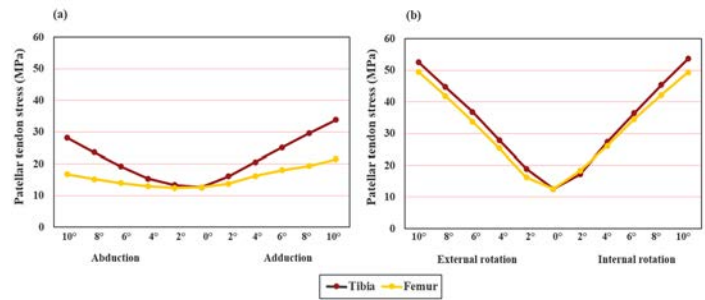


**Figure 3:** Peak patellar tendon principal stress resulting from femur and tibia rotations in frontal (a) and transverse (b) planes.

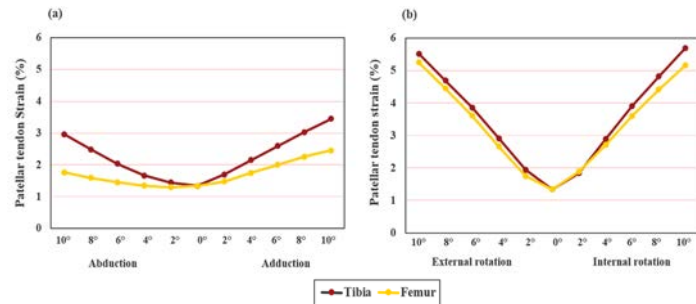


**Figure 4:** Peak patellar tendon principal strain resulting from femur and tibia rotations in frontal (a) and transverse (b) planes.

## CONCLUSIONS

Femur and tibia rotations in frontal and transverse planes result in increased peak patellar tendon stress and strain. In particular, patellar tendon stress and strain appear to be more sensitive to transverse plane motions as opposed to frontal plane motions. The findings of this study suggest that altered lower extremity kinematics in the frontal and transverse planes may contribute to patellar tendinopathy.

## REFERENCES

1. Lian OB, et al. *Am J Sports Med* **33**, 561-567, 2005.
2. Edwards S, et al. *Med Sci Sports Exerc* **42**, 2072-2080, 2010.
3. Janssen I, et al. *Med Sci Sports Exerc* **45**, 927-934, 2013.
4. Farrokhi S, et al. *Osteoarthritis Cartilage* **19**, 287-294, 2011.
5. Liao TC, et al. *Med Sci Sports Exerc* **47**, 1775-1780, 2015.
6. Rawson SD, et al. *Biomech Model Mechanobiol* **14**, 123-133, 2015.

# ANTHROPOMETRIC SCALING OF MUSCULOSKELETAL MODELS

<sup>1</sup> Paulien E. Roos, and <sup>1</sup> Xianlian Zhou\*

<sup>1</sup> CFD Research Corporation, Huntsville, AL, USA

\*email: alex.zhou@cfdr.com, web: <http://www.cfdr.com/>

## INTRODUCTION

There is a need for anthropometrically scaled musculoskeletal (MSK) models in research areas such as ergonomics, medical and military applications. Such scaled models should take into account gender and the shape of the human body and adjust muscle strength accordingly. Here we introduce a method that takes body measurements as input to estimate anthropometry and scale MSK models.

## METHODS

For the development of our scaling method we have gained access to 3D body models of the ANSUR II database [1]. Among a larger survey of military personnel, 4,802 male and 1,986 female were selected and their 3D whole body scans were used to generate digital 3D body shapes. Two sets of data were provided to us (one male and one female), including a mean surface model,  $\pm 3SD$  (standard deviation from the mean surface) principal shapes for selected principal component or Eigen vectors, and variances for each vector, all derived from principal component analysis (PCA) of the 3D body scans. The male dataset includes 34 principal component (PC) vectors, covering about 98% of total variance, and the female dataset 40 PCs covering about 98% of the total variance.

We developed an Anthropometry Model Generating (AMG) GUI software that reads in a mean surface model, PCA variances, and PCs and link them to anthropometry features (or virtual measurements) derived from 3D body shapes [2]. These features include, but are not limited to, height, weight, torso, neck and head width, depth, length and circumference. They are mostly calculated with assistance from body landmarks identified on the 3D body shape. Within the software, the values of

these features can be adjusted and the corresponding body shape will be generated accordingly. Body weight is a special feature calculated as the multiplication of body volume and density, and we chose densities for the male and female ( $1014\text{kg/m}^3$ ;  $973\text{kg/m}^3$ ) such that the mean male and female calculated weights are equal to the measured mean weights exactly. The 3D body model was voxelized and segmented into different body parts, mass and inertia properties of each segment are calculated [2]. In general, voxelized geometry will slightly overestimate the volume. We compensate for this by scaling mass and inertia with a volume ratio between the real volume (calculated based on closed triangular surface) and the voxelized volume.

Joint center locations and axes were calculated using the body (skin) landmarks and the plug-in-gait method with some adjustments. Given an MSK model fitted within skin, its joints and body segments were linked to these calculated locations and axes. Its segment inertia properties were linked to voxelized body segmentations and muscle path is scaled according to segment scaling factors.

To obtain an MSK model with appropriate muscle strength, we first scaled an MSK model to 50<sup>th</sup> percentile male dimensions and tuned muscle maximum isometric force (via optimization) such that the model's moment generating capacity agrees with that reported for 50<sup>th</sup> percentile males in literature. This model is used as a template in the AMG software for scaling with 3D body shape. A template 50<sup>th</sup> percentile female model is created similarly using literature available.

## RESULTS AND DISCUSSION

To demonstrate capabilities of our software, we present the results of male and female neck models derived from the neck model by Vasavada et al. [3].

Four anthropometric models were created based on body height, mass, and neck circumference specifications corresponding to a 5<sup>th</sup> and 95<sup>th</sup> percentile male and female from the ANSUR II database (Table 1; Fig. 1).

**Table 1:** Parameters used for anthropometric models.

	Height (m)	Mass (kg)	Neck circum. (m)
5 <sup>th</sup> M	1.65	64.4	0.40
5 <sup>th</sup> F	1.53	51.3	0.34
50 <sup>th</sup> M	1.76	84.6	0.43
50 <sup>th</sup> F	1.63	66.8	0.37
95 <sup>th</sup> M	1.97	110.7	0.48
95 <sup>th</sup> F	1.74	97.1	0.41

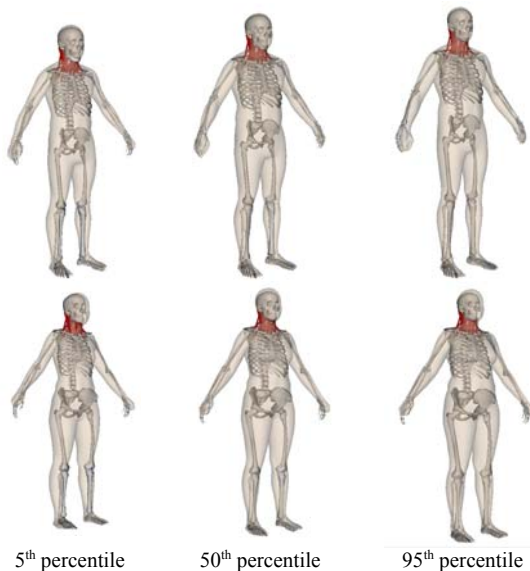


**Figure 1:** Scaled male and female models.

During scaling, muscle maximum isometric force is scaled with mass. Fig. 2 presents moment generating capacity of the scaled male and female models. As expected, the 95<sup>th</sup> percentile model is strongest in all directions and the 5<sup>th</sup> percentile model the weakest. It can be seen that male and female strength has been scaled differently; the 5<sup>th</sup> percentile male has similar extensor strength as the 50<sup>th</sup> percentile female, but is stronger in flexion, lateral bending and axial rotation, for which it is more similar to the 95<sup>th</sup> percentile female. This is because the 50<sup>th</sup> percentile male model was tuned to male strength data and the female model to female strength data.

In conclusion, we successfully created a GUI based software to scale MSK models based on anthropometry and gender that only requires simple body measurements as input. The software also provides tools to further optimize the strength of generated anthropometric MSK models. Similar approach was also utilized to generate lumbar and shoulder MSK anthropometric models.

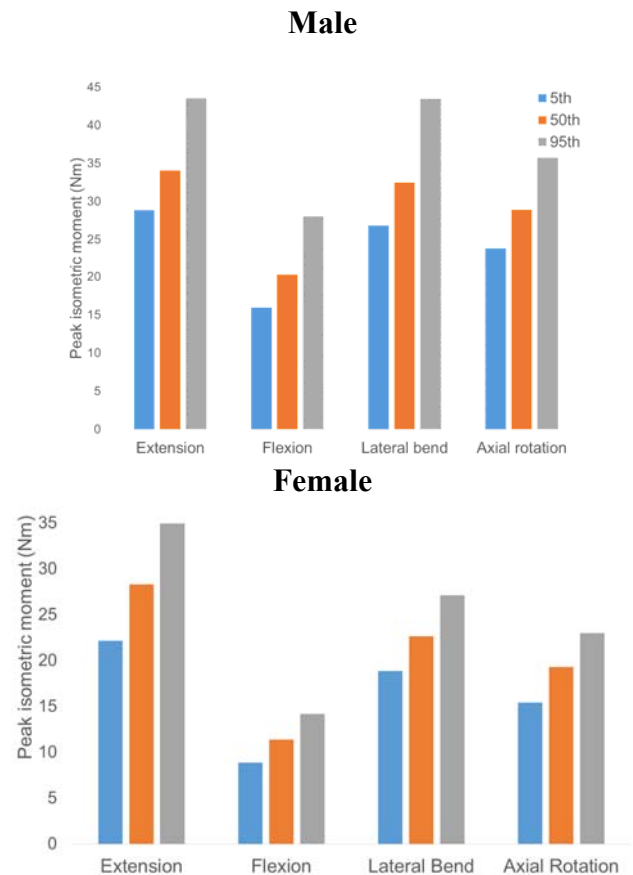


**Figure 2:** Comparison of the maximum isometric neck strength of the three generated male (top) and female (bottom) models.

## REFERENCES

1. Gordon CC, et al., Natick TR-15/007, 2012.
2. Zhou X., et al., *Anthropometry Model Generation Based on ANSUR II Database*, *Int J Digital Human*, in press.
3. Vasavada AN, et al., *Spine*, **23(4)**, 1998.

## ACKNOWLEDGMENTS

Drs. Vasavada for so generously sharing her neck model.

# AUTOMATION OF VOLUMETRIC MESH GENERATION, MESH ASSEMBLY AND MODEL INPUT FROM SURFACE REPRESENTATIONS OF TISSUE STRUCTURES

Ben Landis, Ahmet Erdemir, PhD

Computational Biomodeling (CoBi) Core and Department of Biomedical Engineering, Lerner Research Institute, Cleveland Clinic, Cleveland, OH, USA

email: [landisb@ccf.org](mailto:landisb@ccf.org) website: <https://simtk.org/projects/openknee>

## INTRODUCTION

Finite element analysis has become an increasingly routine and essential component of biomechanics research [1]. However the development of quality virtual representations for finite element analysis is a laborious task, even after image segmentation is completed and surface representations of tissue structures are available. The volumes of geometries need be individually meshed. Then the user interactively selects mesh regions, specifically node, element and surface sets, to facilitate defining the model. Finally meshes of different tissues are combined and the mesh sets are utilized to define constraints and interactions between tissue components and to apply the appropriate boundary conditions. The resultant model then needs to be stored in a markup compatible with the simulation software of preference, e.g. Abaqus (Simulia, Johnston, RI) and FEBio [2], common solvers in biomechanics [3]. The goal of this study is automate all these processes in order to provide an unsupervised workflow for volumetric mesh generation, mesh assembly and model input file generation starting with surface representations of tissue structures.

## METHODS

A Python script was designed, using free and open source Salome [4], to streamline the process of meshing and model assembly through automation. An input XML document contains the hierarchy of the anatomy of interest, that is the tissue components, pointer to tissue surface geometry, and connectivity and interactions, e.g., ties and contacts (Figure 1). The hierarchical structure of this format is general and flexible enough to be applicable to a wide variety of biomedical areas. Upon execution of

the script, the surfaces are loaded and Salome generates volumetric finite element meshes. In following, groups of nodes, faces and elements are automatically defined based on connectivity description provided in the XML document, the characteristic length of the input geometry segments, and the inter-part proximity, e.g. euclidean norm between nodal positions of different tissues. Thresholds for proximity can be adjusted by the user by setting a multiplier. The script provides a warning to the user should they introduce non-reciprocated conditions for contact and ties.

```
<Tibia multiplier = "0.9">
  <file> oks001_MRC_TBB_LVTIT_10.stl</file>
  <material> rigid </material>
  <Contact>
    <MCL multiplier = "0.7"/>
    <PatellarLigament/>
  </Contact>
  <Tie>
    <MCL multiplier = "0.5"/>
    <ACL/>
    <PCL/>
    <PatellarLigament/>
    <MedialMeniscus/>
    <LateralMeniscus/>
    <TibialMedialCartilage/>
    <TibialLateralCartilage/>
    <Fibula multiplier = "1.5"/>
  </Tie>
</Tibia>
```

**Figure 1:** An sample connectivity file for the tibia. The proximity calculation can be adjusted by the multiplier parameter.

The script then creates assemblies of the these parts, specifying ties and contacts in the specific language of the simulation software packages. The currently available options these include specific formatting for Abaqus (Simulia, Johnston, RI),

Febio[2], and the SOFA Framework [5], and could be extended to other formats with only moderate effort.

The script was tested on a set of geometries from the Open Knee(s) [6]. Various models were assembled for the knee, incrementally increasing the fidelity of the simulation by adding/removing parts to the assembly such as the menisci. To test of changing the geometric parts of the assembly, simplified models of the knee (femur-anterior cruciate ligament-tibia) were generated with coarse and fine meshes.

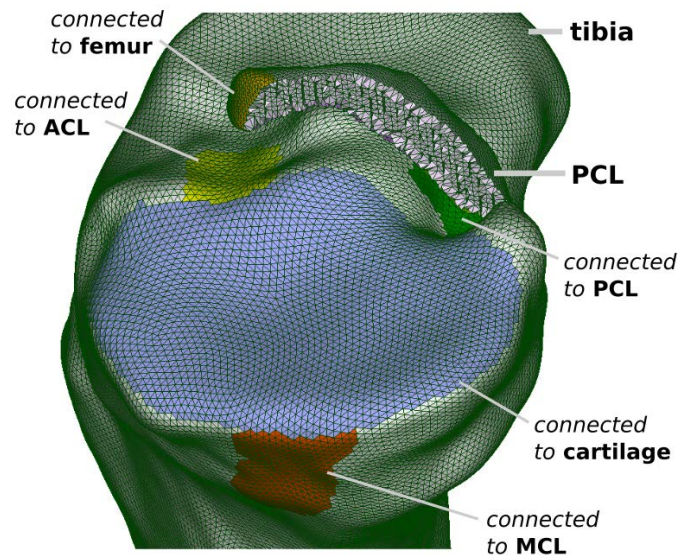


**Figure 2:** A completed mesh of the tibia, showing the color identified locations of the ligaments and cartilage groups that were automatically created to utilize for connectivity constraints.

## RESULTS AND DISCUSSION

Figure 2 shows the sets created on the tibia when using the ligaments, cartilage and bones as input to connectivity file. The automated assembly makes studies of mesh refinement easily accomplished by replacing the pointers to the files associated with each part and re-running the script (Figure 3). This same feature can also be used for swapping healthy tissue representation with a diseased or artificial part, with the limitation that both parts geometries need to have been defined in the same coordinate system. Additionally the generation of model input for different solvers can facilitate simulations in a alternative software packages to compare or confirm results.

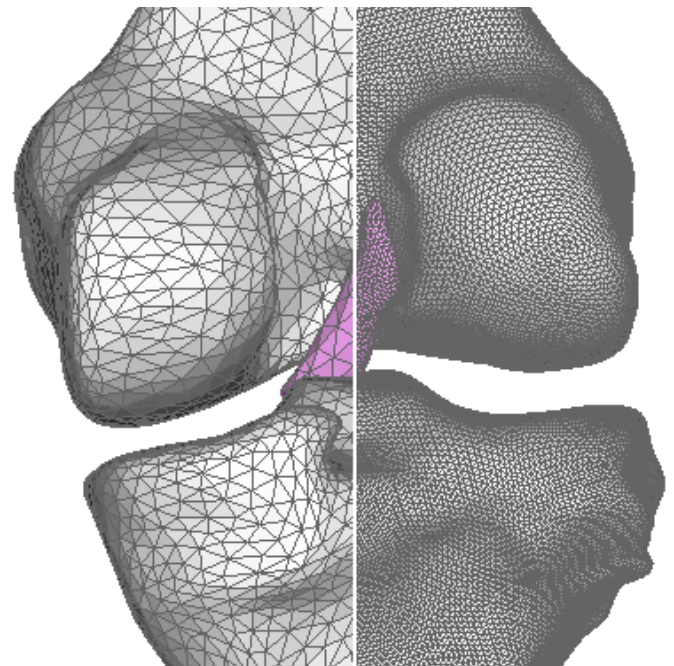


**Figure 3:** The automated model assembly allows for rapid mesh refinement studies by providing the means to quickly replace geometry. Healthy representations of the tissue can be interchanged easily with diseased or artificial parts.

## CONCLUSIONS

This paper presented an automated workflow for combining tissue parts for finite element analysis and feeding the outcome to model input formats of simulation software packages. This high throughput approach removes the model assembly bottleneck of finite element analysis.

## REFERENCES

1. Erdemir, A. et al., *J Biomech*, 45, 625-33, 2012.
2. FEBio. <https://febio.org/>.
3. Meng, Q. et al., *Proc Inst Mech Eng H*, 227, 1009-19, 2013.
4. Salome. <http://www.salome-platform.org>.
5. SOFA Framework. <https://www.sofa-framework.org/>.
6. Open Knee(s). <https://simtk.org/projects/openknee>.

## ACKNOWLEDGMENTS

This study has been supported by NIGMS, NIH (R01GM104139) and USAMRMC (W81XWH-15-1-0232).

# A THREE-DIMENSIONAL MESH WRAPPING MODEL OF THE GLUTEUS MAXIMUS

<sup>1</sup>Andrew D. Vigotsky and <sup>2</sup>Andrew P. Kraszewski

<sup>1</sup>Department of Biomedical Engineering, Northwestern University, Evanston, IL

<sup>2</sup>Leon Root, M.D. Motion Analysis Laboratory, Hospital for Special Surgery, New York, NY  
email: avigotsky@gmail.com

## INTRODUCTION

The use of commercial and open-source interactive musculoskeletal modeling software has allowed for greater understanding into the function muscles play in locomotion; for example, the role of the gluteus maximus. Early and current models make simplified assumptions, such as utilizing single line segments from origin to insertion or line-independent wrapping techniques. In 2005, Blemker, et al. [1] developed a highly sophisticated finite-element model of the gluteus maximus [2, 3]. It is considered a gold-standard by the authors.

Although Blemker & Delp's model has demonstrated accuracy, it requires substantial resources and computational energy to create. In addition, it is not compatible with any musculoskeletal modeling programs, such as OpenSim. Therefore, there is a need for an intermediate model, wherein not only are its moment arm (MA) estimates accurate, but it can also be used clinically, in programs like OpenSim.

The objectives of this work were to: 1) describe our mesh wrapping approach to modeling the gluteus maximus muscle and 2) compare hip extension MA to the wrapping model in OpenSim [2], and a reference model [1] over a 90° range of hip flexion.

## METHODS

Our approach introduces muscle fiber lines of action connected both longitudinally and transversely, effectively creating a 2D rectangular grid or mesh of 1D line elements (Figure 1). The origin and insertion points of the gluteus maximus were taken from Arnold, et al. [2] and were linearly interpolated to five longitudinal lines of action rather than three. Five transverse lines were used between origin and insertion. Also, a wrapping sphere, unlike an ellipsoid in Arnold's model, was used. In addition, a

sacrospinous ligament was modeled to help anchor the gluteus maximus.

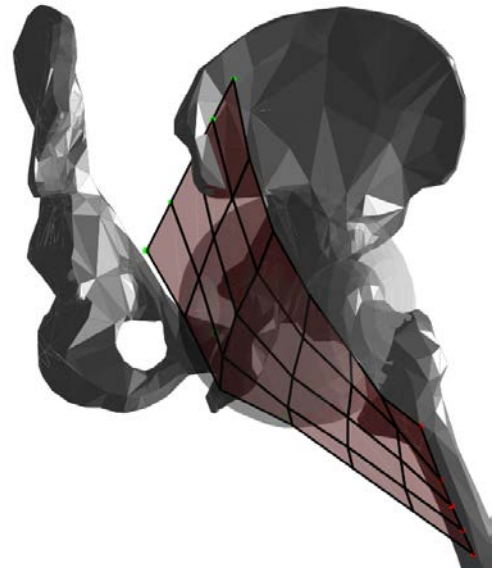


**Figure 1.** 3D surface plot of the gluteus maximus mesh model (red). Black lines are longitudinal and transverse elements. Wrapping object is the semi-transparent sphere.

Each element was modeled as a linear elastic spring with a stiffness and slack length. Two stiffness values were used:  $k_{\text{long}} = 3 \times 10^6 \text{ N} \cdot \text{m}^{-1}$  and  $k_{\text{trans}} = k_{\text{lig}} = 4 \times 10^6 \text{ N} \cdot \text{m}^{-1}$ . Slack lengths were calculated as 75% of the average muscle length over a 0° to 30° flexion range, using the stiffness parameters only. The mesh node coordinates were calculated by minimizing mesh elastic energy and constrained so as not to penetrate the sphere. The mesh was solved from 0° to 90° hip flexion in 2° increments. All calculations were performed in MATLAB.

Muscle length versus flexion angle were extracted and a cubic regression was fit to each line,  $\ell_i(\theta)$ . Instantaneous MA lengths were calculated analytically [5]:

$$MA_i(\theta) = \frac{d\ell_i}{d\theta}$$

MAs from Arnold, et al. [2] were exported from OpenSim. In addition, MA ranges reported by Blemker, et al. [1] were obtained using cubic regressions of the reported values. The MA results of Blemker & Delp's finite-element model were presumed to be the most accurate and used as reference [1]. Average root mean square errors (RMSE) were calculated for Arnold's model and our mesh model against Blemker's data for the entire hip flexion range.

## RESULTS AND DISCUSSION

The mesh muscle length cubic regression fits were excellent, where for any line,  $R_i^2 > 0.999$ . The MA results of our model, compared with those of Blemker, et al. [1] and Arnold, et al. [2], can be seen in Figure 2. The total RMSE for our model and Arnold's model relative to Blemker's model can be found in Table 1.

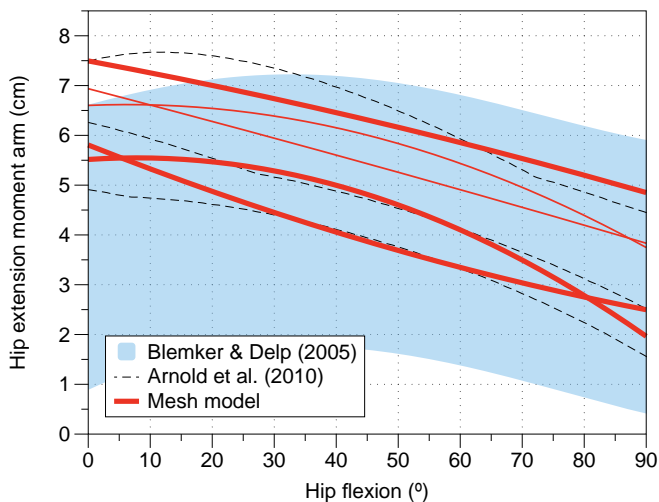


**Figure 2.** Hip extension moment arms of the gluteus maximus of the mesh model compared to the current OpenSim model [2] and Blemker, et al. [1]'s finite-element model. Bold red lines correspond to Arnold's original three lines of actions.

Based on RMSE values, the interdependent line wrapping model is superior to the independent line wrapping algorithms currently utilized by a standard OpenSim model. As computational power of standard workstations increases, so does the ability to utilize more accurate, higher resolution models. Although finite-element models are still out of reach for routine subject-specific and dynamic modeling,

the mesh wrapping approach may be an appropriate stepping-stone for muscles with complex geometries, such as the gluteus maximus.

	RMSE (cm)	$\Delta$
<b>Arnold et al. (2010)</b>	0.211	
<b>Mesh model (3 lines)</b>	0.129	-38.83%
<b>Mesh model (5 lines)</b>	0.103	-51.47%

**Table 1.** RMSE relative to Blemker's model. Mesh model (3 lines) refers to the original three lines utilized by Arnold's model.  $\Delta$  represents change relative to Arnold's RMSE.

## CONCLUSIONS

We have presented a new mesh model for use in musculoskeletal modeling. This gluteus maximus model has decreased the MA error found in a standard OpenSim model by ~40–50% throughout hip flexion. There remains room for improvement and further verification and validation in other planes of motion. The mesh model requires less computational power and resources than finite-element models. By further parameterizing and optimizing our model, it may prove to be an accurate alternative to standard independent line-wrapping models. Future work will explore their utility in dynamic simulations.

## REFERENCES

1. Blemker, et al., *Ann. Biomed. Eng.* **33(5)**, 661-73, 2005.
2. Arnold, et al., *Ann. Biomed. Eng.* **38(2)**, 269-79, 2010.
3. Delp, et al., *IEEE Trans. Biomed. Eng.* **37(8)**, 757-67, 1990.
4. Modenese, et al., *J. Biomech.* **44(12)**, 2185-93, 2011.
5. An, et al., *J. Biomech. Eng.* **106(3)**, 280-2, 1984.

# VALIDATING SUBJECT-SPECIFIC MUSCLE ARCHITECTURE DATA FOR MUSCULOSKELETAL MODELS USING DIFFUSION TENSOR MRI

<sup>1</sup> James P Charles, <sup>2</sup> Chan Hong Moon and <sup>1</sup> William Anderst

<sup>1</sup> Biodynamics Lab, Department of Orthopaedic Surgery, University of Pittsburgh, PA, USA.

<sup>2</sup> Magnetic Resonance Research Center, Department of Radiology, University of Pittsburgh, PA, USA.  
email: JPC110@pitt.edu, web: www.bdl.pitt.edu

## INTRODUCTION

Musculoskeletal models and simulations have become a valuable platform on which it is possible to investigate the intricacies of human movement in great detail. Recent studies have shown that incorporating subject specific data into these models, rather than the traditional method of scaling a generic model [1], may greatly affect their output [2]. This level of specificity in musculoskeletal models potentially increases their utility for various research or clinical tasks, such as tailoring rehabilitation from musculoskeletal injuries or simulating orthopaedic surgical procedures. However, for a model to be considered truly subject specific, it should include the muscle architecture (muscle force generating properties) data of the subject upon which the model is based. Recent studies have shown that diffusion tensor magnetic resonance imaging (DTI) can be used to reconstruct muscle fiber trajectories in skeletal muscle [3], which, when combined with other anatomical MRI sequences (i.e. T1), allows muscle architectural characteristics such as mass, fiber lengths and pennation angles to be gathered from live subjects non-destructively. As yet there is no standardized method of tracking muscle fibers, and furthermore there has been no comprehensive validation of the precision with which this method can reconstruct muscle fibers and estimate muscle force generating properties for use in musculoskeletal models.

Here we aim to perform a novel validation of the DTI technique to measure muscle architecture data, by directly comparing MRI-based data to those gathered from dissections of human cadaveric lower limbs. Once rigorously validated, the ability to gather muscle architecture data from live human subjects has the potential to greatly improve the accuracy of

musculoskeletal models by making them truly subject-specific.

## METHODS

MR images of one cadaveric right lower limb (hemipelvectomy, Female, 22 y/o) were acquired (3T Siemens Biograph mMR) using T1 turbo spin echo (TSE; voxel size  $0.47 \times 0.47 \times 6.5 \text{mm}^3$ , repetition time [TR] 650ms, echo time [TE] 23ms) and diffusion weighted echo planar sequences (voxel size  $2.96 \times 2.96 \times 6.5 \text{mm}^3$ , TR/TE 7900/65ms, 12 direction diffusion gradients, b value- 0 &  $400 \text{s/mm}^2$ , spectral attenuated inversion recovery). The images were acquired in axial slice orientation and repeated for a total five beds, in order to image from the iliac crest to the ankle joint. The fibers of 21 muscles of the lower limb were tracked with the DTI images using Camino software (Fig. 1) [4]. A custom Matlab script was used to estimate the length of each fiber, and pennation angle was measured using ImageJ (U.S. National Institutes of Health, Bethesda, MD, USA). Muscle masses were calculated from the volume of 3D muscle meshes created through digital segmentation of T1 anatomical images. All these architecture data were used to calculate physiological cross sectional area (PCSA,  $\text{mm}^2$ ), a major determinant of muscle force generation, using the equation:

$$\text{PCSA} = (M_m * \cos\theta) / (L_f * \rho),$$

where  $M_m$  is muscle (belly) mass (g),  $L_f$  is muscle fiber length (mm),  $\theta$  is muscle fiber pennation angle and  $\rho$  is the density of mammalian skeletal muscle ( $0.001056 \text{gmm}^{-3}$ ).

These data were then manually measured from the same 21 muscles from the same cadaver through dissections. Here, each muscle was dissected out and cleaned of fat and fascia before measurement.



**Figure 1.** The fibers of the Vastus medialis (A) and Tibialis anterior (B) muscles, tracked from diffusion tensor magnetic resonance images (DTI) and Camino software.

Muscle mass was measured using a digital scale (accurate to 1g), and fiber lengths were measured using 12" precision dial calipers (accurate to 1mm). Photographs were taken of each muscle, and fiber pennation angle was measured from these using ImageJ. For fiber length and pennation angles, five measurements were taken at different areas of each muscle, and the mean value calculated.

## RESULTS

Across the 21 muscles analyzed, mean fiber lengths measured using DTI were on average 7.96mm longer than those measured using dissections (5.8% of mean fiber length from dissections; Fig. 2). However, both mass and PCSA were estimated by MRI to be lower than when measured through dissections, with differences of 15g (7.9% of mean mass) and 225mm<sup>2</sup> (14.86% of mean PCSA) respectively. Measured pennation angles were more variable, with a mean difference of 3.78° (28.4% of mean value) found.

## DISCUSSION

The muscle architecture data measured from both MR images and manual dissections match well in terms of muscle mass, fiber lengths and PCSA across most of the muscles analyzed here. The tendency for the DTI fiber tracking to slightly over-estimate fiber lengths, and for the T1 anatomical segmentation to slightly underestimate muscle mass, compound to underestimate PCSA, and by extension muscle force output.

Fiber pennation angle was the most variable measurement between the MRI and dissection

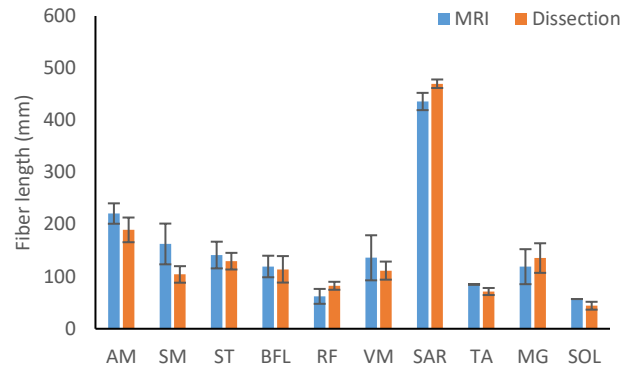


**Figure 2.** Select mean muscle fiber lengths, as estimated from diffusion tensor magnetic resonance images (DTI) and measured from dissections. Error bars= ±1S.D.

measurements. However, this factor is heavily influenced by the level of stretch in the muscle, although fortunately musculoskeletal model sensitivity analyses have shown that pennation angle has little effect on muscle output [5].

## CONCLUSIONS

Overall, based on novel validation from one cadaveric limb, we can be tentatively confident that the method of using diffusion tensor and T1 anatomical MRI to gather muscle architecture data from live subjects is a promising technique to improve the accuracy of subject specific musculoskeletal models and simulations of human movement. To bolster this confidence, we plan to use these methods to gather these same data from additional cadaver specimens, to further investigate the accuracy of this technique in representing muscle architecture.

## REFERENCES

1. Arnold EM, et al. *Ann Biomed Eng.* **38**, 269-279. 2010.
2. Prinold, JAI, et al. *Ann Biomed Eng.* **44**, 247-257. 2016
3. Damon BM, et al. *NMR Biomed.* DOI: 10.1002/nbm.3563. 2016.
4. Cook PA, et al. *14th Scientific Meeting of the International Society for Magnetic Resonance in Medicine, Seattle, WA, USA.* 2759. 2006.
5. Charles JP, et al. *J. Anat.* **229**, 514-535. 2016.

# REDUCING PASSIVE MUSCLE FORCE: A PROCESS FOR PATIENT SPECIFIC MUSCLE MODEL PARAMETER CALIBRATION IN RTSA PATIENTS

<sup>1</sup> Kayla M. Pariser, <sup>2</sup> David R. Walker, <sup>1</sup> Allison L. Kinney

<sup>1</sup> University of Dayton, Dayton, OH, USA

<sup>2</sup> Rehoboth Innovations, LLC., Miami, FL, USA

email: pariserk1@udayton.edu

## INTRODUCTION

A reverse total shoulder arthroplasty (RTSA) is a common treatment used to stabilize the shoulder and improve range of motion in patients with rotator cuff muscle tears or severe arthritis. The RTSA implant is designed to enable the deltoid muscle to become the primary stabilizer thereby increasing the stability of the joint [1]. To improve stability, RTSAs increase the deltoid muscle moment arm and decrease the required deltoid force to achieve the required torque about the glenohumeral joint for shoulder movement. Previous research suggests that a more medial and inferior placement of the center of rotation for the RTSA implant is ideal, however, implant placement is complex given the multiple degrees of freedom of the shoulder joint [2]. In addition, there is no standardized, objective way for a surgeon to position an implant on a specific patient.

Simulation and optimization methods have been used to understand moment arms and their effect on muscle function, to predict muscle forces, and to analyze how surgeries affect the muscle moment arms with general models [3]. However, the effect of patient-specific muscle parameters on modeling realistic muscle function in this population is unknown. Calibration of patient-specific parameters via optimization is feasible, but can be time consuming. Due to the fast workplace environment, surgeons cannot afford to wait a long time for optimizations to converge. In order to decrease convergence time and apply these tools clinically, muscle parameter optimizations must be provided a realistic initial guess that is representative of the patient's muscle function. To our knowledge, previous studies have not established guidelines for adjusting muscle parameter values from literature, especially across a group of subjects. Reduction of

passive force produced by muscles may be a mechanism for adjusting parameters values. Therefore, the purpose of this study is to investigate how much deviation from the literature muscle parameter values is necessary in order to reduce passive force and produce more realistic muscle activations for patient-specific cases.

## METHODS

Eight subjects with two different RTSA implants participated in this study (age:  $73 \pm 6$  years, height:  $65.63 \pm 2.85$  in, mass:  $77.28 \pm 9.62$  kg). EMG, motion capture, and fluoroscopic data were collected previously [4-5]. Fluoroscopic and motion capture data defined the motion in patient-specific shoulder models scaled using the subjects' heights. Muscle moment arms, joint moments, and musculotendon lengths were calculated in OpenSim [6].

The optimal fiber length and tendon slack length values of the three deltoid muscles were modified from the literature values [7] using scaling factors. Scaling factors were chosen manually with the goal of determining common factors for each deltoid muscle across all of the subjects so that the muscle tendon length (IMtilda) values were within the active force range, 0.5-1.0, on the force length curve.

MATLAB was used to generate plots of the IMtilda values, predicted muscle activation as compared to the experimental EMG data, and force contribution from each of the three deltoid muscles before and after the literature parameter values were modified.

## RESULTS AND DISCUSSION

For all eight subjects, reduction of passive force produced more realistic muscle forces and

activations. Common scaling factors were found for the medial (DELTA2) and posterior (DELTA3) deltoids, but not for the anterior (DELTA1) deltoid. The DELTA1 scaling factor for six of the eight subjects was 1.5, but was 1.79 and 2.22 for the other two subjects. DELTA2 and DELTA3 had scaling factors of 1.13 and 1.25 respectively. The ranges for the average IMtilda values across all eight subjects for each of the deltoid muscles prior to adjusting the parameters were: DELTA1: 1.4-3.05, DELTA2: 0.85-1.05, and DELTA3: 0.84-1.08. After adjusting the parameters, the IMtilda ranges were: DELTA1: 0.7-0.91, DELTA2: 0.625-0.82, DELTA3 0.675-0.84. Some of the subjects had IMtilda values for one or more deltoids within the desired range prior to adjustment, but others, as depicted by the ranges, produced large passive forces. There was an inconsistency amongst the subjects as to which deltoid required the most parameter adjustment, thus emphasizing the importance of patient-specific muscle parameter adjustment.

Using the literature parameter values, many subjects displayed a trend in which the muscle activation was minimal, but the predicted muscle force was very high. Once the parameters were adjusted, however, the muscle activation and force contribution became more realistic for all three deltoid muscles for all eight subjects. For example, Figure 1 shows the influence of adjusted parameter values for a representative subject's DELTA1 muscle. With the literature values, DELTA1 produced purely passive force during the motion, requiring no activation from the muscle. By adjusting the parameters to reduce passive force production, the muscle activation and force are more realistic. In addition, the resulting muscle activation mimics the trend observed in the experimental EMG data.

## CONCLUSIONS

RTSA patients have varying height, weight, and muscle function. Therefore, it is important that RTSA implants be placed in patient-specific locations to have optimal deltoid muscle function after surgery. To determine patient-specific implant placement, patient-specific models are needed. It is not adequate to scale the models in terms of the subjects' heights only. This study illustrates the need

for adjustment to the commonly used literature muscle parameter values to generate patient-specific models that more accurately reflect a patient's muscle activation and muscle force contribution. Reduction of passive force appears to be a feasible process to adjust muscle model parameter values and improve patient-specific calibration of models. Future work should focus on automating the calibration process and continuing to test passive force reduction as mechanism for producing realistic results in a larger patient population.

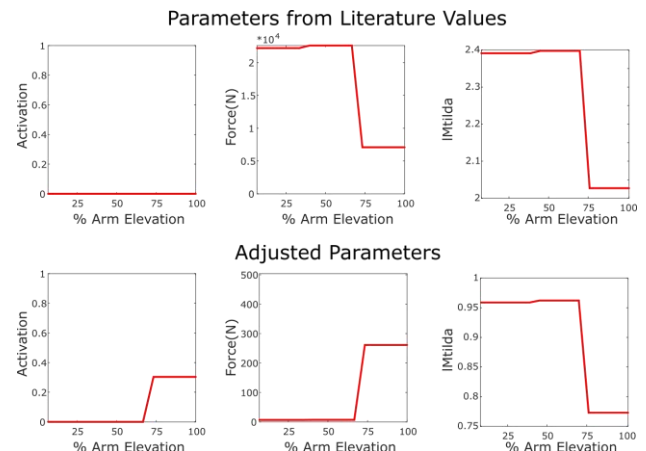


**Figure 1.** DELTA1 activation, force, and IMtilda for literature and adjusted muscle parameters for a representative subject.

## REFERENCES

1. Ackland DC, et al. *J Anat.* **213**, 383-390, 2008.
2. Hoenecke H., et al. *J Shoulder Elbow Surg.* **23**, 1128-1135, 2014.
3. Pandy M.G., et al. *Annu Rev Biomed Eng.* **12**, 401-433, 2010.
4. Walker D., et al. *J Shoulder Elbow Surg.* **24**, 1129-1134, 2015.
5. Walker D., et al. *J Shoulder Elbow Surg.* **23**, 166-172, 2014.
6. Delp, S., et al. *IEEE Trans Biomed Eng.* **54**, 1940-1950, 2007.
7. Saul K., et al *Comput Methods Biomech Biomed Engin.* **5842**, 1-14, 2014.

## ACKNOWLEDGMENTS

Funding for this project was provided by the Berry Family Foundation and the University of Dayton University Honors Program.

# KNEE CONTACT FORCE PREDICTIONS ALTERED BY OBJECTIVE FUNCTIONS DURING OPTIMIZATION

<sup>1</sup> Elijah C. Kuska and <sup>1</sup> Allison L. Kinney

<sup>1</sup> University of Dayton, Dayton, OH, USA  
email: kuskae1@udayton.edu

## INTRODUCTION

Persons with musculoskeletal disorders may have mobility limitations. The level of impairment experienced is patient-specific. Because of this, the rehabilitation the individual needs should also be unique. However, current rehabilitation techniques are generalized for the many rather than the few. The knowledge of patient-specific muscle forces may help to create individual rehabilitation techniques.

Muscle forces must be computationally predicted because they are difficult to measure experimentally. In order to predict these forces, optimization is needed because the musculoskeletal system is under-constrained (# muscles >> # degrees of freedom). Optimizations are reliant on objective functions to converge to a unique solution. Previous studies have examined objective functions and their influence on muscle force predictions [1]. Validation of these predictions are limited because of the *in vivo* nature of muscle forces. Validation may be improved by the use of *in vivo* knee contact force data [2]. The purpose of this study was to investigate how knee contact force predictions are altered by objective function choice during optimizations of self-selected speed and modified walking gait.

## METHODS

Optimizations of 8 different complete walking gait cycles (5 self-selected speed, 3 modified) were generated using data from the 3<sup>rd</sup> Grand Challenge Competition to Predict In Vivo Knee Contact Loads. Data were collected from a single female subject with a force measuring knee implant (left knee, age 68 years, mass 79 kg, height 1.3 m) [2]. Data used in this study includes left leg CT images, motion capture data, ground reaction force data, and *in vivo* knee contact data (forces and torques along all three

axes). The knee contact data were gathered from the subject's force measuring knee implant.

A full leg model containing the patient's bones and implant components was created in OpenSim [3] from the CT images. Muscle geometry and parameters were obtained from a generic model for the 44 Hill-type muscles [4]. Joint kinematics and joint torques were calculated in OpenSim. All optimizations incorporated inverse skeletal dynamics and forward activation and contraction dynamics.

Optimizations were conducted in MATLAB using software designed for direct collocation optimal control: GPOPS-II [5] and ADiGator [6]. All optimizations were performed with constraints such that the sum of the muscle force contributions to the inverse dynamics torques matched the experimental inverse dynamics torques. Muscle forces were optimized while minimizing objective functions over the simulation time  $T$  with the generic form:

$$J = \int_0^T \sum_{i=1}^m u_i^p dt$$

where  $u$  represents the category of muscular effort (excitation, activation, force, or stress) for the number of muscles  $m$  and  $p$  represents the exponent (1, 2, 3, or 4). This resulted in a total of 16 objective functions to be run for each of the 8 gait cycles. Optimizations were performed on a 3.3 GHz Intel Xeon processor with 16 GB RAM. Convergence time and experimental data replication accuracy were analyzed across all optimizations for all gait cycles.

## RESULTS AND DISCUSSION

For all gait cycles, all 16 objective functions matched the inverse dynamic data and converged. Thus, they can be deemed valid and feasible. All of the objective functions averaged a convergence time of less than 8

minutes across all gait cycles. The fastest converging category of muscular effort was activation and the fastest converging power was the 2<sup>nd</sup>. Excitation to the second was the fastest converging objective function (1.49 minutes).

All 16 objective functions had relatively accurate total knee contact force replication. The best replicating category of muscular effort was activation and the best power was the 3<sup>rd</sup>. Stress to the third was the best replicating overall with an average (across all gait cycles) R<sup>2</sup> value of 0.860. This value surpasses previous studies that predicted knee contact forces [7].

Muscular force predictions across all objective functions per trial were similar and some trends were noticed. The first trend noticed was between categories of muscle effort during the self-selected walking trials. Non-force containing objective functions (excitation/activation) favored bi-articular muscles while force containing objective functions (force/stress) favored muscle with larger maximum isometric forces and cross-sectional areas (Figure 1). The trend was similar but not exact during the modified gait trials. During the modified gait trials the force and stress objective functions still favored the larger and more powerful muscles, but the excitation and activation objective functions did not favor the bi-articular muscles as much. This differences between the self-selected gait trials and the modified gait trials may reflect altered muscle control when performing a more demanding task.

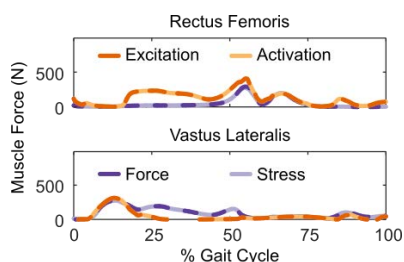


**Figure 1.** Optimized muscle forces from objective functions across categories of muscular effort.

Another trend that occurred was based on the power the objective function was raised to: higher powers favored more shared muscular effort. This meant that as the exponents increased the predictions became more fatigue-like [1]. In addition, as the objective function's power increased, they better predicted the

*in vivo* knee contact data. This may indicate that as the objective functions became more fatigue-like they better represent muscle coordination strategies used by humans.

## CONCLUSIONS

Results of this study provide insight into the muscle coordination strategies used by humans during self-selected and modified walking gaits. Continuation of this study will need to look at other subjects and other non-walking motions. This would assist with determining if our methods are patient or walking-gait specific. If proven, this could create a quantitative tool to assess movement impairments in individuals and allow clinicians to design effective patient specific rehabilitation techniques.

For future use, a best objective function needs to be identified. Though time efficiency is important for clinicians, we believe that differences in time between functions is not considerable enough to justify using excitation squared. We believe the objective function that best replicates the data should be used: stress cubed. The stress cubed objective function should be used in clinical applications to create effective rehabilitation techniques.

## REFERENCES

1. Ackermann, M, et al. *J Biomech* **43**, 1055–1060, 2010.
2. Fregly, BJ, et al. *J Orthop Res* **30**, 503–513, 2012.
3. Delp, SL, et al. *IEEE Trans Biomed Eng* **54**, 1940–1950, 2007.
4. Arnold, EM, et al. *Ann Biomed Eng* **38**, 269–279, 2010.
5. Patterson, MA, et al. *ACM Trans Math Softw* **41**, 1–37, 2014.
6. Patterson, MA, et al. *ACM Trans Math Softw* **39**, 1–17, 2013.
7. Kinney, AL, et al. *J Biomech Eng* **135**, 021012, 2013.

## ACKNOWLEDGEMENTS

Funding for this study was provided by the University of Dayton Research Council Seed Grant, Honors Program, and SURE Program.

# UPPER EXTREMITY MODEL SENSITIVITY TO LIGAMENT ATTACHMENT POINTS

Clarissa LeVasseur, Molly Meyer, Michelle B. Sabick

Department of Biomedical Engineering, Saint Louis University, St. Louis, MO  
email: sabickmb@slu.edu, web: <http://parks.slu.edu/departments/bme/>

## INTRODUCTION

Due to the complexity and lack of bony stability in the shoulder, 1.7% of the population will suffer from shoulder instability [1]. Multiple factors including the individual shoulder geometry, weakness in the rotator cuff muscles, subluxed glenohumeral ligaments, or a reduced intrarticular pressure can lead to instability. Upper extremity musculoskeletal models would provide an excellent tool for examining the individual contributions of these factors to instability, but most existing musculoskeletal models only allow three rotational degrees of freedom (DOF) of the glenohumeral joint [2]. Therefore, realistic six DOF glenohumeral kinematics cannot be studied.

Updating computational shoulder models to include translational degrees of freedom requires including realistic ligament models to provide joint stability, especially in the extreme ranges of motion. However, modeling ligaments requires making informed decisions regarding appropriate material properties and attachment point locations that make sense anatomically and provide convergent solutions in simulations. Understanding how sensitive the model is to these parameters helps guide appropriate choices and assess the robustness of model predictions. The purpose of this study is to quantitatively analyze the sensitivity of an existing upper extremity model to changes in locations of the origin and insertion of two simulated ligaments.

## METHODS

The open-sourced Open-Sim (version 3.3, Stanford University, Stanford, CA USA) model, MoBL\_ARMS [2], was updated to include three translational DOF at the shoulder in addition to the rotational DOF. Ligament representations of the coracohumeral ligament (CHL), superior

glenohumeral ligament (SGHL), and the middle and inferior glenohumeral ligaments and the posterior capsule were modeled as nonlinear elastic bands with attachment points at their anatomical locations as described in Boulet et. al. [3]

The CHL and SGHL were then disabled one at a time while the other ligament attachment points were adjusted in 1 mm increments from 1-3 mm. On the scapula, adjustments were made in the anterior/posterior and superior/inferior directions, while adjustments on the humerus were made in the lateral/medial and superior/inferior directions (Fig. 1). All muscle elements were disabled, and only the translational degrees of freedom were allowed. Forward dynamics simulations were then completed under the influence of gravity, allowing the solution to stabilize over a simulation period of 6 seconds. Overall humeral displacement relative to the glenoid in each simulation was obtained and linear regression analysis was performed to quantify the sensitivity of displacement to ligament attachment location.

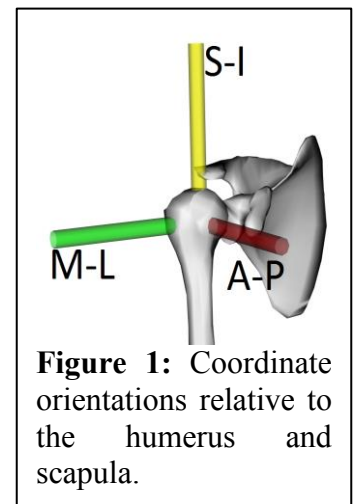


**Figure 1:** Coordinate orientations relative to the humerus and scapula.

## RESULTS AND DISCUSSION

A linear relationship exists between a change in attachment point location and the humeral displacement for each ligament and direction, though the magnitude of that change varies depending on the ligament. Additionally, an inferior attachment point change on the scapula provided the same results as superior change on the humerus for both ligaments (Table. 2). The linear relationship is

understandable as the ligaments are acting in the linear range of their force-length curves.

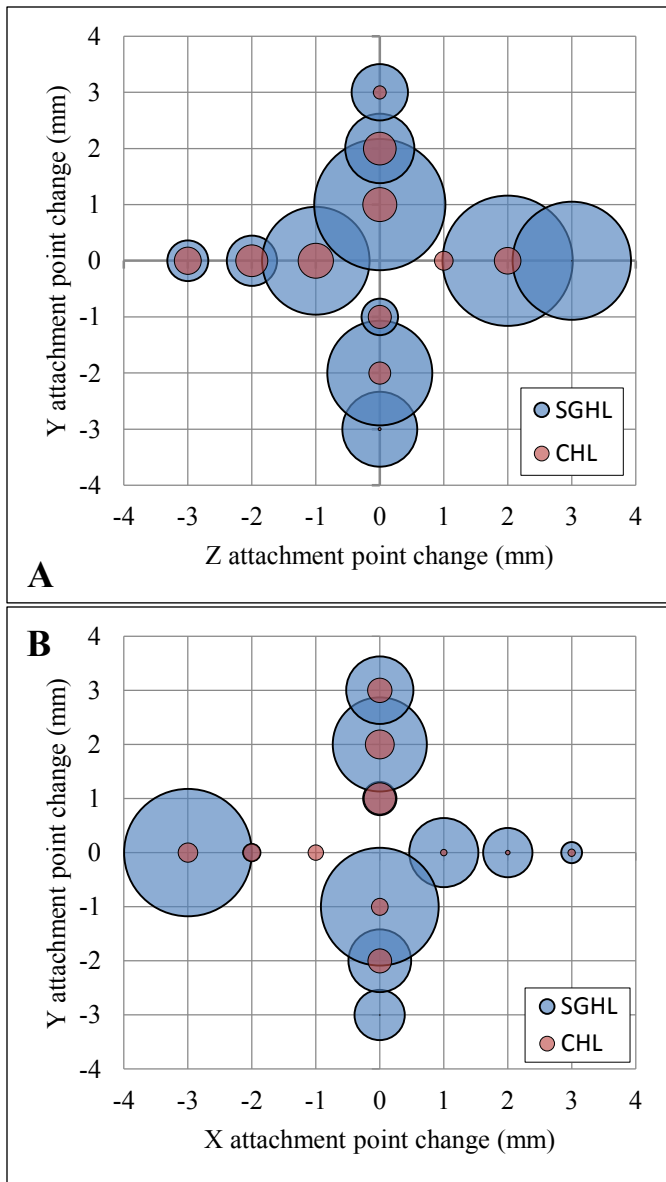


**Figure 2:** Change in displacement of the glenohumeral joint relative to attachment point change on the humerus (A) and on the scapula (B).

The differences in displacement are related to the shape of the wrapping surface of the ligaments on the humerus. These slight deviations can be seen with the SGHL A-P attachment point change on the scapula (Fig. 2B). The differences in magnitudes of the insertion/displacement relationship between the ligaments are due to the relative contribution of the CHL and the SGHL to stability. With a change in the SGHL attachment point, the model responded

with a greater change of glenohumeral displacement than when the CHL attachment point was implemented (Fig. 2). At its neutral attachment point, the CHL allows a displacement of 29.0 mm, whereas the SGHL will only allow the system to displace 22.3mm.

**Table 1:** Displacement of the glenohumeral joint at each attachment point location change (mm).

	CHL				SGHL			
	Scapula		Humerus		Scapula		Humerus	
	AP	SI	ML	SI	AP	SI	ML	SI
-3	27.6	30.1	30.2	26.7	18.4	28.6	27.2	17
-2	28.1	30.1	30.1	27.3	21.9	27.2	26.2	18.9
-1	28.6	29.4	29.5	28.1	22.3	25.5	25.0	21.4
0	29.0	29.0	29.0	29.0	22.3	22.3	22.3	22.3
1	29.1	28.1	28.1	29.4	24.2	21.4	22.3	25.5
2	29.3	27.3	27.3	30.1	25.5	18.9	19.1	27.2
3	29.5	26.7	27.0	30.1	26.1	17.0	16.2	28.6

## CONCLUSIONS

Understanding the sensitivity of the model's outputs relative to the attachment point of the ligaments is an important step in beginning to accurately model ligaments in OpenSim, and eventually understanding the stability of the shoulder. The elasticity of the ligaments will have a large effect on the magnitude of the insertion/displacement relationship, but without the ligament's resting length properly modeled, the elastic properties will not accurately represent the ligament. Regardless, attachment point placement can alter a model output greatly: a few millimeters change on either bone can cause a large change to the overall force applied on the system. Great consideration must be taken when choosing where to place the ligaments on the model.

## REFERENCES

1. Ladermann A., et al. *Medicine*, **95**, 2016.
2. Saul KR., et al. *Comput Methods Biomech Biomed Engin*, **18**, 1445-1458, 2015.
3. Boulet C., et al. *Can Assoc Radiol J* **63**, 79-86, 2012

# SIMULATING THE EFFECTS OF SQUATTING ON PELVIC KINEMATICS TO BETTER UNDERSTAND IMPLICATIONS DURING CHILDBIRTH

<sup>1</sup>Andrea Hemmerich, <sup>1</sup>Emily Geens, <sup>1</sup>Tara Diesbourg, <sup>2</sup>Teresa Bandrowska, <sup>1</sup>Geneviève A. Dumas

<sup>1</sup>Queen's University, Kingston, ON, Canada

<sup>2</sup>Ottawa Birth and Wellness Centre, Ottawa, ON, Canada

email: a.hemmerich@alumni.utoronto.ca

## INTRODUCTION

Upright birthing positions such as squatting are associated with clinical benefits, such as shorter labor and fewer assisted deliveries [1], and have demonstrated a widening of transverse pelvic dimensions [2]. The mechanics of various birthing positions are still poorly understood and most women still deliver lying on their backs (in the lithotomy position), which may be attributed to caregiver preference and constraints imposed by medical procedures, rather than comfort of the mother. Further insight into the mechanics of upright birthing positions may promote natural delivery under complicated circumstances for which medical interventions, such as forceps or Caesarean delivery, have traditionally been recommended. Our objective was to use a computational model to determine the effects of joint loading in the squat position on pelvic alignment.

## METHODS

Two female subjects, one 32-weeks pregnant (mass = 78.9 kg) and an age- and height-matched non-pregnant control subject (mass = 44.5 kg), were recruited for this study. The non-pregnant subject was positioned in supine in a 3.0-T magnetic resonance imaging (MRI) scanner (Magnetom TrioTim, Siemens, Erlangen, Germany) with legs raised to resemble the lithotomy position. A pelvic region coronal scan was acquired from which pelvic bones were segmented using Mimics™ segmentation software (Materialise, Belgium).

A three-dimensional model of the pelvic region, including bones and major ligaments as shown in Figure 1, was constructed and then imported into a multibody dynamic simulation package (RecurDyn™, FunctionBay Inc., Seoul, Korea).

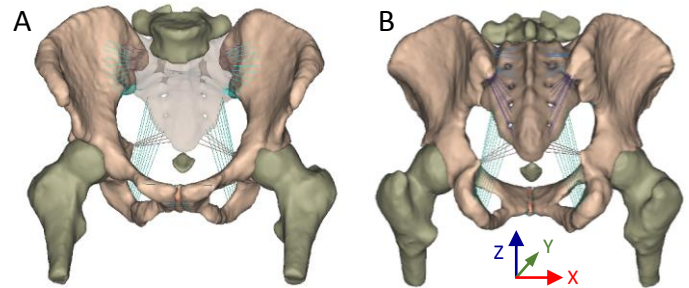


**Figure 1:** Anterior (A) and Posterior (B) views of pelvic model (with orientation of coordinate system) generated from MRI. Bones include L5 vertebra, left and right innominate bones, sacrum, coccyx, and proximal segments of left and right femurs. Ligaments include sacroiliac ventral, short posterior, long posterior, and interosseous, sacrotuberous and sacrospinous ligaments, and superior, inferior, anterior, and posterior pubic ligaments.

The L5 vertebra was fixed, while the femurs were permitted linear translation along the global x-axis; this permitted the hip joints to diverge or converge as needed. Sacroiliac and pubic symphysis joints were left unconstrained.

Torques used to actuate the simulation at the lumbosacral and hip joints were determined using standard motion analysis techniques during five squatting trials for each subject. Two force platforms (Bertec, Columbus, OH) and 13 optical cameras (Oqus 300+, Qualisys, Gothenburg, Sweden) captured data at 120 Hz that were analyzed using an inverse dynamics approach in Visual3D (C-Motion Inc., Germantown, MD). Ligaments were modeled as springs with piecewise linear stiffness approximations; material properties were determined from the literature [3].

The simulation was validated by comparing model measurements against those calculated from a second MRI scan acquired with the non-pregnant subject in a kneeling-squat position (Figure 2) and values from the literature [2].



**Figure 2:** The KneelSquat posture adopted by the non-pregnant subject in the MRI scanner. This was also the position used by subjects in the study conducted by Reitter *et al.* and represented the most upright position possible within the confines of the bore.

## RESULTS AND DISCUSSION

Mean joint reaction moments calculated for the pregnant and non-pregnant subjects in the squat position are listed in Table 1. Moments were determined about the pelvic axes shown in Figure 1. Though most of the difference between pregnant and non-pregnant joint moments may be attributed to subject mass, posture may also be a factor since the pregnant subject adopted a wider squatting stance.

When applied to the computational model, these joint moments increased all pelvic measurements and primarily opened the pelvic outlet in the anterior-posterior (AP) and transverse directions (Figure 3). This trend matched the measurements in the KneelSquat MRI posture; however, the increase in AP Outlet diameter determined from the non-pregnant simulation squat was substantially larger than the KneelSquat MRI measurement.

The differences in measurements between both pregnant and non-pregnant simulation squats and non-pregnant MRI results were within the range of difference between our non-pregnant subject's measurements and the mean values from the non-pregnant subject group in the study by Reitter *et al.* [2]. Results should be interpreted with caution due to model simplifications.

**Table 1:** Moments [Nm] calculated at hip and lumbosacral joints in the resting squat position. Hip moment magnitudes were averaged between left and right sides and are reported using the sign for the right hip.

	Hip			L5-S1
	X	Y	Z	X
Non-Pregnant	-20.5	14.1	-0.6	-53.7
Pregnant	-35.1	43.9	2.9	-77.7

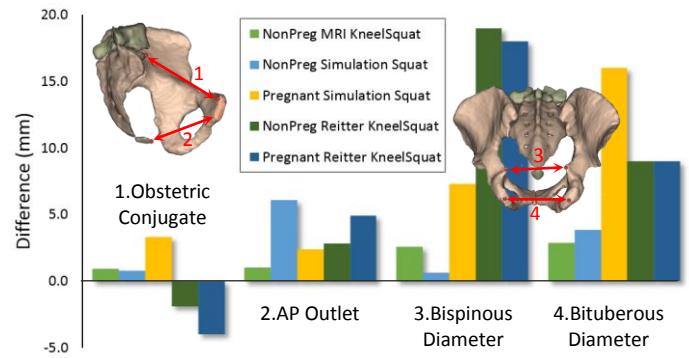


**Figure 3:** The difference in pelvimetry measurements as compared to the supine MRI position. Mean group differences from Reitter *et al.* [2] are also included.

## CONCLUSIONS

In this study, a computational model was developed to simulate the effects of hip and lumbosacral joint moments during squatting on pelvic kinematics and was validated against MRI measurements in a single subject. Joint moments estimated in both pregnant and non-pregnant subjects during squatting produced an increase in anterior-posterior and transverse pelvic outlet measurements comparable to results in the literature.

Results suggest that benefits of squatting likely extend beyond gravity acting on the fetus to advantageous maternal joint loading that could open the outlet of the birth canal and potentially facilitate delivery. The substantial increase in ligament laxity experienced during pregnancy would furthermore enhance this effect. Such evidence may improve medical intervention during childbirth; for example, maneuvers used to assist delivery may be performed more effectively or eliminated altogether by having the mother adopt an upright position and making the most of these biomechanical advantages.

## REFERENCES

1. Gupta JK, et al. *Cochrane Database Syst Rev.* **5**:CD002006, 2012.
2. Reitter A, et al. *Am J Obstet Gynecol.* **211**(6); p.662.e1–662.e9, 2014.
3. Eichenseer PH, et al. *Spine.* **36**(22); p.E1446-E1452, 2011.

## ACKNOWLEDGMENTS

Thanks to Betty-Anne Daviss, Pat Costigan, Kevin Deluzio, Daniel Benoit, and Linda McLean. Funding: NSERC, Queen's University.

# A DATABASE FOR MUSCULOSKELETAL SEGMENT LENGTH AND CIRCUMFERENCES FOR INDIVIDUALIZED ANTHROPOMETRIC REPRESENTATION

<sup>1</sup>Tammy M. Owings, <sup>1</sup>Erica E. Morrill, <sup>1</sup>Tyler Schimmoeller, <sup>1</sup>Tara F. Bonner, <sup>1</sup>Robb W. Colbrunn, <sup>1</sup>Benjamin Landis, <sup>2</sup>John E. Jelovsek, and <sup>1</sup>Ahmet Erdemir

<sup>1</sup>Department of Biomedical Engineering, Lerner Research Institute, Cleveland Clinic, Cleveland, OH, USA  
<sup>2</sup>Obstetrics, Gynecology & Women's Health Institute, Cleveland Clinic, Cleveland, OH, USA  
email: [owingst@ccf.org](mailto:owingst@ccf.org); website: <https://simtk.org/projects/multis>

## INTRODUCTION

Anthropometry data provides useful information regarding health status, disease risk, and body composition [1], but is also used to develop or refine anatomical representation in computer models for biomechanics. Most studies collecting anthropometric data of the arms and legs record only one circumference location along each segment, generally at the midpoint or at the maximal girth of the segment [1].

The data reported for this study is part of a larger study to acquire anatomical and mechanical data for creating computer models of multi-layer tissue architecture of the musculoskeletal extremities. The purpose of this portion of the study was to acquire anthropometric measurements (length and circumference) of the arms and legs. While other studies have collected similar anthropometric data, albeit in a restricted number of locations on the segment, our data, in combination with the acquisition of tissue thickness data [2], will allow for the development of multi-layer tissue models based on data from the same subject.

## METHODS

Fifty adult subjects were recruited to participate in this study, which was approved by the Cleveland Clinic Institutional Review Board and the Human Research Protection Office of the U.S. Army (USAMRMC ORP HRPO). Subject specific information including age, mass, height, gender, race, ethnicity, and activity level were obtained. Specific regions for anthropometric data collection included right upper and lower arms and legs. With subjects lying supine, reference marks were made on

landmarks of the extremities using a washable marker. The length of each segment was measured between the following landmarks: the lateral acromion and the humeral lateral epicondyle (upper arm), the humeral lateral epicondyle and the ulnar styloid process (lower arm), the greater trochanter and the lateral tibial plateau (upper leg), and the lateral tibial plateau and the lateral malleolus (lower leg). Three circumference measurements at the distal, central, and proximal sections were recorded. For the arm, circumferences were drawn at the distal

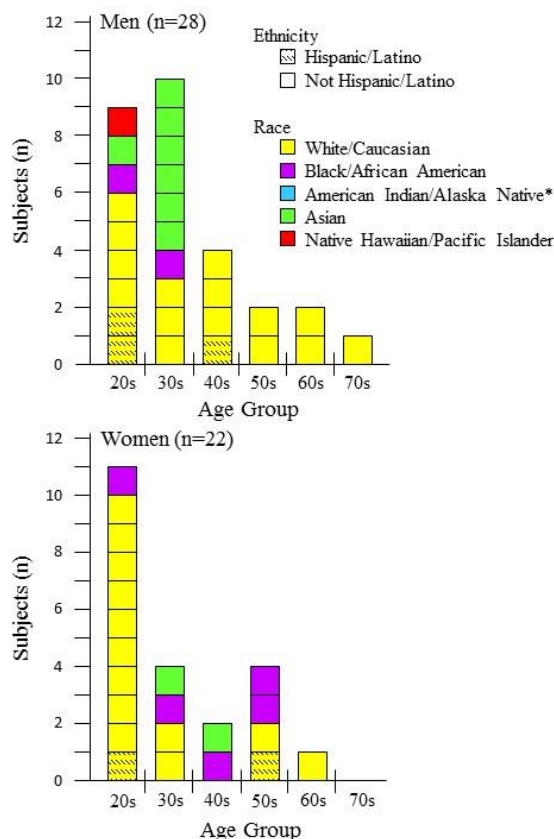


**Figure 1:** Age, gender, ethnic, and racial distribution of participants. \*None of the participants were part of the American Indian/Alaska Native racial group.

axillary, the distal shaft of the humerus, and the midpoint between these locations, as well as at the level of the proximal shaft, the distal shaft of the ulna-radius, and the midpoint between these locations. For the leg, circumferences were drawn at the top of the inner thigh, the distal shaft of the femur and the midpoint between these locations, as well as at the distal tibial tuberosity, the distal shaft of the tibia, and the midpoint between these locations. Circumference measurements were taken along with the distance of the measurement location from the nearest superior landmark. All measurements were recorded to the nearest millimeter by the same investigator, using a cloth tape measure.

## RESULTS AND DISCUSSION

The demographics of current subject sample population are reported in Figure 1. The mean ( $\pm$ SD) age, height, mass, and body mass index were  $26.8 \pm 13.6$  years,  $170 \pm 8.7$  cm,  $78 \pm 17.6$  kg, and  $26.8 \pm 5.6$  kg/m<sup>2</sup>, respectively. Mean ( $\pm$ SD) and range of segment length and circumferences were grouped according to gender (Table 1). Following data dissemination of the database, individualized data can be extracted for further analysis.

As can be seen from the results (Table 1), circumference values change throughout the length of the extremity. In contrast to having a single circumference measurement, having circumferences from multiple locations with a segment increases the

detail in shape descriptors and therefore will improve the fidelity of anatomical and inertial representation, e.g., in musculoskeletal models [3]. The geometry of external volume of segments, when supported by individual tissue thicknesses [2], will allow for detailed volumetric representation of tissue composition, i.e., that of skin, fat, and muscle.

## CONCLUSIONS

This database, which will be publicly accessible, provides anthropometric data from a group of subjects with a variety of demographic parameters. Variations in the circumference measurements within an individual segment indicate the need for data to elaborate on gross shape descriptors of the segment and enhance individualized models of anthropometry.

## REFERENCES

1. Fryar CD, et al. *Nat Health Stat Reports* 3(39), 1-39, 2016.
2. Morrill EE, et al. *Abstract submitted to 41<sup>st</sup> Annual ASB meeting*, 2017.
3. Erdemir, A, et al. *Clin Biomech* 22(2), 131-54, 2007.

## ACKNOWLEDGMENTS

This study has been supported by USAMRMC (W81XWH-15-1-0232).

**Table 1:** Segment length and circumference (in centimeters) for men and women

		Men (n=28)		Women (n=22)	
		Mean (SD)	Range (min-max)	Mean (SD)	Range (min-max)
Upper arm	Length	31.5 (2.3)	24.4 – 35.3	29.5 (1.9)	25.9 – 32.9
	Proximal circumference	34.6 (3.7)	26.3 – 41.2	33.0 (5.2)	25.8 – 43.2
	Central circumference	31.0 (3.6)	22.9 – 37.7	29.2 (5.1)	22.9 – 43.5
	Distal circumference	27.5 (2.8)	21.3 – 33.6	26.2 (3.9)	21.3 – 37.9
Lower arm	Length	26.0 (1.4)	22.4 – 28.6	24.1 (1.4)	20.6 – 26.7
	Proximal circumference	27.8 (2.3)	22.4 – 32.5	25.2 (2.2)	21.4 – 29.5
	Central circumference	24.0 (2.3)	19.7 – 28.0	21.7 (2.2)	17.7 – 27.3
	Distal circumference	17.4 (1.2)	14.8 – 19.3	15.9 (1.4)	14.1 – 18.6
Upper leg	Length	39.9 (3.2)	34.6 – 47.3	38.8 (4.4)	31.7 – 52.4
	Proximal circumference	57.6 (4.3)	46.0 – 65.8	63.5 (9.1)	47.7 – 84.9
	Central circumference	49.7 (4.2)	39.0 – 58.7	54.3 (9.0)	41.9 – 82.5
	Distal circumference	40.5 (3.5)	31.2 – 48.0	42.8 (7.0)	35.0 – 63.7
Lower leg	Length	44.2 (2.7)	39.8 – 49.5	40.7 (1.8)	37.2 – 43.3
	Proximal circumference	35.8 (3.0)	27.7 – 42.2	37.3 (4.0)	32.0 – 47.9
	Central circumference	32.0 (3.4)	24.2 – 39.0	32.0 (2.7)	27.3 – 37.5
	Distal circumference	21.9 (1.4)	18.9 – 24.3	21.5 (1.9)	18.5 – 26.8

# COMPARING SUBJECT SPECIFIC AND SCALED GENERIC MUSCULOSKELETAL MODELS FOR STUDYING KNEE BIOMECHANICS

<sup>1</sup>James P Charles and <sup>1</sup>William Anderst

<sup>1</sup>Biodynamics Lab, Department of Orthopaedic Surgery, University of Pittsburgh, PA, USA.  
email: JPC110@pitt.edu, web: www.bdl.pitt.edu

## INTRODUCTION

The wealth of research into the human musculoskeletal system using biomechanical modeling has mainly relied upon generic models, built upon the muscle architecture (which determine muscle force generating properties) and musculoskeletal geometry (bone morphology and muscle attachment points) of cadaveric specimens. These parameters are then often scaled by various anthropometric measures to match individual subjects [1]. However, the accuracy of these scaled generic models in various functional analyses has been questioned, with several studies showing that incorporating subject specific musculoskeletal geometry into these models has a potentially large impact on their output [2]. The effects of adding subject specific muscle architecture to musculoskeletal models have yet to be investigated in detail.

One possible use for musculoskeletal models, and particularly models incorporating subject specific musculoskeletal properties, is predicting the functional outcomes from surgical procedures, which could potentially allow clinicians to tailor rehabilitation programs to individual patients. Knee ligament reconstructions, for example, are commonly performed on athletes, and require lengthy periods of rehabilitation before normal sporting activity can resume. Using subject specific musculoskeletal models, which include detailed knee joint bone geometries, muscle force generating properties, as well as muscle and ligament attachment points, to predict how individuals might respond to these surgeries has the potential to speed up the rehabilitation process or even improve functional outcome, particularly by reducing the risk of secondary injuries or osteoarthritis [3].

Here we propose to create subject specific musculoskeletal models and simulations of the lower limb (with a specific focus on the knee joint), and

compare the functional outputs to those from scaled generic musculoskeletal models, during both walking and running. This analysis will give valuable insight into the necessity of incorporating such detailed subject specific muscle properties and bone geometry into musculoskeletal models, and potentially increase the utility of biomechanical models to both researchers and clinicians.

## METHODS

One 13 musculotendon unit actuated right lower limb musculoskeletal model was created in OpenSim software [1], based on the musculoskeletal geometry and muscle architecture of a healthy subject (Male, 24y/o. Fig. 1). These data were gathered from three magnetic resonance imaging (MRI) sequences. A T1 turbo spin echo (TSE; axial, voxel size  $0.47 \times 0.47 \times 6.5 \text{mm}^3$ , repetition time [TR] 650ms, echo time [TE] 23ms) sequence was used scan the entire lower limb, from hip to foot. This scan was used to create 3D meshes of bones and muscles and to determine muscle attachment sites. A T2 (sagittal,  $0.29 \times 0.29 \times 0.59 \text{mm}^3$ , TR/TE 29/16) sequence was used to scan the knee joint ( $\pm 7.5$  cm from the joint line). This scan was used create detailed 3D meshes of the distal femur, the proximal tibia and fibula,

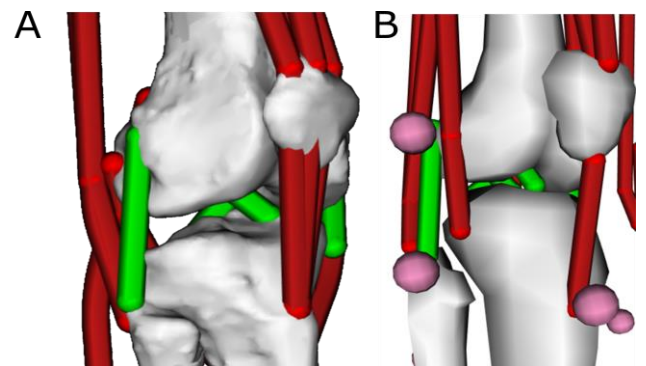


**Figure 1.** Subject specific musculoskeletal model (A), with subject-specific muscle force generating properties, attachment sites and bone geometries, compared to a generic, scaled musculoskeletal model [4] (B).

knee ligaments, menisci and associated cartilage. Finally, diffusion weighted echo planar sequences (voxel size  $2.96 \times 2.96 \times 6.5 \text{ mm}^3$ , TR/TE 7900/65ms, 12 direction diffusion gradients, b value- 0 &  $400 \text{ s/mm}^2$ , spectral attenuated inversion recovery) were used to gather muscle architecture data through the tracking of muscle fibers [4]. These data define the force generating properties of the muscles within the musculoskeletal model. A second, generic lower limb musculoskeletal model [5] was scaled to approximately match the anthropometry of the same subject (Fig. 1).

To simulate motion within both models, kinematic data for treadmill walking and running were gathered using a combination of marker based motion capture (Vicon; 100Hz walking, 150Hz running) and biplane radiography system (100Hz/150Hz). Ground reaction force data (GRF) were recorded with a dual belt instrumented treadmill (Bertec, 1000Hz).

The inverse kinematics tool within OpenSim was used to generate motions for two walking and running gait cycles for the both the subject specific lower limb model and the scaled generic model. The residual reduction algorithm (RRA) tool was applied to both models to reduce residuals, and to adjust the models to make them more dynamically consistent with the applied ground reaction forces. Inverse dynamics analyses were then used to predict the net (flexor-extensor, adduction-abduction, internal-external rotation) moments (Nm) around each lower limb joint during both walking and running.

## RESULTS AND DISCUSSION

The inverse dynamics analyses predicted smaller peak knee extension moments during both walking and running in the subject specific model, relative to the generic model (Fig. 2).

These initial results from inverse dynamics analyses give considerable credence to the notion that incorporating subject specific musculoskeletal geometry and muscle force generating properties into biomechanical models greatly affects their output, although the degree of this effect depends on the movement analyzed. The difference in knee extension moment between the subject specific model and the scaled generic model suggests that using biomechanical modeling techniques for clinical purposes, such as informing patient

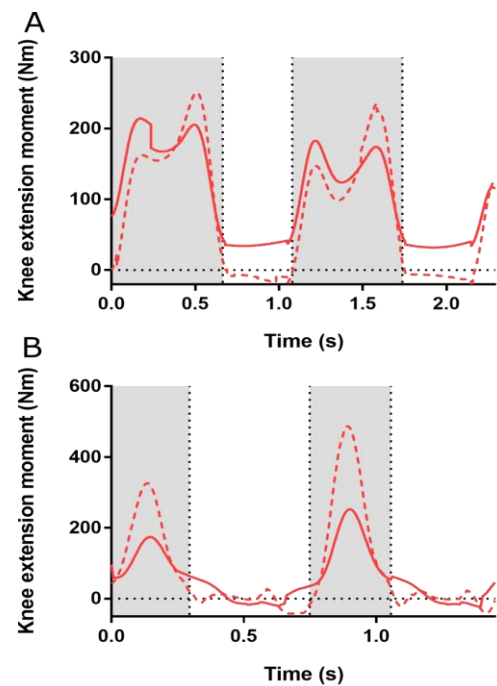


**Figure 2.** Net knee extension moments in the subject specific (solid line) and the scaled generic (dashed line) models, during walking (A) and running (B). Shaded areas indicate stance phase.

rehabilitation or simulating orthopaedic surgical procedures, may greatly benefit from the addition of subject specific data. To bolster the confidence of this claim, we plan to perform more in depth analyses, such as Computed Muscle Control (CMC) and Joint Reaction Analysis, to test for any differences in muscle forces or activations, as well as joint contact forces, between the subject specific or scaled generic models.

Further development of these models may also improve the comparisons made here. Detailed knee joint kinematics from biplane radiography will be incorporated into the models to more accurately represent the motion of the femur and tibia during walking and running.

## REFERENCES

1. Delp SL, et al. *IEEE Trans Biomed Eng.* **54**. 1940-1950. 2007
2. Prinold, JAI, et al. *Ann Biomed Eng.* **44**, 247-257. 2016.
3. Schmitt LC, et al. *Am J Sports Med.* **47**. 1426-1434. 2014
4. Damon BM, et al. *NMR Biomed.* DOI: 10.1002/nbm.3563. 2016.
5. Xu H, et al. *Comput Methods Biomech Biomed Eng.* **18**. 1217-1224. 2015.

# MUSCULOSKELETAL MODELS SCALED WITH CT IMAGES VERSUS SKIN MARKERS IN A POPULATION WITH HIP DEFORMITY COMPARED TO CONTROLS

<sup>1</sup> Ke Song, <sup>2</sup> Andrew E. Anderson, <sup>2</sup> Jeffrey A. Weiss, and <sup>1</sup> Michael D. Harris

<sup>1</sup> Washington University in St. Louis, St. Louis, MO, USA

<sup>2</sup> University of Utah, Salt Lake City, UT, USA

Email: harrismi@wustl.edu

## INTRODUCTION

Subject-specific musculoskeletal modeling relies on accurate estimation of joint center locations and proper scaling of model geometry. Sensitivity studies of model estimates, such as hip joint reaction forces (JRFs) and muscle function, have generally reported low to moderate differences between models with subject-specific versus generic geometry, but cautioned the effects may depend on the population and variables being studied [1, 2]. Indeed, models incorporating abnormal proximal femur geometry have shown significant differences in hip joint forces with increased deformity [3, 4]. Model sensitivity for hips with abnormal pelvic geometry, as in cases of hip dysplasia, is unknown but potentially important because altered hip joint geometry and loads may contribute to soft tissue damage in the joint [5]. Also, while models can be refined by incorporating more details, it is usually beneficial to find a balance between specificity and feasibility to facilitate large-scale musculoskeletal modeling research. Thus, the objective of this study was to compare hip joint center (HJC) location, JRFs and muscle forces between musculoskeletal models scaled using 3D reconstructions from computed tomography (CT) images and models scaled solely with skin markers, for individuals with and without hip dysplasia. We hypothesized intra-subject, inter-model differences to be more prominent for subjects with hip dysplasia.

## METHODS

Eighteen subjects participated after informed consent and IRB approval. Nine subjects had symptomatic hip dysplasia (DYSP; 3M, 6F, 26±7 y/o, 22.7±3.1 BMI) while the other 9 were healthy controls (CONT; 3M, 6F, 26±4 y/o, 23.8±4.5 BMI). Subject-specific pelvis geometries were reconstructed from CT images; kinematic and kinetic gait data were also collected and processed for OpenSim, as described previously [6]. A 23 degree-of-freedom model with

pelvis, lower limbs, torso, head segments and 96 muscle-tendon actuators (**Fig. 1A**) was scaled to each subject via two methods (as described below):

*Method 1. Marker-based uniform pelvis scaling – “Generic model”:* All segments were scaled based on anthropometric measurements derived from skin markers at bony landmarks. Pelvis geometry was scaled uniformly based on differences between virtual and experimental markers placed on anterior and posterior superior iliac splines (ASIS, PSIS).

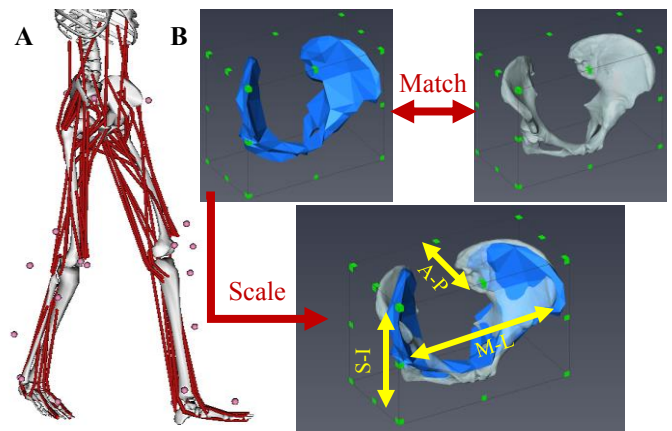


**Figure 1:** (A) OpenSim baseline model; (B) for CT-scaled model, dimensions of generic pelvis geometry (blue) were measured and scaled to match CT 3D reconstruction (gray).

*Method 2. CT-based non-uniform pelvis scaling – “CT-scaled model”:* The baseline OpenSim model pelvis was aligned in Amira with 3D-reconstructed pelvis geometry of each subject. The dimensions of the pelvises were measured as: horizontal distance between ASIS and PSIS, vertical distance between top of iliac crest and lower border of ischial tuberosity, and lateral distance between left and right iliac crests (**Fig. 1B**). The baseline pelvis was then scaled non-uniformly in OpenSim using the three dimensional ratios between baseline and CT geometries. The other segments were scaled with virtual and experimental markers.

For both models, hip joint angles were calculated by inverse kinematics and joint moments by inverse dynamics. After a residual reduction algorithm, individual and grouped (e.g. hip flexors) muscle forces were calculated by static optimization; JRFs were then computed. Data for a representative trial of each subject were interpolated to 0-100% of gait. For each trial, the peak JRFs in early stance (JRF1) and mid-stance (JRF2) were determined. Hip joint angles, moments, JRFs, and muscle forces at these two time points, and HJC location were statistically ( $\alpha=0.05$ ) analyzed between CT-scaled and Generic models, using paired *t*-tests or Wilcoxon signed-rank tests as appropriate. Inter-model comparisons were made for CONT and DYSP subjects separately.

## RESULTS

For DYSP subjects, HJC location in CT-scaled models was more posterior ( $-73\pm 7$  vs.  $-67\pm 4$  mm), inferior ( $-65\pm 4$  vs.  $-63\pm 3$  mm) and lateral ( $82\pm 6$  vs.  $80\pm 4$  mm) versus Generic models, but significant only posteriorly ( $p=0.03$ ). For CONT, HJC location in CT-scaled models was equally posterior ( $-73\pm 4$  vs.  $-73\pm 5$  mm), more superior ( $-66\pm 5$  vs.  $-68\pm 5$  mm) and more lateral ( $87\pm 5$  vs.  $86\pm 6$  mm) versus Generic, but differences were not significant. Hip JRFs, angles and moments were not different between CT-scaled and Generic models at JRF1 or JRF2 for either group.

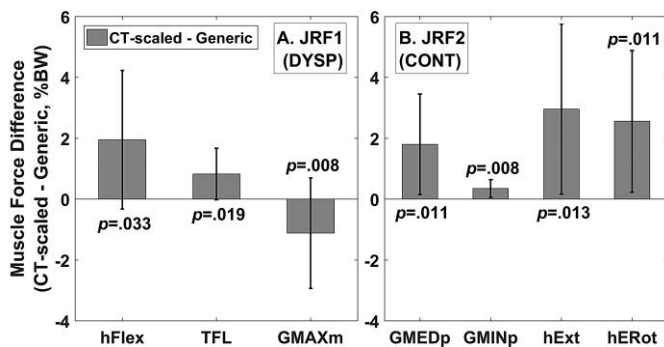


**Figure 2:** Inter-model muscle force differences at (A) JRF1 and (B) JRF2. Error bar =  $\pm 1$  SD of difference.

At JRF1 (**Fig. 2A**): for DYSP, CT-scaled models estimated larger forces for hip flexor group (*hFlex*) and tensor fasciae latae (*TFL*), and smaller force for gluteus maximus middle fibers (*GMAXm*) compared to Generic. No inter-model differences were found for CONT. At JRF2 (**Fig. 2B**): for CONT, CT-scaled models estimated larger forces for gluteus medius posterior fibers (*GMEDp*), gluteus minimus posterior fibers (*GMINp*), hip extensor group (*hExt*) and hip

external rotator group (*hERot*) compared to Generic. No inter-model differences were found for DYSP.

## DISCUSSION & CONCLUSIONS

Despite producing more accurate pelvis sizes by directly scaling to the skeletal dimensions of each subject and bypassing marker placement errors, the CT-scaled models did not estimate different hip JRFs, angles or moments compared to Generic models. The insensitivity of JRFs between subject-specific and generic models is supported by some past studies [1, 2] and may suggest that either method is suitable to estimate resultant joint forces. However, pelvis geometry for both CT-scaled and Generic models was derived from a single baseline. Since neither model incorporated true subject-specific pelvic geometry, both methods may have omitted important traits such as unique muscle paths and HJC locations. Differences in muscle forces seen here (**Fig. 2**) may stem not only from pelvis scaling, but also from muscle activation estimated by static optimization to equilibrate model torques. Without accessing true subject-specific geometry of the hip or experimental muscle activation data, it cannot be verified that muscle paths and forces from CT-scaled models are more accurate than Generic. We showed recently that highly subject-specific pelvis models can delineate JRF differences between dysplastic and healthy hips, but those models required full access to subject-specific bony geometry and HJC location [6]. The current study lays groundwork for future work to determine the level of model specificity required to reliably estimate joint mechanics, yet also feasible for most research projects. In conclusion, musculoskeletal models with pelvis geometry non-uniformly scaled from CT images were not different versus models uniformly scaled with skin markers, and both methods may underestimate differences in subjects with hip deformity compared to controls.

## REFERENCES

1. Correa TA, et al. *J Biomech* **44**, 2096-2105, 2011
2. Valente G, et al. *PLoS One* **9**, e112625. 2014
3. Lenaerts G, et al. *J Biomech* **41**, 1243-1252, 2008
4. Heller MO, et al. *Clin Biomech* **16**, 644-649, 2001
5. Henak CR, et al. *Osteo Cart* **22**, 210-217, 2014
6. Harris MD, et al. *J Biomech* (in press), 2017

## ACKNOWLEDGMENTS

NIH R01AR05344, R01EB016701, R21AR3466184.

# ASSESSMENT OF SPASTICITY BY A NOVEL STRETCH REFLEX ACTIVATION MODEL

<sup>1</sup>Moon Jeong Kang, <sup>1</sup>Young Nam Jo, and <sup>1</sup>Hong Hee Yoo

<sup>1</sup>Hanyang University, Seoul, Republic of Korea  
email: hhyoo@hanyang.ac.kr

## INTRODUCTION

Spasticity is a motor disorder characterized by a velocity-dependent increase in the tonic stretch reflex [1]. The diagnosis and assessment of spasticity requires a neurologic assessment of patient, including reflexes, muscle tone. Despite of much effort to understand and improve treatments for patients, there are only a limited number of studies on spasticity.

The pendulum test models are one of a method to measure spasticity. During the test, the leg is fully extended, and then allowed to swing freely. For patients with spasticity, specific swing pattern is observed. There are some mathematical model to evaluate the swing pattern of patients with spasticity. He et al. developed the model including time delay, threshold, and gain [2].

In this study, we developed the stretch reflex activation model, and assess the spasticity by the model. Proposed model considered muscle type.

## METHODS

We simulated the pendulum test of patients with spasticity and assessed spasticity with parameters used in simulation. First, the equation of motion was derived considering muscle force induced by stretch reflex model. We assumed the pendulum motion of a leg as a sagittal motion. The knee joint is modeled as a revolute joint (Fig. 1). Equation of motion of the pendulum motion is as follows.

$$I\dot{u} + cu + MLg \sin q - F_m D = 0 \quad (1)$$

Where  $I$  is moment of inertia of a leg,  $c$  is damping coefficient,  $M$  is mass of a leg,  $L$  is a length of a leg,  $F_m$  is muscle force,  $D$  is moment arm of  $F_Q$ , and  $q, u, \dot{u}$  are joint angle, angular velocity, and angular

acceleration. Joint angle could be calculated by simulation. Optimization method which minimized difference of joint angle from simulation and experiment was used.

Muscle force induced by stretch reflex could be calculated with Hill-type muscle model as follows [3].

$$\begin{aligned} \tilde{F}^m &= \{f_a(a, \tilde{l}^m, \tilde{v}^m) + f_p(\tilde{l}^m)\} \cos \phi(\tilde{l}^m) \\ \tilde{F}^m &= F^m / F_o^m, \quad \tilde{l}^m = l^m / l_o^m \end{aligned} \quad (2)$$

where  $a$  is muscle activation,  $\phi$  is pennation angle,  $F_o^m$  is optimal muscle force, and  $l_o^m$  is optimal muscle length. During the test, muscle force by stretch reflex is only generated. Therefore we considered muscle force induced by the stretch reflex with suggested stretch reflex activation model. We developed the stretch reflex activation model considering muscle type. The model was based on the study of He et al. [2]. The model consists of threshold, and gain as

$$\begin{aligned} a(t) &= \sigma \left[ \frac{w_1}{T_L} (L_F - T_L) + \frac{w_2}{T_V} (\dot{L}_F - T_V) \right] \\ \text{where, } T_L &= \lambda_1 L_o^m, \quad T_V = \lambda_2 V_{\max} \end{aligned} \quad (3)$$

where  $u$  is muscle activation,  $w_1, w_2$  are the ratio of

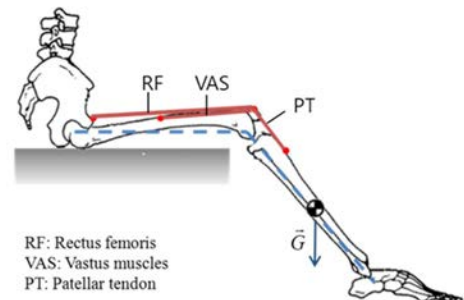


**Figure 1:** Musculoskeletal model.

the slow twitch fiber and fast twitch fiber,  $L_F, \dot{L}_F$  is muscle length and velocity,  $L_o^m$  is optimal muscle length,  $V_{max}$  is maximum muscle contraction velocity, and  $\lambda_1, \lambda_2$  are subject dependent parameters. As the muscle length and stretch velocity exceed the each threshold, muscle is activated as equation (3). It is assumed that the former is related with muscle length, and the latter is related with muscle stretch velocity. If a muscle has same portion of muscle type,  $w_1 = w_2 = 0.5$ . For validating the model, we did pendulum test with healthy adults. For the experimental data of spasticity, results in study of Fowler were used [4].

## RESULTS AND DISCUSSION

For the validation, we compared the knee joint angle and the muscle activation with experiment results of joint angle and EMG signal (Fig. 2). Different with healthy subjects, the knee joint angle has small range of motion. There are 5 parameters in the model. We focused on variation of the parameters as increasing level of spasticity. Muscle activation and knee joint angle were calculated from simulation.  $\lambda_2$  and  $w_2$  were varied with the level of spasticity (Table 1). For the results of spasticity,  $\lambda_2$  decreased. It means that velocity threshold decreased for spasticity. In other word, stretch reflex can be easily induced and is sensitive to muscle stretch velocity for spasticity. However,  $w_2$  increased for simulation of pendulum motion of spasticity. It seems that ratio of muscle type also affects the motion of patient with spasticity.

## CONCLUSIONS

In this study, we developed the stretch reflex activation model, and simulate the pendulum motion of patients with spasticity. For the patients with spasticity, the parameters related with muscle stretch velocity and muscle type were different from that of healthy adults. It seems that muscle stretch

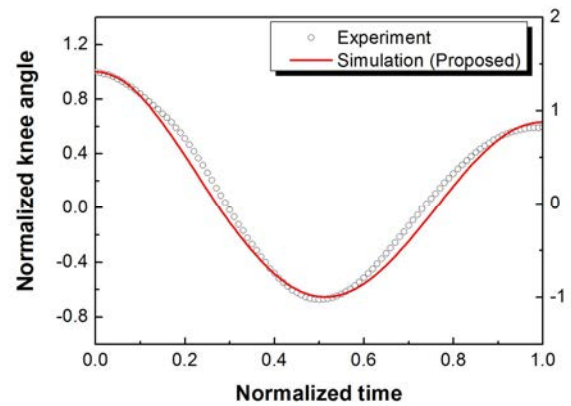


**Figure 2:** Knee angle trajectories of experiment and simulation.

velocity and muscle type affect the level of spasticity.

## REFERENCES

1. Brashear A and Elovic E. *Spasticity: diagnosis and management*, Demos medical publishing, 2010.
2. He J, et al. *IEEE Trans Biomed Eng* 44, 175-187, 1997.
3. Zajac FE, et al. *muscle and tendon: properties, models scaling, and application to biomechanics and motor control*, Crit Rev Biomed Eng, 17, 359-411, 1988.
4. Fowler EG, et al. *Sensitivity of the pendulum test for assessing spasticity in persons with cerebral palsy*, Develop Med Chi Neurol, 42, 182-189, 2000.

## ACKNOWLEDGMENTS

This work was supported by the research fund of Survivability Technology Defense Research Center of Agency for Defense Development of Korea (No. UD1500131D).

**Table 1:** Stretch reflex activation model parameters for healthy subject and patient with spasticity

Muscle	Healthy subjects				Patients with spasticity			
	$w_1$	$w_2$	$\lambda_1$	$\lambda_2$	$w_1$	$w_2$	$\lambda_1$	$\lambda_2$
<b>Rectus femoris</b>	0.45	0.55	0.232	0.250	0.44	0.56	0.230	0.280
<b>Vastus muscles</b>	0.48	0.52	0.346	0.367	0.45	0.55	0.346	0.450

# JOINT CONTACT IS SENSITIVE TO GEOMETRY COARSENESS AND STIFFNESS IN OPENSIM

<sup>1</sup> Michelle R. Krach, <sup>1</sup> Michael W. Hast, and <sup>1</sup> Josh R. Baxter

<sup>1</sup> University of Pennsylvania, Philadelphia, PA, USA

email: [josh.baxter@uphs.upenn.edu](mailto:josh.baxter@uphs.upenn.edu), web: <https://www.med.upenn.edu/motionlab/>

## INTRODUCTION

End-stage joint arthritis is commonly treated with total joint replacement, which was performed on more than 1 million Americans in 2011. Patient outcomes are influenced by surgical and implant factors, but testing this multi-factorial space in clinical studies is not always practical. Finite element modeling allows researchers to isolate the biomechanical effects of modifiable parameters; however, many commercially available software packages are costly, require a great deal of expertise to use effectively, and require substantial amounts of time to create simulations.

OpenSim is a free and open-source musculoskeletal platform that is well accepted in the biomechanics community [1]. While joints of the body are traditionally represented with prescribed kinematic mechanisms in OpenSim, they can also be modeled by relying upon articulating joint contact. To date, the OpenSim contact modeling paradigms are not fully documented and the implications of geometry mesh size and material properties on computation time and fidelity are not clearly defined.

The purpose of this study was to characterize the effects of simulation contact parameters – stiffness and geometry coarseness – on computation time and component penetration. This was achieved by simulating contact between the tibial and femoral components of a total knee replacement.

## METHODS

Tibiofemoral contact was simulated with a forward dynamic model in OpenSim to quantify the relationships between computation time, implant penetration, material stiffness, and geometry coarseness. Briefly, the femoral component was placed 1 mm above the tibial component and ‘drop and settle’ motions were simulated for 1 second. (Fig 1) High-resolution CAD files of a cruciate-retaining

total knee replacement (eTibia) were used in the model and the number of faces used to represent the tibial component was resampled to 100, 500, 1,000, 2,500, and 5,000 faces using MeshLab. The femoral component mesh remained constant at 10,000 faces across all simulations. Additionally, seven stiffness values (ranging between  $10^9$  to  $10^{15}$  N/m), and 3 femoral component masses (1, 10, and 100kg) were used in the simulations. The simulation was repeated 105 times to explore all possible combinations of the aforementioned variables of interest.

Simulation performance was quantified as computation time and component penetration. Component penetration was calculated as the vertical change in position of the femoral component center of mass from the point of initial component contact to the final settling position.

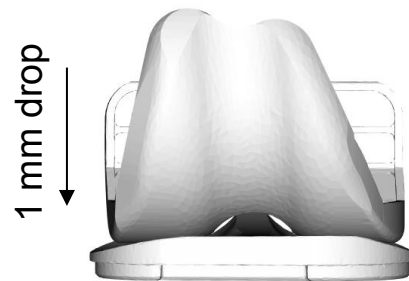


**Fig. 1.** Tibiofemoral contact was simulated by dropping the femoral component from a height of 1 mm above the tibial component. Tibial mesh size and stiffness were changed and tested at 3 femoral masses to characterize the effects of these model parameters on computation time and component penetration.

## RESULTS AND DISCUSSION

Simulated implant penetration was most physiologic ( $< 0.3$  mm) and computation time was minimized ( $< 25$  s) when stiffness was set at  $10^{10}$  N/m and a finer mesh geometry (1000 or greater faces) was utilized (Fig. 2). Computation time was sensitive to both stiffness and loading magnitude but independent of the contact mesh coarseness (Figure 2).

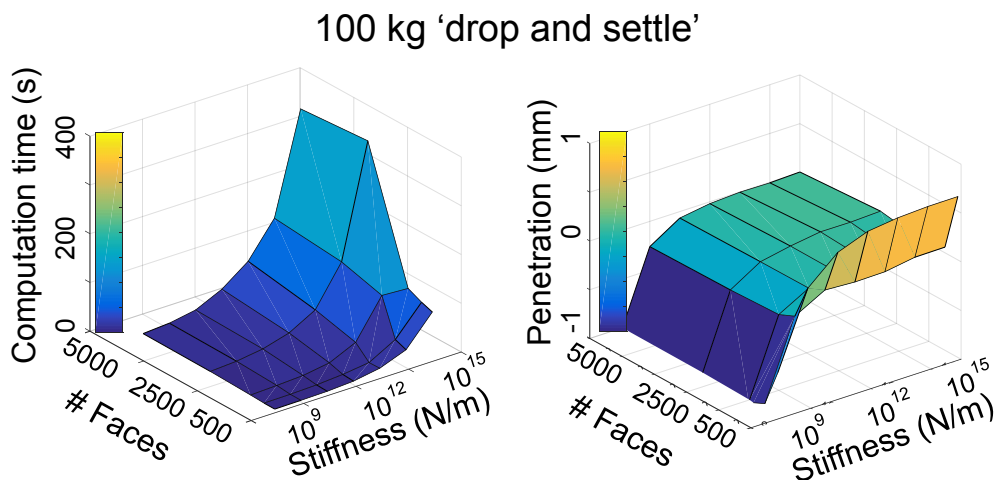


**Fig. 1.** Material stiffness and mesh density both affected computation time and component penetration during all ‘drop and settle’ simulations. Increasing the material stiffness parameter resulted in computation times 20-30 times greater than models with a stiffness of  $10^{10}$  N/m. Component penetration was affected mostly by low stiffness values and coarse meshes.

The expected penetration for weight bearing simulations (100 kg) was assumed to be between 0.1-0.3mm. This was based on an implant retrieval study indicating this degree of permanent deformation after years of loading [2]. Lack of penetration (negative values) can be explained by two phenomena: 1) incomplete settling of the femoral component caused by overly stiff components, or 2) unrealistic protrusions of contact geometry caused by coarse meshing.

Stiffness values outside of the bounds of this experiment (less than  $10^{10}$  and greater than  $10^{12}$  N/m) caused undesirable simulation behavior. For example, overly compliant models resulted in implant penetration approaching 1 mm while overly stiff models resulted in unsettled simulations consisting of very small integrator time-steps. Initial simulations included stiffness values of  $10^7$  and  $10^8$  N/m, but were excluded as the femoral component fell through the tibia at higher loading magnitudes. Stiffer models took much shorter time steps (up to 34 times smaller) than the best performing models, which explains both the increased computation time and oscillating reaction loads in stiffer simulations.

This simple sensitivity analysis of the elastic foundation contact algorithm within OpenSim has several limitations. The results have not been validated with a physical experiment. We are actively pursuing a validation study where we test the identical component geometry under computational

and benchtop testing conditions. Additionally, the loading profile was derived from a constant mass being acted upon by gravity rather than the dynamic loads that drive human motion. The preliminary findings of this study will be used to optimize more rigorous musculoskeletal models to test the effects of implant geometry on knee biomechanics during clinically relevant activities like walking, rising from a chair, and navigating stairs.

## CONCLUSIONS

Finite element models provide unparalleled amounts of information about contact mechanics within a joint, but they require considerable amounts of time and expertise to execute. In comparison, simulating joint contact using the native elastic foundation paradigm within OpenSim is relatively quick and easy. Depending on the application, this approach may provide enough information for testing clinically relevant parameters with regards to implant selection, placement, and performance. To this end, the current study has provided rudimentary guidelines for utilizing this tool in a quick and effective manner.

## REFERENCES

1. Delp SL, et al. *IEEE Transactions on Biomedical Engineering* **54**, 1940-1950, 2007.
2. Liu, T, et al. *Clinical Orthopaedics and Related Research* **474**, 107-116, 2016.

# USING MUSCULOSKELETAL MODELS TO ESTIMATE THE PASSIVE JOINT STIFFNESS

<sup>1</sup> Andrea Zonnino, <sup>1</sup> Fabrizio Sergi

<sup>1</sup>Department of Biomedical Engineering, University of Delaware, Newark DE

## INTRODUCTION

Joint stiffness is actively modulated by healthy humans during tasks requiring interaction with the environment [1]. For individuals with neuromotor dysfunctions, however, the response of the neuromuscular system to exogenous perturbations is compromised [2]. As such, analysis of joint stiffness during manipulation could be important both for basic research in motor neuroscience, and for clinical assessment purposes.

Joint stiffness can be described by two different components: active and passive. The active component is related to the force generating capability of muscles; the passive component is an intrinsic property that depends on the passive elastic behavior of the muscles.

Although experimental approaches to the computation of the passive joint stiffness have been presented [3], the complexity and the length of the experiments limit the number of postures in which joint stiffness can be computed. Musculoskeletal models (MSMs) could extend the results of human subject experiments, and estimate the stiffness of different joints across their entire workspace. However, MSMs have not been developed for joint stiffness analysis; even the simplest models can be characterized by unstable values of stiffness that are not physiologically accurate [4].

This work develops a framework to analyze joint stiffness in MSMs and presents a procedure to minimally modify some of the muscles parameters of a MSM to obtain stable and physiologically accurate values of passive joint stiffness.

## METHODS

In static conditions, joint stiffness ( $K_\theta$ ) is the derivative of the multivariate torque ( $\tau$ ) vs. angle ( $\theta$ ) relationship:

$$K_\theta = \frac{\partial \tau}{\partial \theta} \quad (1)$$

where  $\tau$  is a function of the musculotendinous forces ( $f^{MT}$ ) and the muscle Jacobian ( $J$ ) (i.e.  $\tau = J^T f^{MT}$ ).

Assuming that muscles are modeled with a Hill-type model, and considering only the muscle's passive component, it is possible to express  $f^{MT}$  as:

$$f^{MT} = f^T = f^M = f^{PE} (l^{PE}) \cos(\alpha) \quad (2)$$

where  $f^T$  and  $f^M$  are the forces along the tendon and muscle respectively;  $\alpha$  is the pennation angle.

It is possible to show that:

$$K_\theta = J^T \frac{1}{c} \frac{K^{PE} K^T}{K^{PE} + K^T} J - \frac{\partial J^T}{\partial \theta} f \cos(\alpha) + J^T f \sin(\alpha) \frac{\partial \alpha}{\partial \theta} \quad (3)$$

where  $c = \left(1 + \frac{l^{PE}}{\partial l^{PE}} \frac{\partial \cos(\alpha)}{\cos(\alpha)}\right)$ . We consider a joint unstable if at least one of the eigenvalues of  $K_\theta$  is negative.

Since the first term of (3) is always positive, negative (i.e. unstable) values of stiffness can only be introduced by the second and third terms. The parameters that influence stability are then the moment arm ( $J$ ), its derivative ( $\frac{\partial J}{\partial \theta}$ ), the muscle force ( $f^{PE}$ ), the pennation angle ( $\alpha$ ) and its derivative ( $\frac{\partial \alpha}{\partial \theta}$ ). Preliminary analysis shows that the third term of (3) influences the final value of stiffness by only 0.1%. As such, we consider the moment arm and the muscle force as the only relevant parameters.

We applied the described analysis to study the stiffness of the wrist joint implemented in the upper limb model proposed by Holzbaur et al. [5]. We used a simplified version of the model where only five muscles (ECRL, ECRB, ECU, FCR, FCU) were considered. We calculated stiffness in a 2D workspace defined by two wrist rotations, flexion/extension (FE) with a range of  $-50^\circ$  (extension) to  $50^\circ$  (flexion), and radial/ulnar deviation (RUD), ranging from  $-25^\circ$  (radial deviation) to  $10^\circ$  (ulnar deviation).

Since the model is unstable in certain regions of the workspace (see results), we developed a framework to determine how to minimally modify the model to obtain stability. As both the moment arm [6] and the tendon slack length [7] are highly variable between individuals and cannot be measured

accurately, we hypothesized that that small modifications to these parameters could yield equally accurate MSMs, which are also stable and suitable for the analysis of dynamic interaction with the environment.

We conducted an exhaustive search on the space defined by each muscle attachment point and tendon slack length, and used optimization to find a set of parameters that achieves stability in all workspace postures while minimally changing model behavior. Our analysis seeks to minimize the following function:

$$\Phi = a_1 \frac{A_{unst}}{A_{tot}} + a_2 \frac{\Delta L_{ts}}{\Delta L_{ts_{MAX}}} + a_3 \frac{\Delta \rho_{IP}}{\Delta \rho_{IP_{MAX}}} + a_4 \frac{A_{sl} - A_{sl_0}}{A_{tot}},$$

where  $A_{unst}$  and  $A_{sl}$  are the area of the unstable portion and of the slack portion of the workspace, respectively;  $\Delta L_{ts}$  is the tendon slack length variation;  $\Delta \rho_{IP}$  is the insertion point displacement. A preliminary analysis showed that, by keeping the flexors unloaded in the entire workspace, as proposed by [5] and shown in Fig. 1A, the model presents a partial area where all the muscles are slack. Considering this a non-physiological condition, we forced to the FCR and FCU to decrease the slack area by 20% (i.e. the same amount of modification required to stabilize the ECRL and ECRB).

## RESULTS

### Model stability analysis:

We analyzed joint stability separately for each muscle of the model, and created the stability maps reported in Fig. 1A, which demonstrated the presence of a large unstable region in the workspace. The instability was caused by two muscles (ECRL and ECRB) that, if stretched, are always unstable.

### Stabilization of unstable muscles:

With the optimization procedure, the attachment points and tendon slack length of the unstable muscles were modified to achieve stability throughout the workspace for each muscle and for the entire model (Fig. 1B). Muscle moment arms for the stabilized muscles were changed substantially only for ECRB in the RUD axis, for which the average change in moment arm required for model stabilization was 280%.

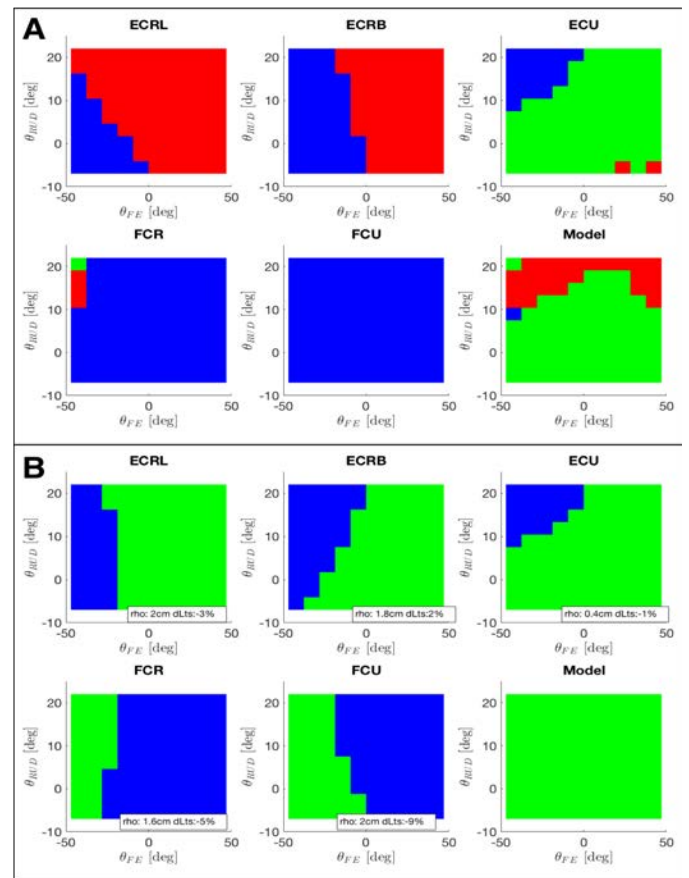


**Figure 1:** Stability maps for each muscle individually and for the entire model: (A) original model based on [5], (B) optimized model. In each map the green area is the stable area, the red area is the unstable area and the blue area is the slack area.

## CONCLUSIONS

Using a musculoskeletal model to investigate the joint stiffness is valuable, as it may allow for the exhaustive analysis of the joint stiffness properties.

Even though MSMs have not been developed to analyze the joint stiffness and can show unstable behavior, we developed a novel method that allows stability to be achieved through minimal parameter changes of the MSM. With proper experimental validation, this method may allow to use current MSMs to study joint stiffness to optimize human-robot interaction and/or to quantify the evolution of disease in neuromotor disorders.

## REFERENCES

1. T. Flash et al. (1990), *Exp. Brain Res.*, 82(2), 315–326.
2. D. Burke et al. (2013), *Neurology*, 80(3), S20–S26.
3. D. Formica et al. (2012), *J. Neurophysiol.*, 108(4) 1158–1166.
4. M. Dornay et al. (1993), *Neural Networks*, 6(9) 1045–1059.
5. K. Holzbaur et al. (2005), *Ann. Biomed. Eng.*, 33(6), 829–840.
6. M. Sherman et al. (2013), *Proc ASME Des Eng Tech Conf.*
7. K. Manal et al. (2004), *J Appl Biomech* 20(2): 195-203

# Investigating Uncertainty in Constitutive Modeling of Components of the Human Head

Patrick Brewick and Kirubel Teferra

US Naval Research Laboratory, Washington, DC, USA  
email: patrick.brewick@nrl.navy.mil; kirubel.teferra@nrl.navy.mil

## INTRODUCTION

Detailed finite element (FE) modeling of the human head provides an invaluable resource for quantifying the mechanical response within the brain during a blast loading event. The exact connections between loading patterns, tissue mechanical response, and injury/physiological effects are still quite unknown; however, the exceedance of specified threshold values based on direct and derived measures of stress, strain, pressure, and acceleration within the brain have been shown to be useful injury criteria. The utility of these thresholds is somewhat mitigated by the fact that preliminary parametric studies have shown significant variation in the predicted injury response, indicating that the exact relationship between model geometry, material properties, and mechanics-based injury response metrics has not yet been established.

The use of stress and strain measurements as indicators of or criteria for injury necessitates accurate material models for the many constitutive components of an FE model of the human head. Identifying an appropriate constitutive model form and optimal parameter values for biological tissues is an enormous challenge hindered by large epistemic uncertainties. This work lies within a larger effort to quantify the uncertainty encountered during modeling of the human head.

## METHODS

The biomaterial components within the human head model, *e.g.*, white matter, gray matter, skin, and bone, were primarily described with the constitutive model forms for hyperelastic, viscoelastic, and hyper-viscoelastic materials. This study was primarily concerned with fitting parameters for the Ogden model of hyperelasticity and the Maxwell model for viscoelasticity. The strain energy density function for an Ogden model is given by Eq. (1)

$$W = \sum_{i=1}^N \frac{2\mu_i}{\alpha_i^2} (\lambda_1^{\alpha_i} + \lambda_2^{\alpha_i} + \lambda_3^{\alpha_i} - 3) \quad (1)$$

where  $N$  is the model order,  $\lambda$  is the principal stretch, and  $\alpha$  and  $\mu$  are model-specific parameters.

Each model form contains parameters that must be estimated by fitting to experimental data. Available data sets are often limited due to the many vagaries associated with testing biomaterials, but sophisticated models must be calibrated and validated based on these narrow data sets. For some materials data must be aggregated from a series of unrelated studies in order to create a complete data set, but combining disparate data sets typically requires numerous assumptions about experiments performed under different conditions and using different equipment.

Typically the experimental data was provided in the form of stress-strain curves; stress may be easily derived for the Ogden model in Eq. (1) and strain is directly relatable to  $\lambda$ . The actual fitting may be performed through an optimization process, but the nonlinearity of the model forms and the necessary constraints on the model parameters meant that the result from a single optimization trial would not necessarily capture the ideal result. For instance, one crucial but complex constraint was Drucker stability [1], a physics-based requirement relating changes in stress to changes in strain. Therefore, an emphasis was placed on the posterior distributions for each parameter instead of individual parameter estimates.

The posterior distributions were based on adopting a Bayesian approach, using the familiar form of Eq. (2)

$$p(\theta|d) = \frac{p(d|\theta)p(\theta)}{\int_{\Theta} p(d,\theta)d\theta} \quad (2)$$

where  $\theta$  represents the unknown model parameters, *e.g.*,  $\alpha$  and  $\mu$ , and  $d$  represents the experimental data.

$p(\theta|d)$  is the desired posterior distribution and  $p(d|\theta)$  may be considered the likelihood function, which models the error between the model predictions and experimental data.  $p(\theta)$  is simply the prior distribution for the unknown parameters. Given the complex form of the models, the posterior distribution cannot be easily solved analytically, especially for larger models. Thus, Markov Chain Monte Carlo methods [2] were employed as they allowed for heuristic parameter bounds, inequality constraints on certain parameter sets, as well as nonlinear functional constraints on the constitutive model forms, such as that for Drucker stability.

## RESULTS AND DISCUSSION

The advantage of this Bayesian approach is that the posterior distributions provide an estimated density for the region of optimal values, as opposed to the maximum likelihood estimate provided during optimization. This becomes important when addressing the inherent uncertainty in experimental data. When calibrating a purely hyperelastic model for the pia mater with a simple, single-term Ogden model ( $N = 1$ ), the posterior distributions showed a marked dependence on the assumed variance in the error between the model prediction and experimental data,  $\sigma_\varepsilon$ . This may be easily seen in Fig. 1.

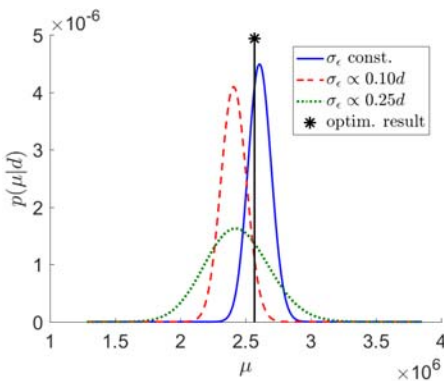


**Figure 1:** Comparison of posterior distributions for  $\mu$  from a single-term Ogden model for pia mater.

The different distributions for  $\mu$  in Fig. 1 are generated by simply changing how  $\sigma_\varepsilon$  is treated. Assuming the variance is constant across all measurements results in a relatively narrow

distribution whose mean lies near the optimal result. However, assuming that the error variance at a given measurement point is directly proportional to its measurement value, *e.g.*, by 10% or 25%, results in much different distributions with shifted mean values. A similar plot may be generated for  $\alpha$ .

The results shown in Fig. 1 are merely for the simplest model class and one of the simplest biomaterials in terms of data sets. More complex materials, such as brain matter, bone, and skin, require significantly more detailed models with greater numbers of parameters (and thus greater dimensionality) and comprise much larger data sets that often span orders-of-magnitude in both stress and strain. Thus, these materials will ultimately produce more complex distributions.

## CONCLUSIONS

This study emphasizes the important role uncertainty plays in biomechanics modeling. It was shown that even small changes to the assumed degree of error in the model can lead to much broader uncertainty in the parameter estimates. However, the degree of uncertainty varies from parameter to parameter.

The uncertainty within the parameters represents only the beginning of this investigation as the main goal of this long-term study is to investigate how these parameter uncertainties propagate through the greater FE model. Future work will focus on analyzing the influence and correlation of parametric uncertainties with TBI prediction.

## REFERENCES

1. Drucker DC. *J Appl Mech* **26**, 101-106, 1959.
2. Neal RM. *Handbook of Markov Chain Monte Carlo*, CRC Press, 2011.
3. Holzapfel GA. *Nonlinear Solid Mechanics*, John Wiley & Sons, Ltd., 2000.

## ACKNOWLEDGMENTS

Funding for this project was provided by the Office of Naval Research (ONR) through the Naval Research Laboratory Basic Research Program.

# VALIDATION OF A MUSCULOSKELETAL MODEL INCLUDING THE LOWER LIMBS AND LUMBAR SPINE USING INTRADISCAL PRESSURE MEASUREMENTS

<sup>1</sup> Jason A. Actis, <sup>1</sup> Jasmin D. Honegger, <sup>2</sup> Deanna H. Gates, <sup>1</sup> Anthony J. Petrella, <sup>2</sup> Luis A. Nolasco, and <sup>1</sup> Anne K. Silverman

<sup>1</sup> Department of Mechanical Engineering, Colorado School of Mines, Golden, CO, USA

<sup>2</sup> School of Kinesiology, University of Michigan, Ann Arbor, MI, USA

email: jactis@mymail.mines.edu, web: fbl.mines.edu

## INTRODUCTION

Altered biomechanical loading in the lumbar spine has been suggested as a contributing factor to the greater prevalence of low back pain in certain populations, such as people with a transtibial amputation (TTA) [1]. Musculoskeletal modeling and simulation techniques allow for estimation of muscle and joint contact forces that are difficult or impossible to measure *in vivo*. Reliable estimates of *in vivo* spinal loading from musculoskeletal models can provide insight into potential mechanisms for low back pain development without the need for invasive measurements. However, when developing musculoskeletal models and simulations, validation of the metrics of interest is critical. Thus, the purpose of this study was to develop and validate a whole-body musculoskeletal model with detail of the lumbar spine during planar trunk-pelvis movements for people with and without TTA.

## METHODS

A musculoskeletal model of the trunk and lower limbs with detail of the lumbar spine was developed in OpenSim 3.3. This model included the lower body from [2], the lumbar spine and torso from [3], muscle strengths from [4], and body mass distributions from [5]. The model included 294 Hill-type musculotendon actuators, five lumbar vertebrae and eight additional body segments. The model had 23 degrees of freedom as in [2], with the motion of the five lumbar intervertebral joints defined with a linear function based on overall trunk-pelvis motion. The model was adapted to represent a person with TTA by removing twelve muscles crossing the affected leg ankle joint, reducing the residual shank mass, and shifting residual shank center-of-mass location proximally.

Four male participants (mean(SD): 35(15 yrs, 1.82(0.05) m, 85.4(2.9) kg, one with a left unilateral transtibial amputation), and two female participants (21-25 yrs, 1.64 m, 58.9-79.2 kg, no amputations) were analyzed during four trunk-pelvis range of motion (ROM) trials. Participants began the trials from a neutral standing posture. Sagittal plane flexion, sagittal plane extension, frontal plane lateral bending to the right, and transverse plane axial rotation to the left were completed. Kinematics were collected at 120 Hz with a 20-camera motion capture system and a full-body marker set including markers placed at C7, T8, xyphoid process, and bilaterally at the acromion, PSIS, ASIS, iliac crest, and greater trochanter. Electromyography (EMG) sensors were placed bilaterally on the upper erector spinae and lumbar paraspinal muscles. Ground reaction force and EMG data were collected at 1200 Hz.

Kinematics and GRFs were low-pass filtered with a 4<sup>th</sup>-order Butterworth filter with cutoff frequencies of 6 Hz and 10 Hz, respectively. EMG data were band pass filtered between 6 and 20 Hz. An eight-segment Visual3D model was used to determine the inverse kinematics solution, and to scaled models to each participant. Each analysis began with a static, standing posture of at least 0.5s. Then, a static optimization algorithm solved the muscle recruitment problem at each time step by minimizing an objective function of the sum of muscle activations squared. Estimated back muscle forces from static optimization were compared with the timing of collected EMG data. Net joint contact loads were calculated at L4-L5, low-pass filtered at 1 Hz and converted to intradiscal pressure based on [4] and average L4-L5 intervertebral disc cross-sectional areas (CSA) from [6,7]:

$$\text{Disc Pressure} = \frac{\text{Compressive Force}}{\text{CSA} \times 0.66}$$

## RESULTS AND DISCUSSION

Timing of model muscle activations corresponded well with measured EMG data (example flexion trial, Fig. 1). Disc pressures calculated in the model also generally agreed with those found in [6] and [7] (no significant difference between standing pressures, Fig. 2). The two female participants had the largest ROM of the six participants in flexion, lateral bending (Fig. 2) and extension (not pictured). Greater ROM from females may be attributed to effects of anatomy on trunk and pelvis tracking. Notably, the data from [6] and [7] are from male participants, and thus may be less relevant to females. The decrease in disc pressure at 20-30° of lateral bending was attributed to muscle deactivation in [6], but our loading estimates were higher at these positions. Higher loading from the model relative to [6] may also suggest greater spinal loading in the facet joints. In the model, facet and disc loading are both included in the net contact force, while facet joint loading was unknown in [6].

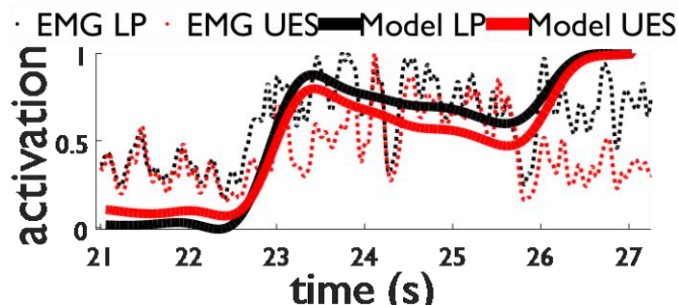


**Figure 1:** Summed model muscle activation estimates (solid) for lumbar paraspinals (LP: multifidus, quadratus lumborum, longissimus pars lumborum, iliocostalis pars lumborum) and upper erector spinae (UES: longissimus pars thoracis, iliocostalis pars thoracis) compared with processed LP and UES EMG signals (dashed) during trunk flexion. Model activations and EMG signals were normalized to their peak filtered value.

## CONCLUSIONS

Estimates of lumbar spine loads during trunk ROM trials in this study were consistent with prior *in vivo* measurements. Future work will further investigate loading differences between males and females and in people with low back pain.

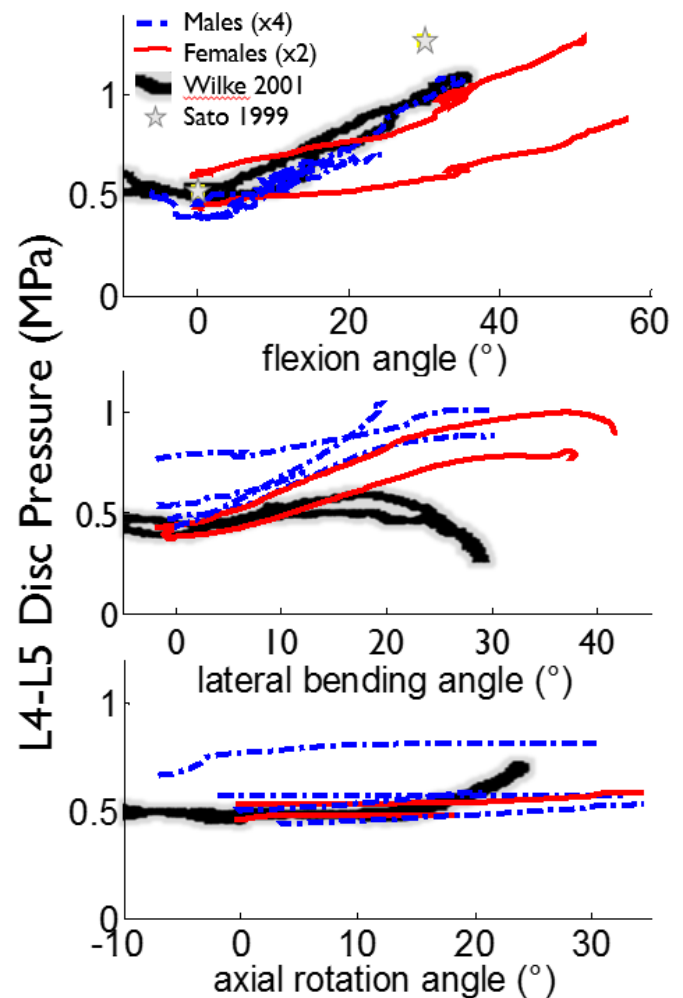


**Figure 2:** Calculated intradiscal pressures during ROM trials for all participants, intradiscal pressures from [6] (black solid line), and average pressures from [7] (gray stars, 8 participants). Data were scaled to body mass in [6].

## REFERENCES

1. Yoder AJ, *et al. Gait Posture*, **41**, 757–762, 2015.
2. Delp SL, *et al. IEEE Trans Biomed Eng*, **37**, 757–767, 1990.
3. Christophy M, *et al. Biomech. Model. Mechanobiol*, **11**, pp. 19-34, 2012.
4. Bruno, *et al. J. Biomech. Eng.*, **137**, 81003, 2015.
5. Winter DA, *Biomechanics and motor control of human movement*, Wiley, 2009.
6. Wilke HJ, *et al. Clin. Biomech.*, **16**, S111-S126 2001.
7. Sato K, *et al. Spine*, **24**, 2468–2474, 1999.

# DEVELOPMENT OF A MULTISCALE MODEL OF THE LUMBAR SPINE: CASE STUDY ON A SIT-TO-STAND MOVEMENT

<sup>1</sup>Jasmin D. Honegger, <sup>1</sup>Jason A. Actis, <sup>2</sup>Luis A. Nolasco, <sup>2</sup>Deanna H. Gates,  
<sup>1</sup>Anne K. Silverman, and <sup>1</sup>Anthony J. Petrella

<sup>1</sup>Department of Mechanical Engineering, Colorado School of Mines, Golden, CO, USA

<sup>2</sup>School of Kinesiology, University of Michigan, Ann Arbor, MI, USA

email: jasminhonegger@mines.edu, web: cbg.mines.edu

## INTRODUCTION

Low back pain (LBP) is a common problem in the general population [1] and has many potential causes. Abnormal whole-body kinematics may lead to increased and/or asymmetric lumbar spine loading, both of which are potential causes of pain. Although LBP is a multifactorial condition, abnormal biomechanics may be an important cause of pain at the tissue-level in locations such as the intervertebral discs or facet joint capsules [2].

Computational modeling techniques can be used to obtain estimates of biomechanical parameters related to LBP that are difficult or impossible to measure *in vivo*. Dynamic rigid-body simulations of human movement can be performed with musculoskeletal models to estimate muscle forces and joint loading. Finite element (FE) models can be used to simulate certain regions of the body and estimate tissue-level mechanics. Separately, both techniques have certain limitations such as lack of constitutive detail in musculoskeletal models and computational expense in FE models. To our knowledge, no previous study has combined the benefits of these two modeling techniques to investigate tissue-level metrics commonly associated with LBP during dynamic movements. The purpose of this study was to develop a multiscale model of the human lumbar spine, including the whole-body-level and tissue-level (lumbar spine L1-L5), and evaluate the model with a case study focused on a sit-to-stand motion.

## METHODS

A whole-body musculoskeletal model with lumbar spine fidelity was created using OpenSim 3.3 (OS). A detailed model of the lumbar spine and torso [3]

was combined with a lower extremity model [4]. A validated FE model of the lumbar spine created in Abaqus/Standard [5] was used to replace the L1-L5 geometry of the OS model and was adapted to match the OS model's global reference frame (Fig. 1a). Lumbar spine muscle attachment locations were obtained using a plugin developed for OS [6] and were transferred from OS to the FE model (Fig. 1b). The fixed centers-of-rotation for each OS model intervertebral joint were implemented in the FE model to constrain the motion of the joints to 3 rotational degrees of freedom (DOF) (Fig. 1c).

One participant was recruited for the case study to test the multiscale model during a sit-to-stand motion (male, 27 yrs, 69.88 kg, 1.75m). The participant was initially positioned in a backless chair with knees and hips at 90° flexion and ankles hip-width apart in a neutral position. The participant's arms were folded across his chest as he progressed to upright standing. Ground reaction forces were collected on two force plates at 1200 Hz and kinematics were collected at 120 Hz using a 20-camera motion capture system.

An inverse kinematics solution was determined using least-squares optimization algorithm with an eight-segment model in Visual3D and used as an input to the OS model. The orientation of the L5 vertebra at each increment of the motion was determined from the OS model and applied to the FE model (Fig. 1d). Using optimization that minimized the sum of muscle activations squared, the force developed by each lumbar spine muscle was estimated at each time increment of the motion and applied to the FE model. Joint contact forces and moments were also determined for the joint between the torso and L1 in the OS model and applied to the FE model for dynamic consistency (Fig. 1e). To evaluate the

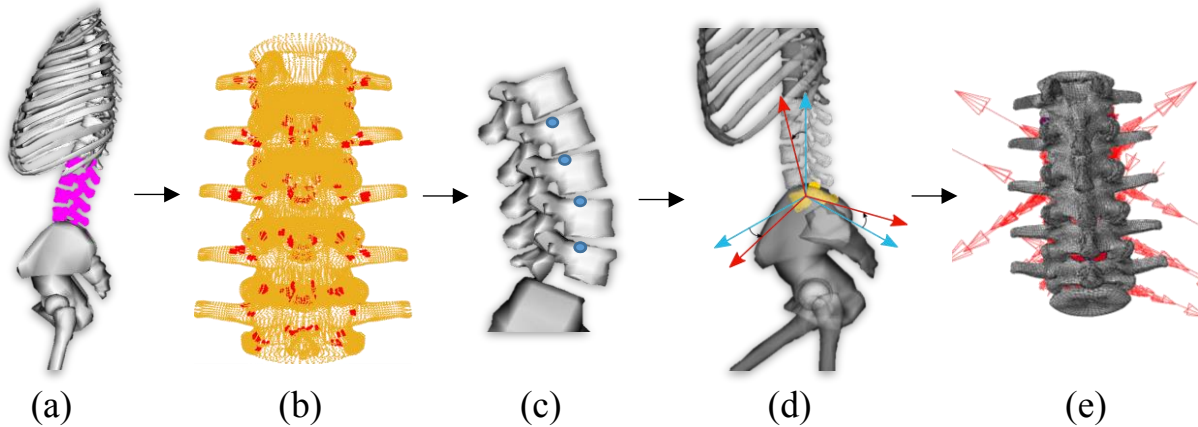


**Figure 1:** Workflow of the multiscale model development (specific step details described in the text).

transfer of muscle forces and consistency of the models at the two length scales, FE output kinematics were compared to the OS input kinematics.

## RESULTS AND DISCUSSION

Total lumbar spine motion (L1-L5) was compared for the 3 rotational DOF (Fig. 2). Flexion exhibited the greatest difference in kinematics ( $8.6^\circ$ ) near the initiation of the sit-to-stand motion.

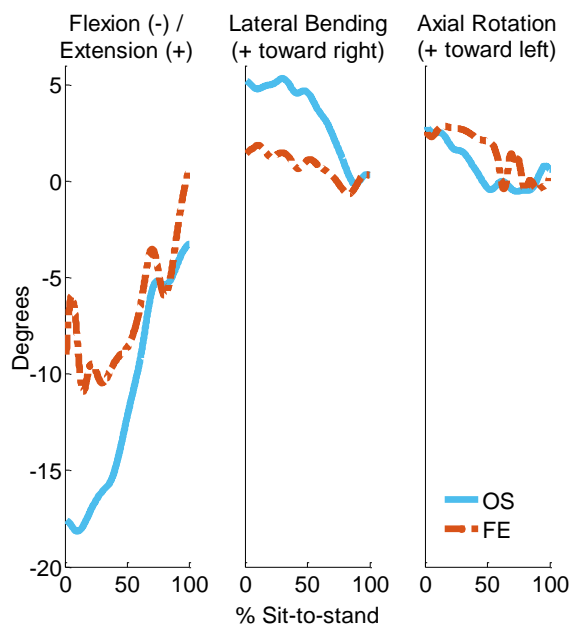


**Figure 2:** Multiscale lumbar spine kinematic evaluation between the OS input and FE output kinematics.

In this multiscale framework, the FE model played the role of sensor to deliver tissue-level metrics (disc stress, facet contact pressure, etc) not represented by the OS model. The validated FE model [5] had sagittally symmetric geometry (Fig. 1b) and generalized material properties for all soft tissues (annulus, nucleus, ligaments, facet cartilage) to represent an average male lumbar spine. This generality in size, shape, and lumbar mechanics was consistent with the OS model (Fig. 1a). Nevertheless, the whole-body OS model (including lumbar joints) was displacement-controlled, whereas the tissue-level FE model was force-controlled. In light of this mechanical difference between the model scales, it can be argued that the kinematic agreement demonstrated in Fig. 2 is quite good, and the FE model is reasonably able to represent variations in tissue-level metrics that are driven by biomechanical abnormalities measurable at the whole-body-level. The broader aim of this research to use the multiscale framework for this purpose – to help clarify how changes in whole-body biomechanics may relate to tissue-level sources of LBP.

## REFERENCES

1. Smith DG, et al. *CORR*, **361**, 29-38, 1999.
2. Bogduk N., Elsevier/Churchill Livingstone, 2012.
3. Christophy M., et al. *Biomech Modeling Mechanobiol*, **11**, 19-34, 2012.
4. Delp, SL., et al. *IEEE TBE*, **37**, 757-767, 1990.
5. Campbell JQ, et al. *J Biomech*, **49**, 2669-76, 2016.
6. Modenese, L., et al. *Accessed: Jan 16 2012*, 2013.

# EFFECT OF MODELING APPROACHES ON NECK MUSCLE MOMENT ARM CALCULATIONS

<sup>1,2</sup> Bethany L. Suderman, <sup>1</sup> Anita Vasavada

<sup>1</sup> Washington State University, Pullman, WA, USA

<sup>2</sup> Guidance Engineering and Applied Research, Seattle, WA, USA

email: vasavada@wsu.edu

## INTRODUCTION

Musculoskeletal models of the cervical spine commonly represent neck muscles with straight paths. However, the curvature of neck muscles affects biomechanical predictions. In this study, we calculated the moment arms of neck muscles *in vivo*, when their paths are constrained naturally by underlying and overlying soft tissues.

The purpose of this study was to compare moment arms of curved and straight neck muscle paths for head and neck flexion and extension, and to compare moment arm calculation methods (tendon excursion, geometric and effective torque methods). We hypothesize that (1) moment arms of curved muscle paths will be significantly different from straight paths; and (2) the three methods will produce significantly different moment arm estimates for curved muscle paths, but not straight.

## METHODS

Magnetic resonance images (MRI) were acquired for two 50th percentile males in 5 sagittal plane postures: 30° and 15° flexion, neutral, 15° and 30° extension. Subjects provided informed consent, and the protocol was approved by the ethics board at the University of British Columbia. Fifteen neck muscle pairs were examined from the MRI data.

The curved path of each muscle was determined from the centroids on each MRI slice, and the straight path was defined between the first and last point (Fig. 1A&B). The muscle paths were also modeled in SIMM (Musculographics, Santa Rosa, CA) using moving muscle points that moved relative to each vertebral body (Fig. 1C) [1]. MRI paths were defined in the five imaged postures, whereas model paths were defined over the range of motion.

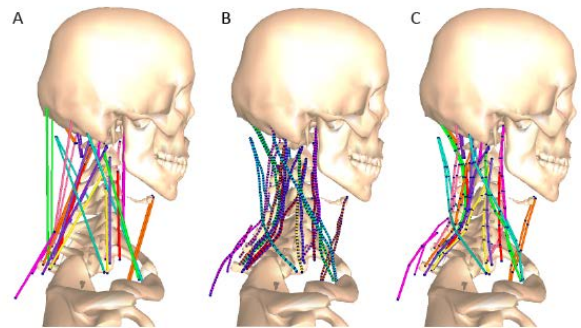


Figure 1: Subject-specific model in the neutral posture. A: Straight muscle paths. B: Curved paths from MRI centroid points. C: Curved paths with moving muscle points.

Five moment arm estimates were determined for each of the straight and curved paths: geometric method for MRI and model paths, tendon excursion for MRI and model, and effective torque for the model. **Geometric (Geo):** The center of rotation (COR) of the head with respect to the sternal notch was calculated using the Rouleaux method [2]. Geometric moment arm was defined as the perpendicular distance from the COR to the straight path; or to a tangent vector through the muscle point closest to the COR in the curved path [3]. **Tendon excursion (TE):** Muscle length was fit with a cubic polynomial, and moment arms were calculated as the derivative of muscle length with respect to joint angle. **Effective torque (ET):** Moment arms were estimated in SIMM as the effective torque: the torque that would produce the same motion as an applied force. Moment arm is the effective torque for a unit muscle force [4].

Moment arm estimates were compared using a two-way ANOVA with repeated measures comparing two factors: muscle path (straight and curved), and moment arm method (model geometric, model tendon excursion, MRI tendon excursion and model effective torque). Root mean square (RMS)



# SCALING OF SUBJECT MUSCLE FORCES FOR USE IN OPTIMIZATION

<sup>1</sup>Jenna Burnett and <sup>1</sup>Timothy R. Derrick

<sup>1</sup>Iowa State University, Ames, IA, USA

email: [jburnet@iastate.edu](mailto:jburnet@iastate.edu), web: <http://www.kin.hs.iastate.edu/>

## INTRODUCTION

Scaling a musculoskeletal model to the properties of an individual can be time consuming if the strength at each joint must be assessed, but the model can be inaccurate if default parameters are used. We sought a compromise that adequately estimated the strength the muscles need to produce torques at selected joints in the lower extremity, and was not time consuming in the data collection process. Therefore, the purpose of this research was to test a procedure that adjusted the scaling factor for maximal static muscle forces to ensuring adequate muscle strength. This method was compared to a method that used a set scaling factor to estimate muscle strength.

## METHODS

Seven young adult recreational runners (3 males, age: 21.3±2.1 yr; body mass: 68.9±6.7 kg; height: 1.84±0.07 m and 4 females, age: 25.3±5.2 yr; body mass: 56.6±11.3 kg; height: 1.64±0.08 m) participated in this study. The runners ran across a force platform (1000 Hz) at 3.5 m/s while 8 cameras recorded the kinematic data (200 Hz). Inverse dynamics and rigid body assumptions were used to estimate 3D joint moments at the hip, knee and ankle. A musculoskeletal model [1] estimated the maximal dynamic muscle forces and moment arms for each of 44 lower extremity muscles. The maximum isometric muscle forces were first scaled by body mass and then increased by a factor of 1.5. This scaling factor is the suggested value to get the model to walk with adequate strength using OpenSIM software [2]. The isometric forces were adjusted by length and velocity during each frame of the activity to obtain maximal dynamic muscle forces. These were then used as input to an optimization procedure that estimated the actual muscle forces during the running. The optimization procedure selected muscle forces that minimized the sum of the squared muscle stresses while constraining the solution such that the

muscles produced torques estimated from the inverse dynamics, if possible. The selected constraints were the sagittal plane hip, knee, and ankle torques as well as the frontal and transverse plane hip torques. The optimization was run a second time, and instead of a scaling factor of 1.5, a variable scaling factor was used. This value was estimated such that the muscles had enough strength to produce the joint torques of the given running trial. During each frame of data, the maximum dynamic muscle forces were multiplied by the muscle moment arms and the resulting torques were compared to the inverse dynamic forces during the trial. If they were not adequate, the muscle forces were increased to a level that insured the actual joint torques could be matched.

## RESULTS AND DISCUSSION

The set max force condition with a scaling factor of 1.5 did not create muscle forces that could produce the inverse dynamics torques during running (Figure 1). The average variable scaling factor was 2.5±0.27. Each joint had a statistically significant reduction in the RMSE for the variable scaling factor condition (Table 1).

Table 1: RMSE for the set and variable factors (\* indicates significance).

Joint Torque	RMSE SF (N)	RMSE VF (N)
Sagittal Hip Torque	7.7±3.3	3.3±1.1*
Frontal Hip Torque	18.3±7.5	4.3±1.5*
Transverse Hip Torque	2.2±1.2	1.4±0.7*
Sagittal Knee Torque	19.5±9.8	3.5±1.1*
Sagittal Ankle Torque	26.2±7.7	3.1±2.1*

It should be noted that the RMSE for the variable factor condition was not reduced to zero. This is likely because co-contractions can reduce the ability of the muscles to produce their maximum joint

torque. This may need to be taken into account when estimating the scaling factor in future research. Further refinement of this method might include a separate scaling factor for each joint, with biarticular muscles taking the larger scaling factor of the two joints. It might be argued that all that is needed is to increase the set scaling factor from 1.5 to 2.5. This may work but it reduces the advantage of selecting a scaling factor based on individual strength.

### CONCLUSIONS

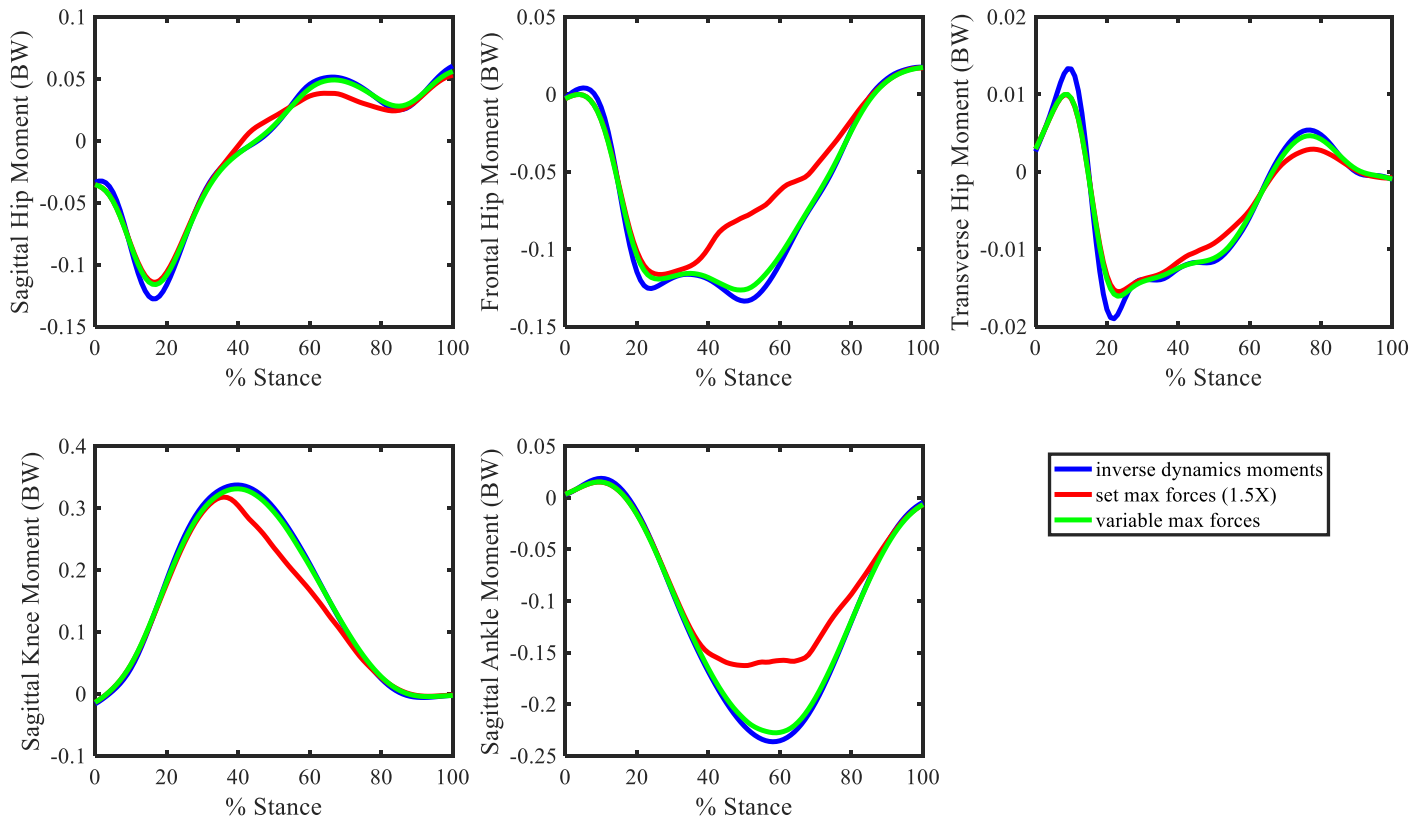
The variable scaling factor technique successfully ensured that the muscles adequately produced the inverse dynamics torques for a particular activity.

This may be a better technique than applying a set scaling factor to all of the subjects. At the very least it ensures that muscle torques are not underestimated by the optimization process.

### REFERENCES

1. Arnold, EM, et al. *Ann Biomed Eng*, **38**, 269-279, 2010.
2. Delp, S.L., et al. *IEEE transactions on biomedical engineering*, **54**, 1940-1950, 2007.

Figure 1: Maximal muscle moments in the hip, knee, and ankle for the set factor, variable factor and inverse dynamics



# INCLUSION OF MENISCI IN FINITE ELEMENT MODELS OF THE KNEE JOINT: IMPLICATIONS ON CARTILAGE CONTACT PRESSURE AND ACL STRAIN

<sup>1</sup>S Sadeqi, <sup>1</sup>R Summers, <sup>1</sup>M Ingels, <sup>2</sup>TE Hewett, and <sup>1</sup>V Goel

<sup>1</sup>Engineering Center for Orthopaedic Research Excellence, University of Toledo, Toledo, OH, USA

<sup>2</sup>Center for Sports Medicine, Mayo Clinic, MN, USA

email: vijay.goel@utoledo.edu

## INTRODUCTION

The menisci play an important role with respect to knee kinematics and loading, but to date, many finite element (FE) knee models omit the menisci [1]. The purpose of this study was to simulate knee joint loading scenarios during bipedal landing from a jump associated with anterior cruciate ligament (ACL) injury using finite element models with and without menisci to investigate the contribution of the menisci to resulting knee kinematic, cartilage pressure and ACL strain.

## METHODS

MR images from one, healthy, 21 year old male were converted to 3D models of bone and soft tissue using Mimics (Materialise, Leuven, Belgium). Meshes of C3D4 elements were constructed in Hypermesh (Altair, MI, USA) before final assembly in Abaqus/Explicit 6.14-5 (Simulia, RI, USA). Cruciate and collateral ligaments were modeled as Holzapfel-Gasser-Ogden hyperelastic materials. The remaining joint capsule was modeled with uniaxial connector elements. Bone and cartilage were modeled as linear elastic materials. Menisci were modeled as transversely isotropic. The meniscal horns were modeled as nonlinear axial connector elements with an effective stiffness of 2000 N/mm [2].

Surface to surface contacts between the menisci and opposing cartilage surfaces were defined. The contacts were frictionless with a “hard contact” pressure overclosure relationship to prevent penetration of the master surface into the slave. The menisci were removed from the model for simulations without menisci.

Simulations were done at 25° flexion with 1200 N quadriceps and 800 N hamstrings loads. Four loading scenarios were considered: 268 N anterior shear force (ASF), 60 Nm internal tibial rotation moment (ITM), 75 Nm knee abduction moment, and all three loads combined. All load cases were followed by an impact step representative of a bipedal landing (half body-weight) from a height of 30 cm.

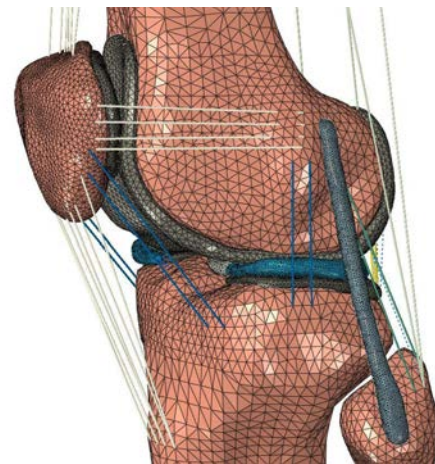


**Figure 1:** Finite element knee model with intact menisci shown in light blue.

## RESULTS AND DISCUSSION

Internal tibial rotation and knee valgus angle tended to increase in simulations without the menisci, most notably in the isolated loading conditions. Little difference was seen for ACL strain and anterior tibial translation with and without menisci cases. Although the data for both with and without menisci were similar, the data for simulations with menisci were in better agreement with the mean values reported by Kiapour et al [3] for cadaveric assessment of ACL injury mechanisms.

Maximum contact pressure on the lateral (LTC) and medial (MTC) tibial cartilages were computed, Table 1. Peak contact pressure increased for all loading cases after the menisci were removed from the models. In ASF and ITM loadings the maximum contact pressure was observed on the medial tibial cartilage while in KAM and combined loading maximum contact pressure was on the lateral tibial cartilage. Figure 2 shows the contact pressure contours for pure ATS loading condition.

## CONCLUSIONS

The emphasis of this study was on the impact that modelling the menisci in FE models of the knee joint has in predicting ACL strain and resulting kinematics and contact pressures. The results presented herein showed a moderate impact on the kinematics at the knee joint under loads and impact representative of bipedal landing. Results showed increased contact pressure on the tibial cartilages in all cases.

Future efforts, including a more robust sample size, expanded loading conditions over larger ranges of

flexion, and varied material properties of the menisci (representative of pathology and variation inherent in the population) are warranted to further study the impact of the menisci on the knee joint as well as the relevance of their inclusion in finite element models of the knee. A total of three models were developed over the course of this study and will be included in future works. Our data suggest that due to decrease in cartilage pressure in the presence of menisci, healthy menisci in athletes may be helpful in preventing/delaying the onset of OA.

## REFERENCES

1. Hull et al, J Biomech Eng. 2002
2. Haut Donahue et al, J Biomech Eng. 2003
3. Kiapour et al, J BiomechEng, 2014

## ACKNOWLEDGMENTS

Supported in part by NIH (R01 AR056259-06-TEH) and by an allocation from the Ohio Supercomputer Center.

**Table 1:** Peak contact pressures on the tibial cartilages for each load case with and without menisci present in the model.

	268 N ATS		75 Nm KAM		60 Nm ITM		Combined loading	
	With menisci	Without menisci	With menisci	Without menisci	With menisci	Without menisci	With menisci	Without menisci
<b>Contact Pressure (Mpa)</b>	5.36/MTC	7.35/MTC	6.24/LTC	7.76/LTC	8.04/MTC	9.9/MTC	5.66/LTC	7.19/LTC

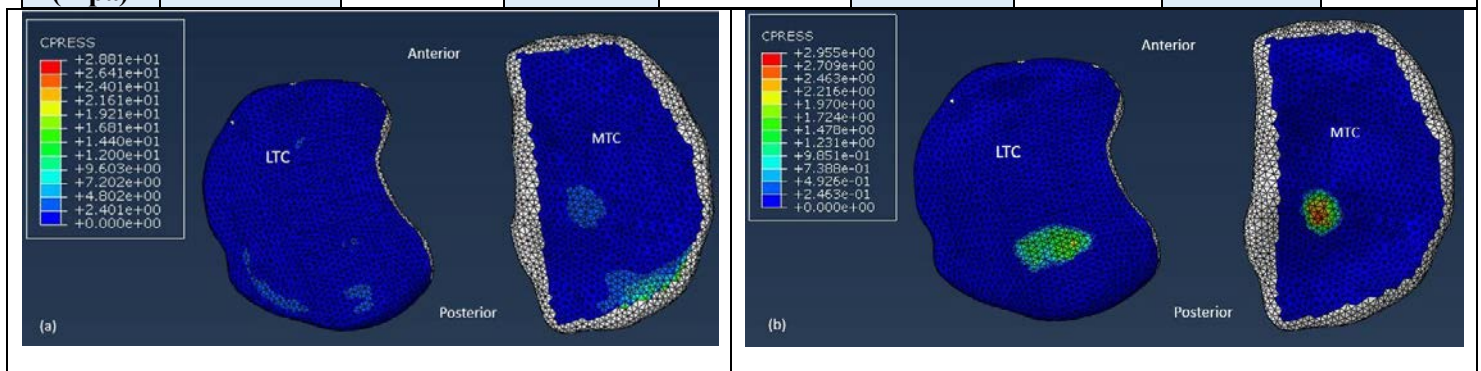


**Figure 2** - Contact pressure contour on medial and lateral tibial cartilages in the ATS only loading condition in (a) model with menisci (b) model without menisci

# A 3D MODEL OF THE MEDIAL GASTROCNEMIUS CREATED BASED ON *EX VIVO* ARCHITECTURAL MEASUREMENTS

<sup>1</sup> Adrienne Williams, <sup>1</sup> Xiao Hu, <sup>2</sup> Samuel Ward, <sup>2</sup> Richard Lieber, and <sup>1</sup> Silvia Blemker

<sup>1</sup> University of Virginia, Charlottesville, VA, USA

<sup>2</sup> University of California, San Diego, CA, USA

email: afw6gf@virginia.edu, web: <http://bme.virginia.edu/muscle/>

## INTRODUCTION

The quality of magnetic resonance- and ultrasound-based three-dimensional (3D) models in biomechanics research relies heavily on the ability to accurately represent muscle architecture in these models. It is important to investigate the accuracy, usefulness/functionality and validity of these biomedical image-based models, to ensure that they parallel biological conditions, since conclusions made from these models are often used to inform medical treatments and surgeries. Simple models are an excellent means by which to conduct preliminary research, as they allow for method refinement before investing resources into further MRI and ultrasound image acquisition, processing and complex model building.

The aim of this study was to demonstrate how a simple 3D computer aided drawing (CAD) muscle model can be created to match available architectural data of an *ex vivo* specimen. This method will be demonstrated with human medial gastrocnemius (MG) data measured *ex vivo* by anatomical inspection and ultrasound [1-3].

## METHODS

Lower limb muscle architecture data was collected from the cadaver of a 52 y-o, male subject (ht = 170.18 cm, wt = 74.84 kg) during a previous study [1]. At the time of data collection, photographs were taken of each muscle with tendons intact. A photograph of the medial gastrocnemius (MG) was imported into Autodesk Inventor (Autodesk Inc., San Rafael, CA) and a 2D outline of the muscle was made using interpolated splines, to obtain the frontal shape of the muscle. The drawing was scaled according to the muscle and tendon lengths in Table 1 (below). The 2D drawing was extruded to create an 11.43 mm thick 3D object. This thickness was selected based on the mean thickness

of an *ex vivo* MG from a 62 y-o male, measured by anatomical inspection [3]. The model was divided into 3 parts (proximal, central and distal) by two 0.5 mm cuts that a) ran from one-third the length of the proximal to one-third the length of the distal tendon and b) ran parallel to the first, and halved the remaining 2/3<sup>rds</sup> of both tendons (Figure 1B).

**Table 1:** *Ex vivo* medial gastrocnemius architectural data used to create the simple model.  $L_M$  = muscle length,  $L_{TIP}$  = length internal proximal tendon,  $L_{TID}$  = length internal distal tendon

Architectural Property	Measurement
Mass <sub>NoTendon</sub> (g)	175.73
$L_M$ (mm)	276.73
$L_{TIP}$ (mm)	210.80
$L_{TID}$ (mm)	211.35

These planes served as “flow guides” when the volume was exported to Simulation CFD (Autodesk Inc., San Rafael, CA), a computational fluid dynamics (CFD) software used as a Laplacian approach for defining muscle fiber tractography [4]. CFD material parameters were set to incompressible with fluid density and viscosity set to: 1 g/cm<sup>3</sup> and 1000 Pa-s, respectively, to ensure laminar flow. To simulate muscle fascicles running from tendon to tendon, inlet boundary conditions of 1 Pa pressure was set at proximal aponeurosis and an outlet condition of 0 Pa pressure at distal aponeurosis. All other surfaces were given a slip condition, which ensured laminar flow. The program’s automatic mesh function was used to generate a fine mesh for which fluid velocity vectors were obtained at each element upon completion of the flow simulation. Fiber tracts (lengths) were determined in MATLAB (Mathworks, MA) by calculating the lengths of streamlines generated from seed points set along the central YZ plane of the model (Figure 1C).

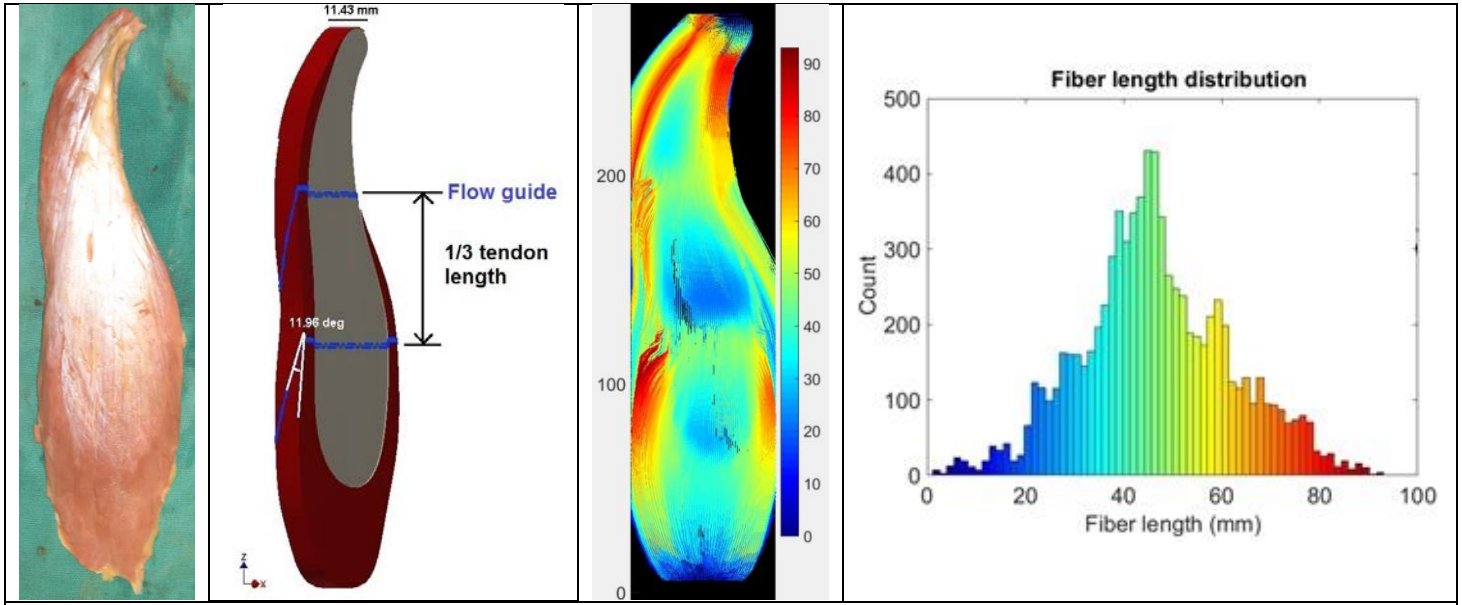


**Figure 1:** A) Photograph of *ex vivo* medial gastrocnemius (MG), B) 3D CAD model of MG, created using photograph and scaled to architectural measurements from same specimen, C) Fiber tracts throughout 3D MG model determined by computational fluid dynamics simulation, and D) fiber length distribution of all tracts in model

Fiber lengths were visually estimated from the simple model in three locations similar to those recorded in the *ex vivo* specimen [1]. The mass of the specimen was used to calculate its volume, assuming that density of muscle is  $1.056 \text{ g/cm}^3$ . The CSA of the coronal face of the model was used to find its volume. After model construction, pennation angle ( $\theta$ ) of the model was determined as the angle between the flow guides and the coronal face of the model. PCSA was calculated using the following formula [2], taking into account  $\theta$ :

$$PCSA (\text{cm}^2) = \frac{M (\text{g})}{\rho (\text{g/cm}^3)} \times \frac{\cos \theta}{Lf (\text{cm})}$$

## RESULTS AND DISCUSSION

The simple model captured the average fiber length and PCSA of the *ex vivo* specimen very well (Table 2). The average Lf was 52 mm for both the specimen and the model, thus the Lf/Lm ratio was the same at 0.19. The smaller volume of the model compared to the 52 y-o specimen volume was likely because the model's thickness measurement came from the more atrophied muscle of a 62 y-o specimen. The differences in pennation angles were attributed to the constraints of the CFD flow guides and the uniform thickness of the model. The model's angle is a function of its thickness, since the guides must dissect both the proximal and distal

tendons into thirds. Despite the model's smaller pennation angle, the PCSA of the model was  $29 \text{ cm}^2$  compared to  $31 \text{ cm}^2$  of the model, thus very similar.

**Table 2:** Comparison of the *ex vivo* medial gastrocnemius (MG) data and parameters of the simple model.  $Lf_{\text{ave}}$  = average fiber length of 3 different locations

Source	Volume ( $\text{g/cm}^3$ )	$Lf_{\text{ave}}$ (mm)	$\theta$ ( $^\circ$ )	PCSA ( $\text{cm}^2$ )
<i>Ex vivo</i> MG	166.41	51.86	18.33	30.52
Simple model	153.10	51.67	11.96	28.99

This study shows that a simple CAD model can recapitulate *ex vivo* architectural data very similarly and may be useful in the initial stages of image-based muscle modeling research for fine-tuning and sensitivity analyses of dynamic and finite element simulations, for example. Other muscles with different architectural arrangements should be modeled similarly to determine if this method is applicable to all muscles.

## REFERENCES

1. Ward SR, et al. *Clin Orthop Relat Res* **467**: 1074–1082, 2009.
2. Wickiewicz TL, et al. *Clin Orthop* **179**: 275–283, 1983.
3. Narici MV, et al. *J Physiol* **496.1**: 287–297, 1996.
4. Inouye JM, et al. (2015) *Proc Summer Sim Multi-Conf*, 2015

## ACKNOWLEDGEMENTS

We thank Geoffrey Handsfield for his helpful feedback.

# STRAIN ANALYSIS ON THE FEMORAL NECK USING FINITE ELEMENT MODEL DURING STAIR NAVIGATION

<sup>1</sup>Chen Deng, <sup>1</sup>Jason C. Gillette, <sup>1</sup>Timothy R. Derrick

<sup>1</sup>Iowa State University, Ames, IA, USA

email: [chend@iastate.edu](mailto:chend@iastate.edu), web: [http:// www.kin.hs.iastate.edu/](http://www.kin.hs.iastate.edu/)

## INTRODUCTION

Femoral neck stress fractures are among the most serious of all types of stress fractures [1,2]. Understanding the loading environment is a crucial factor for reducing their incidence [3,4]. The loading at the femoral neck can be estimated by applying activity specific loading, (muscle forces and joint contact forces) to the finite element model of the femur. In this study, the purpose was to analyze both tensile and compressive strains at the femoral neck during stair ascent and descent.

## METHODS

17 older adults (7 males, age:  $60 \pm 6$  yr, body mass:  $75 \pm 14$  kg, height:  $1.73 \pm 0.05$  m; 10 females, age:  $57 \pm 5$  yr, body mass:  $67 \pm 8$  kg, height:  $1.67 \pm 0.05$  m) with no lower limb injuries volunteered to participate. All subjects performed 5 successful trials of stair ascent and the same number trials of descent with a 3-stair staircase. Motion capture data (120 Hz, Vicon MX, Vicon, Centennial, CO, USA) and force data (120 Hz, AMTI, Watertown, MA) were collected during each trial.

Raw force data and motion capture data were input into Matlab programs and low-pass filtered at 6 Hz. Inverse dynamics and rigid body assumptions were used to calculate 3-D joint moments and reaction forces at the hip, knee and ankle of the right leg. A musculoskeletal model was used to obtain maximal dynamic muscle forces, muscle moment arms and orientations for 44 lower limb muscles [5]. Static optimization was used to select a set of muscle forces that minimized the sum of the squared muscle stresses and balanced the sagittal plane hip, knee and ankle moments, frontal plane hip moment, and the transverse plane hip and ankle moments with the external moments for each frame of data. Muscle forces and joint reaction forces were summed to estimate the 3-D hip joint contact forces.

Hip joint contact forces and 27 muscle forces attaching on the femur were used in the Matlab program to write input model files for FEBio software, which ran the finite element analysis for the entire femur during peak resultant hip joint contact forces for both first and second half of the stance phase.

The maximum compressive and tensile strains during the two hip joint contact force peaks on the cross-section of femoral neck were identified. Differences in maximum tensile and compressive strains during hip joint contact force peaks between stair ascent and descent were assessed by paired t-tests with 2 tails ( $\alpha = 0.05$ ).

## RESULTS AND DISCUSSION

Both of the compressive and tensile maximum strains were reported at the time of peak hip joint contact force during stair ascent and descent.

For the compressive strains, stair descent produced greater maximum strains than stair ascent at peak 1 of the hip joint contact force (stair ascent:  $-853.2 \pm 381.2$   $\mu\text{s}$ , stair descent:  $-1133.6 \pm 883.0$   $\mu\text{s}$ ,  $p = .0079$ ) and peak 2 (stair ascent:  $-781.8 \pm 372.4$   $\mu\text{s}$ , stair descent:  $-1120.4 \pm 939.8$   $\mu\text{s}$ ,  $p < .001$ ).

The increased compressive strains during stair descent could be caused by the impact of the initial foot contact on the ground at peak 1, and greater acceleration during push off at peak 2.

In Figure 1.1, greater compressive strain was located at the superior-posterior side for stair ascent, while the inferior side had more compressive strains for stair descent.

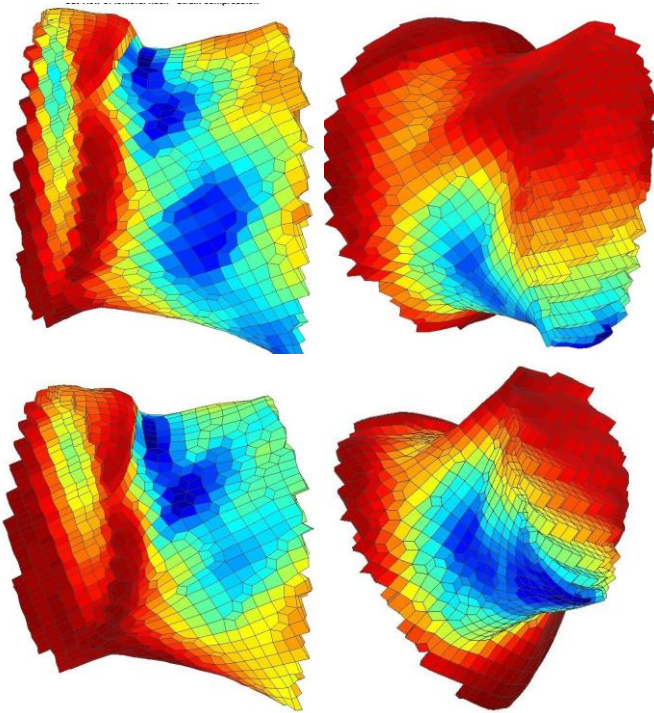


**Figure 1.1:** The compressive strain distribution for the femoral neck: top-left (peak 1 for stair ascent, posterior view), top-right (peak 1 for stair descent, posterior-lateral view), bottom-left (peak 2 for stair ascent, posterior view), bottom-right (peak 2 for stair descent, posterior-lateral-inferior view).

There was no statistical difference for the tensile strains at both peaks of the hip joint contact force between stair ascent and descent (peak 1:  $p = 0.374$ , peak 2:  $p = 0.967$ ). The tensile strains were similar between stair ascent and descent for both peak 1 (stair ascent:  $1769.2 \pm 810.9 \mu\text{s}$ , stair descent:  $1574.1 \pm 1476.9 \mu\text{s}$ ) and peak 2 (stair ascent:  $1544.4 \pm 713.6 \mu\text{s}$ , stair descent:  $1519.9 \pm 1568.3 \mu\text{s}$ ).

It is likely that stair ascent and descent did not produce tensile loading on the femoral neck differently. This may be due to the activities of the hip abductor muscles, which could counter the large adductor torque caused by the torso weight.

In Figure 1.2, greater tensile strain was located at the superior-posterior side for stair ascent, while the maximum tensile strains occurred at the superior side for stair descent.

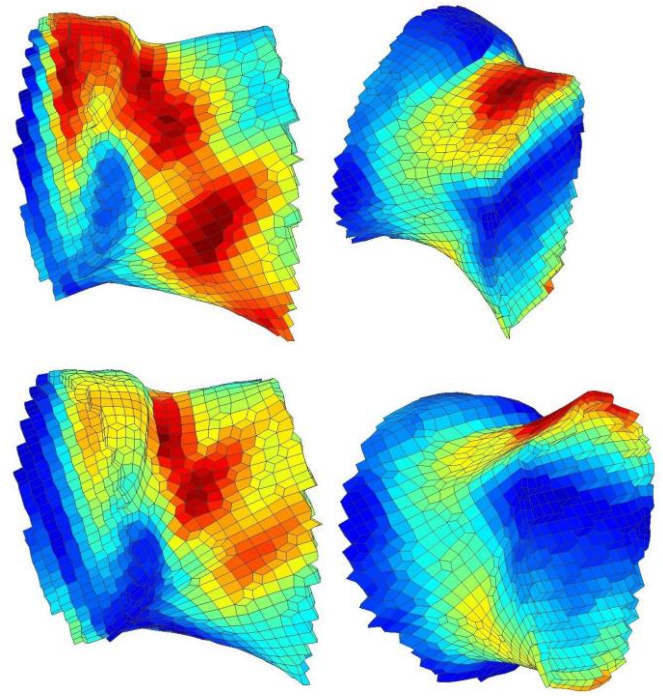


**Figure 1.2:** The tensile strain distribution for the femoral neck: top-left (peak 1 for stair ascent, posterior view), top-right (peak 1 for stair descent, posterior-lateral-anterior view), bottom-left (peak 2 for stair ascent, posterior view), bottom-right (peak 2 for stair descent, posterior-lateral-inferior view).

## CONCLUSIONS

At the femoral neck, the compressive strains increased during stair descent compared to ascent, while the tensile strains did not change. Since the finite element (FE) model was based on only one cadaver, the FE model with more individualized bone geometry and material properties (CT or MRI) could improve estimates of bone strain.

## REFERENCES

1. Center JR, et al. *The Lancet*, 353(9156), 878-882, 1999.
2. Nieves JW, et al. *Osteoporosis Int*, 21(3), 399-408, 2010.
3. Bergmann G, et al. *J Biomech*, 26, 969-990, 1993.
4. Rohlmann A, et al. *J. Biomed.* 4, 241-246, 1982.
5. Arnold, EM, et al. *Ann Biomed Eng* 38(2), 269-279, 2010.

# A Zero-Feedback and Stable Running Model Controlled by a Central Pattern Generator

Samuel Masters, Justin Wager, and John Challis

The Pennsylvania State University, University Park, PA, USA  
email: sem361@psu.edu

## INTRODUCTION

The trajectory of the whole-body center of mass (COM) during human running is similar to that of a spring-loaded inverted pendulum (SLIP). Humans passively store and release energy, and actively produce energy during running. The triceps surae are the main contributors to propulsion during running [1]. The gross motion of the center of mass during the stance phase is mostly due to knee and hip kinematics. Thus, a simple two-body SLIP model that represents the lower and upper bodies and has an active propulsive phase should be sufficient to capture many aspects of human running.

Stability has been studied in human locomotion. However, the majority of these studies center around human walking and their asymptotically stable robotic and model counterparts. Human running does not have an asymptotically stable model counterpart. We will propose and analyze an asymptotically stable running model that can be used to study the stability and energetics of human running.

## METHODS

The SLIP model contained two masses, a spring connecting the upper body to the lower body, and a spring-damper connecting the lower body to the ground (Fig. 1). The springs had a constant stiffness and nonlinear dampening. The dampening was a function of the dampening constant, spring compression, and spring compression velocity.

The SLIP model was powered by an external moment at the spring-ground interface and a propulsive force (PF) that accelerated the whole system COM. The moment was directly proportional to the PF. The propulsive phase of the gait cycle

started when the COM was past vertical and ended when the spring connecting the ground to the lower leg approached its resting length. A tanh function was utilized in order to enforce a zero PF and external moment before and after the propulsive phase.

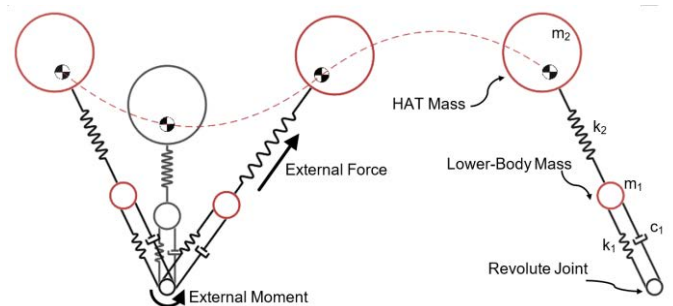


**Figure 1:** Two-mass SLIP model of running with a stance and flight phase.

Stance phase kinematics and vertical ground reaction forces (GRFs) from 10 college-aged male subjects were used to determine the parameters of the model. The COM vertical position and velocity were fitted with a sine wave to enforce smoothness and cyclical kinematics. A particle swarm optimization was utilized to determine the best set of parameters for matching the modeled fit for each subject's kinematics and the magnitude and timing of the impact and active force peaks of the vertical GRF. Following the optimization, the SLIP model was simulated until its step cycle converged to a period-one gait cycle.

The PF and initial ground-contact angle were tuned such that the horizontal velocity of the model match that of each subject during stance phase. The flight-phase kinematics were determined using constant acceleration equations of motion and the next stance cycle proceeded when the COM height was at the experimental COM height during foot-ground contact.

A simple measure of stability was utilized to assess the SLIP model's performance. The spring attaching the lower body to the ground was increased in stiffness by 100% for a single step cycle to simulate a local change in the stiffness in terrain. The number of steps that the model took until the COM velocity kinematics converged to within  $10^{-3} \text{ m}\cdot\text{s}^{-1}$  of the period-one gait cycle were counted (Fig. 3).

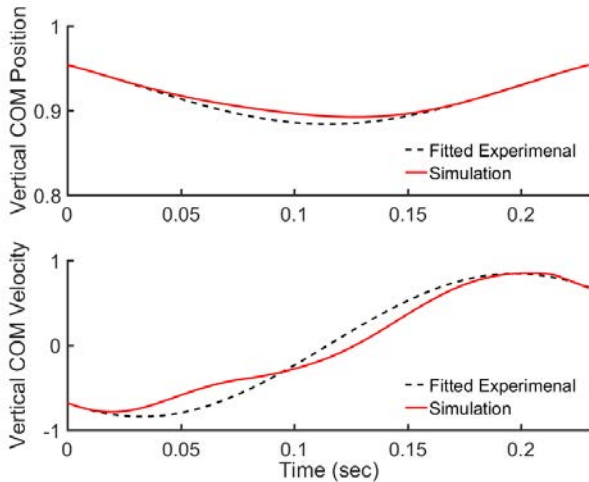


**Figure 2:** The stance phase vertical COM trajectory for a typical experimental trial (black, dotted line) and the SLIP model (red, solid line).

## RESULTS AND DISCUSSION

All units containing force were normalized with respect to subject body weight (BW). The mean spring stiffness for the lower and upper springs were  $309 \pm 27 \text{ BW}\cdot\text{m}^{-1}$  and  $224 \text{ BW}\cdot\text{m}^{-1}$ , respectively. The dampening constant was  $18.8 \pm 5.1 \text{ BW}\cdot\text{s}\cdot\text{m}^{-1}$ . The mean PF and PM were  $7.2 \pm 1.5 \text{ BW}$  and  $2.1 \pm 1.0 \text{ BW}\cdot\text{m}$ . The weight of the lower and upper bodies were 0.165 BW and 0.835 BWs.

The vertical COM position and velocity of the SLIP model matched that of the fitted experimental data

(Fig. 2). The vertical COM position of the SLIP model was always within 10% of the experimental data. The mean horizontal velocity was  $2.9 \text{ m}\cdot\text{s}^{-1}$  and vertical velocity at foot-ground contact was  $0.72 \text{ m}\cdot\text{s}^{-1}$ . On average, the magnitude of the impact and active peaks of the GRF were within 9.1% and 8.5% of the experimental vertical GRF.

None of the models failed to converge following a perturbation to the lower body spring stiffness. The mean number of steps that each model took before converging to the limit cycle was 31.4 steps (Fig. 3). Generally, the models with a higher spring stiffness took longer to converge.

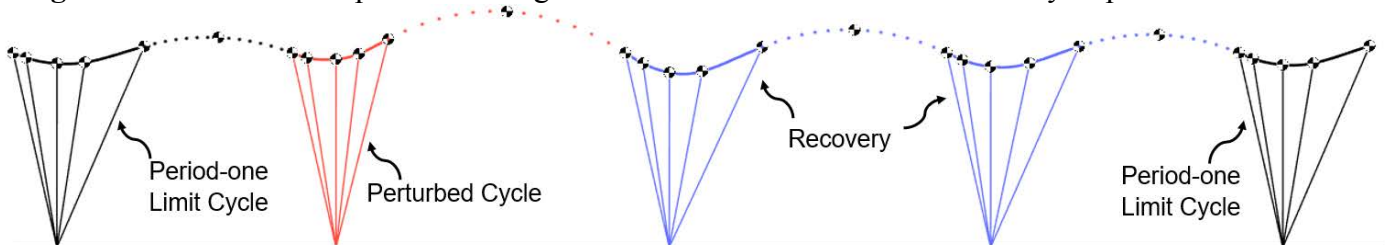
Due to the simplicity of the model and the exclusion of a feedback controller, it can be used to study many of the same aspects that we study in simple, bipedal walkers. Some of those aspects include local, orbital, and global stability measures (e.g., Lyapunov Exponents, Floquet multipliers, and the basin of attraction), the energetics of running (e.g., dissipation, storage, and return of energy), and the whole-body or segmented body COM trajectories during running (e.g. control strategies for locomotion).

We have introduced a model of running that expands on the SLIP model of running [2] to include a CPG. The model is asymptotically stable, requires no control feedback for sufficiently small perturbations, and can mimic the kinematics and dynamics of the COM during human running.

## REFERENCES

1. Hamner SR, et al. *J Biomech* **43**, 2709-2716, 2010.
2. Blickhan R. *J Biomech* **22**, 1217-1227, 1989.

**Figure 3:** Center of mass position during a simulated trial. Some of the recovery steps have been removed.



# GROUND CONTACT MODEL FOR VERTICAL JUMPING OF KANGAROO RATS

<sup>1</sup> Mehrdad Javidi, <sup>2</sup> Jeffrey Rankin, <sup>2</sup> Craig McGowan, and <sup>2</sup> David Lin

<sup>1</sup> Washington State University, Pullman, WA, USA

<sup>2</sup> University of Idaho, Moscow, ID, USA

Email: mehrdad.javidi@wsu.edu

## INTRODUCTION

A ground contact model is essential for forward dynamic simulations because it determines the forces applied to the skeletal system to generate a movement. A previous strategy has been to model the ground contact of human walking with viscoelastic elements which generate force as the foot penetrates the surface in forward dynamic simulation [1]. The viscoelastic model is physically based upon the material properties of the shoe, ground surface and foot [2]. Although this model is able to produce accurate results, development and verification of the model has to be done within the context of forward dynamic simulations and errors can be masked by an array of other uncertainties within the simulation. Moreover, the previous model is for humans and cannot be applied to other animals. Thus, a ground contact model which is linked to the joint kinematics could be developed and verified more easily.

A focus of our research is to elucidate the mechanisms of extreme jumping performance in kangaroo rats. To perform forward dynamic simulations of vertical jumping, we need to develop a ground contact model. Ideally, there would be only one viscoelastic element that is linked to the joint kinematics, so that it could be developed and verified through experimental data. To this end, we defined a virtual displacement for foot segment based upon midfoot angle and then calculated force by applying this displacement to a viscoelastic element. We found model parameters from experimental data and assessed model accuracy using different experimental trials with a range of jump heights.

## METHODS

### *Experimental Data*

Kinematic and kinetic data of a kangaroo rat (weight 0.11 kg) were collected during 5 different vertical jumps over barriers 30 to 40 cm in height. A high

speed video system (250 Hz) recorded the kinematics of the jump, which was used to calculate joint angles. Ground reaction force data were collected simultaneously by using a force platform (600 Hz).

### *Ground Contact Model*

We chose to link the viscoelastic model to rotation of the metatarsal-phalangeal (MTP) segment for two reasons: empirically, the MTP kinematics was most closely correlated to the time-course of the ground reaction force; and theoretically, the MTP joint could act as a passive rotational spring due to the anatomy of the kangaroo rat foot. Contact force between the toe and the ground was generated by one viscoelastic element attached to the toe at a distance of  $r$  from MTP joint. The amount of virtual motion of the viscoelastic element has determined by rotation of the MTP joint minus the amount of vertical motion of the MTP joint (*i.e.*, movement away from the ground). This amount was calculated according to:

$$z = -(\cos(\theta))^2(r \cdot \sin(\theta) - z_{midfoot\ joint}) \quad (1)$$

where  $r$  = distance of attachment point to MTP joint (15 mm),  $\theta$  = angle of MTP segment (relative to horizontal) minus the initial MTP angle (*i.e.*, the change in angle from the initial posture) and  $z_{midfoot\ joint}$  = MTP joint vertical coordinates. Note that the additional cosine term is to account for less contact area of toe segment on the ground (*i.e.*, less contact with the viscoelastic element).

Force produced by the viscoelastic element was calculated as:

$$F = C_f(c_1z + c_2\dot{z}) \quad (2)$$

where  $F$  = change in vertical force from the initial ground reaction force (equaling body weight) and  $c_1$  and  $c_2$  are foot specific parameters of the viscoelastic element.  $C_f$  is a correction factor that is based on initial posture:

$$C_f = 1 + \theta(t = 0) \quad (3)$$

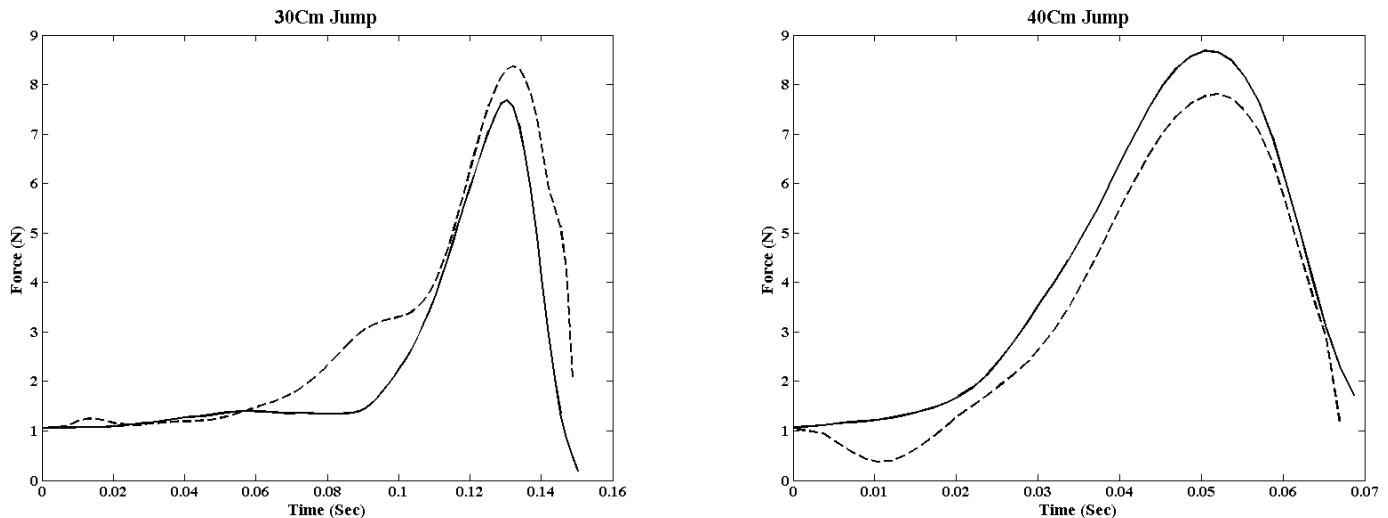


**Figure 1.** Experiment (solid line) and simulation (dashed line) force for lowest and highest jump heights.

This correction factor was necessary because the model only used MTP rotation and vertical position, so more extended initial postures needed larger viscoelastic coefficients to maintain body weight. The correction factor ranged from 1.13 to 1.52. The model coefficients in equation (2) were optimized to fit the simulation force with experimental data according to least squared error, and they were kept constant for all trials.

## RESULTS AND DISCUSSION

Model coefficients were optimized as  $c_1 = -1200 \text{ N/m}$  and  $c_2 = -1.5 \text{ N.s/m}$ . Simulated and experimental force compared well across the range of jump heights (Fig. 1). To assess the accuracy of the simulation, we used temporal and amplitude metrics. For temporal accuracy, the average difference between the time of the simulated and experimental peak force was found to be 3.9 ms. For amplitude accuracy, the average difference in peak magnitude was 0.7 N (equivalent to 9.8% error compared to the experimental value). Overall, the simulations also showed the same shape over time as the experimental data.

The physical premise of the model was that the MTP joint acts like a rotational spring that generates the ground reaction force. Our results indicate that the rotational spring analogy might be a reasonable approximation of the mechanics of the kangaroo rat

foot, which has an anatomy distinctive to many bipedal hoppers.

## CONCLUSIONS

In this study, ground contact forces produced by vertical jumps of a kangaroo rat were predicted from the rotation and vertical displacement of the MTP segment. A disadvantage of this model was the need for a correction factor based upon initial posture. However, the correction factor could indicate a change in foot mechanics as the initial posture changes. In conclusion, this strategy would be useful in forward dynamic simulations because:

- The predictions are computationally efficient with only the MTP joint kinematics involved.
- It predicted the time of the peak ground reaction force accurately and provided a reasonable estimate of the magnitude of the peak ground reaction forces.

## REFERENCES

1. Gilchrist LA and Winter, DA *J. Biomech.*, **29**: 795–8, 1996.
2. Neptune, RR, *et al.* *Comput. Methods Biomech. Biomed. Engin.*, **3**: 321–334, 2000.

## ACKNOWLEDGEMENTS

Funding provided by Army Research Office Grant # W911NF-15-1-0204.

# VERBAL FEEDBACK DURING A SINGLE RUNNING RETRAINING SESSION: BIOMECHANICAL EVIDENCE OF A POSITIVE OUTCOME

Katherine Sharp, Julianne Stewart, Jenny Anne Maun, Kimberly Rowe, and Marilyn Wyatt  
Naval Medical Center San Diego, San Diego, CA USA  
email: katherine.sharp5.ctr@mail.mil

## INTRODUCTION

The Intrepid Dynamic Exoskeletal Orthosis (IDEO®) is a carbon fiber ankle-foot orthosis designed to return the wounded service member to a high level of functional activity. When a patient receives this custom-made orthosis, participation in the Return to Run (RTR) program is mandatory. This program teaches patients many skills which include running with a midfoot strike pattern to both maximize energy return from the brace and protect the knee from hyperextension [1]. The process of converting to a midfoot strike pattern can be challenging and time-consuming, and a majority of runners are natural heel strikers [2, 3]. Therefore, the purpose of this case study was to investigate the immediate impact of a single, brief running retraining session on foot strike pattern and kinematics of an IDEO user.

## METHODS

A portable motion capture system was used to capture overground running data on a male (age 40y/o; height 1.8m; weight 87.54kg) active-duty service member using the IDEO due to a pilon fracture secondary to a 60ft fall while repelling. The patient completed the RTR program before this biomechanical evaluation. A full-body six degrees of freedom marker set was used and 12 motion capture cameras (Motion Analysis Corp., Santa Rosa, CA, USA) collected kinematic data at 300 frames per second while the patient ran down a 50m runway at his self-selected speed. Data were post-processed using Visual 3D (C-Motion Inc., Germantown, MD, USA), and a fourth-order, low-pass Butterworth filter with a cutoff frequency of 8Hz was used.

Motion data were captured before (PRE) and after (POST) a retraining session. No form-related

instructions were given during the data capture sessions. Upon completion of the PRE session, it was apparent that the patient was landing with excessive knee extension at initial contact and maintaining this position throughout the stance phase (Fig. 1). This information was then used to structure the brief retraining session.



**Figure 1:** Patient exhibits excessive knee extension at initial contact and throughout the stance phase prior to gait retraining.

A verbal retraining session was performed on a standard treadmill without motion capture. This session consisted of the patient warming-up for five minutes at his self-selected speed followed by researchers and clinicians providing feedback for an additional five minutes. The feedback consisted of verbal cues to shorten step length (i.e. “take shorter steps”) and to increase step rate (i.e. “quicker turnover”). Both modifications were successfully accomplished during this period of time.

## RESULTS AND DISCUSSION

The patient ran at similar velocities during the PRE and POST testing sessions indicating differences were not due to a change in velocity (Table 1). He successfully increased his step rate by 3.3 steps/min and decreased his stride length by 0.2m in response to verbal feedback from PRE to POST.

Additionally, the patient's step length symmetry improved (Table 1).

This patient is similar to most runners in that the transition from a heel strike to a midfoot strike pattern while running presented difficulty. However, initiating a focused, long-term retraining program was not an option because the patient is active-duty military and stationed an hour from the biomechanics laboratory. The retraining technique used in this study was inspired by Wood & Kipp (2014) who successfully reduced tibial peak positive acceleration in runners after five minutes of audio biofeedback. Similarly, after the brief retraining session using verbal feedback, the patient successfully landed with a flexed knee at initial contact (Fig. 2), which drastically improved his knee kinematics throughout the gait cycle (Fig. 3).



**Figure 2:** Patient exhibits improved knee flexion at initial contact following a brief retraining session.

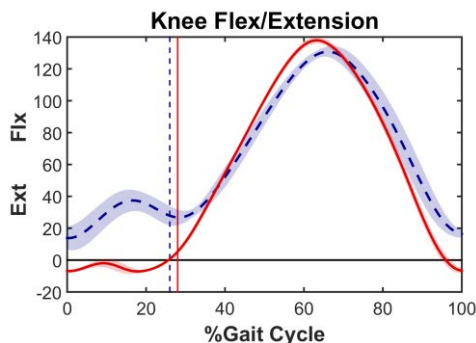


**Figure 3:** Average knee flexion/extension on the right (IDEO) side over 100% of the gait cycle during pre-training (red solid line) and post-training (blue dashed line). Vertical lines represent toe-off.

Considering the patient's reported daily use of the IDEO for work and recreation, maintenance of his increased knee flexion at initial contact, increased step rate, and decreased stride length should lower his risk for injury [3].

## CONCLUSIONS

The brief patient retraining session used verbal feedback that focused on stride length and step rate while the patient ran on a treadmill. Subsequently, during overground running, improvements were found in his foot strike pattern and knee kinematics. The patient was provided feedback on these positive outcomes and will participate in a future study to see if improvements have been maintained. Understanding the value of brief retraining sessions compared to longer, more involved retraining programs is a question for continued research.

## REFERENCES

1. Owens JG, et al. *J. Trauma* **71**, S120-S124, 2011.
2. Hasegawa H, et al. *J Strength Cond Res* **21**, 888-893, 2007.
3. Heidersheit BC, et al. *Med Sci Sports Exer* **43**, 296-302, 2011.
4. Wood CM, & Kipp K. *J Biomech* **47**, 1739-1741, 2014.

## ACKNOWLEDGMENTS

The authors would like to thank Tatiana Djafar, Trevor Kingsbury, and Noel Guerrero for their technical support. Project was supported by Navy Bureau of Medicine and Surgery, Wounded, Ill, and Injured Program (W239) and DoD-VA Extremity Trauma and Amputation Center of Excellence (EACE).

DISCLOSURE STATEMENT: There are no conflicts of interest to disclose by any of the authors. The views expressed in the abstract do not necessarily reflect those of the Department of the Navy, Department of Defense or U.S. Government.

**Table 1:** Time-distance parameters of both the pre- and post-training conditions.

	Velocity (m/sec)	Step rate (steps/min)	Stride Length (m)	Step Length (m)	
				R	L
<b>Pre-Training</b>	4.48	183.6	2.94	1.41	1.53
<b>Post-Training</b>	4.23	186.9	2.74	1.39	1.36

# INFLUENCE OF ILIOTIBIAL BAND SYNDROME ON PELVIS – THIGH COUPLING AND COUPLING VARIABILITY DURING RUNNING

<sup>1</sup>Eric Foch, <sup>2</sup>David Ebaugh, and <sup>2</sup>Clare E. Milner

<sup>1</sup>Central Washington University, Ellensburg, WA, USA

<sup>2</sup>Drexel University, Philadelphia, PA, USA

email: [eric.foch@cwu.edu](mailto:eric.foch@cwu.edu)

## INTRODUCTION

Healthy running involves inter-segmental coupling variability. However, too much or too little variability may result in abnormal soft tissue strains resulting in overuse running injuries [1] such as iliotibial band syndrome (ITBS). Typically, iliotibial band mechanics during running are inferred from the peak hip adduction angle [2, 3]. Yet, discrete analysis does not indicate if contralateral pelvic drop or thigh adduction contributes more to hip adduction and how pelvis – thigh coupling varies during stance.

Vector coding provides a continuous measure of pelvis – thigh coupling angles. Coupling angles and coupling variability can be determined via two vector coding approaches [4, 5]. However, it is unknown if the two approaches yield similar results. Therefore, the purpose of this study was to determine if contralateral pelvis drop/elevation – thigh abduction/adduction coupling and coupling variability differed among female runners with current ITBS, previous ITBS, and controls according to the vector coding approach used. We hypothesized that contralateral pelvis drop/elevation – thigh abduction/adduction coupling would be similar among groups with both vector coding methods. Second, we hypothesized that runners with current ITBS would exhibit less variability than runners with previous ITBS and controls regardless of the vector coding approach.

## METHODS

The Institution's Human Subjects Review Board approved all procedures prior to beginning the study. Twenty-seven female runners between the ages of 18 and 45 provided written informed consent. Runners comprised three equal groups: current ITBS (age: 26.2 (7.9) yrs; height: 1.64 (0.04) m; mass: 53.3 (3.7) kg), previous ITBS (age: 24.7 (5.2) yrs; height: 1.68

(0.03) m; mass: 61.7 (9.9) kg), and controls (age: 25.3 (7.0) yrs; height: 1.71 (0.05) m; mass: 59.6 (5.2) kg) [3]. A secondary analysis of an existing running data set was performed [3]. The two vector coding approaches computed the coupling angle from 0° – 90° (VC90) [4] or 0° – 360° (VC360) [5]. The stance phase was normalized to 100%. Pelvis – thigh coupling angles were determined from relative motion plots. Relative motion plots were divided into four periods: Period 1 (0-20%), Period 2 (~20-50%), Period 3 (~50-75%), and Period 4 (75-100%). At each percent of stance for the five trials, the coupling angle was computed. Coupling angles were averaged across trials, and the mean coupling angle was determined for each period of stance. Coupling variability was computed as the standard deviation of the pelvis – thigh coupling angles for each percent of stance across the five trials [4, 5]. For VC90, a coupling angle <45° indicated greater pelvis motion relative to the thigh. Whereas a coupling angle >45° indicated greater thigh motion relative to the pelvis. In-phase coupling (pelvis and thigh move equal amounts) was exactly 45°. [4] VC360 defines pelvis phase (337°-22.5° and 157.5°-202.5°), thigh phase (67.5°-112.5° and 247.5°-292.5°), and in-phase couplings (22.5°-67.5° and 202.5°-247.5°) on the entire unit circle. Additionally, VC360 defines anti-phase coupling relationships (pelvis and thigh move in opposite directions; 112.5°-157.5° and 292.5°-337.5°), whereas VC90 cannot define this pattern. [5] Two multivariate analysis of variance (MANOVA) were performed: 1) coupling angles for each period of stance; 2) coupling variability for each period of stance. *Post hoc* Fisher's test was used when a main effect was found ( $\alpha = 0.05$ ).

## RESULTS AND DISCUSSION

Contralateral pelvis drop/elevation – thigh abduction/adduction coupling angles were similar among groups during each period of stance for VC90

and VC360 (Table 1). However, coupling variability was different among groups via the VC90 approach during initial loading (Period 1;  $P = 0.004$ ) and late stance (Period 4;  $P = 0.002$ ). During initial loading and late stance, runners with previous ITBS demonstrated greater coupling variability compared to the current ITBS ( $P = 0.002$  and  $P = 0.003$ , respectively) and control ( $P = 0.006$  and  $P = 0.001$ , respectively) groups. Coupling variability was similar among groups via the VC360 approach.

No pelvis – thigh coupling differences among groups suggests ITBS injury status does not affect frontal plane inter-segmental motion during stance. Similarly, hip adduction/abduction – hip internal/external rotation coupling angles did not differ between women with current ITBS and controls during stance via the VC90 approach [2]. Differences in frontal plane pelvis – thigh coupling and transverse – frontal plane hip coupling may not be associated with ITBS. However, the pelvis – thigh phase relationships differ between VC90 and VC360 approaches. The average coupling angle computed via VC90 indicated a pelvis phase throughout stance. Whereas all groups exhibited in-phase pelvis – thigh coupling from ~50-75% of stance via VC360. During late stance, the average coupling angle indicated anti-phase pelvis – thigh coupling among groups.

During initial loading and late stance, absolute mean variability differences across groups between VC90

and VC360 ranged from  $0.3^\circ$  to  $1.7^\circ$  and  $2.4^\circ$  to  $8.6^\circ$ , respectively. Thus, small mean differences may indicate the greater variability demonstrated by runners with previous ITBS via VC90 but not VC360 was due to chance. No previous ITBS study has reported VC360 coupling variability. However, the patellofemoral pain literature indicates VC360 knee – rearfoot coupling variability differences between women with and without patellofemoral pain is the exception rather than the norm [1].

## CONCLUSIONS

Contralateral pelvis drop/elevation – thigh abduction/adduction coupling angles were similar among runners via VC90 and VC360 approaches. However, VC360 provided additional detail compared to VC90 by classifying two additional phases: in-phase and anti-phase pelvis – thigh coupling. Greater pelvis – thigh coupling variability in the previous ITBS group identified via VC90 but not VC360 should be interpreted with caution.

## REFERENCES

1. Cunningham T, et al. *Clin Biomech* **29**, 317-322, 2014.
2. Brown A, et al. *Clin Biomech* **39**, 84-90, 2016.
3. Foch E, et al. *Gait Posture* **41**, 706-710, 2015.
4. Ferber R, et al. *J Biomech* **38**, 477-483, 2005.
5. Needham R, et al. *J Biomech* **47**, 1020-1026, 2014.

**Table 1:** The mean (standard deviation) for contralateral pelvis drop/elevation – thigh abduction/adduction coupling angles and variability for the four periods of stance. The  $P$  value indicates the multivariate effect.

	Vector Coding 90°					Vector Coding 360°			
	Stance Period	Current ITBS	Previous ITBS	Controls	$P$	Current ITBS	Previous ITBS	Controls	$P$
Pelvis – Thigh Coupling Angle (°)	1	21.9 (14.7)	30.5 (12.7)	16.5 (10.7)	0.370	183.1 (15.3)	206.9 (29.2)	183.0 (18.4)	0.369
	2	36.7 (20.8)	40.7 (13.8)	38.2 (12.0)		183.5 (61.0)	178.1 (44.4)	186.7 (41.5)	
	3	23.0 (9.5)	29.7 (16.9)	19.7 (4.1)		216.1 (80.0)	206.1 (90.1)	216.2 (111.2)	
	4	25.5 (13.1)	31.5 (8.9)	21.0 (12.8)		128.5 (90.5)	130.6 (83.8)	113.6 (113.4)	
Coupling Angle Variability (°)	1	8.4(5.6) <sup>α</sup>	15.9(4.3) <sup>αβ</sup>	9.3(3.8) <sup>β</sup>	0.004	10.1(6.4)	16.9(5.6)	9.0(3.5)	0.100
	2	13.9 (6.2)	16.8(7.6)	16.2(4.9)		24.4(10.9)	27.1(11.6)	22.3(10.1)	
	3	10.4 (5.1)	12.4(6.5)	8.5(4.1)		13.5(9.4)	17.0(12.8)	9.9(6.4)	
	4	9.8(4.1) <sup>α</sup>	17.1(5.9) <sup>αβ</sup>	8.7(3.7) <sup>β</sup>		12.4(6.1)	25.3(14.7)	11.1(5.9)	

<sup>α, β</sup> Significant difference between the groups indicated.

# Changes in Limb Symmetry during a 2 Mile Outdoor Run

<sup>1</sup> Kristen Renner, <sup>1</sup> Robin Queen

<sup>1</sup> Department of Biomedical Engineering and Mechanics, Kevin Granata Biomechanics Lab, Virginia Tech, Blacksburg, VA

Email: hulbertk@vt.edu, web: <http://www.beam.vt.edu/granatalab/index.html>

## INTRODUCTION

The presence of side-to-side asymmetry is known to increase injury risk during running and other dynamic activities. Additionally, fatigue has been shown to affect the body's loading patterns over the course of a high-endurance run<sup>1</sup>. Previous research has focused on the use of instrumented treadmills to collect running data during long distance runs with no previous work examining these changes during prolonged overground running<sup>2</sup>. Reports have proven that joint mechanics, loading, and temporal variables differ on a treadmill compared to an overground environment<sup>3</sup>, including the peak value of the ground reaction forces<sup>4</sup>.

Despite the various studies pertaining to asymmetry in runners, the impact that fatigue has on side-to-side asymmetry has never been assessed in an overground running study. Therefore, this study investigated the impact of fatigue on loading symmetry during a 2 mile run on an outdoor course. We hypothesize that the LSI will increase during the run as the subject begins to fatigue.

## METHODS

27 subjects (Table 1) completed a 2 mile overground run wearing single-sensor, load monitoring insoles (pedoped, Novel Electronics, St. Paul, MN). These measured the subjects' normal in-shoe ground reaction forces sampled at 100 Hz throughout the duration of the run. An iPod Touch (5<sup>th</sup> generation, Apple Inc, Cupertino, CA) was used to collect the vGRF data via Bluetooth connection while being secured to the runner in a running pouch worn on the waist in a position that was comfortable for each subject. Each subject ran the same 2 mile course.

Subjects were allowed to run in their own training shoes to decrease the influence of a novel shoe condition. The forces from twenty-step intervals were pulled for each limb at 25%, 50%, and 75% of the run to determine how limb symmetry changed

throughout the run. Using a custom Matlab script (Mathworks, Natick, MA), the overall peak and impact peak (when present) was identified for each step. For each subject, a limb symmetry index (LSI) was calculated for each step for both the impact peak and the overall peak using the equation below. The LSI values were then averaged at each time point (25%, 50%, and 75% of the run) for each subject.

$$LSI = \frac{|Left\ Peak - Right\ Peak|}{0.5 * (Left\ Peak + Right\ Peak)}$$

To analyze the results, the LSI values were first tested for normality using the Shapiro-Wilks test. Then either a 1x3 repeated measures ANOVA or a non-parametric Wilcoxon test was conducted to determine differences in symmetry across time (JMP, SAS, Cary, NC). Finally, a non-parametric Wilcoxon signed rank test was completed to determine differences between the LSI impact peak and the LSI overall peak at each time point individually. For all statistical tests, a type I error rate of  $\alpha=0.05$  was used to determine statistical significance. A gender comparison was not completed on this data as we would like to have a greater number of subjects, 20 males and 20 females, before analyzing the potential differences between male and female runners.

**Table 1:** Subject Demographics

	Male (n=16: 59.2%)	Females (n=11: 40.7%)
Age (years)	22.93 ± 2.93	21.92 ± 3.04
Height (m)	1.81 ± 0.07	1.66 ± 0.05
Weight (kg)	77.78 ± 9.54	59.73 ± 4.34
Weekly Mileage (miles)	10 ± 6	16 ± 9

## RESULTS AND DISCUSSION

The mean time taken to complete the 2 mile run was 14:52 ± 1:51 minutes for men and 15:38 ± 1:26

minutes. Our limb symmetry indexes are reported in Figure 1. Previously reported symmetry indexes are 3.1% for the peak vertical GRF and 12.6% for the vertical impact peak for a short (25m) indoor run over force platforms<sup>5</sup>. While our LSI values are higher than what has been reported, the previous articles all considered indoor or treadmill running which provides a consistent and predictable running environment compared to outdoor overground running.

The LSI values calculated from the overall peak load were not normally distributed while the LSI values from the impact peak were normally distributed. Therefore, overall peak LSI analyses will be completed with non-parametric tests and the impact peak LSI analyses will use parametric tests. There was no difference in overall peak load LSI across time ( $p>0.229$ ) as determined through non-parametric statistics. In addition, no differences in impact load LSI existed across time ( $p=0.207$ ) (Figure 1).

When the LSI values calculated from the impact load were compared to the values calculated by the overall peak load, we found a significant difference between groups, with the impact peak LSI being greater ( $p<0.001$ ). While the impact peak LSI values are higher than those previously reported, the results of the current study are similar to previous work that indicated that the LSI was greater for the impact peak LSI than for the overall peak LSI<sup>5</sup>.

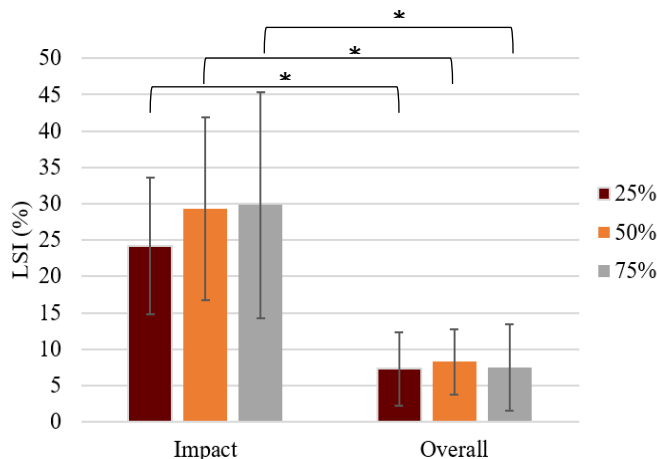


**Figure 1:** The mean LSI value and standard deviation for each time point (25%, 50% and 75%) of the run is shown above. The \* indicates a difference between the impact LSI and overall LSI values.

The lack of change in LSI across time does not support the study hypothesis. At the end of each run, we spoke to the participants about the difficulty of the run and their level of fatigue. During these discussions it was clear that most of the participants were experienced runners who were currently training for 10K, half marathons and full marathons races. Therefore, it is likely that the 2 mile course that was being completed was not challenging enough to result in changes in loading symmetry due to fatigue. In future studies that are designed to assess the impact of fatigue on loading symmetry might need to be completed on a more challenging course, require that the subjects complete the course in a pace that is similar to their race speed or have the subjects complete a longer run in order to increase the level of fatigue. In addition, future work could include the assessment of a rate of perceived excursion at the end of the run to be able to include this measure as a covariate in the statistical analysis.

## CONCLUSION

We did not see any difference in LSI across time using either the impact peak or the overall peak values. There was a difference between the LSI collected at the impact peak and the LSI determined from the overall peak value. These results indicate that the subjects use a portion of the stance phase after the impact peak to alter the loading pattern in order to improve their limb asymmetry by the time they reach the peak overall load during running.

## REFERENCES

1. Pappas, E. *Journal of Science and Medicine in Sport*, **15**, 87-92, 2012.
2. Giandolini, M. *PLoS ONE*. **11**, 2016.
3. Alton, F. *Clinical Biomechanics*. **13**, 434-440. 1998.
4. Riley, P. *Medicine & Science in Sports and Exercise*. **40**(6), 1093, 2008.
5. Zifchock, R. *J of Biomechanics*. **39**(15), 2792-2797, 2005.

# Knees Presenting Varus Thrust do not Increase Knee Adduction when Running with Body Borne Load

<sup>1</sup>Tyler N. Brown, <sup>2</sup>Jon T. Kaplan, <sup>2</sup>Sarah Cameron, <sup>1</sup>Kayla D. Seymore, <sup>2</sup>John W. Ramsay

<sup>1</sup>Dept. of Kinesiology, Boise State University, Boise, ID, USA

<sup>2</sup>Natick Soldier Research, Development and Engineering Center (NSRDEC) Natick, MA, USA  
email: tynbrown@boisestate.edu

## INTRODUCTION

Knee osteoarthritis (OA) is a common occupational hazard for members of the armed services. In fact, the incidence of knee OA in service members has recently increased [1]. Knee OA develops by repeatedly placing abnormal loads on the joint during weight-bearing activity, such as locomotion. Specifically, knee OA is associated with greater lateral knee motion (i.e., varus thrust) and subsequent loading of the medial knee joint compartment during weight-bearing activities [2, 3]. During weight-bearing, varus thrust (i.e., an abrupt increase in the knee adduction angle of 3° or more) increases the incidence, progression and severity of OA [2, 3]. During military activities, service members routinely run with body borne loads that exceed 30% of their body weight. These body borne loads produce significant adaptations in lower limb biomechanical profile, elevating the loads placed on the knee joint during locomotion [4]. The elevated loads may contribute to the increased incidence of OA by exaggerating lateral motion and medial compartment loading for service members that present varus thrust. With that in mind, the purpose of this study was to quantify how body borne load impacts knee biomechanics for participants who present varus thrust during running.

## METHODS

Eighteen male military personnel (age:  $20.2 \pm 3.3$  yrs, height:  $1.8 \pm 0.6$  m, weight  $19.0 \pm 10.8$  kg) had 3D knee joint biomechanical data recorded during an over-ground run task. Each participant performed the run task with three load conditions: light (NL), medium (ML) and heavy (HL). For the NL, participants wore equipment (helmet, boots and mock weapon) that weighs ~ 6 kg. For ML (15% of BW) and HL (30% of BW), participants wore a weighted vest (WeightVest.com Inc. Rexburg, ID, USA) that was adjusted to have the total load (vest plus NL equipment) equal either 15% or 30% of their

BW. With each load, participants performed three successful runs. Each run required participants run at 4.0 m/s down a 10-m walkway and contact a force plate (Optima, AMTI, Watertown, MA, USA) with their dominant limb.

During each run, knee biomechanics were quantified from 3D trajectories of 36 reflective markers recorded with twelve high-speed (240 fps) optical cameras (Opus, Qualysis AB, Gothenburg, Sweden). After securing each marker on the participant, a stationary recording was taken to create a kinematic model with seven skeletal segments (bilateral foot, shank and thigh, and pelvis segments) and 24 DoF. During each run, synchronous GRF data and marker trajectories were low pass filtered with a fourth-order Butterworth filter (12 Hz). The filtered marker trajectories were processed to solve joint rotations at each time frame, and filtered kinematic and GRF data were processed to obtain knee joint moments using Visual 3D (C-Motion, Rockville, MD).

Each participant had varus thrust quantified as the range of knee adduction motion exhibited from heel strike to mid-stance (0% - 51%) during the NL run. Varus participants (VAR, N = 9) exhibited knee adduction equal to or greater than 3° [2, 4]; whereas, control participants (CON, N = 9) exhibited less than 3° of knee adduction motion.

For analysis, dominant limb peak knee adduction joint angle and moment exhibited during weight-bearing (0% - 51%) were quantified. Subject-based means for each measure were calculated and submitted to a RM ANOVA to test the main effects of and possible interactions between load (NL, ML and HL) and group (VAR vs CON). Where statistically significant ( $p < 0.05$ ) differences were observed, a modified Bonferroni procedure was used. Significant interactions were submitted to 1-way ANOVA stratified by group and followed by *t*-tests to test main effects.

## RESULTS AND DISCUSSION

The ANOVA revealed a significant 2-way interaction for peak knee adduction angle ( $p = 0.001$ ) (Fig. 1). Specifically, VAR participants exhibited greater knee adduction compared to the CON participants with the NL ( $p = 0.001$ ) condition, but a significant difference in knee adduction was not evident between groups with either ML ( $p = 0.741$ ) or HL ( $p = 0.142$ ) conditions. Although VAR participants exhibited excessive knee adduction motion during the NL runs, the addition of body borne load did not further increase their use of knee biomechanics linked to OA. The VAR participants, in fact, exhibited a significant reduction in peak knee adduction with the addition of the HL ( $p = 0.023$ ). Conversely, the CON participants exhibited a significant increase in peak knee adduction during the HL runs ( $p = 0.037$ ). For the CON participants, the addition of a heavy borne load may increase their risk of developing knee OA during military service by causing them to rely upon greater knee adduction motion during locomotion.

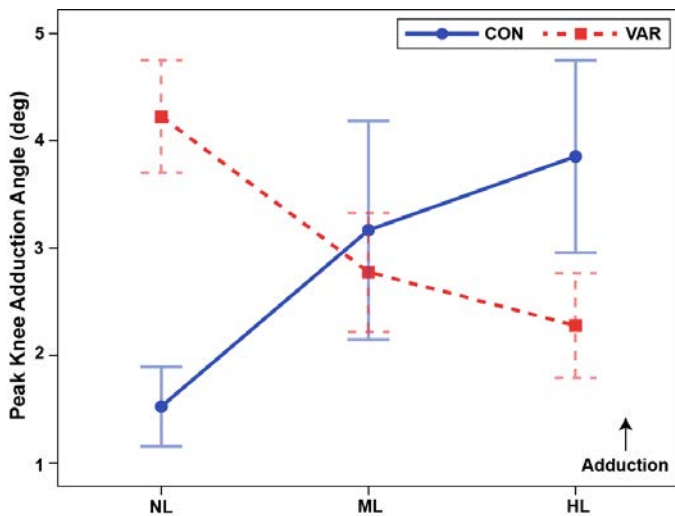


**Figure 1:** Peak (mean  $\pm$  SE) knee adduction joint angle exhibited by the VAR and CON participants with each load condition.

A significant 2-way interaction was also evident for peak knee adduction moment ( $p < 0.001$ ) (Fig. 2). For CON participants, running with the heavy borne load increased the knee adduction moment and load placed on the medial knee joint compartment. Specifically, the CON participants exhibited a

significant increase in knee adduction moment with HL compared to NL ( $p = 0.006$ ) and ML ( $p = 0.031$ ), but no significant difference was evident between the ML and NL ( $p = 0.079$ ) conditions. The VAR participants, however, exhibited no significant difference in knee adduction moment between any load condition ( $p = 0.174$ ). Further work is need to determine why the CON, but not VAR participants exhibited significant increase in peak knee adduction moment with the addition of a heavy borne load.

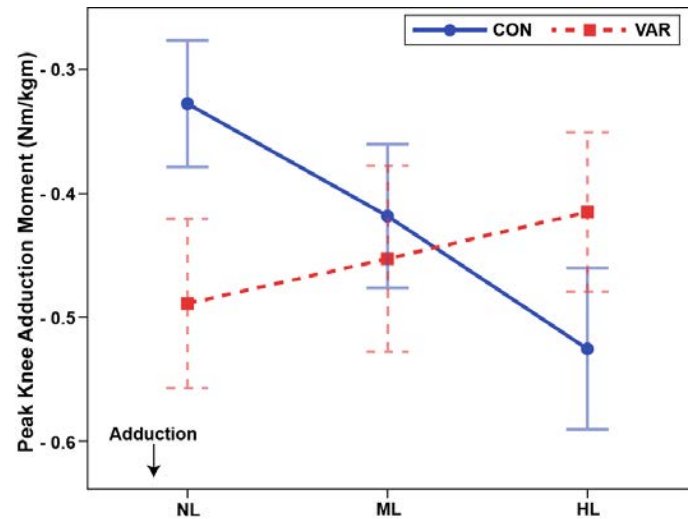


**Figure 2:** Peak (mean  $\pm$  SE) knee adduction joint moment exhibited by the VAR and CON participants with each load condition.

## CONCLUSIONS

Participants that exhibit varus thrust when running with the lightest body borne load did not increase knee biomechanical patterns related to the incidence of knee OA with the addition of a heavy body borne load. Control participants, however, increased peak knee adduction joint angle and moment, biomechanical patterns related to the development of knee OA, with the addition of a heavy borne load. Further research is warranted to understand why certain individuals exhibit frontal plane knee instability with the addition of body borne load.

## REFERENCES

1. Showery JE, et al. *J Arthroplasty* **31**, 2108 – 14, 2016.
2. Chang AH, et al. *OA & Cartilage* **21**, 1668 – 73, 2013
3. Kuroyanagi Y, et al. *Knee* **19**, 130 – 4, 2012.
4. Brown TN, et al. *Gait & Posture* **40**, 237 - 42 2014.

# TIBIAL SHOCK DURING TREADMILL AND OUTDOOR RUNNING: ARE THEY THE SAME?

<sup>1,2</sup> Steve T. Jamison, <sup>1,2</sup> Matthew C. Ruder, <sup>1,2</sup> Adam S. Tenforde, <sup>3</sup> Marian T Hannan and <sup>1,2</sup> Irene S. Davis

<sup>1</sup> Harvard Medical School, Boston, MA, USA

<sup>2</sup> Spaulding National Running Center, Cambridge, MA, USA

<sup>3</sup> TH Chan School of Public Health, Harvard University, Cambridge, MA  
email: stevetjamison@gmail.com, web: <http://runsnrc.org/>

## INTRODUCTION

Studies relating running mechanics to running injuries are most often conducted in the laboratory environment. Further, due to space constraints and ease of analysis, many of these studies are performed on a treadmill. However, most distance and recreational runners complete the majority of their miles outdoors, not on a treadmill.

There has been a proliferation of wearable devices, such as inertial measurement units (IMUs) available to the running and research community. These IMUs allow the measurement of tibial shock (TS; also known as tibial acceleration) while running outdoors, TS has been linked to overuse running injuries in the laboratory setting [1]. However, it is unknown if TS is similar between laboratory treadmill running and running outside where the majority of runners complete their training. Stride length has been reported to be shorter, and cadence higher, during treadmill compared to over-ground running [2]. These differences in mechanics may result in higher tibial shock while running outdoors.

The purpose of this study was to determine if tibial shock is different between treadmill and outdoor running. We hypothesized that TS would be lower for treadmill running than for outdoor running.

## METHODS

254 runners participating in a marathon were recruited. Each subject wore a 3-axis accelerometer attached to their distal medial, right tibia collecting data at 1kHz while they ran on a treadmill and while running an outdoor road marathon (race).

Subjects ran on a treadmill one to three days prior to the marathon at 90% of target marathon speed. The

lower treadmill speed was chosen to avoid compromising race readiness. Subjects were given 3 minutes to warm up on the treadmill in their own way. Once the target speed was reached, 30 seconds of data were used for analysis.

Subjects also completed the same race wearing the accelerometer. Marks were placed on the participants' leg and accelerometer strap during the treadmill testing to assist participants in consistent location and attachment pressure on race morning. Data for approximately the entire seventh kilometer of the marathon were used as this was the earliest flat kilometer of the race. We chose this as the point of comparison as the runners were fresh and the terrain similar to that of the treadmill.

Subjects who reported pain >3/10 on a numeric rating scale prior to the seventh kilometer of the race or who were wearing different shoes between the treadmill and the race conditions were excluded. Additionally, we excluded subjects without complete race and treadmill data. The resulting 192 subjects were used in our analysis [105 males, 87 females; age=44.9±10.8yrs]. Foot strike patterns (determined during the treadmill running) and footwear varied widely within the population. 142 subjects were rearfoot strikers, 30 midfoot strikers and 20 forefoot strikers. Footwear was categorized based upon stack height. 19 wore maximally cushioned, 92 traditional and 54 wore partially minimal shoes, with 8 barefoot or in minimal shoes. 19 runners wore shoes that fell into categories in-between these.

Resultant acceleration was calculated as the root sum of squares of the acceleration from the three axes. Tibial shock (TS) was determined as the peak

resultant acceleration for each right foot fall, averaged for reach subject over the time periods described (Treadmill: 30 seconds after warmup; Race: entire 7<sup>th</sup> km of a marathon). Acceleration due to gravity [ $g=9.81\text{m/s}^2$ ], was subtracted from the resultant accelerations, and then used to normalize TS to units of gravity, g.

Correlation analyses and paired t-tests were used to evaluate differences in TS recorded during treadmill ( $TS_{TM}$ ) and race ( $TS_R$ ) running.

## RESULTS AND DISCUSSION

Treadmill TS ( $TS_{TM}$ ) was significantly correlated with race TS ( $TS_R$ ;  $r^2=0.35$ ,  $p<0.001$ , Fig1 left) but significantly lower than  $TS_R$  ( $p<0.001$ ; Fig1 right).

These results are not surprising, given that TS is strongly correlated with speed [3], and treadmill speeds were significantly lower than race speeds ( $p<0.001$ ; Fig1 middle & right). Using a previously determined association between speed and TS ( $5.26 \frac{g}{m/s}$ ),  $TS_{TM}$  were adjusted to account for their slower speeds. Speed-adjusted treadmill TS ( $TS_{SA-TM}$ ) were more strongly correlated to  $TS_R$  ( $r^2=0.40$ ,  $p<0.001$ ; Fig1 left) but were still significantly lower than  $TS_R$  ( $p<0.001$ ; Fig1 right).

Tibial shocks may be inherently different while running an outdoor race than while running on a treadmill, even when accounting for speed

differences. Differences may also be a function of altered running mechanics (i.e. decreased cadence, increased stride length), device placement and attachment pressure, or surface compliance. We attempted to minimize device fixation variance by developing a method to verify correct placement and tension as described above. Still, strap tightness may have been altered for comfort before the race and the location could have differed slightly. The treadmill used is more compliant than asphalt, which could also contribute to TS differences. However, previous work has shown that stiffer foot-ground interfaces tend to reduce leg stiffness [4] and impact forces [5] rather than increase them.

## CONCLUSIONS

Tibial shocks appear to be significantly lower when running on a treadmill than when running in an outdoor race. Future studies should incorporate the measures of cadence and stride length in order to further understand the source of the higher impacts when running outdoors.

## REFERENCES

1. Milner CE, et al. *MSSE* **38**(2), 323-328, 2006.
2. Riley PO, et al. *MSSE* **40**(6), 1093-1100, 2008.
3. Jamison ST, et al. *Proceedings of ACSM 2017*, Denver, CO, USA, 2017.
4. Ferris DP, et al. *J Biomech* **32**(8), 787-794, 1999.
5. Baltich J, et al. *PLoS One* **10**(4), e0125196, 2015.

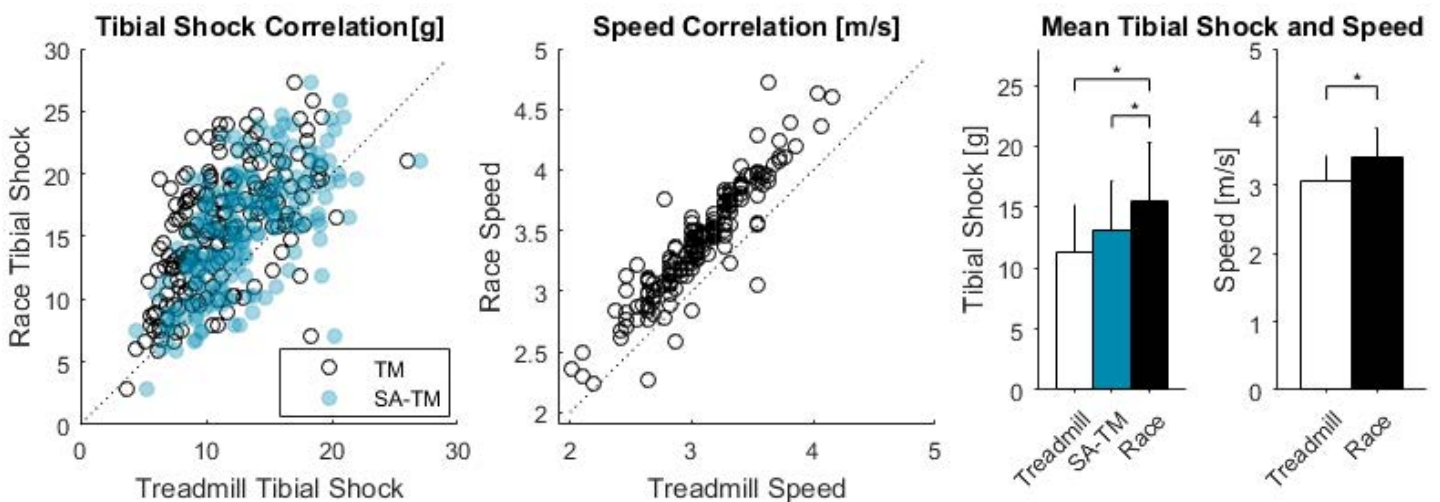


**Figure 1:** LEFT: Correlation between treadmill (TM) and race running tibial shocks (TS). MIDDLE: Correlation between TM and race running speeds. RIGHT: Mean TS (left) and speed (right). NOTES: Dashed lines denote  $x=y$ . Error bars represent standard deviations. Brackets with \* indicate significant differences ( $p<0.001$ ). Blue designate speed-adjusted treadmill TS ( $TS_{SA-TM}$ ).

# DOES WASTED IMPULSE EXPLAIN METABOLIC POWER DURING DOWNHILL RUNNING?

<sup>1</sup>Emily K. Southern, <sup>1</sup>Jana R. Jeffers, and <sup>1,2</sup>Alena M. Grabowski

<sup>1</sup>University of Colorado Boulder, CO, USA

<sup>2</sup>VA Eastern Colorado Healthcare System, Denver, CO, USA

email: emily.southern@colorado.edu

## INTRODUCTION

Previous studies have related the biomechanics and metabolic costs of running over level ground [1,2], but the link between biomechanics and metabolic costs for non-level running is less clear [3]. The metabolic cost of running has been explained by the mechanical work involved; rates of positive mechanical work and metabolic energy both increase linearly with speed [4]. However, this approach produces muscular efficiencies of 40-50%, which are much higher than physiologically possible (25%) [4]. Even greater efficiencies are obtained when including negative mechanical work. Applying the mechanical work model to non-level running would generate even more unreasonable efficiencies, as external work must be done to raise or lower the center of mass. The spring-mass model was created in part to explain the high efficiency values observed during running. It models the leg as a massless linear spring that stores and returns elastic energy, and thus performs mechanical work. However, elastic energy utilization of the leg spring is jeopardized during non-level running [5].

The metabolic cost of running on level ground is primarily due to generating force to support body weight [6]. The cost of generating force hypothesis posits that metabolic cost is inversely proportional to contact time during running [1]. [7] showed that active peak ground reaction forces (GRFs) applied perpendicular to the surface and contact times were not significantly different between level and downhill running at one speed. This suggests that metabolic cost remains constant regardless of slope when running at the same speed. However, metabolic cost decreases to a minimum on downhill slopes between  $-6^\circ$  and  $-9^\circ$  [8].

In addition to the metabolic cost of generating force to support body weight, there is a metabolic cost of

propelling body mass while running [9]. During level-ground running at a constant speed, the magnitudes of parallel braking and propulsive impulses are equal and opposite, resulting in a net zero parallel impulse [7]. Parallel impulses incur a metabolic cost but do not have a net effect of propelling the runner forward. Thus, the sum of the absolute values of the braking and propulsive impulses has been termed wasted impulse [3]. During non-level running, a component of the total parallel impulse is due to gravity; therefore, a portion of the parallel impulse is no longer considered “wasted” because it compensates for this gravitational impulse. [3] found that wasted impulse decreased exponentially ( $R^2=0.89$ ) when running uphill due to decreases in negative external work (braking), and that wasted impulse explains a portion of the metabolic cost of running. Here, we predict that wasted impulse will also decrease when running downhill, due to decreases in positive external work (propulsion). We hypothesize that changes in wasted impulse will be strongly correlated ( $r>0.70$ ) to changes in metabolic cost during downhill running at different speeds.

## METHODS

20 healthy runners (12 M, 8 F; mean±S.D. age: 26.6±6.2 yrs, mass: 68.7±8.4 kg, and height: 175.8±8.9 cm) participated and provided written informed consent according to a VAECHCS Human Subjects IRB approved protocol. Subjects reported no cardiovascular, pulmonary, or neurological disease or disorder, and no musculoskeletal injuries.

Subjects performed 12, 5-min trials on a 3D force-instrumented treadmill (Treadmetrix, USA) over two visits. Subjects ran at three speeds (2.25, 2.50, 3.00 m/s) on four slopes ( $0^\circ$ ,  $-2^\circ$ ,  $-4^\circ$ ,  $-6^\circ$ ). Each visit began with a 5-min standing trial, followed by 6 running trials in randomized order with at least 2

min rest between trials. We measured rates of oxygen consumption and carbon dioxide production throughout each trial using indirect calorimetry (ParvoMedics TrueOne2400, Sandy, UT, USA) and averaged these rates over the last 2 min of each trial. We ensured subjects utilized primarily oxidative metabolism from respiratory exchange ratios <1.0. We calculated metabolic power using a standard equation [10] and determined net metabolic power ( $P_{met}$ ) by subtracting the metabolic power during standing from each trial's metabolic power.

During a third visit, subjects performed all 12 running trials on the force treadmill (1000 Hz) for 30-sec each. We digitally filtered GRFs using a 4th-order low-pass Butterworth filter with a 30 Hz cutoff and analyzed 15 consecutive strides per trial. We used a 20N perpendicular GRF threshold to determine foot-ground contact.

Parallel impulses were computed by integrating all negative (braking) or positive (propelling) GRFs during each ground contact period. Wasted impulse per step ( $I_{wasted}$ ) was calculated from the sum of the absolute values of the parallel braking ( $I_{brake}$ ) and propulsive impulses ( $I_{prop}$ ) minus the parallel component of the gravitational impulse ( $I_{gravity}$ ):

$$I_{wasted} = |I_{brake}| + |I_{prop}| - |I_{gravity}|$$

We calculated  $I_{gravity}$  using mass ( $m$ ), gravity ( $g$ ), treadmill slope ( $\theta$ ), and time between two consecutive foot strikes ( $t_{step}$ ):

$$I_{gravity} = m * g * \sin \theta * t_{step}$$

We divided  $I_{wasted}$  by body mass and calculated a mean value for each condition. We used Pearson's product-moment correlation ( $r$ ) to determine the relationship between  $I_{wasted}$  and  $P_{met}$  with a significance level of 0.05.

## RESULTS AND DISCUSSION

$I_{wasted}$  decreased when running downhill compared to level-ground. For 2.25, 2.50, and 3.00 m/s, respectively, at  $-2^\circ$   $I_{wasted}$  was 26%, 27%, and 25% lower, at  $-4^\circ$   $I_{wasted}$  was 82%, 78%, and 72% lower, and at  $-6^\circ$   $I_{wasted}$  was 271%, 223%, and 182% lower compared to level-ground running.

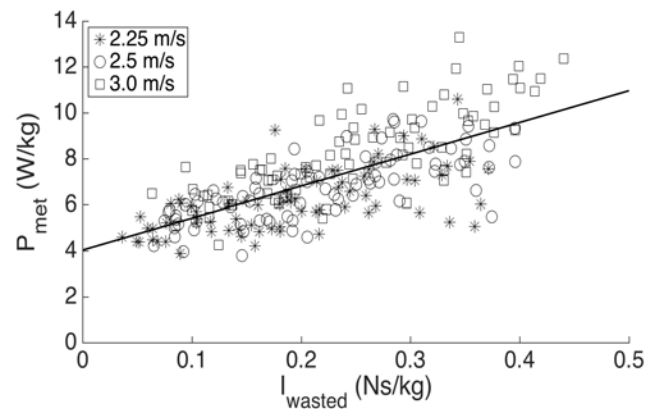


**Figure 1.** The relationship between  $I_{wasted}$  and  $P_{met}$  ( $R^2=0.52$ ).

There was a significant correlation between  $I_{wasted}$  and  $P_{met}$  ( $r(231)=0.72$ ;  $p<0.0001$ ) (Fig. 1).  $I_{wasted}$  alone explained 52% of the variance in  $P_{met}$ . [9] found that the metabolic cost of generating parallel propulsive forces accounts for about one-third of the total metabolic cost of running on level-ground, and when pulling forward on the runner, metabolic cost decreased despite an increase in braking forces. The greater proportion of metabolic energy consumption explained by  $I_{wasted}$  in the present study suggests that all three parallel impulses ( $I_{brake}$ ,  $I_{prop}$ , and  $I_{gravity}$ ) are important when evaluating the cost of braking and propelling body mass parallel to the surface during downhill running.

## CONCLUSIONS

$I_{wasted}$  is an important factor for predicting metabolic energy consumption during downhill running. Additionally, the cost of braking and propelling body mass parallel to the running surface may contribute more to total metabolic energy cost during downhill running than level-ground running.

## REFERENCES

1. Kram R & Taylor CR. *Nature* **346**, 265-267, 1990.
2. Roberts TJ, et al. *J Exp Biol* **201**, 2745-2751, 1998.
3. Hoogkamer W, et al. *PeerJ* **2**, e482, 2014.
4. Cavagna GA, et al. *J Appl Physiol* **19**, 249-256, 1964.
5. DeWolf AH, et al. *J Exp Biol* **219**, 2276-2288, 2016.
6. Teunissen LPJ, et al. *J Exp Biol* **210**, 4418-4427, 2007.
7. Gottschall JS & Kram R. *J Biomech* **38**, 445-452, 2005.
8. Minetti AE, et al. *J Exp Biol* **195**, 211-225, 1994.
9. Chang YH & Kram R. *J Appl Physiol* **86**, 1657-1662, 1999.
10. Brockway JM. *Hum Nutr Clin Nutr* **41C**, 463-471, 1987.

# THE EFFECT OF GRADE ON THE BIOMECHANICS OF DOWNHILL RUNNING IN FEMALE DISTANCE RUNNERS

<sup>1</sup> Meredith Wells, <sup>1</sup> D. Clark Dickin, <sup>1</sup> Jennifer Popp, and <sup>1</sup> Henry Wang

<sup>1</sup> Ball State University, Muncie, IN, USA  
email: mdwells@bsu.edu

## INTRODUCTION

Vast numbers of people run because it provides a variety of health benefits and can be done anywhere. Long distance runners have an increased likelihood of running up and down hills during long runs, and hill training is a key technique used to build strength and speed. Despite the health benefits of long distance running, anywhere from 27 to 79 percent of distance runners will sustain an overuse injury over the course of a year [1].

Kinetic variables such as high vertical ground reaction forces (GRF), and high impact loading rates have been linked to overuse injuries in runners [2]. Some of the most common overuse running injuries are patellofemoral pain syndrome (PFPS) and stress fractures [3]. The most likely cause of stress fractures and PFPS are high GRFs [4,5].

Although numerous studies have been conducted on level running, there is limited research available regarding downhill running. No downhill running studies have been conducted looking at specifically females, yet females are at an increased risk of injury due to anatomical differences [6]. Therefore, the purpose of this study was to analyze the biomechanics of female distance runners at four different downhill grades compared to level with regards to the risk of injury. It was hypothesized that the steeper declines would show greater vertical GRFs, higher loading rates, and increased knee and hip extension at initial contact, leading to an increased risk for injury.

## METHODS

Fifteen healthy, female distance runners (Age: 23.5 ± 4.9 years, Ht: 1.7 ± .06m, Wt: 57.8 ± 6.8kg, weekly mileage: 35 ± 13 miles) participated in this

study. All participants signed an informed consent, and IRB approval was received. Participants were provided compression clothing and standardized athletic shoes. Anthropometric measurements were taken, and reflective markers were placed on anatomical landmarks following a modified plug-in-gait model.

Participants warmed up for 5-10 minutes on a level surface before being fit with a harness attached to the ceiling as a safety precaution. Each participant ran on an AMTI force-instrumented treadmill (Advanced Mechanical Technology, Inc., Watertown, MA, USA) at 0%, -5%, -10%, -15%, and -20% grades for 1-2 minutes at 4.0 m/s in a randomized order. Participants were given 3-5 minutes of rest between each condition.

Kinematic data were collected using 15 VICON infrared cameras (Oxford Metrics, Oxford, UK), sampling at 200 Hz. Kinetic data was sampled at 2000 Hz. Vicon Nexus 2.5, Visual 3D, and Matlab were used to process the data and calibrate the treadmill. Statistical significance was determined using a repeated measure MANOVA in SPSS with an alpha level of .05.

## RESULTS AND DISCUSSION

The GRF at -15% and -20% were both significantly greater compared to each of the other grades ( $p < .001$ ). There was also a dose-response relationship in 10% increments. The -15% grade was greater than -5%, and -20% was greater than -10%. The average and peak loading rates were significantly greater in each of the downhill grades compared to the level condition, and there was a dose-response relationship seen ( $p < .001$ ). However, 0% and -5% were not significantly different from each other (Table 1).

Knee and hip flexion at initial contact decreased significantly in each of the downhill grades compared to the level condition ( $p < .001$ ) (Fig. 1).

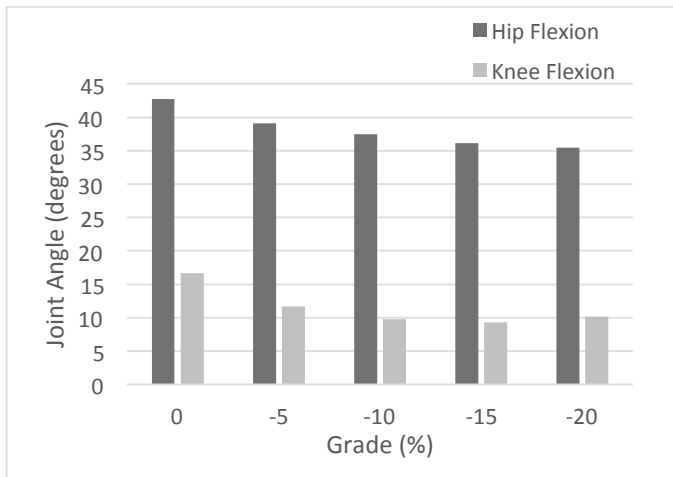


**Figure 1:** Hip and knee joint angles at initial contact.

Musculoskeletal injuries occur due to forces being applied to a structure beyond the capabilities of that structure. Repetitive forces that are small in magnitude and high in number are likely to cause an overuse injury [7]. Distance runners are highly prone to stress fractures due to the repetitive loading of the lower extremity [8]. The risk of sustaining a stress fracture increases when the magnitude of the load being applied increases, as was seen in our results. Running down steep hills involves landing from a greater vertical height, which can lead to a greater vertical GRF, and decreased knee and hip flexion [9], as was illustrated in our results.

High GRFs and landing in greater knee extension have been found to increase the likelihood of sustaining PFPS [4,10]. Increased GRFs and a high rate of loading may also increase the risk of stress fractures. Therefore, the results from our study indicate that running downhill may increase the risk

of injury. Additionally, the steeper the grade is, the greater the risk of injury becomes.

## CONCLUSIONS

There is a chance that running downhill at steep grades for an extended period of time may increase the risk of sustaining a running related injury. It is important for runners and coaches to be aware of these potential risks when running downhill so that training may be modified to avoid injury.

## REFERENCES

1. Lun V, et al. *Br J Sports Med* **38**, 576–580, 2004.
2. Hreljac A, et al. *Med Sci Sports Exerc* **32**, 1635–1641, 2000.
3. Taunton JE, et al. *Br J Sports Med* **36**, 95–101, 2002.
4. Ferber R, et al. *Clin Biomech* **18**, 350-357, 2003.
5. Lorimer A, et al. *Sports Med* **44**, 1459–1472, 2014.
6. van Gent R, et al. *Br J Sports Med* **41**, 469–480, 2007.
7. Hreljac A, et al. *Int J Sports Med* **7**, 98–108, 2006.
8. Edwards W, et al. *Med Sci Sports Exerc* **41**, 2177–2184, 2009.
9. Ali N, et al. *J Hum Kinet* **37**, 27–38, 2013.
10. Rolf C. *Scand J Med Sci Sports* **5**, 181–190, 1995.

## ACKNOWLEDGEMENTS

Ball State University Graduate Student ASPIRE Grant.

**Table 1:** Vertical GRF and loading rate normalized to body weight (mean  $\pm$  standard deviation)

	Grade				
	0%	-5%	-10%	-15%	-20%
<b>Peak vertical GRF (BW)</b>	2.48 $\pm$ 0.16	2.47 $\pm$ 0.16	2.53 $\pm$ 0.20	2.76 $\pm$ 0.24	3.01 $\pm$ 0.31
<b>Average loading rate (BW/s)</b>	2.45 $\pm$ 0.37	3.00 $\pm$ 1.15	5.65 $\pm$ 2.46	7.69 $\pm$ 2.20	8.74 $\pm$ 2.17
<b>Peak loading rate (BW/s)</b>	10.52 $\pm$ 2.53	12.11 $\pm$ 2.64	13.04 $\pm$ 3.63	14.51 $\pm$ 5.16	15.95 $\pm$ 5.21

# FOOTSTRIKE PATTERN EFFECTS ON LOADING IN RUNNERS WITH TRANSTIBIAL AMPUTATION: PRELIMINARY RESULTS

Tatiana Djafar, Katherine Sharp, Julianne Stewart, Jenny Anne Maun, Kimberly Rowe, and Marilyn Wyatt  
Naval Medical Center San Diego, San Diego, CA, USA  
email: tatiana.e.djafar.ctr@mail.mil

## INTRODUCTION

Runners with amputation have higher reported rates of injury than their able-bodied counterparts, with the most common injuries documented as overuse injuries in the intact limb [1]. Research has shown a positive relationship between greater vertical average loading rates (vALR), defined as how fast vertical ground reaction force (vGRF) rises to its first peak, and lower extremity injury rates in running [2]. Additionally, footstrike pattern has been reported to affect the magnitude of vALR, with a forefoot strike pattern (FFS) resulting in a lower vALR than a rearfoot strike pattern (RFS) [3]. However, there has been limited research examining these effects on persons with amputation. Therefore, the purpose of this pilot study was to compare the vertical loading of runners with amputation using FFS to those using RFS with their intact, unaffected limb. It was hypothesized that the vALR of the affected limb would show no differences between the groups due to the consistency of footstrike pattern in a running specific prosthesis while the vALR of the unaffected limb would be greater in the RFS group. Consequently, it was expected that the difference of vALR between the affected and unaffected limbs within groups would be greater in the RFS group as well.

## METHODS

Five subjects (age  $30 \pm 8$  years; height  $1.7 \pm 0.1$  m; weight  $79.3 \pm 13.9$  kg) with unilateral, transtibial amputation were studied using a mobile, overground motion capture system. All subjects had been cleared for high-level activity by their providers and were prescribed the same running specific prosthesis (Össur® Flex-Run™).

Data were collected with a set-up that included four portable force plates (Kistler Instrument Corp., Amherst, NY, USA) embedded within a portable

walkway, and frontal and sagittal high-speed videos (Nikon Corp., Tokyo, Japan) were taken for reference purposes. Analog data were sampled at 1800 Hz, and a fourth-order, low-pass Butterworth filter with a cut-off frequency of 50 Hz was subsequently applied.

Subjects ran through the capture volume at  $3.5 \text{ m} \cdot \text{s}^{-1} \pm 5\%$  during data collection, which concluded after a minimum of three clean force plate strikes per leg were recorded within the specified velocity range. Strike index calculation of the intact limb determined group designation for four subjects (FFS  $> 33\%$ , RFS  $\leq 33\%$ ). Initial contact with the forefoot or midfoot was considered FFS while initial contact with the heel or hindfoot was considered RFS. Sagittal reference videos confirmed calculated footstrike patterns and were also used to solely determine the footstrike pattern of one subject for whom strike index was unavailable. Kinetic data were processed using Visual 3D software (C-Motion Inc., Germantown, MD, USA), and vALR was calculated as the first derivative of vGRF between 20% and 80% of the impact peak, defined as the first peak of vGRF.

## RESULTS AND DISCUSSION

Two subjects were identified as using FFS, while the remaining three were found to be using RFS on their unaffected side. As expected, the vALR of the affected limbs were nearly identical between groups, while the unaffected limbs showed large differences compared to each other (Fig. 1, Table 1). When comparing the affected and unaffected limbs within groups, differences in vALR were found for both groups. However, differences with RFS were more than five times greater than differences with FFS (Fig. 1, Table 1). It is evident that loading in this subject group is asymmetric regardless of footstrike pattern, but limb-to-limb vALR differences within a runner are greatly

decreased when using FFS with the intact limb (Fig. 1, Fig. 2, Table 1).

As previously mentioned, vALR has been suggested as an important indicator of injury risk, with greater rates considered a possible cause of overuse running injuries [2]. While the results of this pilot study are preliminary in nature, there is evidence to consider footstrike pattern conversion as a clinical intervention to reduce vALR in the intact limb of runners with amputation. The injury risk may not be eliminated as vALR asymmetry was still observed with FFS, but it could potentially be reduced.

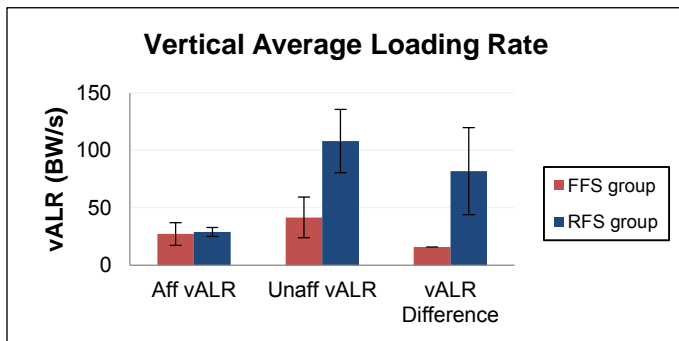


**Figure 1:** Mean  $\pm$  1 standard deviation vALR of the affected (Aff) limb, unaffected (Unaff) limb, and difference between limbs

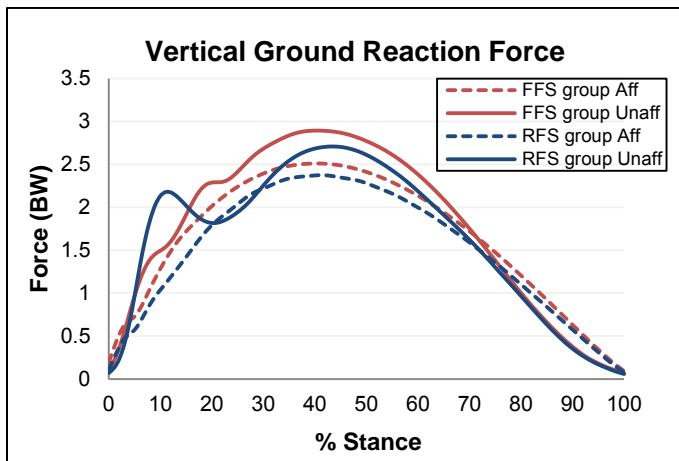


**Figure 2:** Mean vGRF normalized to stance for the affected (Aff) and unaffected (Unaff) limbs between groups

Additionally, these preliminary results have implications for other studies investigating running mechanics of persons with amputation. Future research efforts may want to consider categorizing

subjects with unilateral amputation by footstrike pattern depending on their variables of interest due to the inherent differences in loading observed here.

Despite a large effect size of the vALR differences between limbs (2.47), the main limitation of this study is the sample size. The wide range of running experience among this small group may account for the variable vALR and, thus, the larger standard deviations. A post-hoc power analysis calculation determined that a sample size of eight, with four subjects in each group, would be necessary to achieve 80% power. In addition to increasing the sample size, future work will aim to determine where footstrike patterns may further influence asymmetries within kinematics and other kinetic parameters. It would be beneficial to incorporate able-bodied runners with both footstrike patterns for comparison as well.

## CONCLUSIONS

The limited research on the effects of footstrike pattern on loading in runners with amputation warrant the need for further study of the running mechanics of this population, and though preliminary, the results presented here support this need. Decreasing the loading rate of the intact limb can potentially reduce the risk of overuse injury, and clinicians and coaches may facilitate this goal by training these runners to adopt a FFS pattern.

## REFERENCES

- Hobara H, et al. *Jpn J Biomech in Sports Exerc* **17**, 53-61, 2013.
- Zadpoor A, Nikooyan AA. *J Clin Biomech* **26**, 23-28, 2011.
- Almeida MO, et al. *J Orthop Sports Phys Ther* **45**, 738-51, 2015.

## ACKNOWLEDGMENTS

The authors thank Trevor Kingsbury, Noel Guerrero, and John David Collins for their assistance with data collection and overall technical support. Project was supported by Navy Bureau of Medicine and Surgery, Wounded, Ill, and Injured Program (W239) and in part with resources provided by Extremity Trauma & Amputation Center of Excellence.

**Table 1:** Descriptive statistics for the affected and unaffected limbs of the FFS and RFS groups

	FFS Group		RFS Group	
	Affected	Unaffected	Affected	Unaffected
vALR (BW/s)	27.10 $\pm$ 9.96	41.54 $\pm$ 17.76	28.57 $\pm$ 4.01	108.25 $\pm$ 27.68
vALR Difference (BW/s)	15.73 $\pm$ 0.01		81.89 $\pm$ 37.94	

# STEP FREQUENCY IN ELITE ULTRA-MARATHONERS DURING A 100-KM ROAD RACE

<sup>1</sup> Geoffrey T. Burns, <sup>1</sup> Jessica Deneweth Zender, and <sup>1</sup> Ronald F. Zernicke

<sup>1</sup> University of Michigan, Ann Arbor, MI, USA  
email: gtburns@umich.edu

## INTRODUCTION

The step frequency, or cadence, of a runner has been the subject of great interest in the context of both injury prevention and performance optimization [1-5]. While humans have been shown to self-optimize their step frequency to that which is the most energetically efficient [3,4], manipulating step frequency has been explored as a method to reduce peak impact forces [5-7]. Furthermore, experienced runners have been found to self-select higher step frequencies than novice runners [8], but varied results have been reported regarding the effect, if any, that fatigue has on self-selected step frequency [2,9].

Given the fundamental nature of this kinematic variable, there is a need for normative, field-based data on the characteristics of step frequency across individuals, ranges of paces, and levels of fatigue. The ultra-marathon has been proposed as model to study the consequences of muscular fatigue and prolonged stress in running [10], and studies on healthy, elite runners can provide insights into highly experienced individuals who have “self-optimized” their biomechanics. Therefore, examining step frequency during an elite road ultra-marathon over repeated, level-terrain could provide insight into the step frequencies of experienced runners across a range of speeds and levels of fatigue in a relatively controlled, yet field-based environment.

## METHODS

To characterize the step frequency in elite ultramarathon runners, wrist-based accelerometry data were collected from competitors in the 2016 IAU 100-kilometer World Championship in Los Alcazeres, Spain. The race consisted of 10 loops of a 10-km circuit on city roads with 5 m of elevation

gain and loss. Nineteen individuals (12 males and 7 females), all finishing in the top 25 places of the race, provided the researchers with the file recorded from his or her accelerometer-embedded wrist-based GPS device for the step frequency analysis. Speed and pace were recorded at 10-km intervals from the race’s official lap reports, and the average step frequency for each lap was calculated.

To analyze changes throughout the race in the runners’ step frequencies and paces and to explore the relations between the two variables, mixed-model linear regressions were performed on each variable. Distance into the race and sex were used as fixed predictors, and within-subject changes across distance were modeled treating subjects as random effects. Coefficients of the model were assessed for significance using t-tests at a p-value < 0.05. All data processing and statistical analysis were performed in R 3.2.2 (R Foundation for Statistical Computing, Austria).

## RESULTS AND DISCUSSION

The mean step frequency of all competitors during the race was  $182.0 \pm 12.4$  steps per minute (spm), corresponding to a stride frequency of 1.52 Hz. Female competitors had a significantly higher step frequency than male competitors: 189.5 spm vs. 177.6 spm ( $p < 0.001$ ). Within all competitors, step frequency did not significantly change over the course the 100-km race (Beta = -0.016 spm per km;  $p = 0.19$ ) (Fig. 1). However, pace significantly slowed over the course of the race (Beta = 0.01 min/km per km;  $p < 0.001$ ) (Fig. 2). Finally, there was no significant relation between step frequency and pace after controlling for the sex difference (-2.2 spm per min/km;  $p = 0.47$ ).

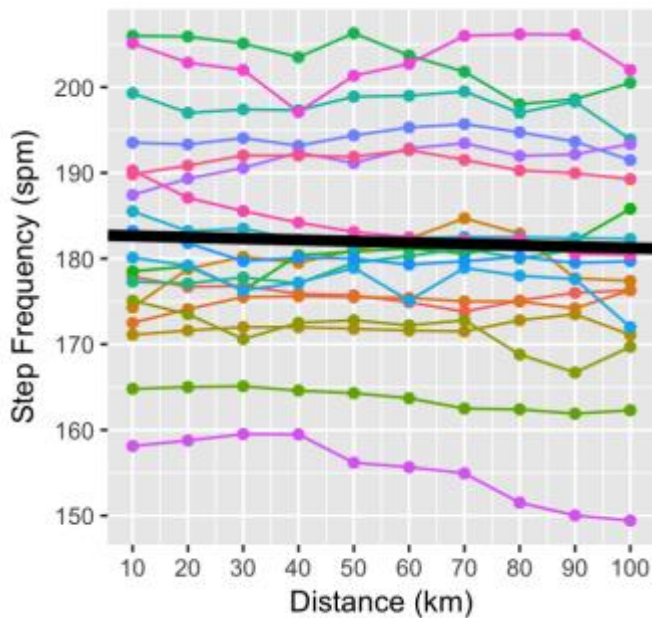


**Figure 1:** Step frequencies of individual runners over the course of a 100-km race with the regression line of step frequency across distance. Note that the slope of the line is not significantly different from zero.

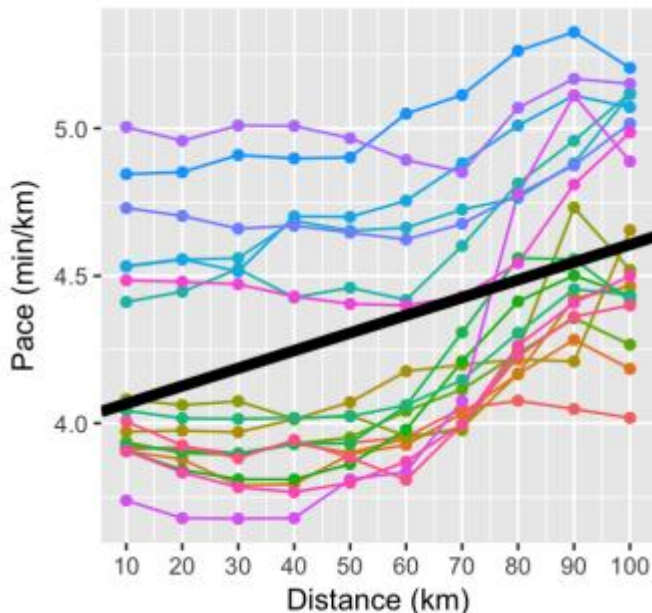


**Figure 2:** Paces of individual runners over the course of a 100-km race with the regression line of pace across distance.

## CONCLUSIONS

In elite ultra-marathoners, step frequency did not change over the course of a 100-km race despite a significant slowing of pace. Significant gender differences existed, with women running 12 spm more than men. Furthermore, step frequency did not significantly change with pace. This study provides field-based evidence that step frequency is relatively independent of pace across varied levels of fatigue in highly experienced long-distance runners.

## REFERENCES

- Schubert AG, et al. *Sports Health* **6**(3), 210-217. 2014.
- Lieberman DE, et al. *J Exp Biology*, **218**(21), 3406-3414. 2015.
- Cavanagh PR. et al. *Med Sci Sports Exerc*, **14**(1), 30-35, 1982.
- Cavanagh PR, et al. *Med Sci Sports Exerc*, **21**(4), 467-79. 1989.
- Hamill J, et al. *Human Movement Sci* **14**(1), 45-60. 1995.
- Heiderscheit BC, et al. *Med Sci Sports Exerc* **43**(2), 296-302. 2011.
- Edwards WB, et al. *Med Sci Sports Exerc* **41**(12), 2177-2184. 2009.
- Nelson RC, et al. *Research Quarterly. AAHPER* **47**(3), 417-428. 1976
- Morin JB, et al. *J Biomech* **44**(6), 1104-1107. 2011.
- Millet GP, et al. *BMC Med* **10**(1), 77. 2012.

## ACKNOWLEDGMENTS

The investigators thank all participants of the 2016 IAU 100-km World Championship who responded to requests for data to support this research.

# KNEE JOINT STIFFNESS AS A NEUROMUSCULAR COMPONENT OF PREFERRED SPEED

Jacqueline Morgan, Bhushan Thakkar, Kathryn Harrison, Gregory Crosswell, Robert Tickes, D.S. Blaise Williams III

VCU RUN LAB, Virginia Commonwealth University, Richmond, VA, USA  
email: [morganj3@mymail.vcu.edu](mailto:morganj3@mymail.vcu.edu) web: <https://khs.vcu.edu/about/vcu-run-lab>

## INTRODUCTION

Preferred running speed is commonly utilized in clinical practice and research to best represent a runner's normal gait mechanics. A physiological reason for choosing a preferred speed is to create an energy-efficient stride (6). Preferred stride frequencies have been found to be economically similar to optimal stride frequencies during non-fatiguing running (3). Another important contributor to running performance is lower extremity stiffness. Torsional joint stiffness at the knee (KS) and ankle (AS) are associated with improved performance through the elastic energy storage and return theory (7).

Traditionally, KS and AS are calculated as the slope of the moment-angle plot during force absorption (2). Typically, changes in joint moments and angles are expressed as differences between peak values and initial contact. Peak values of the knee and ankle, however, do not occur simultaneously or during similar phases of stance. Hence, calculating joint stiffness from the linear component of the moment-angle curve may better estimate the forces absorbed by the lower extremity joints. Throughout the absorption phase, torsional stiffness changes relative to changes in force and displacement and thus this is not a strictly linear measurement.

Calculating torsional stiffness during the stance phase (instantaneous stiffness) may provide a unique method for examining the motor control parameters of preferred running and its relationship to joint stiffness. Therefore, the purpose of our study was to examine the relationship between preferred running speed and joint stiffness (KS, AS), along with the timing and magnitude of peak instantaneous stiffness at the knee (%K, KIS) and ankle (%A, AIS).

## METHODS

Thirty-three healthy female runners between 18 and 50 years old [mean age 29.8 (7.5) years, height 1.64 (0.06) m, weight 61.8 (9.6) kg] volunteered. Passive retroreflective markers were affixed to bilateral lower extremities using a modified Cleveland Clinic marker set.

Gait analysis was performed on an instrumented treadmill (Treadmetrix, Park City, UT) using a 5-camera motion analysis system (Qualisys, Goteborg, Sweden). Static calibration was performed with the subject in a dual support, upright standing posture. Following calibration, joint markers were removed and each participant ran at a preferred speed [mean velocity 2.83 (0.287) m/s]. Analysis was collected for 30 seconds and the data analysis was performed.

Visual3D software (C-Motion, Germantown, MD) was used to compute kinematic and kinetic variables of joint angles and moments. KS and AS were calculated as a simple-spring model, during the linear component of the moment-angle curve. KIS and AIS were calculated as peak joint stiffness between 20% of stance and peak joint moment. %K and %A were assessed at the percent of stance associated with peak instantaneous stiffness.

A forward step-wise multiple linear regression analysis was employed to examine the association between preferred running speed and six potential independent variable gait measures. Variables of KS, AS, KIS, AIS, %K, %A were fit into a best-fit model utilizing the Akaike Information Criterion (AIC) selection criteria. Analysis was performed using JMP® Pro 12.2.0, SAS Institute Inc, 2015. Significance was set at  $\alpha < 0.05$ .

## RESULTS

Six covariates of gait stiffness variables were fit into a best-fit forward step-wise linear regression model. The AIC selection criteria resulted in a best fit model using covariates of KS, KIS, and %K. The results of the regression model found a significant positive association between preferred speed and both knee stiffness variables (Adj  $R^2 = 0.304$ ,  $p = 0.004$ ), with KS and KIS explaining 30.4% of the variance in preferred speed. Post hoc analysis showed KS was positively associated with preferred speed (slope = 9.26), while KIS was negatively associated with speed (slope = -1.77) (Figure 1a-b).

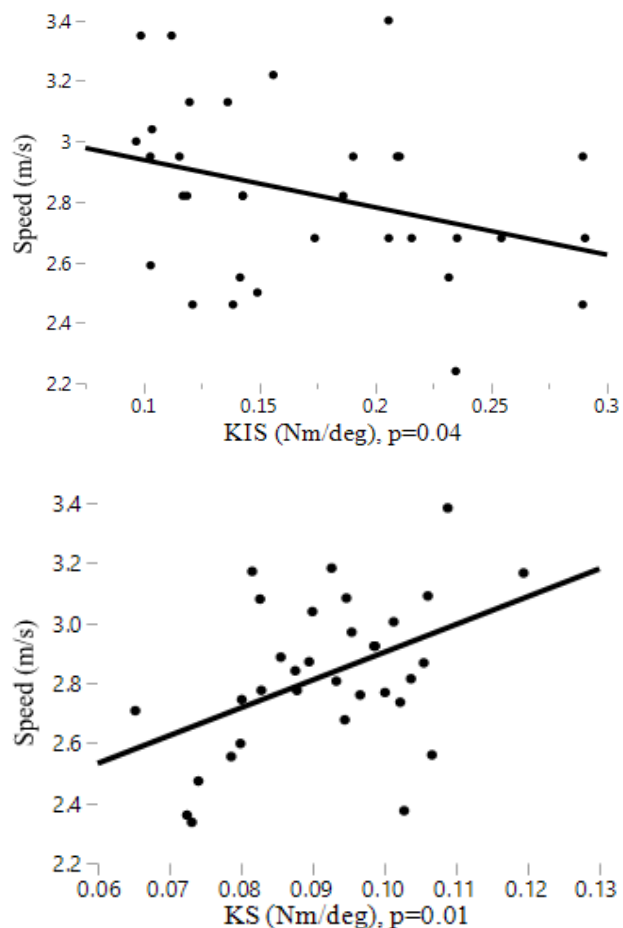


**Figure 1:** The correlation between preferred speed and KIS (1a), and KS (1b).

## DISCUSSION

Stiffness variables of the knee and ankle were examined for their relationship to preferred running speed. Only knee stiffness variables (KS, KIS) were found to be significantly correlated to preferred

speed. Previous research has found increases in speed to be significantly associated with increases in knee stiffness (1,4), when stiffness was assessed across previously determined speed. KIS was found to be inversely associated with faster self-selected speeds, suggesting that torsional stiffness parameters that are more consistent across stance with damped peaks may allow for greater control of movement during running and a faster more efficient gait.

The results of our finding are novel and suggest that knee stiffness may be a motor control parameter used to generate a neuromuscularly efficient gait. Implications from our findings suggest runners may have an optimal knee stiffness during preferred running to provide the runner with a “comfortable” gait (5). The runners recruited in our study were recreational runners. Therefore, improving neuromuscular performance through the generation of preferred stiffness may help to temper any reductions in maximal predictors of performance ( $VO_{2max}$ ).

Physiological measures were not collected for this study, however, future studies would benefit from examining the relationship between joint stiffness, running economy, and motor control to better understand the recreational runner. Investigations into the optimal joint stiffness may aid future researchers and clinicians when examining deficiencies in stiffness, injury risk, and potential intervention to address those impairments.

## REFERENCES

1. Arampatzis, A., et al. *Journal of Biomechanics*, 32, 1349-1353, 1999.
2. Butler, R., et al. *Clinical Biomechanics*, 18:511-517, 2003.
3. Hunter, I., et al. *European Journal of Applied Physiology*, 100:653, 2007.
4. Kuitunen, S., et al. *Medicine & Science in Sports & Exercise*, 34(1):166-173, 2002.
5. Lussiana, T., et al. *Biology Open*, 5:45-48, 2016.
6. Rathkey, J., et al. *American Journal of Physical Anthropology*, 1-9, 2017.
7. Stefanyshyn, D., et al. *Journal of Applied Biomechanics*, 14(3):292-299, 1998

# EFFECT OF SLOPE AND SPEED ON KINETICS OF JOGGING WITH A BACKPACK

Philippe Malcolm<sup>3</sup>, Fausto A. Panizzolo<sup>1,2</sup>, Jozefien Speeckaert<sup>1,2,4</sup>, Jinsoo Kim<sup>1,2</sup>, Hao Su<sup>1,2</sup>, Giuk Lee<sup>1,2</sup>, Ignacio Galiana<sup>1,2</sup>, Kenneth G. Holt<sup>5</sup>, Conor J. Walsh<sup>1,2</sup>

<sup>1</sup> John A. Paulson School of Engineering and Applied Sciences and

<sup>2</sup> Wyss Institute for Biologically Inspired Engineering, Harvard University, Cambridge, MA 02138, USA

<sup>3</sup> Department of Biomechanics and Center for Research in Human Movement Variability, University of Nebraska Omaha, Omaha, NE, 68182, USA

<sup>4</sup> Department of Movement and Sport Sciences, Ghent University, Ghent, B9000, Belgium

<sup>5</sup> Sargent College of Health and Rehabilitation Science, Boston University, Boston, MA 02215, USA

email: [walsh@seas.harvard.edu](mailto:walsh@seas.harvard.edu), web: <http://biodesign.seas.harvard.edu/>, <http://coe.unomaha.edu/brb>

## INTRODUCTION

Running while carrying a load under different conditions such as slopes and speeds is a part of military training [1], trail running [2], commuting and conditioning exercises [3]. There have been different studies on effects of slope [4–6], speed [7,8] and load [3,9,10] on biomechanics of running. However, only a limited number of studies analyzed the effects of multiple parameters in interaction (e.g. [3]) and, to the best of our knowledge, there has been no study on the effects of slope and speed during jogging with a relevant military load at slow speeds that are likely to occur at such slope and load combinations. Knowledge about the effects of slope and speed on the joint kinetics can be useful for understanding the performance requirements of different types of terrain and for preparing accordingly. Our aim is to study the effects of slope and speed on joint kinetics during slow jogging with a military relevant backpack load. We hypothesize that uphill jogging will increase positive work (mostly at the hip and ankle) [5, 6] and reduce negative work and that faster jogging will increase both positive and negative work (mostly at the hip and ankle) [3,7,8].

## METHODS

We tested 10 healthy male participants ( $29 \pm 2$  yrs;  $76 \pm 3$  kg;  $1.79 \pm 0.02$ m; mean  $\pm$  s.e.m.) during jogging on a treadmill (Bertec) at 15 combinations of slope ( $-8$ ,  $-4$ ,  $0$ ,  $+4$  and  $+8^\circ$ ) and speed (2, 2.5 and  $3 \text{ m s}^{-1}$ ) with a 15kg backpack. We measured joint kinetics using motion capture (Vicon). We calculated rates of positive and negative work for each joint by integrating positive and negative

power portions and dividing by stride time. Next, we evaluated the linear, second order and interaction effects of slope and speed on each metric using mixed-model ANOVA with stepwise elimination.

## RESULTS AND DISCUSSION

As hypothesized, we found that an increase in slope leads to an increase in positive work rate at the hip and ankle joint (similar to [5] and [6]) and to a decrease in negative work rate mostly at the knee joint and for the sum of all joints (Figure 1). Furthermore, we found that an increase in speed led to an increase in positive work rate at all joints, but at the knee this effect is very small. We also found that an increase in speed led to an increase in negative work rate for all joints. We found significant interactions for the effect of slope and speed in all joints for positive work rate but only in the knee for negative work rate (Table 1).

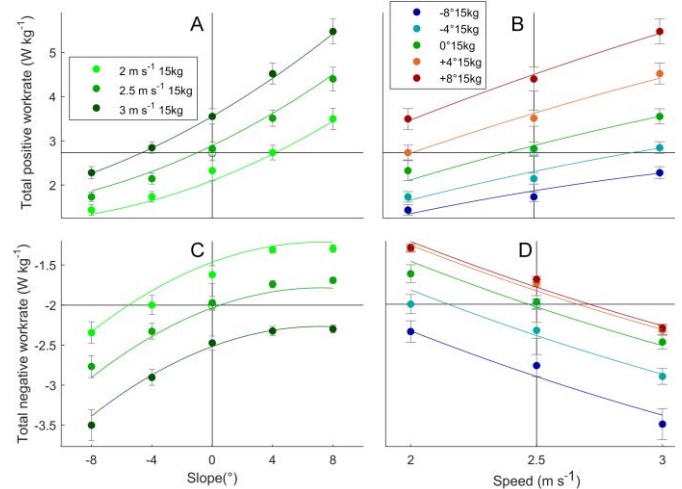


**Figure 1:** Effects of speed (a,c) and slope (b,d) on total positive (a,b) and negative (c,d) work from the hip knee and ankle. Dots and error bars are mean  $\pm$  s.e.m. Lines show curve fits from ANOVA.

## CONCLUSIONS

These results quantitatively show that fast uphill loaded jogging is strenuous, not only because positive joint work rate increases with slope and speed, but also because the interaction between slope and speed further magnifies these effects. Results also show that the combination of fast downhill jogging leads to high negative work at the knee because of the effect of slope, the effect of speed and that this is further magnified by interaction of slope and speed. Knowledge of these effects can be useful for choosing pacing strategies, course selection, estimating injury risk, optimizing training and rehabilitation and for selecting and developing orthotic or assistive devices. For example, an assistive exoskeleton for running [11] could be programmed to change its assistance magnitude based on the equations in table 1 to mimic human responses to changes in slope and speed.

## ACKNOWLEDGMENTS

This work was funded by Defense Advanced Research Projects Agency (DARPA), Warrior Web Program (Contract No. W911NF-14-C-0051), NSF (Grant No. CNS-1446464), Wyss Institute, John A. Paulson School of Engineering and Applied Sciences at Harvard University. We thank Adham Meguid, Andrew Long, Asa Eckert-Erdheim and Lauren Baker for their help.

## REFERENCES

1. Knapik J, et al. *Mil. Med.* 2004;
2. Knoth C, et al. *Extrem. Physiol. Med.* 2012; **1**:13.
3. Liew BXW, et al. *J. Biomech.* 2016;8–13.
4. Buczek FL, et al. *Med. Sci. Sports Exerc.* 1990. 669–77.
5. Swanson SC, et al. *Med. Sci. Sports Exerc.* 2000; **32**:1146–55.
6. Roberts TJ, Belliveau R. *J. Exp. Biol.* 2005; **208**:1963–70.
7. Schache AG, et al. *Med. Sci. Sport. Exerc.* 2011; **43**:1260.
8. Dorn TW et al. *J. Exp. Biol.* 2012; **215**: 1944 – 56.
9. Brown TN, et al. *Gait Posture.* 2014; **40**: 237 – 42.
10. Silder A, et al. *J. Biomech.*; 2015;1–6.
11. Elliott G, et al. *Int Conf Rehabil Robot.* Seattle: IEEE; 2013. 6650418.

**Table 1:** Coefficients of mixed-model ANOVA for each outcome metric. Only significant terms were retained (p-values < 0.05). Outcome metric = intercept + a · slope + b · slope<sup>2</sup> + c · speed + d · speed<sup>2</sup> + e · (speed · slope) with slope in ° and speed in m s<sup>-1</sup>.

	Intercept	a (slope)	b (slope <sup>2</sup> )	c (speed)	d (speed <sup>2</sup> )	e (speed · slope)	R <sup>2</sup>
Positive hip work rate (W kg <sup>-1</sup> )	0.518		0.004	-0.409	0.237	0.034	0.946
Positive knee work rate (W kg <sup>-1</sup> )	-0.684		0.001	0.891	-0.163	0.007	0.689
Positive ankle work rate (W kg <sup>-1</sup> )	-2.195			2.248	-0.330	0.026	0.913
Negative hip work rate (W kg <sup>-1</sup> )	-0.022	0.005	-0.001		-0.022		0.587
Negative knee work rate (W kg <sup>-1</sup> )	0.333	0.029	-0.003	-0.572		0.009	0.901
Negative ankle work rate (W kg <sup>-1</sup> )	1.293	0.014	-0.001	-1.273	0.178		0.883
Total positive work rate (W kg <sup>-1</sup> )	-2.341		0.005	2.731	-0.256	0.066	0.953
Total negative work rate (W kg <sup>-1</sup> )	1.700	0.070	-0.005	-1.938	0.177		0.929

# RELATIONSHIP BETWEEN RUNNING ECONOMY AND KINEMATICS OF THE UPPER EXTREMITY AND TRUNK

Grace Rhodehouse, Shane P. Murphy, Barbara J. Schornstein, Abbie E. Ferris,  
Gary D. Heise, and Jeremy D. Smith

School of Sport & Exercise Science, University of Northern Colorado, Greeley, CO, USA  
email: grace.rhodehouse@unco.edu web: www.unco.edu/biomechanics

## INTRODUCTION

Variability in running economy has been reported in homogenous groups (based on maximal aerobic capacity or race performance) of trained distance runners. Lower extremity kinematics such as increased shank angle and increased knee flexion have been shown to improve steady state economy (i.e., lower  $\text{VO}_2$  consumption), but have not fully explained the variations seen in the homogenous groups [1].

Previous research has also suggested that upper extremity motions such as decreased trunk angle and decreased wrist excursion path lead to improved running economy [2], but it is unclear whether variability in upper extremity mechanics can provide further insights into the differences in running economy among similarly trained runners.

The purpose of this present study was to determine whether upper extremity and trunk kinematics were related to running economy. It was hypothesized that greater motion of the upper extremity and trunk, as well as increased variability of these measures within a participant would lead to increased steady state  $\text{VO}_2$  during running.

## METHODS

Eleven healthy, highly trained female runners ( $21 \pm 3$  years,  $1.69 \pm 0.05$  m,  $58.5 \pm 3.6$  kg) with 5k or 10k times between 19-24 or 40-45 minutes, respectively, and training at least 15 miles per week participated in the study. Participants visited the Biomechanics Lab on two separate occasions, completing a  $\text{VO}_{2\text{max}}$  test (Visit 1) and a steady state running protocol (Visit 2). During both visits, participants ran on an instrumented treadmill

(AMTI, Watertown, MA) while expired gases were collected using a metabolic cart (Parvo Medics, Sandy, UT). A ramped protocol was used for the  $\text{VO}_{2\text{max}}$  test, with participants running at  $3.1 \text{ m}\cdot\text{s}^{-1}$  for the entire test. Treadmill grade was increased by  $2^\circ$  every two minutes, until voluntary exhaustion [3]. During Visit 2, steady state  $\text{VO}_2$  was measured during a six-minute run at  $3.5 \text{ m}\cdot\text{s}^{-1}$ . Whole body and segmental anthropometrics were measured following guidelines of VICON's Plug-In-Gait Model. Retroreflective markers were positioned bilaterally on anatomical landmarks according to this model. Marker coordinate data (100 Hz) were captured during each running trial (VICON, Englewood, CO).

Metabolic data were averaged over the last 60 s of the six minute treadmill bout. Kinematic data were also identified during this last 60 s of the trial. Left arm kinematics of 10 strides during steady state running were analyzed. (Visual 3D, C-Motion, Germantown, MD). Resultant wrist excursion length, and range of motion (ROM) and angular velocities for the shoulder, elbow, and trunk were calculated in all three planes. Stride-to-stride variability during the 10 strides for each participant was also determined for each measure. A Pearson Product Moment Correlation analysis was used to determine relationships between steady state  $\text{VO}_2$  and upper body kinematics. Significant relationships were those with  $r > 0.602$ .

## RESULTS AND DISCUSSION

The  $\text{VO}_{2\text{max}}$  test was designed to have participants reach maximum effort, however the majority of subjects reached voluntary exhaustion before exceeding an RER value of 1.1. Therefore, we will refer to the max value from these tests as  $\text{VO}_{2\text{peak}}$ .

$VO_{2peak}$  ranged between 49.9 - 71.6  $mL \cdot kg^{-1} \cdot min^{-1}$ , with a group mean of  $60.9 \pm 6.6 mL \cdot kg^{-1} \cdot min^{-1}$  (time to exhaustion  $9.6 \pm 1.9$  minutes). The steady state protocol in Visit 2 was performed at a high intensity in comparison to measured  $VO_{2peak}$  for each participant ( $79 \pm 9\%$  of  $VO_{2peak}$ ). This relatively high intensity level reflects an effort expected of a highly trained runner in an intense workout or race setting.

No significant relationships were observed between any measures of stride-to-stride variability and  $VO_2$ . A significant correlation was observed between trunk rotational angular velocity and  $VO_2$  ( $r = 0.713$  and  $r = 0.756$  for rotation to the right and left, respectively). During the steady state run, less economical runners (i.e., higher  $VO_2$ ) had increased rotational trunk velocity (Fig. 1A). A significant correlation was also observed between wrist velocity in the vertical direction and  $VO_2$  ( $r = 0.660$ ). As downward wrist velocity increased,  $VO_2$  increased (Fig. 1B).

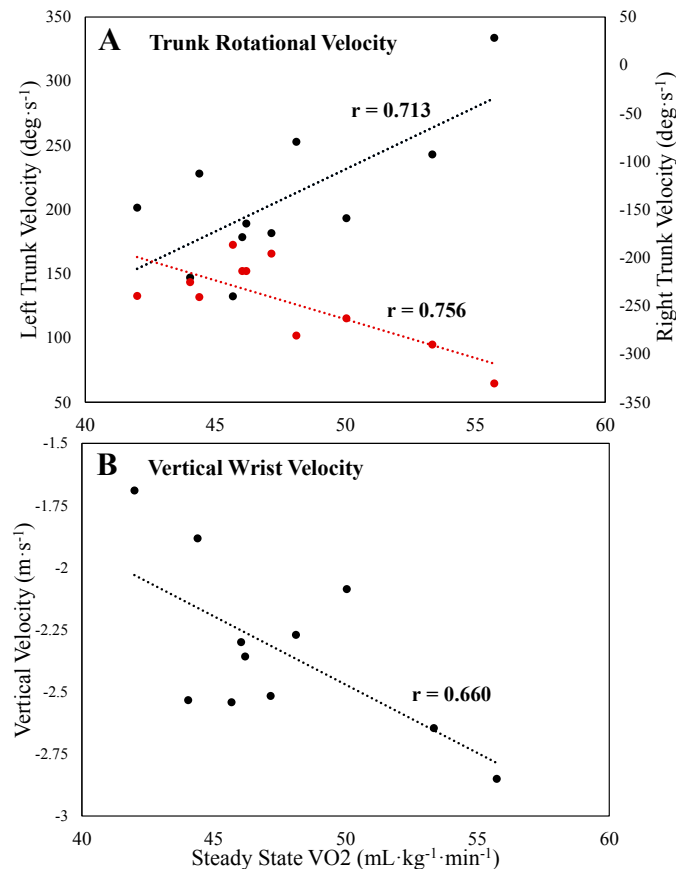


**Figure 1:** Relationships between steady  $VO_2$  and rotational trunk velocity (A) and vertical wrist velocity (B). Right trunk rotation (red) is plotted using the right vertical axis and left trunk rotation (black) is plotted using the left vertical axis of panel A.

Increased rotational trunk velocity and increased vertical wrist velocity may contribute to increased muscle actions of the trunk and elbow to slow down and speed up the segment's motion. This increased muscle action likely leads to increased metabolic energy expenditure during running.

Trunk flexibility has previously been shown to be related to running economy [4]. Greater trunk rotation flexibility is related to higher steady state  $VO_2$  during running. In the current study, trunk ROM, about the vertical axis, approached the critical value ( $r = 0.578$ ). Thus, during dynamic activity, increased rotational motion of the trunk also appears to increase  $VO_2$ . It is likely that the motion of the trunk is controlled significantly by active muscle rather than more passive mechanisms that might arise with each contact with the ground.

Left wrist excursion path length also approached the critical value ( $r^2 = 0.2965$ ). Runners displaying longer path lengths were less economical during steady state running. Although we were unable to determine a significant relationship between wrist excursion and  $VO_2$ , previous research has found longer wrist excursion path lengths among less economical runners, during steady state running [1], which is consistent with the trend we observed.

## CONCLUSIONS

Stride-to-stride variability of the upper extremity and trunk kinematics was not related to running economy. However, more economical runners (lower  $VO_2$ ) had lower rotational trunk velocities and slower vertical velocities of the wrist. Limiting trunk and wrist motions may lead to lower energy expenditures during steady state running.

## REFERENCES

1. Williams KR, & Cavanagh, PR. *J Appl Physiol*, **63**(3), 1236-1245, 1987
2. Arellano CJ, & Kram, R. *J Exp Biol*, **217**, 2456-2461, 2014.
3. Maksud MG & Coutts, KD. *Med Sci Sports*, **3**(2), 63-65, 1971.
4. Gleim GW, et al. *J Ortho Res*, **8**, 814-823, 1990.

# THE EFFECT OF TRANSITIONING FROM A REARFOOT STRIKE PATTERN TO A NON-REARFOOT STRIKE PATTERN ON RUNNING IMPULSES

Adam Reynolds, Erin Florkiewicz, Donald Goss, Gregory Freisinger

United States Military Academy, West Point, NY, USA

email: [gregory.freisinger@usma.edu](mailto:gregory.freisinger@usma.edu), web: <http://www.usma.edu/cme/SitePages/Home.aspx>

## INTRODUCTION

Annual running injury incidence has been reported between 19-79% with approximately 40% of all running-related injuries occurring at the knee [1]. Several popular strategies have been proposed to reduce lower extremity injury risk while running, to include minimalist footwear and alterations in running form [2].

Previous studies have shown a rearfoot strike pattern to be associated with a greater incidence of repetitive stress injuries when compared to a forefoot strike pattern [3]. Much of this research has focused on vertical loading rate and peak vertical load, but less has focused on the effects on the impulse, or time integral of applied force, which the individual experiences. The purpose of this study was to further investigate the changes in impulse when transitioning from a rearfoot strike (RFS) to a non-rearfoot strike (NRFS) running style.

Acceleration in running results from an imbalance of posterior and anterior impulses [4]. This study investigated running at a constant pace in which a balance must exist between these two impulses. We hypothesized that following the transition from RFS to NRFS, a decrease in the magnitude of the posterior and anterior impulses will be observed. We also hypothesized that vertical impulse will decrease, while medial and lateral impulses remain unchanged, following running style transition.

## METHODS

Nine patients were recruited from the Arvin Cadet Physical Therapy Clinic at West Point, NY for the 10-week transition program and provided IRB approved informed consent. Participants were cadets with previous running experience and their demographics are shown in Table 1. All participants met each of the 6 inclusion criteria: 1) previously a RFS runner; 2) recovering from a lower extremity

injury; 3) able to walk pain free for 2 miles; 4) dorsiflexion range of motion of at least 80% symmetry; 5) capable of performing 20 unassisted single leg heel raises; 6) able to perform a single leg hop for distance with at least 80% symmetry. These participants were clinically diagnosed and recovering from one of the following lower extremity injuries: patellofemoral pain syndrome (3), lower leg stress injury (2), lower leg fracture (1), plantar fasciitis (1), and anterior cruciate ligament reconstruction (2).

Sex	5 Male : 4 Female
Age, years	20.3 ± 2.2
Height, cm	170.7 ± 13.8
Mass, kg	71.7 ± 14.9
*All values are means ± standard deviations	

The running transition program began with a private 30 minute training session to encourage transition from a RFS to a NRFS running pattern. Training focused on soft landing off of the heel, a cadence of approximately 180 steps/minute, forward trunk lean and strict adherence to a gradual walk to run progression. Participants met with their study assigned medical provider once a week post-training for the first 4 weeks, then again at weeks 6, 8, and 10 upon which the training focuses were reinforced.

Prior to the training program and at week 10 post-training, each participant's running ground reaction force were assessed. Participants ran at a self-selected speed for 5 minutes on an instrumented treadmill [Bertec; Columbus, OH]. Speed was kept constant throughout the study. Foot-strike pattern was assessed utilizing a high speed digital camera [Casio EX-ZR200; Tokyo, Japan] recording at 240 frames per second. Ground reaction forces were sampled at 1000Hz, low-pass Butterworth filtered at 35Hz, and normalized as a percentage of each

participant's bodyweight (BW). This data was used to calculate impulse in the vertical (vImp), anterior (aImp), posterior (pImp), medial (mImp) and lateral (lImp) directions for each step. Ensemble averages were calculated from five left and right stance phases, then the left and right foot data were also averaged. Cadence was determined based on the vertical ground reaction force data. Subjective measures of running ability were assessed using the Patient Specific Functional Scale (PSFS) and Single Assessment Numeric Evaluation (SANE) averaged scores. PSFS measures functional running ability on a scale from 0 (unable to perform running) to 10 (able to perform running at the same level as before injury), whereas SANE assesses how normal their injured body part feels from 0% to 100%.

Paired t-tests were used to identify differences between the initial and 10 week assessments for the impulse calculations, cadence, and PSFS measures. A significance level of  $\alpha = 0.05$  was used.

## RESULTS AND DISCUSSION

All 9 subjects successfully transitioned to a NRFS running style as verified by high speed camera. Cadence increased from an average of  $170.2 \pm 10.1$  to  $179.8 \pm 6.4$  steps per minute ( $p < 0.05$ ). Average PSFS and SANE scores also increased by approximately 50% ( $p < 0.01$ ) and 25% ( $p < 0.01$ ) respectively, suggesting increased running ability and decreased discomfort (Table 1).

Contrary to our hypothesis, our results demonstrated a significant increase in the average pImp ( $p < 0.01$ ) and a matching increase in aImp ( $p < 0.01$ ). The average magnitude of change increased

approximately 10% bodyweight-seconds (BW-s) for each pImp and aImp. This suggests there is overall greater total impulse in the anterior-posterior dimension when patients transition from a RFS to NRFS per step. We also found no change in the vImp, contrary to our original hypothesis. No statistically significant changes were found in the mImp or lImp. The impulse values for the initial and 10 week assessment are shown in Table 2.

## CONCLUSIONS

We have observed approximately a 10% increase in the magnitudes of the anterior and posterior impulses, in the short-term, after transitioning habitual RFS runners to a NRFS pattern. This is accompanied by a strong increase in PSFS and SANE scores, showing an increase in subjective functional running ability. No significant changes in impulse were observed in the medial, vertical, or lateral directions. Additional work is necessary to identify the long-term effects of increased impulse when transitioning to a NRFS following injury.

## REFERENCES

1. Van Gent RN, et al. *Br J Sports Med* 41, 469-480, 2007.
2. McDougall, *Born to Run*, Alfred A. Knopf, 2009.
3. Daoud, et al. *Medicine & Science in Sports & Exercise* 44.7: 1325-334. 2012.
4. Van Caekenberghe et al. *J R Soc Interface* 10: 20130222 2013.

## ACKNOWLEDGEMENTS

Funding for this study was provided by United States Military Academy Center for Innovation and Engineering.

**Table 2:** Impulses, cadence, PSFS, and SANE data for the 9 participants at initial test and at week 10.

	Anterior Impulse (BW-s)	Posterior Impulse (BW-s)	Medial Impulse (BW-s)	Lateral Impulse (BW-s)	Vertical Impulse (BW-s)	Cadence (steps/min)	PSFS (0-10)	SANE (0-100)
Initial Test	-0.019 ± 0.003	0.018 ± 0.004	-0.007 ± 0.005	0.007 ± 0.005	0.350 ± 0.304	170.2 ± 10.1	6.1 ± 1.0	75.0 ± 13.5
Week 10	-0.022 ± 0.002	0.020 ± 0.003	-0.007 ± 0.004	0.005 ± 0.003	0.343 ± 0.293	179.8 ± 6.4	9.3 ± 0.9	95.9 ± 6.8
p-value	<0.01*	<0.01*	0.67	0.14	0.51	<0.01*	<0.01*	<0.01*

\*indicates a statistically significant difference. All values are mean ± standard deviation. Patient Specific Functional Scale (PSFS); Single Assessment Numeric Evaluation (SANE)

# COORDINATION AND COORDINATIVE VARIABILITY OF THE LOWER LIMBS IN COMPETITIVE MALE DISTANCE RUNNERS

<sup>1</sup> Richard C. Franzese, <sup>2</sup> Julie A. Stebbins, <sup>1</sup> Amy B. Zavatsky

<sup>1</sup> University of Oxford, UK

<sup>2</sup> Oxford Gait Laboratory, UK

email: richard.c.franzese@gmail.com

## INTRODUCTION

This work quantifies coordination and coordinative variability in lower-limb motion, using continuous relative phase (CRP) [1] and CRP variability (vCRP), for a population of uninjured, competitive male distance runners. The effects of velocity and footwear are considered, with stride-specific foot-strike angle (FSA) as a covariate. Barefoot (BF) and shod (SD) conditions are studied because they mark mechanical boundary conditions for affecting running biomechanics.

Segmental coordination is different to joint kinematics; joint kinematics may change whilst coordination patterns for the segments involved do not. vCRP decreases with higher competitive standards [2] and may also decrease with injury [3]. Therefore quantifying CRP and vCRP for a trained population, under conditions which reflect training, may inform on future studies in untrained or recreational populations.

We hypothesize that CRP and vCRP vary with velocity and footwear use, and that FSA is a significant covariate during impact phase.

## METHODS

Segmental sagittal plane coupling, rather than joint angle coupling, was studied for pelvis-thigh, thigh-tibia (ThiTib), tibia-rearfoot, and rearfoot-forefoot. Hindfoot segment frontal-tibia segment transverse plane coupling (EVTIR) was also measured.

Nineteen habitually SD male distance runners (1500 m personal record: mean (st. dev.) = 3.59.8 (10.0); age: median = 21, min = 19, max = 31) were recruited from a College cross country club. Participants ran BF, then SD, on a treadmill (Ultim8 Fitness Ltd, UK) for at least 3 minutes per trial at

12.9 km h<sup>-1</sup>, 14.3 km h<sup>-1</sup>, and 16.0 km h<sup>-1</sup> in a randomized order for BF and SD conditions. Twelve MX cameras (Vicon, Oxford, UK) captured lower-limb kinematics data at 200 Hz. Pelvis and thigh segments were defined according to the Plug in Gait model, whilst tibia, rearfoot, and forefoot segments were defined using the Oxford Foot Model. Based on available data, between 15 and 31 consecutive strides per trial were analyzed.

The discrete Hilbert transform, implemented in MATLAB, was applied to the entire time series ( $O(10^3)$  points) of consecutive gait cycles as part of CRP calculation. Heel and toe marker trajectories were used to determine foot-strike [4] and toe-off [5] events. Swing and stance phase CRP time series were time normalized to 51 points, with impact phase defined as 0-16% of stance phase. Omitting the first and last gait cycles was sufficient to eliminate edge effects, and any remaining waveforms were omitted if they exhibited limit cycle oscillations upon visual inspection. Trials which contained 5 or more gait cycles were used for statistical analysis.

CRP was calculated per stride for the three periods as the circular mean. Given all time normalized gait cycles per trial, vCRP was calculated as the point-wise circular standard deviation across all valid gait cycles, thus generating a single waveform per trial. From this, the circular mean was calculated for each time period. The median FSA for which vCRP data was valid was used as the summary FSA.

Statistical analysis was performed using MATLAB and R. Hierarchical linear mixed-effects models (LMM) with saturated fixed effects were used. The inclusion of velocity, footwear, or an intercept as subject-level random effects was determined using likelihood ratio tests with  $p < 0.05$ . LMM are more

flexible than ANOVA analyses because they allow correlations between random effects to be modeled, may account for missing data, and quantify between-subject variability (BSV). A Bonferroni correction, owing to three comparisons per coupling relationship, was applied in tests for statistical significance such that  $p < 0.017$  was significant.

## RESULTS AND DISCUSSION

Footwear was a random effect for all six applicable statistical tests. This may reflect subject-specific responses to footwear as compared to BF running. Footwear was a significant fixed effect for ThiTib CRP during impact phase, such that CRP was more in-phase for SD running. However, when accounting for BSV in the effect of footwear, 13% of subjects were more out-of-phase for slow SD versus slow BF running. Generally, the magnitude of BSV was comparable to the size of the associated significant fixed effect. Therefore, whilst statistically significant, changes may be of limited biomechanical significance. However, CRP was more robust to changes in velocity and differences in FSA for SD running, possibly from habituation to the SD condition. Also, FSA was a significant covariate for all CRP couplings during impact.

vCRP magnitudes were smaller than for previous studies. This may reflect skill development, or arise from different phase space construction methods. vCRP for ThiTib reduced as velocity increased, but velocity, condition, and FSA were not significant for other vCRP coupling relationships.

Transient phase locking between segments for EVTIR CRP appears to emerge at higher velocities for BF running (Figure 1). This coincides with higher vCRP around mid-stance. This may arise from changes in rearfoot segment motion. However, EVTIR data from several trials were omitted because limit cycle oscillations were present in the CRP signal. The Hilbert transform is susceptible to oscillations due to feedback because it is an infinite impulse response filter. Therefore it is unclear whether this observation reflects a mechanism utilized by the foot to address an increased

functional demand of pronation, or arises from a signal processing artifact.

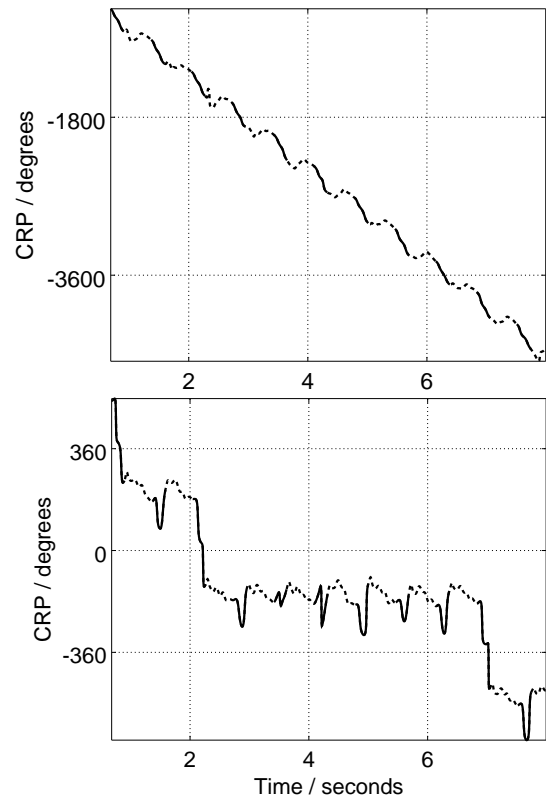


**Figure 1:** EVTIR CRP for a single subject running BF at 12.9 km h<sup>-1</sup> (top) and 14.3 km h<sup>-1</sup> (bottom), with stance phases as solid lines.

## CONCLUSIONS

Future studies of CRP should account for differences in velocity, footwear and FSA. Where studies use a variety of footwear, LMM for hypothesis testing is recommended, such that footwear may be modeled as a random effect. Further study of EVTIR with a larger population is encouraged, to ascertain whether a coordinative adaption occurs with changes in velocity.

## REFERENCES

1. Lamb PF and Stöckl M. *Clin Biomech* **29** 484-93, 2014
2. Cazzola D et al. *JSHS* **5** 35-43, 2016
3. Hamill J et al. *Clin Biomech* **14** 297-308, 1999
4. O'Connor CM et al. *Gait Posture* **25** 469-74, 2007
5. Maiwald C et al. *Proc 22<sup>nd</sup> Conf ISB* Cape Town, South Africa, 2009

## Lower Limb Segmental Variability During a 40-Min Prolonged Run

<sup>1</sup>Julia Freedman Silvernail, <sup>1</sup>Kristyne Wiegand, <sup>2</sup>Max R. Paquette

<sup>1</sup>UNLV, Department of Kinesiology, Las Vegas, NV, USA

<sup>2</sup>University of Memphis, School of Health Studies, Memphis, TN, USA  
email: [jfs@unlv.edu](mailto:jfs@unlv.edu)

### INTRODUCTION

The high frequency of knee injuries in runners has inspired scientists to study a number of running biomechanical variables. Discrete variables relative to joint motion and loading have been identified as possible risk factors for running knee injuries [1,2]. More sensitive metrics have been developed to assess the underlying organization of movement. Coordination variability, one such metric, has the ability to assess how an individual alters their movement organization throughout an entire movement each time they repeat a cyclical task. This provides insight to the adaptability and perhaps health of the individual's movement.

To date, the majority of biomechanical studies have assessed injury-related variables during either a one-time non-fatigued or exhaustive laboratory test. However, runners often complete submaximal runs during their regular training. Thus, the clinical implications of injury-related variables may be better understood if studied following a typical training run.

The purpose of this work was to compare lower limb segmental couples throughout a 40min submaximal run in runners of all levels. We expected that as the run progressed, runners would have a less flexible system resulting in a freezing of degrees of freedom as indicated by a decrease in coordination variability.

### METHODS

Fourty-four runners (24 men; 30±8 yrs; 68.1±11.4 kg; 1.74±0.1 m; 34.3±13.9 miles/week; 9.9±5.2 years of running experience) participated in the

study. Written consent approved by the IRB was obtained for all participants before testing begun.

Before testing, neoprene wraps were secured on both thighs and shanks and around the waist. Runners then ran at an easy effort on the treadmill for 5 minutes to allow the wraps to set into place. A 9-camera motion capture system (240Hz, Qualisys AB, Sweden) was used to collect kinematic data during running. Anatomical markers and tracking marker clusters were placed on both lower extremities to define segment coordinate systems. Following a standing calibration trial, only anatomical markers were removed and runners completed a 40-minute treadmill run. The run speed was set to 75% of the runners' best 10 km race time in the past 5 years to ensure a moderate run effort based on running ability (6.7±1.2 miles/hour). Four 6-second motion capture trials were collected after 10, 20, 30 and 40 minutes to obtain 3D lower limb kinematics during the run.

Visual3D biomechanical software (C-Motion, Germantown, MD, USA) was used to process and analyze all data. Kinematic data were interpolated using a least-squares fit of a 3rd order polynomial with a three data point fitting and a maximum gap of 10 frames. Data were then filtered using a fourth-order Butterworth low-pass filter at 8 Hz. The start and end of stance phase were identified using the minimal vertical pelvis velocity with a 15ms offset [3] and peak knee extension [4], respectively. Using a modified vector coding technique [5] coordination variability was assessed for early, mid and late stance of segment coordination at the knee. This was assessed for thigh-shank sagittal plane coupled motion and the thigh sagittal and shank transverse plane coupled rotation. The average variability for

each phase of stance of five steps was taken at each of the four collection times. These participant averages were used for analysis.

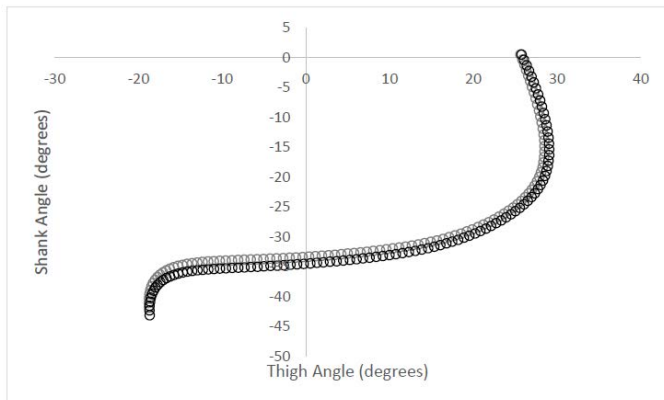


**Fig 1.** Sample Angle-Angle plot utilized for vector coding analysis.

Repeated measures ANOVAs with Time as the within-subject factor were used to evaluate all couples (23.0 SPSS, Chicago, IL, USA). Significance was set at an alpha level of 0.05.

## RESULTS AND DISCUSSION

There were no differences in coordination variability over time in any of the measured couples (Figure 2).

Although fatigue has previously been connected to changes in movement, these occurred during an exhaustive run [6]. We observed no effect of run time on coordination variability during this submaximal 40min run. There are a few factors that likely relate to this discrepancy between the current study and previous research. The runners in this study were well trained (i.e., ~35 miles/week) and a 40 minute run at a sub-maximal pace was in line with their normal training regimen. Furthermore, while this run was prolonged, it was not an exhaustive run. In these individuals performing a typical training run, they were able to maintain flexibility and adaptability in their movement. Perhaps if this were a novel task to the runners we would may have observed a decrease in variability over the course of the run.

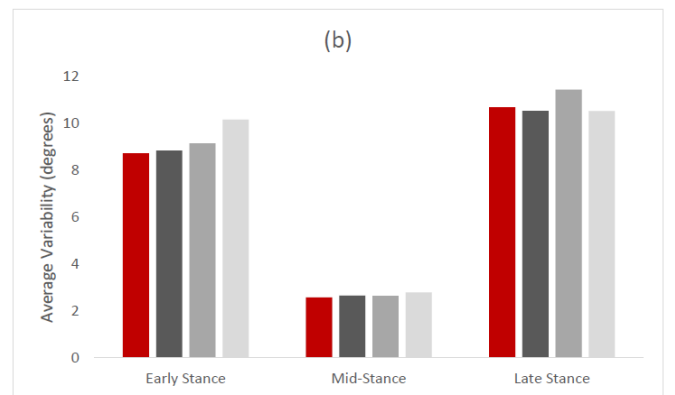
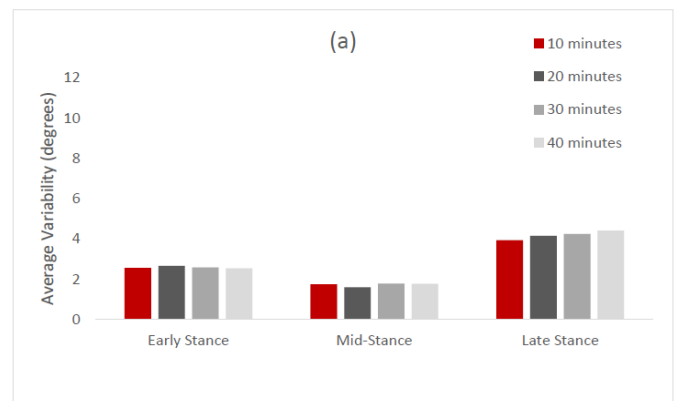


**Fig 2.** Average Thigh Shank Coordination Variability during the Stance Phase of Running. (a) Sagittal plane motion of both segments. (b) Sagittal plane motion of the thigh coupled with transverse plane motion of the shank.

## CONCLUSIONS

These findings suggest that in well trained male and female runners, the completion of a submaximal prolonged run does not affect the adaptability of their system as evidenced by the unchanged coordination variability throughout the run. Future studies are needed as the current findings may be different in novice runners with less running experience or when completing a longer fatiguing run.

## REFERENCES

- Ott B, et al. *J Electr Kinesiol*, **21**, 631-637, 2011.
- Dierks TA, et al. *J Orthop Sports Phys Ther*, **38**, 448-456, 2008.
- Milner et al. *J Biomech*, **18**, 3502-3505, 2015.
- Fellin et al. *J Sc Med Sp*, **13**, 646-650, 2010.
- Freedman Silvernail et al. *MSSE*, **10**, 2175-2180, 2015.
- Derrick et al. *MSSE*, **34**, 998-1002, 2002.

# EFFECT OF RUNNING SPEED ON FOOT STRIKE INDEX, SPATIO-TEMPORAL PARAMETERS AND REARFOOT PRONATION IN RUNNERS

<sup>1</sup>Reginaldo K. Fukuchi, <sup>2</sup>Claudiane A. Fukuchi and <sup>1,2</sup>Marcos Duarte

<sup>1</sup>Biomedical Engineering Program, Federal University of ABC

<sup>2</sup>Neuroscience and Cognition, Federal University of ABC, Brazil

email: reginaldo.fukuchi@ufabc.edu.br, web: <http://demotu.org/>

## INTRODUCTION

Improving the knowledge related to gait biomechanics across a range of running speeds may help to understand the contributing factors related to both running performance and running injuries. In fact, excessive running pace has been considered to be a risk factor for running injuries [1] but its influence on gait biomechanical variables remains poorly understood. For instance, rearfoot pronation and foot strike patterns have been associated to running injuries [2, 3] despite the fact that few studies have attempted to examine their behavior under different running speeds.

Regarding the spatiotemporal parameters, to our knowledge, no studies have examined the effect of increased running pace on stride width despite the fact that a narrow stride width has been associated with increased loading of the tibia during running. Therefore, the aim of this study was to investigate the effect of different running speed on foot strike index (FSI), spatio-temporal parameters and rearfoot pronation in competitive runners. We hypothesized that an increase in stride length, cadence and rearfoot pronation would be observed with increased running speed. In addition, we hypothesized that a shift towards forefoot strike as well as a narrower stride width would be present at higher speeds.

## METHODS

The data used in the present study were obtained from a public repository available at Figshare (DOI: [10.6084/m9.figshare.4543435](https://doi.org/10.6084/m9.figshare.4543435)). Briefly, twenty-eight competitive runners (27 males and 1 female) were analyzed. The information about demographics, anthropometrics and running habits can be accessed in the public repository. Three-

dimensional kinematics and kinetics data were obtained by a 12-camera motion capture system (Motion Analysis) and an instrumented treadmill (FIT, Bertec), while the subjects ran at 2.5 m/s, 3.5 m/s, and 4.5 m/s. The sampling frequency was 150 Hz for the kinematics and 300 Hz for the kinetics data. The FSI was calculated according to [4]. The data processing and data analysis were performed in Visual 3D software (C-motion). Either one-way ANOVAs or Kruskal-Wallis tests were performed to examine the effect of running speed considering the homogeneity of variances assumption. Post hoc pairwise comparisons were performed with Bonferroni adjustments whenever a main effect was observed. The level of significance was 0.05.

## RESULTS AND DISCUSSION

A main effect of running speed on stride length ( $X^2=71.33$ ;  $p<0.001$ ) and cadence ( $F=26.72$ ;  $p<0.001$ ) were observed. The post hoc analysis revealed that both stride length and cadence were significantly higher as the gait speed increased (Figure 1). It is possible to observe in Figure 1 that stride length increased at a greater extent compared to cadence, suggesting that runners may choose to rely more on larger strides than on more steps to cope with higher running speeds, particularly, within this range of gait speed (2.5 to 4.5 m/s). The peak eversion angle was also affected by gait speed ( $F=6.28$ ;  $p=0.003$ ), however, only when the extreme speed values were compared (2.5 m/s vs. 4.5 m/s) as displayed in Figure 1. Similar results have been reported in recreational runners during treadmill running at comfortable speeds [5]. Despite the fact that both rearfoot pronation and increased pace have been linked with running injuries, this relationship remains poorly understood and needs to be addressed in future studies.

Contrary to our hypothesis, no difference was observed for stride width ( $F=2.60$ ;  $p=0.08$ ) and FSI ( $F=0.217$ ;  $p=0.81$ ) which indicates that gait speed did not influence these variables. The lack of studies investigating similar question prevented any comparison. In regards to the effect of running speed on FSI, previous studies have produced contrasting results with some evidence suggesting the existence of an anterior shift of the center of pressure (as a result of increased speed); and others revealing lack of changes in foot strike patterns. The lack of agreement across studies may be explained by the differences related to the range of selected gait speeds, the method to calculate strike index and the controlled laboratory conditions (treadmill vs. overground). Future studies need to further address these issues.

## CONCLUSIONS

The results demonstrated that increased running pace was related to an increase in stride length,

cadence and rearfoot pronation. In contrast, stride width and FSI were not affected by running speed.

## REFERENCES

1. Nielsen RO, et al. *Int J Sports Phys Ther* 8:172-179, 2013.
2. Nigg BM, et al. *Br J Sports Med* 49:1290-4, 2015.
3. Hamill J, et al. *J Sport Health Sci*. In Press, 2017.
4. Cavanagh PR, et al. *J Biomech* 13: 397-406, 1980.
5. Munoz-Jimenez M, et al. *J Sports Sci* 33:2035-2042, 2015.

## ACKNOWLEDGMENTS

To Fundação de Amparo à Pesquisa do Estado de São Paulo (FAPESP) (#13/26829-1, #14/13502-7 and #14/13247-7) e Conselho Nacional de Desenvolvimento Científico e Tecnológico (CNPq) (#487490/2013-4).

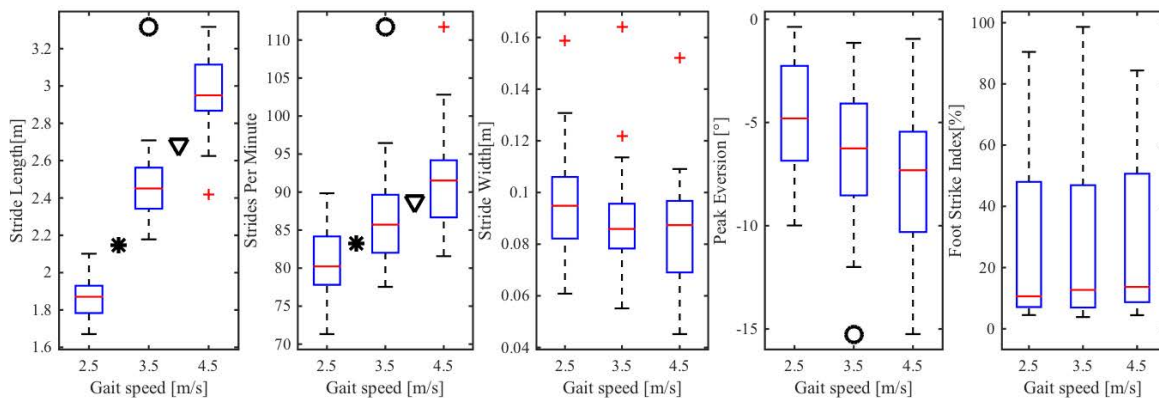


**Figure 1.** Distribution of stride length, cadence, stride width, rearfoot eversion and FSI across gait speeds. The symbols \*, °, Δ, comprises 2.5 vs. 3.5 m/s; 2.5 vs. 4.5 m/s; 3.5 vs. 4.5 m/s, respectively, for the post hoc comparisons.

# THE COUPLING OF FOOTSTRIKE AND STRIDE LENGTH IN RUNNING

<sup>1</sup> Melissa Thompson, and <sup>2,3</sup> Kristine Hoffman

<sup>1</sup> Fort Lewis College, Durango, CO, USA

<sup>2</sup> Denver Health Medical Center, Denver, CO, USA

<sup>3</sup> University of Colorado School of Medicine, Denver, CO, USA

email: mathompson@fortlewis.edu

## INTRODUCTION

Running is one of the most popular recreational activities worldwide, yet runners exhibit some of the greatest rates of overuse injuries. The gait parameters footstrike and stride length have received considerable attention in the scientific literature due to implications for running related overuse injuries.

Increased stride length has been associated with greater ground reaction forces, joint moments, impact accelerations, and energy absorption, factors that have been associated with an increased risk of running-related overuse injuries. Research has indicated that reducing stride length may decrease the risk of tibial stress fracture [1]. In terms of footstrike, running with a rear footstrike (RFS) pattern requires the tibialis anterior to decelerate plantar flexion as the foot contacts the ground. Correspondingly, running with a RFS has been associated with increased pressures in the anterior compartment of the lower leg. Alternatively, the triceps surae muscles are active to slow dorsiflexion when runners adopt a fore/mid footstrike (F/MFS) pattern. Hence, F/MFS running has been associated with higher Achilles tendon strain and plantar flexor moments [2].

While mechanical alterations and corresponding clinical implications are evident with alterations in both stride length and footstrike, these variables have been treated as independent factors in the literature. However, studies have reported data indicating flatter foot placement as stride length is decreased [3], which indicates that the variables of footstrike and stride length may be coupled. Therefore, the purpose of this study was to examine the relationship between footstrike and stride length in running, and to determine if these variables could be independently manipulated.

## METHODS

11 healthy active subjects (5 female, 6 male); mass:  $65.9 \pm 9.8$  kg; age:  $24 \pm 1.65$  years participated in this study. Participants completed two testing sessions that were separated by at least 24 h. Session 1 was used to determine the participant's preferred stride length and velocity. In Session 2, participants ran with their stride length manipulated to  $\pm 5\%$  and  $\pm 10\%$  of their preferred stride length. Participants completed these manipulated stride length trials with their self-selected footstrike (SSFS), as well as attempting to both RFS and F/MFS. 10 trials were completed for each stride length/footstrike condition.

To control running velocity to that of the preferred condition, subjects matched their speed to a marker on a motor driven pulley system located parallel to the runway. Stride length was controlled by having participants match foot falls to strips of tape placed along the runway.

3-dimensional motion analysis (Vicon, Oxford Metrics Ltd., UK) was captured as subjects ran across a 20m runway. Footstrike was determined from footstrike angle (FSA) based on the following:  $FSA > 0^\circ$  was defined as RFS, and  $FSA \leq 0^\circ$  was defined as F/MFS [4]. Participants also completed a brief questionnaire indicating the level of difficulty with adopting the RFS and F/MFS foot strike conditions.

A Pearson product moment correlation was conducted to examine the relationship between FSA and stride length. Repeated measures ANOVA tests were performed to examine the differences in FSA between the preferred condition and manipulated footstrike (SSFS, RFS, F/MFS) / stride length (-10%, -5%, +5%, +10%) conditions. Statistical significance was defined as  $p < 0.05$ .

## RESULTS AND DISCUSSION

All but two participants were natural RFS runners as indicated by positive FSAs in the preferred condition. In the longer (+5% and +10%) stride length conditions nearly all participants continued to RFS. The two natural F/MFS strike runners were the only runners who did not adopt a RFS pattern with the longer stride length conditions. Thus, there was no significant difference in FSA between the +5%, +10% and preferred conditions ( $p > 0.05$ ). In the shorter stride length conditions all participants adopted a F/MFS position (Fig 1). FSAs for the -5% and -10% conditions differed significantly from the preferred condition (both  $p << 0.001$ ).

The correlation for the relationship between foot strike and stride length was low ( $r = 0.16$ ) and non-significant ( $p = 0.41$ ). This is likely due to the fact FSA did not continue to increase as stride length increased. At longer stride lengths runners adopted a RFS position and remained in a similar RFS position as stride length continued to increase.

Participants were able to adopt the imposed foot strike positions (F/MFS & RFS) at both longer and shorter stride lengths (Table 1). FSA was significantly different for the F/MFS condition at the longer stride lengths ( $p = 0.01$ ) and for the RFS condition at the shorter stride lengths ( $p = 0.02$ ). However, there was considerably more variability in FSA for the imposed foot strike conditions (Table 1). Additionally, participants reported greater difficulty with the reduced stride length RFS conditions.

**Table 1:** Footstrike angle for the stride length ( $\pm 5\%$  and  $10\%$ ) and footstrike conditions (SSFS, RFS, F/MFS). FSA  $> 0^\circ$  is RFS, and FSA  $< 0^\circ$  is F/MFS. \* Indicates a significant difference in FSA from the preferred condition, ^ indicates a significant difference in FSA from the other footstrike conditions (SSFS, RFS, F/MFS) at a given stride length.

	Footstrike	Stride Length Condition				
		-10%	-5%	Preferred	+5%	+10%
Footstrike Angle (deg)	SSFS	$-11.3 \pm 4.1^*$	$-11.1 \pm 3.9^*$	$7.2 \pm 7.0$	$6.8 \pm 9.3$	$8.6 \pm 9.0$
	RFS	$3.1 \pm 7.7^{\wedge}$	$3.2 \pm 8.3^{\wedge}$		$6.1 \pm 6.6$	$6.9 \pm 7.1$
	F/MFS	$-10.9 \pm 6.8$	$-8.5 \pm 7.2$		$-3.8 \pm 7.3^{\wedge}$	$-4.5 \pm 6.3^{\wedge}$

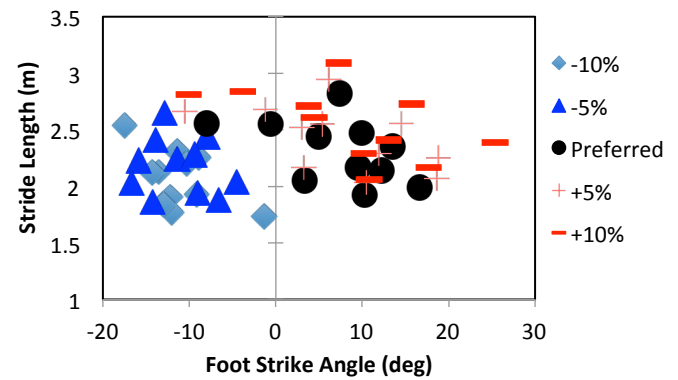


**Figure 1:** Foot strike angle (FSA) as a function of stride length for the preferred and SSFS altered stride length conditions. FSAs for the -5% and -10% differed significantly from the preferred condition ( $p < 0.05$ ).

## CONCLUSIONS

The results presented here indicate that footstrike and stride length are coupled, i.e. changing stride length leads to a corresponding change in footstrike. It is possible for individuals to uncouple these parameters, however it is done with difficulty and results in greater gait variability. When suggesting alterations in stride length or foot strike, clinicians should be aware of the associated changes in the coupled variable.

## REFERENCES

1. Edwards BW, et al. *Med Sci Sports Exerc*, **41**, 2177-2184, 2009.
2. Perl DP, et al. *Med Sci Sports Exerc*, **44**, 1335-1343, 2012.
3. Heiderscheidt BC, et al. *Med Sci Sports Exerc* **43**, 296-302, 2011.
4. Altman AR & Davis IS. *Gait Posture* **35**, 298-300, 2012

# PREDICTION EQUATIONS FOR LEG KINEMATICS AND KINETICS DURING SLOPE RUNNING

<sup>1</sup>Anat Shkedy Rabani, <sup>2</sup>Gregory S. Sawicki, <sup>1</sup>Raziel Riemer

<sup>1</sup>Ben-Gurion University of the Negev, Israel

<sup>2</sup>North Carolina State University and University of North Carolina, NC, USA

Email: rriemer@bgu.ac.il,

## INTRODUCTION

Kinematic and kinetic data describing the dynamics of lower-limb joints are critical for understanding the neuromechanics and energetics of human locomotion, and for guiding the design of assistive devices (e.g. lower-limb exoskeletons). From a basic science perspective, studies have provided insight into the sources of metabolic energy consumption by relating joint kinetics to whole-body oxygen consumption [1]. From an applied science perspective, kinematic and kinetic data are important for the geometric and material properties of lower-limb orthoses [2] and of motors sizing for powered exoskeletons and prostheses [3], as well as for guiding control software in both powered exoskeletons [4] and prostheses [5].

Combining experimental approaches like motion capture and force measurements with rigid body models (i.e. inverse dynamics) provides a means for obtaining lower-limb joint kinematics and kinetics data. Many studies have addressed walking or running at typical speeds on level ground [1,6]. Yet data acquisition is expensive and time-consuming, and therefore available joint-level data is limited to only a small subset of speeds. The same holds for data from locomotion uphill and downhill. Additionally, relationships describing how lower-limb joint kinematics and kinetics depend on the phase of gait have not been documented using parametric-equations, which if developed could help fill in data gaps in the literature without requiring exhaustive data acquisition.

Using an experimental data set, our aim was thus to develop a comprehensive parametric model of lower-extremity joint kinematics and kinetics during human running up and down slopes.

## METHODS

In two separate experiments, at two different labs (BGU and NCSU), sixteen healthy adults (6 females; 10 males; age =  $24.56 \pm 3.16$  years; height =  $1.73 \pm 0.09$  m; mass =  $68.01 \pm 13.98$  kg) ran on an instrumented split belt treadmill (FIT, Bertec, Columbus, OH, USA) at 2.25 m/s at nine grades (-10%, -7.5% -5%, -2.5%, 0%, +2.5% +5%, +7.5%, +10%). In each of the experimental conditions, force and motion data of at least 7 gait cycles (average = 20) were collected (MX40+, VICON, Oxford, UK or Oqus, Qualisys Medical AB®, Gothenburg, Sweden). Then the kinematics and kinetics of the leg joints were calculated using Visual3D software (C-motion Inc., Germantown, MD, USA). All kinematics and kinetics were normalized in time as percentages of one gait cycle. In addition, torque and power were normalized by the subject's height and weight.

Then based on a method by Mizrachi et al. [7] we developed the prediction equations for running in different slopes using data from randomly selected 14 subjects (7 from each group). Each of the above equations was developed in two phases: First, an equation was fitted for each of the five training slopes (-10%, -5%, 0%, 5%, 10%) separately (45 equations = 3 joint\*5 slope\*[angle, torque, power]), where for each joint and given slope the equation's input was the percentage of the gait cycle. Since gait exhibits periodic behavior, we used a Fourier series in the form of sine and cosine with  $\omega = 2\pi / 100$  to model these equations. Then, in the second phase, we modeled the change in value of each of the Fourier series coefficients as a function of the slope, using a polynomial. For both phases we developed an algorithm that found the best fit (Adjusted  $R^2$ ), using the lowest order of series/polynomial. To test the prediction equations, we examined the two subjects who were not used in developing the equations. Also, we tested several slopes that were not included in the training set (-

7.5%, -2.5%, 2.5%, 7.5%). If the results of the test data fell within 3 standard deviations (SD) from the fit, we considered it as a successful fit. The 3SDs were calculated using the training data.

## RESULTS AND DISCUSSION

The prediction equations had an Adjusted  $R^2$  for the leg joint kinematics and kinetics ranging from 0.943 to 0.997. We also show that newly presented data (either for new subjects or new slopes), which were not used for the equations fitting, in most cases fell within 3 standard deviations from the prediction. Figure 1 is an example for the knee, at 5% slope of new subjects' data, and Figure 2 is an example for prediction on untrained subjects and slopes.

In addition, from our analysis we did not see differences between the male's and female's data. Furthermore, since the equations were developed based on data that were collected in two different sites, with different motion capture systems and with similar but not identical marker placements, we believe prediction equations are a good representation of the general healthy adult population.

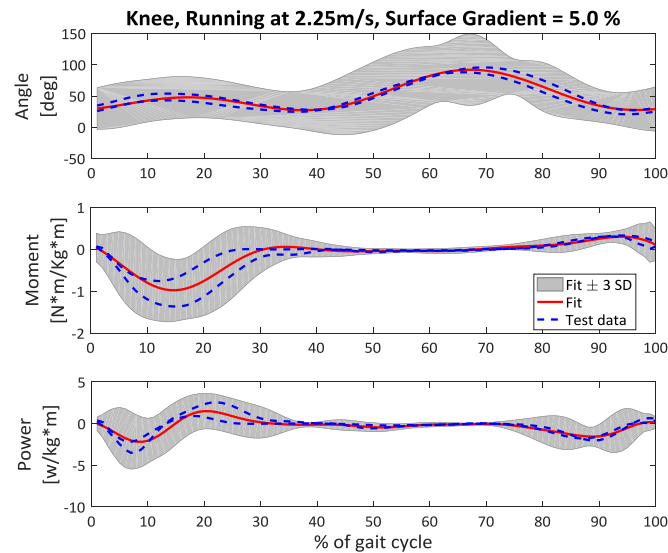


**Figure 1:** Test of the predictions using new subjects at a 5% slope. The red curve represents the prediction equation, and the grey area  $\pm 3$  SD of the training set. The dashed lines represent the test subjects.

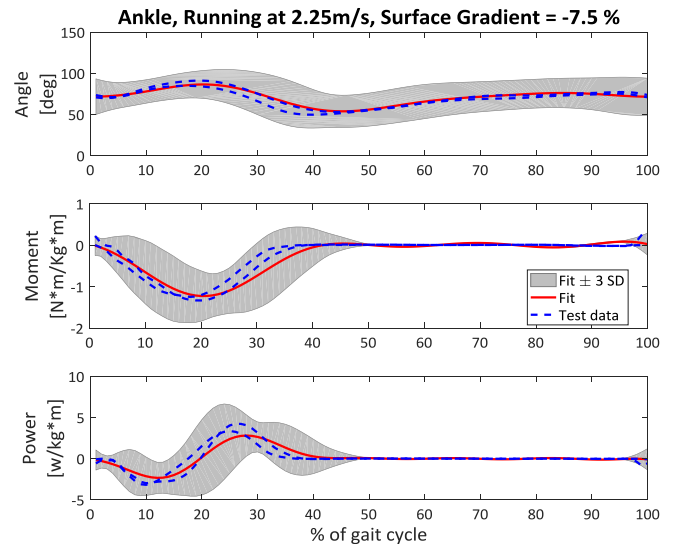


**Figure 2:** Test of the predictions using new slopes of -7.5% slope. The red curve represents the fit, and the grey area  $\pm 3$  SD. The dashed lines represent test data.

## CONCLUSIONS

The prediction equations enable predicting the leg joint angle, torque, and power during running as functions of the slope and percentage in the gait cycle. This set of equations could be used to gain a better understanding of locomotion, and may be helpful in the development of assistive devices such as prostheses and wearable robots.

## REFERENCES

1. Farris DJ, et al. *J R Soc Interface* **9**, 110-118, 2012.
2. Faustini MC, et al. *IEEE Trans Biomed Eng* **55**, 784-790, 2008.
3. Hitt J, et al. *Ind Robot* **36**, 441-447, 2009.
4. Zoss AB, et al. *IEEE/ASME Trans Mechatronics* **11**, 128-138, 2006.
5. Markowitz J, et al. *Philos Trans R Soc Lond B Biol Sci* **366**, 1621-1631, 2011.
6. Devita P. *J Biomech* **27**, 501-508, 1994.
7. Mizrachi S, et al. *World Congress of Biomechanics*, Boston, MA, USA, 2014.

## ACKNOWLEDGMENTS

This study was partially supported by the Helmsley Charitable Trust through the Agricultural, Biological and Cognitive Robotics Initiative of Ben-Gurion University of the Negev.

# EFFECT OF TRANSITIONING RUNNING STYLE FROM A REARFOOT TO A NON-REARFOOT STRIKE PATTERN ON IMPULSE PER UNIT DISTANCE

Alec J. Smith, Erin M. Florkiewicz, Donald L. Goss, Gregory M. Freisinger

United States Military Academy, West Point, NY, USA

Email: [gregory.freisinger@usma.edu](mailto:gregory.freisinger@usma.edu)

## INTRODUCTION

Running is a primary form of physical conditioning and point of evaluation for military personnel. Lower extremity injuries are common in military training due to the frequency and dynamic nature of the associated loads [1]. Several approaches have been taken to mitigate running injuries among athletes and military personnel alike. One approach is the modification of a runner's foot strike pattern (FSP).

Transitioning runners from a rearfoot strike (RFS) to a non-rearfoot strike (NRFS) pattern has been shown to influence several factors related to running injuries, to include a reduction in average vertical loading rate (AVLR) [2]. This idea is well established, but there are likely other factors influencing running related injuries including cadence and the influence of total impulse.

The purpose of this study was to analyze the effect of a NRFS running program on overall impulses per unit distance. We hypothesized that impulse per unit distance will remain constant in the vertical, anterior, posterior, medial, and lateral directions following a running transition programs.

## METHODS

Nine runners recovering from lower extremity injuries at the United States Military Academy were recruited to participate in this study after providing IRB approved consent. All participants were cadets with previous running experience (5 males:4 females; mean age:  $20.3 \pm 2.2$  yrs; mean height:  $170.7 \pm 13.8$  cm; mean weight  $71.7 \pm 14.9$  kg).

Participants met each of the following six inclusion criteria: 1) previously a RFS runner; 2) recovering from a lower extremity injury; 3) able to walk pain free for 2 miles; 4) dorsiflexion range of motion of at

least 80% symmetry; 5) capable of performing 20 unassisted single leg heel raises; 6) able to perform a single leg hop for distance with at least 80% symmetry. These participants were clinically diagnosed and recovering from one of the following lower extremity injuries: patellofemoral pain syndrome (3), lower leg stress injury (2), lower leg fracture (1), plantar fasciitis (1), and anterior cruciate ligament reconstruction (2).

To encourage a transition to a RFS pattern subjects underwent an initial 30 minute training session. Training focused on soft landings, an increase in cadence, forward trunk lean and their strict adherence to a gradual walk-to-run progression. They then met with an assigned medical provider once a week for the first 4 weeks, then again at weeks 6, 8, and 10 upon which the training focuses were reinforced and PSFS (Patient Specific Functional Scale) data were collected. Initial and 10 week assessments were conducted before and after the 10-week training program. Assessments consisted of subjects running at a self-selected pace for five minutes. Speed was kept constant for both the initial and follow up assessment. Two-dimensional video was collected at 240 Hz [Casio, EX-ZR200; Tokyo, Japan] in the sagittal plane to confirm FSP. Ground reaction force data were collected on an instrumented treadmill [Bertec; Columbus, OH] at 1000 Hz, low-pass Butterworth filtered at 35 Hz, and normalized to bodyweight.

Impulse was calculated in the vertical, anterior, posterior, medial and lateral directions for five stance phases on each foot. The ensemble average of five stance phases for the left and right were used in further analyses. Average impulses were multiplied by the respective runner's cadence (in right foot steps per minute) and divided by their treadmill speed (in meters per second). Unit conversions yielded impulses per unit distance which was multiplied by

1000 meters to find impulse measured in bodyweight\*seconds per kilometer.

A paired t-test was used to test for statistical difference between the initial and follow-up assessments for the impulse variables and subjective measures. A significance level alpha = 0.05 was used.

## RESULTS/DISCUSSION

The transition from RFS to NRFS was verified by the high speed video for all subjects. Initial, follow up and change data are shown in Table 1 for the variables of interest. PSFS and running cadence significantly increased as expected following the running transition protocol.

Contrary to our hypotheses, significant differences were found in anterior, posterior and lateral impulses per km ( $p < 0.01$ ,  $p < 0.05$ ,  $p < 0.05$  respectively). However no differences were found in the vertical or medial directions. Boxplots for the percent changes in impulse per km are displayed in Figure 1.

Average individual anterior and posterior impulse per km increased by 26.3% and 14.3%, respectively, while vertical impulse did not increase. Our NRFS transition program emphasized increased running cadence, therefore resulting in a larger number of foot strikes per unit distance. While NRFS has shown a significant reduction in vertical loading rate compared to RFS, our results indicate an increase in total braking and propulsive impulse per unit distance. This increase in total impulse may influence running injury risk over the long-term.

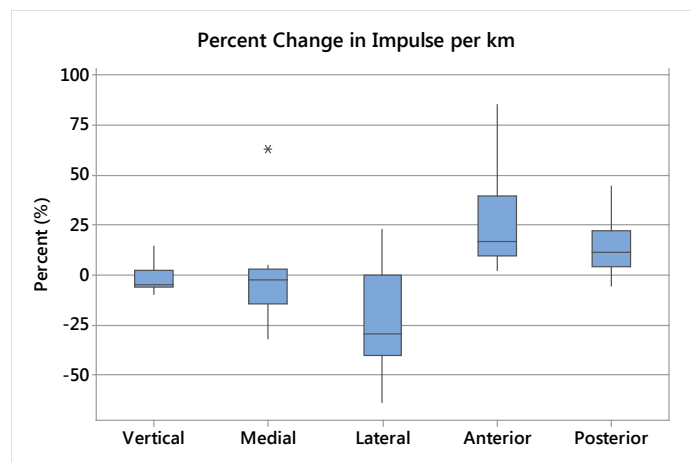


**Figure 1:** Box plot of average percent change in impulse per kilometer.

## CONCLUSION

Anterior, posterior and lateral impulses per unit distance increased following a running transition program. Transitioning from a RFS to a NRFS improved subjective functional scores, however it is unknown how increased total impulse per unit distance may impact running injury risk. Additional research is necessary to further identify the long-term effects of kinetic changes induced from modifying running foot strike pattern.

## REFERENCES

- 1) van Gent RN, et al. *Br J Sports Med* 41, 469-480, 2007.
- 2) Crowell et al. *Clinical biomechanics* 26.1: 78-83, 2011.

## ACKNOWLEDGEMENTS

Funding for this study was provided by the United States Military Academy Center for Innovation and Engineering.

**Table 1:** Average impulse per unit distance, PSFS, and cadence before and after running transition.

	Impulse Type per km (BW-s/km)										PSFS		Cadence	
	Vertical		Anterior		Posterior		Medial		Lateral					
	Mean	Std.	Mean	Std.	Mean	Std.	Mean	Std.	Mean	Std.	Mean	Std.	Mean	Std.
<b>Initial</b>	349.9	16.5	18.4	2.8	18.0	3.5	7.4	1.1	7.0	1.3	6.1	1.0	170.2	10.1
<b>Follow Up</b>	343.4	23.8	22.7	2.0	20.2	2.2	7.3	1.4	5.3	1.4	9.3	0.9	179.8	6.4
<b>Change</b>	-6.4	25.4	4.3	3.6	2.2	2.1	-0.2	1.7	-1.8	2.0	3.1	1.1	9.6	8.1
<b>p-Value</b>	0.469		<b>0.007*</b>		<b>0.013*</b>		0.777		<b>0.027*</b>		<b>p&lt;0.001*</b>		<b>p&lt;0.001*</b>	

*Bold and (\*) indicate a significant p-value < 0.05. PSFS: Patient-Specific Function Scale.*

# A BIOMECHANICAL INVESTIGATION OF COMPENSATION STRATEGIES USED BY RUNNERS IN RESPONSE TO REDUCED CORE STABILITY

Margaret E Raabe and Ajit MW Chaudhari  
The Ohio State University, Columbus, OH, USA

email: margaret.e.raabe@gmail.com, web: <http://u.osu.edu/osusportsbiomechanics/>

## INTRODUCTION

Insufficient core stability is believed to lead to less efficient movements and ultimately musculoskeletal injury, despite minimal scientific evidence supporting this theory. Additionally, compensation strategies that may be utilized by runners lacking sufficient core stability have yet to be investigated.

Altering movement patterns may be one strategy to compensate for poor core stability (kinematic compensation strategy, KIN). Another possibility would be to alter only muscular activation strategies (neuromuscular compensation strategy, NM). The compensation strategy chosen by a runner lacking sufficient core stability may be driven by a number of factors including energy cost, as the minimization of energy expenditure is believed to play a large part in locomotion [1]. Understanding the advantages and disadvantages of these strategies could ultimately provide insight into the influence of core stability on injury risk.

The purpose of this study, therefore, was to identify the biomechanical consequences associated with possible compensation strategies for reduced core stability during running using subject-specific musculoskeletal simulations.

## METHODS

Eight novice runners jogged overground in a motion capture laboratory before and after performing a fatiguing core stability knockdown protocol (CSKP) [2]. All runners in this subset of a previously-reported in vivo study [3] had a significant difference in at least one hip or knee kinematic variable post-CSKP. Four runners experienced experimentally reduced core stability and increased core muscle fatigue following the CSKP (CS group) and the remaining four experienced only core muscle fatigue and no change in core stability

following the CSKP (NCS group). Subject-specific kinematically-driven jogging simulations (Fig. 1) were developed in OpenSim [4] for each participant in four different conditions (pre-CSKP kinematics, no core fatigue; pre-CSKP kinematics, core fatigue; post-CSKP kinematics, no core fatigue; post-CSKP kinematics, core fatigue) in order to isolate and fully characterize the effect of utilizing either the KIN or NM strategy on lower extremity (LE) variables previously associated with running injuries.

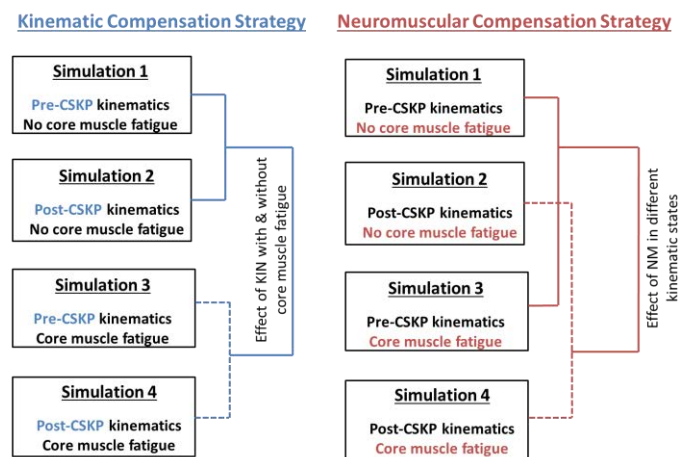


Figure 1. Schematic describing the four subject-specific simulations developed for each participant.

Linear mixed-models were used to test for a significant effect of a KIN or NM strategy in response to core muscle fatigue on the primary variables. The kinematic state (pre-CSKP, post-CSKP), the core fatigue state (none, fatigue), and their interaction were treated as fixed effects and participant was treated as a random effect ( $\alpha=0.05$ ). Results trending toward significance ( $0.05 \leq p \leq 0.1$ ) were also reported. These analyses were conducted separately for the CS and NCS groups to provide insight into which biomechanical changes may be driven by reduced core stability vs. core muscle fatigue. Loading variables presented are internal.

## RESULTS AND DISCUSSION

### Kinematic Compensation Strategy

Runners with experimentally reduced core stability following the CSKP adopted a KIN associated with reduced energy consumption estimated as total cubed muscle stress ( $3249.3 \pm 1317.5 \text{ MPa}^3$  vs  $3009.9 \pm 1259.1 \text{ MPa}^3$ ,  $p=0.059$ ), cumulative lumbar spinal compression ( $p \leq 0.06$ ), and peak core muscle force production (non-dominant psoas (NDom PS),  $p=0.06$ ; NDom internal oblique (IO),  $p=0.027$ ). However, these changes were accompanied by an increased peak patellofemoral joint reaction force ( $6.2 \pm 1.0 \text{ BW}$  vs  $6.6 \pm 0.7 \text{ BW}$ ,  $p=0.029$ ), peak knee abduction moment ( $4.3 \pm 0.9 \text{ \%BW} \cdot \text{h}$  vs  $5.1 \pm 0.8 \text{ \%BW} \cdot \text{h}$ ,  $p=0.01$ ), knee abduction impulse ( $0.6 \pm 0.2 \text{ \%BW} \cdot \text{h} \cdot \text{s}$  vs  $0.7 \pm 0.3 \text{ \%BW} \cdot \text{h} \cdot \text{s}$ ,  $p=0.02$ ), and peak knee extension moment ( $16.4 \pm 1.5 \text{ \%BW} \cdot \text{h}$  vs  $17.2 \pm 2.4 \text{ \%BW} \cdot \text{h}$ ,  $p=0.09$ ) during the stance phase of running (Figure 2). These LE loading changes have previously been associated with increased running injury risk.

	CS group N=4	NCS group N=4
peak patellofemoral joint reaction force	↑ $p=0.029$	$p=0.85$
peak knee abduction moment and impulse	↑ $p=0.01$ ↑ $p=0.02$	↓ $p=0.003$ ↓ $p=0.001$
peak knee extension moment	↑ $p=0.09$	$p=0.58$
estimated energy consumption	↓ $p=0.059$	$p=0.51$
lumbar spine compression force impulse	↓ $p \leq 0.06$	$p \geq 0.1$
peak core muscle force production (IO, PS)	↓ $p \leq 0.06$	$p \geq 0.1$

Figure 2. Biomechanical variables affected by a kinematic (KIN) compensation strategy in response to an experimental core muscle fatiguing protocol. The arrows indicate changes in parameters with a change in kinematics.

### Neuromuscular Compensation Strategy

An NM strategy adopted in response to simulated core muscle fatigue was associated with decreased compressive lumbar spinal loading (CS group: peak compression,  $p \leq 0.04$ ; compression force impulse,  $p \leq 0.06$ ; NCS group: compression force impulse,  $p \leq 0.08$ ), decreased superficial peak core muscle force production (CS and NCS group: Dom and NDom rectus abdominis (RA) and IO and Dom external oblique (EO),  $p \leq 0.033$ ) and increased peak deep core muscle force production (CS group: NDom multifidus (MF),  $p=0.18$ ; NDom quadratus lumborum (QL),  $p=0.18$ ; NCS group: Dom QL,

$p=0.21$ ; NDom PS,  $p=0.18$ ) (Figure 3). NM was not associated with significant changes in estimated energy consumption or LE loading during the stance phase of running, suggesting NM may be preferable to a KIN strategy that potentially results in increased LE loading and injury risk.

	CS group N=4	NCS group N=4
peak lumbar compression force	↓ $p \leq 0.047$	$p \geq 0.1$
lumbar compression force impulse	↓ $p \leq 0.06$	↓ $p \leq 0.08$
estimated energy consumption	$p=0.21$	$p=0.36$
lower extremity loading	$p \geq 0.1$	$p \geq 0.1$
peak superficial core muscle force (RA, EO, IO)	↓ $p < 0.05$	↓ $p < 0.05$
peak deep core muscle force production	↑ Ndom MF $p=0.18$ ↑ Ndom QL $p=0.18$	↑ Dom QL $p=0.21$ ↑ Ndom PS $p=0.18$

Figure 3. Biomechanical variables affected by a neuromuscular (NM) compensation strategy adopted in response to simulated core muscle fatigue. Arrows indicate changes in parameters with changes in core muscle fatigue.

### CONCLUSIONS

Results from this study suggest that novice runners with insufficient core stability may adopt altered movement patterns associated with increased lower extremity loading and ultimately a higher risk of sustaining a running-related injury. Since the only apparent adjustment required to utilize an NM strategy was an increase in force production of the deep core musculature, proper training of these muscles may give runners the ability to utilize lower-risk compensation strategies in the presence of core muscle fatigue and/or poor core stability. Future work may consider developing a neuromuscular training program specifically for runners and determining if this program can reduce LE loading during running and thereby reduce running injury incidence.

### REFERENCES

- Alexander RM. *American Scientist*, 72(4): 348-354, 1984.
- Raabe ME, et al. *Proceedings of 2015 ASB* 39(452), 2015.
- Raabe ME, et al. *Proceedings of 2016 ASB* 40(XXX), 2016.
- Raabe ME, et al. *J Biomech* 49(7):1238-43, 2016.

## Trunk Kinematics Changes With Age and Running Speed

<sup>1</sup>Rumit Singh Kakar, <sup>1</sup>Joshua M. Tome, <sup>1</sup>Zach Finer, <sup>1</sup>Natalie Knight, <sup>2</sup>Kathy J. Simpson

<sup>1</sup>Department of Physical Therapy, Ithaca College, Ithaca, NY

<sup>3</sup>Department of Kinesiology, University of Georgia, Athens, GA

email: [rkakar@ithaca.edu](mailto:rkakar@ithaca.edu), web: <http://www.ithaca.edu/hshp/clinics/movementlab/>

### INTRODUCTION

Our limited understanding of the trunk's role in producing running locomotion is partly due to lack of knowledge of the intra-trunk motions and how these motions change with running speed. [1, 2] Most studies have concentrated on lower lumbar and pelvic mechanics or represented the trunk as a single rigid unit which potentially dilutes the effect of individual trunk segments. [3]

Also, we have very little understanding of movement pattern changes in the trunk, if any, observed among middle-age runners even though changes in certain gait parameters and lower limb mechanics in walking and running have been reported in elderly runners. [4] Multiple studies have reported relationships between various musculoskeletal injuries and age, with more complex or multiple running related injuries documented especially for middle age runners [4], but their relation to altered trunk mechanics is not clear.

Thus, the purpose of the study was to determine if intra-trunk displacements change with increase in running speed and how these differ in middle age runners compared to younger runners. It was hypothesized that intra-trunk motions will increase with age and at faster running speeds, particularly for segments with lower anatomical constraints like the lumbar spine [5].

### METHODS

Sixteen young adult (YA) runners under the age of 40 (age: 32.7±4.9 yrs, mass:71.6±15.8 kg, height:1.70±0.09 m, 21.1±6.1 miles/week) and 14 middle age (MA) runners over 40 (54.6±7.9 yrs, 69.3±13.1 kg, 1.72±0.10 m, 20.2±9.5 miles/week) participated in this study. Locations of 24 reflective markers placed on the trunk and the pelvis were captured by a 7-camera system (120 Hz; Vicon) and was used to collect kinematic data during treadmill (PreCor C954) running. Participants ran at their self-selected jogging (JOG) and maximal (MAX)

treadmill running speeds for 10 minutes at JOG speed and about 15 sec at MAX. Data was collected for 10 sec during the runs. At the completion of running trials for each speed, participants rated their perceived exertion (RPE) using the Borg scale (6-20). Relative angles between adjacent trunk segments (upper [UP]: C7 to T8; middle [MID]: T9 to T12; lower [LOW]: L1 to L5; and pelvis [PEL] were calculated; maximum angular displacements were averaged across 10 strides. Displacements in the 3 planes of motion were compared between groups using a mixed-design ANOVA with speed (JOG and MAX) as the within-subject factor and age (YA and MA) as the between-subject factor ( $p<0.05$ ). *Post-hoc* comparisons with Bonferroni corrections were used to compare means when main effects were observed.

### RESULTS AND DISCUSSION

Speed ( $p = <0.001$ ) and age ( $p = 0.009$ ) main effects were observed for running speed as MA ran slower than YA runners at JOG and MAX paces (**Table 1**). This finding is consistent with those previously reported in the literature [6].

A speed main effect was also observed for Borg RPE ( $p=<0.001$ ; **Table 1**). This effect is due to higher RPE at the JOG and MAX speeds in MA compared to YA. These RPE results suggest both groups were able to reach their maximal efforts on a treadmill making the kinematic comparisons more meaningful and consistent.

The only interaction effect observed from the joint kinematic variables was observed for angular displacements of LOW-PEL joint in the transverse plane ( $p=0.015$ ; **Table 1**). No other interaction effects were observed. Age main effects were observed for all comparisons except for UP-MID angular displacements in the sagittal and frontal planes (**Table 1**). Generally, displacements were greater for MA compared to YA groups for both

running speeds. Speed main effects were observed mainly in the frontal plane for all 3 relative angles and in transverse plane for Low-Pel (lumbo-pelvic) angle (**Table 1**). Displacements decreased in the proximal 2 angles (UP-MID and MID-LOW) in the frontal plane, while it increased in the LOW-PEL for both frontal and transverse plane. This suggests that lumbo-pelvic (LOW-PEL) segmental arrangement potentially contributes the most towards net trunk angular, as the individuals increase their pace regardless of the age.

Overall, both MA and YA groups display greater angular displacements at slower speeds (MA > YA) especially in the transverse plane. Possible explanations include increase in trunk momenta to help cancel some of the greater total body angular momenta[1,7]; appropriately position the pelvis to allow increased leg rotations and longer step lengths[8]; transfer or generate mechanical energy to/from extremities[9]; and/or minimize nonessential center of mass (COM) motion via compensatory shifting of intra-trunk mass [10].

As the running speed increases, trunk mechanics is shifted to minimizing the nonessential COM motion at superior trunk segments (UP-MID and MID-LOW) and limiting the angular momentum and torque production at the lumbar spine (LOW-PEL). This could potentially be a compensatory strategy to increase efficiency of mechanical energy transfers between trunk-pelvis-lower extremity segments.[11] Minimal differences were observed in the UP-MID

joint potentially due to existing anatomical constraints restricting contributions to total body/trunk angular momentum [4]. Also, the observed differences in most comparisons were of small magnitude and should be interpreted with caution, giving full consideration to inter-participant variabilities in running speed ranges, skills and habituation towards running on a treadmill.

## CONCLUSIONS

These findings suggest that runners adapt to changes in speed and advancing age by modifying their trunk kinematics to be able to successfully achieve the performance goals. Future studies warrant including older adult runners (>60 years) to understand if the trend for change in mechanics continues and how it effects running performance.

## REFERENCES

1. Hinrichs RN, et al. *Int J Sport Biomech.*, 3: 242-263, 1987.
2. Ford KR, et al. *Med Sci Sports Exerc.*, 45: 1125-1130, 2013.
3. Schache AG, et al.. *Hum Mov Sci* 21( 2):73-293, 2002
4. Nielsen RO. *Orthop J Sports Med*, 1(1):1-7, 2013.
5. Parke et al. *Rothman-Simeone The Spine*, 6<sup>th</sup>, Saunders & Elsevier, 2006.
6. Kuhman et al. *Eur J Sp Sci*, 16(4):433-440, 2015.
7. Bennett et al. *Hum. Mov. Sci.*, 29:114-124, 2010.
8. Saunders et al..*Clin Biomech.*, 20:784-793, 2005.
9. Gracovetsky. *Spine in Ssports*, CV Mosby, 1990.
10. Simpson KJ, et al. *25th ISB Proceedings*, 2015.
11. Novacheck TF. *Gait Posture*, 7(1):77-95, 1998.

**Table 1.** Trunk kinematics for young (YA) and middle age (MA) runners at JOG and MAX speeds (mean ± SD)

Variables	JOG		MAX		p-values			
	YA	MA	YA	MA	Age	Speed	Inter	
Borg (unitless) <sup>b</sup>	10.8 ± 1.4	11.8 ± 0.9	16.6 ± 1.4	16.6 ± 1.2	0.173	0.000*	0.059	
Running speed (m/s) <sup>a,b</sup>	2.8 ± 0.3	2.5 ± 0.3	4.0 ± 0.6	3.5 ± 0.5	0.009*	0.000*	0.192	
UP-MID (°)	Sagittal	8.8 ± 6.1	8.4 ± 6.1	5.5 ± 1.8	5.9 ± 2.4	0.090	0.887	0.148
	Frontal <sup>b</sup>	8.8 ± 4.7	9.3 ± 5.8	6.2 ± 2.3	7.6 ± 2.9	0.173	0.007*	0.153
	Transverse <sup>a</sup>	13.0 ± 8.7	13.7 ± 6.7	8.4 ± 2.4	8.9 ± 3.3	0.034*	0.422	0.899
MID-LOW (°)	Sagittal <sup>a</sup>	16.6 ± 8.2	17.1 ± 6.8	8.3 ± 3.8	9.2 ± 3.5	0.001*	0.325	0.735
	Frontal <sup>a,b</sup>	12.1 ± 4.9	13.3 ± 4.9	8.4 ± 1.7	10.4 ± 2.8	0.025*	0.001*	0.355
	Transverse <sup>a</sup>	19.9 ± 8.2	20.6 ± 5.8	12.3 ± 5.6	14.1 ± 5.9	0.004*	0.104	0.469
LOW-PEL (°)	Sagittal <sup>a</sup>	16.0 ± 5.7	15.4 ± 4.9	8.9 ± 3.8	9.1 ± 3.2	0.000*	0.777	0.555
	Frontal <sup>a,b,c</sup>	7.7 ± 2.6	7.7 ± 2.5	9.6 ± 4.1	10.8 ± 4.1	0.047*	0.027*	0.015*
	Transverse <sup>a,b</sup>	9.9 ± 3.3	10.4 ± 3.3	13.9 ± 6.1	15.7 ± 6.9	0.015*	0.005*	0.111

Notes: <sup>a</sup>: Group main effect; <sup>b</sup>: Speed main effect; <sup>c</sup>: Group x Speed interaction; \*: Speed difference within Group.

# Lower Limb Joint Kinematics In Young and Middle-Aged Runners

<sup>1</sup> Rumit Singh Kakar, <sup>2</sup> Rachael A Arnwine, <sup>1</sup> Joshua M Tome, <sup>2</sup> Max R Paquette

<sup>1</sup> Ithaca College, Ithaca, NY

<sup>2</sup> School of Health Studies, University of Memphis, Memphis, TN

email: [rkakar@ithaca.edu](mailto:rkakar@ithaca.edu), web: <http://www.ithaca.edu/hshp/clinics/movementlab/>

## INTRODUCTION

The high injury incidences associated with running are well reported. Research suggests that more complex or multiple running-related injuries are observed in middle age runners [1]. Changes in certain running gait parameters have been reported in *older* (i.e., 60+ years) compared to younger runners (i.e., 20s) [1,2] and may play a role in injury development. However, little is known regarding movement patterns observed among *middle-age* runners (i.e., 40-59years). Predictive regression equation suggests decreased stride length, running velocity and peak knee flexion angles with age, while peak hip and ankle sagittal angles in the stance phase were not considered significant predictors [3]. To date, few running biomechanics studies in aging runners have tested more than one running speed.

Increases in running speed can alter running biomechanics. Specifically, increases in peak knee and ankle sagittal plane angles and ranges of motion (ROM) have been reported with increase in running speed. [4] Comparing running biomechanics between young and middle age runners at different speeds will help improve our understanding of age-related running gait patterns.

The objective of this study was to compare lower limb joint kinematics between young and middle age runners during treadmill running at self-selected jogging and maximal speeds. It was hypothesized, that peak knee and ankle angles will increase with increase in speed but minimal change in mechanics was expected between age groups.

## METHODS

Twelve young adult (YA) runners under the age of 40 (10 women; 32.8±4.9 yrs, 69.8±16.3 kg, 1.68±0.08 m, 21.1±6.1 miles/week) and 12 middle

age (MA) runners over 40 (7 women; 54.6±8.3 yrs, 68.0±13.8 kg, 1.68±0.08 m, 20.2±9.5 miles/week) participated in this study. A 7-camera motion capture system (120Hz, Vicon) was used to collect kinematic data during treadmill (PreCor C954) running. Participants ran at their self-selected jogging (JOG) and maximal (MAX) treadmill running speeds for 10 minutes at JOG speed and about 15 sec at MAX. Data was collected for 10 sec during the runs. At the completion of running trials for each speed, participants rated their perceived exertion (RPE) using the Borg scale (6-20). Sagittal plane joint angular kinematics (peaks and ranges of motion (ROM)) of the hip, knee and ankle were calculated for the right side only. The average of each angular kinematic variable for 7 consecutive strides were included in statistical analyses.

A mixed-design ANOVA was used with speed (JOG and MAX) as the within-subject factor and age (YA and MA) as the between-subject factor ( $p<0.05$ ). Paired t-tests with least significant difference were used to compare means when speed main effects were observed. Independent t-tests were used to compare means when age main effects were observed.

## RESULTS AND DISCUSSION

A speed main effect was observed for running speed as MA (5.4±2.1 m/s) ran slower than YA runners (7.2±2.1 m/s;  $p=0.019$ ). This finding is consistent with those previously reported in the literature [4]. Cadence was not different between YA and MA (Table 1). This finding suggests that higher cadence in older runners [2,3] is not a kinematic strategy used by middle age runners. An interaction effect was observed for Borg RPE ( $p=0.022$ ; **Table 1**). The lower RPE at MAX speed in MA compared to YA may suggest that MA runners were unable to achieve a maximal effort perhaps because they were

afraid to reach their true maximal speed on the treadmill.

The only interaction effect observed from the joint kinematic variables was for peak dorsiflexion ( $p=0.021$ ). YA generally had greater peak dorsiflexion than MA and, peak dorsiflexion was only reduced for YA for MAX compared to JOG speed (**Figure 1**). This findings suggests that increased running speed does not affect peak dorsiflexion in MA runners. This may be related to limited sagittal plane ankle mobility in MA. Smaller peak dorsiflexion would suggest a shorter lever arm for the ground reaction force which would explain the lower peak internal plantarflexion moment observed in runners in their 50s compared to runners in their 20s [3]. Contrary to that reported in the literature [3,6,7], knee ROM was similar between YA and MA (**Table 1**). These findings suggest that although older runners run with less knee flexion than young runners, MA runners still retain similar knee flexion during stance as YA runners. Since less knee flexion is generally paralleled by higher knee joint stiffness [7], the unchanged knee flexion in MA runners may suggest similar joint stiffness compared to YA runners. A group main effect was observed for hip extension ROM from foot strike to toe-off (**Table 1**). MA runners ran on average with less hip extension ROM compared YA. Lesser hip extension despite comparatively high cadence explains the slower speeds observed in MA compared to YA.

Finally, speed effects were observed for dorsiflexion excursion and hip extension at toe-off (**Table 1**). Greater dorsiflexion excursion, hip extension ROM and hip extension at toe-off were observed at MAX vs JOG speeds. This may be a

**Table 1.** Kinematics for young (YA) and middle age (MA) runners at JOG and MAX speeds (mean  $\pm$  SD)

Variables	JOG		MAX		p-values		
	YA	MA	YA	MA	Group	Speed	Inter.
Borg (unitless) <sup>a,b,c</sup>	10.8 $\pm$ 1.5*	11.8 $\pm$ 1.0*	17.0 $\pm$ 1.0	16.5 $\pm$ 1.2	0.60	<0.001	0.022
Cadence (steps/min)	164.8 $\pm$ 10.3	163.1 $\pm$ 13.9	186.7 $\pm$ 11.7	185.2 $\pm$ 15.9	0.90	<0.001	0.93
Dorsiflexion ROM ( $^{\circ}$ ) <sup>b</sup>	15.6 $\pm$ 4.2	14.7 $\pm$ 2.6	17.0 $\pm$ 4.8	16.7 $\pm$ 2.5	0.69	0.002	0.55
Knee Flex. ROM ( $^{\circ}$ )	14.6 $\pm$ 5.1	14.4 $\pm$ 5.7	15.1 $\pm$ 4.6	15.5 $\pm$ 7.0	0.96	0.22	0.66
Peak Knee Flex. ( $^{\circ}$ )	37.8 $\pm$ 5.2	34.0 $\pm$ 6.3	37.5 $\pm$ 6.1	34.9 $\pm$ 5.8	0.19	0.57	0.25
Hip Ext. ROM ( $^{\circ}$ ) <sup>a,b</sup>	39.4 $\pm$ 4.7	35.2 $\pm$ 4.8	47.4 $\pm$ 5.8	41.3 $\pm$ 6.1	0.011	<0.001	0.44
Hip Ext. Toe-Off ( $^{\circ}$ ) <sup>b</sup>	7.2 $\pm$ 7.1	0.7 $\pm$ 9.6	10.9 $\pm$ 7.2	4.2 $\pm$ 10.9	0.075	<0.001	0.90

Notes: <sup>a</sup>: Group main effect; <sup>b</sup>: Speed main effect; <sup>c</sup>: Group x Speed interaction; \*: Speed difference within Group.

compensatory mechanism to unchanged peak knee flexion between groups to maintain cadence while speed is increased.

## CONCLUSIONS

These findings suggest that lower limb joint kinematics are generally not different between young and middle age runners. Only peak dorsiflexion and hip extension ROM were smaller in middle compared to young runners. The age by speed interaction for peak dorsiflexion suggests that middle age runners respond differently to an increase in running speed compared to young runners. We hope to add to these preliminary findings by including running biomechanics data from older runners (i.e., over 60 years).

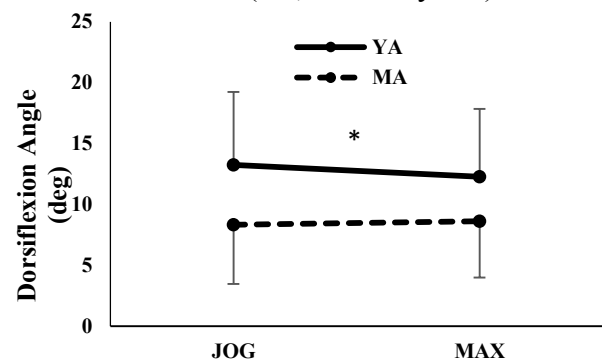


**Fig 1:** Peak dorsiflexion for both age groups at both running speeds (mean  $\pm$  SD). \*: speed different within YA group.

## REFERENCES

1. Nielsen RO. *Orthop J Sports Med*, 1(1):1–7, 2013.
2. Fukuchi, et al. *J Sport Sci*, 26(13), 1447–54, 2008.
3. DeVita, et al. *MSSE*, 48(1), 98–106, 2016.
4. Kuhman et al. *Eur J Sp Sci*, 16(4):433–440, 2015.
5. Fukuchi, et al. *Clin Biomech*, 29(3):304–10, 2014.
6. Bus SA. *MSSE*, 35(7):1167–75, 2003.
7. Powell DW, et al. *JSCR*, Ahead of Press, 2017

# ESTIMATION OF TRUNK MUSCLE ACTIVATION DURING OVERGROUND RUNNING

<sup>1</sup> Jeffrey McClellan, <sup>1</sup> Tim Derrick

<sup>1</sup> Iowa State University, Ames, IA, USA  
email: jeffmc@iastate.edu

## INTRODUCTION

The low back is a commonly studied area of the body due to injury risk during tasks involving bending and/or lifting. Modeling research has been performed which estimates the compressive load on the lumbar spine during bending and lifting tasks, as well as during walking [1].

During running, research has been performed which estimates the joint reaction force at the L5-S1 joint [2], however there is no current research which examines the muscular contribution to lumbar compressive forces during running.

Thus, the purpose of this study was to 1) develop a musculoskeletal model which can estimate, via optimization, the magnitude and timing of lumbar muscle contractions during running, and 2) compare the timing of the modeled muscle activation to EMG recordings of trunk musculature.

## METHODS

Five runners (27.8±8.9 y, 81.2±16.8 kg, 1.79±0.06 m, 25.4±10.3 km/w) were recruited to participate in this study. Informed consent was obtained from all participants, after which they were instrumented with electromyography (EMG) electrodes (2000 Hz, Delsys, Natick, MA) on the erector spinae, and obliques. 26 retro-reflective markers were then placed on the right shoe, leg, pelvis, trunk and left shoe. Participants completed 8 successful running trials over a force platform (2000 Hz, AMTI, Watertown, MA) at 4.25 m/s while wearing lab provided test shoes. Kinematic, Force, and EMG data were collected concurrently using a three dimensional motion analysis system (200 Hz, Vicon MX, Vicon, Centennial, CO).

All analyses were performed using custom matlab programs. Kinematic and kinetic data were low-

pass filtered at 20 Hz [3]. A rigid body model was used with inverse dynamics to estimate 3D joint moments, and reaction forces at the L5-S1 joint. Cylindrical ellipsoids were used to estimate trunk and pelvis volumes, while segment densities, centers of mass, and moments of inertia were calculated according to Pearsall [4]. A musculo-skeletal model was used to estimate muscle insertion, origin, fiber length, tendon slack length, and maximum contractile force, for the right and left erector spinae, internal obliques, and external obliques [5], while an approximation of the L5-S1 joint center was calculated as a point lying 5% along a line between the external location of L5-S1, and the midpoint between the right and left Anterior Superior Iliac Spine.

Muscle forces were calculated by first estimating dynamic muscle moment arms based upon 3D L5-S1 joint kinematics, and the pre-defined muscle origins and insertions. An optimization routine was then run using the muscle parameters, dynamic moment arms, and 3D L5-S1 joint moments in order to calculate the minimum muscle force needed to recreate the 3D joint moment.

Muscle forces calculated via optimization were compared to the recorded EMG signal, which was used as an estimation of muscle activation, with the internal and external oblique forces being combined. The EMG was processed by removing the DC offset, rectifying the signal, and applying a low-pass filter at 10 Hz. Since signal amplitude was not being considered, resultant EMG signals and muscle forces were expressed as a percent of the max recorded force/amplitude during the first 50 percent of stance. Group ensemble averages for muscle forces and the filtered EMG signal were created (Fig. 1), while average correlations between the conditions were calculated for each subject, and on the ensemble averages.

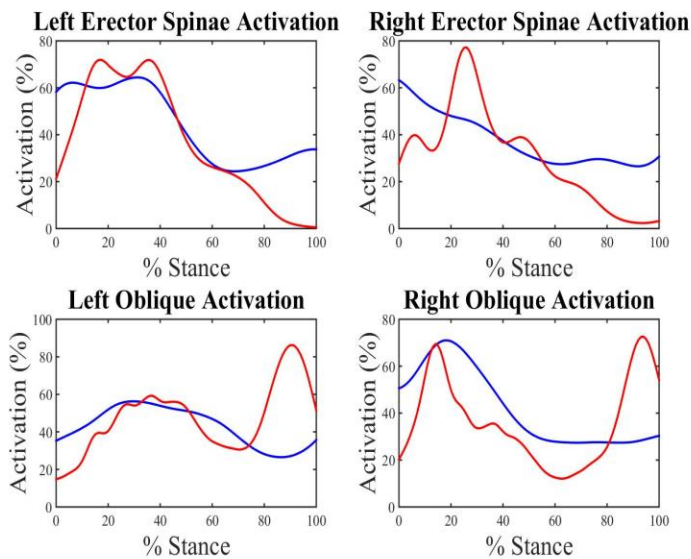


**Figure 1:** Group ensemble averages derived via EMG (blue) and optimization (red).

## RESULTS AND DISCUSSION

R-values for each individual subject/muscle group were quite variable, with correlations ranging from being moderate and negative, to strong and positive. Group ensemble averages tended to have stronger correlations between the conditions although R-values for the left obliques were negative (Table 1).

It should be noted that the muscle activation derived via optimization accounts for all flexor and extensor activation crossing L5-S1, while the muscle activation derived via EMG is location specific. This can lead to activation from additional muscles, which were not accounted for in our model, being attributed to either the erector spinae or the obliques. It is likely that this occurred among the obliques, as a flexor torque at the end of stance resulted in optimization generating large amounts of muscle activation that is not evident when viewing the EMG. It is possible that the rectus abdominis or the psoas muscles could have been active at this same point in time, producing the associated flexor torque.

The right erector spinae may have been similarly affected, as deeper multifidus activation could account for torque production not recorded by the EMG. Individual subject variability may also play a

role, as some individuals displayed EMG patterns that more closely resembled those derived via optimization.

High levels of EMG activation at ground contact and toe off not seen during optimization highlight the potential that some co-contraction is unaccounted for when performing optimization routines, which would lead to an underestimation of the muscular force produced.

**Table 1:** R-values comparing EMG activation and activation derived via optimization

Subject	Left ES	Right ES	Left Obl	Right Obl
1	0.43	0.33	-0.27	0.12
2	0.75	0.33	0.36	0.58
3	0.18	0.46	-0.41	-0.29
4	0.21	0.31	-0.18	0.16
5	0.77	0.24	0.19	0.52
Ensemble	0.85	0.64	-0.17	0.39

## CONCLUSIONS

The optimization method applied appears to do a reasonable job of approximating the timing of muscle activation during the first half of stance at the group level, but may not accurately depict the timing for individual subjects/trials. Additional muscle groups could be added to the optimization routine in order to more accurately depict muscle activation at the end of stance, although it is unknown if this addition would result in a marked difference in the extensor or flexor forces produced.

## REFERENCES

1. Callaghan JP, et al. *Clin Biomech* **14**, 203-216, 1999.
2. Seay J, et al. *J Sports Sci* **26**, 1519-1529, 2008.
3. Bisseling RW, Hof AL. *J Biomech* **39**, 2438-2444, 2006.
4. Pearsall DJ, et al. *Ann Biomed Eng* **24**, 198-210, 1996.
5. Delp S L, et al. *IEEE Trans Biomed Eng* **54**, 1940-1950, 2007.

# Effects of Prolonged Running and Training on Tibial Acceleration and Movement Quality

<sup>1</sup>Max R. Paquette, <sup>1</sup>Kris Camelio, <sup>2</sup>Allison Gruber, <sup>1</sup>Rachael Arnwine, <sup>1</sup>Douglas W. Powell

<sup>1</sup>Musculoskeletal Analysis Laboratory, University of Memphis, Memphis, TN, USA

<sup>2</sup>Biomechanics Laboratory, Indiana University, Bloomington, IN, USA

email: [mrpquette@memphis.edu](mailto:mrpquette@memphis.edu); web: <http://www.memphis.edu/shs/research/mal.php>

## INTRODUCTION

Stress fractures account for the greatest loss of training days among military recruits [1]. Among tibial stress fractures (TSF) risk factors, peak positive tibial axial acceleration (PTA) during running has been found to be higher in runners with a history of TSF [2,3]. PTA can be measured in the field using inexpensive accelerometers. For clinicians, assessing movement strategy can also offer insight into injury risks in runners. The Functional Movement Screen (FMS) is an assessment of several fundamental actions of the human locomotor system [4]. FMS has identified higher risk for injury in male runners who score lower on both the deep squat and active straight leg raise tests versus those who score higher [5].

In novice runners, PTA increases after a single prolonged run to fatigue as measured by gas exchange [6]. In highly trained runners, PTA does not increase over the course of 20min runs at lactate threshold pace (i.e., submaximal) [7]. Training and training-induced muscle damage may alter joint properties associated with shock attenuation [8]. Given that prolonged running alters motor control [6] and training can alter FMS scores [9], FMS test scores may be altered by a single bout of prolonged running and after cumulative training exposure.

Understanding the effects of prolonged running and cumulative training on PTA and FMS scores will provide important information on the appropriate timing of screening tests for injury risk. This may allow for more sensitive results when screening for injury risks to ultimately help reduce injury development. The **purpose** of this study is to assess the effects of prolonged running and cumulative running training on PTA and FMS deep squat and active straight leg raise in novice runners. We expected an increase in PTA and a decrease in FMS scores following both a prolonged run and a 3-week running training program in novice runners.

## METHODS

Sixteen novice runners were recruited for this study. However, only 9 were able to complete the entire study protocol (5 women; 26±7yrs; 73.0±16.3kg; 1.70±0.12m; 11.2±2.7 miles/week; 13.6±7.2 months of running experience). All participants read and agreed to IRB documents before participating.

Participants were instructed to reduce their training volume by at least 80% the week prior to the first testing session. During the first testing session, overall and lower limb fatigue was recorded using a visual analog scale (VAS; 0-10). Participants then performed two FMS exercises: deep squat (DS) and bilateral active straight leg raise (ASLR). The ASLR of each leg was scored out of a possible 6 points, while the DS was scored out of a possible 18 points. Following the FMS, a 3D accelerometer (480Hz, PCB Piezotronics, USA) was attached to the distal anteromedial aspect of the right tibia and aligned with its longitudinal (Z) axis [7] to collect PTA during running. Participants then completed a 30-min run at a preferred running pace (10.0±1.5 min/mile) on a treadmill (C962i, Precor, Woodinville, WA, USA). Tibial acceleration data were gathered after 4 min (Pre-Run), 15 min (Mid-Run), and 30 min (Post-Run) using motion capture software (QTM, Qualisys AB, Sweden). Immediately following the run, overall and lower limb fatigue and the FMS tests were performed once again.

For the next three weeks, participants followed a progressive training program. The program consisted of aggressive weekly mileage increases of 25% based on 3–6 runs per week. Participants were encouraged to run at their preferred training pace as long as the prescribed weekly running volume was met. Participants returned to the lab the week following the conclusion of the training program for the post-training testing session. Overall and lower

limb fatigue using the VAS and PTA were measured after a 5-min treadmill running.

Visual 3D software (C-Motion, Germantown, MD) was used to process and analyze PTA. Accelerometer data were filtered using a fourth-order Butterworth low-pass filter with a cutoff frequency of 60 Hz. The peak positive acceleration immediately following foot strike was extracted. The average of PTA from five consecutive foot strikes were included in the analysis. Repeated measures ANOVA with time as the within-subject factor were used to compare means ( $p < 0.05$ ).

## RESULTS AND DISCUSSION

Contrary to our hypotheses, PTA and FMS scores in novice runners were unchanged following the baseline run and the 3-week training program ( $p > 0.05$ ; **Table 1**). These results suggest that fatigue is required to cause a change in PTA over a 30-min acute run or prolonged running training. Cadence was also unaffected by the run and the training program and may explain the unchanged PTA. The findings suggest that submaximal running and an aggressive increase in running volume over a 3-week period did not alter PTA. Thus, some novice runners may not be at a higher risk of TSF because of rapid increases in mileage. However, risk of developing other injuries may be increased considering that some participants sustained an injury ( $n=2$ ) or became ill ( $n=3$ ) during the 3-week training period. The findings suggests that some novice runners are likely more resilient against injury risk factors when it comes to large increases

in running volume. Novice runners may be able to reduce their risk of injury development related to PTA by only performing easy, submaximal runs during training. A longer training period may be needed to induce a cumulative effect on training that alters PTA in an unfatigued state.

## CONCLUSIONS

These preliminary findings suggest that a submaximal run and a 3-week training program with large mileage increase did not alter PTA or movement quality in novice runners. Further study is needed to determine how quickly novice runners can progress to more exhausting runs, which may be able to help guide ‘couch to race’ training programs for beginners. We will add a group of experienced runners and a control population as we continue this line of research.

## REFERENCES

1. Zadpoor A.A. and Nikooyan A.A. *Clin Biomech*, 26: 23-28, 2011
2. Milner C.E. et al. *MSSE*, 38: 323, 2006.
3. Meardon S.A. et al. *Clin Biomech*, 30: 895-902, 2015.
4. Cook G. et al. *Int J Sports Phys Ther*, 9: 396-409, 2014a.
5. Hotta T. et al. *JSCR*, 29: 2808-2815, 2015.
6. Mizrahi J. et al. *Hmn Mvmnt Sci*, 19: 139-151, 2000.
7. Clansey A.C. et al. *J App Biomech*, 32, 2016.
8. de Paula Simola RI et al. *Sports Tech*, 1-9, 2016.
9. Bodden J.G. et al. *JSCR*, 29: 219-225, 2015.

**Table 1.** Peak tibial acceleration (PTA), cadence and, FMS scores at each time point (mean  $\pm$  SD).

Variables	Pre-Run	Mid-Run	Post-Run	Post-Training	<i>p</i> -values
PTA (g)	3.4 $\pm$ 1.6	3.4 $\pm$ 1.7	3.9 $\pm$ 1.4	3.1 $\pm$ 1.1	0.73
Cadence (steps/min)	159 $\pm$ 8	157 $\pm$ 9	159 $\pm$ 8	160 $\pm$ 10	0.31
FMS					
Deep Squat	6.4 $\pm$ 1.7	-	6.0 $\pm$ 1.7	6.4 $\pm$ 1.7	0.49
ASLR Right	4.4 $\pm$ 1.7	-	4.7 $\pm$ 1.0	4.4 $\pm$ 0.9	0.57
ASLR Left	4.2 $\pm$ 1.2	-	3.8 $\pm$ 1.6	4.7 $\pm$ 1.0	0.24
Aggregate Score	15.1 $\pm$ 3.5	-	14.4 $\pm$ 3.3	15.6 $\pm$ 3.1	0.36

Notes: <sup>a</sup>: Time main effect. FMS: functional movement screen; ASLR: active straight leg raise; Aggregate score: sum of Deep Squat and, average of ASLR right and left.

# BIOMECHANICAL DIFFERENCES BETWEEN KNEE DISARTICULATION AND TRANSFEMORAL AMPUTATION WHILE RUNNING: A CASE STUDY

<sup>1</sup>Jenny Anne Maun, <sup>1</sup>Katherine Sharp, <sup>1</sup>Julianne Stewart, <sup>1</sup>Kimberly Rowe,  
<sup>1,2</sup>John-David Collins, and <sup>1</sup>Marilynn Wyatt

<sup>1</sup>Naval Medical Center San Diego, San Diego, CA, USA

<sup>2</sup>BADER Consortium, University of Delaware, Newark, DE, USA

email: jennyanne.c.maun.ctr@mail.mil

## INTRODUCTION

Running biomechanics are widely studied in adult subjects with unilateral transtibial amputation. While a few studies investigate the running mechanics of subjects with unilateral transfemoral amputation (TFA), even fewer investigate knee disarticulation (KD). KD differs from TFA in that the amputation is at the level of the knee joint, preserving most of the thigh muscles and the distal femur [1]. Previous literature found gait differences between KD and TFA: subjects with KD showed to have fewer running gait deviations over those with TFA due to the advantages of a longer lever arm such as better balance and more natural hip joint range-of-motion, notably in hip flexion [1]. Typical running deviations with TFA include minimal trunk flexion, decreased trunk rotation, and hip hiking [2]. Previous running research has lacked a comparison between KD and TFA, especially within the same patient. The purpose of this study was to describe the differences in overground running in a patient who transitioned from a unilateral KD to a unilateral TFA by comparing velocity, step width, trunk forward flexion and rotation, pelvic obliquity, and hip flexion/extension.

## METHODS

Overground running data at self-selected jogging speeds were collected at two different amputation levels from a 26-year old retired U.S. Marine Corps service member who sustained a right traumatic unilateral amputation. The first running study occurred 28 months after undergoing KD (height: 1.77m; weight: 82.2kg). The patient ran on an Ottobock® Modular Sports™ knee with an Össur® Flex-Run™ foot. The second study occurred 16 months after elective TFA following 44 months as KD (height: 1.75m; weight: 79kg). The patient ran

on an Ottobock® RS640 knee with an Össur® Flex-Run™ foot. Before both studies, the patient had been moderately active utilizing his running leg.

Equipment, set-up, and routine were the same across conditions: 50m straightaway on a track with 12 Raptor-E cameras (Motion Analysis Corp., Santa Rosa, CA, USA) used for marker tracking. Kinematic data were collected at 300Hz. A full-body, six degrees-of-freedom marker set was used with 32 markers. A successful session required a minimum of five strides for each leg. Target data were processed in Visual 3D (C-Motion Inc., Germantown, MD, USA) using a fourth-order, Butterworth filter with a cut-off frequency at 6Hz.

## RESULTS AND DISCUSSION

The patient ran at a slightly faster velocity with TFA than with KD (Table 1). The patient's step width increased by 0.137m with TFA (Table 1). The kinematic measures (Fig. 1A-D) did not surpass a clinically meaningful difference, however in trunk flexion (Fig. 1A) there is a large difference in peak flexion in mid-swing (3.8°), marked with a dot.

The velocity increase from KD to TFA conditions was small enough that it should not cause significant biomechanical changes. A possible explanation for TFA wider base of support could be due to poor balance and stability [1] or a discomfort caused by the proximal socket which extends further toward the pelvis with a TFA. Peak trunk flexion in mid-swing occurred at the same time as contralateral limb weight acceptance in the TFA condition. This will require further investigation.

Despite not finding any clinically meaningful differences, one limitation in this case study was the duration of time from surgery to the data collection and the amount of completed physical therapy

sessions. The patient had KD for 28 months prior to data collection and the most recent running data was collected 16 months after elective TFA. The addition of physical therapy sessions completed from his TFA surgery to his current running study collection may contribute to why differences were not seen between the two amputation levels. Additionally, the kinematics of the contralateral limb was excluded from analysis.

## CONCLUSIONS

This case study aimed to identify the temporal-spatial and kinematic differences in overground running from a patient who transitioned from a unilateral KD to a unilateral TFA. Literature has implied a preference for KD over TFA, however these findings suggest that differences might be minimal in terms of functional performance. It is interesting how similar the two conditions were,

given the different amputation levels. Future work will expand on these results and consider kinetics of this patient between KD and TFA.

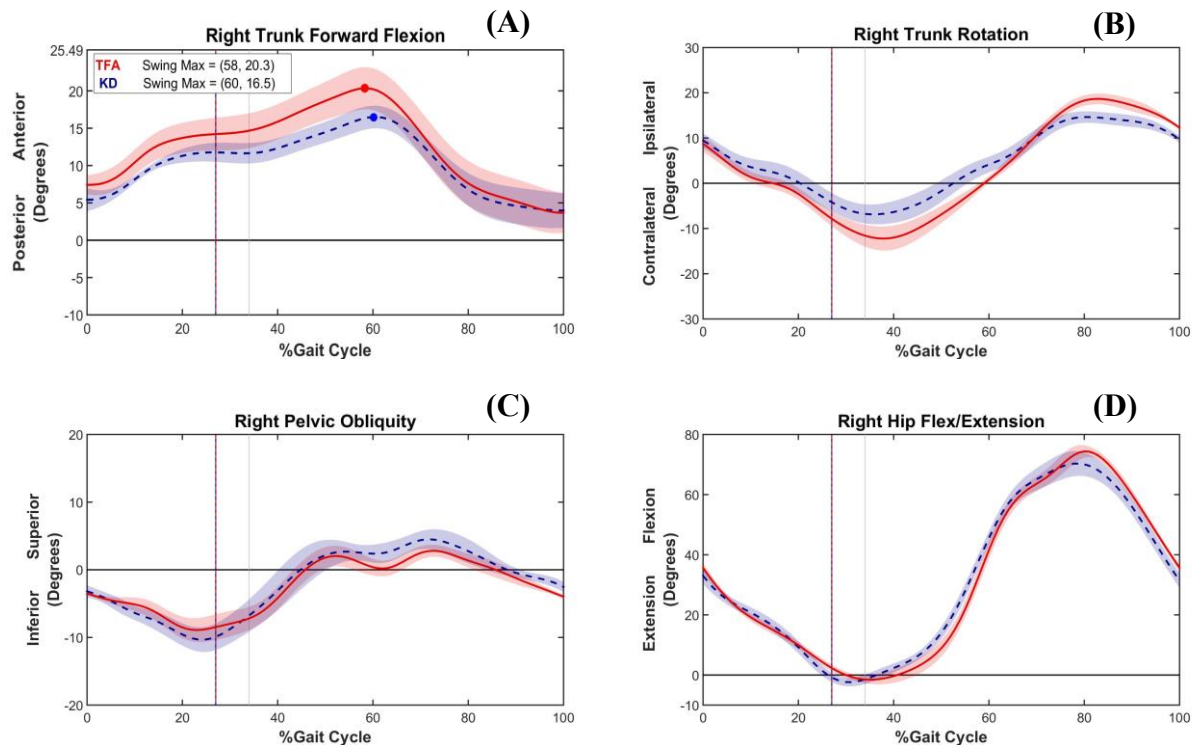
## REFERENCES

1. Baumgartner RF. *Prosthet Orthot Int*, **3** 15-19, 1979.
2. Gailey RS & Clark CR. *O&P Virtual Library*, 2002.

## ACKNOWLEDGMENTS

The authors would like to thank Tatiana Djafar, Trevor Kingsbury, and Noel Guerrero for guidance and technical support. Project was supported by Navy Bureau of Medicine and Surgery, Wounded, Ill, and Injured Program (W239) and in part with resources provided by Extremity Trauma and Amputation Center of Excellence.

**DISCLOSURE STATEMENT:** All authors have no conflicts of interest to disclose. The views expressed in the abstract do not necessarily reflect those of the Department of the Navy, Department of Defense or U.S. Government.



**Figures 1A-D:** Trunk and hip kinematic graphs of the affected side (right) over 100% of the running gait cycle of KD (blue-dashed line) and TFA (red solid line) conditions. The following graphs going clockwise from top-left are: (A) trunk flexion, (B) trunk rotation, (c) pelvic obliquity, and (d) hip flexion/extension. Dots in (A) are max flexion peaks.

**Table 1:** Temporal-spatial measures of KD and TFA conditions

Amputation Type	Residual Limb Length (m)	Velocity (m/s)	Step Width (m)
KD	0.57	4.56	0.109
TFA	0.46	4.74	0.246

# Asymmetric Step Frequencies Increase the Metabolic Cost of Running

<sup>1</sup>Eric N. Azua, <sup>1</sup>Owen N. Beck, and <sup>1,2</sup>Alena M. Grabowski

<sup>1</sup>University of Colorado Boulder, CO, USA

<sup>2</sup>Department of Veterans Affairs, Eastern Colorado Healthcare System, Denver, CO, USA

Email: eric.azua@colorado.edu

## INTRODUCTION

While considering other factors, reducing the metabolic cost of running improves distance running performance [1]. Altered biomechanics, such as contact time, vertical and horizontal ground reaction force (GRF), stride frequency, and leg stiffness change the muscular demands and consequentially influence the metabolic cost of running [2].

Many individuals such as athletes with a leg injury, people with a leg amputation, and people with pathological gait, exhibit asymmetrical biomechanics during running. Yet, despite the prevalence of biomechanical asymmetries, it is unknown how asymmetries affect running performance. Thus, we sought to address whether asymmetric step frequency affects the metabolic cost of running. We hypothesized that greater biomechanical asymmetries between legs would increase the metabolic cost of running.

## METHODS

Ten healthy runners completed two testing sessions on two separate days. Subjects began each session by standing in place while we measured their metabolic rates and then completed seven running trials. First, subjects performed a 12-minute habituation trial at their preferred step frequency (PSF). PSF was then used for subsequent trials. For the remaining trials, subjects were instructed to run for 6 minutes while initiating ground contact with each beat of an audible metronome. Subjects ran two additional habituation trials, with symmetric PSF and 21% step frequency asymmetries, respectively. Subjects then ran 4 additional trials at different randomly selected asymmetric step frequencies, which were 0, 7, 14, and 21% of the absolute value of the symmetry index (SI) (Eq. 1) compared to their PSF (symmetric). For all trials, stride frequency (one stride = two steps) remained constant, and running speed was 2.8 m/s.

We measured GRFs at 1000 Hz for 30 seconds during minutes 3 and 5 of each running trial, filtered the GRFs, and used a 10 N vertical GRF threshold to calculate stride kinematics (step frequency, ground contact time), kinetics (stance average vertical GRF, peak vertical GRF, peak horizontal GRFs), and leg stiffness. We measured rates of oxygen consumption and carbon dioxide production using indirect calorimetry, and averaged these rates over the last two minutes of each trial. We used a standard equation [3] to calculate metabolic power for each trial, and then subtracted this metabolic power from standing to yield net metabolic power.

Biomechanical variable (BV) asymmetries were calculated using the absolute value of the SI and were expressed as a percentage (Eq. 1).

$$SI = \left| \frac{BV(\text{leg1}) - BV(\text{leg2})}{0.5 (BV(\text{leg1}) + BV(\text{leg2}))} \right| \times 100\% \quad \text{Eq. 1}$$

We only analyzed asymmetric running trials where runners achieved a step frequency asymmetry steady-state, which we defined as a change in step frequency asymmetry between minutes 3 and 5 that was within  $\pm$  two standard deviations of the average difference elicited during the PSF trial. We used independent linear mixed models to test the influence of each BV on the increase in the percentage of net metabolic power compared to the PSF trial. Significance was set at  $p < 0.05$ .

## RESULTS AND DISCUSSION

The main goal of this study was to examine the effects of step frequency asymmetries on the metabolic cost of running. We found that for every 10% increase in step frequency asymmetry, net metabolic power increased 3.5% ( $p < 0.001$ ) (Fig. 1). A previous study of walking also associated similar increases in metabolic cost to asymmetric biomechanics. Specifically, they found that step



# CHANGES IN SURFACE STIFFNESS ELICIT VERTICAL STIFFNESS CHANGES WITHOUT CHANGES IN METABOLIC DEMAND DURING BILATERAL HOPPING

<sup>1</sup>Jonathan S. Goodwin, PT, DPT; <sup>2</sup>Michael D. Lewek, PT, PhD; <sup>3</sup>J. Troy Blackburn, PhD, ATC;

<sup>1</sup> Program in Human Movement Science, University of North Carolina at Chapel Hill, Chapel Hill, NC, USA;

<sup>2</sup> Division of Physical Therapy, University of North Carolina at Chapel Hill, Chapel Hill, NC, USA <sup>3</sup>Exercise and Sport Science, University of North Carolina at Chapel Hill, Chapel Hill, NC, USA;

email: [fjgoodwin@unc.edu](mailto:fjgoodwin@unc.edu)

## INTRODUCTION

Running is an increasingly popular physical activity that is associated with reduced disability and mortality [1]. However, as with any physical activity, there is injury risk. Lower extremity injuries occur in 19%-79% runners whose training or race distance exceeds 5 kilometers [2]. Lower extremity stiffness and loading rate are positively correlated and play a role in injury development. Greater loading rate is associated with bony injuries, while lesser loading rates may contribute to soft tissue injuries [3-5]. Additionally, lower extremity stiffness is modified automatically during each ground contact during running and hopping [6, 7]. Greater lower extremity stiffness has been shown to be associated with lesser metabolic demand during running [8]. However, it is unknown if changes in lower extremity stiffness affect metabolic demand. Therefore, the purpose of this study is to induce lower extremity stiffness changes and analyze any resultant metabolic demand changes during bilateral hopping.

## METHODS

12 runners (8 females, 4 males, 22.91 ± 5.99 y.o, 1.70 ± 0.12 m, 66.5 ± 10.83 kg, 25 ± 7.46 miles run/week ) volunteered for participation in the study. Subjects were required to be injury free for 6 months and run a minimum of 15 miles per week. Subjects were fit with a portable metabolic analyzer (K4b2, Cosmed) and whole body retroreflective markers (Vicon). Subjects completed bilateral hopping at 2 Hz on 3 different surfaces with unique stiffness characteristics. These included a “soft” (Airex foam pad), “medium” (Medium density foam), “hard” (Bertec force plate) condition. The order of the conditions was controlled via a balanced Latin square design to remove potential order effect. Subjects were required to hop for 4 minutes on each surface to achieve metabolic steady state and given a

5 minute seated rest to ensure metabolic demand returned to baseline between conditions. 3D lower extremity kinematics and kinetics were sampled throughout along with metabolic demand. Metabolic demand was averaged over the final 30 seconds of each four minute hopping trial. Vertical stiffness was calculated as the maximum vertical force divided by the change in center of mass depression during ground contact ( $F_{max}/\Delta y$ ) and averaged over 10 successive hops within the last 30 seconds of each 4 minute hopping trial [9]. Vertical stiffness was further normalized to subject’s body weight and standing center of mass position [ $(F_{max}/BW)/(\Delta y/y)$ ] [10]. Repeated measures ANOVAs were evaluated for the effect of surface stiffness on both metabolic demand and vertical stiffness during bilateral hopping. A priori alpha level set at 0.05.

## RESULTS

Metabolic demand was not statistically different across three different surface conditions ( $p = 0.265$ , Table 1)

Table 1: Metabolic demand and surface stiffness.  
Values expressed as mean ± SD.

Surface Condition	Metabolic Demand (O <sub>2</sub> ml/kg/min)
Hard	32.207 ± 4.25
Medium	32.778 ± 4.28
Soft	32.877 ± 3.74

Normalized vertical stiffness was statistically significantly different between surface conditions ( $p < 0.015$ ,  $F=6.804$ ). Bonferroni post-hoc test revealed that normalized stiffness differed significantly between soft and hard surface condition with greater vertical stiffness observed with the soft surface condition ( $p < 0.049$ , Table 2).

Table 2: Stiffness and surface condition. Values expressed as mean  $\pm$  SD. ‘\*’ = statistically significantly different ( $p < 0.05$ ).

Surface Condition	Vertical Stiffness (KN/m)	Normalized Stiffness
Hard	50.61 $\pm$ 26.89	.0402 $\pm$ .01*
Medium	50.74 $\pm$ 26.52	.0408 $\pm$ .01
Soft	59.00 $\pm$ 37.22	.0479 $\pm$ .02*

## DISCUSSION

Normalized vertical stiffness was significantly lower during the hard compared to the soft condition during bilateral hopping. This decrease in vertical stiffness was achieved without a significant metabolic compensation. This compensation in vertical stiffness is expected given the subjects were required to overcome the soft surface deformation to maintain the 2 Hz hopping frequency [11]. We did not see a significant difference in vertical stiffness between the medium and hard surface conditions. We also did not see any change with metabolic demand across all surface conditions.

## CONCLUSION

Inadequate and/or excessive lower extremity stiffness is linked with musculoskeletal injury and it is modified automatically to accommodate different surface conditions. Our subjects displayed greater stiffness to overcome the soft surface condition without significant metabolic compensation. This accommodation could have been completed by altering landing posture or increased reliance on non-

metabolic tissues (i.e. increased elastic energy return from tendons) while maintaining previous level of metabolic demand. Maintaining lower extremity stiffness while minimizing increases in metabolic demand is important given athletes display poorer lower extremity biomechanics that may expose them to a greater injury risk when fatigued [12]. This information can be applied practically by intervening with shoe modification (i.e. greater cushioning) to potentially increase or maintain lower extremity stiffness during running without a significant amount of metabolic compensation. Further analysis is needed to examine the non-metabolic methods and behaviors through which subjects are able to alter their stiffness values. This could lead to individual training programs to find the ideal lower extremity stiffness value while minimizing injury risk.

## REFERENCES

1. Lee, D.-c., et al. *Journal of the American College of Cardiology*, 2014. **64**(5): p. 472-481.
2. van Gent, R.N., et al., *British Journal of Sports Medicine*, 2007. **41**(8): p. 469-480.
3. Williams, D.S., 3rd, et al. *Clin Biomech (Bristol, Avon)*, 2001. **16**(4): p. 341-7.
4. Williams, D.S., et al., *Gait & posture*, 2004. **19**(3): p. 263-269.
5. Radin, E.L., et al., *Journal of Orthopaedic Research*, 1984. **2**(3): p. 221-234.
6. Ferris, D.P., et al, *Journal of biomechanics*, 1999. **32**: p. 787-794.
7. Morin, J.B., et al., *Journal of Biomechanics*, 2011. **44**(6): p. 1104-1107.
8. Dalleau, G., et al., *European Journal of Applied Physiology*, 1998. **77**(3): p. 257-263.
9. McMahon, T.A. and G.C. Cheng, *Journal of Biomechanics*, 1990. **23**: p. 65-78.
10. Blickhan, R. and R.J. Full, *Journal of Comparative Physiology A*, 1993. **173**: p. 509-517.
11. Ferris, D.P. and C.T. Farley., *Journal of applied physiology*, 1997. **82**: p. 15-22
12. Liederbach, M., et al., *The American Journal of Sports Medicine*, 2014. **42**(5): p. 1089-1095.

# JOINT TORQUE REQUIREMENTS AND CAPACITIES DURING RUNNING

<sup>1</sup> Timothy R. Derrick, <sup>2</sup> Elizabeth R. Boyer

<sup>1</sup> Iowa State University, Ames, IA, USA

<sup>2</sup> Gillette Children's Hospital, St. Paul, MN, USA

email: [tderrick@iastate.edu](mailto:tderrick@iastate.edu), web: <http://www.kin.hs.iastate.edu/>

## INTRODUCTION

Any situation that reduces the maximal dynamic muscle force capability – ageing, fatigue, lack of training, fiber damage etc. – might reduce maximum torque production below the requirements of the activity. This forces runner's muscles to approach their physiological capacity and may result in an altered running style. It is, therefore, useful to know which torques are closest to their dynamic capacity so that specific steps can be taken to insure an adequate reserve and enable the runner to maintain optimal running form. It is the purpose of this research to identify joint torques that approach their maximum dynamic limits during running and to determine when in the stance phase of the running cycle these relative weaknesses occur. We will also examine if the limitations are due to length or velocity constraints.

## METHODS

Seven young adults recreational runners (3 males, age: 21.3±2.1 yr; body mass: 68.9±6.7 kg; height: 1.84±0.07 m and 4 females, age: 25.3±5.2 yr; body mass: 56.6±11.3 kg; height: 1.64±0.08 m) participated in this study. All runners were healthy and currently free of injury. Reflective markers were placed on the right foot, leg, thigh and the pelvis in order to track the motion while runners ran at 3.5 m/s on a 30 m runway. They landed on a force platform (AMTI, 1000 Hz) with their right foot making contact with their preferred strike pattern while 8 cameras (Vicon, 200 Hz) recorded the location of the reflective markers.

Segment rotation matrices were calculated relative to a static trial using a least squares fit [1]. Anthropometrics were derived using geometric solids [2]. Three dimensional joint moments and

reaction forces were estimated using rigid body assumptions and standard inverse dynamics procedures. A 44-muscle, scaled musculoskeletal model [3] implemented in Matlab used the segment rotation matrices as input to derive length and velocity adjusted maximal dynamic muscle forces and moment arms for each frame of data. Multiplying these muscle forces by their moment arms allowed the estimation of maximal dynamic torque producing capacity at a joint. Actual dynamic muscle forces were estimated using static optimization by constraining the muscle forces to be less than the maximum dynamic muscle forces, and equal to the joint moments (3D hip joint moments, knee sagittal plane joint moment, and ankle sagittal plane joint moment). The solution that met these constraints and minimized the sum of the squared muscle stresses was selected as the actual dynamic muscle forces. Multiplying the actual muscle forces by their respective moment arms gave an estimate of the joint torque requirements of the task.

## RESULTS AND DISCUSSION

Regions in which the joint torque requirements were within .06BW of capacity for more than 5% of stance were identified by a shaded region (Figure 1). The sagittal plane hip moment is the only one in which the inverse dynamics estimate muscle torques did not approach the limitations of the joint muscles. However, the frontal and transverse plane hip moments did approach these limits.

It should be noted that the maximum positive and negative limitations identified in figure 1 were modelled and not measure directly. Direct measurement would allow a subject specific comparison but the major advantage of the current method is that the estimates of the limitations are

length and velocity dependent. This can be seen in the sagittal plane ankle moment when the plantar flexor (maximum negative moment) limitation approaches zero toward the end of the stance period. At this time the length and velocity of the plantar flexors drastically reduce their ability to produce torque.

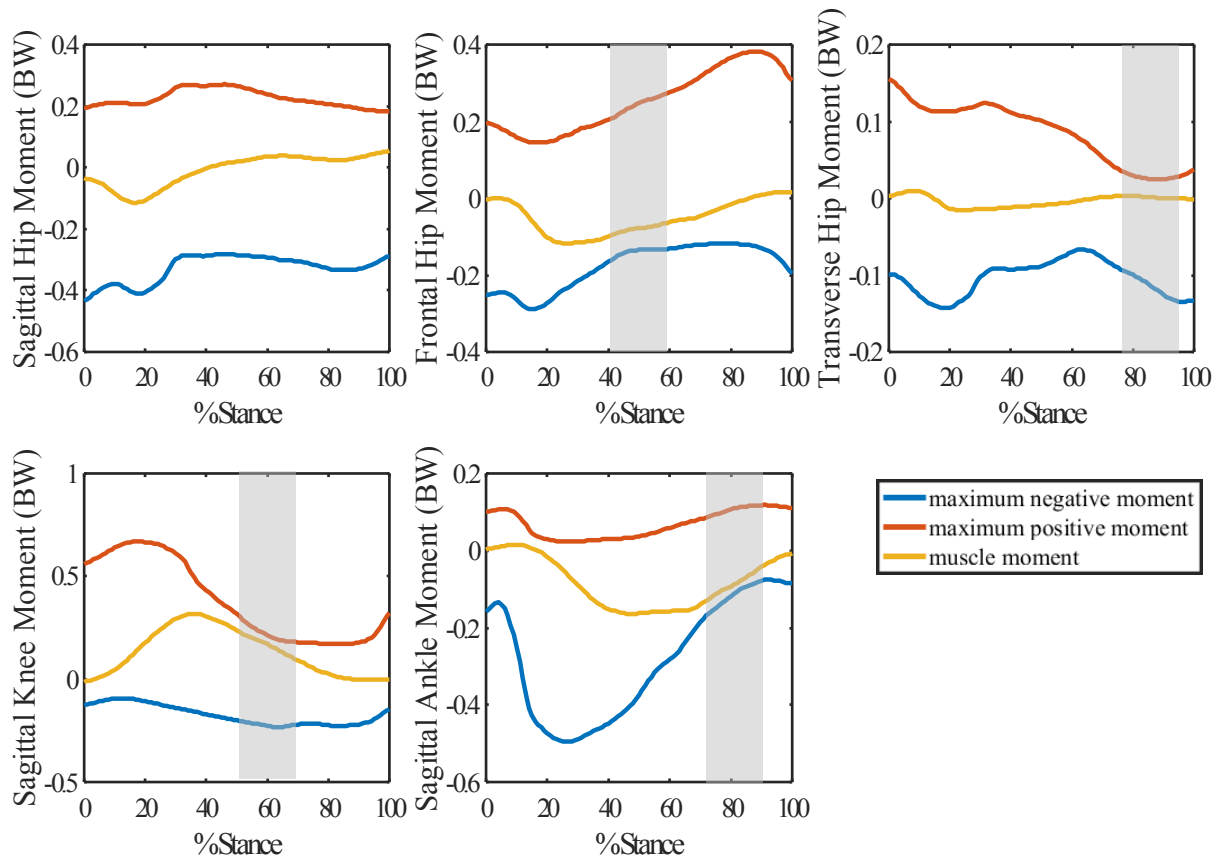
## CONCLUSIONS

This technique of comparing moments created by the joints during running to the maximum capabilities of the joint holds promise for identifying weak links in the lower extremity. As the torques approach their

limits at the joint, compensations take place that may put the runner in jeopardy of injury. This analysis is also useful at identifying which muscle groups should be strengthened or maintained to run effectively.

## REFERENCES

1. Soderkvist, I, et al. *J of Biomech*, **26**, 1473-1477, 1993.
2. Hanavan, E. *Tech. Rep. Wright-Patterson*, 1964.
3. Arnold, EM, et al. *Ann Biomed Eng*, **38**, 269-279, 2010.



# Distance Running Sagittal Plane Hip and Knee Variability During Early and Late Stance and Swing

<sup>1</sup>Brady DeCouto, <sup>1</sup>Robert A. Paxton, <sup>1</sup>Christopher Robertson, <sup>2</sup>Reed Ferber and <sup>1</sup>Jeff T. Wight

<sup>1</sup>Jacksonville University, Jacksonville, FL, USA

<sup>2</sup>University of Calgary, Calgary, AB, Canada  
email: bdecout@ju.edu

## INTRODUCTION

The consistency of a distance runner's biomechanical gait pattern may be relevant to injury and performance as variability measures may serve as important indicators. For example, Ferber [1] studied stride-to-stride variability in runners with patellofemoral pain syndrome and reported decreased stride-to-stride variability after three weeks of hip abductor strengthening.

For variability, it is important to determine which joints, phases, and critical instants are the most important to focus on for cohorts of interest. For both the stance and swing phases of running gait, the biomechanical patterns are very different. During early stance, the weight is accepted until the knee is maximally flexed, and the muscles are eccentrically loaded. During late stance, propulsion occurs (knee and hip extension), and the muscles are concentrically loaded. During early swing, the hip is flexed until the knee reaches its maximum height. Then, during late swing, the leg lowers with gravity. These drastically different biomechanics may cause significant differences in variability.

Therefore, the purpose of this study was to determine if there are significant differences in sagittal knee and hip joint variability between the early and late stance and swing phases for slow and fast running.

## METHODS

Participants were 24 highly trained runners (8 females, 16 males;  $36.1 \pm 10.8$  years; 30-80 miles per week). Six posterior-mounted Vicon Bonita cameras were used to assess treadmill running using a standard marker set-up [3]. Runners completed their preferred warmup and then ran 3-minutes at their "long run pace" (slow) and "half-marathon pace" (fast). Data were collected for 25 seconds during the final minute of each pace. Stance and swing data were normalized to 100 data points, and sagittal plane hip and knee joint angles were assessed.

The early swing phase was defined from toe-off to maximum hip flexion and late swing from maximum hip flexion to foot contact. Early stance phase was defined as foot contact to maximum knee flexion and late stance from maximum knee flexion to toe-off. Variability was assessed for each condition using two steps. First, the standard deviation was calculated on a point-by-point basis across the 10 strides. Second, the overall standard deviation for each individual phase was averaged.

A 4x2x2 ANOVA was used to test for significant main effects and interaction. The factors were the phase (early swing, late swing, early stance, late stance), joint (hip, knee), and speed (slow, fast). Secondary t-test comparisons were completed with Bonferoni corrections for multiple comparisons.

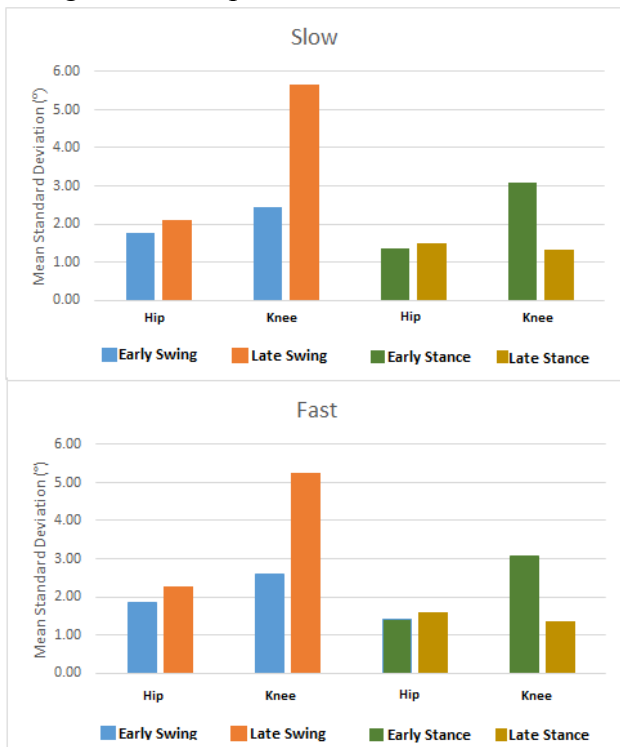
## RESULTS AND DISCUSSION

Overall, the runners in this study appeared to have consistent hip and knee kinematics for all phases as

evidenced by the overall low standard deviations (ranging from 1.33°-5.65°).

Interestingly, for running speed, there was no significant effect ( $p=0.40$ ) on joint variability (Figure 1) and for both the knee and hip, results appear to be very similar for both speeds (Figure 1). Running speed appears to have minimal impact on joint variability. Similar findings have been reported for running reliability. For example, Queen [4] analyzed 35 kinematic and kinetic variables at self-selected and standardized running speeds and found only two to have significant differences.

**Figure 1:** Hip and knee variability in early and late swing and stance phase.



For the knee, increased variability ( $p<0.001$ ) was observed during the early stance and late swing (Table 1) and knee variability more than doubled between early and late phases for both stance and swing with late swing and early stance exhibiting

**Table 1: Overall standard deviations (°).**

	Early Swing	Late Swing	Early Stance	Late Stance
Hip (slow)	1.76 ± 1.02	2.11 ± 1.23	1.35 ± 0.58	1.48 ± 0.86
Hip (fast)	1.86 ± 0.93	*2.26 ± 1.31	1.39 ± 0.47	1.58 ± 0.83
Knee (slow)	2.45 ± 1.24	*5.65 ± 4.18	3.08 ± 2.06	*1.33 ± 0.53
Knee (fast)	2.60 ± 1.12	*5.25 ± 3.79	3.06 ± 1.82	*1.36 ± 0.48

\* indicates significant difference between early and late phases

significant differences in knee variability across speed.

For the hip, there were no significant differences between the early and late stance phase. During swing, the hip exhibited increased variability ( $p<0.01$ ) during the late phase for both speeds; however, the differences were minimal (approximately 0.4°).

## CONCLUSIONS

Running speed had few effects on joint variability across four different phases of stance and swing and between a fast and slow running speed. Overall, the hip showed small changes in variability for the early and late phases and the knee had notable increases in variability for early stance and late swing. These findings are consistent with the literature on running reliability measures.

This study also revealed that variability can be phase dependent, which is similar to previous studies showing that continuous relative phase variability measures varied throughout the stance phase [2]. Future prospective research is necessary to determine the relevance of variability measures to injury.

## REFERENCES

1. Ferber R, et al. *Journal of Athletic Training*, 46(2), 142-149.
2. Hein, T, et al. *Human Movement Science* **31**, 683-694, 2012.
3. Pohl et al., *Gait Posture*, **32**, , 559-563, 2010
4. Queen RM, et al. *Gait & Posture*, **23**, 282-287, 2006.

# USING PHYSICAL EDUCATION AS A PEDAGOGICAL TOOL TO ENHANCE UNDERSTANDING OF BIOMECHANICS IN MIDDLE SCHOOL CHILDREN

<sup>1</sup> Kimberly A. Fournier, <sup>1</sup> Emily D. Clapham, and <sup>2</sup> Karie L. Orendorff

<sup>1</sup> University of Rhode Island, Kingston, RI, USA

<sup>2</sup> University of South Carolina, Columbia, SC, USA

Email: kimfournier@uri.edu

## INTRODUCTION

If we are to encourage students to pursue careers in integrative disciplines such as biomechanics, we must engage students as early as middle school and develop innovative projects that emphasize how STEM sciences (Science, Technology, Engineering, and Mathematics) can be applied and are relevant to their everyday lives.

There is an established relationship between academic achievement and physical activity in school-aged children [1, 2]. However, the scientific principles that underscore the specific physical activities employed in these studies often do not coincide with the specific measure of academic achievement or content being assessed. Instead, the focus is on physical fitness and its effect on test scores and cognitive processes such as executive function, concentration, and attention [2].

The Next Generation Science Standards (NGSS) are designed to engage students in multidisciplinary practices that enhance their understanding of core ideas in science [3]. Some of the core ideas emphasized at the middle school level for the physical sciences are related to *mechanics* (PS2.A: forces & motion; PS2.B: types of force interactions) and for the life sciences (*biology*) are related to structure and function of nerves (LS1.A: Structure and function and LS1.D: Information processing). The Society of Health and Physical Educators (SHAPE America) physical education standards are designed to deliver high quality physical education and develop knowledge and skills that will lead to a physically active lifestyle (Standard 1: Demonstrating competency in movement and Standard 2: Applying movement concepts to learning and the development of motor skills) [4].

As a unique contribution to the area of physical activity and academic achievement, we aimed to simultaneously engage middle school students in science standards (NGSS) and physical education standards (SHAPE America). We employed targeted physical activities that concurrently emphasized both SHAPE America physical education and NGSS standards in an effort to improve middle school level students' understanding of biomechanical principles. Herein, the activities administered during the inaugural National Biomechanics Day (NBD: April 7, 2016) at the University of Rhode Island (URI) are evaluated.

## METHODS

Fourteen 8<sup>th</sup> grade children (age 12-14 years; 9 female, 5 male) participated in the NBD activities. As a group, students first participated in physical activities designed to emphasize principles related to forces (Human Bowling, Balance Poses, Sumo) and life science principles related to neuromuscular control of movement (You're Getting on my Nerves). Students were then divided into 2 smaller groups in order to rotate through 2 additional sessions designed to quantify/analyze movement. In the first session, students learned to analyze movement using simple methodology such as 1) recording the progression of balance using agility balls and 2) using vertical jump measuring equipment. In the second session, students visited the Motion Analysis Laboratory for an interactive demonstration of sophisticated methodology used to analyze movement such as 1) motion capture, 2) forceplates, and 3) electromyograms (EMG).

Prior to participating in the activities, students completed an 8 question quiz (pre-quiz) designed to

assess prior knowledge related to vectors, forces, net force, biomechanics equipment and the neuromuscular control of muscle contractions. Students completed the same quiz again (post-quiz), once all activities had been completed.

A one-way MANOVA with 2 levels of time and an a priori alpha level of 0.05 was performed to assess change in quiz scores as a result of participating in the NBD activities. All statistical tests were performed using SPSS 16.0 for Windows (Chicago, Illinois). The protocol for the study was approved by an institutional review board and the parents or legal guardians authorized the informed consent for all children included in the study.

## RESULTS AND DISCUSSION

We hypothesized that physical education activities that explicitly emphasized elements of physical and life sciences would help provide 8<sup>th</sup> grade students with a more meaningful understanding of the content. By using physical education activities as a pedagogical tool; we hypothesized that students would enjoy learning and would make meaningful, real-world connections between biomechanics and everyday interests.

Most children had knowledge of forces and vectors (Q1-Q3b) prior to participating in the NBD activities. However, for questions related to neuromuscular control and application to real world activities (Q4-Q6), most students were unable to answer on the pre-quiz (Table 1). Quiz scores on those questions improved significantly after completing the activities. Overall, students improved their total score by 65.9%. When asked which NBD activity they preferred the most 85.7% (n=12) of students reported one of the physical education activities. The other two students reported enjoying “everything.”

Research indicates that individuals who are physically active perform better in school [1-2]. However, federal mandates aimed at improving student competencies in reading, mathematics, and science have resulted in less emphasis being placed on health and physical education in the curricula. Exposing students to multiple STEM disciplines via physical activity provides a unique opportunity for students to improve academic performance and make meaningful “real-world” connections in those same areas while simultaneously maintaining an emphasis on health and physical fitness.

## CONCLUSIONS

By using movement to understand the science of movement, children were able to improve their knowledge of interrelated STEM areas. Targeted physical activities emphasizing biomechanical principles appear to be viable pedagogical tool for enhancing the understanding of physical and life sciences in middle school curricula.

## ACKNOWLEDGMENTS

Thank you to Martha Barbera and Curtis Corner Middle School. This research was funded by the Dr. Thomas Manfredi Student Research Fund.

## REFERENCES

1. Donnelly, JE, et al. *Medicine & Science in Sports & Exercise*, **48**(6), 1197-222, 2016
2. Castelli DM, et al. *Journal of Sport and Exercise Psychology*, **29**, 239-252, 2007.
3. NGSS Lead States. *Next Generation Science Standards: For states, by states*. Washington, DC: The National Academies Press, 2013.
4. SHAPE America. *National Standards for K-12 Physical Education*. Reston, VA. 2013.

**Table 1:** Mean scores ( $\pm$  standard deviations) for each question answered on the pre- and post-quiz.

(n=14)	Points								
	Q1 (1)	Q2 (1)	Q3a (1)	Q3b (1)	Q4 (1)	Q5a (1)	Q5b (1)	Q6 (1)	Total (8)
<b>Pre-quiz</b>	1.0 $\pm$ 0.0	0.5 $\pm$ 0.5	1.0 $\pm$ 0.0	0.9 $\pm$ 0.4	0.3 $\pm$ 0.5	0.2 $\pm$ 0.2	0.0 $\pm$ 0.1	0.2 $\pm$ 0.3	4.1 $\pm$ 1.3
<b>Post-quiz</b>	1.0 $\pm$ 0.0	0.9 $\pm$ 0.3	0.9 $\pm$ 0.4	0.7 $\pm$ 0.5	0.8 $\pm$ 0.4	1.0 $\pm$ 0.0	0.9 $\pm$ 0.4	0.7 $\pm$ 0.2	6.8 $\pm$ 0.7
<b>p value</b>	NA	0.01*	0.15	0.38	0.01*	0.00*	0.00*	0.00*	0.00*

\* Significant at  $p < 0.05$

# ASSESSING MOTIVATION AND LEARNING STRATEGIES IN UNDERGRADUATE BIOMECHANICS STUDENTS

<sup>1</sup>Kimberly A. Fournier

<sup>1</sup>University of Rhode Island, Kingston, RI, USA  
email: kimfournier@uri.edu

## INTRODUCTION

Without the knowledge of the mechanics, it is difficult for kinesiology students to explain many of the phenomena they observe when studying human movement [1]. As most students fail to appreciate the relevance of biomechanical concepts underlying human movement, establishing meaningful and “real world” relevancy of biomechanics content is of critical importance, particularly when asking students to engage with challenging material (mathematics, physics, and applied anatomy). Therefore, in order to better serve kinesiology students in biomechanics by deepening their learning, instructors must first understand how students engage with the material.

Self-regulated learning theory (SR) defines learners as metacognitively, motivationally, and behaviorally engaged in their own learning [2]. Student learning is therefore influenced by a variety of factors including cognitive strategies, resource management, goals, values, and expectancies [3]. The Motivated Strategies for Learning Questionnaire (MSLQ) is a validated survey consisting of 81 Likert-type questions (15 subscales) that assess these cognitive, affective, and behavioral measures related to engagement [3].

In order to assess core biomechanics competencies, a Biomechanics Concept Inventory (BCI3) consisting of 25 multiple questions has been developed and validated [4]. Recently, the BCI3 has been used to investigate the influence of academic ability, interest, and study habits on learning [5]. While these factors accounted for a moderate amount of learning, a large amount of variance was still unaccounted for [5]. Therefore, factors related to learning biomechanics are likely complex and dependent on other cognitive processes [5].

The purpose of the current investigation was to build on previous work by quantifying learning strategies and barriers that influence student success when learning biomechanics. It was hypothesized that cognitive, affective, and behavioral measures collected with the MSLQ would help explain variance in learning core biomechanics concepts.

## METHODS

Sixty three college students (36 female; male; 27; 1 freshman; 28 sophomores; 26 juniors, 8 seniors) enrolled in two sections of an undergraduate biomechanics course (same instructor) completed the BCI3 during the first week of the Spring 2017 semester to assess baseline knowledge. The BCI3 will be administered again at the end of the semester. The course consists of four units (linear motion, angular motion, functional anatomy, and “hands on” analysis of movement) that are delivered using a variety of pedagogical strategies (lecture, applied calculations, active learning activities, and application of theory to practical analyses). The MSLQ will be administered prior to each of the four unit exams (same exam in both sections) to assess motivation and learning strategies with respect to the pedagogical approaches used to teach core competencies throughout the semester. Herein, preliminary data collected during the first unit of the Spring 2017 semester are evaluated.

Two, two-way mixed ANOVAs were used to evaluate scores from the three sections on exam 1 (A: algebra & trigonometry review; B: theory; C: applied calculations) and demographic factors (gender, classification year). Next, two one-way MANOVAs were used to evaluate MSLQ scores based on demographic factors (gender, classification year). Finally, two one-way

ANOVAs were used to evaluate BCI3 scores based on demographic factors (gender, classification year). A linear regression was performed to evaluate the relationship between BCI3 and exam 1 scores and multiple linear regressions were used to evaluate the MSLQ subscales and the three sections on exam 1. An a priori alpha level of 0.05 was set for all statistical tests and were performed using SPSS 16.0 (Chicago, Illinois). This protocol was approved by an institutional review board.

## RESULTS AND DISCUSSION

BCI3, MSLQ and exam 1 scores did not significantly differ based on classification year. BCI3 scores did not significantly differ based on gender (Table 1). An interaction was observed between the sections of exam 1 and gender ( $p = 0.015$ ); female students performed better on part B and part C, but not part A (Table 1). BCI3 scores were positively associated with exam 1 scores ( $p = 0.014$ ). MSLQ subscales were different based on gender ( $p = 0.023$ ); female students reported higher scores on L3 (Organization), L6 (Time & Environment), and L9 (Help Seeking) subscales (Table 1). MSLQ subscales were observed to be associated with scores on the sections of exam 1 ( $p = 0.005$ ), where L6 was positively associated with part B ( $\beta_1 = 0.44, p = 0.004$ ).

The hypothesis that the MSLQ would provide additional insight into learning biomechanics was supported. Students had a similar amount of baseline knowledge when compared to previously reported data [4]. No differences in initial BCI3 scores were observed based on demographics. Not surprisingly, students who scored higher on the BCI also scored higher on the first exam. The total score on exam 1 increased by 0.32% for every 1% increase on the BCI3. Similarly to previous research, gender appears to play a role in learning

biomechanics [5], where female students performed 6.4% better on theory and 16.1% better on applied calculation questions but not on basic algebra and trigonometry review questions.

MSLQ subscales assess skills that are critical to success in an undergraduate biomechanics course. While the motivational subscales (e.g. metacognition, critical thinking, self-efficacy) were not different based on demographics, gender differences were revealed for three learning strategies. Female students reported a greater ability to establish meaningful connections between the information being learned (clustering, outlining), a greater ability to regulate their time (effective use of time, setting realistic goals) and their study environment (organized, quiet, no distractions), and a greater ability to recognize when to seek help.

## CONCLUSIONS

A greater ability to organize information indicates that female students in the current study may be experiencing deeper learning. However, the ability to regulate one's time and environment is what appears to predict performance on the first exam.

## REFERENCES

1. Hamill J. *Quest*, **59**, 25-33, 2007.
2. Zimmerman B. *J Educ Psychol* **81**, 329-339, 1989.
3. Pintrich P, et al. *Educ Psychol Meas* **53**, 801-813, 1993.
4. Knudson D, et al. *Sports Biomechanics* **2**(2), 267-277, 2003.
5. Hsieh C & Knudson D. *Sports Biomechanics* **7**(3), 398-402, 2008.

## ACKNOWLEDGMENTS

Supported by the 2017 Innovation Fund at URI.

**Table 1:** Mean Scores ( $\pm$  standard deviations) for Concept Inventory, Exam Sections, and Learning Strategies.

	BCI (%)	Unit Exam 1 (%)			MSLQ		
		Part A	Part B	Part C	L3	L6	L9
<b>Females</b>	42.0 $\pm$ 8.3	95.6 $\pm$ 9.6	86.7 $\pm$ 8.5	82.0 $\pm$ 17.5	5.3 $\pm$ 1.2	5.7 $\pm$ 0.7	4.6 $\pm$ 1.0
<b>Males</b>	41.3 $\pm$ 10.0	96.8 $\pm$ 8.3	81.5 $\pm$ 12.2	70.6 $\pm$ 21.3	4.5 $\pm$ 1.1	5.2 $\pm$ 0.9	3.7 $\pm$ 1.2
<b>p value</b>	0.772	0.606	0.049*	0.023*	0.023*	0.026*	0.004*

\* Significant at  $p < 0.050$

# HIGH SCHOOL BIOMECHANICS COURSE DURING SUMMER STEM PROGRAM

<sup>1</sup> Antonia Zaferiou and <sup>2</sup> George Delagrammatikas

<sup>1</sup> Rush University Medical Center, IL, USA

<sup>2</sup> The Cooper Union, NY, USA

email: Antonia\_Zaferiou@rush.edu

## INTRODUCTION

The Cooper Union Summer STEM Program is a six-week engineering program offered to rising juniors and seniors in high school. The goals of the program are to expose high school students to STEM topics taught through hands-on project-based courses, increase STEM competency, build communication skills, expose high school students to a college environment, and introduce potential STEM careers.

During July and August 2016, a biomechanics, or “Body Physics” course was offered and summarized in this abstract.

## METHODS

21 high school students (12 male, 9 female) participated in the Body Physics course among the 212 students enrolled in the Summer STEM Program. Three undergraduate students participated as course teaching assistants. The course took place in a standard classroom, and the majority of the course focused on engineering design challenges that used every-day materials (e.g., cardboard, string, rubber bands, paper, etc.), following the approach of Iridescent Learning [1]. The final project leveraged the engineering school’s 3D printing, laser cutting, and machine-shop capabilities and resources in order to improve a prototype made first with every-day materials. The course also included activities in a computer lab using both open-source and technical software, and a free field trip to the Natural History Museum. Materials purchased for this course, including reusable equipment (e.g., inertial measurement unit sensors, motors, circuit board chips, etc.) cost approximately \$2,250.

In an informal and anonymous entry survey, students were asked why they were in this course, six of 15 of these open-ended responses included the words “combine”, “relationship”, “both”, or “together”, referring to how they hoped that a course on Body Physics would assist them in understanding the relationship between biology/anatomy and physics.

During the first class, students participated in Alan Alda’s science communication improvisational activities in order to meet their classmates and become more aware of their presentation and body language habits [2]. Following this introductory class, the three chapters of the course included: *Cardiovascular System, Motion Analysis, and Prostheses/Exoskeletons*. Each chapter included hands-on learning activities, a virtual visit from an expert in the field, iteratively building and testing prototypes, and peer-reviewed presentations.

## RESULTS AND DISCUSSION

*Presentations and Peer Review:* Throughout the course, students presented their work with their peers in order to improve their prototypes and presentation skills. Presentations included informal demonstrations for the whole class and to other classes touring through the classroom (as in a science fair), and formal presentations using Prezi, PowerPoint, Google Slides, Keynote, or video-based “PowToon”. Peer review was verbal or written, using the format “I like, but I wish...” (Fig 1).

		Presenter 1	Presenter 2 ...
Student 3	I like...	The design of your cardiovascular system.	How you made it more complex by adding more cups so the water would flow continuously.
	But I wish....	You showed more pictures.	There were less words in your presentation.
Student 4	I like...	how you had a strong presentation and added many pictures to support your claims	I like how you used Prezi to direct your presentation because it allowed for a very dynamic presentation that continuously engaged me
	But I wish....	you could limit the manual labor needed to use your prototype	you included more pictures on the major slide and limited the amount of text so I could visualize how your project functioned without imagining an incorrect version in my head
..			

**Figure 1:** Example peer-review of presentation via live google sheets in a computer lab, using the format “I like...but I wish...” for critical feedback.



**Figure 2:** Final prototype of an artificial arm mimicking deltoid and biceps functions using a set of programmed motors that rotate one direction to flex at the shoulder joint and the other direction to flex the elbow joint.

*Cardiovascular System:* Fluid-flow lab activities and a sheep heart dissection introduced students to the relationship between structure and function. The engineering design process was introduced to students via a skype interview of an engineer who makes fetal pacemakers, who stressed the importance of learning iteratively through multiple prototypes. Students concluded this chapter by building artificial cardiovascular system prototypes made out of every-day materials.

*Motion Analysis:* Introductory activities included an interactive review of Newton's Laws applied to skateboarding, inertial measurement unit (IMU) lab activity, Natural History Museum field trip, and center of mass/balance hands-on activities. Next, students used the computer lab to prepare and present about how biomechanics applies to their favorite hobbies. Finally, students used sports videos to calculate the body's acceleration and draw free body

diagrams at different movement events. Approximate center of mass movement was tracked and exported via PhysMo (open-source movement analysis program for Macs) and data were processed using Excel. One virtual visitor shared how the gaming industry uses motion capture and coding.

*Prostheses and Exoskeletons:* Students built, tested, and presented prototypes of prostheses or exoskeletons out of every-day materials. Virtual visitors included an implant design engineer and a robotic-surgery engineer.

*Final Project:* students self-selected groups based on which prototype project they wanted to further develop using more sophisticated building techniques and materials. Example projects included artificial arms (Fig 2), artificial legs, an exoskeleton arm (Fig 3), and an IMU sensor knee brace.

Educators can find these lessons on the ASB Teaching Repository website.

## REFERENCES

1. Engineering activities: IridescentLearning.org
2. <http://www.centerforcommunicatingscience.org/an-alda-2/>

## ACKNOWLEDGMENTS

Funding for this project was provided by The Albert Nerken School of Engineering, The Consolidated Edison Company of New York, and The New York Building Congress. Lessons plans were created with support from Body Engineering Los Angeles (NSF DGE 1045595), the USC Biomechanics Laboratory, Iridescent Learning, and the USC-Endowed Myronis Fellowship.



**Figure 3:** Sample exoskeleton prototyping from using every-day material (upper left) to using laser-cut acrylic and 3D printed parts in final prototype (bottom pictures and right picture).

# A HANDS-OFF APPROACH TO STUDENT-CENTERED LEARNING OF BIOMECHANICS AND RESEARCH METHODS

Louis A. DiBerardino, III

Ohio Northern University, Ada, OH, USA  
email: l-diberardino@onu.edu

## INTRODUCTION

Active learning has become increasingly prevalent in the university classroom. Problem-based collaborative learning has been shown to be more effective than traditional lecture-based teaching, especially in the engineering disciplines [1]. Further, there are efforts to incorporate entrepreneurial-minded learning into engineering programs, including customer awareness and value creation. [2]. This focus allows for unique opportunities to assign projects that push students outside their typical engineering comfort zones while also applying what they have learned in new ways. In the spring semester of 2016 I developed a new elective course, ME4421 – Biomechanical Engineering, structured around problem-based entrepreneurial-minded learning approaches. This course is an elective for engineering students in their junior or senior year, with a single prerequisite of ENGR 2141 – Dynamics, taken sophomore year for Mechanical Engineering students. The course topics include application of engineering principles to clinical, occupational, and sports biomechanics, with focus on kinematics and kinetics of human movement, including experimental methods, analysis, and design. The course was taken by 16 students (14 males, 2 females), all of whom were mechanical engineering majors (6 juniors, 10 seniors). This presentation will outline a culminating project that I developed for the course, which gave students an opportunity to take ownership of their work while instilling the entrepreneurial mindset with collaborative problem-based learning.

## METHODS

In the final third of the semester, the “Accelerometers” project was assigned, giving students approximately four weeks for completion.

Students worked in pairs using a three-axis accelerometer to measure and analyze a task of their choosing related to human movement biomechanics. The assignment was purposely left open-ended, and little guidance was provided. The students had to learn how to effectively use the accelerometers to record data with no assistance from the instructor. They then were required to determine a *need* for its use in the realm of movement biomechanics, identifying how the accelerometer might be used to benefit the biomechanics community. Students were required to substantiate their claims with data and facts, and discuss how their use of the accelerometer *created value* for biomechanical engineers. Projects were presented as both written reports and oral presentations to the class. Students were evaluated based on the novelty of their application, experimental methods, discussion of value added, and the quality of their report and presentation.

The instructions given to the students were intentionally vague, and detailed discussion of current accelerometer use in biomechanics was omitted from the course. This allowed the students to experience the following entrepreneurial-minded learning outcomes from the project: apply creative thinking to ambiguous problems, identify opportunities to create value, and explore a contrarian view of accepted solutions, among other more standard engineering learning outcomes.

## RESULTS AND DISCUSSION

Students performed particularly well on this assignment. Of the eight teams, five received a grade of A, three received a B, and one a C. Students showed creativity in the topics they chose: kick force for normal vs. underinflated soccer ball, calculating stride frequency during running and walking, comparing foot accelerations for normal and

hypermobile ankles, soccer kick force for standing vs one-step lead-up, calculation of elbow moment while throwing a softball, tibial acceleration for forefoot vs. flatfoot landing during a basketball jump shot, head acceleration vs. ball inflation for a soccer header, and the effect of riding position on body acceleration when riding a bicycle over a speed bump. Five of the eight teams attempted more advanced calculations and analysis than simply comparing acceleration peaks. However, in most cases these more advanced calculations were incorrect to some degree. In terms of their discussion of the value their application has added to the field, one team provided an exceptional discussion, three teams were acceptable, three marginal, and one team did not discuss value at all.

Engaging students in entrepreneurial-minded learning forced them to utilize their own knowledge and curiosity to identify the usefulness of the tool and the value that their application provided. The students took more ownership over their work than I see on a typical class project, likely because they could choose a topic they were interested in exploring. I was very pleased with the quality of work that the students showed, especially considering how vague the task was. Many teams went beyond simply comparing amplitude peaks, which was an unexpected benefit to the project. While many of those more advanced calculations and analyses were incorrect to some degree, I did not harshly penalize the teams because their action of going beyond using the basic data was more important to the assignment outcomes than how correctly they were performed. The most important part of this project was how well students were able to identify the value they were adding to the field of biomechanics, whether it be a new technique/finding, or improvements over existing techniques that use more expensive hardware. As mentioned above, not all teams gave a satisfactory discussion of the value their project added to the field, but it was apparent that they had at least thought about it to some extent.

Students rated this course very favorably, and several specifically mentioned their satisfaction with the

project. The only negative comment I received regarding this assignment was that there should be clearer expectations. However, the project was designed in a manner to be purposely unclear. In my experience, there is usually much more negative feedback regarding projects, especially when the steps to complete the project are unclear. Students' positive comments reinforce that this project was well designed to foster higher-level learning outcomes while maintaining student interest.

While the project was a success, there are certain improvements that can be made. Now that I have experience with it, I plan to begin the project much earlier in the semester. This will allow students to create a detailed preliminary proposal so that I can discuss potential methodological issues with them, resulting in more sound experimentation and analysis. Many groups did not provide a literature review or comparison of the results to literature, so this should be made clear as a requirement. Finally, clearer expectations should be provided regarding how their application adds value to biomechanics.

## CONCLUSIONS

The accelerometer project was largely a success in achieving the stated learning objectives, and in positively engaging students in the experimental process of human movement biomechanics. Other instructors could use this project with various experimental equipment to achieve the same objectives. However, I would caution that the project success may be largely dependent on the grade level of the students.

## REFERENCES

1. Prince M. *J Eng Educ* **93**, 223-231, 2004.
2. Melton DE. *KEEN'zine* **3**, 6-9, 2015.  
URL: <http://online.fliphtml5.com/zyet/hofr/#p=7>.

## ACKNOWLEDGMENTS

This work was supported by funding from the Kern Family Foundation.

# **PUTTING FUNCTION BACK INTO FUNCTIONAL ANATOMY: USING ACTIVE LEARNING TECHNIQUES TO EMPHASIZE HIGHER-ORDER THINKING TASKS**

Erin Feser & Tannah Broman

Arizona State University, Phoenix, AZ, USA  
email: erinfeser@asu.edu

## **INTRODUCTION**

A functional anatomy course is often incorporated into the curriculum of an exercise science or kinesiology undergraduate program. It is important for students to understand the anatomical structures related to human movement. Furthermore, it is vital for the students to be able to apply their knowledge in subsequent coursework and in the field. Knowing the value of the knowledge gained from this course it is important to ensure sound retention of course material and, furthermore, provide learning experiences that allow students to further their ability to apply the knowledge gained.

Faculty have many choices when it comes to deciding how to deliver course content. Active learning is a teaching technique that has repeatedly shown better learning and course performance measures when compared to traditional lecture [1]. Active learning suggests that students must do more than just listen [2]. Students should be engaged in higher-order thinking tasks such as analysis, synthesis, and evaluation. Therefore, instructional activities promoting active learning should involve students in doing things and thinking about what they are doing [3].

The Kinesiology degree program at Arizona State University has focused on incorporating active learning techniques into the required functional anatomy course to ensure students are challenged with higher-order thinking tasks. Many universities that offer a functional anatomy course may be interested in focusing on challenging the students through higher-order thinking tasks and would therefore benefit from learning more about our

experience with incorporating active learning into a functional anatomy course.

## **COURSE DESIGN**

This course, entitled KIN 334 Functional Anatomy and Kinesiology, is regularly delivered as an in-person lecture with a maximum enrollment of 40 students. There is no laboratory component. The course objectives state that after the course the students will be able to:

- Identify the joint type and ligaments of each of the major joints of the body
- Identify origin and insertion points for the muscles that produce primary human movements
- Classify the muscles that produce the primary movement for each of the major joints of the body
- Analyze basic movement in terms of muscle actions
- Analyze what muscles are involved in basic exercises and movements

Course content is divided into eight units. Each corresponding to a section of the body (e.g., shoulder joint). Following are a sample of the activities utilized within each unit of the course to target one or more of the objectives above.

**Palpation Activity** – Students are introduced to each muscle included in the unit through discovery rather than instructor led lecture. Students work with a partner to identify the origin and insertion of each muscle on the body and then work to palpate the muscle using the provided instructions. This activity leads to a more applied understanding of muscle locations since the focus is on using a real body over working off a skeleton or images from a textbook.

Contribution Analysis Activity – Students work in small groups to identify the joint actions two which each muscle might contribute. This requires students to incorporate prior knowledge such as location and line of pull of the muscle and the movement capabilities of the joint type. Instructor reviews the answers to the activity before the end of the class.

Effects of Origin and Insertion Activity – Students are asked to describe the specific aspects of a muscle's origin and/or insertion that allow for a given joint action (e.g. insertion on the radius as opposed to the ulna allows the biceps brachii but not the brachialis to contribute to supination). This activity requires students to employ higher-order analytical skills as opposed to less effective recall skills when learning muscle origins and insertions.

Movement Analysis Activity – Students work in small groups to identify the primary joint actions and muscles that contribute to everyday and exercise movements. Everyday movements are emphasized as these are more likely than sport movements to be encountered in clinical settings. This activity allows students to engage in a higher-order evaluation of movements and apply course content to relevant real-life settings.

## **BEST PRACTICES**

Success of these active learning techniques within the context of a functional anatomy course is dependent on proper implementation centered on effective evidence-based teaching strategies. Many of these activities benefit from the advantages of peer-learning as the students work in small groups. Compared to individual learning, peer-learning has shown positive effects on student academic success and performance on transfer tasks [4]. While the small group work is largely unstructured in this course, it is important to note the value it holds. Students problem solve as a team, encounter new material together, and feel more comfortable asking their peers questions than their professor. Additionally, students can engage as little or as much as they choose with whomever they choose. Thus, allowing for both introverts and extroverts to find a comfortable learning environment.

In addition, it is important to recognize that many of the activities are low stakes assignments graded primarily on in-class attendance and participation. Within a given unit, stakes are gradually increased with each activity, allowing students to build skills and knowledge and learn what is expected of them before being more formally assessed through end-of-unit quizzes and exams. The activity frequency is high which encourages student attendance, helps students stay on task during class, and facilitates regular practice of course material throughout the duration of the semester.

Lastly, traditional lecture is limited to only one short 10-20 minute introductory lecture at the beginning of each unit. The instructor plays a supportive and interactive role in the activities as opposed to being the “sage on a stage”. This allows for the majority of the class time to be devoted to student engagement in higher-order thinking tasks.

## **CONCLUSIONS**

Utilization of active learning techniques has initiated a large transformation to the student experience for this course. Instead of simply observing and passively listening to the instructor, the students can be more fully involved in the content. Naturally, this reinforces lecture material and permits higher-order learning objectives.

Active learning environments have been identified and empirically validated for increasing student performance and are often recommended over traditional lecturing as a teaching method [4]. Functional anatomy courses offer a great opportunity to incorporate active learning techniques throughout the course content to advance student performance and transfer capabilities.

## **REFERENCES**

1. Freeman et al. *Proceedings of the NAS*, **III**(23), 8410-8415, 2014.
2. Chickering A & Gamson Z. *AAHE Bulletin*, **3**, 3-7, 1987.
3. Bonwell C & Eison J. *ASHE-ERIC Higher Ed Reports*, **1**, 1-121, 1991.
4. Pai et al. *Edu Psychol Rev*, **27**, 79-102, 2015.

# SIMULATOR TRAINING LEADS TO IMPROVED WIRE NAVIGATION IN FIREST YEAR ORTHOPAEDIC RESIDENTS

Steven Long, Geb Thomas, Madison Chrisman, Anna Rodriguez, Matthew Karam, and Donald D. Anderson

The University of Iowa, Iowa City, IA, USA

Email: [steven-long@uiowa.edu](mailto:steven-long@uiowa.edu), web: <http://www.uiowa.edu/uiobl>

## INTRODUCTION

The use of simulation training for the development of surgical skills is increasing, because of the opportunities such training affords for reducing training costs, standardizing training opportunities and assessments, and improving patient safety. Recent studies demonstrate that simulator training can improve performance in the operating room (OR), at least for laparoscopic surgery [1]. Orthopaedic surgery has been slower to fully adopt simulation training into its culture. This is perhaps due to the lack of literature conclusively showing that practice on an orthopaedic simulator can lead to improvements in the OR [2]. This project seeks to remedy this, at least for one essential orthopaedic skill: wire navigation.

Orthopedic surgeons often use intraoperative, 2D fluoroscopic images to navigate a wire along a predetermined trajectory through bone. One common application is in the treatment of intertrochanteric hip fractures. The study presented here aims to demonstrate that orthopaedic residents who train on a wire navigation simulator achieve greater levels of performance when compared to those who receive more conventional forms of instruction. In addition, this study also aims to demonstrate that the type of practice on the simulator can impact the amount of improvement shown.

## METHODS

Forty-two first-year orthopaedic surgery residents participated in this study. Participants included residents from the University of Iowa, University of Minnesota, the Mayo Clinic, and the University of Nebraska, all members in the Midwest Orthopaedic Surgical Skills (MOSS) Consortium. Residents were split into three different cohorts that each received varying levels of training.

The twenty-three residents in Cohort 1 received traditional training followed by a performance assessment. The traditional training included a didactic PowerPoint presentation on placing a guide wire in the treatment of an intertrochanteric hip fracture, then a video from the ABOS module on *Fluoroscopic Knowledge and Skills* demonstrating the proper technique for placing the guide wire. The performance assessment measured their ability to place the wire through the femoral neck and into the femoral head in a mock OR (Fig. 1).



**Figure 1** – A resident is shown placing a wire in the mock OR environment.

The thirteen residents in Cohort 2 received the same traditional training, then simulator training, then a performance assessment. Simulator training included 30 minutes to practice the task using the wire navigation simulator [3]. The simulator (Fig. 2) provided real-time feedback to the residents on their wire position relative to the ideal wire position while they practiced navigating the wire.

## RESULTS AND DISCUSSION

Both Cohorts 2 and 3 demonstrated significant improvement in their TAD compared to Cohort 1 (Table 1), indicating that training improved performance. Cohort 3 attained the best average TAD, roughly half that of Cohort 1, but at the cost of more fluoroscopic images and procedure time, suggesting that the training to proficiency changed Cohort 3's speed-accuracy tradeoff. These results indicate the effect that the different styles of training had on each group. In Cohort 2, simulator practice repeated the same procedure several times, possibly leading to a quick, decisive approach. Cohort 3 was taught to approach the task in a more analytical and algorithmic fashion. Possibly this cohort needed more time and more images in the assessment because they were being more analytical in their approach yielding higher mean TAD, arguably the most clinically relevant metric for surgical success. Perhaps with even more time to practice, Cohort 3 would be able to further streamline their technique to reduce their time and fluoroscopic images while still maintaining low TAD values.

## REFERENCES

1. Sroka G, et al. *Am J Surg* **199**, 115-120, 2010.
2. Aim F, et al. *J Arthro* **32**, 224-332, 2016.
3. Long SA, et al. *J Med Devices*, **10**(3):030921-030921-2. 2016.
4. Baumgaertner MR, et al. *J Bone Joint Surg Am*, **77**, 1058-1064, 1995.

## ACKNOWLEDGMENTS

This work was partially supported by grants from the Orthopaedic Research and Education Foundation, the American Board of Orthopaedic Surgeons, and the Agency for Healthcare Research and Quality.

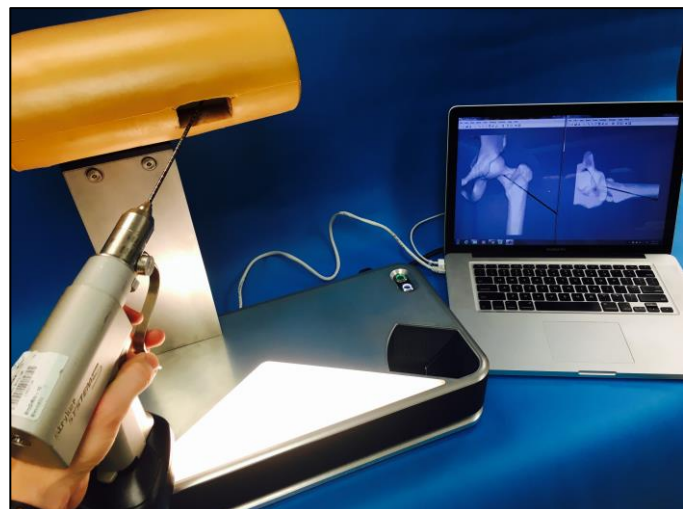


**Figure 2** – The wire navigation simulator is shown here. Virtual fluoroscopy on the laptop screen reflects the actual wire position in a surrogate bone.

The six residents in Cohort 3 received the traditional training, then proficiency-based training, followed by a performance assessment. The proficiency-based training began with a computerized task identifying the correct wire entry point and end point on a series of fluoroscopic images, followed by guided simulator practice breaking down the task into sub-components, including identifying the proper starting point and wire trajectory in both AP and lateral images. Each element was rehearsed until a designated level of proficiency was attained. The third cohort was assessed in the same manner as the other two cohorts.

The performance assessment measured the wire's tip-apex distance (TAD), the number of fluoroscopy images taken, and the total time used during the procedure. The TAD describes the distance from the tip of the wire to the apex of the femoral head, and it has been clinically shown that smaller TAD values have less probability of failure following surgery [4].

**Table 1:** Mock OR results for each cohort. The p values indicated are tested against Cohort 1.

Cohort	TAD (mm)	P	Time (sec)	P	Images	P
1	23.6 ± 7.3		242 ± 124		21 ± 11.9	
2	17.1 ± 5.3	0.005	226 ± 101	0.69	17 ± 5.9	0.15
3	12.6 ± 2.8	< 0.001	357 ± 104	0.06	27 ± 11.4	0.37

# SOFTWARE-BASED TRAINING TO ENHANCE STUDENT LEARNING IN BIOMECHANICS

<sup>1</sup> Kota Z. Takahashi, <sup>1</sup> Angel Gonzalez, <sup>1</sup> Sidney Baudendistel, <sup>1</sup> Amelia Lanier, and <sup>1</sup> Nealy F. Grandgenett

<sup>1</sup> University of Nebraska at Omaha, Omaha, NE, USA  
email: ktakahashi@unomaha.edu

## INTRODUCTION

As the study of Biomechanics is inherently interdisciplinary, Biomechanics may be valuable for promoting STEM education in undergraduate students. For example, students with interests in health-related professions could gain a new perspective on how the human body produces movement by learning basic principles of physics and applied mechanics. Similarly, students with interests in technology, engineering, physics, or mathematics could gain an appreciation for the health-related professions by learning to apply Biomechanics principles. With the growing popularity of Biomechanics, evidenced by the establishment of the National Biomechanics Day, it is critical that teaching approaches continue to evolve such that Biomechanics can reach students and spark interests within various STEM-related backgrounds.

At the University of Nebraska at Omaha (UNO), we are currently implementing software-based training to supplement traditional lecture-based teaching. We have redesigned an existing course that traditionally enrolls students from background in Exercise Science, Physical Education, Athletic Training, and Biomechanics. The students of this class typically enter the semester without a strong quantitative background (i.e., no prior enrollment in Statics, Dynamics, Calculus-based Physics, etc). Thus, our goal for the software-based modules was to encourage rigorous problem-solving skills. While lecture-based teachings are fundamental to a student's learning, we felt that a complementary software-based training approach could facilitate real-world application of Biomechanics.

The purpose of this study was to examine the effects of software-based training of Biomechanics on undergraduate student performance. We hypothesized that following the completion of this

software-integrated course, students will: 1) show greater awareness of Biomechanics' role in STEM related fields, and 2) exhibit improved self-confidence of fundamental Biomechanics' concepts.

## METHODS

We have redesigned an existing course in undergraduate Biomechanics at UNO. The redesigned course was offered starting in Fall 2016. The class offers an hour lecture twice a week, as well as a two-hour weekly laboratory session. The laboratory sessions included introduction of Visual3D software (C-Motion Inc., Germantown, MD). The laboratory sessions were designed such that students were exposed to new topics each week, related to Biomechanics-based computation in Visual3D software.

Once students were exposed to the basic features of the software, the semester progressed with assignments that were designed to challenge the students' critical thinking skills. For example, students were asked to compare and contrast human walking versus running. The students were also asked to analyze the effects of a simulated reduced gravity environment on human walking. The students concluded the semester with a Final Project involving a Clinical Gait Analysis Study. For the project, students were given actual walking data from patients with unique movement disorders. The students were then asked to synthesize the patient's movement limitations, using Visual3D software and Biomechanics-based concepts.

To evaluate student performance, we developed a questionnaire to assess the students' overall knowledge of Biomechanics and the students' awareness of Biomechanics' role in STEM related fields. The questionnaire included a narrative response, as well as questions based on a Likert scale. The students were asked to complete the

questionnaire at the beginning and at the end of the semester.

## RESULTS AND DISCUSSION

To date, 67 students consented to participate in this study. 24 students have completed the pre and post-semester questionnaire (from Fall 2016), and another 37 students have completed the pre-semester questionnaire (Spring 2017 ongoing). We are currently developing a scoring rubric to assess the narrative responses related to the students' awareness of Biomechanics' role in STEM related fields.

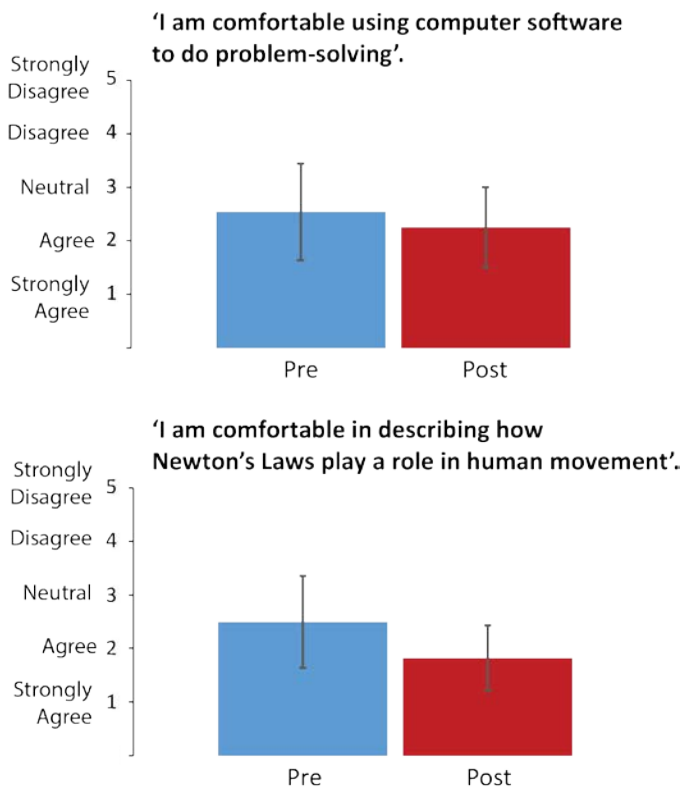


**Figure 1:** Following the completion of the software-integrated course, students became slightly more comfortable in computer-based problem solving and concepts fundamental to Biomechanics (N = 24). The questionnaires were completed at pre (blue) and post-semester (red).

Our preliminary results from 24 students show that our software-based training may improve student's confidence in performing problem-solving activities and understanding how Newton's Laws play a role in human movement (Figure 1). Furthermore, students have indicated that using Visual3D software has contributed to their understanding of Biomechanics,

and that students would like to be more proficient in the software in the future (Figure 2).

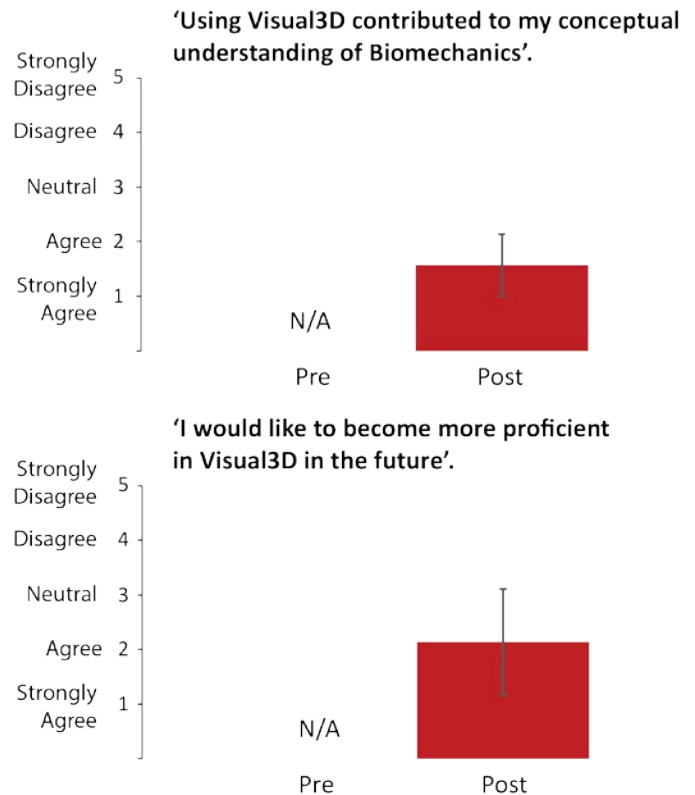


**Figure 2:** Following the completion of the software-integrated course (post-semester in red), students generally agreed that the use of Visual3D software contributed to their overall understanding of Biomechanics, and that students would like to become more proficient in the software in the future (N=24).

## CONCLUSIONS

Our preliminary results revealed that a software-integrated course in undergraduate Biomechanics can positively influence student performance.

## ACKNOWLEDGMENTS

This work was supported by funding from NASA Nebraska Space Grant and by the University Committee for the Advancement of Teaching at UNO. We would like to thank C-Motion Inc., and Dr. Saryn Goldberg for sharing data files.

# ASYMMETRICAL POSTURAL SWAY AS QUANTIFIED BY THE HURST EXPONENT USING AN ACCELEROMETER

<sup>1</sup> Dave P. Heller, <sup>1,2</sup> Kelsi Rempe, and <sup>1</sup>Brittany Oppland

<sup>1</sup> Rockhurst University, Kansas City, MO, USA

<sup>2</sup> Des Moines University, Des Moines, IA, USA

email: dave.heller@rockhurst.edu, web: <https://ruexerciseandsportscience.wordpress.com/>

## INTRODUCTION

The human body is an inherently unstable mechanical system requiring constant correction to maintain equilibrium in a gravitational field. The resulting kinematics of these corrections, known as postural sway, can characterize the dynamics governing the task of maintaining upright balance. Discrepancies in parameters quantifying postural sway can be clinical indicators of psychological, musculoskeletal, or neurological pathologies such as bi-polar disorder, multiple sclerosis, or concussion. Often these parameters include traditional measures of variability such as standard deviation (SD), range, normalized path length, etc. [2].

Postural sway measured using center of pressure (CoP) data from a force plate in the anteroposterior (AP) and mediolateral (ML) directions has been shown to exhibit non-linear properties. Non-linear parameters, such as the Hurst exponent (H), may therefore be more appropriate quantifiers of sway compared to traditional measures of variability. An increasingly popular way to measure postural sway is by tracking the AP and ML acceleration of the center of mass using an accelerometer (see Fig. 1). While a handful of studies (e.g., [1]) have applied non-linear analysis to CoP data, to our knowledge, this type of analysis has not been performed using acceleration data obtained from an accelerometer.

Therefore, the purpose of this analysis was to compare the Hurst exponents of postural sway acceleration data obtained from an accelerometer in the anteroposterior (AP) and mediolateral (ML) dimensions and compare them with traditional variability parameters.

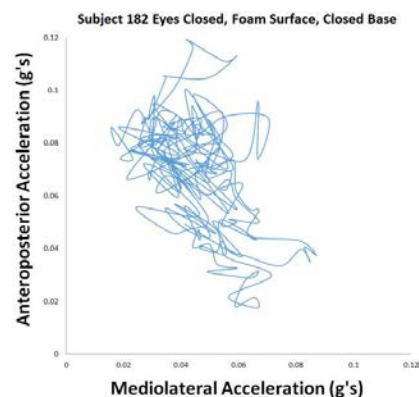


**Figure 1:** Example plot of ML vs. AP acceleration.

## METHODS

13 participants (9 females, 4 males;  $20.2 \pm 1.1$  y,  $1.75 \pm 0.11$  m,  $74.5 \pm 14.1$  kg) from a group recruited for a previous study were used for the current analysis [2]. Participants stood wearing socks for 25 seconds (s) in 18 randomized stances combining eyes open or closed, bipedal stances that were closed, open, or tandem, unipedal stances on the dominant or non-dominant foot, on tile or foam surfaces. A smartphone containing an accelerometer application (iPhone app: acceleration sensor logger v 1.2; Regrex, Inc., Osaka, Japan) was secured with a Neoprene running belt at approximately the level of the subject's center of mass. Acceleration in g's in the X-, Y-, and Z-dimensions were measured at a sampling frequency of 10 Hz with an accuracy of 0.006 g, and a precision of  $\pm 0.005$  g [2].

The middle 20 s of data was analyzed to eliminate starting and ending effects. X-, Y-, and Z-acceleration values in g's were trigonometrically normalized with the gravitational vector and aligned with the participants' longitudinal, ML, and AP axes, respectively, using the method described by Moe-

Nilssen and Helbostad [3]. Hurst exponents in both the AP ( $H_{AP}$ ) and ML ( $H_{ML}$ ) directions were found using Rescaled Range Analysis described by Qian and Rasheed [4].  $H$  was quantified by finding the slope of the regression line of the log-log plot of the rescaled range (Range/SD) vs.  $n$ , where  $n = 200$ -,  $100$ -,  $50$ -,  $25$ -, and  $10$ -data point intervals [4].

Paired t-tests were used to find differences between  $H_{AP}$  and  $H_{ML}$  as well as between  $SD_{AP}$  and  $SD_{ML}$ .

## RESULTS AND DISCUSSION

$H_{AP}$  were found to be statistically significantly larger than  $H_{ML}$  during the same condition (mean  $\pm$  SD:  $0.989 \pm 0.028$  vs.  $0.871 \pm 0.031$ ;  $t = 21.3191$ ,  $p < 0.001$ , mean difference =  $0.115$ , 95% confidence interval:  $0.104$  to  $0.127$ ).  $SD_{AP}$ , however, were not statistically significantly different than  $SD_{ML}$  during the same condition (mean  $\pm$  SD:  $0.019 \pm 0.004g$  vs.  $0.017 \pm 0.004g$ ;  $t = 1.149$ ,  $p = 0.273$ , mean difference =  $0.001$ , 95% confidence interval:  $-0.003$  to  $0.001$ ).

The Hurst exponent quantifies how “persistent” the data is.  $H = 0.5$  represents a random pattern in the data.  $H < 0.5$  represents anti-persistence: a high value is followed by a low value.  $1 > H > 0.5$  represents persistence: a low value followed by another low value [3]. In the present study, for acceleration values measured over 20 s of quiet stance, both  $H_{AP}$  and  $H_{ML}$  exhibited persistent trends: e.g. low acceleration values tended to be followed by another low acceleration value. This is expected in the present analysis since the subject was able to maintain stability for the entire 20 s. However, one might expect to see anti-persistent trends on smaller time scales to counter transient perturbations.

In this study, over all conditions, mean  $H_{AP}$  was found to be significantly greater than mean  $H_{ML}$  ( $0.989 \pm 0.028$  vs.  $0.871 \pm 0.031$ ) meaning this persistent trend was smaller in the ML direction. The mechanism for this difference is unknown. It could be an indicator of a different strategy of postural control in the ML direction. The variability of postural sway in the ML direction was not significantly different than in the AP direction which could indicate that the Hurst exponent is a more

discriminating parameter of differing control strategies in the AP and ML directions.

Previous studies using CoP data to quantify postural sway give a wide range of  $H_{AP}$  and  $H_{ML}$  values ( $0.01$ - $0.93$ ). To our knowledge, only one of these studies has compared the two dimensions statistically finding no difference in  $H_{AP}$  and  $H_{ML}$  in healthy young participants [1]. Additionally, this is the first study to compare  $H_{AP}$  and  $H_{ML}$  of postural sway data using acceleration from an accelerometer.

## CONCLUSIONS

Mean  $H_{AP}$  of acceleration taken during eighteen different quiet stance conditions in a college-aged population was found to be significantly larger than mean  $H_{ML}$  values, while a mean measure of variability (SD) was not significantly different in the AP and ML directions. This could indicate that non-linear parameters such as the Hurst exponent are more discriminating descriptors of postural sway. This difference could also be an indicator of differing control strategies in the AP and ML directions while maintaining upright stability.

Future analysis will focus on possible differences in non-linear measures of postural sway due to gender, concussion status, visual condition, surface condition, and stance.

## REFERENCES

1. Borg FG. & Laxåback G. *J NeuroEng & Rehab* **7**, 1-11, 2010.
2. Heller DP. et al. *Proceedings of ACSM Annual Meeting*, San Diego, CA, USA, 2015.
3. Moe-Nilssen R. & Helbostad JL. *Gait and Posture* **16**, 60-68, 2002.
4. Qian B. & Rasheed K. *Proceedings of IASTED conference on FEA*, Cambridge, MA, USA, 2004.

## ACKNOWLEDGEMENTS

This study was supported by a Dean’s Undergraduate Fellowship Grant from Rockhurst University. Thanks to Rachel Burns and Pandongo Secka for help with data analysis.

# VALIDATION OF INERTIAL MEASUREMENT UNITS

Leah Taylor, Emily Miller, Kenton R. Kaufman

Mayo Clinic, Rochester, MN, USA  
email: kaufman.kenton@mayo.edu

## INTRODUCTION

While optical motion capture systems provide a reliable analysis of human motion, they limit collection to a laboratory based setting. Technological advancements have led to the development of wearable devices such as Inertial Measurement Units (IMUs) as alternative tools to study human kinematics. Advantages of these devices include portability, allowing them to be used outside of a laboratory setting.

The objective of this study was to establish accuracy and precision metrics for a commercially available IMU. The sensor output was validated against the gold standard measures of custom made mechanical testing apparatuses rather than an optical system. This validation provides performance assessment of the IMU capabilities independent of external system error.

## METHODS

Commercially available IMUs were used (Opal version 2, APDM Inc., Portland, Oregon). These sensors contain tri-axial accelerometers, gyroscopes, and magnetometers. Validation testing was done to establish the accuracy and precision of the IMUs in static and dynamic conditions. The custom made testing apparatuses were used as the gold standard comparison for the sensor output.

A testing apparatus (Fig. 1A) was used to establish the sensors' performance during small angular displacements. The testing apparatus consisted of a movable arm utilizing a spring-loaded post to lock the arm into notches on a fixed base with an accuracy of 0.02 degrees for each notch. The sensor was rotated to each notch (0, 1, 3, 6, 10, and 15 degrees) and data was collected for 10 seconds at each position. This protocol was repeated five times for the three different sensor orientations. The three sensor orientations represented rotation about each of the sensors' axes. Fifteen trials were repeated for each of eight sensors.

A separate testing apparatus was used for large angular displacements (Fig. 1B). The device consisted of a rotating wheel with a spring-loaded post mechanism with notches at every 10 degree increment with an accuracy of 0.02 degrees. The sensor was rotated from 0 to 180 degrees in 10 degree increments with data collected for 10 seconds at each increment.

The dynamic testing device (Fig. 1C) was used to establish the sensors' angular velocity performance. The system was able to provide a known rotational speed within 0.003 degrees/second (dps). For testing, the angular velocity inputs for rotation about the X-and Y-axes were: 6, 150, 300, 600, 900, 1,200, 1,500, 1,800, and 2,000 dps. The inputs for rotation about the Z-axis were: 6, 150, 300, 600, 900, 1,200, and 1,500 dps. The same eight sensors used for static testing were included in the dynamic testing. Each of the eight sensors underwent five trials in each of the three positions. A trial consisted of the sensor being rotated at each of the above velocities for 10 seconds.

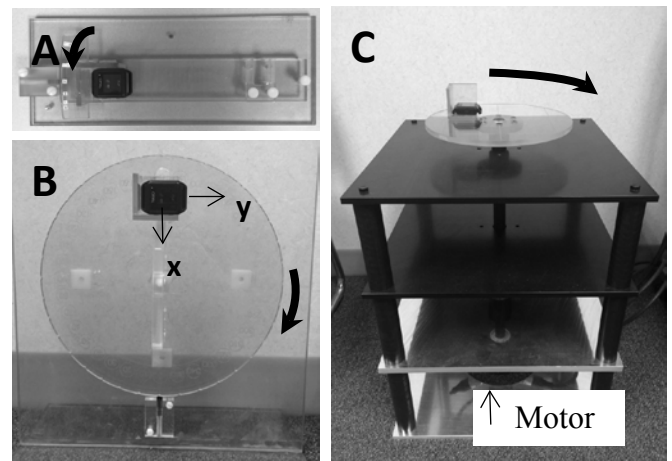


**Figure 1:** Testing apparatus for (A) small angular displacements (B) large angular displacements and (C) dynamic testing at fixed angular speeds. The sensor is in the position representing rotation about the Z-axis.

To evaluate static and dynamic sensor performance, accuracy and precision were assessed for the axis of rotation. Accuracy is reported as the absolute value of the difference between the test apparatus and the sensor output value. Precision was calculated using the standard deviation of each measurement point (angle or degrees per second) between trials. The difference (accuracy) and standard deviation (precision) were averaged across trials for each sensor and averaged for all sensors.

## RESULTS AND DISCUSSION

For both the large and small angular displacement testing; the average sensor output accuracy (Fig. 2A&B) was within  $0.6 \pm 0.1$  degrees of the true value.

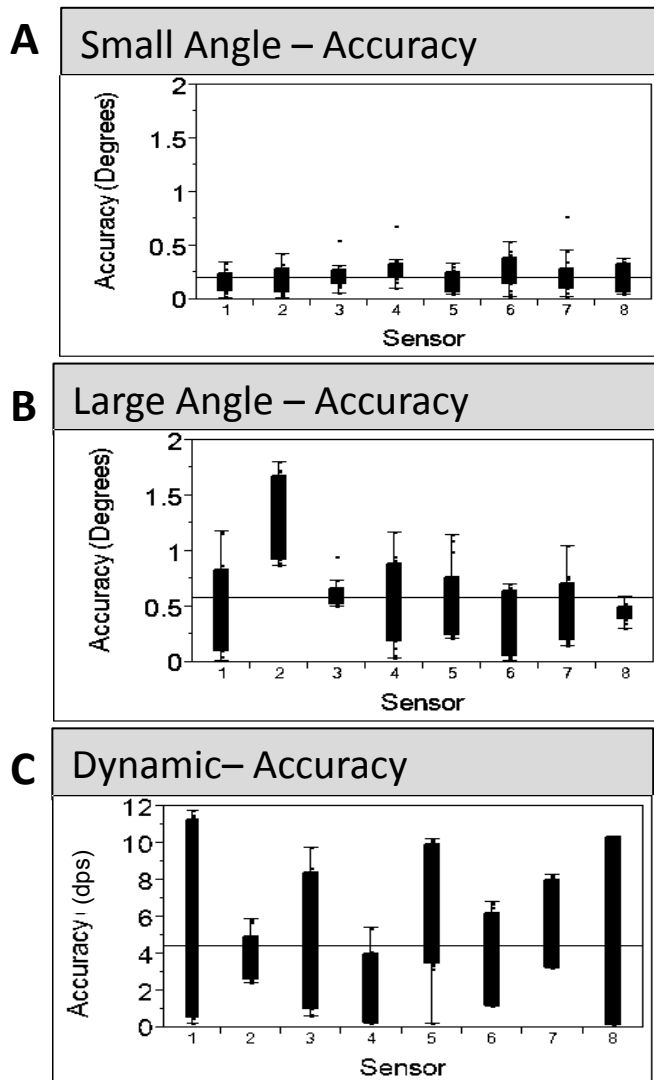


**Figure 2:** Box plots indicating the accuracy for (A) small angular displacements, (B) Large angular displacements, and (C) dynamic velocities.

The sensors had equal precision on the static apparatuses with average precision of  $0.1 \pm 0.1$  degrees. An increase in angular velocity results in an increase in the difference between the testing device input and IMU output. The average percent error for a dynamic trial of a sensor was less than 1.5 dps. The dynamic testing average accuracy for all eight sensors was  $4.4 \pm 0.2$  dps (Fig. 2C) and precision was  $0.2 \pm 0.3$  dps.

This study demonstrated that a commercially available IMU has excellent utility and reliability. Under controlled static testing conditions, the IMUs showed exceptional accuracy and precision, average accuracy and precision was within  $\pm 1.0^\circ$ . This is superior to the manufacturer's reported static orientation accuracy estimates of 1.15 degrees (roll/pitch) and 1.50 degrees (heading) ([www.apdm.com](http://www.apdm.com)). These results have slightly lower accuracy and higher precision than the study by Lebel et al. comparing APDM Opal to Optotrak motion capture orientation at static positions (accuracy  $0.01^\circ \pm 2.9^\circ$ ) [1].

## CONCLUSIONS

The IMUs provide an accurate (within 0.6 degrees) and precise (within 0.1 degrees) measurement of static sensor orientation. The IMUs also provide an accurate (within 4.4 degrees per second) and precise (within 0.2 degrees per second) representation of angular velocity. The sensors are more accurate at lower velocities, but percent error remains relatively constant across angular velocities. When determining whether IMUs are the appropriate tool, it is important to consider the application specific demands and necessary reliability.

## REFERENCES

1. Lebel, K, et al. *PLOS One* 11, e79945, 2013.

## ACKNOWLEDGMENTS

Funding for the project was provided by the Department of Defense grant # W81XWH-15-2-0071. The views expressed are those of the authors and do not reflect the official policy or position of the Department of Defense or the US Government.

# Comparing Inertial Measurement Unit and Optical Infrared Passive Marker-Based Motion Capture Systems for Injury Prevention

Rafael Valbuena, Rebekah Koehn, and Craig M. Goehler

Department of Mechanical Engineering, Valparaiso University, Valparaiso, IN, USA  
email: [craig.goehler@valpo.edu](mailto:craig.goehler@valpo.edu)

## INTRODUCTION

Currently, several measurement systems for recording human motion kinematics exist, with the two most popular being camera-based motion capture (MoCap) and inertial measurement units (IMUs). The user may decide to select one system over the other depending on preferred accuracy and resolution of the data. MoCap is generally regarded as a more accurate measurement system [1], but there are often gaps in the data, which require the investigator to spend time in post-processing. While IMUs are anecdotally believed to provide less accurate information, the data requires little or no additional processing by the investigator and thus it is viewed as a more user-friendly measurement system.

Studies have been run in order to validate the use of IMUs in place of MoCap in specific applications [2]. However, the desired accuracy of the data differs from study to study and the exact nature of the differences between MoCap and IMU data is not explicitly stated. This study will take the first steps to determine if it is appropriate to use IMUs to collect joint kinematic data while completing a previously developed injury prevention protocol [3].

## METHODS

For this preliminary study, 1 male subject, age 21, participated in an IRB approved study that compared two quantitative techniques for human movement data collection. The subject was affixed with 28 passive reflective

markers on both the upper and lower extremities based on the anatomical locations specified in a previous study [3], and 17 IMUs at locations specified by XSens. The subject completed a series of predetermined tests that utilized a variety of lower extremity movements. The subject performed each test three times.

MoCap data was collected using 11 VICON Bonita cameras. This data was processed, filtered, exported, and converted to ensure compatibility with OpenSim. A subject-specific full-body model was used to calculate the inverse kinematics for each trial. IMU data was collected using the XSens Awinda station and MVN Studio. Kinematics data was calculated using the internal model and exported directly from MVN Studio.

## RESULTS AND DISCUSSION

For this abstract, the results from the left and right in-line lunges were analyzed and compared between the two measurement systems. These results were plotted against normalized time in order to compare across the various trials. Figure 1 shows the corresponding knee and hip flexion angles for both tests. Both the MoCap and IMU systems produced curves with very similar shapes. The knee flexion results are consistent across all trials for each measurement system, with the exception of the peaks where the IMUs exceed the maximum angle of the MoCap data in three of the four knee flexion plots. Although the hip flexion plots also show very similar

trends, the difference in maximum angles was more pronounced than in knee flexion.

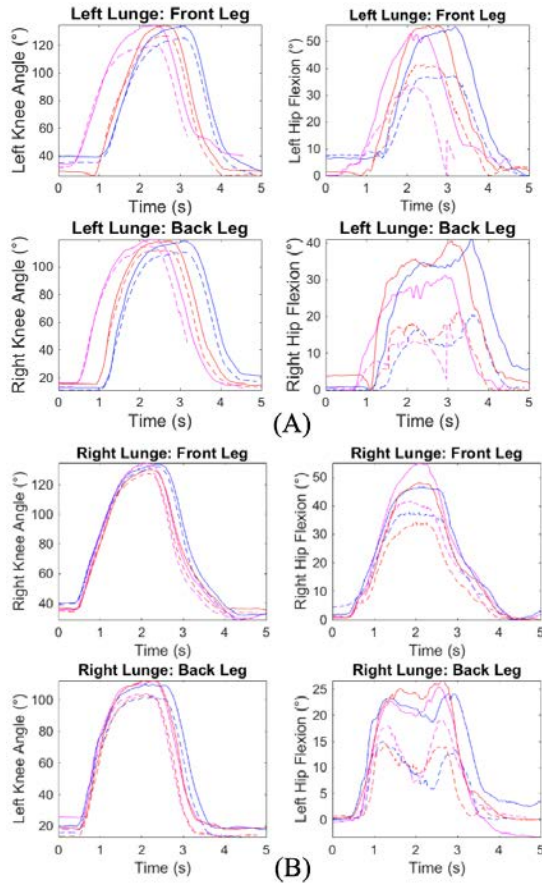


**Figure 1:** Comparison of knee and hip flexion versus time for MoCap (VICON), represented with solid lines, and IMU (XSens), represented with dashed lines, during (A) left and (B) right in-line lunge tests.

A statistical analysis of the data was performed to quantitatively confirm what the plots qualitatively demonstrate. As seen in Table 1, the IMU system showed a higher estimate of the maximum flexion angle than the MoCap system for all trials.

**Table 1:** The average (SD) maximum knee and hip flexion angles across all trials of the in-line lunge tests. The results from both the MoCap and IMU system are shown.

	Right Lunge				Left Lunge			
	Front Leg		Back Leg		Front Leg		Back Leg	
	Knee Flexion	Hip Flexion						
<b>MoCap (Vicon)</b>	130.87 (3.00)	37.92 (3.81)	103.01 (0.92)	16.30 (2.56)	123.86 (3.80)	37.44 (3.79)	112.41 (2.18)	19.89 (1.69)
<b>IMU (Xsens)</b>	132.98 (2.47)	49.89 (4.47)	111.51 (1.15)	26.90 (2.80)	134.10 (0.19)	54.70 (1.50)	118.83 (0.54)	37.58 (5.42)
<b>% Difference</b>	1.61	31.57	8.25	65.03	8.27	46.10	5.71	88.94

Interestingly, the relative difference in peak knee flexion between the two systems ranged between about 1% and 8%, while the relative difference in hip flexion measurements ranged between about 30% and 90%. This suggests that the hip flexion data is difficult to directly compare between the two systems, potentially due to differences in the kinematic models used in both cases.

These results indicate that the use of IMUs for recording information about human kinematics might be plausible for some of our applications with an appropriate calibration that accounts for the offset, but it depends highly on the desired measurement variable and allowable margin of error.

Future work will utilize a goniometer as a common standard in order to quantify the difference in accuracy between the two systems. We will also analyze additional joints across multiple motions to see if the observed trends are consistent. Furthermore, we will study the same movements with the subject moving at slower speeds in order to discard any possible discrepancy due to the speed and momentum issues that may be present with the IMUs.

## REFERENCES

1. Eichelberger P, et al. *Journal of Biomechanics*, **49(10)**, 2085-2088, 2016.
2. Skogstad A, et al. *SMC Conference 2011*
3. Kozłowski A, et al. *Annual Meeting of ASB 2015*.

# Assessing the Effect of Soldier Clothing and Individual Equipment (CIE) on Road March Biomechanics with IMUs

Clifford L. Hancock and Leif Hasselquist

U.S. Army Natick Soldier Research, Development and Engineering Center, Natick, MA, USA

Email: Clifford.L.Hancock4.civ@mail.mil

## INTRODUCTION

The U.S. Army continually seeks to improve soldier CIE. Next-generation CIE is often examined via human factors evaluations or indoor laboratory testing. However, conducting experimentation in operationally relevant conditions is also beneficial since the equipment is evaluated where and how soldiers will realistically use the equipment. When assessing the effects of equipment on biomechanics in operationally relevant conditions, inertial measurement units (IMUs) are particularly useful tools since they can be worn underneath equipment and, unlike optical motion capture, are not confined to small capture volumes. Therefore, the purpose of this study was to assess the effect of various equipment configurations on the biomechanics of soldiers performing two identical road marches during an operationally relevant scenario with IMUs.

## METHODS

Twenty-six U.S. Army enlisted male soldiers' ( $23.9 \pm 3.81$  years;  $1.743 \pm 0.08$  m;  $77.5 \pm 12.04$  kg) IMU (APDM, USA) data was analyzed from the march portions of an operationally relevant scenario. The scenario consisted of 6 sections: 1) a baseline marksmanship test, 2) a 3-mile march, 3) the Load Effects Assessment Program-Army (LEAP-A) obstacles, 4) a room clearing exercise, 5) a second 3-mile march, and 6) a second marksmanship test. The LEAP-A, in particular, was a strenuous activity that was intended to fatigue test participants in between road marches.

Each test participant individually completed the entire scenario three times but on separate days. Each day, test participants were outfitted with IMUs on their feet (secured to the boot laces), pelvis (secured near the sacrum), and sternum. Afterwards, the participants donned one of three randomly assigned equipment conditions. Specifically for the scenario's march sections, equipment condition 1 consisted of a

uniform, helmet, boots, and a mock weapon (7.3 kg). Equipment condition 2 consisted of the components of condition 1 plus body armor and a backpack (47 kg). Equipment condition 3 consisted of the components of condition 1 plus heavier body armor and a backpack (52 kg). March speed was monitored by GPS watches (Garmin, USA) and was maintained at 3 mph. Each hour long IMU march signal was divided into three 20 minute intervals (A=0-20, B=20-40, and C=40-60 minutes). Each interval was processed with a custom gait analysis algorithm developed by the University of Michigan [1].

As in previous research, dependent variables were calculated during each time interval of each march and included: 1) mean anterior-posterior (AP) lean angle of the torso, 2) standard deviation AP lean angle, 3) mean medial-lateral (ML) lean angle, 3) standard deviation ML lean angle, 4) principal components analysis (PCA) of the pelvis, 5) PCA of the feet, and 6) mean stride length [2].

For analysis, subject-based means were calculated for each dependent measure during each time interval. A repeated measures two-way ANOVA examined the main effects of and possible interactions between marches (pre and post) and equipment conditions (1, 2, and 3). When significant interactions were observed, tests of simple effects were utilized to compare all possible pairs of march conditions to each equipment condition.

## RESULTS AND DISCUSSION

For mean AP lean angle during time interval A, the ANOVA revealed a significant main effect of equipment condition ( $p < 0.000$ ). During time interval A, mean AP lean angle for equipment conditions 2 and 3 was  $9.05^\circ$  ( $p < 0.000$ ) and  $11.39^\circ$  ( $p < 0.000$ ) greater than for equipment condition 1, respectively (Figure 1). Time intervals B and C showed similar results, except mean AP lean angle for equipment condition 3 was also  $3.00^\circ$  ( $p = 0.032$ ) and  $2.75^\circ$

( $p=0.035$ ) greater than for equipment condition 2 during time intervals B and C, respectively.

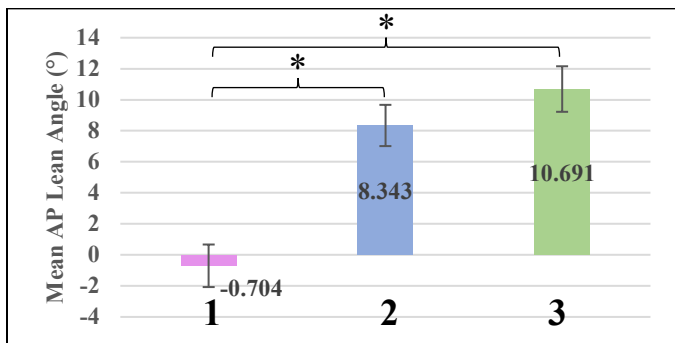


Figure 1 – Marginal means of Mean AP Lean Angle (time interval A) for the equipment conditions (1, 2, and 3) collapsed over march conditions. Positive values indicate forward lean. \* denotes  $p<0.05$ .

While there were no significant differences for mean ML lean angle ( $p>0.05$ ), there were significant interactions for standard deviation AP and ML lean angles during each time interval. The increase in weight from equipment conditions 1 to 3 caused increased mean forward lean angle and more variation about that mean. Additionally, for equipment conditions 2 and 3, standard deviation AP and ML lean angles were greater during the post-march than the pre-march during each time interval. The fatigue developed during the LEAP-A portion of the scenario, particularly while wearing equipment conditions 2 and 3, likely caused the increased variation about the mean during the post-march in both the AP and ML directions.

The ANOVA also revealed a significant interaction for  $PCA_{feet}$  during time intervals A ( $p=0.002$ ) and B ( $p<0.000$ ). During time interval A of the post-march, equipment condition 1 had 0.703% greater  $PCA_{feet}$  than equipment condition 2 ( $p=0.041$ ). While wearing equipment conditions 2 and 3 during time interval A,  $PCA_{feet}$  was greater in the pre-march than the post-march by 0.528% ( $p=0.007$ ) and 0.712% ( $p<0.000$ ), respectively. Time interval B showed similar results. The  $PCA_{feet}$  analyses revealed that when participants wore greater load, or fatigued between marches, the movement of the feet became less planar indicating a slightly altered, compensatory, movement strategy.

The  $PCA_{pelvis}$  analysis revealed a significant main effect of equipment condition for each time interval ( $p<0.001$ ), and pairwise comparisons showed that

equipment conditions 2 and 3 displayed less sagittal plane movement of the sacrum IMU as compared to equipment condition 1. The additional load caused participants to alter their pelvis motion during gait, resulting in greater out of sagittal plane movement. However, despite statistical differences, the small percentage differences evident for both  $PCA_{feet}$  and  $PCA_{pelvis}$  were likely not operationally meaningful.

A previous study concluded that increased equipment load caused decreased transverse pelvic rotation which was likely a result of higher stride frequency and shorter stride length [3]. However, the present study did not reveal any significant differences in stride length ( $p>0.05$ ) despite increased load. Additionally, the  $PCA_{pelvis}$  analysis revealed that additional motion occurred out of the sagittal plane as equipment load increased which may have shifted to the transverse plane. Further analysis is required to determine if pelvic motion has shifted to the frontal, transverse, or a combination of both planes. In the present study, the fact that participants also carried weapons likely influenced pelvic and torso motion since carrying weapons has been shown to alter trunk range of motion and transverse rotation [4].

## CONCLUSION

The present study demonstrated that IMUs are a promising tool when evaluating the effect of soldier equipment on biomechanics during operationally relevant scenarios. While a relatively small number of dependent variables were presented, additional metrics could be derived from the raw IMU signals to develop a more complete understanding of the effect of a particular piece of equipment. As further algorithms are developed to translate raw IMU signals into meaningful and valuable measures, the analysis of equipment effects on soldier biomechanics will become more comprehensive, allowing the U.S. Army to better design and select the optimal equipment for the future soldier.

## REFERENCES

1. McLean S. (Contract W911QY-13-C-0011)
2. Cain SM. Dynamic Walking 2014. Zurich, CH.
3. LaFiandra M. Jour of Biomech: 36 (2003) 87-95.
4. Seay J. Ergonomics: 54, No. 2, (2011) 187-196.

**PROOF-OF-CONCEPT:  
ACCELEROMETER-BASED METRICS PREDICT INJURY IN NCAA RUNNERS**

<sup>1</sup> Dovin Kiernan, <sup>1</sup> Laura Oelsner, <sup>1</sup> Martin Manoukian, <sup>1</sup> Madeline McKallip, <sup>1</sup> Crystal Coolbaugh,  
<sup>1</sup> Charles Caskey, and <sup>1</sup> David Hawkins

<sup>1</sup> University of California Davis, CA, USA  
email: dahawkins@ucdavis.edu, web: <http://hpl.ucdavis.edu/>

## INTRODUCTION

Running is associated with high rates of injury: up to 92.4% of runners sustain a musculoskeletal injury each year [1]. Thus, developing metrics to predict and prevent running injury is integral to preserving the musculoskeletal health of the ~55 million Americans who run regularly [2].

Theory posits that combinations of high magnitudes and numbers of vertical ground reaction forces (vGRFs) contribute to injury; however, in spite of much research, the relationship between vGRF and injury remains unclear [e.g., 3]. This lack of clarity may be due, in part, to the fact that measuring vGRFs typically requires costly equipment and expertise and is largely restricted to laboratory and clinical settings. These constraints limit the amount of data that can be collected and the ecological validity of that data, requiring inferences about overall loading profiles to be made based on limited and potentially biased samples. Extrapolation of these laboratory-based results may not realistically represent the number or magnitude of loads experienced by runners.

To overcome these constraints, our lab previously developed a model that estimates peak vGRFs from hip acceleration data, participant mass, and the type of locomotion (walk or run) [4]. The mean absolute difference between model-predicted and force plate-observed vGRFs was 8.3%, supporting this technique's potential to quantify the peak magnitude of vGRFs during running.

Building on this model, the current study quantifies the magnitude and number of loads experienced by competitive runners and compares those measures with reported pain/fatigue and injury. Runners with high magnitudes and numbers of loads were predicted to report higher pain/fatigue and injury.

## METHODS

Nine male NCAA Division I middle and long distance track runners were followed for 60 days ( $18.7 \pm 1.0$  years old,  $64.2 \pm 7.3$  kg,  $178.4 \pm 4.6$  cm; mean  $\pm$  SD). Coaches provided prescribed daily running distances/times for each participant. Participants completed daily questionnaires describing overall post-training pain/fatigue on a scale from 1 (none) to 9 (extreme) and reported the location and severity of any injuries.

During training runs each participant wore a tri-axial linear accelerometer (ADXL345, Analog Devices, Norwood, MA;  $\pm 8$  g, 48.4 – 52.4 Hz,) on their right hip. Custom MATLAB scripts (R2016a, The MathWorks, Natick, MA) were used to filter the gravity component from the acceleration signal. Steady-state portions ( $>10$  strides) were isolated, and the number and magnitude of right-side acceleration peaks were calculated. Magnitudes were then converted to peak vGRF estimates [4].

19.3% of accelerometer and 29.2% of pain/injury data were missing due to item non-response (e.g., participant removed accelerometer during run). Missing data were multiply imputed using prescribed training, anthropometrics, and all analysis variables and assuming that values were missing at random. Fifty imputed data sets were generated with SPSS (v24.0, IBM Corp., Armonk, NY) and pooled for analysis using Rubin's rules [5].

Injured and uninjured participant mean pain/fatigue, mean estimated peak vGRF, mean strides per run, mean cumulative loading per run (strides\*vGRF), and rate of load accumulation (cumulative load across two-weeks) were entered into independent samples t-tests. Significance was set at  $p < 0.05$  and corrected with a False Discovery Rate to mitigate chance of Type I error.

## RESULTS AND DISCUSSION

Across the 60-day study, three participants (33%) lost training time due to injury (self-reported foot, adductor, and hamstring injuries with 7, 10, and 33 days lost). Injured and uninjured participants did not report significantly different pain/fatigue ( $p = 0.346$ ) suggesting that our pain/fatigue questionnaire, and/or runners themselves, were insensitive to impending injury; thus, underscoring the need for additional objective metrics.

In contrast, while the mean number of strides per run did not differ between injured and uninjured participants ( $p = 0.828$ ; Fig 1a), injured participants had significantly greater peak vGRFs ( $p < 0.001$ ; Fig 1b) and cumulative loading per run ( $p = 0.006$ ; Fig 2a). Injured runners also demonstrated a trend toward faster rates of load accumulation ( $p = 0.079$ ; Fig 2b) and outlying peak vGRF vs. mean strides per run values, suggesting greater injury risk at high load magnitude-number combinations (Fig 3).

## CONCLUSIONS

Although limited by a small sample size, the present results suggest that the accelerometer-based model used here is capable of capturing inter-participant differences in loading profiles that may be predictive of running injury.

## REFERENCES

1. Lopes AD, et al. *Sports Med* **42(10)**, 891-905, 2012.
2. Outdoor Foundation. *Outdoor Participation Report*, 2014.
3. Zadpoor AA & Nikooyan AA. *Clinical Biomech* **26**, 23-28, 2011.
4. Neugebauer JM, et al. *PLoS ONE* **9(6)**, 1-8, 2014.
5. Rubin DB. *Multiple Imputation for Nonresponse in Surveys*, John Wiley & Sons, 1987

## ACKNOWLEDGMENTS

Thanks to Coach Drew Wartenburg and the UC Davis men's NCAA track and field team for their participation, and to Henry Luk, Amar Dholakia, and Shonit Sharma for contributions to earlier work.

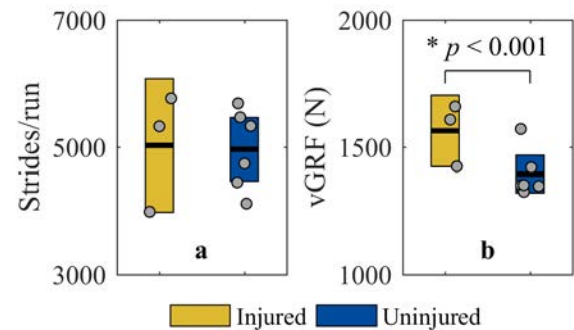


**Figure 1:** Mean (black bar) and 95% CI (shaded area) of (a) Mean number of strides per run, and (b) Mean estimated peak vGRF. Gray dots represent participant means.

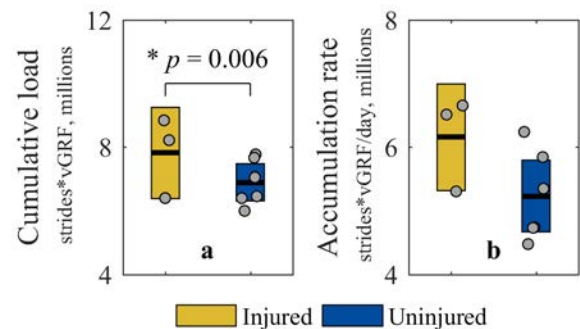


**Figure 2:** Mean (black bar) and 95% CI (shaded area) of (a) Mean cumulative loading per run, and (b) Rate of load accumulation two-weeks prior to injury (or matched temporal period for uninjured participants). Gray dots represent participant means.

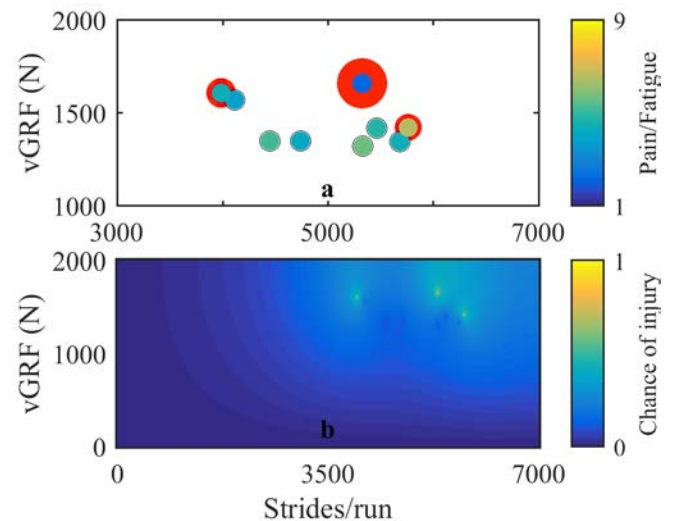


**Figure 3:** (a) Each participant's vGRF vs. strides per run. Color represents mean reported pain/fatigue. Thickness of encircling red line represents time lost due to injury (if any). (b) Chance of injury over two-months. Empirical data interpolated to conceptualize injury risk across a generalizable range.

# THE USE OF A SINGLE INERTIAL SENSOR TO ESTIMATE 3-DIMENSIONAL GROUND REACTION FORCE DURING ACCELERATIVE RUNNING TASKS

<sup>1</sup> Reed D. Gurchiek, <sup>2</sup> Ryan S. McGinnis, <sup>1</sup> Alan R. Needle, <sup>1</sup> Jeffrey M. McBride, <sup>1</sup> Herman van Werkhoven

<sup>1</sup> Appalachian State University, Boone, NC, USA

<sup>2</sup> University of Vermont, Burlington, VT, USA

email: [gurchiekrd@appstate.edu](mailto:gurchiekrd@appstate.edu)

## INTRODUCTION

The magnitude and orientation of the ground reaction force vector ( $F$ ) are often used as an index to assess performance in linear acceleration and change of direction tasks [1, 2]. In-ground force plates (FP) are considered the gold standard for measuring  $F$ , however, their use in the field is limited by their cost and the constraints they place on movement.

To overcome these limitations, previous studies have investigated the use of a single wearable accelerometer for estimating kinetic parameters during accelerative tasks [3, 4]. The sensor is typically placed close to the body's center of mass (COM) thus enabling estimation of  $F$  via Newton's 2<sup>nd</sup> Law with knowledge of the subject's mass. These studies suggest that misalignment of the accelerometer measurement axes relative to the FP may underlie some of the observed error. Inertial measurement units (IMUs) are equipped with on-board sensors that allow them to determine the orientation of the IMU relative to an inertial reference frame (and thus also the FP frame assuming the FP vertical axis is aligned with the gravity vector) and compensate for the aforementioned frame misalignment.

Previous studies have not attempted to compensate for this potential error source using IMUs. Thus, the purpose of this study was to assess the validity of 3-D  $F$  estimates from a single IMU during accelerative running tasks by comparison to a force plate.

## METHODS

Fifteen subjects (12 male, 3 female, age:  $23.20 \pm 2.11$  yrs) volunteered to participate in this study. The movement tasks assessed were:

1. A linear standing sprint start (SS), and
2. A 45° change of direction task (COD)

Subjects performed six trials of the SS task (three to assess  $F$  during the initial push from stance and three to assess  $F$  during the first foot contact after the initial push). Subjects also performed six trials of the COD task (three to the left and three to the right) to assess  $F$  during the first foot contact after the initial push (i.e. the plant foot).

The IMU was attached to the sacral region of the subjects using an elastic strap and double-sided tape (Fig 1). Subjects were positioned with their hips pointed straight forward in order to align the forward axes of the IMU and FP. This allowed the determination of the FP heading (angular deviation of horizontal plane axes) relative to the local

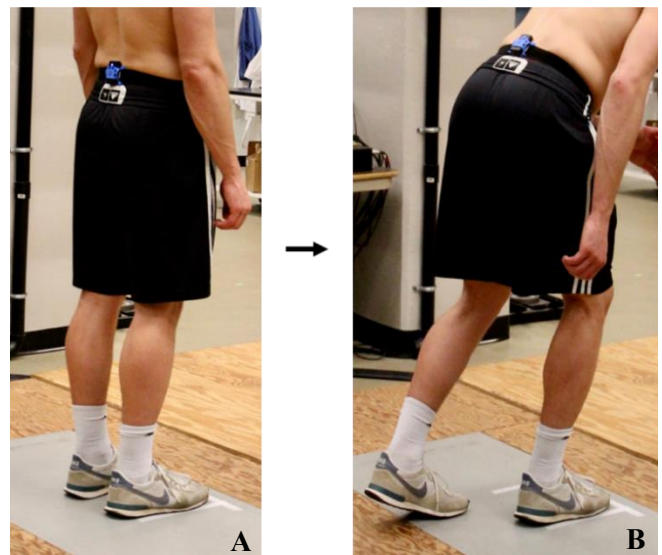


**Figure 1:** Subject on force plate with IMU attached to sacral region. **A.** Static orientation trial - hips aligned with forward axis of the force plate. **B.** Subject assumed standing sprint start stance.

magnetic field vector. Subjects then assumed their stance for three seconds before performing the task. Average accelerometer and magnetometer output during stance was used to determine IMU attitude and heading relative to the FP. The attitude and heading allowed the construction of the composite quaternion representing the orientation of the IMU relative to FP. The angular rate signal measured by the gyroscope was then used to time-integrate the quaternion orientation at each instant during the movement. The acceleration vector measured by the IMU was then resolved in the FP frame and scaled by the subject's mass to provide an estimate of  $\mathbf{F}$ .

Step average  $\mathbf{F}$  ( $\bar{\mathbf{F}}$ ) was determined for the IMU and FP by averaging the  $\mathbf{F}$  estimates measured during foot contact (when FP measured  $F_z > 10$  N). IMU estimates of  $\bar{\mathbf{F}}$  and instantaneous  $\mathbf{F}$  were compared to the same measured by FP. The ratio of the forward component of  $\mathbf{F}$  ( $F_x$ ) relative to  $F_{res}$  expressed as a percentage ( $RF$ ) was also compared between IMU and FP to consider the potential application of the IMU method to assess linear acceleration performance [1]. Error in the IMU estimates of  $\mathbf{F}$  was quantified using root mean square error (RMSE), relative error (absolute percent difference), and Pearson's product moment correlation coefficient ( $r$ ).

## RESULTS AND DISCUSSION

The IMU method gave valid estimates of  $\bar{F}_x$ ,  $\bar{F}_z$ ,  $\bar{F}_{res}$ ,

and  $RF$  during SS and  $\bar{F}_z$  and  $\bar{F}_{res}$  during COD suggested by significant correlations, low relative error, and low RMSE (Table 1). Despite large absolute errors in the IMU estimate of the other components, correlations with FP estimates were significant for all components of  $\bar{\mathbf{F}}$  except  $\bar{F}_y$  during SS suggesting the IMU estimate may be able to detect similar changes in measured values compared to FP over time. The IMU did not provide accurate estimates of instantaneous  $\mathbf{F}$  for any components for the SS task (RMSE: 376.64 N to 476.57 N) nor for the COD task (RMSE: 436.44 N to 632.54 N). The average angular error of the IMU estimate of  $\bar{\mathbf{F}}$  during both SS and COD was less than  $10^\circ$  suggesting the IMU can provide valid estimates of the orientation of  $\bar{\mathbf{F}}$ .

The ability to accurately estimate directional step-averaged  $\mathbf{F}$  during athletic tasks is useful when evaluating performance [1, 2]. The results of this study broaden the scope of IMU applications to perform field-based human movement analyses.

## REFERENCES

1. Rabita G, et al. *Scand J Med Sci Sports* **25**, 583-594, 2015.
2. Dos'Santos T, et al. *J Strength Cond Res* **31**, 696-705, 2017.
3. Howard R, et al. *Proceedings of ISSC '14 and CIICT '14*, Limerick, Ireland, 2014.
4. Wundersitz DWT, et al. *Sports Biomechanics* **12**, 403-412, 2013.

**Table 1:** Comparing IMU and FP estimates of  $\bar{\mathbf{F}}$  and  $RF$  during SS (top) and COD (bottom).

		IMU	Force Plate			
		Mean $\pm$ SD [N]	Mean $\pm$ SD [N]	RMSE [N]	Relative Error [%]	$r$ (p value)
SS	$\bar{F}_x$	219.00 $\pm$ 83.50	220.82 $\pm$ 68.83	45.17	12.88	0.84 (<0.01)
	$\bar{F}_y$	-11.22 $\pm$ 44.23	6.54 $\pm$ 35.07	66.15	341.20	-0.33 (0.08)
	$\bar{F}_z$	785.84 $\pm$ 152.02	821.34 $\pm$ 156.89	77.32	6.82	0.90 (<0.01)
	$\bar{F}_{res}$	821.16 $\pm$ 156.43	853.41 $\pm$ 162.07	75.71	6.51	0.91 (<0.01)
	$RF$	26.75 $\pm$ 8.44	25.87 $\pm$ 6.44	4.53	12.28	0.85 (<0.01)
COD	$\bar{F}_x$	152.45 $\pm$ 90.98	70.88 $\pm$ 52.58	100.93	218.02	0.77 (<0.01)
	$\bar{F}_y$ (Right)	-289.70 $\pm$ 96.58	-388.73 $\pm$ 89.99	132.18	28.42	0.53 (0.04)
	$\bar{F}_y$ (Left)	229.11 $\pm$ 121.54	368.02 $\pm$ 92.45	169.91	38.90	0.58 (0.02)
	$\bar{F}_z$	945.76 $\pm$ 165.99	964.27 $\pm$ 145.10	60.01	5.20	0.94 (<0.01)
	$\bar{F}_{res}$	1002.27 $\pm$ 177.51	1041.72 $\pm$ 159.88	77.12	6.49	0.91 (<0.01)

# Use of Inertial Measurement Units (IMUs) in the Analysis of Bounding Rush Performance in Soldiers

Meghan P. O'Donovan, Jonathan T. Kaplan, Clifford L. Hancock and <sup>1</sup>Leif Hasselquist

<sup>1</sup>Natick Soldier Research, Development, and Engineering Center, Natick, MA, USA

e-mail: meghan.p.odonovan.civ@mail.mil, web: <https://www.nsrdec.army.mil/>

## INTRODUCTION

Realistic operations for military personnel can be difficult to recreate in laboratory settings. To draw meaningful conclusions about Soldier performance, laboratory assessments try to match the tasks and environments Soldiers operate in as closely as possible. The military is investigating the use of wearable technologies, such as Inertial Measurement Units (IMUs), to gather information about Soldier performance directly from the operational tasks Soldiers conduct in the field. The purpose of this study was to: 1. Analyze the performance of Soldiers conducting a bounding rush task in the field and 2. Determine if IMU derived measures relate to overall performance of a bounding rush task.

## METHODS

Forty male Soldiers (ht:  $1.74 \pm 0.07$  m, wt:  $78.5 \pm 11.5$  kg, age:  $23.9 \pm 3.81$  yrs) participated in this study. Each participant conducted the bounding rush task as part of a military obstacle course completed in the field. Participants completed the bounding rush task in the following load configurations: Level I consisted of uniform, boots, helmet, and simulated weapon (M4 carbine) for a total weight of 7.3 kg; Level II consisted of Level I components with the addition of a body armor vest for a total weight of 31 kg; and Level III consisted of Level II components with additional ballistic-protection added to the armor vest for a total weight of 36 kg. An IMU (APDM, USA) sampling at 128 Hz was affixed to the sacrum of each participant prior to the start of the course. The bounding rush task was the 7<sup>th</sup> obstacle of the course and began with the participant standing upright, rushing 2.1 m forward, dropping to a prone position, completing four diagonal 4.6 m rush-to-prone repetitions, and lastly, rushing 3.0 m toward the finish (Figure 1). In each prone position, the participant was required to acquire a sight picture of a target placed near the finish before proceeding. Participants were instructed to complete the bounding rushes as quickly as possible to maximize

effort and task performance. Only the four 4.6 m rushes that included prone-to-prone transitions were analyzed.

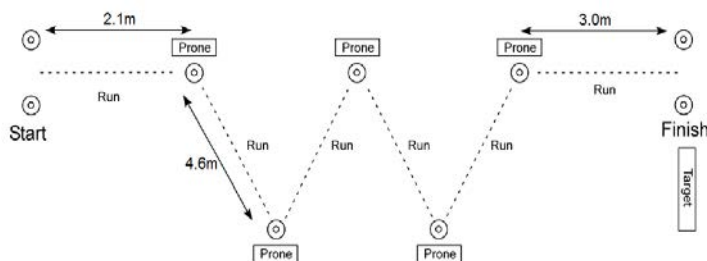


**Figure 1:** Schematic of the bounding rush task.

Dependent measures were averaged across the four rush repetitions. Timing data, including total time (time to complete the bounding rush) and time to standing (time to reach the maximum vertical displacement of the sacrum), was collected via the sacral mounted IMU. In addition, maximum sacral velocity (both horizontal and vertical) was recorded and averaged for each rushing bout. IMU derived measures were analyzed via dedicated algorithms (University of Michigan, MI, USA) [1]. A one-way repeated measures ANOVA was run for the three configurations (I, II, and III) to determine if there was a significant effect of load configuration on the dependent measures. A subsequent regression analysis was conducted to determine the strength of the linear relationship between total time (rush performance) and the other IMU derived measures.

## RESULTS AND DISCUSSION

ANOVA results showed a significant effect of load configuration on total time ( $p < 0.001$ ). Post-hoc pairwise comparisons revealed that increased load significantly increased total time to complete the bounding rush task (I:  $4.95s \pm 0.78$ , II:  $6.59s \pm 1.11$ , III:  $7.12s \pm 1.26$ ), thus decreasing task performance ( $p < 0.05$  for all comparisons tested). This agrees with previous work examining the effects of load on sprint performance [2] and indicates a clear difference in performance between the three load configurations.

ANOVA results also indicated a significant effect of load configuration on other IMU derived measures. Specifically, time to standing in the Level I configuration was significantly faster than both the Level II ( $p<0.001$ ) and the Level III ( $p<0.001$ ) configurations. However, there was no significant difference between Levels II and III ( $p=0.21$ ). Maximum horizontal sacral velocity in the Level I configuration was significantly greater than in both the Level II ( $p<0.001$ ) and the Level III ( $p<0.001$ ) configurations. However, there was no significant difference in max horizontal sacral velocity between the Level II and III configurations ( $p=0.486$ ). Maximum vertical sacral velocity in the Level I configuration was significantly greater than in both the Level II ( $p<0.001$ ) and III configurations ( $p<0.001$ ). Max vertical sacral velocity was also significantly higher in the Level II configuration than in the Level III configuration ( $p<0.023$ ).

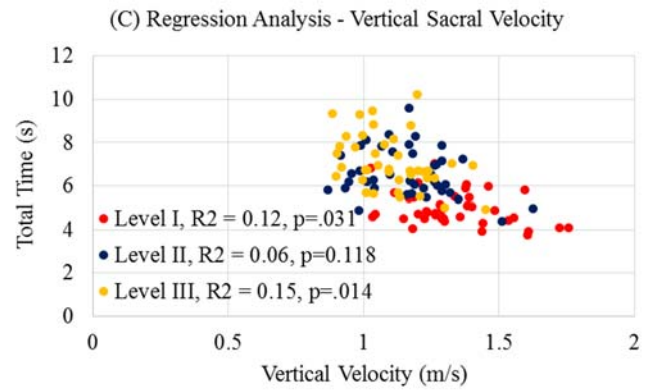


**Figure 2:** Regression plots for IMU derived metrics including (A) time to standing, (B) max horizontal sacral velocity, and (C) max vertical sacral velocity.

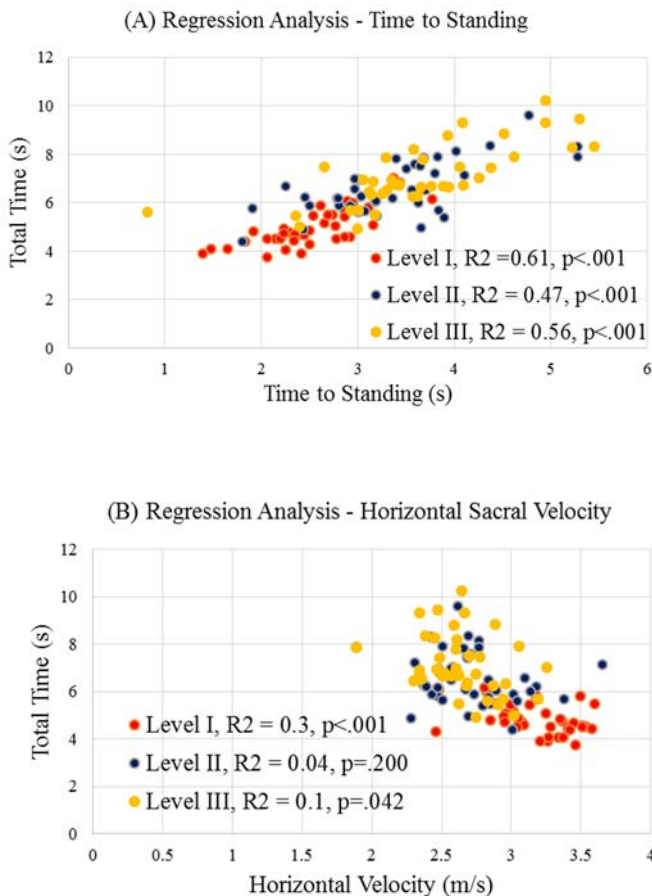
Load configurations I and III displayed significant negative correlations between max horizontal and vertical sacral velocity and total time ( $p<0.05$ ) but with low coefficients of determination. There was no significant correlation between horizontal nor vertical sacral velocity and total time for the Level II configuration. All three load configurations displayed significant, positive correlations between time to standing and total time ( $p<0.001$ ) with higher coefficients of variation (Figure 2A). The regression results indicate that performance on the bounding rush task was best predicted by the transition time from prone to standing while the ANOVA results indicate that max vertical sacral velocity was the most sensitive to changes in load configuration.

## CONCLUSIONS

This study indicated that increased load resulted in greater time to complete a bounding rush task, thus reducing maneuverability in the field. This study has also shown, through several significant correlations between the IMU metrics and task performance, that IMU-derived measures have the potential to be an effective tool to analyze task performance strategies for operationally relevant maneuvers in the field. It is important to note that additional IMU derived measures (e.g., sacral accelerations, sprinting time, footfall distance, etc.) not included in this analysis could also be used to quantify task performance and require further investigation.

## REFERENCES

1. Hasselquist L, et al. *DTIC NATICK/TR-12/014*, 2012.
2. Cain, SM, et al. *Dynamic Walking 2014*, June 10-13, Zurich, Switzerland.



# VALIDATION OF GOPRO CAMERA VIDEO ANALYSIS SYSTEM WITH INERTIAL MAGNETIC SENSORS FOR UNDERWATER AND LAND APPLICATIONS

<sup>1</sup> Mostafa Yaghoubi, <sup>1</sup> Philip Fink, <sup>1</sup> Wyatt Page, and <sup>1</sup> Sarah Shultz

<sup>1</sup> School of Sport and Exercise, Massey University, Wellington, New Zealand  
email: m.yaghoubi@massey.ac.nz

## INTRODUCTION

The ability to analyze human movement in different environments (water and land) is an essential tool of biomechanical analysis for sport and rehabilitation applications. Most of the previous research regarding kinematic effects of aquatic exercises has used video analysis [1]. However, the reliance on video analysis for kinematic parameters in aquatic environment has been questioned as the surrounding water induces differences in the refractive index in comparison to air, which can increase the risk of image geometric distortion and/or parallax error [2]. Additionally, underwater optical motion capture systems are expensive, complicated, and limited to laboratory settings [4]. The use of inertial motion sensors has become popular among researchers when tracking human movement in aquatic environments. The sensors potentially provide a wider field of acquisition, faster set-up, and a practical calibration, with a reliable accuracy reported in analyzing the joint kinematic in sagittal plane [3]. However, wireless inertial motion sensors cannot be used for underwater applications that require high sample rates (>128Hz) or real-time data monitoring.

This paper covers the validation of a GoPro sports camera motion capture system as an inexpensive and reliable way to capture underwater movement.

## METHODS

A single GoPro Hero 4 Black (image rate 240 Hz; image resolution 1280x720 pixels) camera enclosed in a modified waterproof housing, was used. The GoPro Wi-Fi signal was boosted with a passively coupled range extender (TP-Link AC750), permitting a cable to be extended out of the water to a small aerial. This set-up enabled wireless control and monitoring of the camera from a nearby laptop computer using the GoPro camera control software (version 2.0.5 for windows).

A waterproof chessboard was used to perform 2D plate calibration in dry and aquatic conditions [5]. A physical cylindrical segment model was developed to stimulate the human leg movement pivoting in sagittal plane (i.e. Hip extension and flexion). The model was set in a 3 × 1.5 × 2 m pool.

Kinematic data measured from analysis of the GoPro video was compared to data from three tri-axial inertial motion units (accelerometers + gyroscopes + magnetometers; Emerald, APDM, Portland, OR, USA). The units were fixed along the leg segment model and the model was attached to a turning force with a fixture arm to both sides of the pool. The direction of movement of the model and its range of motion simulated hip flexion-extension of a stiffened leg. The angular velocities of power-head (Biodex isokinetic dynamometer) used to drive the model were set to 30°/s and 10°/s for air and underwater conditions respectively. Reflective markers were attached exactly on the centre of the inertial motion units on each segment of the leg model in order to be able to track the movement in the sagittal plane. An analogue clock with a smooth sweep second hand (100 twitches per second, 31 cm diameter, Time Company) was also used as part of the camera validation. The angular velocity of the clock's second-hand was measured from the GoPro video during five cycles of 60 seconds in water and dry-land conditions. A reflective marker was attached to the tail of the second hand to track the movement. One samples T-tests were used to compare measured velocities in air and water to the expected angular velocity of the clock and the leg segment model. Pearson's cross-correlation analysis was used to compare measurements between the inertial sensors and the markers placed on the segmental leg model. Statistical significant was set at  $p < 0.05$ .

## RESULTS AND DISCUSSION

The results are presented in Table 1. The nonlinear direct linear transformation (DLT) showed a mean re-projection error of 0.21 and 0.28 for air and underwater conditions respectively. This is within an acceptable range for the pixel accuracy in both conditions. The expected mean angular velocity of the wall clock's second-hand ( $6^\circ/s$ ) was not significantly different to the values measured in air ( $p < 0.626$ ) and underwater ( $p < 0.157$ ). Similarly, the angular velocity measured along the leg model was not significantly different for marker ( $p < 0.852$ ) and sensor ( $p < 0.578$ ) when compared to the expected velocity of  $30^\circ/s$ ; likewise, marker ( $p < 0.927$ ) and sensor ( $p < 0.673$ ) measurements were similar to expected  $10^\circ/s$  underwater velocity.

Figure 1 shows a comparison between the measured angular velocity on the leg model from one of the inertial motion sensor and the optically tracked markers for both the air and underwater conditions. The result of cross correlation analysis between the measured angular velocity from the three inertial motion sensor and the corresponding optically tracked markers is shown in Table 2. In all cases, there is a very high correlation between each pair of measurements. This study examined the validity using a GoPro Hero4 Black camera in the video analysis of kinematic data on human leg model during simulated hip flexion-extension in underwater and air conditions. The results indicate that the GoPro camera with manual digitization provides an inexpensive system to measure movement in air and underwater conditions. The system provided accurate and reliable kinematic data when compared to the results of inertial motion

sensors and also for known motion of a second-hand on a clock.

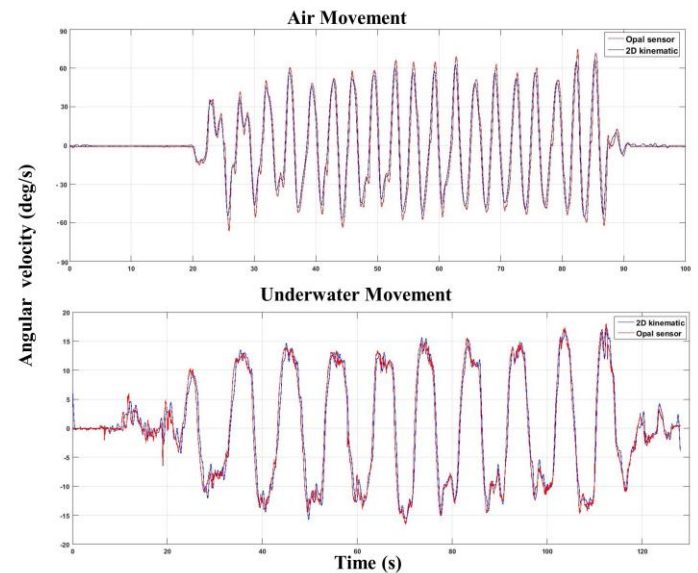


**Figure 1:** Measured angular velocity on the leg model of the inertial motion sensor (red) and markers (blue) in air and underwater conditions.

## REFERENCES

1. Alberton CL, et al. *J Hum Kinet* **49**, 5-14, 2015.
2. Severin AC, et al. *J Fitness Research* **5**, 48-62, 2016.
3. Brodie MA, et al. *Comput Methods Biomech Biomed Engin* **11**, 641-648, 2008.
4. Weinhandl JT, et al. *J Biomech* **43**, 1437-1440, 2010.
5. Zhang Z. *J IEEE Trans Pattern* **22**, 1330-1334 2000.

**Table 1:** Mean ( $\pm$  SD) angular velocity for markers and inertial motion sensors and clock's second-hand, in air and underwater conditions

Condition	Angular velocity (deg/s)		
	Clock second-hand	Model - Marker	Model - Sensor
Air	$5.990 \pm 0.039$	$29.895 \pm 1.794$	$30.190 \pm 1.045$
Underwater	$6.085 \pm 0.049$	$9.970 \pm 0.727$	$10.091 \pm 0.681$

**Table 2:** Cross-correlation analysis between angular velocity of sensors and markers in air and underwater conditions.

Condition	Cross-correlation		
	Sensor 1 & Marker 1	Sensor 2 & Marker 2	Sensor 3 & Marker 3
Air	0.992*	0.985*	0.980*
Underwater	0.996*	0.994*	0.991*

\* $p < 0.001$

# ANALYZING THE APPLICABILITY OF WEARABLE SENSORS TO MEASURING ROWING PERFORMANCE – A PILOT STUDY

<sup>1</sup>Aaron Schlenker, <sup>2</sup>Angela Boynton, <sup>2</sup>Jennifer Neugebauer, <sup>1</sup>Rebecca Zifchock, <sup>1</sup>Gregory Freisinger,

<sup>1</sup>United States Military Academy, West Point, NY, USA

<sup>2</sup>Army Research Laboratory, Aberdeen Proving Ground, MD, USA

email: aaron.schlenker@usma.edu, web: <http://www.usma.edu/cme/SitePages/Home.aspx>

## INTRODUCTION

This project seeks to apply wearable sensors to rowing on an indoor stationary rowing ergometer. An existing body of research describes and analyzes the biomechanical aspects of the motion. Buckeridge et al. found approximately 35% of variance in force applied to the footboard on the drive can be attributed to hip flexion range of motion [1]. Performance improves when lumbar flexion at the catch is minimized, as this allows the force to be transmitted more effectively from the leg drive to the back. Kawalek et al. focused on joint mobility as a key to performance and decreased injury risk, particularly with regard to the lumbosacral joint [2]. Force is applied quickly with the legs in a relatively flexed lumbar spine at the initial point of the drive, and repeated over hundreds or thousands of repetitions. This repeated loading can lead to back trauma and disc herniation. The authors reason that increased hip flexion at the catch will reduce the required flexion in the lumbosacral joint and consequently reduce the stress in the spine.

The purpose of this project was to develop a method to collect and process data from wearable sensors to predict rowing performance. From the background research, it was hypothesized that minimizing the difference between lumbar and hip flexion will improve performance.

## METHODS

A variety of sensors were selected after hypothesizing which factors may influence performance. These included a Zephyr™ Bioharness™ 3 [Annapolis, MD] and an IMeasureU™ [Auckland, New Zealand] inertial measurement unit (IMU).

Sensor selection and proof of concept was initially determined through a series of six self-tests of 500m

ergometer [Concept2®; Morrisville, VA] rowing trials performed at 90% perceived effort. Two trials were rowed at each of the following strokes rates: 24 strokes per minute (spm), 26 spm, and 28 spm. For each pair of tests, the first trial was rowed with the best possible form, while the second trial was intentionally rowed with poor form, primarily initial hip displacement without proper force application to the handle. Ample rest time (>3 minutes) was allowed between trials. The ergometer was used to collect time to complete 500 m, known as 500 m split time and average force through the ergometer handle. Back angle was calculated using data from the 9 axis IMU which was sampled at 500 Hz. Only one IMU device was used during this first iteration as a proof of concept in order to develop the angle algorithm and calculate range of motion. Average heart rate and posture were collected from the Bioharness at a sampling rate of 1 Hz. The preliminary proof of concept data is shown below in Table 1.

Stroke Rating (spm)	Form	Split Time (s)	Avg Handle Force (lb)	Back ROM (deg)	HR (bpm)
24	Good	105	148	72.4	147.2
	Poor	111.2	113	63.3	140
26	Good	101.4	150	69.42	149.4
	Poor	107.8	133	46.14	144.4
28	Good	97.3	160	83.22	156.5
	Poor	105	126	54.26	146.9

We were able to effectively measure back angle by utilizing the wireless IMU, however the resolution of the Bioharness was too low to quantify posture rowing characteristics. Therefore we removed it from further analysis.

The second test session focused solely on the difference between lumbar and hip flexion using the two IMU sensors. Initial analysis of three male collegiate rowers, between the ages of 20 and 22, are reported in this pilot study. Two trials were rowed at 24 spm, and 28 spm, with similar conditions. One IMU sensor was placed under the right armpit and another placed at hip level below the iliac crest. Each subject rowed with constant perceived effort (between 70-90%). Ample rest time (>3 minutes) was allowed between trials.

MATLAB was used to translate the raw data from the IMU to relative range of motion. The code first employed Sebastian Madgwick’s implementation of Robert Mahoney’s Direct Complementary Filter to convert 9-axis IMU data into Euler angles. The filter incorporates quaternions, information about the earth’s magnetic field and magnetic flux, and normalization and integration techniques [3]. Only sagittal rotation about the mediolateral axis was investigated in this analysis. Conditional looping and the “findpeaks” MATLAB function were used to find the peak flexion and extension angles of each stroke. These peaks were then averaged and subtracted to determine the average angular range of motion (ROM) for the back and the hip during each trial. These average ROM variables were subtracted to find the difference between the back and hip for each trial.

No statistical analysis was performed at this time due to the limited sample and pilot nature of this investigation.

## RESULTS AND DISCUSSION

The results from the three participants are shown in Table 2. While limited, some information can be drawn from the data. The difference between Back ROM and Hip ROM tends to be larger during the poor form trial when compared to the good form trial. This is expected given that poor form creates a disconnection between the hips and the back. This increased difference aligns with an increase in split time and a decrease in average handle force, which indicates poorer performance. These differences do vary substantially between participants; which may be due to differences in personal rowing form between the participants.

**Table 2: Data – Second Pilot Test Session**

n	Stroke Rate	Form	Back ROM	Hip ROM	Diff	Split Time	Handle Force
1	24	Good	44.8	42.6	2.2	112.4	127
		Poor	64.0	57.1	6.9	115.5	123
	28	Good	49.9	46.9	3	107.7	133
		Poor	55.6	48.4	7.2	109.9	126
2	24	Good	77.8	17.9	59.9	111.6	105
		Poor	99.9	15.2	84.7	113.2	99
	28	Good	79.8	16.7	63.1	106.9	103
		Poor	101.2	19.5	81.7	110.4	90
3	24	Good	151.8	36.2	115.6	108.6	133
		Poor	160.8	30.6	130.2	112.7	120
	28	Good	135.3	29.8	105.5	101.3	138
		Poor	145.3	33.6	111.7	106.3	-

All data displayed as means for entire 500m rowing trial. Range of Motion (ROM); Difference (Diff)

## CONCLUSIONS

While hip and back ranges of motion varied substantially between rowers, the relative differences between these remained moderately consistent for each rower. Further testing on a larger and more diverse sample population is necessary to confirm these results and validate the original hypothesis. However, the primary concern of this pilot study was to develop a method for measuring, recording, and processing data from wearable sensors that could effectively analyze rowing mechanics and performance. The results indicate that this was achieved and further testing is planned.

## REFERENCES

1. Buckeridge, E., et al. *SJMSS*, **25**, e179-e183, 1996.
2. Kawalek, K., et al. *TRENDS in Sport Sciences*, **2(22)**, 61-69. 2015
3. Madgwick, S. 2010. “An efficient orientation filter for inertial and inertial/magnetic sensor arrays” <http://x-io.co.uk/open-source-imu-and-ahrs-algorithms/>

## ACKNOWLEDGEMENTS

Funding for this study was provided by United States Military Academy Center for Innovation and Engineering.

# INFLUENCE OF ACCELEROMETER RANGE ON ACCURACY OF FOOT-MOUNTED IMU BASED RUNNING VELOCITY ESTIMATION

Michael V. Potter, Lauro Ojeda, Noel C. Perkins, and Stephen M. Cain

University of Michigan, Ann Arbor, MI, USA  
email: mvpotter@umich.edu

## INTRODUCTION

Miniature inertial measurement units (IMUs) are an attractive option for analyzing human performance due to their low cost, light weight, and relatively simple setup. Unlike optical-based motion capture, IMUs allow researchers to collect data in the field, where measurements are not restricted by limited capture volumes.

One application of this technology is to use foot-mounted IMUs to estimate a subject's running velocity in over ground running. Foot-mounted IMUs are an attractive option for this application because the foot is essentially stationary during specific times in the stance phase, which allows the application of zero velocity updates (ZUPTs) [2]. Commercially available IMUs offer a wide variety of sensor specifications (e.g. sampling rate and accelerometer and gyro ranges) that can greatly affect the quality of IMU-derived estimates for gait parameters. Bailey, et al. [1], examined the effect of sampling frequency and accelerometer ranges on estimations of average stride velocity and foot clearance. However, their evaluation was limited to a small range of speeds (2.3 - 3.4 m·s<sup>-1</sup>, much slower than competitive running) and two accelerometer ranges (16g and 100g).

In this pilot study, we investigate the effect of sensor accelerometer range (100, 75, 50, 24, 16, 10, and 6g) on estimates of average running velocity (up to 7.6 m·s<sup>-1</sup>). Doing so provides researchers information necessary to knowledgably select IMUs with the appropriate sensor specifications to meet study goals.

## METHODS

Two healthy male subjects were recruited for this University of Michigan IRB approved pilot study.

Each subject was equipped with two IMUs (Opal, APDM, 128 Hz, ±200g, ±2000 deg·s<sup>-1</sup>). One IMU was placed on each shoe on top of the lower laces and secured with athletic tape to prevent shifting. An instrumented treadmill (Quasar, h/p/cosmos) capable of speeds above 8 m·s<sup>-1</sup> was used to establish a ground truth measurement of gait speed.

After familiarization with the treadmill, each subject completed the following trials, each 20 seconds in duration: walking at speeds of 0.89, 1.79, and 2.24 m·s<sup>-1</sup> and running at speeds of 1.79, 2.24, 3.13, 4.02, 4.92, 5.81, 6.71, and 7.60 m·s<sup>-1</sup>. The subject rested as needed between trials. Neither subject was able to run the full 20 seconds at 7.60 m·s<sup>-1</sup> (stopped at 10 and 15 seconds) but they completed all other trials successfully.

Foot trajectory estimates for each foot and each trial were obtained by integrating a single IMU's sensor data and applying a ZUPT algorithm similar to that used in [2]. Zero velocity points were selected as the time of minimum angular rate magnitude during foot contact. Strides were then segmented by these zero velocity points. Each stride's length was calculated as the total calculated planar displacement of the foot between the beginning and end of the stride. We selected only strides in which the subject was fully on the treadmill (not holding the side rails) for analysis. For each trial the average velocity of each foot,  $v_{calc}$ , was calculated by summing the selected stride lengths of that foot and dividing this by the time elapsed during these strides. Velocity error,  $VE$ , was calculated as:

$$VE = \frac{v_{calc} - v_{treadmill}}{v_{treadmill}} \times 100 \quad (1)$$

where  $v_{treadmill}$  is the speed of the treadmill. This calculation was then repeated (without changing

selection of steady state speed period) but by artificially modifying the accelerometer's range to typical commercial ranges of 100, 75, 50, 24, 16, 10, and 6g. This mimics the effect that using a sensor with these ranges would have on velocity estimation using this technique. This was accomplished by truncating the acceleration to that limit (e.g. any reading  $>50g$  or  $<-50g$  set to  $+50g$  or  $-50g$  respectively). The average error of the four calculated velocities at each speed (two subjects with two feet each) was then compared with respect to change in speed and change in accelerometer range.

## RESULTS AND DISCUSSION

The maximum acceleration measured along any sensor axis in this study was less than  $75g$ , therefore the velocity error in all  $100g$  and  $75g$  calculations was identical. Figure 1 shows mean velocity error vs. treadmill speed for each artificially enforced accelerometer range. It can be readily observed that in general, the IMU-estimated velocity using the aforementioned technique degrades with increasing running speed regardless of accelerometer range. A linear fit to the data for a  $100g$  accelerometer (velocity error vs. treadmill speed) yields a slope of  $-1.27\% \cdot s \cdot m^{-1}$ . This may be attributed to limitations in sampling frequency of the IMUs used in this study that could have a greater influence at higher speeds. Additionally, the zero velocity assumption may be invalid at these speeds or the zero velocity point may be misidentified during foot contact. Even at the highest speed tested, the difference in velocity error between a  $100g$  accelerometer and a  $16g$  accelerometer is only  $5.2\%$ , suggesting that for many running studies, where speeds are significantly lower than this, there may not be a significant benefit to having an accelerometer over  $16g$ . However, the velocity estimation severely degrades for an accelerometer range lower than  $16g$ . For example, at  $6g$  a linear fit to the velocity error vs. treadmill speed has a slope of  $-6.89\% \cdot s \cdot m^{-1}$ .

In comparing the walking vs. running trials at  $1.79$  and  $2.24 m \cdot s^{-1}$ , in six of the eight cases (2 subjects, 2 feet, 2 speeds) the average velocity estimated during walking had slightly lower error than that calculated during running. On average, walking trials produced a velocity error that was  $0.94\%$  better. More subjects

are necessary to determine whether this difference is significant.

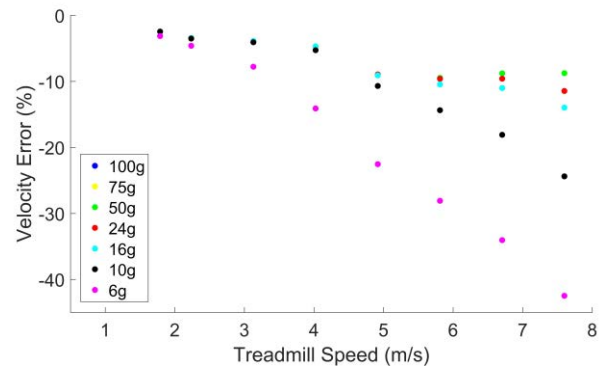


**Figure 1:** Effect of accelerometer range on error in calculated mean velocity at various running speeds. Note that for almost all speeds, results of  $100g$ ,  $75g$ , and  $50g$  accelerometer are identical.

## CONCLUSIONS

Our pilot study demonstrates that velocity estimation using the ZUPT technique presented degrades with increased running speed and with lower accelerometer ranges (especially below  $16g$ ). Future work will require an expanded subject population to more fully describe the relationship between velocity estimation, speed, and accelerometer range. This expanded subject pool will also allow us to more fully determine whether walking vs. running has a significant impact on velocity estimation at the same speeds using the described techniques. Additionally, IMUs with higher sampling rates will be used to test the impact of sampling rate on velocity estimation at high speeds.

## REFERENCES

1. Bailey GP, et al. *icSPORTS*, 154-161, 2014.
2. Ojeda L, et al. *J of Navigation* **60**, 391-407, 2007.

## ACKNOWLEDGMENTS

This material is based upon work supported by the US Army Contracting Command-APG, Natick Contracting Division, Natick, MA, under contract W911QY-15-C-0053.

# Quantifications of the Relative Motion Between the Body and the Soldier Plate Carrier System: Applications of Accelerometry

Logan Leahy, Gabriela Barrera, Matthew Vest, Tyler Weaver, Gregory Freisinger and Becky Zifchock  
The United States Military Academy, West Point, NY, USA  
email: logan.leahy@usma.edu

## INTRODUCTION

As warfare has evolved, the amount of weight soldiers have been asked to carry has increased (Fig. 1) [1]. For those serving in the infantry or similar dismounted units, carrying heavy loads is required. The typical U.S. Rifleman carries a 29kg fighting load; however, during long marches approaching an objective, a soldier will carry approximately 43kg, or 94.6lbs [2].

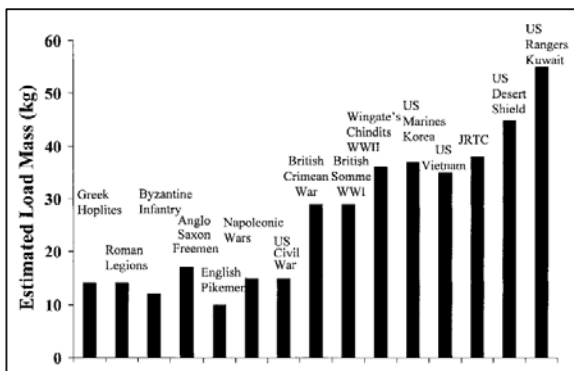


Fig. 1. Loads carried on the march by various infantry units throughout history [1].

In order to decrease the amount of compressive loads felt on the spine and lower back, there is a need for a device that redistributes weight. With more load redistribution devices undergoing research, and eventually reaching the market, there is also a need to evaluate the effectiveness of such devices. One such way is by the relative motion between the carried load and the torso. Load stability is important to soldiers, and could be used to gauge the effectiveness of loadbearing equipment. The movement of a heavy load with each step may not be in sync with the movement of the trunk, leading to cyclic loading of the spinal column [1]. This cyclic loading could lead to fatigue and overuse injuries with the potential to lead to further, more serious complications [1].

In an effort to evaluate passive load redistribution devices, the goal of this study was to quantify the relative acceleration between the torso and body armor with and without a hip-borne load redistribution device. The hypothesis was that the load redistribution device would decrease relative motion.

## METHODS

Data for seven participants has been collected, to date, for this IRB-approved study. Of the seven, 2 were female, 5 were male, and the average height and mass of the participants was 179 ( $\pm 9$ ) cm and 82 ( $\pm 10$ ) kg, respectively. All participants were active duty military.

Two inertial measurement units (IMUs) [IMeasureU: New Zealand] were used to measure the relative acceleration between the torso and the body armor. The IMUs output acceleration in three axes (x, y, and z) at a full scale range of  $\pm 16g$  at a 16 bit resolution. The IMUs were mounted to the torso at C7, and at the top, back side of the body armor (Fig 2a). They were secured in place by using adhesive sport spray and medical tape on the skin, and a sewn strap on the body armor. The mounting positions attempt to align the 3 axes of the IMUs as closely as possible (Fig 2b).



Figure 2a: Load Redistribution Device (ATLAS) and Figure 2b: IMU mounting locations and axes

Data was collected from each IMU simultaneously at 500 Hz during the final two minutes of each of two seven-minute treadmill walking trials: with and without the ATLAS device. Walking speed was standardized to 1.5 m/s.

The raw data in the x, y, and z axes was first processed in LabView [National Instruments; Austin, TX] using a low-pass Butterworth filter with a cutoff value of 10 Hz. After filtering, the data analysis was conducted using a custom code written in MATLAB [MathWorks, Inc.; Natick, MA]. For each condition (with/without ATLAS), the root mean squared error (RMSE) was calculated for each respective axis of the simultaneously-sampled IMUs, which is shown by Equation (1).

$$(1) RMSE = \sqrt{\frac{\sum_{t=1}^n (a_{armor} - a_{torso})^2}{n}}$$

$$(2) a_{Res} = \sqrt{(a_{torso_x} - a_{body_x})^2 + (a_{torso_y} - a_{body_y})^2 + (a_{torso_z} - a_{body_z})^2}$$

$$(3) RMSE_{Res} = \sqrt{\frac{\sum_{t=1}^n (a_{res})^2}{n}}$$

Figure 3: Equation Definitions

To calculate the RMSE for the difference of the resultant acceleration, the difference vector for resultant acceleration was created by using Equation (2). This value illustrates general the difference in motion in all three axes. Equation (3) was then used to calculate the resultant RMSE. RMSE values were then compared between two conditions using paired t-tests.

## RESULTS AND DISCUSSION

The results are displayed in figure 4. The t-test values do not support the initial hypothesis, and in fact support the opposite of the initial hypothesis in the y axis and resultant with P values of 0.04 and 0.02, respectively. The P values for the x and z axes do not support the null hypothesis, but do suggest a possible trend because of the effect size values of 0.50 and 0.59, respectively.

The results suggest the opposite of the initial hypothesis. A contributing factor could be the nature of the design. The ATLAS device lifts the body armor off the body, which may result in the additional motion between the torso and body armor.

## CONCLUSIONS

This study suggests that the ATLAS device and possibly other load redistribution devices that displace the load away from the body create greater relative motion between the torso of the wearer and the body armor. The clinical implications of this are unclear, however, it is possible that devices that create greater relative motion could create additional torques on the musculoskeletal system.

## REFERENCES

1. Knapik et al., *Mil. Med*, 2004; 169: 45-56.
2. Dean CE, *Army Center for Lessons Learned*, 2004.

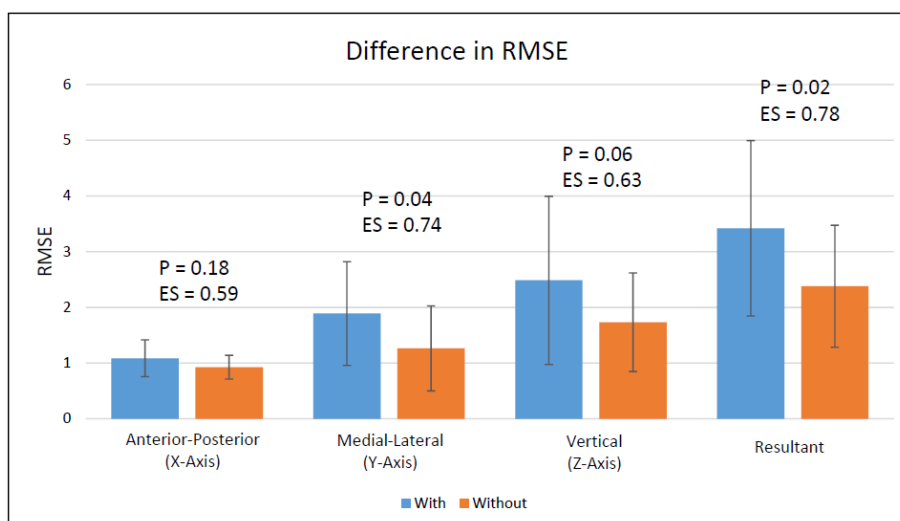


Figure 3: RMSE Difference (With ATLAS – Without ATLAS) for all seven participants for: x, y, z-axes and resultant.

# Assessing the Validity of the G-Walk BTS on Individuals with Unilateral Transtibial Amputations

<sup>1</sup>Daniel Courtney, <sup>2</sup>Corey Koller, BS, <sup>3</sup>Cory Cacciola, <sup>4</sup>John Horne, CPO, <sup>2,5</sup>J. Megan Sions, PhD, DPT, PT, <sup>1,2</sup>Elisa S. Arch, PhD

<sup>1</sup>Kinesiology and Applied Physiology, <sup>2</sup>Biomechanics and Movement Science Interdisciplinary Program, <sup>3</sup>Mechanical Engineering, <sup>5</sup>Physical Therapy, University of Delaware, Newark, DE, USA  
<sup>4</sup>Independence Prosthetics-Orthotics, Inc., Newark, DE, USA  
email: dcourt@udel.edu

## INTRODUCTION

Spatiotemporal parameters of gait can be used to assess an individual's walking performance [1]. For prosthetic users, walking performance can be an indicator used to guide prosthesis prescription, as well as assess prosthetic fit and rehabilitation outcomes [2]. The most accurate method to quantify spatiotemporal parameters is to conduct an instrumented gait analysis using force platforms and motion analysis cameras. However, the time and cost associated with conducting a gait analysis often makes it prohibitive for use in clinical practice.

Newer accelerometer-based technology provides a potential tool to assess spatiotemporal parameters of gait in a clinical setting. For example, the G-Walk BTS® is a small, portable device that uses tri-axial accelerometers, gyroscopes, and magnetometers to measure various spatiotemporal parameters of gait [3]. The G-Walk rests on the fifth lumbar vertebra and transmits data via Bluetooth technology, allowing for quick and easy data collections. However, the accuracy of G-Walk's spatiotemporal parameters has not yet been assessed for individuals with lower-limb amputations. The aim of this study was to determine the accuracy of the G-Walk BTS® for individuals with unilateral transtibial amputations.

## METHODS

Nine prosthetic users with unilateral transtibial amputations (6 males, 60.9 ±11.4 years, 1.74 ±0.11 meters, 85.9 ±25.7 kilograms) participated in this IRB-approved study. Upon arrival to the laboratory, subjects completed a 10 Meter Walk test to determine their self-selected walking speed. Then, subjects underwent an instrumented gait

analysis with concurrent data collected from the G-Walk BTS®.

For the instrumented gait analysis, retro-reflective markers were placed on the pelvis and lower extremities. Kinematics and kinetic data were collected at 240 Hz and 1200 Hz, respectively, using a six-camera optical motion capture system (Motion Analysis Corporation, Santa Rosa, CA, USA) and two force plates embedded in the floor (AMTI, Watertown, MA, USA). As per manufacturer's instruction, the G-Walk BTS® was placed at the fifth lumbar vertebra by use of Velcro belt supplied with the device [3]. Data were recorded from the G-Walk on a laptop via Bluetooth technology. With this equipment in place, subjects were asked to walk across a designated laboratory pathway approximately six meters long, which contained the embedded force plates, at their self-selected walking speed. Photocell beams were used to measure velocity for each trial, and subjects were given verbal cues to guide them to their self-selected speed as determined by the 10 Meter Walk Test. A minimum of three acceptable trials were collected (self-selected speed ±0.2 statures/sec with contact of feet entirely on the force plates).

Cadence, walking speed, step length on both the prosthetic and sound limbs and gait cycle duration on both the prosthetic and sound limbs were calculated from the instrumented gait analysis data using Visual 3D (C-Motion Inc., Germantown, MD, USA). Each parameter was averaged within trials for each subject. The same spatiotemporal parameters were automatically calculated in the software supplied with the G-Walk. To assess the G-Walk's accuracy, the percent error in each parameter as measured by G-Walk (compared to the

instrumented gait analysis as the gold standard) was calculated ( $\%_{error} = \frac{G-Walk - Gait\ Analysis}{Gait\ Analysis} \times 100\%$ ).

This percent error was calculated for each trial, then the absolute percent difference was averaged across trials and then across subjects for each parameter.

## RESULTS AND DISCUSSION

Out of the spatiotemporal parameters assessed, all but one parameter had less than 10% error when measured by the G-Walk BTS® compared to the gold standard. All of the spatiotemporal parameters were within the 10-15% error threshold deemed acceptable for clinical use [4]. The G-Walk's measure of cadence (steps/min) was the most accurate, with an average error of  $1.43 \pm 1.28\%$  (Table 1). The G-Walk's measure of gait cycle duration and step length for both limbs also had less than 10% error. Interestingly, the G-Walk BTS® was more accurate in measuring gait cycle for the prosthetic limb than the sound limb. For the step length, there was negligible difference in the level of error between limbs measured by the G-Walk BTS®. Speed as measured by the G-Walk had the greatest error with a mean percent error of  $14.56 \pm 11.10\%$ .

Spatiotemporal Parameter	Absolute Average Percent Error (%)
Cadence (steps/min)	$1.43 \pm 1.28$
Speed (m/s)	$14.56 \pm 11.10$
Gait Cycle Duration (Prosthetic Limb) (s)	$3.07 \pm 5.00$
Gait Cycle Duration (Sound Limb) (s)	$6.53 \pm 9.45$
Step Length (Prosthetic Limb) (m)	$7.32 \pm 4.85$
Step Length (Sound Limb) (m)	$7.38 \pm 5.32$

**Table 1:** Absolute average percent difference in spatiotemporal parameters between the gait analysis and G-Walk (mean  $\pm$ SD).

## CONCLUSIONS

Validation is a necessary step in all research when implementing a new technology. Given that a clinically acceptable level of error is 10-15%, results from this study suggest the G-Walk BTS® is an accurate tool for collecting spatiotemporal parameters of gait assessed in this study for individuals with unilateral transtibial amputations during forward walking at a self-selected speed. While results supported accuracy of this device, this study was limited in that it only assessed the G-Walk's validity during a short data collection. Before wide scale implementation, this device should be validated over a longer period (both distance and time) as well as on a more diverse population of prosthetic users (transfemoral amputations, bilateral amputations, etc.). Ultimately, if thoroughly validated, the G-Walk BTS® may provide a clinically-viable tool to facilitate prostheses prescription as well as assess prosthetic fit and rehabilitation progress.

## REFERENCES

- Balasubramanian, CK. *Gait & Posture* **29.3** (2009): 408–414. *PMC*.
- Esquenazi, A. *Physical Medicine and Rehabilitation Clinics of North America* **25.1** (2014): 153-67.
- "BTS G-WALK." *BTS Bioengineering*. N.p., n.d. Web. 06 Mar. 2017.
- De Wit, DCM. *Clinical Rehabilitation* **18** (2004): 550-57.

# EVALUATION OF AN ACCELEROMETER TO ASSESS SAGITTAL PLANE KNEE MECHANICS DURING A DROP LANDING

Alexander M. Morgan and Kristian M. O'Connor

Department of Kinesiology  
University of Wisconsin-Milwaukee, Milwaukee, WI, USA  
email: morgan28@uwm.edu

## INTRODUCTION

Non-contact anterior cruciate ligament (ACL) injuries account for around 70% of all ACL injuries annually and are two to eight times more prevalent in women [1]. Prior studies have examined neuro-mechanical factors that contribute to this prevalence and have found decreased knee flexion angles, increased posterior ground reaction force, and increased internal knee extension moments to be contributors to developing an ACL injury [2,3]. Furthermore, inertial measurement units (IMUs) have been used previously to reliably assess knee flexion during a drop landing task [4]. A biofeedback protocol using this IMU system that intended to increase knee flexion was successful in doing so and decreased further risk factors for ACL injury [5]. However, the IMUs being utilized above contain both an accelerometer and a gyroscope, and as such are more expensive. A less expensive IMU measuring only accelerations may also be useful in evaluating ACL injury risk.

Thus, the purpose of this study was to compare accelerations in the sagittal plane near the knee during a drop landing maneuver with commonly assessed kinetic risk factors for ACL injury across three landing conditions using only an accelerometer.

## METHODS

Eighteen subjects (six male and twelve female) participated in this study (average: 23.7 years, 1.68 m, 65.9 kg). Three-dimensional kinematic data were collected for the right leg using a Motion Analysis Eagle motion capture system (Santa Rosa, CA) at 200 Hz. Kinetic data were collected with a Bertec force plate (Columbus, OH) at 1000 Hz. Anterior-posterior accelerations at the tibial tuberosity of the

right leg were collected using a Noraxon DTS 3D Accelerometer (Scottsdale, AZ) at 1000 Hz. Positive accelerations indicated acceleration of the knee posteriorly. Reflective markers were placed on the pelvis and dominant leg at relevant anatomical landmarks for three-dimensional kinematic analysis.

A standing calibration trial was captured, after which subjects were instructed to stand on a 30-cm tall box located next to the force plate. Subjects were instructed to perform a bilateral drop landing task in which the individual stepped off the box and landed on the ground. Subjects were instructed to land with the foot of the right leg on the force plate, with the left foot off the force plate. Three landing conditions were implemented, with ten drop landing trials collected for each condition. Subjects were instructed to land in preferred, soft, and stiff manners. Soft landings were described as occurring with knees flexed, while stiff landings were described as occurring with knees extended.

All data reported occurred in the sagittal plane. Differences in peak positive knee acceleration, knee angle at initial contact, peak internal knee extension moment, and maximum knee flexion across the three conditions were reported. Pearson product-moment correlation coefficients were computed to assess the linear relationship between peak internal knee extension moment and peak positive acceleration during the preferred condition. Average correlation coefficients were computed to assess the relationship between peak positive accelerations and peak knee extension moments within subjects and across conditions.

## RESULTS AND DISCUSSION

Significant differences in average knee flexion at initial contact, maximum knee flexion, peak internal

knee extension moment, and peak positive acceleration were found across conditions (Table 1). Furthermore, a significant correlation between peak internal knee extension moment and peak positive accelerations was found for the preferred condition (Figure 1). Peak values were found within the first 30 ms after initial contact (Figure 2). This suggests that, as the knee accelerates more towards extension, a larger peak internal extension moment during landing will be present. A strong positive association ( $R^2 = 0.76$ ) was found between peak internal knee extension moment and peak positive acceleration across conditions within subjects, when averaged across all subjects. This indicates that, on average, both variables increase or decrease from preferred values during stiff or soft landings, respectively. Overall, it appears that peak positive knee acceleration predicts peak internal knee extension moment both within and across subjects.

## CONCLUSIONS

Knee accelerations were related both within and across subjects to peak internal knee extension

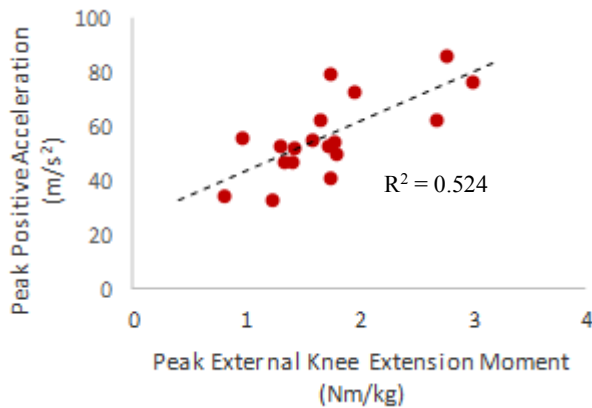


**Figure 1:** Peak positive acceleration displays a significant correlation with peak internal knee extension moment during preferred landings.

**Table 1:** Significant differences in sagittal plane knee kinematics and kinetics between landing conditions. Like letters are not significantly different ( $p < .05$ )

	Soft	Preferred	Stiff
Flexion at Initial Contact (°)	22.2 <sup>a</sup>	14.5 <sup>b</sup>	12.2 <sup>b</sup>
Maximum Flexion (°)	94.5 <sup>a</sup>	70.8 <sup>b</sup>	56.1 <sup>c</sup>
Peak Internal Extension Moment (Nm/kg)	1.4 <sup>a</sup>	1.7 <sup>a,b</sup>	2 <sup>b</sup>
Peak Positive Acceleration (m/s <sup>2</sup> )	38.3 <sup>a</sup>	56.5 <sup>b</sup>	68.1 <sup>c</sup>

moments across different landing conditions. It was hypothesized that sagittal plane acceleration of the knee might predict kinetics at the knee associated with ACL injury based on previous work associating knee flexion with these same kinetic variables [2]. This was indicated in the reported findings. As such it appears that accelerometer data is effective in detecting both within- and between-subject variation in sagittal plane moments for different landing mechanics. Future work should examine the applicability of using an accelerometer to assess ACL injury risk and alter landing mechanics to decrease risk for injury.

## REFERENCES

1. Agel J, et al. *Am J Sport Med* **33**(4), 524-531.
2. Yu B, et al. *Clin Biomech* **21**(3), 297-305.
3. Dai B, et al. *Am J Sport Med* **43**(2), 466-474.
4. Dowling AV, et al. *J Biomech Eng* **133**(7), 071008.
5. Dowling AV, et al. *Am J Sport Med* **40**(5), 1075-1083.

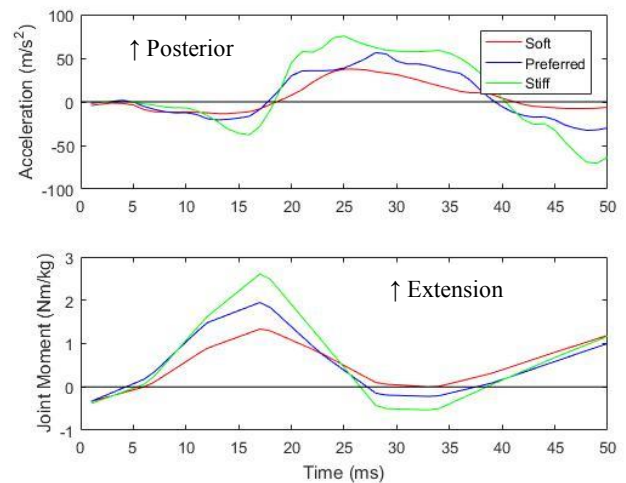


**Figure 2:** Exemplar trials displaying knee acceleration and joint moment in the sagittal plane in one subject for 50 ms following initial contact. Peak posterior acceleration and knee extension moment occur within the first 30 ms and increase with stiff landing patterns.

# CALIBRATION AND VALIDATION OF A NOVEL FORCE MEASUREMENT GLOVE: APPLICATIONS IN QUANTIFYING UPPER EXTREMITY LOADING IN MANUAL WHEELCHAIR USERS

<sup>1</sup> Alexander W Hooke, <sup>1</sup> Anthony Anderson, <sup>2</sup> Chandrasekaran Jayaraman, <sup>1</sup> Emma Fortune, <sup>3</sup> Adam J Burns,  
<sup>3</sup> Jacob J Sosnoff, <sup>1</sup> Melissa M Morrow

<sup>1</sup> Mayo Clinic, Rochester, MN, <sup>2</sup> Rehabilitation Institute of Chicago, Chicago, IL <sup>3</sup> University of Illinois at Urbana-  
Champaign, Urbana, IL  
email: hooke.alexander@mayo.edu

## INTRODUCTION

Upper extremity pain and injury are highly prevalent in manual wheelchair users [1]. While upper extremity loading in manual wheelchair users (MWUs) can be analyzed in the laboratory environment, previous studies have shown that clinically relevant biomechanical variables differ significantly in community settings [2].

While Force Sensitive Resistors (FSRs) have been implemented in many areas of biomechanics research, they have a number of issues that must be accounted for during calibration. Traditionally, these sensors have been considered to be more qualitative devices, as they can lack repeatability, accuracy, and display considerable hysteresis and time drift. Though there are concerns, it has been suggested that these effects can be minimized with quality sensors and proper calibration techniques [3]. Instrumented force gloves with adequate technical performance would provide the ability to capture loading experienced at the hand in manual wheelchair users outside of the laboratory. Therefore, the purpose of this study is to calibrate and validate a custom instrumented glove for measuring high and low upper extremity loading in manual wheelchair users.

## METHODS

*Glove Description:* Each instrumented glove system consisted of a glove and data-logging box. Each glove had 4 FSRs (40mm diameter, sensing range 0.1-150kg) stitched into its palm and was connected to a data logging box which was stored in sleeve on the users forearm (Figure 1). The data logging box contains a custom circuit board and is capable of collecting load data from each of the 4 sensors at 20Hz for 18 continuous hours. Data is recorded onto a microSD card and can be exported as a .csv file [4].

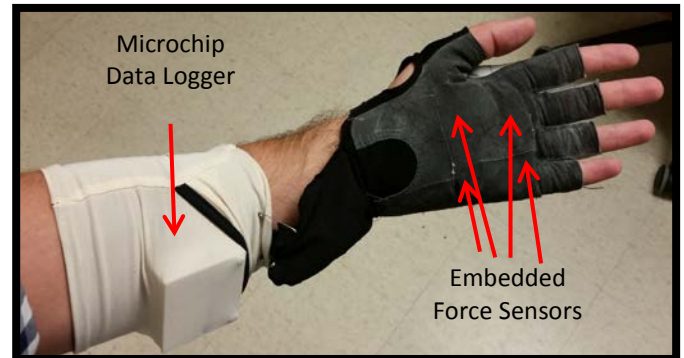


Figure 1: Instrumented glove with data logging box in arm sleeve

*Calibration:* Three factors known to influence the accuracy of an FSR's calibration were investigated: the load application method, the substrate on which the FSR is calibrated, and the temperature of the FSR. Gloves were loaded using a servo-hydraulic test system (MTS 858 Mini Bionix II) at 80N static load intervals from 80-800N. Each load was applied and released for 10 seconds. Loads were applied to the gloves using two applicators of varied size and shape. 1) A round applicator with a flat contact surface (110mm diameter) applied the calibration loads to all sensors simultaneously. 2) A custom force applicator built from a generic wheelchair rim applied the calibration loads to all sensors simultaneously.

To replicate the glove-hand interface that will be experienced during use, two substrate materials were tested by placing them inside of the glove during calibration: (1) a ballistic gelatin and (2) a synthetic flesh (Syndaver Labs, Tampa, USA). Both materials were cut into palm-sized, rectangular shapes and placed in the glove during calibration. To replicate the temperature that will be experienced during use, calibration trials were carried out at both room temperature and 35 °C via a flexible 5V DC heating pad inserted into the glove. A linear fit was performed on each set of calibration conditions.

*Validation:* The predictive power of each tested calibration method was determined via the use of the FSR equipped gloves while operating a wheelchair equipped with Smartwheel rims (Three Rivers Holdings Inc., Mesa, AZ). Each linear calibration was applied to a series of 12 level-ground propulsions and 9 weight reliefs performed using the Smartwheel rims. The RMSE comparing the Smartwheel resultant force and force recorded at the FSR equipped gloves was then computed for each calibration method.

## RESULTS AND DISCUSSION

All calibration techniques that were investigated showed a strong linear fit with all techniques having an  $R^2$  value over 0.97 with no statistically significant difference between them (Table 1). A series of exponential and polynomial fits were also attempted, but pilot results showed notably lower correlation vs. the linear fits during calibration and these techniques were not pursued further.

Applicator	Substrate	Temp	$R^2$
Flat	Ballistic Gel	Room	0.978
Flat	Ballistic Gel	Body	0.982
Rim	Ballistic Gel	Room	0.984
Flat	Syn. Flesh	Room	0.993
Flat	Syn. Flesh	Body	0.981

Table 1: Results of linear fits for tested calibration techniques

A representative weight relief trial displaying the Smartwheel values and the corresponding calibrated glove values are shown in Figure 2. The validation of the FSR equipped gloves showed that all calibration techniques using flat applicator were significantly more accurate than the rim applicator. The error of the gloves during peak loading could be brought down to ~30% during propulsion and ~15% during weight relief with the strongest calibration identified as the flat applicator combined with the ballistic gel at room temperature (Table 2). While more advanced calibration techniques will continue to be developed, these values are likely close to the optimal level of accuracy attainable given the limitations of both the

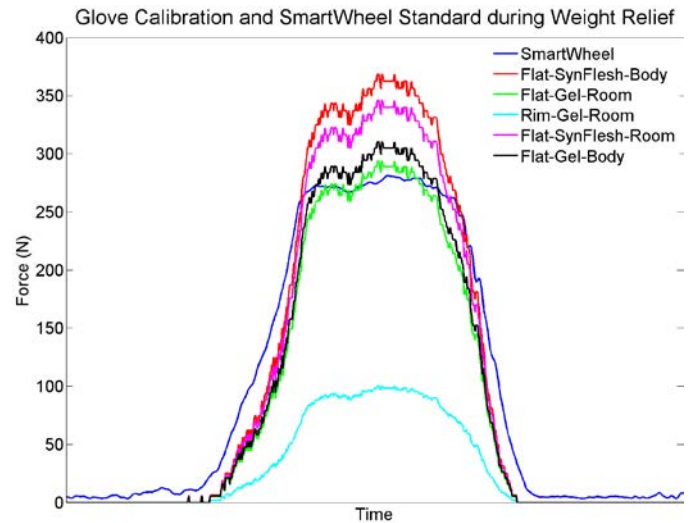


Figure 2: Representative weight relief trial. The Smartwheel values and glove values with each of 5 calibration techniques are shown.

FSRs deployed and the desirable form factor of the gloves for in-field data collections during daily living.

## CONCLUSIONS

The development of the instrumented force glove and identification of a valid calibration technique will enable the collection of in-field data for extended periods of time.

## REFERENCES

1. Bayley, J.C., et al., *JBJS*. **69**, 676-8. 1987
2. Hurd, W.J., et al., *J Electromyol Kinesiol* **19**, 942-7, 2009.
3. Schofield, J.S., et al., *J Biomech* **49**, 786-92, 2016.
4. Burns, A.J. and Jayaraman, C. U.S. Patent Appl. No. 15/449,103, (filing date Mar. 7, 2017)

## ACKNOWLEDGMENTS

This study was funded by NIH Grant R01HD084423 and supported by the Materials and Structural Testing Research Core at Mayo Clinic

Applicator	Substrate	Temp	Propulsion		Weight Relief	
			RMSE (N)	RMSE (% max)	RMSE (N)	RMSE (% max)
Flat	Ballistic Gel	Room	19.89	20.60	24.06	8.54
Flat	Ballistic Gel	Body	21.41	22.16	50.35	17.87
Rim	Ballistic Gel	Room	33.37	34.55	97.04	34.45
Flat	Syn. Flesh	Room	20.48	21.20	40.34	14.32
Flat	Syn. Flesh	Body	19.83	20.53	27.46	9.75

Table 2: Results of validation of calibration techniques during propulsion and weight relief tasks. RMSE values represent the absolute and relative error comparing the calibrated glove to the Smartwheel loads with relative values computed as absolute RMSE / peak load during the trial.

# ACCURATE AND ROBUST GAIT EVENT DETECTION USING FOOT-MOUNTED INERTIAL MEASUREMENT UNITS

Stephen M. Cain, Michael V. Potter, Lauro Ojeda, and Noel C. Perkins

The University of Michigan, Ann Arbor, MI, USA  
email: smcain@umich.edu

## INTRODUCTION

Detection of foot contact with the ground is critical for determining temporal gait characteristics and for the analysis of kinematic, kinetic, and physiologic signals during stride cycles. In addition, detecting when the feet are in contact with the ground can aid the identification of appropriate zero velocity update (ZUPT) locations (when the foot is close to or at zero velocity during its contact with the ground). ZUPTs are used for calculating drift-corrected estimates of foot trajectories, which enable calculation of spatiotemporal gait metrics [1, 2].

Typically, accurate detection of ground contact requires foot-switches, insole pressure sensors, motion capture, or an instrumented treadmill. However, researchers have demonstrated that gait events can be detected reliably with inertial measurement units (IMUs) [3-5]. IMUs do not confine data collection to a capture volume or treadmill and are not subject size specific. However, many methods require known orientation of IMUs on body segments, are limited to specific types of gaits or gait speeds, and expect certain kinematic features to be present in the measurements.

The goal of this study was to demonstrate that our gait event detection algorithm is accurate relative to an instrumented treadmill and is robust to changes in gait type, gait speed, sensor type, and subject.

## METHODS

We recruited two healthy male subjects for this University of Michigan IRB approved pilot study. For each trial, we secured an IMU to the instep of each foot on top of the subject's chosen footwear, using athletic tape to prevent shifting. Two types of IMUs were used for this study: 1) APDM Opal (128

Hz,  $\pm 200g$ ,  $\pm 2000\text{deg/s}$ ) and 2) Yost Labs 3-Space (400Hz,  $\pm 24g$ ,  $\pm 2000\text{deg/s}$ ). Both subjects completed the following trials twice (once with each type of IMU): walking at speeds of 0.89, 1.79, and 2.24m/s and running at speeds of 1.79, 2.24, 3.13, 4.02, 4.92, 5.81, 6.71, and 7.60m/s. Trials were 20 seconds in duration and subjects rested as needed between trials. An instrumented treadmill (quasar, h/p/cosmos, 100Hz) recorded the vertical ground reaction force (VGRF) for each foot during each trial. VGRFs were used to determine foot contact with ground ( $\text{VGRF} > 0$ ) and therefore ground truth times for initial contacts (ICs) and terminal contacts (TCs). The systems (IMU and treadmill) were synchronized using data from synchronization events (foot stomps) at the beginning and end of each data collection period; we used decimation to match the sampling rate of the IMUs to that of the treadmill.

Data from a given IMU was used to identify ICs and TCs by locating times in which the acceleration and angular velocity measured by the IMU contained significant high frequency content; this is based on the idea that there are sudden changes in the force acting on the foot when the foot hits/leaves the ground, and that the sudden changes will cause rapid (high frequency) changes in the acceleration and angular velocity signals. We identified times with high frequency content by first performing a separate continuous wavelet transform (CWT) using FFT (cwtft, MATLAB, MathWorks) on each measured signal of acceleration and angular velocity (six total). For each signal, we summed the CWT coefficients for frequencies above 20Hz and divided this result by the total sum of the CWT coefficients, yielding a measure of the frequency content above 20Hz for each signal. By summing the measures of frequency content for the six signals, we obtained a single resulting output signal suitable for detecting ICs and TCs (Fig. 1).

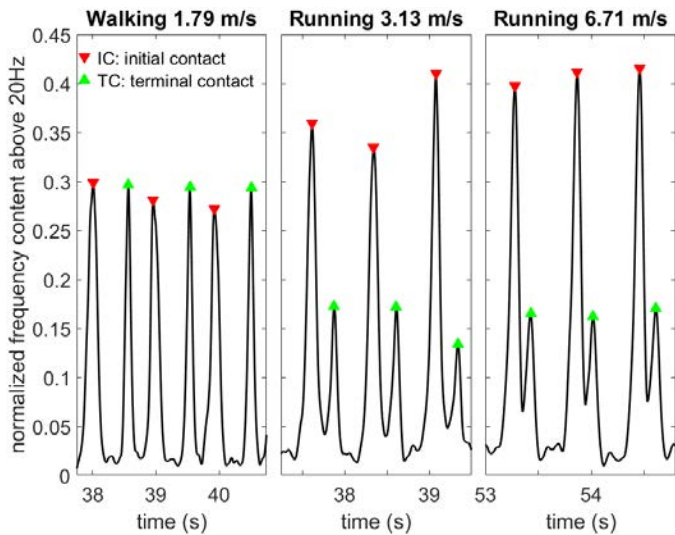


**Figure 1:** Normalized frequency content above 20Hz versus time for three sample gaits.

As illustrated in Fig. 1, we used the peaks of the resulting output signal from our CWT algorithm to identify ICs and TCs. Note that our methodology uses no information about IMU orientation and does not expect certain gait patterns to help identify candidate ICs and TCs.

To evaluate the accuracy of our gait event detection algorithm relative to the instrumented treadmill, we chose to compare stride times, stance times, and swing times; this allowed us to exclude differences due to imperfect synchronization of the IMUs with the treadmill. Significant differences in these parameters were detected using t-tests. For this pilot study, we used 95% confidence intervals to explore effects of gait type, speed, sensor type, and subject.

## RESULTS AND DISCUSSION

Results are illustrated in Fig. 2. There were no significant differences between IMU and treadmill-derived stride times ( $t = 0.51$ ,  $p = 0.61$ ). IMU-derived stance times were significantly less than ( $t = -11.49$ ,  $p < 0.001$ ) and swing times were significantly greater than ( $t = 11.29$ ,  $p < 0.001$ ) those calculated using the treadmill. Gait speed had no effect on the accuracy of any of the gait parameters. Our pilot data suggests that gait type, sensor type, and subject have no effect on stride time estimates, but may have small effects on stance and swing times. Despite these differences, we believe our approach is accurate and robust enough to be used to study gait that may challenge

existing gait event detection algorithms. In particular, our approach will enable accurate detection of ZUPTs (and therefore calculation of spatiotemporal gait parameters) during sprinting, irregular gaits, or other highly dynamic gaits in real-world environments. Data from additional subjects will allow us to more fully characterize our gait event detection approach.

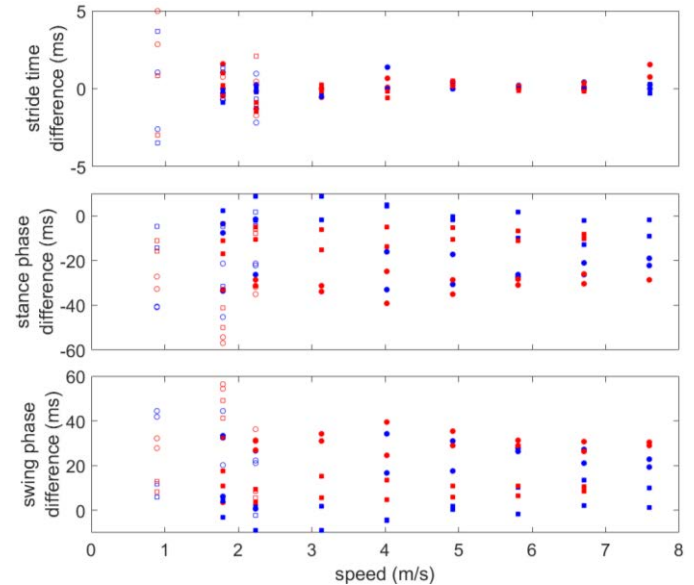


**Figure 2:** Differences (in milliseconds) between instrumented treadmill and IMU-derived stride, stance, and swing times versus gait speed. Symbols are used as follows: circle/square (subject 1/subject 2), open/filled (walk/run), blue/red (APDM/Yost).

## REFERENCES

1. Ojeda L and Borenstein J, *J of Navigation* **60**, 391-407, 2007.
2. Rebula JR, et al. *Gait Posture* **38**, 974-980, 2013.
3. Sabatini AM, et al. *IEEE Trans Biomed Eng* **52**, 486-494, 2005.
4. Lee JB, et al. *J Sci Med Sport* **13**, 270-273, 2010.
5. Rueterbories J, et al. *Med Eng Phys* **32**, 545-552, 2010.

## ACKNOWLEDGMENTS

This material is based upon work supported by the US Army Contracting Command-APG, Natick Contracting Division, Natick, MA, under contract W911QY-15-C-0053.

# EVALUATION OF GROUND REACTION FORCE ASYMMETRY IN WALKING AND RUNNING USING FORCE PLATES VS. ACCELEROMETER

Rana Karimpour, Rebecca L. Krupenevich, Kyung Koh, Ross H. Miller, and Jae Kun Shim

University of Maryland, College Park, MD, USA  
email: ranakp@umd.edu, <https://sph.umd.edu/neuromechanics>

## INTRODUCTION

Evaluation of gait asymmetry is of interest in both human movement research and clinical settings. Specifically, force asymmetry is frequently attributed to the risk or presence of pathologies and injuries [1]. Evaluation of gait asymmetry with a wearable device, such as an accelerometer, will provide a tool for the objective assessment of rehabilitation progress, and diagnosis of pathologies associated with force asymmetries during locomotion under free-living conditions, without the requirement of laboratory settings.

Considering the previously reported effect of the speed and mode of locomotion on the accelerometer readings [2], the purpose of this study was to investigate and compare the relationship between asymmetries measured from ground reaction forces (GRF) and accelerometer data during walking and running.

## METHODS

A total of 25 young healthy adults (5 male and 20 female, 20.8±0.76yrs, 1.64±0.13m, 67.18±8.96kg) volunteered to participate in the study after giving written informed consent. Participants performed three trials under each of six conditions: normal gait at their preferred speed of walking and running (average: 1.53±0.17m/s, 2.7±0.17m/s respectively), and five conditions of simulated asymmetry. During simulated asymmetry trials, participants walked/ran at ±5% of the preferred speed established during normal trials. To simulate asymmetry, the subjects were told to move their dominant leg differently (e.g. swinging it more strongly) compared to their non-dominant leg.

Linear acceleration was measured at 1000 Hz with a lightweight tri-axial wireless accelerometer sensor

(Trigno; Delsys, Boston, MA, USA) placed on the skin near the L3 vertebrae. Ground reaction forces were measured at 1000 Hz using eight force plates (Kistler, Switzerland) embedded in a 12-m long platform. Locomotion speed was determined using electronic timing gates located on either side of the force plates.

The 3D resultant magnitudes of the acceleration and GRF signals were calculated in Matlab. Peak values were used in the calculation of the left/right asymmetry index (AI), using Eq. 1 which was developed by Robinson et al. [3] and has been widely used to quantify gait asymmetry:

$$AI = \frac{(R-L)}{0.5*(R+L)} \quad (1)$$

where R and L are the peak 3D magnitudes of the signals in the right or left stance leg, respectively.

To account for the differences in the number of trials with complete GRF per participant (e.g. range: 9-22, mean±SD: 18.7±2.9 in walking), from the correlation coefficients between accelerometer and GRF AIs in individual participants a weighted average was calculated. To test the statistical significance of the overall correlation coefficient, we conducted Student's *t*-test on its corresponding Fisher-transformed *z*-score.

In addition, to assess the disparity between accelerometer AI and the gold standard (GRF AI) root identity squared deviation (RISD) was calculated using Eq. 2.

$$RISD = \sqrt{\frac{\sum_i d_i^2}{n}} \quad (2)$$

where  $n$  is the number of trials, and  $d_i$  is the distance between the measured accelerometer AI from the identity function (GRF AI = accelerometer AI).

## RESULTS AND DISCUSSION

In both walking and running there was a significant positive correlation between accelerometer AI and GRF AI ( $r = 0.70$  and  $0.91$  in walking and running respectively). The 99% confidence interval was  $r = 0.63-0.76$  for walking, and  $r = 0.88-0.93$  for running.

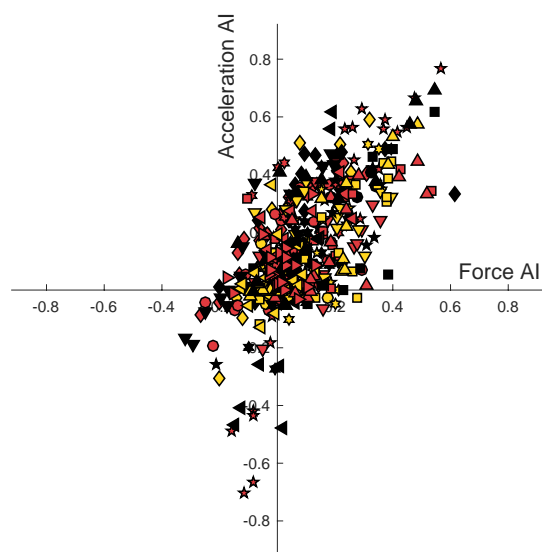


**Figure 1:** The relationship between the asymmetry indices calculated from GRF and accelerometer data in all conditions for all the participants during walking. Each point represents one trial. Colors and markers do not signify any particular condition.

Although running exhibited a stronger positive correlation compared to walking ( $r = 0.91$  vs.  $r = 0.70$ , respectively), the one-to-one identical mapping between the two AI measures -assessed by the RISD- was weaker. A greater RISD in running (average across participants =  $0.27 \pm 0.1$ ) compared to walking (average =  $0.11 \pm 0.4$ ) indicates that the accelerometer AI may not be an immediate measure of force asymmetry during gait particularly in running.

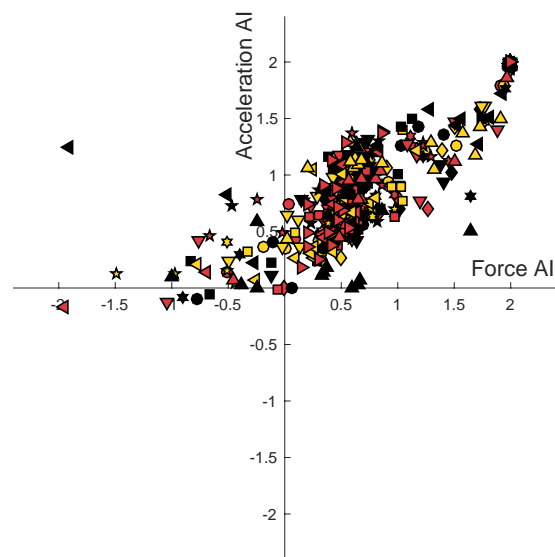


**Figure 2:** The relationship between the asymmetry indices calculated from GRF and accelerometer data in all conditions for all the participants during running. Each point represents one trial. Colors and markers do not signify any particular condition.

## CONCLUSIONS

There is a strong positive relationship between the AI calculated from an accelerometer and the AI calculated from GRF during both walking and running. This preliminary finding suggests that an accelerometer may be a feasible tool for measuring force asymmetry in clinical settings. Further investigation of the factors contributing to this relationship may have practical implications regarding the clinical evaluation of gait asymmetry during walking and the assessment of asymmetry during gait in daily living. Investigating the sources of between and within subject variations in future studies may help provide a more accurate predictive relationship.

## REFERENCES

1. Kramers-de Quervain IA, et al. *Eur Spine J* **13**:449–56, 2004.
2. Neugebauer JM, et al. *PLOS ONE* **7**(10): e48182.
3. Robinson RO, et al. *J Manipulative Physiol Ther* **10**:172–6, 1987.

# VALIDATION OF AN EMBEDDED INERTIAL MEASUREMENT UNIT FOR TRUNK MEASUREMENTS DURING SIMULATED SITTING AND STANDING POSTURES

Jonathan Park, Lois A Sy, Mamiko Noguchi, Jack P Callaghan

University of Waterloo, Waterloo, ON, CA  
E-mail: j56park@uwaterloo.ca

## INTRODUCTION

Globally, low back pain (LBP) is considered the leading cause of disability [1]. Characterizing physical exposures related to occupationally relevant low back disorders is important for implementing appropriate ergonomic interventions for prevention of injury and reoccurrences [2]. Several posture-based measurement techniques (e.g., direct, observational, and self-report) have been previously developed for assessing physical exposures during occupational work [2 – 4]. Optoelectronic motion capture (OMC) systems have been deemed the gold standard for direct, non-invasive trunk kinematic measurements [5]. Generally, OMC systems are restricted to laboratory simulations of occupational work [6]. This may result in potential disagreements between laboratory and on-field physical exposures [7]. However, on-field occupational measurements outside the laboratory with OMC systems are limited by the equipment's practicality [2, 5, 8].

Researchers have shown interest in inertial measurement units (IMUs) for direct measurements of trunk kinematics [2, 5, 8]. This interest is due to IMU's lightweight, portable, wireless, and integrated sensing characteristics from various electromechanical sensors [5, 8]. A commercially available device, called the Myo™ gesture control armband (MYO) (Thalmic Labs Inc., Waterloo, ON), encapsulates an IMU and surface electromyography (sEMG) system. The validity of an IMU is specific to the anatomical site and task being assessed [5]. Determining MYO's validity against a gold standard system is a necessary step to determine its validity for field use. Thus, the aim of this study was to investigate the concurrent validity of the MYO armband's IMU system with a laboratory-based motion capture system during simulated sitting and standing office workplace postures.

## METHODS

Sixteen healthy, asymptomatic participants, 8 females (age =  $21.3 \pm 1.1$  years; height =  $1.67 \pm 0.04$  m; mass =  $64.3 \pm 11.6$  kg) and 8 males (age =  $22.3 \pm 1.5$  years; height =  $1.77 \pm 0.07$  m; mass =  $75.6 \pm 5.9$  kg), were recruited from the university population.

The MYO armband contains eight pods. One pod comprises of a nine-axis IMU, which encapsulates a three-axis accelerometer, gyroscope, and magnetometer. The MYO armband was repurposed and secured around the torso with the IMU-containing pod (POD) overlying the participant's T12 spinous process. Trunk angular displacement estimates from the IMU were reported in quaternion values (via manufacturer proprietary sensor fusion algorithms) and retrieved via wireless Bluetooth® connection.

A laboratory-based OMC system (Optotrak Certus®, NDI, Waterloo, Canada) was used as the reference system. A rigid body of smart markers were superimposed onto the POD. Both the MYO and OMC system were sampled at 50 Hz.

Participants were instructed to adopt 8 sitting and 7 standing postures, in a randomized order, for 30 seconds each. These simulated office workplace postures were previously observed in the literature [9, 10]. Each posture was repeated 3 times.

The quaternion values obtained from the MYO armband were converted into Cardan angles using custom code in Matlab R2016a (The Mathworks, Natick, MA, USA) in the corresponding Cardan rotation sequence of flexion/extension (sagittal), abduction/adduction (frontal) and axial rotation (transverse). Kinematic data from Optotrak Certus® was imported into Visual 3D™ software (Version 5, C-Motion, Inc., Germantown, MD, USA) and smoothed with a low-pass filter (Butterworth, 2nd

order, dual-pass) with a cut-off frequency of 3 Hz. Cardan angles were then calculated with the same rotation sequence used for the MYO armband. The two systems were synced in Matlab using custom correlation code based on three transient perturbations applied to the MYO armband during the collection. The 20 second midmost trial of each posture was used for further data analysis.

Concurrent validity was assessed by calculating the root mean squared error (RMSE) and Bland-Altman (BA) plot analysis. RMSE was calculated for each posture trial in each participant. Data were then averaged and collapsed across all postures and participants to achieve a single averaged RMSE value in each posture category (sitting or standing) and cardinal plane. BA plots were generated and analysed using methods previously outlined [11].

## RESULTS AND DISCUSSION

Overall, trunk angles during sitting and standing postures in the sagittal and frontal plane exhibited less RMSE ( $1.17^\circ - 2.37^\circ$ ) and standard deviation ( $\pm 0.78^\circ - \pm 1.55^\circ$ ), relative to the transverse plane ( $6.04^\circ - 6.63^\circ$ ) ( $\pm 3.56^\circ - \pm 4.68^\circ$ ). Except for the transverse plane, the averaged RMSE results compare well in sagittal/frontal planes with previous literature on trunk angular displacement and validity of IMU with an OMC system [2, 8, 12]. These studies reported the following: 1)  $4.1^\circ - 6.6^\circ$  [2]; 2)  $1.8^\circ - 5.9^\circ$  [8]; and 3)  $\leq 2.1^\circ - 3.1^\circ$  [12]. However, these studies did not include axial rotation.

The BA analysis reveals the MYO armband over- or under-estimates trunk angular displacement relative to the OMC system (Table 1). Similarly, a previous study found mean difference varied across several sitting and standing tasks with a different device [6]. Although mean differences between the two systems are low, the 95% limits of agreement revealed the

cardinal plane of least to greatest error: sagittal, frontal, and transverse planes. For instance, 95% of measurements in the sagittal plane can be expected to be between  $-3.66^\circ$  and  $5.07^\circ$ , relative to the reference system. Whereas 95% of measurements in the transverse plane can be expected to be between  $-16.22^\circ$  and  $19.8^\circ$ .

## CONCLUSIONS

These findings suggest that depending on the magnitude of accuracy chosen for one's purpose, the MYO armband can be used in the field to estimate the sagittal and frontal planes of trunk motion with an "acceptable" magnitude of error [2, 8, 12]. However, transverse plane trunk measurements should be used with caution, as the results demonstrated a large magnitude of error during the postures chosen for this study.

## REFERENCES

- Hoy D, et al. *Ann Rheum Dis* **73**, 968-74, 2014.
- Schall MC et al. *Ergo* **139**, 1-12, 2015.
- Li G et al. *Ergo* **42**, 674-95, 1999.
- David GC. *Occup Med* **55**, 190-99, 2014.
- Cuesta-Vargas AI, et al. *PTR* **15**, 462-73, 2010.
- O'Sullivan K, et al. *Man Ther* **17**, 77-83, 2012.
- van Dieën JH, et al. *Ergo* **53**, 792-800, 2010.
- Bauer CM, et al. *J Electro Kinesi* **25**, 782-90, 2015.
- Whitstance RS, et al. *Ergo* **38**, 2485-503, 1995.
- Hendriks HM, et al. *Ergo* **49**, 1611-626, 2006.
- Giavarina D. *Biochemia Medica* **25**, 141-51, 2015.
- Wong WY, et al. *Eur Spine J* **17**, 743-53, 2008.

## ACKNOWLEDGMENTS

The authors would like to thank the participants and Thalmic Labs Inc. for access to their device for this study. Study design, execution, analysis, and interpretation were the sole product of the authors.

**Table 1:** Mean difference, confidence intervals (CI), and limits of agreement (LOA) of Bland-Altman plots for the trunk angle ( $^\circ$ ) in all cardinal planes. SD = standard deviation; LL = Lower limit; UL = Upper limit

Plane	Mean Difference (SD)	95% CI – UL	95% CI – LL	95% LOA – UL	95% LOA – LL
Flex/Ext	0.70 (2.23)	0.88	0.53	5.07	-3.66
Abd/Add	0.23 (2.59)	0.43	0.02	5.3	-4.85
Axial rotation	1.79 (9.19)	2.52	1.06	19.8	-16.22

# ACCURATE ESTIMATION OF THE KINEMATICS USING AN IMU-BASED MOTION CAPTURE SYSTEM

Wyatt Hahn, Tyler Marr, Mohammad Moein Nazifi, and Pilwon Hur

Department of Mechanical Engineering, Texas A&M University, College Station, TX, USA  
email: {wyatt\_hahn,marres,moeinnazifi,pilwonhur}@tamu.edu, web: <http://hurgroup.net/members>

## INTRODUCTION

Optical motion capture systems (MCSs) are widely used to capture the kinematics of different motor-tasks. However, optical MCSs are often expensive and require long and complicated preparation/collection procedures. An alternative method, however, is to use inertia measurement units (IMUs). IMUs are significantly cost-effective and convenient compared to the optical MCSs. Moreover, unlike optical MCSs, an IMU-based MCSs will not be limited to the vision field of the surrounding cameras or be disrupted by its markers being hidden. Lastly, IMUs do not require labeling/cleaning, making them even more convenient.

The objective of this study is to develop an IMU-based MCSs with graphical user interface (GUI) that can facilitate the accurate biomechanical kinematic analyses of the human and/or animal movement. Successful accomplishment of this application will enable a more affordable, accessible, and portable biomechanics lab of human movement analysis for researchers and provide simple ways for clinicians to diagnose pathological movements of their patients.

## METHODS

The motion capture system developed in this study comprises 16 wireless IM sensors (Delsys Trigno, Natick, MA) bilaterally attached to major upper and lower extremity links as follows: Back of the shoulders (scapula), upper arms, forearms, back of the hands, thighs, shanks, feet, and unilateral at lumbar (L3), and sternum. IMUs captured three-dimensional angular velocity (gyroscope), acceleration (accelerometer), and magnetic field (magnetometer) at 60 Hz. The incoming data was low-pass filtered using a third-order zero-lag Butterworth with a cutoff frequency of 5 Hz [1]. The algorithm built quaternions from the gyroscope data and mathematically rotated the vector representing the corresponding link to which the sensor was attached. Since this rotation was performed only on the vector from the previous time step, the system was susceptible to drift due to the existing noises. To account for this drift, the algorithm simultaneously used the magnetometer and accelerometer data to create a right handed coordinate system using cross products. At each

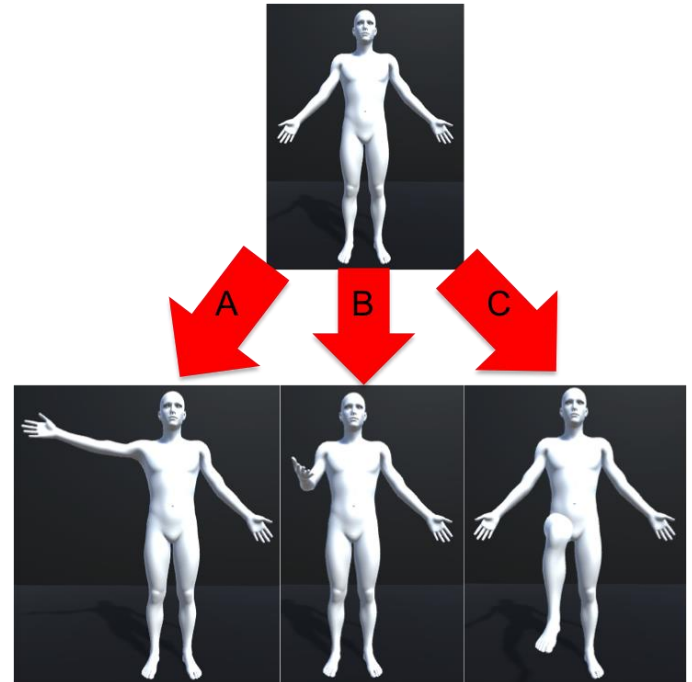


**Figure 1:** The tasks performed by the subject.

time step, a new coordinate system was created in the same manner. The rotation was found from the new coordinate system to the initial coordinate system, and was applied to the initial position of the vector. The rotated orientations found from both methods were then averaged. The result from the magnetometer and accelerometer readings were only viable for low accelerometer readings where the total acceleration was close to that of the gravity. Thus, the algorithm implements calculations to only use the magnetometer and accelerometer data at low to zero angular rates to rid the system of drift and use more of the gyroscope data when accelerometer readings were high.

To test the accuracy of this novel system, we simultaneously collected kinematic data using our device along with an optical motion capture system (Qualisys Oqus, Göteborg, Sweden). The optical motion capture had 30 markers on the bony landmarks of the body to collect the full-body kinematics at 100Hz. The markers were placed bilaterally on toe tip, heel, medial/lateral malleolus, medial/lateral condyle of tibia, trochanter, ASIS, PSIS, acromion, medial/lateral humeral epicondyle, and ulnar/radial styloid process, plus unilateral C7 and T10 markers. One recruited subject

performed three tasks (Fig. 1, A, B, C). Starting from reference anatomic position, task A encompassed ten consecutive bilateral shoulder abduction/adductions (90 degrees), task B included ten bilateral elbow flexion/extension (90 degrees), and task C was to perform ten hip flexion/extensions (90 degrees, right limb first then left limb). During each task, subject were asked to keep other parts as still as possible.

The IMU data was processed using Microsoft C# (Redmond, WA) and used to calculate joint angles. The data was then filtered (4<sup>th</sup> order zero-lag Butterworth, cutoff 1Hz) using MATLAB (v2016a, Mathworks, Natick, MA) [2]. Optical motion capture data was processed offline using MATLAB and the corresponding joint angles were calculated using costume codes.

Finally, the RMS error and the Pearson's correlation coefficients ( $r$ ) were calculated to reveal the accuracy of the IMU-based motion capture system.

## RESULTS AND DISCUSSION

**Table 1:** RMS errors (deg) and  $r$  values.

Task	Right Shoulder		Left Shoulder	
	RMSE	Correlation	RMSE	Correlation
A	10.73	0.95	2.56	0.99
B	Right Elbow		Left Elbow	
	RMSE	Correlation	RMSE	Correlation
	9.00	0.99	8.55	0.99
C	Right Knee		Left Knee	
	RMSE	Correlation	RMSE	Correlation
	5.93	0.99	5.58	0.99

Results revealed small RMS errors as well as a strong correlation between the majorly activated joints (Table 1) of each task (e.g. shoulder in task A). The IMU-based MCS was able to calculate the joint angles with less than 10° of error and a correlation over 95% in all cases.

Other non-essential joints for each test showed a lower correlation due to the noticeable noise. However, this happened only when the body segment has no significant movement or is stationary. When the body segment is moving, we saw the high correlation between the two systems (Fig. 2). Note that unilateral plots were chosen due to the symmetry.

The errors can be due to the inappropriate filtering (e.g., too low cutoff frequency) and misalignment of local coordinate systems between the optical MCS and the IMU-based MCS. Further refinement and calibration will be performed to enhance the accuracy of the IMU-based MCS. More experimental validation with various tasks including walking will be tested.

## CONCLUSIONS

The system developed in this study uses IMU sensors to capture human kinematics. The preliminary test involving shoulder abduction, elbow flexion, and hip flexion revealed strong correlations and minimal RMSE values. These results substantiate feasibility of usage of IMU-based MCSs due to their ease of use with their only draw-back being their minor inaccuracy. Future works will include refinement of filtering and examination of various tasks including walking trials and more elaborate motor-tasks. Upon completion, the codes will be made open-source for public use and desired customizations.

## REFERENCES

1. Pavol MJ, *Journal of Gerontology: Medical Sciences* **59**, 2004.
2. Parijat P, *Annals of Biomedical Engineering* **40**, 2012.

## ACKNOWLEDGMENTS

This MCS was developed and tested by undergraduate students (Tyler Marr, Wyatt Hahn) in the Department of Mechanical Engineering at Texas A&M University.

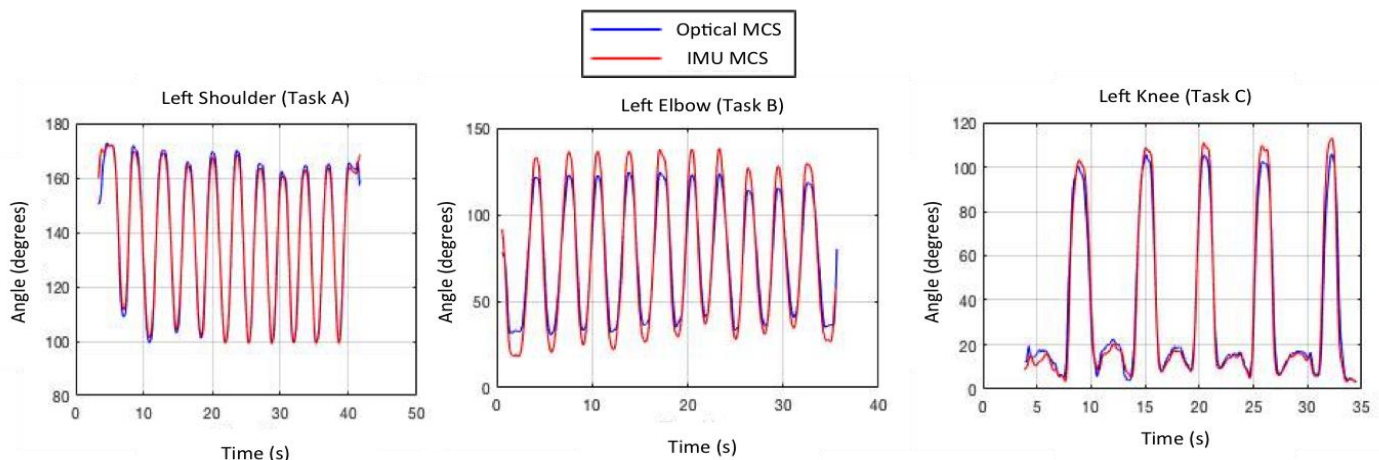


**Figure 2:** The major joint angles during each task.

# AGE-RELATED DIFFERENCES IN POSTURAL CONTROL: EFFECTS OF DIFFERENT VISUAL MANIPULATIONS ON DYNAMIC BALANCE RESPONSES

Andresa M. C. Germano\*, Daniel Schmidt, Claudio Zippenfennig, and Thomas L. Milani

Chemnitz University of Technology, Department of Human Locomotion, Chemnitz, Saxony, Germany

\*email: andresa.germano@hsw.tu-chemnitz.de, web: <https://www.tu-chemnitz.de/index.html.en>

## INTRODUCTION

Assumptions that balance control is based on the integration of afferent inputs and that this integration process changes with age are well accepted [1,2]. Studies have confirmed that the elderly are more susceptible to balance instability after visual manipulation [2]. Different manipulation approaches have been used to investigate the importance of visual inputs on balance, e.g. eyes closed, dark glasses, and different visual surroundings [3,4]. Therefore, we examined whether different approaches of visual manipulation would affect dynamic balance responses differently, and whether balance responses of young and older adults would be affected differently by visual manipulation. Greater instability was expected for the various visual manipulation conditions compared to eyes open and for older compared to younger adults. In addition, no changes within visual manipulation conditions (Eyes Closed, Blackout Glasses, Dark Room) were expected.

## METHODS

36 healthy subjects participated and were divided into two groups: 20 young (mean±SD: 22.9±2.5yrs, 70.9±11.8kg, 1.8±0.08m) and 16 older adults (mean±SD: 69.3±4.2yrs, 73.8±10.4kg, 1.7±0.10m). All procedures were conducted according to the recommendations of the Declaration of Helsinki.

To induce unexpected perturbations, the horizontally moveable bottom platform of a Posturomed device (Haider Bioswing GmbH, Germany) was deflected by 20mm and released by triggering an electromagnet. A GK-1000-Koordinator force platform was affixed to the bottom platform (IMM Holding GmbH, Germany; sampling rate 1kHz). The protocol consisted of three trials performed in antero-

posterior perturbation direction for each randomized condition: Eyes Open (EO), Eyes Closed (EC), Blackout Glasses (BG), and Dark Room (DR). During BG and DR conditions, subjects kept their eyes open. Prior to the tests, subjects had an acclimatization period of 10min (room temperature 23±2°C) and performed three training trials to become familiar with the apparatus. Total center of pressure excursions (COP) as well as medio-lateral (ML) and antero-posterior (AP) ranges were calculated to quantify balance ability. In this study, all data were analyzed in two intervals: anticipatory responses (-200ms to 0ms (trigger) pre perturbation) and compensatory responses (70ms to 260ms post perturbation). Normal distribution was tested using the Shapiro-Wilk test. Differences within conditions were examined using ANOVA repeated measures following a Bonferroni post-hoc test (parametrical data), and Friedmann test following Wilcoxon test (non-parametrical data). Differences within groups were analyzed using the Mann-Whitney-U test. Level of significance for all tests was  $\alpha=0.05$ .

## RESULTS AND DISCUSSION

Changes in COP are presented in Fig. 1 (a and b), while ML and AP ranges are shown in Table 1. When comparing groups, larger AP ranges were found for older compared to young adults, but only for BG and DR. Surprisingly, COP and ML range showed no significant differences between young and older adults for any analyzed condition. This was contrary to previous studies, which showed differences between young and older adults, especially when the visual system was deprived [5]. However, more than 65% of our older adults were physically active, which may explain these results, since physical activity may improve sensory integration for balance control [2]. Regarding the comparison within groups, no differences were found between EC, BG, and DR

for either age group. This may be because the amount of information available during those situations was similar [4]. Hafström et al. [4] also found no differences between balance responses comparing eyes closed with eyes open in darkness. As expected, most of the significant differences in the current study were present when comparing EO with EC or BG, in which eyes open was the more stable balance condition. This is in accordance with Hafström et al., since visual inputs play a dominant role as contributor during balance control [4]. Surprisingly, decreased stability after visual manipulation was not evident in all comparisons. For example, older adults presented no differences between any of the analyzed conditions during compensatory responses. Note that the most challenging postural task was present during compensatory responses due to the unexpected perturbation. In the case of an additional balance challenge, afferent re-weighting and integration are needed. For example, in the case of reduced visual information, other available afferent inputs may be re-weighted to compensate the unavailable information to maintain balance [4]. Although this re-weighting process declines with age

[2], this was probably not the case in our older subjects. They were still capable of successfully controlling dynamic balance even without the presence of visual inputs. It is unclear whether this is due to this group's level of physical activity. For our young subjects, it seems that the amount of challenge during compensatory responses was not high enough to require changes in integration processes. Hence, differences between EO and EC or BG were present.

Further studies should investigate age and physical activity factors related to possible changes in afferent information reweighting.

## REFERENCES

1. Mergner T and Rosemeier T. *Brain Res Rev*, **28**, 118–35, 1998.
2. Prioli AC et al. *Gerontology* **51**, 145–148, 2005.
3. Vrieling AH, et al. *Gait Posture* **28**, 222–228, 2008.
4. Hafström A, et al. *Acta Otolaryngol* **122**: 392–397, 2002.
5. Toledo DR & Barela JA. *Exp Barin Res* **232**, 493–502, 2014.

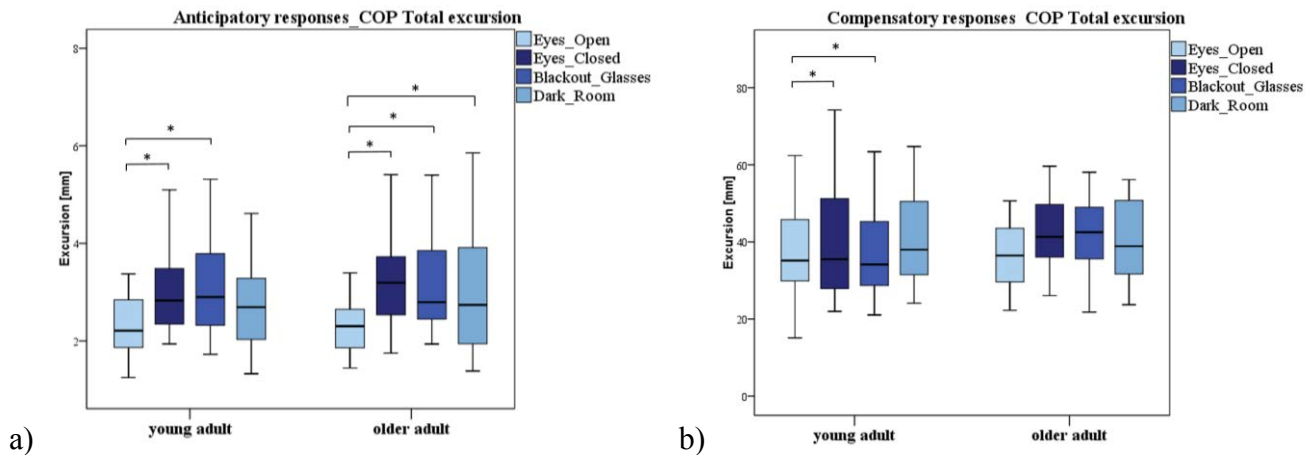


**Figure 1:** COP total excursions for young and older adults in four conditions during a) anticipatory responses and b) compensatory responses. Significant differences: \*  $p < 0.05$

**Table 1:** Mean±SD [mm] of medio-lateral and antero-posterior COP ranges for all groups and conditions

	ML-Range				AP-Range			
	Anticipatory responses		Compensatory responses		Anticipatory responses		Compensatory responses	
	young adult	older adult	young adult	older adult	young adult	older adult	young adult	older adult
Eyes Open	1.02±0.51 <sup>§</sup>	0.93±0.44 <sup>*ϕ</sup>	7.96±5.98	7.01±3.67	1.18±0.48	1.32±0.45 <sup>#</sup>	23.2±10.2	27.5±9.6
Eyes Closed	1.17±0.53	1.32±0.71 <sup>*</sup>	7.84±6.08	8.56±4.97	1.80±0.81	2.11±0.92 <sup>#</sup>	26.4±11.9	34.6±8.2
Blackout Glasses	1.29±0.65 <sup>§</sup>	1.28±0.63 <sup>ϕ</sup>	8.29±8.07	7.17±2.91	2.07±1.41	2.04±0.82 <sup>#</sup>	24.9±9.5 <sup>A</sup>	34.2±9.4 <sup>A</sup>
Dark Room	1.28±0.64	1.29±0.85	8.54±4.82	7.55±4.28	2.09±2.13	1.65±0.91	26.7±11.0 <sup>B</sup>	33.0±9.6 <sup>B</sup>

Significant differences: comparison within groups §; \*, ϕ; #; #̄; p<0.05; and comparison between groups A, B: p<0.05.

# EFFECTS OF LOWER LIMB DOMINANCE AND HEMIPARESIS IN POSTURAL CONTROL DURING QUIET STANDING

<sup>1</sup>Ji-Eun Cho, <sup>1</sup>Sangwoo Cho, <sup>1</sup>Dohoon Koo, <sup>1</sup>Joon-Ho Shin, and <sup>1</sup>Hogene Kim

<sup>1</sup>National Rehabilitation Center, Seoul, South Korea

email: wldms880226@korea.kr, web: <http://www.nrc.go.kr/nrc/english/>

## INTRODUCTION

Survivors with post-stroke hemiparesis have impaired balance control during quiet standing [1]. The typical characteristics of early stage post-stroke standing balance are increasing sway and asymmetrical lower limb weight distribution during quiet standing. A decreased weight bearing on the paretic side causes asymmetrical weight distribution and may be a compensatory strategy to overcome muscle weakness and perceptual deficits. Previous studies showed that the area of center of foot pressure (COP) sway pattern was significantly increased in stroke patients, particularly in the mediolateral (ML) direction [2]. Recent studies revealed weight-bearing asymmetry and reduced amplitude of COP fluctuation under the paretic compared with the non-paretic limb.

In studies on upper limb rehabilitation, a significant portion of stroke patients are forced to change their dominant hand after stroke because of their severe weakness of dominant hand and the increased neural activity in unaffected hemisphere [3]. So the dominant side of paretic upper limb is considered during conventional therapies. However the limb dominance has been negligible in lower limb rehabilitation since only paretic side is considered in conventional lower limb rehabilitation.

Therefore the objective of this study was to show the differences in postural symmetry and COP displacement during 30 second quiet standing between dominant and non-dominant paretic groups in chronic post-stroke survivors before and after the 3-D ankle movement training (AMT).

## METHODS

Fourteen patients with post-stroke hemiparesis (5 women; duration 119.8 months (from 36.5 to 277.4); age 64.9 years (from 52 to 78); Right-paretic 5;

Right-dominant 14, were volunteered in this study. All patients walked independently with and without ankle foot orthosis and walking assistive devices. Inclusion criteria were normal gait pattern before first-ever stroke and Functional Ambulation Category score of 3 or more. Patients were excluded with any presence of neurologic or orthopedic disorder. Recruitment and informed consent procedures were approved by National Rehabilitation Center ethics commission of South Korea (NRC2015-03-020).

All patients performed AMT, 30 minutes a session, 3 times a week for 4 weeks. 3-D ankle movements using AMT were constituted in simple (20 dorsiflexion-plantarflexion; 20 inversion-eversion) and constrained movements (40 everted dorsiflexion-plantarflexion; 40 dorsiflexed inversion-eversion) at 30 degrees per seconds. The symmetry index measured from ground reaction forces (GRF) and displacement of COP from paretic and non-paretic limbs were measured during 30 seconds bipedal standing with both eyes-open (EO) and eyes-closed (EC) condition before and after AMT intervention.

Kolmogorov-Smirnov test was used to validate normal distribution of measured data. The training effects for each group were analyzed using paired t-test (SPSS ver. 21.0, IBM, Armonk, NY, USA). The difference was considered to be significant at  $p < 0.05$ .

## RESULTS AND DISCUSSION

In the weight shift percent of measured from GRF, both the dominant hemi-paralysis group (DP) and the non-dominant hemi-paralysis group (nDP) showed the increases in weight bearing distribution in the dominant limb in before and after the AMT training (**Table1**).

In the COP displacement, the results after AMT

training in patients with stroke did not show a significant difference between dominant paralysis and non-dominant paralysis (**Table2**). However, there was a tendency that the COP displacement increases more in non-paretic than paretic side, more in EC than EO condition, and the COP of DP tends to increase in both lower limbs than the COP of nDP.

**Table1:** Weight shift percent in ground reaction force between dominant and non-dominant limbs

(%)		Pre-EO	Post-EO	<i>p</i>	Pre-EC	Post-EC	<i>p</i>
DP	D	50.5	51.9	.35	50.1	51.2	.4
	nD	49.5	48.1	.35	49.9	48.8	.4
nDP	D	52.3	53.8	.57	53.9	55.4	.55
	nD	47.7	46.2	.57	46.1	44.6	.55

Abbreviations: DP, dominant hemi-paralysis group; nDP, non-dominant hemi-paralysis group; D, dominant side; nD, non-dominant side, Pre-EO, pre-test eyes open; post-EO, post-test eyes open; pre-EC, pre-test eyes closed; post-EC, post-test eyes closed.

The movement of the lower limb is mostly in the closed chain and walking is a rhythmic and alternating movement. For that reason, the factor of dominant side has a small impact on the strategy for maintaining the balance during gait and quiet standing. Although the dominant side of the lower limb is likely to have a minor effect, this study suggest that the symmetry index measured from ground reaction forces and the COP displacement during quiet standing is related to dominant paralysis.

This study was conducted only 14 patients with

**Table2:** Movement distance according to COP direction

(cm)		Pre-EO	Post-EO	<i>p</i>	Pre-EC	Post-EC	<i>p</i>	(cm)	Pre-EO	Post-EO	<i>p</i>	Pre-EC	Post-EC	<i>p</i>	
DP: dominant side (paretic)	A	.79	.69	.46	.94	.75	.40	DP: non- dominant side	A	2.42	2.28	.62	2.51	2.51	.99
	P	.74	.80	.79	.79	2.53	.24		P	2.57	2.37	.64	2.53	.98	.15
	M	.27	.33	.36	.27	.31	.65		M	.45	.55	.54	.51	.59	.73
	L	.31	.30	.88	.37	.29	.46		L	.46	.43	.80	.43	.53	.32
nDP: dominant side	A*	2.06	2.03	.93	<b>2.68</b>	<b>2.22</b>	<b>.04</b>	nDP: non- dominant (paretic)	A	.57	.60	.74	.78	1.23	.40
	P	2.80	2.17	.09	2.80	3.04	.20		P	.57	.58	.88	.69	1.22	.17
	M	.75	.65	.32	.74	.86	.25		M	.23	.19	.59	.27	.35	.33
	L	.74	.56	.57	.53	.55	.79		L	.19	.21	.45	.25	.45	.22

Abbreviations: DP, dominant hemi-paralysis group; nDP, non-dominant hemi-paralysis group; A, Anterior displacement; P, Posterior displacement; M, medial displacement; L, lateral displacement Pre-EO, pre-test eyes open; post-EO, post-test eyes open; pre-EC, pre-test eyes closed; post-EC, post-test eyes closed(\* denotes  $p < 0.05$ ).

chronic stroke who had an average onset of 10 years, which may have affected the results. However, considering there is a dominant side both with the lower limbs and upper limbs, and most of the stroke patients have been used to the dominant side on their lifetime, we propose that the rehabilitation program of the stroke patients considers not only the paralyzed side but also the dominant side.

## CONCLUSIONS

There was a tendency but not significant difference in increase of the symmetry index measured from GRF the COP displacement of dominant paralysis compared with non-dominant paralysis during quiet standing in post-stroke hemiparesis. Therefore, in the lower limb rehabilitation program, not only paretic side but also dominant side is considerable as a factor that contributes to postural control in quiet standing.

## REFERENCES

1. Mansfield A et al. *Neurorehabil Neural Repair*. 2012 Jul-Aug;26(6):627-35.
2. Patterson KK et al. *Gait & posture*. 2010 Feb;31(2):241-6.
3. Jang S and Jang W. *Medicine*. 2016 Feb; 95(6)

## ACKNOWLEDGMENTS

Translational Research Center for Rehabilitation Robots, Korea National Rehabilitation Center, Ministry of Health & Welfare, Korea (#NRCTR-IN16003,NRCTR-IN17004)

# INFLUENCE OF SHORT-TERM VISUAL DEPRIVATION AND REDUCED AUDITORY CAPABILITY ON QUASI-STATIC BALANCE PERFORMANCE IN HEALTHY ADULTS

Tina Drechsel\*, Daniel Schmidt, Thomas L. Milani

Chemnitz University of Technology, Department of Human Locomotion, Chemnitz, Saxony, Germany

\*email: tina.drechsel@hsw.tu-chemnitz.de, web: <https://www.tu-chemnitz.de/index.html>

## INTRODUCTION

Human balance performance is based on interactions of different sensory systems, namely visual, somatosensory (e.g. plantar mechanoreceptors), and vestibular inputs [1]. Visual cues are important for maintaining balance [2]. Various studies have investigated long-term [3] and acute [4] effects of blindness on balance. Furthermore, studies have also examined how auditory cues contribute to balance regulation, which is, however, still controversial (e.g. [5]). Therefore, this study aimed to investigate acute adapting effects of short-term visual deprivation and reduced auditory capability on quasi-static balance performance. It was hypothesized that balance ability would decrease more when visual and auditory cues were deprived compared to only visual deprivation.

## METHODS

Forty-eight healthy subjects participated in this study. In some subjects, plantar temperatures varied considerably ( $>5^{\circ}\text{C}$ ), which was shown to deteriorate plantar sensitivity [6]. Therefore, only 23 subjects (11♀, 12♂; mean±SD: 24.1±3.3yrs; 172.7±8.7cm; 70.8±10.1kg) were included. Participants were informed about the aim of this study and were instructed to stop trials if they experienced discomfort. All measurements were conducted according to the recommendations of the Declaration of Helsinki. The protocol is presented in Fig. 1. Subjects completed three measurement sessions: before (pre1, pre2) and after (post) the intervention. The following parameters were evaluated during each measurement session: a) single-leg quasi-static balance performance (B, 10s) using a force plate (IMM Holding GmbH, Germany; 1kHz); b) plantar vibration sensitivity (S) at the first Metatarsal head (Met I) and Hallux using a TiraVib vibration exciter (Model TV 51075, Germany, 200Hz). During balance and sensitivity tests subjects wore ear

protectors and blackout glasses. Plantar temperatures (Hallux, Met I) were monitored using an infrared thermometer (UNI-T UT301C).

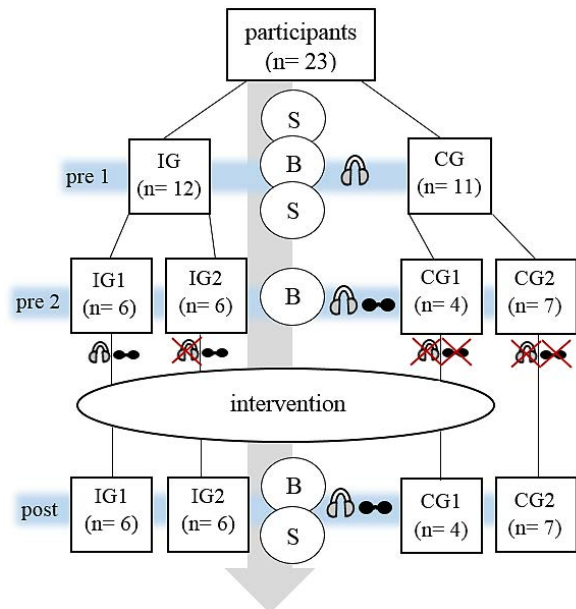


**Figure 1:** Both intervention groups (IG1, IG2) and control group 1 (CG1) performed the intervention: IG1: deaf & blind; IG2: hearing & blind; CG1: hearing & sighted. Control group 2 (CG2) did not attend the intervention and remained seated in the laboratory wearing neoprene socks (hearing & sighted); S foot sensitivity, B balance performance.

Subjects were randomly divided into the intervention (IG1, IG2) or control groups (CG1, CG2) (Fig.1). The intervention consisted of a standardized outdoor-walk (30min) on different surfaces (e.g. grass, grit, stairs), during which different balance exercises (e.g. balancing over curb) were executed. Participants wore thin neoprene socks to stimulate plantar mechanoreceptors, but also to protect the feet. Subjects were guided by a band held by the examiner. Information regarding obstacles etc. were only given through tactile cues using the band. For all parameters, three trials were collected and the median was used for further analysis. Center of

pressure (COP) total excursions were analyzed to examine balance. Vibration perception thresholds (VPTs) were calculated to examine plantar sensitivity. Statistical analysis was performed using SPSS (IBM SPSS Statistics 24). The Shapiro-Wilk-Test was used to determine distribution of data ( $\alpha=0.05$ ). The Wilcoxon Signed-Rank Test, Mann-Whitney-U-Test, Median-Test, and Sign-Test were used for further analysis. For VPTs, due to the two anatomical locations investigated, the level of significance was corrected to  $\alpha=0.05/2=0.025$ .

## RESULTS AND DISCUSSION

Comparing between the measurement sessions, only COP total excursions at pre2 and post were significantly greater compared to pre1 for all four groups (see Fig. 2). The deteriorating effect of blindness on balance was shown by Horak et al. [1]. Our study showed no significant differences for pre1 or pre2 when comparing the four groups within each measurement session (Fig. 2).

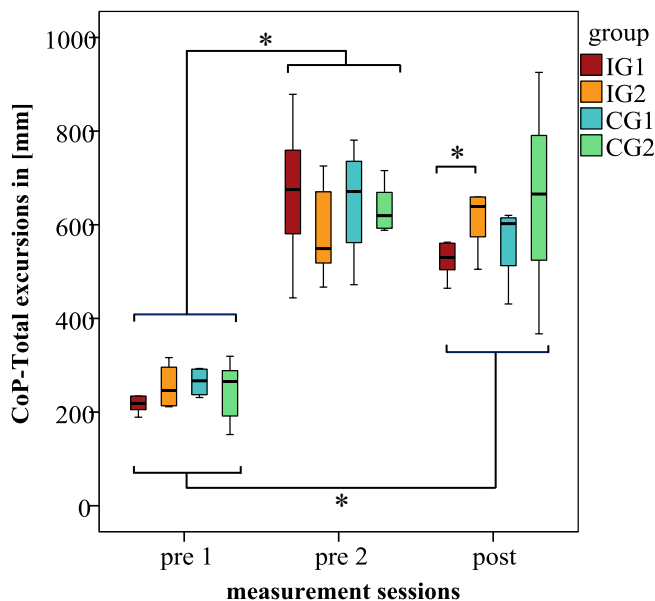


**Figure 2:** COP total excursions for all intervention (IG1, IG2) and control groups (CG1, CG2) before (pre1, pre2) and after (post) the intervention. Significant differences:  $*p \leq 0.05$ ,  $\alpha = 0.05$ .

For post, however, COP total excursions for IG1 were significantly smaller compared to IG2. This means that subjects performing the intervention deaf and blind exhibited improved balance ability

compared to subjects performing the intervention blind only. This is supported by our findings that IG2 remained constant when comparing pre2 vs. post, and that IG1 exhibited a trend-like decrease at post. The absence of auditory cues seemed to help the subjects focus on the new sensory condition and, therefore, improve their balance performance after the 30min outdoor walk. In other words, hearing ambient noise may have decreased balance ability in IG2. Similarly, it was also shown that blindness may cause conflicts in processing auditory cues [7]. Hence, it is possible that auditory cues were not processed properly for IG2 in order to provide supportive input for balance control.

VPTs for Met I and Hallux revealed no significant differences in any of the comparisons. We did not expect this finding, since daily step activity may increase plantar sensitivity [8], which in turn contributes to balance regulation. The thin neoprene socks used on various stimulating undergrounds did not change plantar sensitivity in our study, although plantar temperature changes were small (Hallux:  $0.7^{\circ}\text{C}$ ; Met I:  $2.1^{\circ}\text{C}$ ).

This study showed that balance ability deteriorates when vision is deprived; and that subjects with deprived vision and auditory inputs exhibited improved balance performance compared to subjects with deprived vision only. Further research is necessary to strengthen these results with a larger sample size.

## REFERENCES

1. Horak FB, et al. *Exp BrainRes* **82**, 167-177, 1990.
2. Grace Gaerlan M, et al. *J Am Acad Nurse Pract* **24**, 375-381, 2012.
3. Ray CT, et al. *Gait & Posture* **28**, 58-61, 2008.
4. Friedrich M, et al. *Exp Brain Res* **186**, 305-314, 2008.
5. Palm HG, et al. *Gait & Posture* **30**, 328-333, 2009.
6. Schlee G, et al. *Clinical Neurophysiology* **120**, 1548-1551, 2009.
7. Gori M, et al. *Brain* **137**, 288-293, 2014.
8. Alfuth M, Rosenbaum D. *Neuroscience Letters* **504**, 247-251, 2011.

# CORRELATION BETWEEN PLANTAR VIBRATION SENSITIVITY AND COP-PARAMETERS DURING DYNAMIC BALANCE

Bert Wynands\*, Claudio Zippenfennig, Andresa M.C. Germano, Daniel Schmidt, Tina Drechsel, and Thomas L. Milani

Chemnitz University of Technology, Department of Human Locomotion, Chemnitz, Saxony, Germany

\*email: bert.wynands@hsw.tu-chemnitz.de, web: <https://www.tu-chemnitz.de/index/html.en>

## INTRODUCTION

It is known that the mechanoreceptors in the foot sole play an important role in postural control. It has been reported that decreased plantar sensitivity results in greater instability in quasi-static balance tasks [1]. However, since 70% of human foot sole receptors are rapidly adapting receptors [2] that code dynamic events [3], it is reasonable to assume that plantar afferents might also play a dominant role in dynamic balance ability. However, to our knowledge, no study has analyzed the relationship between plantar sensitivity and Center of Pressure (CoP) parameters for dynamic balance tasks. Therefore, our aim was to examine whether a correlation exists between plantar vibration thresholds (VTs) and CoP-parameters during unexpected perturbations. We hypothesized that participants with low plantar sensitivity show larger CoP-excursions than those with high sensitivity.

## METHODS

Forty (20♀, 20♂) healthy subjects (mean±SD: 22.7±2.2yrs, 73.5±12kg, 1.76±0.08m) participated in this study. Prior to the test, subjects were informed about the study's purpose and were instructed to stop at any point if experiencing discomfort. All procedures were conducted according to the recommendations of the Declaration of Helsinki. Before the trials started, subjects underwent a 10min barefoot acclimatization on a temperature plate (25°C). To test plantar sensitivity, VTs were collected at the first metatarsal head (MET1) and the heel of the left foot using a TiraVib vibration exciter (Model TV 51075, Germany, 200Hz). Subjects sat with their feet resting on a box, with their knees and hips at a 90° angle. They wore noise cancelling earphones (Quiet comfort 20i, Bose, Framingham, USA)

which played pink noise to mask any distracting sounds of the vibration exciter or the environment. Pressure against the vibrating probe (diameter 7.8mm, elevation 2mm above box level) was controlled via a single axis force transducer. To acquire VTs, we used the Method of Limits (MoL) protocol described by [5]. The mean of five consecutive trials was calculated for heel and MET1. To test dynamic balance, a force plate (IMM Holding GmbH, Germany, 1kHz) was attached to the bottom platform of a customized Posturomed device (Haider Bioswing GmbH, Germany). Using an electromagnet, the platform of the Posturomed was released, resulting in an unexpected perturbation of the subject. Subjects stood on their left leg and were randomly perturbed in the antero-posterior (AP) and medio-lateral (ML) directions. For each perturbation direction, the mean of three consecutive trials was analyzed. We acquired four CoP-parameters (CoP total, ML-range, AP-range and CoP-velocity) in both directions for compensatory response, which extends from 90ms to 260ms after perturbation [6]. The Shapiro-Wilk-test was used to test for normality ( $\alpha=0.05$ ). To study differences between genders, Mann-Whitney-U-tests and Median-tests were used ( $\alpha=0.05$ , respectively). Pearson correlations were performed to investigate the relation between VTs and CoP-parameters ( $\alpha=0.05$ ).

## RESULTS AND DISCUSSION

Since VT and CoP data did not show any differences between genders, all data were examined altogether. Table 1 presents mean±SD for all parameters and the correlation coefficients between VTs and CoP data. At MET1, four of eight correlation analyses produced significant results (Table 1). Surprisingly, correlation coefficients were negative, implying that high VTs are linked to

small CoP-excursions. However, all coefficients lie between -0.3 and -0.35, which is considered a weak correlation [7] and probably not relevant. VTs at the heel did not demonstrate any significant correlations with balance parameters. The data do not support our hypothesis that subjects with low plantar sensitivity also feature higher CoP-excursions during a dynamic balance task, like perturbation. In contrast to our study, other investigations found positive correlations between balance and plantar sensitivity in quasi-static balance tasks [8,9]. It could be reasoned that plantar sensitivity is more influential in quasi-static than in dynamic tasks. However, subjects in [8] and [9] had some form of sensitivity impairment, which may have been large enough to influence balance ability and cause a correlation. Subjects in our study represent unimpaired sensitivity, which covers a comparatively small range of sensitivity, due to the low variation between subjects (Table 1). Such small variations may not have an effect on balance, possibly explaining why we could not find the expected correlation. A clear limitation of this study is that we did not investigate the sensitivity of FA1-receptors. Therefore, our results are only expressive for FA2-receptors.

## CONCLUSIONS

In conclusion, weak correlations were found between VTs (200Hz) and CoP-parameters during

perturbation. Most correlation analyses did not find any interaction, which suggests that small sensitivity variations in healthy subjects do not influence dynamic balance ability during perturbation as much as originally thought. Moreover, CoP-parameters may not be sufficient parameters for dynamic balance studies. Future studies should include the sensitivity of FA1-receptors to get a better understanding of the influence of rapidly adapting plantar afferents on dynamic events.

## REFERENCES

1. Oddsson LI, et al. *Experimental Brain research* **156**, 505-512, 2004.
2. Höhne A, et al. *Clinical biomechanics* **24**, 308-313, 2009.
3. Lowrey CR, et al. *Journal of neurophysiology* **109**, 839-850, 2013
4. Perry SD, et al. *Brain Research* **877**, 401-406, 2000.
5. Mildren RL, et al. *Gait & Posture* **43**, 87-92, 2016
6. Germano AM, et al. *BMC Neuroscience* **17**, 1-14, 2016.
7. Brosius F. *SPSS 21*, MITP Verlags GmbH & Co. KG, 2013.
8. Ducic I, et al. *Annals of plastic surgery* **52**, 535-540, 2004.
9. Hämmäläinen H, et al. *Human Movement Science* **11**, 549-561, 1992.

**Table 1:** Mean±SD of all sensitivity and CoP-parameters; correlation coefficients between VTs and CoP-parameters. Superscripted symbols represent significant correlations ( $\alpha=0.05$ ).

Parameter		MW ± SD	Correlation coefficient with VT MET 1	Correlation coefficient with VT Heel
VT Met 1		1.4 ± 0.3µm	/	/
VT Heel		2.4 ± 0.5µm	/	/
Perturbation in AP-direction	CoP total	39.0 ± 12.8mm	-0.32*	-0.06
	AP range	26.8 ± 11.1mm	-0.33*	-0.05
	ML range	5.2 ± 1.9mm	-0.15	-0.15
	CoP velocity	18.0 ± 2.4mm/s	-0.01	-0.13
Perturbation in ML-direction	CoP total	33.3 ± 7.7mm	-0.32*	-0.25
	AP range	11.9 ± 4.5mm	-0.20	-0.17
	ML range	18.8 ± 3.9mm	-0.35*	-0.30
	CoP velocity	18.6 ± 3.8mm/s	-0.09	0.03

# ASSESSING CHANGES IN THE REACTIVE CONTROL OF BALANCE DUE TO MODIFICATIONS OF STEP LENGTH ASYMMETRY

Chang Liu<sup>1</sup> and James M. Finley<sup>1</sup>

<sup>1</sup>University of Southern California, Los Angeles, CA, USA  
Email: jmfinley@usc.edu

## INTRODUCTION

One of the primary challenges for human locomotion is to maintain balance when faced with unexpected perturbations. The ability to maintain dynamic balance in these situations relies on proper reactive control strategies to restore the center of mass (COM) within the base of support. One established metric used to characterize dynamic balance is whole-body angular momentum. This measure reflects the net contribution of all body segments to the body's rotation about a given axis, commonly taken to project through the COM. Specifically, whole-body angular momentum ( $L$ ) is highly regulated during human locomotion (Herr & Popovic, 2008) due to momentum cancellation between the limbs.

Here, we are interested in understanding how reactive control of balance is influenced by gait asymmetries. Recent studies have demonstrated that people post-stroke have impaired control of whole-body dynamics as captured by higher peak-to-peak ranges of angular momentum (Vistamehr et al., 2015; Nott et al., 2014). However, no studies have quantified how direct modification of asymmetry influences reactive balance control.

In this study, we used a biofeedback paradigm that allows participants to systematically adopt different levels of asymmetry to test the hypothesis that walking asymmetrically impairs reactive control of balance. Perturbation recovery was quantified using measures of integrated angular momentum ( $\int L$ ) and step length asymmetry (SLA) to understand how performance and whole-body posture change pre- and post-perturbation. We hypothesized that asymmetry would be associated with a higher angular momentum than walking symmetrically and may also lead to increased recovery time following the perturbations.

## METHODS

Ten healthy individuals were instructed to walk on a split-belt treadmill at 1 m/s. After conducting a baseline evaluation to find their natural step length, visual feedback was provided to induce symmetric walking (0% SLA) and asymmetric walking ( $\pm 10\%$  SLA,  $\pm 15\%$  SLA). SLA is defined as follows:

$$SLA = 100 * \frac{\text{left step length} - \text{right step length}}{\text{left step length} + \text{right step length}}$$

During each trial, 10 unexpected perturbations where the treadmill accelerated to 1.5 m/s were randomly applied to each side (right or left) at heel strike. Full body kinematics were captured using a 10-camera Qualisys Oqus system (Qualisys, Sweden) and a set of reflective markers. From this data, whole-body angular momentum ( $L$ ) as well as  $\int L$  over each step cycle were calculated about a mediolateral axis projecting through the COM for analysis of pre- and post-perturbation steps.

$$L = \frac{\sum_i [M_i (R_{CM-i}^i \times V_{CM-i}^i) + I^i \omega^i]}{MVH}$$

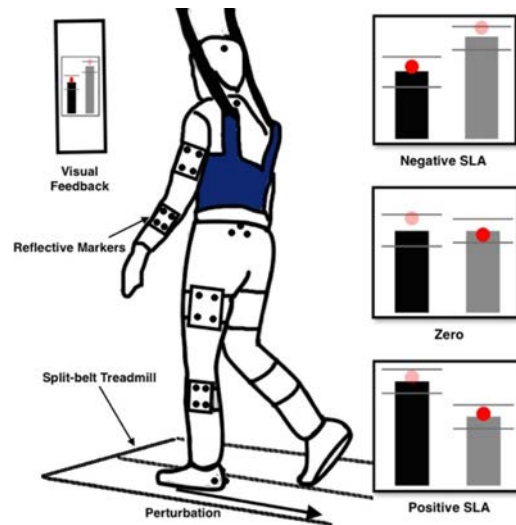
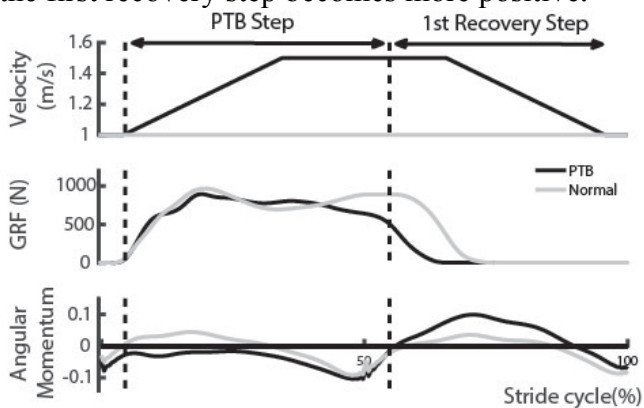


Fig 1: Experiment Setup

The number of recovery steps was also determined as the point when the participant's asymmetry was restored within  $\pm 5\%$  of the assigned SLA.

## RESULTS AND DISCUSSION

Our pre-perturbation measures of angular momentum during symmetric walking were similar to previous reports (Herr & Popovic, 2008). We found systematic variations in perturbation recovery in response to changes in step length asymmetry. A representative example illustrates the change in angular momentum during a perturbation and subsequent recovery step (Fig 2). Momentum was more negative compared to the pre-perturbation condition due to the participant's forward rotation. In order to regain balance, angular momentum for the first recovery step becomes more positive.



**Fig 2.** Treadmill speed, ground reaction force, and whole-body angular momentum across a stride.

Integrated angular momentum at the perturbation step was lowest during symmetric walking for perturbation to the dominant limb (Fig 3a). The magnitude of the integrated angular momentum was increased by 12.84% (SLA -15%), 8.4% (SLA -10%), 1.5% (SLA 10%), and 5.5% (SLA 15%), respectively, when compared to symmetric walking patterns.

Furthermore, the number of recovery strides varied with the direction of asymmetry and the side of the perturbation. One additional recovery stride was necessary when the perturbed side possessed a longer step length (Fig 3b).

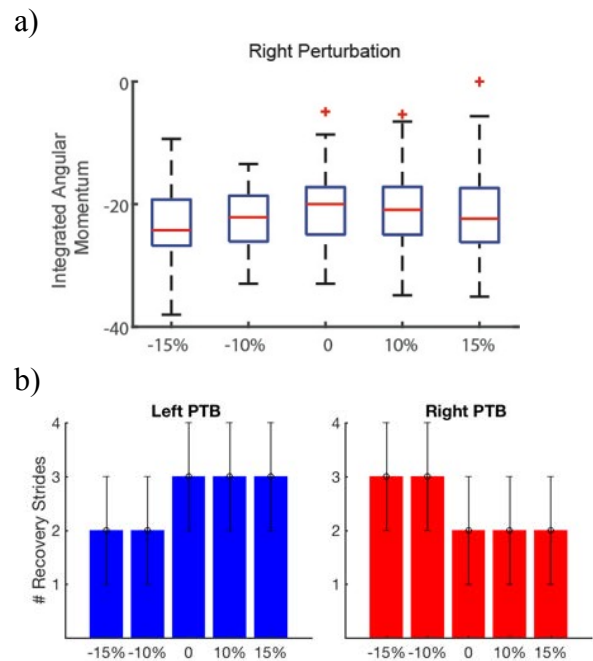


**Fig 3.** a) Integrated angular momentum at the perturbation step for different asymmetries and b) # of recovery strides for left and right perturbations.

## CONCLUSIONS

To our knowledge, this study is the first to test how modification of step length asymmetry affects the reactive control of balance during walking. For healthy individuals, symmetric walking patterns may reduce the destabilizing effects of unexpected perturbations, while asymmetrical patterns impair balance. Future studies will address how asymmetry influences segmental contributions and limb coordination strategies to recovery from perturbations.

## REFERENCES

- Herr, H., Popovic, M. (2008). *The Journal of Experimental Biology*, 211(Pt 4), 467-481
- Nott, C. R., Neptune, R. R., & Kautz, S. A. (2014). *Gait & Posture*, 39(1), 129-134. doi:10.1016/j.gaitpost.2013.06.008
- Vistamehr, A., Kautz, S. A., Bowden, M. G., & Neptune, R. R. (2016). *J. Biomech.* 49 (2016) 396–400

# GESTATIONAL LUMBAR LORDOSIS INTERACTIONS WITH DYNAMIC BALANCE CONTROL DURING PREGNANCY

W. Connor Wolcott, Christopher P. Connolly, Robert D. Catena,

Washington State University, Pullman, WA, USA

email: [robert.catena@wsu.edu](mailto:robert.catena@wsu.edu), web: <https://labs.wsu.edu/biomechanics/>

## INTRODUCTION

Fall rates among pregnant women reach levels comparable to individuals over the age 70 [1]. Falls pose a serious threat to the mother and unborn child, however we still don't fully understand the underlying causes toward increased fall rates. Our ongoing research indicates that mass changes contribute only partially to balance changes during pregnancy. Moreover, the literature describing dynamic balance control changes during pregnancy is thin.

When describing dynamic balance control, we often discuss the center of mass (COM) and base of support (BOS) interactions that occur during a moving task (e.g. gait). Considering the unique changes to the body that pregnancy causes, we could expect that any change that influences the position or motion of the COM in relation to the BOS would influence dynamic balance control.

It has been previously reported that the lumbar curvature of pregnant women increased steadily as gestation progresses [2]. This occurs exclusively in bipedal hominids as it readjusts the COM posteriorly over the hips in response to ventral fetal weight gain. It is currently unknown if, and how, dynamic balance is correlated with these lumbar curvature changes. Presumably, not all pregnant women experience lumbar change to the same degree. Is more change better for dynamic balance in terms of repositioning the COM or detrimental to dynamic balance because of the altered rotational kinetics at surrounding joints? In this study, we examined the correlations between lumbar curvature and dynamic balance control throughout pregnancy.

## METHODS

We have recruited 33 participants total to our study, however due to the longitudinal nature of our testing, data from only 6 of those participants is included here. Our participants' mean age was 27.7 (sd = 4.14) with a mean gestational age at start of testing of 14.5 weeks (sd = 39.9 days).

Testing sessions were conducted monthly, involving full body anthropometry measurements followed by a static standing trial and a 60 second walking trial on a treadmill at a self-selected pace. We utilized a forty-eight retroreflective marker set captured by a ten-camera motion capture system at 100 Hz using Cortex and Biosuite software (Motionanalysis Corp., Santa Rosa, CA) and then low-pass filtered at a 6 Hz cutoff. The entire sixty-second capture was split into individual gait cycles at right heel strikes. The body COM was calculated using a 13-segment anthropometric model; supported by currently in-review findings. COM data were then passed through a custom MatLab program that calculated COM and BOS interactions as well as step width and other balance measures. Average lumbar angle while standing and walking was calculated from markers at the approximate levels of T12, L2, L4 and S2.

Statistical analysis was carried out using a stepwise multiple regression analysis in SPSS v23 to determine correlations between lumbar angle, step width, and balance measures.

## RESULTS AND DISCUSSION

Moderate positive correlations were found between lumbar curvature and measures of balance. In other

words, as lumbar curvature increases during pregnancy, the minimum distance of the center of gravity (COG) to the BOS is greater (Tables 1 and 2). In most cases, we describe a smaller separation of the COG to the BOS as reduced dynamic balance control. From our data it appears that the increase in lumbar curvature that occurs during pregnancy aids in dynamic balance control.

**Table 1.** Step-wise regression of correlates to minimum distance from the center of gravity to the forefoot border

Model	R	R Square	Adjusted R Square	Std. Error
1	.407 <sup>a</sup>	.165	.165	13.42
2	.455 <sup>b</sup>	.207	.206	13.08
3	.461 <sup>c</sup>	.213	.212	13.04
4	.499 <sup>d</sup>	.249	.248	12.73

a. Predictors Back ROM during walking (BRW)

b. Predictors: BRW, Days to birth (Days)

c. Predictors BRW, Days, Back angle average in walking (BAW)

d. Predictors: BRW, Days, BAW, Back angle average in standing (BAS)

**Table 2.** Step-wise regression of correlates to minimum distance from the center of gravity to the rearfoot border

Model	R	R Square	Adjusted R Square	Std. Error
1	.375 <sup>a</sup>	.141	.140	23.67
2	.546 <sup>b</sup>	.298	.297	21.41
3	.578 <sup>c</sup>	.334	.333	20.86
4	.605 <sup>d</sup>	.366	.364	20.36

a. Predictors: BAS

b. Predictors: BAS, BAW

c. Predictors: BAS, BAW, BRW

d. Predictors: BAS, BAW, BRW, Days2Birth

We also observed correlations between the angular range of motion of the COM around the ankle joint during stance in the sagittal plane and lumbar curvature. This suggests that individuals are taking shorter steps as pregnancy progresses. One explanation is that this may be another alteration to improve balance. Alternatively, shorter steps during pregnancy may be a result of a cascading effect of increased lumbar curvature on the moment arms and

lengths of muscles involved in gait performance. So whereas increased lumbar curvature may improve balance control, the trade-off may be that forward gait progression is adversely affected. We discovered that not every participant experienced the same change in lumbar curvature. Future study will involve comparing the balance measures of individuals, who do experience curvature changes throughout pregnancy versus those who do not. Furthermore, we intend to examine correlations between muscular strength to the occurrence of lumbar curvature change.

## CONCLUSIONS

Lumbar curvature changes during pregnancy may be adaptive to increase dynamic balance control. As we increase our analysis sample size we will be able to determine if curvature changes result in diminished gait progression or if gait progression changes naturally occur with gestation. Furthermore, lumbar curvature changes occur at differing magnitudes between women, potentially creating varying balance effects. These effects, in addition to the contribution of muscular strength to the development of gestational lumbar lordosis, should be studied further.

## REFERENCES

1. Dunning, K. et al. *Maternal and Child Health*, **14**,720-725. 2010.
2. Whitcome, K. et al. *Nature*, **450**, 1075-1080. 2007.
3. Lugade, V. et al. *Gait & Posture* **33**, 406-411. 2011.

## ACKNOWLEDGMENTS

This study was funded through a WSU College of Education faculty funding award and a WSU New Faculty award.

# POSTURAL INSTABILITY IN PATIENTS WITH IDIOPATHIC NORMAL PRESSURE HYDROCEPHALUS: EFFECT OF SHUNTING

<sup>1</sup> Tobias Hess\*, <sup>1</sup> Christian Mitschke, <sup>1</sup> Thomas L. Milani, <sup>2</sup> Jürgen Meixensberger, <sup>2</sup> Matthias Krause

<sup>1</sup> Chemnitz University of Technology, Department of Human Locomotion, Chemnitz, Germany

<sup>2</sup> University Hospital, Department of Neurosurgery, Leipzig, Germany

\*email: tobias.hess@hsw.tu-chemnitz.de, web: <https://www.tu-chemnitz.de/index.html.en>

## INTRODUCTION

Idiopathic normal pressure hydrocephalus (iNPH) is generally known as a pathological process with abnormal intracranial fluid dynamics resulting in progressive ventricular enlargement and reduced intracranial compliance [1]. The symptomatic of this disease is usually characterized as a triad of progressing dementia, urinary incontinence, and movement disorders, which are frequently the first and most prominent symptoms [2]. Besides gait disturbance, postural instability is a clinical challenge, because of the associated risk of falling [3]. Commonly, iNPH is treated via surgical implantation of a ventriculoperitoneal shunt to normalize intracranial fluid dynamics and consequently ease symptoms. Hence, clinical balance scales (e.g. Berg Functional Balance Scale, Functional Reach Test) are frequently applied for diagnosis and to determine and assess posturographic changes after shunt treatments. However, these tests often lack objectivity, sensitivity, and specificity compared to data collected with force or pressure distribution platforms [4]. Therefore, the aim of this study was to investigate postural instability in patients with iNPH in contrast to healthy control subjects using computerized methods. Furthermore, we aimed to analyze the impact of a shunt treatment in hydrocephalic patients. Based on comparable study findings [3,5,6] it was hypothesized that patients with iNPH have poorer postural stability compared to healthy controls, whereas shunting improves balance performance.

## METHODS

All procedures were conducted according to the recommendations of the Declaration of Helsinki and were approved by the local ethics committee. This study comprised three groups: iNPH, consisting of

19 diagnosed patients (12 male, 7 female; age: 72.9±5.5 years, height: 168.5±8.9 cm, weight: 79.2±16.1 kg); HC, consisting of 19 healthy control subjects matched for sex, age, and anthropometrics (12 male 7 female; age: 72.1±6.1 years, height: 171.5±10.7 cm, weight: 78.5±11.6 kg); and iNPH shunt, comprising 16 iNPH patients, which had already undergone shunt surgery previous to this study (12 male, 4 female; age: 72.7±6.5 years, height: 173.5±6.8 cm, weight: 84.5±13.3 kg). Additionally, seven hydrocephalic patients were evaluated both pre and 3-12 months post operatively to investigate the intrasubjective effect of shunting. Patients were diagnosed with iNPH by positive clinical testing, including invasive and non-invasive measures according to the previously published protocol [7]. Furthermore, ventricular enlargement was proved by standard cMRI scan. Aqueductal stenosis and other secondary pathologies were excluded. A pressure distribution platform (Zebris FDM 1.5, Medical GmbH, Isny Germany) was used for measuring postural performance during quite stance. Therefore, all participants were instructed to stand upright as still as possible with both feet next to each other on the platform, pointing their gaze ahead with both arms hanging down loosely. To ensure reproducibility for the repeated pre vs. post shunt measurements, foot distance and rotation angle were controlled. Two trials of 30 seconds each were collected at 100 Hz for each participant. Pressure distribution data were analyzed using MATLAB (R2008b, MathWorks, Massachusetts) to calculate the mean of the center of pressure (COP) parameters: COP area of the 95% confidence ellipse, COP path length, and mean COP velocity. SPSS Statistics 24 (IBM) was used to compare between groups with a Kruskal-Wallis-Test followed by post hoc-tests. Due to the three investigated parameters, the level of significance was Bonferroni adjusted to  $\alpha=0.0166$ .

## RESULTS AND DISCUSSION

Table 1 displays the results of the group comparison. All COP parameters showed statistically significant differences between HC vs. iNPH and HC vs. iNPH shunt. Healthy control subjects revealed significantly lower COP areas, path lengths, and mean velocities compared to hydrocephalic patients without (iNPH) and with shunt (iNPH shunt). Higher COP values are generally associated with less postural stability. This implies poorer postural stability in patients with iNPH, regardless of whether they have a shunt or not, compared to healthy subjects. Nevertheless, iNPH patients with shunts showed a tendency toward better postural control, due to lower COP values compared to patients without shunt. Despite improvement, shunted iNPH patients still have worse postural stability than healthy subjects.

The intrasubjective pre vs. post shunt comparison revealed diminished COP areas for all seven patients, indicating improved postural control (Figure 1). The mean values of this specific parameter decreased from  $922.5 \pm 676.1 \text{ mm}^2$  to  $441.2 \pm 329.5 \text{ mm}^2$ , which indicates an overall reduction of 52.2%. Noteworthy, not all patients showed equal improvements: patients with higher pre shunt COP areas improved more than patients with smaller pre shunt COP areas. However, six out of the seven patients reduced their COP area >25 %, and therefore can be considered as positive shunt responders. Our findings are in accordance with those of other studies [3,5,6]. Their results revealed equal postural deficits for patients with iNPH compared to healthy controls. They also characterized hydrocephalic postural instability in quiet stance with increased COP areas and velocities [3,6]. After shunt surgery, Czerwoszcz et al. [3] found reductions for the COP area of approximately 75 %, meaning substantial improvement in postural control. Considering all results of the present study, the stated hypotheses can be confirmed.

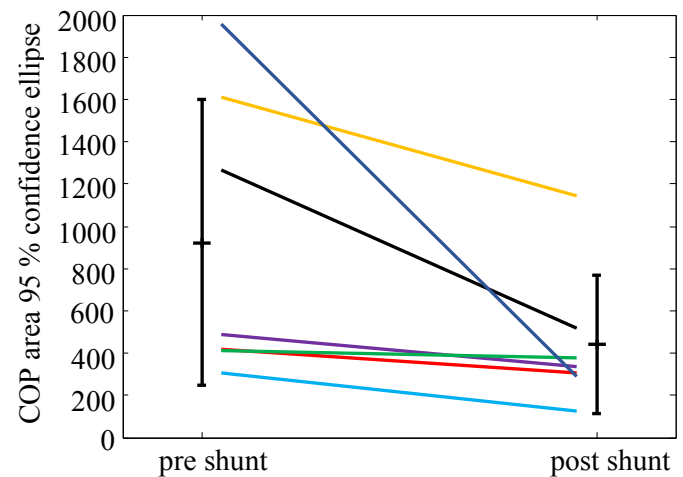


**Figure 1:** Pre vs post shunt changes of the COP area for all seven iNPH patients separately and together (mean  $\pm$  standard deviation).

## CONCLUSIONS

Patients with iNPH suffer from poorer postural stability in quiet stance compared to healthy controls. Shunting positively effects postural control. Computerized posturography in quiet stance may be used as a quantitative, valuable tool for diagnostics, treatment, and rehabilitation purposes in iNPH.

## REFERENCES

1. Relkin N., et al. *Neurosurgery* **S2-4-S2-16**, 2005.
2. Krauss JK., et al. *Acta Neurochir* **146(4):379–88**, 2004.
3. Czerwoszcz L, et al., *Eur J Med Res* **14(Suppl. IV): 53-58**, 2009.
4. Mancini M & Horak F B, *Eur J Phys Rehabil Med.* **46(2): 239–248**, 2010.
5. Lundin F., et al. *Clinical Neurology and Neurosurgery* **115 1626-1631**, 2013.
6. Blomsterwall E, et al., *Acta Neurol Scand:* **102: 284-291**, 2000.
7. Mahr CV, et al., *J Neurosurg* **125:591-597**, 2016.

**Table 1:** COP parameters; mean  $\pm$  standard deviation

	HC (n=19)	iNPH (n=19)	iNPH shunt (n=16)
<b>COP area [mm<sup>2</sup>]</b>	230.9 $\pm$ 123.2*†	567.8 $\pm$ 575.0*	427.6 $\pm$ 207.9†
<b>COP path length [mm]</b>	470.2 $\pm$ 58.8**††	787.8 $\pm$ 413.5**	594.5 $\pm$ 147.5††
<b>mean COP velocity [mm/s]</b>	16.3 $\pm$ 2.1***†††	27.2 $\pm$ 14.3***	20.5 $\pm$ 5.1†††

Significant differences: HC vs. iNPH: \*(p=0.003); \*\*(p=0.000); \*\*\*(p=0.000)

HC vs. iNPH shunt: †(p=0.001); ††(p=0.006); †††(p=0.007)

# EFFECTS OF A HIGH INTENSITY PLYOMETRIC TRAINING REGIMEN ON POSTURAL CONTROL OF YOUNG ADULTS

Malavika Suresh, Shaniel Bowen, Alexandros N. Mathioudakis, and Krystyna Gielo-Perzczak, Ph.D.

Department of Biomedical Engineering, University of Connecticut, Storrs, CT, USA

Corresponding author email: [malavika.suresh@uconn.edu](mailto:malavika.suresh@uconn.edu); Lab website: <http://msml.uconn.edu>

## INTRODUCTION

From a mechanical perspective, human vertical posture is regarded as an unstable system requiring control mechanisms to maintain center of gravity, and therefore postural control [1]. Standing without assistance is a fundamental skill for independent mobility. Previous studies [1-3] suggest multiple muscles are involved in quiet standing balance, and the degree of activation of muscle synergies is a good indication of postural stability.

Plyometric training (PT) is popular amongst trained athletes, and involves exercises such as hopping and jumping over a short period of time [2]. These exercises utilize the elastic energy stored in the stretching phase of the lower limb muscles as they undergo stretch-shortening contractions [2]. PT has been shown to positively impact numerous biomechanical, sensory acuity, and motor control, measures; such as balance control, aerobic/anaerobic power, and capacity [2]. Most plyometric training studies explored low impact training. The very few, high intensity training programs which positively impacted dynamic measures and vertical jump performance involved trained athletes, such as soccer players [2].

The aim of this study was to investigate the effects of a ten-week, high intensity bilateral plyometric training program on young adults to observe and characterize changes in their performance, motor control and postural stability. This is the first part of a larger study, which aims to investigate these measures in adults with impaired standing balance. We hypothesized that over time, there would be a reduction in the overall center of pressure (CoP) velocity, postural sway and 95% ellipse area. Our second aim was to determine the effect of this training on muscle activity in the lower limbs by evaluating vertical jump performance, EMG-EMG coherence of synergistic muscles, and gross innervation input of a select muscle for the task.

## METHODS

### *Participants*

Ten healthy, young participants (Age:  $20.1 \pm 1.4$  years; Group 1: 2 Females, Body Mass:  $49.70 \pm 7.77$  kg, Height:  $1.58 \pm 0.04$  m; Group 2: 4 Males, Body Mass:  $67.80 \pm 0.80$  kg, Height:  $1.65 \pm 0.04$  m; Group 3: 4 Males, Body Mass:  $85.90 \pm 12.70$  kg, Height:  $1.91 \pm 0.04$  m) provided written informed consent to participate in this protocol, which was approved by the local institutional review board.

### *Procedures*

This ten-week study consisted of three plyometric training sessions a week, per person. The experiment consisted of two independent, bilateral standing measurements (pre-exercise and post-exercise), which involved analyzing CoP measurements using a portable force platform (AMTI AccuSway, Watertown, MA) sampled at 500 Hz, and muscle activity measurements using six surface wireless Electromyography (EMG) sensors (Trigno, Delsys Inc. Natick, MA), sampled at 1926 Hz. Participants were instructed to stand with feet shoulder width apart on the force platform with eyes open for 90s, with the EMG sensors placed on the right and left muscle bellies of the vastus lateralis (VL), biceps femoris (BF) and lateral gastrocnemius (GL). These muscles were chosen as they are known to affect postural sway and do not require filtering against cardiac artifacts [3]. After this pre-test recording, the participants were led through a short warm-up, before beginning the exercises. The training itself consisted of four sets of stationary hopping for 30s as fast and as high as possible (maximal effort) with 60s rest in between each set. This was followed by a cool down for 5 minutes and slow walking. Post-test measures were then taken, using the same pre-test procedure as described above. Vertical jump performance was recorded bi-weekly throughout the study to monitor and evaluate the ability to generate multi-joint power in the lower extremities [2].

## RESULTS AND DISCUSSION

Data analysis was performed using MATLAB R2015a (Mathworks Inc., Natick, MA). CoP and muscle activity measures were pre-processed, synchronized and normalized as described in [3]. Significant differences in CoP velocity and 95% ellipse area were found across all three groups of participants, especially *Group 2* (Fig. 1):

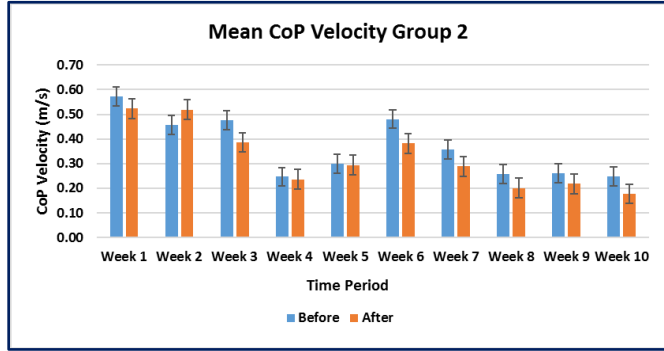


**Figure 1:** Mean CoP velocity comparison *Group 2*

A 61.40% decrease in the overall mean CoP velocity in both directions show increased stability. Postural sway in the medio-lateral and anterior-posterior directions did not show substantial differences, but stabilized after week five.

EMG-EMG coherence estimations using the Welch method [2-3] was used to analyze the coordination between synergistic pairs of muscles:

$$|R_{xy}(\lambda)|^2 = \frac{|f_{xy}(\lambda)|^2}{|f_{xx}(\lambda)f_{yy}(\lambda)|} \quad (1)$$

where  $R_{xy}(\lambda)$  is the intermuscular coherence,  $f_{xy}(\lambda)$  is the cross-spectrum between both EMG signals,  $f_{xx}(\lambda)$  is the auto-spectrum of the first EMG signal, and  $f_{yy}(\lambda)$  is the auto-spectrum of the second. Higher amplitudes of muscle activity were observed in lower frequencies, and overall coherence of muscle pairs increased over time ( $\sim 0.63$ ). Mean EMG root-mean-square (RMS) comparisons between different muscle groups assessed the gross innervation input of select muscles during both testing conditions. All groups

showed a reduction in the mean RMS ( $\sim 0.60\mu V$ ), especially *Group 2* (Fig. 2):

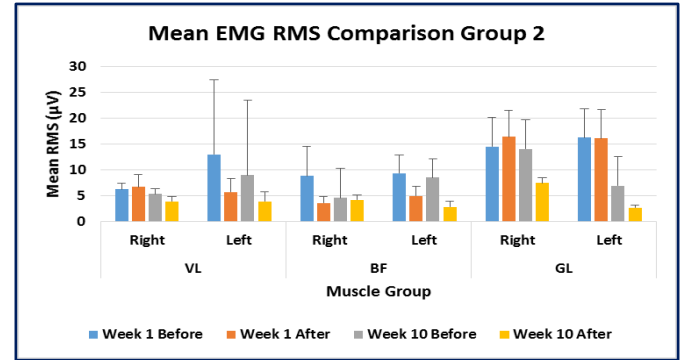


**Figure 2:** Mean EMG RMS comparison *Group 2*

Improved vertical jump performance (Table 1) further validates significant adaptation in lower limb power, as high impact forces are produced during these movements.

## CONCLUSIONS

This ten-week high intensity plyometric training program consisting of maximal intensity bilateral exercises in young adults induced major improvements in lower extremity power and postural control. This decrease in muscle activation/force production can be associated with neural components of adaptation accompanied by improved intermuscular coordination and/or changes in the mechanical characteristics of the muscle-tendon complex [1-3]. High intensity PT provides an alternative approach in treating impaired standing balance and improving postural control. This could potentially provide a training regimen to be incorporated into rehabilitation programs.

## REFERENCES

1. X. García-Massó, et al. *Experimental Brain Research*, vol. **234**, no. 7, pp. 1977-1986, 2016
2. M. Vácz, et al. *Journal of Human Kinetics*, vol. **36**, no. 1, 2013
3. J. Jacobs, et al. *Neuroscience*, vol. **298**, pp. 1-11, 2015

**Table 1:** Effects of the 10-week plyometric training regime on vertical jump performance

	Week 1		Week 10		Change in vertical jump (%)
	Mean (m)	SD (m)	Mean (m)	SD (m)	
<b>Group 1</b>	2.32	± 0.14	2.41	± 0.10	+ 3.83
<b>Group 2</b>	2.79	± 0.07	2.94	± 0.04	+ 5.23
<b>Group 3</b>	2.91	± 0.09	3.01	± 0.08	+ 3.49

# TIME EVOLUTION OF FRONTAL-PLANE DYNAMICAL BALANCE DURING LOCOMOTOR TRANSITIONS OF ALTERED ANTICIPATION AND COMPLEXITY

<sup>1</sup> Wentao Li, <sup>2</sup> Nathaniel T. Pickle, and <sup>1,2,3</sup> Nicholas P. Fey

<sup>1</sup> Department of Mechanical Engineering, University of Texas at Dallas, Richardson, TX, USA

<sup>2</sup> Department of Bioengineering, University of Texas at Dallas, Richardson, TX, USA

<sup>3</sup> Department of Physical Medicine and Rehabilitation, UT Southwestern Medical Center, Dallas, TX, USA

email: wentao.li1@utdallas.edu, web: <http://me.utdallas.edu/people/fey.html/>

## INTRODUCTION

During locomotion, humans often make cognitive decisions and respond to external stimuli that result in cuts (changing direction), transitions to uneven terrain, or complex combinations thereof. The mechanics of these destabilizing locomotor transitions are also affected by whether a change in direction is made towards (crossover) or away from (sidestep) the leading, implanted leg [1]. Finally, these tasks are influenced by cognitive factors such as if a task is unanticipated—conditions in which neuromotor task planning is interrupted. During running, unanticipated cuts influence ground-reaction forces, joint angles, joint moments, and muscle activity, which are thought to lead to knee loading mechanics that are deleterious to knee ligament strain [e.g., 2]. However, during walking, it is unknown how specific contextual factors influence dynamic balance of locomotor transitions, which could inform how we assess balance deficits of fall-prone individuals or inform device interventions to target specific destabilizing and non-steady locomotor scenarios.

One metric to assess dynamic balance of walking is whole-body angular momentum ( $H$ ), which has been shown to be tightly regulated by unimpaired individuals [3] via the generation of appropriate muscle forces [4]. The purpose of this study was to apportion the effects of task anticipation, cutting style, and complexity on the time evolution of frontal-plane dynamic balance during locomotor transitions of healthy, unimpaired individuals. We hypothesized that the magnitude of  $H$  would be larger during unanticipated conditions of increased complexity (i.e., combined cut/stair-ascent).

## METHODS

Data were collected from five healthy unimpaired subjects (27.7±3.8 years; 52.6±5.0 kg; 1.68±0.09 m). Straight-line walking (STR), crossover (CO), sidestep (SS), crossover/stair-ascent (COS), and sidestep/stair-ascent (SSS) were performed overground under anticipated and unanticipated conditions. First, each participant completed 10 baseline STR trials, followed by 20 anticipated cut trials (5 of each style and complexity), and a subsequent 30 unanticipated trials (5 cuts of each style and complexity and 5 STR corresponding to either left or right leg leading). In unanticipated trials, a randomized auditory cue of “stair”, “cut”, or “walk” was given at the initiation of single-leg support of the leading leg, approximately one-half step preceding a visible transition point. The lab setup consisted of an overground straight-line walkway, a level-ground cutting (45°) direction to the right, and a mobile staircase at 45° to the left for cut/stair-ascent.

A 10-camera motion capture system (Motion Lab Systems, Inc.) was used to track body segment movement. An 8-segment model of each subject (torso, pelvis, thighs, shanks, and feet) was constructed using Visual3D (C-Motion, Inc.).  $H$  about the body center-of-mass was calculated using a standard kinematic formulation [e.g., 3] and normalized by body mass and height of each subject. To analyze the time evolution of  $H$ , consecutive maxima and minima of  $H$  were computed during two consecutive strides spanning each condition. These metrics were compared statistically ( $\alpha=0.05$ ) with two, two-way ANOVAs (anticipation, complexity; anticipation, cutting style).

## RESULTS AND DISCUSSION

Anticipatory changes in frontal-plane balance were influenced by style, but not complexity. Prior to the trailing-leg toe-off (i.e., cue onset in unanticipated conditions), a significant style main effect and anticipation by style interaction effect were observed (P1, Fig. 1).  $H$  in anticipated crossovers was more positively directed toward the leading foot (the cutting direction), while  $H$  in sidesteps was reduced to approximately zero momentum (away from the cut), relative to walking and unanticipated conditions. These changes suggest that in the frontal plane, anticipating upcoming demands associated with modifying walking direction is of greater value for task planning than changes in surface.

Our hypothesis was largely supported. However, specific combinations of contextual factors showed unique magnitudes of dynamic balance. In the subsequent heel-strike after the cue, anticipation, complexity, and style main effects and an anticipation by style interaction effect were found (N1, Fig. 2). Unanticipated sidestep had the largest magnitude of negative  $H$  (Fig. 1), possibly due to inability to fully execute a sidestep cut within the available response time, which resulted in a mixed style that most resembled a crossover. In the second stride of the transition, complexity and style main effects were observed (P2, Fig. 1), and anticipated and unanticipated crossover/stair-ascent resulted in the largest frontal-plane  $H$  toward the cut direction (P2, Fig. 1). Later in the second stride of the

transition, anticipation, complexity, and style main effects and anticipation by complexity and anticipation by style interaction effects were found (N2, Fig. 1), with unanticipated sidestep/stair-ascent resulting in the largest negative  $H$  (away from the leading leg toward the cut direction). Collectively, these findings suggest there are adverse downstream effects of unanticipated states on dynamic balance.

## CONCLUSIONS

Anticipatory modifications of balance, transient changes in balance immediately following the interruption of task planning, and subsequent adverse effects were observed by altering task anticipation. All of these changes appear to be important when negotiating locomotor transitions, with respect to frontal-plane balance, and could be targeted in balance-impaired individuals through training or device interventions. However, with respect to only anticipatory modifications, healthy individuals appear to prioritize directional changes over changes in walking surface.

## REFERENCES

1. Potter D, et al. *Int J Sports Phys Ther* **9**, 617-627, 2014
2. Kim JH, et al. *Am J Sports Med* **42**, 1985-1992, 2014.
3. Herr H, et al. *J Exp Biol* **211**, 467-481, 2008.
4. Neptune RR, et al. *J Biomech* **44**, 6-12, 2011.

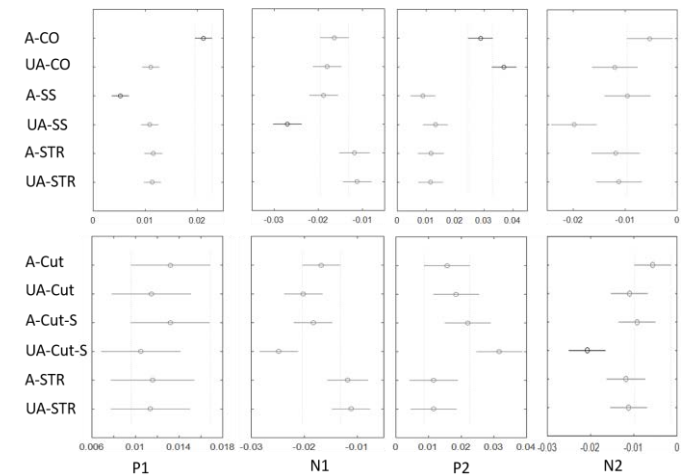
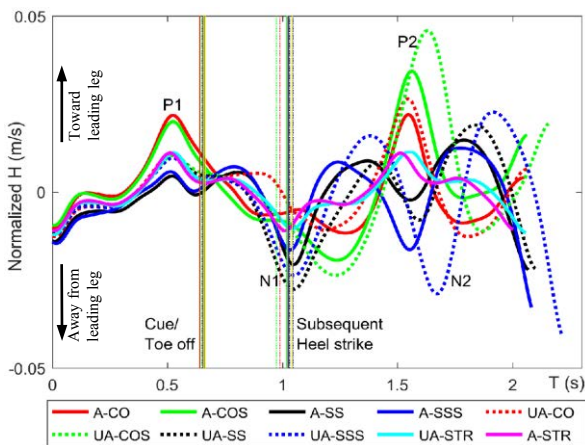


**Figure 1:** Time evolution of group-averaged frontal-plane  $H$  (left) expressed over average time of two consecutive strides of the trailing leg spanning each transition condition. Positive values indicate rotation toward the direction of the implanted, leading foot during each cut. P1, N1, P2, N2 are consecutive maxima and minima of the time series. Confidence interval (95%) of the population mean of frontal-plane  $H$  metrics are also shown for each condition (right).

# VELOCITY-BASED CONTROL OF POSTURAL SWAY IN PEOPLE WITH A UNILATERAL TRANSTIBIAL AMPUTATION

<sup>1</sup>Jenny A Kent, <sup>1</sup>Kota Z Takahashi, <sup>1</sup>Vivien Marmelat, and <sup>1,2</sup>Nicholas Stergiou

<sup>1</sup>Dept. of Biomechanics, University of Nebraska at Omaha, Omaha, NE, USA

<sup>2</sup>University of Nebraska Medical Center, Omaha, NE, USA

email: [jkent@unomaha.edu](mailto:jkent@unomaha.edu), web: [coe.unomaha.edu/biomechanics](http://coe.unomaha.edu/biomechanics)

## INTRODUCTION

The ability to stand is requisite for performing many activities of daily living. The active control of standing balance is known to be facilitated by a wealth of sensorimotor processes [1]. The manner in which the center of pressure (COP) moves over time during quiet standing may be revealing of these underlying control processes.

Postural sway can be characterized according to its velocity patterns. For example, sway may be described to exhibit ‘persistence’ when a COP velocity change in one direction is more likely to be followed by a change in the same direction. Conversely, sway may exhibit ‘anti-persistence’, when a change in one direction is more likely to be followed by a change in the opposite direction. Intriguingly, sway patterns of healthy young adults demonstrate both persistent and anti-persistent behavior, but at different timescales [2]. When examining the patterns within small time increments (i.e. within 1 second) the fluctuations are persistent, whereas at longer time scales (i.e. over several seconds) the fluctuations are anti-persistent. It has been postulated that this transition from ‘short term persistence’ to ‘long term anti-persistence’ reflects the action of a control mechanism that evokes a directional change when a threshold of velocity is exceeded [2].

Given that cutaneous receptors beneath the foot are ideally positioned to detect these movements, it seems reasonable to speculate that their sensory contributions may play a direct role in the mediation of this velocity-based control mechanism. We aimed to test this by comparing the COP velocity patterns of adults with no impairments to individuals with a unilateral transtibial amputation. Following a

unilateral lower extremity amputation, the tactile sensation from one foot will be absent resulting in an asymmetric sensory deficit. We hypothesized that, due to this sensory loss, amputees would exhibit less short term persistence and less long term anti-persistence. In effect, this would be illustrated with a convergence towards similar dynamics at both timescales.

## METHODS

Eleven individuals with a unilateral transtibial amputation ( $60.2 \pm 15.9$  yrs,  $1.8 \pm 0.1$  m,  $98.8 \pm 13.7$  kg) and seven individuals with no impairment ( $40.6 \pm 9.7$  yrs,  $1.7 \pm 0.1$  m,  $85.3 \pm 24.3$  kg) consented to participate. Participants stood for 90 s with their feet on parallel force plates (Optima, AMTI, Watertown, MA), with their feet ‘as close together as possible’ and arms crossed in front of their torso, fixating on a wall-mounted target. COP trajectories at 60 Hz were computed from the two force plates, low-pass filtered at 10Hz and differenced to obtain COPv.

Detrended fluctuation analysis (DFA [3]) was used to quantify persistence in COPv in anterior-posterior (AP) and medial-lateral (ML) directions. DFA estimates the relationship between the size of fluctuations  $F(n)$  within a time series for windows of observation of size  $n$ . A linear slope in bi-logarithmic coordinates reveals a power-law relationship, such that  $F(n) \sim n^\alpha$ , where  $\alpha$  is the slope or scaling exponent. An  $\alpha > 0.5$  reflects persistent fluctuations while  $\alpha < 0.5$  reflects anti-persistent fluctuations, and  $\alpha = 0.5$  indicates randomness. Short and long term exponents were estimated over approximately 0.2-0.6 seconds ( $\alpha_{\text{short}}$ ) and 1.8-11.3 seconds ( $\alpha_{\text{long}}$ ), respectively. This velocity-based control mechanism would be indicated by  $\alpha_{\text{short}} > 0.5$  and  $\alpha_{\text{short}} < 0.5$ . Group differences between individuals with and

without an amputation were determined using Welch's t-tests for unequal variances in R (R core team, Vienna, Austria).

## RESULTS AND DISCUSSION

In partial support of our hypothesis, in the AP direction the participants with transtibial amputation exhibited less persistent sway patterns at the short timescale in comparison to controls ( $\alpha_{\text{short}} = 1.2 \pm 0.2$  vs  $1.4 \pm 0.1$ ,  $p = 0.04$ ). However, reduced persistence (i.e. increased antipersistence) was similarly observed at long timescales ( $\alpha_{\text{long}} = 0.2 \pm 0.1$  vs  $0.4 \pm 0.1$ ,  $p = 0.01$ ). There was no difference between groups in the ML direction ( $\alpha_{\text{short}}$ :  $p = 0.36$ ;  $\alpha_{\text{long}}$ :  $p = 0.53$ ).

Although group differences were observed in the AP direction, the marked disparity between short term persistence and long term anti-persistence remained evident in both AP and ML directions of the individuals with amputation, potentially indicating similar velocity-based control. The lack of a group difference in the ML direction was surprising given the absence of cutaneous plantar sensation from half of the base of the support in prosthesis users.

## CONCLUSIONS

The overall trend to exhibit 'short-term persistence' and 'long-term antipersistence' in the COP velocity was preserved in unilateral transtibial amputees despite the deficit in sensation from one foot. Our results indicate that cutaneous plantar sensation may only play a minor role in the mediation of the proposed COP velocity-based control mechanism (change in direction is exerted when a velocity threshold is exceeded). Alternatively, the residual limb may be able to take on a greater sensory role than we anticipated. We are currently exploring these possibilities.

## REFERENCES

1. Horak FB. *Age Ageing*; **35**(2), ii7-ii11, 2006.
2. Delignières D, et al. *PLoS Comput Biol*, **7**(2), e1001089, 2011.
3. Peng CK, et al. *Chaos*, **5**(1), 82-87, 1995.

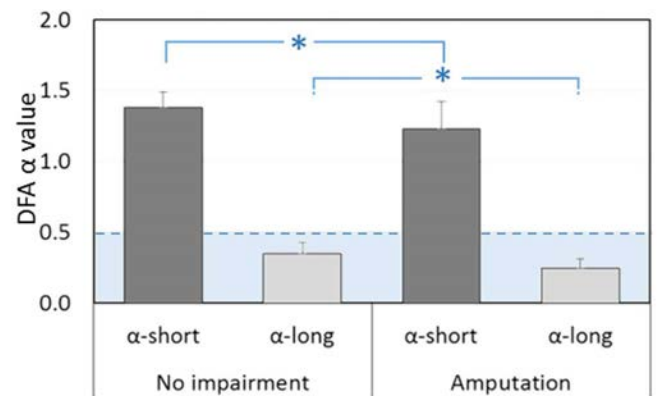


**Figure 1:** AP fluctuations in center of pressure velocity. Individuals with amputation exhibited greater antipersistence at short and long timescales. \*group differences significant at  $p < 0.05$ . Both groups exhibited marked differences between short term (persistent;  $\alpha > 0.5$ ) and long term (antipersistent;  $\alpha < 0.5$ ) behavior.  $\alpha = 0.5$  (dotted line) indicates randomness.

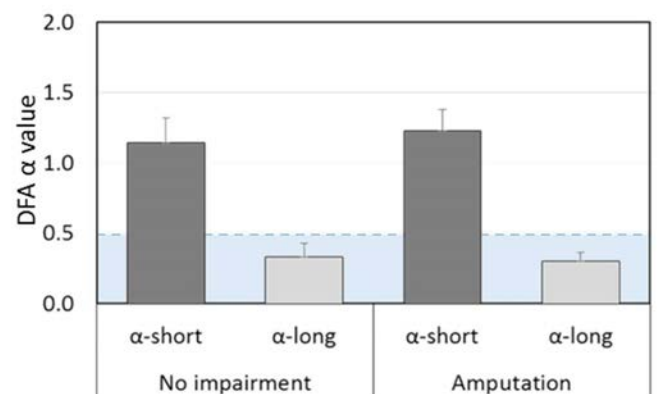


**Figure 2:** ML fluctuations in center of pressure velocity. There was no difference between groups in short and long term persistence ( $\alpha_{\text{short}}$ :  $p = 0.36$ ;  $\alpha_{\text{long}}$ :  $p = 0.53$ ). Both groups exhibited marked differences between short term (persistent;  $\alpha > 0.5$ ) and long term (antipersistent;  $\alpha < 0.5$ ) behavior.  $\alpha = 0.5$  (dotted line) indicates randomness.

## ACKNOWLEDGMENTS

This work was supported by NIH P20GM109090 and NIH R15HD08682.

# STANDING BALANCE RESPONSES TO PROJECTED SENSORY STIMULI IN BELOW-KNEE AMPUTEES

<sup>1</sup> Courtney Shell, <sup>2,3</sup> Hamid Charkhkar, <sup>2,3</sup> Dustin Tyler, <sup>1,2</sup> Paul Marasco, and <sup>2,3</sup> Ron Triolo

<sup>1</sup> Lerner Research Institute, Cleveland Clinic, Cleveland, OH, USA

<sup>2</sup> Advanced Platform Technology Center, Louis Stokes Cleveland VA Medical Center, Cleveland, OH, USA

<sup>3</sup> Case Western Reserve University, Cleveland, OH, USA

email: shellc@ccf.org

## INTRODUCTION

While able-bodied individuals use both vision and proprioception to control posture, amputees rely more heavily on vision [1]. Reliance on vision increases attention required to safely complete tasks and hinders mobility in poor lighting conditions and when terrain is uncertain or variable.

In a below-knee human amputee, we have developed a system that can provide natural sensory feedback perceived as coming from the lost limb by stimulation of sciatic, tibial, and common peroneal nerves through nerve cuff electrodes implanted in the popliteal fossa. Although a similar technology has been previously used to elicit sensation in upper limb amputees [2], we report, for the first time, the feasibility of this technology to restore sensation in people with lower limb amputation. Based on our preliminary observations, the stimulation signal delivered to the nerves can be finely tuned to elicit sensations of toe movement in the missing limb.

As a first step toward understanding how natural sensation can be used to improve functional performance, we examined responses during standing balance to randomly-timed stimuli that induced the sensation of toe movement.

## METHODS

A volunteer who had undergone below-knee amputation 48 years ago as a result of trauma on his left leg (male, 67 years old, 234 pounds) was implanted with 16-contact nerve cuff electrodes around the sciatic, tibial and fibular nerves above the knee in his residual limb in an IRB-approved surgical procedure. Stimulation applied to different

contacts in the cuffs elicited sensations of touch or movement projected to discrete locations on his missing limb. Specific contacts and stimulation parameters (pulse amplitude and duration) that produced four distinct sensations of toe movement (medial toes moving down, lateral toes moving down, medial toes lifting, and lateral toes lifting) were identified and subsequently utilized during quiet stance.

The subject stood wearing his conventional prosthesis with eyes closed, arms by his side, and feet positioned on two different force plates (OR6-6, AMTI). Body position was recorded using a 16-camera motion capture system and the Plug-In Gait marker set (collection Nexus 1.6.1, post-processing Nexus 1.8.5, Vicon). An interactive pen display screen in front of the subject provided cues and recorded drawn responses (CINTIQ, WACOM).

The set of stimulation parameters corresponding to each of the four perceived toe movements was applied at least five times in a random sequence with catch trials where no stimulation was applied interspersed. The subject took breaks to sit every 10-15 minutes to limit fatigue. The sensation of toe movement was induced much like a perturbation by applying stimulation for a random 5 second interval during a 20 second trial with eyes closed. Thus the subject was unaware of the timing and intended sensation defined by stimulation. Having completed a trial, the subject described any sensation felt along with its location and intensity.

Postural sway in response to sensory stimulation was characterized by the range of the net center of pressure (COP) in the anteroposterior (AP) and mediolateral (ML) directions as well as COP path

length. These values were averaged across trials with similar perceived sensations (MATLAB, MathWorks, Inc.). Differences caused by stimulation (5 levels) were assessed using one-way analysis of variance ( $\alpha = 0.05$ ).

## RESULTS AND DISCUSSION

A trend towards greater fore-aft sway, as measured by the range of AP COP, was observed when stimulation inducing the sensation of movement was applied compared to no stimulation (Figure 1). Similarly, COP path length tended to increase with sensory stimulation (Figure 1). With the perception of the medial toes lifting, the ML COP range was slightly lower than the other conditions (Figure 1). None of these differences were large enough to be statistically significant.

In able-bodied individuals, AP COP is controlled by pushing or lifting the toes through adjustments at the ankle [3]. The perturbation-like sensations we provided were similar to sensations that are felt in able-bodied adjustments to AP COP, so the observed changes are consistent with strategies used to control variations in AP COP. The greater range of AP than ML COP in all conditions is consistent with previous standing balance studies in lower-limb amputees and able-bodied individuals [1, 3].

While the changes observed were not statistically significant, trends show that slight postural adjustments were made as a result of sensation. Future work will explore this effect at further post-implantation times, in additional subjects, and in more challenging conditions (e.g., standing with eyes closed on foam). Our system, which allows us to direct sensory feedback by electrical stimulation through nerve cuff electrodes, provides a unique opportunity to study the role of proprioception in amputee balance control tasks.

## REFERENCES

1. Ku PX, et al. *Gait Posture*, **39**, 672-682, 2014.
2. Tan DW, et al. *Sci Transl Med*, **6**, 257ra138(1-11), 2014.
3. Winter DA et al. *J Neurophys*, **75**, 2334-2343, 1996.

## ACKNOWLEDGMENTS

This work was sponsored by the Defense Advanced Research Projects Agency (DARPA) BTO under the auspices of Dr. Doug Weber through the Space and Naval Warfare Systems Center, Pacific Grant/Contract No. N66001-15-C-4038. This material is the result of work supported with resources and the use of facilities at the Louis Stokes Cleveland VA Medical Center.

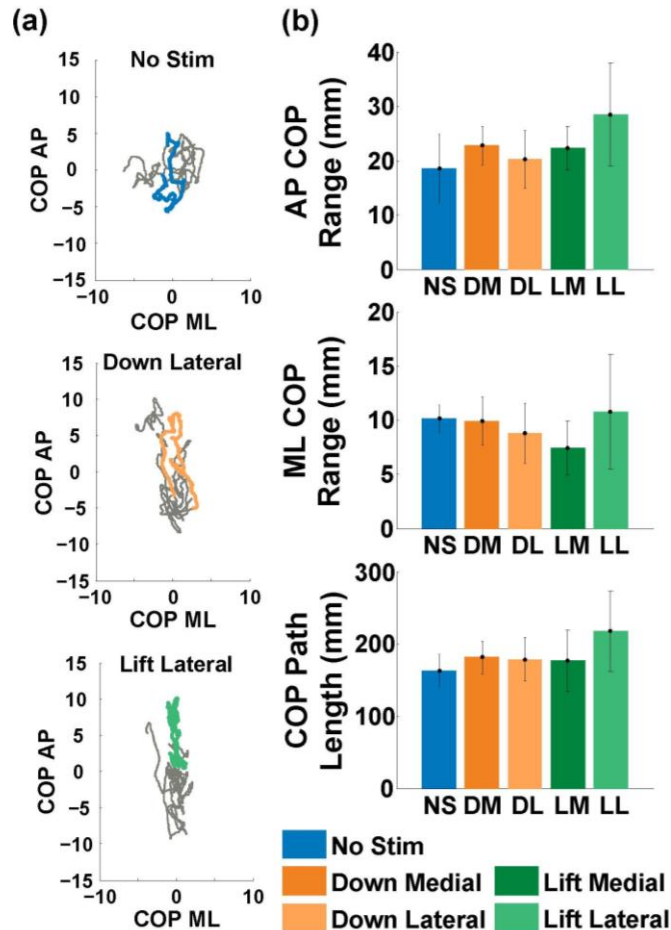


**Figure 1:** (a) Example stabilograms for all 20 seconds from a single standing trial (grey) with the 5 second perturbation period (without stimulation (top), stimulation causing sensations of toes pushing down (middle) and toes lifting (bottom)) highlighted in bold and colored. (b) Anteroposterior (top) and mediolateral (middle) range of center of pressure (COP) as well as path length (bottom) in five different conditions while standing with eyes closed (no stimulation (No Stim) and stimulation causing the sensation of the medial toes moving down (DM), lateral toes moving down (DL), medial toes lifting (LM), and lateral toes lifting (LL)).

# USING APPROXIMATE AND SAMPLE ENTROPY TO MEASURE POSTURAL CONTROL IN INDIVIDUALS WITH ERTL AND NON-ERTL TRANSTIBIAL AMPUTATIONS

<sup>1</sup> Shane P. Murphy, <sup>1</sup> Abbie E. Ferris, <sup>1</sup> Gary D. Heise, <sup>2</sup> Cory L. Christiansen, and <sup>1</sup> Jeremy D. Smith

<sup>1</sup> School of Sport & Exercise Science, University of Northern Colorado, Greeley, CO, USA

<sup>2</sup> Department of Physical Medicine and Rehabilitation, University of Colorado, Aurora, CO, USA

email: shane.murphy@unco.edu

web: www.unco.edu/biomechanics

## INTRODUCTION

Nonlinear methods such as approximate (ApEn) and sample (SampEn) entropy have been used as a measure of regularity to quantify the complexity of the center of pressure (CoP) trajectory in those with lower extremity amputations [1,2]. More complex and irregular CoP trajectories result in higher ApEn or SampEn values, which is often interpreted as more randomness and less neuromuscular control of movements. Lower entropy values have been reported for the affected side of those with unilateral, transtibial amputation (TTA) [1], which is indicative of greater neuromuscular control of the affected limb [3].

The structural properties within the residual limb of a TTA may also play a role in how well the affected limb adapts to changes in surface or visual input. The osteomyoplastic procedure (Ertl) creates a “bone-bridge” between the tibia and fibula, while a Non-Ertl procedure leaves the two bones free floating within the residual limb. The bone bridge in the Ertl technique may provide more structural support and assist with postural control, but little evidence of this exists in the current literature.

It was hypothesized that the affected limb would exhibit lower ApEn and SampEn values compared to the unaffected limb during quiet standing. It was further hypothesized that standing on a rigid surface compared to a compliant surface and standing with eyes open rather than with eyes closed would result in higher entropy values, indicating more complexity and less neuromuscular control. Finally, it was also hypothesized that ApEn and SampEn would be similar for Ertl and Non-Ertl amputation groups.

## METHODS

Fifteen participants with unilateral, TTA were recruited from two groups: Ertl ( $n = 9$ ,  $49 \pm 10$  years,  $75.0 \pm 15.3$  kg,  $1.76 \pm 0.07$  m); Non-Ertl ( $n = 6$ ,  $56 \pm 8$  years,  $85.1 \pm 14.8$  kg,  $1.76 \pm 0.06$  m). Participants gave their informed written consent prior to participation. Participants were asked to stand comfortably with each foot on an individual force plate. Foot placement was measured with respect to the force plates to provide consistent foot positioning when standing on both surfaces. CoP data were collected (2000 Hz) for 30 seconds in four conditions: 1) rigid surface eyes open (RSEO), 2) rigid surface eyes closed (RSEC), 3) compliant surface eyes open (CSEO), and 4) compliant surface eyes closed (CSEC).

The raw CoP data were down sampled to 100 Hz for consistency with common sampling frequencies reported in the literature for quiet standing analyses. The middle 20 s of each trial was used for analysis because participants began each trial with the arms outstretched and the shoulders abducted to 90°. In the last few seconds of each trial, participants were asked to abduct their shoulder to 90° again. So the middle 20 s were data from when the arms were not moving and participants were standing quietly with arms at their side.

ApEn and SampEn were calculated for the anteroposterior (AP) and mediolateral (ML) CoP trajectories (Matlab, MathWorks, Inc., Natick, MA). Entropy parameters for the time series embedded dimension ( $m = 2$ ), tolerance ( $r = 0.2 * \text{stdev}$ ), and time delay ( $\tau = 1$ ) were chosen in accordance with previous literature [4]. A MANOVA ( $\alpha = .05$ ) with a Bonferroni adjustment was performed to identify

significant effects due to limb, surface, vision, and amputation technique, (SPSS 23, IBM, USA).

## RESULTS AND DISCUSSION

Limb ( $p < .001$ ), surface ( $p = .004$ ), and amputation type ( $p < .001$ ) exhibited significant effects at the multivariate level. No significant vision ( $p = .871$ ) or interaction effects were observed.

In both the AP and ML directions, the affected limb had significantly lower ApEn ( $p < .001$ ) and SampEn ( $p < .001$ ) than the unaffected limb. This is similar to results of Wurdeman et al. [1] suggesting that the affected limb requires more neuromuscular control. Comparing across directions, ApEn and SampEn values were larger in the AP direction than the ML direction suggesting a greater level of complexity and lower attentional control in the AP direction. It should be noted that the entropy values in the AP direction are larger than previously reported [5].

The Ertl group had significantly lower entropy values than the Non-Ertl group in the AP direction (Fig. 1) for both ApEn ( $p = .005$ ) and SampEn ( $p = .006$ ). This indicates the Ertl group showed more control than the Non-Ertl group. Considering this outcome in combination with the limb effect from above, the difference between groups appears to be driven by differences between the unaffected limbs rather than differences between affected limbs.

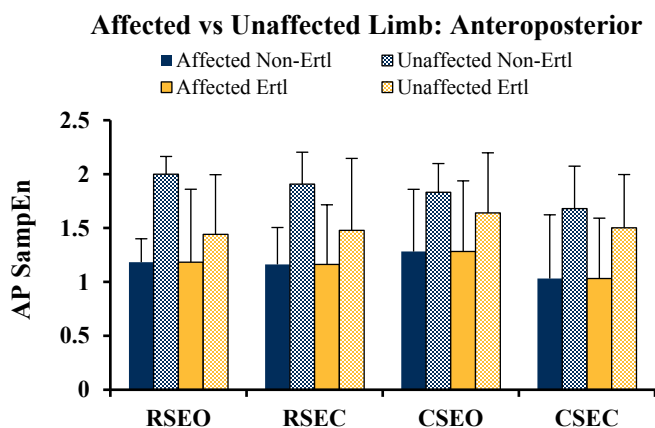


**Figure 1:** Mean SampEn in the AP direction across the four conditions for Non-Ertl (blue) and Ertl (yellow) amputation groups. Errors bars indicate standard deviations.

## Affected vs Unaffected Limb: Mediolateral

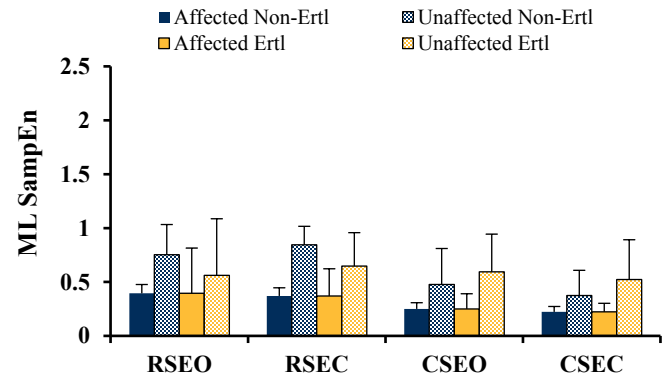


**Figure 2:** Mean SampEn in the ML direction across the four conditions for Non-Ertl (blue) and Ertl (yellow) amputation groups. Errors bars indicate standard deviations.

The compliant surface resulted in significantly lower entropy values compared to the rigid surface in the ML direction (Fig. 2) for both ApEn ( $p = .004$ ) and SampEn ( $p = .001$ ). This suggests that the standing on the compliant surface requires greater neuromuscular control.

Increased entropy values in the current study are likely due to the low standard deviations in the AP direction observed for our groups. Entropy values are sensitive to changes in the tolerance ( $r$ ), which is an input to the model for entropy and depends on the standard deviation of the time series data being analyzed.

## CONCLUSIONS

Consistent with our hypothesis, the affected limb exhibited greater attentional control, based on lower entropy values, than the unaffected limb. Removing vision and standing on a more compliant surface resulted in lower entropy values, which was also consistent with our hypotheses. Contrary to our hypothesis, however, SampEn and ApEn values were different between groups for the unaffected limbs, but similar between the affected limbs.

## REFERENCES

1. Wurdeman SR, et al. *Chaos*. **24**(1), 2014.
2. Hlavackova P, et al. *PLoS ONE*. **6**(5), 2011.
3. Roerdink M, et al. *Exp Brain Res*. **174**, 256-269, 2005.
4. Yentes JM, et al. *Ann Biomech Eng*. **41**(2), 349-365, 2013.
5. Sadeghisani M, et al. *J Ortho*. **13**, 152-156, 2016.

# UNIQUE BALANCE DOMAINS FOR BESS (BALANCE ERROR SCORING SYSTEM) AND Y-BALANCE TESTS

<sup>1</sup> Michael Orendurff, PhD; <sup>2</sup> Christopher Villarosa, BS <sup>3</sup> Joseph Smith, MS, ATC; <sup>3</sup> Charles Chan, MD;  
<sup>1</sup> Carey Hintze, PT, DPT; <sup>1</sup> Kevin Dinglasan, ATC, MS; <sup>1</sup> Kerry Peterson, ATC, MA;

<sup>1</sup> Motion & Sports Performance Laboratory, Stanford Children's Health, Palo Alto, CA, USA

<sup>2</sup> Program in Physical Therapy, University of Washington, Seattle, WA, USA

<sup>3</sup> Stanford Children's Orthopedic & Sports Medicine Center, Palo Alto, CA, USA

Email: [moren@stanford.edu](mailto:moren@stanford.edu), web: <http://www.stanfordchildrens.org>

## INTRODUCTION

Balance is an important element of mobility and functional performance, and errors in balance may contribute to injury risk and hinder locomotor success. Several effective injury prevention programs appear to improve dynamic balance and the resistance to falls from perturbations such as collisions with objects or other individuals that can result in injuries[1]. Evaluating the mechanisms by which fall prevention programs reduce injuries is difficult because strength and balance improvements overlap. Several tests of balance have been developed, but each represents a complex construct of essentially static movements where excessive movements are ranked as errors. Some tests involve maintaining static balance near the base of support, and some tests explore the limits of static stability in more challenging ways. These tests may evaluate covariate domains of balance that are complementary or they may represent unique domains of balance that are differently influenced by injury prevention programs. The purpose of this project was to evaluate the covariance relationship between two commonly used balance evaluation measures: the Balance Error Scoring System (BESS) and the Y-Balance test.

## METHODS

Sixteen healthy, recreationally active adults gave informed consent to participant in this IRB-approved protocol (9 females, 7 males 29 +/-5 yrs; low to high intensity exerciser 2-6 x week). Over a 10-day period, each participant completed the BESS and the Y-Balance protocol four times following a standardized warm up (Figure 1). The total error score on the BESS test for both firm and foam

surfaces was compared to the total distance achieved in the anterior, posteriolateral and posteromedial directions on the Y-Balance test on each day using simple linear regression. It was hypothesized that the  $R^2$  would be in the 0.25 to 0.50 range, indicating some overlap in balance construct domains evaluated by the Y-Balance and BESS tests.



**Figure 1.** Balance Error Scoring System (BESS) and Y-Balance tests.

## RESULTS AND DISCUSSION

Contrary to the hypothesis, the combined data over all 4 days produced an  $R^2 = 0.0000013$ , with a slope of  $-0.00007$  ( $n = 60$ ;  $P = 0.99$ ; Figure 2). Individual day comparisons produced similar results (Figure 3). Day 1:  $R^2 = 0.0295$ ; Day 2:  $R^2 = 0.0290$ ; Day 3:  $R^2 = 0.0039$ ; Day 4:  $R^2 = 0.040$ .

These data suggest that there was no construct covariance between these two balance tests in this small cohort of recreationally active adults. The range of motion achieved on the Y-Balance test and the requirement to remain stable at the extreme end range of motion in all three directions appears to have little relationship to the BESS error scores

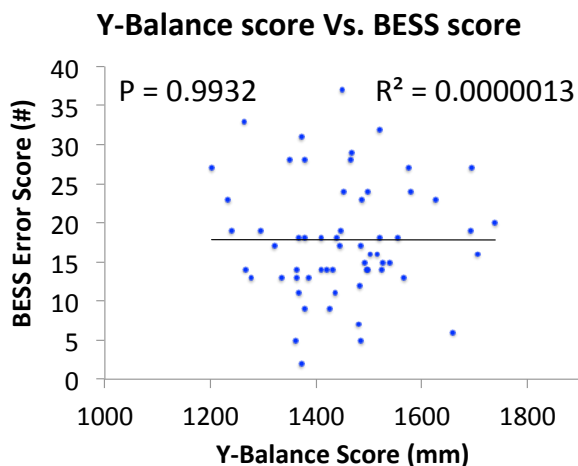


**Figure 2.** Y-Balance scores vs. BESS scores for 16 subjects over 4 days.

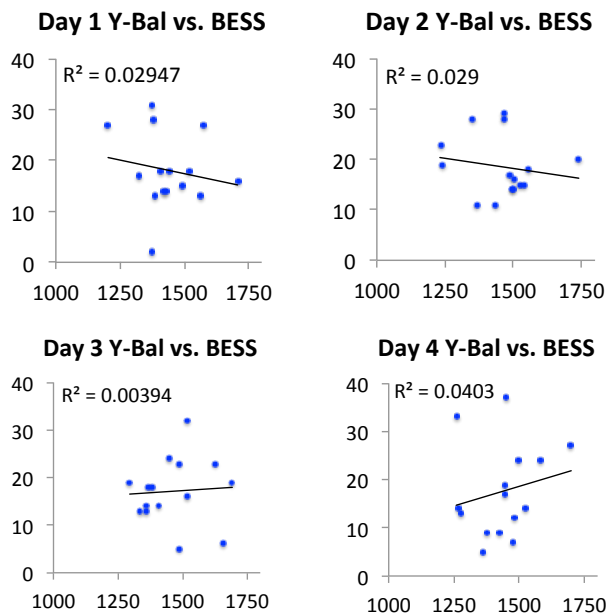


**Figure 3.** Y-Balance vs. BESS for each day.

during static standing balance on firm and foam surfaces. The Y-Balance test is likely to have a much larger strength component, especially for the knee and ankle joints. Greater quadriceps strength may improve performance in Y-Balance test scores but may not be a factor for the BESS test errors. These data suggest that the Y-Balance and BESS tests are unique domains of the complex construct of balance.

Dynamic balance may be improved with injury prevention programs, as demonstrated by risk reductions for both lower and upper extremity injuries that often occurs as a result of collisions

with other individuals[1]. These programs include exercises to improve core strength, lower extremity strength, drills with planned collisions with a teammate in a controlled setting, and drills designed to increase awareness of other players in close proximity. Since injury prevention programs have been shown to produce statistically significant and substantial reductions in injuries to the chest, spine, neck, shoulder, elbow, wrist, and hand this suggest that collision-related falls occur less often after implementation.

Neither the BESS nor the Y-Balance are dynamic balance tests that demand joint moment or power production on the time scale that real world impact perturbations must require. It is very likely that preparatory muscle activation in anticipation of potential collisions is one aspect of the effectiveness of an injury prevention program. This likely plays an interactive roll with the core and lower limb muscle strengthening achieved by the injury prevention program. Therefore, the interaction of increased muscle strength and more rapid force production, improved balance, and increased awareness of potential collisions are likely to contribute to the effectiveness of injury prevention programs. If these interactions could be better understood, more effective injury prevention programs could be designed.

It is possible that an additional dynamic balance test may need to be developed that more closely mimic the improvements in balance that appear to occur when injury prevention programs are implemented.

## CONCLUSIONS

The BESS and Y-Balance tests appear to evaluate distinctly separate domains of the complex construct of balance.

## REFERENCES

1. Silvers-Granelli H, et al. *Am J Sports Med*; 43, 2628-37, 2015.

## DISCLOSURE

This research was funded by a grant from E2 Technologies who had no influence on the design, conduct, data collection, interpretation or decision to analyze or publish these results.

# POSTURAL STABILITY DURING QUIET STANDING IN PERSONS WITH ERTL AND NON-ERTL TRANSTIBIAL AMPUTATIONS

<sup>1</sup>Gabrielle Rentuma, <sup>1</sup>Abbie E. Ferris, <sup>1</sup>Vanessa A. Kellems, <sup>1</sup>Gary D. Heise,  
<sup>2</sup>Cory L. Christiansen, & <sup>1</sup>Jeremy D. Smith

<sup>1</sup>School of Sport & Exercise Science, University of Northern Colorado, Greeley, CO

<sup>2</sup>Interdisciplinary Movement Science Lab, University of Colorado, Anschutz Medical Campus, Denver, CO  
email: [abbie.ferris@unco.edu](mailto:abbie.ferris@unco.edu); website: <http://www.unco.edu/biomechanics>

## INTRODUCTION

Quiet standing under various conditions is often assessed in order to understand postural deficits in various populations [1]. Individuals with transtibial amputation (TTA) are at an increased risk of falling due to functional deficits created by the amputation [2]. During quiet standing with both feet on one force plate, persons with TTA exhibit increased center of pressure (COP) displacements and increased COP velocities compared to non-amputees [2-4]. The increase in these measures is often associated with increased instability. Differences between limbs, however, cannot be assessed with both feet on a single force plate.

Two primary TTA amputation techniques are used; Non-Ertl and osteomyoplastic amputation (Ertl). Non-Ertl amputations leave the tibia and fibula disconnected, whereas a bone bridge connect the tibia to the fibula in the Ertl technique [5]. Due to the differences in these two amputation techniques, functional differences may exist between the groups.

The purpose of this study was to compare postural control of individuals with Ertl and Non-Ertl transtibial amputations during quiet standing under two surface and two vision conditions. Our goal was to establish if a difference exists between the two groups. To this end, we established the null hypothesis there would be no differences in COP displacements, velocities, or frequencies between Ertl and Non-Ertl techniques. However, we hypothesized that both groups would be more unstable as surfaces changed from rigid to compliant and vision was removed. Additionally, we hypothesized that the affected limb would be more unstable than the unaffected limb, as reflected by increased COP measures.

## METHODS

Individuals with Ertl ( $n = 9$ ,  $49 \pm 10$  years,  $75.0 \pm 15.3$  kg,  $1.8 \pm 0.1$  m) and Non-Ertl amputations ( $n = 6$ ,  $56 \pm 8$  years,  $85.1 \pm 13.5$  kg, height  $1.8 \pm 0.1$  m) participated in this study. Inclusion criteria included: amputation resulting from trauma, no concomitant musculoskeletal injuries, no neurological or visual impairments, physically active at least 3 days a week, and classified as K3 or above.

Participants stood shod with each foot positioned on separate force plates. Vertical ground reaction force (GRF, 2000 Hz) and center of pressure (COP) data were collected during each trial. Participants maintained a quiet standing position for 30 s under four separate conditions: 1) rigid surface, eyes open (RSEO), 2) rigid surface, eyes closed (RSEC), 3) compliant surface, eyes open (CSEO), and 4) compliant surface, eyes closed (CSEC). Vertical GRFs and COP data were down sampled at 100 Hz which is a common sampling frequency for quiet standing. Only the middle 20 s of each 30 s trial were analyzed to remove the influence of the upper extremities at the beginning and end of the trial. Dependent variables were calculated according to methods described by Prieto et al. [1] in both the mediolateral (ML) and anteroposterior (AP) directions. Weight distribution was expressed as the average vertical GRF under the foot, divided by the sum of vertical GRF under both feet. A 4-factor MANOVA (amputation technique x vision x surface x leg,  $\alpha = .05$ ) with Bonferoni adjustment was used to evaluate differences in dependent variables.

## RESULTS AND DISCUSSION

There was a significant multivariate effect observed between amputation type, vision, surface, and leg

conditions ( $p < 0.001$ ). No interaction effects were identified.

The affected limb was found to bear significantly ( $p = .005$ ) more weight than the unaffected limb across all conditions (Ertl:  $50.9 \pm 4.1\%$  vs  $48.0 \pm 4.2\%$ ; Non-Ertl:  $50.2 \pm 4.6\%$  vs  $48.6 \pm 4.4\%$ ).

The mean AP (Fig.1) and ML COP velocities increased from rigid to compliant surface ( $p < .001$ , AP;  $p = .004$ , ML) and from eyes open to eyes closed conditions ( $p < .001$ , AP;  $p = .020$ , ML). Mean COP velocity was higher in the affected limb than the unaffected limb for both groups ( $p < .001$ , AP and ML). The Ertl group had higher mean COP velocities in both the AP and ML directions than the Non-Ertl group across all conditions ( $p < .001$ ). The larger COP velocity in the Ertl group suggests they were less stable than the Non-Ertls.

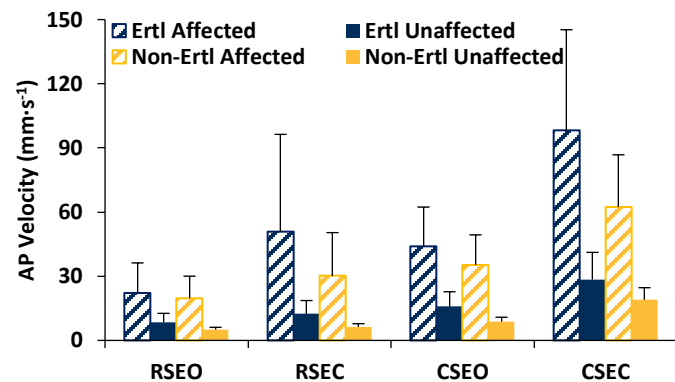


Figure 1. Mean (sd) COP AP velocities for each condition.

Both groups increased mean ML frequency ( $p < .001$ ) and mean AP frequency ( $p < .001$ ) with eyes closed. The Ertl group had higher frequencies in the AP ( $p = .011$ ) and ML ( $p < .001$ ) directions compared to the Non-Ertl group across all conditions. The affected limb exhibited higher AP ( $p = .009$ ) and ML ( $p < .001$ ) frequencies than the unaffected limb. Only the ML frequency increased between surfaces ( $p = .005$ ). Again frequency analysis suggests the Ertl group was adjusting posture more than the Non-Ertl group, suggesting greater instability for the Ertl group.

The 95% confidence ellipse area (95% CE area; Fig. 2) was larger in the affected limb compared to the unaffected limb ( $p = .001$ ). Both groups had a larger 95% CE area when their eyes were closed ( $p = .012$ )

and on a compliant surface ( $p < .001$ ). The Ertl group had a significantly larger 95% CE area across all conditions than the Non-Ertl ( $p = .001$ ), again suggesting greater postural instability in the Ertl group.

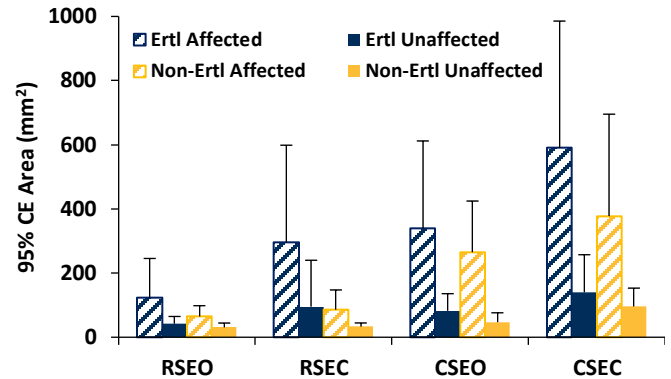


Figure 2. Mean (sd) 95% CE area for all four conditions.

## CONCLUSION

In general, both groups showed increased COP velocities, 95% CE area, and frequencies when their eyes were closed or on the compliant surface, supporting our hypothesis. This would suggest that closing one's eyes or standing on uneven surfaces increases instability. It is not unexpected to see increased instability during these tasks as the proprioceptive or visual feedback has been altered; this has been demonstrated in multiple populations [6, 7]. Our results support our hypothesis that differences between the affected and unaffected limbs exist and that these differences are exacerbated by standing on unstable surfaces and closing the eyes.

However, it was surprising to note the Ertl group showed a tendency to be more unstable than the Non-Ertl group contrary to our hypothesis. Further investigation into the mechanisms behind the differences between these two amputation techniques is needed.

## REFERENCES

- Prieto, T.E., *et al.* IEEE Trans Biomed Eng, 1996. **43**(9): p. 956-66.
- Buckley, J.G., *et al.* Am J Phys Med Rehabil, 2002. **81**(1): p. 13-20.
- Mayer, Á., *et al.* BMC Musculoskel Disord, 2011. **12**(1): p. 118.
- Hlavackova, P., *et al.* PLOS ONE, 2011. **6**(5): p. e19661.
- Ertl, J., *et al.* February 15, 2013
- Mackey, D.C., *et al.* Clin Biomech, 2005. **20**(8): p. 776-83.
- Szczepeńska-Gieracha, J., *et al.* Am J Alzheimer's Dis Other Dementias, 2015: p. 1.

# STRENGTH AND SKELETAL MUSCLE TROPONIN IN POSTURAL CONTROL

<sup>1</sup>Gregory W. King, <sup>1</sup>Eduardo L. Abreu, <sup>1</sup>Patricia J. Kelly, and <sup>2</sup>Marco Brotto

<sup>1</sup>University of Missouri – Kansas City, Kansas City, MO, USA

<sup>2</sup>University of Texas at Arlington, Arlington, TX, USA

email: kinggr@umkc.edu

## INTRODUCTION

It is well known that postural control declines with age, as evidenced by age-related changes in center of pressure (COP) metrics during postural sway. Several authors have modeled the postural control system as an inverted pendulum with proportional-integral-derivative (PID) feedback control, which produces ankle torque to maintain stable positioning of the body's center of mass (COM). Such models have demonstrated effects consistent with age-related changes in COP, including increased postural stiffness and damping, noise, and sensory delay time [1-3]. Age-related declines in strength likely play a role in these observations. In our previous work, we investigated the use of skeletal muscle-specific troponin T (sTnT), a binding site for  $Ca^{2+}$  ions enabling formation of actin-myosin crossbridges, as a biomarker for age-related strength loss and sarcopenia. Initial results suggest that blood levels of sTnT were negatively correlated with grip strength [4] and with scores on a balance assessment instrument [5]. Still, the mechanisms by which strength declines affect postural sway are not fully understood. To investigate this, we tested the hypothesis that control parameters derived from an inverted pendulum sway model would be positively correlated with blood levels of sTnT, and negatively correlated with grip strength.

## METHODS

Eleven female older adults (M=88.3, SD=4.6 years) and eight female young adults (M=22.4, SD= 3.1 years) were recruited for the study, which was approved by UMKC's Institutional Review Board. A phlebotomist collected blood samples, from which sTnT levels were measured using an ELISA kit (USCN Life Science Inc., Houston, TX, USA). Maximum grip force for subjects' left ( $F_L$ ) and right

( $F_R$ ) hands were measured with a grip strength dynamometer (Detecto Scale Company, Web City, MO, USA). Subjects performed quiet stance trials under both eyes open (EO) and eyes closed (EC) conditions while standing on a force platform (AMTI, Watertown, MA, USA), which measured COP time series at a sampling rate of 1 kHz. Each subject was modeled as a single-link inverted pendulum with PID ankle torque feedback (Fig. 1). Models were characterized by PID controller gains

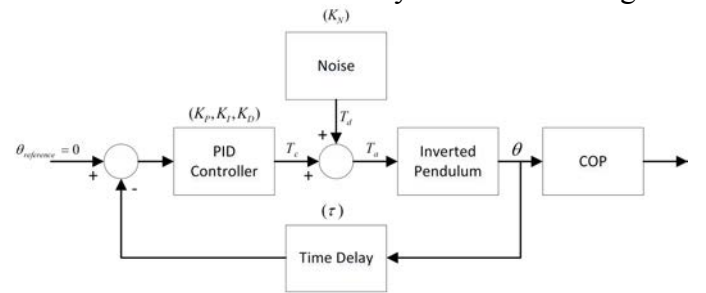


**Figure 1:** Inverted pendulum model and controller:  $T_c$ , control torque;  $T_d$ , disturbance torque;  $T_a$ , applied ankle torque;  $\theta$ , sway angle.

$K_p$ ,  $K_i$ , and  $K_d$ , disturbance torque noise gain  $K_N$ , and time delay  $\tau$ . Initial model simulations were run iteratively to find, using a genetic algorithm, control parameters that minimized the error between simulated and experimental COP metrics as quantified by the cost function:

$$E = \sum_{i=1}^N \left( \frac{C_{sim,i} - C_{exp,i}}{C_{exp,i}} \right)^2$$

where  $C_{sim}$  and  $C_{exp}$  are simulated and experimental COP metrics, respectively and  $N = 7$  represents the number of COP metrics included in the cost function (including root-mean-squared distance, mean velocity, centroidal frequency, frequency dispersion, and short-term scaling coefficient, critical point time, and critical point amplitude derived from

stabilogram – diffusion analysis [1]). Following paired-samples t-tests to confirm that no significant differences existed between  $C_{sim}$  and  $C_{exp}$  metrics, bivariate correlation analyses were performed between control parameters and sTnT metrics. For comparisons exhibiting significant correlations, follow-up stepwise regression analyses were performed with sTnT level as the dependent variable and control parameters ( $K_P$ ,  $K_I$ ,  $K_D$ ,  $K_N$ , and  $\tau$ ) as the predictor variables. All COP analyses and modeling were performed with MATLAB R2014a (The Mathworks, Inc., Natick, MA, USA), and statistical analyses were performed with IBM SPSS Statistics (IBM Corporation, Armonk, NY, USA).

## RESULTS AND DISCUSSION

In the EO condition, regression analysis revealed that  $K_I$  significantly predicts both  $F_L$  ( $b=-391.99$ ,  $p=.011$ ) and  $F_R$  ( $b=-416.99$ ,  $p=.027$ ). In the EC condition, regression analysis revealed that  $K_D$  significantly predicts sTnT level ( $b=263.51$ ,  $p=.026$ ), both  $K_P$  ( $b=-43.84$ ,  $p<.001$ ) and  $K_N$  ( $b=0.11$ ,  $p=.021$ ) significantly predict  $F_L$ , and that both  $K_P$  ( $b=-51.95$ ,  $p<.001$ ) and  $K_N$  ( $b=0.14$ ,  $p=.011$ ) significantly predict  $F_R$ .

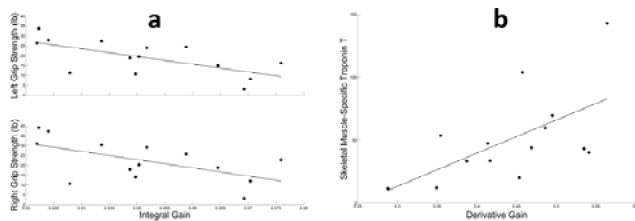


**Figure 2:** Regression plots depicting: (a) relationship between  $K_I$  and grip strength force for EO; (b) relationship between  $K_D$  and sTnT for EC.

These results suggest at least some relationship between postural control parameters and muscle-related measures of strength. Grip strength force was significantly predicted by  $K_I$  in the EO condition, and by  $K_P$  and  $K_N$  in the EC condition. The strong negative correlation between  $K_P$  and grip strength may indicate a compensation mechanism serving to increase postural stiffness, and thus decrease sway amplitude, in the presence of reduced strength. This result is consistent with other work reporting age-related increases in postural stiffness [1]. The modest positive correlation between  $K_N$  and grip strength

may indicate that increases in strength available for postural control are accompanied by slight reductions in the postural control system's sensitivity to changes in sway. Interestingly, the association between  $K_P$ ,  $K_N$ , and grip strength was only observed in EC conditions, suggesting that the presence of visual input in the EO condition eclipsed any association that may have been present. However,  $K_I$  was observed to have a negative correlation with grip strength force in the EO condition. Since  $K_I$  controls steady state error, it is possible that the observed correlation may again represent a compensation mechanism, this time serving to minimize COP-COM error in the presence of reduced strength. Our results also demonstrate that sTnT levels are significantly predicted by  $K_D$ . This suggests that declines in muscle contraction strength and efficiency that presumably accompany an increase in sTnT levels are at least partially compensated for by increased postural damping, which serves to minimize overshoot and ultimately minimize COP-COM error. Again this effect was only observed in the EC condition, suggesting that such a compensation mechanism is not needed or possibly obscured in the presence of visual input.

## CONCLUSIONS

In this study, we demonstrated relationships between strength-related measures and postural control parameters, providing further insight into the role of muscle strength in postural sway and balance impairment. Our results were primarily apparent in the EC condition, suggesting that any strength-related performance declines were not severe enough to be observable with visual input available. Our work provides new evidence for the potential utility of both grip strength testing and skeletal muscle-specific troponin T as biomarkers of strength-related declines of postural sway and balance impairment.

## REFERENCES

1. Maurer C, et al. *J Neurophysiol* **93**, 189-200, 2005.
2. Qu X, et al. *J Biomech* **40**, 3590-3597, 2007.
3. Qu X, et al. *Gait Posture* **30**, 518-522, 2009.
4. Abreu AL, et al. *Nurs Res* **63**, 75-82, 2014.
5. King GW, et al. *Oncotarget* **7**, 13297-13306, 2016.

# ASSESSMENT OF SINGLE LEG POSTURAL CONTROL USING A STABILOGRAM DIFFUSION ANALYSIS AFTER STABILIZING FROM A FORWARD OR SIDEWAYS HOP

<sup>1</sup>K. Otto Buchholz, <sup>1</sup>Nathan J. Robey, <sup>2</sup>Sutton B. Richmond, <sup>1</sup>Abbie E. Ferris, <sup>1</sup>Jeremy D. Smith, and <sup>1</sup>Gary D. Heise

<sup>1</sup>University of Northern Colorado, Greeley, CO, USA

<sup>2</sup>Colorado State University, Fort Collins, CO, USA

email: [otto.buchholz@unco.edu](mailto:otto.buchholz@unco.edu) web: <http://www.unco.edu/biomechanics/>

## INTRODUCTION

Analysis of postural control attempts to gain insight into systemic control strategies. Center of pressure (COP) movement during quiet standing is commonly analyzed to understand postural control. Collins and DeLuca [1] proposed a stabilogram analysis method which attempts to yield more physiologically meaningful results. Stabilogram-diffusion analysis (SDA), assumes that COP trajectories can be modeled as a system of one- and two-dimensional random walks. SDA computes mean squared displacement between COP coordinates at various time intervals to determine displacement (Figure 1). A critical point is identified as the point where the steep initial slope transitions to a shallower slope as the time interval between points increases. It is thought that the critical point is related to short-term (ST) and long-term (LT) postural control strategies. A linear plot in the time domain produces associated diffusion coefficients (D) and a log-log plot of this data produces scaling exponents (H) for each timeframe. These coefficients provide insight into the variability (D values) and randomness (H values) of the measure being analyzed. Implications are then made about the use of open- or closed-loop control.

SDA is regularly applied to single- and double-leg quiet stance [1], however, it is unclear if quiet stance is immediately preceded by a dynamic task, such as hopping, whether results would be similar to these previous quiet stance tasks. Direction may also be important, as Wikstrom et al. [2] showed that single-leg stability decreases as the direction of the hop changed from forward to lateral.

Leg dominance is also commonly considered regarding postural control, as the general belief is that control strategies differ by leg dominance. Yet, Huurnink et al. [3] reported that leg dominance is

task specific and did not produce significant differences when analyzing postural stability.

The current study investigated differences between SDA values after stability was attained during single leg quiet stance after landing from a hop. Differences were analyzed based on the hop direction and the leg used. We aimed to provide insight into how static stance is controlled after a dynamic task.

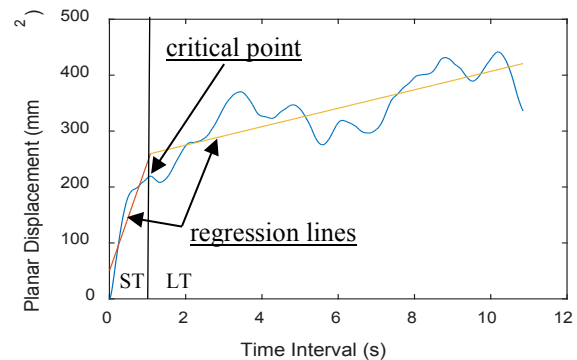


**Figure 1:** A representative SDA plot (mean square planar displacement ( $\text{mm}^2$ ) vs time interval) of a single hop from one participant in the present study. The vertical line denotes the time interval at which the critical point occurs.

## METHODS

Nineteen healthy, recreationally active men ( $n = 8$ ) and women ( $n = 11$ ) volunteered for this study ( $26 \pm 5$  yrs,  $70.3 \pm 9.8$  kg,  $172.7 \pm 9.4$  cm). Participants (all right leg dominant) completed four barefoot hopping tasks onto an AMTI force platform, one with each leg, from both the forward and sideways directions. For the forward hop, the participant took two steps forward and hopped from 50% of their leg length. They took off from the second step on the contralateral foot and landed on the test leg. For the sideways hop, the participant hopped laterally onto the plate from 10 cm away, starting in a single leg stance on the test leg and landing on the same leg. Participants were instructed to remain balanced on the single leg for 20 s after landing.

Ground reaction forces (GRF) were collected at 1000 Hz. To analyze the mean square displacement, the values for the current study were processed to remove the initial COP deviation away from center due to landing, starting the analysis at the point of stability. Stability was defined when vertical GRF was within 5% of body weight for the remainder of the trial. SDA was then used to calculate the critical point to identify the short- and long-term regions and resulting D and H values.  $D_S$  and  $D_L$  were calculated as one-half the slope of each least-squares linear fit of the linear plot (Figure 1). Similarly,  $H_S$  and  $H_L$  were calculated from log-log plots of the data [1]. A two-factor (leg, hop direction) MANOVA was used to test for differences in the critical point, D, and H values between conditions ( $\alpha = .05$ ).

## RESULTS AND DISCUSSION

No significant main effect of leg or direction was observed for any values, nor was there an interaction effect between the main factors. As no difference was found between legs, which agrees with prior findings [3], the means presented (critical point, D, H) are pooled to include both legs per directional condition.

**Table 1:** Mean(SD) SDA diffusion coefficients (D,  $\text{mm}^2 \cdot \text{s}^{-1}$ ) and scaling exponents (H) for the short- (S) and long-term (L) regions.

Hop	$D_S$	$D_L$	$H_S$	$H_L$
Forward	94.91 (41.9)	8.7 (9.66)	.58 (.08)	.15 (.13)
Sideways	94.34 (52.7)	9.57 (10.46)	.56 (.1)	.17 (.13)
<b>Comparative Data</b>				
Heise[4]	450.59	36.86	0.49	0.13
Collins[1a]	6.74	1.76	0.76	0.28
Collins[1b]	11.21	3.05	0.76	0.34

Note: Mean values of current study represent both legs ( $n = 38$ ). Means from Collins [1] are from two different groups (a – 30 x 30 s trials, b – 10 x 30 s trials) during a static bipedal stance. Heise [4] represents a forward step-step-hop task from 100% of leg length.

The mean critical point occurred at (1.13 s, 173.8  $\text{mm}^2$ ) in the forward direction, and at (1.29 s, 193.1  $\text{mm}^2$ ) in the sideways direction, which was not significantly different between directions. This is contrary to results from Wikstrom et al. [2] indicating that mediolateral stability decreases as a hop task becomes more lateral. However, the absolute mean values did trend in the direction of Wikstrom et al. [2].

Critical points in the current study occurred at a longer time intervals than previously reported for a forward hop (0.72 s, 587  $\text{mm}^2$ ) reported by Heise et

al. [4]. Differences from Heise et al. [4] are due to methodological differences. The forward hop distance was from 100% of leg length [4] and the analysis started immediately after ground contact, as opposed to the current study's time of stability starting point. Interestingly, our time interval for the critical point of the forward hop was more consistent with the critical point (1.04 s, 13  $\text{mm}^2$ ) reported by Collins and De Luca [1] for double legged quiet standing. Thus, the process of stabilizing may switch from open loop control to closed loop control at shorter time intervals compared to standing quietly.

In general, the diffusion coefficients (D) were greater when compared to static tests [1], but were lower than the values from a similar forward hop [4]. The data from the present study and comparison data are shown in Table 1.

The scaling exponents for both hop directions in the short-term region were trending towards pure Brownian motion ( $H = 0.5$ ), indicating postural control was mostly random. This is supported by the high D values as well, indicating high variability. In comparison, the low  $H_L$  values, combined with low D values, indicate closed-loop control of posture in the long-term region. These long term scaling exponents are smaller compared to those of Collins and DeLuca [1] for double legged stance, but similar to values of forward hops reported by Heise et al. [4]. Thus, regardless of what occurred immediately prior to stability being achieved, it appears that control of single-leg stance over short time intervals is more randomly controlled compared to double legged quiet stance.

## CONCLUSIONS

SDA illustrated that once postural stability was gained following a single-leg hop, there were no significant differences between the direction of the hop or the leg used in terms of measures of variability and randomness within the postural control system.

## REFERENCES

1. Collins JJ, DeLuca CJ. *Exp Brain Res* **95**, 308-318, 1993.
2. Wikstrom EA, et al. *J Sci Med Sport* **11**, 106-11, 2008.
3. Huurnink A, et al. *J Biomech.* **47**, 308-12, 2014.
4. Heise GD, Smith JD, Liu K. *ASB Abstract*, 2012.

# EFFECTS OF SURFACE TYPE ON SINGLE-LEG STANCE UTILIZING STABILGRAM DIFFUSION ANALYSIS

<sup>1</sup>Nathan J. Robey, <sup>1</sup>Otto Buchholz, <sup>2</sup>Sutton B. Richmond, <sup>1</sup>Abbie E. Ferris,  
<sup>1</sup>Jeremy D. Smith, and <sup>1</sup>Gary D. Heise

<sup>1</sup>University of Northern Colorado, Greeley, CO, USA

<sup>2</sup>Colorado State University, Fort Collins, CO, USA

email: [nathan.robey@unco.edu](mailto:nathan.robey@unco.edu), web: <http://www.unco.edu/biomechanics>

## INTRODUCTION

Postural control during quiet stance is often portrayed as corrective responses to small perturbations caused by the inverted pendulum nature of the body. These corrective responses, otherwise known as postural sway, have been used to assess postural stability [1]. Static postural stability is frequently challenged by changes in sensory input (e.g., surface or vision) and/or perturbations during quiet stance. Leg dominance has also been suggested as a potential influencer for postural stability. It is believed that the dominant leg may display increased postural control during single-leg stability tasks. However, previous work has indicated that leg dominance had no significant effect on postural stability [2].

Center-of-pressure (COP) trajectories during quiet stance are commonly used to assess postural stability [3]. Temporal displacements provide a traditional understanding of stability, but offers minimal insight into the physiological meaning of the variables.

Collins and De Luca [4] presented the stabilogram-diffusion analysis (SDA) as a method to physiologically interpret COP trajectories. SDA models the COP during quiet stance as a system of coupled, correlated random walks [4]. A stabilogram-diffusion plot is created by plotting the mean square displacement between COP coordinates against various time intervals between successive points (Fig. 1) [4]. The critical point in this analysis is defined as the point where the initial steep slope changes to a more shallow slope. Collins and De Luca suggested that the critical point represents where the postural control system changes from open-loop to closed-loop control. Collins and De Luca proposed that the critical point may be

representative of pre-programmed central commands that are used during quiet stance [4].

The purpose of this investigation was to use SDA to determine differences in postural control strategies during single-legged quiet standing on rigid and compliant surfaces. The effect of leg dominance during single-leg quiet standing as assessed by SDA, was also evaluated.

## METHODS

Nineteen healthy, recreationally active men (n=8) and women (n=11) volunteered for this study ( $26 \pm 5$  years,  $70.3 \pm 9.8$  kg,  $172.7 \pm 9.4$  cm). For all trials participants (all right leg dominant) were asked to stand barefoot, with their eyes open on an AMTI force platform (Watertown MA, USA) under two conditions: rigid and compliant surfaces.

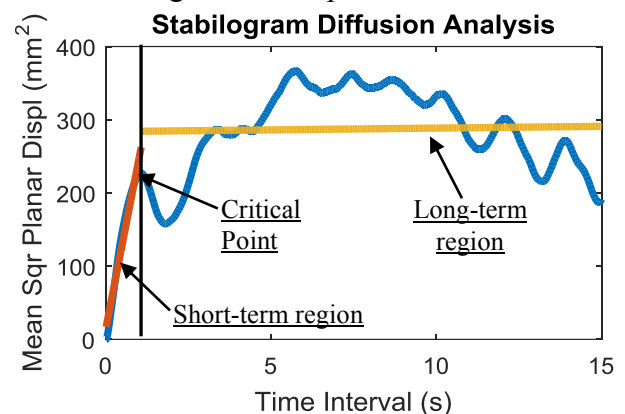


**Figure 1.** A stabilogram-diffusion plot of one representative participant during quiet standing on a compliant surface. Least squares linear fits are shown in each region.

Ground reaction force data were collected at 1000 Hz for 30 s. SDA [4] was then applied to the COP trajectories to create a stabilogram-diffusion plot (Fig. 1). Diffusion coefficients were computed using their respective slopes (short-term,  $D_s$ ; and long-term,  $D_L$ ) for the COP displacement versus time

intervals [4]. Scaling coefficients (short term,  $H_s$ ; long term,  $H_L$ ) were determined from log-log plots of the mean square displacement against time curves [4]. Critical point values, diffusion coefficients and scaling exponents were compared to double leg static stability results [4,5]. A two-factor MANOVA ( $\alpha = 0.05$ ) was performed to identify any significant effects of leg dominance and surface type on SDA values (SPSS 23, IBM, USA).

## RESULTS AND DISCUSSION

Means between each leg were analyzed to compare the effect of leg dominance on postural control using the SDA. However, no significant differences were found between legs, which is in agreement with previous research [2]. This variable was collapsed and taken as a collective average for the rest of the analysis. Surface type revealed a significant difference between  $D_s$  ( $p = 0.003$ ),  $H_L$  ( $p < 0.001$ ), and critical point ( $p < 0.001$ ) indicating a difference between rigid and compliant surfaces.

The mean critical point coordinates were (1.23 s, 134 mm<sup>2</sup>) for the rigid surface and (1.14 s, 297 mm<sup>2</sup>) for the compliant averaged across both legs. Compared to (1.03 s, 13 mm<sup>2</sup>) from Collins and DeLuca [4] and (1.02 s, 16 mm<sup>2</sup>) from Doyle et al. [5] the values for single-leg standing were greater. These critical time intervals have been proposed to represent the transition of the postural control system from open-loop to closed-loop control [4]. Compared to double-legged quiet standing, single-leg standing transitions to closed-loop control occurred at longer time intervals on both rigid and compliant surfaces. However, the increased instability created by the compliant surface in single leg standing appears to result in transition to closed-loop control at shorter time intervals.

Furthermore, both the mean square displacement for the critical point and diffusion coefficients are greater than those seen in Collins and De Luca [4] and Doyle et al. [5] which analyzed double-leg static stability. The increased mean square displacement is likely due to the increased COP sway during single-leg static stability. A significant difference was also

noted over the  $D_s$  coefficients between surface types. This suggests compliant surfaces demonstrated increased levels of variability about the base of support during single-leg static stance.

Short-term scaling exponents ( $H_s$ ) resulted in a value for rigid surface of 0.58, while compliant surface was 0.60. These values are trending towards the value of 0.5 where COP movements over short-term intervals are said to be purely random based on Brownian motion. For the long-term scaling exponent ( $H_L$ ) the rigid surface resulted in a value of 0.12, while compliant demonstrated a value of 0.07. Significance was noted for the scaling coefficient of  $H_L$  indicating a difference between surface types. Thus, these scaling coefficients suggest that posture during single-leg standing was more tightly controlled than double-legged standing, with even tighter control of posture while standing on a compliant surface.

**Table 1:** Mean and standard deviation diffusion coefficients ( $D$ , mm<sup>2</sup>·s<sup>-1</sup>) and scaling exponents ( $H$ ) for the short- (S) and long-term (L) regions of the SDA.

	$D_s$	$D_L$	$H_s$	$H_L$
<b>Compliant</b>	171.39 ± 91.03	3.71 ± 6.19	0.60 ± 0.07	0.07 ± 0.07
<b>Rigid</b>	71.83 ± 0.08	4.01 ± 4.73	0.58 ± 0.09	0.12 ± 0.09
<b>[Collins(a)]</b>	6.74	1.76	0.76	0.28
<b>[Collins(b)]</b>	11.21	3.05	0.76	0.34
<b>[Doyle]</b>	11.00	2.10	0.80	0.24

Note: Mean values from [Collins] are from two different groups a (30 trials, n = 10), b (10 trials, n = 15), mean values from [Doyle] are from 30 s trials (they also analyzed data after 60 and 90 s).

## CONCLUSIONS

Single-legged standing transitions from open-loop control occur at increased time intervals compared to double-leg standing. Changing from a rigid surface to a compliant surface during single-leg standing suggests the transition to closed-loop control occurs over slightly shorter time intervals. Leg dominance does not influence postural control.

## REFERENCES

1. Patel M, et al. *Gait & Posture* **28**, 649-656, 2008.
2. Huurnik A, et al. *J Biomech.* **47**, 308-12, 2014
3. Prieto TE, et al. *IEEE Trans Biomed Eng* **43**, 956-966, 1996.
4. Collins JJ, De Luca CJ. *Exp Brain Res* **95**, 308-318, 1993.
5. Doyle RJ, et al. *Gait & Posture* **27**, 223-230, 2008

# IMPACT OF BABY CARRYING METHOD ON POSTURAL SWAY IN PROLONGED STANDING

<sup>1,2\*</sup>Erin M. Mannen, <sup>1</sup>Alexandra Kahney

<sup>1</sup>University of Denver, Denver, CO; <sup>2</sup>University of Arkansas for Medical Sciences, Little Rock, AR

\*Corresponding Author Email: erinmannen@gmail.com

## INTRODUCTION

Babywearing, the practice of carrying an infant or young child on the caregiver's body in a carrier, has been shown to have numerous emotional, physical, and physiological benefits for babies [1]. The practice of babywearing is becoming more common as parents reap the benefits of close-proximity to their children while remaining "hands-free".

It is known that increased postural sway and asymmetrical loading are linked to pain and increased fall risk [2,3]. While several studies have documented the impacts of backpack load-carriage for military applications and schoolchildren, women are under-represented in load-carriage studies despite research showing women have increased risk of musculoskeletal injuries compared to men [4]. During their lifetimes, many women serve as primary caregivers to children, so a child is a common and relevant load to study. However, no research has been done to analyze the impact of child-carrying methods on the biomechanics of a woman's body. *The purpose of this study is to quantify the impact of two infant carrying methods on a woman's postural sway during prolonged standing.*

## METHODS

Ten female subjects (age:  $27.4 \pm 4.1$  years; BMI:  $21.5 \pm 2.5$  kg/m<sup>2</sup>) with no ongoing musculoskeletal problems and no previous babywearing experience were enrolled in the IRB-approved study. Men, pregnant women, or those with a pregnancy within the past nine months were excluded. Participants underwent testing in the Human Dynamics Lab at the University of Denver.

Each subject completed fifteen-minute quiet standing tasks with each foot placed on a separate force plate (Bertec Corporation, Columbus, OH) for three conditions: **unloaded**, holding a 9-month old infant sized mannequin (Dietz, Freiburg, Germany) **in-arms**, and wearing a 9-month old infant sized mannequin in a baby carrier (**in-carrier**) (Ergobaby,

Inc., Los Angeles, CA) (Figure 1). For the in-carrier trial, subjects watched an instructional video from a certified babywearing professional, and self-fit the baby carrier with the infant mannequin inward-facing. Subjects were instructed to quietly stand for the fifteen minute trials while keeping each foot on its respective force plate. Subjects rested between fatigue trials, and conditions were performed in a random order.

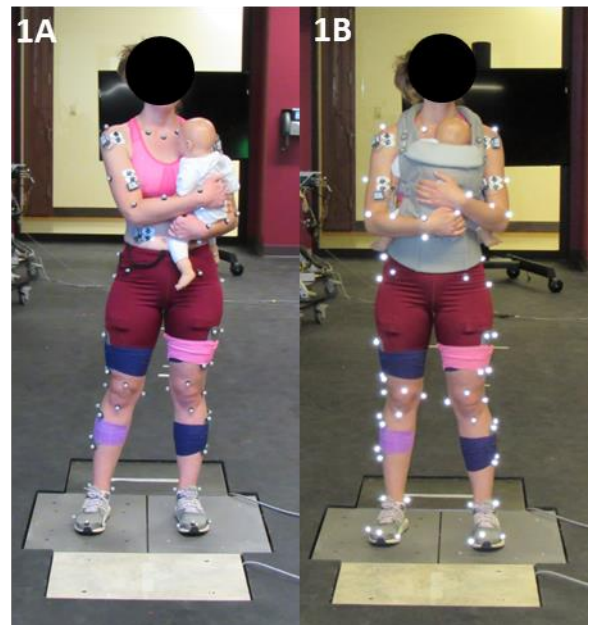


**Figure 1:** In-arms condition (1A) and in-carrier condition (1B).

Data was analyzed at three separate four-minute intervals within the fifteen minute trials: first (0:30 to 4:30), second (5:30 to 9:30), and third (10:30 to 14:30). Custom code (MathWorks, Natick, MA) was written to evaluate postural sway parameters including center-of-pressure (COP) path length, 95% confidence ellipse sway area, medial-lateral (ML) sway variability [root mean square (RMS)], anterior-posterior (AP) sway variability (RMS), and percentage of time of uneven weight distribution (>65% total weight on one limb) for each time period

for each condition. Multiple paired Student's t-tests ( $p < 0.05$ ) were used to compare between conditions (unloaded, in-arms, and in-carrier).

## RESULTS AND DISCUSSION

Baby carrying method was found to impact postural sway parameters during prolonged standing (Table 1). Sway area was 53.3% and 41.3% greater during the in-arms trials v. unloaded trials for the second and third time periods, while the in-carrier condition was not significantly different from the unloaded trials (Figure 2A). Time spent in unequal standing was 2 times greater for the in-arms condition compared to the unloaded condition across all time periods (Figure 2B). ML RMS of the in-arms condition was up to 78% higher than the unloaded condition, while the in-carrier condition was not significantly different than the unloaded condition.

There is greater motion of the COP and more time spent in an asymmetrical stance while carrying an infant in-arms. Both increased COP motion and asymmetric loading have been linked to pain and increased fall risk [2,3]. One goal should be to improve the biomechanics of baby carrying methods to limit COP motion and asymmetry. The current study is limited by sample size, yet significant findings and trends are clear with only ten subjects. Future work will include testing more subjects and performing additional analyses using whole-body motion capture and muscle fatigue using electromyography.

## CONCLUSIONS

Babywearing may offer more postural stability to the caregiver than carrying a baby in-arms, reducing the risks for pain and falls.

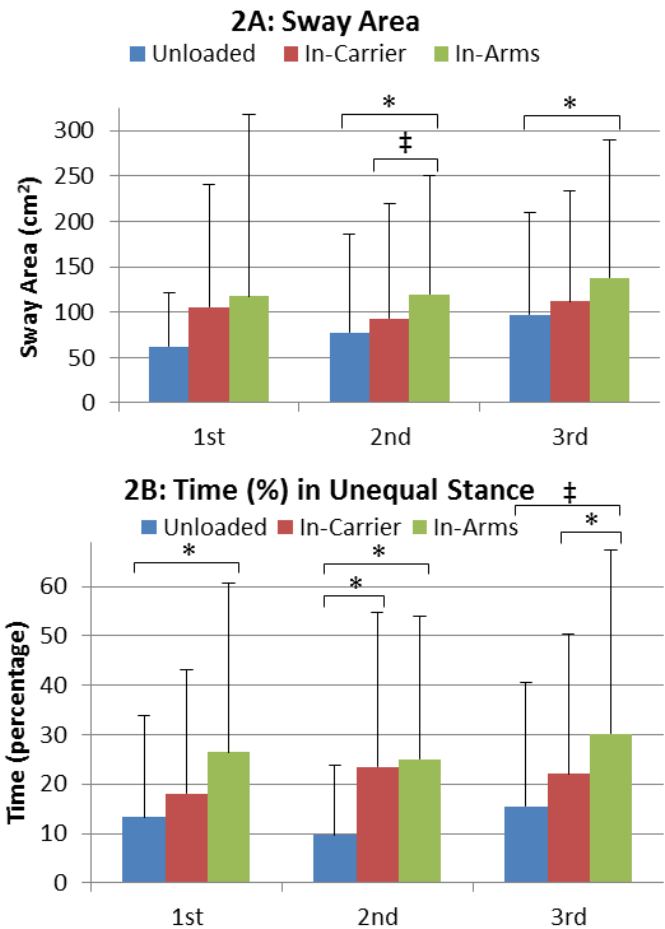


**Figure 2:** Sway area (2A) and time spent in unequal stance (2B) for each condition over all three time periods. \* $p < 0.05$  ‡ $p < 0.1$

## REFERENCES

1. Anisfeld E, et al. *Child Dev* **61**, 1617-1627, 1990.
2. Maki B, et al. *J Gerontol.* **49**(2), M72-84, 1994.
3. Bettany-Saltikov J, Cole L. *Stud Health Technol Inform.* **176**, 117-121, 2012.
4. Beck TF, et al. *Bone* **27**, 437-444, 2000.

## ACKNOWLEDGMENTS

This project was funded by Ergobaby, Inc.

**Table 1:** Postural sway parameters for unloaded, in-carrier, and in-arms conditions for all time periods. (a) indicates significance v. the unloaded condition, (b) v. in-carrier condition, and (c) v. in-arms condition (**bold**  $p < 0.05$ , normal  $p < 0.10$ ) [center-of-pressure (COP); medial-lateral (ML); anterior-posterior (AP); root mean square (RMS)].

	Unloaded			In-Carrier			In-Arms		
	1st	2nd	3rd	1st	2nd	3rd	1st	2nd	3rd
Sway Area (cm <sup>2</sup> )	61.8 (59.9)	77.7 (108.5) <sup>c</sup>	97.3 (112.2) <sup>c</sup>	105.8 (134.5)	92.7 (127.6) <sup>c</sup>	111.8 (121.9)	117.7 (199.6)	119.3 (131.8) <sup>a, b</sup>	137.5 (151.9) <sup>a</sup>
Unequal Stance (%)	13.3 (20.6) <sup>c</sup>	9.7 (14.2) <sup>b, c</sup>	15.5 (25.0) <sup>c</sup>	18.1 (25.0)	23.5 (31.2) <sup>a</sup>	22.1 (28.4) <sup>c</sup>	26.5 (34.3)	25.1 (28.8)	30.2 (37.2) <sup>a, b</sup>
COP Path (m)	7.5 (2.1)	8.3 (3.6)	9.9 (4.9)	8.8 (6.0)	10.0 (7.1)	10.0 (7.0)	10.5 (9.5)	11.6 (7.7)	13.0 (12.5)
ML RMS (mm)	22.3 (20.1)	20.5 (17.6) <sup>c</sup>	26.5 (27.3) <sup>c</sup>	30.4 (30.1)	30.6 (32.4)	33.3 (31.8) <sup>c</sup>	31.1 (33.0)	36.5 (31.8) <sup>a</sup>	43.1 (36.9) <sup>a, b</sup>
AP RMS (mm)	12.4 (5.7)	15.8 (7.3) <sup>b</sup>	16.7 (6.6)	13.6 (7.2)	13.0 (5.4) <sup>a</sup>	15.4 (6.1)	13.4 (9.8)	14.4 (5.7)	15.9 (6.3)

# EFFECTS OF MECHANICAL STEP WIDTH MANIPULATION ON DYNAMIC STABILITY

<sup>1</sup> Landi Wilson, <sup>2</sup> Nicholas Reimold, <sup>1,2</sup> Jesse Dean

<sup>1</sup> Ralph H. Johnson VA Medical Center, Charleston, SC, USA

<sup>2</sup> Medical University of South Carolina, Charleston, SC, USA  
email: wilsolan@musc.edu

## INTRODUCTION

Mediolateral stability during human walking is influenced by the active control of center of mass (COM) trajectory and step-to-step adjustments in foot placement [1]. Based on the inverted pendulum model, margin of stability (MOS) has been proposed as a measure to quantify walking balance. Dynamic MOS is defined as the distance between the lateral margin of the base of support and the extrapolated center of mass (xCOM) – a metric that accounts for COM position and velocity [1]. Based on this model, a smaller MOS would indicate a decreased ability to resist mediolateral perturbations, resulting in an increased risk of a loss of balance.

Individuals with gait deficits often walk with wider steps, generally thought to be a compensatory strategy to maintain lateral stability. Surprisingly, the direct effects of increased step width on lateral stability are not entirely understood. In young healthy controls, *instructed* increases in step width increase mediolateral MOS, presumably increasing stability [2]. However, the natural preference for wider steps among stroke survivors is not accompanied by larger mediolateral MOS values [3-4]. While this discrepancy may be due to the altered control of mediolateral stability in stroke survivors, it could alternatively be an artifact of the difference between instructed and naturally preferred increases in step width.

The purpose of this study was to determine if manipulating the preferred step width in healthy controls would influence the control of mediolateral stability. We hypothesized that encouraging (not prescribing or instructing) wider steps would increase the mediolateral margin of stability.

## METHODS

The preferred step width was manipulated using a novel elastic force-field described previously [5]. Briefly, steel wires in series with extension springs ran parallel to our treadmill belts, and allowed mediolateral forces to be exerted on the legs during swing without affecting forward progression.

Eleven healthy adult subjects (8F/3M; age=25±1 yrs; height=169±9 cm; mass=68±13 kg) completed 7 randomized-order, 6-minute treadmill walking trials. One trial involved normal (no force-field) walking. In three trials, participants interfaced with a “strong” (mediolateral stiffness = 250 N/m) force-field set to encourage step widths of 15, 22.5, or 30 cm. In the remaining three trials, participants interfaced with a “weak” (125 N/m) force-field set to encourage the same range of step widths.

A 16-camera motion capture system (PhaseSpace, Inc.) was used to measure kinematic data at 120 Hz from LED markers placed on the pelvis and feet. Mean step width was calculated as the mediolateral distance between the heel markers upon heel-strike. Center of mass displacement and velocity were estimated using the average location of bilateral ASIS and PSIS markers. Mediolateral margin of stability was calculated as the difference between the xCOM and the lateral boundary of the base of support upon heel-strike. All outcome measures were calculated across the last 3 minutes of each trial.

We used repeated measures ANOVAs to test for significant effects of walking condition on several kinematic measures (mean step width; mediolateral mean COM displacement and velocity upon heel-strike; mean MOS; step-by-step MOS variability).

## RESULTS AND DISCUSSION

The force-field was effective in manipulating preferred step width (Fig. 1A). Significant ( $p < 0.05$ ) increases in step width were observed with the strong force-field set to 22.5 or 30 cm, and with the weak force-field set to 30 cm. Across walking conditions, wider steps were accompanied by significantly ( $p < 0.05$ ) larger mediolateral COM displacements and velocities upon heel-strike.

The combination of these changes in COM displacement and velocity produced a net effect on mediolateral MOS. While a trend was observed for larger MOS with wider steps, this only reached significance ( $p < 0.05$ ) for the condition with the widest steps (Fig. 1B). For this walking condition, the step-by-step variability in MOS was also significantly increased relative to normal walking (Fig. 1C).

Our results match the previous finding that increasing step width in healthy controls causes an increase in MOS and MOS variability [2]. Therefore, this prior result was not simply an artifact of verbally instructing participants to walk with wider steps.

One possible interpretation of these results is that wider steps are subject to greater step-by-step errors, as evidenced by increased MOS variability. In response, humans may choose to actively increase their average margin of stability to reduce the risk of a lateral loss of balance (e.g. by restraining COM

motion). While this explanation is reasonable, the opposite interpretation can also be proposed. Specifically, the larger average margins of stability that accompany wider steps may allow humans to “slack” in the precision of their active control over foot placement location, thus increasing MOS variability. Future work will seek to distinguish between these two distinctly different possible explanations for the observed behavior, and to extend this work to clinical populations.

## CONCLUSIONS

Step width manipulation affects common measures of mediolateral balance. Further investigation of the mechanism underlying changes in margin of stability measures may provide insight into fall risk and gait instability within clinical populations.

## REFERENCES

1. Hof AL et al. *J Biomech* **38**, 1-8, 2005.
2. McAndrew Young PM and Dingwell JB. *Gait & Posture* **36**, 219-224, 2012.
3. Hak L et al. *Clin Biomech* **28**, 1041-1048, 2013.
4. Kao PC et al. *Gait & Posture*, **40**, 457-463, 2014.
5. Nyberg ET et al. *IEEE Trans Neural Syst Rehabil Eng*. In Press.

## ACKNOWLEDGMENTS

This work was partially supported by a grant from the National Science Foundation (#1603391).

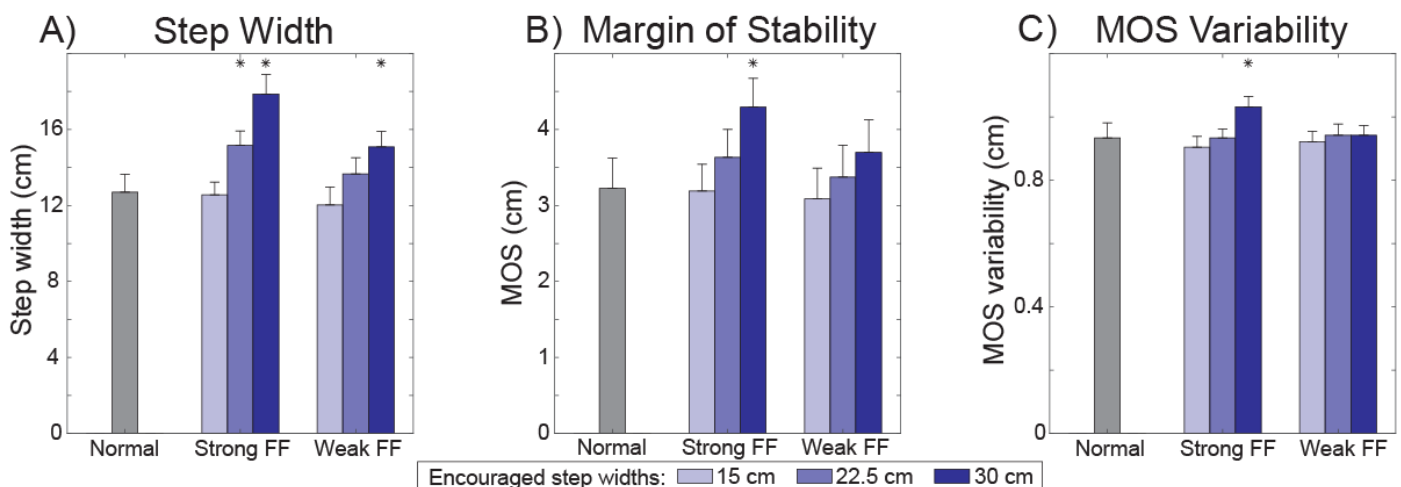


**Figure 1.** Effects of force-field (FF) condition on metrics of mediolateral gait motion. Error bars indicate standard errors, while asterisks indicate a significant ( $p < 0.05$ ) difference from the normal walking condition.

# EFFECTS OF LOCAL MUSCLE FATIGUE ON DYNAMIC POSTURAL CONTROL: A PILOT STUDY

Toshiyuki Kurihara, Tadao Isaka  
Ritsumeikan University, Kusatsu, Shiga, Japan  
Email: t-kuri-a@st.ritsumei.ac.jp

## INTRODUCTION

Muscle fatigue, defined as an acute impairment to produce maximum force, has been shown to impair postural control in single leg stance.<sup>1</sup> Whereas, Shirazi et al.<sup>2</sup> indicated that localized muscle fatigue caused deficits in postural control regardless of the location of fatigue. Winter et al.<sup>3</sup> showed that, in order to control postural stability, human utilize two separate mechanisms: ankle strategy and hip strategy.<sup>3</sup> They explained that the ankle plantar flexors and dorsiflexors play a large role in minimizing anterior-posterior (A/P) movements while the hip abductors and adductors control medio-lateral sway of COP.<sup>3</sup> In addition, the constraint of the great toe deteriorated the A/P weight shifting on dynamic balance.<sup>4</sup>

Common techniques to assess dynamic postural control is a clinical assessment known as the Star Excursion Balance Test (SEBT).<sup>5</sup> The SEBT evaluates the ability to maintain a stable base of support in single limb stance while the opposite limb performs maximal reach excursions in various reach directions. The directional dependency of the muscle activation during SEBT depends on the muscle.<sup>6,7</sup> For example, biceps femoris (BF) electromyographic (EMG) activity was higher during the posterior, posterolateral, and lateral excursions than during the anterior and anteromedial excursions.<sup>6</sup> While, vastus lateralis (VL) activity was less during the lateral excursion than all other directions.<sup>6</sup> Gluteus medius (GM) activity was greater in the anterior and medial directions than in the posteromedial direction.<sup>7</sup>

The purpose of this study was to examine the effects of localized muscle fatigue on dynamic postural control. We choose the fatiguing tasks for the hip abductors, ankle plantar flexors, and toe plantar flexors. It was hypothesized that the each localized fatigue would be effective in each specific direction.

## METHODS

Seven healthy young men free from pain and lower extremity injury were recruited for the study (Age:  $21.1 \pm 0.9$  years; Height  $172.7 \pm 6.0$  cm; Weight:  $67.0 \pm 7.3$  kg) according to guidelines by the Institutional Review Board.

The SEBT is a series of single limb stance using the nonstance limb to touch a point along the lines arranged in a grid that extends from a center point and are  $45^\circ$  from one another. The reaching directions are named in orientation to the stance limb as anterior, anteromedial, anterolateral, medial, lateral, posterior, posteromedial, and posterolateral. While standing on a single limb, the participant reaches as far as possible; lightly touches the line without shifting weight to the reaching limb; and then returns the reaching limb to the center of the grid, reassuming a bilateral stance. Mean reach distance was normalized by the leg length. The participant performed 3 trials in every directions before and after the completion of the fatiguing tasks. The order of the reach directions during the SEBT was randomized for each participant.

Muscular fatigue was induced in either the hip abductors, ankle plantar flexors, or toe plantar flexors with repeated maximum voluntary isometric contractions (MVICs). A maximal load was first determined, and after sufficient rest the participants were asked to perform repeated MVICs following the beat of a metronome (15 contractions/min: 2sec contraction/2sec rest) as many times as possible until peak-torque values declined below 70% MVIC for 2 consecutive trials.

Surface electromyography (EMG) was collected from 11 muscles: erector spinae (ES), adductor magnus (ADD), GM, BF, VL, rectus femoris (RF), gastrocnemius medialis (GS), soleus (SOL),

peroneus longus (PER), tibialis anterior (TA), and abductor hallucis (ABDH). EMG data were collected at 1000 Hz using a wireless system (KinAnalyser, Kissei Comtec co., Japan). Average of rectified EMG signal was calculated over single limb stance phase and normalized to the maximal voluntary contractions of manual muscle testing.

A paired t-test was conducted to test the changes of the SEBT and muscle activities after fatiguing protocols. The level of significance was set at 0.05

## RESULTS AND DISCUSSION

Table 1. summarizes the results of the change of the SEBT, and averaged EMG of 11 muscles after the fatiguing tasks.

After fatiguing hip abductors, SEBT significantly decreased in medial and posteromedial directions, with significantly decreasing VL and GS activities in posteromedial and GM activity in medial. After fatiguing ankle plantar flexors, SEBT significantly decreased in medial, posteromedial, and posterior directions, with decreasing ABDH in posterior and posteromedial directions and a tendency in increased GM activity in posterior and RF activity in posteromedial. After fatiguing toe plantar flexors, SEBT significantly decreased in posterior medial directions with no significant change in muscle activities.

Interestingly, after fatiguing ankle plantar flexors and toe plantar flexors, there was a tendency to increase GM, BF, ADD, VL, and RF. Which implies that the impairment of the distal muscles could be compensated by the activity of the proximal muscles. These compensation did not observe after fatiguing hip abductors.

a)	SEBT	ES	GM	BF	ADD	VL	RF	GS	SOL	PER	TA	ABDH
Hip												
Ante	98 (3)	84 (55)	100 (19)	96 (38)	86 (24)	79 (13)	86 (50)	104 (31)	94 (26)	97 (57)	98 (67)	88 (33)
Ante Med	98 (2)	88 (44)	97 (19)	80 (17)	95 (23)	87 (18)	84 (25)	77 (10)	76 (11)	91 (21)	92 (31)	79 (22)
Med	96 (2)	77 (25)	90 (8)	99 (29)	98 (27)	87 (22)	91 (30)	94 (35)	112 (27)	82 (32)	90 (36)	
Post Med	95 (4)	79 (28)	96 (14)	93 (18)	99 (41)	83 (13)	91 (22)	90 (7)	92 (18)	92 (32)	92 (31)	
Post	97 (3)	76 (23)	81 (21)	99 (23)	99 (34)	87 (19)	70 (25)	81 (14)	88 (16)	105 (26)	91 (43)	102 (26)
Post Lat	99 (3)	63 (15)	125 (89)	112 (29)	103 (28)	88 (15)	73 (22)	80 (21)	83 (18)	107 (49)	71 (20)	81 (28)
Lat	100 (5)	68 (20)	107 (39)	97 (17)	95 (28)	89 (18)	83 (27)	99 (40)	98 (17)	108 (30)	73 (31)	92 (33)
Ante Lat	99 (4)	76 (36)	95 (25)	97 (50)	86 (16)	102 (10)	102 (26)	88 (22)	89 (17)	100 (20)	78 (30)	80 (36)

b)	SEBT	ES	GM	BF	ADD	VL	RF	GS	SOL	PER	TA	ABDH
Ankle												
Ante	97 (4)	91 (16)	128 (44)	125 (45)	93 (45)	104 (25)	119 (27)	92 (18)	120 (72)	114 (26)	99 (44)	79 (24)
Ante Med	98 (2)	78 (14)	101 (23)	99 (30)	109 (66)	106 (43)	118 (22)	95 (29)	121 (71)	98 (24)	102 (73)	82 (33)
Med	96 (2)	86 (24)	106 (40)	102 (46)	78 (25)	87 (29)	104 (34)	75 (16)	111 (70)	122 (22)	93 (33)	73 (33)
Post Med	97 (2)	100 (24)	112 (38)	105 (43)	141 (155)	96 (29)	118 (23)	93 (21)	116 (69)	125 (75)	114 (47)	70 (24)
Post	95 (3)	90 (17)	125 (58)	118 (81)	86 (28)	93 (27)	89 (13)	89 (14)	120 (69)	124 (69)	96 (56)	80 (17)
Post Lat	97 (4)	105 (34)	122 (40)	117 (57)	119 (78)	97 (41)	115 (41)	90 (27)	124 (73)	108 (25)	97 (40)	73 (26)
Lat	97 (4)	84 (26)	127 (45)	121 (57)	76 (21)	87 (23)	91 (26)	87 (22)	114 (54)	100 (35)	87 (38)	77 (32)
Ante Lat	96 (6)	96 (15)	110 (33)	115 (31)	90 (45)	91 (39)	81 (21)	89 (16)	121 (95)	101 (48)	90 (26)	82 (17)

c)	SEBT	ES	GM	BF	ADD	VL	RF	GS	SOL	PER	TA	ABDH
Toe												
Ante	97 (4)	78 (17)	108 (36)	117 (38)	105 (9)	105 (18)	120 (32)	78 (18)	102 (32)	90 (15)	97 (23)	70 (18)
Ante Med	97 (2)	89 (28)	118 (34)	133 (51)	116 (32)	115 (43)	117 (19)	84 (24)	104 (31)	87 (23)	98 (17)	88 (48)
Med	98 (2)	102 (43)	121 (53)	125 (48)	106 (24)	108 (44)	111 (43)	90 (32)	98 (34)	84 (33)	98 (30)	79 (30)
Post Med	98 (2)	91 (35)	121 (49)	115 (41)	96 (19)	105 (42)	99 (17)	91 (25)	104 (34)	95 (24)	91 (23)	82 (35)
Post	97 (4)	102 (38)	124 (53)	118 (39)	93 (16)	108 (33)	101 (14)	97 (33)	115 (43)	92 (32)	93 (21)	87 (37)
Post Lat	98 (2)	103 (20)	141 (53)	116 (29)	101 (16)	116 (39)	131 (50)	87 (32)	105 (32)	101 (18)	102 (31)	81 (20)
Lat	97 (2)	93 (17)	122 (58)	104 (58)	100 (20)	108 (18)	115 (41)	87 (21)	108 (31)	95 (25)	94 (18)	80 (29)
Ante Lat	99 (3)	91 (30)	153 (168)	115 (52)	73 (34)	105 (22)	120 (24)	84 (28)	98 (30)	83 (14)	90 (17)	70 (14)

p < 0.05 p < 0.1

**Table.1:** The change of the SEBT and averaged EMG of muscles in each direction after fatiguing tasks compared to that of before the tasks (%), mean (standard deviation). Fatiguing on a) hip abductors, b) ankle flexors, and c) toe plantar flexors. Bold indicates > 100%.

## CONCLUSIONS

Our results indicate that the localized muscle fatigue affect the dynamic postural control in a specific direction.

## REFERENCES

1. Bisson E et al., *Gait Posture* **33**, 83-7, 2011.
2. Shirazi Z and Jahromi F, *Niger Med J* **54**, 306-9, 2013.
3. Winter D et al., *J Neurophysiol* **75**, 2334-343, 1996.
4. Chou S et al., *J Orthop Res* **27**, 549-54, 2009.
5. Gribble P, et al., *J Athl Train* **47**, 339-57, 2012.
6. Earl J and Hertel J, *J Sport Rehabil* **10**, 93-104, 2001.
7. Norris B and Trudelle-Jackson E, *J Sport Rehabil* **20**, 428-41, 2011.

## ACKNOWLEDGMENTS

This work was supported by JSPS KAKENHI, Grant-in-Aid for Young Scientists (B) (#JP26350825).

# DECREASED PLANTAR SENSATION WORSENS POSTURAL CONTROL

<sup>1</sup>Toyin Ajisafe, <sup>1</sup>Ferdinand Delgado, <sup>1</sup>Poonam Mankar, Mikaela Boham<sup>1</sup>

<sup>1</sup>Texas A&M University, Corpus Christi, TX, USA.

email: toyin.ajisafe@tamucc.edu

## PURPOSE

A review (2) recently concluded that although plantar cooling decreases tactile sensitivity, it did not affect postural sway in healthy young adults during static sensorimotor tasks, including single limb stance with eyes closed. The authors concluded that sensory redundancy, e.g., visual and vestibular systems, appeared to have sufficiently compensated for the deficits in decreased plantar sensation.

It is unclear whether decreased plantar cutaneous sensation impacts postural response during dynamic non-locomotor tasks that involve propulsion using the feet's plantar surface. This study investigated the effect of decreased plantar sensation on postural response during bilateral standing calf raise.

## METHODS

Eleven young adults (four females and seven males) ( $24.18 \pm 4.35$  years;  $171.58 \pm 8.21$  cm;  $76.64 \pm 18.25$  kg) participated in this study.

There were two conditions: no icing and icing.

In the no icing condition, subjects stood barefoot in the middle of an AMTI force plate and performed standing calf raises at a cadence of 48 beats per minute for 90 seconds. The force plate acquired anterior-posterior (AP) and medial-lateral (ML) center of pressure (CoP) excursion area. Participants were asked to maximally push up and stand on their toes at each audible beat of a metronome, then lower back down in readiness for the next.

In the icing condition, participants' forefeet were cooled on bagged ice (while seated) until their forefoot plantar temperature read  $6^{\circ}\text{C}$  on an infrared thermometer. Icing was immediately intervened by the foregoing movement task on the force plate. The order of conditions was

randomized. Participants returned to the lab after 24 hours to complete the second condition.

CoP excursion area was estimated by calculating the 95% prediction ellipse area of CoP stabilogram in MATLAB(1). The area ( $A$ ) of an ellipse is the dot product of pi and its principal axes ( $a$ ,  $b$ ) (equation 1).

$$A(\text{ellip}) = \pi ab \quad (1)$$

We calculated a paired-samples t-test to determine the effect of decreased plantar sensation on CoP excursion area. Statistical significance was set at  $p < .05$ .

## RESULTS AND DISCUSSION

A paired-samples t-test ( $t(10) = -2.526$ ,  $P = .030$ ) showed a significant difference in CoP excursion area between the conditions (Fig. 1).

Previous research found that young adults shifted CoP trajectory away from the insensate region of the foot during walking (3). The current study imposed a constraint such that the insensate foot region (forefoot) could not be avoided and had to be used for propulsion.

Although it was previously reported that plantar cooling did not affect postural sway in healthy young adults (2), the current research found greater CoP excursion area following forefoot cooling (Fig. 2).

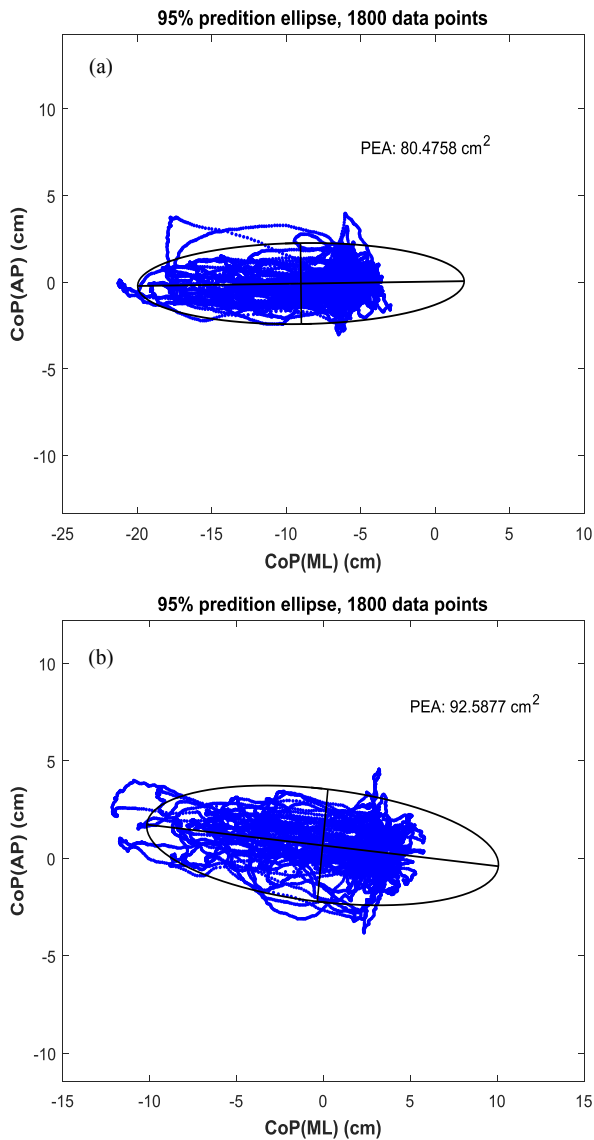


**Fig. 1:** A subject's CoP excursion area (95% prediction ellipse) (a) no plantar cooling, (b) plantar cooling.

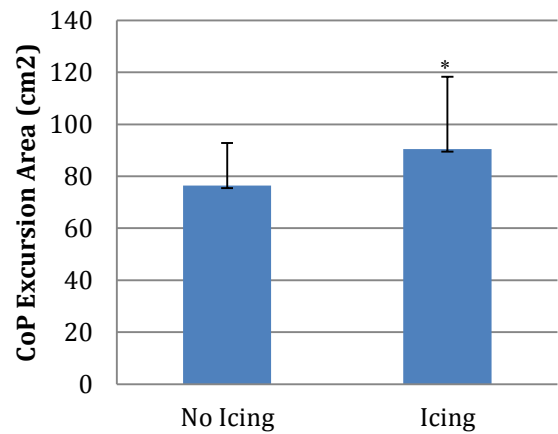


**Fig. 2:** Mean CoP Stabilogram Area. \* Indicates significant difference between conditions.

## CONCLUSION

It is concluded that in spite of sensory redundancy, decreased plantar sensation deteriorates postural control in intact young adults during bilateral standing calf raise.

This finding demonstrates a clear influence of plantar cutaneous sensation on postural control during a non-locomotor task that involves propulsion at the plantar surface of the foot. This may have implications for conditions like obesity that have been associated with decreased plantar cutaneous sensation, and the confidence and capacity to engage in physical activity.

## REFERENCES

1. Duarte M. (Schubert and Kirchner). *Gait Posture* **39**, 518-522, 2014.
2. Matthew C. Hoch, et al. *Gait Posture* **43**, 1-8. 2016.
3. Nurse MA, et al. *Clin Biomech (Bristol, Avon)* **16**, 719-27. 2001.

# A DATABASE OF SOFT TISSUE LAYER THICKNESSES IN MUSCULOSKELETAL EXTREMITIES

<sup>1</sup>Erica E. Morrill, MS, <sup>1</sup>Tammy M. Owings, DEng, <sup>1</sup>Tyler Schimmoeller, BS, <sup>1</sup>Robb Colbrunn, DEng, <sup>1</sup>Tara Bonner, MS, <sup>1</sup>Benjamin Landis, MS, <sup>2</sup>J. Eric Jelovsek, MD, MMEd, <sup>1</sup>Ahmet Erdemir, PhD

<sup>1</sup>Department of Biomedical Engineering, Lerner Research Institute, Cleveland Clinic, Cleveland, OH, USA

<sup>2</sup>Obstetrics, Gynecology & Women's Health Institute, Cleveland Clinic, Cleveland, OH, USA

email: [morrile2@ccf.org](mailto:morrile2@ccf.org); url: <https://simtk.org/projects/multis>

## INTRODUCTION

Musculoskeletal extremities exhibit a multi-layer tissue structure that is composed of skin, fat, and muscle tissue. Anatomical measurements of these tissues provide an understanding of body composition, which is used to assess health status, diagnose disease severity, and identify potential health risks [1,2]. In addition, biomechanical models rely on such data for accurate representation of limb structure and material properties [3]. However, there is a lack of data describing limb soft tissue variations across diverse populations. Therefore, the goal of this study is to provide a publicly available database of skin, fat, and muscle tissue thicknesses for *in vivo* human musculoskeletal extremities. Ultrasound [4,5], an inexpensive imaging modality, will be leveraged to visualize the layered soft tissue structure along limbs for a large group of subjects. With its portability, this imaging modality will facilitate expansion of measurements to the field.

## METHODS

A total of 50 subjects were tested (22 female, 28 male). The mean ( $\pm$ SD) age, height, mass, and body mass index were  $26.8 \pm 13.6$  yrs (range of 20 to 70 yrs),  $170 \pm 8.7$  cm,  $78 \pm 17.6$  kg, and  $26.8 \pm 5.6$  kg/m<sup>2</sup>, respectively. Activity level, ethnicity and race were also noted for each subject. The study was approved by the Cleveland Clinic Institutional Review Board and the Human Research Protection Office of the U.S. Army (USAMRMC ORP HRPO) and participant consent was received prior to data collection.

A custom load transducer instrumented ultrasound device was used to image skin, fat, and muscle

layers in the upper and lower extremities (Acuson S3000, Siemens, USA) [6]. The ultrasound probe (14L5 or 9L4) was attached to a 6-axis load transducer (Nano25, ATI Industrial Automation, USA), to ensure that the bulk tissue was minimally loaded (force magnitude  $< 2.2$  N) during imaging. Four segments (upper/lower arm/leg) of the right extremities were imaged along posterior, anterior, medial, and lateral locations (proximally, centrally, and distally), giving a total of 48 collection sites. The lower leg segment was imaged to the fibula, except for posterior locations (tibia) and the lower arm segment was imaged to the radius, except for medial locations (ulna).

Skin, fat, and muscle thicknesses were measured from the B-mode ultrasound images using a custom graphical user interface developed in Python. The analyst manually dragged markers to each tissue boundary (transducer/skin, skin/fat, fat/muscle, and muscle/bone) (Figure 1). The tissue thicknesses and forces were extracted and recorded for the frame corresponding to the minimum force.

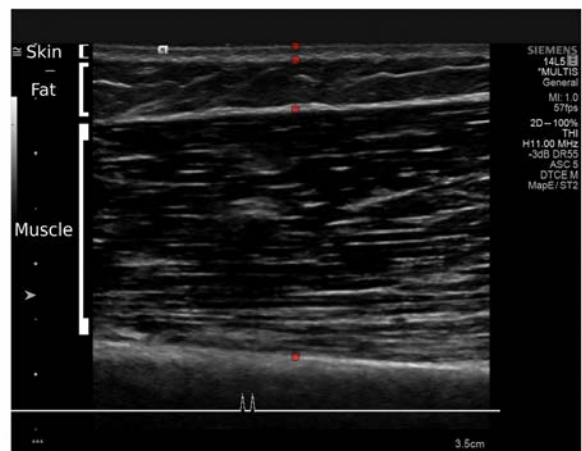


**Figure 1:** Sample ultrasound image of the central anterior upper arm. Red dots show the tissue boundaries.

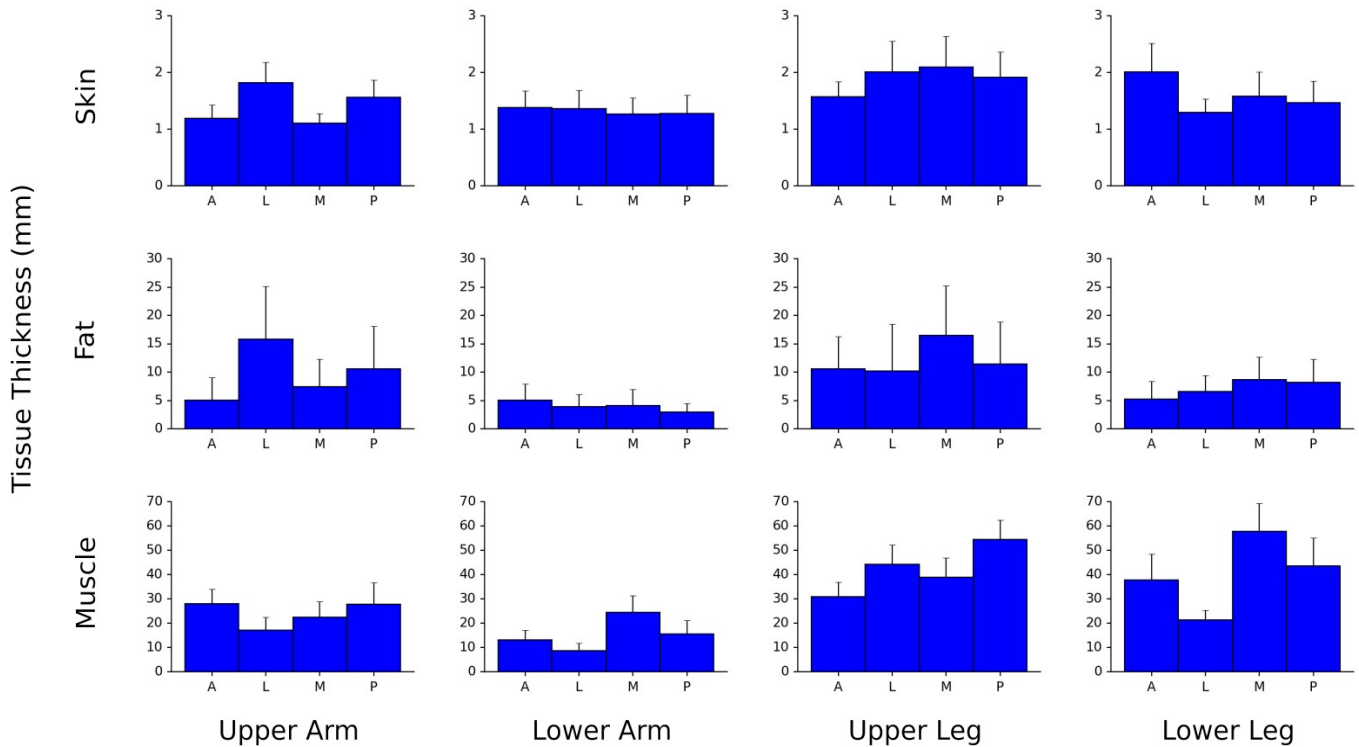


**Figure 2:** Mean ( $\pm$ SD) skin, fat, and muscle thicknesses for the central locations of the arms and legs (N = 50). Horizontal axis key: A = anterior, L = lateral, M = medial, P = posterior.

## RESULTS AND DISCUSSION

Mean ( $\pm$ SD) thicknesses of skin, fat and muscle tissues for the central locations are shown in Figure 2. Results from the proximal and distal locations are not shown, but will be available after data dissemination (visit project website for updates [7]).

During ultrasound imaging there were several bone boundaries that were difficult to locate (i.e. outside of rated probe depth or weak ultrasound signal). In addition, the fat/muscle boundary was difficult to distinguish in some areas, specifically when the image was not taken perpendicular to the muscle fascia plane. Such limitations were documented for each subject that was tested [7].

## CONCLUSIONS

This study has established a site-specific tissue thickness database of musculoskeletal extremities. Future work will include expansion of this database

to include 100 subjects with data dissemination on a publicly available online platform.

## REFERENCES

- [1] Duren, DL, et al., *J Diabetes Sci Technol*, 2(6), 1139-46, 2008.
- [2] Vulcano, DSB, et al., *Acta Cir Bras*, 28(10), 733-9, 2013.
- [3] Hart, NH, et al., *J Sports Sci Med*, 14(3), 620-6, 2015.
- [4] Kelso, A, et al., *Eur J Sport Sci*, 1-10, 2017.
- [5] Chapple, LS, et al., *Crit Care Resusc*, 19(1), 29-36, 2017.
- [6] Schimmoeller, T, et al., submitted to ASB'17, Boulder, CO, USA, 2017.
- [7] <https://simtk.org/projects/multis>.

## ACKNOWLEDGMENTS

This study has been supported by USAMRMC (W81XWH-15-1-0232). The views, opinions and/or findings contained in this document are those of the authors and do not necessarily reflect the views of the funding agency. The authors would also like to thank Siemens Medical Solutions USA, Inc. for loaning the ultrasound equipment and Dr. Patricia Delzell, MD of the Cleveland Clinic for her guidance on the ultrasound image analysis.

# CORRELATION BETWEEN TIBIAL SLOPE AND LIGAMENT STRAIN DURING *IN VIVO* LANDING SIMULATION

<sup>1</sup> Maria C. Mejia Jaramillo, <sup>1</sup> Manuela Vargas Gonzalez, <sup>1</sup> April L. McPherson, <sup>1</sup> Nathaniel A. Bates, <sup>1</sup> Nathan D. Schilaty, <sup>1</sup> Christopher V. Nagelli, <sup>1</sup> Aaron J. Krych, and <sup>1</sup> Timothy E. Hewett

<sup>1</sup> Mayo Clinic, Rochester, MN, USA  
email: [mcperson.april@mayo.edu](mailto:mcperson.april@mayo.edu)

## INTRODUCTION

Intrinsic factors, including hormonal and anatomical measures, have been identified as risk factors for anterior cruciate ligament (ACL) injury.[1] The sagittal plane tibial slope angle is an anatomical measure that can contribute to an increased ACL injury risk due to its effects on loading of the ACL.[2] Increased tibial slope angle has been shown to lead to increased anterior tibial translation; a 10° increase in tibial slope angle can lead to 6 mm of increased anterior tibial translation.[2] Increased anterior tibial translation increases the load on the ACL, making it more vulnerable to injury. The aims of this study were 1) to determine the reliability of an MRI-based method of tibial slope measurement and 2) to evaluate the relationship between tibial slope angle and ligament strain measured during an *in vitro* landing simulation. We hypothesized that the measurement method would exhibit excellent reliability and that tibial slope would be a predictive factor for ACL strain in our simulation model.

## METHODS

Thirty-five cadaveric lower extremity specimens were obtained from an anatomical donations program. Magnetic resonance images (MRI) were obtained on 34 specimens prior to testing. After MRI acquisition, a novel mechanical simulator was used to simulate the impulse ground reaction force generated during an *in vivo* drop vertical jump (DVJ) landing.[3] External knee abduction moment, anterior shear, and internal tibial rotation loads were applied to the specimen via pneumatic actuators. Differential variable reluctance transducers (DVRTs) were implanted on the ACL and MCL to record ligament strains.

Two researchers measured tibial slope three times

for each specimen in RadiAnt DICOM (Medixant; Poznan, Poland).[4] Tibial slope was defined as the angle between the perpendicular line and the parallel line of the diaphysis axis and the line that goes through the osseous tibial plateau peaks. (Figure 1).[4] Sagittal plane anterior/posterior tibial slope in the medial and lateral compartments, and coronal plane tibial slope were evaluated for reliability using interclass correlation coefficients (ICC). Inter-rater (ICC (2, 1)) and intra-rater (ICC (2, k)) correlations were performed. Classifications of ICC values were: ICC < 0.4 poor, 0.4 < ICC < 0.75 fair-to-good, and ICC > 0.75 excellent.[5] Pearson correlations were used to determine significant relationships ( $p < 0.05$ ) between tibial slope angle and ligament strain. To be included in a predictive model for ACL injury risk,  $r^2 = 0.2$  was the linear cutoff criteria.[6]

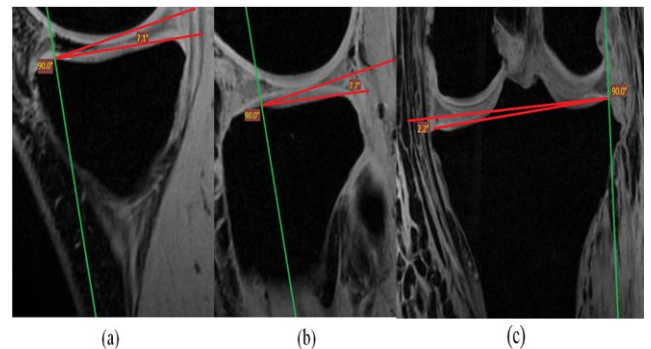


**Figure 1:** Anatomical landmarks used for tibial slope measurements. a) Medial tibial slope b) Lateral tibial slope and c) Coronal tibial slope.

## RESULTS AND DISCUSSION

A published method to measure tibial slope angle from MRI images demonstrated excellent intra-rater reliability and fair-to-good inter-rater reliability. For the sagittal plane anterior/posterior tibial slope, both intra-tester and inter-tester reliability for the medial compartment were excellent (ICC  $\geq 0.823$ ). Lateral

compartment tibial slope demonstrated excellent intra-tester (ICC  $\geq 0.761$ ) and fair-to-good inter-tester (ICC = 0.631) reliability (**Table 1**). Coronal measurements were less reliable than the frontal plane, as intra-tester was fair-to-good (average ICC = 0.739) and the inter-tester was poor (ICC = 0.309).

**Table 1:** Intra- and inter-rater reliability for sagittal and coronal plane tibial slope measurements.

Intra-tester			
	Medial	Lateral	Coronal
<b>Rater 1</b>	0.916	0.867	0.756
<b>Rater 2</b>	0.906	0.761	0.722
<b>Mean</b>	0.911	0.814	0.739
Inter-tester			
	Medial	Lateral	Coronal
	0.823	0.631	0.309

Correlations between tibial slope angle and maximum ACL strain were statistically significant ( $p < 0.015$ ) for both the medial and lateral tibial slope angles. Correlation with the coronal tibial slope was not significant nor did it reach the  $r^2 = 0.2$  linear regression cutoff criterion (**Table 2**).

The positive correlations between tibial slope angle and ACL strain indicate that sagittal plane medial and lateral compartment tibial slope accounts for at least 20% of the variance in ACL strain during a simulated landing. Therefore, tibial slope could be incorporated as a factor in models to predict ACL injury risk (**Figure 2**). This supports previous research that reported increased tibial slope angle corresponded to increased ACL loading.[2]

The current study is not without limitations. The measurement of the tibial slope angle was affected by the specimen orientation during MRI acquisition as well as the image quality of the MRIs.

**Table 2:** Correlations between tibial slope angle and maximum ACL strain.

	R <sup>2</sup> rater 1	p value	R <sup>2</sup> rater 2	p value
<b>Medial</b>	0.220	0.010	0.322	0.001
<b>Lateral</b>	0.213	0.012	0.201	0.015
<b>Coronal</b>	0.061	0.199	0.022	0.439

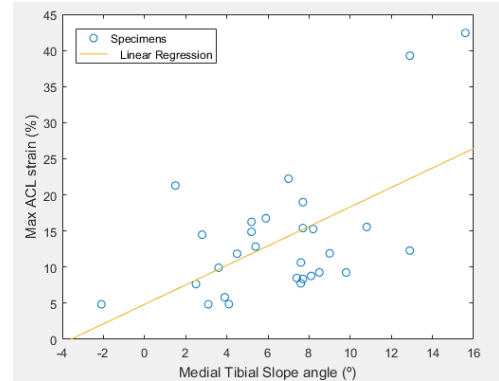


**Figure 2:** Correlation between medial tibial slope and ACL strain.

Furthermore, DVRTs are known to have significant variability when implanted in soft tissue structures. The current analysis did not investigate anterior tibial translation directly; however, the increased strain that was measured during the simulated DVJ may be caused by increased anterior tibial translation.

## CONCLUSIONS

The method proposed by Hashemi et. al [3] demonstrated excellent reliability for the sagittal plane medial and lateral tibial slope measurements; however, the coronal plane demonstrated poor reliability between testers. Correlations between tibial slope angle and ACL strain reported in this study support previous findings that indicate increased tibial slope may be a risk factor for ACL injury due to increased ACL strain.

## REFERENCES

- Hewett TE, et al. *Am J Sports Med.* **34**, 299-311. 2006.
- Webb JM, et al. *Am J Sports Med.* **41**, 2800-2804. 2013.
- Bates NA, et al. *Submitted for Publication.* 2017.
- Hashemi J, et al. *J Bone Joint Surg Am.* **90**, 2724-2734. 2008.
- Bates NA, et al. *Submitted for Publication.* 2016.
- Hewett TE, et al. *Am J Sports Med.* **33**, 492-501. 2005.

## ACKNOWLEDGMENTS

NIH grant funding R01AR049735, R01AR056259, R01AR055563, T32AR056950, and L30AR07027

# Preliminary Biomechanical Analysis of Superior Capsular Reconstruction Grafts

<sup>1</sup> Andrea Simi, <sup>1</sup> Matthew Chin, <sup>1</sup> John Kelly IV, <sup>1</sup> Josh Baxter, and <sup>1</sup> Michael Hast  
<sup>1</sup> University of Pennsylvania, Philadelphia, PA, USA  
email: [hast@upenn.edu](mailto:hast@upenn.edu)

## INTRODUCTION

Rotator cuff tears are painful and often debilitating injuries that are especially prevalent in older adults [1]. While many cuff tears can be surgically repaired, massive ‘irreparable’ tears present a special challenge for patients and shoulder surgeons alike. Recently, a superior capsular reconstruction (SCR) technique has been developed to address this problem, which utilizes a dermal allograft spanning the superior region of the glenohumeral joint that inserts into the glenoid rim and the greater tuberosity of the humerus. While SCR does not restore the cuff, the graft reinforces the superior capsule – thereby providing leverage and support to the proximal humerus that is normally provided by cuff tendons [2]. Preliminary studies indicate that SCR is effective in improving shoulder function [2,3]; however, the biomechanical limitations of this repair technique have yet to be sufficiently explored.

The goal of this study was to identify physical activities that may overburden the implanted graft and cause premature failure. To achieve this task, results from an in vitro experiment and an in vivo 3-D motion tracking session were used as inputs for the development of a musculoskeletal model (Fig 1).

A single cadaveric upper extremity (female, 96 y.o.) was used in this experiment. The specimen was skeletonized such that all muscle, tendon, and capsule tissues surrounding the shoulder joint were removed. The SCR repair was performed by an experienced surgeon using a single-row suturing technique. The scapula was secured to a test frame (TA ElectroForce 3550) and the potted humerus was secured to the actuator in the anatomic position. The humerus was driven superiorly at a rate of 0.5 mm/s until failure of the graft occurred.

Upper extremity kinematics during activities of daily living were captured using motion analysis on a young male (22 y.o.). Reflective markers were adhered the xyphoid process, sternum, C7 vertebra, right acromion, medial and lateral condyles of the elbow, radius and ulna of the wrist, and back of the hand. The subject performed six activities of daily living: combing his hair, a forward reach, an overhead reach, tucking the back of his shirt, washing his back, and washing his opposite shoulder, and marker traces were used to inform the computational model of upper extremity motions in 3-D space.

The musculoskeletal model of an SCR shoulder was developed in OpenSim and was based on a previously published upper extremity model [4]. The model consisted of 6 segments (thorax, clavicle, scapula, humerus, forearm, hand) and had 13 degrees of freedom. No active muscles were included, as this study was purely a kinematic assessment of glenohumeral motions to make estimations of strain and loads imparted onto the SCR graft.

The graft was modeled with four parallel ligament elements that were attached on the rim of the glenoid and the greater tuberosity to mimic the cadaveric insertion points. A wrapping sphere was used to represent the humeral head. Ligament resting

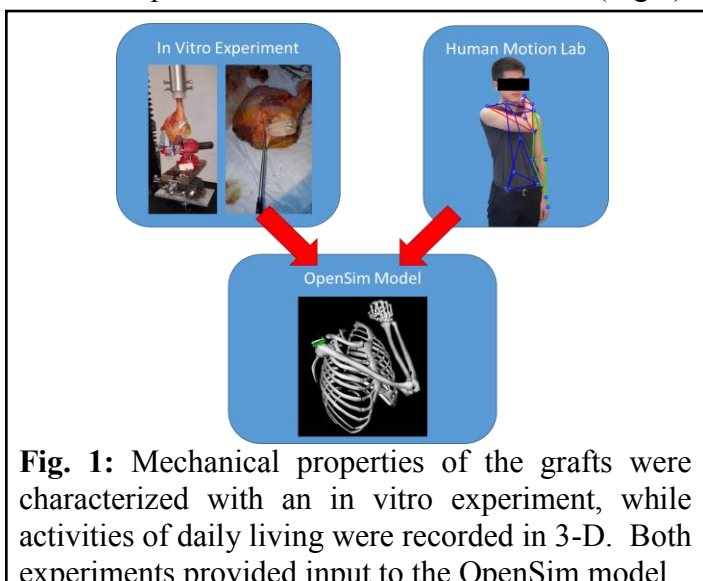


**Fig. 1:** Mechanical properties of the grafts were characterized with an in vitro experiment, while activities of daily living were recorded in 3-D. Both experiments provided input to the OpenSim model.

## METHODS

lengths were based on fiber lengths when the shoulder was in the anatomic position. A simple simulation consisting of prescribed superior translation of the humerus at a rate of 0.5 mm/s was performed to mimic the in vitro experiment. Physiological cross sectional area forces and normalized force-length curves were adjusted to reproduce the force displacement data that was measured experimentally.

Joint kinematics were calculated using the OpenSim inverse kinematics tool to track in vivo data collected using motion analysis. Individual ligament forces and lengths, as well as average fiber lengths and total graft forces were quantified for each motion.

## RESULTS AND DISCUSSION

Activities involving ligament-lengthening posterior shoulder rotation (back washing and shirt tucking) excessively loaded the graft, which may cause graft failure. Throughout these motions the average fiber length exceeded the experimentally determined ultimate strain (dashed line, Fig. 2A). Simulated graft failure is shown as sharp decreases of total force near 180N (Fig. 2B). These values are slightly lower than the experimentally measured ultimate force of 216N. This is explained by the fact that individual fiber lengths differed during motions, causing some fibers to reach ultimate strains and “break” while others remained intact. Fibers did not exceed their failure points during hair combing, forward reaching, overhead reaching, or shoulder washing motions.

This study was preliminary in nature and has several limitations. While the results suggest that this model is capable of identifying high-risk activities, the small sample size precludes our ability to make strong conclusions about its efficacy. Additionally, the modeling could be improved by including muscle forces and articular joint contact, so that the influence of internal and external loads on the shoulder joint could be assessed. Finally, failure of the in vitro graft occurred at the glenoid insertion, so graft failure biomechanics could be improved with stronger fixation (i.e. double-row suture techniques).

## CONCLUSIONS

While SCR has shown promise as a repair strategy for massive irreparable rotator cuff tears, the biomechanical limitations of the grafts are still not

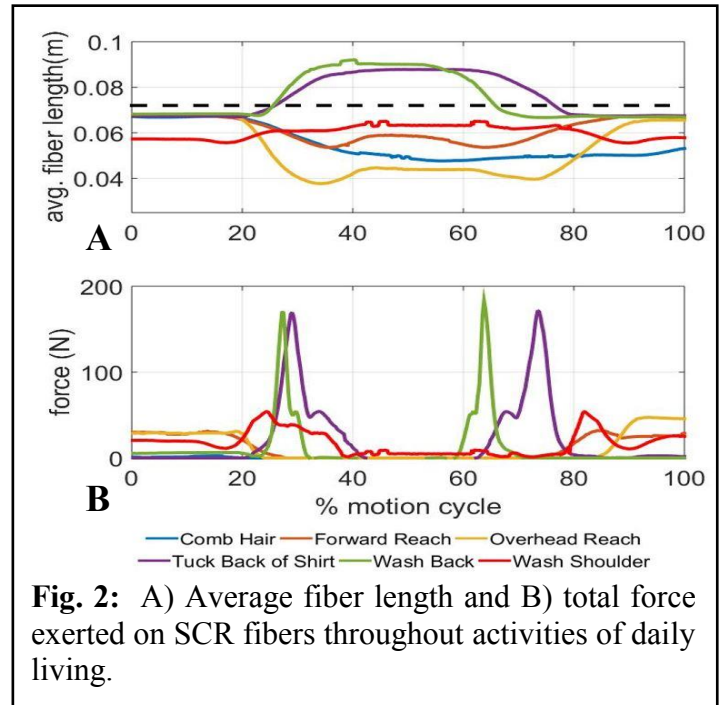


**Fig. 2:** A) Average fiber length and B) total force exerted on SCR fibers throughout activities of daily living.

well-defined. This model identified post-surgical activity limitations that may better inform surgical outcome expectations. These preliminary results also demonstrate the capacity of coupling in vitro, in vivo, and in silico modeling techniques in one cohesive experiment. This approach has potential to provide valuable information to clinicians and rehabilitative specialists to manage patient expectations and guide rehabilitation.

More work is needed to explore the full implications of this preliminary study. In future experiments, we intend to repeat cadaveric simulations, assign validated biomechanical properties to our model ligaments, and validate the model with motion capture data collected in patients treated with SCR.

## REFERENCES

1. Templhof S, et al. *J Shoulder Elbow Surg.* **8**, 296-99; 1999.
2. Hirahara AM, et al. *Arthroscopy Tech.* **4**, e637-41; 2015.
3. Burkhart SS, et al. *Arthroscopy Tech.* **5**, e1407-18; 2016.
4. Saul KR, et al. *Comp. Meth. Biomech. Biomed. Eng.* **18**, 1445-58; 2015.

## ACKNOWLEDGMENT

This study was funded by the University of Pennsylvania McCabe Pilot Award.

# EFFECTS OF PHOTOBIMODULATION THERAPY ON ACHILLES TENDON STRUCTURE

<sup>1</sup> Patrick Corrigan, <sup>2</sup> Daniel H. Cortes, <sup>1</sup> Jennifer A. Zellers, <sup>1</sup> Andrew Sprague, <sup>1</sup> Karin Grävare Silbernagel

<sup>1</sup> University of Delaware, Newark, DE, USA

<sup>2</sup> The Pennsylvania State University, University Park, PA, USA

email: dpwc@udel.edu

## INTRODUCTION

One of the most common overuse injuries is midportion Achilles tendinopathy. This clinical syndrome is characterized by pain during loading activities, impaired athletic performance, and tissue degeneration (tendinosis). Progressive tendon-loading programs, which promote increased collagen synthesis and improved viscoelastic properties, are currently the treatment of choice. However, evidence indicates that symptoms may be better addressed by supplementing these programs with laser-induced photobiomodulation therapy [1]. Despite these positive results, it remains unknown if there are immediate effects of a single photobiomodulation treatment on tendon morphology and viscoelastic properties, which may influence the effects of a loading program.

The purpose of this study was therefore to evaluate the immediate effects of photobiomodulation therapy on tendon morphology and viscoelastic properties in a healthy subjects. Additionally, we investigated change with photobiomodulation in individuals with Achilles tendinosis.

## METHODS

To evaluate the effects of photobiomodulation therapy on healthy tendon, 19 healthy subjects (9 females; 10 males) with a mean (SD) age of 28 (4) years and weight of 81 (18) kg were enrolled after a clinical examination and ultrasound screening was performed to ensure tendons were healthy. Blinded subjects received an active photobiomodulation treatment following an established protocol [1] to one side (Laser) and a sham treatment to the other side (Sham). The side and order of treatment application were randomized. Average tendon thickness (mm), cross-sectional area (CSA) (cm<sup>2</sup>), shear modulus (kPa) and viscosity (Pa\*s) were

quantified using three long-axis and short-axis B-mode ultrasound images obtained with a LOGIQ *e* Ultrasound system (GE Healthcare, Chicago, IL) at the midportion of the Achilles tendon and three trials of continuous shear wave elastography [2] at the same location. Each outcome variable has been shown to have good-excellent test-retest reliability (ICC=0.67-0.99). These procedures were performed on both the laser and sham side before, immediately post, 2 hours post, and 4 hours post treatment.

To describe the effects of photobiomodulation therapy on degenerative tendons, 3 subjects (1 female; 2 males) with a mean (SD) age of 62 (14) years, weight of 83 (15) kg, and confirmed Achilles tendinosis were enrolled in this preliminary study. All procedures remained identical to the healthy cohort, except the treatment was completed on the side of the greatest symptoms and tendinosis.

To analyze differences in tendon morphology and viscoelastic properties between laser and sham treatments and between the four time points in healthy subjects, a 2x4 repeated measures ANOVA was performed for each variable. To begin analyzing the effects of photobiomodulation therapy in subjects with Achilles tendinosis, descriptive statistics were used to describe the laser side. Descriptive statistics for both cohorts are presented in mean (SD) baseline values and change from baseline for the three post-treatment time points. These changes were then compared against the minimal detectable change (MDC<sub>(95%)</sub>) for each variable, which were calculated using measures obtained from baseline and immediate post treatment on the sham side for the healthy cohort. All statistical analyses were performed with IBM SPSS Statistics 24 at a significance level of  $p < 0.05$ .

## RESULTS AND DISCUSSION

In the healthy cohort, there were no significant main effects of treatment side ( $p=0.12-0.98$ ;  $\eta^2_{\text{Partial}}=0.01-0.13$ ) or time ( $p=0.51-0.93$ ;  $\eta^2_{\text{Partial}}=0.01-0.04$ ) and no significant treatment by time interaction effects ( $p=0.37-0.89$ ;  $\eta^2_{\text{Partial}}=0.01-0.06$ ) for all outcome variables (Table 1). Additionally, there were no changes in morphology or viscoelastic properties greater than the  $MDC_{(95\%)}$ , other than thickness on the laser side at the 2 hour time point.

In our preliminary analysis of 3 subjects with Achilles tendinosis, we observed an increase in tendon thickness greater than the  $MDC_{(95\%)}$  (0.12 mm) immediately and 2 hours post treatment (Table 2). Conversely, we found a decrease in CSA that was greater than the  $MDC_{(95\%)}$  (0.01  $\text{cm}^2$ ) at all post treatment time points. Looking at changes in viscoelastic properties, shear modulus reduced greater than the  $MDC_{(95\%)}$  (6.0 kPa) immediately and 4 hours post treatment, but no changes in viscosity were greater than the  $MDC_{(95\%)}$  (3.8  $\text{Pa}\cdot\text{s}$ ).

## CONCLUSIONS

Our results indicate a single photobiomodulation treatment does not have immediate effects on tendon morphology or viscoelastic properties in healthy Achilles tendons. However, in patients with Achilles tendinosis, we observed greater changes in tendon morphology and shear modulus compared to the healthy cohort. This suggests that greater effects of photobiomodulation therapy may be observed in degenerative tendons, however a larger sample size is needed to confirm this speculation.

## REFERENCES

1. Tumilty S, et al. *Lasers Med Sci*, **31**, 127-135, 2016.
2. Cortes DH, et al. *Ultrasound Med Biol*, **41**, 1518-1529, 2015.

## ACKNOWLEDGMENTS

This research was supported by the National Institutes of Health under Award number P30-GM103333, R21AR06739 and the Delaware Bioscience Center for Advanced Technology.

**Table 1:** Tendon morphology and viscoelastic properties in healthy subjects when treated with photobiomodulation therapy. Baseline and change from baseline are presented in Mean (SD). **Bold**  $>MDC_{(95\%)}$

	Treatment	Baseline	$\Delta$ Immediately After Treatment	$\Delta$ 2 Hours After Treatment	$\Delta$ 4 Hours After Treatment
<b>Thickness (mm)</b>	Laser	4.67 (0.62)	0.01 (0.31)	<b>0.13 (0.37)</b>	-0.06 (0.27)
	Sham	4.60 (0.53)	0.01 (0.39)	-0.01 (0.32)	-0.01 (0.48)
<b>CSA (<math>\text{cm}^2</math>)</b>	Laser	0.56 (0.13)	-0.002 (0.03)	-0.009 (0.03)	-0.004 (0.03)
	Sham	0.55 (0.13)	0.003 (0.03)	-0.002 (0.04)	0.004 (0.04)
<b>Shear Modulus (kPa)</b>	Laser	90.7 (15.1)	-1.7 (20.3)	2.7 (18.1)	1.5 (16.9)
	Sham	94.8 (16.4)	0.3 (16.4)	-0.2 (19.8)	-0.3 (21.7)
<b>Viscosity (<math>\text{Pa}\cdot\text{s}</math>)</b>	Laser	56.8 (10.9)	0.001 (0.013)	0.002 (0.013)	0.001 (0.014)
	Sham	57.8 (13.6)	-0.002 (0.011)	0.001 (0.010)	0.001 (0.012)

**Table 2:** Tendon morphology and viscoelastic properties in subjects with Achilles tendinosis when treated with photobiomodulation therapy. Baseline and change from baseline are presented in Mean (SD). **Bold**  $>MDC_{(95\%)}$

	Baseline	$\Delta$ Immediately After Treatment	$\Delta$ 2 Hours After Treatment	$\Delta$ 4 Hours After Treatment
<b>Thickness (mm)</b>	8.46 (2.31)	<b>0.18 (0.33)</b>	<b>0.24 (0.55)</b>	0.08 (0.95)
<b>CSA (<math>\text{cm}^2</math>)</b>	1.06 (0.27)	<b>-0.02 (0.05)</b>	<b>-0.05 (0.13)</b>	<b>-0.02 (0.09)</b>
<b>Shear Modulus (kPa)</b>	113.0 (20.7)	<b>-15.1 (13.8)</b>	-4.0 (11.5)	<b>-8.8 (8.8)</b>
<b>Viscosity (<math>\text{Pa}\cdot\text{s}</math>)</b>	59.5 (7.8)	-0.3 (4.3)	3.0 (4.1)	1.9 (5.1)

# EFFECT OF PRESSURE ON THE FORMATION OF CREASES IN A SOFT TISSUE

Mir Jalil Razavi, Xianqiao Wang

<sup>1</sup> College of Engineering, University of Georgia, Athens, GA, USA  
email: mjrazavi@uga.edu

## INTRODUCTION

When a soft material without a hard skin is compressed, creases with sharp edges usually form on the free surface of the material. Critical condition for the onset of creases cannot be determined by classical linear perturbation analysis, in stark contrast to the conditions for the onset of wrinkles [1]. Creasing in soft biological tissues, in contrast to wrinkling, has not been thoroughly explored and addressed before. Hence, it is essential to study crease formation in soft tissues and set up a systematic approach to quantify the phenomenon. Among different parameters that may have effects on crease formation, our current focus is the effect of pressure. External pressure or internal pressure from intraluminal fluids exist to a greater or lesser extent in organs like airways, esophagi, and brain. Recent studies have shown that internal or external pressure has effects on the critical growth rate and mode number of surface wrinkling in soft tissues [2,3]. Here, the main goal of this work is to find a simple way to demonstrate pressure effect in crease formation of a compressed soft material, and then as a case study to show how theoretical formulation can be applied to the creasing of a soft growing tissue.

## METHODS

**Analytical.** When a block of neo-Hookean hyperelastic incompressible material is compressed under the plane-strain condition, creases develop on the free surface of the block after a certain amount of compression (strain). A study showed that as long as the length and width of the block are large enough compared with crease size, the critical compressive strain for the initiation of creases is  $\varepsilon_0 \approx 0.35$ , and this value does not depend on the shear modulus of the material [1]. In this situation, the principal stretch ratio of the normal and

compression directions should be larger than  $\lambda_3/\lambda_1 \gtrsim 2.4$ . For this derivation, it is supposed that the free surface of the block is pressure-free and the block is compressed from a free state. Here, we want to incorporate the effect of the free surface normal pressure on the critical compressive strain required for the onset of creasing. By a lengthy derivation, we have

$$\lambda_{ext} = \sqrt{\frac{\alpha + \sqrt{\alpha^2 + 4}}{2}}, \quad \varepsilon_{ext} = \lambda_{ext} - 1 \quad (1)$$

where  $\alpha = P/\mu$  and  $P$  and  $\mu$  are the normal pressure and shear modulus of material, respectively.  $\lambda_{ext}$  and  $\varepsilon_{ext}$  are extra stretch and strain in compression direction that show the contribution of the normal pressure. If just the absolute value of the strains are considered,  $\varepsilon_{ext}$  should be added to the critical strain without pressure,  $\varepsilon_0$ , to find the critical strain  $\varepsilon_c$  when there is a normal pressure on the free surface of the block

$$\varepsilon_c = \varepsilon_0 + \varepsilon_{ext} \quad (2)$$

Figure 1 shows that the presence of pressure on the surface retards crease formation, and also that the critical strain is a function of both pressure and material modulus.

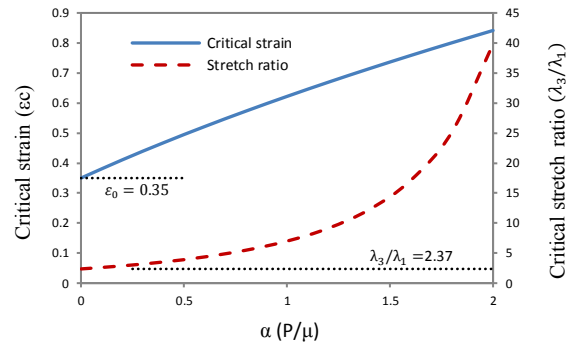


**Figure 1:** Effect of pressure on the critical strain required for the initiation of crease formation in a compressed soft neo-Hookean material.

**Numerical.** Nonlinear finite element (FE) analysis is performed to show the postsecondary morphological evolution after the system reaches

the critical growth ratio predicted from the theoretical analyses.

## RESULTS AND DISCUSSION

Consider a neo-Hookean bilayer tubular soft tissue growing in the plane-strain condition with a pressure applied on the free surface of the inner layer, as demonstrated in Figure 2. The outer layer of the tissue is supposed to be traction-free. In the presence of pressure, we strive to find the critical growth ratio for triggering crease formation at the free surface of the inner layer.

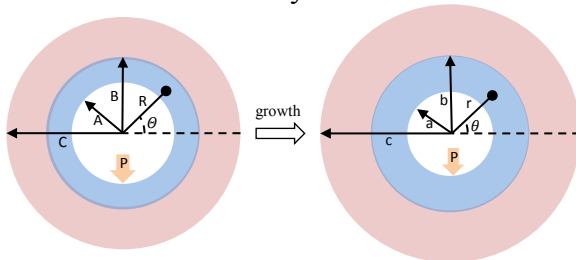


**Figure 2:** Initial and current states of a growing soft bilayer tube in the presence of internal pressure.

By applying the continuum growth theory [4] along with the cylindrical coordinates for this specific case, both stretch ratios and deformation field can be determined. Figure 3 shows the dependency of the stretch ratio at the free surface of the inner layer on the growth ratio and internal pressure for a special case with  $A/C = 0.5$ ,  $B/C = 0.7$  and  $\mu_2/\mu_1 = 50$ , where  $\alpha$  is defined as  $\alpha = P/\mu_1$ . Figure 3 also shows the relevant critical growth ratio for each certain internal pressure. From Figure 2, the critical stretch ratio ( $\lambda_r/\lambda_\theta$ ) for  $\alpha = 0, 0.5$ , and 1 are 2.37, 3.73, and 7, respectively. When these values intersect their counterparts on the growth ratio-stretch ratio graph, the critical growth ratios are obtained. For example, when  $\alpha = 0.5$ , the critical stretch ratio from Figure 2 is 3.73, from

Figure 3 the critical growth ratio is given as  $g_c = 1.32$ . Results show higher internal pressure leads to a higher critical growth ratio required for the formation of creases.

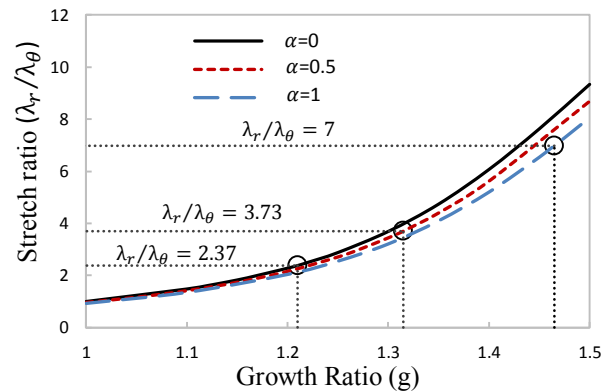


**Figure 3:** Dependency of stretch ratios and deformation of structure on growth ratio and internal pressure,  $A/C = 0.5$ ,  $B/C = 0.7$ ,  $\mu_2/\mu_1 = 50$ .

FE models also predict the same result for the growth and crease formation of the structure, as shown in Figure 4. When the growth ratio of the inner layer reaches the critical value, the system starts to lose stability and form creases at the free surface of the inner layer. This happens in order to partially release the elastic energy in the system and therefore reach a more stable configuration.

## REFERENCES

1. Hong W, et al. *Appl Phys Lett* **95**, 111901, 2009.
2. Xie WH, et al. *J Mech Behav Biomed Mater* **29**, 594-601, 2014.
3. Moulton D, et al. *J Mech Phys Solids* **59**, 525-537, 2011.
4. Rodriguez EK, et al. *J Biomech* **27**, 455-467, 1994.

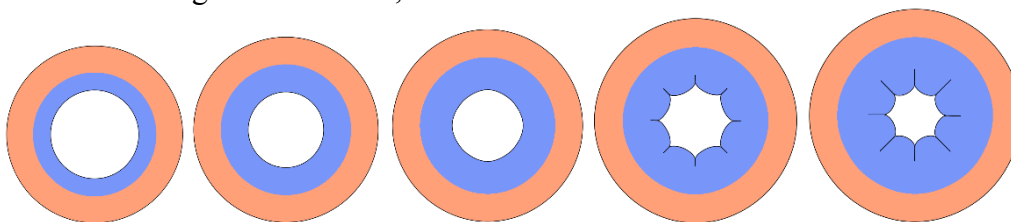


**Figure 4:** From left to right: step by step morphological evolution of a growing bilayer. Growth takes place in only the inner layer and  $\alpha = 0$ ,  $A/C = 0.5$ ,  $B/C = 0.7$ ,  $\mu_2/\mu_1 = 50$ .

# Comparison of Hip Joint Suction Seal in Simulated Labrum Tear

<sup>1</sup>Melinda Choi, <sup>1</sup>Mark Bowers, <sup>1,2</sup>Linda McGrady, <sup>1</sup>Patrick Birmingham, and <sup>1,2</sup>Mei Wang

<sup>1</sup> Department of Orthopaedic Surgery, Medical College of Wisconsin, Milwaukee, WI, USA

<sup>3</sup>Orthopaedic & Rehabilitation Engineering Center, Marquette University, Milwaukee, WI, USA

<sup>3</sup>NorthShore Orthopaedic Institute, Chicago, IL, USA

email: meiwang@mcw.edu

## INTRODUCTION

Hip joint stability is inherently provided by the bony articulation between the femoral head and quasi-sphere acetabulum. Function in conjunction with bony components of the hip, soft tissues, such as joint capsule, labrum, and ligamentum teres, constrain excessive translations during complex joint movements. Acetabular labrum tears are often diagnosed in the young athletic population. Acetabular labral repair or reconstruction is a surgical method addressing this clinical issue.

Biomechanically, the labrum has been shown to create a seal against fluid flow in and out of the hip joint, and thereby regulating fluid pressurization and stress distribution of the joint [1]. The negative pressure (or vacuum) the seal maintained also help resist distraction of the femoral head from its socket [2]. A tear or significant loss of the labrum may play a significant role in altering mechanical environment of intra-articular cartilage and potentially causing early onset of osteoarthritis.

The objective of this study was to quantify the peak suction force during manual pullout to dislocate the hip joint as a measure of sealing function of the labrum, and assess the effect of labral tear and repair.

## METHODS

Four pairs of cadaveric hemi-pelvic specimens with proximal femur were obtained from skeletally normal donors (mean age: 55.5 yrs, range 46-61 yrs, two males and two females), and stored at -30°C till the day of testing. Full pelvis specimens were first skeletonized and potted in the upright position (with ASIS and the pubic symphysis were aligned in the

same frontal plane) onto a custom mounting jig secured at the iliac wings using bolts and dental cement. The joint capsules were removed, but the ligamentum teres was preserved.

The manual pullout tests were performed by the same investigator on all specimens. With the mounted pelvis raised to a height just above the investigator's shoulder, a pullout handle with a 6-axis load cell (AMTI, Watertown, MA) on board was secured in the lateral aspect of the femur, 1-inch below the greater trochanter. Manual pullout was performed along the axis of femoral neck in a steady fashion until the hip dislocated. Suction force induced by the negative pressure was measured by the load cell during the process. Loadcell data were collected at a rate of 100Hz. Prior to the tests, approximately 1ml of baby oil gel (Johnson & Johnson's) was applied to the femoral head surface to mimic the synovial fluid. Several trials were repeatedly performed until a consistent peak force was achieved.

The experiment was conducted in three stages: 1) with native labrum, 2) following simulated labral tear by releasing the labrum directly off the bony acetabular edge from the 11 o'clock position to the 2 o'clock position (12 o'clock is the superior); 3) following labral repair using five suture anchors with one simple suture per anchor (Fig.1). The size of the labrum was measured with a ruler at 12 o'clock position in its native condition and again after simulated labrum tear. The labrum length was defined as the width from bony edge of the acetabulum to the tip of the labrum. The differences in peak suction force before the hip dislocation were analyzed using repeated measures ANOVA followed by Fisher's PLSD pair-wised comparison. Significant level was set at 5% for all tests.

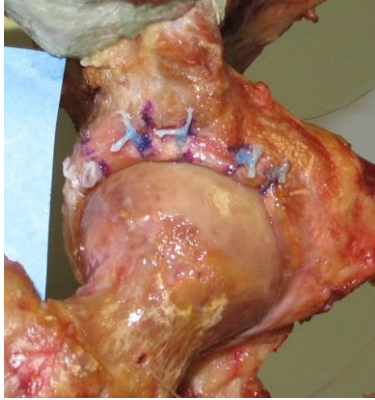


**Figure 1:** Labrum repair with five suture anchors.

## RESULTS

The size of the labrum varied considerably among the eight specimens (Fig. 2). The mean length of the labrums was  $6.1 \pm 4.0$  mm. The peak suction forces measured from the 6-axis load cell was  $52.9 \pm 32.1$  N in the native stage,  $18.5 \pm 8.4$  N after labrum was torn, and  $44.5 \pm 24.4$  N after labrum was repaired (Fig. 3). The peak force obtained from the torn labrum was significantly smaller than those from the native intact ( $p < 0.01$ ) and the repaired labrum ( $p < 0.04$ ), while difference between the intact and repaired labrums was not statistically significant. The suction force data also showed large inter-specimen variations. However, no significant correlation was found between the labrum length and the peak suction force in any labral conditions. When normalized the peak forces with respect to the value of individual intact labrum, there was a mean 54% reduction in peak force with the torn labrum. The mean percentile peak force of the repaired labrum was 91% of the intact.

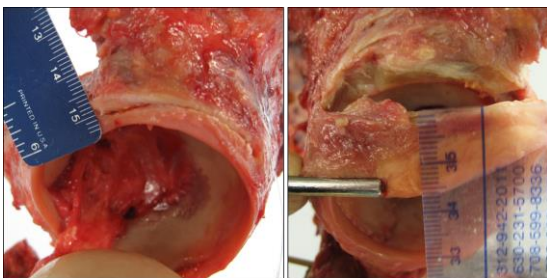


**Figure 2:** Large variations in size of the labrum between specimens.

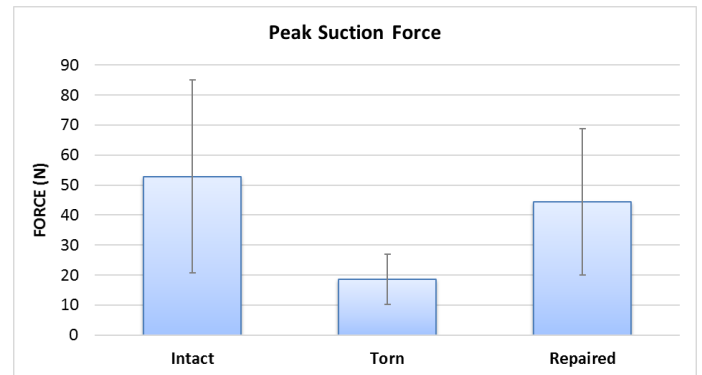


**Figure 3:** The mean (sd) peak suction force for the three labrum conditions: intact, torn, and repaired.

## DISCUSSION

The present study investigated the role of acetabular labrum in resisting distraction of the hip joint in a cadaver model consisted of middle-aged donors. Results demonstrated that labral tear had significant impact on labral seal. A typical tear from 11-2 o'clock can cause over 50% reduction in the vacuum seal. Labral repair can restore significant level of sealing function of the native hip.

Large morphologic variations were found in the specimens included in this study, but no correlation was found between the size of the labrum and peak suction force. This may have been due to the small sample size of this study. Further investigations are needed.

Young patients with compromised or absent labrums are at risk for the development of early arthritis of the hip. The ability to reconstruct the labrum and restore the mechanics of the hip joint could potentially alter the natural history of early hip osteoarthritis in this population.

## REFERENCES

1. Ferguson SJ, et al. *J Biomech* **36**, 171-178, 2003.
2. Terayama K, et al. *Eng Med* **9**, 66-74, 1980.

## ACKNOWLEDGMENTS

This study was supported by a research grant from the Musculoskeletal Transplant Foundation.

# EFFECTS OF BULLET SPEED AND THE DISTANCE BETWEEN SHOT POSITION AND AN ARTERY ON ARTERY RUPTURE PROBABILITY OF A HUMAN THIGH BY GUNSHOT

<sup>1</sup> Young Nam Jo, <sup>1</sup> Gil Ho Yoon, <sup>1</sup> Moon Jeong Kang, and <sup>1</sup> Hong Hee Yoo

<sup>1</sup> Hanyang University, Seoul, Korea

email: hhyoo@hanyang.ac.kr, web: <http://hydyn.hanyang.ac.kr/>

## INTRODUCTION

Gunshot wounds are one of the major injuries of combatants on the battlefield. In Operation Iraq Freedom and Operation Enduring Freedom, about 20% of all injuries were caused by gunshot wounds and over 90% in the civil war [1]. In addition, about 54% of all combat wounds were in the extremities [1]. If someone is shot on their extremities, excessive bleeding due to artery rupture is usually the major cause of death. But previous studies about gunshot wound simulation usually focused on the human mandible or cranium. Because most of death by firearms are caused by suicide. Therefore, the objective of this study is to conduct gunshot wounds simulation for a human thigh using a finite element method and to predict artery rupture probability depending on bullet speed and the distance between shot position and an artery.

## METHODS

In this study, a finite element method was used to predict artery rupture by a gunshot wound. A human thigh including two major arteries was modeled based on human 3D scan data. The model was simplified to conical shape to minimize computational effort assuming that detailed shape of the thigh has little effect on artery rupture. Properties of thigh muscle were assumed to be equal to those of 10% gelatin. Kelvin solid model and Maxwell fluid model were used as linear viscoelastic model. Mie Gruneisen equation of state and Johnson Cook failure model were also used. Explicit solver (ANSYS AUTODYN) was used for finite element simulation. The simulation method was verified by comparing the gelatin penetration analysis results with experimental results (figure 1) [2].

We decided whether the arteries are ruptured or not by comparing analysis results of the artery maximum strain with experimental results of artery yield strain [3]. In other words, the artery rupture probability is the probability that artery yield strain is less than the artery maximum strain. Artery rupture probability can be calculated from below equation.

$$P = \int_{-\infty}^x f_Y(x) dx$$

$x$  : maximum strain of the artery

$f_Y$  : probability density function of artery yield strain

Probability density function of artery yield strain is obtained from fourteen yield strain experimental results. The arteries were removed within 5 hours post-mortem from fourteen healthy male individuals.

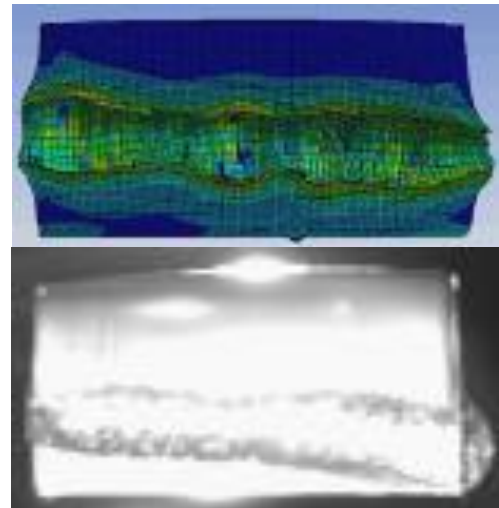


**Figure 1:** A comparison of an analysis result with an experimental result.

## RESULTS AND DISCUSSION

Artery rupture probabilities depending on the distance between shot position and an artery were obtained (Figure 2). Bullet speed is 345m/s and angular speed is 8400rad/s. As shown in the figure, artery rupture probabilities decreased in the quadratic form as the distance increased. In addition, artery rupture probabilities depending on the bullet speed were obtained (Figure 3). Angular speed of bullet was assumed to be changed at the same rate as the bullet speed. Also in this case, artery rupture probabilities increased in the quadratic form as the bullet speed increased. Since the kinetic energy increases in the quadratic form as speed increases, this result seems to be physically reasonable.

## CONCLUSIONS

In this study, the artery rupture probabilities considering various shot location and bullet speed were predicted. However, validation of the simulation results is limited because it is impossible to experiment on a human body. But we were able to find out the qualitative characteristics of artery rupture probability depending on gunshot conditions. This research can be used to predict survivability of combatants who perform combat mission through battlefield simulation.

## REFERENCES

1. Owens BD, et al. *J Trauma Acute Care Surg* **64**, 295-299, 2008.
2. Yoon GH, et al. *J Mech Sci technol* **29**, 3747-3759, 2015
3. Karimi A, et al. *Mater Sci Eng C-Mater Biol Appl* **33**, 2550-2554, 2013.

## ACKNOWLEDGMENTS

This work was supported by the Research fund of Survivability Technology Defense Research Center of Agency for Defense Development of Korea (No. UD150013ID).

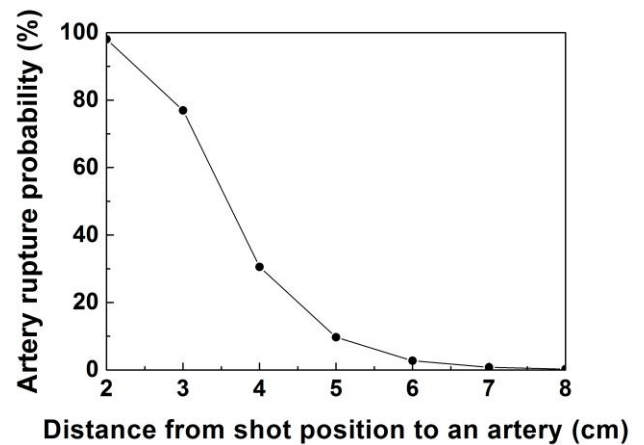


**Figure 2:** Artery rupture probability vs. distance from shot position to the artery.

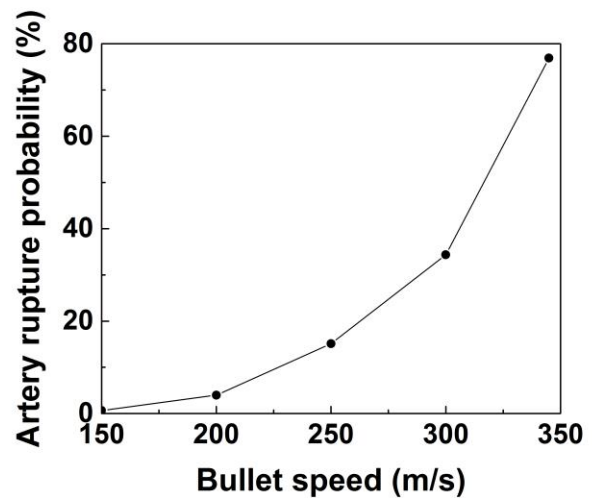


**Figure 3:** Artery rupture probability vs. bullet speed.

# OBSERVATION PERIOD HAS AN IMPACT ON THE OUTCOME OF SOFT TISSUE MATERIAL PROPERTIES IN VIVO. A COMPARISON OF THE INFLUENCE OF RUNNING IN MINIMAL SHOES FOR 8 AND 24 WEEKS.

Freddy Sichting, and Florian Ebrecht

Chemnitz University of Technology, Department of Human Locomotion, Chemnitz, Saxony, Germany  
email: [freddy.sichting@hsw.tu-chemnitz.de](mailto:freddy.sichting@hsw.tu-chemnitz.de)

## INTRODUCTION

Prospective longitudinal research study designs are often used in the field of biomechanics. This involves repeated observations of the same variables over longer periods of time to uncover adaptational effects of certain interventions or predictors of certain diseases. The chosen observation period has an important influence on later discussions of the data. As the adaptation processes and responses of the human body are highly variable, inadequate observation periods can favor misinterpretation. This study used a minimal-shoe running intervention to investigate how the observation period impacts the outcome measures. Specifically, we measured the change of foot muscle size and mechanical properties of selected soft tissues of the foot over a time period of 8 and 24 weeks. We hypothesized that all measures show a gradual positive or negative progression over time.

## METHODS

A total of 13 subjects (6 female, 7 male) participated in this study. The longitudinal 24-week study included a 30-minute running protocol twice a week. The training intensity was gradually increased during the first six weeks. A cross sectional area (CSA) of the m. abductor hallucis (ABH) was measured using ultrasound prior to, during (week 8), and after the intervention (week 24). To evaluate the effect of the intervention on selected tissue properties of the foot, we measured the stiffness parameters of the m. gastrocnemius, Achilles tendon, plantar heel pad, plantar aponeurosis, and ABH using myometric measures. Due to the limited number of participants, we performed descriptive data evaluation only.

## RESULTS AND DISCUSSION

Our hypothesized gradual progression over time was confirmed for the CSA measurement of ABH. The CSA of ABH increased steadily by 22.77% over the observation period of 24 weeks. Over the first eight weeks, the CSA increased by 13.01%, followed by a further but less pronounced increase of 8.64% between week 8 and week 24 (Fig. 1). This data are in accordance with existing literature [1, 2]. Consistent series of reliable ultrasound recordings of all three measurement points were only available for six subjects. However, all six showed the same progression regarding the change of CSA in ABH. This is in contrast to the measured stiffness properties.

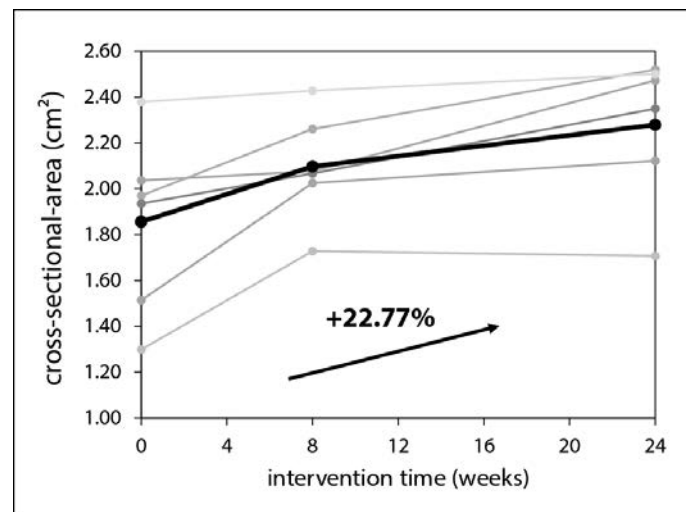


**Figure 1:** Influence of minimal-shoe running on the cross-sectional-area of the m. abductor hallucis. The black line represents the mean value, grey lines represent individual values.

Our hypothesized gradual progression over time must be rejected for the stiffness properties of m. gastrocnemius, Achilles tendon, plantar heel pad,

plantar aponeurosis, and ABH. With the exception of the plantar heel pad, all selected tissues showed a non-gradual progression over the time period of 24 weeks (Fig. 2). Even though the mean stiffness properties of the heel pad showed a gradual increase, the individual analysis showed a rather non-uniform pattern. Only 5 of 13 subjects followed the mean progression. This non-uniformity by the individual subjects also held true for the m. gastrocnemius (5 of 13), plantar aponeurosis (6 of 13), and ABH (6 of 13). We presume that this mismatch between the mean and the individual course limits further general data interpretation.

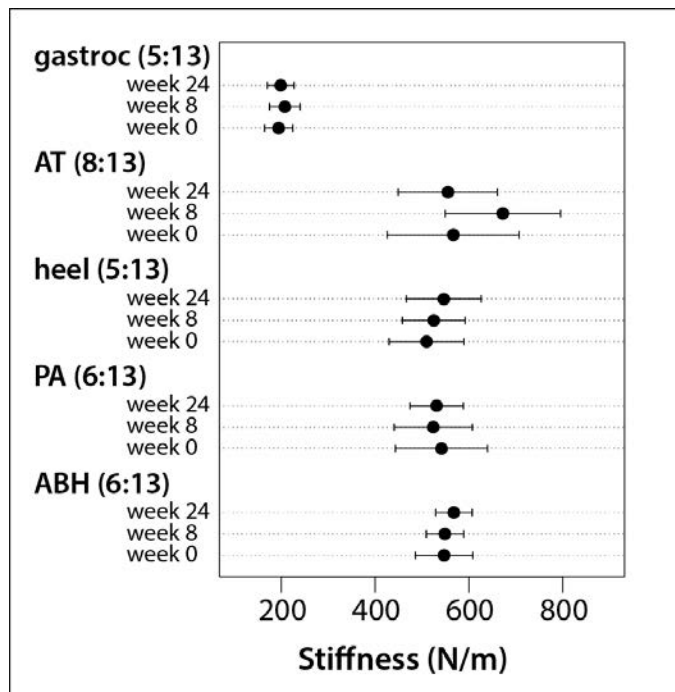


**Figure 2:** Influence of minimal-shoe running on stiffness properties of soft tissues (gastroc - m. gastrocnemius, AT – Achilles tendon, heel – plantar heel pad, PA – plantar aponeurosis, ABH – m. abductor hallucis). Dots represents mean values, error bars represent standard deviations. Numbers in parenthesis state the number of individuals that follow the mean progression, e.g. (5:13) – 5 of 13 subjects.

Only the mean course of the Achilles tendon stiffness was shared by most individual datasets (8 of 13). Interestingly, the AT stiffness increased over the first eight weeks (week 0:  $566.6 \pm 141.6$  N/m vs. week 8  $672.5 \pm 124.1$  N/m) but subsequently decreased

almost to the initial value (week 0:  $566.6 \pm 141.6$  N/m vs. week 24:  $555.1 \pm 107.0$  N/m). Running in minimal shoes for the first time might have caused a temporary increase in the muscle tone of m. gastrocnemius. The increased muscle tone may have increased Achilles tendon tension and thereby changed the stiffness properties. Over time, the subjects adapted to the additional stress of minimal-shoe running and thus the tension of the Achilles tendon, represented by the stiffness value, decreased again.

## CONCLUSIONS

The course of the Achilles tendon stiffness highlights the importance of an appropriate observation period. In contrast to the CSA of ABH, Achilles tendon stiffness did not show a gradual course over the observation time of 24 weeks. Regarding the CSA data, eight weeks seem to be sufficient to show the long-term effects of running in minimal shoes on muscle size. In contrast, eight weeks do not seem to be sufficient to draw clear conclusions regarding changes in the material properties of soft tissues of the foot when running in minimal shoes. Without the data from the measurements after 24 weeks, the increase in Achilles tendon stiffness after 8 weeks cannot be associated with a clear underlying mechanism. This might be misleading with regard to the further progression of Achilles tendon stiffness. In conclusion, we found that changes in the material properties of soft tissues, such as tendons and ligaments, require observation periods that exceed eight weeks.

## REFERENCES

1. Chen TL, et al. Clin Biomech (Bristol, Avon) 36, 8-13, 2016.
2. Miller EE, et al. J Sport Health Sci 3(2), 74-85, 2014.

# DYNAMIC RESPONSE OF THE HUMAN PENIS TO TENSILE LOADING AT VARIOUS STRAIN RATES

Blake Johnson, MS; Naira Campbell-Kyureghyan, PhD  
University of Wisconsin-Milwaukee, Milwaukee, WI, USA  
Email: john2742@uwm.edu

## INTRODUCTION

External genitourinary injury is increasing among soldiers [1]. This shift from internal to external injury can be contributed to improvements in internal injury protection as well as the increase in the use of explosives in the battlefield [2]. Although penile injuries have risen, little research has been conducted to help protect this organ from such traumatic events.

One reason for such limited research in this area could be that there is a lack of finite element models developed to investigate these types of injuries for the human penis. Previous penile finite element models have focused on analyzing normal function, prosthesis function, and Peyronie's disease [3,4,5]. What could be preventing finite element modeling of this organ to shift to traumatic injury prevention is the lack of material properties. Currently there is very limited research in the material properties of the human penis, and no studies have attempted to capture the material properties of the human penis at various dynamic loading rates.

The goal of this study is to determine the compressive and tensile material properties at various dynamic loading rates for the human penis. It is expected that the material properties will exhibit loading rate dependence.

## METHODS

Three penises were procured from donated cadavers. The specimens were removed from the body by severing it at the base of the shaft.

Each penis was dynamically tension tested using an MTS (Plymouth, MN) material testing system. The penises were tested until failure at rates of 25% $S^{-1}$ , 100% $S^{-1}$ , and 500% $S^{-1}$ . Initial failure was defined at the point where force first dropped and complete failure was defined when the force dropped to 0 N.

Forces and displacements were recorded and converted into stress and strains.

After failure testing on the complete specimens, non-destructive testing was conducted on samples that were cut out of the portions of the penises that were not involved in the failures. Non-destructive compression tests were done at the rate of 1% $S^{-1}$ , 10% $S^{-1}$ , and 25% $S^{-1}$ . The secant slope of the stress strain curve was calculated to determine the elastic modulus.

A general linear model ANOVA was used to determine if differences in elastic moduli at different strain rates were statistically significant at a 5% level. A Tukey's post hoc test was used to determine the statistical difference between the three strain rates.

## RESULTS AND DISCUSSION

The human penis exhibited strain rate dependent behavior. The average elastic modulus was 51% higher ( $p=.019$ ) at 25% $S^{-1}$  (.044 MPa) versus 1% $S^{-1}$  (.029 MPa). For every specimen, the elastic moduli increased from 1% $S^{-1}$  to 10% $S^{-1}$ , and from 10% $S^{-1}$  (.033 MPa) to 25% $S^{-1}$ , but the differences were not statistically significant. The elastic moduli ranged from .015 MPa to .068 MPa.

The measured failure stress and strain are presented in Table 1. Large differences were seen between the 25% $S^{-1}$  condition versus the 100% $S^{-1}$  condition. Initial failure stress was over 5 times greater and the failure strain was 41% lower at 100%  $S^{-1}$ . Similarly, complete failure stress at 100% $S^{-1}$  was over twice the value and strain was 23% lower than at 25% $S^{-1}$ . Differences in initial and complete failure stress and strain also existed between the 100% and 500% conditions. The initial and complete failure stresses were 0.24 MPa (12%) and 1.45 MPa (116%) greater in the 500% condition. The difference in initial and complete failure strain varied between 100% $S^{-1}$  and

500% $S^{-1}$  with an increase of 28% for initial failure stress and a decrease of 23% for complete failure strain. This could suggest that at higher rates the strain rate dependency diminishes.

Table 1: Failure stress and strain of the human penis at different loading rates

Specimen	1	2	3
Strain Rate (% $S^{-1}$ )	25	100	500
Initial Failure Stress (MPa)	0.37	2.06	2.3
Initial Failure Strain	136%	80%	102%
Complete Failure Stress (MPa)	0.502	1.15	2.6
Complete Failure Strain	237%	183%	140%

The larger difference in complete failure stress versus initial failure stress between specimens 2 and 3 (100% $S^{-1}$  and 500% $S^{-1}$ ) was possibly due to how the specimen initially failed. Specimen 2 severed most of the skin and corpus cavernosum at the initial failure, causing a large drop in stress (Figure 1). Specimen 3 only ruptured the surrounding skin of the penis at the initial failure, causing the stress to continue to increase with only a minor drop.

With the increased knowledge of penis material properties, better and more accurate models can be developed. Using the properties found at the appropriate strain rates and the knowledge that strain rate dependency seemingly diminishes as rate increases, scientists can create models to better understand injuries from traumatic events. Data

regarding how the penial tissue fails under these loading conditions can lead to creation of better personal protective equipment.

## CONCLUSION

This study determined the dynamic material properties of the human penis under compression and tension testing at various rates. At lower levels and under compression, the tissue behavior is highly reliant on strain rate, but this dependency decreases as strain rate increases. Such knowledge will enable scientists to build more accurate and efficient models to study mechanisms of injury for this organ, but more testing is needed to establish the full range of properties.

## REFERENCES

1. Janak J, et al. *J. of Urol*, **197**, 414-419, 2017.
2. Hudak S, et al. *Urol*, **65**, 1041-1046, 2005.
3. Linden-Ganz E, et al. *Ann of the New York Aca of Sci.*, **1101**, 464-476, 2007.
4. Gefen A, et al. *Med and Bio Eng and Com* **37**, 625-631, 1999.
5. Gefen A. *J of Biomech*, **33**, 1739-1744, 2000.

## ACKNOWLEDGMENTS

This study was funded by US Department of Defense grant No. 4892-ARMY-DHP -ELVIS Ph II.

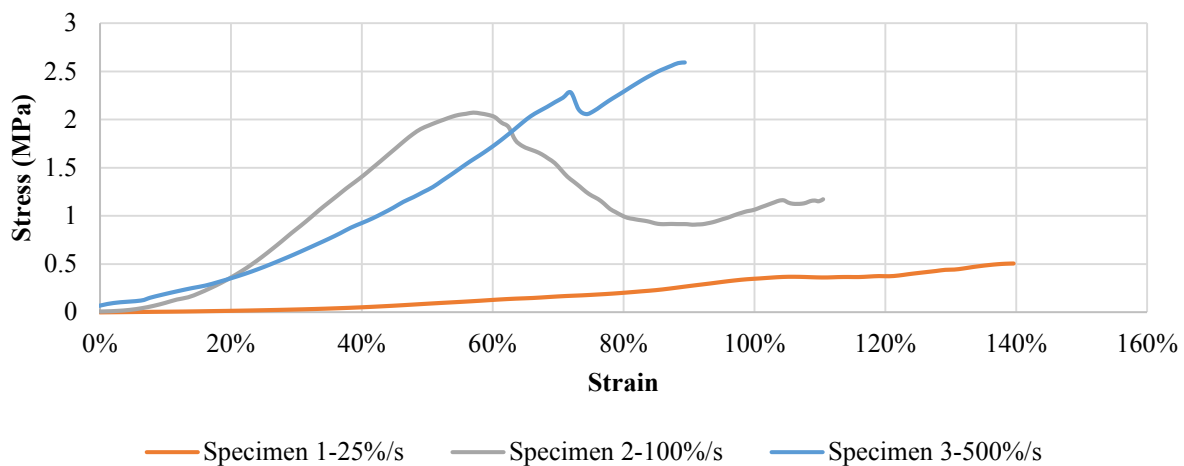


Figure 1: Stress versus strain curve for human penis at different tensile loading rates

# THE CORRELATION OF BONE MINERAL DENSITY AND CUMULATIVE DYNAMIC SKELETAL LOADING

<sup>1</sup> Bethany Lowndes, <sup>2</sup> Kenton Kaufman, and <sup>1</sup> Emma Fortune

<sup>1</sup> Robert D. and Patricia E. Kern Center for the Science of Health Care Delivery, Mayo Clinic, Rochester, MN

<sup>2</sup> Motion Analysis Laboratory, Division of Orthopedic Research, Mayo Clinic, Rochester, MN

email: Fortune.Emma@mayo.edu

## INTRODUCTION

Osteoporosis and low bone mass are major health problems affecting 50% of adults over 50 years old and 30% of postmenopausal women in the U.S. [1, 2]. Osteoporotic fractures are a major cause of morbidity and disability, and incur costs of nearly \$20 billion annually in the U.S.. Hip fractures account for the majority of the disability, morbidity, and financial burden of osteoporosis [3], and can lead to premature death [2]. Hip fracture incidence increases exponentially with age and manifests disproportionately in women over men [4].

Dual-energy X-ray absorptiometry (DXA) is the clinical standard for measuring bone mineral density (BMD) and allows physicians to diagnose osteoporosis. While BMD is an important biomarker of fracture risk, as a standalone measure it lacks information on modifiable causal factors. Convincing evidence indicates that physical activity with both low and high impact forces is beneficial in the prevention of osteoporotic fractures and is one of the main modifiable risk factors [5].

A well-defined relationship between physical activity and hip BMD has not been determined. Quantifying hip BMD and physical activity-based cumulative estimates of skeletal dynamic loading in the free-living environment could provide a biomarker for tracking and prescribing physical activity changes in high risk patients.

## METHODS

Fourteen post-menopausal women (age: 64.7 (7.2) yrs, BMI: 26.0 (3.9) kg/m<sup>2</sup>) were included in this study. Exclusion criteria include current use of prescribed medication which could result in BMD

changes, use of an assistive device while walking, any amputations or use of orthotics, and a history of hip surgery or hip or knee joint replacement on the non-dominant side. The study protocol was approved by the Mayo Clinic IRB and written informed consent was obtained prior to subject participation. To develop a dynamic loading estimation method for use in the free-living environment, tri-axial acceleration and ground reaction force (GRF) data were collected as subjects each performed 30 to 50 walking trials barefoot in the lab at slow, normal, and fast self-selected speeds. Continuous acceleration data were collected at 100 Hz from ActiGraph GT3X+ (ActiGraph LLC, USA) activity monitors worn on the bilateral ankles. GRF data were collected at 600 Hz for one to three steps per trial using three force plates (AMTI, USA; Kistler Instruments, Switzerland) and continuous video data were simultaneously acquired at 60 Hz. Linear regression was used to develop a general peak vertical GRF equation based on peak vertical acceleration data from all 14 subjects.

The same 14 subjects received DXA scans using the Lunar iDEXA (GE Medical Systems, USA) to measure total hip BMD on the non-dominant side and wore the activity monitors for 7 days in their free-living environments. Steps taken in the free-living environment were detected from ankle acceleration data using our previously developed and validated step detection algorithm [6] in MATLAB (Mathworks, USA). Peak vertical GRF, in units of body weight (BW), was calculated for each step using the GRF equation derived from the lab data. A bone density index (BDI), an index of cumulative loading, for each day was determined as the cumulative sum of the peak vertical GRF estimated for each detected step [7]:

$$BDI = [\sum_{i=1}^n (\beta \cdot GRF_i)^m]^{1/2m} \quad (1).$$

$\beta$  is the ratio of the individual subject's BW to the cohort's mean BW and  $n$  is the daily step count. The exponent  $m$  weights the relative importance of force magnitude and loading cycles and was set to a value of 6 [7]. Linear regression with Pearson correlation analysis was used to assess correlations of peak vertical GRF with peak vertical acceleration and of each subject's BMD with their mean BDI.

## RESULTS AND DISCUSSION

Peak vertical GRF had a strong and significant correlation with peak vertical acceleration across all subjects (Fig 1).

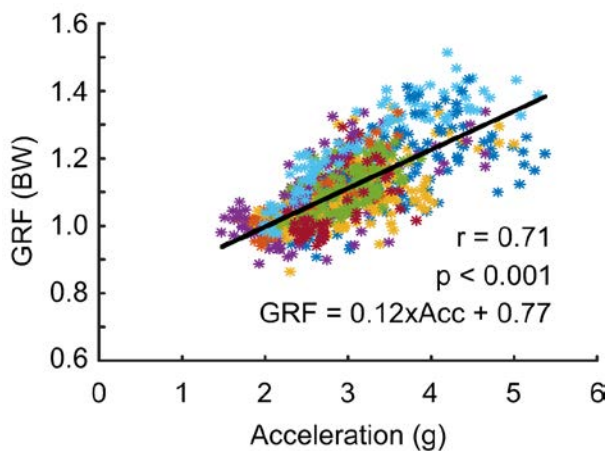


**Figure 1:** Lab data demonstrating the relationship between peak vertical ground reaction force (GRF) and peak vertical ankle acceleration. Each subject is denoted by a different color,

In this study, we observed an RMS error of 0.078 BW and a mean (SD) absolute difference of 5.4% (4.2%) for GRF estimations. These results are similar to our previous study utilizing the same lab-based methods on younger adults [8]. In comparison, a much larger RMS error of 0.185 BW was obtained in a study using the NASA GRF activity monitor [9].

The mean (SD) daily step counts across participants were 10257 (3942). BMD had a moderate and significant correlation with BDI with 51% of the variance accounted for (Fig. 2) compared to 19% for two previous studies using less accurate methods

[7, 9]. Data is currently being collected on an additional 56 participants for further algorithm development and validation. Future work will determine if this ankle acceleration-based BDI tool can be used to predict BMD changes.

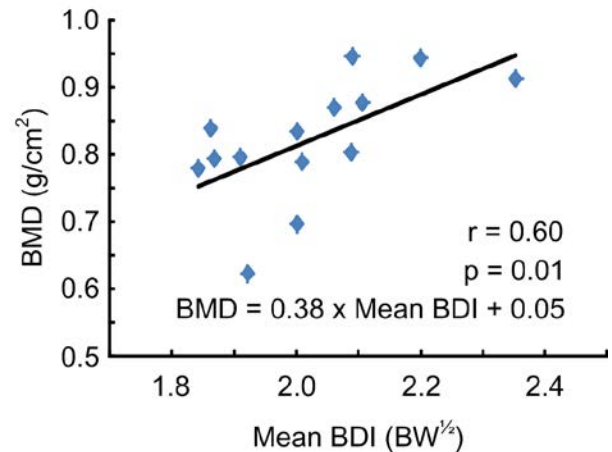


**Figure 2:** Free-living data demonstrating the relationship between each subject's bone mineral density (BMD) and their mean acceleration-based bone density index (BDI).

## CONCLUSIONS

The results strongly suggest that accelerometers worn at the ankle could be a very useful tool for relating cumulative dynamic loading in the free-living environment to bone health.

## REFERENCES

1. Lim L et al. *Am J Prev Med*, **36**, 366-75, 2009.
2. Kanis J. *Osteoporosis International*, **4**, 368-81, 1994.
3. Johnell O. *Am J Med*, **103**, S20-S26, 1997.
4. Khosla S. *New Eng J Med*, **356**, 2293-300, 2007.
5. Basse E. *Age Ageing*, **30**, 29-31, 2001.
6. Fortune E et al. *Physiol Meas*, **36**, 2519, 2016.
7. Boyer K et al. *Osteoporos Int*, **22**, 2981-8, 2011.
8. Fortune E et al. *J Appl Biomech*, **30**, 668-74, 2014.
9. Bowley S, Whalen R, *Ortho Res Soc*, 0063, 2001.

## ACKNOWLEDGMENTS

Funding is provided by NIH R21 AR066643. Stacy Loushin assisted with subject recruitment.

# RELATIONSHIP BETWEEN METATARSAL BONE MINERAL CONTENT AND METATARSAL LOADING DURING GAIT

<sup>1</sup> Jessica L. Downs, <sup>1</sup> Audrey E. Westbrook, <sup>1</sup> Anh-Dung Nguyen, <sup>1</sup> James M. Smoliga, <sup>1</sup> Jeffrey B. Taylor, <sup>2</sup> David R. Sinacore, <sup>1</sup> Kevin R. Ford

<sup>1</sup> High Point University, High Point, NC, USA

<sup>2</sup> Washington University School of Medicine, St. Louis, MO, USA  
email: biomechanics@highpoint.edu

## INTRODUCTION

The ability to adapt to applied mechanical loads is an important characteristic which determines the architecture and strength of bone (Wolff's Law). Specifically, the magnitude of load and number of loading cycles influence whole body and site-specific bone mineral density and bone mineral content (BMC). The individual bones in the foot have been shown to respond to a reloading program and relate specifically to gait loading pattern [1]. While loading plays an important positive role in bone health, bone stress injuries (BSI) will occur when the bone can no longer withstand the loading [2]. The prevalence of BSI in athletes may be due to rapid increases in the duration and frequency of loading with certain sports and physical activities. BSI risk may relate to site-specific bone strength characteristics. Furthermore, the relationship between loading and site-specific BMC may help identify potential risk for both acute and overuse foot injuries. A method to measure metatarsal BMC was recently developed using dual x-ray absorptiometry (DXA) [3]. Therefore, the purpose of this study was to identify differences in metatarsal BMC and whether metatarsal BMC differences elicit different relative metatarsal loading patterns during gait in young athletes.

## METHODS

72 participants were included in the study (26M, 46F, age:  $17.0 \pm 4.8y$  and BMI:  $22.5 \pm 5.7kg/m^2$ ). The participants participated primarily in the following sport categories: basketball (n=19), dance (n=13), soccer (n=24), and running (n=16). A DXA method was used to scan the left foot second (MET2) and fifth (MET5) metatarsals (Figure 1) to calculate BMC for the proximal and shaft regions.

Each participant also performed barefoot gait at a self-selected speed over a 6m walkway to collect plantar pressure distribution. An emed-x system (novel) was mounted in the middle of the walkway and level with the surface. Three separate trials were collected for the left foot and averaged. The platform consisted of a matrix of capacitive sensors (4 sensors/cm<sup>2</sup>) that was sampled at 100Hz. Force-time integral for each metatarsal region (Figure 1) was calculated. The force-time integral in each individual region was divided by the force-time integral for the total foot surface to determine the relative load in each metatarsal region.

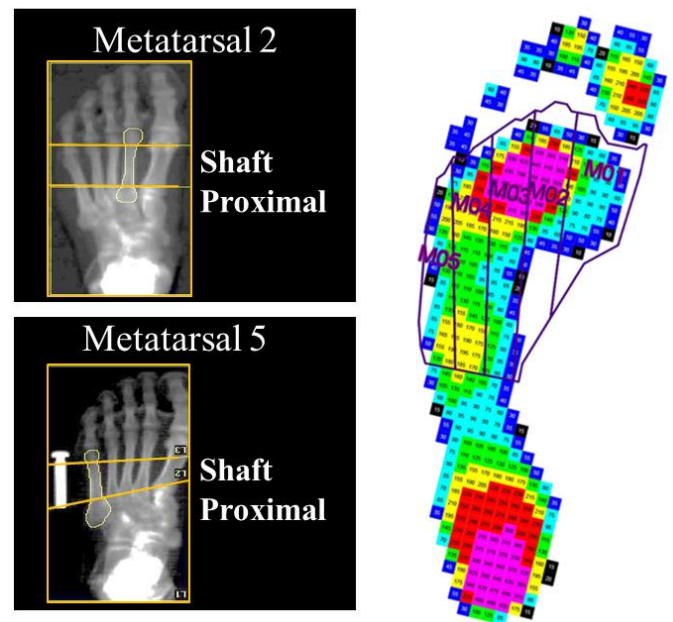


**Figure 1.** Left: DXA image of proximal and shaft regions of the 2<sup>nd</sup> and 5<sup>th</sup> metatarsals. Right: Representative example of emed plantar pressure distribution. Five metatarsal regions were defined based on width and length percentages.

BMC asymmetry between the proximal MET2 and MET5 was established based on the calculated ratio (MET2/MET5). The MET2/MET5 proximal ratio was utilized to classify high asymmetry, moderate asymmetry, and low asymmetry groups based on an equal tertile distribution. Paired t-tests ( $p < 0.05$ ) were used to determine if differences existed between MET2 and MET5 BMC in both the shaft and proximal regions. One-way ANOVA was used to determine if relative loading differences existed among asymmetry groups.

## RESULTS AND DISCUSSION

The proximal MET5 (1.55g) had significantly greater BMC compared to MET2 (1.09g;  $p < 0.001$ ). The shaft was not different between MET5 (1.12g) and MET2 (1.21g;  $p = 0.13$ ). The ratio of MET2/MET5 was significantly different in proximal (0.77) and shaft (1.14) regions ( $p < 0.001$ ) indicating the higher relative BMC in the proximal MET5 compared to the MET2.

Metatarsal relative loading was analyzed from barefoot pressure distribution (Figure 2). A main effect of asymmetry group was found in relative loading of the MET5 ( $p = 0.002$ ). There were no significant group differences between the relative loads of the first, second, third and fourth metatarsals. Post-hoc pairwise comparison indicated that the high ( $7.5 \pm 3.2\%$ ) asymmetry group had significantly greater relative load than both the moderate ( $5.5 \pm 1.8\%$ ;  $p = 0.02$ ) and low ( $5.0 \pm 2.0\%$ ;  $p = 0.002$ ) asymmetry groups. While gait loading may help explain the differences in BMC asymmetry, sport-related loading may play a larger role depending on the type of movements. For instance, various types of loading patterns observed during different sports such as jumping, cutting, and running may provide the mechanical stimuli necessary to increase BMC [4]. In our study, the distribution of primary sport participation was significantly different among asymmetry groups ( $\chi^2 = 32.4$   $p < 0.001$ , Figure 3). 79% of the basketball players were classified as high asymmetry, indicating higher bone mineral content of the proximal MET5 compared to MET2. Future investigations within different sports may be useful to determine sport-related risk of BSI.

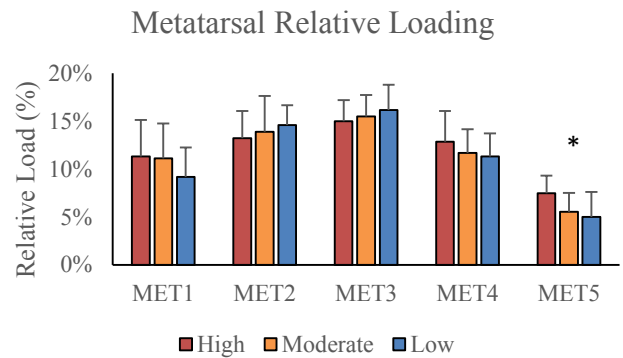


**Figure 2.** Relative loading during gait in the metatarsal regions (MET1-5.) Group main effect \* $p = 0.002$ .

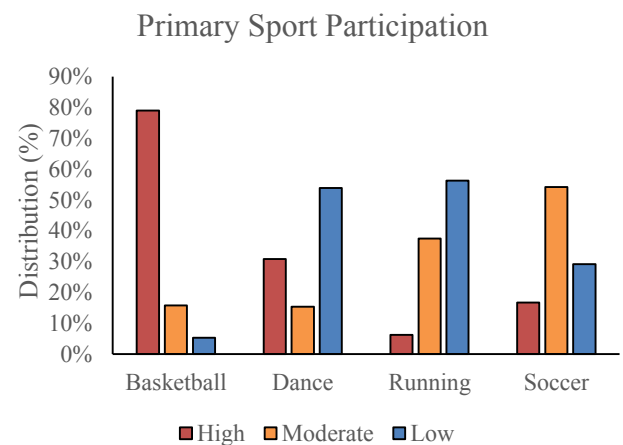


**Figure 3.** Distribution of primary sport participation among high, moderate, and low asymmetry groups.

## CONCLUSIONS

The proximal area of the MET5 overall had higher BMC compared to the MET2. Greater lateral metatarsal loading during gait was found in individuals with greater magnitude of metatarsals BMC asymmetry. The functional relationship among metatarsal mechanical loading, bone characteristics, and bone stress injury should be prospectively investigated.

## REFERENCES

- Hastings MK, et al. *Phys Ther*, **88**(6), 766-779, 2008
- Warden SJ, et al. *J Orthop Sports Phys Ther*, **44**(10), 749-65, 2014
- Bohnert KL, et al. *Foot*, **23**(2-3) 63-9, 2013
- Nordstrom P, et al. *J Bone Min Research*, **13**(7), 1141-1148, 1998

# THE EFFECT OF INFLAMMATION ON THE BIOMECHANICAL PROPERTIES OF THE INTERVERTEBRAL DISC

Brigitte Laird<sup>1</sup>, Matthew Guerreiro<sup>2</sup>, Stephanie DeWitte-Orr<sup>2,3</sup>, Diane Gregory<sup>1,3</sup>,  
<sup>1</sup>Kinesiology, <sup>2</sup>Biology, <sup>3</sup>Health Sciences, Wilfrid Laurier University, Waterloo, ON, CAN  
lair8260@mylaurier.ca

## INTRODUCTION

The intervertebral disc (IVD) is composed of the annulus fibrosus (AF), which surrounds and contains the nucleus pulposus (NP). The IVD is an immune privileged site, meaning in a healthy IVD, the NP is isolated from the adaptive immune system [1]. In addition, the IVD is largely avascular and therefore lacks the capacity to effectively repair itself once damaged. It is hypothesized that when the IVD becomes injured, in the case of IVD herniation, a localized innate immune response is initiated. This response causes the production of pro-inflammatory cytokines at the site of injury leading to macrophage recruitment, inflammation and likely further tissue degradation [2]. Although the presence of pro-inflammatory cytokines in injured IVDs has been well documented, the extent to which inflammation affects the mechanical properties of the IVD remains poorly understood. The aim of this study was to evaluate how the initiation of the innate immune response alters the mechanical properties of the IVD.

## METHODS

Up to four motion segments (bone-IVD-bone) were dissected and removed from the tails of eleven Sprague Dawley rats (42 motion segments in total). In half of the motion segments (2 from each animal), a full AF puncture model (19G) was used to mimic IVD herniation. Further, from each tail, one punctured and one non-punctured IVD were cultured in control media containing DMEM, Penicillin-Streptomycin (1%), Fetal Bovine Serum (10%) and HEPES free acid (25mM). The remaining punctured and non-punctured IVDs were placed in media containing the same concentrations as previously listed with the addition of 10ug/mL of lipopolysaccharide (LPS). LPS is an endotoxin found in the outer membrane of gram-negative bacteria, is an innate immune stimulant, and is pro-

inflammatory. [3]. Through pilot testing, it was confirmed that IVD cells exposed to LPS produce over 100x increase in cytokine production compared to regular media which is supported in previous research [3]. LPS was therefore used to create an inflammatory environment for the motion segments. After 6 days in culture, motion segments were removed and mechanically tested in order to determine changes in IVD mechanics as a result of exposure to inflammation and/or IVD puncture.

A quasi-randomization protocol was used in order to decrease the effects that IVD level may have on the outcome parameters. All motion segments were subject to a preconditioning cycle followed by 20 phases of cyclic mechanical loading in compression and in tension (0.1mm/sec) using a displacement controlled protocol (UStretch, CellScale, Waterloo, Ontario) (Fig.1). From the load displacement data obtained, the neutral zone (NZ) size (mm) and stiffness (N/mm<sup>2</sup>) of the 20<sup>th</sup> cycle was calculated and compared across the conditions. A two way ANOVA was run in order to determine the effect of damage (puncture/ no puncture) and inflammation (LPS media/ control media) on NZ size and stiffness.



**Figure 1:** Image of a mounted motion segment; each sample was subjected to 20 phases of cyclic compression/tension.

## RESULTS

There was no main effect of damage (puncture vs. no puncture) on NZ size or stiffness ( $p=0.38$ ). There was, however, a significant main effect of inflammation (LPS vs. control media) (Fig. 2). When collapsed across damage (puncture vs. no puncture), IVDs cultured with LPS showed a 37% drop in NZ stiffness compared to those in the control media ( $\bar{x} = 0.130\text{N/mm}^2$  (control) vs.  $\bar{x} = 0.081\text{N/mm}^2$  (LPS);  $p=0.019$ ). No interaction was observed between damage and inflammation for NZ stiffness. Further, no significant change in NZ size in any of the groups was observed ( $p=0.384$ ) (Fig. 3).

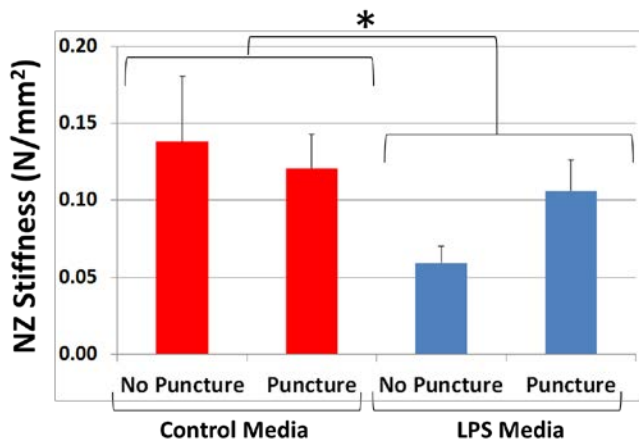


**Figure 2:** Average NZ stiffness ( $\text{N/mm}^2$ ) and standard error in all four conditions. Significant differences denoted by a \*. Red bars indicate regular media; blue bars indicate LPS media. Standard error bars shown.

## DISCUSSION

Based on current analysis it appears as though the mounting of an inflammatory response has a destabilizing effect on the spinal joint marked by a decrease in NZ stiffness in the LPS group compared to the control group. This destabilization may be indicative of tissue degradation in response to inflammation. Interestingly, after 6 days in culture, the puncture did not appear to have a significant effect on the mechanics of the IVD as indicated by the non-significant main effect of damage. It is

possible that the puncture affected the mechanical properties of the IVD immediately following the damage, but that by the 6-day mark it was no longer evident. Further research is needed to confirm this.

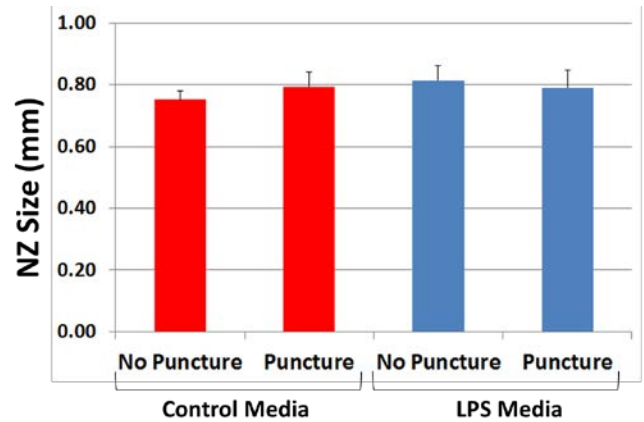


**Figure 3:** Average NZ size (mm) and standard error in all four conditions. No significant differences were observed. Red bars indicate regular media; blue bars indicate LPS media. Standard error bars shown.

## CONCLUSION

Understanding the complex interaction between inflammation and IVD mechanics is a critical step in the overall knowledge base of IVD damage and the development of low back pain. This research will help bolster the growing foundation of research required to eventually develop adequate treatment and rehabilitation options for those affected by low back pain.

## REFERENCES

- [1] Sun, Z. *et al.*, (2013). *Int J Clin Exp Pathol*, 6(6), 1009-1014.
- [2] Walter, B. A. *et al.*, (2015). *PloS One*, 10(3), 1-16.
- [3] Kim, J., *et al.*, (2013). *J Cell Physiol*. 228(9): 10.1002.

# THE MATERIAL PROPERTIES OF STABILIZING ROTATOR CUFF TENDONS RELEVANT IN REVERSE SHOULDER ARTHROPLASTY

Vijay Permeswaran, M. James Rudert, Donald D. Anderson, Carolyn Hettrich, Jessica E. Goetz

The University of Iowa, Iowa City, IA, USA  
email: vijay-permeswaran@uiowa.edu, web: <https://uiowa.edu/uiobl/>

## INTRODUCTION

Reverse shoulder arthroplasty (RSA) is an effective treatment for relieving pain and restoring function to individuals suffering from glenohumeral arthritis secondary to rotator cuff deficiency [1]. However, instability is a commonly reported complication after RSA. In order to study instability following RSA using finite element analysis [2, 3], accurate representation of stabilizing soft tissues must be included. We therefore measured the material properties of individual rotator cuff (subscapularis, infraspinatus, and teres minor) tendons.

## METHODS

Two fresh-frozen female cadaveric shoulders were dissected and prepared for testing. The scapular attachments of the subscapularis, infraspinatus, and teres minor muscles were removed, and the muscle bellies were bluntly dissected away from the tendons. The distal humerus was transected 13 cm distal to the lesser tubercle and potted in PMMA bone cement while maintaining the humeral insertions. The subscapularis and infraspinatus tendons were dissected into two equal-width superior and inferior sections, duly respecting fiber orientation and bundles.

The tendon segments were tested using an MTS 858 Bionix Material Testing System (MTS Systems Corporation, Eden Prairie, MN). The potted section of the humerus was held in a custom machined fixture and oriented perpendicular to the loading direction. This allowed the tendons to be tested in a direction parallel to their primary fiber axis. The fixture was attached to an x-y table, allowing the humerus to float freely in a plane perpendicular to

the loading. The proximal end of each tendon was fixed in a serpentine clamp that was connected to a thrust bearing, allowing free rotation about the direction of pull.

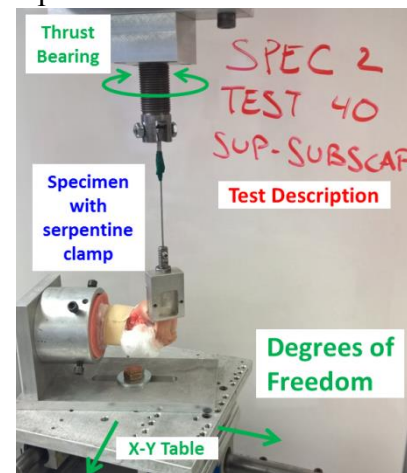
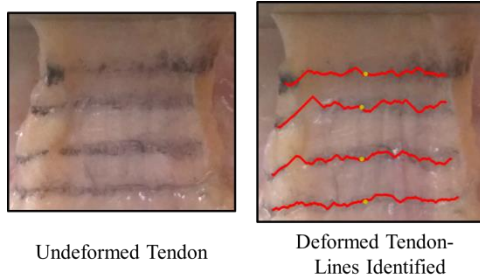


Figure 1: Physical testing setup

A tensile pre-load of 10 N was placed on the tendon, and a suture coated in ink was used to create 3-4 fiducial lines across the tendon specimen, perpendicular to the loading direction. The specimen was then hydrated copiously in saline and tested. The subscapularis and infraspinatus tendon sections were tested in load control over 10 seconds at a rate of 30 N/s for three tests. The loading was then increased to 40 N/s and 50 N/s over 10 seconds for three tests each until the final loading was achieved or failure occurred, whichever happened first. The teres minor, due to its small cross sectional area, was tested starting at 20N/ s, but followed the same testing pattern.

Video was recorded for all tests at 1080p, 30 frames/second using a Nokia Lumia Icon 929 (Microsoft Corporation, Redmond, WA). During testing, audio queues were created for every 50 N of additional load placed on the tendon. Videos were

later analyzed in Matlab (MathWorks, Natick, MA). The ink lines were first identified manually on 6-10 representative frames. The video was split into individual sections for each fiduciary line, and then lines were identified using a Dijkstra's algorithm automated method (Figure 2).



**Figure 2:** Identification of fiduciary lines in video

The centroids of each line were used to calculate strain in the tendons, with the zero-length defined by the distance between adjacent centroids at the initial frame of the video. The strain data were synched to the MTS load data through the audio queues. The tendon stress was defined simply as the load divided by the tendon cross sectional areas. Elastic modulus values were calculated as the best fit line to the linear portions of each stress-strain curve. The moduli values were compared using ANOVA.

## RESULTS AND DISCUSSION

Both shoulder specimens demonstrated clear patterns in elastic moduli values (Figure 3) for the posterior rotator cuff. The superior infraspinatus was found to have significantly stiffer material properties than the inferior infraspinatus ( $223 \pm 88$  vs.  $81 \pm 31$  MPa,  $p < .001$ ), the teres minor was found to be stiffer than the inferior infraspinatus ( $202 \pm 63$  vs.  $81 \pm 31$  MPa,  $p < .001$ ), and no statistically significant difference was found between the stiffness values of the superior infraspinatus and teres minor ( $223 \pm 88$  vs.  $202 \pm 63$  MPa,  $p = .427$ ).

Less clear trends emerged from the subscapularis sections, primarily due to the failure of the inferior subscapularis section on the first trial of specimen 1. No statistically significant difference was observed between the inferior and superior sections of the subscapularis ( $204 \pm 98$  vs.  $176 \pm 64$  MPa,  $p = .481$ ).

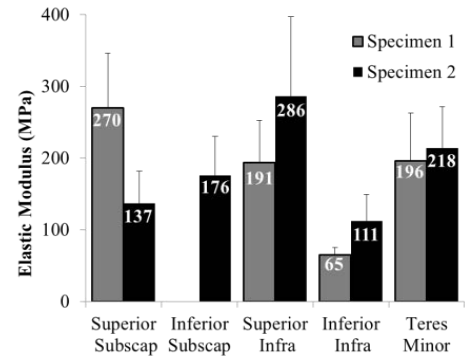


**Figure 3:** Elastic modulus values for the tendon sections tested of both specimens across all tests.

These results indicate that the stiffness and elastic moduli values for the rotator cuff tendons are much higher than previously reported [4, 5]. For example, the teres minor tissue was found to be much stiffer than values reported in Halder et al. ( $201 \pm 63$  vs.  $17 \pm 10$  MPa). In our study, we utilized video measurements of strain in order to isolate any deflection of the humeral bone or testing construct, which may explain why our values are much stiffer. The stiffness of our construct was  $49 \pm 8$  MPa, underscoring the importance of testing soft tissue strain visually.

## CONCLUSIONS

We tested the elastic moduli of rotator cuff tendons present following RSA using video techniques to measure strain. The values calculated were much stiffer than previously reported. We plan to use these data to inform a FE model studying instability in RSA.

## REFERENCES

1. Boileau et al. *JSES*, 2006. **15**(5): 527-40
2. Hettrich et al. *JSES*, 2015. **24**(11): 1774-81
3. Permeswaran et al. *J Biomech*, 2016. **49**(13): 3069-3073
4. Halder et al. *JOR*, 2000. **18**(5):829-34
5. Halder et al. *Clin Biomech*, 2000. **15**(6):456-62

## ACKNOWLEDGEMENTS

This research was generously funded by the University of Iowa Graduate College as well as the University of Iowa Carver College of Medicine.

# SPORT-RELATED LOADING IN ATHLETES PREDICTS BONE MINERAL CONTENT OF THE FIFTH METATARSAL

<sup>1</sup> Audrey E. Westbrook, <sup>1</sup> Anh-Dung Nguyen, <sup>1</sup> James M. Smoliga, <sup>1</sup> Jeffrey B. Taylor,  
<sup>2</sup> David R. Sinacore, <sup>1</sup> Kevin R. Ford

<sup>1</sup> High Point University, High Point, NC, USA

<sup>2</sup> Washington University School of Medicine, St. Louis, MO, USA  
email: awestbro@highpoint.edu

## INTRODUCTION

Exercise is widely known to play an important role in improving bone health to prevent injury, while more sedentary lifestyles are often associated with bone loss. Regular physical activity, especially weight-bearing exercise, provides a positive influence on bone health [1]. Wolff's law helps explain this, stating that bone formation and remodeling occurs as a result of the stress or mechanical load applied to the body, and therefore bone adapts to meet its mechanical demands [2]. Athletes that participate in sports involving weight-bearing exercise such as basketball, soccer or running tend to have higher bone mineral content (BMC) than those who do not (i.e. swimmers or cyclists) [3]. This is likely due to various types of loading patterns observed amongst different sports and leads to the conclusion that activities such as jumping, cutting, and running provide the mechanical stimuli necessary to increase BMC [4].

Previous studies have reported how loading can affect site specific BMC, though few have measured that of the metatarsals. While foot, ankle, and knee injuries during sports are common, an increasingly serious injury with significant participation time loss involves acute and overuse fracture to the proximal 5<sup>th</sup> metatarsal (met5). In-shoe and barefoot plantar loading are methodologies that may help identify risk factors that predispose an athlete to this type of devastating injury. Our long-term goal is to reduce foot injuries in athletes. The objective of this study was to determine the relationship of both in-shoe loading during sport-related tasks and barefoot plantar loading during walking on proximal met5 BMC in basketball players, soccer players, and recreational runners.

## METHODS

Fifty-two athletes (26M, 30F, age:  $18.7 \pm 2.5$  yrs, height:  $173.3 \pm 12.3$  cm, weight:  $70.1 \pm 13.5$  kg) were included in this study and divided into subcategory by sport: basketball (n=18), soccer (n=19), and running (n=15). BMC of met5 was calculated using dual-energy X-ray absorptiometry (DXA) on a Hologic Discovery System (Figure 1). Dynamic plantar pressure distribution was obtained as each participant walked barefoot at a self-selected pace over a platform emed-x system (novel). Three separate trials of barefoot walking were collected for the left foot and averaged.

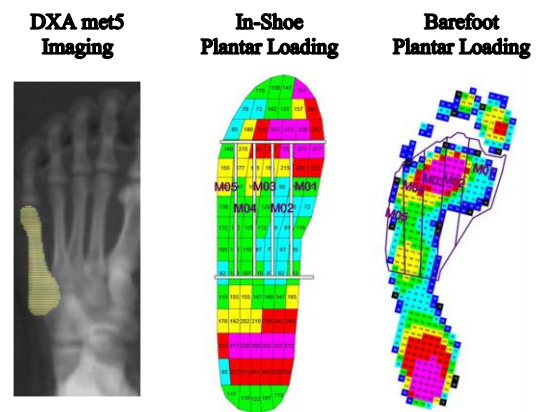


**Figure 1:** DXA scan of the left foot. Regions of interest were masked to the size of the pedar insole and to the size of each participant's foot.

A flexible in-shoe pressure distribution measuring insole was inserted into the left shoe (pedar-x, novel) to calculate in-shoe loading during sport-related tasks for each type of athlete. These tasks included a single leg side drop jump, an unanticipated cutting task, and running at a self-selected speed for basketball players, soccer players, and runners, respectively. A regional analysis of the foot was performed utilizing separate

“masks,” or areas, of the foot consisting of the 5 metatarsal regions using predefined areas in barefoot and in-shoe data (Figure 1). Force time integral for each region was calculated and divided by the force time integral for the total foot surface to determine the relative load in each region.

## RESULTS AND DISCUSSION

A stepwise linear regression was performed (SPSS) to determine the predictors of proximal BMC of met5. Relative loading during stance phase from all 5 metatarsal regions of the sport-related tasks and barefoot walking were included as independent predictor variables as well as sport type. The relative loading of the met5 region during sport-related tasks was significantly predictive of proximal met5 BMC ( $R^2=0.426$ ,  $p<0.001$ ); with a secondary predictor of met5 loading during barefoot walking ( $R^2_{\text{change}}=0.055$ ,  $p=0.027$ ;  $R^2_{\text{Total}}=0.482$ , Adjusted  $R^2=0.460$ ,  $SEE=0.434$ ; Figure 3).

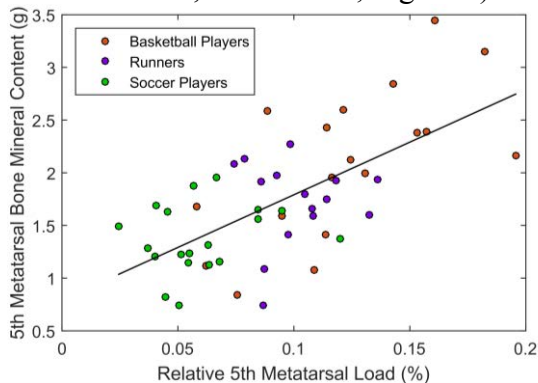


**Figure 3:** Proximal met5 BMC and relative in-shoe loading during sport-related tasks.

Differences in proximal met5 BMC and in-shoe plantar loading of met5 were determined among the three different sport groups using an analysis of variance (ANOVA) with a Bonferroni correction. A main effect for sport group was found in the proximal met5 BMC ( $p<0.001$ ) (basketball:  $2.10\pm0.70\text{g}$ , soccer:  $1.38\pm0.32\text{g}$ , runners:  $1.73\pm0.40\text{g}$ ). However, when controlling for potential covariates (ANCOVA: age, height, mass) the main effect of sport in met5 BMC was not significantly different ( $p=0.14$ ). A main effect was found for relative in-shoe loading of met5 during sport-related tasks when controlling for age, height and mass ( $p<0.001$ ). Specifically, higher met5 in-shoe loading was found in the basketball sport-

related task compared to the soccer sport-related task ( $p=0.002$ ) and running compared to soccer ( $p<0.001$ ) (basketball:  $12.2\pm3.9\%$ , soccer:  $6.0\pm2.3\%$ , runners:  $10.2\pm1.8\%$ ; Figure 4).

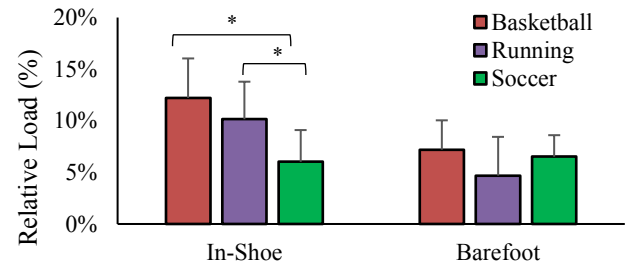


**Figure 4:** Relative load of the met5 region during sport-related tasks and barefoot walking.  $*p<0.05$

Plantar loading of met5 during sport-related tasks was a better independent predictor ( $R=0.653$ ) of met5 BMC than plantar loading during barefoot walking ( $R=0.360$ ). Furthermore, tasks more specific to basketball players resulted in higher loading of met5 than those specific to soccer players or runners, possibly relating to higher BMC in that region. The results of this study imply not only does loading of the foot help explain BMC, but the type and location of loading may be important.

## CONCLUSIONS

The results should be cautiously interpreted due to the cross-sectional nature of the study design. However, bone appears to adapt to site specific in-shoe loading during sport-related tasks. Furthermore, this is highlighted in basketball players that appear to load the met5 region more which may increase the risk of proximal met5 fracture if the loading exceeds the threshold dependent strength of the bone which may occur with extreme changes in training.

## REFERENCES

- Wallace BA, et al. *Calcif Tissue Int*, **67**, 10-18, 2000.
- Chen JH, et al. *J Biomech*, **43**(1), 108-118, 2010.
- Etherington J, et al. *J Bone Min Research*, **11**(9), 1333-1338, 1996.
- Nordstrom P, et al. *J Bone Min Research*, **13**(7), 1141-1148, 1998.

# ASSESSING FRACTURE SEVERITY IN THE TMJ: CAN FRACTURE ENERGY BE COMPUTED USING CBCT?

Kevin N. Dibbern, Kyungsup Shin, Megan Andrew, and Donald D. Anderson

The University of Iowa, Iowa City, IA, USA

email: kevin-dibbern@uiowa.edu, web: <https://uiowa.edu/uiobl/>

## INTRODUCTION

Assessing injury severity is a critical step in treating articular fractures, with important implications in both clinical and surgical decision making. One of the treatment goals is to forestall the development of post-traumatic osteoarthritis (PTOA). This is of particular concern in temporomandibular fractures, as the etiology of temporomandibular joint (TMJ) arthritis is not well understood [1]. Fracture energy has been utilized previously as an objective method for assessing fracture severity in the lower extremities and predicting PTOA risk [2].

Prior assessments of fracture energy have relied upon a standard CT scan, with its calibrated Hounsfield Unit (HU) values, to estimate location-specific bone density. Most TMJ fractures at our institution are scanned instead utilizing a Cone Beam CT (CBCT) system. CBCT systems acquire scans in a fundamentally different manner and do not obtain the same uniform image reconstructions. Therefore, they do not directly provide calibrated HUs with which to estimate bone density. Fortunately, Reeves et al. previously established a linear relationship between HU values and the grey-level intensities derived from CBCT machines [3]. This study aims to determine if automatic HU correction built into a CBCT system enables reliable fracture energy computation.

## METHODS

Fracture energies were computed on a sample of convenience – the first 2 standard CT and 5 CBCT scans to come available after having been acquired to evaluate a TMJ fracture. Patients were consented and enrolled in this IRB approved study. The standard CT scans were performed using a Siemens Somatom Definition AS+ while the CBCT scans were performed in a Xoran Technologies scanner

that automatically applies a rescaling factor to approximate HU intensity values.

The fracture energy computation involves scaling interfragmentary surface area by location-specific densities of the fractured bone. To obtain the interfragmentary surfaces of the bone, the CT scan data are segmented to provide 3D surface models of the fracture fragments. The interfragmentary surfaces are then identified using an automated classifier (Fig. 1) [4]. The location-specific density of the interfragmentary surface is derived directly from the HU values in the CT scans. Finally, the fracture energy is computed by summing the product of the local bone density and an empirically derived fracture energy release rate, which is a function of the bone density.

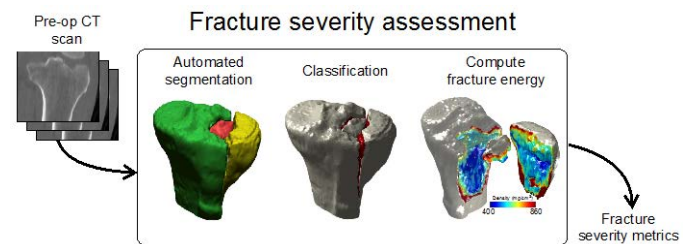


Figure 1. Methods for computing fracture severity.

Fracture energies were computed for all of the fractures, and the fracture energy values were then compared between cases for which standard and CB CT scans were acquired. Additionally, as the interfragmentary surface area is independent of the CT scanner, the average fracture energy release rates for the standard and CB CT scans were directly compared.

## RESULTS AND DISCUSSION

The average fracture energy from the two standard CT scans was  $11.0 \pm 5.5$  J, while the average fracture energy for the five CBCT scans was  $4.8 \pm 1.1$ . These data suggest a large difference between the fracture energies calculated from standard CT vs. CBCT (Fig. 2). However, controlling for area by examining the energy release rates directly, there was no significant difference observed between the different scanner types. The average energy release rate was  $3.31 \pm 0.15$  mJ/mm<sup>2</sup> for the standard CT scans and  $3.42 \pm 0.24$  mJ/mm<sup>2</sup> for CBCT. Therefore, the average energy release rates demonstrated that perceived differences in fracture energy values obtained from the different CT scanners were more attributable to underlying differences in the injuries studied. This observation is further supported by an examination of disparate fractures analyzed using the CBCT scan vs. that of the standard CT (Fig. 3).

## CONCLUSIONS

The automatic rescaling factor by the Xoran Technology's CBCT scans of temporomandibular fractures at our institution produced similar fracture energy release rates when compared to normal

medical CT scans. This indicates that CBCT scans with a HU intensity correction can be utilized to evaluate fracture energy. Fracture energies calculated in this manner have the potential to objectively predict PTOA development in the TMJ with standard of care CBCT scans at our institution.

## REFERENCES

1. Shalender S, et al. *Natl J Maxillofac Surg.* **2**(2): 116-119, 2011.
2. Dibbern KN et al. *J Orthop Research*, doi:10.1002/jor.23359 2016.
3. Reeves TE et al. *Dentomaxillofac Radiol*, 41(6):500-8, 2012.
4. Dibbern KN, et al. *63rd Annual Meeting of the ORS*, March 19–22, 2017.

## ACKNOWLEDGMENTS

The research reported in this abstract was supported by the National Institute of Arthritis and Musculoskeletal and Skin Diseases of the National Institutes of Health under award number R21 AR061808. Dr. Kyungsup Shin and the University of Iowa New Faculty Start-up Fund from College of Dentistry & Clinics also contributed to this research.

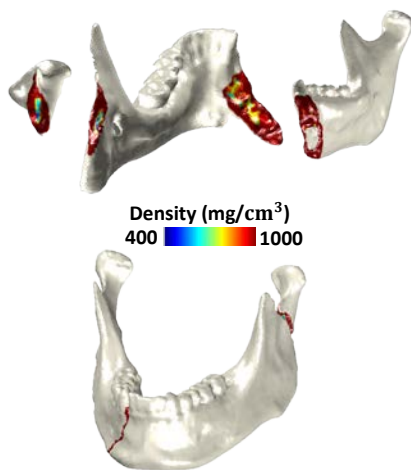


**Figure 2.** 3D model of a temporomandibular fracture with an exploded view (top) of the fragments. Interfragmentary bone is colored according to its density distribution.

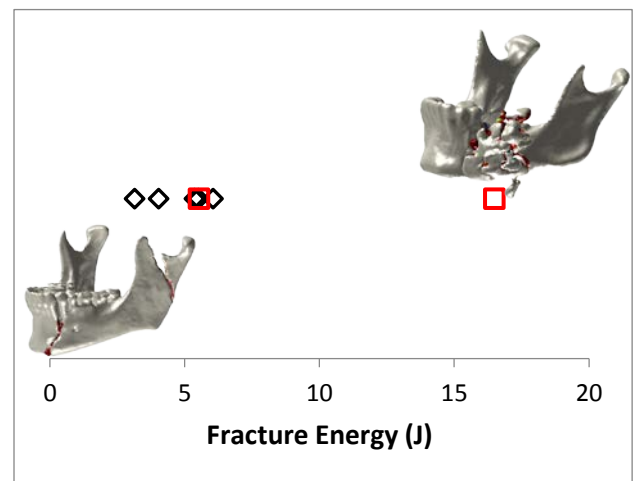


**Figure 3.** Fracture Energy range for CBCT (black) and standard CT (red) with highest (top right) and lowest (bottom left) energy fractures displayed.

# RELATIONSHIP BETWEEN TIBIAL BONE STRESS AND BIOMECHANICAL FACTORS ASSOCIATED WITH STRESS FRACTURE

<sup>1</sup> Stacey Meardon, <sup>1</sup>Zach Blank, <sup>2</sup>Timothy Derrick, <sup>1</sup>John Willson, <sup>1</sup>Michael Baggaley and <sup>1</sup>Richard Willy

<sup>1</sup> East Carolina University, Greenville, NC, USA

<sup>2</sup>Iowa State University, Ames, IA, USA

email: [meardons@ecu.edu](mailto:meardons@ecu.edu) <http://blog.ecu.edu/sites/hmal/>

## INTRODUCTION

Tibial stress fracture (TSF) is common in both running and military populations [1, 2]. Elevated levels of tibial bone stress, which is influenced by both bone geometry and bone loads, has been observed during running in individuals with a history of TSF [3]. Regardless of sex, TSF is more common in individuals with smaller bone geometries [2, 4]. Specific gait dynamics have also been linked with TSF [5, 6]. Together, smaller bone geometry and greater dynamic loads may explain reports of elevated bone stress in runners with a history of TSF [3]. However, the relationship between TSF-related bone structure, running dynamics and tibial stress has not been explicitly examined. Understanding factors that directly contribute to stress applied to the tibia during running may better guide interventions. As a first step to this, we evaluated the relationship between both structural and dynamic biomechanical factors associated with TSF and distal tibial bone stress during running.

## METHODS

20 female runners (25.2±3.3 yrs; 168.1±6.2 cm; 57±9.3 kg; 32.8±18.5 km/wk; 2.82 m/s preferred pace) and 20 male runners (24.9±4.4 yrs; 181.3±6.1 cm; 80.1±8.4 kg; 14.6±7.6 mi/wk; 2.97 m/s preferred pace) participated in this study. All participants were currently free of injury. During an 8-minute progressive warm up and accommodation period on an instrumented treadmill (Bertec, Worthington, OH), each participant's self-selected running speed was determined. Self-selected running speed was operationally defined as the pace utilized during a standard, endurance-paced training run. Once determined, biomechanical data were collected for 15 sec. Kinematic data (Qualysis, Gothenburg,

SWE) and force plate data were sampled at 200 Hz and 1000 Hz, respectively, using a real-time data acquisition system (Innovative Sports, Inc., Chicago, Ill). Marker trajectory and ground reaction force data were filtered with a 4th order, zero lag low-pass Butterworth filter with a 15 Hz cutoff and exported for analyses. 10 stance phases were extracted for analysis. To develop subject-specific bone models, participants then underwent MR imaging of their right tibia (Philips Achieva 1.5T, Best, NLD). The MRI axial slice corresponding to the distal 1/3 location, a common site of TSF [1] was extracted for analysis. A cross-sectional finite element mesh, represented by 600 elements, was created using VA-Batts software [7].

For 10 stance phases, 3D kinematics and kinematics were input to a musculoskeletal model that estimated 3D internal tibia forces and moments at a level corresponding to the distal 1/3 tibia. Internal bone forces and moments at this site were estimated at each 1% of stance and served as inputs to a cross-sectional finite element model. VA-Batts software was used to obtain normal and shear stresses across the stance phase in each element of the bone mesh [8]. Peak normal and shear stresses during the stance phase of running of each trial were extracted and averaged for statistical analysis.

Tibial cross sectional area (CSA), maximum and minimum moment of inertia ( $I_{max}$  and  $I_{min}$ ), and polar moment of inertia (J) have been associated with TSF [2, 4]. These bone geometries were obtained via the VA-Batts software and served as structural inputs for regression analyses. Based on the TSF literature [5, 6], the following running related factors were extracted for analysis to serve as dynamic inputs to the regression analyses: peak hip adduction (HADD), knee adduction (KADD and internal

rotation (KIR), rearfoot eversion (RFEV), instantaneous loading rate of the vertical ground reaction force (VLR), and tibial frontal plane angle at peak vertical ground reaction force (TFA).

For each directional component of bone stress, linear regression analyses were performed to identify key structural and dynamic indicators of peak bone stress (IBM SPSS Statistics 22, Armonk, NY). Co-linearity among predictors was assessed during each iteration of analysis. When the variance inflation factor exceeded 5, one or more of the violating predictors was removed from the regression model. The proportion of the variation in dependent variables explained by independent variables was then adjusted based on the number of independent variables in the model (Adjusted R<sup>2</sup>).

## RESULTS AND DISCUSSION

Peak compression (-201.0±98.3 MPa) occurred posterior-medially, tension (145.9±84.5 MPa) anterior-laterally and shear (21.7±7.8 MPa) medially during mid stance. The most meaningful combination of factors acting together to increase posterior-medial tibial compression were CSA, KADD, VLR, and REV (R<sup>2</sup>=.47, p<.001). For tension, KADD, REV, HADD and VLR were most strongly associated with bone stress (R<sup>2</sup>=.55, p<.001). A combination of bone structure (I<sub>min</sub>) and dynamics (KADD; R<sup>2</sup>=.40, p <.001) best predicted shear stress.

Bone structural characteristics and dynamic biomechanical factors associated with TSF in previous studies of injured populations appear to act in concert to increase distal tibial bone stress during running. Although, a fair portion of bone stress variance remains unexplained. Smaller CSA combined with higher vertical loading rates, knee adduction and reduced rearfoot eversion appear to contribute to higher compressive stress. Tension increased with hip and knee adduction and reduced rearfoot eversion. Like compression, shear was influenced by bone geometry and dynamics. Low bending strength along the narrowest aspect of the

tibia combined with knee adduction resulted in increased shear stress.

Bone stress appeared to be consistently related to frontal plane motion of the lower extremity and loading. Frontal plane motion of the lower extremity during running has been linked to the free moment [8] potentially influencing tibial bending and torsional angles [9]. The free moment has been associated with TSF [5] but was not examined here due to methodological constraints with use of an instrumented force treadmill. Other limitations include assumptions inherent to musculoskeletal modeling and lack of stratification by sex. Future work will examine sex-specific associations as well as associations runners with recent TSF.

## CONCLUSIONS

Overall, this analysis suggests a combination of bone structure and running dynamics contribute to elevated bone stress. Individuals with small bone geometry, excessive frontal plane running mechanics and high loading rates were more likely to experience elevated tibial stress during running. Interventions to address frontal plane running mechanics and loading rates as well as to increase bone size through targeted exercise programs may be beneficial in reducing risk of TSF.

## REFERENCES

1. Nattiv A, et al. *Am J Sports Med* **41**, 1930-1941, 2013
2. Cosman F, et al. *Bone* **55**, 359-366, 2013.
3. Meardon SA, et al., *Clin Biomech* **30**, 895-902, 2015.
4. Franklyn M, et al. *Am J Sports Med* **36**, 1179-1189, 2008.
5. Pohl MB, et al. *J Biomech*, **41**, 1160-1165, 2008.
6. Creaby MW., et al. (2008). *Med Sci Sports Exerc*, **40**(9), 1669-1674.
7. Kourtis LC, et al. *Comp Meth Biomech and Biomed Eng*, **11**, 463-476, 2008
8. Yang P, et al. *PLoS one*, **9**, e94525, 2014.
9. Willawacher S, et al. *Footwear Sci*, **8**, 1-11, 2016.

# VALIDATING THE USE OF pQCT OF PERIPHERAL BONE SITES TO PREDICT THE RISK OF FEMORAL NECK FRACTURES

<sup>1</sup> Rachel Alba, <sup>2</sup> Emily Southmayd, <sup>1</sup> Sarah E. Froehlich, <sup>2</sup> Mary Jane De Souza, and <sup>1</sup> Allison R. Altman-Singles

<sup>1</sup> The Pennsylvania State University, Reading, PA, USA

<sup>2</sup> The Pennsylvania State University, University Park, PA, USA

email: ara5093@psu.edu

## INTRODUCTION

As our population ages, the incidence of osteoporosis and osteoporosis-related fractures increases along with the associated costs and challenges to our health care system. Hip fractures are associated with high medical costs and decreased quality of life following fracture [1].

Currently, the best tool available for predicting risk of hip fracture is a dual x-ray absorptiometry (DXA) scan to calculate bone mineral density (BMD) of the whole body, spine, and hip regions [1]. While this measure gives a general measure of fracture risk, the sensitivity of the imaging to differences in bone sizes and subtle changes in bone structure is low. One study recently suggested that the addition of more specific femoral BMD measures to standard DXA derived BMD provided an improved capacity to predict femoral fractures [2].

Various forms of computed tomography (CT) can assess these more bone-specific BMD measures, and improve upon the sensitivity of DXA-derived measures. However, assessing the BMD at the femoral neck and head exposes the patient to a large amount of radiation. Peripheral quantitative CT (pQCT) offers the best compromise between image clarity and minimal radiation. The pQCT can achieve an image clear enough to distinguish the cortical and trabecular bone compartments, however it is a quick scan and performed on peripheral bone sites, such as the distal tibia or radius, which will be less affected by radiation compared to the more central bone sites [2].

The purpose of this study is to assess the predictive strength of distal bone measures for replacing

femoral BMD values in predicting hip fracture risk. We hypothesize that a regression model using the distal radius and tibia measures derived from pQCT will be able to predict specific BMD of each bone compartment at the femoral head and neck.

## METHODS

The bones from seven cadavers were dissected and used for this study. All available sets of femora, radii, and tibia were dissected and scanned using a Stratec XCT3000 pQCT scanner (Remeda, Zurich, Switzerland). Radial and tibial scans were taken at clinically standardized locations at the distal end calculated as a percentage of total length (33% and 4% respectively). The femoral head, neck, and greater trochanter were scanned along the direction of the femoral neck. The femoral head was defined as the distal most portion with the largest diameter, the neck was the narrowest diameter, and the trochanter was identified as the region where the trochanteric protuberance was greatest along the axis of the femoral neck.

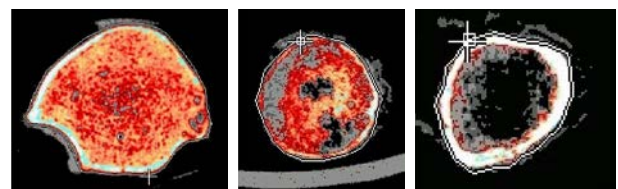


Figure 1: Representative scans of the distal 4% scan of the tibia, femoral head, and femoral neck, respectively.

The scanner software was used to calculate all parameters of interest for each bone after semi-automatic bone contouring to distinguish cortical and trabecular compartments (Figure 1). For the radius, the cross-sectional moment of inertia ( $R\_xMOI$ ), polar moment of inertia ( $R\_pMOI$ ) and

orthogonal sectional stress-strain indices (R\_XSSSI, R\_YSSSI), total bone mineral content (R\_totBMC), total BMD (R\_totBMD), and trabecular BMD (R\_tBMD) were calculated. For the tibia, similar parameters were calculated (T\_XSSSI, T\_YSSSI, T\_totBMD). For the femur the BMD at the trochanteric region and neck region were calculated (F\_BMD.t and F\_BMD.n). In addition, the trabecular BMD was calculated at the trochanteric, neck, and head regions (F\_tBMD.t, F\_tBMD.n, F\_tBMD.h). Each femoral parameter chosen has been previously shown to be predictive of femoral neck fractures [3-4].

Regression models were generated for each femoral parameter using backward stepwise regression analysis (entry  $p < 0.05$ , removal  $p < 0.1$ ).

## RESULTS AND DISCUSSION

The seven cadavers (4 male, 3 female) had an average age of  $78.4 \pm 7.3$  yrs, height of  $1.64 \pm 0.12$  m, and mass of  $71.2 \pm 26.6$  kg. A wide range of causes of death were present, including vascular, renal, pulmonary, and immune related illnesses.

A combination of parameters from both tibia and radius resulted in the best prediction of most femoral parameters (Table 1). Only F\_BMD.t incorporated only one tibial parameter, T\_XSSSI. Indicating the likelihood that trochanteric fractures are more related to the bone structure inferred by another weight bearing bone than by any other factor. All other predictive models included both mechanical strength indicators such as the moment of inertia or stress-strain index and compositional parameters such as BMD or BMC. Interestingly, only F\_tBMD.t required a trabecular bone predictor

(R\_tBMD), otherwise all other predictions were sufficient with total BMD or BMC. These results agree with the existing predictive models relating tibial [2] and radial [5] parameters separately with femoral parameters.

The findings from this study provide evidence that a combination of imaging parameters can be used to predict specific femoral BMD at various fracture-prone sites. In combination with standard DXA-derived BMD the additional knowledge provided by these specific femoral BMD values provides a more complete prediction of hip fracture. The additional information provided in the present study may allow investigators to bypass the challenging process of obtaining femoral-specific BMDs. These pQCT measures can be attained easily from a distal bone site using a small, lower-cost imaging option, which exposes the patient to less radiation than other conventional measures.

## CONCLUSIONS

pQCT of distal bone sites may be used to supplement conventional DXA to provide an improved potential for osteoporotic fracture risk prediction.

## REFERENCES

1. Boehm HF & Link TM. Curr Osteoporos Rep, 2, 41-46, 2004.
2. Sheu et al., JBMR, 26(1), 63-71, 2011.
3. Museyko et al., Osteoporos Int, 23(3), 1137-1147, 2015.
4. Kukla et al., Injury, 33, 427-433 2002.
5. Augat et al., JBMR, 11(9), 1356-1363, 1996.

Table 1: Regression equations using both tibia and radial parameters are shown below for all five femoral parameters. All models reached statistical significance  $p < 0.05$ .

Femoral Parameter	R <sup>2</sup>	Regression Equation
F_BMD.t	0.64	$0.069 (T\_XSSSI) + 167.327$
F_BMD.n	0.82	$0.252 (R\_xMOI) + 1.676 (R\_totBMC) - 0.134 (T\_YSSSI) + 247.577$
F_tBMD.t	0.99	$-0.769 (T\_totBMD) + 0.140 (R\_xMOI) + 0.378 (R\_totBMD) + 0.801 (R\_tBMD) - 0.078 (T\_YSSSI) + 0.085 (T\_XSSSI) - 88.843$
F_tBMD.n	0.98	$1.260 (T\_totBMD) + 0.342 (R\_xMOI) + 4.330 (R\_totBMC) - 0.483 (R\_totBMD) - 0.427 (T\_XSSSI) + 326.041$
F_tBMD.h	0.93	$0.464 (R\_xMOI) + 3.792 (R\_totBMC) - 0.361 (T\_XSSSI) + 238.097$

# A METHOD FOR ASSESSING MANDIBLE BLUNT IMPACT BIOMECHANICS DURING ANTERIOR-POSTERIOR IMPACTS TO A RESTRAINED JAW

<sup>1,2</sup> Charles A. Weisenbach, <sup>1,3</sup> Tyler Bonts, <sup>1,3</sup> Andrea Winegar, <sup>1,2</sup> Danielle Rhodes, <sup>1,2</sup> Ray W. Daniel, <sup>1</sup> Kyle Rybarczyk, <sup>1</sup> Fredrick T. Brozoski, and <sup>1</sup> Valeta Carol Chancey

<sup>1</sup> U.S. Army Aeromedical Research Laboratory, Fort Rucker, AL, USA

<sup>2</sup> Lulima Government Solutions, LLC, Orlando, FL USA

<sup>3</sup> Oak Ridge Institute for Science and Education, Oak Ridge, TN USA

email: valeta.c.chancey.civ@mail.mil, web: <http://www.usaarl.army.mil/>

## INTRODUCTION

Injury risk functions and biofidelity corridors for the human mandible are critical for the evaluation of maxillofacial protection devices that are under development. Currently the mandible is the only facial bone without any injury criterion for use with the Facial and Ocular Countermeasures Safety (FOCUS) headform. Previous attempts to develop an injury criterion for anterior-posterior (A-P) impacts to the mandible have been unsuccessful due to the mandible opening when impacted [1]. In order to investigate the fracture tolerance of the mandible to A-P impact and determine a mandible injury criterion for the FOCUS headform, a closed jaw boundary condition was needed to mitigate the previous limitation. Additionally, the proposed condition would be representative of a helmeted population (military, athletics, etc.), where movement of the mandible is restricted by headgear.

## METHODS

A restraint fixture was designed to prevent the jaw from opening during blunt impacts using a Monorail Drop Tower (MDT). The restraint consisted of an angled ridge aluminum plate (2.5 cm wide, 15.2 cm long) with beveled edges positioned against the body of the mandible. The aluminum plate was connected to a six degree of freedom load cell (Humanetics) and braced against the MDT (Fig. 1). The load cell was used to measure any forces transferred through the mandible into the restraint fixture and allowed for the angle of the aluminum plate to be adjusted. The entire restraint fixture was designed to be adjustable in the vertical and

horizontal directions, allowing the aluminum plate to be aligned with the mandible of the specimen.

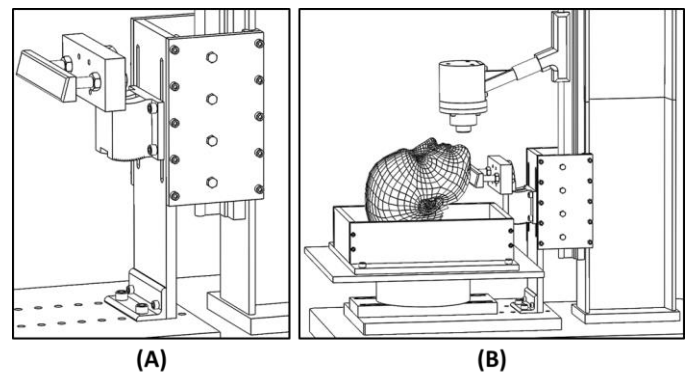


**Figure 1:** (A) Restraint fixture attached to MDT. (B) Experimental test setup with restraint fixture aligned with the mandible.

Two fresh-frozen male cadaveric heads (IBD012, 67 yrs; IBD016, 69 yrs) were used to assess proof of concept in accordance with the Army Policy for Use of Human Cadavers [2]. Each specimen was sectioned between the C2 and C3 vertebrae to keep the foramen magnum from being exposed. Extraneous tissue was removed. The specimen was potted in a polyurethane resin (Golden West Manufacturing) using screws and polymethylmethacrylate. To align the specimen while potting, the Frankfurt plane was identified by the exterior auditory meatus and the infraorbital foramen and oriented vertically, ensuring reproducibility and a natural position of the head. The mandible of each specimen was instrumented at both rami with strain gauges and acoustic emission sensors to assist with fracture detection. The specimen's jaw was exercised by hand before being closed with a 10 N force using the restraint fixture. Impacts were performed at 5 J increments until

fracture was detected using a guided impactor mass with a circular 6.45 cm<sup>2</sup> impact area. After each test, the presence of fractures was detected using specimen mounted sensors, x-ray imaging, and palpation. Additionally, 5 J baseline impacts were conducted to aid in fracture detection. The presence of a fracture was verified using a computed tomography (CT) scan and then the dissection of the mandible. During each test, impact velocity was recorded using a velocimeter (GHI Systems). Impact force and acceleration were measured using a load cell (Honeywell, NJ) and accelerometer (Endevco) on the impactor mass. Force transmitted through the specimen to the base of the MDT was measured using a load cell (Humanetics). Data were collected at 1 MHz using a Synergy Data Acquisition System (Hi-Techniques Inc.) and analyzed using MATLAB (MathWorks) scripts. All data were filtered using a 4<sup>th</sup> order low-pass Butterworth filter with a 500 Hz cutoff frequency. High-speed video was collected for all tests using a MIRO and a Phantom v9 (Vision Research Inc.) camera at 2,000 frames per second.

## RESULTS AND DISCUSSION

A total of sixteen impacts were conducted on the two specimens. The tested impact energies ranged from 4.6 J to 22.4 J. Test velocities ranged from 1.7 m/s to 3.4 m/s. Fracture was observed in the strain data collected (Figure 2) during testing. Post-test CT imaging and dissection confirmed the presence of fractures in both specimens. Specimen IBD012 had a subcondylar non-displaced transverse linear fracture on the left side of the mandible. Specimen IBD016 had a commuted transverse liner fracture of the right mandible condyle. Fracture patterns were consistent with those reported in the literature [2]. Measured impact peak force (Table 1) for both fracture cases compared well with fractures produced during previous work examining A-P

mandible impacts [3] and mandible impacts directed through the temporomandibular joint [4].

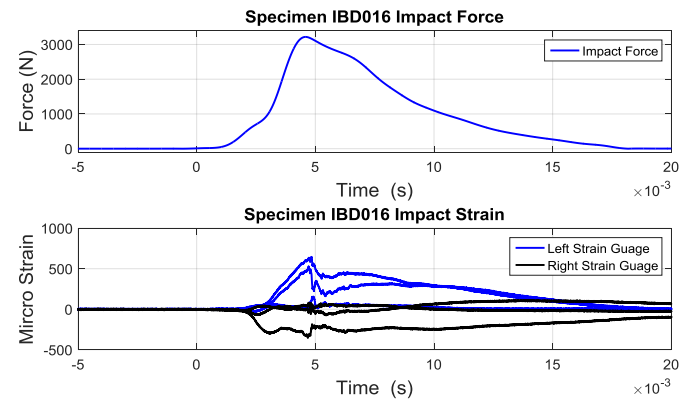


**Figure 2:** Impact force and strain recorded for specimen IBD016.

## CONCLUSIONS

A method has been developed that is able to reliably allow for the creation of mandible fractures during A-P impacts. Future investigation of mandible impact biomechanics will focus on evaluation of mandible fracture tolerance and the development of an injury criterion for the FOCUS headform.

## REFERENCES

1. Cormier J, *Doctoral Dissertation*, Virginia Polytechnic Institute and State, 2008.
2. United States Army, *Army Policy for Use of Human Cadavers for Research, Development, Test and Evaluation, Education or Training*, 2012
3. Viano DC, et al. *J Trauma Acute Care Surg* **56**, 1305–1311, 2004.
4. Craig M, et al. *J Biomech* **41**, 2972–2980, 2008.

## ACKNOWLEDGMENTS

The authors would like to thank Dr. McGhee, Mr. Rooks, Ms. Logsdon, Ms. Vasquez, Mr. Fralish, Mr. McEntire and the Lyster Army Health Clinic.

**Table 1:** Fracture impact test conditions

Test Number	Specimen	Impactor Mass (kg)	Energy (J)	Velocity (m/s)	Peak Force (N)	Loading Rate* (kN/s)
MDT000010	IBD012	3.7 kg	22.0	3.5	3059.4	1261.1
MDT000150	IBD016	3.2 kg	22.4	3.5	3217.0	1267.3

\* Calculated from slope between 20% peak force and 80% of peak force

# DEVELOPMENT OF A STRUCTURAL STOCHASTIC FINITE ELEMENT MODEL OF TRABECULAR BONE

<sup>1</sup> Saif Alrafeek, <sup>2,3</sup> James R. Jastifer, <sup>1,2</sup> Peter A. Gustafson

<sup>1</sup> Western Michigan University, College of Engineering and Applied Sciences, MI, USA

<sup>2</sup> Western Michigan University, Homer Stryker M.D. School of Medicine, MI, USA

<sup>3</sup> Borgess Hospital, MI, USA

email: saifghazyfais.alrafeek@wmich.edu, web: <https://wmich.edu>

## INTRODUCTION

Bone can be described as a multi-level composite arranged in a hierarchical form. At the macrostructure scale, bone is grouped into two types: cortical bone (also known as compact bone or dense bone) and trabecular bone (known as cancellous bone or spongy bone) [1]. Generally, cortical bone surrounds trabecular bone. While cortical bone has a porosity of five to fifteen percent, trabecular bone has a porosity that varies from forty to more than ninety percent [1]. Because cortical bone has low porosity, continuum based finite element methods have been used for most FE modelling. Similarly, homogenized continuum methods have been used for trabecular bone. Recent FE approaches have meshed the trabecular architecture (i.e., non-homogenized) using continuum elements, however, these meshes are difficult to produce, may require detail CT or MRI imaging, and are costly to solve. The proposed paper studies a representation of the trabecular micro-architecture using beam elements. The proposed approach may permit lower meshing and computational cost while capturing the behavior sought with detailed trabecular models. Further, the proposed approach readily admits stochastic analysis incorporating both porosity level and other inputs and model outputs. The FE models in this work will be compared to published biomechanical experiments and cadaver studies [2].

## METHODS

Trabecular bone consists of a three-dimensional network structure mainly composed of rod-shaped and plate-shaped fundamental units named “trabeculae.” In this work, the trabeculae were

modelled as beam elements. Two methods were investigated using differing assumptions. The first method assumed repetition of beam elements arranged as hexagonal unit-cells (henceforth, Hexagonal Network Model or HNM) over a cubic trabecular bone specimen with 4 mm sides. The second method assumed randomly oriented beams (henceforth, Random Beam Method or RBM) also within a 4 mm cube. The cross section of the beams for the hexagonal network method was defined as a circular shape with a 0.1 mm radius. For the random beam method, beams were created algorithmically so that beam properties could be applied stochastically, Fig. (1). The algorithm is general to apply a stochastic approach to all beam properties. However, in this article, stochastic properties included length and orientation while the cross section was assumed to be a circular shape with a 0.025 mm radius. For both methods, the beam element type was a 2-node linear beam element (B31). Abaqus (V. 6.14, Simulia Ltd) was used as an FE solver.

Boundary conditions were applied on the beam structure using multi-point constraints (MPCs). These constraints were placed on two parallel faces of the cubic structure. The MPCs rigidly connected the nodes of the face to a control node. All degrees of freedom were fixed for one control node and a concentrated force load was applied on the opposite face’s control node. Apparent stress was calculated by dividing the applied force by the apparent area of the relevant face. Apparent strain was obtained by calculating the ratio of resulting displacement of the moving control node to the distance between the control nodes (i.e., change in length over length), Fig (1). Apparent moduli were computed from apparent stress and apparent strain. Apparent

densities were calculated by obtaining the ratio of the beams' mass to the volume of the unit cube. The models' materials were assumed orthotropic for the purpose of material property extraction and three moduli (representing an orthogonal set of normal-normal stress-strain relationships) were extracted.

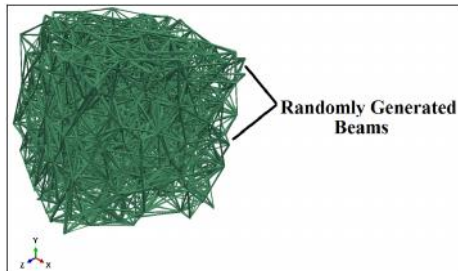


**Figure 1:** Trabecular bone (representative model).

## RESULTS AND DISCUSSION

The Individual FE models created in this study exhibited the mechanical properties listed in Table (1). Each model demonstrated effective moduli within published ranges of trabecular bone [3]. For the HNM, the three apparent moduli varied by hundreds of megapascals as is consistent with the directionality of the unit cell beam orientations. Apparent  $E_{xx}$  and  $E_{yy}$  in the RBM were similar in value as is consistent with the random nature of the beam orientations. The apparent densities of the current models are also within the published ranges [1, 3]. In the present work, the apparent density of the HMN model is slightly greater than that of the RBM model. In a fully random stochastic model with a sufficient number of randomly oriented beams, the effective moduli should produce approximately isotropic effective properties. In models with a finite number of beam elements randomly oriented, the effective moduli will not be isotropic but will not have predictable preferred directions. Trabecular bone has been reported to be

anisotropic material with preferred directions in line with mechanical loads [3]. Such anisotropy can be introduced into the stochastic model by controlling the parameters such that they are not fully random. Rather, they should follow some stochastic process with a distribution of properties that resulting in anisotropy. For example, the beam elements can have a distribution of orientations centered on a preferred orientation. The apparent densities of the FE models are dependent on the number of beams and on their cross sections which were dissimilar between the models. Future models will emphasize cross sections and lengths that are consistent with the nominal (and stochastic) geometry of physical trabecular architecture.

## CONCLUSIONS

The stochastically driven beam element approach may prove useful for efficiently modeling trabecular bone, structural open cell foams, grid stiffened core composites, and other structures. The need for efficiencies in meshing and computation are particularly relevant for current areas of interest to the composites and medical communities including the modeling of mechanical fasteners and bonding, damage evolution, and the modeling of aging. The proposed paper may provide a detailed description of the methodology in future research.

## REFERENCES

1. Bartel, D., et al. Orthopaedic Biomechanics, New Jersey; Pearson Prentice Hall, 2006.
2. Jastifer, J., Alrafeek, S. et al., *American Orthopaedic Foot and Ankle Society*, **37(4)**: 419-426, 2015.
3. Dalstra, M., et al., *J Biomech* **26**, 523 – 535, 1993

**Table 1:** Independent Elastic Constants, Apparent Density and beams circular section radii.

I	FE Models		Literature	
	HNM	RBM	Bartel D.L [1]	Dalstra [3]
<b><math>E_{xx}</math> (MPa)</b>	858.5	40.98	237	96.4
<b><math>E_{yy}</math> (MPa)</b>	246.06	43.7	309	49.1
<b><math>E_{zz}</math> (MPa)</b>	1199.04	67.22	823	25.2
<b>Apparent Density (g/cm<sup>3</sup>)</b>	1.625	1.18	0.09~1	0.1~0.959
<b>Beams circular section radius (mm)</b>	0.1	0.025	-	-

# PASSIVE VISCOELASTIC FINGER STIFFNESS CHANGES MINIMALLY IN INDIVIDUALS WITH CHRONIC HEMIPARETIC STROKE

<sup>1,2,4</sup>Benjamin I Binder-Markey, <sup>1,2,3</sup>Julius PA Dewald, and <sup>1,2,3,4,5</sup>Wendy M Murray

Departments of <sup>1</sup>Biomedical Engineering, <sup>2</sup>Physical Therapy and Human Movement Sciences, <sup>3</sup>Physical Medicine and Rehabilitation, Northwestern University, Chicago, IL, USA

<sup>4</sup>Shirley Ryan AbilityLab (Formerly RIC), Chicago, IL, USA

<sup>5</sup>Edward Hines, Jr. VA Hospital, Hines, IL, USA

Email: [bbinder@u.northwestern.edu](mailto:bbinder@u.northwestern.edu), Website: <http://smpp.northwestern.edu/research/arms/>

## INTRODUCTION

Impairments of the arm and hand are the most common disability post-stroke [1]. These impairments are related to a loss of descending corticofugal neural tracts that cause motor impairments (weakness, hypertonicity, and loss of independent joint control). In addition to these motor impairments, secondary musculoskeletal changes may result in increased passive joint stiffness [2].

Increases in stiffness at the hand, as seen about the elbow and ankle [3, 4], could make hand opening and function exceedingly difficult, yet there are no studies showing how passive joint stiffness changes at the hand of individuals with chronic hemiparetic stroke.

Therefore we aim to determine how the passive stiffness of the structures about the fingers alter post-stroke to aid in the development of targeted interventions that may prevent its development.

## METHODS

Passive torques about the 4 MCP joints were quantified in the paretic and nonparetic hand of 9 subjects ( $\mu=64.3\pm 7.9$  yrs old,  $\mu=13.2\pm 8.0$  yrs post-stroke) with moderate hand impairments based on their Chedoke-McMaster Stroke Assessment hand scores (CMSA-HS 4-5,  $n=9$ ).

Due to hypertonicity of the paretic muscles, torques were quantified while the subjects were in a sleep or near sleep state using a custom built device (Fig. 1). Additionally, EMGs were continuously monitored to ensure no muscle activity. The torques about the

MCP joints were collected throughout the MCP ( $\theta$ ) joint's range of motion in static 15 degree increments at 9 randomized wrist postures ( $\omega$ ) from 60° flexion to 60° extension in 15 degree increments.

The PIP & DIP joints were splinted to prevent distal movements. Measured MCP torques were normalized to forearm volume. Forearm volume was estimated as the volume of a conical cylinder measured by the length of the forearm, wrist circumference, and largest circumference of the forearm.

For each subject the normalized torque data throughout all wrist and MCP postures were fit to an exponential analytical model [5]:

$$T_t(\theta, \omega) = T_{sj}(\theta) + T_e(\theta, \omega)$$

The model is comprised of two components. The first component consists of the torques contributed by the single-joint structures,  $T_{sj}(\theta)$ , (intrinsic muscles, skin, ligaments, joint capsules, etc.) assumed to be a function of MCP joint posture only. The other component contributed by the extrinsic finger muscles,  $T_e(\theta, \omega)$ , is a function of both MCP and wrist posture.

Stiffness was calculated as the derivative of the analytical model. Significant differences between the stiffness of the paretic and non-paretic hands for each impairment level were analyzed using a linear-mixed model analysis.

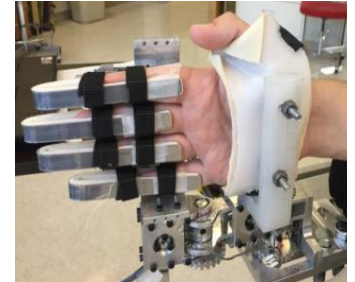


**Figure 1:** Image of the device and splinted fingers

## RESULTS AND DISCUSSION

We found significant differences ( $p=2.17e-4$ ) in the total, normalized, MCP joint stiffness between the paretic and non-paretic hands across all wrist angles using a linear mixed model analysis (Fig 2a-c). However, contrary to previous studies that report up to 200% increases in ankle and elbow stiffness in the paretic vs. nonparetic limb following stroke, we observed relatively small increases in total MCP joint stiffness between limbs. The most notable increases were observed when the wrist was fully extended (Fig 2a). At neutral and flexed wrist postures, changes in stiffness were limited, with a maximum increase of 40% near the limits of MCP extension (Fig 2b&c). We expect the clinical significance of these changes is relatively small, given the active strength deficits we measured in the same paretic hands, were as large as 75%.

Neither the single joint structures nor extrinsic finger muscles demonstrated significant changes when analyzed using a linear mixed model analysis (Fig 2d-f). Only the stiffness of the extrinsic muscles in an extended wrist posture demonstrated a trend towards small increases in stiffness (Fig 2e).

## CONCLUSIONS

Potential increases in the stiffness of the hand post stroke could make hand opening and function

exceedingly difficult. Yet, prior to this study there were no studies showing how passive joint stiffness changes in chronic stroke individuals. We found that there were significant changes in total joint stiffness but these changes were relatively small and most prominent near limits of wrist or MCP ranges of motion. These results indicate that impairments of the hand in individuals with chronic hemiparetic stroke are not likely related to altered passive stiffness of the musculoskeletal structures within the hand. The impairments observed are more possibly due to impaired involuntary neural drive and resulting hypertonicity. These finding indicate that future rehabilitation interventions of the hand should focus on decreasing the effects of hypertonicity while facilitating voluntary neural motor control.

## REFERENCES

1. Lawrence, E.S., et al., *Stroke*, 2001. **32**(6): p. 1279-84.
2. Kamper, D.G., et al., *Muscle Nerve*, 2003. **28**(3): p. 309-18.
3. Nelson, C.M., et al. *APTA CSM*. 2015. Indianapolis, IN.
4. Gao, F., et al., *Arch Phys Med Rehabil*, 2009. **90**(5): p. 819-26.
5. Knutson, J.S., et al., *J Biomech*, 2000. **33**(12): p. 1675-81.

## ACKNOWLEDGMENTS

Vikram Darbhe for his assistance with the experimental set up and device calibration. Funding Sources: AHA: Pre-Doctoral Fellowship: 16PRE30970010; Foundation for PT: PODS II Award; NIH: T32EB009406, 1R01HD084009-01A

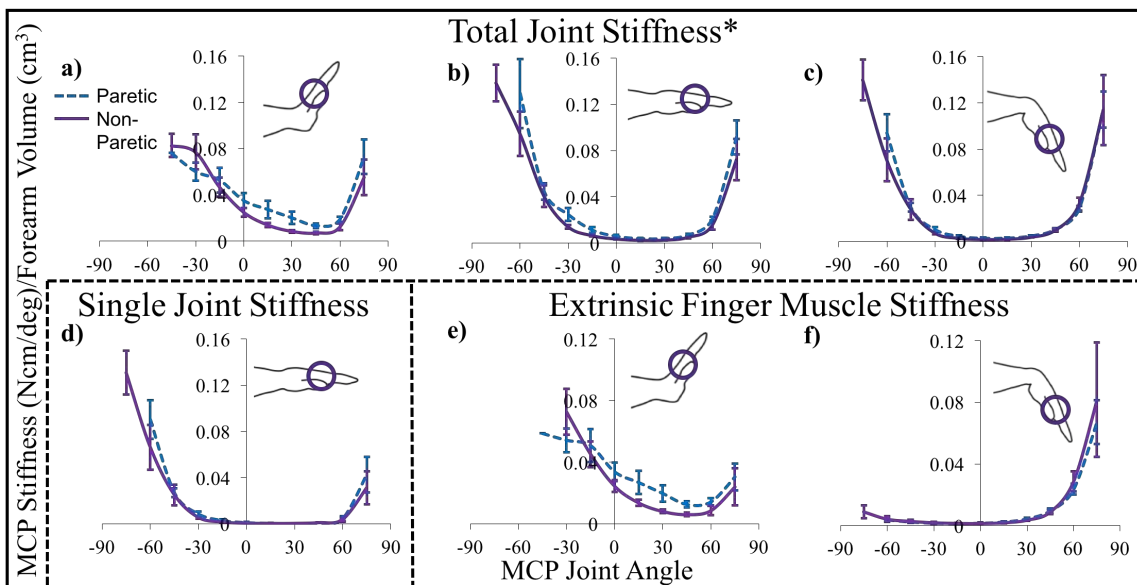


**Figure 2:** Plots of the paretic (blue dashed) and non-paretic (purple solid) total (a-c), single joint structure (d), and extrinsic finger muscle (e-f) stiffness at the MCP joints normalized by forearm volume with standard error bars. \*indicates significant difference  $p < 0.05$ .

# A NOVEL TEMPERATURE CONTROLLED WHEELCHAIR CUSHION FOR PRESSURE ULCER PREVENTION

Ali Ersen, En-Szu Liao, Linda Adams, Mike Richardson, Myla Quiben and Metin Yavuz

University of North Texas Health Science Center, Fort Worth, TX, USA  
email: [metin.yavuz@unthsc.edu](mailto:metin.yavuz@unthsc.edu) , <https://sites.google.com/site/dryavuzlab/>

## INTRODUCTION

For many wheelchair users, the combination of reduced mobility and impaired sensation, including but not limited to neurological insults, vascular issues, decreased cognition, and morbid obesity, results in a life-time risk of pressure ulcer development. Pressure ulcers are a type of wound that results from a breakdown of tissue over bony prominences due to localized ischemia caused by constant pressure. The compromised blood circulation along with reduced airflow results in an accumulation of heat in the tissue over the bony prominence which accelerates the tissue breakdown. Using an animal model under constant vertical loading, researchers have shown that higher temperatures amplified the tissue damage caused by mechanical strain and limited blood circulation [1]. Contemporary wheelchair cushions usually employ thick foam type materials, which provide a higher quality of pressure distribution [2] but poor heat dissipation.

In this study, we designed and tested a custom-built cushion that circulates chilled water. Effectiveness of the cushion was evaluated by measuring buttocks surface temperatures and peak pressures around the ischial tuberosity, with a targeted maximum temperature and pressure of 28°C and 60mmHg, respectively.

## METHODS

We modified a commercially available non-motorized wheelchair (Drive, 16 Medical Silver Sport 2) and equipped it with a custom built cushion that circulated chilled water (Fig.1A). We used two cooling units attached serially (one's output to other's input). A mini water pump circulated the water through the cooling units into the cushion and back to the cooling units. All elements (two cooling

units and one pump) can be operated separately via control buttons (Fig.1B).



**Figure 1:** The cooling wheelchair A) cushion, B) control buttons

All study procedures were approved by the institutional review board (IRB) prior to recruitment and testing, and informed consent was obtained from subjects prior to testing. In this ongoing proof-of-concept study, we have recruited three healthy male subjects, who did not have any physical disabilities or functional deficits. The average age was 29.7±2.1 (mean ± standard deviation). All subjects' forehead temperature was measured (36.6±0.4°C) prior to testing in order to confirm that the subject did not have an abnormal body temperature. All subjects wore standard spandex tights. The room temperature was measured as 22.9±0.1°C during the test. A thermal image of each subject's buttocks was captured using an Infrared (IR) thermal camera (Flir, T650sc). We placed thermocouple sensors (K-type) at the tissue-cushion interface and at the outlet of the cooling units, which recorded temperatures at various intervals (t=0, 1 min, 10 mins, 20 mins and 30 mins). After obtaining the baseline (t=0) and first temperature (t=1 min) recordings, we asked the subjects to actively propel the wheelchair in the hallway. At the end of active use (t=30 mins), we asked the subjects to stand up and then captured another thermal image of each subject's buttocks (post-activity). Interface pressures were acquired via a pressure mat (Tekscan, CONFORMat® 1 System) that was placed on the top of the cooling cushion.

## RESULTS AND DISCUSSION

The recorded tissue-cushion interface and water temperatures from three subjects are provided in Table 1. During the active use, water temperature was maintained around  $21.7 \pm 0.3^\circ\text{C}$ . The interface temperature initially increased to  $27.1 \pm 0.4^\circ\text{C}$  from  $23.0 \pm 0.4^\circ\text{C}$ . Interface temperature dropped down to  $25.1 \pm 1^\circ\text{C}$  at  $t = 30$  minutes.

**Table 1:** Temperature values (mean $\pm$ S.D.) taken with the thermocouple over 30 minutes for  $n=3$

Time (min)	Tissue-cushion Temperature ( $^\circ\text{C}$ )	Water Temperature ( $^\circ\text{C}$ )
0	$23.0 \pm 0.4$	$21.8 \pm 0.4$
1	$27.1 \pm 0.4$	$21.6 \pm 0.1$
10	$26.6 \pm 1$	$21.6 \pm 0.2$
20	$26.0 \pm 1$	$21.7 \pm 0.1$
30	$25.1 \pm 1$	$21.6 \pm 0.5$

These temperature values were confirmed with the IR thermal camera images. Baseline and post activity thermal images of a representative subject are provided in Fig.2. The temperature reduction was calculated as  $4.5^\circ\text{C}$  at the thermocouple location. At this location (white spot in Fig.2) baseline temperature was  $29.5^\circ\text{C}$  whereas post-activity temperature was  $25.0^\circ\text{C}$ . The average temperature reduction at the thermocouple location was  $4.3 \pm 0.3^\circ\text{C}$  in three subjects.

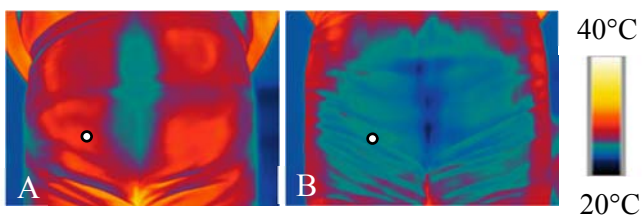


**Figure 2:** Representative thermal images taken by an IR thermal camera, A) baseline (prior to sitting), B) post activity. White spots indicate the location of thermocouple sensors. (Colored scale bar= 20 to  $40^\circ\text{C}$ )

The interface pressure distribution in a representative subject is given in Fig.3. The peak pressure occurred at the right ischial tuberosity and quantified as  $100\text{mmHg}$  while the average pressure was  $39\text{mmHg}$ . The average peak pressure was  $102 \pm 5\text{mmHg}$  for three subjects.

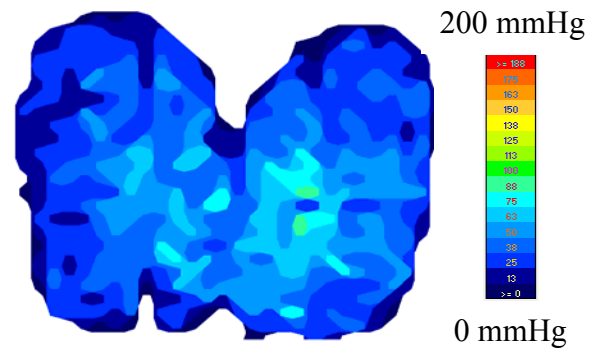


**Figure 3:** Pressure distribution of a representative subject provided by Tekscan ConforMat. The peak pressure is detected as  $100\text{mmHg}$  while the average pressure is  $39\text{mmHg}$ . (Colored scale bar= 0 to  $200\text{mmHg}$ )

## CONCLUSIONS

The custom-built cooling cushion consistently maintained buttocks temperatures below  $28^\circ\text{C}$  in all three subjects. However, the cushion was not able to reduce peak pressures down to the desired value  $60\text{mmHg}$ . Further investigation and modification of the wheelchair cushion design are required to achieve the success criterion for peak pressure.

## REFERENCES

1. Kokate JY et al. *Arch Phys Med Rehabil.* 1995;**76**(7):666-73.
2. Crane B et al. *Arch Phys Med Rehabil.* 2016;**97**(11):1872-9.

## ACKNOWLEDGMENTS

Research reported in this study was supported by the National Center for Advancing Translational Sciences of the National Institutes of Health under the Center for Translational Medicine's award number UL1TR001105. The content is solely the responsibility of the authors and does not necessarily represent the official views of the NIH.

# FINITE ELEMENT ANALYSIS OF THE TIBIAL TUBEROSITY OSTEOTOMY WITH ANTEROMEDIALIZATION PROCEDURE FOR PATELLA INSTABILITY

<sup>1</sup>Jennifer Bagwell, <sup>2</sup>Kai-Yu Ho, and <sup>3</sup>Christopher Powers

<sup>1</sup>Creighton University, Omaha, NE, USA

<sup>2</sup>University of Nevada Las Vegas, Las Vegas, NV, USA

<sup>3</sup>University of Southern California, Los Angeles, CA, USA

email: jennybagwell@creighton.edu

## INTRODUCTION

The tibial tuberosity osteotomy (TTO) with antero-medialization is a surgical procedure utilized in persons with persistent patella instability and patellofemoral pain. The surgery involves moving the tibial tuberosity antero-medially which is thought to decrease the laterally directed forces acting on the patella [1]. The anterior translation of the tibial tuberosity also increases the moment arm of the quadriceps muscles, thereby potentially decreasing the knee extensor demand and the patellofemoral joint compressive forces. Although good clinical outcomes have been reported with this surgery [2], the influence of this procedure on patella cartilage loading remains unclear. The purpose of this study was to assess the influence of the TTO procedure on lateral patella and femur cartilage hydrostatic pressure using finite element analysis.

## METHODS

A 3D finite element (FE) model of the knee joint was developed from a healthy female participant (24 years of age). Subject-specific input parameters included 1) patellofemoral joint (PFJ) geometry, 2) weight bearing PFJ kinematics, and 3) quadriceps muscle forces. Subject-specific PFJ geometry and morphology, weight-bearing PFJ alignment, and quadriceps muscle morphology were obtained from magnetic resonance imaging. Lower extremity biomechanics data (kinematics, kinetics, and EMG) were collected during a squatting task (15° of knee flexion).

Detailed descriptions of subject-specific inputs for the FE model have been described in previous publications [3]. The patellar tendon was modeled as

homogeneous elastic and transversely isotropic using tetrahedral continuum elements. Elastic constants for patellar tendon were determined based on the data obtained by Rawson et al [4].

The FE model was modified to simulate the TTO procedure. Specifically, the tibial tuberosity was moved 5 mm medially and 10 mm anteriorly. To account for the change in the quadriceps muscle moment arm associated with the anterior translation of the tibial tuberosity, the new moment arm was estimated and was utilized to determine the modified quadriceps muscle forces used as input in the TTO model. Three models (initial, TTO, and TTO with modified forces) were run using Abaqus software (Fig. 1 and Fig. 2).

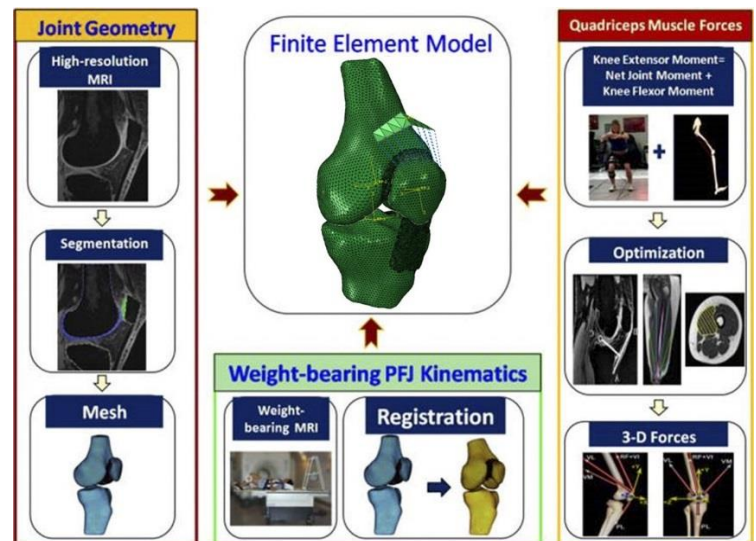
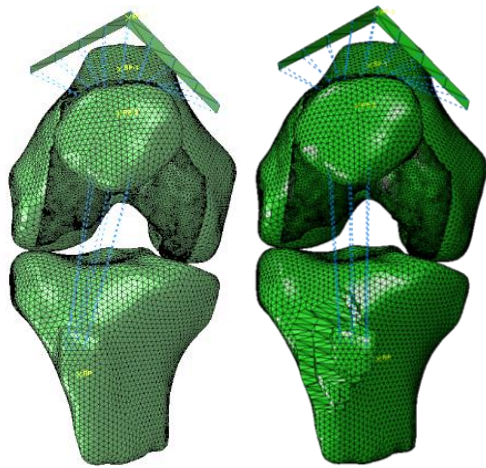


Figure 1: 3D subject-specific finite element model framework.

Mean von Mises stress at the lateral patella and femur chondro-osseous interfaces were the primary variables of interest.



**Figure 2:** Finite element model of the subject specific mesh from the initial model (left) and the tibial tuberosity osteotomy model (right)

## RESULTS AND DISCUSSION

Compared to the initial model, the TTO procedure resulted in a decrease in mean lateral von Mises stress (12% reduction at patella chondro-osseous interface (0.90 MPa vs. 0.79 MPa) and 16% at the femur chondro-osseous interface (0.63 MPa vs. 0.53 MPa) (Fig. 3)). This decrease was even greater when forces were modified to account for the altered quadriceps muscle moment arm (30% reduction at patella chondro-osseous interface (0.90 MPa vs. 0.63

MPa) and 32% reduction at the femur chondro-osseous interface (0.63 MPa vs. 0.43 MPa) (Fig. 3)).

The observed decrease in lateral patella and femur stress with the TTO procedure was the result of an increase in total contact area between the patella and femur. In addition, the decreased quadriceps muscle demand secondary to an increase in the quadriceps muscle moment arm (TTO model with modified forces) contributed to a greater decrease in stress compared to the TTO model.

## CONCLUSIONS

The TTO procedure appears to be effective in reducing lateral patella and femur cartilage stress. The observed changes in cartilage stress may, in part, explain the improved clinical outcomes associated with this surgery.

## REFERENCES

1. Farr J, et al. *J Knee Surg* **20**, 120-128, 2007.
2. Pritisch T, et al. *Knee Surg Sports Traumatol Arthrosc* **15**, 994-1002, 2007.
3. Farrokhi S, et al. *Osteoarthritis Cartilage* **19**, 287-294, 2011.
4. Rawson SD, et al. *Biomech Model Mechanobiol* **14**, 123-133, 2015.

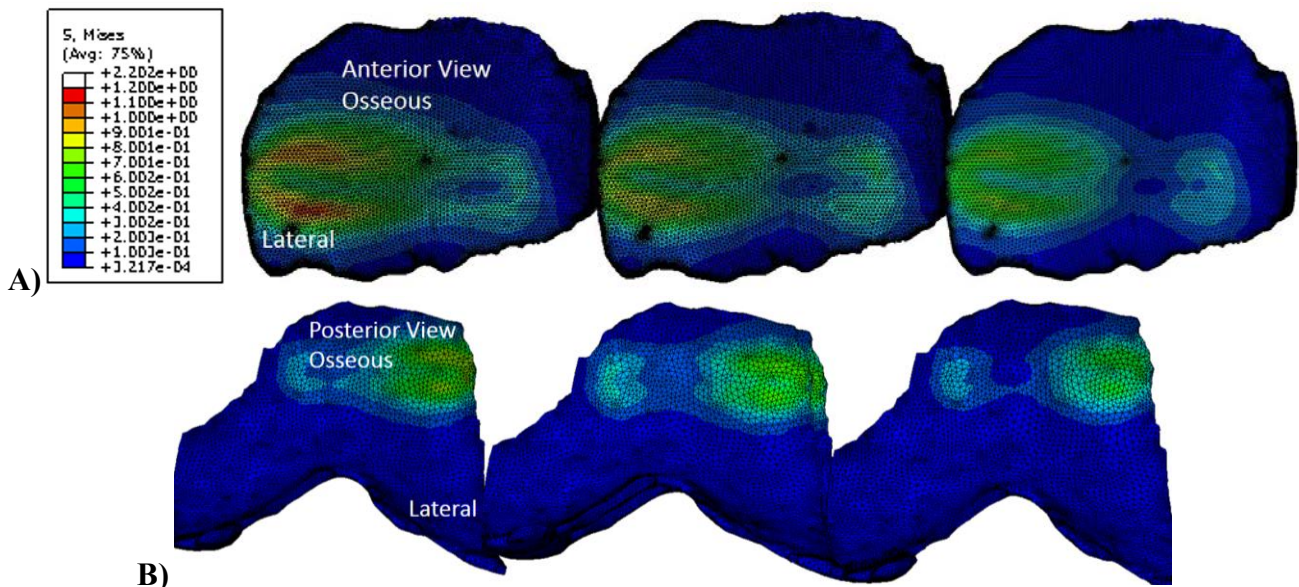


**Figure 3:** Stress profiles of the patella (A) and femur (B) at the chondro-osseous interface. Initial model (left), the tibial tuberosity osteotomy (TTO) model (center), and the TTO with modified forces model (right)

# Localized Fracture Risk Under Gait Cycle Loading Correlates Poorly with High Mirels' Scores in Metastatic Lesions to the Proximal Femur

Palani Permeswaran, Benjamin J. Miller, Jessica E. Goetz  
Orthopedics Biomechanics Research Laboratory, University of Iowa, Iowa City, IA  
email: palani-permeswaran@uiowa.edu, web: <https://uiowa.edu/uiobl/>

## INTRODUCTION

While primary cancers of the bone are relatively rare and highly variable in presentation, metastatic bone disease is an unfortunate and common complication of many more frequently encountered cancers. It has been estimated that the prevalence of metastatic disease in the United States is approximately 280,000,<sup>1</sup> and treatment of metastatic disease accounts for a substantial portion of the practice of most orthopaedic oncologists. Evaluation of metastatic lesions frequently involves scoring the lesion using the scoring system developed by Mirels. In this system, a lesion is given a score of 1, 2, or 3 in the four different categories of lesion site, size of cortical involvement, lesion type, and pain. Lesions that score >8 are recommended for prophylactic stabilization to prevent pathologic fracture, and lesions scoring 7 or lower are considered unlikely to progress to fracture.<sup>2</sup>

Unfortunately, there are no clear recommendations for patients who score an 8, and the obvious subjectivity of the pain category can lead to challenging decisions to be made about the need to prophylactically stabilize a lesion. The goal of this work was to use patient specific computational modeling to determine if the stresses developing around a metastatic lesion correlated with the Mirels' score.

## METHODS

Under IRB approval, 10 patients with metastatic lesions to the proximal femur, rated >8 on the Mirels' system, were retrospectively identified. Mirels' score distribution among identified patients is as follows: 2-Mirels' 9, 2-Mirels' 10, 4-Mirels' 11, 2-Mirels' 12. Femoral geometry was obtained from the patient's CT scans and the resulting point cloud, converted to a tetrahedral element mesh aligned to the Bergmann coordinate system. CT-based material properties

were assigned to each model and a Bergmann walking gait cycle load, applied.<sup>3</sup> Abaqus Standard finite element analysis software was used to solve the stresses for each model. Individual elemental von Mises stresses were exported for analysis at each gait step<sup>4</sup> and the ratio of the CT-based yield stress over the von Mises stress during gait was calculated on an element-by-element basis. This ratio is known as the element's factor of safety (FOS) with a value <1 indicating element failure. To determine the likelihood of localized fracture, contiguous sets of failed elements were analyzed. These sets were obtained by, first, determining the failed element at each step of gait which had the smallest FOS; this indicates the element which yielded the greatest. Adjacent failed elements were then continuously added to the set. The total volume of the contiguous failed element set was divided by the critical volume of failed elements shown to predict fracture.<sup>5</sup> This ratio represents a model's likelihood of localized fracture at each step of the gait cycle. Elements contained within the lesion were excluded from this analysis as they were seen to experience relatively small stresses during loading and fail rarely, if ever. Percentage of contiguous failed elements volume over the critical volume required for fracture was calculated and correlated with the model's Mirels' scores. Scores were assigned by the patient's orthopaedic oncologist.

## RESULTS AND DISCUSSION

Each model's percentage of critical volume failure during gait can be seen in Figures 1-A and 1-B. Several models experienced little to no fracture and are obscured from view. Little correlation is seen at any steps of gait between percentage of critical volume failure and Mirels' (Table 1). The changes in percentage of critical volume failure over the full walking gait cycle were highly variable and dependent upon progression through gait. Localized

fracture seems to occur precipitously; models either experience large amounts of localized fracture or none. This would be expected as the complicated and unpredictable nature of metastases in bone, graphically represented in Figure 3, can cause portions of the femoral head and neck best suited for carrying load during certain times during gait to be compromised in models with lower Mirels' scores but intact in models with higher Mirels' scores.

expanding the range over which the correlation can be made. However, it was clear that high Mirels' scores do not directly relate to specific mechanical risks.

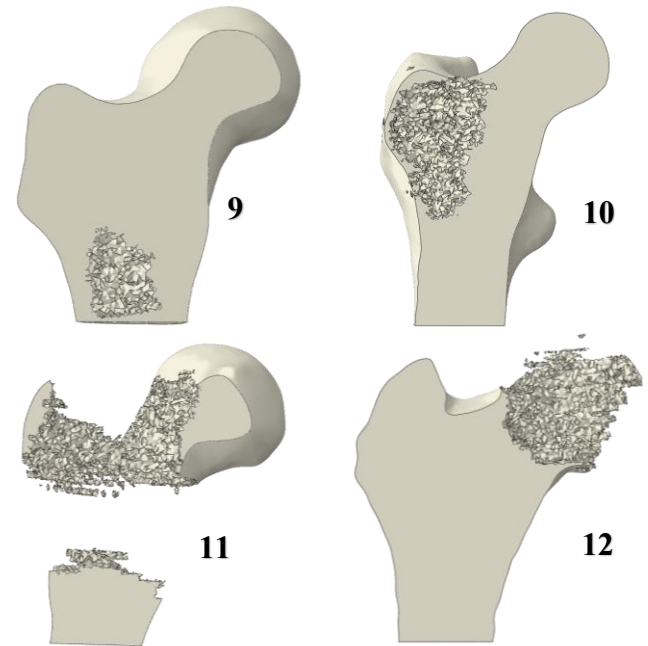


**Figure 3:** Varying Mirels' Scores Less Lesion Elements.

## CONCLUSIONS

Clinicians should use care when interpreting Mirels' scores, as Mirels' scores in isolation appear not to correlate with direct mechanical compromise of the affected bone. Additionally, in-depth, patient specific mechanical analyses may be of great use in this extremely vulnerable population.

## REFERENCES

1. Li S, et al. (2012). *Clin Epidemiol.* **4**, 87-93.
2. Mirels H. (1989). *Clin Ortho Relat Res* 256-264.
3. Permeswaran, et al. (2017). *MWASB*.
4. Keyak, et al. (2000). *J of Biomech.* **33(2)**: 209-14.
5. Keyak, et al. (2001). *Med Eng & Phys.* **23(9)**: 657-664.

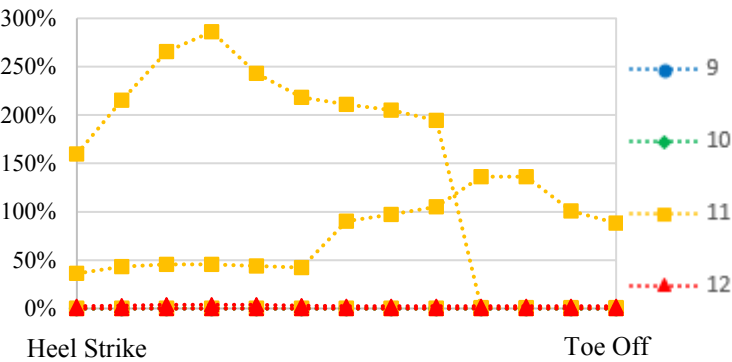


**Figure 1-A:** Percentage of Critical Volume Failure during Gait.

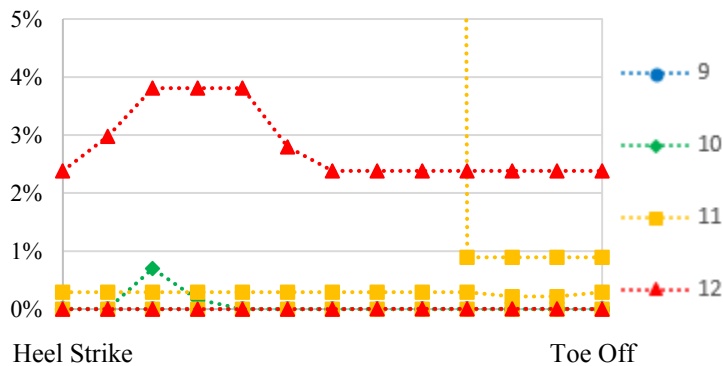


**Figure 1-B:** Percentage of Critical Volume Failure during Gait magnified to 0-5%.

A limitation to this work was that all of the patients studied had Mirels' scores that were high and indicative of fracture. It is possible that the inclusion of additional patients with lower risk lesions to the proximal femur may result in a better correlation between stresses and Mirels' score by

**Table 1:** Correlation of Mirels' Scores and Percentage of Critical Volume Failure at each Gait Cycle Step

Gait Step #	1	2	3	4	5	6	7	8	9	10	11	12	13
R <sup>2</sup>	0.028	0.027	0.026	0.025	0.026	0.027	0.034	0.035	0.037	0.020	0.020	0.021	0.021

# A TASK PROGRESS-BASED PERFORMANCE MEASURE FOR TRACING

Tim Eakin

The University of Texas at Austin, Austin, TX, USA  
email: eakin@austin.utexas.edu

## INTRODUCTION

A common biomechanical task structure for assessment of motor skills is template tracing in which a performer establishes a position, either from movement of the body or from transduced force production causing movement of an external object such as a cursor on a computer screen, with an objective of matching a target position.

Typically the performer and target positions are recorded in a sequence of data samplings, each with a geometry similar to that shown in Fig.1.

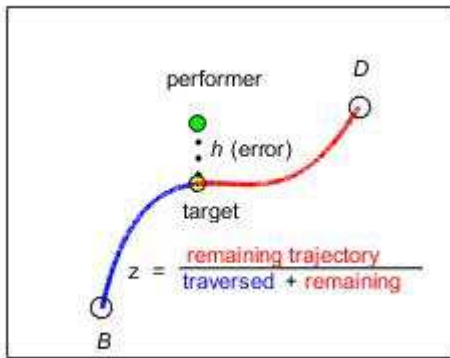


**Figure 1:** Data sampling instance of a tracing task. The target moves from  $B$  to  $D$ , its position being the closest point on the template to the performer's position;  $z$  is the fractional remaining trajectory distance; and the error  $h$  is the distance between the performer and the target.

Performance is evaluated by an error variable constructed from those values, for example the commonly used root mean square error (*RMSE*). Such a measure is a good proxy for accuracy, but does not reflect performance quickness in tasks such as template tracing in which the location of the current target position is determined by the performer position. Conversely, the measurement of task duration is a suitable proxy for average speed in self-paced tasks, but it does not reflect accuracy during performance. It is thus desirable to

construct a quantitative spatiotemporal dependent variable from a sequence of performer and target positions that will reflect both speed and accuracy (or equivalently error and duration) and by which the relative skill levels can be ordered within a set of individual task performances.

## METHODS

The approach to constructing a measure sensitive to task progress as well as geometric error, whose magnitude inversely correlates with accuracy and speed, begins with the generic structure

$$\text{Performance score} = F \left[ \frac{1}{N} \sum_{n=1}^N g(n, z_n) f(h_n) \right]$$

where  $N$  is the total number of data samplings,  $n$  is the index of a particular sampling,  $h$  is the distance error from performer position to target position,  $z$  is the fractional distance yet to be traversed along the target template line,  $f$  is a function of the distance error,  $g$  is a weighting function dependent on the ordinal position of a sampling and the fractional remaining distance for that sampling, and the function  $F$  is the inverse operation of error function  $f$ . If  $g$  is chosen to be 1 for all  $n$  and  $z_n$  and if  $f$  is chosen to be the square of the distance error then the performance score is reduced to the commonly used *RMSE*. However, in order to ensure an increase in the summation magnitude with each additional sampling needed before task completion, the function  $f$  is chosen to be the exponential of the distance error,  $\exp(h_n)$ , rather than its square and thus  $F$  is the operation of taking the natural logarithm of the mean rather than taking the square root. The weighting function  $g$  is chosen such that it amplifies contributions to the score based on the accrued number of data samplings and attenuates contributions to the score based on target position proximity to its end destination. It is of the form

$g(n, z_n) = [a + b \log(n)] \cdot \exp(z_n)$  with the parameters  $a$  and  $b$  chosen to satisfy the desired constraints that every term in the score's summation factor be positive and that the mean of  $N+1$  terms cannot be less than the mean of  $N$  terms. Accordingly the value of  $a$  is chosen to be 1 and the value of  $b$  is chosen to be  $\exp(1)$ . Thus,

$$\text{Performance score} = \log \left\{ \frac{1}{N} \sum_{n=1}^N [1 + e^1 \log(n)] e^{z_n} e^{h_n} \right\}.$$

In analogy with the *RMSE* acronym, this “Logarithm of the Mean Weighted Exponential Error” has the acronym *LMWEE*.

## RESULTS AND DISCUSSION

The character of this alternative *LMWEE* metric can be demonstrated by evaluating it for some hypothetical tracing task performances. One example is a tracing task performed with perfect geometric accuracy and with uniform target progress toward its destination. In such a performance the *RMSE* is zero regardless of the number  $N$  of accrued data samplings at task completion, but the *LMWEE* value increases with an increase in  $N$  so that quicker performances will have a lower score. This is shown in Fig 2.

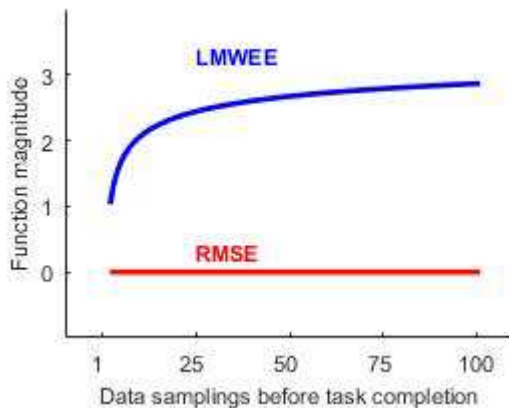


**Figure 2:** *LMWEE* and *RMSE* for a tracing task with perfect geometric accuracy and uniform progress as a function of accrued data sampling number at task completion.

The character of *LMWEE* can be illustrated further with a set of hypothetical tracing task performances

having a constant geometric error and equal samplings  $N$  but in which one performance has a constant acceleration of the target positions toward the destination, one has uniform progress, and one has constant deceleration. This is shown in Fig. 3 where it can be seen that although the *RMSE* remains the same in all cases, the *LMWEE* value decreases as the average position of the target is closer to the destination. The *LMWEE* score is thus attenuated by target proximity to its destination.

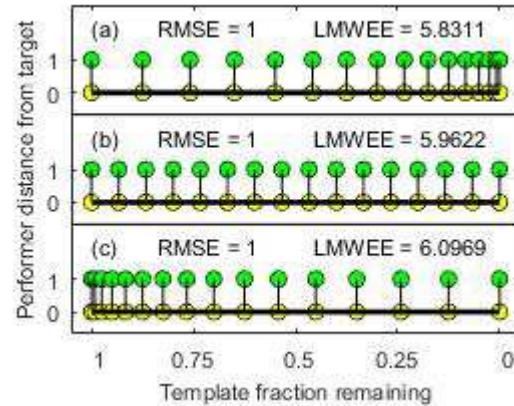


**Figure 3:** *LMWEE* and *RMSE* for tracing tasks with a constant error of one unit but with differing progress of target position toward the destination: (a) constant deceleration; (b) uniform velocity/progress; (c) constant acceleration.

An additional objective for this spatiotemporal evaluation metric was that it have a dimensionality the same as that of the performer displacement variable – be it length, force, or some dimensionless scaled or normalized construct. Another objective was to keep the mathematical structure of the measure as simple as possible for conceptual ease, transparency, and tractability in computation. To a large extent the *LMWEE* variable as constructed conforms to these objectives.

## CONCLUSION

The *LMWEE* measure provides a spatiotemporal assessment tool whereby tracing task performances having identical geometric error but differing target position distributions can be ordered in terms of quality or skill level when timeliness of task progress is a goal in addition to accuracy.

# SIMPLIFIED CENTER OF MASS TRACKING IN ANKLE OSTEOARTHRITIS PATIENTS

<sup>1</sup>Jonathan R. Gladish, <sup>2</sup>Douglas W. Powell, and <sup>1</sup>Robin M. Queen

<sup>1</sup> Department of Biomedical Engineering and Mechanics, Kevin Granata Biomechanics Lab, Virginia Tech, Blacksburg, VA, USA

<sup>2</sup>School of Health Sciences, University of Memphis, Memphis, TN, USA  
email: [jrgladish@hotmail.com](mailto:jrgladish@hotmail.com), web: <http://beam.vt.edu/granatalab>

## INTRODUCTION

Maintaining control of the whole-body center of mass (COM) is paramount in maintaining steady, quiet stance. Lack of stability in COM position may indicate postural control deficits, which have been linked to increased fall risk [1]. While center of pressure measures are often used to evaluate postural stability, calculation of such measures requires a force platform and substantial post-processing of data. Furthermore, it has been suggested that COM may more accurately indicate success of postural control [2].

The location of the human COM is most often calculated using the “segmental method”, which requires full kinematic data collection and intensive post-processing. Double integration of ground reaction force data has been established as a reliable alternative, but still requires an expensive force platform and some data processing. A simplified method characterized by tracking a single point on the lower back has been suggested as an alternative that has been successfully tested in slow walking conditions [3]. If effective in static balance, this would allow clinicians to evaluate postural stability of patients quickly and diagnose balance-related disorders or injuries, such as ankle osteoarthritis. Severe ankle osteoarthritis patients were chosen for this analysis due to the often excessive body sway they experience. Other clinical populations with similarly high sway magnitudes could benefit from the use of this method for clinical assessment of outcomes.

To our knowledge, no previous study has investigated the use of single-marker COM tracking method in a patient population performing static balance tasks. Therefore, the purpose of this study was to evaluate the effectiveness of a simplified method of tracking the whole-body COM in the

assessment of static balance in ankle osteoarthritis patients. We hypothesize that the two methods (double integration and single marker tracking of the COM movement) will produce similar outcome measures and show positive correlation in both anteroposterior and mediolateral directions.

## METHODS

This study was a secondary analysis of previously collected data from 391 ankle osteoarthritis patients. All subjects had end-stage ankle arthritis as diagnosed by a foot and ankle trained orthopedic surgeon and were scheduled for a total ankle replacement within two weeks of initial testing. In order to participate in the study, all subjects had to be capable of independent ambulation without the use of an assistive device and be able to maintain bilateral, quiet, upright stance for 10 seconds. Prior to study initiation, all subjects signed informed consent that was approved by the institutional review board.

Each patient was asked to perform three 10-second, quiet standing trials in two conditions. Trials were conducted with patients standing barefoot on two force plates sampling at 1200 Hz (AMTI, Watertown, MA, USA) with feet together and shoulder-width apart. Lower-body kinematic data were collected using an 8-camera motion capture system sampling at 120 Hz (Motion Analysis, Santa Rosa, CA, USA). COM was calculated for both conditions in two methods: using double integrated force platform data as described by Chan [4], and by tracking the position of a single marker placed on the L4/L5 vertebral joint. Both methods represent center of mass displacement relative to the initial location and not absolute COM locations in the global coordinate system. Coefficients of multiple determination (CMDs) of the mean time series of

each task and intraclass correlation coefficients (ICCs) of the mean COM positions during each task were calculated. Negative CMDs were set equal to 0. Mean COM positions were tested for normality using a Shapiro-Wilks test and found to be not normal. Therefore, the methods were compared for each task with Mann-Whitney tests of the mean anteroposterior (AP) and mediolateral (ML) COM positions ( $p < 0.05$ ).

## RESULTS AND DISCUSSION

Figure 1 is a graphical representation of the mean anteroposterior and mediolateral position of the COM in the feet together (FT) and shoulder width (SW) task as measured by both methods. Mann-Whitney tests revealed significant differences between the location of the two methods in the ML direction only (FT:  $p = 0.0027$ ; SW:  $p < 0.001$ ).

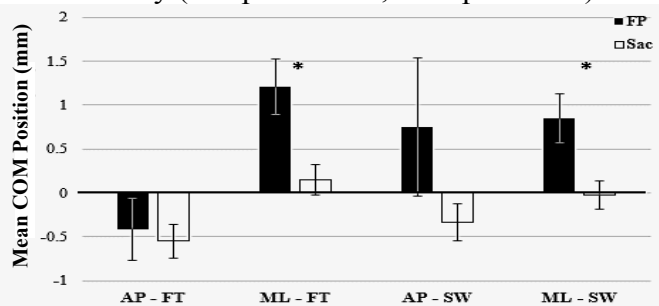


Figure 1: Mean (+/- std. error) COM positions for feet together (FT) and shoulder width (SW) task in AP and ML direction. FP: Force plate integration; Sac: Sacral marker - \* indicates significant difference between methods

Table 1 reports the mean CMD and ICC values for each task and direction. These value indicate that there is limited association between the two measurement methods in the AP and ML directions for the FT and SW tasks.

Taking into account the mostly weak correlations and differences in mean positions, we conclude that the data does not support our hypothesis. These results could indicate that the single-marker method for COM tracking is not suitable for assessing COM

movement during these tasks. However, positive results were achieved in other studies using similar methods in healthy subjects performing more dynamic tasks [3,5]. Other possibilities are that the force platform integration method proposed by Chan is not reliable, or that the tasks in this study have COM movement that cannot be differentiated from signal noise. However, since other studies have employed Chan's method with success [6,7], the former is not a likely explanation. Therefore, calculation of COM from force platform data with this method may not be advisable in patient populations.

## CONCLUSION

The findings of this study suggest that the single-marker sacral method for tracking COM is not reliable in static balance tasks. Due to the lack of whole-body motion capture data in this study, the proposed method was compared to a force-platform double integration method which, while considered an acceptable substitute for the gold-standard segmental method, may not provide reliable data in tasks with lower amplitudes of COM excursion such as those described in this study. Further research is needed to compare this method to the gold standard in patient populations.

## REFERENCES

- Morrison S, et al. *Gait Posture* **49**, 148-154, 2016.
- Gladish JR, et al. *Unpublished Manuscript*, Virginia Tech, 2017.
- Yang F & Pai YC. *J Biomech* **47**, 3807-3812, 2014.
- Chan RB. *Proceedings of BMES/EMBS Serving Humanity, Advancing Technology '99*, Atlanta, GA, USA, 1999.
- Tisserand R, et. al. *Gait Posture* **48**, 64-67, 2016.
- Fournier, KA, et al. *Gait Posture* **32**, 6-9, 2010.
- Wikstrom, EA, et al. *Gait Posture* **32**, 82-86, 2010.

Table 1: Average CMD and ICC values for FT and SW task in AP and ML direction

Task	AP				ML			
	CMD		ICC		CMD		ICC	
	Mean	Std. Err.						
FT	0.407	0.018	0.253	0.0386	0.406	0.018	0.338	0.008
SW	0.515	0.018	0.175	0.083	0.207	0.014	0.169	0.032

# ARE GAIT KINEMATICS SIMILAR BETWEEN ENSEMBLE AVERAGE AND REPRESENTATIVE CYCLE?

Richard Pimentel, Colton Sauer, James Carollo

Center for Gait and Movement Analysis, Children's Hospital Colorado, Aurora, CO  
email: Richard.Pimentel@childrenscolorado.org

## INTRODUCTION

Kinematic data from an instrumented gait analysis (IGA) is typically portrayed in kinematic plots to envision the joint angles and general walking ability of the subject. Given the large amount and complexity of IGA data, these curves typically contain information from either a single representative cycle (RC) or an ensemble average (EA) of the cycles. During an IGA, multiple walking trials are collected and an EA of all the valid gait cycles is computed. Using the EA, a single RC that closely resembles the EA can also be selected for use in clinical interpretation and decision making.

The benefits of using an EA are: 1) it contains summed information of all the gait cycles present during various trials; 2) the gait variability measurements provide additional information about the subject's gait [1]; and 3) the averaged waveform is more reliable than a single cycle [1]. The benefits of using the RC are: 1) it is an intact cycle, coming from one definitive gait cycle; 2) gait features (minima & maxima) are unchanged, these features may be lost during EA; 3) the waveform is not affected by any of the other gait cycles.

These two techniques are mutually exclusive; the benefits of one are the drawbacks of the other. While it has been said that the EA forms the basis of clinical assessments [1], a carefully-selected RC may also serve that purpose. The goal of the study was to compare the RC and EA across the kinematic root mean square (RMS) error between waveforms and how those differences may affect overall quality of gait measured by gait deviation index (GDI) [2]. These were assessed between a group with cerebral palsy (CP) and an age-matched normative group (AMN).

## METHODS

Thirty-two participants were included, 16 with CP and 16 AMNs (16 females and 16 males). Mean characteristics for the groups are shown below.

	N	Age (yr)		Height (cm)		Weight (kg)	
		Mean	SD	Mean	SD	Mean	SD
AMN	16	13.7	4.8	156.9	16.7	49.2	20.5
CP	16	13.8	4.8	152.8	16.1	44.6	14.7
<i>P</i>		0.942		0.482		0.468	

Participants started from standstill and walked through the capture volume at a self-selected pace. The first stride on each side was excluded due to initiation of locomotion. An average of 14 valid strides was collected over at least 4 walking trials for each participant. Kinematics were collected using the Newington-Helen Hayes lower body marker set and captured in Vicon Nexus (Oxford, UK). The Plug-in-Gait model was applied after gap filling and filtering [3]. Using Matlab (v R2015A, Mathworks, Natick, MA, USA), kinematics were parsed from gait events and interpolated to 2% increments of the gait cycle. Lower body kinematics only included those used by GDI [2].

In order for the RC to contain an actual intact gait cycle, RCs were selected primarily on the side with lower GDI and then the contralateral side was chosen from the cycle directly before or after the ipsilateral cycle closest to the EA. Each subject had only one RC and EA across the multiple trials collected.

RMS error was the absolute error between waveforms and GDI difference was calculated as EA minus RC. ANOVAs were used to test for significance in EA-RC difference between the two groups and across body segments/joints. Statistical significance was set at  $\alpha = 0.05$ . All outliers, except for a single extreme outlier, were kept in the sample.

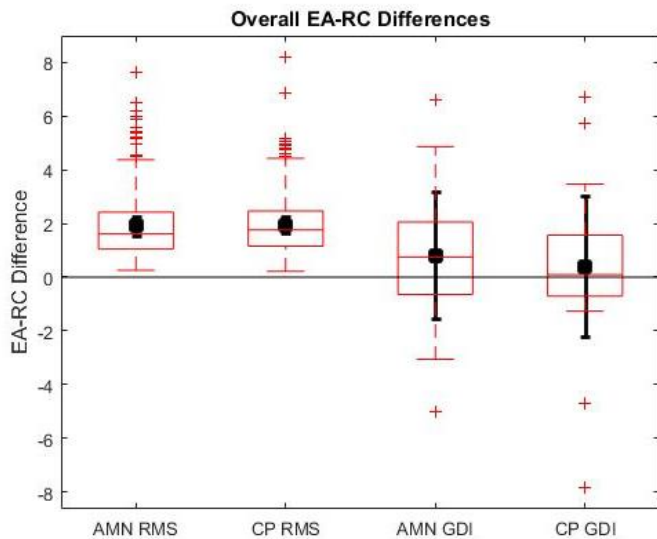


**Figure 1:** EA and RC are similar between groups in terms of RMS error and GDI ( $P \geq 0.500$ ). RMS error is the mean RMS difference in degrees between EA-RC waveforms, averaged across all lower extremity joints. GDI is unit-less (score based). Black represents the mean and SD, while the red box plots represent the median, IQR, bounds, and outliers of the sample (same for Fig 2).

## RESULTS AND DISCUSSION

There were no significant differences between the CP and AMN groups in age, height, or weight ( $P \geq .468$ ). Mean RMS error between EA and RC was similar between AMN and CP groups (Figure 1). GDI scores between EA and RC were similar between groups for both sides (Figure 1). RMS error was not uniform across the various lower body kinematics (Figure 2).

Representative gait cycles or ensemble averages of the gait cycles can be used to portray a person's kinematic curves. While neither version is incorrect, it is important to understand the pros and cons of each data type and how each technique may affect data before making clinical decisions from that technique.

## CONCLUSIONS

The purpose was to determine if there are differences between EA and RC data representation techniques. Overall, EA and RC are similar in accuracy to

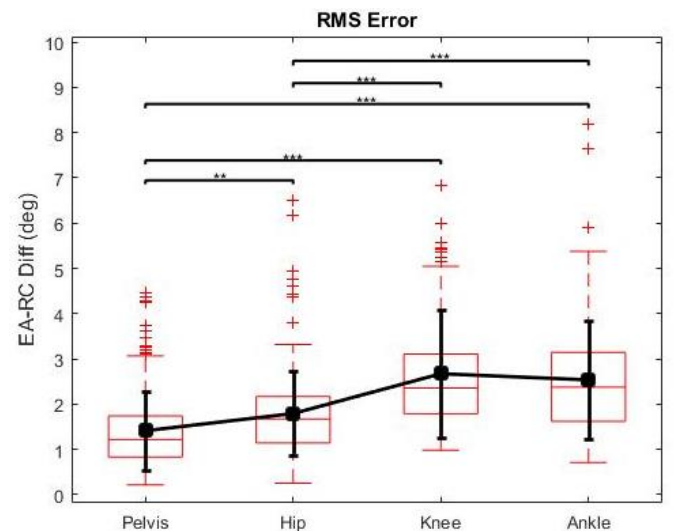


**Figure 2:** RMS error between EA and RC by body segment across the whole group. Hip, knee, and ankle RMS error were higher than the pelvis ( $P \leq 0.0027$ ). Knee and ankle RMS error were greater than the hip ( $P < 0.001$ ). \*\* indicates  $P < 0.01$ , \*\*\* indicates  $P < 0.001$ .

approximately  $2^\circ$  on average and gait quality (GDI) is preserved in both techniques. However, distal kinematics (knee and ankle) show greater differences between EA and RC than proximal kinematics. This may be due to attenuation of local maxima and minima, as the distal joints have larger ranges of movement. In summary, gait kinematics can be accurately depicted in either manner but the data may not be as comparable for distal kinematics.

## REFERENCES

1. Winter DA. *Biomechanics and Motor Control of Human Movement*, Fourth Ed. John Wiley & Sons Inc. 2009.
2. Schwartz MH et al. *Gait Posture*. **28**:351–357. 2008.
3. Woltring HJ. *Adv Eng Softw*. **8**:104–113. 1986.

## ACKNOWLEDGMENTS

Funding for this project was received from NIH/NINDS SBIR Grant # 1R43NS090756-01. We acknowledge the ongoing support of the J. T. Tai & Company Foundation and the support provided by the technical and clinical teams at CGMA.

# COMPARISON OF PATIENT-REPORTED OUTCOMES AND PERFORMANCE-BASED OUTCOME MEASURES OVER MULTIPLE TIME POINTS

<sup>1,2</sup> Amanda Wingate, <sup>2</sup> Julianne Stewart, <sup>1,2</sup> John-David Collins, <sup>2</sup> Trevor Kingsbury and <sup>2</sup> Marilyn Wyatt

<sup>1</sup> BADER Consortium, University of Delaware, Newark, DE

<sup>2</sup> Naval Medical Center San Diego, San Diego, CA

email: amanda.f.wingate.ctr@mail.mil

## INTRODUCTION

Patient-reported outcome (PRO) and performance based, functional outcome measures are important parameters to track during rehabilitation of servicemembers (SMs) with lower extremity amputation(s). Presently, little research has looked at the effect of time throughout rehabilitation on PROs and functional outcome measures and whether any potential correlations exist between qualitative and quantitative measures. At the Naval Medical Center San Diego (NMCS D) Gait Analysis Laboratory, quantitative and qualitative measures are collected at multiple time points as part of routine patient care to support the rehabilitation process and document outcomes.

Two qualitative measures are used to evaluate a patient's overall opinion of his or her health: the PROMIS® Global Health, a 10-item instrument scored into two subscales: physical health and mental health [1] and the Short Musculoskeletal Function Assessment (SMFA), a 46-item instrument that measures perceived functional status by two subscales, one a dysfunction index and the other a bother index [2]. The Four Square Step Test (FSST) is a functional outcome measure that is used to quantify the physical balance and agility of patients and is a sensitive and specific test for impaired mobility [3]. Gait velocity is another parameter used in a clinical setting to assess walking ability and is predictive of community ambulation and the ability to perform higher level tasks in the future [4].

The primary purpose of this study was to evaluate the effect of time through rehabilitation on PRO and functional outcome measures for SMs with amputation(s). Correlations between PRO and performance measures were investigated to see if

there are predictable behaviors of good rehabilitation outcomes.

## METHODS

Thirteen male SMs who underwent amputation (one bilateral transfemoral, three unilateral transfemoral and nine unilateral transtibial) after a traumatic injury were identified through an IRB approved retrospective analysis of 2014-2017 clinical records at NMCS D. As part of their clinical rehabilitation process, SMs underwent gait analysis, FSST, and PRO collection at baseline (initiation of unassisted walking), and at six weeks, three months, and six months after baseline. Nine patients successfully completed their six month visit and were included in this study. At baseline, patients were  $28.5 \pm 6.5$  years old and  $3.3 \pm 0.7$  months from amputation (height  $178.7 \pm 6.7$  cm and weight  $89.5 \pm 16.2$  kg). During each visit, patients completed two qualitative PROs: SMFA and PROMIS® Global Health; and two quantitative functional measures: FSST and self-selected walking velocity collected during gait analysis. One way ANOVAs were performed to examine the effect of time on each PRO and functional measure with a  $p < 0.05$ . If a main effect was found, Tukey post hoc tests were used to determine where differences occurred. Additionally, Pearson correlation coefficients were computed for all PRO and functional outcome variables.

## RESULTS AND DISCUSSION

Descriptive statistics are reported in Table 1. There was not a main effect of time through rehabilitation for any of the PRO measures (SMFA Dysfunction  $p = 0.81$ , SMFA Bother  $p = 0.21$ , PROMIS PH  $p = 0.42$ , and PROMIS MH  $p = 0.76$ ). There was a

significant effect of time on the functional measures (FSST  $p < 0.01$  and Velocity  $p < 0.01$ ). Post hoc tests determined a significant improvement in both quantitative measures at the 6 month time point ( $p < .01$  for both). A significant strong correlation was found between FSST and velocity ( $P = -0.65$ ). Additionally, there were significant strong correlations between all PRO measures. Notably, PROMIS mental health score was strongly negatively correlated with SMFA dysfunction ( $P = -0.81$ ).

## CONCLUSIONS

The purpose of this study was to report on PRO and functional outcome measures throughout rehabilitation and to determine how the qualitative and quantitative measures may correlate with each other. Functional outcome measures significantly improved from baseline to the six month time point. None of the PRO measures were significantly improved, however all SMs reported scores were trending toward improvement throughout rehabilitation. It appears that the functional measures have better sensitivity to change compared to the PRO measures in relatively low patient numbers. As more patients are added to this preliminary study, some of the trends toward PRO improvement may become statistically significant. FSST and velocity were correlated which was expected. While no PRO measures were correlated to any functional measures, it was noteworthy that

as PROMIS mental health worsened, the SMFA Dysfunction increased (worsened), indicating that as patient-reported mental health worsens, SMs perception of his or her dysfunction worsens, and vice-versa. In addition to attempting to understand the relationship between PRO measures and functional outcomes, future research could examine more closely the relationship between mental health scores and perceived dysfunction. That in turn may help explain the changes, or lack thereof, in the SMFA across time in rehabilitation in SMs with amputation(s).

## REFERENCES

1. Hayes RD, et al. Qual Life Res **18**, 873-80, 2009.
2. Swiontkowski MF, et al. J Bone Joint Surg **81**, 1245-60, 1999.
3. Dite W, et al. Arch Phys Med Rehabil, **83**, 1566-71, 2002.
4. Bohannon RW. Age Ageing, **26**, 15-9, 1997.

## DISCLOSURE STATEMENT

The views expressed herein are those of the author(s) and do not necessarily reflect the official policy or position of the Department of the Navy, Department of Defense, or the United States Government. All data collection and analysis was performed under IRB protocol NMCS.D.2014.0026.

**Table 1:** Descriptive statistics (mean  $\pm$  standard deviation) of performance-based and patient-reported outcomes over gait visits. Bold/italic indicates significant differences  $p < 0.05$ .

	FSST (s)	Velocity (m/s)	SMFA Dysfunction	SMFA Bother	PROMIS Physical Health (t-score)	PROMIS Mental Health (t-score)
<b>Baseline</b>	9.06 $\pm$ 2.52	1.19 $\pm$ 0.12	23.5 $\pm$ 11.91	20.8 $\pm$ 15.02	45 $\pm$ 2.69	49.7 $\pm$ 3.12
<b>6 Weeks</b>	7.44 $\pm$ 1.61	1.25 $\pm$ 0.14	21.8 $\pm$ 10.6	15.9 $\pm$ 12.84	47.4 $\pm$ 2.2	48.9 $\pm$ 3.49
<b>3 Months</b>	6.96 $\pm$ 1.92	1.32 $\pm$ 0.12	21.5 $\pm$ 13.85	15.1 $\pm$ 13.74	48.9 $\pm$ 2.87	52.5 $\pm$ 3.43
<b>6 Months</b>	<b>6.01 <math>\pm</math> 0.94</b>	<b>1.39 <math>\pm</math> 0.13</b>	18.3 $\pm$ 8.83	8.8 $\pm$ 9.71	50.5 $\pm$ 2.11	51.7 $\pm$ 3

# INSTRUMENTATION FOR MEASUREMENT OF PROBE FORCES AND ORIENTATION DURING FREEHAND ULTRASOUND

<sup>1</sup>Tyler Schimmoeller, <sup>1</sup>Robb Colbrunn, <sup>1</sup>Tara Bonner, <sup>1</sup>Mark Lobosky, <sup>1</sup>Erica E. Morrill, <sup>1</sup>Tammy M. Owings, <sup>1</sup>Benjamin Landis, <sup>2</sup>J. Eric Jelovsek, <sup>1</sup>Ahmet Erdemir

<sup>1</sup>Department of Biomedical Engineering, Cleveland Clinic, Cleveland, OH, USA

<sup>2</sup>Obstetrics, Gynecology & Women's Health Institute, Cleveland Clinic, Cleveland, OH, USA

email: [schimmt@ccf.org](mailto:schimmt@ccf.org) web: <https://simtk.org/projects/multis>

## INTRODUCTION

Ultrasound is a non-invasive diagnostic tool commonly used for medical imaging. Most ultrasound imaging is performed freehand where the sonographer holds the probe in contact with the skin, adjusting the probe's orientation until the target region is located. During anatomical imaging, the force exerted by the probe on the tissue must be minimized to view the tissue in a more anatomically correct, undeformed state. During mechanical manipulation, e.g. indentation, quantifying the forces would enable clinicians and researchers to characterize the mechanics of the tissue. Researchers have previously proposed methods to measure force and orientation, and compensate for gravity (weight of the probe) [1,2]. However, these methods lack design modularity and their feasibility for clinical use has not been established. A more automated and adaptable system appears to be an emerging need.

This paper presents a methodology for instrumenting any ultrasound system to measure probe forces and orientation while meeting the previously stated needs by including the following features: 1) automatic association and temporal synchronization of data collected from multiple systems 2) gravity compensation, 3) easily interchangeable probes, and 4) extensibility to include additional instrumentation.

## METHODS

A device (Fig. 1) was designed to measure forces and orientation during freehand ultrasound use (Acuson S3000, Siemens, USA). The device compensates for gravity by using an inertial measurement unit (VN-100, VectorNav, USA) and a 6-axis load cell (Nano25, ATI Industrial Automation, USA), relying on a custom LabVIEW program (LabVIEW, National Instruments, USA) in

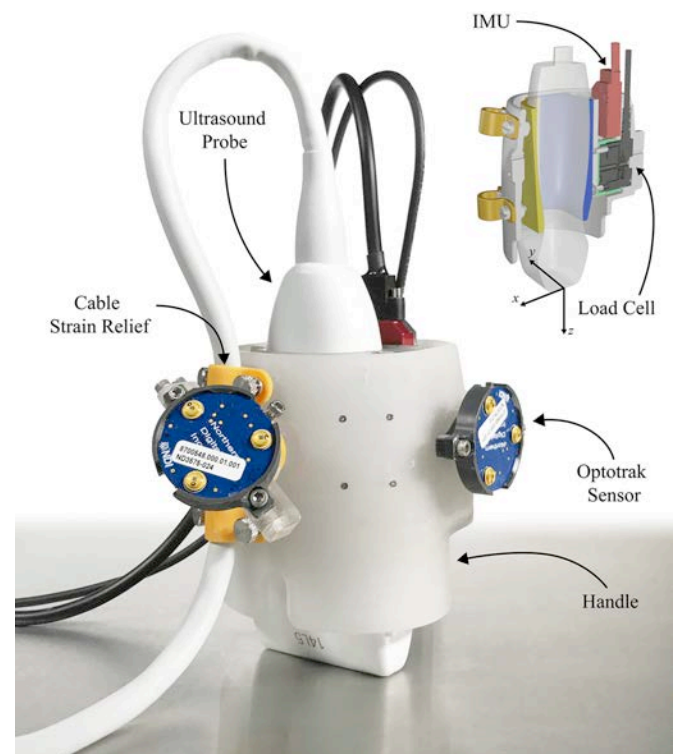


**Figure 1.** The instrumented ultrasound system. The Optotrak sensors (NDI, Canada) are an example of additional instrumentation.

conjunction with a mechatronic toolkit (SSCAD Toolkit, Cleveland Clinic, USA). An analog signal unique to a trial supports association and temporal synchronization of data collected by separate systems (ultrasound images, probe forces, and orientation). This signal was similar to an electrocardiogram (EKG) waveform and was sent simultaneously to the force data acquisition system and ultrasound EKG input (Pulse in Fig. 2), where the time instants of signal peaks were stored in the image metadata. A custom Python script was used to associate the ultrasound and force data files based on this information to determine the time difference between data acquisition systems. All force and orientation data were collected using the same custom LabVIEW program on a single computer, making temporal synchronization innate.

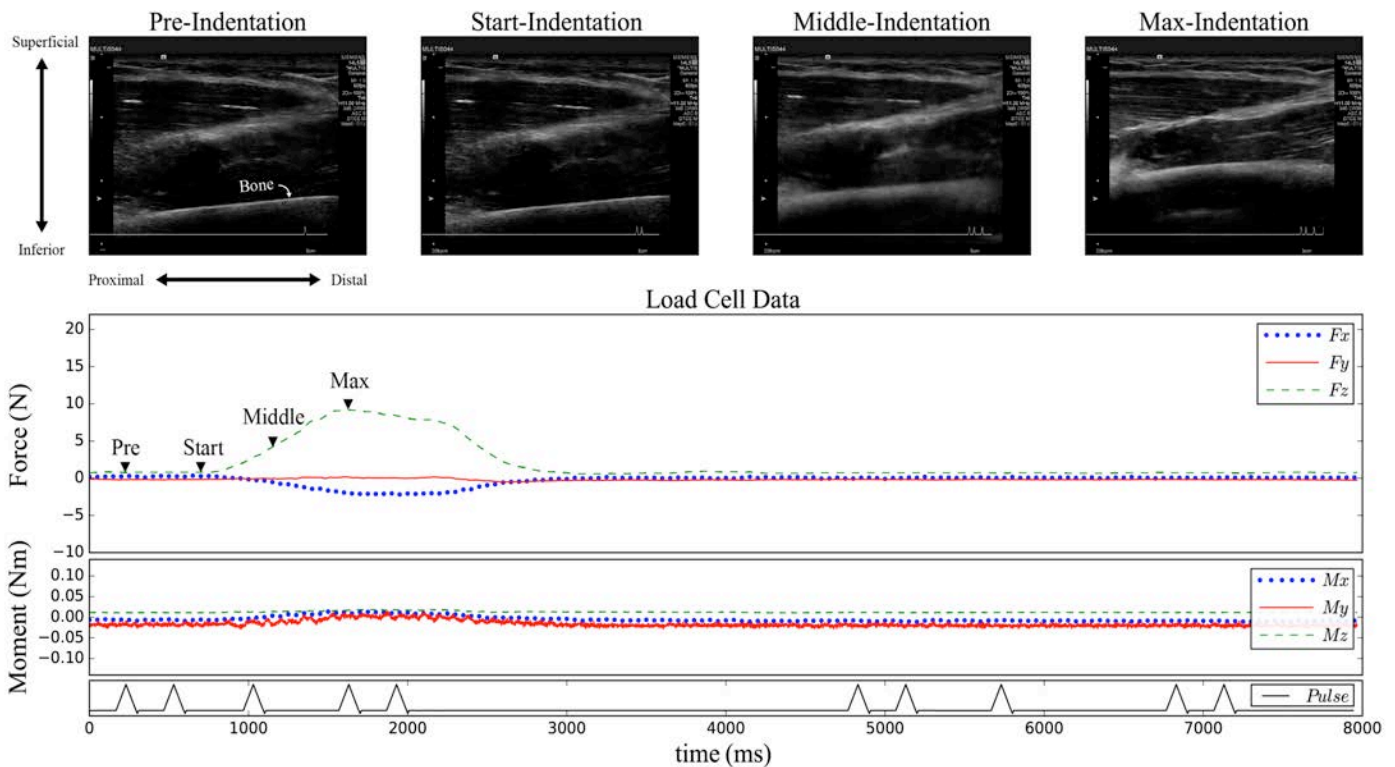


**Figure 2.** A time synchronized trial is shown with the corresponding forces, moments, and ultrasound images. All forces and moments were transformed to the ultrasound probe tip after gravity compensation. Location: lower arm, anterior, central.

An experiment was performed for demonstration purposes, where the device was used *in vivo* for anatomical imaging and to collect a series of images during indentation. The experiment was performed freehand by the sonographer on the right extremities of a 26 year old caucasian male subject (height 183 cm, weight 90 kg). A total of 24 locations were imaged on each extremity using either the 14L5 or 9L4 ultrasound probes (Siemens), depending on the depth of bone boundary. For anatomical imaging, each location was imaged with minimal resultant force (<2.2 N). Indentation trials were performed immediately after minimal force trials at 4 of the 24 locations on each extremity. This study was approved by the Cleveland Clinic Institutional Review Board and the Human Research Protection Office of the U.S. Army.

## RESULTS AND DISCUSSION

Data files from all locations were automatically associated and time synchronized. The results from a single trial can be seen in Fig. 2, showing four events throughout an indentation. All forces and moments were transformed to the ultrasound probe tip after gravity compensation. The force  $F_z$  represents the predominant loading axis (perpendicular to the probe tip). Shear loading ( $F_x$  &  $F_y$ ) is expected due to the freehand operation and

the heterogeneous nature of musculoskeletal tissue. Performance of gravity compensation strategy was demonstrated by the near zero-load state before and after indentation.

## CONCLUSIONS

A robust instrumentation system was developed that can fully integrate with any existing ultrasound machine that has an EKG input, increasing the accessibility and adaptability of instrumented ultrasound systems. The device may be equipped with additional instruments, including motion capture sensors to track its orientation and position relative to a specimen and other devices (Fig. 1). This methodology is being utilized in a separate study to measure *in vivo* tissue thicknesses of musculoskeletal extremities for a large group of subjects[3].

## REFERENCES

- [1] Burcher, M. R., *et al.*, *IEEE Trans Ultrason Ferroelectr Freq Control*, 52(8), 1330-1342, 2005. [2] Noh, Y., *et al.*, *Conf Proc IEEE Eng Med Bio Soc*, Milan, 2015, 5773-5776.
- [3] Morril, E., *et al.*, submitted to *ASB'17*, Boulder, CO, USA, 2017.

## ACKNOWLEDGMENTS

This study has been supported by USAMRMC (W81XWH-15-1-0232). The authors would like to thank Siemens Medical Solutions USA, Inc. for loaning the ultrasound equipment.

# IMPROVED HIP JOINT CENTER PREDICTION

<sup>1</sup> Emily Miller and <sup>1</sup> Kenton Kaufman

<sup>1</sup> Mayo Clinic Motion Analysis Laboratory, Rochester, MN, USA  
email: Kaufman.Kenton@mayo.edu

## INTRODUCTION

In biomechanical modeling for motion analysis, the hip joint center (HJC) is used to define the proximal location of the thigh segment. This is the point about which the hip moments are calculated and the point that defines the orientation of the thigh segment, which determines hip and knee kinematics. The HJC cannot be palpated. For modeling purposes, its location must be calculated. Functional methods for HJC prediction have been shown to be accurate [1], but are difficult to perform for clinical populations with neuromuscular deficits. Therefore, regression based methods are preferred. However, these methods have been shown to yield large degrees of error. Most prediction methods utilize the pelvic landmarks (i.e. the anterior and posterior superior iliac spines) to calculate the location of the HJC [2-4]; Excessive adipose tissue can make these landmarks difficult to locate correctly. A new regression equation utilizing leg length has been shown to improve the accuracy of locating the HJC in cadavers [5]. The Hara regression method has been shown to have considerably less error than the Bell [2] or Davis [3] methods and comparable error to the Harrington method [4]. The purpose of this study was to compare the accuracy of the HJC location calculated with the Harrington method and the Hara method. These two methods were compared to a gold standard digital full-leg coronal radiograph.

## METHODS

Clinical patients (5/8 female;  $23.8 \pm 22.7$  years; BMI =  $20.4 \pm 5.4$ ) visiting the lab for a standard gait analysis and patients (5/8 female;  $69.4 \pm 4.8$  years; BMI =  $29.6 \pm 6$ ) undergoing total knee arthroplasty (TKA) enrolled in a larger post-operative follow-up study were used for this analysis. For the clinical patients both knees were included, while for the

TKA patients only the pre-operative surgical knee was included in the comparison.

Tibiofemoral angles, calculated using standard digital full-leg coronal radiographs were used as the 'gold standard' for comparison. An angle measurement tool (QREADS: Clinical Image Viewer, Mayo Clinic, Rochester, MN) was used to create vectors from the center of the femoral head to the midpoint of the tibial spines and from the midpoint of the tibial spines to the midpoint of the malleoli. The tibiofemoral angle was calculated as the lateral angle between the femoral and tibial vectors minus 180, where a positive angle was a varus knee and a negative angle was a valgus knee.

The motion analysis knee valgus-varus angles were collected from a static trial. Kinematic parameters were acquired with a motion analysis system utilizing ten infrared cameras (Raptor-12 cameras, Motion Analysis Corporation, Santa Rosa, CA). A set of retro-reflective, 3D markers were placed on the body of each subject as described by Kadaba, et al [6]. The 3D coordinates of the marker data were used as input to a commercial software program (Visual3D 5.02.27, C-Motion, Inc., Germantown, MD) to calculate the joint kinematics. The HJCs were defined using the regression equations developed by Harrington [4] and Hara [5]. The knee center was found on a vector directed medially from the knee marker and at a distance one-half of the measured knee width. Similarly, the ankle center was located by a vector directed medially from the lateral malleolus marker at one half the distance of the measured ankle width.

## RESULTS AND DISCUSSION

This study demonstrated that the Hara regression method results in an improved estimate of the HJC

(Fig. 1). The Hara HJC is both more accurate and precise (Fig. 2). The mean error between the gold standard x-ray measurement and the motion analysis calculation for the Harrington HJC regression method was 6.0 degrees (95% CI: 4.4, 7.6) and for the Hara HJC regression method was 1.8 degrees (95% CI: 0.54, 3.0). The mean errors between the two methods were statistically different (P-value = 0.000), however the mean error for the Hara method was still not zero.

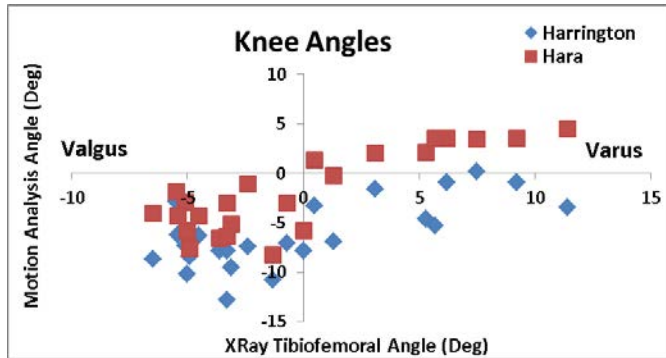


**Figure 1:** Harrington and Hara HJC knee valgus-varus angles versus x-ray tibiofemoral angles.

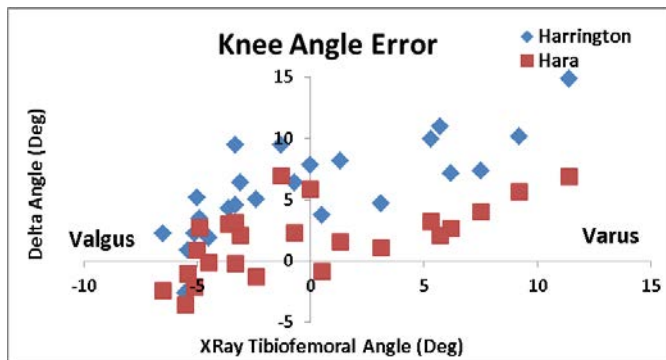


**Figure 2:** Error between motion analysis Harrington HJC and Hara HJC knee valgus-varus angles versus x-ray tibiofemoral angles.

In the findings reported by Hara [5], the Harrington HJC regression model and the Hara HJC regression model had similar error. However, the Harrington method utilizes the pelvic depth distance in the model. This measurement has been shown to have larger errors in a clinical setting compared to medical imaging, which may be contributing to the superior performance of the Hara method to the Harrington method in this in-vivo population.

The Hara method was based upon cadaver estimates. The patients included in this study include children and young adults with neuromuscular pathology and adults with osteoarthritis. This study confirms that the method is reliable and valid in an in-vivo setting.

## CONCLUSIONS

Accurately modeling the HJC is critical for data interpretation and patient care. This study confirms that the Hara HJC regression method is reliable and valid in an in-vivo setting.

## REFERENCES

1. Piazza, S, et al. *J Biomech* **34**, 967-973, 2001.
2. Bell, A, et al. *J Biomech* **23**, 617-621, 1990.
3. Davis, R, et al. *Human Movement Science* **10**, 575-587, 1991.
4. Harrington, M, et al. *J Biomech* **40**, 595-602, 2006.
5. Hara, R, et al. *Scientific Reports*, DOI:10.1038/srep37707, 2016.
6. Kadaba, M, et al. *J Orth Res* **8**, 383-392, 1990.

# Foot Pressure Masking Accuracy and Reliability in Children with Unilateral Clubfoot

<sup>1-2</sup>Juanita Wallace, <sup>1-2</sup>Hank White, <sup>1</sup>Sam Augsburg, <sup>1-2</sup>Henry Iwinski, <sup>2</sup>Robert Shapiro and <sup>1-2</sup>Janet Walker

<sup>1</sup>Shriners Hospitals for Children – Lexington, KY, USA

<sup>2</sup>University of Kentucky, Lexington, KY, USA

email: jjwa234@uky.edu

## INTRODUCTION

Previous research has shown that data from the whole footprint does not give a complete picture of the forces affecting the foot when walking [1]. Clinically it is more beneficial to examine pressure under specific regions of interest (ROI) instead of the total foot [2]. The justification for having an automated masking technique is that it is standardized [2, 3]. However, previous research has found that automated ROI masking techniques are not as accurate with deformity [2]. Therefore, it may be necessary to either edit the pre-defined mask to eliminate inaccuracies or forgo automated masking techniques altogether and mask the ROI based on visual analysis of the foot print (manual masking). Both manual masking and adjusting a predefined mask are based on the subjective interpretation of the clinician[2]. The purposes of this study were to: 1. Report the common inaccuracies found in masking; 2. Report intra-masker reliability when editing a 10 area mask; 3. Report intra-masker reliability when manually masking a 10 area mask; 4. Report inter-masker reliability between a novice and experienced masker.

## METHODS

Twenty-six children, ages 2.6-12.9 years, diagnosed with unilateral clubfoot underwent pedobarographs. Foot pressure analysis was collected for both the affected and unaffected sides using Novel Emed®X platform and Novel Database Pro M v.23.3.52 (Novel Electronics, Munich Germany). Three trials per side were collected for a total of 156 foot pressure trials. The mask used in this study is a 10 area ROI mask (PRC) mask (Figure 1)[4]. One investigator, with 8 years' experience using Novel software, performed all post processing.

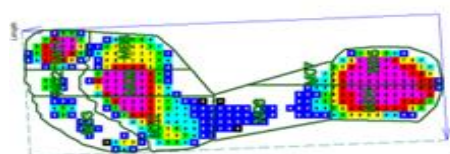


Figure 1. The 10 area PRC mask.

### *Masking Accuracy*

Automated masking of the 156 foot pressure trials was completed using the PRC mask. The 156 foot pressure trials were split into affected and unaffected sides. The foot print was assessed visually for the presence of the four inaccuracies listed in Figure 2. These four inaccuracies are caused by five common foot deformities present in clubfeet. These inaccuracies do not occur in isolation, children with clubfoot can exhibit more than one inaccuracy. The presence of at least one inaccuracy classified a trial as inaccurate.



Figure 2: Common Deformities and Common Inaccuracies when masking clubfeet.

### *Intra-Masker Reliability*

A subset of 10 subjects was chosen at random for the intra-masker reliability. Only one trial for each subject was chosen for a total of 20 foot pressure trials. The PRC mask was applied using automated masking and then edited based on the masker's ability to identify the four common inaccuracies. This was completed for the 20 foot pressure trials on two consecutive days. Values for the contact area (CA) of the 10 ROI were exported for analysis.

The same masker then manually masked the 20 foot pressure trials, using the 10 area PRC mask description as a guide[4]. This was also completed on 2 consecutive days and values for the CA were exported. Interclass correlation coefficients (ICC) were reported.

*Inter-Masker Reliability*

For inter-masker reliability, one investigator, with little to no experience masking, identified inaccuracies and made corrections to the automated masking technique for the 20 foot pressure trials. The investigator was given the description of the PRC mask and was given a tutorial by the experienced investigator. ICC values between the novel masker and the experienced masker were calculated.

**RESULTS AND DISCUSSION**

*Accuracy*

For the unaffected side, 3/78 trials (4%) were identified as inaccurate. Whereas, 19/78 (24%) trials were identified as inaccurate for the affected side. Inaccurate toe mask identification was the most common inaccuracy, where 18/78 had the hallux included in the first metatarsal mask. In addition, 10/78 trials had rotation of the vertical dividing lines.

*Intra- and Inter-Masker Reliability*

ICC values for CA of the 10 regions of interest for intra-masker reliably when editing the automated masking technique, for intra-masker reliability when manually masking, and for inter-masker reliability between a novice and experienced masker are presented in Table 1. Results indicate that the deformities present in clubfoot hinder the automated

masking techniques ability to accurately identify ROI.

Intra- and inter-masker ICC values report excellent reliability (>0.75) for the CA in all regions of the foot except for 2<sup>nd</sup> toe for both inter-masker and intra-masker manual masking and for the 3<sup>rd</sup>-5<sup>th</sup> toes in inter-masker reliability. The low ICC values in the 2<sup>nd</sup> toe and the 3<sup>rd</sup>-5<sup>th</sup> toes can be explained because these are the two smallest areas of the foot print, reliability has been found to be lower in less loaded and smaller areas[5].

**CONCLUSIONS**

This is the first study to report the reliability and accuracy of masking in a pediatric unilateral clubfoot population. The results of this study show that intra- and inter-masking reliability is high for CA in almost all ROI. In addition, automated masking techniques are less accurate for clubfeet than in feet without deformity. Taking into account the excellent reliability for between maskers and between days, it would be safe to conclude that inaccuracies to the automated masking can be reliably corrected by both novice and experienced maskers.

**REFERENCES**

1. Hayafune NY. The Foot, 1999. 9: p. 88-92.
2. Stebbins J. Gait and Posture, 2005. 22: p. 372-376.
3. Deschamps, K. Gait and Posture, 2009. 30: p. 379-382.
4. Novelgmbh. 24 ed. 2014, Munich.
5. Gurney, J. Gait and Posture, 2008. 27(4): p. 706-709.

	<i>Inter-Masker</i>	<i>Intra-Masker Mask Editing</i>	<i>Inter-Masker Manual Masking</i>		<i>Inter-Masker</i>	<i>Intra-Masker Mask Editing</i>	<i>Inter-Masker Manual Masking</i>
<b>Medial Hindfoot</b>	0.667*	0.971*	0.977*	<b>2nd Metatarsal</b>	0.687*	0.985*	0.934*
<b>Lateral Hindfoot</b>	0.767*	0.975*	0.983*	<b>3rd-5th Metatarsal</b>	0.842*	0.987*	0.915*
<b>Medial Midfoot</b>	0.823*	0.998*	0.877*	<b>Hallux</b>	0.906*	1	1
<b>Lateral Midfoot</b>	0.884*	0.992*	0.951*	<b>2nd Toe</b>	0.426^	0.970*	0.142
<b>1st Metatarsal</b>	0.906*	0.993*	0.926*	<b>3rd-5th Toes</b>	0.315	0.994*	0.925*

Table 1: ICC values for the CA of the 10 ROI. \*P<0.001 ^p<0.05

# ACCURACY OF SIMPLER AND LOWER-COST TECHNOLOGIES TO MEASURE THE INITIAL LEAN ANGLE FOR FORWARD LEAN RELEASES IN A CLINICAL SETTING

<sup>1,2</sup> Evelyne Carbonneau, <sup>1,3</sup> Kevin Lalanne, <sup>1,3</sup> Guillaume Léonard and <sup>1,2</sup> Cécile Smeesters

<sup>1</sup> Research Center on Aging, Sherbrooke, QC, Canada

<sup>2</sup> Department of Mechanical Engineering, Université de Sherbrooke, Sherbrooke, QC, Canada

<sup>3</sup> School of Rehabilitation, Université de Sherbrooke, Sherbrooke, QC, Canada

e-mail: [Cecile.Smeesters@USherbrooke.ca](mailto:Cecile.Smeesters@USherbrooke.ca), web: <http://www.usherbrooke.ca/gmecanique>

## INTRODUCTION

The ability to recover balance and avoid a fall decreases exponentially with age, falling below one standard deviation (SD) of the mean value of 18-year-olds, above 51.0yrs for forward lean releases [1]. Moreover, in a recent 12-month prospective falls evaluation, while the maximum forward lean angle was shown to significantly predict a future fall in community-dwelling older adults (65-90yrs), postural sway and timed up and go measures were not predictive [2]. Unfortunately, current technologies to measure the maximum forward lean angle are neither simple nor cheap, making it difficult to use in a clinical setting to identify individuals at risk of falls or to evaluate the effectiveness of exercise-based fall prevention programs. Therefore, the purpose of this study was to determine the accuracy of four alternative initial lean angle measurement methods, of various complexity and cost, compared to the current gold standard for forward lean releases.

## METHODS

Twelve healthy adults (mean±SD=27.4±10.1yrs; range=20-48yrs, 50% women) were instructed to recover balance using a single step, after first being leaned forward and then suddenly released from six randomly ordered initial lean angles (5-30deg or 10-35%BW in 5deg or 5%BW increments), using four different measurement methods:

a) The initial lean angle was calculated live in degrees by a **LabVIEW** (National Instruments Corporation, Austin TX) program from 3D marker positions, as captured by four optoelectronic position sensors (Optotrak, NDI, Waterloo ON) at 100Hz [1].

It was measured as the sagittal plane angle between the vertical and the line connecting the midpoints of the two lateral malleoli and the two greater trochanters prior to lean release.

b) The initial lean angle was measured live in percentage of body weight (%BW) by a single degree of freedom **load cell** (FD-2, AMTI, Newton MA) at 1000Hz attached to the lean cable [2,3]. It was then converted to degrees in post-processing by Thelen et al.'s static equilibrium equation using Matlab (Mathworks, Natick MA) and the ground reaction forces under each foot prior to lean release, as captured by two force platforms (OR6-7, AMTI, Newton MA) at 1000Hz [3].

c) The initial lean angle was measured live in degrees by the experimenter leaning the participant, using a digital **inclinometer** (1886-000, Johnson Level & Tool, Mequon WI) attached to the mid-thigh of the step leg of the participant with Velcro elastic straps.

d) The initial lean angle was measured live in degrees by the experimenter acquiring the electronic data, using a giant **protractor** with 5deg increments printed on a poster (60in x 96in) positioned in the sagittal plane 1m "behind" the participant and aligned on the participant's malleoli. This experimenter was blinded to the initial lean angle to be set at each trial to minimize bias.

Finally, the **gold standard** initial lean angle was calculated in degrees in post-processing using Matlab, measuring it as explained in method "a". Furthermore, whichever of the four methods was used by the experimenter leaning the participant to set the initial lean angle, it was then also measured using the other three methods to increase sample size.

## RESULTS AND DISCUSSION

Unconditional growth linear regressions showed that, despite some residual SD ( $p_{\text{ResidualSD}} < 0.001$ , Table 1), the four initial lean angle measurement methods were strongly correlated ( $p_{\text{Slope}} < 0.001$ , Pseudo  $R^2 > 0.966$ ) with the initial lean angle calculated using Matlab (gold standard). As expected, the LabVIEW angle (a) had the smallest residual SD (0.6-0.9deg) and the strongest correlation (99.5%). The load cell angle (b) had the second strongest correlation (97.4%), but the largest residual SD (2.0-4.2deg) as well as significant intercept ( $p_{\text{Intercept}} < 0.001$ ) and inter-individual covariance ( $p_{\sigma_{10}} = 0.030$ ). Surprisingly, the inclinometer (c) and protractor (d, Figure 1) angles had very acceptable residual SD (1.7-2.6deg and 1.6-2.5deg) and correlations (96.6% and 96.7%).

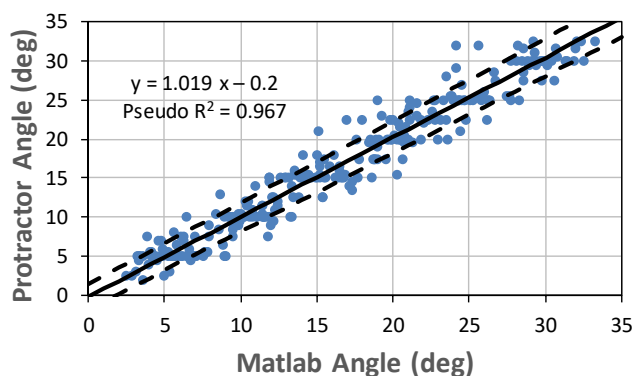


**Figure 1:** Unconditional growth linear regression (mean $\pm$ SD) between the protractor initial lean angle measurement (d) and the initial lean angle calculated using Matlab (gold standard).

The most complex method was the load cell method (b), as the %BW easily fluctuated while setting the initial lean angle, and it required the conversion of the initial lean angle from %BW to degrees in post-processing from ground reaction forces. The second

most complex method was the LabVIEW method (a), as it required calculation of the initial lean angle from 3D marker positions. The inclinometer method (c) was the next one in complexity, as it was slow to display the initial lean angle and required zero resetting at nearly every trial. The protractor method (d) was the easiest but required some training of the experimenter, as he had to position himself perpendicular to the protractor to avoid distortions due to parallax. These distortions could have been reduced by bringing the protractor closer to the participant, but this would have obstructed the optoelectronic position sensors.

Finally, the LabVIEW method is the most expensive one (a $\approx$ 100k\$), followed by the load cell (b $\approx$ 10k\$ in degrees, 1k\$ in %BW), inclinometer (c $\approx$ 100\$) and protractor (d $\approx$ 10\$) methods.

## CONCLUSIONS

Therefore, to measure the maximum forward lean angle accurately in a clinical setting, the protractor method appears to be the simplest and least expensive alternative to current technologies. Lean releases could thus be used to identify individuals at risk of falls or to evaluate the effectiveness of exercise-based fall prevention programs.

## REFERENCES

1. Carbonneau E, Smeesters C. *Gait Posture* **39**, 365-371, 2014.
2. Carty CP, et al. *Age Ageing* **44**, 109-115, 2015.
3. Thelen DG, et al., *J Gerontol* **52A**, M8-13, 1997.

## ACKNOWLEDGMENTS

Antoine Guillerand for technical assistance, as well as a grant from the Ministère des Relations Internationales et de la Francophonie of the Quebec government for financial support.

**Table 1:** Unconditional growth linear regressions between each of the four initial lean angle measurement methods and the initial lean angle calculated using Matlab (gold standard)

Initial lean angle measurement method	Equation	Residual SD	p-value			
			Intercept	Slope	Residual SD	Pseudo $R^2$
a) LabVIEW	$y = 1.000x - 0.1$	0.6-0.9	0.588	<b>&lt;0.001</b>	<b>&lt;0.001</b>	0.995
b) Load Cell	$y = 1.211x + 2.3$	2.0-4.2	<b>&lt;0.001</b>	<b>&lt;0.001</b>	<b>&lt;0.001</b>	0.974
c) Inclinometer	$y = 0.960x + 0.3$	1.7-2.6	0.319	<b>&lt;0.001</b>	<b>&lt;0.001</b>	0.966
d) Protractor	$y = 1.019x - 0.2$	1.6-2.5	0.557	<b>&lt;0.001</b>	<b>&lt;0.001</b>	0.967

Significant p-values ( $p \leq 0.05$ ) are **bolded**. N=286/288 (2 Matlab initial lean angles discarded due to post-processing errors).

# ACCURACY OF THE MILWAUKEE FOOT MODEL WITHOUT THE USE OF X-RAY OFFSET MEASUREMENTS

<sup>1</sup> Karen Kruger, <sup>1</sup> Jessica Fritz, <sup>1</sup> Karl Canseco, <sup>2</sup> Jason Long <sup>1,3</sup> Gerald Harris

<sup>1</sup> Marquette University/Medical College of Wisconsin, Milwaukee, WI, <sup>2</sup> Cincinnati Children's Hospital, Cincinnati, OH, <sup>3</sup> Shriners Hospitals for Children, Chicago, IL,  
email: karen.kruger@marquette.edu, web: <http://www.marquette.edu/orec/>

## INTRODUCTION

Multiple marker sets and models are currently available for assessing foot and ankle kinematics in gait. The Milwaukee Foot Model (MFM) is one of only two validated models [1, 2]. It is a four-segment model which has been validated for adult and pediatric populations and uses a series of weight-bearing foot/ankle radiographs to index the motion of skin-mounted markers to the underlying bony anatomy, thus quantifying multi-segmental foot kinematics during gait. These radiographs greatly improve the accuracy of the model, particularly when deformities are involved [3]. However, x-rays are not always available in all gait labs. The purpose of this study was to determine the amount of error associated with the MFM when radiographic offset measurements are not available.

## METHODS

A group of 36 healthy subjects (23M, 13F) with no prior surgical treatment to the foot that may have altered its anatomy or function was used for this study. Motion data were collected using Vicon Motion Analysis System (Oxford, UK) at 120 Hz. Data were collected during walking trials at self-selected speed along a 6-meter walkway and processed using the Milwaukee Foot Model (MFM).

During the static trial, a foot position template was made by having the subject stand on a rectangular piece of cardboard and tracing both feet. After the gait analysis, this tracing was used during full weight-bearing radiographs (anterior/posterior, lateral, and modified coronal views) to ensure that the same alignment was achieved. Specific offset measurements were obtained from the radiographs with respect to global reference lines to allow for calculation of the transformation from marker-based to bone-based axis systems. All measurements were

made by the same investigator. The angles were measured for each segment relative to the global reference frame. The average offset of the entire group for each measurement collected was also calculated.

The motion data and radiographic offset measurements were input into a custom software model (MathWorks, Natick, MA). The model calculates a marker-based axis system using marker locations from the static trial and a bone-based axis system using the radiographic offset angles. A transformation matrix is computed to relate the two axis systems. Full details of the model were reported by Long et al [4].

The model was run for each subject with both with the patient-specific offsets and the group average offsets. A paired t-test was used to compare the output (minimum, maximum, and range of motion for each joint) of each simulation.

## RESULTS AND DISCUSSION

Average error in range of motion for each segment analyzed is shown in Table 1. Errors were generally within 1-2 degrees with the exception of the coronal tibia, which showed a 6.1° error on average.

Table 1: Average Range of Motion Error. \* indicates statistically significant differences between the two simulations

<i>Segment</i>	<i>Sagittal Plane</i>	<i>Coronal Plane</i>	<i>Transverse Plane</i>
<i>Tibia</i>	2.2°	6.1°*	1.5°*
<i>Hindfoot</i>	0.5°	0.9°	0.4°
<i>Forefoot</i>	0.7°	0.8°	0.5°
<i>Hallux</i>	1.4°*	1.6°	1.1°*

The joint positions (as measured by maximum and minimum excursions) showed the most error in the coronal plane. Average errors in position were 6.3°,

4.7°, 3.7, and 4.8° for the tibia, hindfoot, forefoot, and hallux segments, respectively. Representative data for a selected subject are shown in Figure 1.

A previous parametric study by our group showed that when the hindfoot orientation angles were perturbed as little as 2° from their true orientation, significant changes to the kinematic output resulted [5]. The effect is most significant in the plane of the perturbation, but significant non-zero effects have also been reported in the transverse plane secondary to perturbations in the coronal plane. This emphasizes the need for repeatable and reliable x-ray measurements in the current model. It also highlights the importance of using bony measurements.

## CONCLUSIONS

This paper illustrated the amount of error that can be expected when using the MFM for analysis of segmental foot kinematics without x-ray offsets. The

importance of having accurate, subject-specific x-ray offset measurements was demonstrated, particularly in the coronal plane. However, these results can also be used as justification for using the MFM without x-ray offsets for certain applications when x-rays may not be available, such as analyzing sagittal range of motion.

## REFERENCES

- [1] Bishop et al. J Biomech 45(2012)2185–2194.
- [2] Rankine et al. Crit Rev Biomed Eng 2008; 36(2-3):127-81.
- [3] Kruger et al. Gait & Posture. 2017. In Press.
- [4] Long et al. J Exp Clin Med 2011;3(5):239e244.
- [5] Long et al. Conf Proc IEEE Eng Med Biol Soc. 2008;2008:879-82.

## ACKNOWLEDGMENTS

The contents of this abstract were developed under NIDILRR grant 90AR5022-01-00.

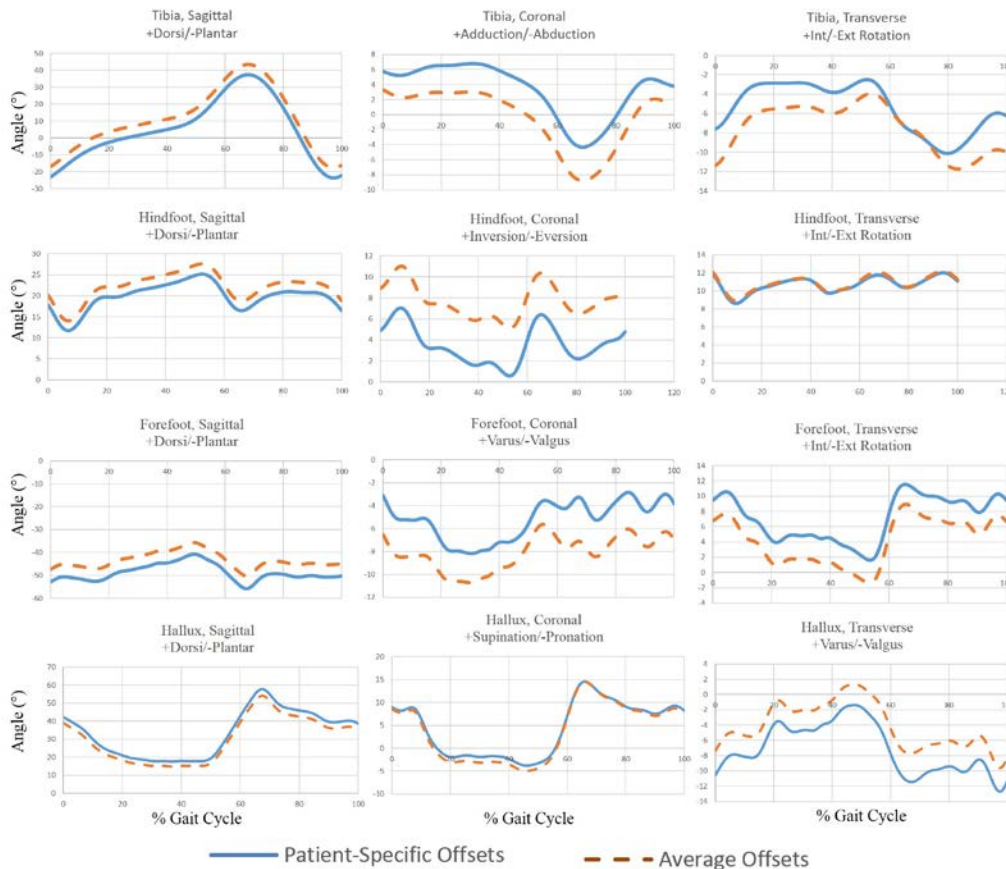


**Figure 1:** MFM kinematics for an example subject. Angles are defined as tibia relative to the global coordinate system, hindfoot relative to tibia, forefoot relative to hindfoot, and hallux relative to forefoot. Solid line indicates model output using patient-specific offset measurements and dashed line indicates output using average offset measurements.

# ERRORS IN MARGINS OF STABILITY ASSOCIATED WITH THE USE OF SIMPLIFIED BODY MODELS DURING WALKING AND TURNING

Kathryn L. Havens, Tatri Mukherjee, James M. Finley

Division of Biokinesiology and Physical Therapy  
University of Southern California, Los Angeles, CA, USA  
Email: khavens@pt.usc.edu, web: [http://pt.usc.edu/Locomotor\\_Control\\_Lab](http://pt.usc.edu/Locomotor_Control_Lab)

## INTRODUCTION

Falls and fall-related injuries are a major public health concern, particularly for older populations and those with neurological disabilities. Prevention of falls relies on an understanding of dynamic balance control. Considering that approximately half of all falls occur during locomotion [1], understanding how stability is controlled and maintained during walking is vital.

During tasks that involve ongoing motion, balance control involves not only control of the position of the center of mass (COM) but also its velocity [2]. To account for both of these factors, Hof et al. proposed a variable, extrapolated center of mass (eCOM) as a metric to characterize dynamic balance. The horizontal distance between the eCOM and the base of support was termed the margin of stability (MoS) [3]. The margin of stability has been used recently to measure dynamic stability during normal walking and during walking with perturbations [4].

Quantification of the MoS requires estimates of the whole body's center of mass. Estimating the whole body center of mass involves quantifying COM locations of all body segments and estimating anthropometrics and distribution of mass. While the gold standard is to use a full body marker set, this method is time-consuming. Studies have therefore used approximations of the COM, such a limited number of pelvic markers [4] or reduced kinematic model of typically available segments when collecting lower extremity kinematics with or without the trunk [5,6]. However, it is unclear whether these methods are appropriate for estimating the COM or how much they affect the margin of stability estimates. Further, the error in

these methods could be exaggerated in certain walking tasks such as turning.

Thus, the purpose of this study was to evaluate the error associated with reduced marker sets in estimating fore-aft and medial-lateral margins of stability during walking and turning tasks.

## METHODS

Thirteen healthy young adults (6 males) participated in this study. Average age, height, and weight were  $26 \pm 3$  yr,  $169 \pm 9$  cm,  $67 \pm 14$  kg, respectively.

Subjects performed straight walking and turning tasks. For straight walking, subjects walked overground for 8 meters. For turning, subjects walked 4 m, performed a 90-degree turn to the right or left and continued walking 4 m. Task order was randomized. Subjects were not constrained to turn type, and performed both step turns (i.e., planting with one foot and turning to the opposite direction of the plant foot) and spin turns (i.e., planting with one foot and turning to the same direction of the plant foot). All trials were conducted at participant's self-selected walking speed.

Three-dimensional kinematics were collected using a 10-camera motion capture system (Qualisys, Inc. Sweden), 250 Hz. Whole body COM was calculated using five methods: 1) as the weighted sum of the COM of all 15 modeled segments using a full body marker set (Visual3D, C-Motion, Inc., Rockville, MD, USA); 2) as the position of a single marker placed on L5-S1 (L5); 3) as the average of four markers on the pelvis (PAM) [4]; 4) as the weighted sum of the COM of the lower extremity (LE); 5) as the weighted sum of the COM of the lower extremity and trunk segments (LETr) [5].

Margins of stability were calculated in the fore-aft and mediolateral directions as described by Hof et al. [3]. The anterior border of the base of support was estimated as the marker placed on the second toe. The lateral border was estimated based on the lateral heel marker. The error between the whole body COM and simplified representations of COM was calculated as the mean difference.

Agreement between whole body COM and simplified methods was quantified using the 95% limits of agreement (LoA) method for repeated measures [7]. The sign test was used to determine whether the error significantly differed from zero. Significance was set at  $\alpha \leq 0.05$ . Upper and lower limits of agreement are shown as mean  $\pm 1.96SD$ .

## RESULTS AND DISCUSSION

In general, the simplified COM models demonstrated a bias for walking and turning tasks. In the mediolateral direction, the bars display bias in different directions (Figure 1), with error bars indicating limits of agreement. For straight walking, only the PAM method exhibited no bias ( $p=0.388$ ). For spin turns, L5 ( $p=0.388$ ) and for step turns, PAM ( $p=0.065$ ) did not demonstrate bias. In the fore-aft direction, all methods tend to overestimate the MoS (positive error) compared to the gold

standard. For straight walking, the PAM method did not demonstrate bias ( $p=0.146$ ).

Large limits of agreement (and thus large bias variability) were found in some methods and tasks, but are not compared statistically. However, while some methods may not be biased (i.e., L5 for ML MoS during spin turns), the large variability suggests that the agreement with the gold standard may not be adequate.

This study suggests that simplified marker sets used to estimate the COM often introduce bias and variability in calculations of margins of stability. Small bias was found in LETr model, and consistent bias could theoretically be corrected. However, additional statistical analysis is necessary to compare errors between methods and tasks.

## REFERENCES

- Gabell A, et al. *Ergonomics* **28**, 965-975, 1985.
- Pai YC & Patton J. *J Biomech* **30**, 347-354. 1997.
- Hof AF, et al *J Biomech* **38**, 1-8. 2005
- McAndrew Young PM et al. *J Biomech* **45**, 1053-1059. 2012.
- Vanrennerghem J et al. *Gait Posture* **31**, 517-21, 2010.
- Suptitz F, et al. *Human Movement Sci* **32**, 1404-1414. 2013.
- Bland JM, Altman DG. *Stat Methods Med Res* **8**, 135-60. 1999.

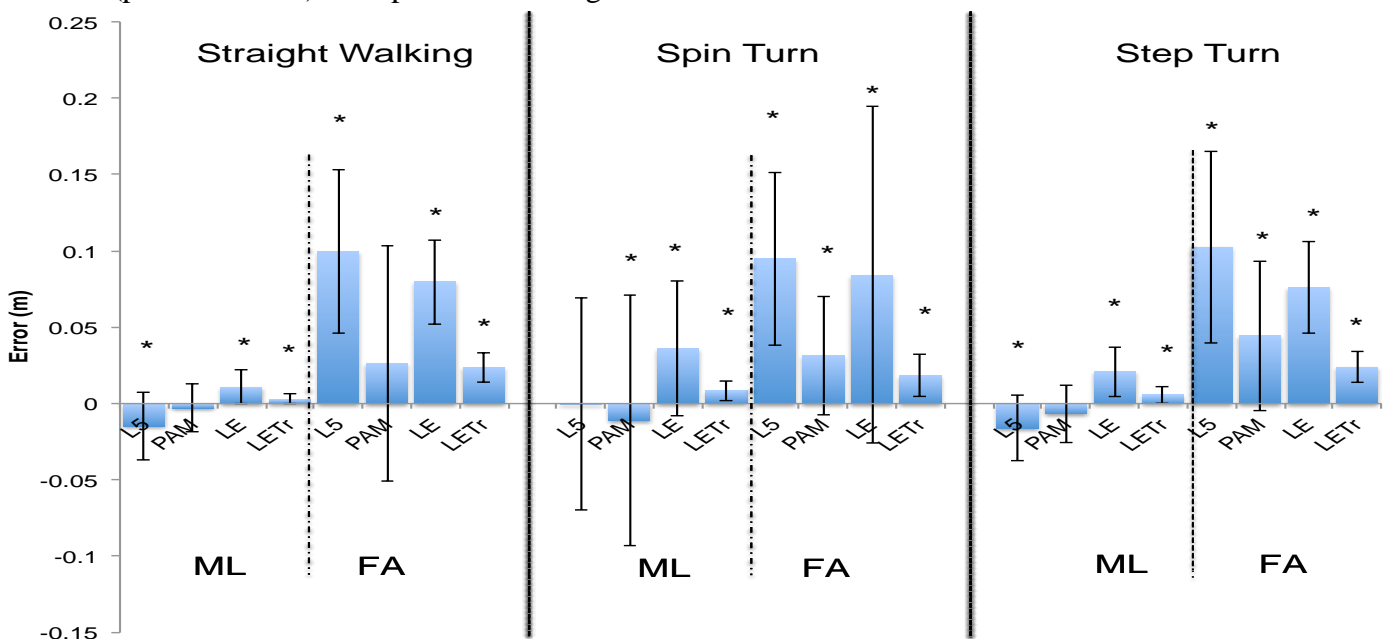


**Figure 1:** Average and limits of agreement for margin of stability error in mediolateral (ML) and fore-aft (FA) directions using simplified COM representations of L5, PAM, LE, and LETr, relative to the whole body COM for straight walking, spin turns, and step turns. \* indicate significant bias ( $p < 0.05$ )

# VALIDATING A NOVEL 3D SCANNER APPROACH FOR MEASURING LEG SWELLING DURING PROLONGED STANDING

John Driggers<sup>1</sup>, Shea McMurtry<sup>2</sup>, Stephanie Wiltman<sup>1</sup>, April Chambers, PhD<sup>1</sup>

Human Movement and Balance Laboratory

<sup>1</sup>University of Pittsburgh Department of Bioengineering, Oakland, PA, USA

<sup>2</sup>University of Pittsburgh Department of Health and Physical Activity, Oakland, PA, USA  
jwd30@pitt.edu

## INTRODUCTION

Out of the top ten occupations in the United States, over half involve prolonged standing [1]. This translates to nearly 3.2 million people whose occupations predispose them to chronic injury due to continual and repeated exposure to blood pooling and muscle fatigue in the lower extremities [2]. Because of this, prolonged standing has been a popular biomechanics research area in the hopes of decreasing injury due to standing.

Prolonged standing causes an increase of blood pooling in the lower extremities due to the decrease in venous return, resulting in volume changes of 3 – 12% [3]. The current “gold standard” for finding anatomical volume measurements is water displacement. However, the water displacement method is subject to a number of inherent issues. Water displacement requires immersing part of the body in water, making it difficult to measure volume while conducting additional tests—especially when using electronics. Furthermore, lifting the leg and transferring it into a bucket of water increases venous return, lending itself to error. Although volume measurements can be taken before and after tests, it is challenging to determine how volume changes over time. In addition, the process is time consuming and unfit for patients in the immediate postoperative period [3]. Because of these challenges, various methods of indirect volume measurements have been proposed, including circumference measurements which are not extremely accurate [3]. As a result, the goal of this study is to validate the use of a 3D

scanner to measure leg volume changes during prolonged standing.

Utilizing a 3D scanner to calculate volume can provide multiple benefits over other methods. Most importantly, using the 3D scanning method requires no subject movement and no potential circulation impedance that may occur by using volume displacement or circumference measurements. Furthermore, a 3D scanner is much cleaner than the water displacement method and allows for the use of EMG’s, force plate, and near infrared technology without the potential of damaging electronic equipment during volume measurements. By using cropping tools in 3D modeling software, it is easy to consistently find limb segment volume in addition to the entire limb. The scanner would also allow for direct volume measurement, which provides a benefit over indirect measurements such as tracking circumference changes.

By comparing volume measurements of objects with known volume with volumes obtained using a 3D scanner, the goal of this study is to validate a novel 3D scanner approach to accurately and precisely measure the volume of known geometric shapes, with the intended goal of calculating volume changes in the limbs, such as leg volume changes during standing.

## METHODS

An EinScan-Pro™ handheld 3D scanner was used to scan a cylinder and hexagonal prism. Three scans of both shapes were taken. The scanner was used to



**Figure 1:** Original picture next to 3D models of the shapes. Bumps on each shape are artifacts left over from adhesive markers the software uses to stitch the image together.

capture the real dimensions of the object and convert it into a digital 3D model. The scanner was accurate to 0.3 mm and can take a full scan of the object in under 3 minutes. The scan was outputted as a “watertight” closed 3D model with real dimensions.

The volume of a scan was found using 3D Computer Aided Design software by modeling it as a solid. The volumes were found 3 times each and averaged. Additionally, the volumes of the blocks were found using their measured dimensions as well as water displacement.

## RESULTS AND DISCUSSION

Volume measurements were first calculated using the 3D scanner. Figure 1 shows each shape next to the final 3D model that was used to calculate the volume. The volume measurements are summarized in Table 1.

The standard deviations for both blocks are small enough for this method to provide adequate repeatability in most cases, specifically in leg volume

changes during standing where changes are on the order of 3% to 12% [2]. The percent error of 1% for the cylinder was also low enough to provide reasonable accuracy for similar applications.

The relatively high percent error of 5.5% for the hexagonal prism could be attributed to the way the scan was taken. The scanner did not pick up the sharp corners of the prism as well as the smooth sides of the cylinder, which could have been a source of error.

## CONCLUSIONS

Using a 3D scanner is a reasonable method to calculate the volume of solid objects. It is best suited for smooth continuous shapes. It may also work as a convenient method to calculate direct anatomical volume changes, although further studies must be done to assure the accuracy of anatomical measurements. Future tests will use a dummy’s leg and a human’s leg to compare the accuracy of the scanner to the other volumetric methods. Applications of this method include quickly finding volume changes in the extremities while performing additional static tests or for patients in the immediate postoperative period [3].

## REFERENCES

- [1] Occupational Employment Statistics, U. S. B. o. L., 2014.
- [2] Cham R and Redfern MS. *Human Factors*, **43**, 737-741, 1999.
- [3] Sukul DK et al. *J Biomed Eng*, **15**, 477-480, 1993.

## ACKNOWLEDGMENTS

Funding for this research has been provided by the National Institutes of Health grant number K01OH010759.

**Table 1:** Volume measurements of shapes using 3D scanner, water displacement, and caliper measurements.

	Average Scan Volume	Water Displacement Volume	Caliper Volume	% STD	% Error
<b>Cylinder</b>	353.9 cm <sup>3</sup>	350.5 cm <sup>3</sup>	346.1 cm <sup>3</sup>	1.17	0.97
<b>Hexagonal Prism</b>	302.9 cm <sup>3</sup>	287.0 cm <sup>3</sup>	289.2 cm <sup>3</sup>	1.04	5.54

# INFLUENCE OF PELVIC SEGMENT DEFINITION USING LANDMARKS PALPATED IN A HIGH FLEXION POSTURE ON JOINT ANGLES AND MOMENTS

<sup>1</sup> Andrea Hemmerich, <sup>2</sup> Rajani Mullerpatan, <sup>1</sup> Tara Diesbourg, <sup>2</sup> Bela Agarwal,  
<sup>1</sup> Emily Geens, <sup>2</sup> Triveni Shetty, and <sup>1</sup> Geneviève A. Dumas

<sup>1</sup> Queen's University, Kingston, ON, Canada

<sup>2</sup> MGM Centre of Human Movement Science, MGM Institute of Health Sciences, Navi Mumbai, India  
email: a.hemmerich@alumni.utoronto.ca

## INTRODUCTION

While several studies have focused on skin motion artifact associated with high impact movements and their inertial effects on activities such as running, little data is available quantifying the influence of soft tissue movement on analyses of high range-of-motion activities [1].

The objective of this study was to compare joint angles and moments at the distal and proximal ends of the pelvis (i.e. hip and lumbosacral joints, respectively) when calculated from anatomical landmarks palpated and digitized in a squat posture versus routine motion analysis techniques where skin markers are affixed to the pelvis in standing.

## METHODS

Data from five female subjects who participated in a related investigation were included in this study (height  $1.66 \pm 0.08$  m, weight  $52.9 \pm 9.5$  kg). Force and motion data were recorded using standard optoelectronic motion capture systems and force platforms. A plug-in-gait marker set was modified by adding tracking markers to the pelvis (iliac crests), thigh, and shank segments; the lumbar spine was tracked via four markers on the L2-L5 vertebral spinous processes.

For each subject, static trials were taken in both standing and deep squat postures. In addition, since tracking markers typically move away from anatomical landmarks as a result of skin motion, anterior superior iliac spine (ASIS) and posterior superior iliac spines (PSIS) landmarks were re-palpated and digitized in the squatting position. Subjects were then asked to perform several deep

squatting dynamic trials in which the squat posture was held for approximately two seconds.

Data were analyzed using Visual3D software (C-Motion Inc., Germantown, MD). The pelvis segment model was based on the CODA algorithm in which hip joint centers are determined from ASIS and PSIS landmarks [2]. Two models were created: one using a pelvis segment defined by the ASIS and PSIS markers in the standing posture, the second defined the pelvis using the ASIS and PSIS landmarks that had been palpated and digitized in the squat position.

Mean three-dimensional hip and sagittal plane lumbosacral joint angles and moments were calculated for the resting position of the same three squat trials for each subject using the two different models; joint angles and moments were averaged across the five subjects, assessed for normal distribution, and compared using a paired samples *t*-test.

## RESULTS AND DISCUSSION

Figure 1 shows the effect of the change in pelvis definition based on palpated anatomical landmarks versus skin markers on three-dimensional hip angles and lumbosacral joint angles.

The decrease in flexion angle at the hip joints for the palpated pelvis model is offset by the increase in lumbosacral flexion when compared to the skin marker model. This exchange in flexion angle at the distal and proximal ends of the pelvis is attributed to the change in orientation of the pelvis segment (modeled as a cylinder) when defined using palpated landmarks instead of skin markers (Fig. 2).

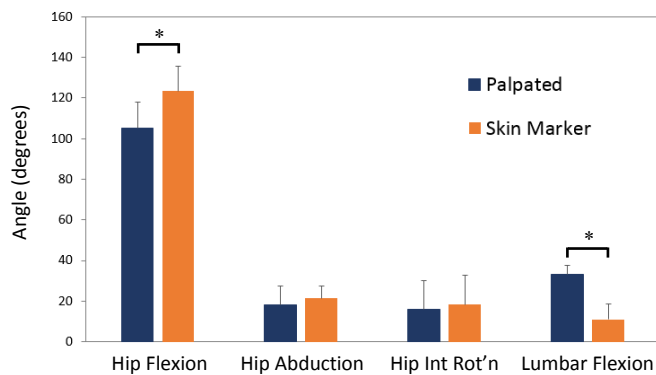


**Figure 1:** Hip and lumbosacral joint angles in the squat position calculated using palpated digitized landmark and skin marker pelvis models (\* $p < 0.05$ ).

Markers placed on PSIS landmarks in standing move superior to the anatomical landmarks in the squat position, generating an artificial anterior tilt of the pelvis segment. Since the positions of the hip joint centers are determined using the ASIS and PSIS landmarks, they are also affected, in turn (slightly) changing the orientation of the thigh segments.

These results are consistent with the findings by Kuo *et al.* [3] who similarly demonstrated hip and lumbar flexion errors in a high-flexed sitting posture due to a superior shift in PSIS markers.

The significant changes observed when comparing joint angles in the sagittal plane were not replicated in the comparison of moments between the two pelvis segment models (Figure 3).

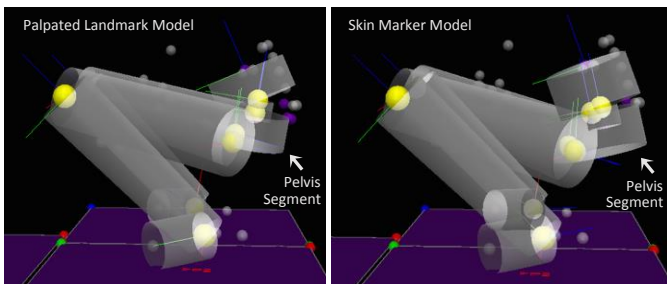


**Figure 2:** Sagittal plane views of the models defined by palpated landmarks (left) and skin markers (right) clearly demonstrate the different orientations of the pelvis segments that account for changes in hip and L5/S1 flexion angles.

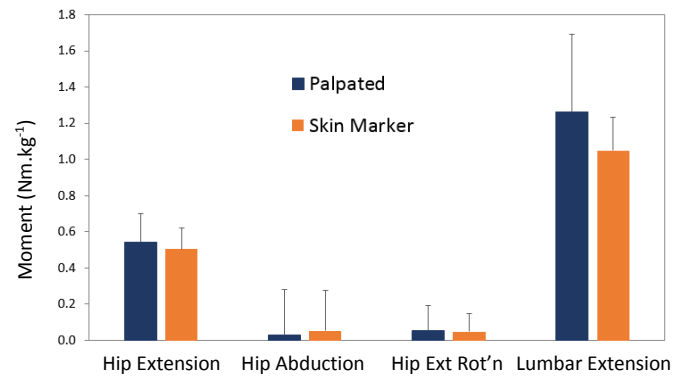


**Figure 3:** Hip and lumbosacral joint moments in the squat position calculated using the palpated digitized landmark and skin marker pelvis models.

This may be due to a relatively consistent center-of-mass position and inertial properties of the pelvis segment between the two models despite its change in orientation.

## CONCLUSIONS

This study has demonstrated how pelvis marker placement is affected by skin motion in a high range-of-motion squatting posture. By comparing two pelvis models generated from standing marker positions and palpated anatomical landmarks in squatting, we can see that hip and lumbosacral angles are significantly altered in the sagittal plane. Although no significant differences were demonstrated in the joint moments, this result should be confirmed with a greater number of subjects. Our findings suggest that skin motion artifact should be taken into consideration primarily during kinematic analysis of high range-of-motion activities.

## REFERENCES

1. Leardini A, et al. *Gait Posture* **21**, 212-225, 2005.
2. Bell AL, et al. *Hum. Movement Sci.* **8**, 3-16. 1989.
3. Kuo Y-L, et al. *Gait Posture* **27**, 264-270, 2008.

## ACKNOWLEDGMENTS

The authors gratefully acknowledge contributions made by Prof. Pat Costigan, the Natural Sciences and Engineering Research Council Canada, Queen's University, MGM Institute of Health Sciences, and the Shastri Indo-Canadian Institute.

# Measurement of Interjoint Pressure in the Midfoot using Novel Sensors

<sup>1</sup> Julia Noginova, <sup>1</sup> Emily Hartley, <sup>1</sup> Matthew Hoch, and <sup>1</sup> Stacie I. Ringleb  
<sup>1</sup> Old Dominion University, Norfolk, VA, USA  
email: sringleb@odu.edu

## INTRODUCTION

Contractile and non-contractile structures within the foot such as ligaments and muscles function to support and provide stability to the bones and joints. Injuries and diseases often cause changes to the loading characteristics of the foot and ankle, such as an increase of peak pressure or shifting of loading to major joints of the foot, such as the talocrural and midfoot joints [1-4]. Understanding how the joints are loaded normally and what changes may occur due to injuries may assist with the development of further prevention and treatment strategies to decrease excess pressure on the joints. In healthy intact feet, the contact pressure in the calcaneocuboid and talonavicular joints increased with an increase in dorsiflexion angle when measured with Tekscan (Tekscan Inc., Boston, MA) 6900 I-scan sensors [2]. This dorsiflexion model closely reflects the weight bearing foot positions found during the late stance phase of the gait cycle. The Novel Pliance Sensors (Novel Inc., Munich, Germany) are also made to be placed inside of a joint. Their pressure sensing technology is based on capacitive transducers and calibration occurs with applied pressure in a standard system, while the Tekscan sensors are made out of semiconductors and recommend a variety of calibration methods based on the application. One of the largest differences between the sensors is that Novel Pliance sensors are much thicker than the Tekscan sensors (1.2 mm vs 0.102 mm thickness, respectively).

Due to our interest in understanding the changes in internal joint pressure that occur with injury and/or disease and their treatments, the goal of this study is to determine if Novel's Pliance sensors measure similar changes in pressures in the calcaneocuboid and talonavicular joints during dorsiflexion, as measured previously with the Tekscan sensors.

## METHODS

A below-knee cadaver specimen with no visible deformities (left foot, female, 65 years old) was fixed into a custom-built device capable of loading the foot while in neutral stance. Minimal amounts of skin and tissue were cut so that a Novel strip sensor could be inserted through the midfoot through an incision on the medial side of the foot (Figure 1). One strip sensor was inserted across both the talonavicular and calcaneocuboid joints, simultaneously, as it was not possible to fit a sensor into the talonavicular joint laterally due to its thickness. The contact pressures were measured across the calcaneocuboid and talonavicular joints while different loading conditions (no load, 10 lbs, 20 lbs) were applied to the top of the foot during different stances (neutral and 30 degrees of dorsiflexion).

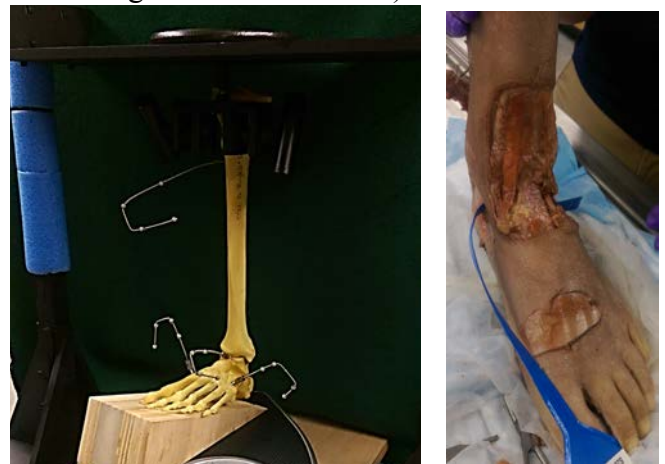


**Figure 1.** a) Custom built ankle positioning and loading device and b) View of Novel strip sensor inserted through the midfoot from the medial side.

The mean and peak pressures of each stance were exported from the Novel Pliance software and plotted for all three load conditions.

## RESULTS AND DISCUSSION

The mean pressure across the calcaneocuboid and talonavicular joints increased minimally when load was applied while the foot was in neutral. However,

while the foot was in dorsiflexion, a greater increase in mean pressure occurred. The largest increase occurred when 10lbs was applied, while a smaller increase occurred at 20 lbs of loading.

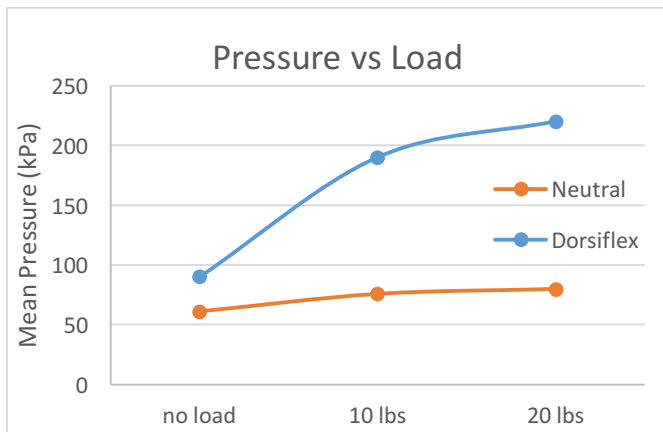


**Figure 2:** Mean pressures recorded during neutral and dorsiflexed stance at three different load conditions.

The peak pressures were reported from the talonavicular (n=11) and calcaneocuboid (n=12) joints with Tekscan I-scan sensors when the tibia was axially loaded to 700 N (157.366 lbs), the Achilles tendon was loaded with 400 N (89.92 lbs) and the posterior tibial tendon was loaded with 200 N (44.96 lbs) of force [2] (Table 1). While the exact pressure values cannot be compared due to significantly different loading conditions, both studies observed an increase in peak pressures from neutral to 30 degrees of dorsiflexion.

The greatest amount of mean contact pressure in the present study occurred when the foot was fully loaded in dorsiflexion compared to when in neutral. The substantial pressure during the late stance of gait while the foot is dorsiflexed is thought to cause serious joint deterioration [2]. At 30 degrees of dorsiflexion, the highest ankle angle seen in normal

gait, the mean pressure in the midfoot is over twice that as seen in neutral stance (Fig. 2). These results support the hypothesis that injuries or diseases that increase pressure can cause further break down of the joints, especially when moving through activities of daily living (e.g., walking).

The Novel Pliance strip sensor provided limitations to measuring pressure in the joints. Due to the thickness of the sensor and limited joint space, the sensor could not be inserted laterally into the joint. Another limitation is due to its current design which includes a grommet for suturing it in place. If one sensors was inserted medially and one laterally, the part of the sensors with the grommets would collide and prevent full insertion of the sensors into the joints. Therefore, our current sensors make it impossible to measure talonavicular and calcaneocuboid joint pressures individually. An additional limitation within the study was that joint pressures were measured in neutral and dorsiflexion only. Future studies should consider investigating the joint pressures within a more global range of possible foot positions (i.e., planterflexion, inversion, eversion).

## CONCLUSIONS

The Novel sensors can be used to measure pressure across the talonavicular and calcaneocuboid joints. The limitation being that the calcaneocuboid and talonavicular joint pressures were not isolated. In future work, different degrees of dorsiflexion (0, 10, 20, 30) and additional loading will be investigated.

## REFERENCES

1. Lee, DG et al. Foot Ankle Intr 30,767-772, 2009.
2. Jung, HG et al. Foot Ankle Intr 28,103-108, 2007.
3. Suckel, A et al. BMC Musculoskelet Disord 8, 1-9, 2007.
4. Momberger, N et al. Foot Ankle Intr 21,730-735, 2000.

**Table 1:** Comparison of peak pressure between that found in Jung et al and this study, where the medial and lateral sides of the Novel sensor approximated the talonavicular and calcaneocuboid joints, respectively.

Degrees	Joint Peak Pressures (kPa)			
	Talonavicular [2]	Calcaneocuboid [2]	Medial	Lateral
0 (neutral)	678.3	493.8	220	100
30 (dorsiflexion)	800.5	702.8	240	200

# A Novel Image-Based Non-Invasive Tracking Technique for In-Vivo Surface Kinematics of the Temporomandibular Joint

Xiangjun Hu<sup>1</sup>, Xiaoqi Zhong<sup>2</sup>, Pei Shen<sup>2</sup>, Jisi Zheng<sup>2</sup>, Shaobai Wang<sup>3</sup>, Kerong Dai<sup>1,2</sup>, Shanyong Zhang<sup>2</sup>, Tsung-Yuan Tsai<sup>1</sup>

<sup>1</sup> School of Biomedical Engineering, Shanghai Jiao Tong University, Shanghai, China, <sup>2</sup> Shanghai Ninth People's Hospital, Shanghai, China, <sup>3</sup> Key Laboratory of Exercise and Health Sciences of Ministry of Education, Shanghai University of Sport, Shanghai, China  
email: tytsai@sjtu.edu.cn

## INTRODUCTION

Temporomandibular joint (TMJ) is the only joint in the maxillofacial region. It with the surrounding muscles is responsible for various fundamental movements, e.g. chewing, biting, clenching, and yawning<sup>[1, 2]</sup>. Measurement of the TMJ kinematics facilitates diagnoses of TMJ disorder/disease and assessment of treatment effects. However, few studies directly assess in-vivo TMJ kinematics during functional activities. This study aimed to propose a new image-based tracking technique for measurement of in-vivo 6 degrees-of-freedom (6-DOF) TMJ kinematics during maximum mouth opening and closing movement (MOCM) and to evaluate the symmetry of mandibular movement in a typical health subject.

## METHODS

In this Institutional Review Board approved study, a healthy individual (Male, 23 years, BMI 21.5) with no history of any surgical, maxillofacial trauma and orthodontic treatment was recruited. Two custom-made stands for fixation of 6 infrared retro-reflective markers to the upper and lower jaws were 3D printed (Fig. 1A) with Medvance PANGU 4.1 (Meditool, Shanghai, China). The subject with the two 3D printed stands then received a cone-beam computer tomography (CBCT, i-CAT, Imaging Sciences International, Hartsfield, PA, USA) scan for the creation of surface models of temporal bone, mandible and the markers. The local coordinate systems were defined using the mandibular bony landmarks (Fig. 1B)<sup>[3]</sup>. The TMJ motion was tracked via the markers using a portable motion capture system (V120:Trio, Optitrack, NaturalPoint,

Inc., USA) during MOCM (Fig. 2). The 3D TMJ angles and the movement trajectories of the mandibular head centers (MHC), and central incisor (CINC) were calculated in MATLAB (The MathWorks, Natick, USA).

## RESULTS

The TMJ rotations showed an asymmetric pattern between opening and closing paths (Fig. 1C). The maximum mandibular axial rotation angle was up to 4.5°. The maximum mandibular title angles were 3.2° and 1.7° for closing and opening movement, respectively. The translations of CINC were apparently asymmetric between opening and closing paths (Fig. 1D). The trajectories of the bilateral MHC were found to be largely asymmetric during MOCM (Fig. 1E&F). The mouth closing movement did not follow the kinematic path during opening. The return trajectories of the left MHC in anterior/posterior and elevation/depression directions were similar to the opening, while the right MHC differed widely.

## DISCUSSION

This study successfully demonstrated the feasibility of the novel CBCT-based tracking technique for quantification of the TMJ kinematics. This technique allowed non-invasive determination of in-vivo 6-DOF TMJ motion and provided detailed surface kinematics of the condyles and opposing fossae. The obvious asymmetric mandibular motion was observed between the mouth opening and closing movement, showing complex TMJ motion characteristics and the importance of individualized medicine for TMJ. Further studies are required to

evaluate the accuracy and precision of this technique before extensive clinical applications.

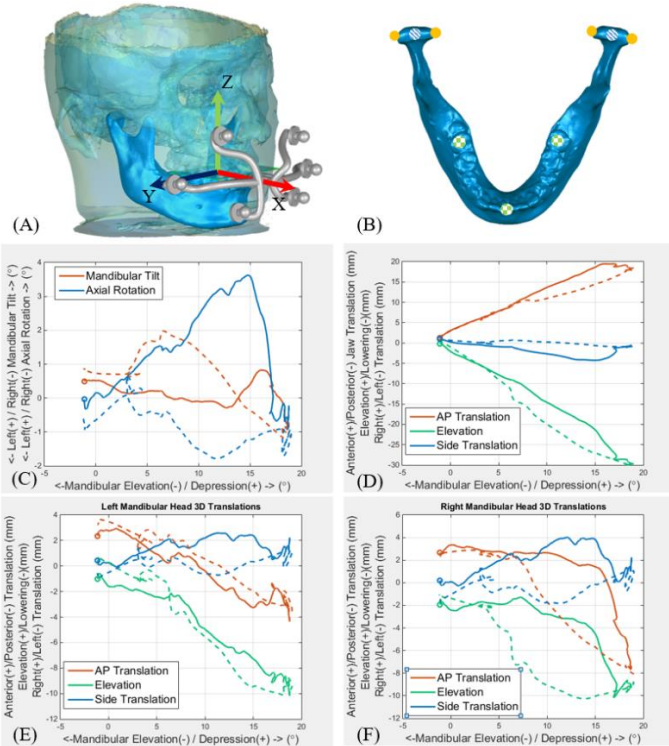


**Figure 1.** (A) CBCT-based 3D models of skull and mandible with anatomical coordinate systems and two 3D printed stands for fixation of 6 infrared reflective markers, (B) Bony landmarks for construction of anatomical coordinate system of the mandible, (C) TMJ rotations and tilts against mandibular elevation/depression, and (D) 3D translations of the central incisor against mandibular elevation/depression. 3D translations of the (E) left and (F) right mandibular head with respect to the mandibular elevation/depression. The obvious asymmetric mandibular motion was observed between the mouth opening (solid lines) and closing (dashed lines) movement.

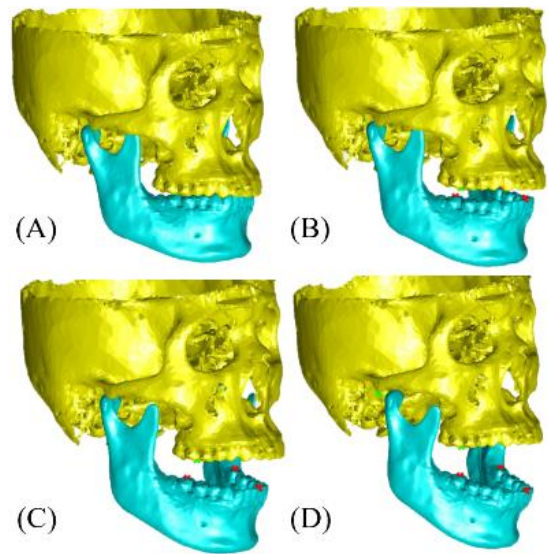


**Figure 2.** 3D TMJ movement tracked using image-based non-invasive tracking technique during maximum mouth opening movement. (A) 0%, (B) 33%, (C) 66%, and (D) 100% of mouth opening movement.

## REFERENCES

1. Kim YK, Kim SG, Kim JH, et al. J Craniomaxillofac Surg 2013, 4(15):e83-e86.
2. Ueki K, Nakagawa K, Marukawa K, et al. Eur J Orthod, 2010, 32(5):522-529.
3. CC Chen, CC Lin, TW Lu, C Hao, YJ Chen. J Dent Sci., 2013, 8(2):151-159.

# THE RELIABILITY OF ULTRASOUND IMAGING TO IDENTIFY CARTILAGE THICKNESS AMONG CLINICAL POPULATIONS

<sup>1</sup> Dylan Barrow, <sup>2</sup> Karen J Mickle, <sup>3</sup> Max R Paquette, <sup>1</sup> Sarah P Shultz

<sup>1</sup> Massey University, Wellington, New Zealand

<sup>2</sup> Victoria University, Melbourne, Australia

<sup>3</sup> University of Memphis, TN, USA

Email: d.barrow@massey.ac.nz

## INTRODUCTION

A reduction in articular cartilage thickness has been identified as a risk factor for the development of osteoarthritis (OA) (3). Magnetic resonance imaging (MRI) has typically been used to determine cartilage thickness in clinical populations. While MRI scans provide detailed images of cartilage thickness, they are expensive, require specialist equipment and extensive training to administer. Ultrasound imaging has emerged as a less invasive, more cost-effective alternative to MRI that can be used to assess cartilage thickness (2).

While ultrasound has been shown to be reliable in healthy and osteoarthritic populations (1, 4), its efficacy is less certain in other clinical populations. Yet, this tool could be extremely valuable in obese and Type 2 diabetic populations, who have an increased risk for developing OA but may currently be asymptomatic. The reliability of ultrasonography is particularly important in these cohorts, due to the increase in soft tissue surrounding the joints.

Therefore, the purpose of this study is to investigate the reliability of ultrasound scans in determining cartilage thickness in a clinical population. The ability to use ultrasound scans to determine articular cartilage thickness would make this measurement more accessible to researchers thus helping to provide further insight into changes in cartilage thickness in more research. We believe that ultrasound scans will be a reliable method in investigating cartilage thickness in clinical populations.

## METHODS

Six healthy (Age  $37 \pm 14$  yrs;  $78.08 \pm 6.15$ kg) and six Type II diabetics ( $56 \pm 2$  yrs;  $99.84 \pm 13.94$ kg) participated in the reliability assessments, which were conducted in the Sport and Exercise Science

Lab at Massey University, Wellington. Ultrasound assessment techniques were adapted from EULAR guidelines (2). To determine femoral cartilage thickness, participants were required to lay supine with their knee bent as much as possible. While full knee flexion was encouraged, it was not required, as some participants found this position difficult to achieve due to increased thigh circumference. Ultrasound scans were taken using a portable ultrasound system (Sonosite MicroMaxx, USA) equipped with a 13-6 MHz bandwidth transducer. The ultrasound probe was placed transverse to the leg and perpendicular to the bony surface, just superior to the proximal aspect of the patella. Three images were captured on the right leg of each participant during one testing session. The probe remained in the selected spot for each image that was captured. The assessment was repeated within 24-36 hours later.



**Figure 1:** Ultrasound image of femoral articular cartilage: showing medial condyle, intercondylar notch, and lateral condyle.

Cartilage thickness was measured from the thin hyper-echoic line at the cartilage-bone interface using Image J software. Measurements were taken at the medial condyle, intercondylar notch, and the

lateral condyle (Fig 1). The measurements for each of the three trials per site were averaged and intra-class coefficients (ICC) were calculated to assess inter-day reliability (SPSS, Version 24.0. Armonk, NY: IBM Corp). An independent t-test was also performed to compare the mass of each participant group. Statistical significance was set at  $p < 0.05$ .

## RESULTS AND DISCUSSION

ICC values can be found in Table 1. Scans for both populations showed high reliability between days (i.e.,  $ICC > 0.7$ ). The medial condyle in the clinical group had the lowest ICC (i.e., 0.797) but was still above the threshold for high reliability. These findings suggest that measurements of femoral cartilage thickness from images taken from diagnostic ultrasound have high day-to-day reliability in both healthy and diabetic patients. The ICC results found in this study were greater than other reliability studies such as that by Abraham et al (1) where ICC values of 0.42 – 0.68 were reported.

Finally, an independent t-test showed that the clinical group carried more mass than the healthy control group ( $p = 0.015$ ). Where it may have been thought that excessive mass and therefore excessive fatty tissue would inhibit accurate ultrasound measurements, this study provides evidence that ultrasound measurements were of similar reliability in the clinical group when compared to the healthy group. Given that overweight individuals are at greater risk for joint disease such as OA, reliable ultrasound methods could provide a more convenient assessment of OA progression.

Average Measures	ICC		
	Medial	Notch	Lateral
<b>Healthy Control</b>	.989	1.000	.974
<b>Clinical Group</b>	.797	.990	.969

**Table 1:** Intraclass correlation coefficient results for the healthy control and clinical group.

## CONCLUSIONS

The purpose of this study was to determine whether ultrasound imaging is a reliable tool in assessing

cartilage thickness in clinical populations. The current results provide evidence that ultrasound imaging is a reliable assessment tool to measure articular cartilage thickness amongst healthy adults and diabetic patients. Future studies should assess the reliability of ultrasound imaging for cartilage thickness measures in obese adults considering that obesity is a major risk factor for knee osteoarthritis.

## REFERENCES

1. Abraham AM, Goff I, Pearce MS, Francis RM, Birrell F. Reliability and validity of ultrasound imaging of features of knee osteoarthritis in the community. *BMC Musculoskeletal Disorders*. 2011;**12**:70.
2. Backhaus M, Burmester GR, Gerber T et al. Guidelines for musculoskeletal ultrasound in rheumatology. *Ann Rheum Dis*. 2001;**60**:641-9.
3. Edd SN, Favre J, Blazek K, Omoumi P, Asay JL, Andriacchi TP. Altered gait mechanics and elevated serum pro-inflammatory cytokines in asymptomatic patients with MRI evidence of knee cartilage loss. *Osteoarthritis Cartilage*. 2017.
4. Spannow AH, Pfeiffer-Jensen M, Andersen NT, Stenbog E, Herlin T. Inter -and intraobserver variation of ultrasonographic cartilage thickness assessments in small and large joints in healthy children. *Pediatric Rheumatology Online J*. 2009;**7**:12.

# OPTIMIZING A FORCE SENSITIVE RESISTOR SYSTEM FOR WHEELCHAIR INSTRUMENTATION

<sup>1</sup>Cesar Lopez, <sup>1,2</sup>Beth Cloud, <sup>1</sup>Andrew Thoreson, and <sup>1</sup>Kristin Zhao

<sup>1</sup>Rehabilitation Medicine Research Center, Department of Physical Medicine and Rehabilitation, Mayo Clinic, Rochester, MN, USA

<sup>2</sup> Program in Physical Therapy, Mayo Clinic School of Health Sciences, Mayo Clinic College of Medicine and Science, Rochester, MN, USA  
email: zhao.kristin@mayo.edu

## INTRODUCTION

Individuals with spinal cord injury have been reported to have upper limb pain in rates as high as 70% [1]. It is believed that this high prevalence of pain is related to an increased reliance on the upper limbs for mobility. Work is ongoing to understand what specific activities or conditions are most detrimental. This includes an evaluation of both kinematics and forces exerted during tasks.

Activities performed from a wheelchair base, particularly transfers and other weight bearing activities, may be performed with variable hand positioning (e.g. one person may place their hands on the armrest and another on the frame of the wheelchair). This variability in technique necessitates a force sensing approach that can be applied to these various surfaces.

The purpose of this study was to optimize instrumentation of wheelchair components with an array of force sensing resistors (FSR's). We hypothesized that agreement between the FSR array and the gold standard measurements would be dependent on array configuration and the hardness of the surface to which they are applied.

## METHODS

Four circular 12.5-mm diameter FSR's (Interlink 402) were connected to a custom-built signal conditioner (LM358N operational-amplifier with 500  $\Omega$  resistors powered by a 5V regulated power supply). Each FSR was laid on a rigid surface and calibrated with a series of reference masses (500, 1000, 2000, and 7000 grams). FSR's were applied to four different surfaces: a rigid, flat wood plate; a

vinyl-covered wheelchair armrest; and a vinyl-covered cushion foam and a second vinyl covered foam of lower stiffness. Surfaces were selected to replicate components with which wheelchair users may interact during daily activities including manipulating objects and load transfers. FSR's were applied to the surface in three different patterns: straight line (Fig 1A), staggered (Fig 1B), and 4-corners (Fig 1C).

Additionally, FSR's were attached to a 25-mm diameter PVC tube in both straight line and staggered patterns (Fig 1D and 1E, respectively). All materials were mounted on top of a load cell (MLP-150, Transducer Techniques) which was used to capture actual loading applied (Figure 2A).

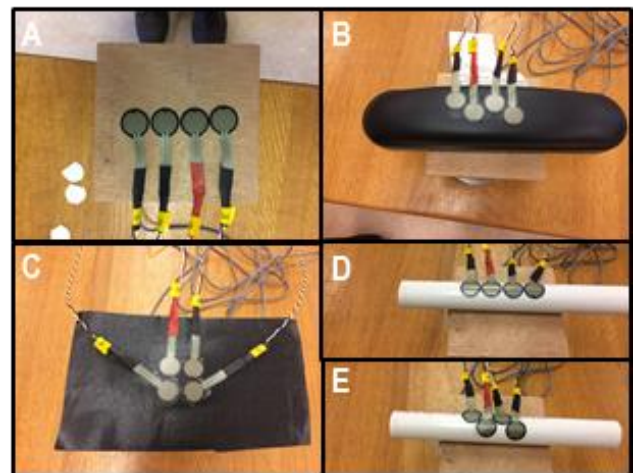


**Figure 1:** Representative FSR configurations: A) straight line on rigid, wood surface, B) staggered on wheelchair armrest, C) 4-corners on cushioned surface, D) straight line on pipe & E) staggered on pipe.

Force measurements were collected from three subjects, each exerting self-directed low, medium,

and high pressures for three trials to each configuration (Fig 2B). Data from each FSR and the load cell were captured simultaneously at a sample rate of 120 Hz.

For each trial, the peak force from the sum of all FSR's was selected, which were compared with the peak load from the gold standard load cell data. For each configuration the Pearson correlation coefficient was assessed, a straight line was fit to the data with linear regression and associated coefficients of determination were calculated, and Bland-Altman plots of agreement were generated [2].

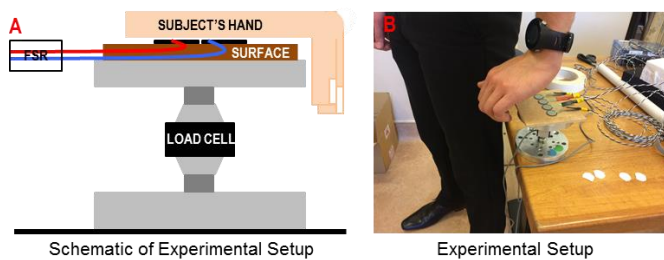


**Figure 2:** A) Schematic of experimental setup B) subjects applying load to instrumented surfaces.

## RESULTS AND DISCUSSION

The Pearson correlation coefficient ranged between 0.63 and 0.98 over all configurations, with the straight line configuration most consistently showing high correlations over the different test surfaces. Slopes of best fit lines ranged between 0.19 and 0.54; with the straight line pattern consistently performing better than other configurations across all test surfaces (Table 1). Bland-Altman plots indicated the best agreement between FSR and load cell data occurred for straight configuration as the smallest range of 95% limits of agreement over different test surfaces was observed.

**Table 1:** Statistical results for all configurations. Data displayed as Pearson correlation coefficient (PCC), slope (m), and coefficient of determination ( $R^2$ ).

	WOOD			WHITE FOAM			BLACK FOAM			ARMREST			PIPE		
	PCC	m	$R^2$	PCC	m	$R^2$	PCC	m	$R^2$	PCC	m	$R^2$	PCC	m	$R^2$
Straight	0.88	0.43	0.77	0.79	0.32	0.62	0.80	0.27	0.64	0.98	0.46	0.97	0.98	0.54	0.95
Stagger	0.90	0.39	0.80	0.63	0.19	0.40	0.82	0.26	0.67	0.98	0.42	0.96	0.96	0.50	0.91
4-corner	0.81	0.42	0.65	0.64	0.19	0.40	0.84	0.35	0.70	0.86	0.35	0.73	<i>not tested</i>		

The analysis shows that, at most, the FSR array is seeing just under 50% of the applied load. One reason for this may be that the FSR arrays were not large enough or dispersed appropriately to capture all contact of the subjects' hands with the surface. The straight line configuration appears to have performed best in this respect, but addition of sensors extending the capture area of this pattern may improve results. When applied to piping, the straight line patterns appear to perform slightly better than the staggered, but only just over 50% of the applied load is captured.

Despite the sensors consistently not capturing the full load applied, correlations for most configurations were quite strong, supporting use of this system as a qualitative, if not quantitative tool.

## CONCLUSIONS

The straight configuration of FSR's consistently correlated well with the applied loading over all surfaces tested, thus we feel it can be used for qualitative assessment of reaction forces of select tasks of wheelchair users.

## REFERENCES

1. Dyson-Hudson TA, Kirshblum SC. *J Spinal Cord Med.* **27**, 4-17, 2004.
2. Altman DG, et al. *The statistician* **32**, 307-317, 1983.

## ACKNOWLEDGMENTS

This work was possible by funding from the Craig H. Neilsen Fund for Spinal Cord Injury Care and Research honoring Robert D. Brown, Jr., M.D.

# 3D SCANNING: AN INNOVATIVE METHOD TO PERSONALIZE BODY SEGMENT PARAMETER CALCULATIONS

Marco Avalos, Mohammad Hasan, Young-Hoo Kwon

Biomechanics Laboratory, Texas Woman's University, Denton, Texas, USA  
email: mavalos1@twu.edu, web: <http://www.twu.edu/kinesiology/biomechanics.asp>

## INTRODUCTION

Motion analysis is commonly used in biomechanics for calculation of various kinematic and kinetic variables. A pre-requisite of an accurate kinetic analysis in motion analysis is an accurate estimation of the body segment parameters (BSP) such as masses, center-of-mass (CM) locations, and principle moments of inertia (MOI) of the segments. [1]. Models to determine these parameters primarily relied on the use of cadavers [2], or technology that results in high costs and the parameters obtained are often not generalizable. Segmentation of the human body into various segments and estimation of the individualized BSPs requires a large number of anthropometric parameters [3]. Modeling of body segments as cascades of simple geometric shapes and use of accompanied equations [4] allows calculation of individualized BSP.

In this study, we propose the use of 3D scanning as a method of measurement for the body segments on a model consisting of 16 segments and a total of 61 geometrical shapes.

## METHODS

Markers were placed on nine female participants ( $20.88 \pm 1.46$  years old) according to the body model (Figure 1). This model consist is mainly composed by elliptical solid and elliptical columns. Upper and lower body scans were performed using a 360° rotating display stand and a 3D scanner (Kinect, Microsoft Corp., Redmond, WA). The upper and lower scans were merged into one and digitally measured using NetFabb 7.0 (Parsberg, Germany). Assuming symmetry, unilateral manual measurements were also collected. Medirolateral length, circumference and height of segmental shapes were taken 3 times. The segmental BSP's

were calculated using a MatLab code. Intra-class correlation coefficient (ICC) of the total mass of the 3D scan, and manual and real measurement were estimated through SPSS v.22.

## RESULTS

The ICC (0.927) between the two measuring methods and the real total mass were consistent in all the participants. Measurements obtained using 3D scan were consistently higher than the real mass, while measurements obtained using the manual method were consistently lower than the real mass. The upper body measurements show no significant differences ( $p=0.262$ ) when using either the 3D scan method or the manual method. However, both methods show significant differences in the lower body ( $p=0.023$ ) and torso ( $p<0.001$ ) measurements.

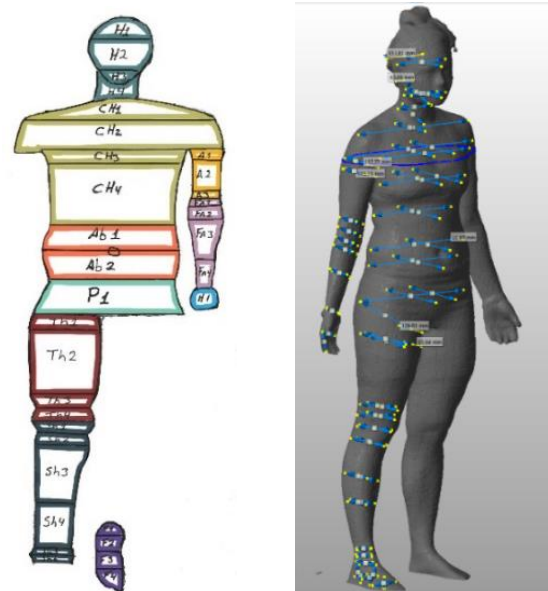


**Figure 1:** a) Proposed body model segmentation, b) 3D scan measurements on participant according to proposed body model.

## DISCUSSION

The 3D scan camera used was adapted from first-generation videogame equipment, new technology cameras would allow for better quality imaging. Scanning participants in one swipe would allow better definition and avoid possible distortion created while merging the images. When measuring the circumferences, it was necessary to tighten the measuring tape in order for it not to move from the marker line. This slight compression may explain the reduction in volume and mass of each segment. The

female gynoid body composition may explain why the measurement around the torso and lower extremities resulted in decreased volume when taking circumferential measurements manually.

## REFERENCES

1. Drilli, et al. *Art Limbs*, **8(1)**, 44-66, 1964.
2. Clauser, et al. *Antioch Coll Yellow Springs*, OH, 1969.
3. Hatze, *J Biomech*, **13(10)**, 833-843, 1980.
4. Zatsiorsky, *Contemporary Problems of Biomech*, 272-291, 1980.

**Table 1:** Participants average mass in kilograms. (WB = Whole body mass, UExt = Mass of upper extremities, LExt = Mass of lower extremities, Torso = Torso mass, \_Real = Real measurement taken on data collection day, \_3D= Estimation using 3D scan method, \_Man= Estimation using manual method)

	WB_Real	WB_3D	WB_Man	UExt_3D	UExt_Man	LExt_3D	LExt_Man	Torso_3D	Torso_Man
<b>Average</b>	55.24	59.09	50.14	4.19	3.96	23.79	21.22	31.11	24.97
<b>St. Dev.</b>	7.93	7.11	7.31	0.59	0.88	3.34	3.22	3.95	3.48

# DAY-TO-DAY RELIABILITY OF GAIT CHARACTERISTICS AND COORDINATION IN RATS

<sup>1</sup> Peter C. Raffalt, <sup>1</sup> Louise R. Nielsen, <sup>2</sup> Stefan Madsen,  
<sup>2</sup> Laurits Munk Højberg, <sup>2</sup> Jacob Wienecke and <sup>1</sup> Tine Alkjær

<sup>1</sup> Department of Biomedical Sciences, University of Copenhagen, Copenhagen, Denmark

<sup>2</sup> Department of Nutrition, Exercise and Sports, University of Copenhagen, Copenhagen, Denmark  
email: raffalt@sund.ku.dk

## INTRODUCTION

Animal models (e.g. rodents and cats) are widely used in applied research of various neurological diseases (e.g. cerebral palsy). Such diseases will often cause impaired gait function. Thus, reliable quantification of the animal gait pattern is vital for the assessment of the functional impact of the diseases and the evaluation of rehabilitation protocols. Gait pattern in rodents can be quantified using kinematic analysis of the stride characteristics (e.g. stride/step length, stride/step time, step width) and lower limb joint angles (1). While these measures provide valuable information of the movement pattern, they do not quantify the inter-segment coordination. In human locomotion research, lower limb segment coordination and coordination variability have been quantified using continuous relative phase (CRP) and deviation phase (DP), respectively (2). Applying these measures in gait analysis of rodents could provide additional information of the impact of pathology on the limb coordination during locomotion.

The present study investigated the day-to-day reliability of selected gait parameters in rats during walking at three different speeds. In addition, the CRP and DP were introduced as outcome measures of the lower limb coordination pattern and the coordination variability.

## METHODS

Twenty-six Sprague Dawley rats with a body mass of  $437 \pm 61$ g were included in the present study. Sagittal plane lower limb 2D kinematics were recorded using one infrared camera (Qualisys) operated at 120 Hz. After careful shaving of the left hind limb, four reflecting markers were attached on bone landmarks (ilia crest, greater trochanter, knee

joint center, lateral malleolus and the head of the 5<sup>th</sup> metatarsal bone). On two separate days, each rat walked on a motorized treadmill at three different speeds (8 m/min, 12 m/min and 16 m/min) for at least 45 seconds. Trials were accepted when 15 successful strides were obtained. The following variables were extracted from the kinematic data: stride length, swing phase duration, stance phase duration, hip, knee and ankle joint angle range of motion (ROM), mean CRP and mean DP for the shank-thigh coupling and paw-shank coupling (figure 1).

In order to estimate the day-to-day reliability, intra-class correlation (ICC 1.1) was applied. This ICC assumes that all within subject variability is due to measurement error. In addition, the absolute reliability was quantified by the square root of the mean square error assessed by a two way ANOVA. The statistical analyses were conducted in SPSS. ICC above 0.75 were considered excellent, between 0.60 and 0.74 good, between 0.40 and 0.59 fair and below 0.40 poor.

## RESULTS AND DISCUSSION

The ten investigated variables of the present study included three different stride characteristics (stride length, swing phase duration and stance phase duration), three different joint angle parameters (hip, knee and ankle joint angle ROM) and four coordination measures (shank-thigh mean CRP, paw-shank mean CRP, shank-thigh mean DP and paw-shank mean DP). Across the three walking speeds, joint angle parameters appeared to have good or excellent reliability in more cases (6 out of 9) compared to stride characteristics (4 out of 9) and coordination measures (4 out of 10) (table 1).

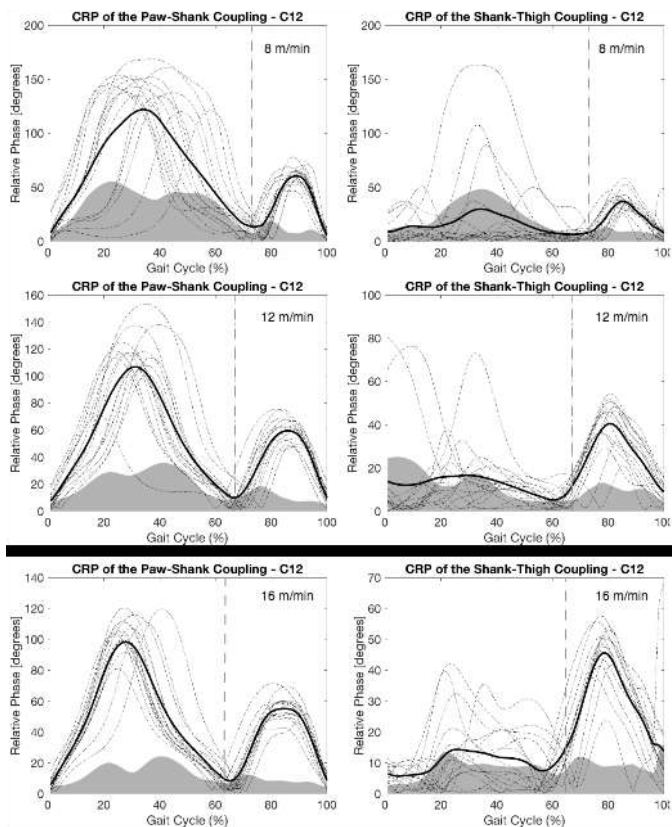


**Figure 1:** CRP of the paw-shank and shank-thigh coupling (average CRP curve: solid, each stride: dashed) for one rat (C12) and DP (gray area). Vertical dashed line indicate paw off. Mean CRP was calculated as the mean of the average CRP curve and mean DP was calculated as the mean of the DP across the gait cycle.

Furthermore, across walking speeds stride characteristics appeared to have good reliability in

more cases compared to the coordination measures (table 1).

Based on the measurement error (table 1), speed did not appear to influence the absolute reliability of the investigated parameters.

## CONCLUSIONS

The present study assessed the day-to-day reliability of a number of gait pattern parameters in rats during walking at different speeds. Based on the result, it can be concluded that joint angle parameters in general had good reliability in more cases compared to stride characteristics and coordination measures.

The absolute size of the day-to-day reliability includes both methodological inaccuracies (e.g. skin movements and marker placement) and the inherent biological variation in the rat gait pattern and does not appear to be influenced by walking speed.

Although, the introduced coordination measures CRP and DP potentially provide valuable information of the coordination pattern during walking in rats, interpretation of the measures should be made with caution in light of the reported reliability of the present study.

## REFERENCES

1. Lakes EH. et al. *Osteoarthritis Cartilage* **24**, 1837-1849, 2016.
2. Hamill J. et al. *Clin Biomech* **14**, 297-308, 1999.

**Table 1:** Intraclass correlation (ICC) and measurement error for each variable at the three walking speeds.

Walking speed	ICC (1,1)			Measurement error		
	8m/min	12m/min	16m/min	8m/min	12m/min	16m/min
Stride length	0.66	0.55	0.72	0.63 (cm)	0.72 (cm)	0.51 (cm)
Swing phase duration	0.63	0.39	0.52	0.01 (s)	0.01 (s)	0.01 (s)
Stance phase duration	0.34	0.42	0.60	0.06 (s)	0.04 (s)	0.02 (s)
Hip angle ROM	0.80	0.48	0.60	2.01 (°)	3.37 (°)	3.09 (°)
Knee angle ROM	0.62	0.61	0.53	4.06 (°)	3.61 (°)	3.97 (°)
Ankle angle ROM	0.71	0.71	0.67	4.48 (°)	3.91 (°)	4.12 (°)
Shank-thigh mean CRP	0.53	0.72	0.53	5.19 (°)	3.29 (°)	4.55 (°)
Paw-shank mean CRP	0.52	0.64	0.73	6.00 (°)	3.53 (°)	3.24 (°)
Shank-thigh mean DP	0.42	0.65	0.43	5.81 (°)	3.58 (°)	4.87 (°)
Paw-shank mean DP	0.48	0.15	0.06	3.64 (°)	3.73 (°)	4.21 (°)

# RELIABILITY OF BIOMECHANICAL VARIABLES ASSOCIATED WITH KNEE OSTEOARTHRITIS DURING WALKING

Jillian L. Hawkins, Richard A. Brindle, Clare E. Milner

Drexel University, Philadelphia, PA, USA  
email: jh3266@drexel.edu

## INTRODUCTION

Knee osteoarthritis is one of the most prevalent musculoskeletal diseases, affecting 14 million people in the United States [1]. Osteoarthritis is associated with difficulty in physical function and poor quality of life [2]. Specifically, knee osteoarthritis affects walking and daily movement.

Biomechanical variables measured during walking are often studied in individuals with or at risk for knee osteoarthritis and compared to healthy controls. In particular, peak knee flexion and adduction angles and peak knee extension and abduction moments have been measured previously and differences between knee osteoarthritis and control groups were reported [3,4]. However, the measurement errors associated with the dependent variables were not provided.

The purpose of this study was to test within-day and between-day reliability and minimum detectable difference (MDD) of knee variables often associated with knee osteoarthritis. We hypothesized that peak knee flexion angle, peak knee adduction angle, peak internal knee extension moment, and peak internal knee abduction moment during walking would have good or excellent within-day and between-day reliability.

## METHODS

Eighteen healthy adult men between 18 and 50 years old participated in this study. All participants ran at least 10 miles per week for a year or more, were uninjured at the time of testing and did not have a previous severe lower extremity injury. Prior to participating, each participant gave his written informed consent.

An eight-camera motion capture system recorded three-dimensional kinematics at 200 Hz in synchronization with a force plate which recorded ground reaction forces at 1000 Hz. Participants changed into athletic shorts and had their height and weight measured. Retro-reflective markers were attached to the participants' pelvis and lower extremity for defining and tracking segments. Participants wore standard laboratory footwear and a static standing trial was recorded. Following the static trial, anatomical markers were removed and five good walking trials were collected. Walking speed was standardized to  $1.25\text{ms}^{-1}$  ( $\pm 5\%$ ). All participants returned to the laboratory a second time at least 5 days after their first visit, and the walking gait analysis protocol was repeated.

Data were processed using rigid body analysis software. A 20 N vertical ground reaction force threshold indicated the beginning and end of the stance phase. Raw data were filtered at 6 Hz using a low pass 4<sup>th</sup> order Butterworth filter. Knee angles were calculated using the joint coordinate system, and internal joint moments were calculated using inverse dynamics. Peak values during the first 60% of stance were determined using custom software.

Within-day and between-day reliability were analyzed using intra-class correlation coefficients ( $\text{ICC}_{(1,1)}$  and  $\text{ICC}_{(3,5)}$ , respectively). The standard error of measurement (SEM), and MDD values for 95% of a normal distribution were also calculated. Reliability was considered to be excellent if the ICC was greater than 0.90, and good if the ICC was greater than 0.75 [5].

## RESULTS AND DISCUSSION

The purpose of this study was to test within-day and between-day reliability and MDD of variables

associated with knee osteoarthritis. Our hypotheses were supported by the results as all variables had either good or excellent within-day and between-day reliability. (Table 1).

Within-day and between-day MDD values for all variables of interest were about the same. Within-day reliability indicates variability within the individuals measured, such as differences in stride-to-stride movements. Since the data were all collected within the same session, the effect of the rater is minimized. Between-day reliability reflects the reliability of the rater in placing markers between sessions in addition to stride-to-stride and day-to-day differences in the individuals measured. Between-day MDD values can be used to interpret differences in interventional or longitudinal data.

The between-day reliability of several of the variables of interest in healthy young adults was reported recently [6]. The ICCs and MDDs for peak knee flexion angle, extension moment and abduction moment were comparable to our results. Unfortunately, magnitude of these variables were not reported, so we cannot confirm that the peaks are comparable. We have extended the previous findings by reporting the reliability and MDD of peak knee adduction angle, plus the within-day reliability and MDD of all variables of interest. The agreement with existing literature for the common variables is encouraging and suggests that the additional findings we report are also representative of young healthy adults. Thus, we suggest that these findings can be used in future power calculations

for these variables in healthy young men. We anticipate that the findings may be extended to healthy young women as well, because variability during walking is similar in healthy young men and women [7]. Furthermore, the previous reliability study reported on a group of men and women with similar findings to the present study for the common variables [6]. However, these data may not generalize to reliability in other populations, such as older adults and individuals with knee osteoarthritis. We suggest that future studies should determine reliability and MDD using samples representative of these populations.

## CONCLUSIONS

Biomechanical variables often studied in association with knee osteoarthritis during gait have good to excellent within-day and between-day reliability. The MDD values can be used to inform future studies in healthy young men. Caution should be used in extending these data to other populations.

## REFERENCES

1. Deshpande et al. *Arthritis Care Res* 1-31, 2016.
2. Alkan et al. *Mod Rheumatol* **24**,166-171, 2014.
3. Kaufman et al. *J Biomech* **34**, 907-915, 2001.
4. Kumar et al. *Osteoarthritis Cartilage* **21**, 298-305, 2013.
5. Portney & Watkins. *Foundations of Clinical Research* Pearson Education, Inc., 2009.
6. Wilken et al. *Gait Posture* **35**, 301-307, 2012.
7. Barrett et al. *J Motor Behav*, **40**, 62-70, 2008.

**Table 1:** Reliability (ICC) and minimum detectable difference (MDD) for knee variables of interest

	First visit	ICC <sub>(1,1)</sub> (CI)	Within-day MDD (SEM)	Second visit	ICC <sub>(3,5)</sub> (CI)	Between-day MDD (SEM)
Peak knee flexion angle (°)	15.5 (6.3)	0.88 (0.78-0.95)	6.0 (2.2)	15.0 (7.2)	0.90 (0.74-0.96)	5.8 (2.1)
Peak knee adduction angle (°)	1.9 (3.1)	0.97 (0.94-0.99)	1.6 (0.6)	2.0 (2.6)	0.93 (0.81-0.97)	2.1 (0.8)
Peak knee extension moment (Nm/kg)	0.50 (0.24)	0.82 (0.68-0.92)	0.30 (0.11)	0.46 (0.30)	0.85 (0.60-0.94)	0.29 (0.11)
Peak knee abduction moment (Nm/kg)	0.50 (0.16)	0.94 (0.89-0.98)	0.10 (0.4)	0.50 (0.15)	0.95 (0.87-0.98)	0.10 (0.03)

CI – confidence interval; SEM – standard error of measurement

# RELIABILITY OF RETROREFLECTIVE MARKERS IN MEASURING SAGITTAL SPINE CURVATURE AND PELVIC TILT AND COMPARISON WITH NON-RADIOGRAPHIC METHODS

<sup>1,2</sup> Seyed Javad Mousavi, <sup>1</sup> Rebecca Tromp, <sup>1,3</sup> Julie Tevenan, <sup>1,2</sup> Dennis E. Anderson

<sup>1</sup> Beth Israel Deaconess Medical Center, Boston, MA, USA; <sup>2</sup> Harvard Medical School, Boston, MA, USA;

<sup>3</sup> Worcester Polytechnic Institute, Worcester, MA, USA

email: smousavi@bidmc.harvard.edu, web: <http://bouxseinlab.org/>

## INTRODUCTION

The measurement of thoracolumbar spine curvature and motion is of interest for study of conditions such as back pain, adolescent idiopathic scoliosis, and age-related spinal deformity. Opto-electronic motion capture systems may allow non-invasive evaluation of spine curvature and dynamic motion with appropriate sets of markers applied to the spine. Such marker sets have been of increasing interest recently, for example with studies of soft tissue artifacts in the back [1] and spine motion in scoliotic and healthy adolescents [2]. However, the between-session reliability of these marker sets for evaluating sagittal spinal curvature has not been evaluated. Thus, the aim of this study was to determine the reliability of the retroreflective marker-based measurements of thoracic kyphosis, lumbar lordosis and pelvic tilt, and compare these measures with corresponding non-radiographic clinical measurements.

## METHODS

A reliability study was conducted on 19 healthy adults (11 men, 8 women) aged between 20 and 74 years. Each subject visited the motion analysis lab and underwent the same set of measurements on two separate occasions an average of 7 days apart (range 2-14 days).

Marker-based measurements were based on a set of 4-marker clusters placed on the skin overlying the T1, T4, T5, T8, T9, T12 and L1 spinous processes, with additional single markers on C7 and the posterior (PSIS) and anterior (ASIS) superior iliac spines (Figure 1). In each session, marker positions were captured using a 10-camera Vicon motion capture system during two static trials in the neutral

upright standing posture (2 sec each). Angle calculations were performed on the mean positions of the markers in the sagittal plane using a custom MATLAB program. For spine curvature, circles were fit to thoracic and lumbar segments [2], then thoracic kyphosis and lumbar lordosis were calculated as angles between T1-T12 and L1 - Sacrum, respectively. Pelvic tilt was defined by the markers placed on the PSIS and ASIS.



**Figure 1:** The set of single and cluster retroreflective markers placed on the back.

Non-radiographic measures were made using established measurement tools reported to have good reliability: the flexicurve for spine curvature [3] and the palpation meter (PALM) for pelvic tilt [4]. A single rater tested each participant in both sessions. Flexicurve angle was calculated for thoracic kyphosis and lumbar lordosis. The PALM measurement was based on the angle between PSIS and ASIS, with a forward tilt defined as negative angle.

Test-retest reliability of each measurement was examined using intraclass correlation coefficients (ICC). Reliability is poor for ICCs < 0.4, fair to good if between 0.4 to 0.75 and excellent if above 0.75. Pearson’s correlation coefficients were calculated to compare marker-based measurements and corresponding flexicurve and PALM measurements. Analyses were performed with Stata/IC 13.1 (StataCorp LP, College Station, TX).

## RESULTS AND DISCUSSION

For thoracic kyphosis, marker-based measurements showed excellent between-session reliability (ICC = 0.95), comparing favorably with the flexicurve measurement (ICC= 0.83) (Table 1). A same-day ICC of 0.94 has been reported for average sagittal thoracic curve during gait cycles in non-scoliotic adolescents [2]. While not directly comparable, this supports the current finding that marker-based measures are highly reliable. We also found a significant positive correlation ( $r = 0.795$ ) between marker-based thoracic kyphosis measurement and flexicurve angle, reflecting good criterion validity of the markers in thoracic curvature measurement (Table 1). This compares well with reported correlations between marker-, and MRI-based measurement of thoracic kyphosis ( $R^2$  of 0.385, [1]), and between flexicurve and radiologic Cobb angle of ( $R^2$  of 0.57, [3]).

For lumbar lordosis, the marker-based ICC value of 0.86 was comparable with the value of 0.84 for flexicurve measurement, both showing excellent between-session reliability (Table 1). Schmid et al. [2] reported the ICC values of 0.90 (CI; 0.80, 0.97) for marker-based sagittal lumbar curve analysis that was averaged during a gait cycle in a same day trial. We also found a significant positive correlation ( $r = 0.643$ ) between marker-based and flexicurve lumbar

lordosis measurement, showing satisfactory criterion validity of markers for lumbar lordosis measurement (Table 1). Again, this compares well with correlations between marker-, and MRI-based measurement of lumbar lordosis ( $R^2$  of 0.552, [1]).

Reliability of marker-based pelvic tilt measurement (ICC; 0.40) was considerably lower than the PALM value (ICC; 0.76). The correlation between marker-based pelvic tilt angle and PALM data was not significant ( $r = 0.345$ ) (Table 1).

## CONCLUSIONS

Marker-based measurements of sagittal spine curvature were very reliable between sessions, and compare quite favorably with frequently used non-radiologic methods. On the other hand, pelvic tilt was not reliably captured, but it may be more sensitive to errors in marker placement as it was based on only four markers. Overall, this study supports opto-electronic motion capture with an appropriate spinal marker set as a reliable non-invasive method for evaluating spine curvature and potentially spinal motion.

## REFERENCES

1. Zemp R, et al. *PLoS One* **18**, e95426, 2014.
2. Schmid S, et al. *Gait Posture* **44**, 231-237, 2016.
3. Greendale GA, et al. *Osteoporos Int* **22**, 1897-1905, 2011.
4. Azevedo DC, et al. *J Bodyw Mov Ther* **18**, 210-214, 2014.

## ACKNOWLEDGMENTS

Our thanks to Stefan Schmid for sharing MATLAB code. This study was supported by the National Institute on Aging (R00AG042458) and by the Department of Orthopaedic Surgery at Beth Israel Deaconess Medical Center.

**Table 1:** Mean (SD) values and ICCs for between-days test-retest reliability of marker-based and flexicurve / PALM measurements of spinal curvature and pelvic tilt, and correlations between corresponding measurements.

Measurement	Marker-based		Flexicurve / PALM		Correlation (p-value)
	Mean (SD)	ICC (95% CI)	Mean (SD)	ICC (95% CI)	
Thoracic kyphosis	45.9 (10.8)	0.95 (0.87-0.98)	23.9 (6.3)	0.83 (0.58-0.94)	0.795 (<0.001)
Lumbar Lordosis	33.6 (10.3)	0.86 (0.63-0.95)	22.0 (9.0)	0.84 (0.60-0.94)	0.643 (<0.001)
Pelvic Tilt	-4.7 (4.9)	0.40 (-0.17-0.76)	-2.2 (3.8)	0.76 (0.44-0.91)	0.345 (0.067)

# PIEZO ELECTRIC DEVICE FOR PERIPHERAL STOCHASTIC SUBSENSORY VIBRATION

<sup>1</sup> John D Zunker, <sup>1</sup> Samuel A Acuña, and <sup>1</sup> Darryl G Thelen,

<sup>1</sup> The University of Wisconsin–Madison, Madison, WI, USA  
email: jzunker@wisc.edu, web: <http://uwnmb1.engr.wisc.edu>

## INTRODUCTION

More than a third of older adults fall each year, and the risk of falling drastically reduces an older adult's mobility, independence, and quality of life [1]. Postural control is dependent on proprioceptive feedback of the lower limbs, but this sensation declines with age, and this decline has been identified as a risk factor for falls [2]. Thus, therapeutic technology that can enhance these degrading proprioceptive signals is of great interest to research.

An emerging mode of intervention utilizes the phenomenon of stochastic resonance (SR), whereby a weak or imperceptible stimulus is detected in the presence of an optimal amount of noise. In humans, externally applied vibratory noise increases action potential generation in the mechanoreceptors under the skin, and can enhance perception of tactile and proprioceptive stimuli [3]. Accordingly, SR vibration has been shown to improve postural control when applied to the feet [4] and ankles [5].

Although there is strong potential for this technology, application has been limited because tuning to the proper amount of noise for each subject is challenging. Too much noise will washout the stimulus signal, yet too little will provide no enhancement. The skin mechanoreceptors are sensitive to frequencies between 100–300 Hz [6], and activation of the SR effect requires a consistent level of noise across these frequencies. Potential SR actuators must be able to modulate noise levels without biasing the vibration signal towards any specific frequencies.

Several studies have measured SR postural control using electromechanical C-2 and C-3 tactors (Engineering Acoustics, Winter Park, FL) to produce the mechanical noise signal [5, 7]. These

tactors function like an audio speaker whereby a diaphragm attached to a magnet is situated in an inductor (Fig. 1A). Due to this construction, the diaphragm is easily impeded and its displacement is highly sensitive to the applied pressure of the tactor against the skin. The C-2 and C-3 tactors have also been specifically designed to exhibit resonance behavior between 250–300 Hz, making the production of white noise in the desired frequency band challenging. These characteristics render the tactor problematic for use in SR applications.

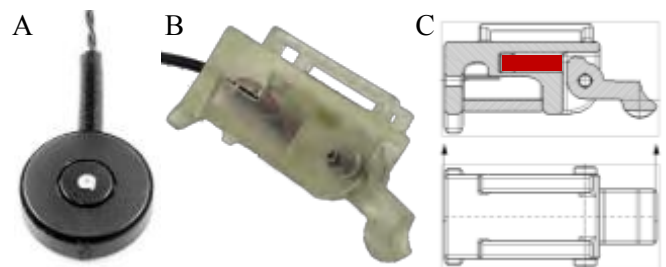


**Figure 1:** A) C-3 tactor. B) Our designed piezo lever device. C) Cross sectional view reveals inner cavity where piezoelectric stack (red) resides.

Piezoelectric actuators have also been used in SR research [4, 8], but unlike tactors which can easily be taped to the skin, the geometry of most piezoelectric actuators require some sort of housing to hold the actuator and transfer vibration to the skin. SR studies using piezoelectric actuators have not well described this housing [4, 8]. We have developed a piezoelectric lever device (PLD) which amplifies the displacement of a piezoelectric stack (PK4JQP2, Thor Labs, Newton, NJ) embedded within the housing (Fig. 1B,C). As the piezo will vibrate under an applied load (<144 N) and exhibits resonance at 60 kHz, the PLD should be suitable for producing predictable amplitudes of noise in the required frequency band. The goal of this research was to compare 100–300 Hz vibrational noise when using a C-3 tactor and the PLD.

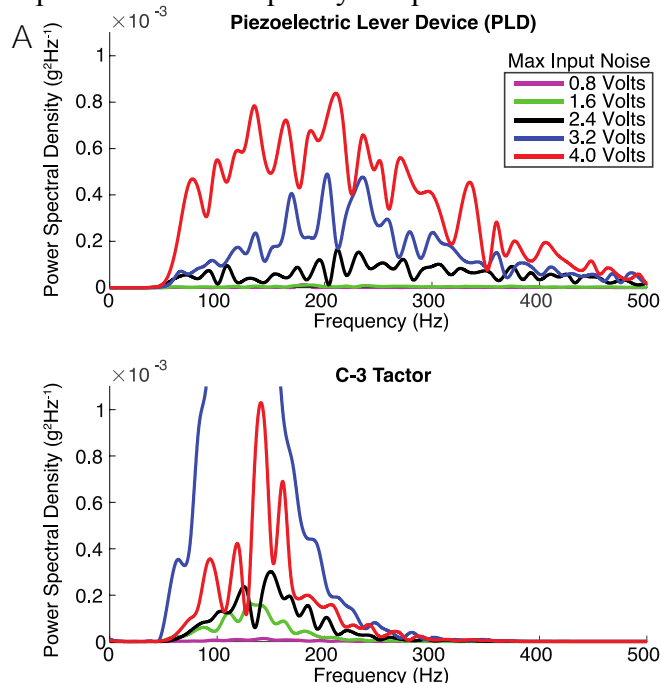
## METHODS

A C-3 tactor and the PLD were secured to a compliant cylinder testbed (simulating skin) using medical tape. An accelerometer (352C23, PCB, Depew, NY) was positioned over the actuators as vibration was driven at 100-300 Hz using a noise signal generated in LabVIEW. Accelerometer data was collected for 10 seconds at 20 discrete levels of input noise, spanning 0.2–4 V in 0.2 V increments, and then analyzed using MATLAB. Each collection was detrended and filtered using a zero-phase digital bandpass filter from 50–500 Hz. The power spectral density was calculated for increasing levels of noise, and the root-mean-squared acceleration was calculated for both 100–200 and 200–300 Hz.

## RESULTS AND DISCUSSION

The PLD demonstrated consistent vibrational noise across 100–300 Hz for all noise levels, but the C-3 tactor exhibited resonance in the 100-200 Hz range (Fig 2A). Analysis of the frequency domain shows that the tactor device did not accurately reproduce a consistent 100–300 Hz noise signal necessary to activate the SR effect across all mechanoreceptors. Attenuation occurred after 200 Hz (Fig 2B).

Comparatively, the PLD responses scaled as expected. The frequency responses were much



flatter across the 100–300 Hz region, with the frequency response extending out to 500 Hz. The PLD has a more predictable response in the driving frequencies compared to the C-3 tactor device.

## CONCLUSIONS

Vibrational SR devices are a promising technology to enhancing lower limb proprioception and improve postural control in older adults. Due to higher force characteristics and more accurate frequency responses, our findings suggest it may be preferable to use piezoelectric actuators rather than traditional tactor devices for lower limb SR applications. Further development of piezoelectric actuated devices will optimize interfaces for specific musculoskeletal geometries (e.g. Achilles tendon), which will be useful in future gait analysis research.

## REFERENCES

1. Rubenstein LZ, et al. *Age Aging* **35**, 37-41, 2006.
2. Soriano TA, et al. *Clin Int Aging* **2**, 545-54, 2007.
3. Onorato I, et al. *Plos One* **11**, 1-12, 2016.
4. Lipsitz LA, *Arc Phys Med Rehab* **96**, 432-9, 2015.
5. Borel L, et al. *Exp Brain Res* **234**, 2305-14, 2016.
6. Kwak K, et al. *Biomed Eng Let* **6**, 16-25, 2016.
7. Priplata AA, et al. *Lancet* **362**, 1123-4, 2003.
8. Miranda DL, et al. *MedSci Sport Ex* **48**, 860-8, 2016.

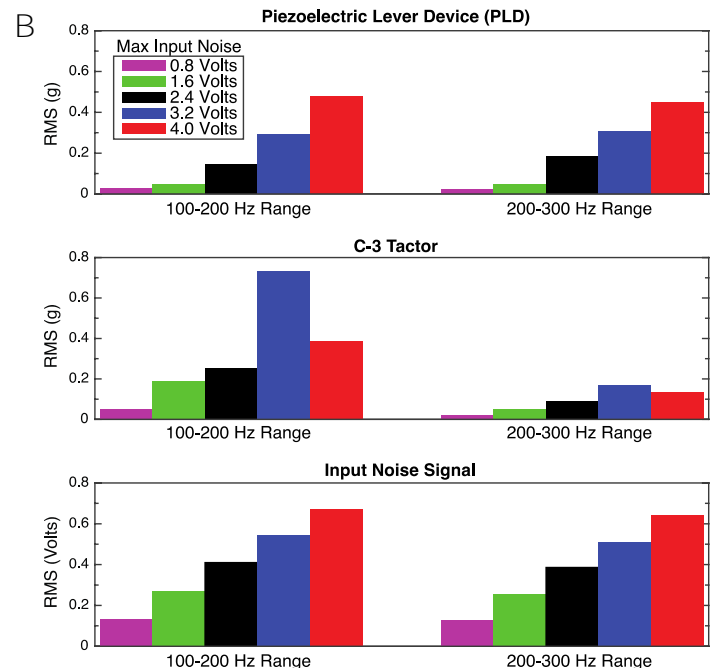


**Figure 2:** A) Frequency response of the PLD and C-3 tactor. B) RMS acceleration by frequency range.

# FORCE AND CENTER OF PRESSURE ERROR ANALYSIS FOR A FORCE-PLATE MOUNTED STAIR CASE: IMPLICATIONS FOR BIOMECHANICAL ANALYSIS OF STAIR CLIMBING

Joshua D. Roth, Scott C. Brandon, Emily M. Keuler, and Darryl G. Thelen

University of Wisconsin-Madison, Madison, WI, USA  
email: jdroth2@wisc.edu, web: <http://uwnmbl.engr.wisc.edu/>

## INTRODUCTION

Stair climbing is a common activity of daily living. It requires greater knee flexion and joint torques than level walking<sup>1</sup>. Thus, biomechanics during stair climbing are especially of interest when studying patient populations with musculoskeletal or neuromuscular impairments. Biomechanical analysis of stair climbing (e.g., inverse dynamics and dynamic multibody musculoskeletal simulations) is important for both clinicians tracking rehabilitation progress and researchers evaluating innovative treatments. However, biomechanical analyses require accurate inputs in terms of ground reaction force (GRF) and center of pressure (CoP) to give meaningful results.

An attractive option to measure ground reaction force and center of pressure during stair climbing is a force-plate-mounted staircase (e.g., FP-Stairs<sup>2</sup>, AMTI, Watertown, MA) (Figure 1). Previous studies have shown that force-plate-mounted staircases do not introduce errors in the vertical component of the GRF or the CoP under purely vertical loads<sup>2-4</sup>. However, the anterior-posterior (A-P) and medial-lateral (M-L) loads present during stair climbing<sup>1</sup> might create errors in the GRF and/or CoP.

Accordingly, the objectives were to (1) characterize the errors in GRF and CoP created by A-P and M-L forces and (2) present and validate a method to reduce these errors.

## METHODS

Forces were applied using an instrumented pole<sup>5</sup> at four locations spanning the width of each of the three steps of a commercially available force-plate-mounted staircase (FP-Stairs<sup>2</sup>, AMTI, Watertown, MA) (Figure 1). Forces were also applied to the surface of each force plate at 8 locations covering the entire surface. The instrumented pole included both an inline load cell (Futek FSH02633, 11 N non-

linearity) and four retroreflective markers. Data were recorded at each location (motion capture at 100 Hz and forces at 2000 Hz) while rotating the instrumented pole about a fixed location to create vertical forces ranging from 150 to 400 N and horizontal (A-P and M-L) forces ranging between  $\pm 100$  N. The motion capture data of the instrumented pole markers were used to determine the applied CoP and orientation of the applied force, and the force data from the instrumented pole load cell determined the magnitude of the applied force. The GRF and CoP were simultaneously estimated from the in-ground force plates (BP400600, AMTI, Watertown, MA) using the sensitivity matrices determined with a previous calibration (surface calibration) using an instrumented pole<sup>5</sup>.

To characterize the errors in GRF and CoP created by the A-P and M-L forces, the difference between

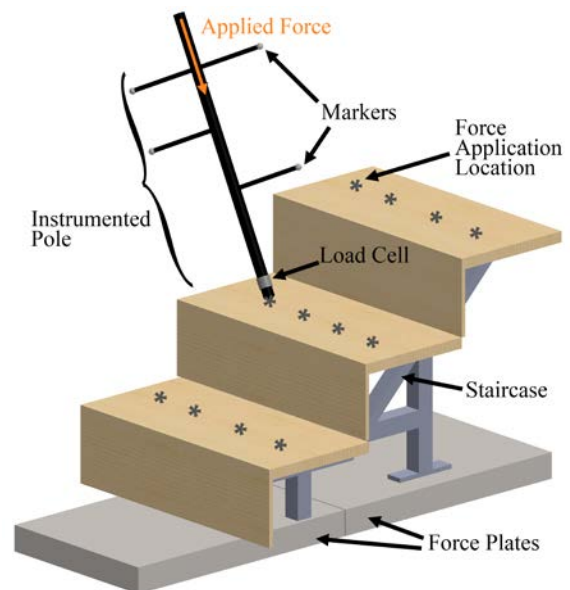


Figure 1. Instrumented pole used to apply a known force at a known location on each stair. The pointed tip of the pole rests in a conical detent in a base plate (not shown) to maintain a fixed force application location (\*) during each trial.

the computed GRF and CoP (force plate) using the surface calibration and the applied GRF and CoP (instrumented pole), respectively was determined for the (1) plate surface (surface calibration): loads applied directly to the surface of the in-ground force plates, and (2) stair surface (surface calibration) loads applied to the surface of the stairs.

To reduce these errors, the data from each stair were used to determine a stair-specific sensitivity matrix that minimized the difference between the applied and computed GRF and CoP for each stair surface (stair-specific calibration). To validate this error reduction method, the errors between the computed GRF and COP and the applied GRF and CoP on each stair surface were recomputed using the stair-specific calibration.

## RESULTS AND DISCUSSION

Errors, mainly bias, in both CoP and GRF were quite large when computed on the stair surface using surface calibration. The bias in the M-L and A-P coordinates of the CoP were one to two orders of magnitude greater than those for the plate surface using the surface calibration (Table 1). When using the stair-specific calibration, the errors in CoP were similar to those for the plate surface using the surface calibration (Table 1). The bias in the M-L, A-P, and inferior-superior (I-S) components of the GRF were about one order of magnitude greater than those for the plate surface using the surface calibration (Table 2). As with the CoP, when using the stair-specific calibration, the errors in GRF were similar to those for the plate surface using the surface calibration (Table 2). The large errors in both CoP and GRF might be due to the stair surfaces being far outside of the region used for the surface calibration. Hence the errors are greatly reduced with the stair-specific calibration because the region of the calibration matches the region where forces are applied.

Table 2. Absolute bias (mean of the magnitude of the bias) and precision (standard deviation) of the errors in the M-L, A-P, and I-S components of the GRF

	M-L GRF Error [N]		A-P GRF Error [N]		I-S GRF Error [N]	
	Absolute Bias	Precision	Absolute Bias	Precision	Absolute Bias	Precision
Plate Surface (Surface Calibration)	0.0	0.5	0.0	0.6	0.1	1.0
Stair Surface (Surface Calibration)	25.6	1.3	7.4	2.2	242.3	1.9
Stair Surface (Stair-Specific Calibration)	0.0	1.2	0.0	2.1	0.1	2.5

Table 1. Absolute bias (mean of the magnitude of the bias) and precision (standard deviation) of the errors in the M-L and A-P coordinates of the CoP

	M-L CoP Error [mm]		A-P COP Error [mm]	
	Absolute Bias	Precision	Absolute Bias	Precision
Plate Surface (Surface Calibration)	0.0	0.6	0.1	0.9
Stair Surface (Surface Calibration)	20.9	5.9	120.5	9.8
Stair Surface (Stair-specific Calibration)	0.2	2.2	0.1	1.1

## CONCLUSIONS

These findings indicate that with a stair-specific calibration, the errors in GRF and CoP using a force-plate-mounted staircase are similar to those when using the in-ground force plates with a surface calibration. Thus, anyone collecting data using force-plate-mounted staircase should perform a stair-specific calibration to minimize the errors in later biomechanical analyses. Errors in the biomechanical analyses might lead to erroneous conclusions about rehabilitation progress and evaluations of innovative treatments<sup>6</sup>.

## REFERENCES

1. Riener, R., et al., Gait Posture, 2002.
2. Della Croce, U., et al., J Biomech, 2007.
3. Whatling, G.M., et al., Comput Methods Biomech Biomed Engin, 2010.
4. Yu, B., et al., J Biomech, 1996.
5. Collins, S.H., et al., Gait Posture, 2009.
6. McCaw, S.T., et al., J Biomech, 1995.

## ACKNOWLEDGMENTS

We acknowledge the support of THINK Surgical and the National Institute on Aging (T32AG000213-25).

# ESTIMATING BODY SEGMENT INERTIAL PARAMETERS USING A KINECT V2

Pawel Kudzia, Erika Jackson, Geneviève Dumas

Queen's University, Kingston, ON, Canada

Email: pawel.kudzia@queensu.ca

## INTRODUCTION

When studying human motion, inverse dynamics is an approach used for the analysis of human movement. Despite being widely used, it is known to have inherent errors [1]. One such error stems from the estimation of body segment inertial parameters (BSIPs) i.e. mass, center-of-mass (CoM) and moments of inertia (MOI). One of the difficulties in approximating BSIP's resides in the quantification of the geometric characteristics of the human body. Current methods in estimating these parameters such as mathematical, medical imaging or cadaver can be time consuming [2], expensive [3], and lack the ability adequately represent the geometric variation of human bodies [4]. Importantly, BSIP estimation is sensitive to how the geometric approximations of the bodily segments represent the true anatomical structures.

In recent years, an inexpensive depth camera the Kinect™ (Microsoft, USA), has shown potential in this application. With 3D imaging capabilities the device has the potential to address some of the limitations associated with current methods [5]. With this in mind, we developed and evaluated a method of employing the Kinect™ (Version 2) to estimate BSIPs. Specifically, the goals of the study were to evaluate the proposed method for scan repeatability, body segmentation repeatability and ease of use. Additionally, we compared the results to a validated approach known as the elliptical cylinder method (ECM) [6] and also to mass estimates obtained from scale values.

## METHODS

Twenty-one subjects (11F, 70±8kg 22±2y; 10M, 73±4kg 23±2y) were recruited for the study. Subjects signed a written consent form approved by the Queen's University Ethics Committee. Subjects

were outfitted into form-fitting attire and weight was taken on a calibrated medical scale. Two-dimensional body markers were placed onto anatomical landmarks to identify individual limb segmentation boundaries [7]. Two scanning protocols were then successively executed. First, following the ECM protocol [6] subject data was collected. Subsequently, subjects were asked to stand as still as possible on an elevated platform with their arms abducted (Fig.1). The Kinect device, tethered via USB 3.0 to a desktop operating system (software: 3D Builder, OS Windows 10; 30Hz) was revolved around the subject following an outlined scanning perimeter (Fig.1). This procedure was repeated until 3 scans were acquired per subject.

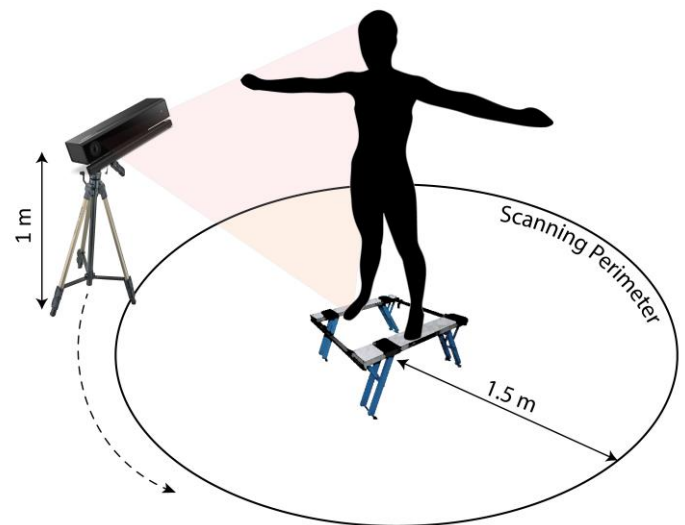


**Figure 1:** Kinect experimental setup

In post processing, Kinect scans were exported to open source software MeshLab (64-bit v.1.3.4) where the 3D data files were cleaned of irrelevant data (e.g. floor) and the body was segmented into a 16-segment model using the body markers as segmentation guidelines (Fig 2-B). Following body segmentation, all data was imported into MATLAB (v2016a, Mathworks, Natick, MA) where BSIPs

were evaluated using a custom written script. ECM data was processed and evaluated using an available software [8]. For analysis purposes, data was grouped into male and female cohorts.

Two one-way repeated measures ANOVA were used ( $\alpha < 0.05$ ) to evaluate the repeatability of body volume estimates obtained from repeated scans and of limb segmentation volumes obtained from repeated segmentations. To compare the mass values collected from the medical scale to the total body mass estimates obtained with the proposed method and with ECM, each segment volume was multiplied by a corresponding uniform density [9], [10]. A one-way repeated measures ANOVA was then used to evaluate the mass estimates.

## RESULTS AND DISCUSSION

No significant differences were observed ( $p > 0.05$ ) between the repeated scans and between repeated segmentations for both males and females. Similarly, there were no significant differences between the scale, ECM and Kinect scans when comparing body mass estimates for the males. For the females, the Kinect overestimated the total body mass by  $5 \pm 2\%$  ( $p < 0.05$ ) when compared to the scale and ECM results. CoM and MOI data were also computed following the proposed methodology. While full analysis of these parameters is still ongoing the capability of estimating these BSIPs has shown to be efficacious.

These results suggest the potential of the proposed method for subject specific BSIP estimation without gender, age or morphological restrictions. With the ability to acquire consistent volumetric estimates and easily modify density inputs, the possibility of reducing errors in estimating BSIPs exists. Motion artifact during 3D scanning, concave surfaces (e.g. cupping palms or cleavage) or steep edges (e.g. between the arms and thighs) may have contributed to unwanted 3D points, which could result in a discrepancy in the total volume. Although this did not appear to be the case in the male participants, perhaps it may explain some of the overestimations seen in the female participants. Further work understanding and reducing these errors will need to be complete.

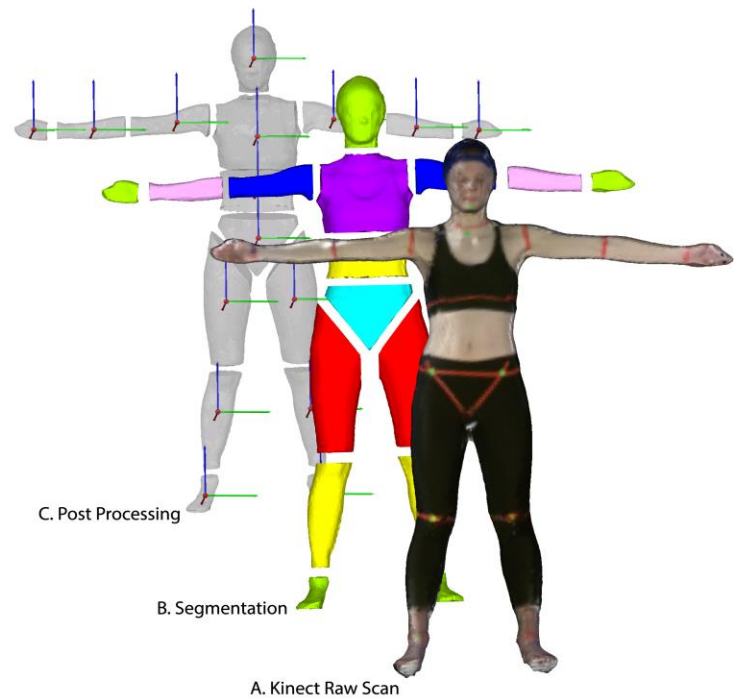


**Figure 2:** Sequence of proposed methodology: **A.** Raw scan **B.** Segmentation and **C.** BSIP evaluation.

## CONCLUSIONS

This study demonstrates the potential for using a Kinect sensor as a tool for body segment parameter estimation and also establishes a methodology for post processing 3D scans. With repeatable volume estimates and the ability to estimate a wide range of subject specific parameters, the opportunity for such a system is promising. Ongoing work will focus on evaluating the remainder of the BSIPs which were not fully evaluated (i.e. CoM and MOI).

## REFERENCES

- [1] R. Riemer et al. *Gait Posture*, vol. 27 2008.
- [2] M. Yeadon, *J. Biomech.*, vol. 21, 1990.
- [3] M. K. Lee, et al. *J. Biomech.*, vol. 42, 2009.
- [4] Dempster, vol. 22, 1963.
- [5] S. Clarkson et al. *4th IEEE Workshop* 2014.
- [6] J. Wicke et al. *J. Appl. Biomech.*, 2003.
- [7] V. Zatsiorsky et al. *Eight Int Con Biomec*, pp. 1152–1159, 1983.
- [8] J. McIlwain, “Slicer.” Sudbury, ON, 1998.
- [9] C. Clauser et al. 1969.
- [10] D. J. Pearsall et al. *Ann. Biomed. Eng.*, vol. 22, 1994.

# VALIDATION OF A DATA ANALYSIS METHOD FOR USE WITH A GAZE TRACKER

<sup>1</sup> Mark Cullen, <sup>2</sup> Michael Granatosky, <sup>3</sup> Michael Platt, <sup>1</sup> Daniel Schmitt, and <sup>1</sup> Roxanne Larsen

<sup>1</sup> Department of Evolutionary Anthropology, Duke University, Durham, NC, USA

<sup>2</sup> Department of Organismal Biology and Anatomy, University of Chicago, Chicago, IL, USA

<sup>3</sup> Department of Neuroscience, University of Pennsylvania, Philadelphia, PA, 19104

email: mmc46@duke.edu

## INTRODUCTION

Gaze-tracking technology provides a first person point of view of the visual field while measuring direct eye movements, allowing researchers to quantify and describe where an individual is directing their gaze [1]. This has been essential to research in psychology, neurobiology, and animal behavior [2]. Yet, most applications of this technology have been applied to monitoring humans during stationary tasks, with a few exceptions including long jumping and walking [3, 4]. Most of the research on humans has focused on walking, which has indicated obstacle fixations increase as walkers approach obstacles and walkers tend to focus on areas where they eventually will step [4, 6]. These studies have advanced our understanding of visual attention during locomotion in humans; however, methods for tracking gaze during rapid dynamic behaviors have been limited and subjective, and whether these approaches can be used during running and when encountering obstacles is understudied.

The overarching goal of this project was to develop an appropriate method for analyzing gaze while the study subject was in motion, particularly when running and navigating an obstacle in a path [7]. For this, we chose a telemetric gaze-tracker, which provided good spatial and temporal resolution and was lightweight and minimally obstructive for participants. These trackers determine where gaze is directed and collects pupil position data by monitoring the cornea and corneal reflections on a mirror with a small camera. Pupillary movements are then superimposed as a crosshair onto video from a camera mounted on the subject's head [1].

To design an automated and accurate method for identifying gaze fixations, models of error (MoEs) that incorporated the innate spatial error of the gaze tracker and the potential error introduced during digitizing were developed. These MoEs were compared to independent raters scores of the same video to determine the best MoE to analyze gaze-tracker data in a dynamic and complex setting.

## METHODS

The data from 1 male (21 yrs, 1.8 m, 83.9 kg) and 1 female (21 yrs, 1.6 m, 56.7 kg) were used to validate the raters' crosshair tracking method and that of the MoEs. Running participants were recreational runners with no history of injury in the past six months. The gaze tracker (60 Hz, "Omniview," ISCAN Inc., Woburn, MA, USA) was placed on each participant's head, and calibrations from 5.18 m, 3.05 m, and 1.52 m were conducted to confirm the runners' gaze and the crosshair were tracking accurately in the video from the field of view of the runner [8]. Each participant ran on a 20 m sidewalk path, intended to mimic a common urban running environment. After warming up, participants were allowed to run at their self-selected speed for up to 15 laps along the sidewalk path. At about 15 meters into the run, participants encountered and cleared a typical sidewalk curb (0.15 m high). Six trials were chosen from each runner for final analyses. All protocols were approved by Duke University IRB.

To analyze data, the crosshair and curb were digitized in each frame in MATLAB using DLTdv5 [9]. To incorporate the change in relative size of the curb as the runner approached the curb, and to account for error in digitizing and the gaze tracker

itself, an algorithm to create MoEs was developed. The MoEs created polygons around the original curb digitization by adding error rates to the X and Y coordinates of the digitized curb. The result was three scenarios: MoE 0.0 (original digitized curb), MoE 0.75 (added error of 0.99% in the X and 1.44% in the Y direction), and MoE 1.5 (added error of 1.97% in the X and 2.88% in the Y direction; Fig. 1). These rates were chosen based on previous studies [8]. The MoEs were then used to identify if the crosshair was within the area of the different sized polygons in each scenario. An absence/presence tally across the running trials (for each MoE) was used to determine when and how many times the runner looked at the curb.

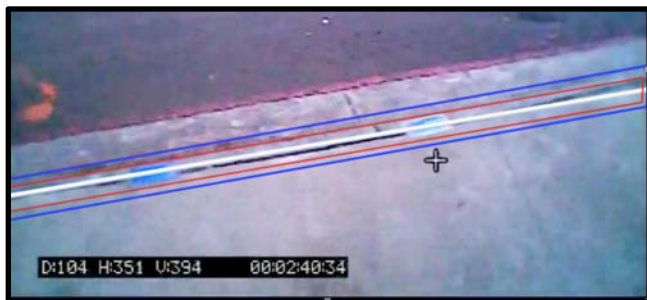


**Figure 1:** Sidewalk curb with superimposed MoEs represented as blue (MoE 1.5), red (MoE 0.75), and white (MoE 0.0) lines. Crosshair indicated by white cross.

To determine the effectiveness of the different MoEs and to obtain a reliability estimate of them, 10 frames from each of the running participants were chosen and provided to seven independent raters. These raters made decisions of whether the crosshair was on the curb in these 20 frames. Their scores were also tallied as absence/presence. Absence/presence results from the three MoEs and the seven raters were compared.

## RESULTS AND DISCUSSION

As values for MoE increased, so did the frequency of fixations scored at the curb (Fig. 2). The average rater frequency (0.34) fell between MoE 0.75 and 1.5 (Fig. 3) and thus those MoEs best captured the gaze fixation of the runners.

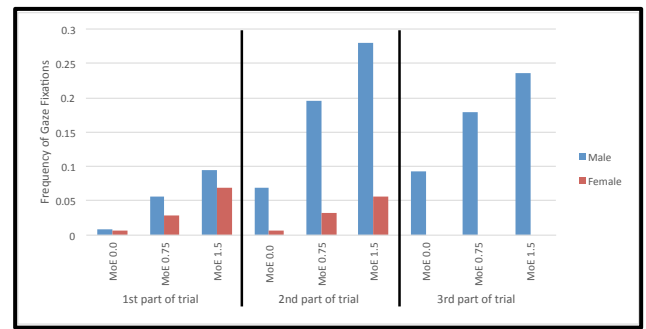


**Figure 2:** Frequency of gaze fixations at the curb over the course of runners' trials (broken into thirds, indicated by vertical lines). Models of error (MoEs) are also represented.

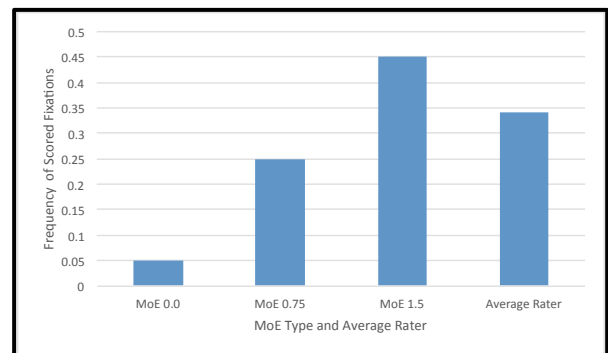


**Figure 3:** Total frequency of gaze fixations at the curb comparing the different MoEs and the average rater.

## CONCLUSIONS

A gaze tracker is an effective means of capturing how individuals observe their environment while running outdoors and navigating obstacles. Using MoEs that scale to a region of interest as a runner moves through the environment allowed us to effectively characterize the gaze fixations of the runner. We were able to determine the best MoE to quickly, efficiently, and reliably analyze gaze-tracker data in a dynamic and complex setting.

## REFERENCES

1. Olson JS, & Kellogg WA. *Ways of knowing in HCI*, Springer New York, 2014.
2. Shepherd SV & Platt ML. *Methods* **38**, 185-194, 2006.
3. Land MF. *Prog Retin Eye Res* **25**, 296-324, 2006.
4. Warren, Jr. WH. *Ecol Psychol* **10**, 177-219, 1998.
5. Patla AP, & Vickers JN. *Neuroreport* **8**, 3661-3665, 1997.
6. Patla AP, & Greig M. *Neurosci Lett* **397**, 110-114, 2006.
7. Larsen RJ, et al. *Hum Mov Sci* **49**, 186-195, 2016.
8. Kano F, & Tomonaga M. *PLoS ONE*. **8**, e59785, 2013.
9. Hedrick TL. *Bioinspir Biomim* **3**, 034001, 2008.

# Feasibility of Optical Motion Capture to Compute Head Impact Kinematics

Sean Quisenberry, Mark Jesunathadas, Scott Piland, and Trenton Gould

University of Southern Mississippi, Hattiesburg, MS, USA  
email: trent.gould@usm.edu, web: <https://www.usm.edu/kinesiology>

## INTRODUCTION

The risks of brain injury associated with an impact are often based on measurements of the acceleration of the center of gravity (CG) of an anthropometric test dummy (ATD) headform during a simulated impact. However, translational accelerations experienced by the brain are not confined to the CG and potentially differ vastly from those measured at the CG. Optical motion capture has the potential to measure accelerations of the head at a variety of locations within its volume. However, the accuracy with which optical motion capture can accurately measure accelerations of the head at the CG, much less other locations, is yet to be determined. Thus, the purpose of this study is to confirm the ability of an optical motion capture system to accurately replicate the accelerations of the CG of an ATD headform as measured by an accelerometer during a drop impact.

## METHODS

A National Operating Committee on Standards for Athletic Equipment (NOCSAE) headform was impacted at the top position using a Cadex Inc. (Quebec, Canada) monorail drop impactor. The headform was dropped 10 times each from seven drop heights (20, 30, 40, 50, 60, 70, 80cm) onto a 1-inch modular elastomer programmer (MEP).

Reference acceleration data during the impact was measured with a triaxial accelerometer (PCB Piezotronics, Inc. Depew, NY; sampling rate = 6000 Hz) located at the CG of the ATD headform. Reference acceleration data was processed in accordance with SAE J211a (channel frequency class 1000)<sup>1</sup>. A 10-camera optical motion capture system (Oqus 7+ series, Qualisys, Sweden; sampling rate 3000 Hz) was used to determine acceleration of the ATD from position data of 11 (12.9mm) markers (6 retroreflective tracking, 5 virtual) on the surface of

the ATD headform. Accelerometer data was synchronized with optical motion capture data by an external optical trigger that was activated just prior to the ATD headform impacting the MEP pad.

Marker and accelerometer data were processed and analyzed in MATLAB R2016b (Mathworks Inc., Natick MA). Marker position data from impact events were low-pass filtered with a second-order zero phase lag Butterworth filter. Cut-off frequencies were 20Hz for the perpendicular axis to sagittal and coronal planes, and 200-400Hz for the perpendicular axis to the transverse plane of motion. The filtered position data was numerically differentiated to compute acceleration at the geometric center of the markers corresponding to the CG. Peak translational acceleration from each axis was collected from both the accelerometer and optical motion capture system to calculate resultant peak linear acceleration (peak g).

We performed simple linear regression analysis between the reference and optimal motion capture acceleration peak g values. The strength of the relationship is reported as the coefficient of determination ( $R^2$ ). Additionally, a Bland-Altman plot (difference of the two-paired measurements plotted against the mean of the two measurements) was used to quantify the agreement between the accelerometer and optical motion capture system techniques. Mean absolute percent error (MAPE) was also calculated for each drop height and across all impacts.

## RESULTS AND DISCUSSION

Linear regression results showed a strong association between optical motion capture acceleration data and reference accelerometer acceleration data for peak g ( $R^2 = 0.99$ ; Figure 1). On average, the optical motion capture system presented a bias of -11g [95% CI:

-28 – 5.3 g], and the agreement limit of 17 g (Figure 2). The mean  $\pm$  SD MAPE values ranged from  $2.6 \pm 1.9\%$  at a drop height of 20 cm to  $8.2 \pm 1.8\%$  at a drop height of 80 cm.

Overall there was a high correlation between measures of acceleration between the optical motion capture system and reference accelerometer. However, an observed increase in the variance of peak g values measured with the optical motion capture system as drop height increased (Figure 2). Thus, as impact velocity increases optical motion capture becomes a less precise means to measure peak translational acceleration during impact.

Differences between optical motion capture acceleration measures and those recorded by the reference accelerometer may have been because an appropriate low-pass filter cut-off frequency for the optical motion capture position data was difficult to establish. While a balance had to be made between signal distortion and noise reduction, an optimal cut-off frequency has yet to be determined.

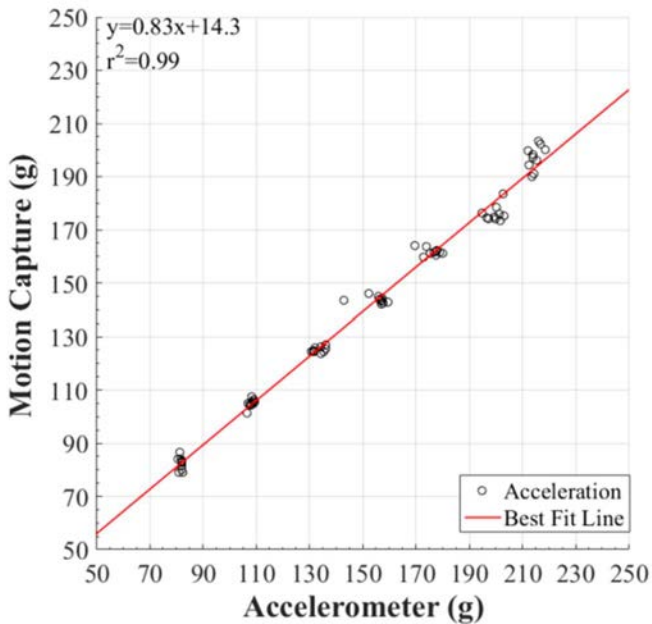


**Figure 1:** Linear regression analysis between accelerometer compared to optical motion capture data for peak linear acceleration. The solid red line corresponds to the ordinary least squares (OLS) best fit line.

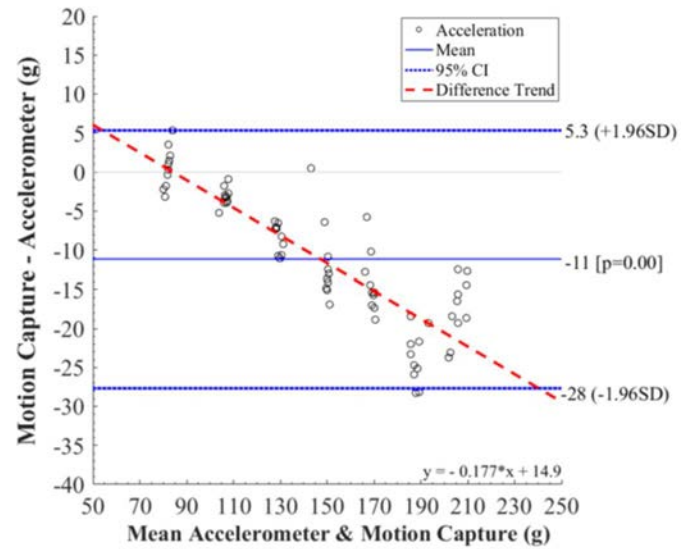


**Figure 2:** Bland-Altman plot for peak linear acceleration of the NOCSAE headform. The solid blue line represented the mean peak linear acceleration difference between the two measurement systems, dotted blue lines represent the 95% CI, and dashed red line illustrates the acceleration difference trend.

## CONCLUSIONS

Preliminary findings indicate potential for the utilization of optical motion capture technology as an additional tool to measure the translational acceleration of ATD during impact events. Additional testing is warranted to fully assess, and expand the use of, optical motion capture technology to calculate head impact kinematic variables (e.g., peak linear acceleration, peak rotational acceleration, GSI, HIC).

## REFERENCES

1. SAE. *Instrumentation for Impact Test, Part 1: Electronic Instrumentation*, Society of Automotive Engineers, 2007.

## ACKNOWLEDGMENTS

The authors would like to thank Elizabeth D. Edward for assistance with data collection and organization.

# REAL-TIME FEEDBACK TO IMPROVE MARKER PLACEMENT CONSISTENCY AMONG NOVICE EXAMINERS

<sup>1</sup> Charles A.J. Macaulay, <sup>2</sup> Sean T. Osis, <sup>1</sup> Christian Clermont, and <sup>1,2</sup> Reed Ferber

<sup>1</sup> University of Calgary, Calgary, AB, Canada

<sup>2</sup> Running Injury Clinic, Calgary, Canada

email: cajmacau@ucalgary.ca

## INTRODUCTION

Marker-based three-dimensional gait analysis (3DGA) is one of the most common methods for analyzing athletic performance and pathological gait in both clinical and research settings. Recently, it has been shown that errors in marker placement constitute the largest source of error in the repeated measurement of kinematic data [1]. With the increasing popularity of 3DGA, and its wide range of applications, there is a growing need to develop novel methods to improve data quality. However, prior attempts have yielded inconsistent results or clinically impractical protocols.

Osis et al. [2] introduced an expert-based software tool that provides real-time feedback to improve marker placement accuracy in considerably less time than previous marker placement devices, and without the need for initial marker placement to be completed by an expert. Preliminary studies showed the use of the tool lead to a reduction in marker placement deviation for novice users, relative to an expert. These results were encouraging however limited by the small sample size ( $n = 6$ ), and the protocol did not allow for between-day comparisons [3].

Building on the pilot work of Osis et al. [3], the purpose of this investigation was to determine if the real-time feedback tool would improve consistency in gait kinematic data collected by a larger cohort of novice examiners, and whether a similar level of improvement would be observed during a one-week follow-up session. The authors hypothesized that the

real-time feedback tool would decrease the 95% confidence interval (CI) range of mean joint angle data compared to trials without feedback.

## METHODS

All 3DGA trials were conducted on a single runner (male, 24 years, 188 cm, 75 kg). Twelve kinesiology students from a university campus assumed the role of examiner. The novice examiners had completed courses in human anatomy, and introductory biomechanics, however, none had any experience locating anatomical landmarks for the purpose of 3DGA.

Aided by a schematic of the target anatomical landmarks, the novice examiners placed retroreflective markers on the runner. A brief written description of landmark location accompanied the schematic, along with minimal verbal instruction.

Following the first static trial collection, marker data were imported to the real-time feedback software tool, which calculated the inter-quartile range ratio (IQRR) for each marker location relative to a morphometric norm, and displayed a standardized 3D plot. The examiner was instructed to use his/her judgement to adjust the markers, according to the direction and magnitude of deviation observed on the plot. No scale or measurement information were displayed. Next, a second static trial was collected, followed by a 60 second running trial which was processed using both static trial conditions collected prior to and following use of the marker check

feedback program. Set-up and protocol from day one was repeated for day two, resulting in four static trial conditions: PRE feedback day one, POST feedback day one, PRE feedback day two, and POST feedback day two.

Mean joint angle was reported to be a sensitive indicator of kinematic similarity between conditions that can provide a single representative value of the entire stride [1]. While the mean joint angle was not expected to differ with feedback, it was expected that the 95% CI range of mean joint angle would be reduced as a result of increased marker placement consistency.

## RESULTS AND DISCUSSION

On day one, the use of the real-time feedback tool reduced the 95% CI range for eight out of nine joint angles by an average of 27.45%. The ankle transverse, knee frontal, hip frontal, and hip sagittal planes showed the greatest reduction (Figure 1). On day two, use of the real-time feedback tool reduced the range of the 95% CI for five out of nine joint angles by an average of 24.73%. Consistent with day one, the greatest reductions were seen in the ankle transverse, knee frontal, hip frontal, and hip sagittal planes (Figure 1). Eight out of nine joint angles showed a reduced range of 95% CI in the POST2 condition, relative to PRE1, by an average of 28.36% (Figure 1).

In support of the hypothesis, the use of the feedback tool reduced the 95% CI of mean joint angle data, due to improved marker placement consistency for the group of novice examiners.

The results of this study agree with those of the marker placement simulation by Osis et al. [2], as mean joint kinematics in the ankle transverse, knee frontal, and hip frontal plane were among the variables that were most positively influenced by use of the feedback tool.

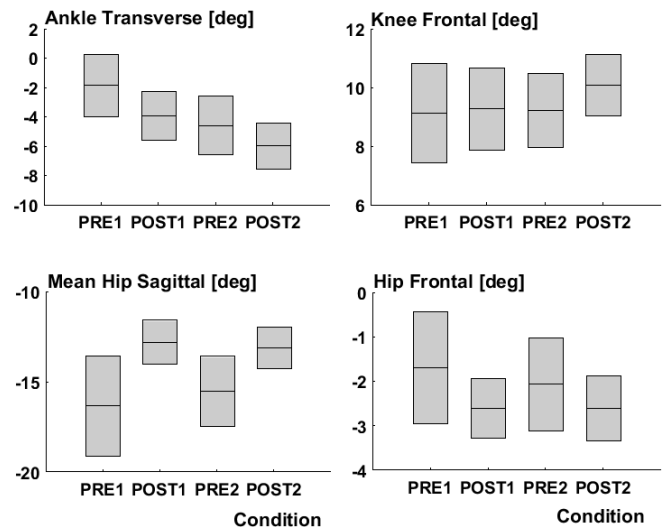


**Figure 1:** Visual representation of 95% CI for select joint angles pre- and post- feedback on days one and two. Static trial condition is displayed on x-axis.

## CONCLUSIONS

The feedback tool presented in this study improves upon previous attempts at reducing marker placement deviation by allowing for real-time feedback. It improves upon standardized training protocols by providing continuous monitoring of the examiner's placement consistency, as opposed to an infrequent training session. The findings of the current study indicate that a real-time feedback software tool improves the consistency of marker placement for a group of novice examiners, leading to improved consistency in 3DGA data.

While further refinement of the tool is encouraged, the results of this study demonstrate its benefit as a teaching and training tool in both a clinical and research gait biomechanics laboratory setting.

## REFERENCES

- <sup>1</sup> Gorton GE, et al. *Gait & Posture* **29**, 398-402, 2009.
- <sup>2</sup> Osis ST, et al. *Computer Methods in Biomechanics and Biomedical Engineering*, 37-41, 2014.
- <sup>3</sup> Osis ST, et al. *Plos One*, **11**, 2016.

# RELIABILITY OF ULTRASOUND ELASTOGRAPHY MEASUREMENTS OF THE SEMITENDINOSUS TENDON

<sup>1</sup>Zachary J. Domire, <sup>1</sup>Clara Amat-Fernandez, and <sup>1</sup>Anthony S. Kulas

<sup>1</sup>East Carolina University, Greenville, NC, USA  
email: domiez@ecu.edu

## INTRODUCTION

Measurement of tendon material properties is of interest to determine energy storage capacity, track healing, and possibly determine injury risk. Shear wave elastography (figure 1) is an attractive option to take in vivo measurements. Most studies examining ultrasound elastography as a tool to measure tendon have focused on either the Achilles or patellar tendon, and have often showed questionable reliability.<sup>1,2</sup>



**Figure 1:** Schematic of shear wave elastography. The technique uses a focused ultrasound pulse to generate a shear wave in the tissue of interest and b-mode imaging is used to measure the wave speed, which is inverted to calculate shear modulus.

Reliability of typical shear wave elastography measurements of the semitendinosus tendon has not been assessed. The semitendinosus tendon is of particular interest to measure as it is the most used type of graft for ACL reconstructions. Revision rates for semitendinosus graft surgeries are higher than for patellar tendon surgeries.<sup>3</sup> Measurement of material properties of the tendon prior to surgery may be a useful tool to help identify individuals who may have poor outcomes following ACL reconstruction using the semitendinosus tendon and help reduce revision rates.

The purpose of this research is to determine the reliability of shear modulus measurements using ultrasound elastography in healthy individuals.

## METHODS

For this study 7 (mean age=21.9 years; SD±4.5 years) healthy recreationally active individuals with no prior history of hamstring or knee injuries were recruited.

ST tendon shear wave elastography (figure 2) measurements were taken using an ultrasound device (AIXPLORER MultiWave, SuperSonic Imagine S.A., France). Height and weight were also collected during data collection.

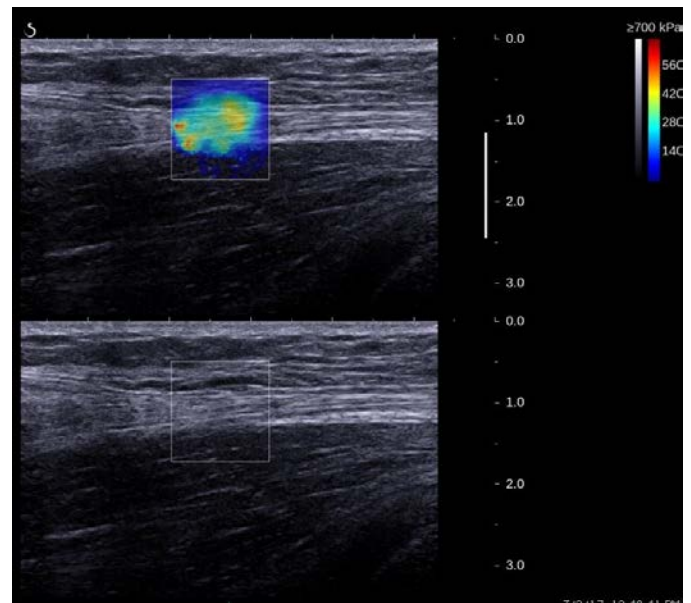


**Figure 2:** Ultrasound image of the semitendinosus to the myotendinous junction. Top: Elastogram centered over the tendon. Bottom: B-Mode image with the elastogram region shown.

Measurements were taken with the participant in a prone position with the knee fully extended. ST tendon measurements were taken just at the 50% mark between the medial epicondyle and the myotendinous junction placing the probe

longitudinally across the tissue. Measurements in the ST muscle were taken longitudinally in the middle of the muscle belly. All measurements were taken bilaterally.

Data was recorded as the mean of the values within a 2mm diameter circumference situated in the middle of the tendon. A two-way single measure intraclass correlation (ICC(2,1)) was calculated to establish the reliability of the measurement. Additionally, standard error of the measurement was calculated in absolute and relative to the mean values.

## RESULTS AND DISCUSSION

The difference between mean modulus from trial 1 to trial 2 was approximately 4kPa (Table1). There was high variability in modulus between subjects. However the reliability of the measurement was excellent (ICC=0.96). The standard error of the measurement was approximately 10% of the mean value.

Shear modulus for the current study was determined from a single measurement. It is common to report the value from an average of two or three measurements<sup>4</sup>. Doing so would likely improve the reliability of the measure.

Reliability in the current study is much better than what has been previously reported for the Achilles or patellar tendon.<sup>1,2</sup> A likely reason for questionable reliability in these studies is that the values for modulus were at or possibly above the maximum measurement capacity of the system. While there was considerable inter-subject variability in the value of modulus, even the stiffest tendons were less than 600kPa, and far below the measurement capacity.

The Achilles and patellar tendons are loaded more frequently and with higher loads than most tendons in the body. These tendons may have specialized adaptations that increase their material stiffness beyond other tendons.

## CONCLUSIONS

ICC's for tendon shear modulus were very high indicating good reliability for this measure. There was high inter-subject variability. This wide range of values possibly indicates that some tendons may be better suited as ACL grafts than others.

## REFERENCES

1. Aubry S, et al. *Skeletal Radiol*, **42** , 1143-1150, 2013.
2. Peltz CD, et al. *Skeletal Radiol*, **42** , 1151-1156, 2013.
3. Rahr-Wagner L, et al. *Am J Sports Med* **42**, 278-84, 2014.
4. Seymore KD, et al. *Eur J Appl Physiol* epub ahead of print.

## ACKNOWLEDGMENTS

We would like to acknowledge Ms. Alison Ratti and Ms. Jenna Pate for their assistance with data collection.

	Trial 1			Trial 2			ICC(2,1)	SEM	%SEM
	Mean	±	SD	Mean	±	SD			
<b>Semitendinosus tendon shear modulus (kPa)</b>	343.7	±	185	347.6	±	184	0.96	36.6	10.6%

**Table 1:** Mean ± SD for Semitendinosus shear modulus, Interclass correlation, absolute standard error, and relative standard error.

# PASSIVE IMPLANTED MECHANISM TO IMPROVE FOOT-ARCH RESTORATION FOR ADULT ACQUIRED FLATFOOT DISORDER: VALIDATION THROUGH GAIT ANALYSIS

Hantao Ling, Ravi Balasubramanian

Oregon State University, Corvallis, OR, USA

Email: ravi.balasubramanian@oregonstate.edu. Web: <http://web.engr.oregonstate.edu/~balasubr/>

## INTRODUCTION

Adult-acquired flatfoot deformity is commonly treated with a tendon transfer surgery, where the flexor digitorum longus (FDL) tendon is transferred to the attachment point of the posterior tibial (PT) tendon on the inferior side of the navicular bone to restore the forces applied to the foot arch [1] (see Fig. 1). While previous studies have shown that this treatment provides a partial improvement, the current surgery does not restore the foot arch completely. This is evidenced by a medial shift in the foot's ground reaction forces (GRF) when compared with a healthy foot's GRF [2]. This is due to the reduced force capability of the FDL muscle (about one-third of the PT's force capability) [2]. Inspired by a recent approach that surgically implants passive mechanisms in the forearm to improve grasping capability following high median-ulnar nerve palsy [3], this paper explores the use of a passive pulley between the FDL muscle and the foot arch to transfer larger forces to the foot arch. Previously, we have shown using biomechanical simulations that a passive implanted pulley creates a lateral shift of GRF (closer to the force distribution in a healthy foot) in a statically loaded flatfoot [4]. This paper now uses biomechanical simulation to show that the implant also helps shift the center of GRF laterally during the stance phase of gait.

## METHODS

Biomechanical models of a healthy foot and flatfoot with five contact spheres were developed in the OpenSim software platform [5] where the feet were divided into quadrants by the metatarsophalangeal joints and by the sagittal plane (see [6], [7] for comparable models; see Fig. 2). In the healthy foot model, 39.7% of the body weight is distributed to the medial side and 60.3% is distributed to the lateral side [8]. For the flatfoot model, 49.3% is distributed

medially and 50.7% is distributed laterally [9]. The models enabled a study of the force distribution between the medial and lateral sides of the foot during the stance phase of gait while also allowing the flexibility needed for the motion. The flatfoot model was modified twice more to represent the foot after the traditional tendon transfer surgery, where the FDL tendon is transferred to the PT tendon, and after the implant-based tendon transfer surgery, which uses a pulley to scale up the FDL muscle force (see Fig. 3).

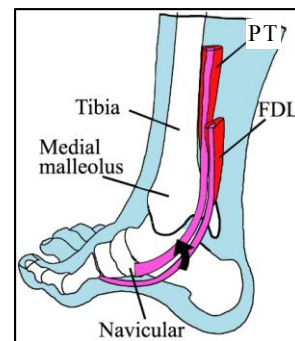


**Figure 1.** Drawing of a foot showing the relative locations of the PT and FDL tendons, and the navicular bone.

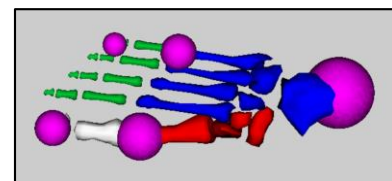


**Figure 2.** Foot model (top view). Showing four quadrants (blue, red, green, white) and five contact spheres (pink).

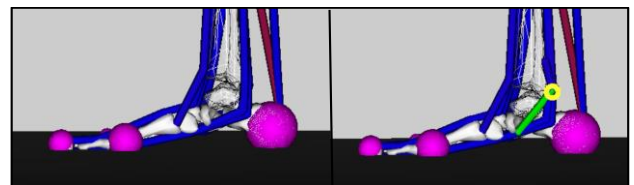


**Figure 3.** Biomechanical models representing (A) a flatfoot or a flatfoot with FDL tendon transfer and (B) a flatfoot with FDL tendon transfer and a passive implanted mechanism.

For each of the four models and simulations, the tibia was held fixed in space while a ground plane moved

relative to it to create the kinematics of a single cycle of the stance phase of gait from heel strike to toe off. While the ground plane moved, nine lower limb muscles were activated based on data generated by the Robotic Gait Simulator [10], and the GRF generated by the five contact spheres was recorded. The force data collected from the spheres on the medial toe and medial mid-foot was compiled into the medial GRF for each model. The same was done for the two spheres on the lateral toe and lateral mid-foot to produce the lateral GRF for each model.

## RESULTS AND DISCUSSION

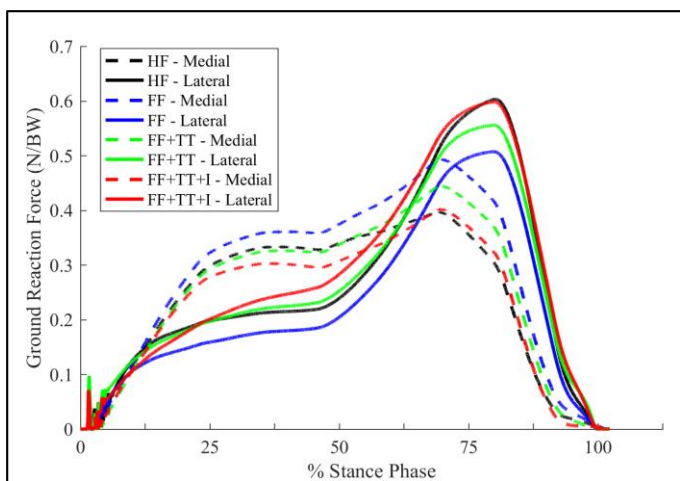


**Figure 4.** Normalized ground reaction forces of the medial and lateral sides of the foot over the stance phase of gait for a healthy foot (HF), flatfoot (FF), flatfoot with tendon transfer surgery (FF+TT), and flatfoot with tendon transfer surgery and implant (FF+TT+I).

Fig. 4 shows the shift in normalized GRF from the medial to the lateral side of the foot through the entirety of the stance phase of gait in the tendon transfer surgery models. The double peak profiles characteristic of the stance phase of gait and the GRF produced by the heel of the model were identical for each model and were left out of the plot for clarity. While the flatfoot without surgery experienced a large amount of GRF shifted medially (50.7% lateral), the traditional tendon transfer surgery model saw the force distribution shift laterally (55.6%), and

the implant-based tendon transfer surgery model caused a the most drastic lateral shift of the normalized GRF (59.8% lateral). The simulation results are summarized in Table 1. The significant transfer of GRF laterally following the implant-based surgery can be attributed to the force-scaling provided by the implant through the transferred FDL tendon. Specifically, the increase in force transferred by the FDL tendon to the navicular bone results in a lifting force acting on the foot arch that shifts the center of pressure of the foot laterally during the stance phase of gait. This matches what has been observed through cadaveric experiments [11]. Creating accurate biomechanical simulations of the flatfoot condition provides a quicker method of validating implant-based surgery when compared with cadaver studies. Future work will focus on conducting sensitivity studies on how implant location and tendon routing impacts the shifting of the center location of GRF.

## REFERENCES

1. Myerson MS, et al. *Foot and Ankle Int* **25.7**, 445-450, 2004.
2. Rosenfeld PF, et al. *Foot and Ankle Int* **26.9**, 671-674, 2005.
3. Mardula KL, et al. *Hand* **10**, 116-122, 2014.
4. Ling H, et al. *Proceedings of ASB40*, Raleigh, NC, USA, 2016.
5. Delp S, et al. *Biomed Engr*, IEEE Trans **54.11**, 1940-1950, 2007
6. Arnold EM, et al. *Ann Biomed Eng* **38.2**, 269-279, 2010.
7. Kapti OK. *Biocybern Biomed Eng* **34.2**, 132-138, 2014.
8. Chang H, et al. *PLoS ONE* **9.4**, 1-7, 2014.
9. Tang SF, et al. *Clin Neurol Nerosurg* **129**, S8-S11, 2015.
10. Aubin PM, *The Robotic Gait Simulator*, University of Washington, 2010.
11. Pihl CM, et al. *Orthopedic Research Society*, 2015.

**Table 1.** Difference in the peak medial and lateral normalized ground reaction forces (GRF) for each of the three flatfoot models.

	Healthy Foot	Flatfoot	Flatfoot with Tendon Transfer	Flatfoot with Tendon Transfer and Implant
Percentage of Ground Reaction Force on Medial Foot	39.7%	49.3%	44.4%	40.2%
Percentage of Ground Reaction Force on Lateral Foot	60.3%	50.7%	55.6%	59.8%

# EFFECT OF PROPHYLACTIC KNEE BRACING ON LOWER EXTREMITY KINEMATICS IN RUNNING AND JUMPING

Mitchell L Stephenson and Jason C Gillette

Iowa State University, Ames, IA, USA  
email: mitch.stephenson@gmail.com, web: www.kin.hs.iastate.edu

## INTRODUCTION

Knee braces have become increasingly popular in recreational and professional sport. While many braces are suggested or prescribed as part of rehabilitation post-injury [1], prophylactic use has also become more common [2]. Many recent braces from different manufacturers claim certain levels of effectiveness in preventing non-contact knee (particularly anterior cruciate ligament; ACL) injuries, but do not provide a biomechanical basis for this claim.

The current analysis compares landing biomechanics of a cross-section of recent and popular knee brace designs in two movements chosen to exacerbate non-contact ACL load. It was expected that more structurally-rigid brace designs would limit peak knee angles during ground contact [3].

## METHODS

Nine physically-active, uninjured recreational athletes (6 females and 3 males;  $21.4 \pm 1.2$  years;  $1.68 \pm 0.06$  m tall;  $71.4 \pm 8.1$  kg) have volunteered for the ongoing study. Participants provided informed consent, executed a warm-up protocol, and then performed a series of successful practice trials before the series of block-counterbalanced recorded trials.

Kinematics of 28 retroreflective markers placed on the lower extremity, pelvis, and torso were recorded via 8 Vicon cameras at 160Hz through Vicon Nexus 1.8.2 (Vicon Corp, Oxford, UK). Four brace designs were tested: a soft support, a soft hinged, a rigid hinged, and a new hybrid semi-rigid hinged design.

Participants performed a total of three recorded trials for three separate movements in an unbraced and four braced conditions. The brace was worn on the

right leg. The first movement consisted of jumping forward from a 30cm tall block, landing bilaterally with the right foot on an AMTI force platform sampling at 1600Hz, and then fluidly performing a left jump at  $60^\circ$  from anterior for maximum distance. The second movement was identical to the first, but jumped  $60^\circ$  to the right.

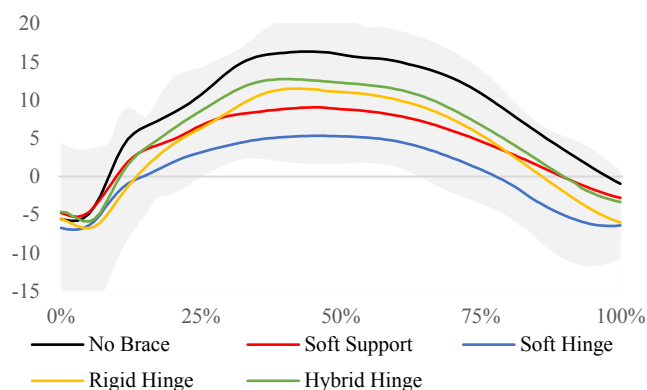


**Figure 1:** Mean knee valgus angle across percentage time in contact with the force platform for each knee brace while jumping left. Gray area represents standard deviation of measures.

The third movement consisted of participants running at a consistent self-selected pace along a 10m path, whereas at the end of the 10m, they placed their right foot on the force platform and sidestepped to the left at  $30^\circ$ . Starting position was manipulated to assure the right foot's strike on the force platform was within normal gait patterns.

Peak knee valgus, varus, and flexion angles during foot contact with the landing force platform were calculated. A repeated-measures analysis of variance was performed to compare the effect of the braces on the knee kinematics for each movement.

## RESULTS AND DISCUSSION

No significant main effects were indicated by the analysis of variance ( $p > 0.15$ ). As demonstrated in Table 1, mean peak knee angles were illustratively different, but moderately variable amongst participants. While some previous research did identify successful reduction in knee valgus angles while wearing prophylactic braces, this change was relatively minor, and the authors concluded little overall prophylactic effect from bracing [4].

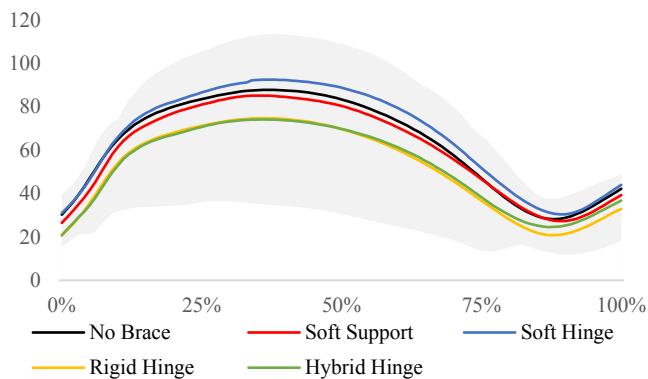


**Figure 2:** Mean knee flexion angle across percentage time in contact with the force platform for each knee brace while jumping left. Gray area represents standard deviation of measures.

It is possible that the analyzed sample was not large enough to demonstrate significant differences that may indeed exist. As seen in Figures 1 and 2, a systemic offset in knee angles between the braces is

apparent and may be clinically-relevant. In addition, a more challenging testing protocol might elicit larger differences between the knee braces and no brace.

## CONCLUSIONS

Superficially, it appears that prophylactic bracing, independent of design, may not significantly influence cutting and sidestep kinematics in healthy, active participants. This provides a dichotomy in implications: The preserved peak knee flexion and varus angles may not decrease performance or hinder ACL protective mechanisms, but the braces also did not limit peak valgus angles associated with ACL injury [5]. Further investigation is ongoing to determine effects with a larger sample size.

## REFERENCES

1. Brandsson S, et al. *Scand J Med Sci Sports*, **11**, 110-114, 2001
2. Rishiraj, JN, et al. *Sports Med*, **39**, 937-960, 2009
3. Vailas J & Pink M. *Sports Med*, **15**, 210-218, 1993
4. Teng P, et al. *Procedia Eng*, **60**, 300-306, 2013
5. Krosshaug T, et al. *Am J Sports Med*, **35**, 359-367, 2007

## ACKNOWLEDGEMENTS

The authors would like to thank United Sports Brands for providing the braces for testing.

**Table 1:** Peak knee angles (Mean  $\pm$  SE) for each brace condition during foot contact with the ground in the three movement tasks. No significant differences identified between any brace.

		No Brace	Soft Support	Soft Hinge	Rigid Hinge	Hybrid Hinge
Jump Left	Valgus ( $^{\circ}$ )	11.5 $\pm$ 3.7	8.3 $\pm$ 2.3	1.7 $\pm$ 1.3	5.9 $\pm$ 3.1	10.4 $\pm$ 3.4
	Varus ( $^{\circ}$ )	0.4 $\pm$ 3.0	2.2 $\pm$ 1.3	4.2 $\pm$ 1.3	5.5 $\pm$ 1.7	0.1 $\pm$ 1.2
	Flexion ( $^{\circ}$ )	87.8 $\pm$ 4.3	85.2 $\pm$ 3.9	92.5 $\pm$ 3.6	74.8 $\pm$ 3.3	74.2 $\pm$ 3.1
Jump Right	Valgus ( $^{\circ}$ )	16.4 $\pm$ 3.8	9.1 $\pm$ 2.8	5.3 $\pm$ 2.0	11.5 $\pm$ 3.7	12.8 $\pm$ 4.2
	Varus ( $^{\circ}$ )	5.8 $\pm$ 2.2	5.3 $\pm$ 1.2	7.0 $\pm$ 1.0	6.8 $\pm$ 1.7	5.9 $\pm$ 1.2
	Flexion ( $^{\circ}$ )	99.5 $\pm$ 3.5	91.5 $\pm$ 3.2	98.5 $\pm$ 3.5	93.4 $\pm$ 3.9	89.8 $\pm$ 3.9
Sidestep Left	Valgus ( $^{\circ}$ )	5.5 $\pm$ 2.4	5.9 $\pm$ 1.4	5.4 $\pm$ 1.6	0.0 $\pm$ 1.5	4.6 $\pm$ 0.8
	Varus ( $^{\circ}$ )	4.2 $\pm$ 1.6	2.2 $\pm$ 1.3	1.8 $\pm$ 1.3	7.0 $\pm$ 1.5	2.3 $\pm$ 0.8
	Flexion ( $^{\circ}$ )	59.8 $\pm$ 2.0	61.1 $\pm$ 1.9	64.8 $\pm$ 3.3	53.8 $\pm$ 2.2	54.6 $\pm$ 1.4

# EFFECT OF FUNCTIONAL 3D SOCKS ON THE ARCH OF THE FOOT

Misaki Wakamiya, Akinori Nagano

Ritsumeikan University, Kusatsu, Shiga, Japan  
email: [ec0240ps@ed.ritsumei.ac.jp](mailto:ec0240ps@ed.ritsumei.ac.jp)

## INTRODUCTION

The foot is the only body part to contact the ground in normal locomotion. The mechanical interaction between the foot and the ground plays an integral role. In the foot, there are characteristic structures, i.e., the arches of the foot. The arches of the foot have significant roles in the transmission of forces and absorption of shocks [1].

When the arch of the foot falls, the condition is often called “flat foot”. Flat foot is usually associated with excessive subtalar joint pronation; in the case of flat foot, instability of the lower extremity causes hypermobility and passive instability, and more neurological control by the neuromuscular system is required to maintain balance. Thus, the instability resulting from a flat foot could cause pathomechanical problems [2]. As well, the ability of balance control is hampered with flat foot. Previous research has also suggested increased incidences of injury in people with flat foot [3].

Recently, several functional socks to support the foot have been developed. The function of those socks has been studied in terms of comfort, performance enhancement and blister prevention [4, 5]. However, no study has yet clarified the effects of socks on the arch of the foot.

Therefore, the purpose of this study was to examine the effect of functional 3D socks on the arch of the foot.

## METHODS

Five healthy subjects participated in this study. The subjects were  $24 \pm 0.4$  years (mean  $\pm$  SD),  $1.72 \pm 0.03$  m and  $65.6 \pm 3.2$  kg, foot size  $27.2 \pm 1.1$  cm.

The subjects were requested to remain in the natural static standing position for 4 min wearing two types of socks: Normal type Socks (NS) and Functional 3D type Socks (3DS) (Cooma Ltd., Japan) (Fig. 1).



**Figure 1:** Functional 3D type Socks (3DS) used in this study.

Pressure measurement film (PRESCALE, FUJIFILM Ltd., Japan) was used for the measurement, placed under the right foot of the subjects. The color of the area of the film where pressure was applied turned red, and the color depth

was dependent on the intensity of the applied pressure. The image was scanned for further analysis. The scanned image was analyzed by using dedicated analysis software (FPD-8010J, FUJIFILM Ltd.). The regions of analysis were determined by referring to the position of metatarsal phalangeal joint and medial malleolus; from metatarsal phalangeal joint to the tip of the toe (Toe), from metatarsal phalangeal joint to medial malleolus (Arch), from medial malleolus to the tip of the heel (Heel) (Fig. 2).

The size of pressure areas was compared using a paired *t* test between the Normal type Socks (NS) and Functional 3D type Socks (3DS). The level of significance for all statistical analyses was set at  $P = .05$ .

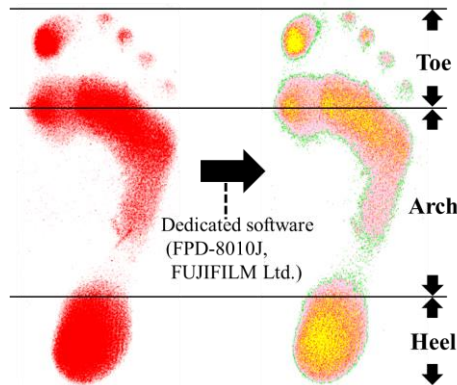


**Figure 2:** Analysis method  
Left side: Scanned image  
Right side: Foot pressure distribution

## RESULTS AND DISCUSSION

The size of pressure areas was smaller in the 3DS condition compared to the NS condition, in the Arch, Heel, and Total regions of the foot (Fig. 3 and Table 1).

**Table 1:** Summary of the pressure area

	Pressure area (mm <sup>2</sup> )		
	NS	3DS	
Toe	1902.8 ± 329.9	1526.4 ± 309.8	N.S.
Arch	3103.2 ± 563.1	2025.4 ± 665.0	P<0.05
Heel	2335.4 ± 405.4	2094.8 ± 392.5	P<0.05
Total	7341.4 ± 654.5	5603.4 ± 1047.9	P<0.05



**Figure 3:** Foot pressure distribution  
Left side: Normal Socks (NS)  
Right side: Functional 3D type Socks (3DS)

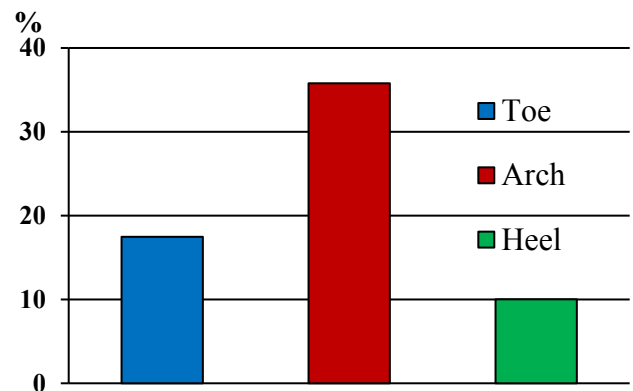


**Figure 4:** Reduction rate of the pressure area

The result suggested that the foot arch was supported by the 3DS. Especially, reduction rate of the pressure area in the 3DS condition was greater than 30% in the Arch of the foot (Fig. 4).

These results suggest that the 3D socks used in this study have a function to support the arches of the foot.

## REFERENCES

1. Robbins SE, Hanna AM. *Med Sci Sports Exerc* 19:148–156, 1987.
2. Franco AH. *Phys Ther* 67: 688-694, 1987.
3. Paul S. *The foot* 26: 58–63, 2016.
4. Bogerd CP et al. *Ann Occup Hyg* 56 (4): 481-488, 2012.
5. Blackmore T et al. *Clinical Biomechanics* 28: 825–830, 2013.

# Effect Of Foot Orthotics On Force Distribution In The Ankle And Subtalar Joint: A Cadaveric Study.

<sup>1</sup> Aron Lechtig, <sup>1,2</sup> Patrick Williamson, <sup>1</sup> Philip Hanna, <sup>1</sup> Stephen Okajima, <sup>1</sup> Peter Biggane, <sup>1</sup> Michael Nasr, <sup>3</sup> Naven Duggal, <sup>1</sup> Ara Nazarian

<sup>1</sup> Center for Advanced Orthopaedic Studies, Beth Israel Deaconess Medical Center, Harvard Medical School. Boston, MA, USA

<sup>2</sup> Department of Mechanical Engineering, Boston University, Boston, MA, USA

<sup>3</sup> Syracuse Orthopaedic Specialists, Department of General Orthopedics and Trauma, Foot and Ankle Division

## INTRODUCTION

Foot orthotics are used to treat a variety of disorders that affect the lower limb and can be purchased as generic over the counter (OTC) or patient-specific products after proper evaluation. The popularity of orthotics has increased over time, and is estimated to reach a market size of \$3.5 Billion by 2020 from \$2.5 Billion in 2014<sup>1</sup>. This allows patients to buy orthotics empirically as a means to alleviate lower limb pain and discomfort. Given the number of orthotic options and anatomical variances, it is unlikely that the patient chooses the correct orthotic.

The foot habitus is the foundation of the lower limb, which depends on its mechanics, orientation and force distribution to maintain a balanced and correlated system. Incorrect modification of the foot habitus can trigger a chain reaction of mechanical events which can cause negative impact on articular cartilage<sup>2</sup>. This study aims to compare the pressure distribution in the ankle and subtalar joint with and without orthotics.

## METHODS

Five fresh-frozen lower limb cadaveric specimens without known skeletal conditions were used. The femoral head was potted with poly (methyl methacrylate) (PMMA) for positioning it against the loading apparatus. Two TekScan pressure sensors (model 6900; TekScan, South Boston, MA, USA) were inserted into the ankle and subtalar joint. Specimens were placed on a custom jig composed of a steel scissor jack equipped with a load cell (model LTH400 rated for 1000 lb, Futek, Irvine, CA, USA) mounted on the in-house made metal box frame to apply Cranio-caudal force on the femoral head of a supine leg. This allowed for modulated

loading of the leg; 75lb load (half-body-weight)<sup>3</sup> applied at the femoral head while the foot was supported against a fixed-plate keeping the ankle in neutral position.

Testing was conducted by placing orthotics underneath the medial half of the sole at the level of the Talo-navicular joint. Mean pressure (MP), peak pressure (PP), contact area (CA), and center of force (COF) were measured in the previously mentioned 2 joints under three conditions; barefoot (BASE), with 1.5cm (ORT1) and 3cm (ORT2) height orthotics.

Each condition was tested three times per specimen; the results were averaged per specimen and used for final analysis. Displacement of the COF was calculated relative to its location at baseline. The absolute vector displacement, medial/lateral and anterior/posterior displacement values were also calculated.

## RESULTS AND DISCUSSION

With ORT1 and ORT2, the COF was significantly displaced from its location at BASE as can be seen in **Table 1** at the ankle by  $0.38 \pm 0.24\text{cm}$  and  $0.30 \pm 0.12\text{cm}$  (Mean  $\pm$  SD) respectively ( $p < 0.05$ ) and at the subtalar joint by  $0.23 \pm 0.18\text{cm}$  and  $0.76 \pm 0.48\text{cm}$  (Mean  $\pm$  SD) respectively ( $p < 0.05$ ), shown in **Figure 1** below.

There was no significant difference among BASE, ORT1 and ORT2 regarding the MP, PP and CA ( $p > 0.05$ ).

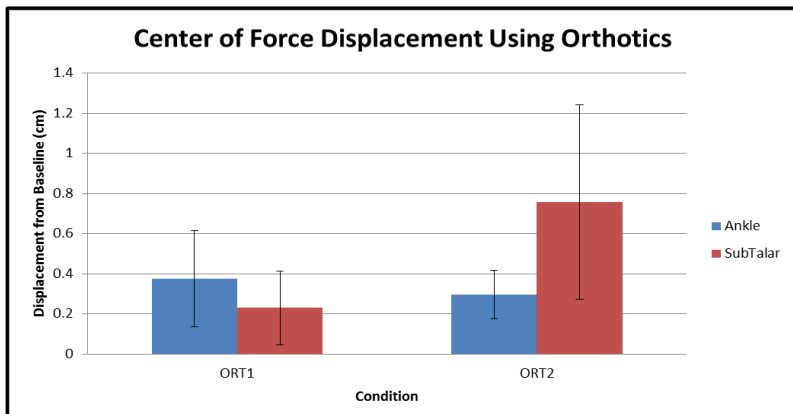


**Figure 1.** Mean and SD of the absolute displacement values from baseline (0) of the center of force in the Ankle and Subtalar joint under ORT1 and ORT2 conditions.

The mechanical impact of orthotics depends on the shape, material and height; which are highly variable parameters among the commercially available orthotics.

Based on our findings, the placement of a solid material between the foot and the ground could modify the location of the COF within the lower limb joints. We believe that this is the result of the alteration on the foot habitus and joint orientation.

Further, *Krause et al.* shows that changes in joint orientation and non-physiological location of the COF are related to the development of articular degenerative changes<sup>4</sup>. We argue that improper use of orthotics has the potential to lead to similar adverse effects, due to their ability to change COF.

Many studies have shown the improvement on biomechanics and quality of life after the proper use of orthotics, nonetheless the high variability between subjects, conditions and available orthotics require a careful evaluation for each patient to achieve positive results with orthotics<sup>5,6</sup>.

We encourage further investigation of the effect of foot orthotics in a larger sample size as well as their potential adverse effect on joints within the lower limb.

## CONCLUSIONS

Based on our findings, previous studies and the accepted mechanism of articular degenerative conditions development, we believe that the unsupervised use of orthotics can lead to negative articular consequences with prolonged use. We recommend the use of foot orthotics under supervision after a rigorous evaluation of the patient.

## REFERENCES

1. IndustryARC. Foot Orthotic Insoles Market to Reach 3.5 USD Billion By 2020. 2016.
2. Steffensmeier S, Berbaum K, Brown T. Effects of medial and lateral displacement calcaneal osteotomies on tibiotalar joint contact stresses. *J Orthop Res.* 1996;14(6):980-985.
3. Krause FG, Sutter D, Waehnert D, Windolf M, Schwieger K, Weber M. Ankle joint pressure changes in a pes cavovarus model after lateralizing calcaneal osteotomies. *Foot Ankle Int.* 2010;31(9):741-746.
4. Krause F, Windolf M, Schwieger K, Weber M. Ankle joint pressure in pes cavovarus. *Bone Joint J.* 2007;89(12):1660-1665.
5. Marks R, Penton L. Are foot orthotics efficacious for treating painful medial compartment knee osteoarthritis? A review of the literature. *International journal of clinical practice.* Jan 2004;58(1):49-57.
6. Nigg BM, Stergiou P, Cole G, Stefanyshyn D, Mundermann A, Humble N. Effect of shoe inserts on kinematics, center of pressure, and leg joint moments during running. *Med Sci Sports Exerc.* Feb 2003;35(2):314-319.

**Table 1.** Statistically significant *p* values for the comparison of COF displacement between orthotics conditions and baseline in the ankle and subtalar joint.

Joint	Ankle		Subtalar Joint	
Condition	ORT1	ORT2	ORT1	ORT2
BASE	0.012	0.003	0.024	0.012

# EFFECTS OF WATER IMMERSION ON PLANTAR SKIN PROPERTIES AND SENSITIVITY

Daniel Schmidt\*, Andresa M.C. Germano, Tina Drechsel, Thomas L. Milani

Chemnitz University of Technology, Department of Human Locomotion, Chemnitz, Saxony, Germany

\*email: daniel.schmidt@hsw.tu-chemnitz.de, web: <https://www.tu-chemnitz.de/index.html.en>

## INTRODUCTION

Skin is the largest organ in the human body, and has many important functions like protecting from dehydration and preventing the intrusion of microorganisms or chemicals [1]. Recent studies showed that certain external factors negatively influence the protective skin function and increase the likelihood of (plantar) ulcer formation [2, 3], affecting quality of life. One of these factors is long-term water exposure. To our knowledge, effects of a shorter duration of water exposure (<1h) have not been reported. Furthermore, assessing plantar skin sensitivity (e.g. vibration perception thresholds, VPTs) may be desirable, since decreased sensitivity is known to facilitate ulcers formation. Decreased sensitivity could also result from water immersion, since water softens the skin [3] and may damp vibration stimuli. Therefore, the present study investigated the effects of short-term water immersion (45min) on various plantar skin properties and sensitivity. We hypothesized increased elasticity and softness, as well as decreased deformation resistance and sensitivity.

## METHODS

18 healthy subjects (mean±SD: 23.8±2.7yrs, 176.1±9.4cm, 69.5±9.5kg) participated in this study. Subjects were informed about the aim of this study and gave written informed consent. If subjects experienced any discomfort, they were free to withdraw from this study at any time. Furthermore, all measurements were conducted according to the recommendations of the Declaration of Helsinki.

First, subjects acclimatized to room temperature (23±2°C) for 10min (barefoot). Then, various plantar skin properties were measured at the Hallux of both feet prior to the intervention (pre): a) skin temperature using an infrared thermometer

(UT301C, Uni-T, China); b) the logarithmic decrement (log D) of the natural oscillation to characterize the tissue's elasticity using the MyotonPRO device (Myoton AS, Estonia); c) the tissue's deformation resistance using a durometer (AD-100-OO, Checkline Europe, Germany) and stiffness (S) readings using the MyotonPRO; and d) skin sensitivity (VPTs) using a TiraVib vibration exciter (Model TV51075, Germany, 200Hz).

The participants' right or left foot was randomly assigned as either control (CF) or intervention foot (IF). During the intervention, subjects sat in a chair and the IF was immersed completely in water (45min, adjusted according to initial Hallux temperature). Meanwhile, the CF remained untreated resting on an insulating foam surface. After the water intervention (post), all of the above-mentioned skin properties were measured again in the same manner. A standardized protocol for all measurements was applied.

Three trials were collected for all analyzed skin properties (except skin temperature), respectively. The mean from those trials was calculated for further analysis (performed R, The R Foundation for Statistical Computing, Austria). The Shapiro-Wilk-Test was used to test for normality of data ( $\alpha=0.05$ ). Pairwise comparisons of each of the skin properties were performed using a dependent t-test and Wilcoxon test for normally and not normally distributed data, respectively ( $\alpha=0.05$ ).

## RESULTS AND DISCUSSION

Although we tried to maintain all temperatures at constant levels, post water temperatures were slightly decreased resulting in slightly decreased post skin temperatures: 1.5°C (CF) and 1.8°C (IF). However, such differences are not expected to influence skin sensitivity [4].

Water immersion significantly reduced both log D and durometer readings (Fig. 1), confirming our hypothesis. The other skin properties (VPTs; S), however, remained unaffected by the intervention (Table 1), contradicting our hypothesis. Since log D is inversely proportional to the tissue's elasticity [5], water immersion increased the skin's elasticity. This was also evident by decreased durometer readings, suggesting a softening of the skin.

The softening effect of water on skin was already confirmed in an earlier study [3]. Mayrovitz et al. [3] also found that the vulnerability of blood vessels to pressure-induced blood flow reductions was increased, hence facilitating ulcer formation after long-term (5.5h) water exposure [3]. Additionally, another study showed that skin wetting increased abrasion damage, skin permeability, and microbial growth [2]. Although skin sensitivity did not decrease in this study, some of the other developments found in previous examinations were

already present after our short-term exposure (45min), e.g. skin softening. As reported above, this could have similar detrimental effects regarding ulcer formation, and might especially be the case in subjects with impaired skin recovery capabilities.

## REFERENCES

1. Forooz A, et al. *Sci World J* **2012**, 1-5, 2012.
2. Zimmerer R, et al. *Pediatr Dermatology* **3**, 95-101, 1986.
3. Mayrovitz H & Sims N. *Adv Skin Wound Care* **14**, 302-308, 2001.
4. Schlee G, et al. *Clin Neurophysiol* **120**, 1548-1551, 2009.
5. Chuang LL, et al. *Stroke Res Treat* **2012**, 1-7, 2012.

## ACKNOWLEDGMENTS

Special thanks are directed to the Sächsische Aufbaubank (SAB) for providing scholarship.

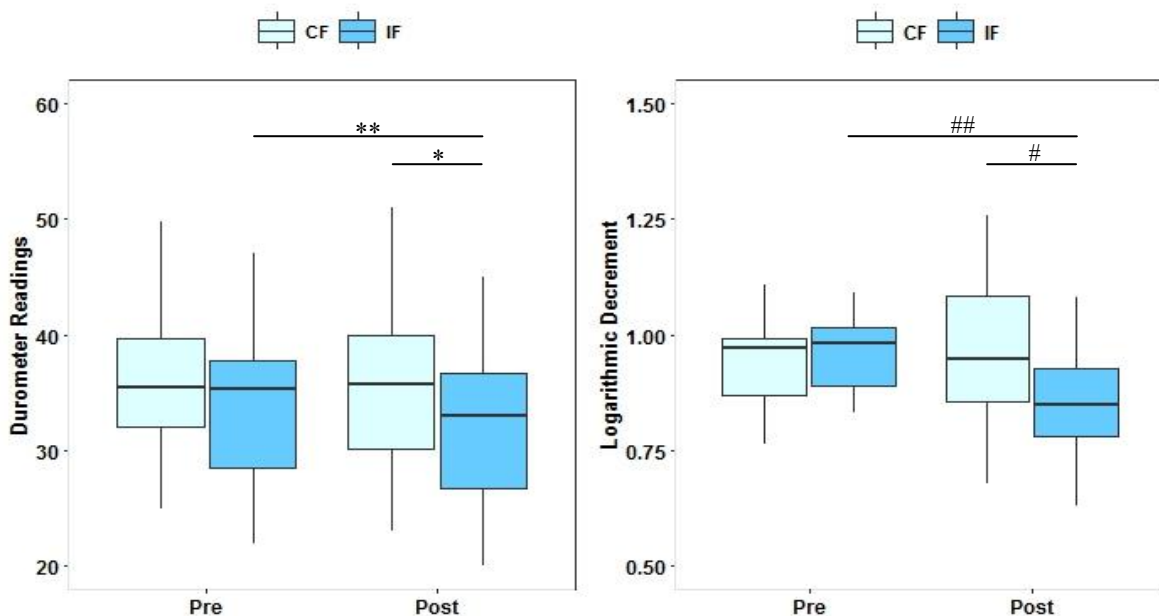


**Figure 1:** Durometer readings and logarithmic decrements pre and post intervention for the control foot (CF) and intervention foot (IF) at the Hallux. Significant differences: \* $p=0.037$ , \*\* $p=0.008$ , # $p=0.006$ , ## $p=0.013$ .

**Table 1:** Mean±SD of vibration perception thresholds (VPTs) and stiffness (S) pre and post intervention for the control foot (CF) and intervention foot (IF) at the Hallux. No significant differences were found.

	Pre		Post	
	CF	IF	CF	IF
VPTs [ $\mu\text{m}$ ]	2.3±2.7	2.1±2.2	1.9±1.5	1.9±1.6
S [N/m]	491.5±40.0	480.2±45.8	492.4±51.3	480.5±56.4

# THIGH-CALF CONTACT DURING SIX HIGH KNEE FLEXION MOVEMENTS: ONSET, RANGE OF MOTION, MAGNITUDE, AND CONTACT AREA

David C Kingston, Stacey M Acker

University of Waterloo, ON, Canada

E-mail: [stacey.acker@uwaterloo.ca](mailto:stacey.acker@uwaterloo.ca) Web: <https://uwaterloo.ca/biomechanics-of-human-mobility-lab/>

## INTRODUCTION

Limited data are available to define parameters of contact force between the thigh and calf during high knee flexion ( $>120^\circ$ ) postures [1]. Given the elevated incidence of degenerative knee diseases in populations that regularly assume these postures, further insight to refine injury mechanisms is needed [2]. Currently, no known three-dimensional musculoskeletal models incorporate thigh-calf contact parameters when estimating knee joint contact loads. Therefore, the purpose of this study was to quantify contact force, area, onset, and maximum angle between the thigh and calf during six high knee flexion postures.

## METHODS

Twenty-eight males ( $23.7 \pm 3.8$  yrs,  $1.77 \pm 0.1$  m,  $77.2 \pm 15.6$  kg) and 30 females ( $21.0 \pm 3.8$  yrs,  $1.63 \pm 0.1$  m,  $61.7 \pm 10.3$  kg) performed five repetitions of transitions to six high knee flexion postures. Postures were heels-up squat, flatfoot squat, dorsiflexed kneel, plantarflexed kneel, dorsiflexed asymmetric kneel, and plantarflexed asymmetric kneel. Trial order was fully randomized. Kinematics were recorded at 64 Hz (3020/Certus, NDI, Waterloo, ON) for the right foot, shank, thigh, and the pelvis. Thigh-calf contact total force and area were recorded simultaneously at 64 Hz with a sensor (3005E, Tekscan, South Boston, MA) attached to the posterior right thigh.

At the frame where  $110^\circ$  of knee flexion angle occurred, the average of force data from a 10-frame window ('baseline') and SD were calculated. Onset (Figure 1 – left black vertical line) was defined as the frame where force data exceeded baseline by two SD. Max angle was manually selected for each trial where the knee flexion angle plateaued (Figure 1 – right black vertical line).

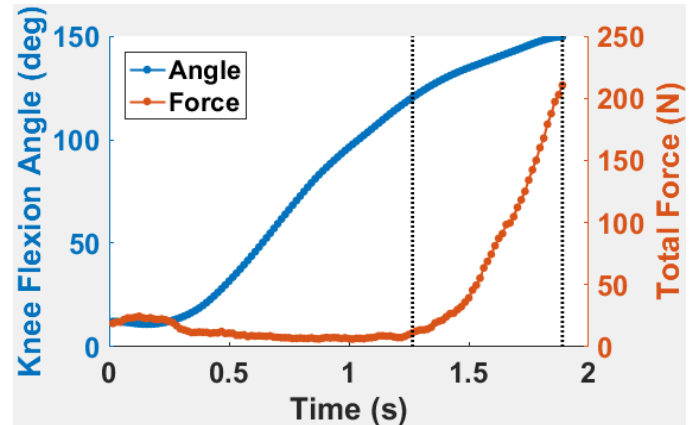


**Figure 1:** Thigh-calf contact onset (left black vertical line) and max angle (right black vertical line) during a heels-up squat.

A linear mixed-model, with a-priori alpha set to 0.05, was used with fixed variables of sex and posture to assess differences between postures for onset, max angle, force, and area. Bonferroni corrections were made on pairwise post-hoc tests to adjust  $\alpha$  levels.

## RESULTS AND DISCUSSION

Mean values from all participants are reported in Table 1. Of the 58 participants, only 23 (11M/12F) were able to achieve thigh-calf contact in the flatfoot squat posture. A main effect of posture ( $p < 0.001$ ) occurred for onset with post-hoc comparisons indicating differences only in the pair of asymmetric kneeling tasks; plantarflexed asymmetric kneel onset being  $4.4^\circ$  earlier than dorsiflexed asymmetric kneel ( $p = 0.001$ ). A main effect of sex ( $p = 0.011$ ) also occurred in onset with females ( $124.1^\circ$ ) achieving thigh-calf contact  $3.1^\circ$  later than males ( $121.0^\circ$ ).

A main effect of posture ( $p < 0.001$ ) occurred in max angle with plantarflexed kneeling being  $3.2^\circ$  higher than flatfoot squat. A main effect of sex ( $p = 0.001$ ) also occurred in max angle with females

(154.4°) having 7.0° higher flexion than males (147.4°).

The only main effect in force was posture ( $p < 0.001$ ). The posture with the highest total contact force (DAK) was 139.08N higher than FS.

Finally, there was an interaction of posture by sex for contact area ( $p = 0.013$ ). Simple main effects indicated that, when performing plantarflexed kneel, females (155.6 cm<sup>2</sup>) had 18.3 cm<sup>2</sup> larger contact area than males (137.3 cm<sup>2</sup>).

These results indicate that there is considerable force transfer between the thigh and calf during high knee flexion postures. Therefore, incorporating these parameters in a model of the knee would decrease compressive joint contact force estimates. Given that females achieved higher knee flexion angles, and no effect of sex was found in force, it would suggest that females would experience more unloading than males when normalizing force estimates to percentage body mass. In addition, these findings suggest that future predictive efforts need only focus on a single posture, from each of the three postural pairs (e.g. squatting, kneeling, asymmetric kneeling), since the effect of ankle position appears to be minimal for these outcome measures.

Experimental findings of onset differ from previously reported data (heels-up squat and dorsiflexed kneeling postures from 10 participants) [1]. Onset occurred approximately 10° and 15° earlier

in squatting and kneeling respectively. This discrepancy is likely because previous work used a pressure sensor designed for seating applications (Conformat #5330, Tekscan, South Boston, MA) which has a non-sensing border around the sensor. Similarly, previous work did not use standardized anatomical coordinate systems to define knee flexion angles as only three markers were used; the greater trochanter, lateral epicondyle, and lateral malleolus.

Only ≈40% of participants achieved thigh-calf contact during the flatfoot squat posture. For many North American populations, this posture is not commonly practiced [3]. Therefore, applicability of these data to groups who assume these postures regularly (e.g. East Asian or Middle Eastern) should be done with caution.

Future work will investigate the feasibility of predicting these parameters using anthropometric based regression and incorporation into a three dimensional musculoskeletal joint contact model of the knee to account for unloading effects. Fluoroscopic data are needed to verify joint angle findings and better estimate tibiofemoral translation when assuming maximal range of motion postures.

## REFERENCES

1. Zelle J, et al. *Clin Biomech* **22**, 821-826, 2007.
2. Bombardier C, et al. *Arthritis Alliance of Canada*, 2011.
3. Chong, et al. *Knee*. **24**(2): 271-279, 2017

**Table 1:** Mean values ( $\pm 1$  SD) of high knee flexion parameters. † and ‡ indicate main effects of posture or sex respectively, \* is an interaction of posture and sex. Values sharing superscripts are not different ( $p < 0.05$ ).

Posture	Onset (deg)†‡	Max Angle (deg)†‡	Force (N)†	Area (cm <sup>2</sup> )†*
<b>Heels-up Squat</b>	125.0 $\pm$ 7.5 <sup>a</sup>	149.6 $\pm$ 9.0 <sup>a</sup>	73.6 $\pm$ 54.2 <sup>c</sup>	90.5 $\pm$ 31.3 <sup>d</sup>
<b>Flatfoot Squat</b>	128.1 $\pm$ 7.7 <sup>a</sup>	149.5 $\pm$ 7.5 <sup>c</sup>	51.1 $\pm$ 34.7 <sup>d</sup>	77.1 $\pm$ 28.3 <sup>e</sup>
<b>Dorsiflexed Kneel</b>	122.1 $\pm$ 7.3 <sup>bc</sup>	151.8 $\pm$ 9.6 <sup>b</sup>	118.6 $\pm$ 68.6 <sup>a</sup>	125.2 $\pm$ 37.5 <sup>a</sup>
<b>Plantarflexed Kneel</b>	119.7 $\pm$ 6.4 <sup>b</sup>	152.7 $\pm$ 8.8 <sup>b</sup>	114.2 $\pm$ 62.0 <sup>a</sup>	124.2 $\pm$ 34.5 <sup>ab</sup>
<b>Dorsiflexed Asymmetric Kneel</b>	124.3 $\pm$ 7.8 <sup>b</sup>	151.4 $\pm$ 10.4 <sup>a</sup>	190.2 $\pm$ 99.7 <sup>b</sup>	152.9 $\pm$ 46.7 <sup>bc</sup>
<b>Plantarflexed Asymmetric Kneel</b>	119.9 $\pm$ 6.5 <sup>c</sup>	149.9 $\pm$ 10.5 <sup>b</sup>	169.4 $\pm$ 99.5 <sup>b</sup>	134.5 $\pm$ 44.6 <sup>c</sup>

# BIOMECHANICAL COMPARISON OF WARM-UP PROCEDURES FOR ACHILLES TENDON

<sup>1</sup> Ya Hsun Shen, <sup>2</sup> Shuo Ju Chiang, <sup>3</sup> Chih Hwa Chen, <sup>1</sup> Hsiang Ho Chen

<sup>1</sup>Taipei Medical University, TAIPEI, TAIWAN

<sup>2</sup> Taipei City Hospital, TAIPEI, TAIWAN

<sup>3</sup> Taipei Medical University Hospital, TAIPEI, TAIWAN

email: hchen@tmu.edu.tw

## INTRODUCTION

With the development of the society, leisure activities and exercises, especially jogging, are becoming more popular. More and more females participate in sports, virtually evolving into a trend. However, many people are busy and warm up exercises can be ignored easily, which may result in sports injuries. Achilles tendon (AT), commonly known as the calcaneus tendon, is located in the back of the calf. At the end of the gastrocnemius, it tapers off and becomes tendon tissue connecting to the calcaneus, serving as the connection between muscle and bone. AT is the body's thickest, largest, and strongest tendon, with an average length of 15 centimeters. Its flexibility is critical during exercise, as it can withstand 8 times the body's weight while running and jumping. Repeated stretching causes the AT to become fatigued, leading to rupture [1]. This study focuses on the effects of two different warm up routines on the AT of females who exercise regularly. We utilize jogging and hot compresses as the two warm up methods and then analyze the risk of injury posed to the AT.

## METHODS

Ten untrained female amateurs, who regularly participated in recreational running and were able to comfortably run 2 kilometers, volunteered to participate in this study. Candidates with any history of AT injuries or other major injuries to the lower limbs that impeded normal gait were excluded from the study.

During the two-week period of the experiment, we conducted trials on the first, the fourth, and the eleventh day. The baseline test was performed on the first day. We marked Soles muscle-tendon junction (Soles MTJ) as point A and Gastrocnemius muscle-

tendon junction (Gastrocnemius MTJ) as point B. A mechanical properties test and ultrasound scan were performed immediately. On the fourth day, we set the treadmills in Taipei Medical University's recreational center to 11.3-14.5 kilometers per hour (adjusted in accordance with each participant's height). After participants ran for 15 minutes, we immediately performed a mechanical properties test and ultrasound scan. On the eleventh day, we used heat padding on the participants. We set electric blankets (iLove, New Taipei City, Taiwan) to 45 degrees Celsius and covered participants' legs from the knees down until the calcaneus. Then we let participants ran for 15 minutes, after that the same tests were performed.

We built spring pedals to perform the mechanical properties tests. The ankle torque was set at 27N-m (50% MVC, maximal voluntary contraction), and the spring pedal board was placed flat on the ground. Participants sat with their knees bent at 90 degrees and used their dominant foot to step on the board, affixed with a girdle, at 50% MVC in the plantar flexion position. To ensure accuracy, the two points underwent three isometric contractions and simultaneous ultrasound scans. Throughout the process, the probe remained at the same position for two seconds at a time.

We used the GE Vivid I ultrasonography machine, coupled with the GE linear probe 12L-RS to perform 2D ultrasonography manually, followed by tissue speckle tracking using the Echopac software in order to determine movement of the MTJ, strain rate, mechanical parameters, etc. A two-way ANOVA and post hoc analyses were conducted by SPSS at  $p=0.05$ .

## RESULTS AND DISCUSSION

The displacement of two points (A and B) were measured and represented lengthening of three tissues (free tendon, soleus tendon and Gastrocnemius tendon) in three warm-up conditions (Table 1). The strain rate of three tissues were measured and compared among three warm-up conditions (Table 2). The two-way ANOVA test revealed that there were differences in lengthening and strain rate of tendon tissues for different tissue types. The post hoc test showed there were differences between lengthening of Gastrocnemius tendon and Soleus tendon in the control group and the hot-compress treatment group. It was also found that the strain rate of the single tendon and the Gastrocnemius tendon were significantly different in the control group and the hot-compress group. The strain rates of the single tendon and the Soleus tendon were significantly different in the control group and the hot-compress group.

The results indicate that elasticities of tissues were significantly different in the situations without warm-up and with hot-compress treatment. There was no significant difference between tissues after warm-up by jogging. Different mechanical behavior between tissues might induce injury during being stretched.

## CONCLUSIONS

**Table 1. The displacement (mm) of three tendon tissues were compared among three warm-up conditions**

	Free tendon			Gastrocnemius tendon			Soleus tendon (between two MTJs)		
	Control	Warm	Jogging	Control	Warm	Jogging	Control	Warm	Jogging
Mean( $\pm$ SD)	0.27 $\pm$ 0.31	0.22 $\pm$ 0.18	0.33 $\pm$ 0.28	0.37 $\pm$ 0.21	0.37 $\pm$ 0.21	0.49 $\pm$ 0.45	0.16 $\pm$ 0.29	0.15 $\pm$ 0.31	0.21 $\pm$ 0.51

**Table 2. The strain rate (1/sec) of three tendon tissues were compared among three warm-up conditions**

	Free tendon			Gastrocnemius tendon			Soleus tendon (between two MTJs)		
	Control	Warm	Jogging	Control	Warm	Jogging	Control	Warm	Jogging
Mean( $\pm$ SD)	0.02 $\pm$ 0.01	0.03 $\pm$ 0.04	0.10 $\pm$ 0.21	0.11 $\pm$ 0.07	0.07 $\pm$ 0.05	0.11 $\pm$ 0.11	0.08 $\pm$ 0.07	0.04 $\pm$ 0.07	0.00 $\pm$ 0.26

The present study found that Achilles tendon tissues after treatment with hot-compress were similar to tendon tissues without any warmup. However, jogging caused no difference between tendon tissues. The contribution of warming up towards performance is still controversy. Numerous authors have attributed the protective benefits of warming up in increasing range of motion or body temperature to causing a decrease in AT flexibility [2]. However, there is no literature which can specify that muscle and tendon contractions lead AT to Stretch-Shortening-Cycle (SSC) during warmup exercises. If athletes could know more about this phenomenon, they will be able to better protect their AT and improve their performances.

## REFERENCES

1. Lichtwark et al. Journal of Experimental Biology, 216: 4388-4394, 2013.
2. Peltonen et al. Journal of Experimental Biology, 215: 3665-3671, 2012.

## ACKNOWLEDGMENTS

This study is supported by a ROC research grant of MOST 105-2221-E-038-016.

# EFFECTS OF KINEMATICS ON THE SURFACE WEAR SCARRING AND WEAR DEBRIS IN A TOTAL ANKLE REPLACEMENT

<sup>1</sup> Nathan Webb, <sup>1</sup> Jesse Fleming, <sup>2</sup> Fabrizio Billi, <sup>1</sup> Jon Moseley, <sup>1</sup> Doug Linton

<sup>1</sup> Wright Medical, Memphis, TN

<sup>2</sup> Dept. of Orthopaedic Surgery, David Geffen School of Medicine, UCLA, Los Angeles, CA  
email: nathan.webb@wright.com web: www.wright.com

## INTRODUCTION

Wear particles of ultra-high-molecular-weight-polyethylene (UHMWPE) are a cause of implant loosening in total joint arthroplasty [1]. A previous ankle simulator wear study demonstrated no reduction in wear rate for a vitamin E-stabilized, crosslinked UHMWPE when compared to conventional UHMWPE when using an anterior/posterior motion of +/- 0.3mm. When the anterior/posterior motion was increased to +/- 1.5 mm (with all other parameters unchanged), the wear rate increased by 121% for conventional polyethylene but only by 43% for the crosslinked material [2]. In this study, the surface wear scarring and wear debris are analyzed and discussed.

## METHODS

Six TAR wear couples were mounted in a Shore Western Knee Wear Simulator modified for ankle wear. Three control tibial inserts were manufactured from Ticona GUR1020 UHMWPE (INBONE® II, Wright Medical, Memphis, TN). Three inserts, geometrically identical to the controls, were manufactured from Ticona GUR1020-E, a UHMWPE resin blended with 0.1%  $\alpha$ -tocopherol (w/w), which had been crosslinked with 65 kGy e-beam radiation. The insert with conventional UHMWPE is marketed for sale internationally. The crosslinked insert is not an approved medical device and was manufactured for research purposes only. All samples were sterilized with ethylene oxide gas.

Wear was conducted in 25% bovine serum, with EDTA and sodium azide. All samples were preconditioned in the lubricant for 48 hours prior to initial weighing.

The kinematic profiles used for wear testing was previously described [2]. The initial 2 million cycles had an anterior/posterior motion that varied from

0.3mm anterior to 0.3mm posterior ("Low A/P"). From 2M to 4M cycles, this motion was increased to 1.5mm anterior to 1.5mm posterior ("High A/P"). Inserts were rotated to a different wear station every million cycles. Mass loss and dimensional change have been previously presented.

At 2M, 3M, and 4M cycles, the surface of the inserts were marked with different colors of ink based on the appearance of the surface. Four surface textures were marked: pitting, scratching, polishing, and undamaged (visible machine marks). Marking was conducted with the aid of a stereo microscope (6.5x–8x). Photographs of the wear scars were taken with a ruler visible in the image. ImageJ (National Institutes of Health, United States) was used to measure the area of each wear scar type, using the ruler for calibration of the area measurement. Two-sample t-tests were used to determine statistical significance between groups ( $p \leq 0.05$ ).

Wear particles were characterized using the method outlined in [3]. Serum samples from the fluid changes at 0.5M cycles and 2.5M cycles were analyzed. One sample (2.5M cycle, conventional UHMWPE) out of the three collected was discarded due to a wear simulator station failure mid-test.

## RESULTS AND DISCUSSION

The wear scarring summary is shown in Figure 1. With conventional UHMWPE inserts, the increase in the A/P motion increased the area of scratching on the surface of the insert by 135% ( $p = 0.004$ ). This trend was also present in the crosslinked inserts, although not significant ( $p=0.086$ ).

Pitting in the crosslinked inserts at the high A/P was less than pitting observed in the conventional inserts, although this did not reach the level of significance chosen for this test ( $p = 0.094$ ).

Similarly, the area of the insert that showed scratching scars in the crosslinked inserts was less than that of the conventional inserts ( $p = 0.089$ ).

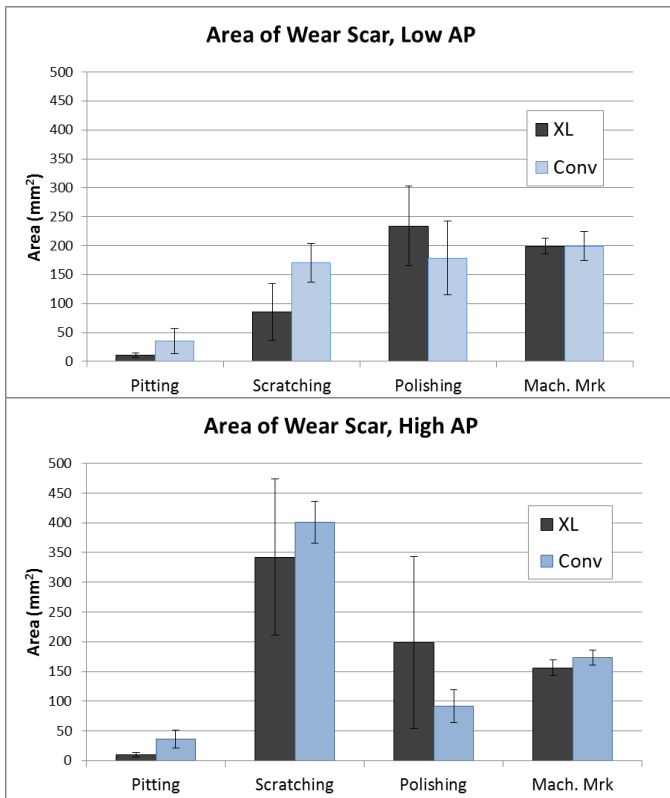


**Figure 1:** Area of wear scarring types. Low AP wear scarring was measured at 2M cycles, High AP at 4M cycles.

Although the gravimetric wear rate in the crosslinked group was 32% less than the conventional group for the high AP condition, this difference was not observed in the total number of particles generated. Figure 2 shows the number of particles measured (normalized per million cycles).

The average maximum dimension of wear particles, and equivalent circular diameter (the diameter at which the area of a circle is equal to that of the 2D representation of the particle image) showed no significant differences between groups. Results are shown in Table 1 and Figure 1.

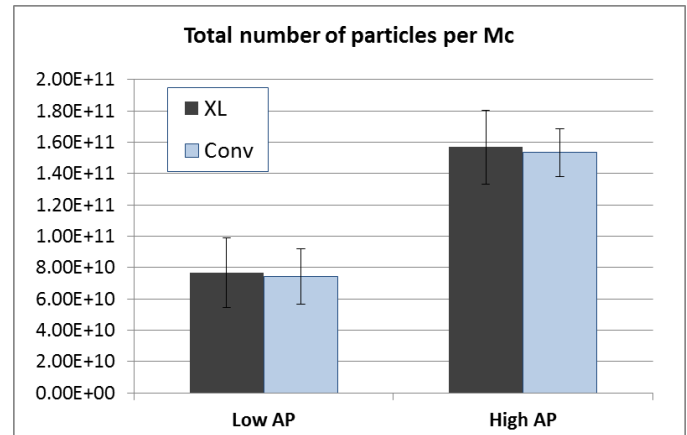


**Figure 2:** Particles measured from 0M to 0.5M (low A/P) and 2M to 2.5M cycles (high A/P). The crosslinked, high AP sample had 2 specimens, due to wear simulator station malfunction.

This study has demonstrated that increasing the anterior/posterior motion during wear simulation will increase the amount of scratching on total ankle insert surfaces, and will generate more particles compared to a gait cycle with lower A/P motion. This study has also shown that with this implant geometry, there is no significant difference between conventional vs a vitamin E-stabilized crosslinked UHMWPE insert in wear scarring or number of particles generated.

## REFERENCES

1. Kurtz et al, *UHMWPE Biomaterials Handbook*, 3rd edition, pp 61 and 147.
2. Webb et al, *Wear of a Stabilized Crosslinked UHMWPE Total Ankle Replacement*, poster at ASB 2016
3. Billi et al, *The John Charnley Award: An Accurate and Extremely Sensitive Method to Separate, Display, and Characterize Wear Debris*, CORR 470(2):329-38

## ACKNOWLEDGMENTS

The authors would like to thank Mr. John DeHarte and Ms. Amy Koury for help with data reduction and analysis.

**Table 1:** The average particle maximum dimension and equivalent circular diameter

Metric	$D_{max}, \mu m$		ECD, $\mu m$	
	Low A/P	High A/P	Low A/P	High A/P
<b>Kinematic Profile</b>				
<b>Crosslinked</b>	$0.311 \pm 0.120$	$0.302 \pm 0.178$	$0.162 \pm 0.023$	$0.151 \pm 0.074$
<b>Conventional</b>	$0.203 \pm 0.025$	$0.343 \pm 0.168$	$0.096 \pm 0.011$	$0.160 \pm 0.063$

# A BRIEF LOWER EXTREMITY GRADING SYSTEM (LEGS) TO EVALUATE BASELINE LOWER EXTREMITY ANALYTICS IN HIGH SCHOOL ATHLETES

<sup>1</sup> Joseph Smith, MS, ATC, OTC, NREMT; <sup>2</sup> Nick DePhillipo, MS, ATC, OTC, CSCS;  
<sup>1</sup> Shannon Azizi, MS, ATC; <sup>1</sup> Andrew McCabe, MAT, ATC, ROT; <sup>1</sup> Courtney Beverine, MA, ATC, ROT,  
<sup>1</sup> Michael Orendurff, PhD; <sup>1</sup> Stephanie Pun, MD, and <sup>1</sup> Charles Chan, MD.

<sup>1</sup> Stanford Children's Orthopedic & Sports Medicine Center, Stanford, CA, USA

<sup>2</sup> Steadman Clinic, Vail, CO, USA

Email: JosephSmith@StanfordChildrens.org, web: <http://www.stanfordchildrens.org>

## INTRODUCTION

In the United States of America, more than half of all high school students participate in some form of athletics each year, making up a population of over 7 million adolescent student-athletes.<sup>1</sup> High school athletes sustain an estimated 1.5 million injuries each year with the ankle and knee being the most common sites of injury.<sup>2-5</sup>

Acute non-contact lower extremity injuries result in impairments in balance, power of the single limb, and jump-landing mechanics. Evidence supports that it is important to assess neuromuscular impairments following injury and for safe return to sport after injury rehabilitation. Currently, no brief comprehensive clinical tool exists for this purpose.

The purpose of this study was to describe and provide the initial data for the establishing age-specific scores of a novel, brief clinical lower extremity grading system (LEGS) of neuromuscular components as a baseline pre-season assessment for United States' high school-aged sports participants to assess risk of injury and performance potential. Additionally, the LEGS may also add utility as an additional measure to help clinicians identify neuromuscular status of the lower extremity following injury rehabilitation.

Baseline assessments with LEGS may also offer a practical clinical data tool which would allow for comparison during the rehabilitation phases of injury management of lower extremity acute non-contact injuries and for return to sport decision making.

## METHODS

Two hundred and fourteen male (n=91) and female (n=123) athletes between the ages of 12 and 17 years were recruited from San Francisco bay area public schools. Sample size was determined by performing a *priori* power analysis using G\*Power statistical software (Version 3.1.9.2) with power set at 0.8. As participants in high school athletics, all subjects played at least one of three sports: soccer (n=101), cheerleading (n=29), or basketball (n=84). These specific sports were selected based upon the common occurrence of noncontact acute lower extremity injuries involved with sport participation and high-risk maneuvers.<sup>2</sup>

The LEGS employed in this study consisted of brief assessments in the following three domains: (1) dynamic balance, (2) jump-landing mechanics, and (3) lower limb power as measured by the Y-balance test (YBT), drop-jump video test (DJVT), and triple crossover hop for distance test (TXHD), respectively.



All subjects completed pre-participation health history questionnaires to rule out current pathological conditions (any condition that would prohibit clearance to participate in athletics). Exclusionary criteria included incomplete pre-participation physical exam, and/or inability to physically perform any of the required assessments. Prior to study participation all procedures were explained to each subject. Subjects and their parents/guardians read and signed assent and consent forms and video assent and consent forms that were approved by the Stanford University institutional review board for human subjects.

Standard normal distribution was calculated for all scores to enable percentile rankings to be established for all participants. Each participant's score was also averaged to present an overall LEGS percentage score. Scores were also used in analysis and correlated to sex, gender, body mass index, age, and sport.

## RESULTS AND DISCUSSION

The three directions from the YBT were averaged for each limb, normalized for limb length, then an average was taken between limbs to describe dynamic stability of the stance leg. The highest score for boys and girls was 114 and 119 cm, respectively.

From the DJVT, the highest possible score (knee separation distance/hip separation distance) from the DJVT was 100 for both boys and girls. Highest averaged scores for boys' and girls' TXHD test were 683 and 538 cm, respectively.

Overall mean YBT value was 94.6 cm with a standard deviation of 9.1 cm. Overall mean DJVT value was 80.2 cm with a standard deviation of 15.2 cm. Overall mean TXHD value was 453.4 cm with

a standard deviation of 88.7 cm.

Percentile rankings for all participants were calculated for each test score and overall averages of percentile rankings ranged from 8% to 89%. This method provides initial data for age and sports specific values for future comparison and further scientific analyses.

## CONCLUSIONS

The Lower Extremity Grading System (LEGS) is presented as a clinical tool used for evaluating neuromuscular control analytics for use during baseline or return to play decision making process in adolescent athletes.

## REFERENCES

1. Centers for Disease Control and Prevention. *Guidelines for school and community programs to promote lifelong physical activity among young people*. MMWR Recomm Rep, 1997. **46**(RR-6):1-36.
2. Darrow CJ, et al. Epidemiology of severe injuries among United States high school athletes. *Am J Sports Med*. 2009;**37**(9):1798-805.
3. Rechel JA, Yard EE, Comstock RD. An epidemiologic comparison of high school sports injuries sustained in practice and competition. *J Athl Train*. 2008;**43**(2):197-204.
4. Le Gall F, Carling C, Reilly T. Injuries in young elite female soccer players: an 8-season prospective study. *Am J Sports Med*. 2008;**36**(2):276-84.
5. Nelson AJ, et al. Ankle injuries among United States high school sports athletes 2005-2006. *J Athl Train*. 2007;**42**(3):381-7.

## ACKNOWLEDGMENTS

The research team would like to extend our sincere gratitude to the administration, athletic departments, and student-athletes of the San Mateo Unified High School District, especially Matthew Smith, MA, ATC; and Sara Golec, MS, ATC.

# FOOT MORPHOLOGY OF SCHOOL AGED CHILDREN IN A DEVELOPMENTAL RESEARCH SCHOOL

P.T. Williams<sup>2</sup>, C.M. Wilburn<sup>2</sup>, M.E. Dupiton<sup>1</sup>, M.A. Morris<sup>1</sup>, J.E. Mcroy<sup>1</sup>, S.L. Price<sup>1</sup>, W.H. Weimar<sup>2</sup>

<sup>1</sup>Florida A&M University, Tallahassee, FL, USA

<sup>2</sup>Auburn University, Auburn, AL, USA

## INTRODUCTION

The foot is a complex structure that endures ongoing development throughout life. Its purpose is to support, stabilize and diminish the impact of forces on the lower limb during locomotion. During the developing stages, internal and external factors can influence the formation of specific foot architecture. The morphological processes of specific architectural components of the foot, such as the medial longitudinal arch, are vital for adequate function. While medial architectural characteristics of height and stiffness serve as important indicators of healthy and pathological function of the lower extremity, limited research regarding the developmental processes remain limited. Specifically, literature regarding foot morphology using the arch height index measurement system among African-American school aged children in K-12 is lacking. The aim of this study was to assess changes in foot morphology for school aged children in a developmental research school, to determine when the foot components of foot girth (FG), arch height index (AHI) and arch height stiffness (AHS) stabilize and become more consistent.

## METHODS

Seventy-eight participants (52 females, 26 males in grade levels (1<sup>st</sup> – 9<sup>th</sup>) volunteered to participate in this study. Prior to conducting any measurements, parents/guardians provided informed consent and the participants provided assent. Foot anthropometric measurements of total foot length, truncated foot length, and maximal dorsal height were taken with the Arch Height Index Measurement System to achieve the arch height and arch height stiffness measures. Arch height was computed by dividing the maximal dorsal height by truncated foot length.

Further, arch height stiffness was computed by dividing the change of arch height by body mass. An additional anthropometric assessment of foot girth was taken using a measuring tape while the participant was seated. The foot girth was defined as the circumferential distance between the first metatarsophalangeal head and the fifth metatarsophalangeal head.

## RESULTS AND DISCUSSION

A one way mixed model ANOVA was employed to determine if significant differences existed in these measures across grades. Significant differences were noted for the following comparisons: Left foot girth (LFG) (Figure 1) in the following grade levels: First grade vs 5<sup>th</sup> ( $p=.005$ ), 6<sup>th</sup> ( $p=.002$ ), 7<sup>th</sup> ( $p<.001$ ), 8<sup>th</sup> ( $p<.001$ ), 9<sup>th</sup> ( $p<.001$ ). Second grade vs 5<sup>th</sup> ( $p=.001$ ), 6<sup>th</sup> ( $p=.015$ ), 7<sup>th</sup> ( $p=.005$ ), 8<sup>th</sup> ( $p=.001$ ), 9<sup>th</sup> ( $p<.001$ ). Third grade vs 5<sup>th</sup> ( $p=.024$ ), and 9<sup>th</sup> ( $p=.001$ ). Fifth grade vs 2<sup>nd</sup> ( $p=.001$ ) and 3<sup>rd</sup> ( $p=.024$ ).

Right foot girth (RFG) (Figure 1): first grade vs 5<sup>th</sup> ( $p=.035$ ), 6<sup>th</sup> ( $p=.037$ ), and 9<sup>th</sup> ( $p=.006$ ). Second grade vs 4<sup>th</sup> ( $p=.007$ ), 5<sup>th</sup> ( $p<.001$ ), 6<sup>th</sup> ( $p<.001$ ), 7<sup>th</sup> ( $p=.002$ ), 8<sup>th</sup> ( $p<.001$ ) and 9<sup>th</sup> ( $p<.001$ ).

Left arch height stiffness (LAHS) (Figure 2) in first vs 6<sup>th</sup> ( $p=.026$ ) and 7<sup>th</sup> ( $p=.017$ ).

Right arch height stiffness (RAHS) (Figure 2) in first vs 5<sup>th</sup> ( $p=.029$ ), 7<sup>th</sup> ( $p=.001$ ) and 8<sup>th</sup> ( $p=.005$ ); second vs 7<sup>th</sup> ( $p=.040$ ).

No significant differences were noted between arch height index (AHI) (Figure 3) for either foot in any grade. Neither was there a difference in the measures of LFG, RFG before the fifth grade and after the ninth. While LAHS and RAHS seem to

stabilize in the late middle to early high school years.

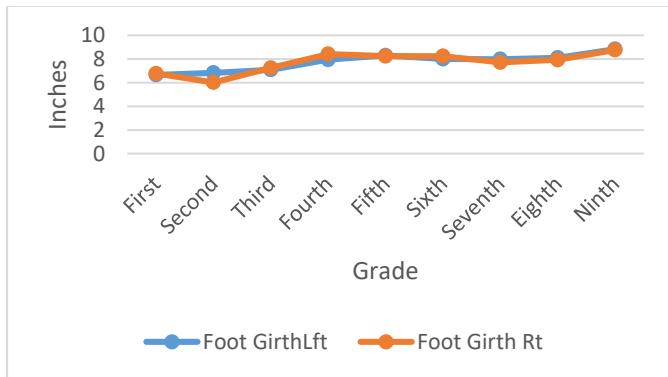


**Figure 1:** Left & Right Foot Girth

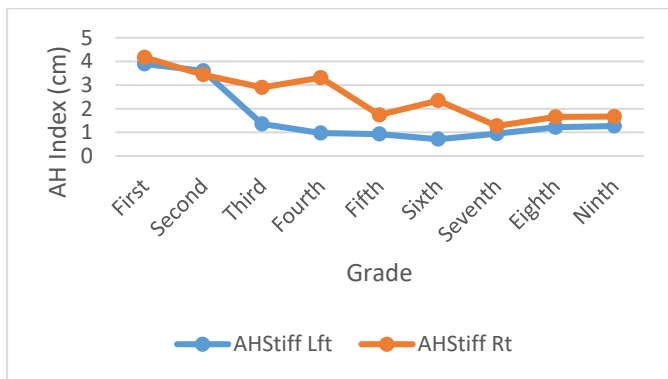


**Figure 2:** Left & Right Arch Height Stiffness

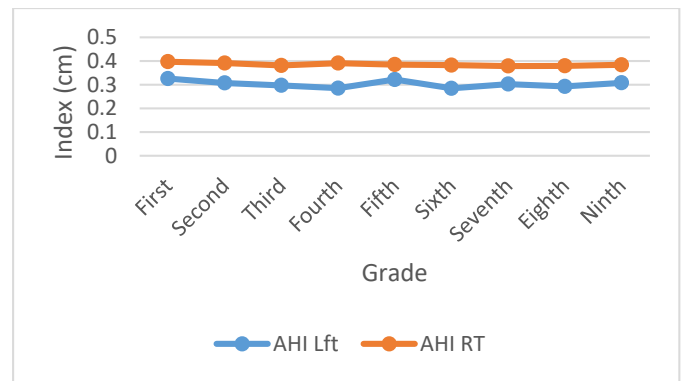


**Figure 3:** Left & Right Arch Height Index

## CONCLUSIONS

In the current study, the foot morphology characteristics of arch height index, arch height stiffness and foot girth, can experience dramatic changes from early childhood to fifth grade and throughout the middle school years until early high school grade levels. The lack of a significant finding for AHI suggests that the proportional relationship between foot components does not change significantly as the child grows and develops. Further research is needed to determine how maturation; weight or gender may influence arch development.

## REFERENCES

1. Krauss, I., et al. *Ergonomics* **54**, 294-300, 2011.
2. Mickle, KJ., et al. *J Am Geriatr Soc* **58**, 1936-1940, 2010
3. Scott, G., et al. *Gait Posture* **26**, 68-75, 2007.
4. Tomassoni, D., et al. *Maturitas* **79**, 421-427, 2014.

# ACTIVITY RELATED PLANTAR TEMPERATURE INCREASE IN HEALTHY SUBJECTS

Linda S. Adams, Ali Ersen and Metin Yavuz

University of North Texas Health Science Center, Fort Worth, TX, USA  
email: Metin.Yavuz@unthsc.edu, web: [www.sites.google.com/site/dryavuzlab/](http://www.sites.google.com/site/dryavuzlab/)

## INTRODUCTION

Skin temperature has long been studied as a causative factor in formation of pressure ulcers (i.e., decubitus ulcers). For example, in a swine model, Kokate et al applied constant pressure of 13.3 kPa for 5 hours with constant temperatures of 25°C, 35°C, 40°C and 45°C [1]. The results indicated that no tissue damage was observed at the 25°C sites, but substantial deep tissue damage and necrosis was observed at the sites of 35°C and above. Investigators studying diabetic foot ulcers have hypothesized that prolonged application of mechanical stresses, not only plantar pressure but also shear, leads to an inflammatory response, increased temperature, and ultimately tissue necrosis [2]: as Brand suggests, “the foot would heat up before breaking down” [3]. A study by Armstrong et al demonstrated that monitoring skin temperatures and limiting physical activity in the event of a bilateral temperature difference of  $> 2.2^{\circ}\text{C}$  could prevent ulceration [4]. Several researchers including, recently, Yavuz et al [5] reported a significant increase in the mean foot temperatures of diabetic neuropathic patients compared to control subjects. Moreover, based on studies in healthy adults, we believe that the plantar temperatures in diabetic subjects could be even greater after activity; Yavuz and associates reported a  $5.3^{\circ}\text{C}$  temperature increase on the foot sole in healthy individuals as a result of walking only for 10 minutes at 3.2km/h [6]. The purpose of this study was to quantify temperature increase in healthy subjects after 20 minutes of treadmill activity and after 70% of typical daily activity, as measured by steps. Further advancements in the treatment and prevention of diabetic ulcers demands a more comprehensive understanding of the multifactorial nature of ulcer development that will only result from a study of the following interrelated factors: plantar stresses, activity and acute and chronic plantar temperature increases.

## METHODS

This is an ongoing observational case-control study that involves analysis of temperature, shear and activity in healthy and both neuropathic and non-neuropathic diabetic subjects. Temperature data from both feet of the first 5 healthy subjects was analyzed. Subjects visited the research lab in the morning and were fitted with a FitBit®. After walking a minimum of 2400 steps, subjects returned to the laboratory. In the afternoon, subjects engaged in two bouts of treadmill walking, each lasting 10 minutes. The total estimated steps including study activities such as treadmill walking was 4800 steps or about 70% of typical daily activity in healthy individuals. Plantar temperatures were measured in the morning and twice in the afternoon, before and after treadmill activity, using a FLIR T650sc infrared thermal camera. Average temperatures were determined for the whole plantar foot, excluding lesser toes. Final maximum temperatures were obtained.

## RESULTS AND DISCUSSION

Three males and two females, three subjects between the ages of 24 and 27 and one aged 41, were tested. Average and maximum temperatures are shown in Table 1 and a representative subject’s thermal image is shown in Figure 1. Combining results from both left and right feet, the difference between morning and post-treadmill plantar temperatures ranged from  $2.6^{\circ}\text{C}$  to  $7.8^{\circ}\text{C}$  with a mean difference of  $6.0^{\circ}\text{C}$  and a standard deviation (SD) of  $1.7^{\circ}\text{C}$ . The difference between pre-treadmill and post-treadmill plantar temperatures ranged from  $0.0^{\circ}\text{C}$  to  $7.7^{\circ}\text{C}$  with a mean difference of  $2.8^{\circ}\text{C}$  (SD  $2.7^{\circ}\text{C}$ ). Maximum plantar temperatures after completion of the 2<sup>nd</sup> treadmill bout averaged  $35.2^{\circ}\text{C}$  (SD  $1.1^{\circ}\text{C}$ ) with 60% of subjects having plantar temperatures above  $35^{\circ}\text{C}$ , the critical value for tissue breakdown as demonstrated by Kokate et al.

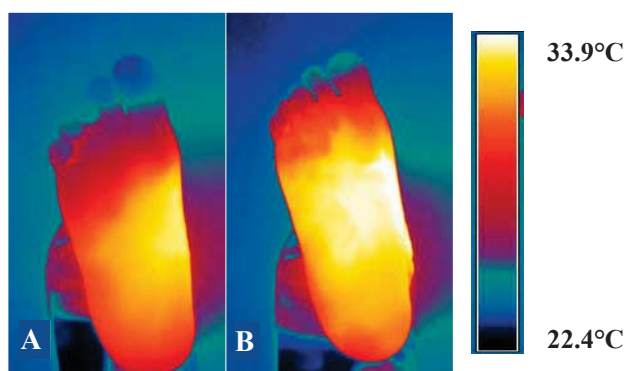


**Figure 1.** Representative thermal profile. Average plantar temperature excluding lesser toes was 28.4°C prior to treadmill activity (A) and 31.7°C after (B).

While the change in temperature resulting from the in-lab treadmill exercise doesn't confirm the 5.3°C increase after 10 minutes of treadmill walking, as previously reported by Yavuz et al., 60% of the final resulting temperatures are above 35°C, the threshold temperature established by Brand for the increased risk of tissue breakdown. Also there is evidence that the pre-tread plantar temperatures were already elevated from activity between the morning and afternoon sessions. The pre-tread plantar temperatures were taken after subjects had completed the required FitBit® steps and several subjects returned to the lab sweaty, suggesting recent physical activity and elevated core temperature. Current results are limited by the small sample size and lack of age diversity. This ongoing study involving about 30 subjects in each subject group will look at temperature increases as a result of both daily activity, as simulated by the overall number of steps taken during the study, and acute activity associated with the treadmill walking. Furthermore, temperature data will be analyzed in relationship to plantar stresses (pressure and shear), which will be taken barefoot and

in-shoe during treadmill walking. In a recent article by Yavuz et al, the relationship between plantar stress and temperature is explored and a distinction is made between chronically elevated plantar temperatures resulting from prolonged activity and an inflammatory response in the body and acute elevated temperatures that result from activity such as walking [5]. The authors state that chronic thermal response results from prolonged exposure to repetitive stresses and is characterized by inflammation. In the case of the diabetic, it is believed that both this chronic and acute temperature increase contributes to tissue breakdown. As seen in this study, the effect of daily and acute activity combined may lead to temperatures in the plantar foot of healthy individuals that is above a critical threshold for tissue breakdown. In the diabetic, these final temperatures may be even higher due to higher resting temperatures, increased inflammation, higher plantar stresses and the highly insulating properties of diabetic footwear. Such information about the diabetic foot may lead to improved ulcer prediction and prevention methods.

*This research was possible due to support from the National Institutes of Health (R15DK104257 and UL1TR001105).*

## REFERENCES

1. Kokate JU, et al. *Arch Phys Med Rehabil* 76(7), 666-673, 1995.
2. Bergtholdt, et al. *Leprosy Rev*, 47(3), 211, 1976.
3. Boulton, *Diabetes-Metab Res*, 28(1), 3-7, 2012.
4. Armstrong D., et al. *Am J Med*, 120(12), 1042-6, 2007.
5. Yavuz M, et al. *Diabetes Care*, dc15-1147, 2015.
6. Yavuz M., et al. *J. Biomech*, 47(15), 3767-70, 2014.

**Table 1. Plantar Temperatures per Subject, Morning and Afternoon Pre- and Post- Treadmill\* (°C)**

Right Foot Averages			Left Foot Averages			Right Foot Change		Left Foot Change		Right Aft. Max	Left Aft. Max
Morn.	1 <sup>st</sup> Aft.	2 <sup>nd</sup> Aft.	Morn.	1 <sup>st</sup> Aft.	2 <sup>nd</sup> Aft.	2 <sup>nd</sup> Aft. Vs. Morn.	2 <sup>nd</sup> Aft. Vs. 1 <sup>st</sup> Aft.	2 <sup>nd</sup> Aft. Vs. Morn.	2 <sup>nd</sup> Aft. Vs. 1 <sup>st</sup> Aft.	2 <sup>nd</sup> Aft.	2 <sup>nd</sup> Aft.
25	30.0	31.8	24.8	29.6	31.7	6.8	1.8	6.9	2.1	34.5	34.1
28.2	28.4	31.7	27.8	27.4	30.4	3.5	3.3	2.6	3.0	34.7	33.1
26.8	32.1	33.8	26.8	31.8	32.7	7.0	1.7	5.9	0.9	35.7	36.1
29.0	34.0	34.0	27.3	34.1	34.1	5.0	0	6.8	0	35.3	35.7
28.0	28.1	35.5	27.3	27.4	35.1	7.5	7.4	7.8	7.7	36.9	36.3

\* All temperatures exclude lesser toes. Abbreviations: "morn." – morning; "aft." – afternoon

# NET ENERGY TRANSFER VIA BIARTICULAR MUSCLES DURING PEDALING FLOWS DISTAL-TO-PROXIMAL DUE TO HAMSTRINGS ACTIVITY

<sup>1</sup> Alexis (Lex) D. Gidley and <sup>2</sup> Brian R. Umberger

<sup>1</sup> Brigham Young University – Idaho, Rexburg, Idaho, USA

<sup>2</sup> University of Massachusetts, Amherst, MA, USA

email: gidleya@byui.edu

## INTRODUCTION

The unique actions of biarticular muscles have been scrutinized for years. While all muscles contribute to the flow of segmental energy, biarticular muscles have the unique ability to transfer mechanical energy generated at one joint to a neighboring joint [1,2]. For example, when the knee and hip are both extending, the rectus femoris is lengthening at the hip and shortening at the knee, which may cause work generated by uniarticular hip extensor muscles to appear as joint work at the knee.

From this joint-level perspective, during the push-off phase of running and jumping net energy transferred via biarticular muscles flows from proximal-to-distal joints [2]. Specifically, rectus femoris (RECT) and gastrocnemius (GAST) dominate the energy flow in the proximal-to-distal direction, while the hamstrings (HAMS) transfer a small amount of energy from the knee to the hip [2]. While the coordination of biarticular muscles has been shown to be critical to performance in running and jumping, similar analyses have not been performed in a wide range of other activities.

In pedaling, there is a similar power generation phase to running and jumping when the hip and knee extend simultaneously. However, in contrast to running and jumping, during seated pedaling the trunk is relatively fixed and the path of the foot is constrained, which could influence biarticular muscle contributions to energy transfer. Therefore, the purpose of this study was to examine the transfer of energy via biarticular muscles during pedaling.

## METHODS

A musculoskeletal model with 9 muscles per leg (3 biarticular: HAMS, RECT and GAST), a fixed hip and 3-degrees of freedom was used to generate

forward-dynamics planar simulations of pedaling (200W, 80 RPM) using simulated annealing. Each muscle was modeled as a two-element Hill-type muscle tendon unit (MTU) with a contractile element parameterized by fiber type distribution, optimal length, maximal force, and force-length-velocity properties, and a series elastic element parameterized by the tendon slack length.

Power transferred by a biarticular muscle was calculated from the product of the torque produced by the muscle (muscle force  $\times$  moment arm) at the joints it crosses and the angular velocities of those joints [1]. Work was determined by integrating power with respect to time. Note that in calculating the energy transferred by biarticular muscles, the work at the two joints, while opposite in sign, may not be equal in magnitude because the instantaneous moment arms and angular velocities at the two joints will usually be different.

## RESULTS AND DISCUSSION

RECT, HAMS and GAST each transferred energy between the joints they cross during the pedal cycle, with the greatest amount transferred during the downstroke. (Figure 1a-c). During the downstroke, net energy was transferred in the distal-to-proximal direction (8.12 J) (Figure 1a & b). RECT transferred a small amount of energy from the hip to the knee (2.27 J) (Figures 1d & e), which is in the same direction as the push-off phase of running and jumping [2], but of a considerably smaller magnitude. This energy transfer to the knee coincides with the critical knee extension during the transition phase near top dead center and into the downstroke [4]. Very little energy (0.39 J) was transferred from the knee to the ankle by GAST during the downstroke. This energy flow through GAST plays a

crucial role in running and jumping [2], but contributes little to pedaling.

The dominant energy transfer was due to HAMS, which transferred substantial energy (10.78 J) from the knee to the hip, mostly during the second half of the downstroke (Figure 1d & e). This distal-to-proximal energy transfer by HAMS in pedaling is the same in running and jumping [2], but of a much greater magnitude. This flow of energy through HAMS enhanced hip and reduced knee extension joint powers mostly when the foot moved back under the hip to follow the pedal trajectory. Thus, HAMS dominated energy flow primarily during the second half of the leg extension phase, which is likely related to its role in controlling the direction the force on the pedal [5].

During the upstroke, GAST transfers a modest amount of energy (3.32 J) from the ankle to the knee, contributing to knee flexion (Figure 1e & f). There is also some energy transferred from the knee to the hip via RECT (2.50 J), contributing to hip flexion (Figure 1d & e). This direction of energy flow through RECT is similar to the swing phase of running when the knee and hip are also flexing [6]. HAMS transfers only a small amount of energy (1.01 J) from the hip to the knee, resulting in a net distal-to-proximal energy flow during the upstroke (4.81 J). Thus, pedaling differs from running in that net

energy transfer via biarticular muscles is distal-to-proximal in both the propulsive *and* recovery phases.

Finally, we note that while joint power flows proximal-to-distal in activities like jumping, segment power flows distal-to-proximal [3]. Interestingly, we find just the opposite in pedaling, with joint power flowing distal-to-proximal, while segment power flows proximal-to-distal [7].

## CONCLUSIONS

We conclude that net energy transferred via biarticular muscles during pedaling flows distal-to-proximal, but individual muscle flow directions are identical to that of running and jumping. The net distal-to-proximal energy flow during pedaling is due to the dominance of HAMS during the downstroke, which reflects the unique task constraints of pedaling associated with the fixed hip and the need for directing force on the moving pedal.

## REFERENCES

1. Bobbert, M et al. *J Physiol* **129**, 672-684, 1986
2. Jacobs, R et al. *J Biomech* **29**, 513-523, 1996
3. Pandy, M & Zajac F *J Biomech* **24**, 1-10, 1991
4. Raasch, C et al. *J Biomech* **30**, 595-602, 1997
5. Schenau, G *Hum Mvmt Sci* **8**, 301-337, 1989
6. Barrett, R *Proc of ISB XVIII*, Zurich, Sui, 2001
7. Kautz, S & Neptune R *ESSR*, **30**, 159-165, 2002

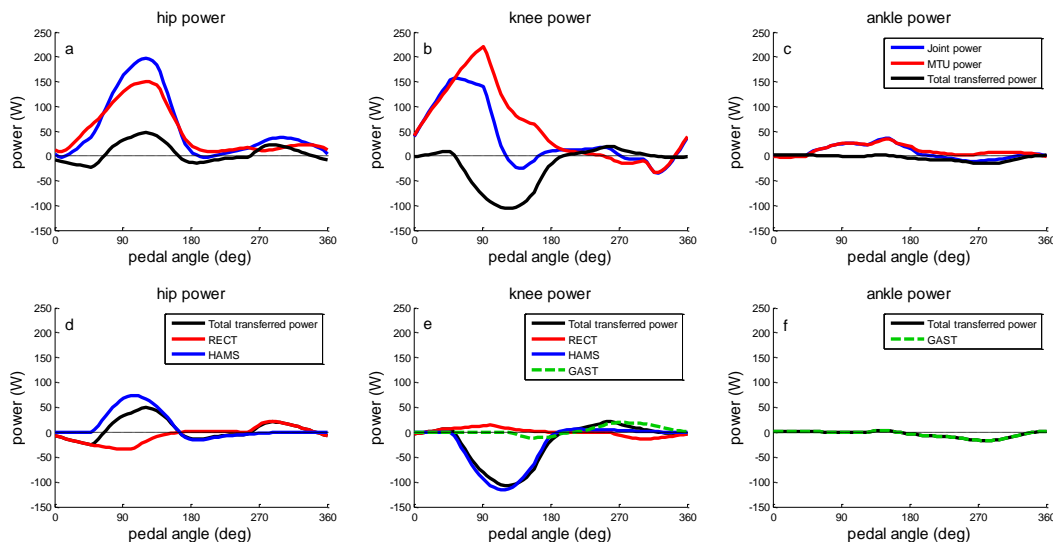


Figure 1 (a-c): Joint power (blue), muscle-tendon power (red), and power transfer (black) to or from that joint (positive and negative, respectively) at the hip, knee and ankle. (d-f): Individual biarticular muscle contributions to power transfer at the hip, knee and ankle.

# BICEPS FEMORIS AND RECTUS FEMORIS ACTIVATION DURING FOUR POSTURES OF HIGH KNEE FLEXION

<sup>1</sup> Annemarie F. Laudanski, <sup>1</sup>Helen C. Chong, <sup>1</sup> Stacey M. Acker

<sup>1</sup> University of Waterloo, ON, Canada

Email: [alaudanski@uwaterloo.ca](mailto:alaudanski@uwaterloo.ca) <https://uwaterloo.ca/biomechanics-of-human-mobility-lab/>

## INTRODUCTION

In North America, postures involving high knee flexion, such as kneeling and squatting (with a knee flexion angle of  $>120^\circ$ ) are most commonly adopted in occupational settings (e.g. tiling, roofing, childcare). In contrast, East Asian cultures, including Chinese, Japanese, Korean, and Vietnamese nationalities, tend to use these postures frequently during activities of daily living for socializing, eating, rest, and religious practices [1]. These high flexion postures have been associated with increased prevalence of knee osteoarthritis (OA) [2, 3].

While it has been theorized that the risk associated with high knee flexion postures results from high moments about the knee during these postures [4, 5], a comparison of muscle contributions associated with high flexion moments has yet to be explored. Therefore the primary objective of this study was to compare rectus femoris and biceps femoris muscle activity coincident with peak flexion moments in kneeling and squatting postures. Additionally, a comparison between ethnicities and sexes was conducted to determine whether any group might adopt different muscle recruitment strategies in these postures.

## METHODS

Thirty-one participants were studied in this retrospective cohort study: twenty-one (eleven males) of European descent (Caucasian group) and ten (seven males) of East Asian (Chinese, Japanese, Korean, or Vietnamese) descent (East Asian group). All were raised in Canada. The study was approved by the university's ethics board and all participants provided informed consent prior to participation.

Four postures were studied: flat foot squatting (FS), heels raised squatting (FxS), dorsiflexed kneeling (FK), and plantarflexed kneeling (FxK). Participants completed randomized trials until 5 trials of each posture were obtained. Participants transitioned from standing into each pose (descent phase), then held the fully flexed pose for 8 seconds (static phase), then transitioned back to standing (ascent phase). Kneeling transitions were performed asymmetrically so that one knee (the "trail" leg) made contact with the force platform before the other (the "lead" leg).

An 18-camera motion capture system (Optotrak, Northern Digital Inc., Waterloo, ON, Canada) was used to collect kinematic data at 64 Hz. Infrared markers were secured to the foot, shank, and thigh of participants' lead leg, as well as to their sacrum. Two AMTI force platforms (Advanced Mechanical Technology Inc. Watertown, MA, USA) were used to collect ground reaction data at 2048 Hz. Wireless EMG electrodes (Wave Plus EMG, Cometa, Cisliano, Italy) were placed on the rectus femoris and biceps femoris of the lead leg, and sampled at 2048 Hz in order to record muscle activity. Two trials of maximum voluntary contractions (MVC) were collected per muscle group and used for EMG normalization purposes [6].

Knee joint moments were expressed in the tibial coordinate system [7]. During the descent and ascent phases for each trial, the EMG activations during peak flexion moment were calculated and then averaged across trials; while for the static phase, the mean EMG activations were calculated and again averaged across trials. Statistics were run using 3-way mixed model (pose (4) x ethnicity (2) x sex (2)) ANOVAs on the descending, ascending, and static phases for the biceps femoris and rectus femoris activations (a total of 6 ANOVAs). In cases where a significant main effect was detected, a post-hoc

Tukey test was performed in order to determine significant differences. A critical value of 0.05 was used in all tests to determine statistical significance.

## RESULTS AND DISCUSSION

Results for biceps femoris and rectus femoris activation during descent, static, and ascent phases for all postures can be found in Figure 1. Rectus femoris activation was found to be most elevated in all three phases of flat foot squatting. Through post-hoc analysis, East-Asian males were found to have the lowest biceps femoris activations across all postures while females were found to have significantly higher muscle activation than males during the heels raised squat (43.1 ( $\pm$ 20) %MVC in comparison to 23.1 ( $\pm$ 20) %MVC for males).

The highest levels of both biceps femoris and rectus femoris activations were found to occur during squatting. Biceps femoris activity, while ascending from a heels raised squat, nearly doubled the activation recorded during any other posture (13.7 ( $\pm$ 3.8) %MVC compared to an average of 7.2 ( $\pm$ 5.1). Ascending from a heels raised squat also required the

highest recruitment of rectus femoris activation (31.8 ( $\pm$ 21) %MVC). Muscle recruitment was not found to be statistically different during any phases for plantarflexed kneeling and dorsiflexed kneeling.

This retrospective cohort study sought to analyze a subgroup of participants from a larger currently unpublished study in which flat foot squatting was found to elicit significantly lower peak knee flexion moments in comparison to the three alternative high knee flexion postures. However, results from this study suggest that during descent and static phases of flat foot squatting, rectus femoris activation is highest, as the quadriceps are recruited in order to regulate knee flexion angles. The results of the current study therefore suggest that while squatting activities could prove beneficial for building strength in the rectus femoris, for individuals who suffer from OA leading to pain during compression of the knee or individuals with quadriceps weakness or injury [8], a kneeling posture, rather than a squat, should be recommended in order to minimize rectus femoris activity. Further consideration of additional exposure measures and person-specific factors will therefore be required in order to best protect the knee from the risks associated with high knee flexion postures.

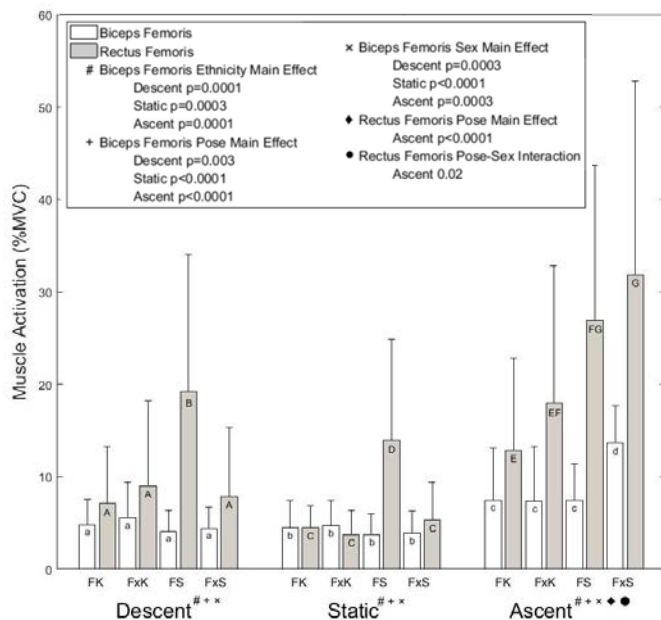


**Figure 1:** Biceps femoris and rectus femoris activation during flat foot squat, heels raised squat, dorsiflexed knee, and plantarflexed knee. Pose main effects have been marked in lower-case for biceps femoris and in upper-case for rectus femoris.

## REFERENCES

1. Akagi, M. *Total Knee Arthroplasty: A Guide to Get Better Performance*, 311–316, 2005.
2. Amin, S, et al. *J Rheumatol* **35**, 1645-1649, 2008.
3. Chokkhanchitchai, S, et al. *Clin Rheumatol* **29**, 39-44, 2010
4. Nagura, T, et al. *J Appl Biomech* **22**, 305-313, 2006
5. Pollard, J, et al. *J. Appl Biomech* **27**, 233-241, 2011
6. Burden, A, et al. *J Electromyogr Kinesiol* **13**, 519-532, 2003
7. Mundermann, A, et al. *Arthritis Rheum.* **50**, 1172-1178, 2004
8. Slemenda, C, et al. *Ann Intern Med.* **127**, 97-104, 1997

## ACKNOWLEDGMENTS

Funding for this study was provided by the Natural Sciences and Engineering Research Council (NSERC) [grant number 418647] as well as the Queen Elizabeth II Graduate Scholarship in Science and Technology (QEII-GSST)

# METATARSOPHALANGEAL JOINT STIFFNESS AT DIFFERENT RUNNING SPEEDS

<sup>1,2</sup> Evan M. Day, <sup>1,2</sup> Michael E. Hahn

<sup>1</sup> Bowerman Sports Science Clinic, <sup>2</sup>Neuromechanics Lab, University of Oregon, Eugene, OR, USA  
email: eday5@uoregon.edu, web: <http://bssc.uoregon.edu>

## INTRODUCTION

The metatarsophalangeal joint (MTP) has been reported to absorb large amounts of energy while generating very little during running [1]. Multiple studies have assessed the effects of the longitudinal bending stiffness of footwear on MTP mechanics and energetics [1,2]. However, these studies reported only the material bending stiffness of the shoe, and did not report MTP joint stiffness during running.

Joint stiffness affects the neuromuscular control of movement, injury risk, and performance. During gait it is commonly calculated as the change in moment divided by the change in angle during the energy absorption phase of stance [3]. The MTP joint does not follow a similar energy absorption and generation pattern as the ankle and knee that are commonly modeled as a spring-mass system. The MTP dorsiflexes throughout most of stance phase peaking during late stance, instead of mid-stance [4]. Despite eliciting a phase dependent stiffness curve, only one portion of the angular load-displacement relationship has been quantified for the MTP joint [5]. There is not currently a common methodology for reporting MTP stiffness. This study investigates MTP stiffness properties during running, and presents initial interpretation of what function each portion of the MTP load-displacement curve represents.

## METHODS

To date, three male runners (average 20yr, 175cm, 58.5kg, 15:20min 5000m best, 67mi/wk) have been enrolled in this ongoing study. Written informed consent was given by the subjects prior to the IRB-approved protocol. Running trials were conducted at 3.89, 4.44, 5.00, 5.56, and 6.11 m/s on an instrumented split-belt treadmill (Bertec, Inc., Columbus, OH). These velocities were chosen as

they are representative of relevant training and racing paces for competitive distance runners. Rest between conditions was self-selected, with subjects instructed to start the next condition when they felt no effects of fatigue. Subjects all wore the same footwear (Brooks Launch 4) to control for the effects of varied longitudinal bending stiffness among shoe types. Windows were cut in the shoes at the hallux, first and fifth metatarsals, and the medial, lateral and posterior calcaneus, to allow for direct application of retro-reflective markers to the skin. Marker coordinate data were collected at 200Hz using an 8-camera motion capture system (Motion Analysis Corp., Santa Rosa, CA). Ground reaction force data were collected at 2000Hz using the force-instrumented treadmill and then imported from Cortex to Visual3D for kinematic and kinetic analysis. A two-segment foot model was defined, with an MTP pin joint defined by a vector between the 1<sup>st</sup> and 5<sup>th</sup> metatarsal markers.

Two separate measures of MTP joint stiffness were defined by plotting the change in angle against the change in moment of the MTP joint. Active stiffness ( $K_{active}$ ), was calculated as the change in moment divided by the change in angle within a phase defined from initial dorsiflexion to peak plantar flexor moment. Critical stiffness ( $K_{cr}$ ) was calculated as the change in moment over the change in angle within the prolonged phase from initial dorsiflexion to peak dorsiflexion, similar to [5].

## RESULTS AND DISCUSSION

Data presented from three of the five running speeds are preliminary and part of an ongoing study. Joint stiffness values represent the combined effects of the foot-shoe complex. The defined stiffness quantities from two portions of the MTP load-displacement curve are discussed with respect to functions related to injury or performance.

The active stiffness ( $K_{active}$ ) was much higher at the fastest running speed, but did not consistently trend upward (Table 1). The active stiffness is representative of when the musculotendinous structures crossing the plantar surface of the MTP joint are storing elastic energy from initial dorsiflexion to the time of peak plantar flexor moment and is the portion of stance when the maximum elastic energy is stored. From an injury perspective,  $K_{active}$  indicates how the MTP joint is attenuating the ground reaction force.

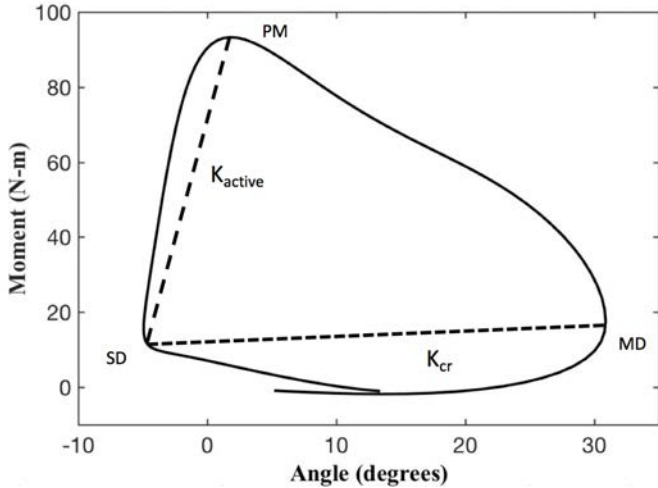


**Figure 1:** Representation of joint stiffness calculations. SD: initial dorsiflexion, PM: peak plantar flexor moment, MD: max dorsiflexion.

The critical stiffness ( $K_{cr}$ ) showed a decreasing trend as running speed increases (Table 1). Previous research defines  $K_{cr}$  as representing the threshold of the elastic benefit of shoe stiffness [5]. We propose that  $K_{cr}$  is also an indicator of the ability of the MTP joint to utilize stored elastic energy. The large hysteresis response suggests that while the initial energy storage ( $K_{active}$ ) is substantial, the hysteresis portion of the curve (PM to MD) indicates dissipation of a large amount of that energy while the MTP joint continues to dorsiflex, reducing the amount of elastic energy for the MTP to utilize

during plantar flexion at terminal stance to assist in forward propulsion. Thus, critical stiffness may be an important performance metric to consider.

The ratio between  $K_{active}$  and  $K_{cr}$  could be used as an indicator of the effectiveness of the stretch shortening cycle of the toe-flexor muscles. Effective stretch-shortening response requires quick loading and release. In a standard spring-mass model, a stiffer joint effectively stores and returns more elastic energy than a compliant joint. Though the toe-flexor muscles continue to experience strain while dorsiflexing, the moment value is decreasing, effectively dissipating the stored energy during the active stiffness phase.

## CONCLUSIONS

Initial examination of these preliminary findings indicates that MTP joint stiffness may be analyzed by two separate functions; active attenuation and utilization of stored energy. Continued analysis of the results from this ongoing study may help to identify injury mechanisms and performance enhancement.

## REFERENCES

1. Roy J, Stefanyshyn D. *Med & Sci in Sports & Ex* **38**, 562-569, 2006
2. Willwacher S, et al. *JoAB* **29**, 583-592, 2013
3. Hamill J. et al. *Eur. J. Sport Sci* **14**, 130-136, 2014
4. Oleson M. et al. *J Biomech* **38**, 1886-1894, 2005
5. Oh K, Park S. *J Biomech* **53**, 127-135, 2017

## ACKNOWLEDGMENTS

Thank you to Brooks Sports for donating footwear for this study.

**Table 1:** Stiffness profiles across running velocities (n=3)

Stiffness Parameter (N-m/degree)	Running Speed (m/s)		
	3.89	5.00	6.11
Critical Stiffness ( $K_{cr}$ )	2.15 ± 0.08	0.75 ± 0.56	0.07 ± 0.29
Active Stiffness ( $K_{active}$ )	7.13 ± 3.05	5.40 ± 1.56	11.70 ± 13.99

# ARCH STRUCTURE AND LOADING PATTERN MAY PREDICT RUNNING FOOT MECHANICS

<sup>1</sup> Adrienne D. Henderson, <sup>2</sup> Joaquin A. Barrios, <sup>1</sup> Dustin A. Bruening,

<sup>1</sup> Brigham Young University, Provo, UT, USA

<sup>2</sup> University of Dayton, Dayton, OH, USA  
email: adriennedhenderson@gmail.com

## INTRODUCTION

Foot structure has long been implicated as a factor in running related injuries and used as a predictor in functional interventions, such as footwear and orthotic prescriptions. While arch height has been associated with passive foot mobility (i.e. higher arch corresponding to higher passive midfoot stiffness) [1], a relationship between foot structure and dynamic foot function has proved elusive. Studies exploring static to dynamic relationships have focused almost exclusively on ankle and midfoot joint kinematics. Positive findings, such as low arched runners landing in a more everted ankle position [2] reflect a relationship between structure and posture as opposed to structure and function. On the other hand, functional range of motion (ROM) measures appear to be similar between foot types [2].

One reason that a true static/dynamic relationship has been so elusive is that foot kinematics may be greatly influenced by variations in foot loading. For example, passive mobility is generally assessed by comparing foot posture between sitting and standing. However, in standing, the center of pressure is generally posterior to the midfoot, while during running, the center of mass travels the length of the foot, creating a much larger torque on the midfoot joints. Additionally, the combination of frontal plane hindfoot position and midfoot torque can affect midfoot motion via the midtarsal locking theory, which postulates that hindfoot inversion reduces flexibility across the joints of the midfoot.

The purposes of this study were to explore relationships between static foot structure and foot mechanics in running by incorporating loading variables into the analysis. We first controlled foot strike pattern, evaluating both rearfoot strike (RFS) and forefoot strike (FFS) patterns. In a FFS, the hindfoot is less everted throughout stance, and midtarsal loading occurs much earlier [3]. We also included several novel kinetic measures of foot

function, hypothesizing that midfoot stiffness and midfoot power absorption would be correlated with measures of foot structure.

## METHODS

Eighteen female runners (25±4 yrs., 1.65±0.06 m, 61±7 kg) were tested. Static structure was assessed using the Foot Posture Index (FPI) [4] as well as standing arch height and arch stiffness from the Arch Height Index Measurement System (AHI) [5]. Dynamic function was assessed as subjects ran over ground at 3.7 m/s with both rearfoot (RFS) and forefoot (FFS) strike patterns. Subjects wore minimalist shoes with cut-outs and reflective markers were placed directly on the skin according to a modified kinetic multi-segment foot model [6]. Marker trajectories and force plate data were collected at 150 and 1,500 Hz respectively.

The ankle and midtarsal joints were modeled in Visual 3D software [6]. Joint angles were extracted using a typical Euler sequence. Joint moments and powers were calculated by first partitioning the ground reaction force to each segment sequentially using the center of pressure [7]. Analysis focused on loading phase only, which was defined from initial contact to peak midtarsal dorsiflexion. Extracted metrics consisted of: ankle eversion ROM, tri-planar midtarsal ROM, peak midtarsal angular velocity magnitude, midtarsal negative work (integral of power), and midtarsal stiffness (slope of the linear portion of the sagittal plane moment / angle graph). Each of these seven functional metrics was then correlated ( $\alpha = 0.05$ ) to the three structure metrics (FPI, standing AHI, and AHI stiffness).

## RESULTS AND DISCUSSION

Of the 42 tested relationships, only 5 were significantly correlated, with four of these five confined to the FFS pattern. It is possible that a FFS increases the ability to detect a static/dynamic relationship for several possible reasons. First,

Barnes et al. [1] hypothesized that low arched feet do not show increased ROMs because they are naturally already approaching an end-range. A FFS position, where the hindfoot is not on the ground, may influence this end-range effect. In addition, the reduced hindfoot eversion accompanying FFS [3] may stiffen the midfoot, potentially also reducing this end-range effect, or reducing the inter-subject variability in midtarsal mechanics.

Arch height index was negatively correlated with midtarsal dorsiflexion ROM in FFS. This supports findings relating arch structure to passive arch stiffness [1], but has not been shown before. Encouragingly, RFS may have also been significant if a larger sample size had been used ( $p=0.0683$ ). A correlation was found with FPI and the traditionally assumed frontal plane ankle motion (e.g. increased eversion in flatfeet), however, our results suggest that midfoot dorsiflexion may be a more sensitive measure, regardless of loading pattern.

AHI was also negatively correlated with sagittal plane midtarsal stiffness. Previous studies have used ROM as a surrogate for stiffness, assuming that a more compliant joint would result in more motion. However, this ignores the effects of loading. The stiffness calculated in this study comprises both motion and loading into one variable, and results suggest that this variable should be employed in future studies.

There were no significant correlations found with the AHI stiffness measurement. AHI stiffness measures the statically loaded foot, but may not replicate dynamic loading conditions.

FPI was negatively correlated to both ankle eversion ROM and midtarsal inversion/ eversion ROM. These two variables are coupled (i.e. with the forefoot on the ground, ankle eversion should result in midtarsal inversion). The only RFS correlation, that of midtarsal ab/adduction ROM, was also found with FPI. The differences between FPI and AHI correlations demonstrate that these measurements reflect different aspects of foot structure.

Our subject sample was fairly homogenous. Sixteen of 18 subjects had normal arches, the other 2 qualifying as low arches according to Zifchock et al's AHI criteria [8]. Future study should investigate these same variables in a larger sample that includes both high and low arch subjects.

## CONCLUSIONS

Despite the homogenous sample, several variables show promise in connecting static and dynamic foot stiffness. These variables showed up primarily in FFS suggesting that loading pattern affects this relationship. Future studies should expand the sample size and scope to better assess these relationships.

## REFERENCES

1. Barnes et al. Foot Ank Int, 2011. **32**(7): 710-716.
2. Powell et al. Hum Move Sc, 2011. **30**(1): 105-114.
3. Pohl et al. Clin Biomech, 2008. **23**(3): 334-341.
4. Barton, et al. J Foot Ankle Res, 2011. **4**(1): 1-8.
5. Butler et al. J Am Pod Med Ass, 2008. **98**(2): 102-06.
6. Bruening et al. Gait Posture, 2012. **35**(4): 529-534.
7. Stefanyshyn et al. J Biomech, 1997. **30**(11): 1081-1085.
8. Zifchock et al. Foot Ank Int, 2006. **27**(5): 367-372.

**Table 1:**

Measure:		AHI		FPI	
		r	p	r	p
Ankle Eversion ROM	FFS	0.08931	0.7245	-0.51104	0.0302*
	RFS	0.06776	0.7894	-0.38181	0.1179
Midfoot Dorsiflexion ROM	FFS	-0.5225	0.0261*	0.12026	0.6345
	RFS	-0.43915	0.0683	0.07916	0.7549
Midfoot Inversion/ Eversion ROM	FFS	0.3846	0.115	-0.69169	0.0015*
	RFS	0.36068	0.1415	0.07665	0.7624
Midfoot Ab/ Adduction ROM	FFS	-0.1565	0.5352	-0.29452	0.2355
	RFS	0.13661	0.5888	-0.50789	0.0314*
Midfoot Sagittal Plane Stiffness	FFS	-0.46854	0.0499*	0.05418	0.8309
	RFS	-0.35425	0.1492	0.08505	0.7372

# EFFECTIVE AVERAGE ANKLE MOMENT ARM AT VARIOUS SPEEDS

<sup>1</sup> Luke Steinbach, <sup>2</sup> Peter G. Adamczyk

<sup>1</sup>Department of Mechanical Engineering, University of Wisconsin, Madison, WI, USA  
Email: [lsteinbach@wisc.edu](mailto:lsteinbach@wisc.edu)

## INTRODUCTION

Control of the ankle-foot complex in walking is dominated by a heel-to-toe rolling motion, whereas in running at high speeds, the ankle and foot are part of the spring like behavior of the leg. These differences represent a shift toward more forefoot-dominated ground interaction at the higher speeds. This shift has been shown through changes in the center of pressure (COP) at initial ground contact [1]. However, instantaneous COP location at a specific time may not capture the full effect of changes in overall ankle control. An understanding of such changes is important for efforts to design and analyze biomimetic assistive devices such as foot-ankle prostheses, which may not adapt appropriately to different speeds.

This study investigates ankle control across a range of speeds including both walking and running. We hypothesize that ground reaction forces will show an overall forward shift as speed increases, representing a more forefoot-dominated strategy. We use a new metric to evaluate this overall shift, which incorporates a weighted average of center of pressure throughout the stance phase. We term this metric the “effective average ankle moment arm” (EAAMA). This parameter estimates the average sagittal moment arm of ground reaction forces about the ankle joint, across an entire stance phase of walking or running. EAAMA is designed to identify kinematic aspects of ankle control related to dorsiflexion/plantarflexion posture and hindfoot vs. forefoot-dominated ground interaction. Results across different speeds are intended to identify the average change in pressure distribution over the plantar surface as locomotive speed changes. We

also compare and contrast this metric to a simple initial-contact COP measurement. *We hypothesize that as locomotive speed increases, both EAAMA and initial COP will translate anteriorly.* The results of this study may influence biomimetic design and control of lower limb assistive devices.

## METHODS

Pressure insoles (Novel GmbH) were placed in the shoes of 8 subjects. Each insole has 99 transducers to measure localized pressure data across the foot. Data were recorded at 4, 6, 8, and 10 mph for each subject on a treadmill, for 20 seconds at each speed. Data processing to find the EAAMA used following steps:

- Assign ankle position to 30% of total in-sole length from the rear of the in-sole.
- Calculate instantaneous COP and total normal ground reaction force at each sample time.
- Integrate the total force impulse and total ankle moment impulse within each trial.
- Calculate EAAMA, defined as moment impulse divided by force impulse.

Take the average of both feet if acceptable cycles were present.

## RESULTS AND DISCUSSION

The EAAMA for each subject resulted in an anterior translation in the sagittal plane on the plantar surface, with an average translation across all subjects of 38% (Fig. 1). All subjects had a walking speed moment arm of 10% to 20% of the in-sole size forward of the ankle. This corresponds to the mean plantar moment found by Winter (reported in [2]) thus offering validation of our results for walking speeds.

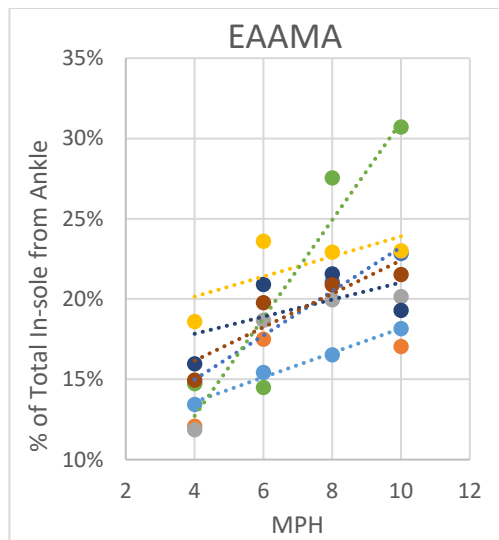


**FIG. 1:** The EAAMA of 8 subjects (different color dots). The ordinate represents how far forward of the ankle the EAAMA is, normalized by in-sole size.

Instantaneous COP at initial ground contact (IGC) was also examined for comparison against results from the EAAMA. If the COP at IGC shows anterior translation, then the EAAMA at the same speed cannot show a posterior, or no, translation since more force is being applied away from the heel.

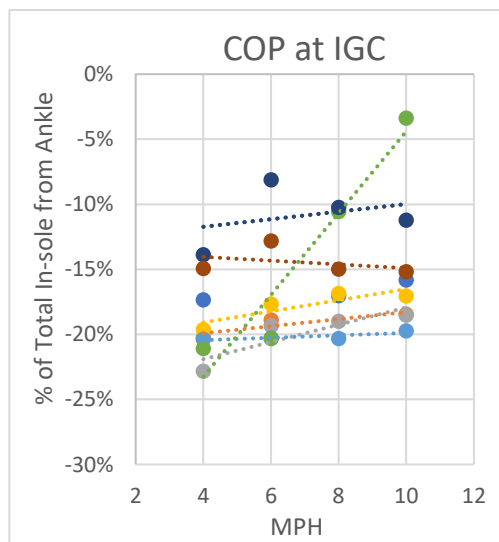


**FIG. 2:** The COP at IGC for 8 subjects (different color dots). The ordinate represents how far behind the ankle the COP is, normalized by in-sole size.

Fig. 1 and Fig. 2 share different ordinate ranges because the COP in Fig. 2 is only at initial ground contact at the beginning of the stance phase. The negative ordinate represents ground reaction forces behind the ankle (heel contact). There is not a direct correlation between Fig. 1 and Fig. 2 as a few of the subjects show a posterior, or insignificant, translation of the COP at IGC, yet a definitive anterior translation for the EAAMA. This could mean that those subjects are exerting much more force on toe-off at running speeds in order to bias the EAAMA anteriorly, while still maintaining, or translating posteriorly, the initial ground contact. These results support the hypothesis that ground interaction forces move forward to become more forefoot-dominated as speed increases, even if initial ground contact location does not change. Future testing with stricter protocols will discern the details of the discrepancy between these measures.

## CONCLUSIONS

The effective average ankle moment arm across different speeds appears to capture a new aspect of ankle-foot control across changes in speed. The slight discrepancy between the EAAMA and the COP at IGC may yield interesting information after further testing. Technical improvements in future testing will be focused on improving robustness to sensor noise in the pressure insoles, which was a significant challenge in this pilot study. Future work will include a higher number of subjects, the same type of running shoe for all subjects, and an instrumented split-belt treadmill to verify in-sole data.

## REFERENCES

1. Breine *et al*, *Med. Sci. Sports Exerc.* **46**. 1595-1603, 2014.
2. Rodgers, *Phys Ther.* **68**. 1822-1830.

# PLANUS FIRST METATARSOPHALANGEAL JOINT LOADING AFTER CHEILECTOMY AND MOBERG OSTEOTOMY: A STUDY OF SIX FINITE ELEMENT MODELS

<sup>1</sup> Oliver J Morgan, <sup>1</sup> Jennifer L Martay, <sup>2</sup> Howard J Hillstrom, <sup>2</sup> Matthew F Koff, <sup>2</sup> Scott J Ellis,  
<sup>2</sup> Jonathan T Deland, and <sup>1,2</sup> Rajshree Hillstrom

<sup>1</sup> Anglia Ruskin University, Chelmsford, Essex, UK

<sup>2</sup> Hospital for Special Surgery, New York, NY, USA

email: oliver.morgan@anglia.ac.uk

## INTRODUCTION

Osteoarthritis (OA) of the first metatarsophalangeal (1<sup>st</sup> MTP) joint is the most common form of degenerative disease in the foot. Increased joint loading and concomitant stress are considered important factors in OA onset and progression. Radiographically-confirmed OA has been quantitatively associated with a lower-arch (planus) alignment [1]. Presence of 1<sup>st</sup> MTP joint OA has been reported in 27% and 34% of men and women over 50 years of age, respectively [2].

Degeneration of the 1<sup>st</sup> MTP joint presents as a reduction in dorsiflexion from >60° for healthy; >40° for hallux limitus; [3] and <20° for end-stage, hallux rigidus [2]. Outcomes for end-of-stage salvage procedures are either unpredictable or limit normal biomechanical function. Joint sparing procedures for mild to moderate disease are favorable to delay OA progression and reduce the economic cost and biomechanical concessions associated with current end-of-stage-treatments. First MTP joint cheilectomy combined with proximal phalangeal dorsiflexion osteotomy (Moberg) is one such treatment. However, postoperative contact mechanics are not fully understood.

The aim of the combined surgery is to remove osteophytes at the dorsal aspect of the 1<sup>st</sup> MTP joint and to dorsiflex the hallux, thereby, freeing up space for the joint to recover range of motion. The goal of this study is to compare the effect of cheilectomy with different Moberg osteotomy geometries on 1<sup>st</sup> MTP joint contact mechanics.

## METHODS

Six cadaveric-specific finite-element (FE) models of the first ray (including metatarsal, sesamoids, proximal phalanx and distal phalanx, as well as associated cartilage and plantar fascia) were developed. All specimens were free of cartilage defects.

Each specimen was imaged, using a 3T MRI-scanner. Three-dimensional (3D) geometrical models were created, where each tissue was segmented in Mimics (Materialise, Belgium), assembled in CATIA (Dassault Systèmes, France) and meshed in Abaqus (Dassault Systèmes, France). The Bones (E=7.3GPa,  $\nu$ =0.4) and cartilage (E=25MPa,  $\nu$ =0.4) were modelled as linear elastic parts for explicit, dynamic analysis. Fourteen ligaments (tension-only ‘wires’; E=260MPa,  $\nu$ =0.4) and the plantar fascia (E=350MPa,  $\nu$ =0.4) were also modelled.

Model geometry was then modified (Fig. 1) to simulate a cheilectomy only, and a cheilectomy combined with 1-mm and 3-mm Moberg osteotomy. The metatarsal bone of each model was rotated in a physiological manner to simulate a planus arch-alignment. Loading conditions were determined during prior cadaveric testing for experimental validation of the computational models. Loads of 28 N, 20 N and 20 N were applied beneath the hallux, lateral sesamoid and medial sesamoid, respectively, to represent one quarter scale of the ground reaction forces during gait. The plantar fascia was loaded with ~150 N to balance moments created by the ground reactions forces.

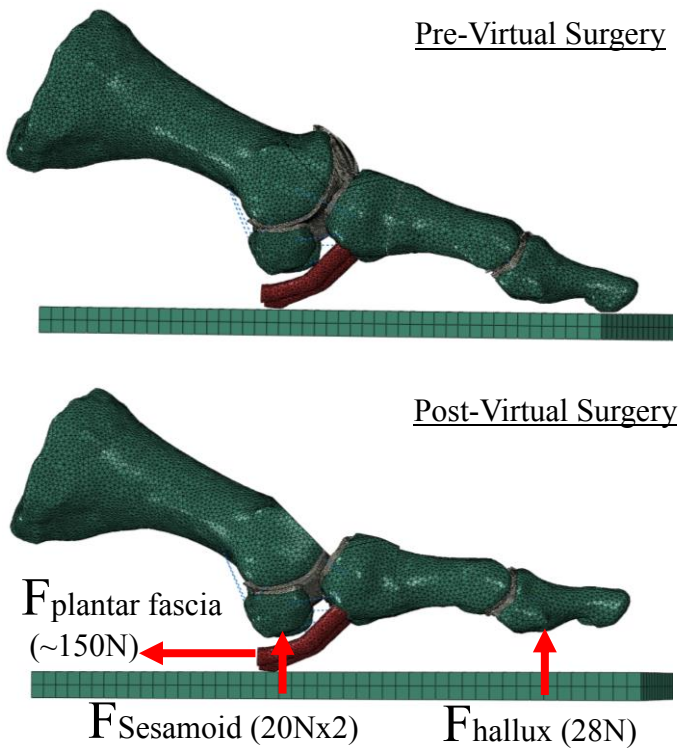


**Figure 1.** FE model of a first ray (with loading conditions) pre- and post-virtual cheilectomy and 3-mm Moberg osteotomy titration.

## RESULTS AND DISCUSSION

Six cadaveric-specific FE models of the first ray were developed to compare 1<sup>st</sup> MTP joint peak shear stress and location of peak shear stress. Stress analyses were performed pre- and post-cheilectomy, without and with Moberg osteotomies, titrated to 1-mm and 3-mm. The computationally-predicted peak shear stress at the 1<sup>st</sup> MTP joint phalangeal base cartilage is shown in Fig. 2. FE analyses demonstrated plantar shifting and increased magnitude of peak shear stress post-cheilectomy.

## CONCLUSIONS

The ability to calculate unique stress distributions before and after virtual surgery suggests that FE model-based analysis is sensitive to the effect of different size and shape specimens. This series of models can be used to develop insight into current

and future surgical techniques at a subject-specific level.

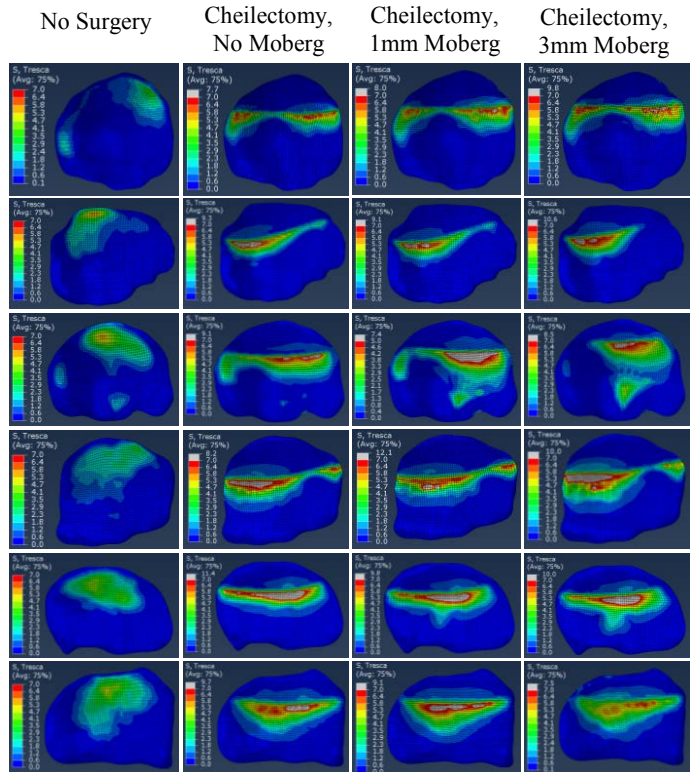


**Figure 2:** Shear stress distributions in the proximal phalanx base cartilage for each first ray specimen presenting with no surgery; cheilectomy and no Moberg osteotomy; cheilectomy and 1-mm Moberg osteotomy and; cheilectomy and 3-mm Moberg osteotomy.

The next phase of this research will be to increase the loading conditions applied to each FE model to represent the full scale ground reaction forces experienced beneath the 1<sup>st</sup> ray during gait.

## REFERENCES

1. Menz, HB. *Osteoarthritis and Cartilage*. 2015.
2. van Saase, JL. *Annals Rheum Disease*. 1989.
3. Buell, T. *J Am Podiatr Med Assoc*. 1988.

## ACKNOWLEDGMENTS

HSS Foot and Ankle Research Fund.

# JOINT LOADING ASYMMETRIES REFLECT PRIMARY OSTEOARTHRITIS INCIDENCE

<sup>1</sup>Toyin Ajisafe, <sup>2</sup>HsinChen Fanchiang, <sup>1</sup>Andrea Gilson, <sup>1,3</sup>Emily Kennedy

<sup>1</sup>Texas A&M University, Corpus Christi, TX, USA.

<sup>2</sup>National Taiwan Sport University, Taoyuan, Taiwan.

<sup>3</sup>University of North Alabama, Florence, AL, USA

email: toyin.ajisafe@tamucc.edu

## INTRODUCTION

Primary (idiopathic) osteoarthritis (OA) of the knee and hip are considerably more prevalent (approximately 20-30% of adults across numerous populations) [1] than the ankle's (less than 1% among adults) [2-3]. Despite suggested links between mechanical loading, articular tissue degeneration, and the risk of OA, it is unclear whether loading asymmetry differences between lower extremity joints is consistent with reported differences in OA incidence between these joints. This study investigated the effect of physical activity rigor on loading asymmetry between lower extremity joints.

## METHODS

13 young adults (7 males and 6 females) (21.7±2.3 years; 170.6±6.9 cm; 65.2±7.9 kg) participated in this study.

Horizontal drop jumps from 41 (low), 56 (moderate), and 71 (intense) cm were implemented as proxies for varying levels of physical activity rigor. Participants were instructed to stand on a box, drop vertically, and jump as far forward as they could upon contacting the force plate below. A 12-camera VICON motion capture system and AMTI force plate acquired joint kinetics and kinematics.

Sagittal joint moments at the hip, knee, and ankle were calculated using inverse dynamics. Moments were averaged across five trials per condition. Cross-correlation coefficients were calculated to estimate loading (moment) symmetry between bilateral homologous joints (equation 1).

$$\text{Corr} - \text{norm } x, y = \frac{\sum_{n=0}^{N-1} x[n] y[n]}{\sqrt{\sum_{n=0}^{N-1} x^2[n] \sum_{n=0}^{N-1} y^2[n]}} \quad (1)$$

Where N is the length of the signal, and x and y are independent in-phase signals. Vector outputs from cross-correlation calculations were normalized to the signal energy (denominator in equation 1).

Movement initiation was delineated as the first non-zero vertical center of mass velocity (vCOM). Touchdown and takeoff from the force plate were defined as the instants vertical ground reaction force exceeded and fell below 40N, respectively.

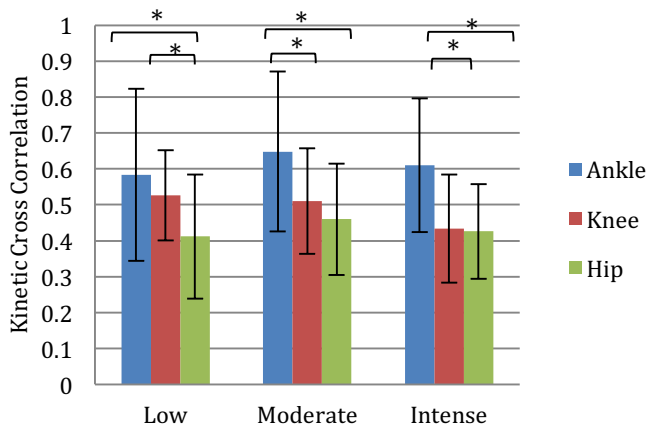
Movement termination was delineated as the last zero vCoM velocity. A 3 (drop height) x 3 (joint) ANOVA with repeated measures was calculated to determine the effects of both factors on loading symmetry. Alpha level was  $p \leq .05$ .

## RESULTS AND DISCUSSION

The knee ( $p = 0.020$ ), ( $p = 0.001$ ), and hip ( $p = 0.002$ ), ( $p = 0.001$ ), showed greater loading asymmetry than the ankle with increased physical activity rigor, i.e., when subjects dropped from 56 cm and 71 cm, respectively.

The hip showed greater kinetic asymmetry than both the ankle ( $p = 0.003$ ) and knee ( $p = 0.004$ ) with decreased physical activity rigor, i.e., when subjects dropped from 41 cm.

Previously, young adult females showed greater loading asymmetry at the knee and hip compared to the ankle during the sit-to-stand task [2].



3. Forczek W, et al. *J Hum Kinet.* **35**, 47-57. 2012.

**Figure 1:** Loading asymmetry between the ankle, hip, and knee joints during low, moderate, and intense physical activity. \* Indicates significant difference between joints.

Despite differences in methodology, this finding is consistent with the observation that greater joint structural stability, which likely imposes greater kinematic constraint, may necessitate more bilaterally uneven moment contributions (increased asymmetry) at the hip and knee compared to the ankle [3].

## CONCLUSIONS

The risk for excessive loading and associated articular tissue degeneration may be greater at the hip than the ankle irrespective of physical activity rigor. Conversely, this risk seems greater at the knee than the ankle only with increased physical activity rigor.

These findings are consistent with previous reports of higher primary OA incidence at the hip and knee compared to the ankle in general adult populations. Therefore, the relationship between physical activity rigor and primary osteoarthritis incidence needs to be further researched, particularly at the knee.

## REFERENCES

1. Neogi T, et al. *Rheum Dis Clin North Am.* **39**, 1-19. 2013.
2. Lundin TM, et al. *J Biomech.* **28**, 109-112. 1995.

# DECREASED PLANTAR SENSATION IS ASSOCIATED WITH INCREASED LOADING

<sup>1</sup>Toyin Ajisafe, <sup>1</sup>Ferdinand Delgado, <sup>2</sup>Hsin-Chen Fanchiang

<sup>1</sup>Texas A&M University, Corpus Christi, TX, USA.

<sup>2</sup>National Taiwan Sport University, Taoyuan, Taiwan.

email: toyin.ajisafe@tamucc.edu

## INTRODUCTION

Decreased plantar cutaneous sensation is associated with a number of conditions, including obesity [1]. Individuals with obesity have greater plantar pressure than those with healthy weight [1].

Interestingly, individuals with overweight and obesity are thought to experience increased ground reaction forces solely due to increased body weight. It is unclear whether decreased plantar cutaneous sensation might engender any compensatory changes to vertical ground reaction forces and impulse during a dynamic non-locomotor task (standing calf raise).

## METHODS

Eleven young adults (four females and seven males) ( $24.18 \pm 4.35$  years;  $171.58 \pm 8.21$  cm;  $76.64 \pm 18.25$  kg) participated in this study.

There were two conditions: no icing and icing.

In the no icing condition, subjects stood barefoot in the middle of an AMTI force plate and performed standing calf raises at a cadence of 48 beats per minute for 90 seconds. The force plate acquired vertical ground reaction forces. Participants were asked to maximally push up and stand on their toes, then lower back down at each audible beat of a metronome.

In the icing condition, participants' forefeet were cooled on bagged ice (while seated) until their forefoot plantar temperature read  $6^{\circ}\text{C}$  on an infrared thermometer. Icing was immediately intervened by the foregoing movement task on the force plate. The order of conditions was randomized. Participants returned to the lab after 24

hours to complete the second condition. Vertical ground reaction force peaks were estimated and averaged across 90 seconds. In addition, we estimated vertical ground reaction force impulse ( $J$ ) by integrating vertical ground reaction force time series ( $F$ ) data over time ( $t$ ), using MATLAB (equation 1).

$$J = \int_{t_0}^{t_{90}} F(t) dt \quad (1)$$

We calculated a paired-samples t-test to determine the effect of forefoot cooling on vertical ground reaction force and impulse. Statistical significance was set at  $p < .05$ .

## RESULTS AND DISCUSSION

A set of paired-samples t-tests, showed significant differences in vertical ground reaction force ( $t(10) = -2.563, p = .028$ ) and impulse ( $t(7) = -2.806, p = .019$ ) between the conditions (Fig. 1).

To our knowledge, there has not been any previous research on the influence of decreased plantar cutaneous sensation on ground reaction force and impulse.

Intact young adults increased vertical ground reaction force and impulse following forefoot cooling (Fig. 1a and 1b) in this study. It is plausible that the observed increase in loading is compensation engendered by deficits in plantar sensation.

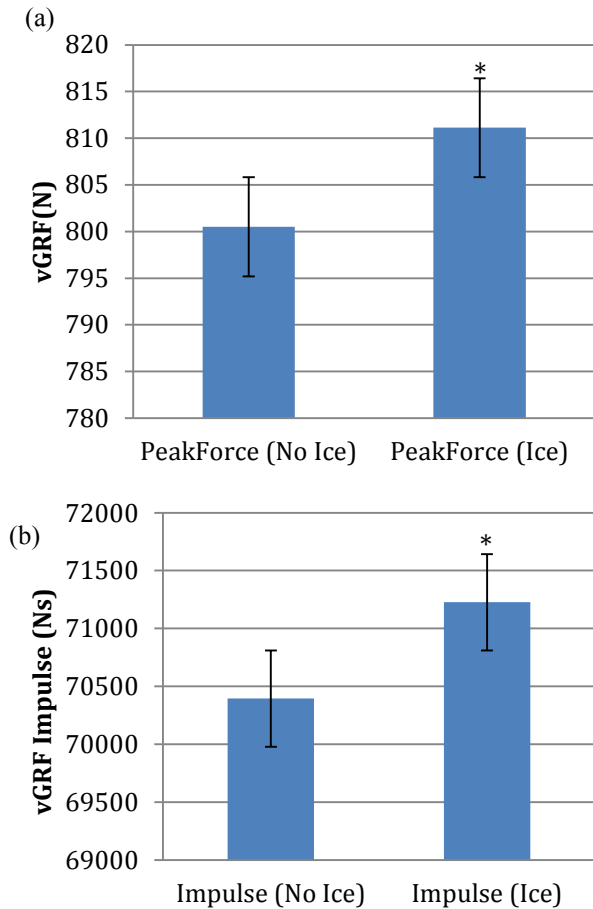


**Fig. 1:** (a) mean vertical ground reaction force (vGRF), (b) mean vertical ground reaction force impulse. \* indicates significant difference between conditions.

## CONCLUSION

The finding of increased loading and its temporal properties following forefoot cooling suggests that decreased plantar sensation may cause increased loading. This may have implications in conditions that are associated with decreased plantar sensation, including obesity.

The association between increased loading and decreased plantar sensation warrants further investigation, especially considering that obesity has been linked with greater plantar pressure and incidence of foot-related injuries/discomfort.

## REFERENCES

1. da Rocha ES, et al. *Clin Biomech (Bristol, Avon)*. **29**, 822-827. 2014.

# Factors influencing visuomotor tracking performance in healthy adults

<sup>1</sup> Anthony C. Santago II, <sup>1</sup> Michael S. Fine, <sup>1</sup> Jennifer Bleck, <sup>1</sup> Elizabeth B. Brokaw

<sup>1</sup> The MITRE Corporation, McLean VA, USA; email: [asantago@mitre.org](mailto:asantago@mitre.org) website: [www.mitre.org](http://www.mitre.org)

Approved for Public Release; Distribution Unlimited. 17-0545; © The MITRE Corporation ALL RIGHTS RESERVED

## INTRODUCTION

Mild traumatic brain injury (mTBI) is a global health concern with an estimated 42 million individuals worldwide receiving an mTBI each year [1]. Recent work has demonstrated that a 3 minute visuomotor tracking (VMT) test can classify mTBI with comparable to or better accuracy than several standard clinical scales, in less time [2]. This may be a result of the VMT test simultaneously evaluating several processes which are often impaired after mTBI such as fine motor performance, reaction time, and spatial processing.

Understanding normal variability in VMT performance can help improve mTBI classification. The goals of this study were to: 1) quantify normative performance on the VMT task, 2) determine if there are human factors associated with differences in task performance and 3) quantify the relationship between VMT performance and standard assessments of fine motor control, reaction time, and spatial processing.

## METHODS

### Visuomotor tracking task

VMT performance was quantified using a novel device [2], adapted to run on an iPad (Fig. 1).

Participants were asked to squeeze a hand dynamometer, and vary their grip force to match an unpredictably-changing target force for 3 minutes. Target force was scaled to their age and sex-based maximum grip force [3]. Previous work demonstrated a model of participants' feedback response (Eq. 1) – how participants changed their grip force in response to errors in force and force velocity – could classify mTBI with a sensitivity of 87% and a specificity of 93% [2].

$$\dot{x}_{(t)} - \dot{x}_{T(t-\tau)} = -K_p(x_{(t-\tau)} - x_{T(t-\tau)}) - K_d(\dot{x}_{(t-\tau)} - \dot{x}_{T(t-\tau)}) \quad \text{Eq. 1}$$

In Eq. 1,  $x$  equals a participant's grip force (given by the position of the vertical bar in Fig. 1).  $x_T$  represents the target grip force (given by the position of the horizontal bar in Fig. 1).  $\tau$  captures



sensorimotor processing delays, and is quantified as the time difference which minimizes the root-mean-square (RMS) error between a participant's grip force and the target grip force.  $K_p$  and  $K_d$  act as a gain on errors in force and force velocity respectively, similar to stiffness and viscosity in a mechanical system, quantifying how each participant responded to error at time  $t$  to update grip force at time  $t + \tau$ .

### Participant recruitment and study design

A total of 125 participants were recruited from the attendees of the 2016 American Society of Biomechanics Meeting (70M 30.2±8.9 years; 55F; 27.3±6.3 years). The study was approved by the MITRE IRB and the ASB executive committee. Demographic information, including history of head injury, were recorded. Participants completed the VMT task followed by standard assessments of cognitive and motor function: Trail Making Test A (TMA) to assess spatial processing [3]; nine-hole peg (NHP) test [4] to assess fine motor performance; and a mouse-click reaction time (RT) test to assess simple RT [5]. VMT data was collected at 240Hz and filtered using a 2<sup>nd</sup> order Butterworth filter with a 2Hz cutoff. Time to completion was measured for both TMA and NHP tests. RT was quantified as the average across 50 trials. VMT parameters  $K_p$ ,  $K_d$ , and  $\tau$  were calculated for each participant (Eq. 1). Three statistical models were constructed to determine if variability in each clinical measure (TMA, NHP, and RT) could be explained by the independent variables  $K_p$ ,  $K_d$ , and  $\tau$ ; sex was also included as an independent variable. Student's t-tests were used to determine if human factors affect performance.

## RESULTS AND DISCUSSION

### Visuomotor tracking performance

Normative VMT performance is shown in Fig. 2. RMS error is represented in pixels to account for differences in the ratio of pixels to lbs for each participant, due to age and sex differences in maximum grip force. The variability in healthy performance is likely indicative that a baseline assessment would be beneficial when evaluating an individual for mTBI. Females had significantly higher  $K_d$  ( $p=0.046$ ) and RMS error ( $p=0.010$ ).  $K_p$

( $p=0.090$ ) and  $\tau$  ( $p=0.055$ ) were not significantly different. The results suggest that men and women respond differently to the VMT task and adding sex to the mTBI classifier [2], should be considered.

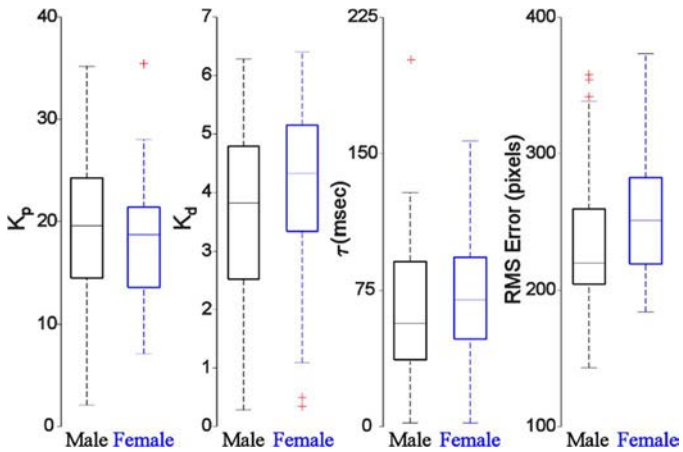


**Fig 2:** Box and whisker plots of the VMT parameters

### Clinical assessments

Regarding the conventional clinical assessments, in general, our population was faster, had smaller inter-subject variability, and reduced overall range relative to the previously reported age- and population-based norms (Fig. 3) [4,5,6]. Females were significantly faster than males at completing the NHP test ( $p<0.001$ ) but had slower RT ( $p<0.001$ ). Since RT has been used to evaluate mTBI, our data supports considering sex when using these tools.

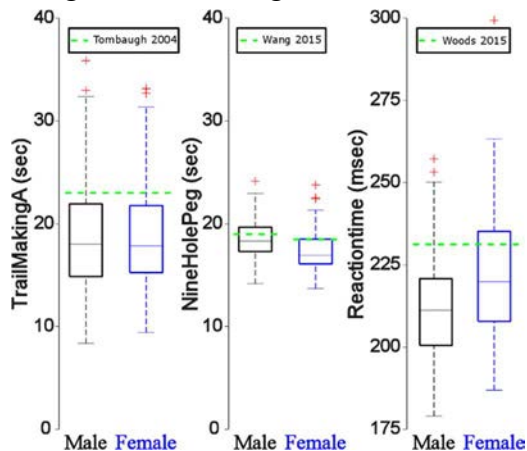


**Fig 3:** Box and whisker plots of the clinical parameters with previous measured norms in green

### Statistical models

Although all statistical models were significant, the VMT parameters only captured a small portion of the variability in spatial processing, fine motor performance, and reaction time: TMA (adjusted  $r^2 = 0.121$ ;  $p<0.001$ ); NHP (adjusted  $r^2 = 0.073$ ;  $p=0.011$ ); RT (adjusted  $r^2 = 0.281$ ;  $p<0.001$ ). This

implies that VMT parameters are capturing more of the variability in participants' reaction time than the variability in participants' spatial processing or fine motor control abilities, quantified by these assessments. In addition, the weak correlation between VMT parameters and performance on the NHP test suggests that fine motor performance in prehensile tasks is significantly distinct from fine motor grasp modulation.

### Effect of history of head injury

Other factors may also affect VMT performance. Individuals with a self-reported history of head injury ( $N=36$ ) performed significantly slower on the NHP test compared to individuals without a history of head injury ( $N=88$ ,  $p=0.023$ ). A self-reported loss of consciousness (LOC) ( $N=9$ ) in the last injury further increased population differences. Participants with LOC were slower on the NHP test ( $p=0.016$ ), and trended higher on  $K_d$  ( $p = 0.051$ ), [2], than those without a self-reported history of head injury. Higher  $K_d$  has previously been shown to indicate more mTBI like VMT performance [2].

## CONCLUSIONS

This study revealed substantial variability in normative VMT performance, suggesting a baseline assessment and the inclusion of sex would improve mTBI classification. VMT parameters marginally explained variation in the clinical assessment signifying the VMT model may not be capturing the cognitive and motor processes explored within this study. Our finding that previous head injuries alters task performance suggests that medical history may also need to be considered by a mTBI classifier. Future studies should explore a larger age-range and consider other human factors that could potentially affect mTBI diagnosis and monitoring with VMT such as age and education.

## REFERENCES

1. Gardner, R & Yaffe, K., *Mol Cell. Neuro.* **66**, 2015
2. Fine, M, et al., *Exp Brain Res.* **11**,2016
3. Massey-Westropp, N, et al., *BMC Res. Notes* **4**, 2011
4. Tombaugh, T, *Clin Neuropsych.* **19**, 2004.
5. Wang, Y, et al. *J Hand Therapy.* **28**, 2015
6. Woods, D, et al. *Front Human Neuros.* **9**, 2015

## ACKNOWLEDGEMENTS

Funding was provided by The MITRE Corporation Research and Development Program. We would like to thank all of the ASB 2016 attendees who participated.

# APPLICATION OF A NOVEL ELASTIC FORCE-FIELD TO INFLUENCE LATERAL GAIT STABILIZATION STRATEGY

<sup>1</sup> Meghan M. Bowman, <sup>1</sup> Kyle T. Maynard, <sup>1,2</sup> Jesse C. Dean

<sup>1</sup>Medical University of South Carolina, Charleston, SC, USA

<sup>2</sup>Ralph H. Johnson VA Medical Center, Charleston, SC, USA  
email: deaje@musc.edu

## INTRODUCTION

Bipedal walking requires the active control of lateral stability [1]. Neurologically uninjured humans accomplish this goal largely through step-by-step adjustments in step width. Briefly, step width is actively controlled based on the mechanical state of the pelvis or center of mass [2-3].

The apparent ease of ensuring lateral stability in healthy controls does not extend to many clinical populations, as lateral losses of balance are often a challenge to mobility. For example, the typical stabilization strategy of actively modulating foot placement is disrupted in a subpopulation of chronic stroke survivors classified as at an increased risk for falls [4]. Unfortunately, no rehabilitation methods currently exist to retrain appropriate step-by-step adjustments in mediolateral foot placement.

In the long term, our goal is to develop a device able to retrain the typical stabilization strategy using either assistive or perturbing methods. The purpose of the present study was to test whether our elastic force-field [5] can influence this strategy in healthy controls. We hypothesized that assistive methods would strengthen the relationship between pelvis mechanics and step width, but only while the force-field was active. We also hypothesized that perturbing methods would produce after-effects in which step width was more tightly controlled.

## METHODS

This work involved a custom-built elastic force-field [5]. This novel device can exert controllable mediolateral forces on the swing leg during walking, without interfering with forward progression. The device is interfaced with a motion capture system,

allowing near real-time control based on participant kinematics (measured using active LED markers). Based on prior studies of sensorimotor adaptation using split-belt walking [6] or other force-fields [7], several control modes were applied:

- 1) *Transparent*. The force-field remained aligned with the leg, minimizing mediolateral forces.
- 2) *Assistive*. At the start of each step, we predicted the upcoming step width based on pelvis mechanics. The force-field pushed the swing leg toward this location.
- 3) *Perturbing*. We predicted step width at the start of each step, but the force-field pushed the swing leg away from this location (e.g. encouraging a narrow step when a wide step was predicted).

24 healthy controls (16F/8 M; age=24±2 yrs; height=172±11 cm; mass=74±13 kg) participated in this experiment, and were randomly assigned to *assistive* or *perturbing* groups (n=12). Participants performed seven random-order treadmill walking trials at 1.2 m/s: no force-field (5-min); *transparent* (5-min); five 10-minute trials in which the force-field switched from *assistive/perturbing* to *transparent* mode at the 5-minute mark. These five trials differed only in the pelvis mechanics parameters used to predict the upcoming step width. As no significant differences were observed between these trials, they were combined for the purpose of the present analyses.

Our primary analysis focused on the strength of the relationship between pelvis mechanics at the start of a step and subsequent step width. To quantify this relationship, we performed multiple regressions to predict step width from mediolateral pelvis velocity and displacement from the stance foot (for each minute of walking). Higher R<sup>2</sup> values would indicate a stronger relationship. We used ANOVAs to detect significant changes in R<sup>2</sup> magnitude from baseline.

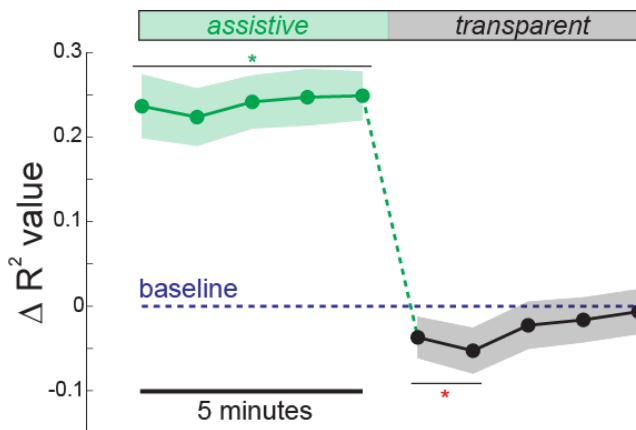


**Figure 1:** Effects of *assistive*-mode force-field on mechanics-dependent control of step width. Shaded regions indicate 95% confidence intervals, and asterisks indicate a significant ( $p < 0.05$ ) post-hoc differences from baseline.

## RESULTS AND DISCUSSION

Our metric of gait stabilization strategy ( $R^2$  value) was nearly identical between normal ( $0.50 \pm 0.09$ ) and *transparent* ( $0.49 \pm 0.08$ ) walking conditions ( $p = 0.40$ ). This result indicates that our force-field does not interfere with the step-by-step control of step width when in *transparent* mode.

With the force-field in *assistive* mode, the relationship between pelvis mechanics and step width was clearly strengthened (Fig. 1). However, the switch to transparent mode caused short-lived after-effects, as the  $R^2$  magnitude was significantly reduced for the next 2-minutes of walking.

With the force-field in *perturbing* mode, the relationship between pelvis mechanics and step width was slightly weakened (Fig. 2). The switch to transparent mode elicited tighter control over step width (evidenced by an increased  $R^2$ ) for the next minute of walking.

The present results demonstrate that our force-field can influence the step width control strategy used by uninjured adults. *Assistive* methods appear to promote “slacking” [8], transiently reducing active control over the assisted gait behavior. In contrast, *perturbing* methods appear to produce beneficial after-effects, likely due to sustained use of the greater active control required to prevent a loss of balance.

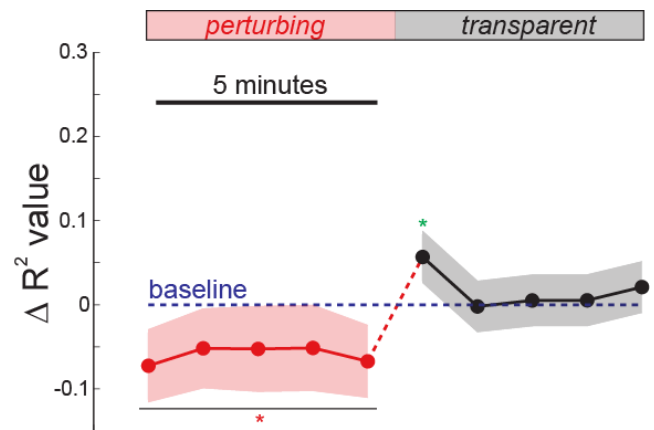


**Figure 2:** Effects of *perturbing*-mode force-field on mechanics-dependent control of step width.

Future work will investigate whether similar methods can be used to retrain the typical lateral stabilization strategy in chronic stroke survivors. The relative effectiveness of our control methods may be influenced by participants’ baseline functional level, with more limited individuals benefiting more from *assistance* [7]. As with split-belt walking, multiple exposures may be needed to affect gait behavior [6].

## CONCLUSIONS

Our novel elastic force-field can influence the lateral stabilization strategy during gait. The device may have potential to serve as a rehabilitation tool for patients with reduced mobility due to gait instability.

## REFERENCES

1. Kuo AD. *Int J Rob Res* **18**, 917-930, 1999.
2. Wang Y, et al. *Biol Lett* **10**:20140405, 2014.
3. Rankin BL, et al. *J Neurophys* **112**, 374-383, 2014.
4. Dean JC, et al. *J Rehab Res Dev* **52**, 577-590, 2015.
5. Nyberg ET, et al. *IEEE Trans Neur Syst Rehab Eng* In Press.
6. Reisman DS, et al. *Neurorehab Neur Repair* **27**, 460, 2013.
7. Milot M, et al. *Exp Brain Res* **201**, 119-131, 2010.
8. Reinkensmeyer DJ, et al. *Conf Proc IEEE Eng Med Biol Soc* **2009**, 2129-2132, 2009.

## ACKNOWLEDGMENTS

This work was supported by a grant from the National Science Foundation (#1603391).

# Muscle Synergy Extraction from EMG (Electro Myogram) data: A comparison of algorithms (PCA, NMF, pICA)

<sup>1</sup> Rajat Emanuel Singh, <sup>2</sup> Kamran Iqbal, <sup>2</sup> Ghulam Rasool, <sup>2</sup> Gannon White <sup>3</sup> Shelby Wingate <sup>3</sup> Hazel Hutchinson  
<sup>1</sup> University of Arkansas at Little Rock, Ar, USA.  
email: resingh@ualr.edu, kxiqbal@ualr.edu

## INTRODUCTION

Muscle Synergies is defined as the pattern of co activation of muscles recruited by a single neural command [1]. The concept of Muscle Synergy has been effectively utilized in myoelectric control for prosthesis [2]. The mathematical model of muscle synergies is in two forms a) time variant b) time invariant [3].

The Synergies are extracted in the form of matrix from the (Electro Myogram) EMG data using different blind source separation algorithm. The Matrix extracted can reconstruct the EMG signal by linearly recombining several time invariant synergies, each activated by a time dependent activation coefficient [1]. It has been hypothesized, if the reconstructed muscle activation pattern for specific task is produced with an artificial limb it is more likely to produce similar biomechanical movement for the specific subtask since muscle synergies represent motor modules recruited by the nervous systems [5], which will allow an amputee with prosthetic limbs to make task specific movements. In this study, we will compare different algorithmic approach to extract muscle synergies for myoelectric prosthesis.

## METHODS

For Muscle Synergy extraction, raw EMG data from Rasool *et al* is used. The data were collected from 12 participants with height  $171.4 \pm 8.8$  cm and age  $28.2 \pm 6.5$  years (mean  $\pm$  std. dev) from wrist muscles. Preprocessing on raw EMG data included removal of the transient part of EMG signal with a ctp (contraction time percentage) of 50%-70% followed by segmentation of the signal into non-overlapping 250ms windows [2]. It has been shown that 200-300ms windows are optimal to retain maximum information, and taking greater than

300ms windows segmentation decreases the amount of information. Root mean square (RMS) values of the EMG signal were obtained and the data were separated into n bins based on the number of stimulus (movement tasks) [2]. After preprocessing, extraction of Muscle Synergies with different blind source separation (BSS) algorithms was performed. A muscle activation pattern is mathematically deduced in the following form represented below, where  $C$  represents activation coefficient, n represent number of muscles, m represent length of activation pattern and  $W$  represent Synergy matrix.

$$M^{n \times m} = W^{n \times s} \times C^{s \times m}$$

$$M = \begin{bmatrix} M_1(t) \\ \vdots \\ M_m(t) \end{bmatrix}, \quad W = \begin{bmatrix} W_{11} & \dots & W_{s1} \\ \vdots & \ddots & \vdots \\ W_{1m} & \dots & W_{sm} \end{bmatrix},$$
$$C = \begin{bmatrix} C_1(t) \\ \vdots \\ C_s(t) \end{bmatrix},$$

MATLAB 2014a is used for extraction of muscle synergies. The separation scheme involves extracting a synergy matrix  $W$  from the EMG data, on running PCA on the processed data, there was a reduction in the dimensionality of output matrix. Similarly, with NMF the dimensional reduction can be achieved. We used MATLAB toolbox for Principle Component Analysis (PCA), Probabilistic Independent Component Analysis (pICA), Non-Negative Matrix Factorization Algorithm (NNMF/NMF). updating the code to run our data model. The EMG data matrix is  $n \times m$  where  $n$  is the number of sensors and  $m$  is the samples. The output Synergy Matrix ( $W$ ) has a reduced dimension for NMF and PCA ie. ( $n \times d$ ) where  $d$  is the number of components selected, i.e., the number of synergies (we selected only 2 synergies). But for pICA, the output Synergy Matrix ( $W$  matrix) is in the form  $d \times m$ , so a PCA algorithm on the MATLAB code is

run first, followed by pICA which changes the dimensionality to the form of  $n \times d$ . In order to find the performance of each algorithm a simulated data set is used. A MATLAB code for NNMF, PCA and pICA is run. The following results are produced that has been discussed below.

## RESULTS AND DISCUSSIONS

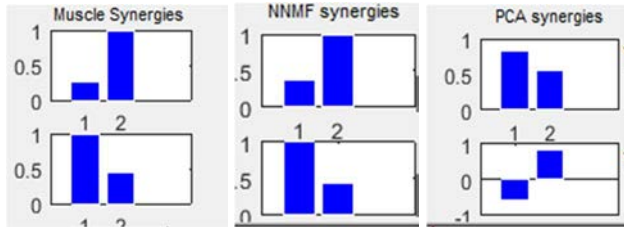


**Fig 2:** Reconstructed Synergies compared with actual Synergies using NNMF and PCA.

The reconstruction of the muscle synergies with NNMF approach is done on MATLAB on the simulated data set, which showed that NNMF was more precise as compared to PCA. On the other hand, the pICA performs better than the NNMF [2]. The result also provides us the understanding of the orthogonality of both PCA and NNMF. In particular, the result shows that the PCA is orthogonal where as NNMF is not.

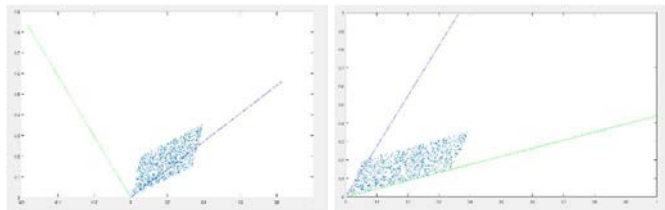


**Fig 3:** Vectors of the PCA (Left) and NMF (Right) for the reconstructed muscle Synergies.

## CONCLUSIONS

The extraction of Muscle Synergy is very important in myoelectric prosthesis. The solutions we obtain from extraction of muscle Synergy are not unique because of the non-convexity. From the above results and discussion, it can be assumed that the performance of pICA for the extraction of muscle Synergy is highest among the three algorithms followed by NNMF and PCA. For the agonistic and antagonistic relationship in the simulated data set PCA shows the relationship but does not allow proper reconstruction [3]. Researching further for the

proper reconstruction of agonistic-antagonistic relationship between muscles autoencoder algorithm has been evaluated which gave better result when compared to other algorithms [4]. There is an another alternate to NNMF which is FA (Factor Analysis). The FA algorithms performs better than the NNMF but not superior to pICA [4].

## REFERENCES

- [1]. Torres Oviedo, G *et al J Neurophysiology*, **96 (3)**, 1530–46, 2006.
- [2]. G. Rasool, K. Iqbal, “Real-time multi degree-of-freedom task discrimination for myoelectric control employing task-specific muscle synergies”, *IEEE Trans. Neural and Rehab. Eng.*, Jan 2016.
- [3]. Mathew C. Tresch. *et al J Neurophysiology*, **95**, 2199-2212, 2006.
- [4]. Alessandro E.P. Villa, et al. *Artificial Neural Networks and Machine Learning-ICANN 2016*, Springer Ltd, 2016.
- [5]. Safavynia SA, Torres-Oviedo G, *et al. Topics in spinal cord injury rehabilitation*. **17(1)**:16-24, 2011.
- [6]. Cheung VCK, Piron L, Agostini M, Silvoni S, Turolla A, Bizzi E. Stability of muscle synergies for voluntary actions after cortical stroke in humans. *Proceedings of the National Academy of Sciences of the United States of America*. 2009;106(46):19563-19568.

**Table:** An EMG data with 8 sensors ( $n$ ) and 200 samples ( $m$ ) is used for 2 muscles Synergy Extraction ( $d$ ).

Algorithm	Input (Data matrix/Emg Data)	Output (Synergy Matrix)
PCA	8 x 2000	8x2
NNMF	8 x 2000	8x2
pICA	8 x 2000	8x2000
PCA-pICA	8 x 2000	8x2

# CENTER OF MASS CONTROL AND MULTI-SEGMENT COORDINATION IN CHILDREN DURING AND AFTER WHOLE BODY VIBRATION

Huaqing Liang and Jianhua Wu

Georgia State University, Atlanta, Georgia, USA. Email: hliang2@gsu.edu

## INTRODUCTION

Maintaining upright posture under external perturbations requires the coordination between the nervous system and the musculoskeletal system, and it is a milestone of motor development in early childhood [1]. Whole-body vibration (WBV) has acute effect on postural control and muscular activation during standing, resulting in an increased sway velocity and sway area of center-of-mass (COM), and the residual effect usually vanish within 20 minutes after the vibration exposure [2]. In quiet standing, a human body can be considered as a multi-segment linked system, and the uncontrolled manifold (UCM) approach has been used to examine how this multi-joint motor redundancy is utilized to achieve postural control of the body [3]. The aim of study was to compare the joint variance partitioning pattern between children and adults while controlling the COM before, during, and after WBV disturbance.

## METHODS

*Subjects:* Fifteen children (6M/9F) and fourteen young adults (6M/8F) participated in the study. Mean (SD) age of the children (TD group) was 8.1 (1.8) years, height 1.32 (0.10) m, and mass 30.2 (6.7) kg. Mean (SD) age of the adults (YA group) was 24.5 (3.9) years, height 1.68 (0.12) m, and mass 70.6 (13.4) kg.

*Experimental design:* An 8-camera Vicon motion capture system and the Vicon full-body PSIS model were used for data collection. A Soloflex platform was used to provide WBV with the frequency of 28 Hz and the amplitude of <1mm, resulting in a vertical acceleration of 0.5g ( $g=9.81\text{m/s}^2$ ). Subjects were asked to stand upright with feet hip width apart 4 times: before vibration (phase *Pre*), during vibration (phase *Vib*), immediately after vibration (phase *Post\_0*), and 5 minutes after vibration (phase

*Post\_5*). Each standing trial lasted for 40 seconds. There were also 2 visual conditions: eyes open (EO) and eyes closed (EC). The order of the conditions was randomized and at least 5 minutes of rest was provided between conditions.

*Data analysis:* The COM data was obtained based on the position of all the markers. The root-mean-square (RMS) of COM in the anterior-posterior (AP) direction was calculated and normalized by each subject's height. Markers on the right side of the body were used for the UCM approach and a geometric model was built that associated the COM movement with the following 8 segment angles: foot, shank, thigh, pelvis, trunk, head, upper-arm, and forearm [1]. The movement on the sagittal plane was examined and all the angles were defined as the segmental angle with respect to the horizontal. The variability of the segment angles can be partitioned into two subspaces: the UCM subspace within which the variability helps maintain the mean COM position, and the orthogonal (ORT) subspace within which the variability causes the deviation of the COM [3, 4]. For a coordinated postural control, the variability in the UCM subspace is larger than that in the ORT subspace [1, 3]. Customized MATLAB program was used to calculate the variance in the UCM ( $V_{UCM}$ ) and ORT subspace ( $V_{ORT}$ ) separately. The UCM ratio was further defined as:

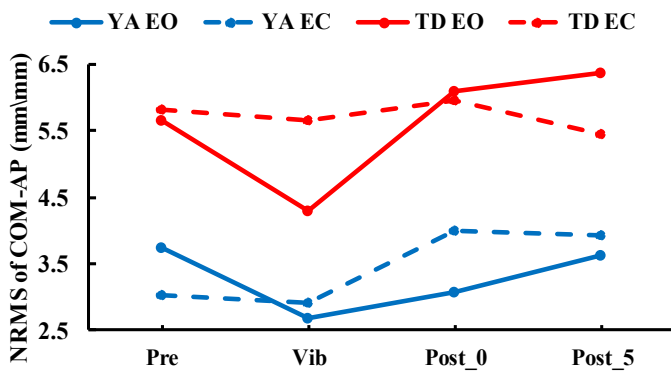
$$UCM\ ratio = \ln(V_{UCM} / V_{ORT})$$

*Statistical analysis:* A 4-way (2 group x 2 visual x 4 phase x 2 component) ANOVA with repeated measures were conducted on variance in the two subspaces. A series of 3-way (2 group x 2 visual x 4 phase) ANOVA with repeated measures were conducted on RMS of COM-AP and UCM ratio. Post-hoc pairwise comparisons with Bonferroni adjustments were conducted when appropriate. Statistical significance was set at  $\alpha = 0.05$ .

## RESULTS AND DISCUSSION

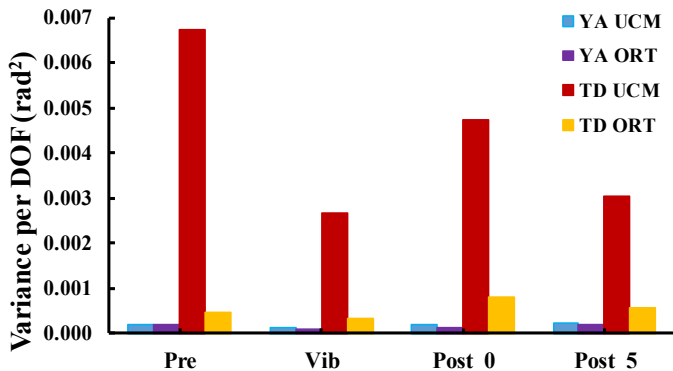
The TD group showed a larger RMS of COM-AP than the YA group. Both groups also displayed a decrease of RMS from *Pre* to *Vib* phase, but increased to *Pre*-level immediately after vibration (Fig. 1). There was a group effect ( $p<0.001$ ) and a phase effect ( $p=0.014$ ). When there was vibration disturbance, both groups constrained their COM sway within a narrower range to adapt to the mechanical vibration, which was more prominent in the TD group.

**Fig. 1** Normalized RMS of COM-AP



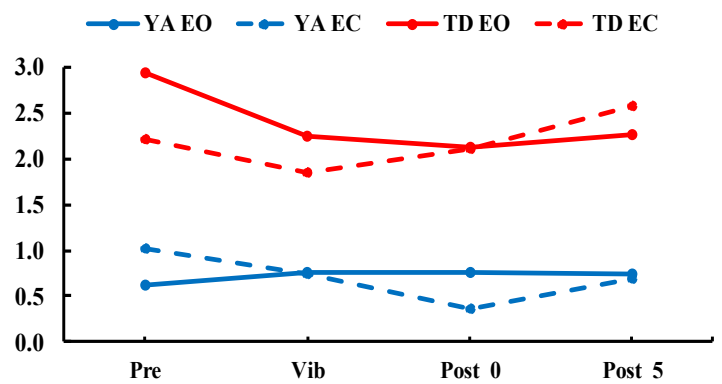
The TD group displayed a larger variance than YA group in both UCM and ORT subspaces. For both groups, a larger variance was generated in the UCM compared to the ORT subspace (Fig. 2). There was a group by component interaction ( $p<0.001$ ). Post-hoc analysis revealed that the difference in variance between two subspaces was greater in the TD group than in the YA group. No visual or phase effect was found for either group.

**Fig. 2** Eyes Open



The TD group exhibited a larger UCM ratio than the YA group across all phases at both visual conditions (group effect,  $p<0.001$ ) (Fig. 3). Both groups displayed a UCM ratio greater than zero, suggesting that more variance was partitioned into the UCM subspace to assist the control of COM for the standing task before, during, and after WBV. The greater UCM ratios observed in the TD group were majorly resulted from the larger difference in variance between two subspaces compared to the YA group. No phase effect was found for both groups, suggesting that even though total variance decreased and increased at different phases, the structure of variance partition remained the same for YA and TD.

**Fig. 3** UCM Ratio



## CONCLUSIONS

Both groups displayed a decrease in overall COM-AP sway variance during WBV, but returned to baseline level immediately after the cessation of vibration. In terms of the structure of variance partition, both groups distributed more variability in the UCM than ORT subspace across all phases although the TD group had a greater variance. This suggests that the TD group may have developed a postural control strategy similar to that observed in YA to regulate variance partition.

## REFERENCES

1. Wu J, et al. *Exp Brain Res* **196**, 329-339, 2009.
2. Dickin DC, et al. *J Appl Biomech* **30**, 529-533, 2014.
3. Scholz J, et al. *Exp Brain Res* **180** 163-179, 2007.
4. Scholz J, et al. *Exp Brain Res* **126** 289-306, 1999.

# Rate Coding and Recruitment of Elbow Flexion Agonists

<sup>1</sup> Zachary Adams, <sup>2</sup> Robert Akins, and <sup>1</sup> Thomas Buchanan

<sup>1</sup> University of Delaware, Newark, DE, USA

<sup>2</sup> Nemours-AI DuPont Hospital for Children, Wilmington, DE, USA

email: buchanan@udel.edu

## INTRODUCTION

One of the interesting problems in motor control is the redundancy of motor action across a single joint. This allows for an array of complex motions with many possible solutions. While this topic has been well studied with respect to biomechanical solutions the relationship of muscle activity to central processing is not yet understood. With the rise of high-yield decomposition it has now become possible to analyze motor activity not as just a simple gain but as a summation of neural inputs.

The purpose of this study was to determine motor unit (MU) characteristics within agonist muscles to determine recruitment differences during contraction. In addition this study aimed to determine specific relationships between MU behavior that would provide a better understanding of the redundancies of the neuromuscular system.

## METHODS

Eleven subjects (5 male, 6 female, 22-31yrs) participated in an isometric elbow flexion force tracking task, during which surface electromyography (EMG) was collected on the right biceps brachii (BB) and right brachioradialis (BRA). Their arms were restrained horizontally at 90 degrees elbow flexion. A force matching task was performed for three low force levels: 20, 30, and 40 percent of their maximal trials (MVIC).

The surface EMG was decomposed using specialized software (Delsys Inc., Boston MA) into individual MU spike trains [1]. Recruitment and rate coding characteristics were extracted from these spike trains and compared across force levels. Only spike trains whose accuracy was reported as 90% by the software was used for analysis.

## RESULTS AND DISCUSSION

Recruitment and rate coding were defined by specific parameters obtained from the force trace in combination with the decomposed MU trains. Recruitment was defined by recruitment threshold (force level at recruitment, %MVC), the initial firing rate (firing rate at recruitment), and recruitment time. Rate coding was defined by the average peak firing rate (defined hereafter as 'peak firing rate').

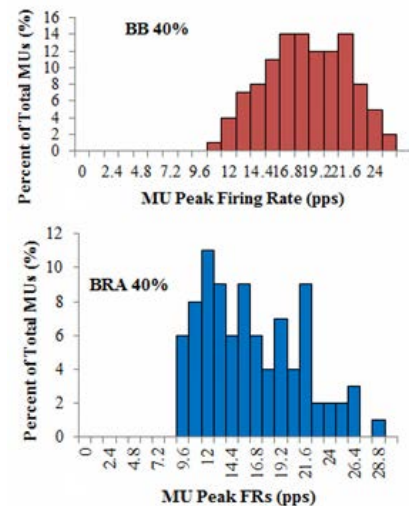


**Figure 1:** Sample MU distributions for a subject at 40% MVC.

All subjects showed an expected increase in BB MU peak firing rate with a corresponding increase in force contraction ( $p < 0.05$ ). This trend was not seen in the BRA peak firing rates. In addition BB and BRA peak firing rate distributions were quite different as well (Fig 1). The BB distribution followed a more standard 'bell shaped', while the BRA distribution is better described as a 'lop sided hill'. This was mostly consistent across all subjects and the distribution for both muscles did not significantly change shape across force levels.

To get a broader perspective of the firing rate behavior of the pool related to recruitment we compared the initial firing rate and peak firing rate for each MU. For both BB and BRA there was an expected increase in firing rate with the increase in initial firing rate. Linear fits were calculated for each force level. Earlier recruited MUs with higher peak firing rates had greater initial firing rates [2,3]. An increase in force was accompanied by an increase in the slope of the linear fit for both muscles. This was expected with the BB due to its increased peak firing rates with an increase in force, but was unexpected in the BRA. Even more confounding was that the linear fits for the BB were much worse than for the BRA ( $R^2_{BB}=.213$ ,  $R^2_{BRA}=.633$ ). This indicates that the BRA MUs have more regulated rate coding than those of the BB.

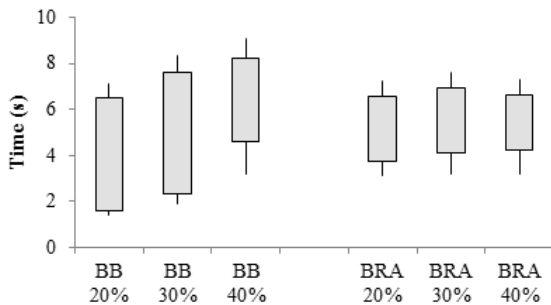


**Figure 2:** MU Firing Times for a single subject. Bottom of the box represents recruitment time, top represents when MU reached peak firing rate.

BB and BRA data for all subjects also showed a difference in motor unit recruitment timings. For all force levels BB MUs were recruited earlier than BRA MUs (Fig 2). In addition it seems as though the time from recruitment to peak firing rate corresponded with the relationship between peak firing rate and force for the BB. BRA MUs, which had no relative change in peak firing rate across force levels, reached their peak at about the same time. Both of these concepts are observed in Figure 2. Because each force contraction was performed at a consistent rate (10% MVC/sec) this may suggest a relationship between rate coding and force rate.

The recruitment threshold distribution mean was positively correlated with force contraction level for both BB and BRA ( $p<0.05$ ,  $p<0.05$ ). This is not unexpected; it is assumed that at lower force levels

not all MUs have been recruited, and muscles will recruit MUs gradually with force until a specific force level [3,4]. Coupling MU's recruitment thresholds with their corresponding initial firing rates should be a more accurate representation of recruitment assuming the muscle is fairly homogenous in firing behavior. A negative relationship exists between initial firing rate and the recruitment threshold within subjects across all force levels and both muscles ( $R^2_{BB}=.35$ ,  $R^2_{BRA}=.41$ : average fits for all subjects). This being said, there was no global relationship across all subjects in recruitment threshold mean, linear fit slope or intercept.

All data presented here define two very different control schemes for both the BB and BRA. One possible explanation is that the BB acts as a force producer while the BRA acts as a force regulator. Precise control is not required if the goal is to produce force, and is represented by the early recruitment times and less organized methods of rate coding seen in the BB. Meanwhile the BRA has much more organized rate coding and does not change its firing rate behavior with respect to force, implying that the force is not its goal.

This recruitment data indicates that each subject has their own specific MU force-firing rate characteristics, most likely represented in physiological differences between subject's muscles. All previous firing rate relationships and data have been true across and hold their significance throughout the population. This may mean that recruitment is a function of subject-specific muscle parameters while rate coding is a function of a common neural drive across the population.

## REFERENCES

1. Nawab SH, et al. *Clin. Neurophysiol.* **121**, 1602–1615, 2010.
2. Henneman E, *Science* **57**, 1345–1347, 1957.
3. DeLuca CJ, Contessa P. *J. Neurophysiol.* **107**, 178–195, 2012.
4. Monster AW, Chan H. *J. Neurophysiol.* **40**, 1432–1443, 1977.

# RELIABILITY OF A NOVEL SEATED BALANCE EXPERIMENT TO ASSESS TRUNK CONTROL

<sup>1</sup> Ahmed Ramadan, <sup>1</sup> Jacek Cholewicki, <sup>1</sup> Clark J. Radcliffe, <sup>1</sup> John M. Popovich Jr., <sup>1</sup> N. Peter Reeves, and <sup>2</sup> Jongeun Choi

<sup>1</sup> Michigan State University, East Lansing, MI, USA

<sup>2</sup> Yonsei University, Seoul, Republic of Korea

email: ramadana@msu.edu, web: http://orthopedicresearch.msu.edu/

## INTRODUCTION

Trunk motor control has been studied using a traditional hemisphere-balance seat [1]. However, such a task has no deterministic input signal to the subject. To improve upon methods of assessing trunk motor control, we recently developed a novel seated balance task (**Figure 1**) that applies known torque perturbations (input) to the subject's pelvis while balancing on a robotic-controlled seat. While this setup improves the signal-to-noise ratio compared to the traditional setup, experimental measurements must be deemed reliable before future implementation. Therefore, this study investigated the reliability of the nonparametric descriptors of the seated balance task depicted in **Figure 1**.

balance task in three visits separated by at least 23 hours. Each visit included three testing conditions: eyes open (EO), eyes closed (EC), and eyes closed with vibration to the lumbar region (VIB). Each testing condition consisted of four practice trials (30s each) and three full trials (30s each).

**Table 1:** Subjects' demographic characteristics.

	Females (n=19)	Males (n=11)
<b>Height (m)</b>	1.63±0.05	1.78±0.07
<b>Weight (kg)</b>	70.6±12.8	86.1±11.5
<b>Age (years)</b>	34.7±12.0	30.7±12.3

The data collected was the input perturbation torque ( $T$ ), and the output lower and upper body angles ( $\alpha_1, \alpha_2$ ).  $T$  was a pseudorandom ternary sequence generated from a motor.  $\alpha_1$  was recorded by an encoder in the motor, while  $\alpha_2$  was recorded using string potentiometers. The motor also provided stiffness and damping response according to the measurement of  $\alpha_1$ . Both the amplitude of  $T$  and the seat stiffness were calibrated for each subject before the trials to make the level of task difficulty similar between subjects.

To assess trunk motor control accuracy in the time and frequency domains, root mean square error (RMSE) and mean bandpass error energy ( $E_{mb}$ ) [2] were computed. The frequency passband region (for  $E_{mb}$ ) was 0.1-1.6 Hz. The subjects were assumed to minimize the error  $e = w_1\alpha_1 + w_2\alpha_2$ , where  $w_1$  and  $w_2$  are scalar weights. The weights were estimated from the static equilibrium, of the system shown in **Figure 1**, given by  $M_1l_1\sin(\alpha_1) + M_2[l_2\sin(\alpha_1) + l_3\sin(\alpha_2)] + T = 0$ . By approximation, we have  $\text{mean}(T) \cong 0$  and  $\sin(\alpha) \cong \alpha$ . Therefore,  $[M_1l_1 + M_2l_2]\alpha_1 + [M_2l_3]\alpha_2 \cong 0$ . The error was then estimated to be  $e = 0.89\alpha_1 + 0.45\alpha_2$ .

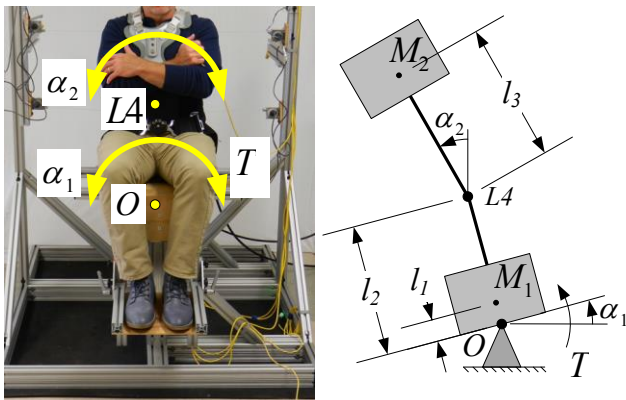


**Figure 1:** The novel seated balance task utilizes a perturbation torque ( $T$ ). The physical model has two degrees of freedom ( $\alpha_1, \alpha_2$ ).

## METHODS

30 healthy subjects (**Table 1**) participated in the study. They had no history of back pain lasting more than three days or a neurological condition affecting motor control. The subjects performed the seated

Intra-class correlation coefficients ICC(3,k) along with 95% confidence intervals (CI) were computed for both RMSE and  $E_{mb}$  to assess between-day reliability. Coefficient of multiple correlations (CMC) of  $E_{mb}$  were calculated to assess both within-day and between-day reliability. The CMCs were computed from the empirical transfer function estimate (ETF) [3] of a single trial., The ETFs were computed from  $T$  to  $\alpha_1$  and from  $T$  to  $\alpha_2$ , and so were the CMCs.

## RESULTS AND DISCUSSION

The between-day ICCs, listed in **Table 2**, show excellent reliability ( $ICC \geq 0.94$ ) and narrow confidence intervals. The CMCs are listed in **Table 3**. Both within-day and between-day reliability are excellent with  $CMC \geq 0.93$  and  $CMC \geq 0.89$ , respectively.

**Table 2:** Between-day reliability as ICC(3,k) and 95% CI.

Task	ICC of RMSE	ICC of $E_{mb}$
EO	0.95 (CI 0.92-0.98)	0.95 (CI 0.91-0.97)
EC	0.96 (CI 0.92-0.98)	0.95 (CI 0.91-0.98)
VIB	0.95 (CI 0.91-0.98)	0.94 (CI 0.90-0.97)

The results agree with the excellent reliability reported in previous studies [1], [4] of unstable seated balance. In [1], RMS of the distance travelled by the center of pressure was used, and reliability was assessed using correlation coefficient ( $R=0.90$ ). In [4], RMS of the seat angle (the error) was used to assess reliability in the form of dependability coefficient ( $\phi=0.77$ ).

On the other hand, another study [5] reported poor to fair ICCs (0.29–0.56). It might be due to (1) low signal-to-noise ratio since there is no deterministic perturbation signal, or (2) the coupled dynamics of

the anterior-posterior and the lateral directions in [5]. In our experiment, the perturbations were applied solely in the lateral direction. Moreover, it was reported that the ICCs increased with the task difficulty level [5]. So, the differences in the results might be due to the different task difficulty.

The limitations of the reported results are as follows. The ETFE uses averaging which improves the precision (less variance), but increases the bias (more deviation from the true mean). The  $E_{mb}$  calculation used the same averaging technique in frequency-domain.

## CONCLUSIONS

The novel seated balance task (**Figure 1**) is reliable and the resulting measurements are reproducible. Therefore, it can be used to assess trunk motor control.

## REFERENCES

1. Cholewicki J, et al. *J. Biomech* **33**, 1733-1737, 2000.
2. Popovich JM, Jr., et al. *J. Biomech* **48**, 549-554, 2015.
3. Ljung L. *System identification: theory for the user*, PTR Prentice Hall, 1999.
4. Larivière C, et al. *J. Electromyogr. Kinesiol* **23**, 899-907, 2013.
5. Lee H, et al. *Clin. Biomech* **23**, 735-742, 2008.

## ACKNOWLEDGMENTS

This publication was made possible in part by grant number U19 AT006057 from the National Center for Complementary and Integrative Health (NCCIH) at the National Institutes of Health. Its contents are solely the responsibility of the authors and do not necessarily represent the official views of NCCIH.

**Table 3:** Within-day and between-day reliability as CMC (mean  $\pm$  standard deviation).

Task	Within-day CMC		Between-day CMC	
	$T \rightarrow \alpha_1$	$T \rightarrow \alpha_2$	$T \rightarrow \alpha_1$	$T \rightarrow \alpha_2$
EO	0.97 $\pm$ 0.02	0.94 $\pm$ 0.05	0.96 $\pm$ 0.02	0.89 $\pm$ 0.11
EC	0.97 $\pm$ 0.01	0.93 $\pm$ 0.05	0.96 $\pm$ 0.02	0.89 $\pm$ 0.07
VIB	0.97 $\pm$ 0.02	0.93 $\pm$ 0.05	0.96 $\pm$ 0.02	0.91 $\pm$ 0.06

# MUSCULAR FATIGUE INFLUENCES MOTOR SYNERGIES DURING PUSH-UPS

Elizabeth M. Bell, Kyung Koh, Ross H. Miller and Jae Kun Shim

University of Maryland, College Park, MD, USA

email: lizbell@terpmail.umd.edu, web: <https://sph.umd.edu/neuromechanics>

## INTRODUCTION

The conventional push-up is a popular exercise used by the American College of Sports Medicine to test muscular endurance [1] and is required in the Army Physical Fitness Test [2]. The push-up is an effective way to improve muscle performance of the shoulder, arm and trunk<sup>3</sup>, is a popular, easy-to-learn exercise that normally requires no equipment [3]. Despite the popularity and importance of push-ups in exercise programs and return-to-duty military requirements, motor control mechanisms of this motion are relatively unknown. Push-ups require changes in the ground reaction forces generated at each point of contact with the ground (all four extremities) which are achieved through muscular contractions.

Research focusing on uninjured push-up performance exists [3] but it is unknown how muscular fatigue influences synergistic actions between the forces produced by hands and feet. It is important to look at the synergistic mechanisms used by the whole body to produce movements of the center of mass.

This work aims to investigate the neuromechanical adaptations that occur, and to determine if performing push-ups to volitional fatigue induces common synergistic changes between extremities.

## METHODS

Volunteers participated in a single motion capture data collection after completing informed consent procedures approved by the local Institutional Review Board. Each participant was instructed on how to complete conventional push-ups<sup>3</sup> with their hands shoulder width apart (Fig. 1). Participants were instructed on how to arrange themselves in a plank position with each extremity within the bounds of an embedded force platform (Kistler Instrument Corp., NY, USA). Audio feedback via metronome

(50bpm) and pre-trial instructions were provided to participants in order to establish the controlled, three-beat tempo of 24 push-ups per minute. On the first beat participants started downward movement, on the second they pushed upward and on the third they held a plank position.

Analog data was collected from four force plates at a rate of 1000Hz as participants completed one trial where they performed as many push-ups as possible, stopping at self-determined failure.

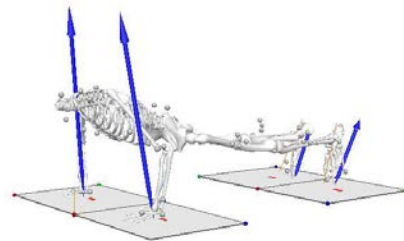


**Figure 1:** 3D representation of participant orientation on force plates.

The start of each push-up cycle was defined as the point at which the whole-body center of mass began to move downward from the plank position and the cycle ended when the center of mass returned to the start position. The push-up cycle was broken into the following phases: downward motion (DOWN) upward motion (UP) and plank (PLANK). Phase determinations were based on movement of the center of mass. Force signals were processed using a Butterworth low-pass filter with a cut off frequency of 50Hz.

An index of synergy ( $SYN_i$ ) was calculated for every DOWN, UP, and PLANK motion for each push-up repetition within a trial:

$$SYN_i = \frac{\sum_{j \neq i}^n \text{corr}(vGRF_i, vGRF_j)}{n} [1]$$

where  $i = \{\text{left hand, right hand, left foot, right foot}\}$  and  $vGRF_i$  is the vertical ground reaction force normalized to bodyweight (BW) at  $i^{th}$  limb and  $n=3$ , or the number of limbs not equal to  $i$ .

Since participants completed a different number of push-ups within the trial,  $SYN_i$  from all repetitions for all 14 participants were plotted with respect to the % of trial completion. A Pearson correlation test with significance at  $p \leq 0.05$  (MatLab 2016A, Natick, MA, USA) was used to determine if the slope of the line of best fit ( $\Delta SYN_i / \Delta \% Trial$ ) was different than zero.

Data was collected from 14 participants (9F, 5M; Table 1).

**Table 1.** Participant demographics

	Mean	(SD)
Age (yr.)	22.0	(3.8)
Body mass (kg)	72.3	(13.4)
Height (m)	171.7	(9.1)
Number of pushups or repetitions completed (#)	22.7	(6.4)

## RESULTS AND DISCUSSION

The slope each line of best fit can be seen in table 2.

**Table 2.** Average rate of change of  $SYN_i$  normalized to trial time

	$\frac{\Delta SYN_{LH}}{\Delta \% Trial}$	$\frac{\Delta SYN_{RH}}{\Delta \% Trial}$	$\frac{\Delta SYN_{LF}}{\Delta \% Trial}$	$\frac{\Delta SYN_{RF}}{\Delta \% Trial}$
DOWN	8.1E-04	-9.3E-05	-2.4E-03	-1.4E-03
UP	-1.6E-03*	-1.8E-03*	-4.0E-03*	-1.9E-03*
PLANK	-2.1E-03*	-2.8E-03*	-3.5E-03*	-2.8E-03*

\* indicates  $\Delta SYN_i / \Delta \% Trial$  was significantly different than zero ( $*p \leq 0.05$ ). LH: left hand, RH: right hand, LF: left foot, RF: right foot.

During DOWN motion  $SYN_i$  did not significantly change (all  $p \geq 0.21$ ). In DOWN the main muscles involved in this action (triceps brachii, pectoralis major) were lengthening.

Initial measures of  $SYN_i$  during UP and PLANK phases were positive indicating that vGRF forces of all limbs were co-varied in order to increase whole body force. In other words, limbs were working together to produce increases or decreased in vGRF needed for COM movement. Significant changes in  $SYN_i$  over the trial were seen during UP (all  $*p \leq 0.01$ ) and PLANK (all  $*p \leq 0.01$ ) phases (Fig. 2).

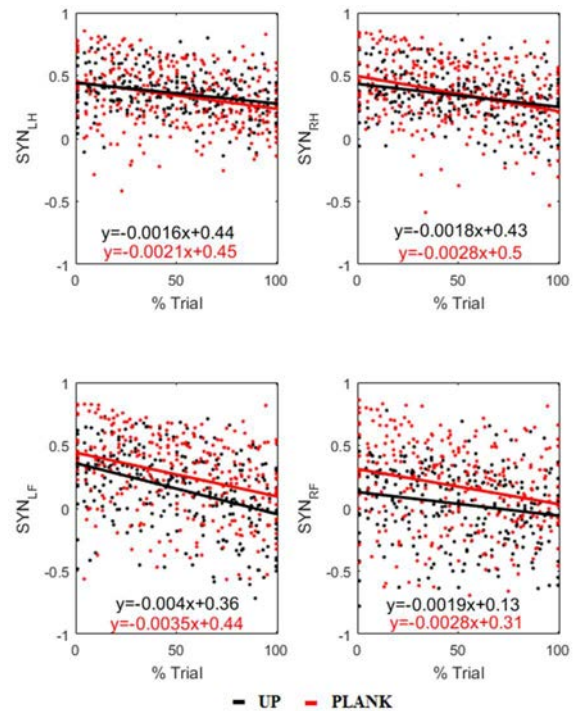


**Figure 2.** Index of synergy ( $SYN_i$ ) measures and linear best fit for data from all participants during upward motion (UP) (black) and PLANK (red) phases of each push-up.

## CONCLUSIONS

We investigated the effect of fatigue on synergistic actions as participants performed push-ups to volitional fatigue. We found that muscular fatigue affected the synergistic actions between limbs in upward motion and plank while not in downward motion. This result indicates that after muscular fatigue the limbs were not working together to produce movement of the COM.

## REFERENCES

1. American College of Sports Medicine. *ACSM's Guidelines for Exercise Testing and Prescription*. 2014. 9th ed. / Philadelphia: Wolters
2. Dept. of the Army *Regulation 40-501: Standards of Medical Fitness*. 2016
3. Youdas JW, et al. *J Strength Cond Res*. 24.12 (2010): 3352-62.

## ACKNOWLEDGMENTS

The authors would like to thank Ms. Emily Finkelstein for her contributions to data collection.

# TALES FROM THE UNINVOLVED LIMB: MOTOR CONTROL IN UNILATERAL ACHILLES TENDINOPATHY

Abigail L Fietzer and Kornelia Kulig

University of Southern California, Los Angeles, CA, USA  
email: fietzer@usc.edu, web: <http://pt.usc.edu/labs/mbrl/>

## INTRODUCTION

Variability is not simply noise or the failure of an imperfect human movement system; it is present even in elite athletes [1]. The magnitude of movement variability shifts with changing skill level, and a certain degree of variability is required in order to be adaptable to small changes in the task or within the performer [1-2]. Movement variability is altered in cases of pathology; some studies indicate greater variability is associated with pathology while others indicate a decrement [3-6].

Uncontrolled manifold (UCM) analysis divides variability into destabilizing ( $V_{ORT}$ ) and stabilizing ( $V_{UCM}$ ) subspaces, testing contributions of variance in elemental variables to variance in a task level variable [2]. Where  $V_{UCM} > V_{ORT}$ , the elemental variables are controlled to inter-compensate and stabilize the task level variable.

Unipedal hopping is a tightly-controlled ankle-drive task useful in modeling aspects of other ecologically relevant bouncing gaits such as running, which is an activity commonly associated with Achilles tendinopathy. While numerous studies have been conducted seeking risk factors for Achilles tendinopathy development, the motor control aspects of this pathology have been grossly ignored in the literature. The purpose of this study was to investigate potential differences in hopping control strategy between the involved and uninvolved limb in persons with unilateral Achilles tendinopathy and healthy controls.

## METHODS

Twenty-five healthy adults (age 23-55, 15 female) and nine otherwise healthy adults (age 24-60, 4 female) with unilateral Achilles tendinopathy participated. Participants with Achilles tendinopathy

had been fully participating in their recreational activity of choice symptom-free for  $\geq 1$ mo at the time of testing, and remained symptom-free during testing. Motion capture was conducted for  $\geq 25$  unipedal hops per leg, with arms constrained by holding a dowel across the shoulders. Testing was performed at 1.7Hz, which is slower than typical self-selected hopping rate (2.0-2.3Hz). Hopping at this rate remains an ankle-driven task but highlights supraspinal control [7].

We sought to discover if differences in the control of elemental variables (individual foot, shank and thigh positions) to stabilize the task level variable of overall vertical leg length were apparent between the different limb types (tendinopathic, uninvolved and control). UCM analysis was performed for every 1% of time-normalized stance phase. Stance was divided into 7 equal bins, with bins 1-3 representing early, mid-, and late impact absorption, bin 4 the most crouched position, and bins 5-7 early, mid-, and late propulsion toward flight. Control limbs were pooled bilaterally. Due to the small sample size of tendinopathic subjects, T-tests were run between control and tendinopathic limbs at each bin, and between control and uninvolved limbs at each bin ( $\alpha=0.05$ ).

## RESULTS AND DISCUSSION

Tendinopathic limbs demonstrated a trend toward lesser  $V_{UCM}$  than control limbs during mid- ( $p=0.13$ ) and late ( $p=0.15$ ) impact absorption (Fig. 1). There was no difference between tendinopathic and control limbs in  $V_{ORT}$  throughout stance.

Uninvolved limbs demonstrated lesser or lesser-trending  $V_{UCM}$  than control limbs during mid- ( $p<0.01$ ) and late- ( $p=0.04$ ) impact absorption, the most crouched position ( $p=0.02$ ), and early- ( $p=0.06$ ) and mid- ( $p=0.11$ ) propulsion (Fig. 2).

Uninvolved limbs also demonstrated lesser or lesser-trending  $V_{ORT}$  than control limbs during early- ( $p=0.03$ ), mid- ( $p<0.01$ ) and late- ( $p=0.02$ ) impact absorption, the most crouched position ( $p=0.02$ ), and early- ( $p=0.14$ ) propulsion.

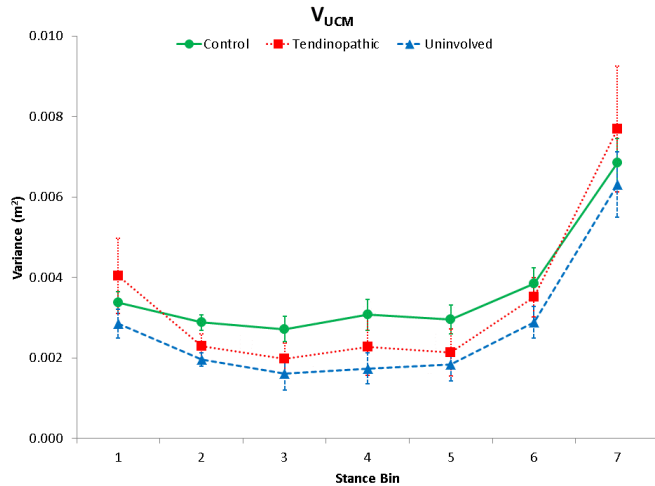


**Figure 1:** Average stabilizing variability ( $V_{UCM}$ ) for the control (green circles), tendinopathic (red squares) & uninvolved (blue triangles) limbs across 7 stance bins. Whiskers represent standard error.

Uninvolved limbs express less of both types of variability (stabilizing  $V_{UCM}$  and destabilizing  $V_{ORT}$ ), thereby likely maintaining a similar  $V_{UCM}$  to  $V_{ORT}$  ratio and thus a similar overall degree of vertical leg length stabilization during single-legged hopping as healthy controls. Tendinopathic limbs express less stabilizing ( $V_{UCM}$ ) variability, but similar levels of destabilizing ( $V_{ORT}$ ) variability as control limbs. This likely corresponds to a lesser  $V_{UCM}$  to  $V_{ORT}$  ratio and thus a decreased overall degree of vertical leg length stabilization during single-legged hopping compared to healthy controls.

## CONCLUSIONS

Results of this study indicate that both the tendinopathic and uninvolved limbs of participants with currently-asymptomatic unilateral Achilles tendinopathy demonstrate a different control

strategy than healthy controls during slow-paced single-legged hopping. Future studies to test whether these control strategies are mutable within this population are warranted with an eye toward the development of interventions directed at the prevention of Achilles tendinopathy development or progression.

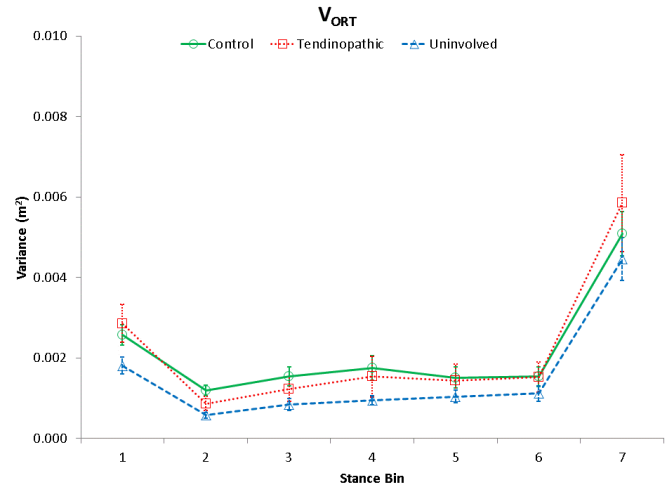


**Figure 2:** Average destabilizing variability ( $V_{ORT}$ ) for the control (green circles), tendinopathic (red squares) & uninvolved (blue triangles) limbs across 7 stance bins. Whiskers represent standard error.

## REFERENCES

1. Bartlett RM. *Int J Sports Sci Coach* **3**, 113-124, 2008.
2. Latash ML, et al. *Mot Contr* **11**, 276-308, 2007.
3. Brown C, et al. *Clin Biomech* **27**, 52-63, 2012.
4. Cote JN, et al. *Clin Biomech* **20**, 581-590, 2005.
5. James CR, et al. *Med Sci Sports Exerc* **32**, 1833-1844, 2000.
6. Seay JF, et al. *Clin Biomech* **26**, 572-578, 2011.
7. Zuur AT, et al. *J Physiol* **588**, 799-807, 2010.

## ACKNOWLEDGMENTS

Funding provided by the Foundation for Physical Therapy's Promotion of Doctoral Studies Scholarship.

# GENERALIZATION OF SPLIT-BELT LOCOMOTOR ADAPTATION: MOTORIZED TREADMILL AFTEREFFECTS ARE PRESERVED AFTER WASHOUT ON A NON-MOTORIZED TREADMILL

<sup>1</sup> Daniel L. Gregory, <sup>2</sup> Frank C. Sup, <sup>1</sup> Julia T. Choi

<sup>1</sup> Department of Kinesiology and <sup>2</sup> Department of Mechanical and Industrial Engineering, University of Massachusetts Amherst, Amherst, MA, USA

email: dgregory@umass.edu, web: <http://blogs.umass.edu/jtchoi/>

## INTRODUCTION

The locomotor system is constantly adapting to environmental changes. Once a locomotor pattern is adapted, the changes (after-effects) are stored until they are actively washed out. To what extent can a newly adapted locomotor pattern be transferred between different contexts? Here we used a motorized split-belt treadmill to independently control the speed of each leg, causing spatial and temporal perturbations that must be adapted to improve walking symmetry [1]. The specific objective of this study is to determine whether adaptations to walking symmetry on a motorized split-belt treadmill (MT) are generalizable to walking on a self-regulated non-motorized split-belt treadmill (NMT). If so, it may be possible to utilize a low-cost non-motorized split-belt treadmill for long-term training in a home-based setting to improve transfer of adaptive locomotor training to other relevant contexts (e.g. over ground walking).

## METHODS

Six subjects participated (5 female, 1 male; age  $26.6 \pm 5.5$  years). For this study, we designed and built a self-regulated non-motorized split-belt treadmill (**Fig. 1a**) that utilizes gravity ( $13^\circ$  incline) to assist subjects driving the symmetrically resisted but independently controlled belt speed. The training paradigm (**Fig. 1b**) consisted of walking in both MT and NMT conditions. To drive adaptation of inter-limb coordination, subjects walked on the MT at a 2:1 speed perturbation (0.67 and 1.33 m/s) for 10 minutes. To assess transfer and washout of after-effects, subjects walked at their preferred speed on the NMT and the slow speed (0.67 m/s) on the MT during the Transfer and Washout periods. Finally, subjects walked at preferred speed on the NMT (Post) to assess any residual after-effects.

Step-length and double support symmetry were calculated for each stride [1]. Step length and double

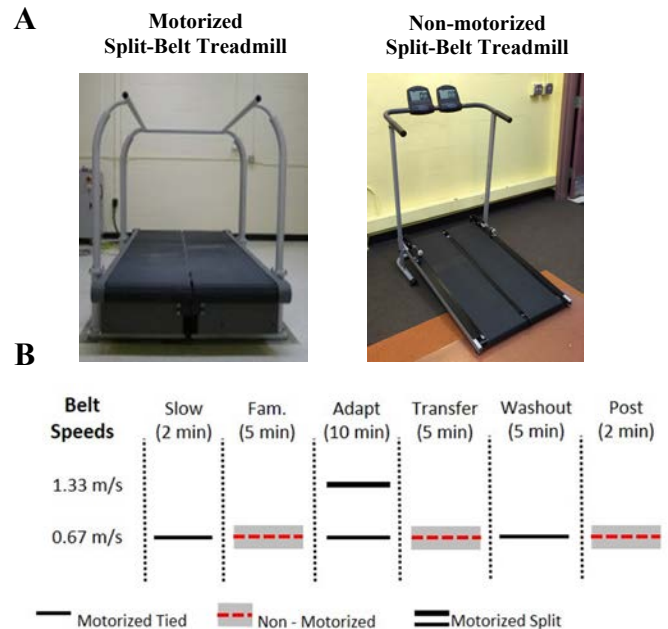


**Figure 1:** A) Motorized (MT) and non-motorized (NMT) split-belt treadmills. B) Study design required subjects to switch between MT and NMT conditions without stepping.

support adaptation magnitudes were calculated as the difference between early (strides 3-5) and late (final three) adaptation. Transfer and washout indexes were defined as the ratio of the magnitude of after-effects to the magnitude of split-belt learning. To determine the relationship between after-effect size and belt speed [2], mean NMT belt speed was calculated as the mean speed of the ankle marker during single-leg stance for strides 3-5 during transfer. The after-effect magnitude is the mean of after-effects during the same period. EMG data were collected at 2000 Hz (Trigno, Delsys Inc.) from bilateral medial gastrocnemius (MG) muscles. EMG data was high-pass filtered at 45 Hz (3<sup>rd</sup> order Butterworth), demeaned, rectified, and low-pass filtered at 35 Hz (3<sup>rd</sup> order). Stride time was normalized to 100% of the gait cycle. EMG amplitude was normalized to the peak averaged EMG during baseline walking. Subject 1 EMG was

not included in the analysis due to poor recording quality.

## RESULTS AND DISCUSSION

**Fig. 2a** shows that subjects adapted inter-limb coordination on the MT. During transfer, subjects showed pronounced after-effects on the NMT (transfer index: double support =  $0.87 \pm 0.65$ , step-length =  $0.9 \pm 0.7$ ), that gradually faded. Similarly, upon returning to the MT during washout, after-effects persisted (washout index: double support =  $1.32 \pm 0.68$ , step length =  $1.38 \pm 0.93$ ) and gradually washed out. There were no after-effects on the return to the NMT.

Transfer index was larger in this study relative to over-ground transfer for both double support (0.87 vs 0.3) and step length (0.9 vs 0.3) [1]. After-effect size is an indication of neural network sharing between contexts, where large aftereffects are expected [1, 2]. Here we show that MT adaptations are generalizable to NMT walking, indicating a potential use in gait rehabilitation.

After-effect magnitude has been shown to be greatest at speeds matched to the slow belt during adaptation, with abating aftereffects in either direction [2]. **Fig. 2b** shows diminishing aftereffects size as slow NMT belt speed moves further from the MT slow belt speed (0.67 m/s; vertical dashed line) for each subject, indicating that belt speed represents an important contextual relationship for transfer that needs further investigation.

Group average MG EMG traces in **Fig. 2c** shows after-effects during transfer and washout. During the transfer period, the slow MG activity increased while the fast MG activity decreased around mid-stance (20% - 40% stride cycle) compared to baseline NMT walking. The MG EMG after-effects were washed out by the end of the transfer period. During the washout period, the after-effects were expressed as additional MG EMG bursts during early stance in the slow leg (10% - 20% stride cycle) and fast leg (0% - 10% stride cycle). The after-effects washed out after 5 minutes of MT walking.

In summary, robust kinematics and EMG after-effects during NMT walking demonstrates that a low-cost split-belt NMT can be used as part of a gait re-training protocol. To promote optimal locomotor learning and generalization, future studies will explore treadmill design, slow belt-speed matching, learning style and changes in muscle activity related to changes in kinematics.

## REFERENCES

1. Reisman DS, et al. *Neurorehab*, 23(7), 735-44, 2009.
2. Vasudevan and Bastian. *J Neurophys*, 103, 183-191, 2010.

## ACKNOWLEDGMENTS

Research supported by the Initiative for Maximizing Student Development (IMSD, UMASS Amherst) NSF (grant #1264752) and UMass Faculty Research Grant.

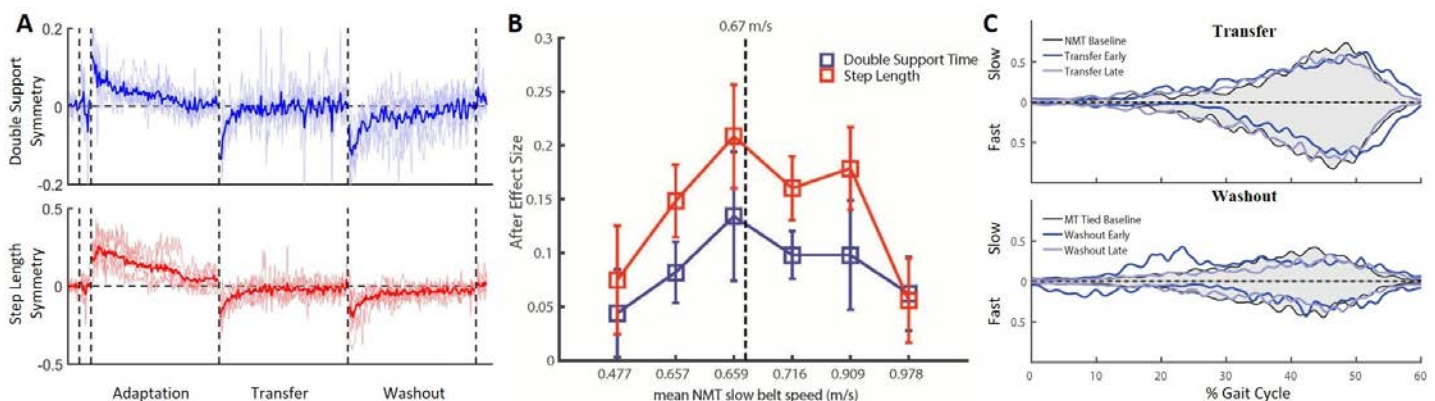


**Figure 2:** **A)** Stride-by-stride step length and double support symmetry. Dark lines represent group average, light lines represent individual subjects. **B)** After-effect magnitude plotted against slow belt speed. Mean and standard deviation of strides 3-5 during transfer period for each subject. **C)** After-effects in medial gastrocnemius EMG for the slow leg (positive) and fast leg (negative) during Transfer and Washout periods, compared to baseline NMT and MT walking (grey area).

# MOTOR UNIT ACTIVATION OF MUSCLE SYNERGISTS DURING CYCLIC UPPER-LIMB MOVEMENTS

<sup>1</sup>Joshua C. Kline, <sup>1</sup>Paola Contessa, <sup>1,2</sup>Serge H. Roy and <sup>1</sup>Gianluca De Luca

<sup>1</sup>Delsys, Inc. and Altec, Inc, Natick, USA

<sup>2</sup>Sargent College of Health and Rehabilitation Sciences, Boston University, Boston, Massachusetts, USA

email: [jkline@delsys.com](mailto:jkline@delsys.com), web: <http://www.delsys.com/altec/>

## INTRODUCTION

Studies of motor unit firing behavior have begun to improve our understanding of the strategies employed by the central nervous system to coordinate groups of muscles and generate force. For example, findings of the fundamental property of “common drive” to the motoneuron pool have revealed that motor unit firing rates within and across muscles are regulated with varying degrees of correlation depending on whether the muscles are acting as synergists or antagonists during different contraction tasks [1]. But such work has been limited to studies of isometric contractions or to the use of intramuscular sensors that are not practical for studying motor control during normal human movement. Consequently, the mechanisms used by the central nervous system to control non-isometric movements remain unknown. Therefore, we developed a non-invasive system of surface electromyographic (sEMG) sensors and software algorithms for measuring motor unit firing behavior during dynamic activities and used this system to investigate the activation of motor units in groups of muscles during movements of the upper-limb.

## METHODS

Experiments were conducted on 6 subjects (3 male and 3 female; 40±16 yrs.) with no known history of neuromuscular health conditions. Non-invasive dEMG sensors (Delsys Inc, Natick, MA) were placed on the extensor digitorum, flexor digitorum profundus, pronator teres and biceps brachii muscles to record high-fidelity sEMG signals produced during voluntary dynamic activities including: flexion/extension of the fingers, pronation/supination of the forearm and object grasping. The finger force, the finger joint angle and the inertial measurements of the wrist were measured

during the execution of each task using Trigno™ auxiliary sensors (Delsys, Inc. Natick, MA). Data recorded during the different movements were processed by the dEMG dynamic decomposition algorithms to extract action potentials and firing times of the active motor units [2]. The motor unit data were validated for accuracy and analyzed to investigate the firing behavior during voluntary movement activity.

## RESULTS AND DISCUSSION

Throughout cyclic dynamic movements in the upper-limb, the firing behavior of all motor units was governed by the same underlying control mechanisms: 1) the firing rates were ordered in an inverse hierarchical relationship relative to the motor unit action potential amplitude as previously described by the “onion-skin” phenomenon; and 2) the firing rates of motor units within each muscle were correlated with respect to one-another and with the output movement in accordance with the

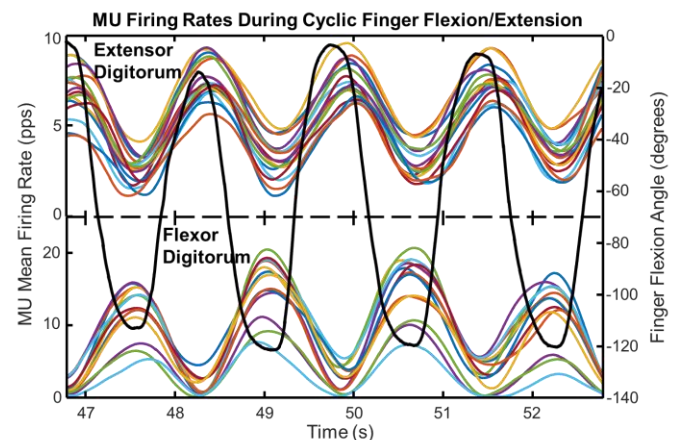


**Figure 1:** Motor unit (MU) mean firing rates (colored lines) measured from the finger extensor and flexor muscles during four cycles of opening and closing of the hand (black line).

common drive [2]. When comparing the motor unit firing behavior across muscles, we observed that the firing rates maintained a relatively high correlation but the latency of the correlation shifted depending on the activity being performed. Specifically, when two muscles acted as antagonists, the correlation of the motor unit firing rates across muscles manifested a relatively greater latency (Figure 1) compared to when the muscles were coactivated during more synergistic tasks.

## CONCLUSIONS

Our data indicate that motor units within each muscle studied under dynamic conditions are governed by the same underlying control properties of the onion-skin and common drive that have been well documented and established in the literature for isometric tasks [2]. Depending on the movement activity, motor units across muscles acting as synergists have positively correlated firing rates, whereas those across muscles acting as antagonists

have negatively correlated firing rates. This would indicate that the central nervous system drives the motor units in a manner that utilizes that same underlying control scheme by shifting the latency between the motor unit firing rates across the two muscles.

## REFERENCES

1. De Luca CJ, et al. *Journal of Neurophysiology*. **87**:2200-2204, 2001.
2. De Luca CJ, et al. *Journal of Neurophysiology*. **113**:1941-1951, 2015.

## ACKNOWLEDGMENTS

Research reported in this abstract was supported in part by the De Luca Foundation and by two grants from the National Institute of Neurological Disorders and Stroke of the National Institutes of Health under awards R44NS077526 and R43NS09365

# STABILIZATION OF LEG LENGTH AND ORIENTATION ACROSS DIFFERENT HOPPING FREQUENCIES IN CHILDREN AND ADULTS: A UCM ANALYSIS

Matthew Beerse and Jianhua Wu

Georgia State University, Atlanta, GA, USA. Email: [mbeersel@student.gsu.edu](mailto:mbeersel@student.gsu.edu)

## INTRODUCTION

Adults coordinate their lower limb joints to stabilize leg length and leg orientation during single-leg hopping in-place with a pattern that is maintained across different frequencies [1]. Children modulate whole-body vertical stiffness and horizontal center-of-mass movement similarly to adults when increasing hopping frequency, but not as effectively [2]. It is unknown if children accomplish hopping at different frequencies with a similar pattern of joint coordination as adults. This study aimed to compare the interjoint coordination strategies during single-leg hopping at different frequencies between children and young adults.

## METHODS

*Participants:* 16 young adults, 8F/8M, aged 24.56 (SD 3.45) years with height of 1.68 (0.10) m and body mass of 73.75 (15.17) kg and fourteen children, 5F/9M aged 8.70 (1.81) years with height of 1.34 (0.08) m and body mass of 32.97 (7.95) kg participated in this study.

*Experimental design:* Subjects completed four frequency conditions established by the subject's preferred frequency. We calculated the subject's preferred frequency as the average self-selected frequency during three 20-second trials. A metronome was used to guide the frequency conditions and was set to the subject's *preferred* frequency, a 20% increase (*moderate*), a 40% increase (*fast*), and a 20% decrease (*slow*).

*Data collection:* Subjects hopped on their dominant leg in-place on an AMTI force for 20-second trials. We used an 8-camera Vicon motion capture system and a full-body PSIS marker set to collect kinematic data at 100Hz. Three child subjects were unable to complete the *fast* condition.

*Data analysis:* We calculated four joint segment angles, foot, shank, thigh, and pelvis, in relation to the horizontal using the kinematic marker position. These joint segment angles were used to create geometric models of a leg length vector (the anterior/posterior and vertical distance between the toe and anterior superior iliac spine), and leg orientation with respect to the ground [1]. The geometric models allowed for the assessment of the variability of the joint configurations related to task variables, leg length and leg orientation, within an uncontrolled manifold (UCM) analysis. We normalized each hopping cycle to 100% and completed UCM analyses for each 1%.

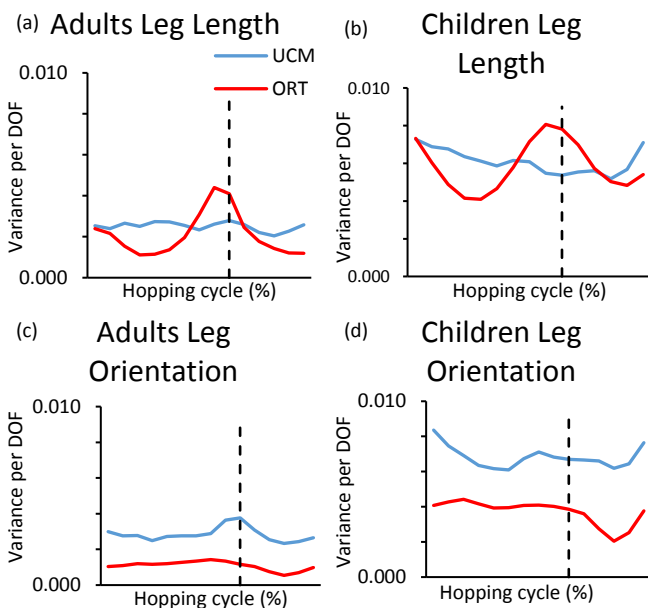
The average joint configuration at each percentage were used as the reference configuration. The two geometrical models were linearized into Jacobian matrices and used to find the null space [3]. Variance of joint configuration was partitioned into two subspaces: a UCM subspace that maintains the mean of a task variable, and an ORT subspace that deviates a task variable from its mean. We calculated the amount of variance per degree of freedom for each subspace. We then calculated an index of motor abundance (IMA) by dividing the difference of the UCM and ORT variances by the total variance [4]. The total variance was calculated as the diagonal sum of the covariance matrix per degree of freedom of the four joint segment angles. We averaged IMA across the entire hopping cycle at each frequency condition. A positive IMA value (UCM>ORT) indicated a stabilization of the task variable. A negative IMA values (UCM<ORT) indicated destabilization.

*Statistical analysis:* Repeated measures two-way ANOVAs (2 group x 4 frequency) were conducted on average IMA values for both leg length and leg orientation. Post-hoc pairwise comparisons with Bonferroni adjustment were completed when necessary. A significance level was set at  $\alpha=0.05$ .

## RESULTS AND DISCUSSION

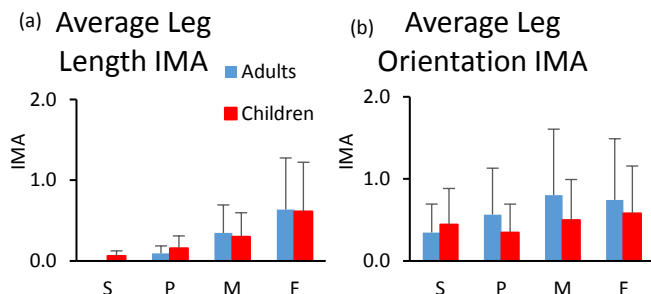
Figure 1 presents average pattern of variance across the hopping cycle for the *preferred* frequency condition. For leg length, both children and adults illustrate a pattern of stabilization around mid-stance and destabilization around take-off (dashed line) (Fig. 1a-b). For leg orientation, both groups stabilized throughout the hopping cycle with greater stabilization around take-off, and less stabilization around mid-stance (Fig. 1c-d). Children demonstrated a greater amount of total variance compared to adults.

Fig.1



Note: Charts for preferred frequency. Vertical dashed line indicates take-off.

Fig.2



Note: S for *slow*, P for *preferred*, M for *moderate*, and F for *fast* frequency condition.

Average leg length IMA across the hopping cycle increased with hopping frequency in both groups (condition effect,  $p < 0.001$ ; Fig. 2a). Post-hoc

analysis demonstrated increases from *slow* to *moderate*, *slow* to *fast*, *preferred* to *fast*, and *moderate* to *fast*. No group difference was found in average leg length IMA. Average leg orientation IMA demonstrated a group by frequency interaction ( $p = 0.035$ ) (Fig. 2b). Children did not change their average leg orientation IMA values across frequencies, however, adults increased with hopping frequency.

During single-leg hopping in-place, children demonstrate similar patterns of interjoint coordination when modulating hopping frequency. However, children do not decrease leg orientation stabilization when hopping 20% slower than preferred (*slow*), as found in adults. Hopping slower than preferred challenges the balance control of children [2]. Therefore, our results may indicate a necessity to maintain leg orientation stabilization to support balance during the *slow* frequency condition.

While children demonstrate greater total variance during single-leg hopping, UCM analysis allows for the classification of the variance into subspaces affecting and not affecting performance. Our results indicate that children single-leg hop with a similar interjoint coordination strategy throughout the entire hopping cycle compared to adults. Specifically, leg length and leg orientation are out of phase during the hopping cycle with peak leg length around mid-stance and leg orientation around take-off.

## CONCLUSIONS

While having greater total variance, children use a similar interjoint coordination strategy to stabilize leg length and leg orientation for single-leg hopping in-place.

## REFERENCES

1. Auyang AG, et al. *Exp Brain Res* **192**, 253-264, 2009.
2. Beerse M & Wu J. *J Biomech* **49**, 3306-3312, 2016.
3. Scholz JP & Schoner G. *Exp Brain Res* **126**, 289-306, 1999.
4. Yen JT & Change YH. *J Soc Interface* **7**, 801-810, 2010

# MOVEMENT VARIABILITY AND SENSORIMOTOR CORTICAL ACTIVATION DURING FORWARD AND BACKWARD WALKING

<sup>1</sup> Boman Groff, <sup>1</sup> Prokopios Antonellis, <sup>1</sup> Brian Knarr, and <sup>1,2</sup> Nicholas Stergiou

<sup>1</sup>Dept. Of Biomechanics, University of Nebraska at Omaha, Omaha, NE, USA

<sup>2</sup>University of Nebraska Medical Center, Omaha, NE, USA

email: [bgroff@unomaha.edu](mailto:bgroff@unomaha.edu), web: <http://coe.unomaha.edu/brb>

## INTRODUCTION

Using functional near-infrared spectroscopy (fNIRS), previous research by Kurz et al. [1] has shown that there is greater hemodynamic activation in motor areas of the cortex while walking backward compared to walking forward. Additionally, stride time variability during forward walking was found to positively correlate with sensorimotor cortical activation [1]. Previous research has also shown that motion artifacts in fNIRS data correlates to the magnitude of head movement [2]. If fNIRS is used to examine cortical activation during walking, it may be necessary to account for differences in head movement between conditions.

The purpose of our study was to extend the work of Kurz et al. [1] by examining sensorimotor cortical activation during forward and backward walking conditions, while also quantifying head movement. We hypothesized that our results would be consistent with previous findings, and greater hemodynamic response during backward walking would be concurrent with increased head movement.

## METHODS

Ten healthy participants (age  $22.1 \pm 1.4$  y, 6 males and 4 females) performed a forward and backward walking trial. Each trial consisted of 30 seconds of walking followed by 30 seconds of rest, repeated 5 times continuously.

The fNIRS was placed over regions of interest (supplementary motor area: SMA, pre-central gyrus: PreCG, post-central gyrus: PostCG, and superior parietal lobule: SPL) based on the International 10/20 System for EEG [1, 3]. Average maximum oxygenated (oxyHb) and average minimum

deoxygenated (deoxyHb) hemoglobin concentrations were compared relative to condition specific baselines. Maximum oxyHb and minimum deoxyHb are associated with cortical activation and have been used in previous walking studies [1].

Heel strikes and toe offs were recorded using pressure sensors. This data was used to calculate inter-stride interval (ISI) during walking, which was defined as the time in between heel-strikes for the same foot. Mean, standard deviation, and coefficient of variation (CoV) were calculated for ISI.

Motion capture markers were placed on head, neck, and sternum to quantify head movement during walking conditions. Range of motion and line path were calculated for the anterior-posterior, medial-lateral, and vertical directions for each head marker.

Wilcoxon sign-ranked tests were performed to determine if there was a difference in oxyHb, deoxyHb, ISI, range of marker movement, and marker line path between walking conditions. Spearman's rank correlations were used to determine if average maximum oxyHb correlated with ISI coefficient of variation, mean, or standard deviation for walking conditions.

## RESULTS AND DISCUSSION

ISI coefficient of variation was significantly greater during backward walking compared to forward walking ( $P = 0.004$ ). Mean ISI was significantly greater during forward walking ( $P = 0.004$ ) and there was no significant difference in ISI standard deviation ( $P = 0.113$ ) (Fig. 1). These results suggest that the greater ISI coefficient of variation during backward walking was due to shorter stride time intervals, not significantly greater variability.

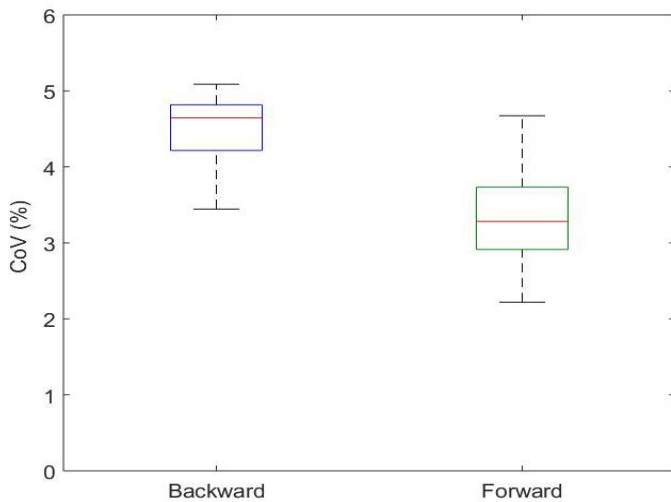


**Figure 1:** ISI coefficient of variation for forward and backward walking ( $P = 0.004$ ).

Range of movement and line path were calculated for the marker on the left temple. Anterior-posterior range of head movement was significantly greater during backward walking ( $P = 0.004$ ). There was no significant difference in range of movement in the medial-lateral ( $P = 0.432$ ) or vertical ( $P = 0.322$ ) directions. The total line path of the head marker (line integral) was not significantly different between walking trials ( $P = 0.233$ ). This indicates that the increased head movement during backward walking was due to slow anterior-posterior drift, which would not influence fNIRS results.

For all four regions of interest, there were no significant differences in maximum oxyHb concentration between backward and forward walking ( $P > 0.05$ ). Minimum deoxyHb concentration in the SMA was significantly lower during backward walking ( $P = 0.020$ ). There were no significant differences in minimum deoxyHb concentrations for the PreCG ( $P = 0.375$ ), PostCG ( $P = 0.846$ ), or SPL ( $P = 0.375$ ).

For forward walking, there was a significant positive correlation between maximum oxyHb in the PreCG and ISI standard deviation ( $r = 0.66$ ,  $P = 0.044$ ) (Fig. 2). There was also a significant correlation between maximum oxyHb in the SPL and ISI mean for forward walking ( $r = 0.66$ ,  $P = 0.044$ ).

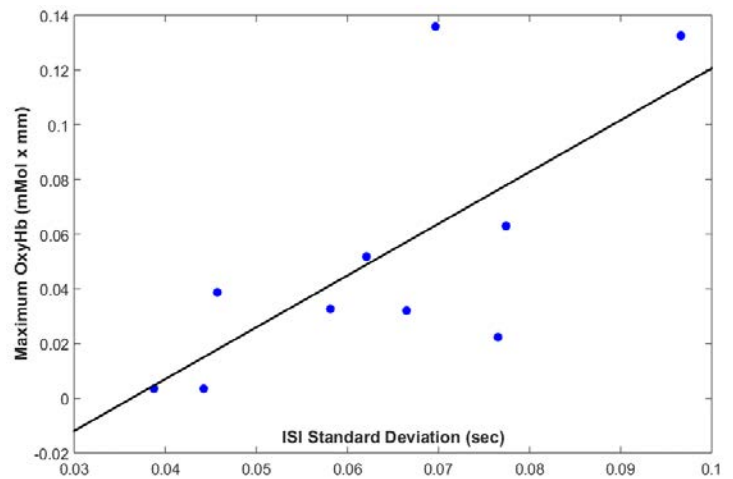


**Figure 2:** Correlation between PreCG activation and ISI standard deviation during forward walking ( $r = 0.66$ ,  $P = 0.044$ ).

## CONCLUSIONS

Based on the measures of this experiment, stride time variability and sensorimotor cortical activation did not differ between forward and backward walking. Differences in hemodynamic activation may be more apparent in subcortical regions [4]. Head movement did not affect the results of this study, but should be taken into account for future fNIRS studies examining walking. The positive correlation between stride time variation and cortical activation suggests that the primary motor cortex (PreCG) may be implicated in forward walking variability.

## REFERENCES

1. Kurz MJ, et al. *NeuroImage*, **59**, 1602-1607, 2012.
2. Ciu X, et al. *J Neuroscience Methods*, **245**, 37-43, 2015.
3. Okamoto MD, et al. *NeuroImage*, **21**, 99-111, 2004.
4. Koenraadt KLM, et al. *NeuroImage*, **85**, 415-422, 2014.

## ACKNOWLEDGMENTS

This work was supported by the Center for Research in Human Movement Variability of the University of Nebraska at Omaha and NIH grant (P20GM109090).

# ESTIMATION OF CHANGES IN LUMBAR SEGMENTAL KINEMATICS ASSOCIATED WITH ALTERATIONS IN TRUNK NEUROMUSCULAR STRATEGY

<sup>1</sup>Iman Shojaei, <sup>2</sup>Navid Arjmand, <sup>3</sup>Jude Meakin, and <sup>1</sup>Babak Bazrgari

<sup>1</sup>University of Kentucky, Lexington, KY, USA

<sup>2</sup> Sharif University of Technology, Tehran, Iran

<sup>3</sup> University of Exeter, Exeter, United Kingdom

Email: shojaei.iman@uky.edu

## INTRODUCTION

With regard to the low back pain problem, imaging is used to detect potential structural and geometrical abnormalities in the lumbar spine. The geometrical information from imaging, if combined with proper mechanical models, may provide a unique platform for the personalized assessment of trunk neuromuscular abnormalities in patients with LBP. Particularly, if changes in lumbar spine kinematics due to abnormalities in trunk neuromuscular behavior can be captured by the current imaging techniques, it may be possible to use image-based kinematics in kinematics-driven computational models to detect potential abnormalities in trunk neuromuscular behavior through personalized estimation of trunk muscle forces.

Recently, we have used a kinematics-driven finite element (FE) model of the spine (Fig. 1) within a heuristic optimization procedure to estimate lumbar kinematics under a trunk neuromuscular strategy that minimized sum of squared stress across all trunk muscles [1, 2]. The resultant kinematics of lumbar spine for a trunk forward bending task were consistent with image-based reports of lumbar spine kinematics of asymptomatic individuals. Using the same approach, estimation of lumbar segmental kinematics for various neuromuscular strategy assumptions is possible. Therefore, the objective of this feasibility study is to determine changes in lumbar segmental kinematics due to alterations in trunk neuromuscular strategy and to verify if such changes are within the reported precision of current imaging techniques.

## METHODS

Five different trunk neuromuscular strategies, each represented by a distinct cost function for the above mentioned heuristic optimization procedure, were selected to either represent the trunk neuromuscular

strategy of asymptomatic persons or a neuromuscular abnormality that minimizes loading on a specific aspect of lower back tissues (i.e., muscles, ligaments, intervertebral discs, and facet joints).

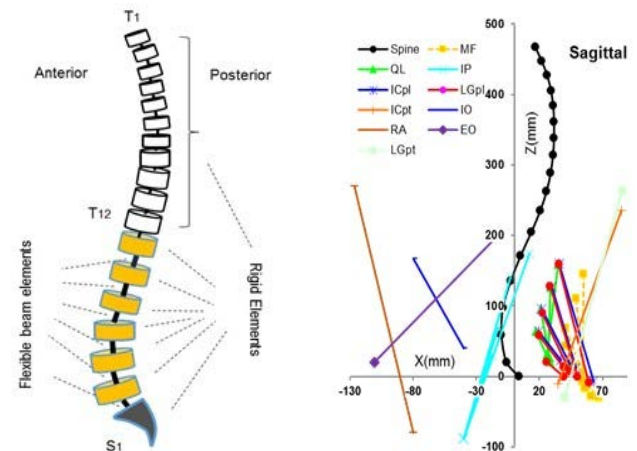


**Figure 1:** A schematic FE model of the spine and its components (left), the musculatures in the sagittal (right) plane in upright posture, and the dimensions (mm) were presented.

A neuromuscular strategy associated with the minimum value of sum of squared muscle stresses across the entire trunk muscles has been reported to be consistent with the electromyography measures of trunk muscles and disc pressure in asymptomatic persons, hence, was regarded to represent a normal neuromuscular strategy. On the other hand, abnormal neuromuscular strategies that minimize loads in muscles, ligaments, intervertebral discs, and facet joints were represented by strategies that respectively minimize sum of muscle forces across the entire trunk muscles, passive moment, compression, and shearing force at the L5-S1 intervertebral disc. For each neuromuscular strategy, kinematics of the lumbar spine (i.e., the axial and angular deformations of each motion segment) were obtained for a static trunk flexed posture involving, respectively, 40° and 10° of thoracic and pelvic

rotations in the sagittal plane. Details of the computational methods for the estimation of lumbar segmental kinematics associated with a given neuromuscular strategy can be found elsewhere [1, 2]. In summary, however, the heuristic optimization procedure searches for a set of lumbar segmental kinematics that when prescribed into the kinematics-driven FE model results in prediction of a neuromuscular strategy that minimizes the associated cost function (Fig. 2).

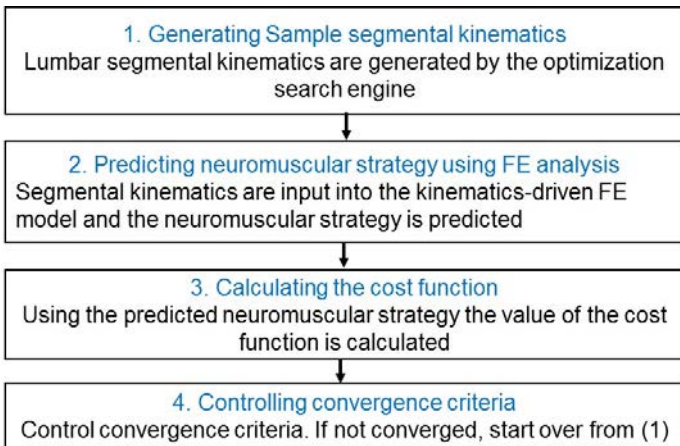


**Figure 2:** The algorithm used for the estimation of lumbar segmental kinematics associated with a given neuromuscular strategy.

## RESULTS AND DISCUSSION

The estimated angular and axial deformations of lumbar motion segments for the five neuromuscular strategies studied here are presented in the Table 1. Minimum changes in the angular and axial deformations of a motion segment with alterations in

neuromuscular strategy ranged from 0° (L2-L3 segment) to 0.5° (L4-L5 segment) and 0 mm (L1-L2 and L2-L3) to 0.04 mm (L4-L5), respectively (Table 1). Similarly, maximum changes in the angular and axial deformations of a motion segment with alterations in neuromuscular strategy ranged from 2.4° (L2-L3 segment) to 7.5° (L5-S1 segment) and 0.11 mm (L2-L3) to 0.39 mm (L3-L4), respectively (Table 1). The differences in kinematics of at least five (out of twelve) cases between each two neuromuscular strategies are detectable by current imaging techniques whose precision have been reported to be ~ 0.1 mm and ~ 0.1° [3]. Particularly, the differences in kinematics of lumbar segments between each combination of two neuromuscular strategies (10 possible combinations) are detectable in 97% of cases for angular deformation and 55% of cases for axial deformation. Therefore, combined imaging and computational modeling appears to have potentials for predicting abnormalities in neuromuscular strategies. Specifically, a geometrically and materially subject-specified model of the spine can be used in future to obtain the neuromuscular strategy that generates the closest lumbar kinematics to those measured from imaging. The accuracy of such assessment strategy can further be improved by implementing dynamic rather than static assessment tasks.

## REFERENCES

1. Shojaei I, et al. *Clin Biomech* **32**, 157-163, 2016
2. Shojaei I, et al. *Int J Numer Method Biomed Eng* **31**, 1-14, 2015
3. Ochia, R.S, et al, *Spine* **31**, 2073-2078, 2006

**Table 1:** Angular (°) and axial (mm) deformations of lumbar segments in the sagitta plane estimated for neuromuscular strategies that minimize 1) sum of squared muscle stresses, 2) sum of muscle forces, 3) the L5-S1 compression force, 4) the L5-S1 anterior-posterior shearing force, and 5) the L5-S1 passive moment.

	Angular deformations						Axial deformations					
	T12-L1	L1-2	L2-3	L3-4	L4-5	L5-S1	T12-L1	L1-L2	L2-L3	L3-L4	L4-L5	L5-S1
Sum of squared muscle stress	3.0	5.1	4.8	3.6	5.7	7.5	0.70	1.10	1.22	1.24	1.48	0.75
Sum of muscle forces	7.8	7.5	4.8	1.5	2.4	5.7	0.97	1.19	1.22	1.09	1.20	0.70
Compression force	7.9	6.8	6	2.1	1.9	5.6	0.97	1.10	1.24	1.07	1.15	0.69
Shearing force	5.7	3.3	5.1	7.5	7.8	0.9	0.89	0.96	1.21	1.37	1.52	0.81
L5-S1 passive moment	4.2	6.6	7.2	7.8	4.2	0.0	0.87	1.18	1.32	1.46	1.44	0.86
Minimum change	0.1	0.2	0	0.3	0.5	0.1	0.02	0	0	0.02	0.04	0.01
Maximum change	4.9	4.2	2.4	6.3	5.9	7.5	0.27	0.23	0.11	0.39	0.37	0.17

# EXPLORING HAPTIC FEEDBACK ON KINESTHETIC AWARENESS: A CASE STUDY

Jo Shattuck, Jack Ransone,  
University of Nebraska and the Nebraska Athletic Performance Laboratory, NE, USA  
Email: [joshattuck@huskers.unl](mailto:joshattuck@huskers.unl), website: <http://www.huskers.com>

## INTRODUCTION

Proprioception (kinesthetic awareness), of the precise joint angles of the effector is especially critical in the cognitive and associative stages of motor learning [1]. The ability to replicate an effector angle in any skill involving a ball and target is crucial for successful ball control. In order to replicate and correct a movement, the subject must have accurate and consistent knowledge of the body's position. Kinesthetic awareness training (KAT) provides the addition of haptic feedback in real time, to introduce secondary discriminatory system information into kinesthetic processing to improve kinesthetic awareness. We propose that haptic feedback through KAT will improve the ability to replicate a joint angle in multi-joint movements [2]. We tested this hypothesis on multiple movements. This dataset refers only to forearm angle replication during shot preparation movement in basketball.

## METHODS

We assessed peripheral limb control, specifically the vertical angle of the right forearm during a basketball shot measured with and without real-time haptic feedback. Four participants, (3 males, 1 female, each was either 20 or 21 years old), wore a miniature motion-capture and feedback device with internal sensors that recorded continual position data in 8 axes at approximately 16Hz. The target angle was determined by the subject, who held the basketball in their desired shot preparation position for 2 full seconds. The precise angle was then captured into the KAT tool through the smartphone app. A researcher then bounce-passed the basketball to the subject from 12 feet away; the subject was asked catch the ball, then return to the shot preparation pose as quickly and accurately as possible, as if preparing to shoot. The device was programmed to automatically provide haptic vibrations while the forearm angle was replicated.

To maintain a 'real-world' basketball environment, the subject could choose to whether or not to shoot the ball. Our outcome measures were:

- 1) Time-to-target: samples needed to replicate shot preparation forearm angle after catching the ball. A beginning reference point began when the angle was within 40 degrees of the target. Angle was considered IN when within 4 degrees of the target.
- 2) HIT/MISS rate: For each trial, a HIT was recorded if the subject held the angle for 2 consecutive samples. A MISS was recorded if the target angle was not reached for 2 consecutive samples. MISSES/HITS is the MISS rate.



**Figure 1:** Forearm at target angle.



**Figure 2:** KAT placement.

The subject wore the KAT on the forearm continually as we collected three sets of five trials: a pre-training baseline set, a KAT condition set with haptic feedback, and a post-test set without-feedback, for a total of 15 trials per person. It is important to note that the goal was not to achieve any *particular* forearm angle across subjects, nor to test the effectiveness of any *particular* angle on shooting success, but instead, to test each subject's ability to replicate their chosen effector angle, that they determined for themselves before the task.

## RESULTS AND DISCUSSION

Single-tail paired T-tests of pre and post KAT in within-subject comparisons showed significant differences in time-to-target, in 2 of the 4 subjects. ( $p = 0.02$  and  $p = 0.03$  for subjects 3 and 4). One notable effect was the HIT/MISS ratio across all subjects in both conditions. The MISS rate in the KAT conditions was lower than in non-KAT sets (5% misses in KAT sets and % 26 misses in non-KAT sets).

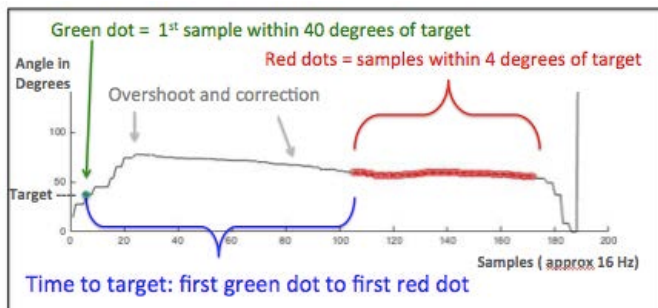


**Figure 3:** Outcome measure in a single trial.

This data is part of an ongoing study testing motor performance simple and complex movements. In this subset of data two of the within-person comparisons showed significant improvement in time needed to replicate the target angle with KAT. Also, the total MISS rate was 5 times lower in the non-KAT sets when compared to the KAT sets.

Our sample size is not large enough to show meaningful differences in angle replication, however, this case study reports on the findings regarding motor behavior when haptic feedback is implemented in a motor task. Visible overshoots and undershoots of the target angle happened more frequently in the KAT conditions, presumably the reflecting the kinesthetic awareness as the subject 'explored' the effector position and felt the haptic feedback. Logically, subjects spent more time in the target angle in the KAT conditions, although this was not part of the instructions to the subject. In future studies, improvements to the methods will include a larger sample size, more trials per set, and two groups design, one with feedback, and one without, instead of alternating conditions, to better control the practice effect.

Further experiments are warranted to determine if KAT training can improve kinesthetic awareness, and more importantly, if the improvement translates to increased performance of a motor skill.

## CONCLUSIONS

This effort was the first use of a novel feedback/monitoring device. The study was not intended to determine the *optimal forearm angle of a basketball shot*, but instead to test angle replication skill, reflecting our measure of kinesthetic awareness. The results show that a miniature motion capture device could be used to test biomechanical techniques in motor skill in real-life situations, without the restraints of in-laboratory multi-camera marker systems.

It is logical that a device that offers vibratory corrective feedback, at the exact instant the correct angle is replicated, would lead to that angle indeed, being replicated, during a movement. The larger purpose is to investigate haptic feedback as an intervention in human movement. Real-world applications include basic motor skill acquisition [2], clinical rehabilitation, post-trauma physical therapy, movement disorders, neurosensory motor dysfunction, and/or other rehabilitative populations with kinesthetic awareness deficits.

## REFERENCES

1. Sigrist R, Rauter G, Riener R, Wolf P *Psychon Bull Rev* 20:21–53, 2013
2. Marchal-Crespo L, Van Raaij M, Rauter G, Wolf P, Riener, *Exp Br Res* 231, 277:291-3, 2013

## ACKNOWLEDGMENTS

Thank you to the University of Nebraska, and Nebraska Athletic Performance Laboratory.

*Disclosure: The kinesthetic awareness training device/technique is provisionally patented by the principle investigator and PANTHER: Principles of Athletics and Neuroscience Toward Human ExpeRtise.*

# KINEMATIC MEASUREMENT AND ANALYSIS OF LIMB MOVEMENT DURING MOTOR LEARNING

<sup>1</sup> Qi Xing, <sup>2</sup> Weiwei Zhou, <sup>3</sup> Sang-Hoon Yeo <sup>2</sup> Wilssan Joiner and <sup>2</sup> Qi Wei

<sup>1</sup> Department of Computer Science, George Mason University, Fairfax, VA, USA

<sup>2</sup> Department of Bioengineering, George Mason University, Fairfax, VA, USA

<sup>3</sup> School of Sport, Exercise, and Rehabilitation Sciences at the University of Birmingham, Edgbaston, Birmingham, B15 2TT, UK  
email: qwei2@gmu.edu

## INTRODUCTION

The human motor system is capable of a range of actions that are modified through experience. Motor learning has been actively studied to examine exactly how humans learn a motor skill by building sensorimotor maps that transform the sensory inputs into the motor output [1]. One of the crucial problems involved in this transformation is the “degrees of freedom problem”, a problem of effectively eliminating the redundancy of transforming high-dimensional joint space motor commands to the three-dimensional operational (endpoint) space movement [2]. However, in many studies on computational motor control, this degree of freedom problem has been substantially simplified or overlooked, and the primary focus has been put on the behavior in the operational space only. For instance, to examine the error-based mechanisms underlying motor learning, researchers have been using robotic manipulators [3, 4] to conduct human behavior studies on arm reaching movements. Typically, the only kinematic information provided and measured by these manipulators is the position and velocity of the manipulandum's handle, while the variability in the joint space induced by the coordinated movement of trunk, limb, and the wrist is purposely eliminated using restraint devices such as harness seat belt, air sled and arm casts. Likewise, the biomechanical models of the arm incorporated in the studies also have been drastically simplified as a planar two-link system of the elbow and the shoulder only, or simply as a linear point-mass system. Although these studies are successful in revealing the mechanisms of skill acquisition, an important component concerning how this adaptation is achieved within the kinematic redundancy is currently missing.

Due to the reasons discussed above, we believe the redundant kinematic factors should be concurrently and systematically assessed, rather than constrained, in motor learning studies. In addition to the endpoint trajectory (hand position and velocity in arm reaching experiments), analyzing kinematic changes in the joint space can provide useful information on brain's coordination strategy, such as the coordinate system used by the motor system during learning, the mechanical aspect of the motor cost function, and the control preference in multiple muscle coordination. To accomplish this goal, we incorporated 3D motion capture and musculoskeletal models with standard motor learning studies. Collectively, through the development of motion capture and modeling methods, our long-term goal is to perform biomechanical simulation of musculoskeletal models of the upper limb in order to provide a comprehensive representation of how the neural and motor systems synergistically accomplish the learning of new motor behaviors.

In this short report we describe our preliminary study that examined the kinematic factors in an arm reaching motor learning task. We hypothesized that the motor system exploits the redundant degrees of freedom to fine-tune the secondary factors of the motor cost, such as manipulability and dexterity. Specifically, we hypothesized that during a two-dimensional force adaptation task, subjects would systematically alter the elbow elevation over the course of motor learning, which is the only redundant degree of freedom when the hand is constrained to move within the horizontal plane. In addition, we expected to determine the mechanical implication of this change through biomechanical analysis, and to further elucidate the brain's strategy to solve the degrees of freedom problem.

## MATERIALS AND METHODS

Fig. 1 shows our system setup. We integrated two Bumblebee2 Stereo Vision Camera Systems (Point Grey Research) with the KINARM robotic manipulandum (Bkin Technologies) to track the arm motion from the lateral side of the subject. Four videos (640 X 480) were acquired at 48 frames per second from the four cameras and streamed to a desktop through firewire. Twelve infrared reflective markers (1cm diameter) fixed to 3D-printed bases were taped to the upper torso, upper arm, lower arm and hand of subject. Markers were also attached to the robot handle whose motion data was used to temporally synchronize the cameras to KINARM. We developed programs to calibrate the two stereo cameras and calculate 3D positions of the markers from the video data.

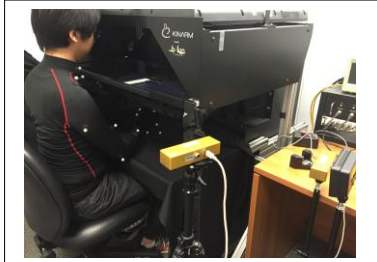


**Fig. 1:** The user manipulates the KINARM robotic handle while performing a motor learning task. We used two stereo cameras to concurrently measure upper limb kinematics.

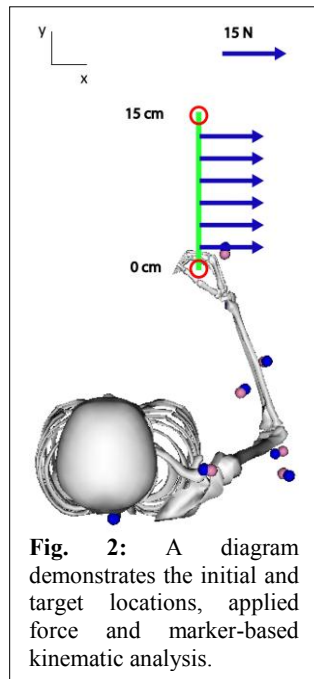


**Fig. 2:** A diagram demonstrates the initial and target locations, applied force and marker-based kinematic analysis.

Each subject performed five blocks of reaching movements. The first and the last blocks consisted of null trials with no force perturbation. In the other blocks, a constant force of 15N perpendicular to the

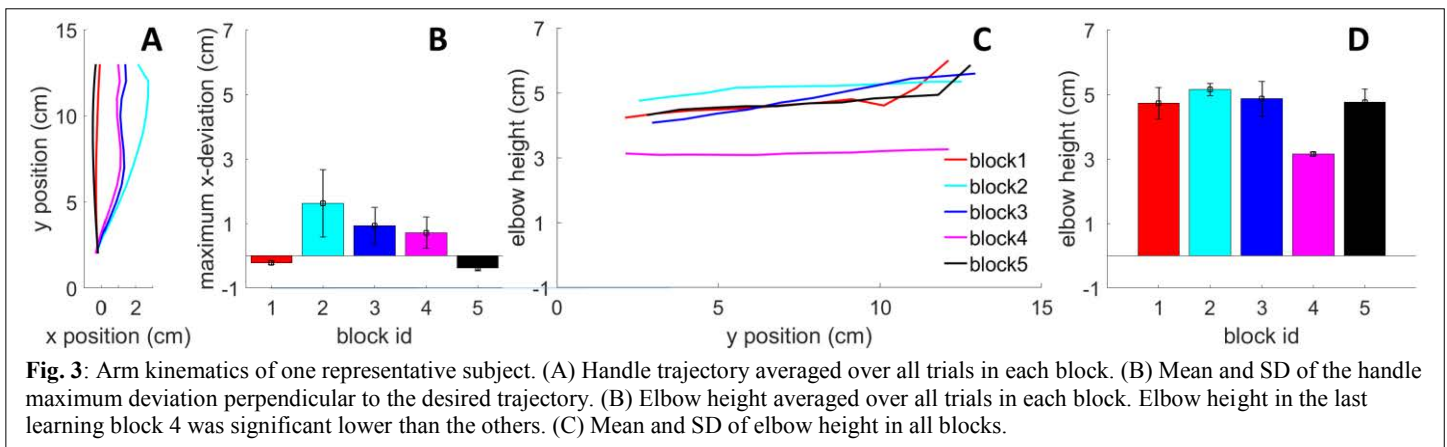
desired handle trajectory (x-direction in Fig. 2) was applied to the handle. More details on similar experiments can be found in [4]. An OpenSim arm model [5] was used to carry out subject-specific kinematic analysis. The pink markers in Fig. 2 are the template markers and the blue markers are the experimentally measured markers. Inverse kinematics was performed in OpenSim and arm kinematics of all reaching movement were examined.

## RESULTS AND DISCUSSION

Four subjects were recruited for the study. Fig. 3 showed analysis of one subject to describe the analysis. The subject was able to gradually learn the task, shown by the decreasing maximum trajectory deviation in blocks 2-4 (Fig. 3B). The subject first elevated his elbow at the beginning of learning (in block 2) then lowered his elbow during subsequent learning (in blocks 3 and 4). Other subjects also showed variable elbow height during learning trials that was significantly different from the elbow height in the null trials. Our preliminary analysis showed the feasibility of the proposed framework in studying the kinematic factors in motor learning. In the future, we plan to carry out more data collection and analysis to systematically test our hypothesis that changes in elbow angle correlates with the motor adaptation throughout the test session.

## REFERENCES

1. Braun DA, et al. *Curr. Biol.* **19**, 352-357, 2009.
2. Bernshtein NA, et al. *Oxford*. Pergamon Press, 1967.
3. Howard IS, et al. *J. Neurosci.* **181**, 199-211, 2009.
4. Joiner WM, et al. *J. Neurophysiol.* **100**, 2948-2955, 2008.
5. Saul KR, et al. *Comput. Methods Biomech. Biomed. Engin.* **18**, 1445-1458, 2014.



# Anticipatory Behaviors in Lateral Weight Shifting

Jackson Fox, Kevin O'Brien and James P. Schmiedeler

Aerospace and Mechanical Engineering, University of Notre Dame, Notre Dame, IN, USA

E-mail: [jfox10@nd.edu](mailto:jfox10@nd.edu), [kobrie23@nd.edu](mailto:kobrie23@nd.edu), [schmiedeler.4@nd.edu](mailto:schmiedeler.4@nd.edu)

## INTRODUCTION

Research on human postural control has typically emphasized quiet standing, but standing balance also requires the ability to dynamically shift ones weight in order to modulate center of pressure (CoP) position in performing functional activities [1]. Prior to voluntary balance adjustments or the initiation of walking, the human body exhibits anticipatory actions to maintain stability throughout the dynamic motion [2]. Implications of the anticipatory actions include improved resistance to falls during these voluntary movements. The present study investigates how shift strategy and CoP positioning during a lateral weight-shifting task are affected by shift direction and prior knowledge of an upcoming shift that enables anticipation.

## METHODS

Eighteen healthy subjects, 5 male and 13 female, ages 18-21 participated in this study. All subjects gave their informed consent prior to the study, which was approved by the appropriate Institutional Review Board. Using the Nintendo Wii Balance Board and the WeHab software [3] to provide visual feedback at approximately 60 Hz on a large computer monitor positioned at eye level, each subject was instructed to shift his/her CoP such that the small circle displaying its position overlaid on a background image of a Balance Board was within a target region. See Figure 1. Subjects completed nine 3-minute tasks and were instructed to shift into as many displayed targets as possible in the allotted time. The shaded rectangular targets (width equal to twice the CoP indicator's diameter) appeared at the center, on the right side, and on the left side of the board, with each lateral shift followed by a return shift to center. The lateral targets were positioned at a distance from neutral such that the subject had to support 70% of her/his weight on the corresponding

foot. The location of the target following a central target was randomized. As a result, subjects were able to anticipate the direction of shifts to the center, but not the direction of lateral shifts. Once the subject had shifted his/her CoP into the target, the CoP had to remain continuously in the target for three seconds before the target disappeared and the next appeared. Subjects were able to see the three-second numeric countdown on the visual display.

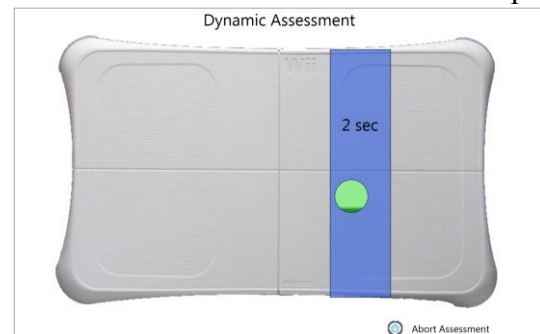


Figure 1: Visual feedback with CoP and target.

For each shift, the mean position of the subject's CoP in the lateral direction relative to the center of the target was computed for the 100 milliseconds prior to the target changing location. (The mean position in the anterior-posterior direction was also computed, but analysis revealed no significant trends.) Negative mean values indicate the side of the target closest to the location of the next target. A multi-factor ANOVA tested the effect of the subject number, the shift number for each subject, and the shift type on the mean position of the CoP prior to the shift. Shift type was defined by the starting and ending locations as type 1: left-to-center; type 2: right-to-center; type 3: center-to-right; and type 4: center-to-left.

## RESULTS AND DISCUSSION

Figure 2 plots the mean CoP positions relative to the target centers across all subjects for each of the four shift types. The ANOVA results indicated that

shift type was a significant main effect. A linear regression between shift type and mean CoP position revealed no statistically significant difference between the type 1 and type 2 shifts ( $p > 0.05$ ) back to center, while all other comparisons indicated statistically significant differences ( $p < 0.001$ ). This similarity in pre-shift behavior for type 1 and type 2 shifts was further investigated.

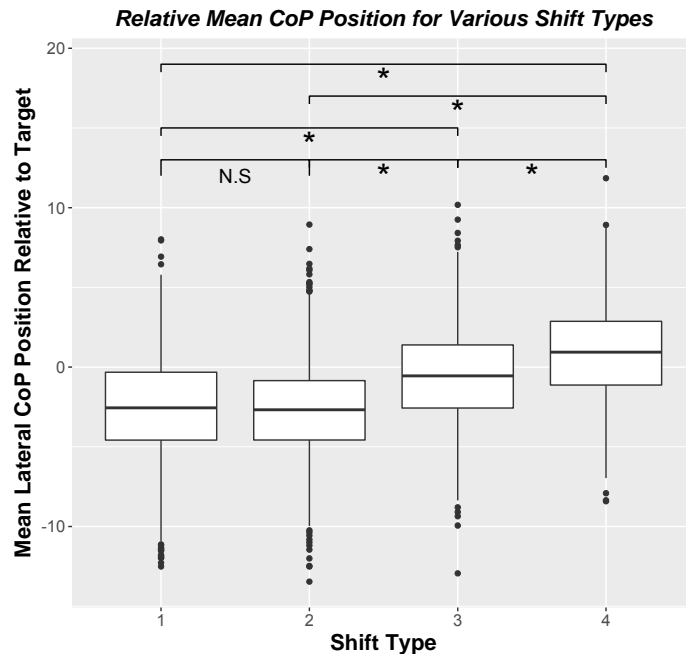


Figure 2: Mean lateral CoP position prior to shift initiation across all subjects for shift types: 1 left-to-center; 2 right-to-center; 3 center-to-right; and 4 center-to-left. (\* indicates  $p < 0.001$ ).

All subjects demonstrated a preference for a mean location in the “inside” half of the offset targets (closer to center). Of the 18 subjects, 13 had at least 75% of their shifts begin from the inside half of the target, with a minimum of 62% of the shifts, a maximum of 98%, and an average of 81.3%. While some subjects exhibited clear preferences for one side in type 3 and type 4 shifts out from center, there was no consistency among the group as a whole, and not all showed a clear pattern, as they did for the type 1 and type 2 shifts.

The subjects’ uniform preference for maintaining the CoP in the inside half of the target prior to shifting from an offset target inward could result from a number of factors. As the offset targets require the subject to support more weight on one

foot to even enter the target, the inside position could simply be preferred for comfort – it reduces the load on the outside leg within the task constraints. As the shifts from center involve moving from a neutral position, no comfort bias would be expected there. Alternatively, the difference could result from the anticipatory effects of shifting from offset targets to center that are not present in the shifts from center out because of the randomized offset target locations. The inside position should modestly reduce the time required to shift back to neutral, consistent with the instructions to complete as many shifts as possible. Furthermore, a shift to any target requires the CoP to first move opposite the target direction as the subjects pushes off [4]. Positioning the CoP closer to the inside target boundary provides a larger buffer to prevent the CoP from moving outside the target during its initial movement. This could be important if subjects started shifting prior to the new target appearing because moving the CoP out of the target too soon would reset the 3-second counter. This characteristic was not found for shifts away from center, perhaps because subjects were unable to anticipate the location of the next target.

## CONCLUSIONS

Young, healthy subjects consistently preferred to maintain an inside mean CoP position within an offset target prior to a visually guided, anticipated weight shift to neutral, which may be explained by maximizing comfort and/or shift speed within the task constraints. Future studies could further examine the role of anticipation by removing the visible timer and randomizing the required time spent in a target. Additionally, more target locations could be included to examine the effects of the subject knowing the direction but not the magnitude of an upcoming shift.

## REFERENCES

- [1] Huxham FE et. al., *Australian Journal of Physiotherapy*, **47(2)**, 89-100, 2001.
- [2] Horak FB *Age and Ageing* **35(2)**, ii7-ii11, 2006.
- [3] Kennedy MW et al., *IEEE Healthcom International Conference*, 162-168, 2011.
- [4] Kennedy MW et al., *Gait Posture*, **40(1)**, 134-139, 2014.

# MUSCLE RECRUITMENT AND COORDINATION DURING COMMON CLINICAL UPPER-EXTREMITY FUNCTIONAL TESTS

<sup>1</sup> Keshia M. Peters, <sup>1</sup> Valerie E. Kelly, <sup>1</sup> Tasha Chang, <sup>1</sup> Madeline C. Weismann, <sup>1</sup> Sarah Westcott-McCoy, and <sup>1</sup> Katherine M. Steele

<sup>1</sup> University of Washington, WA, USA

email: rumbek@uw.edu, web: <http://depts.washington.edu/uwsteele>

## INTRODUCTION

Electromyography (EMG) can provide quantification of muscle recruitment and coordination during dynamic tasks. In research, EMG data are often used to evaluate muscle coordination during highly constrained tasks [1]. Conversely, in rehabilitation settings, clinical tests involving unconstrained movements are commonly used to simulate tasks of daily living and evaluate function [2]. However, EMG data are seldom used during these tasks to quantify patient-specific deficits. A need exists to evaluate unconstrained movements to facilitate the translation of experimental research to clinical practice.

The aim of this study was to evaluate how unimpaired individuals recruit and coordinate their muscles during clinical tests. Specifically, we sought to identify which muscles are used to execute common upper-extremity tasks and whether co-contraction levels are similar across muscle groups and tasks. Establishing normative patterns of recruitment and coordination may assist in identifying patient-specific deficits and opportunities for intervention.

## METHODS

The Jebsen-Taylor Hand Function Test (JTT) was performed by 20 unimpaired participants, 12 males, 8 females (avg  $\pm$  std) age  $27 \pm 5.7$ , height  $174.4 \pm 9.1$  cm, weight  $72.6 \pm 11.0$  kg. The JTT is a timed test that evaluates unilateral movement during simulated tasks in the following order: 1. writing, 2. card turning, 3. picking up small objects, 4. feeding, 5. stacking checkers, 6. moving light cans, and 7. moving heavy cans.

Surface EMG data were recorded from 8 upper-limb muscles for the dominant side: biceps brachii, triceps lateral head, extensor carpi radialis longus (ECRL), flexor carpi ulnaris (FCU), extensor digitorum (ExtD), brachioradialis, anterior deltoid, and posterior deltoid (Trigno Wireless EMG Systems; Delsys, Boston, MA, USA). Maximum voluntary isometric contractions (MVICs) were collected for normalization. EMG data were processed in MATLAB (MathWorks, Inc., Natick, MA, USA) and included high-pass filtering (40Hz), rectification, and low-pass filtering (40Hz) each muscle to calculate a linear envelope.

Percent co-contraction (%COCON) was calculated by comparing the over-lapping integrated areas of the linear envelopes relative to the total integrated area of both muscles [3]. We evaluated %COCON for four muscle pairings: anterior and posterior deltoid (AP), biceps and triceps (BT), brachioradialis and triceps (BrT), and flexor carpi ulnaris and extensor carpi radialis longus (FE). A one-way ANOVA with post-hoc t-tests, with Bonferroni correction for multiple comparisons were conducted to compare %COCON of each muscle pairing, as well as average MVIC of individual muscles across tasks ( $\alpha = 0.002$ ).

## RESULTS AND DISCUSSION

Two distal arm muscles, ExtD and FCU, exhibited greater recruitment than other muscles across most JTT tasks, demonstrating that the JTT places a greater demand on forearm muscles (Fig. 1, Left). The ExtD had significantly greater recruitment (relative to %MVIC) than shoulder and elbow muscles for tasks 1, 2, and 3, and all muscles for tasks 4, 5, 6, and 7. The high activation level of the ExtD demonstrates the relative demand placed on

this smaller muscle and the necessity of finger extension during tasks of daily living, an ability often impaired after stroke. Other muscles that span the wrist may also serve as wrist stabilizers. For example, in the heavy cans task, the ExtD may function as the primary mover, and the remaining wrist movers, FCU and ECRL, may function to stabilize the wrist.

No differences were found in %COCON of muscle pairings across tasks. Average %COCON across tasks were  $35.8 \pm 3.3\%$ ,  $44.0 \pm 3.3\%$ ,  $55.1 \pm 4.5\%$ , and  $49.1 \pm 3.3\%$  for the AP, BT, BrT, and FE, respectively. BrT had significantly greater %COCON than the shoulder (AP) and forearm (EF) during tasks 3 – 7, suggesting the importance of stabilizing the elbow during these tasks. Recent research found a positive correlation between BT and BrT co-contraction levels and speed during the deceleration phase of elbow extension [3], which may also indicate elbow co-contraction is important during timed and targeted tasks like the JTT.

Muscle recruitment during tasks was independent of the time required to complete the task for unimpaired individuals (Fig. 1, Right). For example, the writing task took the longest to complete and had low levels of recruitment in the proximal arm muscles. However, the ExtD and FCU had a significantly higher mean recruitment level than the shoulder and elbow flexors ( $p < 0.0002$ ). Conversely,

the checkers task was completed in  $4.3 \pm 0.8$  seconds and had the lowest mean recruitment level across tasks and most muscles, likely due to the relatively small working space. There was greater inter-subject variability in muscle recruitment than time to complete each task.

## CONCLUSIONS

Quantifying muscle recruitment and coordination during unconstrained clinical assessments in unimpaired individuals provides a set of baseline measurements that can be used to evaluate muscle-specific deficits for individuals with neurologic impairments, such as stroke or cerebral palsy. Such assessments may be used to track recovery, inform therapy, and accelerate rehabilitation.

## REFERENCES

1. Sarcher A, et al. *Clin Neurophys* **128**, 4-13, 2017.
2. Beebe JA, Lang CE. *Stroke* **40**, 1772-1779, 2009.
3. Winter DA. *Biomechanics and Motor Control of Human Movement, 4th ed.*, John Wiley & Sons, Inc., 2009.

## ACKNOWLEDGMENTS

The authors thank George Patrick Cummings for assistance with data collection. Research reported in this abstract was supported by the National Institutes of Health under award R01EB02193.

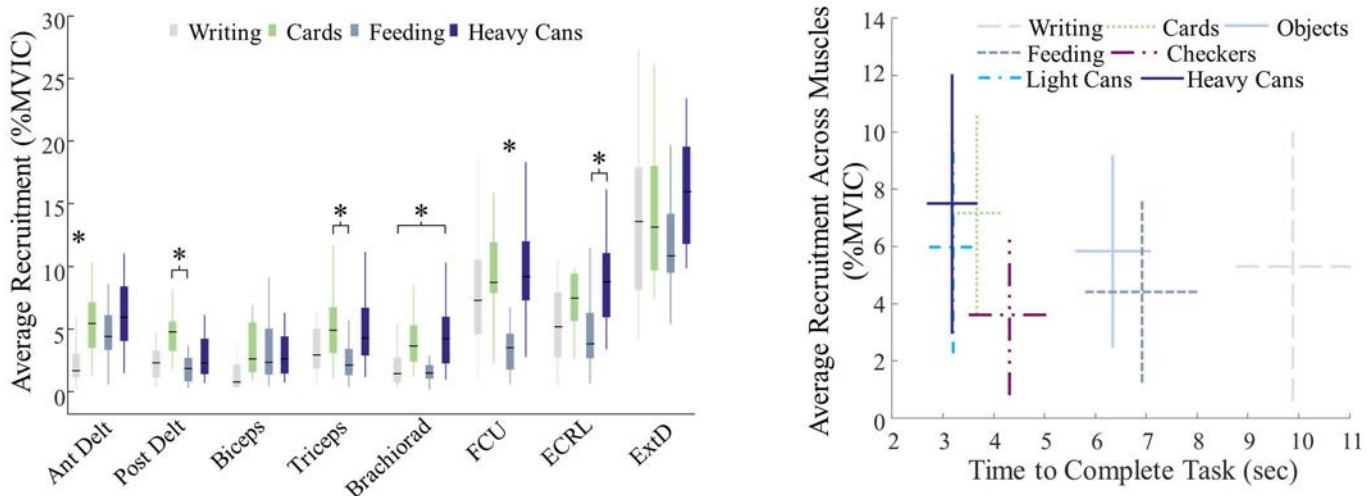


**Figure 1:** Comparison of the temporal and myoelectric demands of each task. **Left.** Average recruitment of each muscle for four tasks of JTT across all participants (outliers > 2SD omitted). \* indicates a significant difference between tasks, and brackets indicate significance between two tasks. **Right.** Ave  $\pm$  one SD across all participants of time to complete each task of the JTT versus average recruitment over all eight muscles.

# REDUCTION IN STABILITY OF MANUAL BEHAVIOR IN UNCERTAIN CONDITIONS

Mitchell A. Tillman and Satyajit S. Ambike

Purdue University, West Lafayette, IN, USA

email: [sambike@purdue.edu](mailto:sambike@purdue.edu). web: [www.purdue.edu/hhs/hk/Biomechanics-MotorBehavior/](http://www.purdue.edu/hhs/hk/Biomechanics-MotorBehavior/)

## INTRODUCTION

Ensuring the stability of motor action is critical for executing successful movements. However, maximizing stability is not always desirable [1]. For example, a transition between motor states must be preceded by the destabilization of the prior state. *Anticipatory synergy adjustments* describe the destabilization of a motor state that begins ~300 ms before the intended change in that state is observed [2]. Similarly, when rapid movement is expected in the near future, the motor system must manage two contrasting objectives: (1) ensure the stability of the current state, and (2) achieve rapid transitions to new states, if required. We argue that the stability of the current motor state is modulated to lower values to account for uncertain task requirements and to achieve dexterous task switching.

Here, we verify if stability reduction enables the dexterous use of the fingers. Subjects performed four-finger, isometric, constant force production tasks in two conditions. In the first (stable) condition, subjects produced one constant target force and had a-priori knowledge of the target's invariance. In the other (dexterous) condition, subjects tracked a longer, unknown, randomly varying trajectory that included the constant-force target as an integral part. We hypothesize that the stability computed during the constant force-production phases in the two conditions (1) will be maximal for the stable condition, and (2) will be progressively lower as the task demands increase.

## METHODS

Twenty-five healthy subjects (6 male, 20.4±2.5 yrs) participated in the study after providing informed consent. Subjects were seated comfortably in a chair with their forearms resting on top of a table. They placed the distal phalanx of each finger of their dominant hand on one force transducer (Nano-17;

ATI Automation). The transducers recorded each finger's downward vertical force at 1000 Hz. Visual feedback on the total force,  $F_T$ , was provided for all trials via a computer screen placed in front of the subject.  $F_T$  was computed as the sum of the vertical downward forces of all fingers ( $F_T = \sum F_i$ ;  $i=1$  to 4).

For the stable condition (Task 1), subjects produced a constant  $F_T$  value (10% of maximum voluntary contraction - MVC) for 7 s with the knowledge of the target's invariant location. This task was repeated 16 times [2]. For the dexterous condition (Tasks 2 and 3), the subjects modulated their total finger force and tracked an  $F_T$  target that randomly changed its vertical position on the screen. The target  $F_T$  profiles lasted for 30 s and consisted of smooth transitions between varying durations and magnitudes of constant  $F_T$ , including one instance of 10% MVC which lasted for at least 4 s. There were 8 distinct target  $F_T$  profiles for Tasks 2 and 3 each, which were repeated once to obtain a set of 16 trials for each task type. The target moved faster for Task 3 compared to Task 2, making Task 3 harder. The trials were randomized within each task, and the tasks were block randomized across subjects.

The last 4 s of Task 1 (Fig. 1A), and the first 4 s of Tasks 2 and 3 were used for further analysis, after the data were time aligned to match the start of the 10% MVC portion (Fig. 1B). The individual finger forces ( $F_i$ ) were filtered using a zero-lag, 4<sup>th</sup>-order, low-pass Butterworth filter (10-Hz cut-off). The stability of behavior was quantified using the uncontrolled manifold (UCM) analysis [3]. The UCM analysis partitions the variability in the input finger forces into a component along the UCM which does not affect the output force (*good* variance:  $V_U$ ), and variability orthogonal to the UCM that affects  $F_T$  (*bad* variance:  $V_O$ ). The relative amount of good variance, normalized by the total variance  $V_T$ , computed per degree of freedom, yields the synergy index:  $\Delta V = (V_U/3 - V_O)/(V_T/4)$ .  $\Delta V$  is z-transformed

to yield  $\Delta V_z$  for statistical analysis.  $\Delta V_z > 0.549$  indicates that the fingers covary to stabilize  $F_T$ , i.e., if one finger force increases, others compensate by reducing their force to maintain  $F_T$ . A *synergy* exists between the fingers, and a greater  $\Delta V_z$  indicates a stronger synergy and higher stability. Conversely,  $\Delta V_z < 0.549$  implies covariation between the fingers that destabilizes  $F_T$ .  $\Delta V_z$  was computed within each trial using a 250 ms sliding window.  $\Delta V_z$  values for two Phases (Phase 1: 2-3 seconds and Phase 2: 3 to 3.875 seconds) were averaged within those time bins for each subject and subjected 2-way, repeated-measures ANOVAs with factors *Phase* (2 levels) and *Task Type* (3 levels). Bonferroni corrections were used for pair-wise comparisons.

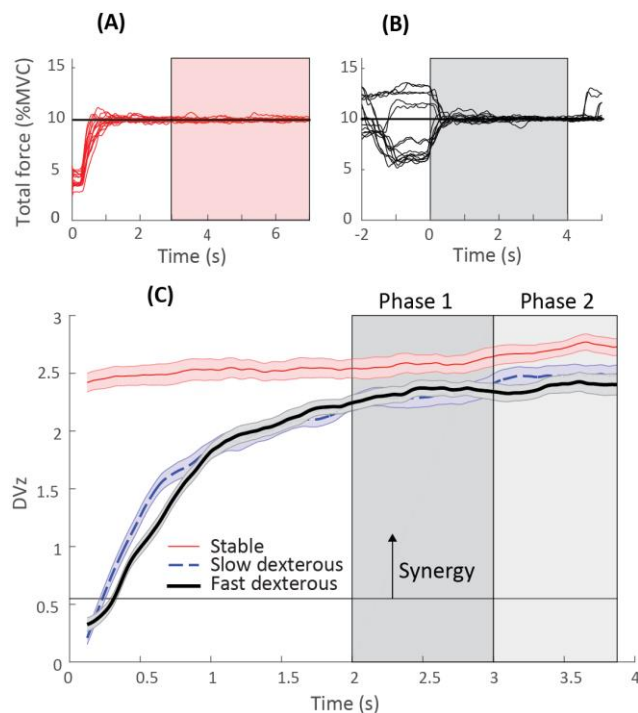


**Figure 1:** Representative data for Task 1 (A) and Task 2 (B). Data in the shaded rectangles is used for computing the synergy index. Across-subject and trial mean $\pm$ SE of the synergy index (C).

## RESULTS AND DISCUSSION

The total force,  $F_T$ , in the 4 s window for Task 1 (Fig. 1A) shows fluctuations about the 10% MVC target. In contrast,  $F_T$  in the 4 s window for Tasks 2 and 3 (Fig. 1B) contain an initial period when force trajectories converge to the 10% MVC target from different previous states. So  $\Delta V_z$  for Task 1 displays a near-constant value, but  $\Delta V_z$  for Tasks 2 and 3

show a period (up to  $\sim 0.3$  s) of covariation that achieves  $F_T$  convergence to 10% MVC ( $\Delta V_z < 0.549$ ; Fig. 1C). Then,  $\Delta V_z$  gradually increases reflecting an increasing tendency to stabilize  $F_T$ . The key observation is that  $\Delta V_z$  values for the slow and fast dexterous tasks (Tasks 2 and 3) always remain lower than those for the stable task (Task 1).

The ANOVA revealed a significant effect of *Task Type* [ $F_{(2,48)}=10.721$ ;  $p < 0.01$ ]. Pair-wise comparisons revealed  $\Delta V_{z\text{stable}} (2.63 \pm 0.07) > \Delta V_{z\text{slow-dexterous}} (2.37 \pm 0.07)$ , and  $\Delta V_{z\text{stable}} > \Delta V_{z\text{fast-dexterous}} (2.35 \pm 0.07)$ . There was also a significant *Phase* effect [ $F_{(1,24)}=39.403$ ;  $p < 0.01$ ]. Pair-wise comparisons revealed  $\Delta V_{z\text{Phase-1}} (2.39 \pm 0.06) < \Delta V_{z\text{Phase-2}} (2.51 \pm 0.06)$ . The interaction was close to significant [ $F_{(2,48)} = 3.041$ ;  $p = 0.058$ ], and it suggested that the increase in  $\Delta V_z$  across the phases tends to be slower for fast dexterous task compared to the other two tasks.

Our first hypothesis was supported by the data. The stability associated with the constant  $F_T$  is reduced ( $\sim 10\%$ ) when subjects expect to produce force changes of unknown direction and magnitude at an unknown time in the near future. Although the drop in  $\Delta V_z$  was similar for Tasks 2 and 3, it tended to last longer for Task 3 (near-significant *Task*  $\times$  *Phase* interaction). These  $\Delta V_z$  changes are anticipatory synergy adjustments, but with two prominent differences: (1) they lasts over 8 times longer than the previously reported ( $\sim 300$  ms), and (2) we show limited destabilization that facilitates movement if and when required. In contrast, earlier work reports progressive destabilization of the current state that is necessarily followed by a state change in *self-paced actions* that do not involve uncertainty [2]. The relation between stability modulation and task performance remains to be established in our study. However, this is the first demonstration of task-specific stability reduction in hand function, and our results have implications for the understanding and the clinical assessment of manual dexterity.

## REFERENCES

1. Hasan Z. *J Mot Behav* **37**, 484-493, 2005.
2. Zhou T, et al. *Exp Brain Res* **226**, 565-573, 2013.
3. Scholz J, et al. *Exp Brain Res* **126**, 126-306, 1999.

# EXPECTATION OF REWARD DISCOUNTS THE COST OF EFFORT IN HUMAN REACHING

<sup>1</sup>Erik Summerside, <sup>1</sup>Ali Nikooyan, Reza Shadmehr<sup>2</sup>, and <sup>1</sup>Alaa Ahmed

<sup>1</sup>Department of Integrative Physiology, University of Colorado, Boulder, CO USA

<sup>2</sup>Department of Biomedical Engineering, Johns Hopkins University, Baltimore, MD USA  
email: erik.summerside@colorado.edu

## INTRODUCTION

Kinematics of many of our most common movements such as saccades and reaching have historically been explained exclusively through the minimization of implicit motor costs [1, 2]. Surprisingly, these sensorimotor control models do not consider important external variables such as the amount of reward available in the environment. If we assume that the purpose of a movement is to acquire a more rewarding state, and that time discounts the value of that reward, then movements are affected by a cost of time. More recent models propose that kinematics may be modulated according to the overall expected utility of the movement, with motor costs being discounted by the rewards associated with the movement outcome [3]. According to this framework, the speed of a movement is optimized according to competing effort and reward costs (slower=less effort, faster=more reward). These predictions are supported experimentally with humans and other animals making faster saccades to targets paired with an increased reward [4,5]. The current study investigated how kinematics in a *reaching* task can be modulated by reward. Furthermore, we probed the specificity of these effects both within a movement and across subsequent non-rewarding movements. We hypothesized that when reward is at stake, individuals would exert more effort. We found that expectation of reward coincided with greater peak velocity and reach extent, and shorter reaction time.

## METHODS

Twenty naïve participants (27.5 years, 11M, 9F) used a robotic handle to control an invisible cursor that interacted with a virtual environment displayed on an LCD monitor. The task consisted of moving the cursor from a middle home circle towards

different quadrants with the direction indicated by a marker displayed in one of four locations (Figure 1A, 45, 135, 225, or 315 degrees from the home circle). For each out-then-return reaching movement, we measured reaction time, peak outward velocity, movement duration, maximum excursion, distance to target, and peak return velocity (Figure 1B). The protocol consisted of a 40 trial baseline block followed by 4 experimental blocks of 100 trials. During baseline, participants reached to the four quadrants at self-selected speeds. This behavior continued during each experimental block, but with one of the quadrants now being paired with a reward (audible beep, exploding target, 4 arbitrary points). At the end of the block, the reward location was changed to a new quadrant so that a unique location was rewarded for each block (Figure 1C, 4 quadrants, 4 blocks).

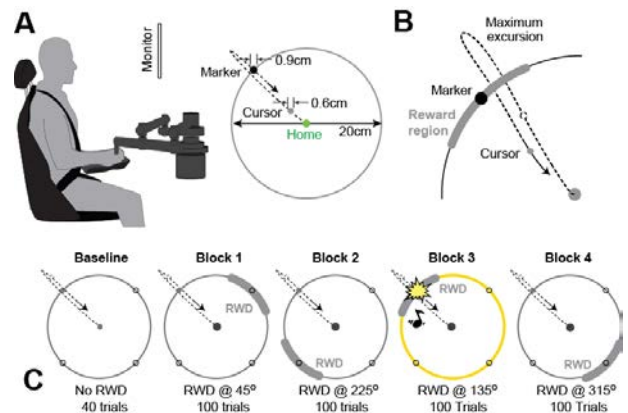


**Figure 1:** Experimental design. A) Set-up: Participants sat in a chair while grasping the handle of a robotic arm that controlled a cursor on a monitor located at eye level. B) Schematic of movement kinematics measured each trial. Distance to marker was calculated as absolute angle between marker and where cursor crossed outer ring. C) Protocol timeline: The order of rewarded blocks was identical for six participants and pseudo-randomized for the remaining fourteen.

Participants were neither aware of the total number of trials remaining in a block nor when a new block began. The only information they received regarding the progress of the experiment was that the experiment would end after an undisclosed amount of points were acquired. Using paired t-tests, we measured the changes in kinematics due to increased reward. To test for specificity in the effects of reward, we compared average kinematics for rewarded trials against non-rewarded trials preceding (two trials) and following (three) reward. Finally, we measured whether the effect of reward persisted through the return component of a reaching movement by comparing return velocity between rewarded and non-rewarded trials.

## RESULTS AND DISCUSSION

Individuals moved with higher outward peak velocity, greater maximum excursion, faster reaction time, and shorter duration when reaching towards targets associated with reward (Figure 2). Peak velocity increased by 2% ( $p=0.023$ ), maximum excursion increased 4% ( $p<0.001$ ), reaction time decreased by 5% ( $p<0.001$ ) and duration decreased by 2% ( $p=0.023$ ). There was no change in distance to marker ( $p=0.220$ ). This suggests, that similar to saccades, as the value of the movement outcome increased (more reward), people exerted more effort in those movements. When looking at the specificity of reward's effects on kinematics, we found that peak velocity and maximum excursion returned to pre-reward levels immediately following the rewarded trial. Duration and reaction time however, had a slightly exaggerated slowing in the trial immediately following reward, when compared to pre-rewarded trials and later post-rewarded trials ( $p's<0.05$ ). This suggests that reward may delay movement initiation and execution in non-rewarded movements immediately following reward.

Reward was attained as the hand crossed the outer ring. However, the movement continued as the hand returned the cursor to the center location. We found that expectation of reward affected only the center-out velocity of the movement, but not the velocity of the return phase back to center. This finding

demonstrates that expectation of reward discounts the effort that is expended before reward is attained, and not the effort that may be expended afterwards.

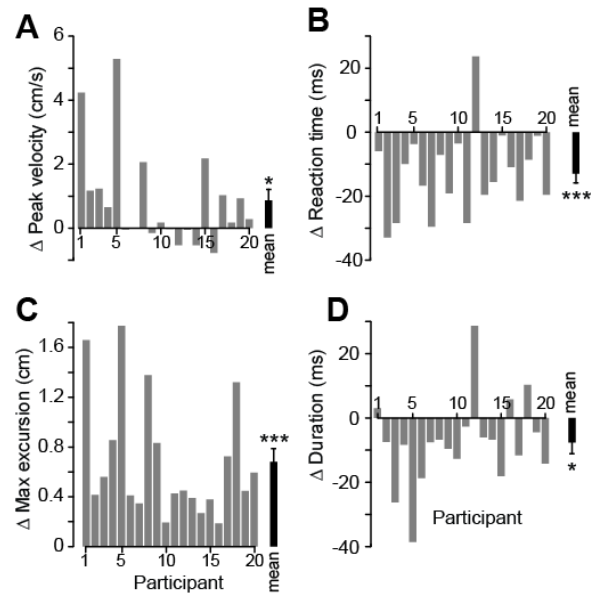


**Figure 2:** Changes in A) peak velocity, B) reaction time, C) maximum excursion, and D) duration as a result of heightened reward ( $*p<0.05$ ,  $***p<0.001$ ). Grey bars represent individual participants and black bars represent group means and SE.

## CONCLUSIONS

We found that humans altered the kinematics of their reaching movements under the expectation of reward. Expectation of reward appeared to discount the effort that the brain was willing to expend in performing a reaching movement.

## REFERENCES

1. Bahill et al. *Math Biosci*, **24**, 191-204, 1975.
2. Harris & Wolpert *Nature*, **394**, 780-784, 1998.
3. Shadmehr et al. *Curr Biol*, **26**, 1929-1934, 2016
4. Takikawa et al. *Exp Brain Res*, **142**, 284-291, 2002
5. Xu-Wilson et al. *Exp Brain Res*, **196**, 475-481, 2009.

## ACKNOWLEDGMENTS

We would like to acknowledge our funding sources: NIH NS078311 (RS) and NSF SES1230933, CMMI1200830 (AA)

# THE EFFECT OF PROLONGED STANDING ON WEIGHT-BEARING AND MUSCLE ACTIVATION ASYMMETRIES

Kylie M. Soliday<sup>1</sup>, Wayne J. Board<sup>2</sup>, Erika Nelson-Wong<sup>3</sup>, Raoul F. Reiser II<sup>1,2</sup>

<sup>1</sup>School of Biomedical Engineering, Colorado State University, Fort Collins, CO

<sup>2</sup>Department of Health and Exercise Science, Colorado State University, Fort Collins, CO

<sup>3</sup>School of Physical Therapy, Regis University, Denver, CO

Email: kysolid@gmail.com

## INTRODUCTION

Quiet stance (QS) is typically used to examine postural control through assessment of the center of pressure (CoP). However, weight bearing asymmetries (WBAs) may also be of value and have relationships to postural alignment and low back pain [1], although it's not fully understood how WBAs relate to the muscle activity and asymmetries at the trunk level. If WBAs do correlate back to the musculature at the hip and lumbar area, it may provide support for use of this measure, as WBAs are easier to collect than muscle activation asymmetries (MAAs). A previous study has indicated sex differences in muscle activation strategies, with women having more motion originate from the hip rather than the trunk during trunk flexion-extension movements [2]. These differences could potentially be related to the differences in core muscle use, size, and fiber type percentage between men and women [2,3,4]. Throughout a typical day, most individuals are on their feet, with prolonged standing (PS) becoming more highly recommended in the work place [5]. Most PS studies are 1-2 hours in length [6,7], however, a more brief 30 minute study may be more representative of the short bursts of time that individuals are on their feet throughout the day. The goal of this study was to examine the relationship between WBAs and MAAs during QS both immediately prior to and post 30 minutes of PS, the effects of PS on this correlation, and sex related differences within healthy young adults during QS.

## METHODS

Twenty-four healthy, pain-free subjects (12 male, 12 female) voluntarily participated in the study (age =  $22.3 \pm 2.4$  years, height =  $1.70 \pm 0.09$  m, mass =  $69.89 \pm 11.31$  kg, BMI =  $24.1 \pm 2.5$  kg/m<sup>2</sup> [mean  $\pm$  SD]). All subjects verified that they could stand comfortably for 30 minutes. Subjects performed two 60 sec. QS trials (pre-PS & post-PS) separated by one 30 min. free-standing trial. For the QS trial,

each subject had a set stance width of 10% of their standing height and were instructed to have a quiet, relaxed stance. For the 30 min. free-standing trial, subjects could shift their feet and sway to keep comfortable, as long as their feet didn't cross over onto the opposite force platform. Bilateral ground reaction forces under each foot were measured during each trial. Surface electromyography of each lumbar erector spinae (ES), gluteus medius (GM), internal obliquus, and external obliquus were also measured each trial. Muscle activity was normalized to a reference contraction (%ref) conducted at the start of the study [6,8]. WBAs and MAAs were calculated by subtracting the non-dominant limb (ND) from their dominant limb (D) using the %SI equation (Equation 1)[9].

$$\%SI = \frac{D-ND}{\frac{1}{2}(D+ND)} * 100 \quad (\text{Equation 1})$$

## RESULTS AND DISCUSSION

There were no differences in WBA or MAA between the pre-PS and post-PS trials, nor between the men and the women ( $p > 0.05$ ) (Figure 1). In both of the QS trials, there were no significant differences between the D and ND limbs ( $p > 0.05$ ).

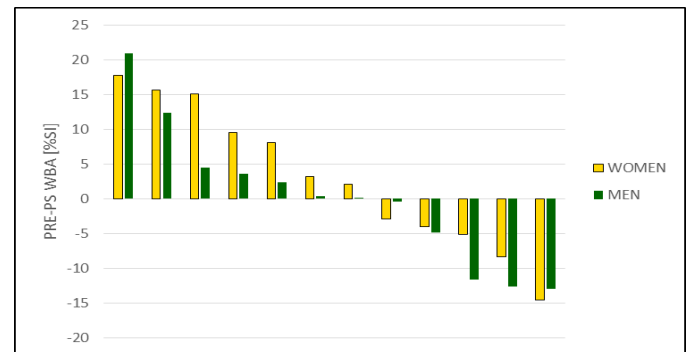


**Figure 1:** Individual subject WBA during the pre-PS trial ranked from highest (most weight on D limb) to lowest (most weight on ND limb). Post-PS WBAs behaved similarly.

Typically, the direction of the WBA stayed similar between the pre-PS and post-PS trials, and were significantly correlated (women  $p=0.016$  &  $r=0.676$ ; men  $p=0.002$  &  $r=0.807$ ).

The women had overall higher GM activity than the men (women =  $7.58 \pm 3.44$  %ref, men =  $4.79 \pm 2.93$  %ref;  $p=0.041$ ) (Figure 2). Overall ES activity decreased from the pre to the post-PS trial for the men, but not the women (women =  $2.08 \pm 1.03$  %ref, pre-PS men =  $2.56 \pm 1.82$  %ref, post-PS men  $1.79 \pm 1.46$  %ref;  $p=0.002$ ) (Figure 3).

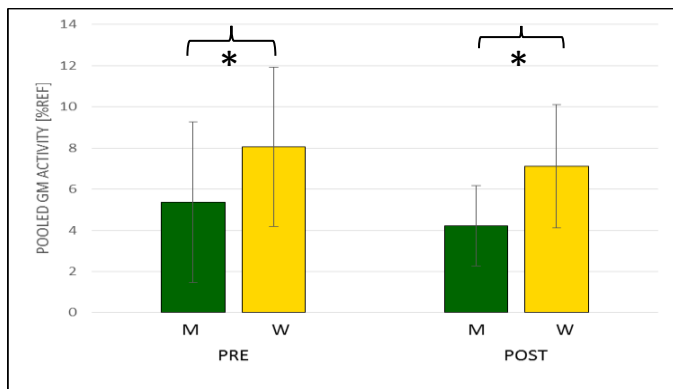


**Figure 2:** Glutes Medius (GM) activity levels with the D and ND sides pooled. Error bars indicate first SD. \*main effect  $p<0.05$  between men and women.

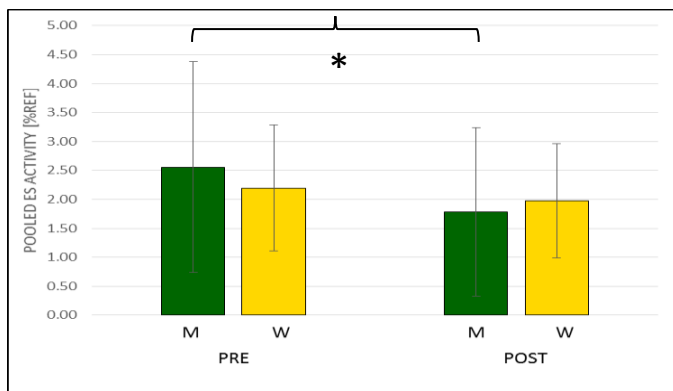


**Figure 3:** Erector Spinae (ES) activity levels with the D and ND sides pooled. Error bars indicate first SD. \*interaction  $p<0.05$  with men dropping pre-post.

During the pre-PS trial, there was a significant, although weak, correlation between the WBA and the GM asymmetry for the women ( $r = 0.615$ ,  $p = 0.044$ ) but not the men ( $r = 0.354$ ,  $p = 0.259$ ). This correlation was not significant in women during the post-PS trial ( $p=0.903$ ). The majority of the MAAs

were significantly correlated between the pre-PS and post-PS trials (women  $p\leq 0.001$  &  $r\geq 0.836$ , men  $p\leq 0.002$  &  $r\geq 0.802$ ), with the only exception being the ES asymmetry for the men ( $p=0.211$  &  $r=0.433$ ).

## CONCLUSIONS

While these results suggest that PS does not have an effect on WBA or MAAs during QS, a small amount of individual variation does exist. There also appears to be sex related differences in both muscle activity and possible changes in muscle use. Previous studies have also indicated sex related differences at the hip and trunk level, with woman activating hip muscles prior to trunk muscles during flexion-extension exercises [2]. These sex related findings could be related to the musculoskeletal differences between men and women [2,3,4]. The relationship between WBAs and GM MAAs changing from pre-PS to post-PS shows that a subject being rested versus unrested does matter for collecting these measurements. Furthermore, these results may potentially relate to what is occurring during the 30 minutes of PS, since the subjects could shift their weight and move around somewhat naturally during the trial. The 30 min data is currently being processed and analyzed.

## REFERENCES

- Childs JD, et al. *Manual Therapy* **8**, 166-169, 2003.
- Nelson-Wong, E, et al. *Clinical Biomechanics*, **27**, 994-998, 2012.
- Gallagher, KM, et al. *Gait & Posture*, **37**, 313-318, 2013
- Mannion, AF, et al. *Journal of Anatomy*, **190**, 505-513, 1997.
- Plotnikoff, R. & Karunamuni, N., *Archives of Environmental and Occupational Health*, **67**(3), 125-127, 2012.
- Nelson-Wong, E, et al. *Ergonomics* **53**(9), 1117-1128, 2010.
- Nelson-Wong, E, et al. *Clinical Biomechanics*, **23**, 545-553, 2008.
- Dankaerts, W, et al. *Journal of Electromyography and Kinesiology*, **14**, 333-342, 2004.
- Robinson, RO, et al. *Journal of Manipulative and Physiological Therapeutics* **10**(4), 172-176, 1987.

# ESTIMATION OF HUMAN ANKLE IMPEDANCE IN LATE STANCE AND IMPLICATIONS IN NEUROMOTOR CONTROL

<sup>1,2</sup> Amanda Shorter and <sup>1,2</sup> Elliott Rouse

<sup>1</sup> Northwestern University, Evanston, IL, USA; <sup>2</sup> Rehabilitation Institute of Chicago, Chicago, IL, USA

email: erouse@northwestern.edu, web: <http://neurobionics.smpp.northwestern.edu>

## INTRODUCTION

The mechanical impedance of human joints is fundamental to our ability to interact with the world. These properties describe the stiffness and damping characteristics of a joint and are actively regulated by the nervous system for adaptation to unexpected changes in task dynamics [1]. However, mechanical and analytical challenges have hindered the study of joint impedance during dynamic tasks, such as walking. Characterizing ankle impedance is critical to our understanding of how the nervous system regulates the mechanics of locomotion, and is needed to provide a basis for the development of biomimetic assistive technologies and their control systems.

Methods have recently been developed to overcome the challenges in estimation of ankle impedance during walking. Rouse *et al.* accurately estimated ankle impedance during the controlled dorsiflexion region of the stance phase of walking [1], while Lee *et al.* have characterized ankle impedance during swing phase and early loading response [3]. However, a gap remains in our knowledge of ankle impedance in late stance phase—or *push off*—when the calf muscle contracts to propel the body forward. This is a particularly important region of the gait cycle, when the majority of mechanical work is provided by the legs [4]. Estimating ankle impedance during late stance phase is challenging because quantifying ankle torque is more sophisticated due to motion and deformation of the midfoot segments following heel rise. Fortunately, motion capture studies have analyzed how the fore-foot, midfoot, and rear-foot segments move relative to each other, the shank, and the ground [5]; but these data have not previously been used in conjunction with joint impedance identification.

The ankle is essential to the energetics of human locomotion, producing the majority of mechanical power [4]. By separating total ankle work into the contributions due to elastic energy storage or return, and displacement of the virtual equilibrium position

of the biological controller, we can improve our understanding of how energy is stored, added, or removed during gait. Understanding energetic contributions to joint dynamics is essential for emulating natural gait in biomimetic assistive technologies.

This study quantifies ankle impedance during this crucial portion of stance phase, and evaluates energy transfer within an impedance framework that may represent aspects of the neuromotor control system. Analysis during late stance provides insight into how active power generation in locomotion affects joint mechanics and neuromotor control modalities.

## METHODS

The purpose of this study is to determine the mechanical impedance of the ankle during the late stance phase of walking using mechanical perturbations and measuring the joint's torque response. To this end, ten healthy subjects participated (6 male, 4 female, age  $25 \pm 4$  years, weight  $73 \pm 13$  kg), with no history of neurological impairments. Two degree angular perturbations in both the plantarflexion and dorsiflexion direction were applied to the ankle at two distinct time points in late stance phase, using a single degree of freedom platform robot [1]. Relevant force data were measured using a force platform included within the robot. The perturbation-induced changes in ankle angle were related to the resulting joint torque response by a second-order parametric model comprised of stiffness, damping and inertia components. Least-squares system identification was used to estimate impedance. Using data from aforementioned motion capture studies, a novel time varying, subject specific transformation was developed to resolve the ground reaction force to the ankle, allowing for accurate and robust torque measurements during mid-foot deformation.

Using an impedance control framework, parameterized by (1), we represented the instantaneous kinetic, kinematic and impedance aspects of human walking [1]. The equilibrium position ( $\theta_0$ ) of the stiffness element governing ankle torque was calculated for each subject by solving (1) using the non-perturbed ankle angle and torque information.

$$T_w = b_a \dot{\theta}_w + k_a (\theta_w - \theta_0) \quad (1)$$

The mechanical energetics of the ankle can be represented as a combination of energy storage and return ( $W_S$ ), and work due to displacement of the equilibrium position ( $W_D$ ). These contributions are estimated using numerical integration of (2) and (3) respectively, and their sum defines total ankle work.

$$W_S = \int k_a (\theta_w) d(\theta_w - \theta_0) \quad (2)$$

$$W_D = \int T d\theta_0 \quad (3)$$

## RESULTS

The second-order model comprised of stiffness, damping, and inertia accurately characterized ankle mechanics during late stance phase (variance accounted for =  $90 \pm 7.7\%$ ).

The stiffness component of impedance decreased linearly throughout late stance from  $3.84 \text{ Nm/rad/kg}$  to  $2.25 \text{ Nm/rad/kg}$ . Mean damping estimates during late stance were found to be relatively constant around  $0.03 \text{ Nms/rad/kg}$ . Mean ankle-foot inertia values were consistent across time points and matched previously reported values during gait [7].

The results of the equilibrium position analysis show equilibrium position to increase linearly from  $0.2$  to  $0.4 \pm 0.06$  radians in late stance. Using (2) and (3), spring work and displacement of equilibrium position contributions were found to be  $45 \pm 4\%$  and  $17 \pm 1\%$  of total work respectively.

## DISCUSSION

Stiffness decreased from values reported pre-heel rise to the relatively low stiffness found during swing phase [7] (Fig. 1). Furthermore, damping estimates increased during late stance when compared to damping values found in early and mid-stance (Fig 1). These findings are in agreement with previously reported work showing increased damping in preparation for toe-off [5].

Comparing ankle work throughout the gait cycle, there are observable differences in system energy.

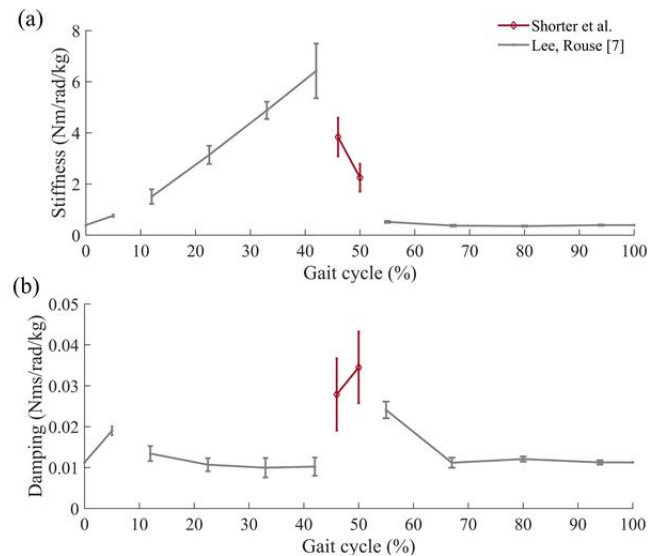


**Fig. 1:** Body weight normalized ankle stiffness (a) and damping (b) reported across the gait cycle modified from [7]. Red indicates average results across perturbation direction during late stance.

In early-mid stance equilibrium position has been shown to be constant, indicating ankle work is entirely due to spring energy [1]. Work in early-mid stance was determined using reported stiffness and equilibrium angle estimates made previously using the platform robot [1]. Less than  $2.3 \pm 0.7\%$  of work done in early-mid stance is attributed to equilibrium angle position. These results contrast results of work done in late stance, wherespring work and work due to equilibrium angle displacement both added to total work ( $45\%$  and  $17\%$  respectively). The method by which energy is been added or removed changes throughout the gait cycle. Subsequent research is required to discern the neural control strategy behind changes in energetics.

## REFERENCES

1. E. J. Rouse, *Transactions on Neural Systems and Rehabilitation Engineering*, **22**, 870-878, 2014.
2. E. J. Rouse, *Transactions on Biomedical Engineering*, **60**, 562-568, 2013.
3. H. Lee, *International Conference on Robotics and Automation*, 2651-2656, 2013.
4. D. A. Winter, *Critical reviews in biomedical engineering*, **9**, 287-314, 1984.
5. A. Leardini, *Gait & Posture*, **25**, 453-462, 2007.
6. E. J. Rouse, *IEEE 13th ICORR*, 1-6, 2013.
7. H. Lee, *Journal of translational engineering in health and medicine*, **4**, 1-7, 2016.
8. V. Lugade, *Gait Posture*, **33**, 406-11, Mar 2011.

# IDENTIFYING NEUROPHYSIOLOGICAL CONTROL PARAMETERS OF THE KNEE

<sup>1</sup> John M. Popovich Jr., <sup>1</sup> Ahmed Ramadan, <sup>1</sup> Joshua D. Hubert, <sup>1</sup> Victoria L. Davis, <sup>2</sup> Martin J. Weaver, <sup>1</sup> Tiffany C. Marchewka, and <sup>3</sup> Jongeun Choi

<sup>1</sup> Michigan State University, East Lansing, MI, USA

<sup>2</sup> Saginaw Valley State University, Saginaw, MI, USA

<sup>3</sup> Yonsei University, Seoul, Republic of Korea

email: popovi16@msu.edu, web: <http://orthopedicresearch.msu.edu/>

## INTRODUCTION

Tracking tasks are commonly used in biomechanics and motor control research. Quantitative measures of these tasks often include tracking accuracy (e.g., error) and steadiness (e.g., variability). Such measures aid in determining task performance, which may aid in classifying or differentiating groups, but understanding where differences in control manifests is not possible. Applying control systems engineering and system identification techniques to understand the biomechanics and control of human systems is a possible solution. Such an approach typically involves a response (output) to an external stimulus (input), such as visual targets or external perturbations. These responses can then be modeled in a closed-loop system that incorporates biomechanical and neurophysiological parameters. Implementing such modeling techniques can be used to non-invasively estimate biomechanical and neurophysiological factors governing human movement.

While trajectory-tracking tasks have been used to study impairments related to the lower extremity [1], [2], most studies do not employ a control systems approach. Therefore, the purpose of this study was to determine if changes in neurophysiological control parameters are identifiable during a knee trajectory-tracking task when given two distinct instructions. We hypothesized that differences in control parameters would exist between the two conditions, which would provide insight into the neurophysiological mechanisms associated with control of the knee.

## METHODS

Twenty-seven individuals (n=11 women, n=16 men) participated in this study. Michigan State

University's Biomedical and Health Institutional Review Board approved the research protocol. All participants signed an informed consent form.

For the knee trajectory-tracking tasks, participants were seated upright in a chair, with their knee positioned at 90 degrees. Their shank was instrumented with a lightweight bracket that allowed the attachment of two string potentiometers (model SM2, Measurement Specialties, Inc., Chatsworth, CA) to record angular position of the knee joint (**Figure 1A**). The knee trajectory-tracking input signal was comprised of 4 step inputs with amplitudes of either 2 degrees or 4 degrees and duration of 5 seconds each. The input signal was displayed on a computer monitor and participants were to respond to the step input by flexing and extending their knee joint. Two sets of instructions were provided: 1) perform the task as fast and accurate as possible (FAP), and 2) perform the task as fast and accurate as possible, but without overshooting (WOS) the displayed target (input signal). Participants performed all trajectory-tracking tasks while seated in an upright posture, arms crossed, and thigh strapped to the chair. Three trials of each condition were performed on each limb, always finishing with the three WOS trials.

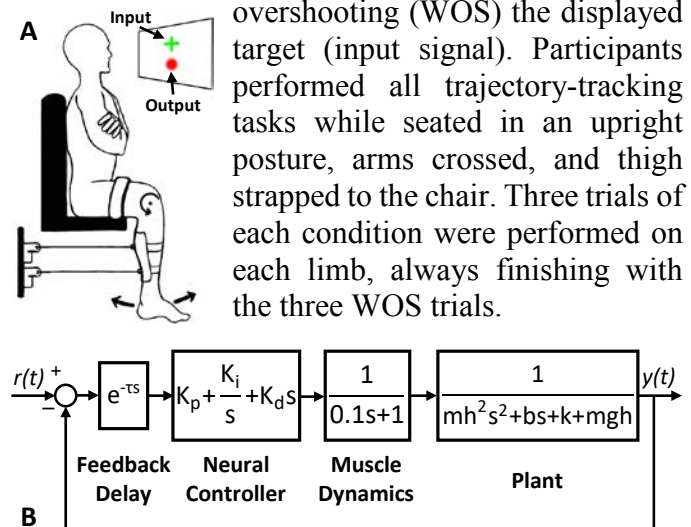


**Figure 1:** A) Experimental setup. B) Block diagram representation of a closed-loop system where  $r(t)$  and  $y(t)$  are the input and output, respectively.

To determine differences in control parameters between the two conditions, the experiment was modeled as presented in **Figure 1B**. This model included a PID-controller to represent a neural controller [3], [4], muscle dynamics [4], [5], plant (simple pendulum with stiffness and damping [5], [6]), and feedback delay. PID-controller gains ( $K_p$ ,  $K_i$ ,  $K_d$ ) and feedback delay ( $\tau$ ) were estimated for each condition by nonlinear least squares. Each trial was divided into eight sections such that a section contained 1s before a step and 4s after that step. Thus, eight different parameter sets were estimated per trial and then averaged across trials and limbs.

Variance accounted for (VAF) was used to determine the quality of the modeled time-domain data fit to the experimental data (0-100%; where higher VAF indicates better model fit). Additional non-parametric variables (i.e., RMS error, delay time, rise time, % overshoot, and settling time) were calculated to characterize the recorded response (across trials and limbs). Paired t-tests were used to determine differences between conditions for both non-parametric and parametric variables. Statistical analyses were performed in SPSS (V.23, Armonk, NY) with a significance level set at  $p < 0.05$ .

## RESULTS AND DISCUSSION

The response of both tasks demonstrated second order behavior, where the FAP response exhibited characteristics of an underdamped second order system and the WOS response was similar to being critically damped or overdamped (**Figure 2**). The overall mean VAF for both conditions was 98.9% ( $\pm 1.2\%$ ), indicating excellent model fits.

All non-parametric variables were significantly different between FAP and WOS (**Table 1**). The neural controller gains and feedback delay were also significantly different between conditions (**Table 2**).

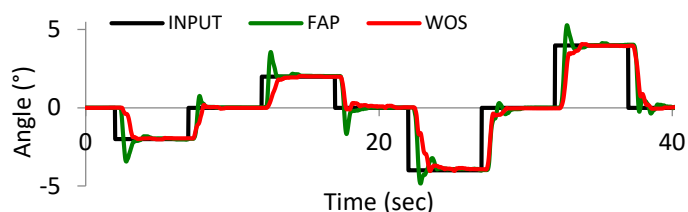


**Figure 2:** An example of the experimental time-series data for both FAP and WOS conditions.

**Table 1:** Calculated non-parametric variables.

	FAP	WOS	% Diff.	$p$ value
<b>RMSE (deg)</b>	0.019	0.020	4.35	<0.001
<b>Delay Time (s)</b>	0.387	0.412	6.70	<0.001
<b>Rise Time (s)</b>	0.375	0.571	52.5	<0.001
<b>Overshoot (%)</b>	30.9	11.2	-63.8	<0.001
<b>Settling Time (s)</b>	3.017	2.900	-3.89	0.025

**Table 2:** Parametric estimates of gains and delay.

	FAP	WOS	% Diff.	$p$ value
<b><math>K_p</math></b>	7.94	5.33	-32.7	<0.001
<b><math>K_i</math></b>	43.49	31.38	-27.8	<0.001
<b><math>K_d</math></b>	0.459	0.211	-53.9	<0.001
<b><math>\tau</math> (s)</b>	0.352	0.366	3.84	<0.001

It is clear from both non-parametric and parametric analyses that individuals were able to alter the control of their knee for the two conditions. In particular, FAP showed improved performance (i.e., shorter delay and rise times) by an aggressive controller (i.e., higher  $K_p$  and  $K_i$ ), while WOS provides improved relative stability (i.e., smaller overshoot) by a less aggressive controller (i.e., lower  $K_p$  and  $K_i$ ). Identifying changes in gains and feedback delays of knee control is consistent with modeling of other body regions, though research considering the response to other inputs is needed.

## CONCLUSIONS

Control of the knee is influenced by task instruction. Neural controller parameters (gains, delays) can be identified using a control systems approach.

## REFERENCES

1. Hortobágyi, T, et al. *Arthritis Rheum.* 2004.
2. Maffiuletti, NA, et al. *Neurosci Lett.* 2005.
3. Peterka, R, et al. *J. Neurophysiol.* 2004.
4. Priess, MC, et al. *Proc. ASME DSCC/MVC.* 2012.
5. Peterson, BW, et al. *Ann. N.Y. Acad. Sci.* 2001.
6. Stein, RB, et al. *IEEE Trans Rehabil Eng.* 1996.

# EXPERIMENTAL EVALUATION OF A FEEDBACK CONTROL SYSTEM TO ADOPT TASK-DEPENDENT POSTURES IN AN IMPLANTED STANDING NEUROPROSTHESIS

<sup>1,2</sup> Brooke Odle, <sup>1,2</sup> Musa Audu, <sup>2</sup> Lisa Lombardo, and <sup>1,2</sup> Ronald Triolo

<sup>1</sup> Case Western Reserve University, Cleveland, OH, USA

<sup>2</sup> Louis Stokes Cleveland Department of Veteran Affairs Medical Center, Cleveland, OH, USA  
email: bmo13@case.edu

## INTRODUCTION

Implanted neuroprostheses utilizing functional neuromuscular stimulation can restore standing function after paralysis due to spinal cord injury (SCI) by supplying constant open-loop (OL) stimulation to the trunk, hip, and knee extensors [1]. With these systems, users are unable to set a task-specific posture to prepare for a functional activity. To address this issue, we developed the posture follower controller (PFC). It is a closed-loop control system that continuously modulates muscle activation according to changes in the projection of whole-body center of mass (CoM) on the base of support. The objective of this study was to implement and assess the performance of the PFC experimentally with one recipient of an implanted neuroprosthesis. For proof-of-concept, center of pressure (CoP), which can be readily obtained from force plate data in the laboratory, was used as a surrogate for CoM as the feedback signal. We hypothesize that the UE load exerted as the user moves from one posture to another with the PFC will be the same as the UE load exerted with OL stimulation.

## METHODS

A 60 year-old male with T4 paraplegia (AIS B) participated in the experiments. At the time of testing, he was approximately 216 cm tall and weighed 63.5 kg. He was well conditioned and actively using a 24 channel surgically implanted neuroprosthesis for standing and exercise at home at the time of data collection. The muscles targeted by the implanted system for standing included: gluteus maximus, semimembranosus, and vastus lateralis. Prior to participating in the experiments, the subject signed informed consent forms approved by the

Institutional Review Board of the Louis Stokes Cleveland Veterans Affairs Medical Center.

As the user adjusted from a nominal erect posture, the controller continuously tracked CoP location and proportionately modulated stimulation, according to the change in CoP location, to the bilateral gluteus medius, posterior portion of the adductor magnus, and gastrocnemius. Activation to the muscles the subject required for standing was not modulated. The controller was tuned over the course of several sessions in the laboratory, prior to experimental evaluation with the subject.

The subject stood erect on force plates (AMTI, Watertown, MA) within a custom walker (80/20, Columbia City, IN) instrumented with load cells to measure hand reaction forces (AMTI). Using visual feedback, he adjusted his resultant CoP to targets located at the extremes of his standing workspace in the forward (FO), forward-right (FR), and forward-left (FL) directions. As the subject adjusted posture, UE force and CoP location were recorded. A total of 12 cycles of movement were collected, in random order, for each leaning posture and control system. To compare standing performance with the PFC to OL control, the mean total resultant UE forces were computed for the deploy phase of each leaning posture. Statistical differences were assessed by applying t-tests at significance level 0.05.

## RESULTS AND DISCUSSION

The PFC did not negatively impact leaning performance over OL standing. No significant differences between the UE loads exerted with OL stimulation and the PFC were observed for any of the leaning postures. The mean total resultant UE forces exerted while the subject adjusted posture with both control systems, represented as a

percentage of the subject's body-weight (BW), are displayed in **Figure 1**.

For postural adjustments in the FO direction, the mean total resultant UE load exerted with OL stimulation was  $29.6 (\pm 5.4)$  % BW and  $29.4 (\pm 5.1)$  % BW with the PFC. When the subject adjusted posture in the FR direction, the mean total resultant UE load exerted was  $28.1 (\pm 7.0)$  % BW with OL stimulation and  $31.6 (\pm 3.1)$  % BW with the PFC. For postural adjustments in the FL direction, the mean total resultant UE loads exerted with OL stimulation was  $34.0 (\pm 3.8)$  % BW and  $36.2 (\pm 4.1)$  % BW with the PFC. These represent mean changes in UE load of 1%, 12% and 2% for FO, FR and FL, respectively.

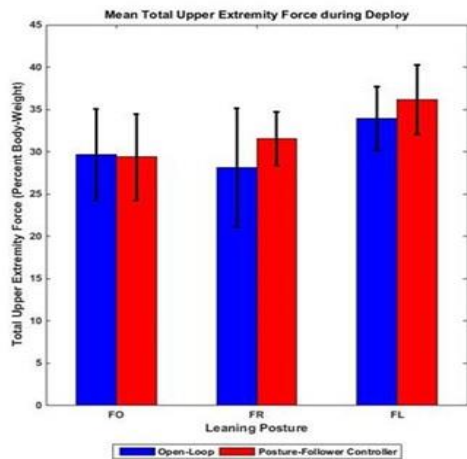


**Figure 1:** Mean total resultant UE forces exerted as the subject adjusted posture with OL stimulation and PFC for the deploy phase.

While the mean total UE loads were not different across controllers, they were nominal in all cases and typically less than 30% BW on average. Changes in UE exertion with the PFC from already small OL values may be difficult to detect with such a small sample and effect size, particularly since the metric was averaged across the deploy phase of the movement from baseline to target. Comparisons instantaneously on a sample-by-sample basis of OL and PFC conditions, peak values during the movement, or root-mean-squared tracking errors on the trajectories from baseline to target may be more sensitive measures. Furthermore, UE effort may be under-estimated in the OL trials since the plantar flexor muscles were not active and the subject did

not have to actively work against them during forward or diagonal leans. Moreover, the UE effort may be over-estimated in the PFC trials since the plantar flexor muscles were at maximum activation as the subject approached the extremes of his standing workspace. It is possible that the plantar flexor muscles pushed the subject backwards as he approached the targets. Working against the active muscles, he pushed down on the walker.

Future investigations will entail the collection and analysis of repeated measures with additional subjects. In these experiments, the location of the targets and the maximum plantar flexor activation will be reduced. As posture is adjusted, the direction of the individual UE forces exerted will be assessed as well. Also, both deploy and return phases of the movement will be explored, along with the additional measures listed above. Subjective measures of user preference, ease of use and safety will also be acquired.

## CONCLUSIONS

The PFC, an advanced control system designed to allow a neuroprosthesis user to change standing posture was implemented and evaluated with an individual with SCI. Standing performance in terms of UE effort to change posture with the PFC was compared to that with an OL control system. Preliminary results suggest that standing performance with the PFC is similar to OL control. Such advanced control systems may enable neuroprosthesis recipients to adopt task-dependent, user-specified postures at those new set-points to reach and manipulate objects in their standing workspace.

## REFERENCES

1. Davis JA, et al. *JRRD*, **38**, 609-617, 2001.

## ACKNOWLEDGMENTS

This work is funded by NIH R01NS040547. This material is the result of work supported with resources and the use of facilities at the Louis Stokes Cleveland VA Medical Center in Cleveland, OH.

# NEUROMECHANICAL IMPLICATIONS OF POSTURAL CHANGES TO MOTOR LEARNING AND PERFORMANCE

<sup>1</sup>Brian Cohn, <sup>3</sup>Kian Jalaeddini, and <sup>2,3</sup>Francisco J Valero-Cuevas

<sup>1</sup>Department of Computer Science, <sup>2</sup>Department of Biomedical Engineering, <sup>3</sup>Division of Biokinesiology and Physical Therapy. University of Southern California, Los Angeles, CA, USA.  
email: brian.cohn@usc.edu, web: <https://valerolab.org/>

## INTRODUCTION

There exist analytical formulations for the transmission of muscle force to endpoint force in tendon-driven limbs, and how it changes nonlinearly with posture [1]. However, how this information is encoded by the nervous system to control limbs remains unknown. The neuroscience literature proposes neural control based both on deterministic (e.g., internal models, optimal control, synergies, etc) and probabilistic (e.g., Bayesian) models of limb physics and environment. To evaluate the neuromechanical advantages of probabilistic control, we characterized the statistical structure of the transmission of muscle forces for multiple postures of a tendon-driven mechanical finger.

## METHODS

We firmly connected the index fingertip of a Utah/M.I.T hand [2] to a 6-DOF load cell to produce static forces (Fig 1). The load cell was affixed to the endpoint of an AdeptSix300 robot that was moved to change finger posture. Seven index finger tendons were actuated by DC brushless motors [3], routed through pulleys.

The robot moved the limb endpoint to 100 randomly selected endpoint postures on an arc (Fig 2). At each posture, the motors applied 100 force combinations across tendons uniformly at random (spanning 3 to 12N range). The duration of each trial was 0.8s— sufficient for forces to settle. We sampled fingertip and tendon forces at 1kHz.

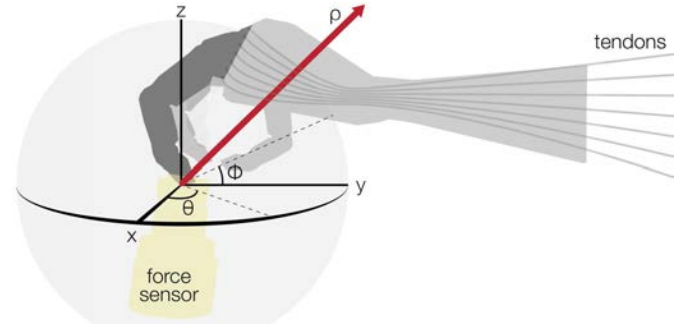


**Figure 1:** Forces at the tip of the mechanical finger were recorded as motors produced known tendon forces, at different postures. The resulting endpoint force vectors (red) were described in spherical coordinates ( $\rho$ ,  $\theta$ ,  $\phi$ ) in the common frame of reference of the fingertip and sensor.

We calculated the force steady-state of each trial by averaging the last 0.2s. For each posture, we identified the linear static  $3 \times 7$  model ( $A^i$ ) that transforms tendon tensions to endpoint forces using linear regression:

$$\begin{bmatrix} F_x^i(1) & F_y^i(1) & F_z^i(1) \\ \vdots & \ddots & \vdots \\ F_x^i(100) & F_y^i(100) & F_z^i(100) \end{bmatrix} = \begin{bmatrix} F_{m_1}^i(1) & \cdots & F_{m_7}^i(1) \\ \vdots & \ddots & \vdots \\ F_{m_1}^i(100) & \cdots & F_{m_7}^i(100) \end{bmatrix} A^i$$

$$A^i = \begin{bmatrix} a_{m_1,x}^i & a_{m_1,y}^i & a_{m_1,z}^i \\ \vdots & \vdots & \vdots \\ a_{m_7,x}^i & a_{m_7,y}^i & a_{m_7,z}^i \end{bmatrix} = [A_{m_1}^i \cdots A_{m_7}^i]^T$$

Note this mapping does not consider torques at the endpoint of the finger [1] and serves as a worst-case scenario for model performance.

## RESULTS AND DISCUSSION

For all individual postures, a linear model  $A^i$ , accurately predicted endpoint force as a function of tendon forces, (i.e., high percentage of variance-accounted-for, %VAF, Fig 2). In addition, the negligible residual error did not have a structure

across posture (Fig 2a).

As could be expected given the nonlinear changes in the finger's Jacobian [1], posture had a profound effect on the  $A^i$  matrices that map tension to endpoint force. Interestingly, the effect of posture in fingertip force strength ( $\rho$ , in N) and direction differed widely across muscles. While  $m_2$  had a consistent  $\rho$  across all postures,  $m_3$  had higher variability (Fig 3, left). As for direction,  $m_2$ 's direction in the  $zy$  plane ( $\phi$ ) was consistent across postures— $m_3$  was more variable (Fig 3, right).

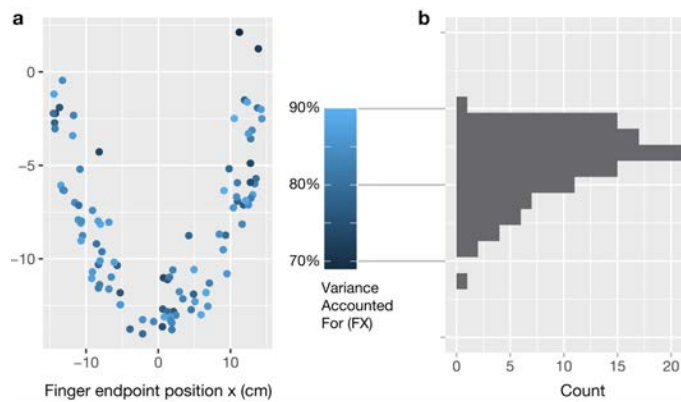


**Figure 2:** For each of 100 postures, the color in (a) represents how each  $A^i$  matrix predicts endpoint force in the  $x$  direction (FX), while (b) shows the performance histogram across all postures.

We conclude that linear models (i.e.,  $A^i$  matrices) do not perform uniformly well across postures. Yet

effective neural control of tendon driven limbs should work well across the workspace [4]. Interestingly, our results suggest small changes in posture can lead to large changes in the mechanical actions of muscles—therefore  $A^i$  matrices likely do not generalize well across regions of the workspace. We speculate that the full mechanical output of the limb should be considered (i.e., endpoint torque output), and that exploration of the full workspace is preferable as interpolation will likely not work. Thus, the mechanical structure of the tendinous apparatus can influence motor learning. Moreover, disruption of learning or recall of these mappings can easily lead to motor pathologies.

## REFERENCES

1. Valero-Cuevas, FJ. Fundamentals of neuromechanics. Vol. 8. Springer, 2015.
2. Jacobsen S, et al. *Proceedings of ICRA'86*, San Francisco, CA, USA, 1986.
3. Pigeon P, et al. *J. Biomech* 29, 1365-1370, 1996.
4. Inouye, J, and Valero-Cuevas FJ. *PLoS Comput Biol* 12.2 (2016): e1004737.

## ACKNOWLEDGMENTS

This project is supported by NIH NIAMS R01 AR050520 and R01 AR052345 to FVC.

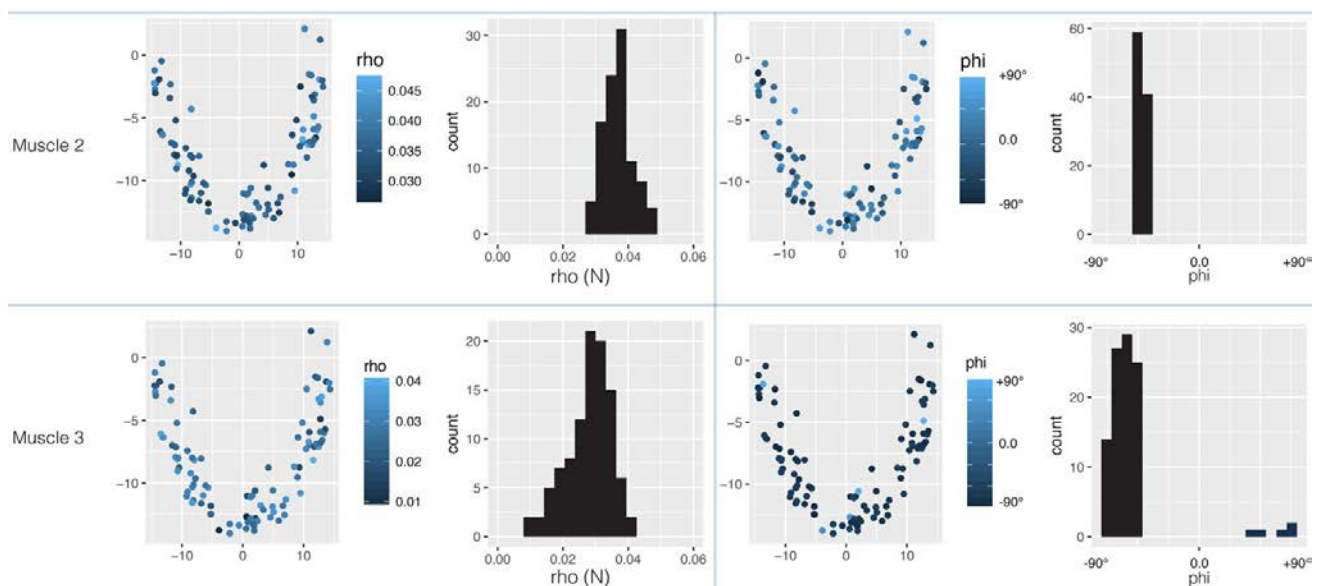


**Figure 3:**  $A^i$  has a vector of force for each muscle at each posture— $\rho$  represents the muscle's endpoint vector strength (N), and  $\phi$  is the angle in the  $F_z/F_y$  plane. This figure highlights 8 of the 42 visualizations.

# Reverse Engineering the Dynamics of Human Pursuit Strategies

<sup>1</sup>Dheepak Arumukhom Revi and <sup>1</sup>Manoj Srinivasan

<sup>1</sup>Mechanical and Aerospace Engineering, The Ohio State University

email: arumukhom-revi.1@osu.edu, srinivasan.88@osu.edu

## INTRODUCTION

Pursuit and evasion are behavioral traits in many animals and often determines the likelihood of its survival in the wild. While most modern humans do not explicitly have to hunt or evade predators, it maybe that, pursuit and evasion strategies were invaluable during our evolutionary past and may still be inherent in guiding our dynamics. Here, we perform human subject experiments to characterize the control strategies used by a human pursuer to intercept a human evader. Understanding the behavioral dynamics of pursuit or evasion can be useful in a wide range of applications, from sports planning, to missile guidance control.

Military airplanes and missiles have long been using intercepting (pursuit) and maneuvering (evasion) strategies on the battlefield. The three most common types of pursuit maneuvers an airplane pilot can do to catch a target are: pure pursuit<sup>2,3</sup>, where the velocity vector of pursuer ( $\vec{V}_p$ ) is always directly aligned towards evader's velocity vector ( $\vec{V}_e$ ); lead pursuit<sup>2</sup>, where the  $\vec{V}_p$  is always directly ahead of the  $\vec{V}_e$  and lag pursuit<sup>2</sup>, where the  $\vec{V}_p$  is always directly behind the evader's velocity vector  $\vec{V}_e$ . Other common pursuit strategy used in homing missiles is true proportional navigation<sup>1</sup>, where the pursuer acceleration ( $\vec{a}_p$ ) is normal to the vector from pursuer to evader ( $PE$ ) and is made proportional to the rotation rate of the vector  $PE$  ( $\dot{\theta}_{PE}$ ) and the pursuer speed ( $|\vec{V}_p|$ ). All of the described strategies are illustrated in figure 1.

## METHODS

We recruited nine pairs of human subjects (6 male pair and 3 female pair between the ages of 20 -25) and assigned either the role of the pursuer or the evader. Each pair participated in five pursuit-evasion scenarios, differing only in how the evader is allowed to move: moving in a straight line (protocol 1), a circle (protocol 4), or free-form (protocol 3), and

being able to change direction or not (when on a straight line (protocol 2) or circle (protocol 5)), as illustrated in figure 2. In all experiments both pursuer and the evader knew each other constrains.

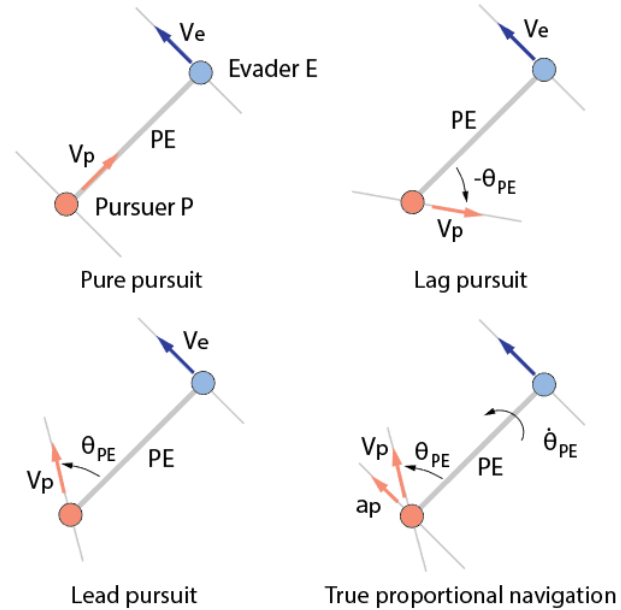


**Figure 1:** Intercept strategies that can be used by the pursuer during pursuit-evasion scenarios

For each of these protocols, we performed at least 10 trials, with the pursuer starting at different initial positions relative to the evader, presented to subjects in randomized order. In each trial, the pursuer is instructed to catch the evader as soon as possible, and the evader is instructed to avoid the pursuer for as long as possible. In all five protocols, the pursuer was allowed to move however they wished within room available. We used three video cameras to collect visual (video data) of the entire event from three different viewpoints. The raw data was processed using computer vision toolbox in Matlab to yield position data of the pursuer and the evader. We then computed the velocity and acceleration data using finite differencing, and smoothing the obtained derivatives to remove measurement noise. In total, each subject pair performed 102 or fewer trials, with an average number of trials at 78 trials and a standard deviation of 34 trials. Each trial on average was 2.6 sec with standard deviation of 1.2 sec.

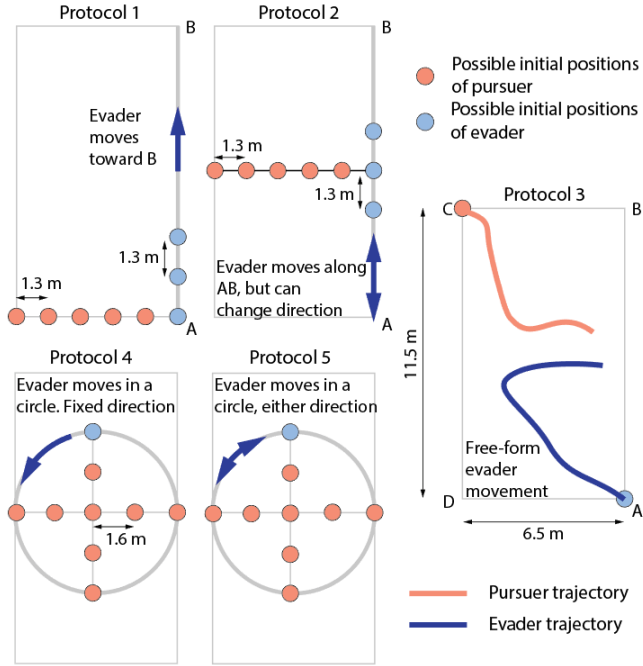


**Figure 2:** Five different protocols with possible starting conditions of both pursuer and evader.

## RESULTS AND DISCUSSION

If we imagine that the pursuer is performing either pure, lead or lag pursuit, we can then examine this strategy using the angle between the pursuer velocity vector ( $\vec{V}_p$ ) and PE vector ( $\theta_{PE}$ ).

$$\theta_{PE} = \sin^{-1} \left( \frac{|\vec{PE} \times \vec{V}_p|}{|\vec{PE}| |\vec{V}_p|} \right) \frac{|\vec{V}_p \times \vec{V}_e|}{|\vec{V}_p| |\vec{V}_e|}$$

Using table 1, we see that as we decrease the constraints applied on the evader, i.e. from being bound to a line (P1, P2) or circle (P4, P5) to freeform (P3) the median theta value decreases. This means that if you constrain the evader and therefore make the evader more predictable, the pursuer will choose a lead strategy. Likewise, if the evader is not constrained (less predictable), the pursuer will choose a lag strategy. A formulation of the true proportional navigation strategy was poor at explaining the pursuer dynamics.

To explain the pursuer dynamics (i.e. pursuer speed ( $V_p$ ) and relative heading angle ( $\theta_{PE}$ )) we formulated

**Table 1:** Theta angle and  $R^2$  values of prescribed models

	Protocol 1	Protocol 2	Protocol 3	Protocol 4	Protocol 5
Theta Angle ( $^\circ$ )	$25.3 \pm 25.5$	$8.6 \pm 20.9$	$-3.0 \pm 23.1$	$22.0 \pm 26.7$	$19.0 \pm 28.3$
$R^2$ for pursuer speed model	0.630	0.352	0.345	0.436	0.307
$R^2$ for pursuer heading model	0.631	0.445	0.424	0.572	0.496

a model of the pursuer based on the motion of the evader (i.e. evader speed ( $V_e$ ) and evader relative heading angle ( $\beta_{PE}$ )) and the relative distance between the pursuer-evader ( $PE$ ).

$$V_p = \lambda_1 V_e + \lambda_2 PE + \lambda_3 PE^2 + \lambda_4$$

$$\theta_{PE} = \lambda_5 V_e + \lambda_6 PE + \lambda_7 \beta_{PE} + \lambda_8$$

where  $\lambda_1 \dots \lambda_8$  are constant coefficients.

The model when tested against the experimental data, yield  $R^2$  values as high as 0.631 (Protocol 1) and as low as 0.307 (Protocol 5). Higher order models with more terms and building models using a symbolic regression algorithm<sup>4</sup> yield a slightly better fit (with  $R^2$  at most increased by 0.156), but none of model is simple enough for the improvements in  $R^2$ .

## CONCLUSIONS

In conclusion, we have experimentally characterized the strategies used by humans in pursuing an evading target and compared our experimental data with few pursuit strategies. During pursuit, people use a combination of pure, lead and lag strategy to catch an evading target. The degree of this lead or lag pursuit versus pure pursuit seems to be based on how constrained or predictable the evader's motion is. We found that a simple model that depended linearly on evader speed and quadratic on the pursuer-evader distance explained at worst 31% and at best 63% of the variance in the pursuer speed. We also found that modeling the relative pursuer angle using a simple model that depended linearly on evader speed, pursuer-evader distance and relative evader angle explained at worst 42% and at best 63% of the variance in pursuer angle, depending on evader motion constraints.

## REFERENCES

- <sup>1</sup> D. Ghose. *National Programme on Technology Enhanced Learning*, online, 2012.
- <sup>2</sup> E. Lynch. *SimHQ*, online, 1998.
- <sup>3</sup> P. J. Nahin. *Princeton University Press*, Princeton, 2012
- <sup>4</sup> Searson, A.H. Gandomi et al., (Eds.), *Springer*, New York, NY, 2015.

# PREDICTION OF MUSCLE ACTIVATIONS FOR REACHING MOVEMENTS USING DEEP NEURAL NETWORKS

Najeeb Khan and Ian Stavness

University of Saskatchewan, Saskatoon, SK, Canada  
email: [ian.stavness@usask.ca](mailto:ian.stavness@usask.ca), web: <http://biglab.ca/>

## INTRODUCTION

The motor control problem involves determining the time-varying muscle activation trajectories required to accomplish a given movement. Muscle redundancy makes motor control a challenging task: there are many possible activation trajectories that accomplish the same movement. Despite this redundancy, most movements are accomplished in highly stereotypical ways. For example, point-to-point reaching movements are almost universally performed with very similar smooth trajectories [1].

Optimization methods are commonly used to predict muscle forces for measured movements [2]. However, these approaches require computationally expensive simulations and are sensitive to the chosen optimality criteria and regularization. Linear dimensionality reduction has also been proposed to identify low-dimensional motor modules that can account for stereotyped movements [3]. However, musculoskeletal systems are highly non-linear, making linear methods less reliable.

Deep neural networks (DNNs) are biologically inspired models that can be employed for non-linear dimensionality reduction. Deep autoencoders are DNN models that can automatically learn successively low dimensional features by transforming the input data through different layers of non-linearity. DNNs have been used to predict torque trajectories from initial and final state information in [4]. However, DNNs have yet to be applied to predict time varying muscle activations, in which the redundancy problem exists.

In this work, we investigate deep autoencoders for the prediction of muscle activation trajectories for point-to-point reaching movements. We evaluate our DNN predictions with simulated reaches and two methods to generate the muscle activations:

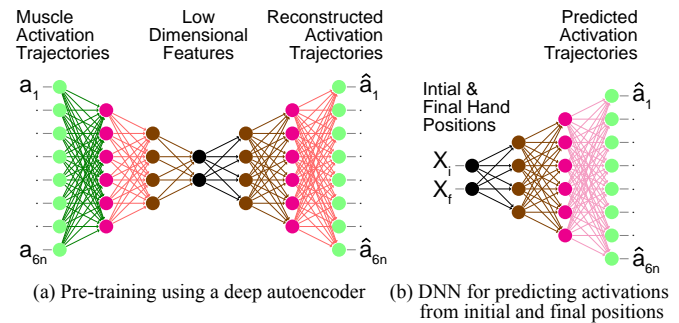


**Figure 1:** A deep autoencoder is trained to learn low-dimensional features that are used to map initial and final hand positions to muscle activations.

inverse dynamics (ID) and optimal control (OC) criteria. We also investigate optimal network parameters and training criteria to improve the accuracy of the predictions.

## METHODS

*Simulated reaches:* Random initial points for the end-effector of a two-link, six-muscle arm [5] were uniformly sampled in a 50 cm x 20 cm rectangular region in the hand-space. A random direction was chosen for each initial point and a final point for the reaching movement was uniformly selected in that direction within 10 cm. The data set consisted of 4500 pairs of initial/final points for training and 500 pairs for testing.

*Inverse Dynamics:* The initial and final points were connected by a time sampled minimum-jerk trajectory with a duration of 1 second. A sampling rate of 50 samples per second was used for sampling the min-jerk path. For each of the points in the minimum-jerk trajectory a torque control vector was calculated by using inverse kinematics and inverse dynamics of the arm model. 300-dimensional muscle activations for the six muscles were computed by minimizing the quadratic norm of the activations under the target torque constraint.

**Optimal Control:** For each pair of initial/final points, 50-dimensional torque control signals were generated for each joint using the iterative Linear-Quadratic-Gaussian (iLQG) method [5]. Muscle activations were computed using static optimization with a quadratic cost.

**Network Training:** For each control type, we trained an autoencoder with layer dimensions 300-150-50-4-50-150-300 (Figure 1a). Layer-wise pre-training [6] was used to train the network with the muscle activation trajectories as the inputs and outputs. The decoder part of the autoencoder (Figure 1b) with dimensions 4-50-150-300 was then retrained on the inputs as the initial/final end-effector positions, and outputs as the muscle activations. Both the networks were trained by minimizing the cross-entropy loss between predicted and desired output using the conjugate gradient descent method.

## RESULTS AND DISCUSSION

Muscle activations predicted with the DNN matched well with the actual trajectories for both the ID and OC conditions (Figure 2). RMS error in the activation trajectories was 0.0048 and 0.0067 for the ID and OC reaches, respectively.

Simulated hand trajectories, when the arm model is driven with DNN-predicted muscle activations, also matched well with the original hand trajectories (Figure 3). The average error in reaching the target was 0.125 cm and 0.127 cm for the ID and OC reaches, respectively.

Previously, DNNs for predicting joint torques used mean squared error (MSE) as the training criteria and canonical optimization for minimization [4]. We found that using cross entropy loss instead of MSE as the training criteria and using conjugate gradient descent for minimization with mini-batch training outperformed [4]. Even with the problem extended from torques to activations, our predictions resulted in an average endpoint error of 0.127 cm, whereas [4] reported an endpoint error of 0.347 cm. Also, we performed a comprehensive evaluation of our methods and reported our results with 500 samples as compared to only 14 in [4].

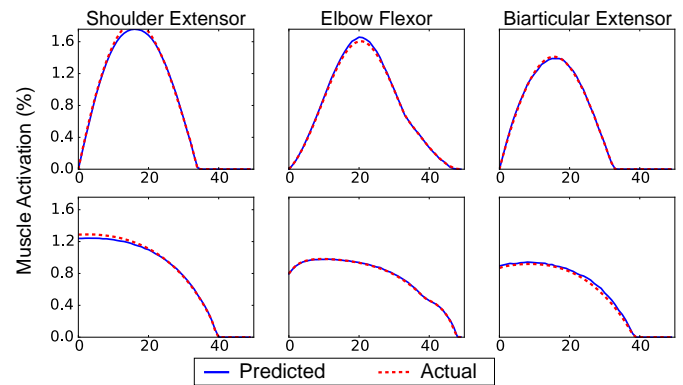


**Figure 2:** DNN predicted activations for 3 muscles for a reaching movement generated by inverse-dynamics (top) and optimal control (bottom).

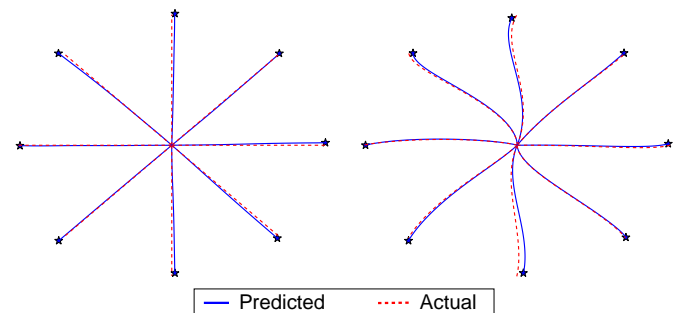


**Figure 3:** Hand trajectories (from center outward) driven by DNN predicted activations for inverse-dynamics (left) and optimal control (right).

## SUMMARY

In this study, we demonstrated that with proper learning criteria and training methods, DNNs can accurately generate simulated muscle-driven reaches with both inverse-dynamics and optimal control based activation trajectories. Our work provides a proof of concept that DNNs can be used for more complex biomechanical models. As future work, we plan to investigate recurrent neural networks to model variable duration reaches.

## REFERENCES

1. Sabes, *CO in Neurobio* **10.6**, 740-746, 2000.
2. Erdemir et al. *Clin Biomech*, **22(2)**, 131-54, 2007.
3. Ting et al. *CO in Neurobio* **17.6**, 622-628, 2007.
4. Berniker et al. *Front in Comp Neurosci* **9** 2015.
5. Todorov et al. *IEEE Am Control Conf*, 2005.
6. Bengio, Y, et al. *NIPS* **19**, 153, 2007.

# Hand-object Kinematics and Gaze Fixation During Bimanual Tasks

Alireza Haji Fathaliyan, Xiaoyu Wang, Sahn Bazargan, and Veronica J. Santos

University of California, Los Angeles, CA, USA

e-mail: [vjsantos@ucla.edu](mailto:vjsantos@ucla.edu) web: <http://BiomechatronicsLab.ucla.edu>

## INTRODUCTION

Many activities of daily living (ADL) involve bimanual tasks. Eye gaze fixations play a large role in gathering visual cues for successful task completion [1]. Prior research on coordination of upper extremities and eye gaze has been reported (e.g. [2]). However, much of this work has focused on unimanual grasp and manipulation. Many daily tasks involve bimanual grasping and bilateral manipulation which is the focus of this study. Few studies have precisely located gaze direction in 3D space or used pupillometry to parameterize the subject's attention shifts during daily tasks (e.g. [3]). The objective of this study is to investigate human hand-eye coordination and vision-based predictors of human intent by quantifying and characterizing spatiotemporal relationships between left- and right-hand palm positions and orientations, hand-object orientation, gaze fixation, and upper limb joint angles in bimanual tasks. The long term goals of this work are to identify kinematic and gaze-based indicators of human intent, and to identify underlying principles of bimanual manipulation.

## METHODS

According to a protocol approved by the UCLA Institutional Review Board, each subject is instructed to perform four bimanual tasks involving everyday objects and actions: lifting, opening, closing, screwing, unscrewing, stirring, scooping, pouring. Objects were selected from the benchmark Yale-CMU-Berkeley (YCB) Object Set: mug, pitcher, spoon, soft scrub bottle, coffee can, sponge, windex spray bottle. Each task is repeated four times; subjects were instructed to narrate their actions during two randomly chosen trials for a parallel study relating action to natural language.

Six T-Series cameras (Vicon, Culver City, CA) are used to track the motion of the objects and subjects' shoulders, upper arms, forearms, and palms (Figure 1). Object and palm kinematics are tracked so that hand-hand and hand-object interactions can be quantified. Subjects are instructed to wear an ETL-500 binocular, head-mounted eye tracker (ISCAN, Inc., Woburn, MA) that tracks subjects' point of regard (POR), pupil dilation, and saccades. 3D gaze vectors are reconstructed from the eye tracker data and combined with YCB object point clouds to produce 3D saliency maps for each object and task.



**Figure 1:** Experimental set-up with motion capture cameras, YCB objects, and subject wearing retro-reflective markers and an eye tracker.

## RESULTS AND DISCUSSION

Preliminary results are shown for the task of making a cup of instant coffee. Data collection for the present study is ongoing, and so data from a single representative subject (female, 23 yrs) are discussed here. Figure 2 shows a subject's point of regard overlaid on a screenshot from the head-mounted eye tracker webcam. In one experimental condition, the subject was instructed to remove the lid of a pitcher, transfer some of the liquid contents of the pitcher to a mug using a spoon, and then to pour from the pitcher into the mug. As expected, the subject fixated on different objects in the scene (pitcher in Fig. 2a, spoon in Fig. 2b), depending on the subtask. As we hypothesized based on a 2D gaze fixation

study [4], the subject fixated on different regions of the same object depending on the task. For instance, the subject fixated on the pitcher lid when the subtask was to remove the lid from the pitcher (Fig. 2a), but fixated on the pitcher spout when the subtask was to pour from the pitcher (Fig. 2c). Interestingly, it was noted that the subject repetitively alternated between the spout of the pitcher and the mug (Fig. 2c,d) during the pouring action.

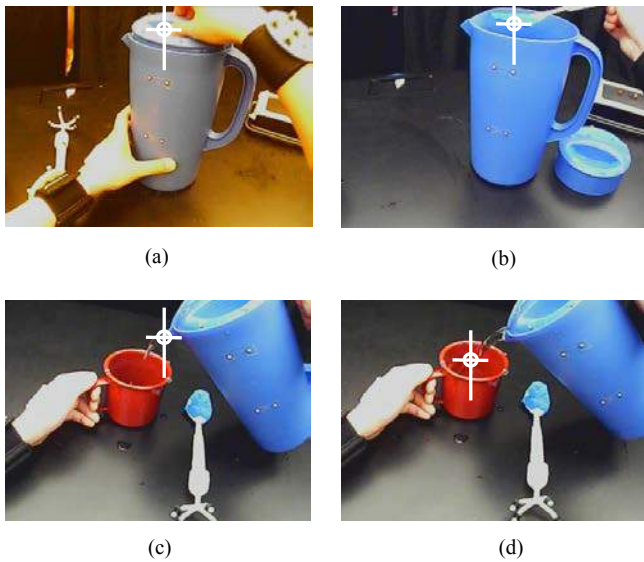


**Figure 2:** The subject's visual point of regard (white cross) is shown on objects during (a) removal of a pitcher lid, (b) transfer of a liquid via spoon, and (c,d) pouring of a liquid from a pitcher to a mug.

Figure 3 shows a subject's pupil area during the subtask of pouring from a pitcher to a mug. The color coded trajectory shows that the subject alternates between fixating on the pitcher and the mug as the liquid is carefully poured from one container to the other. Insets of 3D saliency maps show more specifically where the subject was looking (pitcher spout, inner surface of mug) and for how long (integrated over the pouring period).

Pupil dilation is an indicator of visual detection and attention shift. The saccades shown in Figure 3 occur either as the subject's attention shifts to a new object or to a different location on the same object. Pupil area increases prior to all saccades, which indicates the need for visual cues to proceed to next action such as: location of action-relevant objects

and their geometry features required for motor preparation [5].

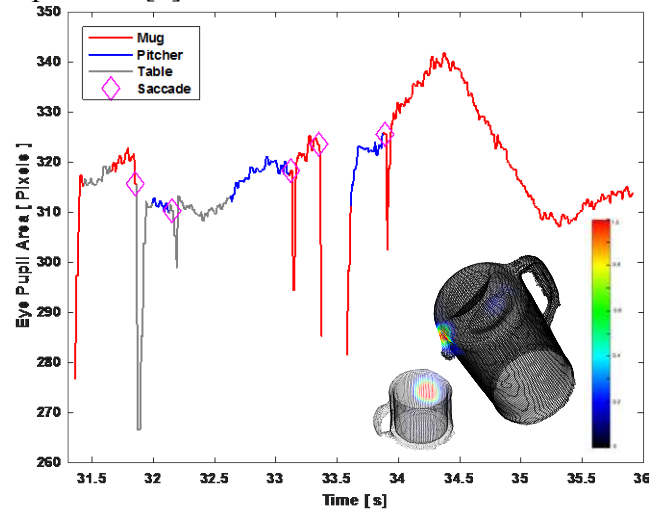


**Figure 3:** A subject's pupil area is shown for the subtask of pouring. Different colors of the trajectory indicate whether the object of interest is the pitcher (blue) or mug (red). Magenta diamonds indicate saccades. 3D saliency maps indicate gaze fixation on the pitcher spout and inner surface of the mug.

Future work includes the completion of data collection, kinematic analyses of hand-hand and hand-object interactions, and the creation of population-based 3D saliency maps. 3D gaze fixation information, specifically which features of different objects are of interest, could be used to infer human intent. Inference of human intent could reduce the cognitive burden on teleoperators of complex robotic systems, and improve human-robot collaborations in the home, on the manufacturing line, or in high-risk environments.

## REFERENCES

- [1] M. Land, et al. *Perception*, vol. 28, no. 11, pp. 1311–1328, Nov. 1999.
- [2] R. S. Johansson, et al. *J. Neurosci.*, vol. 21, no. 17, pp. 6917–6932, 2001.
- [3] B. Laeng, et al. *Perspect. Psychol. Sci.*, vol. 7, no. 1, pp. 18–27, Jan. 2012.
- [4] A. Belardinelli, et al. *Vision Res.*, vol. 106, pp. 47–57, Jan. 2015.
- [5] S. Jainta, et al. *Front. Hum. Neurosci.*, vol. 5, 2011.

# RELATIONSHIP BETWEEN RESIDUAL FORCE ENHANCEMENT AND MUSCLE FATIGUE

<sup>1,2,3</sup> Atsuki Fukutani, <sup>1</sup> Walter Herzog

<sup>1</sup> The University of Calgary, AB, Canada

<sup>2</sup> Japan Society for the Promotion of Science, Tokyo, Japan

<sup>3</sup> Ritsumeikan University, Shiga, Japan

email: atsukifukutani@gmail.com

## INTRODUCTION

The steady-state, isometric muscle force attained after active stretch is larger than that attained in a purely isometric contraction at the corresponding muscle length. This property of skeletal muscle is referred to as residual force enhancement (RFE). At present, a primary factor thought to contribute to RFE is the modulation of titin elasticity by  $\text{Ca}^{2+}$  release and active stretch [1]. Muscle fatigue is associated with a decreasing force generating capability of muscle [2], possibly caused by a decreasing proportion of attached cross bridges and/or changes in the cross bridge kinetics.

Considering that RFE may be caused by a titin-based passive force, and is independent of the proportion of attached cross bridges, RFE may be preserved in muscle fatigue despite a decrease in force generating potential. We evaluated the magnitude of residual force enhancement in the non-fatigued and fatigued states, and hypothesized that the absolute magnitude of RFE is preserved in fatigue, and thus, the relative amount of RFE (normalized to the isometric reference force) is increased in fatigued compared to non-fatigued muscles.

## METHODS

Skinned fibers of rabbit psoas muscle (N=45) were used for all testing. Three experimental conditions were evaluated. For the first condition (N=15), muscle fatigue was mimicked by a low  $\text{Ca}^{2+}$  concentration (pCa6.0). For the second condition (N=15), muscle fatigue was produced using a low pH (pH6.0) level. For the third condition (N=15), muscle fatigue was induced by adding 20mM butanedione monoxime (BDM) to the activating solution. Typical examples of the experimental trials are shown in Figure 1. In the non-fatigued (Normal, upper panel

Figure 1) and fatigued (Fatigue, lower panel Figure 1) state, RFE trial (blue line) and Control trial (orange line) were conducted. The Normal state was always tested first. In the RFE trial, fibres were actively stretched from an average sarcomere length of 2.4  $\mu\text{m}$  to 3.0  $\mu\text{m}$  in 2 s. The isometric muscle force attained 15 s after the end of active stretching was used for analysis. Then, the control trial was conducted. Fibers were passively stretched from an average sarcomere length of 2.4  $\mu\text{m}$  to 3.0  $\mu\text{m}$  in 2 s. Then, fibers were activated isometrically at this length. This purely isometric force was used for analysis. After that, identical trials were conducted in the Fatigue state. The absolute magnitude of RFE was calculated by subtracting isometric force of the Control trial from that of the RFE trial. The relative RFE was obtained by expressing the absolute RFE as a percentage of the isometric Control force.

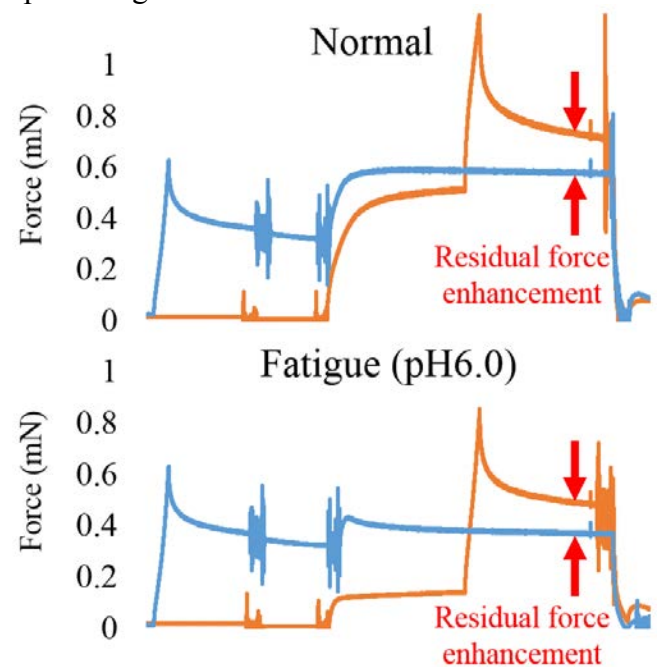


**Figure 1:** Example of force responses in the Normal (upper panel) and Fatigue states (lower panel). Blue traces represent Control trials and orange traces represent RFE trials.

## RESULTS AND DISCUSSION

Isometric muscle forces at 2.4  $\mu\text{m}$  in the Fatigue states were smaller by  $76 \pm 14\%$  for pCa6.0,  $54 \pm 7\%$  for pH6.0, and  $62 \pm 12\%$  for BDM20mM compared to those in the Normal states. These results indicate that we successfully reduced muscle forces, thereby mimicking Fatigue.

The absolute value for RFE was similar for Normal and Fatigue states using pH6.0 and BDM20mM. The relative value for RFE for these two conditions was significantly greater than that obtained for the Normal condition. For the pCa6.0 condition, the absolute and relative RFE were greater than the corresponding Normal values (Figure 2). The increase in absolute RFE in pCa6.0 compared to Normal cannot be explained with an increase in the proportion of attached cross-bridges, but might be caused by an increase in passive forces contributed by structural proteins, such as titin.

In the pCa6.0 condition, the decrease in force compared to the Normal conditions is caused by a decrease in the number of attached cross bridges without major effects on the cross bridge kinetics, which is similar to what happens in central fatigue. In contrast, in the low pH and BDM conditions, a

decrease in muscle force is caused primarily by changes to the cross bridge kinetics, which is similar to what is observed in peripheral fatigue. Thus, our findings may be transferable to the physiological conditions of central and peripheral fatigue.

## CONCLUSIONS

The absolute RFE in all fatigue states was similar to that in the non-fatigued muscle. This finding suggests that RFE may prevent excessive loss of force in fatigued muscles that undergo active stretching.

## REFERENCES

1. Herzog W, et al. *Physiology (Bethesda)* **31** 300-312, 2016.
2. Enoka and Duchateau. *Med Sci Sports Exerc* **48**, 2228-2238, 2016.

## ACKNOWLEDGMENTS

This study was partly supported by the Grant-in-Aid for Challenging Exploratory Research (16K13009) and Postdoctoral Fellowship for Research Abroad (183), CIHR, NSERC of Canada, The Canada Research Chair Programme and the Killam Foundation.

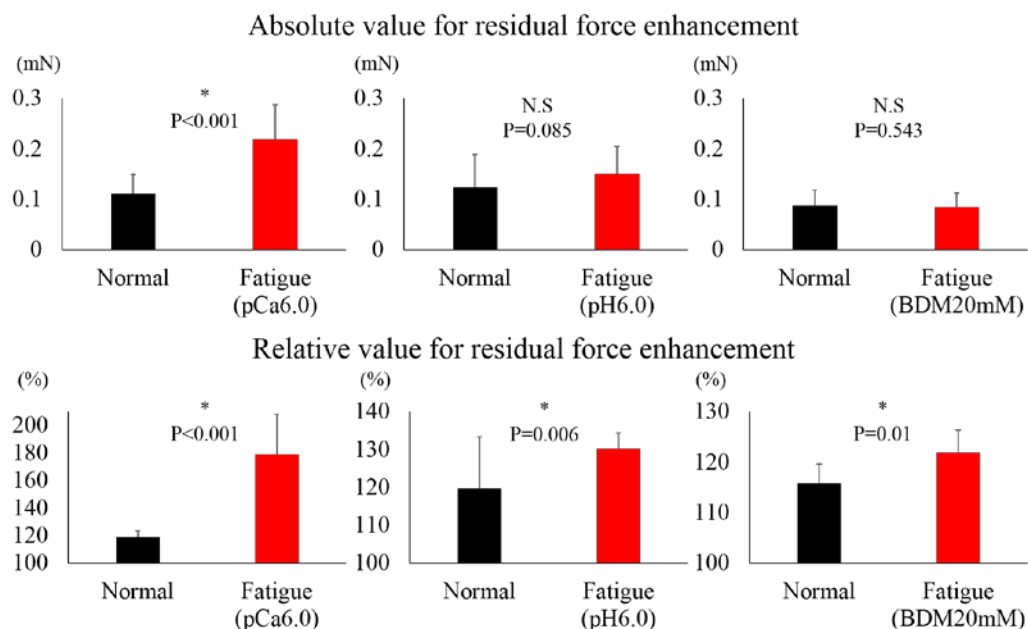


**Figure 2:** The magnitude of residual force enhancement in the Normal and Fatigue states calculated as the absolute RFE (upper panel) and the relative RFE (lower panel).

# RELATIONSHIP BETWEEN YOUNG'S MODULUS, SHEAR MODULUS, AND VISCOSITY IN HEALTHY ACHILLES TENDON

<sup>1</sup> Jennifer A. Zellers, <sup>1</sup> Phoebe Balascio, <sup>1</sup> Patrick Corrigan, <sup>2</sup> Daniel H. Cortes, and <sup>1</sup> Karin Grävare Silbernagel

<sup>1</sup> University of Delaware, Newark, DE, USA

<sup>2</sup> The Pennsylvania State University, University Park, PA, USA

email: jzellers@udel.edu

## INTRODUCTION

Tendon mechanical properties have been of great interest as a measure of tendon structure. In the context of tendon injury, animal studies investigating outcomes following Achilles tendon rupture have found tendon mechanical properties to be responsive to treatment strategy as well as levels of weight-bearing [1]. Quantification of tendon mechanical properties has presented a unique set of challenges, however. While methods involving voluntary contraction have been used to measure Young's modulus *in vivo*, the application of these techniques to an injured population has limitations. Specifically, decreased volitional recruitment of the triceps surae in comparison to the plantar flexors of the deep compartment of the lower leg may result in an overestimation of stress using these methodologies.

Continuous shear wave elastography is a non-invasive method to measure tendon shear modulus and viscosity that does not rely on voluntary contraction [2]. While this technique has been applied to injured tendons [2, 3] the relationship between tendon shear modulus and viscosity compared to *in vivo* methods of measuring Young's modulus has not been described. Therefore, the purpose of this study is to establish the relationship between tendon shear modulus and viscosity measured using cSWE, with Young's modulus.

## METHODS

Participants with healthy Achilles tendons were included in this study. Participants were excluded if they had recent Achilles tendon pain or signs of midportion tendinosis on B-mode ultrasound imaging. Participant's activity level was measured using the Physical Activity Scale [4]. Leg dominance

was determined as the participant's self-reported "kicking" leg. Only right lower extremities were examined.

Shear modulus and viscosity was measured using cSWE as previously described [2]. Strain was measured by measuring the peak displacement of the gastrocnemius myotendinous junction during an isometric contraction using B-mode ultrasound imaging. Stress was simultaneously measured using a KinCom dynamometer. For both cSWE, stress, and strain measurements, the subject was positioned in prone with the foot in four different angles – 20 degrees of plantar flexion, 10 degrees of plantar flexion, neutral (0 degrees of plantar flexion), and 10 degrees of dorsiflexion (-10). The position order was randomized for each participant, and participants were given a 2-minute walking break between positions. Tendon length was measured using extended field of view B-mode ultrasound imaging with the foot in a resting position. Tendon cross-sectional area was measured using B-mode ultrasound imaging with the Achilles tendon in short axis, at a point immediately distal to the soleus myotendinous junction. For all tendon mechanical property and B-mode measurements, the average of 3 trials was used in data analysis. Tendon moment arm was measured using a tape measure from the midpoint of the lateral malleolus to the most superficial aspect of the Achilles tendon.

Young's modulus was calculated as follows:

$$\left( \left( \frac{\tau}{MA} \right) (Lo) \right) / (A\Delta L)$$

Where  $\tau$  is peak torque,  $MA$  is moment arm,  $Lo$  is tendon length from the calcaneal notch to the gastrocnemius myotendinous junction,  $A$  is cross-

sectional area, and  $\Delta L$  is the peak displacement of the gastrocnemius myotendinous junction.

Descriptive statistics were performed for all variables of interest. Pearson correlation analysis was used to determine the strength of the relationship between properties.

## RESULTS AND DISCUSSION

Five subjects are included in this preliminary analysis. Participants were a mean(SD) age of 20(1) years, weighed 58.4(9.6)kg and were a height of 1.66(0.08)m. Participant's activity level ranged from 4-6 on the 6-point Physical Activity Scale. The right lower extremity was the dominant leg in 4 participants. Mean(SD) Achilles tendon length to the gastrocnemius was 18.4(2.5)cm. Descriptive statistics for shear modulus, viscosity, and Young's modulus are listed in Table 1. A significant correlation was observed between viscosity and Young's modulus ( $R = 0.986$ ,  $p = 0.014$ ) as well as between shear modulus and Young's modulus (Figure 1).

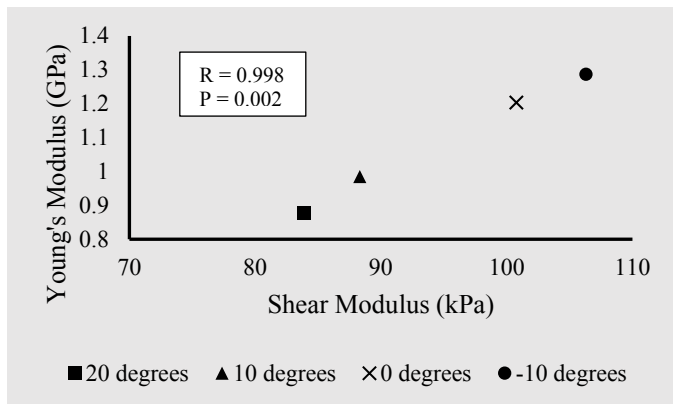


**Figure 1:** Relationship between shear modulus (kPa) and Young's modulus (GPa) at 4 foot angles.

## CONCLUSIONS

The results of this study suggest that mechanical properties quantified using cSWE are strongly related to *in vivo* measurements of Young's modulus in healthy Achilles tendons. The findings of this study support the use of cSWE as an alternative measure that does not require a voluntary contraction of the triceps surae, which may be of interest when examining tendon healing in populations where muscle recruitment may be altered. The results of this study are limited by the small number of subjects.

## REFERENCES

1. Freedman BR, et al. *J Ortho Res* **34**, 2172-2180, 2016.
2. Cortes DH, et al. *Ultrasound in Med & Biol* **41**, 1518-1529, 2015.
3. Zellers JA, et al. *Int J Sports Phys Ther* **11**, 1150-1159, 2016.
4. Grimby G. *Acta Med Scand* **711**, 233-237, 1986.

## ACKNOWLEDGMENTS

Research reported in this publication was supported by the National Institutes of Health under Award numbers P30-GM103333 and R21AR067390, the Foundation for Physical Therapy and the University of Delaware Research Foundation

**Table 1:** Tendon Mechanical Properties at Varying Foot Angles.

Mechanical Property	Foot Angle			
	20 degrees	10 degrees	0 degrees	-10 degrees
Shear Modulus (kPa)	83.9 ± 8.0	88.3 ± 7.1	100.8 ± 14.1	106.3 ± 16.3
Viscosity (Pa*s)	27.7 ± 5.5	31.5 ± 8.2	39.6 ± 3.3	39.8 ± 8.9
Young's Modulus (GPa)	0.877 ± 0.456	0.985 ± 0.418	1.204 ± 0.736	1.287 ± 0.341

# SHEAR WAVE ELASTOGRAPHY OF EXERCISE-TRAINED HAMSTRING MUSCLES

<sup>1</sup> Sarah Eby, <sup>2</sup> Stephen Wisniewski, <sup>2</sup> Kristin Zhao

<sup>1</sup> Mayo Clinic Medical Scientist Training Program, Rochester, MN, USA

<sup>2</sup> Department of Physical Medicine and Rehabilitation, Mayo Clinic, Rochester, MN, USA

email: eby.sarah@mayo.edu

## INTRODUCTION

Exercise-trained skeletal muscle shows a variety of adaptations when compared to sedentary muscle, including reduced active musculotendinous stiffness coupled with increased passive stiffness, and increased collagen turnover [1-3]. These tissue responses to mechanical stress undoubtedly protect muscle from the high demands of physical activity, though injuries still occur, leading to acute changes in stiffness and strength [4].

Shear wave elastography (SWE) is a quantitative and reliable measure of skeletal muscle stiffness [5,6], with notable applications in pediatric populations, aging, and a variety of pathologies. Despite its significant potential, SWE has yet to be utilized in sports medicine applications.

The purpose of this study was to establish baseline shear modulus values for healthy, exercise-trained hamstring muscles throughout normal range of motion.

## METHODS

27 healthy, exercise-trained individuals (11 males) participated in this study. The mean age was 32.3 years (range: 13-57 years). Inclusion criteria were: 1) healthy individuals over 13 years of age; 2) normal function of both legs; 3) at least 30 minutes of moderate to vigorous exercise at least 3 days per week. Exclusion criteria were history of: 1) hamstring muscle injury; 2) neuromuscular disease or stroke; 3) leg, ankle, or foot surgery; 4) statin medication within the past 6 months. All study procedures were approved by the Mayo Clinic Institutional Review Board (Rochester, MN). Prior to testing, all subjects completed a questionnaire

that included basic demographic information, as well as exercise frequency, intensity, and mode.

We collected SWE images of the biceps femoris long head and semitendinosus while subjects were in side-lying position with the hips flexed to 90° and the knee of the testing leg flexed 80°, 60°, and 30°. We acquired all ultrasound images using the SL10-2 linear array transducer on the Aixplorer (Supersonic Imagine, Aix-en-Provence, France) in SWE mode. Images were collected with the ultrasound transducer oriented parallel with the long axis of the muscle, using liberal coupling gel, and minimal pressure on the skin surface. Surface electromyography confirmed the muscles were relaxed throughout testing. Three SWE images were collected at each location for the three knee angles bilaterally, for a total of 36 SWE images per subject.

SWE images were analyzed in OsiriX (Pixmeo, Geneva, Switzerland) to obtain Young's modulus values for the largest possible high-quality region of interest (ROI) for each image (mean (SD) area: 204.2 mm<sup>2</sup> (3.24)). As muscle is anisotropic, we manually converted the mean Young's modulus ( $E$ ) values for each ROI back to shear modulus ( $G$ ) using Eq (1):

$$G = \frac{E}{2(1+\nu)} \quad (1)$$

where  $G$  is shear modulus,  $E$  is Young's modulus, and where Poisson's ratio,  $\nu$  is very close to 0.5 if we assume the tissue is incompressible. For statistical analysis, we used the median shear modulus value from the set of three images at each knee angle.

We used a full-factorial repeated measures ANOVA (JMP, SAS Institute, Inc., Cary, USA) using sex and exercise frequency as within-subjects factors; muscle and knee angle were between-subjects factors; shear modulus was the response variable.

## RESULTS AND DISCUSSION

Of the 27 subjects, 9 self-reported exercising at a vigorous intensity 3-4 times per week; 18 reported participating in such activities 5 or more times per week. Mean biceps femoris shear modulus values by decade are provided in Table 1.

Full-factorial repeated measures analysis revealed a significant effect for knee angle; Tukey post-hoc analyses found shear modulus values for each knee angle were significantly different. We also found a

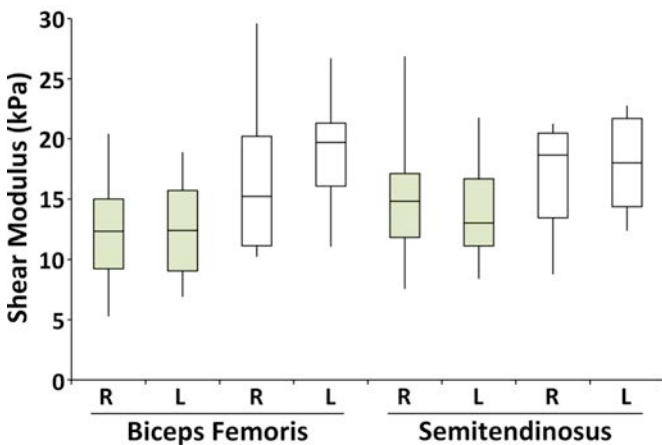


**Figure 1:** Shear modulus values for 30° knee flexion. Green indicates subgroup exercising 5 times or more per week; white indicates subgroup exercising 3-4 times per week. R: right leg; L: left leg.

**Table 1.** Shear modulus values for biceps femoris across age groups. Shear modulus given in kPa, displayed as mean (standard deviation). *n*: number of subjects in each age group; R: right leg; L: left leg.

Ages	<i>n</i> (males)	80° knee flexion		60° knee flexion		30° knee flexion	
		R	L	R	L	R	L
13-19	4 (0)	5.8 (1.8)	5.7 (1.3)	8.3 (1.8)	7.0 (1.4)	12.5 (2.8)	13.3 (3.6)
20-29	9 (4)	5.2 (1.1)	5.7 (1.4)	6.9 (2.0)	7.6 (1.2)	13.4 (3.7)	14.3 (4.4)
30-39	6 (2)	5.3 (1.5)	5.0 (0.9)	8.2 (2.7)	7.7 (1.8)	14.8 (7.7)	16.5 (6.5)
40-49	4 (3)	5.4 (1.4)	5.5 (1.5)	7.7 (1.9)	8.7 (2.1)	15.0 (4.8)	16.3 (2.8)
50-59	4 (2)	5.4 (2.3)	5.0 (1.1)	7.2 (2.5)	6.5 (1.1)	12.1 (5.0)	11.7 (3.0)

significant interaction for exercise frequency and knee angle, with significantly lower shear modulus values at 30° knee flexion for the more frequent exercise group when compared to those exercising 3-4 times per week. Mean shear modulus values by exercise group are shown in Figure 1.

## CONCLUSIONS

As expected, shear modulus varied significantly with knee angle. The most notable study population differences emerged at greater muscle lengths, as with previous investigations of SWE [7].

Study limitations include a relatively small sample size of subjects across a range of ages, with a variety of training regimens.

SWE demonstrates significant potential for evaluating exercise-trained skeletal muscle. Further work should evaluate shear modulus response to a variety of modalities, including stretch, endurance, and strength training, as well as response to injury.

## REFERENCES

1. Fouré A, et al. *Eur J Appl Physiol* **111**, 539-48, 2011.
2. Ducomps C, et al. *Acta Physiol Scand* **178**, 215-4, 2003.
3. Gosselin LE, et al. *J Appl Physiol* **85**, 1011-6, 1998.
4. Howell JN, et al. *J Physiol* **464**, 183-96, 1993.
5. Leong HT, et al. *PLoS ONE* **8**, e67199, 2013.
6. Gennisson JL, et al. *J Biomech* **38**, 1543-50, 2005.
7. Eby SF, et al. *Clin Biomech* **30**, 22-7, 2015.

# Shortening-induced force depression is modulated in a time- and speed-dependent manner following a stretch-shortening cycle

<sup>1</sup> Rafael Fortuna, <sup>2</sup> Martin Groeber, <sup>2</sup> Wolfgang Seiberl, <sup>3</sup> Geoffrey A. Power, and <sup>1</sup> Walter Herzog

<sup>1</sup> Human Performance Laboratory, University of Calgary, Alberta, Canada

<sup>2</sup> Technische Universität München, Germany

<sup>3</sup> University of Guelph, Ontario, Canada

## INTRODUCTION

Steady-state isometric force following an active shortening or lengthening contraction is smaller (force depression; FD) or greater (residual force enhancement; RFE) compared to a purely isometric contraction at the corresponding muscle length and same level of activation<sup>1</sup>. Despite muscles undergoing stretch-shortening cycles (SSC) on a regular basis, few studies have investigated the effects SSC on FD and RFE.

It has been shown that stretch preceding shortening does not affect the resulting FD<sup>2</sup>, while recent evidence suggests it might<sup>3</sup>. We hypothesized from the results of these initial studies that stretch might affect force depression in a time-dependent manner, and that the effects of stretch on FD disappear if sufficient time is given between the end of stretching and the end of shortening in SSC.

Therefore, the purpose of the present study was to perform SSC where the time between the end of stretch and the end of shortening was manipulated by (i) adding a pause between the stretch and shortening phases and (ii) by performing the shortening contractions at different speeds.

## METHODS

Subjects: Sixteen healthy subjects (8 male and 8 female; 25±2 years; 170±9 cm; 67±8 kg) participated in protocol 1, and 15 subjects (6 male and 9 female; 26±4 years; 173±7 cm; 69±9 kg) participated in protocol 2.

Experimental setup: Thumb adduction forces and carpometacarpal angular displacements were

measured using a custom-designed dynamometer, with 0° defined as the highest degree of thumb adduction. The Ulnar nerve was electrically stimulated (50 Hz) to evoke 50-60% of the maximum voluntary contraction (MVC) of the adductor pollicis muscle for 7s.

Protocol 1: For FD, the muscle was held isometrically for 1s at 30°, followed by 1s of shortening over a 30° joint excursion at 30°/s. The muscle was then held isometrically at 0° for 5s. Following FD, a purely isometric reference contraction was performed at 0° for 7s.

For the SSCs, the muscle was held isometrically for 1s at 0° and stretched to 30°. Following stretching, the muscle was either immediately shortened back to 0° at 30°/s (SSC\_0s), held isometrically for 0.5s (SSC\_0.5s) then shortened back to 0°, or held isometrically for 1s (SSC\_1s) then shortened back to 0°. Following shortening, muscles were held isometrically at 0° for 4, 3.5, and 3s, respectively for a total stimulation time of 7s for all conditions (protocol 1).

Protocol 2: FD was performed in a similar manner as in protocol 1. For SSCs, the muscle was held isometrically for 1s at 0° and stretched to 30° joint excursion at 30°/s. Following stretching, the muscle was shortened immediately to 0° at either 15°/s (SSC\_15°/s), 20°/s (SSC\_20°/s), 30°/s (SSC\_30°/s), and 60°/s (SSC\_60°/s) and held isometrically at 0° for 3, 3.5, 4, and 4.5s, respectively for a total stimulation time of 7s for all conditions.

Following SSCs, a 7s isometric reference contraction and a MVC at a thumb adduction angle of 0° was performed.

A one-way ANOVA was used to test for differences between mean steady-state isometric forces following SSCs ( $\alpha=0.05$ ).

## RESULTS AND DISCUSSION

The mean electrically evoked isometric contraction force at a  $0^\circ$  thumb adduction angle was 52% of the MVC force.

Protocol 1: The steady-state isometric force was significantly depressed ( $20.6\pm6.6\%$ ) following active shortening (FD) compared to the isometric reference contraction at the corresponding thumb angle and same level of activation. For the SSCs, force depression was significantly smaller for SSC\_0s and SSC\_0.5s compared to the pure FD conditions ( $13.7\pm7.4\%$  and  $15.5\pm2.9\%$ , respectively), while force depression for SSC\_1s ( $17.6\pm6.1\%$  force depression) was not statistically different from the pure shortening (FD) contractions (Fig. 1).

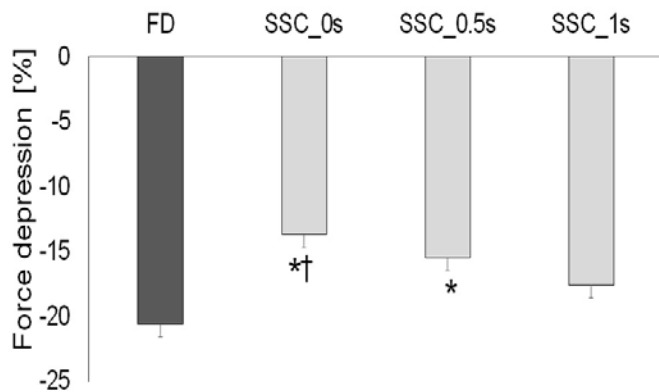


**Figure 1:** Mean ( $\pm$ SEM) values of force depression for a pure shortening contraction (FD) and for the contractions involving SSCs with 0, 0.5, and 1s interval between the stretching and the shortening phase. Force depression is normalized relative to the reference isometric contraction at the corresponding angle. (\* compared to FD; † compared to SSC\_1s).

Protocol 2: The steady-state isometric force was significantly depressed by  $20.3\pm1.4\%$  following active shortening (FD) compared to the isometric

reference contractions at the corresponding thumb angle and same level of activation. Force depression in SSC\_60°/s and SSC\_30°/s was significantly reduced compared to the pure FD condition ( $13.2\pm1.3\%$  and  $16.8\pm1.2\%$ , respectively), while FD for SSC\_20°/s and SSC\_15°/s ( $19.6\pm2.1\%$  and  $20.3\pm1.5\%$ ) were similar to the pure FD values (Fig. 2).

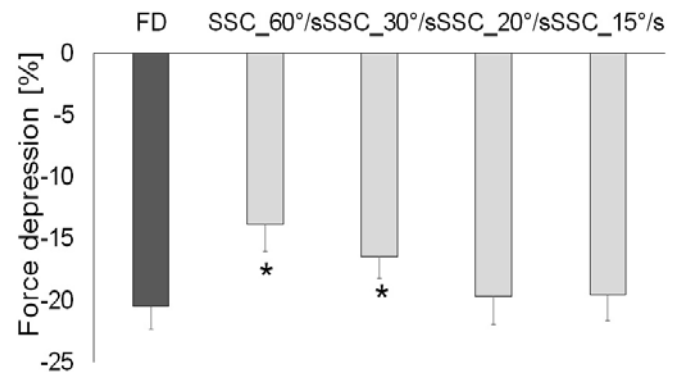


**Figure 2:** Mean ( $\pm$ SEM) values of force depression for the pure shortening contraction (FD) and for the SSCs with the shortening speeds of 60, 30, 20, and  $15^\circ$ /s. Shortening in all cases followed stretching without a pause (\* compared to FD).

## CONCLUSIONS

The results of this study support our hypothesis that stretch preceding shortening affects FD in a time-dependent manner. Given sufficient time between the end of stretching and the end of shortening, the effect of stretch on FD is eliminated. This finding provides crucial new information on the potential mechanisms of RFE and FD, as the events occurring during active muscle stretching either inhibit full development of force depression or offset FD in some hitherto unknown manner.

## REFERENCES

1. Abbott & Aubert., *J Physiol.* **117**(1), 77-86, 1952.
2. Herzog & Leonard., *J Biomech* **33**:531-542, 2000.
3. Seiberl et al., *Physiol Report.* **3**(5):1-12, 2015.

# FINITE ELEMENT ANALYSIS OF INTRAMUSCULAR PRESSURE IN THE HUMAN TIBIALIS ANTERIOR

<sup>1</sup> Benjamin Wheatley, <sup>2</sup> Gregory Odegard, <sup>3</sup> Kenton Kaufman, <sup>1</sup> Tammy Haut Donahue

<sup>1</sup> Colorado State University, Fort Collins, CO

<sup>2</sup> Michigan Technological University, Houghton, MI

<sup>3</sup> Mayo Clinic, Rochester, MN

email: tammy.donahue@colostate.edu

## INTRODUCTION

The strong correlation between muscle force and intramuscular pressure (IMP) provides an opportunity to utilize IMP for measurement of muscle force *in vivo*. However, proper implementation of a pressure microsensor to measure IMP requires knowledge of pressure distributions within the muscle.

Finite element analysis has been previously used to study IMP under passive stretch conditions in an animal model [1]. However, the force-pressure relationship under contractile conditions in humans is of clinical interest, particularly under sub-maximal contraction levels where gait and locomotion typically occur. Thus, there are three primary goals of this work: 1) investigate potential causes for regional variability of intramuscular pressure with muscle, 2) identify the region of minimal IMP gradient, and 3) model the IMP-force relationship in sub-maximally contracting skeletal muscle.

## METHODS

Eight (n=8) healthy young adults were recruited for simultaneous force-IMP measurements in the human tibialis anterior under isometric activation [2]. Each subject performed isometric contractions to 50% maximum voluntary contraction (MVC) at a rate of 10% per second over fifteen trials.

A previously validated hyper-visco-poroelastic constitutive approach for skeletal muscle [1] was implemented within a finite element model of an idealized human tibialis anterior (Figure 1). To study variability of intramuscular pressure, four different muscle lengths and two different specific tension values were utilized (8.5 and 15.5 N/cm<sup>2</sup>)

based on previously published literature data [3-5]. Muscle lengths of 255.5, 254, 252.5, and 251 mm were simulated by applying boundary conditions to the un-deformed model length of 260 mm and contraction level was scaled to 50%.

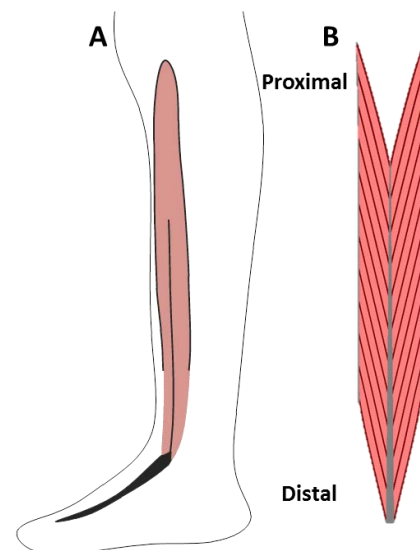


**Figure 1:** A) Drawing of bipennate human tibialis anterior. B) Idealized finite element model.

## RESULTS AND DISCUSSION

Fluid pressure in the finite element model showed a nonlinear increase as a function of contraction level (Figure 2) similar to experimental data. Statistical agreement between model and experimental data ranged from less than 7% normalized root mean square error (NRMSE) to 95% NRMSE for individual pressure-contraction curves. Both muscle length and specific tension affected model fluid pressure (Figure 2). Predicted fluid pressure distribution within the model showed the highest IMP gradients at the distal and proximal regions through a color map (Figure 3A) and graphical analysis (Figure 3B).

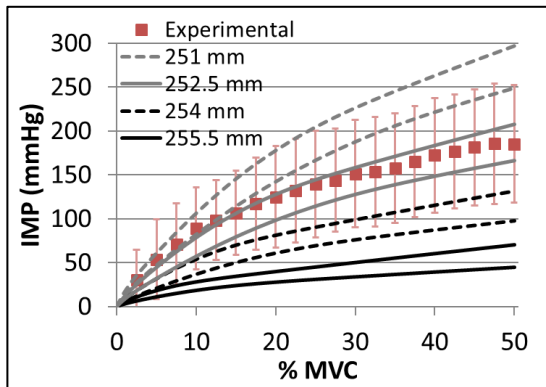


**Figure 2:** Experimental data ( $\pm$  standard error bars) and model outputs as a function of muscle length (shown in legend) and specific tension (top and bottom curves for 7.75 and 4.25 N/cm<sup>2</sup>, respectively).

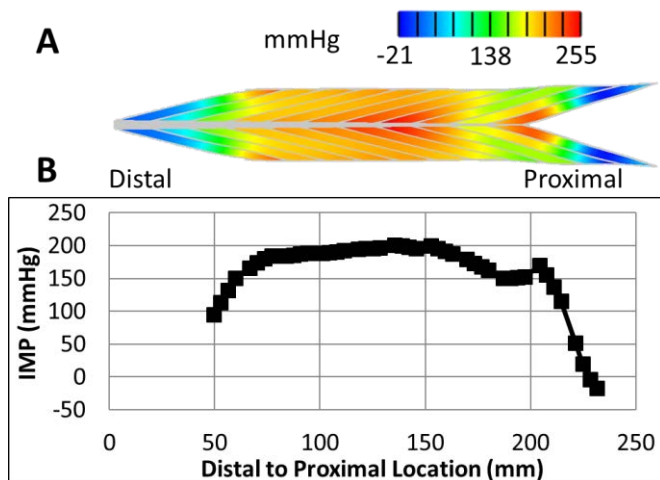


**Figure 3:** A) Color map of model fluid pressure shows high gradients in the distal and proximal regions. B) This is confirmed by plotting pressure values as a function of distal to proximal location.

The data presented in Figures 2 and 3 provide insight into possible contributions to the variability of IMP measurements *in vivo*. While the correlation between muscle force and IMP is strong, variations in relative IMP can make muscle force estimations from multiple patients and muscles more challenging *in vivo*. The model results suggest that fluid pressurization increases as isometric muscle length decreases. While specific tension also yielded changes in pressurization, it appeared to play less of a role than length. Understanding the mechanisms which contribute to IMP allow for

greater confidence in interpreting muscle force through these measurements.

The modeling results also suggest use of pressure microsensors to measure IMP in the muscle midbelly, away from the large pressure gradients observed in the distal and proximal regions (Figure 3). Sensor insertion into regions of high pressure gradients would also contribute to variability of IMP measurements and thus yield inconsistent data.

This work presents the first finite element model of skeletal muscle to study intramuscular pressure at submaximal conditions. The nonlinear pressure-contraction shape observed within the model agreed with the overall shape of experimental data (Figure 2). Specifically, this nonlinear shape showed decreases in change in pressure with increases in contraction. The pressure values at 25% MVC were  $\sim$ 150 mmHg, while the values at 50% MVC were only  $\sim$ 200 mmHg. This further supports the accuracy of this modeling approach in studying intramuscular pressure.

## CONCLUSIONS

This work utilized finite element analysis to study intramuscular pressure in the human tibialis anterior. This was the first study to model IMP in human muscle and at submaximal contraction levels. Modeling results suggested the muscle midbelly is ideal for sensor location due to small pressure gradients. Additionally, muscle length may play a role in variability of IMP *in vivo*. Finally, the model showed good predictability across variable contraction levels from 0-50% MVC.

## REFERENCES

1. Wheatley BB, et al. *Biomech Model Mechanobiol* 2016. DOI 10.1007/s10237-016-0869-z
2. Go S. [Dissertation] Mayo Clinic, 2016
3. Fukunaga T, et al. *J Appl Physiol* **80**, 158-165, 1996.
4. Maganaris CN, et al. *J Appl Physiol* **90**, 865-872, 2001.
5. Koo TK, et al. *Clin Biomech* **29**, 33-39, 2014.

## ACKNOWLEDGMENTS

This work was funded by the NIH: National Institute of Child Health & Human Development [R01HD31476].

# BIOMECHANICAL EVALUATION OF THE SUITABILITY OF MOUSE MODELS FOR HUMAN NEUROMUSCULAR DISEASE

<sup>1</sup> Xiao Hu, <sup>2</sup> James P. Charles, <sup>3</sup> John R. Hutchinson, and <sup>1</sup> Silvia S. Blemker

<sup>1</sup> University of Virginia, VA, USA; <sup>2</sup> University of Pittsburgh, PA, USA

<sup>3</sup> Royal Veterinary College, Hatfield, UK

email: xiaohu@virginia.edu

## INTRODUCTION

Mice are one of the most widely used animal models to study neuromuscular diseases and test new treatments. However, findings from mouse studies often fail to translate to humans due to various factors, including the biomechanical differences between mice and humans.

The biomechanical differences may possibly relate to the differed phenotype appearing in mouse models of neuromuscular diseases and whether exercise studies performed in mouse models are relevant to humans' muscle physiology. For example, in the widely used mouse model (*mdx* mice) of Duchenne Muscular Dystrophy (DMD), a genetic, muscle degenerative disorder affecting 1 in 3500 male births, the limb muscles have much milder phenotype than those in humans [1]. Differences in muscle length changes during daily locomotion, such walking and running, between mice and human may contribute to this milder phenotype in mice [2]. However, whether muscle length changes of mice during walking differ from humans remains unknown.

We hypothesized that the feasible ranges of fiber operating lengths of human lower limb muscles in

walking are larger than those of mouse hindlimb muscles. To test this hypothesis, we used newly published musculoskeletal models of the mouse hindlimb [3] and human lower limb [4] to run dynamic simulations, and calculated fiber operating lengths of 25 muscle homologues in these two species.

## METHODS

Dynamic simulations of muscle-tendon dynamics were developed in OpenSim version 3.2 [5] to estimate possible muscle fiber operating lengths in mice and humans during walking. Two newly published musculoskeletal models were used. The first model describes the 3-dimensional (3D) musculoskeletal geometry of a mouse hindlimb [3], and the second model describes the 3D musculoskeletal geometry of the human lower limbs [4]. In both models, each muscle was approximated with one or more line segments from origin to insertion and was represented with a Hill-type muscle model [6]. Joint kinematics measured from 16 mice [7] and 5 human subjects [8] walking on treadmills were prescribed in the simulations. To consider the influences from muscle activation to the possible ranges of fiber operating lengths, two

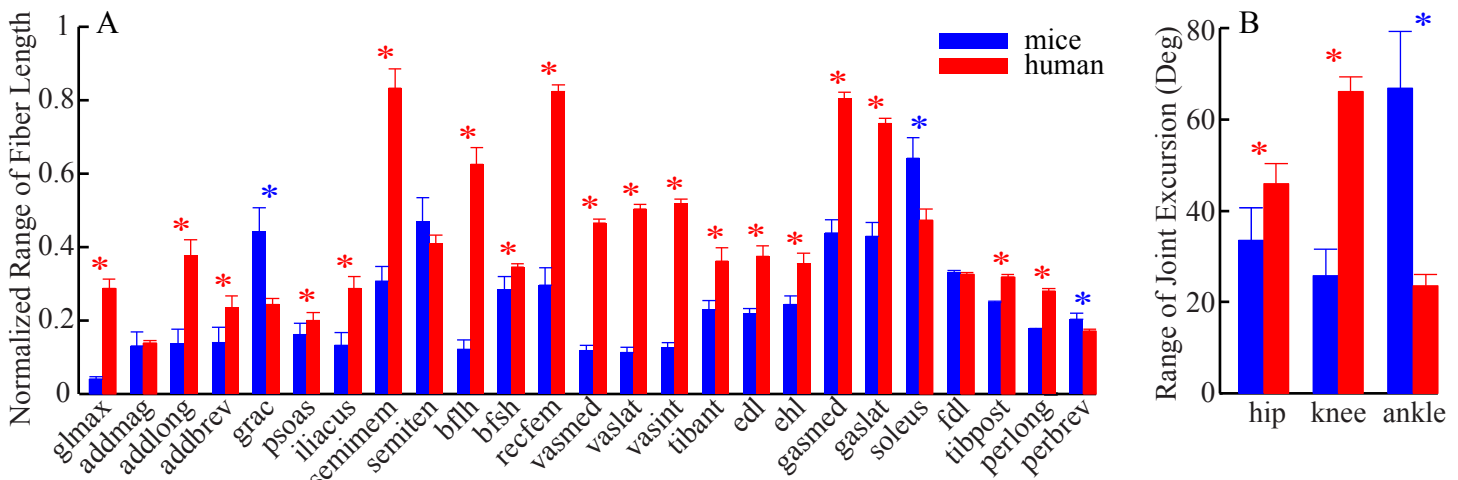


**Figure 1:** Comparison of the feasible ranges of fiber length (A) and joint excursions (B) during walking between mice and humans. Blue stars indicate mice have larger ranges, while red stars indicate humans have larger ranges ( $p < 0.05$ ).

activation cases were also prescribed: maximum activation in which activation was 1 in all muscles; and minimum activation in which activation was 0.05. Forward dynamic simulations were then run to calculate muscle fiber lengths that satisfied these prescribed constraints.

Fiber length changes during one gait cycle were estimated for maximum and minimum activation cases separately, and were then normalized to each muscle's optimal fiber length. The feasible range of fiber operating length in walking was defined as the difference between the maximum fiber length when activation was 0.05 and the minimum fiber length when activation was 1. Feasible fiber ranges of 25 muscles that have homologues in the two species were compared using a *t*-test with *p* value set at 0.05.

To understand any potential causes of the differences in feasible ranges of fiber operating lengths in walking, ranges of excursions for the hip, knee and ankle joints were computed based on the prescribed kinematics in the simulations. In addition, mean muscle flexion/extension moment arms at the hip, knee and ankle in one gait cycle were calculated and normalized by each muscle's optimal fiber length.

## RESULTS AND DISCUSSION

In general during walking, muscles of the human lower limb have larger feasible ranges of operating lengths than those of mice (Fig. 1A). Out of 25 muscles compared, 19 muscles have significantly larger feasible range of operating lengths in humans than in mice. In contrast, only 3 muscles have significantly larger ranges in mice than in humans. Three muscles have comparable ranges. These results suggest that the majority of mouse hindlimb muscles undergo smaller length changes during walking. This biomechanical difference could potentially contribute to the milder phenotype seen in the *mdx* mice, as muscle lengthening may adversely affect the progress of DMD [2].

Both the ranges of joint excursion and mean moment arms in walking contribute to the larger feasible ranges of fiber operating lengths in most muscles in humans than in mice. Humans have significant larger ranges of joint excursion at the hip and knee (Fig. 1B). In addition, humans have larger normalized moment arms in most muscles acting across the hip

and knee (Fig. 2). These two factors are linked to larger muscle length changes at the hip and knee in humans as compared to mice. Although mice have larger ankle excursions in walking, humans have larger mean moment arms in muscles across the ankle, which counteracts the effect from larger ankle motions in mice.

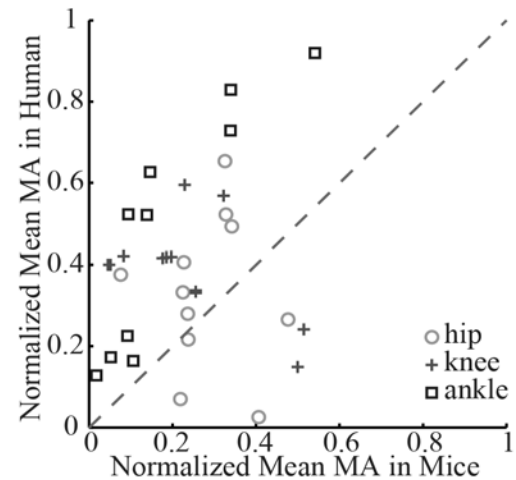


**Figure 2:** Comparison of mean moment arms (MA) in walking. Each symbol is one muscle. The dashed line is the unity line.

## CONCLUSIONS

Our simulation results demonstrated that biomechanical differences could contribute to the differed disease state in *mdx* mice and humans with DMD. By understanding and accounting for these differences, experiments in mice may be better designed to gain knowledge that could be translated to humans.

## REFERENCES

1. Stedman HH, et al. *Nature* **352**, 536-539, 1991.
2. Hu X, et al. *Muscle Nerve* **52**, 174-182, 2015.
3. Charles JP, et al. *J Anatomy* **229**, 514-535, 2016.
4. Rajagopal A, et al. *IEEE Trans. Biomed. Eng.*, **63**, 2068-2079, 2016.
5. Delp SL, et al. *IEEE Trans. Biomed. Eng.*, **54**, 1940-1950, 2007.
6. Millard M, et al. *J. Biomech. Eng.*, **135**, 2013.
7. Akay T, et al. *Proc. Natl. Acad. Sci. USA*. **111**, 16877-16882, 2014.
8. Arnold EM, et al. *J Exp Bio*, **216**, 2150-2160, 2013.

## ACKNOWLEDGMENTS

The authors would like to thank Turgay Akay for sharing data and Dominic Wells for input as well as NIH grants R21AR068562 and U01AR069393 and BBSRC grant BB/J021504/1.

# TOO MUCH WORK: REVISITING ULTRASOUND-BASED ESTIMATES OF ACHILLES TENDON ENERGY STORAGE AND RETURN

Jason R. Franz<sup>1</sup> and Karl E. Zelik<sup>2</sup>

<sup>1</sup>University of North Carolina at Chapel Hill and North Carolina State University    <sup>2</sup>Vanderbilt University  
 email: [jrf Franz@email.unc.edu](mailto:jrf Franz@email.unc.edu)    web1: [abl.bme.unc.edu](http://abl.bme.unc.edu)    web2: [my.vanderbilt.edu/batlab/](http://my.vanderbilt.edu/batlab/)

## INTRODUCTION

Ultrasound imaging is increasingly used with motion and force data to quantify tendon dynamics and to understand the functional role of tendons during human and other animal movement. Frequently, tendon dynamics are estimated indirectly from measures of muscle kinematics (by subtracting muscle length from muscle-tendon unit length), but there is mounting evidence that this approach, which we term the *Indirect* method, yields implausible tendon work loops (tendon force vs. elongation) [e.g., 1-2]. Since tendons are passive, viscoelastic structures, they should exhibit negative work loops (i.e., net negative work over a loading-unloading cycle). However, prior studies using Indirect estimates of tendon kinematics report large positive work loops, estimating that tendons return 100-400% more energy than they store [e.g., 1-2]. More direct ultrasound methods have emerged that estimate tendon elongation by tracking either the muscle-tendon junction (termed the *Direct MTJ* method) or localized tendon tissue stretch (termed the *Direct Tendon* method) [3]. However, it is unclear if these Direct estimates yield more plausible tendon work loops. Here, we estimated tendon work loops and hysteresis using these two Direct tendon kinematics estimates during human walking, then compared these results to previously reported values using Indirect kinematics estimates.

## METHODS

We reanalyzed human walking data from our prior work ( $N=8$ , mean  $\pm$  standard deviation, age:  $23.9 \pm 4.6$  years) [3]. Subjects completed two 2-minute walking trials at three walking speeds (0.75, 1.00, and 1.25 m/s) - one trial for each of two probe locations. We collected human motion and force data using standard gait analysis procedures. Simultaneously, we collected raw radiofrequency

(RF) data from longitudinal cross-sections through the right plantarflexor MTU using a 10-MHz, 38-mm linear array transducer (L14-5W/38, Ultrasonix, Richmond, BC) secured using an orthotic. For the Direct MTJ estimate, we recorded (128 frames/s) through a 3 cm depth from a probe centered on the distal lateral gastrocnemius (LG) MTJ, from which we estimated local MTJ displacements. For the Direct Tendon estimate, we recorded (155 frames/s) through a 2 cm depth from a probe on the distal free Achilles tendon. Custom 2D speckle-tracking estimated longitudinal free Achilles tendon tissue

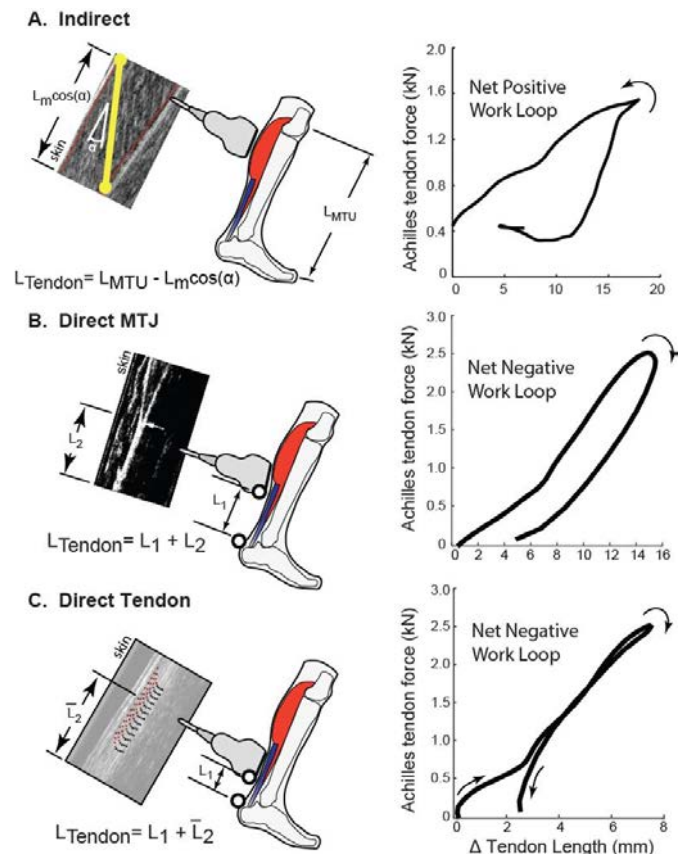


**Figure 1.** Tendon kinematic measurements and group-average tendon work loops during walking. (A) Indirect estimates from digitized published data [1] and Direct estimates via the (B) lateral gastrocnemius MTJ and (C) Achilles free tendon.

displacements [3]. Achilles tendon elongations were then estimated by co-registering local LG MTJ (Direct MTJ) and Achilles free tendon (Direct Tendon) displacements with the calcaneus marker position. Finally, we estimated Achilles tendon force as the net ankle moment divided by subject-specific measures of the Achilles tendon moment arm to create stance phase tendon work loops (tendon force vs. elongation). We integrated tendon work loops to calculate: (i) net stance phase work (J) and (ii) hysteresis (%), defined as one minus the positive work (energy returned during tendon unloading) divided by negative work (energy stored during loading). Tendon hysteresis from Direct MTJ and Direct Tendon methods were compared to Indirect values from literature [e.g., 1-2].

## RESULTS AND DISCUSSION

Based on digitized data from previously published studies [e.g., 1-2], tendon length changes estimated from measured muscle fascicle kinematics consistently produced positive tendon work loops. For example, Achilles tendon hysteresis during walking derived indirectly from soleus and gastrocnemius fascicle kinematics elicited values of approximately -130% and -200%, respectively, indicating considerable but physiologically implausible net positive work performed by the tendon (Fig. 1A) [1].

In contrast to Indirect estimates, we found that both Direct methods yielded, on average, negative tendon work loops and thus positive tendon hysteresis values during the stance phase of walking. Across the range of speeds tested, peak Achilles tendon force during the stance phase averaged 2.2-2.7 kN. This range of peak forces was associated with tendon length changes of 14.3-15.2 mm estimated via LG Direct MTJ and 7.1-7.8 mm estimated via Direct Tendon approaches. Direct MTJ tendon hysteresis (net work) averaged 49.7% (-8.9 J), 37.9% (-8.2 J), and 9.2% (-5.1 J) for walking at 0.75, 1.00, and 1.25 m/s, respectively (Fig. 1B). Direct Tendon estimates averaged 32.9% (-3.4 J), 11.0% (-2.0 J), and 2.1% (-1.2 J), respectively (Fig. 1C). Net tendon work (main effect,  $p=0.04$ ), but not hysteresis (main effect,  $p=0.34$ ), differed significantly between the two

Direct measurement techniques. Finally, both outcome measures decreased significantly and progressively with increasing walking speed (main effect,  $p<0.01$ ). That hysteresis estimates were walking speed-dependent requires further study.

## CONCLUSIONS

As we advance our scientific understanding of movement biomechanics, it is important to continue advancing and validating our experimental methods. It remains unclear which fundamental assumptions or measurement inaccuracies result in the substantial positive tendon work loops obtained from Indirect tendon estimates. Nevertheless, compared to Indirect tendon estimates, Direct estimates may be preferable for understanding tendon dynamics such as energy storage and return, especially during dynamic activities such as walking. The accuracy and completeness of our biomechanical estimates affect our scientific interpretations as well as our applied interventions. Indeed, our results are highly relevant to the degree to which tendon elastic energy storage and return facilitate economical locomotion, and to the bio-inspired design and prescription of assistive devices that seek to restore/augment human calf muscle-tendon function. Musculoskeletal simulations also rely on accurate empirical biomechanical estimates, either as direct inputs or indirectly for validation. Ultimately, we must understand the accuracy, precision, benefits, drawbacks, and assumptions of each measurement approach in order to appropriately interpret the functional role of muscle-tendon dynamics during movement.

## REFERENCES

1. Ishikawa M, et al., *J Appl Physiol.* **99**: 603-608, 2005.
2. Sakuma J, et al., *Eur J Appl Physiol.* **112**: 887-898, 2012.
3. Franz JR, et al., *Gait Posture.* **41**: 192-197, 2015.

## ACKNOWLEDGMENTS

Supported in part by NIH: K12HD073945 awarded to KEZ, F32AG044904 and R01AG051748 awarded to JRF.

# SPATIAL TUNING OF MUSCLE ELASTICITY AND ELECTROMYOGRAPHY ACTIVITY FOR THE STERNOCLEIDOMASTOID MUSCLES

Bhillie Luciani, David M. Desmet, Amani Alkayyali, David B. Lipps

School of Kinesiology, University of Michigan, Ann Arbor, MI, USA  
email: dlipps@umich.edu, web: www.kines.umich.edu/research/mbil

## INTRODUCTION

The neck is composed of a complex layering of musculature to move and generate force in three dimensions. Each neck muscle is precisely tuned to have preferred directions where their muscle activity is greatest during isometric or dynamic tasks [1-3]. Tracking the spatial tuning of muscle activations has clinical utility, as the directional specificity of the sternocleidomastoid (SCM) muscles are reduced in patients with chronic neck pain [2], likely producing increased muscle stiffness [4]. Increased *in situ* muscle stiffness is produced at greater muscle activation levels [5], but direct assessments of *in vivo* muscle stiffness are clinically limited to qualitative assessments (e.g. tissue palpation). Recent advances in ultrasound shear wave elastography (SWE) allow for direct measures of muscle elasticity [6]. Our study utilized SWE to determine if the spatial tuning of muscle elasticity and EMG activity are similar within the SCM muscles of healthy participants.

## METHODS

Fifteen healthy adults (8 males; mean (SD) age = 23.6 (2.6) yrs) with no history of neck dysfunction were enrolled. Surface electromyography (EMG) electrodes (Bagnoli, Delsys, Natick, MA) were placed bilaterally on the SCM, upper trapezius (UT), and splenius capitis (SPL) muscles (Fig. 1A). Participants were seated with their head secured within a wall-mounted aluminum halo attached to a biaxial load cell (Fig. 1A) with their torso and pelvis secured to the backrest using straps.

Maximum voluntary contractions (MVCs) were collected in flexion, extension, left flexion, and right flexion. Visual feedback was provided to assist subjects in matching their isometric force production to 16 axially-directed targets scaled to 20% of their maximal MVC (extension in all participants) (Fig. 1B). Participants completed practice trials to familiarize themselves with the force matching task

before completing two blocks of 16 targets in a randomized order.

After collecting EMG data during these trials, the electrodes over the bilateral SCMs were removed to accommodate an ultrasound transducer. SWE ultrasound images were acquired from the muscle bellies of both SCM muscles using a Supersonic Imagine Aixplorer system (Fig. 1C). Images were acquired as subjects performed the same isometric force matching task (two blocks of 16 randomized targets). Muscle elasticity was estimated as the mean shear wave velocity within the SWE color map.

The EMG data was collected at 1 kHz, gained at 1 or 10 kHz, detrended, rectified, and low-pass filtered (7 Hz). EMG values during each contraction were averaged over 500 ms. Tuning curves were generated to compute the directional specificity of muscle

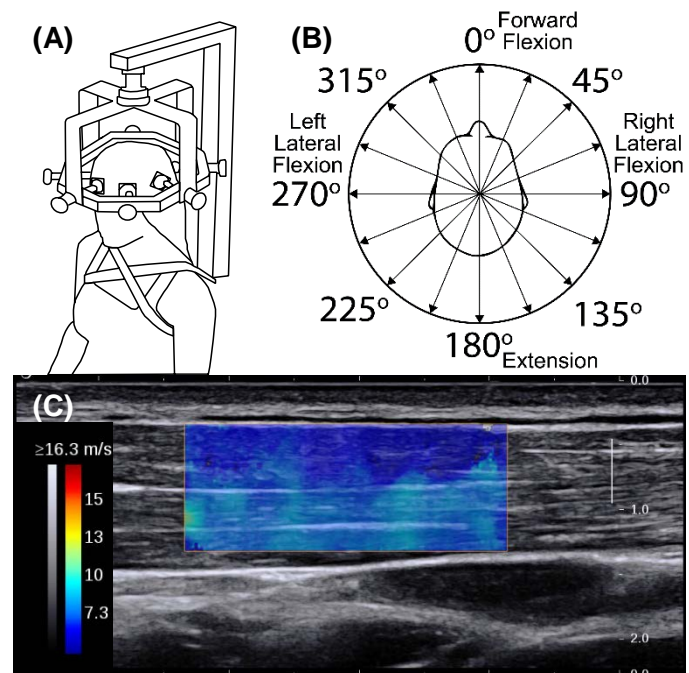


**Figure 1:** (A) Metal halo with embedded force sensor. (B) Experimental procedure involves generating isometric forces in 1 of 16 directions. (C) A representative image of the SCM muscle using ultrasound shear wave elastography. The B-mode image is superimposed with a color map of shear wave velocity, which is directed related to muscle elasticity.

activity of the bilateral SCM, UT, and SPL muscles and muscle elasticity from the shear wave velocity data collected from the bilateral SCMs. Specificity was computed as the mean vector direction of the tuning curve [3], e.g. the vector sum of the normalized EMG or raw SWE data across all force target directions. Differences in the directional specificity of muscle activity and muscle elasticity for the left and right SCMs were assessed using a paired t-test with a significance level of  $P < 0.05$ . A repeated measures ANOVA assessed if the EMG activity specificity for the bilateral UT and SPL muscles differed between the EMG and SWE tasks to insure consistent co-activation patterns.

## RESULTS AND DISCUSSION

Representative EMG and SWE tuning curves for the left and right SCM muscles are shown in Figure 2. Different direction specificities between the left and right SCMs were shown for muscle activity and muscle elasticity. Within each muscle, similar directional specificity patterns between muscle activity and muscle elasticity were observed.

Across subjects, the mean  $\pm$  SD vector direction for the left SCM was  $347^\circ \pm 17^\circ$  for EMG activity and  $332^\circ \pm 24^\circ$  for muscle elasticity ( $p = 0.013$ ). For the right SCM, the mean vector direction was  $12.2^\circ \pm 15^\circ$  for EMG activity and  $22.1^\circ \pm 19^\circ$  for muscle elasticity ( $p = 0.003$ ). The directional specificity of both the left and right SCM were consistent, with both muscles showing preferred activation and elasticity when producing forces in forward and ipsilateral flexion. The mean vector direction for muscle elasticity was significantly more directed towards ipsilateral flexion than the mean vector for muscle activity for both SCMs.

We posited this statistically significant difference in directional specificity could occur due to participants performing the isometric task differently between the EMG and SWE collections. Since the EMG electrodes over the SCM muscles were removed to perform ultrasound SWE, we examined how the specificity of the UT and SPL muscles differed between the EMG and SWE tasks. The directional specificity of the bilateral UT and SPL muscles' EMG activity exhibited no significant task by muscle interactions (left:  $p = 0.809$ ; right:  $p = 0.913$ ) or task main effects (left:  $p = 0.936$ ; right:  $p = 0.707$ ). These

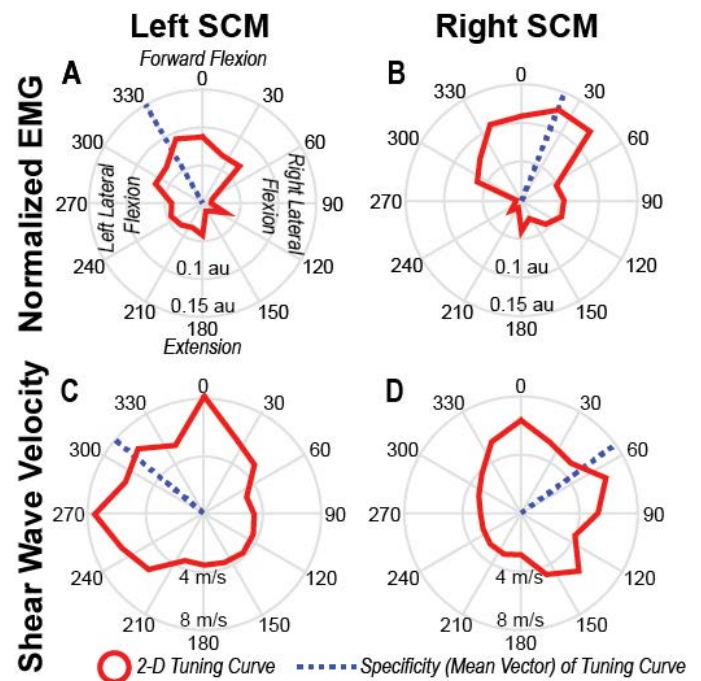


**Figure 2:** Representative tuning curves (red) of (a-b) normalized EMG activity and (c-d) mean shear wave velocity for the left and right SCM muscles for one subject. Dashed blue lines indicate directional specificity for each curve.

findings suggest patients utilized similar muscle co-activation patterns throughout the entire experiment.

The current study provides new insights into healthy neck neuromechanics. The directional specificities of SCM muscle activity were consistent with prior studies [3]. For the first time, we showed that the preferred directions of muscle activity and elasticity are similar for the SCM muscles. This is consistent with greater muscle stiffness at higher activation levels [6]. Future work will investigate if learning adaptations or muscle architecture can explain our observed statistical difference between SCM activity and elasticity. We will also investigate how neck pathologies manifest in regards to underlying changes in muscle elasticity and muscle activity.

## CONCLUSIONS

The SCM muscles exhibit a small but statistically significant difference between the preferred directions of muscle activity and muscle elasticity.

## REFERENCES

1. Blouin JS et al. *J Neurophysiol*, **98**, 920-8, 2007.
2. Falla D et al. *Eur J Pain*, **17**, 1517-28, 2013.
3. Vasavada AN et al. *Exp Brain Res*, **147**, 437-48, 2002.
4. Kuo WH et al. *Ultrasound Med Biol*, **39**, 1356-61, 2013.
5. Rack PM, Westbury DR. *J Physiol*, **240**, 331-50, 1974.
6. Nordez A, Hug F. *J Appl Physiol*, **108**, 1389-94, 2010.

## **HMB preserves strength in contralateral but not in Botox-injected musculature in rabbits**

<sup>1</sup> Rafael Fortuna, <sup>1</sup> Andrew Sawatsky, <sup>2</sup> John Fuller, <sup>1</sup> Walter Herzog

<sup>1</sup> Human Performance Laboratory, University of Calgary, Canada

<sup>2</sup> Metabolic Technologies, Inc., Ames, IA, USA

Email: fortuna.rafael@gmail.com

### **INTRODUCTION**

Botulinum toxin type-A (Botox) induces a dose-dependent muscle paralysis by preventing acetylcholine release at the neuromuscular junctions<sup>1</sup>.

Currently, Botox injections have been applied in clinical settings with the primary aim to relax hyperexcitability of peripheral nerve terminals, such as in patients with cerebral palsy or following a stroke<sup>2</sup>. Additionally, Botox can be used in experimental settings to mimic muscle weakness as seen following injury or in the elderly<sup>3</sup>. Botox-induced muscle weakness models can also be used to test strategies for preventing or reversing loss of strength and muscle mass.

$\beta$ -Hydroxy- $\beta$ -methylbutyrate (HMB) is produced in animals and humans from the amino acid leucine. Studies have shown that HMB supplementation can slow muscle protein breakdown following resistance exercise, and produce gains in lean body mass and strength in a dose-dependent manner. Additionally, HMB is being used as a dietary supplement during rehabilitation following injury, prolonged bed rest, and for hospitalized patients in order to mitigate loss in strength and muscle mass<sup>4</sup>. Despite its ever growing popularity as a diet supplement to prevent muscle wasting, there have been conflicting results regarding the efficacy of HMB to prevent muscle weakness under conditions producing muscle atrophy.

The purpose of the present study was to determine the effects of dietary HMB supplementation on strength and muscle mass following a single Botox injection into the quadriceps femoris muscles of New Zealand white (NZW) rabbits.

### **METHODS**

Twenty-one, one year old female NZW rabbits were divided into: (1) Control (n=7); (2) Botox (n=7); and (3) Botox + HMB (n=7) groups. The Control group received an equal volume of saline injections as the experimental group rabbits, which received a single intramuscular Botox injection (3.5U/kg) unilaterally into the quadriceps femoris musculature.

Two months following the injections, rabbits were evaluated for primary outcome measurements of muscle mass and knee extensor strength in the injected and contralateral non-injected muscles. Muscle mass was assessed by weighing the muscles and maximal isometric knee extensor strength was measured via maximal femoral nerve stimulation at 200 Hz.

The data were analyzed using Proc GLM in SAS (SAS for Windows 9.4, SAS Institute, Inc., Cary, NC) using one-way ANOVA with treatment as the main effect and body weight as a covariate. Data are presented as mean and standard error of the mean (SEM). The level of significance was chosen as  $\alpha=0.05$  a priori.

### **RESULTS AND DISCUSSION**

There was no difference in muscle strength between saline and contralateral non-injected limbs of the control rabbits. However, there was a significant reduction in strength of the injected limbs of the Botox group compared to the control group, but no difference in strength between the injected Botox and Botox + HMB group rabbits was observed (Fig. 1).

Muscle strength on the contralateral non-injected limb of Botox group rabbits was decreased compared to control group rabbits. The Botox +

HMB group had significantly higher strength values than the Botox group and did not differ from the values obtained from the control group rabbits (Fig. 1).

Muscle mass between saline and contralateral non-injected limbs of control group rabbits was not different; however, there was a significant loss of muscle mass in muscles of the injected limbs of the Botox and Botox + HMB groups, with no difference in muscle mass between these two groups (Fig. 2).

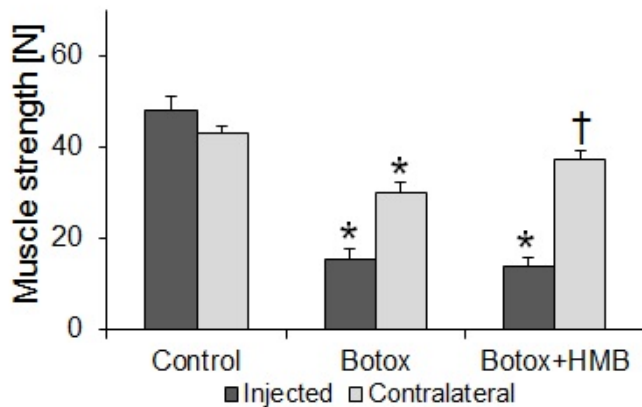


**Figure 1:** Mean muscle strength ( $\pm$ SEM) for injected (dark bars) and contralateral non-injected (light bars) for control, Botox, and Botox + HMB group rabbits (\* compared to control, † compared to Botox).

While muscle mass of the contralateral musculature as a whole was not different between Botox and Botox + HMB group rabbits, the muscle mass of the contralateral rectus femoris in the Botox + HMB group was significantly greater than in the Botox group rabbits (result not shown).

Muscle strength was reduced by about 60% in Botox and Botox + HMB group rabbits compared to control, while muscle mass was reduced by only about 40%. This result suggests that either the muscle structure was also compromised in the two Botox injected rabbit groups, or that Botox inhibition at the neuromuscular junction during the strength testing affected the strength results. Direct muscle stimulation, rather than nerve stimulation, could possibly provide the conclusive answer to this question as this would bypass any residual Botox effect on the neuromuscular junction.

The contralateral muscle strength of the Botox + HMB rabbits was greater than for the Botox alone group, while muscle masses were similar. This finding may indicate that the HMB supplement might have prevented some structural degeneration typically observed in non-target muscles of Botox injected rabbits<sup>5</sup>, thereby maintaining better strength despite equal mass. Follow up histological assessment of our samples will clarify this issue unequivocally.



**Figure 2:** Mean muscle mass ( $\pm$ SEM) for injected (dark bars) and contralateral non-injected (light bars) for control, Botox, and Botox + HMB group rabbits (\* compared to control).

## CONCLUSIONS

While HMB supplementation did not prevent loss of muscle strength and muscle mass in the Botox-injected musculature, HMB did prevent strength loss in the contralateral non-injected muscle. In conclusion, HMB resulted in maintenance of strength in the contralateral musculature which would be important for overall recovery after an immobilizing injury.

## REFERENCES

1. Brin MF., *Muscle & Nerve*. **20**:S146-168, 1997.
2. Gibson *et al.*, *Disabil Rehabil*. **29**(3):1799-1805, 2007.
3. Longino *et al.*, *J Orthop Res*. **23**(6):1411-1418, 2005.
4. Wilson *et al.*, *J Int Soc Sports Nutr*. **10**(6):1-14, 2013.
5. Fortuna *et al.*, *J Biomech*. **4**(44):39-44, 2011.

# FROM HOPPING ON LAND TO TREADING IN WATER: UNDERSTANDING LIMITS ON MUSCLE-TENDON PERFORMANCE IN CHANGING ENVIRONMENTS

<sup>1</sup>Jonathan A. Doering and <sup>1</sup>Gregory S. Sawicki

<sup>1</sup>North Carolina State University, Raleigh, NC, USA  
email: jadoerin@ncsu.edu

## INTRODUCTION

Efficient locomotion requires that the neuromuscular system can quickly adapt to internal and external changes [1]. In many terrestrial animals, the external environment in which locomotion occurs may change instantly (*i.e.*, from land to water), resulting in altered locomotion patterns [2]. Determining whether shifts in locomotion behavior are the result of adapted neural commands versus intrinsic mechanics (*e.g.*, shifts in operating point on the FL and FV curves) is difficult to determine *in vivo*.

The goal of this study was to develop a computer model to understand the muscle vs. tendon contributions to locomotion performance when changing from terrestrial to a fluid environment.

We hypothesized that with no change in motor control, in the terrestrial environment muscle (CE) would act as a rigid strut, while in fluids the CE would act as a work producing motor. Additionally, increasing or decreasing the driving frequency in a fluid would increase or decrease the net work produced by the CE, respectively.

## METHODS

A mass connected to a muscle-tendon unit (MTU) model containing a contractile element (CE), a

parallel elastic element (PEE), and a series elastic element (SEE) was employed (Fig 1A.). The MTU acted through a mechanical advantage to control the motion of a foot. In terrestrial conditions, the mass experienced constant gravitational forces, simulating MTU dynamics of ankle extensors in hopping. In fluid conditions, the mass also experienced a buoyant force, and drag forces at the foot, simulating a treading body in a fluid. Additionally, in the fluid, an antagonist muscle was used to restore the MTU back to longer lengths after a power stroke. Force was generated in the CE by a Hill-type muscle with classic force-length and -velocity relationships and a stimulation modeled as a square wave pulse with a duty of 10% relative to the cycle period. Both the PEE and SEE had non-linear force-displacement relationships taken from the literature. The buoyant force was modeled by:  $F_{buoy} = \rho A_x ((h/2) - dx)$ , where  $\rho$  was the density of the fluid,  $A_x$  was the surface area of the mass and  $dx$  was the change in position of the mass over time. We set  $A_x$  to result in a neutrally buoyant case with half the mass above water when  $dx=0$ . Drag force experienced by the foot was modeled by:  $F_{drag} = -Kv^2$ , where  $v$  was the velocity of the foot, and  $K$  was the lumped drag coefficient (kg/m). Drag only acted when the MTU was shortening, and diminished to zero when the system

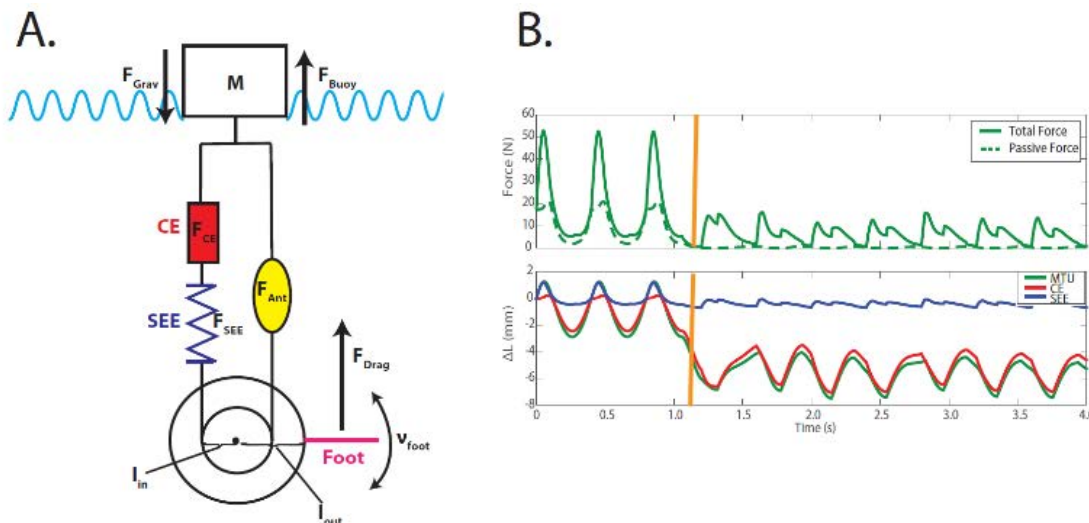


**Figure 1. (A) Hopping/Treading Model, (B) Force and length change of the MTU during a terrestrial to fluid transition.** A body mass/MTU in gravity operating with a fixed mechanical advantage simulates MTU dynamics during cyclic contractions. In terrestrial states, we set drag coefficient to be sufficiently high to allow hopping like behavior. In fluid, drag coefficient is markedly reduced and the mass experiences a buoyant force to assist the restoration of oscillatory behavior (A). In a transition simulation, the MTU operates at longer lengths and higher passive forces in terrestrial vs. fluid state (*i.e.*, before and after the orange line) (B).

reset due to the action of the antagonist muscle. The action of the antagonist muscle was modeled as an acceleration acting to re-lengthen the MTU,  $dV_{MTU}/dt = \alpha * (\Delta L_{MTU})$ , where  $\Delta L_{MTU}$  is the length of the MTU relative to its slack length, and  $\alpha$  is a rate constant. To address the role of environmental changes on MTU dynamics, we drove the system at 2.5 Hz, the passive resonant frequency ( $\omega_0$ ) of the system in terrestrial conditions (*i.e.*, gravity only), in both terrestrial and fluid environments. We then shifted the driving frequency to  $\pm 20\%$  of  $\omega_0$  in fluid to simulate different treading frequencies. To address the hypothesis, we compared the force, length, power dynamics, and work contributions from a steady state contraction in all conditions.

## RESULTS

In the terrestrial environment, we observed higher MTU forces with larger passive contribution, longer muscle (CE) operating lengths and higher tendon (SEE) strains than in the fluid (Fig. 1B). In terrestrial simulations, the CE performed isometrically early in the cycle, facilitating large elastic energy cycling to and from the SEE (Fig 2A, B). In fluid simulations, the CE always shortened on stimulation with increasing velocity and force leading to higher power output at higher and higher driving frequencies. higher power outputs (Fig 2A). In fluid, the majority of the MTU work is produced by the CE, rather than the SEE (Fig 2B).

## CONCLUSIONS

These results support our hypothesis that (1) muscle (CE) should generate net positive work (*i.e.*, act as a motor) in fluid, and generate zero net work (*i.e.*, act as a strut) while in terrestrial conditions and (2) the net work produced by the MTU can be directly modulated by increasing neural drive in a fluid. Our results demonstrate that spontaneous changes in MTU mechanical function can be mediated directly through changes in the environment dynamics without any adjustment in motor control. Interestingly, in terms of maximizing peak power output of the MTU, driving the system under optimal conditions on land (*i.e.*, at the resonant frequency) when in a fluid results in suboptimal performance. Finding a MTU morphology that can maximize power output in both terrestrial and fluid environments without shifts in motor control may be exceedingly difficult. Future experiments will explore how changes in environmental dynamics influence MTU mechanical function *in vitro* on the benchtop using biological MTUs attached to a 'smart' feedback controlled force ergometer.

## REFERENCES

1. Biewener, A.A. and M.A. Daley., *J Exp Biol*, 2007. **210**: 2949-2960.
2. Ijspeert, A.J., *Robotics and Neuroscience*, 2008. **214**: p 642-653.
3. Robertson, B.D. and G.S. Sawicki., *J Theor Biol*, 2014. **353**: p 121-132.

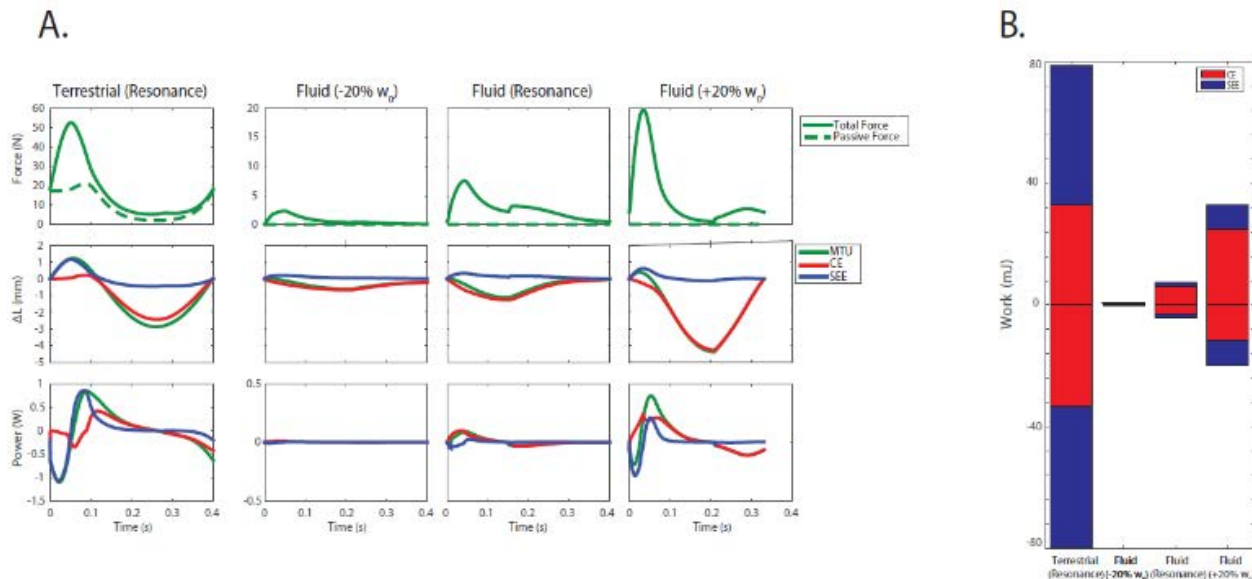


**Figure 2. Force, length, and power responses during environmental simulations (A), and work contributions (B).** In terrestrial environments, the MTU demonstrates high total and passive forces, isometric behavior during contraction, and increased power output compared to fluid conditions. When driving at increasing frequencies in fluid, the MTU generates greater force while undergoing greater length changes and power production (A). On land there is greater elastic cycling of the SEE, while in a fluid, the majority of the MTU work is produced by the CE, rather than the SEE (B). When driving at increasing frequencies in fluid, CE net work also increases.

# CONFOUNDING FACTORS WHEN ANALYZING MOTOR UNIT FIRING ADAPTATIONS DURING MUSCLE FATIGUE

<sup>1</sup> Paola Contessa and <sup>1</sup>Joshua C. Kline

<sup>1</sup>Delsys Inc. and Altec Inc., Natick, USA

email: [pcontessa@delsys.com](mailto:pcontessa@delsys.com), web: <http://www.delsys.com/altec/>

## INTRODUCTION

The control of motor units (MU) during fatiguing contractions has been the subject of debate for decades. Conflicting observations on the firing behavior of MUs during muscle fatigue have reported decreases [1,2] and increases [3] in MU firing rate. The inconsistencies among the observations are often accompanied by differences in the methods used to analyze the MU data. For instance, changes in MU firing rate during repeated isometric contractions are often investigated as a function of MU recruitment threshold. However, this practice may confound the analysis of MU firing adaptations because recruitment threshold itself has been reported to decrease as muscle fatigue develops [1,3]. MU data are also often grouped and averaged across different subjects. Yet, this practice may obscure subject-specific changes in firing rate [2,3]. In this study, we investigated the influence of these analytic approaches on analyzing MU firing adaptations during a fatigue protocol performed with the Vastus Lateralis (VL) muscle.

## METHODS

Five healthy subjects (3 males and 2 females, 24-33 yrs.) performed a series of isometric knee-extension contractions sustained at 30% maximal voluntary contraction (MVC) force and repeated until the endurance limit. Torque and surface electromyographic (EMG) signals from the VL muscle during knee extension were recorded during each contraction (dEMG System, Delsys Inc., Natick, MA). Surface EMG signals were decomposed into the constituent MU action potentials (MUAPs) [4]. The firing rate of MUs in subsequent contractions of the fatigue protocol were analyzed:

- 1) As a function of MU recruitment threshold vs. as a function of MUAP amplitude (to highlight the possible confounding effect of decreasing recruitment threshold with fatigue).

- 2) For MU data grouped across subjects vs. for MU data from individual subjects (to highlight the possible confounding effect of neglecting subject-specific firing adaptations).

## RESULTS AND DISCUSSION

When we assessed the changes in MU firing rate as a function of MU recruitment threshold, we observed a decrease in firing rates during subsequent contractions of the fatigue protocol (Figure 1A). But when the same MU data were analyzed as a function of MUAP amplitude, we found a clear indication that MU firing rates progressively increased throughout the series of fatiguing contractions (Figure 1B). When we assessed the changes in MU firing rate for MU data grouped across all subjects, there was no clear trend in MU firing rate during the fatigue protocol (Figure 1C). But when the same MU data were analyzed for each individual subject, a clear trend for firing rates to progressively increase with

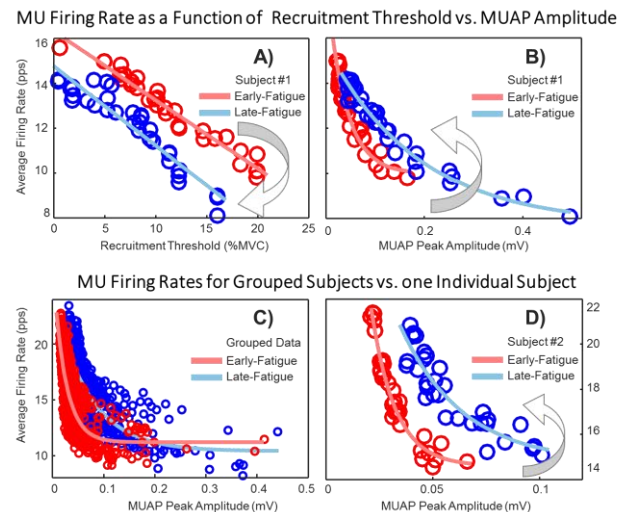


**Figure 1:** Fatigue-induced firing adaptations as a function of recruitment threshold (A) vs. MUAP amplitude (B); and for grouped data (C) vs. a representative subject (D).

fatigue was observed consistently in all subjects (Figure 1D).

Figure 1A and 1B show that the practice of analyzing MU firing rates as a function of recruitment threshold reverses the actual pattern in MU firing adaptation with fatigue that occurs when firing rates are analyzed with respect to MUAP amplitude. The shift to lower frequencies can be considered an epiphenomenon as it is likely caused by the progressive decrease in MU recruitment threshold that occurs during muscle fatigue, which has been suggested to compensate for the progressive decrease in force generation capacity [1,2]. Therefore, as MU recruitment threshold decreases, higher-threshold MUs are recruited at progressively lower forces. Because higher-threshold MUs fire at lower firing rates [3], MU firing rates shift to lower frequencies with muscle fatigue. In contrast, the actual increase in MU firing rate during subsequent contractions is maintained when firing rates are analyzed as a function of MUAP amplitude. Even though MUAP amplitude has also been reported to decrease with fatigue [5], the increase in MU firing rate would only be underestimated but not reversed as a result of a fatigue-induced decrease in MUAP amplitude.

Figure 1C and 1D provide evidence that the practice of grouping MU data across subjects obscures subject-specific firing adaptations with fatigue, which are consistent in trend but differ in magnitude among subjects. Subject-specific differences in the magnitude of the firing adaptations are likely due to

individual differences in muscle mechanical and biochemical characteristics.

## CONCLUSIONS

Our study shows that analyzing MU firing rate as a function of recruitment threshold and grouping MU data across subjects may confound our understanding of MU behavior during muscle fatigue. Analysis practices should be carefully considered when investigating fatigue-induced MU firing adaptations or interpreting conflicting results in the literature.

## REFERENCES

1. McManus L, et al., *J Neurophysiol.* **113**:3186-96, 2015.
2. Vila-Chã C, et al., *Med Sci Sports Exerc.* **44**:616-24, 2012.
3. Contessa P, et al., *J Neurophysiol.* **116**:1579-85, 2016.
4. Nawab S, et al., *Clin Neurophysiol.* **121**:1602-15, 2010.
5. Klein CS, et al., *J Physiol.* **573**:161-71, 2006.

## ACKNOWLEDGMENTS

This work was funded in part by the De Luca Foundation and the National Institute of Neurological Disorders and Stroke of the National Institutes of Health under award number R44NS077526 and R43NS093651. We thank Prof. Carlo J. De Luca (Boston University, Delsys Inc.) for substantial contributions to this work.

# Evidence That Tuning of Muscle Spindles Can Be Decoupled from Muscle Activation

<sup>1</sup>Kian Jalaieddini, <sup>1</sup>Akira Nagamori, <sup>1</sup>Christopher M. Laine, <sup>2</sup>Mahsa A. Golkar  
<sup>2</sup>Robert E. Kearney, <sup>1</sup>Francisco J Valero-Cuevas

<sup>1</sup>University of Southern California, Los Angeles, CA, USA

<sup>2</sup>McGill University, Montreal, QC, Canada

email: jalaiedd@usc.edu, web: <http://valerolab.org/>

## INTRODUCTION

Physiological tremor is the involuntary, rhythmic contraction of muscles in the frequency range of 5-12 Hz. Among other factors, spinal reflex loops have been proposed to lie at the heart of generation, amplification, and persistence of healthy and pathologic tremor [1].

In particular, some reports suggest a strong coupling between physiological tremor and the stretch reflex response—as well as the dependence of stretch reflex amplitude on muscle length [1,2]. Thus, given that stretch reflex amplitude increases with muscle stretch, we hypothesized that muscle stretch would also increase the amplitude of physiological tremor. We tested this hypothesis in the human gastrocnemius muscle by measuring the dependence of physiological tremor on the ankle joint angle.

## METHODS

Seven subjects (2 female) with no history of neuromuscular disease gave informed consent to the experimental procedure approved by the McGill University Institutional Review Board. They lay supine and were instructed to generate tonic, voluntary contractions at 30% of *Maximal Voluntary Contraction* (MVC) of ankle torque aided by real-time visual feedback. Ankle torque and EMG signal from the gastrocnemius muscle were recorded. Three trials lasting 30s each were recorded at three angles (20° plantarflexion, and 5.7° and 8.6° dorsiflexion) in block random order.

Ankle torque was first high-pass filtered at 5 Hz, and its power spectral density was integrated in the physiological tremor range (5-12 Hz) to give the physiological tremor torque power. Also, magnitude-squared coherence between full-wave rectified EMG and torque was calculated to estimate the coupling between muscle activity and torque.

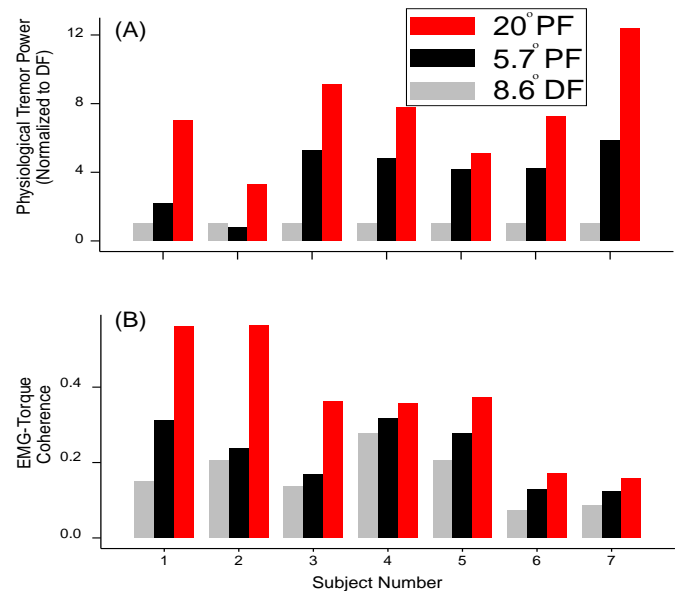


**Figure 1:** Experimental results: (A) physiological tremor and (B) EMG-torque coherence increase from dorsiflexed to plantarflexed angle.

Lastly, a computational model was used to disambiguate neuromechanical contributions to modulation of physiological tremor. This published model has successfully replicated physiological tremor by including muscle-tendon, muscle spindle, Golgi tendon organ and signal dependent noise modules [1]. Given the dynamic and stochastic elements of the model, each isometric gastrocnemius muscle force at 30% MVC was simulated 10 times at each experimental condition. The simulation data were processed using analyses similar to those explained for the experimental data.

## RESULTS AND DISCUSSION

Figure 1A shows that physiological tremor torque power changed consistently as a function of ankle angle; but was always larger in the plantarflexed angle compared to mid and dorsiflexed angles. Thus, physiological tremor was inversely related to muscle

length (i.e., Figure 1A, shorter muscle lengths leads to larger physiological tremor) which contradicts our original hypothesis.

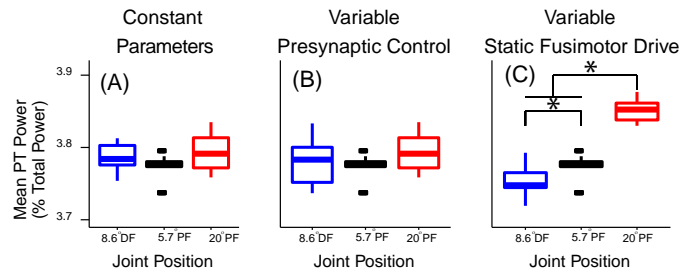


**Figure 2:** Simulations of physiological tremor as a function of joint angle: (A) all the model parameters except muscle-tendon length were kept constant; (B) presynaptic inhibition increased at the dorsiflexed angle; (C)  $\gamma$ -static fusimotor drive increased from the dorsiflexed to plantarflexed angles. Modulation of  $\gamma$ -static fusimotor sufficed to replicate the experimental observations.

Figure 1B shows that EMG-torque coherence, in the physiological tremor frequency range, also consistently increased with plantarflexion. Thus, the coupling between EMG and torque increased with the tremor torque power. Consequently, changes in physiological tremor were likely of neural origin.

We used our model to explore the relationship between physiological tremor and muscle length. First, we held all model parameters constant—except for muscle-tendon length. We found no consistent dependence of tremor on muscle length, indicating that our experimental observations could not be explained solely by changes in joint angle and the induced change in the activity of muscle afferents (Figure 2A).

Then we explored neural factors by varying the gains of the afferent feedback using presynaptic inhibition (i.e. spinal gains, Figure 2B) and fusimotor control (i.e. spindle tuning, Figure 2C) [3]. We implemented the effect of increasing presynaptic inhibition with dorsiflexion angle as has been reported in previous H-reflex studies [4]. This modulation had little impact on physiological tremor as Figure 2B demonstrates. We then tested the effect of fusimotor drive and found that increasing the  $\gamma$ -static fusimotor drive produced an increase in physiological tremor with plantarflexion (i.e., muscle shortening, Figure 2

C). Modulation of  $\gamma$ -dynamic fusimotor drive had no effect.

## CONCLUSIONS

In contrast to the understanding of the relationship between stretch reflex and physiological tremor in the literature, we found that tremor amplitude increased when muscle was shortened. A published computational model of afferented muscle-tendon systems could only replicate these experimental results when  $\gamma$ -static fusimotor drive (but not  $\gamma$ -dynamic) increased as the muscle shortened. This describes a novel mechanism for the control of  $\gamma$  fusimotor drive, which deviates from the widely-accepted  $\alpha$ - $\gamma$  co-activation hypothesis. This work provides a mechanistic approach to interrogate the details of such deviation in future studies. These new findings will also begin to fill important gaps in our knowledge of fusimotor activity that has important clinical implications. By providing a long-needed noninvasive experimental means to probe the fusimotor activity, it is now possible to understand the role of healthy and pathological reflex-driven mechanisms in health and multiple neurological conditions.

## REFERENCES

1. Laine CM, et al. *Front Comput Neurosci*, 10, 2016.
2. Mirbagheri MM, et al. JG, et al. *Exp. Brain Res* 4, 2000.
3. Pierrot-Deseilligny E and Mazevet D, *Neurophysiol Clin*, 30, 2000.
4. Hwang IS, *J of Electromyogr Kinesiol*, 12, 2002.

## ACKNOWLEDGMENTS

This study was supported by NIH-NIAMS under award numbers R01AR050520 and R01AR052345 grants to FVC. The contents of this endeavor is solely the responsibility of the authors and does not necessarily represent the official views of the National Institutes of Health. This work was also supported by the Canadian Institutes of Health Research to REK and the Fonds Québécois de la Recherche sur la Nature et les Technologies to KJ and MAG.

# ARE YOU STIFF ENOUGH TO RESPOND TO FOAM ROLLING? A DEPENDENCY ON TISSUE PROPERTIES

Nicolai Kram\*, René Schrader, Thomas L. Milani, Freddy Sichtung

Chemnitz University of Technology, Department of Human Locomotion, Chemnitz, Saxony, Germany

\*email: nicolai.kram@hsw.tu-chemnitz.de, web: <https://www.tu-chemnitz.de/index.html>

## INTRODUCTION

The application of foam rolls in therapeutic settings is increasing continuously, although the mechanisms inside the human body are not yet fully understood. It is thought that a so-called self-myofascial release (SMR) can reduce the tensional state of muscles and fibrous connective tissues which could highlight the importance of foam rolling for medical conditions, e.g. plantar fasciitis [1,2]. However, there are currently no studies on basic research on this topic.

We hypothesize that eight weeks of whole-body SMR can reduce stiffness properties of plantar fascia, Achilles tendon and M. gastrocnemius.

## METHODS

This longitudinal study included 76 healthy subjects (26 men, 50 women, age  $24.7 \pm 4$  yrs, weight  $68.6 \pm 15$  kg, height  $174 \pm 9.5$  cm). They were divided into a control (CG,  $n = 38$ ) and a foam rolling group (FRG,  $n = 38$ ). Participants with a body mass index greater than  $25 \text{ kg/m}^2$  were excluded.

Stiffness [N/m] was measured non-invasively for the following structures using myometry (MyotonPro, Myoton AS, Estonia) in a lying position:

- Plantar fascia (PF), about 15cm posterior from the calcaneus on the medial portion of PF
- Achilles tendon (AT), between the medial and lateral malleoli
- M. gastrocnemius (MG), 20cm above AT

The measurements were realized within one week before and one week after eight weeks of whole-

body SMR with focus on the lower extremities. The 16 sessions (2 sessions à 20 min per week) were instructed by the examiners. The standardization of the foam rolling was ensured by a speed of five seconds per direction for each structure and a pain scale.

Wilcoxon test and regression analysis were used for statistical evaluation.

## RESULTS AND DISCUSSION

After eight weeks, foam rolling causes a significant decrease of 7.4% for PF stiffness ( $p < 0.05$ ). Further, a significant reduction of 4.8% was observed for MG ( $p < 0.05$ ), while no difference was found for AT (-1.4%). The control group remained at constant levels.

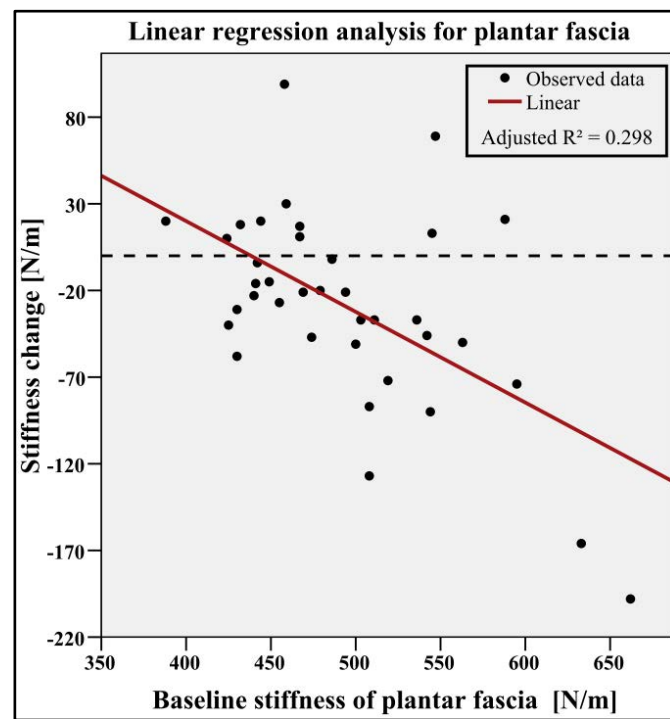


**Figure 1:** Linear regression of the stiffness change of PF of the FRG ( $p = 0.0003$ )

The regression analysis of the baseline stiffness and its change after eight weeks results in an adjusted coefficient of determination ( $R^2$ ) of 0.3 for PF (Fig. 1) and 0.26 for MG (both  $p < 0.05$ ). After the subdivision of the data of the FRG in low, middle and high stiffness groups, a clear trend is obvious for PF and MG. PF shows reductions of 2.5% to 4.2% to 9.8% while MG stiffness decreases by 0.8% to 4.4% to 7.5% (Table 1). Again, the CG shows no difference.

**Table 1:** Descriptive statistics of the influence of low, middle and high tissue stiffness levels on the outcome of an SMR intervention.

	<b>Low</b> (n = 12)	<b>Middle</b> (n = 13)	<b>High</b> (n = 13)
<b>PF</b>	-2.5%	-4.2%	-9.8%
<b>MG</b>	-0.8%	-4.4%	-7.5%
<b>AT</b>	1.4%	1.6%	-3.5%

Eight weeks of SMR with foam rollers provide evidence for the first time that stiffness of MG and PF can be reduced. In contrast, the AT shows no change. Thus, there are no consistent results for the connective tissues (PF, AT).

To better understand the tissue response, we further examined whether the effect of a SMR is influenced by the baseline value of tissue stiffness. The adjusted  $R^2$  for both PF and MG shows an obvious influence of foam rolling on tissue stiffness in dependence on the tissue's baseline value (Fig. 1). The formed groups of high, middle and low stiffness also support our assumption (Table 1).

These findings demonstrate for the first time that fibrous connective tissues and muscles may react to a given stimulus in a stiffness-dependent way: The stiffer the tissue, the greater the impact of an SMR intervention, except for the AT. An explanation might be an insufficient stimulus to trigger adaptation processes of the AT as it is the strongest tendon of the human body [3]. The decrease of PF stiffness may be explained by mechanotransduction pathways of fibroblasts [4,5,6], while the reduction of MG stiffness could be due to change in muscle tone. More research is necessary to explain the mechanisms behind our results.

## CONCLUSIONS

Especially the reduction of high tissue stiffness may be important to treat or prevent medical conditions like plantar fasciitis [2].

It is important to understand how the human body reacts to different stimuli like foam rolling to better understand adaptation processes. Therefore, stiffness properties of fibrous connective tissues and muscles are important for tissue reactions and should be in the focus of future studies.

## REFERENCES

1. Beardsley, C & Škarabot, J. *J Bodyw Mov Ther* **19**, 747-758, 2015.
2. Wearing, S et al. *Sports Med* **36**, 585-611, 2006.
3. Doral, MN et al. *Knee Surg Sports Traumatol Arthrosc* **18**(5), 638-643, 2010.
4. He, Y et al. *Connect Tissue Res* **45**, 28-39, 2004.
5. Archambault, J et al. *J Biomech* **35**, 303-309, 2002.
6. Zheng, L et al. *J Biomech* **45**, 2368-2375, 2012

# NOVEL COUPLED FRAMEWORK OF IN VITRO AND IN SITU ANALYSIS FOR INVESTIGATING INTRAMUSCULAR FORCE TRANSMISSION WITH AND WITHOUT INJURY

<sup>1</sup> Amanda M. Meppelink, <sup>1</sup> J. David Remer, <sup>1</sup> Xiao Hu, <sup>1</sup> Juliana A. Passipieri,  
<sup>1</sup> George J. Christ and <sup>1</sup> Silvia S. Blemker

<sup>1</sup> University of Virginia, VA, USA  
 email: ssblemker@virginia.edu

## INTRODUCTION

Volumetric muscle loss (VML) injuries can occur in a variety of traumatic injuries and congenital diseases where there is a permanent loss of muscle function. Current treatment options for VML injury are limited to physical therapy and functional free muscle transfer, in which a healthy muscle from the patient is transplanted to the injury site to restore motor function and joint movement. However, these procedures are associated with poor engraftment and donor site morbidity. Alternative therapies are being developed, but the lack of mechanistic insight greatly limits development of therapeutic strategies.

The latissimus dorsi (LD) muscle of rodents is a well-established model for VML injuries, and the current standard for assessing functional recovery after VML injury is to quantify muscle force using an organ bath system after muscle excision [1]. Although this system provides consistent results, only a portion of the muscle is fixed longitudinally. However, a more physiologically relevant characterization of the

muscle force can be achieved using the *in situ* method, where the LD is maintained and anchored in its native environment [2]. We used both testing methods in combination with biomechanical analysis to understand the mechanisms of force transmission in un-injured and injured muscles.

## METHODS

Volumetric muscle loss injuries of size 1.5 x 1.2 cm were assessed in the latissimus dorsi muscle of rats. After 2 months, unrepaired VML injuries were compared to native muscles in 20-week rats. In the *in vitro* method, whole LD muscles were explanted and studied using an organ bath system [1]. The muscles were mounted in an organ bath chamber containing Krebs-Ringer bicarbonate buffer. The distal tendon was attached to a fixed support, and the proximal tendon was attached to the lever arm of a force transducer. Maximum isometric force was determined based on applying direct muscle electrical stimulation at varying frequencies.

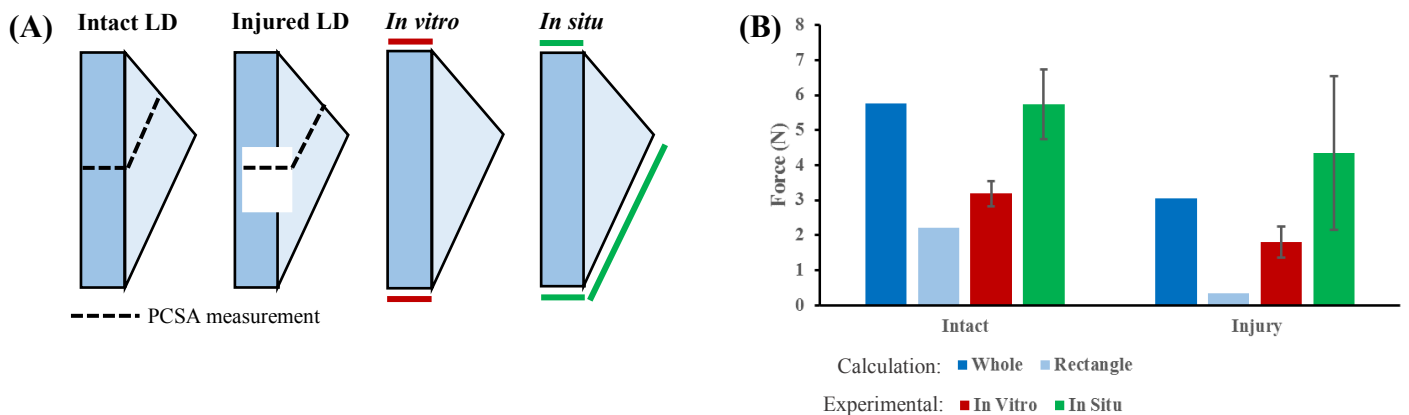


**Figure 1:** (A) Schematics of the rat LD represented as rectangle and fan parts and different fixation methods. VML injury, shown as a white rectangle, is in both parts. (B) Calculated LD forces reveal mechanisms of force production measured experimentally.

In the *in situ* method, the LD muscle was minimally dissected and maintained in its native environment with blood supply and nerve innervation. A nerve cuff was placed around the motor nerve and the muscle's distal tendon was attached to the lever arm of a force transducer. The nerve was then stimulated and the peak isometric forces were measured at a range of stimulation frequencies.

To better understand the biomechanical mechanisms of the two different experimental methods, we developed a simplified geometric representation of the muscle to calculate the contractile force, assuming all forces measured were transmitted longitudinally along the length of the muscle fibers (Fig. 1A). To do these calculations, the muscle was simplified as polygonal geometry, consisting of a rectangle portion and triangular portion. Size and thickness were determined based on dissected LD muscles from 20-week rats. In the mid-section of both portions, the physiological cross-sectional area (PCSA) was calculated. Then using a specific tension ( $\sigma_o$ ) of 0.115 N/mm<sup>2</sup>, the total force was determined for each portion (Eqn 1) as well as the entire muscle (Eqn 2).

$$F = PCSA * \sigma_o \quad (1)$$

$$F_{whole} = F_{rect} + (F_{fan} * \cos(28.16^\circ)) \quad (2)$$

## RESULTS AND DISCUSSION

The *in situ* force measurements were approximately twice as large as the *in vitro* forces for intact and injured muscles (Fig. 1B). The *in vitro* setup anchored only the rectangular portion of the muscle and was expected to capture the longitudinal force production. The *in situ* setup anchored both the longitudinal and pennate fibers of the muscle, and given that a much larger portion of the muscle was anchored, it was expected to produce larger forces than the *in vitro* setup. With an injury, nearly the entire rectangular portion of the muscle was removed, yet both testing methods revealed

substantial force production. This observation of the *in vitro* data pointed toward lateral transmission as the underlying mechanism of force production.

The calculated force (assuming all longitudinal force transmission) for the whole LD in the intact muscles was consistent with the *in situ* measurement, suggesting that when all areas of attachment are fixed, longitudinal force transmission dominates force production (Fig. 1B). The calculated force for the injured LD was within one standard deviation of the measurements, though the average was approximately 30% lower than *in situ* measurements. In the intact muscle, the *in vitro* force production (3.19 N) was higher than the rectangular portion (2.21 N), suggesting that the untied fan portion of the muscle likely contributes to the measured force via lateral force transmission. Further, the *in vitro* method (1.8 N) measured a force significantly larger than the rectangular portion (0.33 N), even though only the longitudinal portion was fixed during testing. Therefore, lateral force production from the fan was inferred to be contributing to force production. Moving forward, the observations from this study can be further explored and developed using finite-element modeling.

## CONCLUSIONS

The experimental testing differences between *in vitro* and *in situ* analysis allowed force production to be measured in both longitudinal fibers alone or in combination with pennate fibers. Capitalizing on this distinction, we were able to demonstrate through experimental and biomechanical analysis that lateral force transmission likely affects force production in the cases where not all fibers are fixed end-to-end.

## REFERENCES

1. Corona, et al. *Tissue Eng Part A* **18**, 1213-1228, 2012.
2. Chen, et al. *J Plast Reconstr Aesthet Surg* **66**, 1750-1758, 2013.

# ELASTIC SHAPE CHANGE AND MECHANICAL BEHAVIOR IN THE APONEUROSSES OF JUMPING AND LANDING TURKEYS

<sup>1</sup> Christopher J. Arellano, <sup>2,3</sup> Nicholas J. Gidmark, <sup>2</sup> Nicolai Konow, and <sup>2</sup> Thomas J. Roberts

<sup>1</sup> University of Houston, Houston, TX, USA

<sup>2</sup> Brown University, RI, USA

<sup>3</sup> Knox College, IL, USA

email: [carellano@uh.edu](mailto:carellano@uh.edu), web: <http://uh.edu/class/hhp/people/cjarellano>

## INTRODUCTION

Aponeuroses are sheet-like elastic structures that undergo complex patterns of biaxial shape change during muscle contractions [1]. In our recent work [2], we suggested that the force resulting from radial expansion (i.e. muscle bulging) of shortening muscle fibers *in situ* drives an increase in aponeurosis width, having the potential to influence its mechanical behavior in the longitudinal direction (along the muscle's line of action).

Elastic mechanisms such as tendons serve the important function of amplifying and attenuating power output and input into muscle, modulating the directional flow of energy that allows animals to perform an array of locomotor activities [3]. Aponeurosis shape change is a prime candidate for such a mechanism because it can modulate its longitudinal stiffness and influence the amount of elastic energy storage and release [2]. We tested two hypotheses: **1)** longitudinal stiffness is reduced when aponeurosis width decreases and because elastic energy (EE) storage is inversely proportional to longitudinal stiffness, **2)** a lower longitudinal stiffness will yield greater elastic energy storage for a given amount of force. Our hypotheses were guided by Hooke's law, which for a linear spring states that force is proportional to stiffness and amount of stretch:

$$F = kx$$

Moreover, the elastic energy stored in the spring is the integral of work performed to stretch the spring:

$$EE = \int_i^f kx dx = \frac{1}{2} kx^2$$

Since we are interested in the amount of EE storage for a given amount of force, we substitute  $x = F/k$  into the previous equation to yield:

$$EE = \frac{1}{2} k \left( \frac{F}{k} \right)^2 = \frac{1}{2} \frac{F^2}{k}$$

Therefore, if the force required to stretch the spring is constant, the EE stored in the spring will be inversely proportional to its longitudinal stiffness:

$$EE \propto \frac{1}{k}$$

## METHODS

Following established methods [1,3], small (0.8-1.0 mm diameter) radiopaque markers were surgically implanted along muscle fibers and on the aponeurosis of the lateral gastrocnemius (LG) muscle of three wild turkeys, *Meleagris gallopavo* (Fig. 1). Strain gauges were also implanted on the calcified region of the distal tendon [4].

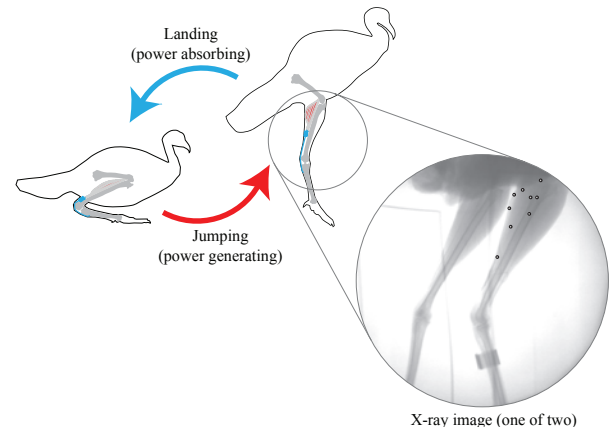


**Figure 1:** In combination with x-ray video, an *in vivo* preparation allowed us to quantify the mechanical behavior of the aponeurosis in landing and jumping turkeys.

*In vivo* measurements of muscle force were combined with high-speed biplanar x-ray video for a series of landing ( $n=16$ ) and jumping ( $n=14$ ) trials. For each trial, radiopaque marker positions were tracked using an established marker-based workflow [3]. We measured the amount of EE storage by plotting MTU force as a function of aponeurosis length and then integrated the area

underneath the curve during the period of force rise from 30N-130N. The linear slope of MTU force versus aponeurosis length during this period was calculated to yield longitudinal stiffness.

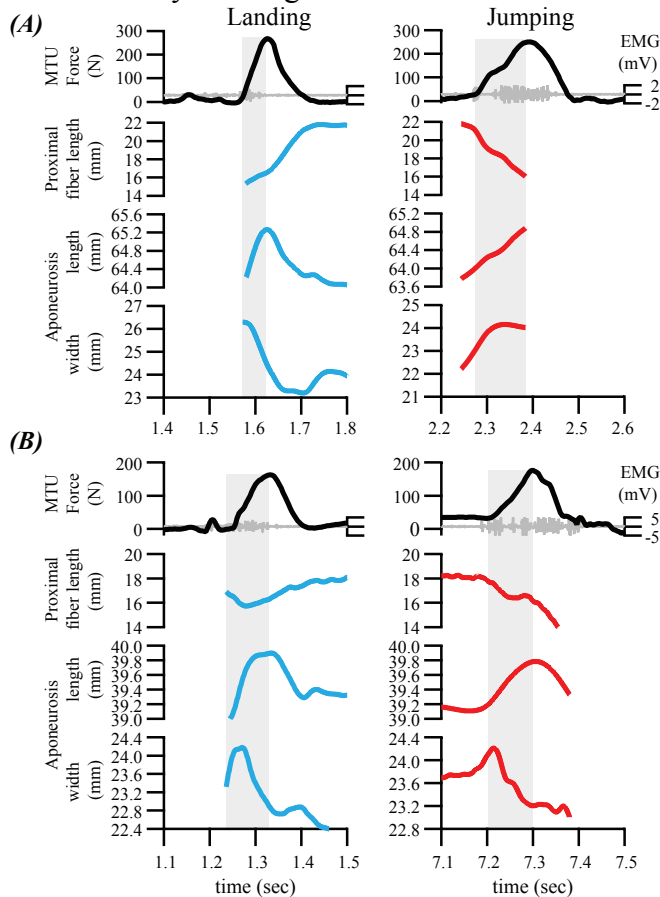


**Figure 2:** Representative trials for two birds (*A and B*). We captured muscle-tendon unit (MTU) force, fiber length, aponeurosis length and width during power absorbing (landing) and power generating (jumping) activities. Shaded regions indicate period of total MTU force rise.

## RESULTS AND DISCUSSION

During MTU force rise, aponeurosis width either increased or decreased. During landing for one bird (Fig. 2A), fiber length increased slightly while aponeurosis length increased and width decreased. During jumping, muscle fibers shortened while aponeurosis length and width increased. Another bird (Fig. 2B) shows the same fiber and aponeurosis behavior during landing. During jumping, however, fibers shortened while aponeurosis length increased and width decreased. To understand the influence of aponeurosis width on the mechanical behavior in the longitudinal direction, we compared trials where aponeurosis width either increased or decreased, irrespective of whether the bird jumped or landed.

*EE Storage and Longitudinal Stiffness:* When aponeurosis width decreased during periods of MTU force rise (Fig. 3A), the elastic energy stored in the aponeurosis was 28% higher ( $p=0.041$ , Fig. 3B) and its longitudinal stiffness was 31% lower ( $p=0.005$ , Fig. 3C) when compared to trials where aponeurosis width increased.

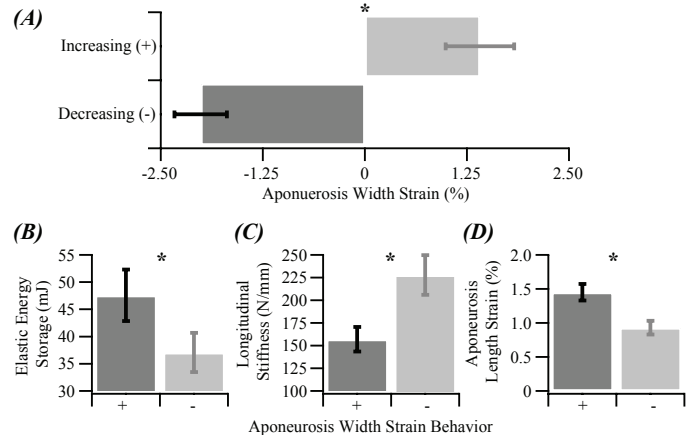


**Figure 3:** Data represent means  $\pm$  S.E.M. for aponeurosis width strain (*A*), elastic energy storage (*B*), longitudinal stiffness (*C*), and aponeurosis length strain (*D*).  $p < 0.05$ .

## CONCLUSIONS

Our findings support our hypotheses that longitudinal stiffness decreases when aponeurosis width decreases and thus, this biological spring has the capacity to store greater amounts of elastic energy. These data reveal that distinct changes in aponeurosis width during periods of MTU force rise *in vivo* have a profound influence on the mechanical behavior of the aponeurosis in the longitudinal direction

## REFERENCES

1. Azizi and Roberts. *J Physiol* **17**, 4309-4318, 2009.
2. Arellano et al. *J Biomech* **49**, 1812-1817, 2016
3. Roberts and Azizi. *J Exp Biol* **214**, 353-361, 2011.
4. Roberts et al. *Science* **275**, 1113-1115, 1997.

## ACKNOWLEDGMENTS

The authors thank Trovov Walker and Benjamin Scott for their assistance on this project. The National Institutes of Health research grant [AR055295] awarded to TJR and University of Houston's CLASS Research Progress Grant awarded to CJA supported this research.

# Atrophy and Fatty Infiltration of Paretic Elbow Muscles in Individuals with Chronic Hemiparetic Stroke: Preliminary Findings

<sup>1,2</sup>Lindsay Garmirian, <sup>1</sup>Ryan Schmid, <sup>1</sup>Ana Maria Acosta, and <sup>1,2</sup>Julius Dewald

<sup>1</sup>Department of Physical Therapy and Human Movement Sciences, Feinberg School of Medicine, Northwestern University, Chicago, IL

<sup>2</sup>Department of Biomedical Engineering, Northwestern University, Evanston, IL  
Email: Lindsay.Garmirian@u.northwestern.edu

## Introduction

The long-term effects of motor impairments on upper limb muscle architecture are unknown post stroke. It is hypothesized that motor impairments may cause decreased use of the paretic upper limb which, over time, may cause muscle atrophy and fatty infiltration. The aim of this research is to quantify long-term changes in muscle volume and intramuscular fat following hemiparetic stroke in the paretic elbow.

## Methods

Eight participants post stroke, five males and three females were recruited to participate in the study. The average age of the participants was 61 years and the average time since stroke was 13 years. The participants were moderate to severely impaired, with an average score of 23 out of 66 on the upper extremity Fugl-Meyer Assessment of Motor Recovery (range: 12/66 to 33/66).

Magnetic resonance images were acquired using a 3D gradient echo pulse sequence of the upper limb (TR=7ms, flip angle=12°, matrix size = 256x216, slice thickness = 3mm). The Dixon method was used to estimate percent fat using an echotime (TE) of 2.39ms, when water and fat are in phase and a TE of 4.77ms, when water and fat are out of phase. Using AnalyzeDirect, manual segmentation of the biceps, triceps and brachialis was done to measure muscle volume and percent intramuscular fat. Percent fat was calculated using a ratio of the intensity of the fat image compared to the intensity of the water image. The volume of intramuscular fat was calculated for each muscle by multiplying the muscle volume by percent fat. The volume of contractile tissue was determined by subtracting the

volume of intramuscular fat from the total muscle volume.

## Results and Discussion

For all three muscles of interest, the volume of contractile element was significantly larger ( $P<0.05$ ) in the non-paretic limb compared to the paretic (Fig. 1). The non-paretic biceps was 33% larger than the paretic, the triceps was 30% larger and the brachialis was 12% larger.

For all three muscles, the percent intramuscular fat was significantly greater ( $P<0.05$ ) in the paretic limb compared to the non-paretic (Fig 2). The percent intramuscular fat for the non-paretic biceps, triceps and brachialis were 7.2%, 7.0% and 8.1%, respectively. The percent intramuscular fat for the paretic biceps, triceps and brachialis were 9.1%, 9.1% and 10.9%, respectively.

The volume of intramuscular fat, however, was similar between the paretic and non-paretic limbs, for all three muscles (Fig. 3). For the biceps and triceps, the volume of intramuscular fat was greater in the non-paretic limb compared to the paretic. The volume of intramuscular fat was 9.97, 24.91 and 9.82 cm<sup>3</sup> for the non-paretic biceps, triceps and brachialis, respectively. The volume of intramuscular fat was 7.79, 22.24 and 11.04 cm<sup>3</sup> for the paretic biceps, triceps and brachialis, respectively.

This study brings new insight to the way in which intramuscular fat is reported. Intramuscular fat is often reported as a percentage of muscle volume [1,2]. However, this study shows that this can be misleading by suggesting an increase in intramuscular fat, reported as a percentage, may be

due to a decrease in muscle volume not an increase in fat volume.

### Conclusions

The triceps, biceps and brachioradialis muscle volumes in the paretic limb were reduced compared to the non-paretic limb. This was mostly due to a difference in contractile element volume and not a difference in intramuscular fat.

Detailed information about the pattern of atrophy and changes (if any) in intramuscular fat after stroke will help guide and improve rehabilitation. The methods developed in this study can be used as highly sensitive outcome measures to track the efficacy of rehabilitation techniques aimed at reducing and preventing muscle atrophy. Additionally, the muscle volume measures obtained from this study can be used to improve stroke specific musculoskeletal models, since muscle volume is one parameter relied upon for the accurate prediction of joint torques.

Future work involves the study of changes in volumetric measures at more distal muscles. Since distal joints, like the wrist, often experience greater deficits [3] post stroke, changes in muscle and intramuscular fat volumes may be more pronounced for muscles that cross these joints.

### References:

1. Smith AC, Knikou M, Yelick KL, et al. MRI measures of fat infiltration in the lower extremities following motor incomplete spinal cord injury: Reliability and potential implications for muscle activation. *IEEE*; 2016:5451-5456.
2. Goutallier D, Postel J-M, Bernageau J, Lavau L, Voisin M-C. Fatty Muscle Degeneration in Cuff Ruptures: Pre- and Postoperative Evaluation by CT Scan. *Clinical Orthopaedics and Related Research*. 1994;304:78.
3. Kamper DG, Fischer HC, Cruz EG, Rymer WZ. Weakness Is the Primary Contributor to Finger Impairment in Chronic Stroke. *Arch Phys Med Rehabil*. 2006;87(9):1262-1269.

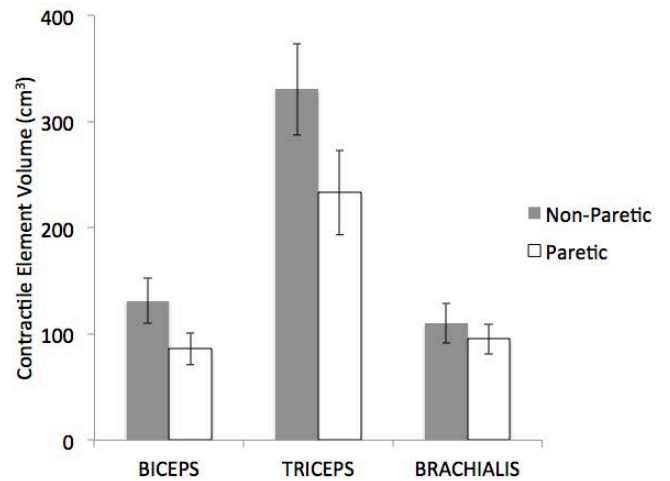


**Figure 1.** Contractile element volume of the biceps, triceps and brachialis muscles in the non-paretic limb compared to the paretic limb.

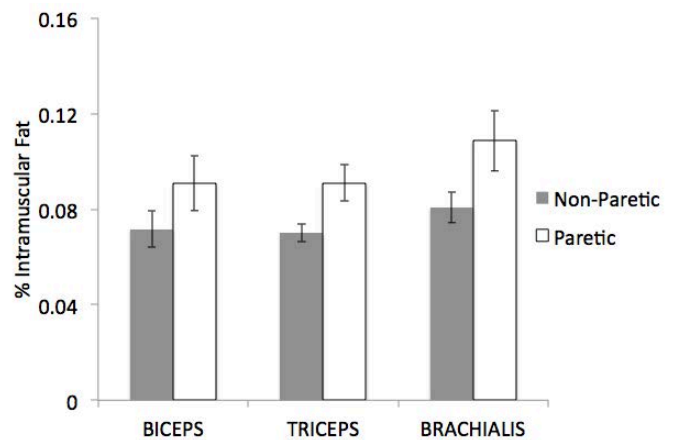


**Figure 2.** Percent intramuscular fat of the biceps, triceps and brachialis muscles in the non-paretic limb compared to the paretic limb.

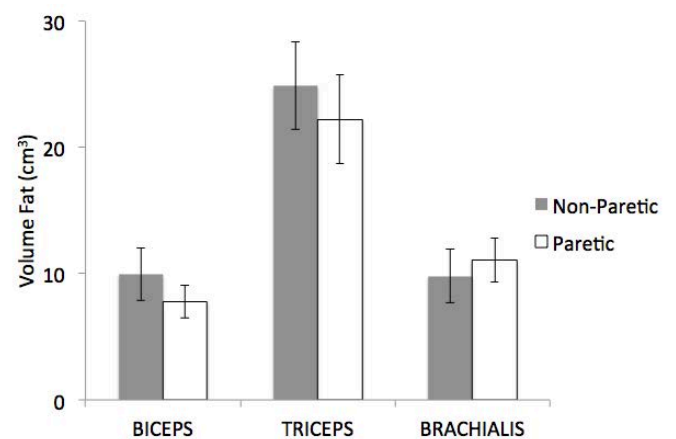


**Figure 3.** Fat volume of the biceps, triceps and brachialis muscles in the non-paretic limb compared to the paretic limb.

# Short Versus Typical Resting Pectoralis Minor Muscle Length: An Investigation of Muscle Elongation and Muscle Length Changes During Overhead Reaching

Jason Mohring, Travis Pollen, Kelly Gerrity, Noel Goodstadt, Margaret Finley, and David Ebaugh

ReHAB Group, Drexel University, Philadelphia, PA, USA

email: [jhm54@drexel.edu](mailto:jhm54@drexel.edu), web: <http://drexel.edu/cnhp/academics/departments/Physical-Therapy/>

## INTRODUCTION

Aberrant scapular position and movement are believed to contribute to shoulder pain and dysfunction which is a common reason for seeking medical attention [1]. Resting pectoralis minor muscle (PMm) length has been proposed to be a contributing factor to shoulder pain as length of this muscle is thought to influence positioning and movement of the scapula on the thorax [1-3].

Previous research has found that individuals with a short resting PMm length demonstrate scapular kinematics similar to individuals with shoulder impingement syndrome [2]. These researchers theorized that PMm passive tension may be a cause of these aberrant movements; however, PMm elongation (amount the muscle can be stretched) was not measured in their study. The purposes of this research were to determine if: 1) active and passive PMm elongation differed in individuals with short and typical resting PMm lengths, and 2) PMm length change during an overhead reaching task differed between groups.

## METHODS

Twenty-six participants (17 females, age =  $26 \pm 4$  years, height =  $1.69 \pm 0.08$  m, mass =  $66.3 \pm 10.4$  kg), who were asymptomatic for shoulder pathology, volunteered for this study. The study was approved by Drexel University's Institutional Review Board and participants provided written informed consent. PMm length at rest and during active and passive stretch conditions (Figure 1) was measured using a Palpation Meter (Performance Attainment Associates, St. Paul, MN). PMm length was measured as the distance between the coracoid process and the inferior medial aspect of the fourth rib. For active stretch condition, participants were asked to maximally elevate and retract their scapula

(Figure 1B). The passive stretch condition was performed by a physical therapist. The participants arm was placed in approximately  $30^\circ$  of flexion. The therapist placed their hand on the distal humerus and, while stabilizing the participant's spine, pushed their shoulder in a superior/posterior direction until firm tissue resistance was encountered (Figure 1C). Previous research has shown excellent intra- and inter-rater reliability for all measurement conditions [4]. Intra- and inter-rater reliability for resting, active and passive PMm length measures ranged from  $ICC_{3,2} = 0.84-0.92$  and  $ICC_{2,2} = 0.80-0.90$ , respectively. Resting PMm length was normalized to height to calculate the pectoralis minor index (PMI) which was used to assign subjects to groups: short ( $PMI < 8.9$ ) and typical ( $8.9 \leq PMI < 10.5$ ) [2]. PMm muscle elongation (percent change) was determined by  $[(\text{active or passive length} - \text{resting length})/\text{resting length}] * 100$ .

Three-dimensional shoulder girdle kinematics were collected at 100Hz with the Flock of Birds electromagnetic motion capture system (Ascension Technology Corporation, Shelburne, VT) and The Motion Monitor™ software (Innovative Sports Training, Inc., Chicago, IL). Sensor placement was based on the International Society of Biomechanics recommendations for shoulder kinematics [5]. Additional landmarks of the coracoid process and fourth rib were digitized to measure PMm length. Three trials of dominant side scapular plane humeral elevation were used for data analysis. A custom Matlab (MathWorks, Natick, MA) program was used for data processing. PMm length change during overhead reaching was defined as the change in length from rest to  $120^\circ$  of humeral elevation. PMm length change (percent change) was determined by  $[(\text{PMm length at } 120^\circ \text{ of humeral elevation} - \text{PMm length at rest})/\text{PMm length at rest}] * 100$ .

PMm elongation during active and passive lengthening, and PMm length change during overhead reaching, respectively, were compared between groups with separate independent t-tests ( $p < 0.05$ ).

## RESULTS AND DISCUSSION

Active and passive PMm elongation and PMm length change during overhead reaching were similar between groups (Table 1).

**Table 1:** PMm elongation and overhead length changes (mean  $\pm$  standard deviation).

Variable	Short	Typical	P-Value
Active Elongation	14.7 $\pm$ 5.5%	14.0 $\pm$ 7.3%	0.80
Passive Elongation	19.2 $\pm$ 7.6%	19.1 $\pm$ 6.4%	0.95
Overhead Length Change	16.6 $\pm$ 0.4%	16.0 $\pm$ 0.7%	0.80

To the best of our knowledge we are the first to report PMm active and passive elongation values and muscle length change during overhead reaching. Our results indicate that those with short resting PMm length exhibit similar muscle elongation and muscle length changes during overhead motions as those with typical resting PMm length. Borstad and Ludwig found that individuals

with a short PMm displayed increased scapular internal rotation and reduced posterior tilt compared to individuals with a long PMm [2]. They hypothesized that passive tension of the PMm may have contributed to altered scapulothoracic motion [2]. However, the present findings cast doubt upon the belief that individuals with a short resting PMm length have PMm tightness. Populations differed between the two studies. In our study, individuals with short and typical resting PMm length were compared, whereas Borstad and Ludwig compared short versus long resting PMm length.

## CONCLUSIONS

No differences were found in PMm elongation or length change during overhead motions between individuals with short and typical resting PMm lengths. These findings indicate that resting PMm length is not appropriate for determining whether or not the PMm is tight.

## REFERENCES

1. Morais N, Cruz J. *Phys Ther Sport* **17**, 1-13, 2016.
2. Borstad JD, Ludwig PM. *J Orthop Sports Phys Ther* **35**, 227-238, 2005.
3. Ludwig PM, Reynolds JE. *J Orthop Sports Phys Ther* **39**, 90-104, 2009.
4. Finley, M. *Braz J Phys Ther*, 2017. In Press.
5. Wu G, et al. *J Biomech* **38**, 981-992, 2005.

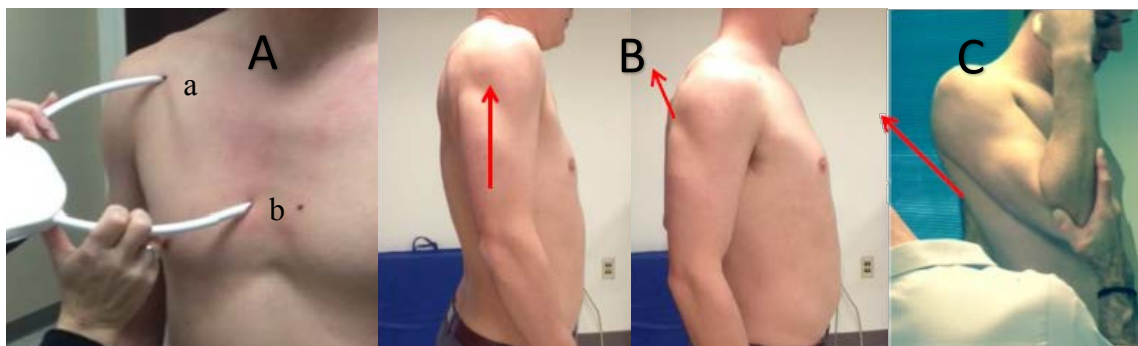


**Figure 1:** Pectoralis minor muscle (PMm) length measurements are taken from the coracoid process (a) to the 4<sup>th</sup> rib (b). (A) Resting PMm length. (B) Actively stretched PMm. (C) Passively stretched PMm.

# ULTRASOUND-BASED ESTIMATES OF ACHILLES TENDON MOMENT ARM DEPEND ON THE METHOD OF JOINT AXIS IDENTIFICATION

<sup>1</sup>Francesca E. Wade, <sup>2</sup>Gregory S. Lewis, and <sup>1</sup>Stephen J. Piazza

<sup>1</sup>The Pennsylvania State University, University Park, PA

<sup>2</sup> Penn State College of Medicine & Milton S. Hershey Medical Center, Hershey, PA  
email: piazza@psu.edu web: www.biomechanics.psu.edu

## INTRODUCTION

The plantarflexion moment arm of the Achilles tendon (ATma) influences the mechanical advantage of the triceps surae and is thus a critical determinant of the mechanics of push-off during walking. ATma may be measured *in vivo* from magnetic resonance images as the planar distance from the center of talocrural joint rotation (determined from relative bone motions) to the tendon line of action [1] or by quantifying tendon excursing using ultrasound and relating it to joint rotation [2]. More recently, a hybrid technique has been described in which ATMA is found as the 3D distance from the tendon line of action to the ankle joint center [3,4]. In this technique, the ankle joint center is approximated by the midpoint of the transmalleolar axis, located using retroreflective markers placed over the malleoli. The tendon is located using an ultrasound imaging probe with markers affixed to it in order to locate the tendon within the laboratory.

There is some question, however, as to whether the transmalleolar midpoint or transmalleolar axis are adequate representations of the center or axis of ankle rotation. Roentgen stereophotogrammetric studies of bone motions have revealed the axis of talocrural rotation to differ from the transmalleolar axis and move during dynamic tasks [5]. An approach in which measured motion of the foot with respect to the shank is used to locate the center or axis of rotation may provide better estimates of ATma in the hybrid technique. For example, finite helical axis decomposition of foot-shank rotations may yield improved estimates of the axis of rotation.

The purpose of this study is to quantify ATma using an ultrasound-based geometric method similar to the hybrid approach, with (1) the axis of rotation taken to be the transmalleolar axis (TA); (2) the center of rotation taken to be the transmalleolar midpoint (TM); and (3) a “functional” axis of rotation determined from finite helical axis decomposition

(FA). We hypothesized that ATma estimated using the FA will differ from those obtained using TA and TM, and that ATma computed from TM will be larger than those found from TA.

## METHODS

Eight participants (3 men, 5 women, age:  $27 \pm 6$  years, height:  $1.70 \pm 0.07$  m, mass:  $69 \pm 11$  kg) were recruited for the study. All experimental procedures had the approval of the Institutional Review Board of The Pennsylvania State University. A LogicScan 128 ultrasound probe (HL9.0/60/128Z-2; Telemed) was strapped in place with Coban (3M) elastic wrap over the right Achilles tendon below the musculotendinous junction, with four markers attached to the probe. Additional markers were placed on the right lateral and medial femoral epicondyles and malleoli, and clusters of four markers each were placed on the shank and the heel.

The participants were instructed to rise and lower on their toes in time to a 1 Hz metronome for three seconds, and each of these trials was repeated three times. This was followed by unloaded trials in which the subject stood on the left leg while performing right foot plantar- and dorsiflexion motions at 1 Hz, with the knee fully extended. Marker motions were captured with six Eagle cameras (Motion Analysis Corp.) operating at 100 Hz, whilst the synchronized ultrasound image data were sampled at 15 Hz.

Data processing and image analysis were performed using custom-written routines in MATLAB (MathWorks, Inc.). For the TA and FA methods, ATma was computed as the shortest distance between each axis and the tendon line of action, identified from ultrasound images and transformed to the ground reference frame. For the TM method, ATma was found as the shortest distance between the transmalleolar midpoint and the tendon line of action. Ankle joint angles were computed using Euler/Cardan angles and a modified version of the

ISB joint coordinate system recommendations for the ankle [6].

Each ATma was plotted against plantarflexion-dorsiflexion angle. A second-order polynomial was fit to the ATma versus angle points and these fits were used to estimate moment arms in neutral position (0°) and 15° plantarflexion. Pearson's correlations were computed to quantify relationships between the ATma, and repeated-measures two-way ANOVAs were used to determine differences in ATma at neutral and 15° PF between methods (TA, TM, FA) and loading conditions (loaded, unloaded) in SPSS (v23, IBM, USA) with  $\alpha = 0.05$ .

## RESULTS AND DISCUSSION

ATma in neutral position and 15° PF computed using FA were larger than corresponding values computed from TA or TM (all  $p < 0.05$ ) (Fig. 1). ATma computed from FA in neutral position were strongly correlated with both TM ( $r = 0.72$ ,  $p < 0.05$ ) and TA ( $r = 0.69$ ,  $p = 0.06$ ), but ATma from FA was more closely approximated by ATma from TM and was underestimated by ATma from TA (Fig. 2).

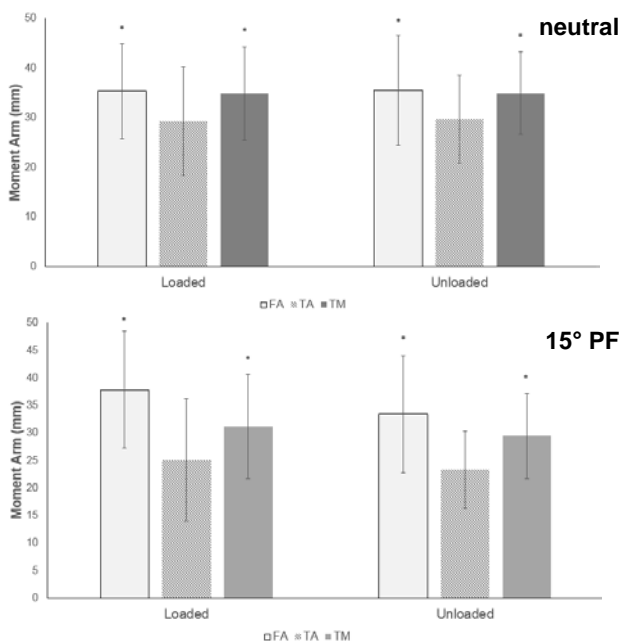


**Figure 1.** Achilles tendon moment arm for loaded and unloaded trials with the ankle in neutral position (top) and 15° PF (bottom). Asterisks denotes significant differences when compared with TA.

ATma computed from FA or TM in the loaded condition were similar in magnitude to those previously reported for the hybrid technique [3]. ATma from FA in the loaded condition increased

with plantarflexion, following a pattern previously measured using MR imaging [1]. This pattern was not observed, however, with ATma from TA or TM. These results suggest that the combination of ultrasound, motion capture, and a joint axis determined via helical axis decomposition may provide a reasonable approximation of ATma measured using MR imaging.

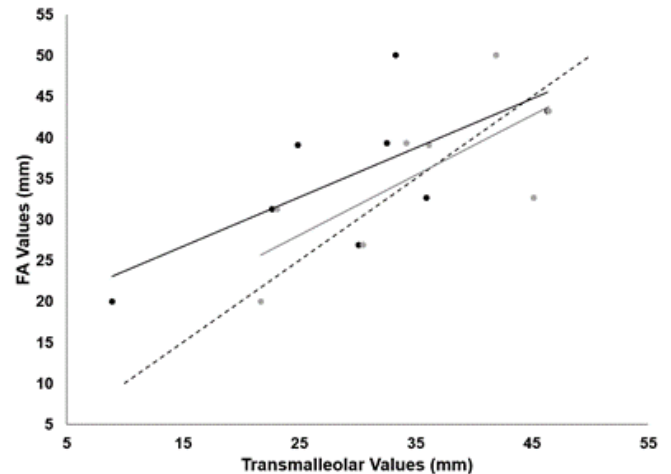


**Figure 2.** ATma at neutral position from FA plotted versus ATma from TA (black) and versus ATma from TM (gray). The dashed line represents  $y = x$ .

## CONCLUSION

The FA and TM methods give ATma similar to each other and to values previously reported. ATma from FA varies with joint angle in a manner consistent with ATma computed from MR imaging, whilst ATma from TM did not. Using ultrasound and motion capture to estimate ATma is an easier and cost-effective alternative to MRI, but the manner in which the joint center or axis is characterized may affect moment arm estimates in important ways.

These results imply that using ultrasound and a FA approximation of talocrural rotation may be a low-cost and portable method of obtaining three-dimensional ATma, providing insight into locomotor mechanics that may not otherwise be possible.

## REFERENCES

1. Maganaris C, et al. *J Physiol* **510**, 977-985, 1998
2. Fath F, et al. *J Appl Physiol* **109** 1644-1652, 2010
3. Manal K, et al. *Physiol Reports* **1**, e00139, 2013.
4. Rasske K, et al. *Comput Methods Biomech Biomed Engin* **20**, 201-205, 2016.
5. Lundberg A, et al. *J Bone Jt Surg* **71**, 94-99, 1989.
6. Wu G, et al *J Biomech* **35**, 543-548, 2002.

# COMPARISON BETWEEN INTRAOPERATIVE MEASUREMENT AND BIOMECHANICAL MODELING TO DETERMINE HUMAN VASTI SARCOMERE LENGTH

<sup>1</sup>Jongsang Son, <sup>2</sup>Andy Indresano, <sup>2</sup>K. Sheppard, <sup>2</sup>Samuel R. Ward, and <sup>1,2</sup>Richard Lieber

<sup>1</sup>Rehabilitation Institute of Chicago, Chicago, IL, USA

<sup>2</sup>University of California, San Diego, CA, USA

email: rlieber@ric.org

## INTRODUCTION

Elucidating the design and function of human skeletal muscles is required to understand normal function and pathological conditions, and to suggest surgical interventions to recover function after injury. One of the most important structures that can be used to elucidate muscle design is the sarcomere [1], the functional unit of force generation in muscle whose length is an excellent predictor of active muscle force [2].

Biomechanical models, based on previously published muscle, joint and tendon properties, is one approach used to understand musculoskeletal function. However, the vast majority of these theoretical models are not validated against primary experimental data. It is also fair to critique most human experimental measurements as not being explained theoretically using models to provide a mechanistic understanding of experimental results.

Thus, the purpose of this study was to compare human vasti sarcomere lengths measured intraoperatively during knee flexion in joint replacement patients to biomechanically-determined sarcomere lengths determined using a theoretical model generated from independent muscle and joint measurements on cadaveric specimens.

## METHODS

Sarcomere length was measured from human patients ( $n=7$ ) using a protocol approved by the Committee on the Use of Human Subjects at the University of California, San Diego and the Department of Veterans Affairs, San Diego. Measurements were performed on vastus lateralis (VL) and vastus medialis (VM) muscles of patients

undergoing total knee replacement. After exposing the VL and VM, a muscle clamp was used to obtain a sample when the knee was flexed to  $45^\circ$  ( $0^\circ$  is full extension) and with the knee flexed to  $90^\circ$  taking care to maintain natural muscle planes and lengths. Sarcomere length was measured by diffraction [3].

To provide independent input data for a biomechanical model, cadaveric lower extremities were used for determination of moment arm and muscle architecture ( $n=10$ ). Tendon excursion of patellar tendon and knee joint angle was measured as described in [4] while the knee was passively ranged from  $0-100^\circ$  of flexion. Then, muscle architectural measurements, such as muscle mass, muscle length, fiber length, pennation angle, and sarcomere length, were measured as in [5].

To predict sarcomere length with respect to knee joint angle, a modified Hill-type musculotendon model [6] for each VL and VM was created for each cadaveric specimen. Muscle-tendon length was determined from tendon excursion data and measured muscle length.

To compare intraoperatively-measured and predicted sarcomere VL and VM length, a paired  $t$ -test was performed with a significance level ( $\alpha$ ) of 0.05, using SPSS Statistics (version 21, IBM, Chicago).

## RESULTS AND DISCUSSION

Intraoperatively-measured sarcomere length in the VM was significantly longer, by about  $0.5 \mu\text{m}$ , than VL ( $p<0.01$ ), for both joint angles, and sarcomere length increased by  $\sim 0.5 \mu\text{m}$  when the knee was flexed from  $45^\circ$  to  $90^\circ$  (Figure 1). These data demonstrate that sarcomere length is consistent among humans for a given muscle and that

sarcomere length for VM is consistently longer than that of the VL.

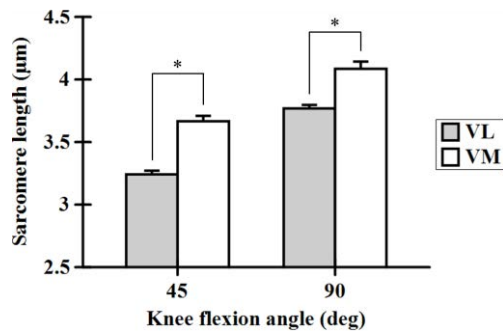


**Figure 1:** Vastus lateralis (VL) and vastus medialis (VM) sarcomere length measured intraoperatively. Asterisk (\*) indicates significant difference between muscles ( $p < 0.01$ ).

Predicted sarcomere length, generated from the model, agreed very well with measured sarcomere length for the VL (Figure 2A), but not as well for the VM (Figure 2B). For the VL, as the knee was flexed from full extension ( $0^\circ$ ) to flexion ( $90^\circ$ ) sarcomere length was predicted to increase from  $\sim 2.3$  to  $\sim 3.6$   $\mu\text{m}$ , which was within a standard error of those measured intraoperatively (Figure 2A). For the VM, predicted sarcomere length ranged from  $\sim 2.2$   $\mu\text{m}$  with the knee fully extended to  $\sim 3.5$   $\mu\text{m}$  with the knee flexed to  $90^\circ$ . However, the measured sarcomere length was  $\sim 3.7$   $\mu\text{m}$  at  $45^\circ$  (compared to a model prediction of  $\sim 3$   $\mu\text{m}$ ) and  $\sim 4.1$   $\mu\text{m}$  at  $90^\circ$ . Thus, intraoperatively-measured values were  $\sim 5$  standard errors away from model predictions. Possible reasons for this disparity are: (1) Intraoperative VM data were obtained from patients undergoing total knee replacement whereas cadaveric data were obtained from subjects without known orthopedic problems. Considering that the range of motion (ROM) of patients is limited, it is possible that the limited ROM resulted in an adaptation of muscle to more extended knee joint angles and/or (2) intraoperative VM data were taken from distal pole of the VM, also known as the vastus medialis obliquus (VMO), since limited surgical exposure made it impossible to obtain samples more proximally. The VMO clearly has different morphology compared to the more proximal VM and thus, VMO properties may not fairly represent whole VM anatomy and function.

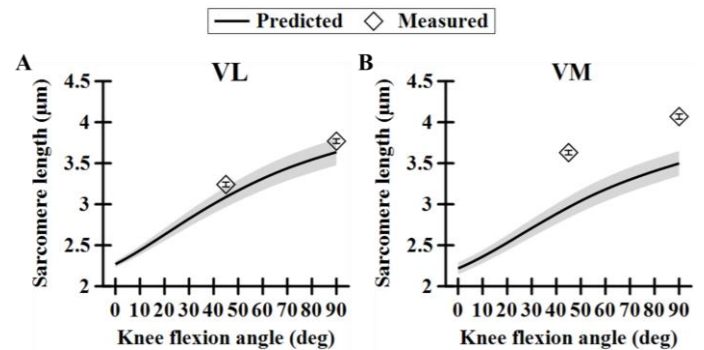


**Figure 2:** Comparison between predicted (solid line) and measured (diamond markers) sarcomere lengths of (A) VL and (B) VM. Crosses in diamond markers and shaded regions around lines represent one standard error of the mean.

## CONCLUSIONS

The fact that experimental and theoretical data agree very well for the VL but not for the VM requires a thoughtful consideration of the nature of independent validation experiments, the specific anatomy of these two muscles and the significance of these findings for vastus physiological function. These types of cross-validation experiments must be implemented widely in order to provide support for the application of models to the fields of surgery, sports medicine and kinesiology.

## REFERENCES

- Lieber RL et al. *Philos Trans R Soc Lond B Biol Sci* **366**, 1466-1476, 2011.
- Gordon AM et al. *J Physiol* **184**, 170-792, 1966.
- Ward SR et al. *J Biomech* **42**, 193-196, 2009.
- An KN et al. *J Biomech* **16**, 419-425, 1983.
- Ward SR et al. *Clin Orthop Relat Res* **467**, 1074-1082, 2009.
- Thelen DG. *J Biomech Eng* **125**, 70-77, 2003.

## ACKNOWLEDGMENTS

This work was supported by NIH grant R24 HD050837

# RELATION BETWEEN FORCE STEADINESS AND EMG AMPLITUDE: EFFECT OF SIGNAL PROCESSING

Jeffrey Peterson and Kevin Keenan

University of Wisconsin-Milwaukee, Milwaukee, WI, USA  
email: peter724@uwm.edu

## INTRODUCTION

Functional limitations, including walking, climbing stairs, and maintaining balance, become increasingly prevalent as adults age. Performance on force steadiness [1] and maximal strength [2] tasks have been related to functional limitations in older adults. However, the underlying neural mechanisms driving the change in performance with aging remain unclear. Changes in electromyogram (EMG) amplitude may be related to performance, and although EMG amplitudes are frequently reported to increase in older vs. young adults [3], few studies examine the relationship between force steadiness and increased EMG amplitude in older adults. This limitation may be due to the inherent variability of single bipolar EMG to estimate muscle activity.

High-density surface EMG can increase the accuracy of muscle force estimation compared to single bipolar EMG, with multichannel bipolar signals reported to more accurately estimate force than monopolar signals [4]. However, whether high-density surface EMG can improve upon the ability of bipolar EMG to predict force steadiness remains unclear. Therefore, the purpose of our study was to examine the differences in EMG amplitude and force steadiness between young and older adults during a 5% maximum voluntary contraction (MVC) dorsiflexion task, to examine the relationship between EMG amplitude and force steadiness, and to examine how processing of the EMG signal influences the strength of this relationship. We also examined differences in dorsiflexion strength and if strength was related to dorsiflexion force steadiness.

## METHODS

17 young ( $26.5 \pm 4.7$  years, 10 females) and 18 older ( $73.9 \pm 7.6$  years, 8 females) adults performed a

dorsiflexion task with the left knee extended and ankle in a neutral position. Participants performed a series of MVCs followed by two 30 s trials of the steadiness task at 5% MVC. Performance was quantified as the coefficient of variation of force.

High-density surface EMG was collected from tibialis anterior using a 64-channel electrode matrix (OTBioelettronica, Torino, IT) in monopolar mode. EMG recordings were visually inspected and bad quality signals (i.e., low signal to noise ratio, 1.2% of all channels collected) were replaced by inter- or extrapolation. Signals were then rectified and normalized to EMG amplitude during the MVC trials. Three sets of EMG signals were obtained from the collected data: (1) a monopolar matrix of 64 channels (Fig. 1A), (2) a bipolar matrix of 59 channels calculated as the difference between neighboring channels in the longitudinal direction of the matrix (Fig 1B), and (3) a single bipolar pair of simulated electrodes each formed by averaging the signals from 5 neighboring electrodes (Fig. 1C) [4]. EMG amplitudes for the multichannel sets (Fig. 1A & B) were averaged across all channels. Results are reported as mean  $\pm$  standard deviation.

## RESULTS

Student's t-tests indicated increased force fluctuations for the older adults compared with the young adults ( $3.5 \pm 1.6\%$  and  $2.3 \pm 1.0\%$ , respectively,  $p = .013$ ) and increased EMG amplitude for the older adults compared with the young adults for all EMG sets ( $p < .001$ , Table 1). Moreover, there was a positive relationship between the coefficient of variation of force and EMG amplitude during the steadiness task in both age groups for all EMG sets ( $p < .05$ ), except in the monopolar matrix for young adults ( $p = .24$ ; Table 1). Dorsiflexion strength was

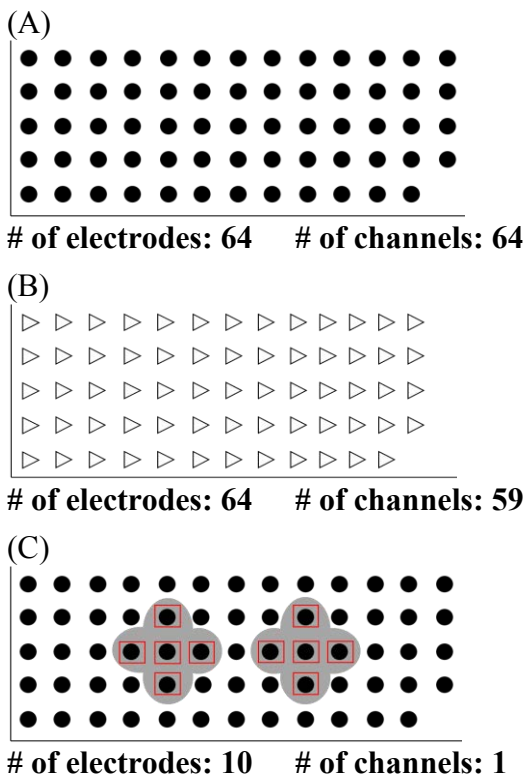


**Figure 1:** Configurations for the monopolar matrix (A), bipolar matrix (B), and conventional pair of bipolar electrodes (C). Monopolar channels are represented with closed circles and bipolar channels with triangles. Red squares in lower panel identify channels used to simulate conventional bipolar electrodes. The shape of the recording area of the conventional bipolar electrodes is shown in gray.

greater in the young adults than in the older adults ( $243 \pm 108$  N and  $157 \pm 97$  N, respectively,  $p < .001$ ) but was not related to performance on the steadiness task in the young ( $p = .22$ ) or older adults ( $p = .9$ ).

## DISCUSSION

In contrast to previous studies [3,5], force steadiness and dorsiflexion strength were impaired in older adults compared to in young adults. However, there

was not a relationship between dorsiflexion strength and steadiness in either age group. Performance on the force steadiness task was related to increased activation of tibialis anterior. Moreover, this relationship was influenced by the way in which the EMG was processed. Specifically, no relation with performance was found in the young adults using the monopolar matrix and the relationship was strongest in older adults using the bipolar matrix. This finding is consistent with previous research which has found that that high-density surface EMG improved force estimation compared to conventional bipolar electrodes [4]. These findings also suggest that the collection of a greater number of independent signals improves the ability of EMG to accurately estimate force and performance in a force steadiness task.

Future studies should investigate the mechanisms influencing increased muscle activity (e.g., altered motor unit activity within and across synergist muscles) and whether interventions to reduce the higher levels of muscle activity in older adults can improve performance.

## REFERENCES

1. Kouzaki M and Shinohara M. *Muscle & nerve* **42**, 78-87, 2010.
2. Lord SR and Fitzpatrick RC. *Series A: J. Gerontol. Ser. A-Biol. Sci. Med. Sci.* **56**, M627-M632, 2001.
3. Griffin E, et al. *J Appl Physiol* **108**, 1510-1519, 2010.
4. Staudenmann D, et al. *J Electromyogr Kinesiol* **15**, 1-11, 2005.
5. Tracy B. *Eur J Appl Physiol* **101**, 629-636, 2007.

## ACKNOWLEDGMENTS

This research was supported by a College of Health Sciences Student Research Grant Award from the University of Wisconsin – Milwaukee.

**Table 1:** EMG amplitude and its relation to performance during the dorsiflexion steadiness task.

		Monopolar	Bipolar Matrix	Single Bipolar
Young	Amplitude (%)	$1.9 \pm 0.6$	$2.4 \pm 0.7$	$2.3 \pm 0.9$
	$r^2$	ns	0.37 ( $p = .009$ )	0.34 ( $p = .01$ )
Older	Amplitude (%)	$3.4 \pm 1.4$	$4.2 \pm 1.7$	$4.2 \pm 1.9$
	$r^2$	0.31 ( $p = .01$ )	0.45 ( $p = .002$ )	0.35 ( $p = .009$ )

# COMPARING THORACIC ERECTOR SPINAE MUSCLE THICKNESS AND FIBRE ANGLE BETWEEN ULTRASOUND AND MRI

Brian C. Nairn<sup>1</sup>, Colin McKinnon<sup>2</sup>, Graham Mayberry<sup>2</sup>, Jack P. Callaghan<sup>2</sup>, and Janessa D.M. Drake<sup>1</sup>

<sup>1</sup>York University, Toronto, ON, Canada  
<sup>2</sup>University of Waterloo, Waterloo, ON, Canada  
email: jdrake@yorku.ca

## INTRODUCTION

Ultrasound imaging (USI) has been shown to be a reliable tool to measure the thickness of trunk muscles including: lumbar multifidus and erector spinae (ES) [1], rhomboid major [2], and lower trapezius [3]. USI was also shown to be comparable to magnetic resonance imaging (MRI) for lumbar ES muscle thickness measurements [1].

The thoracic spine is suspected of playing a key role in the load transfer from the shoulder to the low back. Specifically in the upper-thoracic region at the T4 level, the ES act as the upper trunk extensors while providing support for the rib cage, and are deep to the rhomboid major and trapezius muscle groups. Further, the TES have been shown to be active during both trunk and arm movements.

While LES measures are well established, the quantification of the TES architecture has not been validated between USI and MRI. Specifically, it is not known if USI measures can accurately quantify this muscle, compared to MRI, given its relatively deep location as compared to lumbar ES. Therefore, the purpose of this study was to assess the reliability and level of agreement between USI and MRI measurements of TES thickness and fibre angle.

## METHODS

A total of 20 participants (10 male, 10 female) were recruited, all free of neck, back, and shoulder pain. The mean(*SD*) age, height, and weight for the males were: 25(2) y, 1.77(0.07) m, and 80.0(8.5) kg; and for the females: 26(4) y, 1.67(0.08) m, and 65.8(8.9) kg respectively.

The spinous process of T4 was located via palpation from C7, and marked on the skin laterally. The participant was then strapped supine on a transfer board placed on top of a custom-built MR-safe wheeled gurney. The upper right side of the board had a cutout to access the participant's back with the ultrasound transducer. Strapping the participant to the board minimized gross participant movement during transfer to the MR bore.

Sagittal plane USIs were taken using a SonoSite M-Turbo ultrasound system with a linear transducer model HFL38x, 13-6 MHz (SonoSite Canada Inc., Toronto, Canada) to allow for both thickness and fibre angles to be measured. One image was taken per participant. A vitamin E capsule was adhered to the skin at the cutout edge at the level the image was taken to provide a measureable landmark without creating MR interference. Participants were then wheeled to the MR room and scans were taken using a 3T Magnetom Trio system (Siemens Healthcare, Erlangen, Germany).

All imaging processing was done offline using eFilm software (Merge Healthcare, Chicago, USA). Orthogonal MRI slices were generated using eFilm's Multi-Planar Reformatting technique to match the orientation of the USI. Thickness and angle measures were repeated three times each: once per day for three consecutive days (Figure 1). The same MRI slice was used for between day analyses, but both USI and MRI were presented in a randomized order each day.

Differences of means for each dependent measure (angle and thickness) were compared using a 2x2 (Imaging Method x Sex) mixed-model ANOVA, with  $\alpha=0.05$ . The overall between day intra-rater reliability was assessed by intraclass correlation coefficient (ICC) for each method and measure

using model (3,1). The ICC ranges for reliability adopted were: poor (<0.40), moderate (0.40-0.59), good (0.60-0.74), or excellent (>0.75), based on previous imaging studies [1]. The standard error of measurement (SEM) was also calculated. The level of agreement between USI and MRI measurements was determined using Bland-Altman plots. All statistical analyses were conducted using SPSS v.24 (IBM Corporation, Armonk, USA)

## RESULTS AND DISCUSSION

No differences were found between either the angle mean (Figure 2) or thickness mean measures ( $F(1,18)<3.67, p>0.07$ ). The ICC and SEM results were found to have moderate to excellent reliability (Table 1). The Bland-Altman analyses indicated good agreement, with the mean difference (USI-MRI) for thickness and angle being 0.025 cm and 0.78°, respectively. Also, the upper and lower limits of agreement for both measures were within 10% of the mean difference.

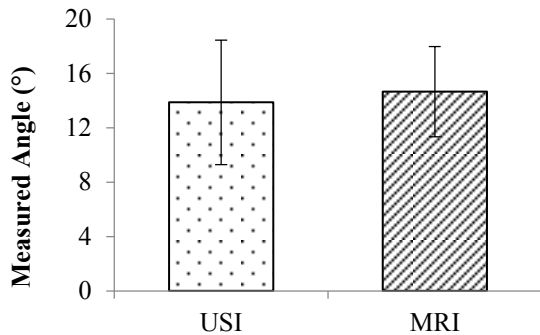


**Figure 2:** Mean(SD) of angle measurements between USI and MRI.

Overall there was good agreement between USI and MRI thickness measurements, but with a lower

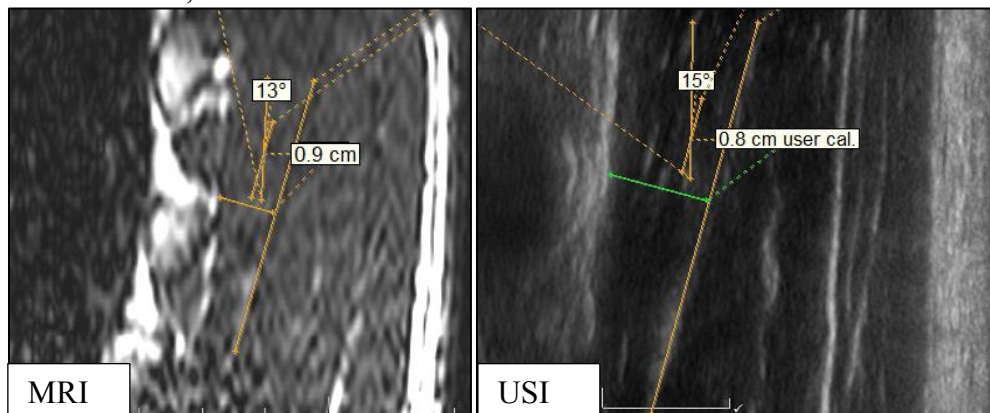


**Figure 1:** Representative images of one participant showing the thickness and angles measures.

(moderate) ultrasound ICC value. While the limits of agreement showed larger ranges for the angle measurement, the USI showed higher (excellent) reliability.

**Table 1:** Results of reliability analyses.

	Modality	ICC (3,1)	SEM
Thickness (cm)	USI	0.509	0.20
	MRI	0.772	0.15
Angle (°)	USI	0.765	2.39
	MRI	0.526	2.75

## CONCLUSIONS

USI can be used to reliably measure muscle architecture of TES. Future work will use USI to analyze changes in thickness and angle during upper-extremity and trunk extension movements, and relate findings to muscle activation. The current and future work will determine the role the TES plays during functional tasks.

## REFERENCES

1. Belavý DL, et al. *Physiol Meas* **36**, 2285-2299, 2015.
2. Jeong JR, et al. *Clin Physiol Funct Imaging* **36**, 134-138, 2016.
3. Talbott NR & Witt DW. *Physiother Theory Pract* **30**, 360-366, 2014.

## ACKNOWLEDGMENTS

Joy Williams provided technical MRI and imaging support.

# SIMILARITY OF FORCE DEVELOPMENT AND DECLINE IN THE STRETCH-SHORTEN CYCLE

<sup>1</sup> John Fox, <sup>2</sup> Jay Patel, <sup>3</sup> Braden Romer, <sup>4</sup> Jared Rehm, and <sup>5</sup> Wendi Weimar

<sup>1</sup> Methodist University, Fayetteville, NC, USA

<sup>2</sup> Palmetto Health, Columbia, SC, USA

<sup>3</sup> High Point University, High Point, NC, USA

<sup>4</sup> Huntingdon College, Montgomery, AL, USA

<sup>5</sup> Auburn University, Auburn, AL, USA

email: jfox@methodist.edu

## INTRODUCTION

A spring-mass model can be used to characterize common movements like running and hopping. During a stride or a hop, the musculoskeletal system is able to store and release elastic energy contributing to center of mass movement [1]. Given the sinusoidal motion of the center of mass in the countermovement jump, the spring-mass model has also been used to explain stiffness in vertical jumping [2]. If a spring-mass system is a valuable model for stretch-shorten cycle type movements, the force-time curve should exhibit symmetry. That is the force development (FD) phase and force attrition (FA) phase should match. This study examined the force development phase and force decline phase for similarity in 3 ballistic upper extremity movements.

## METHODS

Twenty male participants (83.7±7.4kg; height, 1.8±0.07m) were recruited. The ground reaction force (GRF) was measured during plyometric pushups from the modified push-up position under 3 conditions: 1) The nCM was performed from a pre-determined elbow flexed position; 2) the CM, similar to a countermovement jump, involved beginning in the modified push-up position then lowering and pushing vertically; and 3) D, beginning from the modified push-up position participants lifted their hands from the ground and fell into a countermovement.

Once the GRF was obtained, force in equilibrium position was subtracted. The FD phase and FA phase were extracted. These two signals were examined for similarity using dynamic time warping (DTW) [3].

The difference between the two phases was computed by constructing a warping matrix where

$$d(i, j) = \sqrt{(FD_i - FA_j)^2}$$

is the distance between each element of each array. The warping path is the path through the matrix that minimizes the cost of alignment between the two arrays. The path is determined by

$$D(i, j) = d(i, j) + \min \left\{ \begin{array}{l} D(i-1, j-1) \\ D(i-1, j) \\ D(i, j-1) \end{array} \right\}$$

Finally the time-normalized minimum cost of alignment is

$$C = \frac{D(I, J)}{I + J}$$

where  $I$  is the number of rows and  $J$  is the number of columns in the matrix.

## RESULTS AND DISCUSSION

The minimum warping cost values were analyzed using a one-way repeated measures ANOVA. The results of the analysis showed that FD and FA in stretch-shorten cycle conditions are significantly different when compared for similarity using DTW ( $F(2,38) = 6.19, p = 0.0047$ ). The cost of alignment was least for nCM, and CM was less than D (Fig. 1). Post-hoc analyses showed that the cost of alignment was significantly different between nCM and CM ( $p = 0.0066$ ) and between CM and D ( $p = 0.0222$ ).

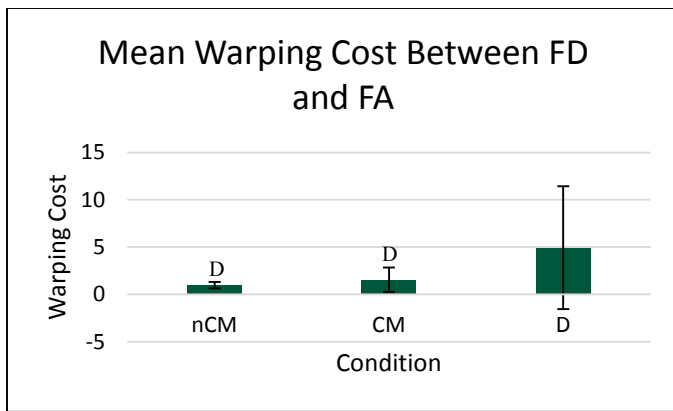


**Figure 1.** Bar height represents the mean warping cost for each condition. Error bars denote the standard deviations. D denotes a significant difference from D with an alpha level of 0.05.

Results indicate that nCM had the least warping cost followed by CM and D, respectively. Therefore, FD and FA were most similar in nCM followed by CM and D, respectively. Given that force development and force attrition are symmetrical in a spring-mass system, the results of this study imply that nCM and CM are movements that closely mimic the dynamics of a spring-mass system, compared to D. The fact that nCM and CM were not significantly different, is possibly a demonstration of equivalent muscular storage and reutilization of elastic potential energy seen in non-countermovement and countermovement vertical jumps [4]. If movements with and without a stretch-shorten cycle are equivalent in terms of storage and utilization of elastic energy, one can expect a lack of warping to match FD and FA in nCM

and CM compared to D. However, FD is necessarily warped to align with FA. Furthermore the more complex the movement the greater warping necessary to align FD and FA. This suggests that in multi-joint movements of increasing complexity the internal dynamics are not clearly reflected by the external dynamics.

## CONCLUSIONS

In this study force development and force attrition phases were examined for similarity in nCM, CM and D. The greatest similarity was seen in nCM followed by CM and D, respectively. However, perfect similarity expected from a simple spring-mass system was not seen. Therefore multi-joint movements should be studied utilizing models of greater complexity.

## REFERENCES

1. Blickhan R. *J Biomech*, **22**, 1217-1227, 1989.
2. Arampatzis A., et al. *J of Electromyogr Kines*, **11**, 355-364, 2001.
3. Keogh E. & Ratanamahatana C., *Knowl Inf Syst*, **7**, 358-386, 2004.
4. Anderson, F. C. & Pandy, M. G. *J Biomech*, **26**, 1413-1427, 1993.

# Interactions between Tendon Stiffness and Spindle Afferent Feedback Determine the Magnitude of Involuntary Force Variability

<sup>1</sup>Akira Nagamori, <sup>1</sup>Christopher M Laine, <sup>1</sup>Kian Jalaeddini, and <sup>1</sup>Francisco J Valero-Cuevas

<sup>1</sup> University of Southern California, Los Angeles, CA, USA  
email: nagamori@usc.edu, web: <http://bbdl.usc.edu/>

## INTRODUCTION

Tendons influence the transmission of muscle contractions [1]. Moreover, the relative mechanical properties of tendon and muscle determine the changes of muscle and tendon lengths. Therefore, tendon stiffness plays a critical role in the neural control of limb motions and forces [3,4], and is a major factor influencing proprioceptive feedback [2,3].

A basic and popular metric of ‘precision’ in motor control is the ability to produce a constant isometric force. During such tasks, involuntary force variability is an informative and fundamental component of current theories of motor control [5]. We have shown that a closed-loop simulation of peripheral neuromuscular elements can replicate cardinal features of force variability, and can be used to test mechanistic hypotheses about its healthy and pathologic generation/modulation [6]. Thus, we hypothesized that alterations in tendon stiffness would have a distinct influence on the nature of involuntary force variability, and its relationship with proprioceptive feedback.

## METHODS

We used a published physiologically-grounded closed-loop simulation of afferented muscle model [6]. The model includes a musculotendon unit, muscle spindle, Golgi tendon organ, and a force-tracking controller, which enables this system to perform force-tracking tasks. In this study, we modeled *gastrocnemius* muscle, and decreased and increased its tendon stiffness by 50% from a default value. We simulated 20 isometric force trials lasting 100s at 20% of maximal voluntary contraction (MVC) for each level of tendon stiffness. We repeated these trials at different levels of spindle

feedback gain. The generated force during the last 90s was analyzed in the time and frequency domains.

## RESULTS AND DISCUSSION

As expected, lower tendon stiffness reduced MVC (208 N, 202 N, and 185 N for high, default, and low tendon stiffness) [1].

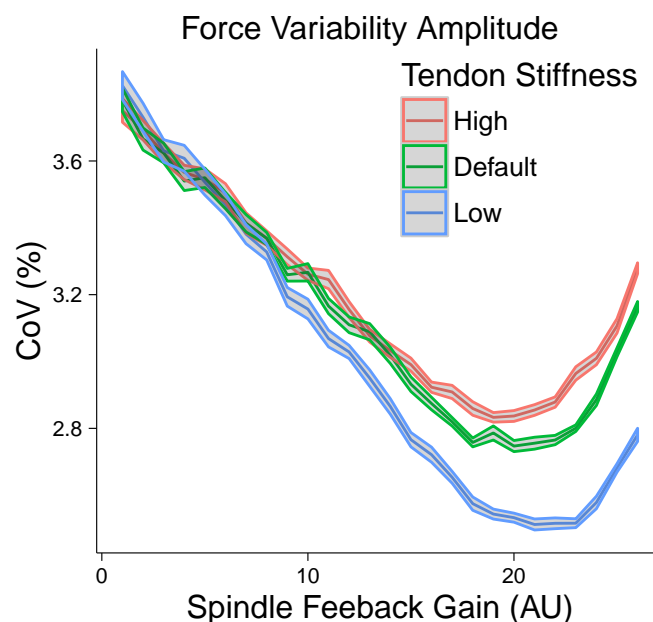


**Figure 1:** Force variability amplitude as per coefficient of variation (CoV) is determined by interactions between tendon stiffness and spindle feedback gain.

Figure 1 shows that the overall amplitude of involuntary force variability depended on spindle feedback gain and tendon stiffness in a non-linear manner. In addition, low tendon stiffness resulted in larger reduction in involuntary force variability amplitude at increased spindle feedback gains. Importantly, tendon stiffness had no effect on force variability at lower spindle feedback gains.

These results demonstrate that tendon stiffness, via changes in spindle feedback gain, affect the regulation of involuntary force variability, and agree with suggestions that compliant tendons improve the control of isometric forces [2-4]. This further suggests that decreased or increased stiffness due to musculoskeletal injuries [7] or aging may require adaptation in neural control and coordination among muscles [8].

We also found frequency-specific effects of interactions between tendon stiffness and spindle feedback gain. Decreases in tendon stiffness led to lower high-frequency (5-12 Hz) force variability across spindle feedback gains (Figure 2).

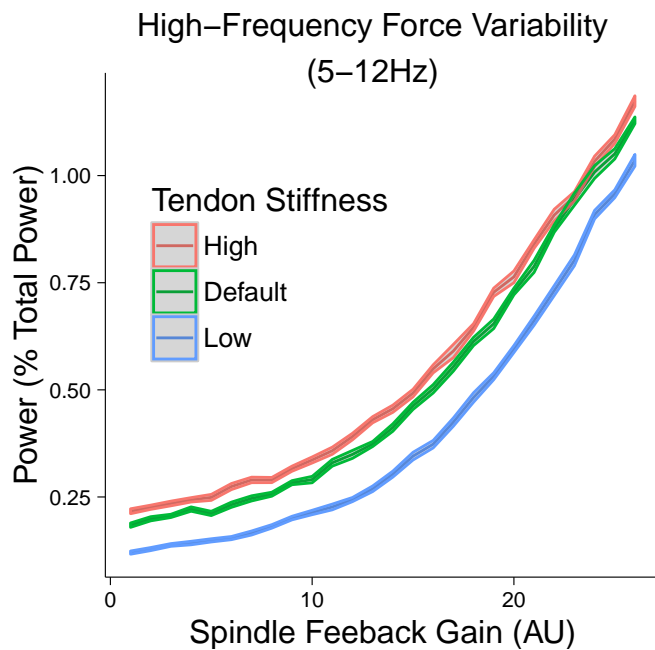


**Figure 2:** Increases in high-frequency force variability as a function of spindle feedback gain is offset by decreases in tendon stiffness.

This result implies that high-frequency involuntary force variability, often called physiological tremor, might provide insight into peripheral neuromechanical interactions. Importantly, pathological tremor, such as occurs in Parkinson's disease (4-6 Hz), may be exacerbated by the

stiffening of tendons which both accompanies aging and is characteristic of the pathology [9].

## CONCLUSIONS

Our work emphasizes that, as previously suggested [1-4], the mechanical properties of tendons could be an important—yet overlooked—aspect of force control. Moreover, our physiologically-grounded simulations begin to explain this in a mechanistic way that extends our understanding of healthy and pathologic involuntary force variability. These findings suggest that tendon properties may contribute to the mechanisms of disrupted motor control within certain pathologies, and may therefore represent promising targets for treatment/intervention.

## REFERENCES

1. Zajac, FE. *Critical reviews in biomedical engineering*, **17**(4), 359-411, 1989.
2. Biewener AA & Roberts TJ. *Exercise and sport sciences reviews*, **28**(3), 99,107, 2000.
3. Rack PM & Ross HF. *Journal of Physiology*, **99**, 351, 1984.
4. Lieber RL, *Skeletal muscle structure, function, and plasticity*, Lippincott Williams & Wilkins, 2002.
5. Faisal AA, Selen LP, Wolpert DM. *Nature reviews neuroscience*, **9**(4), 292-303, 2008.
6. Laine et al., *Frontiers in Computational Neuroscience*, **10**, 2016.
7. Arya S, & Kulig K. *Journal of applied physiology*, **108**(3) 670-675, 2010.
8. Latash ML, Scholz JP, & Schönner G, *Exercise and sport sciences reviews*, **30**(1), 26-31, 2002
9. Marusiak, Jarosław, et al., *Movement Disorders*, **26**(11), 2119-2122, 2011

## ACKNOWLEDGMENTS

This study was supported by NIH-NIAMS under award numbers R01AR050520 and R01AR052345 grants to FVC.

# EFFECTS OF CONSTRAINED FORCE APPLICATION ON MUSCLE WORK AND EFFICIENCY

<sup>1</sup> Franziska Onasch, <sup>1</sup> Rafael Fortuna, and <sup>1</sup> Walter Herzog

<sup>1</sup> University of Calgary, Calgary, AB, Canada  
Email: franziska.onasch@ucalgary.ca

## INTRODUCTION

While the outcome of a bike race certainly depends on the strength and endurance of an athlete, as well as the equipment used, there is also an important technical component to cycling:

Looking at the force applied to the pedals, only the component that is directed perpendicular to the crank results in propulsion, and is therefore often referred to as the “effective force”. The final cycling performance depends, at least in part, on the way the rider directs the pedaling forces [1, 2].

One approach to maximize pedaling efficiency is to constrain and instruct cyclists to practice and direct all the applied force perpendicular to the crank only. Cycling coaches and cycling manuals propose this as the optimal cycling technique, as no force applied to the pedals goes to waste. However, it is also known that applying a force in a specific direction may constrain the relative contributions that muscles can make to a movement [3], and thus might negatively affect performance. The purpose of this study was to analyze muscle activity and force output in cycling using a constrained and a non-constrained condition. In the constrained condition, subjects had to apply the pedal force in a direction perpendicular to the crank in the power phase of cycling, while in the unconstrained condition, forces could be applied any way the subject felt most comfortable.

We hypothesized that subjects would be more efficient in the constrained compared to the non-constrained condition, but less effective due to a decrease in force output and muscle activation for the constrained condition.

## METHODS

Twenty healthy subjects (28±4 years, 1.77±0.05 m, 74±8 kg; 5 female, 15 male) were recruited for this study. They performed the following two test protocols:

Non-constrained (NC): Five maximum isometric voluntary contractions (MIVC) in randomized order at 5 different crank angles (30, 60, 90, 120, and 150° from top dead center, Fig. 1), for 5s each. The first angle was repeated in a sixth trial to assess fatigue.

Constrained (C): The same crank angles as for the NC condition were tested in the same order. However, subjects were asked to produce MIVC perpendicular to the crank. Continuous feedback about the force direction was provided. An index of efficiency (EI) was calculated as:  $EI = \frac{Force_{effective}}{Force_{resultant}}$ ,

Where  $Force_{effective}$  is the force component perpendicular to the crank, and  $Force_{resultant}$  is the total force applied to the pedal.

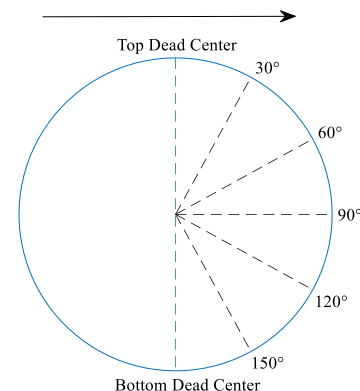


**Figure 1:** Orientation of the tested crank angles with the arrow indicating the direction of pedaling.

Electromyography (EMG) and instrumented pedals (Sensix, Poitiers, France) were used to measure muscle activity of seven lower extremity muscles and the three dimensional pedal forces, respectively.

Differences in force and EMG between non-constrained and constrained condition were analyzed with Wilcoxon tests for paired samples and Bonferroni correction for multiple comparisons.

## RESULTS AND DISCUSSION

The effective force in the non-constrained condition (NC) was significantly higher than in the constrained condition (C) for all crank angles (Fig. 2,  $p < .001$ ). The efficiency index (EI) was significantly greater in C than in NC, except for  $60^\circ$  ( $p < .001$ , Fig. 3).

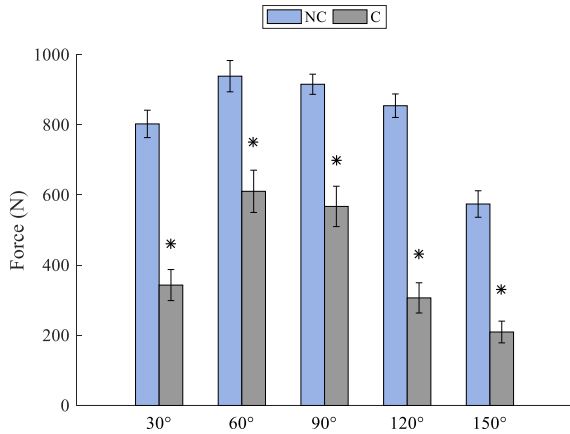


**Figure 2:** Mean ( $\pm$ SEM) of the effective forces for non-constrained (NC) and constrained (C) conditions at all crank angles. (\* significantly different from NC at the corresponding crank angle)

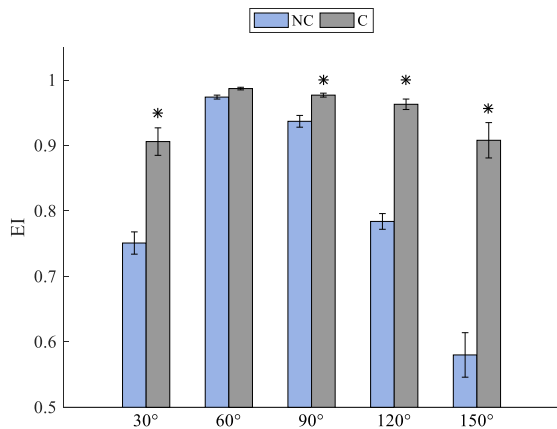


**Figure 3:** Efficiency index ( $\pm$ SEM) for non-constrained and constrained conditions (\* significantly different from NC at the corresponding crank angle).

There was greater muscle activation in NC compared to C. However, these differences were only significant for certain combinations of muscles and angles.

Furthermore, looking at the different crank angles, Figure 4 displays a distinct muscle activation pattern for the different angles. These patterns seem to become more pronounced when switching from the NC to the C condition.

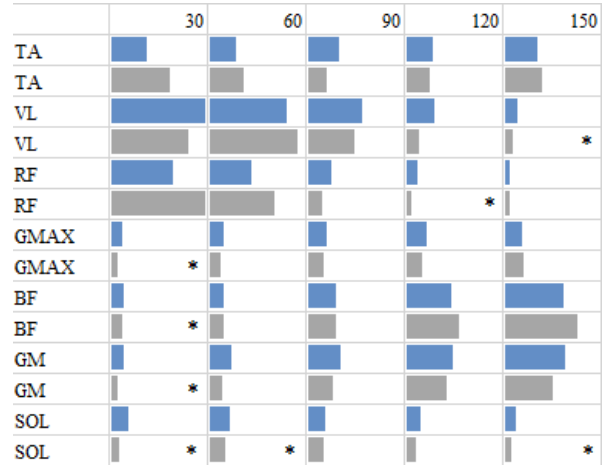


**Figure 4:** Root mean square EMGs of all seven muscles (left column) recorded at the different crank angles (top row) for the NC (blue bars) and the C (grey bars) conditions. (\* significantly different from NC at the corresponding crank angle)

## CONCLUSIONS

We conclude from the results of this study that the coaching wisdom of applying force perpendicular to the crank in the power phase of cycling decreases performance, and thus should not be given. The decrease in force in the C compared to the NC condition is associated with the specific geometry and muscle properties of the lower limb muscles. Therefore, using an optimal technique based on mechanical considerations exclusively is dangerous, and the specific musculoskeletal geometry and muscle properties should always be incorporated when providing athletes with technical advice.

## REFERENCES

1. Cavanagh PR, et al. In ER Burke (ed.). *Science of Cycling*, 91-122, Human Kinetics, 1986.
2. Gregor RJ, et al. *Exerc Sport Sci Rev* **19**(1), 127-170, 1991.
3. Kaya M, et al. *J Biomech* **39**, 2752-2766, 2006.

## ACKNOWLEDGMENTS

Andrzej Stano, technical support.

# OPTIMAL FASCICLE LENGTH CHANGES BASED ON SUBMAXIMAL FORCE OR ACTIVATION

<sup>1</sup>Zackary Scalyer and <sup>1</sup>Benjamin W. Infantolino

<sup>1</sup>The Pennsylvania State University - Berks, Reading, PA, USA  
email: bwi100@psu.edu

## INTRODUCTION

de Brito Fontana and Herzog (2016) described the submaximal force-length relationship of the vastus lateralis muscle obtained using force and muscle activation criteria [1]. It was shown that optimal fascicle length shifts towards longer lengths with respect to the maximal force condition when the submaximal measurement criteria is muscle force. However, when muscle activation was the submaximal measurement criteria optimal fascicle length did not shift from the maximal activation condition.

Since the vastus lateralis is one of four muscles to act to extend the knee and one of those muscles acts at the hip it is possible that the knee joint torque is not directly related to the vastus lateralis activation and fascicle lengths. Since it is impossible to separate out individual muscle forces for each of the quadriceps muscles it is possible that different quadriceps muscles produce more knee joint torque throughout knee range of motion.

The first dorsal interosseous muscle (FDI) primarily acts to abduct the second metacarpophalangeal joint and is the only muscle to do so, eliminating the effect of other muscles at that joint. Previous studies have measured the force length curve of the FDI *in vivo* [2]. The purpose of this study was to investigate the phenomena described by de Brito Fontana and Herzog in the FDI.

## METHODS

Two male subjects were used in this study (mean age: 29.5 years, mean height: 175cm, mean mass: 66kg). The right FDI of each subject was tested. A wireless EMG electrode (Trigno mini sensor, Delsys, Natic, MA) was placed over the second metacarpal head of

the FDI. Ultrasound videos were collected using a 10 MHz ultrasound probe (EchoBlaster 128, Telemed, Lithuania). A standoff pad was used in conjunction with the ultrasound probe head to produce a clear image and to avoid letting ultrasound gel touch the EMG electrode.

The subject placed their hand in a custom made apparatus which constrained the thumb and third through fifth fingers, only allowing the second metacarpophalangeal joint to move. The second finger pressed against a force sensor which was fixed a known joint angles (0°, 5°, 10°, 15°, 20°). The subject was instructed to contract from rest to maximal force in a 3 second interval while producing a steady force increase. During this time the force applied to the sensor, the muscle activity of the FDI, and an ultrasound video of the muscle fascicles were recorded during the duration of the trials.

Data were analyzed using custom written Matlab code based on the method described by de Brito Fontana and Herzog [1]. Force and activation data were filtered then normalized to the maximum respective value for each joint angle. Submaximal data points for 20%, 40%, 60%, 80%, and 100% of maximal force and activation for reach joint angle were located. At these points, the corresponding frame from the ultrasound video was manually digitized to determine fascicle length.

Fascicle length and force data were normalized by the respective maximum values for each subject across joint angles and contraction levels. Subject data were averaged together then the average data were fit to a force-length curve using a least squares method with the following equation:

$$F_L(L_F) = 1 - \left( \frac{(L_F - L_{F,OPT})}{w \cdot L_{F,OPT}} \right)^2$$

Where  $L_F$  is the range of fascicle lengths,  $L_{F,OPT}$  is the optimal fascicle length, and  $w$  indicates the width of the force length curve. This produced estimates for the values of maximal muscle force, optimal fascicle length, and the width parameter.

## RESULTS AND DISCUSSION

The results were generally in agreement with that of de Brito Fontana and Herzog (figures 1 and 2). The trend of increasing optimal fascicle length seen during the force condition was present. The trend in the activation condition was not as clear however.

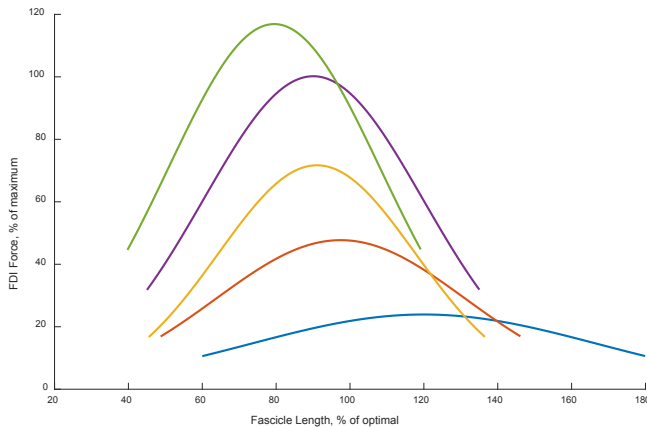


Figure 1. Muscle force length curves based on percent of maximal force.

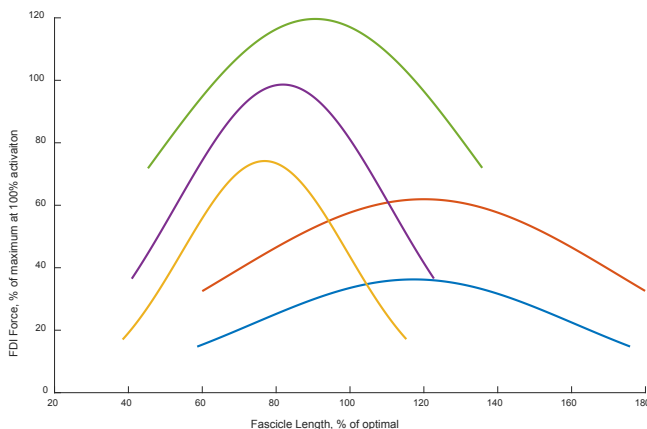


Figure 2. Muscle force length curves based on percent of maximal activation.

Due to low sample size, statistical tests could not be used to better compare the current results with those of the previous study. These findings suggest that even in a muscle with a small range of motion the effect of different measurement criteria has an influence on submaximal optimal fascicle length. Additionally, the current results suggest that difficulty in separating the force contributions of the vastus lateralis through knee range of motion does not have a large effect on the phenomena observed by de Brito Fontana and Herzog.

Limitations with this study include a small sample size and the small range of motion of the FDI. The small range of motion of the FDI made determining the parameters of the force-length difficult since a large range of fascicle lengths could not be directly measured. Using a muscle with a larger range of motion at a joint with fewer muscle acting would help to further clarify the differences in optimal fascicle length based on submaximal measurement criteria.

The results of this study demonstrated that the optimal fascicle length for submaximal conditions will vary depending on the submaximal measurement criteria, either submaximal force or activation.

## REFERENCES

1. de Brito Fontana H and Herzog W, *Eur J Appl Physiol*, **116**, 1267-1277, 2016
2. Infantolino BW and Challis JH, *Ann Biomed Eng* **42**(6) 1331-1339.

# TWO COST-EFFECTIVE METHODS FOR SLIP TRAINING IMPROVE RECOVERY RATE FOLLOWING LABORATORY-INDUCED SLIPS

<sup>1</sup> Leigh J. Allin, <sup>2</sup> Maury A. Nussbaum, and <sup>1</sup> Michael L. Madigan

<sup>1</sup> Texas A&M University, College Station, TX, USA

<sup>2</sup> Virginia Tech, Blacksburg, VA, USA

email: lallin@tamu.edu, web: <http://mobl.tamu.edu>

## INTRODUCTION

Repeated slip training (RST) is a task-specific training methodology that involves practicing the motor skills necessary to avoid a fall following an unexpected slip. Researchers have explored RST as a fall prevention intervention by exposing subjects to slips or slip-like perturbations in a safe, controlled manner. RST has been found to be effective in improving both proactive and reactive responses to subsequent slips [1]. However, current methods for RST require substantial financial resources. More cost-effective methods for implementing RST may improve its potential for adoption.

The purpose of this study was to investigate the efficacy of two cost-effective methods for RST at increasing recovery rate following laboratory-induced slips. Three groups were exposed to either unexpected slip training (UST), expected slip training (EST), or a control condition. Gait characteristics, slip severity, and kinematics of the slipping and trailing feet were compared between the three groups. We hypothesized that UST and EST would exhibit a higher recovery rate, reduced slip severity, and altered trailing limb responses, compared to the control group.

## METHODS

Thirty-six adults (18-31 years, BMI 17.1-34.9 kg/m<sup>2</sup>, 18 female) completed the study. Exclusion criteria included any self-reported musculoskeletal conditions that could affect their balance or gait, participating in  $\geq 30$  minutes of exercise more than four times per week, or participating in  $\geq 30$  minutes of vigorous exercise (e.g. running or jogging) more than two times per week. The study was approved

by the university institutional review board, and written consent was obtained from all subjects.

The study employed a three-group posttest-only design, which involved one training session and one unexpected slip induced while walking on the following day. Six males and six females were randomly assigned to each group: UST, EST, or control. The training session for the control group involved simply walking 20 times along a straight walkway covered in vinyl tile. UST sessions involved 20 unexpected slips while walking across the walkway. Slips were induced by placing a 1 x 1 m polyethylene sheet onto the walkway, which provided a low-friction interface. EST sessions involved repeated slip-like perturbations while walking over a known slippery surface. Subjects were instructed to step onto nylon fabric placed over a polycarbonate sheet (which provided a low-friction interface), simulate a slip, and then recover their balance by stepping with the trailing limb (80 repetitions). The session on the following day was the same for all subjects, during which they were exposed to one unexpected slip while walking by stepping onto a contaminated surface [2]. Subjects wore a safety harness to prevent falls to the floor during all sessions.

Segmental kinematics were sampled at 100 Hz using an 8-camera motion capture system (Qualisys North America, Inc., Buffalo Grove, IL). Ground reaction force during walking and forces applied to the harness rope were sampled at 1000 Hz using a force platform (Bertec Corporation, Columbus, OH) and a uniaxial load cell (Cooper Instruments and Systems, Warrenton, VA), respectively. Slip outcome was determined based on forces applied to the harness rope [3]. During slip trials, gait characteristics (gait speed and step length), slip severity (slip distance and peak slip speed), and

spatial characteristics of the slipping heel and trailing toe at trailing foot lift-off (LO) and touch-down (TD) were measured. Spatial characteristics included slipping heel trailing toe positions, both relative to the sacrum (expressed as percent body height, %bh). During walking trials prior to the slip, step length, heel contact angle (between the foot and floor at heel contact), and required coefficient of friction (RCOF) were measured. A Fisher's exact test was used to compare recovery rates between groups, and analyses of variance (ANOVA) to compare continuous variables between groups. Tukey's HSD test was used for pairwise comparisons between groups where relevant. Statistical analyses were performed using JMP Pro 12 (SAS Institute Inc., Cary, NC) and a significance level of  $\alpha=0.05$ .

## RESULTS AND DISCUSSION

Recovery rates differed between the three groups, in that seven UST subjects, eight EST subjects, and two control group subjects recovered their balance ( $p=0.039$ ). Gait speed ( $1.28\pm0.06$  m/s) and step length ( $0.71\pm0.04$  m) did not differ between groups.

Subjects in the UST group exhibited more cautious gait prior to the slip, and the slipping heel was less anterior to the sacrum at LO and TD (Fig. 1). Compared to the control group, heel contact angle was 4.1 degrees less ( $p=0.030$ ), RCOF was 0.035 lower ( $p=0.003$ ), AP slipping heel position at LO was 4.0%bh less anterior to the sacrum ( $p=0.024$ ), and AP slipping heel position at TD was 8.3%bh less anterior to the sacrum ( $p=0.011$ ).

Subjects in the EST group experienced less severe slips compared to the control group, and their slipping heel was less anterior to the sacrum at TD. Peak slip speed was 0.71 m/s slower ( $p=0.023$ ), slip distance was 21.3 cm shorter ( $p=0.011$ ), and AP slipping heel position at TD was 6.8%bh less anterior to the sacrum ( $p=0.0496$ ), compared to the control group.

There were no significant differences in gait characteristics, slip severity, or slipping and trailing foot kinematics between the UST and EST groups.

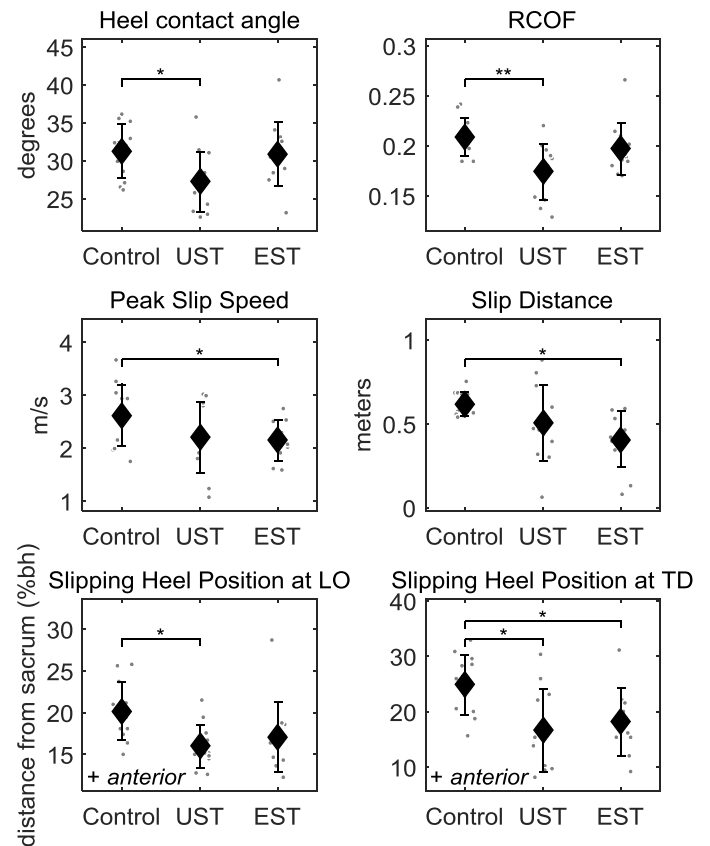


**Figure 1:** Variables that differed between groups (mean and standard deviation, \* $p<0.05$ , \*\* $p<0.01$ )

Compared to the control condition, both interventions resulted in a higher recovery rate in response to laboratory-induced slips. Both interventions also resulted in slipping heel positions less anterior to the sacrum during a slip, which is associated with increased stability. Relative to controls, the UST group exhibited proactive changes in gait, evidenced by reduced heel contact angle and RCOF, while the EST group experienced less severe slips. Since no proactive changes in gait were detected for the EST group, this latter outcome is likely due to an improved reactive response to slipping. Based on these results, both UST and EST appear to have potential use as cost-effective methods for reducing the number of falls due to slipping.

## REFERENCES

1. Pai Y-C, Bhatt TS. *Phys Ther* **87**, 1478-91, 2007.
2. Allin LA, et al. *J Biomech* **49**, 678-83, 2016.
3. Yang F and Pai Y-C. *J Biomech* **44**, 2243-9, 2016.

# STATIC PERTURBATION TRAINING TO IMPROVE DYNAMIC STABILITY DURING OVERGROUND SLIP IN YOUNG ADULTS

<sup>1</sup> Fabricio Saucedo & <sup>2</sup> Feng Yang

<sup>1</sup> The University of Texas at El Paso, El Paso, TX, USA

<sup>2</sup> Georgia State University, Atlanta, GA, USA

email: [fyang@gsu.edu](mailto:fyang@gsu.edu)

## INTRODUCTION

Falls are one of the leading causes of accidental or injury-related death in the aging population and people with neurological disorders. Dynamic gait stability has been identified as a key factor of slip-related falls [1]. Treadmill-based perturbation training has recently emerged as a new modality to reduce falls. It was shown that perturbation training could be effective in improving dynamic stability responding to a slip induced in gait [2].

Most previous studies examining the effects of perturbation training were conducted during walking on a treadmill, which requires that participants walk independently for a long walking distance. Given that limited mobility is common in frail older adults and individuals affected by neurological dysfunctions, some participants may not be willing or able to comply with this training paradigm. Therefore, a simple perturbation-based training program would be of particular interest to those who lack sufficient mobility.

Perturbation training performed during standing could be one of the simple modalities. However, it remains unknown if a static perturbation training program on a treadmill could improve dynamic stability when adults are exposed to an unexpected slip perturbation over ground. The primary purpose of this study was to examine if and to what extent a standing-perturbation training program on a treadmill could improve dynamic stability in response to an unexpected slip perturbation during overground gait among young adults.

## METHODS

Twenty healthy young participants were recruited for the study after providing written informed consent

approved by the Institutional Review Board. Participants were randomly divided into a control ( $n = 10$ , age:  $22.6 \pm 3.09$  years; body height:  $1.68 \pm 0.09$  m; body mass:  $73.36 \pm 15.98$  kg, 3 females) and a training group ( $n = 10$ , age:  $22.33 \pm 1.65$  years; body height:  $1.70 \pm 0.13$  m; body mass:  $73.87 \pm 20.19$  kg, 3 females).

The training group underwent a treadmill-based static perturbation training protocol which consisted of 5 normal walking trials and then 8 slips induced when subjects were standing on the treadmill. The slip was created by moving the treadmill belt rapidly forward for a distance of 24 cm within 200 ms. The control group was exposed to a placebo training protocol on the same treadmill but consisting of 13 normal walking trials. After either training protocol, both groups were exposed to an identical, unannounced slip when they walked over a 14-m walkway. Such an overground slip was induced by a customized sliding device embedded in the middle of the walkway. This device included a movable platform which could travel along a 1.5-m linear track smoothly. When subjects' right foot was in contact with the platform, it slides forward with the foot, creating a real-life slip perturbation. Participants were protected by a safety harness during all trials.

The responses to the unexpected overground slip were recorded from 27 reflective markers attached to the body (26) and the platform (1) using an 8-camera motion capture system (Vicon, UK) at 120 Hz. Marker paths were low-pass filtered at marker-specific cut-off frequencies (ranging from 4.5 to 9 Hz) using fourth-order, zero-lag Butterworth filters [3]. Locations of joint centers, heels, and toes were computed from the filtered marker positions. The body center of mass (COM) kinematics were calculated using the joint center data based on a 13-

segment model [4]. The two components of the COM motion state, i.e. its position and velocity, were calculated relative to the rear of the BOS (i.e., the leading heel) and normalized by the foot length and  $\sqrt{g \times bh}$ , respectively, where  $g$  is the gravitational acceleration and  $bh$  the body height. Dynamic stability was calculated as the shortest distance from the COM motion state to the limit of stability [5] at three consecutive events: the slipping (or right) foot touchdown (RTD), the recovery (or left) foot liftoff (LLO) and its touchdown (LTD). These three events were determined from the foot kinematics. Independent  $t$ -tests were applied to compare dynamic stability between groups at all three events. All statistical analyses were performed using SPSS 21.0 (IBM, NY), and a significance level of 0.05 was implemented throughout.

## RESULTS

At RTD and LLO during the overground slip, dynamic stability was comparable between groups (Fig. 1,  $-0.17 \pm 0.06$  vs.  $-0.19 \pm 0.04$ ,  $p > 0.05$  for RTD;  $-0.26 \pm 0.11$  vs.  $-0.25 \pm 0.17$ ,  $p > 0.05$  for LLO). Nevertheless, the training group was less unstable against backward balance loss than the control group at LTD after the slip onset ( $-0.33 \pm 0.39$  vs.  $-0.57 \pm 0.16$ ,  $p < 0.05$ ).

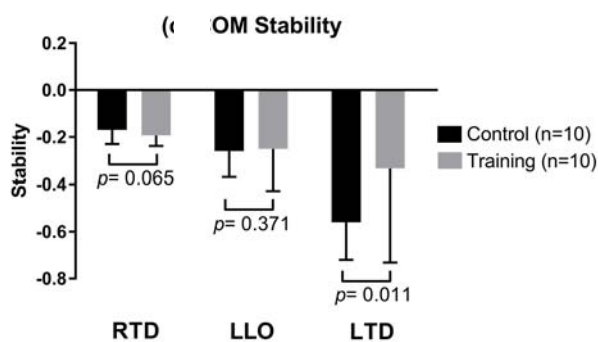


**Figure 1:** Comparison of dynamic stability between the training and control groups during the overground slip at the right touchdown (RTD), left liftoff (LLO), and left touchdown (LTD).

## DISCUSSION

The overall objective of this study was to examine the efficacy of a static treadmill-based perturbation training program on improving dynamic stability in

response to an unexpected overground slip in young adults. The results indicated that participants in the training group exhibited better dynamic stability control than those in the control group at the recovery foot touchdown when exposed to a large-scale, unannounced overground slip. The observed improvement in dynamic stability implies that static treadmill perturbations may serve as an effective means to strengthen one's resistance to slips and falls. Our results demonstrated that a reduced perturbation training intensity (i.e., the perturbation is induced during static standing instead of during dynamic walking) could still incur motor adaptations that can be transferred to improve falls recovery upon the exposure to an overground slip. More studies based on a large sample size and other populations are desired to comprehensively understand the effectiveness, generalizability, and safety of this training modality in reducing falls. The comparison of the training effects between standing-perturbation and gait-perturbation training programs deserves further investigations as well.

## CONCLUSIONS

In summary, the static treadmill-slip training could improve the reactive COM dynamic stability control in response to a real-life like slip perturbation. The finding from this study introduces a new paradigm, which could potentially present numerous benefits to populations with limited mobility to reduce their likelihood of falls.

## REFERENCES

1. Yang F, et al., *J Biomech* **42**, 1903-1908, 2009.
2. Yang F, et al. *J Biomech* **46**, 63-69, 2013.
3. Winter DA. *Biomechanics and Motor Control of Human Movement*, John Wiley & Sons, Ltd., 2009.
4. De Leva P. *J Biomech* **29**, 1223-1230, 1996.
5. Patton JL, et al. *Gait Posture* **9**, 38-49, 1999.

## ACKNOWLEDGMENTS

This study was partially funded by a Research Grant (2014-070 to FY) from The Retirement Research Foundation. The authors thank Patrick Cereceres, Joshua Padilla, and Christina Carrera for assistance in data collection.

# AGE AND FALLS HISTORY EFFECTS ON ANTAGONIST LEG MUSCLE COACTIVATION DURING WALKING WITH OPTICAL FLOW PERTURBATIONS

Jessica D. Thompson and Jason R. Franz

University of North Carolina at Chapel Hill and North Carolina State University, Chapel Hill, NC, USA  
Email: jdtthomp4@email.unc.edu, web: <http://abl.bme.unc.edu/>

## INTRODUCTION

Sensory perturbations are increasingly used to study balance control mechanisms in walking due to their ability to elicit corrective motor responses from step to step [1,2]. Advanced age increases the reliance on visual feedback for motor planning and execution [3]. Thus, optical flow perturbations in particular may represent a promising diagnostic tool for age-associated falls risk [2]. Antagonist leg muscle coactivation, a well-documented phenomenon in motor control thought to increase leg stiffness to improve joint stability, increases with age [4] and may further increase during walking to mitigate the effects of perturbations. Therefore, the purpose of this study was to investigate age and falls history effects on antagonist leg muscle coactivation during walking with and without optical flow perturbations of different amplitudes. We hypothesized that: (1) compared to young adults, aging and falls history would increase antagonist muscle coactivation during walking, and (2) these differences would increase in the presence of optical flow perturbations.

## METHODS

11 healthy young adults (mean±sd, age: 24.8±4.8 years), 11 healthy older adults (age: 75.3±5.4 years) and 11 older adults with a history of falls (age: 78±7.6 years) walked on an instrumented dual belt treadmill (Bertec Cor., Columbus, OH). Older adults were considered to have a fall history if they had experienced one or more unanticipated falls within the last year. Young adults walked on the treadmill at 1.25 m/s while both groups of older adults walked at their preferred walking speed (Nonfallers: 1.19±0.20 m/s, Fallers: 1.03±0.22 m/s). While walking, subjects watched a speed-matched, virtual hallway rear projected onto a semi-circular screen surrounding the treadmill with and without continuous mediolateral oscillations of optical flow. In randomized order, subjects walked for two minutes normally and with optical flow perturbations at amplitudes of 20, 35, and 50 cm. We collected electromyographic (EMG) recordings from wireless electrodes (Delsys, Inc.) placed over five right leg muscles: medial gastrocnemius (MG), soleus (SOL),

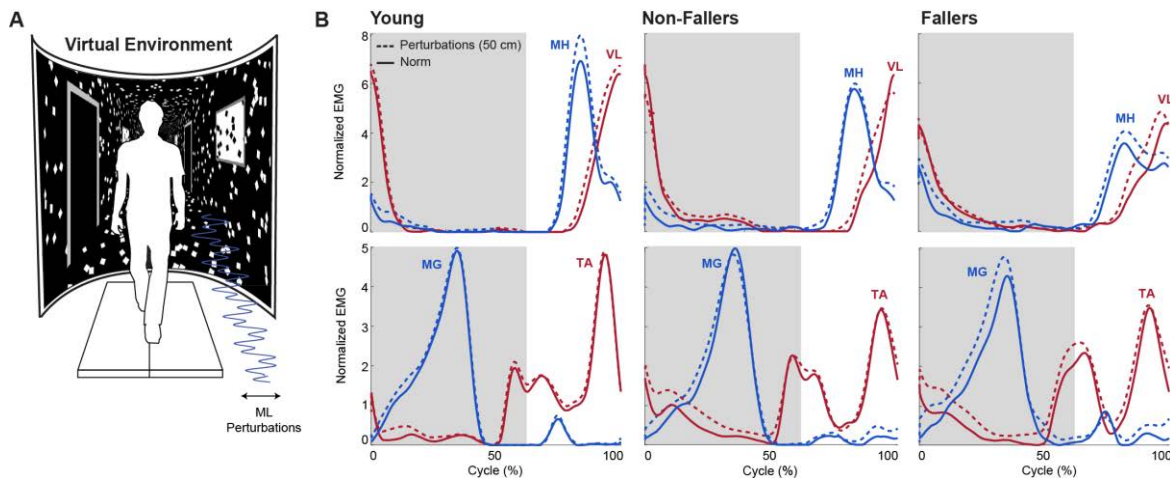


**Figure 1.** (A) Virtual Environment. (B) Normalized EMG linear envelopes for normal and perturbed walking. MH/VL coactivation on the top panel and MG/TA coactivation on the bottom. Shaded area indicates stance.

tibialis anterior (TA), vastus lateralis (VL) and medial hamstring (MH). We bandpass (20-450 Hz) filtered and rectified the data before normalizing the amplitudes to the mean values during normal walking. We then used 10 Hz linear envelopes to calculate antagonist muscle coactivation indices as the normalized shared area of overlap of activations between three muscle pairs: MG/TA, SOL/TA, and VL/MH. A two-way repeated measures ANOVA tested for main effects of perturbation amplitude and muscle coactivation for each subject group during stance and during leg swing. Exploratory independent t-tests compared fallers and non-fallers during walking with and without perturbations.

## RESULTS AND DISCUSSION

Age, independent of falls history, significantly increased stance phase lower leg antagonist muscle coactivation compared to young adults, by an average of 138% for MG/TA and 125% for SOL/TA ( $p < 0.05$ ) (Fig. 2BC). Compared to walking normally, optical flow perturbations had no significant effect on leg muscle coactivation in

young adults. In contrast, in both older adult groups, perturbations significantly increased TA/SOL antagonist coactivation, by on average up to 56% during stance and 170% during swing compared to normal, unperturbed walking (Fig. 2C). Perturbations also revealed age-related differences in swing phase TA/SOL antagonist coactivation that were not otherwise apparent during normal walking (Fig. 2C). Although modest compared to non-fallers, only in older fallers did perturbations significantly increase TA/MG antagonist coactivation, by up to 54% during stance and up to 106% during swing (Fig. 2B). Finally, we found no significant difference between older fallers and non-fallers for any measure of antagonist coactivation during unperturbed walking. However, perturbations revealed up to 109% more stance phase VL/MH coactivation in older fallers compared to non-fallers (Fig. 2A).

## CONCLUSIONS

In partial support of our hypotheses, lower leg antagonist leg muscle coactivation during walking increased with age, independent of falls history. Also, as hypothesized, these effects were larger in the presence of optical flow perturbations. One interpretation of this finding is that older adults rely more on increased leg joint stiffness than young adults to accommodate balance challenges during walking. Moreover, elevated antagonist upper leg muscle coactivation at larger perturbation amplitudes, unique to older adults with a history of falls, may allude to an increased susceptibility to optical flow perturbations that requires further study.

## REFERENCES

1. O'Connor SM, et al. *J Neurophysiology* **102**, 1411-1419, 2009.
2. Franz JR, et al. *Human Movement Sci* **40**, 381-392, 2015.
3. Jeka JJ, et al. *J Motor Behavior* **42**, 197-208, 2010.
4. Franz JR, et al. *Gait & Posture* **37(3)**, 374-284, 2013.

## ACKNOWLEDGMENTS

Supported in part by the National Center for Advancing Translational Sciences (UL1TR001111).

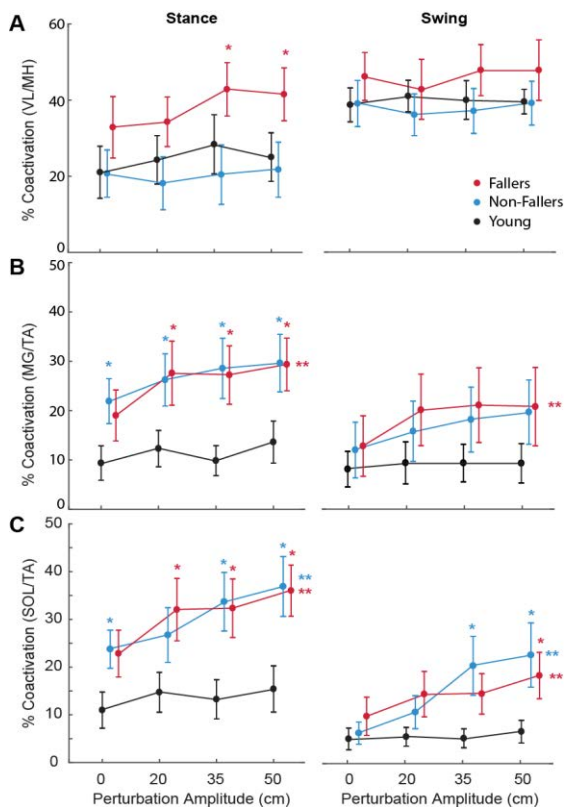


**Figure 2.** Mean (S.E.) antagonist leg muscle coactivation versus perturbation amplitude.

# QUANTIFYING THE CONTRIBUTION OF COUNTER-ROTATION MOVEMENTS DURING FALL RECOVERY: A VALIDATION STUDY

<sup>1</sup> Elizabeth A. Rapp, <sup>1</sup> R. Tyler Richardson, <sup>1</sup> Benjamin C. Conner, <sup>1</sup> Drew A. Petersen, <sup>1</sup> Jamie Pigman, <sup>1</sup> Jeremy R. Crenshaw

<sup>1</sup> University of Delaware, Newark, DE, USA  
email: crenshaw@udel.edu

## INTRODUCTION

Standing balance is maintained by 1) moving the center of pressure under the base of support, 2) applying an external force, and 3) counter-rotating segments about the whole-body COM [1]. Rapid shoulder flexion or extension can serve as a counter-rotation strategy to recover from a fall [2,3]. Although joint angles and velocities can characterize this strategy, the contribution of such movements to fall recovery depends upon the motion timing and influence of other mechanisms. Hof [1] and Halvorsen [4] have proposed a method to specifically quantify the contribution of counter-rotations to balance maintenance. Still, these contributions have not been evaluated during fall recovery after an external perturbation, nor have specific upper extremity contributions been identified.

The purpose of this study was to evaluate the construct validity of measures that quantify the counter-rotation contribution to recovery from a posterior fall. We evaluated a measure that included whole-body counter-rotation [1,4] as well as a modified measure that focused on upper extremity rotations. As a form of treatment validation, we hypothesized that counter-rotation contributions would be reduced during fall-recovery responses in which arm motion was constrained. As a form of convergent validation, we hypothesized that arm contributions would be positively correlated with peak shoulder flexion velocities.

## METHODS

Five healthy adults (age:  $21.8 \pm 1.3$ ; BMI:  $22.3 \pm 4.3$ ) stood on a microprocessor-controlled treadmill (Active Step<sup>®</sup>, Simbex, Lebanon, NH) and proceeded through a single-stepping threshold protocol [5]. Increasingly larger disturbances were delivered as subjects attempted to recover with a

feet-in-place response. This protocol was performed under two conditions: 1) unconstrained (no limitations to arm motion) and 2) arms constrained (both hands holding a rope behind the back). The trials representing the largest disturbance magnitude in which a step was prevented in both conditions were analyzed for each subject.

Trials were recorded with motion capture technology (Motion Analysis<sup>®</sup>, Santa Rosa, CA: 120 Hz). Thirty-five markers facilitated the definition of thirteen body segments (Visual3D, C-Motion<sup>®</sup>, Germantown, MD). Marker trajectories were low-pass filtered at 6 Hz before calculating segment positions, orientations, and accelerations, as well as whole-body angular momentum.

Balance mechanisms were calculated with custom LabVIEW software (National Instruments<sup>®</sup>, Austin, TX) utilizing the following equation [3]:

$$\frac{(r_{COP} - r_{COM}) \times F_G}{M_1} - \frac{d}{dt} \frac{H}{M_2} = \frac{(r_{COM} - r_{COM'}) \times m a_{COM} + I_{BODY} \alpha_{COM}}{M_{TOTAL}}$$

where  $r_{COP}$  is the center of pressure,  $r_{COM}$  is the COM position,  $r_{COM'}$  is the vertical projection of the COM onto the treadmill,  $F_G$  is the force due to gravity,  $\frac{d}{dt}H$  is the rate of change of whole-body angular momentum about its COM,  $m$  is body mass,  $a_{COM}$  is the linear acceleration of the COM,  $I_{BODY}$  is the whole-body moment of inertia and  $\alpha_{COM}$  is the angular acceleration of the COM about the ankle joint center. The contribution of counter-rotation ( $M_2$ ) was calculated as the slope of the total least squares regression [6] of  $M_2$  onto  $M_{TOTAL}$ . Arm-specific counter-rotation contribution was calculated as the slope of the total least squares regression of  $M_{ARMS}$  on  $M_{TOTAL}$ , where  $M_{ARMS}$  equals the rate of change of arm angular momentum about the whole-

body COM. Data were analyzed from the three-second period after the initiation of recovery, defined as a change in direction of  $M_{TOTAL}$  (Fig. 1). To evaluate the construct validity of the contribution measures, constrained and unconstrained conditions were compared using percent changes and effect sizes. To evaluate the convergent validity, Pearson correlations were calculated between peak shoulder flexion velocity and contribution measures in the unconstrained condition.

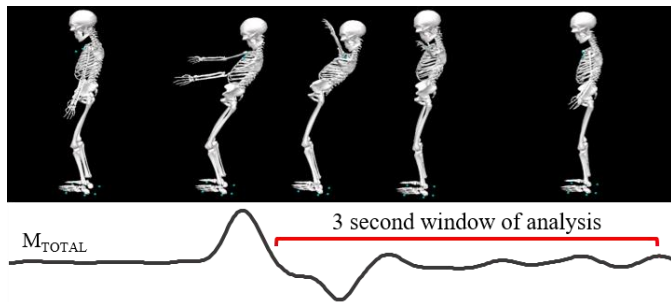


**Figure 1:** Subject model and graph depiction of a trial with the recovery segment highlighted to indicate window of regression analysis.

## RESULTS AND DISCUSSION

*Treatment validity:* The effects of arm constraint on counter-rotation contributions were small. Four out of five subjects demonstrated less counter-rotation (Fig. 2A) and all subjects demonstrated less arm-specific counter-rotation (Fig. 2B) in the arms constrained condition. Arm-specific contributions were low in the unconstrained condition (<11%), suggesting that the arms may not play a major role in recovering from these types of disturbances. Given

this limitation, we were unable to support the treatment validity of our contribution measures.

*Convergent validity:* The correlation between peak shoulder flexion velocity (range = 22 - 326 deg/s) and whole-body counter-rotation contribution was small and negative ( $r = -0.26$ ). In contrast, the correlation between peak flexion velocity and arm-specific counter-rotation was strong ( $r = 0.78$ ). This result supports the convergent validity of our arm-specific contribution measure.

## CONCLUSIONS

- Constraining the arms did not notably reduce the contribution of counter-rotations to fall recovery in this study.
- An arm-specific contribution measure more adequately reflected the use of the arms during fall recovery than a whole-body measure.

## REFERENCES

1. Hof AL. *J Biomech* **40**, 451-7, 2007.
2. Cheng KB et al. *J Biomech* **48**, 3155-62, 2015.
3. Troy KL et al. *J Biomech* **42**, 1339-44, 2009.
4. Halvorsen K, et al. *J Biomech* **43**, 3244-50, 2010.
5. Crenshaw JR, Kaufman KR. *Gait Posture* **39**, 810-15, 2014.
6. Van Huffel S, Vandewalle J. *Phila - SIAM*, 1987.

## ACKNOWLEDGMENTS

This project was supported in part by NIGMS/NIH: 2P20 GM103446

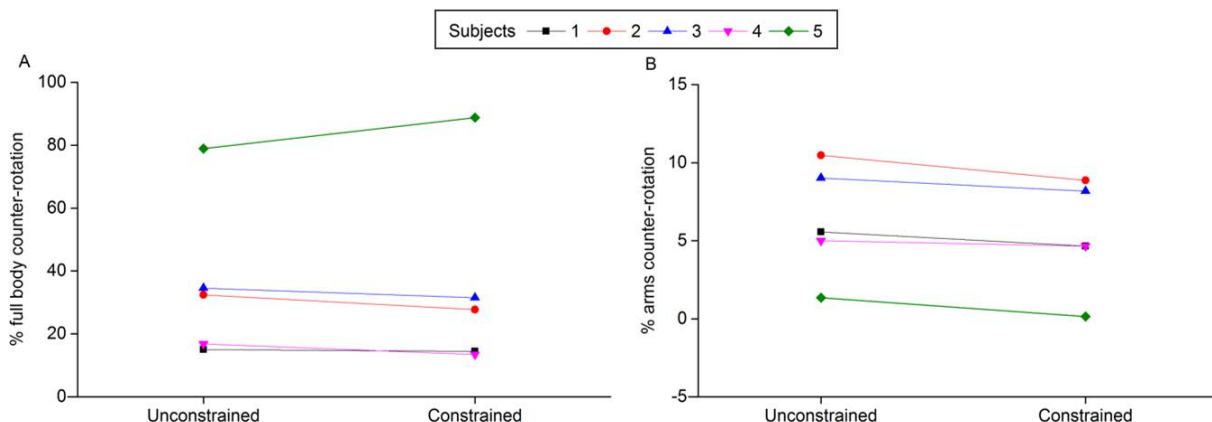


**Figure 2:** **A)** Whole-body contribution (%) of counter-rotation to fall recovery with no constraints and with the arms constrained. The constrained condition was associated with a +9.8% to -4.8% change in contribution ( $d = 0.13$ ). **B)** Arm-specific contribution (%) of counter-rotation to fall recovery. The constrained condition was associated with a -0.3% to -1.6% change in contribution ( $d = 0.27$ ).

# POSTERIOR FALL-RECOVERY TRAINING OF INDIVIDUALS WITH CHRONIC STROKE: PRELIMINARY RESULTS

<sup>1</sup> Jamie Pigman, <sup>1</sup> Drew Petersen, <sup>1</sup> Benjamin C. Conner, <sup>1</sup> Darcy S. Reisman, and <sup>1</sup> Jeremy R. Crenshaw

<sup>1</sup> University of Delaware, Newark, DE, USA  
email: crenshaw@udel.edu

## INTRODUCTION

Individuals living with chronic stroke have a risk of falling that is twice that of age- and gender-matched controls [1]. A third of all post-stroke falls are a result of a trip or a slip [2]. Therefore, interventions that focus specifically on the stepping response necessary to recover from a slip may reduce fall incidence and fall-related injury for this population.

Perturbation-based balance training has significantly reduced falls in other populations including older adults and individuals with Parkinson's disease [3]. Fall-recovery training focused on slip-recovery has reduced fall rates in a laboratory setting by 50% for unimpaired adults [4]. The extent to which the posterior fall-recovery response is modifiable in individuals with chronic stroke is not known. The purpose of this study was to quantify the within-training adaptations to posterior fall recovery over the course of six sessions. We focused on initial step placement relative to the whole-body center of mass (CoM) due the variable's documented importance to slip-recovery [5] and impairment for individuals with chronic stroke [6,7]. We hypothesized that, from the first to last training session, the initial recovery step would be placed more posteriorly and medially relative to the CoM. As another indicator of performance, we also evaluated the percentage of successful trials within the first and last training session. We hypothesized that the proportion of successful trials would increase from the first to last session.

## METHODS

We recruited six participants (age:  $58 \pm 16.6$  yrs, BMI:  $29.2 \pm 5.2$  kg/m<sup>2</sup>, Fugl-Meyer LE  $24.1 \pm 2.4$ ) for this IRB-approved study. Participants performed

six fall-recovery training sessions. Each session consisted of simulated slips delivered as the participants stood on a computer-controlled treadmill (ActiveStep<sup>®</sup>, Simbex, Lebanon, NH; Figure 1). Participants were instructed to "try to recover in a single step". Two progressively challenging, 7-minute series of disturbances were delivered within each session. In the first series, participants were instructed to initially step with their non-paretic limb. In the second series, the participants were instructed to initially step with the paretic limb. Initial belt accelerations ranged from 0.5-6.5 m/s<sup>2</sup> over a 200 ms period, with belt displacements ranging from 1-13 cm. For each trial, subsequent initial accelerations were incremented or reduced by 0.5 m/s<sup>2</sup>, depending on successful fall recovery. Failure was defined as stepping with the wrong limb, taking more than one step to recover, or recording more than 20% of body weight support from an instrumented harness system (Dillon, Fairmont, MN) [8]. The trajectories of a whole-body, reflective marker set were recorded using motion capture technology (Motion Analysis Corp., Santa Rosa CA; 120 Hz).

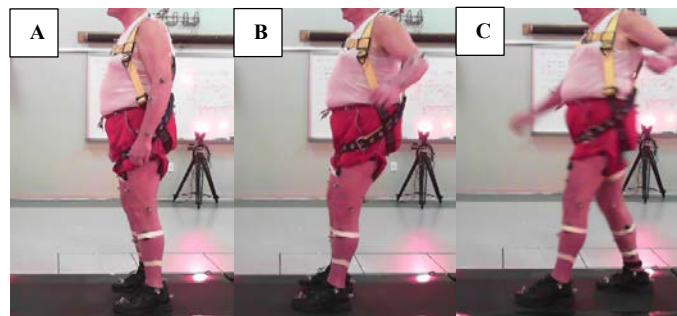


**Figure 1:** A simulated slip (initial belt acceleration 6.5 m/s<sup>2</sup>) (A) pre-disturbance onset, (B) disturbance onset, (C) successful stepping response with the non-paretic limb.

Dependent variables were evaluated for the first and last training session. Recovery kinematics were evaluated at the highest disturbance magnitude common across sessions and stepping limb.

Separate repeated measures 2 x 2 factorial ANOVA's were conducted to evaluate the effects of stepping limb and training day on the lateral and posterior distances between the stepping foot and the whole-body CoM, as well as the percentage of successful trials within each session.

## RESULTS AND DISCUSSION

### Step Kinematics

The paretic limb step was placed significantly wider than the non-paretic limb (Figure 2). However, the effect of the training day on this lateral distance was weak.

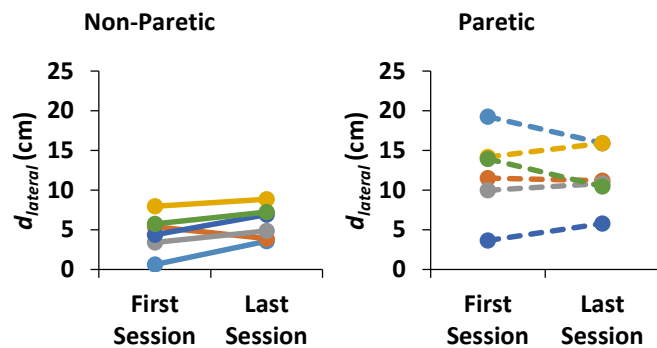


**Figure 2:** The lateral distance ( $d_{lateral}$ ) between the whole-body CoM and the non-paretic or paretic stepping foot. Steps with the paretic limb were significantly wider than steps with the non-paretic limb ( $p = 0.03$ ). There were no apparent changes in this distance from the first to the last session (*Cohen's d* < 0.20;  $p = 0.44$ ).

There were no significant effects or interactions of the training day or stepping limb in the posterior step distance ( $p > 0.32$ ). Against our expectations, we observed a moderate (*Cohen's d* > 0.37) shortening of this distance from the first ( $232.8 \pm 27.0$  cm) to last ( $204.4 \pm 8.0$  cm) sessions.

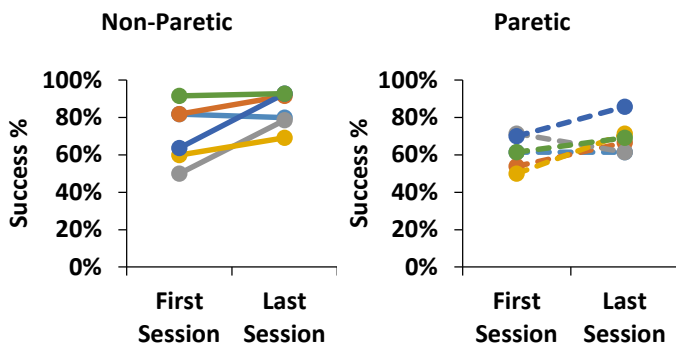


**Figure 3:** The percentage of trials in which balance was recovered successfully in a single step. There were significant increases in success from the first to last training session ( $p = 0.03$ ).

### Fall-Recovery Success

Despite a lack of strong evidence supporting a training benefit in step placement, other evidence suggests that fall-recovery improved. On the last day of training, a higher percentage of trials were performed successfully (Figure 3).

## CONCLUSIONS

- Individuals with chronic stroke demonstrated a wider paretic limb step compared to that with the non-paretic limb. A wider step decreases the likelihood of successful slip recovery in individuals that have not had a stroke [5].
- With six training sessions, the effects on step placement were, at most moderate. We plan to extend the number of sessions and within-session time to ensure that training exposure was not a limiting factor.
- On the last training session, there was an increase in the percentage of successfully performed trials. Improvements were most notably achieved by reducing the number of steps needed to recover.
- In order to avoid a “ceiling effect” of training, we aim to enroll participants who have lower functional capabilities. Work is in progress to evaluate the benefits of this training on clinical balance, balance confidence, and walking activity.

## REFERENCES

1. Jorgensen L, et al. *Stroke* **33**, 542-7, 2002.
2. Schmid A, et al. *J Rehabil Res Dev* **50**, 1277-86, 2013.
3. Mansfield A, et al. *Phys Ther* **95**, 700-9, 2015.
4. Yang F, et al. *J Biomech* **46**, 63-9, 2013.
5. Troy KL, et al. *Gait Posture* **28**, 461-5, 2008.
6. Salot P, et al. *Phys Ther* **96**, 338-347, 2016.
7. Kajrolikar T, et al. *J Biomech* **49**, 2702-08, 2016.
8. Cyr MA-A, et al. *J Biomech* **42**, 1566-9, 2009.

## ACKNOWLEDGMENTS

This project was supported by the University of Delaware Research Foundation, the ASB Junior Faculty Research Award, and a grant from the National Institute of General Medical Sciences (2P20 GM103446) from the National Institutes of Health.

# CONSTRAINING THE ARMS REDUCES POSTERIOR, BUT NOT ANTERIOR, SINGLE-STEPPING THRESHOLDS OF FALL RECOVERY

<sup>1</sup> Drew A. Petersen, <sup>1</sup> Jamie Pigman, <sup>1</sup> Benjamin C. Conner, <sup>1</sup> Jeremy R. Crenshaw

<sup>1</sup> The University of Delaware, Newark, DE, USA  
email: crenshaw@udel.edu

## INTRODUCTION

Rapid arm movements have been reported to play a substantial role during successful fall recovery [1, 2]. When arm motion is constrained, the success of a feet-in-place fall-recovery response is reduced and the duration of recovery is prolonged [1].

Anterior and posterior single stepping thresholds, defined as the minimum disturbance magnitudes that consistently elicit a compensatory step, quantify a person's ability to recover from a fall. These measures are reliable [3], decline with age [4], and evaluate the feet-in-place response that is prospectively related to falls in older adults [5]. It is not known, however, if arm motion influences performance on this assessment of fall-recovery.

The purpose of this study was to determine if arm motion benefitted single-stepping thresholds. Our hypothesis was that thresholds would be reduced by constraining arm motion. In the case that our hypothesis was supported, we evaluated the resulting dynamic stability [6] of the feet-in-place response as a means to explain observed differences.

## METHODS

We recruited six healthy participants, (age:  $21.83 \pm 1.33$  years; BMI:  $22.49 \pm 3.87$  kg/m<sup>2</sup>) for this IRB approved study.

**Single-Stepping Thresholds:** Participants stood on a computer-controlled treadmill (ActiveStep<sup>®</sup>, Simbex, Lebanon, NH) and were instructed to "try to prevent a step" in response to rapid 400 ms belt movements. Initial belt accelerations began at 0.5 m/s<sup>2</sup>, resulting in a 1 cm displacement. For subsequent trials, the initial accelerations were increased or decreased by 0.5 m/s<sup>2</sup> depending on the response, success or failure, respectively. The

progression continued until anterior and posterior thresholds were identified, as evident by four failed attempts at a given disturbance magnitude. Thresholds were expressed as the ankle torque (N·m) necessary to maintain an upright posture [3]:

$$\tau = |m \cdot \ddot{x} \cdot l|$$

where  $m$  is the participant's mass,  $\ddot{x}$  is the initial acceleration of the treadmill belt, and  $l$  is the estimated length of the inverted pendulum representing the participant ( $l = 0.586 \cdot \text{height}$ ) [7].

Stepping thresholds were evaluated under two conditions: unconstrained (Figure 1A) and with arms constrained by holding a rope with both hands behind the participant (Figure 1B).

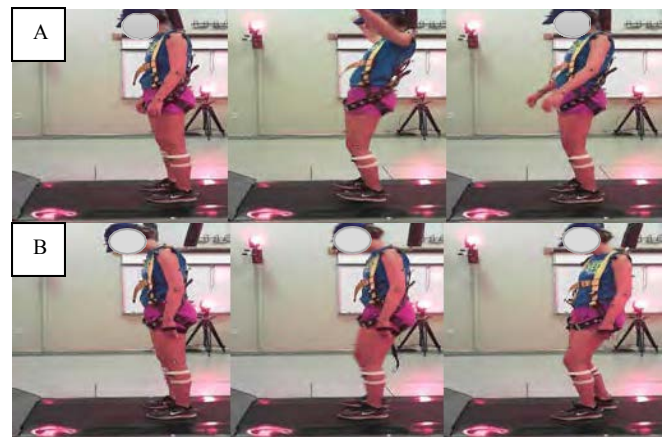


**Figure 1:** Posterior disturbances at a magnitude of ( $\ddot{x} = 3$  m/s<sup>2</sup>). (A) A successful posterior recovery with the arms unconstrained. (B) A failed posterior recovery with the arms constrained.

**Dynamic Stability Measures:** For all trials, the trajectories of 35 markers placed on the extremities, pelvis, trunk, and head were recorded with motion capture technology (Motion Analysis, Santa Rosa, CA; 120 Hz). Dynamic stability, represented as the margin of stability (MoS) [6], was calculated for disturbances as follows:

$$MoS = d + \frac{v}{\sqrt{\frac{g}{l}}}$$

Where  $d$  is the anteroposterior distance between the whole body center of mass and the toe or heel marker, and  $v$  is the velocity of the center of mass relative to that marker. The term  $g$  represents gravity ( $9.81 \text{ m/s}^2$ ), and  $l$  again represents the inverted pendulum length. The minimum MoS (i.e. most negative value,  $MoS_{\min}$ ) as well as the time from this minimum MoS value to a positive stability state ( $t_{MoS}$ ) was determined for each trial (Figure 2) using custom software (National Instruments, Austin, TX).

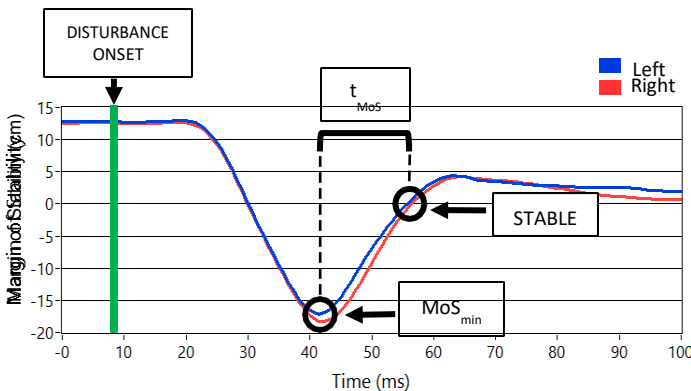


**Figure 2.** Depiction of posterior margin of stability in the arms constrained condition. The difference in time between the  $MoS_{\min}$  and where the MoS becomes stable again ( $MoS > 0$ ) represents  $t_{MoS}$ .

For both anterior and posterior stepping thresholds, constrained and unconstrained conditions were compared using repeated-measures t-tests and effect sizes. In the case that thresholds were different between conditions, dynamic stability measures were compared for the largest disturbance magnitude achieved without stepping across conditions.

## RESULTS AND DISCUSSION

**Single Stepping Thresholds:** Posterior thresholds were lower when the arms were constrained (Figure 3). No differences in anterior stepping thresholds were apparent between constrained ( $290.429 \pm 93.586 \text{ N}\cdot\text{m}$ ) and unconstrained ( $281.194 \pm 91.071 \text{ N}\cdot\text{m}$ ) conditions ( $p = 0.599$ , Cohen's  $d = 0.266$ ).

**Dynamic Stability Measures:** In the posterior direction, no significant differences were found in the minimum margin of stability ( $p=0.284$ , Cohen's  $d=0.171$ ) between the unconstrained ( $-13.919 \pm$

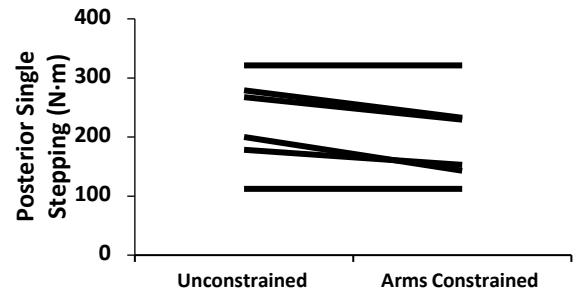


**Figure 3.** Posterior thresholds between the unconstrained ( $226.391 \pm 76.783 \text{ N}\cdot\text{m}$ ) and arms constrained ( $198.499 \pm 77.161 \text{ N}\cdot\text{m}$ ) conditions. Constraining the arms resulted in lower thresholds ( $p = 0.019$ , Cohen's  $d = 1.164$ ).

$8.771 \text{ cm}$ ) and arms constrained ( $-14.131 \pm 9.204 \text{ cm}$ ) conditions. There were no significant differences in duration of recovery ( $p= 0.638$ , Cohen's  $d= 0.231$ ) between unconstrained ( $93 \pm 45 \text{ ms}$ ) and arms constrained ( $87 \pm 51 \text{ ms}$ ) conditions.

## CONCLUSIONS

Constraining the arms reduced performance in fall recovery in the posterior direction, but not in the anterior direction. At a given posterior disturbance magnitude, there were no apparent differences in the level of instability experienced between the two conditions. For this reason, we cannot conclude that the arms altered the ability to prevent or recover from dynamic instability. Thus, between-condition differences may be a result of non-mechanical influences, such as a lower self-efficacy, which may have led to a more conservative stepping strategy.

## REFERENCES

1. Cheng KB, et al. *J Biomech* **48**, 3155-62, 2015.
2. Troy KL, et al. *J Biomech* **42**, 1339-1344. 2009.
3. Crenshaw JR, Kaufman KR. *Gait&Posture* **39**, 810-15, 2014.
4. Crenshaw JR, Grabiner MD. *Gait&Posture* **40**, 363-68. 2014.
5. Sturnieks DL, et al. *PLoS One* **8**, 2013.
6. Hof AL. *J Biomech* **38**, 1-8, 2005.
7. Clauser CE, et al. *Weight, Volume, and Center of Mass of Segments of the Human Body*, 1969.

## ACKNOWLEDGMENTS

This project was supported in part by a grant from the National Institute of General Medical Sciences (2P20 GM103446) from the National Institutes of Health.

# WALKING MUSCLE SYNERGIES INFLUENCE PROPENSITY OF SEVERE SLIPPING

<sup>1</sup> Mohammad Moein Nazifi, <sup>2</sup> Kurt Beschorner, PhD, <sup>2</sup> Rakie Cham, PhD and <sup>1</sup> Pilwon Hur, PhD

<sup>1</sup> Department of Mechanical Engineering, Texas A&M University, College Station, TX, USA

<sup>2</sup> Department of Bioengineering, University of Pittsburgh, Pittsburgh, PA, USA

email: {moeinnazifi,pilwonhur}@tamu.edu, {beschorn,rcham}@pitt.edu, web: <http://hurgroup.net>

## INTRODUCTION

Annually, injuries caused by slips, trips, and falls contribute to the loss of over \$16 billion [1]. Slips and resulting falls contribute to a significant share of these injuries [2]. Understanding how gait patterns influence the risk of a severe slip may lead to new methods of targeting and developing slip prevention strategies.

Previous research suggests that the control of gait may influence an individual's risk of experiencing a slip. For example, kinematic gait metrics like shoe-floor angle, step length and cadence are known to be associated with slip severity [3]. The kinematics of gait are effected predominantly by muscle activation patterns in the lower extremities. It has been suggested that the central nervous system may control the gait and slipping using a lower dimensional organization of muscle synergies [5]. Therefore, a logical next step in understanding how gait patterns influence slipping risk is to quantify differences in gait synergies between individuals whose gait leads to high severity slips versus those who did not.

The objective of this study is to compare the walking muscle synergies of the mild and severe slippers to find the possible inter-group discrepancies.

## METHODS

A total number of twenty healthy subjects (11 male/9 female, age (mean  $\pm$  SD): 23.6  $\pm$  2.52), free of walking disorders, were asked to walk at their self-selected speed in a pathway with an embedded force plate. The starting location of each subject was altered in a way to secure a foot strike on the force plate. Subjects were fitted with appropriate size PVC-soled shoes and donned an overhead safety harness and gave written consent prior to participation in this IRB-approved study at University of Pittsburgh. The data analysis was done at Texas A&M University upon approval of the IRB of both institutions.

Throughout the experiment, EMG signals were recorded at 1080 Hz from medial hamstring (*MH*), tibialis anterior (*TA*), vastus lateralis (*VL*), and medial gastrocnemius (*MG*) on both limbs (right/trailing/non-slipping leg (*NS*) and left/leading/slipping leg (*S*)). The slipping leg refers to the leg that experienced a slip in the following trial since EMG data was only collected from baseline walking conditions. A motion capture system

(Vicon 612, Oxford, UK) was utilized to capture heel kinematics at 120 Hz.

Subjects first performed a normal walking trial in which the data was recorded for synergy extraction. After the normal walking trials, without informing the subjects of a change in walkway condition, a slippery solution (75% glycerol, 25% water) was applied to the surface and a "slip trial" was recorded. The peak heel velocity (PHV) of each subject was used as representative of slip severity: Persons with a PHV higher than 1.44 m/s were considered severe slippers [4].

EMG signals were processed (demeaned, rectified, filtered) for the walking trial according to the procedures in [5]. The gait duration was then normalized to 100 points (0 being right heel strike) and a matrix factorization technique was used to extract four walking synergies and their coefficients from the normalized gait cycle for each subject [5]. Muscle synergies of each severity group were then sorted and ordered according to their similarity using correlation coefficients (*r*) [5]. An independent *t*-test ( $\alpha=0.05$ ) was used (SPSS v21, IBM, Chicago, IL) to detect the significant differences in gain coefficient and muscle activation levels between mild and severe slippers' synergies.

## RESULTS AND DISCUSSION

PHV measurement classified twelve subjects as mild slippers. No significant differences were found in sex, height, mass, and age across severity levels. Statistical analysis revealed significant differences in both walking synergies and their activation coefficients (Fig.1). Significant differences in gains of three muscles were found. *MH\_S* and *VL\_NS* activation were significantly higher for mild slippers while *TA\_S* activation was significantly higher in severe slippers (Fig. 1, W1 and W3). The inter-group comparison also found differences in activation of the first and the third walking synergies (Fig. 1, C1 and C3). The first synergy coefficient 'C1', was statistically different between mild and severe slippers from 10<sup>th</sup> until 18<sup>th</sup> percent (Fig.1) of the gait cycle (Table 1). Also, the activation coefficient of the third muscle synergy, 'C3', was found to be different for the two groups from 37<sup>th</sup> percent to 46<sup>th</sup> percent (Fig. 1) of the gait cycle (Table 1).

**Table 1** Significant differences according to the *t*-test

Variable		p-value	Variable		p-value
W1	VL_NS	0.003	C1	18 <sup>th</sup>	0.043
W3	MH_S	0.010	C3	37 <sup>th</sup>	0.019
	TA_S	0.009		38 <sup>th</sup>	0.008
C1	10 <sup>th</sup>	0.037		39 <sup>th</sup>	0.007
	11 <sup>th</sup>	0.015		40 <sup>th</sup>	0.029
	12 <sup>th</sup>	0.011		41 <sup>st</sup>	0.023
	13 <sup>th</sup>	0.008		42 <sup>nd</sup>	0.019
	14 <sup>th</sup>	0.008		43 <sup>rd</sup>	0.012
	15 <sup>th</sup>	0.012		44 <sup>th</sup>	0.010
	16 <sup>th</sup>	0.025		45 <sup>th</sup>	0.023
	17 <sup>th</sup>	0.026		46 <sup>th</sup>	0.033

According to the results, it can be argued that a higher activation of the *MH* muscle right before the heel strike is associated with less severe slips. This point can be seen in both higher contribution of *MH\_S* in the third synergy (W3), and in its higher activation coefficient (C3), right before the *S* limb's heel strike (which happens at 50%). Hamstring muscle is known to be involved in deceleration of the swing leg in terminal swing phase [6], hence, contributing to less slip severity.

Moreover, the results suggest that a higher activation of the *VL* muscle right after the heel strike is associated with less severity in slips. This conclusion was made upon observation of a higher contribution of *VL\_NS* in W1 along with a higher activation in C1, right after the *NS* limb's heel strike (which happens at 0%, Fig. 1). Considering the role of *VL* in load acceptance, this conclusion stays consistent with existing studies claiming that a late activation of the *VL* may reduce the forward velocity of the center of mass relative to the base of support, resulting in less stability [7].

The results also revealed an association between higher activation of the *TA* muscle before the heel strike and high slip severity. *TA\_S* muscle has both a higher contribution in the third muscle synergy (W3) and a higher activation coefficient (C3) before the *S* limb's heel strike (at 50%). High activation of *TA* may increase

the foot-floor-angle (FFA) which is known to be associated with severe slips [3]. To verify that, using our markers data we calculate the FFA for both mild and severe slippers and found that FFA at heel strike was significantly lower for mild slippers from 25<sup>th</sup> to 49<sup>th</sup> percent of the gait ( $p < 0.05$ ). It is also known that a zero FFA (i.e. flat-foot walking) is a strategy used by individuals to increase dynamic stability of the gait [8] that substantiates our findings.

## CONCLUSION

Our study investigated the walking differences between mild and severe slippers using a muscle synergy approach. We found that mild slippers and severe slippers have different muscle contributions and activation pattern in their normal walking muscle synergies. The findings of this study may have identified underlying gait control patterns that influence slip risk. Future studies would assess the efficacy of these methods in identification severe slippers and developing strategies that modify their gait control.

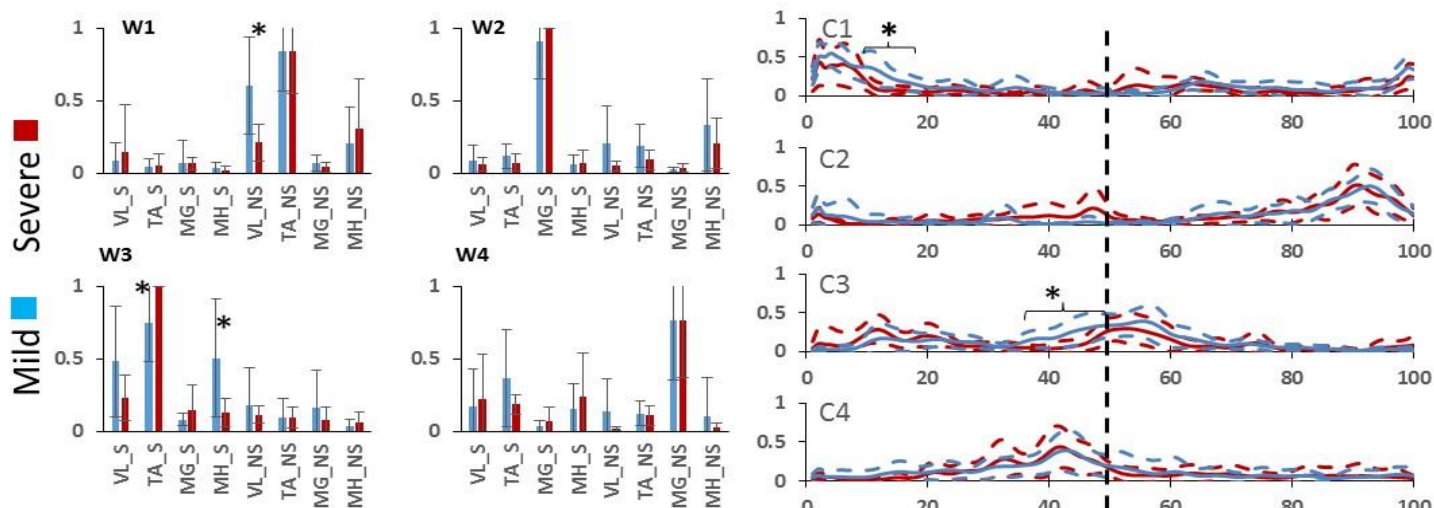
## REFERENCES

1. Liberty Mutual Research Institute for Safety, *Liberty Mutual Workplace Safety Index*. Hopkinton, MA, 2014.
2. Courtney TK, et al. *Ergonomics* **44**, 2001.
3. Moyer BE, et al. *Gait Posture* **29**, 2009.
4. Lockhart TE, et al. *Ergonomics* **46**, 2003.
5. Nazifi MM, et al. *Frontiers in Human Neuroscience*, 2017.
6. Beschorner KE, et al. *Ergonomics* **51**, 2008.
7. Chambers AJ, et al. *Gait and Posture* **25**, 2007
8. Marigold DS, et al. *J Neurophysiol* **88**, 2002.

## ACKNOWLEDGMENTS

The experimental data used in this abstract was collected by Dr. Raki Cham under NIOSH R01 grant (R01 OH007592).

**Figure 1** Walking muscle synergies and their coefficients (averaged) for each severity group. Error bars indicate Standard Error. Asterisks indicate significant differences. (Right/NS heel strike at 0%, Left/S heel strike at 50% (dashed line))



# TRANSLATING A QUANTIFIED MEASURE OF FALL RISK TO CLINICAL USE: DEFINING EXPECTED VARIABILITY

Lise Worthen-Chaudhari<sup>1</sup>, Scott M. Monfort<sup>2</sup>, Courtney Bland<sup>1</sup>, Xueliang Pan<sup>3</sup>, Ajit Chaudhari<sup>2,4</sup>

The Ohio State University, <sup>1</sup> Department of Physical Medicine and Rehabilitation; <sup>2</sup> Department of Mechanical and Aerospace Engineering; <sup>3</sup> Center for Biostatistics; <sup>4</sup> School of Health and Rehabilitation Sciences - Division of Physical Therapy, Columbus, OH, USA

email: [lise.worthen-chaudhari@osumc.edu](mailto:lise.worthen-chaudhari@osumc.edu)

## INTRODUCTION

Despite demonstrated need to reduce the incidence of falls among older Americans [1], clinicians lack quantifiable measures of falls risk that can be used to identify and track those at risk *before* they suffer a first fall. In 1994, Maki et al. reported a biomechanical measure of balance control that identified individuals at risk for falls before they fell: the variability of a person's sway in the medial-lateral direction during comfortable, quiet standing with eyes closed (RMSx\_EC) with those showing more than 2.3mm of RMSx\_EC being at greater risk of falling within the year [2]. RMSx\_EC is a simple measure, collected on equipment that has become relatively affordable of late, that shows promise to identify those at risk of falls before they happen and assess progress over the course of interventions intended to be preventative. Barriers remain, however, to clinical implementation of this quantified measure for the purpose of longitudinal tracking and assessment of patients.

One such challenge is a dearth of information about the *expected variability* (EV) over time, or the variability that normally occurs in balance control within-subject from day to day. Clinicians see patients intermittently and record outcome measures even less frequently. To interpret their measures, and conclude that balance control has/has not improved post treatment on any given day, change due to intervention must exceed expected, day-to-day variability. Past studies have revealed group changes in RMSx\_EC over time [3], however translating this knowledge to clinical care necessitates a consideration of EV. The EV concept is related to both minimum detectable change (MDC) and minimum clinically important

difference (MCID), but is distinct from both. The purpose of this study was to characterize EV over multiple days in RMSx\_EC for a group of healthy middle-aged adults. This information furthers our ultimate goal of identifying a quantified measure of balance control that can be used in clinical settings to identify and longitudinally track falls risk for individual patients.

## METHODS

This research was reviewed and approved by The Ohio State University Institutional Review Board. Thirteen middle-aged adults without neurologic or orthopedic impairment consented to participate (55 +/-9 years; 76 +/- 18 kg; 11 females/2 males). Balance data were recorded (1000 Hz) during quiet standing with eyes closed. Recordings were taken on 6 different days, for 5 minutes each day, in 1 minute intervals as follows: participants stood on a balance board (Bertec Corp), feet comfortable width apart and hands clasped in front of the body, as if they were in a "line up" [2]. At the end of each 1 minute interval, participants were instructed to open their eyes, "get their bearings" by sighting a point approximately 8 ft in front of them at eye level, and close their eyes when ready. Once the participant closed their eyes on their own timing, we commenced the next 1 minute data collection interval. At the beginning of testing on the first day, each participant's foot position was traced on paper that was affixed to the force platform with paper tape, labeled with their study code, and used to ensure that the participant's feet did not move from their original position on the platform between trials [2] or over the course of the study.

Data were filtered (4<sup>th</sup> order, 20 Hz low pass, Butterworth) and RMSx\_EC was calculated as the root-mean-squared of center of pressure (COP) excursion within the frontal plane of motion (i.e., postural sway in the medial-lateral direction) over the course of each 1 minute collection period [2].

For this analysis the first minute of quiet standing data per day was not included, consistent with Maki et al [2]. Variance components analysis was performed on minutes 2-5 to determine the relative variances coming from (A) between subjects, (B) within-subject minute-to-minute variations, (C) within-subject day-to-day variations, and (D) residual variations. To get an estimate of within-subject standard deviation over multiple days in RMSx\_EC, the square root of the sum of variances B-D was calculated. The 95% confidence interval of the within-subject between-day difference (EV) was then calculated as (SD \* 1.96).

## RESULTS AND DISCUSSION

The output for the variance component analysis identified that between-subject variability was greater than within-subject day-to-day variations, which exceeded, within-subject minute-to-minute variations (Table 1).

**Table 1.** Variance component analysis of RMSx\_EC.

Variance Component	Variance (mm <sup>2</sup> )
A. Between Subjects	0.597
B. Minute-to-Minute	0.027
C. Day-to-Day	0.111
D. Residual	0.409

Within-subject standard deviation over multiple days in RMSx was calculated to be 0.74mm and EV to be 1.45mm. **Thus, changes in balance control (as measured by RMSx\_EC) above 1.45mm are expected to represent more change than could be explained by typical day-to-day variability among a middle-aged, healthy participant.** This represents a starting point for determining whether an observed change within-subject is real or simply reflects expected minute-to-minute and day-to-day variability in the measure.

## CONCLUSIONS

Medial-lateral balance control, as measured by a force platform, continues to be a promising measure for identifying those at risk of falling *before* they suffer their first fall and assessing their progress as clinicians intervene to improve their balance control. Quiet standing with eyes closed for up to 5 minutes is a feasible and reasonable quantified test for patients to undergo within standard clinical care. While MCID for this measure remains to be determined, identifying the EV is an important first step toward implementing this measure clinically to impact and improve patient's lives.

## REFERENCES

- [www.cdc.gov/media/releases/2016/p0922-older-adults-falls.html](http://www.cdc.gov/media/releases/2016/p0922-older-adults-falls.html)
- Maki et al. *Journal of gerontology*, **49**(2), M72-M84, 1994.
- Monfort et al. *Gait & Posture*, **48**, 237-242, 2016.
- Doyle et al. *Gait & Posture*, **25**, 166-171, 2007.

# ASSESSING FALL STATUS IN PATIENTS WITH MULTIPLE SCLEROSIS USING A WII BALANCE BOARD

<sup>1</sup> Monica Paliwal, <sup>1</sup> Laura Frey-Law, <sup>1</sup> E. Torage Shivapour, and <sup>2</sup> Sergio Mendoza-Lattes

<sup>1</sup> University of Iowa, Iowa City, IA, USA

<sup>2</sup> Duke University, Durham, NC, USA

email: monicapaliwall@gmail.com

## INTRODUCTION

Balance disorders and falls are highly prevalent among patients with Multiple Sclerosis (MS) and other neuromuscular pathologies with an estimated \$31 billion spent on fall-related injuries in 2015 [1]. Despite its socio-economic burden, current clinical assessment of balance and fall risk relies heavily on functional tests such as the Berg balance test that show limited accuracy and association with fall risk [2]. In contrast, Center of Pressure (COP)-based assessment of balance via force plates is accurate but isn't always feasible in clinical settings. So while COP-based balance parameters are related to increased fall risk, there are no known demarcation thresholds that are indicative of clinically-relevant balance deterioration and fall risk.

The purpose of this study was to examine the ability of a Wii Balance Board (WBB) to predict fall status and determine optimal parameter thresholds that identify increased fall risk in patients with MS.

## METHODS

A subset of 19 patients with reported fall histories were included from a total of 35 patients with MS, recruited from University of Iowa. Patients with other major medical or neurological conditions such as diabetes, stroke, Parkinson's, spinal deformities etc. were excluded. Patients were asked to report any occurrences of fall(s) in the last year. Three fall status levels were defined as: 1. Non-fallers (0 falls), 2. Non-recurrent fallers (1-2 falls), 3. Recurrent fallers ( $\geq 3$  falls).

Subjects were asked to stand independently on the WBB to record COP measurements for 30 seconds.

Path length (total vector distance covered by the COP signal) was calculated.

Receiver operating characteristic (ROC) analysis was performed using two fall status criteria:  $\geq 1$  falls (all fallers vs. non-fallers) and  $\geq 3$  (recurrent fallers vs. all others). Overall test accuracy of the WBB was evaluated using area under the ROC curve (AUC). For each cut-off value used to generate the ROC curve, sensitivity, specificity, positive predictive value (PPV), negative predictive value (NPV) and the Youden Index ( $J = \text{sensitivity} + \text{specificity} - 1$  [3]) were calculated.

One-way Analysis of Variance (ANOVA) was conducted to assess for differences in path length between fall status groups, 1. non-fallers, 2. non-recurrent fallers, 3. recurrent fallers.

## RESULTS AND DISCUSSION

The patients consisted of 17 females and 2 males; mean age:  $43.7 \pm 10.9$  years; BMI:  $26.5 \pm 4.9$  kg/m<sup>2</sup>; 6 with no falls, 4 with 1-2 falls and 9 with  $\geq 3$  falls.

The WBB assessed path length was highly accurate in identifying fallers ( $\geq 1$  falls) from non-fallers and discerning recurrent fallers from all others (91% and 92% accuracy, respectively) (Fig 1). Choice of the optimal cut-off is a trade-off between sensitivity and specificity (Table 1). For example, at cut-off path length of 28.8 cm, the WBB test correctly identified all fallers (sensitivity = 1), but misclassified 33% of non-fallers as fallers (specificity = 0.67). Conversely, increasing the cut-off path length to 39.2 cm improved the specificity (100%) but 31% of fallers were misclassified as non-fallers (false negatives). The cut-off of 35 cm provided a reasonable tradeoff,

resulting in nearly equal, high sensitivity (85%) and specificity (83%).

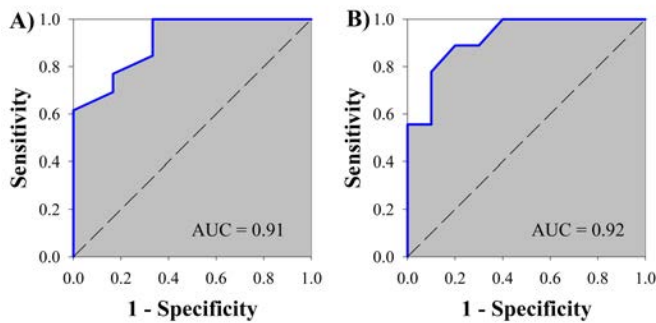


**Figure 1:** ROC curves for path length (cm) considering A)  $\geq 1$  fall(s) in the last year (fallers compared to non-fallers) B)  $\geq 3$  falls in the last year (recurrent fallers from others).

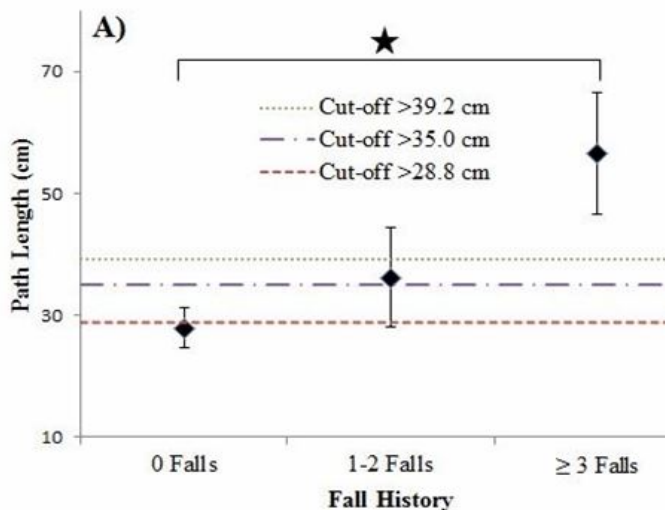


**Figure 2:** Mean (SE) path length in patients with MS who reported no falls, 1-2 falls, or  $\geq 3$  falls in the past year. \*Denotes significant differences ( $p \leq 0.05$ ).

Standing balance deteriorates with a positive history of falls (Fig 2). Path length for patients who reported recurrent falls ( $\geq 3$  falls) was approximately twice as high as those who reported no falls. The cut-off path lengths indicate that if a subject has fallen once or twice, there is a 85% probability that he/she has a path length greater than 35.0 cm, but if a subject reported 3 or more falls, there is a 100% probability that their path length will be higher than 35 cm. Additionally, 89% of the recurrent fallers have path length higher than 39.2 cm and 90% of non-recurrent fallers have a path length lower than 39.2cm.

## CONCLUSIONS

This study demonstrates that quantitative balance assessment using a WBB in patients with MS is highly accurate in discerning increased fall risk based on fall history. Cut-off path length of 35 cm shows excellent sensitivity and specificity in identifying patients with MS who have sustained a fall in the last year. However, future prospective studies investigating its accuracy in predicting fall risk are needed. The WBB test could provide a clinically feasible, practical assessment of fall risk and may be indicative for rehabilitation interventions.

## REFERENCES

- Alexander BH, et al. *Am J Public Health* **82**, 1020–1023, 1992.
- Martina M, et al. *Eur J Phys Rehabil Med* **46**, 239–248, 2010.
- Youden WJ. *Cancer* **3**, 32–35, 1950.

**Table 1:** Optimum cut-off path lengths (for classifying fallers from non-fallers and recurrent fallers from others) and their corresponding Youden Indices, sensitivity, specificity, positive and negative predictive values.

	Cut- off Path length	Youden Index (J)	Sensitivity	Specificity	PPV	NPV
<b>Fallers vs. Non-fallers</b>	28.8 cm	0.67	1	0.67	0.87	1
	35.0 cm	0.68	0.85	0.83	0.92	0.71
	39.2 cm	0.69	0.69	1	1	0.6
<b>Recurrent-Fallers vs. Others</b>	28.8 cm	0.40	1	0.40	0.60	1
	35.0 cm	0.70	1	0.70	0.75	1
	39.2 cm	0.79	0.89	0.90	0.89	0.9

# Effects of Lower Extremity Muscle Fatigue on Dual-Task Obstacle-Crossing

Szu-Hua (Teresa) Chen, Jocelyn Taylor, and Li-Shan Chou

Department of Human Physiology, University of Oregon, OR, USA  
email: [chou@uoregon.edu](mailto:chou@uoregon.edu); web: <http://choulab.uoregon.edu>

## INTRODUCTION

Lower limb muscle fatigue has been shown to cause motor adjustments during walking and obstacle crossing [1]. Walking and simultaneously performing an attention demanding task could take place with the presence of fatigue, especially at the end of a working day. Tripping over an obstacle during walking is one of the most frequently mentioned causes of falls [2]. Although previous studies have demonstrated how a concurrent cognitive task and muscle fatigue affects walking performance [3], the effect of muscle fatigue on dual-task obstacle-crossing remains unclear. The purpose of this study was to examine changes in gait balance control and concurrent working memory task performance in healthy young adults when lower extremity muscles are fatigued.

## METHODS

Ten healthy adults (4 females, 21.5±2.6 yrs) performed the following three tasks before and after a muscle fatigue protocol with a random order: 1) walking and crossing over an obstacle with height set at 10% of body height (OC), 2) sitting and performing a 3-back test, in which participants listened a series of digits over a loud speaker and were instructed to verbally respond “yes” whenever a digit is heard that is the same as presented three positions back in the series (Nback), 3) Obstacle-crossing and performing a 3-back test simultaneously (OC+Nback).

A 30-minutes sit-to-stand task at a pace of 0.5 Hz was performed to induce the muscle fatigue as indicated by the participant’s response of inability to continue or when the movement frequency falling below 0.5 Hz after the examiner’s encouragement. The maximal voluntary isometric strength of knee extensors was assessed using a dynamometer immediately before and after the fatigue protocol and at the completion of the entire study protocol.

Whole body motion data were collected from a set of 29 retro-reflective markers placed on bony landmarks with a 10-camera motion system. The whole-body center of mass (CoM) was calculated as the weighted sum of 13 body segments. Measurements during crossing stride, defined as the gait cycle during stepping over the obstacle between heel strikes of the trailing foot immediately before and after crossing the obstacle were analyzed. Gait speeds were calculated as the average forward CoM velocity during a gait cycle. Gait balance control was examined using the total medial-lateral center of mass displacement (M-LCoM) and peak forward velocity of center of mass (vCoM). Dependent variables for crossing characteristics included the toe-obstacle clearance and foot placements. Toe-obstacle clearance (TC) was calculated as the vertical distance between the obstacle and toe marker at the time of crossing. Foot placements (FP) of trailing foot and leading foot were measured as the horizontal distance between the obstacle and toe marker and heel marker, respectively.

Two-way ANOVA with repeated measures and with the gait velocity as a covariate was used to examine effects of fatigue (pre- and post-fatigue) and gait condition (single- and dual-tasks). Alpha level was set at .05.

## RESULTS AND DISCUSSION

An average of 20.7% knee extensor strength reduction was observed immediately after the completion of fatigue protocol, and it was recovered to approximately 16.2% by the completion of study protocol. The average time-to-fatigue during the sit-to-stand task was 24.3 minutes.

Gait speeds showed a significant main effect of gait condition. Participants crossed over the obstacle

significantly slower when responding concurrent 3-back task than they did under single task condition.

Accuracy of working memory task and M-L CoM were not affected by muscle fatigue or gait condition. Peak forward CoM velocity showed a significant interaction effect. After fatigue, vCoM was significantly slower in the dual-task condition than in the single-task condition. Interestingly, a significantly faster vCoM after fatigue was observed in the single-task condition (**Figure 1**).

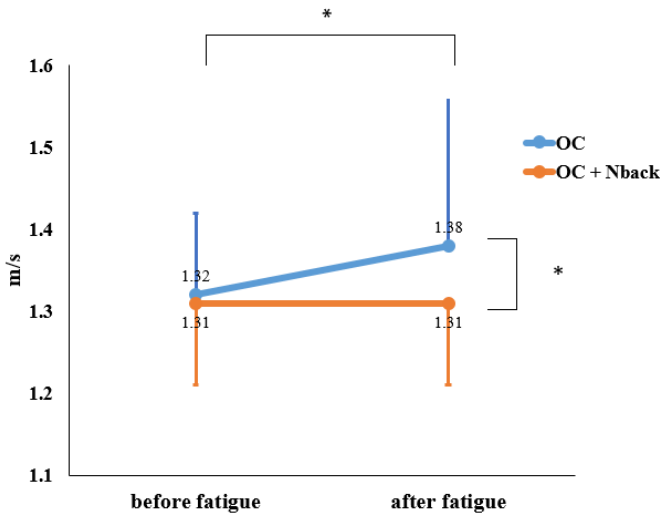


**Figure 1:** Peak forward CoM velocity across gait conditions before and after muscle fatigue. \*  $p < .05$ .

Toe-clearances were not affected by the fatigue or gait condition. However, muscle fatigue significantly decreased foot placement of leading foot after crossing an obstacle and increased foot placement of trailing foot before crossing. (**Figure 2**).

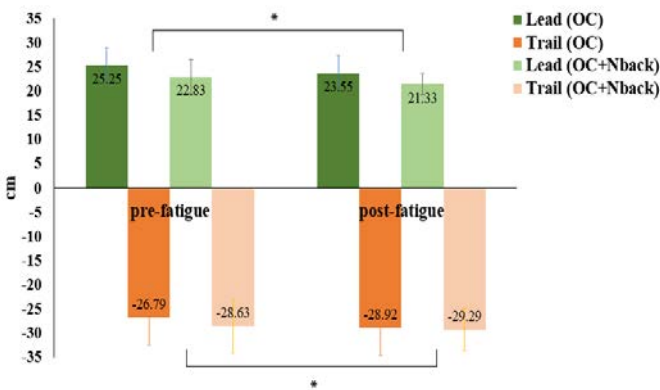


**Figure 2:** Foot placements of leading (top) and trailing (bottom) feet across different conditions before and after muscle fatigue. \*significant main effect.

## CONCLUSIONS

Findings from this study indicated that the acute muscle fatigue induced in this study did not affect the frontal plane balance control or accuracy of concurrent working memory test during obstacle crossing. Instead, sagittal plane CoM momentum control and foot placements were affected by muscle fatigue. This may be due to the selected sit-to-stand fatigue protocol that is more effectively in fatiguing the knee extensors.

## REFERENCES

1. Barbieri FA et al. *Gait Posture* **39**, 985–990, 2014.
2. Berg WP et al. *Age Ageing* **26**, 261–268, 1997.
3. Granacher U et al. *Journal of NeuroEngineering and Rehabilitation* **7**, 56, 2010.

## ACKNOWLEDGMENTS

This work was funded by the UROP Mini-grant Program in University of Oregon.

# EFFECTS OF A VERBAL FLUENCY TASK ON STABILITY WHILE WALKING AND OBSTACLE CROSSING IN AGING

Sarah A. Brinkerhoff, Tiphonie E. Raffegeau, Grace Kellaher, Matthew J. Terza, Jaimie A. Roper, Lori J. Altmann, and Chris J. Hass  
University of Florida, Gainesville, FL, USA  
email: sbrinkerhoff@ufl.edu

## INTRODUCTION

Older adults (OA) exhibit impaired performance during tasks that simultaneously challenge cognitive and motor resources [1]. Dual-task studies frequently challenge executive function using a concurrent verbal fluency task [2] while participants perform mobility tasks such as walking and stepping over obstacles [3].

One goal during walking is to maintain some minimum margin of stability (minMOS) [4]. Thus, evaluating alterations in minMOS may provide insight into control of stability as motor demands rise. Although gait kinematics have been reported in dual-task walking and obstacle crossing (OC), dynamic stability changes in these constraints remain unclear. Therefore, the purpose of this study was to observe changes in dynamic stability (minMOS) with increasing motor complexity and cognitive load in older adults. Further, we aimed to better understand the relationship between cognitive performance and changes in stability.

## METHODS

Thirty-six community-dwelling older adults (12 females,  $72 \pm 1$  yr) participated as part of a larger intervention study and provided informed consent. Validated clinical cognitive assessments were administered during the first visit. In the second visit, participants performed four walking conditions in the order: self-selected walk (SS Walk), walking while generating words from an assigned word category (Fluency Walk), walking and stepping over a 10-cm obstacle (SS OC), and walking and stepping over an obstacle while generating words (Fluency OC).

Whole-body three-dimensional kinematics (10 camera Vicon Motion System, 120 Hz) were collected while participants performed each task. In addition to foot placement, the anterior minMOS was determined as described previously [5]. Anterior

minMOS was analyzed because crossing an obstacle generally perturbs the A/P direction more so than the M/L [5]. This measure quantifies the extent the extrapolated center of mass (xCOM) approaches the anterior boundary of the base of support (BOS). When anterior MOS is negative, the xCOM is past the BOS and therefore represents an unstable position. In walk trials, right and left legs were matched to the participant's lead and trail limbs in OC to directly compare each phase of an over ground step to the step over the obstacle. Results are presented in order of events: trail limb single support, lead limb double support, lead limb single support, and trail limb double support.

Repeated measures MANOVA evaluated the effect of condition on foot placement in OC. A  $2 \times 2$  (Motor task  $\times$  Condition) repeated measures MANOVA analyzed differences in anterior minMOS. Post-hocs with Bonferroni adjustments were used to determine the direction of significant differences in anterior minMOS. In addition to evaluating minMOS, obstacle crossing costs (OCC) were calculated for self-selected  $\left(\frac{SS\ Walk - SS\ OC}{SS\ Walk}\right)$  and fluency  $\left(\frac{Fluency\ Walk - Fluency\ OC}{Fluency\ Walk}\right)$  conditions. The OCC represent the adjustments to stability in each condition as an obstacle is introduced. A repeated measures MANOVA determined differences between SS and Fluency OCC. Two-tailed partial bivariate correlations (controlling for Age, Education, & Gender) evaluated the relationship between SS and Fluency OCC and cognitive measures. Significance was set at  $p=.05$ .

## RESULTS AND DISCUSSION

Compared to SS OC, Fluency OC displayed a higher vertical toe clearance (lead limb  $p<0.001$ , trail limb  $p=0.006$ ) and closer distance after crossing the obstacle (lead limb  $p<0.001$ , trail limb  $p<0.001$ ). Approach steps were not significantly affected by the cognitive task.

The 2x2 MANOVA revealed a significant effect of condition ( $F(24, 12)=3.271, p=.007$ ) and motor task ( $F(24, 12)=25.033, p<0.001$ ). A significant interaction of condition and motor task ( $F(24, 12)=4.736, p=.001$ ) supported that stability performance was affected by task and condition manipulations and these differences were interdependent. Participants displayed lower anterior minMOS scores (less stability) in SS Walk than in Fluency Walk and lower anterior minMOS scores in SS OC than in Fluency OC. As expected, both SS OC and Fluency OC had significantly lower anterior minMOS than their respective walk trials in trail limb single support (SS  $p=0.04$ , fluency  $p<0.001$ ) and lead limb single support (SS  $p<0.001$ , fluency  $p<0.001$ ). Anterior minMOS was lower in trail limb double support in SS OC than in SS Walk ( $p=0.046$ ) and anterior minMOS trended towards significantly lower in Fluency OC than in Fluency Walk ( $p=0.08$ ). In all phases but lead limb double support, participants exhibited lower anterior minMOS scores (less stability) when crossing an obstacle compared to walking over ground with or without a dual-task. Only in lead limb double support did anterior minMOS increase from SS Walk to SS OC ( $p<0.001$ ) and Fluency Walk to Fluency OC ( $p<0.001$ ), indicating a more stable step over the obstacle. Increased stability in lead limb double support in OC may be due to the fact that forward momentum is arrested while the obstacle is in between the lower limbs, restraining the COM to closer to the anterior BOS. Importantly, the added verbal fluency condition limited the anterior minMOS excursion in both walk and OC.

The MANOVA comparing OCC in SS and Fluency show that OCC for SS were smaller than Fluency only in trail limb single support ( $p=0.005$ ). This may be due to a lower (more unstable) anterior minMOS in SS Walk than in Fluency Walk. SS Walk allowed for more excursion in anterior minMOS than Fluency

Walk resulting in a smaller difference between SS Walk and SS OC. Because Fluency resulted in more stable walking, larger changes in anterior minMOS occurred when an obstacle was in the path. Double support showed no significant differences in trail and lead limbs between SS and Fluency. Rather, an additional cognitive load exaggerated changes to anterior minMOS in single support when adjusting steps to cross an obstacle.

The partial bivariate correlations showed that OCC in SS was not related to executive functions. However, the OCC during Fluency was related to several measures of executive function. Clinical cognitive tests related to OCC in Fluency measure global executive function (Montreal Cognitive Assessment,  $r=.39, p=.027$ ), inhibition (Stroop Color Word,  $r=0.455, p=0.009$ ), working memory (Forward digit span,  $r=0.385, p=0.03$ ), and set-switching (Trails B,  $r=-0.624, p<0.001$ ). Overall, greater changes in OCC with a dual-task are related to better executive function. Thus, the aptitude of these aspects of cognition is related to the ability to modulate dynamic stability in order to perform a more complex motor task while generating words.

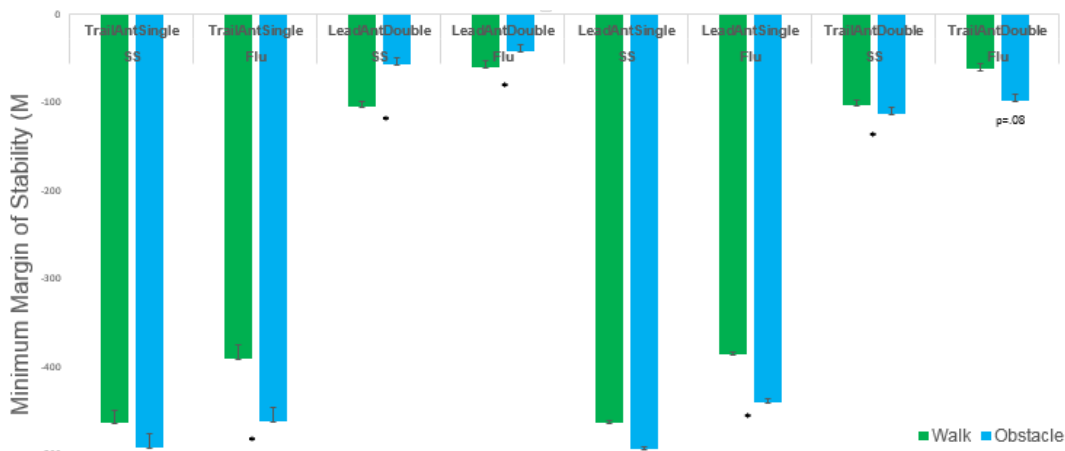
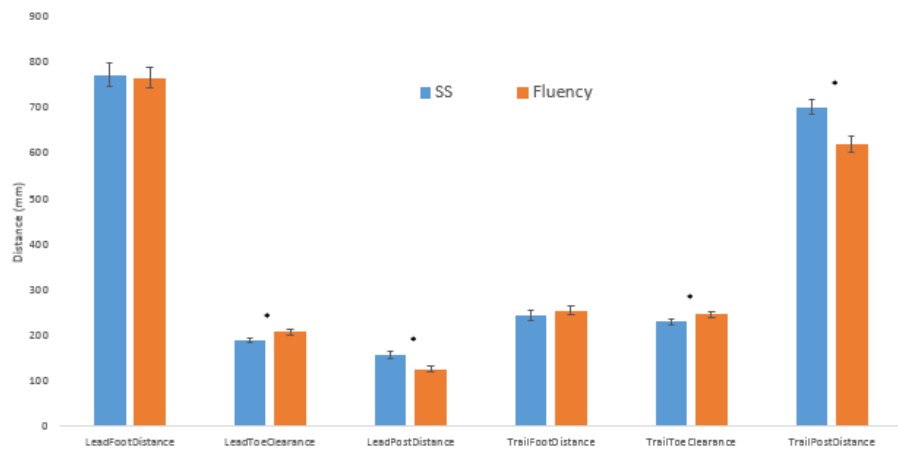
## CONCLUSIONS

Dynamic stability changes due to increasing motor complexity and a cognitive load provide insight into mobility impairments in OA. We determined that anterior minMOS is more tightly controlled during walking when a cognitive task is added. This may be because walking is less dynamically challenging than OC. Therefore, stability changes are limited in OC with a cognitive load in community-dwelling older adults.

## REFERENCES

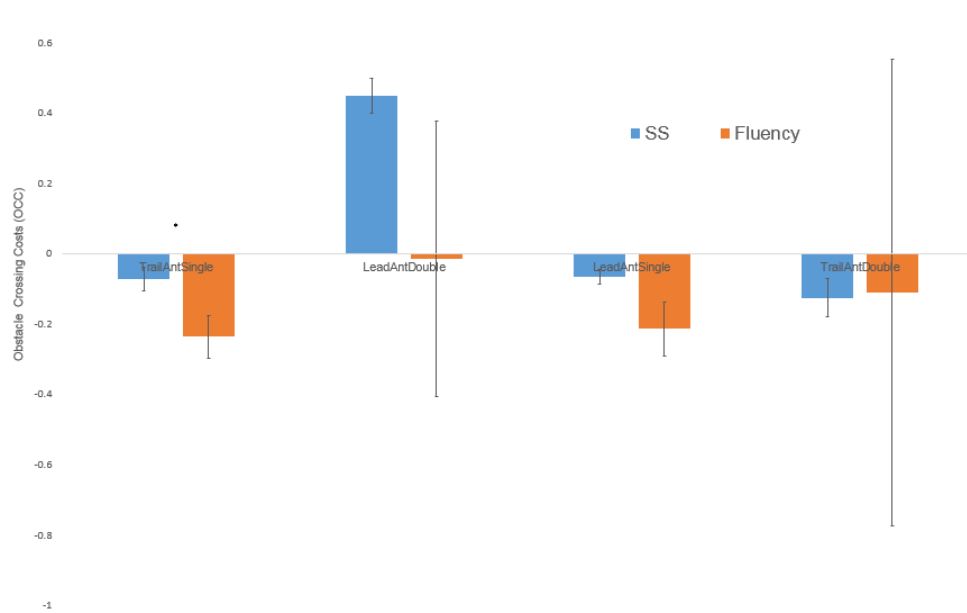
1. Faulkner K.A. et al., (2007). *Journal of the American Geriatrics Society* 55, 570-576.
2. Frith C.D., (1991). *Neuropsychologia*, 29, 1137-1148.
3. Plummer-D'Amato, P. et al., (2012). *Journal of Aging Research*.
4. McAndrew Young P.M. et al., (2012). *J Biomech*, 45, 1053-1059.
5. Stegemoller E.L. et al., (2012). *Archives of Physical and Rehabilitation* 93, 703-709.

Fluency Task Affects Foot Placement during Obstacle Crossing



Motor Task Complexity and Dual-Tasks Affect Stability

Condition Affects Stability During Obstacle Crossing



# TURN PERFORMANCE OF INDIVIDUALS WITH LOWER-LIMB LOSS: WITHIN-SUBJECT COMPARISONS AMONG FALLERS AND NONFALLERS

Jonathan Akins and Samantha Eigenbrot

Widener University, Chester, PA, USA  
email: [jsakins@widener.edu](mailto:jsakins@widener.edu), web: [www.widener.edu](http://www.widener.edu)

## INTRODUCTION

Turns comprises 8-50% of all steps taken during a typical day [1] and occur at a rate of 65-70 turns per hour [2, 3]. Turning gait of individuals with lower-limb loss has been studied during tasks of steady state curved-path walking and transient turns. Comparison in these studies were between individuals with lower-limb loss and controls, prosthetic componentry (torsion adapters), and limb-loss etiology. A limitation among the existing turn literature is the lack of within-subject comparisons between turns towards the sound side and turns towards the prosthetic side. Turns toward the prosthetic limb are likely more challenging for individuals with unilateral lower-limb loss because specific gait characteristics are required. The stride length of the inner leg decreases and the stride length of the outer leg increases as compared to straight-path walking. Simultaneously, the body's center of mass shifts to the inner leg and stance time of the inner leg increases. The ability to successfully shift the body's center of mass over the prosthetic limb may be more difficult given decreased balance confidence and gait asymmetries.

The purpose of this study was to investigate within-subject comparisons of turn performance when turning towards the sound limb and when turning towards the prosthetic limb. We hypothesized that individuals with a history of falls would have decreased turn performance when turning towards the prosthetic limb compared to the sound limb.

## METHODS

Participants: Individuals with unilateral transtibial (TT) and transfemoral (TF) lower-limb amputation using a prosthetic were recruited to participate in this IRB approved study.

Instrumentation: Fall history was assess by asking "How many times have you fallen to the ground in the past year?" Participants were categorized as nonfaller (0 falls in the past year) and faller ( $\geq 1$  fall in the past year). Four wireless inertial sensors (Opal, APDM, Inc., Portland, OR) were secured to the sternum, lumbar spine, and feet using elastic straps. Each sensor recorded at 128 Hz.

Experimental Procedures: Participants walked as quickly and smoothly as possible around a pair of cones (spaced 1.525 m apart) in a figure-of-8. Two laps were performed without pausing, which resulted in two turns towards the sound limb and two turns towards the prosthetic limb.

Data Reduction: Angular velocity in the transverse plane at the lumbar spine (L5) was measured with the gyroscope of the inertial sensor. Data from each turn were segmented from the time series using  $0^\circ/\text{s}$  as a cut point. Turn performance of each turn was quantified using measures of central tendency, variability, and frequency content. Central tendency measures included mean and peak angular velocity, variability included variance and standard deviation of angular velocity, and frequency included 1<sup>st</sup> and 2<sup>nd</sup> dominant frequencies of the angular velocity signal. Turn performance was calculated for each turn and the mean of turns in each direction were used in the analysis.

Statistical Analysis: Related-samples Wilcoxon Signed Rank tests were performed to obtain within-subject comparisons (turns towards the sound limb and turns toward the prosthetic limb) for each participant group: TT nonfallers, TT fallers, TF nonfallers, and TF fallers. Alpha was set to 0.05 *a priori*.

## RESULTS AND DISCUSSION

Sixty-nine individuals with unilateral lower-limb amputation completed the study procedures (Table 1).

**Table 1:** Demographic data

	Transtibial		Transfemoral	
n	36		33	
Gender (M / F)	19	/ 17	21	/ 12
Fallers / Nonfallers	15	/ 21	22	/ 11
Age (years)	47.0	± 14.3	42.8	± 12.9
Height (cm)	174.9	± 10.3	174.2	± 11.2
Mass (kg)	92.7	± 21.0	82.7	± 16.4

**TT nonfallers:** Turn performance was not significantly different when turning towards the sound and prosthetic limb (Table 2). **TT Fallers:** Mean angular velocity was significantly increased when turn towards the sound limb ( $p = .027$ ). Variability was significantly greater when turning towards the sound limb ( $p \leq .015$ ). Turning towards the sound limb was significantly slower ( $p = .020$ ). **TF Nonfallers:** Mean and peak angular velocity were significantly greater when turning toward the sound limb ( $p \leq .033$ ). Variability was significantly greater when turning towards the sound limb ( $p \leq .010$ ). Turning towards the sound limb was significantly slower ( $p = .008$ ). **TF Fallers:** Peak angular velocity was significantly greater when turning towards the sound limb ( $p = .007$ ). Variability was significantly greater when during towards the sound limb ( $p \leq$

.002). The 1<sup>st</sup> dominant frequency was significantly higher when turning towards the sound limb ( $p = .004$ ). No difference in turning times ( $p = .144$ ).

Increased variability when turning towards the sound limb was found for all groups except for TT nonfallers. A possible explanation is that a mechanical (or electromechanical) device was the inner limb when turning towards the prosthetic limb as compared to a biological limb with active control and degrees of freedom when turning towards the sound limb. Increased stability of the prosthetic limb to promote better balance and gait may, in fact, reduce needed variability during curved path walking.

## CONCLUSIONS

Turn performance was quantified using central tendency, variability, and frequency content of the angular velocity signal measured at the lumbar spine. TT nonfallers had no significant differences in turn performance. Signals in addition to angular velocity of the lumbar spine should be explored to further explain these findings.

## REFERENCES

1. Glaister, et al. *Gait Posture* **25**, 289-294, 2007.
2. El-Gohary, et al. *Sensors* **14**, 356-360, 2014.
3. Mancini et al., *Neurorehabil* **37**, 3-10, 2015.

**Table 2:** Within-subject comparisons of turn performance metrics based on angular velocity (AV) and turn time

	TT Nonfaller					TT Fallers				
	Toward Sound		Toward Prosthetic		P	Toward Sound		Toward Prosthetic		P
	Median	IQR	Median	IQR		Median	IQR	Median	IQR	
Mean AV (°/s)	77.9	± 35.8	79.3	± 35.4	0.903	69.3	± 26.7	67.5	± 29.7	0.027*
Peak AV (°/s)	169.7	± 71.7	161.5	± 69.4	0.140	171.2	± 67.4	152.8	± 73.4	0.053
Variance AV (°/s)	2473.9	± 2396.1	1959.1	± 1848.5	0.068	2555.4	± 1444.4	1475.9	± 1660.0	0.012*
SD of AV (°/s)	49.7	± 22.6	44.2	± 19.5	0.058	50.4	± 14.3	38.1	± 18.4	0.015*
1st Dom Freq (Hz)	0.37	± 0.19	0.37	± 0.24	0.986	0.62	± 0.47	0.33	± 0.25	0.069
2nd Dom Freq (Hz)	1.46	± 1.25	1.56	± 0.90	0.876	0.83	± 0.72	0.86	± 1.22	0.140
Turn Time (s)	3.00	± 1.33	2.96	± 1.44	0.848	3.4	± 1.5	3.5	± 2.3	0.020*

	TF Nonfallers				TF Fallers					
	Toward Sound		Toward Prosthetic		P	Toward Sound		Toward Prosthetic		P
	Median	IQR	Median	IQR		Median	IQR	Median	IQR	
Mean AV (°/s)	68.1	± 17.2	66.1	± 24.6	0.033*	67.6	± 15.1	62.7	± 15.2	0.101
Peak AV (°/s)	198.7	± 59.7	155.3	± 82.6	0.008*	176.0	± 66.0	168.1	± 46.5	0.007*
Variance AV (°/s)	3605.6	± 2765.0	1687.5	± 2147.3	0.010*	3244.4	± 2029.4	2326.4	± 1187.7	0.002*
SD of AV (°/s)	59.7	± 22.3	41.1	± 24.0	0.008*	56.7	± 18.0	48.2	± 13.3	0.001*
1st Dom Freq (Hz)	0.66	± 0.40	0.40	± 0.33	0.328	0.73	± 0.43	0.49	± 0.40	0.004*
2nd Dom Freq (Hz)	1.74	± 2.25	1.01	± 1.31	0.110	0.81	± 1.28	1.07	± 0.77	0.733
Turn Time (s)	3.3	± 1.1	3.7	± 1.8	0.008*	3.5	± 1.0	3.7	± 1.1	0.144